11TH INTERNATIONAL SYMPOSIUM ON PROCESS SYSTEMS ENGINEERING

PART A

Edited by

I.A. KARIMI AND R. SRINIVASAN

COMPUTER-AIDED CHEMICAL ENGINEERING, 31

PSE 2012

11th INTERNATIONAL SYMPOSIUM ON PROCESS SYSTEMS ENGINEERING

COMPUTER-AIDED CHEMICAL ENGINEERING
Advisory Editor: R. Gani and E.N. Pistikopoulos

Volume 1: Distillation Design in Practice (L.M. Rose)
Volume 2: The Art of Chemical Process Design (G.L. Wells and L.M. Rose)
Volume 3: Computer Programming Examples for Chemical Engineers (G. Ross)
Volume 4: Analysis and Synthesis of Chemical Process Systems (K. Hartmann and K. Kaplick)
Volume 5: Studies in Computer-Aided Modelling. Design and Operation
Part A: Unite Operations (I. Pallai and Z. Fonyó, Editors)
Part B: Systems (I. Pallai and G.E. Veress, Editors)
Volume 6: Neural Networks for Chemical Engineers (A.B. Bulsari, Editor)
Volume 7: Material and Energy Balancing in the Process Industries - From Microscopic Balances to Large Plants (V.V. Veverka and F. Madron)
Volume 8: European Symposium on Computer Aided Process Engineering-10 (S. Pierucci, Editor)
Volume 9: European Symposium on Computer Aided Process Engineering-11 (R. Gani and S.B. Jørgensen, Editors)
Volume 10: European Symposium on Computer Aided Process Engineering-12 (J. Grievink and J. van Schijndel, Editors)
Volume 11: Software Architectures and Tools for Computer Aided Process Engineering (B. Braunschweig and R. Gani, Editors)
Volume 12: Computer Aided Molecular Design: Theory and Practice (L.E.K. Achenie, R. Gani and V. Venkatasubramanian, Editors)
Volume 13: Integrated Design and Simulation of Chemical Processes (A.C. Dimian)
Volume 14: European Symposium on Computer Aided Process Engineering-13 (A. Kraslawski and I. Turunen, Editors)
Volume 15: Process Systems Engineering 2003 (Bingzhen Chen and A.W. Westerberg, Editors)
Volume 16: Dynamic Model Development: Methods, Theory and Applications (S.P. Asprey and S. Macchietto, Editors)
Volume 17: The Integration of Process Design and Control (P. Seferlis and M.C. Georgiadis, Editors)
Volume 18: European Symposium on Computer-Aided Process Engineering-14 (A. Barbosa-Póvoa and H. Matos, Editors)
Volume 19: Computer Aided Property Estimation for Process and Product Design (M. Kontogeorgis and R. Gani, Editors)
Volume 20: European Symposium on Computer-Aided Process Engineering-15 (L. Puigjaner and A. Espuña, Editors)
Volume 21: 16th European Symposium on Computer Aided Process Engineering and 9th International Symposium on Process Systems Engineering (W. Marquardt and C. Pantelides)
Volume 22: Multiscale Modelling of Polymer Properties (M. Laso and E.A. Perpète)
Volume 23: Chemical Product Design: Towards a Perspective through Case Studies (K.M. Ng, R. Gani and K. Dam-Johansen, Editors)
Volume 24: 17th European Symposium on Computer Aided Process Engineering (V. Plesu and P.S. Agachi, Editors)
Volume 25: 18th European Symposium on Computer Aided Process Engineering (B. Braunschweig and X. Joulia, Editors)
Volume 26: 19th European Symposium on Computer Aided Process Engineering (Jacek Je owski and Jan Thullie, Editors)
Volume 27: 10th International Symposium on Process Systems Engineering (Rita Maria de Brito Alves, Claudio Augusto Oller do Nascimento and Evaristo Chalbaud Biscaia, Editors)
Volume 28: 20th European Symposium on Computer Aided Process Engineering (S. Pierucci and G. Buzzi Ferraris, Editors)
Volume 29: 21st European Symposium on Computer Aided Process Engineering (E.N. Pistikopoulos, M.C. Georgiadis and A.C. Kokossis, Editors)
Volume 30: 22nd European Symposium on Computer Aided Process Engineering (David Bogle and Michael Fairweather)

COMPUTER-AIDED CHEMICAL ENGINEERING, 31

11th INTERNATIONAL SYMPOSIUM ON PROCESS SYSTEMS ENGINEERING

PART A

Edited by

Iftekhar A. Karimi
Department of Chemical & Biomolecular Engineering
National University of Singapore, Singapore

Rajagopalan Srinivasan
Department of Chemical & Biomolecular Engineering
National University of Singapore, Singapore

ELSEVIER

Amsterdam – Boston – Heidelberg – London – New York – Oxford
Paris – San Diego – San Francisco – Singapore – Sydney – Tokyo

Elsevier
Radarweg 29, PO Box 211, 1000 AE Amsterdam, The Netherlands
The Boulevard, Langford Lane, Kidlington, Oxford OX5 1GB, UK

First edition 2012

British Library Cataloguing in Publication Data
A catalogue record for this book is available from the British Library

Library of Congress Cataloging-in-Publication Data
A catalog record for this book is available from the Library of Congress

ISBN (Part A): 978-0-444-59507-2
ISBN (Set): 978-0-444-59505-8
ISSN: 1570-7946

Printed and bound in Great Britain

12 13 14 15 16 10 9 8 7 6 5 4 3 2 1

Contents

Highlights on Modeling & Simulation

Highlights on Process & Product Design

Highlights on Process Supervision

Highlights on Process Control

Highlights on Energy

Highlights on Environment & Sustainability

Highlights on Trends in PSE

Highlights on Process Operations

Posters

PART B

Bioprocessing & Biotechnology

Computational Fluid Dynamics

Parameter Estimation

Education

Energy

Enterprise Optimization

Planning & Scheduling

Industrial Applications

Pharmaceutical Systems

Process Design

Process Simulation

Process Monitoring

Process Operations

Product Design

Sustainability & Environment

Water

Oil & Gas

Optimization

Alarms & Sensors

Heat Integration

Distillation

Model Predictive Control

Control Strategies

Modeling and Analysis

Process Synthesis

Biomedical Applications

Preface

The International Symposia on Process Systems Engineering (PSE) have been a triennial tradition since 1982. The series has been organized by the International Organization for Process Systems Engineering with representations from the Asia Pacific Confederation of Chemical Engineering, the European Federation of Chemical Engineering, and the Inter-American Confederation of Chemical Engineering. It has proved to be an attractive global platform for the PSE academics, researchers, and practitioners from all corners of the world for sharing advances in PSE education, research, and application. PSE2012, the 11^{th} in the series, was held in the global village of Singapore during July 15-19, 2012. This 2-part book presents the various plenary, keynote, oral, and poster papers that featured in PSE2012.

While the PSE community continues its focus on understanding, synthesizing, modeling, designing, simulating, analyzing, diagnosing, operating, controlling, managing, and optimizing a host of chemical and related industries using the systems approach, the boundaries of PSE research have expanded considerably over the years. While the early PSE research concerned largely with individual units and plants, the current research spans wide ranges of scales in size (molecules to processing units to plants to global multinational enterprises to global supply chain networks; biological cells to ecological webs) and time (instantaneous molecular interactions to months of plant operation to years of strategic planning). The changes and challenges brought about by the increasing globalization and common global issues of water, energy, sustainability, and environment provided the motivation for the theme of PSE2012: Process Systems Engineering and Decision Support for the Flat World.

PSE2012 involved nearly 340 contributions on modeling, simulation, design, optimization, operations, control, water, energy, environment, sustainability, biosystems, oil and gas, pharmaceuticals, education, industrial applications, and others. Part A includes the plenary, keynote, short oral, and poster contributions, while Part B comprises the full oral presentations.

We are indebted to many from the PSE community, who contributed their invaluable time and effort as members of the three main committees of PSE2012, namely the International Program Committee (IPC), the Local Organizing Committee (LOC), and the Graduate Organizing Committee (GOC). The LOC reviewed nearly 580 initial abstracts and also full-length papers. The IPC members provided at least two timely and critical reviews for each contributed full-length paper. Finally, the GOC led by Naresh Susarla and Mohammad Sadegh Tavallali accomplished the many tedious and challenging tasks required in bringing this book to its current form. We are grateful to the members of all three committees for their voluntary contributions in various capacities.

We hope that this book serves as a useful reference for the PSE community to advance the science and application of Process Systems Engineering.

I A Karimi and Rajagopalan Srinivasan
Chairs, PSE2012

PSE2012 Committees

Symposium Chairs

I A Karimi / R Srinivasan National University of Singapore (NUS)

International Program Committee

L Achenie	Virginia Tech	C Adjiman	Imperial College
R Agrawal	Purdue University	E Almutairi	King Fahd University of Petroleum & Minerals
R M B Alves	University of Sao Paulo	M H Azlan	University of Malaya
B S Babji	ABB Corporate Research	M J Bagajewicz	University of Oklahoma
A Barbosa-Povoa	Universidade Tecnica de Lisboa	P Barton	Massachusetts Institute of Technology
R Batres	Toyohashi University of Technology	M Bhushan	Indian Institute of Technology, Bombay
L T Biegler	Carnegie Mellon University	D Bogle	University College London
P Bongers	Unilever Research	W Budhi Yogi	Bandung Institute of Technology
J Cerda	CONICET-Universidad Nacional del Litoral	C-T Chang	National Cheng Kung University
C-L Chen	National Taiwan University	I-L Chien	National Taiwan University
M A A S Choudhury	Bangladesh University of Engineering and Tehnology	M Doherty	University of California, Santa Barbara
M R Eden	Auburn University	T Edgar	University of Texas, Austin
M M El-Halwagi	Texas A & M University	S Engell	Technische Universitat Dortmund
A Espuna	Universitat Politecnica de Catalunya	X Feng	Xi'an Jiaotong University
C Floudas	Princeton University	D Foo	University Of Nottingham, Malaysia
R Gani	Technical University of Denmark	M Georgiadis	Aristotle University of Thessaloniki
I E Grossmann	Carnegie Mellon University	S K Gupta	Indian Institute of Technology, Kanpur
C Han	Seoul National University	S Hasebe	Kyoto University
G Henning	CONICET-Universidad Nacional del Litoral	G Heyen	University of Liege
M Hirao	University of Tokyo	D B Huang	University of Alberta
H-P Huang	National Taiwan University	D C W Hui	Hong Kong University of Science and Technology
M Ierapetritou	Rutgers University	X Joulia	Procedes Systemes Industriels
N Kaishta	Indian Institute of Technology, Kanpur	J Klemes	University of Pannonia
A Kokossis	National Technical University of Athens	A Kraslawski	Lappeenranta University of Technology
Z Kravanja	University of Maribor	I B Lee	Pohang University of Science and Technology
P Linke	Texas A&M Qatar	A Linninger	University of Illinois at Chicago
S Mahadzir	Universiti Teknologi Petronas	T Majozi	University of Pretoria
Z A Manan	Universiti Teknologi Malaysia	D Manca	Politecnico di Milano

C Maravelias	University of Wisconsin	F Marechal	Ecole polytechnique federale de Lausanne
W Marquardt	Aachener Verfahrenstechnik	H A Matos	Technical University of Lisbon
N Menshutine	Mendeleev University of Chemical Technology of Russia	I Moon	Yonsei university
I M Mujtaba	University of Bradford	C Nascimento	University of Sao Paulo
S Narasimhan	Indian Institute of Technology, Madras	K M Ng	Hong Kong University of Science and Technology
H Nishitani	Nara Institute of Science and Technology	M Noda	Nara Institute of Science and Technology
S Park	Korea Advanced Institute of Science & Technology	S Pierucci	Politecnico di Milano
J M Pinto	Praxair	E Pistikopoulos	Imperial College
V Plesu	University Politehnica of Bucharest	H A Preisig	Norwegian University of Science and Technology
G Reklaitis	Purdue University	J A Romagnoli	Louisiana State University
P K Saha	Indian Institute of Technology, Guwahati	Y Samyudia	Curtin University of Technology
W Seider	University of Pennsylvania	S Shah	GE Oil & Gas
M A Shaik	Indian Institute of Technology, Delhi	D Shin	Myongji University
J Siirola	Sandia National Laboratories	G Sin	Technical University of Denmark
S Skogestad	Norwegian University of Science and Technology	G Stephanopoulos	Massachusetts Institute of Technology
M O Tade	Curtin University of Technology	R Tan	De La Salle University
Y Tsuge	Kyushu University	M Turkay	Koc University
V Venkatasubramanian	Purdue University	S-Q Wang	Zhejiang University
M Wogsri	Chulalongkorn University	D S-H Wong	National Tsing-Hua University
Y Yamashita	Tokyo University of Agriculture and Technology	E S Yoon	Seoul National University
X-G Yuan	Tianjin University	J Zhao	Tsinghua University
K V Dam	Imperial College	E Zondervan	Eindhoven University of Technology

Local Organizing Committee (Singapore)

G P Rangaiah	NUS	M-S Chiu	NUS
D-Y Lee	NUS	P Linga	NUS
A Rajendran	NTU	P Sharratt	ICES
A Adhitya	ICES	BBalagurunathan	ICES
J Eades	Ispahan	S Huang	SUTD

Graduate Organizing Committee (National University of Singapore)

K S Ang	G Krishna
H P Veluswamy	M C Lau
M Kandpal	M Lakshmanan
M S Tavallali	N Susarla
P V Babu	M Sha
S Sharma	Q Su
V K Kamaraju	

I.A. Karimi and Rajagopalan Srinivasan (Editors), Proceedings of the 11th International Symposium on Process Systems Engineering, 15-19 July 2012, Singapore.

A Perspective on Energy and Sustainability

Jeffrey J. Siirola

Purdue University, West Lafayette, Indiana 47907 and Carnegie Mellon University, Pittsburgh, Pennsylvania 15213, USA

Abstract

There is much interest in concepts of sustainability within the chemical industry, especially related to health, safety, and environmental performance, product stewardship, value chain management, efficient use of resources, and mitigation of potential climate change. However, perhaps the greatest sustainability challenges are those associated with energy production and consumption. Energy consumption directly contributes to the majority of carbon dioxide emissions, and recent estimates of future economic growth imply that global energy consumption may more than triple over the coming decades. Since at present carbon capture and sequestration technologies are very expensive, in difficult economic times emphasis will be given first to energy conservation and fuel switching as primary carbon management approaches. A number of current issues will be discussed including economic limitations to implementing energy conservation in retrofit situations, new approaches to the optimal control of energy during process operations, techniques to hasten the utilization of biomass energy sources, and the impacts of shale gas development.

Keywords: carbon management, energy conservation, fuel switching, biomass torrefaction, smart manufacturing

1. Introduction

While contemplating the near and longer term future of the chemical industry, it is instructive to examine the recent past. For the organic chemical industry, it appears that especially for the half-century from 1940 and the advent of synthetic polymers, the industry was driven by substitution and in particular by the substitution by polymeric fibers, films, and plastics for metals, stone, brick, cotton, wool, linen, and paper. As that period of materials substitution matured, the growth rate in the chemical industry instead tended to more closely reflect general economic activity. That activity in turn is related to population size and increases in the standard of living within each region.

The global population has been steadily expanding and has just reached seven billion. However, many projections estimate that over the coming decades it will stabilize, probably at a level just below ten billion. Over the same period, the standard of living as measured by per capita gross economic product, especially in areas currently less well off, is projected to significantly improve largely because of technology. The result of both of these factors is that the global gross economic product is expected to increase by a factor of six-seven over the next five decades. Based on past trends, such an increase would also result in an increased demand for material commodities including the products made by the chemical industry by perhaps a factor of five and an increase

in overall energy demand by more than a factor of three but an electrical energy demand by perhaps a factor of seven. A legitimate concern is raised whether such a magnitude of materials and energy demand increase, even if only approximately accurate, can be sustainably satisfied. That is, can such a demand be satisfied without compromising the ability of future generations to meet their quality of life aspirations?

The current interest in sustainability focuses on a number of areas including environmental protection, health and safety, energy efficiency, product stewardship, industrial ecology, renewable resources, water management, green chemistry, and national security. But perhaps the greatest challenges to sustainability are the issues of climate change and carbon management, and especially those associated with energy production and consumption.

About eighty-five percent of all energy consumed throughout the world today is derived from carbonaceous fossil fuels (natural gas, shale gas, crude oil, coal, lignite, and peat). Coal is the most abundant and the fuel used most for the production of electricity. Oil is the most common source for the production of transportation fuels. Gas is globally the least abundant and is difficult to transport except by pipeline, but is easy to clean, has the greatest energy content per unit of carbon, and traditionally has commanded the highest price.

The present burning of fossil fuels for the production of energy results in the release of carbon dioxide, a portion of which dissolves in the ocean, but the remainder of which adds to the inventory in the atmosphere, currently increasing the CO_2 concentration by a little more than 2ppm per year. Recent atmospheric CO_2 concentrations have exceeded 395ppm compared with the pre-industrial-revolution level of 280ppm. The level is expected to continue to increase at an accelerating rate as annual fossil fuel combustion to meet growing global energy demand continues to grow. There is widespread concern that the increased CO_2 concentration may interfere with nocturnal radiative emission which could lead to increased average temperatures, altered weather patterns, more severe storms, expanded periods and regions of drought, and other manifestations of global climate change. In any event, such a rise in concentration of any atmospheric constituent is in itself a cause for concern.

The present emission of carbon from the combustion of fossil fuel is on the order of 8 billion tons carbon (30 billion tons CO_2) per year. If over the coming decades the global demand for energy more than triples and if the same mix of fossil fuels continues to be burned even with population stabilization, living standard maturity, and a fair amount of energy conservation awareness, these annual emissions could increase to on the order of 30 billion tons carbon (100 billion tons CO_2) per year at which time atmospheric CO_2 concentration could be increasing at something like 7ppm per year to a total concentration between 600 and 700ppm.

Although there may be significant error in these concentration estimates and in the climatic impact of such concentrations, the atmospheric addition of even only a few tons CO_2 per year clearly is not sustainable and as a result policymakers are likely to mandate some kind of fossil fuel combustion restrictions or carbon emission restrictions in the near future. In anticipation of this possibility, a number of reduction and control strategies are being evaluated by governments, research institutions, and companies around the world.

2. Carbon Management

A number of approaches to carbon management have emerged including carbon emissions reduction, carbon capture and permanent storage, and carbon offsetting or recycling. Common carbon capture approaches from flues and other sources of CO_2 include absorption, adsorption, membrane separation, and others. In general, the captured CO_2 is then recovered from the capturing media and then prepared for storage for example as a supercritical liquid in saline aquifers or in depleted oil and gas reservoirs, or adsorbed in coal seams too thin to mine, or dissolved in oceanic waters. Each of the capture methods is sensitive to the CO_2 partial pressure of the source, and each of the storage methods has its own concerns including acidification, stability, leakage, etc. Although the US Government has targets that carbon management should not increase the cost of electricity to consumers by more than 50%, current estimates for base case absorption, recovery, and compression technologies for coal-fired power plants are several times greater than the target. The Carbon Capture Utilization and Storage program was initiated by the US Department of Energy to directly address capture and storage technology and economic performance, risk, and uncertainty in an attempt to accelerate the timeline in which carbon capture and storage could be considered commercially available by a factor of three. Much current research in the component Carbon Capture Simulation Initiative and the National Risk Assessment Partnership is directed to accelerating all phases of carbon capture and storage technology from development through deployment using a framework of science based and valuated performance simulation, technical and financial uncertainty quantification, and risk adjusted decision making.

3. Emissions Reduction

Nevertheless, at the present time, carbon capture and storage appears extremely expensive and no full scale capture systems on commercial power plants have been installed. Therefore, it is expected that first response to any control restrictions or mandates will most likely take the form of engineered emissions reductions. Within the chemical industry these reductions may be approached from several directions. One is energy conservation.

Energy conservation has long been studied within the process systems community. Topics range from simple operational efficiency considerations (turning out unneeded lighting, optimal insulation thickness to minimize heat losses from pipes, proper matching of driver power to machine requirement, etc.) to greater use of energy recovery and reuse (heat exchanger networks, waste incinerators and heat recovery boilers, etc.) to more aggressive conservation consideration during the process design phase (operating condition selection to maximize the opportunities for heat integration especially of latent heats, use of multi-effect configurations in evaporation and distillation, thermally-coupled distillation, process electricity utility and process steam utility cogeneration, etc.). Typical energy savings range from a few percent for operational policies to ten to twenty percent for the incorporation of heat recovery networks to fifty percent or more for multi-effect separations.

Unfortunately, as large as some of these energy savings are, they are most times difficult or impossible to justify economically as retrofit projects, unless other aspects of the project also result in additional manufacturing capacity and additional sales volume potential. Only in these cases does the potential for additional income (in addition to the energy cost savings) offset the capital costs of the energy-conserving process improvement modifications. There have been many studies where it was speculated that a certain rise in energy costs (or perhaps a future energy or carbon tax) alone could justify the new energy conservation capital (calculated from recent equipment cost experience). However, these studies have been almost never borne out, as it is now more widely recognized that chemical plant equipment costs correlate almost exactly with energy (especially crude oil) prices (with a several year delay), and have done so consistently for more than a century. Any study projecting at what future energy price the capital investment for a particular energy-saving technology will finally be justified must carefully consider that the current equipment cost indices will also escalate by a similar ratio. It is because of this effect that energy conserving retrofit projects rarely can be justified in the absence of additional product sales revenue.

4. Smart Manufacturing

However, there is now under consideration a new paradigm called Smart Manufacturing that may also have an important impact on energy conservation. Smart manufacturing is a proposal to use massive amounts of process data and extensive computational resources to enable a dramatically intensified knowledge-enabled chemical process enterprise in which all business and operating actions are executed to achieve significantly enhanced safety, health, environmental, economic, sustainability, and energy performance. Among the concepts included within smart manufacturing especially for energy-intensive industries like the processing industries are greater use of process sensors, much larger stores of process data, the necessary computational infrastructure to allow real-time reconciliation, analysis, and interpretation of process data, and the process modeling and other generation of knowledge needed to make on-line plant-wide optimal control decisions considering the multiple objectives of fitness-for-use, safety, environmental protection, economics, and energy.

In addition to obviously massive computational and IT requirements and installation of many more process sensors, it is anticipated that process engineering modifications will also need to be invented in order to increase the number of control degrees of freedom so that other smart manufacturing objectives and in particular energy consumption may also be optimized in addition to the usual requirements for product fitness-for-use and public safety.

In the present process systems engineering paradigm, it is common practice to design for energy conservation. During process synthesis, lower energy consuming equipment or configuration alternatives can be selected and operating conditions to minimize energy use and maximize heat recovery opportunity can be chosen. However, during actual operation, energy minimization is less often a control objective. Quite to the contrary, if a fitness-for-use specification (for example, product purity) is being missed, it is often the reflux ratio (and energy consumption) that is first increased in an attempt

to return to specification. Likewise, it is to the utility system that control disturbances are rejected (and in doing so generally resulting in increased energy consumption).

One of the aims of the smart manufacturing initiative in the processing industries is to design for and use additional operational degrees of freedom so that with the aid of increased amount of process data and large-scale on-line computational capability, product fitness-for-use goals can be met while at the same time actively optimizing other sustainability objectives including energy minimization. As an example, consider a distillation column fitted with some futuristic additional engineering infrastructure that would allow active sensing and control of phase mixing or approach to flooding (and hence efficiency) on each tray. In such a case, even though the reflux ratio is still used to control product purity, active control of tray efficiency could simultaneously lower that required reflux ratio even though the existing number of trays remains fixed.

5. Fuel Switching

Different carbonaceous fuels have different heats of combustion depending on their composition. The lower heating value heat of combustion (product water remains as a vapor) per carbon atom can readily be estimated from the average "oxidation state" of carbon in the fuel which is turn can be estimated from the molecular formula and considering the constituents in the fuel that will be converted to a mass of water upon combustion. With this scheme, it is readily seen that the heat of combustion per carbon atom of natural gas is about twice that of coal, and that of most liquid hydrocarbon fuels lies about half way in between. This also means that for the same heat production, the amount of CO_2 emissions from burning gas are about half those from burning coal.

That also means that fuel switching will likely be another early approach to carbon emissions reduction. In the US, coal accounts for approximately half of all electricity generation. Although electrical generation is the largest consumer of coal by about an order of magnitude, significant amounts are also burned in heating plants for large institutions (such as universities) and utility boilers (including some in the chemical industry).

In the past, natural gas consumption in the US for electricity generation was limited by both policy and economics. However, policy began to change two decades ago, which has led to many new natural gas electrical generators, especially to meet peaking demand. At the time these new peaking plants first came on line, the available supply of gas could not increase with the result that gas prices rose. This price increase had several effects which included rejection of gas for most base load demand, a much steeper price for peak-hour electricity (leading to more widespread adoption of time-of-day electricity pricing), and decrease use of natural gas as a feedstock in the US chemical industry (except for the production of hydrogen). Under these economic conditions, few users would consider replacing base-load coal even though it has high CO_2 coproduction.

However, high gas prices also encouraged the development of two new production technologies, directional (horizontal) drilling and hydraulic fracturing. These technologies in turn have enabled the exploitation of shale gas, gas contained in

relatively thin and impermeable shale rock formations. Previously, as no extraction technology was known to be practical, shale gas was not even counted among gas reserves. In the US, there are perhaps two dozen shale gas fields, some of them very large. The first to be developed with horizontal drilling and fracturing were so productive, that now official gas reserves in the country have been doubled. This increased production has also fundamentally changed gas pricing structure which has decreased from its historical ratio to the price of both oil and coal on an energy basis by a factor of four. This means natural gas has gone from the most expensive fossil fuel to being the least expensive as well as being the fuel with the greatest combustion energy per unit CO_2 emissions. Natural gas turbines, in addition to being favored for peaking plants is also useful as a backup electricity generation for intermittent wind farms and solar photovoltaic installations because of relative ease in starting and dynamic load following.

With new natural gas economic realities, it may be that a relatively simple carbon emissions reduction technique will be fuel switching of natural gas into existing coal-fired boilers (many pulverized versions of which already have natural gas burners for pilots). Such a conversion requires only minimal capital, but can almost halve carbon emissions (firing a coal-designed boiler with gas results in some derating of output because the ratio of the size of the convective heat section to the radiant heat section is low compared to what it would be in a purpose-designed gas-fired boiler). If low shale-gas-inspired prices continue, the pace of such fuel switching may even accelerate until either gas prices re-equilibrate to some higher value, or virtually all coal firing is eliminated.

A related feature that will further reduce CO_2 emissions from the electricity generation sector is the further installation of natural gas combined cycle (NGCC) technology. This technology combines a very high temperature Brayton cycle gas turbine with a conventional Rankine waste heat bottoming cycle steam turbine and achieves an electrical generation efficiency approaching 60% (compared to 35-40% for coal-fired power plants). This increased electrical generation efficiency combined with the higher heat of combustion per carbon atom means that new NGCC plants could reduce carbon emissions from the coal part of the electric power generation industry by something close to 70% before implementation of capture and storage technology.

6. Biofuel

Another approach to carbon dioxide emissions reduction is the substitution of biofuels for fossil fuels. Biofuels are considered to be carbon neutral, at least after an equal amount of replacement biomass is regrown. Most current biofuels involve conversion of one specific component in the biomass (for example starch or oil) into a specific compound (ethanol or fatty ester methyl ester) typically for use as a liquid fuel for the transportation sector. Much of the remaining energy content in the biomass feedstock is not used.

However, another option which may in fact have a larger and more immediate impact on CO_2 emissions reduction is the direct combustion of biomass in power plants especially as a partial or total replacement for coal. The oxidation state of carbon in

most biomass is about the same as that of the carbon in coal. Per carbon atom, biomass has about the same heat of combustion as coal. However, unlike coal, biomass also carries with it two kinds of water in the form of bulk moisture and in the "hydrate" part of the carbohydrate components starch, cellulose, and hemicellulose. This water not only takes up weight, but its heat of vaporization detracts from the heat of combustion. In addition, it may be difficult to burn bulk biomass in a boiler designed to burn coal. The additional water lowers combustion temperatures which in turn derates boiler capacity. Economizers in boilers designed for coal in particular are undersized when the same boiler burns biomass.

Nevertheless, in regions where significant biomass is available and underutilized including some hardwood and softwood forests and agricultural residues, biomass could be sustainably harvested for coal substitution for electricity production. In addition, some pretreatment technologies, such as the mild form of pyrolysis known as torrefaction, have been proposed which can remove all of the bulk moisture and some of the "hydrate" part of the carbohydrate components producing a dark, relatively dense, hydrophilic, and brittle material that can even be ground and burned in pulverized coal boilers using existing equipment. Depending on the specific nature of the biomass, the torrefaction process can also produce volatile organic coproducts which could be recovered and used to fuel the torrefaction pyrolysis process itself. Torrefied biomass is another way to extract value from the existing coal-fired power generation assets and infrastructure while significantly reducing net carbon dioxide emissions by substituting a carbon neutral fuel for what is now the most CO_2 inefficient fuel.

7. Conclusions

Although there is growing interest in chemical industry sustainability issues such as health, safety, and environmental performance, perhaps the greatest process systems sustainability challenges are those associated with energy production. Energy production directly contributes to the majority of carbon dioxide emissions of growing concern. As presently known carbon capture and sequestration technologies are very expensive, in difficult economic times carbon management emphasis will first take the form of engineered emissions reduction. Emissions reduction by capital retrofit energy conservation techniques have proven to be difficult to economically justify in the absence of increased product sales revenue. Instead, emissions reductions are likely to implemented first by fuel switching especially increasingly plentiful shale gas for coal in electrical power production, and also by increased substitution of whole biomass and especially torrefied biomass for coal which may prove to have a greater environmental impact that the production and use of bioderived transportation fuels. Implementation of the data rich and computing intense smart manufacturing paradigm may also allow energy minimization to be included along with product fitness-for-use objectives in the optimal control of operating chemical facilities.

I.A. Karimi and Rajagopalan Srinivasan (Editors), Proceedings of the 11th International Symposium on Process Systems Engineering, 15-19 July 2012, Singapore.

Optimizing the end-to-end value chain through demand shaping and advanced customer analytics

Brenda Dietrich, Markus Ettl, Roger D. Lederman, Marek Petrik

IBM Research, Yorktown Heights, NY 10598, USA

Abstract

As supply chains become increasingly outsourced, the end-to-end supply network is often spread across multiple enterprises. In addition, increasing focus on lean inventory can often create significant supply/demand imbalances over a multi-enterprise supply chain. This paper discusses a set of integrated analytics for supply/demand synchronization with a new emphasis on customer facing actions called demand shaping. Demand shaping is the ability to sense changing demand patterns, evaluate and optimize an enterprise supply plan to best support market demand and opportunity, and execute a number of demand shaping actions to "steer" demand to align with an optimized plan. First, we describe a multi-enterprise cloud-based data model called the Demand Signal Repository (DSR) that includes a tightly linked end-to-end product dependency structure as well as a trusted source of demand and supply levels across the extended supply chain. Secondly, we present a suite of mathematical optimization models that enable on demand up-selling, alternative-selling and down-selling to better integrate the supply chain horizontally, connecting the interaction of customers, business partners and sales teams to procurement and manufacturing capabilities of a firm. And finally, we describe findings and managerial insights from real-life experiences with demand shaping in a server computer manufacturing environment.

Keywords: Demand shaping, product substitution, configure-to-order, mixed choice models, supply chain visibility.

1. Introduction

In today's competitive and dynamic business environment, companies need to continually evaluate the effectiveness of their supply chain and look for ways to transform business processes to achieve superior customer service and higher profitability. Imbalances between supply and demand are the primary reason for degraded supply chain efficiency, often resulting in delinquent customer orders, missed revenue, and excess inventory. This paper describes a novel supply chain planning and execution process that incorporates demand shaping and profitable demand response to drive better operational efficiency of the supply chain. The proposed methodology aims at finding marketable product alternatives that replace demand on supply-constrained products while minimizing expected stock-out costs for unfilled product demand and holding costs for left-over inventory. While most prior related literature focuses on the concept of Available-To-Promise (ATP) where a scheduling system determines a particular product's availability, this paper proposes a customer-centric approach based on customer choice modeling and demand shaping to dynamically incorporate product substitutions and up-sell opportunities into the supply-demand planning process.

Demand shaping is a demand-driven, customer centric approach to supply chain planning and execution. The aim is to align customer's demand patterns with a firm's supply and capacity constraints through better understanding of customer's preferences which helps influencing customer's demand towards products that the firm can supply easily and profitably. Demand shaping can be accomplished through the levers of price,

promotions, sales incentives, product recommendations, or on the spot upgrades / discounts to enables sales teams to close deals for in-stock products.

The underlying principles of demand shaping are centered on three competencies:

- Customer preference and demand pattern recognition
- Supply capability analysis that provides improved visibility to the sales force on in-stock and out-of-stock products
- Optimal demand shaping based on advanced customer analytics that estimate propensities of customers to purchase alternate products so that the sales force can guide customers to "next-best" product options

Detecting customer preferences and demand patterns relies heavily on predictive analytics and automated gathering of sales data from every customer touch point, including retailer point-of-sales data, channel partner data, and shopping basket or checkout data from e-Commerce sales portals. Such data is often stored in a so-called Demand Signal Repository (DSR), a cross-enterprise database that stores sales data in a format that allows for easy retrieval of information so that a firm can easily query the database to identify what's selling, where, when and how. Supply capability analysis provides timely information on available product supply to identify imbalances between customer demand and available supply. The third competency of optimal demand shaping is to steer customer demand to a preferred set of products that optimizes the firm's profitability and revenue while increasing overall serviceability and customer satisfaction.

In this paper, we propose a methodology for demand shaping based on mathematical models that aim at finding marketable product alternatives in a product portfolio that best utilize inventory surplus and replace demand on supply-constrained products. We explicitly analyze customer expectations in a dynamic setting utilizing a customer choice model that determines how customers evaluate product substitutions if their initial product selection is unavailable. Moreover, we present numerical results that attempt to quantify the business value of demand shaping in a configure-to-order (CTO) supply chain where end products are configured from pluggable components, such as hard disks, microprocessors, video cards, etc., an environment where demand shaping is most effective.

2. Related Literature

The demand shaping approach we discuss in this paper has connections to several problems in related literature streams. Ervolina and Dietrich (2001) describe an application of the implosion technology for order promising in a configure-to-order (CTO) manufacturing environment. Building on this approach, Dietrich et al. (2005) develop a deterministic implosion model that identifies suitable product configurations for an Available-to-Sell process that consume the most surplus inventory and require minimal additional component purchasing costs. Market demand, customer preferences, or product substitution policies are not considered in their model. Chen-Ritzo (2006) studies a similar availability management problem in a CTO supply chain with order configuration uncertainty. Ervolina et al. (2009) employ integer programming to identify marketable product alternatives in a product portfolio that best utilize inventory surplus and replace demand on supply-constrained products. Yunes et al. (2007) apply a

customer migration model in conjunction with mixed-integer programming to determine the optimal product portfolio at John Deere and Company. A customer migration list contains alternative product configuration choices if a customer's preferred product selection is unavailable. Balakrishnan et al. (2005) apply concepts from revenue management to investigate how a firm can maximize profits by shaping demand through dynamic pricing. Liu and van Ryzin (2008) discuss choice-based optimization in the context of network revenue management, and present a static linear programming approximation that relates to the approximate dynamic programming formulation presented in this paper. Dong et al. (2009) employ a stochastic dynamic programming formulation to study inventory control of substitutable products. Finally, Bernstein et al. (2011) present a model of assortment customization, similar to the choice-set manipulation that we model as a possible lever for demand shaping.

3. Customer Choice Model

In addition to the product-level demand patterns that can be derived from sales data collected at customer touch points, demand shaping requires a detailed model of customer decision-making that can be used to predict the success rate of various shaping actions. We model customers' product choices using a discrete-choice framework that casts the likelihood of all possible purchase decisions within a parametric form. Our framework incorporates product attributes, customer characteristics, and additional market signals that may effect customer decisions. The resulting *customer choice model* depicts latent inter-product relationships, and is combined with up-to-date product-level forecasts to give a full picture of demand.

Product demand forecasts and customer choice modeling are integrated into a two-stage decision process for customer purchases. The first stage occurs prior to demand shaping and involves determination of an *unshaped product choice* for each customer. Our assumption is that the distribution of unshaped product choices is, with the exception of some random forecast error, represented accurately by product demand forecasts that are generated through the traditional planning process. We then allow for a second decision stage in which some portion of this forecasted demand is re-allocated by various shaping actions that are applied across the product portfolio. The end result is a *shaped demand* that we expect to observe post-shaping. The customer choice model is used to predict the degree of redistribution that can be achieved through each possible set of shaping actions.

3.1. Representation of Substitution Probabilities

Customer choice analytics support optimization of shaping actions by generating a matrix of *substitution probabilities* to reflect the rate of demand redistribution between product pairs for any potential collection of shaping actions. To start, customers are segmented by a combination of customer characteristics and unshaped product choice. The set Y provides a collection of observable customer profiles, used to group customers by attributes such as, e.g., sales channel, industry segment, length of relationship, etc. For each type $y \in Y$, we obtain at time $t \in T$ an unshaped forecast F_{tyj} of demand for each product j in the product portfolio J. This allows a further segmentation by unshaped product choice, so that shaping actions are targeted at a

segment $s \in Y \times J$, with a forecasted segment size n_{st} equal to the corresponding unshaped forecast. Let $S = Y \times J$ and partition so that S_y contains those segments with customer type *y*.

For each segment s, we operate within a set A_s of admissible shaping actions. An example of a possible shaping action in A_s is to "offer product *i* to segment *s* customers at a 20% discount". As each segment relates to a specific unshaped product choice *j,* actions for that product are intended to redistribute some portion of product *j*'s demand to elsewhere in the portfolio. Since multiple actions may be applied simultaneously, we define an *action profile* $h_s \in H_s \subseteq 2^{A_s}$ to characterize the full set of shaping activities targeted at segment *s*. For each action profile, we provide the optimizer with the following representation of demand redistribution:

$V_s(h_s)$: a |J|-vector of substitution probabilities, such that V_{si} is the proportion of the unshaped demand from segment *s* that is redistributed to product *i* when the action profile h_s is applied.

As a result, we are able to represent the predicted shaped demand for any set of segment-specific action profiles as $\tilde{F}_{ty}(\{h_s\}_{s \in S}) = \sum_{s \in S_y} n_{st} V_s(h_s)$, where $\tilde{F}_{yt}$ itself is a |J|-vector of shaped product demands.

As is often done in the discrete-choice literature (Kök and Fisher 2007), we can decompose the vector $V_s(h_s)$ into the product of a substitution-structure vector $B_s(h_s)$, and a substitution-rate parameter $\delta \in [0,1]$. The parameter δ is an important measure of the overall substitutability between products in the market. In our numerical tests, we will explore the degree to which effective shaping is dependent on a high value of δ. First, we discuss the estimation of $B_s(\cdot)$ from historical orders and customer data.

3.2. Estimation with Mixed Logit Models

For any significant number of products and actions, the large number of required substitution probabilities makes direct estimation of these values prohibitive. Instead, we derive all of the necessary terms from a discrete-choice model containing far fewer parameters. An important element of this model is the ability to accurately represent customer heterogeneity. In particular, substitution patterns reflect the degree to which products draw from overlapping customer pools, which can only be captured meaningfully through a heterogeneous model. To this end, we employ a mixed logit model of demand (McFadden and Train 2000), which extends the standard logit model (McFadden 1974) to incorporate variation in customer preferences.

We fit a demand model for each customer type *y*, using historical orders from the customer set K_y over the time horizon, T_{Hist}. As with the standard logit model, the mixed logit model predicts order probabilities as a function of product attributes. At time *t*, customer *k* has a stochastic valuation of each product *j*, denoted $u_{kjt} = \alpha_k^T x_j + \beta_k z_{kjt} + \varepsilon_{kjt}$, where x_j contains product attributes, z_{kjt} contains information on shaping actions applied at time *t*, $\{\alpha_k, \beta_k\}$ are model parameters to be estimated, and ε_{kjt} is a stochastic error term. In the server environment that we model, attributes in x_j include, e.g., CPU speed, hard drive capacity, hard drive speed, and GB of memory. The second data term, z_{kjt}, contains factors impacting purchasing that may be manipulating through shaping actions. In the simplest case z_{kjt} equals the price p_{kjt}, but this vector can be expanded to encompass quoted order lead-times, marketing intensity, and other relevant factors.

Under the logit assumption that ε_{kjt} are i.i.d. extreme-value distributed, the likelihood of purchase for product *j*, assuming a choice-set J_{kt} of available products, is:

$$L_{kjt|J_{kt}}(\alpha, \beta, x, z) = e^{\alpha_k^T x_j + \beta_k z_{kjt}} / (1 + \sum_{i \in J_{kt}} e^{\alpha_k^T x_i + \beta_k z_{kit}}).$$

Whereas, in the standard logit model, α and β are constant across customers, the mixed logit model allows for these values to vary across the population according to a specified mixing distribution $G_y(\alpha, \beta \mid \theta)$, whose parameters can in turn be estimated. This can be a continuous distribution, i.e. a normal or lognormal distribution, or a discrete distribution, which then gives rise to distinct latent customer segments. In practice, we combine a discrete component of preference variation, which introduces multi-modality into our preference distribution, with a continuous component that is more economical in its use of parameters. The full parameter vector θ is then estimated along with α and β using a maximum likelihood procedure with our historical order set. In this case, simulation must be used to evaluate $E_{G_y}[L_{kjt|J_{kt}}]$, since this quantity no longer has a closed form.

Under the mixed model of demand, customers' unshaped product choices reflect on their personal values of α and β, giving insight into each customer's sensitivity to shaping actions, and the likelihood of accepting specific substitutes. By conditioning the mixing distribution on each customer's unshaped product choice *j* (e.g., Revelt and Train (1999)), or more generally, on their history of product choices, we obtain an individualized mixing distribution, $G_{y|j}$, that is used to assess various targeted action profiles. In particular, we associate, with each action profile h_s, a shaping attribute vector $\tilde{z}(h_s)$ and an alternative product set $\tilde{J}(h_s)$. The likelihood of a segment *s* customer, where this dictates a type *y* and unshaped choice *j,* accepting substitute *i*

when shaping profile h_s is applied, is then provided by the expected value $E_{G_{yij}}[\, L_{kit\tilde{J}_{kt}(h_s)}(\alpha,\beta,x,\tilde{z}(h_s))]$.

This quantity is computed to populate the i^{th} entry in $B_s(h_s)$.

4. Demand Shaping Optimization

Having outlined customer behavior and the effects of shaping actions, we turn in this section to a description of the optimization model that selects our recommended shaping actions. The optimization is based on a stochastic view of demand forecasts and is formulated as a Markov decision process. Because of the large size of the model, we solve it using approximate dynamic programming.

As described above, demand is shaped in the context of a manufacturer which purchases and inventories individual components and then uses them to assemble and sell products. The demand is shaped over a sequence of time periods, which is indexed as $t = 1,2,\ldots$. The set of all component types is denoted by C and the set of all products, as above, is denoted by J. The bill of material is represented by U; that is each product $j \in J$ is assembled of $U(j,c)$ components of type c. Components that are not sold are inventoried; the inventory of a component c at time *t* is denoted $I_t(c)$.

The planning horizon is infinite and future returns are discounted by a given discount factor γ. The purchase of each component is subject to a moderate lead-time l, which we assume to be identical across components. The order size cannot be changed once it is placed.

Demand shaping, as considered in this paper, can address two main types of the supply-demand imbalance: 1) deterministic imbalance, and 2) stochastic imbalance. A deterministic imbalance is known in advance of the lead time for most components, but the supply constraints do not allow to fully satisfy the demand. This kind of imbalance typically occurs after an introduction of a new product or during a long-term component shortage and it may be mitigated deterministically in advance. Stochastic imbalance is not known in advance and only becomes known after it is too late to adjust component supply. This kind of imbalance can be caused by an incorrect demand forecast, an unexpected last-minute supply disruption, or incorrect planning.

Deterministic and stochastic imbalances in the supply chain not only have separate causes, but also require different solution approaches. Since a deterministic imbalance is known within the lead-time of most components, the demand can be shaped into other products and the supply can be adjusted accordingly. Since a stochastic imbalance occurs only after it is too late to modify the component supply, it can only be mitigated by keeping appropriate inventories and shaping the excess demand into products that are available in the inventory. The model described here addresses both deterministic and stochastic supply-demand imbalances.

Components are ordered based on a build-to-order supply policy—that is the supply matches the expected demand. This assumption is made to simplify the model; in most actual applications, the orders would be based on the solution of a newsvendor optimization problem. The actual solution that we use is based on approximate dynamic programming and in essence generalizes the news-vendor solution to multiple stages. Since the supply is assumed to match the product demand, we can ignore component supplies in our model. In addition, all unused components are automatically inventoried with no expiration.

We model the customers using the customer-choice model defined above. In particular, the set S represents the customer segments with a forecasted size n_{st} at time t for a segment s. The forecast is assumed to be made at time $t-l$, the latest time when the supply can be adjusted. Because the forecast must be made in advance, we allow for stochastic disturbances Δ_t in demand, which will lead to imbalances between supply and the unshaped demands. As a result, the realized segment size is a random variable N_{st} with mean n_{st}. The realization of this value at time t becomes known only at time $t+1$.

The realized demand disturbances are normally distributed with mean 0. The distribution used in the model can be arbitrary and can be fit to historical data. The variance of this distribution depends on an external stochastic process of demand variability. Here, we consider a single-dimensional model of variability, denoted ϑ. The variability itself evolves as a normally distributed martingale with fixed variance and zero mean. The demand disturbances Δ across the products are usually negatively correlated with a larger variance in individual products than the total demand. We use Δ_ϑ to denote the covariance matrix.

The realized, unshaped customer demand is modified by taking shaping actions from the set H_s; which includes a no-shaping action option. As described above, the probability of a customer from segment s buying a product i after a shaping action h_s is taken is $V_{si}(h_s)$. Applying action profiles $\{h_s\}_{s\in S}$ at time t results in a realized, shaped demand of $\tilde{D}_{ty} = \sum_{s\in S_y} N_{st} V_s(h_s)$. At the start of the horizon, $\tilde{D}_{ty}$ is a random vector, whose realization will depend on realized values of N_{st} for $s \in S_y$.

The inventory of component type c is subject to a per-item holding cost $c_H(c)$. Taking any shaping action h carries a fixed cost $c_S(h)$—such as the cost of advertising—and variable costs $c_V(h)$—such as product discounts—which are a function of the segment size. The marginal profit for a product j is $c_M(j)$. Finally, the customer model assumes no backlogging---all demand that cannot be satisfied is lost. The overall objective is then to minimize the sum of lost sales due to the product being unavailable, the cost of shaping actions, and the holding costs.

We are now ready to formulate the stochastic optimization problem. If desired, we allow for specific action profiles to be applied to only a portion of a segment. As such, our decision variables π_t represent the probability of taking each shaping action h_s at every time step t for each segment s. These probabilities are denoted as $\pi_t(s, h_s)$.

The main optimization problem in demand-shaping is stochastic due to the uncertain nature of the demand forecasts and can be modeled as a Markov decision process (MDP) (Puterman 2005). The Markov state at time t is represented by the inventory of all products, the demand variability, and the demand forecast. Demand forecast evolves stochastically as described above; the demand variability evolves as a martingale. The Bellman optimality condition for a value function $v_t(I_t, \vartheta_t, n_t)$ is as follows:

$$v_t(I_t, \vartheta_t, n_t) = \min_{\pi_1, q_1} E\left[\begin{array}{l} \sum_{c\in C} c_H(c)\cdot I_t(c) + \sum_{j\in J} c_M(j)\cdot \min\{q_t(j), \sum_{y\in Y} \tilde{D}_{tyj}\} + \\ + \sum_{s\in S}\sum_{h\in H} \pi_1(s,h_s)\cdot(c_S(h_s) + c_V(h_s)\cdot N_{s,1}) + \\ + \gamma\cdot v_{t+1}(I_{t+1}, \vartheta_{t+1}, n_{t+1}) \end{array}\right] \quad (1)$$

Here, we use $q_t(j)$ to represent how many products can be build from the available components and $\gamma \in (0,1)$ to represent the discount factor.

The optimization variables in the problem above are constrained as follows. The first constraint ensures that the shaped demands $\tilde{D}$ are based on the shaping action probabilities π:

$$\tilde{D}_{tyj} = \sum_{s\in S_y}\sum_{h_s\in H_s} N_{st}\cdot V_{sj}(h_s)\cdot \pi_t(s,h_s) \quad \text{for all } y\in Y \text{ and } j\in J.$$

The second constraint ensures that the number of the products sold corresponds to the inventory of each component type:

$$q_t(j)\cdot U(j,c) \le I_t(c) \qquad \text{for all } j\in J \text{ and } c\in C.$$

Note that due to the assumption of the supply matching the deterministic demand n, we can assume that the demand with no shaping is 0. This assumption allows us to study the effects of stochastic imbalances alone and can be easily relaxed. There are additional constraints that ensure that the probabilities of shaping actions in each segment sum to 1 and that the inventories are correctly tracked across time periods.

The optimization problem in Eq. (1) is too large to be solved directly because the value function is defined for continuously many states. Instead, we solve the MDP using approximate linear programming, which is a version of approximate dynamic programming (Powell 2008). Normal distributions are approximated by the Gauss-Hermite quadrature. The shaping decisions are then chosen greedily with respect to the approximate value function.

5. Numerical Experiments

In this section, we evaluate the effectiveness of demand shaping, as it is depicted in Sections 3 and 4, in minimizing backlogging costs that result in the presence of unbalanced supply and demand. We simulate a production/sales environment that is modeled on a realistic problem setting taken from IBM's server supply chain. The simulation has two parameters – the demand variability ϑ and the substitution rate δ – that may be altered to create alternative settings. Within this two dimensional space, we compare the expected backlogging costs that arise both with and without shaping to assess the value of shaping optimization, and to highlight its sensitivity to the two control parameters.

The details of our simulation are as follows: we begin with true historical forecasts and realized customer orders from the hard drive options portfolio supporting IBM's System X line of servers. We link the forecasts directly into the above model to populate F, while we use customer and order data to estimate a substitution structure framework B. We assume a baseline level of supply that exactly covers the forecasted demand, but simulate the stochastic process Δ of demand disturbances to induce supply imbalances, with the potential to correct these through shaping. Our product set consists of 16 hard drives, and we model customer decisions on the basis of hard drive capacity, speed, interface type, and – a potential shaping lever - price. We assume that any unfilled demand will result in lost sales, and evaluate supply chain performance by the percentage of sales that are lost. Results are averaged across 15 simulation runs for each setting. Simulations cover a 30 week horizon, with a discount rate $\gamma = 5\%$ and a cost of 1% of unit revenue for holding inventory across periods.

Figure 1 plots the percentage of sales lost across a range of simulation environments. Each curve is generated at a particular δ (i.e. low, moderate, or high substitutability), and ϑ is varied from zero up to a setting with a coefficient of variation of 22.5% for each product demand. The $\delta = 0$ case provides a baseline where no demand can be shaped, and the improvement from this case illustrates the *value of shaping* in each setting.

The directions of performance improvement for our shaping optimization are quite intuitive. As variability is increased, there is a greater inherent mismatch between forecasts and realized demand. This increases lost sales in all settings, but also presents a larger opportunity to increase performance through shaping. As such, the value of shaping, measured by the performance gap from the $\delta = 0$ case, widens with increasing ϑ. In conjunction, shaping actions become more effective as the degree of substitutability between products is increased, so that the value of shaping increases in the direction of δ as well. When both variability and substitutability are high, the impact of shaping can be dramatic. For example, with high variability and $\delta = 1$, we observe a reduction in lost sales from 13.1% down to only 2.4% with shaping.

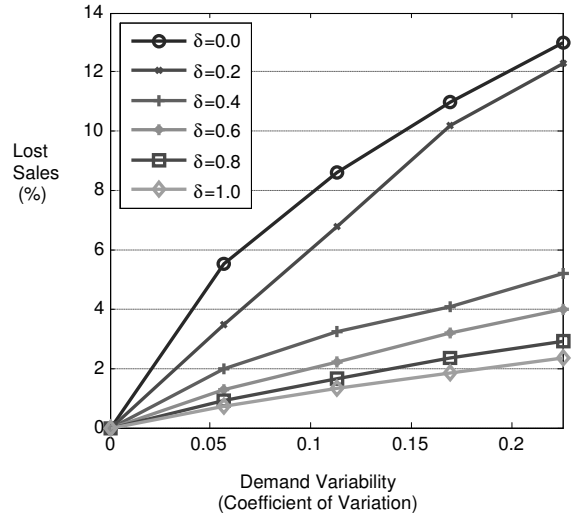

Figure 1: Percentage of sales lost in simulated experiments with demand shaping.

As substitutability is increased from 0, we observe a sharp jump downwards in lost sales resulting from only weak substitutability. For example, in the high variability case, shaping with a conservative substitution rate of $\delta = 0.4$ delivers a relative reduction of 60% in lost sales compared to not shaping. It thus appears, from a product assortment perspective, that only a modest amount of substitutability is needed to successfully implement demand shaping. Interestingly, this result provides something of a demand-side analog to the result of Jordan and Graves (1995) on the steepness of initial returns to production flexibility. A deeper analysis of the interactions between demand shaping and production flexibility may indeed prove worthwhile for future study.

With regards to variability, we observe that the gap in lost sales between each δ curve and the no-shaping curve will increase with ϑ in most cases (the exception is with $\delta = 0.2$, where the gap increases at first, before reaching a threshold where it seems that potential shaping actions are being exploited fully). Despite this trend in performance, it is apparent that additional variability drives a steady increase in lost sales percentage along each curve. Thus, while shaping can soften the deleterious effects of mismatched supply, a comprehensive approach aimed at improved forecast accuracy and/or reduced lead-times is most beneficial. To this end, however, we note that demand shaping will often be the simplest of available measures to implement, and may come at a relatively small cost to the manufacturer. With a strictly supply-side focus, the investment required to achieve a comparable reduction in lost sales can often be prohibitive.

6. Conclusion

In this paper, we have described a mathematical model for demand shaping that aims at finding marketable product alternatives in a product portfolio that best utilize inventory surplus and replace demand on supply-constrained products. We outlined demand shaping actions that improve inventory positions with early and efficient actions to

address surplus materials, and shift demand to available and profitable products through dynamic pricing. Our numerical results showed that more flexible customers are more profitable customers. Market intelligence and data analytics can identify these more flexible customers via market models. For example, a very price-sensitive client may only be presented with two sales recommendations – both of which are alternative-sells or one alternative sell and one down sell. A more price insensitive client may be presented with five dynamic sales recommendations – three are up-sells and two are alternative sells (no down sells). This stratification of clients by price sensitivity and the approach to dynamic sales recommendations will be essential to achieving the business results we have identified.

References

Balakrishnan, A., Y. Xia and B. Zhang. 2005. Shaping Demand to Match Anticipated Supply. In: Proc. Manufacturing & Services Operations Management Conference. Northwestern University.

Bernstein, F., A.G. Kök., L.Xie. 2011. Dynamic assortment customization with limited inventories. Working paper. Fuqua School of Business, Duke University, Durham, NC.

Chen-Ritzo, C.-H. 2006. Availability Management for Configure-to-Order Supply Chain Systems. PhD Dissertation. Pennsylvania State University.

Dietrich, B., D. Connors, T. Ervolina, J.P. Fasano, R. Lougee-Heimer and R. Wittrock. 2005. Applications of Implosion in Manufacturing. In: An, C. and H. Fromm (eds.). Supply Chain Management on Demand. Springer. 97-115.

Dong, L., P. Kouvelis, Z. Tian. 2009. Dynamic pricing and inventory control of substitute products. Manufacturing and Service Operations Management, 11(2), 317-339.

Ervolina, T., M. Ettl, Y.M. Lee and D.J. Peters. 2009. Managing Product Availability in an Assemble-To-Order Supply Chain with Multiple Customer Segments. OR Spectrum, 31, 257-280.

Ervolina, T. and B. Dietrich. 2001. Moving Toward Dynamic Available-to-Promise. In: Gass, S. and Jones. A.T. (eds.) Supply Chain Management Practice and Research: Status and Future Directions. 1-19.

Jordan W., S.C. Graves. 1995. Principles on the benefits of manufacturing process flexibility. Management Science, 41(4), 577-594.

Kök, A.G., M.L. Fisher. 2007. Demand estimation and assortment optimization under substitution: Methodology and application. *Operations Research,* **55**(6), 1001-1021.

Liu, Q., G. van Ryzin. 2008. On the choice-based linear programming model for network revenue management. Manufacturing and Service Operations Management, 10(2), 288-310.

McFadden, D. 1974. Conditional logit analysis of qualitative choice behavior. In: P. Zarembka (ed.), *Frontiers of Econometrics*, Academic Press, New York, NY.

McFadden, D., K. Train. 2000. Mixed MNL models of discrete response. *Journal of Applied Econometrics*, **15**(5), 447-470.

Powell, W. B. 2011. Approximate dynamic programming: Solving the curses of dimensionality. 2nd ed., John Wiley & Sons.

Puterman, M. L. 2005. Markov decision processes: Discrete stochastic dynamic programming. John Wiley & Sons.

Revelt, D., K. Train. 1999. Customer-specific taste parameters and mixed logit: Households' choice of electricity supplier. Working Paper No. E00-274, Department of Economics, University of California, Berkeley, CA.

Yunes, T.H., D. Napolitano, A. Scheller-Wolf and S. Tayur. 2007. Building Efficient Product Portfolios at John Deere and Company. Operations Research 55, 4, 615-629.

I.A. Karimi and Rajagopalan Srinivasan (Editors), Proceedings of the 11th International Symposium on Process Systems Engineering, 15-19 July 2012, Singapore.

Bio-based Value Chains of the Future – An Opportunity for Process Systems Engineering

Wolfgang Marquardt, Andreas Harwardt, Sebastian Recker,
Joern Viell, Anna Voll

AVT–Process Systems Engineering, RWTH Aachen University, 52064 Aachen, Germany

Abstract

This paper argues for a paradigm shift to properly address the requirements of model-based design of future bio-based value chains. Rather than focusing on the process with emphasis on separations and heat integration, the decisions on the molecular level require much more attention. A rough sketch of a systematic sequential and iterative model-based design strategy is presented and illustrated by a few examples related to the manufacturing of future bio-based fuels.

Keywords: Bioeconomy, biofuels, bio-based chemicals, process synthesis, process design, molecular sciences, reaction pathways, reactor synthesis

1. Introduction

Different scenarios have been published recently which predict the depletion of fossil carbon resources for the production of fuels, chemicals and materials in face of the increasing demand of a growing world population. The substitution of fossil by biorenewable carbon feedstock seems to be inevitable to stop the increase of the average surface temperature on our planet by equilibrating global CO_2 binding and release.

The shift from fossil to biorenewable carbon offers a unique opportunity to design new value chains, which are tailored to the feedstock properties while exploring a novel product range (Marquardt et al., 2010). The first opportunity is the exploitation of the rich molecular structure of biomass to the extent possible (Sanders et al., 2007). Rather than breaking its molecular structure into C_1 building blocks, either by gasification to synthesis gas (CO, H_2) or by anaerobic fermentation to a methane-rich gas (CH_4, CO_2, H_2), the synthesis power of nature should be preserved by exploiting and refunctionalizing the native molecular structures in the feedstock into new chemicals, materials and fuels. A second opportunity is the replacement of existing molecular products by novel products of comparable performance in a desired application. Current molecular products contain little oxygen because they are derived from oxygen-free fossil carbon feedstock. In contrast, future bio-based products should contain higher oxygen content to reduce the amount of oxygen to be released during processing as either CO_2 or H_2O. While the former alternative reduces carbon efficiency and contributes to the climate problem, the latter requires large amounts of hydrogen, which has to be produced sustainably.

Such a perspective of the future calls for a radical change in chemical and biochemical catalysis, in the associated process technologies, and in the strategies towards novel molecular and functional products. A holistic systems approach orchestrating experimental and model-based methods and tools across disciplines in a complementary manner offers an enormous potential for sustainable, first-time-right solutions (Bakshi & Fiksel, 2003). Process systems engineering (PSE) is in a perfect position to address

this challenge by *extending its scope* to become a leader in implementing this transition in the next decades. This way, our field can effectively contribute to address the global challenges our society is facing (Glenn & Gordon, 2007).
This contribution will focus on opportunities for *process design and synthesis*. In particular, we will motivate a paradigm shift in process design in Section 2: Rather than taking raw materials, products, reactions and reaction pathways as well as a first process flowsheet for granted, these choices should become part of integrated and rational, ideally model-based decision-making to achieve an optimum in terms of sustainability. Following the PSE tradition, all significant aspects might be cast into an optimization problem which is solved to global optimality. Obviously, model complexity and limitations of numerical optimization methods prevent such a strategy. Rather, decomposition of the multi-faceted design problem is unavoidable to arrive at manageable subproblems. A first sketch of such a strategy is presented in Section 3. A brief outlook on future research needs is finally given in Section 4.

2. Designing bio-based processes – need for a paradigm shift?

Established process design usually starts off when the raw materials and the products have been fixed and a promising reaction pathway has been identified (Douglas, 1988). Stoichiometry and yield of this sequence of reactions fix the material flows from raw materials to target and side products. The given pathway is then translated into a flowsheet consisting of interconnected reactors and unit operations. While flowsheet design is a creative work process largely driven by experience, mass and energy balancing, the choice of suitable unit operations, heat integration or the estimation of cost and expected revenue constitute routine engineering tasks. All these tasks are well-supported by process design software, which is routinely employed in industrial practice. As a consequence of this established approach, process economics is largely determined by the often rational, but typically not model-based selection of the reaction pathway by chemists and the process flowsheet by process engineers. A similar strategy is also followed in process revamping: while aiming, e.g., at an improvement of reaction selectivity and conversion or at the debottlenecking of existing process units the reaction pathway and (basic) flowsheet structure are typically not questioned. Consequently, early design decisions – being often heuristic and experience-based – run at risk to bias the technological development and to miss promising research results in chemistry or process engineering which could enable innovative process concepts.
The history of the Organosolv process for the pretreatment of native biomass as part of future biorefineries can serve as an educating example to underline this argument. Originally invented by chemists as early as 1931 (Kleinert & v. Tayenthal, 1931), this process relies on some aqueous-organic solvent mixture to produce pulp from wood or to fractionate wood into its components lignin, hemicellulose, and cellulose. Despite the continuous improvements to realize environmentally friendly reaction conditions, the concept has been discredited when a pilot plant had to be shut down due to technical and economical deficits in the early 1990s (Hergert, 1998). However, the potential of the Organosolv process as a first step toward the production of bio-based chemicals, materials or fuels from the variety of available lignocellulosic feedstock lead to a revival of this technology. Recent cooperative research has led to an impressing technology readiness level (Michels & Wagemann, 2010), though conceptual process design and model-based analysis have largely been neglected. Consequently, the developed process may still be economically unviable and may face scale-up pitfalls.

Obviously, model-based analysis and scale-up studies carried out prior to building a large-scale pilot plant would reduce the risk of unsatisfactory plant performance which might even jeopardize the success of the biorefinery concept as a whole. Our recent conceptual design study of the Organosolv process has identified significant room for improvement. For example, the energy demand of the costly solvent recovery system can be reduced by heat integration by 89 % (Viell et al., 2012). An economic analysis shows that the improved process can be profitably operated even at capacities well below that of current world-scale plants. Still, our systematic analysis identifies serious deficits inherent to the Organsolv process, such as large solvent streams and a high energy demand of the separation system. While the latter can be tackled by yet not fully exploited heat integration, the efficiency of the Organosolv process is still much lower than that of fossil refinery processes.

Radical improvement might be materialized, if tailored solvents and reaction media are employed to facilitate innovative process concepts off the beaten track. For example, a biphasic aqueous-organic electrolytic solvent system could be chosen to facilitate lignocellulose fractionation solvent recovery in an integrated process (vom Stein et al. 2011). Such a concept encourages integrated reaction and separation in a single unit which constitutes the core of a highly integrated pulping process. Unfortunately, the reaction mechanisms and kinetics of this and related biomass pretreatment processes are not yet adequately understood to support model-based design. Intensive research is required to unveil new promising mechanisms for wood pretreatment, such as chemical disintegration and fractionation by means of ionic liquids (Viell & Marquardt, 2011) or by their mixtures with molecular solvents (Rinaldi, 2011).

This example motivates that an innovative formulation of the process design problem should not only address reaction, separation and recycling strategies on the flowsheet level, but should rather include decision-making on the molecular level (e.g., Bardow et al. (2010)). Such extended design strategies not only require intense collaboration between chemists and process engineers, but also a shift in the research agenda to overcome inherent methodological limitations. For example, complex reaction chemistry and phase behaviour (i.e., organic-aqueous electrolyte mixtures or non-aqueous electrolyte systems with various dissolved macromolecular species) cannot yet be described by available property models at desirable accuracy. Moreover, experiments have to be carried out to allow for quantitative (reaction kinetics) modelling, following for example, the concept of model-based experimental analysis (Marquardt, 2005).

3. Toward an incremental strategy for integrated design of value chains

State-of-the-art process design focuses on the degrees of freedom available after the reaction pathway has largely been fixed. Such an approach will inevitably miss the true potential buried in the reaction (sequence), catalyst systems and reaction solvents. Though integration of chemistry- and process-related decision-making practiced in industry to some extent, systems-oriented methods and tools are largely lacking. Rather, design problems are currently often approached pragmatically, hence, running at risk to miss truly innovative solutions as demonstrated by example in the previous section.

The predicted manifold capacity increase in chemical industries and the advent of bio-based value chains emphasize the necessity to integrate process and molecular level decision-making. Rather than waiting for the “pull” of the evolving bioeconomy and applying established, but inadequate design methodologies, researchers in PSE should shift their attention and develop appropriate methodologies which systematically

address molecular degrees of freedom in addition to those on the process level. Due to the complex nature of biobased raw materials as well as the increasing importance of sustainability, decisions on the most promising reaction steps and pathways, on proper compartmentalization of reactions, on efficient catalysts and reaction solvents, on non-standard (often multi-phase) reactor systems, and on an integration of reaction and separation in either a single multi-functional unit or in non-standard reaction-separation flowsheet structure have to be routinely addressed during design. Such an extended scope of systematic, model-based process design and optimization results in a design problem of unprecedented complexity, because it spans multiple scales from the molecular level to the level of the process, the site or even the complete value chain. Since an "all-in-one" formulation and model-based solution of such a design problem does not seem to be tractable, an incremental strategy is suggested to comprehensively address the requirements of designing future bio-based value chains.

The proposed concept assumes given raw material and target product molecules, though product and raw material design could be integrated into process design. The design problem is addressed here on three levels: the reaction, the device and the flowsheet level. The decision on a reaction pathway on the *reaction level* is based on a material-flow analysis of a set of promising pathways through a network of chemical compounds linking raw materials and target products. The reactions (and material flows) are not yet associated to a "physical" reaction compartment. This decision constitutes the first step of the *device level*, where a reaction kinetic model is used to decide on a network of reaction compartments to refine the yield-based approach employed on the reaction level. At the same time, the number and interconnection of reaction and separation subsystems is determined for specified target split factors and/or recoveries. In a second step, separation system variants are generated and evaluated for feasibility and effort using shortcut methods. This decision making process results in a spatially resolved allocation of the reaction or separation tasks to a device in the spirit of task-based design (Menon et al., 2007), thus proposing a first flowsheet configuration. The realization of the devices in concrete pieces of equipment and their connectivity to a process flowsheet are decided on *the flowsheet level*. Major equipment design parameters are optimized rigorously by minimizing total annualized cost subject to mass and energy balances and rigorous physical property and reaction kinetic models.

On each level, the number of possible alternatives is reduced, while the degree of detail is refined in order to obtain a sustainable process, thus generalizing the process synthesis framework of Marquardt et al. (2008) to reaction-separation processes. Furthermore, the uncertainties on the different levels are addressed systematically by propagating available results to the following more detailed steps. Since assumptions in a previous step may be disproved in a subsequent step, iterations are not only unavoidable but also desirable. The incremental refinement and improvement can be stopped once the postulated design targets are fulfilled.

In the following, the individual design levels and their relations are introduced and sketched from a methodological perspective. They are illustrated in parallel by means of exemplary design problems arising in the context of designing a process for the production of the novel biofuel candidate 2-methyltetrahydrofuran (2-MTHF).

3.1. Reaction level

The objective on the reaction level is to assess possible reaction pathways for the molecular transformation of a given raw material to a desired molecular product from a process perspective. Relevant design decisions are pointed out, including the selection of (a few) favourable pathways for a more detailed analysis regarding energy and raw

material demand, carbon footprint, product yield and selectivity or production cost. Consequently, the reaction level is designed to link the traditional areas of bio-/chemo-catalysis and conceptual process design, thus bridging the disciplinary gap between chemistry and process engineering. This early design stage is characterized by many reaction pathway alternatives and, at the same time, by very little data on reactions and fairly uncertain property predictions. Under these circumstances, the use of established conceptual process design methods is not only very time-consuming, if possible at all, but also not very informative in face of the lack of valid information on reactions, material properties and process performance. To reduce the reaction pathway alternatives to a manageable number, fast screening methodologies are required to accomplish a first crude characterization of the target production process. Even though the analysis of large reaction networks is well established in metabolic pathway analysis (Varma & Palsson, 1994), and the design of reaction networks in the context of chemical synthesis has been discussed for a long time (e.g., Mavrovouniotis & Bonvin (1995) or Broadbelt et al. (2004)), systematic screening strategies for the assessment of reaction pathways in the context of process design are still scarce, but have received some attention recently in the context of biorenewables processing (Cherubini & Stromman, 2010; Pham & El-Halwagi, 2011).

Motivated by metabolic pathway analysis and by the challenges of designing innovative bio-based value chains, a novel reaction scouting method called "Reaction Network Flux Analysis" (or RNFA for short) has been developed to assist model-based selection of promising reaction pathways in the early stage of process design (Besler et al., 2009, Voll & Marquardt, 2011). All relevant reactions are summarized in a network including all known reaction alternatives in the sense of a superstructure such that stoichiometric material balances can be formulated for all the substances to result in a set of linear equations. This basic model can be extended by yield constraints or by selected performance models to predict, for example, the overall product yield, the use of main and auxiliary reactants such as H_2, or the formation of (undesired) by-products such as CO_2 or H_2O. It is also possible to estimate indicators for investment and operating cost or for process sustainability such as carbon or energy efficiencies and environmental impact without having completed the process design process. The promising reaction pathways can be found as the multiple solutions of a mixed-integer optimization problem which minimizes or maximizes a given objective function reflecting multiple selected performance criteria. Finally, the different reaction pathways can be compared according to even additional evaluation criteria. The analysis not only reveals most promising pathways, but also identifies single reaction steps which have tremendous impact on performance and hence require further attention – either in the following investigation on the device level (to reduce uncertainty in the assumptions on yield or selectivity) or in catalysis research (to search for catalyst systems with higher turnover number).

The RNFA methodology has recently been used to evaluate reaction networks for the production of 10 novel biofuel candidates and to compare them to those of more common biofuels like ethanol or butanol (Voll & Marquardt, 2012). Assuming that the same amount of fuel energy should be produced by each pathway, a multi-objective optimization problem accounting for environmental impact and total annualized cost has been solved for each fuel candidate to identify the most competitive fuel product and corresponding reaction pathways. This model-based screening suggests 2-MTHF as a target biofuel and the pathway shown in Fig. 1. Starting from glucose, 2-MTHF can be synthesized via hydroxymethylfurfural (HMF) and levulinic acid (LA) followed by a

sequence of hydrogenation and dehydration reactions (Geilen et al., 2010). According to lab experience, the reaction pathway can be subdivided into two reaction systems, namely A for converting glucose to LA and B synthesizing 2-MTHF from LA. The yield of the acid-catalysed reaction system A limited by decomposition of glucose and HMF to humines. The reaction forming 2-MTHF is catalyzed by a ruthenium-based catalyst with a triphos-ligand and a p-toluene sulfonic acid additive. Selectivity towards 2-MTHF is high at 95%, with pentanol being the major by-product. The aqueous-organic mixture exhibits a miscibility gap, which can be exploited for separation. However, a simple liquid-liquid phase split does not result in the product purity, because the water produced in the dehydration has to be completely removed from 2-MTHF for fuel application.

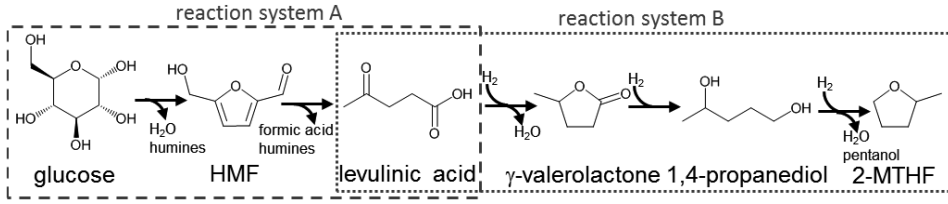

Figure 1: Reaction pathway for the production of 2-methyltetrahydrofuran

3.2. Device level

The goal on the device level is to close the gap between the reaction level and the flowsheet level by evaluating the assumptions made on the reaction level, optimizing the reactions, deciding on reaction compartments, and validating the feasibility of the chosen separation strategies. The result of this step is a network of *devices* which assign an abstract reaction or separation task to a physical compartment without deciding on its technical realization. This is similar to the first steps of the (heuristic) hierarchical framework for conceptual design introduced by Douglas (1988). In particular, the Douglas methodology starts with clustering the reactions of the network into groups of reactions which can take place in the same *reaction device*. Starting from the results obtained on the reaction level, a single or a set of contiguous reaction steps is mapped to an *"elementary process"* (using the terminology of Douglas). The result is a partial decoupling of the reaction pathway into sequences of reactions carried out in individual *reaction devices*, which are possibly structured into *reaction compartments*, and which are typically separated by *separation devices*. While reaction compartments are modeled by well-mixed, homogeneous volume elements, the separation devices are represented by splitters with given target split factors. Although such modular frameworks have been suggested before in process synthesis (Papalexandri & Pistikopoulos (1996) and later work), they either restrict the achievable product composition to reaction equilibrium (Ismail et al., 2001) or they use superstructure-based methods to account for different flowsheet options (Linke & Kokossis, 2003).

For an assessment of the validity of the assumptions on the reaction level regarding reaction yield and selectivity, for the optimal choice the reaction conditions and for the decision on the network of reaction and separation devices, a classical mass-exchange network is used to model the interconnections of the reaction and separation devices. Each reaction device is structured and represented by a network of reaction compartments, which is subject to structural optimization. There are various possible formulations to derive candidate networks of interconnected reaction and separation devices. For example, Peschel et al. (2010) uses the concept of elementary process functions. A fluid element is tracked on its way along a (spatial or temporal) reaction

coordinate. During its travel, the state of the fluid element defined by concentrations, temperature, and pressure, for example, can be manipulated by reaction and heat and mass transfer fluxes. Thus, an optimal state trajectory of the element in thermodynamic state space can be decided. An analysis of this trajectory provides insight into the choice of promising device networks. While largely neglecting the separations, Peschel et al. (2010) decide on the type of reactor system by experience and refine it by a model-based approach. In contrast, we prefer to use nonlinear programming to first decide on the compartment structure of a reaction device embedded in a postulated network of reaction and separation devices (Recker & Marquardt, 2012). This way, reaction device performance can be assessed at an optimal operating point accounting for relevant external (feed and effluent) streams without fixing the type of reactor a priori.

Deciding on the internal structure of each reaction device requires knowledge about the kinetics of the reactions in the relevant part of the pathway including undesired side reactions. Hence, in contrast to the reaction level, a number of decisions regarding molecular transformations have to be fixed to allow postulating a likely reaction mechanism, which is a prerequisite for reaction kinetic modeling. Consequently, reaction solvent selection, catalyst design, reaction kinetic experiments as well as reaction kinetic modeling have to be carried out before the calculations on the device level become possible. The objective used for deciding on the compartment network of the reaction device can be the same as the one employed in RNFA. Then, the results obtained on the device level (for possibly different chemistries) can be abstracted into yields, which may be fed back to the reaction level to repeat the RNFA with refined assumptions to revise the rating of the reaction pathway alternatives.

The described approach has been used to structure the reaction device implementing the elementary process A from glucose to LA in Fig. 1 using reaction kinetics and side reactions of an acid-catalyzed pathway proposed by Girisuta et al. (2007). A single compartment is found to constitute the optimal device structure, because the rates of the side reactions are an order of magnitude slower than those of the main reactions. The elementary process exhibits a yield of 77 %, which is beyond the yields reported in literature (Huber et al., 2006) and assumed in RNFA analysis on the reaction level.

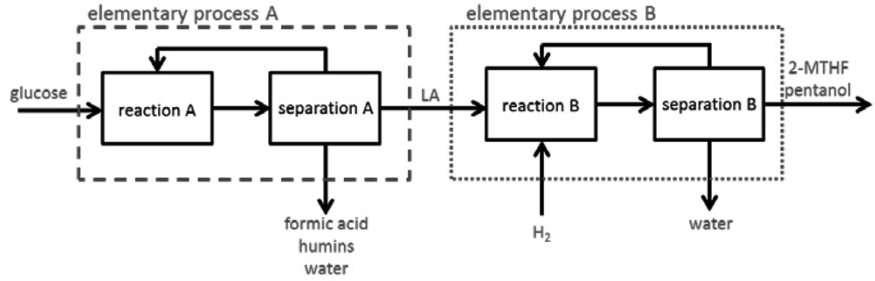

Figure 2: Device network for the production of 2-MTHF

After a device network of the process has been optimized assuming ideal separation (see Fig. 2 for 2-MTHF process), the thermodynamic and economic feasibility of the separations have to be investigated. Candidate separation sequences are constructed (manually) based on insight into the thermodynamic mixture behavior and process specifications. Separation sequence alternatives can efficiently be rated by means of shortcut methods. The separation is always analyzed in combination with the structured reactor device to properly handle the coupling of reaction and separation. Exemplarily, the separation system for elementary process B is designed to separate 2-MTHF from

the reactor effluent containing water, pentanol and 2-MTHF (cf. Fig. 2). Three different flowsheet variants have been created based on a thermodynamic analysis of the mixture and have been screened using the feed pinch shortcut method of Kraemer et al. (2010).

3.3. Flowsheet level

The device structure determined on the device level is the starting point for the development of candidate flowsheets and their rigorous optimization on the flowsheet level. Consequently, the network of separation and reaction devices is refined to a process flowsheet constituting of concrete concrete reactors and unit operations. In particular, the structured reactor device has to be mapped to concrete reactors and the separation sequences have to be detailed with respect to their technical realization. The large number of structural and continuous degrees of freedom cannot be adequately addressed by heuristic rules, process simulation and sensitivity analysis (Barnicki & Siirola, 2004). Therefore, the promising sequences are optimized by means of deterministic mixed-integer optimization minimizing total annualized cost. Each of the separation variants is detailed by a superstructure to capture additional technical detail, for example the number of trays and the feed and sidestream trays in a distillation column (Viswanathan & Grossmann 1990) which is part of the separation sequence. A similar approach could be used to detail the design of the reactor systems.

The mixed-integer optimization problem can robustly be solved by employing the results from shortcut evaluation on the device level for efficient initialization and by its reformulation into a continuous optimization problem (Kraemer et al., 2009). Still, these difficult problems can only be solved if robust formulations and solution strategies are available. For example, the switching from two to three phases on the trays in heteroazeotropic distillation has been tackled successfully only recently (Skiborowski et al., 2012) by tailored sequential and simultaneous optimization strategies. All models used on the flowsheet level rely on rigorous property prediction models in addition to reaction kinetic models. Since model parameters are often not available to predict the behaviour of the complex mixtures arising in biorenewables processing, the missing parameters have to be determined experimentally or need to be estimated by some computational chemistry approach such as molecular dynamics, CosmoRS, group contribution methods or quantitative structure-property relationships.

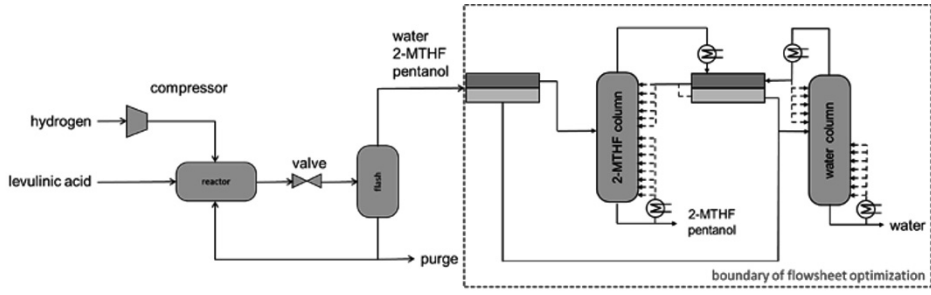

Figure 3: Process flow diagram with superstructure for the optimization of the 2-MTHF purification

The most promising flowsheet variant found on the device level for elementary process B (cf. Fig. 1) consists of two decanters and two distillation columns; the corresponding superstructure is shown in Fig. 3. The vaporous reactor effluent is first condensed and split into two liquid fractions, each of which is fed to a distillation column. In both columns, the product is withdrawn at the bottom at high purity. The composition at the top corresponds to the vapour line of the miscibility gap, which starts at the minimum

boiling heteroazetrope of 2-MTHF and water. Rigorous mixed-integer optimization is used to minimize for total annualized cost by fixing the column designs and the operating point. A total energy demand of about 2.6% of the energy content of the fuel (Geilen et al., 2010) was determined for the cost-optimal design. The cost of separation can further be reduced by heat integration. In particular, recompression of the top vapour can be used to provide the heat of vaporization, which allows for a reduction of 75% in energy demand and of 54% in cost. Hence, the resulting energy demand is an order of magnitude lower than that of bioethanol production (Vane, 2008).

4. Conclusions

This paper presents a first and rough sketch of a process design methodology which extends the scope of traditional PSE from decision-making on the flowsheet to the molecular level in order to address the multiple and often competing objectives of sustainability in the emerging bioeconomy. The extended scope of process design introduces a number of complications, including the need of improved models to predict molecular phenomena, which can be integrated into reactor system and flowsheet design as well as proper formulations of the multi-scale and multi-objective decision-making problem. Since a direct solution of the design problem will not be possible, decomposition and iterative refinement of promising alternatives for the subproblems become mandatory. As always, decomposition runs at risk to miss important interdependencies. This trade-off between the desired holistic treatment and the inevitable decomposition of the design problem as well as the existing limitations of model-based design approaches will constitute the major future research challenges. Interdisciplinary cooperation between PSE and the molecular sciences seems to be a key to success, because truly innovative process solutions are typically initiated on the molecular level. Vice versa, the tradition of quantification in PSE has to offer a lot to the exploratory research in the molecular sciences. In particular, model-based approaches can provide focus and orientation in the discovery process to systematically track down the truly golden “needles in the haystack”.

Acknowledgements

This work was performed as part of the Cluster of Excellence “Tailor-Made Fuels from Biomass”, which is funded by the Excellence Initiative by the German federal and state governments to promote science and research at German universities and by the European Community’s Seventh Framework Programme [FP7/2007-2013] for SYNFLOW under grant agreement n° NMP2-LA-2010-246461.

References

B. R. Bakshi, J. Fiksel, 2003, The quest for sustainability: Challenges for process systems engineering, AIChE Journal, 49, 1350-1358

A. Bardow, K. Steur, J. Gross, 2010, Continuous molecular targeting for integrated process and solvent design, Ind. Eng. Chem. Res.. 49, 2834–2840

A. Besler, A. Harwardt, W. Marquardt, 2009, Reaction networks – A rapid screening method, In: J. Jeszowski, J. Thullie (Eds.) Proc. 19th European Symposium on Computer Aided Process Engineering, Elsevier, 243-248

L. Broadbelt, J. Pfaendtner, 2005, Lexicography of kinetic modeling of complex reaction networks, AIChE Journal, 51, 8, 2112 – 2121

F. Cherubini, A. Stromman, 2010, Production of biofuels and biochemicals from lignocellulosic biomass: Estimation of maximum theoretical yields and efficiencies using matrix algebra, Energy Fuels, 24, 4, 2657–2666

J. M. Douglas, 1988, Conceptual Design of Chemical Processes, McGraw-Hill, New York
F. Geilen, B. Engendahl, A. Harwardt, W. Marquardt, J. Klankermayer, W. Leitner, 2010, Selective and flexible transformation of biomass-derived platform chemicals by a multifunctional catalytic system, Angew. Chem., 49, 5510-5514
B. Girisuta, L. P. B. M. Janssen, H. J. Heeres, 2007, Kinetic study on the acid-catalyzed hydrolysis of cellulose to levulinic acid. Ind. Eng. Chem. Res., 46, 1696-1708
J. C. Glenn, T. J. Gordon, 2007, State of the Future, the Millennium Project. United Nations Publications
H. L. Hergert, 1998, Developments in Organosolv pulping – An overview, In: R. A. Young, M. Akhtar (Eds.), Environmentally Friendly Technologies for the Pulp and Paper Industry, 5-68
G. W. Huber, S. Iborra, A. Corma, 2006, Synthesis of Transportation Fuels from Biomass: Chemistry, Catalysts, and Engineering, Chem. Rev., 106, 4044-4098
S. R. Ismail, P. Proios, E. N. Pistikopoulos, 2001, Modular synthesis framework for combined separation/ reaction systems. AIChE Journal, 47,3, 629-649
T. Kleinert, K. v. Tayenthal, 1931, Über neuere Versuche zur Trennung von Cellulose und Inkrusten verschiedener Hölzer, Angewandte Chemie, 44, 788-791
K. Kraemer, S. Kossack, and W. Marquardt, 2009, Effficient optimization-based design of distillation processes for homogenous azeotropic mixtures. Ind. Eng. Chem. Res., 48, 14, 6749–6764
K. Kraemer, A. Harwardt, M. Skiborowski, S. Mitra, W. Marquardt, 2011, Shortcut-based design of multicomponent heteroazeotropic distillation. Chem. Eng. Res. Design, 89, 8, 1168 – 1189
P. Linke, A. Kokossis, 2003, Attainable reaction and separation processes from a superstructure-based method. AIChE Journal, 49, 6, 1451-1470
W. Marquardt, 2005, Model-based experimental analysis of kinetic phenomena in multi-phase reactive systems, Chem. Eng. Res. Design, 83, 561–573
W. Marquardt, S. Kossack, K. Kraemer, 2008, A framework for the systematic design of hybrid separation processes, Chin. J. Chem. Eng., 16, 3, 333–342
W. Marquardt, A. Harwardt, M. Hechinger, K. Kraemer, J. Viell, A. Voll, 2010, The biorenewables opportunity - toward next generation process and product systems, AIChE Journal, 56, 2228-2235
M. Mavrovouniotis, D. Bonvin, 1995, Towards design of reaction pathways, AIChE Symposium Series, 304, 91, 41-51
A. R. Menon, A. A. Pande, H. J. M. Kramer, P. J. Jansens, J. Grievink, 2007, A task-based synthesis approach toward the design of industrial crystallization process units, Ind. Eng. Chem. Res., 46, 3979-3996
J. Michels, K. Wagemann, 2010, The German lignocellulose feedstock biorefinery project, Biofuels Bioproducts & Biorefining 2010, 4, 263–267
K.P. Papalexandri, E.N. Pistikopoulos, 1996, Generalized modular representation framework for process synthesis. AIChE Journal, 42, 4, 1010-1032
V. Pham, M. El-Halwagi, 2011, Process synthesis and optimization of biorefinery configurations, AIChE Journal, doi: 10.1002/aic.126040
A. Peschel, H. Freund, K. Sundmacher, 2010, Methodology for the design of optimal chemical reactors based on the concept of elementary process function. Ind. Eng. Chem. Res., 49, 10535-10548
S. Recker, W. Marquardt, 2012, A nonlinear programming approach to conceptual design of reaction-separation systems, In: I. D. Lockhart Bogle, M. Fairweather (Eds.), Proc. 22nd European Symposium on Computer Aided Process Engineering, in press
R. Rinaldi, 2011, Instantaneous dissolution of cellulose in organic electrolyte solutions, Chemical Communications, 47, 511-513
J. Sanders, E. Scott, R. Weusthuis, H. Mooibroek, 2007, Bio-refinery as the bio-inspired process to bulk chemicals, Macromolecular Bioscinece, 7, 105-117
M. Skiborowski, A. Harwardt, R. Hannemann, K. Kraemer, W. Marquardt, manuscript in preparation
L. M. Vane, 2008, Separation technologies for the recovery and dehydration of alcohols from fermentation broths. Biofuels, Bioproducts and Biorefining, 2, 6, 553–588.
A. Varma, B. Palsson, 1994, Metabolic Flux Balancing – Basic concepts, scientific and practical use, Bio-Technology 12, 10, 994-998
J. Viell, W. Marquardt, 2011, Disintegration and dissolution kinetics of wood chips in ionic liquids, Holzforschung, 65, 519-525
J. Viell, A. Harwardt, J. Seiler, W. Marquardt, 2012, manuscript in preparation
A. Voll, W. Marquardt, 2011, Reaction network flux analysis: Optimization-based evaluation of reaction pathways for biorenewables processing, AIChE Journal, doi: 10.1002/aic.12704
A. Voll, W. Marquardt, 2012, Benchmarking of next-generation biofuels from a process perspective, Biofuels, Bioprod. Bioref., doi: 10.1002/bbb.1325
T. vom Stein, P.M. Grande, H. Kayser, F. Sibilla, W. Leitner, P. Dominguez de Maria, 2011, From biomass to feedstock: one-step fractionation of lignocellulose components by the selective organic acid-catalyzed depolymerization of hemicellulose in a biphasic system, Green Chemistry, 13, 1772-1777

I.A. Karimi and Rajagopalan Srinivasan (Editors), Proceedings of the 11th International Symposium on Process Systems Engineering, 15-19 July 2012, Singapore.

Process Systems Engineering: Quo Vadis?

G V Rex Reklaitis [a]

[a]*Purdue Univeristy, West Lafayette IN, USA*

Abstract

Process systems engineering, which in content if not in title has a history almost as old as the chemical engineering discipline itself, can rightly be proud of having had a remarkable and sustained impact on the chemical and related industries. Model based methodologies for process design, process control and operations have become firmly imbedded in industrial practice world-wide, with focused teams regularly applying these approaches and tools in virtually all major CPI corporations (Stephanopoulos and Reklaitis, 2011). Within academic environments, instruction in process design and control likewise was firmly embedded as a core part of the chemical engineering curriculum, beginning in the mid 60's. However, in the 90's through the early years after the turn of the century, this core gradually eroded, especially in US universities. While the US ABET criteria continue to emphasize that the chemical engineering curriculum should" enable graduates to design, analyze, and control physical, chemical, and biological processes", many departments gradually lost the in-house capabilities to provide the appropriate process engineering educational experience, have relied on adjunct faculty to meet those critical needs, and in some cases have simply scaled-back in delivering this educational experience. This was on the one hand driven by exciting developments in nanoscale materials and applied biological sciences and growth in associated research funding which stimulated departments to add faculty who could contribute to such efforts. On the other hand, declines in available research funding for PSE methodology from US R&D funding agencies coupled with reduction of industrial support for academic research in PSE areas, at least in part as a result of reduced capital investments within the developed world, caused departments to see PSE faculty candidates as less attractive contributors to the departmental research funding portfolio. Accordingly, faculty numbers in PSE declined while industry demand for engineers trained in PSE was sustained in part as a result of the needs in associated industries such as semiconductors and pharmaceuticals.

However, in the past five years, the rising cost of petroleum and associated increasing cost of transportation fuels and core chemical building blocks, the mounting shortages of potable water in many parts of the world , and the concerns to at least restrain the growth of CO2 in the atmosphere, have driven a resurgence of research in process innovations, such as in technologies to exploit renewable energy sources and in the invention of process pathways towards biologically sourced organic chemical building blocks. In parallel, the healthcare needs of the aging populations of the developed economies and burgeoning healthcare needs of developing economies that required cost-effective solutions, have stimulated research and developments in products and processes for meeting those needs. Most recently, the economic downturn and loss of manufacturing jobs in the developed countries have awakened governments to the importance of advanced manufacturing to their economies both in terms of economic output and in creation of good quality jobs. These factors have impacted demands for PSE trained graduates both from industry and increasingly to staff university departments. It thus seems that the scene has been set for a period of growth in the PSE discipline.

In parallel with these economic drivers, the enabling technologies on which the PSE discipline can build its model-based applications have also seen tremendous growth in capabilities and scope. Four major technology drivers of particular note are massive low cost data storage, cheap and powerful computing, near universal connectivity and innovative multimode man-machine interfaces. The PSE community is already exploiting this growth in power to address large scale process problems. We are seeing applications such as the dynamic grade change optimization of a chemical plant in which the optimization formulation involves some 6+ million differential algebraic equations (Hartwick and Marquardt, 2010) and integrated production planning and scheduling applications involving tens of thousands of discrete variables (Grossmann, 2012). An important and interesting question is where can and will these capabilities take us in the next decade?

It can be predicted with certainty that PSE algorithms and tools will be enhanced to take advantage of computing and data management capabilities. Global optimization and treatment of stochastic decision problems certainly are among the methodology domains of highest potential and need. For instance, such decision problems readily arise in product development pipeline management which involve large scale multi-stage stochastic decision problems of very challenging dimensions (Lainez et al., 2012). Certainly the capabilities to store, manage and access Big Data, developments in which science applications in biology and physics have dominated to date, will allow the PSE community to effectively exploit massive process and product historical data to better model process and product performance but also to better understand and mitigate abnormal process behavior along the lines advanced by Seider and coworkers to extract, characterize and learn from process near misses (Pariyani et al 2012). The management of the information, models and knowledge, which constitute the intellectual capital of an enterprise is another area of great potential. For instance, effective knowledge management over the life cycle of pharmaceuticals is recognized as central to the quality by design process promulgated by the FDA (Junker et al 2011). While the financial and commercial worlds are already exploiting wireless connectivity and highly intuitive graphical interfaces that use visual, tactile and audio inputs and outputs to support real time distributed decision making, there is tremendous promise for applications to real time process management, extending from the plant to the supply chain.

These technologies will also allow considerable expansion of the scope of PSE problems that it will be possible to attack, ranging from design and operation of smart manufacturing systems and enterprise-wide decision support systems to socio-technical systems such as regional power and water distribution grids. Such expansions in temporal and special dimensions will be matched by PSE support for modeling and design synthesis at micro and nano scales in biological and materials applications. It is interesting to speculate whether the PSE community can establish a valued role in these application domains where scientific discovery is the driver but PSE support tools and analysis are needed to support and guide that discovery process. Developments in the discovery, manufacture and delivery of medicines for personalized treatment and developments of innovative chemical pathways to the processing biologically derived feedstocks, both of which require multiscale approaches spanning the molecular to the process scale, seem to offer significant promise challenge.

In this paper we will offer speculations and predictions on such future directions along with opinions on prospects for success and impact. It certainly seems that the PSE area of chemical engineering is on an exciting path towards reestablishing its central role in chemical engineering.

References

I. Grossmann, "Advances in Mathematical Programming Models for Enterprise-wide Optimization", FOCAPO 2012, Savannah, GA, January 8-11, 2012.

A. Hartwich and W. Marquardt, "Dynamic optimization of the load change of a large-scale chemical plant by adaptive single shooting", Comp.& Chem.Engr, 34, 1873–1889 (2010)

J. M. Laínez-Aguirre, E. Schaefer, and G. V. Reklaitis," Challenges and Opportunities in Enterprise-wide Optimization in the Pharmaceutical Industry", FOCAPO 2012, Savannah, GA, January 8-11, 2012.

B. Junker, G. Maheshwari, T. Ranheim, et al., "Design-for-Six-Sigma To Develop a Bioprocess Knowledge Management Framework", PDA J Pharm Sci and Tech 65 140-165 (2011)

A. Pariyani, W. D. Seider, U.G.Oktem and M.Soroush, "Dynamic Risk Analysis Using Alarm Databases to Improve Process Safety and Product Quality: Part I—Data Compaction", AIChE J, 58, 812-825 (2012)

G. Stephanopoulos, and G.V. Reklaitis, "Process systems engineering: From Solvay to modern bio- and nanotechnology. A history of development, successes and prospects for the future", Chem Eng Sci 66, 4272-4306 (2011)

I.A. Karimi and Rajagopalan Srinivasan (Editors), Proceedings of the 11th International Symposium on Process Systems Engineering, 15-19 July 2012, Singapore.

Process Intensification in Water and Wastewater Treatment Systems

Yatin Tayalia[a] and Vijaysai P[b]

[a]*Regional Product Sales Manager – Asia Pacific, GE Power & Water, Singapore*
[b]*Engineering Manager, GE Power & Water, GE ITC Pvt.Ltd. Bangalore, India*

Abstract

Demand for fresh water is continuously growing worldwide and more than half of the world would be under water stress by 2015 [1]. As the gap between available fresh water and demand widens, the current water and wastewater treatment technologies are challenged to treat tougher waters and meet stringent environmental regulations at affordable cost. Conventional treatment technologies have been successful within limits of feed water quality, contaminant removal efficiencies, recoveries and treatment cost. However, to manage this global crisis, a holistic approach to water treatment needs to be adopted to provide a robust and cost effective solution for lot more demanding requirements. This paper focuses on key trends in water treatment technology, from both the component and system design perspective that significantly impact the total solution and ability to meet the overall requirements. Also specific developments in desalination and wastewater treatment technologies like Reverse Osmosis, Ultrafiltration, energy recovery devices and Membrane bioreactors are discussed that have significantly widened the capability envelope. An integrated multi-scale approach to system design leveraging various technologies can provide the viable alternatives and meet this global challenge in sustainable way.

Keywords: Process Intensification in water, Novel water solution, Cost of water, Evolution in water technology

1. Introduction

Water quality and quantity issues are certainly one of the biggest challenges that the world is facing at present. Water consumption is constantly increasing and has increased six times in the last 100 years and is expected to double again by 2050 [1]. Population growth, rapid industrialization and urbanization have been key factors driving increase in consumption. There are 1.2 billion people who live in regions experiencing water scarcity, and the situation is expected to worsen for individuals as well as companies which operate in many emerging economies. To make situation worse, water quality of surface water and aquifers has deteriorated in certain regions due to indiscriminate discharge of wastewater without adequate treatments. Environmental regulations pertaining to water discharge and usage are becoming tighter. Both, drinking and wastewater infrastructure either are ageing or require new development in most part of the world. The multitude of water related issues means water industry has to do more with less.

Traditional water treatment approaches are not able to meet afore mentioned growing needs and there is need to look beyond conventional methods of water treatment [2]. The new approaches should either be able to treat more contaminated water as source, or allow alternative sources of water with increasing salinity at affordable cost, or treat

tougher wastewater to meet discharge standards and to reuse. These should also be able to work without ageing or non-existent infrastructure like point-of-source supply, point of discharge and point-of-use systems. The management of this global crisis requires a holistic approach to water treatment solution that is more robust and cost effective for growing requirements.

Process Intensification is an innovation strategy that has greatly benefitted process industry in making the process more efficient, safer, flexible, smaller, cheaper and more environment-friendly [3]. It defines a holistic approach starting with an analysis of economic constraints followed by the selection or development of a production process.. Process intensification also aims at taking a systemic approach towards performance improvements of each process. In a few words, this strategy aims to "Produce much more with much less" [4] for more sustainable industrial processes. This in the context of water treatment industry could mean reducing energy consumption, increasing recovery, reducing the foot-print, reducing the waste or even generating the value from the waste, more flexible processes that meets varying feed water qualities, shorter time to market, lower lifecycle costs or combination of these objectives.

This paper essentially seeks to address the relevance and realization of process intensification in water and waste water treatment at various levels including development of new materials, equipment design and plant design. It also discusses cases of successfully commercialized technologies that demonstrate the paradigm shift in designing water treatment solutions. Within this context, the process intensification in following five categories is discussed:

(1) Surface Water Treatment
(2) Desalination
(3) Wastewater Treatment and Reuse
(4) Waste to Value
(5) Zero Liquid Discharge

2. Surface Water Treatment

Surface water like river or reservoir water is increasingly used in the production of potable water or industrial process water. Surface water is characterized by high degree of suspended solids and microbial contamination [4]. A conventional surface water treatment plant comprises of a multi-step process based on physico-chemical processes including screen-filtration, ozonisation, coagulation and flocculation, sedimentation, media filtration, and usually disinfection as a last step. The process is fairly complex and each step of this process has to be controlled to get an optimal performance of the overall process. The use of chemicals like ozone, flocculants, hydrogen peroxide, lime and chlorine requires special precautions for safety purposes [5]. As the surface water quality gets further deteriorated, the conventional process is really limited in its ability to meet treated water specifications. Recent advances in Ultra Filtration (UF) have enabled direct filtration of surface water after a course filtration step without cost intensive pretreatment [6, 23].

It is to be noted that conventional media filtration worked on the basic principle of depth filtration while ultrafiltration works on the principle of surface filtration. The term ultrafiltration is used to describe a membrane filter, ideally with a pore size of 100 nanometers or less [6]. This is smaller than bacteria, rejecting virtually all non-dissolved particles on its surface. They have capability to produce 6 log reductions in bacteria and considerable reduction in viruses too.

The UF membrane filtration process provides several advantages such as superior quality of water and ease of operation over the conventional process. Simplicity in the process allows automation to be effective. Furthermore, fluctuations in the demand and changing river water quality can be managed through modular construction, offering higher degree of flexibility. Except for cleaning of membranes, excessive use of chemicals is avoided thus enabling significant reduction in residues and by-products. The ultrafiltration also serves to reduce the risk of biofouling and particulate fouling in subsequent operations such as nano-filtration and reverse osmosis. A more efficient performance of UF is also complemented with the reduced foot print of the plant, which is primarily achieved through elimination of large settling tanks. .

Large plants are most often managed by well trained and qualified engineers, which is seldom the case with decentralized facilities and remote areas [7]. Fully automated UF systems aptly fit into these conditions and their reliability could further be improved through remote monitoring and diagnostics.

Ultrafiltration Plants are also increasingly used for retrofitting existing conventional drinking water plants that demands higher capacity within existing footprint, or as a decentralized water treatment solution

The increased usage of Ultrafiltration for surface water treatment for industrial and municipal applications with above mentioned benefits is a great example of process intensification in water treatment.

3. Desalination

Desalination through membrane processes represents one of the unique successes in water treatment technology and is probably one of the distinct examples today of the success of process intensification in the water industry..

Seawater and saline aquifers account for 97.5% of all water on the Earth. Hence capturing even a tiny fraction could have a huge impact on water scarcity. Until recently, seawater desalination was only limited to desert areas like Middle East but now it has expanded its use in coastal areas owing to all technological developments and decrease in cost [8]. Two basic types of technologies have been widely used to separate salts from ocean water: thermal evaporation and membrane separation [15]. Over the past ten years, seawater desalination using semi-permeable sea water reverse osmosis (SWRO) membranes has gained momentum and currently dominates desalination markets. Membrane treatment process is more efficient, requires less physical space and is less energy consuming than vaporization or distillation [22].

A key factor which has contributed to the noteworthy reduction in seawater desalination costs is the advancement of the SWRO membrane technology [21]. Today's high-productivity membrane elements are designed with higher surface area, enhanced permeability and denser membrane packing. Increasing active membrane leaf surface area and permeability allows it to gain higher flux and hence significant productivity improvement is achieved using the same size (diameter) membrane element. The total active surface area in a membrane element is also increased by increasing the membrane size. Although 8 inch SWRO membrane elements are still the 'standard' size most widely used in full-scale applications, larger 16 inch and 18 inch size SWRO membrane elements have become commercially available over the past three years, and have already found full-scale implementation in SWRO projects worldwide[9]. The above mentioned factors result in significantly reduced footprint, piping, pressure vessels and associated costs [25].

Advances in the technology and equipment allowing the recovery and reuse of energy applied for seawater desalination, have resulted in a reduction of 80% of the energy used for water production over the last 20 years. While few years ago, the majority of the existing seawater desalination plants used Pelton-Wheel based technology to recover energy from the SWRO concentrate, today the pressure exchanger-based energy recovery systems dominate most desalination facility designs. The key feature of this technology is that the residual energy exchange between the concentrate and fresh seawater intake to the SWRO system. . Pressure exchanger technology typically yields 5-15% higher energy recovery savings than the Pelton-Wheel based systems. The specific (per unit of produced potable water) energy of desalination has been reduced from over 20kWh/m3 in the 1970s to below 3 kWh/m3 [10].

Further efficient desalination processes can be achieved through integrated membrane systems. Integrating different membrane technologies for minimizing the limits of the single membrane units and for increasing the efficiency of the overall system offers significant benefits. Feed water to RO systems needs pretreatment to remove inorganic and organic membrane foulants. Conventional pretreatment process is complex and has a high operating cost. There is a growing trend to replace all of this equipment with ultrafiltration. These membrane pre-treatment processes can handle a large variation in raw water quality and still produce water for the RO unit that is of better quality than water produced by the conventional technology [11]. Membrane pretreatment systems are also more compact and have lower operating costs than the conventional processes. Membrane based pretreatment allows RO design to be operated at higher fluxes, more compact membranes (440 ft2 vs. 400 ft2) and significantly reduces the fouling occurrence in RO system thus further making the design more efficient and robust.

Extending the capability of desalination further, integrated systems have been developed to push the recovery up for brackish water systems. High Efficiency Reverse Osmosis (HERO™) is one such proprietary system originally developed to provide ultrapure water to the microelectronics industry [12]. Ultrapure water is critical in a number of industrial applications, such as power generation, semiconductor manufacturing, and pharmaceutical formulation. Besides greater water recovery (95-99% vs. 75% from conventional RO), it also has other advantages like higher quality permeate, higher operating flux (gallons per square foot of membrane per day), and generally lower costs. HERO™ systems are ideally suited for applications with challenging feed water (e.g., with silica content greater than 20 ppm) or in areas with high water costs, limited available water, high water quality requirements, or zero liquid discharge requirements. It produces water that is higher in quality than necessary for potable use.

In HERO™, the membrane process is operated at higher pH thus eliminating microbiological fouling and making membranes self-cleaning. Due to the use of high pH, the hardness of the feed is reduced to less than 0.1mg/litre using hardness and alkalinity removal stage through weak and strong acid cation exchanger upstream. HERO™ does not use anti-scalant chemicals and requires less cleaning and maintenance than conventional RO. HERO™ also has limited self-healing properties, so small problems tend not to cause major system disruptions. In addition, there are the environmental benefits of saving water and energy [12].

Electro-deionization (EDI) is another such technology developed that combines ion-exchange resins, ion-exchange membranes and electric field. This has the capability to make ultrapure water using permeate from RO process [13]. Traditionally, ion exchange has been used to provide ultrapure water in these industries. EDI process can provide very high levels of demineralization and offer the advantage of continuous operation.

Moreover, these are not as mechanically complex as ion-exchange systems, and they require no acid and caustic regeneration, nor waste neutralization. Thus there is no need to store or handle bulk chemicals on the site.
All these technologies are well integrated and now available in pre-engineered packaged plants or even containerized mobile plants. This significantly reduces the footprint, overall cost and it can be installed in very short times to the point that they are used routinely for providing even emergency services.

4. Wastewater Treatment and Reuse

As the regulations and environment compliance parameters are being tightened and as concerns are mounting over the deteriorating quality and quantity of water supply, water reuse is recognized as more viable and sustainable source of water both for municipal and industrial applications [14]. The treatment and reuse of wastewater has two fold advantages as it reduces the quantity of wastewater to be discharged and it reduces the requirement of fresh water.
Reclaimed municipal or industrial wastewater must meet very stringent treatment standards to be acceptable to regulatory agencies and the end-users. In addition to removal of conventional pollutants such as Total Suspended Solids (TSS) and BOD, the elimination of all waterborne pathogens is required, as well as the reduction of nutrients such as total nitrogen and phosphorous . Membrane Bioreactor (MBR) systems provide this high effluent quality in a greatly simplified process. This requires only head works, biological processes, membrane filtration and disinfection to meet the most stringent water quality standards. In comparison, conventional process requires additional primary treatment, secondary clarifiers, enhanced nutrient removal and media filtration. The main advantage of the MBR process is that it reduces for the burden of biomass sedimentation, thus allowing a significantly smaller tank to be used for the bio-treatment process [24]. The operations can be conducted at higher mixed liquor concentrations (commonly 8,000-18,000 mg/l) as compared to conventional systems (around 2000 mg/l); this significantly reduces the footprint required as well as improves the removal of dissolved constituents. MBR designs will require only 30- 50% of the space required for conventional systems designed to meet the even more stringent treatment goals. This improved space efficiency benefits not only for new facilities but allows expansion and upgrade of existing facilities up to 3-5 times existing capacity without additional treatment volume or site footprint.
MBR systems also provide more flexibility in coping with flow rate and feed quality variation as hydraulic retention time (a function of flow rate) can be decoupled from sludge retention time (a function of biological reaction processes and sludge setting rates). They are also simpler, with fewer process components and maintenance requirements. Common maintenance is still required on mechanical components, but operators can now avoid difficulties in operation tied to sludge settling and clarifier sludge blankets. Besides, these can be easily automated and instrumented to measure performance. It allows systems to be remotely operated and monitored, thus significantly reducing operator attendance. The modular nature of the membrane system allows more efficient phasing of facilities. Membrane modules can be delivered on a "just in time" basis, thus reducing the need for large and costly initial construction to meet long-term projections.
The holy grail of reclamation and reuse of water is to capture water directly from non-traditional sources such as industrial or municipal wastewaters and restore it to direct useable quality either for potable or industrial purpose. Since the large part of the cost

of water is pumping, transport and storage, recovering water at or close to the point of use is the most efficient. Decentralized systems allows remote treatment of wastewater, thereby alleviating the need for expanding centralized sewage systems and long distance pipelines, which can be disruptive and costly. However, there has been a historic concern about the robustness, cost and operational effectiveness, creating the need for treatment solutions that deliver reduced complexity and provide affordability for the customer, as well as allow regulators to ensure high operation and maintenance standards. Also, wastewater treatment plants have historically required a significant amount of land to construct the necessary tanks and infrastructure for the required levels of treatment. MBR technology greatly addresses the concerns and makes it ideal choice for decentralized systems.

It offers ability to meet more stringent effluent water quality requirements, space constraints, lower operator involvement, modular expansion characteristics and consistent effluent water quality capabilities. Thus MBR technology meets the Process Intensification Criterions laid out earlier.

5. Waste-to-value

There is a conceptual shift from today's pollution prevention towards resource recovery. For instance, organics (COD) in water can be used as source of methane rather than having them destroyed aerobically by adding fossil energy. The same concept can be applied to nutrients such as phosphorous, nitrogen and potassium. Rather than removing or draining nutrients, we can make products out of them.

Water can be treated through aerobic process (oxidation) which consumes energy, or anaerobic digestion (reduction) which generates energy in the form of methane. Aerobic process consumes 1-2 MJ/kg of COD, while anaerobic digestion delivers about 12 MJ per kg of COD consumed. As the name suggests, anaerobic digestion demands the system to be completely isolated from air (oxygen) and maintain a redox potential of less than -250 mV. Ideally, anaerobic digestion is recommended on higher strength wastewater (COD>3000) whereas the aerobic process is suitable for a lower strength waste.

The waste-to-value concept discussed in this paper focuses on two different schemes both aiming at deriving energy/power from the organics followed by reusable water. The first scheme is applicable for the wastewater with higher COD loading. With necessary pretreatment, the water is fed to the anaerobic digester, followed by optional TSS removal unit, MBR and RO. The biogas thus generated is typically used for generating steam or electricity in gas engines. This integrated approach also seeks to treat the concentrate produced from MBR/RO with the help of waste heat of the flue gas. This strategy is more suitable for high strength wastewater from food and beverage industries. The second scheme is typically more applicable for wastewater laden with higher amount of volatile suspended solids. The water is initially clarifier to separate the solids whereas the supernatant from the clarifier is fed to the MBR. The solids from clarifier and the sludge from the MBR are fed to the anaerobic digester. The biogas from the digester produces captive power driving the entire system towards energy neutral condition.

In addition to the power and water, both the above mentioned integrated solutions can be designed to bring-down the concentration of the nutrients in the treated wastewater below the dischargeable limits. These solutions defeat the notion of wastewater treatment being cost intensive but on the contrary make the economics more attractive for the customer.

The holistic approach to wastewater treatment and shift towards resource recovery again highlights the process intensification trend in wastewater management.

6. Zero Liquid Discharge

Many industries, power plants, oil and gas exploration companies and even municipalities are facing with problems on the disposal of the liquid waste generated by their operations. In most of these plants, the ultimate goal is salt or total dissolved solids (TDS) reduction using economical process and minimization of liquid wastewater. As a result, Zero liquid discharge (ZLD) systems have become more prevalent. The goal of a well-designed system is to minimize the volume of liquid waste that requires treatment while also producing a clean stream suitable for use elsewhere in the plant processes.

Energy companies involved in development of unconventional gases and oil sands are facing severe challenges in managing the wastewater on site. Extraction of gas sources like Coal Bed Methane, Shale rock deposits and tight sand gas deposits requires fracturing to create openings in the deposits. The fracking process is enormously water-intensive, with up to five million gallons of water being required for a single well. Anywhere from 5% to 60% of this water flows back to the surface. In addition, water that is naturally found in the rock formations will flow from the well over the course of its proactive life, which is known as "Produced Water". Besides, in enhanced oil recovery process (EOR) using steam assisted gravity drainage (SAGD), 100% quality steam is injected into the well to heat-up the formation and get the heavy oil to flow. Produced water is highly variable and evolves over time, so a new well will produce smaller volumes of water than an older well. For treatment technology to be effective in produced water market, it must be robust to work efficiently under varying conditions and with variable flow rates. It must be versatile to remove a variety of contaminants and process a wide range of waters. It must be serviceable for easy O&M and most importantly, it must be economical.

In EOR process, huge water demand and ultimate conversion to steam requires the maximum amount of recycle potential from the water. Oil and condensed steam are brought to the surface where the oil is separated, and the condensate, or produced water, is treated and recycled to produce the steam. The traditional de-oiling, softening, filtration, and ion exchange produced water treatment scheme is complex, costly, produces several waste streams requiring disposal, is labor intensive, requires the use of steam generator, and requires vapor/liquid separation systems (to produce the required 100% steam quality for SAGD process). Evaporation through novel evaporators provides an alternate approach to produced water treatment which is simpler, more cost effective, more reliable, and reduces the size and complexity of the steam generation system significantly.

Novel design of evaporators and crystallizers has greatly facilitated the Zero Liquid Discharge solutions even with significantly challenging conditions like in gas fields with significantly reduced complexity and in cost effective way.

7. Integrated System Design Framework

There have been numerous technical advancements in water and wastewater treatment technologies as discussed in sections above. The holistic approach to water management requires evaluation of water treatment solution on various technical, economic, social and environmental parameters. The overall solution is integrated part of larger system that could be an industrial process or residential communities and has the capability to significantly influence it. For example, for industrial process, water and wastewater

treatment solution can influence the choice of technology with regard to water consumption, effluent discharge quality and quantity and overall economics. Likewise, for municipal process, water treatment solution clearly influences the water quality and quantity of the potable water, water tariffs and development in the territory. The evaluation of various options at various levels including using existing water source or desalination or wastewater reuse as an option requires an integrated framework. This framework should provide capability to evaluate the solution on various technical, economic, social and environmental parameters. This requires development of predictive process models for various water treatment unit operations, capability to integrate various unit operations, cost models for CAPEX, OPEX and lifecycle cost analysis, all on one platform. The predictive capability needs to be for specific water quality parameters, product flow rate, system recovery, energy consumption and several other parameters discussed in sections above. Likewise, these models should be able to predict in wide range of operating conditions, account for all the variability in the system, and allow designers to carry out what-if and sensitivity studies [16]. Besides, this also should be able to provide framework for optimization during design as well as operations phase. The choice of water treatment technologies and their capabilities are so numerous that even a knowledge management based decision support tool is required to help design flow-sheet and configuration to reach an optimum solution.
There is huge opportunity from Process Systems Engineering standpoint to develop this integrated framework that allows city planners, industrial process engineers or even residential communities to come up with the optimum solution that works within the constraints defined by them and also meet their overall requirements.

8. Conclusion

The developments of new technologies that follow the process intensification principles are critical to solve the current water and wastewater treatment challenges. This in the context of water treatment industry could mean reducing energy consumption, increasing recovery, reducing the foot-print, generating the value from the waste, more flexible processes that meets varying feed water qualities, shorter time to market, lower lifecycle costs or combination of these objectives. The new processes like membrane based ultrafiltration treatment, seawater desalination processes, membrane bio-reactors are lot more process efficient, safer, flexible, smaller, lower cost and more environment-friendly as compared to conventional processes and have the capability to meet the challenging requirements in the current scenario. The shift in approach towards resource recovery from pollution prevention is a good example of benefits of holistic approach and system level thinking. There is also a need for integrated design framework that allows evaluation of multiple options on economical, technical and environmental parameters, has the capability to integrate advanced and conventional technologies and evaluate various process configurations to design optimum solution.

References

1. GE Reports (2011, April 6), Water Reuse Gains as Urban and Industrial Demand is Set to Double, Retrieved from http://www.gereports.com/water-reuse-gains-as-urban-industrial-demand-is-set-to-double/
2. Roni Kasher (2009), Membrane-based water treatment technologies: Recent achievements,and new challenges for a chemist, *Bulletin of the Israel Chemical Society* (24), 10-18.

3. Charpentier, J.C. (2007), "Modern Chemical Engineering in the Framework of Globalization, Sustainability, and Technical Innovation", *Ind. Eng. Chem. Res.,*(46), 3465-3485.
4. F. Berne and J. Cordonnier, Industrial water treatment, Gulf Publishing Company, 1995.
5. U.S. Environmental Protection Agency, *The Environmental Protection Agency's White Paper on Peroxone* (EPA Guidance Manual, 1999; http://www.epa.gov/ogwdw/mdbp/pdf/alter/chapt_7.pdf
6. G.K. Pearce (2007), The case for UF/MF pretreatment to RO in seawater applications, *Desalination.*(203), 286-295
7. World bank report (2011,Sep), India Rural Water Supply, Retrieved from http://www.worldbank.org.in/WBSITE/EXTERNAL/COUNTRIES/SOUTHASIAEXT/
8. Mark Wilt, Craig Bartels (2005), Optimization of seawater RO systems design, *Desalination* (173), 1-12
9. Membrane Filtration (2008, Aug) Large-diameter RO elements only for large scale plants? http://waterwastewaterasia.com/WWA_archive/JulAug08/32t34.pdf
10. Baltasar Peñate and Lourdes García-Rodríguez, Current trends and future prospects in the design of seawater reverse osmosis desalination technology, *Desalination* (284), 1-8
11. Lauren F. Greenlee, Desmond F. Lawler, Benny D. Freeman, Benoit Marrot, and Philippe Moulin (2009), Reverse osmosis desalination: Water sources,
12. Science Direct, 2011, Expanded licensing agreement enables GE to incorporate HERO systems in more products, *Membrane Technology* (2011), Retrieved from http://www.sciencedirect.com/science/journal/09582118/2011/3
13. Y.Tanaka(2007), Chapter 4 Electro-deionization, *Membrane Science and Technology* (12), 437-460
14. Venkatesh Madyastha, Vijaysai P and Venkatram Mahendraker (2011), Reduced Order Model for Monitoring and Control of a Membrane Bioreactor System via Delayed Measurements, *Water Science & Technology* (64), 1675-1684
15. A.M. Helal, A.M. El-Nashar, E. Al-Katheeri, S. Al-Malek (2003), Optimal design of hybrid RO/MSF desalination plants Part I: Modeling and algorithms, *Desalination,* (154) 43-66
16. GE Water (2012), Winflows Membrane System Design Software, Retrieved from http://gewater.com/winflows.jsp
17. Raymond R. Tan, Dominic Chwan Yee Foo, Kathleen B. Aviso, Denny Kok Sum Ng (2009), The use of graphical pinch analysis for visualizing water footprint constraints in biofuel production, *Applied Energy,*(86), 605-609
18. Alessandra Criscuoli and Enrico Drioli (2007), New Metrics for Evaluating the Performance of Membrane Operations in the Logic of Process Intensification, *Ind. Eng. Chem. Res.*(46), 2268-2271
19. *Global Trends 2015,* NIC 2000-02, National Intelligence Council, Washington, DC, December 2000, p. 27
20. Mark Wilf and Kenneth Klinko (2001), Optimization of Sea Water RO Systems Design, *Desalination*, (138), 299-306.
21. K.V.Reddy and N.Ghaffour (2007), Overview of the cost of desalinated water and costing methodologies , *Desalination*, (205), 340-353
22. Ioannis C. Karagiannis and Petros G Soldatos (2008), Water desalination cost literature: review and assessment , *Desalination*, (223), 448-456
23. Enrico Drioli, Andrzej I. Stankiewicz, and Francesca Macedonio (2011), Membrane engineering in process intensification—An overview, *Journal of Membrane Science*, (380), 1-8
24. Thomas Buer and Jeff Cumin (2010), MBR Module Design and Operation (250), 1073-1077
25. Nikolay Vouchkow (2008), Sea Water Reverse Osmosis Design and Optimization, Advanced Membrane Technologies,

I.A. Karimi and Rajagopalan Srinivasan (Editors), Proceedings of the 11th International Symposium on Process Systems Engineering, 15-19 July 2012, Singapore.

Applications of Technology Roadmapping to Planning and Building Systems for Medicine and Vaccine Manufacturing

Anando A. Chowdhury[a], Michael P. Thien[a]

[a]*Global Science Technology & Commercialization, Merck Manufacturing Division, Merck/MSD, Whitehouse Station, NJ 08889*

Abstract

Health and sustainability are two of the most daunting global challenges facing humankind today. The need to preserve and improve human life in new and more robust ways is at the core of these global challenges. Process systems engineering (PSE) when applied to the manufacturing and distribution of medicines and vaccines has the capacity to impact these global issues for the better, but it must be effective at size scales that span global enterprises and supply chains and time scales that cross multi-year long range planning. Technology roadmapping is a process that has been applied effectively to the identification, selection, acquisition, development, exploitation, and protection of technologies in a variety of industries. We explain how this method combined with PSE can be used to design and enact complex technological change at the size and time scales needed to transform a global manufacturing operation.

Keywords: manufacturing technology roadmap pharmaceuticals vaccines biologics.

1. Introduction

Technology roadmapping is a process that has been applied effectively to the identification, selection, acquisition, development, exploitation, and protection of technologies in a variety of industries. In this paper we describe an approach taken at our company that allows this technique to be used to drive process systems engineering (PSE) activities across a size scale that spans a global manufacturing operation with hundreds of connected supply chains and time scales that cover multiple years into the future. When driven at the global operation level, technology roadmapping provides the only viable way to align thousands of technological, organizational and business model changes to systematically transform and coordinate PSE activities across the organization. This is especially critical in our business sector where our global operations deal with the manufacture and distribution of medicines and vaccines that preserve or improve human life and animal health. We have defined **technology** as a system comprised of scientific/technical knowledge, processes and equipment that is used to accomplish a specific goal. The knowledge encompasses the understanding of fundamental principles and relationships that provide the foundation of the technology. The processes are the procedures, techniques and best practices associated with the technology. The equipment is the physical manifestation of the technology as devices, instruments and machinery. Given this definition, **manufacturing technologies** are combinations of knowledge, process and equipment that transform raw materials into products and deliver them in a useful form to our patients & customers. Additionally, **product configurations** are changes in format to a product that a customer would see

or perceive – for example formulation platforms or packaging configurations that manufacturing technologies enable.

Our approach follows this reasoning in a fairly linear way. Initially we create global operations level systems views, allowing for holistic management and consideration of systems changes. This creates the visual of the larger system that is the subject of transformation and deployment of technologies. Stakeholder maps are created that account for the external and internal constituencies, clearly identifying the key stakeholder groups involved in global systems level transformation. The changing global trends are then mapped inwards from the customer market and societal needs and outwards from the business drivers and requirements from the manufacturer. In this paper, we focus on the some significant shifts in the health and sustainability areas. This stakeholder mapping also allows for the development of key performance indicators (KPIs) for the global system, thus collapsing the trends and drivers identified into workable and measurable goals. These KPIs result in very precise operational definitions around which global operations level changes can be made. During the needs and requirements definition, technology inventories can be created simultaneously by technology subject matter experts that become repositories of internal and external technology efforts and innovations. The two streams of efforts combine when the KPIs, trends and drivers are used to prioritize the technologies in time that are most important. This allows for the initial creation of technology roadmaps. Individual technologies are generally at the single and multi-phase system and process unit level, and thus visualization on roadmaps allow for plant, site and enterprise level integration and planning. Interactions between different global pathways can be analyzed utilizing dependency structure matrix (DSM) analysis. This creates a portfolio of PSE projects that can be managed through maturity by an enterprise-wide technology management process and governance, with information and knowledge being refreshed on an annual basis as the transformation and implementation progresses.

2. Global Operations Level Systems Views

A simple schematic of all the possible pathways of manufacturing possible at the global operations level was created. This is depicted in Exhibit 1 below.

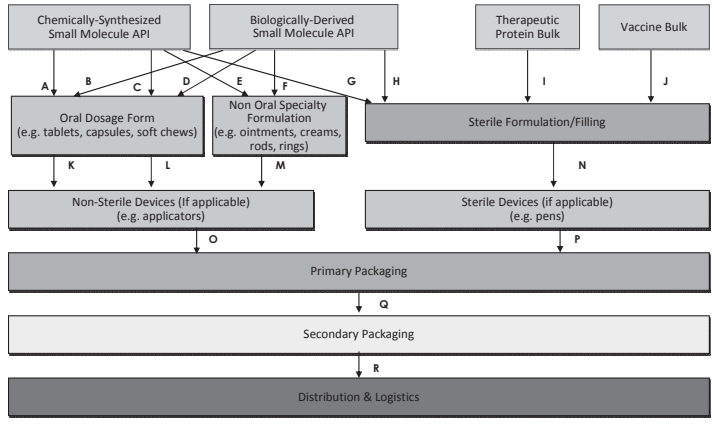

Exhibit 1: Global operations level system view

In this global view, process unit systems up to plant scales can exist within each box, while site and enterprise level integration occurs along pathways defined by connections of different boxes. An example of a pathway is AKOQR, which represents the pathway for a small molecule pharmaceutical oral dosage form. It is clear that from even this view, PSE models for enterprise optimization such as those discussed by Sahinidis (Sahinidis et al, 1989) or Grossman and Biegler (Biegler et al., 1997) can be applied to pathways such as AKOQR, and that the evolution of technologies within any given node of box would inform the variables, constants and coefficients of the models from the current pathways to future pathways. Each processing unit box can be further blown out as necessary, but the overarching scheme allows for taxonomy of future roadmaps for each node and each pathway.

3. Stakeholder maps, trends, drivers and key performance indicators

Having a clear way of representing all the stakeholders of the global operation is incredibly important as it allows for segmentation of needs and ultimate definition of key performance indicators by constituency. A high level stakeholder map from our work is shown in Exhibit 2.

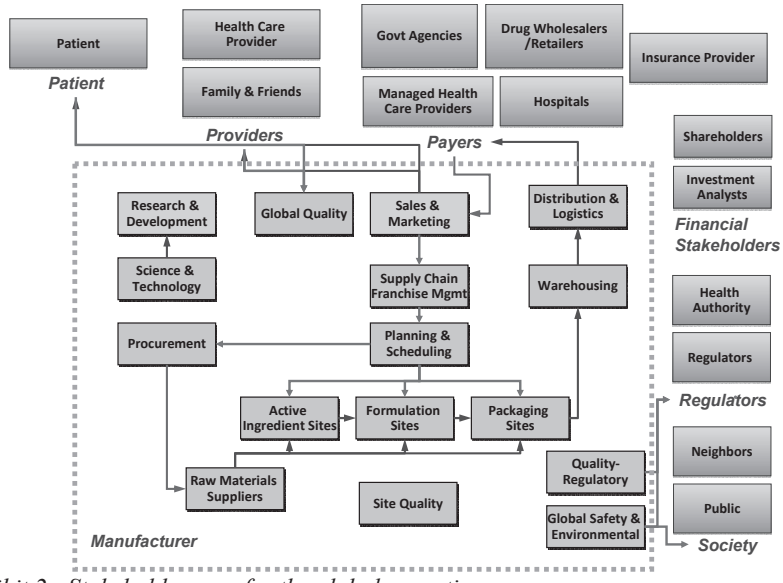

Exhibit 2: Stakeholder map for the global operation

As global operations-level transformation occurs, there are multiple interests that must be met. Patients and consumers must benefit from the appropriate use of our products and services and challenges such as affordability and adherence must be met. Different configurations that allow for convenient and safe use as well as protect the product from human and environmental threats must be introduced. On the other side of the stakeholder map, we serve our society, from the local communities in which we operate to the national and international levels, by supporting and promoting environmental sustainability. This leads to processes designed to be green with respect to emissions and waste and sustainable packaging designs and configurations.

MAJOR PARAMETER		KEY PERFORMANCE PARAMETER	MEASURE DEFINITION	STAKEHOLDER WHO CARES	SAMPLE TRENDS & DRIVERS FOR THE NEXT 5 YEARS
PRODUCT	A winning product fashioned with the customer value drivers in mind and continues to deliver this value consistently.	Safety & Tolerability	The safety profile of the medicine.	Patient, Provider, Payer, Regulator	More potent compounds
		Efficacy	How effective is the medicine in effecting the disease target, generally measured by bioavailability over time.	Patient, Provider, Payer, Regulator	Variety of different dosage forms to achieve delivery optimums
		Features	Attributes that signify the non-biological elements of the product, like integrity and elegance of the medicine, the ease of use of the packaging etc.	Patient, Provider, Payer, Regulator	Increased set of market and customer-specific requirements
PROCESS	Sustainable and profitable business/manufacturing system to create and deliver the product robustly, wherever they are needed while building and leveraging institutional wisdom seamlessly.	Manufacturing Efficiency and Robustness Measures	All the manufacturing parameters that are part of being a world class supplier including inventory stock turns, process capability (CpK), overall equipment effectiveness (OEE), right first time (RFT), on time in full (OTIF), and cycle times.	Manufacturer, Regulator	Need to do substantially better in all manufacturing effectiveness measures
		Standard Cost to Make Product	The manufacturing cost to create a certain number of units of the product.	Manufacturer	Appropriate reductions to assit with affordability of medications for more customers
		Flexibility to Continuously Improve	The measure of how rigid or flexible the process is to learning and then instituting improvements based on that learning.	Manufacturer	The need for flexible process technologies are going
		Sustainability and Environmental Factor	The inherent operational safety and the green-ness or environmental friendliness and sustainability of the process.	Manufacturer, Society, Regulator	Much greater global need for on green sustainable solutions
		Global Access	Increased global access for medicines is important and this parameter represents the technologies ability to be operable in various markets around the globe.	Patient, Society, Manufacturer	Desire to expand access to previously unserved patients and customers
		Scalability and Continuity of Technology from R&D to Manufacturing	This measures the continuity of the technology from bench scale and pilot scale models to manufacturing allowing for knowledge to be built over time and across different products using the same platform.	Manufacturer, Regulator	The need to have and demonstrate continuous learning from development through to manufacturing is vital

Exhibit 3: Stylized stakeholder, KPI, trend and driver mapping

It is important to reflect the needs and requirements of the various stakeholders in precise terms, with operational definitions and maps that can establish precise sub-factors that can be targeted by the global operation for improvement. Exhibit 3 is a generic global operations level stakeholder needs and requirements mapping that shows a stylized representation of the stakeholder, KPI, trend and driver mapping.

4. Technology inventories

While the work of defining key performance indicators are being established for the technologies, parallel work can and should be occurring to gain common and universal enterprise level visibility to all technologies being considered or potentially of interest. An important connection between advances in technology achieved at local levels in the enterprise and the higher level technology strategy should be the development and maintenance of a **technology inventory**. The technology inventories should be a primary reference source whenever an effort to resolve a stakeholder-driven set of needs or requirement via manufacturing technology is undertaken. The inventory serves as one avenue to connect technology advances in manufacturing, research and all manufacturing businesses to the customers and business. Leaders of technical organizations should assign functional areas to have one or more representatives keep the technology inventory current so that it may be a continuously useful tool for technology roadmapping. Local groups in research and manufacturing can have updating the inventory as a standing objective for technologies in their scope of work. We have found that customer field visits, and reports from conferences, visits to partner companies and industrial collaborations may serve as key sources of contributions to the inventory. Individuals within each area of the enterprise should appoint an appropriate function or group of individuals to periodically check to ensure the inventory is kept current, at least, on an annual basis.

5. Technology Management Process

A stylized example of a technology roadmap is shown in Exhibit 4, and does not differ much from conceptual examples presented by Phaal (Phaal, 2004) and other manifestations of roadmaps going back to their initial use in Corning and Motorola in the 1980s. The top of the roadmaps are representations of product or business strategies while the bottom represents investments in the most critical enabling technology projects. The horizontal axis represents multi-year transformation time scales while the dotted line ties from the top to the bottom represent a visually simple way of showing the most critical ties. It is important to note that these roadmap visuals constitute a graphical summary of much more complex and interrelated connections that are best managed through multi-domain matrices as will be discussed in the last section.

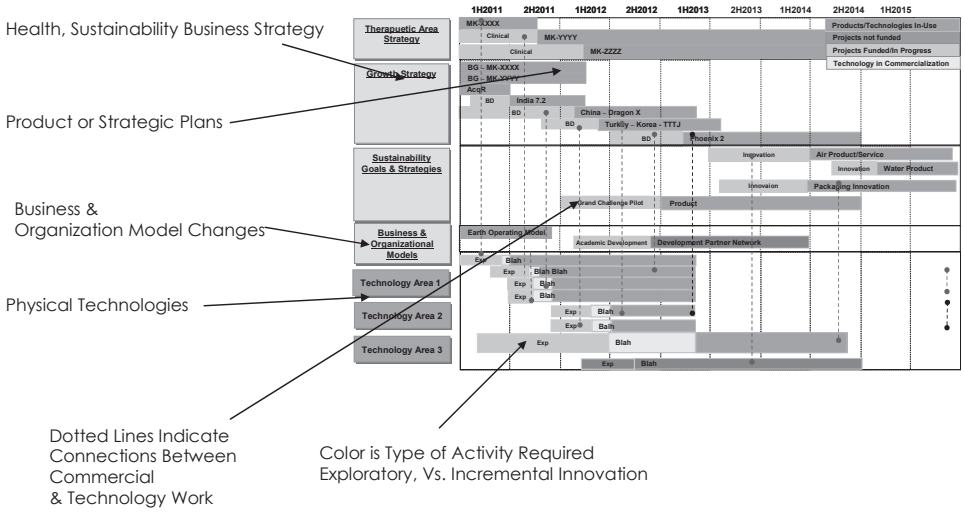

Exhibit 4: Stylized example of a technology roadmap.

The subsystems we have spoken of so far become a part of an integrated technology management process that has these roadmaps at the center, and this concept we have depicted in Exhibit 5. We have chosen to adopt the European Institute of Technology Management (EITM) definition of technology management as that which "addresses the effective identification, selection, acquisition, development, exploitation and protection of technologies (product, process and infrastructural) needed to maintain (and grow) a market position and business performance in accordance with the company's objectives." (Phaal, 2004). This must be managed by an organizational structure that has clear accountabilities and decision rights established. Most importantly, an overarching ability of tracking and responding to process health metrics and realization indicators are extremely important. Each section and its roles are described.

5.1 **F1 – Technology inventory system –** This part of the process ensures that the enterprise can consistently track and update the technologies it has in its inventories from the inside and outside as the business learns more. The sub-process gives access to all technologists to help maintain and access these inventories.

Appropriate guidelines for an intellectual property strategy are embedded in this section.

5.2 **F2 – Product planning system –** Access for the latest product plans for every health area and market are embedded here. The means of transforming these product plans into a way the technology roadmaps can consume and use them are defined in this sub-system.

5.3 **F3 – Customer & business needs/reqts system –** It is critical that a firm link is created between the clinical and marketing portions of the business and the customer need-sensing and translation processes are established so that observations can be translated into business requirements and goals. This sub-system also assures that we stay in touch with the business needs and requirements that are independent of customer needs.

5.4 **P1 – Technology roadmap mgmt –** This part of the system establishes how the enterprise manages the actual roadmaps, including gathering changing information, augmenting investment choices, socializing the recommendations, and making decisions on the overall maps and investments. **T**he maps are made visible and visualized on an ongoing basis.

5.5 **P2 – The gated technology process –** The mapping of technology and technical systems to roadmaps allows for global tracking of technologies at each stage of maturity. This is an important concept as different investment postures need to be taken based on different maturity states of the technologies. A clear map of the decision rights at all levels of the enterprise for progressing technologies through must be created, the broader and more externally facing the technology is, the more challenging decision rights can become. Additionally, the enterprise must account for technologies that "pop in" at a gate, that is acquired from the outside or working with a partner. Each gate should have the standard ways to kill projects as well as clear way to map the overall health of the process.

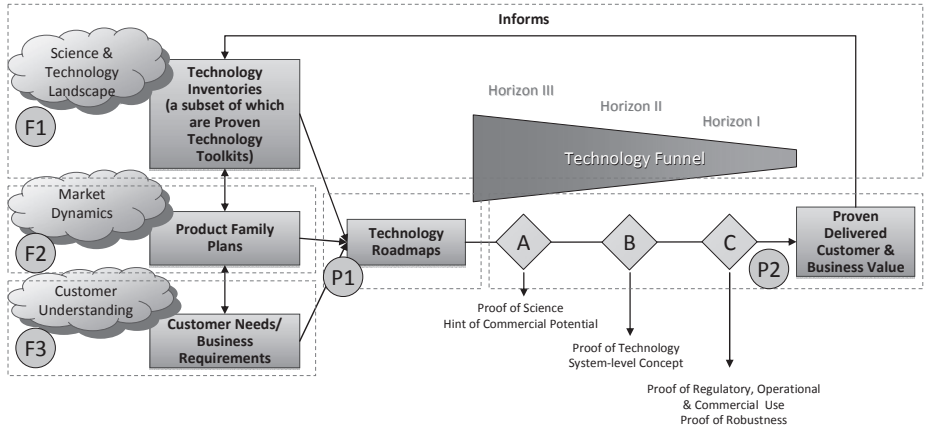

Exhibit 5: Conceptual design of an enterprise level technology management process.

The progression of technologies through the various phases of maturity is critical and linking technology development with the knowledge and capability level of the organization is vital. In this we have proposed using **horizons** of maturity (Cournoyer, 2003, Chowdhury, 2009, Kukura, 2012). **Horizon I** technologies refer to incremental

improvements in currently commercialized or near commercialized technologies. They are implementable in the near term. **Horizon II** technologies are in the middle part of the adoption curve (potential technology), the physical principles have been demonstrated either in our industry or elsewhere - we need to adapt the solution for our needs. These are medium term solutions 2-3 years out. **Horizon III** technologies are much further out and likely the physical principles have not yet been demonstrated. They require some fundamental knowledge work and are a ways from being commercialized. These are longer term solutions.

This maturity level assessment, which is also depicted in Exhibit 5 in the part of the diagram labelled the "technology funnel", can be married up with a needs assessment. As the various stakeholder needs, and for our purposes those that contribute to transforming human health and driving sustainability globally, some will be well articulated (i.e. a problem looking for a solution) and others will not be (i.e. a solution looking for a big way to impact a problem). As we assess transformation at a global operational level, it is important that our efforts have a combination of these types of technologies and these types of defined value drivers. These dual dimensions and the trade space that is created by examining them are represented in Exhibit 6.

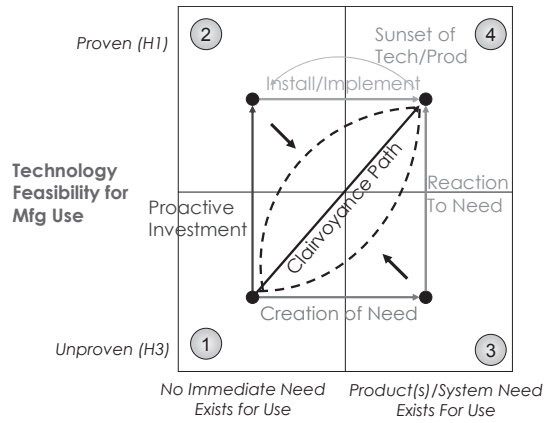

Exhibit 6: Technology Maturity by Extent of Need

In the y-axis, the technology maturity as represented by the different horizons is shown while the extent of known and identifiable need is shown on the x-axis. Theoretically, technologies can traverse from zone 1 to zone 2, where we make proactive investment in a technology without a well articulated need or move from zone 2 to zone 3 where we are implementing a proven technology as a need is articulated. They can theoretically traverse from zone 1 to zone 3 where we work to create a need for an unproven technology or (where most mental models around technology development reside), move from zone 3 to zone 4 where we develop a technology for a particular need. In reality technologies traverse this trade space in multiple and diverse trajectories and at different speeds. They are can start within any zone and can stay within a zone and never go anywhere and die. The idea of technology roadmapping as a means to build large scale systems or transform them essentially looks to solve the most difficult problem of moving technologies from zone 1 to zone 4 in a more methodical, integrated

and predictive way. We represent this concept in the diagram as the "path of clairvoyance". Theoretically, well fashioned roadmaps that are refreshed with technical knowledge would deliver a straight line from zone 1 to zone 4. In reality this is impossible, but this thinking does provide some helpful principles as the enterprise puts in place an overarching technology process.

6. The Technology and PSE portfolio and network management

The final leg of the process is to actually manage the technologies and PSE efforts that are born of the technology roadmaps. One of the key issues around technology management is the lack of visibility of how different efforts touch each other and need information or data from one another to make a larger, more holistic transformation possible. In helping to manage these interdependencies, the concept of the multi-domain matrix (MDM) has been applied (Crawley et al, 2004). A mock version of an MDM is shown in Exhibit 7 for the manufacturing pathway AKOQR discussed in Section 2 that has been applied to our efforts in managing technologies and PSE efforts at an enterprise scale. The MDM is laid out to show relationships within like elements (such as the process to process connections dependency structure matrix (DSM) in the red box, or the operand to operand connections DSM within the blue box or across unlike elements such as operand to initiative, as shown in the area labeled zone 1.

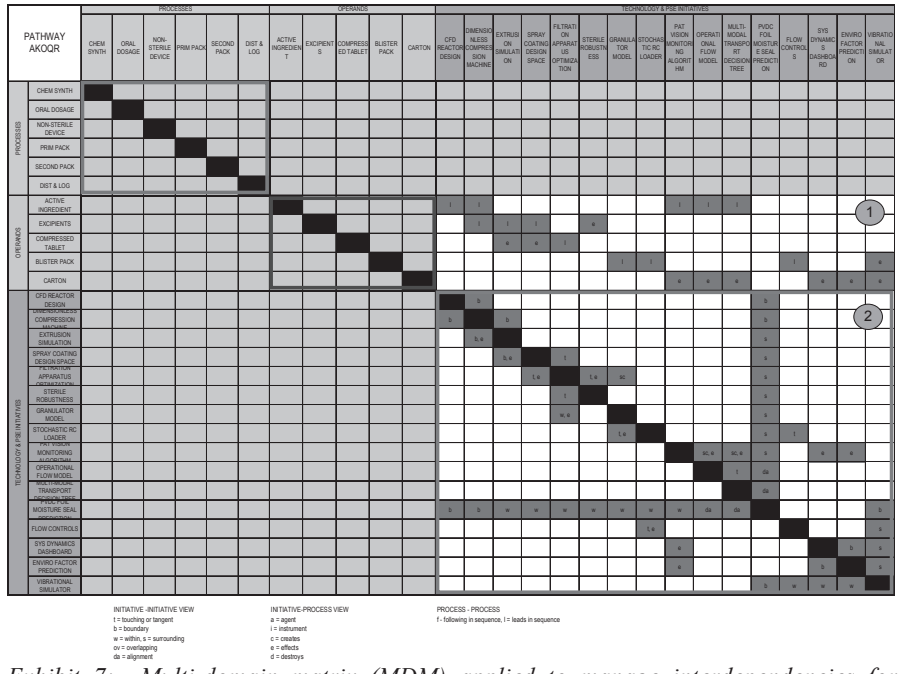

Exhibit 7: Multi-domain matrix (MDM) applied to manage interdependencies for technology and PSE initiatives.

Understanding the relationships between some of the most important potential efforts and the process or operands at the enterprise level is critical to help manage multi-year efforts and to foster the right knowledge sharing and hard connections required as

internal and external resources execute on the portfolio of choices. The cross hairs within the matrix can represent the nature of the connection, e.g. "supporting", "connected" to or "integral". In this mock example, we see that the following projects are in the portfolio: CFD reactor design, dimensionless compression machine, extrusion simulation, spray coating design space, filtration, apparatus optimization, sterile robustness, granulator model, stochastic RC loader, PAT vision monitoring algorithm, operational flow model, multi-modal transport decision tree, monitoring algorithm, PVDC foil moisture seal prediction, flow controls, sys dynamics dashboard, enviro factor prediction, and vibration simulator. First and foremost, the importance of these PSE initiatives and their ability to address multiple needs at the global operational level would not be seen if were not for the roadmapping effort. The MDM analysis brings to light for example that the PAT vision monitoring project as creating datasets that are needed for the system dynamics dashboard or the enviro factor prediction model. These interconnections can then me mapped to intended resource connections through a process called organizational network analysis where people resources are mapped with their current structured technical and data sharing relationships (Cross et al, 2009). This leads to being able to visualize the resource connections between technical resources working on various programs and drive management of needed connections. An actual mapping of technical resource connections working in on the pathway AKOQR is shown in Exhibit 8.

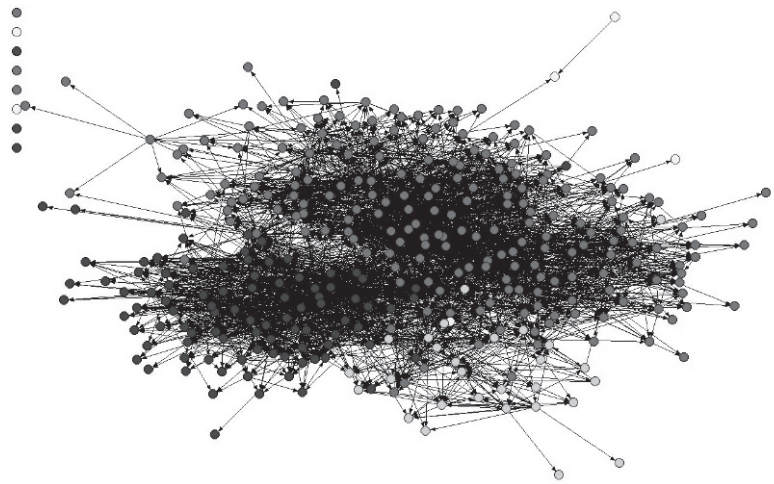

Exhibit 8: Organizational network analysis of connections between technical resources working on technology/PSE initiatives

7. Conclusion

The ability to impact human health and global sustainability requires enterprise transformation at size scales of global operations and time scales that traverse multi-year planning cycles. We have introduced a systematic method that has been pressure tested in our enterprise that combines technology roadmapping, portfolio management, multi-domain matrix and network analysis to methodical management of technology and PSE initiatives in an integrated and interdependent way.

References

Ansel, H.C., Loyd, A.V., and Popovich, N.G. (2005), "Ansel's Pharmaceutical Dosage Forms and Drug Delivery Systems 8th Edition", Lippencott Williams & Wilkins.

Biegler, L.T., Ignacio E.G., and Westerberg. A.W. (1997), "Systematic Methods of Chemical Process Design", Prentice Hall PTR.

Chowdhury, A. (2009), "Technology Strategy Papers 15.965 #1-4, Pharmaceutical Manufacturing Technology Platforms," Individual Paper Assignments for partial fulfillment of requirements of Fellowship, System Design & Management, Massachusetts Institute of Technology.

Cournoyer, R. et al (2003), "Growth Initiatives Technology Framework", Eastman Kodak Company.

Crawley, E., de Weck, O., Eppinger, S., Magee, C., Moses, J., Seering, W., Schindall, J., Wallace, D., and Whitney, D. (2004), "The Influence of Architecture in Engineering Systems", MIT Engineering Systems Division Monograph.

Cross, R., Thomas, R.J., (2009), "Driving Results through Social Networks: How Top Organizations Leverage Networks for Performance and Growth." John Wiley & Sons.

Cross, R., Singer, J., Zehner, D., and Vossen, D. (2009), "Global Pharmaceutical Commercialization Organizational Network Analysis Final Report." Merck Internal Document, Merck & Co., Inc., Whitehouse Station, NJ.

IBM Business Consulting Services (2005), "Transforming Industrialization: A new paradigm for pharmaceutical development."

Kukura, J. (2012), "Strategic Manufacturing Technology Management in the Pharmaceutical Industry", Cornell University Lecture, Policy Analysis and Management in the Pharmaceutical Industry.

Kukura, J., Starbuck, C., and Chowdhury, A. et al (2007), "Merck Commercialization Technical Forum White Paper on a Framework and Guidance for Distinguishing Core and Non‐Core Technologies.", Merck Internal Document, Merck & Co., Inc., Whitehouse Station, NJ.

Moore, G.A. (2002), "Crossing the Chasm: Marketing and Selling Disruptive Products to Mainstream Customers", HarperBusiness Essentials.

Nelson, R.R. (2003), "Physical and Social Technologies and Their Evolution.," Columbia University working paper available from the author, Columbia University.

Phaal, R., Farrukh, C.J.P. and Probert, D.R. (2004), "Technology roadmapping - a planning framework for evolution and revolution." Technological Forecasting and Social Change, 71. pp. 526. ISSN 0040-1625.

Phaal, R., Farrukh, C.J.P., and Probert, D.R. (2004), "A framework for supporting the management of technological knowledge." International Journal of Technology Management, 27. pp. 1-15. ISSN 0267-5730

Phaal, R., Farrukh, C., Mitchell, R. and Probert, D. (2003) "Starting-up roadmapping fast." IEEE Engineering Management Review, 31. pp. 54-60. ISSN 0360-8581

Phaal, R. (2003), "Strategic roadmapping: linking technology resources to business objectives." International Journal of Technology Management, 26. ISSN 0267-5730

Ravasz, E., Somera, A.L., Mongru, D.A., Oltvai, Z.N., Barabási1, A-L., (2002). Hierarchical Organization of Modularity in Metabolic Networks. Science.

Rogers, E.M. (1962), "Diffusion of Innovations", Simon & Schuster.

Sahinidis, N.V., Grossman, I.E., Fornari, R.E., and Chatharthi, M. (1989), "Optimization model for long range planning in the chemical industry", Computers & Chemical Engineering.

I.A. Karimi and Rajagopalan Srinivasan (Editors), Proceedings of the 11th International Symposium on Process Systems Engineering, 15-19 July 2012, Singapore.

Multi-scale Optimization for Advanced Energy Processes

Lorenz T. Biegler[1] and Yi-dong Lang

Department of Chemical Engineering; Carnegie Mellon University; Pittsburgh, PA USA 15213

Abstract

Advanced energy systems demand powerful and systematic optimization strategies for analysis, high performance design and efficient operation. Such processes are modeled through a heterogeneous collection of device-scale and process scale models, which contain distributed and lumped parameter models of varying complexity. This work addresses the integration and optimization of advanced energy models through multi-scale optimization strategies. In particular, we consider the optimal design of advanced energy processes by merging device-scale (e.g., CFD) models with flowsheet simulation models through sophisticated model reduction strategies. Recent developments in surrogate-based optimization have led to a general decomposition framework with multiple scales and convergence guarantees to the overall multi-scale optimum. Here, we sketch two trust region-based algorithms, one requiring gradients from the detailed model and one that is derivative-free; both demonstrate multi-scale optimization of advanced energy processes. Motivated by an advanced Integrated Gasification Combined Cycle (IGCC) process, we present two case studies that include PSA models for carbon capture and CFD models for gasification and combustion.

Keywords: model reduction, nonlinear programming, proper orthogonal decomposition (POD), trust region methods, IGCC power plants, carbon capture

1. Introduction and Motivation

Increasing pressures and awareness of critical energy systems demand powerful and systematic optimization strategies for their design and operation. These demands present a number of challenges, particularly as emerging energy processes incorporate advanced technologies that are described by complex process, nonconventional, multi-scale process models. In this study, we discuss the development of a multi-scale optimization framework that addresses these challenges. This framework is enabled through rapid advances in optimization models and solution strategies over the past decade. Nonlinear optimization algorithms can now solve models with millions of decision variables and constraints. Correspondingly, the computational cost of solving discrete optimization problems has been reduced by *nine orders of magnitude* (Biegler and Grossmann, 2004; Biegler, 2010). These algorithmic advances have been realized through software/design frameworks that integrate these optimization models through nonlinear and mixed-integer nonlinear programs (NLPs, MINLPs). On the other hand, it is essential to note that these benefits arise because these frameworks permit (indeed require) optimization models to be formulated carefully as well-posed, well-conditioned problems with exact first and second derivatives.

[1] biegler@cmu.edu

To extend these tools to multi-scale energy processes, we require the integration of efficient and accurate model reduction strategies within the optimization framework, leading to simple analytic descriptions that we term *reduced order models* (ROMs). Moreover, the development of efficient and accurate model reduction strategies allows the capture of multi-scale, multi-fidelity model behavior within an optimization framework. As described in Chung et al. (2011), these strategies can be applied within a cascaded network that link multi-scale models (from atomic to enterprise scales) along with optimization formulations that provide the "glue" to exploit synergies among these systems through ROMs.

With this goal in mind, a number of important research questions arise. First, how should reduced models be constructed and how do we balance accuracy with computational cost for the model construction phase? Second, does the multi-scale optimization framework converge to the optimum of the original system models? Third, can multi-scale optimization be performed efficiently without frequent recourse to the original models? To motivate these questions and describe our recent research, we consider the advanced IGCC process with carbon capture, shown in Fig. 1.

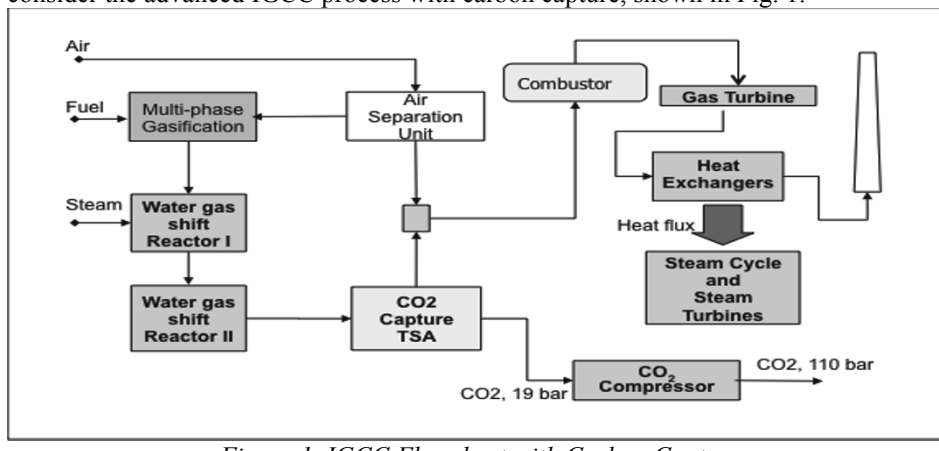

Figure 1. IGCC Flowsheet with Carbon Capture

The advanced IGCC process is described in a detailed case study prepared by TNO (Kessel et al., 1998). The gasifier converts feeds for fuel, water and oxygen into syngas; the effluent CO in the syngas is converted into H_2 and CO_2 in two cascaded water-shift reactors, and the syngas becomes an H_2-rich stream, with 90% of the CO_2 in the stream captured by a temperature-swing adsorption (TSA) unit. The CO_2 is compressed for subsequent storage and sequestration. On the other hand, after mixing with nitrogen and oxygen, the H_2-rich gas enters the combustor of the gas turbine to produce electricity. The energy in the turbine exhaust is recovered by driving the steam turbines in the steam cycle. This process model comprises lumped parameter (algebraic) models for heat exchange and compression, distributed, dynamic (differential-algebraic) models for the TSA unit and distributed, multi-phase (partial differential-algebraic) CFD models for the gasification and combined cycle units. To provide the optimization capability for the overall process model, our strategy converts these heterogeneous (AE, DAE, PDAE) models to equation-based optimization models through model reduction and nonlinear programming. In this way we capture the phenomena of multi-phase flow, particle mechanics, and dynamic operation within the process optimization. In addition, we

describe a framework that allows the optimum of the original, heterogeneous process model to be obtained.

The next section discusses previous model reduction developments, challenges for ROM-based optimization and the extension of these methods for integrated flowsheet optimization with heterogeneous models. The third section describes a ROM-based optimization method that requires gradients from the detailed model. A case study based on the optimization of a pressure swing adsorption (PSA) process demonstrates the performance of this method. In the fourth section we describe a derivative free alternative for ROM-based optimization for the integrated optimization of the IGCC process in Figure 1. Here we develop an optimization strategy based on a trust region framework that guarantees convergence to the rigorous optimum with minimum recourse to detailed models. Conclusions and future work are discussed in the fifth section.

2. Paradigm for Reduced Order Models

Model reduction is a widespread practice that extends over many engineering disciplines, and over several decades. In process systems engineering, early work on model reduction includes the use of reduced models for physical properties that require detailed thermodynamics and transport models (see Leesley and Heyen, 1977; Boston and Britt, 1978, Barrett and Walsh, 1979). These early strategies provide a vision for reduced models that extend beyond physical property models to a wide range of process engineering tasks. In fact, Caballero and Grossmann (2008) applied a related ROM-based strategy for distillation models in flowsheet optimization.

Similarly, in the PDE modeling community, reduced order modeling strategies have been developed and include multi-grid methods, proper orthogonal decomposition (POD) and state-space ROMs based on data-driven modeling and principal component analysis (PCA). To adapt ROMs to process optimization, a typical strategy is to match the ROM to rigorous models at specific points, usually over the course of the optimization path, and to rely on the constructed ROM for gradient information needed for optimization. However, it is well-known that such a strategy cannot be guaranteed to converge to the optimal solution of the detailed model (Biegler, et al., 1985; Brdys, et al., 1987; Gao and Engell, 2005), as gradients from the original model are needed to satisfy optimality conditions. Instead, ROM-based optimization strategies centered on trust region strategies (Conn, Gould, Toint, 2000) provide effective communication between the original model and the ROM, as well as convergence guarantees.

Model reduction strategies coupled with optimization generally cover two approaches. The first approach is based on model reduction that retains most of the structure of original equations but leads to simpler and smaller models. Examples include shortcut models based on physical phenomena, coarsening of discretization (finite difference, element, volume) steps and the use of spectral-based strategies such as POD. The second approach is based on data driven model reduction that leads to the construction of input-output models used in the optimization problem. Issues for the construction of these ROMs include experimental design for model reduction, well-posedness and conditioning of the constructed ROM (known as poisedness) and the choice of basis functions (e.g., specific regression models, artificial neural networks, radial basis functions and Kriging). Often the reduced models from the data-driven approach are used as surrogate models within a derivative-free optimization (DFO) strategy.

Additional requirements arise when adding multiple ROMs within an overall process optimization model. Here, well-conditioned algebraic ROMs need to be incorporated within the optimization framework with exact derivatives provided from the ROMs. This implementation allows the use of equation-based models, fast optimization algorithms and greater robustness in the optimization (e.g., intermediate failures of CFD models are avoided). On the other hand, over the course of the optimization process, ROMs may need to be reconstructed from the original models, often leading to the dominant computational cost. For example, when coupling CFD to flowsheeting models, the former may require CPU hours or days, while the ROM-based flowsheet optimization requires only a few CPU minutes. As a result, recourse to the original model needs to be minimized; this is enabled through the ROM's predictive capability.

Finally, to guarantee convergence of the ROM-based optimization to the optimum of the detailed model, two general trust region frameworks have been developed. The first framework assumes that accurate gradients are available from the detailed model. This allows the ROM to be formulated within a *model NLP,* which is solved within a trust region to generate a search direction for the original model. A key property is that *both* functions and gradients from the original model match the basepoint on the model NLP, i.e*., first order consistency*. This trust-region framework was developed for unconstrained problems by Alexandrov et al. (1998) and is sketched in Figure 2. They also introduced scaled (i.e., corrected) objective functions in the trust-region subproblem to enforce consistency conditions. Fahl (2000) extended this approach by relaxing the consistency conditions and solving the trust-region subproblem inexactly. Finally, Agarwal and Biegler (2012) extended Alexandrov's approach through a filter trust region approach, which greatly reduces the need for gradients from the detailed model.

The second approach does not require gradients from the detailed model and is based on concepts of trust-region-based DFO methods (Conn, Scheinberg, Vicente, 2009). In the context of unconstrained optimization, convergence to a stationary point requires the ROM to have the *fully linear property,* i.e., $\left\|\nabla f(x)-\nabla f^R(x)\right\| \le \kappa_g \Delta$, where $f(x)$ and $f^R(x)$ are objective functions related to the original and reduced models, respectively, and Δ is the size of the trust region. The trust region then proceeds according to Fig. 4 and requires the trust region Δ to vanish upon convergence. Convergence properties of the trust region method with fully linear and fully quadratic ROMs were developed in Conn, Scheinberg and Vicente (2009). Wild et al. (2008) developed conditions for ROMs constructed with Radial Basis Functions (RBFs) that satisfy the fully linear property and lead to well-conditioned models. March and Willcox (2012) recently extended their approach to Kriging models and demonstrated the effectiveness of this approach over conventional unconstrained methods. More detail on this approach is presented in Section 4.

3. ROM-based Optimization with Detailed Model Gradients

For ROM-based trust region methods we consider the following *constrained* nonlinear programming problem:

$$Min\ f(x),\ s.t.,\ c_E(x) = 0,\ c_I(x) \le 0,\ x_L \le x \le x_U \qquad (1)$$

where the objective and constraint functions $f(x)$, $c_E(x)$, $c_I(x)$ are assumed to be at least twice differentiable functions. At iteration k of the optimization cycle, a ROM is

constructed at x_k, and this is used to build the following ROM-based trust-region subproblem at iteration k:

$$Min\ f^R(x_k + s),\ s.t.,\ c^R_E(x_k + s) = 0,\ c^R_I(x_k + s) \le 0,\ x_L \le x_k + s \le x_U,\ ||s|| \le \Delta_k \qquad (2)$$

where $f^R(x_k + s)$, $c^R_E(x_k + s)$, $c^R_I(x_k + s)$ are the ROM objective and constraint functions and the trust region Δ_k is a (l_∞) box that restricts the step size s.

3.1 ROM-based Algorithm Development

To simplify the construction of ROMs, model functions are derived by using local corrections that correspond to the current iterate k. Additive correction schemes for the objective and constraints of (2) are given by:

Zero Order Correction (ZOC)

$$\tilde{\Phi}^R_k(x) = \Phi^R_k(x) + (\Phi(x_k) - \Phi^R_k(x_k)) \qquad (3)$$

First Order Correction (FOC)

$$\tilde{\Phi}^R_k(x) = \Phi^R_k(x) + (\Phi(x_k) - \Phi^R_k(x_k)) + (\nabla\Phi(x_k) - \nabla\Phi^R_k(x_k))^T(x - x_k) \qquad (4)$$

with $\Phi(x) = f(x), c_i(x)$ and $\Phi^R_k(x) = f^R_k(x), c^R_{i,k}(x) \qquad i \in \{E, I\}.$

Here ZOC matches basepoint functions only, while FOC matches both functions and gradients at the basepoint. In terms of corrected objective and constraint values, subproblem (2) becomes:

$$Min\ \tilde{f}^R_k(x_k + s),\ s.t.\ \tilde{c}^R_{E,k}(x_k + s) = 0,\ \tilde{c}^R_{I,k}(x_k + s) \le 0,\ x^L \le x_k + s \le x^U,\ \|s\|_\infty \le \Delta_k \qquad (5)$$

Subproblem (5) is then solved using only functions and derivatives from the ROM. On the other hand, functions and derivatives from the detailed model are calculated for the construction of the ROM values in (5), using ZOC and FOC. The algorithm proceeds by choosing step sizes that satisfy a sufficient decrease condition for an exact penalty function of problem (5):

$$\psi^R(x_k + s) = \tilde{f}^R_k(x_k + s) + \mu\left[\left\|\tilde{c}^R_{E,k}(x_k + s)\right\| + \sum_j \max(0, \tilde{c}^R_{I,k,j}(x_k + s))\right] \qquad (6)$$

The corresponding decrease of the penalty function of problem (1) leads to the metric:

$$\rho_k = ared / pred = (\psi(x_k + s) - \psi(x_k)) / (\psi^R(x_k + s) - \psi^R(x_k)) \qquad (7)$$

which determines the increase or decrease of the trust region Δ_k. The resulting trust region algorithm is shown in Fig. 2. Note that the algorithm expands or shrinks the trust region based on how well the ROM-based subproblem follows the original problem surface. Also, the algorithm may terminate with $\Delta_k \rightarrow 0$ if ZOC is applied and detailed model gradients are not provided. On the other hand, if FOC is applied, the algorithm is guaranteed to converge with $||s|| \rightarrow 0$ and a stationary point (where the norms of the directional derivatives $||D_s\psi^R(x^*)|| = ||D_s\psi^R(x^*)|| = 0$) is found for the original problem (1). More details of this approach can be found in Agarwal and Biegler (2012). In addition to the algorithm below, Agarwal and Biegler developed a more detailed filter-based trust region algorithm, which is not sensitive to the penalty parameter μ in (6) and leads to faster performance.

3.2 PSA Case Study

The ROM-based trust-region algorithm was applied in Agarwal and Biegler (2012) to optimize a two-bed four-step pressure swing adsorption process with an 85%-15% N_2-CO_2 feed mixture, as shown in Fig. 3. Although this process cannot be applied directly to the IGCC process in Fig. 1, PSA models have a similar structure to the TSA process and the optimization strategy applies in a straightforward way. The operation consists of four distinct operating steps; pressurization, adsorption, depressurization (counter-current), and light reflux (or desorption). We maximize CO_2 recovery subject to a constraint on CO_2 purity and consider five decision variables, high pressure P_h, low pressure P_l, step times t_p and t_a and adsorption feed velocity u_a according to:

$$\begin{aligned} \max \quad & CO_2 \text{ recovery} \\ \text{s.t.} \quad & CO_2 \text{ purity} \geq 50\% \quad 0.1 \text{ m/s} \leq u_a \leq 0.3 \text{ m/s} \\ & 1 \text{ bar} \leq P_h \leq 3 \text{ bar} \quad 0.4 \text{ bar} \leq P_l \leq 1 \text{ bar} \\ & 35 \text{ sec} \leq t_p \leq 150 \text{ sec} \quad 50 \text{ sec} \leq t_a \leq 400 \text{ sec} \end{aligned} \tag{8}$$

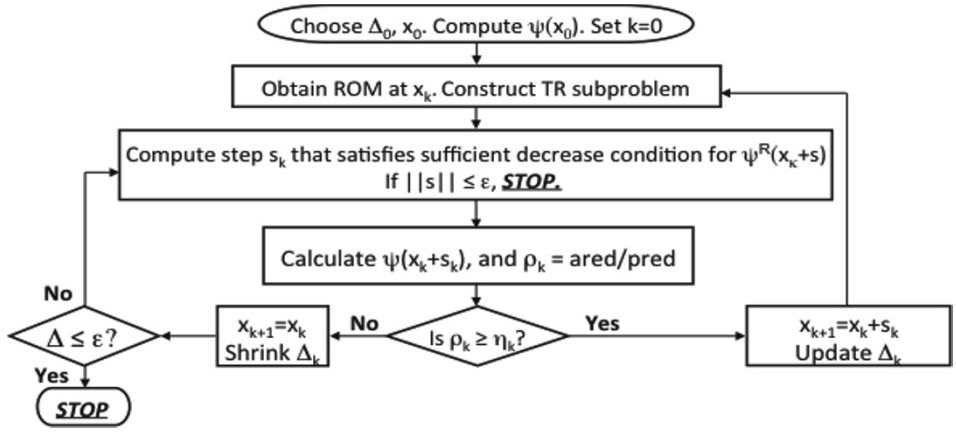

Figure 2. Trust Region Method with Detailed Model Gradients

For the PSA process, the ROM is based on POD applied to the bed equations (as described in Agarwal and Biegler, 2009). The algorithm in Fig. 2 includes the solution of subproblem (5), using the POD-based ROM and IPOPT (Waechter and Biegler, 2006) in an equation-based environment. Also, evaluating the detailed bed models can be done efficiently as part of the generation of the ROM, but here gradient evaluation of the detailed models is done through finite differences. The algorithm requires the solution of 105 trust region subproblems (using IPOPT) and 2.47 CPU h (Intel Quad Core 2.4 GHz processor). It should be noted that if the filter-based trust region algorithm is used, only 51 trust region subproblems and only 1.36 CPU h are required. Moreover, using finite difference gradients we conclude that the algorithm converges to a local optimum. More information on these models and algorithms is given in Agarwal and Biegler (2012).

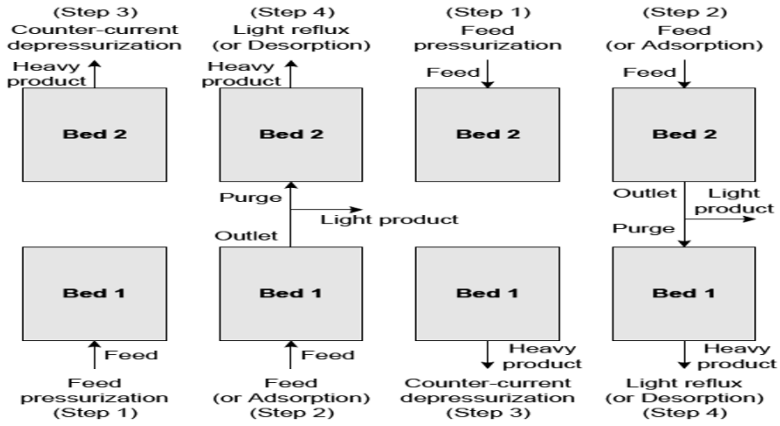

Figure 3: A two-bed four-step PSA cycle

4. ROM-based Optimization without Detailed Model Gradients

Obtaining gradients from detailed CFD models is often prohibitively expensive; hence, the algorithms in Fig. 2 can no longer be used and modifications are needed. In this case convergence guarantees are available if the following properties hold for the ROM. The *fully linear* and *fully quadratic* properties are given by:

$$\left\|\nabla\Phi(x)-\nabla\Phi^R(x)\right\| \le \kappa_g\Delta \text{ and } \left\|\nabla^2\Phi(x)-\nabla^2\Phi^R(x)\right\| \le \kappa_h\Delta, \text{ respectively.}$$

If the *fully linear* property is satisfied, ROM-based trust region algorithms can be constructed that guarantee convergence to a stationary point, satisfying first order optimality conditions. Stronger guarantees for convergence to locally optimal solutions require *fully quadratic* ROMs. Moreover, for ROMs based on radial basis functions (such as Kriging) the fully linear property can be satisfied *only if at least* n+1 *interpolation points lie within the trust region* Δ, where n is the dimension of the degrees of freedom in problem (1).

For fully linear ROMs, a derivative free trust region algorithm was developed and analyzed in Conn et al., 2009) and is sketched in Fig. 4. As with the algorithm in Fig. 2, this algorithm constructs and solves trust region subproblems (such as (5)), updates the trust region based on agreement with the detailed model, and shrinks the trust region if progress is poor. In both cases, frequent recourse is needed to the original detailed model. Moreover, this algorithm has some additional complexities. In particular, note that finding a stationary point for the ROM-based subproblem is *not* sufficient for convergence. Instead, termination of the algorithm occurs if either $\|D_s\psi^R(x^k)\| \rightarrow 0$ or $\Delta_k \rightarrow 0$ *and the ROM remains fully linear*. With a shrinking trust region, the fully linear property therefore needs to be monitored and the ROM needs to be updated. This update step may require more frequent recourse to the original model.

4.1 ROM-based Algorithm Development

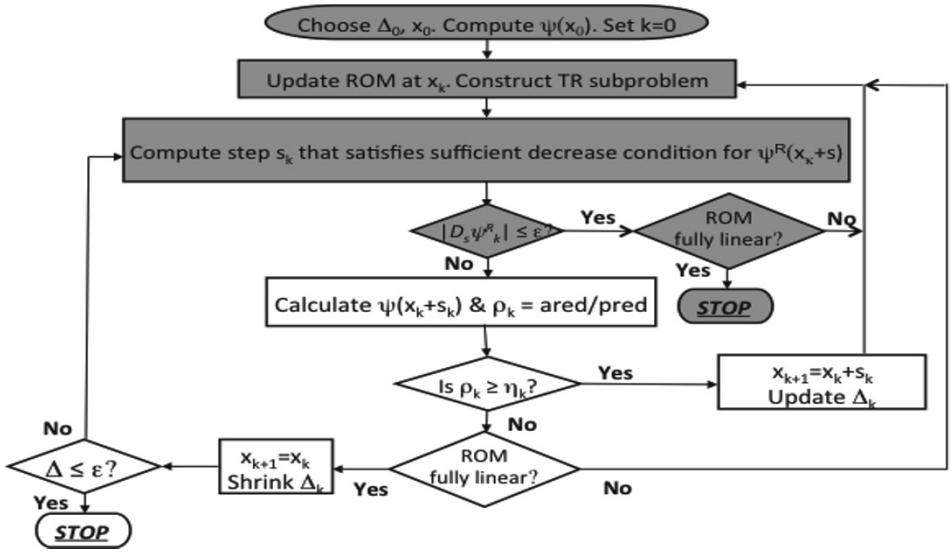

Figure 4. Trust Region Method without Detailed Model Gradients

Now consider the flowsheet optimization problem with heterogeneous models, as illustrated by the IGCC process in Figure 1. Here, it is particularly clear that recourse to the original CFD models during the optimization step is prohibitively expensive. In fact, checking the CFD model at the *solution* of the ROM-based flowsheeting optimization problem may be all that the computing budget allows. To deal with this challenging restriction, we develop ROMs from efficient space-filling experimental designs. We also ensure that ROMs are poised (sampling points are chosen and ROMs are well-posed and well-conditioned). Kriging models with RBFs are a good choice for this. Finally, the ROM-based trust region subproblem (5) comprises the overall flowsheeting model with an initial large trust region, and this subproblem is solved to convergence.

The above characteristics greatly simplify the algorithm in Figure 4. In fact, since the ROM-based model is always fully converged and $\|D_s\psi^R(x^k)\| \le \varepsilon$, only the grayed steps apply and the trust region management steps are bypassed. Moreover, once the ROM-based optimization is determined, the remaining concern is maintaining the fully linear property of the ROM. We propose to address this concern with the following approach:

1. Based on the number and location of sampling points as well as the Lipschitz constants of the original model, determine the smallest value of κ_g that defines a fully linear ROM.
2. Armed with the value of κ_g and a specified tolerance, ε, determine the largest trust region size Δ_{min} that satisfies the convergence criterion.
3. Solve subproblem (5) and locate the number of sampling points within distance Δ_{min} from the solution of (5).
4. If at least n+1 sampling points are within Δ_{min}, convergence is achieved. Else, update the ROMs with additional sampling points and return to step 1.

4.2 ROM-based Process Optimization coupled with CFD Models

We now demonstrate the above approach with the optimization of the advanced IGCC

process shown in Figure 1. In addition to lumped parameter flowsheeting models, the process model contains two CFD models, for the gasifier and combustor. As described in Lang et al. (2009) and Lang et al. (2012), ROMs were developed for both CFD models using Latin Hypercube Sampling for the experimental design and PCA-based reduction of the snapshots of their vector fields at each sampling point. For the combustor ROM, a Kriging model was developed to map the process inputs to the output streams, while an artificial neural network (ANN) ROM was developed for input-output mapping of the gasification unit. Cross-validation on both ROMs showed excellent predictive capabilities over the entire input space. Both output temperatures and compositions were typically predicted with relative errors of less than 1%. Full details of the ROM construction and validation of these models are given in Lang et al. (2009). It is notable that sampling points of the CFD combustor model required over 30 CPU min, while the CFD gasifier model required as much as 20 CPU h. On the other hand, each of the resulting ROMs could be executed within 1 CPU s.

As detailed in Lang et al. (2012), the ROM models were integrated within an equation-based version of the Aspen Plus simulator using the USER3 protocol. This allowed fast, equation-based NLP solvers to be applied directly. For the process optimization, we select four independent variables that relate to the gasifier and the combustor, i.e. fuel distribution, steam and oxygen ratios for the gasifier, and the split fraction that determines the flowrate of the oxidant stream supplied to the combustor. In addition, three independent variables are selected from the process variables in the flowsheet: mass flowrate feeding the water gas shift (WGS) reactors; mass flowrate of the makeup stream recycle within the steam cycle and heat allocation ratio of the high pressure turbine to the medium pressure turbine. The flowsheet optimization problem included ROMs for the for the combustor and gasifier and the objective is to maximize the power generated by the IGCC plant. The problem formulation consists of 3747 variables; solution of the ROM-based optimization problem (9) requires no more than 15 iterations and less than 3 CPU seconds by DMO, the default solver available in Aspen Plus. With an additional $n+1 = 8$ CFD simulations, one can verify the detailed model optimality of these results. The optimization with the ROMs derived from CFD models improves the objective function by a total of 23.22 MWe or 6.8%. This result demonstrates the advantages of process optimization through conversion of ROMs from CFD models into EO process models. With the CFD-derived process models, the process optimization clearly improves the objective function, and provides greater process accuracy. This result shows that ROM-based process modules overcome the prohibitive computational requirements of CFD models and are effective surrogate models for process simulation and optimization.

5. Conclusions and Future Work

Large-scale process optimization of advanced energy systems needs to consider a heterogeneous collection of device-scale and process scale models, with distributed and lumped parameter models of varying complexity. The integrated optimization of these models through multi-scale optimization strategies is enabled by state of the art, equation oriented optimization algorithms along with management of reduced order models. Recent developments in surrogate-based optimization have led to a powerful decomposition framework with multiple scales and convergence guarantees to the overall multi-scale optimum. Here, we also develop an efficient framework that requires infrequent recourse to the original detailed model. Motivated by an advanced IGCC process, we present two case studies that include PSA models for carbon capture and

CFD models for gasification and combustion. In particular, integrated optimization of the IGCC process (including ROMs derived from CFD models) shows that the power output of the process increases by 7% compared to an optimization model that does not consider degrees of freedom in the gasifier and combustion units. This implies that ROM-based flowsheet optimization can significantly increase the efficiency of energy processes. Moreover, the ROM-based optimization framework extends across a wide range of engineering disciplines that include multiple scales and model types. Future work will deal with a detailed analysis of convergence properties for ROM-based trust region methods, particularly with the development and application of fully linear and fully quadratic ROMs. We also plan to improve methods to develop accurate and efficient ROMs from detailed models that arise at device and molecular scales, as well as their integration and validation within multi-scale optimization environments.

References

Agarwal, A., Biegler, L. T., Zitney, S. E. (2009). *Ind. Eng. Chem. Res., 48,* 2327.
Agarwal, A., Biegler, L. T. (2012). *Optim. Eng.,* in press, doi: 10.1007/s11081-011-9164-0
Alexandrov, N. M., Dennis Jr., J. E., Lewis, R. M., Torczon, V. (1998) *Struct. Optim., 15,* 16.
Barrett, A., J.J. Walsh, Comput. Chem. Engng, 3 (1979), p. 397
Biegler, L.T., I.E. Grossmann and A.W. Westerberg, *Comp. Chem. Engr.* 9, 2, p. 201 (1985).
Biegler, L. T., I. E. Grossmann, *Comp. Chem. Eng.* , 28, 8, pp 1169-1192 (2004)
Biegler, L. T. *Nonlinear Programming: Concepts, Algorithms and Applications to Chemical Processes,* SIAM, Philadelphia (2010)
Boston, J. F., H.I. Britt, *Comp. Chem. Eng.*, 2 (1978), p. 109
Brdys, M., P.D. Roberts, *International Journal of Systems Science*, 18, pp. 1305-1322 (1987)
Caballero, J. A. and I. E. Grossmann, *AIChE Journal*, 54, 2633-2649 (2008)
Chung, P. S., M. S. Jhon, L. T. Biegler, *Adv. Chem. Eng*., 40, pp. 59–118 (2011)
Conn, A. R., Gould, N. M., Toint, P. L. (2000). *Trust-region Methods*, *SIAM.* Philadelphia, PA.
Conn, Scheinberg, Vicente, *SIAM J. Opt.,* 20, pp. 387-415, 2009
Fahl, M. (2000). *PhD Thesis.,* Trier Univ.
Gao, W., S. Engell, Comp. Chem. Eng., 29, pp. 1401-1409 (2005)
Kessel, L.B.M. van, J.C.P.L. Saeijs, V. Lalbahadoersing, A.R.J. Arendsen, M. Stavenga, A.B.M. Heesink and H.M.G. Temmink, TNO-Report R98/135 (1998)
Lang, Y-D, A. Malacina, L. T. Biegler, S. Munteanu, J. I. Madsen, S. E. Zitney, *Energy and Fuels,* 23, 1695–1706 (2009)
Lang, Y-D, S. E. Zitney, L. T. Biegler, *Comp. and Chem. Engr.*, 35, pp. 1705 – 1717 (2011)
M.E. Leesley, G. Heyen, Comput. Chem. Engng, 1 (1977), p. 102
March, A. and Willcox, K., AIAA-2010-9198, AIAA/ISSMO Multidisciplinary Analysis and Optimization Conference (2010)
Wächter, A., Biegler, L. T. (2006). *Math. Program., 106,* 25.
Wild, S. M., R. G. Regis, C. A. Shoemaker, *SIAM J.Sci. Comp*. 30, pp. 3197-3219 (2008)

I.A. Karimi and Rajagopalan Srinivasan (Editors), Proceedings of the 11th International Symposium on Process Systems Engineering, 15-19 July 2012, Singapore.

PSE in China: Retrospect and Prospects

Youqi Yang[a] Siwei Cheng[b]

[a]*China National Chemical Information Center,Beijing 100029,China;*
[b]*Research Centre for Virtual Economy, University of Science and Technology of China, Beijing 100049,China;*

Abstract

This is an overview on the developments of Process Systems Engineering (PSE) in China, outlining some viewpoints on future prospects, consisting of four parts:1) Introduction, consisting of progress of the international PSE community and the definitions of PSE from well-known authors;. 2).Retrospect on 20 years of development of PSE in China: Part I describing 5 major PSE contributions: modeling, simulation and optimization for process design and operation; advanced process control and monitoring; process integration for energy conservation and waste reduction; supply chain management for global competition and green PSE for sustainable development, and Part II on problems in development;3).Challenges on future developments for PSE,
4).Future prospects consisting of: two issues: problems in development of PSE in China and future strategies.

Keywords: Process Systems Engineering; Retrospect; Prospects; Overview

1. Introduction

Although the general systems theory could be traced back to the 1930s, system engineering was founded during World War II, when Operation Research (OR) was applied by the Allied Forces to improve logistics. In the 1940s Bell Telephone Laboratory started the large network system theory to meet the requirement of large-scale communication network development. In the 1950s the electronic computer was created and applied in engineering areas, thus providing a sound material basis for systems engineering. In 1954 MIT started offering “systems engineering” as a course, and the well-known book “Engineering Cybernetics” written by H.. S. Tsien（1954） was published in same year. In 1957 the first book titled “Systems Engineering” was published by Goode and Machol (1957).

The development of Process Systems Engineering (PSE) started about 10 years later. The book, “Systems Engineering for the Process Industries”, was published by Williams in 1961. The earliest dynamic process simulator SPEED-UP was developed by Sargent and Westerberg in 1964. In the 1970s PSE began an explosive growth worldwide, along with the rapid growth of the chemical industries, while the first worldwide energy crisis started to challenge energy conservation.

PSE was introduced into China in the late 1970s, several books were written or translated into Chinese (Takamatsu, 1981; Kafarov, 1983; Yang, 1989). Training classes and courses were offered in universities, and teaching-research groups were organized since that time. In 1991 Professor H. S. Tsien recognized as “the father of systems engineering in China”, suggested to Siwei Cheng to organize a PSE society in China. This society was established some 20 years ago as a PSE academic society

covering 11 industries. The major PSE educational and research institutes in main land China is listed on Fig.1.

The Major PSE educational and research institutes in main land China

- Tsinghua University, Institute of PSE in Chemical Engineering Dept.
- Dalian University of Technology, Institute of PSE in School of Chemical Eng.
- East China University of Science and Technology, Eng. Research Center of PSE, sponsored by Ministry of Education
- Qingdao University of Science and Technology, Institute of Computer and Chem. Eng.; Institute of Hi-Tech in Petrochemical Industry
- Tianjing University, Teaching and Research Group of PSE in School of Chem. Eng.
- South China University of Science and Technology, Chem. Eng. Institute in School of Chemistry and Chemical Eng.
- Zhejiang University, The state key laboratory of industrial control technology; National Engineering Research Center for Industrial Automation
- Beijing University of Chemical Technology, School of Chemical Engineering; School of Information Science and Technology
- Wuhan University of Science and Technology, PSE institute of Dept. of Chemical Engineering
- Automation Research and Design Institute of Metallurgical Industry, National Metallurgical Automation Engineering Technology Research Center
- Institute of Process Engineering in Chinese Academy of Science: State Key Lab of Multi-Phase Complex System; Lab for Green Process and Engineering
- Some professors at Beijing University of Petroleum. Xi'an Jiaotong University, Nanjing University of Industry, Nanjing University of Science and Technology are also working involving PSE

Figure1. The list of Major PSE educational and research institutes in main land China

The definition of PSE has witnessed changing since its first definition given by Takamatsu at the first international PSE conference in 1982 (Takamatsu,1983) :
PSE is an academic and technological field related to methodologies for chemical engineering decisions. Such methodologies should be responsible for indicating how to plan, how to design, how to operate, how to control any kind of unit operation, chemical and other production process or chemical industry itself.
This definition emphasized the *multi-scale* concept from the very beginning. Later, Grossmann and Westerberg (2000) extended PSE to chemical supply chains, that is, extended chemical engineering decisions to much larger scope consisting of economics and management. The present authors suggested in 2003 the following definition of PSE:
PSE is a comprehensive science focusing on systems processing mass, energy and information, with its core of studying process system organization, planning, coordination, design, control, operation and management, and aimed at holistic optimization of process system in order to meet the requirements of sustainable development. PSE is broadly applied in industries, such as chemical, pharmaceutical, metallurgical, paper, construction materials, food, etc.

Recently Stephanopoulos and Reklaitis (2011) extended the scope of PSE to (a) processing plants; (b) manufacturing systems producing consumer goods; (c) diagnostic and therapeutic products and processes to treat human diseases;(d) energy production, distribution, and consumption systems; and (e) systems which ensure the quality of environment.

2. Retrospect on 20 years of PSE developments in China

2.1. Contributions of PSE

2.1.1. Simulation and optimization technologies for optimal design and operation of chemical plants

In late 1980s Qingdao Institute of Chemical Technology has developed the second generation Chinese process simulator called "Engineering Chemistry Simulation System, ECSS", which was applied in many design and educational institutes in China. In the new century this technology has been recognized from top leadership of major Chinese petrochemical giants such as Sinopec and PetroChina. For instance, according to report from Sinopec, 3000 people have been trained in 17 enterprises and 8 research/ engineering institutes. 142 plants were simulated in 8 years and 250 million RMB (40MM USD) benefits was gained. (Qi, X., 2007)

An ethylene cracker simulator called EPSOS was developed by corporation between Tsinghua University, Research Institute of Petrochemical Technology under PetroChina and Lanzhou Petrochemical Co. This software is based upon chemical kinetics mechanism model and optimization algorithms, which can predict ethylene yield of the cracker and provide optimal operation guide. (Gao, X., Chen, B., etc.,2010) Operation Training Simulator (OTS) is another area PSE made significant progress in China, most OTS used in China are developed domestically.

2.1.2. Advanced process control and real time monitoring

As China became the world largest iron and steel production country since 1996,the development of process control and monitory technologies in metallurgical industry in China has made significant progresses. For example, the multi-scale close loop hierarchical control system developed by Automation Research and Design Institute of Metallurgical Industry and Baoshan consistent process control system(BPC) are used in China with significant economic benefit. (Sun, G.,2008)

An APC controller based on neural network model predicted control for ethylene cracking furnace was developed at East China University of Science and Technology (Wang, H., Qian, F.. 2011), which can control the outlet temperature from cracking coils keeping the temperature fluctuation range less than 1℃ and the production fluctuation range less than 0.25%.

The Manufacturing Executive System (MES) developed by Zhejiang University, Software Research Institute of Chinese Science Academia and Sinopec is a national key project and the first result SMES 1.0 came out in 2004. As an example, after the installation of SMES in Yanshan Petrochemical Co. the time of material balance calculation of whole enterprise reduced from original 6 days to 6～8 hours, the raw material consume reduced 2% and energy consume reduced about 1%.(Li, D., 2011)

2.1.3. Contributions of process integration for energy conservation

Pinch Technology, as a well-known representative technology of process integration has been broadly promoted in China: energy pinch technology was promoted in 1980s,water

pinch technology in 1990—2000, hydrogen pinch in 2000—2010, cooling water pinch 2010—up to now . In application of those pinch technologies, Chinese scholars have made many progresses (Feng, X.,etc.,2007;Du J., etc..,2010).

2.1.4. Supply chain management technology contributes to increasing competitive capability

Since Sinopec adopting linear programming planning tool PIMS in 35 refineries in 2006 the yield of gasoline/kerosene/diesel increased in 1.03% and the benefit from this is about 291 million RMB per year. In 2007—2010 the application of planning optimization in the deeper integration application phase,19 chemical enterprises and 7 refinery-petrochemical enterprises adopted XPIMS. Not only crude oil for each enterprise but also the intermediates supply for each other's between refinery and chemical plants are also optimized. For instance of Shanghai Petrochemical Co., the benefit from optimization of AGO production planning is about 229 million RMB/a and of naphtha is 187 million RMB.

2.1.5. Green PSE contributes to increasing utilization efficiency of resources and to improving development of ecological industry

EIP is a natural, industrial and social complex, in which the integrations of materials, energy, water and information are all included. PSE provides the theoretical guide for design and construction of EIP in China. (Jin, Y., Arons, J. de. Swaan, 2009)

For example, Tsinghua University was responsible to helping planning and construction of Kaiyang phosphorus-coal chemical eco-industrial basis located in Guiyang,. Through the eco-industry network preliminarily established, the number of product kind is increased to more than 60,total amount of product reached 3 million tons annually and total value of output reach 8000 million RMB per year with average annual growth rate 27.2%. (Hu, S Y., Li, Y., Shen, J., 2003)

2.2. Real problems

The development of simulation and optimization technologies have not satisfied the requirements of industries' growth. Up to now the optimization of chemical process design is still based upon multiple iterations between experience and calculations of simulation tools. Besides, many R/D projects are depending upon big size pilot plants, because the mathematical simulation scale-up methodology has no power to guarantee the results in despite of reduction of pilot experiments.

As we put forwarded "comprehensive integration and holistic optimization" for PSE in order to obtain the whole economic benefit optimal and environment impact minimized results of those large scale petrochemical complexes 12 years ago (Yang, S., Zhou, Z., Hua, B., Chen, S.,1999), but there is seldom expected good results coming out. Application researches of PSE in the strategically important new industries, such as new chemical materials, new energy industry, biochemical industry, clean coal industry, are insufficient.

As mentioned by Klatt, K. U., Marquardt, W., (2009), many good results of PSE only enjoyed published on journals, have not penetrated industrial practice.

The combination of PSE with management science is not close enough. The informatization of process industries needs PSE providing theoretical guide. Another example is the supply chain management of process industry is much lagging behind that of other industries, such as automobile, electronic industries.

3. Challenges for future development of PSE

3.1. Challenges from demands in application

3.1.1. Enterprise-wide operation optimization for cross-country global corporations

The operation of cross-country global corporations depends upon dynamic supply chain management .However, unfortunately the logistic cost of chemical supply chain is the highest among the asset-intensive industries, it cost about 12% of total value of sales, which of pharmaceutical industry and automotive industry is 10% and 9% respectively. The proportion of logistic cost in the net increase value is 43% for petroleum industry; 37% for chemical industry; 30% for paper industry and 28% for automobile industry. (Karimi, I. A. 2009). This is because of the rather low chemical supply chain efficiency.

3.1.2. Challenges of low-carbon sustainable development for process industries

The main tendency of optimization study is extending the scope from internal enterprise to external ecological environment in order to construct a sustainable environment friendly enterprise. Particularly to China, there are following issues should be mentioned: ① Use of renewable resources to replace those fossil resources can play an important role in sustainable development; ② Challenges of clean production: For China, coal as the major primary energy (70% of total energy input) is the main cause of pollution. Therefore the principle task is clean utilization of coal; ③The industrial ecology and eco-industrial parks. In China there are 38 state approved EPI and 319 province approved EPI involving petroleum and chemical industries have been built up to last year. ;④Improving energy efficiency.

3.1.3. Rapid IT progress and emerging development of industrialization and informatization

Since 2010 the chemical industry of China became the largest one in the world. However, the biggest one does not mean the strongest one. So how to turn the large one into strong one is the strategic task in China. Since the new IT innovations commercialized rapidly, such as cloud computation, radio frequency identification (RFID), internet of things are getting popular and will effect on emerging cyber infrastructure. All these progresses will undoubtedly lead to one of the grand challenges of modern PSE.

3.1.4. Small scale production and process intensification

Current production modes are increasingly challenged by decentralization, modularization and miniaturization. Process intensification also tends toward this direction. The micro-chemical technology studies systems within the spatial range of 1—100μm and temporal range of 1—100ms. This kind of systems has many features different from traditional chemical systems(Yang, YQ., 2008): ① The miniaturization of length scale causes significant process intensification: ② Miniaturization brings significant reduction of sample amount required in tests, much faster and more accurate; ③ Inherent safety and good controllability. ④Convenience in scale-up to commercial production of new products; ⑤ Possibility of implementing distributed production mode in chemical industry; ⑥ Pursuing new reaction paths. Combining Micro-chemical Technology with process intensification may create the way of miniaturization of chemical plants. How to design, operate and control this kind of micro-chemical systems is the task of micro scale PSE.

3.1.5. Urbanization causing the need to optimize the infrastructure network of cities

An infrastructure can thus be seen as a complex socio-technical system, the complexity of which is defined by its multi-agent/multi-actor character, the multi-level structure of the system, and the multi-objective optimization. Since PSE field has enabled

tremendous advances in holistic optimization, it is interesting to explore those PSE methods and tools to be applied to infrastructure system design and operations. (Lukszo, Z., etc. 2006).

3.2. Challenges from academic developments

3.2.1. Integration of multi-scale modeling

The simulation scope of PSE is quite different on scales: time scales (10^{-15} to 10^{8} s) and length scales (10^{-9} to 10^{6} m) are used. This large research scope is studied by different disciplines: Atomistic-based simulations such as molecular mechanics (MM), molecular dynamics (MD), and Monte Carlo-based methods (MC) are the area of Computer-Aided Molecular Design (CAMD); for the morphology on scales of 100–1000 nm is the mesoscopic modeling techniques; both of above belong to Computational Chemistry; the scales of 1000nm～10m is the area of Computational Fluid Dynamics (CFD);the scales of 0.1m～10^{4}m is the area of traditional Process System Modeling (PSM), The application ranges of the PSM and CFD methods partly overlap owing to scaling down of the modeled equipment in PSM (Jaworski, Z., Zakzewska, B., 2011).

Each simulation area has its own commercialized tools. As we stressed "comprehensive integration and holistic optimization", the integration approaches of the numerical simulation tools are urgently needed.

3.2.2. Challenges from sustainable development

Simulation and analysis of sustainable development requires extending the scope to include the society–economy–ecology. As Bakshi mentioned (Bakshi, B. R., Fiksel, J., 2003) there are 3 kinds of sustainable business practices that simultaneously benefit both an enterprise and its stakeholders :design for sustainability ,eco-efficient manufacturing and industrial ecology.

3.2.3. The third paradigm of chemical engineering– challenges from product engineering

A classification of chemical products divides all chemical products into three classes: *basic* chemical products (e.g., commodity and specialty chemicals, pharmaceuticals, polymeric materials), *industrial* chemical products (e.g., films, fibers, paper, glass substrates, pastes, creams), and *configured-consumer* chemical products (e.g., light bulbs, hemodialysis devices, labs-on-a-chip). (Seider, W. D., etc. 2009) For *basic* chemical products, emphasis is normally on *process design*, with significant involvement in molecular-structure design – to select the molecules that satisfy customer requirements. Herewith CAMD tools may help a lot. However, for *industrial* and *configured-consumer* products, the key issues probably become to morphology problem. There is no simulation tools and little or no PSE knowledge available for this area.

3.2.4. Nanoscale Process Systems Engineering

With the birth of nano scale process systems engineering, Stephanopoulos (2005) at MIT proposed "nano scale factories" as the next frontier of processing scale and nano scale PSE as the new theory to handle the design, simulation and operation of those active processing systems.,

Yang (2008) pointed out the challenges for PSE. As "molecular factories" is the frontier of next generation manufacturing, traditional PSE is not valid in this area. Nano scale PSE could be realized as a cross-discipline ,where one may find the PSE, system biology, molecular tectonics and molecular computer all fueling the development of nano scale PSE.

4. Future Prospects

4.1. Problems in development of PSE in China

The core competence of PSE used to be related to modeling, simulation and optimization (MSO), methods and tools, which soon became a regular part of chemical engineering studies at the end of the last century. Therefore a risk for PSE is more or less being marginalized. If the PSE community continues limiting efforts to academic research without penetrating industrial practice, PSE is bound to shrink. Risk investment is needed to help transform many good PSE research results into commercial software and routine tools used in industries. This is especially urgent in China.

4.2. Strategies for the future

4.2.1. Upgrade PSE to Multi-scale Product & Process Systems Engineering (MPPSE) to intensify contribution to chemical engineering.

The future challenges in chemical engineering are essentially systems problems, for which PSE could bridge the scales, addressing product design, reaction pathway synthesis as well as equipment and process design in an integrated manner to link user requirements to engineering solution. PSE needs to promote holistic treatment by integrating mature methods/tools from different disciplines into a commercial platform for industrial use, including specialized simulation systems, e.g., for coal-based chemical processes, efficient optimization algorithm packages, etc.

4.2.2. Extend simulation scope — toward virtual plant

Since a plant is accounted as a cost center, cost minimization is the optimization objective. In order to do so, resource and energy/water reduction with quality control is an everyday routine. Should there be a virtual plant based on integration of rigorous models, this would be highly helpful both in operation decision, support and operator training.

4.2.3. Combination with management science — from virtual plant to virtual corporation

Since the headquarter or Strategy Business Unit (SBU) is the benefit center, which accounts every day the net benefits of the whole company dealing with financial flow and financial cost. Therefore, there is a need of combining traditional PSE with management science to simulate the behavior and performance on the corporation level.

If the integrated optimization of a corporation including not only material energy and information flows but also financial flow, the benefit room for the enterprise must be enlarged. The decision support tools are not yet integrated with PSE tools. Once such IT systems were seamlessly integrated with the PSE tools, the competitive power of a corporation would be much improved.

4.2.4. Extend scope of PSE to supply chain — corporation-to-supply-chain optimization

Supply chain management (SCM) extends the enterprise border to enable the enterprise to share information, to cooperate in financial deployment for mutual benefits, and even to establish global manufacturing networks, thus making the enterprise more competitive. Supply chain dynamic optimization avoids, too, *bullwhip effect* and *wave effect*.

4.2.5. Integral simulation of real economy – Virtual Business

Real economy circulation means the entire chain of exchange, production and circulation. The focus of current PSE is production, and the focus of recent e-commerce is exchange (mainly the last exchange). However, virtual business tries to simulate the

whole real economy circulation as a whole by means of advanced information technology together with overall optimization on this basis. Due to extensive use of Internet Protocol Version 6(IPV 6) and network of things the mode of global business will be essentially changed, all presaging the birth of *Virtual Business*.

References

Bakshi,B.R., Fiksel, J., (2003),The Quest for Sustainability: Challenges for Process Systems Engineering, AIChE Journal, 49[6]:1350-1358

Du J., Li X. , Chen, L., Yao,P., (2010),Synthesis of heat integrated mass exchanger networks using step-wise approach based on superstructure, Chinese Journal of Chemical Engineering, 61[10]:2636-2643

Feng, X., Bai, J., Zheng,Z.(2007),On the use of Graphical Method to Determine the Targets of Single-contaminant Regeneration Recycling Water Systems, Chem. Eng. Science, 62 (8) 2127-2138

Gao ,X., Chen, B., He, X., Qiu, T., Li, J., Wang, C., and Zhang, L.,(2008), Multi objective optimization for the periodic operation of the naphtha pyrolysis process, Comput. and Chem. Eng., 32[11] : 2801-2811

Goode, H.,Machol,R.E.,1957, System Engineering, McGraw Hill.

Grossmann, I. E., &Westerberg, A.W. (2000). Research challenges in process systems engineering. AIChE J., 46, 1700–1703.

Hu,SY., Li, Y.,Shen, J.(2003), Integration methodology and applications of Eco-industrial systems(In Chinese), Environment Protection, [1]:16-19

Jin, Y., Arons, J.de.Swaan, (2009), Resource· Energy· Environment· Society —scientific and engineering principles for circular economy, Chemical Industry Press, Beijing.

Karimi,I.A. (2009)., Chemical Logistics—Going Beyond Intra-Plant Excellence Proceedings of 10th Intern.Symposium on PSE—PSE'2009,Elsevier B.V.

Klatt,K.U., Marquardt,W.,(2009), Prospectives for process systems engineering—Personal views from academia and industry, Comp. & Chem. Eng, 33:536-550

Li, DF., (2011) The design and applications of a model driven Manufacture Executive System (MES) for process enterprises, Proceedings of 20 years anniversary conference of PSE, Beijing.

Lukszo, Z., Weijnen, M.P.C., Negenborn,, R.R., Schutter, B. De, Ilić,M., （ 2006 ）, Challenges for process system engineering in infrastructure operation and control, Proceedings of 9th International Symposium on Process Systems Engineering, W. Marquardt, C. Pantelides (Editors) , Elsevier B.V.:95-100

Qi,XZ., (2007),The Status and prospects of informatization construction in Sinopec(in Chinese),Proceedings of 11th annual conference on IT applications in chemical industry CIESC,Xi'ning , China.

Seider, W. D. , Widagdob, S., J.D. Seader, Daniel R. Lewin, (2009), Perspectives on chemical product and process design, Comp. and Chem . Eng., 33 :930–935

Stephanopoulos,N.,Solis, E.O.P. and Stephanopoulos, G.., (2005), Nanoscale process systems engineering: Toward molecular factories, synthetic cells, and adaptive devices, AIChE Jour. 51[7]:1858-1869

Stephanopoulos, G. , Reklaitis, G.V.,(2011).Process systems engineering: From Solvay to modern bio- and nanotechnology. A history of development,successes and prospects for future. Chem. Eng. Science,66:4272-4306

Sun, G.,(2008), The automation technologies for energy conservation in iron and steel industry(In Chinese), Proceedings of annual conference of PSE society of China, Shanghai.

Takamatsu, T. (1983). The nature and role of process systems engineering. Comput. Chem. Engg.,7, 203–218.

Tsien, H. S.,1954, Engineering Cybernetics, McGraw Hill.

Wang, H., Wang, Z., Mei, H., Qian, F.,and Tang, Z.,(2011), Intelligent severity control stabilizes ethylene crackers. Oil and Gas Journal, 109 (6):104-109.

Williams,T.J., 1961, Systems Engineering for the Process Industries, McGraw Hill.

Yang, YQ,1989, Chemical Process Engineering in Practice (In Chinese), Chemical Industry Press, Beijing.

Yang, YQ., (2008), Microscale and nanoscale process systems engineering: Challenge and Progress(In English),The Chinese Journal of Process Engineering, 18, [3] : 616-624,

Yang, S., Zhou, Z., Hua, B., Cheng, SW.,(1999) Comprehensive integration of PSE and management(In Chinese), Modern Chemical Industry(Suppl),:209-214

I.A. Karimi and Rajagopalan Srinivasan (Editors), Proceedings of the 11th International Symposium on Process Systems Engineering, 15-19 July 2012, Singapore.

RECENT DEVELOPMENTS ON PSE EDUCATION AND RESEARCH IN MALAYSIA

Mohd Azlan Hussain[a*], Zainuddin Abdul Manan[b], Norashid Aziz[c]

[a]*Department of Chemical Engineering, Faculty of Engineering,Universiti Malaya, Kuala Lumpur, Malaysia.*

[b]*Process Systems Engineering Centre (PROSPECT), Faculty of Chemical Engineering, Universiti Teknologi Malaysia, 81310 Skudai, Johor, Malaysia.*

[c]*Department of ChemicalEngineering,Faculty of Engineering,Universiti Sains Malaysia, Nibong Tebal, Penang, Malaysia.*

Abstract

Process systems engineering (PSE) is a relatively young area in chemical engineering. The term PSE was used for the first time in the 1961 AICHE symposium series and became more established in Asia in 1982 after the first international symposium in Kyoto, Japan. The development of PSE education and research in Malaysia have taken shape within the last 15 years. PSE has recently evolved into a generic tool for the planning and management of policies as well as resource supply-chain that transcends the process domain. This paper presents the development of PSE education and research in Malaysia. Special highlights are given on the elements of innovation in PSE education and on various research works done by institutions in Malaysia including those that fits the big picture of systems planning and engineering.

Keywords: Chemical Engineering,Process Systems Engineering (PSE), Systems Planning, Engineering education, Malaysia.

1. Introduction

Prof Takamatsu from Kyoto University defined process systems engineering as "...an academic advanced technology field related to methodologies for Chemical Engineering decisions. Such methodologies should be responsible for indicating how to (i) plan (ii) design (iii) operate and (iv) control any kind of unit operation, chemical and other production and chemical industrial processes" [1]. Over the years, this definition has been the basis of many core courses in Chemical Engineering taught in universities around the world including in Malaysia.

The previous definition of Takamatsu falls within the typical and traditional systems engineering concept that is largely confined to the process domain (hence the phrase *process systems engineering)* that is aimed at providing technical solutions for *process industry*. Over the years, systems engineering research has transcended the process industry domain and has, in fact, been used as a tool for the planning and management

[*]azlan@um.edu.my (azlan); zain@cheme.utm.my (zain); chnaziz@eng.usm.my (norashid)

of a nation's policy, resource supply-chain and for facility design and operations [2]. This paper highlights the development of education and research in the field of process systems engineering in Malaysia that fits this big picture of systems engineering that goes beyond the process domain.

2. PSE Education in Malaysia

In Malaysia, the field of Chemical Engineering was introduced in the late 60's at University of Malaya (UM) via the Chemical Technology course, which was established in the Department of Chemistry in 1965. In 1975, Chemical Engineering replaced the Chemical Technology course in University of Malaya [3]. Development of Chemical Engineering programmes with sizable PSE education and R & D elements later took place at Universiti Teknologi Malaysia (UTM), Universiti Kebangsaan Malaysia (UKM), Universiti Sains Malaysia (USM), Universiti Putra Malaysia (UPM), Universiti Teknologi PETRONAS (UTP), Curtin University of Technology and University of Nottingham Malaysia Campus (UNMC).

The area of process systems engineering (PSE) has been widely viewed as the foundation of chemical engineering that provides graduates with the overall, or the systems' perspective to problem solving. This basic foundation in PSE is first introduced in the chemical engineering Material and Energy Balances course. The concept is further strengthened in subsequent courses such as Computational Methods/Computer Programming, Process Simulations and Applications, Chemical Engineering Thermodynamics, Mathematical Methods for Chemical Engineering, Process Dynamics and Control, Reactor Design and Analysis, Product and Process Design and Analysis, Process Integration and Plant Design and Economics.

The Malaysian Chemical Engineering degree is recognised and accredited by the Engineering Accreditation Council (EAC) under the Board of Engineers Malaysia (BEM). As Malaysia is a signatory of the Washington Accord, all engineering degrees in Malaysia including Chemical Engineering is internationally accredited under the Washington Accord. This provides the vital means for benchmarking as well as exposure to international best practices in systems engineering. A few institutions including UM, UKM, UTP and USM have also opted for accreditation by the Institutions of Chemical Engineers of UK (IChemE, UK). USM receives M.Eng accreditation by the IChemE. In order to enhance teaching and learning in PSE, educators in Malaysia have introduced elements of innovations in the PSE modules as highlighted in **Table 1**.

3. Showcase Innovation in PSE Education - Co-operative Problem-Based Learning (CPBL) Approach in Process Control

Extensive innovation in teaching and learning in PSE in Malaysia can be well-exemplified by the successful accomplishments of Mohd-Yusof co-workers from UTM-Process Systems Engineering Centre (PROSPECT) and UTM-Regional Centre on Engineering Education (UTM-RCEE). They introduced, developed and implemented the Co-operative Problem-Based Learning Approach (CPBL) in Process Control and Dynamics Course over a period of ten years. Since the year 2002, teaching and learning in the undergraduate Process Control and Dynamics course at Universiti Teknologi Malaysia has evolved via implementation of tools such as Cooperative Learning (CL),

Problem-based Learning and finally Cooperative Problem-based Learning (CPBL) [4],[5]. CPBL is the integration of CL principles into the PBL cycle to support the implementation of PBL in a typical class setting. Since active learning and solving of practical problems occur in small groups of three to five students before they are taught the necessary concepts, proper support must be given through a functioning learning team. A detailed description of the CPBL framework, and the implementation in the course can be seen Mohd-Yusof et. al. [6].

Table 1: Highlights on the elements of innovation in PSE courses in Malaysia.

PSE-Based Course	Year offered	Elements of Innovation
Introduction to Engineering	1st year	Introduction of principles and applications of engineering and chemical engineering; exposure to, and application of, practical engineering practices through innovative industry and community-related problem-based projects
Material and Energy Balances	1st year	Separation of the material from the energy balance modules to provide more effective learning time for undergraduates
Computational Tools in Chemical Engineering	2nd year	Use of programming tools, simulation software, Matlab/Mathcad and optimization tools/software in Chemical Engineering
Process Control and Dynamics	3rd year	CPBL (see section on innovation in teaching and learning for Process Control an Dynamics Couse)
Product and Process Design/Process Synthesis/Plant Engineering, Process Economics	4th year	Introduction of down-to-earth design concepts and approach through the 7M approach of Chemical Engineering design; use of CPBL. Integration of Process Design and Process Control
Advance Process Control, Process Integration,	4th year & postgraduate	Use of software and patented techniques developed in-house and locally (within Malaysia), and elsewhere.
Design Project	4th year	Industrial visits to process sites related to students projects
Energy Management	4th year (elective) and postgraduate	Job-creation – student are employed as energy auditors to solve problems within the university and present results to the university community.
Industrial Training	3rd year undergraduate, and postgraduate	Integration of undergraduate/postgraduate research projects with industrial training via UNIX (University-Industry Innovation Exchange) programme results in a one year industry-based project.

Efforts to innovate the teaching of the course have brought positive impacts on the students. Research conducted on the implementation of CPBL showed that there were significant increases in students' motivation towards learning the course, as well as their learning strategies and team-based problem solving skills [6]. Consequently, it is not surprising that the final grades for the course also increased significantly. Students' performance in answering the examination questions showed significant improvement in terms of higher class average scores and smaller number of failures (less than 5%) compared to when traditional lectures were used. While grades had improved

tremendously compared to when traditional lectures were given, comparing the different teaching and learning techniques is not the main purpose, knowing that there is a difference in the assessment strategy of the course to ensure constructive alignment. What is vital is that the assessment results show significant learning of the content as well as increased learning motivation and strategies had occurred with CPBL, even when solely measured using written examinations, compared to the dismal grades students used to achieve (at least 30% failures and low average grade) when traditional lectures were

4. Research and Development in PSE in Malaysia

In Malaysia, R & D in systems engineering that exemplifies *the big picture* has begun in earnest over the past few years. The vast majority of the Malaysian institutions however has made noteworthy contributions in the well-established process systems engineering domain of design and synthesis, control and modelling and operations of *processes*. Alongside this, ample progress has been made in the development of holistic and sustainable business model via systems planning and management, facility design and operations within a multi-disciplinary R & D environment beyond the *process* domain. The R & D activities in PSE in Malaysia can be classified under the following sub-areas[2]:

(1) Molecular product design - Design of tailor-made, marketable green products to meet customer requirements.
(2) Facility design, control and operation- Development of models, tools, techniques and products to design, control and operate sustainable facilities and enterprises (process plants and buildings) that are cheaper, safer, cleaner, energy-efficient and operable.
(3) Community, systems and resource planning and management - Development of business models for optimal planning and management of green and smart townships, regions and nations that cover technical and implementation solutions including development of policies and market instruments, educational systems and guidelines as well as development blueprints.

Table 2 highlights the R & D activities in PSE in various institutions in Malaysia.

5. Conclusion

The development of PSE education and research in Malaysia has recently evolved in the direction of a generic tool for systems, policy as well as resource supply-chain planning and management that transcends the process domain. Continuous international benchmarking, networking and world-class R & D works have spurred various innovations in PSE teaching and learning as well as in research.

References

[1] Takamatsu T, Process Systems Engineering, Proceeding of the International Symposium on Process Systems Engineering, Japan, 1982.
[2] Universiti Teknologi Malaysia-Process Systems Engineering Centre (PROSPECT), http://www. Cheme.utm.my/prospect.

[3] Department of Chemical Engineering, Faculty of Engineering, University Malaya.http://engine.um.edu.my/

[4] K. Mohd.-Yusof, Z. Tasir, J. Harun, S. A. Helmi, "Promoting Problem-based Learning (PBL) in Engineering Courses at the Universiti Teknologi Malaysia", Global Journal on Engineering Education, Vol. 9, No. 2, 2005 (page 175 – 184).

[5] Khairiyah Mohd Yusof and S. A. Helmi, "Designing Effective Learning Environment for Cooperative Problem-based Learning (CPBL) for Engineering Courses", ASEE Global Colloquium Proceedings, Paper GC2008-87, Cape Town, South Africa, October 2008.

[6] Khairiyah Mohd-Yusof, Syed Ahmad Helmi, Mohammad-Zamry Jamaluddin and Nor Farida Harun, "Cooperative Problem-based Learning: A Practical Model for Typical Course", International Journal of Emerging Technologies in Learning, Vol. 6, Issue 3, September 2011.

Table 2. Highlights on PSE research and development activities in various Malaysian universities

Institution (Year Established); Group/Centre of Excellences related to PSE	**Current PSE Focus Areas**	**Key Research Themes**
University of Malaya (1975) UMPEDAC www.umpedac.um.edu.my	Process Control, Modeling and Automation	Process Control and Modeling, power electronics, drives, automation and control.
Universiti Teknologi Malaysia (1983); UTM-PROSPECT (Process Systems Engineering Centre), IHE (Institute of Hydrogen Energy) & RCEE (Regional Centre on Engineering Education) www.cheme.utm.my/prospect	Sustainable Systems Planning and Engineering; Hydrogen Energy; Engineering Education	From molecular product design to facility planning and operation and community planning and management; Hydrogen energy and fuel cell energy systems
Universiti Kebangsaan Malaysia (1984); Fuel Cell Institute www.ukm.my/selfuel/	Fuel Cell and Hydrogen Energy	Renewable energy – i.e. solar, hydrogen energy and fuel cell systems
Universiti Sains Malaysia (1992);Process Systems Engineering Group chemical.eng.usm.my/	Process Control and Modeling	Process Control and Modeling, optimization, process integration and intensification.
Universiti Teknologi PETRONAS (1997); Process Systems Engineering Group www.utp.edu.my/index.php?option=com_content&view…	Process Design, Process Integration, Control and Optimisation	Process design and analysis, process integration and control for energy efficiency and environmental protection
Curtin University of Technology (2000); Process Systems Engineering Group http://soes.curtin.edu.my/chemical-engineering/	Sustainable Process Systems and Design	Bioreactor optimization, energy and resource management, optimal pollution prevention and treatment
University of Nottingham (Malaysia) (2000); COE for Green Technologies www.nottingham.edu.my/SPI www.nottingham.edu.my/CEGT	Sustainable Process Integration and Green Technologies	Resource conservation and planning, biorefinery and molecular design

I.A. Karimi and Rajagopalan Srinivasan (Editors), Proceedings of the 11th International Symposium on Process Systems Engineering, 15-19 July 2012, Singapore.

Opportunities for Energy Savings in Azeotropic Separation Processes

I-Lung Chien

Department of Chemical Engineering, National Taiwan University, Taipei 10617, Taiwan.

Abstract

There are various methods in industry which can be used for separating azeotrope. Wise choice of the most effective separation method is very important in saving energy and reducing total annual cost of such processes. In this paper, methods for separating azeotrope via distillation will be overviewed. Industrial applications will be used to demonstrate that large savings of operating energy can be realized by selecting the most effective separation method. Several analytical tools can be used to aid the decision of the selection.

To further save energy of the azeotropic separation processes, several feasible heat integration schemes are explored. These include: feed-effluent heat exchanger, double-effect distillation, and divided-wall column. Industrial examples will be used to illustrate the heat integration applications.

Keywords: Azeotropic Separation, Extractive Distillation, Heterogeneous Azeotropic Distillation, Heat Integration, Divided-Wall Column

1. Introduction

Distillation is the most widely used separation process in chemical industry. In Tyreus (2011), it is estimated that separation processes account for 40-70% of both capital and operating costs in petrochemical processing and that distillation is used to make 90-95% of all separations in the chemical process industry. In Julka, et al. (2009), it is stated that distillation columns and their support facilities can account for about one-third of the total capital cost and more than half of the total energy consumption. Consequently, the design and optimization of the distillation train have a critical impact on the economics of the entire process.

Among all the distillation processes, the mixtures containing azeotrope are most difficult to be separated. Simple distillation cannot be used to achieve complete separation. A recent book by Luyben & Chien (2010) summarizes the feasible ways used in industry to achieve such separation.

Although for a particular azeotropic mixture, there are more than one way to achieve the separation. This paper will address the important issue of how to use analytical tools such as vapor-liquid equilibrium plots, residue curve maps (RCM), and material balance lines to select the most suitable separation method. Two industrial applications will be used to demonstrate that significant energy savings can be realized with proper selection of the most suitable separation method.

To further save energy of the azeotropic separation processes, various heat-integration schemes will be explored. The simplest scheme is via feed-effluent heat exchanger (FEHE) to recover heat from hot product stream. One other ways is to operating two columns in the process at different pressures so that the condenser of the high-pressure column can be combined with the reboiler of the low-pressure column to save energy. This is called the double-effect columns. The other feasible way is to come

up with thermally-coupled (divided-wall) design in the process so that the possible "re-mixing effect" in the column can be eliminated. Another heat-integration method mentioned in open literature is to use vapor recompression scheme so that the vapor from the overhead of a column is compressed as the heat pumping fluid to support energy required for its reboiler in the bottoms of the same column. This is called the internal heat-integrated distillation column (HiDiC). However, this scheme needs to add an expensive compressor to the process thus is not studied in this paper.

2. Azeotropic Separation Processes via Distillation

There are various ways to achieve the separation of azeotrope via distillation. In the following, industrial examples will be used to overview these separation methods.

2.1. Pressure-swing distillation

The distillate stream from a reactive-distillation column to produce *tert*-amyl methyl ether (TAME) is used here as an example (Luyben, 2005). This distillate stream contains several inert C5s and methanol. The purpose is to recover methanol from these C5s and to recycle back to the reactive-distillation column. Let's use iC5-methanol separation as an example to illustrate the concept to achieve the separation. Other inert C5s have the similar property as iC5.

The Txy plots of iC5 and methanol mixture at two different operating pressure are shown in Figure 1. There is difference in azeotropic compositions at these two pressures which permits the use of the design flowsheet in Figure 2 to achieve the separation. The question of how far apart these two azeotropic compositions is very important for determining the competitiveness of this flowsheet versus other separation methods. Large recirculation flow rate will result in larger operating energy as well as large capital cost. From total material and composition balances, it is very easy to estimate the ratio of HP recycle flow rate vs. the fresh feed flow rate.

The usual way for the selection of the operating pressure at LP column is to have a high enough top temperature to permit the use of inexpensive cooling water in the condenser. For the HP column, the decision is usually dependent on the unit price of the steam used in the reboiler. The decision here is to select a high enough pressure but still permit the use of same steam. Other limitation for the HP column is to avoid too high a temperature at reboiler to prevent the forming of oligomer or other problems.

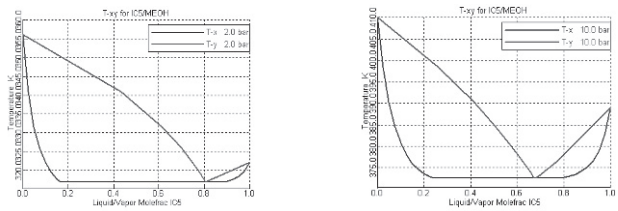

Figure 1. Txy plots of iC5-methanol mixture at two different operating pressures.

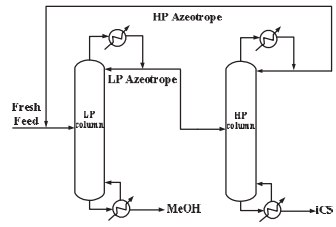

Figure 2. Pressure-swing distillation design flowsheet.

2.2. Heterogeneous Binary Azeotrope Separation

From previous Figure 1, one distinguish characteristics of this mixture can easily be observed. It is found that the azeotrope after condensed to liquid phase can naturally be separated into two liquid phases. The following alternative design flowsheet in Figure 3 takes advantage of the liquid-liquid separation in a decanter to achieve the separation. Note that the methanol-enriched phase can further be separated in a stripper to obtain pure methanol and the iC5-enriched phase can also be separated in another stripper to obtain pure iC5.

Notice that in this design flowsheet the fresh feed is fed into the decanter. The reason is because the feed composition is already in the liquid-liquid splitting region. Luyben & Chien (2010) introduced other applications where the fresh feed can be fed into one of the two strippers. The other choice is the operating pressures of the two strippers. The decision is similar in the pressure-swing distillation to achieve easy vapor-liquid separation and to avoid using more expensive cooling or heating mediums.

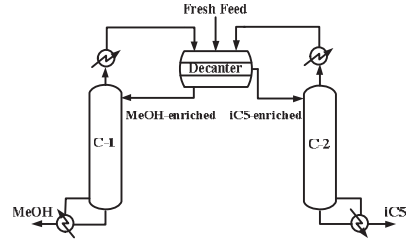

Figure 3. Heterogeneous Binary Azeotrope design flowsheet.

2.3. Heterogeneous Azeotropic Distillation

Another way to separate azeotropic mixture is to add a light entrainer into the system so that an additional azeotrope can be formed that helps in the separation. The most common applications are to form a heterogeneous minimum-temperature azeotrope so that one of the original components can be carried overhead in a distillation column and liquid-liquid splitting in a decanter. Various industrial applications can be found in Chapter 8 of Luyben & Chien (2010). Wu, et al. (2011) illustrated another application where a middle decanter is designed.

Isopropyl alcohol (IPA) dehydration is used here as an example to illustrate the separation principle of this separation system. The residue curve map and liquid-liquid boundary of this system with cyclohexane as an entrainer is shown in Figure 4. The design flowsheet in Figure 5 contains a combined column (served as a pre-concentrator column and also as a recovery column) and another heterogeneous azeotropic distillation column. The conceptual design can be explained by the material balance lines in Figure 4.

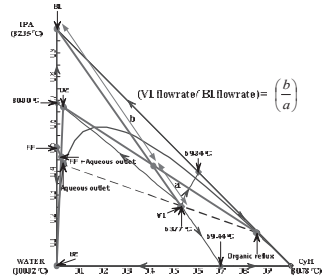

Figure 4. RCM, LLE, and material balance lines of the IPA dehydration system.

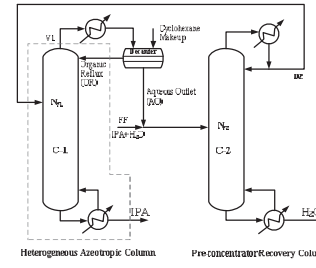

Figure 5. Design flowsheet via heterogeneous azeotropic distillation.

2.4. Extractive Distillation

Another way to separate azeotropic mixture is to add a heavy entrainer into an extractive distillation column so that the relative volatility of the original two components can be greatly enhanced. Thus, one original component can go overhead and the other component will go with the heavy entrainer to the column bottoms. A second entrainer recovery column is designed to separate this stream so that the entrainer can be recycled back to the extractive distillation column. The conceptual design flowsheet of the IPA dehydration system is shown in Figure 6.

The most important decision in this design is to choose a most effective entrainer in order to enhance the relative volatility of the original two components. Chapter 10 in Luyben & Chien (2010) used isovolatility and equivolatility curves to compare candidate entrainers. An even easier plot to generate is shown in Figure 7. In this plot, the starting composition is right at the azeotrope of IPA and water. By gradually adding entrainer into the system, we can calculate the enhancement of relative volatility at various feed ratio. This figure demonstrates that dimethyl sulfoxide (DMSO) is a much more effective entrainer than ethylene glycol (EG) for this separation system.

The way to generate the above plot is very easy by using commercial simulator such as the one from Aspen Technologies, Inc. The way to generate each point in the plot is to use the *Flash2* module in the unit operation library. Without adding entrainer, the relative volatility of a stream at azeotropic composition will be at 1.0. At any other feed ratio, the vapor and liquid composition in equilibrium can be calculated by Aspen Plus under adiabatic flash operating at 1 atm and with negligible vapor flow. Excerpting information about the IPA and water, the relative volatility between these two components can be calculated.

Other factors that affect the entrainer performance are the yx or Txy plots. The yx or Txy plots of the IPA-entrainer pair can be used to determine the ease of separation in the rectifying section of the extractive distillation column. The yx or Txy plots of the water-entrainer pair can be used to determine if the separation in the entrainer recovery column is easy or not. Of course, thermally stable, nontoxic, low price, and other favorable physical properties should also be considered in the entrainer selection.

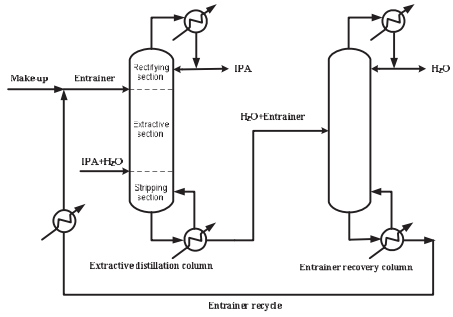

Figure 6. Design flowsheet via extractive distillation.

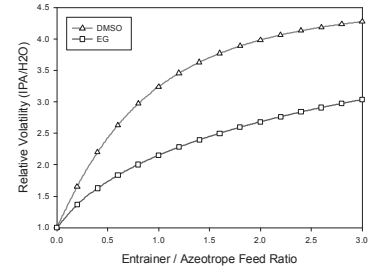

Figure 7. Relative volatility Plots at 1 atm for two heavy entrainers.

2.5. Other Separation Methods

We did not include discussion of other separation methods such as hybrid distillation-adsorption, hybrid distillation-pervaporation in this paper. The main reason is because the efficiency of the separation is highly dependent on the performance of the adsorbent (e.g. molecular sieve) in the adsorption unit or the membrane in the

pervaporation unit. Chapter 14 in Luyben & Chien (2010) showed a hybrid distillation-pervaporation application for the separation of ethanol and water.

Another separation method is to use a reactive intermediate to react away one of the components in the azeotrope in a reactive-distillation (RD) column and then to utilize reverse reaction in another RD column to obtain that component. We also did not include any discussion of this separation method in this paper.

3. Two Industrial Examples via Different Separation Methods

For a particular application, there are usually more than one ways to achieve the separation. In the following, two industrial examples will be used to demonstrate the importance of selecting the most effective separation method in terms of energy savings.

3.1. C5s and Methanol Separation

In previous Sections 2.1 and 2.2, two alternative design flowsheets can be used to achieve the same separation of C5s and methanol. The optimal design flowsheet via pressure-swing distillation in Fig. 2 is obtained in Luyben (2005) while that of the design flowsheet via heterogeneous binary azeotrope in Fig. 3 is obtained in Wu, et al. (2009). In either of the two flowsheets, feed composition and also product specifications are kept the same, thus direct comparison can be made.

Table 1 compares the total annual cost (TAC), the capital and the energy costs of the two alternative design flowsheets. The calculations are based on the cost data in Appendix E of Douglas (1988). From Table 1, it is shown that significant reductions in both the capital and energy costs can be made by choosing the more suitable separation method. Using the design flowsheet in Fig. 3, the capital cost can be cut by 66.2% and the energy cost can be reduced by 81.9%. The main reason for the significant savings is because natural liquid-liquid splitting behavior is utilized in the flowsheet in Fig. 3.

Table 1. TAC and energy cost of C5s and methanol separation.

	Figure 2 design	Figure 3 design
Annualized capital cost (10^6 \$/yr)	1.42	0.48
Annualized energy cost (10^6 \$/yr)	6.92	1.25
TAC (10^6 \$/yr)	8.34	1.73

3.2. Isopropyl Alcohol Dehydration Process

In previous Sections 2.3 and 2.4, two alternative design flowsheets are used to achieve the same separation of IPA and water. The optimal design flowsheet via heterogeneous azeotropic distillation in Fig. 5 is obtained in Arifin & Chien (2007) while via extractive distillation in Fig. 6 is obtained in Arifin & Chien (2008).

Table 2 compares the total annual cost (TAC), the capital and the energy costs of the two alternative design flowsheet. It is observed that 31.2% energy savings can be made by using the design in Figure 6. Significant savings in TAC and the capital cost can also be made by performing the separation via extractive distillation.

The main reason that heterogeneous azeotropic distillation flowsheet is not competitive can be observed from previous Fig. 4. Doing material balance for the heterogeneous azeotropic column indicated in red-dashed envelope in Fig. 5, the flow ratio for the top vapor to the bottoms can be estimated for this column. From Fig. 4, this ratio is approximately to be three. This means large organic reflux flow rate is recycled back to this column as well as large aqueous flow to the entrainer recovery column. These in terms cause large capital and energy costs. This deficiency of using this separation method can easily be found before doing any rigorous simulation.

Table 2. TAC and energy cost of IPA and water separation.

	Figure 5 design	Figure 6 design
Annualized capital cost (10^6 \$/yr)	0.71	0.47
Annualized energy cost (10^6 \$/yr)	0.48	0.33
Entrainer makeup cost (10^6 \$/yr)	nil	nil
TAC (10^6 \$/yr)	1.19	0.80

4. Further Energy Savings via Heat Integration

In this section, other heat-integration methods widely used in industry will be outlined below and applied to azeotropic separation processes.

4.1. Feed-Effluent Heat Exchanger (Economizer)

Since the bottom temperature of a distillation column is at the highest, the simplest method is to utilize this heat to exchange to the feed stream of this column. This is called a feed-effluent heat exchanger (FEHE) design or called an economizer. Implementing this heat-integration method required an additional heat exchanger. The trade off will be the additional investment of this heat exchanger to the savings of the reducing reboiler duty. A typical economizer design for pressure-swing distillation flowsheet is shown in Figure 8. This design concept can also be used in the extractive distillation flowsheet. For the heterogeneous design flowsheet in Fig. 5, the temperature difference between the hot and cold stream is usually not large enough to justify the use of this heat-integration method.

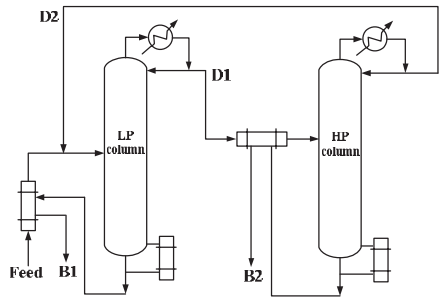

Figure 8. Pressure-swing distillation with two feed-effluent heat exchangers.

4.2. Double-Effect Distillation Columns

This design concept of double-effect distillation is to utilize the heat recovered in a condenser to be used in another reboiler. With this design, a heat exchanger is installed which serves as the condenser for the high-pressure column and also as the reboiler for the low-pressure column. The conceptual design flowsheet of this design with two additional FEHEs is shown in Figure 9. Note that because the heat removal in the condenser should be exactly the same as the heat input in the reboiler, a control degree-of-freedom is lost. Most often, the dynamic and control of this complete heat-integration design will be deteriorated. Another alternative design to trade-off economics/controllability is to install an auxiliary reboiler and/or auxiliary condenser. In this way, partial heat-integration can still be achieved without the lost of one control degree-of-freedom.

This design is not suitable to be used in the flowsheets in Figs. 5 and 6. Although there are also two columns in these two flowsheets, increasing operating pressure in the entrainer recovery column usually will have adverse effect in the ease of separation. For

the extractive distillation system, the bottom temperature may also become too high to prohibit the use of the original heat source.

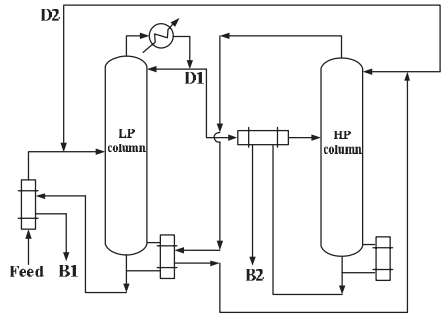

Figure 9. Pressure-swing distillation with two FEHEs and a double-effect arrangement.

4.3. Thermally-Coupled (Divided-Wall) Column

Another method used in industry is to eliminate the remixing effect in a column sequence via thermally coupled two columns. This is also called Petlyuk column or divided-wall column because a special-designed wall can be installed in a column to achieve the same purpose of thermally-coupling two columns together. In this way, besides energy savings the plant site can also be reduced. By observing the four previous separation methods for azeotropes, the extractive distillation column in Fig. 6 exhibited remixing effect in the stripping section of the extractive distillation column. To further save energy of this process, the way is to thermally-coupled the two columns so that the vapor for the extractive distillation column is supplied by a sidedraw from the entrainer recovery column. This design configuration is shown on the left-side of Figure 10. The identical divided-wall column design is illustrated on the right-side of the same figure.

Notice that the number of reboilers of this extractive distillation process is reduced from two to only one. We have studied this design configuration for two chemical systems of IPA-H_2O-DMSO and acetone-methanol-H_2O. The total reboiler duty can always be reduced. However, the total steam cost of this extractive divided-wall column process may not be lower than the original design without divided-wall. The main reason is that the combined reboiler requires a heat medium with higher temperature because a heavy entrainer is used. The question if it is beneficial to use thermally-coupled design can easily be determined by checking the two bottom temperatures in Fig. 6.

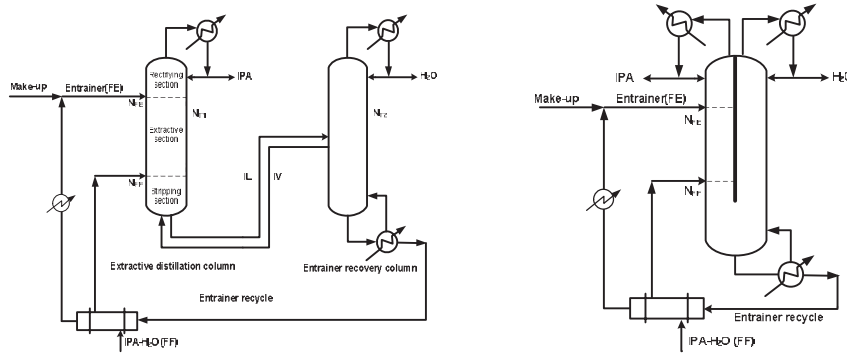

Figure 10. Extractive divided-wall column with FEHE.

5. Conclusions

In this paper, various ways to save operating energy in azeotropic separation process are presented. Two industrial systems illustrated the importance of choosing the most effective separation method. For heterogeneous binary azeotropes, a separation process with a decanter and two strippers should be used to take advantage of the natural liquid-liquid splitting in this system. The disadvantage of the pressure-swing distillation is the necessary recirculation flows of LP and HP azeotropic compositions in the system. This recirculation flow rate can easily be estimated from Txy plots as in Figure 1. The deficiency of the heterogeneous azeotropic distillation presented in this paper is also due to the large recirculation flows in the system. This deficiency can easily be revealed from RCM, LLE, and material balance lines in Figure 4. For extractive distillation process, the key is to select an effective entrainer to greatly enhance the relative volatility of the original two components. This capability can be known with the comparison plot as in Figure 7. Another point needs to be aware is the inherent disadvantage of the heterogeneous azeotropic distillation or extractive distillation of introducing a third component into the system that will appear as impurity in the product streams.

To further save operating energy, FEHE can be used in pressure-swing distillation and extractive distillation systems because of enough temperature difference between the feed and bottoms streams. The double-effect distillation can also be used in pressure-swing distillation process to combine a reboiler and a condenser. However, there is a trade-off between the economics and dynamic controllability. For extractive distillation processes, the thermally-coupled design principle can also be applied to reduce the total reboiler duty. However, the attention should be given to the heat medium used in this system. There are industrial examples where the total steam cost adversely increased by using thermally-coupled design as in Figure 10.

6. Acknowledgment

Research cooperation with Prof. W. L. Luyben on the C5s-methanol separation is gratefully acknowledged. Hard works from my former and current graduate students on the case studies in this paper are also greatly appreciated.

References

S. Arifin & I. L. Chien, 2007, Combined preconcentrator/recovery column design for isopropyl alcohol dehydration process, Ind. Eng. Chem. Res., 46, 2535.

S. Arifin & I. L. Chien, 2008, Design and control of an isopropyl alcohol dehydration process via extractive distillation using dimethyl sulfoxide as an entrainer, Ind. Eng. Chem. Res., 47, 790.

J. M. Douglas, 1988, Conceptual Design of Chemical Processes, McGraw-Hill, New York.

V. Julka, M. Chiplunkar, & L. O'Young, 2009, Selecting entrainers for azeotropic distillation, Chem. Eng. Prog., March, 47.

W. L. Luyben, 2005, Cmoparison of pressure-swing and extractive distillation methods for methanol recovery systems in the TAME reactive-distillation process, Ind. Eng. Chem. Res., 44, 5715.

W. L. Luyben & I. L. Chien, 2010, Design and Control of Distillation Systems for Spearating Azeotropes, Wiley, Hoboken, New Jersey.

B. D. Tyreus, 2011, Distillation–energy conservation and process control, a 35 year perspective, AIChE Annual Meeting, October 16-21, Minneapolis MN, U.S.A.

Y. C. Wu, I. L. Chien, & W. L. Luyben, 2009, Two-stripper/decanter flowsheet for methanol recovery in the TAME reactive-distillation process, Ind. Eng. Chem. Res., 48, 10532.

Y. C. Wu, C. S. Hsu, H. P. Huang, & I. L. Chien, 2011, Design and control of a methyl methacrylate separation process with a middle decanter, Ind. Eng. Chem. Res., 50, 4595.

I.A. Karimi and Rajagopalan Srinivasan (Editors), Proceedings of the 11th International Symposium on Process Systems Engineering, 15-19 July 2012, Singapore.

Process Systems Engineering Approach to Synthesis of Batch Chemical Processes

Thokozani Majozi[a,b]

[a]*Department of Chemical Engineering, University of Pretoria, Pretoria, South Africa*
[b]*Council for Scientific and Industrial Research, Advanced Modelling and Digital Science, Pretoria, South Africa*

Abstract

The problem of batch chemical process synthesis was first posed formally in the seventies. However, it is only in the last 2 decades that significant advances have been made in this regard. The volatility in global market trends that has characterised recent times necessitates that the chemical process of today readily adapts to sudden changes in demand and supply. Unlike their continuous counterparts, batch processes are readily amenable to this situation due to their inherent discreteness of unit operations. Consequently, they continue to remain an obvious choice where competitiveness is paramount. Much credit in understanding and ultimately addressing the idiosyncrasies of batch facilities is attributable to the adoption of a process systems engineering approach in synthesis of these processes. Whilst highlighting challenges that still prevail in this domain, the paper also presents some of the most advanced contributions made in recent years in synthesis of batch facilities. The presentation focuses on scheduling, design, heat integration, as well as water minisation in multipurpose batch processes. Results from various case studies of industrial relevance are presented.

Keywords: Synthesis, Optimisation, Scheduling, Batch, Multipurpose

1. Introduction

The most challenging aspect in optimum synthesis and design of batch chemical processes is the ability to capture the essence of time. This mandates a robust framework which allows accurate treatment of time without steep computational intensity. Early contributions in this regard proposed a discretization of time which is concomitant with enhanced binary dimensions that invariably lead to serious computational difficulties. The mid-nineties were characterised by the introduction of continuous-time frameworks which drastically reduced the binary dimension thereby allowing some of the developments to permeate the practical space. However, the industrial applications of these developments were still limited to very short time horizons which proved insufficient. Very recently, methods that seek to extend the range of time horizons within which these continuous time frameworks could be applied with confidence have been proposed in published literature, albeit at the expense of rigor.

Significant advances in scheduling batch plants followed the work of Kondili et al. (1993), which proposed even discretization of the time horizon. This approach was met with significant computational challenges, due to the extent of the binary dimension. Consequently, Zhang and Sargent (1996) proposed a continuous time formulation based on the concept of the resource task network (RTN) representation. The resulting

formulation led to a MINLP problem later linearized into a large MILP model that was difficult to solve by conventional solvers.
Méndez et al. (2006), Floudas and Lin (2004), Shaik and Floudas (2006) present excellent reviews of the current scheduling techniques based on different time representations and associated challenges. In their review the different models are classified as slot based, event based and precedence based (sequence - based) time representation. In the slot based models (Pinto and Grossmann, 1994, 1995; Lim and Karimi, 2003; Liu and Karimi, 2007, 2008) the time horizon is divided into non-uniform unknown slots with tasks starting and finishing at the same slot. The event based models (Maravelias and Grossmann, 2003; Castro et al., 2004) use uniform unknown events where the time associated with the events is common across all units. On the other hand, the sequence-based or precedence-based representation uses either direct precedence (Méndez and Cerdá, 2000; Hui and Gupta, 2000; Gupta and Karimi, 2003a,b; Liu and Karimi, 2007) or indirect precedence sequencing of pairs of tasks on units (Méndez et al., 2000, 2001; Méndez and Cerdá, 2003, 2004; Ferrer-Nadal et al., 2008).
Another unique contribution in the synthesis of batch plants is the technique based on the so called S-graph framework, which has been reported extensively by Friedler and co-workers (1998, 2002). This framework does not require any presupposition of time points, which renders it truly continuous in time. However, it also experiences challenges in handling Finite Intermediate Storage (FIS) operational policy.
The aforementioned contributions have laid a solid foundation for handling resource conservation problems, like energy optimization and wastewater minimization, in batch chemical plants. Presented in this paper are some of the most recent results in this regard.

2. A brief description of problems addressed

This section gives a brief description of problems addressed in this paper.

Batch process scheduling and synthesis
In its simplest form, the problem of batch process scheduling involves determination of maximum throughput over a given time horizon, or determination of minimum makespan for a given production profile. Both these objectives are achieved through an optimum production schedule, which takes into account the production recipe, the capacity of a unit and the type of tasks the unit can perform, as well as the maximum storage capacity for each material. Although the scheduling problem qualifies as a synthesis problem, since it involves the optimum combination of tasks in the temporal space, the exact synthesis problem is mainly about optimum capacity and number of processing units that satisfy a predefined objective. Figure 1 below shows a typical superstructure used as a basis for the synthesis a minimum capital cost Parahydroxy-Benzoic-Acid (PHBA) facility, whilst Figure 2 shows the optimum design.

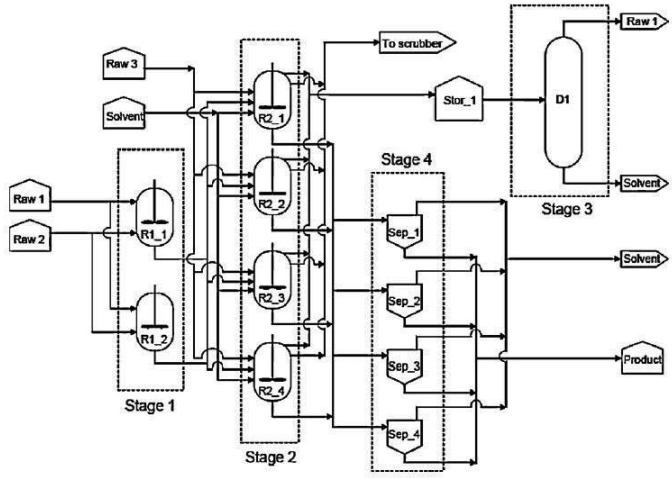

Figure 1: Superstructure for the synthesis of the industrial facility (Pattinson and Majozi, 2010)

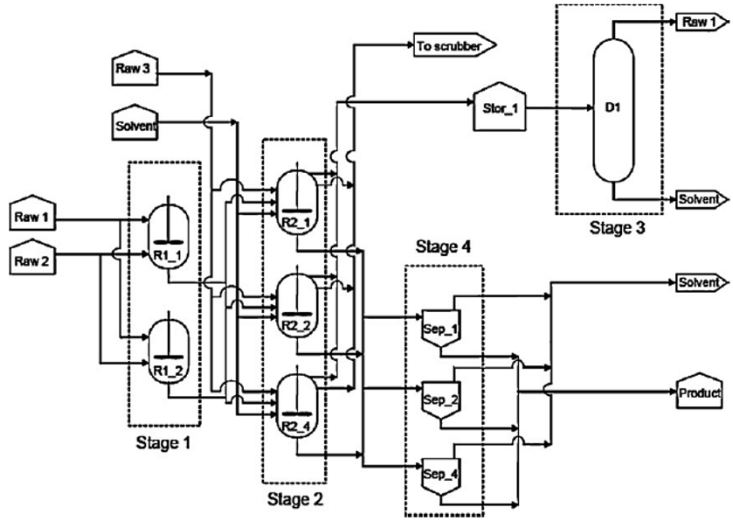

Figure 2: Optimum design (Pattinson and Majozi, 2010)

Energy optimization in batch processes

The problem of energy optimization in batch facilities is fundamentally distinct from a similar problem in continuous processes, due to the inherent time dimension that cannot be readily suppressed. Figure 3 shows a superstructural representation of a typical batch heat integration framework that considers both direct and indirect heat integration. Indirect heat integration involves storage of heat for purposes of bypassing time and utilizing maximum available heat in the process. The work presented in this paper considers one of the most advanced problems in this category, which involves

simultaneous production scheduling and heat integration within a comprehensive framework.

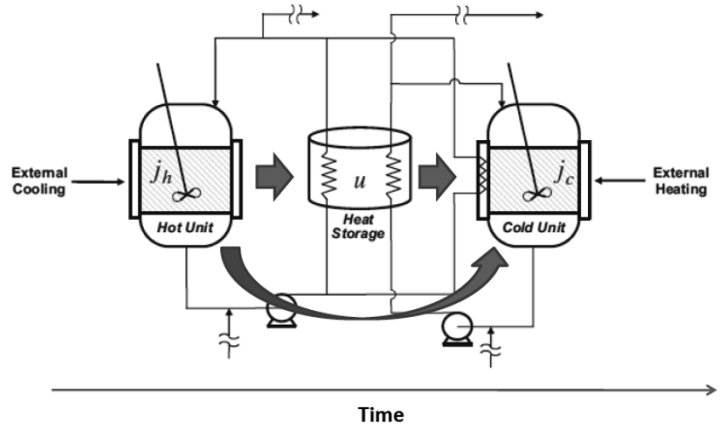

Figure 3: Superstructure for heat integration in batch plants (Stamp and Majozi, 2011)

Water optimization in batch processes

The problem of water optimization in batch processes is similar to the problem of heat integration, except that the source process has to be finished prior to commencement of the sink process. Both cases of direct and indirect water reuse are addressed in this paper. Figure 4 shows a superstructure that forms the basis of most mathematical models that simultaneously address the problem of scheduling and water minimization.

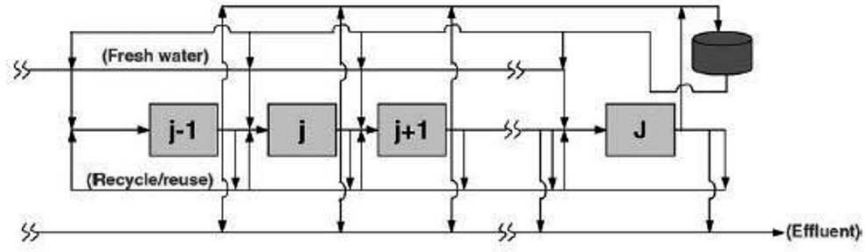

Figure 4: Superstructure for water optimisation in batch plants (Majozi, 2005)

3. Solution procedure

Whilst the paper does not disregard the significance of discrete time formulations, the results presented only consider continuous time formulations.

4. Case study I

Case study I is taken from Susarla et al. (2010). This case study indicates the necessity of non-simultaneous transfer of intermediate into a unit to get a better objective value. This batch plant constitutes six tasks performed in three units and three storages for the

intermediates. The plant produces two products using two different production paths (R1 and R2) as depicted in the STN representation (Figure 5). The processing time for a task, the capacity of the unit to process a task, the storage capacity and the initial inventories for each state are given (Susarla et al., 2010).

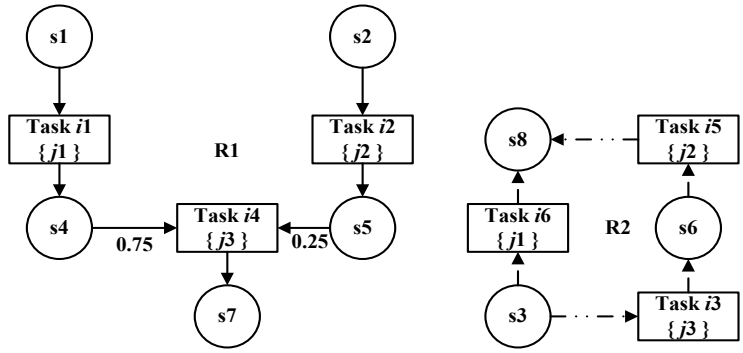

Figure 5: STN representation for case study I

For revenue maximization of the time horizon of 6 h, the models by Maravelias and Grossmann (MG) (2003), Sundaramoorthy and Karimi (SK) (2005) and Shaik and Floudas (SF) (2009) give an optimal solution of $560.The models by Susarla et al. (SLKs) (2010) and the models proposed by Seid and Majozi (SMs) (2011) give a better objective value of $650. The better objective value by SLKs and SMs is because the model allows non-simultaneous material transfers, which means for a task that uses more than one intermediate states, it is possible one state to be stored in a unit that is processing it for a while and wait for the other intermediates to come together to start the task.

In this case task 4 needs state *s*4 and *s*5 to produce *s*7. The 10 kg of *s*5 is produced at 3 h and 30 kg of *s*4 is produced at 4 h (Figure 6). Since *s*5 is produced earlier when compared to *s*4 and there is no enough storage to store *s*5 and later to use together with *s*4, it is required that the state s5 is stored in unit 3 for 1 h and start processing together with *s*4 at 4 h. By doing so we get better revenue since unit 2 transfers the state *s*5 to unit 3 at 3 h and start processing *s*6 at the same time to produce the product state *s*8. The models by SF, SK and MG give sub optimal results since the models do not allow non-simultaneous mass transfer. In this case the state *s*5 produced at 3 h stayed in unit 2 for 1 h until used at 4 h by unit 3; as a result unit 2 is inactive for 1 h. The amount of material processed by each unit, the type of task each unit is conducting and the starting and finishing time of each task are shown in Figure 6.

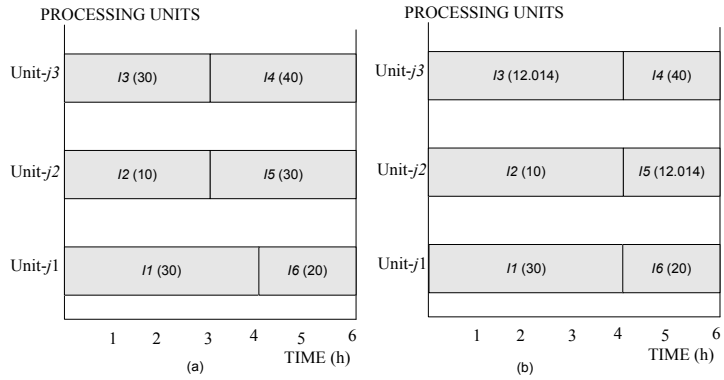

Figure 6: (a) schedule from SLKs and SMs (b) schedule from MG, SK and SF

5. Case study II

This case study has been studied extensively in the literature. It is a simple batch plant requiring only one raw material to get a product as depicted in the STN representation (Figure 7).

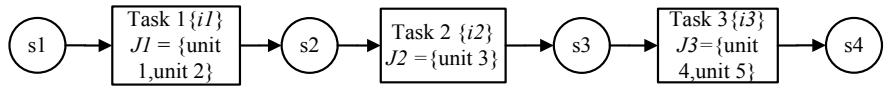

Figure 7: STN representation for case study II

The plant encompasses 5 units and two intermediate storages. The conversion of the raw material into a product is achieved through three sequential processes. The first task can be performed in two units ($j1$and $j2$), the second task can be performed only in unit $j3$ and the third task is suitable for units $j4$ and $j5$. The required data to solve the case study is given (Susarla et al., 2010). The computational performances for the different models are summarised below.

For the time horizon of 10 h, models SMs require 5 slots (p = 6) to get the optimal objective value of 2628.2. Almost all the models get the same optimal objective value in a similar CPU time. For the time horizon of 12 h, the models SMs require 6 slots (p = 7) to get the optimal objective value of 3463.6. These models require 2 slot less when compared to the other models. The models SMs outperform both single grid and multi grid models in terms of CPU time required to get the optimal objective value (0.25 s for SM1and 4.5 s for SM2 vs. 781 s for SLK2, 1492 for SLK1, 585 s SF (Δn = 1), 11.6 s for SK and 10.3 s for MG). In a case where task need not span over multiple time points SF (Δn = 0) and SM1 perform better - 1.88 s for SF (Δn = 0) and 0.25 s for SM1. For the time horizon of 16 h the proposed model SM2 requires 8 slots (p = 9) which is 3 slot less when compared to other models to get the optimal objective value of 5038.2. The models SMs outperform the multi grid models SF and SLKs in terms of CPU time required (75.8 s for SM1 and 60 s for SM2 vs. 10,000 s for SLKs and SF (Δn = 1)). In this case also the models SMs give a better CPU time when compared to the single grid models (377 s for SK and 2431 s for MG).

For makespan minimization two scenarios are taken with product demands of 2000 mu and 4000 mu. In the first scenario the model SM2 gives better objective value of 27.98 in a specified CPU time of 10,000 s when compared to other models. The model SMs

required 12 slots (p = 13) to get an optimal objective value, which is 4 slots less when compared to the other models. For the second scenario, the model SM2 again gives a better objective value of 53.1 when compared to other models in literature which give objective value of 56.432. The superior performance of the proposed models is due to the reduction of the required time points and does not allow task to span over multiple time points to get a better objective value like in the models of SF and SLKs. The Gantt chart for the time horizon of 12 h is shown in Figure 8.

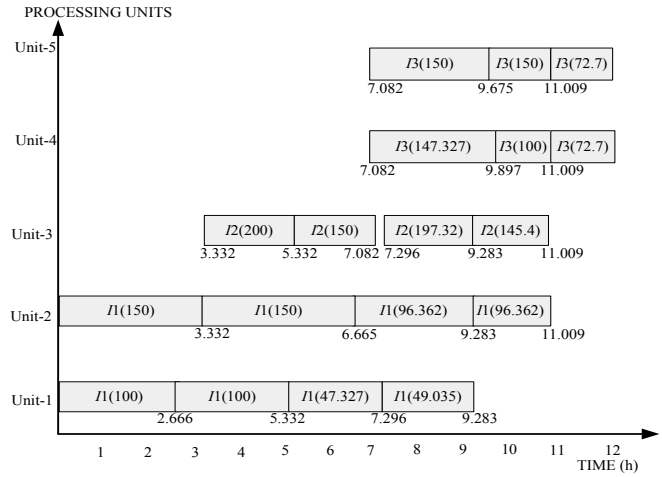

Figure 8: Gantt chart for case study II

6. Conclusion

The results from the various mathematical models on batch chemical process synthesis in published literature have been presented. The paper aims to draw comparisons among various models in terms of performance based on different objective functions. In particular, the paper aims to highlight advances that have been made in the last 2 decades in process systems engineering as applied to synthesis of batch processes.

References

E. Kondili, C.C.Pantelides, R.W.H.Sargent, (1993), A general algorithm for short-term scheduling of batch operations. I. MILP formulation, Comput. Chem. Eng., 17, 211-227

X.Zhang, & R.W.H.Sargent, (1996), The optimal operation of mixed production facilities-a general formulation and some approaches for the solution, Comput. Chem. Eng., 20, 897-904

C.A. Méndez, J. Cerdá, I.E. Grossmann, I. Harjunkoski, M. Fahl, (2006), State of- the-art review of optimization methods for short-term scheduling of batch processes, Comput. Chem. Eng., 30, 913–946

C.A. Floudas, & X. Lin, (2004), Continuous-time versus discrete-time approaches for scheduling of chemical processes: a review. Comput. Chem. Eng., 28, 2109-2129

M.A. Shaik, S.L. Janak, C.A. Floudas, (2006), Continuous-time models for short-term scheduling of multipurpose batch plants: A comparative study, Ind. Eng. Chem. Res., 45, 6190-4209

J.M. Pinto, & I.E. Grossmann, (1994), Optimal cyclic scheduling of multistage continuous multiproduct plants, Comput. Chem. Eng., 18, 797-816

J.M. Pinto, & I.E. Grossmann, (1995), A continuous-time mixed-integer linear programming model for short-term scheduling of multistage batch plants, Ind. Eng. Chem. Res., 34, 3037-3051

M.F. Lim, & I.A. Karimi, (2003), Resource-constrained scheduling of parallel production lines using asynchronous slots, Ind. Eng. Chem. Res., 42, 6832-6842

Y. Liu, & I.A. Karimi, (2007), Novel continuous-time formulations for scheduling multi-stage batch plants with identical parallel units. Comput. Chem. Eng., 31, 1671-1693

Y. Liu, & I.A. Karimi, (2008), Scheduling multistage batch plants with parallel units and no interstage storage. Comput. Chem. Eng., 32, 671-693

C.T. Maravelias, & I.E. Grossmann, (2003), New general continuous-time state-task network formulation for short-term scheduling of multipurpose batch plants, Ind. Eng. Chem. Res., 42, 3056-3074

P. M. Castro, A. P. Barbosa-Povóa, H. A. Matos, A.Q. Novais, (2004), Simple continuous-time formulation for short-term scheduling of batch and continuous processes, Ind. Eng. Chem. Res., 43, 105-118

C.A. Méndez, & J. Cerdá, (2000), Optimal scheduling of a resource-constrained multiproduct batch plant supplying intermediates to nearby end-product facilities, Comput. Chem. Eng., 24, 369-376

C.W. Hui, & A. Gupta, (2000), A novel MILP formulation for short-term scheduling of multi-stage multi-product batch plants, Comput. Chem. Eng., 24, 2705-2717

S. Gupta, & I.A. Karimi, (2003a), Scheduling a two-stage multiproduct process with limited product shelf life in intermediate storage, Ind. Eng. Chem. Res., 42, 490-508

S. Gupta, & I.A. Karimi, (2003b), An improved MILP formulation for scheduling multiproduct, multistage batch plants, Ind. Eng. Chem. Res., 42, 2365-2380

C.A. Méndez, G.P. Henning, J. Cerdá, (2001), An MILP continuous-time approach to short-term scheduling of resource-constrained multistage flowshop batch facilities, Comput. Chem. Eng., 25, 701-711

C.A. Méndez,& J. Cerdá, (2003), An MILP continuous-time framework for short-term scheduling of multipurpose batch processes under different operation strategies, Optim. Eng., 4, 7-22

C.A. Méndez, & J. Cerdá, (2004), Short-term scheduling of multistage batch processes subject to lmited finite resources, Computer Aided Chemical Engineering 15B:984-989

S. Ferrer-Nadal, E. Capón-Garćia, C.A. Méndez, L. Puigjaner, (2008), Material transfer operations in batch scheduling, A critical modeling issue, Ind. Eng. Chem. Res., 47, 7721-7732

N. Susarla, J. Li, I.A. Karimi, (2010), A novel approach to scheduling of multipurpose batch plants using unit slots, AICHE J., 56, 1859-1879

M. Shaik, & C. Floudas, (2009), Novel unified modeling approach for short term scheduling, Ind. Eng. Chem. Res., 48, 2947-2964

R. Seid, & T. Majozi, (2012), A robust mathematical formulation for multipurpose batch plants, Chem. Eng. Sci., 68, 36–53

E. Sanmarti, F. Friedler, L. Puigjaner, (1998), Combinatorial technique for short term scheduling of multipurpose batch plants based on schedule-graph representation, Comput. Chem. Eng., 22, 847-850

E. Sanmarti, T. Holczinger, L. Puigjaner, F. Friedler, (2002), Combinatorial framework for effective scheduling of multipurpose batch plants, AIChE J., 48, 2557-2570

J. Stamp, & T. Majozi (2011), Optimum Heat Storage Design for Heat Integrated Multipurpose Batch Plants, Energy, 36 (8), 5119 – 5131

T. Majozi,(2005), An Effective Technique for Wastewater Minimisation in Batch Processes, J. Clean. Prod., 13(15), 1374-1380

T. Pattinson, & T. Majozi, 2010, Introducing a New Operational Policy: The PIS Operational Policy, Comput. Chem. Eng., 34, 59 – 72

I.A. Karimi and Rajagopalan Srinivasan (Editors), Proceedings of the 11th International Symposium on Process Systems Engineering, 15-19 July 2012, Singapore.

The Role of PSE Community in Meeting Sustainable Freshwater Demand of Tomorrow's World via Desalination

Iqbal M. Mujtaba*

School of Engineering, Design & Technology, University of Bradford, Bradford BD7 1DP, UK. Email: I.M.Mujtaba@Bradford.ac.uk

Abstract

This paper highlights how the Process Systems Engineering (PSE) community and the practitioners of desalination can address sustainable freshwater issue of tomorrow's world via desalination using model based techniques. This paper will focus both on thermal and membrane based desalination techniques but will restrict to only Multistage Flash (MSF) and Reverse Osmosis (RO) processes. State of the art and future challenges in both MSF and RO desalination process will be presented.

Keywords: Freshwater demand, Desalination, MSF, RO, Model based techniques

1. Introduction

Quality water and quality life go hand in hand. The food we eat, the house we live in, the transports we use and the things we cannot do without in 24/7/365 determine our quality of life and require sustainable and steady water supplies (IChemE Technical Roadmap, 2007). Exponential growth in population and improved standards of living (together with water pollution due to industrial use of water) are increasing the freshwater demand and are putting serious strain on the quantity of naturally available freshwater. By the year 2030, the global needs of water would be 6900 billion m^3/day compared to 4500 billion m^3/day required in 2009 (Water Resources Group, 2009). With most of the accessible water around us being saline (94 percent of the world's water), desalination technology is vital for our sustainability.

The commonly used industrial desalination processes can be classified broadly into two groups: (a) thermal processes (b) membrane processes. Although thermal process (mainly MSF) is the oldest and still dominating for large scale production of freshwater, RO process, due to advancement in membrane technology, has been continuously increasing its market share. Numerous researches have been conducted in the past decades to develop more sustainable technological solutions that would meet increasing water demand (Greenlee et al., 2009; Misdan et al., 2011). However, exploitation of the full potential of model based techniques in such solutions can hardly be seen.

Process Systems Engineering (PSE) community makes extensive use of model based techniques in design, operation, control and in designing experiments due to the fact that model based techniques are less expensive compared to any experimental investigation. The yearly event of ***European Symposium on Computer Aided Process Engineering*** (since 1991) and 3-yearly event of ***International Symposium on Process Systems Engineering*** (since 1985) and the ***Computers and Chemical Engineering Journal*** (published by Elsevier since 1979) cover design, operation, control, process integration of many processes but desalination (very limited). Interestingly, most reported literatures on desalination are experimental based and are mostly published in

Desalination Journal (since 1966 by Elsevier) although periodically it publishes some model based research works.
With these in mind, this paper highlights the state of the art in model based techniques and future challenges for the PSE community and the practitioners of desalination to address sustainable freshwater issue of tomorrow's world.

2. State of the Art: MSF Desalination Process

Recently, Mujtaba (2008, 2009) reflected on the state of the art in MSF desalination process. A typical MSF desalination process is shown in Figure 1. Note, many alternative configurations of the MSF process can be generated depending on the way the seawater is fed and brine is recycled (El-Dessouky and Ettouney, 2002).

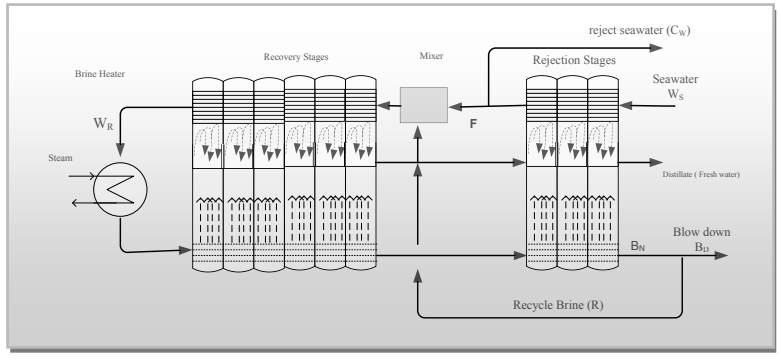

Figure 1: A Typical MSF Desalination Process (adopted from Hawaidi and Mujtaba, 2010)

To date, with a basis of given *fixed or seasonal freshwater demand profile*, *seawater composition*, *seasonal seawater temperature profile* and *fouling profile* the main issues in an MSF process have been to determine the following.

Design parameters: Number of stages, Width and height of the stages, Heat transfer area (number of tubes in the condensers), Materials of construction, Vent line orifice (air and non-condensable), Demister size and materials, inter-stage brine transfer device, Brine heater area, size of freshwater storage tank, etc.

Operation parameters: Steam flow, Top brine temperature, Brine recycle, Seawater rejection and Maintenance schedule.

Cost: Capital, Operating (utilities, cleaning), Pre-treatment and post-treatment (chemicals).

Majority of the experimental or model based study of the past and recent is focused on either to maximise the profitability of operation, or maximise the recovery ratio or maximise the plant performance (GOR – Gained Output Ratio) ratio, or minimise the cost or minimise the external energy input, etc. by optimising design and operating parameters (Rosso et al., 1996; Mussati et al., 2001; Tanvir and Mujtaba, 2008; Hawaidi and Mujtaba, 2010, 2011).

2.1 Steady State and Dynamic Modelling of MSF Desalination Process

Table 1 describes the evolution of steady state MSF process models over the last half century (included only the major developments published in international journals). Table 2 lists the studies using dynamic model. Note, most of these dynamic models are interestingly an extension of the steady state model developed by Helal et al. (1986).

Table 1: Steady State Models for MSF since 1970

Authors, Yr	Type/Description of Model
Mandil & Ghafour, 1970	Approximate Lumped Parameter Model, Constant thermophysical properties
Coleman, 1971	Stage to Stage Model, Linear and simplified TE (boiling point Temperature Elevation) correlation for different temperature range, no fouling/scaling.
Helal et al., 1986	Detailed Stage to Stage Model, Nonlinear TE correlation and other physical properties as function of (Temperature, seawater composition), Temperature loss due to demister included, Heat Transfer Co-efficient (HTC) via polynomial fit (fouling included).
Rosso et al., 1996	Model similar to Helal et al. and carried out different simulation studies. Model validation with plant data
El-Dessouky et al., 1995; El-Dessouky and Ettouney, 2002	Model based on Helal et al. but included: Heat losses to the surroundings, Constant inside/outside tube fouling factors, Pressure drop across demister, Number of tubes in the condenser and tube material, Constant non-equilibrium allowance (measure of stage thermal efficiency).
Mussati et al., 2001	Detailed Stage to Stage Model but with constant thermophysical properties
Tanvir and Mujtaba, 2006, 2008	Model based on Helal et al. (1986) but included NN (Neural Network) based correlation for TE calculation.
Hawaidi and Mujtaba, 2010, 2012	Model based on Helal et al. (1986) but included dynamic brine heater fouling and dynamic seawater temperature profile. Also included dynamic intermediate storage tank to enhance flexibility in operation
Said et al., 2010, 2012	Model based on Helal et al. (1986) but included effect of non-condensable gases (NCGs) and fouling factors on overall HTC. Considered regular (variable) and irregular (variable) water demand
Al-Fulaij et al., 2010, Al-Fulaij, 2011a,b	Rigorous modelling, CFD based demister modelling

Table 2: Use of Dynamic Models in MSF Desalination

Authors, Yr	Purpose/Software
Hussain et al. (1993)	Simulation / SPEEDUP
Maniar & Deshpande (1995)	Control / SPEEDUP
Aly and Marwan (1995)	Simulation
Thomas et al. (1998)	Simulation / SPEEDUP
Mazzotti et al. (2000)	Simulation / LSODA
Shivayyanamath and Tewari (2003)	Startup
Gambier and Badreddin (2004)	Control/MATLAB-SIMULINK
Sowgath (2007)	Simulation / gPROMS
Al-Fulaij et al. (2010, 2011a)	Simulation / gPROMS
Hawaidi and Mujtaba (2011)	Optimisation/ gPROMS
Said et al. (2012)	Optimisation/ gPROMS

2.2 Flexible Scheduling of MSF Desalination Process

Most recently, Tanvir and Mujtaba (2008), Hawaidi and Mujtaba (2010, 2011) observed that, for a fixed or variable freshwater demand, seawater temperature dictates the optimum number of flashing chambers (winter season requiring less number of stages than the summer). This opens up huge opportunities for flexible maintenance and operation schedule throughout the year (without shutting the plant fully for maintenance) and for new way of designing MSF processes.

3. State of the Art: RO Desalination Process

Since 1950s, membrane processes have been rapidly developing and are now surpassing thermal desalination processes (Misdan, et al., 2011). Reverse osmosis is a membrane process commonly used for seawater and brackish water desalination (Figure 2).

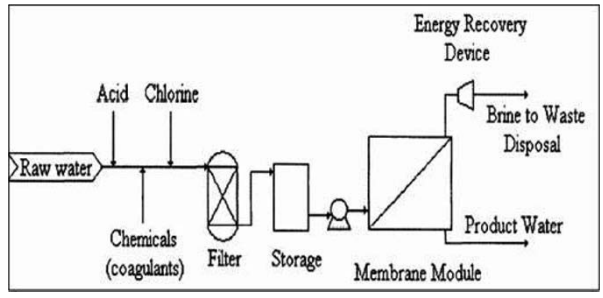

Figure 2. A Typical RO Desalination Process

Table 3: Models for RO membranes since 1958

Authors, Yr	Type/Description of Model
Kedem and Katchalsky, 1958	Model based on irreversible thermodynamics approach and describes the solvent and solute fluxes in terms of pressure and osmotic differences for solvent flux and osmotic variation and average concentration for solute.
Spiegler and Kedem, 1966	Modified Kedem and Katchalsky model and assumed that the solute flux is a combination of diffusion and convection.
Lonsdale et al., 1965	Model assumes that the solvent and solute dissolve in the nonporous and homogeneous surface layers of the membrane.
Sherwood et al., 1967	Modified Lonsdale et al. model and includes pore flow and diffusion of solute and solvent through the membrane.
Michaels, 1968	Analytical Film Theory (FT) model to estimate concentration polarisation (due to build up of solute along the membrane surface)
Sourirajan, 1970	Preferential sorption-capillary flow model - assumes that the separation is due to both surface phenomena (preferential sorption for solvent) and fluid transport through the pores.
Matsuura and Sourirajan, 1981	Modified Sourirajan model and allows characterization and specification of a membrane as a function of pore size distribution along with surface forces.
Song and Yu, 1999	Retained Solute (RS) model to estimate concentration polarisation.
Zhu et al.,1997	Simple model for decay in water flux due to fouling.
Al-Bastaki and Abbas, 2004	Detailed analytical expression to represent decay in water flux due to membrane fouling.
Abbas and Al-Bastaki, 2005	Neural Network based modeling of an RO water desalination process
Wardeh and Morvan, 2008, 2011	CFD model for evaluating fluid flow and concentration polarisations throgh RO membrane channels

3.1 Modelling of RO Desalination Process

Table 3 describes the evolution of RO process models (different component of the process) over the last half century. Kim and Hoek (2005) made a comparative study of different models and found that film theory model accurately predicted experimental permeate flux and salt rejection data. Solution-diffusion model was used in many

membrane applications (Baker, 2004) including desalination (simulation and optimisation by Lu et al., 2007) and Al-Bastaki and Abbas model was used for membrane fouling (used in simulation and optimisation by Sassi and Mujtaba, 2011b). However, Villafafila and Mujtaba (2003) considered simulation and optimisation of RO process using irreversible thermodynamics based transport model.

Most of the dynamic RO models have been obtained by system identification using real data so that they are only valid for a particular plant, working at the selected operating point (Alatiqi et al., 1989; Robertson et al., 1996; Abbas, 2006). There are only few dynamic models based on mass and energy balances and solution-diffusion model available in the literature (Gambier et al., 2007; Bartman et al., 2009).

3.2 Network Optimisation in RO Desalination Process

Generally, the most common arrangements of the membrane modules (Figure 3A) are: a) Series, b) Parallel and c) Tapered arrays. Although applied in RO waste treatment process, El-Halwagi (1992) presented the most comprehensive model based RO network synthesis problem formulation and solution by considering a superstructure configuration (Figure 3B). Zhu et al. (1997) extended El-Halwagi's work by including scheduling aspect and membrane fouling and applied in seawater desalination. See et al. (1999) extended the work of Zhu et al.'s and included membrane cleaning and regeneration. Most recently Sassi and Mujtaba (2011a) considered RO network synthesis problem for a wide range of salinity and seawater temperature.

3.3 Summary

Fritzmann et al. (2007) and Misdan et al. (2011) reviewed the state-of-the-art of RO desalination and have mentioned 'modelling', 'simulation' and 'optimisation' only once or twice in over 100 references (each) with not a single one considering model based techniques. Greenlee et al. (2009) reviewed more than 200 papers on RO desalination and there was only one mention of a model based RO optimisation of Vince et al. (2008). Kim et al. (2009) presented an overview of RO process from Systems Engineering approach and observed that there were only 30 research articles since 1965 which had used model based techniques for simulation and optimisation of RO processes (to some extent). However, only about half of these works included applications in seawater or brackish water desalination.

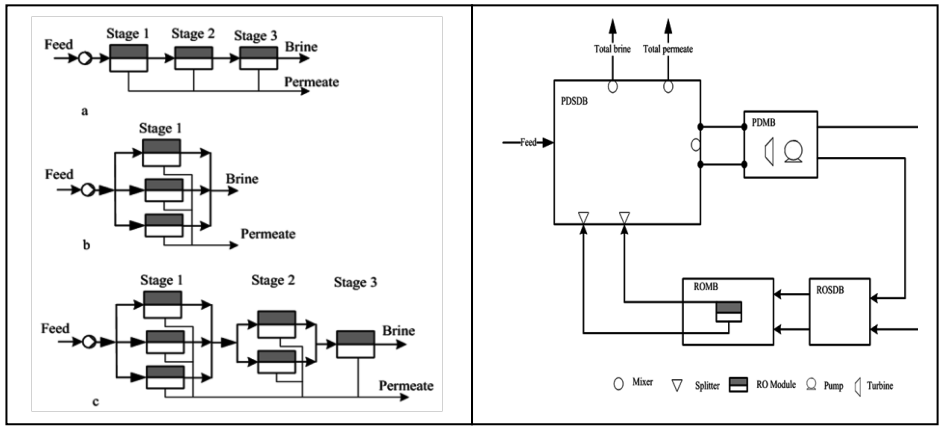

Figure 3: A. Reverse osmosis configuration. a. Series b. Parallel c. Tapered;
B: Superstructure of reverse osmosis configuration (Adapted from El-Halwagi, 1992)

4. State of the Art: Hybrid MSF/RO Desalination Process

Integration of a seawater RO unit with an MSF distiller provides the opportunity to blend the products of the two processes. Such arrangement allows operating the RO unit with relatively high TDS (total dissolved solids) and thus reduces the replacement rate of the membranes (Hamed, 2005). Although the discussions on hybrid MSF/RO date back to 80s, Helal et al. (2003, 2004a,b) and Marcovecchio et al. (2005) presented the detailed model based feasibility studies of hybrid MSF/RO desalination process. Several ways of connecting the RO with MSF process have been considered.

5. State of the Art: Use of Renewable Energy in MSF and RO Process

Rizzuti et al. (2006) edited a book comprising 26 research articles from around the world on desalination coupled to renewable energies (solar and wind), however, with only two articles considering model based MSF process (Bogle et al., 2006) and hybrid MSF/RO process (Fois et al., 2006). Mathioulakis et al. (2007) showed possible combinations of renewable energies to be used in MSF and RO processes (Figure 4) but no model based techniques have been discussed. Model based simulation of renewable energy driven desalination systems has been provided by Koroneos et al. (2007).

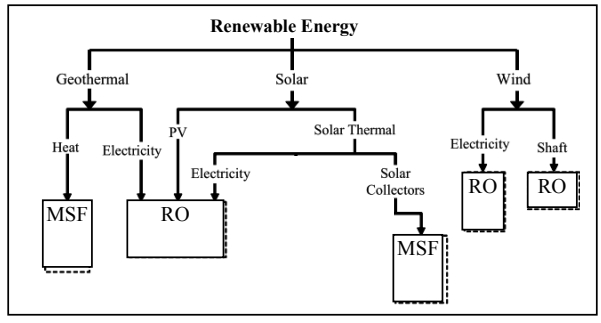

Figure 4: Technological combinations of the renewable energies and desalination methods

6. State of the Art & Future Challenge: Environmental Impact Modelling

Due to increasing environmental legislation (EL), the activities in the area of assessment and quantification of environmental impact (EI) are gaining importance in desalination processes. Sommariva et al. (2004), for the first time, attempted to establish model based relations between the improvement in plant efficiency (PE) and EI in thermal desalination system. Vince et al. (2008a) provided a simple model based LCA (Life Cycle Analysis) tool to provide help at the decision making stage for designing, operating and choosing an appropriate process to minimise EI. Mujtaba (2009) summarised some of the major work since 1999 on quantifying EI in MSF process. In most cases, EI issues are dealt in a reactive mode where EI from an existing process is assessed and, based on the current EL, the operations are adjusted. The preventive mode requires that new design and operations are achieved based on a set/desired EI targets (Vince et al., 2008a). While trial and error based on experimental studies is time consuming and expensive, studying these via model based techniques are less time consuming and inexpensive and remains a future challenge.

7. Opportunities for the PSE Community

Based on the discussions presented in earlier sections, Figure 5 summarised the state of the art in MSF and RO desalination processes. Clearly, the engagement of the PSE community in this very important sector is far away from expectation. Figure 5 also summarises the area of opportunities for the PSE community to be engaged in tackling the world's water crisis of the future by using model based techniques. Development of economically and environmentally efficient desalination processes is the future challenge. This can be achieved by better design, operation and control and model based techniques and the PSE community can play a significant role in this.

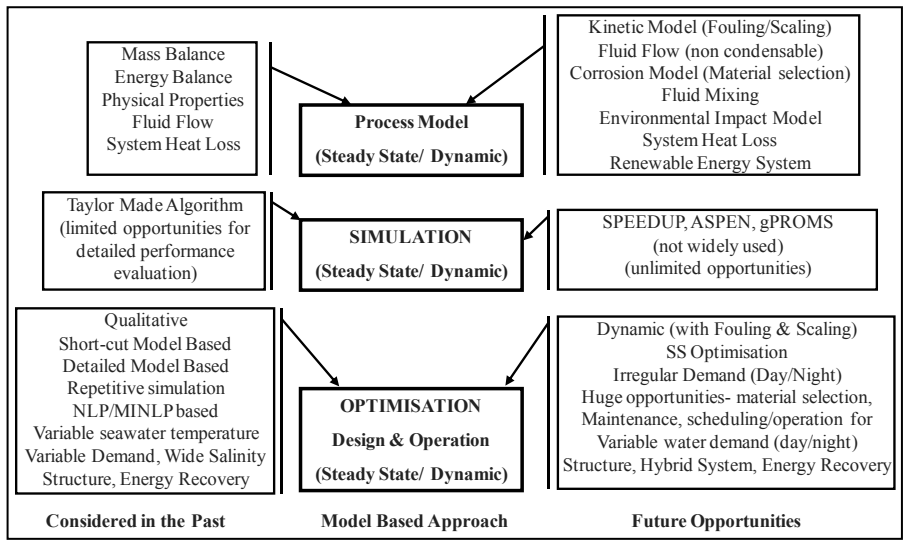

Figure 5: State of the Art and Future opportunities for PSE Community in Desalination

References

A. Abbas (2006), *Desalination*, 194, 268–280
A. Abbas and N. Al-Bastaki (2005), *Chemical Engineering Journal*, 114, 139–143
N. Al-Bastaki, and A. Abbas, A. (2004), *Chemical Engineering and Processing,* 43(4)**,** 555-558.
I. Alatiqi, A. Ghabris, and S. Ebrahim (1989), *Desalination*, 75, 119–140
H.F. Al-Fulaij (2011a), *PhD Thesis*, University College London, UK.
H.F. Al-Fulaij, A. Cipollina, H. Ettouney, D. Bogle, (2011b) *Desalination*, 281, 404–412
H.F. Al-Fulaij, A. Cipollina, D. Bogle, H. Ettouney (2010), *Desalin. Water Treat*.18, 46–60.
N.H. Aly and M.A. Marwan. (1995), *Desalination*, 101, 287-293
J.S. Baker, and L.Y. Dudley, (1998), *Desalination,* 118(1-3)**,** 81-89.
A.R. Bartman, P.D. Christofides, and Y. Cohen (2009), *Ind. Eng. Chem. Res*., 48, 6126–6136
I.D.L. Bogle et al. (2006), *Solar Desalination for the 21st Century*, Eds. L. Rizzuti et al., Spinger.
A.K. Coleman (1971), *Desalination*, 9, 315-331.
H.T. El-Dessouky, and H.M. Ettouney, (2002), *Fundamentals of salt water desalination*, Amsterdam, Elsevier Science Ltd.
H. El-Dessouky, H.I. Shaban, H. Al-Ramadan, *Desalination*, 103, 271-287, 1995
M.M. E1-Halwagi (1992), *AIChE J.*, 38(8), 1185- 1198.
E. Fois et al. (2006), In *Solar Desalination for the 21st Century*, Eds. L. Rizzuti et al., Spinger.
C. Fritzmann, J. Lowenberg, T. Wintgens, and T. Melin, (2007), *Desalination,* 216**:** 1-76.
A. Gambier and E. Badreddin (2004), *Desalination*, 166, 191-204
A. Gambier, A. Krasnik, E. Badreddin (2007), *Proceedings of the 2007 American Control Conference*, New York City, USA, July 11-13, 2007, FrA19.3, 4854-485

L. F. Greenlee et al. (2009), *Water Research.* 43, 2317–2348.
O.A. Hamed (2005), *Desalination*, 186, 207–214
E.A.M. Hawaidi and I.M. Mujtaba (2010), *Chemical Engineering Journal*, 165, 545–553
E.A.M. Hawaidi and I. M. Mujtaba (2011), *Ind. Eng. Chem. Res.*, *50* (18), 10604–10614
A. M. Helal, M.S. Medani, M.A. Soliman and J.R. Flower (1986), *comput. chem. eng*., 10, 327.
A.M. Helal, A.M. El-Nashar, E.S. Al-Katheeri and S.A. Al-Malek (2003), *Desalination*, 154, 66.
A.M. Helal, A.M. El-Nashar, E.S. Al-Katheeri and S.A. Al-Malek (2004a), *Desalination*, 160, 13.
A.M. Helal, A.M. El-Nashar, E.S. Al-Katheeri and S.A. Al-Malek (2004b), *Desalination*, 169, 43
A. Hussain et al. (1993), *Desalination*, 92, 21-41
O. Kedem, and A. Katchalsky, A. (1958), *Biochim Biophys Acta,* 1000**:** 413-30.
C. Koroneos, A. Dompros, G. Roumbas (2007), *Journal of Cleaner Production*, 15, 449-464.
S. Kim, and E.M.V. Hoek, (2005), *Desalination,* 186(1-3): 111-128.
Y.M. Kim, S.J. Kim, Y.S. Kim, S. Lee, I.S. Kim, J.H. Kim (2009), *Desalination* 238, 312–332
H.K. Lonsdale, U. Merten and R.L. Riley (1965), *Appl. Polym. Sci*., 9,1341.
Y.Y. Lu, Y.D. Hu, X.L. Zhang, L.Y. Wu and Q.Z. Liu (2007), *J. Membr. Sci*., 287, 219–229.
M.A. Mandil and E.E.A. Ghafour (1970), *chem. eng. sci* , 25, 611-621.
V.M. Maniar and P.B. Deshpande, *J. Proc. Cont.*, 6, 49-66, 1995
M.G. Marcovecchio et al. (2005). *Desalination*, 182, 111-122.
E. Mathioulakis, V. Belessiotis, E. Delyannis (2007), *Desalination*, 203, 346–365
T. Matsuura, and S. Sourirajan, S. (1981), *Ind. Eng. Chem. Process Des. Dev.*, 20, 273.
M. Mazzotti et al. (2000), *Desalination*, 127, 207-218
A.S. Michaels, (1968), *Chem. Eng. Prog.,* 64**,** 31−43.
N. Misdan, W.J. Lau and A.F. Ismail (2011), *Desalination*, doi:10.1016/j.desal.2011.11.001
I.M. Mujtaba (2008), Keynote lecture, CAPE FORUM 2008, February, Thessaloniki, Greece.
I.M. Mujtaba (2009), In *Dynamic Process Modelling*, Eds. Georgiadis et al., Vol 7, Wiley-VCH
S.F. Mussati, P.A. Aguirre and N.J. Scenna (2001), *Desalination*, 138, 341-347.
L. Rizzuti et al. (2006), *Solar Desalination for the 21st Century*, Spinger.
M. Rosso, A. Beltmmini, M. Mazzotti, and M. Morbidelli (1996), *Desalination*, 108, 365-374
M.W. Robertson et al. (1996), *Desalination*, 104, 59-68
S.A. Said, I.M. Mujtaba and M. Emtir (2010), In *Computer Aided Chemical Engineering- 28*, S. Pierucci and G. Buzzi Ferraris (Editors)., Vol 28, 25-30, Elsevier
S.A. Said, I.M. Mujtaba and M. Emtir (2012), *Proceedings of the 9th International conference on Computational Management*; 18-20 April 2012, London
K.M. Sassi and I.M. Mujtaba (2011a). *Chemical Engineering Transactions*, 25, 1055-1060.
K.M. Sassi and I.M. Mujtaba (2011b), *Chemical Engineering Journal*, 171, 582–593
H.J. See, V.S. Vassiliadis and D.I. Wilson (1999), *Desalination,* 125(1-3): 37-54.
T. Sherwood, P. Brian, R. Fisher, and L. Dresner, (1965), *Ind. Eng, Chem. Fundam.*, 4, 113
S. Shivayyanamath, P.K. Tewari (2003), *Desalination* 155, 277-286
C. Sommariva, H. Hogg and K. Callister (2004), *Desalination*, 167, 439-444
L.F. Song and S.C. Yu (1999), *AIChE Journal,* 45(5), 921-928.
S. Sourirajan (1970), *Reverse Osmosis*, Logos Press*,* London.
M.T. Sowgath (2007), *PhD Thesis*, University of Bradford, UK.
K.S. Spiegler and O. Kedem, (1966), *Desalination,* 1(4)**,** 311-326.
M.S. Tanvir and I.M. Mujtaba (2006), *Desalination*, 195, 251–272
M.S. Tanvir and I.M. Mujtaba (2008), *Desalination,* 222, 419–430
Technical Roadmap, Section 3.5, pp24, IChemE, 2007.
P.J. Thomas, S. Bhattacharyya, A. Patra, A. and G.P. Rao, (1998), *Comput. Chem. Eng*, 22, 1515
A. Villafafila and I.M. Mujtaba (2003). *Desalination*, 155, 1–13.
F. Vince, E. Aoustin, P. Breant and F. Marechal (2008a). *Desalination*, 220, 37–56.
F. Vince, F. Marechal, E. Aoustin, P. Breant (2008). *Desalination* 222 (1–3), 96–118.
S. Wardeh, H.P. Morvan (2008), *Chemical Engineering Research and Design*, 86, 1107–1116.
S. Wardeh, H.P. Morvan (2011), *Chem. Prod. Proc. Modeling*. 6 (2), 1–28
2030 Water Resources Group (2009), *Charting Our Water Future - Economic frameworks to inform decision-making*.
M.J. Zhu, M.M. El-Halwagi, and M. AlAhmad, (1997), *J. Membrane Science,* 129(2), 161-174.

I.A. Karimi and Rajagopalan Srinivasan (Editors), Proceedings of the 11th International Symposium on Process Systems Engineering, 15-19 July 2012, Singapore.

LNG Processing: From Liquefaction to Storage

Chonghun Han and Youngsub Lim

School of Chemical and Biological Engineering, Institute of Chemical Processes, Seoul National University, San 56-1, Shillim-dong, Kwanak-gu, Seoul 151-742, Korea

Abstract

Development of LNG technology has responded to expanding LNG demand. LNG worldwide consumption is expected to increase continuously for the following two or three decades. The LNG value chain includes pretreatment, liquefaction process, shipping and storage of LNG. This paper addresses the process and development of LNG liquefaction plant and receiving terminals. In addition, the role of process systems engineering in the LNG industry is reviewed with future challenges as the concluding remarks.

Keywords: LNG, liquefaction, terminal, BOG

1. Introduction

The rapid growth of Earth population coupled with the industrialization of undeveloped countries has dramatically increased the global energy demand. In the GAS(Golden Age of Gas) Scenario, global primary natural gas demand increases from 3.1 tcm (trillion cubic meters) in 2008 to 5.1 tcm in 2035 – an increase of 62% - the average rate of increase being nearly 2% per year. The reason for this continuous increase of natural gas demand largely arises from its cleanness and economic feasibility. The lower C/H ratio and lower carbon emissions compared to oil and coal, along with reduced emissions of SOx, NOx and particulates, make natural gas a very environmentally attractive option. Furthermore, the costs of processes based on natural gas such as power generation are much lower than those for coal or oil.

Although the usage of LNG (Liquefied Natural Gas) has been increased and its importance as an energy source has been emphasized, the systematic approach to LNG value chain in academia is insufficient rather than other processes. The fundamental of LNG value chain lies in the practical use of phase change of liquefaction and regasification process. That is, it is essentially important to ponder on how to liquefy natural gas into LNG more efficiently in natural gas liquefaction plant and how to regasify LNG into natural gas more safely and effectively in the terminal. The academic approach of process design and operation derived from process systems engineering can give a reasonable solution in this area.

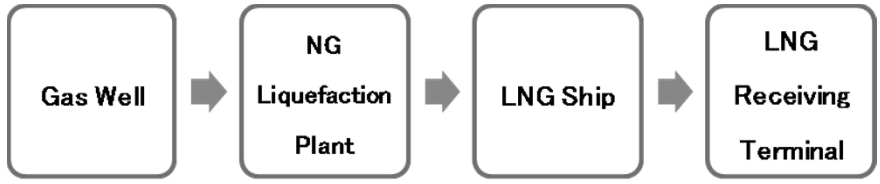

Figure 1 LNG Value Chain

The LNG value chain is well described in Figure 1. The natural gas is extracted from gas field and then transferred to the natural gas liquefaction plant. Them, natural gas is cooled and liquefied to LNG at the plant. LNG is shipped in LNG ship and transported to LNG storage tanks in LNG receiving terminals. At the terminal, it is vaporized to natural gas and sent to end users via pipeline system. The essential reason to utilize LNG value chain is placed on its massive volume shrinkage occurring in liquefaction process, which enables to deliver natural gas to remote demand regions economically rather than PNG (Pipe Natural Gas) which uses pipeline system. In other words, the volume of natural gas is reduced by 1/600 when liquefied, which improves its transportability via LNG ship.

2. Natural Gas Liquefaction

2.1. Liquefaction process

Liquefaction plant is composed of 3 major processes including pretreatment section, liquefaction section and post-treatment section. Pretreatment secion includes acid gas removal unit, dehydration unit and mercury treatment unit. Figure 2 depicts the block diagram of a typical liquefaction plant.

Mercury removal unit is needed to reduce the mercury level in the feed gas usually by adsorption through an activated carbon bed. Failure to reduce mercury levels may result in mechanical failure of downstream plant and equipment made from Aluminium. The role of acid gas removal unit is to remove carbon dioxide from the feed gas stream to less than 50 ppmv to prevent freezing out and blockage in the downstream liquefaction unit. H_2S is a toxic, poisonous gas, which cannot be tolerated in gases that may be used for domestic fuels. In presence of water, H_2S is extremely corrosive and can cause premature failure of valves, pipelind, and pressure vessels. Most pipeline specifications limit H_2S content to about 4 ppm. Water vapor is probably the most undesirable impurity found in untreated natural gas. Water content can affect long-distance transmission of natural gas and can form hydrates that may plug the pipeline and other equipment. Water content also decreases the heating value of natural gas.

Post-treatment section is mainly fractionation unit, which separates the natural gas liquids (NGL) into methane, ethane, propane and other heavy hydrocarbons. Fractionation unit is not needed when dealing with lean natural gas feed.

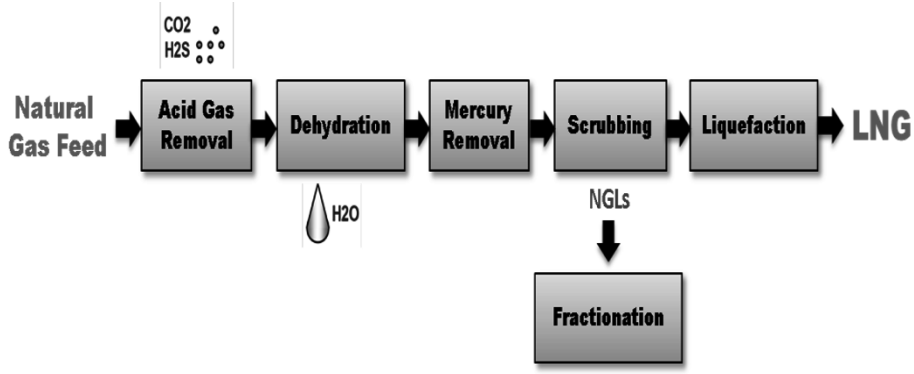

Figure 2 Block diagram of a typical liquefaction plant

2.2. Development of liquefaction processes

LNG industry started with the need of natural gas peak shaving. Cascade cycle wa used in the beginning. Later, mixed refrigerant concept was introduced. Phillips Petroleum invented the cascade liquefaction cycle. This cycle utilizes three refrigerants; propane, ethylene and methane. Air Products applied the mixed refrigerant cycle in the Libya Marsa El Brega LNG Plant in 1970.

For many years, propane precooled mixed refrigerant (C3MR) process developed by Shell and APCI (Air Products and Chemicals International) has remained the dominant liquefaction cycle in the LNG industry. The train capacity with Air Products' main cryogenic heat exchanger (MCHE) is up to 5 million tons per annum (MTPA). Natural gas and the mixed refrigerant are precooled by propane refrigerant cycle to -30°C and then liquefied to around -150°C by thermal contact with mixed refrigerant which mainly consists of methne, ethane, propane and nitrogen in main cryogenic heat exchanger (MCHE).

Recent improvents of the mixed refrigerant cycle, the AP-X^{TM}, can increase train capcity beyong 10 MTPA. Final sub-cooling is not done in the MCHE part and the temperature exiting the exchanger is about -115°C. Final stage of sub-cooling is done using a nitrogen expander loop. However, the AP-X N_2 refrigeration process would not be optimized to perform all three refrigeration system : precooling, liquefaction and subcooling. Many variables such as the number of expanders, pressure and temperature levels must be optimized for process efficiency.

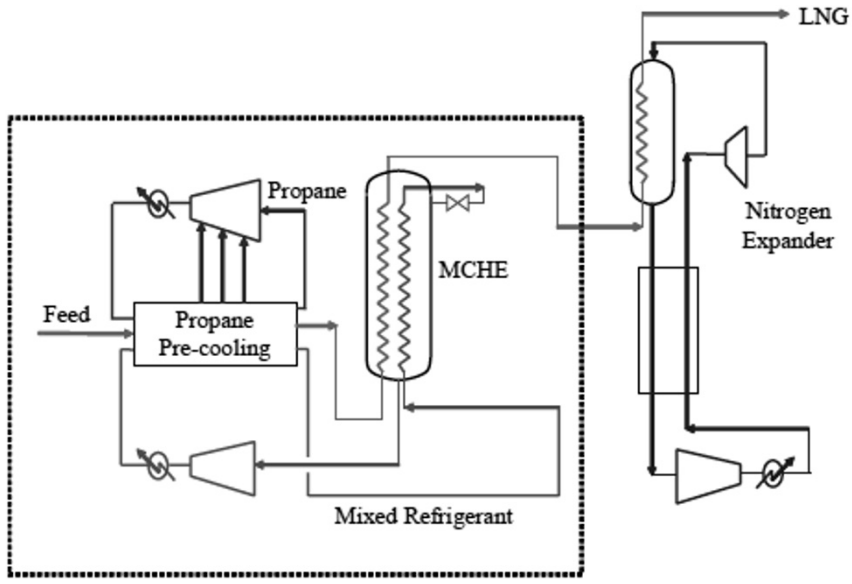

Figure 3 AP-X^{TM} Process

Other developments in recent years include the double mixed refrigerant cycles developed by Shell. Shell also developed the Parallel MR cycle which utilizes the split casing propane compressor arrangement.

New energy-saving developments across the LNG value chain include the use of cryogenic liquid expanders and new concepts including floating LNG plants. Land-based LNG plants must be solved at the debottlenecking: increased capacity, extended

life and operational improvements. Because of environmental issues including global warming, low the CO2 emissions and the treatment of sour gases and impurities are serious problems that cannot be ignored. An LNG liquefaction plant on a floating platform is similar to an onshore LNG plant but has some important differences. The motion of the LNG vessel by the sea conditions is a key issue. Development of new liquefaction process for safety caused flammable component is a problem awaiting solution.

The reverse brayton cycle and the single MR cycle are the most remarked process as a FLNG liquefaction process. The reverse brayton cycle has an object in minimization of flammable inventory for process safety. On the other hand, the single MR cycle is more efficient than the reverse brayton cycle form the power consumption point of view. It is necessary to consider which system is suitable. LNG vessel design and operating scenarios following the sea conditions are also short of study and research.

2.3. LNG Plant R&D Center in Korea

The Korean government initiated LNG Plant R&D program to acquire own technology in the liquefaction process of natural gas according to the Plant Technology Advancement Program in the Ministry of Land, Transport and Maritime Affairs. The main goals are to establish own license through the liquefaction process development and the basic designing of the commercial liquefaction plant. Test-bed construction is in successful progress with a roadmap of base construction for overseas entry in 2014.

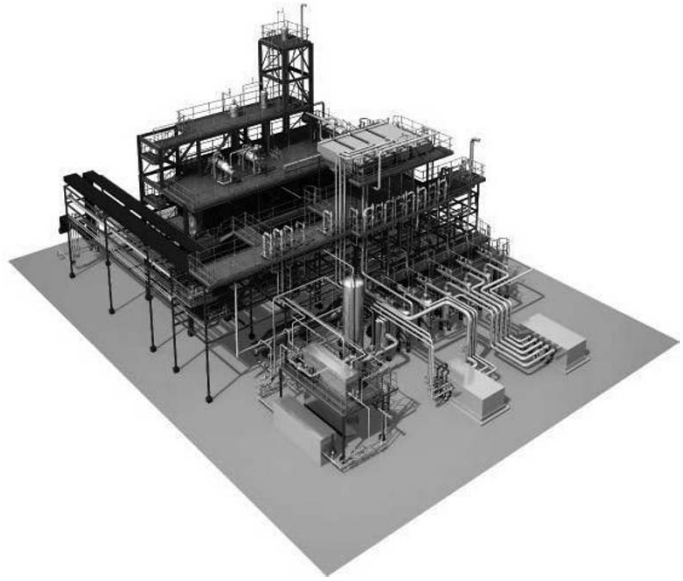

Figure 4 Bird's-eye view of the test bed constructed in Korea

3. LNG Storage and Regasification

The role of LNG receiving terminals in LNG value chain is for LNG storage and sending natural gas to end users as depicted in Figure 1. It generally includes a pipeline, LNG storage tanks, compressors, vaporizers, pumps and so on. LNG is transferred to the storage tank through the unloading pipeline from the LNG carrier ship. Stored LNG is transported to vaporizer process using a pump in the storage tank. Through the vaporization process, the natural gas is supplied to end user.

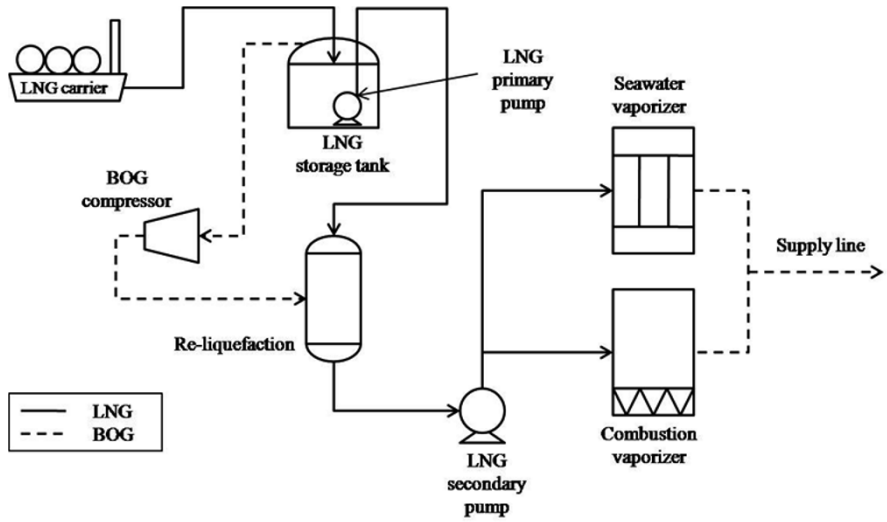

Figure 5 Schematic diagram of LNG receiving terminal (Park et al., 2010)

The LNG unloading operation consists of recirculation, depressurization and unloading. Before LNG unloading, the unloading pipeline needs to be kept cryogenic state to prevent warming of the pipeline. In the recirculation stage, a small amount of LNG from the storage tank circulates continuously through the pipeline to keep the pipeline cool. In the depressurization stage, the pressure of the pipeline is lowered to the appropriate pressure to transfer LNG from the carrier to the storage tank. After unloading stage, the operation move to the first stage of recirculation.

On unloading and storing LNG, the vapor continuously evaporates from LNG because of absorbed heat in the storage tank and in the cryogenic pipelines. This vapor is called boil-off gas (BOG). It can cause a physical damage in the LNG facilities for sudden volume expansion by 600 times. Over-treatment of the BOG causes consumption of excess energy. Hence, proper BOG handling is required for an energy saving. Usual BOG handling methods for LNG receiving terminals include recondensation and direct compression. BOG from the storage tank is compressed to around 10 bar through a BOG compressor and mixed with enough send-out LNG, which is pumped in the recondenser to obtain a liquid mixture. The liquid mixture is compressed to supply pressure in high-pressure (HP) pump and vaporized by seawater. If the LNG rate required in demands is insufficient to condense all of the BOG, it cannot be condensed in the recondenser. The remaining BOG in the recondenser is compressed to the pipeline pressure through the HP compressor and is directly transported to the pipeline mixed with the natural gas (Park et al., 2010). Because the operation of the HP

compressor requires considerable energy, it is desirable to minimize the operation of the HP compressor.

4. Process systems engineering in LNG processing

Many authors have worked on design, modeling, simulation, optimization and monitoring of LNG processing.

Wu and Zhu intoduced method for synthesizing integrated refrigeration system combining mathematical optimization techniques and engineering knowledge. The system includes the refrigeration cycle and heat integration. (Wu and Zhu, 2002) Del Nogal et al. used genetic algorithm to simultaneously solve optimal design of mixed refrigerant cycles. Their consideration of multistage refrigerant compression and application of stochastic optimization algorithm showed better performance compared to previously published works. (Del Nogal et al., 2008) Group of Michelsen et al. showed dynamic modeling and simulation of the TEALARC LNG process, selection of controlled variables of regulatory control layer as linear combination of measurements using self-optimizing control principles, and impact of process design decision on operability and control of the LNG process (Michelsen et al., 2010a, Michelsen et al., 2010b, Michelsen et al., 2010c). Natarajan and Srinivasan published their work on multi-model based process condition minitoring of offshore oil and gas production process. Online fault detection and identifiaction were performed. (Natarajan and Srinivasan, 2010)

Some researches on the LNG receiving terminals have been focused on analyzing the operation of a specific facility in the LNG receiving terminal Lee et al. suggested a reliable unloading operation procedure for a mixed operation of above-ground and in-ground storage tank (Lee et al., 2010). Shin et al. studied on the optimal operation of the BOG compressor at the Pyeoungtaek LNG receiving terminal using industrial data (Shin et al., 2007). Liu et al. proposed the optimal design of a process for the multi-stage recondensation of the BOG based on a thermodynamic analysis (Liu et al., 2010). Studies on optimal operating conditions for a regasification facility have been performed by Dharmadhikari S. (Dharmadhikari, 2004). Park et al. studied on the approach to minimize the cost in terminal operation according to the variation of LNG demand (Park et al., 2010).

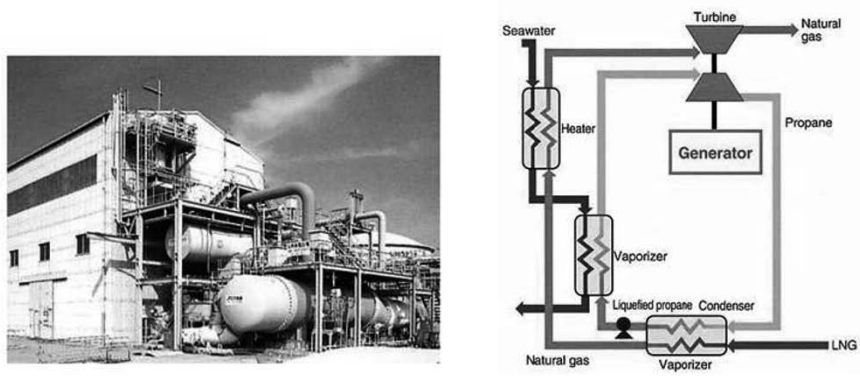

Figure 6 Power generation using LNG cold energy (Otsuka, 2006)

Researches on the utilization of the cold energy of the LNG stream have received attention. Various studies have been proposed a power generation plant using cold energy applied to power cycle as shown Figure 6. Liu and You developed the mathematical model to predict the total heat exergy of LNG stream (Liu and You 1999). The LNG cold energy has been conventionally used for air separation, power generation, and other application. (Otsuka, 2006) Recently, the industry has focused on process integration in industrial complex for LNG cold energy, ethane extraction using LNG cold energy and carbon dioxide liquefaction using the LNG cold energy for utilization of the LNG cold energy.

5. Future challenges

Future growth in LNG industry appears to be marked by an increasing interest in developing remote offshore gas fields. Offshore plants on fixed platforms, Floating Production Storage and Offloading (FPSO) vessels developed for oil production in deep water and Floating Storage and Regasification Unit (FSRU) are the main targets. Challenges for FLNG include weight and space limits, flammable components, corrosion and motion of vessels.

Gas-to-liquids technologies are also improving recently with the need for monetizing significant reserves of non-associated and stranded natural gas. It is also expected that energy efficiency improvements to limit CO_2 emissions is required in LNG value chain design. New design using combined cycle and cogeneration is therefore important.

The main purpose of LNG value chain enhancement has been to increase the LNG production capacity over the last decade. While the limitation of each process unit, such as the maximum capacity of the cold-box, is a major cause of the existing process capacity, the main topic of process research has been the optimization of LNG plants recently. For process systems engineers, hydraulic modeling and dynamic modeling of the cold-box is a field of interest. Integration of refrigeration design with power systems is another challenging issue. Proper driver selection can significantly increase the performance and decrease the capital and operating costs. In the case of FLNG, the steady-state process model is quite similar to land-based LNG process, but the dynamic model shows different behavior from land-based due to the sea condition. Analysis of hydraulic behavior using CFD and vessel design has been achieved recently. The dynamic modeling and simulation of the whole FLNG process is necessary. The unit arrangement which is suitable for installing on board and the development of operating system are the important topics of FLNG research for safety.

6. Conclusion

Worldwide liquefied natural gas consumption will increase steadily, especially in Asian countries. The LNG value chain includes the liquefaction, shipping and storage. Starting from the cascade cycles of liquefaction process, utilization of mixed refrigerants made the train capacity grow up to 5 MTPA and more. Nowadays, dual mixed refrigerant loop or AP-X^{TM} are able to handle up to 10 MTPA production. The LNG receiving terminal is designed for LNG storage and regasification. During the unloading procedure, efficient BOG handling is required for safety and energy saving. Numerous works on design, modeling, optimization, control, operation and monitoring of the LNG processing have been published. Future challenges include the floating liquefaction plants, floating storage and regasification units, gas-to-liquids technology and combined cycles.

Acknowledgment

This research was supported by the second phase of the Brain Korea 21 Program in 2012, Institute of Chemical Processes in Seoul National University, Strategic Technology Development and Energy Efficiency & Resources Development of the Korea Institute of Energy Technology Evaluation and Planning (KETEP) grant funded by the Ministry of Knowledge Economy (MKE) and grant from the LNG Plant R&D Center funded by the Ministry of Land, Transportation and Maritime Affairs (MLTM) of the Korean government.

References

F. Del Nogal, J. Kim, S. Perry, R. Smith, 2008, Optimal Design of Mixed Refrigerant Cycles, Industrial & Engineering Chemistry Research, 47, 8724-8740.

S. Dharmadhikari, 2004, Optimize LNG Vaporizers, Hydrocarbon Processing, 83(10), 95-9.

C. Lee, Y. Lim, C. Park, C. Han, 2010, Optimal Unloading Procedure for a Mixed Operation of Above-ground and In-ground LNG Storage Tank using Dynamic Simulation, *2nd Annual Gas Processing Symposium*, Doha, Qatar, January 11-14.

C. Liu, J. Zhang, Q Xu, J Gossage, 2010, Thermodynamic-Analysis-Based Design and Operation of Boil-Off Gas Flare Minmization at LNG Receiving Terminals, Industrial & Engineering Chemistry Research, 49(16), 7412-20.

H. Liu, L. You, 1999, Characteristics and applications of the cold heat exergy of liquefied natural gas, Energy Conversion and Management, 40(14), 1515-25.

F. A. Michelsen, I. J. Halvorsen, B. F. Lund, 2010, The Impact of Process Design Decisions on Operability and Control of an LNG Process, Journal of Natural Gas Science and Engineering, 183-191.

F. A. Michelsen, I. J. Halvorsen, B. F. Lund, P. E. Wahl, 2010, Modeling and Simulation for Control of the TEALARC Liquified Natural Gas Process, Industrial & Engineering Chemistry Research, 49, 7389-7397.

F. A. Michelsen, B. F. Lund, I. J. Halvorsen, 2010, Selection of Optimal, Controlled Variables for the TEALARC LNG Process, Industrial & Engineering Chemistry Research, 49, 8624-8632.

S. Natarajan, R. Srinivasan, 2010, Multi-model Based Process Condition Monitoring of Offshore Oil and Gas Production Process, Chemical Engineering Research and Design, 88, 572-591.

T. Otsuka, 2006, Evolution of an LNG terminal: Senboku terminal of Osaka gas, 23rd World Gas Conference, Amsterdam.

C. Park, C. Lee, Y. Lim, S. Lee, C. Han, 2010, Optimization of Recirculation Operating in Liquefied Natural Gas Receiving Terminal, J. Taiwan Inst. Chem. Eng., 41(4), 482-491.

M. Shin, D. Shin, S. Choi, E. Yoon, C. Han, 2007, Optimization of the operation of boil-off gas compressors at a liquified natural gas gasification plant, Industrial & Engineering Chemistry Research, 46(20), 6540-5.

G. Wu, X. Zhu, 2002, Design of Integrated Refrigeration Systems, Industrial & Engineering Chemistry Research, 41, 553-571.

I.A. Karimi and Rajagopalan Srinivasan (Editors), Proceedings of the 11th International Symposium on Process Systems Engineering, 15-19 July 2012, Singapore.

Research Challenges in Alarm Management for Safe and Stable Plant Operations in Chemical Process Industries

Masaru Noda[a]

[a]*Nara Institute of Science and Technology, 8916-5 Takayama, Ikoma 630-0192, Japan*

Abstract

Industrial plan alarm systems form an essential part of the operator interfaces for automatically monitoring plant state deviations and for attracting plant operators' attention to changes that require their intervention. To design effective plant alarm systems, it is essential to evaluate their performances. In this presentation, I introduce two methods for evaluating plant alarm systems. The first is the data-based evaluation method that refers to operation and alarm event data in a plant. It uses event correlation analysis to detect statistical similarities among time series data of discrete alarm and operation events. Grouping correlated events on the basis of their degrees of similarity makes it easier to consider countermeasures for reducing frequently generated alarms than merely analyzing individual alarm and operation events. The second is a model-based evaluation method, where an operator model is used to mimic humans' fault detection and identification behaviors. Analyzing simulated fault detection and identification tracks after all assumed malfunctions have occurred in a plant makes it possible to evaluate alarm system performance without human-subject-based experiments. Case study results demonstrated the usefulness of these methods for safe and stable plant operations in the chemical process industries.

Keywords: plant alarm system, event correlation analysis, operator model, behavior simulation, ethylene plant

1. Introduction

An alarm system is a core element in almost all operator interfaces of industrial plants, including oil refineries, power stations, and chemical plants. The progress with distributed control systems (DCSs) in the chemical industry has made it possible to install many alarms easily and inexpensively. Figure 1 shows statistics compiled by the Society of Chemical Engineering of Japan in 2005 indicating that typical Japanese chemical plants had 200 alarms per day and per operator. While most alarms help operators detect abnormalities and identify their causes, some are unnecessary. A poor alarm system might cause floods of alarms and nuisance alarms, which would reduce the ability of operators to cope with abnormalities at plants because critical alarms would be buried under many unnecessary alarms (Nimmo, 2002, Alford, 2005).

The Engineering Equipment and Materials Users' Association (EEMUA, 2007) defined the primary function of an alarm system as directing the operator's attention toward plant conditions requiring timely assessment or action. To achieve this, every alarm should have a defined response and adequate time should be allowed for the operator to carry out this response. The International Society of Automation (ISA, 2009) suggested a standard alarm-management lifecycle covering alarm-system specifications, design, implementation, operation, monitoring, maintenance, and change

activities from initial conception through to decommissioning. The lifecycle model recommends continuously monitoring and assessing operation data to rationalize alarm systems.

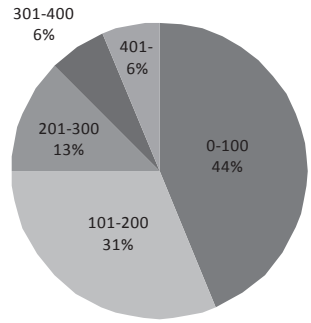

Fig. 1 Generated alarms per day and per operator in Japanese chemical plants (Society of Chemical Engineering of Japan, 2005)

The "top-ten worst alarm method" has been widely used in the Japanese chemical industry to reduce the number of unnecessary alarms. It is used to collect data from the event logs of alarms during operation, and it creates a list of frequently generated alarms. Although this method can effectively reduce the number of alarms triggered at an early stage, it is less effective at reducing them as the proportion of the worst ten alarms decreases. Because the ratio of each alarm in the top-ten worst alarm list is very small in the latter case, effectively further reducing the number of unnecessary alarms becomes difficult.

Kondaveeti *et al*. (2009) proposed the High Density Alarm Plot (HDAP) and the Alarm Similarity Color Map (ASCM) to assess the performance of alarm systems in terms of effectively reducing the number of nuisance alarms. HDAP visualizes the time various alarms occurred, which facilitated the identification of periods when the plant was unstable. ASCM orders alarms in accordance with their degree of Jaccard similarity (Lesot *et al.*, 2009) with other alarms to identify redundant alarms. However, these visualization tools cannot tell whether individual alarms have a defined response, because they only focus on alarms in the operation data.

In 2008, the Japan Society for Promotion of Science established an alarm management workshop comprising members from 29 universities and different firms from the chemical, petrochemical, oil refinery, electrical equipment, electronics, and other industries. The workshop aims to develop new alarm management technology to operate plants safely and sustainably. This paper introduces two methods for evaluating plant alarm systems developed in the workshop, i.e., a model-based evaluation method and a data-based evaluation method.

2. Alarm system evaluation by event correlation analysis

2.1. Event correlation analysis

Nishiguchi and Takai (2010) proposed a method for data-based evaluation that referred to not only alarm event data but also operation event data in the operation data of plants. The operation data recorded in DCS consist of the times of occurrences and the tag names of alarms or operations as listed in Table 1, which we call "events" hereinafter.

Table 1 Example of operation data

Date/Time	Event	Type
2011/01/01 00:08:53	Event 1	Alarm
2011/01/01 00:09:36	Event 2	Operation
2011/01/01 00:11:42	Event 3	Alarm
2011/01/01 00:25:52	Event 1	Alarm
2011/01/01 00:30:34	Event 2	Operation

The operation data are converted into sequential event data $s_i(k)$ by using Eq. (1). When event i occurs between $(k\text{-}1)\Delta t$ and $k\Delta t$, $s_i(k) = 1$, otherwise $s_i(k) = 0$. Here, Δt is the time-window size and k denotes the discrete time.

$$s_i(k) = \begin{cases} 1 \text{ if event } i \text{ occurs between } (k-1)\Delta t \text{ and } k\Delta t \\ 0 \text{ otherwise} \end{cases} \tag{1}$$

The cross correlation function, $c_{ij}(m)$, between $s_i(k)$ and $s_j(k)$ for time lag m is calculated with Eq. (2). Here, K is the maximum time period for lag and T is the time period for complete operation data.

$$c_{ij}(m) = \begin{cases} \sum_{k=1}^{T/\Delta t - m} s_i(k) s_j(k+m) & (0 \le m \le K/\Delta t) \\ c_{ji}(-m) & (-K/\Delta t \le m < 0) \end{cases} \tag{2}$$

Here, we assumed that two events, i and j, are independent of each other. If probability p_{ij} that two events, i and j, will occur simultaneously is very small, the probability distribution that two events will occur simultaneously is approximated by the Poisson distribution. The total probability that two events will occur simultaneously more than c_{ij}^* times, which is the maximum value of the cross correlation function with time lag m is given by Eq. (3), where λ is the expected value of c_{ij} (Mannila and Rusakov, 2001).

$$P(c_{ij}(m) \ge c_{ij}^* \,|\, -K/\Delta t \le m \le K/\Delta t) \cong 1 - \left(\sum_{l=0}^{c_{ij}^*-1} \frac{e^{-\lambda} \lambda^l}{l!} \right)^{2K+1} \tag{3}$$

Finally, the similarity, S_{ij}, between two events, i and j, is calculated with Eq. (4) (Nishiguchi and Takai, 2010).

$$S_{ij} = 1 - P(c_{ij}(m) \ge c_{ij}^* \,|\, -K/\Delta t \le m \le K/\Delta t) \tag{4}$$

If a high degree of similarity between two events is not detected, the time window is doubled in size and is used to reconvert the log data of two events into sequential binary data using (Kurata *et al.*, 2011). The time window continues to be expanded and similarity continues to be recalculated until either a high degree of similarity is detected or the time window becomes larger than the maximum pre-determined size.

A larger similarity means a stronger dependence or closer relationship between the two events. After similarities are calculated between all combinations of any two events in the plant log data, all events are classified into groups with a hierarchical method for clustering. The following four types of nuisance alarms and operations can be found by analyzing the results obtained from clustering.

(1) ***Sequential alarms***: These are when a group contains multiple alarm events that occur sequentially. Changing the alarm settings of sequential alarms may effectively reduce the number of times they occur.

(2) ***Routine operations***: These can be when a group includes many operation events and operation events in the same group appear frequently in the event log data. These operation events can be reduced by automating routine operations using a programmable logic controller.

(3) ***Alarms without corresponding operations***: These can be when a group contains only alarm events and operation events are not included in the same group. As every alarm should have a defined response (EEMUA, 2009), these may be unnecessary and should be eliminated.

(4) ***Alarms after operation***: Operations can cause alarm events to occur after all operation events in a group. These are unnecessary because they are not meaningful or actionable.

2.2. Alarm system evaluation of ethylene plant

Idemitsu Kosan Co. Ltd. started operations at the ethylene plant of their Chiba complex in 1985. Figure 2 is an overview of the ethylene plant, which is operated by two board operators using DCS. The plant log data gathered in one month included 914 types of alarm events and 857 types of operation events, and a total of 51640 events was generated. Figure 3 shows the points at which 1771 types of alarm and operation events occurred.

Fig. 2 Ethylene plant in Idemitsu Kosan Chiba complex. (Higuchi *et al.*, 2009)

Event correlation analysis was applied to the operation data obtained from the ethylene plant (Noda *et al.*, 2012). By using the hierarchical method of clustering, 1771 types of alarms and operation events were classified into 588 groups. Figure 4 is a similarity color map of events in the top 10 worst groups, where the alarm and operation events are ordered in accordance with the group Nos. The red indicates that two events have a high degree of similarity.

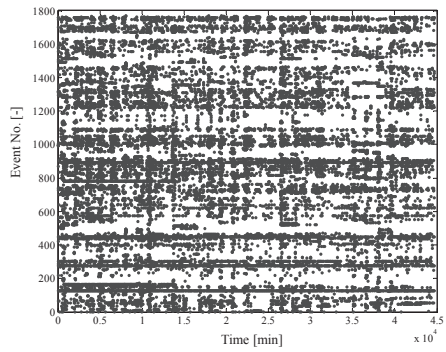

Fig. 3 Operation data of ethylene plant

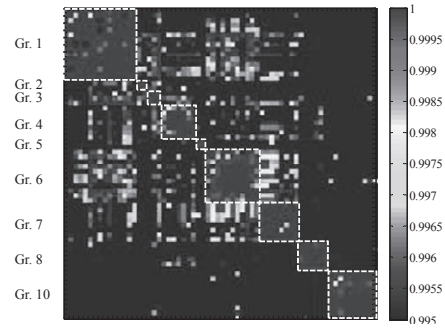

Fig. 4 Similarity color map

The top group contains five types of alarm events and ten types of operation events, and the total number of events in the group accounted for 5.8% of all generated events at the ethylene plant. Although the total number of events in the worst 10 groups accounted for 32.4% of all generated events at the plant, this included only 4.2% of alarm and operation event types. Evaluation results shows that we could effectively identify unnecessary alarms and operations within a large amount of event data by using the method, which should be helpful for reducing the number of unnecessary alarms and operations in other industrial chemical plants.

3. Alarm system evaluation by a virtual subject

3.1. Operator Model

An operator model can be used as a virtual subject in evaluating alarm systems by analyzing their performance during fault detection and identification (FDI) under a set of assumed malfunctions. This evaluation method using a virtual subject makes it possible to check alarm system performance without needing operation data provided by human operators so that the alarm system satisfies the specifications determined by the philosophy, identification, and rationalization stages in the alarm management lifecycle.

The model human processor (Card *et al.*, 1983) explicitly describes human perception, cognition, execution, and memory. The operator model (Liu *et al.*, 2010) shown in Fig. 5 for evaluating alarm systems was built by referring to this processor. In every scenario under abnormal situations, the operator model's main tasks are monitoring plant status with alarms and identifying causes of failure.

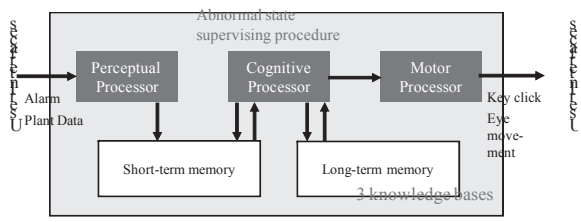

Fig.5 Structure of operator model (Liu *et al.*, 2010)

Human behavior during FDI process is classified into physical and mental subtasks. The latter includes perception, cognition, short-term memory, and long-term memory activities, respective examples of which are reading an alarm message, remembering a previous alarm, searching for a symptom in the knowledge base, and rejecting a cause of failure. An FDI track is an information-flow diagram composed of these subtasks. The FDI track from detecting an alarm to successfully identifying a cause of failure is generated automatically in accordance with the supervising procedure for failure-cause identification in the operator model.

3.2. Numerical example

The boiler plant in Fig. 6 produces 80 tons of superheated steam per hour at 485 ºC. As normal fluctuations, the steam load of the boiler plant randomly changes between 77.9 and 82.4 t/h. Figure 7 shows the overview a graphic panel of DCS. Abnormality propagation diagrams were drawn up for each of the 11 malfunctions assumed in the boiler plant listed in Table 2.

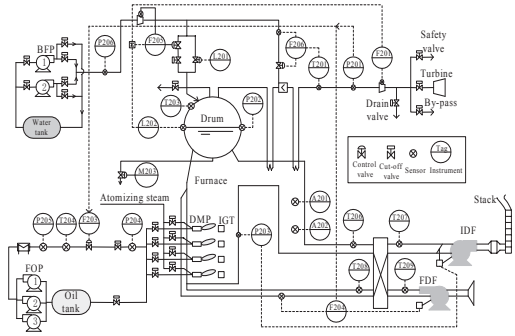

Fig. 6 Boiler plant process flow diagram

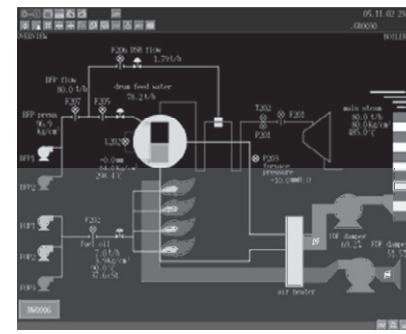

Fig. 7 Overview of graphic pannel of DCS

Table 2 Assumed malfunctions in the boiler plant

Malfunction	Description
1	FDF (forced draft fan) degradation
2	FOP (fuel oil pump) failure
3	Fuel leak
4	Burner's fire extinction
5	O_2 sensor failure
6	Oil heater failure
7	Water tube leak
8	P204 sensor failure
9	Turbine trip
10	BFP (boiler feed pump) trip
11	IDF (induced draft fan) trip

In the case study, we evaluated the actual alarm system of the boiler plant simulator using the following five criteria:

(1) Number of alarms triggered within 10 min of the malfunction
(2) Number of different kinds of alarms triggered within 10 min.
(3) Time the first alarm was triggered after the malfunction
(4) Elapsed time of the FDI process after the first alarm
(5) Total elapsed time of the FDI process after the malfunction

Table 3 shows the evaluation results for the alarm system. The number of alarms triggered within 10 min (Criterion (1)) remained at a low level for most malfunctions, while for an FOP failure malfunction (Mal-2) the number increased to 66 and was still more than 10 for a turbine trip (Mal-9). However, fewer than 10 different kinds of alarms (Criterion (2)) were triggered. The time the virtual subject needed to identify the malfunction (Criterion (5)) was short for most malfunctions, i.e., the subject was able to find the cause of a malfunction fairly quickly. An important alarm was triggered that enabled the operator to judge quickly that a water tube leak (Mal-7) had occurred, and useful alarms that enabled a turbine trip (Mal-9) to be identified were triggered in a timely manner.

Table 3 Alarm system evaluation results by virtual subject

	Malfunction										
Criteria	1	2	3	4	5	6	7	8	9	10	11
(1)	6	66	3	4	2	6	1	8	21	1	2
(2)	5	1	3	4	2	5	1	7	8	1	2
(3)	6	9	24	2	20	13	88	2	6	5	14
(4)	6	4	39	4	213	3	215	81	11	2	6
(5)	12	13	64	6	233	15	303	83	17	8	20

Units for criteria (3), (4), and (5) are in seconds.

4. Conclusion

This presentation introduced quantitative evaluation methods based on operation data and an operator model to rationalize plant alarm systems. Applying an event correlation analysis to operation data of the ethylene plant verified its effectiveness in identifying nuisance alarms and repeating operations occurring within the context of a large amount of event data. The behavior simulation by the virtual subject makes it possible to locate weak points in alarm systems and improve them from the viewpoint of operator workload without human-subject-based experiments. Case study results demonstrated that these two methods can be used to support alarm system design and evaluation. Future work will include using the evaluation results described in this paper to develop a method for redesigning alarm systems.

References

Alford, J. S., K. Kindervater, R. Stankovich, 2005, Alarm Management for Regulated Industries, *Chemical Engineering Progress*, 101, 25-30

Card, S. K., T. P. Moran, and A. Newell, 1983, The Psychology of Human-Computer Interaction, Lawrence Erlbaum Associates, London

Engineering Equipment and Material Users' Association (EEMUA), 2007, Alarm Systems - A Guide to Design, Management and Procurement, EEMUA Publication No.191 2nd Edition, EEMUA, London

Higuchi, F., I. Yamamoto, T. Takai, M. Noda, and H. Nishitani, 2009, Use of Event Correlation Analysis to Reduce Number of Alarms, *Proc. of PSE2009*, 1251-1256

International Society of Automation (ISA), 2009, Management of Alarm Systems for the Process Industries (ANSI/ISA-18.2-2009), ISA, Research Triangle Park, NC

Kondaveeti, S. R., S. L. Shah, and I. Izadi, 2009, Application of multivariate statistics for efficient alarm heneration, *Proc. of the 7th IFAC Symposium of Fault Detection, Supervision and Safety of Technical Processes*, 657-662

Kurata, K., M. Noda, Y. Kikuchi, and M. Hirao, 2011, Extension of Event Correlation Analysis for Rationalization of Plant Alarm Systems (in Japanese), *Kagaku Kogaku Ronbunshu*, 37, 338-343

Lesot, M. J., M. Rifqi, and H. Benhadda, 2009, Similarity measures for binary and numerical data: a survey, *Int. J. Knowledge Engineering and Soft Data Paradigms*, 1, 63-84

Liu, X., M. Noda, and H. Nishitani, 2010, Evaluation of Plant Alarm Systems by Behavior Simulation using a Virtual subject, *Computers & Chemical Engineering*, 34, 374-386

Mannila, H., D. Rusakov, 2001, Decomposition of Event Sequences into Independent Components, *Proc. of 2001 SIAM International Conferences on Data Mining*

Nimmo, I., 2002, Consider Human Factors in Alarm Management, *Chemical Engineering Progress*, 98, 30-38

Nishiguchi, J., and T. Takai, 2010, IPL2 and 3 performance improvement method for process safety using event correlation analysis. *Computers & Chemical Engineering*, 34, 2007-2013

Noda, M., T. Takai, and F. Higuchi, 2012, Operation Analysis of Ethylene Plant by Event Correlation Analysis of Operation Log Data, *Proc.of FOCAPO2012*

Society of Chemical Engineering of Japan, 2005, Report of the Questionnaire Survey of Plant Operations and Skill Transferes (In Japanese)

I.A. Karimi and Rajagopalan Srinivasan (Editors), Proceedings of the 11th International Symposium on Process Systems Engineering, 15-19 July 2012, Singapore.

Uncertainty propagation in condensate stabilization column

M. Askarian[a,b], R. Zarghami[a], F.Jalali[a], N.Mostoufi[a]

[a]*School of Chemical Engineering, College of Engineering, University of Tehran, PO Box 11155-4563, Tehran, Iran*
[b]*Pars Oil and Gas Company, PO Box 141471311, Tehran, Iran*

Abstract

Uncertainties, present in any engineering calculations would impact on decision making. In this work, uncertainty propagation in the simulation of condensate stabilization column in gas refinery is performed by Monte Carlo (MC) and Latin hypercube sampling (LHS) methods. Furthermore, a novel approach of building a statistical emulator of a simulation model for uncertainty analysis is presented. The results showed that the emulator is enormously more efficient than conventional approaches and the LHS is superior to MC due to its convergence in small sampling size.

Keywords: Uncertainty, Emulator, Monte Carlo, Latin Hypercube Sampling, Condensate Stabilization Column

1. Introduction

Process systems typically involve significant uncertainty in their design and operation. Based on the nature of the source of uncertainty in a process, a suitable classification can be proposed as: (i) model-inherent uncertainty which includes kinetic constants, physical properties, transfer coefficients; (ii) process-inherent uncertainty including flow rate, temperature variations and stream quality fluctuations; (iii) external uncertainty including feed stream availability, product demands, prices and environmental conditions; and (iv) discrete uncertainty for equipment availability and other random discrete events [1]. The existence of uncertainty transforms conventional deterministic concepts to stochastic problems, the solution of which remains challenging.

Uncertainty propagation is the computation of the uncertainty in the outputs which is induced by the uncertainty in its inputs. Different techniques have been developed to handle this issue include: (i) random sampling techniques such as Monte Carlo (MC), Latin hypercube (LH) and orthogonal array (OA). Use of MC in uncertainty analysis was introduced by Helton [2]. Iman and Conover took into account the correlation among variables in sampling techniques [3, 4]. Seaholm proposed applying LHS in order to limit the number of runs and account the interaction of model parameters [5]. Applying OA sampling was introduced by Koehler [6]. However, these conventional techniques typically require a large number of runs that demand heavy computation [7, 8]. (ii) emulators as surrogates model including response surface methodology, artificial neural network method, adaptive regression spline, radial basis function approximation and Kriging method. These approaches construct simple and fast approximations of complex computer analyses to minimize the computational expense of runs [9]

In this work, a stabilization column in gas refinery was studied. The purpose of this column (has 13 trays, re-boiler and reflux) is separation of light cuts (C^1-C^4) from C^{5+}. This process decreases vapor pressure of condensate (C^{5+}) to provide feasibility of its export; thus Reid Vapor Pressure (RVP) is considered an important index for the quality of product. Uncertain parameters that would impact on quality and quantity of product are assumed to be process-inherent type. Uncertainty propagation would be studied by three methods; Monte Carlo, Latin hypercube sampling, and Kriging method. Based on the sampling size for each method, their efficiency would be compared. This study would be done by two categories of data: historical data of plant and simulation results.

2. Uncertainty propagation

The conventional approach of expressing non-deterministic parameters is probability distribution or its statistics such as the mean and standard deviation. In the present work, the feed flow rate to stabilization column, steam flow rate of the re-boiler, temperature and pressure of column were treated as uncertain parameters and were assumed to be the sole sources of uncertainty in the stabilizing process. All the remaining parameters and inputs were treated as deterministic quantities. Using historical data of the plant, statistics (mean values and standard deviation) of probability distribution functions for inputs were obtained and showed at Table 1. The impact of these uncertain parameters on quality (RVP and specific gravity of condensate) and quantity (flow rate of condensate and gas) of product was studied.

Table 1: Input uncertain parameters of condensate stabilization column based on historical data

	feed flow rate (m^3/h)	Steam flow rate of re-boiler (Kg/h)	Pressure of column(bar g)	Temperature of column (°C)
Mean	86.2772	4351.8361	6.8970	88.9035
Std	7.374	364.911	0.020	4.354

2.1. Monte Carlo Sampling

In the Monte Carlo simulations, each uncertain parameter was treated as a random variable. Thus random values were generated between 0 and 1, and then multiplied by the available number of historical data. The calculated number indicated random scenario and corresponding inputs (feed flow rate to stabilization column, steam flow rate of the re-boiler, temperature and pressure of column were) were drawn from historical data. In this way, the correlation between parameters is considered inherently. For this scenario, experimental response (RVP, SG and flow rate of condensate and gas) could be drawn from historical data; in addition, simulation response was obtained for each random scenario. In order to study uncertainty propagation, the same procedure was repeated to achieve response distribution (for both experiment and simulation). When stable statistics for response distribution were achieved, the results would be reliable. The computational tractability of Monte Carlo method depends heavily on the number of random variables and complexity of the model [10].

2.2. Latin Hypercube Sampling

The approach of uncertainty propagation by LHS is the same as MC, the only difference is the strategy for generating random values. LHS ensures that all the portions of the uncertain parameters are represented [10]. Consider the case where it is required to

sample *N* points from M uncertain parameters; LHS partitions the parameter space into an N^M grid of bins, with N bins along each axis. Then, the sample points are distributed such that all one-dimensional projections of the samples yield one sample per bin [11].

2.3. Emulator

For obtaining response distribution through the simulator, large number of runs should be taken. To deal with this problem, emulator (response surface model taken based on limited number of run) could be constructed sufficiently accurate to replace the original simulator. The emulator attempts to reduce the number of simulations required for an adequate estimation of uncertainty propagation [7]. This emulator is then used instead of simulation code, facilitating uncertainty quantification (by predicting output from a model at untried inputs), design space exploration, optimization, and reliability analysis [9].

Kriging model as an emulator postulates a combination of a linear model and departures of the form [11]:

$$\hat{y}(x) = \sum_{j=1}^{k} \beta_j y_j(x) + Z(x) \quad (1)$$

Where $\hat{y}(x)$ is an approximate model of y (x), β is the regression factor, and Z(x) is assumed to be a realization of a stochastic process with mean value of zero and spatial correlation function (e.g. exponential, generalized exponential, Gaussian, linear, spherical, cubic spline) given by:

$$\mathrm{Cov}[Z(x_i),Z(x_j)]=\sigma^2 R(x_i,x_j) \quad (2)$$

Where σ^2 is the variance and R is the correlation. Subsequently, Kiging model is generalized to polynomial.

Since approximation models interpolate the sample data, additional validation points are collected for each example to assess the accuracy of each approximation model over the region of interest. For each set of validation points, root mean square error (RMSE) is computed as:

$$RMSE = \sqrt{\frac{\sum_{i=1}^{n}(y_i-\hat{y}_i)^2}{n}} \quad (3)$$

DACE (Design and Analysis of Computer Experiments) software is used to construct Kriging model [11]. The best Kriging model was obtained by zero order polynomial and exponential correlation (RMSE= 0.08) for RVP that is illustrated in Figure 1. Other output parameters would be presented in future works of the authors.

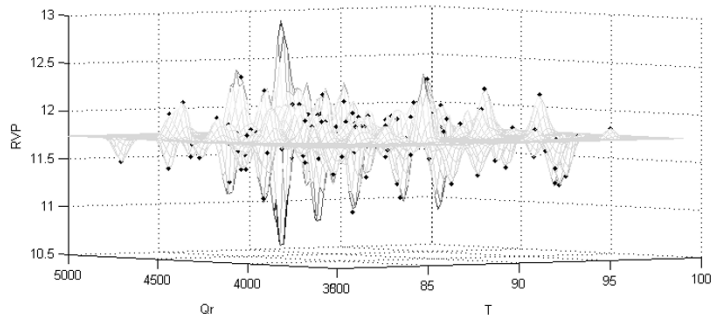

Fig 1: Kriging model for RVP treated by uncertain parameter T_{column} and $Q_{reboiler}$, RMSE=0.08 (bold point is sample point and curve demonstrate untried points)

3. Results

MC, LHS sampling and Kriging method were applied and uncertainty propagation was investigated for output parameters (RVP, SG, Condensate flow rate, and Gas flow rate) of the condensate stabilization column. Figure 2 shows the mean value of experimental RVP for different sample sizes. The data points for the MC, LHS, and Kriging methods have been slightly shifted along the horizontal axis to facilitate viewing of the data. As this figure shows, by getting 300 samples, the mean of RVP predicted by Kriging is converged. Since LHS generates more even distribution of sample points in the parameter space than typically generated with MC, LHS tends to converge in smaller sampling sizes in comparing with MC. On the other hand, the Kriging method by applying stochastic process (Z(x)) appears to be better. In addition it seems three methods converge to same mean value.

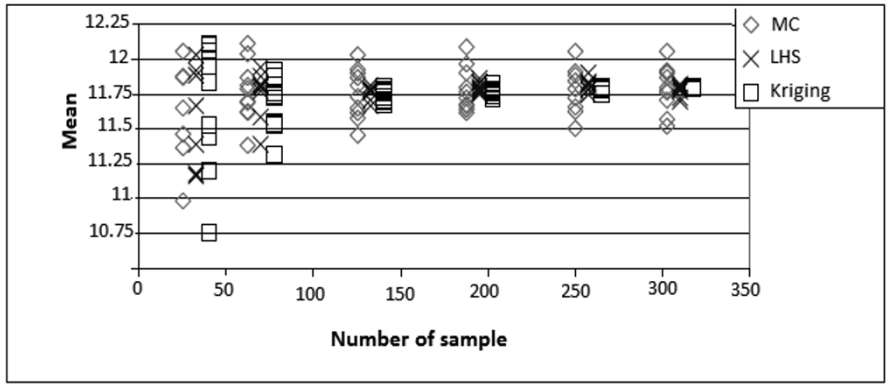

Fig 2: Mean value of RVP for different sample numbers each have eight replicas

However, MC requires more sampling sizes to obtain stable statistics. Propagation of uncertainties to output could be deduced by LHS and Kriging. This result is presented in Table 2. The standard deviation of each parameter obtained from experimental data is larger than that obtained by simulation. It could be caused by external-uncertainty sources (such as an environmental condition) that reflect on data inherently.

Table 2: Propagation of uncertainties to output

		Reid VP of condensate	Specific Gravity of condensate	Condensate flow rate (m^3/h)	Gas flow rate (Nm^3/h)
Experiment	**Mean**	11.760	0.738	33.083	2808.367
	std	0.257	0.002	20.625	640.807
Simulation	**Mean**	11.980	0.731	40.120	2901.231
	std	0.198	0.001	13.540	508.231

4. Conclusion

LHS provides an attractive alternative approach to Monte Carlo by reducing the number of runs required to converge statistics of response variables. However, Kriging method has the advantage of generating a set of samples that more precisely reflect the shape of a sampled distribution than random (Monte Carlo, Latin Hypercube) samples.

Acknowledgement

This research is supported by Pars Oil and Gas Company. Special thanks are directed to Mr.Amir Niko, Mr.Valinejad and Ms.Jafarpour for their guidance.

Reference:

[1] M.G. Ierapetritou, J. Acevedo and E.N.Pistikopoulos, 1996, “An Optimization Approach For Process Engineering Problems Under Uncertainty”, Comp. & Chem. Eng., 20, 703-709

[2] J.C. Halemane, I.E. Grossman, 1983, “Optimal Process Design Under Uncertainty”, ALCHE J. 29(3) 425-433

[3] R.L. Iman, W.J. Conover, 1980, “Small Sample Sensitivity Analysis Techniques for Computer Models,With an Application to Risk Assessment”, Commun, Stats. Theor Meth. A9(17) 1749-1874

[4] R.L. Iman, W.J. Conover, 1982, “A Distribution-free Approch to Including Rank Correlation Among Input Variables”, Commun, Stats. Simulat. Comput. 11(3) 311-334

[5] Susan K. Seaholm, Eugene Ackerman, Shu-Chen Wu, 1988, “ Latin hypercube Sampling and the Sensitivity Analysis of a Monte Carlo Epidemic Model” International Journal of Bio-Medical Computing, 23(1-2) 97-112

[6] Koehler, Owen, 1996, “Handbook of Statistics, Computer Experiments”, Elsevier science, NewYork, P261-308

[7] S. Balakrishnan, M. Ierapetritou;P.G. Georgopoulos, 2001, “Coping with Uncertainty in the Description of Complex Kinetic Mechanisms”, AIChE Annual Meeting, Reno

[8] Brian D.Phenix, Joanna L.Dinaro, Menner A.Tatang, Jefferson W.Tester, Jack B.Howard, and Gregory J.Mcrae, 1998, “Incorporation of Parametric Uncertainty into Complex Kinetic Mechanisms: Application to Hydrogen Oxidation in Supercritical Water", Combustion and Flame 112: 132-146

[9] Timothy W. Simpson, Dennis K. J. Lin, Wei Chen, 2001, “Sampling Strategies for Computer Experiments: Design and Analysis”, International Journal of Reliability and Application

[10] M.D. McKay, W.J. Conover, R.J. Beckman, 1979, “A Comparison of Three Methods For Selecting Values of Input Variables in the Analysis of Output from a Computer Code”, Technometrics, vol.21, no.2

[11] Søren N. Lophaven, Hans Bruun Nielsen, Jacob Søndergaard, 2002, “DACE A MATLAB Kriging Toolbox, Informatics and Mathematical Modeling

I.A. Karimi and Rajagopalan Srinivasan (Editors), Proceedings of the 11th International Symposium on Process Systems Engineering, 15-19 July 2012, Singapore.

A multi-scale model of naphtha pyrolysis process

Lei Zhang,[a] Bingzhen Chen*,[a] Tong Qiu[a]

[a]*Department of Chemical Engineering, Tsinghua University, Beijing, 100084, China*[*]

Abstract

Continuing demand for ethylene, propylene and butadiene makes the naphtha pyrolysis process occupying an important position in the chemical industry. For the accurate prediction of the product yields of given naphtha pyrolysis, it is crucial to establish the naphtha pyrolysis model based on the detailed reaction mechanism. Even though this subject is extensively studied, there are still some remaining unsolved issues in the existing models resulting in a less satisfied accuracy of predicting the product yields. Current challenges include: the detailed reaction mechanism involving a lot of kinetic parameters that are hard to obtain and need to be estimated based on the experimental or real data; a lack of effective method on mapping the feed from commercial indices, such as ASTM boiling curve and PINA fractions, to the conventional components; inefficient method of controlling the scale of the model meeting the required prediction accuracy. This paper develops a multi-scale model of industrial cracker to meet the challenges mentioned above. Here the multi-scale model of the pyrolysis process has been illustrated in detail from microscopic scale to mesoscopic and macroscopic ones. The established multi-scale model has been tested in the plant. Calculated results of the product yields match well with data collected from the plant with satisfied prediction accuracy. Also, based on the established model, an improvement of the performance of an industrial naphtha pyrolysis furnace will be obtained through simulation analysis.

Keywords: multi-scale model, naphtha pyrolysis, radical reaction model, Shannon's maximum entropy theory.

1. Introduction

Naphtha pyrolysis process occupys an important position in the chemical industry. To meet the demands from science and engineering on the depth of revealing the characteristics of a system, a mathematical model may involve relations of properties at different scales of the system (A. Yang, 2009), called multi-scale model. The multi-scale model often consists of nonlinear equations and differential equations that are not easy to solve. And the communication of information between scales is the key factor in the multi-scale model (A. Lucia, 2010).

Reaction network is the kernel part of the multi-scale modeling and nowadays the detailed reaction model is widely used in the simulation of pyrolysis process. Many reasearchers have studied the radical reaction model in depth and described the generation of radical reaction model in detail (E. Ranzi, 2005; R. Fournet, 2001; D. Depeyre, 1991; Z. Belohlav, 2003). Even though this subject is extensively studied, there are still some remaining unsolved issues in the existing models resulting in a less satisfied accuracy of predicting the product yields. Current challenges includes: the detailed reaction mechanism involving a lot of kinetic parameters that are hard to obtain

[*]Corresponding author. Tel.:+86 10 62784572; fax: +86 10 62770304; Email address: dcecbz@tsinghua.edu.cn (B. Chen).

and need to be estimated based on the experimental or real data; a lack of effective method on mapping the feed from commercial indices, such as ASTM boiling curve and PINA fractions, to the conventional components that results in a less satisfied prediction accuracy; ineffcient method of controlling the scale of the model meeting the required prediction accuracy. To meet the challenges mentioned above, a multi-scale model of industrial cracker was developed in this paper, the reaction model contains 125 species and 2424 reactions.

2. Establishment of multi-scale model

2.1. macroscopic scale – process model

Generally speaking, the aspect ratio of tubular reactor for naphtha is greater than 100, so it can be treated as one-dimension reactor. One-dimensional reactor model is used in some commercial steam cracking software, e.g. SPYRO, CRACKER,and COILSIM. The hydrocarbon in the reactor is supposed to be ideal gas, and the reactor is a PFR (Plug Flow Reactor) without axial dispersion and radial temperature and concentration difference. According to the assumptions above, Xu Qiang (Xu, Q., 2001) proposed a process model of pyrolysis:

$$\frac{dN_m}{dL} = \frac{S}{V}\sum_i \upsilon_{im}\, r_i = f_N(T, P, N_m) \tag{1}$$

$$\frac{dP}{dL} = -\frac{f \cdot E(L) \cdot G^2}{5.07 \times \rho \cdot D_i \times 10^4} = f_P(T, P, N_m) \tag{2}$$

$$\frac{dT}{dL} = \frac{k\pi D_o(-\frac{1}{2}\sqrt{\theta_2 - \theta_1} + \frac{1}{2}\sqrt{\theta_1 - \theta_2 + \theta_3} - T) - \sum_m \Delta H^0_{fm} \cdot \frac{dN_m}{dL}}{\sum_m C_{pm} \cdot N_m + C_{\mathrm{pH_2O}}\, N_{\mathrm{H_2O}}} = f_T(T, P, N_m) \tag{3}$$

In equation (1) N_m is the concentration of substance m and L is the corresponding reactor tube length, S is the reactor tube flow passage area, V is the volumetric flow rate, υ_{im} is the reaction stoichiometric coefficient, r_i is the reaction rate for reactrion i. In equation (2) P is the pressure at length L, f is the Fanning friction factor, E(L) is the equivalent length, G is the mass flow rate, ρ is the density, D_i is the inner diameter of the reactor. In equation (3) T is the temperature at length L, k is the heat transfer coefficient, D_o is the outer diameter of the reactor, $\theta_1, \theta_2, \theta_3$ are variables in solving external wall temperature, ΔH^0_{fm} is the formation enthalpy of substance m, C_{pm} is the heat capacity of substance m.

2.2. Mesoscopic scale – reaction model

Reaction model of pyrolysis plays an important role in optimization of production process and process improvement. In equation (1) of process model r_i is the reaction rate equation. For radical reaction A+B→C:

$$r_i = d[C]/dt = k[A][B] \tag{4}$$

So the process model is communicated with reaction model through equation (1). and the multi-scale model can be solved by solving the ordinary differential equations (1-4).

The radical reaction model is proposed by Rice and Herzfeld in 1934. Initiation, propagation and termination reactions are included in a detailed radical reaction model. A detailed radical reaction model can be established based on the four types of reactions above.

Dente proposed the generation of radical reaction model based on large number of experimental data (R. Fournet, 2001). And RMG software as the reaction network

generator was developed (W. Green., 2007). Also graph theory can be used to generate a detailed reaction network (Broadbelt, L. J., 1994, 1996).

2.3. Microscopic scale – radical properties and reaction kinetic parameters

In equation (4) $k = AT^n \exp(-E/RT)$ is the reaction rate constant. Pre-exponential factor A, activation energy E, and heat capacity C_p, enthalpy ΔH in equation (3) are constants that need to be settled. Here, for the key reactions, transition state theory (P. Willems, 1988) can be used to establish a more accurate model.

In addition, thousands of reactions and substances are in the radical reaction model, so the constants are hard to obtain, so quantum chemistry is used to calculate the constants not available.

3. The information communications between different scales

The emphasis of the establishment of the multi-scale model is the information communications between different scales. The relationship of different scales is shown in figure 1.

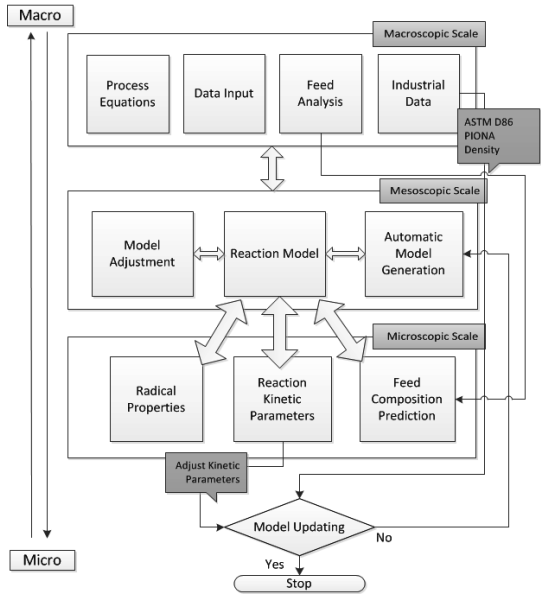

Figure 1: information communications between different scales

3.1. Relationship between macroscopic scale and microscopic scale – feed composition prediction

The input data are important for the pyrolysis simulation, but only ASTM D86, PIONA, and density etc. of the feed property are obtained from industry data. If detailed reaction model is used for the simulation, the feed properties need to be translated into detailed feed information. Shannon's entropy theory is used in the prediction of detailed feed information (K. Geem, 2007). The feed properties prediction problem could be formulated as an optimization problem (L. Zhang, 2012) based on Shannon maximum principle where the objective function max S(x) is Shannon's entropy shown as equation (5), and the relationships between the properties of each substance and mixture properties are the constraints. The calculated results using Shannon's entropy theory are shown in figure 2.

$$\max \quad S(x) = -\sum_{i=1}^{n} x_i \ln x_i \tag{5}$$

3.2. Relationship between macroscopic scale and mesoscopic scale – control of reaction network scale

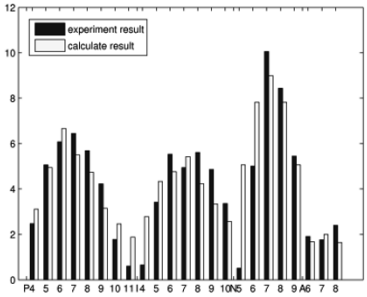

Figure 2: comparision between experimental and calculated results for the feed composition

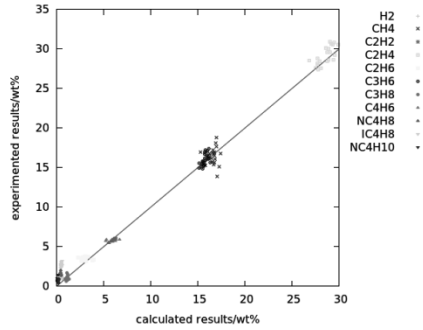

Figure 3: comparision calculated and industrial product yields using the multi-scale modeling

Large number of reactions in the reaction model caused it difficult to solve. So it is necessary to simplify the reaction model on the premise of accuracy. In order to establish an appropriate model that can represent the pyrolysis process, a criterion for controlling characteristics and scale of the radical reaction model based on the difference of industry data and calculate result is derived as follows:

Vajda (S. Vajda, 1985) proposed PCA for the reduction of reaction network. The objective condition for constructing a minimal reaction set:

$$Q(\alpha) = \sum_{j=1}^{q} \sum_{i=1}^{m} \left[(y_{i,j}(\alpha) - y_{i,j}(\alpha^0)) / y_{i,j}(\alpha^0) \right]^2 \tag{6}$$

$y_{i,j}(\alpha) = y_i(t_j, \alpha)$, $\alpha_i = \ln k_i$ in equation (6), k is the rate constant of reaction i, m is the number of substance in the model, and q is the number of selected time points.

According to PCA and perturbation method, the equation (7) can be derived.

$$\sum_i \lambda_i (\ln t) \le mq\xi^2 \tag{7}$$

Where λ_i are the eigenvalues obtained from PCA, $t = k_i / k_i^0$, ξ is the error of calculation result of each product (L. Zhang, 2011).

Equation (7) is considered as a criterion for controlling characteristics and scale of the radical reaction model based on the difference of industry data and calculated result. The right side of equation (7) is known from the macroscopic level, and the eigenvalues can be obtained from the mesoscopic level. So the reaction model can be adjusted to a minimum set of reactions based on equation (7). Besides, the most important reactions in the model can be found using equation (7) for the model adjustment. Therefore, the information transfer between macroscopic scale and mesoscopic scale is the most important issue for model reduction.

3.3. The integration of multi-scale models

Communications of information between different scales as shown in figure 1 are crucial for the establishment of the multi-scale model. The established multi-scale model has been tested in the plant. As the multi-scale model shows the nature of the pyrolysis process, so its simulation results agree well with the industrial data. The calculated product yields for all 22 industrial cases of naphtha pyrolysis match well with that collected from the plant, as shown in figure 3 , which demonstrates the advantage of the proposed model in enhancing the prediction accuracy.

4. Conclusions

In this work a multi-scale model of naphtha pyrolysis process from macroscopic scale to microscopic scale was established and the communication of information between different scales was studied in detail. It has been shown that the modeling results agree well with the industrial data, which demonstrates the advantage of the proposed model in enhancing the prediction accuracy. The proposed multi-scale modeling approach to the naphtha pyrolysis process would be expected to be implemented in modeling of other chemical pyrolysis processes.

Acknowledgments

The authors gratefully acknowledge the financial support from PetroChina Company limeted (Grant No. 20102000079).

References

A. Lucia, 2010, “Multi-scale methods and complex processes : A survey and look ahead”, Comput. Chem. Eng., vol. 34, 1467-1475.

A. Yang and W. Marquardt, 2009, “An ontological conceptualization of multiscale models”, Comput. Chem. Eng., vol. 33, 822-837.

Broadbelt, L. J., Stark, S. M., and Klein, M. T. 1994, “Computer generated reaction networks: on-the-fly generation of species, reactions and rates”, Ind. Eng. Chem. Res., 33, 790-799.

Broadbelt, L. J., Stark, S. M., and Klein, M. T. 1996, “Computer generated reaction modeling: decomposition and encoding algorithms for determining species uniqueness”, Comput. Chem. Eng., 20, 113-129.

D. Depeyre and C. Flicoteaux, 1991, “Modeling of Thermal Steam Cracking of n-Hexadecane”, Ind.Eng.Chem.Res, vol. 30, 1116-1130.

E. Ranzi, A. Frassoldati, S. Granata, and T. Faravelli, 2005, “Wide-Range Kinetic Modeling Study of the Pyrolysis , Partial Oxidation , and Combustion of Heavy n-Alkanes”, Ind. Eng. Chem. Res, vol. 44, 5170-5183.

K Geem, D. Hudebine, M. Franc, J. Verstraete, and G. Marin, 2007, “Molecular reconstruction of naphtha steam cracking feedstocks based on commercial indices,” Comput. Chem. Eng., 31, 1020-1034.

L. Zhang, B. Chen, 2012, “Applications of shannon’s entropy theory to naphtha pyrolysis simulation”, Chem. Eng. Technol., 35, 281-286

L. Zhang, B. Chen, T. Qiu, 2011, “Reaction network model reduction based on PCA”, CIESC Journal (in Chinese), 1, 137-141

P. Willems and G. Froment, 1988, “Kinetic Modeling of the Thermal Cracking of Hydrocarbons. 1. Calculation of Frequency Factors”, Ind. Eng. Chem. Res, vol. 27, 1959-1966.

P. Willems, 1988, “Kinetic modeling of the thermal cracking of hydrocarbons. 2. Calculation of activation energies”, Ind. Eng. Chem. Res, vol. 27, 1966-1971.

R. Fournet, F. Battin-Leclerc, P. Glaude, B. Judenherc, V. Warth, G. Come, G. Scacchi, A. Ristori, G. Pengloan, P. Dagaut, and M. Cathonnet, 2001, “The gas-phase oxidation of n-hexadecane”, International Journal of Chemical Kinetics, vol. 33, 574-586.

R. Fournet, F. Battin-Leclerc, P. Glaude, B. Judenherc, V. Warth, G.M. Come, G. Scacchi, A. Ristori, G. Pengloan, P. Dagaut, and M. Cathonnet, 2001, “The gas-phase oxidation of n-hexadecane”, International Journal of Chemical Kinetics, vol. 33, 574-586.

S. Vajda, 1985, “Principal component analysis of kinetic models”, International Journal of Chemical Kinetics, 14, 55-81.

W. Green. 2007, “Predictive kinetics: A new approach for the 21st century”, Advances in Chem. Eng., 32, 1-51.

Xu, Q., Chen, B. Z., He, X. R., 2001, "Simulation for Naphtha Pyrolysis in Clear Radiation Tube of SRT-IV Cracking Furnace", Comput. and Appl. Chem. (in Chinese), 18(3), 223-228

Z. Belohlav, 2003, “The kinetic model of thermal cracking for olefins production”, Chemical Engineering and Processing, vol. 42, 461-473.

I.A. Karimi and Rajagopalan Srinivasan (Editors), Proceedings of the 11th International Symposium on Process Systems Engineering, 15-19 July 2012, Singapore.

Simulation and Optimization of Saponification Process in Propylene Oxide Plant

Li Xia [a], Xiaoyan Sun [a], you Li [b], Shuguang Xiang [a]

[a] *The Hi-Tech Institute for Petroleum and Chemical Industry，Qingdao University of Science and Technology，Qingdao，266042，Shandong，China*
[b] *China Petroleum Engineering&Construction corporation (CPECC) East-China Design Branch ，Qingdao，266071，Shandong，China*

Abstract

By combining Electrolyte NRTL and the NRTL activity coefficient model, and using the reaction kinetics of propylene chlorohydrins (PC) saponification and propylene oxide (PO) hydrolysis, the simulation of the saponification process in propylene oxide plant is accomplished. In order to reduce the Chemical Oxygen Demand (COD) of wastewater and improve the yield for propylene oxide, the effects of several conditions for the COD of wastewater are studied. The simulation results showed that the yield for propylene oxide has increased 0.47% and the COD of wastewater has reduced 371 mg/l in the case of the optimum condition. Moreover, the unit operation models and thermodynamic models used here had been proved accurately and reliably to simulate the saponification system. So the optimized operating conditions could provide the theoretical basis to the operation of propylene oxide plant.
Keywords: Propylene oxide, Chlorohydrination, Saponification reaction, Simulation

1. Introduction

Propylene oxides are one of the important intermediates in the petroleum and chemical industry. Today, it is produced industrially using multistep manufacturing processes, namely, the antiquated chlorohydrin process and the peroxidation process (Berndt, et al., 2003).In the chlorohydrin process, a large volume of wastewater which contains organic compounds is generated (Steltenpohl & Graczová, 2008). There is an enhanced environmental stress caused by these organic compounds. The COD of wastewater is very important guide posts. It not only directly reflects the status of propylene chlorohydrins saponification and propylene oxide hydrolysis, but also affects the wastewater treatment system. Adopting the suitable operating conditions and reducing the COD of wastewater is crucial.

In this study, a COD-based optimization of the saponification process is presented that develops a detailed simulation model and obtains the optimum operating conditions and equipment configuration.

2. Process Description

The saponification process is shown schematically in Fig. 1. The saponification column from the feed stage is a packed bed and the lower half of the column is a multistage column. The type of multistage part is a sieve tray, and the packed bed is packed irregularly with 4 meters height of ceramic pall rings.

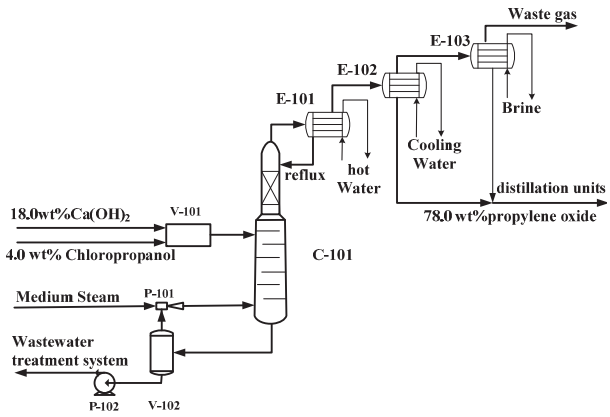

Fig. 1. Process diagram of Saponification Process in Propylene Oxide Plant

2.1. Reaction Kinetics

Choosing the optimal operating conditions for saponification process requires the kinetic parameters for the above reactions involved in the process. In a paper (Carrà, et al., 1979), a kinetic of the reaction involved in the manufacturing of propylene oxide from chlorohydrin have been given in table 1.

Table1. Kinetic parameters for the saponification and hydrolysis reaction

Reaction	Adopted kinetic model	A_i	E_i (kcal/mole)
saponification	$r_{PC} = k_1[PC], k_1 = A_1 \times e^{-E_1/RT}$	$3.02\times10^{9}s^{-1}$	15.86
hydrolysis	$r_{PO} = k_2[PC]\cdot[OH^{-1}], k_1 = A_2 \times e^{-E_2/RT}$	$2.68\times10^{8}mol^{-1}s^{-1}$	16.253

note: A_i :preexponential factors; E_i :activation energy;[OH^{-1}]:OH^{-1} concentration; r:reaction rates; [PC]:propylene chlorohydrins concentration; [PO]:propylene oxide concentration.

2.2. Exchangers, pumps, separators, reactive distillation column models

The saponification process, shown in Figure 1, is modeled using ASPEN PLUS. Standard equipment modules are used for modeling exchangers, pumps, separators, reactive distillation column, etc., given in table 2. Every model is constructed and solved by the sequential modular approach.

2.3. Simulation results

Finally, the material and energy balance for a saponification process is computed in the model. The simulation results are analyzed and compared with actual plant operation data, given in table 3. The results showed that the simulation proposed in this paper is suitable and can be applied to process optimization.

3. Process Optimization

Since the hydrolysis reaction lowers the yields, propylene oxide must be removed as quickly as possible from the reaction environment. For these reasons, the production of propylene oxide is mainly performed in saponification column, and propylene oxide is flashed out with the stream to shorten the contact time and to prevent hydrolysis.

Table2. Modeling in the saponification process

equipment	model in ASPEN PLUS	configuration(mm) diameter×height	thermodynamic model	reaction kinetics
V-101	RPLug	Φ800×1000	Electrolyte NRTL	S. CARRA et al.[5]
pipelines(from V-101 to C-101)	RPLug	Φ300×13800	Electrolyte NRTL	S. CARRA et al.[5]
V-102	Flash2	-	Electrolyte NRTL	-
C-101	RadFrac	Φ2200/3600×25292	Electrolyte NRTL	S. CARRA et al.[5]
E-101/102/103	Heater+Flash2	-	NRTL	-
P-101	Mixer	-	NRTL	-
P-102	Pump	-	Electrolyte NRTL	-

Table3. Comparison of the Simulation Results and the Actual Operating Data

conditions	simulation results	actual operating data
The dilute PC solution flow rate, kmol/h	20837.7	20837.7
$Ca(OH)_2$ solution flow rate , kmol/h	4097.2	4097.2
Top temperature of saponification column, ℃	90.0	92.7
bottom temperature of saponification column, ℃	99.8	100.5
product flow rate (78wt% propylene oxide), kmol/h	274.4	-
The yield for propylene oxide, %	95.87	95.80
The COD of wastewater, mg/l	1218.0	1300.0

3.1. Optimization conditions

On initial analysis, it quickly became apparent that the COD of wastewater were heavily dependent on hydrolysis reaction and separation of the saponification column. To reduce the COD of wastewater, several factors, shown in Table 4, are taken into account separately.

Table4. Optimization decisions regarding saponification

	actual condition	Boundary
Saponification column pressure, kPaA	97.0	67.0~107.0
The number of trays for saponification column	9	9~13
The height of weir, mm	80.0	70.0~110.0
The fresh steam injection rate, 10^3kg/h	23.0	20.0~24.0
The mole ratio of OH^{-1} to the sum of PC and HCl	1.3	1.1~1.5
The saponification reaction temperature, K	349.6	344.6~354.6

3.2. Optimization Results and Discussion

In Figure 2 and Figure 3, the effects of the conditions, shown in Table 4, for the COD of wastewater are studied ordinal. The optimal conditions are determined via a COD-based optimization calculation that minimized the COD of wastewater.

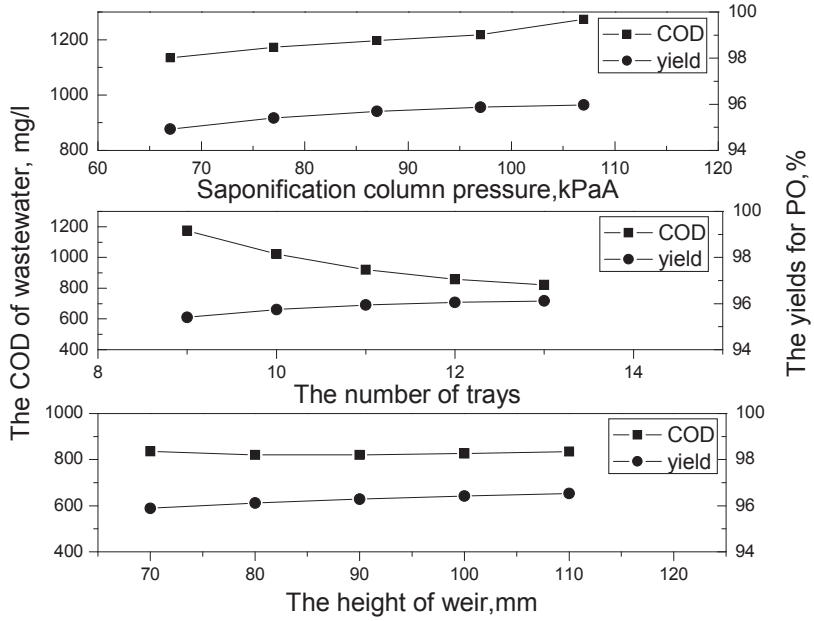

Fig. 2. Top:Trend of saponification column pressure vs the COD and yields. Middle:Trend of the number of trays vs the COD and yields. Bottom: Trend of the height of weir vs the COD and yields.

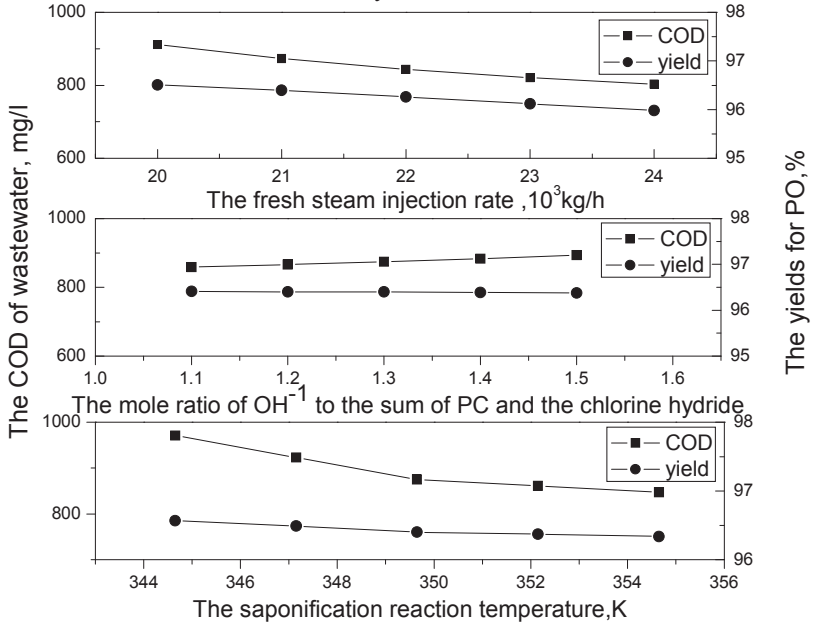

Fig. 3. Top: Trend of the fresh steam injection rate vs the COD and yields. Middle: Trend of the mole ratio of OH^{-1} to the sum of propylene chlorohydrins and chlorine hydride vs the COD and yields. Bottom: Trend of the saponification reaction temperature vs the COD and yields.

Optimization is accomplished which directs appropriate changes in the independent variables to the executive system (H. Martin Rodriguez, et al., 2010). Boundary constraints on the independent variables, shown in Table 5, are checked before performing the computations in the ASPEN PLUS.

Process optimization requires consideration of many trade-offs as a whole. In addition to minimizing the COD of wastewater, the actual situation of the propylene oxide plant must be taken into account: ⑴ Because of restriction of its pumped vacuum system, the lowest of saponification column pressure is 77 kPa(A);⑵ Although increasing the steam consumption can lower the COD of wastewater, fresh steam is 21000kg/h from the economic point of view.

Finally, the optimum conditions are obtained as follows: (1) saponification column pressure is 77kPa(A); (2) the number of trays is 13; (3) the height of weir is 80mm; (4) fresh steam is 21000kg/h; (5) mole ratio of OH^{-1} to the sum of propylene chlorohydrins and chlorine hydride is 1.1; (6) the saponification reaction temperature is 354.6K.

4. Conclusions

During the course of the operation optimization described in this article, the yield for propylene oxide has increased 0.47% and the COD of wastewater has reduced 371 mg/l. In addition to delivering an optimal operation, the project proved that:

- Equipment configuration decisions, such as the height of weir of trays and the volume of the saponification mixer, should be taken into account.
- Models are sufficiently accurate to be able to reflect the effects of small changes in operating condition, for example, saponification column pressure.
- The methods used in this optimization are suitably general and can be applied to any process plant. They are available via commercially-available simulation and modeling tools.

Acknowledgment

Financial support of National Natural Science Foundation, China (Project 21176127), for this work is gratefully acknowledged.

References

Berndt, T., O. Böge, et al., 2003, From Atmospheric Research to an Industrial Process:The Formation of Propylene Oxide, Ind. Eng. Chem. Res.,42,12, 2870-2873.

Steltenpohl, P. and E. Graczová, 2008, Vapor−Liquid Equilibria of Selected Components in Propylene Oxide Production, J. Chem. Eng. Data, 53,7, 1579-1582.

Carrà, S., E. Santacesaria, et al., 1979, Synthesis of propylene oxide from propylene chlorohydrins-I: kinetic aspects of the process, Chem. Eng. Sci., 34,9, 1123-1132.

Carrà, S., M. Morbidelli, et al., 1979, Synthesis of propylene oxide from propylene chlorohydrins-II: Modeling of the distillation with chemical reaction unit, Chem. Eng. Sci.,34,9, 1133-1140.

H. Martin Rodriguez, A. Cano, et al., december 2010, Improve engineering via whole plant design optimization, Hydrocarbon Process., Int. Ed., 43-49.

I.A. Karimi and Rajagopalan Srinivasan (Editors), Proceedings of the 11th International Symposium on Process Systems Engineering, 15-19 July 2012, Singapore.

Simulation Studies and Sensitivity Analysis of Methyl Tert-butyl Ether Reactive Distillation

Sudibyo, M.N. Murat and *N.Aziz

School of Chemical Engineering, Engineering Campus, Universiti Sains Malaysia, 14300 Nibong Tebal, Seberang Perai Selatan, Penang, Malaysia.
**E-mail: chnaziz@eng.usm.my*

Abstract

Methyl Tert-butyl Ether (MTBE) is an important chemical used as an octane booster in gasoline to replace tetra ethyl lead. Maximum production of the MTBE can be achieved using reactive distillation (RD) process that is operated at the optimum operating conditions and column configuration. However, optimizing the column configuration such as tray or catalyst location is experimentally expensive. Therefore, a reliable model of the MTBE reactive distillation is important to find the optimum conditions for MTBE production. In this work, continuous RD processes is simulated based on dynamic model using Aspen Dynamics. The model is then further used in Simulink for the singular value decomposition (SVD) analysis in order to select the best input-output pair for the control implementation. Finally, the step test is conducted in order to observe the sensitivity of the MTBE process toward changes of selected input variables. The results show that the model obtained from the Aspen produced a comparable result with the literature. The results also show that the tray temperature number 3 and 8 are the most sensitive output variables toward changes of reflux flowrate and reboiler duty.

Keywords: Reactive distillation; Dynamic simulation; MTBE, sensitivity analysis

1. Introduction

Separation and reaction processes can be combined in one unit process which is called as reactive distillation (RD). It has been used in several industries especially for the process which have reversible reaction [Sharma and Singh, 2010]. RD can reduce the capital investment, because two process steps can be carried out in the same device [Higler et al., 1999; Taylor and Krishna, 2000; Murat et al., 2003; Mohammed, 2009]. However, it is still difficult to bring a new reactive distillation column into industrial applications because of the complexities in design, synthesis and operability of RD, which is resulting from the interaction of reaction and distillation. [Satyanarayana and Saha, 2005]. Here, MTBE is considered because it is an important chemical that is used as solvent, chemical reagent and antiknock additive to improve octane number of gasoline [Sharma & Singh, 2010]. MTBE can be efficiently produced using RD; with isobutene conversion up to 99 % can be achieved [Taylor and Krishna, 2000].

The purpose of RD control is to maintain the product purity and conversion at a desired value or specified range. However, to control the conversion directly is a difficult task and expensive to be applied in industry. Thus, MTBE purity can be controlled by controlling tray temperature because the MTBE purity can be correlated with tray temperature [Taylor and Krishna, 2000]. Many researchers have modeled or simulated the MTBE RD process using either first principle model or various commercial software such as HYSIS and Aspen [Higler et al., 1999; Taylor and

Krishna, 2000; Murat et al., 2003; Satyanarayana and Saha, 2005; López-Arenas et al., 2006; Mohammed, 2009;]. However, those who used the commercial software were aim for the steady state model. In this work, the industrial RD dynamic process model is developed using Aspen Dynamics which is more feasible to be used for design and verification of process control schemes and safety studies.

At the same time, the SVD analysis and the step test are also carried out in order to evaluate the controllability and sensitivity of the process [Pearson, 2003]. The work is carried out in Simulink and interfacing with Aspen.

2. Description of the MTBE Column

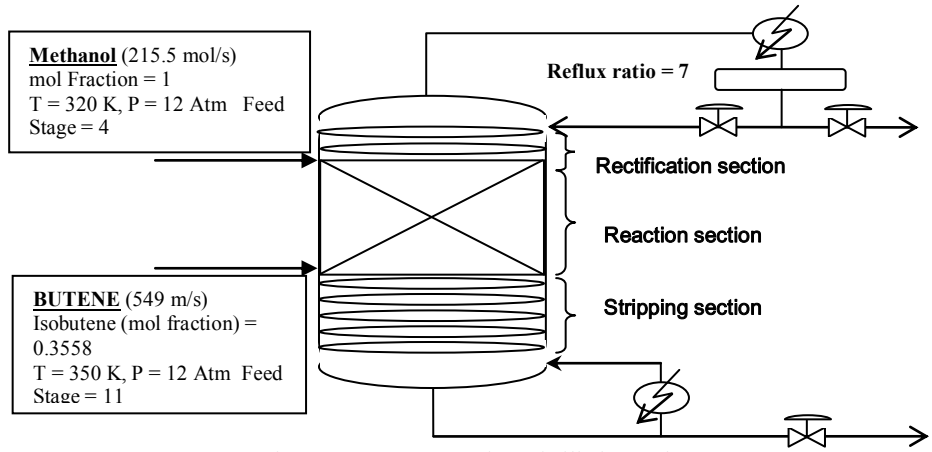

Figure 1. MTBE Reactive Distillation Column

Table 1. Tray and Packed Column Specification [Higler *et al.,* 1999]

Packed column specification		Tray specification		
Parameters	Reaction Section	Parameters	Rectifying Section	Stripping Section
Column Diameter	6 m	Column Diameter	5.95 m	5.019 m
Total column area	28.27 m^2	Total tray area	24.58 m^2	19.78 m^2
Packing height	0.7 m	Number of pass	4	4
Packing size	¼ in	Active area	19.21 m^2	15.32 m^2
Nominal size	0.00635 m	Total hole area	2.12 m^2	1.52 m^2
Packing factor	5249.34	Downcomer area	2.68	2.23

MTBE reactive distillation column consists of three sections: rectification, reaction and stripping as shown in Fig. 1. For this case study, the RD column has 17 stages, including a total condenser and a partial reboiler as given in Fig. 1 [Higler *et al.*, 1999]. The tray and packed column specifications and operation conditions are given in Table 1. The specification used here is similar to the specification used by Higler *et al.* [1999], except the number of passes, the pressure column and location of feed stages are different. In this work, 4 passes and 12 atm of pressure column while Higler *et al.* [1999] have used 5 passes and 11 atm. Meanwhile, the feed, methanol and butane, are fed at stages 4 and 11, respectively (being optimized) in order to get the maximum value of isobutene conversion.

2.1. MTBE Reaction Scheme

The most promising technique of producing MTBE is from methanol and isobutene, where the liquid-phase reaction is catalyzed by ion exchange resin (heterogeneous reaction). The reaction scheme is:

$$i\text{-}C_4H_8 + CH_3\text{-}OH \rightleftharpoons C_5H_{12}O \quad (1)$$

Chemical equilibrium constant for reaction (1) as used in the Aspen is:

$$ln\ k_{eq} = ln\ k_{eq0} + \alpha[(1/T) - (1/T^*)] + \beta\ ln\ (T/T') + \sigma(T - T^*) + \delta\ (T^2 - T^{*2}) + \varepsilon(T^3 - T^{*3}) + \theta(T^4 - T^{*4}) \quad (2)$$

where α is -1.49277 x 10^3, β is -7.74002, γ is 5.07563 x 10^{-1}, δ is -9.12739 x 10^{-4} , ε is 1.10649 x 10^{-6} , θ is -6.27996 x 10^{-10} , T* = 298.315 K , *keq0* = 284 [Murat et al., 2003].

3. Results and Discussion

3.1. Modeling of Reactive Distillation

The results obtained from the RD dynamic model using Aspen dynamics were compared with data available in literature and tabulated in Table 2. From the table, it is found that the simulation results obtained are comparable to the published results which verify that the proposed Aspen Dynamics model is capable to simulate the MTBE reactive distillation process. The small differences observed in the result obtained are due to some different specifications (as mentioned earlier) used in the simulation. The isobutene conversion can reach 99.82% using reactive distillation and which is in a good agreement with the value reported in the literature [Taylor and Krishna, 2000].

Table 2. Model Comparison

	Nijhuis *et al.* 1993	Murat *et al.,* 2003	This Work
i -butene conversion	98.5%	99.5%	99.82%
MTBE Purity	98%	98.6%	95.04%
Software	Aspen	Fortran 90	Aspen Dynamics

3.2. Singular value decomposition (SVD) analysis

Here, the most suitable tray temperature to be paired as controlled variable in respect of manipulated variable changes (reflux flowrate and reboiler duty) was determined using SVD analysis technique. The SVD test was conducted by changing the inputs of manipulated variable with the step magnitude of +0.1% from nominal input value [Luyben , 2006; Imam and Aziz, 2011]. The SVD analysis was performed by SVD command in Matlab which calculated the left singular vectors from SVD analysis result (U_{SVD}) as shown on Fig. 2. From Fig. 2, tray number 3 and 8 show the largest magnitude which signifies that they are the most sensitive trays temperature towards the changes of reflux flowrate and the reboiler duty, respectively.

3.3. Step Test Study

3.3.1. Effect of Reflux Flowrate

The study was performed by introducing several step-tests with different magnitude of manipulated variable (reflux flowrate) and the response on tray temperature (tray number 3) is observed. Fig. 3 shows the effect of reflux flowrate changes on the temperature of tray number 3 and MTBE purity. From Fig. 3a, it is show that the temperature of tray number 3 is decreasing when the reflux flowrate is increasing. The

changes in the reflux flowrate produce an asymmetric form of the output response thus signify that the reactive column is a nonlinear process. The changing of reflux flowrate also affected the MTBE purity as shown in Fig. 3b, where the MTBE purity decrease as the reflux flowrate increase.

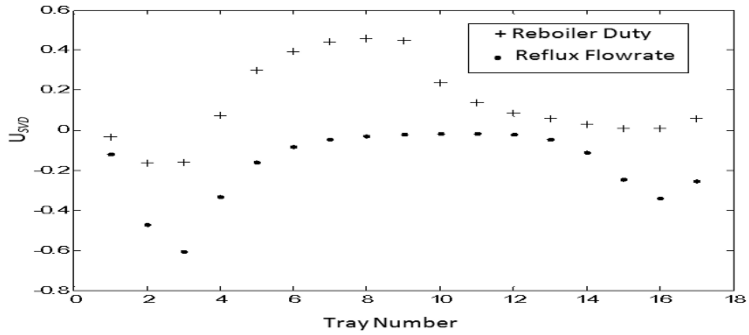

Figure 2. U_{SVD} versus tray number

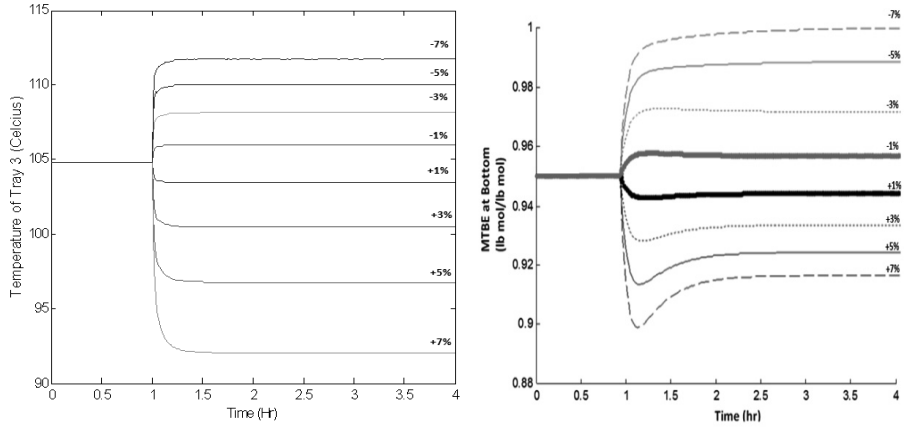

(a) (b)

Figure 3. Effect of reflux flowrate change on (a) 3rd tray temperature (b) MTBE Purity

3.3.2. Effect of Reboiler Duty

The result of step-test on reboiler duty towards the temperature of tray number 8 is shown in Fig. 4. From the figure, the changes in the reflux flowrate produce an asymmetric form on the output response thus again proved that the reactive column is a nonlinear process. Meanwhile, the effect of reboiler duty change on the MTBE purity in the bottom product is shown in Fig. 4a, where the MTBE purity increases as the reboiler duty increases.

4. Conclusion

The dynamic model of MTBE RD has been developed using Aspen Dynamics which has been validated using data available from literature. The singular value decomposition (SVD) analysis show that the tray temperature number 3 and 8 are the most sensitive toward changes of reflux flowrate and reboiler duty. Finally, the step

test results show that MTBE RD is a nonlinear process hence need nonlinear controller to control MTBE reactive distillation.

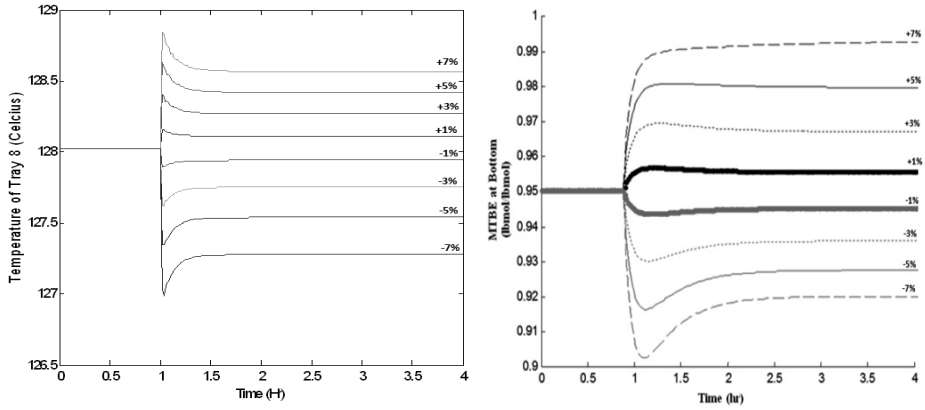

(a) (b)

Figure 4. Effect reboiler duty change on (a) 8th tray temperature (b) MTBE Purity

Acknowledgement

The financial support from Universiti Sains Malaysia through Research University (RU) Grant and Graduate Assistant (GA) to the first author are greatly acknowledged.

References

A.P. Higler, R. Taylor and R. Krishna, 1999, The influence of mass transfer and mixing on the performance of a tray column for reactive distillation, Chem. Eng. Science, 54, 2873-2881.

H. Lin and P.L. Douglas, 2000, Dynamic Simulation and Control of an MTBE Catalytic Distillation Column. Dev. Chem. Eng. Mineral Process, 8(3/4), 375-399.

I.M. Iqbal and N. Aziz, 2011, Comparison of Various Wiener Model Identification Approach in Modelling Nonlinear Process, IEEE Proceedings of the 3rd Conference on Data Mining and Optimization (DMO 2011), 134-140.

M.N. Murat, A.R. Mohamed and S. Bhatia, 2003, Modelling of reactive distillation column: Methyl Tertiary Butyl Ether (MTBE) simulation studies, IIUM Engineering Journal, 4.

N. Sharma and K.Singh, 2010, Control of Reactive Distillation Column: A Review, Int. J. Chemical Reactor Eng., 8, R5.

R.K. Pearson, 2003, Selecting Nonlinear model structures for computer control,Journal of process control, 13,1-26.

R. Taylor and R. Krishna, 2000, Review: Modelling reactive distillation, Chem. Eng. Science, 55, 5183-5229.

S.A. Nijhuis, F.P.J.M. Kerkhof, and A.N.S. Mak, 1993, Multiple steady states during reactive distillation of methyl tert-butyl ether, Ind. and Eng. Chemistry Res., 32, 2767-2774.

T. López-Arenas, S. Eduardo and R. Gani, 2006, Static/dynamic analysis and controllability issues in reactive distillation columns, Computer Aided Chemical Engineering, 21, 1323-1328.

T. Satyanarayana and P. Saha, 2005, Modeling and Control Structure Selection for Reactive Distillation Process using Aspen Custom Modeler, CHEMCON – 05, New Delhi.

W. L. Luyben, 2006, Evaluation of criteria for selecting temperature control trays in distillation columns, Journal of Process Control, 16, 115–134.

Z. M. Mohammed, 2009, Mathematical Modeling and Simulation for Production of MTBE by Reactive Distillation, MSc Thesis, Chemical Eng. Department, Univ. of Technology, Kingdom of Saudi Arabia.

I.A. Karimi and Rajagopalan Srinivasan (Editors), Proceedings of the 11th International Symposium on Process Systems Engineering, 15-19 July 2012, Singapore.

Optimal Design of HMX recrystallization process using supercritical carbon dioxide as antisolvent

Sungho Kim,[a] Shin Je Lee,[a] Hyoun-Soo Kim,[b] Youn-Woo Lee,[a] Jong Min Lee*[a]

[a]*School of Chemical and Biological Engineering, Institute of Chemical Process, Seoul National University, 1 Gwanak-ro, Gwanak-gu, Seoul, 151-744, Republic of Korea*
[b]*High Explosives Team, Agency for Defense Development, 462, Jochiwon-gil, Yuseng-gu, Daejeon 305-600, Republic of Korea*

Abstract

This work studies optimization of a Cyclotetramethylenetetranitramine (HMX) recrystallization process by precipitation. HMX is a powerful and relatively insensitive explosive. Since the shape and particle size are important properties for explosive materials, there have been many efforts to control those properties. Due to their vulnerability to heat and impact traditional methods like milling and solution-based recrystallization are inapplicable. Gas Anti-Solvent (GAS) process with supercritical carbon dioxide as an antisolvent does not have such safety issues and can produce particles with required shape and size distribution. This process, however, has been tested mostly in laboratory scale semi-batch reactors. The main purpose of this study is to develop a process flowsheet model for large-scale GAS processes and determine optimal process economics. The proposed process consists of a reactor, a separator, and recycle of carbon dioxide. An optimal operating point is also determined.

Keywords: Gas antisolvent, supercritical fluid, process optimization.

1. Introduction

Explosives with high energy density require increased performance and stability, and their physical properties are determined by crystal size, shape, and uniformity. Even in recent years, many crystals are produced by conventional milling or recrystallization from solution. Though these processes provide economical, easy, and conventional ways to product powder from the bulk material, heat or impact during the processing can cause unexpected accidents like explosion. Moreover, the conventional processes are known to be ineffective for the control of physical properties.

Gas Anti-Solvent (GAS) process can be considered as an alternative for recrystallization due to its capability to control the particle size distribution (PSD) of the product. It can also satisfy the required quality using various process variables such as antisolvent inlet flow rate and temperature [1]. Furthermore, GAS process is much safer than traditional techniques such as milling.

Experimental studies have shown that several variables like antisolvent addition rate, temperature and agitation speed play a key role in determining PSD. A population balance model is presented to predict PSD for general GAS processes [2]. A GAS process for recrystallization of beclometasone dipropionate using carbon dioxide as antisolvent and acetone as a solvent is analyzed with Muhrer's model [3].

These studies are focused on laboratory-scale reactors, and no studies have been reported for modeling and optimization for an integrated GAS process towards large-scale productions. Since GAS processes using supercritical fluids require large amounts of energy, economic optimization of the process is also necessary.

This work provides a conceptual design and a steady-state optimal operating condition for large-scale recrystallization of Cyclotetramethylenetetranitramine (HMX) where acetone is used as a solvent for HMX and supercritical carbon dioxide as the antisolvent. The proposed model is a scaled-up version of the currently operating laboratory-scale process.

2. GAS process

For scale up of the experiment to a large-scale process, not only the reactor itself but also the entire process including peripheral equipment and necessary unit operations must be specified first. Figure 1 shows a lab-scale GAS process reactor with feeding and separator units in Seoul National University. The process consists of three operations; reaction, separation, and recycle of used carbon dioxide. The process is operated in a fed-batch mode. In the followings , major unit operation steps in the lab-scale process are described.

Figure 1. A lab-scale GAS process including feeding and separator units.

2.1. Reactor

Figure 2 shows reaction steps for a batch cycle. HMX is first dissolved in acetone for recrystallization. The solution is loaded in the reactor before a batch cycle begins. Each batch cycle starts once supercritical carbon dioxide (antisolvent) is fed into the reactor. As carbon dioxide being fed, rapid expansion of solution occurs and the volume of solution and pressure inside the reactor are increased. After carbon dioxide feeding is completed, the mixture stays in the reactor for a few minutes for thermal equilibrium and then outlet flow valve is opened for the product flow to move out to the separator.

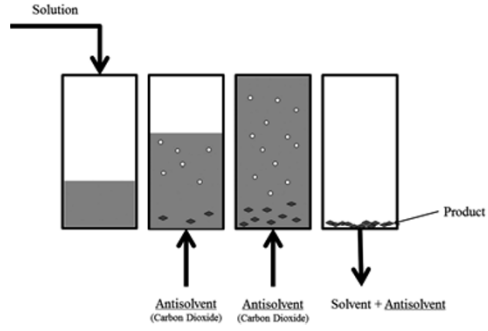

Figure 2. Reaction steps of GAS process in a cycle.

2.2. Separator

In the separation unit, solid HMX is separated first. A fabric filter is installed in the pipe to collect solid HMX in the outlet flow. The filter is removed after each batch cycle to collect solid HMX. Mixture of carbon dioxide and acetone is easily separated because these materials are insoluble and their boiling points differ significantly. Carbon dioxide is recovered from top of the separator and acetone is recovered from the bottom. A small amount of energy is used to minimize the amount of acetone in the top flow.

2.3. Recycle

Used carbon dioxide is recycled to reduce the carbon dioxide emission. Separated carbon dioxide is recompressed and brought back to the reactor inlet stream condition. The carbon dioxide contained in the acetone needs to be recovered before compression. In order to reduce the burden of each unit, compression and cooling are done by two compressors and two coolers, respectively.

3. Base-case design and optimization of the entire process

The three processing units mentioned above are combined and created as a process flowsheet. Aspen Plus V7.2 is used as the flowsheet simulator, and Figure 3 shows the flowsheet and calculation results.

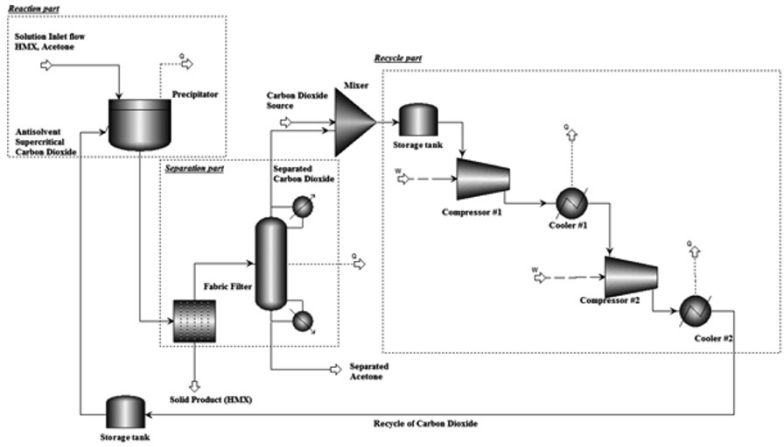

Figure 3. Process flowsheet of GAS process

Material and energy balances are calculated for 5000 ton/year production rate of HMX. UNIQ-RK EOS was chosen as a thermodynamic model. Steady state operation is presumed and dynamic operation for control of PSD of HMX is not considered in this step. Pressure drops in the fabric filter and cooler are neglected.

A batch reactor model is used to simulate the reactor. The reactor is operated at constant temperature of 30℃ and the temperature is controlled by the water jacket. Heat duty of water jacket is estimated by comparing the conditions of inlet and outlet flows. This assumption is valid because no chemical reaction occurs in the process. Batch cycle time of the reactor is one hour and the amount of antisolvent (carbon dioxide) feed

per cycle is 5 times bigger than the amount of HMX-acetone solution to increase the product yield. HMX-acetone solution is at standard temperature and pressure condition (101.325 kPa, 25℃). The condition of the antisolvent are chosen as 10000 kPa and 35℃ [4].

A fabric filter is installed to collect HMX product. Default simulation mode and parameters are used because PSD is not considered in the reactor. Hence, all the solid materials were assumed to be recovered from solvent flow.

For separation of CO_2 and acetone a flash drum is added. For implementation, the Sep2 model in Aspen Plus was employed because this can specify the mole-fraction of each substream and can compute the corresponding pressure and temperature condition. The Sep2 model is useful when the split ratio of each component is the key factor, while details of the separation are not important. Mole fraction of acetone in the bottom product is set to be above 0.999 and in the top product is set to be below 0.001 to avoid condensation of acetone in the recycle flow.

Compression and cooling set-points were specified as the inlet condition of the antisolvent for the reactor, e.g., 10000 kPa and 35 ℃. Storage tanks are also installed on each side of recycle part to store the recycled carbon dioxide between each batch cycle. Properties in the storage tank are assumed to be the same as the recompressed carbon dioxide stream.

Optimal operating points for compressor and coolers were also determined. Optimizer of Aspen HYSYS V7.2 is used for optimization. The objective function is to minimize the sum of heat duties of compressor and cooler. The optimization variables are the ΔP of compressor #1 and ΔT of cooler #1. Efficiency of each unit are was set to be a proper value less than 100% to have convergence. By solving this optimization problem, the optimal operating point and heat duties of each unit were estimated as shown in Tables 1 and 2.

Table 1. Optimal operating points of each unit.

	Compressor #1	Cooler #1	Compressor #2	Cooler #2
ΔP (kPa)	1748		7735	
Pressure Ratio	4.3		4.5	
ΔT (℃)		-42.41		-128.4

Table 2. Heat duty of each process unit.

	Reactor jacket	Solvent separator	Compressor #1	Cooler #1	Compressor #2	Cooler #2
Heat duty (Btu/hr)	7.30×10^4	2.14×10^4	4.17×10^5	1.85×10^6	4.96×10^6	1.27×10^7

It is shown that the cooling process requires most of the energy and thus will contribute to the increased operating cost. In this work carbon dioxide is designed to be fully recycled for environmental consideration, but for economic optimization the recycle ratio of carbon dioxide can be another manipulated variable for reducing operating cost. If carbon dioxide is not fully recycled for each cycle and the additional carbon dioxide for replenishment is increased, reduction of operating cost may be achievable. Detailed analysis for the optimal tradeoff will be done in the future work.

4. Concluding Remark

This work provides a base-case design for an integrated GAS process towards large-scale production of HMX and a steady-state optimal operating point for minimization of energy use. A rigorous population balance model will be incorporated into the reactor model to provide a more rigorous solution to optimal process economics and dynamics of the particle size distributions.

5. Acknowledgement

This work was financially supported by Agency for Defense Development of South Korea

References

[1] P. M. Gallagher, 1991, Gas Anti-Solvent (GAS) Recrystallization: Application to Particle Design, in Particle Design via Crystallization, AIChE symposium.
[2] G. Muhrer and C. Lin, 2002, Modeling the Gas Antisolvent Recrystallization Process, Industrial & Engineering Chemistry Research.
[3] S. Dodds and J. A. Wood, 2007, Modeling of the Gas-Antisolvent (GAS) Process for Crystallization of Beclomethasone Dipropionate Using Carbon Dioxide, Industrial & Engineering Chemistry Research.
[4] B. M. Lee, 2011, Preparation of Micronized β-HMX Using Supercritical Carbon Dioxide as Antisolvent, Industrial & Engineering Chemistry Research.

I.A. Karimi and Rajagopalan Srinivasan (Editors), Proceedings of the 11th International Symposium on Process Systems Engineering, 15-19 July 2012, Singapore.

Thermal integration of a hot process stream on distillation columns through a side-reboiler

Qinglin Chen*, Zhiqiang Wei, Shengyuan Wu, Bingjian Zhang

School of Chemistry and Chemical Engineering/Key Lab of Low-carbon Chemistry & Energy Conservation of Guangdong Province, Sun Yat-Sen University, Guangzhou 510275, China

Abstract

This paper presents a novel procedure to effectively integrate a hot process stream on a distillation column. The original value of the side-reboiler heat duty is identified through a comparison of the available heat duty of the hot process stream with the required heat duty of the side-reboiler. A benzene-toluene column is used to demonstrate the performance of the procedure. The results obtained demonstrate that the available heat duty of the hot process stream, the place location, heat duty of the side-reboiler, and stage number modification for the column could be identified by using the proposed procedure in a relatively simple and reliable way.

Keywords: distillation column, thermal integration, side reboiler, process streams.

1. Introduction

Integrating a hot process stream on distillation columns through side-reboilers is important for either designing an energy-efficient distillation column or improving the energy-use efficiency of chemical processes (Bandyopadhyay, 2007). In practical, when the available heat duty ($Q_{\mathrm{ava,hs}}$), and the inlet temperature ($T_{\mathrm{in,hs}}$) of the hot process stream are specified, a challenge for improving energy-use efficiency is how to effectively integrate the hot process stream with a specific distillation column through side-reboilers. Some approaches for thermal integration of distillation systems have been reported in the literature (Sobočan, 2002; Gadalla, 2003; Cabrera-Ruiz, 2011). Unfortunately, the key issues related to integration of the hot process stream on columns have not been fully addressed up to now. Thus, a novel procedure aimed to effectively integrate the hot process stream on distillation columns is proposed in this paper. Based on the procedure, the available heat duty of the hot process stream, the location and heat duty of the side-reboiler, stage number modification for the column could be easily and effectively identified. A benzene-toluene column is used to demonstrate the performance of the procedure.

2. Available heat duty of a hot process stream

The outlet temperature ($T_{\mathrm{out,hs}}$) and the available heat duty of a hot process stream are calculated through Eqs. (1) and (2), respectively.

$$\Delta T = \frac{\left(T_{in,bs} - T_{out,ss}\right) - \left(T_{out,bs} - T_{in,ss}\right)}{\ln \dfrac{T_{in,bs} - T_{out,ss}}{T_{out,bs} - T_{in,ss}}} \tag{1}$$

* Correspondence author; email: chqlin@mail.sysu.edu.cn.

$$Q_{ava,bs} = CP_{bs} \cdot (T_{out,bs} - T_{in,bs}) \quad (2)$$

Where CP represents heat capacity flowrate, $\triangle T$ is the temperature difference for heat exchanging. The subscripts *in, out, hs* and *ss* represent the inlet temperature, outlet temperature, hot process stream and side-reboiled stream, respectively. In calculating the value of $T_{\text{out,hs}}$, $\triangle T$ is assumed to be 10 K, as the minimum temperature difference.

The arranging location ($N_{\text{side-re},i}$) and required heat duty ($Q_{\text{side-re},i}$) of the side-reboiler are identified through exergy grand composite curve (EGCC) and avoidable exergy destruction curve (AEDC), as proposed by our group (Wei, 2012). Thus, the inlet and outlet temperatures of the side-reboiled stream are identified, and the available heat duty of the hot process stream is calculated through Eqs. (1) and (2). With the value of $Q_{\text{ava,hs},i}$ and $Q_{\text{side-re},i}$, one can conclude whether the heat duty of the hot process stream is sufficient or not for setting a side-reboiler, as is presented in Fig. 1.

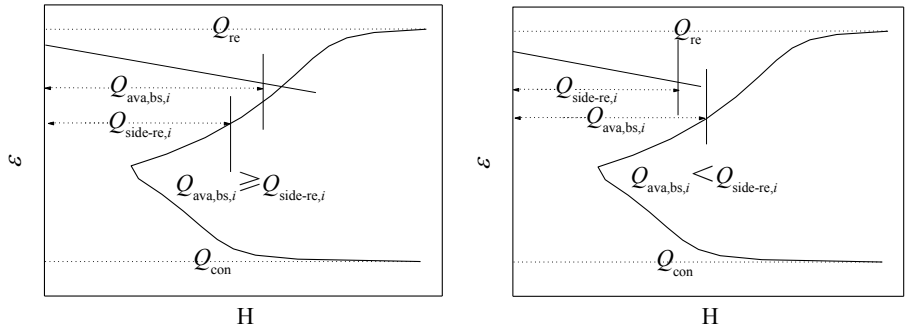

Fig. 1 Schematic of $Q_{\text{ava,hs},0}$ and $Q_{\text{side-re},0}$

As shown in Fig. 1a, the value of $Q_{\text{ava,hs},i}$ is greater than $Q_{\text{side-re},i}$, which suggests that $Q_{\text{ava,hs},i}$ is sufficient for setting a side-reboiler, and the heat duty has a surplus. Then, $Q_{\text{side-re},i}$ and $N_{\text{side-re},i}$ are identified as the original values of the side-reboiler heat duty and location. While in Fig. 1b, $Q_{\text{ava,hs},i}$ is smaller than $Q_{\text{side-re},i}$, which means that $Q_{\text{ava,hs},i}$ is not sufficient for arranging a side-reboiler. In this case, the original value of the side-reboiler heat duty should be reconsidered. In general, the value should be fallen among $Q_{\text{ava,hs},i}$ and $Q_{\text{side-re},i}$. Therefore, stage number between these two boundary values is determined and the corresponding available heat duty $Q_{\text{ava,hs},j}$ is calculated. The maximum value of $Q_{\text{ava,hs},j}$ is treated as the original value of the side-reboiler heat duty, and the corresponding stage is used to arrange the side-reboiler.

3. Calculation procedure

The calculation procedure, illustrates in Fig 2, can effectively integrate the hot process stream with a specific distillation column through arranging a side-reboiler.

1) Identify the optimum feed stage $N_{F,\text{opt}}$ and the optimum reflux ratio $R_{0,\text{ opt}}$.
2) Identify the location $N_{\text{side-re},i}$ and the duty $Q_{\text{side-re},i}$ of a side-reboiler through EGCC and AEDC.
3) Identify the inlet and outlet temperature of the side-reboiled stream, $T_{\text{in,ss},i}$ and $T_{\text{out,ss},i}$.
4) With the values of $T_{\text{in,ss},i}$, $T_{\text{out,ss},i}$ $T_{\text{in,hs},i}$ and CP_{hs}, calculate the outlet temperature of the hot process stream $T_{\text{out,hs},i}$ and the available heat duty $Q_{\text{ava,hs},i}$.
5) If $Q_{\text{ava,hs},i}$ is equal to or greater than $Q_{\text{side-re},i}$, $N_{\text{side-re},i}$ and $Q_{\text{side-re},i}$ are used as the

original values of the location and heat duty for arranging a side-reboiler.
6) Determine the new reflux ratio R_i' after the side-reboiler arranged.

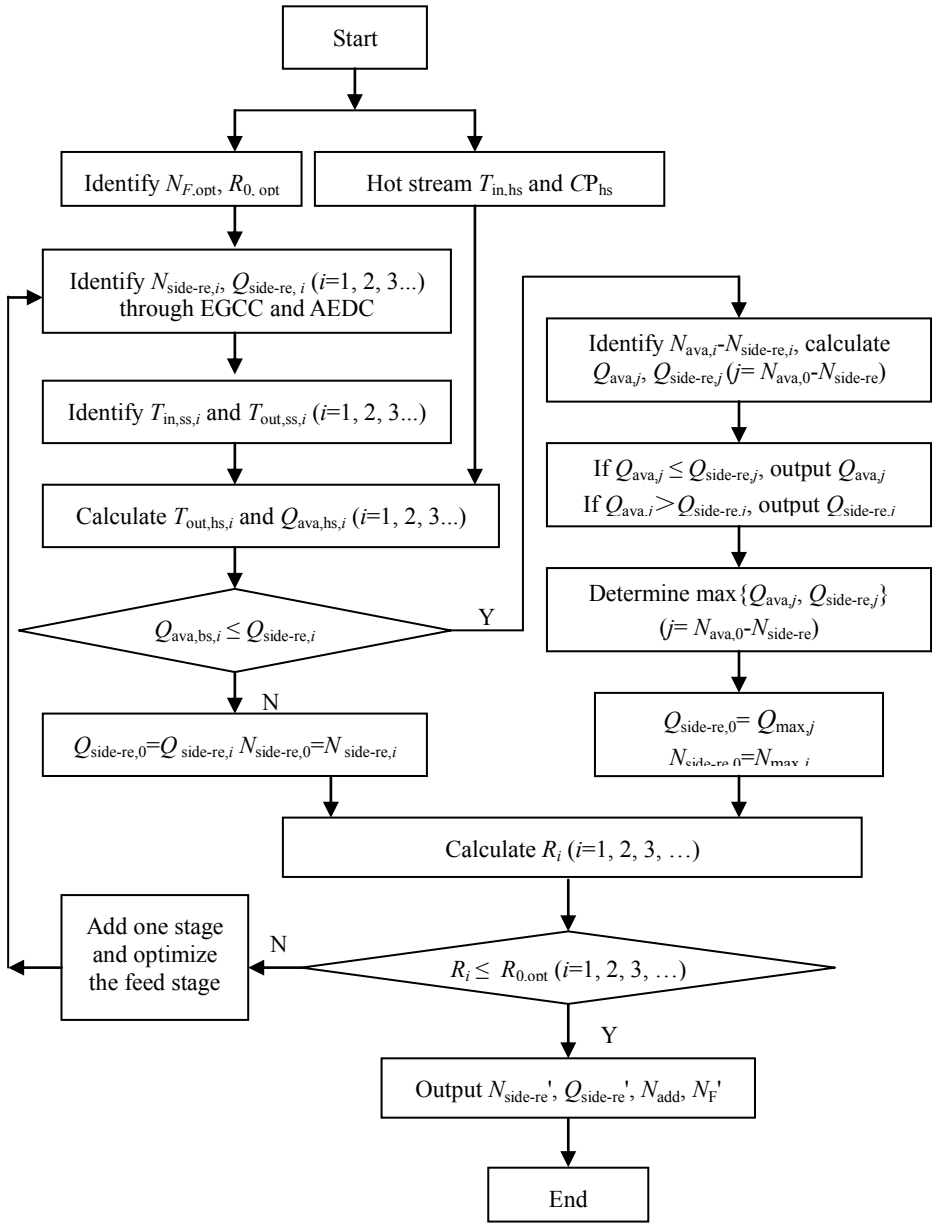

Fig. 2 Calculation procedure to integrate the hot process stream on a distillation column

7) If R_i' is not larger than $R_{0,opt}$, adjust the stage number is unnecessary, and information of the side-reboiler $N_{side\text{-}re}$', $Q_{side\text{-}re}$' can be output and the procedure is ended.
8) If R_i' is greater than $R_{0,opt}$, add one stage to the column, and optimize the feed stage.
9) Return to the second step, recalculate until R_i' is not greater than $R_{0,opt}$, output the information of the side-reboiler $N_{side\text{-}re}$', $Q_{side\text{-}re}$', N_{add}, N_F' and the procedure is ended.

10) If $Q_{ava,hs,i}$ is smaller than $Q_{side\text{-}re,i}$, identify the stages between $N_{ava,i}$ and $N_{side\text{-}re,i}$, and calculate the $Q_{ava,hs,j}$ and $Q_{side\text{-}re,j}$ values for these stages, where the EGCC enthalpy values are treated as the corresponding $Q_{side\text{-}re,j}$ to identify the values of $T_{in,ss,j}$ and $T_{out,ss,j}$.
11) If $Q_{ava,hs,j}$ is not larger than $Q_{side\text{-}re,j}$, the output parameter to the next step is $Q_{ava,hs,j}$, while for $Q_{ava,hs,j}$ is greater than $Q_{side\text{-}re,j}$, the value of $Q_{side\text{-}re,j}$ is taken as an output result to the next step.
12) Determine the maximum value of the results $\{Q_{ava,j}, Q_{side\text{-}re,j}\ (j= N_{ava,0}\text{-}N_{side\text{-}re})\}$, and the original values of the location and heat duty of the side-reboiler are the maximum value $Q_{max,j}$ and the corresponding stage $N_{max,j}$.
13) Repeat the steps 6-9 and output information of the side-reboiler $N_{side\text{-}re}'$, $Q_{side\text{-}re}'$, N_{add}, N_F', and the procedure is ended.

A benzene-toluene column is used to demonstrate the performance of the calculation procedure, and specifications of the column are listed in Table 1. The heat capacity flowrate of the hot process stream is set as 25 kW/K, and the inlet temperature is 393 K.

Table 1 Feed, product, and column specifications

Feed properties		Column characteristics		Feed molar fractions	benzene	0.50
Molar flow kmol/h	100	Stage number	25		toluene	0.50
Temperature K	365	Feed number	12	Column specifications	$x_{D,benzene}$	0.99
Pressure MPa	0.1	Condenser	total		$x_{B,toluene}$	0.99

Table 2 Information for determining the avaliable heat duty of the hot process stream

N_{add}	$N_{side\text{-}re,i}$	$T_{in,ss}$ / K	$T_{out,ss}$ / K	$T_{out,hs}'$ / K	$Q_{side\text{-}re,i}$ / kW	$Q_{ava,hs,i}$ / kW
0	17	375.5	378.0	382.0	495	285
	16	373.0	375.5	378.0	395	380
	15	370.0	373.0	374.0	295	470
1	18	375.5	378.0	382.0	485	285
	17	373.0	376.0	378.0	390	375
	16	370.0	373.0	374.5	290	460
2	19	376.0	378.0	382.0	460	280
	18	373.0	376.0	378.0	360	370

The detailed results of arranging a side-reboiler on the benzene-toluene column are listed in Table 2 and Table 3. It can be seen that in the base case, a 495 kW heat duty is needed on the 17th stage, and only 285 kW heat duty is available. The value of $Q_{ava,hs,i}$ is lower than $Q_{side\text{-}re,i}$. Then, the stages between $Q_{ava,hs,i}$ and $Q_{side\text{-}re,i}$ are identified as the 15th and 16th stages. For the 16th stage, the output heat duty for the side-reboiler is 380 kW, and the heat duty determined in the 15th stage is 295 kW. This means that the 16th stage and a 380 kW heat duty should be identified as the original values for the side-reboiler. The modified reflux ratio is larger than that of the base one, which indicates that one stage should be added, and a new iteration is started. The final results are obtained after three iterations, and the outlet temperature of the hot process stream is 378 K and the available heat duty of the hot process stream is 370 kW. In arranging a side-reboiler, two stages should be added. The feed stage is the 13th stage, the placing location is the 18th stage, and the heat duty is 360 kW.

Table 3 Information of arranging a side-reboiler on the benzene-toluene column

Iteration	R	$N_{F,i}$	$N_{\text{side-re},i}$	$Q_{\text{side-re},i}$ / kW	$N_{\text{add},i}$
Base case	1.66	12	---	---	---
1	1.76	12	16	380	0
2	1.72	13	17	375	1
3	1.65	13	18	360	2

4. Conclusions

A novel procedure is proposed to integrate the hot process stream on a distillation column. According to the procedure, the available heat duty of the hot process stream is calculated, and the original value of the side-reboiler heat duty is identified through a comparison of the available heat duty of the hot process stream with the required heat duty of the side-reboiler. A benzene-toluene column is used to demonstrate the performance of the procedure. The results indicate that the available heat duty of the hot process stream and information of the side-reboiler (i.e. the location and heat duty of the side-reboiler, stage number modification for the column) are related to each other. The procedure proposed can effectively integrate the hot process stream on a distillation column in a relatively simple and systematic way.

Acknowledgement

The authors gratefully acknowledge the financial support from the National Natural Science Foundation of China (No. 20906016, 21076233) and the Major Science and Technology R&D Program of Guangdong Province (No. 2010A080801003).

References

G. Sobočan, P. Glavič, 2002, A simple method for systematic synthesis of thermally integrated distillation sequences, Chem. Eng. J., 89, 1, 155-172

J. Cabrera-Ruiz, A. Jiménez-Gutiérrez, J. G. Segovia-Hernández, 2011, Assessment of the implementation of heat-integrated distillation columns for the separation of ternary mixtures, Chem. Eng. Res. Des., 50, 4, 2176-2181

M. Gadalla, M. Jobson, R. Smith, 2003, Optimization of existing heat-integrated refinery distillation systems, Chem. Eng. Res. Des., 81, A1, 147-152

S. Bandyopadhyay, 2007, Thermal integration of a distillation column through side-excahngers, Chem. Eng. Res. Des., 85, A1, 155-166

Z. Q Wei, S. Y. Wu, B. J. Zhang, Q. L. Chen, 2012, An exergy grand composite curve based procedure for side-exchanger arrangement on distillation columns. 11th International Symposia on Process Systems Engineering.

I.A. Karimi and Rajagopalan Srinivasan (Editors), Proceedings of the 11th International Symposium on Process Systems Engineering, 15-19 July 2012, Singapore.

Forecasting Naphtha Price Crack Using Multiple Regression Analysis

Chaeeun Sung[a], Hweeung Kwon[a], Jinsuk Lee[b], Haesub Yoon[b], Il Moon[a]

[a] *Department of Chemical and Biomolecular Engineering, Yonsei University, 50 Yonsei-ro, Seodaemun-gu, Seoul 120-749, Korea*
[b] *SamsungTotal Corporation 411, Dokgot-ri, Daesan-eup Seosan*-si, *Chungcheongnam-do 356-711, Korea*

Corresponding Author's E-mail: sce0214@yonsei.ac.kr

Abstract

The price of naphtha depends on that of crude oil as naphtha is produced by refining crude oil. Naphtha plays an important role as one of basic petrochemicals for downstream products. Large fluctuation of naphtha price has been intensified along with recent political unrest of Middle East Asia and the growing naphtha demand in developing countries. Thus forecasting naphtha price is becoming more uncertain. The development of models for forecasting naphtha crack (price difference between naphtha and crude oil) will help minimize any loss from naphtha price variations. This study is concerned with the derivation of a set of major parameters affecting naphtha prices and the identification of the most dominating factors. We proposed a model for forecasting naphtha crack based on statistical approach and multiple regression analysis, and R^2 was 0.651. .Naphtha price depends mainly on Asia supply and demand of naphtha as well as naphtha substitute and margin. Actual and predicted variations of naphtha crack were also analyzed. The proposed modeling approach can be extended to forecast prices of other downstream chemicals such as LPG and NGL.

Keywords: Naphtha crack, Multiple regression model, Statistical approach, Forecasting

1. Introduction

In recent years, uncertainty of naphtha price forecasting has increase due to expanding price variability of naphtha affected various factors such as supply and demand, prices, margin of naphtha and petrochemical products, global economy and the operational rate of oil company. Forecasting naphtha crack has been regarded as one of the most important thing of purchasing naphtha. Thus, various models have been depicted to provide the naphtha buyers with more precise predictions.

Several studies for price forecasting have been published. Artificial neural networks (ANN) have been referring to forecasting price. B.R. Szkuta et al. (1999) study the System Marginal Price short-term forecasting using artificial neural networks. P. Pai (2005) presents a hybrid model of the autoregressive integrated moving average (ARIMA) and the support vector machines (SVMs). This model is higher evaluated than the prediction performance of the single ARIMA model and single SVMs model. W. Zhang (2010) researches forecasting agricultural and livestock products price using statistical approach.

In this paper, we develop the multiple regression model to forecasting naphtha crack considering more than 20 factors. This paper shows part of these factors, supply and demand of naphtha, margin, and naphtha substitute. This model verified by comparing actual naphtha crack and predicted naphtha crack from January 2011 to November 2011. Finally, we analyze the percentage of the correct predicted variation of naphtha crack.

2. Problem statement

2.1 Data normalization

The actual data was normalized in this work from 0 to 1 in order to standardize unit and range

$$D_{nor} = \frac{D - D_{min}}{D_{max} - D_{min}} \quad (1)$$

where D_{nor} is the normalized data, D is the actual data, D_{min} is the minimum value of the normalized data, and D_{max} is the maximum value of the normalized data.

2.2 Data preparation

Among the various major factors, we select the three factors, supply and demand, margin and naphtha substitute. These are not the only factors influencing naphtha crack. The major factors were used as independent variables in forecasting naphtha crack. Monthly data for major factors are collected from 2008 to 2010 except from October 2008 to March 2009 to avoid unusual economic effect, Lehman Brothers collapse

Table 1. The major factors from 2008 to 2010

Date	Naphtha crack ($/mt)	Supply/ Demand (mt/month)	Margin ($/mt)	Naphtha substitute ($/mt)	Date	Naphtha crack ($/mt)	Supply/ Demand (mt/month)	Margin ($/mt)	Naphtha substitute ($/mt)
Jan-08	41.760	1545000	146.867	6.205	Oct-09	-22.187	1515000	120.668	-28.261
Feb-08	25.974	1463000	154.385	-52.986	Nov-09	-2.692	1481000	119.573	-1.150
Mar-08	-13.974	1501000	171.540	-52.092	Dec-09	30.952	1586000	121.677	45.012
Apr-08	-35.386	1373000	194.698	-82.716	Jan-10	37.742	1571000	147.853	76.163
May-08	-62.668	1455000	211.831	-106.592	Feb-10	19.538	1438000	147.949	64.250
Jun-08	-40.362	1469000	211.885	-165.369	Mar-10	21.987	1405000	200.023	3.750
Jul-08	-53.882	1537000	158.885	-141.883	Apr-10	-10.251	1430000	179.259	3.750
Aug-08	-20.111	1546000	177.856	-136.538	May-10	8.391	1522000	169.018	-44.103
Sep-08	-31.760	1309000	179.613	-72.432	Jun-10	-9.454	1413000	170.609	-23.944
Apr-09	-140.008	1404000	126.375	-60.000	Jul-10	-34.687	1505000	164.643	-25.840
May-09	-197.908	1490000	178.928	-120.855	Aug-10	-12.185	1496000	128.349	-17.600
Jun-09	-101.827	1426000	173.518	-93.648	Sep-10	-7.097	1425000	100.680	7.013
Jul-09	-31.295	1486000	144.537	-67.293	Oct-10	14.215	1443000	121.843	24.800
Aug-09	21.201	1548000	167.900	-79.118	Nov-10	24.593	1496000	129.176	96.100
Sep-09	-3.973	1477000	112.430	-36.670	Dec-10	36.381	1607000	145.223	163.413

4. Modeling

The general model of multiple regressions is given

$$y = \beta_0 + \beta_1 x_1 + \beta_2 x_2 + \cdots + \beta_p x_p + \varepsilon \quad (2)$$

where y is the predicted trend, $x_1, x_2, \cdots x_p$ are the influence factors of predicted trend, $\beta_0, \beta_1 \cdots \beta_p$ are the regression coefficients, and ε is the residual variable.
In this paper, naphtha crack (C) was assumed as function of supply and demand of naphtha (S), margin (M) and naphtha substitute (N). According to the three major factors, we establish the following multiple regression model equation

$$C = f(S, M, N) = \beta_0 + \beta_1 S + \beta_2 M + \beta_3 N + \varepsilon \quad (3)$$

5. Results

Table 2 shows that correlation coefficients between the naphtha crack and three major factors.

Table 2. Pearson correlation and significance values to naphtha crack

	Pearson Correlation	**Significance**
Supply/Demand (S)	.792	.000
Margin (M)	.358	.026
Naphtha substitute (N)	-.452	.006

Significance values of major factors to naphtha crack are less than the significance level 5%. It means that major factors have very strong correlations with naphtha crack.

Table 3. Coefficients and R^2 in model

Model	**Unstandardized Coefficients**		**Standardized Coefficients**	**Significance**	**R^2**
	β	**Std. Error**	**Beta**		
Constant	.211	.298		.484	.651
Supply/Demand (S)	.404	.076	.734	.000	
Margin (M)	.477	.375	.154	.215	
Naphtha substitute (N)	-.033	.141	-.032	.818	

This table explain the values of multiple regression model. Supply and demand of naphtha is less than the significance level 5% shows that this factor has a large impact on naphtha crack rather than other two factors. From R^2 of this model, we know that 65.1 % of the variations in naphtha crack can be explained by the three major factors.

The regression coefficients of multiple regression model is obtained from β of unstandardized coefficients.

$$C = 0.211 + 0.404S + 0.477M - 0.33N \quad (4)$$

Using this model, actual and predicted variations of the naphtha crack from January 2008 to December 2010 are investigated 48.3%. (The data are not shown) We forecast this model by forecasting naphtha crack from January 2011 to November 2011. Fig. 1 shows actual naphtha crack and predicted naphtha crack from January 2011 to November.

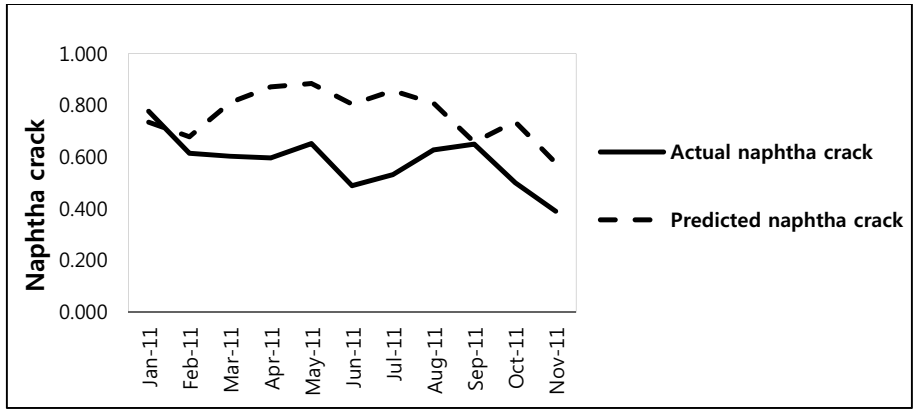

Figure 1. Time series plot of actual naphtha crack and predicted naphtha crack.

In forecasting of naphtha crack, it is important variation more than exactly naphtha crack data. Table 4 shows actual and predicted variations of naphtha crack. From prediction result in table 4, we obtain the percentage of the correct predicted variation. The variation of naphtha crack obtained from the difference between that month and previous month. If both actual and predicted variations of the naphtha crack have the same sign, it indicates that it means that the prediction is same. Owing to 5 same predictions out of total 10 months in table 4, the correct predicted variation is 50%

Table 4. Actual and predicted variations of naphtha crack

Date	Actual naphtha crack variation	Predicted naphtha crack variation	Prediction result
Jan-11	-0.162	-0.057	Same
Feb-11	-0.012	0.133	Different
Mar-11	-0.006	0.061	Different
Apr-11	0.056	0.013	Same
May-11	-0.163	-0.079	Same
Jun-11	0.043	0.052	Same
Jul-11	0.096	-0.048	Different
Aug-11	0.022	-0.151	Different
Sep-11	-0.149	0.079	Different
Oct-11	-0.111	-0.159	Same

6. Conclusion

In this study, we develop the multiple regression models to forecasting naphtha crack. Three major factors influencing naphtha crack have correlation with naphtha crack. Among the major factors, supply and demand of naphtha have strong impact on naphtha crack. From multiple regression models, we could forecast future naphtha crack and analysis the percentage of the correct predicted variation. Through this study, we could more consider major factors influencing naphtha crack for obtaining higher R^2 in model and the percentage of the correct predicted variation.

6. References

B.R. Szkuta, L.A. Sanabria, T.S. Dillon, 1999, Electricity Price Short-Term Forecasting Using Artificial Neural Networks, IEEE Transactions on Power Systems, Vol.14, 854-857

P. Pai, C. Lin, 2005, A hybrid ARIMA and support vector mahines model in stock price forecasting, The International Journal of Management Science, Vol.33, 497-505

W. Zhang, H. Chen, M. Wang, 2010, A forecast model of agricultural and livestock products price, Mechanics and materials 20-23, 1109-1114

A. Ghaffari, S. Zare, 2009, A novel algorithm for prediction of crude oil price variation based on soft computing, Energy economics 31, 4, 531-536

P. Visetsripong, P. Sooraksa, P. Luenam, 2008, Naphtha's Price Forecasting using Neuro-fuzzy System, Society of Instrument and Control Engineers Annual Conference, 659-663

Kim, J., Lee, Y., Moon, .I., 2008, Optimization of a hydrogen supply chain under demand uncertainty, International Journal of Hydrogen Energy, Vol.33, Issue 18, 4715-4729

Kim, J., Moon, .I., 2008, Strategic design of hydrogen infrastructure considering cost and safety using multiobjective optimization, International Journal of Hydrogen Energy, Vol.33, Issue 21, 5887-5896

Kim, J., Moon, .I., 2008, The role of hydrogen in the road transportation sector for a sustainable energy system: a case study of Korea, International Journal of Hydrogen Energy, Vol. 33, No.24, 7326-7337

I.A. Karimi and Rajagopalan Srinivasan (Editors), Proceedings of the 11th International Symposium on Process Systems Engineering, 15-19 July 2012, Singapore.

Model-based development of optimal reaction concepts for plant wide process intensification

Andreas Peschel,[a] *Andreas Jörke*,[b] *Hannsjörg Freund*,[a] *Kai Sundmacher*[a,b]

[a]*Max Planck Institute for Dynamics of Complex Technical Systems, 39106 Magdeburg, Germany.* [b]*Process Systems Engineering, Otto-von-Guericke University, 39106 Magdeburg, Germany*

Abstract

In order to design optimal chemical reactors, the interaction between reactor and process needs to be considered. In this contribution we propose a new method for the design of optimal reactors in the overall process framework by simultaneous determination of the best reaction concept and optimization of the process design parameters. The reaction concept is apparatus independent and optimal state space profiles for composition and temperature are provided along the reaction coordinate.
The oxygen based production of ethylene oxide, one of the most important bulk chemicals, is considered as an example. Here, advanced cooling and distributed dosing of oxygen is identified as best reaction concept from an economical and technological point of view. Applying this innovative reaction concept, the production costs of an average sized plant are reduced by 1.35 Mio \$/a, and the CO_2 emissions are decreased by $2.7 \cdot 10^4$ t/a compared to an optimized reference case. This general method provides a first step towards more economical and greener processes.

Keywords: Reactor, design, optimization, ethylene oxide, process intensification.

1. Introduction and methodological approach

Since selectivity and conversion in the reactor determines the effort of the downstream purification process, the reaction concept offers a large potential to enhance the energy and raw material efficiency of today's chemical processes. To identify the best reaction concept from a process point of view, the interaction between reactor and process needs to be taken into account; otherwise suboptimal reactors are placed in the process. Only a simultaneous optimization of the reaction concept and the plant operation gives rise to the reaction concept that results in the maximum improvement of the overall process. In order to identify the most promising reaction concept, the elementary process functions approach is used to describe the reaction module [1, 2]. Within this approach, optimal profiles of the heat flux and component dosing/removal fluxes are realized in order to obtain the best reaction conditions over the entire residence time and process intensification options are considered by modeling the physico-chemical phenomena. This method constitutes a symbiosis of process intensification and process systems engineering methods as can be seen from the objectives and methods of both disciplines [3].

2. Example process: Oxygen based ethylene oxide synthesis

Ethylene oxide (EO) is one of the most important bulk chemicals and already small improvements in the reactor results in large savings in the running expenses of the process. Due to the undesired total oxidation of ethylene to CO_2 in the reactor and the energy intensive downstream purification process, the EO process is one of the main producers of CO_2 within the chemical industry.

For the synthesis of EO, the oxygen based process is state-of-the-art. However, few publications consider the optimization of the oxygen based EO process and, in particular, the optimal reaction concept has never been determined so far. An earlier publication on the air based EO process [4] shows significant potential for a better reaction concept for the EO synthesis, but the reaction concept was not determined within the overall process. The flowsheet of the oxygen based ethylene oxide process is shown in Fig. 1. Downstream of the reaction section, the produced EO is absorbed using water. Further downstream, part of the CO_2 is removed by absorption in hot potassium carbonate, before the fresh feed is added to the recycle stream.

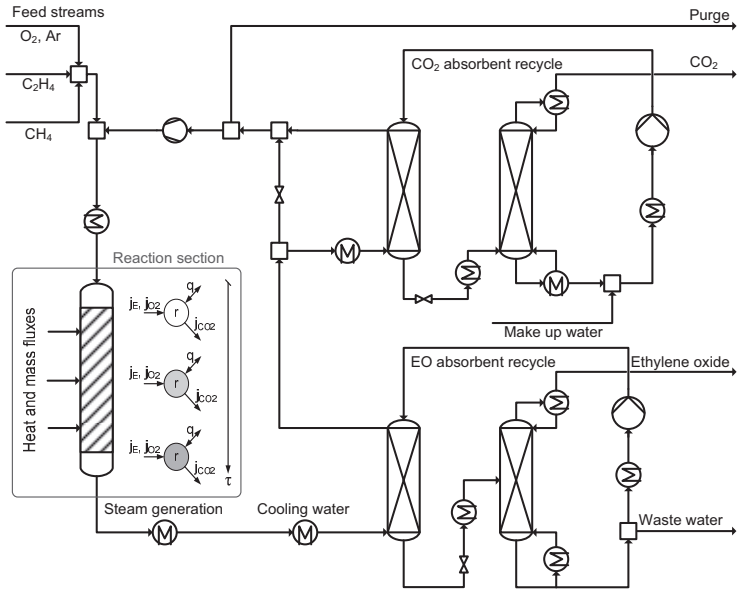

Figure 1: Flowsheet of the oxygen based ethylene oxide process

The overall objective of this work is the minimization of the EO production costs by optimizing the reaction concept and the plant operation simultaneously. Thereby, all raw material (ethylene, oxygen, methane) and utility costs (electricity, steam, cooling water) are taken into account using the most currently available cost data [5].

3. Modeling

The overall process according to Fig. 1 is modeled using a detailed model of the reaction section, tailored models for the EO and CO_2 absorption sections, and short-cut models for the additional process units. This paper is an excerpt of a more comprehensive paper [5], where all model equations are given, the optimization problems are stated, the modeling assumptions are discussed, and a sensitivity analysis is performed to investigate the influence of uncertainties.

3.1. Reaction section

The reaction module is modeled according to the elementary process function approach [1, 2]. Here, a fluid element is tracked and optimal flux profiles are determined in order to obtain the best reaction conditions for this fluid element over its entire residence time. Exemplarily, the component mass balance for the tracked fluid element is given below (n_i=amount in fluid element, a_i=exchange area, j_i=dosing flux, ρ=catalyst density, ε=void fraction, V_{gas}=gas volume of fluid element, r=reaction rate, NR=# of reactions).

$$\frac{dn_i}{dt} = a_i j_i + \rho_{cat} \frac{1-\varepsilon}{\varepsilon} V_{gas} \sum_{j=1}^{NR} \upsilon_{ij} r_j$$

The dosing fluxes j_i are used to manipulate the concentration profile in an optimal manner along the reaction coordinate and they constitute an optimization function in the intensified reaction concepts discussed in Section 4. Different reaction concepts including advanced cooling and distributed dosing of reactants and in-situ removal of CO_2 are considered. The optimal profiles for these fluxes are obtained by solving a dynamic optimization problem, which is constrained by the complete process model for the reaction section and downstream purification. The model of the reaction module consists of the component balances, the energy balance, bounds for the temperature region of the catalyst, a lower limit for the obtained space time yield of 1 mol/(m^3s), the reaction kinetics [7], and intrinsic bounds imposed by the explosion limits of the mixture.

Due to the explosion hazard inside the reactor, the reaction mixture must stay outside the explosive region all along the reaction coordinate. For this purpose, a new model based on literature data for the explosive region, which is developed in [5], is included into the optimization. This model rigorously accounts for the influence of the individual flammable gases (ethylene, methane, ethylene oxide) [8] including the non-idealities arising from the composition [9], as well as the pressure [10, 11] and temperature dependency of the explosive region. A detailed model of the explosive region allows for the optimal manipulation of the composition along the reaction coordinate in order to improve the reactor performance but always keeping clear of the explosive region.

3.2. Downstream process

The downstream process consists of an EO absorption section and a CO_2 separation section. In the former, EO is separated from the gases by physical absorption in water. The absorber is modeled using the Kremser equation and the desorber is described using two flash tanks. The produced EO has a purity of 95% and is send to further distillation to remove the light components. In order to separate the CO_2 from the recycle gas, a hot potassium carbonate solution with piperazine as promoter is used. The chemical equilibrium of this chemisorption is modeled taking all 6 equilibrium reactions and all 10 intermediate species into account [12]. The physical solubility of all gas components are modeled using Henry's law combined with a specialized approach to describe the physical solubility of CO_2 in the potassium carbonate solution. The additional process units (pumps, compressors, heat exchangers, mixers, and splitters) are modeled using common short-cut models as proposed in the literature [13]. Ideal heat integration is assumed in order to determine the minimal utility consumption of the process.

4. Results

Depending on the investigated reaction concept the heat flux (q) as well as the mass fluxes of oxygen (j_{O2}), ethylene (j_E), and CO_2 (j_{CO2}) into or out of the fluid element are optimized along the reaction coordinate. In addition, the feed streams, the reaction pressure, the residence time in the reactor, the temperature of the absorbers and desorbers, the absorbents stream of water and potassium carbonate solution, the split fractions of each splitter are degrees of freedom to be simultaneously optimized to the reaction concept. The optimization problem is constrained by the overall process model including the detailed description of the reaction section and of the downstream process. The distributed balance equations of the reaction section are discretized using orthogonal collocation on finite elements and the overall process model is implemented in *AMPL* yielding a large scale NLP problem which is solved using the state-of-the-art solver *CONOPT*.

The optimization results of all investigated reaction concepts are summarized in Fig. 2. In the reference case (case 1), the reaction conditions are assumed to be isothermal and

no components are dosed in order to manipulate the concentration profiles in the reaction section. This reaction concept refers to the industrially used tube bundle reactor with very effective cooling. The EO production costs of the optimized reference case are 656.3 $/t, which is in good agreement to the published production costs of the oxygen based EO process [5].

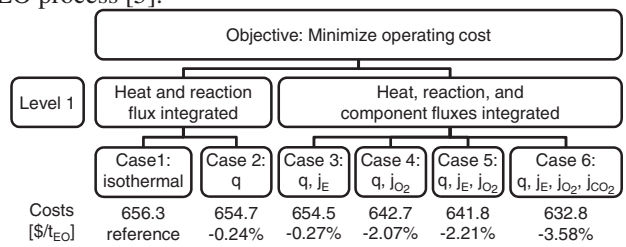

Figure 2: Results overview

Obtaining an optimal temperature profile in the reactor (case 2) as well as optimal cooling combined with distributed dosing of ethylene (case 3), show only small potential for the reduction of the running expenses. However, distributed dosing of oxygen combined with an optimal heat flux profile (case 4) reduces the running expenses of the process by more than 2%. Such a cost reduction refers to annual savings in the order of 1.35 Mio $/a for an average plant capacity of 100 kt/a.

The combined dosing of ethylene and oxygen in combination with in-situ removal of CO2 (case 6) are investigated in order to determine the maximum potential of an optimal reaction concept for the overall process improvement. Even if such an in-situ removal cannot be realized at the moment, the maximum potential of such a case is helpful for guiding further research and development activities. In addition, the combined dosing of ethylene and oxygen (case 5) performs only slightly better than case 4. Since the combined dosing oxygen and ethylene suffers from safety hazards, distributed oxygen dosing combined with an advanced cooling strategy (case 4) is the most promising option from a technical and economic point of view and investigated in more detail. The obtained profiles in the reactor of the reference case (case 1) and the selected case (case 4) are shown in Fig. 3.

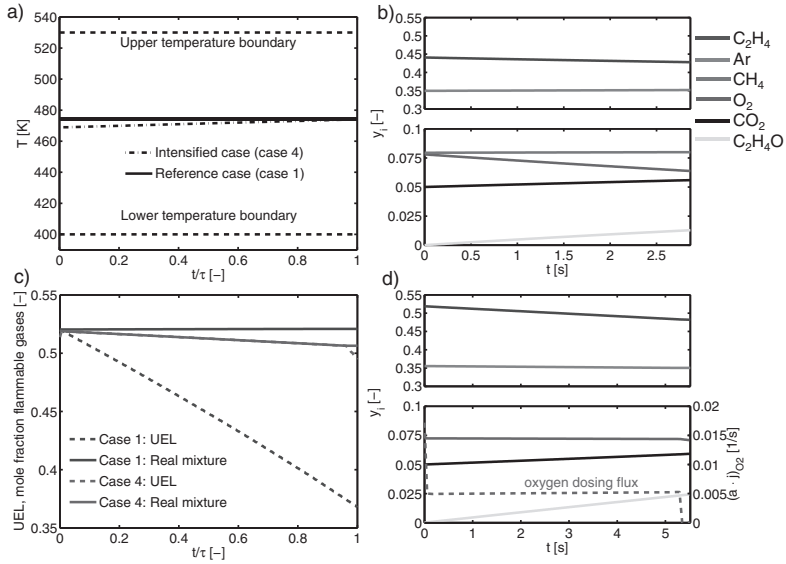

Figure 3: Detailed profile comparison. a) Temperature profiles b) Mole fraction profiles (case 1) c) Explosion limits d) Mole fraction profiles (case 4)

The optimal temperature profile slightly increases (Fig. 3a). By comparing the composition in the reactor (Fig. 3b and Fig. 3d) it can be noted that the ethylene level and the ethylene oxide outlet mole fraction are considerably higher in the intensified case. This leads to a major reduction of the gas recycle stream of 47.4%, which gives rise to smaller apparatuses and lower energy consumption of the overall process. The steam consumption is reduced by 7.0%, the cooling water by 6.9%, and the electricity consumption by 46.3%. In addition, no methane is required in the intensified case to keep the gas composition out of the explosive region. This simplifies the overall process design and control significantly. By dosing oxygen and controlling the temperature profile of the reactor, the composition in the reactor can be kept at the upper explosion limit all along the reaction coordinate, but the mixture is never explosive (refer to Fig. 3c). In the reference case, the composition at the reactor inlet is at the explosion limit, but oxygen depletes and the margin from the explosive region increases. Thereby, the composition falls short of the optimal reaction conditions, which results in a lower process performance. The total CO_2 emissions associated with the purge stream and the utility consumption is reduced by 8.0%, which refers to a reduction of the annual CO_2 emission of $2.7 \cdot 10^4$ t/a for an average sized EO plant.

5. Conclusion

The method proves to be able to determine the optimal reaction concept from an overall process point of view giving rise to a better process performance. The reaction kinetics and complex intrinsic bounds such as explosion limits are directly considered in the model of the reaction section, yielding an accurate model from the thermodynamic and reaction engineering point of view. Based on the determined reaction concept, an optimal tailor-made reactor for this process can be designed [2, 3]. The obtained results proof that the optimal reaction concepts offers significant potential to intensify the overall process; the significant reductions of the production costs, recycle flow rate, and CO_2 emissions give rise to a new generation of more economical and more sustainable chemical processes.

6. Acknowledgments

The authors gratefully acknowledge financial support by BASF SE.

References

[1] H. Freund, K. Sundmacher. Chem. Eng. Process., 2051–2060 (47), 2008.
[2] A. Peschel, H. Freund, K. Sundmacher. Ind. Eng. Chem. Res., 10535–10548 (49), 2010.
[3] J.A. Moulijn, A. Stankiewicz, J. Grievink, A. Górak. Comput. Chem. Eng., 3–11 (32), 2008.
[4] A. Peschel, F. Karst, H. Freund, K. Sundmacher. Chem. Eng. Sci., 6453–6469 (66), 2011.
[5] Nexant-Inc. Ethylene Oxide/Ethylene Glycol. PERP Program 04/05–5, 2006.
[6] A. Peschel, A. Jörke, H. Freund, K. Sundmacher. Chem. Eng. J., submitted.
[7] L. Gan, H. Wang, B. Zhu, S. Xu, Z. Wang. Chem. Ind. Eng., 969–972 (52), 2001.
[8] M. Molnárné, T. Schendler, V. Schröder. Safety Characteristic Data. Volume 2: Explosion Regions of Gas Mixtures. Wirtschaftsverlag NW, Bremerhaven, 2008.
[9] M. Klaubert. PhD thesis, University of Paderborn, Germany, 1998.
[10] F. van den Schoor, F. Verplaetsen. J. Hazard. Mater., 1–9 (128), 2006.
[11] F. van den Schoor, F. Verplaetsen. Int. J. Hydrogen Energ., 2548–2552 (32), 2007.
[12] J.T. Cullinane, G.T. Rochelle. Chem. Eng. Sci., 3619–3630 (59), 2004.
[13] L.T. Biegler, I.E. Grossmann, A.W. Westerberg. Systematic Methods of Chemical Process Design. Prentice Hall, Upper Saddle River, 1999.

I.A. Karimi and Rajagopalan Srinivasan (Editors), Proceedings of the 11th International Symposium on Process Systems Engineering, 15-19 July 2012, Singapore.

Hierarchical simulation of integrated chemical processes with a web based modeling tool

Robert Kraus, Victor Alejandro Merchan, Harvey Arellano-Garcia, Günter Wozny

Chair of Process Dynamics and Operation, Berlin Institute of Technology, Sekr. KWT-9, Straße des 17. Juni 135, D-10623 Berlin, Germany

Abstract

A novel approach for the systematic and hierarchical derivation of process models is presented. Model candidates for different unit phenomena are collected and rated on the basis of the model structure, origin and the modeler's belief. The process model is created as a superstructure with the competing partial models. Thereby, it is possible to determine the best possible combination through optimization with respect to different objective functions. The systematic procedure has been implemented into the online web modeling platform MOSAIC. Based on the superstructure, optimization code for the state-of-the art optimization and simulation software can automatically be created. Based on two case studies, the new approach is demonstrated, namely a process model for the hydroformylation of long-chain olefins and a model for the pressure drop in packed columns with foaming components.

Keywords: model discrimination, integer optimization, code generation.

1. Introduction into hierarchical simulation

As illustrated in Fig. 1, the equation system for a complete chemical process is a combination of different models, which fully describe the different phenomena of all process units, for instance, the pressure drop of a packed column, or a chemical reaction network. These models can be more or less complex and rigorous. The selection and connection of these elementary models is mostly done without the knowledge, which combination of all sub-models is able to describe the whole system in the best possible way. It is possible that the selected models explain single phenomena's very well, but when they are combined, they may fail. Furthermore, it is not known then, if a combination of less complex and more robust models is able to describe the unit with the same accuracy and less effort. Thus, with the possibility to exchange single equations and systems, it is now possible to create a process as a superstructure of different model combinations and to determine the optimal structure through integer optimization with respect to different objective functions, which mainly depend on the designated use of the model.

The approach is implemented and based on the web modeling platform MOSAIC[*], which is an in-house development. It has all the features, which are needed to realize the new modeling approach. The users can in fact work together online. All the models and measurements are centrally stored in libraries. The modeling with MOSAIC is highly modular and each equation and equation system can be reused, shared and exchanged.

[*] www.mosaic-modeling.de.

Generally, MOSAIC is a system-independent simulation and modeling platform where the user can work online through a Java-web applet. Working groups from different departments, who are working in different locations and different software, can use MOSAIC as a common modeling platform. Based on the Models stored in the MOSAIC database, a complete program code can be created for the preferred modeling and simulation environment as for example in Matlab, GAMS, Aspen Custom Modeler, gPROMS and many more as described by Kuntsche et al. (2011). In a second database, measurements are systematically stored, which can be directly connected to the models. Hence, MOSAIC can help to support the collaboration of the modeler and the experimenter. Moreover, the reuse of all elements in a different context and other projects is possible because of its modular structure.

The modeling process in MOSAIC is very close to the structure of a written mathematical model in a publication, which consists mainly of a variable notation, model equations, and descriptions. In MOSAIC, the first modeling step is to define a new, or select an existing, mathematical notation. In this notation, all used base names, superscripts, subscripts and indices have to be defined and described. The consistency of the model is checked and verified in each step against a notation. For the next step, the model equations are created. This can be done with Latex code or via the Microsoft Word Formula editor. Each equation is stored separately as an equation object and can be used in more than one model. The complete equation systems are created by combining the equations and already existing equation systems. The last step is the evaluation of the created equation system, where the values of the variables and parameters are specified and thus the system can be solved or exported to other simulation environments. A description is compulsory for each step and model element, which guaranties a consistent documentation through the whole project.

All modeling elements, such as the notation, the equations and equation systems, are

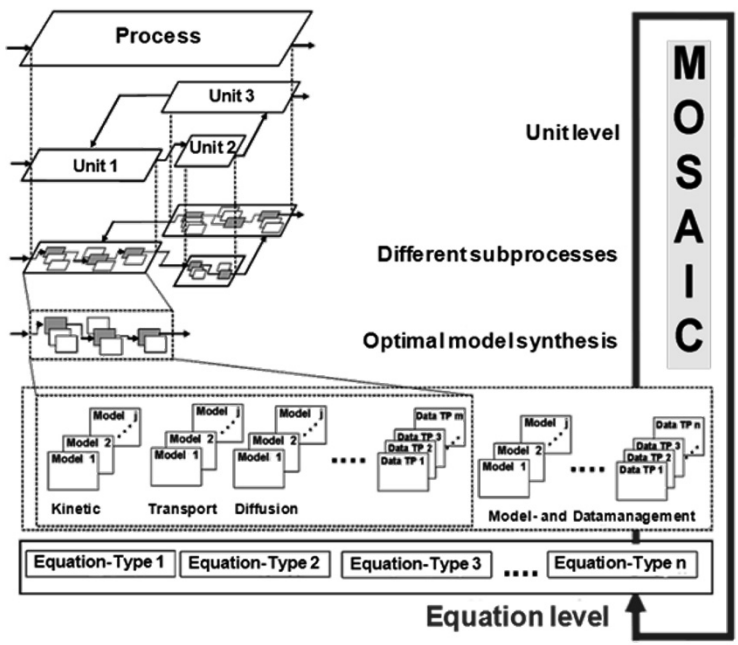

Fig. 1: Hierarchical modeling

stored separately as single objects. Each element can be used in different applications and with a different context. A connection of all elements is always possible, also between different users. This is realized with connectors, which are defined by the user and enable MOSAIC to connect the equation systems between working groups with different notations. The variables in the equations are directly translated and integrated in the corresponding system. In this way, models or even single equations can be easily reused for new purposes. There is no need to enter the same equations more than once. If a model from a publication is already included into the MOSAIC database, it can be directly used together with the knowledge, that it was already tested and the source of errors is minimized.
The connection of modeling and experimental work can be a difficult and error prone task. It can be time consuming for the modeler to follow the changes of the plant setup and to keep his model up to date. The association of measurements to the model variables can be incorrect, or not even possible, if the documentation of the plant was not probably maintained. As a solution, a systematic and central data management module is provided by MOSAIC. It can be directly accessed by the experimenter through an intuitive graphical user interface. It is mandatory to supply a piping and instrumentation diagram for each plant, which has to be updated for every change in the configuration. In this way, a clear identification of the measurement locations in the plant is always guarantied and all changes are well documented and stored. The modeler has the possibility to access all this information directly. It is also possible to connect the model with the measurements by assigning the system variables to measuring points in the plant. Different sets of measurements can be selected by specifying the time scope, which can also have an open end. In this way, values added by the experimenter, are automatically included and added to the model or optimization statement.

2. Workflow for hierarchical modeling in MOSAIC

The workflow and the process of hierarchical modeling are illustrated in Fig. 2 and it consists of two major parts. First, an abstract model of the process is created in MOSAIC, which includes all model candidates and possible combinations. All available partial models are collected, which have been developed by the project participants during a constant process and are stored in the model database. Over the project time, the models are altered and changed. Our policy is to include all versions; otherwise possible informations are lost by simple misjudgment. Based on this collection, the single units and the process are modeled, which is a combination of different models with different degrees of complexity.
The second step is the optimization of the model combination. Program code for state-of-the-art optimization languages such as GAMS, AMPL or Matlab can automatically be created. The superstructure for the MINLP optimization is already stored in the abstract model description. The objective function has to be specified and mainly depends on the designated use. There is mostly a trade-off between the model accuracy and complexity. When the optimization is finished, the optimal model combination is stored in MOSAIC for future use. Finally, the optimal model structure can be exported to the needed simulation environment. In case that new partial models, or measurements are updated, or the objective function changes, the optimization has to be readapted or even repeated. Thus, the hierarchical modeling systematic represents a continuous process.

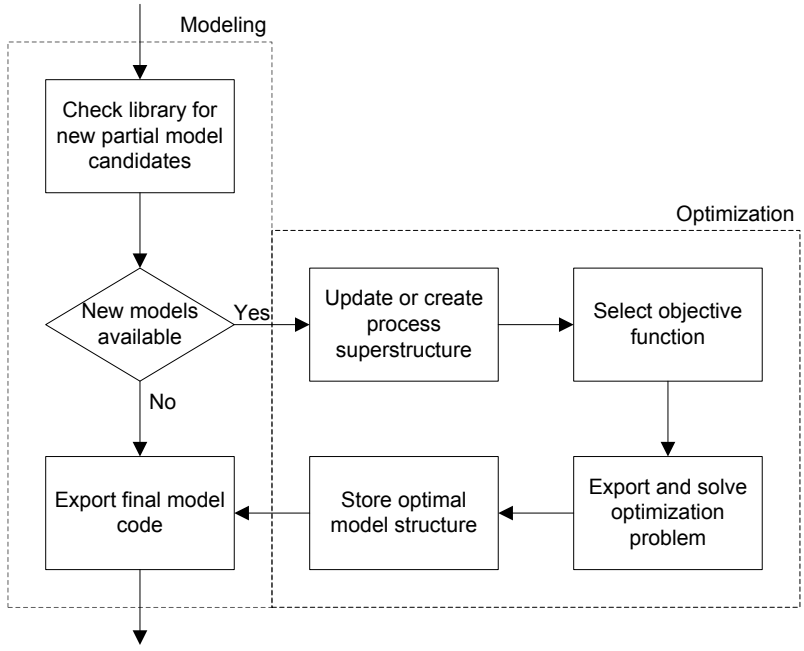

Fig. 2: Hierachical modeling workflow

3. Case studies

The hierarchical modeling systematic is applied to two case studies. In the research project „Integrated Chemical Processes in Liquid Multiphase Systems[*]“, fourteen groups, located at three different universities are working together. The goal is to investigate the hydroformylation of long-chain olefins. Each group is working on different particular aspects of the process. For instance, one of the subprojects concerns the reaction network, where different theories and models are developed with different degrees of complexity. Consequently, the result is a variety of models in different research groups, which have to be selected and properly combined for a complete process model. With MOSAIC, the groups can share their work. Models from the literature and the different user will be combined in a superstructure and based on the algorithm for the hierarchical simulation, the most suitable model combination can finally be determined.

The second case study is the modeling of the pressure drop in packed columns with foaming components. Foam can cause severe problems in distillation and absorption columns and is one of the most frequent malfunctions (Kister, 2003). The main problems are an increased pressure drop and a lower separation efficiency, which leads to a reduced capacity of the separation unit. Up to now, it is not possible to derive a model, which is based on physical parameter of the system like density and viscosity. The hierarchical modeling approach is used to extend existing models for non foaming systems from the literature. In this work, models where used, which have been described in Bravo (1985), Rocha (1993), Billet (1999), Engel (2001), Olujic (2003) and Mackowiak (2010). Therewith, we have a basis of different correlations available

[*] http://www.inprompt.tu-berlin.de.

with different degrees of complexity and accuracy. The next step is the development of different approaches to include the formation of foam and to describe it with a calculated correction factor. A superstructure of the classic literature models for the non foaming area and the new models for the correction factor is created with the aid of MOSAIC. The different model combinations are verified by comparing them to measurements in a packed column for different systems and the optimal model combination is determined by model discrimination. A big advantage is the possibility to determine the parameter for new foaming systems. It is not necessary to run experiments in column, the results of a foam test cell will be then sufficient.

4. Conclusion

A new concept of hierarchical modeling is introduced together with the workflow for a constant improvement of the process model structure. The new methods are implemented in the web simulation environment MOSAIC. Partial models in the database are rated by the user or by MOSAIC on the basis of the model structure, parameter, and degree of nonlinearity. Two case studies show the benefit of the new approach based on a systematic selection and discrimination of models. It is shown how simulations and measurements from different users can be combined and stored over the whole project period. The program keeps track of the development of the partial models and takes all major development steps into consideration. The optimal model combination is then determined depending on the designated use. As a result, an optimized model is available, which can be automatically exported to any equation based simulation environment.

Acknowledgements

This work is part of the Collaborative Research Centre "Integrated Chemical Processes in Liquid Multiphase Systems" coordinated by the Technische Universität Berlin. Financial support by the Deutsche Forschungsgemeinschaft (DFG) is gratefully acknowledged (TRR 63).

References

R. Billet and M. Schultes, 1999, Prediction of mass transfer columns with dumped and arranged packings, Trans IChemE, vol. 77, pp. 498–504.

J. L. Bravo, A. J. Rocha, and J. R. Fair, 1985, Mass transfer in gauze packings, Hydrocarbon Processing, pp. 91–95

G. Buzzi-Ferraris and F. Manenti, 2009, Kinetic models analysis, Chemical Engineering Science, vol. 64, pp. 1061-1074

V. Engel, J. Stichlmair, and W. Geipel, 2001, Fluid Dynamics of Packings for Gas-Liquid Contactors, Chemical Engineering & Technology, vol. 24, pp. 459–462

H. Z. Kister, 2003, What Caused Tower Malfunctions in the Last 50 Years?, Chemical Engineering Research and Design, vol. 81 (1), pp. 5-26

S. Kuntsche, T. Barz, R. Kraus, H. Arellano-Garcia and G. Wozny, 2011, MOSAIC a web-based modeling environment for code generation, Computers & Chemical Engineering, vol. 35, pp. 2257-2273

J. Mackowiak, 2010, Fluid Dynamics of Packed Columns, Springer

Z. Olujic, A. F. Seibert, B. Kaibel, H. Jansen, T. Rietfort, and E. Zich, 2003, Performance characteristics of a new high capacity structured packing, Chemical Engineering and Processing, vol. 42, pp. 55–60

A. J. Rocha, J. L. Bravo, and J. R. Fair, 1993, Distillation columns containing structured packings: a comprehensive model for their performance. 1. Hydraulic models, Industrial & Engineering Chemistry Research, vol. 32, pp. 641–651

I.A. Karimi and Rajagopalan Srinivasan (Editors), Proceedings of the 11th International Symposium on Process Systems Engineering, 15-19 July 2012, Singapore.

Modeling and Simulation of a Catalytic Distillation Process for Production of Ethylene Glycol Monobutyl Ether

W. Z. An [a,*] ,X. Meng[a], D. W. Bi[b] and J. M. Zhu[b]

([a] Department of Chemical Engineering, Ocean University of China, Qingdao 266100; Shandong;China;
[b] Liaoning Oxiranchem Group; Liaoyang 111003; Liaoning; China)

Abstract

The production of ethylene glycol monobutyl ether (EGMBE) from ethylene oxide (EO) and n-butanol was studied in a catalytic distillation (CD) column using a base catalyst immobilized in a structured packing. A pilot plant CD packed column been built up for experimental investigations and a steady-state mathematical model was developed to investigate the basic laws of the CD column. The results revealed that the CD process offers potential advantages for EGMBE production, and a 99% conversion of EO and 91% selectivity of EGMBE could be achieved simultaneously that was otherwise not possible with the traditional reactors.
Keywords: Catalytic distillation; Ethylene Glycol Monobutyl Ether; Ethylene oxide;

1. Introduction

Ethylene glycol monobutyl ether (EGMBE) is an environmentally friendly EO-based solvent and widely used in industries. Traditionally, the route (process) for producing EGMBE consists of two separate unit operations, i.e., synthesis reaction and distillation separations are carried out separately and sequentially(Sulzer technical review, 2001). The disadvantages existed for these traditional processes are obvious, such as a low selectivity of desired product, the high energy consumption, as well as the severe corrosion problem due to the use with homogeneous catalysts. In order to overcome these disadvantages, a catalytic distillation (CD) process, which has been proven to be a very high efficiency process(Malone & Doherty, 2000) was developed at Liaonin Oxiranchem Group in China. In this research a steady-state equilibrium model was developed to investigate the basic laws of the CD process and to obtain the suitable operating parameters. Simulations results for the CD process were discussed and compared with experimental data as well.

2. Process characteristic

2.1. Chemical systems and reaction kinetics

EGMBE is produced commercially by reacting EO with n-butanol($C_4H_{10}O$), i.e., ethoxylation of n-butanol, in the presence of a base or acid catalyst. Based on ethoxylation reaction mechanism (An et al., 2008), the reaction can conveniently be expressed as the following irreversible, consecutive and competing reactions:
Main reaction:

* Corresponding author: awzhong@ouc.edu.cn
Supported by the National Natural Science Foundation of China (20976172).

$C_2H_4O + C_4H_{10}O \rightarrow C_6H_{14}O_2$ (EGMBE) (1)

Undesired side reaction:

$C_2H_4O + C_6H_{14}O_2 \rightarrow C_8H_{18}O_3$ (DEGMBE) (2)

It is noted that the chemical systems exists a large volatility difference between reactants and products. The normal boiling points of the four components is ranged as follows: ethylene oxide 283.6 K; n-butanol 390.81 K; EGMBE 444.47 K; DEGMBE 504.15 K. The difference ensures a rapid separation of EGMBE from reaction zone, which prevents further reaction to yield DEGME, and therefore the selectivity of EGMBE should be improved. The reaction heats of the two reactions are -104.2 and -100.4 kJ· (mol EO)$^{-1}$, respectively, which are considered highly exothermic. The reaction heat of system can also be utilized directly for distillation, thus a natural heat integration can be achieved. Consequently, CD technique is suitable for the studied system.

The rate equations of the two reactions obtained previously in our laboratory by using a sold alkali catalyst can be described by the first order power law with respect to EO and n-butanol as follows(An et al., 2008):

$$r_1 = k_1 C_{cat} C_{EO} C_{C_4H_{10}O} \tag{4}$$

$$r_2 = k_2 C_{cat} C_{EO} C_{C_6H_{12}O_2} \tag{5}$$

The kinetic study has revealed that the two reactions have the approximately same rate constant based on the mechanism of ethoxylation(Serio et al., 2005, An et al., 2008)which are given by the following Arrhenius forms.

$$k_1 = k_2 = 7.2318 \times 10^6 \exp(-63016 / RT) \tag{6}$$

2.2. Phase equilibrium data

Since the presented CD column is operated at low-to-moderate pressures (<0.3Mpa), the vapor phase can be reasonably considered as ideal, thus the vapor-liquid equilibrium constant could be calculated with the liquid phase activity coefficient and the vapor pressure of the pure components. In this work, the Antoine equation is used for the calculation of the saturation vapor pressures of the pure components and the UNIFAC method is employed for description liquid phase non-ideality of the system. The data of the binary interaction parameters for UNIFAC for the pure component are summarized in Table 1.

2.3. Catalytic distillation column configuration

Figure 1 shows a sketch of the CD pilot column bulit in our laboratory. The CD column (100 mm in diameter, 6 m of the overall height, 20 kg/h of bottom product flowrate) was equipped with a total condenser and partial reboiler and consisted of two parts: a reaction section and a stripping section. The stripping section of the column was filled with non-catalytic structured packing, while in the reaction section a base catalyst was immobilized in a structured packing. The geometrical data and HETP of the two types of packings were determined experimentally and given in Figure 1. The mass of dry catalyst per meter of catalytic packing has been determined experimentally to $m_{cat,dry}$ =0.205 kg $_{cat,\ dry}$/$m_{packing}$, whereas the activity of the catalyst has been measured to c_{cat}=0.78 eq/$kg_{cat,dry}$. Due to the nature of EO (a toxic and explosive gas and should not be released into the environment), sampling along the current set-up CD column was

forbidden, and therefore only temperature was measured using thermometers mounted at six different place of column from top to bottom as shown in Figure 1.

Table 1 Parameters for UNIFAC model

Groups		CH_3	CH_2	CH_2O	OH
v_k^i	n-butanol	1	3	0	1
	EO	0	1	1	0
	EGMBE	1	4	1	1
	DEGMBE	1	5	2	1
R_k		0.901	0.674	0.9183	1.000
Q_k		0.848	0.540	0.780	1.200
a_{jk}	CH_3	0	0	251.5	986.5
	CH_2	0	0	251.5	986.5
	CH_2O	83.36	83.36	0	237.7
	OH	156.4	156.4	28.06	0

In the operation of the CD column, n-butanol is supplied to the top of the column, while EO feed is partitioned to two streams which are supplied to the middle and bottom of reaction zone respectively. The motivation for adopting the feed mode is to reduce the concentration of EO in reaction zone since a low concentration of EO is benefit to prevent the generation of more byproducts.

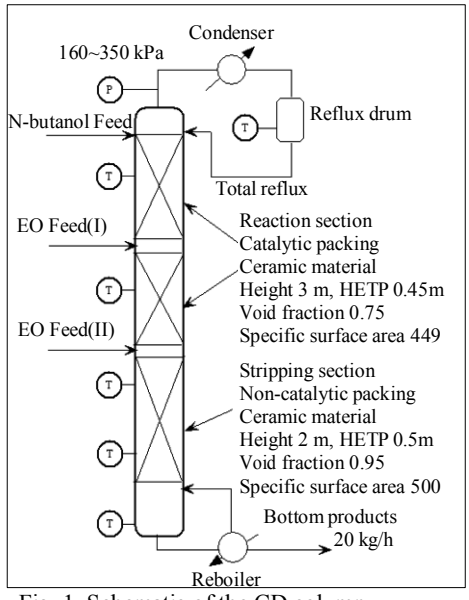

Fig. 1 Schematic of the CD column

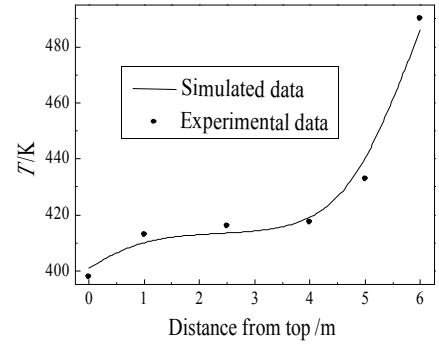

Fig. 2 Temperature profiles along the column

3. Modeling of CD column

In the open literatures there are two types of models for reactive/catalytic distillation, the equilibrium model and non-equilibrium (rate-based) model (Malone &Doherty,

2000; Taylor & Krishna,2000). Although some authors concluded a non-equilibrium model describes better the performance of a reactive distillation process(Peng et al., 2002), it requires accurate estimations of mass transfer coefficients, binary diffusion coefficients, surface tensions values, etc., and as these estimations are a big challenge. Based on these, an equilibrium model, which has been extensively applied for modeling various reactive/catalytic columns (Malone &Doherty, 2000), is adopted in this study to investigate the basic law of a new CD process Future works will attempt to incorporate more complex modeling method in this framework.

The modeling approaches to various CD column have been reported elsewhere (for a review, see Malone &Doherty, 2000), which were developed based on mass and heat balances, vapour-liquid equilibrium and the chemical kinetics on every stage of the reactive distillation column. In the present study Newton's method is used for solving the model equations and a computation program has been formulated using C++ programming language.

4. Results and discussions

4.1. Suitable operating conditions

Based on the model approach described above, detailed simulations are carried out to investigate the influence of selected operating parameters (pressure, boilup ratio, and feed ratio) on the process performance (conversion and selectivity). From both the simulation studies and our current pilot experiments of CD column, the suggested operational parameters of the CD process are summarized in Table 2. From the simulation results it was found that, although the reactants are fed to the column in a nearly stoichiometric ration, it is due to the distillation effect so that unconverted n-butanol is always recycled into the reaction section and EGMBE product is separated for the reaction section simultaneously, thus resulting in the reactive section n-boutanol is in tremendous stoichiometric excess (n-boutanol /EO>300). It is concluded that CD technology not only obtains a high EO conversion but also a high EGMBE selectivity. This seems to contradict with the commonly accepted premise in reaction engineering based on the batch and flow reactors that a higher conversion is always accompanied by a lower selectivity to its intermediate product. However, a higher conversion with a higher selectivity is possible for CD process because of its function of an internally recycled flow reactor (Malone &Doherty, 2000).

Table 2 The suggested operating parameters

Parameters	*Value*	*Parameters*	*Value*
Column pressure, kPa	*200*	*Conversion of EO, %*	*>99.0*
Molar feed ratio of EO to n-butanol	*1.05*	*Selectivity to EGMBE, %*	*91.73*
Bottom rate, kmol/h	*0.178*	*Yield of EGMBE, %*	*91.73*
Boil-up ratio	*10*	*Condenser duty, kW*	*36924*
Mole fraction of EGMBE in bottom	*0.917*	*Reboiler duty, kW*	*27320*

4.2. Model validation

In order to investigate the reliability of simulation, the calculated bottom concentration and temperature profiles along the column are compared with experimental results. Under the given operating conditions as shown in Table 2, the temperature profiles of the six temperature measuring points configured in the CD

column were measured as shown in Figure 2. It can be seen that the agreement between simulated data and experimental data is very good, since the temperature profiles correlate well with an average relative error of 1.22%. Table 3 gives the comparisons of calculated product composition in the bottom stream with experimental results analyzed using gas chromatograph. The agreement between simulation and experiment for both processes is satisfactory. The results presented here demonstrate clearly that the model developed in this paper could predict the steady-stage behavior of this CD process well.

Table 3 The comparison of simulated data and experimental data

Items	*Simulation values*	*Experimental data*
Molar fraction of n-butanol in bottom stream	*0.0413*	*0.0440*
Molar fraction of EO in bottom stream	*1.6843e-10*	*0*
Molar fraction of EGBME in bottom stream	*0.9173*	*0.9118*
Molar fraction of DEGMBE in bottom stream	*0.0410*	*0.0442*
Selectivity of EGMBE, %	*91.73*	*91.18*

5. Conclusion

The production of ethylene glycol monobutyl ether (EGMBE) from ethylene oxide (EO) and n-butanol was studied in a catalytic distillation (CD) column. From both the simulation studies and our current pilot experiments showed that the use of a catalytic distillation offered potential advantages compared with conventional processes. The CD column allowed the use a moderate operation pressure and a lower molar feed ratio of n-butanlo to EO. The reaction heat released can be completely utilized in distillation. The key component EO can be converted completely and a selectivity of 91% toward the desired product EGMBE can be achieved, which is otherwise not possible with conventional processes. The industrial significance of this study lies in the fact that the understanding of the process has been made clearer. The provided results have served as useful guidelines for improving the plant design and operation without need of expensive test runs.

References

J. Peng, S.Lextrait, T.F.Edgar,&R.B. Eldridge, 2002, A comparison of steady-state equilibrium and rate-based models for packed reactive distillation columns. Ind. Eng. Chem. Res., 41: 735-2744

M. D. Serio,R.Tesser, A. Dimiccoli, &E. Santacesaria,2005,Comparison of different reactor types used in the manufacture of ethoxylated, propoxylated products. Ind. Eng. Chem. Res., 44(25): 9482-9489.

M.F. Malone & M.F.Doherty, 2000, Reactive distillation. Ind. Eng. Chem. Res.,39, 3953-3957

R.Taylor, &R. Krishna, 2000, Modelling reactive distillation. Chem.Eng.Sci., 55: 5183-5229.

Sulzer technical review, 2001, A New Technical Solution for Glycol Ether Production. 4: 14-17

W.Z. An, F. L. Dong, Z. B. Liu, & J.M. Zhu, 2008, Kinetics of n-butanol ethoxylation. Journal of Chemical Engineering of Chinese Universities, 22, 4, 612-617

.

I.A. Karimi and Rajagopalan Srinivasan (Editors), Proceedings of the 11th International Symposium on Process Systems Engineering, 15-19 July 2012, Singapore.

Use of reactive distillation for triacetin production from crude glycerol: Simulation and performance analysis

Pimpatthar Siricharnsakunchai, Lida Simasatitkul, Apinan Soottitantawat, Amornchai Arpornwichanop*

Department of Chemical Engineering, Faculty of Engineering, Chulalongkorn University, Bangkok,10330, Thailand
* *Corresponding author (e-mail: Amornchai.a@chula.ac.th)*

Abstract

This study is focused on the use of crude glycerol from biodiesel production to produce triacetin via esterification reaction with acetic acid by using a reactive distillation. In general, a composition of crude glycerol consisting mostly glycerol and methanol varies with biodiesel feedstock and processes. Simulation studies are performed to investigate the effect of using crude glycerol with different fractions of methanol on triacetin production. Three process configurations are considered: (i) direct feed of crude glycerol to reactive distillation, (ii) separation of crude glycerol coupled with reactive distillation and (iii) reactive separation of crude glycerol coupled with reactive distillation.

Keywords: Triacetin production, Crude glycerol, Reactive distillation, Esterification.

1. Introduction

In a conventional process of biodiesel production, glycerol is generated as by-product. Increases in the demand and production of biodiesel enlarge an amount of glycerol produced. Efficient utilization of crude glycerol could lead to significant economic and environmental benefits.

In general, crude glycerol contains mostly glycerol (60-70 wt.%) and other contaminants such as methanol and soap (Thompson and He, 2006), so that the cost of crude glycerol is low. The composition of crude glycerol varies with raw materials and catalyst used for biodiesel production and post-reaction cleanup processes such as acidulation and demethylization (Bohon et al., 2010). To purify crude glycerol for food, pharmaceutical or cosmetics industries, further processing steps such as filtration, chemical additions, fractional vacuum distillation, bleaching and deodorization are required. These purification processes are costly and economically infeasible for small and medium-scale biodiesel producers. To date, a number of studies have been being explored to find useful applications for glycerol via combustion, anaerobic digestion, thermo-chemical process and biological conversion. In addition, glycerol can be used as a raw material to produce high value-added products such as hydrogen, propylene glycol, acetol and 1,3-propanediol.

This study investigates the use of glycerol to produce triacetin, an important chemical used as a plasticizer and a solvent (Wolfson et al., 2009), via esterification with acetic acid. Since the esterification reaction is limited by chemical equilibrium, a reactive distillation is implemented to improve the conversion of glycerol. Crude glycerol with different ratios of methanol is considered and three different process configurations for

Table 1. Kinetic constants for esterification of glycerol and acetic acid

Reaction	$k_{0,i}$ (L mol^{-1}s^{-1})	Ea$_i$ (cal kmol^{-1})	$k_{0,-i}$ (L mol^{-1}s^{-1})	Ea_{-i} (cal kmol^{-1})
1	5.24×10^{-4}	616.8	8.56×10^{-4}	-3864.4
2	9.69×10^{-5}	-1462.3	2.16×10	8701.1
3	6.26×10^{-2}	4964.1	1.86	5137.5

triacetin production are studied.

2. Process Description

In general, triacetin can be produced by the liquid-phase esterification of glycerol and acetic acid in a conventional process consisting of a continuous stirred tank reactor followed by a series of distillation columns. This causes a low conversion of glycerol and high energy consumption. A reactive distillation is potentially an attractive process as reaction and separation tasks can be carried out in a single unit. To analyze the triacetin production process, simulations of a reactive distillation are performed using the RADFRAC module of Aspen Plus. The UNIFAC method is employed to predict thermodynamic properties of substances in the system. The kinetics of esterification of glycerol and acetic acid in the liquid phase proposed by Maria-Isabel et al. (2009) are used as follows:

Glycerol + Acetic Acid ↔ Monoacetin + Water

$$r_1 = k_1 C_{\text{glycerol}} C_{\text{acetic acid}} - k_{-1} C_{\text{mono acetin}} C_{\text{H2O}} \quad (1)$$

Monoacetine + Acetic Acid ↔ Diacetin + Water

$$r_2 = k_2 C_{\text{monoacetine}} C_{\text{acetic acid}} - k_{-2} C_{\text{diacetin}} C_{\text{H2O}} \quad (2)$$

Diacetin + Acetic Acid ↔ Triacetin + Water

$$r_3 = k_3 C_{\text{diacetin}} C_{\text{acetic acid}} - k_{-3} C_{\text{triacetin}} C_{\text{H2O}} \quad (3)$$

Table 1 shows the kinetic constants of the esterification reaction for triacetin production.

2.1. System I: Direct feed of crude glycerol to reactive distillation

In general, a composition of crude glycerol obtained depends on biodiesel feedstock and production process. However, crude glycerol consists of mainly glycerol and methanol. Fig. 1 shows the schematic of a reactive distillation for triacetin production. Acetic acid and crude glycerol at the ratio of 6 are fed to the stage 3 and 2 of the reactive distillation column having a total stage of 17. The column is operated at atmospheric pressure and reflux ratio of 2 and the bottom product is removed at flow rate of 5 kmol/h. The temperature of feed streams is 298 K. Flow rate of crude glycerol is 5 kmol/h

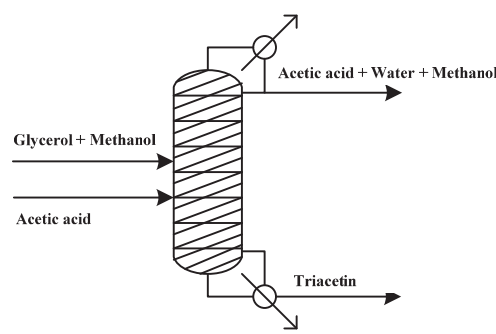

Fig. 1. Direct feed of crude glycerol to reactive distillation.

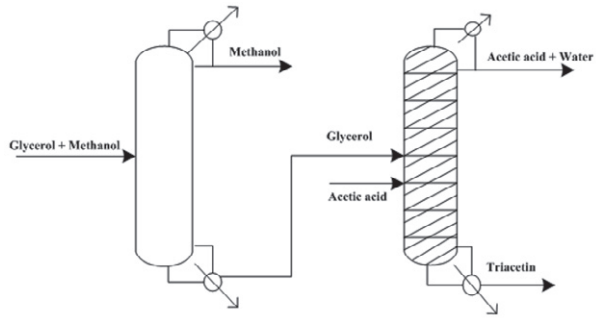

Fig. 2. Separation of crude glycerol coupled with reactive distillation.

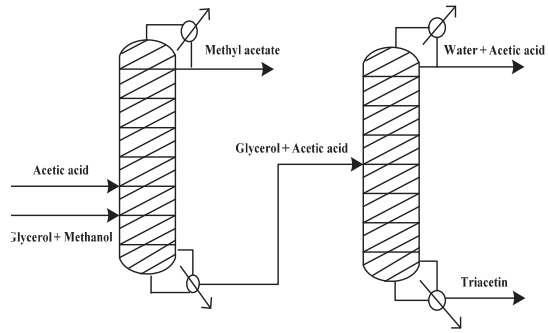

Fig. 3. Reactive separation of crude glycerol coupled with reactive distillation.

2.2. System II: Separation of crude glycerol coupled with reactive distillation

In this process configuration, crude glycerol is first purified to remove methanol using a conventional distillation and pure glycerol is then fed to a reactive distillation to produce triacetin. Crude glycerol is fed to the distillation column at stage 2 (Table 2). The distillation column is operated at reflux ratio of 0.1 and the bottom flow rate is fixed at 5 kmol/h. Pure glycerol obtained and acetic acid are introduced to the reactive distillation at stage 2 and 3, respectively. Reflux ratio of the reactive distillation is 2.3 and the bottom product rate is 5 kmol/h. The acetic acid to glycerol ratio is fixed at 6.

2.3. System III: Reactive separation of crude glycerol coupled with reactive distillation

Two reactive distillations are applied for triacetin production. The first reactive distillation column is used to separate methanol from crude glycerol by reacting with acetic acid via esterification to produce methyl acetate (Song et al., 1998). It consists of a total stage of 38 and is operated at reflux ratio of 2.8 (Table 3). With this process design, crude glycerol can be purified and a valuable product (methyl acetate) is obtained at the same time. The second reactive distillation is employed to convert glycerol to triacetin as mentioned above.

3. Simulation Results

3.1. Direct feed of crude glycerol to reactive distillation

The results show that the fraction of methanol in crude glycerol has a slight effect on the conversion of glycerol. When crude glycerol with 30 wt.% of methanol is used for triacetin production, the triacetin yield of 99.85% is obtained. However, the purity of triacetin obtained reduces when methanol content in crude glycerol increases. Further,

Table 2. Feed conditions and specifications in case of separation of crude glycerol coupled with reactive distillation (System II)

Feed Conditions		Column specifications			
		Distillation column		Reactive distillation column	
Temperature (K)	298	Total stages	10	Total stages	17
Pressure (bar)	1	Pressure (bar)	1	Pressure (bar)	1
Flow rate (kmol/h)		Reflux ratio	0.1	Reflux ratio	2.3
1) acetic acid	30	Bottom rate (kmol/h)	5	Bottom rate (kmol/h)	5
2) glycerol	5	Feed location		Feed location	
Mole fraction		1) glycerol + methanol	2	1) glycerol	2
1) glycerol + methanol	1			2) acetic acid	3

Table 3. Feed conditions and specifications in case of reactive separation of crude glycerol coupled with reactive distillation (System III)

Feed Conditions		Column specifications			
		First reactive distillation		Second reactive distillation	
Temperature (K)	323	Total stages	38	Total stages	17
Pressure (bar)	1	Pressure (bar)	1	Pressure (bar)	1
Flow rate (kmol/h)		Reflux ratio	2.8	Reflux ratio	2
1) acetic acid	280	Bottom rate (kmol/h)	510	Bottom rate (kmol/h)	250
2) glycerol + methanol	280	Feed location		Feed location	
		1) acetic acid	3	1) acetic acid	3
Mole fraction		2) glycerol + methanol	36	2) glycerol + acetic acid	2
1) acetic acid	1				
2) glycerol + methanol	1				

the total energy consumptions of condenser and reboiler decrease with increasing the content of methanol.

3.2. Separation of crude glycerol coupled with reactive distillation

It is found that adding a purification unit to crude glycerol can improve the triacetin production; high conversion of glycerol is achieved even crude glycerol is used. However, the yield of triacetin is reduced to 92.5% in case of using crude glycerol with 30 wt.% of methanol. Increased fraction of methanol in glycerol decreases the molar fraction of triacetin at the bottom stream of the reactive distillation and water at the distillate stream; however, the fraction of acetic acid increases. When crude glycerol with 30 wt.% of methanol is used, the purity of triacetin product is 84%, higher than that the crude glycerol is directly employed for triacetin production. Considering the energy consumption of the system, it is found that the condenser and reboiler duties decrease with increasing the percentage of methanol in crude glycerol. The requirement of energy for this process configuration is more than that for the system I as one more conventional distillation is needed for purifying crude glycerol.

3.3. Reactive separation of crude glycerol coupled with reactive distillation

Considering the first reactive distillation for methyl acetate production, the molar fraction of methyl acetate in the distillate stream increases with the increased amount of methanol in crude glycerol. At 30 wt.% of methanol in crude glycerol, the molar fraction of methyl acetate obtained is 95%. High pure glycerol with slight acetic acid is fed to the second reactive distillation for triacetin production. The molar fraction of triacetin reduces when increasing the percentage of methanol in crude glycerol. The

conversion of glycerol decreases slightly and the yield of triacetin reduces to 99.85% when methanol in crude glycerol is 30 wt.%. It is also found that this process design consumes the highest energy, compared with other ones due to the reactive separation process of crude glycerol to generate methyl acetate causes high energy requirement.

4. Conclusions

This study investigates the potential of using crude glycerol derived from biodiesel production to produce triacetin via an esterification process. Reactive distillation is used to improve the performance of triacetin production. Three process designs: (i) direct feed of crude glycerol to reactive distillation, (ii) separation of crude glycerol coupled with reactive distillation and (iii) reactive separation of crude glycerol coupled with reactive distillation, are proposed. An increase of methanol content in crude glycerol decreases the purity of triacetin product. The conversion of glycerol and yield of triacetin obtained by using crude glycerol are slightly lower than those using pure glycerol. Removal of methanol from crude glycerol before being fed to the reactive distillation causes the highest purity of triacetin when crude glycerol with high methanol content is used. The two productions of methy acetate via a reactive separation of crude glycerol and triacetin via a reactive distillation require the highest energy consumption compared with other process designs.

5. Acknowledgement

Support from the 90th Anniversary of Chulalongkorn University Fund (Ratchadaphiseksomphot Endowment Fund) and the Computational Process Engineering Research Group, the Special Task Force for Activating Research (STAR), Chulalongkorn University Centenary Academic Development Project is gratefully acknowledged.

References

M.D. Bohon, B.A. Metzger, W.P. Linak, C.J. King, W.L. Roberts, 2010, Glycerol combustion and emissions, Proceedings of the Combustion Institute.

G. Maria-Isabel, B. Jordi, S. Romain, R. Jean-Michel, E.P. Alexandra, 2009, From residual to useful oil: Revalorization of glycerine from the biodiesel synthesis, Bioresource Technology 100, 3775-3778.

J.C. Thompson, B. He, 2006, Characterization of crude glycerol from biodiesel production from multiple feedstocks, Applied Engineering in Agriculture 22, 261-265.

W. Song, G. Venimadhavan, J.M. Manning, M.F. Malone, M.F. Doherty, 1998, Measurement of residue curve maps and heterogeneous kinetics in methyl acetate synthesis, Industrial Engineering and Chemical Research 37, 1917-1928.

A. Wolfson, A. Atyya, C. Dlugy, D. Tavor, 2009, Glycerol triacetate as solvent and acyl donor in the production of isoamyl acetate with Candida antarctica lipase, Bioprocess and biosystems engineering 33, 363–366.

I.A. Karimi and Rajagopalan Srinivasan (Editors), Proceedings of the 11th International Symposium on Process Systems Engineering, 15-19 July 2012, Singapore.

Dynamic modeling of direct contact membrane distillation processes

Badr Bin Ashoor[a,b], Hassan Fath[b], Wolfgang Marquardt[a] , Adel Mhamdi[a]

[a]*Lehrstuhl für Prozesstechnik, RWTH Aachen, D-52056 Aachen, Germany*
[b]*Masdar Institute, P.O.Box 54224 Abu Dhabi, United Arab Emirates*

Abstract

Membrane distillation (MD) for desalination is an emerging thermally driven process exhibiting various advantages in comparison with traditional processes. Most of the MD configuration processes have been modeled as steady-state one-dimensional systems using empirical heat and mass transfer equations. Stationary two-dimensional MD models have been considered only in very few studies. In this work, a dynamic model of a direct contact membrane distillation (DCMD) process in plate-and-frame configuration is developed. It aims at giving insight into the underlying coupled physico-chemical phenomena at a level of detail. The model is implemented in the modeling package gPROMS. Numerical simulations are conducted for different operational parameters at the module inlets such as the feed and permeate temperature or feed and permeate flow rate. The results are compared with experimental data published in the literature.

Keywords: direct contact membrane distillation. plate-and-frame configuration. dynamic two-dimensional model. heat and mass transfer. numerical simulation

1. Introduction

Membrane distillation (MD) is a non-isothermal process known for less than fifty years. The first paper was published in 1967 by Findly [1]. MD was considered first as a process that would operate with minimum external energy requirements. The large vapor space required by a conventional distillation column is replaced in MD by the pore volume of a microporous membrane. As a result, the MD process equipment can be much smaller. Membrane distillation may be operated in several configurations [2,3]. In this work, we focus on direct contact MD (DCMD), although the approach may be easily extended to other configurations. Today, we see an enormous number of publications dealing with experimental and modeling issues of MD [4].

In MD, both mass and heat transfer occur simultaneously and both temperature and concentration polarization effects should be taken into consideration. Most modeling works in literature on DCMD processes usually focus on the mass transfer resistance of vapor across a membrane attributed to the membrane characteristics (i.e. pore size, porosity and tortuosity) and heat transfer resistances to obtain the mean temperature on the membrane surface [5]. The concentration polarization phenomena are usually ignored to simplify the calculation procedure. Only few publications use stationary one- or two-dimensional heat-transfer equation to simulate a particular application more accurately. Although many semi-empirical models have been developed, a detailed model for temperature polarization on flat-plate MD processes is still lacking. In this study, we develop a dynamic two-dimensional flat-plate mathematical model for DCMD processes, in order to obtain the temperature and concentration distributions in

the channels and the local mass flux at the membrane surfaces. The availability of such a model for simultaneous energy and mass balances will be an important basis for the analysis, design and optimization of DCMD processes for saline water desalination.

2. Dynamic modeling of a plate-and-frame direct contact MD module

The DCMD to be considered in this study is a flat-sheet membrane module (Figure 1). The module has two adiabatic impermeable walls with the flat-sheet membrane in between. The membrane has two hydrophobic walls permeable for water vapor but impermeable for liquid water.

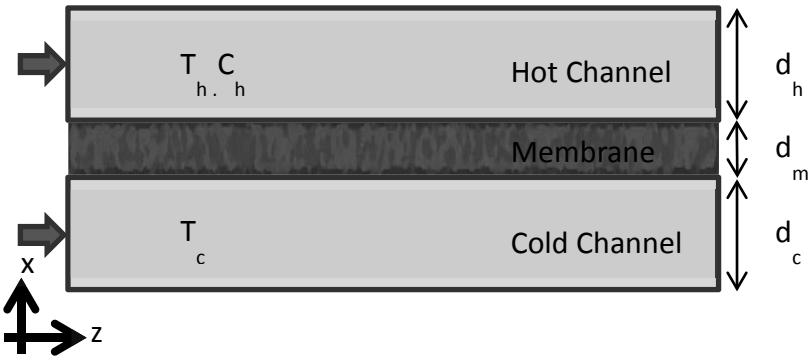

Figure 1. Schematic diagram of a DCMD module in rectangular coordinates.

The work focuses on modeling the heat and mass transport in two spatial dimensions through the three parts of the DCMD module, i.e. membrane, feed and permeate channels. . The model is implemented in the modeling package gPROMS. This allows implementing the model equations in a modular and hierarchical way, such that it is very easy to adapt the model to different plant configurations or operating conditions. Moreover, the model can be used without much effort for parameter estimation, design or optimization studies. In the following subsections, we describe the main equations and assumptions used in the model.

2.1. Vapor transport through the membrane pores

The mass transfer driving force across the membrane is the difference in saturated pressure on both membrane surfaces due to the temperature gradient. Depending on a comparison between the mean free path and pore diameter, there are some models that can be used to describe the mass flux across the hydrophobic porous membrane [6]: the Knudsen diffusion model (due to the larger mean free path of vapor molecules than the membrane pore size), Poiseuille flow model (due to the momentum transfer to the supported membrane) and molecular diffusion model (due to the concentration gradient across the membrane). If the mean free path is: much larger than the pore size, molecule-wall collisions become more important and the gas transport is described using the Knudsen diffusion model. If it is much smaller than the pore size, the molecule motion due to the pressure gradient (i.e. saturated pressure difference across the membrane) becomes the major transport phenomenon and is described using the Poiseuille flow model.

The vapour flux density j across the hydrophobic membrane, can be computed from

$$j = C_m \Delta P^{sat} = C_m (\gamma(X) P_h^{sat} - P_c^{sat}), \quad (1)$$

where P_h^{sat} and P_c^{sat} are the saturated pressure of pure water on the hot and cold channel, respectively. They can be determined from corresponding saturation temperatures using the Antoine equation. The coefficient $\gamma(X)$ accounts for influence of the salt (mole fraction X) in the feed on the saturation pressure. P_h^{sat} and P_c^{sat}.
The membrane coefficient C_m in (1) can be estimated by a weighted sum (via parameters θ_k and θ_p) of the Knudsen diffusion and the Poiseuille (viscous) flow models [6], i.e.

$$C_m = 1.06\,\theta_k \frac{\varepsilon\tau}{\tau\delta_m}\left(\frac{M_w}{RT_m}\right)^{1/2} + 0.125\,\theta_p\,\frac{\varepsilon r^2}{\tau\delta_m}\,\frac{M_w P_m}{\eta_v\, RT_m} \tag{2}$$

The parameters ε , τ and δ_m are the porosity, tortuosity and thickness of the membrane, respectively. M_w is the molecular weight of water, R is the gas constant. T_m is the mean temperature in the membrane ($i.e.$ $(T_h + T_c)/2$). It is related to the mean saturated pressure P_m by the Antoine equation for water, i.e. $\log 10\,(P_m) = A - B/(T_m + C)$.
The heat flux density at the membrane interface between the liquid and the vapor is

$$q_i = j\,\Delta H + k_m\,\frac{T_h - T_c}{\delta_m}, \tag{3}$$

where ΔH is the latent heat of vaporization and k_m the thermal conductivity of the porous membrane. It can be calculated from

$$k_m = \varepsilon\, k_g(T) + (1 - \varepsilon)\, k_s\,, \tag{4}$$

where k_s is the solid membrane thermal conductivity and $k_g(T)$ the temperature-dependent gas pore thermal conductivity.

2.2. Heat and mass transport in the feed and cold channels

Under appropriate assumptions, the general balance equations for mass and energy reduce to the following equations for the distributions of temperature T and salt concentration C_s in each of the hot and cold channels:

$$\rho C_p \frac{\partial T(x,z)}{\partial t} + \rho C_p u(x) \frac{\partial T(x,z)}{\partial z} = k\left(\frac{\partial^2 T(x,z)}{\partial x^2} + \frac{\partial^2 T(x,z)}{\partial z^2}\right), \tag{5}$$

$$\rho \frac{\partial C_s(x,z)}{\partial t} + \rho u(x) \frac{\partial C_s(x,z)}{\partial z} = D\left(\frac{\partial^2 C_s(x,z)}{\partial x^2} + \frac{\partial^2 C_s(x,z)}{\partial z^2}\right). \tag{6}$$

Here ρ, k, C_p, and D are density, thermal conductivity, heat capacity of the fluid and diffusion coefficient, respectively. We assume, for simplicity, a constant or parabolic velocity profile $u(x)$ in the channels. In the permeate channel there is only pure water, such that the mass balance equation (6) is not needed in the model.

2.3. The boundary and initial conditions

At the inlet of the channels, we assume given values for temperature and concentration, T_{in} and $C_{s,in}$ i.e. $T(x,0) = T_{in}$ and $C_s(x,0) = C_{s,in}$. The channel walls are assumed impermeable and adiabatic, so that the corresponding mass and heat fluxes are zero. At the outlet, we use usual outlet conditions.
The boundary conditions in equation

$$k(T)\frac{\partial T(d,z)}{\partial x} = q_i(z)\,,\; D\,\frac{\partial C_s(d,z)}{\partial x} = j(z) \tag{8}$$

link the models for the channels and the membrane. They are obtained via mass and energy balances for the interfaces between liquid and vapor on both sides of the

membrane. d is the channel height, j and q_i are the mass and heat fluxes at the interface given in Eqs. (1) and (3), respectively.

3. Case study

A case study from literature has been investigated. All the data used in our simulations like geometry, physical properties and operating conditions can be found in [5]. Numerical simulations have been conducted for different operational parameters at the module inlets such as the feed and permeate temperature or feed and permeate flow rate. Compared with the stationary experimental data in [5], the computed mass flux densities are in good agreement with the measurements. By varying some of the parameters, we may assess their effects on the trans-membrane flux. For instance, by varying the feed temperature, we observe, as shown in Figure 2, a monotone increase of the MD flux with the increase of the difference between the feed water temperature and the permeate side temperature (ΔT) . This is due to the increase of the vapor pressure of the feed (the driving force) which increase the trans-membrane flux, although the temperature polarization will increase with the increase of the feed temperature. The trans-membrane flux also increases with the flow rate as also shown in Figure 2. The effect of an increasing flow rate is to increase the convective heat transfer coefficient at the feed side of the membrane, to reduce the velocity and temperature boundary layers and to reduce the temperature and concentration polarization effects, thus increasing the trans-membrane flux.

The temperature polarization phenomena dominate the production of water flux in DCMD process. It increases along the flow direction at the feed side which leads to the reduction of the trans-membrane flux. The temperature polarization ratio, which is defined as the ratio of the membrane surface temperature and the bulk feed temperature, increases along the flowing direction at the hot feed side and reduces the temperature difference between the hot and the cold side resulting in reduction of the water flux.

In Figure 3, we plot the temperature distribution at the interface between the hot channel and the membrane along the flow direction at different times. The inlet temperature to the hot channel is 45°C. We observe that after some time, a stationary profile is reached.

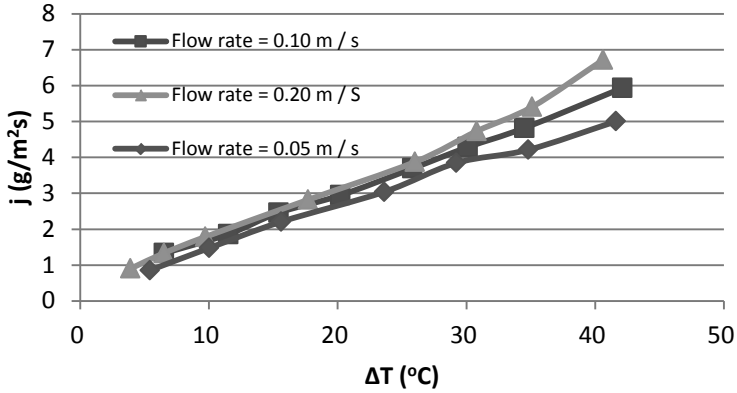

Figure 2. Transmembrane flux increases with increasing ΔT for different flow rates.

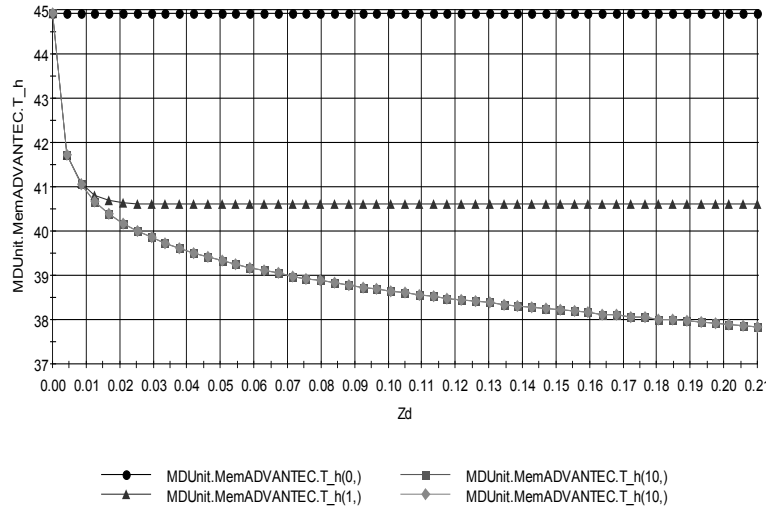

Figure 3. Temperature distribution at the interface hot channel/membrane along the flow direction as a function of time.

4. Conclusions

A dynamic two-dimensional model was developed, describing the flow in the plate-and-frame countercurrent DCMD system. The model has the capabilities of predicting the temperature polarization profile and pure water production. The model is implemented using the modeling package gPROMS.

In our future work, we will on the one hand continue our efforts in enhancing the dynamic model. On the other hand, an experimental setup will be constructed. It will enable us to perform dedicated experiments for the purpose of model validation.

Acknowledgements

The first author would like to thank Masdar Institute for financial support.

References

[1] Findely M.E., Vaporization through porous membranes, 1967, 6, Ind. & Eng. Chem. Process Des. Dev. and ev. 226-237

[2] Lawson K.W., D.R. Lloyd, Review membrane distillation, 1997, 124, J. Membr. Sci. 1-25

[3] El-Bourawi M.S., A framework for better understanding membrane distillation separation process, 2006, 285, J. Membr. Sci. 4-29

[4] Khayet M., Membranes and theoretical modeling of membrane distillation: a review, Adv. in Colloid and Interface Sci., Volume 164, Issues 1–2, 11 May 2011, Pages 56-88

[5] Chen T, Ho C, Yeh H. Theoretical modeling and experimental analysis of direct contact membrane distillation. J Membr Sci 2009;330:279–87.

[6] Schofield R.W., Fane A.G., and Fell C.G.D. 1990, Gas and vapor transport through microporous membrane, J. Membr. Sci 53-159

I.A. Karimi and Rajagopalan Srinivasan (Editors), Proceedings of the 11th International Symposium on Process Systems Engineering, 15-19 July 2012, Singapore.

2-D Population Balance Modelling of Nucleation and Growth of Needle-shape Crystals

A.V. Bekker, T.S. Li, and I. Livk

CSIRO Process Science and Engineering, Minerals Down Under Flagship
PO Box 7229, Karawara WA 6152, Australia

Abstract

Population balance equation models are widely accepted for simulating various particulate processes including crystallization. In this work, a dynamic 2-D population balance equation crystallization model was solved using a finite element method-based numerical algorithm with adaptive mesh and time step for three different cases: i) constant crystal growth rate, ii) constant crystal growth and nucleation rates, and iii) nonlinear crystallization kinetics. The model results obtained for the three different cases clearly demonstrate consistency of the newly developed numerical algorithm for solving 2-D population balance models of crystallization systems that produce crystals with the variable aspect ratio.

Keywords: crystallization modelling, multidimensional population balance equation, crystal aspect ratio, 2-D secondary nucleation, multidimensional crystal growth, FEM.

1. Introduction

A population balance equation (PBE) approach has been widely accepted for modelling particulate processes in various industrial applications including crystallization. In many crystallization applications, the product crystal size distribution (CSD) is a crucial quality parameter, which also makes it a focal point of process modelling. CSD of the crystallization product has been traditionally characterised using a single size dimension, which is the characteristic crystal diameter. The disadvantage of a 1-D description of crystal size is that it can not capture a changing crystal shape. During crystallization, crystals often experience significant changes to their aspect ratio, which requires a two-dimensional population balance model in order to describe the crystal size distribution with respect to the crystal length and width. With the advent of advanced sensing techniques (Bekker, 2011; Khanam, 2011) the crystal size can now be characterised in multiple dimensions. Different approaches for modelling the evolution of multidimensional crystal size, based on fixed mesh high-resolution algorithms, have been reported in literature by various authors (Gunawan, 2004; Sato *et al*., 2008). In this work, we present the development of a finite element method-based solution algorithm, with adaptive mesh and time step, of a 2-D population balance equation-based model to describe the evolution of the size distribution of needle-shape crystals. Secondary nucleation and crystal growth mechanisms are taken into account in the model.

2. 2-D PBE Model Incorporating Crystal Growth and Nucleation Kinetics

For crystals with high aspect ratio, defined as the ratio between crystal length and width, the crystal shape can be approximated as a rectangular prism of length L and equal width and height W, as shown in Fig.1. The volume of crystals can be calculated as $V=LW^2$.

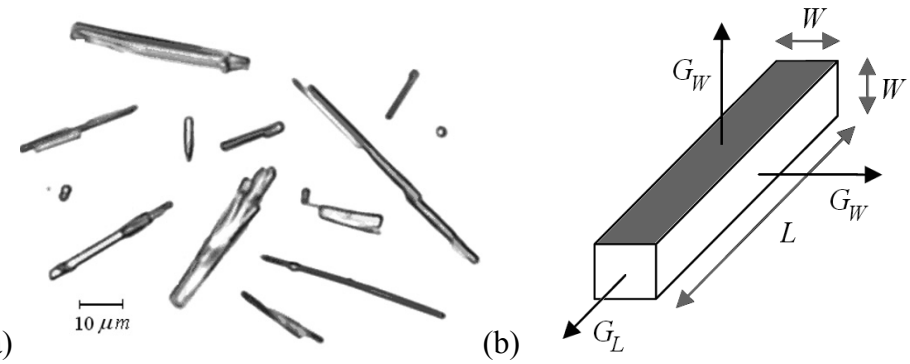

Figure 1. High aspect ratio crystals: (a) an optical microscope image, and (b) a 2-D rectangular approximation of a 3-D needle-shape crystal.

With crystal faces exhibiting different crystal growth rates, due to different supersaturation dependences of the respective growth rate equations, the crystal aspect ratio changes during the crystallization process. Similarly, seed and nuclei crystals can also exhibit a distribution of aspect ratios, which are in general different for the two types of crystals. A 2-D population balance equation model, developed previously for crystal breakage (Sato *et al*., 2008), is adapted in this work to model crystallization with simultaneous supersaturation-dependent 2-D secondary nucleation and crystal growth The resulting dynamic 2-D model can be stated as:

$$\begin{cases} \dfrac{\partial n}{\partial t} + G_W \dfrac{\partial n}{\partial W} + G_L \dfrac{\partial n}{\partial L} = B_u\, n_n(W,L), \quad W \in [0, W_{\max}],\ L \in [0, L_{\max}],\ t \in [t_0, t_{\text{end}}]; \\ \dfrac{d\sigma}{dt} = -\alpha B_u\, \mu_{21}(n_n) - 2\alpha G_W \mu_{11}(n) - \alpha G_L \mu_{20}(n), \\ G_W = k_W \sigma^2,\ G_L = k_L \sigma^4,\ B_u = k_n \sigma^2 \mu_{21}(n),\ \ \mu_{ij}(n) = \int_0^{L_{\max}} \int_0^{W_{\max}} W^i L^j\, n\, dW\, dL\ , \\ n\big|_{\substack{(0,0)-(W_{\max},0) \\ (0,0)-(0,L_{\max})}} = 0, \quad \left.\dfrac{\partial n}{\partial L}\right|_{\substack{(W_{\max},0)-(W_{\max},L_{\max}) \\ (0,L_{\max})-(W_{\max},L_{\max})}} = 0,\ n\big|_{t=0} = n_0(W,L), \qquad \sigma\big|_{t=0} = \sigma_0\,. \end{cases} \tag{1}$$

were n is the number density, σ is the relative supersaturation, t is time, L and W are the crystal length and width, n_0 and n_n are the initial and nuclei CSDs, respectively, σ_0 is the initial relative supersaturation, G_L and G_W are the crystal length and width growth rates, respectively, B_u is the secondary nucleation rate, α is the crystal density, k_L, and k_W are the length and width growth rate constants, respectively, k_n is the nucleation rate constant, and μ_{ij} is the *i-j* cross-moment of the crystal size distribution.

Solving the above dynamic crystallization model enables prediction of the evolution of crystal size distribution and supersaturation in an isothermal batch crystallizer. The two crystal growth rates are assumed to be independent of crystal size. This spatially-homogenous model describes the population of crystals distributed in a two dimensional domain with the crystal length and crystal width as internal coordinates.

3. A Constant Crystal Growth Rate Case

The 2-D nonlinear dynamic model of Eq. 1, is solved numerically for the case of constant crystal growth rates; $G_W = G_L$ = const., and no nucleation; $B_u = 0$. The seed crystals are described by a 2-D Gaussian CSD as

$$n_0(W,L) = \frac{1}{\pi \delta_W \delta_L} e^{-\left(\frac{W-W_S}{\delta W}\right)^2 - \left(\frac{L-L_S}{\delta_L}\right)^2} \quad (2)$$

where δ_W=0.4 μm, δ_L=10 μm are the aspect ratio dispersion coefficients in the width and length directions, respectively. The average seed width, W_S, and the average seed length, L_S, equal to 2 and 20 μm, respectively. As shown in Fig. 2 for the case of constant growth rates, the maximum of the initial CSD travels along the diagonal of the *L-W* plane with a translation distance that is equal to $\Delta=(t-t_0)\sqrt{(G_W^2+G_L^2)}$. The Gaussian shape of the initial crystal number density is closely preserved, as expected for the case with the zero nucleation rate. Generally, the larger the value of the ratio, $\Delta/\min(\delta_W,\delta_L)$, and the higher the dispersion ratio, δ_L/δ_W, deviates from unity, the more difficult it is to numerically solve the model in Eq.1. High values of $\Delta/\min(\delta_W,\delta_L)$=100 and δ_L/δ_W=25 were used to demonstrate the ability of the FEM with adaptive mesh and time step to preserve CSD shape.

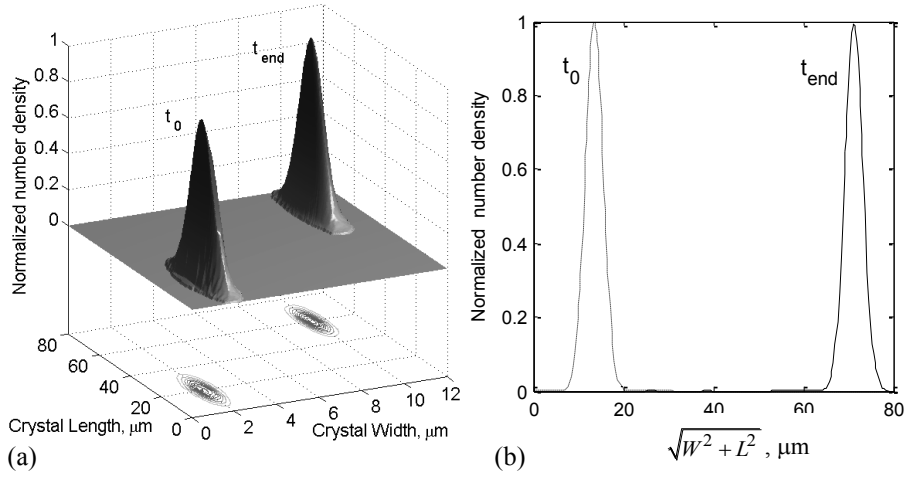

Figure 2. Initial and final normalized number density distributions of needle-shape crystals with the dispersion coefficient ratio, δ_L/δ_W, of 25 for the growth only case: (a) 2-D normalized number density, and (b) 1-D diagonal cross section of the 2-D normalized number density.

4. A Constant Nucleation and Crystal Growth Rate Case

For the case of constant nucleation and crystal growth kinetics; $G_W = G_L = G_0$ = const., and B_u = const., the 2-D dynamic model of Eq.1, with the seed crystals of Eq.2, was solved numerically using the following Gaussian size distribution of nuclei

$$n_n(W,L) = \frac{1}{\pi \delta_W \delta_L} e^{-\left(\frac{W-W_n}{\delta W}\right)^2 - \left(\frac{L-L_n}{\delta_L}\right)^2} \quad (3)$$

An average width of nuclei, W_n, of 2 μm, and average length, L_n, of 20 μm were used in numerical experiments. Although this nuclei size is not realistic for most practical

problems, it was chosen here to demonstrate the principle, which is general and independent of nuclei size. At the same time, an average width of seed crystals, W_S, was 4 μm, and average length, L_S, 30 μm. The same dispersion coefficients of δ_W=0.4 μm and δ_L=10μm were used for both the nuclei and seed crystal size distributions.

Similar to the pure crystal growth case, in the nucleation-growth case the maximum in the initial seed CSD is shifted diagonally on the *L-W* plane, as shown in Fig. 3 (a). At the same time, nuclei of a smaller size than the seed start appearing and grow along the *L-W* direction. The number density resulting from nuclei forms a saddle-like shape with a constant height. As expected, the initial maximum of the seed number density is correctly preserved during crystallization, as shown in Fig.3 (b) with the 1-D cross sections of the initial and final 2-D normalized number densities compared. Also, the predicted increase in the total number of crystals accurately matches the increase in estimated based on the constant nucleation rate multiplied by the crystallization time. Note, however, that the cross section plane presented in this case in Fig.3 (b) is not exactly the same plane as that presented in Fig. 2(b).

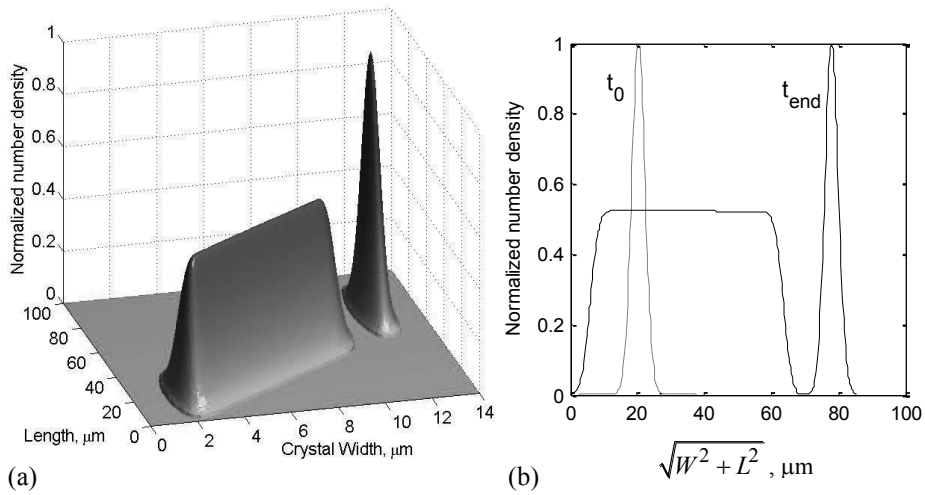

Figure 3. Normalized number density distributions of crystals with seed and nuclei dispersion coefficient ratio, δ_L/δ_W, of 25 for the constant nucleation and growth case: (a) final 2-D normalized number density, (b) initial and final 1-D diagonal cross section of the 2-D number density.

5. A Nonlinear Crystallization Kinetics Case

To test the numerical algorithm for a fully nonlinear kinetic case the number density was coupled with a decreasing supersaturation profile, which lead to decreasing crystal growth and nucleation rates. The statement of Eq.1 was run with the same parameters for the seed and nuclei distribution as those used in the nucleation-growth constant kinetics case. As shown in Fig. 4(a), the final CSD predicted for the nonlinear crystallization kinetic case differs from the one obtained for the constant nucleation-growth kinetic case. However, the maximum and the shape of the CSD of the seed crystals are accurately preserved by the numerical solution, as illustrated in Fig. 4(b). Due to decreasing supersaturation in this case, the travel distance of the maximum in the seed crystal CSD along the diagonal is smaller than in the previous two cases.

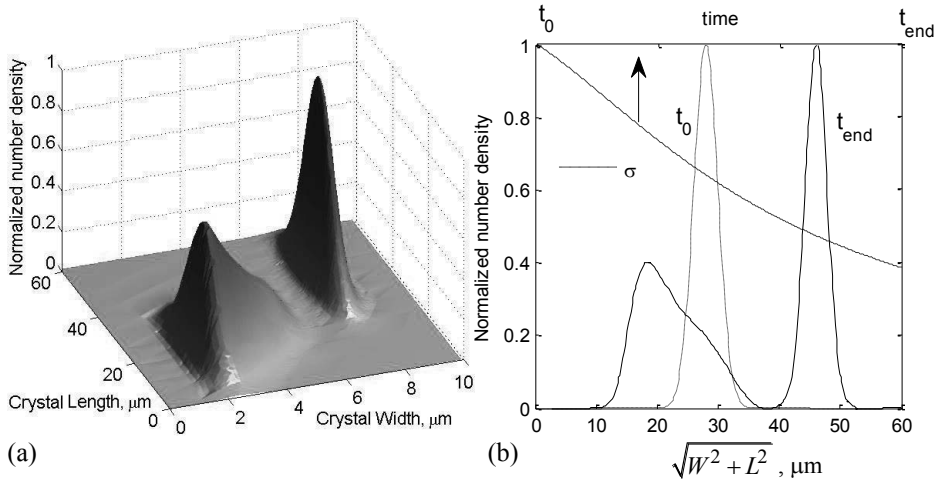

Figure 4. Normalized number density distributions of crystals with seed and nuclei dispersion coefficient ratio, δ_L/δ_W, of 25 for the nonlinear kinetics case: (a) final 2-D number density, and (b) initial and final 1-D diagonal cross section of the 2-D number density shown with the corresponding supersaturation profile.

As shown in Fig. 4(b), the left-hand side part of the normalised number density distribution, the appearance of which is due to the onset of nuclei, exhibits a pyramid-like local maximum forming a shape that differs significantly to the saddle-like shape shown in Fig. 3(b) for the constant nucleation-growth case. Also, in the nonlinear case the height of the pyramid local maximum is lower than the height of the saddle. The results presented in Fig. 4 provide a qualitative demonstration of consistency of the numerical solution of the nonlinear model of Eq.1.

6. Conclusions

A 2-D population balance equation model was solved using a finite element method-based numerical algorithm with adaptive mesh and time step for three different crystallization cases: i) constant crystal growth rate, ii) constant crystal growth and nucleation rates, and iii) nonlinear crystallization kinetics.

The model results obtained for the three different cases clearly demonstrate consistency of the newly developed FEM-based numerical approach for solving dynamic 2-D population balance models of crystallization systems with crystals of variable aspect ratio.

References

A.V. Bekker, J. McShane, D. Bedell and I. Livk, 2011, Image Analysis-based Sizing of Oxalate Crystals, Proceedings of the Chemeca 2011, Sydney, Australia, 18-21 September 2011.

R. Gunawan, I. Fusman and R.D. Braatz, 2004, High Resolution Algorithms for Multidimensional Population Balance Equations, AIChE Journal, 50, 11, 2738-2749.

T. Khanam, M.N. Rahman, A. Rajendran, V. Kariwala, and A.K. Asundi, 2011, Accurate Size Measurement of Needle-shaped Particles Using Digital Holography, Chemical Engineering Science, 66, 12, 2699-2706.

K. Sato, H. Nagai, K. Hasegawa, K. Tomori, H.J.M. Kramer and P.J. Jansens, 2008, Two-Dimensional Population Balance Model with Breakage of High Aspect Ratio Crystals for Batch Crystallization, Chemical Engineering Science, 63, 12, 3271-3278.

I.A. Karimi and Rajagopalan Srinivasan (Editors), Proceedings of the 11th International Symposium on Process Systems Engineering, 15-19 July 2012, Singapore.

Dynamic analysis of reaction kinetics of carton packaging pyrolysis

Larissa M. Alvarenga[a], Thiago P. Xavier[b], Marcos Antonio S. Barrozo[b], Marcelo S. Bacelos[a], Taisa S. Lira[a]

[a] *Departamento de Engenharias e Computação, Programa de Pós-graduação em Energia, Universidade Federal do Espírito Santo,, Rod. BR 101 Norte, km. 60, Bairro Litorâneo, CEP 29932-540, São Mateus- ES, Brazil, email:marcelobacelos@ceunes.ufes.br*

[b] *Programa de Pós-graduação em Engenharia Química, Universidade Federal de Uberlândia, Av. João Naves de Ávila, 2121, Bloco 1K do Campus Santa Mônica, CEP 38408-100, Uberlândia-MG, Brazil*

Abstract

As reported in the literature, the post-consumption carton packaging has been recycled using different process. Pyrolysis can be a promising technology to be used for recovering the aluminum from polyethylene and generating products with high heating value. In this research paper, by using thermogravimetric analysis (TGA), a kinetic study on pyrolysis reactions was performed. Furthermore, the activation energy of pyrolysis reaction was estimated using the methodology proposed by Ozawa (1965).

Keywords: pyrolysis, carton packaging, thermogravimetric analysis.

1. Introduction

A modern solid waste commonly found in urban areas is the post-consumption carton packaging, composed of 75% paper, 20% polyethylene and 5% aluminum. Recycling is one of the alternatives for recovering the long-life packaging. The recycling starts in the paper industry where recycling fibers can be recovered by repulping process. The polyethylene and aluminum separated in a hydropulper can be recovered in three different ways: energy generation from paraffinic oil, recovery of aluminum in pyrolysis ovens, recovery of polyethylene and aluminum by plasma technology, and the processing of the mixtures of polyethylene and metal to obtain high-end plastic lumber products. Among these technologies, pyrolysis highlights to be a good alternative either to separate aluminum from polyethylene or to generate products with high heating value. In the literature, few studies have done on the pyrolysis of carton packaging wastes (de Marco et al., 2009; Korkmaz et al., 2009). Thus, this research aims at analyzing the reaction kinetics of carton-packaging components pyrolysis using thermogravimetric analysis.

2. Methodology

2.1. Thermogravimetric Analysis.

The data were obtained using a thermogravimetric analyzer, TGA-60 (Shimadzu). Table 1 presents operating conditions and sample characteristics used in this research and those reported in the literature.

Table 1: Operating conditions, physical properties, methods and models used.

References	Operating Conditions, physical properties, method and models
Present research	- Continuous flow of nitrogen gas at a rate of 50 mL min^{-1}; - Samples of 6 mg and sieve diameter smaller than 1 mm; - Densities: carton packaging (1.3234g.cm^{-3}), cardboard (1.4893g.cm^{-3}) and polyethylene (0.9414g.cm^{-3}). - Dynamic tests: 25 to 600 °C; heating rates: 5, 10, 20 and 50 °C min^{-1}; - Kinetic model used: Ozawa (1965).
Paik and Kar (2009)	- Continuous flow of nitrogen gas at a rate of 200mL min^{-1} - Average particle diameter: ~20, ~10, ~1μm < 500 nm - Dynamic tests: 40 to 600ºC at heating rates of 5, 10 and 15 ºC/min^{-1} - Kinetic model used: Friedman (Li et al.,1998), Freeman–Carroll (Li et al.,1998), Kissinger (Li and Huang,1999), Kim–Park (1995) and Flynn–Wall (Li and Huang, 1999).
Volker and Rieckman (2002)	- Continuous flow of helium gas at a rate of 1.7 l h^{-1}; - Initial sample masses of 1, 3, 20, 37 and 54 mg and bulk density of 400 and 550 kg m^{-3}; - Dynamic tests performed at heating rates: 0.14, 3, 41 and 105 K min^{-1}. - Kinetic model used is not isoconversional.
Wu and Chang (2001)	- Continuous flow of nitrogen gas at a rate of 50 mL min^{-1}; - Samples of 6±0.5 mg and diameter smaller than 1 mm; - The same properties of this present research. - Dynamic tests performed at heating rates: 5.2, 12.8 and 21.8 K min^{-1}. - Kinetic model used: Friedman (1965).

2.2. Kinetic model

Table 2 shows the set of equations describing the kinetic model used.

Table 2: Kinetic model used for estimating the activation energy.

Conversion of solids

$$X = \frac{m_0 - m}{m_0} \quad (1)$$

m is the solid mass for a given time and m_0 is the initial mass of solid.

Temperature

$$T = T_0 + \beta t \quad (2)$$

β (dT/dt) is the heating rate and T_0 is the initial temperature.

Rate of conversion

$$\frac{dX}{dt} = f(X) \times k(T) \quad (3)$$

f is the conversion function, k is a reaction rate constant.

Arrhenius equation

$$k(T) = Ae^{\frac{-Ea}{RT}} \quad (4)$$

E_a is the activation energy, R is the ideal gas constant, A is the pre-exponential factor and T is the temperature of the sample.

Obtaining Ozawa's model

Based on equations (1), (3) and (4), the expression for degree of solid transformation as function of temperature can be calculated:

$$\frac{dX}{f(X)} = \frac{A}{\beta} e^{\frac{-Ea}{RT}} dT \quad (5)$$

By integrating the Eq.5 from T_0 (corresponding to X_0) to temperature inflection (T_m) (corresponding to X_m), the following equation is obtained:

$$g(X) = \int_{X_0}^{X_m} \frac{dX}{f(X)} = \frac{A}{\beta} \int_{T_0}^{T_m} e^{\frac{-Ea}{RT}} dT \quad (6)$$

Because of the complexity of the pyrolysis reaction, the form of the function $f(X)$ can be simplified assuming that the reaction follows a first order kinetics:

$$f(X) = (1 - X) \quad (7)$$

Ozawa (1965) used an empirical approximation to the integral of Equation 6, which resulted in the following equation:

$$\ln \beta = -1.0518\left[E_a / RT\right] + \left[\ln\left(k_0 E_a / R\right) - \ln g(X) - 5.3305\right] \quad (8)$$

Therefore, a plot of ln β versus $1/T$ should result in a straight line with slope -1.0518 E_a/R, with R = 8.314J/mol.K

3. Results and Discussion

Figures 1a-c show the curves of the rate of mass loss (DTG) as a function of temperature and heating rate, for carton packaging, cardboard and polyethylene, respectively. Comparing the DTG curves for different components, it can be observed that, in general, there are three steps of carton packaging devolatilization.

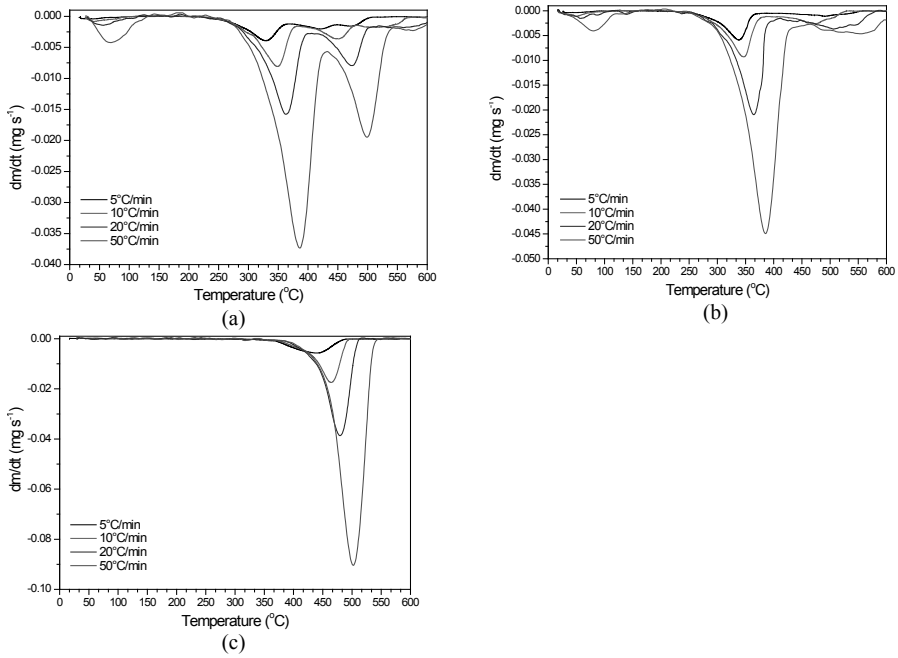

Figure 1: Rate of mass loss as function of reaction temperature and heating rate. (a) Carton packaging, (b) cardboard and (c) polyethylene.

In Figure 1a-b, at low temperatures (T<100°C), the first step is characterized by the significant moisture loss. The second step can be perfectly correlated with the cardboard devolatilization, which occurs at temperatures ranging from 300 to 420°C. Then, the third step it can be associated with the polyethylene devolatilization, occurring in the range of 400 to 550ºC, as shown in Figures 1a and 1c. In addition, in Figure 1a-b, a devolatilization step is also observed at temperature range of 500 to 600°C. This may be probably indexed to either the dye used in manufacturing of both the carton packaging and cardboard or aluminum decomposition. However, the peaks showed in figures 1a-b cannot be related to the decomposition of aluminum as this component is not subject to devolatilization. These findings are in agreement to those reported recently by Korkmaz et al. (2009). These authors verified that only coal and aluminum are the wastes from decomposition of carton packages. Moreover, it can be verified in Figures 1a-c that, for higher temperatures (T>350ºC), as heating rate is increased, the main peaks of mass loss are noticeable. These probably are due to the change in the decomposition mechanism.

Figures 2a-c show the linear regression data for pyrolysis of carton packaging, cardboard and polyethylene using the method proposed by Ozawa (1965), as described in Table 2. For carton packaging, in a range of 10-50% conversion, it can be seen in Figure 2a that the linear fits show approximately the same slop. As well, it is presented a similar behavior of linear fits for cardboard and polyethylene, as shown in figure 2b-c,

in a range of 10-60% and 10-40% conversion, respectively. Such a parallelism of linear fits indicates an analogous kinetic behavior, suggesting that the activation energies are probably similar and the mechanism of reaction can be most likely described and represented by one global step.

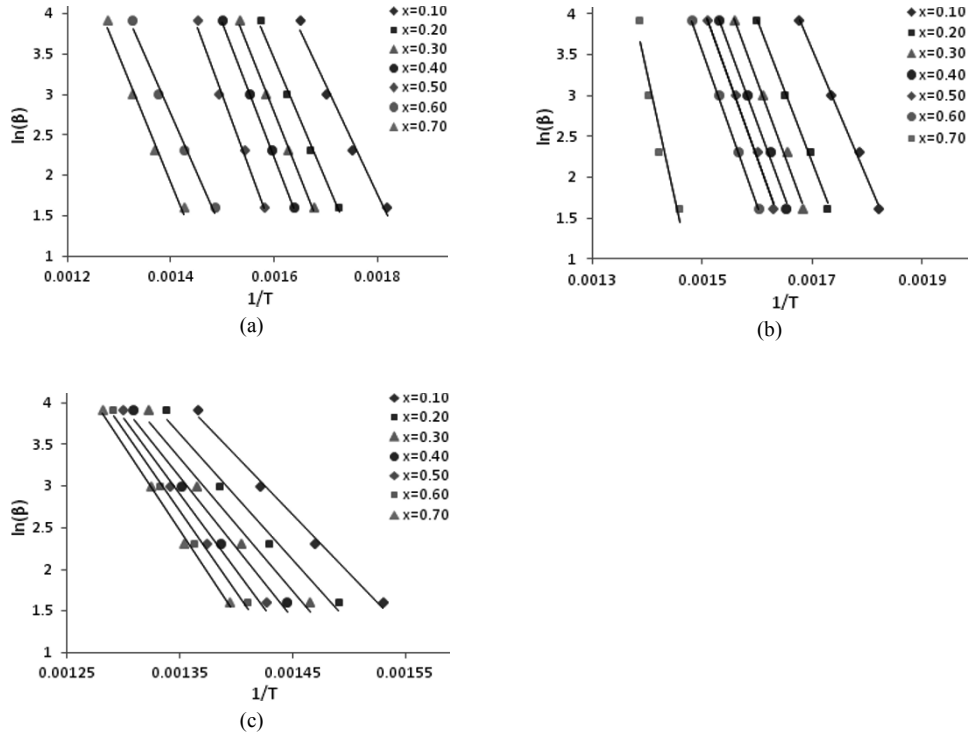

Figure 2: Graph of Ozawa for pyrolysis. (a) carton packaging, (b) cardboard and (c) polyethylene.

However, for higher conversion values, as that 60-70% for carton packaging and 70% for cardboard, a different slopping line is achieved as compared to others, indicating that there is a change in the reaction mechanisms. In addition, for the polyethylene, the lines of the linear fits present comparable behavior for each conversion value achieved, as shown in Figure 2c. Consequently, this leads to similar values of activation energies attained as shown in Table 3.

The Table 3 shows activation energy data (E_a) for each conversion attained in the pyrolysis of carton packaging, cardboard and polyethylene, respectively. For all conversion ranges, the linear fits show highly significant correlation coefficients ($0.93 \leq R^2 \leq 1.0$) and reasonably low values of RMSE ($0.02 \leq \text{RMSE} \leq 0.23$, root-mean-square error). The comparison between E_a averages obtained to those of Literature shows that data are in the same order of magnitude to those of Paik and Kar (2009), Volker and Rieckmann (2002) and Wu and Chang (2001), as shown in Table 3 and 4, even considering either different methods, operating conditions or material physical properties used (see Table 1).

Table 3: Activation energy obtained by the Ozawa's model (1965).

Carton Packaging				Cardboard			Polyethylene		
X	E_a ($kJ.mol^{-1}$)	R^2	RMSE	E_a ($kJ.mol^{-1}$)	R^2	RMSE	E_a ($kJ.mol^{-1}$)	R^2	RMSE
0.1	106.85	0.98	0.11	123.61	0.99	0.06	110.58	0.99	0.08
0.2	119.22	0.99	0.07	138.62	0.99	0.06	118.52	0.98	0.11
0.3	127.17	1.00	0.05	142.62	0.99	0.06	126.36	0.98	0.13
0.4	131.41	1.00	0.02	144.91	0.99	0.07	133.95	0.98	0.13
0.5	136.88	0.99	0.08	148.80	1.00	0.05	144.03	0.98	0.12
0.6	113.21	0.99	0.09	150.65	1.00	0.02	153.82	0.99	0.09
0.7	122.46	0.99	0.09	239.92	0.93	0.22	162.45	1.00	0.05
Mean	**122.46**			**155.59**			**135.67**		
S.D	10.41			38.24			18.84		

Table 4: Activation energy from data obtained by Literature

References	Paik and Kar (2009), for Polyethelene	Volker and Rieckmann (2002), for cardboard	Wu and Chang (2001), for carton packaging
E_a ($kJ.mol^{-1}$)	232.5	244.0	150.0

Conclusions

Based on analysis established in this research the following conclusions can be drawn:

- The carton packaging pyrolysis follows three steps characterized by moisture loss, cardboard and polyethylene devolatilization, respectively.
- For conversion values ranging from 20 to 60%, the pyrolysis reaction probably follows a similar mechanism and can be represented by one global step.
- Considering the high correlation coefficients of linear fit of Ozawa (1965)'model to the experimental data, it can be stated that such a model can be used for satisfactorily estimating the activation energy of pyrolysis reactions of carton packaging, cardboard and polyethylene.

Acknowledgments

The authors wish to express their gratitude to CNPq and FAPES for financial support to carry out this research and, especially, to CAPES for MSc scholarship of L. M. Alvarenga. We also thank to Tetra Pak for providing the samples.

References

KORKMAZ, A.; YANIK, J.; BREBU, M.; VASILE, C., 2009, Pyrolysis of the tetra pak, Waste Management, Vol 29, p. 2836-2841.

OZAWA, T., 1965, A new method of analyzing thermogravimetric data, Bulletin of the Chemical Society of Japan, Vol. 38, p. 1881-1886.

PAIK, P.; KAR, K. K., 2009, Thermal degradation kinetics and estimation of lifetime of polyethylene particles: Effects of particle size", Materials Chemistry and Physics, Vol 113, p. 953-961.

VÖLKER, S.; RIECKMANN, Th. 2002, Thermokinetic investigation of cellulose pyrolysis - impact of initial and final mass on kinetic results", Journal of Analytical and Applied Pyrolysis, Vol 62, p. 165-177.

WU, C.; CHANG, H., 2001, Pyrolysis of tetra pack in municipal solid waste. J. Chem. Technol. Biotechnol., Vol 76, p. 779–792.

de MARCO, I., CABALLERO, B.M., LOPEZ, A., LARESGOITI, M.F., TORRES, A. CHOMON, M.J., 2009, Pyrolysis of the rejects of a waste packaging separation and classification plant, J. Anal. Appl. Pyrolysis 85, 384–391.

I.A. Karimi and Rajagopalan Srinivasan (Editors), Proceedings of the 11th International Symposium on Process Systems Engineering, 15-19 July 2012, Singapore.

A simultaneous synthesis method for combined heat and mass exchange networks

Linlin Liu[a],Jian Du[a*],Mahmoud M.El-Halwagi[b,c],José María Ponce-Ortega[d],Pingjing Yao[a]
[a] *Chemical Engineering Department,Dalian University of Technology,Dalian 116024,China*
[b] *Chemical Engineering Department, Texas A&M University, College Station 77843, TX, USA*
[c] *Adjunct faculty at the Chemical and Materials Engineering Department, King Abdulaziz University, Jeddah, Saudi Arabia,*
[d] *Chemical Engineering Department, Universidad Michoacana de San Nicolás de Hidalgo, Morelia, Mich 58060, Mexico*

Abstract

Mass-exchange operations are highly impacted by heating and cooling. Therefore, there is a natural coupling between the problems of synthesizing mass exchange networks (MENs) and heat exchange networks (HENs). The objective of this paper is to introduce a systematic method for the simultaneous synthesis of combined mass- and heat-exchange networks (CM&HEN). The proposed method is based on a novel approach that integrates the pseudo-T-H diagram approach (PTHDA) for HEN synthesis, with the mass pinch technology (MPT) for MEN synthesis. The applicability of the proposed approach is shown through an example problem, where a significant reduction in the total annual cost is obtained.

Keywords: mass exchange network; heat exchange network; combined mass- and heat-exchange network; simultaneous synthesis.

1. Introduction

Significant conservation of natural resource (mass and energy) can be achieved through the design of MENs and HENs. Because the performance of mass-exchange operations depends on the operating conditions including temperature, there is an important coupling between the synthesis of MENs and HENs. Therefore, systematic methods should be used.

For the simultaneous synthesis of combined mass- and heat-exchange networks (CM&HENs). The design challenges include the need to screen mass-separating agents while accounting for their operating conditions and linking the mass-exchange operations with heat integration among process streams, the rich streams, and the mass-separating agents

Srinivas and El-Halwagi (1994) introduced the problem of combined heat and reactive mass exchange networks and developed a procedure based on optimizing individual mass-exchange temperatures in isothermal unit. Isafiade and Fraser (2007, 2009) presented two approaches for the synthesis of CM&HEN using the mass pinch technology and mathematical programming. Iterative approaches were used to solve the problem. The iterative approach simplifies the solution but does not guarantee the identification of the optimal solution. Du et al. (2010) presented a superstructure based method for the CM&HEN synthesis problem; however, the type of stream for the HEN (hot/cold) is predefined, and this way some potential solutions are eliminated yielding suboptimal solutions.

This paper proposes a new approach for the simultaneous synthesis of CM&HEN considering the multidimensional optimization issue. The proposed approach combines

the mass pinch technology (El-Halwagi and Manousiouthakis, 1989) and the pseudo-T-H diagram (Xiao et al., 2006) methods. The proposed approach considers explicitly the relationships between the MEN and HEN since the synthesis stage eliminating the drawbacks of previously reported methods.

2. Problem Statement

The problem addressed in this paper for the synthesis of CM&HEN can be described as follows: Given are a set of streams that are rich in transferable components, a set of mass-separating agents or lean streams (e.g., solvent streams) that can be used to remove the transferable components, and a set of hot/cold utilities. The task is to synthesize a CM&HEN that considers the tradeoffs between mass transfer and heat exchange at the same time with the objective of minimizing the total annual cost.

To practically solve the CM&HEN synthesis problem, the following assumptions applied for dilute systems are considered (Srinivas and El-Halwagi, 1994): the stream mass flow rates remain constant throughout the network; the mass exchange units operate isothermally; the mass transfer is related to the lean stream temperatures; the coefficient a_n in the equilibrium relationship shown by equation (1) is a monotonic function of temperature.

$$y_n^* = a_n x_n + b_n \qquad (1) \qquad\qquad y_n^* = a_n (x_n + \varepsilon_n) + b_n \qquad (2)$$

In equation (1), y_n^* is the rich stream equilibrium concentration, x_n is the lean stream concentration, and T_n^* is the mass transfer temperature. The minimum concentration difference ε_n ($\varepsilon_n > 0$) is introduced in equation (2) to avoid zero driving forces.

3. Proposed Method

3.1. Method outline

Mass pinch technology and pseudo T-H diagram approach are based on thermodynamic analysis, and both have been used effectively for MEN and HEN synthesis. The simultaneous synthesis method proposed in this paper integrates these two methods to establish a mathematical model for the overall CM&HEN synthesis and optimization. In CM&HEN, HEN provides suitable temperatures for MEN while MEN provides streams for HEN. Therefore, CM&HEN is not merely a simple linkage of single MEN and HEN. This paper follows the coupling approach proposed by Srinivas and El-Halwagi (1994), where the mass exchange temperature for each lean stream remains constant during the mass exchange, and the heat exchange only exists at the two sides of MEN(i.e., pre- and post-mass exchange). To address the simultaneous problem, a synthesis/optimization strategy is explained and detailed in the next section.

3.2. Synthesis and optimization strategy

During the simultaneous synthesis and optimization of CM&HEN, the mass transfer temperatures and the stream flow rates are the linking parameters between the MEN and the HEN, therefore the key point for the simultaneous CM&HEN synthesis problem is to consider the interactions between these variables. It is worth noting that some methods are not suited to satisfy these requirements, because they need to represent the HEN before the optimization. The present paper uses the PTHDA method for the HEN synthesis to avoid the previous complication.

The PTHDA method considers as variables a list of heat transfer temperature difference contribution values T_C for each corresponding stream. These T_Cs may be optimized in a feasible range. Consequently, the PTHDA method does not require identifying and

distinguishing the different types of variables. Based on this feature, the HEN optimization can be coupled with the MEN synthesis by giving every potential hot/cold stream a variable position and identifying it during the optimization process. Hence, it is assumed that there are *i* MEN synthesis variables and at most *j* HEN synthesis variables. When a set of optimization variables are given, all cold/hot streams related can be determined and the treatment of these variables can be represented through the matrix $\boldsymbol{Z}$ as follows:

$$Z=\begin{bmatrix} z_{11}=\text{-1or0}or1 & & & \\ & z_{22}=\text{-1or0}or1 & & \\ & & \cdots & \\ & & & z_{jj}=\text{-1or0}or1 \end{bmatrix}$$

Three types of values can be observed along the diagonal: '-1' means it is a hot stream, '1' means it is a cold stream and '0' means the stream does not exist. The result of Matrix $\boldsymbol{Z}$ dot product with the HEN variables matrix $T_C=\lfloor T_{C1},\ T_{C2},\ \ldots,\ T_{Cj}\rfloor$ is an expression of variables and streams that exchange heat in the HEN. A value of 0 indicates no corresponding streams, non-zero means there is a corresponding streams and the absolute value is the temperature difference contribution value.

This strategy is robust and can be particularly applied to the cases of complex operating units whose hot and cold streams are hard to be determined.

3.3. Objective function

Based on the MPT and the PTHDA, and a sub-network coupling, this paper establishes a minimum total annual cost through a mathematical model for the CM&HEN synthesis. The total annual cost shown in equation (3) is a combination for the costs associated to the sub-MEN and the sub-HEN. For the MEN side, the operating cost considers the use of external lean streams and the capital cost is related to the mass exchanger units. For the HEN, the costs are the requirement of hot/cold utility and the fixed costs of the heat exchanger units. The following is the expression for the total annualized cost:

$$\min \sum_p \sum_m \sum_n N_{mnp}\cdot C_{stage}+\sum_n L_{l,n}\cdot C_{l,n}+\sum_i CF_{cui}+\sum_j CF_{huj}+\sum_k \sum_i \sum_j CF_{ijk}$$

$$+\sum_i C_{cui}\cdot A_{cui}^{B_{cui}}+\sum_j C_{huj}\cdot A_{huj}^{B_{huj}}+\sum_k \sum_i \sum_j C_{ijk}\cdot A_{lijk}^{B_{ijk}}+\sum_i C_{cui}\cdot q_{cui}+\sum_j C_{huj}\cdot q_{huj} \quad (3)$$

4. Case study

This example was taken from Srinivas and El-Halwagi (1994), Isafiade and Fraser (2007), it involves two H_2S-rich gas streams (R_1, R_2), one process lean stream S_1 and one external lean stream S_2. The cost and stream data are listed in Tables 1-3. Notice that each process stream has a certain target temperatures except S_2. The equilibrium relationships for H_2S in lean stream S_1 and S_2 are shown in equations (4) and (5), respectively. Besides, four external hot and cold streams listing in Table 4 are considered in this case study.

$$S_1: m_1=(5.86807\times10^{-8})\times10^{0.01024\times T_1^*} \quad (4)\qquad S_2: m_2=(9.386\times10^{-10})\times10^{0.0215\times T_1^*} \quad (5)$$

First, the HEN optimization variables–the temperature difference contribution values, are determined. There are at most two hot/cold streams that can be generated from S_1, one at most from S_2, thus 7 temperature difference contribution variables in total are required by adding 4 external hot/cold streams.

Table 1. Process parameters for the example

Operating time	8600 h·a^{-1}	Cost of S_2	0.001 \$·kg^{-1}
Column capital cost	4552 \$·stage^{-1}·a^{-1}	Hot utility (HU)	120 \$·kW^{-1}·a^{-1}
Annualizationfactor	0.2	Cold utility 1 (CU_1)	10 \$·kW^{-1}·a^{-1}
Heat exchanger cost	30000+750A$^{0.81}$	Cold utility 2 (CU_2)	30 \$·kW^{-1}·a^{-1}
Annualization factor	0.2	Heat transfer film coefficient	0.2 kW·m^{-2}·K^{-1}

Table 2. Streams data for the example

R_i	G_i/kg·s^{-1}	Y_i^s	Y_i^t	S_j	L_j^{up}/kg·s^{-1}	X_j^s	X_j^t
R_1	104	8.83×10^{-4}	5.00×10^{-6}	S_1	40	0.07557	≤0.115
R_2	442	7.00×10^{-4}	5.00×10^{-6}	S_2	∞	0.001	≤0.01

Table 3. Thermal data for the streams in the example

Streams	T^s/K	T^t/K	T^{low}/K	T^{up}/K	Cp/kJ·kg^{-1}·K^{-1}
R_1	298	298	288	313	1.00
R_2	298	298	288	313	1.00
S_1	368	368	279	368	2.50
S_2	310	-	280	330	2.40
HU	453	452	-	-	-
CU_1	288	298	-	-	-
CU_2	278	283	-	-	-

Table 4. Extra stream data

Streams	FCp/ kW·K^{-1}	T^s /K	T^t/K	h/ kW·m^{-2}·K^{-1}
H_1	10.0	448	318	0.2
H_2	40.0	398	338	0.2
C_1	20.0	293	428	0.2
C_2	15.0	313	385	0.2

The results obtained through the proposed approach are represented in Table 5. It is worth noting that the lean streams S_1 and S_2 appear in the optimal solution, and that the number of the mass separation stages is 26. This produces a higher cost of the MEN than the one previously literature reported (Isafiade and Fraser, 2007), which only involves S_2 and 26 column stages. However, the associated cost for the HEN is 39.6% lower, yielding a reduction for the TAC of the CM&HEN of 2.14%lower than the solution reported in Isafiade and Fraser (2007). In literature, the optimal mass exchange temperature of S1 is 286K, then one hot stream (368K-286K) and one cold stream (286K-368K) with a total heat exchange load of 414 kJ are generated. While in this paper, S_1 and S_2 take part in the mass exchange, and optimal mass exchange temperature of $S_1$is equal to its start and target temperatures, meanwhile there is no target temperature constrain for S_2, finally only one hot stream is formed and its temperatures changes from 310K to 280.8 K with a heat load of 103.7kJ.

Table 5.Results comparison

Options	T_1^*/K	T_2^*/K	L_1/kg·s^{-1}	x_1^{out}	L_2/kg·s^{-1}	x_2^{out}	TAC of MEN /10^3\$·a^{-1}	TAC of HEN /10^3\$·a^{-1}	TAC of Combined networks /10^3\$·a^{-1}
Literature	286	-	10.1	0.1150	0	-	54.6	295.4	350.0
This paper	368	280.8	39.4	0.0853	1.48	0.01	164.2	178.3	342.5

Figure.1 presents the optimal combined network obtained. There are 4 mass exchanger units and 7 heat exchanger units including one heater and two coolers in the structure, stream H_3 in the HEN is the only hot stream generated from S2.

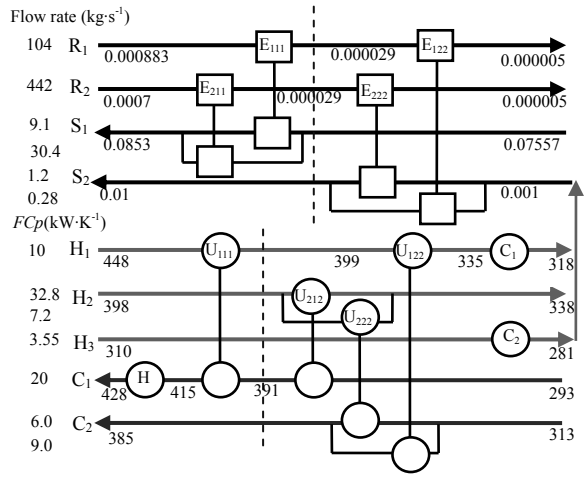

Fig.1 The optimal overall CM&HEN

5. Conclusion

This paper proposes a novel simultaneous synthesis strategy for the synthesis of CM&HEN. Concepts of MPT and PTHDA are adopted and integrated for MEN and HEN integration. An optimization formulation is developed to minimize the total annual cost of the MEN and the HEN while optimizing the selection of the mass-separating agents, the operating temperature of each mass-separating agent, and the assignment of heating and cooling duties. An example was presented to show the applicability and effectiveness of the proposed method with comparison to published results.

6. Acknowledge

The authors gratefully acknowledge the financial support from Natural Science Foundation of China (No. 20976022) and China Scholarship Council. Mahmoud El-Halwagi is thankful to funding from King Abdulaziz University. JoséMaría Ponce-Ortega appreciates funding from CONACyT.

References

A. J. Isafiade, D. M.Fraser, 2007. Optimization of combined heat and mass exchanger networks using pinch technology. Asia-Pacific Journal of Chemical Engineering, 2, 6, 554–565.

A. J. Isafiade, D. M.Fraser, 2009. Interval based MINLP superstructure synthesis of combined heat and mass exchanger networks. Chemical Engineering Research and Design, 87, 11, 1536-1542.

B. K. Srinivas, M. M. El-Halwagi, 1994. Synthesis of combined heat and reactive mass exchange networks . Chemical Engineering Science, 49, 13, 2059–2074.

J. Du, X. F. Li, L. Chen, P. J. Yao, 2010. Simultaneous synthesis of combined mass and heat exchanger networks. 5th International Symposium on Design, Operation and Control of Chemical Processes(PSE Asia 2010), Singapore.

M. M. El-Halwagi, V. Manousiouthakis, 1989. Synthesis of mass exchange networks. AIChE Journal, 35, 8, 1233-1244.

W.Xiao, P. J.Yao, X.Luo, W. Roetzel, 2006. A new and efficient NLP formulation for synthesizing large scale multi-stream heat exchanger networks.Journal of Chinese Institute of Chemical Engineers, 37, 4, 383-394.

I.A. Karimi and Rajagopalan Srinivasan (Editors), Proceedings of the 11th International Symposium on Process Systems Engineering, 15-19 July 2012, Singapore.

A New Method To Determine The Optimum Heat Exchanger Network Approach Temperature

Sharifah Rafidah Wan Alwi,[a] Zainuddin Abdul Manan[a], Sun Kheen Nam[a]

[a]*Process Systems Engineering Centre (PROSPECT), Faculty of Chemical Engineering, Universiti Teknologi Malaysia, 81310 Skudai, Johor, Malaysia.*

Abstract

Supertargeting is a widely used procedure to determine the optimum approach temperature (ΔT_{min}) for heat exchanger networks (HEN). It involves plotting the sum of HEN capital and operating costs, and finding the minimum total cost at an optimum ΔT_{min}. The capital and operating costs are determined from the heat transfer area and the minimum utility targets obtained from the temperature (T) vs enthalpy (H) plot of composited process streams (composite curves (CC)). S*upertargeting* using CC has two key limitations. Firstly, the HEN area calculations are drastically simplified through the assumption that CC segments are pseudo-single hot and cold streams exchanging heat via only one heat exchanger that is governed by a single cost correlation. Secondly, the current *Supertargeting* approach of considering only one hot and one cold utility levels at highest and lowest temperatures respectively is simplistic at best since a plant typically uses multiple levels of utilities. These limitations may lead to a very crude estimation of the total HEN cost and the corresponding ΔT_{min}. This work presents the Stream Temperature vs. Enthalpy Plot *Supertargeting* (STEPS) method that overcomes the aforementioned ΔT_{min} targeting limitations. Multiple utility levels, various heat exchanger types and streams individual heat transfer coefficients can be considered using STEPS. Application of STEPS on two case studies shows that the conventional *supertargeting* method can lead to up to 50% error in the total cost target and poor ΔT_{min} estimation.

Keywords: Pinch Analysis, Streams Temperature Versus Enthalpy Plots (STEP), multiple utilities, supertargeting, Heat Exchanger Network.

1. Introduction

Pinch Analysis has been a well-established tool for the design of maximum heat recovery networks in process plants. Among the important steps in Pinch Analysis is the determination of the optimum approach temperature for heat exchange (ΔT_{min}) to obtain the minimum total annual heat exchanger network (HEN) cost. The total annual HEN cost is affected by the trade-off between HEN capital and the operating costs. Ahmad and Linnhoff [1] introduced *supertargeting*, as a technique to determine the optimum ΔT_{min} that leads to the minimum total cost for HENs based on the composite curves.

Hall *et al*. [2] later developed a method which allows capital cost targets to consider different heat exchanger specifications such as materials of construction, pressure ratings and equipment types. This paper demonstrates that capital cost targets for HEN with different heat exchanger specifications can be predicted with good accuracy using individual stream temperature versus enthalpy plot (STEP). In a later research, Jegede and Polley [3] examined the effects of variations in heat exchanger

specifications on the network cost, and based on this, they developed a general procedure for predicting HEN total cost prior to design. Shenoy *et al*. [4] proposed a methodology to determine the optimum load for multiple utilities considering the cost tradeoffs in energy and capital for HENs. Akbarnia *et al*. [5] developed a method that considered piping costs and include the correlation for estimating piping costs for each stream based on the piping size, materials of construction and pressure rating.

The traditional supertargeting method has two major limitations. Firstly, the HEN area calculations are drastically simplified through the assumption that composite curve (CC) segments are pseudo-single hot and cold streams exchanging heat via only one heat exchanger that is governed by a single cost correlation. Traditionally, a composite stream is also assumed to have a single heat transfer coefficient even though it may consist of many streams, each with unique heat transfer coefficient and set of stream properties. Secondly, the current *Supertargeting* approach of considering only one hot and one cold utility levels at the highest and lowest temperatures respectively is simplistic at best since a plant typically uses multiple levels of utilities. These limitations may lead to a very crude estimation of the total HEN cost and the corresponding ΔT_{min}. These assumptions and limitations may lead to the total HEN cost to be grossly over or underestimated, and the wrong optimum ΔT_{min} selected. This work proposes the new Stream Temperature vs. Enthalpy Plot Supertargeting (STEPS) approach that overcomes all these limitations.

2. Methodology

2.1. Step 1: Data Extraction

The first step is hot and cold streams data extraction. The data required for analysis are primarily heat capacity flowrate, streams supply and target temperatures, and individual heat transfer coefficients, h. **Table 1** shows the extracted stream data for example 1 (Wan Alwi and Manan, 2010).

Table 1: Stream data for example 1 (Wan Alwi and Manan, 2010)

Stream	Supply Temp., T_s (°C)	Target Temp., T_t (°C)	Heat Capacity Flowrate, FCp, (kW/°C)	Enthalpy, ΔH (kW)	Shifted Supply Temp., T_s' (°C)	Shifted Target Temp., T_t' (°C)	Heat transfer coefficient, h, (kW/m^2°C)
Hot 1	300	160	3	-420	290	150	1.3
Hot 2	230	120	7	-770	220	110	1.1
Hot 3	160	60	2	-200	150	50	1.2
Cold 1	40	230	2	380	50	240	1.2
Cold 2	100	230	4	520	110	240	1.2
Cold 3	230	300	3	210	240	310	1.2

2.2. Step 2: Setting the Minimum Utility Targets by Using STEP

The next step is setting the minimum utility targets. In this step, Streams Temperature vs. Enthalpy Plot (STEP) by Wan Alwi and Manan [6] is used to determine the minimum utility targets instead of the traditional composite curves. For more details on STEP construction, readers are referred to Wan Alwi and Manan [6]. The construction of STEP is performed for ΔT_{min} values from 5 to 50°C.

2.3. Step 3: Targeting Multiple Utilities Using the Balanced STEP

Four types of utilities have been included into STEP and drawn as the balanced STEP. The utilities added are cooling water (CW), tempered water (TW), high pressure steam (HPS) and hot oil. The supply temperatures used for the utilities are the closest feasible temperatures relative to the process temperatures. Note that, the supertargeting technique based on composite curves introduced by Khorasany and Fesanghary [7] does not consider multiple utility levels.

2.4. Step 4: Utilities Cost Calculation

The hot and cold utilities determined from **Step 3** are then used to calculate the utility costs.

2.5. Step 5: Area Calculation For Each STEP Segment

The next step is to calculate the area of each heat exchanger. This can be done by observing each segment of STEP. The area for each STEP segment (A_k) can be calculated by using Equation (1). Note that for each composite curves' segment, the area may be calculated from a 'composite', as opposed to an individual stream match. This may lead to the wrong area and capital cost estimations. **Figure 1** shows each heat exchanger match for STEP at ΔT_{min} of 20°C.

$$A_k = \frac{Q_k}{\Delta T_{LMK}}\left(\frac{1}{h_{h,k}} + \frac{1}{h_{c,k}}\right) \quad (1)$$

Where A_k is in m^2, Q_k is the heat transferred (kW), $h_{h,k}$ and $h_{c,k}$ are heat transfer coefficients for hot and cold streams, ΔT_{LMK} is the log-mean temperature difference (K).

2.6. Step 6: Capital Cost Calculation

The double-pipe heat exchanger is assumed to be used for all STEP segments. The capital costs for networks with ΔT_{min} values between 5°C to 50°C are estimated based on the cost correllations from Seider *et al.* [8].

2.7 Step 7: Supertargeting by Constructing Trade-Off Diagram to Determine the Optimum ΔT_{min}

This step involves determining the utility and capital costs for ΔT_{min} values between 5 and 50 ºC. The costs of utilities as well as capital are added together at each ΔT_{min} to obtain the total cost. **Figure 2** shows that the optimum ΔT_{min} obtained is 5 ºC.

3. Case Study 1

The new STEPS method is applied on a Case Study 1 from Linnhoff *et al*. [9]. The results obtained using STEPS are compared with those obtained using the traditional approach. Supertargeting based on composite curves and STEPS both result in an optimum ΔT_{min} of less than 10°C. **Table 2** shows the difference between the total costs obtained via CC supertargeting as well as via STEPS. Note that STEPS result in higher total costs of up to 8.67%.

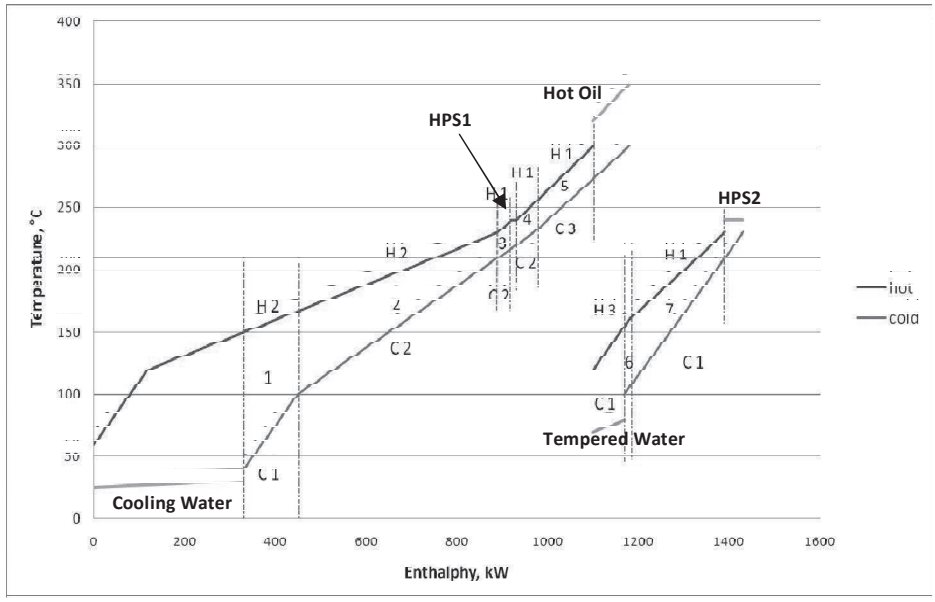

Figure 1: Stream matches for STEP at ΔT_{min} of 20°C (example 1).

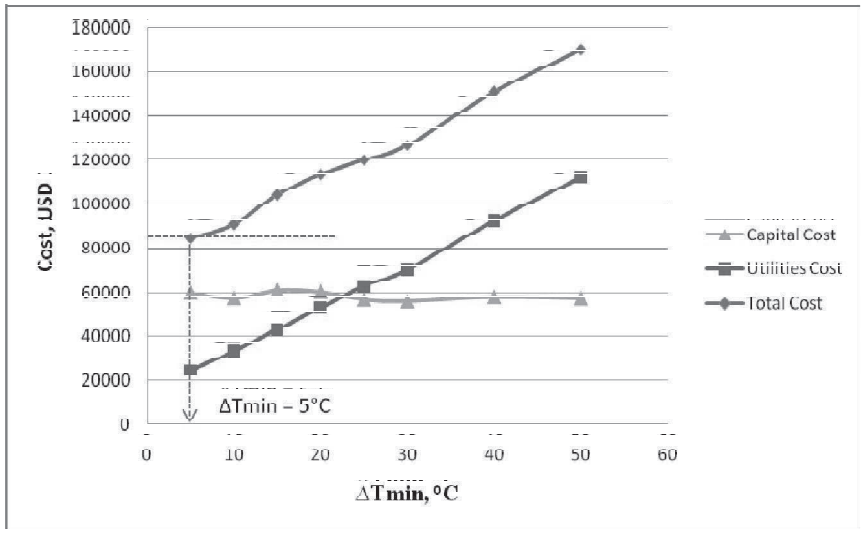

Figure 2: STEP Supertargeting - double-pipe heat exchanger is used for all STEP segments (example 1).

Table 2: Percentage total cost deviations between CC and STEP supertargeting (Case Study 1)

ΔT_{min}, °C	Total Cost, USD/ Yr		Percentage Difference, %
	Composite Curve	STEP	
10	97,755	91,107	6.80
20	104,508	113,572	8.67
30	121,015	126,835	4.81
40	140,534	150,785	7.29
50	159,739	169,877	6.35

4. Conclusion

Supertargeting using CC may lead to inaccurate optimum ΔT_{min} as well as the minimum total cost determination. For the case study considered, an error of up to almost 10% was observed for 6 streams. It is predicted that if there are more composited streams, the error will be bigger. The use of 'composite' to calculate HEN area is the major limitation of the previous methods. The new STEPS method allows the individual heat exchanger capital and utility costs to be considered, leading to an exact total HEN cost calculation. For exact computations of the HEN area, utility costs, the optimum total cost and the optimum ΔT_{min}, supertargeting should be based on the STEP method instead of composite curves.

4. Acknowledgment

The authors would like to thank MOHE (Ministry of Higher Education) Malaysia and UTM for providing the research fund for this project.

References

[1] S. Ahmad, B. Linnhoff, and R. Smith, 1990, Cost Optimum Heat Exchanger Networks-2. Targets and Design for Detailed Capital Cost Models, Computer and Chemical Engineering, 14(7): 751-767.

[2] S. G. Hall, S. Ahmad and R. Smith, 1990, Capital Cost Targets For Heat Exchanger Networks Comprising Mixed Materials Of Construction, Pressure Ratings And Exchanger Types, Computer and Chemical Engineering, Vol. 14, No. 3, pp. 319-335, 1990.

[3] F. 0. Jegede and G. T. Polley, 1992, Capital Cost Targets For Networks With Non-Uniform Heat Exchanger Specifications, Computer and Chemical Engineering, Vol. 16, No. 5, pp. 477-495

[4] U. V. Shenoy, A. Sinha and S. Bandyopadhyay, 1998, Multiple Utilities Targeting For Heat Exchanger Networks, Institution of Chemical Engineers Trans IChemE, Vol 76, Part A.

[5] M. Akbarnia, M. Amidpour and A. Shadaram, 2009, A New Approach In Pinch Technology Considering Piping Costs In Total Cost Targeting For Heat Exchanger Network, Chemical Engineering Research and Design 87 (2009) 357–365.

[6] S. R. Wan Alwi and Z. A. Manan, 2010, STEP - A New Graphical Tool for Simultaneous Targeting and Design of a Heat Exchanger Network, Chemical Engineering Journal, 162, 106–121.

[7] R. Mohammadhasani Khorasanya and M. Fesangharyb, 2009, A Novel Approach for Synthesis of Cost-Optimal Heat Exchanger Networks, Computers and Chemical Engineering, 33, 1363-1370.

[8] W. D. Seider, J. D. Seader and D. R. Lewin, 2010, Product and Process Design Principles-Synthesis, Analysis, and Evaluation. (3rd ed.), John Wiley & Sons (Asia) Pte Ltd.

[9] B. Linnhoff, D. Townsend, D. Boland, G. Hewitt, B. Thomas, A. Guy and R. Marshland, 1982, User Guide on Process Integration for the Efficient Use of Energy (Institute of Chemical Engineers, UK).

I.A. Karimi and Rajagopalan Srinivasan (Editors), Proceedings of the 11th International Symposium on Process Systems Engineering, 15-19 July 2012, Singapore.

Product Driven Process Design Method

Peter M.M. Bongers[a,b], Cristhian Almeida-Rivera[b]

[a]*Chemical Engineering and Chemistry, Eindhoven University of Technology, POBox 513, 5600 MB Eindhoven, peter.bongers@unilever.com*
[b]*Unilever Research and Development, Oliver van Noortlaan 120, POBox 114, 3130 AC Vlaardingen, The Netherlands.*

Abstract

In the last ten years much more processes are being reported to be designed through a process synthesis approach. It has been recognized during those years that (i) processes for structured products are more difficult to design through process synthesis; (ii) process synthesis is disconnected from product development. In a response to those shortfalls a number of authors have described that the gaps need to be filled, however no methodology extension has been proposed.

In this work, we will present extensions to the conceptual process synthesis methodology to include (structured) product design. The whole design methodology spans from how the new product can enlighten the consumer, financial and supply chain boundary conditions, through an optimal flowsheet able to produce the desired product cost effectively. A real case study will be used to illustrate the applicability and scope of the proposed methodology

Keywords: process synthesis, structured products, product development

1. Introduction

All leading fast moving consumer goods companies are rapidly transforming from general manufacturing hubs of loosely connected products to companies delivering health, wellness and nutrition. Manufacturing in a responsible and sustainable way products within strategic areas important for the company imposes technical challenges to work on and requires the development of R&D capabilities. Finding and creating business opportunities to be brought successfully to the market [1] is the response of leading companies to the rapidly changing environment, characterized by slim profit margins and fierce competitiveness. The stage–gate model is a project management tool to effectively manage such initiatives or projects (e.g., new product development, process improvement, business change) throughout companies. Each project is divided into stages separated by gates. At each gate, the continuation of the project is decided. Typically the proceed/re-cycle/stop decision is made by a steering committee. Cooper [2,3] distinguishes five stages: (1) Scoping; (2) Build business case; (3) Development; (4) Testing and validation; (5) Launch. As seen in Figure 1.

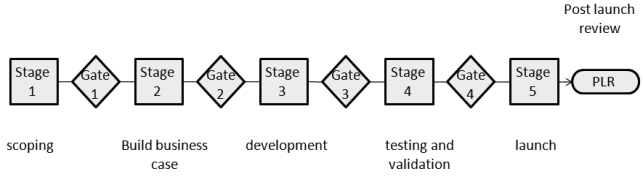

Figure 1 Stage-gate model

The stage-gate model has the clear aim of delivering the right product with all associated benefits at a short time to market and at a reduced manufacturing

expenditure. A key activity in this innovation process (stage-gate model) is the actual creation of the conversion or manufacturing system.
This creative activity referred to as process synthesis (PS), accounts for a cost of 2% of the total design costs and allows fixing 80% of the combined capital and operational costs [4]. In contrast to its relevance, PS is normally carried out by copying existing processes or scaling-up lab scale non-optimized protocols. Our challenge is addressing the PS problem from a systems engineering perspective and proposing a structured approach. Process Synthesis takes place in all conceptual process engineering steps within the innovation process and includes the selection of desired process unit operations, their interconnections and a preliminary design and cost estimation of the major units with key dimensions and operating conditions. Although the definition of PS might suggest a straight-forward and viable activity, the synthesis is complicated by the nontrivial tasks of: (i) identifying and sequencing the physical and chemical tasks to achieve specific transformations; (ii) selecting feasible types of unit operations to perform these tasks; (iii) finding ranges of operating conditions per unit operation; (iv) establishing connectivity between units with respect to mass and energy streams; (v) selecting suitable equipment options and dimensioning; and (vi) control the process operations. Moreover, the synthesis activity increases in complexity due to the combinatorial explosion of potential options. The number of possible combinations can easily run into many thousands [4]. The PS methodology is regarded in this context as a way to beat the problem complexity.

2. A Product-driven Process Synthesis (PDPS) Approach in Foods

It is now well-established by industry and academia that chemical industry focus has shifted from a process- centred orientation to a product-centred one [5]. During the last decades we have experienced how the commodity chemical business is gradually releasing its dominating role towards higher-added value products, such as specialty chemicals and consumer products. This trend is further reflected in the increasing number of scientific publications addressing product and process design [5-8], textbooks [9] and undergraduate/graduate courses in chemical process design [10;11]. In [11] Process Synthesis, for (structured) products is mapped on the stage-gate model as shown in Figure 2.

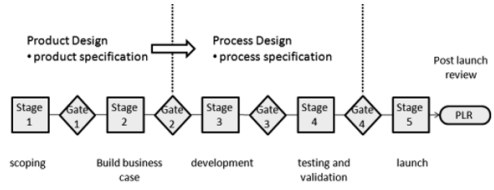

Figure 2 Product-Process design work flow according to [60]

Stretching the boundaries of the synthesis activity towards products has brought challenges for the chemical and process engineers. Those refreshing problems need the development of novel methods and tools, involving areas like the fundamental understanding of the product-process interactions, multi-level modelling of consumer products, property models for products with internal micro-structure, prediction of consumer liking and its dependence on ingredients and processes, etc.
Despite the maturity of most process synthesis approaches for chemical products, they fall short when it comes to extending its scope and applicability to food products. This drawback of current approaches is derived from the intrinsic differences between bulk

chemicals and food products, and include for the case of structure food products: (i) food products are typically structured products where the performance is determined by the internal microstructure of the product (Figure 3); (ii) unit operations are quite different, involving less reaction and separation tasks and more mixing and preservation; (iii) food processes are generally multi product processes, where a same production line can accommodate the manufacturing of different products with different properties; and (iv) cleaning is an essential and non-negotiable task within the operational policy.

Thus, in contrast to bulk chemicals, structured products are characterized not only by the level of each ingredient (i.e. composition, purity, physical state, temperature, pressure, etc.), but also by the relative spatial arrangement of each ingredient and performance behaviour. All these features are responsible for the exclusive attributes of structured products (e.g. creaminess of an ice-cream, spoonability of a mayonnaise, spreadability of a margarine, etc).

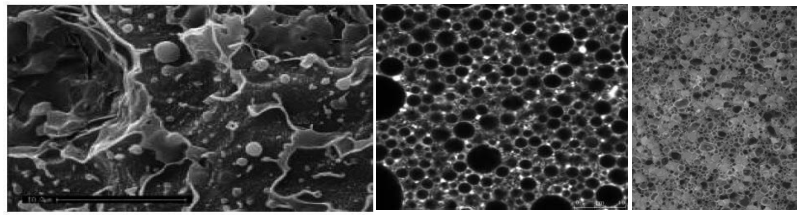

Figure 3. Lamellar structured hair conditioner [5] (left); confocal micrograph of a full-fat O/W emulsion (center); microscope photograph of an ice-cream matrix (right)

Aiming at a more structured approach towards the synthesis of product and processes in the food and drink sector, we proposed a methodology termed product-driven process synthesis (PDPS). This approach exploits the synergy of combining product and process synthesis workstreams and is based on the systems engineering strategy. Thus, it is supported by decomposing the problem into a hierarchy of design levels of increasing refinement (Table 1), where complex and emerging decisions are made to proceed from one level to another.

Table 1. Description of each level of the PDPS approach

Level	Generic description
0	**Framing level**. We embed the design into the overall project. Description of the background of the project and the business context, overall supply chain considerations (product portfolio, demand profiles, regional spread, …)
1	**Consumer wants**. We obtain the consumer wants (consumer likings, focus groups, interviews) in qualitative descriptions and translate them into quantifiable product attributes.
2	**Products.** We identify potential products that meet the consumer wants and map the quantifiable product attributes onto the product properties, which are measurable.
3	**Input-output level.** We make a complete specification of the output. We choose inputs (ingredients) and the descriptors of the output (microstructure, flavour profile and microbiological status). We determine performance parameters such as quality, economic potential, hygienic considerations, flexibility, pumpability, availability...

Table 1 (cont). Description of each level of the PDPS approach

4	**Task network**. We define the fundamental tasks needed to go from input to output, taken from a cluster of tasks and its subgroup. Furthermore, tasks that require a certain sequence or that belong together without any doubt are grouped, to reduce the number of sequencing possibilities. Then, a network is made from the selected tasks and clusters.
5	**Mechanism and operational window**. We select mechanism and principles that can be used to perform a task. This step includes the driving forces and kinetics. Furthermore, the operational window of the problem (time, P, pH, shear, T, etc.) is defined.
6	**Multi product integration**. The outcomes of steps 3 –5 for the different products are compared to look for overlap and possibilities to combine the production.
7	**Equipment selection and design**. The operating units are selected. Integration possibilities (e.g. by combining tasks with the same driving force that are close together in task network) and controllability should be considered. The operational window from step 6 is compared to the operating boundaries of the unit. Then, the final design of the units (only of the key dimension) and final flowchart are made.
8	**Multi product-equipment integration**. We optimise the interaction of the various unit operations in the flowsheet (plant-wide control). Multi-stage scheduling of the multiple products is applied, fed by the run-strategy based on the product demand and portfolio.

Moreover, each level in the PDPS methodology features the same, uniform sequence of activities (scope and knowledge » generate alternatives » analyze performance of alternatives » evaluate and select » report) [12].

The input of the PDPS methodology is a complete and comprehensive specification of the potential raw materials along with any other requirements the process needs to fulfill (e.g. the capacity requirements, cost requirements, hygiene standards, etc).

The method is fed by consumer preference studies and business relevance involving the desired product throughout the whole innovation process (stage-gate model (Figure 4)). In the scoping stage, more effort is put in the “product” design, moving through the gates to the testing and validation stage, more emphasis is put on the “process” design (not neglecting the reality checks with the consumer). This is indicated in bold in Figure 4. Moving through the stage-gate model, the PDPS levels are executed iteratively a number of times. In each iteration, the level of detail will (need to) be increased. For some of the levels, this only means a check if the environment has been changed, and if so, do we need to adapt the product/process.

The output of a process synthesis exercise is a flowsheet structure, along with unit interconnections, operating conditions and key dimensions of key equipment units. Additionally, controllability, reliability and flexibility of the proposed process are accounted for within the methodology. Recent efforts in the development of PDPS methodologies have been focusing on broadening the design scope to consumer preferences, product attributes, process variables and supply chain considerations [12].

The applicability and scope of the proposed methodology has been demonstrated using industrial cases as examples. These case studies include the synthesis of a novel freezing equipment for the production of ice-cream, a novel process for the production of ice-cream premix, a novel process for the production of low-fat starch-free mayonnaise and a bouillon cube manufacturing process.

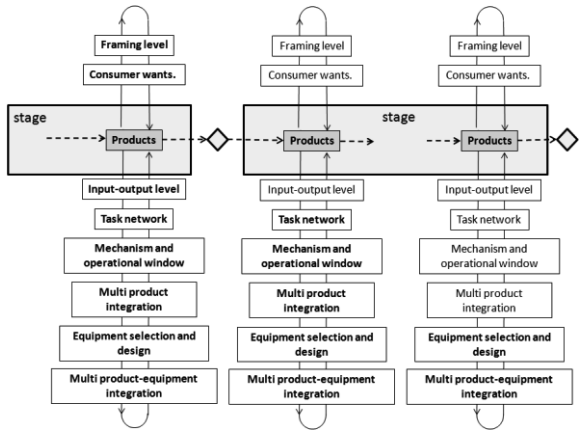

Figure 1. Product Driven Process Synthesis

3. Conclusions

In this contribution we present our approach towards product-driven process synthesis. The proposed methodology is composed of 9 levels of increasing degree of complexity and where complex and emerging decisions are made to proceed from one level to another. The whole methodology spans from how the new product can enlighten the consumer, financial and supply chain boundary conditions, through an optimal flowsheet able to produce the desired product cost effectively. The methodology's applicability and scope have been demonstrated using industrial cases as examples. A model-based strategy was implemented at various levels of the methodology, stressing the relevance of modelling towards more time- and cost-effective process synthesis.

4. References

[1] Verloop, J. (2004). Insight in Innovation - Managing Innovation by Understanding the Laws of Innovation. Amsterdam, Elsevier
[2] Cooper, R.G. (1990). Stage-gate systems: a new tool for managing new products. Business Horizons, p.44-54.
[3] Cooper, R.G. (1996). Overhauling the new product process. Industrial Marketing Management. 25, p.465-482
[4] Douglas, J. (1988). Conceptual design of chemical process. USA, McGraw-Hill
[5] Hill, M. (2004). Product and Process Design for Structured Products. AIChE Journal, 50(8),1656-1661
[6] Gani, R. (2004). Chemical product design: challenges and opportunities. Computers and Chemical Engineering, 28,2441-2457
[7] Edwards, M. F. (2006). Product engineering: Some challenges for Chemical Engineers. Transactions of the Institute of Chemical Engineers - Part A, 84(A4),255-260
[8] Wibowo, C. and Ng, K. M. (2002). Product-Centered Processing: Manufacture of Chemical-Based Consumer Products. AIChE Journal, 48(6),1212-1230
[9] Cussler, E. L. and Moggridge, G. D. (2001). Chemical Product Design. New York, Cambridge Series in Chemical Engineering
[10] Moggridge, G. D. and Cussler, E. L. (2000). An Introduction to Chemical Product Design. Transactions of the Institute of Chemical Engineers - Part A, 78,5-11
[11] Seider, W.D., Seader, J.D., Lewin, D.R., Widagdo, S. (2009) Product and Process Design Principles. Wiley press.
[12] Bongers, P., Almeida-Rivera, C. (2009). Product Driven Process Synthesis Methodology. Computer-Aided Chemical Engineering, 26, 231-236

I.A. Karimi and Rajagopalan Srinivasan (Editors), Proceedings of the 11th International Symposium on Process Systems Engineering, 15-19 July 2012, Singapore.

Sensitivity of Process Design due to Uncertainties in Property Estimates

Amol Hukkerikar[a], Mark Jones[a], Bent Sarup[b], Jens Abildskov[a], Gürkan Sin[a], and Rafiqul Gani[a]
[a] *CAPEC, Department of Chemical and Biochemical Engineering, Technical University of Denmark, DK-2800, Kgs.Lyngby, Denmark.*
[b] *Vegetable Oil Technology Business Unit, Alfa Laval Copenhagen A/S, Maskinvej 5, DK-2860, Søborg, Denmark.*

Abstract

The objective of this paper is to present a systematic methodology for performing analysis of sensitivity of process design due to uncertainties in property estimates. The methodology provides the following results: a) list of properties with critical importance on design; b) acceptable levels of accuracy for different thermo-physical property prediction models; and c) design variables versus properties relationships. The application of the methodology is illustrated through a case study of an extractive distillation process and sensitivity analysis of designs of various unit operations found in chemical processes. Among others vapour pressure accuracy for azeotropic mixtures is critical and needs to be measured or estimated with a ±0.25% accuracy to satisfy acceptable safety levels in design.

Keywords: Process design, sensitivity analysis, uncertainty, property prediction.

1. Introduction

The accuracy and reliability of the process design depends largely on the accurate physical and thermodynamic data and property models employed (Whiting, 1996). Since experimental values of many of the needed pure component and mixture properties cannot be expected to be measured, they must therefore be estimated. Also, process design involving new molecules/mixtures require their properties to be predicted through a suitable model. In such cases, it is important to know the uncertainties of the estimated property values that arise due to uncertainties in the regressed parameters of the selected property model (Hukkerikar et al., 2012). With this information, it is possible to answer the following two questions: (i) what is the effect of uncertainties in the property estimates on the design, and, (ii) which properties are the most sensitive from a process design point of view? These questions, once answered, can provide useful and critical insights into reliability of process design and eventually suggestions for further improvement.

In this paper we present a systematic methodology to establish the sensitivities of process design due to uncertainties in property estimates and to evaluate their effects on the final design; to list the properties based on their sensitivities; to establish acceptable levels of accuracy for different thermo-physical property prediction models; and to provide relationships between design variables and properties.

2. Methodology

The main steps of the systematic methodology for performing the sensitivity analysis for process design are shown in Figure 1.

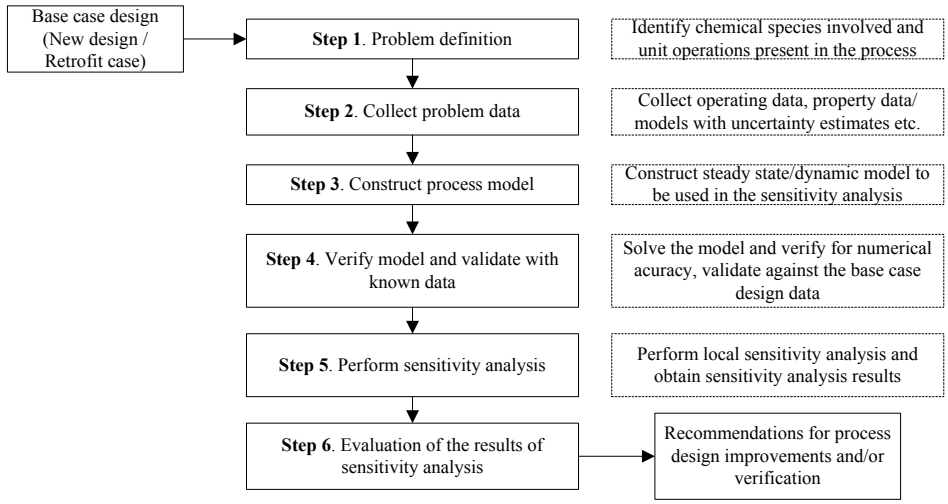

Figure 1. Methodology for performing the sensitivity analysis for process design

2.1. Step 1: Problem definition

In this step, the process (base case) for which sensitivity analysis is to be performed is defined. Information such as the chemical species involved, the unit operations present in the process is also defined.

2.2. Step 2: Collect problem data

The problem data is collected in this step. This includes operating data of the process, desired specifications, kinetics data (if reactions are involved), data related to economic evaluation, equipment data, property data and models of concerned properties together with uncertainties of the predicted property values.

2.3. Step 3: Construct process model

The objective of this step is to construct a model for the process under study so that the effects of change in property estimates can be analysed. The model may be steady state and/or dynamic, depending on the problem definition. Note that the property models belong to the constitutive equations that are part of the process model.

2.4. Step 4: Verify model and validate with known data

The process model is solved. The obtained simulation results are verified for numerical accuracy and validated against base case design data.

2.5. Step 5: Perform sensitivity analysis

Local sensitivity analysis (one-factor-at-a-time approach) is employed. The local sensitivity is the sensitivity of the model output when only one input factor (for example, vapor pressure) is perturbed at a time while keeping all other input factors fixed at their base case design values. The obtained sensitivity analysis results are represented in the form of plots showing relationships between design variables and the properties involved. The y-axis represents the deviation (expressed as relative error in %) of the design variables from its base case design value and the x-axis represents the expected prediction error (in %) in the properties.

2.6. Step 6: Evaluation of the results of sensitivity analysis

The objective of this step is to analyze the relationships between design variables and properties and evaluate the impact of uncertainties in the predicted properties on the design. This involves: (i) examining the slope of plot of design variable versus property

prediction error and identifying the most sensitive properties (a large slope implies that sensitivity of the design variable is high and the uncertainties in the property estimates are significant); (ii) analyzing the possible consequences (such as, effect on capital and operating cost) of property errors on the process design; and (iii) establishing an acceptable level of accuracy for property models based on the maximum allowable deviation (as specified by the user) in the design variable from its base case design value. The analysis carried out in step 6 can be used as an input to a process design tool for improvement in the design. The application of the methodology is illustrated using a case study of process design of extractive distillation.

3. Case Study: Sensitivity of extractive distillation design

3.1. Step 1: Problem definition

It is required to perform sensitivity analysis for design of an extractive distillation process (employed to separate acetone from methanol using water as an entrainer; to obtain a product of at least 99.4% of acetone) subject to uncertainties in the property estimates. Uncertainty estimates of property models are available.

3.2. Step 2: Collect problem data

The operating data of the extractive distillation process is collected from Gil et.al. (2009). The involved single value pure component properties and temperature-dependent properties are collected from the SIMSCI library available in PRO/II®. The UNIQUAC model is employed to calculate the liquid phase activity coefficients while the vapor phase is assumed to behave as an ideal gas.

3.3. Step 3: Construct process model

A steady state simulation model of the extractive distillation process is constructed in PRO/II®. The pure component properties involved in the design calculations are: (i) vapor pressure (P^s), (ii) critical temperature (T_c), (iii) heat of vaporization (H_{vap}), (iv) liquid density (ρ), (v) liquid viscosity (μ), (vi) surface tension (σ), and (vii) activity coefficient (γ). The design variables considered for sensitivity analysis are: (i) number of stages (N), (ii) reflux ratio (R), (iii) binary feed stage (N_f), (iv) entrainer stage (N_s), (v) column diameter (D), and (vi) reboiler (Q_r) and condenser (Q_c) heat duties.

3.4. Step 4: Verify model and validate with known data

The model is solved in PRO/II® and the obtained results are compared and validated against the results given by Gil et.al. (2009). A good match is obtained.

3.5. Step 5: Perform sensitivity analysis

The results of sensitivity analysis for selected design variables with respect to uncertainties in the selected predicted properties are shown in Figure 2. When necessary, chain rule is applied to obtain relationships between the design variables and the properties analysed. For example, to obtain sensitivity of N_s with respect to uncertainties in the predicted P^s, the following chain rule is applied: $[\partial R/\partial P^s]*[\partial N_s/\partial R] = [\partial N_s/\partial P^s]$. In Figure 2, the results are reported for only those simulations in which a converged solution satisfying the desired product purity is obtained from PRO/II®.

3.6. Step 6: Evaluation of the results of sensitivity analysis

Figure 2(a)-2(c) shows that even small errors in the predicted P^s of acetone and water may result in significant uncertainty in the design. The uncertainty (in terms of average relative error) of predicted P^s of acetone from DIPPR correlation used in PRO/II® is ±0.25%. This level of accuracy of P^s is found to have significant impact on the calculation of R, N and N_s (up to 20% deviation from base case). If this level of uncertainty in R, N and N_s is not acceptable then user needs to collect a higher accuracy

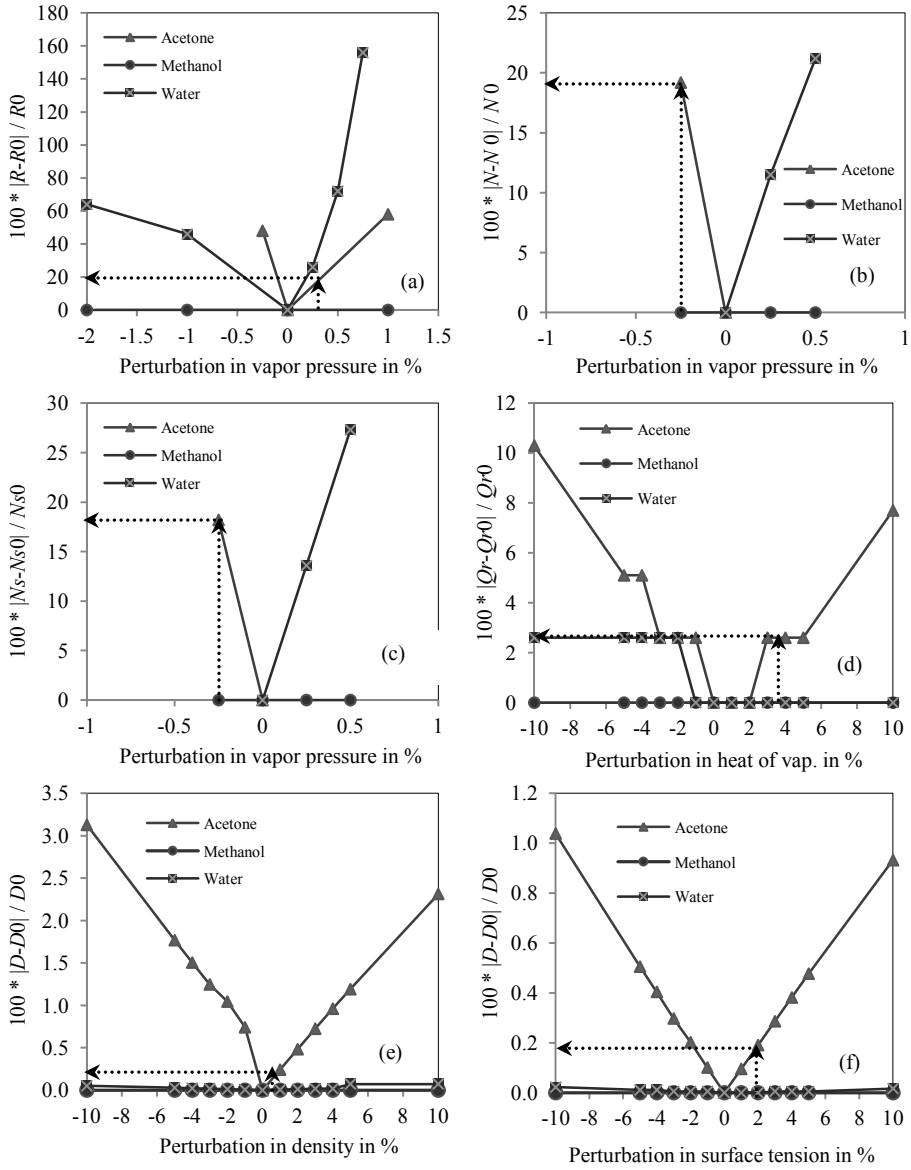

Figure 2. Sensitivity of *R, N, N_s, Q_r,* and *D* with respect to uncertainties in the predicted property values. *R0*, *N0*, N_s0, Q_r0, and *D0* represent the base case values and zero point on the x-axis represents the base case design.

data for P^s and use this data in regression to obtain improved model for P^s with desired accuracy level (i.e. error less than ±0.25%). The uncertainty of predicted H_{vap}, ρ, and σ of acetone from DIPPR correlation used in PRO/II® is ±3.44%, ±0.38%, and ±1.77% respectively. It can be seen from Figure 2(d) that accurate predictions of H_{vap} of acetone is important to reduce the uncertainty in calculation of Q_r. The sensitivities of *D* to prediction errors in ρ and σ are shown in Figures 2(e)-2(f). From Figures 2(a)-2(f), it can be seen that the most sensitive properties are P^s of acetone and water and H_{vap} of acetone. For this case study, process design without the consideration of uncertainties of

the predicted P^s and H_{vap} of acetone and P^s of water may lead to following consequences: (i) an overestimate (+ve or –ve) of R (which is undesirable from an operation point of view); (ii) an overestimate (+ve or –ve) of N and N_s resulting in an inefficient operation; and (iii) an overestimate (+ve or –ve) of Q_r and hence waste of utilities. This information serves as input for a process design tool to carry out further improvements. The uncertainty of design variables R, N, N_s, Q_r and D due to given uncertainties in predicted P^s, H_{vap}, and ρ is 20.0%, 18.0%, 17%, 2.5% and 0.20% respectively. The sensitivity of process design of several other unit operations have also been analysed. The results are summarized in Table 1.

Table 1. Results for sensitivity analysis of process design of unit operations analysed

Unit operation (chemical system involved)	Reference for problem data / required task	Properties inolved in the analysis	Variables considered for sensitivity analysis / most important properties (ranked)
Short-path evaporator (Glycerol + Mono-, Di-, and Tri-glyceride)	Sales-Cruz & Gani (2006) / separate glycerol from the mixture	P^s, T_c, P_c, H_{vap}, μ, specific heat (C_p), acentric factor (ω), and γ	Distillate (glycerol) flow rate / P^s of glycerol, γ of glycerol, ω of di-glyceride, P_c of di-glyceride C_p of glycerol and di-glyceride, T_c of glycerol, H_{vap} of di-glyceride.
Batch distillation (Multicomponent mixture of A, B, C, and D)	ICAS-MoT® / separate A from the mixture	Relative volatality ($\alpha = P^s/P^s_{ref}$)	Purity of A in the distillate / α of component A
Flash process (methanol and water)	ICAS-MoT® / Separate methanol from the mixture	P^s, T_c (used in the correlation for H_{vap}), and ρ	Product (methanol) flow rate / T_c of methanol, P^s of methanol, ρ of methanol Volume of the flash tank / T_c of methanol, ρ of methanol

4. Conclusions

In this work, a systematic methodology to analyze the sensitivity of process design due to uncertainties in property estimates is presented. The application of the methodology is highlighted through several examples. The results of the sensitivity analysis helps to establish relationships between design variables and properties; allows evaluation of the impact of uncertainties in the property estimates on the process design; and helps to identify the most sensitive properties from a process design point of view, thereby, contributing to better-informed and reliable design solutions. Our current and future work is focussed on evaluation of effect of uncertainties of predicted mixture properties (such as, liquid activity coefficient) on the process design.

References

W.B. Whiting, 1996, Journal of Chemical & Engineering Data, 41, 935-941.

A.S. Hukkerikar. B. Sarup, A. Ten Kate, J. Abildskov, G. Sin, and R. Gani, 2012, Fluid Phase Equilibria, 321, 25-43.

Integrated Computer Aided System (ICAS version 14.0), Department of Chemical Engineering, Technical University of Denmark, Lyngby, Denmark, 2010.

I.D. Gil, D.C. Botia, P. Ortiz, and O.F. Sanchez, 2009, Industrial Engineering and Chemical Research, 48, 4858-4865.

M. Sales-Cruz and R. Gani, 2006, Chemical Engineering Research and Design, 84, 583-594.

I.A. Karimi and Rajagopalan Srinivasan (Editors), Proceedings of the 11th International Symposium on Process Systems Engineering, 15-19 July 2012, Singapore.

An integrated quantitative index of stable steady state points in chemical process design

Hangzhou Wang, Bingzhen Chen *, Tong Qiu, Xiaorong He, Jinsong Zhao

Department of Chemical Engineering, Tsinghua University, Beijing 100084, China

Abstract

In order to design inherently safer chemical processes, researchers proposed many methods and strategies, many quantitative indices have been developed to describe the potential hazard and dangerous of different reaction routes and reactants. Because in emergency situation the disturbance may be so large that the system can not return back to the steady state points. For considering both situations under small and large disturbances, this paper proposed a quantitative index (QI), in which disturbance range index (RI) and convergence speed index (SI) were integrated, considering both capability of resistance to disturbances and speed to return to steady state point. Based on the integrated index, this paper proposed an approach for designing a more stable chemical process that can maintain stable within larger region to resist the disturbance and has shorter time to approach to the original stable steady state operation point when disturbance is encountered. The approach is applied to methyl methacrylate polymerization process and a multi-objective optimization problem considering both economic and stability factors were conducted and a Pareto set is obtained.
Keywords: inherently safer; process design; quantitative index; multi-objective optimization

1. Introduction

The concept of inherently safer design was proposed by Kletz, the main concept is that avoids hazards instead of controlling them. Also Kletz proposed many methods and strategies for engineering such designs in practice. Hendershot reviewed the development of inherently safer design strategies in chemical processes. Stability describes the behavior of a system when a disturbance is encountered. Because of the complexity and non-linearity of chemical processes, a system may have multiple steady states and the stabilities of these operating points are different even in the same reaction route. Uppal, Balakotaiah, Yuan and Razon theoretically analyzed the multiple steady state solutions of reactors. Flores-Tlacuahuac, Katariya and Mancusi analyzed more complex chemical processes. Seider also studied multiple steady state solutions of reactors. In the existing related works, only Meel proposed a quantitative index to describe the instability of unstable points. In authors' previous paper a universal quantitative index based on the time for convergence to a stable point under a given small disturbance is introduced. However, even stable steady state operation points have different stabilities from one to another, so it is important to develop a quantitative index of stability for these steady state points. Such an index would play an important role in comparing the stabilities of given operating points or optimizing the process operation conditions.

2. Process design approach

Because in emergency situation the disturbance may be so large that the system can not return back to the steady state points. For considering both situations under small and large disturbances in dynamic model of chemical process

$$\begin{cases} \dfrac{d\mathbf{x}}{dt} = \mathbf{F}(\mathbf{x}) \\ \mathbf{x}(0) = \mathbf{x}^* + \Delta\mathbf{x} \end{cases}$$

Where x* is the steady state solution, $\Delta\mathbf{x}$ is the disturbance. The Jacobian matrix of $\mathbf{F(x)}$ is $\mathbf{F_x}$, and the eigenvalue of $\mathbf{F_x}$ is λ_i. We define disturbance range index

$$RI = \frac{\max(\Delta x^+) + \max(\Delta x^-)}{x^*}$$

where $\Delta x^+ \le x^*$, $\Delta x^- \le x^*$, Δx^+ and Δx^- are positive and negative disturbances of focused variable, respectively. We also define convergence speed index

$$SI = \left| \frac{\prod_{i=1}^{n} \lambda_i}{\sum_{i=1}^{n} \prod_{j=1, j\neq i}^{n} \lambda_i} \right|$$

After normalized RI and SI, we define a quantitative index

$$QI = \min(RI, SI)$$

QI considers both capability of resistance to disturbances and speed to return to steady state point. Based on the integrated index, this paper proposed an approach for designing a more stable chemical process that can maintain stable within larger region to resist the disturbance and has shorter time to approach to the original stable steady state operation point when disturbance is encountered. The detailed steps of this approach are illustrated as follows:

(1) Solve the steady state solution of the dynamic model of chemical process.
(2) Judge the stability of these solutions and distinguish the stability of these solutions, divided the solution curve into parts with different stabilities (stable and unstable).
(3) Calculate RI, the larger RI is the larger convergence range does.
(4) Calculate SI, the larger SI is the faster convergence speed does.
(5) Calculate QI, and QI is better when it is larger.
(6) Use QI for multi-objective process operation optimization.

The approach is applied to methyl methacrylate polymerization reactor process, and a multi-objective optimization problem considering both economic and stability factors was conducted, a Pareto set is obtained. The optimization results provide information that is very important for guiding process design and operation.

3. Case study

Methyl methacrylate (MMA) is an important chemical product and an MMA polymerization reactor is shown in Fig. 1 below.

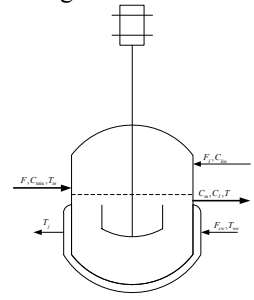

Figure 1 Polymerization reactor flow sheet

For free-radical polymerization, the following elementary reactions are postulated:

Initiation	$I \xrightarrow{k_D} 2R \quad M+R \xrightarrow{k_1} P_1$
Propagation	$P_i + M \xrightarrow{k_p} P_{i+1}$
Monomer transfer	$P_i + M \xrightarrow{k_{fm}} P_i + D_i$
Addition termination	$P_i + P_j \xrightarrow{k_{tc}} D_{i+j}$

Disproportionation termination $P_i + P_j \xrightarrow{k_{td}} D_i + D_j$

where I, P, M, R, and D stand for initiator, polymer, monomer, radicals and dead polymer, respectively. The mathematical model for this reactor is given by:

$$\frac{dC_m}{dt} = -(k_p + k_{fm})C_m P_0 + \frac{F(C_{min} - C_m)}{V}$$
$$\frac{dC_I}{dt} = -k_I C_I + \frac{F_I C_{Iin} - FC_I}{V}$$
$$\frac{dT}{dt} = \frac{-\Delta H k_p C_m}{\rho C_p} P_0 - \frac{UA}{\rho C_p V}(T - T_j) + \frac{F(T_{in} - T)}{V}$$
$$\frac{dD_0}{dt} = (0.5k_{tc} + k_{td})P_0^2 + k_{fm} C_m P_0 - \frac{FD_0}{V}$$
$$\frac{dD_1}{dt} = M_m(k_p + k_{fm})C_m P_0 - \frac{FD_1}{V}$$
$$\frac{dT_j}{dt} = \frac{F_{cw}(T_{w0} - T_j)}{V_0} + \frac{UA(T - T_j)}{\rho_w C_{pw} V_0}$$

where

$$P_0 = \sqrt{\frac{2f^* C_I k_I}{k_{td} + k_{tc}}}$$

$$k_r = A_r e^{\frac{-E_r}{RT}}, \quad \text{r=p, fm, I, td, tc}$$

The parameter values of the model are listed below in Tab. 1.

Table 1. Parameters for the MMA polymerization reactor

Parameter	Value	Unit	Parameter	Value	Unit
F	1.0	m^3/h	M_m	100.12	kg/kmol
F_I	0.0032	m^3/h	f^*	0.58	—
F_{cw}	0.1588	m^3/h	R	8.314	kJ/(kmol K)
C_{min}	6.4678	$kmol/m^3$	$-\Delta H$	57800	kJ/kmol
C_{Iin}	8.0	$kmol/m^3$	E_p	1.8283*10^4	kJ/kmol
T_{in}	350	K	E_I	1.2877*10^5	kJ/kmol
T_{w0}	293.2	K	E_{fm}	7.4478*10^4	kJ/kmol
U	720	kJ/(h K m^2)	E_{tc}	2.9442*10^3	kJ/kmol
A	2.0	m^2	E_{td}	2.9442*10^3	kJ/kmol
V	0.1	m^3	A_p	1.77*10^9	m^3/(kmol h)
V_0	0.02	m^3	A_I	3.792*10^18	1/h
ρ	866	kg/m^3	A_{fm}	1.0067*10^15	m^3/(kmol h)
ρ_w	1000	kg/m^3	A_{tc}	3.8228*10^10	m^3/(kmol h)
C_p	2.0	kJ/(kg K)	A_{td}	3.1457*10^11	m^3/(kmol h)
C_{pw}	4.2	kJ(kg K)			

The steady state operation points for this model are shown in Fig. 2. It can be seen that monomer concentration changes with effluent value, and there are multiple steady states in this process.

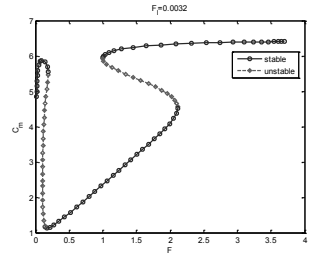

Figure 2 Changes in monomer concentration and temperature with effluent value

Changes in RI, SI and QI with effluent in part 1, 2 and 3 are shown in Fig. 3, 4 and 5.

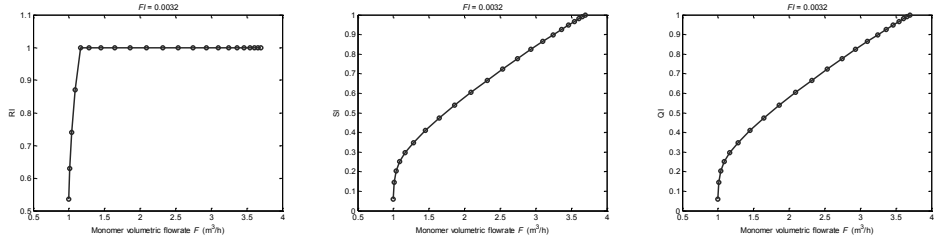

(a) RI with effluent (b) SI with effluent (c) QI with effluent

Figure 3 Changes in RI, SI and QI with effluent(Part 1)

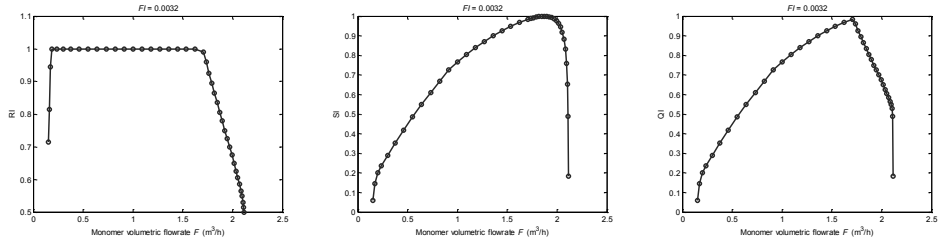

(a) RI with effluent (b) SI with effluent (c) QI with effluent

Figure 4 Changes in RI, SI and QI with effluent(Part 2)

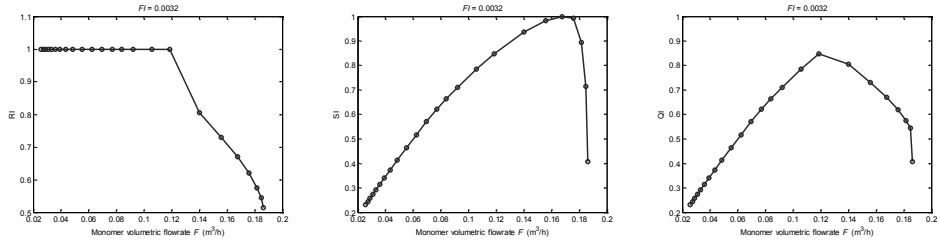

(a) RI with effluent (b) SI with effluent (c) QI with effluent

Figure 5 Changes in RI, SI and QI with effluent(Part 3)

When economy and inherent safety are considered as the main factors in chemical process design, the concentration of monomer indicates the reaction efficiency, and it could indicate process economy. The proposed quantitative stability index could indicate the inherent safety of the reaction. Consequently selecting operation points is a multi-objective (monomer concentration and quantitative stability index) optimization problem. The optimization result is a Pareto set, shown in Fig. 6.

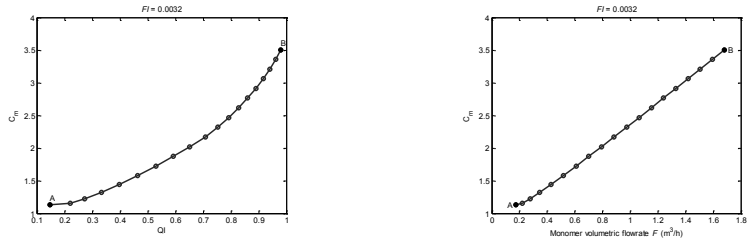

(a) Changes in concentration and quantitative stability indices (b) Changes in concentration with effluent value

Figure 6 Optimization result for the multi-objective: economy and stability (Pareto sets)

Point A is the maximum economic operation point where the monomer with the highest reaction efficiency and point B is the maximum inherent safety point where the convergence time is shortest when a disturbance is encountered and the resistance range of disturbance is the largest at the same time. These values of are listed in Tab. 2.

Table 2. Values of operating points A and B

Points	F	Cm	QI
A	0.173	1.132	0.146
B	1.679	3.505	0.979

In process design the final operation point would be determined from the optimized Pareto set according to the detailed economical and safety requirement.

4. Conclusion

From this study, conclusions can be drawn:

(1) Stability is an important factor in design of an inherently safer chemical process.
(2) Quantitative stability index is useful in multi-objective optimization problem when stability was considered as one of the objectives.

5. Acknowledgements

The authors gratefully acknowledge financial support from National Basic Research Program of China (Grant No. 2012CB720500).

References

V. Balakotaiah, D. Luss, 1984, Global Analysis of the Multiplicity Features of Multi-Reaction Lumped-Parameter Systems. Chemical Engineering Science, 39, 5, 865-881.
E. Gazi, W. D. Seider, L. H. Ungar, 1996, Verification of controllers in the presence of uncertainty: Application to styrene polymerization. Industrial & Engineering Chemistry Research, 35, 7, 2277-2287.
K. S. Gritton, J. D. Seader, W. J. Lin, 2001, Global homotopy continuation procedures for seeking all roots of a nonlinear equation. Computers & Chemical Engineering, 25, 7/8, 1003-1019.
D. C. Hendershot, 2006, An overview of inherently safer design. Process Safety Progress, 25, 2, 98-107.
F. Jalali, J. D. Seader, S. Khaleghi, 2008, Global solution approaches in equilibrium and stability analysis using homotopy continuation in the complex domain. Computers and Chemical Engineering, 32, 10, 2333-2345.
A. Katariya, K. Moudgalya, S. Mahajani, 2006, Nonlinear dynamic effects in reactive distillation for synthesis of TAME. Industrial and Engineering Chemistry Research, 45, 12, 4233-4242.
T. Kletz, 1978, What you don't have, can't leak. Chemistry and Industry, 6, 287-292.
A. Meel, W. D. Seider, M. Soroush, 2006, Game theoretic approach to multiobjective designs: Focus on inherent safety. AIChE Journal, 52, 1, 228-246.
L. F. Razon, 2006, Stabilization of a CSTR in an oscillatory state by varying the thermal characteristics of the reactor vessel. International Journal of Chemical Reactor Engineering, 4, 1320-1329.
W. D. Seider, D. D. Brengel, A. M. Provost, S. Widagdo, 1990, Nonlinear-Analysis in Process Design - Why Overdesign to Avoid Complex Nonlinearities. Industrial and Engineering Chemistry Research, 29, 5, 805-818.
A. K. Trevor, 2003, Inherently Safer Design-Its Scope and Future. Institution of Chemical Engineers Trans IChemE, 81, Part B, 401-405.
H. Z. Wang, Z. H. Yuan, B. Z. Chen, X. R. He, J. S. Zhao, T. Qiu, 2011, Analysis of the stability and controllability of chemical processes. Computers & Chemical Engineering, 35, 6, 1101-1109.
Z. H. Yuan, H. Z. Wang, B. Z. Chen, J. S. Zhao, 2009, Operating zone segregation of chemical reaction systems based on stability and non-minimum phase behavior analysis. Chemical Engineering Journal, 155, 1-2, 304-311.
Q. P. Yuan, Z. M. Qian, 2003, The Study on Static Bifurcation Behavior of the Immobilized Yeast Spherical Beads for Ethanol Production, Journal of Chemical Engineering of Chinese Universities, 17, 5, 527-533.

I.A. Karimi and Rajagopalan Srinivasan (Editors), Proceedings of the 11th International Symposium on Process Systems Engineering, 15-19 July 2012, Singapore.

Applicability of product-driven process synthesis to separation processes in food

Lena Jankowiak[a], Atze J. van der Goot[a], Olivera Trifunovic[b], Peter M.M. Bongers[b], Remko M. Boom[a]

[a]*Laboratory of Food Engineering, Wageningen University, P.O. Box 8129, 6700 EV Wageningen, The Netherlands*
[b]*Unilever Research, P.O. Box 114, 3130 AC Vlaardingen, the Netherlands*

Abstract

The demand for more sustainable processing in the food industry is rising but requires structured methodologies to support the fast implementation of new economic and sustainable processes. Product-driven process synthesis (PDPS) is a recently established methodology facilitating the rapid development of feasible process alternatives for structured products, such as in mayonnaise, ice-cream, or margarine.
Here, we present the application of the PDPS methodology to valorize okara, which is a by-product from soy milk production. It is produced in large amounts, but its use as food or feed is not fully exploited. Besides fibers, protein, and fat, it contains substantial amounts of isoflavones, which are high value components. This paper evaluates the PDPS-methodology for the design of an economic and sustainable process for the production of isoflavones from okara. The main challenge is to adapt the method in such a way that it is able to deal with a complex matrix as starting material. Therefore, the PDPS methodology may require extension. Nevertheless, it promises to be a useful tool also for fractionation of food materials.

Keywords: Product-driven process synthesis, separation, okara, isoflavones.

1. Introduction

During the last decade, conventional product design and process design have been combined into product-oriented process synthesis. An important component of this methodology is aimed at the generation and screening of alternative flow sheets. Conceptualization retards the fixation of a flow sheet, which reduces the risks of irreversible mistakes during the design of a process. However, the process synthesis methodologies have to be updated concomitantly due to the dynamics within the industry, such as a shifting product portfolio, new economic situations, new regulations, and sustainability concerns [1].
Process synthesis has been developed mainly for chemical products until the similarities between complex chemical consumer goods and structured food products were recognized [2-6]. The latter explains the growing interest of the food industry to translate conceptual design methodologies from the chemical sector into the food sector. Therefore, Bongers and Almeida-Rivera (2009) suggested a new methodology combining product and process synthesis based on the systems engineering strategy. This methodology, called product-driven process synthesis (PDPS), eases the complexity of the problem by dividing the problem into several hierarchically ordered

levels. Each level requires important and complex decisions, which allows the user to strategically go from one level to the next one [7, 8].
In this paper we describe in which way PDPS should be further developed to make it applicable for separation processes in food. Refinery of biomaterials is now increasingly important and the separation of high value components is a method to improve the economic potential of bio refinery processes. Okara, a by-product of the soy milk industry, is used as a case study.

2. Applications of PDPS in the food industry

Food microstructure largely determines the properties and, consequently, the consumer acceptance of a food. Contrary to chemical products, spatial distribution of the foods' ingredients is a key attribute of the product, because it largely determines texture, sensory, flavor, and mechanical properties [8, 9].
The PDPS methodology is divided into several levels as described in detail by Bongers and Almeida-Rivera (2009) [8]. The core of the methodology is in levels 1 to 3. Level 1 describes the input and output, level 2 asks for the development of the task network, and level 3 describes the mechanisms and operational window. The most recent application of PDPS is described by Gupta and Bongers (2011) [10]. The authors redesigned a bouillon cube production process by applying PDPS resulting in improved structure of the product, shorter cooling times, and reduction of redundant ingredients. Other examples of structured food products, where the PDPS approaches were practical, are mayonnaise, dressings, and ice-cream [8, 9]. Such food products have one thing in common: they are made by combining single ingredients, and the production process has to consider the interplay of ingredients to obtain the desired end product with the preferred attributes and microstructure.

3. Applicability of PDPS for a separation process

Hostrup et al. (1999) presented an integrated approach of product design and separation process synthesis for chemical processes [11]. The authors used an optimization-based approach combining mathematical modeling with heuristics to design a solvent and a separation process simultaneously. One of the key success factors was the availability of thermodynamic data of the system. However, such approach is difficult to realize for structured food products, since detailed thermodynamic models are generally not available for complex food systems.
The use of PDPS to design a separation process is more complex than for the design of a final structured product. This can be demonstrated by comparing a case in which a three component product is formed, and in which such a product is separated into its building blocks. First, we show how the PDPS methodology works in case a product contains three hypothetical ingredients: A, B and C. In level 1 the input stream and output stream are defined. Thus, the input has to contain component A, component B, and component C. The process can be modified according to the order in which the ingredients are added, but the output is in any case a mixture of component A, B, and C. In the case of a separation process the output is not as straightforward. If the input consists of a structure ABC, the output greatly depends on the process, and the input can result in at least two options for the output. Assuming the main interest is in component A, the options are the following: ABC = A+B+C or ABC = A+BC

The first option can also be obtained by two more options:
ABC = C+AB ➔ C+A+B or ABC = B+AC ➔ B+A+C
The more components the starting material contains, the higher the number of options that should be considered when defining the input and output, and sequences of separation in the task network. The existence of more possibilities for the input/output level is not the only challenge. In case of separation, a component will never be completely separated and will contain certain impurities (e.g. A+*A*BC or A*BC*+BC). Many ratios and combinations of components are possible, which complicates building task networks if limited experimental results are available, and information about the thermodynamics on the process and components is incomplete.

4. Case study: Separation of isoflavones from okara

In contrast to previous approaches where a microstructure had to be established, the starting material in the following case is a structured by-product of the food industry (okara), which has to be decomposed to produce a single ingredient to fully utilize the economic potential of okara.
Being the insoluble part after water extraction of the soybeans, okara contains predominantly insoluble fibers. Additionally, depending on soybean variety and processing conditions, okara contains isoflavones, often present in a range of 0.1-0.2% (db) [12-14]. Isoflavones are minor components belonging to a group of polyphenols and having a high potential economic value due to suspected health benefits [15, 16].
The value of the end product, the isoflavones, can be estimated by comparison to similar, commercially available products. Information about available margins for the process can be obtained by comparing the input value of okara and the output values. Those calculations showed that the economic potential is highest if the output consists of isoflavones in powder form of high purity (>70%).
Further design rules were defined and comprise the following:

- To avoid production of further unutilized waste
- The process should be sustainable regarding energy, water, and chemical usage
- The isoflavone mixture should have a certain purity, be in powder form, food-grade, and microbiological stable

As far as we are aware of, okara is not used as a starting material for isoflavone production yet. Therefore, experiments have to be performed to support decision making during process synthesis.

4.1. Level 1 Input and output

A major difference to the conventional application of PDPS appeared already when the input and output were defined. At this level, the process is only represented with a black box with an incoming stream (input) and an outgoing stream (output).
The only certainty at this stage is the input, namely okara. Moisture content and major components of the material were measured to further characterize the input (Tab.1).

Table 1 Characterization of okara

Moisture (%)	Carbohydrates (% db)		Proteins (% db)	Fat (% db)	Isoflavones (%db)
	Sugars (%)	Uronic acid (%)			
81 ± 0.5	47.5 ± 3.3	6.1 ± 0.2	32.0 ± 0.4	14.6 ± 0.03	0.12 ± 0.01

The output can be twofold. The isoflavones should either be separated in a way that the residual material can still be used, for example as animal feed, thus having the same composition as before only absent of isoflavones. The other option involves separation of several components, which could allow the use of other components as a food ingredient (e.g. soy protein isolate).
The black box representing the process is now evaluated in more detail in the following step, the task network level, as will be described in the following section.

4.2. Level 2 Task network

The basic class of task is defined as separation. We define it as the separation of isoflavones from the rest of the matrix (Fig.1).

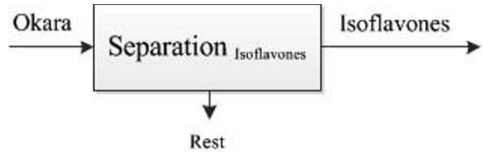

Figure 1 Class of task: separation of isoflavones from okara

To be more specific, a task network could look like in Fig. 2 including some more fundamental tasks.

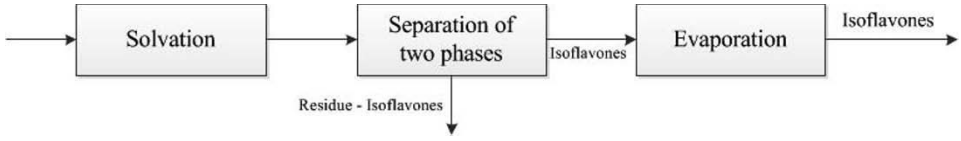

Figure 2 Example of a task network for separation of isoflavones from okara

Okara is a fibrous material, and the isoflavones are in relatively low concentrations present compared to other components. It is assumed that some sort of liquid is available for the disclosure of the isoflavones from the fibrous matrix. Solvation means in this case dissolution of okara in a liquid. Then the liquid, which we assume contains all the isoflavones after some time, has to be separated from the rest of the matrix. Last but not least, one of our design rules says that a dry powder is required. Thus, concentration and solidification (e.g. through evaporation) will be necessary, very likely as the last step of the process. However, at an early stage, there are many possible task networks, and Fig. 2 is only one example. A conservative estimation of the number of possibilities is 12, considering different sequences of separation of the components of okara. This increased number requires insight in the behavior of the materials, and thus, the involvement of experimental experience at an earlier stage compared to the PDPS for a structured product. Experiments are needed to narrow down the possibilities and refine or substitute those fundamental tasks. Thus, an ongoing alternating process between design and experiments seems to be required to reach the final process design.
The PDPS methodology, however, supports and guides the user to be aware of all possibilities and to allow motivated decisions. It becomes even more important to apply a structured approach, and systematically go through different options, when the system becomes more complex.

To summarize, it is possible to apply PDPS to separation processes in the food industry The case discussed above differs from previous cases (mayonnaise, ice-cream, or bouillons) primarily in the fact that there is no existing process describing the separation of isoflavones from okara. Moreover, a separation process can lead to more outcomes than a structuring process and uncertainty in the compositions of the streams. That is why the method needs further development in describing how and when the design process should interact with experimental work to limit the number of possible process design and task networks.

5. Conclusion

Product-driven process synthesis is a useful tool for product and process development in the food industry. The complexity associated with highly structured products can be captured systematically by combining existing product design methodologies with process synthesis. Furthermore, the breakdown of the problem into several levels, and refinement in each level as the design progresses, helps to tackle the problem strategically.
Since the need for a more sustainable use of resources rapidly increases, PDPS is now also used to upgrade a structured by-product of the food industry. Applying the PDPS methodology to an already existing structured food product may require some extensions of the methodology due to the fact that a structure has to be decomposed instead of built. Nevertheless, PDPS is also useful for fractionation of food material even though it requires some further developments, including a continuous information exchange between experimental work and design.

Acknowledgment

The financial support of the Institute for Sustainable Process Technology (ISPT), the Netherlands, is gratefully acknowledged.

References

[1] S.D. Barnicki and J.J. Siirola, Comput. Chem. Eng., 28 (2004)
[2] G.D. Moggridge and E.L. Cussler, Chem. Eng. Res. Des., 78 (2000)
[3] C. Wibowo and K.M. Ng, Aiche J., 47 (2001)
[4] C. Wibowo and K.A. Ng, Aiche J., 48 (2002)
[5] B. Harjo, C. Wibowo and K.M. Ng, Chem. Eng. Res. Des., 82 (2004)
[6] M. Hill, Comput. Chem. Eng., 33 (2009)
[7] J.M. Douglas, Aiche J., 31 (1985)
[8] P.M.M. Bongers and C. Almeida-Rivera, Comput.-Aided Chem. Eng. (2009) 231-236
[9] F.M. Meeuse, J. Grievink, P.J.T. Verheijen and M.L.M. vander Stappen, Aiche Symp. Ser. (2000) 324-328
[10] S. Gupta and P. Bongers, Chem. Eng. Process., 50 (2011)
[11] M. Hostrup, P.M. Harper and R. Gani, Comput. Chem. Eng., 23 (1999)
[12] C.J.C. Jackson, J.P. Dini, C. Lavandier, H.P.V. Rupasinghe, H. Faulkner, V. Poysa, D. Buzzell and S. DeGrandis, Process Biochem., 37 (2002)
[13] V.E.A. Rinaldi, P.K.W. Ng and M.R. Bennink, Cereal Chem., 77 (2000)
[14] H. Wang and P.A. Murphy, J. Agric. Food Chem., 42 (1994)
[15] M.J. Messina, V. Persky, K.D.R. Setchell and S. Barnes, Nutr. Cancer, 21 (1994)
[16] K.D.R. Setchell and A. Cassidy, J. Nutr., 129 (1999)

I.A. Karimi and Rajagopalan Srinivasan (Editors), Proceedings of the 11th International Symposium on Process Systems Engineering, 15-19 July 2012, Singapore.

Simultaneous optimization of hydrogen network with desulfurization processes embedded

Li Zhou, Zuwei Liao, Jingdai Wang, Bingbo Jiang, Yongrong Yang*

Department of Chemical and Biochemical Engineering, Zhejiang University, Zhejiang, China

Abstract

In refineries, hydrogen purification techniques include hydrocarbon removal units and hydrogen sulfide (H_2S) removal units. Hydrocarbon removal units such as membrane separation and pressure swing adsorption (PSA) are frequently employed in the hydrogen network integration (HNI) study. However, the possibility of integrating H_2S removal units into HNI study has been overlooked until recently. In the present work, an improved modeling and optimization approach has been developed to integrate H_2S removal units into HNI. By introducing a desulfurization ratio, $R_{ds_{pl,i}}$, simplified mass exchange network (MEN) is incorporated into hydrogen distribution network. Total annual cost (TAC) is employed as the optimizing object to investigate the tradeoffs between hydrogen distribution network cost and MEN cost. A practical case study is used to illustrate the application and effectiveness of the proposed method.

Key words: hydrogen network; H_2S removal network; desulfurization ratio; total annual cost; optimization.

1. Introduction

Hydrogen network integration has been extensively explored and the studies carried out can simply be classified into two major categories: 1) Pinch analysis approaches, 2) Mathematical programming approaches based on superstructures. The first graphical hydrogen pinch analysis approach was developed by Alves [1,2], who proposed a hydrogen surplus diagram in the purity versus flowrate coordinate system. Later, another coordinate system, the purity versus impurity load system, was employed by Agrawal and Shenoy [3] and Bandyopadhyay [4]. Liao et al. [5] presented a new algebraic method addressing the relationship between pinch simplification and the mathematical model. Recently, pinch analysis for placing purifiers has been improved: optimal placements were obtained for both remove ratio specified [6] and tail gas purity specified [7] purifier models. Pinch analysis methods are useful in giving design targets, while mathematical programming methods are powerful in detailed design. Hallale [8] proposed a MINLP optimization approach. Liao [9] developed a systematic approach for the integration of hydrogen network with purifiers. Considering the life cycle of hydrogenation catalysts, Xuan et al [10] extended the problem formula to cope with the multi-period operation problems. Recently, Jia [11] considered the multi-component effect of hydrogen streams by integrating flash calculations, which made the obtained result more feasible.

However, the incorporation of H_2S removal units into multi-component HNI remains unexplored. In the present work, we aim to develop a systematic optimizing approach that incorporates desulfurization processes with HNI. Desulfurization ratio, $R_{ds_{pl,i}}$, is introduced to connect hydrogen network and the hydrogen sulfide removal network. Total annual cost (TAC) is employed to learn the trade-offs between hydrogen distribution network cost and MEN cost and a real world case study is illustrated.

2. Novel modeling and optimization approach

State-space superstructure [12] is modified in the present work to capture the feature of our desulfurization processes embedded hydrogen network. To be more specific, the hydrogen network in

* Corresponding author. Email: yangyr@zju.edu.cn Fax: + 86 571 87951227

this work is demonstrated as a system of four interconnected blocks as shown in Fig. 1: 1) Hydrogen distribution section; 2) hydrocarbon removal section, where the hydrocarbons get removed and hydrogen concentration of relevant streams get upgraded. 3). Desulfurization section, where the H2S contaminant gets partially removed from the process stream. 4). Compressor section, where the pressure level of streams get upgraded. It's worth noting that the inlets of the purifiers as well as the compressors can serve as hydrogen sinks, while the outlets are considered as hydrogen sources.

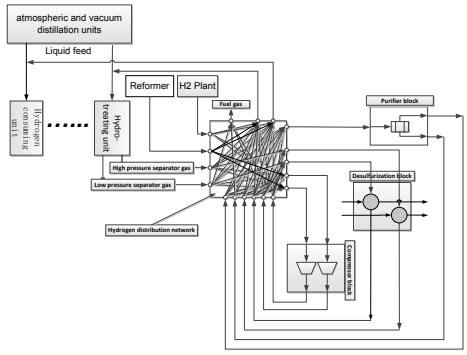

Fig. 1 State-space representation of hydrogen network.

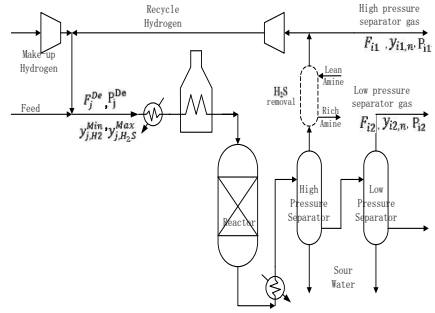

Fig. 2 Schematic diagram of a typical hydrotreating unit.

Fig. 2 represents a typical hydro-treating unit. As is shown, H_2S removal units are optionally installed to remove the overloaded hydrogen sulfide from the HP separator purges in order to reuse the hydrogen. However, there is also reuse potential in the LP separator gases. Though the hydrogen concentrations of these gas streams from LP separator are relatively lower than that of the gas streams from HP separators, while the H_2S concentrations are higher, those streams could be further reused after properly handled with purifiers. In order to hit the ultra-high efficient of hydrogen usage, desulfurization unit is introduced as mass exchange network and incorporated into the hydrogen network integration. It should be stress out that the present work only concerns half of the MEN design, i.e. the distribution of the rich streams and simple design of the desulfurization column.

The inlet and outlet flowrate of the desulfurization column are assumed to be identical:

$$F^{in}_{ds_{pl,i}} = F^{out}_{ds_{pl,i}} \qquad \forall\, pl \in PL, i \epsilon I \tag{1}$$

For the desulfurization column design, the theoretical number of trays N_T is analytically calculated by making use of the Kremser equation [13].

If $A \neq 1$:

$$N_T = \frac{\log\left[\left(y^{in} - mx^{in} - c\right)/\left(y^{out} - mx^{in} - c\right)\left(1 - 1/A\right) + 1/A\right]}{\log A} \tag{2}$$

If $A = 1$:

$$N_T = \frac{\left(y^{in} - y^{out}\right)}{\left(y^{out} - mx^{in} - c\right)} \tag{3}$$

where $A = \frac{L}{mG}$, which is the ratio of the operating line slope to the equilibrium line slope, and is called the absorption factor. In this work, the absorption factor is simply assumed to be 1.

As tradeoffs exist between hydrogen distribution network cost and the MEN cost. The more hydrogen sulfide gets removed in the MEN, the more hydrogen can be reused in the hydrogen distribution

network, while the cost of the MEN will increase and the cost of the hydrogen distribution network will decrease. Consequently, the desulfurization ratio, $R_{ds_{pl,i}}$, is selected as an optimizable variable to investigate the tradeoffs.

$$y_{ds_{pl,i}}^{out} = \left(1 - R_{ds_{pl,i}}\right) y_{ds_{pl,i}}^{in} \qquad \forall\, pl \in PL, i\epsilon I \tag{4}$$

$$1 \le R_{ds_{pl,i}} \le 1 \qquad \forall\, pl \in PL, i\epsilon I \tag{5}$$

Then the following equation can be deduced:

$$N_{T,ds_{pl,i}} = \frac{\left[y_{ds_{pl,i}}^{in} - (1-R_{ds_{pl,i}}) y_{ds_{pl,i}}^{in}\right]}{\left[(1-R_{ds_{pl,i}}) y_{ds_{pl,i}}^{in} - mx^{in} - c\right]} \qquad \forall\, pl \in PL, i\epsilon I \tag{6}$$

The capital cost of a desulfurization column in the present work is simply assumed to be \$4552 per year per stage [14].

$$C_{ds_{pl,i}} = 4552 N_{T,ds_{pl,i}} \qquad \forall pl \in PL,\ \ i \in I \tag{7}$$

As the modeling of other blocks had been widely investigated in HNI study, we will not give a detailed description here subject to the limited space.

3. Case study

A case study with two hydrogen producers and five hydrogen consumers is presented to illustrate the application of the methodology developed. The base case hydrogen network including the placement of the existing pipes and compressors is shown in Fig. 3. Table 1 shows the physical pipe distances between the units, while the inlet stream hydrogen constraints and impurity constraints are illustrated in Table 2.

Table 1 Piping distances between the units for base case.

Source	Sink				
	PE	GHT	G/DHT	PP	DHT
HPlant	400	1900	200	2400	900
RF	1100	1200	900	1700	200
G/DHT	600	2100	0	2600	1100
DHT	1300	1000	1100	1500	0
PSA	1300	1000	900	1500	0

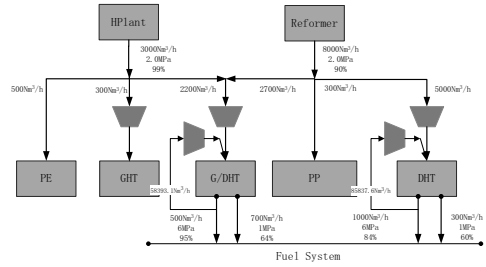

Fig. 3 The existing hydrogen network in the base case.

Table 2 Inlet stream concentration constraints of each hydrogen consumers.

	PE	GHT	G/DHT	PP	DHT
$y_{j,H2}^{Min}$	86%	86%	86%	86%	84%
$y_{j,H2S}^{Max}$	0	0	0.0044	0	0.0045

It is worth noting that there is an idled PSA plant with feed and residual pressure specified at 2 MPa and 0.2 MPa which is not shown in the base case diagram. Since the hydrogen concentration of LP off-gases is not high enough for directly reuse and yet there's recovery potential, the idled PSA plant is considered to be put into use. The recovery ratio and product hydrogen purity of the PSA unit are at 0.9 and 99% respectively. The prices of hydrogen produced by hydrogen plant and catalyst reformer are 0.893 RMB/Nm^3 and 2.054 RMB/ Nm^3 respectively. Electricity costs 0.75 RMB/kw·h, and fuel costs 0.02369 RMB/MJ. The capital cost is annualized in 5 years, with 5% interest rate per year.

As shown in Fig. 3, four purge streams of hydrogen consumers with high hydrogen concentration are released as fuel gas, due to its high content of hydrogen sulfide. In order to take good use of the hydrogen in these streams, desulfurization columns are considered.

The MINLP problem is solved in GAMS software using Baron as solver. The optimal flowsheet from the MINLP optimization is shown in Fig. 4. The optimal result involves two new desulfurization columns, an additional compressor and several pipes, as represented by dashed lines. In the optimum result scheme, the HP purge stream of DHT unit is sent to mix with the HP purge stream of G/DHT unit, and desulfurized in DSH_1. 64.4% of the outlet stream from DSH_1 is sent to the recycle hydrogen compressor of G/DHT unit and reused. While the LP purge stream of G/DHT is sent to mix with the LP purge stream of DHT unit, and desulfurized in DSL_2, the outlet stream is recompressed to 2MPa and then sent to PSA unit. The product from the PSA unit is sent to the make-up hydrogen compressor of DHT unit and reused, while the residual stream served as fuel gas. The optimized desulfurization ratio $R_{ds_{pl,i}}$ and theoretical plate number N_T of each desulfurization column are demonstrated in Table 3. With these new equipments, 82.8% of the purge streams are recovered and reused, contributing to the reduction of 2070.909 Nm^3/h on the hydrogen plant production, thus ￥7.67 million in TAC is saved. It should be noted that the capital cost of PSA is not included in this case. Detailed comparison is illustrated in Table 4. Comparing to the operating cost being saved (9.783 million/a), the additional capital cost (2.113 million/a) is acceptable.

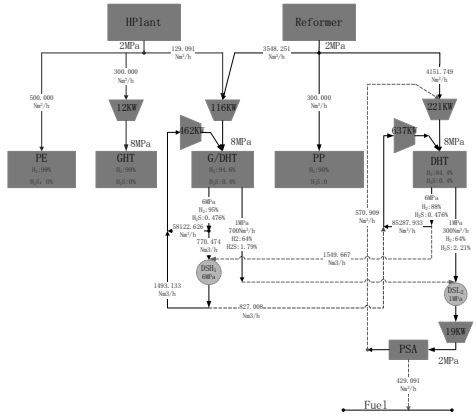

Fig. 4 Optimum retrofitted hydrogen network.

Table3 Optimized design parameter for desulfurization towers.

	DSH_1	DSL_2
$R_{ds_{pl,i}}$	0.814	0.828
$N_{T,ds_{pl,i}}$	5.247	5.020

Table 4 Cost breakdown for the optimal solution of base case.

Existing network	**Optimized network**
Operating cost/RMB·a^{-1}:	**Operating cost/RMB·a^{-1}:**
HPlant: 2.250×10^7($3000Nm^3\cdot h^{-1}$)	HPlant: 6.968×10^6(929.091 $Nm^3\cdot h^{-1}$)
RF: 1.380×10^8(8000 $Nm^3\cdot h^{-1}$)	RF: 1.380×10^8(8000 $Nm^3\cdot h^{-1}$)
Electricity: 1.047×10^7	Electricity: 1.087×10^7
Fuel: -5.252×10^6	Fuel: -3.996×10^5
	Desulfurization: 4.786×10^5

	Capital cost/RMB·a^{-1}:
	DS tower: 1.660×10^{6}
	Compressor: 3.896×10^{5}
	Piping: 0.636×10^{5}
Total annual cost: 1.657×10^{8}	**Total annual cost: 1.580×10^{8}**

4. Conclusions

A new modeling and optimization methodology has been developed to investigate the combination of these two systems. The desulfurization ratio, $R_{ds_{pl,i}}$, is employed to incorporate H_2S removal units into hydrogen distribution networks. The optimization of the case study demonstrates an ultra-high efficient hydrogen usage compared to the original network. The technique can fully account for not only the trade-offs between HNI and MEN, but also the trade-offs between operating cost and investment cost.

References

1. Alves, J. J., 1999. Analysis and design of refinery hydrogen distribution systems. Ph.D. thesis, UMIST, UK, Manchester.
2. Alves, J. J., Towler, G. P., 2002. Analysis of refinery hydrogen distribution systems. Ind Eng Chem Res 41(23), 5759-5769.
3. Agrawal, V., Shenoy, U. V., 2006. Unified conceptual approach to targeting and design of water and hydrogen networks. AIChE J 52(3), 1071-1082.
4. Bandyopadhyay, S., 2006. Source composite curve for waste reduction. Chem Eng J 125(2), 99-110.
5. Liao, Z. W., Rong, G., Wang, J. D., Yang, Y. R., 2011. Rigorous algorithmic targeting methods for hydrogen networks—part Ⅰ: systems with no hydrogen purification. Chem Eng Sci 66(5), 813-820.
6. Liao, Z. W., Rong, G., Wang, J. D., Yang, Y. R., 2011. Rigorous algorithmic targeting methods for hydrogen networks—part Ⅱ: systems with one hydrogen purification unit. Chem Eng Sci 66(5), 821-833.
7. Zhang, Q., Feng, X., Liu, G. L., Chu K. H., 2011. A novel graphical method for the integration of hydrogen distribution systems with purification reuse. Chem Eng Sci 66(4), 797-809.
8. Hallale, N., Liu, F., 2001. Refinery hydrogen management for clean fuels production. Adv Environ Res 6(1), 81-98.
9. Liao Z. W., Wang, J. D., Yang, Y. R., Rong, G., 2010. Integrating purifiers in refinery hydrogen networks: a retrofit case study. J of Clean Prod 18(3), 233-241.
10. Xuan, J., Liao, Z. W., Rong, G., Yang, Y. R., 2010. Hydrogen network retrofit design in refinery based on stochastic programming. CIESC J 61(2), 398-404.
11. Jia, N., Zhang, N., 2011. Multi-component optimization for refinery hydrogen networks. Energy 36(8), 4663-4670.
12. Bagajewicz, M. J., Manousiouthakis, V., 1992. Mass/heat-exchange network representation of distillation networks. AIChE J 38(11), 1769-1800.
13. Treybal, R. E., 1981. Mass transfer operations. 3rd ed. New York, McGraw-Hill.
14. Peters, M. S., Timmerhaus, K. D., 1990. Plant design and economics for chemical engineers, 4th ed. Singapore, McGraw-Hill.

I.A. Karimi and Rajagopalan Srinivasan (Editors), Proceedings of the 11th International Symposium on Process Systems Engineering, 15-19 July 2012, Singapore.

A Systematic Methodology for Design of Emulsion Based Chemical Products

Michele Mattei, Georgios M. Kontogeorgis, Rafiqul Gani

Department of Chemical and Biochemical Egineering, Technical University of Denmark, Søltofts Plads, Building 229, DK-2800 Kongens Lyngby, Denmark

Abstract

A systematic methodology for emulsion based chemical product design is presented. The methodology employs a model-based product synthesis/design stage and a model-experiment based further refinement and/or validation stage. In this paper only the first stage is presented. The methodology employs a hierarchical approach starting with the identification of the needs to be satisfied by the emulsified product and then building up the formulation by adding one-by-one the different classes of chemicals. A structured database together with dedicated property prediction models and evaluation criteria are employed to obtain a list of formulations that satisfy constraints representing the desired needs (target properties). Through a conceptual case study dealing with the design of a sunscreen lotion, the application of this new methodology is illustrated.

Keywords: Emulsions, Formulation, Model-base Method, Product Design, Sunscreen.

1. Emulsion Based Chemical Product Design – An Introduction

The goal of chemical product design is to find a product that exhibits a set of desirable or specified behavior[1]. A chemical product design problem can be summarized as follows: given a set of desired (target) properties, establish a list of chemical formulations satisfying these targets and then choose from them the most appropriate candidate to be verified experimentally[2]. Cussler and Moggridge[3] recommend a four step systematic methodology to solve this kind of problems: define customer needs; generate ideas to fulfill these requirements; select the most advantageous option among those generated; and finally manufacture the product. The chemical product of interest can be a single chemical or a mixture/blend; a formulated product is a mixture that contains different chemicals, active ingredients as well as additives. Cussler and Moggridge[3] distinguish between commodities (pure chemicals), chemical devices (where the attention is on selection and manufacture), molecular products (where focus is on active ingredients at the molecular level) and microstructured products (where the most important part is the structure of the product itself). The term "microstructure" refers to a chemical organization on the scale of micrometers, which belongs to the colloidal domain and incorporates polymer solutions, foams, gels as well as emulsions. The performances of such products are related not only to the presence of active ingredients and additives in the formulation, but also to the product's structural and material properties[4]. A common way to design these structured products is through trial-and-error approaches as predictive mathematical models needed to describe the relationships between product behavior and its performance need to be developed first[5].
A modified procedure[6], which is applicable to the design of emulsified formulated products, is presented in this paper. These emulsified products have a large use in the food and cosmetic industries and are described as mixtures of two normally immiscible liquids (representing the continuous and the dispersed phases), kinetically stabilized by

so called "emulsifiers" that mainly lie on the surface between the two phases. Active ingredients and additives are usually dissolved in the continuous and/or dispersed phases according to the needs of the product. Property models and databases have been developed to support the product (emulsified formulations) design methodology.

2. A Systematic Methodology for Emulsified Product Design

The steps of the modified methodology (Stage-1) for the design of emulsified chemical products are listed in Table 1. Except for Step 1, where consumer assessments are converted into target properties to be used in following steps, and Step 7, where the composition of the formulated product is determined; each step is responsible for the selection of one or more ingredients of the product satisfying one class of needs. To implement the methodology, a database[7] of ingredients, additives, and solvents has been created together with a library of developed/tested property models and a knowledge base of emulsified products and their need-property relations.

Table 1: Step-by-step methodology (Stage-1) in tabular form with necessary inputs for each step, action performed and outputs generated.

Step	Input	Performed Action	Output
Step 1	Information about the product	Understanding of needs, translation into target properties in terms of constraints to match	List of main needs, secondary needs and target properties with boundaries
Step 2	List of main needs	Find chemicals suitable as active ingredient, select the most advantageous	Candidate active ingredient
Step 3	Candidate active ingredient	Find chemicals suitable as dispersed phase solvents, select the most advantageous	Candidate dispersed phase solvent
Step 4	Candidate active ingredient and dispersed phase solvent	Find chemicals suitable as continuous phase solvents, select the most advantageous	Candidate continuous phase solvent
Step 5	Candidate active ingredient dispersed and continuous phase solvents	Find chemicals suitable as emulsifiers, select the most advantageous	Candidate emulsifier
Step 6	List of secondary needs, candidate dispersed and continuous phase solvents	Find chemicals suitable as additives, select the most advantageous	Candidate additives
Step 7	List of constraints on target properties, all ingredients	Find overall composition of selected ingredients	Product to be experimentally verified (Stage-2)

3. A Conceptual Case Study – A Sunscreen Lotion

A sunscreen lotion has been chosen as a conceptual case study to highlight the application of the emulsified product design methodology. This type of product can also be found as a single-phase liquid formulation[6]. However, as an emulsified formulation the product has advantages, such as, with respect to sensorial properties and cost, because of the presence of water in high concentration.

3.1. Problem Definition (Step 1)

From the knowledge base, it is found that consumers want a sunscreen lotion to protect from sunburns and UV radiations (risk of skin cancer and other diseases), to prevent from skin aging, to be water-proof, to have good sensorial properties (color, odor, *etc*.), good stability, low toxicity, easily spray able, and to have a low price. The protection from sunburns and UV radiations are identified as the main need, while the other consumer assessments are classified as secondary needs. This last distinction is crucial when translating consumer needs into target properties. The main needs are satisfied by active ingredients, while secondary needs are matched through appropriate additives as well as through the identification of the most advantageous overall composition of the formulation.

The above needs are converted to the following properties and their corresponding target values based on the information in the knowledge base[6]: properties needed to satisfy low toxicity ($LC_{50} > 3.16$); easy spray ability (kinematic viscosity, $\nu < 75$ cS; and molar volume, 20 kmol/l $< V <$ 50 kmol/l); protection from sunburn and radiation (UV absorbity; filtering); product stability (emulsion properties of surfactant-water mixtures); liquid product (miscibility in water; solubility).

3.2. Identification of Active Ingredients (Step 2)

The main need of a sunscreen lotion is to protect from sunburns and UV radiations. This is achieved by providing protection from both UV-A and UV-B rays. Two UV absorbers are selected in terms of their ability to block one type of UV radiation. In addition, a physical barrier for radiations (UV filter) is added in order to enhance the effectiveness of the formulated product. According to the legislation for sunscreens in EU[8], only 18 chemicals (also available in our database) are found to be suitable. The maximum allowed concentration of the active ingredients are also set at this point, through the knowledge base. From among the 18 UV absorbers[9] and their LC_{50} values, Avobenzone (CAS number 70356-09-1) is chosen as the UV-A absorber, Octyl Salicylate (CAS 118-60-5) as the UV-B absorber and Zinc Oxide (CAS 1314-13-2) as the UV filter.

3.3. Identification of Dispersed Phase Solvent (Step 3)

As the selected active ingredients (AIs) are solid at standard conditions; a suitable solvent is therefore needed to dissolve them, forming a homogeneous liquid phase. According to the database, Zinc Oxide is an insoluble pigment that can only be finely dispersed in the formulation, while the selected UV absorbers are oil-soluble. This is verified through their calculated (with property model from the model library) total Hildebrand solubility parameters (19.4 and 20.4 $MPa^{1/2}$, respectively). A search of the solvent database (from our CAMD-tool) revealed more than 100 chemicals that potentially are applicable as the dispersed phase solvent. Additionally, the solubility is verified by considering (also predicted with models from model library) the Hansen solubility parameters (dispersive, polar and hydrogen-bonding). Solvents matching the following target values of dispersive, polar and hydrogen bonding contribution, respectively, are identified for Avobenzene (0.57, 0.26 and 0.17); and for Octyl

Salicylate (0.49, 0.21 and 0.3). Only 6 chemicals are found to match these targets. Based on effectiveness (in terms of their expected solubility of active ingredients), toxicity and cost, Butyl Acetate (CAS 123-86-4) is chosen as the most appropriate dispersed phase solvent.

3.4. Identification of Continuous Phase Solvent (Step 4)

The identification of the continuous phase solvent is carried out by considering those chemicals that are not likely to dissolve the AIs or be miscible with the dispersed phase solvent. This is achieved by comparing the Hildebrand solubility parameters of the AIs and the solvent, and, checking for stability of the liquid phase (using models from model library). Note that the selected AIs are known to be only oil-soluble and are not miscible with water. Therefore, water is chosen as the most suitable continuous phase solvent. The total Hildebrand solubility parameter of water (δ^T = 48 $MPa^{1/2}$) confirms that the AIs and the dispersed phase solvent would not be miscible with it. Moreover, water is cheap, non-toxic and environmentally friendly.

3.5. Identification of the Emulsifier (Step 5)

The key-player in the formation of an emulsion is the emulsifier, which is often a surfactant. Since an oil-in-water emulsion is needed, the selected emulsifier needs to ensure the formation of this type of emulsion (indicated by a Hydrophilic-Lipophilic Balance value: HLB > 12) and ensure the stability of the desired emulsion for a wide range of temperature. Note that a sunscreen lotion is expected to be exposed to a range of temperatures and it must be stable under these conditions. Accordingly, Octyl Esaethylene Oxide (CAS 27252-75-1) has been identified (from our database of emulsifiers) as the most suitable emulsifier for this product. Its HLB value is 13.4[10], its cloud point (maximum temperature of use) is 73°C[11], and since it is a non-ionic surfactant, it is not affected by the presence of electrolytes in solution. If HLB and cloud point data are not available, they are predicted with models from the model library.

3.6. Identification of Additives (Step 6)

Additives are usually added to enhance the quality of the product, that is, to satisfy the secondary needs. Prevention from skin aging, stability and odor is improved by adding appropriate additives to the formulation. An antioxidant, a preservative and an aroma are needed, respectively and the choice of oil-soluble chemicals would ensure that these properties would not be affected by contact with water (note that the selected AIs are only oil-soluble). Because of the presence of dispersed Zinc Oxide in the formulation, color needs to be white. For this case study, α-Tocopherol (CAS 59-02-9), Heptylparaben (CAS 1085-12-7) and *laevo*-Menthol (CAS 2216-51-5) have been selected based on the available properties in the database. Selection of feasible candidates has been made based on their available prices.

3.7. Identification of Overall Composition (Step 7)

In this last step, the overall composition of the formulated product based on cost and subject to the property constraints (see Step 1) is determined. Also, solubility issues as well as constraints imposed by legislation[8] on use of the AIs are considered. The formulation toxicity parameter, molar volume and cost are calculated using an ideal mixing rule, weighted in terms of the composition of the chemicals in the mixture, as,

$$\zeta = \sum_{i=1}^{NC} x_i \zeta_i \quad (1)$$

Where ζ is a mixture property, x_i is the molar fraction of compound i in the formulation, and ζ_i the corresponding pure compound property.

Formulation viscosity, however, is calculated through a non-linear model[12].

$$\eta_r = 1 + \frac{2\left[5\lambda - 5\left((\lambda-1)\varphi^{7/3}\right)\right]}{4(\lambda-1) - 5(5\lambda-2)\varphi + 42\lambda\varphi^{5/3} - 5(5\lambda-2)\varphi^{7/3} + 4(\lambda-1)\varphi^{10/3}}\varphi \quad (2)$$

Where η_r is the relative viscosity, λ represents the ratio of viscosities of dispersed phase and continuous phase and φ is the dispersed phase volume fraction.
A candidate composition representing the desired sunscreen emulsified product is given in Table 2. This mixture satisfies the critical micelle concentration (calculated with model from the model library) needed to ensure stable emulsions.

Table 2: Candidate overall composition (weight percentage) for a sunscreen emulsion

Active Ingredients	Avobenzone	0.99%	Emulsifier	Octyl Esaethylene Oxide	0.09%
	Octyl Salycilate	1.22%			
	Zinc Oxide	8.56%	Additives	α-Tocopherol	0.34%
Disp. Phase Solvent	Butyl Acetate	32.4%		Heptylparaben	0.59%
Cont. Phase Solvent	Water	54.9%		laevo-Menthol	0.91%

4. Conclusions and Future Work

The work-flow for a systematic methodology for emulsion based chemical product design has been presented and its application has been highlighted through a conceptual case study from the health-care industry. The methodology is generic in the sense that other similar products can also be designed once the needs-property relations are established. Application range is enhanced through addition of data to the database and/or property models in the model library (details of these models can be obtained from the authors). Uncertainties in prediction of the composition of the formulated product are likely, and therefore, a final stage of verification by experiments is necessary. The work-flow of the methodology will now be implemented into the "The Virtual Process-Product Design Laboratory"[13] software to allow virtual (formulation) design and verification of emulsified products. In this way design and development of these products can be made less costly and introduced to the market earlier, while using the experimental resources only for verification of the product.

References

1. Gani R.; Comput. Chem. Eng., 2004; 28 (12): 2441-2457.
2. Gani R.; Chem. Eng. Res. Des., 2004; 82(A11): 1494-1504
3. Cussler E.L., Moggridge G.D., Chemical Product Design. Cambridge Univ Press; 2011.
4. Smith B.V., Ierapepritou M.G.; Comput. Chem. Eng., 2000; 34: 857-865.
5. Wibowo C., Ng K.M.; AIChE J.,, 2002; 48 (6): 1212-1230.
6. Conte E., Gani R., Cheng Y.S., Ng K.M.; AIChE J., 2011; 58(1), 173-189.
7. Nielsen T.L. et al.; J. Chem. Eng. Data, 2001; 46: 1041-1044.
8. Regulation (EC) No 1223-2009 of the European Parliament and of the Council of 30 November 2009 on Cosmetic Products
9. Couteau C., Chammas R., El-Boury S., Choquenet B., Paparis E., Coiffard L.J.M.; Journal of Dermatological Science, 2009; 50, 159-161.
10. Chen M.L., Wang Z.W., Duan H.J.; Journal of Dispersion Science and Technology, 2009; 30(10): 1481-1485.
11. Ren Y. et al.; Journal of Colloid and Interface Science, 2011; 358(1): 202-207.
12. Choi S.J., Schowalter W.R.; Physics of Fluids, 1975; 18(4): 420-427.
13. Conte E., Gani R., Malik T.I.; Fluid Phase Eq., 2011; 302: 294-304.

I.A. Karimi and Rajagopalan Srinivasan (Editors), Proceedings of the 11th International Symposium on Process Systems Engineering, 15-19 July 2012, Singapore.

Molecular Design using Three-Dimensional Signature Descriptors

Robert H. Herring[a], Rudolfs Namikis[a], Nishanth G. Chemmangattuvalappil[a,b], Christopher B. Roberts[a], Mario R. Eden[a]

[a]*Department of Chemical Engineering, Auburn University, USA*
[b]*Department of Chemical and Environmental Eng., University of Nottingham, Malaysia*

Abstract

Integrated process and product design is a useful approach for identifying globally optimal solutions to increasingly demanding problems. Property based process and product design methods are convenient since both sides of the problem can easily be expressed in terms of molecular properties. Property clustering, a technique for tracking stream properties or functionalities through conserved quantities, allows for interpretation of process performance as a function of properties. The molecular signature descriptor is quite effective in this approach as any topological index, which enumerates molecular information for use in QSPRs, can be derived from the molecular signature. Previous works on application of the signature descriptor have been limited to use with topological indices. This contribution outlines an algorithm for including topographical, or three-dimensional, information with the signature descriptor and how to apply this information in the reverse problem formulation (RPF) methodology.

Keywords: Molecular Design, Topographical Descriptors, Molecular Signatures.

1. Theoretical Background

1.1. Topographical Descriptors

A topographic index is a form of 3D molecular characterization that attributes a molecule with a unique number, thus giving a quantitative reference to shape. The advantage of this technique is that topographic indices can enumerate the spatial orientation of a molecule, which might not be fully captured in the conventional 2D methods of developing QSAR/QSPRs. This would be useful for modelling ligand-receptor type interactions and has even been shown to have strong correlations to several physicochemical properties [1]. Most geometrical descriptors are calculated directly using the (x,y,z) coordinates of the atoms in the molecule and others are derived from these coordinates, e.g. inter-atomic distances or distances from an origin. The information content of topographical descriptors typically allows more discrimination power than topological descriptors for similar molecular structures. It is often necessary to include connectivity information in the form of adjacency matrices, molecular graphs, or molecular signatures in this case since topographic indices do not include this data [1]. Another shortcoming of these descriptors is the necessity for geometry optimization, with the global conformational minima overshadowed by several local conformational minima of slightly different energy values. Overall, this remains an effective method of accounting for the shape of a molecular structure, and can even be used to address electrostatic properties in a 3D context [2]. The topographical descriptors utilized in this study are the 3D Wiener index [3,4] and the Van der Waals volume [5].

1.2. Molecular Signatures

The molecular signature descriptor is a representation of the extended valence sequence of the atoms in a molecule [6]. This descriptor is ideal for the RPF approach because of its low degeneracy and ability to capture enough structural information to derive almost any other index, topological [7,8] and now topographical, necessary for a quality QSPR. Another convenient feature of the signature descriptor is the coloring function, which can be tailored to include useful information about the atoms involved. Graph theory [9] is applied to the concept of molecular signatures to ensure that only feasible and complete solution structures are generated. If G is a molecular graph and x is an atom of G, the atomic signature of height h of x is a canonical representation of the sub-graph of G containing all atoms that are at a distance h from x. If k is a constant, ${}^{h}\alpha_G$ is the vector of occurrences of atomic signature of height h and $TI(root({}^{h}\Sigma))$ is the vector of TI values calculated for each root of atomic signature, then:

$$TI(G) = k \cdot {}^{h}\alpha_G \cdot TI(root({}^{h}\Sigma)) \tag{1}$$

1.3. Reverse Problem Formulation (RPF) Technique and Property Operators

The conventional approach to process and molecular design has been to treat both problems separately. Decisions on which components to use are typically made before the design process and are limited to qualitative intuition based on previous experience. The reverse problem formulation allows these two design aspects to be treated simultaneously, which can likely result in a more optimal solution [10]. The strength of this approach is that process design is not tied to any specific molecular components, which allows for a more thorough search for optimal process conditions, and the molecular design aspect considers a wider range of candidate structures. This method essentially creates two reverse problems that can easily communicate through the use of property operators, which are functions of the original properties forced to obey linear mixing rules. The normalized property operator, Ω_{js} is obtained by dividing it by a reference value [11]. If $\psi_j(P_{js})$ is the property operator of the j^{th} property P_{js} of stream s, x_s is the fractional contribution, N_s is the number of streams, then:

$$\Omega_{js} = \frac{\sum_{s=1}^{N_s} x_s \psi_j(P_{js})}{\psi_j^{ref}} \tag{2}$$

2. Signature Descriptors for Molecular Design

2.1. General Problem Statement and Solution Procedure

Design the molecules with the best dominant property which also satisfy the set of property constraints that are identified during the process design.

Stepwise Solution Procedure:

- The property targets for the input molecules to provide the optimum process performance will be calculated using eq. (2).
- Identify QSAR/QSPR/GC (Group Contribution) models that can predict the properties corresponding to the optimum performance.
- Identify the height of molecular signatures corresponding to TI used in QSPR models that matches the diameter (D) of the target molecule as described in section 2.3

- Based on the structural constraints and transformation techniques explained in section 2.3, identify the signatures and generate candidate molecules from signatures based on the algorithm by Faulon *et al*. [12].

2.2. Topographical Indices in Reverse Problem Formulation

The topographical indices applied in this case, 3D Wiener index and Van der Waals volume, can both be derived from the geometric distance matrix. The geometric distance matrix of a molecular graph (G) is a real symmetric nxn matrix, where n represents the number of vertices in the chosen graph or sub-graph. Each entry in this matrix represents the Euclidean distance between two vertices $v_i(G)$ and $v_j(G)$. These values are calculated as shown below:

$$d_{ij} = \sqrt{(x_i - x_j)^2 + (y_i - y_j)^2 + (z_i - z_j)^2} \tag{3}$$

The geometric distance matrix can be used to calculate the 3D Wiener index through a simple summation of values in the upper or lower triangular matrix. The Van der Waals volume of a molecular graph can be calculated by treating each atomic coordinate as the center of a sphere, with the appropriate Van der Waals radius defined by signature coloring, while accounting for sphere overlapping. If r_i and r_j are the Van der Waals radii of two bonded atoms in a molecular graph and n is the total number of vertices in this graph then the volume can be calculated as shown:

$$V = \frac{4}{3}\sum_{i=1}^{n}\pi r_i^3 - \frac{1}{2}\sum_{i\neq j}^{n}\frac{\pi(r_i + r_j - d_{ij})^2(d_{ij}^2 - 2d_{ij}r_j - 3r_j^2 + 2d_{ij}r_i + 6r_i r_j - 3r_i^2)}{12d_{ij}} \tag{4}$$

Starting geometries for each signature were obtained from a stochastic conformational search, utilizing the xSS100 script in BOSS (biochemical and organic simulation system) [13]. The Cartesian coordinates for each vertex of the molecular graph were calculated from gas phase geometry optimizations, utilizing the semi-empirical quantum mechanical model formulation called Austin Model 1 (AM1) [14]. This method was chosen as suitable for small to medium alkane structures because it generates accurate geometries at a fraction of the time required for most ab initio methods.

2.3. Problem Formulation

If θ is the property function of property P, the property operator corresponding to P is estimated as follows:

$$\theta = f(TI) \tag{5}$$

$$TI = \sum_{i=1}^{N} {}^{h}\alpha_i \cdot TI(root({}^{h}\Sigma)) = \sum_{i=1}^{N} {}^{h}\alpha_i L_i \tag{6}$$

$$\Omega(P) = \sum_{i=1}^{N} x_i L_i \tag{7}$$

The dominant property, being expressed in terms of the occurrences of atomic signatures, can be optimized subject to the property constraints. If Ω_j is the property operator corresponding to the dominant property and Ω_{ij} is the normalized property operator of molecule i, an optimization problem can be formulated as follows:

$$Max / Min\ \Omega_j \tag{8}$$

$$\Omega_j^{\min} \le \Omega_j \le \Omega_j^{\max} \tag{9}$$

The geometry matrix can be generated for each signature. In the next step, the diameter and vertex number of the signatures are identified. The diameter (D) of the signature is the largest distance between all pairs of atoms in the signature. The vertex number is the number of vertices in the subgraph. The height of the signature will be decided based on the type of target molecule.

$$\sum n \le Max(D) \tag{10}$$

If eq. (10) is satisfied, generate the geometry matrix from the signature with maximum vertex value. Since all atoms in the molecule, which this signature is part of, are described in the signature, the geometry matrix will be exactly the same as the molecule. Subsequent studies will include derivation of topographic indices from signature combinations.

3. Case Study – Design of Alkyl Substituent for Rice Plant Fungicide

Application of the molecular signature descriptor in accounting for topological, topographical and information indices is illustrated through the optimal substituent selection for dialkyldithiolanylidenemalonate (DD). DD has been shown to have eradicant and protectant activity against rice blast disease. Uchida [15] enumerated the effectiveness of this fungicide in terms of affinity ($\log(V_E)$), mobility ($\log(\mu)$) and retention ($\log(R/(100\text{-}R))$). These three attributes have been linearly related to the lipophilicity ($\log(P_{oct/wat})$) of the chosen substituents. A QSPR was developed [16] to model $\log(P)$ as a function of several different descriptors. Index values are calculated only for the substituent regions of the fungicide and the summation of property values for the two substituents are constrained to values shown in Table 1. Raman and Maranas [17] previously visited this problem while correlating $\log(P)$ values to the first order molecular connectivity index. The same upper and lower bounds on mobility and retention are applied in this study, while the objective function is to maximize substituent affinity to the rice plant.

Table 1. Property Constraints

Property	Upper Bound	Lower Bound
Retention, $\log(R/100\text{-}R)$	-2.04	-2.48
Mobility, $\log(\mu)$	0.3	-0.3
Affinity, $\log(V_E)$	Maximum	

Property models utilized in this study are shown in Table 2. The information content (IC) indices infer a measure of molecular symmetry, and this formulation was originally introduced by Shannon [18]. Another information theoretical invariant utilized in the $\log(P)$ QSPR is the complementary information content (CIC) index [19]. Some of the descriptors, with large structure references, used in the hydrophobicity QSPR were found to be unnecessary based on the height of the solution signature. This case study, formulated as an MILP optimization problem, was solved using a simplex algorithm.

Table 2. Property Models

Property	Property Model
Retention	$\log(R/100-R)=0.72*\log(P)-1.93$
Mobility	$\log(\mu)=-0.64*\log(P)+1.95$
Affinity	$\log(V_E)=0.53*\log(P)-0.24$
Hydrophobicity	$\log(P)=-5.60+0.19(P_{10})-1.46(IC_0)+1.09(CIC_2)-0.77(CIC_3)-1.36({}^{6}\chi^{b})$ $+5.34({}^{0}\chi^{v})-3.41({}^{1}\chi^{v})+0.55({}^{4}\chi^{v})-0.41({}^{3}\chi^{v}_{C})+1.10(V_W)-0.17({}^{3D}W)$

Using height two atomic signatures for acyclic alkanes, of which there are 65, the optimal DD-substituents which satisfy the criteria for this study are found to be ethyl and sec-butyl. This solution was also found in the original case study [17], thus lending credibility to the developed methodology. It should be noted that in this specific case the inclusion of topographical descriptors did not result in a different solution. For alternate studies in which the contribution of three dimensional descriptors might have a more pronounced effect, this technique could lead to unique solutions which were previously unrealized. Overall, use of the signature descriptor as a platform on which to derive any topostructural and information indices is effective within the reverse problem formulation method.

4. Conclusions

The concept of molecular signature descriptors has been extended to include the use of 3D-descriptors. This extension enables us to make use of both 2D and 3D descriptor based QSPR models on the same platform to solve molecular design problems. In the next step, the algorithm will be modified to define three dimensional descriptors as a function of more than one signature building block.

References

[1] R. Todeschini and V. Consonni (2008), Handbook of Molecular Descriptors: Descriptors from Molecular Geometry, 1004
[2] P. Mezey (2008), J. Math. Chem., 45(2)
[3] B. Bogdanov, S. Nikolić, and N.Trinajstic (1989), J. Math. Chem., 3, 299
[4] Y. Malysheva, Y. Papulov, M. Vinogradova, A. Botov, V. Smolyakov (1998), J. Struct. Chem, 39(3)
[5] A. Bondi (1964), J. of Phys. Chem., 68, 441
[6] D.P. Visco Jr., R.S. Pophale, M.D. Rintoul, J.L. Faulon (2002), J. Mol. Graph Model 20
[7] J.L. Faulon, D.P. Visco Jr., R.S. Pophale (2003), J. Chem. Inf. Compt. Sci., 43, 707
[8] N. G. Chemmangattuvalippil, C.C. Solvason, S. Bommareddy, M.R. Eden (2010),Comp. Chem.Eng.,34, 2062
[9] N. Trinajstic (1992), Chemical Graph Theory, 2nd Edition, CRC press, Boca Raton, FL
[10] M.R. Eden, S.B. Jorgensen, R. Gani and M.M. El-Halwagi (2004), Chem. Eng. Process, 43
[11] M.D. Shelley and M.M. El-Halwagi (2000), Comput. Chem. Eng., 24
[12] J.L. Faulon, C.J.Churchwell, D.P. Visco Jr. (2003), J.Chem. Inf. Compt. Sci., 43, 721
[13] W.L. Jorgensen and J. Tirado-Rives (2005), J. Comput. Chem., 26, 1689
[14] M. Dewar, E. Zoebisch, E. Healy, J. Stewart (1985), J. Am. Chem. Soc., 107
[15] M. Uchida (1980), Pesticide Biochemistry and Physiology, 14, 249
[16] S. Basak, B. Gute and G. Grunwald (1996), J. Chem. Inf. Comput. Sci., 36, 1054
[17] V. Raman and C. Maranas (1998), Comp. Chem. Eng., 22, 747
[18] C. Shannon (1948), Bell Sys. Tech. J., 27, 379
[19] S. Basak and V. Magnuson (1983), Arzneim.-Forsch./Drug Res., 33, 501

I.A. Karimi and Rajagopalan Srinivasan (Editors), Proceedings of the 11th International Symposium on Process Systems Engineering, 15-19 July 2012, Singapore.

Optimization design of RO system for water purification

Yanyue Lu,[a] Anping Liao,[a] Yangdong Hu[b]

[a]*Key Laboratory of Chemical and Biological Transforming Process, College of Chemistry and Chemical engineering, Guangxi University for Nationalities, 188, East Daxue Road Nanning, Guangxi, 530006, China*
[b]*College of Chemistry and Chemical Engineering, Ocean University of China, Qingdao, 266003, China*

Abstract

A mathematical model of reverse osmosis (RO) membrane system is presented. The membrane system can be used to product multiple freshwater with different salinity from seawater. Based on the system model, the mathematical programming method is used to optimizing design the RO water purification system, the objective function is to minimize the total annualized cost of the RO system. The cost equation relating the capital and operating cost to the design variables, as well as the structural variables have been introduced in the mathematical programming model. As a results, the various freshwater with different concentration can be supplied simultaneously, it can lead to significant capital cost and energy saving and provide income from the multiple freshwater sales.

Keywords: reverse osmosis, membrane, seawater desalination, optimization design.

1. Introduction

The seawater and brackish desalination is the main source for supplying fresh water in the regions suffering from the scarcity of natural fresh water supplies (Wade, 2001). Reverse osmosis (RO) is the major technologies for large-size plants for desalinating water. The interest in RO is that it is able to meet varying feed water concentration and varying production water quantity and quality requirement through change system construction and operation condition. These characteristic have made the design of RO process more flexible (Marcovecchio, 2005). Considerable efforts for the research of the optimum RO system design have been made. El-Halwagi (1992, 1997) investigated the synthesis of RO networks which involve multiple feed streams for waste reduction. Based on the state-space approach, a structural representation of RO networks has been introduced. Voros et al. (1997) simplified the El-Halwagi's representation by reducing the distribution boxes to junctions.

In this work, a mathematical model of reverse osmosis (RO) membrane system is presented. The membrane system can be used to product multiple freshwater with different salinity from seawater. Based on the system model, the mathematical programming method is used to optimizing design the RO system for water purification. The design results would determine the optimal system structure and operating conditions, and the optimal streams distribution. At the same time, the most appropriately choice of the types of membrane elements in each stages and the optimal number of membrane elements in each pressure vessel (PV) also be given.

2. RO unit model

It is necessary to adopt the appropriate modeling equations that can satisfactorily predict the membrane performance with reasonable computational complexity. The solution diffusion model is the one most commonly used in RO system design. The model is mainly based on two parameters: the water permeability, A, and the solute transport parameter, B. The values for these two parameters are usually specified by membrane manufactures. According to the model, the pure water flux, J_w (kg/m^2.s), and the salt flux, J_s (kg/m^2.s), can be calculated as follow:

$$J_w = A\left[\left(P_f - P_p - \frac{\Delta P_f}{2}\right) - \left(\pi_w - \pi_p\right)\right] \times 10^6 \tag{1}$$

$$J_s = B\left(C_w - C_p\right) \tag{2}$$

$$V_w = \frac{J_w + J_s}{\rho_p} \tag{3}$$

$$Q_p = 3600 \times V_w \times S_m \times m \tag{4}$$

where V_w is the permeate velocity. ρ_p denotes the density of the permeate. S_m is the membrane area. m is the number of the membrane element, it is a continuous variable.

The arrays of pressure vessels (PV) with 1 up to 8 membrane elements per PV consist of a RO stage. In this paper, the optimal PV structure has been researched. Four different types of spiral wound FilmTec reverse osmosis membrane elements have been considered. According to its performance characteristics and the design requirements of a specific desalination application, the optimum selection of types of the membrane element employed in each PV can be determined by the following equations:

$$\sum_{k=1}^{4} Z_k \le 1 \tag{5}$$

$$L_1 \times \left(1 - \sum_{k=1}^{4} Z_k\right) \le Q_{ROf} - x_c \le U_1 \times \sum_{k=1}^{4} Z_k - \varepsilon \tag{6}$$

$$Q_p = \sum_{k=1}^{4} Q_{p,k} \tag{7}$$

$$Q_{p,k} \le U_2 \times Z_k \tag{8}$$

$$m_k \le U_3 \times Z_k \tag{9}$$

where Z_k is the binary variable. It takes the value of 1 when the kth element type is utilized in the PV. L_1 and U_1, are the arbitrary small and large number, respectively. x_c denote the small positive number. Q_{Rof} is the feed flow rate entering a RO stage. For the Eq. (6), when Q_{ROf} takes some value which is larger than x_c, it means the RO stage is presence and one element type should be chosen. Q_p is the permeate flow rate of pressure vessel. While $Q_{p,k}$ denote the permeate flow rate of pressure vessel when the kth element type is utilized in this PV. U_2 and U_3 are large enough positive number so that $Q_{p,k}$ and m_k are not restricted if $Z_k = 1$. By this way the module type and number of stage are chosen simultaneously when the optimization design is performed.

3. RO network representation

Several RO system configurations were investigated (Marcovecchio, 2005) which are common in seawater and brackish desalination applications. In order to describe the possible RO configuration, a simplified superstructure is presented, which incorporates

all the feasible process flow in the RO desalination system with multiple-product output. As shown in Fig. 1, a RO network consists of N_{ps} pressurization stages and N_{RO} reverse osmosis stages. In this configuration, there are three sets of stream nodes employed: N_{ps} mixing junctions, N_{RO} reverse osmosis junctions, N_p outlet junctions of product streams. The junction of N_{ps+1} indicated the brine stream leaving the network. It is assumed that seawater only enter the RO system from stage 1. The mixing streams pressurized by high pressure (HP) pump or not are connected to the corresponding reverse osmosis stages. The RO stages consist of multiple parallel reverse osmosis pressure vessels operating at the same conditions. The mathematical model that describes the superstructure is presented as follow.

$$Q_{ps,1} = Q_f + \sum_{j=1}^{N_{RO}} Q_{ROb,j} \times x_{b,1,j} + \sum_{j=1}^{N_{RO}} Q_{ROp,j} \times x_{p,1,j} \tag{10}$$

$$Q_{ps,1} \times C_{ps,1} = Q_f \times C_f + \sum_{j=1}^{N_{RO}} Q_{ROb,j} \times x_{b,1,j} \times C_{ROb,j} + \sum_{j=1}^{N_{RO}} Q_{ROp,j} \times x_{p,1,j} \times C_{ROp,j} \tag{11}$$

$$Q_{ps,i} = \sum_{j=1}^{N_{RO}} Q_{ROb,j} \times x_{b,i,j} + \sum_{j=1}^{N_{RO}} Q_{ROP,j} \times x_{p,i,j} \qquad i = 2,3,\ldots,N_{ps} \tag{12}$$

$$Q_{ps,i} \times C_{ps,i} = \sum_{j=1}^{N_{RO}} Q_{ROb,j} \times x_{b,i,j} \times C_{ROb,j} + \sum_{j=1}^{N_{RO}} Q_{ROp,j} \times x_{p,i,j} \times C_{ROp,j} \qquad i = 2,3,\ldots,N_{ps} \tag{13}$$

where $Q_{ps,i}$, $C_{ps,i}$ denote the flow rate and concentration of the ith pressurization stage, respectively. $Q_{ROb,j}$, $C_{ROb,j}$ denote the brine flow rate and concentration of the jth RO stage, $Q_{ROp,j}$, $C_{ROp,j}$ denote the permeate flow rate and concentration of the jth RO stage, respectively. $x_{b,i,j}$, $x_{p,i,j}$ indicate the stream split ratios of the brine and permeate, respectively. The values determine the flow rates of brine and permeate leaving the jth RO stage and being linked to the ith pressurization stage.

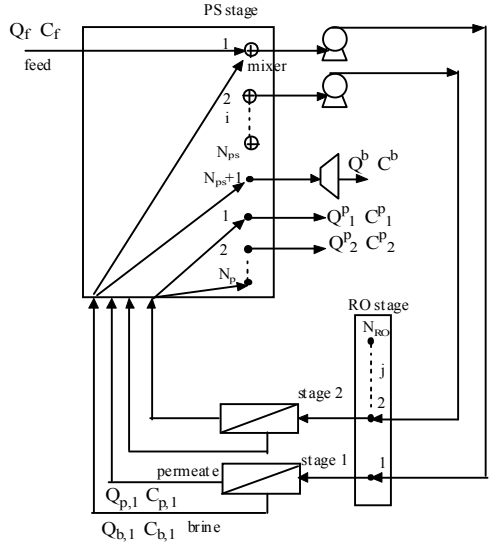

Fig. 1 The representation of the RO network via the superstructure

All the streams connected to the ith pressurization stage firstly mix in the mixer. The outlet pressure from the mixer is the smallest feed pressure. The stream split ratios and the logical expression of stream mixing are employed in this paper, these techniques reduced the number of binary variable and the solving space, therefore the mathematical model may be easily handled.
The overall material balances for the RO network and a set of product quantity and quality constraints concerning the minimum desirable product flow rate, and the maximum allowable product concentration are also needed in the system model.

4. Solution methodology

The optimization design problem is formulated as a mixed-integer nonlinear programming (MINLP) for minimizing the total annualized cost subject to thermodynamic, technical, and flexibility constraints. The MINLP can be solved using the software GAMS. This procedure is carried out by introducing an excessive number of units as an initial guess, while at the optimum certain design variables, such as stream split ratios, are either set to zero or to a value that indicate the absence or presence of the specific stage. Several starting points are used to obtain the best possible solution.

5. Illustrative example

The proposed methodology for RO system optimization design has been applied to deals with the desalination of seawater. In this example, there are three kinds of freshwater required, which subject to different permeate quantity and quality constraints. The minimum desirable product flow rate for these outlets are 200 m^3/h, 100 m^3/h, 50 m^3/h, while the corresponding maximum allowed salt concentration are 100 ppm, 300 ppm, 500 ppm, respectively. Four different types of FilmTec reverse osmosis membrane elements from DOW have been included in the design studies of the current work. They are the low energy, high productivity element SW30XLE-400, the high rejection, high productivity element SW30HR-380, the high rejection, fouling resistant element SW30HR-320, and the high productivity, high rejection brackish RO element BW30-400.
The results of the RO system optimization design were presented in Table 1. The two-stage RO configuration with brine re-processing was employed in design (shown as Fig. 2). This scheme supplies three kinds of freshwater. The first freshwater come from the permeate of stage 1 ($x_{p,5,1}$=0.828) which concentration is lower, while the third freshwater come from the permeate of stage 2 ($x_{p,7,2}$=0.46). The second freshwater consist of partial permeate coming from stage 1 ($x_{p,6,1}$=0.172) and stage 2 ($x_{p,6,2}$=0.54). The total annualized cost of the system is $1,397,600 per year.

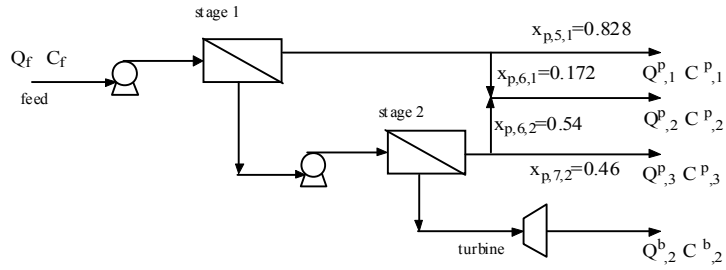

Fig. 2 The optimal RO configuration with multiple-product outlet

6. Conclusions

For a RO system of seawater desalination with multiple-product requirement, the design objective is to identify the most cost effective RO network configuration, the optimal streams distribution and operating conditions, and the optimal arrangement of the membrane elements. A process synthesis method has been applied to the optimal design of RO system with multiple freshwater outlets. The design task has been formulated as an MINLP which minimizes the total annualized cost of the RO system. As a results, in this RO system, the various freshwater with different concentration can be supplied simultaneously, it can lead to significant capital cost and energy saving and provide income from the multiple freshwater sales. A desalination case demonstrated that the design method can meet the requirement for multiple freshwater at the lowest cost.

Table 1 Design and optimization results for the study case

Process flow	two-stage RO system, show as Fig. 2
Seawater feed flow, Q_f (m^3/h)	588
Flow rate of the first freshwater, Q^p_1 (m^3/h)	200
Salt concentration of the first freshwater, C^p_1 (ppm)	100
Flow rate of the second freshwater, Q^p_2 (m^3/h)	100
Salt concentration of the second freshwater, C^p_2 (ppm)	300
Flow rate of the third freshwater, Q^p_3 (m^3/h)	50
Salt concentration of the third freshwater, C^p_3 (ppm)	430
Membrane type in stage 1	SW30HR-320
Number of elements per PV in stage 1	3
Number of PV in stage 1	81
Operating pressure in stage1, P_1 (Mpa)	8.2
Membrane type in stage 2	SW30XLE-400
Number of elements per PV in stage 2	4
Number of PV in stage 2	53
Operating pressure in stage2, P_2 (Mpa)	8.3
The overall system recovery	59%
The total annualized cost, ($)	1,397,600

Acknowledgements

This work was financially supported by the Education Department of Guangxi, China (200812MS084), Project of the Science and Technology Department of Guangxi, China ((No.0992028-13).

References

N.M. Wade, 2001, Distillation Plant Development and Cost Update, Desalination, 136, 3-12.

M.G. Marcovecchio, P.A. Aguirre, 2005, Global Optimal Design of Reverse Osmosis Networks for Seawater Desalination: Modeling and Algorithm, Desalination, 184, 259-271.

M.M. El-Halwagi, 1992, Synthesis of Reverse Osmosis Networks for Waste Reduction, AICHE J, 38, 1185-1198.

M. Zhu, M.M. El-Halwagi, 1997, Optimal Design and Scheduling of Flexible Reverse Osmosis Networks, Journal of membrane science, 129, 161-174.

N.G. Voros, Z.B. Maroulis, 1997, Short-cut Structural Design of Reverse Osmosis Desalination Plants, Journal of membrane science, 127, 47-68.

I.A. Karimi and Rajagopalan Srinivasan (Editors), Proceedings of the 11th International Symposium on Process Systems Engineering, 15-19 July 2012, Singapore.

Retrofit of Heat Exchanger Networks Including the Detailed Equipment Design

Mauro A. S. S. Ravagnani, Aline P. Silva

Chemical Engineering Department – State University of Maringá
Av. Colombo, 5790 – Maringá - CEP 87020900 – Brazil
ravag@deq.uem.br

Abstract

Many studies and methodologies were proposed to minimize the utilities consumption, the number of heat transfer equipment and effluent emissions by synthesizing Heat Exchanger Networks (HEN). Most of these formulations have been developed to the synthesis of new plants. Industrial processes in operation, however, can often be made more energy-efficient and sustainable by a retrofit. In the present paper, a methodology for the retrofit of HEN considering simultaneously the possibilities of reuse of exchangers for different junctions and the inclusion of new units is proposed, both considering the detailed heat exchangers design using TEMA standards. The developed methodology is based on a superstructure simultaneous optimisation model for the HEN synthesis considering stream splitting, with an additional constraint of including all the existent equipment among the possibilities of heat exchanges. The superstructure takes into account the operational and capital costs, by maximizing the recovery of energy and minimizing the installation costs. In the object function the total cost is composed by the costs of utilities used in the HEN and the new equipment. The problem was solved using Particle Swarm Optimization (PSO).

Keywords: heat exchanger networks, retrofit, Particle Swarm Optimization, detailed design, shell and tube heat exchangers.

1. Introduction

Heat exchanger networks (HEN) synthesis is an important field in process systems engineering, and has been the subject of considerable research efforts over the last five decades. Many studies and methodologies were proposed to minimize the utilities consumption, the number of heat transfer equipment and effluent emissions. Most of these formulations have been developed to the synthesis of new plants. Industrial processes in operation, however, can often be made more energy-efficient and sustainable by a retrofit. As a task considerably more arduous than the grassroots design, the retrofit of heat exchanger networks presents a less intense progress. This can be explained because the process must suffer structural modification, considering the reuse of existing heat exchanger equipment and the inclusion of new ones, resulting in increases in process fixed costs. The detailed design of the equipment is also a

subject that can influence in the final cost and in the environmental impact caused by the emissions.

Papers relating retrofit in HEN was first published in the middle of the 1980, using thermodynamic concepts (Tjoe and Linnhoff, 1986, Asante and Zhu, 1996, Nordman e Berntsson, 2009 a,b). Mathematical methods were also proposed (Ciric and Floudas, 1989, Yee and Grosmman, 1990, Ciric and Floudas, 1990, Yee and Grosmman, 1991, Singh and Castillo, 2002, Bjork and Nordman, 2005). Some authors used thermodynamic concepts jointly with Mathematical Programming (Zhu and Asante, 1999, Nie and Zhu, 1999, Panjeh Shahi et al. 2008).

In the present paper it was developed a methodology for the retrofit of HEN including the detailed design of the heat exchangers. A new network is proposed using all the existent equipment. The method is based on the superstructure proposed by Yee and Grossmann (1990).

2. Development

The proposed methodology for the retrofit of HEN consider simultaneously the possibilities of reuse of exchangers for different junctions and the inclusion of new units is proposed, both considering the detailed heat exchangers design using TEMA standards. The developed methodology is based on a superstructure simultaneous optimization model for the HEN synthesis considering stream splitting, with an additional constraint of including all the existent equipment among the possibilities of heat exchanges. This superstructure takes into account the operational and capital costs, by maximizing the recovery of energy and minimizing the installation costs. The object function takes in account the total cost composed by the cost of the utilities used in the HEN and the cost of the new equipment. The heat exchangers are designed using the methodology presented in Ravagnani and Caballero (2007). The standards of TEMA are used, jointly with the Bell-Delaware method for the shell side. The design method is included in the HEN retrofit procedure. The problem was solved using Particle Swarm Optimization (PSO) presented in Ravagnani et al. (2009).

The problem can be formulated as the minimization of the total cost (the summation of the cost of including new heat exchangers and the cost of utilities).

3. Example

An example is used to show the applicability of the developed methodology, presented by Castillo et al. (1998). The current HEN has three heat exchangers (5.69 m^2, 2.55 m^2 and 0.41 m^2, respectively), six heaters and five coolers. Hot and cold utilities consumption are, respectively, 3,100 kW and 4,375 kW. Stream data as well as the cost for additional equipment and the parameters used for PSO are presented in Table 1. Figure 1 shows the existent HEN. The problem is solved using the proposed methodology and the new

HEN is achieved, with sixe heat exchangers (three new and the three old ones, reused), five coolers and no heaters. The stopping criteria used is a fixed number of iterations. Table 2 present the detailed design of the new heat exchangers. Figure 2 present the new HEN and Table 3 show the final costs for the network. Computational effort (@Pentium IV 1.70 GHz) was approximately 600 minutes.

4. Conclusions

In this paper it is proposed a new methodology for the retrofit of HEN. The final network has the minimum cost, considering area and utilities, considering all the existent heat exchangers. The method is based on a superstructure proposed by Yee and Grossmann (1990) and the heat exchangers are designed using the procedure proposed by Ravagnani et al. (2009). The optimisation problem is solved using the PSO algorithm. One example was presented to show the applicability of the proposed methodology.

Results shown that the proposed methodology is very interesting, allowing achieving optimal HEN using all the existent heat exchangers. Computational effort is acceptable, considering the constraints of including all the existent heat exchangers with the detailed design using the Bell-Delaware method.

References

Z. Asante, N. D. K. e Zhu, X. X. (1996). An automated approach for heat exchanger network retrofit featuring minimal topology modifications. *Computers & Chemical Engineering*. 20: S7–S12.

Bjork, K. e Nordman, R. (2005). Solving large-scale retrofit heat exchanger network synthesis problems. *Chemical Engineering and Processing*. 44: 869-876.

Castillo, E., Acevedo, L. e Reververi, A. (1998). Cleaner Production of Nitric Acid by Heat Transfer Optimization: A Case Study. *Chemical & Biochemical Engineering*. 12: 157 – 165**.**

Ciric, A. R., e Floudas, C. A. (1989). A Retrofit Approach for Heat Exchanger Networks. *Computers & Chemical Engineering.* 13(6): 703-715.

Ciric, A. R. e Floudas, C. A. (1990). A Mixed Integer Nonlinear Programming Model for Retrofitting Heat-Exchanger Networks. *Industrial & Engineering Chemistry Research*. 29: 239-251.

Nie, X., R. e Zhu, X. (1999). Heat Exchanger Network Retrofit Considering Pressure Drop and Heat-Transfer Enhancement. *AIChE Journal*. 45(6): 1239-1254.

Nordman, R. e Berntsson, T. (2009a). Use of advanced composite curves for assessing cost-effective HEN retrofit I: Theory and concepts. *Applied Thermal Engineering*. 29: 275–281.

Nordman, R. e Berntsson, T. (2009b). Use of advanced composite curves for assessing cost-effective HEN retrofit II. Case studies. *Applied Thermal Engineering*. 29: 282–289.

Panjeh Shahi, M. H., Ghasemian Langeroudi, E., Tahouni, N. (2008). Retrofit of ammonia plant for improving energy efficiency., *Energy*. 33: 46–64.

Ravagnani, M. A. S. S., and Caballero, J. A. (2007). A MINLP Model For The Rigorous Design Of Shell And Tube Heat Exchangers Using The Tema Standards. *Chemical Engineering Research and Design.* n. 85(A10): 1–13.

Ravagnani, M. A. S. S., Silva, A. P., Biscaia Jr, E. C. e Caballero, J. A. (2009). Optimal Design of Shell-and-Tube Heat Exchangers Using Particle Swarm Optimization. *Industrial & Engineering Chemistry Research.* 48 (6): 2927-2935.

Singh, H. e Castillo, F. (2002). Process life cycle solutions for the case of automated heat exchanger network retrofit. *Applied Thermal Engineering*. 22: 949-958.
Tjoe, T.N. e Linnhoff, B. (1986). Using Pinch Technology for Process Retrofit. *Chemical Engineering*. 28: 47 - 60.
Yee, T. F. e Grossmann, I. E. (1990). Simultaneous Optimization Models for Heat Integration – II Heat Exchanger Network Synthesis. *Computers & Chemical Engineerin*. 14(10): 1165-1184.
Yee, T., F. e Grossmann, I. E. (1991). A Screening and Optimization Approach for the Retrofit of Heat-Exchanger Networks. *Industrial & Engineering Chemistry Research*. 30(1): 146-162.
Zhu, X. X. e Asante, N. D. K. (1999). Diagnosis and Optimization Approach for Heat Exchanger Network Retrofit. *AIChE Journal*. 45(7): 1488-1503.

Table 1 – Inlet data

Stream	*Tin (K)*	*Tout (K)*	*m (kg/s)*	*μ (kg/ms)*	*ρ (kg/m3)*	*Cp (J/kgK)*	*κ (W/mK)*	*ΔP (kPa)*	r_d *(W/mK)*
H1	1113	313	2.033	2.4 E-4	634	2454	0.114	68.95	1.7 E-4
H2	349	318	1.909	2.4 E-4	634	2454	0.114	68.95	1.7 E-4
H3	323	313	0.315	2.4 E-4	634	2454	0.114	68.95	1.7 E-4
H4	453	350	0.249	2.4 E-4	634	2454	0.114	68.95	1.7 E-4
H5	453	452	119.28	2.4 E-4	634	2454	0.114	68.95	1.7 E-4
H6	363	318	1.249	2.4 E-4	634	2454	0.114	68.95	1.7 E-4
C1	297	298	134.39	2.4 E-4	634	2454	0.114	68.95	1.7 E-4
C2	298	343	0.219	2.4 E-4	634	2454	0.114	68.95	1.7 E-4
C3	308	395	1.519	2.4 E-4	634	2454	0.114	68.95	1.7 E-4
C4	363	453	0.248	2.4 E-4	634	2454	0.114	68.95	1.7 E-4
C5	453	454	1051.79	2.4 E-4	634	2454	0.114	68.95	1.7 E-4
UQ	503	503							
UF	293	313							

Area cost = $9094 + 485A^{0.81}$, A em m^2
Pumping cost= 0.7 ($\Delta P_t m_t/\rho_t + \Delta P_s m_s/\rho_s$), ΔP em Pa, m em kg/s e ρ em kg/m^3
Hot utility cost = 110 $/kW ano
Cold utility cost = 15 $/kW ano
c1 = c2 = 1.0 w = 0.65 Npt = 30

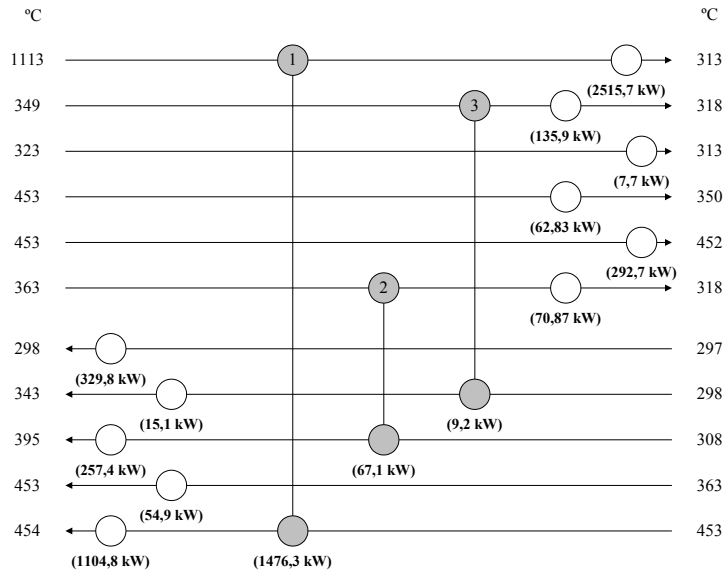

Figure 1 – Actual HEN

Table 2 – New equipment details

	E4	*E5*	*E6*
L (m)	*2.438*	*2.438*	*2.438*
D_c (m)	*0.686*	*0.205*	*0.205*
N_t	*349*	*16*	*14*
d_{ex} (m)	*0.0254*	*0.0191*	*0.0254*
d_{in} (m)	*0.0225*	*0.0122*	*0.0170*
ΔP_t (kPa)	*16587.14*	*63668.32*	*67854.25*
ΔP_c (kPa)	*33.29*	*3.58*	*3.91*
r_d (m^2 KW)	*3.396E-03*	*1.171E-02*	*7.710E-04*
Arrangement	*Triangular*	*triangular*	*triangular*
Hot fluid	*Shell*	*Tube*	*Tube*
Area (m^2)	*6.80*	*0.23*	*0.27*
Cost ($/year)	11,382.53	*9,241.48*	*9,261.94*

Table 3 – Comparison of the global cost

	Cost ($/year) Actual HEN	Cost ($/year) New HEN
HU	193,820	0
CU	46,290	21,240
Area	----------	29,886
Total	240,110	51,126

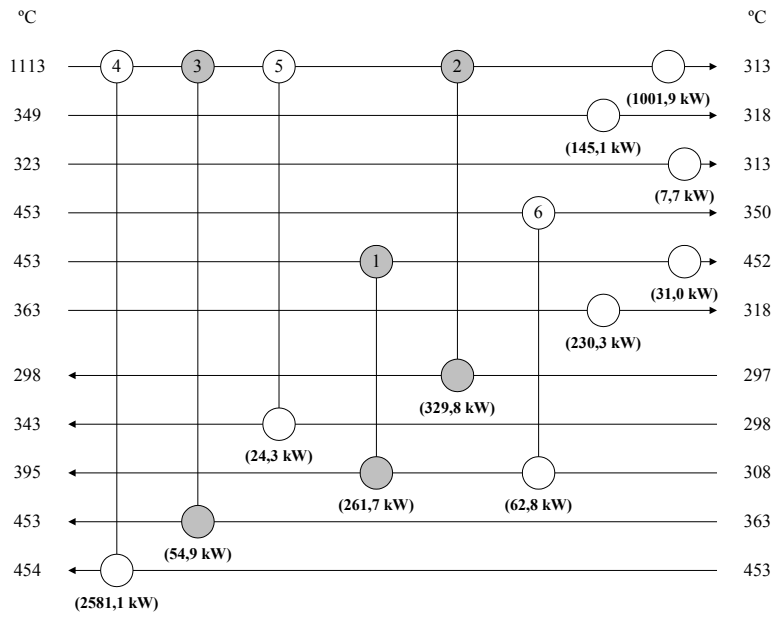

Figure 2 – Final HEN configuration

I.A. Karimi and Rajagopalan Srinivasan (Editors), Proceedings of the 11th International Symposium on Process Systems Engineering, 15-19 July 2012, Singapore.

Production of Cylohexane from Hydrogenation of Benzene using Microreactor Technology

Emmanuel A. Dada,[a] Luke Achenie[b]

[a]*ChemProcess Technologies, LLC, P.O. Box 3046, League City, TX 77573, USA*
[b]*Dept of Chemical Engineering, Virginia Polytechnic Institute & State University, Blacksburg, VA 24061, USA*

Abstract

Cyclohexane is generally used as an intermediate chemical where about 54 percent of its production is used in the production of adipic acid for nylon-6/6, 39 percent for caprolactam for nylon-6, and 7 percent for miscellaneous including solvents, insecticides and plasticizers. The demand for nylon (and hence cyclohexane) in engineering thermoplastics in resins and films is growing at about 6% annually. The production of cyclohexane from hydrogenation of benzene and hydrogen is a highly exothermic reaction where the reactor temperature control is very critical. Consequently, in most conventional commercial cyclohexane processes, multi-stage reactors involving recycling of cyclohexane, inter-reactor cooling to allow efficient removal of the heat of hydrogenation, and staged addition of the benzene feed are employed.

To address the temperature control problem more efficiently, we have taken advantage of the efficient and rapid heat removal characteristics of a microreactor system; our design offers more than two orders of magnitude better temperature removal and control than conventional reactors.. Our design also achieved minimal benzene, methylcyclopentane and other impurities (by-products) in the product thus having less impact on the environment compared with the conventional process. This paper suggests a general microreactor technology framework for the production of cyclohexane and other similar commodity chemicals. The framework is economical and leads to a safer route than the conventional technology.

Keywords: cyclohexane, microreactor, hydrogenation, safe, economical

1. Introduction

Cyclohexane is generally used as an intermediate chemical. Specifically 54 percent of what is produced is used in the production of adipic acid for nylon-6/6, 39 percent for caprolactam for nylon-6, and 7 percent for products including solvents, insecticides and plasticizers. The demand for nylon (and hence cyclohexane) in engineering thermoplastics in resins and films is growing at about 6% annually. Engineering thermoplastics are noted for their outstanding properties of high tensile strength, excellent abrasion, and chemical resistance and heat resistant. They have particular and growing demand in performing mechanical duties that traditionally relied on metal parts. The total world annual capacity of cyclohexane is about 1,800 million gallons of

which the U.S. capacity is about 600 million gallons with the U.S. annual production of Chevron-Phillips of 205 million gallons. Cyclohexane growth rate is estimated to average about 2 percent annually. The demand for cyclohexane in Japan has decreased due to a new production route to adipic acid that employs cyclohexene rather than cyclohexane.

Both patents and technical literature on conventional production of cyclohexane from hydrogenation of benzene have been reviewed. The available processes are very similar but differ by the choice of catalysts to ensure high degree of hydrogenation in order to meet product specifications. The major by-products of hydrogenation of benzene to cyclohexane are n-hexane, methyl-cyclopentane, methyl-cyclohexane, methyl-pentane, n-pentane, and methane. The control of the reactor's temperature and maintaining it at a desired level minimizes by-products formation. One of the major problems encountered in the production of cyclohexane is the deactivation of the reactor's catalyst bed by the CO in the hydrogen source necessitating a pre-treatment reactor unit (methanator) that converts the CO to methane and water before the hydrogen is fed into the main reactor. In the literature, a sensitivity analysis on the temperature control was carried out to investigate the best phase to carry out the reaction. Although most production of cyclohexane is carried out in the vapor phase, there are claims in the open literature that the mixed-vapor (liquid and gas mixture) phase gives the best reactor temperature control. However, when the temperatures and pressures are carefully chosen with the right catalyst, a liquid phase reaction minimizes by-products and gives a good reactor temperature control.

2. Reactor design for Production of Cyclohexane

The design of the reactor is the key to the production of cyclohexane where the temperature control of this highly exothermic reaction is an important determinant in the reactor configuration. We have carried out extensive literature search on many of the industrial processes and found out that most of the processes for the production of cyclohexane were carried out in the vapor phase. Table 2.1 shows the reactor operating conditions for different phases (liquid, liquid + vapor, and vapor). Our results are consistent with the studies reported by John McKetta and William Cunningham, 1978. Although most industrial processes for the production of cyclohexane are carried out in the vapor phase, McKetta and Cunningham suggested that a mixed phase (liquid + vapor) has the advantage of considerable flexibility. In view of these facts we chose to design the reactor for a mixed phase. The operating conditions (temperature of about 200 °C, and pressure of about 40 atms) that we selected for the mixed phase reactor design are very similar to the IFP (US patent 3,202,723). At these operating conditions, the principal side reaction of isomerization of cyclohexane to methyl cyclopentane is minimized.

The mixed phase presents a great challenge for the reactor design; we modeled the mixed phase as separate liquid and vapor phases and applied different kinetics equations to each phase. The work of Konyukhov, et al., appears to be one of the best referenced liquid phase kinetics studies of hydrogenation of benzene to cyclohexane. Likewise the work of Kehoe and Butt appears to be the most relevant vapor phase kinetics studies of hydrogenation of benzene to cyclohexane. Specifically these two pieces of work have

reconciled the many variations of the literature kinetics results in the liquid and vapor phases respectively. Therefore we employed these findings in our preliminary reactor design. In particular, Kehoe and Butt have shown that for a commercial nickel on kieselguhr, Harshaw Ni-0104 P, supplied as a powder and containing 58% wt Ni, equation 2.1 is applicable. Our preliminary reactor design and key results are

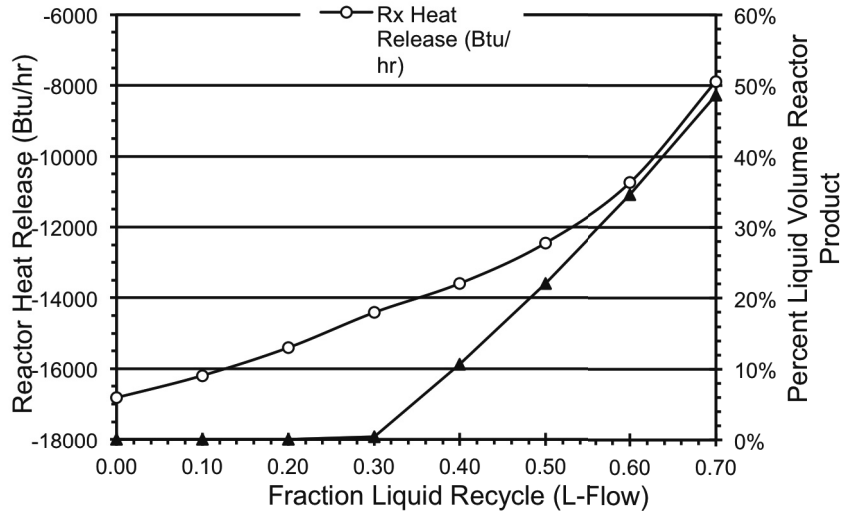

Figure 2.1 Impact of Liquid Recycle on Reactor Heat and Reactor Liquid

Table 2.1 Reactor Operating Conditions

Temperature (F)	Pressure (Psia)	H_2/C_6H_6 (HBR)	Reactor Phase
350 – 500	250 – 500	≥3.5	Vapor
350 – 500	350 – 500	3.05 – 3.5	Vapor + Liquid
350 – 400	≥2500	3.05 – 3.2	Liquid

presented in Figure 2.1.

$$Rate = \{\nu K P_B P_{H2} exp[-(Q+E)/RT]\}/\{1 + K P_B exp(-Q/RT)\} \quad (2.1)$$

Here $\nu = 0.1774$ mol/g catalyst s Torr, $K = 0.000008905$ Torr^{-1} (or 8.905 X10^{-6} Torr^{-1}), $Q = -8.26$ kcal/mol (Heat of adsorption), $E = 12.29$ kcal/mol (activation energy), $P_B =$ Partial Pressure Benzene, Torr, $P_{H2} =$ Partial Pressure Hydrogen, Torr, $T =$ Temperature, deg K, $R = 1.987$ cal/gmol K (gas constant), Torr = (101.325/760) kN/m^2.

3. Process Improvement (i.e. Optimization) Studies

We carried out space-time yield analysis and "optimized" relevant process parameters for the design of the microreactor. The key results are presented here.

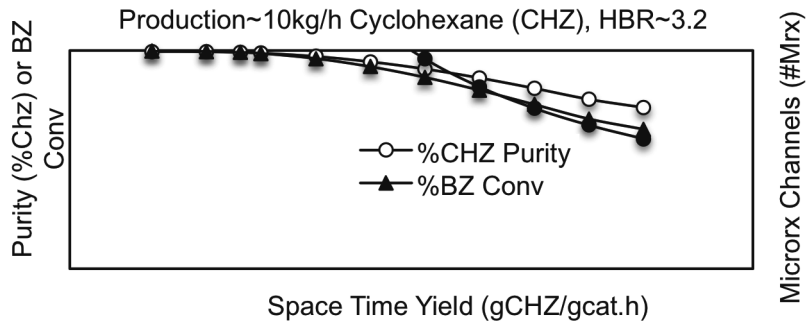

Figure 3.1 Space Time yield vs. Product Purity (3.2 H_2/C6H6 feed ratio)

3.1 Impact of Space Time Yield on product Purity

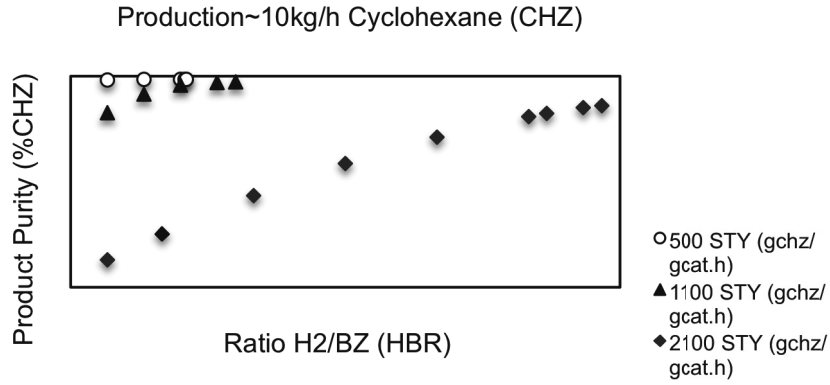

Figure 3.2 Impact of hydrogen to benzene feed ratio (HBR) on Product Purity

As shown in Figure 3.1, a reactor with space-time yield of 600 g Cyclohexane (CHZ)/g cat.h or less is needed to achieve 99wt% or more product purity. For the production of 10 kg/hr of cyclohexane, about 200 or more channels are needed to deliver 99 wt% product purity at hydrogen to benzene feed ratio of 3.2. Each channel is assumed to be of dimensions 500 micron x 500 micron x 6 in.

3.2 Impact of Hydrogen-Benzene Ratio on Product Purity

Figure 3.2 shows that for all space-time yields increasing the hydrogen-benzene ratio will result in higher product purity. As expected, a reactor with moderate to large volume (e.g. 500 - 800 g CHZ/g cat.h (STY) yields high purity product (>99wt %) with moderate amount of hydrogen (3.2- 4.0 HBR). Also, a reactor with small volume (1100-2100 g CHZ/g cat.h STY) will need moderate to large amount of hydrogen (>4.5 HBR) to attain the same product purity.

4. Results and Discussion

In this paper we have presented the design of a microchannel catalytic reactor system for production of cyclohexane from hydrogenation of benzene. The microreactors operate at a combined space-time yield of 500g cyclohexane/g cat.h and at 3.2 molar ratio of hydrogen to benzene. The proposed process involves large and rapid heat transfer, and we have shown that microreactors have promising application for better control and safety because of their large surface to volume ratio better than the conventional reactors.

References

Amend, William J., 1943, "Catalytic Oxidation", US Patent 2316543 assigned to DuPontClement, Thonon, 1965, “Process for the Catalytic Hydrogenation of Aromatic Hydrocarbons”, US patent 3,202,723, assigned to Institut Francais du Petrole.

Felix, Albert; Roques, Yves, 2004, "Method of making adipic acid", US patent 6822117 assigned to Rhodia, Fiber And Resin Intermediates (Courbevoie, FR)

John McKetta and William Cunningham, 1978, Vol. 14 of Encyclopedia of Chemical Processing and Design.

Kehoe and Butt, 1972, “Kinetics of Benzene Hydrogenation by Supported Nickel at Low Temperature”, Journal of Applied Chem. Biotechnol. 22, 23-30

Kirk-Othmer Encyclopedia of Chemical Technology, 1980, Vol. 12, John Wiley & Sons.

Konyukhov, et al., 1987, “Kinetics of Liquid-Phase Hydrogenation of Benzene on Palladium Catalyst and Hydrogenation of Toluene on Palladium and Catalysts”, Kinetika, Vol. 28, No 2, pp. 360-365

Sanderson, John Ronald, et al., 2003, " Manufacture of cyclohexane from benzene and a hydrogen source containing impurities”, US patent application # 20030114723

Srinivas, Darba; Chavan, Suhas; Ratnasamy, Paul, 2003, "Process for the preparation of adipic acid", US Patent 6521789 assigned to Council of Scientific and Industrial Research (New Delhi, IN)

Ullmann's Encyclopedia of Industrial Chemistry, 2005

I.A. Karimi and Rajagopalan Srinivasan (Editors), Proceedings of the 11th International Symposium on Process Systems Engineering, 15-19 July 2012, Singapore.

Synthesis Framework of Biorefinery Systems for Lignocellulosic Biorenewables

Wenkai Li[a], Ramadoss Karthik[b], I A Karimi[b], Wong Pui Kwan[c]

[a] *Graduate School of International Management, International University of Japan, Niigata, Japan 949-7277*
[b] *Department of Chemical and Biomolecular Engineering, National University of Singapore, 4 Engineering Drive 4, Singapore 117576*
[c] *Institute of Chemical and Engineering Sciences, Agency for Science, Technology and Research (A*STAR), No. 1, Pesek Road, Jurong Island, Singapore 627833*

Abstract

In this paper, we present a mathematical framework to design an economically attractive and environmentally friendly biorefinery. We embed various biomass feedstocks, conversion technologies, and products into a novel superstructure of alternative configurations for a general biorefinery. To obtain the optimal configuration and design of the biorefinery, we model each technology block using simplified mass, resource, and energy balance equations. These form the basis for the mathematical model.
Keywords: lignocellulose, biorefinery, process synthesis.

1. Introduction

The world is actively looking for sustainable alternatives to meet increasing energy and product demands. This is amid growing concerns of global warming, fast depletion of petroleum resources, expected increase in crude oil price due to rapid demand growth from China and India, and unstable oil supply due to the turmoil in the Middle East. Although the replacement of carbon-based economy is receiving considerable attention nowadays, mankind's reliance on carbon will continue for the foreseeable future. As the only carbon-rich material source, biorenewables processed in biorefineries are very likely to be the only viable alternative to fossil resources for the production of chemicals and transportation fuels. The development of biorefineries will be "the key for the access to an integrated production of food, feed, chemicals, materials, goods, and fuels of the future" (National Research Council, 2000). Several major research projects are underway worldwide on the development and demonstration of biorefineries. These include BIOCORE in EU, DEFRA in UK, and VACL in Singapore.

2. Literature Review

Based on the types of feedstocks used, Kamm and Kamm (2004) categorize biorefineries into three major systems: the whole-crop biorefinery, the green biorefinery and the lignocellulose feedstock (LCF) biorefinery. LCF biorefinery is considered as the most promising one because of its abundance, renewability, lack of competition with food/crop, and ability to contribute to significant CO_2 emission reduction. Most existing literature study either single product (mostly bioethanol) with some by-products or a single main product (mostly bioethanol) together with 1 or 2 value-added products from the LCF biorefinery. Little research has focused on producing high value-added products where bulk chemicals such as bioethanol are not the main products.

Kamm and Kamm (2006) highlight existing works relevant to process, raw material, product, and technology options. However, a study that integrates all these components using a modeling and optimization approach based on mathematical programming does not exist. Here, we aim to bridge these knowledge gaps by systematically and intelligently proposing and evaluating possible alternatives for a biorefinery configuration.

The attractive future prospects for biorefineries are accompanied by several unique and challenging characteristics. Such challenges mainly include supply chain design and management (decentralized raw material sources, low transport densities, etc.), process design and development (e.g. lack of models and critical data, heterogeneity and complexity of biomass sources and conversion technologies) and intelligent decision making (e.g. uncertainty in markets and prices). Furthermore, in most scenarios, successful process synthesis strategies for conventional refineries do not work for biorefineries. Thus, biorefinery synthesis using advanced systems engineering approaches requires substantial research to design and manage economically viable and environmentally benign biorefineries. Ideally, a holistic lignocellulosic biorefinery should integrate the three major aspects shown in Figure 1.

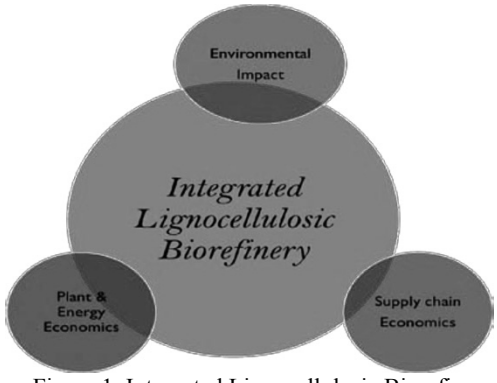

Figure 1. Integrated Lignocellulosic Biorefinery

3. Superstructure for a General Biorefinery

Biomass has a complex composition and can be processed to a plethora of products. Starting from the pre-treatment unit, numerous processing routes and products can exist. We have explored a variety of plausible and promising options for the conversion of cellulose, lignin, and C5 sugars into a slate of potential products using different technologies. The goal was to gather as many "potentially synergistic" alternatives as possible for products, technologies, and processes into a grand pool from which we can synthesize novel, non-intuitive, and best options. We have developed a superstructure (Figure 2) of various alternative configurations for a general VACL biorefinery system. Such a superstructure can enable an objective, systematic, and smart examination of various alternatives through a modeling and optimization approach based on mathematical programming.

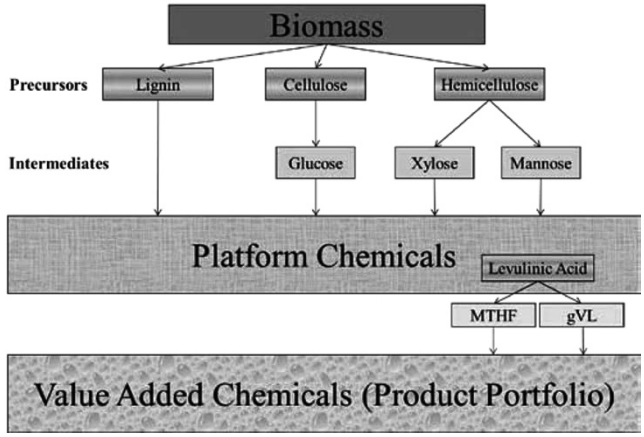

Figure 2. Superstructure For A General Biorefinery

Figure 2 is based on three precursors, namely lignin, cellulose, and

hemicellulose; three intermediate chemicals, namely glucose, xylose, and mannose; and several platform chemicals. Key value-added chemicals from each platform chemical are also identified according to their market importance. Processing routes applying different technologies connecting the precursors, intermediates, platform chemicals, and final value-added chemicals are also identified. The platform chemicals and their derivatives are mainly selected from three major reports in the literature, namely the US DoE Report, the BREW Project report and the FROPTOP white paper. Clearly, the collected pool of options and possibilities is huge and interconnected, making the determination of the optimal configuration of a VACL biorefinery a formidable task.

4. Mathematical Formulation

All operations in the biorefinery are modeled using basic equations. The parameters and values used are based on yearly operation. Some notations are adopted from Oh and Karimi (2004) and Hugo and Pistikopoulos (2005).

4.1. Material Balances

Let m denote all materials (raw materials, products, and utilities) involved in the biorefinery, s denote source, c denote consumer and t denote fiscal year. Let IM_u and OM_u denote sets of input and output materials of unit u respectively and U denote set of all units in the biorefinery. Two special units are used in our model: *Src*, which represents the source of raw materials, and *Market*, which represents the sink of products. The life time of the biorefinery is assumed to be T years. Let f_{msu} denote the flow of material m from unit s to unit u.

As data available in most of the literature are usually based on a primary material to characterize the unit operation, we identify a primary material π_u to be used as the reference for further calculation. The actual consumption/production level of material m can be calculated from the consumption/production level of the primary material π_u.

$$\sum_{m\in OM_s} f_{msu} + \sum_{m\in IM_c} f_{muc} = \rho_{mu}\left(\sum_{\pi_u\in OM_s} f_{\pi_u su} + \sum_{\pi_u\in IM_c} f_{\pi_u uc}\right), u\in U, m\in IM_u \cup OM_u \tag{1}$$

, where ρ_{mu} is the amount of material m needed to process one unit of π_u in unit u.

In addition to the above constraint, the supply of raw materials is limited by its availability in the market, the manufacture of products is limited by its demand in the market, the operation capacity of a unit is restricted by its technological limits, and emissions from the biorefinery should not exceed regulatory limits.

4.2. Environmental Impact Assessment

4.2.1. Goal and Scope

We apply the popular 'cradle-to-gate' approach, in which downstream processing is neglected, to assess the environmental impact of the biorefinery. We employ Eco-indicator 99 score as the environmental performance indicator. The eleven impact categories proposed by Eco-indicator 99 are considered, which are further aggregated into three damage categories.

4.2.2. Inventory Analysis

Let D_{eu} denote the value of impact category e for unit u. Let V denote set of environmental burdens, E denote set of impact categories, W denote set of raw materials and R_u denote set of utilities consumed by unit u. Parameters df_{ve} and ω_{vm} give the damage factor of substance v contributing to impact category e and the amount of substance v generated per unit flow of material m respectively.

$$D_{eu}=\sum_{v\in V}\left[df_{ve}\left(\sum_{\pi_u\in OM_s\in s}f_{\pi_u su}+\sum_{\pi_u\in IM_c\in c}f_{\pi_u uc}\right)\left(\omega_{v\pi_u}+\sum_{m\in W\cup R_u}\omega_{vm}\rho_{mu}\right)\right] \quad (2)$$

4.2.3. Impact Assessment

Let L_{ed} denote set of impact categories e that belong to damage category d and D denote set of damage categories. The values of the impact categories are first normalized and then aggregated into a single Eco-Indicator 99 score using a normalization factor η_d and a weighting factor Ψ_d:

$$Eco\text{-}indicator\ 99=\sum_{d\in D}\left(\Psi_d\eta_d\sum_{e\in L_{ed}}\sum_{u\in U}D_{eu}\right) \quad (3)$$

4.3. Economics

We assume linear relationships between the flow rate of the primary material π_u and both the operation cost $OPEX_{ut}$ and capital investment $CAPEX_{ut}$ of unit u in fiscal year t. All investment costs for unit u are made at the first fiscal year. Also the total capital investment of the biorefinery should not exceed budgetary constraints.

The purchase cost of input materials RC_{ut} of unit u in year t is given by:

$$RC_{ut}=(1+ir)^t\sum_{m\in IM_u}\sum_{m\in OM_s\in s}CIF_{msu}f_{msu},u\in U,t\in T \quad (4)$$

, where ir is the inflation rate and CIF_{msu} is the cost of purchase, insurance, freight, and waste treatment of raw material m from supplier s to unit u.

The cost of utilities UC_{ut} consumed by unit u in year t is given by:

$$UC_{ut}=(1+ir)^t\sum_{r\in R_u}CIF_{r,Src,u}\rho_{ru}\left(\sum_{\pi_u\in OM_s\in s}f_{\pi_u su}+\sum_{\pi_u\in IM_c\in c}f_{\pi_u uc}\right),u\in U,t\in T \quad (5)$$

The selling rate of output materials SR_{ut} of unit u in year t is given by:

$$SR_{ut}=\sum_{m\in OM_u}\sum_{m\in IM_c\in c}P_{muc}f_{muc},u\in U,t\in T \quad (6)$$

, where P_{muc} is the price of product sold from unit u to unit c.

Assuming that the life times of all units start at t=1 and end at t=T, the total capital expenditure CE_{ut} for unit u in year t is given by:

$$CE_{ut}=CAPEX_{ut}+OHC_{ut}-SV_{ut},u\in U,t\in T \quad (7)$$

, where OHC_{ut} is the unit overhead costs and SV_{ut} is the estimated salvage value of the unit at the end of the unit life time. SV_{ut} takes value of zero except at t=T.

The cash flow CF_{ut} of unit u in year t is given by:

$$CF_{ut}=\begin{cases}(SR_{ut}-RC_{ut}-OPEX_{ut}-UC_{ut})(1-TR_{ut})-CE_{ut} & \forall SR_{ut}-RC_{ut}-OPEX_{ut}-UC_{ut}\geq 0\\ (SR_{ut}-RC_{ut}-OPEX_{ut}-UC_{ut})-CE_{ut} & \forall SR_{ut}-RC_{ut}-OPEX_{ut}-UC_{ut}<0\end{cases},u\in U,t\in T \quad (8)$$

, where TR_{ut} is the corporate tax for unit u in year t.

The NPV (Net Present Value) of the biorefinery is given by:

$$NPV=\sum_{u\in U}\sum_{t}\frac{CF_{ut}}{(1+\phi)^t} \quad (9)$$

, where ϕ is the annual interest rate.

4.3.1. Multi-Objective Function

Two objectives, economic (expressed as *NPV*) and environmental (expressed as Eco-Indicator 99 score), are used in VACL biorefinery optimization model:

$$min\begin{pmatrix} -NPV \\ Eco\text{-}Indicator\ 99 \end{pmatrix} \tag{10}$$

Conclusions

We highlighted the need for continued research on the development of biorefineries and the importance of using advanced systems engineering methods to design sustainable biorefineries. We proposed a novel superstructure of various alternative configurations for a general biorefinery, and a general mathematical model to obtain the optimal design and configuration of a biorefinery. Key challenges in the implementation of this novel superstructure are its inherent complexity and unavailability of detailed data for chemicals and processes. We are currently in the process of generating necessary data for the various pathways in the superstructure, development of solution methodology, and testing with appropriate case studies.

References

[1] Biobased Industrial Products, Priorities for Research and Commercialization, National Research Council, National Academic Press, Washington, D.C., 2000.
[2] B. Kamm and M. Kamm, Appl. Microbiol. Biotechnol., No. 64 (2004), 137.
[3] B. Kamm, P.R. Gruber, M. Kamm (eds.), Biorefineries – Industrial Processes and Products, Vols 1 & 2, Wiley-VCH, Weinheim, Germany, 2006.
[4] T. Werpy and G. Petersen (eds.), Top Value Added Chemicals from Biomass Volume I: Results of Screening for Potential Candidates from Sugars and Synthesis Gas, Pacific Northwest National Laboratory and the National Renewable Energy Laboratory, Department of Energy (DoE), USA, 2004.
[5] M.K. Patel (ed.), Medium and Long-term Opportunities and Risks of the Biotechnological Production of Bulk Chemicals from Renewable Resources – The Potential of White Biotechnology – The BREW Report, Utrecht, Netherlands, 2006.
[6] W. Skibar, G. Grogan, J. McDonald and M. Pitts (eds.), UK Expertise for Exploitation of Biomass-Based Platform Chemicals, FROPTOP programme, UK, 2010.
[7] H.C. Oh and I.A. Karimi, Ind. Eng. Chem. Res., No. 43 (2004), 3364.
[8] A. Hugo. and E.N. Pistikopoulos, Journal of Cleaner Production, No. 13 (2005), 1471.

I.A. Karimi and Rajagopalan Srinivasan (Editors), Proceedings of the 11th International Symposium on Process Systems Engineering, 15-19 July 2012, Singapore.

Heat-integrated reactive distillation for biodiesel production from Jatropha oil

Samaporn Phuenduang,[a] Porntida Chatsirisook,[a] Lida Simasatitkul,[a] Woranee Paengjuntuek,[b] Amornchai Arpornwichanop[a,*]

[a] *Department of Chemical Engineering, Faculty of Engineering, Chulalongkorn University, Bangkok 10330, Thailand*
[b] *Department of Chemical Engineering, Faculty of Engineering, Thammasat University, Patumthani 12120, Thailand*
[*] *e-mail: Amornchai.a@chula.ac.th*

Abstract

Minimizing the biodiesel production cost by using inexpensive and inedible feedstock like Jatropha oil is more practical as it is readily available and also not competes with edible oils. However, Jatropha oil contains high free fatty acid content, which causes operational problems in biodiesel production via alkaline-based transesterification reaction. This study aims to design a biodiesel production process from Jatropha oil. A hydrolysis reactor is applied to convert triglyceride in Jatropha oil to fatty acid. The fatty acid obtained then reacts with methanol to produce methyl ester (biodiesel product) using an esterification process. A reactive distillation is employed to intensify reaction and separation tasks for the esterification process. In order to minimize energy consumption, the heat integration of a reactive distillation process is considered. The simulation result using a flowsheet simulator indicates that the heat-integrated reactive distillation can improve the biodiesel production by minimizing the energy requirements, compared with a conventional process.

Keywords: Reactive distillation, Heat integration, Biodiesel production, Jatropha oil

1. Introduction

Biodiesel, a clean renewable fuel, has been considered the best candidate for a petroleum diesel substitute because it can be used in any compression ignition engine without the need for modification (Leung et al., 2010). In general, biodiesel can be produced from natural resources such as vegetable oils, animal fats and algae. A high consumption of edible oils in the world results in a shortage of feedstock for biodiesel production. Alternatively, the use of inedible oils, which are unsuitable for human consumption because of some toxic components in the oils, is an interesting option.

Jatropha curcas is a potential resource for biodiesel production as it contains a high fraction of oils (30-40 wt.%). However, a high amount of free fatty acids (FFAs) in Jatropha oil affects a transesterification process using alkaline catalyst to generate biodiesel. FFAs can react with the alkaline catalyst and form soap, causing a difficulty in the purification of biodiesel product. Accordingly, the development of an efficient process for biodiesel production from oils with high free fatty acid content is required. A two-step biodiesel production has been proposed to deal with such a problem. The first step involves a hydrolysis process where triglycerides in oil are hydrolyzed with water to produce fatty acids and glycerol, whereas all the fatty acids react with methanol via esterification reaction to generate methyl oleate (biodiesel product) and water in the

second step (Chen et al., 2010). However, since the esterification is an equilibrium reaction, the conversion of fatty acid is limited. To improve the performance of biodiesel production, the application of a reactive distillation (RD) in which reaction and separation tasks are carried out in a single unit is an attractive option (Kiss et al., 2008).

This study is focused on the production of biodiesel from Jatropha oil. The two-step method consisting of hydrolysis and esterification sections is studied based on a reactive distillation technology. Process heat integration is considered to improve the energy usage of the biodiesel process.

2. Biodiesel production from Jatropha oil

Since oleic acid is a major component of Jatropha oil, triolein is used to represent a triglyceride in this study. Fig. (1) shows a conventional process for biodiesel production from Jatropha oil. Triolein is first treated with water to produce fatty acid and glycerol (Eq. 1). Fatty acid obtained then reacts with methanol to obtain methyl oleate, biodiesel product, and water (Eq. 2).

$$\begin{array}{l} CH_2-OCOR \\ CH-OCOR \\ CH_2-OCOR \end{array} + 3H2O \leftrightarrows 3RCOOH + \begin{array}{l} CH_2-OH \\ CH-OH \\ CH_2-OH \end{array} \quad (1)$$

(Triolein) (Water) (Oleic acid) (Glycerol)

$$RCOOH + CH_3OH \leftrightarrows RCOOCH_3 + H_2O \quad (2)$$

(Oleic acid) (Methanol) (Methyl oleate) (Water)

The hydrolysis reaction occurs at pressure of 11 MPa and temperature of 563K and reaches equilibrium condition (Chen et al., 2010). The kinetic of esterification (Eq. 2) proposed by Jain and Sharma (2010) is used. The UNIFAC model is selected to estimate thermodynamic properties and simulations are performed using Aspen Plus flowsheet simulator.

A heat integrated reactive distillation process to produce biodiesel is showed in Fig. 2. The esterification reaction of oleic acid and methanol is carried out in a reactive distillation column. The bottom product of the reactive distillation is sent to a conventional distillation to separate methanol from a biodiesel product. The biodiesel product stream is used to preheat methanol and oleic acid feed streams before entering the reactive distillation column.

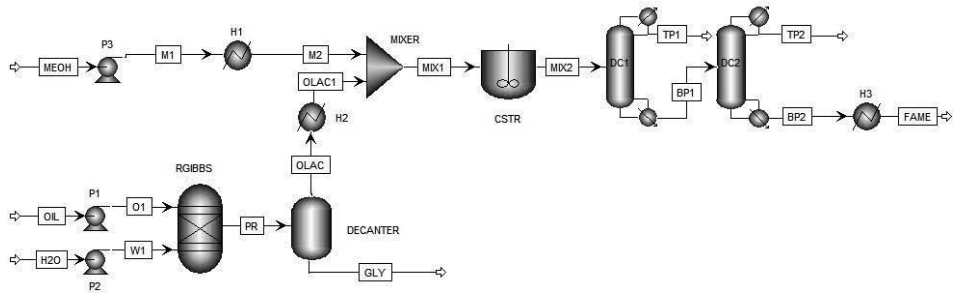

Fig. 1. Conventional process for biodiesel production.

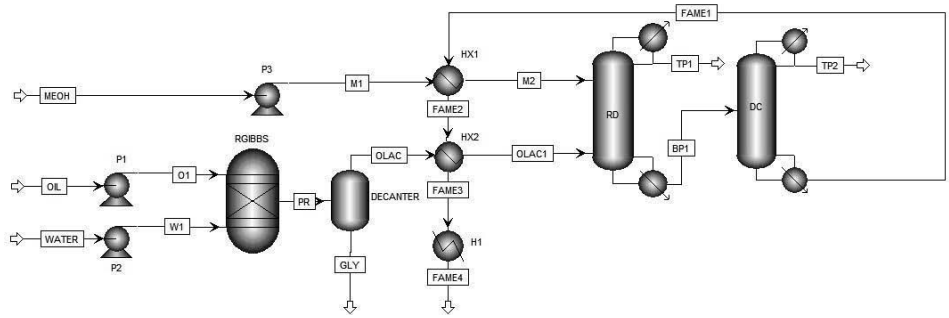

Fig. 2. Heat integrated reactive distillation process for biodiesel production.

Table 1. Specifications and operating conditions for a conventional biodiesel process

Reactor	Hydrolysis	Esterification
Total mole flow (kmol/h)	183.99	496.33
Conversion (mol%)	99.99 (oil)	95.79 (acid)
Heat duty (kW)	2347.75	-3938.16
Temperature (K)	563.15	343.15
Pressure (MPa)	11	0.101325
Decanter		
Temperature (K)	433.15	
Pressure (MPa)	0.101325	
Heat duty (kW)	-4284.97	
Distillation column (DC)	DC 1	DC 2
Stages	25	15
Feed stage	10	6
Distillate to feed mole ratio	0.5	0.3
Reflux ratio	0.6	0.5
Condenser duty (kW)	-3856.32	-1252.39
Reboiler duty (kW)	4794.24	1465.21
Top stage pressure (MPa)	0.101325	0.101325
Biodiesel purity (mol%)	44.39	63.41

3. Simulation results

To perform the simulation of a biodiesel production via a conventional process, the hydrolysis of triolein and the esterification of oleic acid are carried out in equilibrium (RGIBBS) and continuous (CSTR) reactors, respectively. A 46 kmol/h stream of triolein is fed to the equilibrium reactor and reacts with 138 kmol/h of water. Oleic acid and glycerol are generated at the flow rates of 137.94 and 42.88 kmol/h. Then, the oleic acid and methanol are mixed before entering a continuous reactor where the esterificaion reactor is occurred. The reaction product is sent to distillation columns (DC1 and DC2) to purify the methyl oleate product, which is cooled down to temperature of 25 ^{o}C. Table 1 shows the process specifications and conditions of the conventional biodiesel process. Under the standard conditions, the purity of methyl oleate obtained is 63.41 mol%. The overall heat requirement of the conventional process is 25,937 kW.

Table 2. Specifications and operating conditions for a reactive distillation biodiesel process

	RD	DC
Stages	15	15
Molar reflux ratio	0.2	0.5
Methanol feed stage	4	-
Oleic acid feed stage	12	-
BP feed stage	-	7
Reactive stages	2-14	-
Distillate rate (kmol/h)	291.07	80
Condenser duty (kW)	-3799.77	-2970.43
Bottom rate (kmol/h)	200	120
Reboiler duty (kW)	309.57	9656.77
Fatty acid conversion (mol%)	99.99	-
Biodiesel purity (mol%)	68.85	99.80

Table 3. Comparison of energy requirement for different biodiesel processes

	Conventional process	Reactive distillation (RD) process	Heat integrated RD process
Reactor			
Hydrolysis	2347.75	2347.75	2347.75
Esterification	-3938.16	-	-
Distillation column			
Condenser duty	-5108	-2970.43	-2970.43
Reboiler duty	6259.45	9656.77	9656.77
Reactive distillation column			
Condenser duty	-	-3799.77	-3799.77
Reboiler duty	-	309.57	309.57
Additional power			
Pump	245.36	245.36	245.36
Cooler	-2155.16	-7772.61	-1886.68
Heater	5883.87	5883.87	-
Total energy consumption	25937	32986.13	21216.33

Next, the performance of a reactive distillation process to produce biodiesel is presented. The hydrolysis section is similar to the conventional process but the difference is in the esterification section where a reactive distillation is employed. Oleic acid (137.94 kmol/h) and methanol (350 kmol/h) from the hydrolysis section are sent to a reactive distillation at the stage 4 and 12, respectively. The reactive distillation is operated at relatively low molar reflux ratio of 0.2 because the methyl oleate product has much more higher boiling point than methanol and water, so that the separation of these substances can be easily performed. The methyl oleate product is removed at the bottom of the reactive distillation and then sent to a purification section. The purity of methyl oleate obtained is 99.80 mol%. The total energy consumption is 32,986.13 kW, which is higher than the conventional process. Table 2 shows the specification and operating conditions of reactive and conventional distillation columns.

To improve the energy usage, a heat integration of the reactive distillation process for biodiesel production is considered. The methyl oleate product is used as a heat source for preheating the oleic acid and methanol feeds (Fig. 2). Table 3 shows a comparison

of the total energy requirements of biodiesel processes with different configurations. It can be seen that the heat integrated reactive distillation process requires the lowest energy consumptions. The heating and cooling requirements are significantly reduced by 35.7% and 20% when compared with a reactive distillation process without heat integration and a conventional process, respectively.

4. Conclusions

This study presents a biodiesel production using Jatropha oil as feedstock. A two-step biodiesel process consisting of hydrolysis and esterification steps has been studied. A reactive distillation is proposed to improve the performance of the esterification process. In addition, a heat integration of the reactive distillation process is considered for an efficient energy usage. The major benefits of the proposed biodiesel process include increased productivity, reduced investment cost and minimum energy requirement. The results show that the heat integrated reactive distillation can save the energy consumption by 20%, compared with a conventional biodiesel process.

5. Acknowledgement

Support from the Computational Process Engineering Research Group, the Special Task Force for Activating Research (STAR), Chulalongkorn University Centenary Academic Development Project is gratefully acknowledged.

References

C.H. Chen, W.H. Chen, C.M. Chang, S.M. Lai, C.H. Tu 2010, Biodiesel production from supercritical carbon dioxide extracted Jatropha oil using subcritical hydrolysis and supercritical methylation, Journal of Supercritical Fluids 52, 228-234

S. Jain and M.P. Sharma, 2010, Kinetics of acid base catalyzed transesterification of *Jatropha curcas* oil, Bioresource Technology 101, 7701-7706

A.A. Kiss, A.C. Dimian, G. Rothenberg, 2008, Biodiesel by Catalytic Reactive Distillation Powered by Metal Oxides, Energy & Fuels 22, 598-604

D. Leung, X. Wu, M. Leung, 2010**,** A review on biodiesel production using catalyzed transesterification, Applied Energy 87, 1083-1095

I.A. Karimi and Rajagopalan Srinivasan (Editors), Proceedings of the 11th International Symposium on Process Systems Engineering, 15-19 July 2012, Singapore.

Functional modeling applied to HAZOP automation

José Luis de la Mata,[a] Manuel Rodríguez[a]

[a]*Technical University of Madrid, José Gutiérrez Abascal 2, 28006 Madrid, Spain*

Abstract

In this paper we present a new tool to perform guided HAZOP analyses. This tool uses a functional model of the process that merges its functional and its structural information in a natural way. The functional modeling technique used is called D-higraphs. This tool solves some of the problems and drawbacks of other existing methodologies for the automation of HAZOPs. The applicability and easy understanding of the proposed methodology is shown in an industrial case.

Keywords: Functional modeling; HAZOP; Risk assessment.

1. Introduction

Currently, due to economical optimization of process plants, they are working at extreme conditions of pressure and temperature. This situation makes them more likely to fail and, even worse, the consequences of accidents are more severe. In addition, the Chemical Industry is facing tighter regulations and a growing attention of the media towards industrial accidents. Of course, we have also to consider the economical losses associated to accidents in terms of shutdowns, reparations, compensations and fines.

In the design stage of the process plant, Process Hazard Analyses (PHA) are carried out to identify potential sources of accidents and propose some solutions that enhance the safety of the plant. One of the most used of all of the existing PHA techniques is the Hazard and Operability Study (HAZOP) (Zhao et al., 2005). However, this approach consumes a lot of effort, time and, hence, money.

For these reasons, in the last two decades a lot of effort has been devoted to the implementation of tools and methodologies that can lead to the automation of these studies. In this work we present a new tool based on a functional modeling technique called D-higraphs. This approach takes into account in a natural way the structure as well as the functionality of the system (process and control system).

2. D-higraphs: merging function and structure

2.1. Dualization: from Higraphs to D-higraphs

Higraphs were first presented by Harel (1987) and they are a general kind of diagramming that can be understood as a combination and extension of Graphs, Euler/Venn diagrams and the Cartesian Product. They are well suited to specify complex concurrent systems but not process systems.

However, they can be adapted to process specification by the dualization of their properties and relations. This dualization has led to D-higraphs that were first presented in Rodríguez & Sanz (2009). Higraphs and D-higraphs consist of blobs and edges connecting them.

It should be noted that the term ‘dualization’ is used in a different way than the one used in Dual-Graphs or Digraphs; it is only applied to the properties and not to the elements.

2.2. Elements of a D-higraph

A basic blob and its elements are depicted in the left-hand-side of Fig. 1 and the different types of edges are shown in the center of Fig. 1. Blobs represent functions (transitions) that are performed by an ACTOR producing state/s 2 if the state/s 1 is enabled and if the *condition* is true. Edges represent flows of mass, energy, or information, which are responsible of all the interactions in a process system (Lind, 1994). Mass, energy and information edges are depicted differently, but the type of flow does not affect the behavior of the model, it is a just a visual aid.

Disjoint blobs imply an AND relation (both transitions between states take place) while orthogonal blobs represent an OR relation (only one of the transitions takes place). The main properties are:

- *Blob connection*. An edge always links two blobs. Under certain conditions, one of the blobs cannot be represented (elliptic blob), but it exists.
- *Blob inclusion*. Blobs can be included inside of other blobs (Venn diagram inclusion). This means that the inner blob performs a function that is necessary for the function of the outer blob (representation of functions hierarchy).
- *Blob partition*. A blob can be partitioned into orthogonal components, establishing an OR condition between the partitions.

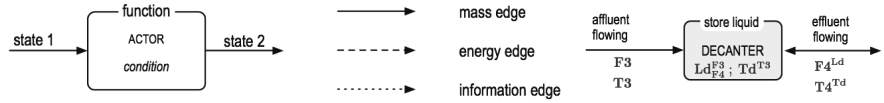

Fig. 1. Basic blob, types of edges, and three layer D-higraph.

2.3. Causality and qualitative reasoning

The main objective of D-higraphs is not only the representation of knowledge about process systems. De la Mata & Rodríguez (2010a,b) provide a series of causation rules relating two events that allow us to track the evolution and propagation of failures across the system. This rules combined with sensor data of the plant enables the possibility of performing FDI analysis using D-higraph models.

However, certain analyses require the use of deviations and not only failures, like HAZOP studies. In a certain way, we need to simulate qualitatively the system in order to propagate these deviations. The description of a system is made in three different layers (Kuipers, 1984):

1. *Structural description*: variables that characterize the system, such as flow (F), pressure (P), temperature (T), composition (x), energy (E), information (I), level (L), valve opening (A), etc. The symbols in brackets will be used in D-higraphs.
2. *Behavioral description*: potential behavior of the system as a network. The M^+ and M^- constraints (Kuipers, 1986) provide this information and they we will use the following compacted compacted notation:

$$Z^{X_1,X_2\ldots X_n}_{Y_1,Y_2\ldots Y_m} \quad \Leftrightarrow \quad M^+(X_i,Z) \wedge M^-(Y_i,Z) \quad \forall i,j \qquad \text{(Eq. 1)}$$

3. *Functional description*: purpose of a structural component of connections; provided by the D-higraphs layout.

The three layers of this representation are shown in the right-hand-side of Fig. 1, where there is a physical device (DECANTER) whose main purpose is to *store liquid*. The decanter has two characteristic variables: level (Ld) and temperature (Td). Ld is affected by the inflow F3 with variations of the same sign (an increment of F3 increases Ld) and by the outflow F4 in the opposite way. In the same way, the flow F4 is affected by the level of the decanter in the same direction (see Eq. 1).

3. D-higraphs environment and HAZOP Assistant

D-higraphs are developed using the environment shown in Fig. 2. The models are implemented using a graphic tool Álvarez (2010). This tool has as input the P&ID of the process and it uses a D-higraphs built in template. Once the model has been developed, it is loaded into the expert system. The HAZOP study is performed feeding the deviations to the reasoning engine. The result of the analysis, a causal tree, is provided to the user and they can be fed back to the modeling tool in order to make changes into the process and/or D-higraph.

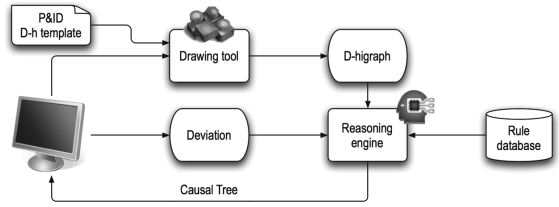

Fig. 2. D-higraphs environment.

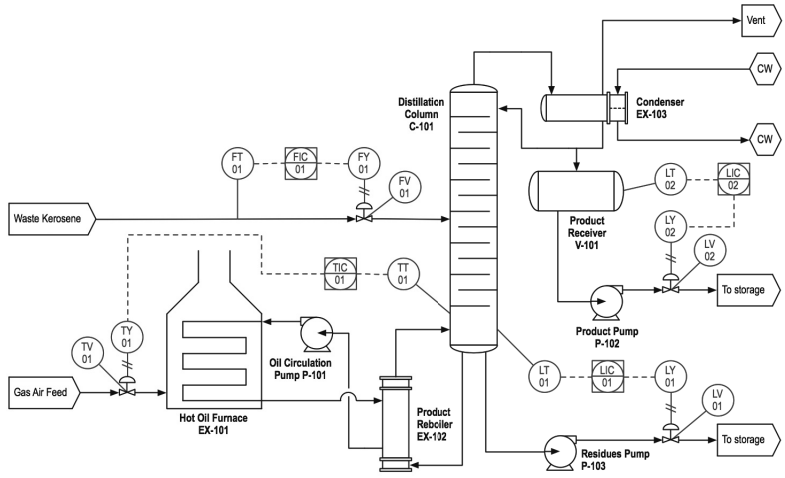

Fig. 3. Kerosene recovery unit.

4. Kerosene recovery unit (case study)

The kerosene recovery unit shown in Fig. 3 is part of a proposal of DOP Refineries Ltd. for the construction of a refinery for the recovery of kerosene from the waste kerosene solvent returned from auto engine repairers. This process and its conventional HAZOP analysis is taken from the "Hazardous Industry Planning Advisory Paper No. 8" (2011).

4.1. Functional decomposition

The main goal of the unit is to recover the kerosene from the waste kerosene solvent. To that end, the system can be decomposed into its subsystems, which perform the necessary subfunctions and subgoals, in the following way: (1) Feed section: provide a constant feed flow, (2) Distillation column: separate the kerosene, (3) Reflux section: provide reflux to the column and remove the recovered kerosene, and (4) Reboiler section: provide energy to the column.

This decomposition can be continued until the desired level of detail. The D-higraph is developed using this decomposition and the P&I diagram. However, in this paper we only show a part of the overall D-higraph due to space constraints. See Fig. 4 for the D-higraph of the reboiler section.

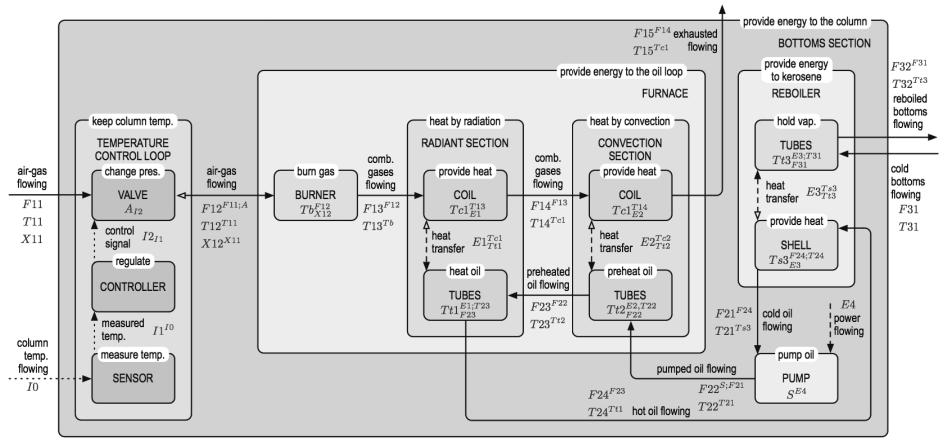

Fig. 4. Reboiler section D-higraph.

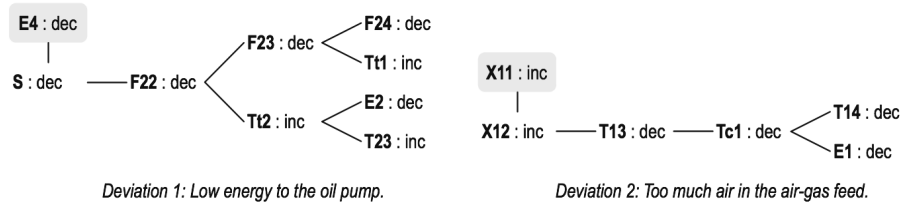

Fig. 5. Consequences trees for the deviations considered.

4.2. Deviation 1: Low energy to the oil pump.

This deviation consists of the variable "power flowing" to the oil pump (E4) and the guide- word "less of". Its consequences tree (with depth 4) are show in Fig. 5. This tree can be expanded to cover all of the D-higraph. The conclusions that can be obtained are: (1) The temperature of the oil can be to high and end in its degradation, (2) the temperature of the reboiled flow would decrease, and (3) the temperature of the exhausted would increase, which means that we are wasting energy.

4.3. Deviation 2: Too much air in the air-gas feed.

This deviation consists of the variable "air-gas composition" (X11) and the guide-word "more of". The consequences tree for this deviation (with depth 4) are shown in Fig. 5. Again, this tree can be expanded to drawn these consequences: (1) low temperature of the oil in its loop, and (2) low temperature of the reboiled flow.

Of course, in both deviations, the trees can be expanded to cover all of the process, only the depth of the tree has to be changed. With this, the analysis can cover all of the plant and not only the node under consideration.

5. Comparison with other methodologies

Conventional HAZOP studies are systematic and a logical way of performing PHA. However, 70% of the time they require is devoted to routine deviations (Venkatasubramanian et al., 2000). The automation of the procedure saves time and hence money. Automating HAZOP, the team can spend their time in analyzing the deviations, causes, consequences and the possible solutions and not in obtaining them. Another advantage of automated HAZOPs is that no nodes are left unexplored. The proposed assistant only needs a model (a D-higraph) of the process and not a model for each node of the HAZOP analysis, like the MFM HAZOP assistant (Rossing et al., 2010). The rule database is also common for all of the process because it is related to the relations between the elements of the model and not to the process itself, like HAZOPExpert (Venkatasubramanian et al., 2000), however, HAZOPExpert is able to deal with batch processes. Another advantage of this approach, when compared with the MFM methodology, is that the conclusions of the study can be directly mapped to the devices and equipment of the process. This is a consequence of the functional and structural integration.

6. Conclusions and further work

We have presented a tool that allows us to perform guided HAZOP studies. This tool uses a functional model, D-higraph, that merges functional and structural information about the process under analysis. This tool has been applied to an industrial case to show its applicability and to compare it with other existing tools. The resulting analyses are more complete, easier to perform and directly related to the process due to the integration of functions and structures. Future work will be devoted to the development of a "translator" between P&IDs and D-higraphs, so the models can be obtained from the diagrams by adding additional information. Further work will also include the integration of this tool with quantitative information and models.

References

Álvarez, M. E. 2010. Diagnosis de fallos en procesos químicos mediante modelos D-higraph. Final Project. Department of Chemical Engineering, Technical University of Madrid.

CLIPS. 2011. CLIPS, A Tool for Building Expert Systems. http://clipsrules.sourceforge.net

De la Mata, J. L., Rodríguez, M. 2010a. Abnormal situation diagnosis using D-higraphs. Proc. of the 20th European Symposium on Computer Aided Process Engineering, pp. 1477-1482.

De la Mata, J. L., Rodríguez, M. 2010b. D-higraphs. ASLab Report. http://www.aslab.org

Department of Planning, State of New South Wales, Australia. 2011. Hazardous Industry Planning Advisory Paper No. 8. HAZOP Guidelines.

Harel, D. 1987. Statecharts: A visual formalism for complex systems. Sci. Comput. Program., 8.

Kuipers, B. 1984. Commonsense reasoning about causality. Artificial Intelligence, 24.

Kuipers, B. 1986. Qualitative simulation. Artifiial Intelligence, 29.

Lind, M. 1994. Modeling goals and functions of complex Industrial plant. Applied Artificial Intelligence, 8 (2).

Lind, M. 2005. Modeling goals and functions of control and safety systems. NKS Report.

Rodríguez, M., Sanz, R. 2009. Development of integrated functional-structural models. Computer Aided Process Engineering, 27.

Rossing, N. L., Lind, M., Jensen, N., Jorgensen, S. B. 2010. A functional HAZOP methodology. Computers and Chemical Engineering, 34 (2).

Venkatasubramanian, V., Zhao, C., Viswanathan, S. 2000. Intelligent systems for HAZOP analysis of complex process plants. Computers and Chemical Engineering, 24 (9-10).

Zhao, C., Bhushan, M, & Venkatasubramanian, V. 2005. PHASuite: An Automated HAZOP Analysis Tool for Chemical Processes. Process Safety and Environment Protection, 83 (6).

I.A. Karimi and Rajagopalan Srinivasan (Editors), Proceedings of the 11th International Symposium on Process Systems Engineering, 15-19 July 2012, Singapore.

Dynamic Flexibility Analysis with Differential Quadratures

Vincentius Surya Kurnia Adi, Chuei-Tin Chang

National Cheng Kung University, University Road 1, Tainan 701, Taiwan

Abstract

Realistic chemical processes are often operated in the presence of complex and uncertain system dynamics. Obviously, flexibility analysis comes into play in designing such systems. In order to build the mixed-integer nonlinear program (MINLP) for computing the flexibility index, the Karush-Kuhn-Tucker (KKT) conditions must be derived from the system model and this model usually consists of a set of differential-algebraic equations (DAEs). A common approach for this task is to replace these DAEs with equality constraints by using a numerical discretization technique. In the present study, the *differential quadratures* (DQs) are adopted to approximate the derivatives in the original system model. The time horizon is discretized at the roots of a Chebyshev polynomial for optimally mimicking the transient profiles of control and state variables. Finally, a novel concept of *temporal flexibility* is also proposed in this paper and a simple system is used to demonstrate its usefulness. All results obtained in case studies show that the proposed approach is convenient and effective for assessing realistic issues in operating complex dynamic chemical processes.

Keywords: dynamic flexibility analysis, temporal flexibility, chemical process design, differential quadrature.

1. Introduction

Dealing with uncertainty is one of the problems in operating the chemical plants. The uncertainties can be considered as variation either in the external parameters (such as the quality of the feed streams, the product demands, and the environmental conditions, etc.), or the internal parameters (such as the heat transfer coefficients, the reaction rate constants, and other physical properties). A satisfactory level of flexibility should be allocated so as to ensure feasible operation over a specified range of every uncertain parameter. Methods for systematic flexibility analysis in the synthesis and design of chemical processes have been developed in the literature (Bansal et al., 1998; Swaney and Grossmann, 1985; Zhou et al., 2009). As suggested by Swaney and Grossmann (1985), a chemical process can be described with the following constraints

$$\mathbf{h}(\mathbf{d},\mathbf{z},\mathbf{x},\boldsymbol{\theta}) = 0 \tag{1}$$

$$\mathbf{g}(\mathbf{d},\mathbf{z},\mathbf{x},\boldsymbol{\theta}) \le 0 \tag{2}$$

where $\dim\{\mathbf{h}\} = \dim\{\mathbf{x}\}$. In eqs. (1) and (2), $\mathbf{h}$ is the vector of equations, i.e., mass and energy balances, and $\mathbf{g}$ is the vector of inequalities, i.e., design specifications or physical operating limits. The variable $\mathbf{d}$ is the vector of design variables, $\mathbf{x}$ is the vector of state variables, $\mathbf{z}$ is the vector of the control variables, and $\boldsymbol{\theta}$ is the vector of the uncertain parameters. Since the state variables in eq. (2) can be implicitly eliminated with eq. (1), the above model can be reduced to

$$\mathbf{g}(\mathbf{d},\mathbf{z},\mathbf{x}(\mathbf{d},\mathbf{z},\boldsymbol{\theta}),\boldsymbol{\theta}) = \mathbf{f}(\mathbf{d},\mathbf{z},\boldsymbol{\theta}) \le 0 \tag{3}$$

Given a set of nominal parameter values $\boldsymbol{\theta}^N$ and the corresponding expected deviations in the positive and negative directions ($\Delta\boldsymbol{\theta}^+$ and $\Delta\boldsymbol{\theta}^{--}$), the space of uncertain parameters can be expressed as

$$\mathbf{T} = (\boldsymbol{\theta} \mid \boldsymbol{\theta}^N - \Delta\boldsymbol{\theta}^- \le \boldsymbol{\theta} \le \boldsymbol{\theta}^N + \Delta\boldsymbol{\theta}^+) \tag{4}$$

A scalar flexibility index can be formulated to quantify the ability of such processes to operate at points other than the nominal point of operation (Swaney and Grossmann, 1985). This flexibility index F represents the largest deviation that the design can accommodate while remaining feasible. $F \ge 1$ clearly indicates that the flexibility target is satisfied.

A modified formulation for the *dynamic flexibility index* was proposed by Dimitriadis and Pistikopoulos, (1995). To perform flexibility analysis on a dynamic system, the following optimization must be solved

$$\begin{aligned} & F = \max \delta \\ & s.t. \max_{\boldsymbol{\theta}(t)\in\mathbf{T}(\delta)} \min_{\mathbf{z}(t)\in\mathbf{Z}(t)} \max_{t\in[0,H]} \mathbf{g}(\mathbf{d},\mathbf{z}(t),\mathbf{x}(t),\boldsymbol{\theta}(t),t) \le 0 \\ & \quad \mathbf{h}(\mathbf{d},\mathbf{z}(t),\mathbf{x}(t),\dot{\mathbf{x}}(t),\boldsymbol{\theta}(t)) = 0,\ \mathbf{x}(0) = \mathbf{x}^0 \\ & \quad \mathbf{T}(\delta) = (\boldsymbol{\theta}(t) \mid \boldsymbol{\theta}^N(t) - \delta\Delta\boldsymbol{\theta}^-(t) \le \boldsymbol{\theta}(t) \le \boldsymbol{\theta}^N(t) + \delta\Delta\boldsymbol{\theta}^+(t)) \end{aligned} \tag{5}$$

The differential quadrature technique (Bellman *et al*., 1972; Quan and Chang, 1989) is used in this study to convert the differential equations in the above model into algebraic ones. It was suggested that Chebyshev polynomial approximation should be applied for discretization of time horizon (Chen, 1996). Therefore, the main issue to be addressed here is mainly concerned with the applicability of DQ in dynamic flexibility analysis for batch processes. The solution procedures can be implemented on GAMS platform to determine the dynamic flexibility F.

The scope of aforementioned dynamic flexibility index obviously covers the entire operation horizon. In practice, there is also a need to determine a "short-term" flexibility index for the purpose of assessing the effectiveness of quick responses. Thus, the concept of *temporal flexibility* is developed in this work. Let us assume that the general dynamic uncertainty space is defined as below,

$$\boldsymbol{\theta}(t)^{\mathrm{N}} - \delta\Delta\boldsymbol{\theta}^-(t) \le \boldsymbol{\theta}(t) \le \boldsymbol{\theta}(t)^{\mathrm{N}} + \delta\Delta\boldsymbol{\theta}^+(t); \quad t_0 \le t \le t_1 \tag{6}$$

For these expected disturbances within an expected time interval $[t_0,t_1]$, one can define the *net* positive and negative deviations as

$$\int_{t=t_0}^{t=t_1} \Delta\boldsymbol{\theta}(t)^- dt = \Delta\boldsymbol{\theta}^-_{temp}, \int_{t=t_0}^{t=t_1} \Delta\boldsymbol{\theta}(t)^+ dt = \Delta\boldsymbol{\theta}^+_{temp} \tag{7}$$

thus

$$\int_{t=0}^{t=t} \boldsymbol{\theta}(t)^{\mathrm{N}} dt - \delta_{temp} \int_{t=t_0}^{t=t_1} \Delta\boldsymbol{\theta}(t)^- dt \le \int_{t=0}^{t=t} \boldsymbol{\theta}(t) dt \le \int_{t=0}^{t=t} \boldsymbol{\theta}(t)^{\mathrm{N}} dt + \delta_{temp} \int_{t=t_0}^{t=t_1} \Delta\boldsymbol{\theta}(t)^+ dt \tag{8}$$

Or in an alternative form

$$\boldsymbol{\theta}^{\mathrm{N}}_{temp} - \delta_{temp}\Delta\boldsymbol{\theta}^-_{temp} \le \boldsymbol{\theta}_{temp}(t) \le \boldsymbol{\theta}^{\mathrm{N}}_{temp} + \delta_{temp}\Delta\boldsymbol{\theta}^+_{temp} \tag{9}$$

Eq. (9) are then imposed together with eq. (5) to calculate the temporal flexibility index for the entire time horizon.

2. Applications

Two examples are first presented in the sequel to demonstrate the applicability of differential quadratures in solving the dynamic flexibility model. Another example is then followed to illustrate the proposed temporal flexibility concept.

2.1. Example 1

Let us consider an exothermic first-order reaction (A→B) in a jacketed batch reactor (Dimitriadis and Pistikopoulos, 1995). The mathematical model is given below in eqs. (10) - (15), while the parameter values can be obtained from Zhou et al. (2009). The heat of reaction, ΔH_r, is assumed to vary between –72500 and –82500 J/mol with nominal value of –77500 J/mol. The cooling water flow rate, F_{cw}, can be adjusted to satisfy operational constraints and end-time specifications and be regarded as the control variable.

$$\frac{\mathrm{d}N_\mathrm{A}}{\mathrm{d}t} = -kN_\mathrm{A};\ N_\mathrm{A}(0) = 20000 \text{ mol} \tag{10}$$

$$\frac{\mathrm{d}N_\mathrm{B}}{\mathrm{d}t} = kN_\mathrm{A};\ N_B(0) = 0 \tag{11}$$

$$C_p(N_\mathrm{A} + N_\mathrm{B})\frac{\mathrm{d}T}{\mathrm{d}t} = kN_A(-\Delta H_r) - Q_{cw} \tag{12}$$

The final reactant conversion must exceed 95%, i.e.

$$\frac{N_A(t=H)}{N_A(t=0)} \le 0.05 \tag{13}$$

The temperature in the reactor cannot exceed a maximum of 400 K at any time during operation,

$$T(t) \le 400 \text{ K},\ 0 \le t \le H \tag{14}$$

The temperature of the reacting mixture at the end of the operation must not exceed 308 K so that discharge and cleaning operations can take place,

$$T(t=H) \le 308 \text{ K} \tag{15}$$

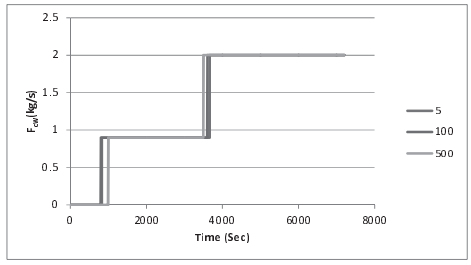

Figure 1. Cooling water flow rate vs. time at the critical point in Example 1; interval 5, 100, 500 s; nodes number = 5

According to Dimitriadis and Pistikopoulos (1995), the initial reaction temperature is fixed at 298 K. The time profile of the cooling water flow rate in 2-h batch cycle is presented in Fig. 1. The dynamic flexibility index and the critical value of the uncertain parameter for different nodes number and a fixed horizon are also presented in Table 1. It can be seen that the node number of differential quadrature method slightly affects the numerical results due to the stepwise nature of the problem. Higher node number can

increase accuracy but the improvement is not significant (see Table 1). N = 5 should be sufficient for adequate accuracy.

Table 1. Dynamic flexibility index and the critical uncertain parameter in Example 1

Node Number	5	10	15
FI (δ)	0.7721	0.7783	0.7788
ΔH_r J/mol	82863	81748	81387

2.2. Example 2

Let us consider the following polymerization reaction that produces a polyol lubricant:

$$C_4H_9OH + (n+1)C_3H_6O \rightarrow C_4H_9(OC_3H_6)nOCH_2CHOHCH_3 + \text{heat}$$

The system description and the model parameters can be found in Zhou et al. (2009). To consider the effect of the uncertain parameters, a 10% uncertainty in the activation energy is introduced as it is assumed that the activation energy is inaccurately measured. The reactor temperature profile for 33.3 h with different interval lengths and fixed node number can be found in Fig. 2. The corresponding dynamic flexibility indices can be found in Table 2. From Fig. 2, it can be seen that the profile associated with 5-min intervals has better detail than those corresponding to the 100-min and 500-min intervals. The resulting dynamic flexibility index obtained for 5-min intervals is also significantly higher.

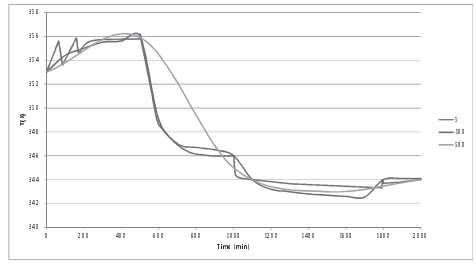

Figure 2. Reactor temperature in Example 2 (node number = 5)

Table 2. Dynamic flexibility indices in Example 2

Interval (min)	5	100	500
FI (δ)	0.8	0.6743	0.5063

2.3. Example 3

To illustrate the proposed temporal flexibility concept, the simple tank in Fig. 3 is analyzed. The dynamic model of this system can be written as

$$A\frac{dh}{dt} = \theta(t) - k\sqrt{h} \tag{16}$$

The model parameters are $\theta(t)^N$ = 0.5 m^3/min, h_{low} = 0m, h_{up} = 10 m, h_{ss} = 5 m, A = 5 m^2, k= $\frac{\sqrt{5}}{10}$, H=2500 min.

The disturbance condition is described that from steady state condition, the inlet flow stops at t = 1500 min, and return back to normal after 250 min. For tank area A = 5 m^2, the temporary dynamic flexibility δ_{temp} is found to be 0.4. From the result, it can be

concluded that the tank does not have enough flexibility to hold up such flow cut. By optimizing the volume of the tank, in this term is by changing A, it is suggested that A should be increased to be 12.5 m^2 and the corresponding δ_{temp} is 1. It can be evaluated in Fig. 3 that water level of A = 5 m^2 is quickly dried out after 100 min, while water level of A = 12.5 m^2 has 250 min time period before it is empty, and after 250 min the inlet flow returns back to normal.

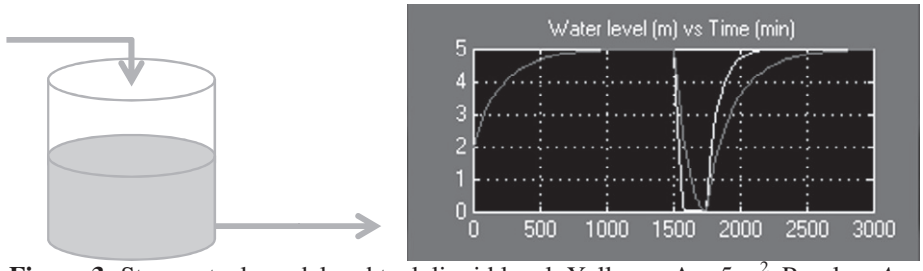

Figure 3: Storage tank model and tank liquid level; Yellow – A = 5 m^2, Purple – A = 12.5 m^2

3. Conclusions

Differential quadrature technique is successfully implemented in computing the dynamic flexibility indices. It is suggested that the node number and the interval length should both be small enough to achieve high accuracy and calculation robustness. The presented approach has been successfully implemented in two examples. Finally, a temporal flexibility concept is also proposed in this work for assessing the need for quick responses.

References

V. Bansal, J. D. Perkins, and E. N. Pistikopoulos, 1998, Flexibility Analysis and Design of Dynamic Processes with Stochastic Parameters, Comput. Chem. Eng., 22, S817

R. Bellman, B. G. Kashef, and J. Casti, 1972, Differential Quadrature: A Technique for The Rapid Solution of Nonlinear Partial Differential Equations, J. Comput. Phys., 10, 40

W. Chen, 1996, Differential Quadrature Method and its Applications in Engineering – Applying Special Matrix Product to Nonlinear Computations and Analysis, PhD Thesis, Shanghai Jiao Tong University, P.R.C.

V. D. Dimitriadis, and E. N. Pistikopoulos, 1995, Flexibility Analysis of Dynamic Systems, Ind. Eng. Chem. Res., 34, 4451

J. R. Quan, and C. T. Chang, 1989, New Insights in Solving Distributed System Equations by The Quadrature Methods – I, Comput. Chem. Eng., 13, 779

J. R. Quan, and C. T. Chang, 1989, New Insights in Solving Distributed System Equations by The Quadrature Methods – II, Comput. Chem. Eng., 13, 1017

R. E. Swaney, and I.E. Grossmann, 1985, An Index for Operational Flexibility in Chemical Process Design. Part I: Formulation and Theory, AIChE. J., 31, 621

R. E. Swaney, and I. E. Grossmann, 1985, An Index for Operational Flexibility in Chemical Process Design. Part II: Computational Algorithms, AIChE. J., 31, 631

H. Zhou, X. X. Li, Y. Qian, Y. Chen, and A. Kraslawski, 2009, Optimizing the Initial Conditions to Improve the Dynamic Flexibility of Batch Processes, Ind. Eng. Chem. Res., 48, 6321

I.A. Karimi and Rajagopalan Srinivasan (Editors), Proceedings of the 11th International Symposium on Process Systems Engineering, 15-19 July 2012, Singapore.

A Method of Designing Plant Alarm Systems with Hierarchical Cause-Effect Model

Takashi Hamaguchi,[a] Kazuhiro Takeda,[b] Masaru Noda,[c] Naoki Kimura[d]

[a] *Graduate School of Engineering, Nagoya Institute of Technology, Gokiso Showa-ku Nagoya, 466-8555, Japan*
[b] *Faculty of Engineering, Shizuoka University, 3-5-1 Johoku Hamamatsu, 432-8561, Japan*
[c] *Graduate School of Information Science, Nara Institute of Science and Technology, 8916-5 Takayama Ikoma, 630-0192, Japan*
[d] *Faculty of Engineering, Kyushu University, 744 Motooka Fukuoka, 819-0395, Japan*

Abstract

Plant alarm systems are important because they enable safe and reliable operations at chemical plants. Takeda *et al*. proposed a method of designing alarm systems for plants based on a plant cause-effect (CE) model. We propose a method of designing alarm systems for plants with a hierarchical CE model to improve the selection of fault origins to distinguish them with the systems and a procedure for designing the systems.

Keywords: Plant alarm system, fault origins, alarm source variables, hierarchical CE model

1. Introduction

Plant alarm systems are important because they enable safe and reliable operations at chemical plants. These alarm systems notify operators through warning tones, warning lights, and messages when the values for process variables move from normal to abnormal ranges. Poorly designed alarm systems cause nuisance, standing, and flooding alarms, and can even result in incidents or accidents. Therefore, new regulations and guidelines for plant safety have been established in the U.S.A. and Europe. The International Society of Automation (ISA, 2009) in the U.S.A. requires strict risk management through plant life cycles, which consists of design, operation, and management phases. The Engineering Equipment and Materials User's Association (EMMUA, 2007) in Europe requires that the philosophy, objectives, and functions of alarm systems be clearly developed, and inadequate alarms be eliminated. However, they have not described any methods of designing alarm systems. Therefore, a systematic method of designing plant alarm systems is needed to detect faults or abnormalities at plants, and to alert, inform and guide the operator during plant upset. Takeda *et al*. (2010) proposed a new method of selecting alarm source variables using a cause-effect (CE) model. They proposed a process of selecting fault origins to distinguish them by using alarm systems based on the grades of fault origins using a risk matrix with their frequencies and impacts of effects. However, it is not an easy task to determine grades in large-scale plants. When alarm systems cannot distinguish origins, this method cannot present useful information to enable problems to be reviewed. We therefore propose a method of designing plant alarm systems with a hierarchical CE model to improve the selection of fault origins to distinguish them by using alarm systems.

2. Hierarchical CE Model

2.1. Structure of Hierarchical CE Model

There is an overview of the method of designing a plant alarm system with the hierarchical CE model in Fig. 1. This model is generated by information from the CE model and it consists of a primitive variable layer, a strongly-connected component layer that enables variable selection of alarm sources, and a group unit layer that enables selection of fault origins.

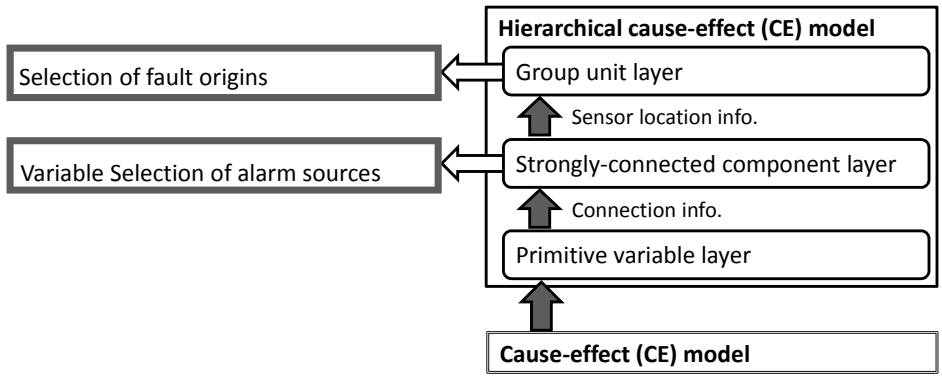

Fig. 1 Overview of method of designing plant alarm system with hierarchical CE model

2.2. CE model and primitive variable layer

Iri et al. (1979) proposed that the structure of a system be represented by a "signed directed graph (SDG)" and its state by "patterns". The SDG in this paper is called a CE model. The CE model is a diagram for the propagation of abnormalities that shows the propagation process for abnormalities after a fault has occurred. The model is based on the material and energy balances of the plant that could be constructed from the plant topology. Consequently, it is easy to maintain the CE model. The state of the system is expressed in terms of the signs "0", "+", and "-", according to the values of the state variables, such as process variables and manipulated variables, which correspond to normal, higher than normal, and lower than normal. The group of signs corresponding to all the state variables is defined as the pattern.

The CE model is composed of nodes and directed branches with a sign. The nodes in the model represent state variables in the plant. The branches represent the directed influence between state variables and each branch is assigned the sign "+" if it represents a positive influence (reinforcement) and the sign "-" if it represents a negative influence (suppression). Let $\boldsymbol{M}$ be a set of all measured variables of state variables and m be the element of $\boldsymbol{M}$. Let $\boldsymbol{N}$ be a set of all unmeasured variables of state variables and n be the element of $\boldsymbol{N}$. Nodes that carry a sign other than "0" are known as "valid nodes", while branches for which the product of the signs on the initial and terminal nodes is the same as the sign of the branch are known as "consistent branches". There are virtually no real systems in which all the state variables are measured. Nodes of a CE model corresponding to the measured state variables are known as "observed nodes" and those corresponding to the unmeasured state variables are known as

"unobserved nodes". In this paper, *s* is an observed node and ***S*** is a set of all observed nodes.

The example plant in Fig. 2(a) is represented as the CE model in Fig. 2(b). Raw material in this plant is fed from outside the boundary to tank 1. Product is discharged to outside the boundary through tank 2. Part of the product is recycled to tank 1. In this paper, *P*, *F*, *L*, and *V* are state variables for pressure, flow rate, liquid level, and valve position. All state variables without *P*1 and *P*2 can be measured. Unobserved nodes are represented by circles with a single line and observed nodes are represented by circles with double lines. Branches with "+" are represented by solid arrows, whereas branches with "-" are represented by dashed arrow. The solid arrow *L*1 to *F*2 represents an enhancing relationship, viz., increasing (or decreasing) *L*1 has a direct effect on increasing (or decreasing) *F*2.

A primitive variable layer is generated from information from the CE model. The primitive variable layer is used to modify the CE model for the alarm system. The primitive variable layer in this example is identical to the CE model in Fig. 2 (b)

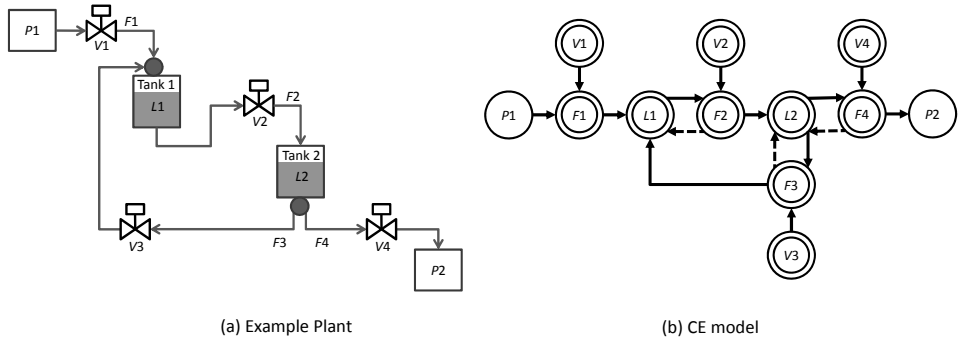

Fig. 2 Example plant and CE model

2.3. Strongly-connected component layer

Strongly-connected components are generated from the connection information in the primitive variable layer in a strongly-connected component layer. When the effect of a fault propagates to a strongly-connected component, then the effect propagates to all variables and loops in the strongly-connected component. Therefore, we selected strongly-connected components as minimal elements for setting fault origins. Fig. 3 has a strongly-connected component layer, which is generated from the primitive variable layer shown in Fig. 2 (b). Strongly-connected components are divided into group unobserved components, which only consist of unobserved nodes, and observed components, which contain some observed nodes. Unobserved components are represented by the rectangles with a single green line and observed components are represented by the rectangles with double green lines.

2.4. Group unit layer

Let ***C*** be a set of fault origins to be distinguished by using the alarm system and *c* be an element of ***C***. Therefore, ***C*** is a subset of all assumed fault origins in the plant. It is assumed that ***C*** could be obtained by process hazard analysis (PHA), like that in the HAZard and Operability (HAZOP) study.

Strongly-connected components in this layer are divided into group units x and y according to the information on their connections and sensor locations. The group unit layer is used to divide $\boldsymbol{C}$ into a subset for each unit x and y to select the fault origins to be distinguished by using the alarm system. Fault origins up to one can be set in group unit x, whereas no fault origins can be set in group unit y. Let $\boldsymbol{X}$ be a set of group unit x. When strongly-connected components can connect from upper strongly-connected components until an observed component is reached by direct branches, then the group of strongly-connected components belongs to group unit x. If a terminal strongly-connected component is an observed component, then the group of strongly-connected components belongs to group unit y. The elements c of $\boldsymbol{C}$ are divided into each group unit.

The group unit layer of the example plant is shown in Fig. 4. Group unit x is represented by the rectangles with double red lines and y is represented by the rectangles with the single blue line. There are six group units x and one group unit y in the example plant. Up to one fault origin can be selected in each group unit x.

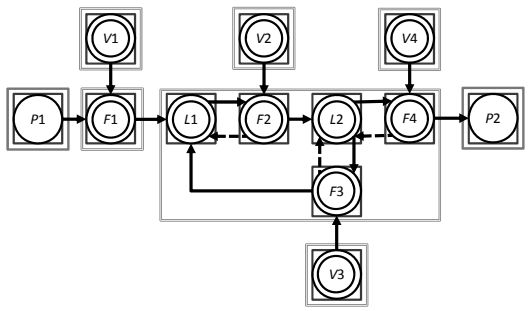

Fig. 3 Strongly-connected layer in example plant

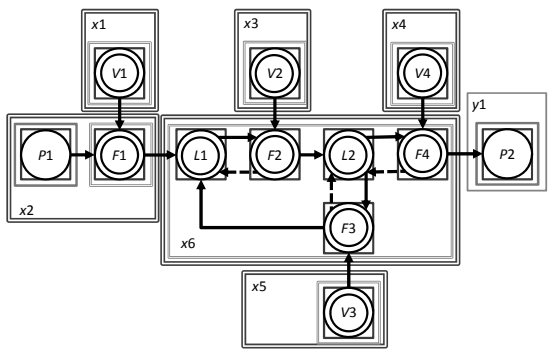

Fig. 4 Group unit layer in example plant

3. Design of Plant Alarm System using Hierarchical Cause-Effect Model

The design of the alarm system is defined in this paper as the selection of alarm source variables from $\boldsymbol{M}$ to distinguish the fault origins of $\boldsymbol{X}$.

The origin of a failure is represented by origin pair z of a node and its sign. Shiozaki *et al*. (1984) proposed the idea of a "consistent rooted tree". If all the branches on an elementary path can be made consistent with either "+" or "-" for unobserved nodes on

the path, then the path is defined as a "consistent path". If there are consistent paths from a node on the CE model to all the valid observed nodes on it, the tree composed of the node and these consistent paths is defined as a consistent rooted tree, and the node is defined as a "root". A consistent rooted tree is also considered to be a representation for the state of propagation of a failure. There may be two or more candidates for the origin of the failure. Therefore, a set of z as candidates for the origin of the failure is defined as candidate pair set $\boldsymbol{Z}$. A set of candidate pairs, which is not a proper subset of all the other sets of candidate pairs for all observed patterns on all observed node $\boldsymbol{S}$, is defined as the greatest set of candidate pairs. Two or more greatest pairs are generally given by the branch and bound method (Shibata and Matsuyama, 1989). If two or more elements of $\boldsymbol{X}$ are not involved in any greatest sets of candidate pairs, then all elements of $\boldsymbol{X}$ can be distinguished in any abnormal situations.

Let $\boldsymbol{A}$ be a set of alarm source variables to distinguish fault origins, which is grouped as group unit x. Set $\boldsymbol{A}$ of alarm source variables can be selected from $\boldsymbol{S}$ as follows. It is assumed that a CE model of the objective plant and the hierarchical CE model have been given.

1. **Determine $\boldsymbol{X}$ of the objective plant**: List up all the fault origins to be distinguished by the alarm system in the objective plant, and map the fault origins to adequate pairs of nodes and the signs of the CE model of the objective plant.
2. **Select alarm source variables**: Select alarm source variables that can distinguish all the elements of $\boldsymbol{X}$. Let $\boldsymbol{Q}$ be a power set of $\boldsymbol{S}$ without an empty set. Calculate a set of greatest sets of candidate pairs when all elements of $\boldsymbol{Q}$ are made into a set of alarm source variables.
3. **Determine monitoring ranges**: Select a fault origin from each group unit x. The monitoring ranges of alarm source variables are adjusted using a dynamic simulator. This step has been omitted from this paper.

4. Conclusion

We proposed a method of designing alarm systems for plants with a hierarchical CE model to improve the selection of fault origins to distinguish them with the systems and a procedure for designing the systems.

References

EEMUA, 2007, ALARM SYSTEMS – A Guide to Design, Management, and Procurement Publication No.191 2nd edn., London

M. Iri, K. Aoki, E. O'shima, and H. Matsuyama, 1979, An Algorithm for Diagnosis of System Failures in the Chemical Process, Comput. Chem. Eng. 3, 489-493

ISA, 2009, Management of Alarms Systems for the Process Industries, North Carolina

J. Shiozaki, B. Shibata, H. Matsuyama, and E. O'shima, 1989, Fault Diagnosis of Chemical Process utilizing Signed Directed Graphs Improvement by using Temporal Information, IEEE Trans. Ind. Electron., 36, 469-474

B. Shibata, and H. Matsuyama, 1989, Evaluation of the Accuracy of the Fault Diagnosis System Based on the Signed Directed Graph, Kagaku Kougaku Ronbunshu, 15, 395-402

K. Takeda, T. Hamaguchi, and M. Noda, 2010, Plant Alarm System Design based on Cause-Effect Model, Kagaku Kougaku Ronbunshu, 36, 136-142

I.A. Karimi and Rajagopalan Srinivasan (Editors), Proceedings of the 11th International Symposium on Process Systems Engineering, 15-19 July 2012, Singapore.

Computer Aided Assessment of Occupationally Healthier Processes during Research and Development Stage

Santha Pandian[a], Mimi H.Hassim[a*], Markku Hurme[b]

[a]*Universiti Teknologi Malaysia, Department of Chemical Engineering, 81310, UTM Johor Bahru, Malaysia*
[b]*Aalto University, Department of Biotechnology and Chemical Technology, P.O. Box 16100, FIN-00076 Aalto, Finland*
*Corresponding email: mimi@cheme.utm.my

Abstract

Each year more people die from occupational related diseases than are killed in industrial accidents. Therefore it is critical to start considering health aspect early when developing a new chemical process. In this paper, computer aided tool for assessing inherent occupational health is proposed for chemical process research and development stage. The method was developed based on the reaction chemistry data, which is the only data available at this stage. Three types of approaches were formulated to calculate the route index value using additive type, average type and worst case type calculations. The tool can be used to rank the alternative chemical synthesis routes by their health properties as well as characterize the hazard level of single process. Finally the tool was applied to six process routes for methyl methacrylate production for demonstration.

Keywords: inherent occupational health, computer aided tool, process design, R&D, CAPE

1. Introduction

Occupational health is the promotion and maintenance of the highest degree of physical, mental and social well-being of workers in all occupations by preventing departures from health, controlling risks and the adaptation of work to people, and people to their jobs (ILO/WHO, 1950). Occupational health hazards are generally more difficult to manage than safety hazards. The causes and consequences of poor safety at work are immediate and often relatively easy to deal with. Meanwhile work-related causes of ill health are more difficult to assess. It often takes some time for health symptoms to develop; therefore the connection between cause, in this case occupational exposure, and worker health effect is less obvious.

In recent years, occupational health issues have become more common and known. In principle it is better to identify health hazards when the proposed plant is still 'on paper'. As the project progresses, the process modifications will be more difficult and more costly and the opportunity to apply inherently healthy design features will become smaller (Hassim and Edwards, 2006).

2. Occupational Health Assessment Methods

There are several methods available for occupational health assessment during design stage. Among the earliest ones is the Occupational Health Hazard Index (OHHI) (Johnson, 2001), which intends to assess and rank chemical synthesis routes in the R&D

stage. The method has several disadvantages including poor assessment of fugitive emissions, which is too brief that the accuracy is questionable. INSET Toolkit (INSIDE Project, 2001) is a comprehensive method which covers assessment of all safety, health and environment (SHE) as well as other feasibility factors. The toolkit however is highly complex besides requiring massive detailed information. Even reading the instruction manual is demanding. Later, Hassim and Edwards (2006) introduced an improved method from the OHHI called the Process Route Healthiness Index (PRHI). However similar to the OHHI, PRHI also suffers from being quite complicated despite claiming for R&D application. The most recent method is by Hassim and Hurme (2010), called the Inherent Occupational Heath Index (IOHI). The method was designed carefully by taking into account all the parameters for health assessment but limited to only those information available in the R&D stage.

All the methods discussed above were created based on manual calculations. This somehow makes them less attractive as industries prefer tools which are simple and swift (Gupta and Edwards, 2002). Besides, most design work is done using CAPE tools now. Therefore, the aim of this research is to develop a computer-aided tool that will assist users in making chemistry pathway selection based on the health hazard level of process candidates using the IOHI method. Such tools are needed since in the R&D stage, large number of routes needs to be screened within a limited time. Computerized tool also avoids incorrect assessment results due to mistakes done in manual calculations.

3. The Inherent Occupational Health Index

Inherent Occupational Health Index (IOHI) comprises of two indexes; Index for Physical and Process Hazards (I_{PPH}) that represents the possibility for workers being exposed to chemicals and Index for Health Hazards (I_{HH}) that characterizes the impacts on health due to the exposure (Hassim and Hurme, 2010). The IOHI for each process route is calculated as a sum of the two indexes:

$$I_{IOHI} = I_{PPH} + I_{HH} \quad [1]$$

The I_{PPH} consists of six subindexes; process mode (I_{PM}), pressure (I_P), and temperature (I_T), materials phase (I_{MS}), boiling point (I_V), and corrosiveness (I_C). For the I_{HH}, two subindexes are included; exposure limit (I_{EL}) and R-phrase (I_R). Each subindex has a range of penalties; a higher penalty represents a higher tendency for exposures or a more severe health impact. Summary of the subindexes and their penalties for the I_{PPH} and I_{HH} are in Hassim and Hurme (2010). The IOHI is reaction-step oriented. Therefore a whole reaction step is considered as one entity. The formula for calculating the IOHI as in Eq. (1) is for each reaction step or here called as subprocess. The index value for a route (may consist of ≥ 1 subprocess) can be calculated using three types of calculation, which are additive type, average type and worst case type. The difference between these evaluations is described by Hassim and Hurme (2010) and is demonstrated in this paper by a case study.

4. Development of Systematic Computer Aided IOHI Tool

A systematic computer-aided tool for inherent occupational health assessment has been developed based on the IOHI using Microsoft Excel. All the subindexes considered in the assessment, penalties system, index formulation etc. are similar to the manual based IOHI (Hassim and Hurme, 2010), therefore will not be elaborated here. The difference

is in the effort of computerizing the IOHI evaluation. An electronic database has been created which consist of 1625 as shown in Fig.1. The database provides chemical properties required for the IOHI calculation, which are the material phase, boiling point, corrositivity, R-phrases value and exposure limit (EL). The first four data were obtained from individual Material Safety Data Sheet (MSDS) provided by ScienceLab. Meanwhile the EL value is the Permissible Exposure Limit (PEL) 8-hour data taken from Schedule 1-Malaysian Regulation.

The proposed tool is very straightforward where the user has to input process related data only i.e. operating pressure, temperature and process mode. Prior to that, user needs to select the chemicals involved in the subprocess from the database. Then the tool will automatically calculate the IOHI value for each subprocess based on the formulation that has been specified using the logical functions in Excel. Once the IOHI for each subprocesses of a routes are calculated, the tool will then calculate the route index value using three approaches i.e additive, average, and worst case type calculation. The tool also is able to characterize the hazard level of process route as either Safe, Moderately Safe, Moderately Hazardous or Hazardous. The details on how the standard for the categorization was developed are described by Hassim and Hurme (2010). To illustrate the proposed approach, an industrial case study on the production of methyl methacrylate (MMA) was used.

5. Case Study on Methyl Methacrylate

The computer aided IOHI tool is demonstrated by a case study of six alternative routes for methyl methacrylate (MMA) manufacture. The routes are:

1. Acetone cyanohydrin based route (ACH)
2. Ethylene via propionaldehyde based route (C2/PA)
3. Ethylene via methyl propionate based route (C2/MP)
4. Propylene based route (C3)
5. Isobutylene based route (i-C4)
6. Tertiary butyl alcohol based route (TBA)

Among these six routes, ACH is the most common and widely used in industries. Details of the routes are in Hassim and Hurme (2010).

5.1. The Index Calculation

Each subprocesses of MMA alternative synthesis routes is assessed for their health properties using the proposed tool. The IOHI index calculations, including the penalties received by each subindex, are summarized by the tool to further ease hazards assessment process. Here only summary of ACH routes is shown (see Fig. 2) due to the space limitation. The index value for the whole route is then calculated using three approaches of additive type, average type and worst case type calculations and presented in Tables 1and 2. Besides tables of results, the tool also generates graphs for each calculation type; the I_{PPH} and I_{HH} as well as the total IOHI values. However due to the limited space, only the IOHI graph for additive calculation is shown here (Fig. 3).

Material	R-Phrases	Boiling Point (°C)	Corrosivity	PEL		Material State	Solid
				8 hrs time weighted	Ceiling limit airborne		
				ppm	ppm		
Acetaldehyde	R12 R36/37/38 R40	21	Stainless Steel	20.00	50.00	Liquid	
Acetamide	R40	223	Non-corrosive in glass	2.07	6.21	Solid	Crystalline Solid
Acetic acid	R10 R35	118.1	Stainless Steel	10.00	30.00	Liquid	
Acetic anhydride	R10 R20/22 R34	139.9	Stainless Steel	5.00	15.00	Liquid	
Acetone	R11 R36	56.2	Stainless Steel	500.00	1500.00	Liquid	

Fig. 1 Overview of the electronic database

Route/Step	I_{PPH}						I_{HH}		I_{IOHI}
	I_{PM}	I_{MS}	I_V	I_P	I_C	I_T	I_{EL}	I_R	
ACH									
2	1	2	2	0	1	0	3	4	13
3		3	0	1	2	1	4	4	15
4		3	1	1	2	1	4	4	16
Total	1	8	3	2	5	2	11	12	44

Fig. 2 Summary of IOHI index calculations for the ACH route

5.2. Results and Discussions

5.2.1. Additive type calculation

The typical way of calculating the process route index is based on the additive method. Based on Table 1 and Fig. 3, it can be seen that the C2/PA and C3 routes have the highest index value compared to the others. This is due to the largest number of subprocesses they have. Additive calculation does affected a lot by the number of subprocess a route has. This somehow indicates that a more complex route (with more subprocesses) has a probability to pose greater hazards due to e.g. the presence of more chemicals etc.

5.2.2. Average type calculation

The average of the IOHI can be calculated for each route to eliminate the influence of the number of subprocess on the final index value (Hassim and Hurme, 2010). Now the results are almost opposite from the additive based approach (see Table 1). Also based on the average IOHI value, the hazard level of a route is determined automatically by the tool; all routes are categorized as moderately hazardous based on the standard developed by Hassim and Hurme (2010).

5.2.3. Worst case type calculation

In the worst case type approach, the highest penalty of each subindex is taken to represent the worst potential hazard of a process. This is to avoid the same 'worst chemical' in different subprocess to be penalized repeatedly (Hassim and Hurme, 2010). Table 2 presents the results obtained based on this approach.

It can be observed from Tables 1 and 2 that all the three calculations give different results as the idea is to provide different perspectives in inherent hazards assessment. However upon a need to integrate the findings, it can be summarized that C2/MP and TBA are the more healthier ones whereas C2/PA and C3 are the least healthier routes among the process candidates for manufacturing MMA.

All the results obtained are similar to those calculated using the manual based IOHI. This is not surprising since the computer aided IOHI tool was developed based on the manual IOHI. Therefore details of the results for all the three calculation types are not discussed here, but are in Hassim and Hurme (2010). Furthermore, the aim of this paper is not to introduce totally a new index but an effort to develop a computer aided tool for the existing IOHI method.

6. Conclusion

This study introduces a computer-aided tool for inherent occupational health assessment of chemical processes in the R&D stage. The tool was developed based on the IOHI but the assessment now becomes so much faster, easier and attractive with the computer tool. Electronic chemical properties database was also constructed for 1625 chemicals. The tool is powerful that it does not only allows swift calculation of the IOHI, but also

Table 1. The Inherent Occupational Health Index for MMA routes (Additive and Average)

Route	No. of steps	Add I_{PPH}	Add I_{HH}	Add I_{IOHI}	Avg I_{PPH}	Avg I_{HH}	Average I_{IOHI}	Status
ACH	3	21	23	44	7.00	7.67	14.67	Moderately hazardous
C2/PA	4	29	28	57	7.25	7.00	14.25	Moderately hazardous
C2/MP	3	25	15	40	8.33	5.00	13.33	Moderately hazardous
C3	4	31	26	57	7.75	6.50	14.25	Moderately hazardous
i-C4	3	23	20	43	7.67	6.67	14.33	Moderately hazardous
TBA	3	21	20	41	7.00	6.67	13.67	Moderately hazardous

Add: Additive-type calculation, Avg: Average-type calculation

Table 2. The Inherent Occupational Health Index values for MMA routes (worst case-type)

Route	Max I_{PPH}	Max I_{HH}	Max I_{IOHI}
ACH	10	8	18
C2/PA	11	8	19
C2/MP	11	6	17
C3	13	7	20
i-C4	11	7	18
TBA	9	7	16

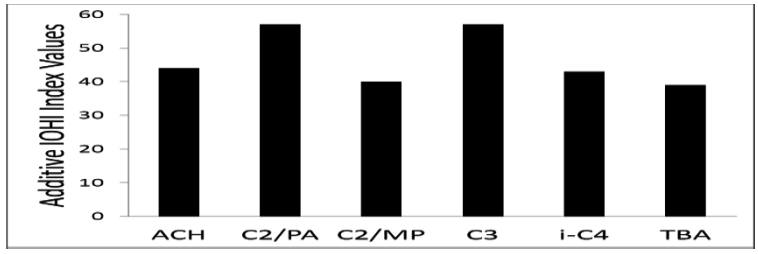

Fig. 3 The IOHI index values for MMA routes (additive-type calculation)

providing users with a summary of results for alternative process routes in terms of tables and graphs, which further ease the hazards assessment process. Furthermore a hazard level of single process can also be determined by the tool.

References

J.P. Gupta, D.W. Edwards, 2002, Inherently Safer Design: Present and Future, Process Saf. Environ. Protect. 80(3) p. 115-125.

M.H. Hassim, D.W. Edwards, 2006, Development of a Methodology for Assessing Inherent Occupational Health Hazards, Process Saf. Environ. Protect. 84(B5) p.378-390.

M.H. Hassim, M. Hurme, 2010, Inherent Occupational Health Assessment During Process Research and Development Stage, J.Loss Prev. Proc. Ind. 23(1) p.127-138.

ILO/WHO, 1950, Joint ILO/WHO Committee on Industrial Hygiene: Report of the First Meeting, ILO, Geneva.

INSIDE Project, 2001, The INSET Toolkit, http://www.aeat-safety-and-risk.com/html/inside.html

V.S. Johnson, 2001, Occupational Health Hazard Index for Proposed Chemical Plant, MSc Thesis, Loughborough University, Loughborough, UK.

I.A. Karimi and Rajagopalan Srinivasan (Editors), Proceedings of the 11th International Symposium on Process Systems Engineering, 15-19 July 2012, Singapore.

A Performance Assessment Method for Feedback Control Loops in Chemical Processes with Distribution Outputs

Jose Munoz and Junghui Chen

Department of Chemical Engineering, Chung-Yuan Christian University, Chung-Li, Taiwan 320, Republic of China

Abstract

Distributions of output quality variables are important in many chemical processes because they significantly affect the product quality and the process performance. A performance assessment method is proposed for feedback control loops in chemical processes with distribution outputs. The method assesses the ability of control loops to minimize the fluctuations in distribution outputs. Presently, due to long delays in obtaining measurements of distribution outputs, fluctuations in distribution outputs are controlled by a non-distribution variable. The non-distribution variable is a process variable that describes the conditions of a chemical process operation. To date, there has been no established method of estimating probability density distribution function (PDF) of a distribution from measured values of non-distribution controlled variable. In this paper, an algorithm is developed to estimate the PDF. An indicator of the performance assessment is defined in terms of the variance of the PDF of the over-all distribution output. This indicator can be used to compare various PDFs of different control loops to determine which control loop yields the optimal PDF.

Keywords: Control loop performance, distribution outputs, feedback control, monitoring and diagnosis

1. Introduction

There are certain chemical processes wherein the controlled variable of interest does not yield a single-value when measured but a distribution consisting of myriad of values. This distribution either gives a description of the quality of the end-product or serves as an indicator of the process operational efficiency. In polymerization, the controlled variable of interest is the molecular weight distribution (MWD) and this represents the different concentrations of polymers of varying molecular weights. It determines the end-use properties of product polymers, such as thermal properties, stress-strain properties, impact resistance, strength and hardness (Crowley & Choi, 1998; Takamatsu, et al., 1988). Clearly, control of process outputs in the form of distribution of values referred to in this paper as distribution outputs is important in producing high quality products and in running efficient plant operations.

Presently, distribution outputs are controlled by a non-distribution variable which is a single-valued variable, and the non-distribution variable has a significant relationship with the distribution output. This non-distribution controlled variable can be measured immediately and independently of the distribution output measurement. In the indirect method of controlling the distribution output, the non-distribution variable can be a process variable describing the conditions of operation. Some polymerization studies show that the first and second moments of MWD are kept within certain ranges as temperature is controlled to lie within a fixed range. The indirect method of controlling

the distribution output is implemented because the direct measurement of output distribution incurs very long delay.

Literature review reveals that there have been some studies done on performance assessment of single-input-single-output and multi-input-multi-output control loops whose controlled variables are non-distribution variables (Desborough & Harris, 1997; Harris, 1989; Harris et al. 1996; Huang et al. 1997). To date, no study has been documented on performance assessment of feedback control loops involving chemical processes with distribution outputs whose control objective is to minimize distribution output fluctuations. This may be due to the absence of a known or established: 1) clear methodology on building a process model used to approximate an actual chemical process, and 2) an acceptable indicator of over-all distribution output fluctuation. In this paper, a method for assessing the performance of feedback control loops used in chemical processes with distribution output is proposed. It can be used to compare the performance of different controllers using non-distribution variables for the distribution process. An algorithm is also developed for analyzing the effects of various control laws, including controller structures and controlled variables, on the resulting distribution outputs. Finally, an indicator of the performance assessment is defined in terms of the variance of the PDF of the over-all distribution output.

2. Modeling of Chemical Processes with Distribution Outputs

Assume that the chemical process with distribution outputs can be represented by a system of nonlinear differential shown as

$$\begin{bmatrix} \dfrac{d\mathbf{s}}{dt} \\ \dfrac{d\boldsymbol{\gamma}}{dt} \end{bmatrix} = \begin{bmatrix} \mathbf{f}_1(\mathbf{s},\boldsymbol{\gamma},u,\boldsymbol{\varepsilon}) \\ \mathbf{f}_2(\mathbf{s},\boldsymbol{\gamma},u,\boldsymbol{\varepsilon}) \end{bmatrix} \tag{1}$$

$\mathbf{s}$ represents the vector of n_s non-distribution state variables and $\boldsymbol{\gamma}$, the vector of N distribution variables at several y locations on the distribution output. For example, location y may refer to a particular molecular weight, crystal or bubble size. u is the control input and $\boldsymbol{\varepsilon}$ is the vector of n_d disturbance variables. $\mathbf{f}_1(\mathbf{s},\boldsymbol{\gamma},u,\boldsymbol{\varepsilon})$ and $\mathbf{f}_2(\mathbf{s},\boldsymbol{\gamma},u,\boldsymbol{\varepsilon})$ are nonlinear functions of $\mathbf{s}$, $\boldsymbol{\gamma}$, u and $\boldsymbol{\varepsilon}$. By means of a Taylor series expansion and the discretization, the distribution process can be represented as

$$\begin{bmatrix} \bar{\mathbf{s}}_{k+1} \\ \bar{\boldsymbol{\gamma}}_{k+1} \end{bmatrix} = \begin{bmatrix} \mathbf{A}_{11} & \mathbf{A}_{12} \\ \mathbf{A}_{21} & \mathbf{A}_{22} \end{bmatrix} \begin{bmatrix} \bar{\mathbf{s}}_k \\ \bar{\boldsymbol{\gamma}}_k \end{bmatrix} + \begin{bmatrix} \mathbf{b}_1 \\ \mathbf{b}_2 \end{bmatrix} \bar{u}_{k-1} + \begin{bmatrix} \mathbf{K}_1 \\ \mathbf{K}_2 \end{bmatrix} \bar{\boldsymbol{\varepsilon}}_k \tag{2}$$

The distribution function $\bar{\boldsymbol{\gamma}}_{k+1}$ is often approximated by a linear combination of m basis functions (Yue et al., 2008). The state space model can be rewritten as

$$\begin{bmatrix} \bar{\mathbf{s}}_{k+1} \\ \bar{\mathbf{v}}_{k+1} \end{bmatrix} = \begin{bmatrix} \mathbf{A}_{11} & \mathbf{A}_{12} \\ \bar{\mathbf{A}}_{21} & \bar{\mathbf{A}}_{22} \end{bmatrix} \begin{bmatrix} \bar{\mathbf{s}}_k \\ \bar{\mathbf{v}}_k \end{bmatrix} + \begin{bmatrix} \mathbf{b}_1 \\ \bar{\mathbf{b}}_2 \end{bmatrix} \bar{u}_k + \begin{bmatrix} \mathbf{K}_1 \\ \bar{\mathbf{K}}_2 \end{bmatrix} \bar{\boldsymbol{\varepsilon}}_k \tag{3}$$

$$\bar{\boldsymbol{\gamma}}_k(\mathbf{y}) = \mathbf{C}(\mathbf{y})\bar{\mathbf{v}}_k$$

3. PDF of the Individual Distribution Values

The fluctuations caused by the control input and disturbances on the non-distribution variables $\bar{\mathbf{s}}$ are obtained and the effects of these fluctuations on the distribution

variables $\bar{\mathbf{v}}$ are evaluated. The transfer function relating the non-distribution variables $\bar{\mathbf{s}}$ to the control input $\bar{u}$ and the disturbance variables $\bar{\boldsymbol{\varepsilon}}$ is found to be

$$\bar{\mathbf{s}}_k = \mathbf{G}_{u,s}\left(z^{-1}\right)\bar{u}_k + \mathbf{G}_{d,s}\left(z^{-1}\right)\bar{\boldsymbol{\varepsilon}}_k \tag{4}$$

The transfer function relating the distribution variables $\bar{\mathbf{v}}$ to the control input $\bar{u}$ and the disturbance variables $\bar{\boldsymbol{\varepsilon}}$ is found to be

$$\bar{\mathbf{v}}_k = \mathbf{G}_{u,v}\left(z^{-1}\right)\bar{u}_k + \mathbf{G}_{d,v}\left(z^{-1}\right)\bar{\boldsymbol{\varepsilon}}_k \tag{5}$$

The derivation of the PDF of each distribution value depends on the non-distribution variable used in the control loop. In the method shown for the assessment of the control loops, the key idea is to determine how a given control law can be rewritten to be expressed in terms of disturbance variables. Let $\bar{s}_l$ be one of the non-distribution variables in $\bar{\mathbf{s}}$, which is taken to be the controlled variable, and the control law be expressed as

$$\bar{u}_k = -G_c\left(z^{-1}\right)\bar{s}_{k,l} \tag{6}$$

Eqn (6) is substituted in Eqn (4) to get a transfer function relating $\bar{u}_k$ to disturbance variables. The transfer function in $\bar{u}_k$ is substituted in Eqn (5) to get a transfer function, which is substituted into Eqn (3) to get $\mathbf{H}_{v,l}\left(z^{-1}\right)$, a transfer function relating individual distribution values to disturbance variables. Each distribution value is computed from the disturbance variables by

$$\bar{\gamma}_k\left(y_l\right) = \mathbf{H}_{v,l}\left(z^{-1}\right)\bar{\boldsymbol{\varepsilon}}_k = \sum_{j=1}^{n_d} H_{v,l,j}\left(z^{-1}\right)\bar{\varepsilon}_{k,j} \tag{7}$$

Each distribution value follows a normal distribution with mean zero and with variance calculated by

$$\sigma_{l,v}^2 = \sum_{j=1}^{n_d}\sum_{p=1}^{\infty}\sigma_j^2 h_{v,l,j,p}^2 \tag{8}$$

4. PDF of the Distribution Output

In a sample considered for constructing PDF of the over-all distribution output, there is no need to make a distinction on which distribution value an observation value comes from. All the values are lumped together to form a PDF for the entire distribution output. Each of N deviation distribution values $\bar{\gamma}\left(y_l\right)$ is considered as a random variable which follows a Gaussian distribution with a zero mean and a variance σ_l^2 computed, so PDF of the over-all distribution output is constructed from the average of PDFs of all the distribution values as shown below

$$\Pr(e) = \frac{1}{N\sqrt{2\pi}}\sum_{l=1}^{N}\frac{1}{\sigma_l}\exp\left[-\frac{e^2}{2\sigma_l^2}\right] \tag{9}$$

In Eqn (9), the random deviation of any distribution value from its set-point is referred to as e and only one PDF can be constructed for a given control law with its specified control parameter values. By varying the control law or the values of the control parameters, various PDF can be constructed; obviously, the control loop yielding the PDF with the smallest variance is the most effective controller.

5. Case Study

The proposed performance assessment method is used to evaluate the performance of temperature control loops using a proportional controller for different controller gains in free radical solution polymerization of styrene. A process variable, temperature, is used as a controlled variable. Due to the space limitation, the mathematical model is listed here and readers can refer to Schmidt & Ray (1981). Most of the parameter values are taken from Hidalgo & Brosilow (1990). The operating conditions are taken from Tatiraju et al. (1999).

The model has the vector of three non-distribution state variables $\mathbf{s} = [C_I \;\; C_M \;\; T]$ (initiator concentration, monomer concentration and temperature) and the vector of $N = 200$ distribution variables at several chain length locations on the MWD output $\boldsymbol{\gamma} = \left[C_{M_2} \;\; C_{M_{2+\Delta n}} \;\; C_{M_{2+2\Delta n}} \;\; C_{M_{2+3\Delta n}} \;\; \cdots \;\; C_{M_{n,\max}} \right]^T$. Q is the heating rate which is the control input, and the vector of two disturbance variables (inlet initiator concentration and inlet temperature) is $\boldsymbol{\varepsilon} = \left[C_{I,i} \;\; T_I \right]^T$. The MWD function $\bar{\gamma}(y)$ is approximated by a linear combination of $m = 35$ B spline cubic wavelet functions. For a temperature proportional controller, the control law is given by

$$\bar{Q}_k = K_p \bar{T}_{k-1} = K_p z^{-1} \bar{T}_k \tag{10}$$

Eqn (10) is substituted into the transfer function relating temperature T to the control input Q and disturbance variable inlet initiator concentration $C_{I,i}$ s and inlet feed temperature T_I to get

$$\bar{T}_k = \left[G_{T,C}\left(z^{-1}\right) \; G_{T,T}\left(z^{-1}\right) \right] \begin{bmatrix} C_{I,i,k} \\ T_{I,k} \end{bmatrix} = \mathbf{G}_T\left(z^{-1}\right) \bar{\boldsymbol{\varepsilon}}_k \tag{11}$$

Eqn (11) shows the relationship between the disturbances and the fluctuations in temperatures for a proportional controller with a specified gain. The disturbances, namely fluctuations in inlet initiator concentration and inlet feed temperature, are assumed to follow a Gaussian distribution with mean zero and standard deviations of 0.06 and 20. The PDF of temperature is based on two controller gains namely -0.8 and -0.08 respectively. Since it assumes that controlling fluctuations in MWD are indirectly done by controlling temperature fluctuations, it is speculated that the MWD fluctuations under the controller with higher gain would be smaller than those with a smaller gain. The overall PDF can be calculated using Eqn (9) shown in Figure 1 and 2. It is found that most of the deviations are very close to zero and that only certain distribution values deviate significantly from the target distribution and the performance for the controller gain of -0.8 is better. Using the proposed method, the conclusion can indeed be obtained and plots of PDFs for overall MWD fluctuations can be obtained together with the variance of the PDF. The PDF curve for the overall MWD fluctuation will be narrower and the variance smaller when the controller has higher gain.

6. Conclusions

The feasibility of using the proposed performance assessment method for feedback control loops in chemical processes with distribution outputs is shown. The proposed method assesses the performance of control loops on the ability to minimize fluctuations of distribution outputs. The control loops indirectly control distribution outputs by a non-distribution variable, so the method uses a state space process model to determine the effects of various control laws on the probability density distribution

function (PDF) of the resulting distribution outputs. Results show that the proposed method is effective in assessing the control loop performance.

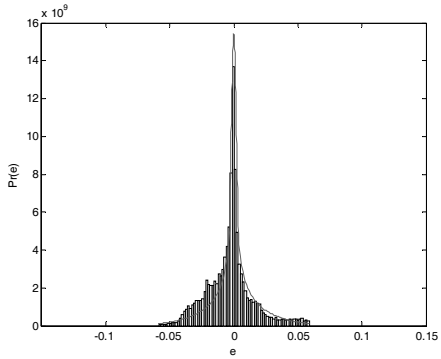

Figure 1 PDF of Distribution Output K=-0.8

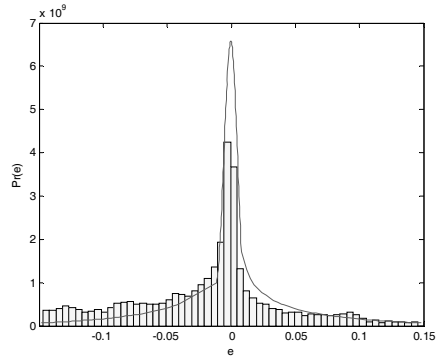

Figure 2 PDF of Distribution Output K=-0.08

References

T.J. Crowley, Y.K. Choi, 1998, Experimental Studies on Optimal Molecular Weight Distribution in a Batch Free Radical Polymerization Process, Chem. Eng. Science, 53, 2769-2790.

T. Takamatsu, S. Shioya, and Y. Okada, 1988, Molecular Weight Distribution Control in a Batch Polymerization Recator, Ind. Eng. Chem. Res., 27, 93-99.

L Desborough, T.J. Harris, 1997, Performance Assessment Measures for Univariate Feedback Control, Canadian J. Chem. Eng., 70, 1186-1197.

T.J. Harris, 1989, Assessment of Control Loop Peformance, Canadian J. Chem. Eng., 67, 856-861.

T.J. Harris, F. Boudreau, and J.F. MacGregor, 1996, Performance Assessment of Multivariable FeedBack Controllers, Automatica,12, 1505-1518.

B. Huang, S.L. Shah, and E.K. Kwok, 1997, Good, Bad or Optimal? Performance Assessment of Multivariable Processes, Automatica, 31, 1175-1183.

H. Yue, H. Wang, and J.F. Zhang, 2008, Shaping of Molecular Weight by Iterative Learning PDF Control Strategies, Proc.IMechE, 227, 639-653.

A.D. Schmidt, W.H. Ray, 1981, The Dynamic Behaviour of Continuous Polymerization Reactors-I, Chem. Eng. Science, 36, 1401-1410.

P.M. Hidalgo, C.B. Brosilow, 1990, Nonlinear Model Predictive Control of Styrene Polymerization at Unstable Operating Points, Comp. Chem. Eng., 4, 481-494.

S. Tatiraju, M. Soroush, and B.A. Ogunnaike, 1999, Multirate Nonlinear State Estimation with Application to a Polymerization Reactor, AIChE J., 45, 769-780.

I.A. Karimi and Rajagopalan Srinivasan (Editors), Proceedings of the 11th International Symposium on Process Systems Engineering, 15-19 July 2012, Singapore

Fault Diagnosis based on *DPCA* and *CA*

Celina Rea, Ruben Morales-Menendez [*], Juan C. Tudón Martínez, Ricardo A. Ramírez Mendoza, Luis E. Garza Castañon

Tecnológico de Monterrey, Campus Monterrey, Av. Eugenio Garza Sada 2501, Col. Tecnológico, 64,849 Monterrey NL, México

Abstract

A comparison of two fault detection methods based in process history data is presented. The selected methods are Dynamic Principal Component Analysis (*DPCA*) and Correspondence Analysis (*CA*). The study is validated with experimental databases taken from an industrial process. The performance of methods is compared using the Receiver Operating Characteristics (*ROC*) graph with respect to several tuning parameters. The diagnosis step for both methods was implemented through Contribution Plots. The effects of each parameter are discussed and some guidelines for using these methods are proposed.

1. Motivation

Industrial process have grown in integration and complexity. Monitoring only by humans is risky and sometimes impossible. Faults are always present, early Fault Detection and Isolation (*FDI*) systems can help operators to avoid abnormal event progression. *DPCA* and *CA* are two techniques based on statistical models coming from experimental data that can be used for fault diagnosis, Detroja et al. (2006b). These approaches are well known in some domains; but, there are several questions in the fault diagnosis. A *ROC* graph is a technique for visualizing, organizing and selecting classifiers based on their performance. *ROC* graph has been extended for use in diagnostic systems. In the published research works, the number of data for model's learning the model, sampling rate, number of principal components/axes, thresholds have not been studied under same experimental databases.

2. Fundamentals

A brief comparative review of both *DPCA* and *CA* approaches is presented focus in modelling, detection and diagnosis.

Modeling for both DPCA and CA. Both methods need a statistical model of the process under normal operating conditions. The data set need be scaled to zero mean and unit variance. *CA* requires n_t observations for p variables having a form of $\mathscr{X}(t) = [X_1(t) \ \ldots X_p(t)\ ]_{(n_t \times p)}$; while *DPCA* additionally includes some past observations (i.e. w-time delay) $\mathscr{X}(t) = [X_1(t) \ \ldots \ X_1(t-w) \ \ldots \ X_p(t) \ \ldots \ X_p(t-w)]_{(n_t \times (p \cdot [w+1]))}$. Based on $\mathscr{X}(t)$ matrix, two subspaces are built. The Principal Subspace captures major faults in the process, and the Residual Subspace considers minor faults and correlation rupture. A SCREE test, determines the number of principal and residual components (axes). By plotting the eigenvalues (singular values) of $\mathscr{X}(t)$ for *DPCA* (*CA*), the principal components (axes) are the first k components (axes) before the inflection point is located, while

[*] rmm@itesm.mx

the remainders are the residuals components (axes). Even *DPCA* and *CA* models cannot be compared. The representation given by *CA* would appear to be better able to capture inter-relationships between variables and samples, Detroja et al. (2006a). Fig. 1 (left) summarizes the model's learning for both methods.

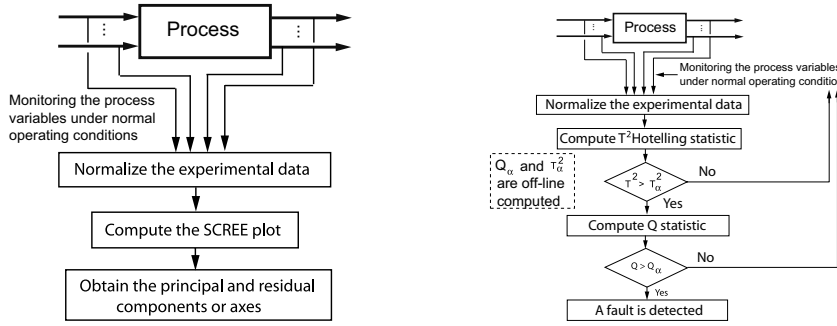

Figure 1. Model's learning algorithm (left) and online detection (right) for DPCA *&* CA.

Detection for DPCA. The variables must be normalized, $\mathscr{X}_S$. Based on the correlation matrix $\mathscr{R}$, the eigenvalues λ_i and eigenvectors $\mathscr{V}_i$ are obtained. The eigenvalues must be organized in decreasing order. The eigenvectors form two matrices: $\mathscr{V}_{[1,k]}$ which is the principal component transformation and $\mathscr{V}_{[k+1,p\cdot[w+1]]}$, known as residual transformation matrix. The projections to the subspaces are based on a linear transformation with no correlation between them. Mapping from multivariate approach to a scalar demands two statistics: T^2 Hotelling and Q statistics. The T^2 measures the deviation of variables in a data set from their mean values. Hotelling T^2 chart is based on the concept of statistical distance and it monitors the change in the mean vector T^2 statistic is obtained by $T^2_{\mathscr{X}_{S_i}}$; a normal operating point can be established as $T^2_\alpha = (n_t-1)F_\alpha(k,n_t-k)/(kn_t-k)$ F_α-distribution with k and n_t-k degrees of freedom, $\alpha = 0.95$. If $T^2 > T^2_\alpha$ a fault is detected. Q statistic will detect changes on the residual directions. The Q statistic is obtained as $Q_{\mathscr{X}_{S_i}} = \mathscr{X}_{S_i} G \mathscr{X}_{S_i}^T$. The threshold for normal operating conditions is given by $Q_\alpha = \theta_1 \left[h_o C_\alpha \sqrt{2\theta_2}/\theta_1 + 1 + \theta_2 h_0(h_0-1)\theta_1^2\right]^{\frac{1}{h_0}}$ If $Q_{\mathscr{X}_{S_i}} > Q_\alpha$ a fault is detected.

Detection for CA. *CA* is an optimization problem with $\mathscr{P} = \mathscr{D}_r^{-1/2}[(1/g)\mathscr{X} - rc^T]\mathscr{D}_c^{-1/2}$ and $\mathscr{A}\mathscr{D}_\mu\mathscr{B}^T = SVD(\mathscr{P})$. For choosing the principal and residual axes, a SCREE plot can be made with the singular values obtained in $\mathscr{D}_\mu$. The Greenacre's criteria was used for selection of k principal axis. The coordinates of the row and column profile points for the new principal axis can be computed by projecting on $\mathscr{A}$ and $\mathscr{B}$, with only the first k columns retained, with $\mathscr{F} = \mathscr{D}_r^{-1/2}\mathscr{A}\mathscr{D}_\mu$ and $\mathscr{G} = \mathscr{D}_c^{-1/2}\mathscr{B}\mathscr{D}_\mu^T$. Matrix $\mathscr{F}$ gives the new row coordinates for the row cloud. Using a new measurement vector $X = [X_1 \ \ldots \ X_m]^T$, the row sum is given by $r = \sum_{i=1}^p X_i$ and the new row score is $f = [r^{-1}x^T\mathscr{G}\mathscr{D}_\mu^{-1}]^T$. The T^2 statistic for *CA* is defined as $T_i^2 = f^T\mathscr{D}_\mu^{-2}f$, where $\mathscr{D}_\mu$ contains the first k-largest singular values. The threshold is computed through T^2_α. For residual axes, Q statistic

allows to detect any significant deviation. Considering $Q_i = Res^T Res$, and the control limit as $Q_\alpha = \mu_Q \pm C_\alpha * \sigma_Q$ where C_α is a confidence limit of 95% according to its normal deviation $\mathcal{N}(\mu_Q, \sigma_Q)$. Fig. 1 (right) shows the scheme for online detection.

Diagnosis for both *DPCA* and *CA*. The T^2 statistic gives a variable which is calculated by using all variables; it shows the changes that occurred in all variables. The T^2 chart does not give information on which variable or variables is faulty. Miller et al. (1998) introduced a method for determining the contribution of each of the p variables in the T^2 computation. Scores of the *PC* are used for monitoring in T^2 chart; upon a faulty signal, first the contribution of each variable in the normalized scores is computed. Then total contributions of each variable are determined and plotted. The plot that shows the contribution of each variable in T^2 chart at time k is called the variable contribution plot, Kosebalaban and Cinar (2001). When T^2 value at time k is above the upper control limit, the variable contribution are calculated and plotted to diagnose the variable(s) that caused the fault alarm in multivariate T^2 chart. The variables with higher contribution, are isolated as the most probable fault: $Cont_i = Z_i^2 / \sum_{j=1}^{n_t} Z_j^2$ where $Z = R_{\gamma_r}$ is a generated residual for *DPCA*. *CA* method cannot diagnose the fault neither; for this purpose, a contribution plot base on the residuals of the Q statistic are used, $Z = Res$. The contribution plots can be plotted over time when a faulty signal alarms, the change in contribution of process variables gives more information about the root cause of the faulty condition at that time period.

3. Experimental Setup

An industrial Heat Exchanger (*HE*) was the test-bed for this research. The *HE* uses steam vapor for heating water. The operating point is 70% of steam vapor flow (FT_2), 38% of water flow (FT_1), and the input water temperature (TT_1) was at 23^{o}C, which give an outlet water temperature (TT_2) of 34^{o}C. More than 20 experimental tests were done. For each sensor an abrupt fault as a bias of $\{ \pm 5, \pm 6, \pm 8 \}\ \sigma$ of the signal were implemented Prakash et al. (2002). Also, the number of data were 200, 500,..., 5000, and the sampling rate: 1,2,...,10.

4. Analysis of the Tuning Parameters.

Number of Principal Components (PC)/axes. Data compression is an important aspect of multivariate statistical tools. SCREE plot indicates the percentage of accumulated information variation versus the components/axes. The components/axes, when the slope of the plot does not change, defines the number of *PC*/axes. Figure 2 (A) shows the percentage accumulated variation information versus the number of components for *DPCA*, and versus number of axes for *CA* is shown in Fig. 2 (B). Each plot includes databases with 100, 200, 500 and 1,000 data vectors. For *DPCA*, 5 *PC* describe 92-94 % of the information; 6 or more components do not contribute significantly. The number of data vector of process variables do not impact in the curve behavior. For *CA* the number of data affects the curve: 100-200 data have lower percentage accumulated variation than 500-1000 data vectors for 1 or 2 axes. After 3 axes there is not difference. According to *Greenacre* criteria, Greenacre and Blasius (1995), three axes are recommended.

Thresholds. A False Negative (*FN*) is when there is a fault, but it is not detected; while a False Positive (*FP*) is when there is no fault, but one is detected. True Positive (*TP*) is when there is a fault, and it is detected; while, True Negative (TN) is when there is no

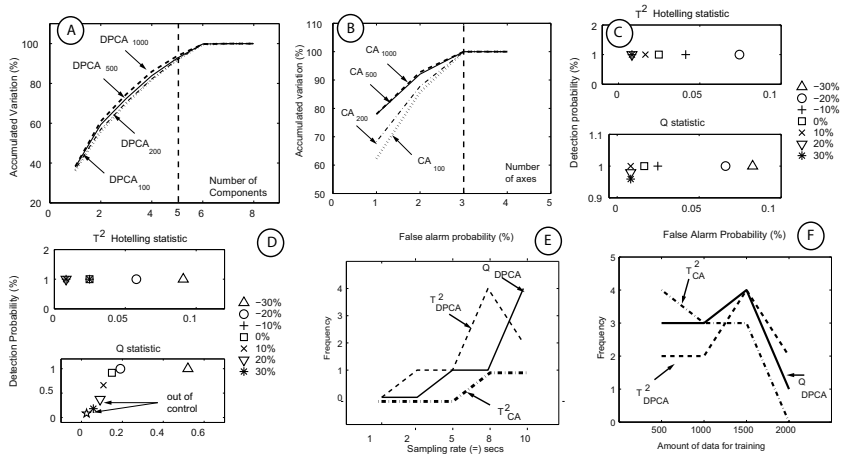

Figure 2. Average variation accumulated versus components for DPCA *(A), and versus number of axes for* CA *(B).* ROC *curves for outlet water temperature (TT_2) transmitter using* DPCA *(C), and for outlet water temperature (TT_2) transmitter* CA *(D). Frequency of errors for different sampling time (E) and for different number of training data (F).*

fault and no fault is detected. The sum of *TP* and *FN* are the total faulty cases (*TFC*) and the sum of *TN* and *FP* are total healthy cases (*THC*). The probability of detection $P_d = \frac{TP}{TFC}$ while the probability of false alarms $P_{fa} = \frac{FP}{THC}$. For every condition, when $[(P_d > 0.9)$ and $(P_{fa} < 0.1)]$, an optimum is achieved by having a good compromise between right detection and minimum false alarms. *ROC* curves show a relation between opportune detection probability P_d versus false alarms probability P_{fa}. Table 1 summarizes the performance of $[(P_d > 0.9)$ and $(P_{fa} < 0.1)]$ criteria for faults sensors. *DPCA* shows successful results; while, *CA* exhibits some troubles mainly with *Q* statistics. Fig. 2 (C and D) shows *ROC* curves, where the thresholds were modified in different percentage. Fig. 2 (C) shows that *DPCA* is successful for both statistics. However, Fig. 2 (D) shows that for *CA* only T^2 statistics works well. *Q* statistics for *CA*, is only based on the residuals axes, which does not capture the variation of the residual per axes, Table 1.

Sampling rate. The process variables were sampled at 1, 2, 5, 8 or 10 s. Fig. 2 (E) shows the number of times that the $[(P_d > 0.9)$ and $(P_{fa} < 0.1)]$ criteria was violated for each statistics for different sampling rate. There is a good performance for both methods when sampling rate is 1 or 2 s; however, the probabilities for missing detections or increasing false alarms grows up for sampling times greater than 5 s. The *Q* statistic for *CA* was avoided because its low performance.

Number of Training Data. Fig. 2 (F) shows the number of times that the $[(P_d > 0.9)$ and $(P_{fa} < 0.1)]$ criteria was violated for each statistics for the number of training data. The number of data is a key issue for learning a statistical model. It can be seen that after 1,500 training data (25 min, 1 s sampling rate) both methods improve their performance.

Table 1. Average performance for different sensors based on ROC *curves.*

Sensor Transmitter	Number Tests	*DPCA-*T^2	*DPCA-Q*	*CA-*T^2	*CA-Q*
TT_2	11	100	100	100	9.09
FT_1	15	100	86.67	40	6.67
FT_2	12	91.67	100	91.67	91.67
TT_1	11	81.82	90.91	81.82	0

Diagnosis. There is a good performance with *DPCA* for the 4 faulty sensors, while *CA* shows 90.9% performance when a fault occurs in (TT_2) and 46.6% if the fault is in (FT_1). Contributions of 4 variables were compared to the same statistic and choose the variables corresponding to the relatively large contributions as the possible causes for faults. Instead of comparing the absolute contribution and the corresponding control limit, the use of the relative contribution is more convenient way to identify faulty variables Choi and Lee (2005).

5. Conclusions

Given experimental data a multivariate statistical model can be learned. SCREE plot and the *Greenacre* criteria guide the complexity of the model based on the minimum number of components/axes. The statistical model for *CA* is more sensible to the number of data than the model for *DPCA*; but, defined the minimum number of components/axes, the number of data does not have influence. The *ROC* graphs are a useful tool for visualizing and evaluating fault detection algorithms. A detection probability ($P_d > 0.9$) and false alarm probability ($P_{fa} < 0.1$.) is a good criteria for choosing the sampling rate, number of data and thresholds. Sampling rate was the most important parameter. Based on *ROC* graphs, *DPCA* outperforms *CA* in fault detection, because the Q statistics does not work well. Diagnosis could be implemented in both methods through contribution plots.

References

Choi, S., Lee, I., 2005. Multiblock PLS-based Localized Process Diagnosis . J of Process Control 15 (3), 295–306.

Detroja, K., Gudi, R., Patwardhan, S., 2006a. Fault Diagnosis using Correspondence Analysis: Implementation Issues and Analysis. In: IEEE Int Conf on Ind Tech. pp. 1374 – 1379.

Detroja, K., Gudi, R., Patwardhan, S., Roy, K., 2006b. Fault Detection and Isolation Using Correspondence Analysis . Ind Eng Chem Res 45, 223 – 235.

Greenacre, M., Blasius, J., 1995. Correspondence Analysis in the Social Sciences. A Press.

Kosebalaban, F., Cinar, A., 2001. Integration of Multivariate SPM and FDD by Parity Space Technique for a Food Pasteurization Process. Computers and Chemical Eng 25, 473–491.

Miller, P., Swanson, R., Heckler, C., 1998. Contribution Plots: A Missing Link in Multivariate Quality Control . Appl. Math. and Comp. 8, 775–792.

Prakash, J., Patwardhan, S., Narasimhan, S., 2002. A Supervisory Approach to Fault-Tolerant Control of Linear Multivariable Systems. Ind. Eng. Chem. Res. 41, 2270–2281.

I.A. Karimi and Rajagopalan Srinivasan (Editors), Proceedings of the 11th International Symposium on Process Systems Engineering, 15-19 July 2012, Singapore.

Design Method of Alarm System for Identifying Possible Malfunctions in a Plant Based on Cause-Effect Model

Makoto Kato[a], Kazuhiro Takeda[b], Masaru Noda[ac], Yasunori Kikuchi[a], Masahiko Hirao[a]

[a]*Department of Chemical System Engineering, University of Tokyo, 7-3-1 Hongo, Bunkyo-ku, Tokyo 113-8656, Japan*
[b]*Department of Material Science and Chemical Engineering, Shizuoka Univeristy, 3-5-1 Johoku, Naka-ku, Hamamatsu, Shizuoka 432-8561, Japan*
[c]*Graduate School of Information Science, Nara Institue of Science and Technology, 8916-5 Takayama-cho, Ikoma 630-0192, Japan*

Abstract

A new alarm system design method is proposed, in which it is assumed that the sign patterns and alarm sequences generated by the alarm system are invariant for each possible plant malfunction in a plant. The proposed method gives the most sets yet provided of plant malfunctions that operators can distinguish using the alarm system. We applied the proposed method to select alarm variables for a simple chemical plant. Results showed that the method provides more alarm variable combinations that can identify possible malfunctions than a previously used method.

Keywords: Plant Alarm System, Design, Cause-Effect Model, Malfunction

1. Introduction

Plant alarm systems form one of the core elements of operator interfaces for automatically monitoring plant state deviations and for alerting plant operators to changes that require their attention in industrial plants such as chemical plants, oil refineries, and power stations. Designing an efficient alarm system that helps operators to quickly identify the causes of abnormalities and respond to abnormal situations is vital to achieve safe and stable plant operations.

Distributed control systems (DCS), which are widely used in chemical industries, utilize control instruments that have process variables (PVs) and manipulated variables (MVs). Plant alarm systems make use of these variables and issue warnings when PV or MV values exceed allowable alarm limits to a degree that is undesirable or potentially unsafe. When a plant situation becomes abnormal, alarm information is reported in the form of flashing icons or buzzing sounds and a text list describing related alarm information appears on an alarm summary panel.

In 2009, the Engineering Equipment and Materials Users' Association (EEMUA) published comprehensive guidelines for the development, procurement, operation, maintenance, and management of industrial alarm systems. While the guidelines mentioned, for example, the key design principle that every alarm (or combination of alarms) presented to the operators should have a response clearly defined by the alarm's designer, some of the design methodologies mentioned in it, such as the selection of alarm variables, are still only conceptual in nature.

Luo *et al.* (2007) proposed a method for selecting a set of alarm variables on the basis of an abnormality propagation diagram that denotes the relations between failure causes and detectable symptoms for all assumed plant malfunctions. The method selects the variables by referring to the number of possible malfunctions that could generate the symptoms. This is because the smaller the number of possible malfunctions that could generate a symptom, the fewer malfunctions an operator needs to check for. However, the method does not theoretically guarantee that operators will be able to identify all malfunctions assumed in the plant by using selected alarm variables.

Takeda *et al.* (2010) proposed using a cause-effect model to derive sets of plant alarm variables for identifying assumed plant malfunctions. The alarm system they designed is theoretically guaranteed to be able to statistically identify all assumed plant malfunctions. However, the number of malfunctions that operators using the system can identify is limited because the method it employs assumes that operators will utilize only alarm variable combinations generated by the system for identifying them.

In this study, we propose a new alarm system design method, in which we assume that the pattern of signs and the sequence of alarms generated by the system are invariant for each possible malfunction. The method gives more plant malfunction sets that operators using an alarm system can identify than have heretofore been provided.

2. Cause-effect model

A cause-effect model is an abnormality propagation diagram that shows the propagation process of abnormalities after malfunctions occur. The signed directed graph in Fig. 1 is used to describe a cause-effect model, where process variables and their causal relations are denoted by nodes and directed braches, respectively (Iri *et al.*, 1979). Node signs are defined as follows:

\+ Positive deviation of process variable from normal condition
0 Process variable is in normal condition
− Negative deviation of process variable from normal condition

The solid and dotted branches in the cause-effect model represent positive (+) and negative (−) influences between two nodes, respectively. A possible plant malfunction is defined by pairs of a state variable and its sign. The cause-effect model of the process is derived by a Hazard and Operability Study or Process Hazard Analysis. In this paper, it is assumed that the cause-effect model of the object plant is given in advance.

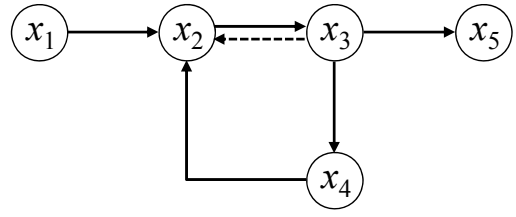

Fig. 1 Example of cause-effect model

3. Alarm variable selection method

3.1. Problem definition

In this paper, the alarm system design problem is how to determine all alarm variable sets that are able to distinguish the true malfunction among all assumed plant malfunctions. Following assumptions are introduced in the method:

- Total number of alarm variables is given
- Multiple malfunctions don't occur simultaneously

3.2. Alarm variable selection method

All measured variables in the cause-effect model can be treated as alarm variables. The proposed method uses the following steps to determine all alarm variable sets that are able to distinguish the true malfunction among all possible plant malfunctions.

Step 1: Generate all alarm variable permutations by selecting measured process variables, where the total number of alarm variables is given.

Step 2: Generate all permutations of pairs of alarm variables and signs by assigning three signs, i.e., "+", "0", and "−", to each alarm variable in all alarm variable permutations. These permutations are called "alarm generation patterns" hereafter.

Step 3: Find directed single paths from the first alarm to each alarm in the alarm generation pattern on which node signs corresponding to alarm variables and signs of directed branches along the directed single path are consistent with each other. If no feasible directed single paths are found, eliminate the alarm generation pattern because there is inconsistency between the pattern and the cause-effect model. Execute the consistency check for all alarm generation patterns with the cause-effect model.

Step 4: Find all assumed malfunctions that can generate the pair of the first alarm and its sign of the alarm generation pattern. If two or more assumed malfunctions that satisfy the above conditions are found, eliminate this pattern because it is not able to distinguish one true malfunction among all assumed plant malfunctions. Eliminate all alarm generation patterns where the first alarm is caused by two or more assumed malfunctions.

Step 5: Derive all alarm variable combinations that are able to identify all assumed plant malfunctions.

4. Case study

4.1. Example process

The proposed method was applied to the alarm system design problem of the simple reaction process with a recycle loop in Fig. 2 (Takeda *et al,* 2010), where P, F, L, and V are state variables of pressure, flow rate, liquid level, and valve position, respectively. All state variables except for P1 and P2 are measured process variables. Therefore, the set of measured process variables is S = {F1, F2, F3, F4, L1, L2, V1, V2, V3, V4}.

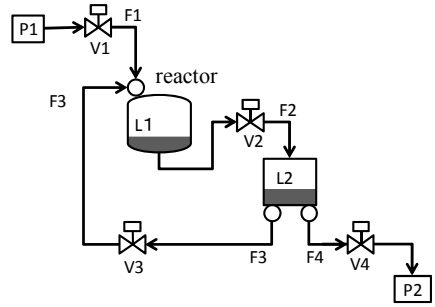

Fig. 2 Example process

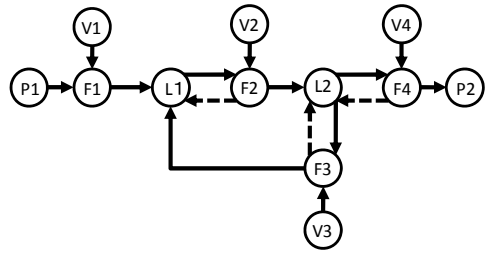

Fig. 3 Cause-effect model

Figure 3 shows the cause-effect model of the objective process. For example, the liquid level of reactor L1 increases when the pressure of feed P1 becomes abnormally high. The following six malfunctions are assumed to occur in the plant.

P1[+]	High feed pressure
P1[−]	Low feed pressure
F2[+]	Leakage from the pipe between reactor and buffer tank
F2[−]	Blockage in the pipe between reactor and buffer tank
V4[+]	Valve stiction at high valve position
V4[−]	Valve stiction at low valve position

The alarm system design problem is how to derive all combinations of alarm variables from S = {F1, F2, F3, F4, L1, L2, V1, V2, V3, V4} that are able to distinguish all assumed malfunctions C = {P1[+], P1[−], F2[+], F2[−], V4[+], V4[−]}.

4.2. Results and discussion

Table 1 shows all alarm variable combinations derived by the proposed method that are able to distinguish all assumed malfunctions for a total of three alarm variables. The table also shows all alarm variable combinations derived by a previously used method. The proposed method found 18 combinations.

5. Conclusion

We have proposed a new alarm system design method in which we assume that the pattern of signs and the sequence of alarms are invariant for each possible malfunction. Theoretical analysis showed that our method is especially effective for isolating the root causes of malfunctions that have corresponding nodes in the connected cause-effect graph.

References

Engineering Equipment & Material Users' Association (EEMUA), ALARM SYSTEMS-A Guide to Design, Management and Procurement, EEMUA Publication No.191 2nd Edition, EEMUA, London (2007)

M. Iri, K. Aoki, E, O'shima, and H. Matsuyama; "An algorithm for diagnosis of system failures in the chemical process," *Comp. Chem. Eng.*, **3(1-4),** 489-493 (1979)

Y. Luo, L. Xiwei, M. Noda, and H. Nishitani, Systematic Design Approach for Plant Alarm Systems, *Journal of Chemical Engineering of Japan*, **40(9)**, 765-772 (2007)

K. Takeda, T. Hamaguchi, and M. Noda; "Plant Alarm System Design based on Cause-Effect Model," *Kagaku Kogaku Ronbunshu*, **36(2)**, 136-142 (2010)

Table 1 Possible alarm variable combinations when total number of alarms is three

Combination of alarm variables
F1, V4, F2
F1, V4, F3
F1, V4, F4
F1, V4, L2
F1, F2, F3
F1, F2, F4
F1, F2, L1
F1, F2, L2
F1, F3, F4
F1, F4, L2
F2, F3, L1
F2, F4, L1
F2, L1, L2
F2, V4, L1
F4, L1, L2
F3, F4, L1
F3, V4, L1
V4, L1, L2

I.A. Karimi and Rajagopalan Srinivasan (Editors), Proceedings of the 11th International Symposium on Process Systems Engineering, 15-19 July 2012, Singapore.

Real-time application of CAPE-OPEN for PTA process monitoring and optimization*

Xiaorui Zhao[a,b], Pengfei Jiang[a], Xi Chen[a], Jun Zhao[a], Zhijiang Shao[a]

[a]*State Key Laboratory of Industrial Control Technology, Institute of Industrial Control, Zhejiang University, 38 Zheda Road, Hangzhou 310027, China*
[b]*Department of Mechanical and Industrial Engineering, University of Illinois at Chicago, Chicago 60607, United States*

Abstract

A computer-aided process engineering (CAPE)-OPEN-based open-architecture application was implemented for the online Purified Terephthalic Acid (PTA) process monitoring and optimization. The framework incorporates independent Process Modeling Components (PMC) that comply with the CAPE-OPEN 1.0 standard: *p*-xylene (PX) oxidation unit operation model, the nonlinear algebraic/nonlinear programming (NLA/NLP) interior point optimizer (IPOPT) solver, as well as the physical properties and the equilibrium calculation engine. All components are seamlessly integrated into the Process Modeling Environment (PME) for process simulation and optimization. The key reaction kinetic constants were estimated using a sequential subproblem strategy and then encapsulated through an *ICapeUnit* interface, with the selective operational parameters exposed for the operation and maintenance requirements. The reactor model can be solved by IPOPT within less than a second through the *ICapeMINLP* interface using an ordinary desktop computer. The convergence reliability in successfully solving the model for a wide-range of operation conditions was subsequently investigated. Based on the developed CAPE-OPEN model, a *de-facto* "Soft-sensing and Optimization System for p-xylene (PX) and acetic acid (HAC) Consumption in the PTA Process" was implemented and successfully used at the Sinopec Yangzi Petrochemical Company in Nanjing, China. The system provides real-time consumption calculation, product quality prediction, and operational guidance for operators. The CAPE-OPEN conceptual design can be applied in industrial settings for real-time applications.

Keywords: CAPE-OPEN, Purified Terephthalic Acid Process, PX Oxidation Reactor, Open Architecture, Real-time Simulation and Optimization

1. Introduction

Purified Terephthalic Acid (PTA) is the important raw material of polyester fibers, polyethylene terephthalate (PET), and insulated paint (Wang, 2005). The current manufacturing method for PTA is based on *p*-xylene (PX) oxidation, which is well known for its highly complex reaction kinetics, thermodynamics, and mass-transfer characteristics.

Environment and safety regulations, as well as growing demand on product quality and increasingly competitive markets, necessitate the continuous improvement of chemical processes in minimal time at minimal cost (Marquadt, 1996). A useful tool based on a

*This work was supported by the 973 Program of China(2012CB720500) and the NSF Program of China(21006086). E-mail address: zjshao@iipc.zju.edu.cn

rigorous model is needed in the process industry to provide operational guidance for production applications. Fortunately, with the rapid development of the computer-aided process engineering (CAPE) technology, the mechanism of PTA manufacture has become well understood and translated into a simulation flowsheet.

In the current work, the PX oxidation kinetics-based continuous stirred-tank reactor (CSTR) model is rewritten and is made CAPE-OPEN compliant. The core kinetic parameters are estimated and encapsulated on a binary level, and the end-users can only access the operational conditions. The reformed model is combined with a CAPE-OPEN compliant numeric algorithm interior point optimizer (IPOPT) and thus can solve itself under a sequential modular (SM) simulation mode. The validated model is then embedded into a PTA manufacturing process steady-state simulation in Aspen Plus as a substitute for the Aspen CSTR model. The validated model is further utilized in an open-architecture simulation and optimization platform being run at the Sinopec Yangzi Petrochemical Company in Nanjing, China. A Microsoft component object model (COM) middleware technology keeps the key model parameters invisible, thereby guaranteeing confidentiality (Banks, 2005).

1.1. PTA Process Introduction

The procedure for the PTA manufacturing process consists of two steps, namely, oxidation and purification. During the oxidation step, the PX oxidation reaction takes place in the liquid phase and is catalyzed by a Co-Mn-Br system at the 150°C to 210°C temperature range, producing crude terephthalic acid (TA).

The reactor unit has four inputs (two for the liquid and oxygen input streams, and two from the cycle loop streams) and two outputs. The vapor phase output of the reactor is passed to the next three-level condenser to feed the subsequent reaction, and the liquid phase output is sent to the crystallizer to be reoxidized.

1.2. PX Oxidation Reactor Model

PX oxidation follows a catalyzed reaction chain (Figure 1) of methyl oxidation to produce the final product, TA.

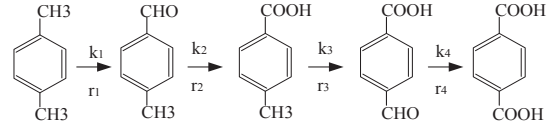

Figure 1. PX oxidation route

The vapor/liquid phase reactants in the tank are assumed to be well-mixed. The main reactions occur in the liquid phase, while the combustion in the gas phase produces side products and releases the CO and CO_2 tail gas. The mathematical model of the PX oxidation unit can be divided into four parts, namely, the reaction kinetics, material balance, physical property and equilibrium calculation, and connectivity equations. The reaction kinetics follows the simplified LHHW (Langmuir-Hinshelwood Hougen-Watson) kinetic equations.

1.3. Kinetic Parameter Estimation

To obtain the rigorous reactor model, the reaction kinetic factors (the K factors in the kinetic factor in LHHW equations) must be precisely estimated. The objective function for estimation is developed using the seven guide concentration variables from the field, namely, TA production, 4-carboxybenzaldehyde (CBA) concentration, acetic acid (HAC) consumption, as well as O_2, CO, CO_2, and crystallizer O_2 tail gases. The objective function is optimized under five typical steady-state operating conditions.

The estimation problem is formulated as formula (1). It has 21,718 variables, and is highly nonlinear. The traditional DMO solver available in Aspen Plus cannot solve the problem easily, especially when the initial values of the optimization variables are far from the optimum.

$$\begin{aligned} & min \sum_{i=1}^{5}\sum_{j=1}^{7}\varphi_{i,j}(y_{i,j}^{pred}-y_{i,j}^{meas})^2 \\ & s.t.\ f(x,y,k)=0 \\ & \quad k=[k_1,k_2,...,k_p] \\ & \quad lb_p \le k_p \le ub_p \\ & \quad p=1,2,...,10 \end{aligned} \tag{1}$$

The authors proposed a sequential subproblem programming strategy for data reconciliation and parameter estimation using multiple datasets (Zhang and Shao et al., 2010). A series of subproblems was constructed based on the objective and the model parameters. The solutions of each subproblem are a good initial estimation of the optimum of the next one. The optimum of the original parameter estimation problem can be derived by solving the series of subproblems.

1.4. Software Interface Implementation

CAPE-OPEN interfaces are used for the simulation under the SM and equation-oriented (EO) modes. The framework is shown in Figure 2.

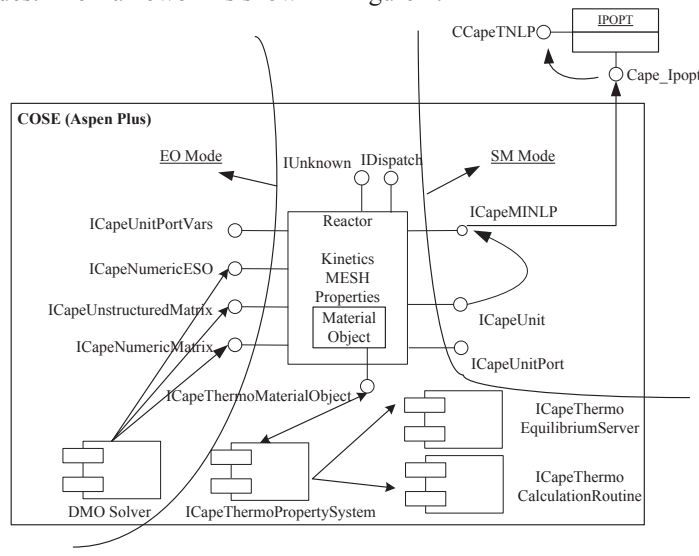

Figure 2. CAPE-OPEN PX oxidation reactor interface implementation

Under the SM mode, each operation unit (OU) should have a self-contained solver and a valid access into the solver to be self-solvable. In the current work, the main *ICapeUnit* interface is generated under the SM mode using the Unit Operation Wizard developed by the CAPE-OPEN Laboratories Network (Co-LaN). The COM-based dynamically linked library component is generated, in which all interfaces are wrapped and used by the simulator **(**Pérez et al., 2005**)**.

The access to the internal property system is provided by a container object, defined as the *ICapeThermoMaterialObject*, which is associated with each port of the OU, has access to the property package server installed within the process PME. The property

component has two functionalities, namely, the physical property and the equilibrium calculation.

The IPOPT solver is adopted to numerically solve the reactor model. IPOPT is a powerful nonlinear programming algorithm developed by the Carnegie Mellon University. It is compatible with the CAPE-OPEN standard through a wrapper (Lang and Biegler, 2005). In the *ICapeUnit_Calculate* routine, the model is defined by an *ICapeMINLP* interface. The wrapper converts the CO-based *ICapeMINLP* model into a nonlinear programming (NLP) problem, which can be solved by the IPOPT solver.

Four EO interfaces are further implemented for the support of any CAPE-OPEN compliant PMEs, which redefine the model into an equation set object (ESO). The EO interfaces contain a mathematical model (through *ICapeNumericESO*), as well as first-order derivatives (through *ICapeNumericUnstructuredMatrix* and *ICapeNumericMatrix*) and stream connectivity mapping information (through *ICapeUnitPortVars*). The validity of the interfaces has been successfully tested in the Aspen Plus simulator under the EO mode.

2. Rigorous Model Validation

The CAPE-OPEN unit is embedded into the PX oxidation section of the PTA manufacturing process to validate the model on a statistical level, and the online operational data are used to determine the accuracy and stability of the model.

The input stream data of the CAPE-OPEN simulation are obtained and processed based on the historical datasets from April to October, 2009 at the PTA manufacturing plant of Sinopec. Five index variables are selected as the key indicators of the production quality (Table 1).

Table 1. Relative errors between real-time process data & CAPE-OPEN simulation

Monthly relative error (%) / Components	Apr.	May	Jun.	Jul.	Aug	Sep.	Oct.
4-CBA	4.66	4.63	5.37	3.47	4.21	4.88	3.76
O_2	1.27	0.91	0.98	1.03	1.17	0.99	0.80
CO	1.73	1.50	1.35	1.81	1.57	1.49	1.19
CO_2	1.44	1.00	0.91	1.05	1.09	1.27	0.91
O_2 after crystallization	3.88	3.20	3.15	3.63	3.55	4.16	3.25

In Table 1, 4-CBA is the most important indicator of the quality of production of the entire process; however, 4-CBA concentration cannot be obtained as an online measurement. The offline sampling and analysis require at least four hours. Meanwhile, the tail gas concentrations are used to estimate the real-time material consumption, which cannot be directly measured either. The CAPE-OPEN model, as a soft sensor, can precisely predict the index variables, the maximum relative errors of which can be bounded within 5.4% through seven months period.

Given its wide-range accuracy and robustness, the CAPE-OPEN model is applied into the field for the online sensing, monitoring, and optimization platform.

3. Online Process Monitoring and Modeling Platform Deployment

Based on the developed CAPE-OPEN model, a *de-facto* "Soft-sensing and Optimization System for PX and HAC Consumption in the PTA Process" was implemented and successfully used at the Sinopec Yangzi Petrochemical Company. As illustrated in Figure 3, the simulation platform fetches streams and operational data from the Honeywell PHD historical data server. The simulation results are sent to the monitoring software for visualization and optimization. Operational instructions are then sent back

to the operators, and all production conditions are visualized by ProcessX, a software package developed by Zhejiang University and Viacontrol Inc. The proposed system provides real-time consumption calculation, product quality prediction, and operation guidance for the operators.

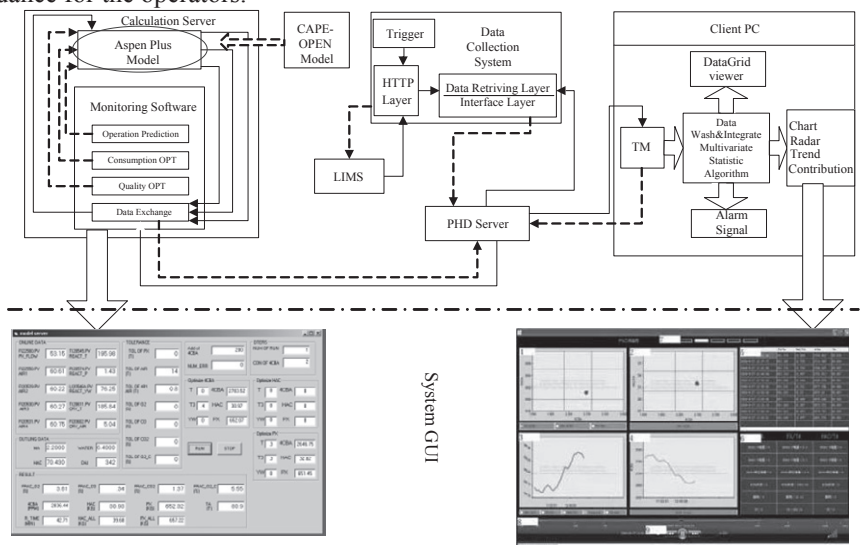

Figure 3. Soft-sensing and optimization system for PX and HAC consumption in the PTA process

4. Conclusion

This paper reports on a CAPE-OPEN solution to process simulation and optimization. Based on an open-architecture prototype, the process simulation has been divided into independent components, of which the PX oxidation reactor core unit of the PTA manufacturing process is developed and applied. The openness and transplant ability of the model are hence demonstrated. The CAPE-OPEN model encapsulates the important kinetic factors to guarantee confidentiality. The online soft-sensing and production quality prediction capability of the CAPE-OPEN conceptual design prove that it can be applied in industrial settings for real-time applications.

References

P. S. Banks, K. A. Irons, M .R. Woodman, 2005, Interoperability of Process Simulation software, Oil and Gas Science and Technology, 60, 4, 607–616

W. Chen, Z. Shao, K. Wang, X. Chen, L. T. Biegler, 2010, Convergence Depth Control for Interior Point Methods, AIChE Journal, 56, 12, 3146–3161

Y. Lang, L. T. Biegler, 2005, Large-scale Nonlinear Programming with a CAPE-OPEN Compliant Interface, Chemical Engineering Research and Design, 83, 718–223

W. Marquardt, 1996, Trends in Computer-Aided Process Modeling, Computers Chemical Engineering, 20(6/7), 591–609

V. L. Pérez, A. O. Domancich, G. E. Vazquez, N. B. Brignole, 2005, A CAPE-OPEN Compliant Simulation Module for an Ammonia Reactor Unit, 2nd Mercosur Congress on Chemical Engineering

L. Wang, 2005, Modeling, Control and Optimization Research on PX Oxidation Process, Doctorate Thesis, Zhejiang University, Hangzhou, China

Z. Zhang, Z. Shao, P. Jiang, X. Chen, Y. Zhao, J. Qian, 2010, Sequential Sub-problem Programming Strategies for Data Reconciliation and Parameter Estimation with Multiple Data Sets, Proceedings of the 49th IEEE Conference on Decision and Control, Atlanta

I.A. Karimi and Rajagopalan Srinivasan (Editors), Proceedings of the 11th International Symposium on Process Systems Engineering, 15-19 July 2012, Singapore.

Towards Holistic Decision Support Systems: Including Human and Organizational Performances in the Loop

Simone Colombo, Salman Nazir, Davide Manca

Politecnico di Milano, Piazza Leonardo da Vinci 32, 20133 Milan, Italy

Abstract

A fundamental challenge and opportunity for risk and operational managers to improve significantly their activity is to adopt a holistic approach to decision-making by grounding their decisions on the effective knowledge, experience and capabilities of operators and their organization. The paper explains why accounting for human and organizational factors is fundamental to strengthen decisions and why doing it in an experimental fashion is the way forward. Further, it is explained that leveraging on human and organizational factors, instead of appealing mainly to the technological ones, opens opportunities to improving decisions and save resources. The manuscript presents an example stemming from a use case developed with one major company of the Oil & Gas sector.

Keywords: Holistic decision-making; Human & organizational factors; Human performance; Process automation; Safety engineering

1. Introduction

Making decisions in complex, safety-critical systems is all but an easy task to accomplish, especially when the decisions relate to Health, Safety and Environmental (HSE) issues. Key Performance Indicators (KPI) used at corporate level, (*e.g.*, *CCPS Guide, 2007*), to depict what the corporate safety level is, to identify what the criticalities are, and, above all, to decide what to improve, *i.e.* where to focus resources, very seldom, for not saying ever, are grounded and traced back to human- and organizational-related parameters reflecting the actual capabilities of the system to respond to critical situations. The reason is threefold: (i) the inherent difficulty to envisaging all the possible alternatives including systematically Human and Organizational Factors (HOF) (*Colombo et al., 2008*), *i.e.* identifying scenarios that might unfold, and enabling even to highlight HOF weaknesses, (ii) the difficulty to estimate the consequences each alternative might bring about (*Manca and Brambilla, 2010*), and (iii) the complexity to verify the consistency between the envisaged scenarios and both (a) the effective resilience of the organizational set-up in place at plant level (*Hollnagel et al., 2006; Costella et al., 2009*), and (b) the effective capabilities of the workforce that has to cope with the unexpected event.

2. Holistic vs. reductionist approach – including systematically HOF

A decision-making process, to be effective, and possibly even efficient, has to be grounded on "pictures" that reflect the entire spectrum of possible alternatives, *i.e.* possible scenarios/stories that might occur, achieved by considering the productive system in a holistic way, *i.e.* as composed by Human, Technological (both hardware and software), and Organizational (HTO) elements tightly interweaved to make the whole.

Typically, for reasons we are going to investigate here to avoid bringing us too far apart from our track, safety analyses are externalized to consultancy companies. New standards, even for safety-related equipment, *e.g.*, *IEC 61508*, do not explicitly prescribe how to calculate the achieved safety but provide just guidelines on "how to", the consequences being that a multitude of safety analyses techniques are used by practitioners, and even approached differently by different industries (*Garrick, 1988*), thus making a (cross-) comparison and the use of their outcomes difficult and demanding (*Rouvroye and van den Bliek, 2002*). This is a further struggle on top of an already delicate, sometime controversial and certainly intensive task that has potentially huge social implications, *i.e.* might bring to major accidents. But this is not all as when it comes to HOF the situation is even worse as many, not all commonly known, accepted and widely used, techniques are applied by practitioners to incorporate HOF in Quantitative Risk Assessment (QRA) (*Skogdalen and Vinnem, 2011a*), whose outcomes are typically the basis for risk managers to make their decisions. And this in the best cases, *i.e.* when HOF techniques are used, because on average it is not so (*Skogdalen and Vinnem, 2011b*), particularly when not explicitly enforced by law.

3. The importance to move to an experimental approach

From the aforementioned context, it should be clear how much important is to verify the realism and completeness of the envisaged scenarios whether they are to be used as a basis for decision-making by risk managers and, more broadly, by operational managers. Further, given the increasing complexity of HTO systems due to the intensification, optimization, and automation processes that are swiftly transforming the (process) industry, relying on an "at-the-desk" verification of the identified scenarios made by expert(s), is not anymore sufficient and an experimental approach becomes necessary. Why? The reason is straightforward: envisaging scenarios in complex industrial settings where HTO factors are tightly interweaved it is a task too complex to be left just to the imagination of analysts; especially when it comes to the identification of HOF-related potential shortcomings. From the research performed in the Virthualis project we came to the conclusion that the verification session requires the support of visually immersive, real-time simulation tools that allow immerging people in Virtual Environments (VE) and experience critical, abnormal working conditions, as they would be in reality. In short, it requires the use of a Plant Simulator (PS). This way it is possible to leveraging not just on people's imagination but also on people's emotions and see how the HTO system behaves lively and effectively while facing the evolution of complex, risky situations. Consequently, the experience of people and the resilience of the organization are built-in the envisaged scenarios that become safer and more effective to use for decision-making purposes.

4. Performance assessment

4.1. Decision-making in process plants

Since the late 80's of last century it was understood that "even in the case of continuous processes monitored from a control room, the operator activity cannot be isolated from the one of the team surrounding him: roundsmen, supervisors, etc." (*De Keyser, 1986*), thus starting to introduce the idea of collective control (*Vidal et al., 2009*). This tells us one simple thing: whatever might be the automation level, *i.e.* the unmanning level, the communication and coordination between the Control Room Operator (CROP) and the Field Operator(s) (FOP), is fundamental to manage the process.

On the aforementioned ground, the Virthualis project was created and brought to the creation of what lately we baptized as PS. And it was following a strand the Virthualis experience has triggered that a piece of software capable to track human beings during operation in VE, with the ultimate goal of supporting decision-making, was created (*Colombo et al., 2011*). This tool, called Performex®, has been conceived and created even capitalizing the experience accumulated in the Virthualis project while performing experiments with field operators of two major companies in the Oil & Gas sector. Performex® is currently fully embedded in a PS used for conducting live experiments.

4.2. Performex® as a decision-making support tool

Performex® enables tracking automatically a set of defined performance indicators according to the four categories of the taxonomy adopted in the Virthualis project, namely (1) Situation Awareness (SA), (2) Decision-Making (DM), (3) Task Management (TM), and (4) Team Communication (TC). Each category has its own elements. SA elements are: (1) Recognition (data Collection), (2) Understanding, and (3) Anticipation. DM elements are: (1) Options Selection, (2) Communication of Options & Intentions, and (3) Options re-evaluation. TM elements are: (1) Planning and Preparation, (2) Tasks Prioritization, (3) Resources Usage. TC elements are: (1) Coping Interruptions, (2) Making Enquiries (info pull), (3) Sending Information (info push).

The number of identified Human Performance Indicators (HPI) is then twelve (12) and each of them has specific behavioral markers measured. As an example, the SA1, which represents the ability of "Recognition" in the SA phase, is measured in terms of different variables, such as (a) time used to reach the state (normally measured as the time elapsed between the system readiness for the operator to perform a specific action and the actual time when the action is performed – if it is performed, else it is "∞"); (b) Number of cues required/checked before reaching the state of recognition; (c) Coherency check.

Each specific HPI is context dependent. This is why the value of the SA1 might vary, even significantly, from one context to another, exactly as it happens when recording the intermediate racing time during a car or ski racing (which clearly depends on the specific raceway). Similarly, even the specific HPI measured depends on the specific task performed in the specific context. However, within the same context, it has to be clearly the same, *i.e.* the benchmark for both teams and individuals.

5. An industrial use case

This section briefly presents the use case developed in cooperation with a major company operating in the Oil & Gas market.

5.1. The decision-making problem

Gas-processing plants daily face the "unavoidable" issue of gas leaks. Gas leaks in the plant might be coarsely separated into small (0.5 kg/s), medium (5 kg/s) and large leakages (50 kg/s). Contrary to intuition, small leakages are the most concerning ones as when a large leak takes place, the decision is straightforward, *i.e.* shutdown the plant, while when a small leak occurs it might turn out to be a big trouble as it is hard to detect (especially in harsh weather conditions) and might create gas clouds that might explode, thus damaging the plant and the surroundings (major accident). Further, the task, in the mind of operators, is strongly traded-off by two contrasting factors: their personal safety and that of colleagues, and the cost of a shutdown (in the order of millions €/day).

Then the decision-making problem for managers is whether installing an automatism to activate the Emergency Shutdown (ESD) system or keeping the ESD system manually

activated by human beings. Fortunately, the management experience on automation systems was extremely high, probably one of the highest one may find, as the plant, where the experiments were made, is highly automated and highly unmanned and the management already knew the limitations and risks the automation might bring about.

5.2. The risk analysis

A preliminary risk analysis was conducted to (a) figure out the spectrum of possible alternatives, *i.e.* stories and type of human failures, (b) identify the conditions to better design the experiments, and (c) to verify the outcomes of the risk analysis already in the hands of the company (and not surprisingly outsourced to an external consultant).

According to the company procedure, the activities of the operators to manage the leak were divided in three phases, namely (1) control room activities with potential involvement of field operator(s) (not involved in case of large leaks), (2) identification and reach of the leak area, (3) shutdown or recovery actions.

Phase 1 produced 3,446 different possible scenarios, *i.e.* different stories for the control room (including the management of spurious signals). Phase 2 produced 56,814 different scenarios (from calling the FOP to asking him/her to identify the leak position). Phase 3 produced 180,951 different scenarios. All these scenarios were then split according to the leak size, *i.e.* small-, medium- and large-related.

Phase 1 comprises (a) 1,416 scenarios for large leaks with 97% probability of shutdown by the CROP, (b) 1,078 scenarios for medium leaks with 40% probability of shutdown by CROP, (c) 952 scenarios for small leaks with 1.4% probability of shutdown by CROP. Phase 2 scenarios are 18,938 evenly shared amongst the three types of leaks. Phase 3 scenarios are (a) 287 scenarios for large leaks with 100% probability to end up with a shutdown, (b) 736 scenarios for medium leaks with 52% probability to conclude with a shutdown, (c) 179,928 scenarios for small leaks with negligible probability to end up with a shutdown.

For each scenario, it was calculated a probability of occurrence and the time required to develop it. This work allowed creating a correlation between the shutdown times and their probability of occurrence. The identified shutdown times span from a fist of seconds for large leaks, independently on whether the shutdown is performed by the CROP or by the FOP, to 22 minutes for small leaks.

5.3. The experiments

Experiments were performed in a PS of the specific plant section with real operators.

From the safety analysis (the one in the hands of the company) the intervention time, *i.e.* the time elapsed from the alarm to the resolution by operators (either shutdown or remedy), was a sharp value estimated in 7 minutes (not clear how). The company thought the decision-making parameter for installing the automatism for the ESD system was the verification of the intervention time. This is why the experiments performed were initially conducted having in mind the verification of the intervention time. Nevertheless, on the way, they allowed to go well beyond and highlight, *i.e.* measuring, strong weaknesses in the organizational elements and, specifically, in the DM capabilities of teams. The decision-making then shifted the attention from the verification of the intervention time highlighted in the safety analyses (by external consultants), to the verification of the realisms and completeness of the scenarios identified. During the verification, the attention focused on the identification of the opportunities to improve the HOF elements of the system, instead of being focused on the Technological ones, thus allowing moving forward and improving the gas leak management activity at the only cost of the simulator and time used to test the scenarios.

6. Conclusions

Adopting both a holistic and experimental approach to decision-making enables plant and corporate managers to make safer and more robust decisions. Specifically, using an experimental approach to grounding decisions on both the effective capabilities of operators and the resilience of the organization, allows to better shape competences on real operational needs and, more broadly, unveiling the huge opportunities given by the improvements in HOF. Opportunities that might allow to save an enormous amount of time and resources, while being safer, by avoiding to unbalancing the decisions towards the adoption of unnecessary, very expensive and potentially risky automation solutions.

References

CCPS Guide, 2007, "Process Safety Leading and Lagging Metrics", Centre for Chemical Process Safety, www.aiche.org/ccps

Colombo S., M. Demichela, 2008, "The systematic integration of human factors into safety analyses: An integrated engineering approach", Reliability Engineering & System Safety, Volume 93, Issue 12, Pages 1911-1921, doi:10.1016/j.ress.2008.03.029

Colombo S., D. Manca, S. Brambilla, R. Totaro and R. Galvagni, 2011, "Towards the Automatic Measurement of Human Performance in Virtual Environement for Industrial Safety", "Proceedings of the ASME 2011 World Conference on Innovative Virtual Reality WINVR 2011, June 27-29, Milano, Italy.

Costella M. F., T. A. Saurin, L. B. de Macedo Guimarães, 2009, "A method for assessing health and safety management systems from the resilience engineering perspective", Safety Science, Volume 47, Issue 8, Pages 1056-1067, doi:10.1016/j.ssci.2008.11.006

De Keyser V., 1986, "Technical Assistance to the Operator in Case of Incident: Some Lines of Thought", Intelligenti Decision Support in Process Environments, NATO ASI Series, Volume 21, Pages 229-253, Springer Verlag, ISBN 3-540-13922-2 / 0-387-13922-2

Garrick B. J., 1988, "The approach to risk analysis in three industries: nuclear power, space systems, and chemical process", Reliability Engineering and System Safety, Volume 23, Issue 3, Pages 195-205, doi:10.1016/0951-8320(88)90109-3

Hollnagel E., D. Woods, N. Leveson, Editors , 2006, "Resilience Engineering: Concepts and Precepts", Ashgate, London, ISBN: 978-0-7546-4641-9

IEC 61508, 2000, "Funcitonal safety of electrical/electronic/programmable electronic safety-related systems", Bureau Centrral de la Commission Electronique International, Genève

Manca D., S. Brambilla, 2010, "Complexity and uncertainty in the assessment of the Viareggio LPG railway accident", Journal of Loss Prevention in the Process Industries, Volume 23, Issue 5, Pages 668-679, doi:10.1016/j.jlp.2010.07.007

Rouvroye J. L., E. G. van den Bliek, 2002, "Comparing Safety Analyses Techniques", Reliability Engineernig and System Safety, Volume 75, Issue 3, Pages 289-294, doi:10.1016/S0951-8320(01)00116-8

Skogdalen J. E., J. E. Vinnem, 2011a, "Quantitative Risk Analysis of Oil and Gas Drilling, Using Deepwater Horizon as Case Study ", Reliability Engineering and System Safety, In Press, doi:10.1016/j.ress.2011.12.002

Skogdalen J. E., J. E. Vinnem, 2011b, "Quantitative risk analysis offshore—Human and organizational factors", Reliability Engineering and System Safety, Volume 96, Issue 4, Pages 468-479, doi:10.1016/j.ress.2010.12.013

Vidal M. C. R., P. V. R. Carvalho, M. S. Santos, I. J. L. dos Santos, 2009, "Collective work and resilience of complex systems", Journal of Loss Prevention in the Process Industries, Volume 22, Issue 4, Pages 516-527, doi:10.1016/j.jlp.2009.04.005

I.A. Karimi and Rajagopalan Srinivasan (Editors), Proceedings of the 11th International Symposium on Process Systems Engineering, 15-19 July 2012, Singapore.

Sensor Location for water systems: A Stochastic Design Approach

Mercedes Carnero,[a] José Hernández,[a] Mabel Sánchez[b]

[a]*Facultad de IngenieriaUNRC, Campus Universitario, 5800 Río Cuarto, Argentina*
[b]*Planta Piloto de Ingeniería Química (UNS- CONICET) Camino La Carrindanga Km 7, (8000) Bahía Blanca, Argentina.*

Abstract

The optimal design of sensor networks consists in selecting the type, number and location of sensors that provide the required quantity and quality of process information by optimizing an appropriate objective. The problem is multimodal and involves many binary variables, therefore a huge combinatorial optimization problem results. In this work, the design for water systems is addressed using metaheuristics. A strategy that combines the advantages of Tabu Search and Estimation of Distribution Algorithms is devised, which is able to solve high scale designs since it can be executed in parallel.

Keywords: Sensor Network design, Combinatorial Optimization, Estimation of distribution algorithms.

1. Introduction

A reliable and complete knowledge of the current system state is essential for implementing monitoring, regulatory and supervisory control, real time optimization, planning and scheduling, and fault diagnosis tasks. The quality and availability of variable estimates strongly depend on the sensor network (SN) installed in the system, the data reconciliation packages used to enhance the precision of estimates during its operation, and the SN maintenance tasks.

The problem of selecting a set of variables to be measured, which is optimal with respect to some specified criteria and simultaneously provides the quantity and quality of information required from the system, is called the sensor network design problem (SNDP). In practice it is necessary to satisfy constraints only on a subset of key variable estimates, therefore a general SNDP arises without knowing in advance the cardinality of the optimal sensor set.

In SND the important decision to be made with regard to each variable is whether to measure it or not. In the first case the sensor is selected from a set of available instruments with certain features, i.e. cost, precision, failure rate, etc. To mathematically formulate these decisions, binary variables are employed which indicate the presence or absence of sensors. The problem is usually multimodal and involves many binary variables, therefore a huge combinatorial optimization problem subject to constraints should be solved.

Different deterministic and stochastic strategies have been presented to address the solution of the SNDP. For the sake of brevity, only some metaheuristics are briefly review in this work given that it is devoted to present a contribution on this particular subject. A metaheuristic is an iterative master process that guides and modifies the operations of subordinates heuristics to efficiently produce high quality solutions.

Regarding the design of general SNs, Benqlilou et al. (2004) applied GAs to solve the design and retrofit of reliable SNs using the GA toolbox of MATLAB program.

Gerkens and Heyen (2005) proposed two ways of parallelizing the GA, namely the global parallelization and the distributed GA, and concluded that the second one is more efficient. Carnero et al. (2005) developed a hybrid procedure based on GAs (HGA) to minimize the instrumentation cost subject to precision constraints on key variables. They used a structured population in the form of neighbourhoods and a local optimizer of the best current solutions, which provide a good balance between the algorithm capabilities of exploration and exploitation. Recently, Gerkens and Heyen (2008) proposed a general approach for designing the cheapest SN able to detect and locate a set of specified faults.

In recent years applications of Tabu Search (TS) metaheuristic for the solution of chemical engineering problems have appeared. Within the framework of TS, a Strategic Oscillation Technique around the feasibility boundary (SO-TS) was reported for solving the SNDP by Carnero et al. (2005). This strategy efficiently searches the solution space, significantly reducing the number of required calls to the evaluation function in comparison with HGA and the Classic TS.

There exist other population-based methodologies that have demonstrated a rewarding performance for solving vehicle routing, knapsack and scheduling problems, and constitute attractive alternatives to GAs. In this regard, Estimation of Distribution Algorithms (EDAs) (Emmendorfer and Pozo, 2009) offers a novel evolutionary paradigm. Within the framework of EDAs approach, Population Based Incremental Learning Algorithms (PBIL) are devised (Baluja, 1994), which introduce the concepts of competitive learning to direct the search. Carnero et al. (2009) presented an efficient strategy for the design of SNs based on PBIL, and implemented a parallel procedure. The comparison between SO-TS and PBIL strategies for solving SNDPs indicates that the first one strongly depends on the structure of the initial solution. If a good starting point is provided it produces a high quality solution with a low computational effort. In contrast, PBIL is more robust. It is capable of making replicas of the best solutions starting from lower quality initial points at the expense of an increment of the computational time. As PBIL can be naturally run in parallel, the total elapsed time can be reduced for a given number of calls. Taking into account this analysis, a new procedure is proposed that combines the advantages of both approaches.

The rest of the paper is structured as follows. In Section 2 a particular design problem, that is, the minimum cost SNDP subject to precision and estimability constraints, is briefly introduced. The new strategy is described in Section 3. Its rewarding performance for the location of sensors in water systems is shown in Section 4 by different case studies of incremental size. A Conclusion section ends this work.

2. Sensor Network Design Problem

The minimum cost SNDP that satisfies precision and estimability constraints for a set of key variable estimates is formulated in Eq. (1), where $\mathbf{q}$ is an n dimensional vector of binary variables such that: $q_i = 1$, if variable i is measured and $q_i = 0$ otherwise; $\mathbf{c}^{\mathbf{T}}$ is the cost vector; is the standard deviation of the j-th variable estimate after a data reconciliation procedure is applied and E_k stands for the degree of estimability of variable k (Bagajewicz and Sánchez,1999). For this formulation E_k is set equal to one, consequently only a variable classification procedure run is needed to check its feasibility. Furthermore S_J and S_K are the set of key process variables with requirements in precision and estimability respectively, and n is the total number of measurable variables. It is assumed that a linear algebraic model represents process operation and measurements are subject to non-correlated normally-distributed random errors. For the

sake of simplicity no instruments' localization restrictions are imposed and it is assumed that there is only one potential measuring device for each measurable variable.

$$
\begin{aligned}
&\textit{Min} && \mathbf{c}^{\mathrm{T}}\mathbf{q} \\
&\textit{s.t.} && \\
& && \hat{\sigma}_j(\mathbf{q}) \le \sigma_j^*(\mathbf{q}) && \forall\ j \in S_J \\
& && E_k(\mathbf{q}) \ge 1 && \forall\ k \in S_K \\
& && \mathbf{q} \in \{0,1\}^n
\end{aligned}
\tag{1}
$$

3. Stochastic Approach

Estimation of Distribution Algorithms are Evolutionary Algorithms that work with a population (P) of candidate solutions. At first an initial P is generated and their members are evaluated using the objective function. Those with better function values are selected to build a probabilistic model of P, and a new set of points is sampled from the model. The process is iterated until a termination criterion is fulfilled.

Therefore EDAs' approach is based on the evolution of a probabilistic model of the solution space. The potential solutions included in P are assumed as realizations of multivariate random variables, whose joint probability distribution can be estimated and updated. If independent variables are considered, the product of their marginal distributions constitutes the joint distribution of all variables, which is the simplest estimation model. This assumption may originate convergence problems for complex systems. To overcome this limitation of simplest EDAs, like PBIL, the use of more complex factorization models, i.e. Bayesian Network learning, the incorporation of niching techniques, and the hybridization with local search mechanisms are reported.

In this work the core of the solution strategy is constituted by the PBIL. The technique explicitly maintains statistics about the search space and uses them to direct its exploration. A real valued probability vector **p** is created, which reveals high quality solution vectors with high probability when sampled. A parallel implementation of PBIL that allows *NPBIL* instances being executed independently is applied. After the *NPBIL* Ps evolve one iteration, their **p** vectors are related by different mechanisms before sampling, in such a way the relevant information from each sub-P is exchanged with the others.

The previous solution scheme performs well for medium scale problems, but exhibits limitations for large ones. In these cases the identification of constructive blocks of high quality solutions and their maintenance during the evolution turn out more relevant. In this work high dimensional problems are addressed by incorporating to the EDAs a local search algorithm, such as SO-TS, that allows taking into account specific process knowledge during the search. This procedure works in a controlled way in certain regions of the search space, which are selected using a metric that groups solutions of structural similarity using a clustering technique. The local search should be performed in a controlled fashion because the number of its calls to the evaluation function has a linear dependence with the problem size. The pseudocode of the proposed algorithm is presented below**.** Each sub-P is characterized by the following variables: PBIL.**p** is the probability vector, PBIL.**V** is its matrix of solutions, PBIL.$\mathbf{V_b}$ contains the best solution in PBIL.**V**.

Initiate PBILs
for *i*=1 to *MaxGenerations*
  for *k*=1 to *NPBIL*
    $PBIL_k$.**V**=*sample*($PBIL_k$.**p**)
    $PBIL_k$.*fit*=*fitness*($PBIL_k$.**V**)
    $PBIL_k$.$\mathbf{V_b}$=best individual in $PBIL_k$.**V**
    if $PBIL_k$ is not tabu and *randnumber*< *pso*
      Divide $PBIL_k$.**V** in *t* clusters
      Apply SO to one indivual/cluster
      Set $PBIL_k$ tabu for *ptabu* iterations
    endif
    Update probability vector $PBIL_k$.**p** with learning rate *LR*
    Update tabu list
  endfor
  if *randnumber*<*Pinteracion*
    Modify **p** vectors by crossover operator
  endif
endfor
Get **SolOut** by applying SO to best individual along all PBILs
Return(**SolOut**)

4. Application Examples

In this section, application results of the proposed methodology to water systems of incremental size are reported. The analysis of results is based on the solution quality and variability, the procedure robustness and its scalability behavior to tackle the SNDP for large scale plants.

Three process flowsheets (Cases 1 - 3) of dimension: 11 units - 28 streams, 19 units - 52 streams, and 47 units – 82 streams, respectively, are considered. The standard deviation of flowmeters is assumed as 2.5%, 2% and 2% of the corresponding true flowrates for Cases 1 – 3, respectively. For the sake of brevity, instrumentation costs, which are different for each case of study, are not provided. Table 1 shows the complexity of the set of constraints imposed on each Case, and Table 2 reports the parameter settings. The next table presents the best solutions of Cases 1-3 for 40 runs of the algorithm. The same values are obtained for all the runs. The average times of each run are 1, 5.8 and 9 minutes for Cases 1 – 3 when the procedure is executed in a PENTIUM (R) 2.4 GHz, 1GB RAM using MatLab Release 14.

Table 1. Set of constraints for Cases 1-3

Case	Constraints
1	$E \geq 1$ for streams 3 8 9 17 20 21 24 25 $\sigma_3^* = 2.23$ $\sigma_8^* = 3.28$ $\sigma_{21}^* = 1.74$ $\sigma_{24}^* = 0.93$
2	$E \geq 1$ for streams 2 5 15 29 31 32 38 39 40 44-52 $\sigma_{15}^* = 12410$ $\sigma_{31}^* = 13750$ $\sigma_{32}^* = 126$ $\sigma_{40}^* = 1378$ $\sigma_{44}^* = 568$ $\sigma_{45}^* = 595$ $\sigma_{46}^* = 716$ $\sigma_{47}^* = 546$ $\sigma_{49}^* = 1442$
3	$E \geq 1$ for streams 4 11 21 24 30 32 35 39 43 44 52 58 60 68 75 80 81 σ_{11}^*=1423, σ_{35}^*=172, σ_{39}^*=1422, σ_{58}^*=27, σ_{60}^*=579, σ_{81}^*=425

Table 2. Parameter Setting

Parameter	Value	Parameter	Value
# PBIL	4	*Ptabu*	25
PBIL_Size	12	*t*	3
LR	0.1	*Pso*	0.05
Pinteraction	0.7	*# Maxiter*	120
# MaxGeneration	200		

Table 3. Results

Case	Optimal Solution	Estimated deviation	cost
1	1,2,4,7,9-11,13-24	$\hat{\sigma}_3$ =2.16 , $\hat{\sigma}_8$ =2.54, $\hat{\sigma}_{21}$ =1.5, $\hat{\sigma}_{24}$ =0.92	1297.39
2	10,16,31-33,35,37,39- 41, 43-48,50- 52	$\hat{\sigma}_{15}$ =2510, $\hat{\sigma}_{31}$ =916, $\hat{\sigma}_{32}$ =84, $\hat{\sigma}_{40}$ =919, $\hat{\sigma}_{44}$ =379, $\hat{\sigma}_{45}$ =397, $\hat{\sigma}_{46}$ =478, $\hat{\sigma}_{47}$ =364, $\hat{\sigma}_{49}$ =566	1154.34
3	1,2,5,15,21,22,25,28,31,33-35,37,44-46,49-51,53-55,60-63,67,68,72-77,79,80-82	$\hat{\sigma}_{11}$ =698, $\hat{\sigma}_{35}$ =172, $\hat{\sigma}_{39}$ =978, $\hat{\sigma}_{58}$ =22, $\hat{\sigma}_{60}$ =443, $\hat{\sigma}_{81}$ =419	107377.00

5. Conclusions

In this work a new methodology, which combines the advantages of SO-TS and EDAs for solving the SNDP is presented. The strategy is robust, produces high quality solutions, and is able to solve high dimensional problems since it can be executed in parallel. The scalability analysis indicates the SO-TS should work in a controlled fashion to avoid an increase of the computational time. The methodology has been successfully applied to the design of SNs of distribution water systems.

References

M. Bagajewicz, M. Sánchez, 1999, Cost Optimal Design and Upgrade of Non-Redundant and Redundant Linear Sensor Networks, AIChE J., 45, 9, 1927-1938.

S. Baluja, 1994, Population-based incremental learning: A method for integrating genetic search based function optimization and competitive learning, Technical Report, CMU, Pittsburgh, USA.

C. Benqlilou, M. Graells, E. Musulin, L. Puigjaner, 2004, Design and Retrofit of Reliable Sensor Networks, Ind. Eng. Chem. Res., 43, 25, 8026-8036.

M. Carnero, J. Hernández, M. Sánchez, J. Bandoni, 2005, On the Solution of the Instrumentation Selection Problem, Ind. Eng. Chem. Res., 44, 2, 358-367.

M. Carnero, J. Hernández, M. Sánchez, 2005, Optimal Sensor Network Design and Upgrade using Tabu Search, Comp. Aided Chem. Eng., 20, 1447-1452.

M. Carnero, J. Hernandez, M. Sanchez, 2009, Design of Sensor Networks for Chemical Plants based on Metaheuristics ALGORITHMS , 2, 1, 259-281.

L. Emmendorfer, A. Ramirez Pozo, 2009, Effective Linkage Learning Using Low – Order Statistics and Clustering. IEEE Transactions on evolutionary Computation, 13, 6, 1233-1246.

C. Gerkens, G. Heyen, 2005, Use of Parallel Computers in Rational Design of Redundant Sensor Networks, Comput. Chem. Eng., 29, 6, 1379-1387.

C. Gerkens, G. Heyen, 2008, Sensor placement for fault detection and localization. Computer Aided Chemical Engineering, 25, 355-360.

I.A. Karimi and Rajagopalan Srinivasan (Editors), Proceedings of the 11th International Symposium on Process Systems Engineering, 15-19 July 2012, Singapore.

Quantitative Risk Analysis of New Energy Stations by CFD-Based Explosion Simulation

Seungkyu Dan[a], Hyunmin Kim[a], Dongil Shin[b], En Sup Yoon[a]

[a]*Seoul National University, 1 Gwanak-ro, Gwanak-gu, Seoul 151-742, Korea*
[b]*Myongji University, Nam-dong, Cheoin-gu, Gyeonggi-do, 449-728, Korea*

Abstract

In this research, we compared the safety of mixture fuel which is composed of 20% new energy and 80% existing gas against existing fuel in the perspective of explosion risk that would be the biggest concern in the operation of new-energy stations. The new mixture will be used in the existing station in Korea without any changing the structure. The explosion risk was analyzed and compared by three representative models: empirical model, phenomenological model, and a CFD-based model, in increased model complexity and computational efforts. Overpressures of explosion of mixture and existing fuel, respectively, showed similar results, in all three models. Thus, it seems like there is no additional risk in using mixture at the existing refueling facilities. CFD-based explosion simulation was useful in finding out the exact overpressure distribution and installation of prevention equipment if necessary. The final results are being adopted as part of new safety regulations for the new and existing mixture stations to be operated in Korea.

Keywords: Explosion Simulation; Quantitative Risk Analysis; Gas Explosion Modeling; HCNG Mixture Fuel; DME-LPG Mixture Fuel

1. Introduction

Since the environmental pollution problems and climate issues related to ever-increasing energy use have been emerging all over the world, developing efficient renewable and/or alternative energy sources are considered as top-priority research agenda [BP, 2009]. Among them, DME (dimethyl ether) has emerged as an attractive, promising, alternative clean fuel for transportation, power generation and household. Korean Government, with the leading role of KOGAS, is promoting commercial introduction of this new clean energy, DME. This research has been conducted as part of the KOGAS's core technology development activities covering from DME synthesis from feedstock, such as natural gas, through utilization of DME as fuel by end users.
Also CNG, one of alternative energy, is used by fuel of bus in Korea. And it is going to be used with hydrogen to prevent the exhaustion of natural gas and air pollution after combustion.
Using the new mixtures still deal with inflammable gas. Therefore, when dealing with new mixtures at the conventional filling stations, safety managements do not become an automatically solved issue. Since the severe accident at Bucheon LPG filling station [Park et al., 2006], operation, expansion and construction of LPG stations are heavily regulated and controlled in Korea. Thus, converting and operating conventional filling stations into new energy stations must be thoroughly analyzed and studied to get the acceptance and approval by local communities and government authorities. The development of a strategy for improving gas explosion models is also highly desirable

[Jiang et al., 2001] as the use of gas as energy sources is expected to grow in near future.

2. Comparison of explosion simulation models

We need an accurate assessment about possible accidents to reduce the loss caused by overpressure shaped by gas explosion. There are many models ranging from calculations using a simple expression to complex numerical formulas using CFD. The more accurate the simulation results, the better confidence we may have in expecting the real situations and the real risk and enforcing the results out of the analysis. However, selecting and using appropriate models for the problem is important as the information requirements and efforts to run the models increase with its model accuracy. The estimation of the explosion risk have been conducted by following three approaches: Empirical models are based on correlations obtained from analysis of experimental data; and phenomenological models are simplified physical models, which is using simple computer software based on emprical correlations, which seek to represent only the essential physics of explosions; and using computer simulation program based on Computational Fluid Dynamics (CFD) models find numerical solutions to the partial differential equations governing the explosion process [Lea, 2002].

2.1. Empirical Model

Empirical models are based on correlations obtained from analysis of experimental data. Among these models, the TNT equivalency model is a representative empirical model and it is very simple and easy to use. TNT equivalency model is based on the assumption that gas explosion is similarly to an explosive of high efficiency. There are many differences between gas explosion and solid explosion, but using the utility factor helps correcting the gap. Eqs. 1 and 2 below calculate overpressure from the explosion effect of TNT. The calculation of scaled distance is necessary to obtain the overpressure out of the calculation from Eq. 1.

$$W = \frac{\eta M E_c}{E_{TNT}} \tag{1}$$

$$Z_G = \frac{R_G}{W^{1/3}} \tag{2}$$

where W is the equivalent mass of TNT (kg or lb), η is an empirical explosion efficiency (unitless), M is the mass of hydrocarbon (kg or lb), E_c is the heat of combustion of flammable gas (kJ/kg or Btu/lb), and E_{TNT} is the heat of combusition of TNT (4437-4765 kJ/kg or 1943-2049 Btu/lb) [CCPS, 1999].

2.2. Phenomenological Model

Phenomenological models are simplified physical models, which seek to represent only the essential physics of explosions. It is made by simplication of the geometry, and it considers a simplified condition for the simulation: wind, temperature, atmospheric pressure, etc. PHAST, which has been selected as the phenomenological model for our research, is a general tool for consequency analysis examining the progress of a chemical process incident from initial release through formation of a cloud or pool to final dispersion; calculating concentration, fire radiation, toxicity and explosion overpressure. PHAST is a comprehensive hazard analysis package, applicable to all stages of design and operation across a range of process and chemical industry sectors.

The VCE in the PHAST is calculating the overpressure based on TNT Equivalency model and is calculated by below Eqs. 3. [DNV, 2007].

$$\log P_0 = 0.2518 (\log z)^2 - 2.0225 (\log z) + 5.8095 \quad (3)$$

2.3. Simulation Based on the CFD Model

Computer simulation programs based on CFD (Computational Fluid Dynamics) models solve patial differential equations, based on Navier-Stokes equations that govern the fliud flow, to calculate the phenomena controlling the explosion process. CFD simulations can offer insight into the flow behavior in situations where it is impractical or impossible to carry out experiments. Its use is being widely accepted for risk analysis of explosion or dispersion.

The using equations in each model are based on Navier-Stokes equation but there are some different ways for calculating results.

In this research, we utilized FLACS (FLame ACceleration Simulator) made by Gexcon in Norway, which is a tool for dispersion and explosion simulations based on CFD [Gexcon, 2010]. CFD-based complicated models are widely acknowledged for enabling to show the necessary accuracy required for the adoption of simulation results for detailed safety reviews and corresponding upgraded design of refilling stations.

For the comparion of aforementioned three models and the proper risk control, we need to predict and estimate exact damages of existing and new energy refueling facilities' explosion by running the simulation for a 3D structure of the refilling station.

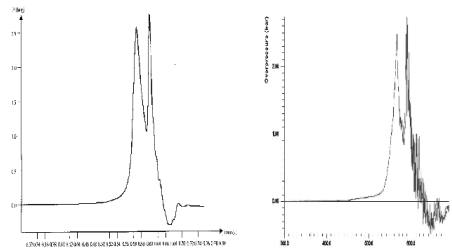

Figure 1: Comparison of Overpressure by Propane Explosion for FLACS and Experiment [Gexcon, 2010]

3. Explosion scenario

DME-LPG refilling stations will begin operating by setting two types of tank. One type of tank is added as new tank which can store 5 ton of DME-LPG mixture gas, and it is located nearby an existing LPG tank. Another way is using an existing tank which can store 40 ton of DME-LPG. Installing tanks is separated by three types: one is pressurized on the ground, another is a refrigeration method on the ground, and the other is pressurized under the ground. Among them, the pressurized tank on the ground was selected as the representative case in this research.

Once a release occurs caused by any accidents, flammable gases are shaped around the refuelling facility. After the release, fire or explosion could happen if an ignition is follwed by that accident, too. Between fire and explosion, we focused on the overpressure hazard out of the explosion.

In the case of CNG or HCNG, because the state of stored fuel is gas, the possible explosion by flammable gas is vapor cloud explosion, and BLEVE is not occurred. Instead of BLEVE, it is possible that the tank is ruptured physically.

4. Results

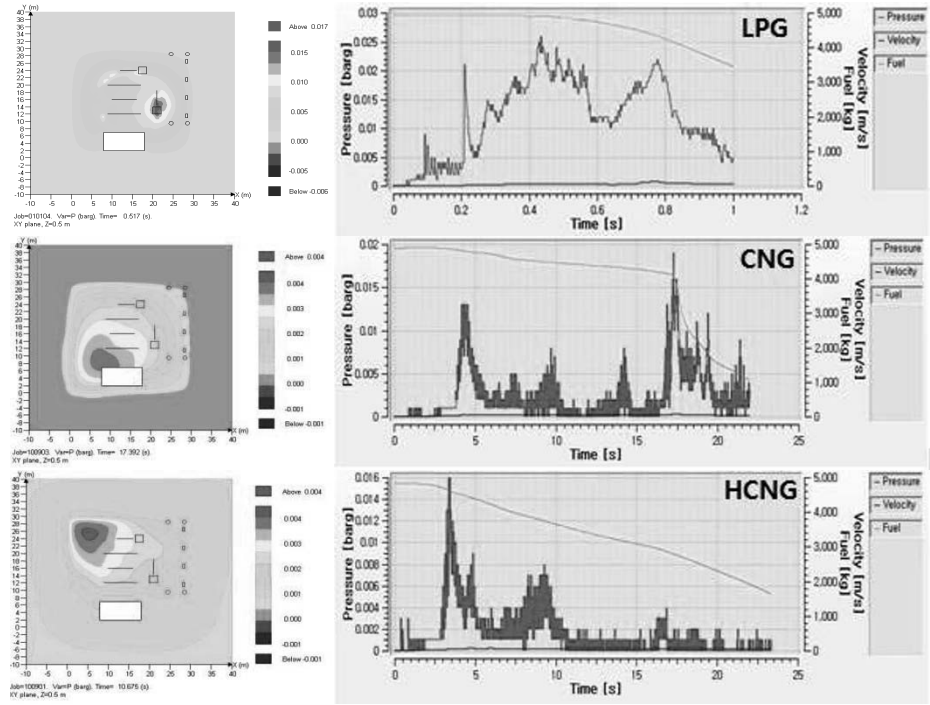

Figure 2: The results of explosion simulation by FLACS

Table 1: Summary of Results (DME-LPG)

Overpressure	**TNT Equivalency Model**	**PHAST**		**FLACS (VCE)**
		VCE	**BLEVE**	
5 ton LPG	5.8 bar at 10 m	1 bar at 10 m	18 bar at 10 m	0.026 bar at 0.43sec after the ignition
	0.13 bar at 50 m	0.4 bar at 50 m	0.1 bar at 50 m	
5 ton DME-LPG	5.3 bar at 10 m	1 bar at 10 m	18 bar at 10 m	
	0.11 bar at 50 m	0.39 bar at 50 m	0.09 bar at 50 m	
40 ton LPG	Over 10 bar at 10 m	1 bar at 10 m	18 bar at 10 m	
	0.76 bar at 50 m	1 bar at 50 m	0.4 bar at 50 m	
40 ton DME-LPG	Over 10 bar at 10 m	1 bar at 10 m	18 bar at 10 m	
	0.70 bar at 50 m	1 bar at 50 m	0.38 bar at 50 m	

Table 2: Summary of Results (HCNG)

Overpressure	**TNT Equivalency Model**	**PHAST** (VCE)	**FLACS (VCE)**
5 ton CNG	Over 10 bar at 10 m	1 bar at 10 m	0.019 at 17sec after the ignition
	0.4 bar at 50 m	0.87 bar at 50 m	
5 ton HCNG	Over 10 bar at 10 m	1 bar at 10 m	0.016 at 0.34sec after the ignition
	0.42 bar at 50 m	0.97 bar at 50 m	
40 ton CNG	Over 10 bar at 10 m	1 bar at 10 m	
	1.79 bar at 50 m	0.87 bar at 100 m	
40 ton HCNG	Over 10 bar at 10 m	1 bar at 10 m	

	1.9 bar at 50 m	0.97 bar at 100 m	

Results of simulations by three models were summarized as Table 1 and Table 2. In the case of LPG and DME-LPG, compared against the TNT equivalency model, PHAST results show a little lower value near to the ignition, but it shows a little bigger value far from the ignition. The FLACS was simulated only for VCE, and comparison of its BLEVE results is still being prepared. In the results of CNG and HCNG, although the results of simulation about hcng mixture is a little higher than the cng, its values are almost same.

5. Conclusions

This study has analyzed and compared the results of explosion risk prediction by three representative models for estimation of explosion consequence, such as the TNT equivalency model, PHAST, and FLACS. First, the three models were used and compared in the explosion risk prediction for the conventional LPG station. When the overpressures of gas explosion for both LPG and DME-LPG mixtures are calculated, there was less difference between the simple TNT equivalency model and PHAST simulation requiring more parameters. Overpressure plots of LPG and DME-LPG mixtures relative to distance were similar to each other. Likewise, in the case of the CNG and HCNG mixtures, the calculated results show almost same overpressure of explosion. So when the HCNG mixtures using in the CNG filling station, it is expected that almost no additional risk.

CFD-based complicated models only showed the necessary accuracy required for the adoption of the simulation results for safety reviews and corresponding upgrade design of refilling stations. Even though some experimental data are available for the explosion characteristics of DME [Mogi and Horiguchi, 2009], we needed to simulate it for the given 3D structure of the recharging station to get the precise view of the explosion consequence. We compared the difference of current LPG station with the one using DME-LPG mixture from the obtained result and investigated how we can reduce the explosion risk effectively, including installation of additional devices for protection. The final results are being adopted as part of new safety regulations for the DME-LPG stations to be operated in Korea.

Also, we are coding a model of explosion by matlab, but it is not perfom properly. So it is required to revise some code to make accurate results of explosion using our model.

References

BP Statistical Review of World Energy 2009, http://www.bp.com/productlanding.do?cate goryId=6929&contentId=7044622

Center for Chemical Process Safety (CCPS), 1999, Guidelines for Chemical Process Quantitative Risk Analysis, 2nd Ed., American Institute of Chemical Engineers.

DNV. Phast User Manual, 2007 (http://www.dnv.com/services/software/products/safeti/ safetihazardanalysis/phast.asp).

Gexcon, 2010, FLACS v9.0 User's Manual (www.gexcon.com).

Lea, C. J. A, 2002, Review of the State-of-the-Art in Gas Explosion Modelling, Health & Safety Laboratory.

Mogi, T. and Horiguchi, S. , 2009, Explosion and detonation characteristics of dimethyl ether, J. Hazardous Materials, 164, 114-119.

Park, K., Mannan, M. S., Jo, Y.-D., Kim, J.-Y., Keren, N. and Wang, Y., 2006, Incident analysis of Bucheon LPG filling station pool fire and BLEVE, J. Hazardous Materials, 137(1), 62-67.

Jiang, J., Liu, Z. G. and Kim, A. K. , 2001, Comparison of blast prediction models for vapor cloud explosion, National Research Council Canada Report, NRCC-44715.

I.A. Karimi and Rajagopalan Srinivasan (Editors), Proceedings of the 11th International Symposium on Process Systems Engineering, 15-19 July 2012, Singapore

Knowledge-based attributes generation for data-driven fault diagnosis in process systems

Yoshiyuki Yamashita *

Department of Chemical Engineering; Tokyo University of Agriculture and Technology; Tokyo 184-8588, Japan

Abstract

Data-driven approaches to fault detection and isolation are widely used for various process systems. The purpose of this paper is to present a new method to improve the performance of fault diagnosis of chemical plant. This method combines simple process knowledge with data-driven diagnosis by introducing new feature variables. Simple method to create new feature variables is proposed. The proposed method was applied to diagnosis of the Tennessee Eastman plant simulation benchmark problem. Fault diagnosis performance on the extended feature sets are compared with the performance on the original dataset. The result shows that addition of new attributes is effective to improve the accuracy of the diagnosis.

Keywords: Fault Detection, Fault Diagnosis, Process Monitoring, Process Knowledge

1. Introduction

Fault diagnosis is of great importance in monitoring of today's industrial chemical plants. Plenty of methods have been reported for fault diagnosis of chemical plants. The methods can be categorized into data-driven, analytical and knowledge-based approaches (Venkatasubramanian et al., 2003a). In industrial plant, data-driven approaches to fault diagnosis are widely used (Venkatasubramanian et al., 2003c). Chemical engineers usually have plenty of knowledge about the target systems. Dimensionless numbers and balance equations are examples of typical tools to extend the description ability of the phenomena. These kind of knowledge must be very useful for fault detection and isolation of process systems, but they have not been used in pure data-driven approaches.

Addition and selection of attribute variables are crucial to obtain good diagnosis result in data-based approaches. It requires engineer's expertise to add and select variables. A systematic methodology to generate new valuable attributes based on the process knowledge is proposed in this paper. Several heuristic rules to add knowledge to the dataset are presented. To examine the appropriateness of this methodology, it was applied to a simulated industrial chemical plant benchmark problem (Downs & Vogel, 1993; Lyman & Georgakis, 1995; Ciang et al., 2001). After generating some new attribute variables, a data-based fault diagnosis method, a decision tree inducer, was applied to the extended dataset. The diagnosis performance on the extended dataset was compared with that on the original dataset. The result shows that addition of new attributes is very effective to improve the accuracy of the diagnosis.

*yama_pse@cc.tuat.ac.jp

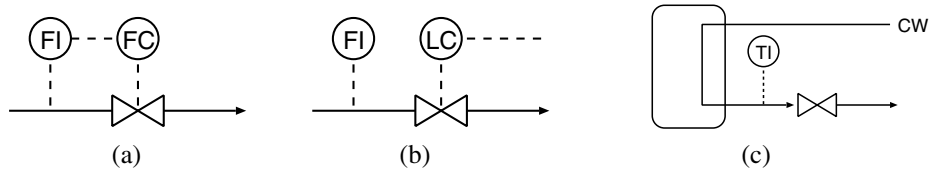

Figure 1. Flowrate and temperature measurement with MV

2. Method

2.1. Addition of Attributes

Chemical Engineer has plenty of knowledge about the target plant. In usual data-based approach for fault diagnosis, these kind of knowledge is not used at all. Model-based approaches for fault diagnosis have been also proposed. But they are not widely used because it usually require time consuming task to develop knowledge model of a plant. In this paper, a simple and easy method to utilize process knowledge for data-based fault diagnosis of a chemical plant is proposed.

The idea of the proposed method is to extend features based on process knowledge. Many kinds of process knowledge can be used for this purpose. Due to the page limit, only two example heuristics to add new features are described here.

1) Flowrate in a Control Loop: Let's think about flowrate measurement through a control valve first. The manipulated variable (MV) of the valve should directly connected to its flowrate for any types of controllers including flow, level and temperature controllers. Therefore, the ratio of flowrate and the MV would provide useful information to diagnose the loop. Typical example configuration of this case are shown in Fig. 1(a) and (b).

2) Temperature in a Control Loop: Temperature measurement of utility flow is considered next. The MV of the valve should closely connected to its outlet temperature. Under the assumption of constant operation, if the utility is a cooling water (CW) as shown in Fig. 1(c), the outlet temperature will decrease as the increase of MV. If the utility is a steam, the outlet temperature will increase as the increase of MV. The ratio of the outlet temperature and the MV would provide useful information to diagnose the line. If the utility flowrate is measured, MV can be replaced by the flowrate.

2.2. Data-based fault diagnosis

After adding extended attributes to the dataset, any usual data-driven fault diagnosis can be applied to the dataset. Various kind of data-driven methods have been proposed for the fault diagnosis of chemical plant (Venkatasubramanian et al., 2003c). Some methods may not suitable for this purpose because they are vulnerable to the increase of the number of attribute variables.

Among various techniques, an well known learning algorithm C4.5 decision-tree inducer is utilized here (Quinlan, 1993). It generates a decision tree from a set of given examples based on the gain ratio of information entropy. In the case study of this paper, Java Implementation of the C4.5 algorithm (known as J48) was applied (Wtten et al., 2011).

Although a problem of fault detection is not treated in this paper, similar idea will also be applied to improve the performance of fault detection on a plant.

Table 1. Selected list of measured, manipulated and extended variables

Variable	Description
XMEAS(1)	A Feed
XMEAS(2)	D Feed
XMEAS(3)	E Feed
XMEAS(4)	Total Feed
XMEAS(10)	Purge Rate
XMEAS(14)	Product Sep Underflow
XMEAS(17)	Stripper Underflow
XMEAS(18)	Stripper Temperature
XMEAS(19)	Stripper Steam Flow
XMEAS(21)	Reactor CW Out Temp
XMEAS(22)	Sep. CW Out Temp
XMV(1)	D Feed Flow
XMV(2)	E Feed Flow
XMV(3)	A Feed Flow
XMV(4)	Total Feed Flow
XMV(5)	Compressor Recycle Valve
XMV(6)	Purge Valve

Variable	Description
XMV(7)	Separator pot liquid flow
XMV(8)	Stripper liquid product flow
XMV(9)	Stripper steam valve
XMV(10)	Reactor CW flow
XMV(11)	Condenser CW flow
XADD(1)	XMEAS(2)/XMV(1)
XADD(2)	XMEAS(3)/XMV(2)
XADD(3)	XMEAS(1)/XMV(3)
XADD(4)	XMEAS(4)/XMV(4)
XADD(5)	XMEAS(10)/XMV(6)
XADD(6)	XMEAS(14)/XMV(7)
XADD(7)	XMEAS(17)/XMV(8)
XADD(8)	XMEAS(19)/XMV(9)
XADD(9)	XMEAS(21)/XMV(10)
XADD(10)	XMEAS(22)/XMV(11)
XADD(11)	XMEAS(18)/XMV(9)
XADD(12)	XMEAS(18)/XMEAS(19)

3. Case Study

3.1. Tennessee Eastman Process

The proposed methodology is tested on the Tennessee Eastman Process (TEP). TEP is a well known benchmark chemical process for fault identification and diagnosis (Downs & Vogel, 1993). Plenty of fault diagnosis methods have been applied to TEP. The process has 41 measured and 12 manipulated variables. Selected list of measured and manipulated variables are shown in Table 1.

The original simulation code is open-loop unstable and should be operated with appropriate control structures. Among various control strategies, decentralized control scheme proposed by Lyman & Georgakis (1995) is used in this study (Lyman & Georgakis, 1995; Ciang et al., 2001).

TEP contains 21 preprogrammed faults as shown in Table 2. For each single fault, training and test datasets are prepared, containing respectively 480 and 800 observations of 3 minutes sampling. Each of the dataset is a matrix consisting of variables XMEAS(1) through XMEAS(41) and XMV(1) through XMV(12).

3.2. Results

At first, 12 new feature variables XADD(1) through XADD(12) are introduced as shown in Table 1 by using heuristics described in the previous section. Here, the last 4 variables are for temperature measurements and the others are for flowrate measurements. These 12 attributes are added to both the training and the test datasets. A decision tree to diagnose all the 21 faults was generated by using the C4.5 algorithm on the extended training dataset. Table 2 summarizes the evaluation result of the trained tree on the test dataset

Table 2. Process faults and diagnosis result

			Diagnosis Accuracy[%]		
Fault	Description	Type	original	extended	Δ
IDV(1)	A/C Feed Ratio, B Comp. Const	Step	98.25	92.88	−5.37
IDV(2)	B Composition, A/C Ratio Const	Step	94.63	93.50	−1.13
IDV(3)	D Feed Temperature	Step	14.63	19.75	5.12
IDV(4)	Reactor CW Inlet Temperature	Step	84.63	82.75	−1.88
IDV(5)	Condenser CW Inlet Temperature	Step	59.75	52.13	−7.62
IDV(6)	A Feed Loss	Step	99.50	99.88	0.38
IDV(7)	C Header Pressure Loss	Step	97.63	100.00	2.37
IDV(8)	A/C Feed Ratio, B Comp. Const	Random	35.00	49.25	**14.25**
IDV(9)	B Composition, A/C Ratio Const	Random	12.25	14.63	2.38
IDV(10)	D Feed Temperature	Random	36.00	39.50	3.50
IDV(11)	Reactor CW Inlet Temperature	Random	66.00	66.50	0.50
IDV(12)	Condenser CW Inlet Temperature	Random	50.88	51.50	0.62
IDV(13)	Reaction Kinetics	Drift	20.00	29.25	**9.25**
IDV(14)	Reactor CW Valve	Sticking	96.00	96.00	0.00
IDV(15)	Condenser CW Valve	Sticking	16.25	13.50	−2.75
IDV(16)	Unknown		33.00	60.25	**27.25**
IDV(17)	Unknown		80.63	84.75	4.12
IDV(18)	Unknown		84.75	82.00	−2.75
IDV(19)	Unknown		59.88	56.75	−3.13
IDV(20)	Unknown		48.38	47.88	−0.5
IDV(21)	Feed Valve was fixed at const	Constant	17.13	24.63	7.50
total			57.39	59.87	2.48

for each fault. In this table, the diagnosis accuracy is defined as the number of correctly identified samples against all the fault samples.

For comparison, evaluation results of a tree trained by the original dataset are also shown in the same table. To clarify the improvement of the extended dataset against the original dataset, the differences of these two diagnosis accuracy are also shown in the last column (Δ). When the value Δ becomes positive, the diagnosis accuracy of the extended dataset is better than that of the original dataset. In total, the diagnosis accuracy was increased 2.48% on the extended dataset. As shown in the table, diagnosis accuracy of IDV(8), IDV(13) and IDV(16) are especially improved. For other faults, the diagnosis accuracy of the extended datasets showed better or worse than that of the original dataset, but the differences between the two datasets are relatively small.

Based on the analysis of the decision tree on the extended dataset, it was found that additional attributes are well utilized in the tree. For example, IDV(6) and IDV(8) can be diagnosed by the value of XADD(3) only. IDV(7) and IDV(18) can be diagnosed by using only the 3 values XADD(3), XADD(4) and XADD(5). On the contrary, the tree generated by the original dataset does not have such a simple structure to diagnose these faults. As the result, the tree on the extended dataset can diagnose IDV(6) abd UDV(7) almost perfectly, and it can diagnose IDV(8) much better than the tree on the original

dataset. For other cases, it is not simple to interpret each result because the decision tree has 830 leaves and the extended attributes are highly integrated in the tree. The tree became a little bit compact and precise by adding extended attributes, while the tree on the original dataset has 856 leaves.

4. Conclusions

Data-driven fault diagnosis of chemical plants have been investigated by many researchers for various plants. Most of them did not use any process knowledge or had difficulty to describe process knowledge. In this paper, a simple method to use process knowledge for data-driven fault diagnosis of chemical plants was proposed. Focused on control valves, which are the most common manipulated variables, two heuristics to add new attribute variables were presented. The original dataset of a plant operation can be easily extended by these heuristics. Based on the extended features dataset, the performance of a data-driven fault diagnosis is improved.

The method was applied to the diagnosis of the Tennessee Eastman process. The proposed heuristics provided twelve new attribute variables for the diagnosis of the plant. Twenty-one faults of the extended dataset was diagnosed by using the C4.5 inductive learning algorithm. The result showed large improvements on the diagnosis accuracy of faults IDV(8), IDV(13) and IDV(16). The result of this application shows effectiveness of the proposed diagnosis method. Investigation of another heuristics and the combination of the extended dataset with another learning method would be interesting.

5. Acknowledgements

This work was supported by Grant-in-Aid for Scientific Research (C) 23560522 from the Ministry of Education, Culture, Sports, Science and Technology, Japan.

References

V. Venkatasubramanian, R. Rengaswamy, K. Yin and S. N. Kavuri, (2003a), A review of process fault detection and diagnosis: Part I, Quantitative model-based methods, *Comput. Chem. Eng.*, **27**, 293–312

V. Venkatasubramanian, R. Rengaswamy, N. Kavuri and K. Yin, (2003b), A review of process fault detection and diagnosis: Part III, Process history based methods, *Comput. Chem. Eng.*, **27**, 327–346

J. J. Downs and E. F. Vogel, (1993), A plant-wide industrial process control problem, *Comput. Chem. Eng.*, **17**, 245–255

P. R. Lyman and C. Georgakis, (1995), Plant-wide control of the Tenessee Eastman process, *Comput. Chem. Eng.*, **19**, 321–331

L. H. Chiang, E. L. Russel and R. D. Braatz, (2001), Fault Detection and Diagnosis in Industrial Systems, Springer, London

J. R. Quinlan, (1993), C4.5: Program for machine Learning, Morgan kaufmann, San Mateo, CA

I. H. Witten, E. Frank and M. A. Hall, (2011), Data Mining: Practical machine learning tools and techniques, 3rd ed., Morgan Kaufmann, Boston, MA

I.A. Karimi and Rajagopalan Srinivasan (Editors), Proceedings of the 11th International Symposium on Process Systems Engineering, 15-19 July 2012, Singapore.

Pattern Recognition using Multivariable Time Series for Fault Detection in a Thermoeletric Unit

Otacílio José Pereira,[a] Luciana de Almeida Pacheco,[b] Sérgio Sá Barreto,[b] Weliton Emanuel,[a] Cristiano Hora de Oliveira Fontes,[a] Carlos Arthur M. Teixeira Cavalcante [a]

[a] *Universidade Federal da Bahia, Escola Politécnica, Rua Aristides Nóvis, 02, Federação, Salvador, BA, CEP 40210-630, Brasil*
[b] *Petróleo Brasileiro S.A. (BA), TIC-BA, Av. ACM, 1113, EDIBA, Itaigara, Salvador, BA, CEP 41856-90, Brasil*

Abstract

This paper presents a methodology for recognition of operating patterns of a gas turbine in a thermoelectric power plant (Brazilian Oil Company). Patterns related to the normal starts (without failure) and starts with failure (trip) were recognized. The process data were obtained from the plant information management system (PIMS) and techniques of data mining suitable for multivariable time series were adopted with emphasis on similarity metrics, linear scan and clustering, among others. The recognized patterns represent important and useful results to support the development of dynamic system for the monitoring and predicting the probability of failure in the equipment.

Keywords: Data mining, Multivariate Time Series, Gas Turbines.

1. Introduction

The advance of information technology (IT) provided the storage and handling of large amount of data. This led to development of methods associated to the Knowledge Discovery in Databases (KDD) and Data Mining (DM) that use data to obtain useful knowledge, adding value to businesses in strategic sectors such as ecommerce, medicine and economy ([1], [2]).

In engineering, the improvements in the technology of instrumentation, control and automation, together with the advance in IT, also built a scenario of high availability of data in industrial plants. While these technologies for data acquisition have been consolidated, the analysis of this information with the appropriate knowledge generation is still an active field of research [3].

In many situations related to industrial plants, data (or objects) are represented by time series that express the dynamics of a given process variable, collected directly from the PIMS [4]. When the object contains more than one time series and the knowledge to be extracted is related to an integrated behavior of these series, there is a problem of pattern recognition in multivariate series. This problem is more complex than the traditional case (static data or univariate time series ([5], [6])) and therefore requires specific techniques ([7-11]).

This paper presents a methodology for the acquisition of knowledge, represented by patterns of operation, from data of an industrial plant. More specifically, patterns of failure in a gas turbine of commercial scale are recognized following a systematic procedure. The turbine represents the main equipment of a thermoelectric unit belonging to the industrial park of the Brazilian Oil Company (Brazil).

The next section presents the industrial unit and the gas turbine. Sections 3 and 4 present and discuss the methodology and results.

2. Application Scenario

The industrial unit analyzed in this work is the Thermoeletric Power Plant Rômulo Almeida (TPP-RA) that is part of the Brazilian Oil Company (Figure 1). It comprises a cogeneration unit that operates in combined cycle producing steam and electricity, with natural gas as raw material.

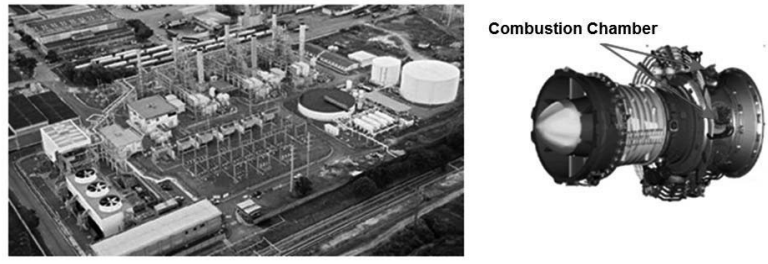

(a) (b)

Figure 1 – (a) UTE-RA [12] e (b) illustration of a gas turbine RB211-G62 DF [13]

The TPP-RA has three gas turbines (GT) Rolls Royce RB211-G62 DF[13], each one coupled to an electric generator of 27 MW, in conjunction with other equipments to drive a total generation capacity of 137 MW of energy and production of 260.3 t/h steam. Trips may occur in the turbines ([14]) and can be caused by some factors such as surge, vibration and temperature dispersion. This work focused on the recognition of patterns of failure during the starting of the turbine caused by temperature dispersion. This trip occurs when the temperature of one of the 17 temperature sensors, distributed radially after the combustion chamber, reaches a temperature value of $\pm$ 150°C different from the average of the others [13].

3. The methodology

The main process variables associated with the turbine operation comprise the flow of natural gas, inlet temperature of the natural gas and temperature of the exhaust gases. The procedure developed is illustrated in Figure 2 and have the following steps:

1. Generation of samples. Occurrences of normal starts and starts with trip caused by temperature dispersion were chronologically identified through operation reports during the period between 2008 and 2010. Two groups were established, namely, one group with 18 objects associated to starts with trip and another group with 57 objects associated to normal starts. This step was supported by the linear scan algorithm [6] which enabled the automatic capture of samples of starting events of the turbine directly from the database.
2. Analysis of similarity within and between groups. This step involved the quantification of the level of homogeneity within each group (starts with and without trip) and the distinction between them. The quantification of similarity between multivariable time series ([7-11]) was used instead of the commonly approaches applied in the univariate case ([5], [6]) in which the euclidean distance, for example, can be used directly. In this paper we used the SPCA (Similarity Factor Principal

Component Analysis) [10] as a measure of similarity which provides a dimensionless index determined from the angles between the principal components of each object.

3. Clustering and pattern recognition. Inspired in the Fuzzy C-Means ([5], [8], [15]), an algorithm suitable for the clustering of multivariable time series and also based on optimization was developed. This algorithm provided different groups of normal starting of the turbine, the degree of membership of each object to each one of these groups and the centers or patterns of each group (or cluster).

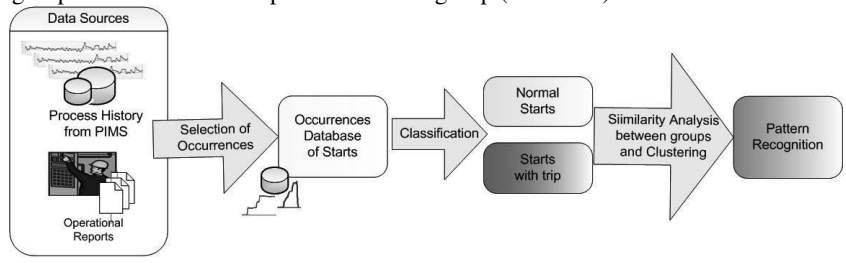

Figure 2 – Overview of the methodology

4. Results

In the analysis of similarity between the two groups (starts with and without trip), some combinations of the three process variables previously selected (flow of natural gas, gas natural inlet temperature and gases exhaust temperature) were tested, considering also the univariate case. The alternative of object with the three variables provided better homogeneity inside the group of starts with trip and better polarization between the two groups of normal starts.

The clustering algorithm was based on these three variables and on the SPCA index to measure the similarity between objects. The algorithm identified two patterns (N1 and N2) for the normal starts group. Despite the homogeneity and the small number of objects in the group of starts with trip, only one pattern was considered. Therefore, the mean object of this cluster was taken as the pattern of trip. Figure 3a presents one of the patterns of normal starts (N2) and Figure 3b, the pattern of trip (T1). Figure 3c ilustrate the distance between the patterns, also based on the SPCA index.

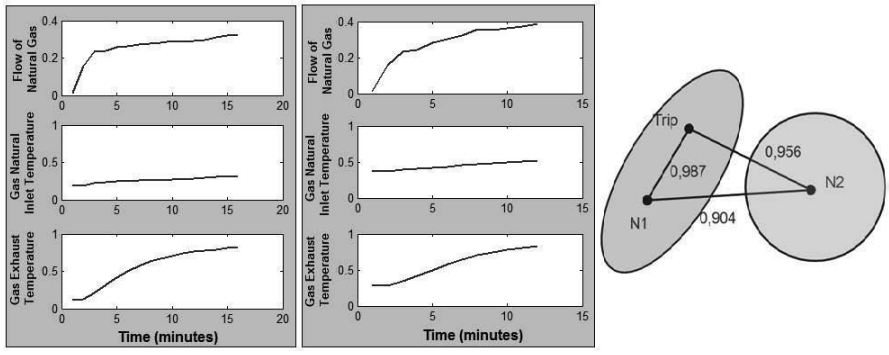

(a) (b) (c)

Figure 3 – (a) One of the patterns of normal start (N2); (b) The pattern of trip (T1) and (c) Distance between patterns

In Figure 4a, the pattern N2 is used as reference and the distances of all objects to this pattern are presented. As expected, the objects belonging to the group N2 are very similar to the pattern of N2. Figure 4b shows the degree of membership of each object of normal starting to the pattern of N2 and a polarized distribution is verified. There are few objects in the center of y-axis which attests that there is little ambiguity or uncertainty in the clustering process.

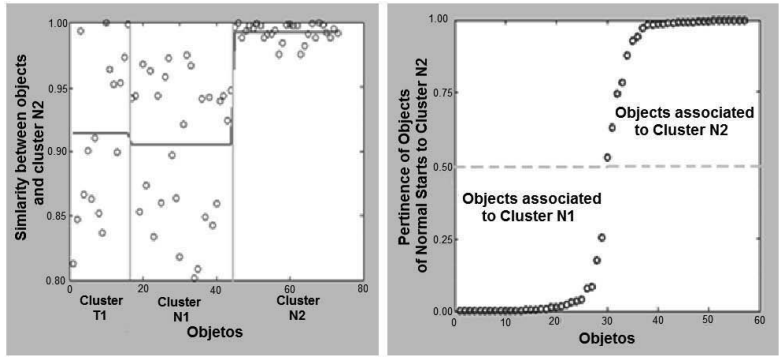

(a) (b)

Figure 4 – (a) Distances of objects to the cluster N2 (b) Objects belonging to cluster N2

Figure 5 shows the gas flow curve in a starting with trip occurrence. Using the moving-window approach [3], the distances between the flow curves of the turbine and each one of the patterns (T1, N1 and N2) are presented. The proximity of the event of failure leads to a rapprochement between the flow curve and the patterns of T1 and N2. This means that the occurrence is closer to the patterns of starting with trip or normal starting N1 and is far from the pattern of N2. It suggests that the pattern N2 represents a safer alternative to starting the turbine.

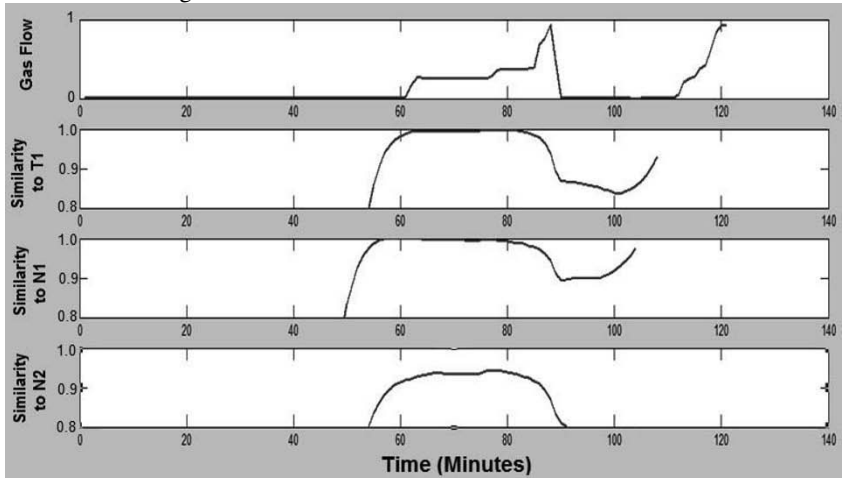

Figure 5 – Dynamic behavior of distances between one starting with trip and the patterns of T1, N1 and N2

5. Conclusion

This paper presents a procedure for recognition of operating patterns in gas turbines in order to provide support to implement a system for fault prediction. In the case studied, techniques based on data mining suitable for multivariate time series allowed the identification of two patterns of normal starts One of them is more distance from the fault pattern and is associated to a safest starting of the turbine.

The solution developed is flexible and portable. Despite its application on the pattern recognition associated to one kind of failure, the tools and techniques employed can be easily adjusted to treat other problems. Other types of failures can be investigated if data and operation reports are available.

References

[1] U.M. Fayyad, G.Piatetsky, P. Smyth, R. Uthurusamy, 1996, Advances in Knowledge Discovery and Data Mining. California: American Association for Artificial Intelligence e MIT Press.

[2] G. Piatetsky, 2007, Data mining and knowledge discovery 1996 to 2005: overcoming the hype and moving from "universty" to "business" and "analystics", Data Mining Knowledge Discovery, 15, 99-105.

[3] A.Singhal, D.E.Seborg, 2002, Pattern Matching in Multivariate Time Series Databases Using a Moving-Window Approach, Industrial and Engineering Chemistry Research, 41, 3822-3838.

[4] F. B. Carvalho, B. S. Torres, M. O. Fonseca, C Seixas Filho, 2003, Sistemas PIMS – Conceituação, Usos e Benefícios, VII Seminário de Automação de Processos da Associação Brasileira de Metalurgia e Materiais – ABM, Santos/SP.

[5] T.W. Liao, 2005, Clustering of time series data - a survey, Science Direct. Pattern Recognition, 38, 1857 – 1874.

[6] M. Vlachos, 2005, A practical Time-Series Tutorial with MATLAB, European Conference on Machine Learning.

[7] H.P.Kriegel, K.M.Borgwardt, P. Kroger, A.Pryakhim, M.Schubert, A.Zimek, 2007, Future Trends in data mining, Data Mining Knowledge Discovery, 15, 87-97.

[8] G.Gan, C. Ma, J. Wu, 2007, Data clustering : theory, algorithms, and applications.ASA-SIAM series on statisticsand applied probability.

[9] X.Wang, A.Wirth, L.Wang, 2007, Structure-based statistical features and multivariate time series clustering, Seventh IEEE Conference on Data Mining, 351-360.

[10] K. Yang, C.Shahabi, 2004, A PCA-based Similarity Measure for Multivariate Time Series, Second ACM International Workshop on Multimedia Databases, ACM-MMDB 2004, Washington, DC, USA, November 13, 2004.

[11] A.Singhal, D.E.Seborg, 2005, Clustering Multivariate Time-series Data, Journal of Chemometrics, 19, 427-438.

[12] S. T. Sá Barreto, 2009, Desenvolvimento de Metodologia para Atualização em Tempo Real de Modelos Matemáticos de Processos Decisõrios. Dissertação de Mestrado em Mecatrônica – PPGM, UFBA, Salvador.

[13] Rolls-Royce. Trainning Manuals of the Gas Turbine RB 211-G62 DF, 2010.

[14] H. I. H. Saravanamutoo, G. F. C. Rogers, H. Cohen, 1996, Gas Turbine Theory. 5.ed. Dorchester: Prentice Hall.`

[15] F. Hoppner, R. Klawonn, R. Kruse, T. Runker, 1999, Fuzzy Cluster Analysis, *Wiley, Chichester*.

I.A. Karimi and Rajagopalan Srinivasan (Editors), Proceedings of the 11th International Symposium on Process Systems Engineering, 15-19 July 2012, Singapore.

Compressive Strength Prediction of Concrete Recycled Aggregates made from Ceramic Tiles using Feedforward Artificial Neural Network (FANN)

Chan Chee Kin,[a] Mashitah Mat Don,[b] Ahmad, Z[c]

[a,b,c]*School of Chemical Engineering, Engineering Campus, Universiti Sains Malaysia, 14300 Nibong Tebal, Seberang Perai Selatan, Penang, Malaysia*

Abstract

In this paper, Feed forward Artificial Neural Network (FANN) model has been used to predict concrete compressive strengths made from ceramics tiles. Multiple regression analysis (MRA) was used to compare the results obtained from FANN. Both models are trained and tested using the available test data of 72 different concrete mix using recycled aggregates derived from homogenous ceramic tiles. The data are arranged in a format of inputs parameters for fine and coarse aggregates that cover the percentage of replacement, water/cement ratio, compacting factor, curing time of 7 and 14 days respectively. The output considered was the compressive strength for curing time of 28 days of the recycle concrete. The r^2 value for fine aggregates was 80% for MRA and 88 % for FANN respectively. In coarse aggregates, the r^2 value was 64 % for MRA and 74 % for FANN respectively. The results showed that FANN is a suitable tool for predicting compressive strength values for different concrete mixtures.

Keywords: **Neural Network Modeling, Concrete Compressive Strength, Multiple Regression Analysis, Ceramic Tiles, Feed Forward Artificial Neural Network**

1. Introduction

Malaysia as a developing country has a very active construction industry. As the construction industry continues to grow, it will generate a large amount of construction wastes which causes significant impacts on the environment. Hassan *et al.* [1] reported that on average, 28.34% of total generated solid wastes came from industrial and construction industry in the central and southern region of Malaysia. These wastes, among which were dependable on many factors, including the stage of construction, type of construction work and practices on site. Instead of dumping it in landfills and dumpsite, recycling and reuses of such wastes is an urgent need for environmental and social benefits. Moreover, conventional crushed stone aggregates reserves are depleting fast. This in turn jeopardized the principle of sustainability and received increasing opposition from environmentalist. Sani *et al.* [2] suggested that recycling of construction wastes could reduce the volume of wastes produced. As a result, the usage of inorganic construction waste will lead to sustainable concrete design and a greener environment. Rao *et al*. [3] reported that recycled aggregate concrete (RAC) have reduction of strength however it should be noted that the extent of reduction is related to the parameters such as type of concrete used, the replacement ratio, water/cement (w/c) ratio and the moisture condition of the recycled aggregates. Previously, Katz [4] found that at a high w/c ratio, the strength of RAC is comparable to that of reference concrete even at a replacement of 75%. The usage of ceramic tile wastes as course aggregates

was first reported by Kaloo in 1995 [5]. He found that crushed tiles concrete had a lower density, higher compressive and flexural strength. However, studies on the use of crushed ceramic tiles as a construction material is scarce [6], though it could provide enormous economical and environmental benefit to the society in general.

It is well recognized that the prediction of concrete strength is important in the modern concrete construction and engineering judgement. Various methods were proposed for predicting the concrete strength. The purpose of this paper is to present a comparison of FANN and MRA while exploring the usage of bootstrap sampling for resampling the limited data for training, testing and validation purposes.

2. Methodology

2.1. Feedforward Artificial Neural Network (FANN)

FANN is an information processing technique that can provide meaningful answers even when the data to be processed include errors or are incomplete, and can process information extremely rapidly when applied to solve real world problems. This FANN architecture considers all neurons of input and output layers in one structure. Prediction results by this architecture could show good results with some test data sets, which has not been used in the training process. In assessing the developed models, mean SSE (MSSE), mean absolute percentage error (MAPE) and the regression of coefficient (r^2) was also calculated to find its accuracy on the unseen validation data is used as the performance criterion. The model is shown as follows:

$$\hat{y}(t) = f[u1(t), u2(t), u3(t), u4(t), u5(t)] \quad (1)$$

where *u1(t)* is the percentage replacement, *u2(t)* is the water/cement ratio, *u3(t)* is the compacting factor, *u4(t)* and *u5(t)* is the compressive strength for curing time of 7 and 14 days respectively. $\hat{y}(t)$ is the predicted process output which is the compressive strength of curing time of 28 days. The model with the smaller MSSE and MAPE and the largest r^2 is considered to be the best where accurately predict the compressive strength of the concrete.

2.2 Multiple Regression Analysis (MRA)

MRA is also known as Ordinary Least Square (OLS) and it assumes that a vector of regression parameters, θ, can be used to determine the system output y, from n measured variables x, through a linear model of the following form:

$$y = x_1\theta_1 + x_{22} + \ldots + x_n\theta_n$$

By using MRA, the model parameter, θ, can be estimated through the following equation:

$$\hat{\theta} = (X^T X)^{-1} X^T Y) \quad (3)$$

where X is the matrix of input variable data and Y is a matrix (or a vector in a single output case) output variable data. For this MLR analysis, X will be the prediction output of the individual networks on the training and testing data and Y is the actual process

output on the training and testing data. Once the model parameters are estimated, it can be applied to the unseen validation data.

2.3 Description of data

Homogenous ceramic tiles were collected from 5 construction sites in the state of Perak and Penang, Malaysia. The tiles were broken manually using a hammer and then fed into a jaw crusher (Model: Retsch BB-200) to acquire aggregates of mesh size 20 mm (Plate 1 and 2). Other materials including ordinary portland cement (OPC), locally available river sand (specific gravity 1.73) and natural crushed stone aggregates of maximum size 20 mm (specific gravity 1.62) were also used for the production of concrete block. In the case of homogenous ceramic tiles waste aggregates, five concrete mixes were prepared by varying the content of ceramic tiles coarse aggregates from 20% to 100%. The concrete block were then demoulded and cured under water at 27° ± 2°C until the test age. The samples were demoulded 24 hours after casting and cured. The blocks were then tested for compression strength at different curing time in days (7, 14 and 28 days). In this study, the percentage of placement, the water/cement (W/C) ratio, compacting factor, and compressive strength at 7 and 14 days were used as inputs and the values of the compressive strength for curing time of 28 days was used as an outputs for fine and coarse aggregates respectively. Herein, all the data were divided into 3 categories which are training, testing and validation data because "early stopping" criteria were used in the neural network training. Then, all data are resampled through bootstrap re-sampling approach to make it 72 data in each category.

3. Result and Discussion

3.1 Feedforward Artificial Neural Network (FANN)

FANN structure with 10 hidden nodes was used in fine and coarse aggregate model respectively. Note that all the results in this study are based on scaled data but afterwards being re-scaled to get the real physical data of compressive strength which is in MPa for all figures. The performance values for the predicted results of the compressive strength were presented in **Table 1**. It can be seen from the table that the MAPE and MSSE were lower. This means that the predicted results were closer to the experimental data. The results of testing phase shows that the FANN was capable of generalizing between input variables and the output and reasonably good predictions.

Table 1: Result for the compressive strength for curing time of 28 days using FANN

Performance values	Coarse Aggregates	Fine Aggregates
$\mathbf{r^2}$	0.74	0.88
MAPE	0.39	0.05
MSSE	0.74	0.38

This proved that the experimental results with the predicted ANN results were all in good agreement. The ANN can learn any relationship, linear or non-linear, as long as there are sufficient large numbers of neurons in the hidden layer. Another remarkable advantage of the ANN is the capability of modelling data of multiple data of multiple inputs and multiple outputs. **Figure 1** supported the previous statement where the actual and predicted output for validation data is reasonably closed respectively.

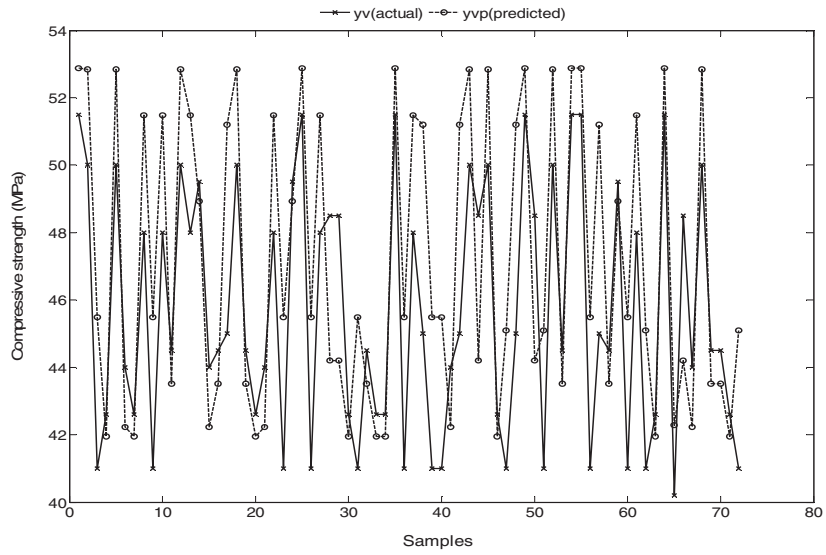

Figure 1: Predicted and measured value of 28 days compressive strength for FANN using coarse aggregates

3.2 Multiple Regression Analysis

Experimental results were satisfactory and gave good agreement to the model used, with the correlation regression coefficient (r^2) values at 0.9128 and 0.9541 respectively. **Table 2** shows the performance values for the predicted results of the compressive strength using the MRA. The MRA is the simplest method for modelling compressive strength. It does not need too complicated computation and all parameters can be tested statically. The MRA has a capability of producing a confidence interval for prediction. However, the MRA cannot be used to model the data with multiple outputs. It is clearly shown in **Figure 2** that MRA is slightly suffered in predicting the compressive strength for fine and coarse aggregates. The actual and predicted values for both outputs are quite different.

Table 2: Results for the compressive strength for curing time of 28 days using MRA

Performance values	Coarse Aggregates	Fine Aggregates
$\mathbf{r^2}$	0.64	0.80
MAPE	0.18	0.04
MSSE	0.64	0.40

4.0 Conclusion

A comparative analysis of two alternative approaches for modelling compressive strength, which are feedforward artificial neural network (FANN) and multiple regression analysis (MRA) has been presented in the present study. It is found that neural network is particularly suitable for learning nonlinear functional relationships and multiple outputs and input relationships which are unknown or cannot be specified

whereas the MRA is suitable for modelling functional relationships which can be specified. This suggests that the FANN is a useful tool for compressive strength of concrete mixture analysis.

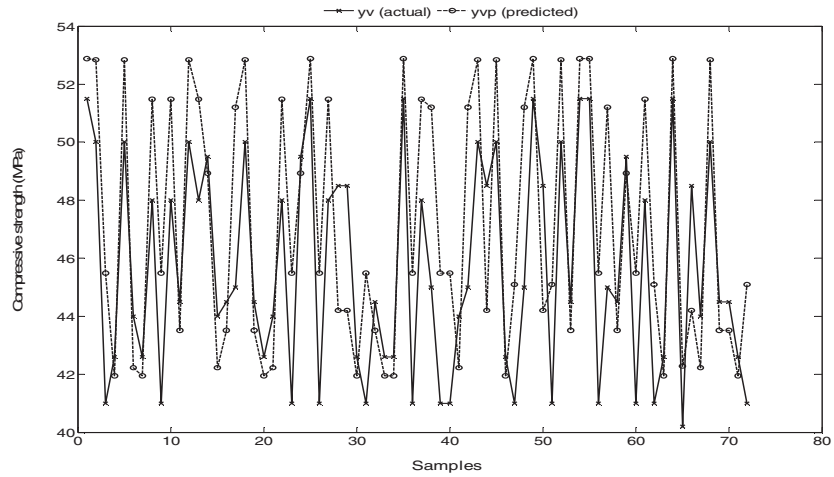

Figure 2 : Predicted and measured value of 28 days compressive strength for MRA using coarse aggregates

5.0 Acknowledgement

The authors are grateful to the Construction Industry and Development Board of Malaysia (CIDB) and Construction Research Institute of Malaysia (CREAM) (Account No.: 6050116) and Universiti Sains Malaysia (USM) for providing the facilities to carry out this study.

References

[1] M.N. Hassan, M.K. Yusoff, M.N.A. Sulaiman, R.A. Rahman, 1998, Issues and problems of solid waste management in Malaysia. Proceedings on national review on environmental quality management in Malaysia: towards the next two decades, Hasan et al. Eds. Institute for Environmental and Development (LESTARI), Universiti Kebangsaan Malaysia.

[2] D. Sani, G. Moriconi, G. Fava, V. Corinaldesi, 2005, Leaching and mechanical behaviour of concrete manufactured with recycled aggregates. Waste Manage., 25, 177-182.

[3] A. Rao, K.N. Jha, S. Misra, 2007, Use of aggregates from recycled construction and demolition waste in concrete, Resour. Conserv. Recycl. 50, 71-81.

[4] A. Katz, 2003, Properties of concrete made with recycled aggregate from partially hydrated old concrete, Cem. Concr. Res. 33, 703-711.

[5] A.R. Khaloo, 1995, Crushed tile coarse aggregate concrete, Cem. Concre. Aggregate 17, 119-125.

[6] C.S. Poon, D. Chan, 2007, Effects of contaminants on the properties of concrete paving blocks prepared with recycled concrete aggregates, Constr. Build. Mater. 21, 164-175.

I.A. Karimi and Rajagopalan Srinivasan (Editors), Proceedings of the 11th International Symposium on Process Systems Engineering, 15-19 July 2012, Singapore.

Control of integrated unit operations

José A. Chinea-Herranz, Manuel Rodríguez [a]

[a] *Autonomous System Laboratory, Universidad Politécnica de Madrid, José Gutierrez Abascal 2, Madrid 28006, Spain.*

Abstract

As a thermal separation method, distillation is one of the most important technologies in the chemical industry. Given its importance, it is no surprise that increasing efforts have been made in reducing its energy inefficiencies. A great deal of research is focused in the design and optimization of the Divided-Wall Column. Its applications are still reduced due to distrust of its controllability. Previous references studied the decentralized control of DWC but still few papers deal about Model Predictive Control. In this work we present a decentralized control of both a DWC column along with its equivalent MPC schema.

Keywords: Process Control, Thermally coupled distillation, Model Predictive Control.

1. Main Text

Basically, in every production process some of the chemicals go through at least one distillation column on their way from raw species to final product. Distillation is and will remain the main separation method in the chemical industry (there are more than 50,000 columns in operation around the world). Despite its flexibility and widespread use, distillation is very energy demanding. It can generate more than 50% of plant operating costs and it is the responsible of 3% of the energy usage in the U.S. (notice that the thermodynamic efficiency of a distillation column is between 5-20%). In order to reduce this drawback new approaches and configurations have appeared.

The divided-wall column (DWC, the name is given because the middle part of the column is split into two sections by a wall) is an important example of process intensification and integration. DWC is very appealing to the chemical industry, with Montz and BASF as the leading companies. Kenig et al. state that there are more than 125 industrial applications nowadays and if the exponential trend continues there will be more than 350 by 2015 [1].

DWC can separate three or more components in one vessel using a single condenser and reboiler, hence reducing capital and operating costs compared to conventional two-column sequences. In fact, DWC can save up to 30% in the capital invested and up to 40% in the energy costs, particularly for close boiling species. DWC is considered to be on the path for energy conservation and green house gases emissions decrease.

DWC is not widespread due to distrust of its controllability. Its control is more difficult than the control of a conventional schema with two columns for the separation of ternary mixtures because there is more interaction among control loops. Besides, the absence of controllability could mean the absence of the energy savings if the optimal operation is not accomplished. The remaining of the paper is organized as follows. Section two discusses thermally coupled distillation columns, making emphasis in DWC columns. Section three presents the control strategies used in the paper. Section four applies decentralized (PID controllers) control and MPC to a ternary system separation. Finally, section five draws conclusions and introduces further work.

2. Energy integration in distillation

Distillation systems have evolved from direct, indirect or distributed column sequences to thermally coupled systems and eventually to Petlyuk configurations [2] and DWC schemes (Fig. 1). Intermediate steps in this path include systems with heat pumps, prefractionators and side-stripers or side-rectifiers. The Petlyuk configuration and the DWC were aimed at the reduction of thermodynamic losses due to mixing streams, especially at the feed tray location.

DWC has more degrees of freedom (DOF) compared to a binary distillation column. This entails a complex design, but also presents extended optimization capabilities. If 3 product specifications are taken into account, DWC has 7 DOF's: distillate and bottoms flowrate, reflux ratio, reboiler duty, side-stream flowrate and vapor and liquid internal split ratios. 5 DOF's are used to stabilize 2 levels and 3 compositions while the remaining 2 DOF's are used for optimization purposes. Traditionally, liquid split ratio ($\alpha_L=L_P/L_M$) and vapor split ratio ($\alpha_V=V_P/V_M$) are optimization variables (Fig. 1c). Vapor split ratio is usually fixed during the design stage because it is given by the pressure drop across both sides of the wall, which in turn depends on the stage type and geometry. The liquid split ratio is used as a control variable during operation by manipulating the flowrates leaving the bottom tray of the rectifying section.

The optimal design is given by the number of stages in the different sections of the DWC. The number of stages at both sides of the wall is usually the same but approaches with different number of plates have been reported. Olujic et al. presents a review on the different design approaches of DWC [3].

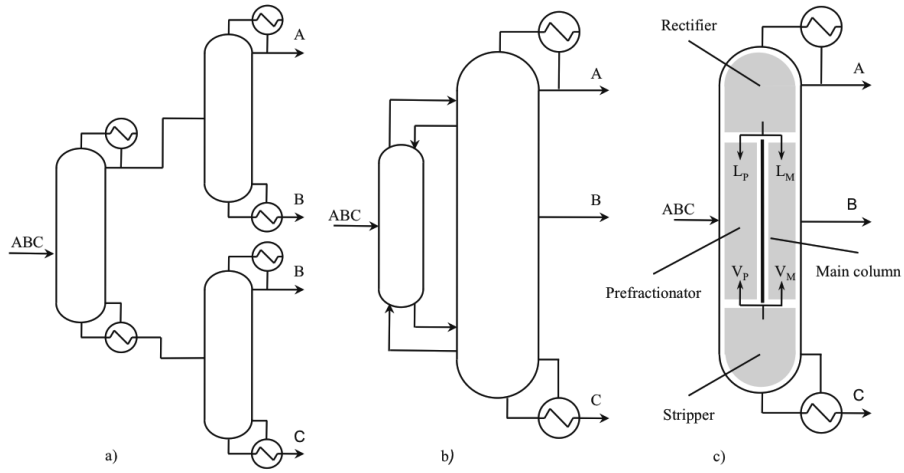

Figure 1. Evolution from a distributed sequence (a) to a Petlyuk configuration (b) and eventually to the DWC (c)

3. Control strategies for Divided-Wall Columns

Past and recent distrust on DWC controllability and flexibility is mainly due to the complex design of a control strategy. Maintaining product specifications while rejecting disturbances and loop interaction are the key concerns together with achieving significant energy savings. Otherwise, DWC advantages might disappear.

Early references on DWC control were focused mainly on decentralized control. The first approaches extended PID control structures of traditional distillation columns by including liquid or even vapor split ratio among the manipulated variables. Wolff & Skogestad [4] demonstrated that three-point control structures were feasible using PID controllers. Mutalib and Smith reported the first experimental application of decentralized control using temperature profile instead of composition measurements [5, 6]. Puigjaner et al. follow a research line in which multiple decentralized control studies are compared by using transfer functions obtained from shortcut modeling and dynamic matrix control is applied to DWC [7-9]. Kim [10] and Adrian [11] are among the first to use model predictive control but their approach is either experimental or shortcut modeling based. DWC has been also applied to complex distillation systems. Wang extended DWC to azeotropic distillation [12], while other references deal with extractive and reactive DWC [13, 14].

4. Process studied

The separation of n-pentane, n-hexane and n-heptane is carried out in a DWC. The rectifying, prefractionator and stripping sections have respectively 7, 12 and 10 stages. The number of stages at both sides of the wall is the same. The feeding stage and side-stream withdraw are located at stage 12 in the prefractionator and main column respectively. The feed is assumed to be 180 kmol/h of a mixture 0.4/0.2/0.4 (C5/C6/C7) in mole fraction at 300 K and product specifications are set at 98%. The operation values are calculated to minimize the reboiler duty. The minimum energy consumption occurs at a liquid split ratio of 0.33 and a vapor split ratio of 0.625. The resulting reflux and boilup ratios are 2.521 and 3.445 respectively. The steady state simulations are performed in Aspen Plus using the rigorous Radfrac model with a Chao-Seader property package. Sizing rules for reflux drum, bottoms and trays are taken from Luyben [15].

4.1. Decentralized control

The main advantage of decentralized control lies in its simple design and tuning. As less time and effort is needed on its development, it might be convenient for simple applications. However, PID ability to reduce interaction among control loops is reduced and as a result settling times and oscillation might compromise stable operation.

In decentralized control, the choice of variable pairings plays a fundamental role in the performance of the system. There are numerous references dealing with the best pairing. Variable pairing depends highly on the chemical system studied, the design and the product specification level. Nevertheless, the best result is traditionally associated to the strategy L/S/V-D/B, meaning that distillate, side-stream and bottoms specifications are controlled by reflux, side-stream and bottoms rate respectively while condenser drum and bottoms levels are maintained by distillate and bottoms rates respectively.

A special reference must be done on a paper by Luyben & Lin applying a four composition PID control scheme [16], which is eventually extended to temperature profile control [17]. Luyben's control scheme minimizes indirectly energy consumption by maintaining heavy component concentration on top of the prefractionator at a minimum value. It is widely accepted that any minimal amount of heaviest component going out the top of the prefractionator causes an irreversible decrease on the side stream purity [4]. The same idea applies if the lightest component crosses the dividing wall at the bottom of the prefractionator, however the influence on product specification is not so important as this component will be present mainly in the vapor phase. As L/S/V-D/B gives the best performance according to most of the references and Luyben's control scheme accomplishes and indirect energy optimization, both

approaches will be used. A PI controller is designed for each control loop, tuning parameters are shown in Table 1.

Table 1. Summary of tunning parameters for decentralized control

	Proportional gain	Integral time	Set point (mole frac.)
Distillate composition control	7.144	63.36	0.98
Side-stream composition control	121.37	38.28	0.98
Bottoms composition control	4.745	35.64	0.98
Prefractionator composition control	0.379	29.04	0.004

4.2. Model Predictive Control (MPC)

There are few applications of MPC to integrated unit operation and especially to DWC. Some references highlight the enhanced performance of MPC while for others PID control gives better results. Relevant experience on the superiority of MPC is still limited. Theoretical and experimental comparisons between MPC and PID controllers should be done for a variety of chemical systems so as to reach a heuristic solution.

MPC present enhanced performance reducing oscillations, loop interactions and settling times. Besides the ability to include optimization constraints allows for the safety improvement. Nevertheless, MPC present several disadvantages: 1) it entails larger development cost and time, 2) it requires a deep knowledge of the process and 3) it requires the availability of a dynamic model representing the main features of the unit operation. The performance of MPC is directly proportional on the accuracy of the dynamic model and the adequate tuning of its parameters.

MPC control of the dynamic model for the DWC is carried out in Matlab with the MPC Toolbox. The step responses obtained from Aspen Dynamics are transformed to the Plant Model using the Systems Identification Toolbox. An ARX linear parametric model is found to represent the plant responses adequately.

The MPC controller is tuned using the Tunning Advisor available in the MPC Toolbox. The Integrated Square Error function is used as the performance function for tuning.

4.3. Performance comparison

The decentralized control scheme has been tested to ±10% disturbances in feed flowrate, temperature and composition as well as a simultaneous set point change in all product purities from 98 to 98.5% (mole frac.). Loop interaction is clearly demonstrated with the set point change experiment (Fig. 2 left). MPC performance is compared to decentralized control by carrying out the same simultaneous set point change.

The results are shown in Fig. 2 and clearly demonstrate the advantage of MPC in eliminating loop interaction and oscillations. Settling times for distillate and bottoms purity are significantly lower. For sidestream purity and prefractionator vapour composition the decentralized control scheme presents lower settling times.

5. Conclusions

In this paper the control of a DWC has been presented applying MPC as well as decentralized control. MPC superiority in eliminating loop coupling has been demonstrated comparing it to a decentralized control scheme. The same comparison has to be done with a decentralized control with decoupling strategies. In this case the development cost and time must be taken into account to compare both strategies

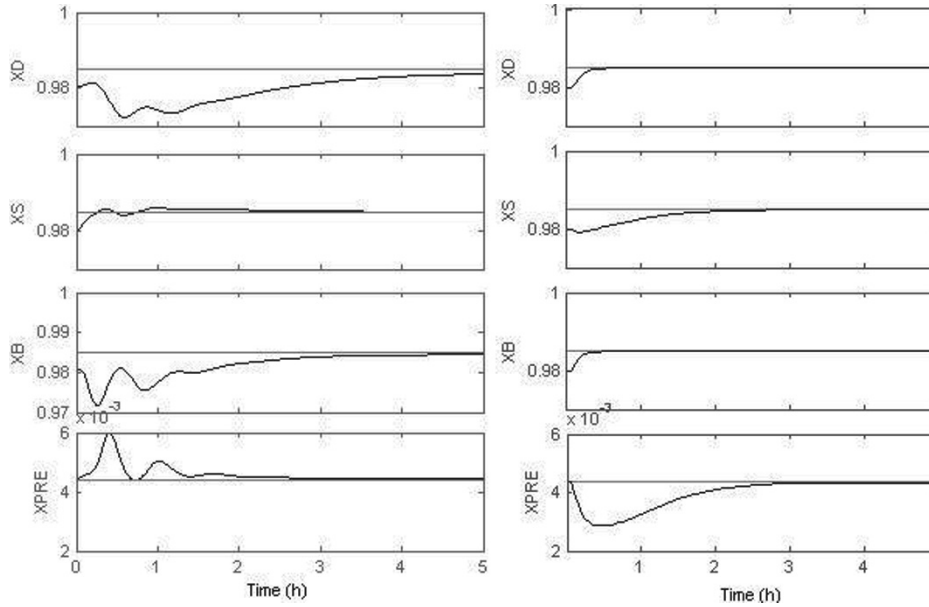

Figure 2. Set point increment of product purities from 98 to 98.5% for a decentralized control (left) and MPC scheme (right)

The industrial application of decentralized or model predictive schemes must be based on temperature profile control to avoid using composition analyzers, which in most of the cases are expensive and present slow responses.

The study of control strategies will be extended to complex schemes such as Kaibel columns, double-wall distillation columns (Sargent arrangements) or Agrawal columns.

References

[1] E. Y. Kenig, O. Yildirim, A. A. Kiss, Sep. Purif. Technol., 80 (2011) 403.
[2] F. B. Petlyuk, V. M. Platonov, V. M. Slavinskii, Int. Chem. Eng. 5 (1965) 555.
[3] Z. Olujic´, I. Dejanović, L. Matijasević, Chem. Eng. Process., 49 (2010) 559.
[4] E. A. Wolff, S. Skogestad, Ind. Eng. Chem. Res., 34 (1995) 2094.
[5] M. Mutalib, M. Smith, Trans. IChemE. 76 Part A (1998) 308.
[6] M. Mutalib, M. Smith, Trans. IChemE. 76 Part A (1998) 319.
[7] L. Puigjaner, M. Serra, A. Espuña, Chem. Eng. Process., 38 (1999) 549.
[8] L. Puigjaner, M. Serra, A. Espuña, Ind. Eng. Chem. Res., 42 (2003) 1773.
[9] L. Puigjaner, M. Serra, A. Espuña, M. Perrier, Comput. Chem. Eng. 25 (2001) 859.
[10] Y. H. Kim, Chem Eng J., 85 (2002) 289.
[11] T. Adrian, H. Schoenmakers, M. Boll, Chem. Eng. Process., 43 (2004), 347.
[12] S. Wang, C. Lee, S. Jang, S. Shieh, J. Process Control, 18 (2008) 45.
[13] C. C. Bravo-Bravo, J. G. Segovia-Hernández, C. Gutiérrez-Antonio, A. L. Duran, A. Bonilla-Petriciolet, A. Briones-Ramírez, Ind. Eng. Chem. Res., 49 (2010) 3672.
[14] A. A. Kiss, H. Pragt, C. van Strien, Chem. Eng. Commun., 196 (2009) 1366.
[15] W. L. Luyben, Distillation design and control using Aspen^{TM} simulation. Bethlehem, Pennsylvania. 2006.
[16] W. L. Luyben, H. Lin, Ind. Eng. Chem. Res., 48 (2009) 6034.
[17] W. L. Luyben, H. Lin, Ind. Eng. Chem. Res., 49 (2010) 189.

I.A. Karimi and Rajagopalan Srinivasan (Editors), Proceedings of the 11th International Symposium on Process Systems Engineering, 15-19 July 2012, Singapore.

Nonlinear Control Strategies for a Micro-Aerobic, Fermentation Process

Emily Liew Wan Teng and Yudi Samyudia

Department of Chemical Engineering, Curtin University, CDT 250, 98009 Miri, Sarawak, Malaysia

Abstract

In this paper, we propose a new strategy to control the yield and productivity of the fermentation process by viewing the fermentation process as a multi-scale process, where the mixing conditions in terms of aeration rate and stirrer speed are considered in studying the bioreactor dynamics. The inclusion of mixing for bioreactor control would allow us to influence the metabolic activities of microorganisms through the distribution of nutrients to the microbial cells. The engagement of both mixing and biological processes, however, would lead to a very complex dynamics of the bioreactor. As a result, the control strategy with a direct use of a nonlinear model will be implemented. Two different modeling techniques to capture the mixing dynamics, namely data-based and kinetics hybrid modeling are proposed. The validated nonlinear models are used in determining the optimal aeration rate and stirrer speed to maintain the desired productivity and yield of the fermentation process for different disturbance scenarios via extensive simulation studies.

Keywords: bioreactor control, mixing, nonlinear model, micro-aerobic fermentation

1. Introduction

A micro-aerobic fermentation process for ethanol production is a complex multi-scale process constituting the dynamic interactions between the microbial cells and the governing environment. The kinetics is the result of microbial metabolic activities at the cellular level within its environmental conditions (i.e. mixing, pH, temperature). The process performance is measured by its productivity and yield, whereby a control system is often used to achieve (and/or maintain) its desired performance. Previous work in controlling this fermentation process (e.g. Schügerl and Bellgardt, 2000; Lane, Schwarz and Evans, 2002; Castillo-Toledo, González-Alvarez and Luna-Gutiérrez, 1999; Cardello and San, 1988;) was mainly focused on the macro bioreactor conditions such as pH, temperature, etc while assuming an ideal mixing condition so that the lumped kinetics models, i.e. Monod type, could be used. The interactions of the microenvironment (i.e. mixing conditions, cellular dynamics) around the microbial cells are not taken into account. In this work, we consider the mixing conditions in developing a new control strategy for the fermentation process. By viewing the process as a multi-scale in nature it would therefore allow us to have additional manipulated variables from which new control strategies for the bioreactor can be developed. It is, however, not easy to get the kinetics model that describes the inhomogeneous conditions of the microorganisms. The aim of the present work is therefore to develop different mathematical models for bioreactor control design by capturing the mixing mechanism within the bioreactor. By analyzing the dynamic behavior of the non-ideally mixed fermentation process, two new manipulated variables, i.e. aeration rate (*AR*) and stirrer speed (*SS*), could be exploited to control the bioreactor's performance, i.e. yield

and productivity. Using these manipulated variables, a nonlinear model-based controller is then designed, where the two different models are compared for the controller design. The closed-loop performances are evaluated for different disturbance scenarios and different models.

2. Modeling and Controller Design

Two process models, i.e. data-based model and kinetics hybrid model, are developed where the mixing phenomena are included via *AR* and *SS*. The data-based model is developed based on linear regression technique to sets of experiment data of *AR, SS*, productivity and yield. The kinetics hybrid model is developed based on Herbert's concept of endogenous metabolism, which is combined with the macro-scale bioreactor model. Herbert's concept is chosen especially in fermentation processes because it could describe the kinetics of the process thoroughly (Starzak et al., 1994). Both data-based model and kinetics hybrid models are developed based on experimental conditions of *AR* (1.0-1.5LPM) and *SS* (150-250rpm).

2.1. Data-Based Model

Suppose that the process yield or productivity is a function of the levels of *AR* (or x_1) and *SS* (or x_2):

$$y = f(x_1, x_2) + \varepsilon \tag{1}$$

where ε represents the error in the response y, i.e. Yield (Y) or Productivity (P). If the expected response is a quadratic function, by applying the regression technique, the data-based model of the fermentation process is obtained as:

$$Y = -29.32 + 42.34 * AR + 0.15 * SS + 0.15 * AR * SS - 26.00 * AR^2 \tag{2}$$

$$P = 0.77 - 0.59 * AR - 0.004 * SS + 0.004 * AR * SS \tag{3}$$

2.2. Kinetics Hybrid Model

A general model of the continuous bioreactor model is given as:

Biomass formation: $dX = -DX + r_x$ (4)

Substrate consumption: $dS = D(S_0 - S) - r_s$ (5)

Product formation: $dP = -DP + r_p$ (6)

where S_0 is the initial substrate concentration (kg/m^3) of the medium, S is the final substrate concentration (kg/m^3) of the medium, P is the final product concentration (kg/m^3) of the medium and X is the final biomass concentration (kg/m^3) of the medium. According to the Herbert's concept, it is assumed that the observed rate of biomass formation comprised of the growth rate and the rate of endogenous metabolism:

$$r_x = (r_x)_{growth} + (r_x)_{end} \tag{7}$$

$$(r_x)_{growth} = \frac{k_1 XS}{k_2 + S} \exp(-k_5 P) \tag{8}$$

It is also assumed that the rates of substrate consumption and product formation are proportional to the biomass growth rate:

$$r_s = (r_s)_{growth} = -k_3 (r_x)_{growth} \tag{9}$$

$$r_p = (r_p)_{growth} = k_4 (r_x)_{growth} \tag{10}$$

The rate of growth due to endogenous metabolism by a linear dependence is given by:

$$(r_x)_{end} = -k_6 X \tag{11}$$

In order to obtain the relationships of k_1 to k_6 with *AR* and *SS*, the regression analysis is applied, whereby experimental data such as substrate and product concentrations, yield

and productivity values will be utilized. By taking *AR* and *SS* into account in the general expression of linear regression, we get:

$$\text{Variable} = \beta_1 + \beta_2 \frac{(r - \bar{r})}{\Delta r} + \beta_3 \frac{(R - \bar{R})}{\Delta R} \tag{12}$$

where "Variable" represents k_1 to k_6, r and R denote the variables taken into account, i.e. *AR* and *SS*, whereas $\bar{r}$ and $\bar{R}$ represent the baseline values for *AR* and *SS*. β_1, β_2 and β_3 values will be obtained through least squared technique. All of these equations signify the kinetic model and it is of interest to investigate whether *AR* and SS can be described without the use of mass transfer coefficient for oxygen and carbon dioxide stripping. Based on the experiment data, the optimum values of β_1, β_2 and β_3 are obtained so that the developed kinetic model is given as:

$$k_1 = 1.4085 - 0.2852X_1 + 0.3692X_2 \tag{13}$$

$$k_2 = 0.0010 \tag{14}$$

$$k_3 = 0.6631 - 0.0.148X_1 + 0.0220X_2 \tag{15}$$

$$k_4 = 0.1040 + 0.0.142X_1 + 0.0128X_2 \tag{16}$$

$$k_5 = 0.7558 - 0.1019X_1 + 0.0211X_2 \tag{17}$$

$$k_6 = 0.0143 - 0.0001X_1 - 0.0019X_2 \tag{18}$$

where $X_1 = (AR - 1.25)/0.25$ and $X_2 = (SS - 200)/50$. Combining equations (13-18) with the continuous bioreactor model of (4-11), we obtain a kinetics hybrid model of the fermentation process.

2.3. Controller Design

To design the controller for the fermentation process, an optimization approach of (Firmansyah and Samyudia, 2010) is employed, where an explicit non-linear model is required in the form of:

$$y_t = f(y_{t-1}, u_{t-1}, \theta) \tag{19}$$

where y_t and y_{t-1} are the current and past predicted outputs; u_{t-1} is the past inputs; Θ is the process parameters. Equation (19) will be used in solving a constrained or unconstrained nonlinear optimization problem that minimizes the following objective function:

$$\Delta u_t^* = \arg\{\min_{\Delta u_t} (\Delta y_t - e_t)^2 + (\Delta u_t)^2\} \tag{20}$$

Subject to:

$$\Delta y_t = y_t - y_{mt} \tag{21}$$

$$u_{\min} \le u_t \le u_{\max} \tag{22}$$

$$\Delta u_{\min} \le \Delta u_t \le \Delta u_{\max} \tag{23}$$

where y_{mt} are the current measurements of the outputs; $u_t = u_{t-1} + \Delta u_t^*$ are the optimal inputs and e_t is the current error trajectory defined as:

$$e_t = k\int_0^T (y_{sp} - y_{mt})dt \tag{24}$$

y_{sp} is the set point of the outputs and k is the tuning parameter for desired closed-loop responses. Note that when there are no constraints, i.e. (22) and (23) do not exist so the optimal solution for the nonlinear optimization will have an explicit form as follows:

$$\Delta u_t^* = -[\Delta y_t - k\int_0^T (y_{sp} - y_{m_t})dt] \tag{25}$$

which is a PI type controller, but the gain is adjusted using the nonlinear model of (19).

3. Simulation Results

The control design objective is to maintain the yield and productivity in the face of disturbances in the feed substrate concentration, S_o and dilution rate, D. The measured yield and productivity will be calculated from the measured biomass, product and substrate concentrations. Table 1 summarizes the steady state conditions for all the input, output and disturbance variables whereas the two scenarios of disturbance step change of $\pm$10% and $\pm$ 30% around their operating conditions are considered. In the closed-loop analysis, we implement the nonlinear controller designed using either the data-based or the hybrid kinetics model to control both yield and productivity in the fermentation process. We compare their performances in the face of the two disturbance scenarios.

Table 11: Summary of Steady State Conditions for All Variables

Description	**Steady State Conditions**
Yield	21.15%
Productivity	0.15g/L.hr ($4.17\text{x}10^{-5}$kg/m^3.s)
Biomass Concentration	30g/L solution (30kg/m^3 solution)
Substrate Concentration	48g/L solution (48kg/m^3 solution)
Product Concentration	5.2g/L solution (5.2kg/m^3 solution)
AR	1.43LPM ($2.38\text{x}10^{-5}$m^3/s)
SS	250rpm (4.17rps)

Fig. 1 shows that both controllers are able to keep the controlled variable in their set-point values, by manipulating both *AR* and *SS*. A step change of +10% is made in S_0 and D at time t=20 hr (72,000s), i.e. both S_0 and D values are changed instantaneously to a new value. From Fig. 1, it can be seen that both controllers perform well, whereby there are not much oscillations observed in the closed-loop dynamics of the yield. More dynamics are observed for the productivity. The kinetics hybrid model controller shows slight oscillations with a higher overshoot, and requires a longer settling time. The use of the simple data-based controller is sufficient to control the bioreactor for this disturbance scenario.

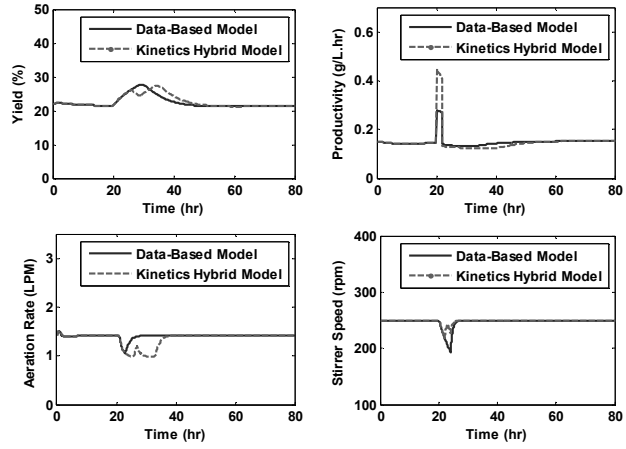

Figure 1: Closed-Loop Responses for 10% Disturbance Scenario.

Our investigation is continued for a larger disturbance scenario exciting more nonlinearity and dynamics of the process. The step perturbation is increased to $\pm$30% from the steady state conditions of S_0 and D. Fig. 2 shows the closed-loop responses for both data-based and kinetics hybrid model-based controllers for the 30% disturbance

change. Both control strategies are able to maintain the controlled variables in the set point values. However, the kinetics hybrid model controller performs much better than the data-based model controller. This could be seen for all the input and output variables. Besides, a higher overshoot can be observed for yield and productivity. Note that the manipulated variables *AR* and *SS* hit their upper limits indicating nonlinear dynamics of the process.

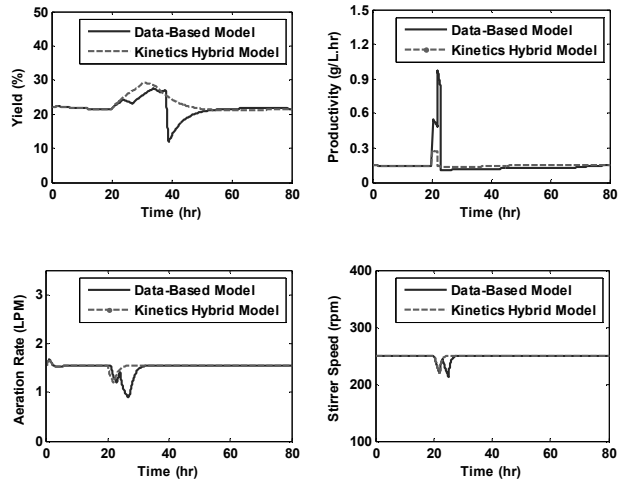

Figure 2: Closed-Loop Responses for 30% Disturbance Scenario

4. Conclusion

A new model-based control design for non-ideally mixed fermentation process has been presented in this paper. Models with different complexity are compared for the controller design. The disturbances of the inlet substrate concentration, S_0 and dilution rate, D, are simulated to study its effectiveness for bioreactor control. Our study revealed that the choice of the nonlinear controller would depend on the expected disturbances on the process. For a relatively small disturbance scenario, the data-based controller should be sufficient; however, for a significantly large disturbance, the kinetics hybrid model-based controller is preferable.

References

B. Castillo-Toledo, V. González-Alvarez and J.A. Luna-Gutiérrez, 1999, Nonlinear robust control of a batch fermentation. Chem. Eng. Technol., vol. 22, pp.675-682.

E.W.T. Liew, J. Nandong and Y. Samyudia, 2010, Optimization of fermentation process using a multi-scale kinetics model, Proc. 5th International Symposium on Design, Operation and Control of Chemical Processes (PSE Asia 2010), pp. 1174-1183, ISBN.978-981-08-6395-1.

G.L. Lane, M.P. Schwarz and G.M. Evans, 2002, Predicting gas-liquid flow in a mechanically stirred tank. Applied Mathematical Modelling, vol. 26, pp.223-235.

K. Schügerl and K.H. Bellgardt, 2000, Bioreaction Engineering, Modeling and Control, Springer-Verlag Berline Heidelberg, New York.

R.J. Cardello and K.Y. San, 1988, The design of controllers for batch bioreactors. Biotechnology and Bioengineering, vol. 32, pp.519-526.

S. Starzak, M. Krzystek, L. Nowicki and H. Michalski, 1994, Macroapproach kinetics of ethanol fermentation by *Saccharomyces cerevisiae*: experimental studies and mathematical modelling. The Chemical Engineering Journal, vol. 54, pp. 221-240.

T. Firmansyah and Y. Samyudia, 2010, Robust Nonlinear Control Systems Design, Lambert Academic Publishing.

I.A. Karimi and Rajagopalan Srinivasan (Editors), Proceedings of the 11th International Symposium on Process Systems Engineering, 15-19 July 2012, Singapore.

Real Time Model Predictive Control of a Four Tank Interacting Storage System

B.Rajasekhara Reddy, Prabirkumar Saha

Department of Chemical Engineering, IIT Guwahati, Assam 781039, INDIA

Abstract

In this paper, two Model Predictive Control algorithms *viz*., Linear and Nonlinear Dynamic Matrix controller (DMC) have been implemented on a four tank interacting liquid storage system. The process is a Two Input Two Output (TITO) nonlinear system and is equipped with data acquisition facility. A mechanisic dynamic model of the process has been developed based on the mass balance equations and model parameters are estimated using experimental data. The performance of the predictive controllers (DMC and NLDMC) have been evaluated through both simulation and experimental studies.

Keywords: Four Tank Interacting Liquid Storage System, Model Predictive Control, Dynamic Matrix Control, Real Time Control.

1. Introduction

Model Predictive Controllers (MPC) have been an attractive research theme by control engineers for decades, however, their use in the real-time control application has been quite limited. Dynamic Matrix Controller (DMC) is a type of MPC which has perhaps been the only MPC that has been applied in the Advanced Process Control (APC) technique in the industrial application (Bequette 2003). Application of other MPCs, especially nonlinear MPCs, would be quite a challenge for control engineers. This research group is actively involved in the investigation for typical bottlenecks which are responsible for hindrance to the comprehensive success of real-time MPC applications. Significance of this work is the development of a complete protocol package (C++ based) for real-time implementation of MPC. This protocol is portable across other process systems with minimum changes required. Customized Object Oriented Program (OOP) can be generated for a nonlinear MPC and readily implemented for any process with minimum or no changes in the main protocol. Initial success has been reported in this work with real-time nonlinear MPC application. Further research is going on for more elaborate study on this issue.

In this paper, DMC and NLDMC have been implemented for a complex and interacting chemical process *viz*., four tank interacting liquid storage system (Patra and Saha, 2012). The process has four interconnected tanks among which two are interacting. The development of model of the process and control laws thereof have been discussed in the subsequent sections. Successful implementation of these control techniques in real-time application would encourage one to try other complex MPC strategies too.

2. Model of Four Tank Liquid Storage System

Fig. 1 demonstrates the four tank liquid storage system. The process consists of four similar sized overflow type cylindrical tanks whose maximum possible level is 25 cm.

Tank 1 and 3 are placed at same height and they are interconnected. Thus they have interacting mutual behaviour. Tank 2 and Tank 1 are in series, whereas Tank 4 and Tank 3 are in series. The tanks are fitted with level measuring transducers that send a signal of 4-20 mA on a linear scale against liquid level. Two metering pumps are also there to feed the tanks at a maximum possible flow rate of 30 L/min. The pumps can be regulated using 4-20 mA signal. The online data is acquired through ADAM 4022T (Advantech® Co. Ltd.) data acquisition card.

Thus the process has two inputs F_1 and F_2 through two pumps. These inputs are bifurcated to serve the Tanks 1 & 4 and Tanks 2 & 3 respectively. Let m and n be the fractions of F_1 and F_2 which are respectively fed to Tanks 1 and 3. Non-interacting outlets of the tanks *viz*., F_{o1}, F_{o2}, F_{o3}, and F_{o4} are proportional to the square roots of their respective liquid heights of the tanks. Interacting outlet of Tank 1 or 3, *viz*. F_{o5} is proportional to the square root of the difference of heights of liquid in Tanks 1 & 3. The direction of flow F_{o5} is dependent upon the liquid height in the tanks 1 & 3. The flow will take place from higher level to the lower level.

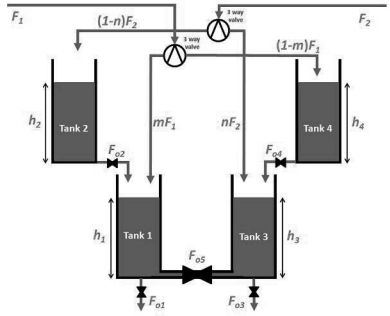

Fig. 1: Four tank storage system

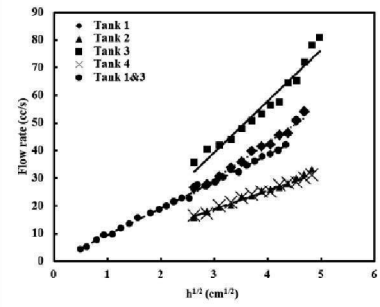

Fig. 2: Data for model parameters c_1-c_5

The model can be developed based on first principles of material balance theory. The relevant ordinary differential equations are summerized as follows:

$$\alpha \frac{dh_1}{dt} = mF_1 + c_2\sqrt{h_2} - fc_5\sqrt{|h_1 - h_3|} - c_1\sqrt{h_1} \quad (1)$$

$$\alpha \frac{dh_2}{dt} = (1-n)F_2 - c_2\sqrt{h_2} \quad (2)$$

$$\alpha \frac{dh_3}{dt} = nF_2 + c_4\sqrt{h_4} + fc_5\sqrt{|h_1 - h_3|} - c_3\sqrt{h_3} \quad (3)$$

$$\alpha \frac{dh_4}{dt} = (1-m)F_1 - c_4\sqrt{h_4} \quad (4)$$

where α is the cross sectional area of the tank(s), c_1-c_5 are the valve constants, $f = 1$ if $h_1 > h_3$ and $f = (-1)$ if $h_1 < h_3$. The diameter of the tank is 9.2 cm and hence the cross sectional area is 66.48 cm^2. In order to estimate the valve constants, various steady state conditions were generated in those tanks and the corresponding flow rates and level measurements were recorded, as plotted in Fig. 2. The figure demonstrates steady state flow rates against the square roots of their corresponding liquid heights in the tank. A linear regression analysis would yield the following values of valve constants: c_1=10.62; c_2=14.53; c_3=6.48; c_4=6.377; c_5=9.613. It is also assumed that both inputs of

the system are equally divided and fed into their respective tanks. Hence, m=n=0.5 for this study.

3. Derivation of DMC controller for Liquid Storage System

The DMC can be designed as per the procedure cited by Bequette (2003). With control horizon of 1 and no weights on control move, the feedback gain matrix for DMC is

$$K = \left(S_f^T S_f\right)^{-1} S_f^T \tag{5}$$

Where S_f is matrix containing step response coefficient. Since deviation variable is used for all manipulated inputs and controlled outputs, the unforced error vector would be $P \times 1$ vector $\left(\bar{h}_{i,sp} - \bar{h}_{is}\right)$ where P is the prediction horizon, $\bar{h}_{i,sp}$ is the setpoint vector. The DMC control law would be

$$F_i = F_{is} + K_j\left(\bar{h}_{j,sp} - \bar{h}_{js}\right) \tag{6}$$

Here $F_{is}, i = 1,2$ are values of flow inputs at steady state, $h_{js}, j \in 1,4$ are liquid levels of tanks 1-4 at steady state, K_j are corresponding feedback gain matrices of DMC. In order to formulate the S_f matrix, step response curves were generated for levels in tanks by introducing small step inputs to F_1 and F_2 at their respective steady state conditions *i.e.* F_{1s} and F_{2s}.

4. Derivation of Nonlinear DMC

Unlike DMC, where step response coefficients are fixed for the entire operation, the nonlinear DMC is operated on the basis of stepwise linearization and re-calculation of step responses at each sampling instant (Gattu and Zafiriou, 1992). For simulation study, the nonlinear meachanistic model, *i.e.* eq. (1) to (4), can be linearized analytically; whereas for real-time control study, numerical derivative can be used if the confidence on the process model is not established. In the present case, analytical linearization is done for both simulation and experimental studies. Using mathematical identity, $|x| \approx \frac{2x}{\pi}\tan^{-1}(kx)$, eqs.(1) to (4) can be linearized as

$$\begin{bmatrix} \frac{dh_1}{dt} \\ \frac{dh_2}{dt} \\ \frac{dh_3}{dt} \\ \frac{dh_4}{dt} \end{bmatrix} = \begin{bmatrix} \left(\frac{-c_1}{2\alpha\sqrt{h_{1s}}} - \frac{c}{\alpha}\right) & \left(\frac{c_2}{2\alpha\sqrt{h_{2s}}}\right) & \left(\frac{c}{\alpha}\right) & 0 \\ 0 & \left(\frac{-c_2}{2\alpha\sqrt{h_{2s}}}\right) & 0 & 0 \\ \left(\frac{c}{\alpha}\right) & 0 & \left(\frac{-c_3}{2\alpha\sqrt{h_{3s}}} - \frac{c}{\alpha}\right) & \left(\frac{c_4}{2\alpha\sqrt{h_{4s}}}\right) \\ 0 & 0 & 0 & \left(\frac{-c_4}{2\alpha\sqrt{h_{4s}}}\right) \end{bmatrix} \begin{bmatrix} h_1 \\ h_2 \\ h_3 \\ h_4 \end{bmatrix} + \begin{bmatrix} \frac{m}{\alpha} & 0 \\ 0 & \frac{1-n}{\alpha} \\ 0 & \frac{n}{\alpha} \\ \frac{1-m}{\alpha} & 0 \end{bmatrix} \begin{bmatrix} F_1 \\ F_2 \end{bmatrix} = A \begin{bmatrix} h_1 \\ h_2 \\ h_3 \\ h_4 \end{bmatrix} + B \begin{bmatrix} F_1 \\ F_2 \end{bmatrix} \tag{7}$$

where,

$$c = fc_5\left\{\frac{1}{\pi\sqrt{|h_{1s}-h_{3s}|}}\right\}\left\{\tan^{-1}(k|h_{1s}-h_{3s}|)\frac{k|h_{1s}-h_{3s}|}{1+(k|h_{1s}-h_{3s}|)^2}\right\} \quad (8)$$

With a sampling period of T and identity matrix I, The state space matrices in eq. (7) is discretized as

$$\Phi = e^{AT} \quad (9)$$

$$\Gamma = A^{-1}(e^{AT} - I)B \quad (10)$$

$$e^{AT} = \sum_{n=0}^{\infty}\frac{(AT)^n}{n!} \quad (11)$$

The step response coefficients can be updated as

$$S_f = \sum_{j=1}^{i} C\Phi^{j-1}\Gamma \; ; i \in 1, P \quad (12)$$

The performance of nonlinear DMC is evaluated through simulation and experimental studies as described in the following section.

5. Results and Discussion

Both the simulation and experimental studies were carried out in a PC with Intel® Core™ 2 Duo CPU P8600 @2.40GHz processor using Windows 7 (64bit) operating system. All the codes have been written in Microsoft® Visual C++(.NET 2003). In this report, the results have been limited to SISO operations only. The level of the Tank 3 has been controlled using pump 1. The prediction and control horizons of DMC has been taken to be 20 and 1 respectively whereas weight on control action is 10.

5.1. Simulation Studies

The Fig.3 shows the simulation results on performance of both DMC and nonlinear DMC.

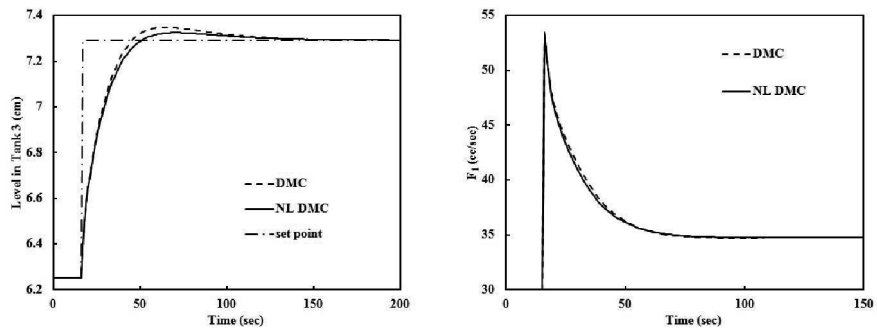

(a) Controlled output (b) Manipulated input

Fig. 3: Closed loop response of level in Tank 3 through simulation

The DMC yields marginally larger overshoot than the nonlinear DMC. The IAE values of DMC and NLDMC performances are 11.49 and 10.99 respectively. However, the IAE values do not show real efficacy of the NLDMC. The merit of the nonlinear controller should be evaluated rather qualitatively than quantitative manner. The profile of manipulated input is almost same for bothe DMC and NLDMC. Not much of advantage is observed by using nonlinear version of DMC.

5.2. Real Time Experimental Studies

The Fig.4 shows the performance of both DMC and nonlinear DMC for real-time control studies on the four tank system.

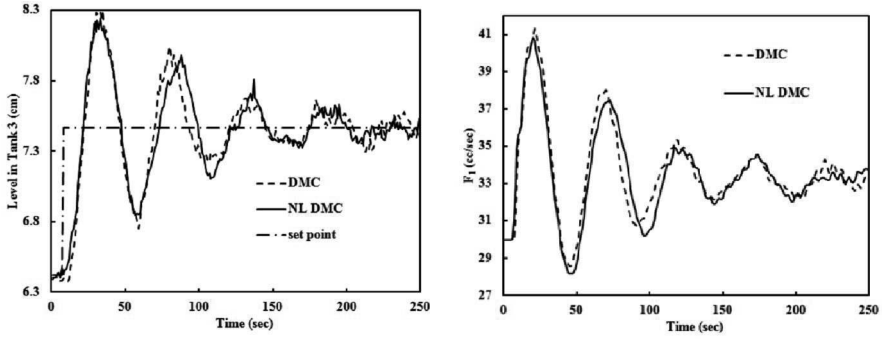

(a) Controlled output (b) Manipulated input

Fig. 4: Real-time closed loop control of level in Tank 3

Unfortunately the performance of NLDMC cannot be claimed to be improved one, though the ISE values show slight improvement (ISE_{DMC}=27.18 and ISE_{NLDMC}=24.27). The unsatisfactory improvement of NLDMC over DMC can be attributed to the physical limitation for actuation by metering pump. It has been observed that full fledged flow would lead to overflow of the tank. This fact compels the operator to put tight and narrow constraint on F_1, thereby limiting the process operation within a fairly linear zone of operation. This problem can be solved by suitable alteration in the process (*e.g.* making bypass line for release of excess water) so that one can employ full range of manipulation and obtain satisfactory improvement of NLDMC over DMC. Moreoever, the analytical linearization of mechanistic model doesn't accurately match with the actual derivative of the process, a numerical derivative could be better option.

6. Conclusion

Two basic structures of model predictive controllers, *viz*., DMC and nonlinear DMC have been employed for controlling a four tank interacting liquid storage system through both simulation and real-time control application. Substantial improvement in controller performance by incorporating nonlinear component hasn't been observed. This limitation can be attributed to the physical limitation for actuation by metering pump. Further modification in the process and/or incorporating numerical derivative would enhance the chance of better performance with nonlinear control application on four-tank system. This paper has been limited only to SISO application, however, MIMO application is under progress which would be reported elsewhere in future.

References

B. W. Bequette, 2003, Process Control-Modelling Desing and Simulation (Prentice Hall, India 2003).

G. Gattu and E. Zafiriou, 1992, Nonlinear Quadratic Dynamic Matrix Control with State Estimation, Ind. Eng. Chem. Res., 31, 4, 1096-1104

S. Patra and P. Saha, 2012, Modeling and Control of a Complex Interacting Process, Advanced Materials Research, 403-408, 3758-3762

I.A. Karimi and Rajagopalan Srinivasan (Editors), Proceedings of the 11th International Symposium on Process Systems Engineering, 15-19 July 2012, Singapore

Approximate Dynamic Programming based control for Water Gas Shift reactor

Sudhakar M Sridharakumar Narasimhan * Niket S Kaisare
Department of Chemical Engineering, IIT Madras, Chennai-36, India.

Abstract

The Water Gas Shift (WGS) reactor is an important component in a fuel processing system. It is necessary to maintain low CO levels during steady state and transient operation of fuel processing system when used onboard in a vehicle. The WGS reactor plays an important role in this regard. The focus of this paper is a model based controller for the regulation of CO level in the presence of the possible disturbances from upstream temperature and flow rate. The use of model based controllers such as nonlinear Model Predictive Control (nMPC) suffers from large computational load. On the other hand Approximate Dynamic Programming (ADP) based controller will result in better performance with lower computational load. In this paper, a non-adiabatic WGS reactor modeled by hyperbolic partial differential equations is considered. The performance of the ADP is illustrated through numerical simulations.

Keywords: Water Gas Shift reactor, Approximate Dynamic Programming, Disturbance rejection

1. Introduction

The Water Gas Shift (WGS) reactor is one of the important reactors in fuel processing system for reducing the carbon monoxide (CO) levels in the reformate which is subsequently required for a PEM Fuel cell. The WGS reaction is mildly exothermic whose conversion is limited by equilibrium temperature. Hence, the reaction is usually carried out in two stages: A high temperature followed by low temperature shift reactor. Alternatively, the WGS reaction could be carried out in a compact, coupled reactor-heat exchanger device, which provides an "optimal" temperature profile to promote the equilibrium-limited WGS reaction [Kim et al. (2005); Baier and Kolb (2007)]. In this paper we have used counter-current reactor with the reactant flowing through one channel and coolant flowing through the other channel.

During the transient operation, the WGS reactor can encounter several disturbances, such as change in the upstream reactant flow rate, temperature and composition. Efficient control of WGS reactor is therefore essential to minimize the effect of the disturbances on CO conversion. Varigonda et al. (2004) have designed Linear Quadratic Regulator (LQR) based control for the nonlinear plant by using a linear model which is linearized at three different operating points to address the nonlinear nature of the plant. Wright and Edgar (1994) have used nMPC for the control of fixed bed WGS reactor and the performance was observed to be superior to that of linear or adaptive controllers. Ling and Edgar (1997) have used model based fuzzy gain scheduling which uses several linear models partitioned in the state space. Nevertheless, all these efforts conclude that use of nonlinear model would have better performance over other approximations with the

*sridharkrn@iitm.ac.in

limitation on excessive online computational load. This paper illustrates the potential of using Approximate Dynamic Programming (ADP) strategy for the control of a coupled WGS reactor resulting in a significant reduction of computational cost.

2. Mathematical model and simulation of WGS Reactor

A 1-D transient model of parallel plate reactor-heat exchanger device is considered. The reactor has the following dimensions with length (l) : 50 mm, breadth (b) :40 mm and height (h): 0.5 mm. The model consists of the following equations for species balance, and energy balances for reacting and coolant streams:

$$\frac{\partial Y_i}{\partial t} = -v_r \frac{\partial Y_i}{\partial x} - \frac{\rho_{cat} r_i}{C} \text{ where } i = \text{CO, } \text{CO}_2\text{, } \text{H}_2\text{, } \text{H}_2\text{O, } \text{N}_2 \tag{1}$$

$$\frac{\partial T_r}{\partial t} = -v_r \frac{\partial T_r}{\partial x} + \frac{Ub}{CAc_{p,r}}(T_c - T_r) + \frac{\rho_{cat} r(-\Delta H_r)}{Cc_{p,r}} \tag{2}$$

$$\frac{\partial T_c}{\partial t} = v_c \frac{\partial T_c}{\partial x} - \frac{Ub}{A\rho_{air} c_{p,air}}(T_c - T_r) \tag{3}$$

where C is the total concentration, U is the overall heat transfer coefficient and Y represents the mole fraction. Note that the axial dispersion and wall conduction have been neglected in the above expressions, resulting in a set of hyperbolic PDEs. The WGS reaction considered is $\text{CO} + \text{H}_2\text{O} \rightarrow \text{CO}_2 + \text{H}_2$; $\Delta H_r = -48.4$ kJ/mol and the kinetics of the WGS reaction is given by (Ref Kim et al. (2005))

$$r = kP_{\text{CO}}P_{\text{H}_2\text{O}}\left(1 - \frac{P_{\text{CO}_2}P_{\text{H}_2}}{KP_{\text{CO}}P_{\text{H}_2\text{O}}}\right), \ \frac{\text{mol}}{\text{g}_{\text{cat}}\ \text{s}} \tag{4}$$

with $k = 0.00225\exp(\frac{-50{,}000}{RT})$ and $K = 9.543 \times 10^{-3}\exp(\frac{39{,}876}{RT})$.

The values of ρ_{cat}, ρ_{air}, $c_{p,air}$, $c_{p,r}$ and U are taken to be 10^3 kg/m^3, 0.883 kg/m^3, 1009 J/kg K, 34 J/mol K and 37 W/m^2 K respectively. The inlet to the reactor is assumed to be of constant composition (mole fraction) typical to that of reformer outlet ($\text{CO} : 0.06$, $\text{CO}_2 : 0.1$, $\text{H}_2 : 0.29$, $\text{H}_2\text{O} : 0.25$, $\text{N}_2 : 0.30$). The inlet steady state reactant temperature and inlet air temperature are 700 K and 450 K respectively. We assume negligible pressure drop in the reactor and the operating pressure is 303 kPa.

3. Online Control using Approximate Dynamic Programming (ADP)

The control objective is to regulate the CO conversion to steady state value using available manipulated inputs in the presence of disturbances. The disturbance considered are changes in inlet reactant flow rate and temperature with inlet air flow rate and inlet steam flow rate considered as manipulated variables. The control problem becomes non-square with two manipulated variables and single control variable (conversion). An additional constraint is that the inlet steam can only be added and not removed from the inlet reactant stream. In order to simplify the analysis, we assume that steam flow rate is linearly related to the inlet air flow rate as long as the steam flow rate is greater than the corresponding nominal steady state flow rate. Hence, in this analysis, the only manipulated variable is the inlet air flow rate and the steam flow rate is a piece wise linear function of the air flow rate.

Model predictive control is a well established model based control technique which depends on open loop model prediction and online optimization at every sampling time step. The typical objective function solved online at k^{th} sampling instant considering infinite horizon prediction length is given by,

$$J(x_k) = \min_{u(k,\ k+1,\ldots)} \sum_{i=k}^{i=\infty} \left(Q(y_{i+1} - y_{sp})^2 + R\Delta U_i^2 \right) \tag{5}$$

where y_{sp} is the desired CO conversion. Since the infinite-horizon control problem is not tractable, a finite horizon nMPC is implemented with prediction horizon p = 25 and input horizon m = 1 and the results are shown in figure 1 for two different disturbances (disturbance 1: 20% step down in inlet temperature and disturbance 2: 20% step down in inlet temperature and inlet flow rate). The computational requirement for 2.5 seconds of closed loop simulation is around 3413.10 seconds and 3303.91 seconds for disturbance 1 and 2 respectively.

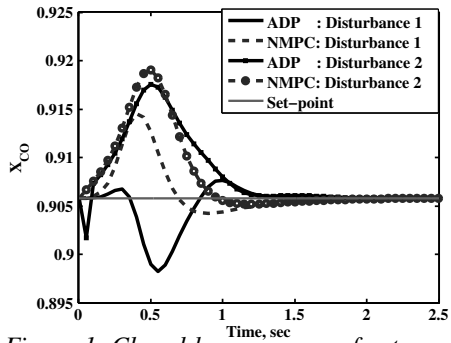

Figure 1. Closed loop response for two disturbances given by ADP and nMPC with $p = 25$ and $m = 1$

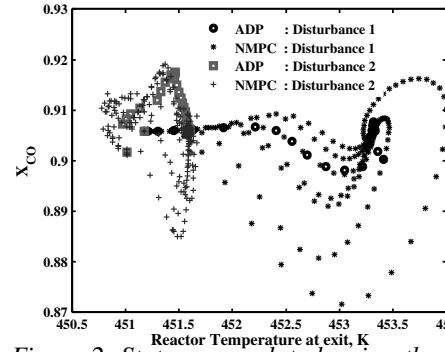

Figure 2. State space plot showing the path traced by the ADP in the operating region

As seen above, the computational requirement for the implementation of nMPC is significant as an open loop, multi-step nonlinear optimization problem has to be solved at every sampling instant. Dynamic Programming (DP) provides an alternate way of solving the infinite-horizon optimization described in equation 5 by solving the following equivalent one-stage problem:

$$J(x_k) = \min_{u_k}(\phi(x_k, u_k) + J(x_{k+1});\ \text{where } \phi = Q(y_{k+1} - y_{sp})^2 + R\Delta U_k^2 \tag{6}$$

here $J(x_{k+1})$ is the "cost-to-go" value starting from x_{k+1} to the setpoint, which is estimated through offline solution of Bellman equation, $J^{opt}(x_k) = \min_{u_k}(\phi(x_k, u_k) + J^{opt}(x_{k+1})$.

The computational load in the calculation of cost-to-go values for all the points in the state space increases exponentially as the state dimension increases, which is referred to as 'curse of dimensionality'. ADP overcomes this problem by identifying smaller region in the state space through the closed loop simulation from sub-optimal controllers like MPC, PID etc and using a function approximator for the interpolation of cost-to-go values. The optimal path in reaching the set-point is assumed to lie within this identified region.

In this paper we have used nMPC as the sub-optimal controller and collected about 579 data for disturbance1 and 546 data for disturbance2 respectively by varying prediction

horizon (sampling time of 0.05 seconds is used). For the purpose of interpolating the cost-to-go values, 'K-nearest neighbour (KNN)' function approximator (with K = 4) which interpolates the cost-to-go values from K nearest neighbors based on distance weighted averaging is used.

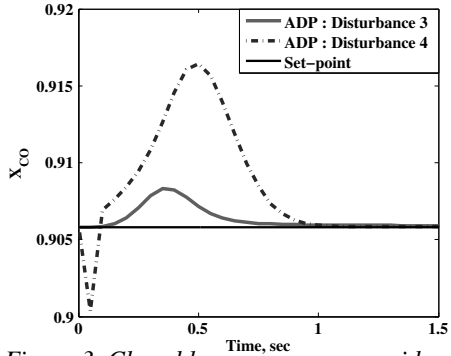

Figure 3. Closed loop response :considering fresh disturbance other than used for generating sub-optimal data

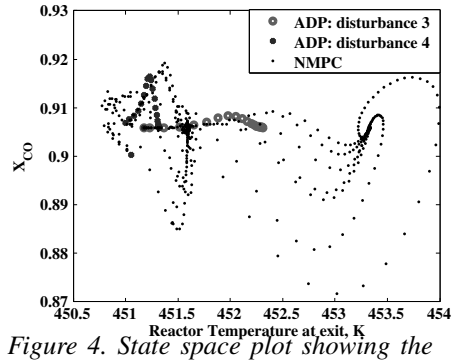

Figure 4. State space plot showing the path traced by the ADP in the operating region with two new setpoints

In order to restrict the search in the region of data density and to avoid excessive extrapolation, quadratic penalty function with Parzen density estimator is used which limits the controller from extrapolating to the region of lower density by assigning higher cost-to-go values to those points outside the region. The Parzen local density estimate for the data set Ω near the query point x_0 is defined as follows,

$$f_\Omega(x_0) = \frac{1}{N}\sum_{i=1}^{KNN}\frac{1}{2\pi\sigma^2}exp\left(\frac{-\|x_0 - x_i\|_2^2}{2\sigma^2}\right);\ \sigma \Rightarrow \text{ user defined parameter} \tag{7}$$

The quadratic penalty function is defined between $\|x_0 - x_i\|_2^2 = \sigma^2$ (with no penalty below this limit) and $\|x_0 - x_i\|_2^2 = 3\sigma^2$ (with maximum penalty, J^{max} after this limit) as follows,

$$J_{penalty}(x_0) = S.H\left(\frac{1}{f_\Omega(x_0)} - \beta\right)\left[\frac{\frac{1}{f_\Omega(x_0)} - \beta}{\beta}\right]^2 \text{ and hence } J(x_0) \Leftarrow J(x_0) + J_{penalty}(x_0) \tag{8}$$

where S is the scaling parameter, β is the threshold value and H is the Heaviside step function. The value of σ is taken as 10 for this study. For further details on the calculation of S, J^{max} and β refer Lee et al. (2006).

The cost-to-go values for the points collected from nMPC are improved by value iteration using the Bellman equation. The one step ahead prediction is obtained by simulating the discretized model equations (20 nodes) and solving the resulting set of ODEs along time in MATLAB. The optimization routine `fmincon` in MATLAB is used for the calculation of minimal cost for each of these points and this cost value is updated at every iteration. The maximum absolute difference between the cost-to-go values of subsequent iteration is monitored for convergence. The final converged cost-to-go values are then used for the online optimization.

The ADP controller is initially tested for the disturbances which was used for the generation of sub-optimal data points. The input(R) and output(Q) weight for online implementation are taken as 10 and 1000 respectively. From the closed loop simulation results

(Refer 1 and 2) and comparison of cost-to-go values (Disturbance 1: 249.83 for ADP and 365.06 for nMPC, Disturbance 2: 1034 for ADP and 1087 for nMPC), it is observed that the performance of ADP is marginally better compared to nMPC. However, the computational load for 2.5 seconds of closed loop simulation is significantly lower: Disturbance 1: 369.98 seconds for ADP and 3413.10 seconds for nMPC, Disturbance 2: 478.5 seconds for ADP and 3303.91 seconds for nMPC.

Next, closed loop performance of the ADP controller is tested for two fresh disturbances (disturbance 3: 15% step down in inlet temperature and disturbance 4: 15% step down in inlet temperature and flow rate) with the same suboptimal data obtained previously. Figures 3 and 4 indicate satisfactory closed loop performance in the presence of these disturbances. This means that given sufficient amount of data considering all the relevant disturbances, ADP could be deployed to reject disturbances in a wide range.

The performance of the ADP controller can be improved by adding relevant data points in the state space. The inclusion of additional points would result in more coverage of state space where optimal path lies and hence the estimate of cost-to-go values for online optimization would be closer to optimal. Although the computational time is considerably lower as compared to nMPC, there is still scope for reducing it further. There are several ways one could address this problem such as use of order reduction techniques, using better function approximation etc.

4. Conclusion

The control of a compact WGS reactor coupled with a heat exchanger is considered. The nonlinear nature of the process and wide operating region necessitates the use of nonlinear model for model based control of the reactor. ADP based controller has been designed for the WGS reactor for disturbance rejection and it has been found that the computational demand of ADP is considerably much smaller than corresponding MPC. Further improvement in computational time is required and the use of Method Of Characteristics (MOC) for model order reduction and prediction is under investigation.

References

Baier, T., Kolb, G., 2007. Temperature control of the water gas shift reaction in microstructured reactors. Chemical Engineering Science 62, 4602–4611.

Kim, G. Y., Mayor, J. R., Ni, J., 2005. Parametric study of microreactor design for water gas shift reactor using an integrated reaction and heat exchange model. Chemical Engineering Journal 110, 1–10.

Lee, J. M., Kaisare, N. S., Lee, J. H., 2006. Choice of approximator and design of penalty function for an approximate dynamic programming based control approach. Journal of Process Control 16, 135 –156.

Ling, C., Edgar, T. F., 1997. Real-time control of a water-gas shift reactor by a model-based fuzzy gain scheduling technique. J. Proc. Cont. 7, 239–253.

Varigonda, S., Eborn, J., Bortoff, S. A., 2004. Multivariable control design for the water gas shift reactor in a fuel processor. In: American Control Conference Proceedings. pp. 840–844.

Wright, G. T., Edgar, T. F., 1994. Nonlinear model predictive control of a fixed-bed water-gas shift reactor: An experimental study. Computers them. Engng 18, 83–102.

I.A. Karimi and Rajagopalan Srinivasan (Editors), Proceedings of the 11th International Symposium on Process Systems Engineering, 15-19 July 2012, Singapore.

Comparison of MIMO MPC and PI Decoupling in Controlling Methyl Tert-butyl Ether Process

Sudibyo, I.M. Iqbal, M.N. Murat and *N.Aziz

School of Chemical Engineering, Engineering Campus, Universiti Sains Malaysia, 14300 Nibong Tebal, Seberang Perai Selatan, Penang, Malaysia.
**E-mail: chnaziz@eng.usm.my*

Abstract

The main control objective of Methyl Tert-butyl Ether (MTBE) reactive distillation is to maintain the MTBE product purity within the desired range at the highest isobutene conversion possible. However, MTBE purity and isobutene conversion have strong interaction, hence need a multiple input – multiple output (MIMO) based control system. In this work, MIMO model Predictive control (MPC) and Proportional Integral (PI) decoupling have been implemented to control both the MTBE purity and isobutene conversion by manipulating the reboiler duty and reflux flowrate. The purity of MTBE is at 99% and the isobutene conversion is at 99.83%. Performance of both controllers are then compared in term of integral absolute error (IAE), integral squared error (ISE), integral of the time-weighted absolute error (ITAE) and settling time. The results showed that the MIMO MPC is better than the PI decoupling.

Keywords: Multivariable processes, PI decoupling, MPC, Reactive distillation; MTBE

1. Introduction

MTBE is well known chemical used as an anti-knock agent to replace tetra ethyl lead [Satyanarayana and Saha, 2005; Sharma and Singh, 2010]. Using reactive distillation, the MTBE conversion can reach up to 99% [Taylor and Krishna, 2000]. The maximum production of the MTBE process can be achieved if the reaction and separation can be kept at the optimum conditions. Therefore, the development of the MTBE reactive distillation control is important to achieve the process which can lead to high yield of MTBE production.

Controlling of this reactive distillation is a challenging task due to its process uncertainties, time delay, strong interactions, the large number of possible control configuration and the complex dynamics arising from the combination of reaction and separation [Satyanarayana and Saha, 2005; Nagya *et al.*, 2007, Kawathekar and Riggs, 2007; Sharma and Singh, 2010]. To control the reactive distillation process, choosing control configuration by selecting the best pairing of manipulated variable (MV) and control variable (CV) is very important [Satyanarayana and Saha, 2005; Nagya *et al.*, 2007]. The degree of the variable interaction and the best pairing of MV and CV can be determined by implementing a singular value decomposition (SVD) test [Luyben, 2006].

Normally, to increase the purity of MTBE and the conversion of isobutene, the reboiler duty and reflux flowrate are manipulated. However, the increase of conversion of isobutene will decrease the MTBE purity, thus this become one of major problem in controlling the MTBE reactive distillation process. PI decoupling and MPC are among

the well known control strategies that can be applied in MTBE reactive distillation control to cater the interaction of the control variables. The aim of this work is to compare the performance of both PI decoupling and MIMO MPC in controlling the MTBE purity and isobutene conversion in the MTBE reactive distillation. Prior to control implementation, the SVD test is carried out to analyze the degree of the variable interaction and also to choose the best pairing of MV and CV.

2. MTBE Reactive distillation

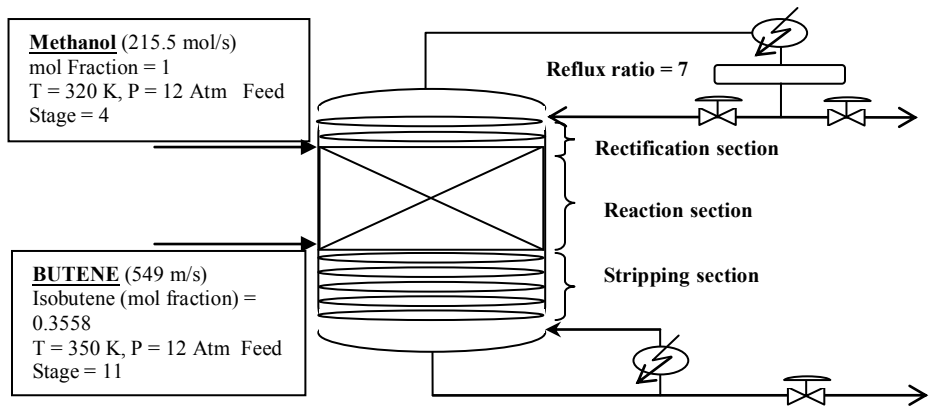

Figure 1. MTBE Reactive Distillation Column Configuration

The specification used here is similar to the specification used by Higler *et al.* [1999], except the number of passes, the pressure column and location of feed stages are different. In this work, 4 passes and 12 atm of pressure column are used while Higler *et al.*[1999] used 5 passes and 11 atm. Meanwhile, the feed, methanol and butane, are fed at stages 4 and 11, respectively. The reaction scheme to produce MTBE is:

$$i\text{-}C_4H_8 + CH_3\text{-}OH \rightleftharpoons C_5H_{12}O \quad (1)$$

In this work, the steady state Aspen simulators were used to simulate the process. Then, the model obtained is exported to Aspen dynamics using flow driven dynamic model.

3. Control Development

3.1. SVD Analysis

SVD test is used to select the best control configuration and to know the degree of interaction among the variables. For SVD test, the reflux flowrate was changed at 0.1 % while the reboiler duty was kept constant and the the reboiler duty was changed at 0.1 % while the reflux flowrate was kept constant [Luyben , 2006]. The result obtained is shown in matrix *k*. Matrix *u* show that the purity of MTBE has the largest magnitude (largest effect) due to reflux flowrate change, while the isobutene conversion has largest magnitude for reboiler duty change. Thus, both pairs of manipulated and control variables are selected. From the SVD analysis (matrix *s*), the condition number was calculated by dividing the large value (8.1×10^{-4}) with the small value (4.5×10^{-6}) of the singular matrix which resulted to 179.4. This means the variable have strong interaction and need the decoupling system to control this process.

$$k = \begin{bmatrix} -6.2764e-4 & 5.0763e-4 \\ 1.11e-5 & -3.2183e-6 \end{bmatrix}; u = \begin{bmatrix} -0.9999 & 0.0132 \\ 0.0132 & 0.9999 \end{bmatrix}; s = \begin{bmatrix} 8.1e-4 & 0 \\ 0 & 4.5e-6 \end{bmatrix}$$

3.2. PI Decoupling scheme

Fig. 2 shows the PI Decoupling scheme for the MTBE process. The decoupling for two inputs and two outputs system are shown below:

$$\begin{bmatrix} T_{1,1(s)} & 0 \\ 0 & T_{2,2\,(s)} \end{bmatrix} = \begin{bmatrix} g_{1,1(s)} & g_{1,2(s)} \\ g_{2,1(s)} & g_{2,2(s)} \end{bmatrix} \times \begin{bmatrix} D_{11(s)} & D_{12(s)} \\ D_{21(s)} & D_{22(s)} \end{bmatrix} \quad (2)$$

where T is the decoupled process matrix, G is the process matrix and D is the decoupling matrix. The input interaction in transfer function G (process) can be eliminated by introducing decoupling matrix D , as shown in figure 3 [Yaghoubi and Shahmansoorian, 2011]. $T_{1,1\,(s)}$ and $T_{2,2\,(s)}$ can be set equal to one, then the matrix D can be determined by choosing two from four element of matrix D as c_1 and c_2. Here, c_1 and c_2 are assumed equal to one. Hence, the matrix D can be obtained as shown below:

$$D = \begin{bmatrix} c_1 & -\frac{g_{12}.c_2}{g_{11}} \\ -\frac{g_{21}.c_1}{g_{22}} & c_2 \end{bmatrix} = \begin{bmatrix} 1 & -\frac{g_{12}.1}{g_{11}} \\ -\frac{g_{21}.1}{g_{22}} & 1 \end{bmatrix} \quad (3)$$

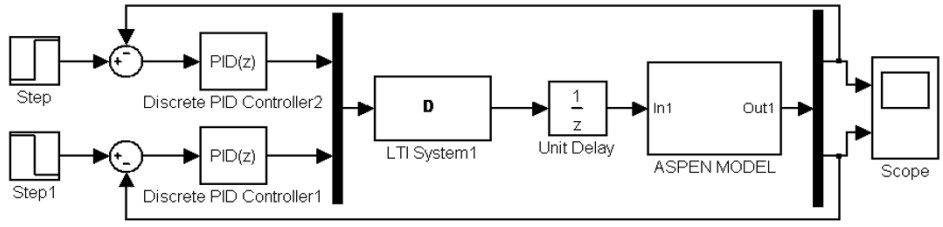

Figure 2. PI Decoupling scheme for the MTBE process

3.3. MIMO MPC Scheme

The MPC objective function (j_k) for two inputs and two outputs (2 x2) is defined as [Kawathekar and Riggs, 2007]:

$$j_k = \sum_{i=1}^{P} \left((y_{f1|k+i} - y_{sp1|k+i})^2 Q_1 + (y_{f2|k+i} - y_{sp2|k+i})^2 . Q_2 \right) + \left(\Delta u_{f1|k+i} \right)^2 . R_1 + \left(\Delta u_{f2|k+i} \right)^2 . R_2 \quad (4)$$

where y_f is a predicted future output, y_{sp} is a set point, Q is an error penalty, R is an input change penalty, Δu_f is a future input change and k is a current sampling time. In this work, for MIMO MPC, the Aspen dynamics model is used to represent the process, the state space equations as the process model and the quadratic programming as an optimizer. The MIMO MPC scheme for MTBE process is shown in figure 3.

3.4. State space model

To generate data for state space model development, two generalized multiple-level noise (GMN) signals are used as input signal to the Aspen dynamics based model which is integrated in Matlab simulink block. One third of 98% process settling time is used as the average switching time for the excitation signal [Arefi *et al., 2008*]. The GMN signal has 11 input levels from +7% to -7% of the input nominal value. In this test, the GMN generate data for 30 hours. The generated data was then used in the system identification to develop the state space model of the process. The state space model obtained is used in both PI decoupling and MIMO MPC. The state space model obtained is:

$$x(t+Ts) = A\,x(t) + B\,u(t) + K\,e(t) \quad (5)$$
$$y(t) = C\,x(t) + D\,u(t) + e(t) \quad (6)$$

where:

$$A = \begin{bmatrix} 0.73897 & -0.042774 & 0.060387 & 0.02007 \\ -0.34542 & 0.7133 & 0.31961 & 0.30447 \\ 0.24956 & 0.44335 & 0.34635 & -0.7272 \\ 0.035443 & 0.059417 & -0.11259 & 0.61541 \end{bmatrix} \quad B = \begin{bmatrix} -1.3786 & 1.5398 \\ -4.2 & 4.1893 \\ 6.4984 & -5.8288 \\ 1.1353 & -0.38649 \end{bmatrix}$$

$$C = \begin{bmatrix} 0.20528 & 0.10429 & 0.10847 & -0.11637 \\ -0.0039021 & 0.0034986 & 0.0019554 & -0.00039005 \end{bmatrix}$$

while D, u and x are matrix zero with size (2x2), (4 x 2) and (4 x 1), respectively.

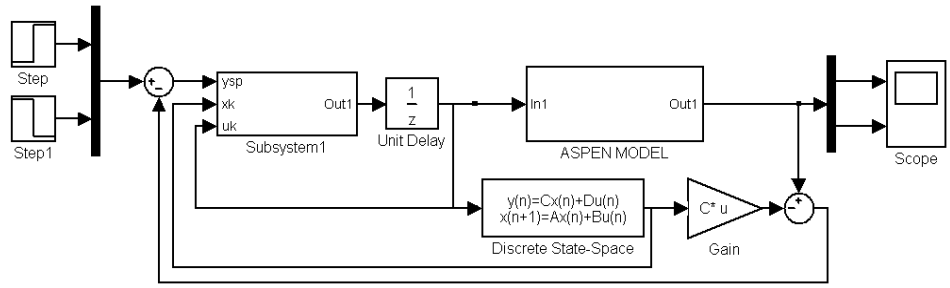

Figure 3. MIMO MPC scheme for MTBE process

4. Results and Discussion

The result of the PI and MIMO MPC tuning is shown in Table 1. CV1 is referring to MTBE purity (set point at 99%) and CV2 is referring to conversion of isobutene (set point at 99.83%). Meanwhile, figure 4 shows the response of both controllers proposed. The figure shows that when using PI decoupling, the settling time for the MTBE process is more than 2 hours from the time when the step setpoint is introduced. Meanwhile less than one hour settling time is required when MIMO MPC is used. For the CV2, the settling time given by PI decoupling and MIMO MPC are 4 and 1 hours, respectively. Table 2 tabulated the value of IAE, ISE and ITAE values for both PI Decoupling and MIMO MPC. The table shows that the MIMO MPC produces lower error value if compared to PI decoupling, thus proved that MIMO MPC better than PI decoupling.

Table 1. PI Decoupling and MIMO MPC setting after tuning

PI Decoupling :	CV 1	CV 2	MIMO MPC :	CV1	CV 2
Proportional (P)	-0.44	-173.45	Penalty error (Q)	2	3
Integral (I)	-53.045	-6446.98	Input changes penalty (R)	0.00015	0.01
			Input change constraint	±10%	±10%

Table 2. Performance of PI decoupling and MIMO MPC

PI Decoupling			MIMO MPC	
	CV1	CV2	CV1	CV2
IAE (%)	3.42	3.20×10^{-2}	0.25	7.83×10^{-3}
ISE (%)	0.10	8.39×10^{-6}	3.56×10^{-3}	6.52×10^{-7}
ITAE (%)	5.61	5.27×10^{-2}	0.47	1.56×10^{-2}
Settling Time	2 hr	4 hr	0.6 hr	1 hr

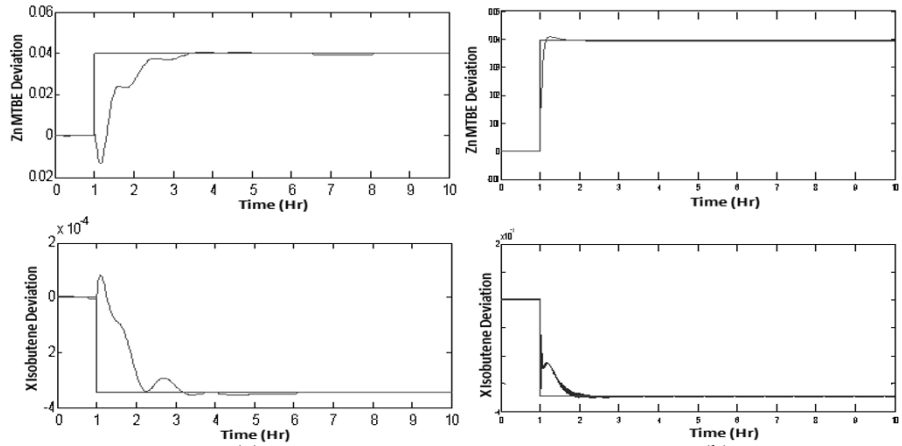

(a) (b)

Figure 4. Response of (a) PI decoupling (b) MIMO MPC

5. Conclusion

PI decoupling and MIMO MPC have successfully designed and implemented to control the MTBE reactive distillation in order to maintain the purity of MTBE at 99% and isobutene conversion at 99.83%. From the results, the MIMO MPC outperformed the PI decoupling in all performances criteria considered.

Acknowledgement

The financial support from Universiti Sains Malaysia through Research University (RU) Grant and Graduate Assistant (GA) to the first author are greatly acknowledged.

References

A.P. Higler, R. Taylor and R. Krishna, 1999, The influence of mass transfer and mixing on the performance of a tray column for reactive distillation, Chem. Eng. Science, 54, 2873-2881

D.E. Seborg, T. F. Edgar, D. A. Mellichamp and F.J. Doyle, 2011, Process dynamics and control, 3rd ed., John Wiley.

M.M. Arefi, A. Montazeri, J. Poshtan and M.R. Jahed-Motlagh, 2008, Wiener-neural identification and predictive control of a more realistic plug-flow tubular reactor, Chemical Eng. Journal, 138, 274-282.

N. Sharma and K.Singh, 2010, Control of Reactive Distillation Column: A Review, Int. J. Chemical Reactor Eng., 8, R5

R.K. Pearson, 2003, Selecting Nonlinear model structures for computer control, Journal of process control, 13, 1-26

R. Kawathekar, J.B. Riggs, 2007, Nonlinear model predictive control of a reactive distillation column, Control Engineering Practice, 15, 231–239

R. Taylor and R. Krishna, 2000, Review: Modelling reactive distillation, Chem. Eng. Science, 55, 5183-5229.

T. Satyanarayana and P. Saha, 2005, Modeling and Control Structure Selection for Reactive Distillation Process using Aspen Custom Modeler, CHEMCON – 05, New Delhi.

W. L. Luyben, 2006, Evaluation of criteria for selecting temperature control trays in distillation columns, Journal of Process Control, 16, 115–134.

Z. Yaghoubi, A. Shahmansoorian , 2011, Inverted decoupler and PID controller design for MIMO processes with time delays, Canadian J. on Electrical and Electronics Eng., 2, No. 6.

I.A. Karimi and Rajagopalan Srinivasan (Editors), Proceedings of the 11th International Symposium on Process Systems Engineering, 15-19 July 2012, Singapore

MPC for LPV systems using perturbation on control input strategy

Pornchai Bumroongsri, Soorathep Kheawhom *

Department of Chemical Engineering, Faculty of Engineering, Chulalongkorn University, Bangkok, Thailand

Abstract

In this paper, a model predictive control (MPC) algorithm for linear parameter varying (LPV) systems is proposed. The proposed algorithm consists of two steps. The first step is derived by using parameter-dependent Lyapunov function and the second step is derived by using the perturbation on control input strategy. An overall algorithm is proved to guarantee robust stability. The controller design is illustrated with a case study of continuous stirred-tank reactor. Comparisons with other MPC algorithms for LPV systems have been undertaken. The results show that the proposed algorithm can achieve better control performance.

Keywords: MPC, LPV, parameter-dependent Lyapunov function, perturbation on control input strategy, continuous stirred-tank reactor

1. Introduction

Model predictive control (MPC) is an effective control algorithm widely used in the chemical processes. At each sampling time, MPC uses an explicit process model to solve an open-loop optimization problem and implements only the first element of input sequence. MPC based on linear model is typically used because the on-line optimization problem can be formulated as the convex optimization problem by either linear programming or quadratic programming (Kothare et al. , 1996). This is a good assumption for typical processes. However, most of the chemical processes are nonlinear. Thus, when the operating conditions undergo significant changes, the performance of linear MPC can deteriorate drastically. Moreover, the stability of the control system cannot be guaranteed.

In Kothare et al. (1996), min-max predictive control strategy was presented. The nonlinear system is approximated by the polytopic uncertain system. The goal is to design a state feedback control law which minimizes the worst-case performance cost. The algorithm is proved to guarantee robust stability. However, the algorithm turns out to be conservative because the nonlinear system is approximated by the polytopic uncertain system. Moreover, the scheduling parameter is not considered in the controller synthesis. In order to reduce the conservativeness, the idea of controlling nonlinear systems by using linear parameter varying (LPV) systems has been widely investigated. At each sampling instant, the scheduling parameter is measured on-line.

In Lu et al. (2000), Quasi-min-max MPC algorithm for LPV systems was presented. The control input is computed by minimizing the quasi-worst-case performance cost. The algorithm is seen as an extension of the algorithm presented in Kothare et al. (1996) by keeping the first control input as a free decision variable. The algorithm is proved to

*soorathep.k@chula.ac.th

guarantee robust stability. However, an invariant ellipsoid constructed to guarantee robust stability is derived by using a single Lyapunov function. Thus, the conservative result is still obtained. A feedback min-max MPC algorithm for LPV systems subject to bounded rates of change of parameters was presented in Casavola et al. (2002) . The algorithm in Lu et al. (2000), where open-loop MPC scheme is limited to one step control horizon, is extended to the general case of control horizon of arbitrary length N. The perturbation on control input strategy is developed in order to improve control performance. However, this strategy cannot guarantee robust stability due to the fact that the constraint on terminal invariant set is not explicitly imposed. Moreover, robust constraint satisfaction before switching horizon N cannot be guaranteed (Ding and Huang , 2007).

In this work, the closed-loop MPC strategy for LPV systems is developed. The proposed algorithm consists of two steps. The first step is derived by using parameter dependent Lyapunov function (Wada et al. , 2006). In the second step, the perturbation on control input strategy is introduced to improve control performance. Moreover, the algorithm in the second step is developed such that it can be implemented with a state feedback gain derived by using parameter-dependent Lyapunov function, and robust stability and constraint satisfaction for the whole algorithm can be guaranteed.

2. Problem Description

The model considered here is the following discrete-time LPV system

$$x(k+1) = A(p(k))x(k) + Bu(k), \tag{1}$$

where $x(k)$ is the state of the plant. $u(k)$ is the control input. We assume that the scheduling parameter $p(k)$ is measurable on-line at each sampling time k. Moreover, we assume that $A(p(k)) \in \Omega, \Omega = Co\{A_1, A_2, ..., A_L\}$, where Ω is the polytope. Co denotes convex hull. A_j are vertices of the convex hull. Any $A(p(k))$ within the polytope Ω is a linear combination of the vertices such that $A(p(k)) = \sum_{j=1}^{L} p_j(k)A_j, \sum_{j=1}^{L} p_j(k) = 1, 0 \leq p_j(k) \leq 1$. Further, let $\chi_K^{k+i}(x(k)) = Co\{\bar{\Phi}_K(p^{k+i-1})x(k)\}$ denotes the closed convex hull of all i-steps state trajectories from x at time k under the state-feedback gain K where $\Phi_K(p(k)) = A(p(k)) + BK$ and $\bar{\Phi}_K(p^{k+i-1}) = \Phi_K(p(k))\Phi_K(p(k+1))\Phi_K(p(k+2))...\Phi_K(p(k+i-1))$.

The above sets can be computed according to $\chi_K^{k+i}(x(k)) = Co\{\Phi_K(p(k+i-1))z, \forall z \in vert\{\chi_K^{k+i-1}(x(k))\}, \forall p(k+i-1) \in P^{K+i-1}\}$, and $P^{K+1} = vert\{Co\{p(k) \pm \Delta p\}\}$, $P^{K+2} = vert\{Co\{p(k+1) \pm \Delta p\}\}$, $P^{K+i-1} = vert\{Co\{p(k+i-2) \pm \Delta p\}\}$, where Δp is the bounded parameter variation and it is assumed to be known and *vert* denotes the vertices of the polytope.

The aim of this research is to find a state feedback regulation $u(k) = g(x(k))$, which stabilizes Eq. 1 and achieves the following performance cost

$$\min_{u(k+i/k)} \max_{A(p(k+i)) \in \Omega, i \geq 0} \sum_{i=0}^{\infty} \begin{vmatrix} x(k+i/k) \\ u(k+i/k) \end{vmatrix}^T \begin{vmatrix} \Theta & 0 \\ 0 & R \end{vmatrix} \begin{vmatrix} x(k+i/k) \\ u(k+i/k) \end{vmatrix}, \tag{2}$$

where $\Theta > 0$ and $R > 0$ are symmetric weighting matrices, subject to constraints

$$|u_h(k+i/k)| \leq u_{h,max}, h = 1, 2, 3, ..., n_u, \tag{3}$$

$$|y_r(k+i/k)| \leq y_{r,max}, r = 1, 2, 3, ..., n_y. \tag{4}$$

3. The proposed MPC algorithm for LPV systems

Algorithm 3.1: Step 1: At any sampling time k, measure $x(k)$ and find $\gamma, K_j = Y_j G_j^{-1}, Q_j$ by solving the following problem (Wada et al. , 2006)

$$\min_{\gamma, Y_j, G_j, Q_j} \gamma, \tag{5}$$

$$\text{s.t.} \begin{vmatrix} 1 & * \\ x(k/k) & Q_j \end{vmatrix} \geq 0, \forall j = 1,2,...,L, \tag{6}$$

$$\begin{vmatrix} G_j + G_j^T - Q_j & * & * & * \\ A_j G_j + B Y_j & Q_l & * & * \\ \Theta^{\frac{1}{2}} G_j & 0 & \gamma I & * \\ R^{\frac{1}{2}} Y_j & 0 & 0 & \gamma I \end{vmatrix} \geq 0, \forall j = 1,2,...,L, \forall l = 1,2,...,L, \tag{7}$$

$$\begin{vmatrix} X & * \\ Y_j^T & G_j + G_j^T - Q_j \end{vmatrix} \geq 0, \forall j = 1,2,...,L, X_{hh} \leq u_{h,\max}^2, h = 1,2,...,n_u, \tag{8}$$

$$\begin{vmatrix} S & * \\ (A_j G_j + B Y_j)^T C^T & G_j + G_j^T - Q_j \end{vmatrix} \geq 0, \forall j = 1,2,...,L, S_{rr} \leq y_{r,\max}^2,$$
$$r = 1,2,...,n_y. \tag{9}$$

Step 2: Given $\gamma, K_j = Y_j G_j^{-1}, Q_j$ from step 1, find $C_{\text{opt}} = C(k+i/k)_{i=0}^{N-1}$ by solving the following problem

$$\min_{J_i, C_{\text{opt}}} \sum_{i=0}^{N} J_i, \tag{10}$$

$$\text{s.t.} \begin{vmatrix} J_N & * \\ z(k+N/k) & \gamma^{-1} Q_j \end{vmatrix}, \forall j = 1,2,...,L, \forall z(k+N/k) \in vert\{\chi_K^{k+N}(x(k))\}, \tag{11}$$

$$J_N \leq \gamma, \tag{12}$$

$$|(K_j z(k+i/k) + c(k+i/k))_h| \leq u_{h,\max}, \forall i \in \{0,1,...,N-1\},$$
$$\forall h \in \{1,2,...,N_u\}, \forall z(k+i/k) \in vert\{\chi_K^{k+i}(x(k))\}, \tag{13}$$

$$|(Cz(k+i/k)_r| \leq y_{r,\max}, \forall i \in \{0,1,...,N-1\}, \forall r \in \{1,2,...,N_y\},$$
$$\forall z(k+i/k) \in vert\{\chi_K^{k+i}(x(k))\}, \tag{14}$$

$$\begin{vmatrix} I & * & * \\ \Theta^{\frac{1}{2}} z(k+i/k) & J_i I_{n_x} & * \\ R^{\frac{1}{2}} c(k+i/k) & 0 & J_i I_{n_u} \end{vmatrix} \geq 0, \forall i \in \{0,1,...,N-1\},$$
$$\forall z(k+i/k) \in vert\{\chi_K^{k+i}(x(k))\}. \tag{15}$$

Feed the plant by $u(k) = K(p(k))x(k) + c(k), K(p(k)) = \sum_{j=1}^{L} p_j(k) K_j$.

Theorem 3.1: The control law provided by the algorithm 3.1 assures robust stability to the closed-loop system.

Proof: By applying Schur complement to Eq.11, with Eq.12, we obtain $z(k+N/k)^T \gamma Q^{-1} z(k+N/k) \leq J_N \leq \gamma$ where $Q = \sum_{j=1}^{L} p_j(k) Q_j$. This is equivalent to $z(k+N/k)^T Q^{-1} z(k+N/k) \leq 1, \forall z(k+N/k) \in vert\{\chi_K^{k+N}(x(k))\}$. Thus, the state $x(k+N/k)$ is restricted to lie in an invariant ellipsoid $\varepsilon = \{x / x^T Q^{-1} x \leq 1\}$ and the control law $u(k+i/k) = K(p(k+i))x(k+i/k), i \geq N$ is able to steer the state $x(k+N/k)$ to the origin.

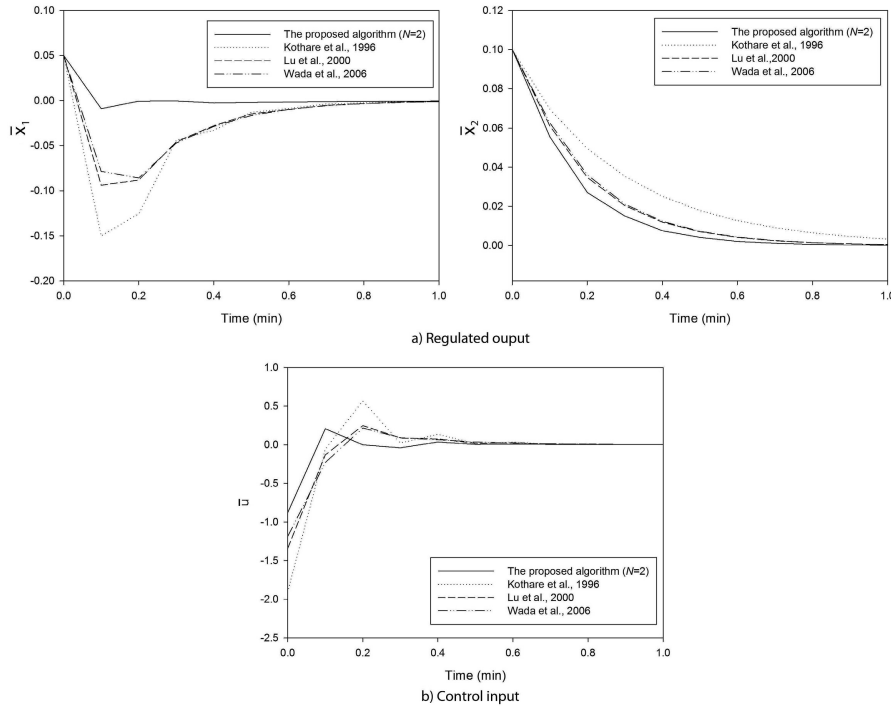

Figure 1. The closed-loop responses of nonlinear CSTR in the case study.

4. Example

The numerical simulations have been performed in Intel Core i-5 (2.4GHz), 2 GB RAM, using YALMIP (Löfberg , 2004) within Matlab R2008a environment.

Consider the following nonlinear model for CSTR where the consecutive reaction $A \rightarrow B \rightarrow C$ takes place

$$\begin{vmatrix} \dot{x_1} \\ \dot{x_2} \end{vmatrix} = \begin{vmatrix} -1-Da_1 & 0 \\ Da_1 & -1-Da_2x_2 \end{vmatrix} \begin{vmatrix} x_1 \\ x_2 \end{vmatrix} + \begin{vmatrix} 1 \\ 0 \end{vmatrix} u, \tag{16}$$

where x_1 and x_2 denote the dimensionless concentration of A and B, respectively. The control input u corresponds to the inlet concentration of A. $Da_1 = 1$ and $Da_2 = 2$ are Damkohler numbers. Here $J_\infty(k)$ is given by Eq. 2 with $\Theta = 10I$ and $R = 0.01$. The objective is to regulate the deviated states $\bar{x}_1$ and $\bar{x}_2$ from 0.05 and 0.1, respectively to the origin by manipulating $\bar{u}$. The input and output constraints are $|\bar{x}_1| \leq 2$, $|\bar{x}_2| \leq 2$ and $|\bar{u}| \leq 2.5$.

Figure 1 shows the closed-loop responses of the system. The proposed algorithm can achieve less conservative result as compared to MPC algorithms of Kothare et al. (1996), Lu et al. (2000) and Wada et al. (2006).

5. Conclusions

In this work, a model predictive control (MPC) algorithm for linear parameter varying (LPV) systems is proposed. The proposed algorithm is derived by using parameter-dependent Lyapunov function with the perturbation on control input strategy. An overall algorithm is proved to guarantee robust stability. The controller design is illustrated with a case study. The results show that the proposed algorithm can achieve better control performance as compared with existing robust MPC algorithms for LPV systems.

Acknowledgement

The authors gratefully acknowledge the financial support provided by the Higher Education Research Promotion and National Research University Project of Thailand, Office of the Higher Education Commission (EN636A)

References

Casavola, A., D. Famularo, G. Franze, 2002. A feedback min-max MPC algorithm for LPV systems subject to bounded rates of change of parameters. IEEE T. Automat. Contr. 47(7), 1147-1152.

Ding, B., B. Huang, 2007. Comments on A feedback min-max MPC algorithm for LPV systems subject to bounded rates of change of parameters. IEEE T. Automat. Contr. 52(5), 970.

Kothare, M.V., V. Balakrishnan, M. Morari, 1996. Robust constrained model predictive control using linear matrix inequalities. Automatica 32 (10), 1361-1379.

L öfberg, J., 2004. YALMIP : A toolbox for modelling and optimization in MATLAB. in Proceedings of the 2004 IEEE international symposium on computer aided control systems design, Taipei, Taiwan, 284-289.

Lu, Y., Y. Arkun, 2000. Quasi-min-max MPC algorithms for LPV systems. Automatica 36 (4), 527-540.

Wada, N., K. Saito, M. Saeki, 2006. Model predictive control for linear parameter varying systems using parameter dependent lyapunov function. IEEE T. Circuits Syst. 53(12), 1446-1450.

I.A. Karimi and Rajagopalan Srinivasan (Editors), Proceedings of the 11th International Symposium on Process Systems Engineering, 15-19 July 2012, Singapore.

Systematic Specification of a Logic Controller for a Delayed Coking Drum[1]

Stephan Fischer,[a] Herbert Teixeira,[b] Sebastian Engell[a]

[a] *Process Dynamics and Operations Group, Department of Biochemical and Chemical Engineering, TU Dortmund, 44221 Dortmund, Germany*
[b] *PETROBRAS / CENPES, Av. Horácio Macedo, 950 - Cidade Universitária, Ilha do Fundão, Rio de Janeiro, 21949-915, Brazil*

Abstract

This paper presents the results of the application of a systematic logic controller design methodology to an industrial case study, the delayed coking drum process. The design process starts from a set of semi-formal documents from which a formal specification of the control requirements is derived. The formal specification is transformed into a logic controller implemented in *Sequential Function Charts* as well as into a timed automata model of the logic controller which in turn is utilized to validate the logic controller by means of simulation and formal verification.

Keywords: Logic Controllers, Systematic Design, Formalization

1. Introduction

In chemical plants, logic controllers play an important role to realize desired sequences in batch processes as well as during start-up and shut-down of continuous plants. The design and the implementation of logic controllers have to be performed by teams of experts from different engineering disciplines: process engineers usually specify the function of the logic controller in natural-language or semi-formal documents and the controller is then implemented by automation engineers in specific programming languages as defined in the standard IEC 61131-3 (IEC (2003)). As the specifications usually are neither complete nor consistent, and often ambiguous, frequent iterations between the two sides are necessary and changes may still be required in the commissioning phase which may cause costly delays and lead to inconsistencies of the documentation and the implementation.

Many different methods for the enhancement of the design of logic controllers have been developed which can be grouped into two classes. The first class consists of methods for the formalization of the requirements or of the specification using a variety of formalisms such as Petri-nets (Ferrarini & Piroddi (2003), Klein et al. (2003)) or automata-based formalisms (Maler et al. (1995), Ramadge & Wonham (1989), and Stursberg (2005)). The formalized specification is then used to (algorithmically) derive logic controllers which are correct by design. The second class of approaches focuses on quality control of the logic controllers at the end of the design process. This class contains methods for the algorithmic generation of test cases (Provost et al. (2009)) or the verification of logic controllers using formalisms like timed automata (Stursberg & Lohmann (2005) and L'Her et al. (2001)) or Petri-nets (Fujino et al. (2000)).

[1] The research reported in this paper was (partly) funded by the European FP7 project MULTIFORM, contract number INFSO-ICT-224249, http://www.ict-multiform.eu. This support is very gratefully acknowledged.

In our recent work (see Fischer et al. (2011)), we have proposed a systematic logic controller design method that combines features of both classes. On the one hand, the design process is supported by providing a transparent and consistent formal specification that is refined into controller code in the programming language *Sequential Function Charts* (SFC) step by step. On the other hand, the final formal specification is transformed into models that are used to verify the controller.
In this contribution we report the application of this *DC/FT* design approach and of the corresponding software tool to an industrial-scale case study, an automation system of delayed coking drum plant, operated by PETROBRAS.

2. Systematic Logic Controller Design

Following industrial practice, the design starts from a set of informal, natural-language requirements that represent a coarse description of the desired behavior of the controlled process. In contrast to a manual conversion, as reported e.g. in Lucas & Tilbury (2004), of more or less structured requirements into logic controller code which is not easily comprehensible to process engineers, in the *DC/FT* approach first a structured and formalized representation of the requirements is generated. The desired functionality is represented in a modular fashion, dividing the sequences of actions into smaller parts. These parts are then further refined until all requirements have been processed and the controller is specified in detail. The approach makes use of three major principles to structure, simplify, and improve the design process:

1. Hierarchy and refinement to reflect the complexity of the controller and to deal with the large amount of information in the different phases of the design process, ranging from abstract representations of the specification and control algorithms (that are required in the early design stages) to very detailed representations in the later design stages and in the implementation phase.
2. Flexibility to be able to react to revisions of the specification that are necessary due to changes or more detailed definition on the requirements of the plant and/or of the controller.
3. Structured documentation of all design decisions to provide a consistent and intuitive representation of all (informal and formal) design parameters and decisions to the design team in all stages of the design process.

2.1. The DC/FT Formalism

The DC/FT structuring formalism consists of two coupled formalisms, the *Dependency Chart* (DC) and the *Function Table* (FT). A DC is a two-dimensional graphical representation of the conceptual design of the logic controller (see Fig. 1). It consists of a set of *Function Blocks* (symbolized by rectangular boxes) and a set of directed connections between the blocks, the *Transitions*. The DC can be seen as an extended version of the Gantt chart formalism that provides an intuitive representation of sequential processes and is used in e.g. scheduling as well as for project management tasks. Hierarchy is introduced to the DC formalism by the refinement of the function blocks of the DC. Each function block holds either a *Function Table* or one or more DCs. In contrast to the original definition of Gantt charts, the DC also supports the concepts of alternative branching (including priorities), loops, and jumps. A FT is inspired by the documentation formats that are used in industry to specify control systems. It consists of a set of *Function Table Entries* (FTE), where each FTE holds an executable action with an assigned qualifier and, if applicable, a Boolean condition that controls the execution of the action. If this condition is empty, the condition of the preceding FTE is used instead, so that two or more actions can be coupled. The conditions and actions are defined by

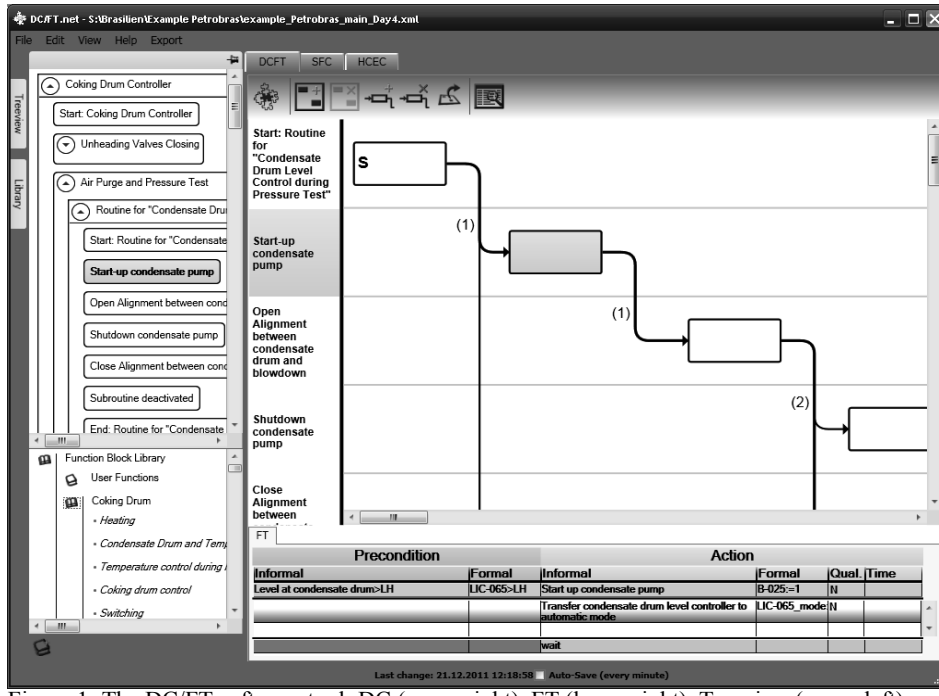

Figure 1: The DC/FT software tool: DC (upper right), FT (lower right), Treeview (upper left), and Library (lower left)

an informal description as well as by a formal specification. The qualifiers assigned to the actions are taken from the set of qualifiers defined in the IEC standard (IEC(2003)) for SFC to facilitate the coupling of DC/FT and SFC. Actions can be executed in a stored mode (qualifiers S, SL, DS, SD) which means that they remain active until the action is reset with the qualifier R, or in a non-stored mode (N, L, D) which means that they are switched off automatically when the following condition evaluates to true; a third group of qualifiers (P, P_0, P_1) executes the action as a pulse. Some of the qualifiers involve time (e.g. to delay the execution of an action). If these qualifiers (D, L, SL, SD, and DS) are assigned to an action, the time span has to be specified in the last column of the function table. The FTEs are executed sequentially without branching or repetition. For more details of the DC/FT formalism and a formal definition we refer to Fischer et al. (2011).

2.2. The DC/FT Software Tool

The *DC/FT* design process is supported by a software tool with an intuitive graphical editor (Fig. 1). The benefit of the tool-based design process is that in addition to the desired logic controller in the format of SFC, a consistent formal specification of the logic controller is obtained. The tool also provides the possibility to export parts of the formalized specification (function blocks or DCs) to a library. Several export filters, notably to the *UPPAAL* model checker (Larsen et al. (1997)) and to the *Compositional Interchange Format for Hybrid Systems* (van Beek et al. (2008)) to which many other model-based design and analysis tools are connected are integrated into the tool, which can be used for analyses of the controller (simulation, testing, formal verification).

3. Example Process

The example process (see Fig. 2), a delayed coking plant consists of pairs of reactors (drums) used for the coking of heavy-oil that are operated in batch mode. The drums are

connected to a fired heater that provides a mixture of steam and bottoms product of a heavy oil fractionator. The process is called delayed as the reaction to coke and shorter olefins is taking place in the drum while the components are mixed before in the fired heater. During operation, a drum is filled with the solid coke until it is filled completely. Since the coking drums are connected to the continuously operating fractionator (distillation column), the reactors are filled and emptied in an alternating fashion. The emptying and preparation procedure consist of the following phases:

1. Purge volatile components to the fractionator using steam
2. Cooling and drainage
3. Decoking using a water lance
4. Purging of air and pressure test
5. Heating to reach the operation temperature

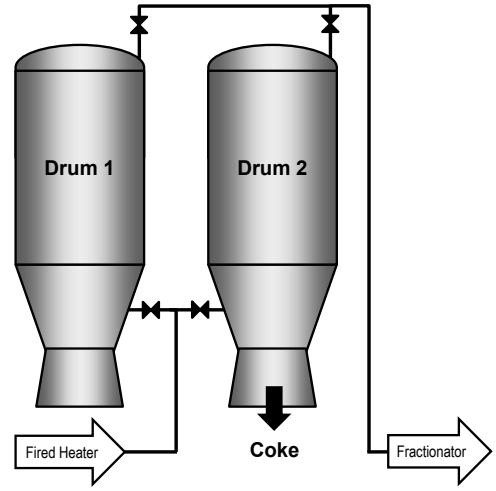

Figure 2: Delayed Coking Drum Process (simplified)

3.1. Formalization of the Control Requirements of the Example Process

At the beginning of the design process the requirements were given in a semi-formal document (~30 pages A4 paper), consisting of description of the process and the desired control system behavior, and *Piping and Instrumentation Diagrams* (PID) of the plant. The sequences of action are given as flow-charts. It was decided to split the requirements into seven function blocks according to the phases described above with one additional block for the coking (operation) and the switching procedure. Each of the blocks was refined further by means of one or more dependency charts that were again refined using function blocks and (in the end) function tables. The function block "Air Purge and Pressure Test" for instance contains three parallel DCs (purge and test sequence and in parallel pressure and condensate level control) that in turn are further refined, etc. The final formal specification consists of more than 350 function blocks on four hierarchy levels, resulting in ~250 function tables at the end of the refinement. The navigation through the large hierarchical structure is realized by means of the treeview (see Fig. 1). During the design process both relatively small parts of the specification like the opening/closing of valves or the waiting for operator permission and larger parts of the specification like the level or pressure control in the drum were frequently reused saving a lot of time and effort.

After all requirements were formalized, a SFC representation is generated which serves as a documentation of the requirements and as basis for the implementation. Parts of the specification were transformed into a *UPPAAL* (timed automata) model and were simulated and verified with regard to certain properties. Particularly, the correctness of the pressure control of the coking drum during the pressure test was verified.

4. Conclusions

By utilizing the DC/FT approach, a formalization of the specification using intuitive data formats replaces the informal and manual implementation procedure. Based on the

formalized specification, all parties involved can discuss the control logic and find possible errors in the specification as well as implementation errors. Furthermore, the hierarchical and modular structure of DC/FT is partly preserved and recognizable in the SFC. Although no real hierarchy is defined for SFC, this well-arranged structure improves the readability and maintainability of the SFC code. The DC/FT paradigm provides an intuitive and systematic approach to the design of logic controllers that covers the complete design sequence, from early specification to implementation.

The explicit documentation of knowledge and expertise of all members of the team, irrespective of their technical background and in a format that is understandable for other design team members, greatly simplifies the detection of design errors and their correction and thus ensures a high quality of the designed controller. The methodology and the prototype tool were proven to have the potential to improve the current design flows by reducing errors and facilitating later changes. The hierarchical and modular structure of the DC/FT formalism enables the designers to reuse parts of the controller code to further improve the efficiency of the development process. The controller can also be exported into the CIF (Sonntag & Fischer (2010)) to validate the controller together with an accurate plant model (including continuous plant dynamics).

References

IEC 61131-3, 2003. Programmable Controllers – Programming Languages.

Ferrarini, L. and Piroddi, L., 2003. Modular Design and Implementation of a Logic Control System for a Batch Process, Computers and Chemical Engineering, 27(7), 983-996.

Klein, S., Frey, G., and Litz, L.,2003. Designing Fault Tolerant Controllers Using SIPN and Model-Checking. Proc. IFAC-Safeprocess, 115-120.

Maler, O., Pnueli, A., and Sifakis, J., 1995. On the Synthesis of Discrete Controllers for Timed Systems. Proc. Theoretical Aspects of Computer Science, STACS'95.

Ramadge, P. and Wonham, W., 1989. The Control of Discrete Event Systems. Proc. of IEEE, 77(1), 81-98.

Stursberg, O., 2005. Supervisory Control of Hybrid Systems Based on Model Abstraction and Guided Search. Nonlinear Analysis, 65(6), 1168-1187.

Provost, J., Roussel, J.M., and Faure, J.M., 2009. Test Sequence Construction from SFC Specification. Proc. Dependable Control of Discrete Systems, 341-346.

Stursberg, O. and Lohmann, S., 2005. Analysis of Logic Controllers by Transformation of SFC into Timed Automata. Proc. CDC/ECC, 7720-7725.

L'Her, D., Le Parc, P., and Marce, L., 2001. Proving Sequential Function Chart Programs Using Timed Automata. Theoretical Computer Science, 267(1-2), 141-155.

Fujino, K., Imafuku, K., Yamashita, Y., and Nishitani, H., 2000. Design and Verification of the SFC Program for Sequential Control. Comp. and Chem. Eng., 24(2-7), 303-308.

Fischer, S.; Hüfner, M.; Sonntag, C.; Engell, S., 2011. Systematic Generation of Logic Controllers in a Model-Based Multi-Formalism Design Environment. Proc. IFAC World Congress, 12490-12495.

Lohmann, S. and Engell, S., 2008. Systematic Logic Controller Design as Sequential Function Chart Starting from Informal Specifications. Chin. Journal of Chem. Eng., 32, 43-47.

Lucas, M.R. and Tilbury, D.M., 2004. The Practice of Industrial Logic Design. Proc. American Control Conference, 1350-1355.

Larsen, K.G., Pettersson, P., and Yi, W., 1997. Uppaal in a Nutshell. International Journal on Software Tools for Technology Transfer, 1(1–2), 134-152.

van Beek, B., Reniers, M.A., Rooda, J.E., and Schiffelers, R.R.H., 2008. Concrete Syntax and Semantics of the Compositional Interchange Format for Hybrid Systems. Proc. IFAC World Congress, 7979–7986.

Sonntag, C.; Fischer, S., 2010 Translating Sequential Function Charts to the Compositional Interchange Format for Hybrid Systems. Proc. CDC, 4250-4256.

I.A. Karimi and Rajagopalan Srinivasan (Editors), Proceedings of the 11th International Symposium on Process Systems Engineering, 15-19 July 2012, Singapore

A Mixed Integer Quadratic Reformulation of the Quadratic Assignment Problem with Rank-1 Matrix

Otto Nissfolk[a] * Ray Pörn[a] Tapio Westerlund[a] Fredrik Jansson[b]

[a] *Center of Excellence in Optimization and Systems Engineering, Åbo Akademi University, Biskopsgatan 8, 20500 Åbo, Finland*

[b] *Department of Physics and Material Sciences Center, Philipps-Universität Marburg, Renthof 6, D-35032 Marburg, Germany*

Abstract

This paper focuses on the formulation and solution of certain quadratic assignment problem (QAP). A new mixed integer quadratic programming (MIQP) formulation of the QAP is presented that is especially well suited for solving instances where the flow or distance matrix is of rank-1. Computational experiments are conducted on some special generated instances as well as on some instances from the QAPLIB (Burkard et al., 1997; QAPLIB, 2012). The QAP is solved using a two-stage procedure. The objective is first simplified as a result of the rank-1 assumption and thereafter the quadratic objective is convexified. The resulting convex MIQP is then solved with a suitable solver.

Keywords: Quadratic assignment problem (QAP), mixed integer quadratic programming (MIQP), semidefinite programming (SDP), quadratic convex reformulation (QCR)

1. Introduction

This paper addresses the important task of solving certain classes of the Quadratic Assignment Problem introduced by Koopmans and Beckmann in 1957. The QAP is a problem where n facilities and n locations are given with specified flows and distances between the facilities and locations, respectively. The cost is a function of the distances and flows between the facilities and an additional cost may be associated with placing a facility at a certain location. The overall objective is to minimize the total cost of placing each facility to a certain location. In addition to facility layout problems, the QAP appears in applications such as backboard wiring (Steinberg, 1961), scheduling (Geoffrion and Graves, 1976), gray pattern generation (Taillard, 1995) and many other.

In its basic form QAP is a non-convex 0-1 quadratic program. A common approach for solving QAPs is based on using different types of linearizations. A linearization procedure overcomes the quadratic structure by introducing a set of new variables and additional linear and binary constraints. Linearization techniques can also be used to obtain bounds for QAP problems. Different heuristics have also proved to be efficient to obtain bounds, but optimality of such solutions cannot be proven (Burkard et al., 1998).

The paper is organized as follows. The different quadratic formulations are introduced in section 2. The set of testproblems and well-known linearizations are presented in section 3. Section 4 contains the solution results and section 5 concludes the paper.

*Otto.Nissfolk@abo.fi

2. Problem formulation

2.1. The Quadratic Assignment Problem

The quadratic assignment problem introduced by Koopmans and Beckmann (1957) has the following form:

$$\min_{x\in X} \sum_{i=1}^{n}\sum_{j=1}^{n}\sum_{k=1}^{n}\sum_{l=1}^{n} f_{ik}d_{jl}x_{ij}x_{kl} + \sum_{i=1}^{n}\sum_{j=1}^{n} c_{ij}x_{ij} \tag{1}$$

$$\text{where } X = \{x| \sum_{j=1}^{n} x_{ij} = 1 \quad i \in N, \sum_{i=1}^{n} x_{ij} = 1 \quad j \in N, x_{ij} \in \{0,1\} \quad i,j \in N\} \tag{2}$$

and f_{ik} is the flow between facilities i and k, d_{jl} is the distance between locations j and l, and c_{ij} is the cost of placing facility i at location j. The variable $x_{ij} = 1$ if facility i is assigned to location j, otherwise, $x_{ij} = 0$ and $N = \{1,2,\ldots,n\}$. With no loss of generality we can assume that $c_{ij} = 0$ and omit the linear term in (1). In this paper we also assume that the flow and distance matrices are symmetric.

2.2. Trace formulation

Another popular formulation of the QAP is the trace formulation (Edwards, 1980). If $\mathbf{F}$ and $\mathbf{D}$ are given flow and distance matrices and $\mathbf{X}$ the permutation matrix with elements defined by (2) the quadratic objective in (1) (with $c_{ij} = 0$) can be expressed using the trace-operator according to

$$\sum_{i=1}^{n}\sum_{j=1}^{n}\sum_{k=1}^{n}\sum_{l=1}^{n} f_{ik}d_{jl}x_{ij}x_{kl} = \text{tr}(\mathbf{DXFX}^T).$$

2.3. QAP with rank-1 flow matrix

We assume that the flow matrix (or distance matrix) is of rank-1, i.e. $\mathbf{F} = \mathbf{qq}^T$ for some vector $\mathbf{q} = (q_1,\ldots,q_n)^T$. The quadratic part of the objective function (1) can, in this case, be restated as

$$\sum_{i=1}^{n}\sum_{j=1}^{n}\sum_{k=1}^{n}\sum_{l=1}^{n} f_{ik}d_{jl}x_{ij}x_{kl} = \text{tr}(\mathbf{DXFX}^T) = \text{tr}(\mathbf{DXqq}^T\mathbf{X}^T) = \text{tr}(\mathbf{Dyy}^T) = \mathbf{y}^T\mathbf{Dy}$$

where **y=Xq**, i.e. $\mathbf{y}$ is a permutation of $\mathbf{q}$. By substituting, $y_i = \sum_{j=1}^{n} q_j x_{ij}$ we then get a quadratic problem of the form

$$\min_{x\in X, y\in\mathbb{R}^n} \mathbf{y}^T\mathbf{Dy} \tag{3}$$

$$\text{subject to } y_i = \sum_{j=1}^{n} x_{ij}q_j \quad \forall i, \quad \sum_{i=1}^{n} y_i = \sum_{j=1}^{n} q_j \tag{4}$$

Problem (3-4) is a mixed integer quadratic optimization problem with n continuous, n^2 binary variables of SOS1-type and $n+1$ linear constraints. The objective function is not necessarily convex.

2.4. Convex QAP with rank-1 flow matrix

In order to efficiently solve the quadratic formulation defined in section 2.3 we have to convexify the objective (3). The convexification can be done, for example, by adding the smallest eigenvalue to the diagonal so that $\text{Diag}(\mathbf{u}) = -\lambda_{min}(\mathbf{D})\mathbf{I}$ or by using the QCR-method (Billionnet et al., 2009). By solving an SDP problem we will get an optimal $\mathbf{u}$-vector so that the lower bounding is as tight as possible. If we add $\mathbf{u}$ to the diagonal of $\mathbf{D}$ then we have to subtract new variables $\mathbf{z}(z_i = y_i^2)$ to obtain the same objective value as in (3).

$$\min_{x\in X,\, y,z\in\mathbb{R}^n} \mathbf{y}^T(\mathbf{D}+\text{Diag}(\mathbf{u}))\mathbf{y} - \mathbf{u}^T\mathbf{z} \tag{5}$$

$$\text{subject to } y_i = \sum_{j=1}^{n} x_{ij}q_j, \quad z_i = \sum_{j=1}^{n} x_{ij}q_j^2 \quad \forall i, \quad \sum_{i=1}^{n} y_i = \sum_{j=1}^{n} q_j \tag{6}$$

Problem (5-6) is a convex MIQP with $2n$ continuous, n^2 binary variables and $4n+1$ constraints (counting SOS1-constraints). This formulation is referred to as QAP-r1. If the vector $\mathbf{q}$ contains many identical elements, an alternative formulation can be derived. Let $\{v_1,\ldots,v_m\}(m \le n)$ be the distinct values in $\mathbf{q}$ and $\{f_1,\ldots,f_m\}$ the corresponding frequencies. This observation leads to a slightly different formulation.

$$\min_{y,z\in\mathbb{R}^n} \mathbf{y}^T(\mathbf{D}+\text{Diag}(\mathbf{u}))\mathbf{y} - \mathbf{u}^T\mathbf{z} \tag{7}$$

$$\text{s.t. } y_i = \sum_{j=1}^{m} x_{ij}v_j,\ z_i = \sum_{j=1}^{m} x_{ij}v_j^2,\ \forall i, \quad \sum_{i=1}^{n} y_i = \sum_{j=1}^{m} f_j v_j,\ f_j = \sum_{i=1}^{n} x_{ij}\ \forall j, \quad \sum_{j=1}^{m} x_{ij} = 1\ \forall i \tag{8}$$

Problem (7-8), referred to as QAP-r1-freq, is also a convex MIQP but with $2n$ continuous, nm binary variables and $3n+m+1$ constraints. Formulation (7-8) does, however, not give the optimal permutation of q only the optimal objective value. If $m << n$ the formulation QAP-r1-freq is considerably smaller than formulation QAP-r1.

3. Testproblems

The problems solved in this paper are gray-scale pattern instances (Taillard, 1995) and rank-1 approximations of all symmetric problems from the QAPLIB (2012). The problems are solved using CPLEX 12.2.0.0 on a Intel i7-930 processor with 6GB RAM running Windows 7.

3.1. Linearizations

The linearizations XYL and GLL (Zhang et al., 2012) are used as comparison to the quadratic formulations of rank-1 QAP. Both XYL and GLL have n^2 continuous variables, n^2 binary variables and $2n^2$ constraints.

3.2. Taixxc-problems

The taixxc problems found in the QAPLIB are of size 8×8 and 16×16. These problems are too large for testing so we created some smaller instances using the formula found

in (Taillard, 1995). The tai36c problem that is used in 4.2 is a grayscale problem of size 6×6. In these instances, the flow and distance matrices are defined as follows:

$$T_{rstu} = \max_{v,w \in \{-1,0,1\}} \frac{1}{(r-t+nv)^2 + (s-u+nw)^2}$$

$$f_{ij} = \begin{cases} 1 & \text{if } i \leq m \text{ and } j \leq m \\ 0 & \text{otherwise} \end{cases}, \quad d_{ij} = d_{n(r-1)+s \quad n(t-1)+u} = T_{rstu}$$

4. Results

4.1. QAPLIB-results

First all symmetric problems, 111 out of 135 in total, from QAPLIB (2012) are approximated as rank-1 problems and then solved for 1800 seconds. The solutions times for the four different formulations are the compared using performance profiles showing the solution time versus number of problems solved. As one can see from figure 1 the QAP-

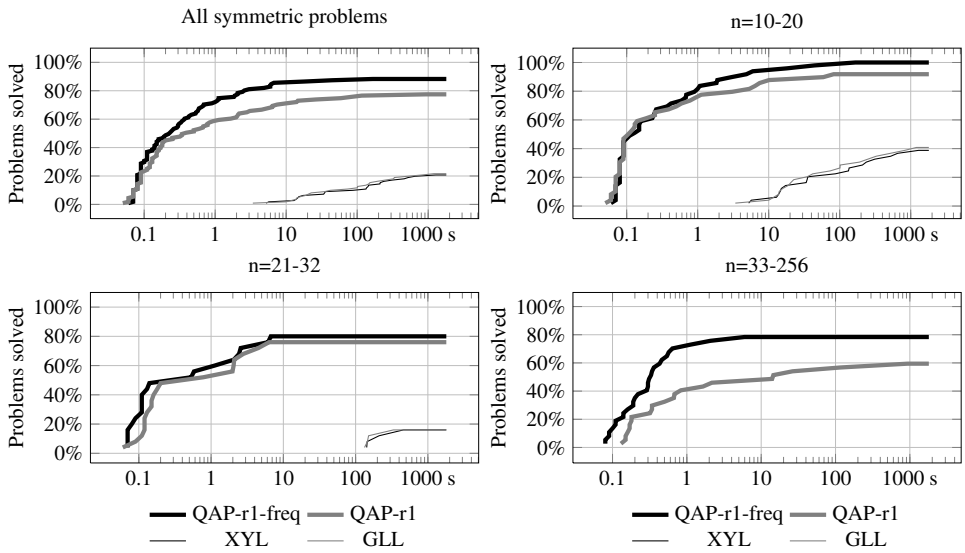

Figure 1. Percentage of problems solved within the timelimit of 1800 s

r1-freq formulation seems to be the best, solving about 90% of all problems followed by QAP-r1 formulation solving a bit over 80% of all problems. As one could expect, the linearizations are quite similar and not as good as the quadratic ones, both solving around 20% of all problems. The linearizations work on small problems but the quadratic formulations are the best approach for these problems.

4.2. Taixxc-results

In figure 2 the results for the tai36c problem are presented. The b-values on the x-axis correspond to different densities of gray where $b = 0$ is all white and $b = 36$ is all black. The timelimit for the solver is set at 1800 seconds. The solution time of instances with gray

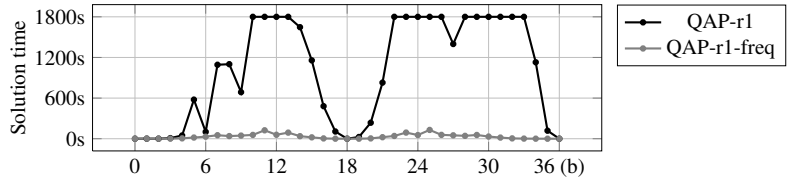

Figure 2. Solution times of the tai36c problem

density close to 50% is very low, since the gray pattern will resemble a checkerboard and therefore there are very few good solutions. Instances with gray density close to 0% and 100% are also easy since they correspond to almost all white and all black, respectively. The intermediate instances are difficult since there exists many near-optimal patterns. The QAP-r1-freq formulation is the better one for solving these problems.

5. Conclusions

In this paper two MIQP formulations of rank-1 QAPs were derived. The results show that the formulations are efficient for solving QAPs with a rank-1 flow matrix. The QAP-r1-freq formulation seems to be the most efficient approach. This is due to a model with fewer binary variables than QAP-r1. The drawback with QAP-r1-freq is that the solution only contains the objective value but no information about the permutation vector.

References

Billionnet, A., Elloumi, S., Plateau, M.-C., March 2009. Improving the performance of standard solvers for quadratic 0-1 programs by a tight convex reformulation: The QCR method. Discrete Appl. Math. 157, 1185–1197.

Burkard, R., Cela, E., Pardalos, P., Pitsoulis, L., 1998. Handbook of Combinatorial Optimization. Vol. 3.

Burkard, R. E., Karisch, S. E., Rendl, F., June 1997. Qaplib – a quadratic assignment problem library. J. of Global Optimization 10, 391–403.

Edwards, C. S., 1980. A branch and bound algorithm for the Koopmans-Beckmann quadratic assignment problem. Combinatorial Optimization II 13, 35–52.

Geoffrion, A., Graves, G., 1976. Scheduling parallel production lines with changeover costs. Operations Research 24, 595–610.

Koopmans, T. C., Beckmann, M., 1957. Assignment problems and the location of economic activities. Econometrica 25 (1), pp. 53–76.

QAPLIB, 2012. http://www.seas.upenn.edu/qaplib/inst.html.

Steinberg, L., 1961. The backboard wiring problem: A placement algorithm. SIAM Review 3 (1), 37–50.

Taillard, D., 1995. Comparison of iterative searches for the quadratic assignment problem. Location Science 3 (2), 87 – 105.

Zhang, H., Beltran-Royo, C., Ma, L., 2012. Solving the quadratic assignment problem by means of general purpose mixed integer linear programming solvers. Annals of Operations Research, 1–18.

I.A. Karimi and Rajagopalan Srinivasan (Editors), Proceedings of the 11th International Symposium on Process Systems Engineering, 15-19 July 2012, Singapore.

Uncertainty evaluation for multivariate industrial processes

Reiner Requião[a], M.A.F. Martins[a], Ricardo de Araújo Kalid[a], Rafael de Pelegrini Soares[b]

[a]*Research Group on Process Uncertainty at theFederal University of Bahia, Rua Aristides Novis, 02, Sala 6.1.18, Federação, Salvador, CEP 40210-630, Brazil*
[b]*Federal University of Rio Grande do Sul (UFRGS), Porto Alegre, Brazil*

Abstract

The paper presents a supplement for the equation-oriented process simulator EMSO - Environment for Modeling Simulation and Optimization – which automatically evaluates the uncertainty of process output variables. Two methods for the evaluation of process uncertainty in multivariate systems have been implemented, namely: MLPU (Multivariate Law of Propagation of Uncertainties) and MLPP (Multivariate Law of Propagation of Probability Density Functions). For illustrative purposes, a comparative analysis of both approaches is carried out in a typical nonlinear industrial process system: a continuous stirred-tank reactor (CSTR). The paper finally closes with a discussion which raises some issues for future work.

Keywords: Propagation of Uncertainties, Multivariate Systems, Probability Density Functions, EMSO.

1. Introduction

Modeling and simulation are common tools in the engineering field and its use often results in multivariate systems (MIMO - Multiple Input Multiple Output). These systems are usually described by implicit nonlinear equations. In general, the simulation software available does not evaluate the uncertainties associated with the variables and rarely discloses the equipment models used, which with some effort allow the calculation of these uncertainties.

On the other hand, the available specialized software for uncertainty evaluation cannot usually handle multivariate systems and are not integrated with the simulators of industrial processes. In order to overcome these limitations, we have developed a new module for the software EMSO - Environment for Modeling Simulation and Optimization – namely *Uncertainty*. This module can evaluate the uncertainties associated with variables of nonlinear multivariate models in the steady-state. EMSO is a general equation-oriented process simulator. It can handle both dynamic and steady-state models and implements its own object-oriented modeling language. The simulator comes with an extensive library of models for chemical processes and allows the user to create new equipment models. Furthermore, it is accompanied by a series of numerical packages for solving a wide range of problems and it also contains modules to perform case studies, sensitivity analysis, optimization, data reconciliation, among others (Soares & Secchi 2003).

The purpose of this paper is to present the *Uncertainty* module developed for EMSO that performs the best estimates and the covariance matrix of output variables of industrial processes through methods based on the MLPU approach - Multivariate Law

of Propagation of Uncertainty (Lira 2002) - and the MLPP approach - Multivariate Law of Propagation of Probability Density Functions (PDF) which uses a Monte Carlo method (MCM) (Martins & Kalid 2011); these two approaches are in accordance withSupplement 2 of the Guide to the Expression of Uncertainty in Measurement (GUM S2) (BIPM et al. 2011).

2. Methods

The problem addressed here consists of a multivariate process model with various output quantities Y_j related directly to several input quantities X_i through known functional relationships of the form

$$\begin{cases} h_1\left(Y_1, \dots, Y_j, \dots Y_K; X_1, \dots, X_i, \dots X_N\right) = 0 \\ \vdots \\ h_K\left(Y_1, \dots, Y_j, \dots Y_K; X_1, \dots, X_i, \dots X_N\right) = 0. \end{cases} \tag{1}$$

The set of model relations (1) is generally determined from phenomenological (conservation laws and constitutive equations) or empiric modeling. In some simple cases the equations may be solved analytically, however, a numerical solution is usually mandatory in cases of nonlinear systems. In matrix notation, (1) can be written in a more compact form as follows:

$$\mathbf{h}(\mathbf{Y};\mathbf{X}) = \mathbf{0}, \tag{2}$$

where $\mathbf{h} = (h_1, \dots h_K)^{\mathrm{T}}$, the symbol $\mathbf{0}$ stands for a column vector with all elements equal to zero. From the formulation set out above, the MLPU and MLPP approaches are outlined in the following two subsections.

2.1. MLPU approach

The MLPU approach consists of propagating the vector of input estimates ($\mathbf{x}$) and its covariance matrix ($\mathbf{U_X}$) through a first-order Taylor series approximation of the process model for evaluating the vector of estimates ($\mathbf{y}$) and the associated covariance matrix ($\mathbf{U_Y}$) of the output quantities (measurands). The key features of this approach are summarized hereafter:

(1) Set up the model process, estimates and associated covariance matrix of the input quantities, $\mathbf{x}$ and $\mathbf{U_X}$, respectively;

(2) Compute the estimates of the output quantities through the solution of multivariate model $\mathbf{h}(\mathbf{y};\mathbf{x}) = \mathbf{0}$;

(3) Compute the sensitivity matrix or both input and output quantities, evaluated at the estimates $\mathbf{y}$ and $\mathbf{x}$:

$$\mathbf{C_X} = \begin{pmatrix} \frac{\partial h_1}{\partial x_1} & \cdots & \frac{\partial h_K}{\partial x_1} \\ \vdots & \ddots & \vdots \\ \frac{\partial h_1}{\partial x_N} & \cdots & \frac{\partial h_K}{\partial x_N} \end{pmatrix} \text{ and } \mathbf{C_Y} = \begin{pmatrix} \frac{\partial h_1}{\partial y_1} & \cdots & \frac{\partial h_K}{\partial y_1} \\ \vdots & \ddots & \vdots \\ \frac{\partial h_1}{\partial y_K} & \cdots & \frac{\partial h_K}{\partial y_K} \end{pmatrix};$$

(4) Compute the covariance matrix associated with the output quantities as follows: $\mathbf{U_Y} = \mathbf{C}^{\mathbf{T}}\mathbf{U_X}\mathbf{C}$, where $\mathbf{C} = (-\mathbf{C_Y^{-1}}\mathbf{C_X})^{\mathbf{T}}$.

2.2. MLPP approach

Compared to MLPU,a more general approach is adopted by MLPP. MLPP treats the numerical evaluation of process uncertainty with a Monte Carlo method (MCM) as an

implementation of the propagation of probability density functions (PDFs). The basic idea of the MLPP approach is to draw random samples from the joint PDF assigned to the input quantities $g_{\mathbf{X}}(\boldsymbol{\xi})$ and propagate these samples through the model (2) to yield the joint PDF associated with the output quantities $\mathrm{g}_{\mathbf{Y}}(\boldsymbol{\eta})$; here the possible values of the input and output quantities are denoted respectively as $\boldsymbol{\xi} = [\xi_1, \ldots, \xi_n]^{\mathrm{T}}$ and $\boldsymbol{\eta} = [\eta_1, \ldots, \eta_K]^{\mathrm{T}}$. An algorithm for this method follows:

(1) Draw a set $\{(\xi_1^1, \ldots, \xi_N^1), \ldots, (\xi_1^M, \ldots, \xi_N^M)\}$ of M independent samples from $g_{\mathbf{X}}(\boldsymbol{\xi})$;

(2) Compute M samples for the output quantities using the model (2), at least 10^4:

$F(\boldsymbol{\eta}^r; \boldsymbol{\xi}^r) = \mathbf{0}, \quad r = 1, \ldots, M$. These samples constitutes a set of independent random deviates from $g_{\mathbf{Y}}(\boldsymbol{\eta})$.

(3) Calculate the estimates y and its covariance matrix $\mathbf{U}_{\mathbf{y}}$ according to equations:

$$y_j = \frac{1}{M}\sum_{r=1}^{M} \eta_j^r, \quad j = 1, \ldots, K \tag{3}$$

$$U_y(i,j) = \frac{1}{M-1}\sum_{r=1}^{M} (\eta_i^r - y_i)(\eta_j^r - y_j), \quad i,j = 1, \ldots, K \tag{4}$$

3. *Uncertainty* module

The *Uncertainty* module is designed to be versatile software, i.e. it allows the user to provide the estimate of the input quantities and its correlation matrix or combined uncertainty or the parameters of their PDF as well as set up the simulation parameters, such as number of simulations of the MCM, tolerance, iterations etc. A general picture of the *Uncertainty* module structure and its components (input and output data) is shown in Figure 1.

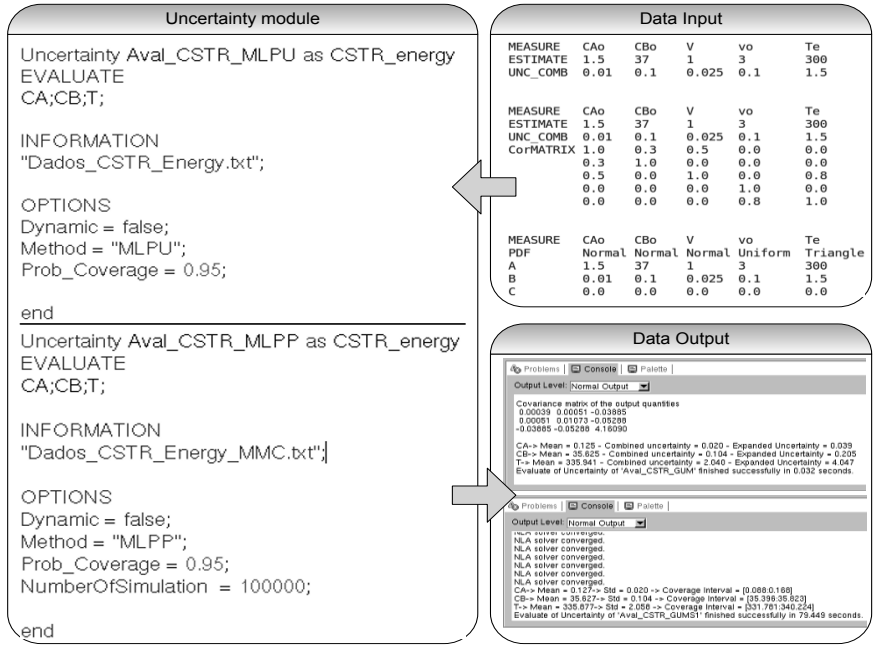

Figure 1.General vision of the *Uncertainty* EMSO module structure and its components.

To use *Uncertainty,* one needs a process model (*FlowSheet*) that runs at steady-state and then this module converts the process equations into a multivariate process model like (2) in order to evaluate the estimate and the covariance (uncertainty) matrix of all output quantities, using both the MPLU and the MLPP approaches.

4. Case Study: a CSTR

CSTR is an industrial equipment that may be described by a system of nonlinear implicit algebraic equations, obtained from mass and energy balances combined with reaction rates:

$$\begin{cases} C_A = \dfrac{v_0 . C_{A0}}{v_0 + V . k_0 . e^{-\frac{E}{R.T}}} \\ C_B = C_{B0} + \nu_2 . (C_{A0} - C_A) \\ \sum_{i=1}^{n} C_{i0} . Cp_i . (T - T_e) + (C_{A0} - C_A) . \nu_i . \left(H^{\circ}_{i,R}(T_R) . Cp_i . (T - T_R) \right) = 0, \end{cases} \quad (5)$$

where C_{i0}, Cp_i e $H^{\circ}_{i,R}$ are the initial concentration, specific heat at constant pressure and formation enthalpy at reference temperature (T_R), respectively, for each substance i; E is the activation energy; R is the universal gas constant; k_0 is the frequency factor; ν_i is the vector of reaction stoichiometric coefficients; these variables are considered parameters with negligible uncertainties. For this particular case, or for more information about reaction modeling in general see (Fogler 2002).

The volumetric flow rate (v_0), reactor volume (V), initial concentration of the reactants A (C_{A0}) and the B (C_{B0}) and inlet temperature (T_e) are input quantities of the process model. For each of these input quantities a Gaussian PDF was assigned with the expectation and standard deviation equal to the estimate and standard uncertainty presented in Table 1, respectively.

Table 1.Estimate and process uncertainties of the input quantities.

Input quantities	C_{A0}/(kmol.m^{-3})	C_{B0}/(kmol.m^{-3})	v_0/(m^3.h^{-1})	V/m^3	T/K
Estimate	1.5×10^{0}	3.7×10^{1}	3.0×10^{0}	1.0×10^{0}	3.0×10^{2}
Standard uncertainty[1]	1.0×10^{-2}	1.0×10^{-1}	1.0×10^{-1}	2.5×10^{-2}	1.5×10^{0}
PDF	Gaussian	Gaussian	Gaussian	Gaussian	Gaussian

[1] This is evaluated according to section 5.1.2 of GUM S1 (BIPM et al. 2008).

The purpose of this case is to evaluate the estimate and the covariance matrix, using the MLPU and MLPP approaches, for the following output quantities: final concentration of A (C_A) and B (C_B) and the discharge temperature (T). These results are shown in Table 2 and 3.

As can be seen for the given case study, the results of the MLPU and MLPP approaches are fairly close in this operating point. Even though the difference in the results of both methods is negligible in this example, the MLPP approach is expected to provide a more reliable uncertainty evaluation than that given by MLPU, mainly when the process model is strongly nonlinear (Martins et al. 2011). Nevertheless, MLPP requires rather more computational effort (see the processing time of both methods in Table 2 and 3), which is proportional to the size of M samples; in addition, it can accumulate numerical errors when the computational algorithm of the random numbers generator is not carefully developed.

5. Conclusions

In this paper, we presented the new *Uncertainty* module developed within the equation-oriented process simulator EMSO. This module evaluates the uncertainties for the output quantities of general process models based on methods recognized internationally for this task, namely MLPU and MLPP. The tool developed here can be used to evaluate uncertainty in process analysis, design of equipment or industrial process optimization considering measurement uncertainty. For future works, our goals for the *Uncertainty* EMSO module are: (i) to build the coverage region associated with the output quantities with support for processes composed of more than 1000 variables; and (ii) to implement other methods for the evaluation of uncertainty, such as the Bayesian and Kragten multivariate methods for either dynamic or steady models.

Table 2.Estimate and standard uncertainties of the output quantities using the MLPU approach.

Output quantities	Estimate	Standard uncertainty	Correlation		
			C_A	C_B	T
$CA/(\mathrm{kmol/m^3})$	125.0×10^{-2}	2.0×10^{-2}	1.00	0.25	-0.96
$CB/(\mathrm{kmol/m^3})$	356.3×10^{-1}	1.0×10^{-1}	0.25	1.00	-0.25
T/K	335.9×10^{0}	2.1×10^{0}	-0.96	-0.25	1.00
Processing Time		0.012 seconds			

Table 3.Estimate and standard uncertainties of the output quantities using the MLPP approach using $M = 10^5$ samples.

Output Quantities	Estimate	Standard Uncertainty	Correlation		
			C_A	C_B	T
$CA/(\mathrm{kmol/m^3})$	127.0×10^{-2}	2.0×10^{-2}	1.00	0.25	-0.96
$CB/(\mathrm{kmol/m^3})$	356.3×10^{-1}	1.0×10^{-1}	0.25	1.00	-0.25
T/K	335.9×10^{0}	2.1×10^{0}	-0.96	-0.25	1.00
Processing Time		71.388 seconds .			

References

BIPM et al., 2011. Evaluation of measurement data – Supplement 2 to the "Guide to the expression of uncertainty in measurement" – Models with any number of output quantities, Joint Committee for Guides in Metrology - JCGM 102:2011.

BIPM et al., 2008. Evaluation of measurement data — Supplement 1 to the "Guide to the expression of uncertainty in measurement" — Propagation of distributions using a Monte Carlo method 1st ed., Joint Committee for Guides in Metrology - JCGM 101:2008.

Fogler, H.S., 2002. Elementos de engenharia das reações químicas 3rd ed., Rio de Janeiro - BRA: LTC.

Lira, I.H., 2002. Evaluating the Measurement Uncertainty: Fundamentals and practical guidance 1st ed., Bristol, UK: Institute of Physics Publishing.

Martins, M.A.F. & Kalid, R.A., 2011. Métodos Clássicos para Avaliação da Incertaza de medição em Sistemas Multivariáveis. Sba: Controle e Automação Sociedade Brasileira de Automatica.

Martins, M.A.F., Requião, R. & Kalid, R.A., 2011. Generalized expressions of second and third order for the evaluation of standard measurement uncertainty. Measurement, 44(9), pp.1526-1530.

Soares, R. de P. & Secchi, A.R., 2003. EMSO: A New Environment for Modelling, Simulation and Optimisation. Computer Aided Chemical Engineering, 14(C), pp.947-952.

I.A. Karimi and Rajagopalan Srinivasan (Editors), Proceedings of the 11th International Symposium on Process Systems Engineering, 15-19 July 2012, Singapore

Frequency and Identification

Heinz A Preisig*
Dept of Chem Engineering; NTNU; Trondheim, Norway

Abstract

Process and model identification are very common operations in chemical engineering applications. Reasons are mainly that we do not have all information of the process and that we model processes only approximately. In the latter case we usually hope that the fitting of the model will smoothed out some of the modelling errors that we cannot avoid, such as approximating a distributed system by a network of lumped systems. The latter definitely implies that our models are usually not providing a good description for the high-frequency behaviour of our processes, which is not a surprise. But is it then clever to put a lot of effort into generating identification signals, excitation signals, that have a very high portion of high frequencies, such as steps, pulses and random switching / binary / multi-valued input signals? The answer is no, because indeed the high frequencies only hurt the estimate.

Keywords: dynamic system, software engineering, computational engineering

1. The issue

Modelling is central to most chemical engineering activities. If possible one uses mechanistic models that build on the conservation principles, but then many of the constituent models may not be white box models, but grey or black box models. The models, being parametrised can often be instantiated with parameters from the literature, but then not always everything is available and thus needs to be acquired through experimental means. Also, in all cases the model is not identical with the process, but is an approximate representation of the behaviour of the plant being modelled. And as such, modelling errors may make it necessary to fit the model to the plant thereby compensating for some of the modelling errors.

This paper is aiming at illustrating the latter problem, namely fitting a model, which we know has the wrong structure. Fitting the wrong model seems rather unreasonable, but it only reflects the fact that we cannot mimic the process in all details, thus we have to live with modelling errors. The objective of this paper is to provoke some thinking towards on how to choose the excitation signal for the model identification having some basic knowledge on where some modelling errors must exist. The paper does not attempt to provide theoretical answers, some of which can be found in the literature. The recent survey summarises many of the theoretical results Gevers et al. (2011). The paper focuses mainly on control. An analysis using wavelets that provides time-local frequency information is absent.

When modelling a process, we usually capture the steady-state behaviour well mainly because this is usually also a requirement, but we do not capture the fast parts accurately. This has many reasons but not at least because of the complexity associated with geometry, uniformity of material and distribution of mass and energy in the plant body.

*Heinz.Preisig@chemeng.ntnu.no

In order to fit of the model to the plant, we perform identification experiments, or experiments for regression, or calibrate the model, three terms being coined by three different communities. Each experiment injects an identification signal, a disturbance, that must be sufficiently exciting to let the process exhibit its properties. Literature coins the term "persistent excitation" (Ljung (1987); Goodwin and Payne (1977)) requesting that all modes are being excited. So the apparently save thing to do is to excite the whole spectrum, from low to high. The step input is satisfies these conditions and is often relatively easy to apply and thus a commonly applied input signal. In some communities one would also use pulse functions that are short but intensive enough to get as close as possible to an impulse. This to get the approximate impulse response, which provides the approximate residence time distribution of the analysed equipment.

Most processes exhibit the behaviour of infinite order, because natural systems are distributed. Making simple, lumped models, or approximating distributed systems as networks of lumped systems, makes it apparent, that these models do not capture the high-frequency behaviour of a the plant. A simple example is the use of overall heat transfer models for a energy being transferred from one fluid to another through a wall, for example in the form of heat: This model has no dynamics, as it assumes zero capacity effect of the physical transfer system.

Using excitation signals that cover the full range, or at least as much as possible, of the frequency range seems a save way of doing things. This contribution shows that this is not the case and that one should pay attention to the frequency range in which the model actually mimics the process relatively accurately.

2. A simple case to illustrate

2.1. The plant and the model

To illustrate the above-sketched problem, we use a nominal case, probably one of the simplest ones: For the process we use a second-order process with two time constants and for the model we use a first-order model. We use standard software, thus no particular sophisticated methods, tricks and no special conditions. The transfer function of the model and the plant are:

$$\text{plant}: \quad g_p(s) := \frac{1}{(T_1 s+1)(T_2 s+1)}, \qquad \text{with } T_1 := 1 \text{ and } T_2 := 0.1 \tag{1}$$

$$\text{model}: \quad g_m(s) := \frac{1}{(\tau_1 s+1)} \qquad \text{with } \tau_1 \text{ to be identified} \tag{2}$$

The Bode plot of the plant has two corner frequencies, one at 1 rad/s and one at 10 rad/s, whilst the model will only have one at the location we are going to identify through our identification experiments.

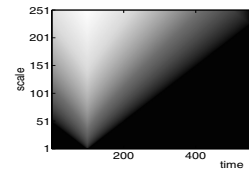

Figure 1. Haar wavelet coefficients for a step at t=100

2.2. Input signal: step

A step signal is the integral of an impulse, with the impulse exciting all the frequencies equally. The step thus also excites all frequencies. A wavelet analysis of the step clearly shows that the high frequencies are most active at the beginning of the step, which is at time 100, whilst the lower frequencies are becoming

more important later. This could also be deducted from a Fourier series representation of a pulse, where the high frequencies compensate each other in the centre of the pulse, whilst adding to form the steep ascent at the beginning and the equally steep decent at the other end.

2.3. Fitting the first-order model

It is apparent that this model, when excited with a step, will respond immediately: the slope at time zero is non-zero, whilst it is zero for our second-order plant. So in terms of the slope, the deviation is relative largest at the beginning and if one looks closer, the difference decreases later for most well-fitted models. The second effect one observes is a shift in the response, a reflection of the phase shift. Also, the extreme phase shift, at high frequencies, is double for the plant compared to the model.

The different frequencies are thus more or less "active" as time progresses when applying a step. In order to get a view on how different frequencies affect the identification, we shall use a package of well-defined frequencies to excite the system, namely a package of 8 sinusoidal functions that are logarithmically spaced in a frequency range.

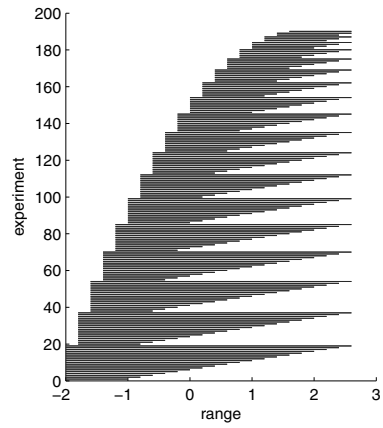

Figure 2. Frequency ranges for the 19 sets of experiments

A number of experiments are performed, whereby the range is changed and the input-output signals are used to fit a first-order model keeping the gain constant to the nominal value. Thus we only adjust the time constant in the identification focusing the dynamics.

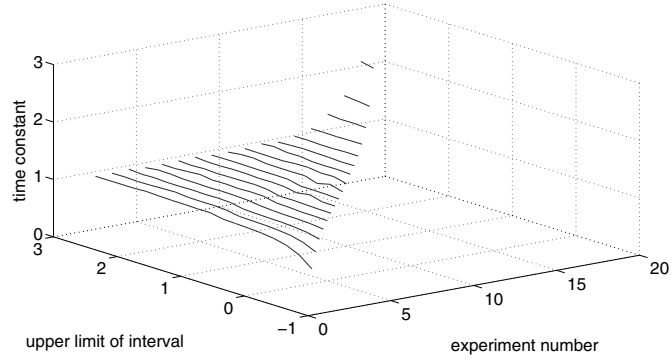

Figure 3. Experiments with packages of 8 sinusoidal. Each line is the set of experiment with range shown in Figure 2 with the upper limit changing.

The range is changed by setting a lower limit well below the first corner (1 rad/s)and extending the range step-wise at the upper end including more and more of the frequencies covering beyond the second corner (10 rad/s) up to 2.7 rad/s.

The upper limit is set to meet the Shanon condition for sampling, as the simulation of the plant is sampled at 0.001 s. Measuring the frequencies relative to the corner frequencies, the experiments begin with packages that are below the lower corner gradually increase the range including both. Next the lower limit is increased and the set of experiments is again performed until the packages cover a range up to the upper limit. The effect is that we get experiments covering only below and above the two corners and different ranges including both and one or the other.

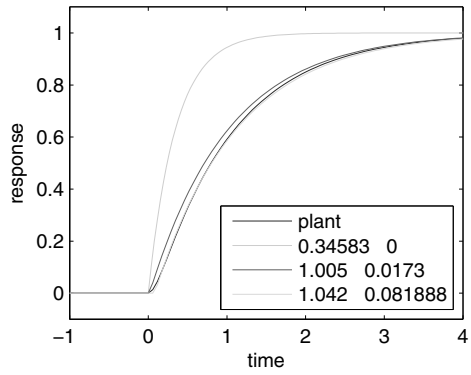

Figure 4. Step responses of different models compared with plant

Looking at the fit in the time domain, the step responses for an under-estimated, a well estimated and an over-estimated model are shown in Figure 4. The difference in the model is apparently large and most likely significant to any application. The figure also clearly reveals the second-order behaviour of the plant, specifically the zero slope at the beginning.

The frequency responses look similarly intriguing. Figure 5 shows the same three models and the plant in Bode plots.

Apparently the phase is not matched as the model's high-frequency phase shift is 90 degrees, whilst the plant has 180 degrees. Most likely, at this point control people would suggest a first-order-plus-dead-time model, which when fitted would do a better job on the phase. Indeed if we use the same experiments as above, this is the case, though only for frequency packages that are below the second time constant. Above things get hairy very quickly and the algorithms fail to provide an estimate. On the lower frequency package side nothing changes, the estimated dead time is zero. Figure 6 shows the situation in the frequency domain. for three models. The

Figure 3 shows the result. Using only a package of relative low frequencies results a time constant smaller than the dominating one. Increasing the range (see first experiment set) the estimate does change less and less, but increasingly monotonically towards the end (left end). The low estimate is due to not having the first corner frequency (located at 0) included in the range. As one moves the package range covering the two corners, the estimates get relatively constant though always increasing with the inclusion of higher frequencies. Once one is over the limit of including the lower corner frequency, which is a 1, the estimated time constant is increasing rapidly.

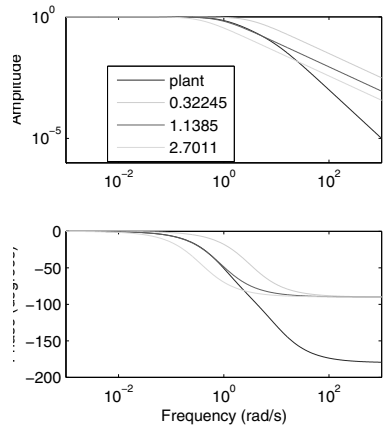

Figure 5. Step responses of different models without dead time compared with plant

three chosen experiments are the very first, thus the package clearly below the dominating time constant (green, top one), the second is the red one (second from the top, down turning in the phase plot) and the third is fitting best (third in the phase plot turning down most quickly). The step responses for the two last estimates look superb, whilst the first is equally bad as shown in Figure 4.

3. Discussion

The choice of frequencies for the excitation affects the model fidelity. The high frequencies for which the model deviates significantly from the plant, have clearly a negative effect on the estimated model parameter. The effect is most visible if one chooses the wrong frequency range. Obviously one would not use such extreme conditions. We did so because we want to make to problem visible. However, using steps or approximate steps or any other excitation signal that contains high frequencies, is not necessarily a good idea. The high frequency parts have clearly a negative effect on the estimate.

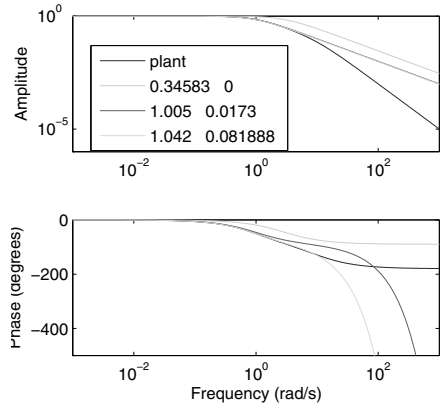

Figure 6. Step responses of different models with dead time compared with plant

Whilst this has the flavour of a negative statement, in reality this is usually quite happy news, because generating high frequency input is usually not easy to realise and in many cases inflicts quite a bit of costs. This because the state of a physical system can only be affected by the transfer of extensive quantity such as mass and energy. The flow is to be controlled with a valve or a corresponding device if it is not volume flow. Fast moving valves are usually more expensive than slow ones and similarly for tracer experiments high frequency injections are not easy to generate reproducible.

4. Conclusions

Spending effort on generating very fast changing inputs for the purpose of exciting the process for model fitting is usually not a good idea. The high frequencies, rather then adding information to the estimated model, actually usually reduce the fidelity of the model. Since we nearly always under-model our physical processes, the frequency range in which the model describes the process well, is limited and should be considered both in the identification task as well as in the utilisation of the model.

References

Gevers, M., Xavier, B., Hildebrand, R., Solari, G., 2011. Optimal design for open and closed-loop system identification. Communications in Information and Systems 11 (3), 197–224.

Goodwin, G. C., Payne, R. L., 1977. Dynamic system identification: Experiment design and data analysis. Academic Press.

Ljung, L., 1987. System Identification Theory for the User. Prentice Hall Inc. Englewood Cliffs, New Jersey.

I.A. Karimi and Rajagopalan Srinivasan (Editors), Proceedings of the 11th International Symposium on Process Systems Engineering, 15-19 July 2012, Singapore.

Real-time optimization of energy systems in sugar and ethanol facilities: a modifier adaptation approach

Fernán Serralunga, Miguel C. Mussati, Pio A. Aguirre

INGAR Instituto de Desarrollo y Diseño (CONICET-UTN), Avellaneda 3657, (S3002GJC) Santa Fe, Argentina.

Abstract

Real-time optimization (RTO) is used to operate industrial processes close to their minimum cost or maximum profit conditions. Model-based RTO needs an adaptation step to update the model under plant/model mismatch. This work proposes a novel RTO approach based on the modifier adaptation strategy, aiming to reduce the dimension of the gradient correction problem. The approach was tested in a model of a heat and power system of a sugar/ethanol facility. It could be also applied to other kind of processes. The results showed a noticeable performance improvement when compared to adaptation strategies without gradient correction.

Keywords: real-time optimization; energy optimization; sugar and alcohol industry.

1. Introduction

Sugarcane is nowadays the most efficient way to produce bioethanol at large scales. Due to improvements in process technology, sugar and ethanol plants have become energy self-sufficient, and they can export electric power by burning surplus bagasse. Optimal operating setpoints for the energy system in these plants can change along time, as result of changes in sugarcane quality, equipment performances (fouling), power price and production level. This encourages the use of real-time strategies to maximize performance or minimize energy costs. A recent work shows industrial application of computer-aided real-time tools for energy management in sugar and alcohol facilities (Mariani et al., 2009).

Real-time optimization (RTO) can be used to continuously improve the performance of an industrial process. Model-based RTO approaches need to deal with parametric and structural plant/model mismatch. Structural mismatch can make the system converge to operating points different to the real plant optimum. Some algorithms (ISOPE, modifier adaptation) have been developed to overcome this difficulty (Chachuat et al., 2009). They incorporate gradient correction terms aiming to match the Karush-Kuhn-Tucker conditions of the plant, making thus the model optimum coincident with the plant optimum, upon convergence.

Real-plant gradient estimation is not a trivial task. Some techniques make use of current and past data (Broyden methods, dual control, dynamic identification), other ones add perturbations to the plant around each steady state (finite forward differences, etc). (Mansour and Ellis, 2003, Srinivasan et al., 2011).

This work proposes a real-time optimization scheme for steam and power generation in a sugar plant with annexed ethanol production. The scheme is based on the modifier adaptation approach. It only adapts specific performance equations, such as those used for calculating boilers and turbines efficiencies and multiple-effect evaporation

coefficients. Data from current and past RTO cycles are used (Yip et. al., 2002). The algorithm is tested under different operating scenarios of the sugar/ethanol facility.

2. Real-Time Optimization

The proposed RTO approach assumes that all the parametric and structural uncertainty is included in a subset of equations, which calculate efficiencies and performances in pieces of equipment. The problem to solve can be stated as:

$$\begin{aligned} &\min_{\mathbf{u}} Q(\mathbf{y},\mathbf{u}) \\ &s.t.\ \ \mathbf{h}(\mathbf{y},\mathbf{u},\boldsymbol{\eta}) = \mathbf{0} \\ &\quad \mathbf{h}_m(\mathbf{u}) = \boldsymbol{\eta} \\ &\quad \mathbf{g}(\mathbf{y},\mathbf{u}) \le \mathbf{0} \\ &\quad \mathbf{u}_l \le \mathbf{u} \le \mathbf{u}_u \end{aligned} \tag{1}$$

where **y** are the process outputs, **u** the process inputs, **h** the process model (mass, energy and entropy balances, considered as free of uncertainty), and **g** inequality equations. $\boldsymbol{\eta}$ are performance or efficiency factors, whose functionality with process inputs is only known by an approximate model $\mathbf{h}_m(\mathbf{u})$.

In a RTO cycle *k*, after measurements validation and data reconciliation, the actual efficiency terms $\boldsymbol{\eta}_k$ can be known without the need of the uncertain equations $\mathbf{h}_m$. Therefore, equations $\mathbf{h}_m$ can be adapted to match the predicted value with the actual one. Modifier adaptation (Chachuat et al., 2009) would adapt the equations as:

$$\boldsymbol{\eta} = \mathbf{h}_m(\mathbf{u}) + \boldsymbol{\beta}_k + \boldsymbol{\lambda}_k^T(\mathbf{u} - \mathbf{u}_k) \tag{2}$$

where $\boldsymbol{\beta}_k = \boldsymbol{\eta}_k - \mathbf{h}_m(\mathbf{u}_k)$ is the so-called constraint modifier. $\boldsymbol{\lambda}_k = [\nabla\boldsymbol{\eta} - \nabla\mathbf{h}_m]_{\mathbf{u}=\mathbf{u}_k}$ is the gradient correction term. Under convergence, this approach matches a KKT point of the plant, and therefore both feasibility and optimality are guaranteed. Constraint adaptation (Chachuat et al., 2008) only includes the term $\boldsymbol{\beta}_k$ and no gradient correction; this guarantees feasibility but not optimality under structural mismatch.

This work proposes the following adaptation:

$$\eta_j = h_{m,j}(\mathbf{u}_k) + \gamma_{jk}(\mathbf{x}_j(\mathbf{u})) \qquad j = 1,2,..nj \tag{3}$$

where each efficiency η_j (being *nj* the total number of adapted equations) has an adaptation term γ_{jk}, which is a linear or quadratic function of a subset of states $\mathbf{x}_j$. Coefficients γ_{jk} are obtained from current and past data by linear regression:

$$\begin{aligned} &\min_{a_k,\mathbf{b}_k,C_k} \sum_{j=1}^{nj} \sum_{i=k-n}^{k} w_i(\beta_{ji} - \gamma_{ji})^2 \\ &s.t.\ \ \beta_{ji} = \eta_{ji} - h_{m,j}(\mathbf{u}_i) \\ &\quad \gamma_{ji} = a_{jk} + \mathbf{b}_{jk}^T \cdot \mathbf{x}_{ji} + \mathbf{x}_{ji}^T C_{ji} \mathbf{x}_{ji} \\ &\quad \mathbf{x}_{ji} = \mathbf{x}_j(\mathbf{u}_i) \\ &\quad a_j^L \le a_{jk} \le a_j^U \qquad\qquad j = 1..nj \\ &\quad \mathbf{b}_j^L \le \mathbf{b}_{jk} \le \mathbf{b}_j^U \qquad\qquad i = (k-n),\ldots,k \\ &\quad C_j^L \le C_{jk} \le C_j^U \end{aligned} \tag{4}$$

where a_{jk}, $\mathbf{b}_{jk}$ and C_{jk} are the coefficients of the regression. w_i is a weight factor that gets smaller as the data gets older and $n+1$ is the number of RTO cycles used in the regression. This allows having a data set with enough elements to eliminate the effect of noise, and at the same time to discard old data that could include different values of process disturbances. If the proposed function is a linear one, the method is similar to modifier adaptation, but using a special update method for the linear (gradient) term.
This method can be useful when each efficiency term is a function of a small subset of states. This situation can often be observed in heat and power systems as the one studied in this work. Indeed, by fixing the steam temperature and pressure, the performance of pieces of equipment like boilers and turbogenerators, is a function of the load, while process disturbances can remain approximately constant if the period analyzed is short.

3. Sugar and ethanol energy system model

A steady state model of a steam system of a sugar and ethanol facility was built. It includes two bagasse boilers, a set of turbines for cane milling, an extraction-condensing turbine for power generation, a 5-effect evaporator with vapor bleeding in the first 3 effects, and a set of steam demanding units (sugar boiling, ethanol distillation, steam deaerator). The diagram of the steam system is shown in Figure 1.

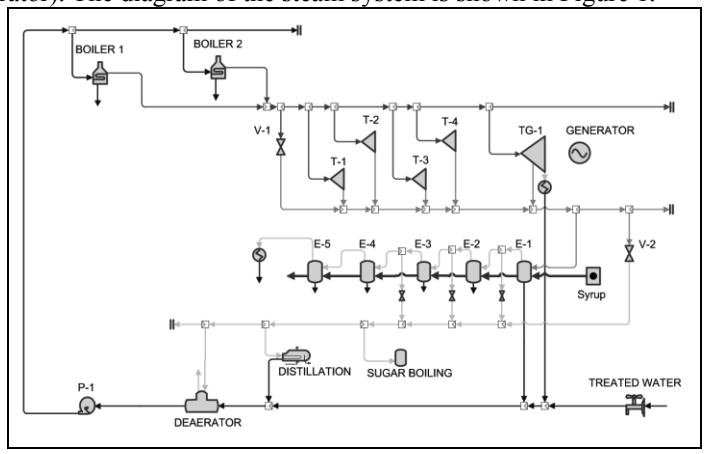

Figure 1. Diagram of the modeled steam system.

The model consists of mass, energy and entropy balances, and a set of equations that predict boiler and turbogenerator efficiencies, and evaporation coefficients in the evaporators. In order to evaluate the performance of the proposed RTO scheme, a different model (called hereafter "real plant") represents the real plant behavior. It consists of the same balance equations and a different set of equations to predict efficiencies and coefficients. Boiling point elevation in evaporator effects is calculated using correlations (Camargo, 1990) and is considered as free of error.
The real plant model is used to evaluate the evolution of the system after applying RTO results, and to provide data to the next RTO cycle. These data are used to adapt the model equations as described in the previous section. In order to simulate measurement errors and perform a data reconciliation step, the real plant simulation outputs are modified with a Gaussian noise prior to RTO calculations.
Table 1 lists RTO and real plant model equations. F_1 and F_2 are boiler steam flows, F_3 and F_4 are TG-1 admission and exhaust flows; T_3 is TG-1 extraction temperature; e is the evaporator effect. X_e and T_e are effect solids fraction and steam temperature.

Table 1. Real and RTO efficiency equations

	Real plant	RTO (h_{mj})
Boiler 1	$90-0.001(145-F_1)^2-10^{-6}F_1^3$	$92-0.005(150-F_1)^2$
Boiler 2	$91-0.001(155-F_2)^2-1.2\times10^{-6}F_2^3$	$93-0.005(150-F_2)^2$
TG-1 stage 1	$53-0.0023(120-F_3)^2+1\times10^{-6}F_3^3$	$70-0.005(130-F_3)^2$
TG-2 stage 2	$66-0.0018(50-F_4)^2+2.2\times10^{-6}F_4^3+10^{-2}T_3$	$70-0.004(41-F_4)^2$
Evaporation coefficients	$(0.0012-0.0001e)(96-X_e)(T_{e-1}-54)$ $-0.2(X_e/100)^2-0.5\exp(-(T_{e-1}-50)/100)$	$0.001(100-X_e)(T_{e-1}-54)$

Efficiency equations are adapted with second-order polynomials, which are functions of the equipment flow (even TG-1 2nd stage efficiency, which is actually also function of temperature). The quadratic terms can be different to zero only after 5 RTO cycles. Evaporation coefficients are adapted with a linear function of the live steam flow consumed in effect 1 (F_V). The optimization problem to solve in a k^{th} RTO cycle is:

$$\min_{\mathbf{u}} Q_1+Q_2-c_1W$$

$$s.t\quad \begin{cases} \mathbf{h}(\mathbf{F},\mathbf{P},\mathbf{T},\mathbf{B},W,Q_1,Q_2,\boldsymbol{\eta})=\mathbf{0} & \\ \eta_j=h_{mj}(F_j)+a_{jk}+b_{jk}F_j+c_{jk}F_j^2, & j=1\ldots4 \\ \eta_j=h_{mj}(F_j)+a_{jk}+b_{jk}F_V & j=5\ldots9 \\ \mathbf{F}_l\le\mathbf{F}\le\mathbf{F}_u & \\ \left\|F_j-F_{j,k}\right\|\le2.5 & j=1,2 \end{cases} \tag{5}$$

where **F, P** and **T** are steam flows, pressures and temperatures, W is the power produced by the turbogenerator. Q_1 and Q_2 are boiler fuel consumptions, **B** are the syrup Brix degrees in all evaporator effects. η_1 to η_4 are boiler and turbine efficiencies according to Table 1, and η_5 to η_9 are evaporation coefficients in effects 1 to 5. c_1 is the power cost. a_{jk}, b_{jk} and C_{jk} are the adaptation parameters (Eq. 4). **u** are the process inputs; in this case they are Boiler productions, TG-1 extraction and vapor bleeding in the evaporators. The last constraint is added to limit the size of changes in each RTO cycle.

4. Results

The performance of the proposed RTO scheme is analyzed under different scenarios. A starting operating point is simulated with the real plant model. After that, Gaussian noise is added to the results, and a data reconciliation step is performed using the RTO model, which allows calculating efficiencies and evaporator coefficients. The adaptation step is then performed, followed by RTO optimization. The calculated optimum inputs are used to simulate the real plant model, calculating the real cost achieved and starting the cycle again with noise addition and the data reconciliation step.

The results considering an evaporator feed of 500 m^3/h, initial and final Brix of 15 and 70, respectively, are shown in Figure 2, and compared with a constraint adaptation (CA) approach. Initial steam demand (distillation and sugar boiling) is of 200 t/h. The model parameters are $c_1=0.018$, $n=10$, $w_i=0.85^{k-i}$. The proposed adaptation shows convergence close to the real plant optimum in noise-free scenarios. When Gaussian noise is present, it shows better performance than CA for both constant and variable steam demand.

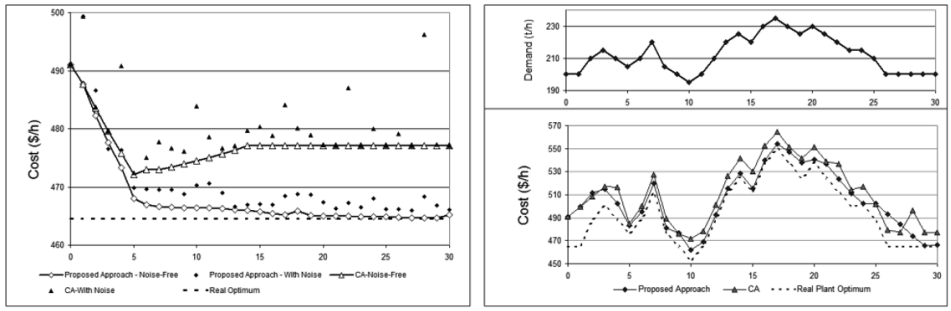

Figure 2. Cost evolution for 30 RTO cycles. Constant steam demand (left). Variable steam demand with noise (right). Gaussian noise standard deviation: Flow = 0.3 t/h, Temperature = 0.5°C, Fuel = 1 Gcal/h, Power = 25 kW.

Such performance comparisons were performed using Extended Design Cost (Zhang et al., 2000), which evaluates the distance from the real plant optimum. For constant demand, the relative costs are: CA without noise: *100*; CA with noise: *127*, proposed approach without noise: *30*, proposed approach with noise: *49*. For variable steam demand, CA: *100*, proposed approach: *62.5*.

5. Conclusions

A RTO approach based on modifier adaptation has been proposed, which has been shown to be efficient through a sugar and alcohol facility steam system. However, it could be applied straightforward to other industrial processes. The performance of the proposed scheme, which includes a correction of model gradients, was better than that using constraint adaptation, in line with theory and results of the mentioned references.
Energy systems in sugar/ethanol plants provide a wide range of opportunities for applying real-time optimization. In this line, the performance of RTO schemes under lack of instrumentation, measurement failures and non-steady behavior will be the objective of further research.

Acknowledgements: The authors gratefully acknowledge the financial support from CONICET and Soteica Latinoamérica S.A.

References

B. Chachuat, B. Srinivasan. and D. Bonvin, 2009, Adaptation strategies for real-time optimization. Computers & Chemical Engineering 33, 1557 – 1567.
B. Chachuat, A. Marchetti, and D. Bonvin, 2008. Process optimization via constraints adaptation. Journal of Process Control, 18(3-4), 244 – 257.
C. Camargo, A. Ushima, A.. Ribeiro, M. Souza, N. dos Santos, Manual de Recomendacões-Conservacão de Energia na Indústria do Açúcar e Álcool, Publicação IPT, São Paulo, 1990.
M. Mansour and J. Ellis, 2003, Comparison of methods for estimating real process derivatives in on-line optimization. Applied Mathematical Modelling 27, 275 – 291.
D. Mariani, . Kihn, and C. Ruiz, 2009. Industrial experience on the implementation of real time on line energy management systems in sugar and alcohol industry. Computer Aided Chemical Engineering, 27, 459 – 464.
B. Srinivasan, G. François and D. Bonvin, 2011, Comparison of Gradient Estimation Methods for Real-Time Optimization. Computer Aided Chemical Engineering, 29, 607-611.
W. Yip and T. Marlin, 2002. Multiple data sets for model updating in real-time operations optimization. Computers & Chemical Engineering, 26(10):1345 – 1362.
Y. Zhang, and J.F. Forbes, 2000, Extended design cost: a performance criterion for real-time optimization systems. Computers & Chemical Engineering 24, 1829 – 1841.

I.A. Karimi and Rajagopalan Srinivasan (Editors), Proceedings of the 11th International Symposium on Process Systems Engineering, 15-19 July 2012, Singapore.

On the Stability and Feasibility of Model Predictive Control

Supriyo K. Mondal,[a] Swapan Paruya,[a] S. S. Rao[b]

[a]*National Institute Technology, Durgapur 713209, India*
[b]*University of Miami, Florida 33124, USA*

Abstract

In this paper, we demonstrate the issues of feasibility, stability and performance of constrained finite receding horizon linear quadratic regulator (RHLQR) problems using primal-dual interior point (PDIP) method developed in FORTRAN. Instead of including path constraints, we have chosen sufficiently long horizon to achieve stability with finite horizon cost leading to Lyapunov function. We observed a significant improvement of stability of model predictive control using PDIP over active set method.
Keywords: feasibility, stability, performance

1. Introduction

The developments of model predictive control (MPC) deal with the existence of solution to optimal control problems. MPC for constrained linear and nonlinear systems essentially uses Lyapunov and Riccati stability theory. Feasibility, stability and performance are the important issues of MPC. It is always challenging to study the issues for making MPC more suitable in real-time applications. Survey of literature indicates that the studies on the issues began late seventy. Kwon and Pearson (1977) found cost function (J_N) to be non-increasing with length of horizon (N) by imposing an end constraints on the state (x(N)=0), which guarantees stability. Based on the exhaustive survey of literatures, Mayne et al. (2000) made generalization for ensuring closed-loop stability of MPC under terminal cost, terminal constraint set and local stabilizing controller. Primbs and Nevistic (2000) proved using the finite horizon cost (acting as a Lyapunov function) that a sufficient long horizon is required for feasibility and stability of a constrained receding horizon (RH) policy. Santos et al. (2008) demonstrated with the help of nonlinear programming techniques that constrained MPC is robustly stable for the case with modeling errors.

In this paper, we focus on the analysis of feasibility, stability and performance of constrained finite receding horizon linear quadratic regulator (RHLQR) problems adopted from published literatures. We do not consider any end constraint or terminal constraint. Instead, we suitably chose sufficiently long horizon to achieve stability with finite horizon cost leading to Lyapunov function. We show how the costly primal-dual interior point (PDIP) method for optimization makes an impact on the feasibility, stability and performance of MPC. As analyzed by Mondal et al. (2011), PDIP has a guaranteed feasibility property due to the barrier function used in PDIP. We expect to an improvement of feasibility and stability of MPC using PDIP. From the analysis, we have also determined the optimal horizon length (N^*).

The performance or cost function of MPC can be expressed as below:

$$\min \phi = [x^T(p)Px(p) + \sum_{k=0}^{p-1} x^T(k)Qx(k) + \sum_{k=0}^{m-1} u^T(k)Ru(k)] \quad (1)$$

Where p is prediction horizon, m is control/input horizon and k is the sampling time step. We consider $p = m = N$. Subject to the linear state space model constraint:

$$x(k+1)=Ax(k)+Bu(k);\ k = 0, 1, 2,\ldots\ldots, N-1 \quad (2)$$

The number of input and state variable are denoted by *ni and ns*. *A* and *B* are the system matrices with the dimension. *P* is the terminal weight and solution of the *P* is to the corresponding Lyapunov equation or discrete-time Riccati equation. *Q* and *R* are the weight matrices. X_k is a system state variable and U_k is the system control / input.

2. Criteria for feasibility and stability

We discuss here the condition related to the feasibility and stability based on which the present analysis has been made. We attempt to identify the feasible region in which the constrained optimal control problem is solvable. For a properly chosen horizon, RH policy always remains in the region. The RH policy can be shown to be capable of retaining feasibility without end constraints (Primbs & Nevistic, 2000).

We consider the following time-invariant linear system. The constraints:

$x(k+1)=Ax(k) + Bu(k),\ x(0) = x_0,$ (3)

s.t: $Ex + Fu \le \psi$ (4)

where $x(k)\in R^n$, $u(k)\in R^m$, $\psi\in R^p$, $E\in R^{p\times n}$ and $F\in R^{p\times m}$ denote the state vector, input vector and constraints respectively.

The cost function of a linear quadratic regulator (LQR) problem may be expressed infinite or finite horizon as follow:

Infinite horizon cost function:

$$J(x_0) = \inf_{u(.)} \sum_{k=0}^{\infty} (x^T(k)Qx(k) + u^T(k)Ru(k)) \tag{5}$$

Finite horizon cost function:

$$J_N(x_0) = \inf_{u(.)} \left[x^T(N)P_0x(N) + \sum_{k=0}^{N-1} \left(x^T(k)Qx(k) + u^T(k)Ru(k) \right) \right] \tag{6}$$

Criteria are based on the following assumptions:

(i) $Q > 0$, $R > 0$ ($[Q^{1/2}, A]$ observable).

(ii) [A, B] controllable.

(iii) $P_0 = Q$ (J_N is monotonically non-decreasing).

(iv) There exists a neighborhood of the origin which is feasible for deadbeat and the unconstrained optimal control.

For any set *W*, let $\overset{0}{W}$ denote its interior, $\overline{W}$ its closure, and W^c its complement. Given two sets *W* and *M*, $W - M = W \cap M^c$. Let L_θ denote the θ sub-level set of the optimal infinite horizon cost J(x) i.e:

$L_\theta = \{x : J(x) \le \theta\}$

2. 1 Computational Schemes for stability parameter

Calculate $\theta = \max_{x\in I} x^T Px$ and define the set $W = \{x: x^T Px \le \theta\}$ and solve the following optimization problems:

$$\tau_N = \max \frac{J_{N+1}(x)}{J_N(x)} \text{ ,s.t } x \in W \tag{7}$$

and $\chi_N = \min \dfrac{x^T Qx}{J_N(x)}$, s.t. $x \in W$ (8)

$$\text{or } \xi_N = \max \frac{J_N(x(1))}{J_N(x(0))}, \text{ s.t. } x \in W \tag{9}$$

3. Numerical results

Here we consider one case study from literature in order to experience and analyse the response, feasibility, stability and performance. We also discuss the numerical results we obtain in relation to the data from the literature. CPU used in our computations is Intel(R) core(TM)2 Duo E7500@2.93 GH_Z. PDIP method and MPC algorithm were implemented using digital visual FORTRAN 5.0.

3.1 Case study 1: The problem adapted from Pistikopoulos et al.

The following discrete state-space model with sampling period of 0.1s is considered:

$$x_{k+1} = \begin{bmatrix} 0.7326 & -0.0861 \\ 0.1722 & 0.9909 \end{bmatrix} x_k + \begin{bmatrix} 0.0609 \\ 0.0064 \end{bmatrix} u(k) \tag{10}$$

$$y_k = \begin{bmatrix} 0 & 1.4142 \end{bmatrix} x_k \tag{11}$$

The constraints on input are as follows:

$$-2 \le u \le 2 \tag{12}$$

And the weight matrices,

$$Q = \begin{bmatrix} 1 & 0 \\ 0 & 1 \end{bmatrix}, R = 1$$

Initial conditions: $x(0) = [1 \quad 1]^T$, N = 2

The system (10-12) was run 40 samplings. We apply the receding horizon policy for optimal control of the system. The optimal control sequence is obtained by minimizing the cost function along with the constraint (12) and $P \geq 0$ is the solution to the corresponding Lyapunov equation which is given below:

$$P = \begin{bmatrix} 3.0485 & -2.5055 \\ -2.5055 & 12.9916 \end{bmatrix}; P \text{ is the terminal weight.}$$

Fig. 1(a) shows the system state response varying with number of sampling. Fig. 1(b) presents the variation of input (control action) with number of samplings. Both the state and the input settle at zero as expected in the regulator problem. While comparing these results with those of Pistikopoulos et al. (2002) using QP, it is observed that the results in the present studies are found to be very close to the later with improved stability with our PDIP method. The method yields faster convergence and better feasibility with continuous variations of states and input, although the number of active constraints in our study is almost equal to those obtained by them using QP method. It is noted that number of iteration for convergence is independent of the size of the problem.

3.1.1. Feasibility of the solutions

Here, we analyse the feasibility of the solution. In order to test the feasibility, we satisfy the following conditions:

$$\mu \ge J(x(0)) \ge J_N(x(0)) \ge J_{N-1}(x(1)) \ge x^T(1)Qx(1) \tag{13}$$

where μ is sub level set and $\mu = x^T P x = 11.029$ with $x(0) = [1 \quad 1]^T$

$J_N(x(0)) = 10.47$ at N = 8

$J_{N-1}(x(1)) = 6.4361$ at N=7

$x^T(1)Qx(1) = 1.5985$

We see most of the condition is fulfilling according to present theorem. So, our solution is in the feasible region.

3.1.2. Stability of the system

Following the procedure outlined in the Section 2.1, the sensitivity of stability parameter ξ_N with horizon length (N) is presented in the Fig. 2 using Eq. (9) and the relevant parameters are tabulated in the Tables 1. The variation of ξ_N is linear. One may note in the Fig. 3 that $\xi_N < 1$ for $N \geq 3$. Specifically, τ_N and χ_N were calculated using Eq. (7) and Eq. (8) respectively.

Although $\omega_N < 1$ or $\xi_N < 1$ determines stability of closed loop, $\xi_N < 1$ is less conservative than ω_N. Considering the results using ω_N, a horizon of 4 is sufficient to guarantee stability. The variation of parameters τ_N and χ_N with N are displayed in Table 1 for reference. These parameters are necessary to calculate ω_N and additionally, τ_N is needed to calculate performance parameter $\prod_N$ in conjunction with both ω_N and ξ_N.

Performance result is presented in Table 1 with the help of Eq. (14) and Eq. (15). With ω_N, a horizon length of 5 is sufficient to guarantee performance in terms of Π_N^{ω}. Similarly under ξ_N, a horizon length of 5 is sufficient to guarantee performance in terms of Π_N^{ξ}. The criteria yield similar results.

Another computation of our results using PDIP with Primbs and Nevistic(1997) shown in Fig. 3 reveals that our PDIP yields improved stability compared to SQP-active set method. ξ_N is well below unity compared to that of Primbs and Nevistic(1997), as evident in the figure. This is due to faster convergence rate and better feasibility properties of PDIP. ξ_N with PDIP appreciably decreases with N (although depending on IC) compared to active set method.

The performance Π_N^{ω} with respect to ω is given by:

$$\Pi_N^{\omega} = \left[1 + \left(\frac{\tau_{N-1} - 1}{\tau_{N-1}}\right)\frac{\omega_N}{1-\omega_N}\right] \tag{14}$$

Π_N^{ξ} with respect to ξ_N is given by:

$$\Pi_N^{\xi} = \left[1 + \left(\frac{\tau_{N-1} - 1}{\tau_{N-1}}\right)\frac{\xi_N}{1-\xi_N}\right] \tag{15}$$

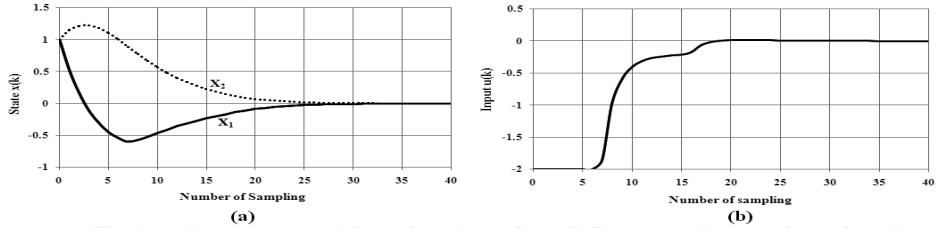

Fig. 1. (a) State response with number of sampling. (b) Response of input with number of sampling.

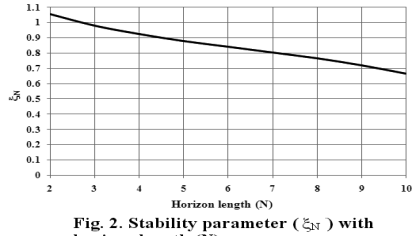

Fig. 2. Stability parameter (ξ_N) with horizon length (N).

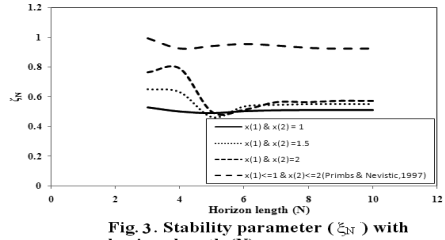

Fig. 3. Stability parameter (ξ_N) with horizon length (N).

Table 1
Stability parameter ω_N and parameters τ_N, χ_N (used to calculate ω_N) and performance results Π_N^{ω} and Π_N^{ξ} (using ω_N and ξ_N).

N	ω_N	τ_N	χ_N	Π_N^{ω}	Π_N^{ξ}
2	-	-	0.093418	-	-
3	1.008164	1.101582	0.084803	-	5.530698325
4	0.933611	1.018414	0.083270	1.25427103	1.225820551
5	0.880265	0.963535	0.086421	0.721769944	0.719103799
6	0.835272	0.921694	0.093763	0.569203025	0.542520512
7	0.792027	0.885790	0.105853	0.508973309	0.465784039
8	0.747602	0.853455	0.124029	0.491401221	0.437606066
9	0.698175	0.822203	0.150849	0.499789514	0.441232071
10	0.638368	0.789217	0.191138	0.528542373	0.471430225

4. Conclusion

We have presented one case study of constrained finite RHLQR problems from the published literature to demonstrate feasibility, stability and performance of MPC developed with FORTRAN. From the analysis, we have determined the optimal horizon length (N). However, stability parameters and performance parameters is observed to have decreased with horizon length. In the case study, we observed that the stability and the feasibility were achieved for $N \geq 3$ and the performance parameter is very close to unity. It is also found that $\xi_N < 1$ for stability seems to be less conservative than $\omega_N < 1$. PDIP method contributes to improve stability compared to active set method.

References

W.H. Kwon, A.E. Pearson, 1977, A modified quadratic cost problem and feedback stabilization of a linear system, IEEE Trans Automat Contr, 22, 838-842

S.K. Mondal, N. Goswami, S. Paruya, S.S. Rao, 2011, Primal-dual interior point (PDIP) for model predictive control – a computational experience, Submitted in J Optimiz Theory App.

L.O. Santos, L.T. Biegler, J.A.A.M. Castro, 2008, A tool to analyse robust stability for constrained nonlinear MPC, J. Process Control, 18, 383-390

J. Primbs, V. Nevistic, 1997, Constrained finite receding horizon linear quadratic control, CDS Technical Memo #CIT-CDS 97-002

J. Primbs, V. Nevistic, 2000, Feasibility and stability of constrained finite receding horizon control, Automatica, 36, 965-971

E.N. Pistikopoulos, V. Dua, N.A. Bozinis, A. Bemporad, M. Morari, 2002, On-line optimization via off-line parametric optimization tools, Comput Chem Eng, 26, 175-185

D.Q. Mayne, J.B. Rawlings, C.V. Rao, P.O.M Scokaert, 2000, Constrained model predictive control: Stability and optimality, Automatica, 36, 789-814

I.A. Karimi and Rajagopalan Srinivasan (Editors), Proceedings of the 11th International Symposium on Process Systems Engineering, 15-19 July 2012, Singapore.

Studying Various Optimal Control Problems in Biodiesel Production in a Batch Reactor under Uncertainty

Pahola T. Benavides1, [a,b] Urmila M. Diwekar, [a,b]
[a]*Department of Industrial Engineering, University of Illinois, Chicago, IL 60607 - USA*
[b]*Center for uncertain Systems: Tools for Optimization & Management (CUSTOM), Vishwamitra Research Institute, Clarendon Hills, IL 60514 – USA*

Abstract

Optimal control problems encountered in biodiesel production can be formulated using various performance indices like maximum concentration, minimum time, and maximum profit. The problems involve determining optimal temperature profile so as to maximize these performance indices. This paper presents these three formulations and analyzes the solutions in biodiesel production. We also present the maximum profit problem where the variability and uncertainties in the feed composition of soybean are considered.

Keywords: batch reactor, biodiesel, optimal control, stochastic optimal control, maximum principle, minimum time, maximum profit.

1. Introduction

Optimal control problems are defined in the time domain and their solution requires establishing a performance index for the system. Because of the dynamic nature of the decision variables encounter, optimal control problems are much more difficult to solve compared to normal optimization where the decision variables are scalars.

Optimization in batch processes can lead to different types of problems depending on the objective of the process. Some of the examples of optimal control problems in batch reactor are presented in Denbigh, 1958; Crescitelli and Nicoletti, 1973; Luus, 1999, and Aziz and Mujtaba, 2001. To solve these problems, dynamic and NLP methods are employed; however, since these types of problem are large, they require large-scale NLP solvers. In this paper, we are proposing an alternative approach that avoids the use of these large-scales NLP solvers. Moreover, we study the three optimal control problems on batch reactors: maximum concentration problem (MCP) of methyl ester, the minimum time problem (MTP), and the maximum profit problem (MPP) for biodiesel production in batch reactor. The MCP and MTP illustrated in this paper are solved using the maximum principle theory, and the approach is based on the Steepest Ascent of Hamiltonian, also shown in Diwekar, 2008. On the other hand, the MPP is solved using an algorithm that combines the maximum principle and NLP techniques. This algorithm is an efficient approach which avoids the solution of the two-point boundary value problem that results in the pure maximum principle or in the solution of the partial differential equations for the pure dynamic programming formulation.

Biodiesel is one of the most well-known examples for alternative energy and is also renewable and domestic resource with an environmentally friendly emission profile (Zhang et al., 2003). This biofuel is derived from vegetables oils produced by transesterification reaction with an alcohol (methanol). Several factors that can affect the process in terms of yield have been investigated. Among of these factors, the most relevant are the alcohol ratio, catalyst concentration, reaction temperature, and reaction time. To mention some important aspects Leung and Guo 2006 has an excellent summary. Here we present the optimal control problem where optimal temperature profile is derived using optimal control theory.

Optimal control problems become more challenging when variability in any parameter or variable is included. In biodiesel production, there are inherent uncertainties that have a significant impact on the product quantity, quality and process economic. One of the most influential uncertainties in this process is the feed composition since the percentage and type of triglycerides in biodiesel composition varies considerable (Linstromberg, 1970). This uncertainty can be modeled using probabilistic techniques, and can be propagated using stochastic modeling iterative procedures (Diwekar and Rubin, 1991). Therefore, at the end of this paper we propose a stochastic maximum profit problem (SMPP) that regards the variability in the feed composition to observe how this uncertainty affects the process economic in the batch reactor.

2. Optimal Control Problem:

Table 1 summarizes the optimization problems presented in this paper.

Table 1 Optimal Control problems in Biodiesel Production

Problem	Concentration	Batch time	Objective
Maximum concentration	Free	Fixed	Maximize C_E
Minimum Time	Fixed	Free	Minimize t_f
Maximum profit	Free	Free	Maximize profit

The kinetic model for biodiesel production presented here is based on Noureddini et al., 1997 and is used to solve the three optimal control problems.

$$F_1 = \frac{dC_{TG}}{dt} = -k_1 C_{TG} C_A + k_2 C_{DG} C_E \quad (1)$$

$$F_2 = \frac{dC_{DG}}{dt} = k_1 C_{TG} C_A - k_2 C_{DG} C_E - k_3 C_{DG} C_A + k_4 C_{MG} C_E \quad (2)$$

$$F_3 = \frac{dC_{MG}}{dt} = k_3 C_{DG} C_A - k_4 C_{MG} C_E - k_5 C_{MG} C_A + k_6 C_{GL} C_E \quad (3)$$

$$F_4 = \frac{dC_E}{dt} = k_1 C_{TG} C_A - k_2 C_{DG} C_E + k_3 C_{DG} C_A - k_4 C_{MG} C_E + k_5 C_{MG} C_A - k_6 C_{GL} C_E \quad (4)$$

$$F_5 = \frac{dC_A}{dt} = -\frac{dC_E}{dt} \quad (5)$$

$$F_6 = \frac{dC_{GL}}{dt} = k_5 C_{MG} C_A - k_6 C_{GL} C_E \quad (6)$$

where C_{TG}, C_{DG}, C_{MG}, C_E, C_A, and C_{GL} are the state variables and represent concentrations of triglycerides, diglycerides, monoglycerides, methyl ester, methanol, and glycerol, respectively. The initial conditions are: $C_i(t_0) = [C_{TG}; 0; 0; 0; C_A; 0]$ [mol/L]. The reaction constant, k_i, is expressed by the Eq.7.

$$k_i = a_i e^{-\frac{b_i}{T}} \quad (7)$$

where T is the reaction temperature (control variable), a_i is the frequency factor and $b_i = E_{ai}/R$ for which E_{ai} is the activation energy for each component i and R is the gas constant.

The objective function for the maximum profit problem is represented by Eq.8 (Kerhof and Vissers, 1978).

$$\max J^{w} = \frac{M_E P_r - B_o C_o}{t + t_s} \quad (8)$$

where M_E is the amount if product (kg), P_r is the sales value of the product ($/kg), B_o is the amount of feed F (kg), C_o is the cost of feed ($/kg), t is batch time (minutes)

and t_s is the setup time for each batch (minutes). However, this equation can be converted as:

$$\max J^{w} = \frac{(\max M_E)P_r - B_o C_o}{t+t_s} \quad (9)$$

Table 2 shows the information needed for profit function calculation. The amount of feed involves the quantity of methanol and triglycerides at the beginning of the reaction while the amount of product is the final concentration of methyl ester which is maximized by finding a temperature profile as a control variable.

Table 2 Information for maximum profit problem

Item	Data
Raw materials [a]	
Soy bean oil (Triglycerides)	\$0.62/kg
Methanol	\$0.320/kg
Product	
Biodiesel (methyl ester)	\$ 3/gallon=\$ 0.9/kg
Additional parameters	
Biodiesel density	0.88 kg/l
Triglyceride density	885.446 kg/l
Methanol density	32.04 kg/l
Setup time (t_s)	10 min
Volume	10000 l

a Chemical Market Reporter (www.icis.com), Zhang et al., 2003

For the MCP and MTP, maximum principle is used to solve the optimal control problem. On the other hand, a combination of maximum principle and nonlinear optimization (NLP) technique based on SQP algorithm is used to solve the MPP.

In the SMPP, the objective function in this problem is subject to fluctuations due to the uncertainty arising in the feedstock content. In a previous work of our group (Benavides and Diwekar, 2012), we showed the uncertainty characterization and the stochastic simulation for the feed stock composition of soybean oil. The interest of these types of problems is to determine the expected value of the maximum profit. Then, the objective function for the SMPP can be formulated as it is shown in Eq. 10.

$$\max J^{w} = E\left[\frac{(\max M_E)P_r - B_o C_o}{t+t_s}\right] \quad (10)$$

where the values of P_r, B_o, C_o and t_s are the same values shown in Table 2.

3. Result and discussion

The results of the three optimal control problems in a batch reactor for biodiesel production are analyzed in this section. Figure 1 shows the concentration profiles obtained for the three optimal control problems and two base cases. To start with, consider the concentration profile of methyl ester for the maximum concentration problem. Here, we are comparing the concentration values at constant temperature (base case 1: 315K and base case 2: 323K) with the values calculated at optimal temperature profile. It can be seen that at 100 minutes of reaction time, the concentration of methyl ester at optimal control temperature reaches its maximum value, 0.7944mol/L; while at constant temperature 315K and 323K, the maximum concentration is 0.7324mol/L and 0.7829mol/L, respectively. This change represents an increase of 8.46 % with base case 1 and 1.47% with base case 2 on the concentration of methyl ester. The increment for the second base case is not significant since the constant profile at 323K belongs to the constant optimal profiles reported in the

literature (Dennis Y.C. L et al., 2010). Moreover, if we fix the concentration at 0.7324mol/L, which is the concentration reached in base case1, the reaction time needed is 30.5 minutes which represents 69.5% less than it was at the beginning (100 minutes) after using optimal control. Compare with base case 2, the reduction on time represents 46% of the original reaction time. This improvement does not affect the behavior of the other components because after 50 minutes their concentration values remain constant. For the MTP, after fixing the concentration of methyl ester to 0.7324mol/L the minimum reaction time reached is around 30.6 minutes when optimal control approach is applied, while for base case 1 and 2 their minimum time is reached at 100 and 54 minutes, respectively. Although, the optimal control profiles shown in Figure 2 for the two optimal control problems are significantly different, their results are similar showing that this problem have multiple solutions.

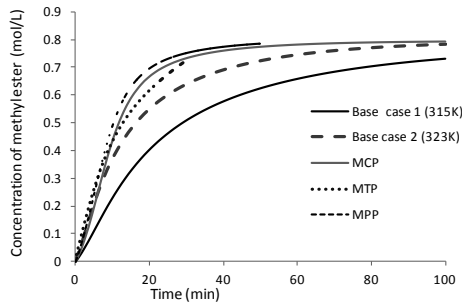

Figure 1 Concentration Profiles for the Three Problems and the Two Base Cases.

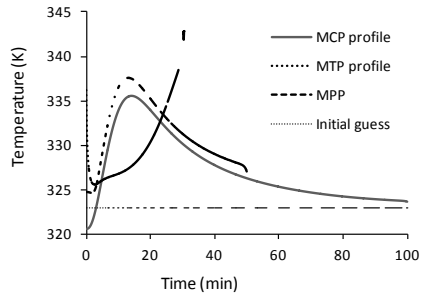

Figure 2 Optimal Temperature Profiles for the Three Problems

For the case of MCP, it can be seen that at 50 of minimum time there is an increase of methyl ester concentration of 25.56% (base case 1) and 8.50% (base case 2). Moreover, if we compute the profit values in the MCP and MTP using Eq. 9 and compare these values with the profit value found in the MPP, there is an increment of 45.32% and 355.58%, respectively; this information is summarized in Table 3.

Table 3 Comparison of the optimal control problems

Parameter	Maximum Concentration	Minimum Time	Maximum Profit
Concentration of Biodiesel (mol/L)	0.7944	0.7324	0.7802
Time (minutes)	100	30.5	50
Profit ($/hr)	103.1005	32.8868	149.8260

Finally, results of these problems regarding uncertainty in the feed composition are shown in Table 4. This table compares between the two bases cases, the deterministic and stochastic optimal control profiles in the face of uncertainties. As it is shown, in stochastic case there is an improvement of 7.69% compare to the deterministic case and a very significant improvement compare with the two base cases. In other words, the SMPP gives 11.499$/hr more than MPP (deterministic case) and 78.458$/hr and 149.67$/hr more than base case 1 and 2, respectively.

Table 4
Comparison between Constant temperature, deterministic and stochastic cases.

Parameter	Base case (315K)	Base case (323K)	Deterministic case	Stochastic case
Concentration of Biodiesel (mol/L)	0.7316	0.7767	0.7799	0.7791
Time (minutes)	100	92.653	50	44.912
Profit ($/hr)	11.197	82.409	149.368	160.867

4. Conclusions

The article presented three operation modes for optimal control problems encounter in biodiesel production. The problems involved determining optimal temperature profile so as to maximize or minimize three performance indices, namely, concentration, time, and profit. For the maximum concentration and minimum time problem, the maximum principle along with the steepest ascent of the Hamiltonian method was used as the solution technique. It was shown that the solution of these two problems results in similar equations for maximum principle and in both cases around 30.5 to 30.6 minutes of reaction time the concentration of methyl ester was the same, 0.7324mol/L. While in the maximum profit, the solution technique used was based on combining the maximum principle and NLP techniques. It was shown that applying optimal control under uncertainty (feed composition) it resulted in better reaction time to produce the same amount of biodiesel which improved the profit value of the problem.

References

Aziz, N.; and Mujtaba, I.M. Optimal control of semi-batch reactors. Computer Aided Chemical Engineering. 9 (2001) 609.

Benavides, P.; Diwekar, U. Optimal Control of Biodiesel Production in a Batch Reactor Part lI: Stochastic Control. Fuel. 94 (2012) 218.

Crescitelli, S.; and Nicoletti, B. Near optimal control of batch reactors. Chem. Eng. Sci. 28 (1973) 463.

Denbigh, K. G. Optimum temperature sequences in reactors. Chem. Eng. Sci. 8 (1958) 125.

Dennis Y.C. L.; Xuan, W.; and Leung, M.K.H. A review on biodiesel production using catalyzed transesterification. Applied Energy 87 (2010) 1083.

Diwekar U, Rubin ES. Stochastic modeling of chemical processes. Comput. Chem. Eng. 15 (1991) 105.

Diwekar, U. Introduction to Applied Optimization. Springer. Second Edition (2008).

Kerkhof, L. H. J.; and Vissers, J. M. On the profit of optimum control in batch distillation. Chem. Eng. Sci. 33 (1978) 961.

Leung, D.Y.C., and Guo, Y. Transesterification of neat and used frying oil: optimization for biodiesel production. Fuel Process Technol. 87 (2006) 883.

Linstromberg WW. Organic chemistry. MA: DC Heath and Co. Lexington. (1970) 129.

Luus, R.; Okongwu, N. O. Towards practical optimal control of batch reactors. Chem. Eng. J. 75 (1999) 1.

Noureddini H, Zhu D. Kinetic of transesterification of soybean oil. J Am Oil Chem Soc. 74 (1997) 1457.

Zhang, Y.; Dube, M.A.; McLean, D.D.; and Kates, M. Biodiesel production from waste cooking oil: 1. Process design and technological assessment. Bioresour. Technol. 89 (2003) 1.

I.A. Karimi and Rajagopalan Srinivasan (Editors), Proceedings of the 11th International Symposium on Process Systems Engineering, 15-19 July 2012, Singapore.

Neural Network Predictive Control of a Tubular Solid Oxide Fuel Cell

S. A. Hajimolana,[a] M. A. Hussain,[a] J. Natesan,[a] S. M. Tonekaboni Moghaddam[a]

[a]*Chemical Engineering Department, Faculty of Engineering, University of Malaya, Kuala Lumpur, Malaysia*

Abstract

The dynamic behavior and control of a tubular solid oxide fuel cell will be studied in this paper. The effect of fuel/air temperature and pressure will be investigated. Controlling the average stack temperature is the final objective of this study due to a high operating temperature of the system. In this case, temperature fluctuation induces thermal stress in the electrodes and electrolyte ceramics; therefore, the cell temperature distribution should be kept as constant as possible. A mathematical modeling based on first principles is developed. The fuel cell is divided into five subsystems and the factors such as mass/energy/momentum transfer, diffusion through porous media, electrochemical reactions, and polarization losses inside the subsystems are presented. Dynamic fuel-cell-tube temperature responses of the cell to step changes in conditions of the feed streams will be presented. A neural network model predictive controller (NNMPC) is then implemented to control the cell-tube temperature through manipulation of the temperature of the inlet air stream. The results show that the control system can successfully reject unmeasured step changes (disturbances) in the load resistance.

Keywords: Neural network predictive control; SOFC; cell-tube temperature.

1. Introduction

Solid oxide fuel cells (SOFCs) have shown promise in the electricity generating sector for stationary applications in the mid-term future. This is due to the fact that the energy efficiency usually achieved in a SOFC is much greater than that obtained from conventional heat engines or any other types of fuel cells. SOFCs offer high power density, low cost, scalability, fuel flexibility, and superior durability. Only few research studies are available on mathematical modelling of NH_3-SOFC (M. Ni et al., 2008). However, in all of these studies the mathematical models were based only on electrochemical models of planar SOFCs and did not cover the entire system. Besides working on fuel cell modeling, some studies on the control of fuel cell systems have been published (F. Jurado, 2006, S. A. Hajimolana et al., 2009). However, controlling the fuel cell temperature by using neural network predictive control has not been done before with these researchers.

In this work a dynamic model of an ammonia fed-tubular solid oxide fuel cell that is based on first principles is developed and presented. A NNMPC system is implemented to control the cell-tube temperature.

2. Model description

The mathematical model used in this study was previously developed by this research group (S.A. hajimolana et al., 2009). The tubular SOFC system under study here is a bank of single tubular SOFCs. Each cell has two tubes, an outer tube and an inner tube.

The outer tube is a cell tube. The outer surface of the outer tube is the anode side of the cell, and its inner surface is the cathode side. Between the anode and cathode sides (surfaces) lies the solid oxide electrolyte. The inner tube is an air injection and guidance tube, from which preheated air is injected into the bottom of the cell tube and flows over the cathode surface of the cell tube through the gap between the injection and the tubes. Fuel gas flows over the anode surface through the gap among the cell tubes. To develop a first-principles model of the SOFC system, a single tubular fuel cell is considered and divided into five subsystems (Hajimolana et al., 2011): Subsystem 1 (SS1): air inside the injection tube; Subsystem 2 (SS2): injection tube; Subsystem 3 (SS3): air inside the space between the cell and injection tubes; Subsystem 4 (SS4): cell tube; and Subsystem 5 (SS5): fuel flow channel. The assumption considered in the mathematical formulation is that the gas boundary layers are very small relative to the corresponding radius; therefore, the equations governing the diffusion processes are written in the Cartesian coordinates. Fluid velocities are averaged along the radial direction. Partial pressures, temperatures, and fluid velocities in each subsystem are uniform in every direction. The mass/momentum and energy balance inside SS1, SS3 and SS5 are given as follows, respectively:

$$L\frac{d\xi^i_j\rho^i_j}{dt} = u^i_{j_{in}}\xi^i_{j_{in}}\rho^i_{j_{in}} - u^i_j\xi^i_j\rho^i_j + \sum N_j M_j\left(\frac{2r_i L}{r_i^2 - r_0^2}\right) + nr_j \tag{1}$$

$$L\frac{d(u_i\rho_i)}{dt} = (u_{i_{in}})^2\rho_{i_{in}} - (u_i)^2\rho_i + \frac{\rho_{i_{in}}R^*T_{i_{in}}}{M_i} - \frac{\rho_i R^*T_i}{M_i} \tag{2}$$

$$L\frac{d(\tilde{H}^i_j\rho^i_j)}{\partial t} = \rho^i_{j_{in}}u^i_{j_{in}}H^i_{j_{in}} - u^i_j\rho^i_j\tilde{H}^i_j + \frac{2Lh_w}{r}\left(T_w - T^i_j\right) \tag{3}$$

i is air flow injection tube, air flow inside cathode side, fuel flow inside anode side, *j* is air, oxygen, nitrogen, ammonia, hydrogen, w is the wall, r_i and r_o is the inner and outer radius respectively, N_j is mass transfer by means of diffusion, *n* is the molar number and r_j is producing or consuming of the components.

This model assumes that the pressure drop caused by the pipe resistance over the distance *L* is negligible. It is also assumed that energy is transferred to the flow streams by convection only. Enthalpy of formation, heat capacities, viscosities, and conductivities of the components of air and the fuel are given in a previous work (Hajimolana et al., 2009).

Energy balance for the solid parts (SS2 and SS4) leads to:

$$m_s\tilde{C}_{p_s}\frac{dT_s}{dt} = \frac{\sigma 2\pi rL}{R_{rad}}\left(T_w^4 - T_j^4\right) + 2\pi rLh_w(T^i_j - T_w) + 2\pi rLh_w\left(T^i_j - T_w\right) + \tag{4}$$

$$\sum H_j N_j\left(\frac{2r_i L}{r_i^2 - r_0^2}\right) + 2r_{ct_o}LR_{NH_3}\Delta H_{R_{NH3}} - 0.001V_{out}I$$

The last three parts are heating transfer by means of diffusion, heating consuming by ammonia decomposition and heating supply by electrochemical reaction, respectively only in SS4. Electrochemical reaction occurs inside the fuel cell (SS4) at the triple phase boundary (*TPB*). Fuel cell voltage output is dependent on gas partial pressures and is adversely affected by concentration, activation, and ohmic losses (polarizations or irreversibilities). The electromotive force, reversible open-circuit cell voltage is given by the Nernst equation. However, the actual cell voltage (*E*) is less than its theoretical open circuit voltage because it is strongly affected by several irreversible losses

including activation losses due to irreversibility of electrochemical reactions at the *TPB*, concentration losses due to mass transport resistance in the electrodes (especially for thick anodes as in an anode-supported SOFC) and ohmic losses due to ionic and electronic charge transfer resistances. Actual voltage is thus given by:

$$E = E^o - \eta_{act_{ano}} - \eta_{conc_{ano}} - \eta_{act_{cat}} - \eta_{conc_{cat}} - \eta_{ohm} \tag{5}$$

The thermal decomposition of ammonia for hydrogen production in the porous anode is solved using the chemical model described as follows. NH_3 thermal decomposition takes place on the anode surface (fuel) channel (SS4) as this process is favored at high temperatures (G. Meng, 2007):

$$r_{NH_3} = z_r \exp\left(-\frac{E_r}{R_{kj}T_{ct}}\right) P_{NH_3} \tag{6}$$

where P_{NH3} is the partial pressure of NH_3. It's considered that the reaction rate is mainly dependent on the partial pressure of NH_3 and the operating temperature. It is assumed here that NH_3, H_2O and N_2 diffuse into the anode at a negligible rate; only H_2 gas diffuses into the anode (SS4).

3. Results and discussion

3.1.1st Model validation

Simulation was done to compare the results with the experimental data of Singhal. In this simulation, the values of fuel and air flow rates were adjusted to match the values of factors given by Singhal. The current–potential plot obtained from this simulation was compared with the experimental data and the predictions from the model developed by Ota and co-workers, 2003, as shown in Fig. 1. Excellent agreement was obtained in the low current density region in comparison to the model developed by Ota et al., 2003, which actually showed some deviation from experimental results. After validating the mathematical model developed in this work with experimental results of Singhal (2000) for H_2-SOFC, the model was improved to account for NH_3-SOFC.

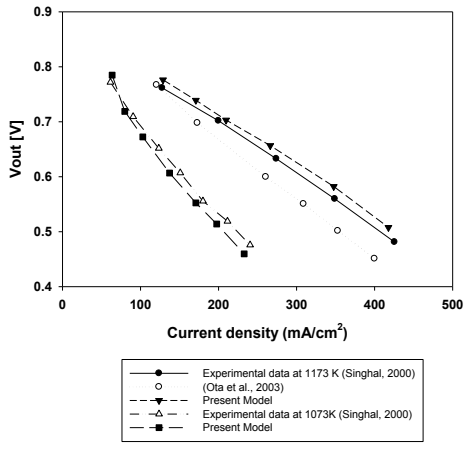

Fig. 1: Comparison of current–potential plots from the present model, model from Ota et al. 2000, and the experimental data available in the literature (Ota et al., 2003).

3.1. 2nd Open-loop Dynamic Cell Rresponses

The dynamic model of the SOFC system derived in the previous section has 20 first order ordinary differential equations, which are integrated numerically using MATLAB. Figure 2 and 3 depict the dynamic responses of the fuel cell to step changes of +5% in the temperature, pressure, and velocity of the inlet fuel and air stream respectively at time t= 100 s. Simulation results show that temperature of the inlet air stream has the strongest effect on the cell performance.

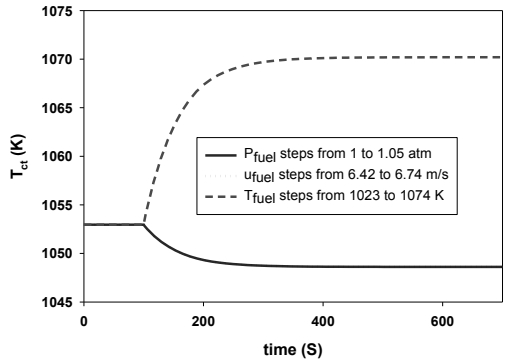

Fig. 2: Open-loop responses of the SOFC to step changes of +5% in the inlet fuel stream

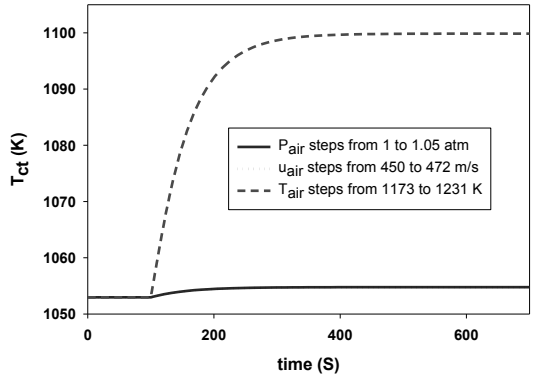

Fig. 3: Open-loop responses of the SOFC to step changes of +5% in the inlet air stream

4. Control of the SOFC System

A SOFC has a problem with regard to the durability of the ceramics used as its cell materials, because its operating temperature is very high, and its cell temperature fluctuation induces thermal stress in the ceramics. Therefore, the cell temperature distribution should be kept as constant as possible. In this case, NNMPC is used to predict future plant responses to control signals. The controller then calculates the control input that will optimize plant performance over a specified future time horizon. The first step in model predictive control is to determine the neural network plant model. Next, the plant model is used by the controller to predict future performance. MPC refers to a class of control algorithms in which a dynamic model of the plant is used to predict and optimize the future behavior of the process. The basic control strategy of the MPC is to select a set of future control horizons and minimize a cost

function based on the desired output trajectory over a prediction horizon with a chosen length. To select the manipulated input that has the strongest effects (in terms of dimensionless steady-state gain) on the controlled output, the open-loop analysis suggests that the cell tube temperature can be paired with the air inlet temperature. Figure 4 shows the performance of the NNMPC in tracking the series of setpoint changes for T_{ct} and satisfactory to reject the unmeasured disturbances.

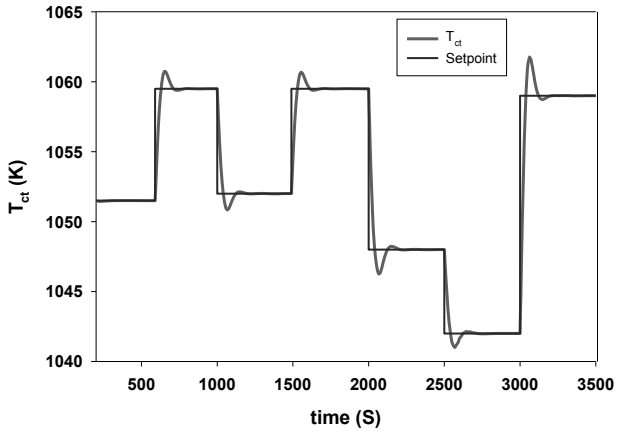

Fig. 4: The performance of the MPC

5. Conlusion

A dynamic model of a tubular solid oxide fuel cell (SOFC) was presented. Simulation results indicate that temperature of the inlet air stream has the strongest effect on the cell performance. The cell-tube temperature was regulated effectively using a NNMPC that manipulates the temperature of the inlet air stream. The performance of the control system was determined to be satisfactory to reject the unmeasured disturbances.

Acknowledgment

The authors are grateful to the University of Malaya Research Grant and the UM Bright Sparks Unit Bsp_App462/11(K) for providing financial assistance for this project.

References

Ni, M. Leung, M.K.H, 2008, Mathematical modelling of ammonia-fed solid oxide fuel cells with different electrolytes. Int. J. of Hydrogen Energy, 88, 33, 5765-5772.

Jurado, F. 2006, Predictive control of solid oxide fuel cells using fuzzy Hammerstein models. J. Pow. Sour, 11, 158, 245-253.

Hajimolana, S.A. Soroush, M, 2009, Dynamics and Control of a Tubular Solid-Oxide Fuel Cell. Ind. Eng. Chem, 23, 48, 6112-6125.

Hajimolana, S.A. , Hussain, M. A. Wan Daud, W. A. Soroush, M. Shamiri, A. 2011, Mathematical modelling of solid oxide fuel cells: A review. Renew. and Sustain. Ener. Rev. 121, 15, 1893-1917.

Meng, G. 2007, Comparative study on the performance of a SDC-based SOFC fueled by ammonia and hydrogen. J. Pow. Sour, 32, 173,189-193.

Singhal, S.C. 2003, Advances in solid oxide fuel cell technology. Sol. St. Ion, 23, 135,305-313.

Ota, T. 2003, Object-based modeling of SOFC system: dynamic behavior of micro-tube SOFC. J. Pow. Sour, 118, 125, 430-439.

I.A. Karimi and Rajagopalan Srinivasan (Editors), Proceedings of the 11th International Symposium on Process Systems Engineering, 15-19 July 2012, Singapore.

Novel MILP-based optimization method for heat exchanger network retrofit considering stream splitting

Ming Pan, Igor Bulatov, Robin Smith

Centre for Process Integration, School of Chemical Engineering and Analytical Science, The University of Manchester, Manchester, M13 9PL, UK

Abstract

This paper presents a novel optimization method for heat exchanger network (HEN) retrofit including stream splitting. A simple mixed integer linear programming (MILP) model and two iterative loops have been developed to effectively deal with the nonlinear computational difficulties associated with logarithmic mean temperature difference (LMTD) and retrofit costs for HEN retrofit problems. In case study, comparison with the existing methods illustrates the validity of the proposed approach.

Keywords: Heat exchanger network (HEN), retrofit, optimization, mixed integer linear programming (MILP), stream splitting

1. Introduction

Mathematical programming techniques have been widely studied in heat exchanger network (HEN) retrofit problems. The published work for HEN retrofit can be divided into two parts, conventional topology modifications and intensified implementation without topology modification.

The HEN retrofit problems addressing topology modifications include the strategies of restructuring heat matches (e.g. exchanger relocating, and stream repiping), adding additional heat transfer area, and installing new exchangers. Most of the relevant models involve MINLP formulations or NLP-MILP combination formulations. To deal with the non-convexities in these models, Ciric & Floudas (1990) used the Generalized Benders Decomposition techniques which can repeatedly update the values of variables in an iterative procedure (primal sub-problem to master sub-problem) until the final solution was found; while Yee & Grossmann (1991) introduced some simplifications to relax nonlinear equations, and replaced logarithmic mean temperature difference (LMTD) with arithmetic mean temperature difference (AMTD). On the other hand, stochastic optimization approaches, simulated annealing (SA) (Athier et al., 1998) and genetic algorithms (GA) (Bochenek & Jezowski, 2006; Rezaei & Shafiei, 2009), have been carried out for handling such NP-hard problems. Implementing intensified techniques in HEN without topology modifications is easily achieved in practice, due to the lower capital cost of during the retrofit in existing HEN and shorter implementation. Pan et al. (2012a, 2012b) have firstly proposed a new MILP-based iterative optimization method to intensify heat transfer in HEN without topology modifications for some literature problems, and then successfully extended the approach to large scale problems.

In this paper, the method proposed by Pan et al. (2012a) is developed to address HEN retrofit with structure modifications (including stream splitting). Distinguished from the previously proposed method, the new model addresses network topology modification and stream splitting, which is more complicated and difficult for optimization.

2. MILP-based iterative method for HEN retrofit

The optimization work is based on a potential superstructure network proposed in this section, where all potential matches are presented. Fig. 1 illustrates a HEN superstructure involving two hot streams and two cold streams. The whole stream region is divided into seven intervals, in which a stream-splitting match locates in interval 4, and no-stream-splitting matches are in the rest.

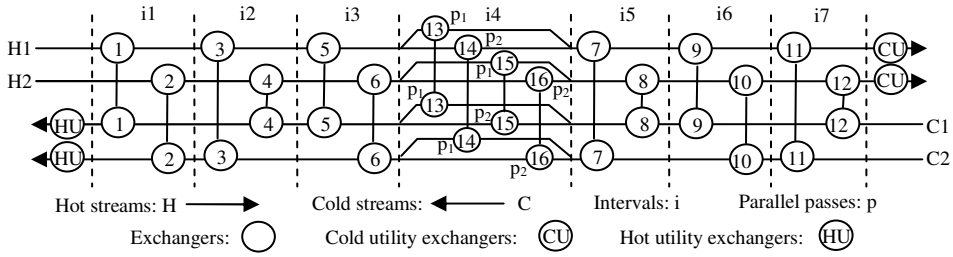

Figure 1. The superstructure network involving two hot streams and two cold streams

2.1. MILP-iteration method for structure optimization

The objective of this stage is to determine the suitable network structure for retrofit scenario. Based on the work proposed by Pan et al. (2012a), LMTD ($LMTD'_{ex}$), heat transfer (HBA_{ex} and HBB_{ex}) and energy balance (AEB_{ex} and BEB_{ex}) in no-stream-splitting matches are formulated in Eqs. (1)-(5).

$$LMTD'_{ex} = \frac{(HTI'_{ex} - CTO'_{ex}) - (HTO'_{ex} - CTI'_{ex})}{\ln[(HTI'_{ex} - CTO'_{ex})/(HTO'_{ex} - CTI'_{ex})]}, \quad \forall ex \in EX \tag{1}$$

$$HBA_{ex} \geq HFCP_{ex} \times (HTI_{ex} - HTO_{ex}) - EXA_{ex} \times U_{ex} \times LMTD'_{ex}, \quad \forall ex \in EX \tag{2}$$

$$HBB_{ex} \geq EXA_{ex} \times U_{ex} \times LMTD'_{ex} - HFCP_{ex} \times (HTI_{ex} - HTO_{ex}), \quad \forall ex \in EX \tag{3}$$

$$AEB_{ex} \geq HFCP_{ex} \times (HTI_{ex} - HTO_{ex}) - CFCP_{ex} \times (CTI_{ex} - CTO_{ex}), \quad \forall ex \in EX \tag{4}$$

$$BEB_{ex} \geq CFCP_{ex} \times (CTI_{ex} - CTO_{ex}) - HFCP_{ex} \times (HTI_{ex} - HTO_{ex}), \quad \forall ex \in EX \tag{5}$$

In stream-splitting match, stream heat-flow capacities ($HFCP_{ex}$ and $CFCP_{ex}$) are variables, thus the stream duties ($HFCP_{ex} \times (HTI_{ex}\text{-}HTO_{ex})$ and $CFCP_{ex} \times (CTI_{ex}\text{-}CTO_{ex})$) have to be linearized. Eqs. (6)-(8) show the first order Taylor series expansions of $HFTI_{ex}$ ($HFCP_{ex} \times HTI_{ex}$), where $HFTI'_{ex}$, $HFCP'_{ex}$ and HTI'_{ex} are the initial values; positive variables, $AHFTI_{ex}$, and $BHFTI_{ex}$, are remainder terms, and should be very small, which is to be formulated in the objective function.

$$HFTI_{ex} = HFTI'_{ex} + HFCP'_{ex} \times (HTI_{ex} - HTI'_{ex}) + HTI'_{ex} \times (HFCP_{ex} - HFCP'_{ex}), \quad \forall ex \in EX \tag{6}$$

$$AHFTI_{ex} \geq HFTI_{ex} - HFTI'_{ex}, \quad BHFTI_{ex} \geq HFTI'_{ex} - HFTI_{ex}, \quad \forall ex \in EX \tag{7, 8}$$

Based on Eqs. (6)-(8), the bilinear term $HFCP_{ex} \times HTI_{ex}$ has been converted into linear terms, and other bilinear terms ($HFCP_{ex} \times HTO_{ex}$, $CFCP_{ex} \times CTI_{ex}$ and $CFCP_{ex} \times CTO_{ex}$) can be linearized in the same way.

To select exchangers in the retrofitted HEN, a set of binary variables is used: $ESEX_{ex}$ is equal to 1, if exchanger ex exists in the retrofitted HEN; otherwise, it is 0. In no-stream-splitting matches, hot-stream temperatures are restricted in Eqs. (9)-(14), where $HSTI_{hs,i}$ and $HSTO_{hs,i}$ are inlet and outlet temperatures of hot stream in the i^{th} interval.

$$HTI_{ex} - M \times (1 - ESEX_{ex}) \leq HSTI_{hs,i} \leq HTI_{ex} + M \times (1 - ESEX_{ex}), \forall hs \in HS, i \in I, ex \in EX_{hs,i} \tag{9, 10}$$

$$HTO_{ex} - M \times (1 - ESEX_{ex}) \leq HSTO_{hs,i} \leq HTO_{ex} + M \times (1 - ESEX_{ex}), \forall hs \in HS, i \in I, ex \in EX_{hs,i} \tag{11, 12}$$

$$HSTI_{hs,i} - M \times ESEX_{ex} \leq HSTO_{hs,i} \leq HSTI_{hs,i} + M \times ESEX_{ex}, \forall hs \in HS, i \in I, ex \in EX_{hs,i} \tag{13, 14}$$

For stream splitting, the outlet temperatures of parallel exchangers ($PTO_{hs,i}$) are given:

$$HTO_{ex} - M \times (1 - ESEX_{ex}) \le PTO_{hs,i,p} \le HTO_{ex} + M \times (1 - ESEX_{ex}), \ \forall p \in P, ex \in EX_{hs,i} \quad (15, 16)$$

$$HSTI_{hs,i} - M \times ESEX_{ex} \le PTO_{hs,i,p} \le HSTI_{hs,i} + M \times ESEX_{ex}, \forall hs \in HS, \ p \in P, ex \in EX_{hs,i} \quad (17, 18)$$

Note that the heat duties of mixing streams after two parallel exchangers are normally described as bilinear terms, such as $HPTO_{hs,i,p} = HFP_{hs,i,p} \times PTO_{hs,i}$ (where $HFP_{hs,i,p}$ is the hot stream (*hs*) heat-flow capacity in the p^{th} parallel pass in the i^{th} interval), thus they can be linearized with first order Taylor series expansions similar to Eqs. (6)-(8). Then heat transfer (PHA_{ex} and PHB_{ex}) balance after two parallel exchangers is obtained:

$$PHA_{hs,i} \ge \sum_{p \in P} HPTO_{hs,i,p} - THF_{hs} \times HSTO_{hs,i}, \quad \forall hs \in HS, \ i \in I \quad (19)$$

$$PHB_{hs,i} \ge THF_{hs} \times HSTO_{hs,i} - \sum_{p \in P} HPTO_{hs,i,p}, \quad \forall hs \in HS, \ i \in I \quad (20)$$

where parameter THF_{hs} is the total heat-flow capacities of hot stream *hs*.

Hot stream inlet and outlet temperatures in each interval are presented as:

$$HSTO_{hs,i} = HSTI_{hs,i+1}, \quad \forall hs \in HS, \ i \in I \quad (21)$$

The cold-stream temperatures in each interval ($CSTI_{cs,i}$ and $CSTO_{cs,i}$) can be treated in the same manner as the hot-stream temperatures in each interval ($HSTI_{hs,i}$ and $HSTO_{hs,}$). Furthermore, Eqs. (22) and (23) show the constraints of minimum temperature difference allowed (ΔT_{min}) in each exchanger.

$$HTI_{ex} \ge CTO_{ex} + \Delta T_{\min}, \quad HTO_{ex} \ge CTI_{ex} + \Delta T_{\min}, \qquad \forall ex \in EX \quad (22, 23)$$

To maximize retrofit profit, the costs of utility consumption (*CU*) is formulated first, where *PHU* and *PCU* are price of hot utility and cold utility, EX_{hu} and EX_{cu} are the set of all hot and cold utility exchangers.

$$CU = PHU \times CFCP_{ex} \times (CTO_{ex} - CTI_{ex}) + PCU \times CFCP_{ex'} \times (CTO_{ex'} - CTI_{ex'}), \forall ex \in EX_{hu}, \ ex' \in EX_{cu} \quad (24)$$

In the structure stage, average area of the existing exchangers (*AVEXA*) is used to estimate the cost of adding exchanger area ($CEXA_{ex}$).

$$PAEXA_{ex} \ge EXA_{ex} - AVEXA, \ \forall ex \in EX \quad (25)$$

Normally, $CEXA_{ex} = \alpha \times (PAEXA_{ex})^{\beta}$, this nonlinear term can be linearized as well by using first order Taylor series expansions. Eq. (26) shows the cost of installing new exchangers (*CNEX*) estimated in the structure stage, where *FCNEX* is the fixed cost of installing new exchanger, and *NE* is the exchanger number in the initial HEN.

$$CNEX = \left(FCNEX + \alpha' \times AVEXA^{\beta'}\right) \times \left(\sum_{ex \in EX} ESEX_{ex} - NE\right) \quad (26)$$

The estimated retrofit profit (*ERP*) in the structure stage can be described as the energy saving costs (*OCU*-2×*CU*) minus the total retrofit cost (*CNEX*+$\sum$*CEXAex*). In Eq. (27), *IFY* is the interest factor in the investment years, *OCU* is the original utility cost in the existing HEN, and *ACF* is the annual cost factor.

$$ERP = IFY \times \left((OCU - 2 \times CU) - \left(CNEX + \sum_{ex \in EX} CEXA_{ex}\right) \times ACF\right) \quad (27)$$

As the HEN structure changes after retrofit, the initial and updated variables before and after solving the MILP model might be different. The objective of the new method is to find a feasible retrofit solution whereby the differences of heat transfers and energy balance, the differences between initial and updated variables, and the remainder terms in the first order Taylor series expansions are minimized close to 0 under the restriction of a certain retrofit profit value (*ERP'*), as shown in Eqs. (28) and (29).

$$ERP \ge ERP' \quad (28)$$

$$Obj = heat\ transfer\ differences + energy\ balance\ differences + variable\ differences + remainder\ terms\ in\ the\ first\ order\ Taylor\ series\ expansions \quad (29)$$

The new MILP-based model for network structure optimization consists of an objective function given in Eq. (29) and other constraints given from Eqs (1)-(28).
The iteration algorithm is mainly based on the work proposed by Pan et al. (2012a), where two iteration loops are proposed to find the optimal solutions for HEN retrofit. The first loop is to find the solution for HEN retrofit under certain retrofit profit, while the second loop is to find the maximum retrofit profit for HEN retrofit.

2.2. MILP-iteration method for investment stage

The first optimization stage is to find the suitable retrofitted structure, and then the accurate investment for retrofitted exchangers is considered in the selected network structure. In this stage, the costs of adding area, new exchanger and exchanger moving can be formulated with accurate parameters. Thus, the average area of the exchangers before retrofit (*AVEXA*) in Eqs. (25) and (26) is replayed with the exchanger area in existing HEN. Then the same iteration algorithm is executed to find the optimal solution with calculated retrofit costs.

3. Case study

A famous example reported in literature is carried out to test the new method. The existing HEN includes two hot streams (H1 and H2) and two cold streams (C1 and C2). The heat-flow capacity of each stream is 30 kW/K (H1), 15 kW/K (H2), 20 kW/K (C1), 40 kW/K (C2), and 94.95 kW/K (CW). Other information include: U = 0.8 kW/m^2·K for all exchangers, cost of area for a new exchanger ($) =1300A$^{0.6}$, cost of adding area for an existing exchanger ($) =1300ΔA$^{0.6}$, fixed cost for a new exchanger ($) =3000, cost of moving an existing exchanger ($) =300; plant life time is 3 years with 33% rate of interest. The original HEN is presented in Fig. 2(a).

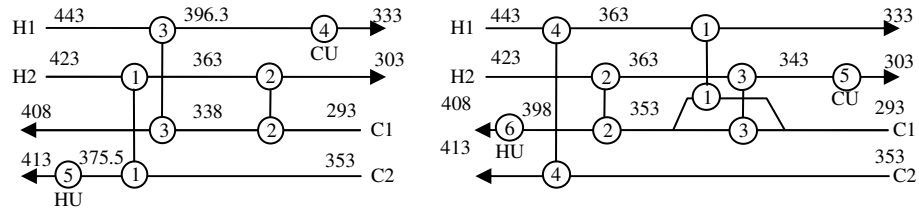

(a) Original HEN (ΔT_{min}=10K) (b) Retrofitted HEN (ΔT_{min}=10K)

Figure 2. Original HEN and retrofitted HEN (ΔT_{min} = 10K)

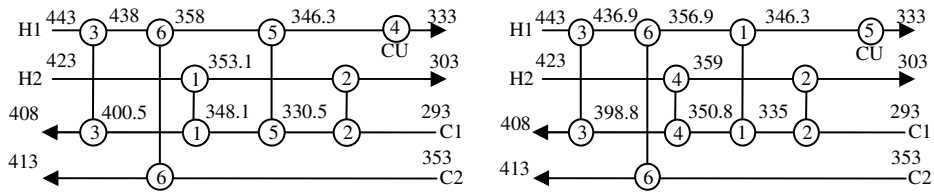

(a) Retrofited HEN (ΔT_{min}=5K) (a) Retrofited HEN (ΔT_{min}=2.7K)

Figure 3. Retrofited HEN (ΔT_{min} = 5K) and Retrofited HEN (ΔT_{min} = 2.7K)

The optimal solutions based on the proposed approach in different ΔT_{min}, such as 10 K, 5 K and 2.7 K, are shown in Fig. 2(b) and Fig. 3. Table 1 presents the retrofit and cost details of each exchanger in the optimal solutions. To prove the advantage of the new method, the solutions obtained in this work are compared with those reported in the

references, as presented in Table 2. The comparison shows that the new method can achieve higher retrofit profit than the existing methods, especially in lower ΔT_{min}.

Table 1. Exchanger details in original and retrofitted scenarios

Scenarios	Exchanger area (m^2)						Cost (10^3×$)			
	1	2	3	4	5	6	Added area	New exchanger	Exchanger moving	Utility
Original	46.7	68.7	38.3	40.2	35.0					158.0
R(10K)	52.0	68.7	15.1	164.8	32.8	5.3	27.0	6.6	1.2	28.0
R(5K)	112.7	60.8	5.2	11.2	34.8	241.4	16.1	38.0	0.6	8.0
R(2.7K)	46.7	65.6	6.3	81.1	11.3	273.4	12.0	40.7	0.9	8.0

Table 2. Comparison of the new and existing methods

ΔT_{min} (K)	Methods	Profit (10^3×$)	Utility (10^3×$)	Cost (10^3×$)			
				Total	Added area	New exchanger	Exchanger moving
10.0	**New**	**336.2**	**28.0**	**34.8**	**27.0**	**6.6**	**1.2**
	Ciric & Floudas (1990)	334.5	28.0	35.5	3.5	30.8	1.2
5.0	**New**	**453.6**	**8.0**	**54.7**	**16.1**	**38.0**	**0.6**
	Yee & Grossmann (1991)	347.7	24.7	41.5	10.1	30.8	0.6
	Athier et al. (1998)	380.9	19.4	45.9	45.3		0.6
	Bochenek & Jezowski (2006)	335.3	28.3	34.3	2.6	30.8	0.9
2.7	**New**	**455.8**	**8.0**	**53.6**	**12.0**	**40.7**	**0.9**
	Rezaei & Shafiei (2009)	442.4	8.0	59.3	58.4		0.9

4. Conclusions

In this paper, the nonlinear computational difficulties of optimizing HEN retrofit problems have been reduced efficiently with the proposed MILP-iteration method. Compared with the existing methods, the proposed approach is able to find suitable retrofitted structures, and requires less modification expense in most cases. Deeper insight on the proposed method, such as global optimization and large scale problems, will be addressed in future work.

Acknowledgement

Financial support from FP7-SME-2010-1 (262205 Intensified Heat Transfer Technologies for Enhanced Heat Recovery - INTHEAT) is gratefully acknowledged.

References

A. R. Ciric, & C. A. Floudas, 1990, A Mixed Integer Nonlinear Programming Model for Retrofitting Heat-Exchanger Networks, Ind. Eng. Chem. Res., 29, 239-251.

E. Rezaei, & S. Shafiei, 2009, Heat Exchanger Networks Retrofit by Coupling Genetic Algorithm with NLP and ILP Methods, Comput. Chem. Eng., 33, 1451-1459.

G. Athier, P. Floquet, L. Pibouleau, & S. Domenech, 1998, A Mixed Method for Retrofiting Heat-Exchanger Networks, Comput. Chem. Eng., 22, S505-S511.

M. Pan, I. Bulatov, R. Smith, & J. K. Kim, 2012a, Novel MILP-Based Iteractive Method for the Retrofit of Heat Exchanger Networks with Intensified Heat Transfer, Comput. Chem. Eng., in press, doi: 10.1016/j.compchemeng.2012.02.002.

M. Pan, I. Bulatov, R. Smith, & J. K. Kim, 2012b, Optimisation for the Retrofit of Large Scale Heat Exchanger Networks with Comprising Different Intensified Heat Transfer Techniques, Appl. Therm. Eng., in press, doi: 10.1016/j.applthemaleng.2012.04.038.

R. Bochenek, & J.M. Jezowski, 2006, Gentic Algorithms Approach for Retrofitting Heat Exchanger Network with Standard Heat Exchangers, Comput. Aided Chem. Eng., 21, 871-876.

T. F. Yee, & I. E. Grossmann, 1991, A Screening and Optimization Approach for the Retrofit of Heat-Exchanger Networks, Ind. Eng. Chem. Res., 30, 146-162.

I.A. Karimi and Rajagopalan Srinivasan (Editors), Proceedings of the 11th International Symposium on Process Systems Engineering, 15-19 July 2012, Singapore.

Simulation based Heuristics Approach for Plantwide Control of Propane Precooled Mixed Refrigerant in Natural Gas Liquefaction Process

Yuli Amalia Husnil[1], Changuk Park[2], Moonyong Lee[1]*

[1]*School of Chemical Engineering, Yeungnam University, Gyeongsan, 712-749, Korea*
[2]*Institute for Advanced Engineering, Yongin, 449-863, Korea*
**Corresponding Author's e-mail: mynlee@ynu.ac.kr*

Abstract

In this paper a simulation based heuristic approach is used to configure the control structure of propane precooled mixed refrigerant (MR) natural gas (NG) liquefaction process. The liquefaction of NG in cryogenic exchanger involves MR stream condensation and vaporization in different sections of cryogenic exchanger. This increases the interactions among MR streams as illustrated using dynamic simulation. To identify these interactions, first the sensitivity analysis of propane precooled MR was carried out and then several heuristic based on dynamic simulation were proposed for disturbance rejection and increased liquefied natural gas (LNG) production rate. Major findings from several case studies suggest that the maximization of available cold energy is possible by utilizing temperature difference between MR streams as set point for controlling LNG production rate.

Keywords: Plantwide control, Cryogenic exchanger, Heuristics, Dynamic simulation, LNG.

1. Introduction

Several Natural gas (NG) liquefaction process are available in world market and Air Products and Chemical, Inc. licensed, propane pre-cooled mixed refrigerant process (C_3MR) accounts for about 80% of worlds baseload liquefied natural gas (LNG) production capacity. Liquefaction of NG in this process is achieved by successive condensation and vaporization of MR in cryogenic heat exchanger. MR with lower boiling and higher boiling components flows in separate loops in cryogenic exchanger to achieve liquefaction. The presence of several MR loops provides difficulty in designing robust control structure which is essential for plant safety and profitable operation. Understanding the hidden nature of interaction that exists between MR loops and other plant variable can overcome the challenging task of robust control design. In this regard, dynamic simulation plays an essential role in giving the insight of inherent process dynamics. In dynamic simulation every independent variable of the plant can be changed arbitrarily to see its effect on the process plant which is not possible in real plant. However, without well structured guideline these tests will fall on the series of trials and errors and consumes a lot of time. Konda et al (2005) proposed an integrated framework of dynamic simulation and heuristics based on Luyben's work (Luyben et al., 1997). This idea is uncommon considering most of the works in plantwide control design utilize dynamic simulation to validate the control structure (Vasbinder et al., 2004). This work of configuring the control structure of C_3MR is also inspired by Luyben's work. First the main disturbances are identified and the best manipulated

variables are correspondingly paired with controlled variables that increase LNG production and plant safety. Based on extensive case studies performed on dynamic simulation of C_3MR process, several general guidelines and heuristics are proposed for robust control and are listed in section 3.6.

2. Description of C_3MR Process Plant

The dynamic model of C_3MR plant was developed in Aspen Hysys® V.7.1 platform and the schematic diagram is illustrated in *Fig 1*. Peng-robinson equation of state was used for thermodynamic property calculation. It should be noted that propane cycle which precools NG to -32.7^{o}C is ignored in this study and MR cycle is considered for control configuration. High pressure NG stream which is mainly methane enters the cryogenic exchanger at -32.7^{o}C and exchange heat with MR in Exchanger 1 & 2 (Exchanger 1 & 2 are in fact hypothetical division of main cryogenic exchanger) and exits at -146.7^{o}C which is flashed to atmospheric pressure before shipping. Other part of MR liquefaction consists of compression and cooling assembly of MR. Compressed MR is flashed and MR vapor and liquid (MRV & MRL) enters the Exchanger 1. MRL after pressure let down in Joule Thompson valve act as cold stream for the other stream in Exchanger 1. Similarly in Exchanger 2 MRV act as cold stream which subcooled and liquefy the NG gas. Compression of MR is achieved in staged compression with intermediate cooling. Presence of several MR loops provides challenge in profitable and safe operation of liquefaction plant. Hence a robust control strategy must be needed and described in section 3.4.

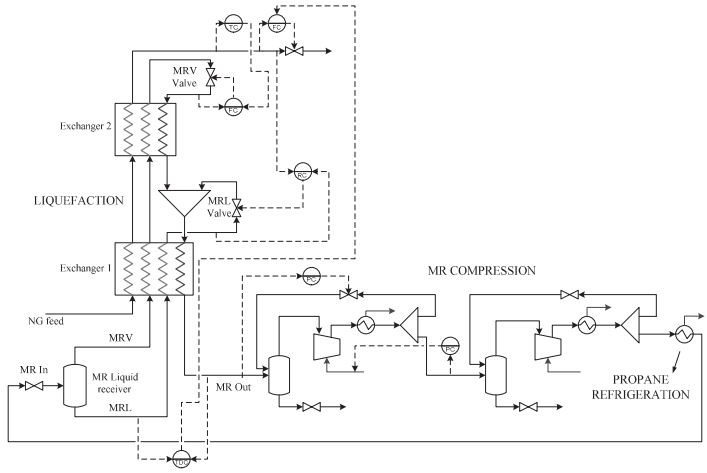

Figure 1. Process flowsheet and control configuration of C_3MR process plant

3. Dynamic Simulation and Heuristic Methods

The simulation based heuristic method is explained in this section. The original method of Konda et al. consists of 8 steps but in this work only the first four are applied with some adjustments. The rest of other steps are considered irrelevant with the respective process. The role of steady-state and dynamic simulation will be involved in most of the steps.

3.1. The Control Objectives

A plant control system can be divided into three levels of hierarchy (Hovd and Skogestad, 1993). From the lowest to the highest level, control objectives of C_3MR

process can be summarized as follows. At the level of *regulatory control* the control objective is to maintain the stability of the operation. Moving to *supervisory control*, the control structure is aimed to maintain the quality of the product and can be obtained by maintaining the temperature of LNG. At the highest level, *plantwide optimization*, the objective is to optimize the usage of cold energy available in MR. Considering above, LNG production rate in C_3MR can be adjusted according to the available cold energy in MR, instead of fixing it at certain value. The difference, between inlet and outlet temperature of MR can be utilized as indicator for the availability of cold energy in the liquefaction. The higher the difference means there is still some cold energy available that can be used to liquefy more natural gas. In contrary, if the difference getting smaller and cross the lower bound then the natural gas throughput should be decreased.

3.2. Control Degrees of Freedom (CDOF) Analysis

CDOF analysis based on Konda et al. (2006) was performed for process under study and the value of 13 variables was come out. Among those variables, flowrate of LNG, MRL, and MRV are selected as manipulated variables. The controlled and manipulated variables are listed on *Table* 1.

Table 1. List of controlled and manipulated variables

Controlled Variables	Manipulated variables
LNG temperature (y_1)	LNG flowrate (u_1)
Temperature Difference between inlet (MRL inlet stream) and outlet MR (y_2)	MRV flowrate (u_2)
	MRL flowrate (u_3)

3.3. Disturbances Identification & controller pairing selection

Based on simulation studies three potential sources of disturbance are identified for the process under study that are NG inlet; temperature, pressure and composition. Among the three disturbance sources, NG pressure and its composition has significant effect to controlled variables. The most interesting result obtained from series of tests in dynamic simulation is the inverse response of LNG temperature when MRV and MRL flowrate were step changed as can be seen from *Fig. 2*. Step change responses of MRL & MRV flowrate have same controller gain but give different time constant. It is expected that pairing MRL flowrate with both controlled variables would give a poor performance and should be avoided.

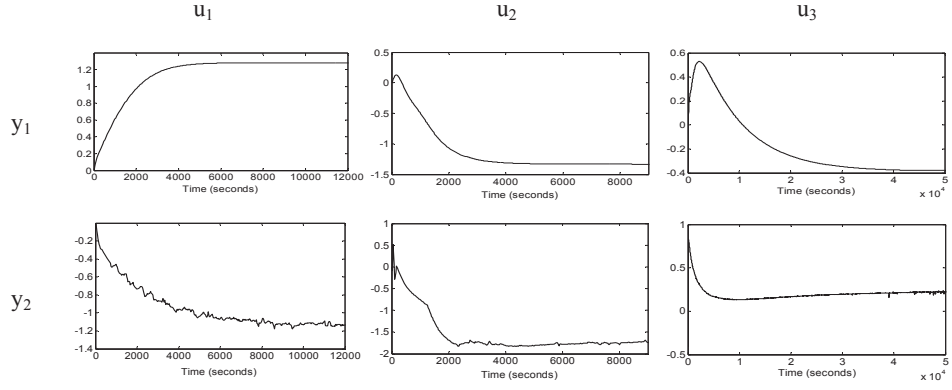

Figure 2. Open loop responses of controlled variables after step changes on manipulated variables

3.4. Selecting Best Pairings

Relative gain array (RGA) is utilized for find best pairing that corresponds to good controller performance. The steady-state gain that is used in pairing analysis purpose is obtained from closed and open loop simulation of the process. The summaries of RGA are shown in *Table 2*.

Table 2. Results from RGA analysis of three different structures

Closed-loop						Open loop					
Structure 1		Structure 2		Structure 3		Structure 1		Structure 2		Structure 3	
u_1-u_2		u_2-u_3		u_1-u_3		u_1-u_2		u_2-u_3		u_1-u_3	
0.67	0.33	0.35	0.65	11.84	-10.84	0.47	0.53	0.45	0.54	-2.71	3.71
0.33	0.67	0.65	0.35	-10.84	11.84	0.53	0.47	0.54	0.45	3.71	-2.71

RGA analysis shows inconsistent results. Closed and open loop RGA recommends different pairing for structure 1. Also, structure 3 has negative RGA in off-diagonal pairing based on closed-loop analysis while in open loop analysis the negative RGA is in diagonal pairing. Despite these contradictions, the negative magnitude of RGA in structure 3 is enough reason to screen it out. It is said earlier, based on analysis of *Fig. 2*, that utilizing MRL flowrate or u_3 as manipulated variable should be avoided because it gives relatively slow response. Since structure 2 contains u_3 as one of manipulated variables therefore this structure is also omitted.

The analysis above left structure 1 as the only candidate for control structure. However it is also not clear whether to select the diagonal or the off-diagonal pairing. Several disturbance tests on simulation studies will provide the answer of which pairing gives better control performance. In case of MRL flowrate, there are two possible ways of utilizing it. One is by utilizing MRL flowrate or MRL valve for controlling liquid level of MR receiver. Second, MRL flowrate is fixed on certain ratio with LNG flowrate using MRL valve as the control element.

Finally, four control structures are left after screening and their description is provided in *Table 3*.

Table 3. List of four final control structures

Manipulated variable	Structure 1 (S_1)		Reverse Structure 1 (RS_1)	
	S_1-LC	S_1-RC	RS_1-LC	RS_1-RC
LNG flowrate	LNG temperature	LNG temperature	Temp. difference	Temp. difference
MRV flowrate	Temp. difference	Temp. difference	LNG temperature	LNG temperature
MRL valve	Liquid level	LNG/MRL ratio	Liquid level	LNG/MRL ratio

3.5. Control Structure Assessment

S_1-RC is discarded from the structure candidate because it fails to maintain controlled variables at their respective setpoints during inlet pressure disturbance. The other three structures are able to reject the disturbance but perform differently. Screening best among the final three structures is based on IAE performance during disturbance rejection and shown in *Fig 3 & 4*. RS_1-RC has the smallest IAE compare to the other structures in both disturbance tests. Therefore, RS_1-RC is selected as the control structure for C_3MR liquefaction process. The control arrangement for RS_1-RC is presented on *Fig. 1*.

3.6. Conclusions

A robust plantwide control strategy for C_3MR process plant was developed based on dynamic simulation and RGA analysis. Preliminary selection among several candidate control configuration was based on RGA analysis. IAE performance was used to choose the best structure and finally RS_1-RC was selected. Based on simulation studies and quantitative analysis performance on C_3MR plant several heuristics are made:

i) LNG outlet temperature should always be paired with MRV flowrate.
ii) MR temperature difference is a good measure for product maximization.
iii) Simulation and quantitative analysis should be used in parallel to get the best controller configuration.
iv) IAE index is a good performance evaluation criterion in liquefaction plant control strategy development.

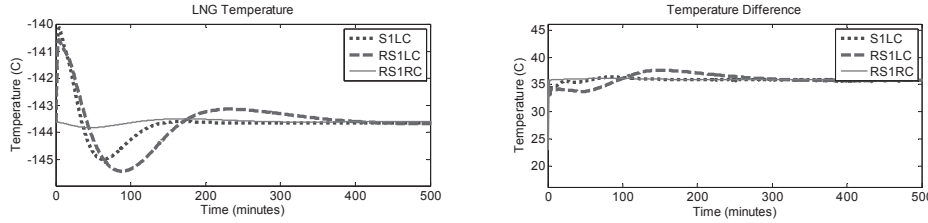

Figure 3. Responses of variables on different structures after NG inlet pressure is increased 1 bar

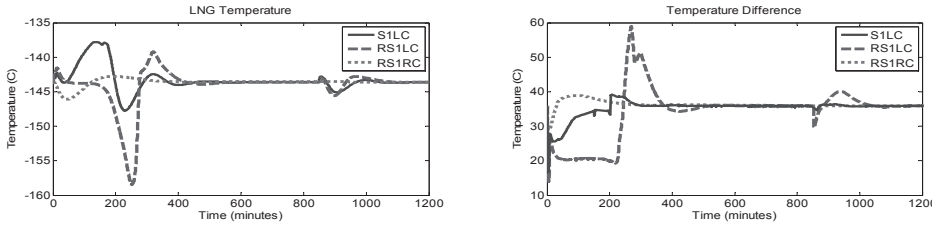

Figure 4. Responses of variables on different structures after composition of NG is changed (reducing 20% of methane and increasing 20% of ethane)

Acknowledgment

This research was supported by a grant from the Gas Plant R&D Center funded by the Ministry of Land, Transportation and Maritime Affairs (MLTM) of the Korean government

References

N. V. S. N. M. Konda, G. P. Rangaiah, P. R. Krishnaswamy, 2006, A Simple and Effective Procedure for Control Degrees of Freedom. Chem. Eng. Sci., 61, 1184-1194.

N. V. S. N. M. Konda, G. P. Rangaiah, P. R. Krishnaswamy, 2005, Plant-Wide Control of Industrial Processes: An Integrated Framework of Simulation and Heuristics, Ind. Eng. Chem. Res., 44, 8300-8313.

M. L. Luyben, B. D. Tyreus, W. L. Luyben, 1997, Plantwide control design procedure, Process Systems Engineering, 43, 3165-3174

M. Hovd, S. Skogestad, 1993, Procedure for Regulatory Control Structure Selection with Application to the FCC Process. AICHE Journal, 39, 1938-1953

E. M. Vasbinder, K. A. Hoo, U. Mann, 2004, Synthesis of Plantwide Control Structures Using a Decision-Based Methodology. In The Integration of Process Design and Control; Seferlis, P., Georgiadis, M. C., Eds; Elsevier: New York, 375-400.

I.A. Karimi and Rajagopalan Srinivasan (Editors), Proceedings of the 11th International Symposium on Process Systems Engineering, 15-19 July 2012, Singapore.

Studying the effect of feed composition variation on typical natural gas liquid (NGL) recovery processes

Mesfin Getu[a], Mohd Shariq Khan[b], Nguyen Van Duc Long[b] and Moonyong Lee[b*]

[a]Chemical Engineering Department, Curtin University of Technology, CDT 250, 98009 Miri, Sarawak, Malaysia.

[b]School of Chemical Engineering, Yeungnam University, 214-1 Dae-dong, Gyeongsan, Gyeongbuk 712-749, Republic of Korea.

*: Corresponding author: mynlee@ynu.ac.kr

Abstract- In this work, the different process schemes used for known NGL recovery methods have been studied with various feed compositions. The original turbo-expander process scheme (ISS) was considered as a base case. The GSP, CRR, RSV and RSVE process schemes are those which focus on improvement at the top of the demethanizer column, while the IPSI-1 and IPSI-2 at the bottom of the demethanizer column. All the process schemes have initially built using ASPEN HYSYS with a common set of operating criteria. Numerous simulation runs have been made later by taking various typical feed compositions classified as lean and rich. Regardless of the common operating conditions set to each process schemes, there exist different performance results obtained from the simulation. Accordingly, the reboiler duty requirement is high for the GSP, CRR, RSV and RSVE due to the need for external refrigeration. However, the IPSI-1 and IPSI-2 simulation result show relatively lower reboiler duty requirement for the self-refrigeration system applied to the systems.

Keywords: Feed composition, lean feed, process scheme, rich feed.

1. INTRODUCTION

Basic technology trends for natural gas liquid (NGL) recovery have emerged since 1970 onwards. A major leap in gas processing industries was the introduction of a turbo-expander design scheme, which is also known as an Industry-Standard Single-stage (ISS) process scheme. The ISS scheme is considered as a major leap development towards gas industry for its better performance compared to the previous oil absorption and refrigeration techniques. However, this process scheme has still certain limitation in terms of operational flexibility and overall recovery performance (Rahman et al., 20004). As a result, a number of various design schemes have evolved after that to improve the process efficiency which can contribute for higher NGL recovery. The Gas sub-cooled process (GSP) scheme was later developed by Campbell and Wilkinson (1981) to solve several problems related to the turbo-expander process scheme. The cold residue-gas recycle (CRR) was introduced in the original design of GSP by Campbell et al. (1989) to improve ethane recovery efficiency. The Recycle split-vapor (RSV) developed by Campbell et al. (1996) was another alternative process scheme for high NGL recovery. A modification of the RSV process scheme, recycle split- vapor

with enrichment (RSVE), was also developed by Campbell et al. (1999). All the GSP, CRR, RSV and RSVE process schemes mainly focus on improving of the reflux stream to the demethanizer column. Unlike those process schemes, an enhanced NGL recovery process (IPSI-1) which was introduced by Yao et al. (1999) gives a process enhancement at the bottom of the demethanizer column. The internal refrigeration for enhanced NGL recovery (IPSI-2), which is introduced recently by Lee et al. (2007), is also another process enhancement which focuses on the bottom of the demethanizer column. The condition for feed composition is an important factor since it determines what kind of process configuration to be employed for recovering NGLs (Jibril et al., 2006). It is also considered as a basic requirement for particular process scheme whether it can accommodate a range of feed composition which varies from time to time. In this work, various feed compositions were considered and characterized under the basic classification of lean and rich feeds. The original turbo-expander process scheme (ISS) is taken as a base case plant. The GSP, CRR, RSV and RSVE are those process schemes those that focus improvement on the top of the demethanizer column. The IPSI-1 and IPSI-2 are those that focus on the bottom of the demethanizer column. Accordingly, HYSYS (Aspen HYSYS V7.1) simulations were made initially for all the process schemes by setting common operating parameters as criteria in order to compare the performance of each scheme. Later, a range of typical feed compositions which are classified as lean and rich feeds are used to study the performance of each process schemes.

2. Case study

2.1. Feed composition and operating conditions

The feed composition is a very vital factor which affects the NGL recovery. Since the feed normally originates from upstream plants, there is a continuous variation of feed composition which increases the instability of the plant operation (Fleshman et al. 2005). Thus, to study the different feed composition types, a typical eight gas feeds are adapted from literatures Jibril et al. (2006) as shown in Table 1. The feeds have been arranged in accordance to increasing order of C_{5+} content (heavier hydrocarbons).

Table 1: Typical feed composition in mole percent (mol %)

Components	Feed 1	Feed 2	Feed 3	Feed 4	Feed 5	Feed 6	Feed 7	Feed 8
C_1	0.9717	0.8457	0.8400	0.8034	0.7260	0.6507	0.6539	0.5952
C_2	0.0189	0.0820	0.0760	0.0693	0.0494	0.1050	0.0504	0.0536
C_3	0.0029	0.0340	0.0200	0.0259	0.0176	0.0497	0.0297	0.0471
iC_4	0.0013	0.0058	0.0000	0.0043	0.0038	0.0095	0.0090	0.0203
C_4	0.0012	0.0086	0.0000	0.0073	0.0067	0.0187	0.0172	0.0239
IC_5	0.0007	0.0028	0.0070	0.0018	0.0031	0.0077	0.0085	0.0180
C_5	0.0005	0.0021	0.0000	0.0015	0.0031	0.0078	0.0084	0.0161
C_6	0.0004	0.0018	0.0030	0.0016	0.0046	0.0125	0.0160	0.0260
C_7	0.0024	0.0012	0.0000	0.0017	0.0167	0.0149	0.0214	0.1998
C_8	0.0000	0.0005	0.0000	0.0018	0.0000	0.0156	0.0243	0.0000
C_9	0.0000	0.0004	0.0000	0.0019	0.0000	0.0108	0.0194	0.0000
C_{10}	0.0000	0.0005	0.0000	0.0005	0.0000	0.0352	0.0652	0.0000
N_2	0.0000	0.0055	0.0540	0.0619	0.1325	0.0349	0.0464	0.0000
CO_2	0.0000	0.0091	0.0000	0.0171	0.0365	0.0270	0.0302	0.0000
Total	1.0000	1.0000	1.0000	1.0000	1.0000	1.0000	1.0000	1.0000

The first five feeds (1 to 5) are classified as lean feeds, while the remaining three feeds (6 to 8) are rich feeds. The classification for lean and rich feed is usually based on the contents of C_2 or C_3 components. Accordingly, if the C_2 content is less than 10% or the C_3 content less than 4%, the feed is considered as lean feed, otherwise it is taken as rich feed. Feed 5 is more close to lean feed property than rich feed even if it does not fulfil to the above requirement due to its large N_2 content (13.25%). It is also important to notice that feed 5 has the maximum contents of N_2 and CO_2 components. The feeds which contain the minimum N_2 content ($N_2 = 0$) are feed 1 and 8. Similarly, the feeds which contain the minimum CO_2 content ($CO_2 = 0$) are feed 1, 3 and 8.

The main step toward a good comparison of the different alternative NGL recovery method is to assess the details of the simulation for each process scheme (Lynch et al., 2007). Due the different types of additional equipment introduced on each process scheme, it may not be possible to have an exact comparison among the processes. However, by tabulating some main operating data, it is possible to identify those key process parameters which have a significant effect on the overall plant performance. The key process operating parameters which are used for comparison purpose are shown in Table 2.

Table 2: common process key parameters taken for comparison

Feed flow (kgmole/h)	5000
Plant inlet gas pressure (psia)	1040
Plant inlet gas temperature (°F)	120
Salesgas outlet pressure (psia)	730
Salesgas outlet temperature (°F)	120
Product specification (C_1/C_2 ratio)	0.02
Theoretical trays including reboiler	41
Compressor/Expander/pump efficiency (%)	75
Demethanizer pressure (psia)	337
Pressure drop across the heat exchangers, shell and tube sides (psi)	10
Property fluid package	Peng Robinson

2.2. Effect of feed composition on various process scheme

The feed energy requirement for each process scheme is shown in Fig. 1. It can be observed from the figure that the feed energy is same for a particular feed regardless of the different process schemes applied. For example, if we consider feed 1, the corresponding feed energy value is -10.56×10^4 kW for all the process schemes. The feed energy is actually obtained by multiplying the enthalpy of the feed and its flow rate. However, the feed flow rate is constant for all the feeds as shown in Table 2. The difference in feed energy for the eight feed types arises due to the variation of the feed compositions shown in Table 1, which in turn changes the values of the enthalpy. Based on Fig. 8, the rich feeds (6-8) normally requires more chilling than the lean feeds (1-5). Hence, mechanical refrigeration which consists of primarily pure refrigerant, such as propane, is mostly used as external refrigeration source especially for GSP, CRR, RSV and RSVE. In addition, a mixed refrigerant and cascade refrigeration cycle may also be used depending on the process requirement. Further cooling of those feeds is also provided by the turbo-expander with appropriate heat exchange.

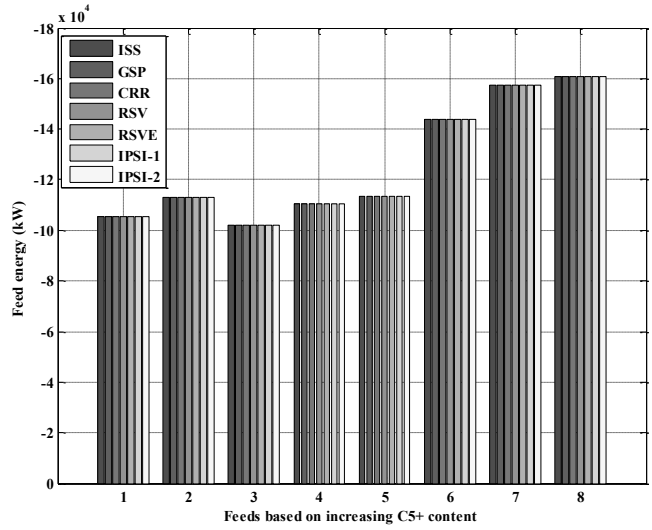

Fig. 1 Energy requirement of feed

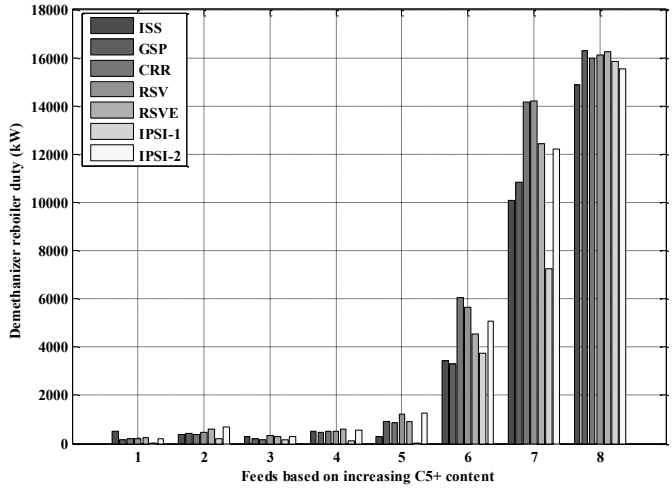

Fig. 2 Energy consumed by demethanizer reboiler

The demethanizer reboiler and salesgas compressor are the major energy consuming units in NGL recovery. The energy consumption of the demethanizer reboiler as the heavier hydrocarbon content increases is shown in Fig. 2. The leaner feeds (1-5) generally give a lower duty than those of the rich feeds (6-8). This is due to the presence of high heavier hydrocarbons (C_{5+}) components in the rich feeds. Propane refrigeration or other external sources is usually used for the rich feeds (6-8) to condense the heavier hydrocarbon (C_{5+}) components. This will maintain the low temperature profile in the demethanizer column by reducing the steam requirement. Referring to Fig.2, the IPSI-1 process scheme has the lowest reboiler duty for the lean feeds (1-5) compared to any of the other process scheme. This is mainly because the advantage of the self refrigeration system which can efficiently reduces energy for such kind of feeds. Even for the rich

feed 6 and 7, the IPSI-1 process scheme has lower reboiler duty. However, for very rich feed, such as feed 8, the IPSI-2 process scheme gives a lower reboiler duty than IPSI-1. One of the limitations of the IPSI-1 process scheme was that when a large amount of external refrigeration is needed, there seems a shortage of refrigeration that can be produced by the self refrigeration system. However, the improved self refrigeration system (open and closed refrigeration cycles) of the IPSI-2 scheme helps to reduce this limitation. Accordingly, the IPSI-2 process scheme lowers the temperature in the demethanizer column and improves the heat integration to cool the rich feed gas through reboiler. This will reduces external heating and refrigeration requirements. In addition, it also reduces the need for external reboiler heat and thereby saves both steam and refrigeration usage.

Conclusion

A simulation study for comparing representatives NGL recovery process has been made by considering a range of various feed composition classified as lean and rich feeds. The effect of feed composition variation and its impact on the economic analysis for the different process schemes have also been assessed. The ISS, GSP, CRR and RSV generally require more refrigeration for rich feeds than lean feeds. Lean feeds give a lower reboiler duty than rich feeds. The self-refrigeration system applied to the IPSI-1 and IPSI-2 has helped in reducing the reboiler duty requirement by avoiding additional external refrigeration as compared to those developments made at the top of the demethanizer column.

Acknowledgment

This research was supported by a grant from the gas plant R&D center funded by the Ministry of Land, Transport & Maritime Affairs (MTLM) of the Korean Government.

References

Campbell, R.E., Wilkinson, J.D.1981. Hydrocarbon gas processing. *U.S. Patent 4,278,45*.

Campbell, R.E., Wilkinson, J.D., Hudson, H.M., 1989. Hydrocarbon gas processing. *U.S. Patent 4,889,545*.

Campbell, R.E., Wilkinson, J.D., Hudson, H.M.,1996, Hydrocarbon gas processing. *U.S. Patent* 5,568,737.

Campbell, R.E., Wilkinson, J.D., Hudson, H.M., Pierce, M.C.,1999, Hydrocarbon gas processing. *U.S. Patent* 5,983,664.

Fleshman, J., Alderton, P., Bahnassi, E., Khori, A.R.,2005, Achieving Product Specifications for Ethane through to Pentane Plus from NGL Fractionation Plants. *Presented on AIChE annual meeting*, Cincinnati, OH.

Jibril, K.L., Al-Humaizi, A.L., Idriss, A.A., Ibrahim, A.A.,2006, Simulation study determines optimum turboexpander process for NGL recovery. *Oil and Gas Journal,* 104, 58-62.

Lee, R.J., Zhang, Y., Yao, J., Chen, J.J and Elliot, D.G.,2007, Internal refrigeration for enhanced NGL recovery. U.S. Patent 7,257,966.

Lynch, J.T., Lousberg, N.B., Pierce, C.M., 2007, How to compare cryogenic process design alternatives for a new NGL project. *Presented at the 86th annual convention of the gas processors association, Denver, Colorado*.

Rahaman, A.A., Yusof, A.A., Wilkinson, J.D., Tyler, L.D.,2004, Improving ethane extraction at the PETRONAS gas GPP-A facilities in Malaysia. *Presented at the 83rd annual convention of the gas processors association* New Orleans, Louisiana.

Yao, J., Chen, J.J., Elliot, D.G.,1999., Enhanced NGL recovery processes, *United states patent number:* 5,992,175.

I.A. Karimi and Rajagopalan Srinivasan (Editors), Proceedings of the 11th International Symposium on Process Systems Engineering, 15-19 July 2012, Singapore.

Techno-Economic Analysis for the Synthesis of Downstream Processes from the Oxidative Coupling of Methane Reaction

Daniel Salerno[a], Harvey Arellano-Garcia[a], Günter Wozny[a]

[a] *Department of Process Dynamics and Operations, Sekr, KWT-9, Berlin Institute of Technology, Strasse des 17 Juni 135, D-10623, Berlin, Germany*

Abstract

Due to the huge methane deposits worldwide and the great need for the chemical process industry to have new alternatives for olefins production, especially ethylene as starting raw material for numerous products, the direct conversion of methane to ethylene has attracted considerable interest. The main reason that motivates the realization of this new approach is to exploit the availability of un-reacted methane, coming from the exit flue gas products of the OCM reactor, and thus, design an alternative process for methanol and formaldehyde production via OCM and the co-generation of electricity that can make the process economically attractive and designed so as to be industrially implemented. The total project investment, based on total equipment cost, as well as variable and fixed operating costs, was developed based on mass and energy balance information taken from Aspen® Process Economic Analyzer simulation results. The feasibility was evaluated in terms of energy savings, CO_2-emission reductions and costs, in comparison to the separate production of methanol with conventional technology alone. Before starting the economic study of the OCM process a preliminary analysis of possible plant locations has been developed. Natural gas is a commodity which price varies strongly from one region to another. Moreover, not only the price of raw materials is affected by the location of the plant but also the costs associated with the production, namely: steam, refrigeration, electricity, fuel, wages, etc., affecting strongly the profitability of a petrochemical project. Due to low natural gas prices in Venezuela, which has the highest production potential in South America, and the highest ethylene sales for the European market, this geographical location has been chosen for economic analysis of this project. Kinetic data of the OCM reaction were taken from the experimental fluidized bed reactor values that has been build in our facilities at TU-Berlin, which reflect promising conversion, selectivity and yield values, testing different catalysts developed at the Institute of Chemistry inside the scope of the UNICAT project. This analysis suggests areas for research focus that might improve the profitability of natural gas conversion, and the results have also been used for the design of the pilot plant which is now being operational at our department.

Keywords: OCM reaction, ethylene production, methanol generation, formaldehyde production, economic evaluation.

1. Introduction

The oxidative coupling of methane (OCM), a heterogeneously catalyzed reaction, is one of the most intensively studied as a promising route for the production of ethylene by utilizing methane, the main constituent of natural gas. Despite the great efforts

dedicated to research better catalysts, so far only a few have achieved promising ethylene conversion values but it was not possible in the past 20 years to achieve yield values more than of 26% (Zavyalova, et al. 2011). There have been major research efforts to solve this problem and achieve higher methane conversions to make this process economically attractive to the industry (Kondratenko and Baerns, 2008). As oil prices rise, it becomes necessary to seek alternative sources of energy, so that for several years has become a concern for scientists to use natural gas as feedstock for the chemical industry; it is more advantageous to convert the natural gas to the useful products and transport the end product to users. Thus, several researchers are currently making great efforts to direct conversion of methane to value added products, such as ethylene (feedstock for petrochemicals), aromatics (ethyl benzene) and liquid hydrocarbon fuels (methanol). With this in mind, the development of a new process that converts directly methane into liquid fuel (e.g., gasoline), rather than through synthetic gas, has been carried out (Graf, 2008). Although great effort has been made on direct CH_4 conversion into oxygenates, the yield for desired products was below an economical value. However, the methane source is a key factor to make this oxidation process for methanol (CH_3OH) and formaldehyde (HCHO) economical achievable. The work presented here describes a feasibility study on the production of ethylene and oxygenated products (methanol and formaldehyde) and and also generation of electricity using the non-reacted methane coming from the OCM reaction.

2. Brief description of the processes

2.1. Original OCM Process

The OCM reaction is a highly exothermic process that is performed on metal oxide catalysts at temperatures between 700 and 900 °C. The process products are C_2H_6, C_2H_4, CO, CO_2, H_2 and H_2O. The COx (CO and CO_2) are formed from the complete combustion of hydrocarbons, which leads to point out the difficulties of achieving high performance in the OCM reaction process (Coronas, 1995). The complete process consists of three main sections: reaction, purification and separation section. Figure 1 shows the flowsheet for this process. The reactor is continuously fed with natural gas and oxygen. The feed gas is preheated to 700 °C, catalytic partial oxidized at pressure of 115 kPa and the reaction is carried out at 850 °C. The exothermic reaction heat has to be immediately removed using the transfer line exchanger to takeaway by vaporization of high-pressure boiler feed water, which is separated in the steam drum and subsequently superheated in the convection section to high-pressure superheated steam. The reaction products are compressed in a multi-compaction section to 1090 kPa and cooled down to 40 °C later on. In the purification section the reactor effluent gasses are cooled and then are fed into the bottom stages of a series of absorber columns that uses monoethanolamine (MEA) as absorbent solution. The MEA solvent is then regenerated in stripper columns thereby releasing the CO_2 captured in a dilute stream with water vapor product. The operation data from a pilot plant at TU Berlin were used to specify feed conditions and unit operation block specifications in the model. Finally, the ethylene separation section consists of two cryogenic distillation columns. The first one is the demethanizer and the unconsumed methane is separated from the product stream (ethylene and ethane). After the removal of light OCM gases, the next column separates the C_2+ components: ethylene at the top and ethane at the bottom.

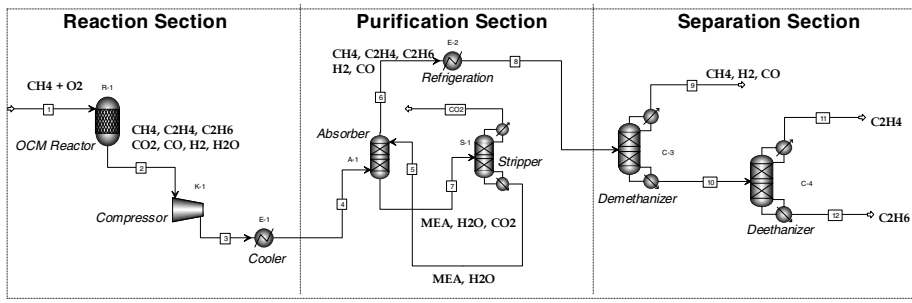

Fig. 1: Flowsheet for the Oxidative Coupling of Methane Process.

2.2. Formaldehyde and methanol process

The designed process is different from a commercial methanol plant based on autothermal reforming of natural gas. It uses the non-reacted methane from the OCM reaction process, a gas phase by-product stream composed by H_2O, CH_4, CO_2, CO and H_2. Although this is a by-products stream with low economic value for the ethylene production process, the amount of CO produced is attractive enough to be used in the production of synthesis gas. First this gases are purified by removing the components that may affect the conversion into synthesis gas (ethylene traces), before being used in the methanol process. The unreacted methane is used as raw material for the formaldehyde reaction. The reactor uses the selective oxidation of methane yielded essentially CH_2O, CO, CO_2, and H_2O, which takes into account chemical kinetics obtained from the fixed-bed reactor experiment (Yang et al. 1998). Additional oxygen as oxidant is required to fulfill the reaction conditions producing the equivalent of 117.1 metric tons of formaldehyde per day. All CH_2O formed in this reactor has been purified using two distillation columns. After the formaldehyde product separation follows the synthesis gas production using the stream coming from the top of the demethanizer column of the formaldehyde purification section. For this section the synthesis gas comes from a fixed-bed reactor for the catalytic partial oxidation of methane at conditions suitable for the production of methanol (De Smet, 2001). Addition of CO_2 (from the OCM purification process with amines) is possible in order to adjust the carbon/hydrogen ratio, which depends on the concentrations of CO and CO_2 from the non-reacted methane. The gas exiting the reformer is cooled with water generating the steam for the reformer. The synthesis gas is compressed to 30 bar by intercooled compressors before entering the synthesis reactor. The reactor operates at 250 °C and the composition of the outlet gas is calculated assuming chemical equilibrium. The chemical equations used in the production of methanol and the kinetic data were taken from Gallucci et al. (2007). The flowsheet of the process is shown in figure 2.

3. Results and discussions

The strategic implications of being able to use natural gas as a feedstock continue to provide an incentive to develop the OCM process. One way forward is to integrate the OCM process with another process, whereby through synergistic effects the combined process can be made economically attractive. The feature of the OCM process that can most obviously be exploited in this context is the large heat of reaction.

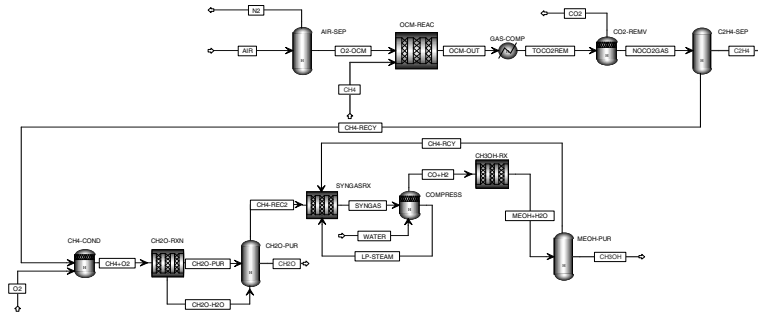

Fig. 2: Simplified flowsheet for oxygenates plant process.

Before deciding what to do with the amount of non-reacted methane in the OCM process, we performed an economic analysis to compare the costs associated with recycling of this methane. Table 1 summarizes the economic overview of this analysis. The steady state flow rates of raw materials, products and by-products streams are summarized in Table 2. Both simulated processes (OCM alone and proposed alternative) consume a 2593 t/d pure methane as feed-stock, resulting in a production of 396 t/d of 99% purity ethylene. The alternative process also produces 117.1 and 204.2 t/d of formaldehyde and methanol respectively. The difference in water production in both processes can be explained because the alternative process goes through more equipment to produce steam to be the raw material for the syngas reaction before its final use in the methanol reactor.

Table 1: OCM Process Economic Results

Investment (Millions €)	OCM Process without CH_4 Recycling	OCM Process with CH_4 Recycling
Total Project Capital Cost	170.67	183.94
Total Operating Cost	266.05	255.34
Total Raw Material Cost	83.77	81.31
Total Utilities Cost	154.89	147.71
Total Products Sales (C_2H_4)	272.40	272.40
Payout Period (Years)	12.16	10.54

4. Conclusions

This analysis shows that it is possible to produce ethylene from the OCM reaction and also oxygenated products, methanol and formaldehyde, from the non-reacted methane coming from the OCM process. The design of the process has taking into consideration the alternative production of valuable chemicals, such as methanol, giving added value to the OCM process, besides the ethylene production made with this use of natural gas. This process can be implemented to enable an optimum utilization of the methane gas based on market demand. The payout period, the expected number of years required to recover the original investment in the project, is 8 years. The process presented here shows that it should be possible to produce ethylene from the OCM reaction that is suitable to satisfy de ethylene demand worldwide as a precursor for the production of other chemicals.

Table 2: OCM and Oxygenated Process Economic Results

	OCM Process Alone	OCM & Oxygenated Process Proposed
Raw Materials	(metric ton/day)	
Methane	2593.2	2593.2
Mono Ethanol Amine	676.7	676.7
Products		
Ethylene	396.0	396.0
Formaldehyde	---	117.1
Methanol	---	204.2
Ethylene purity (mass %)	99.6	99.2
By-products		
H_2O	1438.9	229.2
C_2H_6	19.6	25.7
CO_2	1675.2	518.8
CO	126.5	1512.9
H_2	72.0	108.6
Non-reacted CH_4	1421.1	502.2

The development of integrating the OCM process technology, including reactor considerations, and a materials survey under severe OCM reaction conditions have been conducted in this project. The inclusion of alternative processes to the traditional OCM process to increase its profitability is indeed feasible. Nevertheless, a bigger capital investment is required, and the benefits obtained from this are still overcome by the margins and pay out time periods of the OCM process, due to the increase on capital expenses and operative costs.

Acknowledgment
The authors acknowledge support from the Cluster of Excellency "Unifying Concepts in Catalysis" coordinated by the Berlin Institute of Technology and funded by the German Research Foundation – Deutsche Forschungsgemeinschaft.

References

J. Coronas, 1995, Síntesis de Hidrocarburos por Acoplamiento Oxidativo de Metano. Utilización de Reactores de Membrana. Doctoral Thesis, Universidad de Zaragoza, Departamento de Ingeniería Química y Tecnologías del Medio Ambiente (in Spanish).

F. Gallucci and A. Basile, 2007, A theoretical analysis of methanol synthesis from CO_2 and H_2 in a ceramic membrane reactor, International Journal of Hydrogen Energy, 32, 5050-5058.

P. Graf, PhD Thesis, 2008, University of Twente, Enschede, Netherland.

E. Kondratenko and M. Baerns, 2008, Oxidative Coupling of Methane, Handbook of Heterogeneous Catalysis, Chapter 13, Wiley-VCH, Weinheim, p. 3010-3023.

H. De Smet, H. de Croon, R. Berger, G. Marin and J. Schoten, 2001, Design of adiabatic fixed-bed reactors for the partial oxidation of methane to synthesis gas. Application to production of methanol and hydrogen-for-fuel-cells, Chemical Engineering Science, 56, 4849-4861.

C. Yang, N. Xu and J. Shi, 1998, Experimental and Modeling Study on a Packed-Bed Membrane Reactor for Partial Oxidation of Methane to Formaldehyde. Ind. Eng. Chem. Res. 37, 2601-2610.

U. Zavyalova, M. Holena, R. Schlögl and M. Baerns, 2011, Statistical Analysis of Past Catalytic Data on Oxidative Methane Coupling for New Insights into the Composition of High-Performance Catalysts, ChemCatChem, DOI: 10.1002/cctc.201100186.

I.A. Karimi and Rajagopalan Srinivasan (Editors), Proceedings of the 11th International Symposium on Process Systems Engineering, 15-19 July 2012, Singapore

Targeting industrial heat pump integration in multi-period problems

Helen Becker, * François Maréchal
Industrial Energy Systems Laboratory, Ecole Polytechnique Fédérale de Lausanne (EPFL), Lausanne, Switzerland

Abstract

Process integration aims at optimizing industrial processes by identifying the heat recovery potential and the optimal integration of energy conversion systems. Most industrial processes especially in the food industry are non-continuous problems (batch problems) that are more difficult to tackle with process integration techniques. Process integration of multi-period problems can become complex and often the heat integration is realized by using time averaging approaches. The main disadvantages are that the sizing of equipments becomes more difficult and that the investment cost calculation is almost impossible at the targeting stage, since storage tanks are not included. This work presents a MILP method that targets simultaneously the heat recovery and the integration of energy conversion systems like heat pumps and other utilities in multi-period multi-time problems. In each time slice, the heat cascade constraints are considered together with the flows of the utility streams and the mass balances for storage, which create a link between the different operating times.

Keywords: energy integration, pinch analysis method, utility integration, industrial heat pumps, process design, multi-period, storage units

1. Introduction

Process integration was originally developed for continuous processes. But many processes have non-continuous operation tasks and therefore the approach has to be adapted for multi-period problems. Often pseudo multi-period heat integration is realized by using the time average model (TAM) or the time slice model (TSM) (Linnhoff et al., 1988). The time average model uses average values over all operating time slices. This approach is correct when it is assumed that all batch operations can take place at any time and in any order or when it is assumed that heat storage is available. On the other side, the time slice model cuts the process into several time slices where the process operations are simultaneous. Using the composite curves resulting from the TAM, Krummenacher and Favrat (2001) propose a heuristic targeting method to identify the minimum number of heat storage units for the heat recovery. According to Kemp and Macdonald (1987), the TAM or pseudo-continuous approach is too simple and may give over optimistic results, except when heat storage is available, the TAM results in the theoretical energy efficiency which can be achieved with the maximum heat storage. The authors propose analog to the graphical heat cascade the new "time cascade" to identify energy storage for batch problems. Applying mathematical programming techniques, Grossmann and Santibanez (1980) present a mixed integer linear programming (MILP) formulation for a given number of time slices with different prices and demand fluctuations. The problem

*helen.becker@epfl.ch

not only optimizes the total annual costs but also gives the optimal scheduling solution. Later, Maréchal and Kalitventzeff (2003) developed a methodology, based on the TSM for multi-time problems. The times are only linked with the usage level of utilities but there is no possibility to integrate heat storage. To integrate indirect energy storage of batch problems in the heat exchanger network, Chen and Ciou (2008) use a mixed integer non-linear programming (MINLP) formulation. The problem can become very complex, since the storage tanks are included in the superstructure. Using the TSM and total site approach, Varbanov and Klemeš (2011) integrate heat storage to manage the heat supply from renewables. A systematic approach allows heat storage between process operations but the self-sufficient pockets are not considered, which may miss opportunities for combined heat and power integration. Stoltze et al. (1995) propose a combinatorial method to include the heat storage in the heat exchanger network design. Sadr-Kazemi and Polley (1996) propose an iterative search method based on the composite curves in terms of heat quantities to define the temperature interval. Heat storage and intermediate heat transfer networks enables the process to stay independent and more flexible. As shown from the literature review, heat storage is very important to improve the energy efficiency of a non-continuous process. The TSM seems to be more realistic for integrating multi-period and storage problems, since instant heat loads can be used. The purpose of this paper is to adapt the multi-period targeting method, using the TSM and to include the possibility to integrate heat storage tanks simultaneously with energy conversion units (e.g. heat pumps) to maximize the heat recovery in multi-period problems.

2. Methodology

This paper develops a methodology based on a MILP formulation, which is able to solve multi-scenarios (without storage) and multi-time slices (with storage between time slices). Each period is defined by the operating conditions and the operating time. A multi-time slice problem consists in several successive process operations in a given period. Non-continuous processes can easily be modeled, by dividing them for example into a certain number of typical days and each day is divided into necessary time slices depending on the process schedule (e.g. 12 typical days a year and 24 time slices corresponding to one hour of operation). The approach can also be useful for other application like the optimization of large scale process or urban systems.

2.1. MILP formulation for multi-time problems

A MILP problem that targets simultaneously the heat recovery and the integration of energy conversion systems like heat pumps and other utilities in multi-time problems, is developed. For each time slice, the heat cascade constraints are considered together with the flows of the utility streams and the storage tanks. The storage equations are added and create a link between the different time slices. Utility and storage units are optimized to satisfy the process demand for all time slices simultaneously. The MILP formulation developed for heat exchange restrictions (Becker and Maréchal, 2012) is extended to the time dimension. For a given period, the objective function minimizes the yearly operating costs (e.g. OpC_p from Eq. (1)) or the total costs including the annualized investment costs.

$$min(cy_p \sum_{t=1}^{nt} d_{p,t}(\sum_{f=1}^{nf}(c^{+}_{f,p,t}\sum_{u=1}^{nu} f_{u,p,t}\dot{E}^{+}_{f,u,p,t}) + c^{+}_{el,p,t}\dot{E}^{+}_{el,p,t} - c^{-}_{el,p,t}\dot{E}^{-}_{el,p,t} + \sum_{u=1}^{nu} f_{u,p,t}c_u)) \quad (1)$$

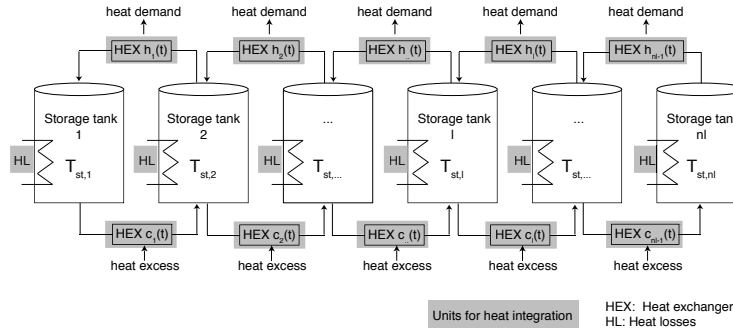

Figure 1. Definition of the storage network

nt is the number of time slices, cy_p is the number of cycles (e.g. number of days a year which can be represented by a chosen typical day), $d_{p,t}$ are the operating hours of time slice t in period p. The other terms concern the operating costs linked to fuel and electricity consumption and additional operating costs. For each time slice, the overall electricity import and the produced electricity in the process are defined. It becomes possible to take into account electricity price variations (e.g. peek hours or night prices). $f_{u,p,t}$ defines the multiplication factor of unit u in time t and period p. A unit can be a process ($f_{u,p,t} = 1$) or a utility ($f_{u,p,t}$ variable) unit. The flow rates of streams belonging to utility units are proportional to the multiplication factor. This factor is limited by a minimum and maximum value and corresponds to the usage level for a given time. The associated integer variable $y_{u,p,t}$ defines if the utility unit u is added to process ($y_{u,p,t} = 1$) or not ($y_{u,p,t} = 0$) in time t and period p. Thus, globally integrated utilities can be activated in a time slice and deactivated in another time slice.

$$y_{u,p,t} \cdot f_u^{min} \leq f_{u,p,t} \leq y_{u,p,t} \cdot f_u^{max} \tag{2}$$

Basically, the equations are extended to include the time dimension. In order to be able to integrate storage units, each time slice needs a link with its previous and next time slice.

2.2. Integration of storage tanks

Although the concept can be easily adapted to any kind of storage, only liquid (sensible) storage will be considered here. A given number of interdependent water tanks at discretized temperature levels can be integrated, as shown in Fig. 1. Water is heated up with available excess heat and will then be stored in a tank at higher temperature. In a following time slice, the water will be cooled down to satisfy a hot demand of the process. The cold water is then stored in a tank at lower temperature. The total maximal amount of water (M_{tot}) and the temperature levels of the tanks are defined as input parameters. The approach includes an estimation of heat losses which is linked to the temperature of the tank. The investment is evaluated as a function of the maximum needed storage capacity.

2.2.1. Mass balance

The overall mass balance is given as the cyclic constraint in Eq. (3), which states that the total stored mass has to be given back to the process. The water content after each time

is calculated for each tank in Eq. (4). $ds_{p,t}$ is the operating time in seconds of time slice t in period p and $\dot{M}$ is the water flow rate. Furthermore, constraints have to be added to guaranty the positive level of the tank, and that the total volume of water is not exceeded.

$$\sum_{t=1}^{nt}(ds_{p,t}\sum_{l=1}^{nl}(\sum_{h_l=1}^{ns_{h,l}} f_{u,p,t}\dot{M}_{h,l,u,p,t} - \sum_{c_l=1}^{ns_{c,l}} f_{u,p,t}\dot{M}_{c,l,u,p,t})) = 0 \tag{3}$$

$$M_{l,p,t} = M_{0,l} + \sum_{t=1}^{t}(ds_{p,t}\sum_{l=1}^{nl}(\sum_{h_l=1}^{ns_{h,l}} f_{u,p,t}\dot{M}_{h,l,u,p,t} - \sum_{c_l=1}^{ns_{c,l}} f_{u,p,t}\dot{M}_{c,l,u,p,t})) \tag{4}$$

2.2.2. Definition of thermal streams for the heat integration

The heat exchange with other process or utility units is shown on Fig. 1. The cold storage stream $c_n(t)$ is heated up by process excess heat and is going from a lower temperature tank l to tank $l+1$. Whereas the hot storage stream $h_n(t)$ corresponds to water coming from a higher temperature level and giving back heat to process units. As an example, a cold stream from tank l to tank $l+1$ is defined with the inlet temperature $T_{in} = T_{st,l}$ and the outlet temperature $T_{out} = T_{st,l+1}$. The corresponding heat amount is calculated with Eq. (5). By analogy the heat load is given for the hot stream.

$$\dot{Q}_{c,l} = f_{u,p,t} \cdot \dot{M}_{c,l,u,p,t} \cdot c_p \cdot (T_{st,l+1} - T_{st,l}) \tag{5}$$

2.2.3. Heat losses in storage tanks

Heat losses can be included, by adding a cold stream which corresponds to maintaining the temperature of each tank. The difficulty is to estimate the heat losses of each tank, especially because the size of tank is an optimization result and not known in advance. Therefore Eq. (6) has been used to estimate the heat losses in the tank. Knowing the current stored mass from Eq. (4), the heat losses can be calculated by Eq. (6).

$$\dot{Q}_{hl,l,p,t} = k_{hl} \cdot \frac{f_{hl} \cdot 4 \cdot M_{l,p,t}}{\rho \cdot d} \cdot (T_{st,l} - T_a) \tag{6}$$

ρ is the density of the considered storage fluid in the tanks in kg/m^3. In the following examples water is used. d is the diameter of the tank in m. k_{hl} is the considered heat loss coefficient and f_{hl} is a factor to account the heat losses on the top and bottom of the storage tank. To model the heat losses, new cold streams corresponding to the heat losses and the associated temperature are added to the heat cascade. The multiplication factor has been fixed to consider the calculated heat losses as heat loads. The advantage of adding the heat losses are on the one hand to make the problem more realistic and on the other side, it ensures that the storage fluid will be used as soon as possible.

3. Example and conclusions

As example, Fig. 2 gives some typical results of the presented methodology. The case study consists in one period with 15 time slices. For each time slice the storage tank levels and the optimal utility usage rates are calculated, which allows to evaluate the corresponding investment costs for new storage and utility equipments in a next step. The above method is generic and can be adapted through the definition of temperature levels, number of tanks and the maximum content. Heat pump integration benefits can be increased when integrating storage units because the heat pump working hours and their profitability can, by this way, be increased.

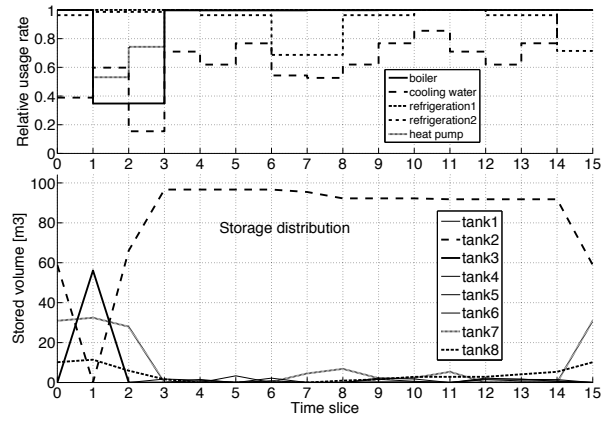

Figure 2. Storage tank distribution and relative utility utilization rate

4. Acknowledgements

The authors wish to thank ECLEER for supporting this research and collaborating in its realization.

References

Becker, H., Maréchal, F., 2012. Energy integration of industrial sites with heat exchange restrictions. Computers and Chemical Engineering 37, 104–118.

Chen, C., Ciou, Y., 2008. Design and optimization of indirect energy storage systems for batch processes. Industrial & Engineering Chemistry Research 47, 4817–4829.

Grossmann, I., Santibanez, J., 1980. Applications of mixed integer linear programming in process synthesis. Computers and Chemical Engineering 4 (4), 205–214.

Kemp, I., Macdonald, E., 1987. Energy and process integration in continuous and batch processes. IChemE Symposium Series (105), 185–200.

Krummenacher, P., Favrat, D., 2001. Indirect and mixed direct-indirect heat integration of batch processes based on pinch analysis. International journal of applied thermodynamics 4 (3), 135–143.

Linnhoff, B., Ashton, G., Obeng, E., 1988. Process integration of batch processes. IChemE Symposium Series (109), 221–237.

Maréchal, F., Kalitventzeff, B., 2003. Targeting the integration of multi-period utility systems for site scale process integration. Applied thermal engineering 23, 1763–1784.

Sadr-Kazemi, N., Polley, G., 1996. Design of energy storage systems for batch process plants. Chemical Engineering Research and Design 74 (5), 584–596.

Stoltze, S., Mikkelsen, J., Lorentzen, B., Petersen, P., Qvale, B., 1995. Waste-heat recovery in batch processes using heat storage. Journal of Energy Resources Technology, Transactions of the ASME 117 (2), 142–149.

Varbanov, P., Klemeš, J., 2011. Integration and management of renewables into total sites with variable supply and demand. Computers and Chemical Engineering 35, 1815–1826.

I.A. Karimi and Rajagopalan Srinivasan (Editors), Proceedings of the 11th International Symposium on Process Systems Engineering, 15-19 July 2012, Singapore.

Thermodynamic analysis of homogeneous non-isothermal mixing influence on the water-using networks' energy target

LUO Yiqing , LUO Sucai, YUAN Xigang

School of Chemical Engineering and Technology,Tianjin University, Tianjin 300072,China

Abstract

In order to take full advantage of non-isothermal mixing in designing a simple and energy efficient water network, this paper has divided streams into three types and has explored the effects of different mixing patterns between the three types of homogeneous streams on the water-using network' utility consumption target based on thermodynamic analysis method. The conclusions for homogeneous non-isothermal mixing in the paper can be used to analyze or optimize the heat exchanger network of a given water-using system.

Keywords: homogeneous non-isothermal mixings, thermodynamic analysis, water-using network, influence mechanism

1. Introduction

There are numerous cases where streams in industrial processes are allowed to be mixed. This is particularly the case with water networks. The energy required by water streams could be supplied indirectly through heat exchangers or directly through streams mixing. The implementation of streams mixing not only permits the reduction of the heat load exchanged in the system and therefore that of the amount and area of heat exchangers, but also changes the number of streams which exchange heat through heat exchangers. However, improper mixing would result in a penalty for energy targets because a larger temperature approach between streams causes energy degradation. Although conceptual methods [1-4] as well as mathematical programming methods [5-8] have studied more about the minimization of water and energy consumption for water-using system, they have mainly focused on network design purpose with the consideration of streams mixing opportunities, rather than understanding the mechanism of energy penalty caused by mixing and how the penalty can be eliminated or avoided. In this paper, the effect of different types of homogeneous non-isothermal mixing on system utility consumption is studied by thermodynamic analysis method, and conclusions obtained can be used to identify whether a homogeneous non-isothermal mixing is beneficial or not to the system utility consumption.

2. The classification of streams and of stream mixing

For the convenience of expression, some temperatures which characterize a stream joined in mixing are defined as follow:

T_{mix}: the temperature of the stream after mixing;

$T_{S,high}$: the supply temperature of the stream with $T_{S,high} > T_{mix}$;

Foundation item: supported by the National Natural Science Fundation of China under Grant 21176178 and the National Basic Research Program of China (973 Program) 2012CB720500

$T_{S,low}$: the supply temperature of the stream with $T_{S,low} < T_{mix}$;

T_P: the pinch temperature of a water-using system before streams mixing;

T_{target}: the temperature of a water-using unit.

Streams joined in mixing could be classified into two main groups:

Non-across-pinch stream. If T_P does not belong to the temperature range from $T_{S,high}$ (or $T_{S,low}$) to T_{mix}, the stream is a non-across-pinch stream. Non-across pinch streams can be further divided into streams above the pinch and streams below the pinch.

Across-pinch stream. If T_P belongs to the temperature range from $T_{S,high}$ (or $T_{S,low}$) to T_{mix}, the stream is an across-pinch stream.

Obviously there is a relationship $T_{S,high} > T_{mix} > T_{S,low} > T_{target}$ for hot-hot streams mixing, and $T_{target} > T_{S,high} > T_{mix} > T_{S,low}$ for cold-cold streams mixing. Therefore the mixing patterns between homogeneous streams (mixing between hot streams or mixing between cold streams) can be classified according to the position of the pinch temperature, as shown in the table 1.

Table1. Mixing patterns for homogeneous streams

Pinch position	Mixing patterns
$T_P \geq T_{S,high}$	Mixing between hot (or cold) streams below the pinch
$T_{S,high} > T_P > T_{mix}$	Mixing between a hot (or cold) stream across the pinch and a hot (or cold) stream below the pinch
$T_{S,high} > T_P = T_{mix}$	Mixing between a hot (or cold) stream above the pinch and a hot (or cold) stream below the pinch
$T_{S,high} > T_{mix} > T_P > T_{S,low}$	Mixing between a hot (or cold) stream across the pinch and a hot (or cold) stream above the pinch
$T_{S,low} \geq T_P$	Mixing between hot (or cold) streams above the pinch

3. The influences of homogeneous stream mixings on water-using network's energy target

In this paper water-using network structure is assumed to be given, and the continuous operation of water usage is considered, each water-using unit operated isothermally without water loss and heat loss, water stream data are available for mass flowrate and operating temperatures. The discharge temperature and the fresh water source are both specified as 30℃. And an equal specific heat capacity 4.2 kJ/kg ℃ for all water streams is assumed. Non-water-using operations are not included in heat recovery. A minimum temperature approach (ΔT_{min}) of 10℃ is assumed for any heat exchanger. After classifying the types of streams and mixing patterns, the influence of different kind of mixing to water-using system's energy target could be studied by thermodynamic analysis according to heat transfer and grade variation caused by stream mixing.

3.1. The mixing between homogeneous streams above the pinch ($T_{S,low} \geq T_P$)

When two hot streams join in mixing, a new stream with temperature (T_{mix}) is generated. If the mixing process is described using stream composite curve in T-H diagram, it can be found the flowrate of hot stream in the temperature range from $T_{S,high}$ to T_{mix} will decrease, and the flowrate in the temperature range of T_{mix} to $T_{S,low}$ will increase. As a result, the gradient of the hot composite curve from the temperature range of $T_{S,high}$ to T_{mix} will increase (in some cases, the hot composite curve in the temperature range may even vanish), while that from T_{mix} to $T_{S,low}$ will decrease, as the gradient of the hot composite curve is in inverse proportion with the stream mass flowrate. Therefore, it can be presumed that after the mixing, if the heat from T_{mix} to T_P (the T_P corresponding

to hot stream) can be totally recovered by cold streams in the temperature range from (T_{mix} – ΔT_{min}) to T_P (the T_P corresponding to cold stream), the system energy consumption will not change. Otherwise, the system energy consumption will increase. The reason for the increase is that part of the heat above the pinch is transferred to cold streams below the pinch after mixing, which will cause the waste of high temperature energy. Similarly, for the mixing between cold streams above the pinch, if the heat of hot streams in the temperature range between (T_{mix}+ ΔT_{min}) and T_P can't be totally recovered by the cold streams in temperature range from T_p to T_{mix}, the residual heat have to be transferred to the cold streams below the pinch, which definitely causes an energy penalty of the system. Otherwise, the hot and cold utilities consumptions of the system will keep still. An example of mixing between hot streams above the pinch with energy penalty is given in Fig.1 for detail illustration.

The water-using network is shown in figure 1a. When indirect heat exchange through exchangers is adopted for the water-using network, the cold and hot composite curves of the system are shown in the Fig. 1b. The pinch temperature is 60℃ (for hot streams) and 50℃ (for cold streams). When the mixing between the stream $F_{1,3}$ and $F_{2,3}$ is adopted, the mixing is between hot streams above the pinch. According to the mass and energy balance for the mixing, T_{mix} is 62.5 ℃. Obviously, the hot stream which can supply heat from 70℃ to 62.5 ℃ disappears, while the flow rate of hot stream supplying heat from 62.5 ℃ to 60 ℃ increases from 5 kg·s-1 to 20 kg·s^{-1}. Namely after the mixing, certain number of heat supplied originally in temperature interval from 70℃to 62.5 ℃ before the mixing now shifts to the temperature interval below 62.5 ℃. However, the heat requirement by cold stream from 50 ℃ to 52.5 ℃ does not change. Therefore after the mixing, there must be a part of the heat above the pinch now used to heat cold streams below the pinch, and the energy penalty of the system must occur. The composite curves of the system after the mixing (Fig. 1c) just demonstrate the result, the hot composite curve from 70 ℃ to 62.5 ℃ disappears after the mixing, while the gradient of the hot composite from 62.5 ℃ to 60 ℃ decreases. What's more, after the mixing the hot and cold utilities consumptions increase to 525kW and 1785kW respectively.

Example1： The mixing between hot streams above the pinch (with energy penalty)

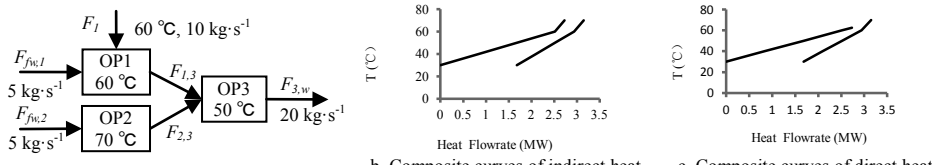

a. Water-using Network

b. Composite curves of indirect heat transfer

c. Composite curves of direct heat transfer

Fig 1. The mixing between hot streams above the pinch

3.2. The mixing between homogeneous streams below the pinch ($T_P \geq T_{S,high}$)

When the mixing between hot streams below the pinch occurs, in the temperature range from $T_{S,high}$ to T_{mix}, hot stream flowrate will decrease, which leads to the gradient of the hot composite curves in this temperature range increase; The flowrate in the temperature range from T_{mix} to $T_{S,low}$ will increase, which leads to the gradient of the hot composite curves in this temperature range decrease; Therefore, the hot composite curve will come closer to the cold composite curve after mixing. If hot streams in temperature range from T_{mix} to T_p can still supply the cold streams between (T_{mix} - ΔT_{min}) and T_p with the heat they need, the system energy consumption will not change; Or else, the system

energy consumption will increase. And the reason for the increase is also because part of heat above the pinch is transferred to cold streams below the pinch after mixing. For the mixing between cold streams below the pinch, if the heat of hot streams between ($T_{mix} + \Delta T_{min}$) and T_P can still meet the needs of cold streams from T_{mix} to T_p after mixing, the system energy performance will keep still. However, if not, the energy penalty occurs.

3.3. The others mixing patterns of homogeneous streams mixing

The other three types of hot-hot streams mixing will inevitably make some heat transferred across the pinch from up to down, and the energy punishment of the system must occur. Take the mixing between a hot stream across the pinch and a hot stream below the pinch for instance, as one of the mixing streams is across the pinch, part of the energy above the pinch will definitely be transferred to the mixing hot stream with a lower temperature below the pinch, which causes a penalty on the system energy consumption. As for the reminder mixing patterns of cold-cold streams mixing, the mixing will inevitably cause a penalty on the system utilities consumption, as part of heat will be transferred across the pinch from up to down.

3.4. Homogeneous mixing influence on water-using system utilities consumption

From analyzing all homogeneous mixing patterns, we can conclude as follows:

(1) For hot-hot steams mixing, three types of mixing will definitely cause energy penalty on water-using system energy consumption, including the mixing between a hot stream across the pinch and a hot stream below the pinch, the mixing between a hot stream above the pinch and a hot stream below the pinch and the mixing between a hot stream across the pinch and a hot stream above the pinch.

(2) For cold-cold streams mixing, three types of mixing will also cause energy penalty, including the mixing between a cold stream across the pinch and a cold stream below the pinch, the mixing between a cold stream above the pinch and a cold stream below the pinch and the mixing between a cold stream across the pinch and a cold stream above the pinch.

(3) The mixing between hot streams above the pinch and the mixing between cold streams above the pinch will cause energy penalty if the energy in the temperature range from T_{mix} to T_p cannot be totally recovered by the cold streams above the pinch, or else the system utilities consumption will keep still.

(4) The mixing between hot streams below the pinch and the mixing between cold streams below the pinch will cause energy penalty if the energy demand by cold streams from T_{mix} to T_p cannot be satisfied by the hot streams below the pinch, otherwise the system utilities consumption will keep still.

4. An application example

The water-using network of Example2 given in Fig.2 has six possibilities of streams mixing at the inlets of unit OP5, OP6, OP7, OP8, OP9 and OP 10. Fig. 3 shows that the pinch temperature of the indirect exchanger network is 100/90℃. The hot and the cold utility consumption are 1890kW and 9240kW respectively. Based on the guidance concluded in the section 3.4, the mixings at the inlet of OP5, OP6 and OP10 has no influence to the system utility consumption. For the mixings at the inlet of OP7 and OP8, they will definitely cause the energy penalty. As to the mixing at the inlet of OP9, which is between a cold and a hot stream belongs to heterogeneous non-isothermal mixing, which we will consider in our future's work. Fig. 4 shows the composite curves after the three types of mixing at the inlet of OP5, OP6 and OP10. Although the composite curves vary, the total energy target keeps still, and this testifies our results.

On the whole, there are three kinds of mixing operations out of the five types of homogeneous mixings we can make use of. Although the three mixings have no energy saving effect, they are still adoptable. Because after mixing the total number of heat exchangers will decrease, which is beneficial to the capital cost.

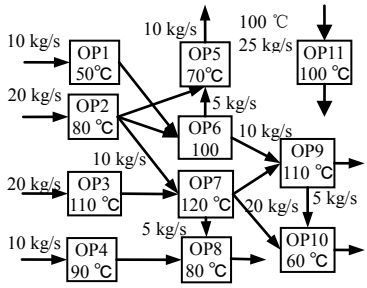

Fig. 2 Water-using Network for example 2

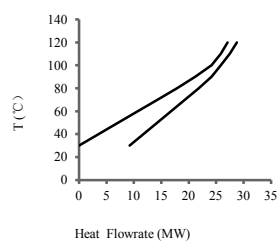

Fig. 3 Composite curves of indirect heat transfer

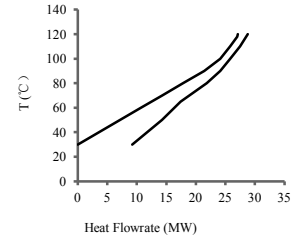

Fig. 4 Composite curves after suitable mixings

5. Conclusions

This paper has classified streams into three types, namely the stream above the pinch, the stream below the pinch and the stream across the pinch. Based on these stream classifications, mixing patterns are defined according to the position of the pinch temperature. Through thermodynamic analysis for homogeneous non-isothermal mixing on system utilities consumption, it has been found that the potential value of homogeneous non-isothermal is to reduce the equipment investment cost. And it will never have energy saving effect. The conclusions for homogeneous non-isothermal mixing in the paper can be used to analyze or optimize the heat exchanger network of a given water-using system. What is more, they may be used establishing a simple model to simultaneously optimize water consumption and energy consumption by mathematical programming method. In terms of the heterogeneous non-isothermal mixing, based on our method, we will explore it in our next work.

References

[1]L.E. Savulescu, M. Sorin, R.Smith, 2002, Direct and indirect heat transfer in water network systems. Applied Thermal Engineering, **22**(8), 981-988.

[2]M. Sorin, L.Savulescu, 2004, On minimization of the number of heat exchangers in water networks, Heat Transfer Engineering, **25**(5), 30-38.

[3]L. Savulescu, J K. Kim, R.Smith, 2005, Studies on simultaneous energy and water minimization-Part II: Systems with maximum re-use of water, Chemical Engineering Science, 60(12), 3291-3308

[4]X. Feng, Y.C Li, X.J. Yu, 2008, Improving energy performance of water allocation networks through appropriate stream merging, Chinese Journal of Chemical Engineering, 16(3):480-484.

[5]M. Bagajewicz, H. Rodera, M. Savelski, 2002, Energy efficient water utilization systems in process plants, Computers and Chemical Engineering, **26**(1), 59-79.

[6]H.G.Dong, C.Y.Lin, C.T. Chang, 2008, Simultaneous optimization approach for integrated water-allocation and heat-exchange networks, Chemical Engineering Science, **63**(14), 3664-3678.

[7]M. Bogataj, M.J. Bagajewicz, 2008, Synthesis of non-isothermal heat integrated water networks in chemical processes, Computers and Chemical Engineering, **32**(12), 3130-3142.

[8]J.Y. Kim, J.K. Kim, J.G. Kim, 2009, A simultaneous optimization approach for the design of wastewater and heat exchange networks based on cost estimation, Journal of Cleaner Production, **17**(2), 162-171.

I.A. Karimi and Rajagopalan Srinivasan (Editors), Proceedings of the 11th International Symposium on Process Systems Engineering, 15-19 July 2012, Singapore.

Optimal Process Configurations of Bioethanol Dehydration for Different Ethanol Inlet Concentrations and Throughputs

Pakkapol Kanchanalai, Matthew J Realff ,Yoshiaki Kawajiri

School of Chemical & Biomolecular Engineering, Georgia Institute of Technology
311 Ferst Drive, Atlanta, GA 30332-0100

Abstract

Purification of low concentration ethanol solutions is an energy intensive process that comprises a significant portion of the overall cost of biobased ethanol. Optimization models of two hybrid ethanol separation processes, distillation-membrane pervaporation process and vapor-compression-membrane-gas-permeation technology, are developed. These options are compared for different feed concentrations and throughputs. Different feed concentrations change the optimal separation process because the top composition of the column using vapor compression is more sensitive to feed concentration than the pervaporation case. The pervaporation annualized capital cost increases more slowly with increasing throughput, but its operating cost increases more quickly, leading to very little impact on scale on the optimal decision at any given feed concentration.

Keywords: Biofuels, ethanol, hybrid separation, optimization, superstructure

1. Introduction

Energy demands, particularly in the form of liquid fuels, have been increasing globally driven by the rise of GDP in rapidly developing countries. This, coupled with concerns about increased atmospheric CO_2 concentrations, has driven the search for other fuels that do not come from fossil hydrocarbons. Biobased ethanol has been considered as a promising and potentially sustainable fuel since it can be used as a gasoline oxygenate, both to increase the octane number and provide a cleaner combustion, as well as being produced from carbon fixed from the atmosphere over relatively short time periods (Huang et al, 2008). However, the cost of biobased ethanol production is relatively high compared to other fuel production, particularly if sourced from lignocellulosic materials. Significant efforts have been undertaken to improve and optimize the biobased ethanol production process. Fuel grade biobased ethanol is above 99 wt %, and requires separation from water above its azeotrope, increasing the energy demand of distillation processes. Beyond distillation, several separation technologies have been proposed such as adsorption and membrane gas and pervaporation separation, as well as hybrid systems with distillation. However, each process has its own advantages and disadvantages – extractive distillation is considered a highly energy intensive process, while membrane separation consumes less energy with higher capital cost (Frolkova & Raeva, 2010). Previous studies have proposed a hybrid system of distillation and membrane separation. The optimization of this hybrid process has been investigated to minimize the total annual cost of the separation process (Szitkai et al, 2002).

Optimal process selections may depend on different ethanol inlet purities which rely on the ethanol conversion process and feed conditions. In addition, the costs of alternative technologies scale differently with production flow rate. The effect of the ethanol inlet

concentration and throughput should therefore be considered to determine the optimal purification process. In this work, the combination of distillation and a membrane system are investigated for two different membrane options, pervaporation and gas permeation. The latter allows vapor compression distillation to be employed. Optimal configurations for each technology that minimize ethanol unit cost are determined for different inlet ethanol concentrations and throughputs by considering rigorous cost optimization models. Superstructures of these two technologies are formulated as mixed integer nonlinear programming (MINLP) models where numerous operating and design parameters are optimized such as the number of stages, feed location, reflux ratio, pressure, and membrane area. The cost model is applied to estimate the capital cost, operating cost and the unit cost of the biobased ethanol (Seider et al, 2010).

2. Process Description

2.1. Distillation-membrane pervaporation process

The first hybrid process considered combines a distillation column with the membrane pervaporation process. The pervaporation network is placed after the distillation column to separate the top product across the azeotropic point after an initial dehydration from the atmospheric distillation column. A superstructure of this hybrid process is obtained by integrating the superstructure of a distillation column and that of a pervaporation network shown in Figure 1a (Malik & Naidu, 2011). The superstructure of the distillation column is used to find the optimal number of theoretical stages, feed stage location, recycle stage location, and reflux ratio by applying logical constraints on binary variables (Viswanathan & Grossmann, 1993). The superstructure of pervaporation contains multiple stages of membranes arranged in series. The ethanol liquid stream from the top distillate is concentrated by partially vaporizing through the hydrophilic membrane. The driving force depends on the partial pressure difference between the liquid and vapor phase (Davis, 2002). The enthalpy of vaporization is provided by the sensible heat of the feed, and hence the driving force of the pervaporation drops along the membrane as the sensible heat converts into the heat of vaporization of the water, lowering the liquid partial pressure. Intermediate heat exchangers are therefore used to reheat the liquid feed and the intermediate streams to below the maximum membrane operating temperature. The appropriate number of membrane stages is investigated by solving several cases. Little improvement is observed when the number of stages is increased from four. Four membrane stages with four interstage heaters are therefore found to be sufficient in this work. The permeates from all stages operated under the same vacuum pressure are combined and condensed by the chilled water before being recycled to the column.

2.2. Vapor-compression-membrane-gas-permeation process

The second hybrid process, illustrated in Figure 1b (Huang et al, 2010), considers a membrane gas permeation system combined with a distillation column. The key point of this process design is that it uses the mechanical work from the compressor to increase the driving force in the membrane and also to provide heat for the vapor stream which enables energy recovery in the column reboiler. The distillation column performs an initial step of separation similar to the pervaporation process; and the membrane is used to concentrate the ethanol of the vapor from the distillate to cross the azeotropic point. The membrane for this system must be able to operate at a high temperature to maintain a vapor phase of the mixture at a high pressure. The superstructure of this system uses a similar distillation column model and integrates it with the gas permeation system. Unlike the pervaporation system, the driving force (partial pressure difference) depends

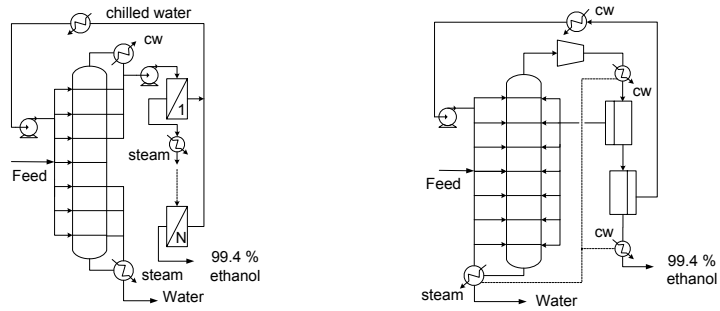

Figure 1. Superstructure of hybrid separation process (a) Distillation - Membrane pervaporation (b) vapor- compression gas permeation

on the pressure difference of vapor stream between the feed and the permeate, as well as the compositions. Therefore, the column may operate under a vacuum to increase this driving force for the membrane separation, since the permeate from the first membrane stage is returned to the column. The vapor stream from the top distillate is compressed and cooled down to below the maximum membrane operating temperature and fed to the membrane unit. This paper considers a vacuum distillation column with two membrane units which allow the system to operate with two different permeate pressures. The permeate stream from the first membrane stage is recycled back to the column and the permeate from the second membrane stage is condensed and return to the column as a reflux. Heat integration between heat exchangers is also considered in this system as shown by the dashed line in Figure 1b.

3. Results

This work uses MINLP model of the superstructure of a distillation column (Viswanathan & Grossmann, 1993) with up to 120 integer variables, and VLE model using NRTL. A high selectivity commercial polyvinyl alcohol membrane is used in the pervaporation process where the permeability correlation comes from Davis (2002), and the maximum operating membrane temperature of 90°C is assumed. In contrast, the gas permeation membrane can operate at a higher temperature, where the maximum of 120°C is used, but with a lower selectivity which is modeled by assuming constant average permeability (Huang et al, 2010). The logarithmic-mean pressure driving force is used in both membrane process (Davis, 2002). The separation costs for both technologies are minimized at different ethanol feed concentration and throughputs based on the best solution found from GAMS/SBB solver with different initial guesses. Ethanol of 99.4wt% purity with 99% recovery is produced, and the unit cost is computed using the capital cost models and all energy costs from Seider et al. (2010) with a discount rate of 7% per year, and 5 year life cycle.

3.1. Effect of ethanol feed concentration

It can be seen from Figure 2 that for both throughputs, the pervaporation technology has lower separation cost than the vapor compression process at a low ethanol feed concentration, but at approximately above ethanol feed at 0.2 w/w and 0.24 w/w for the feed of 10 Mgal/yr and 100 Mgal/yr respectively, the optimal technology switches to vapor compression. Each hybrid technology partitions the separation work between the distillation column and the membrane differently. From Figure 3, the top ethanol concentration in pervaporation is almost constant near the azeotropic point for all inlet

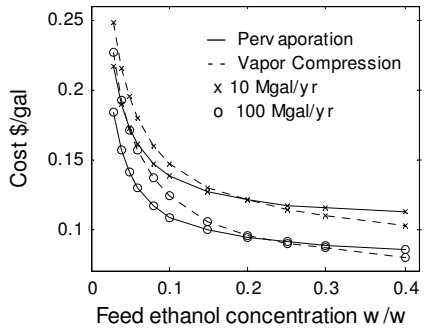

Figure 2. Ethanol cost of pervaporation and vapor compression technologies with different feed concentrations.

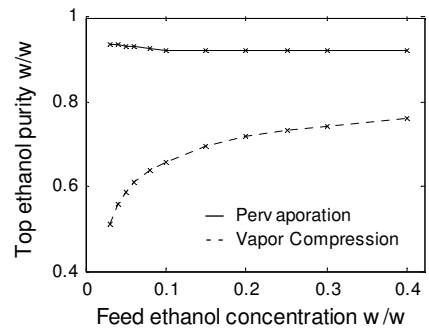

Figure 3. Ethanol concentration from the top of the distillation column with different inlet concentrations at 100 Mgal/year.

concentrations. The optimizer decides to purify the mixture mainly by the distillation column in order to reduce the expensive membrane area. In contrast, the top ethanol concentration in the vapor compression process increases with increasing ethanol feed concentration. The top purity of the distillation column relies on the purity and the liquid flow from the second membrane permeate. It requires a significantly larger membrane area to increase the purity of both the overhead vapor and the second membrane permeate. The optimizer therefore decreases the overhead ethanol content of the distillation column. This requires more membrane separation work and leads to a higher cost than the pervaporation technology at low ethanol feed concentrations.

3.2. Effect of ethanol throughputs

The result from Figure 2 shows that the concentrations at which the costs of the two technologies cross for two different capacities are slightly different – 0.2 w/w for 10 Mgal/yr and 0.24 w/w for 100 Mgal/yr. This concentration range is further investigated for more different throughputs as shown in Figure 4. At ethanol feed of 0.23 w/w, the vapor compression has cheaper separation cost than the pervaporation process at a small plant capacity. When increasing the feed flow rate, the cost of pervaporation technology becomes lower than the vapor compression at above 40 Mgal/yr. This demonstrates that the pervaporation process is slightly more sensitive to the throughputs. This is because the cost components of each technology scale differently. From Figure 5, the pervaporation process has a higher operating cost for all throughputs, but the annualized capital cost is cheaper and overcomes the effect of higher operating cost. This leads to

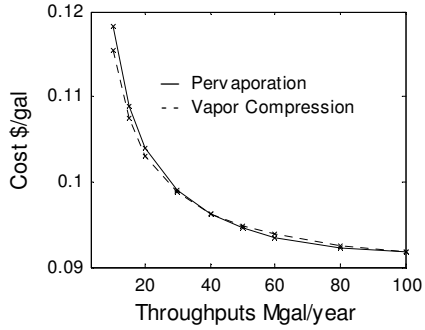

Figure 4. Cost of pervaporation and vapor compression with different feed throughputs at ethanol feed of 0.23 w/w

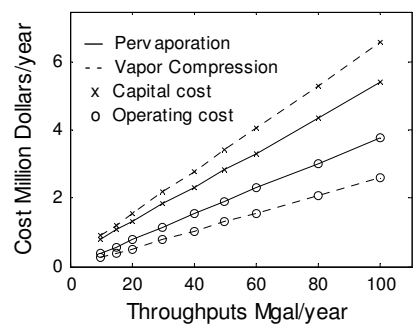

Figure 5. Annualized capital cost and operating cost of two technologies for different feed throughputs at ethanol feed of 0.23 w/w

a lower ethanol unit cost than the vapor compression technology at a higher throughput above 40 Mgal/yr. A more detailed examination of the component costs shows that the pervaporation process requires less membrane area than vapor compression, since the distillation column, a cheap separation unit, in the pervaporation technology can achieve a higher top ethanol concentration. Moreover, the compressor capital cost in the vapor compression technology is a high portion in the capital cost of separation process. The membrane and the compressor cost then increase significantly when the throughputs through the membrane increase. Furthermore, an external investigation reveals that the maximum operating temperature for the membrane also has a significant impact on the cost. These results therefore may change if different membrane is used in the process.

4. Conclusion

Two MINLP models of bioethanol hybrid separation technologies are optimized to compare the purification cost for different inlet concentration and throughputs. Pervaporation technology is optimal at a very low feed concentrations, while vapor compression process, more sensitive to the feed concentration, has a lower separation cost at a higher inlet ethanol concentration. Different throughputs also have an effect on the optimal technology in that the pervaporation process is more sensitive to the plant capacity. Because of the higher operating cost but lower capital cost, the pervaporation process is cheaper than the vapor compression technology at higher throughputs, but only marginally. From these results, the vapor compression process may benefit more from feed pretreatment because of its higher sensitivity to the inlet concentration. Different membrane permeabilities and the maximum membrane operating temperature may also change the results of optimal process configuration and technology; these impacts will be investigated in the future work.

Acknowledgements

The authors are grateful for the financial support from PTT Public Company Limited, Thailand. The second author gratefully acknowledges partial financial support from NSF grant and GOALI program, CBET 0933392.

References

Davis, R.A., Simple gas permeation and pervaporation membrane unit operation models for process simulators. Chemical Engineering & Technology, 2002. 25(7): p. 717-722.

Frolkova, A.K. and V.M. Raeva, Bioethanol dehydration: State of the art. Theoretical Foundations of Chemical Engineering, 2010. 44(4): p. 545-556.

Huang, H. J., Ramaswamy, S., Tschirner, U. W., & Ramarao, B. V., A review of separation technologies in current and future biorefineries. Separation and Purification Technology, 2008. 62(1): p. 1-21.

Huang, Y., R.W. Baker, and L.M. Vane, Low-Energy Distillation-Membrane Separation Process. Industrial & Engineering Chemistry Research, 2010. 49(8): p. 3760-3768.

Malik, R.K. and Y. Naidu, A generalized methodology for optimal configurations of hybrid distillation-pervaporation processes. Chemical Engineering Research & Design, 2011. 89(8A): p. 1348-1361.

Seider, Warren D., J. D. Seader, Daniel R. Lewin, and Soemantri Widagdo. Product and Process Design Principles: Synthesis, Analysis and Design. 3rd ed. Chichester: John Wiley, 2010.

Szitkai, Z., Lelkes, Z., Rev, E., & Fonyo, Z., *Optimization of hybrid ethanol dehydration systems.* Chemical Engineering and Processing, 2002. 41(7): p. 631-646.

Viswanathan, J. and I.E. Grossmann, Optimal Feed Locations and Number of Trays for Distillation-Columns with Multiple Feeds. Industrial & Engineering Chemistry Research, 1993. 32(11): p. 2942-2949.

I.A. Karimi and Rajagopalan Srinivasan (Editors), Proceedings of the 11th International Symposium on Process Systems Engineering, 15-19 July 2012, Singapore.

A comparison between the two balancing regimes of the natural gas market in the Netherlands

Catalin Bucura[*a], Zofia Lukszo[a]

[a]*Delft University of Technology, Faculty of Technology, Policy and Management, Jaffalaan 5, Delft, 2621BX, the Netherlands*
(c.a.bucura; z.lukszo)@tudelft.nl

Abstract

The functioning of the old and new balancing regimes of the natural gas market in the Netherlands is explored using an agent-based model. The two balancing regimes are simulated to determine the participants' cash flows under different behavioral strategies for both regimes. The total system imbalance and the costs associated to the balancing strategies are calculated. Model simulations runs and observation of shippers' cumulative penalties and rewards provide support in understanding the old and new regime.
Keywords: agent-based models, simulation, gas market, balancing regime.

1. Introduction into the Dutch gas market and its balancing regime

The third EU energy package – Third Gas Directive [1] was adopted by the European Parliament in September 2009. The goals of the directive are to increase competition and efficiency, to ensure security of supply and to ensure the freedom of choice of consumers at a fair price. The Dutch natural gas market has formed back in the 1960's when the gas field Groningen in the North of the country has been discovered, and ever since, it has been continuously going through many technical and institutional changes.

Figure 1 presents an overview of the Dutch gas market. The company that operates the gas network is Gas Transport Services B.V. (GTS), also known as the Dutch Transport Service Operator (TSO).

Figure 1: The Dutch Gas market value chain

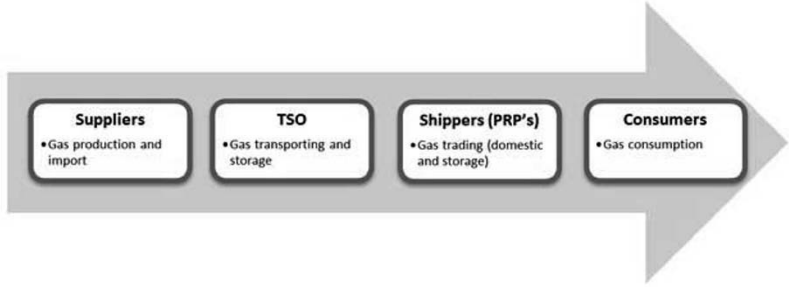

* corresponding author

2. The old and new balancing regime

At abstract level, the functioning of the gas market is fairly simple: suppliers produce the gas, traders commercialize it, customers use it, and the transporter makes sure that gas gets from one side to the other. Transportation of gas must be done according to a set of rules, and it also must be done in a safe and reliable way.

The reliable operation of the Dutch gas network requires that the TSO, maintains pressure in the network within certain limits. The system is considered to be *out of* balance if the pressure in the network falls outside those limits. If the pressure is too low, the system is *short* and *long* if the pressure is too high. The companies which trade the gas are called *shippers*.

2.1. The old balancing regime

In the old balancing regime if the network was out of balance, the first intervention in balancing was done by the TSO. Next, the shipper with contractual rights on almost all assets, took out or injected the amount needed to balance in concordance with the contracts. In case one shipper was out of balance, it had to pay penalties. Not only were those penalties excessively high, but they were applied regardless the position of the shipper (long or short). All these penalties due to the shippers' imbalance were used to pay the costs of balancing the national transport network.

In 2006, the Dutch Parliament decided to change this detrimental situation and requested improvement in the system. On the 1st of April 2011 a *new balancing regime* was adopted.

2.2. The new balancing regime

The design of the new regime relies on a market driven balancing mechanism. All the participants in the balancing system are called Program Responsible Parties (PRP's). They are now responsible for balancing any difference between their forecasted volume of gas to be transported and the actual transported volume. However, a tolerance which is related to the size of their portfolio is applied (i.e. smaller PRP's have a larger tolerance than larger ones) [2].

In the new regime the TSO provides the shippers with two real time information signals: the System Balance Signal (SBS) and Portfolio Imbalance Signal (POS). POS represents the own imbalance of a shipper, whereas the SBS represents as the name suggests, the sum of all POS's [3,4]. A responsible party whose imbalance is the opposite of the total system imbalance is called a *helper*, and respectively, a party with imbalance in the same direction is called a *causer*.

Another new component of the new Dutch gas market balancing regime is the Bid Price Ladder (BPL) mechanism, designed to purchase and sell deficit as well as excess volumes of gas. It also determines the cost of imbalance, unlike in the previous old regime where the penalties were related to the price of transactions on the virtual trading point.

3. Modeling the two balancing regimes of the natural gas market

3.1. Modeling approach

The new balancing regime has come with changes to the existing system. It is now based on penalties and incentives for the shippers. It stimulates them to participate on the market, rather than, like in the old regime, charge them for whichever type of imbalance. Balancing the network becomes now a common task for the shippers. The emergent behavior of such a complex system is not obvious, and its properties are hard

to deduce. The behavior of the whole system is different from the individual behavior of its components.

Complex adaptive systems are systems evolving over time, composed by agents which react with each other according to what the others agents do [5]. Agents are semi-autonomous entities that seek to maximize their objectives by evolving over time. Examples of such complex systems are economies, weather, traffic, social organizations, and most of the infrastructure systems that are composed of heterogeneous actors. One way to explore and understand such complex systems is represented by the use of Agent Based Modeling (ABM).

In ABM, a complex system is decomposed into agents whose actions aim to simulate the behavior of the real life actors. The aggregate behavior as a result of interaction of the individual behaviors allows analyzing the system as a whole. Creating an ABM of the old and new balancing regime aims to provide insight into the operation of this new complex system.

3.2. Goals of the model

The model aims to explore the operation of the two balancing regimes. The model replicates the operation of the gas market in the old and new balancing regime. It simulates the effects of the individual shippers' decisions on the operation of the system as a whole.

3.3. Design of the model

The model simulates the operation of the gas market composed out of several types of agents: suppliers, TSO, shippers and consumers (see Fig. 1 for the sequence). The system is in balance as long as the aggregated system position is between the predefined bounds. When the system is out of balance the TSO buys or sells gas according to the system's state.

The shippers are responsible for balancing. They have to make sure that their own portfolio is balanced and also they must ensure that the total network is balanced, too. In case the network goes out of balance, then the TSO calls the bid ladder. The bid ladder is constructed by using the volumes with their corresponding prices submitted by the PRP's, but not used in the previous transactions. At this stage, only bids that can physically be delivered are accepted. To construct the BPL, the accepted bids are sorted based on the merit order, so that those with the lowest marginal costs are the first ones to be bought. The price of the last bid that satisfies the demand is the price used for the transactions on the BPL.

3.4. Agents

Agent Based Models (ABM) approach usually consists in decomposing the complex system into autonomous agents, which interact with each other. The agents are represented using formalized concepts and definitions. This formalization is represented by the *ontology*. The use of ontologies for conceptualizing domain knowledge has been a standard practice in information science [6]. In ABM, ontology provides a shared vocabulary that can be used to model a socio-technical system: the type of objects and concepts that exist, and their properties and relations [7]. As we built the model of the (new) balancing regime, we created the ontology used later on, as a simplified conceptualization of the real system.

In our ontology, every social node has a physical node attached; every agent owns or operates a technology. The social nodes represent the agents and the physical nodes represent technologies. Agents in the model represent the decision makers in the real world: suppliers, TSO, shippers and consumers (see Fig. 1 for the sequence). Technologies in the ontology are used to describe the physical connections and reflect

the physical constraints. The model is composed of the following agents: demand (commercials, electricity producers, export, households and industry), supply, the TSO and the shippers. Trading of gas takes place, and depending on the total system position and imbalance, the TSO calls the BPL accordingly. Helpers are rewarded whereas causers are penalized according to the BPL mechanism and the settlement price. At this stage of the model, the agents do not learn from their mistakes in the past

4. Model results and insights

In this section we compare and discuss the simulations of the two balancing regimes. The two charts for both simulations - the old and new regime (Figure 2) represent the liquid assets of three types of shippers (represented in the model as 10 different shippers), i.e. with large (shippers 1, 2, 3), medium (shippers 4, 5, 6 and 7) and small portfolio (shippers 8, 9 and 10).

Comparing the two simulations from Figure 1 we observe that in the old regime all shippers pay penalties. Large shippers (2 and 3) pay the highest penalties. In the old regime, without any information about SBS and penalties paid regardless their position, shippers with larger portfolio get higher imbalance and smaller tolerance, and therefore higher penalties. Small size shippers (e.g. shipper 10) also get penalties even if their imbalance is not high. In the real life, most of the transactions were done on a bilateral market, or "over the counter", and for this reason the shippers did not get bankrupt.

In the new regime, even though there is no negotiation between the shippers, they do not always pay penalties (right side of Figure 1). Shipper 2 (blue 'x' in the graph), which has a large portfolio, has negative outcome. On the opposite, the medium size shipper 4 (black triangle in the graph) performs much better in the first half of the simulation. The explanation for this is that shipper 2 overbooks the network, and has a large portfolio which triggers a large imbalance and small tolerance. The medium size shipper 4, turns the imbalance into his own favor and due to his small overbooking, it performs well.

The three types of shippers perform rather different in the two regimes. In the old one, regardless their imbalance all paid penalties. Small shippers paid high penalties in the old regime even though their imbalance is not high. In the new regime, however, medium shippers perform better. The simulations show that for large capacity overbooking, none of the shippers performs well. This is also one of the new regime goals – more efficient capacity utilization. It should be added that we have showed that individual imbalances of a shipper are only relevant in relation to the aggregate system position. For this reason we do not treat shippers individually. [8]

5. Final remarks

In this paper we have presented agent based simulations of the old and new balancing regime of the natural gas market in the Netherlands. The new regime is rather complex and relatively difficult for shipper's operation. Every hour signaling may not be most appropriate way for presenting the system position. There is an expectation that the EU grid code will be published shortly and it will require daily balancing, with limited possibility for within-day actions. The simulations as presented in this paper can give a valuable support in understanding the consequences of the new EU grid code.

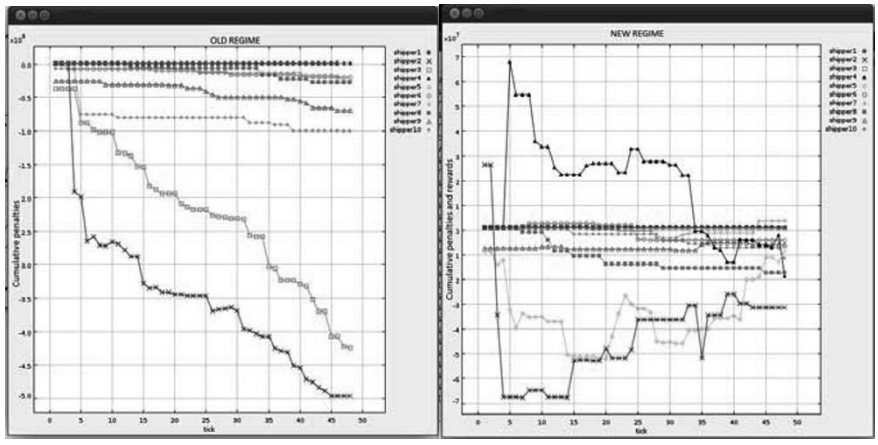

Figure 2. Cumulative penalties of shippers in the old regime (left side) and cumulative penalties and rewards in the new regime (right side)

As is the case with most agent-based models of complex systems, the process of building the model helps to conceptualize the system and to understand it. The aim of this paper is not to measure the performance of any of the two regimes, but to explore and understand them. The model is not yet in the final state. In the future research the real system data will be used and the model will be extended by adding storage facilities.

6. Acknowledgements

This research is funded by the Dutch Energy Delta Gas Research (EDGaR) program. The focus EDGaR is to understand the challenges encountered by the transition of the gas-based energy market to a more liberal, secure, affordable and sustainable state.

References

[1] Directive 2009/73/EC gas – "Third Gas Directive", [last visited on 20.01.2012] http://ec.europa.eu/energy/gas_electricity/legislation/third_legislative_package_en.htm
[2] Procedure qualifying balancing instrument gas transport services, [last visited on 20.01.2012] http://www.gastransportservices.nl/en/balancing/procedure-qualifying-balancing-instrument
[3] Shippers and traders in the Dutch gas market, [last visited on 20.01.2012] http://www.gastransportservices.nl/en/shippers
[4] About POS and SBS, [last visited on 20.01.2012] http://www.gastransportservices.nl/en/balancing/about-pos-and-sbs
[5] Dooley, K. (1996), "A Nominal Definition of CASystems," The ChaosNetwork, 8(1): 2-3.
[6] P. A. Fishwick and J. A. Miller. Ontologies for modeling and simulation: issues and approaches. Winter Simulation Conference, pages 259–264, Washington, D.C., 2004.
[7] K. van Dam. Capturing socio-technical systems with agent-based modelling. PhD thesis, Delft University of Technology, the Netherlands, 2009.
[8] C. Bucura et al., Modeling the new balancing regime of the natural gas market in the Netherlands. ICNSC - IEEE, pages 68-73, the Netherlands, April 2011

I.A. Karimi and Rajagopalan Srinivasan (Editors), Proceedings of the 11th International Symposium on Process Systems Engineering, 15-19 July 2012, Singapore

Model predictive control for BioPower combined heat and power (CHP) plant

Jukka Kortela * Sirkka-Liisa Jämsä-Jounela
Aalto University School of Chemical Technology; PL 16100, FI-00076 Aalto, Finland

Abstract

This paper presents a model predictive control (MPC) development for BioGrate boiler. Amount of fuel and moisture in the furnace are chosen as the state variables for the MPC model in order to take into account fuel quality. To this end, dynamic models for fuel decomposition and water evaporation in the furnace are used. As a result, the drum pressure can be predicted accurately and an efficient stabilization of the plant operations is possible by using the MPC. The performance of the MPC is evaluated using real industrial plant data and compared with the currently used control strategy. Finally, the results are presented, analyzed and discussed.

Keywords: biopower, combustion, biomass, fuel quality, MPC, moisture, advanced control, power plant

1. Introduction

The usage of biomass fuel for heat and power production is growing due to an increasing demand for replacing of fossil energy sources with renewable energy. The fuel is usually a blend of different batches, for example, spruce bark and dry woodchips with varying moisture content between 30% and 55% (Yin et al. (2008)). This varying moisture content of the fuel results in uncertainty in the energy content of the fuel and complicates the operation of combustors. One of the latest developed processes, which can burn biomass fuel with high moisture is BioGrate technology developed by MW Biopower. In the BioGrate system, this is achieved by feeding the fuel onto the center of a grate, thus improving water evaporation due to the heat of the surrounding burning fuel and thermal radiation from the brick walls (Wärtsilä Biopower (2005)).

An important step in the control strategy development for BioGrate boiler has been to develop a method for estimating the furnace fuel flow and combustion power, as shown in theoretical studies and practical tests by Kortela and Lautala (1981). On-line measurements of oxygen consumption were used when a new cascade compensation loop was built to optimally control the fuel flow. It was reported that the amplitude and the settling time of the response of the generator power decreased to about one third of the original.

In addition, advanced combustion control has been applied to control air and fuel. Havlena and Findejs (2005) used model-based predictive control to enable tight dynamical coordination between air and fuel to take into account the variations in power levels. The results showed that this approach enabled boiler to be permanently operated with optimum excess air, resulting in reduced O_2 and a significant increase in the boiler efficiency. Similar results have also been reported for the application of a multivariable long-range predictive control (LRPC) strategy based on a local model network (LMN) in the simulation of a 200

*jukka.kortela@aalto.fi

MW oil-fired drum-boiler thermal plant (Prasad et al. (1998)) and for a scheme presented by Swarnakar et al. (1998) for robust stabilization of a boiler, based on linear matrix inequalities (LMIs). However, there are still some challenges and unattained objectives in the development combustion power control. For example, variations in the moisture of fuel should be considered in order to correct any estimation errors of combustion power.

This paper presents a model predictive control (MPC) development of BioGrate boiler. The paper is organized as follows: Section 2 presents the process description, the MPC control strategy, and the models for the MPC controller for BioPower CHP plant. The test results of MPC control strategy are presented in Section 4, followed by the conclusions in Section 5.

2. Description of the process and model predictive control strategy for Biopower 5 CHP plant

In the BioPower 5 CHP plant, the heat used for steam generation is obtained by burning solid biomass fuel: bark, sawdust and pellets, which are fed to the steam boiler together with combustion air. Heat and flue gases generated in the result of combustion are used to produce steam which accumulates in the drum.

The aim of the control is to keep the energy production at the target level that allows to stabilize the steam pressure in the drum. The suggested MPC control strategy presented in Fig. 1 utilizes fuel flow and fuel moisture soft-sensors and furnace state estimators to handle the inherent large time constants and long time delays of the boiler. In addition, models for fuel decomposition and water evaporation are used to predict the combustion power and to stabilize the drum pressure. This results in a radical reduction of settling time of the drum pressure and enables faster steam load changes, while maintaining the stability of the boiler.

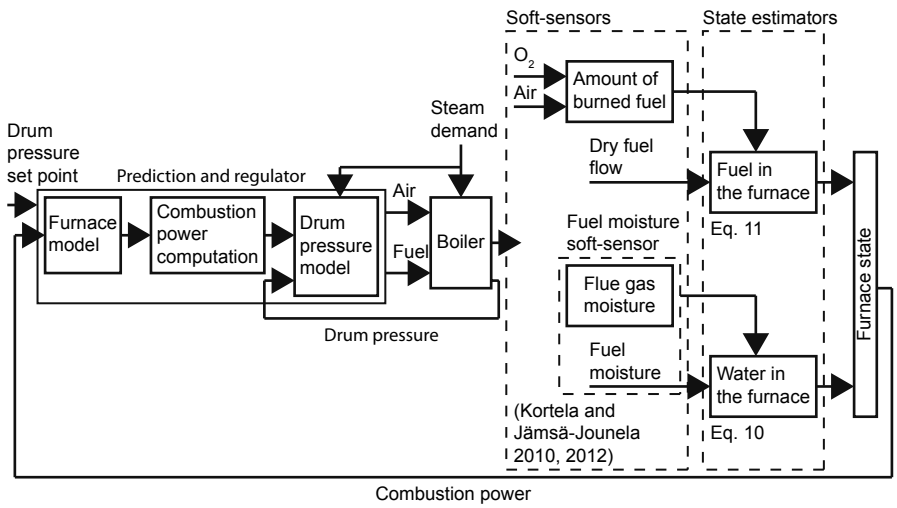

Figure 1. Model predictive control (MPC) strategy of BioGrate boiler

2.1. MPC Controller for BioGrate boiler

The MPC control is used as a master control, manipulating simultaneously set points for air and fuel flows. The configuration of the models is as follows: the fuel flow MV1 and the primary air flow MV2 are the manipulated variables; the fuel moisture DV1 is the estimated disturbance and the steam demand DV2 is the measured disturbance; and the combustion power CV1 and the drum pressure CV2 are controlled variables. The models are stacked into a linear state space system:

$$\begin{aligned} x_{k+1} &= Ax_k + Bu_k + Ed_k \\ z_k &= C_z x_k \end{aligned} \tag{1}$$

where x are the states, u are the manipulated variables (MVs), and d are the measured disturbances. z denote the controlled variables (CVs). Regularized l_2 output tracking problem with input and output constraints is formulated as (Maciejowski (2002))

$$\begin{aligned} \min \phi &= \frac{1}{2}\sum_{k=1}^{N} \|z_k - r_k\|^2_{Q_z} + \frac{1}{2}\|\Delta u_k\|^2_S \\ s.t.\, x_{k+1} &= Ax_k + Bu_k + Ed_k, k = 0,1,\ldots,N-1 \\ z_k &= C_z x_k, k = 0,1,\ldots,N \\ u_{\min} &\leq u_k \leq u_{\max}, k = 0,1,\ldots,N-1 \\ \Delta u_{\min} &\leq \Delta u_k \leq \Delta u_{\max}, k = 0,1,\ldots,N-1 \\ z_{\min} &\leq z_k \leq z_{\max}, k = 1,2,\ldots,N \end{aligned} \tag{2}$$

2.2. Modelling of BioGrate boiler for MPC

Modelling of grate combustion is of great importance, since unknown fuel flow and water evaporation result in uncertainty in the combustion power, and complicate the operation of the boiler. The model is based on two mass balances for water and dry fuel, in which both models are obtained from the literature and their parameters are defined with experimental data. Other models of the boiler include the drum, the primary air, and the secondary air models.

2.2.1. The model for amount of moisture in the furnace

According to (Bauer et al. (2010)), the rate of water evaporation is mainly independent of the primary air flow and the dynamics of the moisture in the furnace m_w is

$$\frac{dm_w}{dt} = -\alpha_{wev} * m_w + m_{w,in}(t - T_d) \tag{3}$$

where α_{wev} is a dimensionless scaling factor, $m_{w,in}$ is the moisture in the fuel feed, and T_d a constant delay.

2.2.2. The model for amount of dry fuel in the furnace

Bauer et al. (2010) showed that the overall effect of the primary air flow rate on the thermal decomposition rate is multiplicative. Therefore, the thermal decomposition of dry fuel is as follows

$$\frac{dm_{ds}}{dt} = -\alpha_{thd} * m_{ds} + m_{ds,in}(t - T_d) - \alpha_{pa} * m_{pa} \tag{4}$$

where α_{thd} is the decomposition rate coefficient of fuel flow, and α_{pa} the decomposition rate coefficient of primary air flow, $m_{ds,in}$ is the stoker speed, and T_d a constant delay.

2.2.3. Drum model

If the drum level is kept at a constant set point, the variations in the steam volume are small. Neglecting these variations, the drum model is (Åström and Bell (2000))

$$\frac{dp}{dt} = \frac{1}{e}(Q - m_f(h_w - h_f) - m_s(h_s - h_w)) \quad (5)$$

$$e \approx \rho_w V_{wt} \frac{\partial h_w}{\partial p} + m_t C_p \frac{\partial T_s}{\partial p} \quad (6)$$

where Q is combustion power (MJ/s), m is mass flow rate (kg/s), h is specific enthalpy $(MJ/kg$, ρ is specific density (kg/m^3), V is volume (m^3), m_t is the total mass of the metal tubes and the drum (kg), C_p is specific heat of the metal (MJ/kgK), and T_s temperature of steam (K). The subscripts f, w, s, refer to feed-water, water, and stem, respectively. Double subscript t denotes total system. The combustion power and fuel moisture soft-sensor are described detailed in (Kortela and Jämsä-Jounela (2010)) and (Kortela and Jämsä-Jounela (2012)).

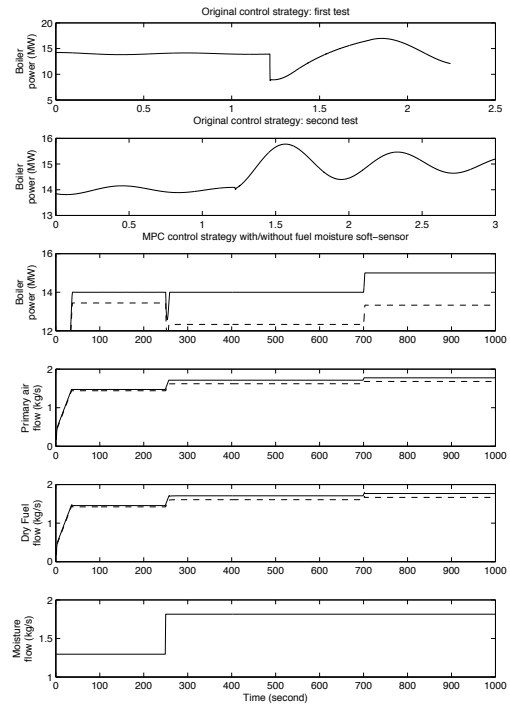

Figure 2. The test results when the MPC control estimates both states: fuel and moisture in the furnace (solid line), and the test results when the MPC control assumes that the moisture content is constant (dashed line). The top two pictures show the boiler power of the original control for the first and the second test.

2.2.4. Models for the primary air and secondary air flows

The primary air and secondary air models represent the dynamics of the regulatory layer PID control loops of air transport.

$$G_{pa}(s) = \frac{1}{\tau_{pa}s + 1} e^{-\alpha s} \quad (7)$$

$$G_{sa}(s) = \frac{1}{\tau_{sa}s + 1} \quad (8)$$

3. Test results of MPC control strategy of BioGrate boiler

The performance of the MPC control strategy was evaluated using real industrial plant data. In the first test scenario, the power demand of the boiler was kept at 14 MW while the moisture content of the fuel flow was changed from 47% to 51% at a time 300 seconds, as shown in Fig. 2. When the MPC control estimates both states: fuel and fuel moisture in the furnace, the boiler power drops by 1.5 MW for a short time. Nevertheless, the power demand and the actual power match really well. To compare, there is an offset in the results when the MPC control assumes that the moisture content in the fuel is constant. With the original plant control, the change in the moisture content caused strong oscillations. In the second scenario, the power demand was changed from 14 MW to 15 MW at a time 700 seconds. The settling time is only 2 minutes with the MPC control strategy, whereas it was about 1.5 hours with the original control.

4. Conclusions

This paper presented model predictive control (MPC) development for BioGrate boiler. The performance of the MPC was evaluated using real industrial plant data and comparison was made with the currently used control strategy. The test results show that the MPC followed power demand better compared with the currently used control strategy while maintaining stability.

References

Bauer, R., Gölles, M., Brunner, T., Dourdoumas, N., Obernberger, I., 2010. Modelling of grate combustion in a medium scale biomass furnace for control purposes. Biomass and Bioenergy 34 (4), 417–427.

Havlena, V., Findejs, J., 2005. Application of model predictive control to advanced combustion control. Control Engineering Practice 13 (6), 671–680.

Kortela, J., Jämsä-Jounela, S.-L., 2010. Fuel quality soft-sensor for control strategy improvement of the Biopower 5 CHP plant. In: Control and Fault-Tolerant Systems (SysTol), 2010. Nice, France, 6-8 October 2010, pp. 221–226.

Kortela, J., Jämsä-Jounela, S.-L., 2012. Fuel moisture soft-sensor and its validation for the industrial Biograte boiler. In: 17th Nordic Process Control Workshop. Kgs Lyngby, Denmark, 25-27 January 2012.

Kortela, U., Lautala, P., 1981. A New Control Concept for a Coal Power Plant. In: Proceedings of the 8th IFAC World Congress. Kyoto, Japan, 1981.

Maciejowski, J. M., 2002. Predictive Control with Constraints. Prentice Hal, Harlow, England.

Prasad, G., Swidenbank, E., Hogg, B. W., 1998. A Local Model Networks Based Multivariable Long-Range Predictive Control Strategy for Thermal Power Plant. Automatica 34 (10), 1185–1204.

Swarnakar, A.,Marquez, H.J., Chen, T. 2007 Robust stabilization of nonlinear interconnected systems with application to an industrial utility boiler. Control Engineering Practice 15(6), 639-654

Yin, C., Rosendahl, L. A., Kær, S. K., 2008. Grate-firing of biomass for heat and power production. Progress in Energy and Combustion Science 34 (6), 725–754.

Wärtsilä Power Plants: Bioenergy solutions. Vaasa: Waasa Graphics; 2005.

Åström, K. J. A., Bell, R. D., 2000. Drum-boiler dynamics. Automatica 36 (3), 363–378.

I.A. Karimi and Rajagopalan Srinivasan (Editors), Proceedings of the 11th International Symposium on Process Systems Engineering, 15-19 July 2012, Singapore.

Exergetic optimization of a refrigeration cycle for natural gas liquefaction

Liza Cipolato,[a] Maria C. A. Lirani,[a] Thiago V. Costa,[a] Francine M. Fábrega,[a] José V. H. d'Angelo[a.]

[a]*School of Chemical Engineering, University of Campinas, Rua Albert Einstein, 500 – Bloco A, Campinas (SP) – 13083-852, Brazil*

Abstract

Natural gas is widely use in many industries as fuel and also as raw material. Although gas pipelines present less transportation losses they become impracticable when distances are too long or when demands are highly variable. The liquefaction of natural gas is then necessary to allow its transportation in great volumes, with little loss of material. This also enables its storage in a more stable way. Natural gas consumption is continuously growing worldwide and consequently, the number of exporter terminals (liquefaction industries) and importer terminals (regasification plants) will increase. The natural gas liquefaction process is based on a sequence of refrigeration cycles, which need to work in an optimized way. The exergetic analysis is a very useful thermodynamic tool to evaluate the efficiency of these cycles. This work aims at an exergetic analysis of a multistage cascade refrigeration cycle applied to a natural gas liquefaction process. Firstly, the process was simulated using commercial software and the results obtained from the simulations were validated with literature data, showing a good agreement. After that, different operational conditions, according to a complete factorial design of experiments, were studied, in order to verify the influence of pressure in six specific points of the cycle. The response variable analyzed is the rate of total exergy destroyed in the cycle. The results showed a new set of operational condition to the refrigeration cycle in which the destroyed exergy rate was reduced by approximately 48% in comparison with literature data.

Keywords: natural gas, liquefaction, exergy, optimization, refrigeration.

1. Introduction

Natural gas consumption is growing worldwide mainly because of its good properties as a fuel. The transportation of natural gas from the producing site to the consumption site is usually done by pipelines, but when the distances are great or the sites are separated by an ocean, the transportation of natural gas in the liquid state is preferred.

Natural gas is in liquid state at temperatures around -150 ^{o}C or lower and pressures varying up to 500 kPa. In order to reach this low temperature refrigeration cycles are used. The most usual liquefaction processes are: multistage cascade liquefaction; mixed refrigerant and turbine-based. Finn *et al.* (1999) and Geist (1983) have presented in detail the advantages and disadvantages of each one of these cycles.

The classical cascade liquefaction cycle was the first one to be applied in natural gas plants. It is based on a three stage refrigeration cycles, each one operating with a different fluid: methane, ethane (or ethylene) and propane. The mixed refrigeration cycle utilizes only one refrigeration fluid using a mixture of refrigerants, which

composition is adjusted in order to have its evaporation temperature similar to the natural gas being liquefied, which can change depending on its origin.

Because of the high costs involved in construction and operation, the feasibility of an industrial site is strictly related to the efficiency of the process. One possible way of reducing thermodynamic losses of the process is to perform an exergetic analysis, to reduce exergy losses, leading to an optimal operation.

The objective of this work is to perform an exergetic analysis of a classical multistage cascade refrigeration cycle applied in the liquefaction of natural gas, in order to propose an optimal operational condition, contributing to reduce the exergy destroyed in the cycle. This analysis will consider the influence of six pressures in different points of the cycle: after the compressor and after the expansion valve of each subcycle.

2. Materials and Methods

2.1. Multistage Cascade Refrigeration Cycle

The multistage cascade refrigeration cycle presents lower energy consumption when compared to the other types, enables flexible operation, as each cycle can be independently operated, and requires smaller heat transfer area in the evaporators. This last characteristic implies in a lower thermodynamic efficiency of the process, which requires higher utilities demand. Another disadvantage is the high installation and maintenance costs, as each cycle has its own compressor and refrigeration fluid storage tank. Figure 1 shows the cascade cycle studied in this paper. For simplification of the figure, only one stage is shown per refrigeration fluid. In this cycle, natural gas is cooled and finally liquefied by a three stage process. In the real cycle, each refrigeration stage has multiple expansion and condensation steps, being each of them operated at three different evaporation temperatures. Details of this multicascade cycle can be found in Kanoglu (2002).

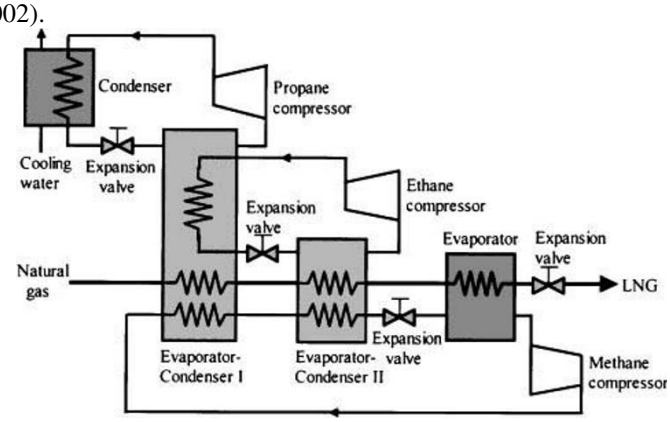

Figure 1-Multistage refrigeration cycle (Kanoglu, 2002).

2.2. Process Simulation

The multistage cascade refrigeration shown in Figure 1 was simulated using Hysys (Aspen Technology, version 3.2), based on the works of Kanoglu (2002) and Filstead (1965). The fluid package chosen to provide thermodynamic properties was the Peng-Robinson equation of state, which is adequate for the refrigerants used in the cycles. Steady state operation and adiabatic equipments were assumed in the simulations. Natural gas molar composition used in the simulation was taken from a Brazilian LNG

plant and is: 90.7% CH_4, 6.8% C_2H_6, 1.3% C_3H_8, 0.3% C_4H_{10}, 0.7% N_2 and 0.2% O_2. Refrigerants selected were: methane, ethane and propane (all 100% pure).

After validation of the simulation by comparison with literature data, obtaining a good agreement, different operational conditions were tested following a full factorial experimental planning. Finally, the results were analyzed by a statistical software, and an optimal operation condition for the process was proposed.

2.3. Exergetic Analysis

Details of how to perform an exergetic analysis may be found in Szargut (1980). The aim of this analysis is to locate and evaluate quantitatively the effect of irreversibilities which reduce thermodynamic efficiency of a process, proposing modifications in order to reduce these irreversibilities, by reducing destroyed exergy. In this work only the physical component of exergy for each process stream was analyzed using Equation (1):

$$ex = (h - h_o) - T_o(s - s_o) \quad (1)$$

where h is enthalpy and s is entropy at temperature and pressure of the process stream and the index "o" indicates the value of the variables at the reference state considered, which is T_o = 298.15 K and P_o = 101.3 kPa. The total destroyed exergy of the multistage cascade refrigeration cycle considered in this work is the sum of the destroyed exergy in each control volume of the cycle, which is obtained through an exergy balance.

2.4. Factorial Experiment Design

To evaluate the influence of pressures at six different process streams of the cycle (after the compressor and after the expansion valve of each refrigeration subcycle) over total destroyed exergy, a 2^6 factorial design was applied. Therefore, 6 factors were analyzed, being 2 levels for each one. Following the experimental design, a minimum number of simulations need to be performed for the minimization of the resulting variable, which is the total destroyed exergy of the system. The experimental design resulted in 64 simulations plus the base case, which is the one studied by Kanoglu (2002).

In the full factorial design, both the individual and the combined influence of the input factors (pressures) in the total destroyed exergy are analyzed. The basis selection for the different pressure levels for the streams was ±10% over the value of the base case. This choice is due to a limited operational range. Table 1 shows the superior and inferior levels for the tested factors. The results obtained from the full factorial experimental planning were evaluated by a statistical analysis with Minitab 15.

Table 1: Planning matrix for the tested factors (pressures, in kPa).

Stream	Description	Cycle	Base case	Inferior	Superior
7	after compressor	Methane	3337	3003	3671
10	after expansion valve	Methane	170	153	187
12	after compressor	Ethane	2069	1862	2276
14	after expansion valve	Ethane	110	99	121
16	after compressor	Propane	1344	1210	1478
18	after expansion valve	Propane	110	99	121

*streams numbers correspond to the ones used in the simulations.

3. Results and Discussion

After 65 simulations, some combinations of the variables have shown cross temperatures in some heat exchangers. In order to avoid this the pressures of the propane cycle were fixed at the base case value and a new full factorial design was constructed, being 4 factors at 2 levels (2^4), resulting in 16 experiments plus the base

case (run #17). Table 2 shows the results obtained for this new experimental design. Run #12 has presented the minimum value for the total destroyed exergy.

Table 2: Results of the full factorial design.

	Process Stream/ Pressure (kPa)				Total destroyed exergy (kJ/h)
Run	7	10	12	14	
1	3003	153	1862	99	132262
2	3671	153	1862	99	10750
3	3003	187	1862	99	250836
4	3671	187	1862	99	10290
5	3003	153	2276	99	134099
6	3671	153	2276	99	10916
7	3003	187	2276	99	254631
8	3671	187	2276	99	10461
9	3003	153	1862	121	130182
10	3671	153	1862	121	10563
11	3003	187	1862	121	246560
12	**3671**	**187**	**1862**	**121**	**10096**
13	3003	153	2276	121	131957
14	3671	153	2276	121	10723
15	3003	187	2276	121	250215
16	3671	187	2276	121	10262
17	3337	170	2069	110	19494

Figure 2 shows the main effects plot for the full factoril design 2^4. From Figure 2, one can see that the factors which individually influence the destroyed exergy are the pressures of streams 7 and 10. As the slope seen in the plot of stream 7 is higher than that of stream 10, it is possible to conclude that the influence of the pressure of stream 7 on the response variable is higher. The pressures of streams 12 and 14 are not statistically significant, when analyzed individually, as the plots of these streams show practically horizontal lines. Figure 3 is the Pareto diagram of the full factorial design and presents the influence of the factors, individually and combined, on the response variable. Figure 3 shows that the destroyed exergy was influenced by factors A, B and AB. That means that the pressures of streams 7, 10 and also the combined effect of these two pressures together influence the destroyed exergy of the cycle. The thin line at 0.05 represents the confidence interval (95%), which is the limit to the significance of the estimated effects.

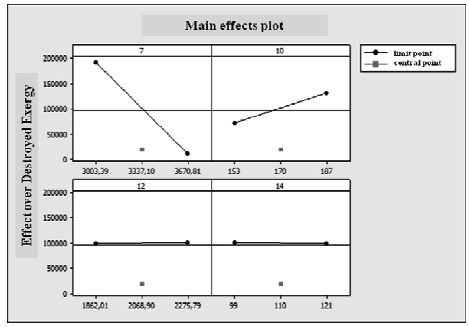

Figure 2: Main effects plot over the total destroyed exergy.

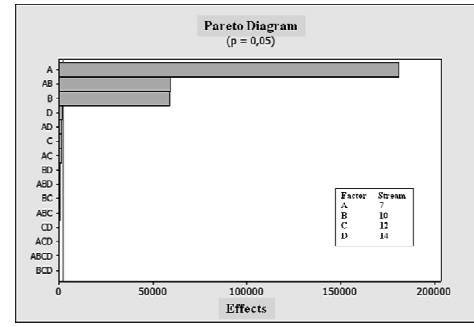

Figure 3: Pareto diagram for total destroyed exergy.

The independent variables and the interactions are statistically significant if the value of the effect is at right side of p = 0.05. Thus the significant effects are the pressures of streams 7, 10 and the combination of pressures 7 and 10.

Figure 4 shows the response surface for the relation between the total destroyed exergy and pressures of streams 7 and 10. Lower values for total destroyed exergy are achieved for high pressure values of streams 7 and 10. It is important to notice that when analyzing the independent influence of the factors on the response variable, Figure 2, one would suggest that the pressure of stream 10 should operate at its minimum value. Nevertheless, when the factors are analyzed together the combined influence of the pressures is higher than the influence of pressure of stream 10 alone, as shown in the Pareto diagram. Therefore, the influence of the pressure of stream 10 alone is disguised by the influence of combined pressures of streams 7 and 10 and as a result, the optimal operation point is at both higher points of streams 7 and 10. Using the optimization tool of Minitab 15, the optimal operation point was determined, which is the one shown in run #12 at Table 2.

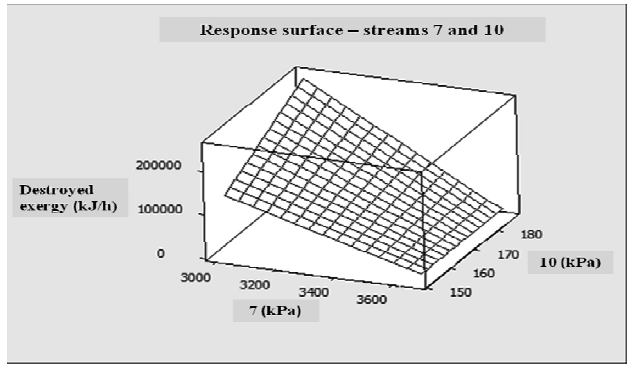

Figure 4: Response surface - relation between destroyed exergy and pressures at streams 7 and10.

4. Results and Discussion

The classical multistage cascade refrigeration cycle applied in the liquefaction of natural gas was studied using an exergetic analysis. The influence of six pressures at six different points of the cycle was evaluated: after the compressor and after the expansion valve of each refrigeration subcycle. The base case scenario has presented a rate of total destroyed exergy of 19494 kJ/h. Through a full factorial design and a statistical analysis a new set of operational conditions based on the analyzed factors resulted in a reduction of 48% of this rate, obtaining a new rate of total destroyed exergy of 10096 kJ/h. Using a thermoeconomic analysis it is possible to check the final benefit of this reduction in the total destroyed exergy. Technically, the modifications proposed are feasible.

References

C.G. Filstead, 1965, Camel LNG Plant: world`s largest, Hydrocarbon Processing, v. 44, n.7, 135-138 pp.

A.J. Finn, G.L. Johnson, T.R. Tomlinson, 1999, Gas processing developments: a special report – developments in natural gas liquefaction, Hydrocarbon Processing, v. 78, n. 4, 47-60 pp.

J.M. Geist, 1983, The role of LNG in energy supply, International Journal of Refrigeration, v. 6, n. 5, 283-297 pp.

M. Kanoglu, 2002, Exergy analysis of multistage cascade refrigeration cycle used for natural gas liquefaction, International Journal of Energy Research, v. 26, 763-774 pp.

J. Szargut, 1980, International progress in second law analysis, Energy, v. 5, 709-718 pp.

I.A. Karimi and Rajagopalan Srinivasan (Editors), Proceedings of the 11th International Symposium on Process Systems Engineering, 15-19 July 2012, Singapore.

Theoretical analysis of a multi-stage membrane reactor for oxidative coupling of methane

Sirikarn Tiraset,[a] Wisitsree Wiyaratn,[b] Suttichai Assabumrungrat,[a] Amornchai Arpornwichanop[a,*]

[a] *Computational Process Engineering, Department of Chemical Engineering, Faculty of Engineering, Chulalongkorn University, Bangkok 10330, Thailand*
[b] *Department of Production Technology Education, Faculty of Industrial Education and Technology, King Mongkut's University of Technology Thonburi 10140, Thailand*
[*] *e-mail: Amornchai.a@chula.ac.th*

Abstract

Oxidative coupling of methane (OCM) is a promising route for the production of ethylene by fully utilizing the abundance of methane feedstock. In this study, a multi-stage dense tubular membrane reactor is investigated to improve the performance of OCM. Mathematical model of the membrane reactor based on conservative equations and detailed OCM kinetic model is employed to analyze the effect of key operating parameters such as temperature and methane to oxygen feed ratio, on the efficiency of the OCM process in terms of CH_4 conversion, C_2H_4 selectivity and C_2H_4 yield. Adjustment of feed distributions at each membrane stage is also studied. The result shows that the multi-stage membrane reactor shows a better performance than the single-stage one. Moreover, a suitable feeding policy can improve the OCM performance.

Keywords: Oxidative coupling of methane, Membrane reactor, Multi-stage reactor, Feed distribution, Performance analysis

1. Introduction

An oxidative coupling of methane (OCM) to produce more valuable hydrocarbons, C_{2+} products, is an attractive technology for fully utilizing the abundance of methane feedstock. The major target product of OCM is ethylene, which is an important petrochemical feedstock. Extensive studies on OCM processes have been conducted and many different reactor concepts, therefore, have been proposed for this process. Due to its technological simplicity, a fixed-bed reactor (FBR) is widely implemented. The operation of this reactor is accidentally prone because of the large amount of heat released during the course of reaction. Furthermore, a poor heat removal from the highly exothermic reaction results in the occurrence of hot spots, affecting the reactor operation such as temperature runaway, catalyst deactivation, undesired side reactions and thermal decomposition of products. The use of a fluidized-bed reactor, which has high heat transfer capacity, shows better heat management and temperature control than a fixed bed reactor system. Talebizadeh et al. (2009) studied the OCM over $Mn/Na_2WO_4/SiO_2$ catalyst in a two-zone fluidized-bed reactor (TZFBR) and its performance was compared with a fluidized-bed reactor. Although the TZFBR gave the C_2 selectivity higher than the fluidized-bed reactor, the C_2 yield was still relatively low (< 20%).

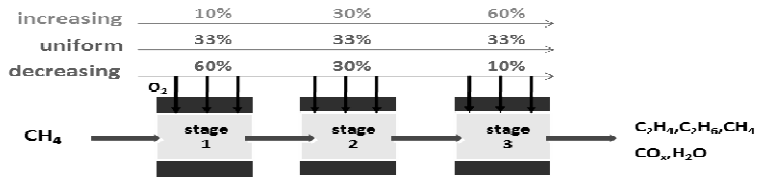

Fig. 1. Schematic diagram of a multi-stage membrane reactor.

The difficulty in the operation of OCM process lies in the fact that the intermediates and target products are higher reactive than the reactant and therefore are prone to deeply oxidize to CO_x. Thus, the oxidation of methane and C_{2+} products seems to be unavoidable when high oxygen content is present in the feed stream. The concept of using an oxygen distribution in a fixed-bed reactor was studied by Zarrinpashne et al. (2004) in order to improve the OCM performance. There are five oxygen feeding points along the reactor with precise control of oxygen flow rate at each point. However, the proposed reactor concept cannot achieve the high yield of ethylene due to the incomplete gas mixing at the oxygen feeding points. This causes high oxygen concentration zones at which the C_{2+} product is easily combusted and its selectivity falls significantly. Omata et al. (1989) initially applied a membrane reactor for the OCM process. The use of the membrane reactor to control oxygen concentration offers a possibility to achieve much higher C_2 hydrocarbons selectivity and yield. Mixed-conducting oxide membranes such as perovskite-type membranes, are well known for their abilities to separate oxygen from air. $Ba_{0.5}Sr_{0.5}Co_{0.8}Fe_{0.2}O_{3-\delta}$ (BSCFO), which was first reported by Shao et al. (2000), is a promising mixed conducting membrane with high oxygen permeability and has proven to be a good candidate for use as an oxygen distributor in the OCM reactor.

In this study, a BSCFO tubular membrane reactor is proposed to improve the performance of the oxidative coupling of methane. A multi-stage membrane reactor is considered and its performance with respect to key operating parameters such as temperature and methane-to-oxygen feed ratio is analyzed. Adjustment of feed distributions at each membrane stage is also studied. The result of applying a multi-stage membrane reactor is compared with a single-stage one.

2. Theory

2.1. Principle

The schematic diagram of a multi-stage membrane reactor is shown in Fig. 1. Three arrangements of oxygen feeding distribution are considered: (i) increased feed, (ii) uniform feed and (iii) decreased feed.

2.2. Reactor model

The mathematical model of a multi-stage membrane reactor is based on the following assumptions: (i) the reactor is under steady-state and isothermal operation, (ii) radial concentration distributions in tube and shell sides of the reactor are negligible and (iii) axial diffusion is neglected. The mass balance of component *i* can be written as:

Tube side (reaction side):

$$\frac{dN_i^t}{dz} = \frac{W}{V} A_{CS} \sum_{j=1}^{n} v_{i,j} r_j + \pi d_2 J_{O_2} \tag{1}$$

Shell side:

$$\frac{dN_{O_2}^s}{dz} = -\pi d_1 J_{O_2} \tag{2}$$

The oxygen flux (Eq. (3)), which was developed by Kim et al. (1998), is used to determine the oxygen permeation through a tubular BSCFO membrane where a bulk diffusion is the controlling step for oxygen permeation.

$$J_{O_2} = \frac{\pi L C_i D_a}{2S \ln(d_1/d_2)} \ln\left(\frac{P_1}{P_2}\right) \tag{3}$$

2.3. Kinetics of oxidative coupling of methane

A comprehensive kinetic model of OCM used in this study was developed by Stansch et al. (1997) for La_2O_3/CaO catalyst. The reaction scheme describing the network of primary reactions for the OCM involves all relevant chemical species as:

Step 1 : $CH_4 + 2O_2 \rightarrow CO_2 + 2H_2O$ (4)
Step 2 : $2CH_4 + 0.5O_2 \rightarrow C_2H_6 + H_2O$ (5)
Step 3 : $CH_4 + O_2 \rightarrow CO + H_2O + H_2$ (6)
Step 4 : $CO + 0.5O_2 \rightarrow CO_2$ (7)
Step 5 : $C_2H_6 + 0.5O_2 \rightarrow C_2H_4 + H_2O$ (8)
Step 6 : $C_2H_4 + 2O_2 \rightarrow 2CO + 2H_2O$ (9)
Step 7 : $C_2H_6 \rightarrow C_2H_4 + H_2$ (10)
Step 8 : $C_2H_4 + 2H_2O \rightarrow 2CO + 4H_2$ (11)
Step 9 : $CO + H_2O \rightarrow CO_2 + H_2$ (12)
Step 10 : $CO_2 + H_2 \rightarrow CO + H_2O$ (13)

The reaction rates for each step are given by Eqs. (14)-(19) and the kinetic parameters are listed in Tabel 1.

$$r_j = \frac{k_{0,j} e^{-E_{a,j}/RT} P_C^{m_j} P_{O_2}^{n_j}}{(1 + K_{j,CO_2} e^{-\Delta H_{ad,CO_2}/RT} P_{CO_2})^2} \qquad j = 1,3-6 \tag{14}$$

$$r_2 = \frac{k_{0,2} e^{-E_{a,2}/RT} (K_{0,O_2} e^{-\Delta H_{ad,O_2}/RT} P_{O_2})^{n_2} P_{CH_4}}{[1 + (K_{0,O_2} e^{-\Delta H_{ad,O_2}/RT} P_{O_2})^{n_2} + K_{j,CO_2} e^{-\Delta H_{ad,CO_2}/RT} P_{CO_2}]^2} \tag{15}$$

$$r_7 = k_{0,7} e^{-E_{a,7}/RT} P_{C_2H_6} \tag{16}$$

$$r_8 = k_{0,8} e^{-E_{a,8}/RT} P_{C_2H_4}^{m_8} P_{H_2O}^{n_8} \tag{17}$$

$$r_9 = k_{0,9} e^{-E_{a,9}/RT} P_{CO}^{m_9} P_{H_2O}^{n_9} \tag{18}$$

$$r_{10} = k_{0,10} e^{-E_{a,10}/RT} P_{CO_2}^{m_{10}} P_{H_2}^{n_{10}} \tag{19}$$

Table 1. Kinetic parameters of the OCM reactions

Step	$K_{0,j}$(mol $g^{-1}s^{-1}$ $Pa^{-(m+n)}$)	$E_{a,j}$ (kJ mol^{-1})	m_j	n_j	$K_{j,CO2}$ (Pa^{-1})	$\Delta H_{ad,CO2}$ (kJ mol^{-1})	$K_{j,O2}$ (Pa^{-1})	$\Delta H_{ad,O2}$ (kJ mol^{-1})
1	0.20×10^{-5}	48	0.24	0.76	0.25×10^{-12}	-175		
2	23.2	182	1.00	0.40	0.83×10^{-13}	-186	0.23×10^{-11}	-124
3	0.52×10^{-6}	68	0.57	0.85	0.36×10^{-13}	-187		
4	0.11×10^{-3}	104	1.00	0.55	0.40×10^{-12}	-168		
5	0.17	157	0.95	0.37	0.45×10^{-12}	-166		
6	0.06	166	1.00	0.96	0.16×10^{-12}	-211		
7	1.2×10^{7} [a]	226						
8	9.3×10^{3}	300	0.97	0				
9	0.19×10^{-3}	173	1.00	1.00				
10	0.26×10^{-1}	220	1.00	1.00				

[a]Units are mol $s^{-1}m^{-3}Pa^{-1}$.

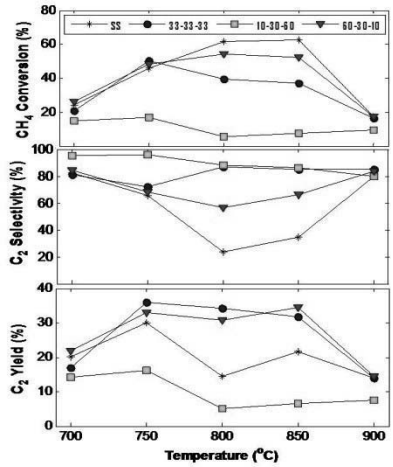

Fig. 2. Effect of operating temperatures on single- and multi-stage membrane reactors (CH_4/O_2 ratio = 1.5 and CH_4 feed flow rate = 1.6×10^{-3} mol/s).

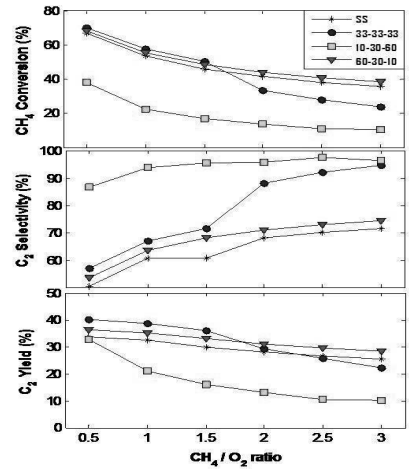

Fig. 3. Effect of CH_4/O_2 ratio on single- and multi-stage membrane reactors (T = 750 °C and CH_4 feed flow rate = 1.6×10^{-3} mol/s).

3. Results and Discussion

The effect of operating temperatures on the performance of single- and multi-stage membrane reactors for the OCM reaction is presented in Fig. 2. It is found that the multi-stage membrane reactor operated under the uniform and decreased feeding policy of oxygen shows higher selectivity and yield of C_2 than the single stage one. The conversion of methane in the single-stage membrane reactor is higher than that in the multi-stage reactor, especially at the temperature higher than 750 °C, because of a higher oxygen permeability. However, the C_2 selectivity of a single stage reactor is lower than a multi-stage reactor because a decrease in the methane partial pressure in the tube side leading to low methane and oxygen ratio (high oxygen content in the reaction side). In case of the multi-stage membrane reactor with increased feed of oxygen, due to the very low CH_4 conversion, the C_2 yield is therefore low even the highest C_2 selectivity is obtained.

Fig. 3 shows the effect of CH_4/O_2 ratio varying from 0.5 to 3 on the performance of the OCM membrane reactor. It can be seen that the performance of the single-stage membrane reactor is quite similar to the multi-stage membrane reactor with a decreased distribution of oxygen. The conversion of CH_4 and the yield of C_2 decrease with increasing the CH_4/O_2 ratio. The C_2 selectivity can be improved by using the multi-stage membrane reactor, especially at high CH_4/O_2 ratio.

Fig. 4a. shows the profiles of oxygen concentration at the tube side, which increases as more oxygen permeates from the shell side. Under the increased oxygen feeding policy, low oxygen content in the first stage of the multi-stage reactor causes relatively low CH_4 conversion and C_2 yield (Fig. 4b and Fig. 4d). The selectivity of C_2 at the outlet of each stage is given in Fig. 4c. The multi-stage membrane reactor with an increased distribution of oxygen shows higher C_2 selectivity than the others. An increase in the oxygen concentration, especially in the third stage, reduces the C_2 selectivity at the outlet due to undesired series reactions.

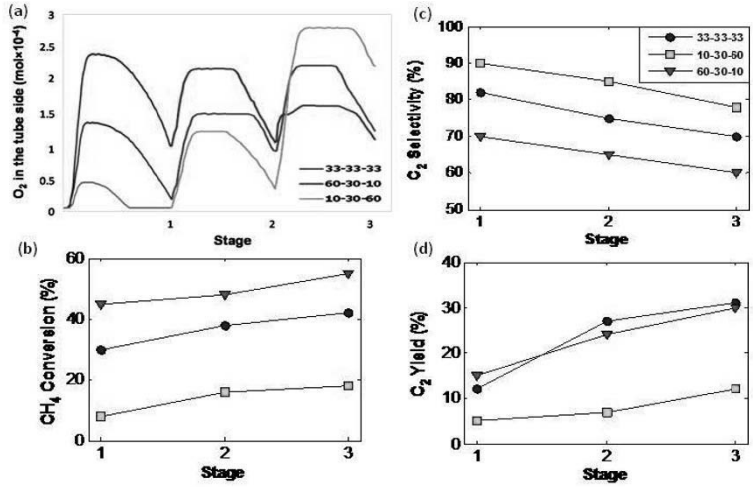

Fig. 4. (a) O_2 concentration profile at the tube side, (b) conversion of CH_4, (c) C_2 selectivity and (d) C_2 yield, at the outlet of each stage of the multi-stage membrane reactor, respectively (T = 800 °C and CH_4/O_2 ratio = 2 and CH_4 feed flow rate = 1.6×10^{-3} mol/s)

4. Conclusions

In this study, the performance of a multi-stage membrane reactor for OCM was investigated via simulation studies. The results have shown that the use of membrane as an oxygen distributor improves the OCM process. In addition, the multi-stage membrane reactor with a distributed feeding policy shows a better performance, in terms of C2 selectivity and yield, compared with a conventional single-stage membrane reactor. This is because the adjustment of oxygen feed distributions at each membrane stage avoid the formation of high oxygen concentration zones.

5. Acknowledgement

Support from the National Research Council of Thailand, the Thailand Research Fund and Commission of Higher Education is also gratefully acknowledged.

References

S. Kim, Y.L. Yang, A.J. Jacobson, B. Abeles, 1998, Diffusion and surface exchange coefficients in mixed ionic electronic conducting oxides from the pressure dependence of oxygen permeation, Solid State Ionics, 106, 189, 95.

K. Omata, S. Hashimoto, H. Tominaga, K. Fujimoto, 1989, Oxidative coupling of methane using a membrane reactor, Appl. Cat., 51, L1-L4.

Z. Shao, W. Yang, Y. Cong, H. Dong, J. Tong, G. Xiong, 2000, Investigation of the permeation behaviour and stability of a $Ba_{0.5}Sr_{0.5}Co_{0.8}Fe_{0.2}O_{3-\delta}$ oxygen membrane, J. Membr. Sci., 172, 177.

Z. Stansch, L. Mleczko, M. Baerns, 1997, Comprehensive kinetics of oxidative coupling of methane over the La_2O_3/CaO catalyst, Ind. Eng. Chem. Res., 36, 2568.

A. Talebizadeh, Y. Mortazavi, A.A. Khodadadi, 2009, Comparative study of the two-zone fluidized-bed reactor and the fluidized-bed reactor for oxidative coupling of methane over $Mn/Na_2WO_4/SiO_2$ catalyst, Fuel Proc. Tech., 90, 1319–1325.

S. Zarrinpashne, J.S. Ahari, R. Ahmadi, 2004, Development of a process for ethylene production from methane by OCM reactions and its commercialization challenges, Research Institute Of Petroleum.

I.A. Karimi and Rajagopalan Srinivasan (Editors), Proceedings of the 11th International Symposium on Process Systems Engineering, 15-19 July 2012, Singapore.

Optimal synthesis for the feed-water-heater network of a Pulverized Coal (PC) power to minimize water consumption

Juan M. Salazar, [a] Urmila M. Diwekar, [a]

[a]*Vishwamitra Research Institute: Center for Uncertain Systems, Tools for Optimization and Management, 368 56th Street, Clarendon Hills, Il 60514, USA*

Abstract

Coal-fired power plants contribute to almost 50% of the United States' total electric power production. At the same time, pulverized coal (PC) power plants are large water consumers to the point that construction and operability of PC power plants have started to be constrained by water availability in some regions of the country. Research efforts have been intensified to reduce the water usage and consumption which are closely related to the water losses associated to the cooling systems and gas purification operations. Two process systems engineering approaches have been studied to minimize the water consumption of power plants. First, a better optimization of nonlinear uncertain systems (BONUS) algorithm has provided solutions to the minimization of water consumption under uncertain atmospheric conditions. The calculated conditions for a 550 MW PC plant predicted reductions of 6.4%, 3.2%, 3.8% and 15.4% in the average water consumption for the four different seasons from fall to summer respectively. A second approach pursues the reduction of the residual heat in the steam cycle of the PC process by formulating an optimal design of the feed water heat exchange network (HEN). The proposed methodology uses Aspen Energy Analyzer (AEA) to determine the mass flowrates of the bleeding streams while generating alternative designs that can potentially reduce the water consumption by reducing the total cooling requirement. The optimization approach to process synthesis involves the selection of an optimal solution from the superstructure with a simulated annealing (SA) capability built in Aspen Plus. Results show at least a 5% reduction in water consumption for the PC power plant via this enhanced HEN synthesis technique
Keywords: Pulverized Coal power plants, water management, stochastic optimization HEN synthesis.

1. Introduction

Water consumption is one of the characteristics that need to be addressed when assessing the generation capabilities of a coal-fired power plant [1] . Makeups, blowdowns, process water and cooling water are responsible for consumption with the evaporative cooling system being the largest water consumer in power plants [2] . Comprehensive simulation models of pulverized coal (PC) power plants have been formulated in Aspen Plus to estimate the performance of the processes including its water consumption[1] . It has been reported that evaporative loses in the cooling tower are significant and they are affected by environmental conditions like air temperature and humidity and design conditions like process efficiency [2] . This implies that computational tools of process analysis should include approaches to account for the influence of uncertain parameters in the models and to improve efficiency of the process.

Stochastic modeling (process modeling under uncertainty), has been used for process analysis in power systems [3] . When including optimization techniques, the resulting non-linear stochastic programming (NLSP) can become highly computationally demanding [4] . These computational expenses have been drastically decreased with the better optimization of non-linear uncertain systems (BONUS) algorithm [4] . Heat exchange network (HEN) synthesis has been employed to improve the efficiency of power cycles [5] . Aspen Energy Analyzer (AEA) is a simulation and design tool that can be employed to generate alternative HENs with the purpose of improving the process performance [6] . In this work, BONUS algorithm has been integrated to Aspen Plus simulator via the advanced engineering co-simulator (APECS) and CAPE-OPEN interface. Also, a HEN synthesis problem is formulated by switching the roles of hot streams to hot utilities and modifying their costs to generate alternative designs with AEA. Finally, an integrated approach of process synthesis under uncertainty is proposed as an efficient alternative to minimize the water consumption of PC processes

2. Process Description

The PC power plant model studied in this paper is based on Case 11 referenced by the DOE/NETL's report on cost and performance of fossil energy plants [1] . This power plant is a re-heating cycle with feed-water heating. The process comprises a boiler section where coal is burned and the combustion heat is transferred to water generating steam, and a steam section where the high pressure steam is expanded through a train of high, intermediate and low pressure turbines. Steam is initially generated in the boiler and expanded in the high pressure (HP) turbine; then, it is re-heated at the boiler for later expansion at the intermediate (IP) and low pressure (LP) turbines. Then, exhausted steam is condensed with liquid water and returned to the boiler while heated with bleeding streams of steam from the turbines (feed-water heater). Cooling water is sent to the cooling tower where heat from the cycle is ultimately rejected to the environment by evaporative cooling.

3. Optimization under uncertainty

3.1. Stochastic Simulation

As it was previously said, water consumption is strongly affected by weather conditions like air temperature and humidity. Detailed information about air conditions for different locations within the US can be obtained from the website (http://www1.eere.energy.gov). Histograms of the frequency distributions were fitted to the appropriate probability density functions to represent the air conditions variability of an average U. S. Midwestern urban center during each of the four seasons [7] . Stochastic simulation is carried out by efficiently sampling these distributions to generate a set of scenarios under which the plant models are evaluated and a corresponding probability distribution of water consumption (output variable) is calculated.

3.2. Stochastic Optimization

Minimization of water consumption in power plants is a stochastic non-linear programming (SNLP) problem where one of the moments (expected value, standard deviation, etc.) of the water consumption's probability distribution is the objective function, the model is the set of constraints and model parameters are the decision variables. BONUS algorithm [4] is a "here and now" approach to solve this problem [8] determining the process conditions under which the expected value of the water

consumption can be reduced compared to the base case originally reported, as shown in Table 1[9] . It can be seen that the reduction on the consumption strongly depends on the season consumption during drastic weather conditions as summer can be reduced by changing some of the parameters of the process.

Table 1 Minimization of average water consumption under uncertain air conditions for a 550 MW PC power plant located at Midwestern US for four different seasons [9] .

Season	Optimal values of decision variables					Savings %
	Par 1 (%)	Par 2 ^{0}F	Par 3 Mass fraction	Par 4 pressure ratio	Par 5 pressure ratio	
Fall	38.9	1160.8	0.31	0.49	0.61	6.4
Summer	48.9	1174	0.42	0.49	0.66	15.4
Spring	35.5	1096.5	0.22	0.36	0.61	3.8
Winter	19.0	1141.9	0.30	0.49	0.79	3.2
	Base case values of decision variables					
All	20	1157	0.3	0.365	0.637	

4. Heat Exchange Network synthesis for water management

4.1. Modified HEN synthesis in AEA

Conventional methodology for the heat exchange network synthesis of the feed water heating system is based on equal enthalpy change on the liquid stream for each of the heaters. Mass flow rates of the bleeding streams are calculated based on such heat load distribution. AEA generates alternative designs with a mixed integer linear programming (MILP) algorithm. The solution of the MILP problem is based on the thermodynamic characteristics of the involved streams and on fixed mass flowrate of the bleeding streams. This approach was modified based on the early work by Linhoff [5] that proposes the employment of pinch technology to define mass flowrates from the bleeding streams for maximum heat recovery and improved cycle efficiency. This cycle efficiency is directly associated to the PC process water consumption through the amount of heat rejected by the cycle.

The main idea of this work is employing the AEA MILP algorithm to determine the mass flowrates of the bleeding streams while generating alternative designs that can potentially reduce the water consumption by reducing the total cooling requirement. For this purpose, the bleeding streams have been treated as utilities (instead of process streams) whose mass flowrates are determined by the calculated heat load assigned to them by the MILP algorithm.

4.2. Cost modification for alternative utility streams

Optimization algorithms based on process costs (as the one used by AEA) yield designs that employ mostly hot streams because they minimize heat transfer area leaving low temperature streams unused. To avoid this situation a cost penalty was assigned to bleeding (utility) streams. The approach assumes that feed water heating is expensive for the process when using high pressure steam and using low pressure steam is inexpensive to the point that some income can be generated. The main reason is that employing large amounts of high pressure steam may decrease the process productivity

and preheating the feed water with low pressure steam will increase the process efficiency. The utility costs were assigned as shown in Table 2(For the description and location within the process of bleeding streams the reader is referred to original work by Linhoff [5]). It can be seen that the highest costs (based on the cost of high pressure steam as utility) is assigned to the bleed stream "bleed 3" and the lowest value corresponds to the coldest bleed as the stream entering the last low-pressure turbine. The other values were assigned as equally spaced values yielding 4 positive values and 4 negative values.

Table 2 Assumed costs of bleeding streams as utilities for the heat integration of feed water heater network

Bleed stream	Temperature (F)	cost index/BTU
bleed 1	773	2.04E-06
bleed 2	660	4.08E-07
bleed 3	929	2.86E-06
deareator stream	720	1.22E-06
bleed 4	568	-4.09E-07
bleed 5	308	-1.23E-06
bleed 6	227	-2.04E-06
bleed 7	146	-2.86E-06
Cooling Water		4.49E-06

The drain streams are mixed and also are used to transfer sensible heat to the feed water. The costs assigned to these drains are naturally related to those shown in Table 2and reported in Table 3. It can be seen that the costs of "Drain1" and "Drain5" are equal to those of "bleed 1" and "bleed 5" respectively. The reason is that these drains are not mixed with any other so their employment as heat sources for the feed water preheating will be associated to that of the corresponding bleeds.

Table 3 Assumed costs of drain streams as utilities for the heat integration of feed water heater network

Drain stream	cost index/BTU	weights		
Drain 1	2.04E-06			
Drain 2	1.39E-06	bleed 1:0.6	bleed 2:0.4	
Drain 3	1.71E-06	bleed 3: 0.5	bleed 1: 0.3	bleed 2: 0.2
Drain 5	-4.09E-07			
Drain 6	-7.35E-07	bleed 4; 0.6	bleed5: 0.4	
Drain 7	-9.80E-07	bleed 4: 0.5	bleed 5: 0.3	bleed 6: 0.2

On the other hand the remaining drain streams are mixtures of two or three drains. Therefore their costs have been assumed to be a weighted average of their bleeding constituents having more weight the cost of the bleed that is more expensive. This formulation of the problem and its solution with AEA yielded interesting alternative designs whose cold utility consumption is lower than that of the base case as shown in Table 4 and it is expected that the water consumption will also be lower.

Table 4 Cooling requirements for designs that consider the bleed streams as utilities

Design	Cooling requirement X 10 7 BTU/h
base case	1.024
Design1	0.627
Design2	0.627
Design3	0.627

5. Conclusion

This paper presents a framework for integrated water management in power systems. It has been found that water consumption depends on the weather conditions and the uncertainties in weather affect the consumption considerably. We presented an optimization under uncertainty problem for savings water consumption. The second approach is heat integration. An algorithmic framework (Figure 1) based on simulated annealing (and OA/ER/AP MINLP) for discrete decisions, BONUS algorithm for the stochastic NLP, and Hammersley sequence sampling for the sampling saved 97% of computational time to solve this problem. Optimization under uncertainty allowed us to save up to 15% in the expected value of water consumption in a PC plant and a pinch technology approach to the heat exchange network synthesis allowed a 38% in cooling requirement which will be translated in water savings as well.

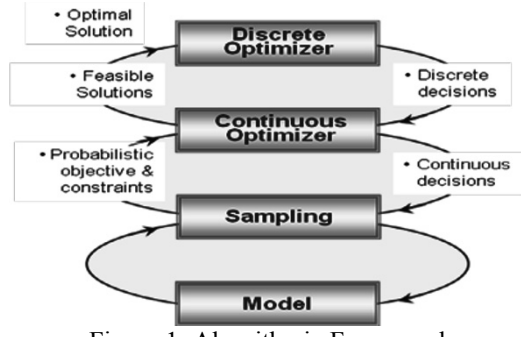

Figure 1: Algorithmic Framework

References

[1]DOE/NETL, Cost and performance baseline for fossil energy plants, (2007). DOE/NETL-2007/1281.
[2]DOE/NETL, Power plant water usage and loss study, (2007).
[3] U. Diwekar and E.S. Rubin, Comput. Chem. Eng. 15 (1991) 105-114.
[4] K. Sahin and U. Diwekar, Annals of Operations Research 132 (2004) 47-68.
[5] B. Linhoff and F.J. Alanis, ASME Advanced Energy Systems 85 (1989) 10-15.
[6] J.M. Salazar, U.M. Diwekar and S.E. Zitney, Comput. Chem. Eng. 35 (2011) 1863-1875.
[7] J.M. Salazar, U.M. Diwekar and S.E. Zitney, Energy Fuels 24 (2010) 4961-4970.
[8] U.M. Diwekar, Introduction to Applied Optimization, 2nd ed., SpringerLink, New York, 2008.
[9] J. Salazar and U. Diwekar. Energy Systems 2 (2011) 263-279.

I.A. Karimi and Rajagopalan Srinivasan (Editors), Proceedings of the 11th International Symposium on Process Systems Engineering, 15-19 July 2012, Singapore.

Techno-economic analysis of coal gasification based co-production systems

Siyu Yang, Hengchong Li, Yu Qian

School of Chemistry and Chemical Engineering, South China University of Technology, Guangzhou 510640, P.R. China

Abstract

Coal gasification based co-production systems are increasing popular in the world because they are assumed to be advantageous in energy efficiency and economic cost. However, there has been seldom researches on quantifying these advantages. In this paper, the co-prouction systems are analyzed from the technical and ecnomic point of views. During the study, the co-production system, of which the products are electricity and methanol, is modeled and simulated. For analysis, the energy analysis model and the economy analysis model are established. Results show that the co-production system has higher energy efficiency and less capital expenditure than tranditional single production systems.

Keywords: Co-production system; Techno-economic analysis; Coal gasification; Combined cycle.

1. Introduction

Coal has been broadly accepted as one of inportant alternatives of petroleum. NBS (NBS 2008) reported that coal provides 70.3% of energy in China. Similar to petroleum, the derivatives of coal include electricity, fuels, and chemicals. Traditional coal based techniques have low energy efficiency. For high energy and resource efficiency, the coal gasification based co-production systems are developed and increasing popular. However, the co-production systems are complex. Till now, there have been many researches on the systems (Yamashitaa & Barretob 2005, Rieger et al. 2008, Liu et al. 2010). However, most of them are limited on the technical analyses. The aim of this paper is to analyze the systems from technical and economic aspects.

2. Conceptual structure of the co-production system

Co-production systems are developed for high energy and resource efficiency. These systems have different configurations through selecting derivative products. The schematic of the co-production system used in this paper is shown in Figure 1.

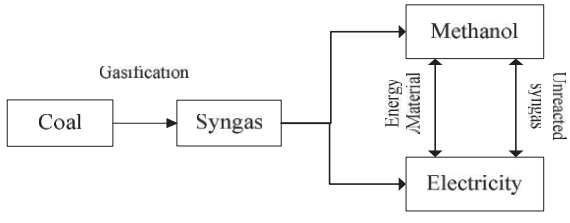

Figure 1 Structure of the co-production system

It can be seen that the co-production system consists of two parts: electricity generation and chemical production. For the former part, the combined cycle process is used due to

China's energy development tendency (i.e. clean energy). For the latter part, methanol is selected as the chemical product. The following sections brief the modeling and simulation of the co-production system.

3. Modeling and simulation of the co-production system

The co-production system (Figure 2) consists of a number of general process units: Air separation unit (ASU), Solid feed preparation and gasification (SPG), Acid gas removal (AGR), CLAUS sulfur recovery (CLAUS); Water gas shift (WGS), Heat recovery steam generation (HRSG), Combined cycle (CC), Methanol synthesis subsystem (MS).

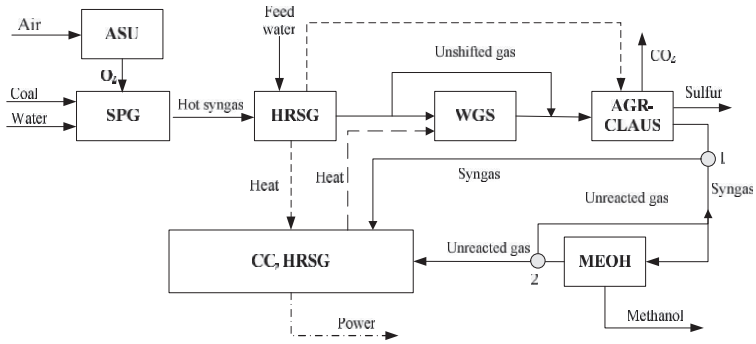

Figure 2 Schematic of the co-production system

As Figure 2 shown, coal slurry is combusted with O_2 in the gasifier to produce syngas. The syngas is cleaned in AGR-CLAUS to remove acid gas and recover elemental S. The H_2/CO ratio is adjusted in WGS by converting CO into H_2. MS is used to synthesize methanol. CC includes the gas turbine and the steam turbine to generate electricity. Heat of the gas is recovered in HRSG to generate steam. Aspen Plus software is used to model and simulate the co-production system. The operational parameters for the system are listed in Table 1.

Table 1. Reference operational parameters of the co-production system

Parameters	Value	Parameters	Value
O_2 supplied mole purity	95%	Gas turbine outlet temperature	1250K
O_2 supplied pressure	40atm	Gas turbine expansion ratio	16
Gasification pressure	42atm	High pressure	120atm
Gasification temperature	1645K	High temperature	838K
CO conversion ratio	47%	Intermediate pressure	40atm
H_2/CO ratio in syngas	0.6	Intermediate temperature	836K
Methanol synthesis temperature	545K	Low pressure	3atm
Methanol synthesis pressure	80atm	Low temperature	516K

4. Analyses of the co-production system

4.1. Energy analysis

Analysis model

In theory, exergy of a system reflects the maximum work that the system can do. Energy efficiency is calculated by using exergy theory as shown in Eq. 1.

$$\eta_{ex} = EX_{out} / EX_{in} \quad (1)$$

Where η_{ex} is the energy efficiency, EX_{out} is the output exergy of a process and EX_{in} is the input exergy of a process. In theory, exergy consists of physical exergy, chemical exergy and exergy change of mixing. Chemical exergy refers to the standard chemical exergy of chemical elements (Kameyama et al. 1982).The exergy of heat stream and work stream is calculated in Aspen Plus. The exergy loss of a process unit is the difference between the input exergy and the output exergy. Exergy loss ratio ξ for the process unit *j* is formulated as.

$$\xi_j = EX_{loss,j} / EX_{in} \quad (2)$$

The coal from Luzhou, China is used in this study. According to the work of Zhong (Zhong 1988), the exergy of raw coal is 27703.3kJ/kg.

Result and discussion

For energy analysis of the co-production system, it is compared with two single produciton sysetms (IGCC and methanol produciton system). For comparision, the co-production system is set to generate the same amount of electricity and methanol as those of the single systems. Through the comparison, the reduction of exergy loss are explored. The results are shown in Table 2.

Table 2. Energy performance of the co-production system and standalone systems

	IGCC		CMS		COME	
	kJ	Ratio (%)	kJ	Ratio (%)	kJ	Ratio (%)
Coal input	13145	100	14682	100	27703	100
Gasification	1840	14.0	1835	12.5	3851	13.9
CC	3154	25	1071	7.1	5153	18.6
WGS	-	-	88	0.6	150	0
MES	-	-	396	1.3	55	0.2
HRSG	1432	10.9	1791	12.2	2937	10.6
ASU	381	2.9	734	5.0	1039	3.75
Others	920	7	1174	8	1662	6
Sum	7729	59.7	7092	46.5	14696	53.05
Electricity	5416	41.3	-	-	5416	19.5
Methanol	-	-	7591	51.7	7591	27.5

The co-production system has the energy efficiency of 47.4% between those of IGCC (40.3%) and CMS (53.5%). Considering exergy loss of process units, it is found that SPG and CC are the main sources for exergy loss. In the gasifier, the exergy loss is caused by irreversibility in the heat transferring of exothermic reactions. In CC, the heat loss in the gas turbine and the steam turbine is the main source of exergy loss. By comparison, the co-production system needs for 27827Kj coal more than that of the single systems. The co-production system has better performance in energy utilization.

4.2. Economic analysis

The economy analysis for the co-production systems is as important as the energy analysis. Understanding their production process from economic viewpoint explores unnecessary expenditures. This paper builds an economic analysis model, in which the cost of the co-production process consists of the static investment and the operating cost.

The static investment of unit j is equal to domestic made factor γ multiplied by the sum of overnight cost $I_{OC,j}$ and the construction interest $I_{IC,j}$. I_{IC} is calculated by multiplying I_{OC} the construction period interest λ (set to 0.12). I_j^{OC} is formulated as:

$$I_{OC,\ j} = \theta I_j^{\ b}\left(S_j / S_j^{\ b}\right)^f \qquad (3)$$

where θ and f indicate the regional factor and the scaling factor, S_j and S_j^b are the practical scale and the reference scale of unit j, and I^b_j is the reference investment of unit j. Depending on the researches(Huang 2008a, Huang 2008b), the above parameters of process units are determined and shown in Table 3.

Table 3. Parameters for estimating static investment

	S^b_j	f	Θ	I^b_j (million \$)	γ
ASU	21.3kg/s (O_2)	0.5	0.5	45.7	0.5
Solid preparation	27.4kg/s (Coal)	0.67	0.65	29.1	0.65
Gasification	39.2kg/s (Coal)	0.67	0.8	78	0.8
WGS	716 MW (Heat)	0.67	0.65	28	0.65
AGR-CLAUS	29.3 mol/s (S)	0.67	0.65	67.34	0.65
Gas turbine[a]	276 MW (Electricity)	0.67	1	83	1
Steam turbine	59.2 MW (Electricity)	0.67	0.65	94.7	0.65
MES	10810mol/s (syngas)	0.67	0.65	20.4	0.65

Besides the static investment, the operating cost is an important indicator to evaluate the process. In this paper, the annual operating cost is the sum of the annual investment I_{CRF} , the material charge I_{MT}, and the matainence cost I_{MC}. According to Li et al (Li et al. 2007) the annual investment is equal to the static investment multiplying the capital recovery factor (CFR), which can be formulated as

$$CRF=i(1-(1+i)^{-n}) \qquad (4)$$

where n denotes the useful life and is set to 30, i means the discount rate and is set to 0.1 in this paper. The maintenance cost here is set to 4% of the overnight cost. The products of the co-production system are 263.3MW electricity and 312.9MW methanol. The annual operation time is set to 8000 hours. Prices of coal in this paper is 2 \$/GJ.

4.2.1. Result and discussion

Depending on the economic model, the investment of the co-production system for 30 years are calculated and shown in Table 4.

Table 4. Economic analysis of the co-production system (million \$)

	IGCC +CME	CFCP
I_{OC}	571	402
I_{CI}	70	49
I_{MT}	60.5	42.5
I_{MC}	84.1	74.2
I_{CRF}	22.8	16.1

As the results shown, the co-production system save 224.6 million \$ investment compared to the single systems. The save is broken down to the static investment 190 million \$ and the operating investment 34.6 million \$.

5. Conclusion

This paper analyzed the co-production systems from technical and economy aspects. The products of the system are electricity and methanol. In the technical analysis, exergy theory is used to calculate the energy efficiency. In the economic analysis, the total investment is estimated by summing the static investment and the operating cost. Comparison with single systems (IGCC and methanol production system) is used for analysis. Result shows that the co-production systems use less energy and spends less investment than single systems. China is now going through a rapid industrialization and economic growth. The demand for energy and capital is larger than ever before. The analysis in this paper is worthwhile to be expanded in other energy and chemical systems.

Acknowledgements

This work is supported by the China NSF key project (No. 21136003), National Basic Research Program (No. 2012CB720504) and Specialized Research Fund for the Doctoral Program of Higher Education (No. 20100172110016).

Reference

B. Lin, J. Liu, 2010, Estimating coal production peak and trends of coal imports in China, Energy Policy, 38 512–519.

C. Yongtaek, G. S. Harvey, 2003, Water gas shift reaction kinetics and reactor modeling for fuel cell grade hydrogen. Journal of Power Sources, 124, 432–439.

H. Huang, 2008, Economic estimation model of IGCC plant, Journal of power plant, 28(4): 633-637.

H. Huang, Estmination model of design, procurement and construction of IGCC plant, Journal of power plant, 28(3): 475-479, 2008.

H. Kameyama, K. Yoshida, S. Yamauchi, K. Fueki, 1982, Evaluation of reference exergies for the elements. Applied Energy, 11(1), 69-83.

M. Rieger, R. Pardemann, H. Rauchfuss, B. Meyer, 2009, Carbon capture and storage power plants; effects of ASU integration on IGCC performance and gas turbine operation. VGB Powertech 88 (3), 102 – 107.

National Bureau of Statistics of China (NBS), 2008 China Statistics Yearbook Beijing: China Statistic Press.

S.M. Zhong, 1989, Handbook of Water and Vapor Character Parameter with Exergy Character, Hydroelectricity Press, Beijing.

I.A. Karimi and Rajagopalan Srinivasan (Editors), Proceedings of the 11th International Symposium on Process Systems Engineering, 15-19 July 2012, Singapore.

A Process Integration Technique for Steam System Synthesis Involving Multiple Levels

[a]Sheldon G. Beangstrom, [a,b]Thokozani Majozi[*]

[a]*University of Pretoria, Lynnwood Rd, Pretoria, 0002, South Africa*
[b]*Modelling and Digital Science, CSIR, Meiring Naude Rd, Pretoria, 0002, South Africa*
[*]*corresponding author: thoko.majozi@up.ac.za*

Abstract

Recent work has shown that process integration techniques can be used to systematically reduce the flowrate of steam through a network. This is achieved by reusing hot condensate as an additional heating medium. This paper presents techniques for the application of process integration techniques to systems with multiple steam levels. The method is limited to a graphical technique as this allows the designer to interact with and guide the technique using one's knowledge of the system.

Application of these techniques to an illustrative example reduced the steam flowrate by 24% and reduced the cost of the steam network by 13%. This is advantageous in establishing new plants as well as debottlenecking old plants.

Keywords: heat exchanger network, synthesis, process integration, pinch analysis

1. Introduction

Given the steady increase in the cost of energy as well as the cost of process equipment, a great emphasis has been placed on finding techniques to reduce the capital and operating costs of a plant. Pinch analysis is well suited to help optimize processes in order to meet these demands.

Pinch analysis was first popularized by Linnhoff and Flower (1978) and Linnhoff and Hindmarsh (1983) in the form of process-process heat integration. In their method, heat is transferred from a hot process stream to a cold process stream, thereby reducing the duties of the external hot and cold utilities. The limit to the amount of energy that can be saved is seen when hot and cold composite curves are shifted together, until at some point the two curves are separated by a predetermined minimum temperature difference for heat exchange. This point is then referred to as the pinch point.

More recently, Kim and Smith (2001) have applied process integration to the optimisation of cooling water networks. Their work was inspired by evidence that the effectiveness of a cooling tower can be improved by reducing the flowrate of cooling water and increasing the return temperature of the water (Bernier, 1994). They developed a method using pinch analysis whereby cooling water is reused from one heat exchanger to another. By adding reuse streams to the Heat Exchanger Network (HEN), the flowrate of cooling water required is reduced. Since the cooling duty remains constant, the return temperature of water also increases. This in turn raises the effectiveness of the cooling tower.

Not much has been done on the topic of process integration as applied to the steam system network, particularly where the use of condensate is considered. Coetzee and Majozi (2008) proposed that the flowrate of steam can be minimised by using the sensible heat of the hot condensate to perform low temperature heating. They present the ground work for a graphical method of targeting the minimum steam flowrate, but

require a linear program to design the layout of the HEN and all the reuse streams. Their work was also limited to a single level of steam. This work was motivated by the fact that the purchase cost of boilers rise rapidly with increasing flowrate.

Price and Majozi (2010) developed a number of models that included the boiler efficiency. Their work aimed to minimise the flowrate of steam while maintaining the boiler efficiency and minimising pressure drop.

In this paper, we outline a graphical method for targeting the minimum steam flowrate and synthesizing the HEN in the presence of multiple steam levels. A method is given in which various composite curves are systematically shifted to target the minimum steam flowrate. Once the target has been determined, the HEN is synthesized using another graphical method.

2. Problem Statement

The problem which the design procedure addresses can be stated as follows.
Given:

1. a set of heat exchangers,
2. the fixed duties of the respective heat exchangers,
3. the limiting inlet and outlet temperatures of the hot utility passing through each heat exchanger,
4. the minimum global driving force ΔT_{min} for all the heat exchangers in the system,
5. the thermophysical properties of all the available steam levels from the boiler(s), and
6. the thermophysical properties and fixed flowrates of all present turbine exhaust streams.

Determine the minimum flowrate of steam required from each steam level and design the layout of the HEN that will achieve this target.

3. Flowrate Targeting

The first task to be completed is to target the minimum steam flowrate across the various steam levels. Once the desired flowrate has been targeted, the HEN can be synthesized to meet this target.

The method by which a single level of steam can be minimized is based on the work by Coetzee and Majozi (2008). First, one must determine the limiting utility profile for each process. In a counter-current heat exchanger, there exists a minimum temperature difference for heat exchange (ΔT_{min}). A hot utility that is ΔT_{min} above the process stream at all points in the heat exchanger represents a feasible lower limit on the utility. To extract this limiting data from the process data, ΔT_{min} must be added to the supply and target temperature of the cold process streams to give the minimum feasible target and supply temperatures of the hot utility respectively. This data is then used to create a limiting utility curve, similar to a composite curve but moving in the opposite direction. This curve represents a feasible boundary, as any utility line that crosses this boundary is in violation of the minimum driving force for heat transfer.

The utility line representing the steam and condensate is composed of two parts: a horizontal segment representing the latent heat, and a slanting segment representing the sensible heat. Fig.1 shows this shape.

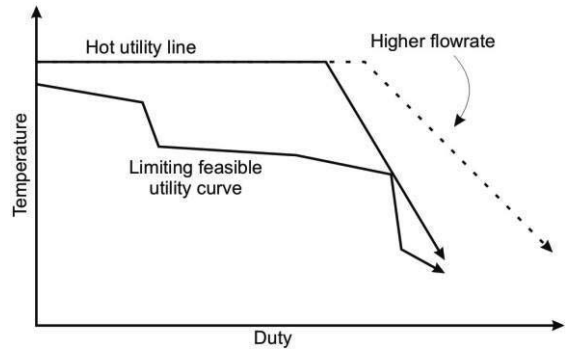

Figure 1: Limiting utility curve and a utility line representing one steam source

The hot utility line is constructed using the standard equations representing the latent and sensible heat of steam. As can be seen in Fig. 1, changing the flowrate not only makes the utility line longer or shorter, but also changes the slope of the sensible heat segment. This will cause a pinch to form at the minimum flowrate. Coetzee and Majozi (2008) show that this represents the minimum feasible steam flowrate that is capable of heating the system. Thus, to target the minimum possible steam flowrate, one needs only to reduce to flowrate until a pinch is observed between the two curves.

To extend this approach to multiple steam level systems, one needs to follow a two-step approach. In the first step, the original limiting utility curve is divided between the intervals created by the different steam level temperatures. The above technique is applied individually to each interval to initially minimize the flowrate of each individual steam level.

The second step involves identifying opportunities for further reductions. This begins in the highest temperature interval and moves downwards. Fig. 2(a) shows the utility lines of two steam levels that have been minimized inside their respective intervals. The highest steam level has been extended into the infeasible region. Where the line crosses the boundary, it is broken and shifted to the right to form a new pinch. The flowrate of the lower steam level can then be minimised further over the unheated region that remains, as shown in Fig 2(b).

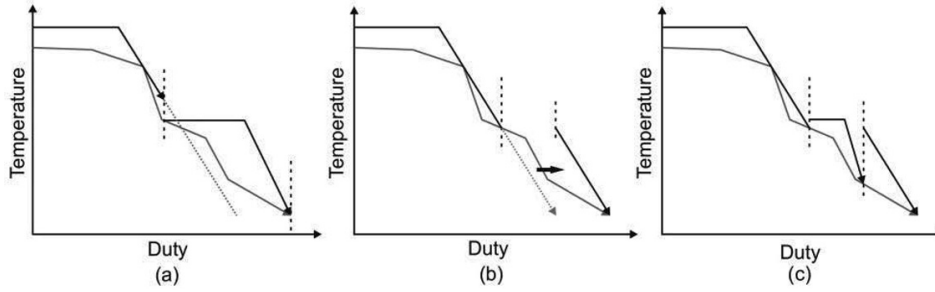

Figure 2: Producing further reductions in steam flowrate. (a) original curves, (b) shifting a segment of the higher steam level curve to form a new pinch, (c) minimising the lower steam level between the new boundaries.

By doing this, the flowrate of the lower level is reduced at no cost to the higher level. This procedure must be repeated over all the lower temperature intervals. Once this is

done, the designer can use these flowrates to specify the size of the boilers, or relax them as needed.

4. HEN Layout

Having targeted the various steam flowrates, the focus is turned to synthesizing the HEN that corresponds to these flowrates, with each steam level requiring its own network. Since both sensible and latent heat is being utilized, the networks will have two distinct regions, as seen in Fig. 3. The set of heat exchanges utilizing latent heat are arranged in parallel. After that, the condensate is passed to the heat exchangers utilizing sensible heat, where series and reuse connections may be required to maintain the flowrate whilst meeting the constraints.

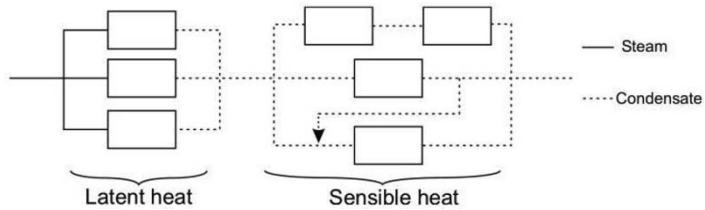

Figure 3: The two regions of a typical HEN for minimum flowrate.

Several mathematical modeling methods exist which can be used to design the layout of the sensible heat region. In this work, an adaptation of the "water mains" method developed by Kim and Smith (2001) is used.

5. Illustrative Example

An illustrative example is presented to demonstrate the targeting and synthesis procedure and to highlight its benefits. A grassroots design must be created for the hot utility system using multiple steam levels. Table 1 gives the limiting minimum supply and target temperatures of a hot utility, based on the supply and target temperatures of 11 cold process streams. A ΔT_{min} of 10 °C was applied to the data. A boiler produces superheated steam at 200 °C, part of which will be used to run a small turbine and the remainder throttled to saturation conditions to heat the process streams. A stream of saturated exhaust steam is produced at 130 °C with a flowrate of 42.2 tons per hour, which acts as a second steam level. Steam tables were used for the thermophysical properties of the water and steam.

The heating network was designed using the conventional design procedures and also using the technique outlined above. In the conventional design, 142.7 ton/h of steam was required. In the new design, only 108.4 ton/h of steam was required, and no cooling water. The minimum steam flowrate obtained using the new technique was confirmed to be the minimum by comparing it to the results obtained using the Mixed Integer Linear Program developed by Price and Majozi (2010). This represents a 24% reduction in steam flowrate. Furthermore cost estimates were used to compare the increase in cost due to additional heat exchangers versus the decrease due to a smaller boiler. The reduction in the steam flowrate resulted in a 57% increase in the heat exchanger costs and a 31% decrease in the boiler cost, giving a total cost reduction of 13%.

Table 1: Limiting hot utility temperatures and duties

Stream	1	2	3	4	5	6	7	8	9	10	11
Supply temp (°C)	106	174	164	142	102	76	106	154	78	194	142
Target temp (°C)	64	174	135	89	71	76	53	30	35	106	64
Duty (kW)	414	15610	5811	912	358	12923	4312	14239	941	13980	3585

6. Conclusion

A graphical method has been presented for targeting the steam flowrate and designing the HEN in the presence of multiple steam levels. Designing a HEN for minimum steam flowrate by reusing hot condensate has a number of advantages. In an existing plant, the technique can be used to debottleneck the boiler and avail steam for use in increased production rates. With a grassroots design, application of this new method can reduce the capital cost of the steam system and allow for a smaller and more efficient boiler to be purchased.

An example is presented to illustrate the use of the new synthesis method, as well as to demonstrate its advantages. A process with 11 cold streams that required heating is used. A boiler supplied steam for heating, as well as to a power generation turbine. By comparing the new design with the traditional design, it was shown that the flowrate of steam could be reduced by 24%, which reduced the capital cost of the network by 13%. The results of the graphical technique were compared with a mathematical programming technique in the open literature, and were found to be accurate. It is concluded that the new synthesis procedure has significant economic benefits.

References

MA Bernier, 1994, Cooling tower performance, *ASHRAE Trans:Reshearch*, 100, 114-121.

WAS Coetzee, T Majozi, 2008, Steam system network synthesis using process integration, *Industrial and Engineering Chemistry Research*, 46(13), 4405-4413.

JK Kim , R Smith, 2001 Cooling water system design, *Chemical Engineering Science*, 56(12), 3641-3658.

B Linnhoff, JR Flower, 1978, Synthesis of heat exchanger networks, *AIChE Journal*, 24(4), 633-654.

B Linnhoff, E Hindmarsh, 1983, The pinch design method for heat exchanger networks, *Chemical Engineering Science*, 38(5), 745-763.

T Majozi, T Price, 2010, On synthesis and Optimization of Steam system networks 1: Sustained boiler efficiency, *Industrial and Engineering Chemistry Research*, 49, 9143-9153.

T Price, T Majozi, 2010, On synthesis and Optimization of Steam system networks 2: Multiple steam levels, *Industrial and Engineering Chemistry Research*, 49, 9154-9164.

T Price, T Majozi, 2010, On synthesis and Optimization of Steam system networks 3: Pressure drop consideration, *Industrial and Engineering Chemistry Research*, 49, 9165-9174.

R Sinnott, G Towler, 2009, *Coulson & Richardson's Chemical Engineering Design,* UK, Butterworth-Heinemann.

I.A. Karimi and Rajagopalan Srinivasan (Editors), Proceedings of the 11th International Symposium on Process Systems Engineering, 15-19 July 2012, Singapore.

Modeling the dissolution of carbonate minerals utilized in Flue Gas Desulfurization scrubbers. A stepwise titration technique applied to low Grashof-Reynolds ratio.

Cataldo De Blasio[a], Claudio Carletti[b], Kurt Lundqvist[b], Loay Saeed[a], Tapio Westerlund[b], Carl-Johan Fogelholm[a].

[a]*Department of Energy Technology, Aalto University, P.O. Box 17800 FI-00076 Aalto, Finland.*
[b]*Department of Chemical Engineering, Åbo Akademi University, Biskopsgatan 8, 20500 Turku, Finland.*

Abstract

Every year a significant amount of Sulfur Dioxide (SO_2) is discarded in the atmosphere. SO_2 can cause indirect ozone depletion, it leads to the formation of acidic rains and a large number of diseases are provoked by contact with sulfur dioxide. Limestone ($CaCO_3$) is widely utilized in Flue Gas Desulfurization (FGD) processes because of its ability to capture the sulfur and precipitate as solid gypsum. The correct evaluation of limestone reactivity is a key aspect for FGD wet scrubbing process design and plant operation. In the present study results from tests to a particular group of samples classified as Sedimentary Limestone and Sedimentary Dolomite are reported.

Keywords: Gas Desulfurization, Limestone Reactivity, Mathematical Modeling, Transport Phenomena.

1. Objective

The sedimentary rocks in our possession are numerous and from different regions of the world, the project aims to classify and evaluate the reactivity of a large amount of samples with a great suitability for wet Flue Gas Desulfurization. A stepwise titration method and a mathematical model for non-steady state conditions allow the very accurate estimation of limestone's reaction rate constant and mass transfer coefficient. The dynamic conditions of an actual Holding Tank in a FGD wet scrubbing process were simulated by a Batch Stirred Tank Reactor (BSTR), in addition the fluid dynamic conditions for complete re-suspension of the solid particles were accurately evaluated.

2. Modeling

The sedimentary rocks were tested in diluted concentrations of hydrochloric acid in order to simulate the acidic conditions of the actual industrial process. The main reaction steps involved in a Limestone-HCl system are described in literature (S. Kiil *et al.,* 1998) where four stages have been considered with final formation of CO_2 and H_2O. The reaction rate for limestone has been reported as proportional to the H^+ ions activity to the first power for *pH* values less than four (Plummer *et al.,* 1978). The general mass balance (macro) for pseudo first order chemical reaction and related to the dissolving component is expressed in Eq.(1):

$$\frac{dC_a}{dt} = -k_r \cdot C_a + \frac{\langle k_c \rangle \cdot S}{V} \cdot \left(C_{ai} - C_a\right), \tag{1}$$

where C_a is the concentration of the carbonate ions (mol/dm^3), V is the reactor volume (dm^3), S represents the surface of reaction (dm^2), k_r and k_c are respectively the reaction rate constant (1/s) and the mass transfer coefficient (dm/s). Dividing the first and second term of Eq.(1) by the concentration value at saturation C_{ai}, it is possible to use a convenient non-dimensional form for the concentration, C_a^*. With the substitution $\tau = V/(\langle kc \rangle \cdot S)$ after integration over the time and C_a^*, the general solution becomes:

$$C_a^* = -\frac{\left(-1+e^{(-k_r - 1/\tau)\, t}\right)}{\tau\,(k_r + 1/\tau)}. \tag{2}$$

The first order chemical kinetic describes accurately the dissolution of limestone (Fig. 2) while dolomite dissolution is well modelled by a first order model only for the first period of the titration steps (Fig. 3, left). A second order model, where the term $(C_a^*)^2$ is used as the multiplier for k_r instead of C_a^* in Eq.(1), approximates the dissolution of dolomite for the entire duration of the titrations (Fig. 3, right). The analytical solution for the second order model is reported as follows:

$$C_a^* = \frac{-B+\sqrt{B}\sqrt{4k_r+B}\,Tanh\left[\frac{1}{2}\left(\sqrt{B}\sqrt{4k_r+B}\,t+2\,ArcTanh\left[\frac{\sqrt{B}}{\sqrt{4k_r+B}}\right]\right)\right]}{2k_r}, \tag{3}$$

where $B = 1/\tau$. In order to estimate the re-suspension of all solid particles belonging to a determinate Particle Size Distribution (PSD), a relation between non-dimensional numbers, Eq.5, is obtained by combining a balance of forces at incipient lift of the particles with the friction velocity as follows (O. Molerus, 1987):

$$\frac{\pi d_p^2}{4}\tau_w = (\rho_s - \rho_F)\frac{\pi d_p^3}{6} g \quad \longleftarrow \quad u_\tau = \sqrt{\frac{\tau_w}{\rho_F}}, \tag{4}$$

in the equations above, d_p is the mean particle's diameter, ρ_s and ρ_F the particle's and the fluid mass density (kg/m^3), g the gravity acceleration (m/s^2) and τ_w the wall shear stress (N m^{-2}). Eqs.4 lead to:

$$\mathrm{Re}_\tau^2 = \left(\frac{d_p u_\tau}{\nu}\right)^2 = \frac{2}{3}\frac{d_p^3 \cdot g}{\nu}\frac{\rho_s - \rho_F}{\rho_F} = \frac{2}{3} Ar, \tag{5}$$

where Re is the Reynolds number, Ar is the Archimedes number, ν is the kinematic viscosity (m^2/s) of the fluid and u_τ is the shear stress velocity (m/s) evaluated by:

$$u_\tau = 0.182\frac{\nu^{0.1} u_\infty^{0.9}}{D^{0.1}}; \tag{6}$$

D is the diameter of the vessel, and u_∞ is defined as the reference velocity evaluated at a distance "large enough" from the center of the vessel. The reference velocity is evaluated as $u_\infty = KD_s\omega$, where D_s is the stirrer diameter, ω is the angular velocity (s^{-1}) and K is a non-dimensional constant which is a function of the system's geometry. The method described above demonstrate that the particles in our experiments were completely immersed in the viscous sub-layer since Re_τ is between 0 and 5, for $0.117 < K < 1$; this is in accordance with O. Molerus in (O. Molerus,1987).

3. Materials and methods

3.1. Analyzed samples with compositions

The samples analyzed in the present study are a part of a series of 25 samples coming from different locations of the world. The samples were crushed and ground in three different size fractions (63-106 μm, 106-150 μm and 150-250 μm). Detailed images were obtained by using a Scanning Electron Microscope (SEM). Figure 1 gives a SEM image of one selected sample and the design of the experimental setup. Table 1 shows the description of four samples, their provenience and bulk composition measured with x-ray fluorescence (XRF).

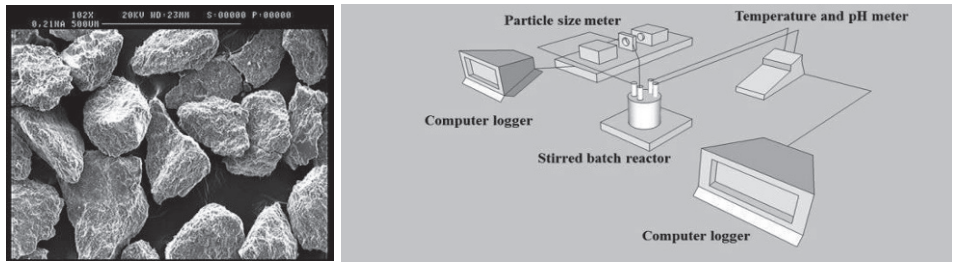

Figure 1. Left: SEM image of Limestone LJJ-27C for the size fraction 150-250 μm. Right: experimental setup.

Table 1. Sample description, provenience, XRF bulk composition for CaO, MgO and SiO_2 (wt%).

Sample	Description/Age	Provenience	CaO %	MgO%	SiO2%
LJJ-27C	Limestone, (416-360Ma)	Röngu, Estonia	53.0	0.52	2.6
LJJ-28C	Dolomite, (416-360 Ma)	Otepää, Estonia	30.8	19.9	1.3
LJJ-29C	Dolomite, (461-444 Ma)	Kore, Estonia	30.8	19.7	1.5
LJJ-30C	Limestone, (444-416 Ma)	Tallin-Tartu, Estonia	52.6	2.5	0.27

3.2. Experimental settings

The experimental set-up consists of a Batch Stirred Tank Reactor (BSTR), a laser diffractometer (Malvern 2600C), a fast electrode *pH* meter with temperature measurement for adjustment (EDT Micro 2) and two computer logger for data collection (Fig. 1, right). The procedure consisted in a step by step titration (J. Ahlbeck *et al.* 1993), a variable amount of particles between 1 – 2.8 g were added to the reactor creating a suspension suitable for particle size distribution measurements.

4. Results and discussion

Following the method described previously the mass transfer rate can be expressed by a parametric function of the constants *kr* and *kc*. The parametric evaluation has been performed for ten titration steps, for each experiment and for all the samples considered by using an implemented software procedure which handles thousands of *pH* values and more than fifty particle's size ranges. The Ca^{2+} concentration over time was evaluated by using *pH* data and the surface of reaction was evaluated considering spherical particles and taking into account the cumulative frequency function obtained from the PSD measurements; the titration stages were performed in sequence for each experiment.

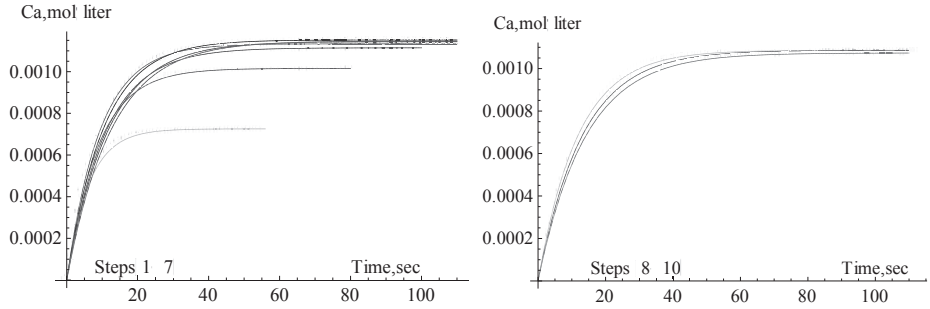

Figure 2. Eq.2 (line) and experimental data (dots) for limestone sample Ljj-27c, titration steps [1-7] (Left) and steps [8-10] (Right).

The following figure shows experimental results concerning the dolomite sample Ljj-28c.

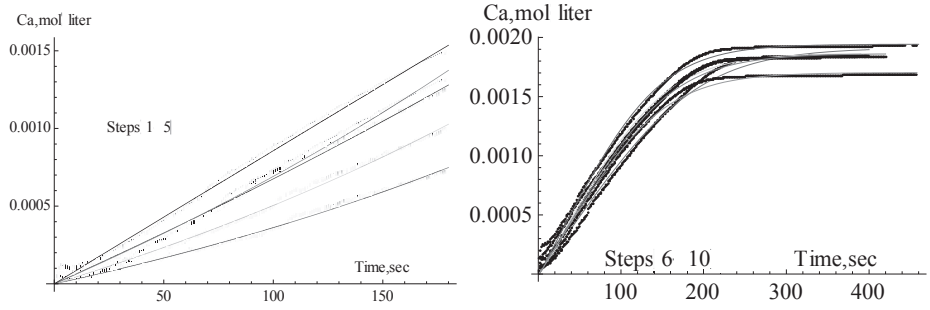

Figure 3. Left: Eq.2 (lines) and experimental data (dots) for dolomite, steps [1-5]. Right: Eq.3 (lines) and experimental data (dots) for dolomite, steps [6-10].

A stabilization of the values for *kr* and *kc* can be observed for both dolomite and limestone, this is in agreement with our expectations since a graining phenomenon can be experimentally observed for the first titration steps and for this reason the surface of reaction is altered, this phenomenon disappears when proceeding with the experiment giving more stable results. The mean reaction rate constant for the sedimentary rocks listed in Table 1 and the particle size distribution versus particle size (μm) for sample Ljj-27c and ten titration steps are reported in the following figure.

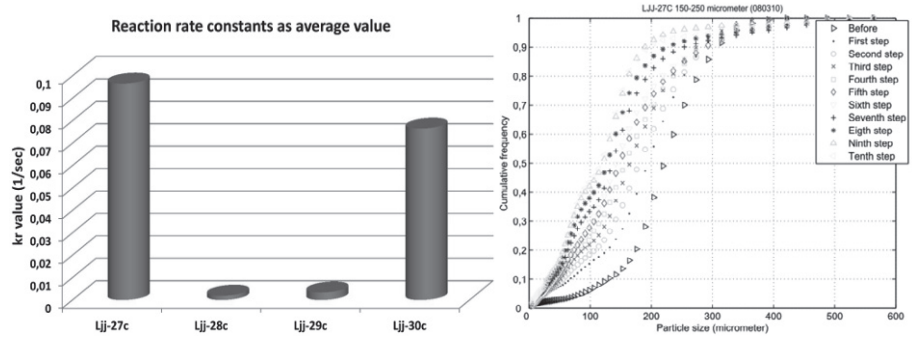

Figure 4. Left: overall reaction rate constants for limestone (Ljj-27,30c) and dolomite (Ljj-28-29c). Right: particle size distribution versus particle size (μm) for LJJ-27C-150-250 μm.

The mean values of the reaction rate constants are evaluated considering a period of three minutes from the titration's start, (Fig.4). In this time range both limestone and dolomite follow a first order model which allows for a suitable comparison of their reactivity. The experimental data related to the limestone samples were fitted by the model (Eq.2) in a really accurate manner (Fig.2). Great difference can be observed between the CaO and MgO content (Tab.1); dolomite is belonging to the Rhombohedral class with a different arrangement for Mg atoms compared to limestone belonging to the Hexagonal Scalenohedral class, hence the different dissolution behavior. The rate of reaction of limestone with hydrochloric acid was much greater than in the case of dolomites in accordance with previous studies (K. Lund *et al.,* 1973). As expected, the reactivity of the dolomite samples was much smaller. Values for the saturation concentration of carbonic ions where taken from literature (Manahan *et al.,* 2005).

5. Conclusions

Since more than one phase is present, the mass transport from phase to phase must be considered in the rate equation (O. Levenspiel, 1999). Thus the rate expression in general will incorporate mass transfer terms in addition to the usual chemical kinetics term, hence the meaning of k_r and k_c. The stepwise titration method allows for a more accurate determination of the above mentioned parameters since more sets of data are obtained for each experiment and for the same sample. The more pure limestone follows a first order model with respect to k_r, while dolomite dissolution is well approximated by a first order model only in the beginning of the titration steps (Fig. 4, left). A second order model, (Fig. 4, right), approximates in a better way the dissolution of dolomite for the entire duration of the titration steps, this is in accordance with previous studies (Chou *et al*., 1989) where is stated that the existence of successive reactions may lead in ideal cases to a reaction order with respect to H^+ of one or two, but not less than one. The obtained values for k_r and k_c for limestone are well in agreement with the case of semi-slow reaction regime (Sharma *et al.*,1984).

6. Acknowledgements

The authors sincerely acknowledge the Laboratory of Energy Engineering and Environmental Protection at Aalto University, the Process Design and Systems Engineering Laboratory and the Department of Geology at Åbo Akademi University in Finland. The CARETECH project under the Akademi of Finland's Sustainable Energy Program (SusEn). M.Sc. Lauri Järvinen is highly acknowledged for his collaboration.

References

S.Kiil, M.L. Michelsen and K. Dam-Johansen. 1998. Ind.Eng.Chem.Res.,37,2792-2806.

Plummer, L.N., Wigley, T.M.L., Parkhurst, D.L., 1978, American Journal of Science, Vol. 278, pp. 179-216.

O. Molerus, 1987, Chem. Eng. Sci. Vol.42, No.6, pp. 1423-1430.

Alhbeck, J., Engman, T., Fältén, S., Vihma, M., 1993, Chemical Engineering Science, Vol. 48, No 20, pp. 3479-3484.

K.Lund, H.S. Fogler, C.C. McCune., 1973. Chem. Eng. Sci, Vol. 28, pp.691-700.

S.E.Manahan, 2005, Environmental Chemistry,8th Edition, Sections 3.7-3.8, CRC Press.

O. Levenspel,1999,Chemical Reaction Engineering,3rd Edition, J.Wiley & Sons.

Chou L., Garrels R. M., and Wollast R., 1989. Comparative study of the kinetics and mechanisms of dissolution of carbonate minerals. Chemical Geology, vol. 78, pp. 269-282.

L. K. Doraiswamy, M.M. Sharma, 1984. Heterogeneous Reactions Analysis Examples and Reactor Design (vol2). United States : John Wiley & Sons. ISBN:0-471-05367-8.

I.A. Karimi and Rajagopalan Srinivasan (Editors), Proceedings of the 11th International Symposium on Process Systems Engineering, 15-19 July 2012, Singapore.

Optimal Multi-Objective Planning of Distributed Biorefinery Systems Involving Economic, Environmental and Social Aspects

José Ezequiel Santibañez-Aguilar,[a] J. Betzabe González-Campos,[a] José María Ponce-Ortega,*[a] Medardo Serna-González[a] and Mahmoud M. El-Halwagi[b,c]

[a]*Universidad Michoacana de San Nicolás de Hidalgo, Morelia 58060, México*
[b]*Texas A&M University, College Station 77843, USA*
[c] *Adjunt faculty at the King Abdulaziz University, Jeddah, Saudi Arabia*

Abstract

This work presents a multi-objective optimization model based on a mathematical programming formulation for the optimal planning of distributed biomass conversion systems. The model considers the optimal selection of feedstocks, processing technologies and products while considering a time horizon. The multi-objective optimization problem simultaneously considers the profit maximization, the environmental impact minimization, as well as the maximization of the social impact benefit through the generation of jobs in rural areas. The economic objective function takes into account the availability of bioresources, processing limits and demand of products, as well as the cost of feedstocks, products and processing routes. The environmental impact is measured through the eco-indicator-99 based on the life cycle analysis methodology. The social impact is measured through the number of jobs generated. This formulation considers the variation of parameters over time. For instance, time-based profiles for raw-material availability and product demand are considered. Although the economic and environmental objectives may contradict each other with an influence on the social impact, by means of the proposed methodology is possible to obtain a set of Pareto curves that identify the set of optimal solutions for each objective. Each Pareto curve shows the compromise between the objectives and enables a better decision about the processing of biomass. The proposed methodology is applied to a case study for planning the production of a biorefinery system in Mexico, where several scenarios that compensate the economic, social and environmental objectives are identified.

Keywords: Biorefineries, Biofuel Supply Chain, Biomass, Environmental Impact, Social Impact, Sustainable Process.

1. Introduction

Nowadays the increasing demand of energy around the world has incremented the demand of petroleum to be used as fuel, increasing its cost and, at the same time, decreasing the proved reserves; consequently, its currently use as fuel will not be feasible in the future. In addition, petroleum fuels have drastically deteriorated the global environment through the huge greenhouse gas emissions (GHGE).This has promoted the research for renewable energy sources to satisfy economically, environmentally and socially efficiently the energy demanded around the world. In this context, biomass as feedstock for energy production has gained great attention because

*jmponce@umich.mx

it has interesting characteristics including: 1) Renewable resource –to guarantee a sustainable production; 2) Significant reduction in the life cycle of GHGE –to guarantee the sustainability for the environment; 3) Competitive costs –to compete with the use of petroleum; 4) Huge abundance in the planet –to guarantee the generation of jobs in marginal areas; and 5) Flexibility to produce a lot of products. In addition, because the flexibility of the biomass to produce several products (biofuels, polymers, specialty chemicals, etc.), the biorefineries have gain a lot of attention. A biorefinery is an industrial facility similar to the petroleum-based refinery, but this uses biomass as feedstock instead of petroleum.

Recently, several papers have been reported for the optimization of supply chain for biofuels production (see, for examples, Aksoy et al., 2008; Sammons et al., 2007; Bowling et al., 2011; Santibañez-Aguilar et al., 2011). However, these methodologies include some drawbacks: a) they have not considered the variation of the availability of the feedstock year-round (a very important fact in countries where the weather drastically changes through the year); b) the interaction between the economic, environmental and social impacts have not been taken into account; and c) the simultaneous consideration for the economies of scales has not been properly considered. Therefore, to overcome these drawbacks, this paper proposes a new multi-objective optimization approach for the optimal planning of a biorefinery system considering the seasonality variation for the feedstock availabilities and product demands as well as the economic, environmental and social objectives. The economic objective considers the total net profit associated to the biorefinery based on a distributed system and considering the economies of scale, while the environmental impact includes the global impact measured through the eco-indicator99 based on the life cycle assessment, this methodology is damage oriented and considers the impacts to the human health, the ecosystem and the resources, and finally the social impact is measured through the jobs generated for the implementation of the biorefinery supply chain.

2. Problem Statement

Figure 1 shows schematically the problem addressed in this paper, which is described as follows. Given are: A set of available bioresources in specific places with given characteristics. It should be noted that the amount available for each bioresource depends on the season of the year and the location. Each bioresource has associated a unit cost, as well as unit environmental and social impacts. Also, there is a set of places where the bioresources can be stored. This work considers a set of processing plants to produce several products through different technologies from several bioresources, these technologies have given conversion factors and unit costs, as well as unit environmental and social impacts. Furthermore, there is a set of storages for products, a set of consumers located in different places with given demands through the year and a set of transportation methods. The objective is to determine the optimal configuration for the planning system that considers the seasonality and simultaneously compensates the economic, environmental and social objectives, identifying the used bioresources, location for production for each season of the year, the products produced as well as the consumers; and the transportation and storage requirements. To account for the economies of scale the formulation presented considers a distributed systems that includes central and hubs processing facilities.

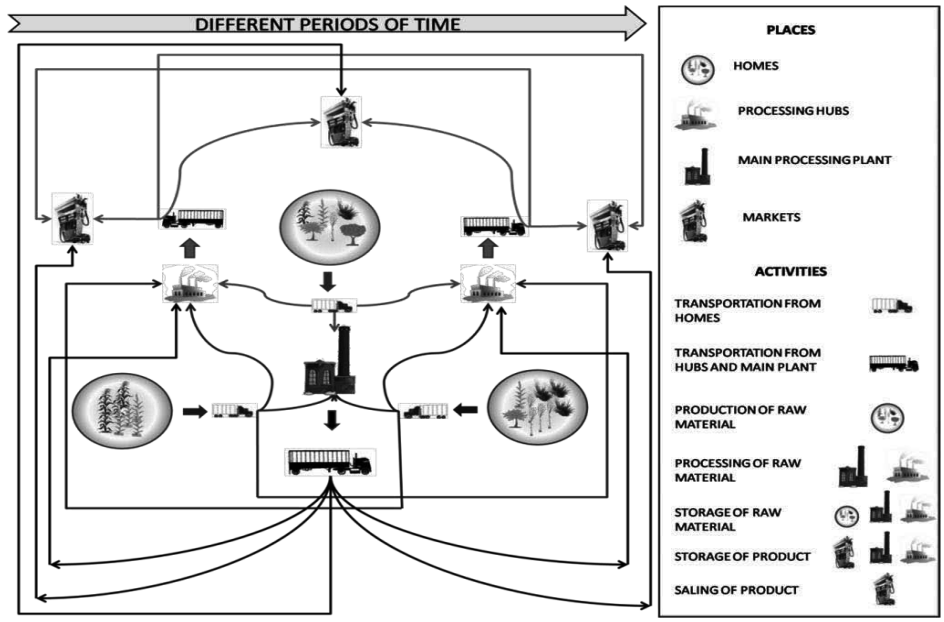

Figure 1. Representation of the addressed problem.

3. Model Formulation

The model is based on a state-task network representation for distributed systems, where the states are represented by the materials in the different places. In this approach, each state such as feedstock in home, feedstock in processing facilities, product in hubs and product in markets is different each other (i.e., each material depends on the location). On the other hand, the tasks are the different activities that consume a given time and divide the states (i.e., sugar cane after harvesting is transported to produce sugar cane in processing plant). Each activity has a binary variable associated because they are time depended; in addition, each activity has associated different economic, environmental and social impact. This way, the model considers mass balances in the homes for the feedstock, mass balances in the hubs, and in the main plants for the feedstock and products, mass balances in the storage, relationships for transportation and processing, and availability constraints. The economic objective function consists in the maximization of the net profit, taking into account the income for the sale of products minus the cost for the processing, transportation, storage and production of raw materials. This economic objective function is stated as follows:

Net Profit=Profit for Sales-Cost for [Processing Hubs+Processing Centralizers+Storage raw materials+Storage product-Transportation raw materials+Transportation product+Raw material production]

Also, there is an environmental objective function that incorporates the environmental impact through the eco-indicator99 considering the life cycle assessment. This function considers the eco-indicator99 for the raw material production, processing, transportation and use of products. This is stated as follows:

Environmental Impact =Eco-indicator for use of products+Eco-indicator for production of raw materials+Eco-indicator for processing in central and hub facilities+Eco-indicator for transportation

Furthermore, the model presented takes into account the social impact through the number of jobs generated for the raw material production, transportation and processing (notice that additional social impacts like the competitive use of bioresources can be included). This objective is difficult to consider because the jobs produced do not impact in the same form; for instance, the jobs generated in the field are different of the jobs for the transportation. However, this objective is very important because it gives a different vision for the biorefinery production. This social objective function is stated as follow:

Social Impact =Jobs production of raw materials+Jobs processing in central and hub facilities+Jobs transportation

To solve properly this problem and to generate a set of Pareto solutions that compensate these objectives, the e-constraint method is implemented. This way the problem is solved for the maximization the net profit for given constraints for the environmental impact and satisfying given requirements for the number of jobs generated.

4. Case Study

To test the proposed approach, a case study for the biofuels production in Mexico is presented. The data for this case were taken from the reports of the Mexican Agriculture Commission accounting for the seasonal variability and dividing the country in 6 regions. The example considers 9 bioresources available in Mexico, 2 products (bioethanol and biodiesel) and several technologies. The economic and environmental data were taken from Santibañez-Aguilar et al. (2011). This example was solved using different constraints for the objectives considered and the Pareto curves are shown in **Figure 2**. The curves represent the set of Pareto solutions for different cases, the upper is the curve without penalty and others have a penalty for the unsatisfied demand. Notice in this figure the interesting relationships between the profit and the environmental impact: for low environmental impact the associated profit is small, whereas for moderate environmental impact the associated profit is high. It is noteworthy that for high environmental impact the associated net profit does not increase significantly. In addition, for this case study, the higher the number of jobs, the higher the environmental impact; also, the number of jobs increases when the net profit increases. These interesting relationships between these contradict objectives allow the decision makers to choose the solution that shows the best compromise between them. It is noteworthy that each point of the Pareto curve represents different bioresources used and product produced in different places and considering the season of the year; for the case that maximizes the profit without considering the environmental and social impacts the main raw materials used are wood chips, african palm and jatropha; whereas for the case where the environmental impact become important the raw materials used are sorghum and sugar cane, with a little amount of wood chips, african palm and jatropha. Finally, the season of the year is very important in the example presented because the used raw materials change drastically through the year, for example the main raw material used in January is sorghum whereas in July it is sugar cane. Each point on the Pareto curves have different value of environmental and economic impacts as well as number of jobs, that is because the selection of different raw materials and places on the time horizon. For example, the number of jobs for point A is 2686, where

these jobs are mainly for the production of raw materials (sugar cane and sorghum), this point A also shows a moderate environmental impact with a huge annual profit.

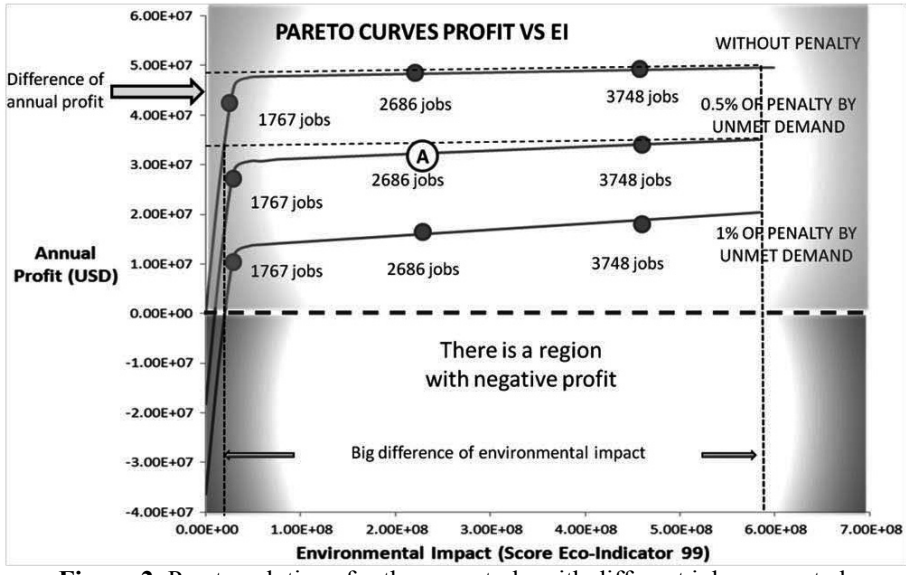

Figure 2. Pareto solutions for the case study with different jobs generated.

5. Conclusions

This paper proposes a new optimization model for the supply chain optimization of biorefinery systems. The proposed approach simultaneously considers the economic, environmental and social objectives; in addition, it allows to take into account the seasonal dependence for the feedstock as well as the economies of scale considering the installation of a distributed systems that includes preprocessing hubs and central facilities. The application of the proposed approach to a case study from Mexico, allows to identify the interaction between these contradict objectives, and gives the opportunity to the decision maker to choose the solution that best satisfy the specific requirements. Finally, the proposed approach is useful to identify the governmental incentives required to yield a given social benefit though the jobs generated in given marginal places.

References

B. Aksoy, H.T. Cullinan, Jr.N.E. Sammons, R.M. Eden, 2008. Identification of optimal poultry litter biorefinery location in Alabama through minimization of feedstock transportation cost. Environmental Progress, 27(4), 515-523.

I.M. Bowling, J.M. Ponce-Ortega, M.M. El-Halwagi, 2011. Facility location and supply chain optimization for a biorefinery. Industrial and Engineering Chemistry Research, 50(10), 6276-6286.

Jr.N. Sammons, R.M. Eden, W. Yuan, H. Cullinan, B. Aksoy. 2007. A flexible framework for optimal biorefinery product allocation. Environmental Progress, 26(4), 349-354.

J.E. Santibañez-Aguila, J.B. González-Campos, J.M. Ponce-Ortega, M. Serna-González, M.M. El-Halwagi, 2011. Industrial and Engineering Chemistry Research, 50 (14), 8558-8570.

F. You, L. Tao, D.J.Graziano, S. W. Snyder, 2011. Optimal design of sustainable cellulosic biofuel supply chains: Multiobjective optimization coupled with life cycle assessment and input–output analysis. AIChE Journal, In press, DOI: 10.1002/aic.12637.

I.A. Karimi and Rajagopalan Srinivasan (Editors), Proceedings of the 11th International Symposium on Process Systems Engineering, 15-19 July 2012, Singapore.

Bi-objective MINLP optimization of an industrial water network via benchmarking

Hella Tokos,[a] Zorka Novak Pintarič,[b] Yongrong Yang[a]

[a] *State Key Laboratory of Chemical Engineering, Department of Chemical and Biochemical Engineering, Zhejiang University, Hangzhou, 310027, P.R. China*
[b] *University of Maribor, Faculty of Chemistry and Chemical Engineering, Smetanova 17, SI–2000 Maribor, Slovenia*

Abstract

This paper presents an approach to water system retrofitting by estimating both the economic and environmental impacts of the water network design using bi-objective optimization. The environmental impact is evaluated via benchmarking. By using benchmarking, the decision maker could obtain insight not only into the environmental impact of a certain design belonging to the Pareto optimal solutions, but also into the competitiveness of the design within a particular production sector. The economic criterion used is the total cost of the water network and involves the freshwater cost, annual investment costs of the storage tank, piping and local treatment unit installation, and wastewater treatment cost. This approach uses a mixed-integer nonlinear programming (MINLP) model that enables water re-use and regeneration re-use in batch and semi-continuous processes. The Pareto front is generated using the Normal-Boundary Intersection (NBI) method. The proposed approach can be used for the separate integration of production sections, but also for joint integration of the sections via temporal decomposition. The proposed approach was applied to an industrial case study in a brewery.

Keywords: bi-objective; retrofit; economic criteria; environmental impact; MINLP.

1. Introduction

Due to increasing awareness about the effects of industrial activities on the environment, along with an ever more demanding legal enforcement, it has become necessary to take into consideration both, the economic and environmental impacts of production sites. Typically, traditional process design and optimization are based on economic objectives, such as capital investment, net present value (NPV), operating cost, and payback period. Water network synthesis is used to minimize the flow rate and cost of freshwater in the water supply systems of industrial plants, by maximizing water reuse and regeneration re-use. Two main approaches are generally used for addressing the issue of freshwater demand minimization within total water networks, i.e. the graphical approach (Liu et al., 2009; Ng and Foo, 2009), and the mathematically-based optimization approach (Li et al., 2010; Tan et al., 2008). The environmental aspect of water networks has recently become more important in water network synthesis, in order to enhance their environmental performances. Process flow diagram (PFD)-based life cycle assessment (LCA) (Lim and Park, 2007), and sustainable process index (Ku-Pineda and Tan, 2006) have been employed to evaluate the environmental impacts of water networks. Also, multi-objective optimization has been studied in order to minimize the total annualized cost and environmental impacts (Erol and Thöming, 2005). A streamlined mathematical

optimization model has been proposed for practically synthesizing an environmentally-friendly water network, by Lim and Park (2008).
In this paper, a bi-objective optimization method is presented that uses the environmental sustainability index to evaluate the environmental impacts of the obtained water networks, and the total annual water network cost as the economic criterion. The proposed approach is used for separate and joint integration of the production sections within a brewery via temporal decomposition.

2. Benchmarking in bi-objective optimization

A given set of indicators provides no information on a company's progress towards sustainable development in relation to other companies within the sector, unless a reference value, such as a benchmark is assigned to each indicator. According to this, the decision maker who uses benchmarking would gain insight, not only into the environmental impact of certain design from the set of Pareto optimal solutions but also into the competitiveness of the design compared to other companies within the production sector. In bi-objective optimization of a water network, the environmental sustainability index is used as the first objective function, with the total cost of the water network as the second objective function. The proposed environmental sustainability index is calculated over four steps:

1) Defining the indicators and benchmarks: The selection of a suitable set of indicators should always be performed in close cooperation with the industry, using for example Global Reporting Initiative (GRI) guidelines. The benchmark values of the selected indicators should be determined based on the values of the best available techniques (BAT), measurements and standards within the company, local legal regulations, GRI reports for specific production sectors, and other relevant documents.
2) Judging the importance of indicators and their normalization: Normalization is necessary for integrating the selected indicators into a composite index, as they are usually expressed in different units. Regarding their influence on the sustainable development, the indicators are divided before normalization into the group of indicators, the increasing values of which have a positive impact on sustainable development (I^+), e.g. water re-use, and those indicators the increasing values of which have negative impact (I^-), e.g. toxic releases into water. When applying distance to a reference method the normalized value is calculated as a ratio between the indicator and the benchmark:

$$I_{N_i}^{+} = \frac{I_i^{+}}{I_i^{Benchmark}} \qquad \forall i \in I \tag{1}$$

$$I_{N_i}^{-} = \frac{I_i^{Benchmark}}{I_i^{-}} \qquad \forall i \in I \tag{2}$$

3) Determination of the indicator weights: The budget allocation process was used to determine the indicator weights. This method calculates the indicator weights based on expert opinion. In order to establish a proper weighting system, it is essential to bring together experts representing a wide spectrum of knowledge and experience, e.g. experts from different production sectors and management within the company.
4) Aggregation of the indicators into the environmental sustainability index: The environmental sustainability index, I_{ES}, is determined by linear aggregation, which is based on summation of weighted and normalized individual indicators:

$$I_{ES} = \sum_i I_{N_i}^{+} \cdot w_i + \sum_i I_{N_i}^{-} \cdot w_i \qquad \sum_i w_i = 1,\ w_i \geq 0 \tag{3}$$

The applied mixed-integer nonlinear programming (MINLP) model is given in Tokos and Pintarič (2009) and enables water re-use and regeneration re-use in batch and semi-continuous processes for known and fixed operating schedules. The Pareto front is generated using the NBI method. This method solves a bi-objective optimization problem by constructing sub-problems with an aggregated objective function using the solution obtained in the previous sub-problem. The proposed approach can be used for the separate integration of water networks within each production section, and for joint integration of water networks within several sections via temporal decomposition. The joint integration is performed in two steps: firstly, both strategies perform simultaneous retrofit of the integrated water system for each working day by identifying the daily water re-use and regeneration re-use connections among water consumers within all sections. At the second step of the first strategy, the design of integrated water system is performed over the entire working week for each section by fixing the identified daily matches between sections. In the second strategy, the freshwater upper and wastewater lower bounds of the integrated processes are modified, and retrofit performed for each production section over the entire working week. More detail about the decomposition method can be found in Tokos et al. (2012).

3. Case study

The described bi-objective optimization strategy was applied to a brewery case study. The environmental sustainability index used as the environmental objective function consisted of five indicators: volume ratio of freshwater consumed to beer production, volume ratio of wastewater discharged from production to beer produced, indirect emission of CO_2 by electricity generation per volume of beer produced, indirect emission of CO by electricity generation per volume of beer produced, indirect emission of NO_x by electricity generation per volume of beer produced (the emissions were calculated based on the electricity needed for pumping water from the wells to/within the production site). The benchmarks for the selected indicators were 3.7 m^3/m^3, 2.89 m^3/m^3, 2.05 kg/m^3, 0.019 kg/m^3 and 0.0067 kg/m^3, respectively. The indicators' weights determined by the budget allocation method were 0.63 for freshwater consumption, 0.1 for wastewater discharge and 0.09 for greenhouse gas emissions. The economic criterion used was the total cost of the water network.

3.1. Separate integrations of the production and the packaging sections

The optimal water network for the weekly schedule in the packaging area at an increasing weight of the environmental criterion would include: wastewater re-use between the can rinser and the pasteurization process, water re-use between the rinser for non-returnable glass bottles and the washer for returnable glass bottles, wastewater re-use from the pasteurization process to the washer for returnable glass bottles, wastewater re-use from the washer for returnable bottles and the crate washer, and water re-use between the rinser for non-returnable glass bottles and the crate washer. Several water networks exist with the same sustainability index but different total costs because in the model formulation, the water consumptions of the operations can vary between the lower and upper bounds. The weekly freshwater consumption could be reduced from 2,233 t to 1,493 t. The environmental sustainability index improved from 0.911 to 0.952. The total annual network cost was between 223,162 €/a (at the environmental criterion weight of 0), and 514,833 €/a (at the environmental criterion weight of 1).

The optimal water network for the weekly schedule in the production area at an increasing weight of environmental criterion would include: re-use of wastewater from filtration as water for pouring the batch material in the cellar or in the brewhouse, regeneration re-use of wastewater from pouring operation in CIP systems. The wastewater purification is carried out by nanofiltration technology. The weekly freshwater consumption could be reduced from 2,592 t to 1,861 t. The environmental sustainability index improved from 0.829 to 0.928. The total annual network cost is between 334,804 €/a (at the environmental criterion weight of 0), and 1,072,521 €/a (at the environmental criterion weight of 1). In case of the highest total annual network cost both batch and semi-continuous local treatment units are included in the water network.
The environmental sustainability index of all networks in the packaging and production sections is lower than 1. This problem can be solved by investing in new technologies with lower freshwater consumption. For example, new washers for returnable glass bottles have lower freshwater consumption, and/or the tunnel pasteurizers could be replaced by flash pasteurizers. Another possibility is joint integration of the production and packaging sections.
The size of the MINLP model was approximately 6,600 constraints, 3,300 continuous variables, and 1,500 binary variables in the case of the packaging area, and approximately 21,500 constraints, 10,500 continuous variables, and 4,600 binary variables for the production area. The model was solved by the GAMS/DICOPT solver using 218 seconds of CPU time at the PC (P4, 2.6 GHz and 512 MB RAM) in the case of the packaging area, and 3,884 seconds in the case of the production area.

3.2. *Joint integration of production and packaging sections*

In the first step of joint integration, the water networks of the production and the packaging sections are simultaneously integrated for each working day by identifying the daily water re-use and regeneration re-use options. By changing the weight coefficient of the environmental criterion between 0.0 and 0.6, one connection is identifiable between the sections, i.e. wastewater from pasteurization in the packaging area is re-used as pouring water for batch material in the brewhouse. A storage tank would be needed for wastewater re-use between the sections. The capacity of the storage tank would be 105 t. Two connections between the sections can be found at higher weight coefficients (0.8 and 1.0): re-use of wastewater from pasteurization in the packaging area as pouring water for batch material in the brewhouse and the cellar. The required storage tank capacity is 210 t.
Two analyses are performed during the second step. A water re-use connection between pasteurization in the packaging area and batch material pouring in brewhouse is fixed in the first evaluation. The optimal water network in the production and the packaging areas contains water re-use and regeneration re-use options as in the case of separated integration. The weekly freshwater consumption could be reduced from 4,725 t to 2,882 t. The environmental sustainability index improved from 0.993 to 1.093. The total annual network cost is between 560,434 €/a (at the environmental criterion weight of 0), and 3,428,927 €/a (at the environmental criterion weight of 1).
Both of the identified connections are fixed in the second evaluation. The optimal water networks include the same connections as in case of separated integration of the production sections. The weekly freshwater consumption could be reduced from 4,725 t to 2,847 t. The environmental sustainability index increases from 1.013 to 1.106. The total annual network cost is between 739,887 €/a, and 4,911,839 €/a.
According to the results, the environmental sustainability index is slightly higher than 1, except in the optimal water network obtained by fixing only one connection at the

environmental criterion weight equal to 0. This means that the company can perform better than the assigned benchmarks by applying one of the obtained optimal water networks.

The size of the MINLP model was up to 16,900 constraints, 8,300 continuous variables and 3,800 binary variables in the case of the first step and the model was solved by the GAMS/DICOPT solver using up to 2,245 seconds of CPU time at the PC (P4, 2.6 GHz and 512 MB RAM). In the case of the second step the model had up to 39,000 constraints, 18,600 continuous variables, and 8,400 binary variables, which were solved using up to 10,907 seconds of CPU time.

4. Conclusion

This paper presented the bi-objective optimization method for retrofitting total water networks, which evaluates the economic and environmental impacts of a water network. The environmental impact is evaluated via benchmarking. The economic criterion used is the total cost of the water network. The approach uses a mixed-integer nonlinear programming (MINLP) model which enables water re-use and regeneration re-use in batch and semi-continuous processes. The Pareto front is generated using the NBI method. The proposed approach was applied to an industrial case study in a brewery. The results obtained show that the benchmark cannot be reached by the individual integrations of two sections, and investment in new technologies with lower freshwater consumption would be needed. The environmental sustainability index rose to slightly above 1 by integrating water networks of the production and the packaging sections, which means that the brewery can achieve better performance than its competitors by using the results of process integration.

References

P. Erol, J. Thöming, 2005, ECO-design of reuse and recycling networks by multi-objective optimization, Journal of Cleaner Production, 13, 15, 1492–1503.

GAMS Beta 22.4. The Solver Manuals. Washington: GAMS Development Corporation. 2007.

V. Ku-Pineda, R. R. Tan, 2006, Environmental performance optimization using process water integration and Sustainable Process Index, Journal of Cleaner Production, 14, 18, 1586–1592.

L-J. Li, R-J. Zhou, H-G. Dong, 2010, State-Time-Space Superstructure-Based MINLP Formulation for Batch Water-Allocation Network Design, Industrial & Engineering Chemistry Research, 49, 1, 236–251.

S-R. Lim, J. M. Park, 2007, Environmental and economic analysis of a water network system using LCA and LCC, AIChE Journal, 53, 12, 3253–3262.

S-R. Lim, J. M. Park, 2008, Synthesis of an environmentally friendly water network system, Industrial & Engineering Chemistry Research, 47, 6, 1988–1994.

Z-Y. Liu, Y-M. Li, Z-H. Liu, Y-J. Wang, 2009, A Simple Method for Design of Water-Using Networks with Multiple Contaminants Involving Regeneration Reuse, AIChE Jounal, 55, 6, 1628–1633.

D. K. S. Ng, D. C. Y. Foo, 2009, Automated Targeting Technique for Single-Impurity Resource Conservation Networks–Part 1 and 2, Industrial & Engineering Chemistry Research, 48, 16, 7637–7661.

R. R. Tan, K. J. Col-long, D. C. Y. Foo, S. Hul, D. K. S. Ng, 2008, A methodology for the design of efficient resource conservation networks using adaptive swarm intelligence, Journal of Cleaner Production, 16, 7, 822–832.

H. Tokos, Z. Novak Pintarič, 2009, Synthesis of batch water network for a brewery plant, Journal of Cleaner Production, 17, 16, 1465–1479.

H. Tokos, Z. Novak Pintarič, Y. Yang, Z. Kravanja, 2012, Multilevel strategies for the retrofit of large-scale industrial water system: a brewery case study, AIChE Journal, 58, 3, 884–898.

I.A. Karimi and Rajagopalan Srinivasan (Editors), Proceedings of the 11th International Symposium on Process Systems Engineering, 15-19 July 2012, Singapore.

A Graphical Approach to Optimal Source-Sink Matching in Carbon Capture and Storage Systems with Reservoir Capacity and Injection Rate Constraints

Raymond R. Tan[a], Raymond Ooi[b], Dominic C. Y. Foo[b], Denny K. S. Ng[b], Kathleen B. Aviso[a], Santanu Bandyopadhyay[c]

[a]*Chemical Engineering Department, De La Salle University, 2401 Taft Avenue, 1004 Manila, Philippines*
[b]*Department of Chemical & Environmental Engineering/Centre of Excellence for Green Technolgies, The University of Nottingham, University of Nottingham, Malaysia, Selangor 43500, Malaysia*
[c]*Department of Energy Science and Engineering, Indian Institute of Technology, Bombay, Powai, Mumbai 400076, India*

Abstract

Carbon capture and storage (CCS) is regarded as an important interim technology for the reduction of carbon dioxide (CO_2) emissions from large industrial facilities such as power plants and refineries. CCS involves capture of concentrated CO_2 streams from industrial flue gases, followed by subsequent secure storage in an appropriate natural reservoir. Such reservoirs include various geological formations such as depleted oil or gas wells, inaccessible coal seams and saline aquifers. In practice, such storage sites will have limitations on both CO_2 storage capacity and injection rate, subject to geological characteristics. In this work, a graphical methodology is proposed for optimally matching multiple CO_2 sources and storage sites or sinks within a predefined geographical region. The technique is developed based on analogies with existing graphical pinch analysis approaches for the synthesis of industrial resource conservation networks. A hypothetical case study is shown to illustrate the methodology. In addition, generalized principles for optimal CO_2 source-sink matching based on pinch analysis insights are discussed.

Keywords: Pinch analysis, carbon capture and storage, source-sink matching.

1. Introduction

In addition to strategies involving energy efficiency enhancement and increased use of low-carbon energy sources, CO_2 capture and storage (CCS) is widely considered as an essential technology for mitigating climate change by reducing industrial greenhouse gas emissions. CCS entails capturing relatively pure CO2 streams from point sources through techniques such as flue gas scrubbing, pre-combustion capture through gasification-based combined cycles and oxy-fuel combustion. The CO_2 may then be stored in various reservoirs such as depleted oil wells, inaccessible coal seams, saline aquifers and other geological structures (Davison et al., 2001). Various systems engineering techniques have been proposed for the planning of the deployment of CCS on a large scale, including insight-based analysis (Tan et al., 2009; Shenoy and Shenoy,

2012), rule-based algorithms (Kazmierczak et al., 2009) and mathematical programming models (Turk et al., 1987; Benson and Ogden, 2003; Middleton and Bielicki, 2009; Pekala et al., 2010; Tan et al., 2010; Fimbres Weihs et al., 2011; Tan et al., 2012a; b).

From a systems standpoint, one key problem in planning the deployment of CCS is matching CO_2 sources with the appropriate sinks. This problem is structurally analogous to the synthesis of resource conservation networks (RCNs). The specific graphical procedure used in this work is the material recovery pinch diagram (MRPD) which was developed independently by El-Halwagi et al. (2003) and Prakash and Shenoy (2005) for targeting of maximum material recovery. However, there are various pinch techniques are described in a recent review by Foo (2009) which are equivalent to MRPD, and may thus be used as alternative solution techniques. Such insight-based approaches have been shown to be an effective complement to mathematical programming based strategies, especially for decomposing difficult problems into computationally tractable subproblems. A formal problem statement is given, followed by a description of the methodology and an illustrative case study. Finally, conclusions and prospects for future work are given.

2. Problem Statement

The formal problem statement addressed in this work is as follows:

- The CCS system is assumed to be comprised of m CO_2 sources, n CO_2 sinks, all of which are available at the start of the planning horizon.
- Each CO_2 source i (i = 1, 2, …, m) is characterized by fixed captured CO_2 flowrate that corresponds to the maximum removal from the plant's flue gas. Furthermore, the operating life of each source i is also defined.
- Each CO_2 sink j (j = 1, 2, …, n) is characterized by an upper limit for CO_2 storage capacity; the maximum rate at which CO_2 may be injected into each sink is also given. Both of these characteristics are based on the geological characteristics of the storage site.
- The objective is to determine the minimum amount of unutilized CO_2 storage capacity by matching CO_2 sources and sinks, given these specified temporal and physical constraints.

3. Methodology

The targeting procedure used in this work is based on the MRPD approach (El-Halwagi et al., 2003; Prakash and Shenoy, 2005), and is hereby referred to as the CO_2 capture and storage pinch diagram (CCSPD). As with all pinch-based techniques, it requires that each source and sink be characterized in terms of "quantity" (amount of CO_2 associated with the source or sink, typically measured in megatons or Mt) and "quality" (the reciprocal of the lifespan of the source or sink, measured in 1/year or y^{-1}). The main steps are as follows:

- The sources are first ranked in order of ascending numerical value of their quality indices. Since the quality index is simply the inverse of duration, the CO_2 with the longest lifespan is ranked first, and the rest are listed based on progressively shorter operating lives.
- The "load" for each source is calculated by multiplying the "quantity" and "quality" index. Note that the resulting value is measured in Mt/y, and is thus actually the CO_2 flow rate of the source.

- The *source composite curve* is drawn using the cumulative "quantity" index as the horizontal axis and the "load" index as the vertical axis. Each segment of this composite curve corresponds to one source. The sources are plotted end to end, in the same manner as with graphical summation of vector quantities.
- These three steps are repeated for the sinks, to generate the *sink composite curve*.
- The relative positions of the two composite curves then provide the basis to determine the system target. The source composite curve must be below and to the right of the sink composite curve. If this geometric condition is not met, then the current solution is infeasible. The target may be determined by shifting the source composite curve horizontally to the right, until the condition is just met. As a result, the two composite curves will be tangent to each other at a pinch point (in some instances there may be multiple pinch points). The distance by which the source composite curve was shifted is the minimum unutilized CO_2 storage capacity in Mt.

The procedure is illustrated in the next section with a simple case study.

4. Case Study

In this example, there are four CO_2 sources and two CO_2 sinks with relevant data as shown in Table 1, respectively. Note that the sources generate a combined 800 Mt of CO_2 throughout the entire planning period, while the combined storage capacity of the sinks is 1,000 Mt. Thus, it may seem at first that it will be possible to capture and store all of the CO_2 in the system.

Table 1. Quantity, quality and load indices of CO_2 sinks and sources

Source	Amount of CO_2 (Mt)	1/Lifespan (y^{-1})	CO_2 Flowrate (Mt/y)
1	200	0.025	5
2	300	0.033	10
3	200	0.04	8
4	100	0.05	5
Total	800		
Sinks	Amount of CO_2 (Mt)	1/Lifespan (y^{-1})	CO_2 Flowrate Limit (Mt/y)
1	750	0.02	15
2	250	0.1	25
Total	1,000		

Following the first four steps described in the previous section results in the CCSPD shown in Figure 1. It can be seen that the relative positions of the composite curves indicate that this is an infeasible solution. An optimal solution may be found by shifting the source composite curve to the right to give a target of 250 Mt, which corresponds to the minimum unutilized storage capacity for the system (Figure 2). As the sinks have a combined 1,000 Mt of storage capacity, this solution implies that 750 Mt of CO_2 can be captured and stored. Note that this targeted amount of CO_2 is 93.75% of the 800 Mt of CO_2 from the sources. Thus, there is 50 Mt of CO_2 which may not be stored in these available sinks. It can be seen that Sources 1 and 2 are below and to the left of the pinch point, while Sources 3 and 4 are above and to its left. The source-sink matching can thus be solved by inspecting the above- and below-pinch regions separately, either by inspection or through the *nearest neighbor algorithm* (Prakash and Shenoy, 2005). The resulting optimal allocation for this system is given in Table 3. This result illustrates

that, below the pinch point, there is surplus storage capacity, and the main bottleneck for CCS is the injection rate limit into the sinks in this region. On the other hand, above the pinch point there is surplus injectivity and, in this case, insufficient storage capacity such that only half of the CO_2 from Source 4 can be stored. One possible interpretation is that Source 4 may be linked to Sink 2 during its first 10 years of operation while an alternative storage site is developed for the remaining 50 Mt to be stored in the final 10 years of the life of this plant.

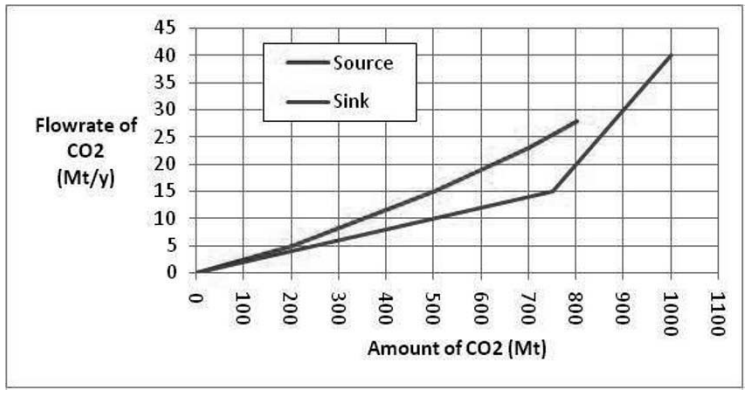

Figure 1. CCSPD showing infeasible initial solution

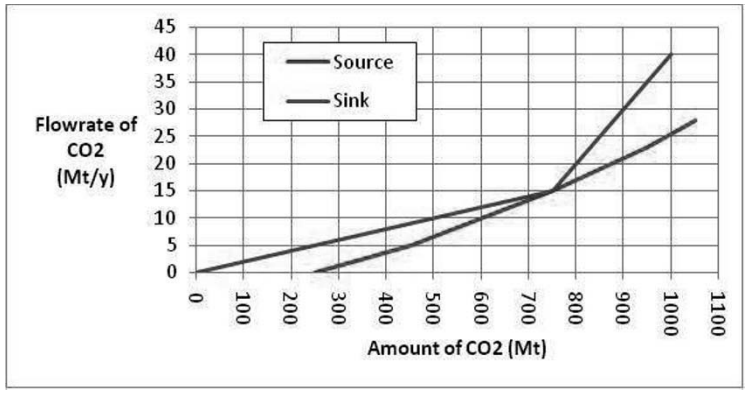

Figure 2. CCSPD showing optimal solution

Table 3. Optimal CO_2 allocation network

	Sink 1	Sink 2	Uncaptured CO_2
Source 1	200	0	0
Source 2	300	0	0
Source 3	0	200	0
Source 4	0	50	50

5. Conclusion

A graphical approach to optimal matching of CO_2 sources and sinks in CCS systems has been developed. This technique is based on pinch analysis methods developed for generic resource conservation networks, and as with such insight-based strategies, allows system targets to be determined based on the physical characteristics of the sources and the sinks. Furthermore, pinch-based insights can be used for problem decomposition to determine general guidelines for the synthesis of the CO_2 network. A simple case study has been used to demonstrate the methodology. In this paper, geographical distances, and hence pipeline costs, between various sources and sink are neglected. Future research works directed to address this issue. Extensions of the methodology developed here will also address uncertainties encountered in CCS planning, such as storage capacity of reservoirs and operating lives of sources and sinks.

References

Benson, H. Y. and Ogden, J. M. (2003). Mathematical programming techniques for designing minimum cost pipeline networks for CO_2 sequestration. Proceedings of the 6th International Conference on Greeenhouse Gas Control Technologies (October 1 – 4, 2002, Kyoto, Japan) p. 627 – 632.

Davison, J., Freund, P. and Smith, A. (2001). Putting carbon back into the ground. International Energy Agency Greenhouse Gas R&D Programme, Cheltenham.

El-Halwagi, M. M., Gabriel, F. and Harrel, D. (2003). Rigorous graphical targeting for resource conservation via material recycle/reuse networks. Industrial & Engineering Chemistry Research 42: 4319 – 4328.

Fimbres Weihs, G. A., Wiley, D. E. and Ho, M. (2011). Steady-state optimisation of CCS pipeline networks for cases with multiple emission sources and injection sites: south-east Queensland case study. Energy Procedia 4: 2748 – 2755.

Foo, D. C. Y. (2009). State-of-the-art review of pinch analysis techniques for water network synthesis. Industrial & Engineering Chemistry Research 48: 5125 – 5159.

Kazmierczak, T., Brandsma, R.,Neele, F. and Hendriks, C. (2009). Algorithm to create a CCS low-cost pipeline network. Energy Procedia 1: 1617 – 1623.

Middleton, R. S. and Bielicki, J. M. (2009). A scalable infrastructure model for carbon capture and storage: SimCCS. Energy Policy 37: 1052 – 1060.

Pekala, L. M., Tan, R. R., Foo, D. C. Y. and Jezowski, J. (2010) Optimal energy planning models with carbon footprint constraints. Applied Energy 87: 1903 – 1910.

Prakash, R. and Shenoy, U. V. (2005). Targeting and design of water networks for fixed flowrate and fixed contaminant load operations. Chemical Engineering Science 60: 255 – 268.

Tan, R. R., Ng, D. K. S. and Foo, D. C. Y. (2009). Pinch Analysis Approach to Carbon-Constrained Planning for Sustainable Power Generation. Journal of Cleaner Production 17: 940 – 944.

Shenoy, A. U. and Shenoy U. V. (2012). Targeting and design of energy allocation networks with carbon capture and storage. Chemical Engineering Science 68: 312 – 327.

Tan, R. R., Ng, D. K. S., Foo, D. C. Y. and Aviso, K. B. (2010). Crisp and fuzzy integer programming models for optimal carbon sequestration retrofit in the power sector. Chemical Engineering Research and Design 88: 1580 – 1588.

Tan, R. R., Aviso, K. B., Bandyopadhyay, S. and Ng, D. K. S. (2012a). Optimal Source-Sink Matching in Carbon Capture and Storage Systems with Time, Injection Rate and Capacity Constraints. Environmental Progress and Sustainable Energy, DOI: 10.1002/ep.11630.

Tan, R. R., Aviso, K. B., Bandyopadhyay, S. and Ng, D. K. S. (2012b). A Continuous-Time Optimization Model for Source-Sink Matching in Carbon Capture and Storage Systems. Industrial and Engineering Chemistry Research, DOI: 10.1021/ie202821r.

Turk, G. A., Cobb, T. B., Jankowski, D. J., Wolsky, A. M. and Sparrow, F. T. (1987). CO_2 transport: A new application of the assignment problem. Energy 12: 123 – 130.

I.A. Karimi and Rajagopalan Srinivasan (Editors), Proceedings of the 11th International Symposium on Process Systems Engineering, 15-19 July 2012, Singapore.

Fugitive Emission Reduction through Optimization

A-Jalil, S.[a*], Hashim, H.[a], Hassim, M. H.[a], Johari, A.
[a]*Process System Engineering Centre(PROSPECT), Faculty of Chemical Engineering, Universiti Teknologi Malaysia, 81310, UTM JB, Johor, Malaysia*

Abstract

Fugitive emissions (FE) nowadays become a great concern around the world due to their negative impacts on productivity, environment and health. This paper presents a mathematical model for reducing fugitive emissions from piping equipment. The problem is formulated as mixed integer linear programming and coded in General Algebra Modeling System (GAMS). The MILP model proposed in this work can be used to identify the most appropriate technologies for fugitive emissions reduction as well as maximize the profit. . Application of this model on the case yields a significant FE reduction up to 82.2 percent, illustrating the effectiveness of the technique.

Keywords: *fugitive emissions, mitigation, valve, GAMS, optimization*

1. Introduction

Fugitive emissions (FE) are spurious leak in an industrial site that comes from the equipment such as valve, pump, pipeline etc. (Lipton and Lynch, 1994). The emissions are not only an environmental and economy issue, but also a concern to health. Despite being very small and mostly invisible, FE are the main sources of the continuous background exposure to workers. It also leads to a substantial impact on global warming problem. Even though the impact on the daily life is a small, but it still can affect if the problem is not resolve from now. The study on the FE has been done widely especially in the United States and Europe country in term of the estimation or quantifying. The regulation regarding this matter had been implemented in both countries.(Kakaiya, S.,1999) However, for the research on the FE mitigation, the research is still few and not much done by the researchers nowadays.

It was found that valve contributed to the higher FE than the other piping equipment. Most of the study conducted by past researcher is related to strategies to overcome the leakage from the valve. They carried out a study on the properties of sealing material used for the valve and also the valve type and maintenance that may be the factor of the leakage (Kakaiya, 1999, Onat, 2008). According to the Cornelsen (2006), there are two problems from valve that causes the emissions which are from the body to bonnet joint which was readily solved and also from the valve stem packing. . It can be concluded that material technologies is the important element for solving the problem. Regardless the study on the sealing material and the successfulness of it to reduce the FE, due to the highly cost of maintenance and services to change the equipment, most of the industry do not see the important of it as the loss on cost is invisible and can be neglected (Szweda, 2000).

According to the report from Australian Government, Department of Climate Change and Energy Efficiency the amount of FE will rapidly growth from 2010 onwards where the projection showed 7 percent of FE is increasing each year. This amount can be reduced if the steps on the reduction are taken now for all the industry around the world.

2. Development of fugitive emissions mitigation model

There are certain technologies that had been developed by certain company in order to comply the regulation from the authorities (Cornelsen, 2006 and Vogel,. 2007) Even though the technologies are successes, due to the cost, most of the companies neglected it and make no change with the reduction of FE. Table 1 shows the relative life cycle cost for potential valve seal types compared with the impact on environment as total emission level (Ellis, 2004).

Table 1: Relative life-cycle cost for potential valve seal types compared with impact on the environment as total emissions level.

Packing types / Parameters	Standard packings	Die-formed packing rings sets	Fugitive emissions packing sets with/without spring loaded gland	Bellows seals with safety packing	Packing sets with lantern rings for leakage collection
Packing System cost	Low	Low to average	Average to high	High	High
Installation efforts/costs	Average	Low	Low to average	Average	High
Maintenance frequency/costs	Average	Average	Low to average	Low	High
Leakage performance	ISO 15848-1 Class B or C	ISO 15848-1 Class B or C	ISO 15848-1 Class A or B, TA-Luft	ISO 15848-1 Class A or TA-Luft	ISO 15848-1 Class A or TA-Luft
Life expectancy (service life)	Low to average	Average	Average to high	High	Average

From the table, it can be seen that the better leakage performance, the higher the cost of the systems. Therefore, in order to find the optimal solution that will satisfy the cost and also the environment regulations, a systematic technique for mitigate the FE which takes in to account cost as the main objective had been developed.

2.1. Superstructure Model and parameter data

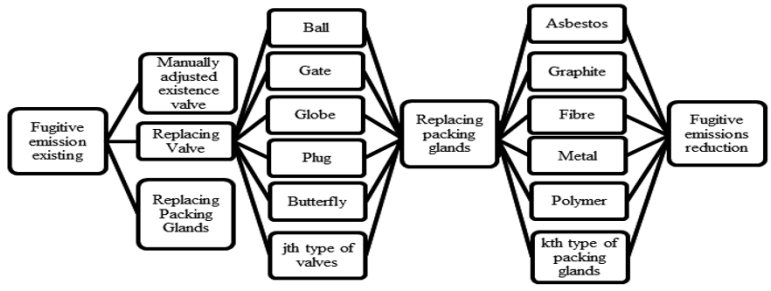

Figure1: The superstructure model describes the methods and the steps for the reductions of fugitive emissions.

There are three available mechanisms that can be implemented for FE reduction as illustrated in Figure 1. These include (i) manually adjusted valve, (ii) replacing valve and (iii) replacing packing glands. Manually adjusted valve is not preferable method as it needs a consistently monitoring on the valve. By replacing the valve and packing glands with the new technologies of valve and packing glands for the minimal emission leakage, it will reduce the emission in the industry. Table 2 shows the data of emission control, maximum operating condition and the cost for each type of valve and packing

glands which will be the constraints for the selection while Table 3 is the data input from the industries.

Table 2: Emission Control, Operating Condition and Cost of each type of valve and packing glands

Type of Valve(jth)	*Emission Control (ppm)*	*T Max (oC)*	*P Max (bar)*	*Cost (RM)*	*Type of Packing(kth)*	*Emission Control (ppm)*	*T Max (oC)*	*P Max (bar)*	*Cost (RM)*
Ball	70	190	20	100	Asbestos	150	200	25	250
Gate	200	200	25	400	Graphite	90	250	30	150
Globe	100	170	15	300	Polymer	100	180	12	300
Butterfly	150	300	20	200	Metal	400	300	20	200
Plug	250	250	30	500	Fibre	250	220	30	450

Table 3: Input data of the current fugitive emission, operating condition and budget provided for each stream from chemical plant.

	Stream 1	*Stream 2*	*Stream 3*	*Stream 4*	*Stream 5*	*Total*
Current FE (ppm)	600	900	1000	600	400	3500
Operational Temperatute, T(°C)	150	120	160	200	200	
Operational Pressure, P(bar)	12	15	25	18	10	
Budget, RM	500	800	900	700	1000	3900

Table 4: List of Variables

Variables	Description
C_{equip}	Cost due to the replacement of each equipment in pipeline
C_m	Cost due to the maintenance/services
C_b	Maximum Budget prepared for the replacement
FE_{ex}	Estimation of currents fugitive emissions in the plant
FE_{red}	Emission control by the equipment (jth, kth)
T^{max}	Maximum temperature of each equipment
p^{max}	Maximum pressure by each equipment(jth, kth)
T^{opt}	Operational temperature in the plant
p^{opt}	Operational pressure in the plant

2.2. Mathematical Modeling

There are 5 main steps involve obtaining the optimal solution for FE reductions where the variables described in table 4 above:

Step 1: Specify or Evaluate the Fugitive Emission Quantification

The fugitive emission (FE) quantification should be known. It can be measured /calculated from existing plant or at the design stage by using the tool of FE quantification. Summation of the fugitive emission from piping equipment i^{th} is the total of FE at the plant.

$$\sum_i FEex(i) = \text{Total FE at the plant} \quad (1)$$

Step 2: Specify Design Operational Condition Constraints

This constraint indicates that the replacement of new equipment such as valves and packing glands must satisfy the operational condition. Two operational conditions that need to be considered are the operational temperature and pressure.

$$T^{\max}(j,k) \geq T^{opt}(i) \quad (2) \qquad P^{\max}(j,k) \geq P^{opt}(i) \quad (3)$$

The above equations indicates that the maximum temperature and pressure of the new equipment $j^{th}$and k^{th} must be higher than the operational temperature and pressure at the piping line i^{th}. This constraint is important as to ensure the equipment will not be harmed if the operational temperature and pressure are higher that the allowable maximum temperature and pressure of the equipment.

Step 3: Specify the Limitation of the Budget for Installation New Equipment

The cost of replacement, maintenances and other services must be lower than the budget provided by the company.

$$\sum_i \sum_j \sum_k C_{equip} + C_m \leq C_b \quad (4)$$

Step 4: Calculate the Maximum Saving Cost After Installation

Equation (5) represents the objective function to maximizing the saving cost of the plant after the installation of the new equipment and also reducing the FE at the plant.

$$\max cost(RM) = \sum [(FEex(i) - FEred(j,k)) * P - (Cequip(j,k) + Cm)] * y(a) * x(b) \quad (5)$$

The choice of the equipment which is valve and packing glands are depends on the target and limitation. From above equation, i^{th} indicates the equipment at the pipe line which consist the FE while j^{th} and k^{th} indicates the new equipment of valve and packing glands which can reduce the existing FE at the plant. The FE which is measure in concentration or part per million(ppm) at the i^{th} can be reduce after installing the new valve and packing glands jth and kth and give a saving cost of emission reduction after multiply by the cost of chemical/substance produce by the plant, *P (RM/ppm)*. *FEred (ppm)* represent the quantity of FE after the installation of the new equipment.

Cost of the equipment chosen after meet the satisfied operational condition and budget limitation will affect the maximum cost. So, the maximum saving cost for this equation is based on the equipment chosen after satisfying the operational condition, budget limitation and will give the minimum cost of replacement/installation compare to other equipment listed.

Step 5: Calculate the Percentage of Emission Reduction

The percentage of emission reduction can be calculated as follows:

$$\%\text{emission reduction} = \frac{\text{Total Existing Emission - Total Emission after installation (ppm)}}{\text{Total Existing Emission (ppm)}} \quad (6)$$

where, total existing emission is the summation of emission at the piping equipment for the whole plant, $\sum FEex(i)$ and total emission after installation is the emission after replacing the chosen equipment at the piping equipment, $\sum FEred(j,k)$

3. Results and Discussions

Figure 2 represents the cost savings analysis and the percentage reduction of FE for each stream while table 4 shows type of valves and packing glands for stream 1. . It is observed that, by replacing t ball valve with graphite can leads to the cost savings up to RM 65750 with 73.3% emission reduction.

The valve and packing glands selected are varies depending on the operating condition for each stream. The results shows that, for the same type of valve and packing glands for stream 1 and 2 , provides about RM110750 profit and 82.2% reductions forFE. . For stream 4, butterfly valve with fibre packing is recommended for the replacement. This is due to the higher temperature of stream 4.

Table 5: Optimal Solution for Valve and Packing Glands for stream 1

	Type of Packing/ Type of Valve	*Asbestos*	*Graphite*	*Polymer*	*Fibre*	*Metal*
STREAM 1	Ball	0	1	0	0	0
	Gate	0	0	0	0	0
	Globe	0	0	0	0	0
	Butterfly	0	0	0	0	0
	Plug	0	0	0	0	0

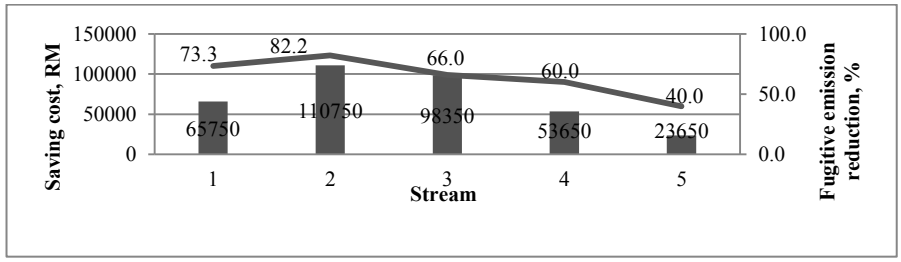

Figure 2: Graph on maximum saving cost (RM) and percentages of emission reduction for each stream in chemical process industry.

4. Conclusion

The systematic technique to determine the best technologies to reduce the FE as well as maximised profits to the industries is developed. This proposed technique is highly in need as it can be used to design the chemical process with more sustainable features through fugitive emissions reduction. It can be used by all the chemical process industry in order to comply the regulation from the authorities and at the same time give a significant cost savings to the process plant.

Acknowledgement

Special thanks to Universiti Teknologi Malaysia and Ministry of High Education for sponsoring my research under Research University Grant (vot: Q.J130000.7125.01H52)

References

Australia's emissions projection 2010. http://www.climatechange.gov.au/publications/projections/australias-emissions-projections/emissions-projection-2010.aspx

Cornelsen, D., (2006). The development of effective fugitive emissions control fro valves. Valve World, February 2006, pages 49-53

Ellis, B. (2004). Developments in EU environmental legislation and the ESA guidance note. Sealing Technologies, Volime 2004, Issues 10, Octover 10, pages 6-8

Kakaiya, S. (1999). Valve fugitive emissions: the challenge ahead. Sealing Technologies, Volume 1999, Number 71, November 1999, Pages 7-9.

Lipton, s. And Lynch, J.(1994). Hnadbook of Health Hazard citrol in Chemical Process Industry. John Wiley and Sons, New York.

Onat, A. (2008). The effects of sealing materials on elimination of fugitive emissions. Material and Design (2008), pages 533-538.

Szweda, R. (2000). Fugitive emissions: The matter of imperfect seals. Sealing Technologies, Volume 2000, Number 83, November 2000, pages 9-11.

Vogel, R., Danner, S., Smith, B. (2007). Fugitive emissions: Guidelines for successful valve upgrades. Valve World, June 2007, pages 80-85

I.A. Karimi and Rajagopalan Srinivasan (Editors), Proceedings of the 11th International Symposium on Process Systems Engineering, 15-19 July 2012, Singapore.

Process modeling and economic analysis of microalgal systems for CO_2 capture and production of chemicals

Rui Vogt Alves da Cruz, Claudio Augusto Oller do Nascimento
Chemical Engineering Department - Escola Politécnica da Universidade de São Paulo, Av. Prof. Luciano Gualberto, trav. 3, n. 380, CEP 05508-900 São Paulo, Brazil

Abstract

The use of microalgae and cyanobacteria for the production of biofuels and other substances of commercial interest has been widely advertised as an extremely promising sustainable technology, due to the high areal productivity, potential for fixation of CO_2, possibility of using non-arable land and alternative sources of nutrients such as brackish water and agricultural and industrial effluents. The commercial production of cyanobacteria in open raceway ponds was studied through the combination of a mathematical model for the algal growth with technical, economical and sustainability evaluations. A macromodel was developed to simulate the ponds, and it was used to assess the impact of environmental variables, such as light and temperature, and to optimize the process conditions for operation and harvesting. A detailed economic analysis demonstrated the impact of capital, operation costs and energy consumption, also highlighting the importance of revenue from high value products to process viability, considering the current technology. The sensitivity analysis and evaluation of both technology improvements and alternative business models enabled the prioritization of future research areas, based on economic and environmental impact.

Keywords: Algae. Economic Analysis. Process Modeling.

1. Introduction

The use of microalgae and cyanobacteria for the production of biofuels and renewable feedstocks has been regarded as an extremely promising sustainable technology [1]. Some of the key advantages are the high areal productivity and lipid content [2], the potential for CO_2 fixation (ca. 1.8 kg CO_2 per kg of biomass produced) [3], the possibility of using non-arable land and the number of high value substances that can also be extracted.

However, there are still challenges for the large scale implementation of this technology, such as, high capital, operation costs and energy consumption, seasonal variations in productivity and contamination risks when using open ponds. The harvesting and extraction steps represent one of the main areas for improvement, accounting for up to 30% of the capital costs [3] and 90% of the total energy demand. A number of studies have described the economic analysis for open and closed systems, describing the current challenges related to economic viability and the dependence on the revenue for high value added products [4].

The mathematical modeling of growth in photobioreactors and open ponds is another challenging task which is extremely important for designing the system, predicting process efficiency and optimizing and controlling operation conditions. Several authors have developed mechanistic and hybrid models for growth of microalgae and cyanobacteria in photobioreactors, or using neural networks or response surface models. However, the development of macromodels for prediction and control of algal growth in open ponds has been much less frequently studied [5-7]. Guterman, Vonshak and Ben-Yaakov [5] developed a model for growth of *Spirulina platensis* in open raceway ponds, capable of simulating the biomass productivity, pH, and growth rate as function of light intensity, temperature, nutrients and other parameters.

2. Model Development and Analytical Methodology

The production system used for the development of the model and subsequent analysis is based in a farm of open raceway ponds, with concrete walls and compacted earth bottoms. The reference system was a total area of 500 ha, split in 80,000 m^2 ponds, 0.4 m deep. The suspension is harvested periodically to an intermediate tank, being afterwards transferred to a cluster of continuous centrifuges and concentrated to 22% solids. The culture medium is recycled to a buffer tank, where nutrients and additional water are made up. The resulting sludge is then dried in belt dries, followed by solvent extraction with n-hexane, extracting the algal oils. The solvent is recycled and the remaining solid biomass goes through a finishing step to remove the residual solvent.

The algal growth model used to simulate the open ponds is based on the equations developed by Guterman, Vonshak and Ben-Yaakov [5] for *Spirulina platensis*, growing in a low cost culture media based on fertilizers and industrial grade salts [8], and was developed in MATLAB R2007b (The Mathworks, Natick, MA). The biomass growth components of the model are summarized by the equations below.

$$\frac{dC(t)}{dt} = \mu_e C(t)$$

$$\mu_e = \mu_p - \mu_r$$

$$\mu_p = \frac{qI_0}{2{,}3OD(t)H}\left[1 - e^{(-2{,}3OD(t)H)}\right]$$

$$\mu_r = \begin{cases} a \cdot T + b, & 15 < T \leq 40^oC \\ 0, & 15^oC \end{cases}$$

Where C(t) is the concentration of algal biomass at a given time, μ_e the effective growth rate, μ_f is the photosynthesis growth rate, μ_r is the respiration growth (consumption) rate, q is the light conversion rate, I_o the light intensity at the surface of the pond, OD(t) the optical density of the suspension at a given time, H the depth of the pond, and a and b are the linear regression parameters for respiration rate as function of temperature.

CO_2 is supplied by dispersors disposed in sumps along the ponds. The reference case considers the use of flue gas from a thermoelectric power plant as the source of CO_2. Figure 1 summarizes the system used in the development of the models and economic analysis.

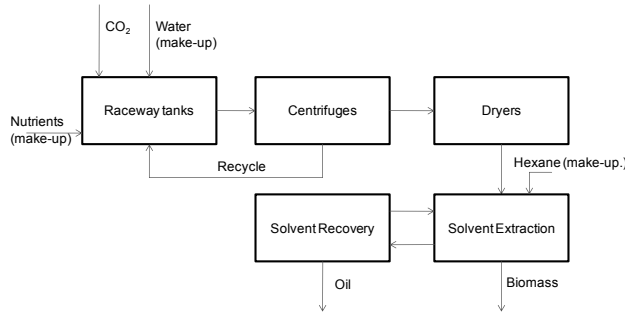

Figure 1 – Block diagram for reference system

The mass balance for water used empirical relations proposed by EPA [9] to estimate typical losses with evaporation. The mass balance for CO_2, biomass and nutrients was based on the stoichiometric relations measured for *Spirulina platensis* by Cornet et al [10]. The cost of equipment, construction and energy demand of unit operations was based in specific equipment specs and quotes or estimated using the charts by Peters, Timmerhaus and West [11]. The additional capital costs (installation, instrumentation, engineering, etc) and the operation costs were calculated using the estimates proposed by Peter, Timmerhaus and West [11] and representative data on labour and utilities costs for a plan in Texas, USA. For each case studied the net present value (NPV) and internal rate of return (IRR) were calculated.

3. Results and Discussion

3.1. Mathematical model for growth in raceway ponds

The model developed was initially used for the study of the main process parameters in growth rate and productivity. The considerable decrease of μ_e for increasing concentrations is a consequence of the light attenuation by the algal suspension (Figure 2). Temperature also has an important effect on the effective growth rates, impacting both the photosynthesis rate but also the respiration rate in the dark zones of the pond (Figure 3). Figure 4 describes the combined effect of pond depth and initial cell concentration in daily areal productivity. The understanding of those effects allows the determination of design and process conditions in order to maximize productivity. It also supports the evaluation of potential locations for the production of microalgae and cyanobacteria, based on the daily and seasonal variation of light and temperature.

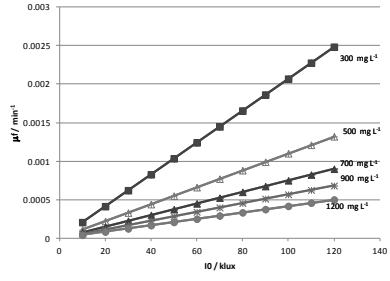

Figure 2 – Effect of light intensity and cell concentration in growth rate

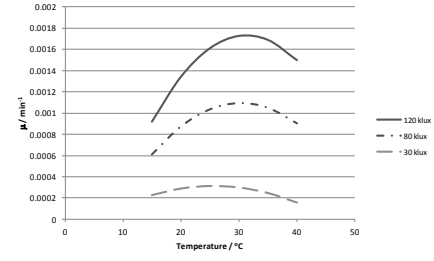

Figure 3 – Effect of temperature and light intensity in growth rate

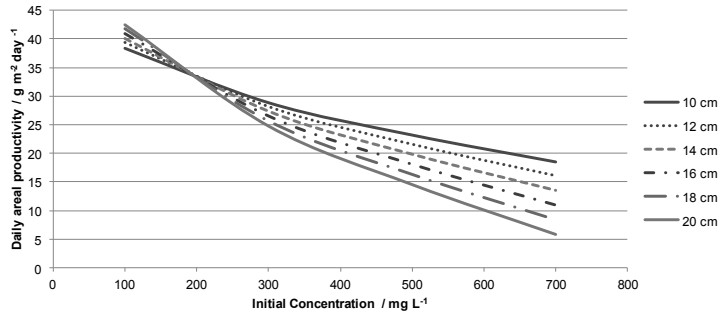

Figure 4 – Effect of pond depth and initial cell concentration in daily areal productivity

The model was also used to optimize operational conditions, especially the maximum concentration before harvesting and the renewal rate (% of total pond volume harvested and replaced by fresh culture medium). Table 1 describes the results of a designed experiment using the model to optimize the above mentioned process parameters. Higher productivities were obtained for higher renewal rates and lower harvesting concentrations, in agreement with experiments in batch photobioreactors [12].

Table 1 – Results of experiment to optimize process conditions. The productivity is calculated for a 1000 m^2 pond, 0.2 m deep, and reported in kg day^{-1}

Harvesting concentration / g L^{-1}	Renewal Rate					
	20%	30%	40%	50%	50%	70%
0.4	31.5	33.4	35.6	36.4	37.8	39.8
0.5	28.5	32.6	31.2	33.2	33.2	37.9
0.6	26.8	28.0	29.0	31.9	32.1	32.8

3.2. Economic analysis

A sensitivity analysis of the simplified economic model is summarized in Figure 5. The main variable impacting the IRR are capital costs and productivity. A detailed analysis, taking into consideration specific equipment costs and consumption of utilities, also highlights the cost of nutrients (30% of operation costs), and energy (up to 14% of operation costs, for electricity and natural gas).

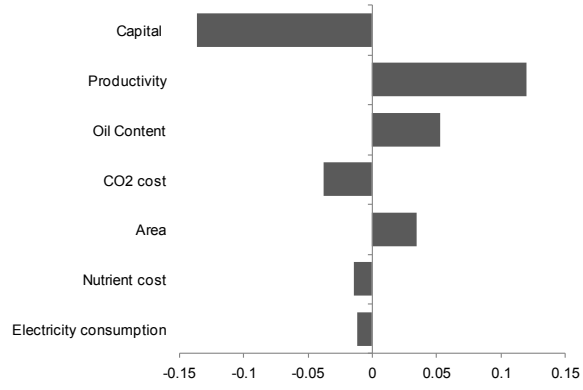

Figure 5 – Normalized effects of variables in the internal rate of return

The detailed economic analysis has also showed the importance of high value products to the total revenue and economic viability, based on the currently available technology. The only alternative cases studied with positive NPVs and an IRR above 15% were based on the sale of a high value specialty apart from the algal oil and biomass. The use of alternative nutrient sources (to reduce operation costs) and the development of improved technologies for harvesting and separation (to reduce capital and energy consumption) were identified as key priorities to improve the economics of microalgae related products.

4. Conclusions

The development of reliable and robust models for the production of microalgae and cyanobacteria in open ponds is critical for designing improved systems and optimizing and controlling process conditions. A detailed economic analysis demonstrated the impact of capital, operation costs and energy consumption, also highlighting the importance of revenue from high value products to process viability, considering the current technology. The sensitivity analysis and evaluation of both technology improvements and alternative business models enabled the prioritization of future research areas, based on economic and environmental impact.

References

[1] Greenwell HC. Laurens LML. Shields RJ. Lovitt RW. Flynn KJ. Placing microalgae on the biofuels priority list: a review of the technological challenges. J R Soc Interface 2010;7:703-26.
[2] Chisti Y. Biodiesel from microalgae. Biotechnol Adv 2007;25:294-306.
[3] Benemann JR. Oswald WJ. Systems and economic analysis of microalgae ponds for conversion of CO2 to biomass. Final report to the Department of Energy. Pittsburgh: Pittsburgh Energy Technology Center; 1996.
[4] Stephens E. Ross IL. King Z. Mussgnug JH. Kruse O. Posten C. Borowitzka. MA. Hankamer B. An economic and technical evaluation of microalgal biofuels. Nat Biotech 2010;28:126-28.
[5] Guterman H. Vonshak A. Ben-Yaakov S. A macromodel for outdoor algal mass production. Biotechnol Bioeng 1990;35:809-819.
[6] Sukenik A. Levy. RS. et al. Optimizing algal biomass in an outdoor pond: a simulation model. J App Phycol 1991; 3:191-201.
[7] James SC. Boriah V. Modeling algae growth in an open-channel raceway. J Comp Biol 2010; 17:895-906.
[8] Raoof V. Kaushik. BD. Prasanna R. Formulation of low-cost medium for mass production of Spirulina. Biomass Bioen 2006; 30:537-542.
[9] EPA. Technical Guidance for Hazard Analysis. U.S. EPA. 1987. http://www.epa.gov/OEM/docs/chem/tech.pdf.
[10] Cornet JF. Dussap. CG. et al.. A structured model for simulation of cultures of cyanobacterium Spirulina platensis in photobioreactors: II. Indentification of kinetic parameters under light and mineral limitations. Biotechnol Bioeng 1992;40:826-834.
[11] Peters M. Timmerhaus K. West R. Plant design for chemical engineers. 5 ed. New York: McGraw-Hill. 2003.
[12] Reichert CC. Reinehr CO. Costa AV. Semicontinous cultivation of the cyanobacterium Spirulina platensis in a closed photobioreactor. Braz J Chem Eng 2006;23:23-28.

I.A. Karimi and Rajagopalan Srinivasan (Editors), Proceedings of the 11th International Symposium on Process Systems Engineering, 15-19 July 2012, Singapore.

Sustainability Assessment of CO2 Capture Process in the Preliminary Process Design: Selection of Solvents

Namjin Jang, [a] Hae-jin Moon, [a] Inhyck Choi,[a] En Sup Yoon [a]

[a] *Seoul National University, Gwanak st. 1, Gwansk-gu, Seoul 154-742, Korea*

Abstract

The sustainable process is drawing attention as the upcoming frontier and alternative works. Sustainable developments of chemical process are one of the core activities to launch the production of chemical materials in the chemical process industries. We introduce a set of indicators that can be used to measure the sustainability performance of chemical process, such as net present value, material intensity, energy intensity, CO2 capture efficiency, global warming, and inherent safety, etc. The evaluation was done by using the 6th alternative of solvents for post-compustion in CO2 capture technologies as a case study. Sustainability in chemical process design can be applied to product and process design to improve sustainable developments that is economic, environmental, and social aspects. Also, it can be considered in order to counteract multidisciplinary change such as environmental responsibility, social concerns, and economic uncertainty, etc.

Keywords: Sustainabiltiy, CO2, post-combustion, solvents, CCS.

1. Introduction

The concept of sustainability was first mentioned in scientific literature by the German Miner Hans Car von Carlowitz referring to sustainable forestry in "Sylvicultura oeconomica" in 1713. Especially, sustainability have recently interested and studied both the society at large and micro scale of process. In this sense, the sustainable process is drawing attention as the upcoming frontier and alternative works. Development of sustainable chemical process is one of the core activities to launch the production of chemical materials in the chemical process industries. Especially, process design and synthesis is the essential engineering activity based on the mathematics, basic science, engineering science, economics, safety, reliability, and social consideration, etc. in the whole process design phases (Kim, 2010; Sigiyama, 2007). Generally, there are three major facets considered in sustainability, such as economic, environment and society/safety to assess sustainability. In the preliminary process design phase, sustainability of alternative process needs to be studied to evaluate improvement options, strategies for development, innovations of process and inherent safety design, etc (Azapagic, 2006).

Removal of carbon dioxide (CO2) is an important industrial operation. CO2 is produced in large quantities by many important industries such as fossil-fuel-fired power plants, steel production, chemical and petrochemical manufacturing, cement production, and natural gas purification. The reasons for the CO2 removal are traditionally technical and economic concerns. Also, environmental concerns, such as global warming, climate change, etc., are now focused as one of the most important and

challenging environmental issues facing the world community (Ma'mun, 2006; Wang et al., 2011).

Carbon dioxide capture by an absorption process is one of the most common industrial technologies today. Recent economic studies (IEA GHG, 2006; Desidere and Corbelli, 1998; Zahraa et al., 2011) indicate that the process will also remain competitive in the future. One of the key improvements under development is new, faster and more energy–efficient absorbents. A chemical to be used as a commercial absorbent must have high net cyclic capacity, high absorption rate for CO2, and good chemical stability. For example, alkanolamines are the most commonly used chemical absorbents for the removal of acidic gases today.

In this paper, we are focused on the chemical absorption process (Zahraa et al., 2011 ; Husebye et al., 2011). Over ten absorbents are developed and researched in the world including alkanolamines, methanol, K2CO3, Ammonia, etc. as represented in Table 37. Especially, we evaluated six absorbents, which is 2-amino-2-methyl-1-propanol (AMP), diethanolamine (DEA), potassium carbonate (K2CO3), monoethanol amine (MEA), methanol and ammonia since these absorbents has studied in pilot plant. Actually, chemical absorption process consists of two mainly equipment which are absorber and stripper. Here, Figure 1 is a flowsheet diagram representing the pilot plant at the University of Texas at Austin for CO2 capture by MEA and the unit operations. The absorber and stripper data for the CO2 capture process by various absorbents.

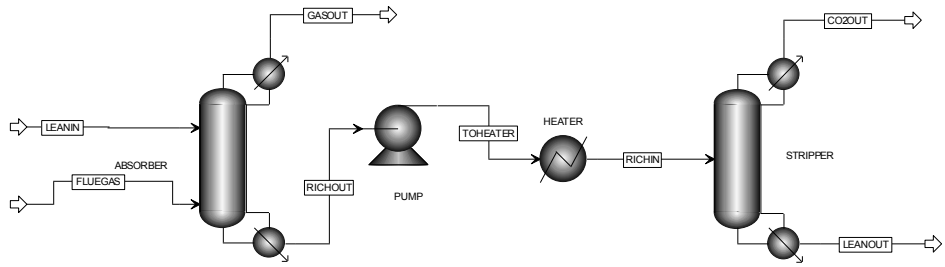

Figure 1. Simple schematic of the CO2 capture process using MEA.

2. Sustainability Assessments

In this paper, we are focused on the three indicators to evaluate sustainability of CO2 capture process, which are CO2 removal efficiency with capital and operating cost as an economic indicator, environmental impact as environmental indicator and inherent safety impact as a safety and social indicator. Here, first of all, we need to identify alternatives and define scope of sustainability. And then, the database is constructed including capital costs, production costs and simulated the process information. Finally, sustainability will be drawn by using graph.

2.1. Economic Impact Assessments

As an economic aspect, in this paper, we proposed efficiency analysis based on cost of production by removing CO2 in the process. It is accounted for costs of raw materials (absorbents) and utilities used in the reaction, separation, waste treatments, etc. of the alternatives based on the CO2 removal quantity in the cost using Eq. (1)

$$Ecc = (AR\_CO2 \times C\_CO2)/TPE \quad (1)$$

Where,

E_{CC} = Cost of Production for CO2 removing

AR_CO2 = CO2 absorption rate [kg/hr]
C_CO2 = Price of CO2 [kg/$]
TPE = Total Product Expense [$/hr]

ECC means the ratio of total product expense to remove CO2 quantity in the process. Also, ECC is normalized using Eq. (2) in order to compare with other indicators in sustainability. Actually, small value of ECC means more economic. We can use this factor, when expense is greater than profit, excluding social benefits.

$$\textit{Cost of Production factor} = \log10\ (1/E_{CC}) \quad (2)$$

Table 1 represents the results of economic analysis of absorbents. Methanol is ranked as a high efficiency material. Also, It means that to remove same quantity of CO2, methanol-based process require small methanol as an absorbent and spend small heat duty for cooling and heating in the absorber and stripper during plant operation time compared with other absorbents-based process. Also, ammonia, MEA and DEA based process is ranked in high efficiency compared with other absorbents.

Table 1. Results of economic analysis of absorbents

	AMP	DEA	K2CO3	MEA	MeOH	NH3
CO2 removal efficiency	2.55	1.79	3.22	1.80	1.17	1.34
Rank	5	3	6	4	1	2

2.2. Environmental Impact Assessments

Environmental impact is one of the key parameter for evaluating sustainability in not only world societies but also chemical process industries. In the environmental analyses, we can evaluate energy consumption, waste generation, global warming effect, and environmental and health impact based on the chemical and physical properties.

M. H. Hassim (Hassim and Ali, 2009) proposed health and environmental criteria such as material state, volatility, chronic toxicity and adverse impact as a health impact and terrestrial toxicity as an environmental impact. In order to show results, the index values are normalized to the same magnitude range of 0 to 10. The absorbents are ranked by their environmental and health index as shown in Figure 2.

The index calculations indicate that the ammonia has the largest potential hazard from environmental and health aspects because ammonia evaporate easily and is very toxic material. K2CO3, on the other hands, is ranked as the best absorbent based on the environmental and health index. K2CO2 existed by dissolved in water. Therefore, K2CO3 has low volatility and toxicity scores in the process.

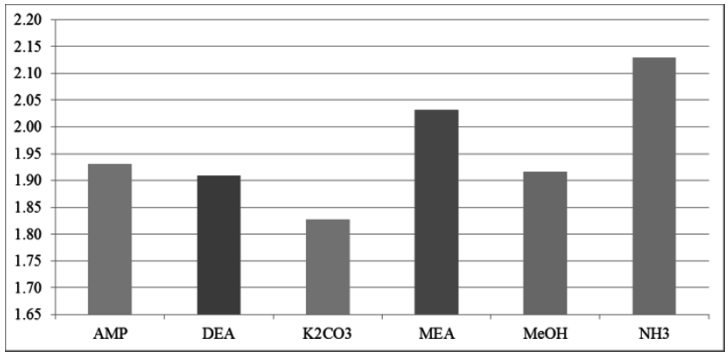

Figure 2. Results of environmental impact of CO2 absorbents.

2.3. Social and safety Impact Assessments

To evaluate inherent safety of absorbents, first of all, we simulate CO2 capture process using Aspen Plus to get process conditions and material data. Also, chemical and physical properties were obtained from Material Safety Data Sheet (MSDS) or literature reports. Results of inherent safety for absorbents are showed in Figure 3. In the results, ammonia, AMP, MEA is determined high ranking in general because of low operating temperature and pressure. In risk-standard rule (fifty-fifty rule), AMP ranks top (1.98) material among the alternatives. And then, NH3 ranked (2.12). However, in risk-aversion rule, the rank is changed. NH3 (2.69) ranks top and then MEA (3.06) ranked. AMP (3.26) is ranked in third.

This result is not quantitative assessment. However, these trends of CO2 absorbents can recommend the inherently safer material to design of chemical process. Also, in the next section, we will evaluate sustainability of CO2 absorbents including economic impact and environmental impact. It can be possible guide to adequate decision to improve sustainability.

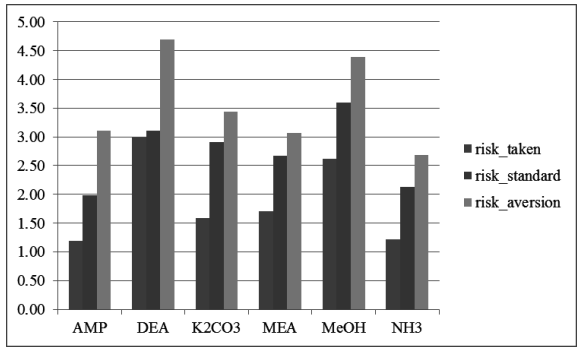

Figure 3. Result of inherent safety evaluation of CO2 absorbents.

2.4. Results of Sustainability Assessments

Figure 4 represents the comparison results of sustainability indicators for CO2 absorbents in normalized value of range 0 to 10. Here, the inherent safety result was based on the risk-standard rule. In the graph, the low value means better process compared with other. In the results, ammonia is ranked in high priority in the aspect of sustainability. And then AMP and MEA have been ranked in second and third. Especially, methanol has low tendency in economic and environmental aspect except for social and safety impact.

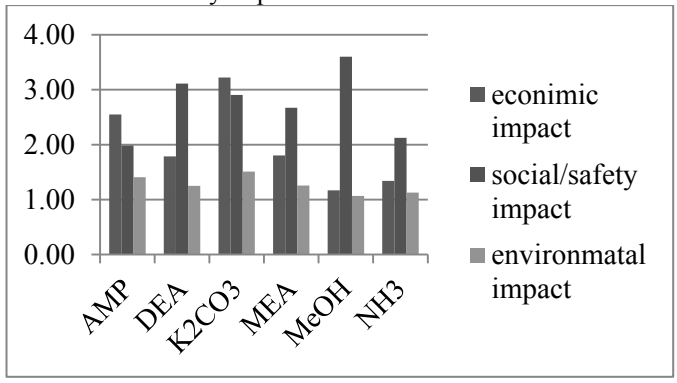

Figure 4. Comparison results of sustainability indicators for CO2 absorbents.

3. Conclusions

The sustainable process is drawing attention as the upcoming frontier and alternative works. Sustainable developments of chemical process are one of the core activities to launch the production of chemical materials in the chemical process industries.

In this paper, the evaluation was done by using the 6th alternative of solvents for post-compustion in CO2 capture technologies as a case study. Here we proposed the framework for sustainability study in the process design. In the case study, we used CO2 capture efficiency based on the Cost of Production analysis of process as an economic aspect. Environmental and health impact study is used as an environmental aspect. Finally, we use inherent safety performance index for evaluating inherent safety of process of case study regarding social and safety aspects.

Sustainability in chemical process design can be applied to product and process design to improve sustainable developments that is economic, environmental, and social aspects. Also, it can be considered in order to counteract multidisciplinary change such as environmental responsibility, social concerns, and economic uncertainty, etc.

References

A. Azpagic, A. Millington and A. Collett, 2006, A Methodology for Integrating Sustainability Considerations into Process Design, Chemical Engineering Research and Design, 84, 439 – 452.

U. Desideri, R. Corbelli, 1998, CO2 Capture in Small Size Cogeneration Plants: Technical and Economic Considerations, Energy Convers. Mgmt., 39, 857–867.

M. H. Hassim and M. W. Ali, 2009, Screening Alternative Chemical Routes based on Inherent Chemical Process Properties Data: Methyl Methacrylate Case Study, Journal the Institution of Engineers, Malaysia, 70, 2-9.

Jo Husebye, Rahul Anantharaman and Stein-Erik Fleten, 2011, Techno-economic Assessment of Flexible Solvent Regeneration & Storage for Base Load Coal-Fired Power Generation with Post Combustion CO2 Capture, Energy Procedia 4, 2612-2619.

IEA Greenhouse Gas R&D Programme (IEA GHG), January, 2006, Estimating future trends in the cost of CO2 capture technologies, 2006/5.

H. S. Kim, 2010, Study of Multiobjective Process Synthesis Based on Generalized Disjunctive Programming and Process Simulator, Doctoral thesis, Seoul National University.

Sholeh Ma'mun, 2006, Selection and Characterization of New Absorbents for Carbon Dioxide Capture", Doctoral thesis, Department of Chemical Engineering, Norwegian University of Science and Technology, Norway.

Hirokazu Sugiyama, 2007, Decision-making Framework for Chemical Process Design including Different Stages of Environmental, Health and Safety (EHS) Assessment, Doctoral thesis, ETH Zurich, Diss. ETH No. 17186.

M. Wang, A. Lawal, P. Stephenson, J. Sidders, and C. Ramshaw, 2011, Post-combustion CO2 capture with chemical absorption: A state-of-the-art review", Chemical Engineering Research and Design, 89, 1609-1624.

Mohammad R. M. Abu Zahraa, Eva Sanchez Fernandezb, Earl L. V. Goetheerb, 2011, Guidelines for Process Development and Future Cost Reduction of CO2 Post-Combustion Capture, Energy Procedia 4, 1051-1057.

Acknowledgement

This paper was supported by the Engineering Research Institute and ASRI (Automation and Systems Research Institute) in Seoul National University.

I.A. Karimi and Rajagopalan Srinivasan (Editors), Proceedings of the 11th International Symposium on Process Systems Engineering, 15-19 July 2012, Singapore.

Characterization of moisture and free air space effects and the optimal operation of a composting process for minimal waste and energy use

Gi Hoon Hong[a], Bettar El Hady[a], Ki Don Joo[a], Dongil Shin[a]

[a]*Department of Chemical Engineering, Myongji University, Yongin 449-728, Korea*

Abstract

Since composting of organic material releases a high amount of CO_2, which is known as a greenhouse gas, it is needed to reduce CO_2 emission to protect our planet from the global warming; in this study we have managed to reduce CO_2 by 23% compared to the previous study. We optimized the quality of compost by changing only one parameter and letting the other parameters be fixed, which permitted us to handle the composting process in easier way. In this work, a new dynamic model of composting process was developed and optimized using SuperPro Designer and Matlab. We studied the influence of air flow rate on oxygen concentration, CO_2, moisture and degradation of volatile solid. It was observed that those parameters depend strongly on air flow rate; for air flow rate at 2,000 kg/hr the temperature and oxygen showed the optimum results.

Keywords: Mathematical modeling, optimization, composting process, reactor modeling, SuperPro Designer.

1. Introduction

Composting is a biological decomposition and stabilization of organic substrates, under conditions that allow development of thermophilic temperatures as a result of biologically-produced heat, to produce a final product that is stable, free of pathogens and plant seeds, and can be beneficially applied to land. This is a largely satisfactory definition, although omission of the high solids aspect of composting means that this description might apply equally to liquid phase aerobic digestion [1]. However, the product stability criterion would not be met in the latter case, since the biological solids produced remain very wet, and thus prone to subsequent anaerobic biological activity. Composting is also a very important element in the successful operation of the recycle and reuse process of valuable resources out of municipal collection of garbage. Since the municipal garbage contains lots of biodegradable materials, proper treating through composting enables easy handling and separation of reuse materials. This research investigates on a dynamic modeling, simulation and optimization of a composting process operated mainly for this purpose (see Fig. 1).

2. Process Description

The most commonly-used type of equipment for composting process is a reactor; before the raw material to be sent to the reactor it is mixed with air in a mixer to upgrade the concentration of oxygen in the raw material. After the reaction is occurred, the product is flowed to a conveyer. By using the conveyer we can transport the reactor output to a centrifuge where we can separate substrates based on their size. Substrates that have size less than 30 mm are mixed with air in mixer, before being sent to generic procedure

where the second reaction occurs [1]. From the high outlet of generic procedure we have the gases and from the second outlet we have the final products; 10% of the products will be recycled and used as an amendment for raw material and the 90% is sent for storage or sold.

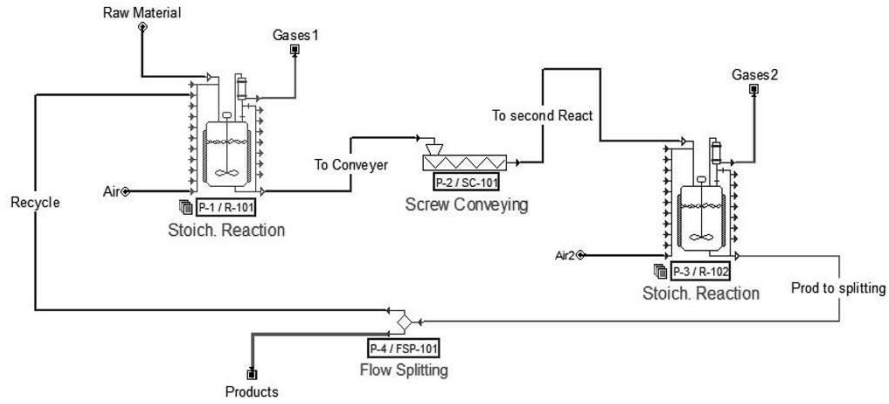

Fig. 1 Schematic diagram of the composting process being simulated

2.1. Raw material

Biodegradable waste is a type of waste, typically originating from plant or animal sources, which may be degraded by other living organisms. Wastes that cannot be broken by other living organisms are called non-biodegradable. Biodegradable waste can be commonly found in municipal solid waste (sometimes called biodegradable municipal waste, or BMW) as green waste, food waste, paper waste and biodegradable plastic.

2.2. Temperature and volatile solid

Because of the strong relationship of temperature with decomposition, temperature provides an important indicator of composting process efficiency [3]. Flow rate of 2,000 kg/h was able to reach the maximum temperature faster than the other flow rates, presumably because increased aeration minimized the oxygen limitation common in the initial phases of composting. The temperature and air flow profiles obtained for control strategy based on air flow regulation from temperature measure are shown in Fig. 2. According to previous studies [8,9], the sensing was placed at a middle layer matrix. It was necessary to begin the simulation with the oxygen controller until the thermophilic temperatures were achieved. Shortly before the third day of process, the maximum air flow rate was applied.

The effect of temperature on the substrate has been adjusted by the KT; the main factors affecting the BVS biodegradation were organic matter component and microorganism succession. During first 14 hr, BVS degradation accumulation was 0.026 kg which was about 0.7% of the total accumulation, so microorganism succession should be the main factor affecting the degradation. The slow degradation rate may be attributed to the inactivity of aboriginal microbes in the raw material when the temperature is rising. At 17 hr, mesophilic bacteria began to grow quickly. Decreasing volatile solid (VS) continued throughout the composting process as microbes degraded the organic material in mixture (see Fig. 3). Decomposition kinetics depends on a variety factors including moisture, oxygen and temperature in ranges appropriate to

support microbial activity [2]. The volatile solid decreased more rapidly at flow rate equal to 2000 kg/h than the other flow rates in the latter half of the composting process. This difference likely resulted from the more optimal moisture at the optimum flow rate at that stage of the process. The relatively high oxygen concentration of the optimum flow rate reactors may also have a positive influence on volatile solid degradation.

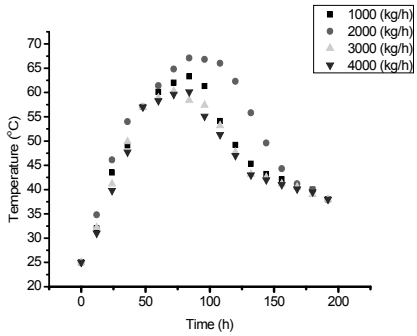

Fig. 2 Profile of substrate temperature with different initial airflow rate

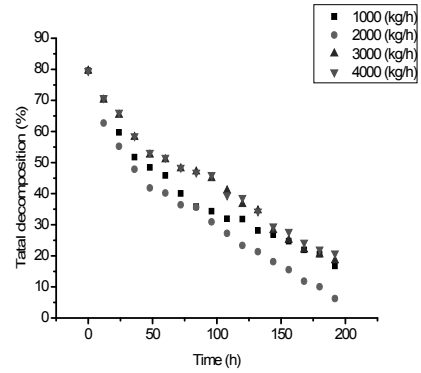

Fig. 3 Profile of substrate VS with different initial airflow rate

2.3. Output of reactors

The simulation results showed that most compost indexes decreased during the composting process. Because the high energy released from the reaction is exothermic, the temperature increases rapidly at the early stage. The oxygen concentration kept stable, showing that function of air supply in this period was mainly cooling compost. As we can see here, an increase in airflow rate led to low temperature and slows the degradation of substrate. Oxygen concentration in the exit gas did not fall below 5% which is the boundary for anaerobic condition. The output values examined were the total material reduction, the total percent reduction, and the maximum biomass concentration in products. For better description of the process, the effect of carbon nitrogen ratio should be included in the model kinetics. Evolved carbohydrate can stay in the solution in form of liquid or gas. Modeling of all possible ways is a very complicated task. For better prediction of carbohydrate we need to use different percentage of both moisture and oxygen concentration [4-7].

3. Emission of Exhaust Gases

3.1. CO_2 emission

Predicted percentages of CO_2 and oxygen in exhaust gas mixture follow qualitatively the simulation results. The deviations found could be explained by opening of the reactor during sampling periods, and they could also be attributed to the variation of the liquid-gas transfer rate as the material is dried. The water soluble fraction is mineralized to CO_2 through a first order reaction at K_{aq} rate. The mineralization rate of water soluble carbon is not expected to be rate-limiting. Therefore, an infinite value can be used for the C_{eq} mineralization rate constant to reflect rapidity of this stage. A fraction of the water-soluble carbon is assumed to convert to CO_2, while the rest is converted to microbial biomass, which is also part of the total solid carbon sink. Due to endogenous decay, a fraction of the microbial biomass is ultimately converted to CO_2 yield coefficient, as used in the model, referring to the mineralization carbon that will be

ultimately converted to CO_2, regardless of the pathway followed. Therefore, this yield coefficient is taken equal to 1, indicating that all initial mineralization carbon will be eventually converted to CO_2.

3.2. Oxygen concentration

Oxygen levels within the pile can also be used as an indicator of how the composting process is developing. As aerobic activity increases, the oxygen consumption should also increase causing the oxygen levels to decrease. Measuring oxygen levels to monitor the composting process is not as accurate as measuring temperatures. Oxygen monitoring is most useful to show that stability has been reached. Oxygen levels remain low during the active composting period. However, as the pile reaches maturity and microbial activity begins to slow, oxygen levels rise. Because CO_2 is a product of aerobic respiration, it can also be used as an indicator of microbial activity. The CO_2 levels should increase as microbial activity develops and decrease as the composting process approaches maturity.

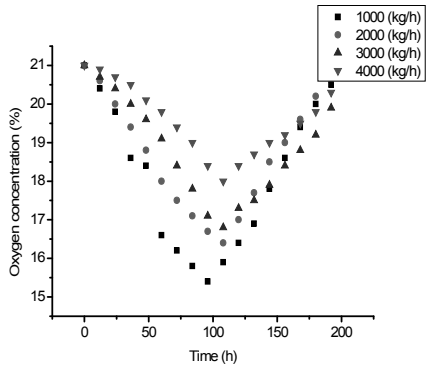

Fig. 4 Oxygen concentration in exhaust gas

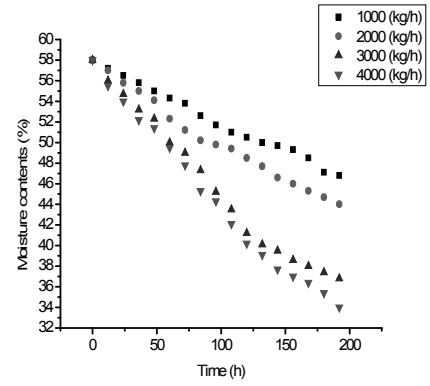

Fig. 5 Moisture contents of substrate with different airflow rate

3.3. Moisture

The measurement of moisture in both initial substrate and composted material allowed the determination of the amount of water accumulated during the composting treatment. Finally, gas monitoring enabled the determination of vapor flow in the incoming and outgoing gas [10,11]. Then, conducting a water balance allowed the calculation of the amount of water produced through bio-degradation of organic matter. As a first approximation, considering that biodegradable organic matter could be described as $C_xH_yO_z$, neglecting nitrogen content, the conversion of biodegradable organic matter during composting can be assumed by its oxidation, then transformation of biodegradable organic matter. Fig. 5 shows the variation of moisture content during the process in both reactors, initial moisture contents of about 62% wet basis decreased during the composting process, heat neglected by biological metabolism and the convective air flow increased water evaporation in the reactors. The compost moisture content in the high flow rate decreased more rapidly than in the low flow rate, in the high flow rate reactor led to low moisture content less than 40%, for 2,000 kg/h the moisture contents is at its optimum, around 46%.

4. Conclusion

This study provided a quantitative explanation for the current experience-based operation of a commercial composting plant for municipal waste and demonstrated the complex interactions which occur in composting processes. Variations of compost indexes, such as volatile solid degradation, temperature fluctuation, moisture exchanges and oxygen concentration were simulated; the decay rate and quality of compost were good due to reaching thermophilic phase in less than 48 hr and the process kept in it for 5 days. In this study, the percentage of cell mass in the mass composition of products was increased to 63% which can give high stability and desired products. The two-reactor system produces more stable compost than a single reactor in less composting time. Internal recirculation of air in the first reactor leads to more homogeneous temperature distribution throughout the composting mass as compared to no-recirculation, resulting in improved organic matter degradation. The model was developed based on several assumptions and simplifications, it could be further improved in the future when the complex reaction among and within the three phases are allowed (this work assumed that the raw materials have high moisture contents and high C/N ratio and free air space is enough to assure the circulation of air). To improve the robustness of the simulation model further studies on the complex transactions are required.

Acknowledgment

This work was supported by the Energy Efficiency & Resources program of the Korea Institute of Energy Technology Evaluation and Planning (KETEP) grant funded by the Korea Government Ministry of Knowledge Economy (*No. 2011T100200023*).

References

1. I.G. Mason, “Mathematic modeling of the composting process: A review”, *Waste Management*, 26, 3-21 (2006).
2. N. Bongochetsakul and T. Ishida, “A new analytical approach to optimizing the design of large scale composting systems”, *Bioresource Technology*, 99, 1630-1641 (2008).
3. A. Vlyssides, S. Mai and E.M. Barampouti, “An integrated mathematical model for composting of agricultural solid wastes with industrial waste water”, *Bioresource Technology*, 100, 4797-4806 (2009).
4. D.P. Komilis, “A kinetic analysis of solid waste composting at optimal conditions”, *Waste Management*, 26, 82-91 (2006).
5. M. Baptista, F. Antunes, M. S. Goncalve, B. Morvan and A. Silveira, “Composting kinetics in full-scale mechanical-biological treatment plants”, *Waste Management,* 30, 1908-1921 (2010).
6. H. Zhang and T. Matsuto, “Mass and element balance in food waste composting facilities”, *Waste Management*, 30, 1477-1485 (2010).
7. I. Petric and V. Selimbasic, “Development and validation of mathematical model for aerobic composting process”, *Chemical Engineering*, 139, 304-317 (2008).
8. M.E. Lang and R.A. Jager, “Evaluation of composting feasibility for regional implementation”, *Waste Management*, 35, 138-145(2009).
9. B. Puyuelo, T. Gea and Antoni Sanchez, “A new control strategy for the composting process based on the oxygen uptake rate”, *Chemical Engineering*, 165, 161-169 (2010).
10. P. Beuno, R. Tapias, F.Lopez and M.J. Diaz, “Optimization composting parameters for nitrogen conservation in composting”, *Bioresource Technology*, 99, 5069-5077 (2008).
11. H.K. Ahn, T.L. Richard and H.L. Choi, “Mass and thermal balance during composting of a poultry manure-wood shavings mixture at different aeration rates”, *Process Biochemistry*, 42, 215-223 (2007)..

I.A. Karimi and Rajagopalan Srinivasan (Editors), Proceedings of the 11th International Symposium on Process Systems Engineering, 15-19 July 2012, Singapore.

Post-Combustion CO_2 Capture Process with Aqueous MEA: An Advanced MEA Process using a Phase Separation Heat Exchanger

Jaeheum Jung[a], Yeong Su Jeong[a], Ung Lee[a], Youngsub Lim[a], Seeyub Yang[a], Chi Seob Lee[b], Jaehyung Kim[b], Chonghun Han[†a]

[a]*School of Chemical and Biological Engineering, Seoul National University, Gwanak-ro 599, Gwanak-gu, Seoul 151-742, South Korea*
[b]*KEPCO Engineering & Construction Company, INC., 2354 Yonggudaero, Giheung-gu, Yongin-si, Gyeongi.do, South Korea*

Abstract

A CO_2 capture process using MEA (Monoethanolamine) scrubbing has been considered a leading technology in the early phase of the CCS (Carbon Capture & Storage) market due to its high CO_2 capture capacity and feasibility of use with existing power plant facilities. In spite of these advantages, this process has a disadvantage of requiring high energy for solvent regeneration in the stripper. For this reason, various improved solvents and process alternatives have been developed to reduce the solvent regeneration energy. This paper suggests an advanced MEA scrubbing process with a PSHE (phase separation heat exchanger) and shows its energy reduction effect using a commercial simulator. The main idea of the PSHE process is to reduce the reflux ratio of the stripper by sacrificing a part of the sensible heat recovery in the heat exchanger. In order to mitigate this sensible heat recovery loss, the PSHE process uses a phase separation heat exchanger. As a result, the PSHE process saves 123MJ/hr of condenser cooling energy while losing 51MJ/hr of sensible heat recovery in the phase separation heat exchanger. Consequently, the net energy reduction is 72 MJ/hr, and the ton CO_2 capture energy decreases about 14%, from 3.31 GJ/ton CO2 to 2.86 GJ/ton CO_2.

Keywords: CO_2 Capture Process, Post Combustion CO_2 Capture, MEA Scrubbing, Split Flow Configuration, Phase Separation Heat Exchanger

1. Introduction

The CO_2 capture process using MEA (Monoethanolamine) scrubbing has been considered as one of the most promising technologies to reduce CO_2 emissions. The MEA process is suitable for treating the flue gas from large CO_2 emission sources because of its high CO_2 capture capacity and feasibility for use with existing coal-fired power plant facilities. This MEA process, however, consumes a lot of heat energy for solvent regeneration in the stripper. In order to overcome this problem, various process alternatives have been developed such as absorber intercooling(Reddy, Johnson et al. 2008), lean vapor compression(Reddy, Johnson et al. 2008), staged feed of the stripper(Le Moullec and Kanniche 2011), split-flow configurations(Chang and Shih 2005), and integration of the power plant and amine scrubbing(Alie, Douglas et al. 2006). This paper suggests an advanced CO_2 capture process using the PSHE (phase separation heat exchanger), which inhibits water vaporization at the top of the stripper.

2. Typical CO_2 Capture Process using Aqueous MEA

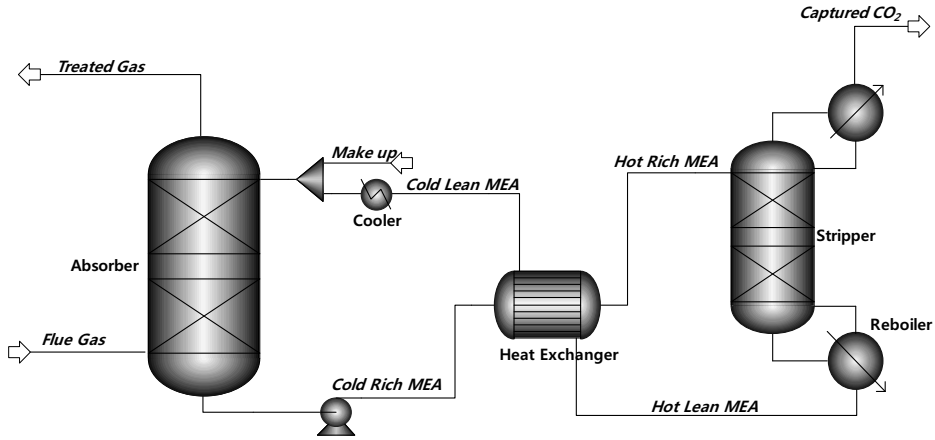

Figure 1. Process flow diagram of the reference process

The typical CO_2 capture process using MEA scrubbing is composed of an absorber and a stripper as indicated in Figure 1. The SO_x free flue gas enters at the bottom of the absorber (Flue gas) and cold lean solvent enters at the top of the absorber (Cold Lean MEA). In the absorber, the lean solvent selectively absorbs CO_2 by exothermic reaction and drains out at the bottom of the absorber (Cold Rich MEA). The remaining flue is purged out the top of the absorber (Treated Gas). The cold rich solvent is preheated by passing through the heat exchanger and enters at top of the stripper (Hot Rich MEA). In the stripper, the hot rich solvent desorbs CO_2 by endothermic reaction at the high temperature condition and drains out at the bottom of the stripper (Hot Lean MEA). The detached CO_2 is cooled by passing through the condenser and is captured at the top of the stripper (Captured CO_2). The hot lean solvent is cooled through the heat exchanger and cooler, and recycled at the top of the absorber to absorb CO_2 in the flue gas. Since the reboiler is the most energy intensive unit in this process, most of advanced MEA scrubbing processes target the reduction of the reboiler heat energy.

Table 1. Main stream information in Reference Process

Stream	Variable	Specification
Flue gas	CO2 composition	0.184 mol%
	Flow rate	18.46 kmol/hr
Solvent	MEA concentration	30 wt%
	Flow rate	2219 kg/hr
	Lean a (mol CO_2/ mol MEA)	0.27

3. Advanced MEA Process using a Phases Separation Heat Exchanger

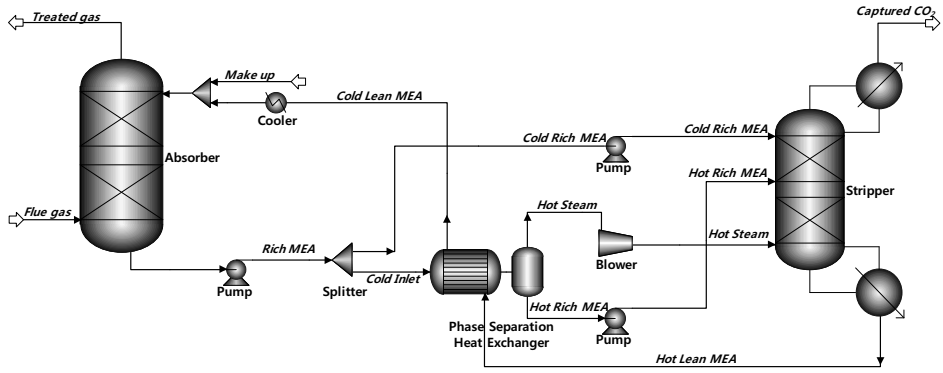

Figure 2. Process flow sheet of the phase separation heat exchanger process

The main idea of the PSHE process is to prevent water vaporization at the top of the stripper by reducing the temperature. In order to reduce this temperature, the cold inlet stream (Rich MEA) is split before it passes through the heat exchanger, as indicated in Figure 2. One of the split streams (Cold Rich MEA) directly enters and cools the top of the stripper. Consequently, this split cold stream prevents water vaporization, which simultaneously reduces both condenser and reboiler heat energy. This split flow configuration, however, diminishes sensible heat recovery in the heat exchanger because the cold stream's heat capacity is decreased by splitting the stream. In order to increase the cold stream's heat capacity, this PSHE process operates a phase separation heat exchanger in low pressure conditions. The cold stream is heated and vaporized in the phase separation heat exchanger. As a result, the cold stream heat capacity increases rapidly, which is increasing the amount of heat recovery in the phase separation heat exchanger. In the flash drum, the vaporized stream (Hot Steam) enters the bottom of the stripper as an energy source after it passes through the blower. The hot liquid (Hot Rich MEA) enters the middle of the stripper after it passes through the pump. As indicated in Table 2, 25% of the cold stream enters and cools the top of the stripper and 75% of the cold stream enters the phase separation heat exchanger for recovering sensible heat.

Table 2. Main process variables in the phase separation heat exchanger process

Unit	Variable	Specification
Heat exchanger	Cold side pressure drop	1.6atm to 1.2atm
Blower	Discharge pressure	2.1atm
Splitter	Split ratio to the top of the stripper	0.25
	Split ratio to the heat exchanger	0.75

4. Simulation Results

The main effect of the PSHE process is to cool the top of the stripper using the split cold stream. Consequently, the temperature at the top of the stripper is reduced from 101°C to 52 °C. Corresponding to this temperature drop, the condenser cooling energy is reduced from 136 MJ/hr to 13 MJ/hr, as indicated in Table 3. On the other hand, the PSHE process recovers less sensible heat in the heat exchanger compared with reference data. The amount of heat recovery loss is 51 MJ/hr which is about 10% decrease. It is commendable performance because only 75% of the cold stream recovers 90% of the sensible heat using the phase separation heat exchanger. Consequently, the net energy reduction is about 72 MJ/hr, and this value is reflected in the regeneration energy. The regeneration energy is summation of blower energy and reboiler energy. In order to convert electrical energy to thermal energy, 10 MJ/hr of blower electrical power is converted to 20 MJ/hr of heat energy. The regeneration energy in the PSHE process is lower than that in the reference process by 61 MJ/hr. The ton CO_2 capture energy decreases about 14%, from 3.31 GJ/ton CO_2 to 2.86 GJ/ton CO_2.

Table 3. Summary of the energy recover and consumption in each unit

	Heat exchanger heat recovery [MJ/hr]	Condenser cooling duty [MJ/hr]	Blower power [MJ/hr]	Reboiler heat duty [MJ/hr]	Ton CO_2 Capture Energy [GJ/ton CO_2]
Reference Process	539	136	-	446	3.31
PSHE Process	488	13	10	365	2.86

5. Conclusion

The MEA scrubbing CO_2 capture process has been considered as one of the most promising techniques to reduce CO_2 emissions. However, this process has a disadvantage of requiring high energy for water vaporization in the stripper, which is a common issue when using aqueous solvent. To overcome this problem, this paper suggests an advanced MEA scrubbing CO_2 capture process, the PSHE process. In the PSHE process, one of the split cold rich streams is fed into the stripper to reduce the reflux ratio, and the other split cold rich stream recovers sensible heat in the phase separation heat exchanger. As a result, the condenser heat energy saving is about 123 MJ/hr, and the sensible heat recovery loss is about 51 MJ/hr. Consequently, the net energy reduction is about 61 MJ/hr, and the ton CO_2 capture energy decreases about 14% compared with the reference process.

6. Acknowledgement

This research was supported by the second phase of the Brain Korea 21 Program in 2012, Institute of Chemical Processes in Seoul National University, Strategic Technology Development and Energy Efficiency & Resources Development of the Korea Institute of Energy Technology Evaluation and Planning (KETEP) grant funded by the Ministry of Knowledge Economy (MKE) and grant from the LNG Plant R&D Center funded by the Ministry of Land, Transportation and Maritime Affairs (MLTM)

of the Korean government.

References

Alie, C., P. Douglas, et al. (2006). Simulation and optimization of a coal-fired power plant with integrated CO2 capture using MEA scrubbing.

Chang, H. and C. M. Shih (2005). "Simulation and Optimization for Power Plant Flue Gas CO2 Absorption-Stripping Systems." Separation science and technology **40**(4): 877-909.

Le Moullec, Y. and M. Kanniche (2011). "Optimization of MEA based post combustion CO2 capture process: Flowsheeting and energetic integration." Energy Procedia **4**: 1303-1309.

Reddy, S., D. Johnson, et al. (2008). Fluor's Econamine FG Plus SM Technology for CO2 Capture at Coal-fired Power Plants.

I.A. Karimi and Rajagopalan Srinivasan (Editors), Proceedings of the 11th International Symposium on Process Systems Engineering, 15-19 July 2012, Singapore.

A superstructure model of water-using network synthesis with multiple contaminants for batch processes and its solution

Xia YANG, Jincai YUE, Shiqing ZHENG

Research Center for Computer and Chemical Engineering, Qingdao University of Science and Technology, Qingdao 266042, China

Abstract

The key contaminant component (KCC) is defined to establish a superstructure model of water-using network synthesis for batch process with multiple contaminants, which uses storage tanks to eliminate the time limitations for water reuse or recycle, and its mathematic programming model is established and solved by nonlinear programming (NLP) method by a two-step solution strategy. Finally, an example is illustrated to show the efficiency of this method.

Keywords: water-using network; multiple contaminants; superstructure model; batch process

1. Introduction

Since Wang and Smith (1994) addressed the minimization of wastewater in the process industries, water-using network synthesis (WNS) targeted for freshwater and/or wastewater minimization in these industries has become an urgent task because these industries not only consume enormous fresh water, but discharge enormous wastewater containing many kinds of dangerous contaminants.

Over decades lots of techniques of WNS for process industries are developed, but it is much less for batch process than for continuous process as batch process is not steady and must be described by (partial) differential equations. R.Grau et. al.(1996) developed a mathematical technique for waste minimization with emphasis on waste generated during changeover. M.Almato´(1999) adopted a mathematical programming to optimize the network and get the assignment coefficient between tank and operation. Yao and Yuan (2000) developed a discrete time mathematical model by optimizing production campaigns. J.K Kim and R. Smith(2004) considered time constraints and the network design and systematically identified minimum cost. D.C. Foo etc.(2005) developed a new two-stage approach to synthesize a batch maximum water recovery network based on pinch technology. T. Majozi.(2005) developed a continuous-time mathematical formulation using central reusable water storage in batch wastewater minimization. Cheng (2007) presented a mathematic programming model for batch WNS with single contaminant, and Yang (2007) developed a time-purity two dimensional graph method to design water network for batch. E. Dogaru and V. Lavric (2011) took a water network for a batch process as a dynamic structure which changes its topology at fixed time intervals delimited by events. M. Bagajewicz (2000) and J. Jezowski (2010) both gave a detailed overview on the subject.

This paper presents a superstructure model of water-using network synthesis for batch process with multiple contaminants (BMWNS) and develops a two-step strategy of solution, the detail is as followed.

2. Model Establishment and Solution

2.1. Key contaminant component definition

Though there are multiple contaminants for a water-using unit j (WU_j), only one contaminant affect the fresh water usage of WU_j, so the key contaminant component (KCC) of the unit, which is denoted as key can be written by the following formula:

$$M_{f,j,key} = \frac{m_{j,key}}{c^{\max}_{j,key,out}} = \max_{i=1}^{C}\left(\frac{m_{i,j}}{c^{\max}_{i,j,out}}\right) \tag{1}$$

In which, M stands for water mass flowrate, ton; m for contaminant mass transfer, kg; C and c stands for the number of contaminants and contaminant concentrations (ppm) respectively, the subscrip f stands for fresh water, and the subscript out stands for the outlet of WU_j.

2.2. Superstructure model establishment

All water-using units (WUs) are sorted firstly according to their water-using starting time, if the WUs with the same starting time are taken as the same sequences; then the KCC of every units are determined by Eq.(1), and by which water sources are determined for every units according to their water-using time sequences. Figure 1 describes partial superstructure of unit j, the cylinders stand for storage tanks, cylinder 0 storages fresh water, cylinder w storages waste water; WU_j has three water sources (including fresh water), its outlet water is used as water sources by two units and the rest is discharged.

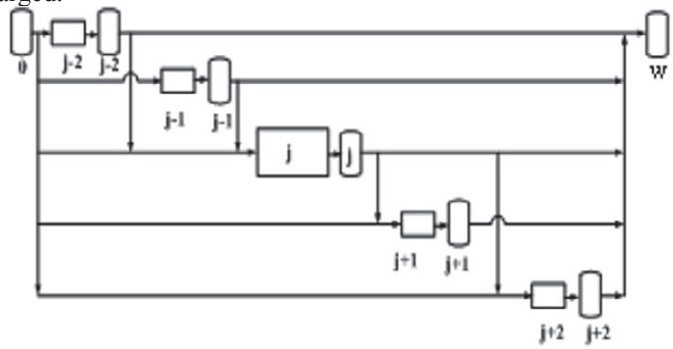

Fig.1 the partial superstructure of WU j for batch

2.3. mathematical model

A double layer mathematical model is developed to describe the superstructure of water-using network for batch, which includes the inner model and the outer model: the former is to find the minimum freshwater of unit j in the current water-using period, and the latter is to find the minimum freshwater of all units in the current water-using period. During a water-using process with N units, there are p ($p \le N$) water sources for WU_j, and its discharged outlet water is taken as q ($q \le N$)water sources. The mathematical model is written as equations from (2) to (14). In which, F stands for water mass flowrate, ton/h, t for water-using time, hour; the superscript $surplus$ for the surplus water in storage tank; and the superscript e, s and new for starting time and end time of the WUs, the new data of the next cycle respectively. It is clear that equation (6) and (7) are not linear so the model is a nonlinear problem (NLP).

Outer model: min $z = \sum_{j=1}^{N} M_{f,j}$ (2)

$$\text{s.t. } M_{f,j,surplus}^{new} = M_{f,j,surplus} - \sum_{j=1}^{N} M_{f,j} \quad (3)$$

Inner model: min $z = M_{f,j}$ (4)

$$s.t.\ M_j = M_{f,j} + \sum_{ij=1(ij\neq j)}^{p} M_{j,ij} \quad (5)$$

$$m_{j,key} = M_j \cdot (c_{j,key,out} - c_{j,key,in}) \quad (6)$$

$$M_j \cdot c_{j,key,in} = \sum_{ij=1(ij\neq j)}^{p} M_{ij,j} \cdot c_{j,key,out} + M_{f,j} \quad (7)$$

$$\sum_{i=1}^{q} M_{j,i} \le M_{j,surplus} \quad (8)$$

$$M_{j,surplus}^{new} = M_{j,surplus} - \sum_{i=1}^{q} M_{j,i} \quad (9)$$

$$M_i = F_i(t_i^e - t_i^s) \quad (10)$$

$$M_{j,i} = F_{j,i}(t_i^e - t_i^s) \quad (11)$$

$$M_{f,i} = F_{f,i}(t_i^e - t_i^s) \quad (12)$$

$$0 \le c_{j,key,in} \le c_{j,key,in}^{\max} \quad (13)$$

$$0 \le c_{j,key,out} \le c_{j,key,out}^{\max} \quad (14)$$

2.4. model solution strategy

2.4.1. the first step

In the first step, time constraints are not considered in the model, so there are only concentration variables for every WUs. The minimum limiting flowrate is introduced as equation (15).

$$F_j^{\min} = \max_N \left(\frac{c_{j,key,out}^{\max} - c_{j,key,in}^{\max}}{c_{j,key,out}^{\max}} \cdot F_j^{\max}\right) \quad (15)$$

The obtained result is an optimum water-using network with only concentration consideration for batch, since a storage tank is connected with every water unit, the obtained water-using structure could be the target network for the problem.

2.4.2. the second step

Time constraints are taken into the model, and the main task is to design storage tanks before the network steady. The water-using network with time consideration is designed in terms of the target network from the first period to the next until the network reaches its steady state.

3. Case study

A water-using process with 3 contaminants and 3 water-using units is illustrated here to demonstrate the practicability of the established model and the efficiency of the presented solution methods, water-using data are listed in table 1. It is seen from table 1 that the total fresh water usage is 128.3ton before WNS, and the original water-using network is as figure 2.

Table 1 Water using data of the case

j	i	$C_{i,in}^{max}$ 10^{-6}	$C_{i,out}^{max}$ 10^{-6}	t^s h	t^e h	m kg
	1	100	400			30
1	2	200	400	1	1.5	20
	3	50	200			15
	1	0	200			8
2	2	0	100	1	1.5	4
	3	0	50			2
	1	100	200			2.5
3	2	50	100	0	0.5	1
	3	50	150			2

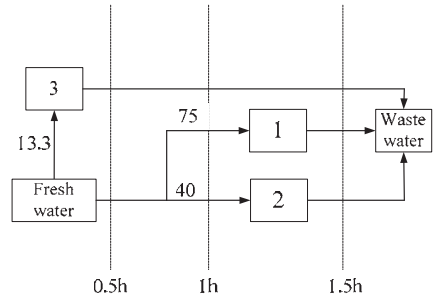

Fig.2 Original network for the case

According to the presented method above, firstly WNS problem is regarded as a pseudo-continuous process without time constraints consideration, the, the optimum water-using network is seen as figure 3, and which is the target network for the case, the minimum fresh water usage is 102.5 ton.

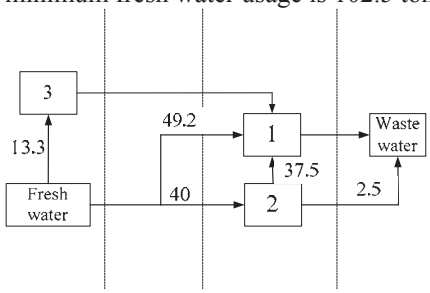

Fig. 3 The target network for the case

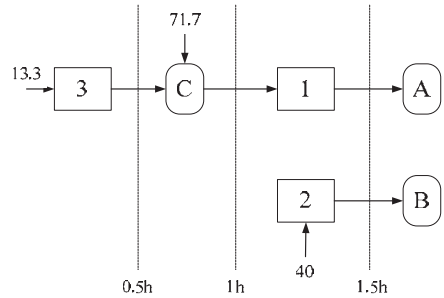

Fig. 4 Water network in the first period

Secondly, time constraints are considered in the model. In the first period, every water-using units are not steady, and no outlet water could be reused, so water sources are only fresh water, so unit 3 could be only use fresh water during 0-0.5h; during 1.0-1.5h, unit 2 is not steady so that its outlet water could not be reused, so unit 2 could only be used fresh water, however unit 1 as the last water-using unit it could be used the outlet water of unit 3; the outlet water of unit 1 and 2 are fed into storage tank A and B respectively, therefore the first period finished and the obtained network is shown as figure 4.

It could be seen that unit 2 and unit 3 are steady by comparison figure 4 with figure 3, but unit 1 is not steady, so the second period must be calculated, and the obtained network is shown as figure 5.

It could be seen that all units are steady by comparison figure 5 with figure 3, so the network is steady and also reached the target fresh water usage 102.5 ton, which reduces 20% compared with the original 128.35 ton.

The final optimum water network is obtained by more optimizing the location and number of storage tanks, which is shown as figure 6.

4. Conclusions

A superstructure model for water-using network synthesis with multiple contaminants for batch process is established in the paper, in which the key contaminant component is defined and adopted. Because of time characteristics of batch the model reduction rules are put forward and a two-step solution method is presented, the first step is to determine the target network for the problem by not considering time constraints, and the second step is to determine the final optimum water-using network by optimizing the storage tanks in terms of the obtained target network. At last, a case is introduced, the calculation results show the model is practical and the solution method is efficient.

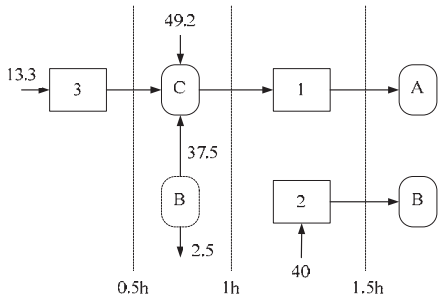

Fig. 5 Water network in second period

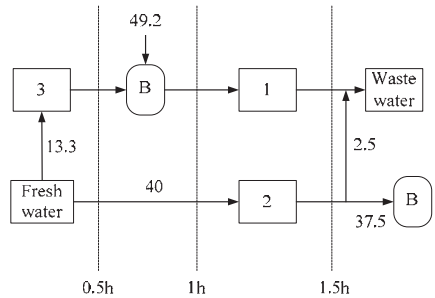

Fig. 6 Final water using network

References

D.C.Y. Foo, Z. A. Manan and Y. L. Tan., 2005, Synthesis of maximum water recovery network for batch process systems. Journal of Cleaner Production, Volume 13, Issue 15, Pages 1381-1394

E. Dogaru,V. Lavric, 2011, Dynamic Water Network Topology Optimization of Batch Processes, Ind. Eng. Chem. Res. Volume 50, Issue 7, Pages 3636–3652

H. N. Cheng, 2007, Fresh water minimization for batch process with single contamination based on linear programming. Journal of Chemical Industry and Engineering (China), Volume 58, Issue 2, Pages 417-424

J. Jezowski, 2010, Review of Water Network Design Methods with Literature Annotations, Ind. Eng. Chem. Res. 2010, Volumn 49, Issue 10, Pages 4475–4516

J.K Kim, R. Smith,2004, Automated design of discontinuous water systems. Transactions of the Institute of Chemical Engineers, Part B, 82(B3), Pages 238-248.

M. Bagajewicz, 2000, A review of recent design procedures for water networks in refineries and process plants, Computers and Chemical Engineering, Volumn 24, Issue 9, Pages 2093–2113

M. Almató, A. Espuña, L. Puigjaner., 1999, Optinization of water use in batch process Industries. Computers and Chemical Engineering, Volume 23, Pages 1427-1437

R. Grau, M. Graells, J. Corominas, A. Espun˜a & L. Puigjaner, 1996, Global strategy for energy and waste analysis in scheduling and planning of multiproduct batch chemical processes. Computers and Chemical Engineering, Volume 20, Pages 853–868.

T. Majozi., 2005, Wastewater minimisation using central reusable water storage in batch plants .Computers & Chemical Engineering, Volume 29, Issue 7, Pages 1631-1646

X. Yang, J.C. Yue, R.S. Bi, et. al., 2007, Single contaminant water network design for batch processes, Journal of Chemical Industry and Engineering(China), Volume 58, Issue 1, Pages 161-167

Y.P. Wang, R. Smith, 1994, Wastewater minimisation. Chemical Engineering Science, Volumn 49, Issue7, Pages 981-1006.

Z. L. Yao, X.G. Yuan, 2000, An approach to optimal design of batch processes with waste minimization. Computers and Chemical Engineering, Volume 24, Pages 1437–1444.

I.A. Karimi and Rajagopalan Srinivasan (Editors), Proceedings of the 11th International Symposium on Process Systems Engineering, 15-19 July 2012, Singapore.

Effects of greenhouse gas emission on decentralized wastewater treatment and reuse system

Hyunjoo Kim[a], Yujin Cheon[a], Ho-Kyung Lee[b] and In-Beum Lee[a]

[a]*Department of Chemical Engineering, POSTECH, Pohang, Kyungbuk 790-784, Republic of Korea*
[b] *LG Chem, Ltd / Research Park, Daejeon 305-380, Republic of Korea*

Abstract

There are growing concerns on greenhouse gas (GHG) emission from wastewater treatment. It is generally known that decentralized treatment of wastewater allows industrial sectors to increase wastewater reuse rate, meanwhile usually consume more energy resulted additional GHG emissions. Therefore the optimized wastewater reuse system can be largely differed when GHG emissions are considered.
We optimized industrial wastewater reuse networks considering GHG emissions. We constructed a mathematical model of wastewater reuse network including intermediate treatment facilities and a final treatment plant. Amount of emission was calculated then converted to monetary terms via carbon price and cost minimization was performed.
An industrial sector with four types of plants was selected as a case study. We figured out changes in the system when installation of intermediate facilities was allowed. If decentralized treatment and reuse were adopted the amount of freshwater consumption were decreased to 65% of the base case; when GHG emissions were considered as additional cost, the freshwater consumption increased to 87%, which is a drawback from the former case. Sensitivity analyses on the GHG expenses were performed which showed importance of pricing scheme on the network formation.

Keywords: wastewater reuse, greenhouse gas, decentralized treatment

1. Introduction

As greenhouse gases (GHG) from human activities are believed to be a main reason of climate change, estimating GHG emission draws strong interests in various fields these days. Water and wastewater treatment is not an exception; water and wastewater plants have been known as one of the most common minor source of GHG emission. In consequence there are growing numbers of researches estimating GHG emission and its impacts in water treatment and utilization. (Shahabadi et al. 2009; Fine and Hadas 2011)
It is generally known that introducing decentralized wastewater treatment encourages industrial sectors as well as urban water systems to increase water reuse ratio with shorter pipe length and easier source/effluent quality control.(Orth 2007) However, decentralized treatment facilities designed for wastetewater recycling and/or reuse usually adopt advanced treatment methods which require relatively more energy. Therefore the optimized wastewater reuse system with decentralized treatment can be largely differed when GHG emissions are considered.
In this research we optimized industrial wastewater reuse networks considering GHG emissions. We constructed a mathematical model of wastewater reuse network including intermediate treatment facilities and a final treatment plant. A wastewater network of an industrial sector was optimized as a case study and results were discussed.

2. Methodology

2.1. GHG emissions in wastewater reuse

GHG emissions from wastewater treatment are generally classified into two categories: (1) direct emissions from biological degradation (2) indirect emissions from energy usage, mainly electricity. While typical secondary treatment facilities show higher direct emission ratio, major part of emissions in advanced treatment methods are from their electricity use since their general aim is to remove metals and recalcitrant organics which do not discharge biological GHGs like methane when removed. (Environment Agency 2009)

2.2. Mathematical formulation of wastewater reuse network

Figure 1 shows general configuration of water network in an industrial sector adopted in this research. The network includes four types of unit process; manufacturing processes, decentralized (intermediate) treatment facilities, final treatment center and reclamation unit as its annex. Flow and mass balance equations were developed and listed in Table 1.

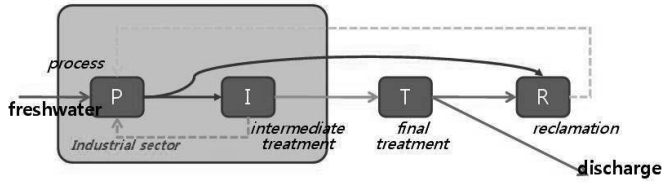

Figure 1. General wastewater reuse network

Table 1. Flowrate and mass balance equations

	Flowrate balance	Mass balance
Manufacturing process	$fw_p + \sum_i rg_{i,p} + rc_p \geq fpin_p$, $fpout_p = \sum_i wwi_{p,i} + wwt_p$	$Cfw_p fw_p + \sum_i Crg_{i,p} rg_{i,p} + Crc_p rc_p \leq Cfpin_p (fw_p + \sum_i rg_{i,p} + rc_p)$, $Cfpout_p = Cwwi_{p,i} = Cwwt_p$
Intermediate treatment	$\sum_p wwi_{p,i} = fiin_i$, $fiin_i = fiout_i$, $fiout_i = \sum_p rg_{i,p} + wwd_i$	$\sum_p Cwwi_{p,i} wwi_{p,i} = Cfiin_i fiin_i$ $Cfiin_i = \chi \cdot Cfiout_i$, $Cfiout_i = Crg_{i,p} = Cwwd_i$
Final treatment	$\sum_p wwt_p = ftin$, $ftin = ftout$, $ftout = wwr + dc$	$\sum_p Cwwt_p wwt_p = Cftin \cdot ftin$, $Cftout = Cwwr = Cdc$
Reclamation unit	$wwr + \sum_i wwd_i = frin$, $frin = frout$, $frout = \sum_p rc_p$	$wwrCwwr + \sum_i Cwwd_i wwd_i = frinCfrin$, $Cfrout = Crc_p$

2.3. Economic evaluations

In developing wastewater reuse network economic evaluation is a must, since cost reduction is one of the main reasons of wastewater reuse. We calculated total annual

expenses of the network with capital and O/M cost including charges for water consumption and wastewater discharge and individual treatment facility operation cost if introduced.
In this research we dealt with different expensing schemes for direct and indirect GHG emissions. For emissions from electricity use from pumping and freshwater consumption a fixed carbon tax was imposed. In the case of emissions from treatment facilities carbon credit method was introduced.

3. Case Study

3.1. System descriptions
We carried out a case study with the mathematical model and optimization strategy. A South Korean industrial sector with 15 plants discharging highly contaminated wastewater with metals and chemicals was selected as a case study. The plants were categorized into four business types (general, cements, chemicals, textile) and standard concentration values were assigned for each category if not specified.

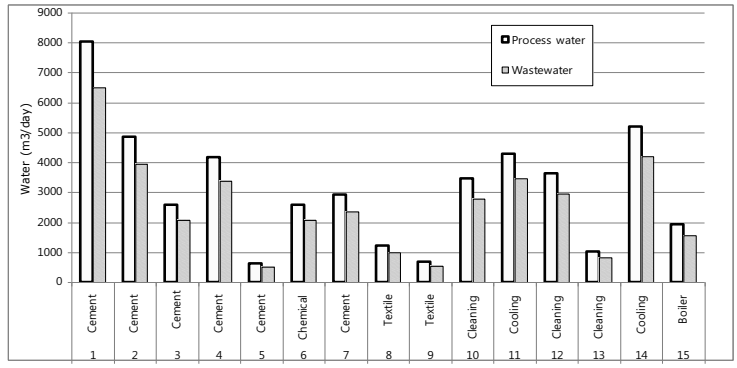

Figure 2. Water/wastewater characteristics of plants in the sector

Two types of intermediate treatment facilities, reverse osmosis (RO) and microfiltration (MF), were considered. Their cost, treatment efficiencies as well as GHG emission were presented in Figure 3.
Cost minimization was performed (1)considering decentralized treatment facilities, without GHG expenses (2) under cost objective function with GHG expenses. Then the results were compared and analyzed.

3.2. Results
While a wastewater reuse network can be formulated without intermediate treatment center, decentralized facilities gave more reuse oppotunities to the system. Amount of wastewater reuse decreased when additional expense from GHG emissions was included. The reuse amount reduction in the latter case was mainly due to the additional GHG expenses, since total GHG emission of the system was decreased to 25% of the second case(9,812,000 to 2,514,000 kgCO_2/day).
As shown in Figure 5, RO was favored in both cases. Better treatment efficiency of RO was the major reason of the preference despite of the higher capital cost. It was also noticeable from figure 4 and 5 that reclaimed water from intermediate facilities was much preferred when GHG emissions were considered.

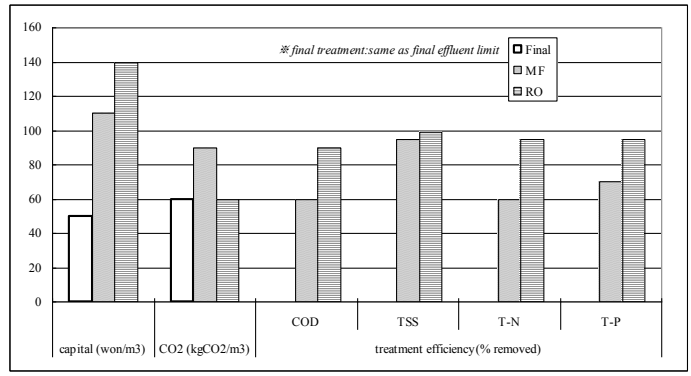

Figure 3. Characteristics of treatment facilities

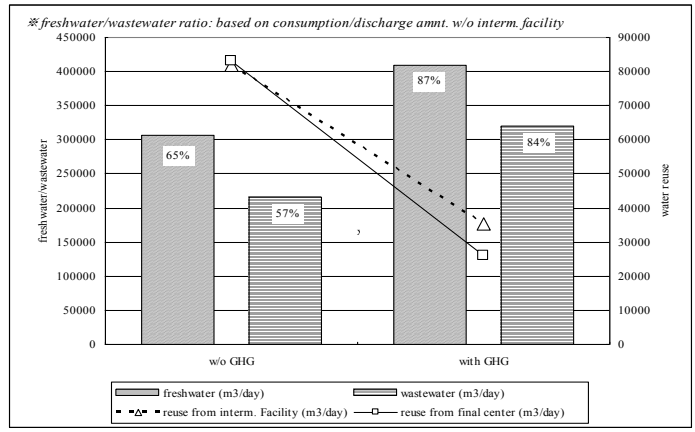

Figure 4. Amount of water consumption/discharge and reuse under different obj. functions

To figure out effects of GHG expense to the system we performed a couple of sensitivity analysis on GHG price. When GHG tax on freshwater increased, amount of reuse was increased to some extent then remained on the same. In the case of carbon capping for facilities, as carbon tax increased amount of reuse from intermediate facilities were decreased.

Based on the sensitivity analyses the pricing rule which enabled maximun amount of reuse can be derived. While the result cannot be adopted directly because of the lack of data validation, it shows that a proper GHG pricing scheme is necessary for developing effective reuse networks.

4. Conclusions

Wastewater reuse network with decentralized treatment facilities were developed and optimized considering GHG emissions from both direct and indirect sources. While decentralized facilities increased reuse potential within the system, additional expenses from GHG emission gave negative effects on wastewater reuse. By modifying GHG pricing scheme the reuse network can be evolved into more efficient one.

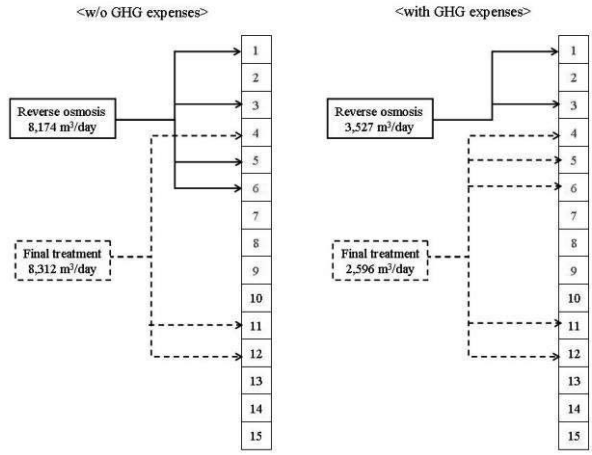

Figure 5. Reclaimed water usage

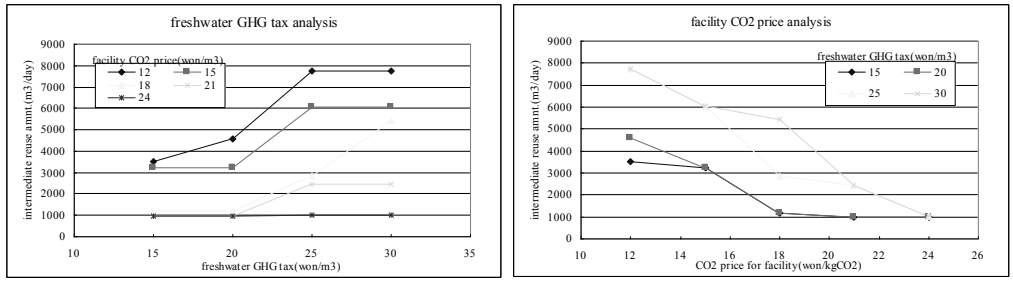

Figure 6. Total freshwater consumptions under different GHG pricing schemes

Nomenclature

p: manufacturing process ; i: intermediate treatment facility ; fw_p: freshwater into process p
$rg_{i,p}$: reclaimed water from intermediate facility i to process p
rc_p: reclaimed water from final reclamation unit to process p
$wwi_{p,i}$: wastewater from process p to intermediate treatment facility i
wwt_p: wastewater from process p to final treatment center
$fiin_i$: wastewater into intermediate facility i ; $fiout_i$: reclaimed water from intermediate facility i
wwd_i: reclaimed water from intermediate facility i to reclamation unit
ftin: wastewater into final treatment center ; ftout: reclaimed water from final treatment center
wwr: reclaimed water from final treatment center to reclamation unit ; dc: discharged water
frin: reclaimed water into reclamation unit ; frout: reclaimed water from reclamation unit

References

M. B. Shahabadi , L. Yerushalmi, F. Haghighat, Impact of Process Design on Greenhouse Gas Generation by Wastewater Treatment Plants, Water Research, 43,10, 2009, 2679-2687

P. Fine, E. Hadas, Options to Reduce Greenhouse Gas Emissions During Wastewater Treatment for Agricultural Use, Science of The Total Environment, 2011, Article in press

Environment Agency, Transforming Wastewater Treatment to Reduce Carbon Emissions, 2009

H. Orth, Centralised versus decentralised wastewater systems?, Water Science & Technology, 56,5, 2007, 259-266

I.A. Karimi and Rajagopalan Srinivasan (Editors), Proceedings of the 11th International Symposium on Process Systems Engineering, 15-19 July 2012, Singapore.

Optimal Membrane Desalination Network Synthesis with Detailed Water Quality Information

Sabla Y. Alnouri, Patrick Linke

Department of Chemical Engineering, Texas A&M University at Qatar, Education City, PO Box 23874, Doha, Qatar,
sabla.alnouri@qatar.tamu.edu; patrick.linke@qatar.tamu.edu

Abstract

This work builds on a previously developed superstructure optimization approach for SWRO desalination network design, and expands the richness of the representation by accounting for multiple water quality parameters, including boron. This involves replacing conventionally-simplified feed solution assumptions, and incorporating multiple water quality parameters into the SWRO network optimization problem. In doing so, simple correlations capable of predicting RO membrane performance, according to salt rejection characteristics, is carried out by exploiting numerical simulation data via the specialized commercial membrane design software such as ROSA Filmtech (Reverse Osmosis Systems Analysis). A number of additional degrees of freedom are introduced into the problem, such as the pH level, since it considerably affects the boron removal efficiency. Moreover, the superstructure representation has been extended to include multiple membrane element choices for the different SWRO units within the network, rather than strictly limiting the network design to a single membrane type, thus allowing the assessment of several choices of membrane types within a single optimization. Moreover, enhanced economic and environmental assessment procedures are adapted, that capture more genuine and accurate design performance predictions. The method is illustrated through a case study example involving a typical seawater feed.

Keywords: *desalination; reverse osmosis; process design; multiple water quality parameters; boron removal*

1. Introduction

Membrane-based water desalination technologies have become increasingly attractive, as well as globally utilized in order sustain the rapid increase in demand for potable water [1]. The design of such desalination processes resembles a network synthesis problem, for which the utilization of a superstructure optimization approach is employed to identify plausible design candidates, given certain desirable performance conditions and constraints. However, it is often realized that many previous approaches, although capable of capturing rich sets of process configurations, generally lack the ability to handle detailed water quality information as part of the process synthesis and optimization problem [2, 3]. This usually presents inconsistency in terms of the richness of the solutions obtained since detailed information is often essential when assessing important operational and product constraints. Handling multiple water quality parameters are of preeminent importance, especially within a desalination network design problem, due to the variable scaling tendency of certain seawater components. Therefore, it is essential to capture multiple water quality parameters when solving a

SWRO network design problem, as opposed to adopting the standard assumption of two pseudo components, i.e. “water” and “total dissolved solids”. This would enable the design impact of important phenomena to be addressed, most importantly membrane scaling and, boron removal.

2. Synthesis Approach

This work adopts a well-defined SWRO network synthesis strategy representation introduced previously [4], that involves two main steps:

2.1. Targeting: The performance target of the system is determined through global optimization of full superstructures, in which the best performing design is extracted and subsequently used as a benchmark whilst assessing different design alternatives.

2.2. Development of Alternative Designs: Reduced superstructures resembling fundamentally distinct design classes are globally optimized, such that design alternatives of increasing complexity can be identified. Therefore, insights for potential performance advantages, any complex designs offer over more simple designs can be analyzed.

3. Accounting multiple water quality parameters

The prediction of membrane desalination process performance in relation to a reflective multiple water quality nature within the network is of imminent importance, since the presence of turbidity and high concentration levels of hardness ions, such as calcium and magnesium, tend to degrade a SWRO plant performance [1]. Therefore, effective knowledge regarding the concentrations of the various sweater components (especially dissolved ions which are usually lumped together as a Total Dissolved Solids “TDS” category) would drastically improve understanding of the behavior of such components in a SWRO network optimization problem. Simplified analytical relations that provide technical membrane performance information, in terms of salt rejection capacities of individual ions are developed accordingly. Such water quality parameter information is extracted from available membrane commercial simulators, such as ROSA Filmtech (Reverse Osmosis Systems Analysis) [5]. All data extracted are in the form of simple linear relationships relating ion-specific rejection characteristics to temperature, and such relevant information pertaining to membrane performance, serve with relatively sufficient accuracy over typical variations in operating conditions.

4. Accounting for boron removal requirements

Standard boron removal techniques, that would effectively achieve low boron levels in the permeate have been previously presented and adopted [6-8]. Therefore, models that predict boron removal efficiency within a SWRO network optimization problem are very imperative for an accurate determination of plausible designs. Operating parameters such as the temperature and pH, affect the levels of boron removed from the permeate stream. Thus, in order to enable accurate predictions for the purpose of screening the various boron removal options, simplified analytical relations are developed for multiple membrane element choices. This enables the superstructure optimization to determine SWRO networks that feature different types of membrane elements in different parts of the network, targeting the removal of specifically important water quality parameters. For each membrane element choice, correlations are using the combined effects of temperature and pH onto boron rejection, as well as all other ions constituting the feedwater, for a number of commercial membrane elements:

BW30-2540, SW30HRLE-4040, SW30-2540 and SW30HRLE-400i. The information regarding these modules has been extracted from ROSA, in order to capture the observed membrane element performance.

5. Enhanced economical assessment considerations

To enable the extraction of meaningful solutions, we have formulated a comprehensive economic objective function, so as to capture the multiple fixed and variable costs associated with real SWRO plants. This is implemented through the use of a thorough cost breakdown assessment procedure, consisting of computations for the Total Annualized Cost (TAC) as function of an annualized form of Total Capital Investment (TCI), involving Direct Capital Costs (DCC), Soft Costs (SC) as well as a Contingency Cost (CC) factor, all added to the Total Operating Cost (TOC) of the system, both Variable O&M Costs (VOC), and Fixed O&M Costs (FOC). [1, 9-13]. A Lang Factor (LF) and a Depreciation (D) value were assumed to be associated with the total capital investment term, over the useful plant lifetime.

6. Mathematical Formulation & Implementation

The problem formulation involves a performance assessment criterion as an objective, relating various operational and capital cost elements to the design variables. System constraints involving mass balance calculations around the inlet process splitter, outlet process mixers, mixers and splitters associated with individual membrane units in the system (both reject and permeate) are formulated. The resulting optimization problem takes the form of a Mixed Integer Non Linear Program (MINLP), in which the aim was to minimize the total annual cost (TAC), subject to process equality and inequality constraints. Given these conditions, the optimization problem is solved using "*what'sBest"* LINDO Mixed-Integer Global Solver for Microsoft Excel [14], so as to keep the implementation simple and user friendly.

7. Case Study

A seawater desalination case study example is carried out using the modified representation, which has been introduced in previous work [4]. The capability of extracting multiple water quality information, boron removal efficiency, and assessing the performance of several membrane element types within the optimization problem is implemented. Table 1 summarizes some of the input parameters for the case study using a typical seawater feed (salinity 34.39 g/L). Figure 1 illustrates an optimal solution example attained using superstructure optimization for a design that incorporates three units, where both exiting streams from first RO unit are treated using both a subsequent stage and pass simultaneously. The solution was obtained in 74s of CPU time on a on a desktop PC (Intel® Core ™ i7-2620M, 2.7 GHz, 8.00 GB RAM). Table 2 summarizes the water quality information extracted, for the network reject and permeate. Therefore, the example illustrates how detailed insights into water quality dependent problem features can be explored within reasonable CPU times using the proposed approach. The total annual cost of the design illustrated was found to be \$0.574/m^3, with an annual fixed cost of \$0.107/ m^3, and an operating cost of \$0.466/m^3 of water produced.

Table 1- Case Study Input Data

Parameter	*Value*
Total inlet feedwater flowrate into the network (m^3/day)	40,000
Minimum permeate flow required in the network (m^3/day)	12000
Maximum allowable TDS in the permeate (ppm)	450
Maximum allowable boron concentration in the permeate (ppm)	0.5
Pressure drop in RO unit j (bar)	1.3
Maximum allowable feed pressure using SW RO elements (bar)	70
Maximum allowable feed pressure using BW RO elements (bar)	15.5
Temperature (^oC)	25
Number of Skids	1
Lang Factor	5
Depreciation (yr)	20
Power Cost ($/kWh)	0.05

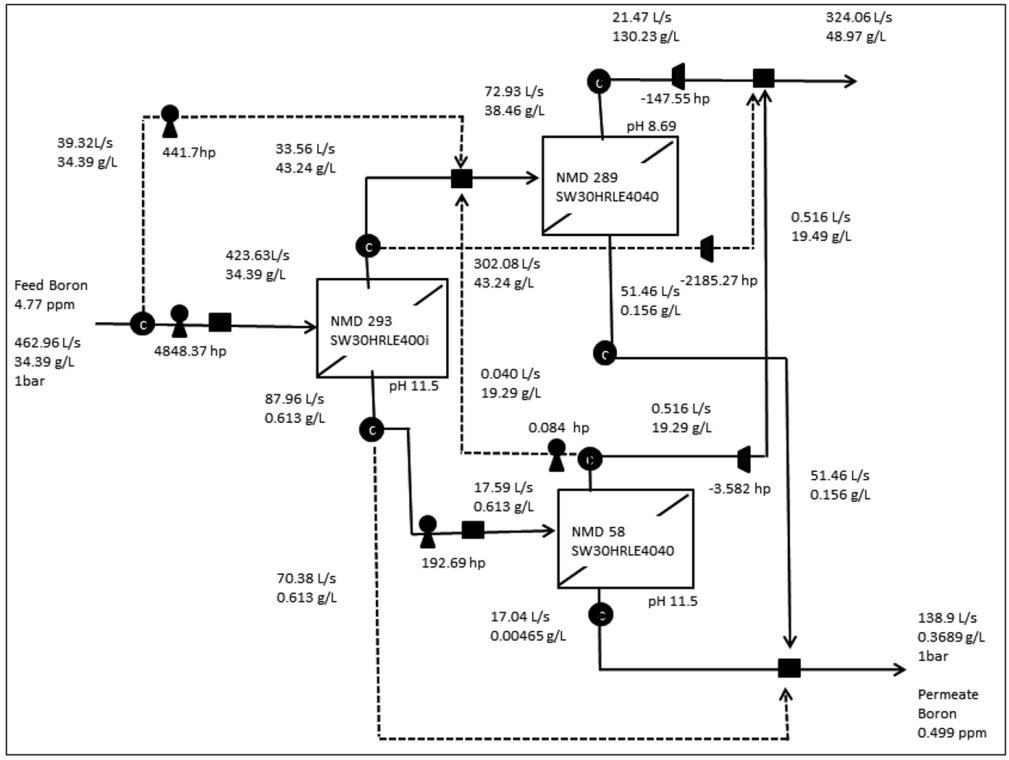

Figure 1. Typical seawater feed, optimal solution example involving a three-unit design case

Table 2. Water quality information extracted

Ions	*Feed (mg/L)*	*Permeate (mg/L)*	*Reject (mg/L)*
K	380	10.68	538.27
Na	10556	246.75	14974
Mg	1262	7.07	1799.8
Ca	400	2.21	570.47
Sr	13	0.07	18.54
HCO3	140	3.20	198.62
SO4	2649	56.91	3760
Cl	18985	42.58	27103
Boron	4.77	0.499	6.60
TDS	34390	368.95	48970

7. Conclusions

This paper involves the utilization of a superstructure optimization approach, and expands the proposed representation so as to incorporate additional water quality parameters, including boron considerations, as well as multiple membrane element choices into the SWRO network optimization problem. Data extracted for various membrane elements, that predict water quality parameters using commercial membrane software, are employed. A case study that illustrates the various features of the problem is demonstrated, and it was shown that the solutions extracted become a lot richer, within reasonable CPU computational timings.

References

1. A. Cipollina, G. Micale, L. Rizzuti, Seawater Desalination Conventional and Renewable Energy Processes (2009), Springer-Verlag Berlin Heidelberg
2. M. El-Halwagi, AIChE Journal, 38 (8) (1992) 1185-1198.
3. Y. Saif, A. Elkamel, M. Pritzker, Ind. Eng. Chem. Res. 47 (1) (2008) 3060-3070.
4. S. Alnouri, P. Linke (2012). Reliable and Efficient Targeting for Optimal Design of SWRO Desalination Processes. In I.D.L. Bogle and M. Fairweather (eds), Proceedings of the 22nd European Symposium on Computer Aided Process Engineering, 17 - 20 June 2012, London, Elsevier
5. http://www.dowwaterandprocess.com/support_training/design_tools/rosa.htm
6. P. Glueckstern, M. Priel, Desalination 156 (1–3) (2003) 219–228.
7. N. Nadav, M. Priel, P. Glueckstern, Desalination 185 (1–3) (2005) 121–129.
8. L.F. Greenlee, et al., Water Research 43 (9) (2009) 2317–2348.
9. M. Wilf, The Guidebook to Membrane Desalination Technology: Reverse Osmosis, Nanofiltrartion and Hybrid Systems: Process Design, Application and Economics (2007), Balaban Desalination
10. S. Frioui, R. Oumeddour, Desalination 223(1) (2008) 457–463
11. I.C. Karagiannis, P.G Soldatos, Desalination 223(1) (2008) 448–456
12. R.T.Vicente, G.R, Lourdes, Desalination 181(1) (2005) 43-59
13. S.C, McCutcheon, J.L, Martin, T.O, Barnwell, Handbood of Hydrology: Water Density as a Function of Temperature and Concentration (1993)
14. http://www.lindo.com/index.php?option=com_content&view=articleReferences

I.A. Karimi and Rajagopalan Srinivasan (Editors), Proceedings of the 11th International Symposium on Process Systems Engineering, 15-19 July 2012, Singapore.

Modeling and Simulation of CO_2 Absorption with Amine Component Solvent

Yanjie Chen[a,b], Yuehua Yao[a,b], Xiangping Zhang[b,*], Chunshan Li[b], Haifeng Dong[b] , Ying Huang[b], Baozeng Ren[a]

[a]*School of Chemical Engineering and Energy, Zhengzhou University,450001,Zhengzhou, China*
[b]*Institute of Process Engineering, Chinese Academy of Sciences, 100190, Beijing, China*

Abstract:Blended amine solvent has been shown unique and predominant performance while used to capture CO_2 compared with the single amine solvent. Calculations were compared with experimental solubility measurements of CO_2 in aqueous ternary and quaternary systems of H_2O, MEA and AMP. Electrolyte non-random two liquid (ENRTL) theory was employed to fit solubility data in three ternary systems CO_2–H_2O–MEA and CO_2–H_2O–AMP. The binary interaction energy parameters for the ionic species were obtained by regression of the experimental solubility data of the ternary systems. A good agreement between the calculated values and the experimental data was achieved. Process simulation for CO_2 removal using an equilibrium approach was performed with newly fitted parameters. The simulation results have been compared with the pilot plant experimental data.

Keywords: CO_2 capture; Blended amine; Electrolyte-NRTL model; Simulation

1. 1 Introduction

The application of CO_2 capture and subsequent geological storage (CCS) is a promising option to significantly reduce the greenhouse gas emissions of coal-fired power plants[1]. In a post combustion CO_2 capture process, CO_2 is separated from the flue gas of the power plant.Recently the use of blended amines (a solution of two or more amines in varying compositions) in gas-treating processes is a subject of potentially major industrial importance.The blended amines, which contain a combination of the absorption characteristics of the amines, such as higher loading capacity and faster reaction rate, brings about a considerable improvement in absorption and a great savings in energy requirements. Over the past two decades, extensive data for the ternary systems CO_2–H_2O–MEA and CO_2–H_2O–AMP have been collected. Many thermodynamic models were proposed in order to reproduce experimental data[2,3].The Electrolyte Non-Random Two Liquid (NRTL) model is a versatile model for the calculation of activity coefficients. Using binary and pair parameters, the model can represent aqueous electrolyte systems as well as mixed solvent electrolyte systems over the entire range of electrolyte concentrations,so the Electrolyte-NRTL model is used in this paper.

This paper focuses on CO_2 capture from flue gas by absorption with mixed amines of monoethanolamine (MEA) and 2-amino-2-methyl-1-propanol (AMP), which appears to be an attractive new blended amine solvent for the gas treating processes. Electrolyte-NRTL equations for equations for electrolytic mixed-solvent solution were applied also and the equilibrium model of gas absorption in the system of CO_2-MEA-AMP-H_2O was established. The parameters in Electrolyte-NRTL equations were carefully selected and

* Corresponding authors. E-mail addresses: xpzhang@home.ipe.ac.cn(X.P. Zhang)

obtained through regression. With the parameters generated from gas absorption equilibrium data, solubilities of CO_2 in the mixed amine solutions can be directly predicted. The process simulation was also carried out with the thermodynamic model. The simulation results are compared with measured data from pilot plant.

2. Thermodynamic Model

2.1. Electrolyte-NRTL model

The CO_2-MEA-AMP-H_2O quaternary system involving different ionic species, the activity coefficient of any species is calculated from the partial derivative of the excess Gibbs energy with respect to the mole number, i.e.

$$\ln\gamma_i = \frac{1}{RT}\left[\frac{\partial(n_t g^{ex})}{\partial n_i}\right]_{T,P,n_{j\neq i}} \tag{1}$$

The electrolyte NRTL model uses the infinite dilution aqueous solution as the reference state for ions[4,5]. The excess Gibbs energy of a mixed solvent electrolyte system can be written as the sum of two contributions; local ion–molecule, ion–ion and molecule–molecule interactions that exist in the immediate neighborhood of any species and long-range ion–ion interactions.

$$g^{ex} = g^{ex,LR} + g^{ex,local} \tag{2}$$

The first term on the right hand side of Eq.(3) is the original Pitzer-Debye-Hu¨ ckel equation while the second term is the Born expressions for excess Gibbs energy:

$$\frac{g^{ex,LR}}{RT} = -\left(\sum_k x_k\left(\frac{1000}{M_s}\right)^{0.5}\left(\frac{4A_\phi I_x}{\rho}\right)\ln\left(1+\rho\sqrt{I}\right)\right) + \frac{e^2}{2kT}\sqrt{\left(\frac{1}{D}-\frac{1}{D_w}\right)}\left(\sum_i \frac{x_i z_i^2}{r_i}\right)\times 10^{-2} \tag{3}$$

The local-composition electrolyte NRTL expression for excess Gibbs energy is given as follows，

$$\frac{g^{ex,local}}{RT} = \sum_m X_m \frac{\sum_j X_j G_{jm}\tau_{jm}}{\sum_k X_k G_{km}} + \sum_c X_c \sum_{a'}\left(\frac{X_{a'}}{\sum_{a''} X_{a''}}\right)\frac{\sum_j X_j G_{jc,a'c}\tau_{jc,a'c}}{\sum_k X_k G_{kc,a'c}} + \sum_a X_a \sum_{c'}\left(\frac{X_{c'}}{\sum_{c''} X_{c''}}\right)\frac{\sum_j X_j G_{ja,c'a}\tau_{ja,c'a}}{\sum_k X_k G_{ka,c'a}} \tag{4}$$

The different terms in Eq.(4), are computed using the following expressions:

$$G_{jm} = \exp(-\alpha_{jm}\tau_{jm}),\ G_{jc,ac} = \exp(-\alpha_{jc,ac}\tau_{jc,ac}),\ G_{ja,ca} = \exp(-\alpha_{ja,ca}\tau_{ja,ca})$$

$\tau_{ca,w}$，$\tau_{w,ca}$，binary interaction parameters are expressed as a function of temperature:

$$\tau_{ca,w} = C_{ca,w} + \frac{D_{ca,w}}{T} \quad \tau_{w,ca} = C_{w,ca} + \frac{D_{w,ca}}{T}$$

The data regression system (DRS) in Aspen Plus allows the use of user experimental data to estimate the model parameters. In this work, the following interaction parameters are fitted from experimental data available in literature. H_2O–$MEACOO^-MEAH^+$, $MEACOO^-MEAH^+$–H_2O, H_2O–HCO_3^-MEAH+ , HCO_3^-MEAH+–H_2O, H_2O–HCO_3^-AMPH+, $HCO_3^-MEAH^+$–H_2O.

2.2. Experimental results

Experimental data are important for the regression of interaction parameters, so the reliability of the data is important. In this work, VLE data of CO_2 in MEA were form

the literature Jou et al[6]. The data has sufficiently covered temperature from 0℃to150℃,CO_2 partial pressure from 0.001-2000 kPa. The VLE data source of CO_2-AMP comes from Seo and Hong, and it covers the blends of MEA and AMP, including the ratio of MEA and AMP is 18 wt%/12 wt%(1:1 in mole)[7].

2.3. Results and discussion

In this work, interaction parameters were fitted using data regression to determine the parameter values was performed using an algorithm reported by Britt and Luecke[8]. The objective function is formulated based on the maximum likelihood principle. Table 1 shows new parameters for the Electrolyte-NRTL. All parameters obtained for the ternary systems, were used for in the quaternary systems.

Table 1 Interaction parameters estimated using Aspen Plus

Value	$C_{w,ca}$ /$C_{ca,w}$	$D_{w,ca}$ /$D_{ca,w}$
H_2O-$MEAH^+$-HCO_3^-	5.3467128	964.48626
$MEAH^+$-HCO_3^- -H_2O	-4.0754512	-11.071867
H_2O- $MEAH^+$-$MEACOO^-$	9.8773762	10.809863
$MEAH^+$-$MEACOO^-$ -H_2O	-4.9595131	0.062485124
H_2O-$AMPH^+$-HCO_3^-	22.531087	-4296.8954
$AMPH^+$-HCO_3^- -H_2O	-11.374142	2248.5915

The model parameters generated from the single amine experimental data were used to predict CO_2 loading in MEA–AMP mixtures without further regression. The model predictions are compared with the experimental values for mixtures of 12 wt%-18 wt%. Fig.1 shows the solubility of CO_2 in the aqueous of MEA and AMP (1:1 in mole) solution at 40℃, and the results are in good agreement with the experimental data.

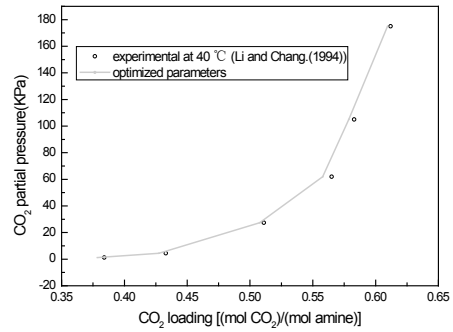

Fig.1 VLE figure of CO_2–blended amine–H_2O with E-NRTL model at 40 ℃.

3. Process simulation

3.1. Pilot plant experiment

The experimental equipment of CO_2 capture by reactive absorption was designed and set up in our laboratory, and the capacity of the gas treatment is $1m^3$/hr. The detailed parameters of the equipments are listed in table 2.

Table 2 Data of the absorber and the desorber in our pilot plant

Parameter	Absorber	Desorber
Diameter (m)	0.05	0.05
Packing height(m)	1.6	1.4
Packing type	Θring 5×5	Θring 5×5
Operation pressure(bar)	<15	<10

The simulated flue gas are made through mixing N_2 and CO_2.The CO_2 gas mixture, with the flow rate of about 0.5 m^3/h and the CO_2 volume concentration about 9%, entering the absorber from the bottom, and the amine solution, with the flow rate of around 3 kg/h and after cooled to 40℃by the cooler, entering the absorber from the top. After absorbing the CO_2 in the flue gas, the purified gas leaves at the top of the absorber. The rich amine solution is pre-heated to 95 °C by the heat exchanger, entering into packed desorber from the top. After heating, the amine solution evaporates and has the liquid-gas mass exchange in the desorber, achieving the desorption process. Consequently, after reaching the steady state, this experimental procedure system is acompletely closed loop system.The experimental run 48 hours, except the data recorded by the computer ,liquid samples were collected from the absorber feed and the outlet to check for CO_2 loading .

3.2. Process simulation for CO_2 absorption with mixed amines

A simulation program was established to simulate the capture and desorption process with software Aspen Plus. The thermodynamic model Electrolyte-NRTL and parameters regressed in this work are used. An equilibrium-stage model was adopted in this work in view of its lesser complexity. The simulation results will be compared with the pilot plant measurement data.

Table 3 Comparison between simulation results and experimental data of absorption column

Item	Value of simulation	Value of experiment
Inlet gas/$Nm^3.h^{-1}$	0.5	0.5
Inlet lean solvent/$l.h^-$	3	3
Flue gas inlet temp/℃	30	30
Outlet gas temp/℃	40	40.1
Lean solvent feed temp/℃	40	39.9
Top pressure/bar	1.1	1.2
Bottom pressure/bar	1.15	1.18
Rich CO_2 loading ($molCO_2$/mol MEA)	0.35	0.34
CO_2 at outlet (mol% wet)	0.7	1

CO_2 recovery(%)	92.9	89.8

Table 4 Comparison between simulation results and experimental data of desorption column

Item	Value of simulation	Value of experiment
Outlet CO_2 gas/$Nm^3.h^{-1}$	0.042	0.40
Inlet rich solvent/$l.h^-$	3	3
Outlet gas temp/℃	40	40.1
Rich solvent feed temp/℃	40	39.9
Top pressure/bar	1.1	1.1
Bottom pressure/bar	1.15	1.12
Lean CO_2 loading (molCO_2/mol MEA)	0.16	0.15

It can be seen from Table3-4 that the predictions of the model are in good agreement with the experimental data. A difference of less than 7% between the models prediction and the pilot plant experimental data has been obtained.

4. Conclusions

Thermodynamic models have been established for calculation of gas solubility of CO_2 in aqueous amine solution with electrolyte-NRTL model equations as the activity coefficient model. The electrolyte-NRTL model parameters generated in the single amine MEA and AMP can be used to predict CO_2 solubility in the mixed amine solutions. The process simulation software is established based on gas solubility thermodynamic models. Simulation prediction results are in good agreement with pilot plant experimental ones. This work will provide some instructions in rational design and simulation of the gas treating units involving blended amine solvent.

References

[1] Hongqun Yang, 2008, Progress in carbon dioxide separation and capture: A review. Journal of Environmental Sciences. 20, 14–27.

[2] Ying Zhang, 2009, Rate-Based Process Modeling Study of CO_2 Capture with Aqueous Monoethanolamine Solution. Ind. Eng.Chem.Res. 48, 9233–9246.

[3] B. P. Mandala, 2001, Removal of carbon dioxide by absorption in mixed amines: modelling of absorption in aqueous MDEA/MEA and AMP/MEA solutions. Chemical Engineering Science. 56, 6217–6224.

[4] M.K. Aroua, 2002, Modelling of carbon dioxide absorption in aqueous solutions of AMP and MDEA and their blends using Aspenplus. Separation and Purification Technology. 29, 153–162.

[5] Yunda Liu, 1999, Representing Vapor-Liquid Equilibrium for an Aqueous MEA-CO_2 System Using the Electrolyte Nonrandom-Two-Liquid Model. Ind. Eng. Chem. Res. 38, 2080-2090.

[6] Fang-Yuan Jou, 1994, Vapor-Liquid Equilibrium of Carbon Dioxide in Aqueous Mixtures of Monoethanolamine and Methyldiethanolamine. Ind. Eng. Chem. Res. 33, 2002-2005.

[7] MengHui Li,1994, Solubilities of Carbon Dioxide in Water+Monoethanolamine +2-Amino-2-methyl-1-propanol. J.Chem. Eng. Data. 39, 448-452.

[8] Aspen Physical Property System,V7.2. Aspen Technology, Inc:Burlington, MA,2010.

I.A. Karimi and Rajagopalan Srinivasan (Editors), Proceedings of the 11th International Symposium on Process Systems Engineering, 15-19 July 2012, Singapore.

Life cycle assessment of coal-based methanol

Hengchong Li, Siyu Yang, Yu Qian

School of Chemistry and Chemical Engineering, South China University of Technology, Guangzhou 510640, P.R. China

Abstract

This paper analyzes the environment impact of methanol production from both product life cycle and process life cycle. Four indicators, global warming, acidification, photochemical oxidant formation and human toxicity, are used for assessment. According to the analysis, the periods that have significant impacts on environmental performance are explored. Several suggestions are provided at the end.

Keywords: Process life cycle; Product life cycle; LCA; Environmental impact.

1. Introduction

Life cycle environmental assessment (LCA) is the cradle to grave analysis. It investigates environmental impacts of a system, a process, or a product. Application of LCA is now expanded and its techniques are used in the evaluation of economic and technical performance. The methodological framework of LCA includes goal and scope definition, inventory analysis, impact assessment and interpretation.

In this paper, LCA is used to assess the environmental impact of the process of coal producing methanol. The reason for selecting this process is due to the dominance of coal in China's energy structure. Methanol is an important platform chemical and can be used to synthesize a large range of derivatives, methanol gasoline and formaldehyde, dimethyl ether, etc. In China, the demand for methanol is increasing. However, the production process of methanol gives environmental impacts. This impact is increasingly worse as the production scale increases. It is therefore important to assess this impact. This paper uses LCA to analyze the production process from both product life cycle and process life cycle. The combination of these two gives a comprehensive assessment on environmental performance of the production process.

2. Goal and scope definition

Four indicators for environmental assessment are used in this paper. They are global warming, acidification, photochemical oxidant formation and human toxicity. As for defining the boundaries, the product life cycle and the process life cycle are considered separately. For the product life cycle, five periods, coal mining, coal transportation, methanol production, methanol utilization and waste disposal, are defined. For process life cycle, there are five periods, building materials production, building materials transportation, factory construction, plant operation and factory disposal. The boundaries are shown in Figure 1. It can be seen that the methanol production period in the product life cycle is equivalent to the plant operation period in the process life cycle.

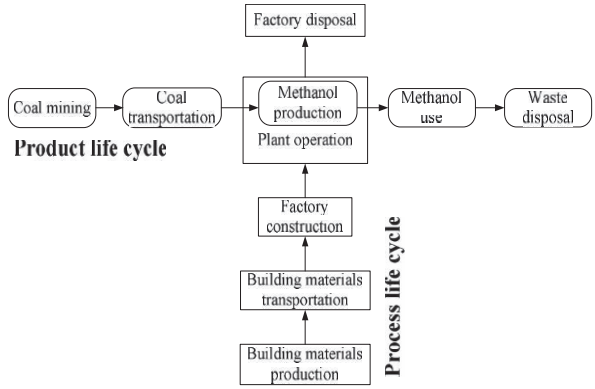

Figure 1. Life cycle boundaries of methanol production processes

3. Inventory analysis

Inventory analysis is the most important step in LCA because of its significant affect on final results. In this paper, eight general pollutant emissions (PM10, SO_X, CO, CO_2, VOC, CH_4, NOX, and N_2O) are collected for inventory. For the methanol utilization period, methanol is used as fuel (M100, Methanol solution without additives) for vehicles. The emitted gases from vehicles are not recycled so there is no waste disposal period in this paper. The production process of methanol involves a large number of material flows and heat flows. It is therefore difficult for data collection for the production period. Aspen Plus is used for modeling and simulating the process. The relevant parameters refer to the Handbook of Modern Coal Chemical Technologies (Xie, 2006). Emissions of the production period are obtained from the simulation results.

For inventory of the process life cycle, we assume that the location of the plant is in Guangzhou, China. We also assume that the building materials are transported from Foshan (40km away from Guangzhou) by diesel trucks. The emissions in the production process of these building materials refer to the literatures (Marono, 2001; Liu, 1998). Data for plant construction and plant disposal was found in Ecoinvent Database (Althaus, 2007). Life length of the plant is set to 30 years. Emissions in the coal mining period are calculated depending on Chinese year book (National Bureau of Statistics of China, 2011). Emissions of the methanol fuel are calculated by GREET model, which is developed by Argonne National Laboratory of US (Wang, 1999). Emissions of the different life cycle periods are listed in Table 1. Depending on this table, Figure 1 is drawn for better showing the distribution of the emissions.

Table 1 Emission of the different life cycle periods ($kg \cdot kg^{-1}$ Me.)

Emission factors	PM10	SO_X	CO	CO_2	CH_4	NO_X	N_2O	VOC
Coal mining	2.65E-03	2.14E-04	7.67E-06	2.48E-02	5.68E-03	1.05E-04	2.50E-06	1.90E-04
Coal transportation	7.05E-07	5.11E-06	4.36E-06	8.58E-04	1.93E-07	3.59E-07	5.12E-06	8.68E-08
Methanol production	0.00E+00	1.10E-05	1.95E-05	1.95E-02	1.63E-04	9.70E-07	0.00E+00	2.67E-07
Methanol use	1.01E-04	8.08E-06	1.06E-02	1.20E+00	2.61E-06	1.54E-05	1.74E-06	1.09E-03
Process life cycle	6.99E-06	1.17E-05	1.35E-06	1.00E-03	5.37E-06	3.05E-06	1.19E-07	1.13E-07
Total	2.76E-03	2.50E-04	1.06E-02	1.25E+00	5.85E-03	1.25E-04	9.48E-06	1.28E-03

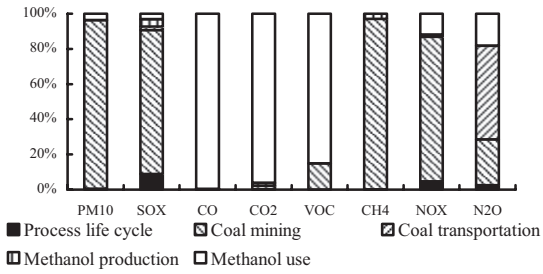

Figure 2. Emission distribution of different life cycle stages

It can be seen that CO, CO_2 and VOC are mainly emitted in the methanol utilization period. In the coal mining period, the emissions are PM10, SO_X, CH_4, and NO_X. Large amount of N_2O is emitted in the coal mining period, the coal transportation period and the methanol utilization period. The emissions of the methanol production period are CO_2, SO_X, and CH_4. Compared to the emissions in the product life cycle, the emissions in the process life cycle are much less.

4. Impact assessment

A three-step model for impact assessment is used in this paper, which includes classification, characterization and quantification. There are many environmental indictors, generally including depletion of nonrenewable resources, biological resources depletion, global warming, ozone depletion, photochemical smog, human toxicity, eco-toxicity, acidification and eutrophication. Four indicators are used in this paper, global warming, acidification, photochemical smog and the human toxicity.

4.1. Global warming

Emission of greenhouse gas (GHG) is the main factor for global warming. The general GHG are CO_2, CH_4, CO, and N_2O. For calculating the global warming potential (GWP) of GHG except for CO_2, the characterized factor model is used and shown as Eq. 1. This model is developed by Intergovernmental Panel on Climate Change (IPCC) (Siebenhuner, 2003). 50 years' average data are used for the calculation,

$$GWP_i = E_i \times CF_{CO_2} \qquad (1)$$

where *i* indicates GHG, *E* denotes the emission quantity and CF_{CO2} means the CO_2 characterized factor.

Table 2. GWP of the methanol life cycle

GHG	CF (kg $CO_{2\text{-eq}}$)	Emission (kg•kg^{-1}Me.)	GWP (kg $CO_{2\text{-eq}}$•kg^{-1}Me.)	Proportion (%)
CO_2	1	1.25E+00	1.25E+00	87.23
CH_4	21	5.85E-03	1.23E-01	8.58
CO	2	1.06E-02	2.12E-02	1.48
NO_X	310	1.25E-04	3.88E-02	2.71
Total	—	—	1.43E+00	100.00

As shown in Table 2, GWP of the methanol life cycle is 1.39kg $CO_{2\text{-eq}}$•kg^{-1}Me. It is mainly aroused by CO_2. Depending on the inventory analysis in Chapter 3, it is known that most of CO_2 is produced in the production period and utilization period. Besides, CO is produced by the incomplete combustion of methanol in the utilization

period. CH_4 is emitted in the coal mining periods. NO_X is mainly emitted in the coal mining period and the methanol utilization period.

4.2. Acidification

Acidification is mainly aroused by the emission of acidic gases. The acidic gases usually contain elements, N, S, and P. They damage soil, change the pH value of water, and finally destruct the living environment of plants and fishes. In LCA of methanol, emitted acidic gases are SO_X and NO_X. Similar to GWP, the calculation of acidification potential (AP) uses SO_2 as the base. The model refers to the report of EPA (EPA, 2000) and is shown in Eq. 2 where CF_{SO2} refers to the SO_2 characterized factor.

$$AP_i = E_i \times CF_{SO_2} \quad (2)$$

Table 3. AP of the methanol life cycle

Acidic gas	CF (kg $SO_{2\text{-eq}}$)	Emission (kg•kg^{-1}Me.)	AP (kg $SO_{2\text{-eq}}$•kg^{-1}Me.)	Proportion (%)
SO_X	1	2.50E-04	2.50E-04	74.10
NO_X	0.7	1.25E-04	8.73E-05	25.90
Total	—	—	3.37E-04	100.00

As shown in Table 3, the total AP is 3.37E-4kg $SO_{2\text{-eq}} \bullet kg^{-1}$Me. This AP has 74.10% from SO_X and 25.90% from NO_X. According to the inventory analysis, most of these two acidic gases are generated in the consumption of fuel for mining tools in the mining period.

4.3. Photochemical smog

Photochemical smog is produced by photolysis of pollutants in atmosphere. The smog mainly consists of CH_4, SO_X, NO_X and VOC. We use photochemical oxide creation potential (POCP) to assess the impacts of photochemical smog. The calculation of POCP is based on the quantity of photochemical smog made by the C_2H_4 (Yan, 2005) and is calculated in Eq. 3 where CF_{C2H2} refers to the C_2H_4 characterized factor.

$$POCP_i = E_i \times CF_{C_2H_4} \quad (3)$$

Table 4. POCP of the methanol life cycle

Photochemical smog gas	CF (kg $C_2H_{4\text{-eq}}$)	Emission (kg•kg^{-1}Me.)	POCP (kg $C_2H_{4\text{-eq}}$•kg^{-1}Me.)	Proportion (%)
CH_4	0.006	5.85E-03	3.51E-05	6.02
SO_X	0.048	2.50E-04	1.20E-05	2.06
NO_X	0.028	1.25E-04	3.50E-06	0.60
VOC	0.416	1.28E-03	5.32E-04	91.31
Total	—	—	5.83E-04	100.00

As shown in Table 4, we find that 91.31% of POCP is aroused from the emission of VOC. This is because VOC is made up by low-carbon hydrocarbons and low-carbon aldehydes. They are the main components of photochemical smog. Depending on the inventory analysis, VOC is mainly emitted in the methanol utilization period.

4.4. Human toxicity

Human toxicity (HT) includes Human Toxicity Potential by Ingestion (HTPI) and Human Toxicity Potential by Inhalation or Dermal Exposure (HTPE). According to Table 1, SO_X, NO_X, CO, and PM10 are classified as the human toxicity substances. The calculation of HT is based on 1, 4-dichlorobenzene (Yan, 2005). The HT of the methanol life cycle is calculated by Eq. 4 where $CF_{1,\ 4\text{-}C6H4Cl2}$ means the 1, 4-$C_6H_4Cl_2$ characterized factor.

$$HTP_i = E_i \times CF_{1,4-C_6H_4Cl_2} \quad (4)$$

Table 5. HTP of the methanol life cycle

HT substances	CF (kg 1,4-$C_6H_4Cl_{2\text{-eq}}$)	Emission (kg•kg^{-1}Me.)	HTP (kg 1, 4-$C_6H_4Cl_{2\text{-eq}}$•kg^{-1}Me.)	Proportion (%)
SO_X	0.096	2.50E-04	2.40E-05	0.94
NO_X	1.2	1.25E-04	1.50E-04	5.85
CO	0.012	1.06E-02	1.27E-04	4.96
PM10	0.82	2.76E-03	2.26E-03	88.25
Total	—	—	2.56E-03	100.00

As shown in Table 5, PM10 occupies 88.25% of HTP. NO_X and CO have the small percentage of HTP. According to Table 1, we can find PM10 mainly generated in the coal mining period.

5. Conclusion

This paper assessed the environmental impact of the coal-generated methanol from the product life cycle and the process life cycle. Four indicators, global warming, acidification, photochemical oxidant formation and human toxicity, were used for the assessment. The substances that affect these indicators are explored. In the result analysis, we identify environmental impacts of the different life periods and their percentages. Due to the importance of coal chemical industry, people are increasingly concerned with LCA of coal-generated chemicals. The analysis results of this work are worthwhile for further researches of other coal-generated chemicals.

Acknowledgements

This work is supported by the National Natural Science Foundation of China (No. 21136003), National Basic Research Program of China (973 Program, No. 2012CB720504) and Specialized Research Fund for the Doctoral Program of Higher Education (No. 20100172110016).

References

Y. He. 2006, Handbook of Modern Coal Chemical Technology, Beijing: Chemical Industry Press.

H. Althaus, M. Chudacoff, S. Hellweg. 2007, Life Cycle Inventories of Chemicals, Ecoinvent Data v2.0, http://www.pre.nl/

S. Liu, Z. Lin, X. Zhang. 1998, Life cycle assessment of portland cement, *China Environmental Science*, 18(4), 328-332.

J. J. Marano, J. P. Ciferno. 2001, Life-cycle Greenhouse-gas Emissions Inventory for Fischer-Tropsch Fuels, National Renewable Energy Laboratory, http://www.netl.doe.gov/technologies/coalpower/gasification/pubs/systems_analyses.html

National Bureau of Statistics of China, 2011, China Statistical Yearbook of 2010, Beijing: China Statistics Press.

M. Wang. 1999, GREET 1.5 Transportation Fuel-Cycle Model Volume II: Appendices of Data and Results, http://greet.anl.gov/publications.html

B. Siebenhuner. 2003, The changing role of nation states in international environmental assessment-the case of the IPCC, *Global Environmental Change*, 13(2), 113-123.

EPA (Enviromental Protection Agency), 2000, Using life cycle assessment to evaluate preferability of product. Framework for responsible environmental decision making, http://www.epa.gov/nrmrl/std/sab/lca/lca_fred.htm.

Z. Yan. 2005, Chemical Product Life Cycle Evaluation of Integrated Environmental and Economic Performance, Guangzhou: South China University of Technology.

I.A. Karimi and Rajagopalan Srinivasan (Editors), Proceedings of the 11th International Symposium on Process Systems Engineering, 15-19 July 2012, Singapore.

Information integration: From P&I diagrams to functional models

Manuel Rodríguez[a], José L. De la Mata[a], M. Eugenia Alvarez

[a]*Autonomous System Laboratory, Universidad Politécnica de Madrid, José Gutierrez Abascal 2, Madrid 28006, Spain*

Abstract

Information integration is a very important topic. Reusing the knowledge and having common and exchangeable representations have been an active research topic in process systems engineering. In this paper we deal with information integration in two different ways, the first one sharing knowledge between different heterogeneous applications and the second one integrating two different (but complementary) types of knowledge: functional and structural. A new architecture to integrate these representation and use for several purposes is presented in this paper.

Keywords: Process representation, functional models, structural models.

1. Introduction

Information integration and exchange has been and still is a very important topic (see ISO standards like 10303-221, 231 or AP233). In the past decades ontologies have got an important role in information representation, some of them have been developed for process systems, as OntoCape (Morbach et al., 2007) and some neutral model formulations have also been presented (as CapeOpen). But these approaches deal only with structural models and with the problem of merging and using information from different software applications (Wiesner et al., 2011). In this paper we present an architecture to integrate the information coming from the structural and the functional views of a single system. The remaining of the paper is organised as follows, section 2 introduces the D-higraph functional modeling methodology, the third section presents the developed tool for the integrated use of structural and functional models, section four shows an application of the proposed architecture and finally section five presents the conclusions of this work.

2. D-higraph functional modeling methodology

This section briefly presents the D-higraph methodology. For further information and deeper understanding of the methodology, the reader is encouraged to have a look at De la Mata & Rodríguez (2010b).

2.1. D-higraph: Dualization of Higraphs

Higraphs are a general kind of diagramming objects well suited to the behavioral specification of complex concurrent systems, presented by Harel (1987). Higraphs consist of two basic elements called blobs (denote states) and edges (denote transitions) connecting the blobs. However, higraphs original formulation is not suited for process systems specifications. Rodríguez & Sanz (2009) first presented D-higraphs as a functional modeling technique that merges functional and structural information of the system modeled.

D-higraphs come from the dualization of Higraphs: blobs representing transitions and edges representing states. Disjoint blobs imply an AND relation, i.e., both transitions between states take place. Orthogonal blobs represent an OR relation, i.e., only one of the transitions takes place.

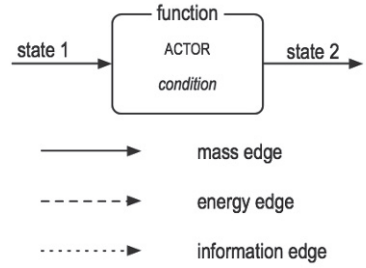

Figure 1. Basic blobs and types of edges

2.2. Main components

Blobs represent functions (transitions) and they include the ACTOR of the function and an optional condition for the transition to fire. As a result a new state is generated. The states are represented by edges coming in or out of a blob. Edges represent flows of mass, energy or information, which are responsible of all of the interactions in a process system (Lind, 1994). Mass, energy and information edges are depicted differently, as shown in the bottom of Fig. 1. However, the type of flow does not affect the behavior of the model, it is a visual aid to represent more information. An additional end of an edge is a hollow arrow which means that the state has influence on the blob pointed by the arrow (although the flow is in the opposite direction).

2.3. Properties

• *Blob connection.* An edge always links two blobs. Under certain conditions one of the blobs can not be represented (elliptic blob) but it exists.

• *Blob inclusion.* Blobs can be included inside of other blobs. This means that the inner blob performs a function that is necessary for the function of the outer blob. This is how hierarchical functions are represented and how structural and functional information is integrated.

• *Partitioning blobs.* A blob can be partitioned into orthogonal components, establishing an OR condition between the partitions.

The main objective of D-higraphs is not only the representation of knowledge about process systems. De la Mata & Rodríguez (2010a,b) provide a series of causation rules that allow to track the evolution and propagation of failures across the system. This rules combined with sensor data of the process enables the possibility of performing FDI analysis using D-higraphs models.

3. Information integration tool

3.1. P&I representation

The available P&I diagram of a process is translated to a steady state model, in this case to an Aspen Plus model. This initial translation is performed manually. The generated model is converted to a dynamic model (Aspen Dynamics / Aspen Custom Modeler). This completes the structural representation of the process.

3.2. D-h tool

The steady state model is automatically translated to a D-higraphs model, additional information regarding the functionality of the different units is provided to the API to perform the creation of the model. The developed tool, Álvarez (2010), allows a visual representation of the goals of the process.

3.3. CLIPS

The D-higraph representation is automatically translated to production (rule based) system (CLIPS, 2011) that will be used to conduct fault diagnosis and HAZOP analysis.

3.4. Architecture

Figure 2 shows all the components of the architecture. The communication between the structural (dynamic) model and the functional one is through an access extension coded as a dll. This dll allows bidirectional communication between the simulation and the functional representation, allowing to study the effects of a fault on the whole process.

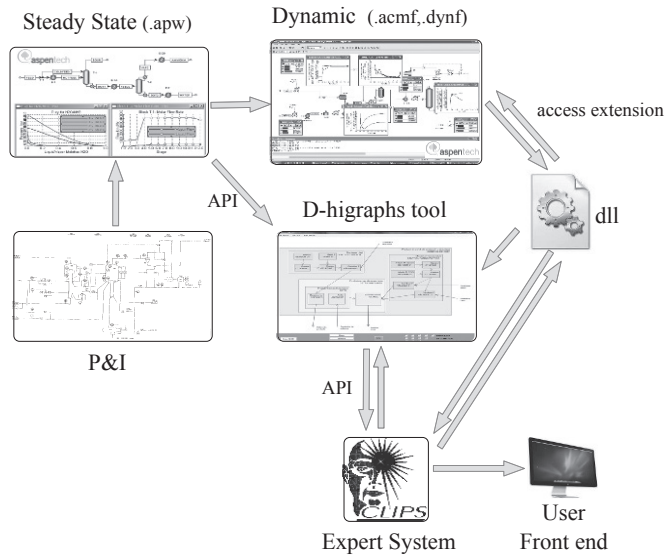

Figure 2. Structural-functional information integration architecture

There are different uses of this environment from conventional simulation to fault diagnosis, sensor validation, control reconfiguration or HAZOP analysis.

4. Application

Amine gas treating is a process that uses an aqueous solution of an amine to remove H_2S and CO_2 from gases. In this case we consider the treatment of an off-gas from a secondary absorber of a FCC in an oil refinery using an aqueous solution of diethanolamine (DEA). In the absorber the DEA solution absorbs H_2S and CO_2 from the incoming off-gas producing a sweetened gas stream and a DEA solution rich in the absorbed acid gases. The sweet gas is sent to the high-pressure gas system of the refinery while the rich amine is routed to the regenerator.

The regenerator is a stripper with a reboiler where the rich amine desorbs H_2S and CO_2 producing a lean amine stream that is recycled to the absorber for reuse. The reboiler is fed with steam to vaporize the DEA solution. The acid gas is sent to a Claus process

while the lean DEA is recycled to the absorber. A make-up DEA stream is needed to keep the amine inventory. The P&ID of the process is shown in Fig 3

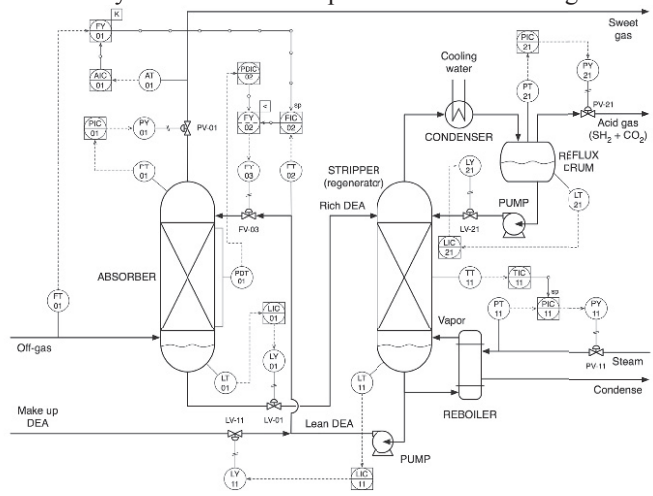

Figure 3. Piping and instrument diagram of the amine gas treating process

For this P&I a steady state model as well as a dynamic model has been created. A functional model has also been generated using the D-higraph tool. Figure 4 shows the D-higraph of a small part of the process, the reflux section of the stripper and the dynamic model generated using Aspen Dynamics.

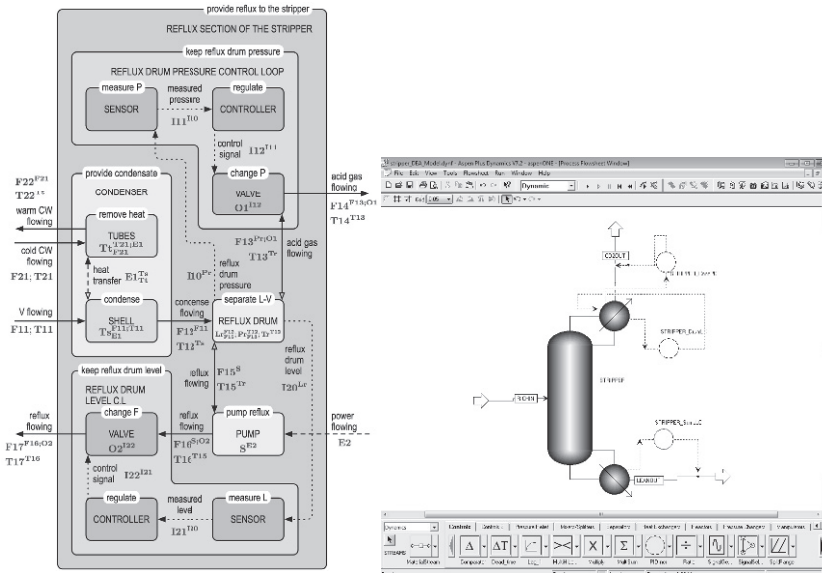

Figure 4. Functional model of the stripper reflux section (left) and the dynamic model (right)

For the first test we have a dynamic model for the stripper, which receives actual input data from the plant. Using the dynamic model, a fault has been identified following De la Mata & Rodríguez (2011). This fault has been input to the functional model, which generates a tree with the consequences of the fault. For the second test a fault has been observed and the functional model has generated the tree of possible causes. The

generated fault is produced in the pressure sensor. Figure 5 shows the set of possible causes (it produces as a possible cause the sensor fault I11 signal in the tree) and the simulated model used to validate and quantify the deviations provided by the functional model.

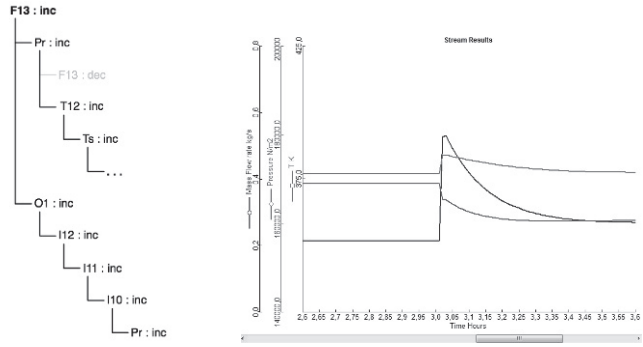

Figure 5. Causal tree and dynamic simulation of the sensor fault

5. Conclusions

In this paper a new architecture to integrate structural as well as functional information has been presented. Functional models are represented using the D-higraphs formalism and its exploitation is made using a production system. Structural (steady state and dynamic) models are generated using the AspenTech software. Communication between both representations is made using a dll component which can control the simulation or generate events for the functional representation. This approach has been tested on an industrial process with satisfactory results. It can be used in many different ways as to validate and quantify functional models, to validate sensors and alarms or to provide control reconfiguration. Future research is being focused on automating all the procedure (including adding functional information directly on the Aspen models) and on testing and creating a procedure for automatic control reconfiguration.

References

Álvarez, M. E. (2010). Diagnosis de fallos en procesos químicos mediante modelos D-higraph. *Final Project, Department of Chemical Engineering, Technical University of Madrid.*

CLIPS (2011). *CLIPS, A Tool for Building Expert Systems.* March, 13, 2011. http://clipsrules.sourceforge.net/

De la Mata, J. L., Rodríguez, M. (2010a). Abnormal Situation Diagnosis Using D-higraphs. *Computer Aided Process Engineering (ESCAPE 20),* pp. 1477-1482.

De la Mata, J. L., Rodríguez, M. (2010b). D-higraphs. *ASLab Report.* http://www.aslab.org

De la Mata, J. L., Rodríguez, M. (2011). Self-learning of fault diagnosis identification. *Proc. of the 21th European Symposium on Computer Aided Process Engineering (ESCAPE 21)*., pp. 885-889

Harel, D. (1987). Statecharts: A Visual Formalism for Complex Systems. *Sci. Comput. Program, 8 (3),* pp. 231-274.

Lind, M. (1994). Modeling Goals and Functions of Complex Industrial Plant. *Applied Artificial Intelligence, 8 (2),* pp. 259-283.

Morbach, J., Yang,A., Marquardt, W. (2007). OntoCAPE-A large-scale ontology for chemical process engineering. *Engineering Applications of Artificial Intelligence*, 20 (2), pp. 147-161.

Rodríguez, M., Sanz, R. (2009). Development of Integrated Functional-Structural Models. *Computer Aided Process Engineering, 27,* pp. 573-578.

Wiesner, A., Morbach, J., Marquardt, W. (2011). Information integration in chemical process engineering based on semantic technologies. *Computers & Chem. Eng.*, 55 (4), pp. 692-708

I.A. Karimi and Rajagopalan Srinivasan (Editors), Proceedings of the 11th International Symposium on Process Systems Engineering, 15-19 July 2012, Singapore

Nonlinear Design of Stimulus Experiments for Optimal Discrimination of Biochemical Systems

Robert J. Flassig,[a*] Kai Sundmacher,[ab]

[a] *Otto-von-Guericke University, Process Systems Engineering, Universitätsplatz 2, D-39106 Magdeburg, Germany*

[b] *Max Planck Institute for Dynamics of Complex Technical Systems, Sandtorstr. 1, D-39106 Magdeburg, Germany*

Abstract

Biochemical reaction networks in the form of coupled ordinary differential equations (ODEs) provide a powerful modeling tool to understand the dynamics of biochemical processes. During the modeling process a pool of competing nonlinear models is generated, from which the most plausible set has to be selected, given distributed model parameters and hence distributed model prediction. At this point, robust (=taking distributed model responses into account) model-based stimulus experiments can be used, to find experimental conditions at which models show maximal dissimilarities to focus experimental efforts. Response variabilities are typically obtained from linearization. Here we compare this method to the nonlinear Sigma-Point approach for a nonlinear, multi-stable model and show its advantage for model discrimination, especially for large parameter variances.

Keywords: optimal stimulus design; nonlinear model discrimination; sigma point method

1. Introduction

Mechanistic ODE models can help to find missing links based on dynamic features of hypothesized mechanisms. However, large biological variability and measurement noise lead to distributed model parameters, which in combination with several hypotheses render model-based prediction highly uncertain. Model-based experimental stimulus design can be used to optimize new experimental data for (i) parameters estimation and/or (ii) model discrimination. Most of the work on optimal experimental stimulus design (OESD) for biochemical systems focuses on parameter estimation. Here, the origin of distributed parameters is solely attributed to suboptimal parameter sensitivities and measurement noise. Natural parameter variations and potentially associated multi-stable states are excluded. For (bio)chemical systems, there exists also work on OESD for model discrimination, e.g., Chen and Asprey (2003); Apgar et al. (2008). As has been illustrated by Chen and Asprey (2003), the consideration of model response variabilities strongly improves discrimination designs. Here, linearization has been used to estimate model response variabilities. However, by using the Sigma-Point method (Julier et al. (2000)), Heine et al. (2008); Schenkendorf et al. (2009) show that a linear OED for best parameter estimation is suboptimal for nonlinear systems. In the case of OESD aimed at model discrimination, we have shown in (Flassig and Sundmacher, 2012), that the Sigma-Point method outperforms linearization with respect to accuracy and discriminative power at same computational costs for nonlinear models. In this work we analyze the behavior of both methods in the presence of multiple stable states using the Schlögl model.

*flassig@mpi-magdeburg.mpg.de

2. Approach

2.1. Modeling

In many situations, the dynamics of a biochemical system with internal states $\mathbf{x}(t,\mathbf{u}(t),\theta_x) \in \mathbb{A}_\mathbf{x} \subset \mathbb{R}^{n_x}$ can be described by the solution of an initial value problem of the form

$$\frac{\mathrm{d}}{\mathrm{d}t}\mathbf{x}(t) = \mathbf{f}(\mathbf{x}(t),\mathbf{u}(t),\theta_\mathbf{x}); \qquad \mathbf{y}_{sim}(t,\theta) = \mathbf{g}(\mathbf{x}(t,\theta_\mathbf{x}),\theta_\mathbf{y}) \tag{1}$$

with initial system state $\mathbf{x}(t_0) = \mathbf{x}_0$ and right hand side function $\mathbf{f}(\mathbf{x}(t),\mathbf{u}(t),\theta_\mathbf{x})$ describing biological interaction mechanisms, which depends on the system states $\mathbf{x}(t)$, (multiple) stimuli $\mathbf{u}(t)$, and kinetic parameters $\theta_\mathbf{x}$. The response signal is determined by the function $\mathbf{g}(\mathbf{x}(t,\theta_\mathbf{x}),\theta_\mathbf{y})$, relating the system states to the readouts of the experiment. All modeling parameters may be lumped to the model parameter vector $\theta = [\theta_\mathbf{x},\theta_\mathbf{y}]^\mathrm{T}$, with redefined $\theta_\mathbf{x} \equiv [\theta_\mathbf{x},\mathbf{x}_0]^\mathrm{T}$. The dynamic model defined by Eq. (1) represents a nonlinear mapping from model parameter space $\mathbb{A}_{\theta_\mathbf{x}} \times \mathbb{A}_{\theta_\mathbf{y}} = \mathbb{A}_\theta \subset \mathbb{R}^{n_\theta}$ to model output space $\mathbb{A}_\mathbf{y} \subset \mathbb{R}^{n_\mathbf{y}}$. Assuming the model parameters to be distributed according to $\rho_\Theta(\theta)$, $\mathbf{y}_{sim}(t,\theta)$ represents a time dependent, distributed variable $\mathbf{Y}$, which can be described by a model response distribution (MRD) $\rho_{m_\mathbf{Y}}(\mathbf{y},t)$.

2.2. Design criterion for model discrimination

The shape of an MRD is determined by the underlying ODEs and applied stimuli. OESD seeks stimuli that minimize similarities of competing MRDs. Similarities of two MRDs, referred to as model overlap, can be measured by the scalar product

$$\Phi(t,\mathbf{u}(t)) = \int_{\mathbb{A}_\mathbf{y}} \rho_{A_\mathbf{Y}}(\mathbf{y},t,\mathbf{u}(t))\rho_{B_\mathbf{Y}}(\mathbf{y},t,\mathbf{u}(t))\mathrm{d}\mathbf{y}. \tag{2}$$

From this, the average model overlap of the time course is

$$O = \langle\Phi(\mathscr{D})\rangle_t = \frac{1}{n_t}\sum_{k=1}^{n_t}\Phi(t_k,\mathbf{u}(t_k)), \tag{3}$$

where $\mathscr{D} \in \mathbb{D} = \mathbb{T}\times\mathbb{U}\times\mathbb{Y}$ represents the experimental design, encompassing for instance selection of discrete measurement time points $t_k \in \mathbb{T}$, stimulus design $\mathbf{u}(t) \in \mathbb{U}$ and readout design $\mathbf{g} \in \mathbb{Y}$. An optimal model discrimination design $\mathscr{D}_\dagger$ minimizes Eq. (3). When approximating the MRD by $\rho_{\mathbf{Y}|m}(\mathbf{y},t,\mathbf{u}(t)) \simeq \mathscr{N}(\mu_{\mathbf{y}|m}(t,\mathbf{u}(t)),\Sigma_{\mathbf{y}|m}(t,\mathbf{u}(t)))$, the integration in Eq. (2) can be performed to yield an analytic expression of the approximate overlap in terms of $\mu_{\mathbf{y}|m}(t,\mathbf{u}(t)),\Sigma_{\mathbf{y}|m}(t,\mathbf{u}(t)))$. For details see Jebara et al. (2004).

2.3. Estimation of the response distribution

If we approximate the parameter distribution $\rho_\Theta(\theta)$ by its first two statistical moments, $\mathbf{E}[\theta]$ and $\mathbf{C}[\theta]$, we can apply the linearization or Sigma-Point method to estimate the first two statistical moments of the resulting time dependent MRD.

Linearization: Applying the chain rule to the readout function in Eq. (1) yields

$$\mathbf{y}^\mathscr{L}(t,\theta) = \mathbf{y}_{sim}(t,\mathbf{E}[\theta]) + \mathbf{S}(t,\mathbf{y})^\mathrm{T}\big|_{\theta=\mathbf{E}[\theta]}(\theta - \mathbf{E}[\theta]), \tag{4}$$

with response sensitivity matrix $\mathbf{S}(t,\mathbf{y}) = \frac{\partial\mathbf{y}_{sim}(t,\theta)}{\partial\mathbf{x}}\mathbf{S}_\mathbf{x}(t,\mathbf{x}) + \frac{\partial\mathbf{y}_{sim}(t,\theta)}{\partial\theta}$ and state sensitivity matrix $\mathbf{S}_\mathbf{x}(t,\mathbf{x}) = \frac{\partial\mathbf{x}}{\partial\theta}$. Then, the linear estimates of expectation and variance-covariances

of the MRD can be calculated as

$$\mathbf{E}_t^{\mathscr{L}}[\mathbf{y}] = \mathbf{y}_{sim}(t, \mathbf{E}[\theta]); \qquad \mathbf{C}_t^{\mathscr{L}}[\mathbf{y}] = \mathbf{S}(t,\mathbf{y})\,\mathbf{C}[\theta]\,\mathbf{S}(t,\mathbf{y})^{\mathrm{T}}. \tag{5}$$

These local estimates may miss parameter dependent coexisting stable states. Further, for nonlinear models, the estimate of the expectation is typically biased, i.e., $\mathrm{Bi} = \mathbf{E}_t^{\mathscr{L}}[\mathbf{y}] - \mu_{\mathbf{y}} \neq \mathbf{0}$. The computational effort is of order $\mathscr{O}(n_{\theta_{\mathbf{x}}})$.

Sigma-Point: According to Julier et al. (2000), the first two statistical moments of nonlinear transformed distribution can be estimated by the following procedure:

1. Select $2n_\theta + 1$ Sigma Points in the original domain according to

$$\theta^{(0)} = \mathbf{E}[\theta]; \qquad \theta^{(i)} = \theta^{(0)} \pm \sqrt{n_\theta + \lambda}\sqrt{\mathbf{C}[\theta]}^{(i)}, \tag{6}$$

2. Propagate these through the model $\mathbf{y}_t^{(i)} = \mathbf{y}_{sim}(t, \theta^{(i)})$.

3. Estimated expectation and variance-covariance of the MRD are given by

$$\mathbf{E}_t^{\mathscr{S}}[\mathbf{y}] = \sum_{i=-n_\theta}^{n_\theta} w^{(i)}\mathbf{y}_t^{(i)}; \quad \mathbf{C}_t^{\mathscr{S}}[\mathbf{y}] = (1-\alpha^2+\beta)\left(\mathbf{y}_t^{(0)} - \mathbf{E}_t[\mathbf{y}]\right)\left(\mathbf{y}_t^{(0)} - \mathbf{E}_t[\mathbf{y}]\right)^{\mathrm{T}} + \\ + \sum_{i=-n_\theta}^{n_\theta} w^{(i)}\left(\mathbf{y}_t^{(i)} - \mathbf{E}_t[\mathbf{y}]\right)\left(\mathbf{y}_t^{(i)} - \mathbf{E}_t[\mathbf{y}]\right)^{\mathrm{T}} \tag{7}$$

with weights $w^{(0)} = \frac{\lambda}{n_\theta+\lambda}$, $w^{(\pm i)} = \frac{1}{2(n_\theta+\lambda)}$ and $\lambda = \alpha^2(n_\theta + \kappa) - n_\theta$. In the case of nonlinear systems, this provides higher order information without any need of derivative information. We may use this method as a Monte-Carlo surrogate to compare the linear estimates of expectation and covariance to, Flassig and Sundmacher (2012). The computational effort is of order $\mathscr{O}(2n_\theta + 1)$.

3. Numerical Analysis

The Schlögl model is a canonical example of a biochemical system exhibiting bi-stability, Schlögl (1972). It describes an autocatalytic, tri-molecular reaction, that occurs in biochemical system such as cell metabolism or signaling. Two model alternatives for the rate of concentration change of specie x are given by

$$\frac{\mathrm{d}}{\mathrm{d}t}x_m(t) = k_1\, a\, s_m(u(t))x_m^2(t) - k_2 x_m^3(t) - k_4 x_m(t) + k_3 b, \tag{8}$$

$$s_A(u(t)) = u(t) \quad \text{or} \quad s_B(u(t)) = \frac{1}{2}(u(t) + u^2(t)) \tag{9}$$

and distributed initial condition $X_0 \propto N(\mathrm{E}[x_0], \eta\mathrm{E}[x_0])$. The model alternatives differ in the input layer $s_m(u(t))$. Parameters a and b represent the concentration of two reaction partners a and b of specie x, which both are assumed to be in constant exchange with a material bath. The parameter values are taken from Vellela and Qian (2009). For an initial, suboptimal experiment with stimulus $u(t) = 1$, models A and B cannot be distinguished, given $y_m(t) = x_m(t) + \theta_\varepsilon$ to be the response signal. Additionally to a distributed initial

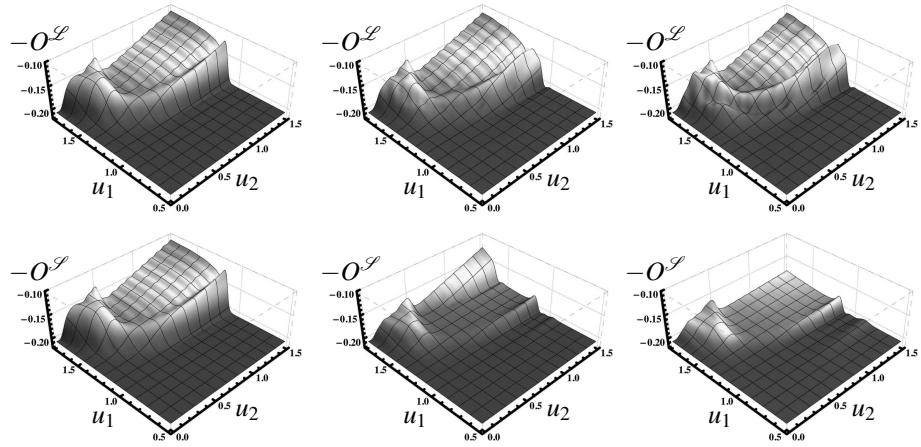

(a) $\eta = 0.01$ (b) $\eta = 0.3$ (c) $\eta = 0.6$

Figure 1: Design $\mathscr{D} = [u_1, u_2]^{\mathrm{T}}$ dependent overlap landscape for three different levels of parameter variances.

condition x_0, we assume a constant additive measurement noise with zero mean and $\sigma_\varepsilon^2 = 0.1$. We parameterize the stimulus as

$$u(t) = u_1 \left(\Theta[u_2 - t] + (1 - \Theta[2u_2 - t]\Theta[3u_2 - t])\right); \quad \Theta[t] = \begin{cases} 1, & \text{if} \quad t \leq 0 \\ 0, & \text{else,} \end{cases} \tag{10}$$

which allows to analyze the overlap landscape as a function of u_1 and u_2. Both parameters are subjected to box constraints mimicking experimental limitations, i.e., $u_{i|lb} \leq u_i \leq u_{i|ub}$. In Fig. 1 we show the design dependent overlap landscape, i.e., Eq. 3 for $n_t = 30$ and different levels of parameter variances derived from $\sigma_{x_0} = \eta \mathrm{E}[x_0]$. For small parameter variances both methods estimate the same overlap landscape, thus same optimal design $\mathscr{D}_\dagger^{\mathscr{E}}$. For $\eta = 0.6$ the best design points $= \max(-O^{\mathscr{E}})$ differ for both methods, i.e., $\mathscr{D}_\dagger^{\mathscr{L}} \neq \mathscr{D}_\dagger^{\mathscr{S}}$. In Fig. 2 we show time courses of the estimated moments (thick/thin lines expectation/std. deviation) for each best designs $\mathscr{D}_\dagger^{\mathscr{E}}$ based on linearization $\mathscr{E} = \mathscr{L}$ and Sigma-Points $\mathscr{E} = \mathscr{S}$. Evaluating the overlap of the optimal linear design with the Sigma-Points reveals a larger expected overlap $O_\dagger^{\mathscr{L}\mathscr{S}} > O_\dagger^{\mathscr{L}\mathscr{L}}$, as linearization misses the spread of the variance and the location of the expected response due to the existence of a second stable state (Fig. 2 (b) vs. (c)). The optimal Sigma-Point design minimizes the overlap by "switching" optimally between the two states while keeping the variance minimal (Fig. 2 (f)). We also see that $O_\dagger^{\mathscr{S}\mathscr{S}} < O_\dagger^{\mathscr{L}\mathscr{S}}$, i.e., the linear design is suboptimal.

4. Conclusion

The behavior of linear and Sigma-Point estimations of nonlinear transformed statistical Gaussian moments, has been analyzed in the framework of OESD in the presence of multiple stable states. As we illustrate, due to the non-local estimation property of the Sigma-Point method, the optimizer can use the bistability for optimal discrimination. Further, the estimated variances of the Sigma-Point method encompass both stable states, whereas the estimated expectation lies between the stable states. In contrast, linearization captures only one of the states, which results into underestimated variances, biased expectation

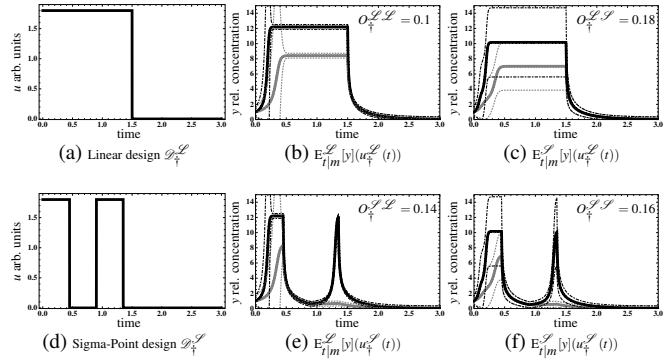

(a) Linear design $\mathscr{D}_{\dagger}^{\mathscr{L}}$ (b) $\mathrm{E}_{t|m}^{\mathscr{L}}[y](u_{\dagger}^{\mathscr{L}}(t))$ (c) $\mathrm{E}_{t|m}^{\mathscr{S}}[y](u_{\dagger}^{\mathscr{L}}(t))$

(d) Sigma-Point design $\mathscr{D}_{\dagger}^{\mathscr{S}}$ (e) $\mathrm{E}_{t|m}^{\mathscr{L}}[y](u_{\dagger}^{\mathscr{S}}(t))$ (f) $\mathrm{E}_{t|m}^{\mathscr{S}}[y](u_{\dagger}^{\mathscr{S}}(t))$

Figure 2: Time course estimates of both models (A gray, B black) for $\eta = 0.6$.

estimates and suboptimal OESD. As both method have the same computational effort, we conclude that the Sigma-Point method provides a powerful estimation method, when designing discrimination experiments for complex, nonlinear biochemical ODE models having widely distributed parameters and associated multiple stable states.

References

Apgar, J. F., Toettcher, J. E., Endy, D., White, F. M., Tidor, B., 2008. Stimulus Design for Model Selection and Validation in Cell Signaling. PLoS Comput Biol 4 (2).

Chen, B. H., Asprey, S. P., 2003. On the Design of Optimally Informative Dynamic Experiments for Model Discrimination in Multiresponse Nonlinear Situations. Industrial & Engineering Chemistry Research 42 (7), 1379–1390.

Flassig, R. J., Sundmacher, K., 2012. Optimal design of stimulus experiments for robust discrimination of biochemical reaction networks. Bioinformatics *submitted*.

Heine, T., Kawohl, A., King, R., 2008. Derivative-free optimal experimental design. Chemical Engineering Science 63 (19), 4873–4880.

Jebara, T., Kondor, R., Howard, A., Bennett, K., Cesa-bianchi, N., 2004. Probability product kernels. Journal of Machine Learning Research 5, 819–844.

Julier, S., Uhlmann, J., Durrant-Whyte, H. F., 2000. A new method for the nonlinear transformation of means and covariances in filters and estimators. IEEE Transactions on Automatic Control 45 (3), 477–482.

Schenkendorf, R., Kremling, A., Mangold, M., 2009. Optimal experimental design with the sigma point method. IET Systems Biology 3 (1), 10–23.

Schlögl, F., 1972. Chemical reaction models for non-equilibrium phase transitions. Zeitschrift für Physik A Hadrons and Nuclei 253, 147–161.

Vellela, M., Qian, H., 2009. Stochastic dynamics and non-equilibrium thermodynamics of a bistable chemical system: the schlögl model revisited. Journal of The Royal Society Interface 6 (39), 925–940.

I.A. Karimi and Rajagopalan Srinivasan (Editors), Proceedings of the 11th International Symposium on Process Systems Engineering, 15-19 July 2012, Singapore.

Multi-scale modeling for prediction of distributed cellular properties in response to substrate spatial gradients in a continuously run microreactor

Rita Lencastre Fernandes[a], Ulrich Krühne[a], Ingmar Nopens[b], Anker D. Jensen[c], Krist V. Gernaey[a]

[a]*Center for Process Engineering and Technology, Technical University of Denmark, 2800 Kgs. Lyngby, Denmark*
[b] *BIOMATH, Department of Mathematical Modelling, Statistics and Bioinformatics, Ghent University, Coupure Links 653, 9000 Ghent, Belgium*
[c] *Center for Combustion and Harmful Emission Control, Department of Chemical and Biochemical Engineering, Technical University of Denmark, 2800 Kgs. Lyngby, Denmark*

Abstract

In large-scale fermentors, non-ideal mixing leads to the development of heterogeneous cell populations. This cell-to-cell variability may explain the differences in e.g. yields for large- and lab-scale cultivations. In this work the anaerobic growth of *Saccharomyces cerevisiae* in a continuously run microbioreactor is simulated. A multi-scale model consisting of the coupling of a population balance model, a kinetic model and a flow model was developed in order to predict simultaneously local concentrations of substrate (glucose), product (ethanol) and biomass, as well as the local cell size distributions.

Keywords: Population Balance Model, Computational Fluid Dynamics, yeast, microreactor, fermentation

1. Introduction

A heterogeneous microbial population consists of cells in different states, which implies a distribution of activities (e.g. respiration, product efficiency), as well as different responses to extracellular stimuli. The existence of a heterogeneous cell population may explain the lower productivities obtained for cultivations in large-scale reactors, where substrate and oxygen gradients are observed, in comparison to cultivations in well-mixed bench scale reactors (Enfors et al, 2001).

Population balance models (PBM) have been used in various applications (e.g. crystallization, granulation, flocculation, polymerization processes, etc.) to predict distributions of certain population properties including particle size, mass or volume, molecular weight,... Similarly, PBM allow for a mathematical description of distributed cell properties within microbial populations (Lencastre Fernandes et al, 2011).

Phenotypic heterogeneity arises as a result of the variability inherent to the metabolic mechanisms of single cells. Cell size is a key feature affecting cellular design, fitness and function (Jorgensen and Tyers, 2004). In fact, cell growth and division are tightly coupled, and this is reflected in the cell's capability of adjusting its growth rate to nutrients' availability (Enfors et al, 2001; Jorgensen and Tyers, 2004). Cell total protein content distributions (a measure of cell size) have been observed to provide a dynamic

picture of the interplay between the cells and surrounding extracellular environment (Alberghina et al, 1998).
The work hereby presented focuses on modeling the development of a microbial population growing in a continuous microbioreactor. The dynamics of single cell total protein content are described by a PBM, the consumption of substrate and production of ethanol are described by simple kinetics (unstructured model), and the transport of the species throughout the reactor is described by a computational fluid dynamics (CFD) model.

2. Case Study

The anaerobic fermentation of *Saccharomyces cerevisiae* in a continuous microreactor is used as case study. As above mentioned, cell growth and division are tightly coupled, and are modulated according to the substrate availability. The regulation of growth ensures that cells attain a critical size before initiating the division process (Rupeš, 2002; Porro et al, 1995). In the particular case of *S. cerevisiae*, two critical sizes corresponding to the regulation points START (committing to budding, or budding transition) and division have been identified. A schematic representation of the cells transition through the cell cycle and the associated cell growth (i.e. size increase) is presented in Fig. 1.
Using cell size as population descriptor allows, thus, for describing the distribution of cellular states. Moreover, a better description of the cellular state is obtained by determining the distribution of cells in cell cycle phases, i.e. by measuring DNA distributions (Alberghina et al, 1998). It was thus found desirable to use a PBM based on cell size as model variable, which is applied to different stages (i.e. subpopulations) corresponding to the non-budding and budding (cell cycle) phases.

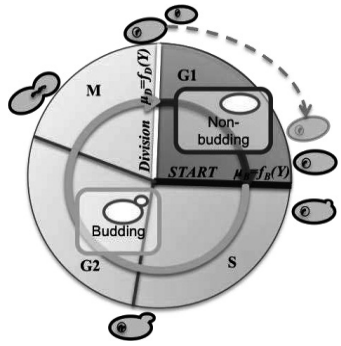

Figure 1 - Schematic representation of the cell cycle during exponential growth. The dark arrow (inside the circle) corresponds to the duration of the non-budding stage (G1phase). Due to their bigger size, G1 phase is shorter for mother cells than for daughter cells (dashed arrow). The *START* point represents the regulation point that defines the inititation of the DNA replication and budding process, i.e. transition to the S phase. The division point corresponds to the completion of the mitotic process and separation of a budding cell into two non-budding ones.

The microreactor consists of a sequence of spherical chambers connected in the center by a channel (Fig. 2). An inlet mass flow rate of $1x10^{-9}$ kg/s, containing glucose (20 g/l), was applied. The ethanol and biomass concentrations at the inlet are 0 g/l. The hydraulic retention time is 783 s.

3. Model Description

Aiming at both describing the distributions of single-cell sizes for the two cell size stages (non-budding and budding), a population balance model was coupled to an unstructured model describing the extracellular environment.

3.1. Population Balance Model

The PBM developed for this study is based on a multi-stage model reported in the literature (Hatzis and Porro, 2006). In this work, the segregated model consists of two

population balance equations (PBE), which describe cell growth, initiation of the budding process, cell division and birth, for both the non-budding and budding stages (Eq. 1 and 2), as well as the corresponding initial and boundary conditions.

$$\frac{\partial N^{NB}(m,t)}{\partial t}+\frac{\partial}{\partial m}\left[r_m(m,Y)N^{NB}(m,t)\right]=-\Gamma_B(m|Y)N^{NB}(m,t)+2\int_m^{\infty}\Gamma_D(m'|Y)P(m,m'|Y)N^B(m',t)dm' \quad \text{(Eq. 1)}$$

$$\frac{\partial N^{B}(m,t)}{\partial t}+\frac{\partial}{\partial m}\left[r_m(m,Y)N^{B}(m,t)\right]=-\Gamma_D(m|Y)N^{B}(m,t)+\Gamma_B(m|Y)N^{NB}(m,t) \quad \text{(Eq. 2)}$$

Here $N^{NB}dm$ and $N^{B}dm$ represent the number of cells in the cell size interval *[m, m+dm]* for the non-budding and budding stages, respectively, *m* is the cell total protein content or cell size (in arbitrary units), and *Y* designates the extracellular environment. The budding and division transitions, Γ_{NB} and Γ_B, are mathematically described as hazard functions (Eq. 3 and 4, for the budding transition) where the probability that a cell of mass *m* initiates the budding process, i.e. transitions to the budding stage, or divides into two new cells is described by a Gaussian probability density function with mean μ_B and μ_D, respectively. The standard deviation was assumed to be the same for the two transition functions and constant along the cultivation.

$$\Gamma_{NB}(m|Y)=r_m(m,Y)\frac{h_{NB}(m|Y)}{1-\int_{m_0}^{m}h_{NB}(m')dm'} \quad \text{(Eq. 3)}$$

$$h_{NB}(m|Y)=N(\mu_{NB}(Y),\sigma_{NB}) \quad \text{(Eq. 4)}$$

$$r_m(m,Y)=k_G m\cdot\lambda(Y) \quad \text{(Eq. 5)}$$

Generally, the link to the extracellular environment is accounted for by including substrate dependency in the growth function as well as transition functions (budding and division) for each of the stages: (i) the growth rate of single cells (r_m, *Eq. 5*) depends on the mass of each cell (first-order kinetics) and on the available concentration of glucose. The substrate factor, λ(Y), can be regarded as a single cell specific growth rate and it is derived from the unstructured model describing the consumption of glucose and formation of ethanol; (ii) concerning the budding and division transitions, the critical transition cell sizes (μ_B and μ_D) are function of the locally available substrate concentration, and mathematically described by Monod type expressions. A mother and a daughter cell are generated upon division, where the ratio of the mother cell size to the daughter cell size is defined by the partitioning function, *P(m,m'| Y)*. This function consists of a symmetrical beta probability density function. The dependence of the partitioning function on the substrate was neglected for this case study.

3.2. Unstructured Model: Description of the extracellular environment

The unstructured model describes the fermentation of glucose (substrate) to ethanol. The local consumption rate is estimated based on an averaged yield of biomass on substrate and the concentration of biomass present at a given location in the microreactor and a given time point. The rate of formation of ethanol is estimated in a similar fashion. This concentration of biomass is calculated as the zeroth moment of the total cell size distribution. The updated concentrations of glucose and ethanol are used for recalculating the substrate factor λ(Y), which serves as input to the PBM.

3.3. Solution methods

The fixed-pivot technique (Kumar and Ramkrishna, 1996) was used to discretize the PBE, using an evenly distributed grid with 20 pivots. The commercial software by ANSYS® CFX (v. 12.1) was used, and PBM was implemented using the expression language (CEL). The geometry was defined with ICEM CFD 12.1, and a hexahedral

mesh with 32159 elements and 36535 nodes was generated. Diffusion was not considered in the simulations.

4. Results and Discussion

The glucose supplied at the inlet is transported through the reactor, allowing for the biomass to grow. The biomass is suspended, and thus is also transported throughout the reactor until it exits the system. The spherical structures allow for a higher retention of the biomass within the reactor in comparison to a plug-flow configuration, preventing a complete wash out of the biomass. The steady-state profiles for glucose, total biomass and ethanol profiles are presented in Figure 2.

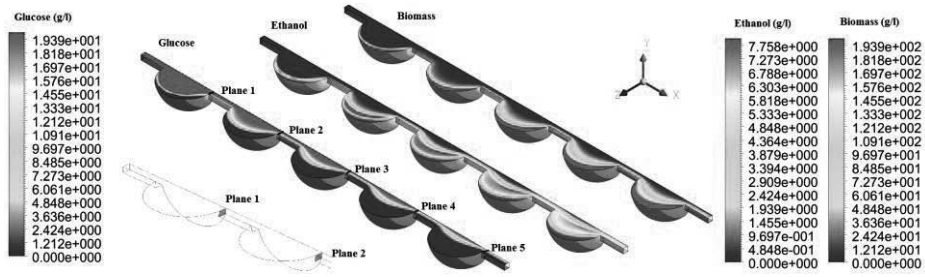

Figure 2 – Glucose, total biomass and ethanol profiles obtained at steady-state. As the reactor is symmetrical along the x- and y-axis, only a quarter of the reactor was simulated and illustrated. The total length of the reactor is 8 mm. The inlet of the reactor is located at the nearest to Plane 1.

The glucose concentration is highest at the inlet and decreases along the reactor. Therefore, the biomass growth rate is highest close to the inlet. The biomass formed in the first compartments is transported along the flow streamlines towards the outlet (Fig. 2). This results in a higher biomass concentration in the compartments closest to the outlet, although the growth rate here is virtually zero. Ethanol cannot be consumed by the cells due to the lack of oxygen. Its concentration is highest at the interface of glucose and the biomass is accumulated in each compartment.

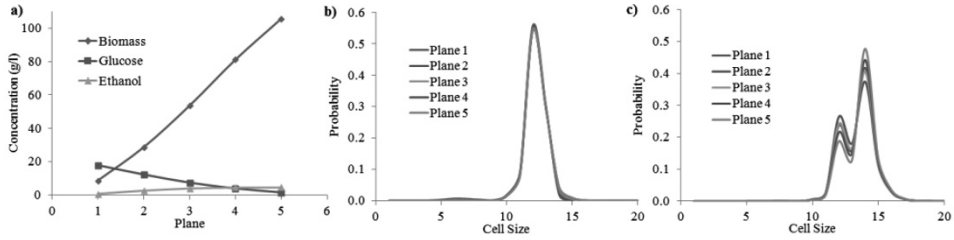

Figure 3 – Comparison of average concentrations and cell size probability density distributions for different location planes in the reactor: a) average concentrations of total biomass, glucose and ethanol b) distribution for the non-budding stage c) distribution for the budding stage. Arbitrary units are used for cell size.

Four different location planes were selected corresponding to the outlets of the spherical compartments (Fig.2) . The average glucose, ethanol and total biomass concentrations corresponding to each location plane are presented in the Figure 3. Additionally, the cell size distributions for the two stages for each of the locations are compared (Fig. 3). While the difference in the distributions is not significant for the non-budding stage, this difference is rather noticeable for the budding stage. If cells were imobilized in the

different compartments, it would be expected that the population in the compartment closest to the inlet (experiencing higher glucose concentration) would contain a higher fraction of bigger cells. Experimentally, the cell size distributions shifts towards smaller sizes when entering stationary phase (Werner-Washburne et al., 1993). This is however not observed in the simulation results, where cells are transported through the reactor. The coupling of a segregated biological model with the fluid dynamic model, increases the complexity of the problem and challenges the interpretation of the results. Different control tests, e.g. continuity check and mass balance closure, have been performed. Further investigation, both *in silico* and experimentally, is required in order to assess the validity of these results.

5. Conclusions

In this case study, a PBM describing the distribution of cell size for cell cycle stages, and its dependence on the available substrate concentration, was coupled to a fluid dynamic model that describes the transport of the supplied substrate and the biomass throughout the reactor. The interpretation of the results is challenging as the transport of the cells along the fluid streams has to be considered together with biological phenomena (growth, budding and division) taking place locally. The study is, nonetheless, a contribution to the development of modeling tools for successful prediction of the dynamic behavior of total protein content distributions of a yeast population under non-ideal mixing conditions, as found in large-scale fermentors as well. In the future a comparison of this more detailed model with simpler ones (e.g. lumped models) should be performed in order to identify the situations where the use of more complex models such as the proposed one is adequate and justifiable.

Acknowledgments

The Danish Council for Strategic Research is acknowledged for financial support in the frame of project number 09-065160.

References

S.-O. Enfors, M. Jahic, A. Rozkov et al. 2001. Physiological responses to mixing in large scale bioreactors. Journal of Biotechnology, 85, 175-185

R. Lencastre Fernandes, M. Nierychlo, L. Lundin et al. 2011. Experimental methods and modeling techniques for description of cell population heterogeneity. Biotechnology Advances, 29, 575-599

L. Alberghina, H.V. Westerhoff eds. 2005. Systems biology. Berlin/Heidelberg: Springer-Verlag. Vol. 13.

L. Alberghina, C. Smeraldi, B.M. Ranzi, D. Porro. 1998. Control by nutrients of growth and cell cycle progression in budding yeast, analyzed by double-tag flow cytometry. Journal of Bacteriology, 180, 3864-3872.

P. Jorgensen, I. Rupeš , J.R. Sharom et al. 2004. A dynamic transcriptional network communicates growth potential to ribosome synthesis and critical cell size. Genes & Development, 18, 2491 -2505.

I. Rupeš. 2002. Checking cell size in yeast. Trends in Genetics, 18, 479-485.

D. Porro, F. Srienc. 1995. Tracking of individual cell cohorts in asynchronous saccharomyces cerevisiae populations. Biotechnology Progress, 11, 342-347.

C. Hatzis, D. Porro. 2006. Morphologically-structured models of growing budding yeast populations. Journal of Biotechnology, 124, 420-438.

S. Kumar, D. Ramkrishna. 1996. On the solution of population balance equations by discretization—i. a fixed pivot technique. Chemical Engineering Science, 51,1311-1332.

M. Werner-Washburne, E. Braun, G.C. Johnston , R. A. Singer. 1993. Stationary phase in the yeast Saccharomyces cerevisiae. Microbiology and Molecular Biology Reviews, 57, 383-401

I.A. Karimi and Rajagopalan Srinivasan (Editors), Proceedings of the 11th International Symposium on Process Systems Engineering, 15-19 July 2012, Singapore.

Development of an integrated model for cobalt solvent extraction using Cyanex 272

Heather A Evans[a], Linh Vu[a], Parisa A Bahri[a] and Keith R. Barnard[b]

[a] *Murdoch University – School of Engineering, South Street, Murdoch, 6150, Australia*
[b] *CSIRO Process Science and Engineering, PO Box 7229 Karawara,WA 6152, Australia*

Abstract

A model of metal extraction based on pH isotherms was generated and applied to a cobalt solvent extraction (SX) circuit. Cyanex 272 (*bis*-(2,4,4-trimethylpentyl) phosphinic acid) was used as the organic extractant due to its selectivity for cobalt over nickel in the extraction process. Experiments were conducted for cobalt, nickel and magnesium extraction, with the latter two representing impurity elements in Co SX. The methods for determining metal extraction incorporated the effects of temperature, solution composition and pH on the equilibrium constant *k*, and hence on the overall extraction extent. This information was applied to a multi-stage mixer-settler model consisting of integrated extraction units. The initial mathematical model for cobalt, which was built in Matlab can be further developed to include the impurity elements and incorporate the scrubbing and stripping units. Future work will focus on using the model for process optimisation.

Keywords: cobalt, solvent extraction, modelling, equilibrium constant, Cyanex 272

1. Solvent Extraction modelling background

1.1. Solvent extraction

Solvent Extraction (SX) is a hydrometallurgical process used to purify and concentrate metal ions of interest from an aqueous phase. It has been used on commercial scale since the 1950's (Sole et al., 2005). Selective extraction of cobalt typically from nickel-rich sulfate solutions using SX became widely possible in the 1980's with the introduction of the organic extractant Cyanex 272, which contains *bis*(2,4,4-trimethyl pentyl) phosphinic acid ('phosphinic acid') as its active component (Bourget et al., 2011). Cobalt SX using this reagent, diluted in a suitable diluent (solvent), is an equilibrium process whereby cobalt is selectively extracted from an aqueous feed solution onto the organic phase, typically by using a series of mixer-settler units. Cobalt loaded onto the organic phase is subsequently recovered by stripping with an acidic aqueous solution. The aqueous cobalt concentration can be increased by judiciously varying the aqueous to organic ratio in both the extraction and stripping stages. Cobalt extraction follows the general form of Equation 1, where RH represents the phosphinic acid.

$$Co^{2+}{}_{(aq)} + 2(RH)_{2\ (Org)} \leftrightarrow Co(R_2H)_{2(org)} + 2H^{+}{}_{(aq)} \quad (1)$$

A typical flowsheet for cobalt recovery using Cyanex 272 as the extractant is shown in Figure 1. The evaluated flowsheet consisted of three stages of counter-current extraction in mixer-settlers to effectively separate the cobalt from the pregnant leach solution (PLS). As the reaction proceeds, hydrogen ions are released from the extractant into solution, lowering the pH of the solution (Equation 1). As the reaction is highly pH dependent, alkali (base) is added to neutralise the hydrogen ions and maintain the desired pH. To minimise the risk of any entrained organic extractant being transferred to the downstream circuit, the aqueous solution leaving the last extract stage (E3) is washed with fresh diluent in the diluent wash (DW) mixer-settler. The cobalt-rich loaded organic (LO) phase leaving the first extract stage (E1) is scrubbed (Sc) to remove any co-extracted impurities such as nickel and calcium, before entering the strip circuit. Cobalt is then progressively stripped from the organic using a combination of aqueous lean electrolyte and acid to produce the loaded strip liquor (LSL) from which Co is recovered. The stripped organic is then washed with water to dilute any entrained cobalt and acid, prior to returning to the extraction circuit. For the purpose of this paper, only the extraction circuit has been modelled in detail.

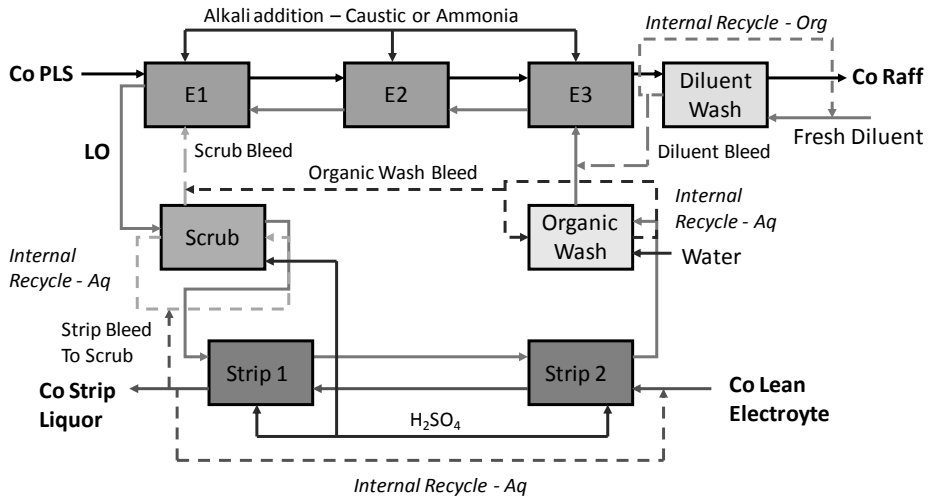

Figure 1: Flowsheet for cobalt solvent extraction using Cyanex 272

1.2. Modelling

Flowsheet modelling is an important area in the metallurgy/chemical engineering disciplines due to the high cost of new metallurgical plants and more complex processing routes being used. Engineers designing new plants and optimising existing circuits need to have a good understanding of the process and what is likely to happen if any of the input variables change during operation. While initial bench scale and pilot scale testwork can provide valuable information regarding the chemistry of the system, the long term testing required is very expensive. Therefore the use of flowsheet modelling to assist in project evaluation is becoming more widespread. The commercial modelling packages are continually being updated as new computational techniques are developed and more is known about the unit operations being modelled.

From the SX perspective, the most developed models are the proprietary modelling packages owned and operated by the reagent suppliers, the most common of which are the Isocalc™ TM (total metallurgy) and and MINCHEM® computer simulation packages developed by Cognis (formally Henkel) and Zeneca (now Cytec) respectively, as tools to assist in simulating copper solvent extraction (CuSX) processes involving sulfuric acid leaching followed by copper extraction using a phenolic oxime extractants. These modelling packages are used to develop circuit layouts, flow options, recovery options, reagent inventory and make-up requirements. Both packages rely on extensive isotherm libraries developed over a number of years covering an extremely wide range of feed and reagent combinations. Outputs from these models include McCabe-Thiele plots, calculations of stage efficiencies and final rich electrolyte and raffinate copper concentrations. These can be used to model alternate plant configurations. Inputs required are stripped organic copper concentration, feed rate and concentration and reagent concentration. However these can be varied to achieve a desired output concentration. These programs are helped by the high selectivity these phenolic oximes show for copper over other metal ions. In recent years Cytec has been adapting the MINCHEM® software for use in cobalt solvent extraction using Cyanex 272 (Bourget et al., 2011). However, this is a challenging task as this reagent can extract multiple cations besides cobalt, and exhibits variable complex stoichiometry.

2. Experimental

To generate the data required for model construction, some experimental work was undertaken. This involved the construction of pH-extraction isotherms for cobalt, nickel and magnesium extraction with Cyanex 272 under various operating conditions (refer Figure 2). The experimental procedure has been discussed elsewhere (Evans et al., 2008), and only the key results will be included here.

2.1. Relationship between log k and extraction extent for cobalt, nickel and magnesium

It is known that cobalt and magnesium tend to form tetrahedrally co-ordinated complex with phosphinic acid and nickel forms a hydrated octahedral complex (Tati, 1993; Badrul et al., 2007). As shown elsewhere (Evans et al., 2008) for the purpose of this work, we can express the extraction extent (ε%) for each metal, which can be readily measured directly, in terms of its equilibrium constant (k) and the free or available phosphinic acid (RH). Based on the resulting coordination complexes for cobalt and magnesium we use Equation 2 and for nickel we use Equation 3.

$$\varepsilon\% = \frac{k[\overline{(RH)_2}]^2}{k[\overline{(RH)_2}]^2+[H^+]^2} \quad (2)$$

$$\varepsilon\% = \frac{k[\overline{(RH)_2}]^3}{k[\overline{(RH)_2}]^3+[H^+]^2} \quad (3)$$

The equilibrium constant was determined for each metal using the experimental data and using least squares regression techniques to solve for log k. Examples of the experimental and calculated isotherms for the three metals are shown in Figure 2.

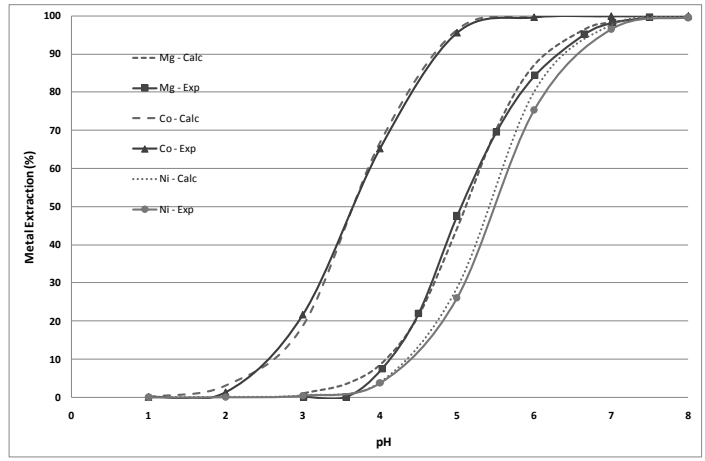

Figure 2: Experimental and calculated isotherms for cobalt, nickel and magnesium as extracted from single metal systems with 20%v/v Cyanex 272 at 35 °C.

3. Model Construction

The steady state model developed for the 3-integrated extraction units is based on the total and component mass balances around the whole system and each unit. For the purpose of the extraction model, each unit has three inlet streams: aqueous phase (A), organic phase (O) and ammonia hydroxide solution (B) used for pH neutralisation. It is assumed that B is soluble in the aqueous phase and no tertiary phases are generated, so that there are only two outlet streams A and O.

Inputs to the model are the feed composition of the aqueous phase (pH, Co, Mg and Ni concentrations), the composition of the barren organic (available RH, any residual loaded metal values Co, Mg and Ni), extraction unit pH, the temperature of the system (in K) and organic and aqueous flow rates (m^3/h). For the purpose of the initial model it is assumed that the mass flowrate of the organic phase does not change throughout the extraction stage. For the three metals studied, it was found that the Arrhenius relationship (Equation 4) could be used to determine the effect of temperature (T) on the equilibrium constant (k).

$$Ln\, k = \frac{A}{T} + B \qquad (4)$$

The two constants A and B were determined for each metal individually and the results are shown in Table 1. The high correlation (R^2) for cobalt and magnesium show that the equilibrium constants for these metals does indeed follow the Arrhenius relationship. However, the R^2 for nickel was significantly lower, indicating that nickel extraction with Cyanex 272 was relatively independent of temperature.

The model also calculates the mass of ammonia hydroxide solution to be added to each unit to maintain the pH of the reaction at a desired set-point, e.g. pH 5.5. If ammonia is not added to the mixer, the pH will drop during the extraction reaction, which lowers the overall metal extraction for the process. If too much ammonia is added, then more impurity metals will be co-extracted, and the risk of metal precipitation also increases.

Table 1: Values for constants A and B determined as a function of operating temperature

Metal	A	B	R^2
Cobalt	-8330.5	10.509	0.9892
Magnesium	-9670.9	9.252	0.9677
Nickel	-2233.4	-18.115	0.6632

The available information and the model equations were applied to develop a steady state model in Matlab code. Using the constants A and B with the temperature of the system allows the determination of the equilibrium constant for each metal. This together with the input values previously mentioned, eg pH, allows the calculation of the available RH and metal content of each stream leaving the extraction unit. As the Matlab solver can only sequentially solve the model equations, the extraction efficiency for units E1, E2 and E3 must be known to recalculate the concentration of RH in the organic phase leaving each unit. The initial model focused only on cobalt extraction using the assumption that ε1 = ε2 = ε3. The value of ε3 can be calculated directly from the pH, initial RH concentration and *k* as per Equation 2. After the first simulation is performed, ε1, ε2 and ε3 must be back-calculated. If their values are significantly different from ε3, the second simulation with updated values for ε1, ε2 and ε3 must be performed and back-calculated until insignificant change in values of ε is achieved.

The initial cobalt only model assumed a feed of 0.5 g/L cobalt at pH of 5.5 with a flow rate of 300 m^3/h, at an O:A ratio of 1. At the high extraction efficiency of 95%, only 2 stages were required to extract the cobalt producing a raffinate of 0.01 g/L Co.

4. Future work

The Matlab model will be updated to include nickel and magnesium. The mathematical model will be transferred to Aspen Custom Modeller (ACM), which with its object oriented features will provide the ability to build a more efficient flowsheet incorporating recycle streams to more accurately reflect a commercial operation. This will then be used for trialling different process configurations and operating parameters leading to the optimisation of the process.

The authors would like to thank the Parker Centre for the initial project funding and CSIRO and Murdoch University for ongoing support.

References

IM Badrul, HM Zahurul, IM Shamsul, 2007, Studies on Cyanex 272 complexes of Mg(II), Ca(II) and Fe(III), Bangladesh Journal of Scientific and Industrial Research, 42, 1, pp 475-482.

C Bourget, M Soderstrom, S Donegan, J Morrison, 2011, Design optimisation of a Cyanex 272 solvent extraction circuit, Proceedings of ISEC 2011, pp 1-9.

Cognis Mining Chemicals Technology, Blue Line Technical Bulletin, www.cognis-us.com access date 31/12/2011.

HA Evans, PA Bahri, JA Rumball & KR Barnard, 2008, Modelling cobalt extraction with Cyanex 272, Proceedings of ISEC 2008, pp 459-466

KC Sole, AM Feather, PM Cole 2005, Solvent extraction in southern Africa: An update of some recent hydrometallurgical operations, Hydrometallurgy, 78, pp52-78.

BK Tait, 1993, Cobalt-nickel separation: the extraction of cobalt(II) and nickel(II) by Cyanex 301, Cyanex 302 and Cyanex 272, Hydrometallurgy, 32, pp 365-372.

I.A. Karimi and Rajagopalan Srinivasan (Editors), Proceedings of the 11th International Symposium on Process Systems Engineering, 15-19 July 2012, Singapore.

Fast simulation of annual optical efficiency of solar tower power plant

Fei Xie, Yuhong Zhao, Lifang Zhou

Department of Control Science & Engineering, Zhejiang University, Hangzhou 310027, China

Abstract

The simulation of annual optical efficiency is important for the design of a solar tower power plant. The acceleration of the efficiency computation is investigated in this paper. An efficient implementation is presented using a Graphics Processing Unit (GPU) for the optical analysis of the heliostat field in the tower power plant and a new code is developed. The efficiency and the general applicability of the proposed method to different field arrangements are verified by the numerical simulations. The speedup of the calculation on a GPU with respect to that on a CPU is significant.
Keywords: solar tower power plant, optical efficiency, GPU computing

1. Introduction

The solar tower power plant is the most economical way to produce solar electricity in large scale. It employs an array of mirrors called heliostat field to focus the sunlight upon a receiver to concentrate solar thermal energy. The heliostat field is an important subsystem because it provides the reflected energy and contributes almost half of the total plant cost. Therefore the optical efficiency needs to be calculated repeatedly to evaluate the performance of the heliostat field during the design and optimization of the heliostat field layout. Although some codes and methods have been developed to simulate the optical efficiency of the heliostat field (Garcia et al., 2008), none of them has a good performance on accuracy, computing speed and versatility simultaneously due to the large amount of computation which is difficult to be handled with CPU.

On the other hand, Graphics Processing Unit (GPU) has become an integral part of today's mainstream computing systems for the purpose of high performance computing since NVIDIA released the Compute Unified Device Architecture (CUDA) toolkit in 2006. With the help of CUDA, GPU can be easily used for general-purpose computing and numerous scientific papers have been published showing moderate to impressive improvements in performance of codes on a GPU over a CPU (Bleichrodt et al., 2011).

CUDA programming model allows programmers to define a C function, called kernel, which can be executed in parallel on a set of GPU threads. The threads are organized into groups called thread blocks. One or more than one blocks consist of a grid. This provides a more efficient architecture with two parallel levels in a kernel function: the coarse-grained parallel (blocks in a grid) and fine-grained parallelism (threads in a block). A detailed introduction to CUDA can be found in NVIDIA, 2011.

In this paper, a new acceleration method for the computation of the optical efficiency of the heliostat field is proposed by exploring the parallel processing capabilities of GPU. The model and the numerical methods adopted are introduced in Section 2. In Section 3, the implementation on CUDA is described in detail. In Section 4, the simulation results are given and the performance of two codes is compared. Finally, conclusions are drawn and the future research is indicated in Section 5.

2. The numerical model of the optical efficiency

The optical efficiency is to measure the energy loss of the heliostat field which is about 47% annually. The loss mainly comes from five parts: the cosine loss (23.4%), the mirror reflectance loss (10%), the atmospheric attenuation loss (6%), the shading and blocking (s&b) loss (5.6%) and the receiver spillage loss (2%) (Wei et al., 2010).
In general, the optical efficiency of the field $\eta_{optical}$ can be given by

$$\eta_{optical} = \rho_{Mirror} \cdot \eta_{cos} \cdot \eta_{Atmosph.Att} \cdot \eta_{s\&b} \cdot \eta_{spillage} \quad (1)$$

where ρ_{Mirror}, η_{cos}, $\eta_{Atmosph.Att}$, $\eta_{s\&b}$ and $\eta_{spillage}$ are the mirror reflectance efficiency, the cosine efficiency, the atmospheric attenuation efficiency, the s&b efficiency and receiver spillage efficiency respectively, which is equivalent to 1 minus the corresponding loss. Since the mirror reflectance loss depends on the heliostat reflective rate, ρ_{Mirror} can be considered as a constant ($\rho_{Mirror} = 0.9$ is adopted in this work). The heliostats are assumed to be perfectly flat and the sunlight is supposed to be parallel in this paper, therefore the receiver spillage loss was not taken into consideration, namely $\eta_{spillage} = 1$. As a result, three types of efficiency need to be computed to determine the optical efficiency.
In fact, in order to obtain the annual optical efficiency of the field, which is based on the hourly performance of each heliostat on certain days during a year (Pitz-Paal et al., 2011), these three efficiencies have to be simulated at hundreds of solar positions (the azimuth angle and the elevation angle of the sun) for thousands of heliostats leading to a large amount of computation and then a long running time. Hence, a parallel computing method is presented to accelerate the procedure of the efficiency calculation.
The calculation method of the three efficiencies for a single heliostat called calculated heliostat which is represented by H with center $O_H(x_{OH},y_{OH},z_{OH})$ is described in this section. The other heliostats can be calculated similarly.

2.1. The cosine efficiency, η_{cos}

The amount of insolation reflected by the heliostat is proportional to the amount of sunlight intercepted. The reflected power is proportional to the cosine of the angle between the heliostat normal and the incident sun rays. Let S be the unit vector with the opposite direction of the incident ray and R be the unit vector of reflected ray of H. Because the angle between S and R is twice of the angle between the heliostat normal and S, the cosine efficiency can be expressed as follows:

$$\eta_{cos} = cos\left[\frac{1}{2} arccos(S \cdot R)\right] \quad (2)$$

2.2. The atmospheric attenuation efficiency, $\eta_{Atmosph.Att}$

Some of the energy of the reflected rays is scattered and absorbed by the atmosphere. This effect is referred to as the atmospheric attenuation loss. The atmospheric attenuation efficiency can be calculated simply as a function of the distance between heliostat and receiver d_{HR} in meter for a visual range of about 40 km (Wei et al., 2007):

$$\eta_{Atmosph.Att} = \begin{cases} 0.99321 - 0.0001176 * d_{HR} + 1.97 * 10^{-8} * d_{HR}^2 & (d_{HR} \leq 1000m) \\ e^{-0.0001106 \times d_{HR}} & (d_{HR} \geq 1000m) \end{cases} \quad (3)$$

2.3. The shading and blocking efficiency, $\eta_{s\&b}$

The shading loss is the part of the reflective area which shadowed by other heliostats. The blocking loss is the fraction of the reflected radiation hitting the back of other heliostats. The s&b loss is mainly caused by adjacent heliostats. Before computing the

s&b efficiency, the heliostats that may cause s&b loss to the calculated heliostat H must be decided. First two rectangles are generated with O_H located at the midpoint of one side of each rectangle as shown in Fig. 1 and the other pair of sides parallel with the incident ray (for judging shading loss) and the reflected ray (for judging blocking loss) separately. The side lengths depend on the relative position of H, the receiver and the sun. The calculation is omitted due to space limitation.

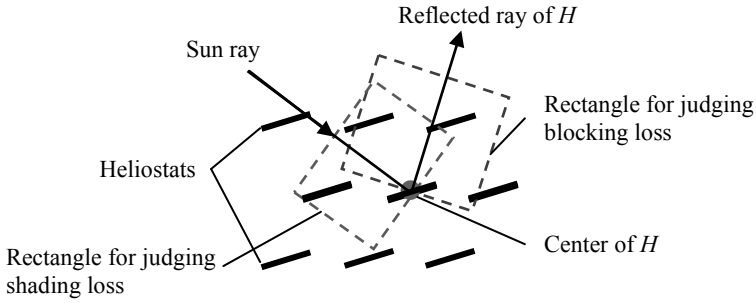

Fig. 1 Diagram of determining the heliostats that may cause shading and blocking loss (from top view in the ground coordinate system)

All the heliostats whose centers locate in the rectangle margin are called projecting heliostats, which may cause s&b loss to H. A projection parallelogram can be formed for each projecting heliostat by projecting the vertices of the projecting heliostat to the plane spanned by H along the direction of the incident ray or the opposite direction of the reflected ray and transforming the results into the coordinate system of H, which is depicted as Fig. 2.

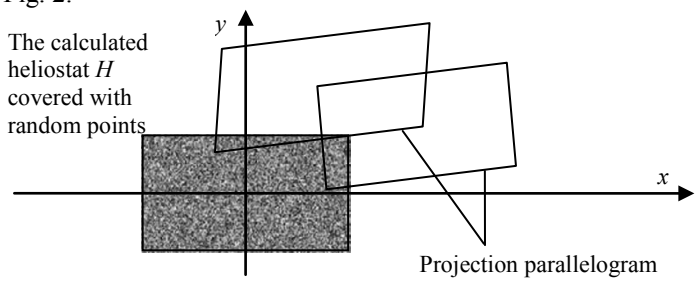

Fig. 2 Diagram of computing the s&b efficiency

The s&b efficiency is the ratio of the area of H that is not covered by any projecting parallelogram to the area of H. Since it is difficult to calculate this irregular area analytically, Monte Carlo method is adopted. Numerous random well-distributed points are generated to cover H. Count the points which are not in any parallelogram and the s&b efficiency can be represented by the ratio of the counter to the total number of random points. The total number determines the accuracy of the derived efficiency.

3. Implementation details

The method described in Section 2 is implemented on CPU and GPU respectively. The main parts of both codes are written in MATLAB. The difference is that the GPU code calls CUDA through the parallel computing toolbox in MATLAB when computing the most computationally intensive part, $\eta_{s\&b}$.

The inputs for both codes are the coordinates in the ground coordinate system of the heliostats and the receiver and the solar position. The unit vectors of the incident ray, the reflected ray and the normal of each heliostat are computed first, followed by η_{cos},

$\eta_{Atmosph.Att}$ and the coordinates of the vertices of each heliostat, and finally $\eta_{s\&b}$ of each heliostat is calculated as following steps:
1) Decide the projecting heliostats;
2) Compute the coordinates for the vertices of the projection parallelogram;
3) Judge the points that are not in any projection and calculate the s&b efficiency.
The key issues of step 1 and 3 are the same, which is to identify whether a point is inside a quadrilateral or not. Different methods are adopted on GPU and CPU to make use of their advantages. As CPU is good at logical affair and serial computing while GPU performs well implementing highly threaded parallel processing tasks, a coordinate judgment method with more logical affair is used on CPU and the Helen Theorem method exhibiting more computationally intensive is used on GPU to achieve the fastest running speed on both codes. The former judges the position relationship between the point and the four vertices of the parallelogram, while the latter computes the areas of the four triangles which are formed by the point with every two adjacent vertices of the parallelogram and compares their sum with the area of the parallelogram. By exploiting the two-level parallel architecture of GPU, each block is used to calculate the efficiency of a different heliostat and the threads in each block are in charge of the related calculation of the same heliostat.

4. Simulation Results

The numerical simulations are implemented on an Inter® Core™ i5-2300 CPU @2.80GHz and a NVIDIA's GTX 570 GPU. The performance comparisons between the codes on CPU and GPU are illustrated in Fig. 3. Both codes are applied to calculate the optical efficiency of a corn-field heliostat field with similar heliostat size and field arrangement to the eSolar's plant at an individual solar position (Schell, 2011). Fig. 3(a) shows the running time comparisons between two codes at different field scales and with different accuracy which is defined as the reciprocal of the number of the random points covering a heliostat. The Grid size used in the GPU code is 10000, which is the product of the block number and the number of threads in each block. In Fig. 3(b), the speedup of the calculation on the GPU with different Grid size with respect to that on CPU is plotted for different field scales with same accuracy of 0.0001. The results manifest that the proposed method behaves much better on GPU than on CPU especially with the increasing of the computation if the Grid size is big enough.

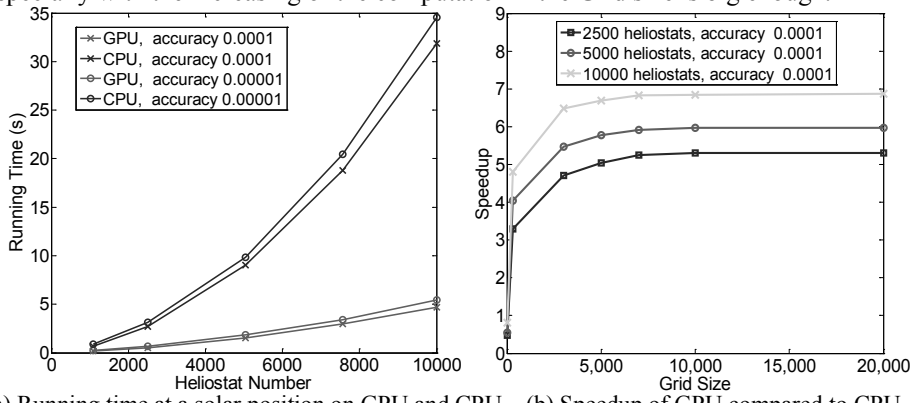

(a) Running time at a solar position on GPU and CPU (b) Speedup of GPU compared to CPU

Fig. 3 Performance comparisons of GPU and CPU

Moreover, the proposed method can be applied to various arrangements. The annual optical efficiencies of two different fields are depicted as Fig. 4. Fig. 4(a) indicates the

result of a corn-field heliostat field consisting of 10000 heliostats and 4(b) indicates the result of a radiate heliostat field consisting of 554 heliostats with an area of $80m^2$(10m*8m) (Siala et al., 2001). The accuracy of both simulations is 0.0001, and the running time is 4.69 seconds for the corn-field heliostat field and 0.52 seconds for the radiate heliostat field at one solar position.

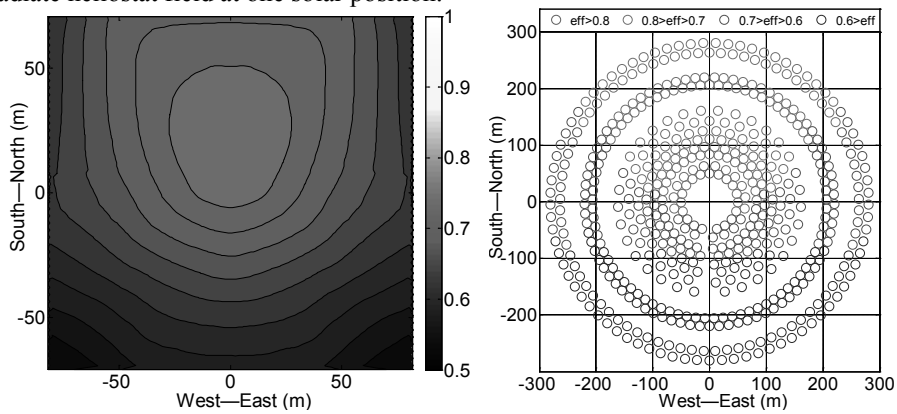

(a) Corn-field heliostat field (b) Radiate heliostat field

Fig. 4 Simulation results of the heliostat fields

5. Conclusion

A new parallel simulation method of the optical efficiency of the heliostat field in a solar tower power plant is presented on GPU using a CUDA implementation. The method is applicable to various field arrangement and scale. The simulation results demonstrate that the speedup compared with the CPU method is significant under the same accuracy. However, the efficiency model used is somewhat simplified and the GPU code is not optimized to be more efficient. The further work will be focused on how to develop a more effective algorithm and a more efficient GPU code considering more practical effects.

Acknowledgements

The authors gratefully acknowledge the financial support of NSFC (61173128, 60974007) and 973 Program of China (2012CB720500).

References

F. Bleichrodt, H.B. Rob, A.D. Henk, 2011, Accelerating a Barotropic Ocean Model Using a GPU, Ocean Modelling, 41, 16–21.

P. Garcia, A. Ferriere, J.J. Bezian, 2008, Codes for Solar Flux Calculation Dedicated to Central Receiver System Applications: A Comparative Review, Solar Energy 82, 189–197.

NVIDIA, 2011, NVIDIA CUDA C Programming Guide, Version 4.0.

R. Pitz-Paal, N.B. Botero, A. Steinfeld, 2011, Heliostat Field Layout Optimization for High-temperature Solar Thermochemical Processing, Solar Energy 85, 334–343.

S. Schell, 2010, Design and Evaluation of eSolar's Heliostat Fields, Solar Energy 85, 614–619.

F.M.F. Siala, M.E. Elayeb, 2001, Mathematical Formulation of a Graphical Method for a No-blocking Heliostat Field Layout, Renewable Energy 23, 77–92.

X.D. Wei, Z.W. Lu, Z. LIN, 2007, Optimization Procedure for Design of Heliostat Field Layout of a 1MWe Solar Tower Thermal Power Plant, Proc. of SPIE 6841, 684119-1–684119-10.

X.D. Wei, Z.W. Lu, W.X. Yu, 2010, A New Code for the Design and Analysis of the Heliostat Field Layout for Power Tower System, Solar Energy 84, 685–690.

I.A. Karimi and Rajagopalan Srinivasan (Editors), Proceedings of the 11th International Symposium on Process Systems Engineering, 15-19 July 2012, Singapore.

A Numerical Analysis for Total Site Sensitivity

Peng Yen Liew[1], Sharifah Rafidah Wan Alwi[1*], Petar Sabev Varbanov[2], Zainuddin Abdul Manan[1], Jiří Jaromír Klemeš[2]

[1]*Process Systems Engineering Centre (PROSPECT), Faculty of Chemical Engineering, Universiti Teknologi Malaysia, 81310 Skudai, Johor, Malaysia.*
[2]*Centre for Process Integration and Intensification – CPI[2], Research Institute of Chemical and Process Engineering, Faculty of IT, University of Pannonia, Egyetem u. 10, H-8200 Veszprém, Hungary. Email: [*]shasha@cheme.utm.my*

Abstract

Total Site Heat Integration (TSHI) is an established method for analysis and mapping of heat sources and sinks of multiple processes linked via a centralised utility system. The TSHI method is very beneficial for analysing a total site's sensitivity to plant maintenance shutdown and production changes that affect integrated heat sources and sinks. This paper presents the Total Site Sensitivity Table (TSST) as a systematic approach for exploring the effects of plant shutdown or production changes. TSST can be used hand in hand with TSHI graphical approaches (Grand Composite Curve, Total Site Profile and Site Composite Curve) or numerical approach (Total Site Problem Table Algorithm). The graphical approach provides better insights while the numerical approach provides faster, easier and accurate calculations. Both approaches have its advantages and disadvantages and it is up to the engineers which approach they prefer or complement. The use of TSST allows a design engineer to clearly see the sensitivity of Total Site (TS) towards operational changes. The best setting for different operation condition in total site context can be selected by exploiting this tool. The worst case scenario can also be explored for the integrated TS system through the use of TSST. This information is useful for exploring the individual plant operational flexibility. Decision for having a backup heat exchanger network according to TSST would increase the energy saving for various TS operating conditions. TSST can be used to consider various *'what if'* scenarios. They allow the determination of the optimum size of utility generation system and backup piping needed to be designed, external utilities that need to be bought and stored. Application of this technique on a case study demonstrates with the assistance of TS-PTA, TSST clearly pinpoint the effects of plant shutdown or production changes on heat distribution and utility generation systems of a Total Site.

Keywords: *Total Site Heat Integration; Pinch analysis; Total Site Problem Table Algorithm (TS-PTA); Total Site Sensitivity Table (TSST); plant sensitivity*

1. Introduction

Total Site Heat Integration (TSHI) is an inter-processes integration method linked by a common site utility system. The concept was first introduced by Dhole and Linnhoff (1993) and Raissi (1994) and further extended by Klemeš et al. (1997) in the form of

designing software. This integration method offers a greater energy saving opportunity compared to single processes integration. Perry et al. (2008) has conceptually extended TSHI to reduce carbon footprint by integrating large community servicing and corporate building as additional heat sinks, and renewable energy as heat sources. However, the variability of heat supply and demand has increased the difficulty in handling and controlling the system. Varbanov and Klemeš (2011) has later introduced Time Slices with heat storage system for solving the variable supply and demand problem in TSHI. Other researches in TSHI include the development of cogeneration targeting by Bandyopadhyay et al. (2010) and Kapil et al. (2011). Varbanov et al. (2012) also revisited the minimum temperature difference (ΔT_{min}) and new software module for TSHI.

In previous methods, the site utility targets are typically obtained from graphical approach, e.g. Total Site Profile (TSP) and Site Composite Curve (SCC). Just recently, Liew et al. (2012) has introduced an alternative approach based on numerical method known as Total Site Problem Table Algorithm (TS-PTA) to target TSHI. This method is easier to construct and gives faster, easier and accurate results as compared to graphical approach which have the tendency of graphical error due to curve shifting.

In this paper, a new tool for exploring TS sensitivity - a Total Site Sensitivity Table (TSST) - is introduced. This tool can be used hand in hand with either the graphical (Dhole and Linnhoff, 1993; Klemeš et al, 1977) or numerical TSHI approaches (Liew et al., 2012). This method allows the effect of process disruption within a TS to be analysed and contingency plans and actions to be taken to avoid affecting other processes. Process disruptions may include shutdowns of one or more plants, scheduled maintenance, production changes or emergency cases. The worst case scenario for the integrated plants can also be determined using TSST, for operational flexibility of the individual plants in the TS system.

2. Methodology

The proposed methodology of TSST is defined as follows:

STEP 1: Determine TS utility requirement using the TSP (Dhole and Linnhoff, 1993; Raissi, 1994; Klemeš et al., 1997) or TS-PTA (Liew et al., 2012) for various 'what if' scenarios e.g. when there are one or more plants shutdown. To do this, the source and demand data of the plant being shut down are omitted in the construction of TSP or TS-PTA.

STEP 2: Construct TSST to show the variation of utility requirement in the TS for the different scenarios.

i. The requirements for different types of utilities during different scenario are recorded in the TSST. All values are stated in positive values for both hot and cool utilities.
ii. The variations between normal operations and the various operating conditions are calculated by subtracting the utility requirements in normal operations from the utility requirements under different operating conditions according to utility types. A positive variance indicates that there is excess utility, while a negative variance represents the deficit of external utility.

iii. If there is excess utility (positive variance), it can be cascaded down to the lower utility level with negative variance to form the "variance after cascade". If there is still excess utility, it could be sold, cooled down or the utility generation can be reduced.

iv. A summary can be made according to the results for each scenario:
- The maximum requirement for each type of utility can be computed by adding the absolute value of the most negative number in the "variance after cascade" with the utility requirement at normal operation. If there are no negative values, the maximum utility requirement is equal to the normal operation utility.
- The minimum utility requirement for each type of utility can be calculated by deducting the most positive value of "variance after cascade" from the utility requirement at normal operation.

3. Demonstration Case Study

The construction of TSST is illustrated using a demonstration case study with four process units - Processes A, B, C and D (see Table 1). The minimum temperature difference between process streams ($\Delta T_{min,pp}$) of 20 °C and the minimum temperature difference between process streams and utility ($\Delta T_{min,up}$) of 10 °C are assumed for the system. The existing available utilities are high pressure steam (HPS) at 270 °C, medium pressure steam (MPS) at 179.93 °C, low pressure steam (LPS) at 199.59 °C and cooling water (CW) at 15-20 °C.

An example of TS-PTA under normal operation is shown in Table 2. Column 8 shows the utility requirement for normal operation of this Total Site. Total Site Pinch is located at between LPS and CW. Total heating and cooling requirement for the system are 4,807 kW and 3,085 kW respectively. Multiple utility targeting at TS-PTA shows that the system requires 1165kW of HPS, 645.5 kW of MPS and 2,996.5 kW of LPS as heating utility for the whole TS. 3,085 kW of CW is required as cooling utility. These values are recorded in the second column of TSST as shown in Table 3.

Table 1: Stream data for Processes A, B, C and D

Stream	T_S (°C)	T_T (°C)	ΔH (kW)	Cp (kW/°C)	T_S' (°C)	T_T' (°C)
Process A						
A1 Hot	200	100	2,000	20	190	90
A2 Hot	150	60	3,600	40	140	50
A3 Cold	50	220	-2,550	15	60	230
A4 Hot	150	130	1,000	50	160	140
Process B						
B1 Hot	200	100	2,000	20	190	90
B2 Cold	50	120	-4,900	70	60	130
B3 Cold	50	200	-750	5	60	210
Process C						
C1 Hot	200	50	450	3	190	40
C2 Hot	200	119	1,863	23	190	109
C3 Cold	30	200	-680	4	40	210
C4 Cold	130	150	-300	15	140	160
Process D						
D1 Hot	240	100	210	1.5	230	90
D2 Cold	50	250	-400	2	60	260
D3 Cold	40	190	-1,500	10	50	200

D4 Cold	109	140	-186	6	119	150

Table 2: TS-PTA at normal operation.

1	2	3	4	5	6	7	8
Utility	Heat Source (kW)	Heat Sink (kW)	Heat Requirement (kW)	Initial Cascade (kW)	Final Cascade (kW)	MU Cascade (kW)	Utility Requirement (kW)
				0	4,807	0	
HPS		1,165	-1,165				1165
				-1,165	3642	0	
MPS	50	695.5	-645.5				645.5
				-1810.5	2,996.5	0	
LPS	1,549	4,545.5	-2996.5				2,996.5
				-4,807	0	0	**Pinch**
CW	3,085		3085				-3085
				-1,722	3,085	0	

The TS utility requirements and THU for various scenarios involving process shut downs and production changes are evaluated using TS-PTA and recorded into TSST. The variances between normal operation and the various scenarios of TS utilities requirement are then determined. For example, when Plant A is run at half of its production rate, the system has extra HPS and CW and requires more MPS and LPS as shown in scenario 3 of Table 3(a).

Table 3(a): Total Site Sensitivity Table (TSST)

Scenario		**1**			**2**			**3**		
Utility	Normal (kW)	A shut down (kW)	Variance (kW)	Variance after cascade (kW)	B shut down (kW)	Variance (kW)	Variance after cascade (kW)	½ A shut down (kW)	Variance (kW)	Variance after cascade (kW)
HPS	1165	565	600	0	1065	100	100	865	300	0
MPS	6,45.5	695.5	-50	0	645.5	0	0	670.5	-25	0
LPS	2,996.5 pinch	4,511.5 pinch	-1,515	-965	pinch 553.5	2,443	2,443	3,754 pinch	-757.5	-482.5
CW	3,085	0	-3,085	-3,085	3085	0	0	1,542.5	1,542.5	1,542.5

Table 3(b): Total Site Sensitivity Table (TSST) (continue)

Scenario		**4**			**5**			**Summary**	
Utility	Normal (kW)	BC shut down (kW)	Variance (kW)	Variance after cascade (kW)	BCD shut down (kW)	Variance (kW)	Variance after cascade (kW)	Maximum requirement (kW)	Minimum requirement (kW)
HPS	1165	885	280	280	600 pinch	565	565	1165	600
MPS	645.5	545.5 pinch	100	100	50	595.5	595.5	645.5	50
LPS	2,996.5 pinch	519.5	2477	2477	1,515	1,481.5	1,481.5	3,961.5	519.5
CW	3,085	3,085	0	0	3085	0	0	3085	1,542.5

After analysing the various 'what if' scenario, the total site integration for the demonstration case study requires a boiler that can produced a maximum capacity of 1,165 kW of HPS, 645.5 of MPS and 3,961.5 kW of LPS, giving a total 5,772 kW of steam production compared to 4,807 kW of steam required during normal operation. A

backup boiler may be a good option to cater for this production changes or the steam requirement can be obtained externally. In worst case, the minimum steam requirement for the system is 1,169.5 kW (summation of each steam types minimum requirement). Normally a boiler would require a turn down ratio of not lower than 50%. Hence assuming the boiler lowest capacity is 2,403.5 kW. It would mean the remaining 1,269 kW of steam needs to be cooled down using cooling water or sold to other plants. Another alternative is to divert the excess steam production for Combined Heat and Power (CHP) system to generate more power.
For cooling water, the maximum capacity required is 3,085 kW and minimum capacity is 1,542.5 kW.

4. Conclusion

The TSST is a simple and systematic tool for accessing the TS sensitivity towards the plant operational changes due to schedule maintenance or emergency shutdown. The tool can be used for both TS-PTA and TSP to develop utility system planning such as determining the maximum boiler size, turn down ratio, backup piping system planning and the heat to be bought or sold. The tool is also able to detect the worst case scenario in the integrated TS system for plants' operational flexibility.

Acknowledgement

The authors would like to thank MOHE (Ministry of Higher Education) Malaysia and UTM in providing the research fund for this project under Vote No. Q.J130000.7125.00H22.

References

A. Kapil, I. Bulatov, R. Smith, J. Kim, 2011, Site-wide low-grade heat recovery with a new cogeneration targeting method. Chemical Engineering Research and Design. doi:10.1016/j.cherd.2011.09.001

J. Klemeš, V. R. Dhole, K. Raissi, S. J. Perry, L. Puigjaner, 1997, Targeting and Design Methodology for Reduction of Fuel, Power and CO_2 on Total Site, Applied Thermal Engineering, vol. 7 , 993–1003.

K. Raissi, 1994, Total Site Integration, PhD Thesis, UMIST, Manchester, U.K.

P. Varbanov, J. Klemeš, 2011, Integration and Management of Renewables into Total Sites with Variable Supply and Demand. Computers & Chemical Engineering, 35(9), 1815-1826.

P. S. Varbanov, Z. Fodor, J. J. Klemeš, 2012, Total Site Targeting with Process Specific ΔT_{min}. Energy. doi: 10.1016/j.energy.2011.12.025

P. Y. Liew, S. R. Wan Alwi, P. S. Varbanov, Z. A. Manan, J. J. Klemeš, 2011, A Numerical Technique for Total Site Sensitivity Analysis, Applied Thermal Engineering. doi: 10.1016/j.applthermaleng.2012.02.026

S. Bandyopadhyay, J. Varghese, and V. .Bansal, 2010, Targeting for Cogeneration Potential Through Total Site Integration, Applied Thermal Engineering, Vol. 30, 6-14.

S. Perry, J. Klemeš, I. Bulatov, 2008, Integrating Waste and Renewable Energy to Reduce The Carbon Footprint of Locally Integrated Energy Sectors, Energy, 33, 1489-1497.

V. R. Dhole, B. Linnhoff, 1993, Total Site Targets for Fuel, Co-generation, Emission and Cooling. Computers and Chemical, 17, S101–S109.

I.A. Karimi and Rajagopalan Srinivasan (Editors), Proceedings of the 11th International Symposium on Process Systems Engineering, 15-19 July 2012, Singapore.

Study on a New type of Gas-Liquid Cyclone used in COIL

BI Rong-shan[a*], WANG Zhen-xing[a], LI Yu-gang[a], TAN Xin-shun[a] , ZHENG Shi-qing[a], LIU Zhen-dong[b], CHEN Wen-wu[b]

[a]*Research Center for Computer and Chemical Engineering, Qingdao University of Science and Technology, Qingdao and 266042,China;*
[b]*Dalian Institute of Chemical Physics, Chinese Academy of Science, Dalian and 116023, Liaoning, China*

Abstract

In order to separate the gas-liquid products from new ejector singlet oxygen generator (SOG) effectively, we designed a new type of gas-liquid cyclone. The classical Muschelknautz cyclone model method, the improved method and computational fluid dynamics (CFD) code's discrete phase model (DPM) and eddy diffusion concept (EDC) were used for the new type separator's calculation and simulation. The results show that: (1) Compared with classical Muschelnautz model, the improved Muschelknautz model can predict the cyclone's separation performance more accurately; (2) On the design conditions, the smaller droplets have more complex trajectories. For droplets larger than 3 μm, their separation efficiency is over 80% in the new separator; (3) The droplets' entrance locations affect the droplets' trajectories and separation efficiency, (4) The residence time which CFD predicts ranges from 1 to 50 ms and decreases with the droplets size increasing (5) The loss of $O_2(^1\triangle)$ in the gas phase is less than 1% and it loses primarily on the gas-liquid contact reaction.

Keywords: gas-liquid cyclone Muschelknautz Model CFD $O_2(^1\triangle)$

1. Introduction

Chemical oxygen-iodine laser (COIL)[1-3] generator can efficiently use the chemical energy and has scale-up effects. With the development of technology, there are bubble-type $O_2(^1\triangle)$ generator, rotating disk $O_2(^1\triangle)$ generators, jet $O_2(^1\triangle)$ generator and uniform droplet generator in the form types[4]. Our team developed a new type of ejector singlet oxygen generator. Because the products from ejector singlet oxygen generator have the characteristic of great gas-liquid ratio, and in order to reduce the separation process of quenching reaction, the droplets residence time in separator should be as short as possible. Besides, we designed a new type of gas-liquid cyclone, as shown in Fig. 1.

Muschelknautz model is based on Professor W. Barth[5](1956)'s research. In the past thirty years, Muschelknautz model has been becoming a perfect model to perform the actual situation of cyclone separator[6], however the gas-liquid transfer is completely different from the gas-liquid's, Muschelknautz model is rarely used for gas-liquid cyclone. The improved Muschelknautz model modified the two-phase fraction factor and limit-loading concentration[7-9]. The classical Muschelknautz cyclone model method,

* Corresponding author. Tel.: +86 532 84022515;
E-mail address: birongshan@163.com

the improved method and DPM and EDC were used for the new type of gas-liquid cyclone's calculation and simulation.

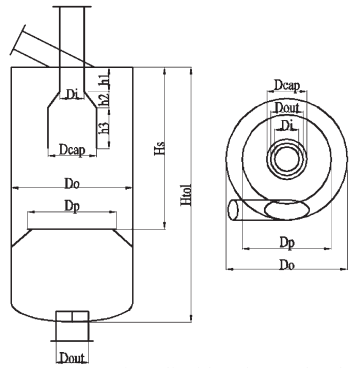

Fig. 1 New type of gas-liquid cyclone's sketch

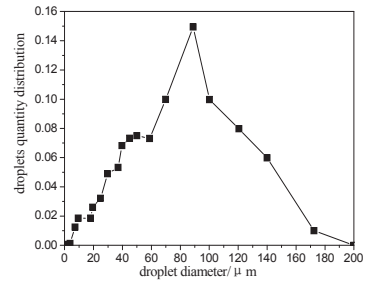

Fig. 2 Droplet diameter distribution

2. Device structure and simulation conditions

2.1. Device structure

In order to take the advantages of Muschelknautz model, the complex gas-liquid cyclone structure was simplified as following:

(1) The declination inlet tube would be a horizontal one, (2) The circular inlet would be a rectangular inlet with the same area, (3) Complex vortex finder would be a simple straight pipe and the new diameter would take the average of the original sizes, (4) Don't study the flow field below the baffle and the gap between the baffle and the wall is the liquid outlet.

2.2. Simulation conditions

The inlet boundary condition is mass-flow-inlet at the mass flow rate of 0.075kg/s. The injection type of particle phase is surface at the inlet. The outlet pressure at the top of vortex finder is 20000kpa. Discrete phase model (DPM)[10-11] was used to simulate the movement of liquid droplets and the particles' size distribution (PSD) can be presented as shown in Fig. 2. The mass rate of liquid phase is 2.6kg/s. The CFD simulation was performed with a Pentium Dual-Core E5300, 2GB RAM-memory, and 250GB hard-disc memory.

3. Result and discussion

3.1. Pressure drop

Fig. 3 shows the pressure drop of new gas-liquid cyclone CFD simulation. The static pressure decreases radically from wall to the cyclone center, and the minimum pressure appears near the top of vortex finder. The greater pressure gradient is below the vortex finder, because of the effect of the quasi-forced vortex. There is little change in static pressure field along the axis below the wide segment of the vortex finder. Besides, a sharp pressure drop appears near the narrow segment in the vortex finder, as the static pressure converts into dynamic pressure rapidly.

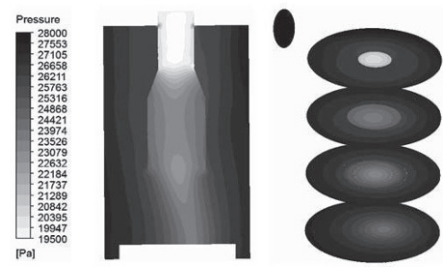

Fig. 3 contours of static pressure calculated using CFD

3.2. Grade efficiency

In this study, similar grade efficiency curves were obtained by using different calculation methods as shown in Fig. 4. The deviations of the cyclone grade efficiency between improved mathematic model and CFD are much smaller than the classic model. When the particle size is over 3μm, the grade efficiency has almost no change. The new gas-liquid cyclone can effectively remove the liquid droplets larger than 5μm and the grade efficiency is almost 100%. However, the new gas-liquid can't effectively remove the liquid droplets less than 5μm which account for a very small mass fraction; this means the new type of gas-liquid cyclone can effectively separate the gas-liquid mixture.

It also can be seen in Fig. 4 that the grade efficiency calculated by improved Muschelknautz model is better than the classic one. This is because the classic Muschelknautz model's total friction factor doesn't suit gas-liquid mixture, which can get an inaccurate tangential velocity at the cylindrical surface.

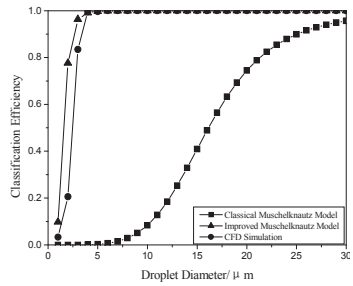

Fig. 4 Classification Efficiency at different models

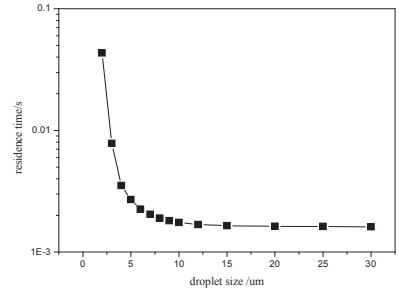

Fig. 5 the residence time of different droplets sizes

3.3. Droplets residence time

In the gas-liquid cyclone separation process, the gas-liquid mixture feeding the cyclone enters though some upstream piping where droplets coalesce into bigger one which is different from solid particles. Professor Wendy Zhang and Silney Nagal[12-13] studied the process of droplets hitting a surface under different surrounding pressure. The results show that the presence of gas is a decision condition to form droplets splashing. The design pressure of ejector singlet oxygen generator is 20kPa which is very similar with the Wendy Zhang's experiment's 17.2kPa. When the droplets hit the wall, they will form a uniform film without serious splash and shed along the wall. The time for droplets reaching the wall was considered the residence time of droplet for the loss of $O_2(^1\triangle)$ mainly happening in the gas-liquid transfer process. Fig. 5 shows the residence time of different droplets sizes calculated by CFD. The residence time which CFD predicts ranges from 1 to 50 ms and decreases with the droplets size increasing, which are in keeping with practical experience and previous laboratory studies. As the droplet size distribution tested by PDPA shown in Fig. 2, most of the droplets residence time is about 1.6ms.

3.4. Particles trajectories

The calculated particles' trajectories with different sizes are shown in the Fig. 6. As shown in the figures, the increase of liquid droplets size raises the collection efficiency since the effect of larger centrifugal force causes a larger advance distance. The particles with larger scale, such as 4μm and 5μm, can quickly spin down along the wall to reach the new separator's baffle. For small particles, the centrifugal force will be less than the drag force between air and droplets, which will make the small particles reach the wall difficultly and do many rotations below the bottom of vortex finder. As for critical particles, 3μm particles has a strong random. If they enter the irregular flow field at the

bottom of gas-liquid cyclone, they have a great chance to escape from the vortex finder.

The droplets' entrance locations can significantly affect the droplets' trajectories and separation efficiency. As shown in Fig. 6's 3μm(b), two 3μm particles enter the new separator from the top of inlet surface. Because the roof affects the top flow field of gas-liquid cyclone, the particles do rotations with almost parallel way at the top of separator. Compared with the 3μm(a) particles can be easily caught, the 3μm(b) particles have more complex trajectories and the less efficiency.

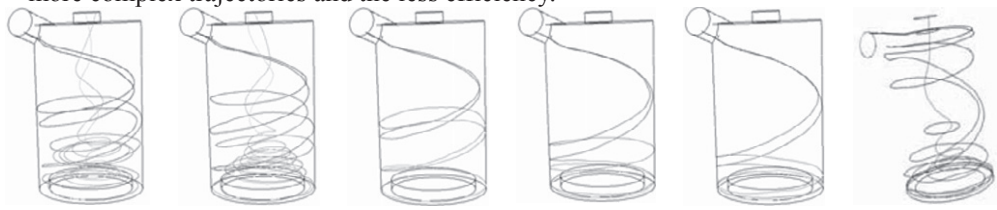

Fig. 6 the track of droplets with different sizes

4. Reaction research

4.1. $O_2(^1\triangle)$ quenching reaction in gas phase

In order to study the details of $O_2(^1\triangle)$ quenching reaction in gas phase, Eddy-Dissipation-Concept(EDC) was used for CFD simulation. The inlet feed is composed of $O_2(^1\triangle)$, Cl_2, He, H_2O(vapor), and their mole fractions are 0.3846, 0.01, 0.6044, 0.001. Fig. 7 shows the mole fraction of $O_2(^1\triangle)$ in the axial section and radial sections with different heights. At the inlet of gas-liquid cyclone separator, the concentration of $O_2(^1\triangle)$ is the highest, with the gas-liquid separation process carrying through, quenching reactions become more and more severe; the bottom of gas-liquid cyclone separator is the position where $O_2(^1\triangle)$ concentration is lowest; when the gas coming from bottom enters into the vortex finder, they mix with the fresh gas from inlet which causes an apparent high level. However, the $O_2(^1\triangle)$ quenching in gas phase is little, just from 38.46% to 38.28%. Most of the quenching occurs in the gas-liquid contact reaction.

4.2. p-τ of gas-liquid cyclone separator

p-τ value was experimentally proved to be a key parameter for the chemical efficiency of the chemical oxygen-iodine laser (COIL). In our COIL device with ejector singlet oxygen generator and chlorine flow rate of 0.5mol/s, the $O_2(^1\Delta)$ absolute yield and p-τ have a good correlation. Here, the $O_2(^1\Delta)$ absolute yield is defined as the converting efficiency from chlorine and measured by PS method[14].

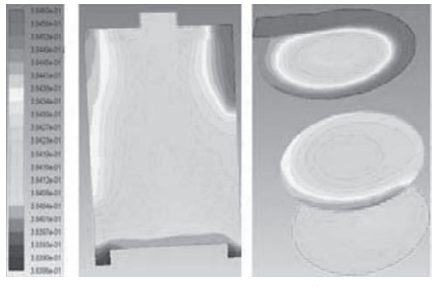

Fig. 7 the mole fraction of $O_2(^1\triangle)$

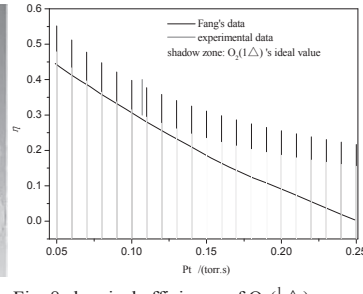

Fig. 8 chemical efficiency of $O_2(^1\triangle)$ vs p-τ value

Fig. 8 shows the relationship between chemical efficiency of $O_2(^1\triangle)$ and p-τ value. Red line is our experimental data obtained in the pilot test system. Compared with Fang's data[15], in the same p-τ value, chemical efficiency of $O_2(^1\triangle)$ is higher than Fang's device ; so it is better than Fang's device. Shadow area is obtained by calculating the chemical efficiency of $O_2(^1\triangle)$ using Fang's empirical formula. As the shadow area is basically on the top of the Fang's data, the new gas-liquid cyclone separator of ejector SOG system is reliable and feasible.

5. Conclusion

In this paper, we designed a new gas-liquid cyclone separator for separating the gas-liquid products from new ejector SOG effectively. The classical Muschelknautz cyclone model, the improved cyclone model, CFD and experiment was used to study the new gas-liquid cyclone separator's performance. The results show that: (1) the improved Muschelknautz cyclone model is very similar to the CFD simulation results; (2) droplet size and inlet position can significantly affect the droplet's separation efficiency; (3) the droplet residence time is inversely proportional to the size of droplets; (4) the loss of $O_2(^1\triangle)$ in the gas phase is less than 1% and it loses primarily on the gas-liquid contact reaction; (5) compared with Fang's experimental data, the new SOG system is reliable and feasible.

References

[1] J.Vetrovee, 1996, Prospects for an industrial chemical oxygen-iodine laser, Proc. SPIE, 3092: 723-726.
[2] W. C. Solomon and D. L. Carroll, 2000, Commercial applications for COIL, Proc. SPIE, 3887: 137-151.
[3] W. P. Latham, K. R. Kendrick and B. Quillen, 2000, Applications of the chemical oxygen-iodine laser, Proc. SPIE, 3887:170-178.
[4] SANG Feng-ting, JIN Yu-qi, DUO Li-ping, 2006, Chemical laser and its application, Chemical Industry Press, Beijing.
[6] Hoffmann A C,Stein L E. 2004, Gas cyclone and swirl tubes: principles, design and operation. Chemical Industry Press, Beijing.
[7] Muschelknautz E,Trefz M. Design and calculation of higher and highest loaded gas cyclones. Proceedings of Second World Congress on Particle Technology[C], Japan,52-71.
[8] Trefz M, Muschelknautz E., 1993, Extended cyclone theory for gas flows with high solids concentration, Chem Eng Techn, 16(3):153-160.
[9] Muschelknautz E,Dahl H D, 1994, Cyclone as Droplet Separators, Chem Ing Techn, 66(2), 223-229.
[10] Elsayed K, Lacor K, 2010, Optimization of the cyclone separator geometry for minimum pressure drop using mathematical models and CFD simulations, Chem Eng Sci, 65(8): 6048-6058.
[11] Fluent Inc., 2003, FLUENT User's Guide, Fluent Inc.
[12] L. Xu, W. Zhang, S. R. Nagel, 2005, Drop Splashing on a Dry Smooth Surface, Phys. Rev. Lett., 94, 184505.
[13] Michelle M. Driscoll, Cacey S. Stevens, and Sidney R. Nagel, 2010, Thin film formation during splashing of viscous liquids, Phys. Rev. E 82, 036302.
[14] Duo L P, Cui T J, Wang Z Q, 2001, Absolute $O_2(^1\Delta)$ concentration measurement in singlet oxygen generator by using the piston source method, Journal of Physical Chemistry A, 105: 281-284.
[15] FANG Ben-jie, WEI Ling-yun, etc, 2002, Experiment investigation of the influence of *p-τ* on COIL, High Power Laser and Particle Beams, 14(1):26-28.

I.A. Karimi and Rajagopalan Srinivasan (Editors), Proceedings of the 11th International Symposium on Process Systems Engineering, 15-19 July 2012, Singapore.

Trend analysis for studies of knowledge flow in research on polymeric materials

Sitarz R.[a,b*], Heneczkowski M. [b], Kraslawski A. [a,c].

[a]*Department of Chemical Technology, Lappeenranta University of Technology, POBox 20, 53851 Lappeenranta, Finland.*
[b]*Faculty of Chemistry,, Rzeszow University of Technology Al. Powstancow Warszawy 6, 35-959 Rzeszów, Poland.*
[c] *Faculty of Process and Environmental Engineering, Technical University of Lodz, Poland*

Abstract

Dynamics of research trends and patenting activity in a given period of time are important factors influencing the composition of the portfolio of the research projects. This article introduces the methods for identification of thematic clusters, determination of their development dynamics and prediction of the short-term trends in a specific research domain. The research on polymeric materials: composites, nanocomposites and blends has been analyzed in this paper. The presented method of structuring is based on clustering of word sets. The financial analysis techniques are applied to identification of dynamics and trend development in the analyzed field of research. The presented analyse is limited to the research papers found in Science Direct database in 1980-2010. The diversified development trends of the identified clusters have been identified e.g. strong development trend of the cluster "Biomedical application", or visible decline of the cluster "Structure of nanocomposites"

Keywords: blends, nanocomposites, composites, technology forecasting, trend analysis

1. Introduction

The assessment of development trends in the given branch of technology is important factor influencing decisions on R&D funding (Zapata et al. 2008, Rajapakse et al. 2005). The number of scientific publications and patents is indirect indicator of importance and growth potential of the specific area of expertise (Fabry et al. 2006). The changing number of publications and patents is an important information facilitating the prediction of the development trends in the analyzed field of research.
This paper analyses the following aspects of research on composites, nanocomposites and blends:

- identification of thematic clusters
- determination of research dynamics
- prediction of the short-term development trends

* Corresponding Author e-mail: robs@prz.edu.pl

2. Method

The identification of the thematic clusters and prediction of the development trend in a given research field is based on the method presented by Sitarz et al. (2010). The structure of the method is given in Fig. 1.

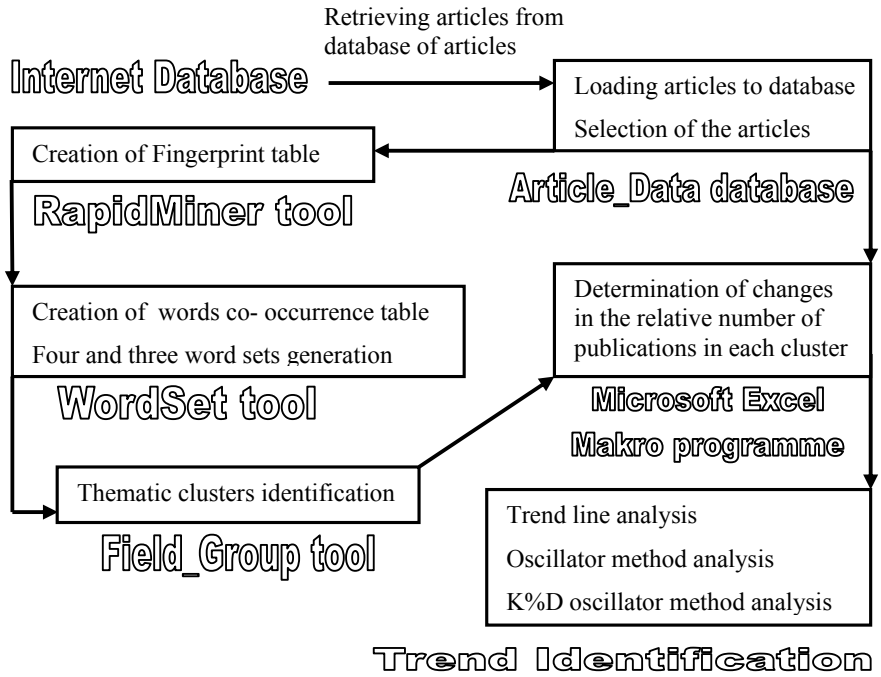

Figure 1. The structure of the method for identification of development trends in a given field of research

The creation of fingerprint table is realized using a dedicated tool: a Rapidminer with TextInput operator (Mierswa et al. 2006). The fingerprint of each paper consists of the set of characteristic words that constitute the meaning of a given paper. The table is created using the statistical analysis of the text and removal of non-specific "stop-list" words, such as "the", "be", "can". The next tasks are realized applying "WordSet" tool. It creates the word co-occurrence table (Ding et al. 2001) and generates four- and three-word sets (Sitarz et al. 2010). The columns and rows of the co-occurrence table are composed of the fingerprint words. The value in each cell shows how many times a given column-row word pair co-occurs. The four-word sets, which determine the seeds of thematic clusters, are generated by checking every possible four-word combination. The combinations satisfying the conditions presented below are selected (Sitarz et al. 2010):

$$D_{wi} \cap D_{wj} \cap D_{wk} \cap D_{wl} \geq ThrA \quad ; \frac{D_{wi} \cap D_{wj} \cap D_{wk} \cap D_{wl}}{\frac{1}{4}\left(D_{wi} + D_{wj} + D_{wk} + D_{wl}\right)} \geq ThrB \qquad (1)$$

where: D_{wi} – number of articles where word wi occurs; ThrA, ThrB – threshold values.

The values of ThrA and ThrB affect the number of word sets. There should be a minimal number of the articles that is greater than ThrA in order to identify only the essential thematic clusters as well as emerging ones. However, only the significant words should be considered, it means characterized by high word co-occurrence between words constituting the same thematic field. In the next step, the four- and three-word sets are grouped into thematic fields by the "Field_Group" tool, applying the agglomerative clustering method (Voorhees 1986).

The similarity between cluster pair (e.g. X and Y) is calculated as follow:

$$MIN\left[\left(\frac{D_{Si} \cap D_{Sj}}{MIN(D_{Si}, D_{Sj})}\right), For \quad i = 1..I, j = 1..J\right] \tag{2}$$

where: Si denotes the word sets belonging to the cluster X, Sj denotes the word sets belonging to the cluster Y, D_{Si} - number of the articles where word set Si co-occurs, I-number of the word sets in the cluster X, J - number of the word sets in the cluster Y,
In the next step, the determination of the yearly distribution of the relative number of the papers belonging to every thematic cluster is performed using Microsoft Excel Makro programme (Sitarz et al. 2010).

The last block, trend identification, is composed of three methods used in the technical analysis of the financial markets (Murphy 1999). The application of the methods (trend line method, oscillator method and K%D stochastic oscillator method) was presented in Sitarz et al. 2010.

3. Results

There were analyzed 17431 papers published in 1980- 2010 and found in Science Direct database using the search query: "blend and (composite or nanocomposite) and polymer". In the next step of the analysis, 13828 papers with the published abstracts were selected. Rapidminer has generated the fingerprint table for 7287 fingerprint words. 1050 four-word sets were identified for ThrA equal 14 and ThrB set as 0.13. The "Field_Group" tool identified 318 thematic clusters for the previously generated word sets for a C threshold value equal to 30%.
Due to the limited space, only the most representative examples are selected to present the most typical trends. Fig. 2 presents the change in the relative number of the papers belonging to the clusters "Biomedical application" and "Sources of electricity – batteries" published between 1980 and 2010, as well as the trend line method (solid lines I, II and III). Fig. 3 and 4 present the results of two oscillator methods for the clusters. On the left side of the figures the oscillator method is presented for x parameters equal 4 (oscillator 4) and 2 (oscillator 2). On the right side of the figures the results of K%D oscillator method are given (%K line for a y parameter equal 4), Murphy 1999.

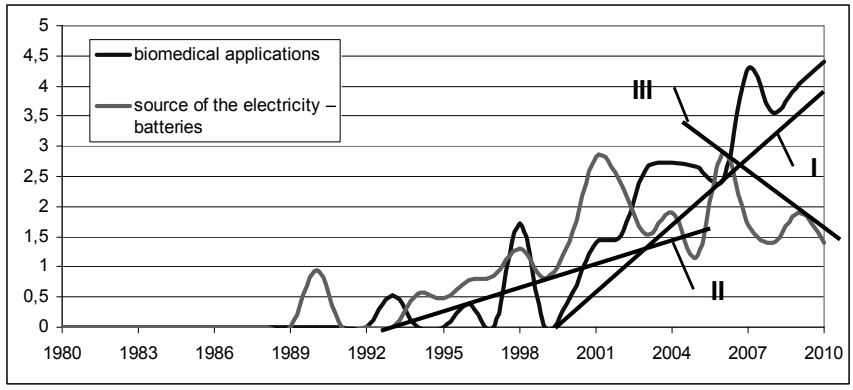

Figure 2. Relative number of publications and trend line method for the clusters "Biomedical application" and "Sources of electricity – batteries"

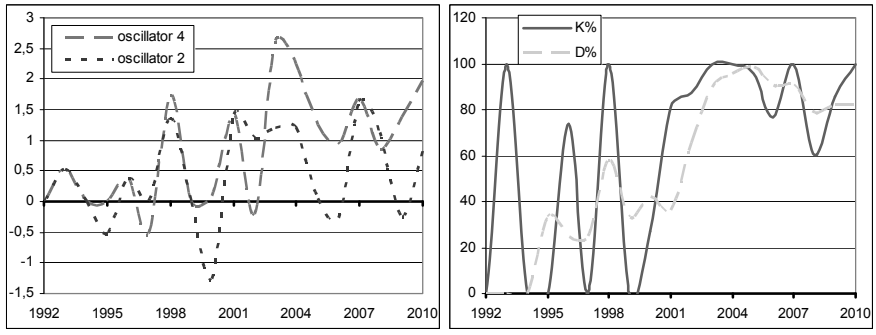

Figure 3. Oscillator and K%D methods for the cluster "Biomedical application"

For the cluster "Biomedical application" an increasing trends from 1999 can be identified, Fig. 2 and Fig. 3. It is illustrated by the increasing trend line I, positive momentum values of both oscillators after 1999, as well as intersection %K and %D lines in 2000.

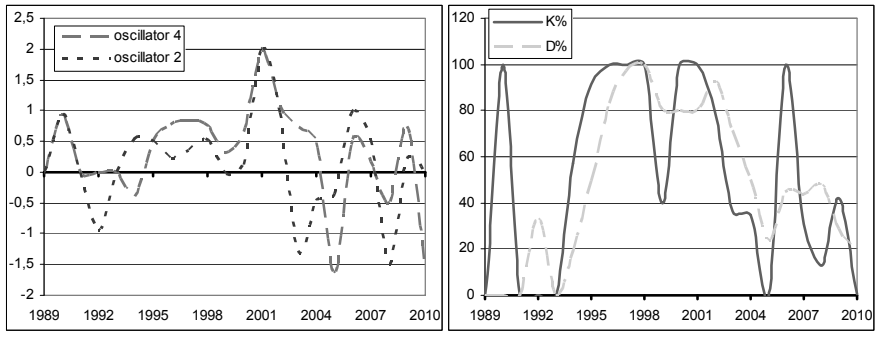

Figure 4. Oscillator and K%D methods for the cluster "Sources of electricity – batteries"

For the second analyzed cluster, the trend line method suggested an increasing trend from 1993 to 2004 (trend line II in Fig. 2), and next the increase of the relative number of publication toward 2006, and the decreasing trend toward 2010 (trend line III in Fig. 2). The momentum values of both oscillator methods were positive between 1994 and 2004, confirming the increasing trend for this period. Afterwards, the momentum values intersected at the zero line several times, forming the increasing trends from 2005 to 2007 and 2009-2010 as well as decreasing trend between 2004 and 2005 and from 2007 to 2009. The intersection of the zero line in 2010 by both momentum lines is a signal of future decreasing trend.
The first presented cluster "Biomedical application" is still developing, but the second one "Sources of electricity – batteries" seems to be declining, despite the peak activity in 2001 and 2006.

4. Summary

The identified clusters have shown the diversified patterns of development. Some clusters, e.g. "Biomedical application", "Carbon nanotubes", "Carbon nanofibers", "Photovoltaic cells", exhibited the increasing trend. The others, e.g. "Structure of nanocomposites", "Thermal resistance", "Hybrid polymers" have shown the signs of decline. The other ones, e.g. "Sources of electricity – batteries", "Fracture and stress cracking", "Tribological properties", have exhibited the long stagnation period.
The presented method identifies potentially interesting areas of research, worth of investments, for which development is forecasted. The method is universal and can be adopted to various research disciplines. The authors have analyzed several research field using the presented method (e.g distillation, filtration) with good predictive performance.

References

Y. Ding, G.G. Chowdhury, S. Foo, 2001, Bibliometric cartography of information retrieval research by using co-word analysis, Information Processing and Management, 37, 817 – 842.
B. Fabry, H. Ernst, J. Langholz, M. Köster, 2006, Patent portfolio analysis as a useful tool for identifying R&D and business opportunities—an empirical application in the nutrition and health industry, World Patent Information, 28, 3, 215-225.
I. Mierswa, M. Wurst, R. Klinkenberg, M. Scholz, T. Euler, 2006, YALE: Rapid Prototyping for Complex Data Mining Tasks, in Proceedings of the 12th ACM SIGKDD International Conference on Knowledge Discovery and Data Mining (KDD-06).
J.J. Murphy, 1999, Technical Analysis of the Financial Markets, New York Institute of Finance.
A. Rajapakse, N.J. Titchener-Hooker, S.S. Farid, 2005, Modelling of the biopharmaceutical drug development pathway and portfolio management, Computers & Chemical Engineering, 29, 1357-1368.
R. Sitarz, A. Kraslawski, J. Jezowski, 2010, Dynamics of Knowledge Flow in Research on Distillation, Computer Aided Chemical Engineering, 28, 583-588.
E.M. Voorhees, 1986, Implementing agglomerative hierarchic clustering algorithms for use in document retrieval, Information Processing & Management, 22, 465-476.
J.C. Zapata, V.A. Varma, G.V. Reklaitis, 2008, Impact of tactical and operational policies in the selection of a new product portfolio, Computers & Chemical Engineering, 32, 307-319.

I.A. Karimi and Rajagopalan Srinivasan (Editors), Proceedings of the 11th International Symposium on Process Systems Engineering, 15-19 July 2012, Singapore.

Multidimensional Monte Carlo Cell Population Dynamics in Virus Replication Systems

Andreas Voigt[a]

[a]*Process Systems Engineering, Otto-von-Guericke-University Magdeburg, Universitätsplatz 2, 39106 Magdeburg, Germany*

Abstract

We present a kinetic Monte Carlo simulation of a discrete cell population model. The model takes into account internal cell properties related to the viral RNA translation and replication. These dynamical changes can be compared to new available experimental data obtained with quantitative real-time reverse transcription PCR. In combination with the virus release from the cells into solution the model couples the internal and external cell environment in one single ansatz. This kind of high dimensional population balance modeling has already shown promising results in other areas of process systems technology, for example particulate processes. Here its application for applied biosystems technology is key to a better understanding of the process as a whole and to possibilities of process optimization and experimental design.

Keywords: Kinetic Monte Carlo Simulation, Cell Population, Virus Replication

1. Introduction

A biotechnological process of virus production using Madin-Darby canine kidney cells (MDCK) has been studied experimentally and theoretically (see e.g. [1,2]). A thorough understanding of the complex interaction of the cell population and the virus replication is important in order to optimize and improve the established process technology. Measurements of different continuous process parameters as well as measurements of internal cell properties enable options to model the complex interaction between the cells and the virus and also the replication mechanism inside the cells [3,4]. One already established model approach is based on the representation of the cell population as a discrete population balance and the simulation with a kinetic Monte Carlo Ansatz [5]. This type of stochastic modeling is well suited for such a system as it is an easy approach to take inot account a larger number of cell properties leading to a high dimensional population model where analytical and differential solvers run often into numerical difficulties. Also the kinetic Monte Carlo approach is typically developed in a modul-like fashion and therefore easy the extend in order to take into account new theoretical ideas or new experimental results. A last but important aspect of the kinetc Monte Carlo Ansatz is the use of a random factor which reflects especially here the underlying variability of any cell population. Recent studies using quantitative real time reverse transcription PCR of the process enables a new and improved validation of the model formulation of the internal dynamics of the virus replication inside cells [6,7,8]. Using this data one is now able to improve the qualitative level of description of the whole process. One can now combine both the internal as well as the external dynamics of the virus replication in the vaccine production. Here we want to present a first model formulation together with qualitative simulation as a starting point for further experimental as well as theoretical analysis of the technical virus production.

2. Model Formulation

Our kinetic Monte Carlo model will consider a population of cells, N, studied dynamically under the influence of a virus infection. Based on previous work, one is interested in the external dynamics, for example the number of virus, replicated throughout the complete process. In order to understand the time evolution of this process property, one would like to know, how cells change internally during the replication cycle. The virus number can be monitored with a hemagglutination assay (HA); the overall internal replication of virus inside a cell can be measured using flow cytometry [4]. More information on the internal replication is now available with a new quantitative real-time reverse transcriptase polymerase chain reaction assay (RT-qPCR). This information will be modeled here by taking into account three different internal cell properties, namely the amount of viral genomic RNA (vRNA), the amount of viral messenger RNA (vmRNA) and the amount of viral complementary RNA (cRNA). These specific molecules were analyzed in [6] even for specific viral segments. The current model will as a starting point only take into account an overall change of these three molecule species. In [7] it has been shown the qualitative time course of the dynamics for the specified segments is comparably similar. For our model formulation we therefore present every cell as a compartment with 3 internal variables, M_{vRNA}, M_{vmRNA} and M_{cRNA}. The dynamical evolution of these three basic molecules leads finally to a situation where the cell internally produces all necessary components for a new virus. Once a sufficient amount of virus components has been accumulated inside a cell, virus is released from a cell and can be observed in the external solution with the HA assay.

In our internal cell model we start with an infection where at first vRNA is initiated from the attacking virus inside the cell. This molecule is either used in a transcription step to produce vmRNA or used for a replication step to produce cRNA. From cRNA more vRNA can be replicated. The change of the molecule numbers of these components is modeled here. Inside the cell more steps for the production of certain virus proteins are taken (see e.g. [3]). The number of M_{vRNA}, M_{vmRNA} and M_{cRNA} can be followed with our model and qualitatively compared to the data from [7] as well as to fluorescence and HA data (for example from [1,2]). The number of accumulated molecules of M_{vRNA}, M_{vmRNA} and M_{cRNA} corresponds to virus proteins numbers and are therefore connected to the ability of the cell to release virus. Keeping track of these numbers on can estimate the time point where virus release will happen from a particular cell.

The internal model dynamics of every cell *i* consist of three basic steps:

1. Replication of cRNA: $M_{cRNA}(i,k+1) = M_{cRNA}(i,k) + p_{cRNA} \cdot M_{vRNA}(i,k)$
2. Transcription of vmRNA: $M_{vmRNA}(i,k+1) = M_{vmRNA}(i,k) + p_{vmRNA} \cdot M_{vRNA}(i,k)$
3. Replication of vRNA: $M_{vRNA}(k+1) = M_{vRNA}(k) + p_{cRNA} \cdot M_{cRNA}(k)$

The internal biological variation of every individual cell is taken into account by a random factor. Each individual step 1-3 is carried out for every cell *i* only with a chance of 0.5 at every time step.

The external dynamic of virus numbers in solution is connected to the internal cell property via a release step once a certain threshold, $p_{release}$, of $M_{vRNA}(i,k)$ molecule numbers has been reached in a given cell *i*:

4. If$(M_{vRNA}(i,k) > p_{release})$: $Vir(k+1) = Vir(k) + rand \cdot (M_{vRNA}(i,k) - p_{release})$

This step 4 decreases the number of M_{vRNA} molecules inside the cell with a certain variability given by a random factor. This release number leads to an external change in the system, namely a corresponding increase of virus in solution. From the experimental

data is deduced, that the release step is connected to a similar release and degradation of certain numbers of M_{vmRNA} and M_{cRNA} molecules inside a cell. We reflect this by including step 5 with a random decrease of p_{deg} molecules of M_{vmRNA} and M_{cRNA}:

5. If($M_{vRNA}(i,k)>p_{release}$): $M_{vmRNA}(i,k) = M_{vmRNA}(i,k) - \text{rand}\cdot(p_{deg}\cdot M_{vmRNA}(i,k))$
   $M_{cRNA}(i,k) = M_{cRNA}(i,k) - \text{rand}\cdot(p_{deg}\cdot M_{cRNA}(i,k))$

For the simulation of the model a MatLab simulation has been developed, where the different steps are represented by discrete time steps of the whole cell population. In the beginning an array for the cell population of size N is defined. As in a typical kinetic Monte Carlo Ansatz at every single time step every cell will change according to the given model rules. Here for every time step, all cells are simulated according to the random internal change of the molecule numbers via steps 1-5. In particular a random number is generated with a selected random number generator provided by MatLab (i.e. Marsaglia, Twister or Congruential) and compared to the specific probability factors. If the random number exceeds the factor, the change of the internal state in the cell is made and recorded in the cell array. Throughout the whole simulation we monitor any change in the internal cell property and calculated from that selected averaged data for the whole cell population. Also a display of different cell property distributions is possible. In order to compare to experimentally available data we select specific average numbers and cell property distributions in the result section.

3. Simulation Results

The new model will be used for a first qualitative comparison to the new information about internal changes of the cells, available from the RT-qPCR data in [7]. We will here address a similar situation within this new model approach.

All simulation results have been checked for statistical validity by varying cell numbers from 100 to 10^4, extended statistics over 10-20 runs and variations of the used random number generators. No significant statistical deviations have been observed and we show therefore typically overlay data for 1000 cells and of 5 runs in order to show the statistical error of the method.

In [7] the experiment has been carried out for MDCK cell where initially a very high multiplicity of infection (MOI=6) was used. This approach was applied in order to ensure that already in the beginning all cell are infected. Therefore our simulation starts with the same situation. All cell are infected at time point t=0 and therefore contain one M_{vRNA} molecule. Now every cell will develop according to the steps 1-5. In Fig. 1 we show the time evolution of our model system for 10 hours. Our simulation time step is 3min; the simulation respectively runs for 200 Monte Carlo steps. The parameters p_{vmRNA}=0.8, p_{cRNA}=0.6 and p_{vRNA}=0.6 reflect the experimental observation qualitatively so that the average molecules numbers $M_{vRNA}(k)$, $M_{vmRNA}(k)$ and $M_{cRNA}(k)$ per cell can be compared to Fig. 1 from [7] qualitatively. If $p_{release}$=1000 is reached (also obtained from [7]) step 4-5 set in. Now cells randomly release virus (and decrease M_{vRNA} respectively) and randomly degrade M_{vmRNA} and M_{cRNA} with p_{deg}=0.05.

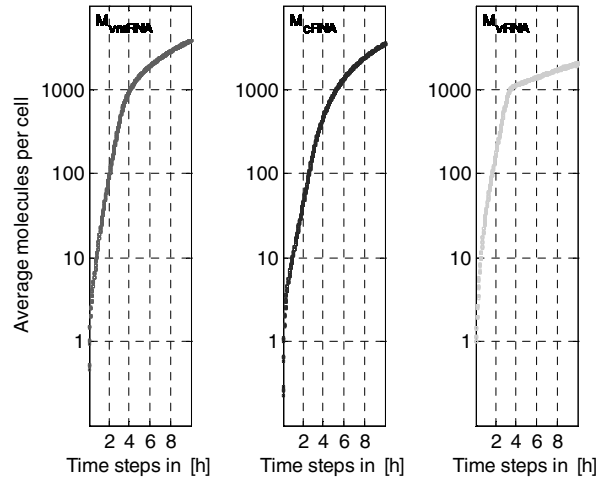

Fig. 1: Time evolution of average molecule numbers of vmRNA, cRNA and vRNA per cell from 5 statistical runs from a population of 1000 cells.

Of interest and may be to be compared with fluorescence measurements are the corresponding cell property distributions. In Fig. 2 we show the molecule number distribution of $M_{vRNA}(i,k)$, $M_{vmRNA}(i,k)$,$M_{cRNA}(i,k)$ at two time points. Time point t=3h (Fig.2, left) corresponds to the situation where no virus has been released yet, according to the HA assay from [7]. At time point t=6h (fig.2, right) virus is released and this is reflected especially in pronounced changes in the M_{vRNA} distribution.

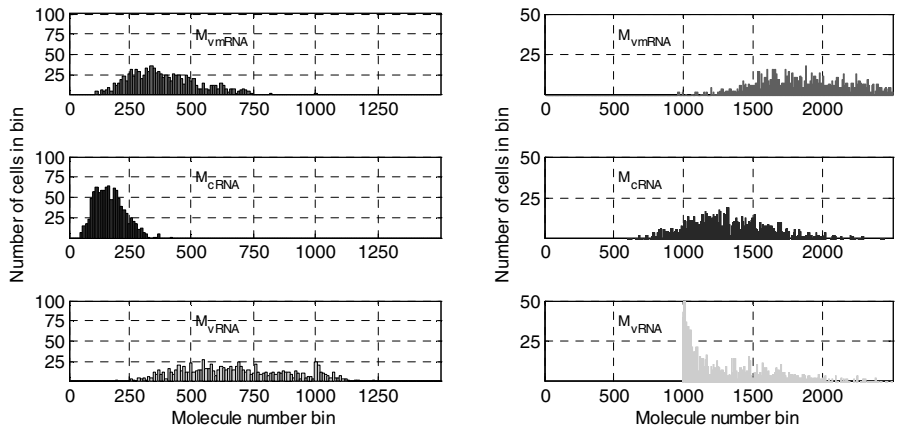

Fig. 2: Molecule number distribution of the cell population at a time point t=3h (left) and (t=6h) for vmRNA, cRNA and vRNA, collected into molecule number bins of width of 10 molecules.

With all the options for data calculation the model can be used to extract cell property distribution, its dynamics, the virus release numbers as well as other quantities of interest. More data from experiments, RT-qPCR, fluorescence data or HA assays, can now be compared in order to judge on the validity of the model representation. Model variations and parameter estimations are another important step for further investigations.

4. Conclusion

We have presented a new model approach to simulate a cell population in a virus production process based on infection of MDCK cells with influenza virus. New data from quantitative real-time reverse transcription PCR enables a comparison of internal cell dynamics from this model with experimental data. The simulation is carried out within a discrete kinetic Monte Carlo method where every cell behaves slightly differently according to given probabilities of cell changes. These changes represent steps in the virus replication cycle where virus RNA is transcribed and replicated so that finally new virus particles can be release by the given cell. A first qualitative analysis shows the applicability of the model approach. The parameters have been adjusted so that a qualitative agreement between data from an experiment (see Fig. 1 from [7]) and model data is achieved. The model can be used to track other properties or to monitor for example certain cell property distributions. These results will help in experimental design and improved understanding of the process. The long term goal should be the simultaneous application of model simulation and experiments in order to improve reliability and efficiency of this technologically very important virus production process.

References

[1] Kalbfuss, B. et al, Monitoring influenza virus content in vaccine production: precise assays for the quantification of hemagglutination and neuraminidase activity, *Biologicals* 36, p.145 (2008).

[2] Schulze-Horsel, J. et al, Infection dynamics and virus induced apoptosis in cell culture based influenza vaccine production flow cytometry and mathematical modeling, *Vaccine* 27, p.2712 (2009).

[3] Sidorenko, Y. and Reichl, U., Structured model of influenza virus replication in MDCK cells, *Biotechnol. Bioeng.* 88, p.1 (2004).

[4] Sidorenko, Y et al, Stochastic population balance modeling of influenza virus replication in vaccine production processes, *Chemical Engineering Science* 63, p. 157 (2008).

[5] Diaz et al, Modeling the Innate Immune Responses of Cells for Vaccine Production, *Chemical Engineering Science* 66, p.3954-3961 (2011).

[6] Robb, N. et al, NS2/NEP protein regulates transcription and replication of the influenza virus RNA genome *J. Gen. Virol.,*90, p.1398-1407 (2009).

[7] Vester, D. et al, Real-time RT-qPCR assay for the analysis of human influenza A virus transcription and replication dynamics, *Journal of Virological Methods* 168, p. 63-71 (2010).

[8] Kawakami, E. et al, Strand-specific real-time RT-PCR for distinguishing influenza vRNA, cRNA and mRNA, *Journal of Virological Methods* , 173, p.1-6 (2011).

I.A. Karimi and Rajagopalan Srinivasan (Editors), Proceedings of the 11th International Symposium on Process Systems Engineering, 15-19 July 2012, Singapore.

CFD Analysis of Cavitation in a Crude Oil Pipeline to an Oil Tanker

Woohyun Kim[a], Munkyu Yoon[b], Moonyong Lee[b], Sunwon Park[a]

[a]*Department of Chemical and Biomolecular Engineering, Korea Advanced Institute of Science and Technology (KAIST), Daejeon, Republic of Korea*
[b] *School of Chemical Engineering, Yeungnam University, Gyeongsan, Republic of Korea*

Abstract

Emission of volatile organic compounds (VOCs) during loading crude oil to oil tankers has become a particularly critical issue because it does not only cause environmental problems but also economic loss. Since a pipeline from a terminal to an oil tanker has a long vertical drop line, the acceleration of the pipe flow by the gravity may cause a sudden pressure drop that stimulates cavitation, the evaporation of the VOCs in crude oil. To analyze the amount of vaporized VOCs and the fluid dynamic behaviors of the two-phase pipe flow, experiments have been conducted with a pilot-scale pipeline and a computational fluid dynamic (CFD) model have been developed based on the experimental result. As crude oil is the complex mixture of various hydrocarbons, a phase transition model based on crude oil assay data has been developed and included in the CFD model. This developed model is capable of predicting the amount of vaporized VOCs and the fluid dynamic behaviors of the pipe flow with different operating conditions, e.g. flow rate, pump pressure, type of crude oil, etc. Thus, it is expected that the model will contribute to analyzing the amount of VOC emission during loading crude oil onto an oil tanker.
Keywords: computational fluid dynamic model; cavitation; crude oil; oil tanker; volatile organic compound

1. Introduction

Emission of volatile organic compounds (VOCs) during loading crude oil to oil tankers has become a particularly critical issue with the growth of maritime transport since it does not only cause environmental problems but also economic losses (Husain et al., 2003). Crude oil is a mixture of various hydrocarbons and VOCs in crude oil generally refers to some light end components that range from C1 to C10. These components can evaporate during loading, transportation, or discharging processes because pressure changes can accelerate evaporation. The amount of VOCs emitted during loading is found to be in the range of 0.08 - 0.15 % of the total volume loaded in an oil tanker (web site of Hamworthy).

In terms of environmental impacts of VOC emission, it is reported that VOCs emitted from crude oil contribute to global warming. Especially, methane in the evaporated VOCs has a strong effect on global warming and various international regulations are imposed and reinforced these days (Endresen et al., 2003).

The VOC emission also causes adverse economic losses. A 130,000-deadweight-ton oil tanker discharging oil 40 times per year emits approximately 5,000 tons of VOCs per year. Since the oil price is around $ 110/bbl, the economic loss of the evaporated crude oil is expected to be about $ 4,000,000, assuming that price and specific gravity of VOCs are equivalent to ones of crude oil.

One of the main causes of the VOC emission is pressure drop along the loading pipe line (Rudd & Hill, 2001). Since a gravity-driven pipe flow runs through the pipe line, a sudden pressure drop can occur. Thus, negative pressure may appear in the oil loading system and it obviously accelerates the vaporization of the VOCs in crude oil.

To design a system to reduce the amount of the VOC emission, a high-fidelity model predicting the phase-transition phenomena will be necessary so we have developed a computational fluid dynamic (CFD) analysis method which is capable of analyzing the amount of vaporized VOCs and the fluid dynamic behaviors of the two-phase pipe flow in this work. Therefore, experiments corresponding to an actual oil loading system have been carried out and a phase transition model based on crude oil assay data has been developed for the accurate CFD model

2. Experiment

2.1. Theoretical Background

Since crude oil contains various organic compounds, light compounds can naturally boil off at ambient temperature and pressure. Plus, if negative pressure, meaning pressure lower than ambient pressure, appears in the oil loading system, the pressure accelerates the evaporation of VOCs, causing cavitation. In this section, physical phenomena of gravity-driven pipe flow and the volatility of crude oil are discussed.

A loading system of an oil tanker has long vertical pipe lines which are generally longer than 20 m (*see* Figure 1). When crude oil running through a horizontal pipe line starts to fall into the vertical drop line, the fluid is suddenly accelerated by the gravity. This acceleration results in drastic decrease in static pressure along the pipe line. This phenomenon is same as the principle of a siphon. Consequently, the low static pressure stimulates the evaporation of VOCs in crude oil so cavitation occurs in the pipe flow.

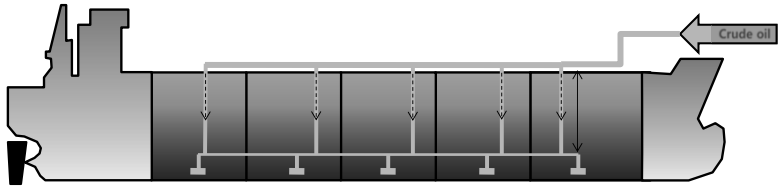

Figure 1. Conceptual design of oil loading pipe lines

To predict the amount of vaporized VOCs, the volatility of crude oil should be analyzed. It is obviously found that the composition of the components in crude oil varies depending on the types of crude oil. When oil with higher content in light components is transported, more amount of VOC emission is expected. Thus, a model based on assay data of crude oil is necessary to predict the phase transition phenomena of crude oil. In this work, we have calculated the vapor volume fraction of crude oil at equilibrium using assay data and Aspen PLUS and the calculated data is used to develop the phase-transition model for the CFD analysis. The calculation procedure is explained as follows:

(1) Gathering assay data of crude oil: Assay data includes average molecular weight, true boiling point (TBP) data, light end components, viscosity, etc.
(2) Calculating vapor volume fraction: Using the assay data, the vapor volume fraction of crude oil at given temperature and pressure can be calculated in Aspen PLUS. Based on the calculated data, we can develop function to predict vapor volume fraction with respect to pressure. This function is combined with the phase transition model in the CFD model.
In the experiment, a pipe line has been designed to observe the fluid dynamic behaviors of the gravity-driven flow and CFD analysis has been carried out based on the experimental data.

2.2. Details of Experiment

In the experiment, we have designed 20-m-high pipe line (see Figure 2). The line is composed of 40A steel pipes.

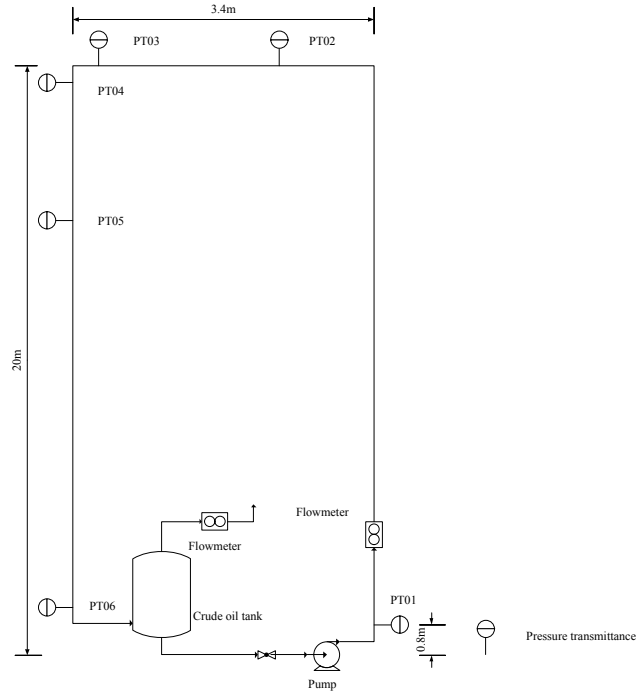

Figure 2. The P&ID chart of the experimental facility

We have tested several cases in the experiment varying the flow rate. The CFD simulation results of the pressure profiles are compared with the experimental data for the model validation. In the experiment, pressure profile is measured by the pressure transmittances (see Figure 2 and Table 1) and vapor flow, which means the amount of vaporized VOCs, is measured by the flow meter located at the top of the tank.

Table 1. The locations of the pressure transmittances

	Pressure transmittances					
	PT01	PT02	PT03	PT04	PT05	PT06
Altitude from the bottom	0.8m	20m	20m	19.9m	13.5m	0.88m
Length from the pump	0.8m	22m	23.1m	23.5m	28.9m	42.4m

3. CFD Analysis

3.1. Phase Transition Model of Crude oil

We have modified an evaporation-condensation model for describing the phase transition phenomena in crude oil with respect to pressure. Since saturated temperature and pressure cannot be determined for mixture, we have used equilibrium vapor volume fraction, which is calculated in Aspen PLUS using the assay data of crude oil. In this model, mass flux between phases is determined based on deviation from the equilibrium vapor volume fraction at given pressure and temperature. The mathematical expression of the model is shown below.

$$\dot{m}_{l\to v} = c_1 \cdot \alpha_l \cdot \rho_l \frac{\alpha_l - \alpha_{l,eq}}{\alpha_{l,eq}} \qquad \text{(1) mass flux from liquid to vapor: vaporization}$$

$$\dot{m}_{v\to l} = c_2 \cdot \alpha_v \cdot \rho_v \frac{\alpha_v - \alpha_{v,eq}}{\alpha_{v,eq}} \qquad \text{(2) mass flux from vapor to liquid: liquefaction}$$

c_1 and c_2: mass flux coefficient
α_l and α_v: current volume fraction of liquid and vapor (subscript *eq* means equilibrium.)

The essential coefficients, c_1 and c_2, are adjusted to make CFD simulation results similar to experimental data. To determine these parameters, we have used the assay data of the crude oil we have used in the experiments. This model is developed as a user-defined function in FLUENT and combined with the momentum balance equation and the continuity equation of the CFD model.

3.2. CFD Model

In this work, we have used FLUENT for CFD analysis. Since the pipe flow has two phases, vapor and liquid, we have selected the mixture model of FLUENT. A turbulent model is also selected because the Reynolds number is high enough. Thus, the k-ε model is used in this work. The standard k-ε model in ANSYS FLUENT is one of the most practical engineering flow calculations. It is a semi-empirical model and the derivation of the model equations relies on phenomenological considerations and empiricism. This model is combined with the momentum balance equation of each phase. In this simulation, we have prepared a 2-D model for fast calculation. Since the system we have analyzed consists of simple pipes without considerable 3-D changes in flow direction, 2-D analysis is assumed to be reasonable. All the simulations are carried out in an Intel Core2 Quad Q9550 processor machine with 4.0 GB RAM.

4. Results

As we observed in the experiment, the lowest static pressure is calculated around the location where the oil starts to fall along the vertical drop line.

Table 2.Comparison between the CFD simulation results and the experimental data

Flow rate		Static pressure measured at each pressure transmittance					
		PT01	PT02	PT03	PT04	PT05	PT06
17 m^3/h	experiment	2.80 bar	-0.24 bar	-0.24 bar	-0.23 bar	-0.06 bar	0.02 bar
	simulation	2.80 bar	-0.15 bar	-0.21 bar	-0.18 bar	-0.10 bar	0.02 bar
15 m^3/h	experiment	2.40 bar	-0.42 bar	-0.44 bar	-0.43 bar	-0.26 bar	0.03 bar
	simulation	2.40 bar	-0.40 bar	-0.42 bar	-0.43 bar	-0.30 bar	0.03 bar

Table 2 shows the comparison between the experimental data and the simulation result in the two different cases. According to the table above, the CFD model is considered to be acceptable.

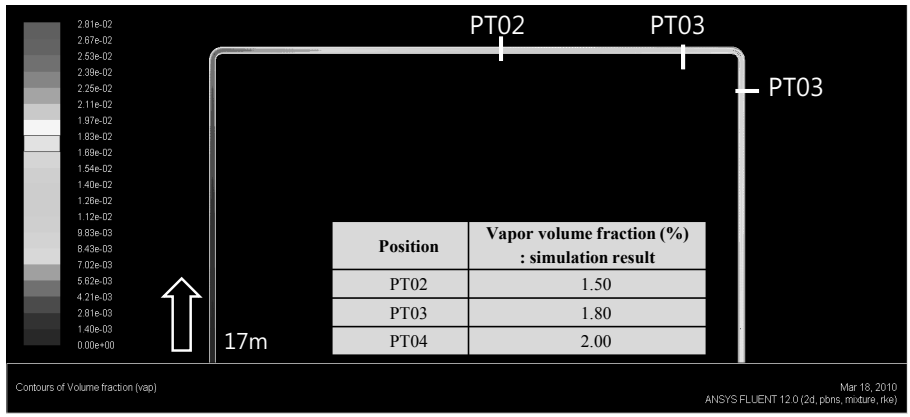

Figure 3. Profile of vapor volume fraction (Flow rate: 15 m^3/h)

Figure 3 shows the predicted vapor volume fraction along the pipe line. In the simulation result, it is observed that the vaporized VOCs are partially liquefied at the bottom of the vertical drop line since the static pressure at the bottom is almost same as the atmospheric pressure. The amount of the vaporized VOCs is predicted as approximately 0.09 % by weight when the flow rate is 15 m^3/h and it is similar to the experimental data (0.1 - 0.12 % by weight). This value is also similar to the amount of crude oil loss in the actual loading process of an oil tanker caused by VOC emission.

5. Conclusions

To analyze the amount of vaporized VOCs and the fluid dynamic behaviors of the two-phase oil flow driven by the gravity, the experiments have been conducted and the CFD model have been developed based on the experimental result. The experiments have been carried so that the negative pressure and the vaporization of VOCs are experimentally observed. The proposed CFD model, which can predict the amount of the vaporization and condensation of the VOCs based on the property data of the crude oil, is also considered to be acceptable since the simulation results of the pressure profiles and the amount of VOC emission have been compared with experimental data. Thus, the model can be used to analyzing the amount of VOC emission during loading crude oil onto an oil tanker under different operating conditions. This modeling approach will contribute to designing a system to reduce the VOC vaporization.

References

Endresen, Ø, Sørgård, E, Sundet, J.K., Dalsøren, S.B., Isaksen, I.S.A., Berglen, T.F., Gravir, G. (2003). Emission from international sea transportation and environmental impact. Journal of Geophysical Research, 108, 4560.

Web site of Hamworthy: http://www.hamworthy.com/Products-Systems/Hamworthy-Marine/Gas-System/VOC-recovery/

Husain, M., Hunter, H., Altshuller, D., Shtepani, E., Luckhardt, S., Lemley, N. W., Daidola, J. C., Aabo, K. and Hirst, D. (2003). Crude oil under negative pressure and hydrocarbons emission containment. Transactions-Society of Naval Architects and Marin Engineers, 111, 584.

Rudd, H.J., Hill, N.A. (2001). AEA TECHNOLOGY Report: Measures to reduce emission of VOCs during loadign and unloading of ships in EU. (Available on the web: http://ec.europa.eu/environment/air/pdf/vocloading.pdf)

I.A. Karimi and Rajagopalan Srinivasan (Editors), Proceedings of the 11th International Symposium on Process Systems Engineering, 15-19 July 2012, Singapore

Utilisation of Computer Science Design Patterns in Chemical Engineering

Heinz A Preisig, and Tore Haug-Warberg
Dept of Chem Engineering; NTNU; Trondheim, Norway

Abstract

Keywords: dynamic system, software engineering, computational engineering

1. Computational chemical engineering

Computer-aided process engineering has been the main source for computational tools that make it possible to experiment with processes, explore and test any scenarios without having to fool around with real processes and their limitations. The tools are essential for our community and their position and usage is only going to grow. Naturally Chem Eng has been focusing on its interests: the project and problems the community have and want to solve whilst benefiting from the increasing computing power and increasing possibilities to polish the user interfaces. This left little room for adjusting the underlying structure whilst in the meantime, computer science also made progress driven by a large growth and diversification of the application market. This should also affect on the structure of our tools.

2. Software considerations

The concept of *design patterns* in computer science is a loosely defined term which addresses the fact that many tasks in object oriented programming (OOP) are quite standard when viewed as semantic operations Gamma et al. (2009, c1995). The implementation into a specific programming language will differ and they are not standard at the syntactic level, but they are mostly independent of the programming language and implementation details. A design pattern is therefore not an algorithmic description of a certain mathematical operation but is more akin to a pattern of programmatic behaviour. This is an interesting observation that lends more to psychology and philosophy than it points to hard evidences in natural sciences. To put it short it can be argued that design patterns in OOP must be lifted from the existing pool of computer programs and that they in some sense are the common denominators of how we organize, structure and solve certain tasks that over the years have become standard in the software industry. Seen from this perspective it is clear that design patterns are not inventions of the human mind but are rather representatives of human nature. Design patterns are therefore not limited in number; new ones will emerge and old ones may die out. Some important patterns (like e.g. the *iterator* pattern) will find their way into the programming languages and become part of the languages themselves or the standard libraries. This process has already become visible in several open source OOP languages like e.g. C++, Perl, Python and Ruby.

The first question is how, or if, the design patterns are useful to software enterprises in mathematics, physics and chemistry. The answer to this question is definitely positive because design patterns conserve somehow the way human thinks. The next question that

pops up is what design patterns we would need to solve our programming tasks connected to: formulation, calculus, analysis, exportation, execution and interfacing.

From what was said above—that design patterns reflect they way we tend to solve routine programmatic problems—we might argue that we have in fact identified six patterns here. Philosophically this is true but not practically. We have not yet reached the abstraction level there it is sufficient to say *model formulation* and let this be instructive for how we choose to implement the model. It may therefore be instructive to see what the computer scientists have come up with over the years and, if this looks promising, borrow their terms to describe our own activity. Design patterns in OOP are currently classified into *creational* (C), *structural* (S) and *behavioural* (B) patterns, see Gamma et al. (2009, c1995). There are at least 23 patterns suggested of which we think around a dozen are sufficiently important to help us describing our task:

C: Factory (creating objects from textual information), Builder (factory for building objects incrementally), Singleton (one-to-one factory for single objects)

S: Decorator (in-situ extension of objects), Adapter/wrapper (interface adaptation) Composite (internal nodes and leave nodes have the same basic interface), Facade (interface to group of objects), Bridge (kind of driver)

B: State (changing behaviour when internal state changes), Interpreter (parsing text according to a grammar), Iterator (accessing objects sequentially)

The process of generating e.g. a thermodynamic run-time library can now be described on a very high level of abstraction. The description is sufficiently accurate to indicate what complexity we are talking about, yet it is insufficient to tell anything about the actual implementation. However, it tells very accurately that any programming language covering the ?? design patterns mentioned above will be adequate for the actual implementation. The answering of that question alone is so important that it by itself "rettferdiggjÃÿr" the design pattern idiom. Looking into the past there are countless examples of engineering software projects that have stranded because the "wrong language" was used. Choosing the right language from the outset is in fact a premise for success in this context.

2.1. Factory

Creates objects without specifying the exact class of objects that it creates.

The factory pattern has a direct application in modelling involving flowsheets that commonly use specific thermodynamic material models and kinetic models. An object-oriented implementation the material model could be equipped with a symbolic and numerical solution engine. It will also have to know the material's composition, specifically what species make up the material and consequently must be modelled. Similarly for the object of a reaction: it requires a kinetic model, and the knowledge of what intensive properties it depends on, not at least the species composition and the relevant intensive quantities, primarily the temperature and pressure. The symbolic and numerical procedures may be taken from different places, whilst the dependencies are likely provided by an ontology.

2.2. Builder

Separate the construction of an object from its representation.

The thermodynamic model are often very complex and in order to capture this complexity we build them recursively as tree structures. This requires the objects to be built incrementally. Typically, one line of code is needed per line of input taken from the textbook description of the model. This one-to-one relationship between programming and textual formatting is important for two reasons: Firstly, it reduces the likelihood of mistakes in the code because the generation of the code line is a linear translation. Secondly, it makes the documentation and maintenance easier because the textbook model can be directly utilised as explanation for the code. A self documenting code is of course the ultimate goal. Whilst it is probably not quite realistic to reach this goal absolutely, tailor-made languages are very helpful auxiliary tools (see discussion of the *Interpreter* below).

2.3. Singleton

Restrict instantiation of a class to one object.

This concept is suitable to capture the basic structures as they are formulated in the associated ontology. In our applications typical elements are conservation equations, transport and kinetics.

2.4. Decorator

Add behaviour to an existing object dynamically.

The decorator is a handy feature when generating different target output. Models may be written in different target languages for there consequent utilisation. The purposes are numerous including: LaTeX for generating automatic documentation; C, C++, Fortran and Matlab for numeric calculations; DOT for visualizing the model hierarchy; and Ruby and Python for object oriented programming and not at least any type of model exchange format such as the mock-interface language currently developed in the Modelica community Modelisar (2012). There are virtually endless options here and for any application, it is essential that the exportation is open to enable interactions with other software components. The structure should be such that the programming effort increases linearly with the number of exported languages. To achieve this goal the decorator pattern is very useful. For example, using abstract syntax trees for the representation of expressions and equations, or for that matter any such information having a tree structure, it is sufficient to renew the definition of one single method called `to_fun()` in each of the classes of which the leave nodes are instances. The decorator pattern is a dynamic feature and thus happens at run-time such that several languages can be exported from the same tree. The tree itself respond to a method called `export()` that invokes the leaf-nodes sequentially using the *Iterator* pattern described below and execute `to_fun()` on each of the node objects. The tree itself is not touched, just the leaf-nodes. In this way it is possible to export the model into any kind of language that does not require external information beyond what can reasonably be supplied as default, or at run-time, values or is already stored in the model graph. The code exportation is basically a linearisation technique in that it takes a complicated tree structure and writes it out as a linear program. A second thought will soon reveal a possible caveat: Not all programming languages are linear in the sense that the information generated by the node objects all go into one place. In LaTeX documents for instance there is a heavy mix of information that goes into the individual parts, chapters and sections.

2.5. State

Considering the fact that executing software is an automaton, it has also a state. The concept *state* can be used exactly the same way as we use state in physics and engineering. It has applications as state of the software but also as state of the process one has implemented in software as well as the abstract state of a model, for example.

2.6. Interpreter

Specifies how to evaluate sentences in a language.

We use this technology in several places in our modelling software. It has a direct application for the implementation of algebraic expression built from basic objects variables and operators, whereby the object variable is extended to various classes such as physical variables. The approach is also used to build and analyse composite type definitions that are utilised by the graphical model editor Preisig (2010, 2011).

The language RGrad Løvfall (2008) was invented by our group to describe the thermodynamic models (or any other models relying on multi-dimensional inner product rules) on a symbolic level. Rather that defining a stand-alone parser for RGrad it was decided to write it as an extension to the Ruby language. In this way we could rely on the rich syntax of the Ruby parser and focus on modelling issues instead. The decision turned out to be highly successful and time–cost effective.

2.7. Iterator

Travers a data container and access the individual elements.

Constructing and storing models makes extensive use of graphs: trees for algebraic expressions, for typing using hierarchical attributes, species in different state of aggregation, reaction schemes, etc. All these containers will have an iterator associated enabling the traversing of the data container.

2.8. Wrapper

Translate one interface for a class onto a compatible interface.

The application is apparent: make software written in one language available in another. The CAPE-OPEN project is a classic representative of this approach. The fact that the wrapped software modules may be binary, enables the utilisation of compiled and proprietary software in different environments. This may be models at various levels, where the physical property calculations are of particular interest in model-supported computational engineering. But also models with built-in solvers are interesting applications.

2.9. Composite

A group of objects are to be treated in the same way as a single instance.

The graphical interface module for the hierarchical tree of systems with the leave nodes being simple control volumes, this concept is directly applicable to handling the tree itself, but also the associated graphics.

2.10. Facade

Provide a simplified interface to e.g. a class library

A typical application is material models. There exists several hundred equations of state, which can be grouped. Putting these models into a library, where groups of models are being realised as packages, with a facade providing a common interface.

2.11. Bridge

Decouples an abstraction from its implementation so that the two can vary independently.

3. Conclusions

The concept or paradigm of "Program to an 'interface', not an 'implementation'." Gamma et al. (2009, c1995) (Gang of Four 1995:18) has been very useful in the generation of high-level modelling software, specifically model structure editor and thermodynamic factory and computational engine.

Many of the OOP design patterns are extremely useful for the implementation of such tools and have certainly made the realisation easier and more structured yielding a much more flexible framework that is easy to maintain given the level of complexity. In general it has been observed that the for any particular problem or need there exists a suitable pattern for the implementation.

References

Gamma, E., Heim, R., Johnson, R., Vlissides, J., 2009, c1995. Design patterns: elements of reusable object-oriented software. No. 37th printing. Addison-Wesley, Boston. 2, 3

Løvfall, B. T., 2008. Computer realisation of thermodynamic models using algebraic objects. Ph.D. thesis, Norway: NTNU. 2.6

Modelisar, 2012.
URL `http://www.functional-mockup-interface.org` 2.4

Preisig, H. A., 2010. Constructing and maintaining proper process models. Comp & Chem Eng 34(9), 1543–1555. 2.6

Preisig, H. A., 2011. A multi-layered ontology for physical-chemical-biological processes. ESCAPE 21 (2011), Porto Carras, Chalkidiki, Greece 1, ISBN 978-0-444-53711-9 (ISBN 978-0-444-53711-9), 101–105. 2.6

I.A. Karimi and Rajagopalan Srinivasan (Editors), Proceedings of the 11th International Symposium on Process Systems Engineering, 15-19 July 2012, Singapore.

NGL Recovery from CO_2–EOR Streams

Maíra C. Barbosa[a], José Luiz de Medeiros[a], Ofélia Q. F. Araújo[a], Giovani Cavalcanti Nunes[b]

[a] *Departament of Chemical Engineering, Escola de Química da Universidade Federal do Rio de Janeiro. Av. Horácio Macedo, 2030, Bloco E - Centro de Tecnologia, Ilha do Fundão, CEP: 21949-900, Rio de Janeiro, Brazil.*
[b] *ENGP/IPP/PMF, Petrobras, Rio de Janeiro, Brazil.*

Abstract

The need to reduce concentration of greenhouse gases has promoted the use of technologies for CO_2 destination. Of particular interest is the use of CO_2 present in natural gas streams in the context of the Brazilian pre-salt fields. This motivation guides the development of CO_2 based processes that attribute extra revenue to the oil and gas production therefore reducing the penalty posed by CO_2 capture. In this work, a feasibility analysis is performed on the process of recovering Natural Gas Liquids (NGL) from CO_2 rich streams used in Enhanced Oil Recovery (EOR). For this purpose, a waste stream from synthetic natural gas production reported in the literature was analyzed. The proposed process arrangement employs natural gas processing techniques to recovering NGL from EOR streams rich in CO_2. Among the technologies available, three are approached and applied to recover propane (C_3), butane (C_4) and natural gasoline (C_{5+}) fractions: (a) Joule Thomson Process, (b) Turbo Expander Process and (c) Cryogenic Process. The comparative study presented includes process simulation in the environment UNISIM DESIGN (Honeywell), and sizing of main equipment for economic analysis, which includes calculation of capital and operational expenditures (CAPEX and OPEX). The study indicates the Cryogenic Process as the most feasible. Based on its superior performance, this process is applied to a case study concerning Tupi Pilot field, belonging to the Brazilian pre-salt layer, even though large uncertainties surround the actual data from the pre-salt reservoirs. With further consideration of revenues from Carbon Credits, the three processes and the case study are found to be economically feasible.

Keywords: greenhouse gases, EOR, pre-salt, NGL Recovery.

1. Purpose

The purpose of the work is to study the technical and economic feasibility of different Natural Gas Liquids (NGL) Recovery Processes from CO_2 rich streams for use in Enhanced Oil Recovery (EOR).

2. Introdution

With the intensification of global climate changes due to global warming associated to increased emissions and consequent atmospheric buildup of Greenhouse Gases (GHG), sustainable processing of oil reserves should pursue GHG emissions reduction targets. Among the various greenhouse gases, CO_2 is identified as the main contributor to global warming.
In Brazil, the environmental concern tends to worsen after the announcements of the discoveries made by Petrobras for oil in the Brazilian Pre-Salt. The oil found in this region is

light, and the associated natural gas presents large amounts of CO_2: preliminary studies indicate an approximate percentage of 10% to 15% CO_2 in these fields (Formigli, 2007).
The projections of the graph in Figure 1 show that, in 2030, this increase in emissions could reach 55% of emissions in 2004:

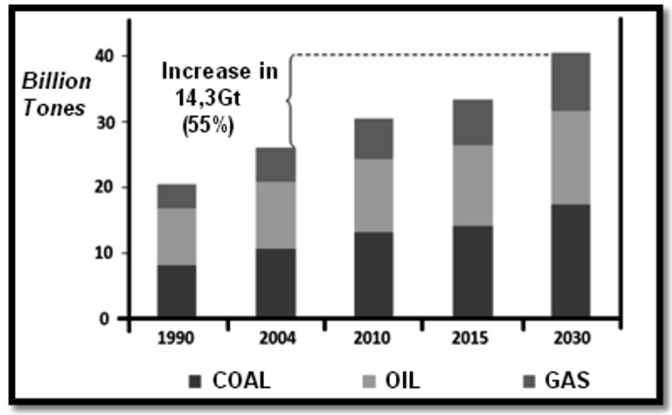

Figure 1: CO_2 emissions in billion tones. SOURCE: Costa, 2009 - adapted by the author

Carbon Capture and Storage (CCS) is currently the most promising solution to the long-term and widespread storage of CO_2, with some projects already underway (Costa, 2009). The technique is characterized by the injection of a liquid or the supercritical CO_2 in geological formations, in order to isolate it from the atmosphere.
Undoubtedly, the alternative of geologic sequestration increases operating costs of production. In this case, uses of CO_2 that generates revenues should hence be prioritized. In this respect, the application of CO_2 in EOR is attractive. In order to minimize even more the cost of CO_2 destination, this study evaluates three processes for NGL recovery from these CO_2 rich streams.
The result of evaluation of NGL recovery process technically and economically feasible for acid gas rich streams is then applied to a case of interest to the Brazilian Oil Sector. Thus, because of the importance of the Tupi Pilot field for history, it was chosen as a case study for this work.

3. Methods

At first glance for process analysis a CO_2 rich stream from synthetic natural gas is adopted as feed to compare NGL Recovery Process.
This waste stream came from the Great Plains Synfuels Plant operated by Dakota Gasification Company which is used for EOR purposes in *Weybum* and *Midale* fields, located in Saskatchewan, Canada (Vargas, 2010).
Among the existing NGL Recovery Process, were evaluated and compared three of them:

1) **Joule Thomson** – this process has the lowest cost but has restricted use because it does not guarantee the sale specification for the Natural Gas (NG) according to ANP. This is basically a process for setting the dew point of the NG. The temperature decreases when the system expands freely while maintaining constant enthalpy. In an industrial plant, this expansion is accomplished in a isenthalpic pressure control valve;

2) **Turbo Expander** – this process is similar to the Joule Thomson procedure but in lieu of being a pressure control valve the expansion takes place in a turbine, which releases energy that is used in the present process. It`s more expensive than the previous process since it has more critical equipment, such as the turbine;
3) **Cryogenic** – this process is more complex than the two previous ones, since it necessarily have a propane refrigerant cycle to decrease the temperature. This has a moderate investment and is capable of generating GN with the sale specification required by ANP.

Figures 2A, 2B and 2C show schematic diagrams of these processes:

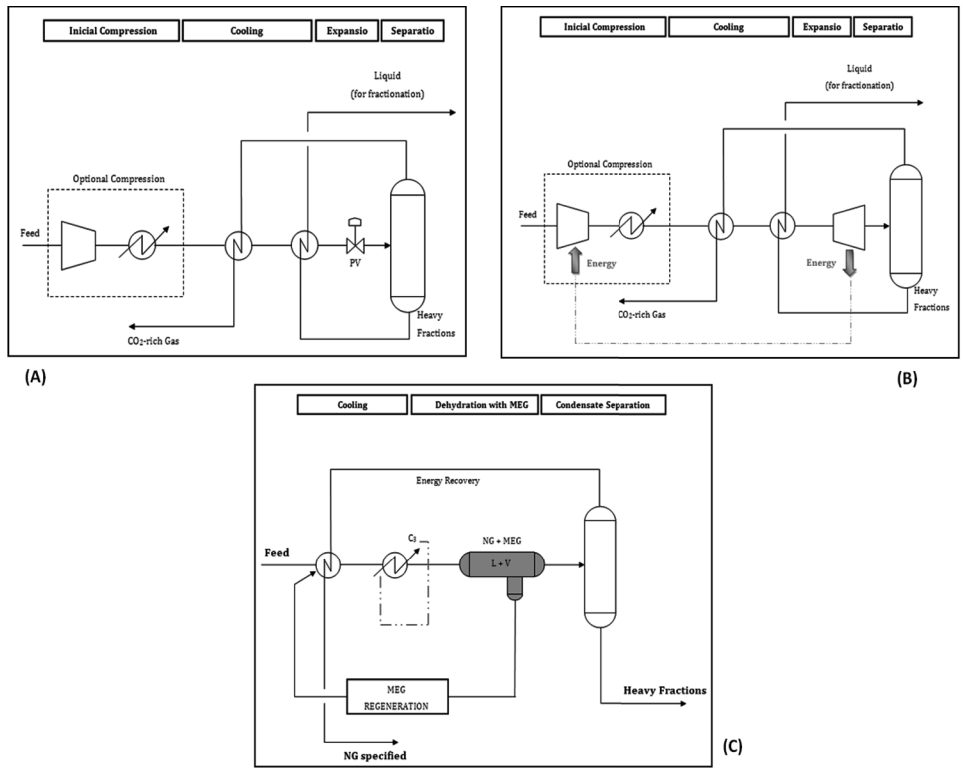

Figure 2: **(A)** Joule Thomson Process; **(B)** Turbo Expander Process; **(C)** Cryogenic Process.
SOURCE: Vaz et al. 2008 - adapted by the author

The proposed flow diagrams in the environment UNISIM DESIGN (Honeywell) include three sections:

a. *Initial Section*, where one of the components of the gas stream migrates to the liquid phase for later recovery. This migration occurs when the process stream is subjected to very low temperatures, around -30°C;
b. *Fractionation Section*, where the liquid fraction obtained in the previous step is directed to a battery of distillation columns, to separate streams for future injection (CO_2 and light components, as C_1 and C_2) and streams for market (C_3, C_4 and C_5^+);
c. *Compression and Injection Section*, where the flow of CO_2 and light components obtained in the previous step is compressed into three stages of compression and then is sent by pipeline to the oil well head.

The processes are simulated using UNISIM DESIGN and the main equipment sizing is performed to calculate capital costs (CAPEX) and operational costs (OPEX).
The methodology used for economic analysis (Turton et al., 2009) sought a preliminary estimate of the cost, which is indicated for comparison of alternatives of the same process, the focus of this work.
The estimated cost of a plant may be done in two ways: from a similar existing plant, for example, in the case of a REVAMP, or can also be made for a new plant ("Grass Roots ").
In the case of an existing plant, the cost of the new plant should be update in relation to the nominal capacity and the date of construction. This update date use Economic Indexes presents in the literature, for example, the CEPCI ("Chemical Engineering Plant Cost Index") or M&S ("Marshall & Swift Equipment Cost Index"). Otherwise, for a new plant, the total capital cost "Grass Roots" is calculated by the cost associated with its main equipment.
In this study, the Guthrie technique introduced in the late 60's and recognized as the best estimate for capital expenditures was used. It calculates the cost in a baseline condition and employs correct factors (adapting the material of construction, pressure, etc.) to find the installed cost of the module (CM).
The last step in this economic analysis is the Cash Flow. The method used was the Discounted Cash Flow (DCF), which is one of the main methods used for economic evaluation. The approach used by the method determines the value of the company through a projected cash flow, discounted by a rate that reflects the risk associated with investment.
The DCF calculated for the three processes are evaluated and then compared on an economic basis for determining the most attractive alternative.
The winner process was applied to the case study of the Tupi Pilot field.

4. Results

The three cases showed very similar mass flow rates for the sale streams and for the injection streams (EOR), which indicates that their recovery efficiencies are equivalent. Two approaches are used for the economic analysis. The first one is a more rigorous analysis, considering NGL sale as the only process revenue. In this analysis, the most profitable process is the Cryogenic alternative, with an investment return around 8 years of operation (figure 3A).
The second analysis accounts for the environmental cost associated with power consumption. In addition, the analysis also considers carbon credits associated with the CO_2 emissions avoided as extra revenue to the LGN sale. Finally, the increased productivity of the well with the activity of EOR is also included in the analysis. In this case, the three cases appear to be attractive, with an investment return occurring within the first 3 years of plant operation (figure 3B).

Figure 3: **(A)** Cash Flow only with NGL sale; **(B)** Cash Flow with new revenues and NGL sale.

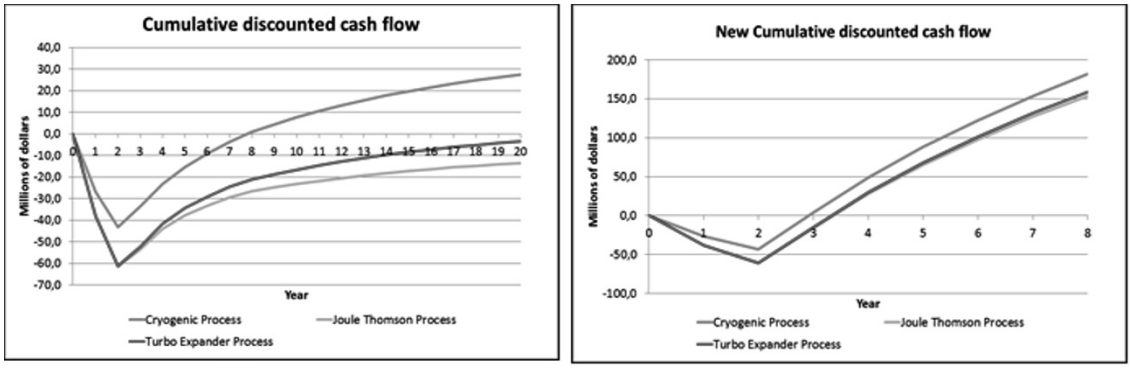

(A) (B)

For the study case with the cryogenic process, the same two approaches are used for the economic analysis. In the first analysis the process was not feasible but in the second analysis the process proved to be profitable with an investment return around 3 years of operation.

5. Conclusions

In the comparative study the economic analysis indicated similar performance in relation to the product flows obtained for the three simulated cases. In a first approach to economic analysis, the cryogenic process showed the best discounted cash flow. However, in a second and more complete analysis, considering carbon credits, the three cases shown to be feasible and attractive.

Finally, for the study case of the Tupi Pilot field the Cryogenic process is feasible only when the carbon credits associated with the CO_2 and the increased productivity of the well with the activity of EOR where considered.

Acknowledgment

Financial support of MCT/FINEP/CTPETRO, Grant No.2460-06 is kindly acknowledged.

References

I. V. L. Costa, 2009, “Análise do Potencial Técnico do Seqüestro Geológico de CO_2 no Setor de Petróleo do Brasil”, Dissertação de Mestrado. Rio de Janeiro, RJ, Brasil : UFRJ - COPPE.

J. Formigli, November 2007, “Pre-Salt Reservoirs Offshore Brazil: Perspectives and Challenges”, Energy Conference, Miami, USA.

IPCC, 2005, “Special Report on Carbon Dioxide Capture and Storage”, United Kingdom and New York: Cambridge University Press.

C. E. M. Vaz, J. L. P. Maia, W. G. Santos, 2008, “Tecnologia da Indústria do Gás Natural”. São Paulo: Blucher.

R. Turton *et al.*, 2009, “Analysis, Synthesis, and Design of Chemical Processes”. Prentice Hall, 3rd. Edition.

K. J. Vargas, 2010, “Refrigeration provides economic process for recovering NGL from CO2-EOR recycle gas”, Oil & Gas Journal. Canada : Falcon EDF Limited.

I.A. Karimi and Rajagopalan Srinivasan (Editors), Proceedings of the 11th International Symposium on Process Systems Engineering, 15-19 July 2012, Singapore.

Integrated Platform at ICES Kilo-Lab for Process Quality by Design

Suat-Teng Tan, David Wang, Iskandar Halim, Soo Khean Teoh, Paul Sharratt, Gabriel Loh, Run Ling Wong, Steven Mun Chun Yee, Chien Ying Loke, Wee Chew*

*Institute of Chemical and Engineering Sciences (ICES), Agency for Science, Technology and Research (A*STAR), 1 Pesek Road, Jurong Island, Singapore 627833, Singapore*

Abstract

The paradigm shift that is attempting to change the way pharmaceutical manufacturing is undertaken in the 21st century has raised practical challenges for the adoption and implementation of the Process Analytical Technology (PAT) framework initiated by the U.S. Food and Drug Administration (FDA). The motive is to engender a science-oriented pharmaceutical manufacturing that is along FDA's pharmaceutical product quality by design (QbD) ideology. One such challenge revolves around the integration of PAT technologies such as varied process analytics (e.g. sensors, spectrometry, chromatography, etc.), multivariate analyses, knowledge management, and process control under a common information exchange and data-logging platform. Such an integrated platform was recently installed and commissioned at the Kilo-Lab in the Institute of Chemical and Engineering Sciences (ICES). Its efficacy was demonstrated through synthesizing 4-D-erythronolactone at kilo-scale using a four-phase hybrid process.

Keywords: Process Analytical Technology (PAT), Quality by Design (QbD), Process Raman Spectroscopy, Supervisory Control and Data Acquisition (SCADA), Multivariate Data Analysis and Management

1. Introduction

With the introduction of two key FDA guidance documents in 2004 along the themes of 21st century pharmaceutical current good manufacturing practice (cGMP) [1] and Process Analytical Technology (PAT) [2], there has been a paradigm shift that is brewing within the pharmaceutical industry and related fields, including R&D carried out in academia and research institutions. The drive is towards achieving innovation in pharmaceutical manufacturing unit operations through process understanding along the FDA ideology of "quality by design" (QbD) [1]. Moreover, the undergirding thrust of process analytical technology (PAT) purports an *integrated systems approach* in the implementation of QbD in PAT pharmaceutical processes [2]. These two FDA initiatives essentially revolve around the tripartite guidelines Q8(R2), Q9 and Q10 by the ICH (International Conference on Harmonisation of the Technical Requirements for Registration of Pharmaceuticals for Human Use), which respectively expound details on pharmaceutical development, risk assessment and quality system [3]. The ICH guidelines are also drawn upon by other deliberations from pharmaceutical professional societies, e.g. ASTM committee E55 documents [4] and Product Quality Lifecycle Implementation (PQLI) roadmap of ISPE (International Society for Pharmaceutical

* chew_wee@ices.a-star.edu.sg

Engineering) [5]. In effect, the aforesaid publications from FDA, ICH, ASTM committee E55 and ISPE PQLI espouse the translation of a cadre of manufacturing philosophy and methodological concepts related to the PAT framework and process innovation [6], e.g. systems approach, risk and knowledge management, quality by design, etc., into practical steps realizable for actual processes within the envisioned 21st century science-based pharmaceutical cGMP.

As with all paradigm shifts, there are gaps and teething issues to overcome in changing the way pharmaceutical manufacturing is carried out [6]. One major hurdle in realizing the aforesaid innovation pharmaceutical manufacturing is the lack of an integrated approach to bridge the various *sub-disciplines* (e.g. process chemistry development, process analytical chemistry, process engineering and design, multivariate chemometrics, chemical process systems and control engineering) and *enabling technologies* (e.g. in situ process analytics, multivariate numerical software, SCADA and expert systems) [6]. Second, the PAT framework suggested four essential tools, namely: (i) multivariate tools for design, data acquisition and analysis, (ii) process analyzers, (iii) process control tools, and (iv) continuous improvement and knowledge management tools [2]. As such, the process data and information communication under this PAT framework is both multi-dimensional and voluminous, and it happens in real-time between (i) in- or on-line process analytics that monitors the state of processes with (ii) supervisory control and data acquisition software (SCADA), and (iii) numerical software handling multivariate data analyses, process models and control strategies. The aforesaid two challenges circumscribe a technological gap to be bridged before PAT validated 21st century pharmaceutical cGMP scenarios can be easily implemented. This void also impacts the real-time release of drugs and time-to-market of new chemical entities or drug formulations.

This contribution describes the use of an *integrated platform* that brings together varied software, process units and IT technologies that can help to resolve the aforesaid impasse. Such an integrated platform was tested on the synthesis of 4-D-erythronolactone (4-DEL) through a four-phase hybrid process (i.e. with batch and continuous processing units) [7].

2. Methodological Framework for Integrated Platform

Implicit in the aforesaid strive towards achieving innovative 21st century pharmaceutical cGMP along the ideology of QbD and the PAT framework is the necessity of reliable and timely process information. This process information, as implied in various professional guidelines and documents, will be multi-dimensional and mixed-type in nature; that is the information contains scalar, arrays (vectors and matrices), and even hyperspectral data types [6]. As such, it is considerably more complex than the usual scalar (univariate) process data, e.g. pH, temperature, flow rates and pressure. Thus, a practical methodological framework had to be conceptualized so as to capture the *intrinsically data-rich information environment* within which the aforesaid integrated platform architecture is to interface and function. Figure 1 schematically shows the scenario of a typical QbD/ PAT validated process (unit operation) that needs to be integrated. It consists of (i) various manual controls and automation (valves, pumps, temperature control, etc.) to regulate process conditions, and (ii) data transmission between analytical instrumentation (sensors, spectroscopic probes, etc.) and the supervisory control and data acquisition (SCADA) or distributed control system (DCS) for monitoring and controlling the process state. However, as the real-time data is intrinsically multi-dimensional and complex, it had to be analyzed using multivariate

analyses (chemometrics models) before returning critical process parameters (e.g. chemical concentrations, abstract principal components information, etc.) to the control algorithms residing in the SCADA/ DCS for initiating process control strategies. Third party numerical software might also be invoked to execute specialized mathematical procedures to aid the process analyses and control.

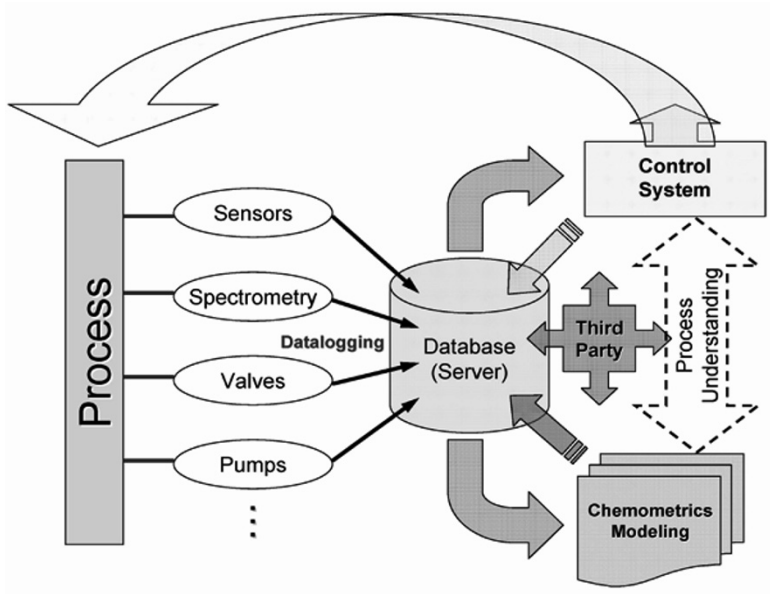

Figure 1 ICES Kilo-Lab vessels and equipment utilized for Integrated Platform

Furthermore, in a science-oriented regulated process scenario described by the FDA PAT guidance [2] and also the ISPE PQLI initiative [6], process analytics, data analysis and control are to be well described within the *design space* and *control strategy* of the process/ unit operation. This implies a *flexible integrated platform* to allow for (i) automated datalogging of process analytical and parameter data, (ii) a secured database server (or historian) that records and maintains the integrity of all data (raw and calculated), and (iii) a flexible software architecture that facilitates the retrieval and inter-exchange of pertinent data from varied software that perform data analyses (e.g. through chemometrics modelling), process modelling (obtained through laboratory and simulation studies), and process control. Modern SCADA/ DCS are able to achieve parts (i) and (ii), with their analytical process measurements and control primarily based on univariate sensors such as temperature, pH, etc. A segment of part (iii), particularly the link between spectroscopic measurements, multivariate chemometrics numerical packages and some form of process control, is presently under development and testing in actual manufacturing facilities by major players in the process system integration and automation industry [6], e.g. ABB Industrial^{IT} eXtended Process Analytical Technology (xPAT) platform, GE Intelligent Platforms Proficy® Process Systems, and Siemens SIPAT™ PAT software that works in conjunction with their SIMATIC WinCC software package. All data flow, analyses and feedback must be governed by science-based process understanding along the QbD ideology, and also compliant to regulatory stipulations (e.g. FDA's 21 CFR electronic records [8]). To the best of our knowledge, such a flexible infrastructure is currently rare, if ever one actually exists, in both industrial and academic R&D facilities; and a full and seamless integration of all

aspects of (i)-(iii) is presently unheard of [6]. Therefore, the ability to set up such a platform would mean a significant step forward to realizing product quality by design (QbD) envisioned by the pharmaceutical fraternity.

3. Implementing an Integrated Platform at the Kilo-Lab Facility of the Institute of Chemical and Engineering Sciences (ICES)

The Kilo-Lab at ICES is the first of its kind within academic research institutions in Southeast Asia. It is geared towards developing new process research techniques and to solve problems of scale-up and manufacturing for the pharmaceutical and specialty chemicals industry sector. The Kilo-Lab is equipped with batch reactor systems and has been building up its continuous processing facilities over the recent few years. Before installing Siemens technologies for the aforementioned integrated platform, the batch process equipment is managed using the GE iFIX SCADA system, whilst the continuous processing skids are separately controlled by the ABB 800xA DCS. To test the integrated platform, a kilo-scale four-phase hybrid processing of 4-DEL was implemented at the ICES Kilo-Lab, which involves (i) salt formation using D-isoascorbic acid and sodium carbonate solutions, (ii) batch oxidation using hydrogen peroxide and (iii) continuous operation of salt formation and oxidation, and (iv) acidification using hydrochloric acid to induce ring closure [7].

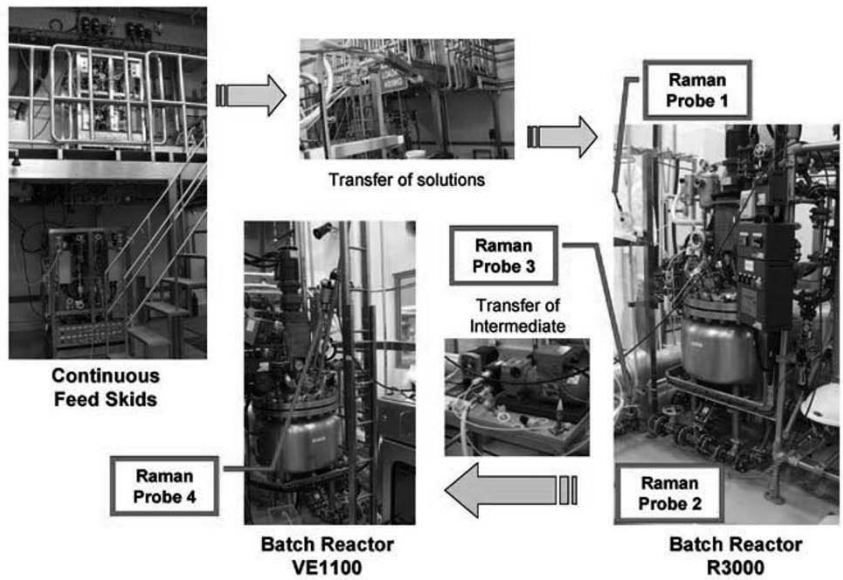

Figure 3 ICES Kilo-Lab vessels and equipment utilized for Integrated Platform

As shown in Figure 3, the kilo-scale implementation of the 4-DEL synthesis involves the use of continuous mobile skids that transfers initial reagents of D-isoascorbic acid, sodium carbonate, hydrogen peroxide in either batch or continuous fashion into the two Hastelloy batch reactors (R3000 and VE1100) that act as either reactors or receivers for different phase of operations. The hydrochloric acid solution (ca. 18% strength) used for ring closure was dosed into VE1100 vessel using a separate pump. The integrated platform is realized through combining Siemens WinCC SCADA and PAT (SIPAT) software technologies, with communication hardwiring using Ethernet lines and the data-exchange through the OLE for Process Control (OPC) protocol. Data acquisition and process control was achieved from the WinCC-SIPAT integrated platform via the

two legacy ABB DCS and GE SCADA systems to control the programmable logic controls (PLCs) of the continuous feed skids and batch reactors.

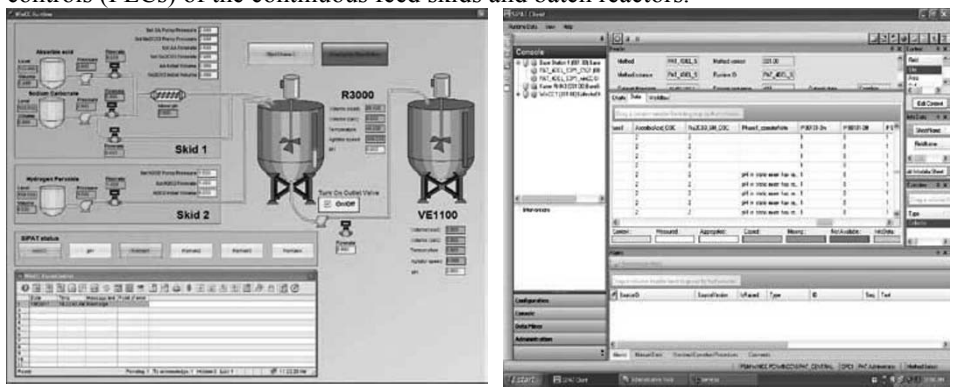

Figure 4 Typical WinCC Graphical User Interface and SIPAT in 4-DEL kilo-scale synthesis

The integrated platform is also directly linked through OPC tags and Ethernet protocol to the in situ Kaiser RamanRXN3 with four multiplexing probes, multivariate chemometrics analyses through MATLAB® and Gensym's G2 monitoring system for real-time process data acquisition and multivariate analyses. In addition, the process understanding acquired from laboratory-scale experimentation was incorporated through programmable scripts in C language for triggering operation logic automation during the kilo-scale operations for all four phases of 4-DEL synthesis. Graphical user interfaces (GUI) for all four phases of operations were also created for simple operator-level command and control with SIPAT displaying real-time process information (e.g. Figure 4). All SIPAT methods development, kilo-scale 4-DEL synthesis runtime data and information such as critical process parameters (CPPs), process alarms, multivariate Raman spectroscopic data and real-time estimates of chemical species concentrations were automatically data-logged into a secured SQL database in compliance to FDA 21 CFR Part 11 requirements.

This successful implementation of the integrated platform at the ICES Kilo-Lab, tested by a four-phase hybrid processing of 4-DEL kilo-scale synthesis, demonstrates great promise as a flexible plug-and-play methodology for facilitating the development and implementation of PAT validated processes.

References

[1] U.S. Food and Drug Administration, September 2004, Pharmaceutical cGMPS for the 21st Century – A Risk-Based Approach (Final Report).

[2] U.S. Food and Drug Administration, September 2004, Guidance for Industry, PAT – A Framework for Innovative Pharmaceutical Development, Manufacturing, and Quality Assurance.

[3] http://www.ich.org/products/guidelines/quality/article/quality-guidelines.html.

[4] http://www.astm.org/COMMIT/COMMITTEE/E55.htm.

[5] T. Garcia, G. Cook, R. Nosal, 2008, PQLI Key Topics - Criticality, Design Space, and Control Strategy, *Journal of Pharmaceutical Innovation*, 3, 60-68.

[6] Chew W. and P. Sharratt, *Analytical Methods* 2 (2010) 1412–1438.

[7] L.L. Wong, R.L. Wong, G. Loh, P.E.W. Tan, S.K. Teoh, S.M. Shaik, P.N. Sharratt, W. Chew, S.T. Tan, D. Wang, Multi-Kilo Synthesis of 4-D-Erythronolactone via Batch and Continuous Processing, *submitted manuscript*.

[8] U.S Food and Drug Administration (FDA), August 2003, Guidance for Industry Part 11, Electronic Records; Electronic Signatures – Scope and Application.

I.A. Karimi and Rajagopalan Srinivasan (Editors), Proceedings of the 11th International Symposium on Process Systems Engineering, 15-19 July 2012, Singapore.

Multiphase CFD simulation of an F-T airlift external loop slurry reactor

Zhenxing Zhu，Jie Yang，Qing Bian

SINOPEC Research Institute of Petroleum Processing，No.18, Xueyuan Road, Haidian District, Beijing, 100083，China

Abstract

F-T Synthesis is a hot spot in the development of new resource. Because of its simple structure and effective heat removal, Slurry bed becomes a most promising technology for F-T Synthesis. But because of its complex hydrodynamics, the reactor is difficult to design and enlarge. Based on the airlift external-loop slurry reactor's cold model, CFD simulations were taken to optimize the gas distributor in a gas-liquid system. Then a study on a gas-liquid-solid system was carried out to observe the flow and distribution of each phase.

Keywords: CFD, F-T Synthesis, Slurry bed, Multiphase Main Text

1. 1. Introduction

As a route converting synthesis gas to liquid fuels or chemical feedstocks, Fischer-Tropsch synthesis (FT Synthesis) has been an interesting topic in reactor design as well as process scale-up.[1] Understanding the flowing status in the designed reactor is of great importance for the design of a specified F-T process because of the complex multiphase flow in FT Synthesis reactor. The flowing status may dramatically change with operation condition and reactor structure.[2] It is well-known that the flow field (such as velocity, pressure, volume fraction of each phase) is closely related to the type of reactor. There are many types of reactors can be used in F-T Synthesis process, such as fixed bed reactor, fluidized bed reactor and slurry bed reactor, among which slurry bed reactor is superior to other beds in many fields, such as heat transfer performance, investment and product yield. Because of the simple structure and effective ability of heat removal, the airlift external-loop slurry bed reactor has been regarded as the most promising technology for F-T synthesis.

The flow in an airlift external-loop slurry bed reactor is quite complicated, because there are three phases inside it, namely gas, liquid and solid. In such fluidization system, bubble dynamics plays a key role in dictating the transport phenomena and ultimately affects the overall rates of reactions. It has been recognized that the bubble wake, when it is present, is the dominant factor governing the system hydrodynamics (Fan and Tsuchiya, 1990).[3] A proper holdup and volume fraction distribution of gas, which is mostly depend on the structure of gas distributor, may be quite important to the process. On the other hand, the existence of solid may be an intractable influence on flowing behavior inside reactor. Unfortunately, the solid motion can not be described directly from experiments because of the lack of measuring instruments.

There are various approaches to the mathematical and physical modeling of multiphase flows. The most widely used methods for CFD are the Eulerian-Eulerian[4] and the Eulerian-Lagrangian approach[5]. In the Eulerian method, both the continuous and dispersed phase(s) are mathematically modeled as interpenetrating fluids, represented by sets of mass, momentum and energy balances. In the Lagrangian approach, a large

number of particles are tracked individually, while the liquid phase is treated as a continuum. The interaction between the particles and the liquid shows up as a source term in the momentum equations. The advantage of the Eulerian method above the Lagrangian way is the void fraction of the dispersed phase is high. While the computational time in the latter approach depends highly on the number of particle trajectories to be calculated, in the Eulerian method the number of equations to be solved remains the same. Interaction terms describing drag, virtual mass and elects of lift forces appear in momentum balances of both phases.[6] Turbulence modeling in three-phase flow is done using the same approach as in single-phase flow.
Two CFD causes using Eulerian method was involved in this article, a simulation of gas-slurry system to optimize the gas distributor and a simulation of gas-liquid-solid system to gain the flowing field and volume fraction of each phase. Both of them was based on and had been verified with a cold model test.

2. 2. Setup and CFD-Approach

In this paper, an Eulerian-Eulerian approach is presented to study the flow in a three-phase external-loop airlift slurry bed reactor. The reactor is shown schematically in Fig. 1. The airlift consists of a riser that is a cylinder tower (H=3000mm, D=280mm) filled with water. A circulating tube (H=2000mm, D=70mm) create a down comer beside the riser. Gas is injected via a distributor on the bottom of the riser. At first, the system is treated as a pseudo-two-phase: the carrier-phase contains liquid with small solid particles, which is modeled as a pseudo single-phase to reduce the calculating time. The gas enters directly into the riser (see Fig. 1) as a dispersed phase. A Reynolds stress models, including source terms due to coupling of the phases, is used for the turbulence and solved simultaneously with the mass and momentum balances. The turbulent kinetic energy and dissipation rate of the dispersed phase are obtained by algebraic relation and are functions of turbulent kinetic energy and dissipation rate of the continuous phase. In the present simulations, interest is merely in steady-state solutions of the two-fluid formulations, throw which the gas distributor may be optimized and the velocity distribution of each phase can be obtained. Then, a gas-liquid-solid system can be simulated by using the information of the two-phase calculation.

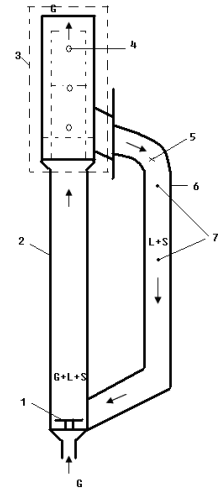

Fig. 1 schematic diagram of external-loop airlift slurry bed reactor

3. 3. Optimization of gas distribution

Through long term experiments, the gas should be better injected down into the reactor. The diameter and the open porosity of gas holes on the distributor were considered in this section. When the average volume fraction of solid is 0.2, the superficial velocity of gas is 0.144m/s, the diameter of gas hole is 2mm, the holdup and velocity distribution of gas at a horizontal plane which is 619mm above the distributor with deferent open porosity can be obtained (see Fig. 2). Under the same conditions, the holdup and velocity distribution of gas at the plane with deferent diameter of gas holes can be obtained by fixing the open porosity on 0.2 (see Fig. 3).

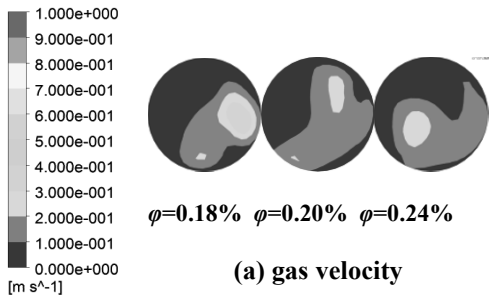

Fig. 2 Velocity and holdup distribution of gas with deferent open porosity

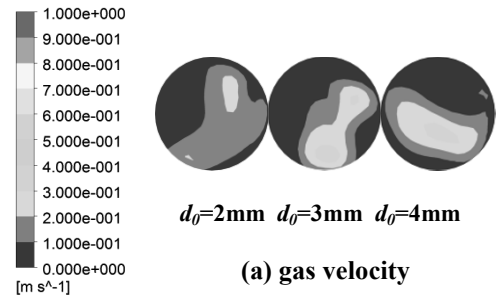

Fig. 3 Velocity and holdup distribution of gas with deferent diameter

It can be found from Fig. 2 and Fig. 3 that gas was distributed uniformly, when the open porosity was 0.2 and diameter is 2mm. It can be inferred that the slurry was also distributed uniformly under the same conditions. Furthermore, the variance of the flowing field of each phase at a horizontal plane which is 619mm above the distributor with deferent open porosity and deferent diameter of gas holes was involved to verify the conclusions (see Table 1 and Table 2). When the open porosity was 0.2 and diameter was 2mm, the variance of gas velocity, slurry velocity and holdup was minimum, which indicated that the most uniform flow was provided.

Table 1 The variance of the flowing field with deferent open porosity

Open porosity of gas holes	φ=0.18%	φ=0.20%	φ=0.24%
Gas velocity	4.78E-03	3.14E-03	3.71E-03
Slurry velocity	1.89E-02	3.25E-03	6.42E-03
Holdup	2.81E-03	2.83E-03	2.88E-03

Table 2 The variance of the flowing field with deferent diameter

Diameter of gas holes	d_0=2mm	d_0=3mm	d_0=4mm
Gas velocity	3.14E-03	6.53E-03	9.03E-03
Slurry velocity	3.25E-03	1.32E-02	4.25E-03
Holdup	2.83E-03	3.40E-03	5.59E-03

4. 4. Gas-liquid-solid CFD simulation

To describe the flow of each phase in details, a gas-liquid-solid CFD simulation was carried out with the results of former section, for example, the gas velocity via holes. The volume fraction of each phase in the reactor can be calculated (see Fig. 4), when the average volume fraction of solid is 0.1, the superficial velocity of gas is 0.054m/s.

（a）Holdup in ZX plane

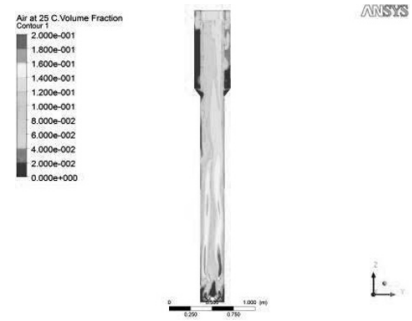

（b）Holdup in ZY plane

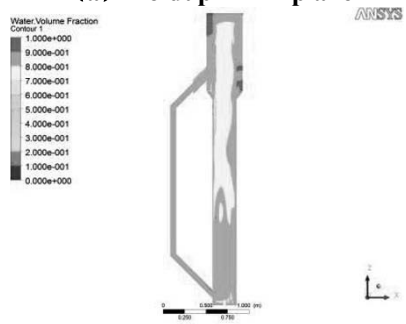

（c）Volume fraction of liquid in ZX plane

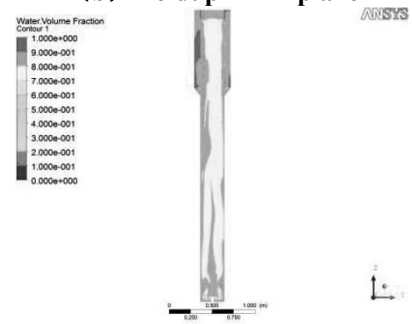

（d）Volume fraction of liquid in ZY plane

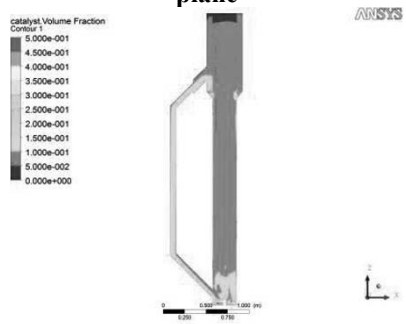

（e）Volume fraction of solid in ZX plane

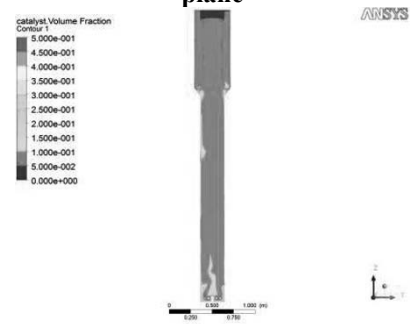

（f）Volume fraction of solid in ZY plane

Fig. 4 The volume fraction distribution of each phase in reactor

It can be seen that the volume fraction distribution of solid and liquid showed a good agreement, a slurry had been formed by these two phases. All of the three phases distributed symmetrically in the view of ZY plane, by which the effects of gas distributor could be confirmed.

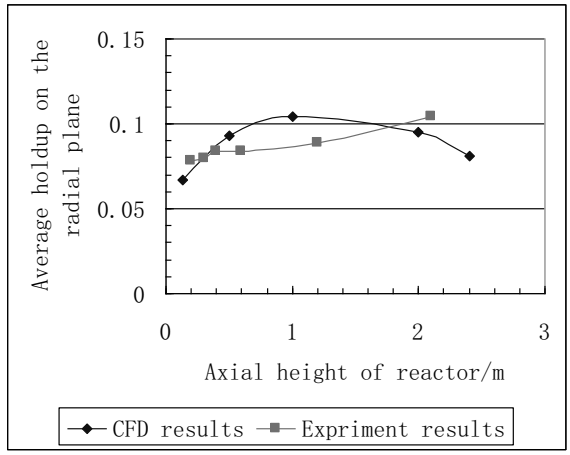

Fig. 5 Average holdup along the axis of reactor

The average gas holdup of radial planes along the axis of reactor was involved to verify the simulation through the results of a cold model test (see Fig. 5). There is a good agreement between simulation and experiment, by which the simulations was proved to be correct. The tiny errors may be cased by neglecting the Coalescence and breakup of bubbles, or gas expansion in reactor.

5. 5. Conclusion

An Eulerian-Eulerian approach was presented to simulate the flow in a multiphase external-loop airlift slurry bed reactor. The gas distributor inside the reactor was optimized by a two-phase simulation. Then, a gas-liquid-solid CFD simulation was performed to observe the flow inside the reactor extensively. The simulation was reasonable through a comparison of the calculating results and the experimental results. Many useful information can be provided from the CFD simulations, according to which, the further researches on the design and scale up of F-T slurry beds must be stepped deeply.

References

[1] R.Krishna, J. M. V.Baten, M. I.Urseanu, J.Ellenberger, 2001, Design and scale up of a bubble column slurry reactor for Fischer-Tropsch synthesis. Chem. Eng.Sci. 56, 537.
[2] B. H. Davis, 2002, Overview of reactors for liquid phase Fischer-Tropsch synthesis. Catal. Today 71, 249.
[3] L.S. Fan, K. Tsuchiya, , 1990. Bubble Wake Dynamics in Liquids and Liquid–Solid Suspensions. Butterworth-Heinemann, Stoneham, MA.
[4] A. Sokolichin, , G. Eigenberger, 1999. Application of the standard k-ε model to the dynamic solution of bubble columns. Chemical Engineering Science, 54, 2273-2284.
[5] S. Lain, S. D. Broder, M. Sommerfeld, 1999. Experimental and numerical studies of the hydrodynamics in a bubble column. Chemical Engineering Science, 54, 4913-4920.
[6] R. T. Jr. Lahey, D. A. Drew, 1992. On the development of multidimensional two-fluid models for vapor/liquid two-phase flows. Chemical Engineering Committee, 118, 125-139.

I.A. Karimi and Rajagopalan Srinivasan (Editors), Proceedings of the 11th International Symposium on Process Systems Engineering, 15-19 July 2012, Singapore.

Multi-scale process and supply chain modelling: from feedstock to process and products

Seyed Ali Hosseini[a] , Atiyeh Abedpour[a], Mingyen Yu[a]

[a]*Center for Process and Information Systems Engineering, University of Surrey, Guildford, GU2 7XH, UK*

Abstract

There is a large body of literature regarding the choice and optimization of different processes for converting feedstock to bioethanol and bio-commodities; moreover, there has been some reasonable technological development in bioconversion methods over the past decade. However, the eventual cost and other important metrics relating to sustainability of biofuel production will be determined not only by the performance of the conversion process, but also by the performance of the entire supply chain from feedstock production to consumption. Moreover, in order to ensure world-class biorefinery performance, both the network and the individual components must be designed appropriately, and allocation of resources over the resulting infrastructure must effectively be performed. The goal of this work is to describe the key challenges in bioenergy supply chain modelling and then to develop a framework and methodology to show how multi-scale modelling can pave the way to answer holistic supply chain questions, such as the prospects for second generation bioenergy crops.
Keywords: Supply chain management, Optimization, Renewable energy

1. Introduction

Although the main global concerns about biofuel are currently limited to sustainability, energy security and prices, each specific bioethanol production plant also faces a wider range of uncertainties, such as which of different processes to choose, which feedstock will be best for the plant, and even the best location for the plant, since all these factors are the main factors that determine cost. In addition to direct cost-determining factors, there are number of indirect effects, such as the effect of the production site and feedstock fields on local communities and the social economy. There is a large body of literature about choice and optimization of different processes for converting feedstock to bioethanol and bio-commodities; however, there is no single best process for all the different feedstocks, and based on the source and composition of the feedstock; there may be several feasible processes. The availability of the right feedstock for the plant is a spatial function of crop production yields, land availability, rainfall, and even the political decisions of local governments. These all imply that all the determining factors for any specific biorefinery are interlinked, and that obtaining the maximum profit for a production site and the maximum benefit for the social economy is only possible by realizing the holistic nature of all the factors and their interrelationship at different scales. These all imply that the eventual cost of biofuel production will be determined not only by the performance of the conversion process, but also by the performance of the entire supply chain from feedstock production to consumption. These relationships can be explained through multiscale modelling.

2. Multiscale Process Modelling and the Supply Chain

There is a large body of literature regarding the choice and optimization of different processes for converting feedstock to bioethanol and bio-commodities; moreover, there has been some reasonable technological development in bioconversion methods over the past decade (Hosseini and Shah, 2009a and 2009b). However, a question that has gone unconsidered in the literature is how technological developments in processing technologies and the life cycle of bioethanol feedstocks will affect the structure of the supply chain. In order to ensure world-class biorefinery performance, both the network and individual components must be designed appropriately, and allocation of resources over the resulting infrastructure must effectively be performed. Shah (2005) has divided all supply chain problems into three categories: (i) supply chain infrastructure (network) design; (ii) supply chain analysis and policy formulation; (iii) supply chain planning and scheduling. Regarding bioenergy, there is a lack of methodology on how to incorporate all the available knowledge into one interconnected network to answer important supply chain questions.The key goal of this work is to develop a framework and methodology to show how multiscale modelling can pave the way to answer holistic supply chain questions; this is illustrated in the figure below.

2.1. Supply Chain Network Design

The bioenergy supply chain network is a direct medium for engaging the end users of bioethanol derivatives and the suppliers of the feedstock; thus, at first glance, the main data required for designing such a network is spatial distribution of biomass supply and energy (fuel, electricity and heat) demand. A great deal of the PSE literature deals with how to handle demand uncertainty, mainly for consumer products (Tsiakis, Shah and Pantelides, 2001a); however, current global biofuel production, specifically in the EU, is much smaller than the desired target. Consequently, at this stage, research focussed on demand forecasting is irrelevant as supply is far lower than current demands. In modelling terms, the authors believe that at this stage, demand should be treated as a deterministic temporally growing spatial function, and not as stochastic.

Classically, location-allocation problems have tended to focus only on logistical aspects (Geoffrion and van Roy, 1979); however, in the process industry supply chain, greater benefits could be achieved by considering logistic and processing aspects simultaneously. The first step in the biofuel supply chain network design should be listing all the possible bioconversion methods for any given biomass. Then, for any specific bioconversion method, a multiperiod spatial optimisation can be built to maximise the total net profit of global network and/or GHG and/or energetic efficiency. This type of model is usually based on technology capital and operating cost as well as distance, capacity and costs of biomass and ethanol; the table below shows one example of the decision spaces for two processing options and three feedstocks. If there are a number of different types of objective functions and trading off between these objectives is difficult, a multi-objective optimisation procedure should be used. Considering these elements together provides opportunities for systems involving distributed pre-processing coupled with centralised processing (Dunnett et al, 2008).

In the optimisation problem, key decision variables can be: mode of transport at each stage, operating mode of equipment in each time period, production and supply of products, number of echelons, number of components in each echelon, and the

connectivity between components in adjacent echelon. The choice of deciding factors usually depends on the availability of data and the complexity of the network; nevertheless, a larger number of decision factors usually lead to more robust network structures, although it makes the optimisation problem more complex. In general, there exists a trade-off between models' precision and complexity; thus, a modeller's skill lies in choosing the right combination. Having developed optimisation problems for each specific biomass and any possible bioconversion methods, one can then easily compare these networks based on metrics such as cost, GHG, capacity, products, etc. In this way, a supply chain network design can be a valuable tool for decision-making.

2.1.1. Fundamental Bioenergy Supply Chain Network

Most of the literature on bioenergy supply chains assumes a given fundamental structure for the network in terms of suppliers, manufacturing plants, warehouses, distribution centres and customers. Thus the design procedure mainly focuses on the number of echelons and the connectivity between adjacent echelons. This is mainly due to the relative youth of the field of supply chain management (SCM), as most of the companies with established supply chain networks traditionally used SCM techniques to increase the efficiency of their already-established network. However, at this stage of development of biofuel production, the fundamental structural elements of the bioenergy supply chain have not yet been established; since these are important aspects of overall efficiency, one of the key challenges in the field is to integrate the different components of supply chains without any prior assumptions about the fundamental structure of the network (e.g. allowing distributed pre-processing).

Tsiakis *et al*. (2001b) addressed this problem in general, and proposed a general framework using the concept of flexible nodes. These nodes can be located at any one of a set of candidate locations, produce one or more products using one or more shared resources, hold inventories of the products as well as of any other materials in the network, and exchange material with other nodes. The functions of these nodes are therefore not specified a priori, and no flow network is superimposed. Consequently, the node functionalities and the flows between nodes are determined as part of the optimisation. Authors believe that applying this methodology to the bioenergy supply chain may result in a leaner network, where storage capacity is only established when necessary. Furthermore, this method provides the possibility of taking advantage of economies of scale in transportation that can result in huge financial savings due to the low energy value of biomass.

2.1.2. Integration of Process Model to Supply Chain Model

It should be mentioned that in the field of operational research and PSE, a very large amount of work has been undertaken to address both the infrastructure network design problem and optimisation of established networks. However in most of the work to date, the potential benefit of including more detail in the manufacturing process has not been established. Since there is huge uncertainty regarding the efficiency of each bio-refining process option in its mature state, at this stage of development these uncertainties should be captured in the global network model, to direct the research in way that most benefits the global network. For example, Hosseini and Shah (2009a) showed that optimising the biomass chip size in a dilute acid pretreatment process achieves average savings equivalent to a 5% improvement in the yield of the biomass-to-ethanol

conversion process. This kind of improvement in processing efficiency can lead to completely different result in global network optimization results; therefore, it is of utmost importance to formulate a methodology incorporating process uncertainty in the global supply chain network.

Although multiscale modelling is a promising technique for integrating all processing aspects at different scales into the biofuel supply chain, computational efficiency is also an intellectual challenge in the PSE area, as computation usually increases exponentially with problem size (Grossmann and Westerberg, 2000). One practical way to address this challenge would be to use conceptual process models from the molecular level up to the unit operation level in order to predict the possible range of operation and efficiency at each unit of operation, and then, in the supply chain model, consider the overall process as a combination of different outcomes, i.e. scenarios from process models at all scales. In other words, it would use characteristic models to run detailed dynamic simulations for each unit operation, and then use the results of these simulations (as "metamodels") in the global network model offline. In this way, it would be possible to consider uncertainty at a process level in the supply chain model; moreover, since these uncertainties are determined by conceptual models, it would be possible to find the root of the uncertainties. For example, if the model predicts a rising cost-purity curve for a specified unit of operation, then it would be possible to integrate this into the supply chain model and chose the appropriate purity for that specific unit of operation in order to maximize overall network efficiency. Therefore, in this approach, instead of considering the process as a black box, it would be possible to consider the process as a set of black boxes (unit operations) with a range of inputs and outputs for each unit of operation. Indeed, this approach would aid in optimizing the interactions between all available unit operations so that opportunities for new flowsheet configurations are facilitated.

2.2. Supply Chain Simulation

As stressed in the previous section, characteristic models are of utmost importance since they are the closest representation of reality and provide a way to find the root of uncertainties at any level. Therefore characteristic models are the most appropriate method for designing a fundamental bioenergy supply chain network. However, simulation models can be used to study the detailed dynamic operation of a fixed configuration under operational uncertainty, and can be used to evaluate expected performance measures for the fixed configuration to a high level of accuracy.Therefore, model-based simulations can have great significance for policy makers, as they can identify the potential socioeconomic effects of the bioenergy supply chain under different operating policies, ahead of actual implementation of any one policy.

2.3. Supply Chain Planning and Scheduling

Supply chain planning starts immediately after designing an infrastructure network and considers a fixed infrastructure over a certain time period, usually up to one year, and seeks to find the best network configuration to respond to forecast supply and demand in an economically efficient manner. In most of the works to date, the focus of researchers has been on identifying the best way to design the best network configuration based on demand uncertainty. However, as discussed earlier, there is not going to be a huge variation in ethanol demand; the main problem will be the variation of biomass supply due to seasonality. Therefore, the main issue for bioenergy supply

chain planning will be finding the best network configuration, using different feedstocks throughout the year to meet constant demand. At this stage of development, most of processes are designed for specific biomass types; it should be emphasized that for a bioenergy network to be economically efficient, biorefineries should be able to use different feedstocks with only minimum changes made to their overall process. For example, processes should be flexible enough so that different operating conditions (i.e., different residence time or temperature in a bioreactor) are enough to process different types of feedstock, and it is not necessary to change the overall process configuration. It should be possible to get the same result from different feedstocks in an economically feasible manner. To conclude, authors believe process intensification –developing processes which are more responsive to market needs whilst responding to changes in process parameters in seconds, rather than several minutes or hours – is essential to designing an efficient global bioenergy network.

3. Conclusion

Over the past few years there has been huge body of literature published addressing challenges for commercial bioenergy production ranging from feedstocks to processes and products. However, there is lack of methodology on how to incorporate all the available knowledge into one interconnected network to answer key supply chain questions holistically. Thus, in this work we have described the key challenges in modelling the bioenergy supply chain and then developed a framework and methodology to show how multi-scale modelling can pave the way to answer holistic supply chain questions, such as how to design fundamental bioenergy supply chain and incorporate process models into supply chain models. The important next steps involve modellers working alongside scientists engaged in fundamental experimental work on biomass production and conversion, ensuring that there is a good fit between the needs of whole systems modelling and the generation of empirical data.

References

Dunnett, A. J, C. S Adjiman, and N. Shah. “A spatially explicit whole-system model of the lignocellulosic bioethanol supply chain: an assessment of decentralised processing potential.” *Biotechnology for biofuels* 1 (2008): 13.

Geoffrion, A. M., & van Roy, T. J. (1979). Caution: Common sense planning methods can be hazardous to your corporate health. *Sloan Management Review*, *20*(4), 31–42.

Grossmann, I. E, and A. W Westerberg (2000). “Research challenges in process systems engineering.” *AIChE Journal* 46, no. 9 (2000): 1700–1703.

Hosseini, Seyed Ali, and Nilay Shah (2009a) . “Multiscale modelling of hydrothermal biomass pretreatment for chip size optimization.” *Bioresource Technology* 100, no. 9 (May 2009): 2621-2628.

Hosseini, Seyed Ali, and Nilay Shah (2009b). “Multiscale modelling of biomass pretreatment for biofuels production.” *Chemical Engineering Research and Design* 87, no. 9 (September 2009): 1251-1260.

Shah, N “Process industry supply chains: Advances and challenges (2005).” *Computer Aided Chemical Engineering* 18 (2004a): 123–138.

Tsiakis, P., Shah, N., & Pantelides, C. C. (2001a). Design of multi-echelon supply chain networks under demand uncertainty. *Industrial and Engineering Chemistry Research*, *40*, 3585–3604.

Tsiakis, P., Shah, N., & Pantelides, C. C. (2001b). Optimal structures for supply chain networks. In *Presented at AIChE annual meeting*.

I.A. Karimi and Rajagopalan Srinivasan (Editors), Proceedings of the 11th International Symposium on Process Systems Engineering, 15-19 July 2012, Singapore.

Performance Assessment of Water Gas Shift Membrane Reactors by a Two-dimensional Model

Marcello De Falco[a], Vincenzo Piemonte[a], Angelo Basile[b]

[a]*Faculty of Engineering, University Campus Bio-Medico of Rome, via Alvaro del Portillo 21, 00128 Rome, Italy*
[b]*CNR-ITM, c/o University of Calabria, Via Pietro Bucci, Cubo 17/C, 87030 Rende (CS,)Italy.*

Abstract

There is currently a large world effort towards developing hydrogen power as the next generation of clean energy for both the transportation and the electricity sectors.
Water gas shift (WGS) is a thermodynamically limited reaction which has to operate at low temperatures, reducing kinetics rate and increasing the amount of catalyst required to reach valuable CO conversions.
It has been widely demonstrated that the integration of hydrogen selective membranes is a promising way to enhance WGS reactors performance: a Pd-based membrane reactor (MR) operated successfully overcoming the thermodynamic constraints of a traditional reactor (TR) thanks to the removal of hydrogen from reaction environment.
In this work, the effect of hydrogen removal in membrane water gas shift reactors will be investigated by a two-dimensional, non-isothermal model in order to analyze the WGS reactor performance.
Keywords: WGS, Mathematical Modeling, Computer Simulations, Hydrogen.

1. Introduction

The water gas shift (WGS) reaction is an important step of hydrogen production in industrial cycles for upgrading H_2 rich streams by CO conversion present in syngas mixtures. In the last few years, significant developments in membrane science and the vision of process intensification by multifunctional reactors have stimulated the academic and industrial research focused on membrane reactor application to chemical processes (Mendes et al., 2010). From these works, the increase of the CO conversion above the equilibrium values appears to be possible when hydrogen is removed through the membrane. The membrane integration inside the WGS reactor leads to two main advantages: firstly, by allowing operation at optimum temperatures, MR improves reaction rates and reduces the need for excess water, improving plant efficiency. Secondly, by providing both reaction and product separation in one process step, a MR can potentially reduce the plant size and thus capital costs.
Membranes integrated in WGS reaction environment are usually dense metallic membranes composed by a Pd-alloy selective layer and a ceramic or Porous Stainless Steel (PSS) support. Composite dense Pd-based membranes are extremely selective and allow the separation of an ultra-pure hydrogen stream from the reaction environment. On the other hand, composite Pd-based membranes suffer for thermal stability problems due to the adherence between selective layer and support, which imposes a temperature constraints (operating temperature < 500°C, Bredesen, 2008). However, it is a worth assessment that the membrane temperature threshold would be coherent with the typical

WGS operating temperature (250-450°C). In this work, a Matlab model was developed to analyze and predict the performance of a WGS membrane reactor for H_2 production.

2. Mathematical Model

The WGS reaction is described as follow:

$$CO + H_2O \Leftrightarrow CO_2 + H_2 \quad (1)$$

The membrane reactor (MR) is composed by a reaction zone, where a catalyst is packed in order to support the WGS reaction, and a permeation zone where a carrier gas is fed to carry out the hydrogen permeated through the Pd-based dense membrane. Therefore, to describe the MR by a mathematical model, mass, energy and momentum balances have to be imposed both in reaction and permeation zones.

The 2D non-isothermal model has been developed by the following assumptions: steady-state conditions; negligible axial dispersion and radial convection; ideal gas behavior; pseudo-homogenous condition inside the reactor; perm-selective of Pd-Ag membrane towards hydrogen 100%; negligible radial dispersion and isobaric conditions in permeation zone.

The model equations, together with boundary conditions, are reported as follows:

2.1. Mass balances

Reaction zone:

$$\frac{\partial(\tilde{u}_z\tilde{c}_i)}{\partial\tilde{z}} = \frac{d_p \cdot L}{Pe_{mr} \cdot r_{i,o}{}^2} \cdot \left(\frac{\partial^2(\tilde{u}_z\tilde{c}_i)}{\partial\tilde{r}^2} + \frac{1}{\tilde{r}} \cdot \frac{\partial(\tilde{u}_z\tilde{c}_i)}{\partial\tilde{r}}\right) - \frac{\rho_{bed} \cdot L}{u_{z,in} c_{CO,in}} \cdot \eta \cdot R_i \quad (2)$$

where $\tilde{u}_z$ and $\tilde{c}_i$ are the dimensionless gas mixture velocity and mole concentration of component i, $u_{z,in}$ and $c_{CO,in}$ inlet velocity and inlet CO concentration, $\tilde{z}$ and $\tilde{r}$ dimensionless axial and radial coordinates, d_p the catalyst particle diameter, L and $r_{i,o}$ reactor length and catalytic bed tube radius respectively, ρ_b is the packed bed density, η and R_i are the effectiveness factor and the intrinsic rate for component i, expressed according to (Criscuoli et al., 2010) and Pe_{mr} is the mass effective radial Peclet number given by (Kulkarni and Doraiswamy, 1980) for Reynolds number greater than 1000.

Permeation zone:

$$\frac{dY_{H_2}}{d\tilde{z}} = \pm \frac{N^m_{H_2} \cdot 2\pi \cdot r_{o,i}}{u_{z,in} \cdot c_{CO,in}} \quad (3)$$

where $Y_{H_2} = \frac{F_{H_2,perm}}{F_{CO,in}}$ is the hydrogen recovered per mole of inlet carbon dioxide, $r_{o,i}$ is the membrane radius and $N^m_{H_2}$ is the hydrogen flux permeating through the membrane, evaluated by the Richardson's law for dense membranes when the limiting step is the diffusion of atomic hydrogen in the metallic layer:

$$N^m_{H_2} = \frac{P_H}{\delta} \cdot \left(p^{0.5}_{H_2,reac} - p^{0.5}_{H_2,perm}\right) \quad (4)$$

where δ is the Pd-based membrane thickness (20 μm in this work), $p_{H_2,reac}$ and $p_{H_2,perm}$ are hydrogen partial pressures in the reaction and permeation zone, respectively, and P_H is the membrane permeability, depending on temperature and

membrane composition (Shu et al., 1994). The sign + or – in is related to co-current or counter-current sweeping gas configuration.

2.2. Energy balances

Reaction zone:

$$\frac{\partial \tilde{T}_R}{\partial \tilde{z}} = \frac{\lambda_{er} \cdot L}{(u_z c_{tot}) \cdot c_{p,mix} \cdot r_{i,o}^{\ 2}} \cdot \left(\frac{\partial^2 \tilde{T}_R}{\partial \tilde{r}^2} + \frac{1}{\tilde{r}} \cdot \frac{\partial \tilde{T}_R}{\partial \tilde{r}}\right) + \frac{\rho_b \cdot L \cdot \eta \cdot R \cdot (-\Delta H)}{(u_z c_{tot}) \cdot c_{p,mix} \cdot T_{R,in}} \quad (5)$$

where $\tilde{T}_R$ and $T_{R,in}$ are the dimensionless reaction zone temperature and the inlet temperature, $c_{p,m}$ is the specific heat of gas mixture, c_{tot} is the total gas concentration, R is the reaction rate of reaction, (-ΔH) is the enthalpy of reaction and λ_{er} is the effective radial thermal conductivity of packed bed and gas mixture, considered as a pseudo-homogeneous phase and calculated according to (Elnashaie and Elshishini, 1993).

Permeation zone:

$$\frac{d\tilde{T}_P}{d\tilde{z}} = \frac{L}{F_{P,tot} \cdot c_{p,perm}} \cdot \frac{1}{T_{R,in}} \cdot \left[U_1 \cdot 2\pi \cdot r_{i,i} \cdot (T_R - T_P) + N_{H_2}^m \cdot \pi \cdot r_{o,i} \cdot \left(h_{H_2,reac} - h_{H_2,perm}\right)\right] \quad (6)$$

where $\tilde{T}_P$ is the dimensionless permeation zone temperature, $c_{p,perm}$ is the specific heat of gas mixture in permeation zone, $F_{P,tot}$ the total flow-rate, $r_{i,i}$ the membrane internal radius, $h_{H_2,reac}$ and $h_{H_2,perm}$ hydrogen enthalpies in the reaction and permeation zone and U_1 the overall heat transfer coefficient between reaction and permeation zone.

2.3. Momentum balances

In the reaction zone, the momentum balance is described by the well-know Ergun equations for packed beds. In the permeation zone, the pressure drop is negligible.

2.4. Boundary conditions

If the co-current MR configuration is imposed, the boundary conditions have to be fixed in the inlet section and at external and internal tubes. The PDEs set will be solved by a numerical method. On the other hand, if the counter-current configuration is imposed, the permeation zone equations boundary conditions will be fixed at $\tilde{z} = 1$ and the problem is a BVP (Boundary Value Problem), to be solved by a shooting method.

3. Results and Comments

In figure 1 the reactor conversion versus the gas hourly space velocity (GHSV) at T=550 - 600 K is reported. The hydrogen conversion both in membrane and conventional reactors decreases increasing space velocity. Moreover, at low space velocities the reactor conversion growth is more evident due to the membrane presence inside the WGS reactor: indeed a higher hydrogen flow crosses the reaction zone towards the permeation zone. Furthermore the reactor conversions are very close to equilibrium conditions for operating temperature of 600 K, while, due to kinetic rate reduction, the reactor conversions obtained at 550 K are far from equilibrium also for low values of the GHSV.

Figure 2 shows the effect of inlet reaction zone temperature on CO. At 600 K there is a maximum on the reactor conversion. It can be seen that, with temperature increasing, the conversions are reduced but drawing ever nearer to equilibrium. At temperatures

above 675 K, the conversion of the membrane reactor appears to be greater than the equilibrium conversion, while the conversion of the traditional reactor (TR) moves toward equilibrium.

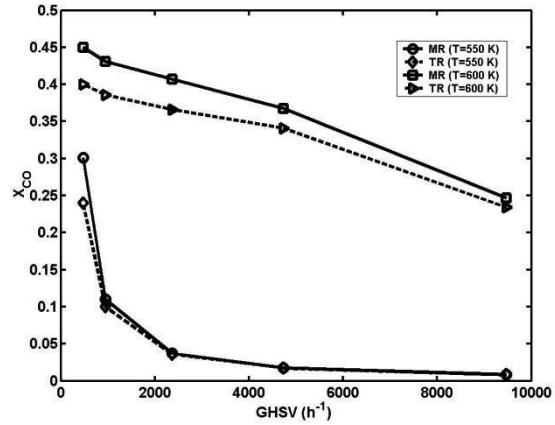

Figure 1 - CO conversion vs GHSV at 550 – 600 K (Reaction pressure = 10 bar, permeation pressure = 1 bar, H2O/CO = 1.1, Equilibrium conversion at 550 K = 0.6, Equilibrium conversion at 600 K = 0.45)

Figure 3 reports the reactor temperature profiles vs. the reactor axial coordinate: at low space velocities, initially there is a large increase of temperature because the reaction is very fast. When the reaction slows, T is reduced because there is a greater amount of outgoing heat due to the ΔT with the wall temperature (outlet temperature is set equal to the inlet temperature, i.e. 600 K) with respect to the amount of heat generated by the reaction.

4. Conclusions

A two-dimensional model was developed to analyze and predict the performance of a WGS membrane reactor for H2 production.

The main advantages of membrane reactors in WGS processes are CO conversion larger than in TR due to hydrogen removal during reaction. The model highlights the effect of the main operating parameters:

• at higher mixture GHSV the CO conversion decreases but the catalyst productivity increases;

• CO conversion profiles in function of operating temperature shows a maximum at 600 K about.

References

R. Bredesen, 2008, Thin Pd-23w%Ag membranes for hydrogen separation, CASTOR workshop, Lyon 22 – 24 January 2008.

A. Criscuoli, A. Basile, E. Drioli, 2000, An analysis of the performance of membrane reactors for the water-gas shift reaction using gas feed mixtures, Catalysis Today, 56 , 53-64.

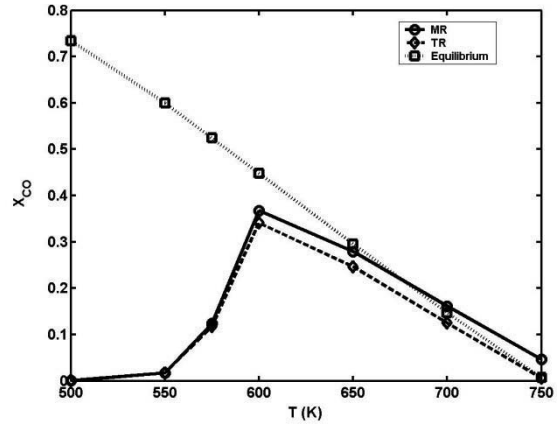

Figure 2 - CO conversion vs T (GHSV = 4750 h^{-1}, Reaction pressure = 10 bar, permeation pressure = 1 bar, H2O/CO = 1.1)

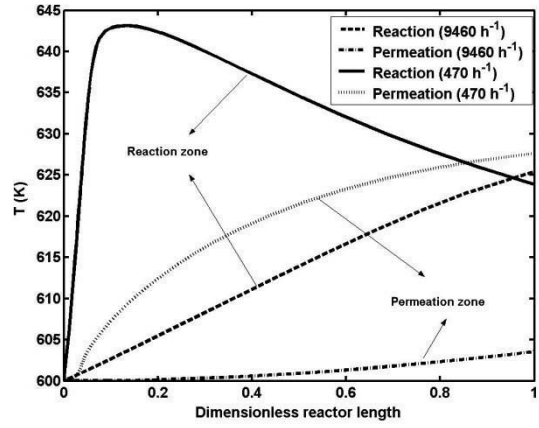

Figure 3 - T vs reactor length (GHSV = 4750 h-1, Reaction pressure = 10 bar, permeation pressure = 1 bar, H2O/CO = 1.1) (De Falco, 2011).

M. De Falco, V. Piemonte, A. Basile, 2011, Simulation of Water Gas Shift Membrane Reactors by a Two-dimensional Model, 21st European Symposium on Computer Aided Process Engineering – ESCAPE 21, in press.

S. Elnashaie, S. Elshishini, 1993, Modelling, simulation and optimization of industrial fixed bed catalytic reactors, Vol. 7 of Topics in Chemical Engineering, Gordon and Breach Science Publisher.

B.D. Kulkarni, L.K. Doraiswamy, 1980, Estimation of effective transport properties in packed bed reactors, Catalysis Reviews: Science and Engineering, 22, 3, 431-483.

D. Mendes, A. Mendes, L.M. Madeira, A. Iulianelli, J.M. Sousa, A. Basile, 2010, The Water-Gas Shift Reaction: From Conventional Catalytic Systems to Pd-based Membrane Reactors – a Review, Asia-Pacific Journal of Chemical Engineering on Membrane Reactors, 5, 111-137.

J. Shu, B. Grandjean, S. Kaliaguine, 1994, Methane steam reforming in asymmetric Pd and Pd-Ag porous SS membrane reactors, Appl. Catal. A: General, 119, 305-325.

I.A. Karimi and Rajagopalan Srinivasan (Editors), Proceedings of the 11th International Symposium on Process Systems Engineering, 15-19 July 2012, Singapore.

A Hybrid Meta-heuristic Method for Optimizing Logistic Networks Subject to Operational Conditions in Practice

Yoshiaki Shimizu and Syota Tsuchiya

[a]*Department of Mechanical Engineering, Toyohashi University of Technology, 1-1 Hibarigaoka, Ten-paku-cho, Toyohashi 441-8580, Japan*

Abstract

Under agile and global manufacturing environment, importance of logistics as a core of supply chain management has been acknowledged increasingly. In this study, we provide a practical hybrid method for a hierarchical logistic network optimization belonging to a tactical level. Since the problem is made of different kinds of NP-hard combinatorial optimization problems, its rigid solution is almost impossible for practical scale problems. Hence, to cope with the problem in practice, we have developed a three-level method in terms of the modified insertion method for VRP with time windows. It is deployed on a basis of Ton-Kilo (load (ton) multiply distance (km)) based evaluation instead of the conventional Kilo (distance only) based one. It also includes a new mechanism that enables us to engage in multi-objective analysis between economics and service of delivery. Validity of thus developed method is examined through numerical experiments.

Keywords: Global combinatorial optimization, Logistics, Vehicle routing, Hybrid method, Tabu search, Insertion method.

1. Introduction

To improve business efficiency for agile and global manufacturing, importance of logistics as a core of supply-chain management has been acknowledged increasingly. Noticing a similarity of hierarchy of decision level, which is popularly classified as long-term, middle-term and short term levels in production planning, this study provides a practical hybrid method for a hierarchical logistic network optimization belonging to a middle-term or a tactical level. Following this category, we classify traditional location problems (Melo, Nickel and Saldanha-da-Gama, 2009) into the long-term planning while vehicle routing problems (VRPs; Yeun, et al., 2008) into the short-term planning. Then the middle-term tries to consider a location problem and VRP at the same time.

Since thus defined problem is made of different kinds of NP-hard combinatorial optimization problems, we have developed a new hierarchical method so as to commonly evaluate transportation cost throughout the levels. For this purpose, we try to develop a modified insertion method that derives a near optimal solution for VRP on a basis of Ton-Kilo (load multiply distance) cost accounting instead of the conventional Kilo basis (only distance). It also includes a new mechanism that enables us to engage in multi-objective analysis between economics and service represented by the term associated with due dates of delivery. Thus developed solution method provides a unique integrated method amenable to practical applications at tactical level.

2. Problem Statements and Basic Idea for Solution

Let us consider a logistics network composed of plants, depots and customers as shown in Fig.1 (left). Then the present problem tries to optimize the selection of available depots, shuttle paths between plants and depots and circular routes covering the client customers of every depot. This problem is formulated as a mixed integer programming problem with an objective function composed of transportation costs, fixed changes of opening depots and serving vehicles, shipping cost at plants and handling cost at depots. As a tactical delivery condition that will link to a certain service, we consider a time window or an admissible delivery interval for every customer.

Conventionally, transportation costs of location problems are counted on a basis both of distance and load (Ton-Kilo base) while just on distance (Kilo base) in VRP. We can claim that the Ton-Kilo base is more realistic than Kilo base since the transportation cost depends not only distance but also weight of loads. Hence, in order to keep consistency of cost accounting for both problems, it makes sense to follow the Ton-Kilo base (Shimizu, 2011). Though thus formulated problem is not only consistent but also practical in cost accounting, such idea has never been considered in previous location-routing problems.

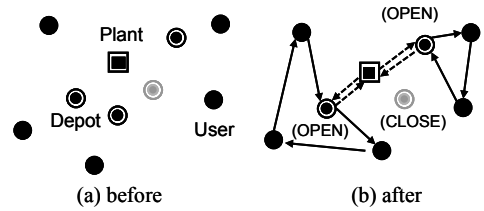

Fig. 1: Logistics network model in concern

Moreover, since the resulting problem refers to an integrated NP-hard problem, it becomes almost impossible to directly solve the mathematical programming model with real-world size. Then, we try to extend our two-level hybrid method of the location problem (Shimizu and Wada, 2004) as shown in Fig.2. The deployed idea is a three-level method and the third level VRP problem starts with searching the circular routes based on the solution of the second level location problem. Letting the customers served by the depot be its clients, we can cope with the multi-depot VRP problems practically. Below, key components of the proposed procedure will be described.

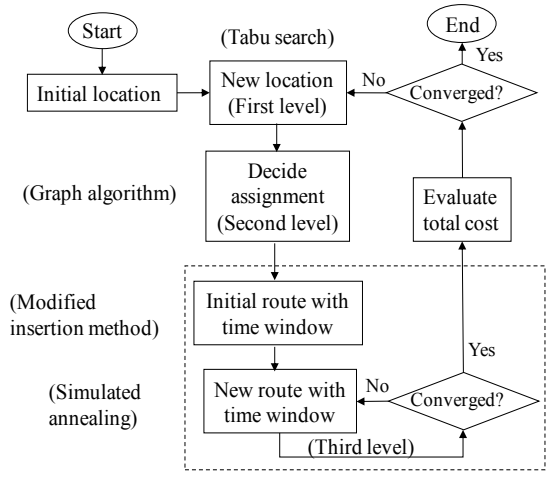

Fig. 2: Flow chart of the algorithm

3. Modified VRP Method with Time Window

3.1. Insertion Method for Ton-Kilo based VRP

Insertion method (Solomon, 1987) has been known as an effective approximation method of VRP together with saving method. For the present Ton-Kilo based case, we extended the original procedure as follows.

Step 1: Select randomly seed customers till the numbers of truck.

Step 2: Decide initial routes by round trip between the depot and each seed customer (Fig.3(a)).
Step 3: List the remaining customers in the descending order of $d_{0k}w_k$ for all k except for the seeds customers, and select one for the next step from the top of the list, in turn.
Step 4: Insert customer k between the node i and j for which Δ_{ij}^k $(=\Delta c_{ij}^k)$ becomes minimum for $\forall i, j$ as long as such insertion will not violate the admissible condition (upper bound for payload of truck) (Fig.3(b)).

$$\Delta c_{ij}^k = w_k(d_{01} + d_{12} + \cdots + d_{i-1,i} + d_{ik}) + (w_j + \cdots + w_n + q)(d_{ik} + d_{kj} - d_{ij}) \qquad (1)$$

where d_{ij}, w_k, q denote distance between nodes i and j (0 means depot), demand at customer k and weight of truck.
If customer k is selected, delete it from the list. Otherwise, go back to Step 3.
Step 5: Repeat the above procedures (Fig.3(c)) until the list becomes empty.
Step 6: Letting the above result as an initial guess, improve it based on simulated annealing (SA) until a certain convergence criterion has been satisfied.

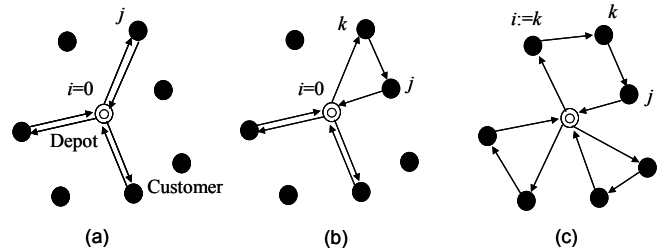

Fig.3: Scheme of insertion method

3.2. Time Window as for Describing Customer Service

To deliver products just on time is one of the essential customer service required for the today's tactical delivery. The idea is deployed as the time window in VRP. Accordingly, besides the payload requirement in Step 4, we must add the one whether the arrival time is on time or not as another admissible condition (hard condition) (See Fig.4). On the other hand, regarding the waiting time for the earlier delivery, we view it as a soft condition and modified the computation in Eq.(1) as Eq.(2).

$$\Delta_{ij}^k = \Delta c_{ij}^k + \alpha \cdot \Delta t_{ij}^k \qquad (2)$$

where Δt_{ij}^k denotes the increment of waiting time at node j when customer k is inserted between node i and j. Moreover, α is a weighting factor between the delivery cost and the waiting time. Generally speaking, shorter waiting time transport needs longer trip distance and spends more vehicles. Since those will increase the cost, and vice verse, there exists a trade-off between them. By solving the problem with a set of weighting factor α, we can engage in the trade-off analysis.

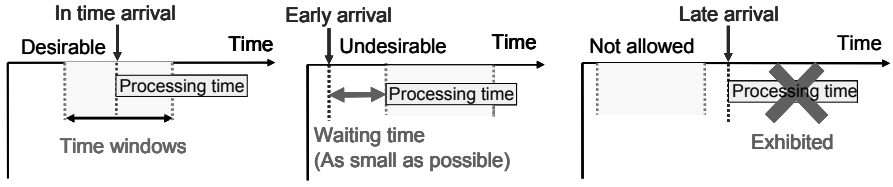

Fig.4: Scheme on time window condition

4. Numerical Experiment

We carried out a numerical experiment for the problem with 5 plants, 10 depots and 100 customers to illustrate the proposed procedure.

Table 1 show the system parameters employed here. Regarding the tuning parameters of SA, we set the initial temperature as 100 and annealing factor as 0.9. The algorithm is applied by using four methods for generating neighbors such as insert, swap, cross exchange and 2-opt operations (See Fig.5) under 50 outer iterations and 100 inner iterations.

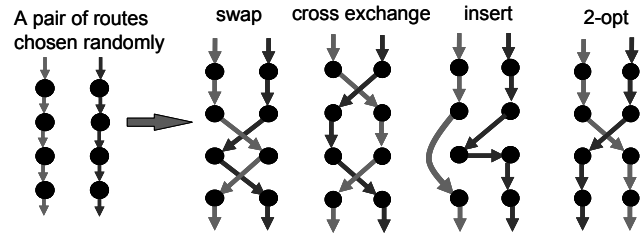

Fig.5: Employed operations for neighbourhoods generation

To validate the performance, we compared the results among three variants of application as shown in Fig.6. The first method is the expedient since none of the previous methods can cope with such a consistency that is considered here in cost accounting. Deriving the circular routes from the conventional or the Kilo-based method, we re-account the cost in terms of the Ton-Kilo basis and continue the solution procedure. Regarding the variants of the proposed approach, the method 2 skips the additional search at VRP by SA. Hence according to the ascending order, the accuracy of solution will increase.

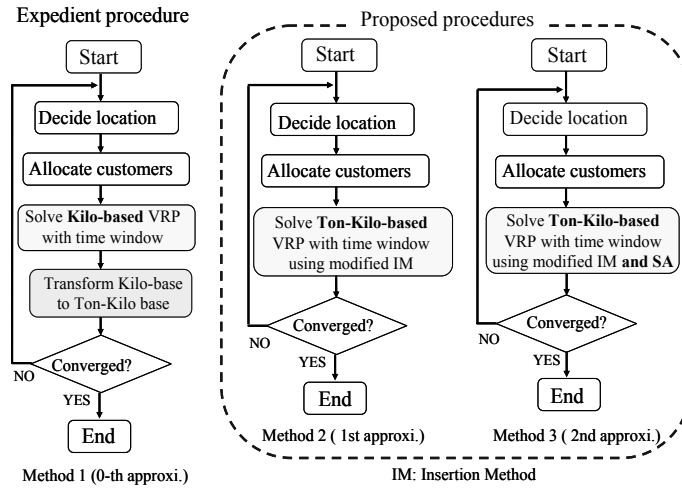

Fig.6: Comparison of applied procedures

In Fig.7, we compare the results by solving each problem with various values of α. Since making α larger means shorter waiting time is more preferred, each solution moves on in southeast direction. Eventually, we can observe the trade-off between the cost and the waiting time, and know the method 3 outperforms the others as expected since its Pareto front sticks out most to the direction of origin.

Table 1 Employed parameter values

Plant	Number = 5	Available supply	[0, 1000]
DC	Number = 10	Holding capacity	[250, 300]
Customer	Number = 100	Demand	[10, 20]
		Earliest time	[8:00, 16:00]
		Latest time	[9:00, 17:00]

Moreover, we can confirm the adequateness of the result if we compare the specified results shown in Fig.8. The route that weights the total cost (Fig.8(a)) will make the travel distance shorter or the cost cheaper while another extreme neglects such effort to reduce the total waiting time.

5. Conclusion

To improve business efficiency for agile and global manufacturing, this study has developed a practical method for a logistic network optimization at a tactical level. Thereat a Ton-Kilo based hybrid method for VRP with time window is proposed so that it can concern with multi-objective analysis between economics and service of delivery. Presenting a general formulation and giving its algorithm, we provided numerical experiments to examine the validity through comparison of multi-objective analysis among the variant applications. Future studies should be devoted to apply the method to real-world problems concerning with multi-objective optimization and parallel computing (Shimizu and Ikeda, 2010) to enhance the solution speed.

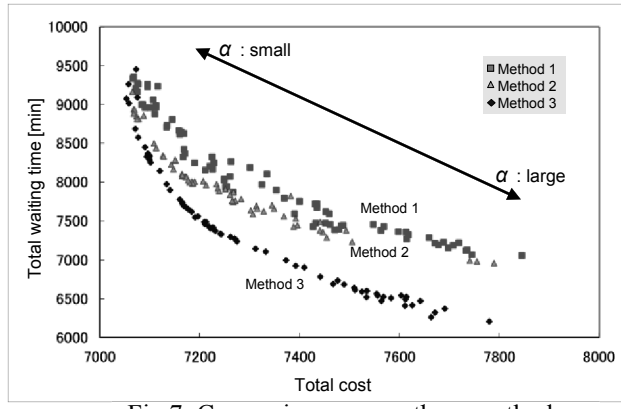

Fig.7: Comparison among three methods

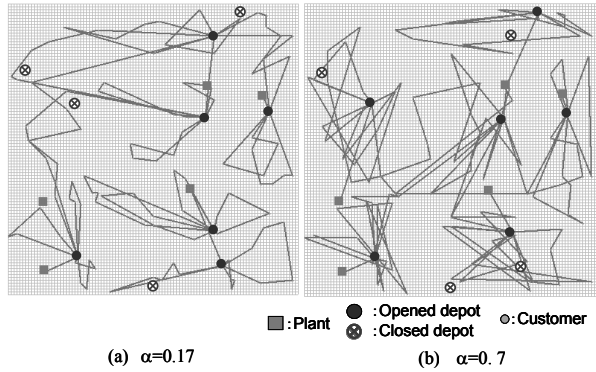

Fig.8: Comparison of routes for the specific α

References

M. T. Melo, S. Nickel and F. Saldanha-da-Gama, 2009, Facility location and supply chain management-A review, European Journal of Operational Research, 196, 401-412

Y. Shimizu, and T. Wada, 2004, Hybrid Tabu Search Approach for Hierarchical Logistics Optimization, Transactions of the Institute of Systems, Control and Information Engineers, 17, 6, 241-248

Y. Shimizu and M. Ikeda, 2010, A Parallel Hybrid Binary PSO for Capacitated Logistics Network Optimization, Journal of Advanced Mechanical Design, Systems, and Manufacturing, 4, 3, 616-626

Y. Shimizu, 2011, A Meta-heuristic approach for variants of VRP in terms of generalized saving method, Transactions of the Institute of Systems, Control and Information Engineers, 24, 12, 287-295

M. M. Solomon, 1987, Algorithms for the Vehicle Routing and Scheduling Problems with Time Window Constraints, Operations Research, 35, 254-265

L. C. Yeun, W. R. Ismail, K. Omar, and M. Zirour, 2008, Vehicle Routing Problem: Models and Solutions, Journal of Quality Measurement and Analysis, 4, 1, 205-218

I.A. Karimi and Rajagopalan Srinivasan (Editors), Proceedings of the 11th International Symposium on Process Systems Engineering, 15-19 July 2012, Singapore.

Application of bee colony algorithm for optimization of CCR reforming process

Majid Sa'idi, Navid Mostoufi , Rahmat Sotudeh-Gharebagh

Oil and Gas Processing Centre of Excellence, School of Chemical Engineering, College of Engineering, University of Tehran, PO Box 11155-4563, Tehran, Iran

Abstract

Swarm intelligence is a member of exploration calculations which is used in different industrial, commercial and engineering fields due to its wide range of applications, easy implementation and capability of reaching the absolute optimum. The bee colony optimization (BCO) algorithm is one of the most recent and efficient swarm intelligence based algorithms which simulates the foraging behavior of honey bee colonies. In this work, BCO algorithm is introduced and used for optimizing continuous catalytic regeneration (CCR) reforming process. The CCR optimization leads to non linear programming that contains non-linear quality constrains such as octane number and coke concentration on catalyst particles. The non-linear optimization problem with process constraints was used to improve the process performance and maximize unit profitability. The BCO algorithm performance was compared with genetic algorithm (GA) for optimizing the CCR process. Modeling and optimization results of the model were validated by industrial data.

Keywords: Bee Colony Optimization algorithm, Genetic algorithm, Kinetic model.

1. Introduction

Continuous catalytic regeneration (CCR) is one of the main refinery and petrochemical process for converting low-octane hydrocarbons to high-octane. According to modes of catalyst regeneration, reforming processes are generally classified into three types: semi-regenerative, cyclic and continuous regenerative process. Nowadays due to high catalyst activity, higher aromatic content and high hydrogen purity, applying of CCR units are very common respect to other type of reforming process.

In this work, Bee Colony Optimization (BCO) algorithm was used for optimizing operating conditions of the reactors of the CCR process. Artificial bees represent agents, which collaboratively solve complex combinatorial optimization problem. The artificial bee colony behaves to some extent similar and to some extent in a different way from bee colonies in nature. They explore through the search space looking for the feasible solutions. In order to discover superior solutions, artificial bees cooperate with each other and exchange information. Therefore, the BCO algorithm can be used as an effective optimization algorithm applying to multi objective engineering problems.

2. Bee Colony Optimization Algorithm

BCO is a bottom-up approach to modeling where special kinds of artificial agents are created by analogy with bees. High speed convergence, independent of the initial solutions, low number of algorithm parameters and accurate solution with lower evaluation of the objective function is characteristics of this algorithm. Colony of artificial bees collaboratively searches for the optimal solution of a given problem. Each

artificial bee generates a solution to the problem. In strategy of finding solution, there are two alternating phases, forward pass and backward pass, constituting single step in the BCO algorithm. Forward pass expresses the process of a forager bee leaving the beehive and flying towards a food source while backward pass denotes the process of a forager bee returning to the beehive and sharing the food source information with other forager bees (role change). In the algorithm, the length of each forward move is determined by NC which represents the number of solution components which is visited by each bee in each forward pass. In a forward movement, the forager bee may evaluate the profitability of every partial route during a foraging trip and in the backward pass upon a return to a hive from a food source, the forager bee must release the food (scheduling solution) and share the food source information with other forager bees. When the bees obtained new partial solutions, they start the backward pass and meet their nest mate in the hive. After evaluating all solutions and according to the quality of solutions, each bee decides whether to abandon its food source and search for another promising flower patch which was selected by her nest mate, continue to forage at the new food source or perform the waggle dance to recruit nest mates. According to above rule, in BCO algorithm, there are two types of bees, scout bee and follower bee. If the profitability of the solution found by the forager bee in the forward move is greater than the expectations of the bee colony, its role would be as a scout in this round and advertises its solution. If the profitability of the solution found by the forager bee in the last forward move is smaller than the expectations of the bee colony, its role would become a follower (Teodorovi, 2009; Davidovic et al. 2011).

For producing initial food source sites according to range of the boundaries of the parameters, the following random function was used:

$$x_{i,j} = x_j^{lowerbound} + rand(0,1)\left(x_j^{upperbound} - x_j^{lowerbound}\right) \tag{1}$$

where i =1... B and j =1... D. B and D are the number of bees and number of optimization parameters respectively. Roulette wheel method was used for producing the initial solutions of bees. As mentioned above, NC determines the number of constructive moves during a forward pass.

$$\text{Number of Forward Passes} = {}^{D}\!/_{NC} \tag{2}$$

Each bee is associated with only one food source site and produces a modification on the solution in its memory depending on its neighboring food source and local information according to:

$$x_{ij}^{'} = x_{ij} + \alpha_{ij}\left(x_{ij} - x_{kj}\right) \tag{3}$$

where k =1... D. In the above function, x_{ij} is a component of solution, x_{kj} is a neighbor of a component and x'_{ij} is a modified value for x_{ij}. If the modified value produced by this operation exceeds its boundaries, the component can be set to an acceptable value, the boundary itself in this work. After producing x'_{ij} within the boundaries, fitness value for a minimization problem can be assigned to the solution x'_{ij} by using equation (4). A greedy selection is applied between x_{ij} and x'_{ij}, then the better one is selected depending on fitness values of the complete solution.

$$fitness\ i = \begin{cases} \dfrac{1}{1+(object\ \ value)_i} & if\ \ (object\ \ value) \geq 0 \\ 1+abs\left[(object\ \ value)_i\right] & if\ \ (object\ \ value) < 0 \end{cases} \tag{4}$$

After completing all solution, the solutions with low fitness values must be identified by using equation (5) and final improvement will be done by Eq. (3) again.

$$p_i = \frac{fitness_{\max} - fitness_i}{fitness_{\max} - fitness_{\min}} \tag{5}$$

3. CCR process modeling

The most common feed to the catalytic reforming unit is the straight-run naphtha, distilled to obtain a narrower cut to be reformed. The most important reactions in the catalytic reforming are dehydrogenation, dehydrocyclization, isomerizatiom, hydrocracking, hydrodealkilation and catalyst deactivation. The hydrocarbon stream flows in the redial direction and the catalyst moves along the axial direction of the reactor. Consequently, conversion of hydrocarbons occurs in the radial direction while the catalyst becomes deactivated while moves down the reactor. Therefore, mass and heat balance equations for each reactor was written for a limited length of the reactor, L, in which the reaction rates ($r_{i,n}$) were assumed to be constant in axial direction (Ancheyta and Villafuerte, 2000).

$$\frac{dF_i}{dR} = (2\pi R\rho_b)\sum_{n=6}^{n=9}\sum_{j=1}^{12}\left(r_{j,n}\nu_{i,j}\right)L, \qquad i = 1\ to\ 26 \tag{6}$$

$$\frac{dT}{dR} = (2\pi R\rho_b)\frac{\sum_{n=6}^{n=9}\sum_{j=1}^{12}\left(-\Delta H_{j,n}r_{j,n}\right)}{\sum_{i=1}^{26}\left(F_i C_{p_i}\right)}L \tag{7}$$

R, ρ_b and $v_{i,j}$ are reactor radius, catalyst bed density and stoichiometic coefficient respectively. The effect of catalyst deactivation is simulated by defining catalyst deactivation factor (η_j).

$$r_j = \eta_j . r_j^0, \qquad 0 \leq \eta_j \leq 1 \tag{8}$$

$$\eta_j = \exp\left(-\alpha_j C_c\right) \tag{9}$$

$$r_c^0 = \frac{dC_c}{d\tau} = \left(k_p P_p + k_A P_A\right) p_{H_2}^{n_1} C_c^{n_2} e^{-k_c C_c} \tag{10}$$

In the above equations Cc is coking content on catalyst particles, n1 and n2 are constants and P_P, P_A and P_{H2} are paraffin, aromatic and hydrogen vapor pressures (Raeev, 2003; Froment, 2001). For parameter estimation the following objective function was minimized by the genetic algorithm and model validation is carried out by another set of industrial data.

$$\text{Objective function} = \sum_{k=1}^{26}\left[\frac{\left(x_{k,model} - x_{k,Ind}\right)}{x_{k,Ind}}\right]^2 + \sum_{m=1}^{4}\left[\frac{\left(T_{m,model} - T_{m,Ind}\right)}{T_{m,Ind}}\right]^2 \tag{11}$$

4. CCR process optimization

For process optimization, there are different viewpoints leading to different objective functions. In this work, the objective function is minimizing energy consumption per unit reformate production and inlet temperature of the reactors were decision variables. The objective function and mole flow rate of fuel consumption were defined as below:

$$F = \min\left[F_{fuel} \Big/ F_{reformate} \right] \tag{14}$$

$$F_{fuel} = \frac{q}{(Eff \times NHV)} \tag{15}$$

Furnace efficiency was considered to be 85% and the net heat value of fuel (NHV) was 40480 (kJ/kmol) in this case. Characterization and parameters of the BCO and the Genetic Algorithm (GA) considered in this work are given in Table 1.

Table1. BCO and GA characterizations

Algorithm	BCO	GA	
Algorithm Parameter Characteristic	B=100	Population=100	Random Selection
	D=4	Single Point Crossover = 0.8	Mutation and Elite units
	NC=4	Stochastic Uniform	Forward Migration
	Number of Evaluation<80000		

5. Results and discussion

Three sets of industrial data were used for determining kinetic model parameters and model validations. The modeling results are compared with an industrial CCR plant data in Table 2 in terms of outlet temperature of reactors. This table indicates that the modeling results are in appropriate agreement with the industrial plant data.

Table2. CCR process modeling results

	Model outlet Temp. (K)	Industrial outlet Temp. (K)	Error
Reactor 1	665.62	661.35	0.65%
Reactor 2	712.14	712.95	0.11%
Reactor 3	739.37	731.45	1.08%
Reactor 4	744.29	744.15	0.02%

Product mole Percent	Model's data	Industrial's data
Paraffins	12.16	11.89
Naphtenes	1.03	0.58
Aromatics	12.30	11.39
Light Components	9.99	9.32
Hydrogen	64.51	66.82

The BCO algorithm optimization results were compared with the values obtained by the GA. According to table 3, the optimum inlet temperature of reactor 1 is higher than the existing industrial value. In contrast, inlet temperature of the fourth reactor should be lower than the existing industrial value. Since the reaction in the first reactor is endothermic, higher reactor inlet temperature increases the rate of reactions. On the contrary, in the fourth reactor, due to occurrence of the exothermic reaction, lower reactor inlet temperature is required.

Table3. Energy function optimization results

	Plant Data	BCO	GA
Reactor1 inlet temperature (K)	776.55	784.3	784.42
Reactor2 inlet temperature (K)	774.25	769.87	788.16
Reactor3 inlet temperature (K)	781.25	764.87	772.31
Reactor4 inlet temperature (K)	781.15	773.67	771.34
RON	98.3	99.01	98.82
Reformate (kmol/hr)	943.97	965.41	949.92
Fuel consumption (kmol/hr)	1285	1159.8	1196.9
Fuel consumption/ Reformate(kmol/ kmol)	1.36	1.20	1.26

As indicated in Table 3, by using BCO and GA, the ratio of fuel consumption to reformate production decreases from 1.36 to 1.20 and 1.26, respectively, while the reformate production rate is increased. Figure 1 represents the performance of BCO and GA in energy optimization. The optimum value of the objective function in the BCO algorithm is reached faster and to a better value with respect to the GA.

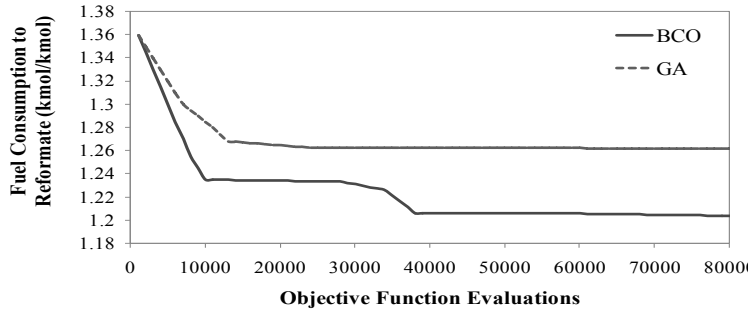

Figure1. CCR process optimization

6. Conclusion

The BCO algorithm was introduced as a new and powerful optimization algorithm for optimizing the chemical processes. The process considered in this work was CCR reforming process and its model is consisted a set of mathematical relations which simulates the kinetics of reforming process based on 48 reactions network and 26 pseudo components and implemented by catalyst deactivation derived from literature. In the process optimization, the fuel consumption in the furnaces per flow of reformate was minimized. Optimization was performed with both BCO and GA. It was shown that the BCO algorithm leads to a significant improvement of the optimum value with respect to the GA and it was found to be considerably faster than the GA. Finally the BCO algorithm can be used for optimizing the other chemical engineering problems.

References

D. Teodorovi, 2009, Bee colony optimization (BCO), Innovations in Swarm Intelligence, 39-60.

G. Froment, 2001, Modeling of catalyst deactivation, APPL CATAL A-GEN. 212, 117-128.

J. Ancheyta, E. Villafuerte, 2000, Kinetic modeling of naphtha catalytic reforming reactions, Energy Fuels. 14, 1032-1037.

S. Raeev, 2003,Thermal and catalytic processes in petroleum refining, marcel Dekker, New York.

T. Davidovic, D. Ramljak, M. Selmic, D. Teodorovic, 2011, Bee colony optimization for the p-center problem, COMPUT OPER RES, 38, 1367-1376.

I.A. Karimi and Rajagopalan Srinivasan (Editors), Proceedings of the 11th International Symposium on Process Systems Engineering, 15-19 July 2012, Singapore.

A scatter search algorithm for the twin roll caster scheduling problem in aluminum industry

Qingxin Guo, Lixin Tang[a,b]

[a]*The Logistics Institute, Northeastern University, Shenyang, 110819, China*
[b]*Liaoning Key Laboratory of Manufacturing System and Logistics, Northeastern University, Shenyang, 110819, China*

Abstract

This paper investigates the scheduling problem in the aluminum twin roll casting process. The ultimate goal is to determine the sequence of aluminum coils considering the sequence-dependent setup cost caused by alloy, width, thickness of the adjacent coils and the orders' specifications. A mixed integer linear programming model considers both the makespan and total tardiness is proposed to describe the problem. Since this problem and the mathematical model are very complex, a scatter search based heuristic is designed to solve the problem. Computational experiments show that the proposed method could get better solutions than the CPLEX software package.

Keywords: twin roll caster scheduling, sequence-dependent setup, makespan and total tardiness, scatter search

1. Introduction

The twin roll caster is a common unit of aluminum production process. In twin roll caster, molten aluminum alloy is fed onto water-cooled rolls, where it solidifies and is then rolled into aluminum coils with various widths and thicknesses. These coils are then rolled to the desired dimensions and properties through cold milling, annealing, surface processing and cutting operations according the customers' orders.

Strip casting using the twin roll caster has many advantages. First of all, the twin roll caster is a very simple process with low equipment cost and low space requirements. Also, the energy consumption of twin roll caster is only 40% of conventional casting method. However, the twin roll caster is not suitable for some aluminum alloys with wide freezing range. Another drawback of the technique is its low productivity due to the low casting speed of the roll caster. So managers are most concerned about how to better preparation of the alloy composition and improve the productivity.

The twin roll caster scheduling problem can be described as follows. There are N orders to be produced by a twin roll caster. The orders have different alloy compositions, due dates, widths, thickness and weights. The task is to decide the scheduling of the orders and the objective is to minimize both the makespan and total tardiness. Because the processing time of an order is only depended on its weight, so the makespan is mainly related with the setup times between two consecutive orders.

The setup time for twin roll caster includes the furnace cleaning and shutdown to adjust the export flow of the shaper. The furnace cleaning may be required while there is an alloy change between two consecutive orders. Specifically, the cleaning is not required to process an order with more composite alloy after an order with pure alloy. But the furnace must be cleaned thoroughly if an order with pure alloy is to be cast after an order with composite alloy. A significant shutdown must be required to adjust the export flow of the shaper if the width or thickness change occurs between two

consecutive orders. In general, it is expected that the cleaning and shutdown occur infrequently since they are both costly and time consuming.

There has been less research on scheduling related to aluminum production process. Bowers et al (1995) proposed a two-phase model for scheduling the aluminum ingot casting process to reduce ingot misapplication/import and maintains low inventory levels. Gravel et al (2002) proposed an ant colony optimization algorithm for the scheduling problem in an aluminum casting center. Prasad et al (2006) present a mixed-integer linear programming model for the optimization of aluminum smelter casthouse operations. Ladurantaye et al (2007) studied the integrated homogenizing furnaces and the mill scheduling problem in aluminum hot rolling mill. Duman et al (2008) presented a mathematical formulation for scheduling casting lines jobs to minimize setup time on production lines for a given time period while balancing workload between production lines to accommodate potential new orders.

The single machine scheduling problem has been extensively studied, but the setup times in our problem are more sophisticated and we consider both makespan and total tardiness in the objective function. The motivation of this paper is to study single machine scheduling problem deeply, the more important is to solve actual aluminum twin roll caster scheduling problem that did not find research works. The remainder of the paper is organized as follows: Section 2 describes the mix-integer linear programming model is formulated. A scatter search algorithm is proposed in Section 3. Section 4 reports the experimental results of the scatter search algorithm compared with the CPLEX solver. Finally, conclusions are stated in Section 5.

2. Mathematical model

We formulate the scheduling problem for the twin roll caster as a mixed-integer linear programming model as follows:

Parameters are described as follows, the set of orders is N (N=$\{0,1,\ldots,n\}$), for each order i or j ($i, j \in N$), the release time of order i is r_i, the alloy composition of the molten aluminum in order i is p_i, the width of order i is w_i, the thickness of order i is g_i, the due date of order i is d_i, the weight of order i is c_i, the processing time of unit weight order is t, the time of hot cleaning is t_w, the adjustment time for the width change is t_c ($t_c < t_w$).

Auxiliary variable

$$P_{ij} = \begin{cases} 1, & \text{if } p_i \neq p_j \\ 0, & \text{otherwise} \end{cases} \qquad W_{ij} = \begin{cases} 2, & (w_i \neq w_j) \wedge (g_i \neq g_j) \\ 1, & (w_i \neq w_j) \vee (g_i \neq g_j) \\ 0, & (w_i = w_j) \wedge (g_i = g_j) \end{cases}$$

Decision variables

$$x_{ij} = \begin{cases} 1, & \text{if order } j \text{ is produced directly after order } i \\ 0, & \text{otherwise} \end{cases}$$

s_i The start time of order i.
e_i The completion time of order i.
$C_{\max}$ makespan.
T_i The tardiness time of order i.

Let λ_1, $\lambda_2 \in [0,1]$ be two preset constants such that $\lambda_1+\lambda_2=1$. Using the above symbols, the model is constructed as follows:

$$\text{Min} \quad \lambda_1 C_{\max} + \lambda_2 \sum_i T_i \tag{1}$$

$$\text{s.t.} \quad \sum_{i=0}^{n} x_{ij} = 1 \qquad j = 0,\ldots,n \tag{2}$$

$$\sum_{j=0}^{n} x_{ij} = 1 \qquad i = 0,\ldots,n \tag{3}$$

$$e_i = s_i + c_i t_i \qquad i = 0,\ldots,n \tag{4}$$

$$T_i \geq e_i - d_i \qquad i = 0,\ldots,n \tag{5}$$

$$s_j = \max\{r_j, e_i\} + \sum_{i=1}^{n} \max\{P_{ij} t_w, W_{ij} t_c\} \cdot x_{ij} \qquad i = 0,\ldots,n \qquad j = 0,\ldots,n \tag{6}$$

$$\mathrm{C}_{\max} \geq e_i \qquad i = 0,\ldots,n \tag{7}$$

$$x_{ij} \in \{0,1\} \qquad i = 0,\ldots,n \qquad j = 0,\ldots,n \tag{8}$$

$$s_i \geq r_i, e_i \geq 0 \qquad i = 0,\ldots,n \tag{9}$$

In this model, objective function (1) consists of two components, the first one is the makespan and the second one is the total tardiness. Constraints (2) ensure that exactly one order is produced before order *j*. Constraints (3) guarantee that exactly one order is produced after order *i*. Constraints (4) mean that the completion time of each batch is equal to its start time plus its processing time. Constraints (5) represent the tardiness of order *i*. Constraints (6) guarantee that two orders can not be produced at the same time; the order *j* can be produced only after its release time is reached and its previous order *i* is completed, the starting time of order *j* equals to the maximum time between its release time and the completion time of order *i* plus the possible wash furnace (width-modulated) time. Constraint (7) detects the maximum completion time. Constraint (8) and (9) impose the binary and nonnegative restrictions on the decision variables.

3. The proposed scatter search algorithm

Scatter search (SS) is an evolutionary method in which solutions are intelligently combined to yield better solutions. Our proposed SS is described in the following discussion.

3.1. Diversification generation method

To guarantee a diversified population of solutions, we use three types of heuristic strategies to construct a subset P of p initial solutions. The first heuristic randomly selects orders from the orders set until it is empty. The orders are sorted as the selection sequence. The second one randomly selects an order for the first position, and then the order with the smallest difference for the second position is chosen from the remaining order set. This process is repeated until the set is empty. And the third one is based on the earliest due-date (EDD) rule which generates one trial solution.

3.2. Improvement method

In scatter search, an improvement method is introduced to transform a trial solution into one or more enhanced trial solutions. In this paper, we use a local search that is a combination of the insert and swap neighborhood. The insert move means removing an order from current position and inserting it into another position. The swap move of two orders means swapping two orders between two positions.

3.3. Reference set update method

The scatter search algorithm builds a reference set (*Refset* for short) of solutions that containing high evaluation to generate new solutions to replace less promising solutions

in the implementation process. A straightforward way to create a reference set *Refset* consists of selecting the two subsets, the first set with high quality solutions and the second set with diverse solutions by selecting the solution that differs by the greatest amount from the current reference set.

As a diversity measure we define $div(s_1, s_2)$ to be the diversification value between two solutions s_1 and s_2 and calculate the value of $div(s_1, s_2)$ as the number of edges in scheduling sequence by which the two solutions differ from each other. Based on the above diversity measure formula, the candidate solutions are included in $Refset_2$ according to the *Maxmin* criterion that maximizes the minimum distance of each candidate solution to all the solutions currently in the reference set.

3.4. Subset generation method

The subset generation method is to operate on the reference set, to produce a subset of its solutions as a basis for creating combined solutions. The most common subset generation consists of creating a list of all pairs (i.e., all 2-element subsets) of reference solutions for which at least one of the solutions is new. A reference solution is new means that it hasn't been used by the combination method. In our work, all possible 2-element subsets are adopted.

3.5. Solution Combination Method

The solution combination method generates one or more new trial solutions for every subset generated in the previous step. In this paper, we adopt directly the first and the third combination methods from the Campos' (2005) ten and also a crossover operator similar to the first method. These methods generate one new trial solution from the combination of two reference solutions.

3.6. The Stopping Criteria

While the iteration of the best solution can not be improved reaches the given maximum consecutive iterations or the computing time reaches the given maximum time, the whole scatter search terminates.

4. Computational experiments

To test the performance of the model and algorithm described in Sections 2 and 3, computational experiments have been conducted on randomly generated problem instances. For the test instances, the parameters are given as follows: the number of orders is chosen from {5, 6, 7, 8, 9, 10, 11, 12, 13, 14, 15, 16, 17, 18, 19}, p_i is randomly generated from uniform distributions of which range was set to be [99.53%, 99.99%]. The range of w_i, g_i and c_i are set to be [900mm, 1100mm], [6mm, 10mm] and [1.25t, 1.55t] by the uniform distributions, respectively. The range of r_i and d_i are set according to the number of orders and the total processing time of these orders. The parameters t, t_w and t_c are taken as 0.2h, 2h and 1h, respectively.

The testing results of scatter search algorithm and CPLEX software are given in Table 1. The first column is the number index of problem instance; the second column is the number of orders; the third column is the objective function value of CPLEX; the fourth column is the objective function value of scatter search; the fifth column is the computation time of CPLEX and the sixth column is the computation time of scatter search. Note that the values of the table are the ratios between the scatter search and CPLEX (taking the values of CPLEX as the divisor).

From table 1, it can be seen that both scatter search and CPLEX can obtain optimal solutions with short computation time for small size instances. As the problem size increases, the computation time of CPLEX increases rapidly and the results of CPLEX

are deteriorated. The scatter search can also obtain satisfactory solutions for large size instances with reasonable computation time.

Table 1 Comparison results between scatter search and CPLEX

Instance	n	Computation results		Computation time (s)	
		CPLEX	Scatter search	CPLEX	Scatter search
1	5	1.0000	1.0000	0.500	1.719
2	6	1.0000	1.0000	1.000	1.547
3	7	1.0000	1.0000	1.760	1.672
4	8	1.0000	1.0000	15.320	1.875
5	9	1.0000	1.0000	34.110	2.062
6	10	1.0000	1.0000	31.890	2.421
7	11	1.0000	0.9968	23.560	2.593
8	12	1.0000	0.9437	25.860	2.781
9	13	1.0000	0.9122	48.360	2.984
10	14	1.0000	0.7620	48.120	3.187
11	15	1.0000	0.7930	54.040	3.562
12	16	1.0000	0.7329	1000	3.797
13	17	1.0000	0.6470	1000	4.125
14	18	1.0000	0.6961	1000	4.407
15	19	1.0000	0.6565	1000	4.687

5. Conclusions

In this paper, we proposed a mixed integer linear programming model for the scheduling problem in the aluminum twin roll casting process. The model considers the actual production constraints as well as both the makespan and total tardiness as the objective function. A scatter search based heuristic is implemented to solve the problem. Computational experiments show that the proposed method outperforms the CPLEX software package.

Acknowledgements

This research is partly supported by State Key Program of National Natural Science Foundation of China (71032004), the Fundamental Research Funds for the Central Universities (N090104002, N100704002)

References

M.R. Bowers, L.A. Kaplan and T.L.Hooker, 1995, A two-phase model for planning the production of aluminum ingot, European Journal of Operational Research, 81(1): 105-114.

M. Gravel, W.L. Price and C. Gaqné, 2002, Scheduling continuous casting of aluminum using a multiple objective ant colony optimization metaheuristic, European Journal of Operational Research, 143(1): 218-229.

P. Prasad, C.T. Maravelias and J. Kelly, 2006, Optimization of aluminum smelter casthouse operations, Industrial & Engineering Chemistry Research, 45: 7603-7617.

D.Ladurantaye, M. Gendreau and J.Y. Potvin, 2007, Scheduling a hot rolling mill, Journal of the Operational Research Society, 58: 288-300.

Duman, E., Yildirim, M.B. and Alkaya, A.F., 2008, Scheduling continuous aluminium casting lines. International Journal of Production Research, 46(20): 5701-5718.

V. Campos, M. Laguna and R. Martı′, 2005, Context-independent scatter and tabu search for permutation problems, INFORMS Journal on Computing, 17(1): 111-122.

I.A. Karimi and Rajagopalan Srinivasan (Editors), Proceedings of the 11th International Symposium on Process Systems Engineering, 15-19 July 2012, Singapore.

Hydrogen Network Integration with both Pressure and Impurity Constraints

Qiao Zhang,[a] Xiao Feng[b*]

[a]*Department of Chemical Engineering, Xi'an Jiaotong University, Xi'an 710049, China*
[b]*College of Chemical Engineering, China University of Petroleum, Beijing 102249, China*

Abstract

For refineries, the minimization of fresh hydrogen consumption is significant to minimize operation cost and maximize profit. To get such effect, in addition to the flow rate and purity of hydrogen sources and sinks, the main constraints are pressure and impurities based on the operation requirements. Based on the existing hydrogen network, by introducing pressure cascade use and impurity diverted path corresponding to pressure and impurity constraints, this paper presents an experiential method for hydrogen network optimization. As complement to integration methodology, the reduction of fresh hydrogen is reliable and attainable. Finally, a refinery case study is used to illustrate the method.

Keywords: hydrogen network, optimization, pressure cascade use, impurity diverted path

1. Introduction

Hydrogen is an expensive utility to oil refineries. In recent years, increasing strictly environmental regulations and the change of crude oil to high-sulfur and/or heavier oil both require increasing processing depth of hydrogen-consuming crafts, resulting in huge deficiency of fresh hydrogen. Thus, effective use and conservation of fresh hydrogen is significant to the profit of petrochemical industries.

For the minimization of fresh hydrogen, process integration is an effective way in refinery hydrogen network optimization. Pinch-based conceptual methods and mathematical programming have been widely used to analyze and optimize the whole network performance. Pinch-based methods have clear concepts and insights to the optimization. Alves and Towler(2002) put forward hydrogen surplus diagram to identify the pinch and minimum fresh hydrogen demand. Successively, material recovery pinch diagram(El-Halwagi et al., 2003; Zhao et al., 2006), and other visual solutions(Agrawal and Shenoy, 2006; Bandyopadhyay, 2006; Foo et al., 2006; Zhang et al., 2011) are also developed to address the fresh hydrogen target and/or network design. Compared to pinch-based methods, mathematical programming is able to deal with complex hydrogen systems and various constraints. Hallale and Liu(2001) put forward a fundamental superstructure with flow rate, hydrogen purity, pressure and purifiers, as well as economic consideration. After this work, Van den Heever and Grossmann(2003), Liu and Zhang(2004), Khajehpour et al.(2009), and Liao et al.(2011a,b) set up respective superstructures and mathematical models, in which important factors, such as purifiers selection, reactive scheduling, production planning, utility system, costs etc., are taken into consideration.

* Corresponding author. Tel.:+86 10 89703991. E-mail address: xfeng@cup.edu.cn.

For hydrogen network retrofit, experiential observation may be very important to give effective guideline in a simple way. In this paper, an experiential method based on observation of pressure cascade use and impurity diverted path is proposed, so as to discover possible direct reuse of hydrogen sources, for pressure and impurity are two main factors influencing on the hydrogen network optimization. Its solution is reliable and easily to be determined.

2. The Method with Pressure Cascade Use and Impurity Diverted Path

2.1. Background

Figure 1 is a typical hydrogen network. In this flow sheet, the X coordinate is the increasing impurity purity direction, and the Y coordinate is the lifting pressure direction. Hence, streams locate at left top position are the highest quality streams both in hydrogen purity and pressure. Conversely, streams locate at the right bottom is the lowest quality streams. Firstly, the fresh hydrogen is with low pressure and high hydrogen purity, so it locates at the left bottom. When pressure is lifted to the required high levels by compressors 1, 2 and 3, it rises to respective high positions (sources 1, 2 and 3). Such high pressure gradually drops as the fresh hydrogen go through the reactors (sinks 1, 2 and 3), separators (1, 2 and 3), purification unit etc. Meanwhile, streams with high hydrogen purity are devalued to low hydrogen purity, accompanied by the stepwise accumulation of impurities, as internal sources (1 and 2) and tail gas generated. In order to reuse the considerable internal sources, a purification unit is introduced to concentrate hydrogen and remove harmful impurities. The purified product is near to fresh hydrogen in quality and returned to the left bottom. For sinks 1, 2 or 3, the thick solid lines with arrows compose such a cycle.

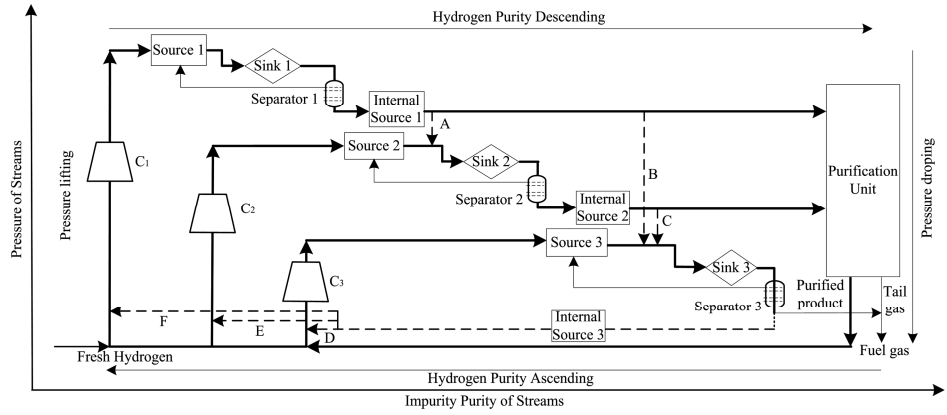

Figure 1. A typical flow sheet of refinery hydrogen network

2.2. Pressure cascade use and impurity diverted path

2.2.1. Pressure cascade use

From Figure 1, internal sources 1 and 2 have high pressure, but they are sent to purification unit. Because the pressure of the purified product is dropped in purification process, it should be lifted again. Such depressurization and repressurization processes result in waste of compressing work. From this point, the sources with high pressure should be directly reused at maximum extent.

Pressure cascade use means that each high pressure internal source is possible to supply hydrogen for all sinks with lower pressures. For an existing hydrogen network, it is probably that some such cascade uses are not included, and should be discovered.

For example, internal source 1 has higher pressure than sinks 2 and 3, and internal source 2 has higher pressure than sink 3. Thus, the three dotted arrows A, B and C are all possible pressure cascade uses which are not included in the hydrogen network. After such complement, the possible pressure cascade uses are complete, and feasible ones can be determined according to practice consideration.

2.2.2. Impurity diverted path

Purification causes not only pressure drop, but also hydrogen loss in terms of tail gas, which is discharged to the fuel gas system. Hence, unnecessary purification should be avoided.

Reasonable mix can increase direct reuse. Impurity diverted path is a way to mix internal sources with each other or fresh hydrogen, which has low purity in any impurity. In this way, internal sources with high impurity purities can be diluted by other sources with low purities of corresponding impurities, so as to make the sources with high impurity purities feasible for direct reuse.

For example, if part of internal source 1 can be mixed with source 2 or source 3 to dilute some impurities, then such part of internal source 1 can be directly sent to sink 2 instead of sent to purification reuse. Similarly, the mixture of internal source 2 and source 3 sent to sink 3 could also be such case.

In addition, there are still some other internal sources, which cannot be directly sent to sinks after mix because of low pressure, such as internal source 3. As there is no other sinks with lower pressure than that of internal source 3, it can only be mixed with fresh hydrogen and then get direct reuse after pressurized by compressors.

Thus, A, B, C, D, E and F are all possible impurity diverted path and feasible ones can be determined according to practice consideration.

With both pressure cascade use and impurity diverted path, the possible direct reuse of hydrogen sources can be taken into consideration, and the fresh hydrogen consumption can be reduced.

3. Case study

This is a refinery case, and the current flow sheet and network is shown in Figure 2(a). The data are extracted and shown in Table 1. This hydrogen network contains eight sources and three sinks, three impurities, H_2S, N and C, six compressors. SR1 is the fresh hydrogen, and its current minimum flow rate is 15385 Nm^3/h.

For this case, all impurity purities of sources are given, and the limiting impurity purities of sinks are also listed. SR3 has high pressure with high purity of impurity C, and thus 3000 Nm^3/h is sent to purification unit. The purified product is suitable to SK3 in pressure and so allocated to it. Although the pressure of SR7 is high enough to direct reuse, the impurity purities restricts the reuse.

By observation, SR3 to SK2 and SR4 to SK3 are two feasible pressure cascade use. For impurity diverted path, the mixture of SR2 and SR3 to supply for sink 2, the mixture of SR3 and SR4 to supply for sink 3, and the mixture of SR6 and fresh hydrogen to supply for all three sinks, are all possible cases.

With the observed pressure cascade use and impurity diverted path, after calculation for flow rate, hydrogen purity and impurity purities requirements, the feed of 3000 Nm^3/h to purification unit and SR6 can both be directly reused completely, and the membrane separation can be eliminated.

After the retrofit, the high quality internal source of 3000 Nm^3/h, 7.0MPa is sent to sink 2 instead of sent to membrane separation, part of SR4 (3000 Nm^3/h, 4.5MPa) is sent to

sink 3, and SR6 is intercepted to three streams, which are separately mixed with fresh hydrogen and then directly reused after pressurization by compressors.
After the improvement of experiential guidelines, the minimum fresh hydrogen demand is reduced from 15385 Nm^3/h to 14500 Nm^3/h.

Table 1. The Current Data of a Refinery Case

Streams	Flow rate (Nm^3/h)	Purity (mol%)	H_2S (ppm)	N (ppm)	C (ppm)	Pressure (Mpa)
Sources (SR1 is the fresh hydrogen)						
SR1	15385	99.9	0	0	0	2.1
SR2	2615	95	2	0	10	2.5
SR3	27000	92.0	10	0	60	7.0
SR4	10000	90.0	30	0	30	4.5
SR5	6000	88.0	70	50	35	2.2
SR6	500	80.0	100	150	100	2.1
SR7	385	71.7	143	0	400	5.0
SR8	1000	60.0	1000	2000	3000	0.5
Sinks						
SK1	36000	≧93.0	≦15	/	/	17.5
SK2	15000	≧90.0	/	/	≦30	6.8
SK3	10000	≧88.0	/	≦50	/	3.8
(/ no requirement)						

The modified flow sheet is shown in Figure 2(b), in which the dotted line shows the difference to Figure 2(a). After modification, 885 Nm^3/h fresh hydrogen, taking up 5.75% of the current demand, can be reduced; only some pipelines and streams interception are needed; membrane separation, an expensive purifier, is eliminated; the inlet flow rate of compressors does not increase. From the retrofit of the network, it can obviously be seen that the improvements are very cost-efficient.

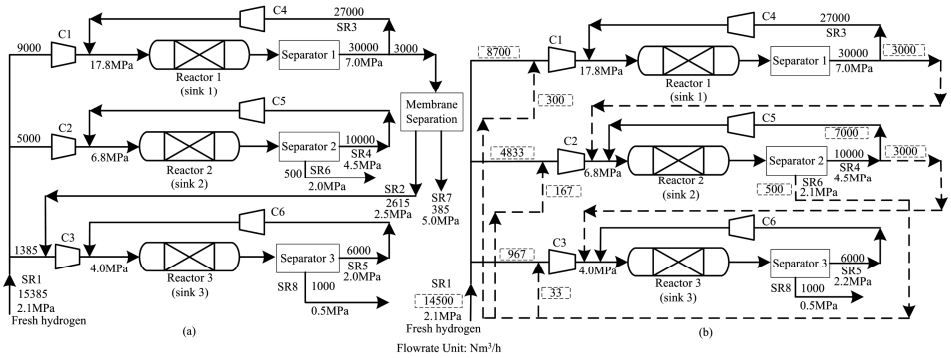

Figure 2. The optimization results. (a) The current network; (b) The modified network.

4. Conclusion

This paper presents an experiential approach to reduce the fresh hydrogen consumption of hydrogen networks with both pressure and impurity constraints. Based on a refinery hydrogen network, experiential rules of pressure cascade use and impurity diverted path are developed to give a simple way to deal with hydrogen network synthesis.

This method is for hydrogen network retrofit. The modification involves the placement of only additional pipelines and the elimination of expensive membrane separation. The reduction of fresh hydrogen is 5.75% of current demand, and thereby the retrofit is very cost-efficient. Although the method is experiential and based on a refinery case, it is more practical, and can probably be extended to a systematic methodology in future work.

Acknowledgement

The financial support for this research provided by the National Basic Research Program of China (973 Program: 2012CB720500) and the National Natural Science Foundation of China under Grant 20936004 is gratefully acknowledged.

References

Agrawal V., Shenoy U.V., 2006, Unified conceptual approach to targeting and design of water and hydrogen networks. *AIChE Journal*, 52 (3), 1071-1082.

Alves J.J., Towler G.P., 2002, Analysis of refinery hydrogen distribution systems, *Industrial & Engineering Chemistry Research*, 41 (23), 5759-5769.

Bandyopadhyay S. Source composite curve for waste reduction. *Chemical Engineering Journal.* 2006;125(2):99-110.

El-Halwagi M.M., Gabriel F., Harell D., 2003, Rigorous graphical targeting for resource conservation via material recycle/reuse networks, *Industrial & Engineering Chemistry Research*, 42 (19), 4319-4328.

Foo D.C.Y., Kazantzi V., El-Halwagi M.M., Manan Z.A., 2006, Surplus diagram and cascade analysis technique for targeting property-based material reuse network, *Chemical Engineering Science*, 61 (8), 2626-2642.

Hallale N., Liu F., 2001, Refinery hydrogen management for clean fuels production. *Advances in Environmental Research*, 6 (1), 81-98.

Khajehpour M., Farhadi F., Pishvaie M.R., 2009, Reduced superstructure solution of MINLP problem in refinery hydrogen management, *International Journal of Hydrogen Energy*, 34 (22), 9233-9238.

Liao Z.W., Rong G., Wang J.D., Yang Y.R., 2011, Rigorous algorithmic targeting methods for hydrogen networks—Part I: Systems with nohydrogen purification, *Chemical Engineering Science*, 66 (5), 813-820.

Liao Z.W., Rong G., Wang J.D., Yang Y.R., 2011, Rigorous algorithmic targeting methods for hydrogen networks—Part II: Systems with one hydrogen purification unit, *Chemical Engineering Science*, 66 (5), 821-833.

Liu F., Zhang N., 2004, Strategy of purifier selection and integration in hydrogen networks, *Chemical Engineering Research & Design*, 82 (A10), 1315-1330.

Van den Heever S., Grossmann I., 2003, A strategy for the integration of production planning and reactive scheduling in the optimization of a hydrogen supply network, *Computers & Chemical Engineering*, 27 (12), 1813-1839.

Zhang Q., Feng X., Liu G.L., Chu K.H., 2011, A novel graphical method for the integration of hydrogen distribution systems with purification reuse, *Chemical Engineering Science,* 66 (4), 797-809.

Zhao Z.H., Liu G.L., Feng X., 2006, New graphical method for the integration of hydrogen distribution systems, *Industrial & Engineering Chemistry Research*, 45 (19), 6512-6517.

I.A. Karimi and Rajagopalan Srinivasan (Editors), Proceedings of the 11th International Symposium on Process Systems Engineering, 15-19 July 2012, Singapore.

Modeling and Solving Batch Scheduling Problems with Various Storage Policies and Operational Policies using Timed Automata

Christian Schoppmeyer [a], Subanatarajan Subbiah [a], Sebastian Engell [a]

[a]*Process Dynamics and Operations Group, Department of Biochemical and Chemical Engineering, Technische Universität Dortmund, 44221 Dortmund, Germany*

Abstract

In this contribution we present the conceptual ideas on modeling deterministic batch scheduling problems with various storage policies and operational policies using timed automata (TA) and on solving them using reachability analysis for TA. We propose a new reduction technique to improve the efficiency of the search algorithm for scheduling problems with non-intermediate storage policy. The performance of the proposed modeling approach and the reduction technique is evaluated by investigating it on benchmark instances from OR literature and on typical batch scheduling problems. The comparative study shows that the proposed modeling approach handles the crucial aspects of the storage policies and operational policies in straightforward way and the new reduction technique increases the overall performance of the solution algorithm.

Keywords: Batch scheduling, storage policies, operational policies, timed automata.

1. Introduction

In multi-product batch processing plants, efficient scheduling of the scarce resources can have a substantial impact on the economic performance of the plant. The availability of storage units and their functional limitations in the plant can have a major impact on the feasibility of schedules and therefore they should be modeled precisely. The state-of-the-art approach to address this type of scheduling problems is to model them as MILP or MINLP and to solve them using solution techniques such as branch-and-bound or cutting-plane methods. The authors in Ferrer-Nadal et al. (2008) demonstrated that several MILP models which either simplify or neglect the storage policies or material transfer times compromise on the feasibility of the schedules and proposed a MILP formulation to address the problem of handling various storage policies. However the efficiency of the solution approach was not quantitatively illustrated.

An alternative approach to handle batch scheduling problems is to model them using timed automata (TA) and to apply the technique of reachability analysis for TA to compute schedules, see Subbiah et al. (2011a). Model building using TA is relatively straightforward due to the graphical nature of the formalism and the modular definition of the elements of the problem. In this contribution, the modeling of scheduling problems with various storage policies and operational policies as TA is discussed, and a new reduction technique is introduced to improve the efficiency of the search algorithm for problems with non-intermediate storage policy.

2. Timed Automata Based Modeling

Fig 1. shows a modular TA model for an example process where two products A and B have to be produced using processing units U_1 and U_2. The operational sequence and the

durations for product A are $(op_1,U_1,5)$ followed by $(op_2,U_2,7)$. Similarly, for product B they are $(op_3,U_2,6)$ followed by $(op_4,U_1,3)$. Details on the modeling procedure and on the solution algorithm using reachability analysis can be found in Subbiah et al. (2011a, 2011b).

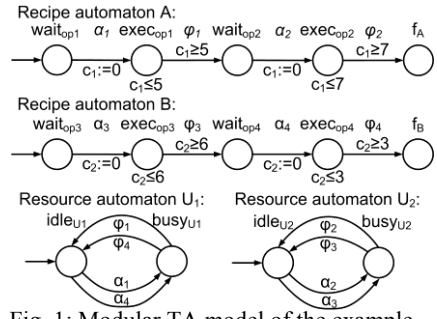

Fig. 1: Modular TA model of the example problem

3. Modeling Storage Policies

Based on the presence of storage units between the process stages the storage policy can be classified into two main categories namely "With intermediate storage (WIS)" and "Non-intermediate storage (NIS)". The WIS policy can be further classified into "Dedicated intermediate storage (DIS)" where the storage unit is allowed to store only one type of material and "Common intermediate storage (CIS)" where the storage unit is allowed to store more than one material. Both the DIS and the CIS are further classified based on their storage capacities.

3.1. Modeling the dedicated-intermediate storage policy

The idea of how to model the dedicate-intermediate storage (DIS) policy is explained by extending the example process by a dedicated storage unit $U_{str\text{-}A}$ to store the intermediate material Int_A of the product A. The modular TA model for the example problem is extended by creating a separate *storage automaton* for the storage unit. The TA for the storage unit $U_{str\text{-}A}$ is shown in Fig. 2. The storage automaton for unit $U_{str\text{-}A}$ consists of a location *empty* $U_{str\text{-}A}$ representing that the storage unit is empty and a location *filled* $U_{str\text{-}A}$ representing that the storage unit is filled with the material Int_A. Draining the material Int_A to the storage unit after finishing the operation op_1 in the upstream unit U_1 is represented by a transition from the location *empty* $U_{str\text{-}A}$ to *filled* $U_{str\text{-}A}$. Pumping the material Int_A from the storage unit to the downstream unit U_2 is represented by a transition from the location *filled* $U_{str\text{-}A}$ to *empty* $U_{str\text{-}A}$. These transitions are synchronized with the corresponding transitions of the recipe automaton. A shared variable S_A is introduced to model the amount of intermediate material Int_A present in the storage. Guards on the transitions of the storage automaton ensure that the amount of material drained to the storage unit $b_{in,A}$ does not exceed the maximum capacity $max(S_A)$ and that the storage automaton switches back to the location *empty* $U_{str\text{-}A}$ when the entire amount of material is pumped to the downstream unit. Additional transitions from the *filled* $U_{str\text{-}A}$ location to itself model the change in the amount of material present in the storage when more than one batch of a product is produced.

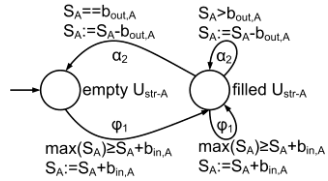

Fig. 2: TA model for the storage

3.2. Modeling the common-intermediate storage policy

The idea of how to model the common-intermediate storage (CIS) policy is explained by extending the example process by a common storage unit shared among both intermediate materials Int_A and Int_B. The modular TA model for the example problem is extended by creating a common *storage automaton*. The TA for the common storage unit is shown in Fig. 3. The storage automaton consists of one

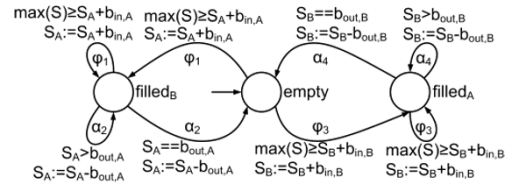

Fig. 3: TA model for the common intermediate storage

empty location representing that the storage unit is empty and one *filled*$_l$ location for each intermediate product $l \in \{Int_A, Int_B\}$ which can be stored in the storage unit representing that the storage unit is partly or completely filled with the corresponding intermediate material. For each intermediate product a shared variable is introduced. The guards and the actions on the corresponding synchronized transitions model the amount of material present in the storage.

3.3. Modeling the non-intermediate storage policy

The idea of how to model the non-intermediate storage policy (NIS) is explained by extending the example process such that no storage units exist in the plant. For each processing unit U_k a shared variable S_k is introduced to model the occupancy of the unit. Each shared variable is initialized with a value of 0 indicating that the unit is not occupied and with a value of 1 if it is holding any amount of processed material. Guards on the shared variables in the recipe automata ensure than an operation can start only if the corresponding unit is unoccupied. The state of the unit is updated by actions on the shared variables when the corresponding transition is taken. The extended TA models for the recipes *A* and *B* are shown in Fig. 4. In production environments with NIS policy a phenomenon called *blocking* may occur when an upstream unit has finished an operation and the downstream unit is busy or occupied then the upstream unit is not allowed to release the material till the downstream unit is free thus blocking the upstream unit.

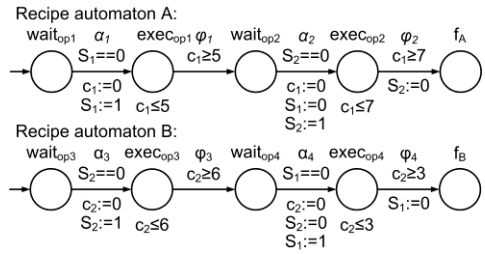

Fig. 4: TA models for the recipes *A* and *B* of the example problem with NIS policy

4. Blocking Reduction

The first part of the reachability tree of the example process with NIS policy is shown in Fig. 5. It can be seen from the figure that there exist four traces that lead to leaf nodes which are not target nodes but deadlocks. These leaf nodes represent partial schedules in which both recipes *A* and *B* have finished the first operation op_1 and op_3, respectively. In this state, neither of the recipes can start the second operation since the needed resource is occupied and thereby blocked by the other recipe. This is known as *mutual blocking*. The computational effort is wasted by exploring traces that lead to mutual blocking and demands for efficient reductions schemes to prune such traces in the search tree. The idea is to compare the sequence of the resources of a recipe order with the sequence of the resources in other recipe orders for which the latter is a swap of the former and to avoid starting an operation that would lead to mutual blocking. The blocking reduction schemes are explained below.

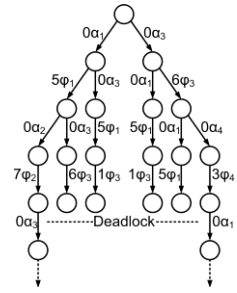

Fig. 5: Reachability tree

4.1. α-φ Reduction

In the reachability tree given a node q with outgoing timed transitions $\tau_1\varphi_i$ and $\tau_2\alpha_j$ where $\tau_1\varphi_i$ denotes finishing of operation i after τ_1 time units and $\tau_2\alpha_j$ denotes starting of operation j after τ_2 time units, the transition $\tau_2\alpha_j$ is removed and all successor nodes are pruned if all the following conditions are satisfied: (1) Operation i and j are not the last operations of their respective recipes, (2) the resource currently executing operation i is the same resource required by the operation $j+1$ where $j+1$ is the operation immediately

succeeding *j* with respect to the recipe it belongs to, and (3) the resource allocated to execute operation *j* is the same resource required by the operation *i+1* where *i+1* is the operation immediately succeeding *i* with respect to the recipe it belongs to.

4.2. α-α Reduction

In the reachability tree given a node *q* with outgoing timed transitions $\tau_1\alpha_i$ and $\tau_2\alpha_j$ where $\tau_1\alpha_i$ denotes starting of operation *i* after τ_1 time units and $\tau_2\alpha_j$ denotes starting of operation *j* after τ_2 time units, the transition $\tau_1\alpha_i$ is removed and all successor nodes are pruned if all the following conditions are satisfied: (1) Operation *i* is not the last operation to be performed to complete the recipe it belongs to and operation *j* is not the first operation to be performed to start the recipe it belongs to, (2) both operations *i* and *j* bid for the same resource, and (3) the resource in which operation *j-1* was executed is the same resource required by operation *i+1* where *j-1* is the operation immediately preceding *j* with respect to the recipe it belong to and *i+1* is the operation immediately succeeding *i* with respect to the recipe it belongs to.

5. Modeling Operational Policies

The different operational policies that are observed in chemical process industries can be classified into three main categories namely "Infinite waiting (IW)", "Finite waiting (FW)" and "Zero waiting (ZW)".

5.1. Modeling finite waiting

The idea of modeling the FW operational policy is explained by extending the example process such that the intermediate material Int_A of recipe *A* has a finite waiting period. The material Int_A has to be stored for at least A_{min} time units before it can be processed in unit U_2 and is allowed to be stored for at most A_{max} time units. The $wait_{op2}$ location of the recipe automaton *A* is extended by an invariant restricting the residence time of Int_A to $A_{max,}$ the outgoing transition α_2 is extended by a guard ensuring a minimum residence time of A_{min}, and the clock is reset on transition φ_1. The extended recipe automaton is shown in Fig. 6.

Fig. 6: TA model of recipe A with FW policy

5.2. Modeling zero waiting

The idea of modeling the zero waiting policy (ZW) is explained by extending the original example process with the ZW policy for the intermediate product Int_A of recipe *A*. The $wait_{op2}$ location of the recipe automaton *A* is marked as an *urgent* location forcing the automaton to leave the location immediately once it is active (i.e. the automaton is not allowed to stay more than 0 time units in the location). Due to the zone abstraction technique used in the reachability analysis, however, the optimal solution for problems with ZW policy may not be found, see Subbiah et al. (2011a).

6. Numerical Results

The blocking reduction schemes were implemented in the TA-based scheduling tool TAOpt developed at our group. The search algorithm chosen is a combination of a depth-first and a best-first search strategy. The reduction techniques safe non-laziness, safe sleep-set method and the MRPT scheme are used in the tests, see Subbiah et al. (2011a, 2011b). The computation equipment used is a Linux machine with 2x2.4 GHz speed and 16GB memory. In order to investigate the performance of the blocking reduction a series of problems with NIS policy were generated using the benchmark instance generator; see Demirkol et al. (1998). Table 1 shows the number of nodes explored and

the computation times required to prove the optimality of the best solution obtained in the reachability analysis for the different reduction techniques The results show that when the number of recipes increases, for the same number of units the search space increases substantially due to an increase in the possible degrees of freedom. Since the search space increases, the computation time also increases. The blocking reduction (BR) reduces the search space for all instances tested compared to the algorithm without the BR. The MRPT-based bounding scheme is efficient in comparison to the BR as the number of nodes explored is less. For all instances tested the MRPT-based bounding in combination with BR could explore the complete search space with minimal computation time. Three case studies proposed in Ferrer-Nadal et al. (2008) are considered for investigation. Table 2 shows the number of nodes explored and the computation times required to prove the optimality of the best solution obtained with different reduction techniques for the case studies. For the cases with ZW policy the optimal solutions could not be found due to the zone abstraction technique, however feasible solutions close to the optimal solutions were found.

Table 1: Comparison results on the generated job-shop instances.

EN – number of nodes explored to prove optimality; T_{CPU} – computation time in CPU seconds required to prove optimality; None – without blocking reduction and bounding scheme; BR – blocking reduction; MRPT – MRPT-based bounding scheme.

Res.	Recp.	None		BR		MRPT		MRPT+BR	
		EN	T_{CPU}	EN	T_{CPU}	EN	T_{CPU}	EN	T_{CPU}
6	4	16775	0.37	14877	0.32	2159	0.19	1867	0.16
	5	136649	3.32	120634	2.89	21296	1.17	17993	1.61
	6	1018063	26.40	917328	24.02	178504	18.13	154398	15.99
	7	5064805	150.47	4485761	135.33	479783	63.18	396756	52.02
7	4	50038	1.26	44621	1.12	4255	0.39	3710	0.36
	5	511087	13.15	466325	12.53	51922	5.72	448361	4.90
	6	3934306	118.32	3462821	103.92	432144	61.32	360107	49.48
	7	10mio*	322.39*	10mio*	323.49*	2354210	376.330	1960728	319.38

* - sub-optimal solution – node limit of 10 million reached.

Table 2: Comparison results on the case studies from Ferrer-Nadal et al. (2008).

EN – number of nodes explored to prove optimality; T_{CPU} – computation time in CPU seconds required to prove optimality; None – without blocking reduction and bounding scheme; BR – blocking reduction; MRPT – MRPT-based bounding scheme.

CS	Policy	None		BR		MRPT		MRPT+BR	
		EN	T_{CPU}	EN	T_{CPU}	EN	T_{CPU}	EN	T_{CPU}
1	UIS	11807	0.23	-	-	699	0.03	-	-
	NIS	6530	0.11	6045	0.10	1071	0.05	983	0.03
2	UIS	1684	0.01	-	-	176	0.01	-	-
	NIS	1283	0.11	1036	0.02	863	0.03	681	0.03
3	UIS	10mio*	468.41	-	-	27600	0.79	-	-
	NIS	10mio*	392.40	5989973	214.19	69421	6.93	38378	3.90

* - sub-optimal solution – node limit of 10 million reached.

7. Conclusions

The conceptual ideas of modeling batch scheduling problems with various storage policies and operational policies have been presented. Furthermore, a new blocking reduction technique was introduced and tested on batch scheduling problems with NIS policy. The results show that the reduction technique increases the efficiency of the reachability algorithm in terms of the number of nodes explored and the computation time required to prove optimality or to find the best schedule. Current work includes the extension of the zone abstraction technique to problems with ZW policy and building a reactive scheduling framework for the TA-based approach.

References

Ferrer-Nadal, S., Capon-Garcia, E., Mendez, C. A., Puigjaner, L., 2008. Material Transfer Operations in Batch Scheduling. A Critical Modeling Issue. Ind. & Eng. Chem. Res. 47(20), 7721-7732.

Subbiah, S., Schoppmeyer, C., Engell, S., 2011a. An Intuitive and Efficient Approach to Process Scheduling with Sequence-Dependent Changeovers Using Timed Automata Models. Ind. & Eng. Chem. Res. 50(9), 5131-5152.

Subbiah, S., Schoppmeyer, C., Engell, S., 2011b. Efficient Scheduling of Batch Plants Using Reachability Tree Search for Timed Automata with Lower Bound Computations. In Proceedings of European Symposium on Computer Aided Process Engineering, 930-934.

Demirkol, E., Mehta, S., Uzsoy, R., 1998. Benchmarks for Shop Scheduling Problems. European Journal of Operations Research 109(1), 137-141.

I.A. Karimi and Rajagopalan Srinivasan (Editors), Proceedings of the 11th International Symposium on Process Systems Engineering, 15-19 July 2012, Singapore.

Optimal design of batch-storage network under sporadic operating time loss

Gyeongbeom Yi[a], Bomsock Lee[b], Euy Soo Lee[c]

[a]*Pukyong National University, 100 San Yongdang-Dong Nam-Gu, Busan 608-739, Korea*
[b]*Kyung hee University, 1732 Dugyoungeaero Gyhung-Gu Yonginsi, Kyunggi 446-701, Korea*
[c]*Dongguk University, 26 3-Ga Pi-Dong Jung-Gu, Seoul 100-715, Korea*

Abstract

The purpose of this study is to find the analytic solution of determining the optimal capacity(lot-size) of batch-storage network to meet the finished product demand under periodic or sporadic operating time losses. Batch processes are bound to random but infrequent operating time losses. Two common remedies for these failures are duplicating another process or increasing process and storage capacity, which are very costly. An optimization model minimizing total cost composed of setup and inventory holding costs as well as the capital costs of constructing processes and storage units is pursued with the framework of batch-storage network of which flows are susceptible to periodic or sporadic operating time losses. The superstructure of the plant consists of a network of serially and/or parallel interlinked batch processes and storage units. The processes transform a set of feedstock materials into another set of products with constant conversion factors. A novel production and inventory analysis method, PSW(Periodic Square Wave) model, is applied. The advantage of PSW model comes from the fact that the model provides a set of simple analytic solution in spite of realistic description of the material flow between processes and storage units. The resulting simple analytic solution can greatly enhance the proper and quick investment decision at the early plant design stage confronted with diverse economic situations.

Keywords: Optimal Lot Size, Process-Inventory Network, Periodic Shutdown, Sporadic Shutdown.

1. Introduction

Periodic or sporadic shutdowns are very common in batch chemical processing. A certain class of production shutdowns caused by planned preventive maintenance such as inspection or replacement of rapidly aging parts and periodic switching of operation mode as well as seasonal production commonly occur in periodical (and sometimes sporadic) pattern. Processes are also susceptible to infrequent random processing failures as well as intentional shutdowns. Random processing failures are usually originated from equipment damage, operator mistakes and process troubles, and irregular and insufficient feedstock delivery or sudden sales fluctuation in the product market. Such failures incur emergency corrective maintenance and therefore sporadic shutdowns. The periodic or sporadic shutdowns cause periodic or sporadic loss of operation or business times as well as maintenance cost. In spite of such operation or business time losses, the customer demand of final products should be satisfied. In

order to supply the customer demand during shutdown or failure period, duplicated processes and/or increased storage capacity are unavoidable. On the contrary, duplicating processes or increasing storage capacity is not easy task any more. It is no doubt that the design and construction cost of the chemical processes is substantially increasing with respect to their total capacities. Nowadays, even the storage facilities are growingly expensive because of increased land value, environmental concern and severe quality control requirement. Moreover, modern plant design concept such as JIT (Just-In-Time) strongly pursues to reduce storage capacity. Therefore, the storage capacity in conjunction with process capacity should be selected carefully to consider the operational characteristics such as frequent or sporadic shutdowns.

In this study, the plant structure is composed of a batch-storage network that can cover most supply chain components, for example raw material purchasing, production, transportation and finished product demand. PSW(Periodic Square Wave) model has been successfully used to find the analytical solution of optimal design of batch-storage network including uncertainty and waste streams[1]. In this study, we modified the previous PSW model to incorporate the periodic shutdowns and sporadic shutdowns. We would not use an ordinary probabilistic analysis of random failures. Instead, we will use a judicious graphical method to find the upper and lower bound of the flows under periodic or sporadic shutdowns. Specially, we focus on obtaining a compact set of analytical solutions with minimally given shutdown information.

2. Problem Formulation

Figure 1 shows two typical flows of periodic shutdown $F(t)$ and sporadic shutdown $\mathbf{F(t)}$.

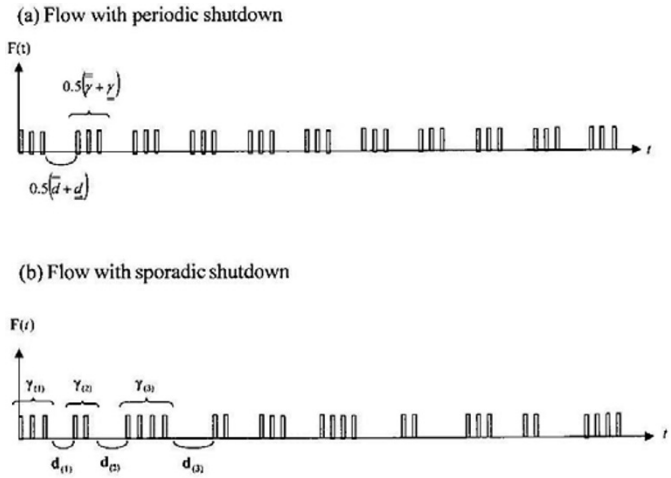

Figure 1. Definition of Uncertainty in Sporadic Shutdown.

The sporadic shutdowns have random characteristics. The random properties of sporadic shutdown are characterized by two random variables $\boldsymbol{\gamma}_{(l)}$ and $\mathbf{d}_{(l)}$ as are shown in Figure 1(b) where subscript **(l)** represent the sequence of occurrence. It is not

necessary to know the exact distribution functions of $\boldsymbol{\gamma}_{(\mathbf{l})}$ and $\mathbf{d}_{(\mathbf{l})}$. We assume that $\boldsymbol{\gamma}_{(\mathbf{l})}$ and $\mathbf{d}_{(\mathbf{l})}$ have symmetrical distribution function with $\underline{\underline{\gamma}} \le \boldsymbol{\gamma}_{(\mathbf{l})} \le \overline{\overline{\gamma}}$ and $\underline{\underline{d}} \le \mathbf{d}_{(\mathbf{l})} \le \overline{\overline{d}}$. That is, the maximum and minimum values of random variables are already known. The mean values of $\boldsymbol{\gamma}_{(\mathbf{l})}$ and $\mathbf{d}_{(\mathbf{l})}$ are $0.5\left(\underline{\underline{\gamma}} + \overline{\overline{\gamma}}\right)$ and $0.5\left(\underline{\underline{d}} + \overline{\overline{d}}\right)$ respectively. Note that $\underline{\underline{\gamma}}, \overline{\overline{\gamma}}$ and $0.5\left(\underline{\underline{\gamma}} + \overline{\overline{\gamma}}\right)$ are all integer values. For $0.5\left(\underline{\underline{\gamma}} + \overline{\overline{\gamma}}\right)$ to be integer, both $\underline{\underline{\gamma}}$ and $\overline{\overline{\gamma}}$ should be odd or even numbers. Suppose that $\boldsymbol{\gamma}_{(\mathbf{l})}$ and $\mathbf{d}_{(\mathbf{l})}$ have identical independent distribution functions with respect to **(l)**. For a given convergence limit $0 < \varepsilon_1, \varepsilon_2 << 1$ and confidence level $0 < \delta_1, \delta_2 << 1$, the weak law of large numbers says that there exists an integer η such that $P\left\{\left|\frac{1}{\eta}\sum_{l=1}^{\eta} \boldsymbol{\gamma}_{(\mathbf{l})} - 0.5\left(\underline{\underline{\gamma}} + \overline{\overline{\gamma}}\right)\right| < \varepsilon_1\right\} \ge 1 - \delta_1$ and $P\left\{\left|\frac{1}{\eta}\sum_{l=1}^{\eta} \mathbf{d}_{(\mathbf{l})} - 0.5\left(\underline{\underline{d}} + \overline{\overline{d}}\right)\right| < \varepsilon_2\right\} \ge 1 - \delta_2$. From Tchebycheff's inequality, $\eta \ge \frac{Var\left(\boldsymbol{\gamma}_{(\mathbf{l})}\right)}{\delta_1 \varepsilon_1^{\,2}}$ and $\eta \ge \frac{Var\left(\mathbf{d}_{(\mathbf{l})}\right)}{\delta_2 \varepsilon_2^{\,2}}$, that is, $\eta = \max\left\{\text{int}\left[\frac{Var\left(\boldsymbol{\gamma}_{(\mathbf{l})}\right)}{\delta_1 \varepsilon_1^{\,2}}\right], \text{int}\left[\frac{Var\left(\mathbf{d}_{(\mathbf{l})}\right)}{\delta_1 \varepsilon_1^{\,2}}\right]\right\} + 1$ if the least integer is chosen.[1] η, called occurrence number, should be an even number in order for 0.5η to be an integer value. The long cycle time in the sporadic shutdown case is different from that in the periodic shutdown case. The time interval during which η number of shutdowns occur is defined as a long cycle time $\tilde{\omega}$. Because the sample means of $\boldsymbol{\gamma}_{(\mathbf{l})}$ and $\mathbf{d}_{(\mathbf{l})}$ converge to their mean values during a long cycle time according to the weak law of large numbers, total number of batches and total shutdown duration during a long cycle time are $0.5\left(\underline{\underline{\gamma}} + \overline{\overline{\gamma}}\right)\eta$ and $0.5\left(\underline{\underline{d}} + \overline{\overline{d}}\right)\eta$ respectively. And thus, $\tilde{\omega} = 0.5\eta\left[\left(\overline{\overline{\gamma}} + \underline{\underline{\gamma}}\right)\omega + \overline{\overline{d}} + \underline{\underline{d}}\right]$. Here, the long cycle time has the meaning of the least period within which all random effects diminish with given confidence level. We note that the flow with sporadic shutdowns has a constant average flow rate $D = \frac{\left(\overline{\overline{\gamma}} + \underline{\underline{\gamma}}\right)B}{\left(\overline{\overline{\gamma}} + \underline{\underline{\gamma}}\right)\omega + \overline{\overline{d}} + \underline{\underline{d}}}$ measured during a long cycle time. This means that in spite of the randomness, the total quantity processed during a long cycle time is a constant. In order to make the optimization formulation, what we need is the upper/lower bound and average inventory level of storage units under sporadic shutdowns. The upper bound of inventory level will be used to compute the storage size; the lower bound of inventory level will be used in the optimization constraint that ensures the inventory level is always nonnegative; and the average inventory level will be used to compute the inventory holding cost of the optimization problem. Two extreme cases of the flow with sporadic shutdowns; (a) Upper bound case and (b) Lower bound case, exist. The

upper bound case has 0.5η times of minimum shutdown duration $\underline{\underline{d}}$ with maximum batch frequency $\overline{\overline{\gamma}}$ and then 0.5η times of maximum shutdown duration $\overline{\overline{d}}$ with minimum batch frequency $\underline{\underline{\gamma}}$ within repeated long cycle times. The lower bound case has 0.5η times of maximum shutdown duration $\overline{\overline{d}}$ with minimum batch frequency $\underline{\underline{\gamma}}$ and then 0.5η times of minimum shutdown duration $\underline{\underline{d}}$ with maximum batch frequency $\overline{\overline{\gamma}}$ within repeated long cycle times. Figure 2 shows the cumulative flow functions of the two cases.

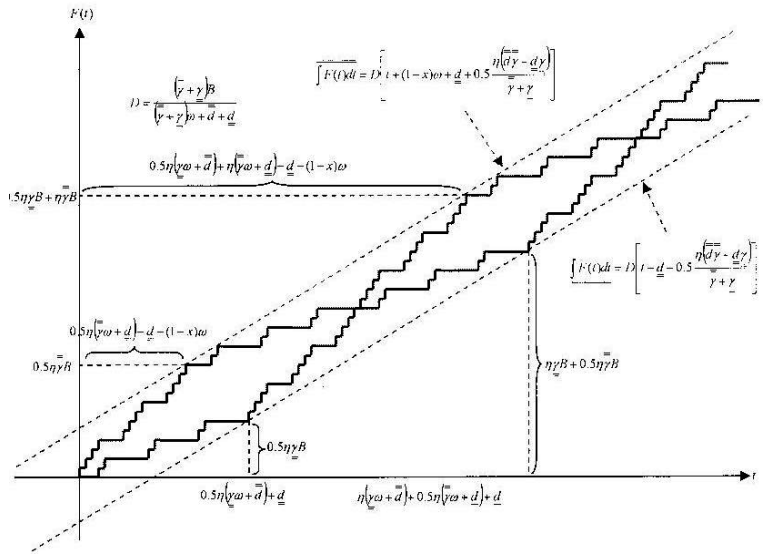

Figure 2. Cumulative Flow Function for Two Extreme Cases.

The dotted lines are the upper and lower bounds of the two extreme cases. All integrals of flows with sporadic shutdowns $\int_0^t \mathbf{F}(t)dt$ exist between the dotted lines whose equations are given in Figure 2.

$$D\left[t+(1-x)\omega+\underline{\underline{d}}+0.5\frac{\eta\left(\overline{\overline{d}}\,\overline{\overline{\gamma}}-\underline{\underline{d}}\,\underline{\underline{\gamma}}\right)}{\overline{\overline{\gamma}}+\underline{\underline{\gamma}}}\right] \geq \int_0^t \mathbf{F}(t)dt \geq D\left[t-\underline{\underline{d}}-0.5\frac{\eta d\left(\overline{\overline{d}}\,\overline{\overline{\gamma}}-\underline{\underline{d}}\,\underline{\underline{\gamma}}\right)}{\overline{\overline{\gamma}}+\underline{\underline{\gamma}}}\right]$$

The upper bound of the inventory level, $\overline{\overline{V^j}}$, is computed by adding the upper bounds of all incoming flow integrals and subtracting the lower bounds of all outgoing flow integrals from the initial inventory. The lower bound of the inventory level, $\underline{\underline{V^j}}$, is computed by adding the lower bounds of all incoming flow integrals and subtracting the upper bounds of all outgoing flow integrals from the initial inventory. Incoming flows are raw material purchase flows and product discharging flows from production

processes. Outgoing flows are feed flows to production processes and finished product demand flows. We can find the upper and lower bounds of inventory level. Note that the overall material balance around a storage unit, still holds for the case with sporadic shutdowns. The average inventory level is highly dependent on the random properties of failures. The exact value of it cannot be obtained without defining the probability distribution function of all random variables, which is a nontrivial work. In this study, we will take an intuitive approach. The average of $\overline{\int_0^t \mathbf{F(t)}dt}$ is selected as the line equidistant from the upper and lower bounds. [1]

$$\overline{\int_0^t \mathbf{F}(t)dt} = D\left[t + 0.5(1-x)\omega\right]$$

The average inventory level of a storage unit is is computed by adding the average of all incoming flow integrals and subtracting the average of all outgoing flow integrals from the initial inventory. The objective function for the design of the batch-storage network is to minimize the annualized expectation of total cost, which consists of the setup cost of processes, the inventory holding cost of storage units, and the capital cost of the processes and storage units at a given minimum/maximum shutdown duration, minimum/maximum batch frequency and occurrence number in a long cycle time of each process.

$$TC = \sum_{j=1}^{|J|}\sum_{k=1}^{|K(j)|}\left[\frac{0.5\eta_k^j\left(\overline{\overline{\gamma}}_k^j + \underline{\underline{\gamma}}_k^j\right)A_k^j}{\widetilde{\omega}_k^j} + a_k^j B_k^j\right] + \sum_{i=1}^{|I|}\left[\frac{0.5\eta_i\left(\overline{\overline{\gamma}}_i + \underline{\underline{\gamma}}_i\right)A_i}{\widetilde{\omega}_i} + a_i B_i\right]$$
$$+ \sum_{j=1}^{|J|}\left[H^j\overline{V^j} + b^j\overline{\overline{V^j}}\right]$$

The constraints of optimization are no depletion of all storage units, $0 \le \underline{\underline{V^j}}$. Optimal cycle times are:

$$\omega_k^j = \sqrt{\frac{A_k^j}{D_k^j\Psi_k^j}} - \frac{\overline{\overline{d}}_k^j + \underline{\underline{d}}_k^j}{\left(\overline{\overline{\gamma}}_k^j + \underline{\underline{\gamma}}_k^j\right)}, \qquad B_k^j = \sqrt{\frac{A_k^j D_k^j}{\Psi_k^j}}$$

$$\omega_i = \sqrt{\frac{A_i}{D_i\Psi_i}} - \frac{\overline{\overline{d}}_i + \underline{\underline{d}}_i}{\left(\overline{\overline{\gamma}}_i + \underline{\underline{\gamma}}_i\right)}, \qquad B = \sqrt{\frac{A_i D_i}{\Psi_i}}$$

References

1. Yi G. 2008 Optimal design of batch-storage network under joint uncertainties. *AIChE J.* 54 p2567

This work was supported by the Pukyong National University Research Fund in 2011(C-D-2011-0197).

I.A. Karimi and Rajagopalan Srinivasan (Editors), Proceedings of the 11th International Symposium on Process Systems Engineering, 15-19 July 2012, Singapore.

Steady-state optimization of an industrial high-density polyethylene slurry process based on an equation-oriented molecular weight distribution model

Zhiliang Zhan[a], Zhijiang Shao[a], Xi Chen[a], Yuhong Zhao[a], Xueping Gu[b], Zhen Yao[b], Lianfang Feng[b]

[a] *Department of Control Science and Engineering, Zhejiang University, Hangzhou, Zhejiang, 310027, P. R .China*
[b]*State Key Laboratory of Chemical Engineering, Department of Chemical and Biological Engineering, Zhejiang University, Hangzhou, Zhejiang, 310027, P. R. China*

Abstract

High-density polyethylene (HDPE) has been widely used as the main material in the film, pipe, and container industries. An equation-oriented molecular weight distribution (MWD) model is developed for an industrial HDPE slurry process using the method of moments and Flory's distribution. The Kriging method is used to establish a surrogate model for the thermodynamic properties. A completely simultaneous approach is proposed to optimize the steady-state process and achieve products with expected MWDs. Two HDPE grades with different MWDs are discussed.
Keywords: High-density polyethylene slurry process; Equation-oriented; Kriging; Optimization; Molecular weight distribution.

1. Introduction

The slurry polymerization process is widely used to produce high-density polyethylene (HDPE). Its major advantages include mild operating conditions, ease of heat removal, high monomer conversion, and relative ease of processing (Hakim and Moballegh 2006; Hakim, Nekoomanesh et al. 2008). Molecular weight distribution (MWD) is a key quality index for polymers, measurement and optimization of MWD is of considerable importance since the microstructural properties determine its mechanical and rheological properties. However, MWD optimization in a polymerization process is always a challenging task because of the large-scale features. Population balances and the method of moments are usually used to describe the mass conservation of polymer components in polymer systems (Soares 2001). On the basis of the moment models, Flory's most probable distribution can be used to describe the instantaneous chain length distribution (CLD) in ethylene polymerization in each reactor (Soares 2001). Changing CLD into MWD is easy by using two simple mathematical transformation steps (Alghyamah and Soares 2009). In the present project, a large-scale, equation-oriented (EO) model with over 140,000 variables is developed for an industrial HDPE slurry process. A simultaneous approach that optimizes the process and produces of different HDPE grades with expected MWDs is then presented.

2. Model development

Fig. 1 shows the flowsheet of an industrial HDPE slurry process with two reactors in a series. A five-site Ziegler-Natta catalyst, with titanium tetrachloride ($TiCl_4$) as the

primary catalyst and triethyl aluminum ($Al(C_2H_5)_3$) as the co-catalyst, is used. The modeling work consists of thermodynamics, kinetics, MWD calculation, and process unit models that include reactors, flash drums, coolers, compressors, and pumps. Unit models other than the reactors are formulated using the general approach and will not be described in detail because of space constraints.

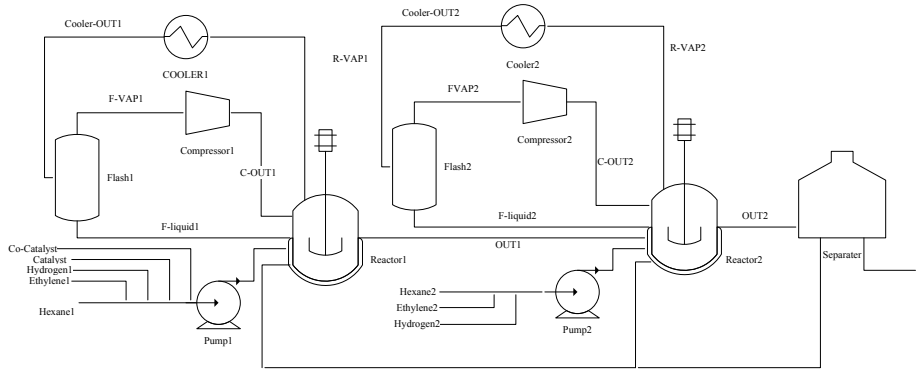

Fig 1. Flow chart of ethylene slurry polymerization process

2.1. Thermodynamic properties based on Kriging

Equation-of-state models are usually used to calculate the thermodynamic properties of polymer systems, among which, the perturbed-chain statistical associating fluid theory (PC-SAFT) is the most accepted one for the polyethylene system (Gross and Sadowski 2001). Given the complexity of the PC-SAFT model, developing an EO model for PC-SAFT is very difficult. To fully exploit the advantages of simultaneous EO optimizations, surrogate models based on the Kriging technique are proposed and developed to describe the relationship between the physical conditions (temperature, pressure, and mole fraction) and the properties (fugacity coefficients, enthalpy, entropy, and density). Kriging models are a family of reduced models that have been used as metamodels (Palmer, Realff 2002). They have also been used in process optimizations (Gomes, Bogle et al. 2006, 2008).

Given the inputs $x=[x_1,x_2,\cdots,x_n]$ and the responses $y=[y_1,y_2,\cdots,y_m]$, the model $\hat{y}(x)$ expresses the deterministic response for an input x as a sum of a regression model and a random function (Lophaven, Nielsen et al. 2002).

$$\hat{y}(x)=f(x)^{\mathrm{T}}\beta^{*}+r(x)^{\mathrm{T}}\gamma^{*} \tag{1}$$

where $f(x)$ is the regression model, $r(x)$ is the correlation model, β^{*} is the regression parameter, and γ^{*} is the correlation parameter. Unlike PC-SAFT, which works for a wide range of conditions, deriving a surrogate model that also covers a wide range is difficult. Considering the features of the simultaneous approach and the huge differences between the streams, a strategy that divides the process into several subsystems and establishes a Kriging model for each subsystem is proposed. In practice, each stream and unit is set as a subsystem. The regression data were generated using the Aspen Property software with PC-SAFT. Up to 3000 data were collected for regression and 10,000 other data for verification. The dimension of the Kriging model is highly related to the data number. Therefore, the surrogate models derived for the thermodynamic properties are in considerably large scales. However, they will not add difficulty in solving the procedure because only direct calculations are involved. The

verification shows that the average errors between the Kriging model and PC-SAFT for all systems in the process model are less than 0.1%, and the maximum relative errors are less than 0.5% for the non-polymer system and 2% for the polymer system. The maximum errors in the properties of the main streams (F-VAP, F-LIQUID, OUT, and VAP) are shown in Table 1. The physical conditions are the inputs to the models for the calculation of these properties, including the enthalpy (H), density (ρ), entropy (S), and fugacity coefficients (φ). The subscript A denotes the co-catalyst. The results prove that the Kriging model can approximate the PC-SAFT for each subsystem well.

Table 1. The regressive results of properties for main streams of both reactors

Stream	Physical conditions	Properties	Max error %	Stream	Physical conditions	Properties	Max error %
F-VAP	T	H	0.224	F-LIQUID	T	H	0.005
	P	φ_{H2}	0.072		P	φ_{H2}	0.191
	x_{H2}	φ_{C2H4}	0.054		x_{H2}	φ_{C2H4}	0.182
	x_{C6H14}	φ_{C6H14}	0.082		x_{C6H14}	φ_{C6H14}	0.265
		S	0.158	R-VAP	T	ρ	0.053
OUT	T	ρ	0.092		P	H	0.035
	P	H	0.007		x_{C2H4}	φ_{H2}	0.034
	x_{H2}	φ_{H2}	1.789		x_{C6H14}	φ_{C2H4}	0.017
	x_{C2H4}	φ_{C2H4}	0.821			φ_{C6H14}	0.057
	x_A	φ_{C6H14}	1.072				
	x_{HDPE}						

2.2. Moment model for polymerization reactor

The reactors are assumed to be continuous stirred tank reactors (CSTR). The kinetics of the polymerization reaction includes catalyst activation, initiation, propagation, transfer, and deactivation. The kinetic parameters can be found in the report by Gu et al. (2008). Population balances and the method of moments are used to describe the mass conservation of the polymer components. The moments of the chain length distribution are calculated for both living and dead polymers.

2.3. The method of instantaneous distribution

The method of instantaneous distribution relies on the assumption that the time-scale for the life of a polymer chain is several times smaller than that for dynamic phenomena taking place. The average lifetime of a polymer chain is in the order of seconds, whereas the time-scale for the reactor and particle dynamics during ethylene polymerization under realistic conditions is generally in the order of several minutes up to hours (Soares 2001). Hence, the use of the method of instantaneous distribution for the HDPE process is fully justified. Associated with the reaction kinetics and the moments of the polymer, the instantaneous CLD for ethylene polymerization at site j is given by a single-parameter equation , Flory's distribution, as follows:

$$w_j(n) = n\tau_j^2 \Big/ (1+\tau_j)^{n+1} \tag{2}$$

where $w_j(n)$ is the weight chain length distribution of the polymer chains with length n, τ is the ratio of all the chain transfer rates to the propagation-rate (calculated from the kinetic model), and j is the site number. Transformations (Alghyamah and Soares 2009) are further performed to convert CLD to MWD in the logarithmic scale, as follows:

$$w_j\left(\log MW\right) = \ln 10 \times MW^2 \left(\tau_j / mw\right)^2 \left(1+\tau_j\right)^{-\left(\frac{MW}{mw}+1\right)} \tag{3}$$

The entire instantaneous distribution of the molecular weight for each reactor can be obtained using the weighted superposition of Flory's distribution for each site.

$$W\left(\log MW\right)=\sum_{j=1}^{Ns} w_j\left(\log MW\right)mf_j \tag{4}$$

where mf_j is the mass fraction of the polymer at site *j*. The MWD of the final product is a combination of the two instantaneous distributions in each reactor, as follows:

$$W_{com}\left(\log MW\right)=\left(m_1W_1\left(\log MW\right)+m_2W_2\left(\log MW\right)\right)/\left(m_1+m_2\right) \tag{5}$$

where m_1 and m_2 are the polymer masses in the first and second reactors, respectively, and can be calculated from the moment models.

3. Results and discussion

Given a designed MWD curve of HDPE as the product quality requirement, an optimization problem can be formulated to minimize the error between the given and predicted distributions by adjusting the process operation conditions, as follows:

$$\begin{aligned}
&\min_{z} \sum_{k=1}^{N_{point}}\left[W_{exp}\left(\log MW^k\right)-W_{com}\left(\log MW^k\right)\right]^2\\
&\text{s.t.}\quad h\left(W_{com}\left(\log MW^k\right),\tau_i,mf_i\right)=0\\
&\qquad g\left(z,\tau_i,mf\right)=0\\
&\qquad z_{lb}\le z\le z_{ub}
\end{aligned} \tag{6}$$

where $W_{exp}\left(\log MW\right)$ is the expected MWD, N_{point} is the curve sampling number (100 in the current project), MW^k is the molecular weight at a discrete point, and *z* is the optimized operational conditions, including the reactor temperatures and pressures and the feed flowrates of hydrogen, ethylene, and hexane in both reactors.

Two MWD curves, one with two peaks and the other with a single peak, are plotted for the optimization. The complete EO model consists of more than 141,101 variables, most of which are the intermediate variables in the Kriging models. The simultaneous approach is used for the optimization using the interior point optimizer (IPOPT) as the solver. Fig. 2 shows that the expected MWDs can be achieved in both cases. The optimized and expected MWDs almost overlap each other. The instantaneous MWDs of the first and second reactors are also shown in the figure. The composite MWD can be very different in shape as a result of the combination of the two reactors. The optimal operation conditions for each case are presented in Table 2.

Table 2. The operation conditions from the optimization

		T(°C)	P (Mpag)	L (%)	H_2 (Nm^3/h)	C_6H_{14} (t/h)	C_2H_4 (t/h)
Twin Peaks	Reactor 1	91.98	0.4516	70.05	49.55	280.23	3.21
	Reactor 2	78.73	0.25	73.36	54.29	23.91	6.82
Single Peak	Reactor 1	80	0.6574	52.34	58.08	80.74	1.3
	Reactor 2	82.1	0.1187	69.66	49.55	282.52	2.32

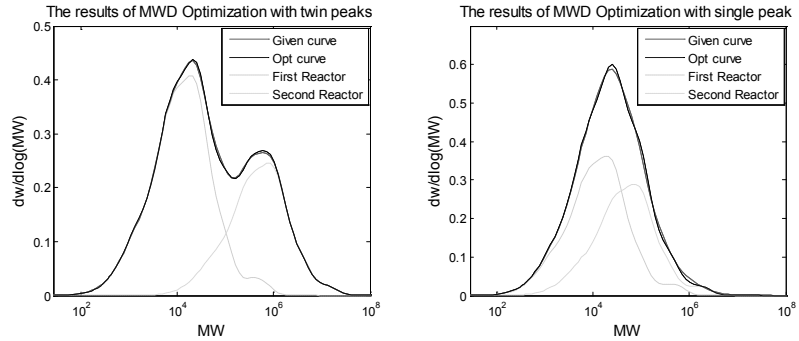

Fig.2 Comparison between MWD optimization results and given curve

4. Conclusion

A steady-state MWD model for the polymerization of ethylene in the slurry process is developed in the present paper. A simultaneous approach is used to optimize the operational conditions and produce polymers with expected MWDs. The optimization results show that good performance can be achieved for different shapes of the MWD curves, thereby providing potential applications in product design.

Acknowledgment

We gratefully acknowledge the financial support of 973 Program (No.2009CB320603), National Natural Science Foundation of China (No. 61074148) and the Fundamental Research Funds for the Central Universities.

References

A. A. Alghyamah, J. B. P. Soares, 2009, Simultaneous Deconvolution of the Bivariate Distribution of Molecular Weight and Chemical Composition of Polyolefins Made with Ziegler-Natta Catalysts, Macromolecular Rapid Communications, 30, 4-5, 384-393

K. Palmer, M. Realff, 2002, Optimization and Validation of Steady-State Flowsheet Simulation Metamodels, Trans IChemE Part A - ChERD, 80, 7, 773-782

J. B. P. Soares, 2001, Mathematical Modelling of the Microstructure of Polyolefins Made by Coordination Polymerization: a Review, Chemical Engineering Science ,56, 13, 4131-4153

J. Gross, G. Sadowski, 2001, Perturbed-chain SAFT: An Equation of State Based on a Perturbation Theory for Chain Molecules, Industrial & Engineering Chemistry Research, 40, 4, 1244-1260

M.V.C.Gomes, I.D.L.Bogle, et al., 2006, An Application of Metamodels for Process Optimisation, Proceedings of the 16th European Symposium on Computer Aided Process Engineering, 1449

M. V. C.Gomes, I. D. L. Bogle, et al., 2008, Using Kriging Models for Real-time Process Optimisation, Computer Aided Chemical Engineering, 25, 361-366

S.Hakim, L. Moballegh, 2006, Simulation of a Series of Industrial SlurryReactors for HDPE Polymerization Process Using Deconvolution of the GPC Graph of Only the First Reactor, Iranian Polymer Journal, 15, 8, 655-666

S. Hakim, M. Nekoomanesh, et al. , 2008, Investigating the Behaviour of a Bi-Supported SiO2/TiCl4/THF/MgCl2 Catalyst in Slurry Ethylene Polymerization: Activity and Molecular Weight, Iranian Polymer Journal, 17, 3, 209-216

S. N.Lophaven, H. B. Nielsen, et al., 2002, DACE: A Matlab Kriging Toolbox, Technical Report IMM-TR-2002-12

X. Gu, L. Feng, et al., 2008, Simulation for Grade Transition of Ethylene Slurry Polymerization Process, Sciencepaper online, 3, 12

I.A. Karimi and Rajagopalan Srinivasan (Editors), Proceedings of the 11th International Symposium on Process Systems Engineering, 15-19 July 2012, Singapore.

Cyclic Scheduling of Cracking Furnaces System with Real Operational Characters

Lijie Su, Lixin Tang,

The Logistics Institute, Northeastern University, *Shenyang 110819*, *Liaoning*, *China*

Abstract

The cyclic scheduling of cracking furnaces is investigated with the practical operational characters, which are concurrent or serial cracking different raw materials in one furnace between its two adjacent decoking operations. This paper presents two mixed-integer nonlinear programming (MINLP) formulations respectively for the two scheduling problems based on a continuous time representation. Valid inequalities and linearization techniques are used, and an improved Outer Approximation (OA) algorithm with parallel strategies is designed for solving the formulations. Numerical experiments demonstrate the efficiency of the models and solution strategies. [1]

Keywords: Cyclic Scheduling, Ethylene Cracking Furnace, MINLP, Outer Approximation

1. Introduction

Ethylene production is multi-stage continuous process with parallel cracking units as illustrated in Figure 1, which operate multi-feedstock and produce few final popular products. Cracking furnaces would need periodical decoking in order to assure the conversion of final products, protect furnace pipes and save fuel. The cyclic scheduling of the process would determine assignment, processing times, and number of subcycles of various feeds on different units during a optimal production cycle. Jain and Grossman(1998) presented a pseudo-convex MINLP formulation for one general scheduling problem. The work of Liu et al(2010) considered the non-simultaneous cleanup constraints. Those two papers are assumed that only one kind of raw materials is processed in one subcycle, and the length of subcycle is between lower and upper bounds dependent on cracked raw materials. However, concurrent or serial cracking different raw materials during one subcycle of same furnace often occurs in practical production. This two operation ways could increase the flexibility of process, ease the shortage of raw materials and avoid shutting down.

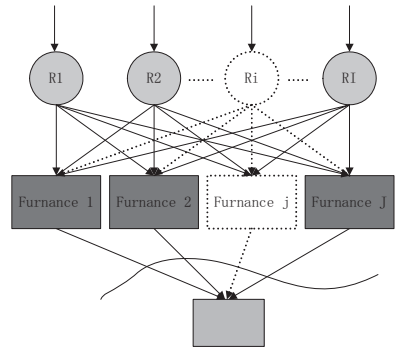

Figure 1 Cracking Process of Ethylene Production

With the concerns of practical operation, this paper presents two formulations for the cyclic scheduling of cracking furnaces with new operational characters. The

This research is partly supported by State Key Program of National Natural Science Foundation of China (71032004), the Fundamental Research Funds for the Central Universities (N090104002，N100704002).

linearization and valid inequalities are designed to reformulate the models. And an improved OA algorithm with some parallel strategies is designed to solve the model. Some cases would demonstrate the efficiency of the presented formulations and improved algorithm.

2. Problems Statement

With non-simultaneous cleanup constraints, the cyclic scheduling problem would also determine decoking times of each furnace during one cycle in order to maximize the net profit value per time. Here, assume (1) regressed cracking yield model based on plant data is reliable; (2) The conversion to final products are assumed as Jain and Grossman(1998). Based on our investigation of real Ethylene plants, two kind of cracking operation for one furnace in one subcycle which would not be considered before often occur.

2.1. Concurrent cracking problem

The minimal producing unit is pipe group in one cracking furnace. For example, there are 4-6 pipe groups in the SRT types. And different pipe groups could operate different feeds with similar cracking condition. For these groups belong to one furnace, the starting and ending times of the subcycles are same, and cleanup must be simultaneous.

2.2. Serial cracking problem

The subcycle length is about 50-80 days in real production. Therefore, processing one kind of feeds in single subcycle must assume sufficient feedstock supply, which is often unavailable in practical process. For one furnace, serially cracking different feeds during one subcycle would relax the strong assumption. Here, assume one raw materials be processed continuously in one subcycle. The processing rate of furnace could be adjusted in some scope, which be considered as a constant before.

3. MINLP Formulations

Two MINLP formulations are presented for the cyclic scheduling problem with different operating rules as described. The definition of production cycle is composed of complete subcycles with their cleanup durations. Continuous-time representing method are applied to determine the boundaries of every subcycle. Distinctive constraints are described as follow and others which are described in Jain and Grossman(1998) or Liu etc(2011) are omitted here, which include some general assignments, integrality, mass balance, non-simultaneous cleanup constraints and objective functions.

3.1. Concurrent cracking model

Except indices of feeds, furnace and subcycle, number of pipe groups in one furnace is introduced as one index. The definition of binary variable X_{ijgk} is that whether assign feed i to the pipe group g of furnace j in subcycle k. Those pipe groups included in one furnace must work synchronously, which lead to the following constraint:

$$|G| \cdot \sum_{i} X_{ijgk} \geq \sum_{i,g} X_{ijgk} \quad \forall j, g, k \tag{1.1}$$

The subcycles must be front closely, that is if one subcycle of a furnace is empty, the following subcycles of that cracking unit should be empty.

$$\sum_{i,g} X_{ijgk} \geq \sum_{i,g} X_{ijgk+1} \quad \forall j,k<K \tag{1.2}$$

The continuous variables Ts_{jk} , Tp_{jk} represent the starting time and duration for subcycle k of furnace j, and Tr_{ijgk} is the duration of feed i cracked in pipe group g of furnace j during its subcycle k. Then constraints (1.3) and (1.4) would insure that pipe groups in one furnace operate synchronously.

$$Tr_{ijgk} \leq Tp_{jk} \quad \forall i,j,g,k \tag{1.3}$$

$$\sum_{i,g} Tr_{ijgk} = |G| \cdot Tp_{jk} \quad \forall g,k \tag{1.4}$$

Cleanup duration of each subcycle for one furnace Tcl_{jk} would be equal to the maximum cleanup one of cracked feeds.

$$\tau_{ij} \cdot X_{ijgk} \leq Tcl_{jk} \quad \forall i,j,g,k \tag{1.5}$$

There are minimal demand rates for different kind of final product.

$$\sum_{i,j,g,k} F_{ijg} \cdot \left[c_{ijl} \cdot Tr_{ijgk} + \frac{a_{ijl}}{b_{ijl}} \left(e^{b_{ijl} \cdot Tr_{ijgk}} - 1 \right) \right] \geq Q_l \cdot T_{cycle} \quad \forall l \tag{1.6}$$

3.2. Serial cracking model

Here, sequence of feeds in one subcycle of a furnace is introduced as one additional index. The sequence in subcycle also is front closely.

$$\sum_{i} X_{ijks} \geq \sum_{i} X_{ijks+1} \quad \forall j,k,s<I \tag{1.7}$$

Using F_{ijk} represents the processing rate, and T_{ijk}^{SC} represents the processing duration of feed in subcycle, which are continuous variables here. Through introducing an auxiliary variable FT_{ijk} and four additional constraints, the mass balance constraint could be linearization, which would avoid the bilinear term in the model. T^L , T^U are lower and upper bounds of continuous processing time of one kind of feeds.

$$FT_{ijk} \geq T^L \cdot F_{ijk} + F_{ij}^L \cdot T_{ijk}^{SC} - T^L \cdot F_{ij}^L \quad \forall i,j,k \tag{1.8}$$

$$FT_{ijk} \geq T^U \cdot F_{ijk} + F_{ij}^U \cdot T_{ijk}^{SC} - T^U \cdot F_{ij}^U \quad \forall i,j,k \tag{1.9}$$

$$FT_{ijk} \leq T^U \cdot F_{ijk} + F_{ij}^L \cdot T_{ijk}^{SC} - T^U \cdot F_{ij}^L \cdot \sum_{s} X_{ijks} \quad \forall i,j,k \tag{1.10}$$

$$FT_{ijk} \leq T^L \cdot F_{ijk} + F_{ij}^U \cdot T_{ijk}^{SC} - T^L \cdot F_{ij}^U \cdot \sum_{s} X_{ijks} \quad \forall i,j,k \tag{1.11}$$

The summation of serial processing durations for different feeds in each subcycle equals to the length of subcycle.

$$\sum_{i} T_{ijk}^{SC} = Tp_{jk} \quad \forall j,k \tag{1.12}$$

The product of coking-velocity coefficient γ_{ij} and cracking duration of one feed stock T_{ijk}^{SC} is described as the cleaning up duration of this feed. Assume the decoking duration of one subcycle Tcl_{jk} is equal to the accumulation of cleaning up duration of some feeds, which are cracked in this subcycle.

$$Tcl_{jk} = \sum_{i} \gamma_{ij} \cdot T_{ijk}^{SC} \quad \forall j,k \tag{1.13}$$

Using lower and upper bound of decoking time determines the length of subcycle.

$$\tau^{L} \cdot \sum_{i} X_{ijks} \le Tcl_{jk} \le \tau^{U} \quad \forall j,k,s=1 \tag{1.14}$$

In order to define the beginning processed time of feed i in subcycle k of furnace j, that is $\tilde{T}s_{ijk}$, introduce another auxiliary variable TX_{ijks} and linearization constraints

$$TX_{ijks} \le T^{U} \cdot X_{ijks} \quad \forall i,j,k,s \tag{1.15}$$

$$TX_{ijks} \le T_{ijk}^{SC} + M \cdot \left(1 - X_{ijks}\right) \quad \forall i,j,k,s \tag{1.16}$$

$$TX_{ijks} \ge T_{ijk}^{SC} - M \cdot \left(1 - X_{ijks}\right) \quad \forall i,j,k,s \tag{1.17}$$

Then

$$\tilde{T}s_{ijk} \ge \sum_{i' \ne i} \sum_{s' < s} TX_{i'jks'} - M \cdot \left(1 - X_{ijks}\right) \quad \forall i,j,k,s \tag{1.18}$$

$$\tilde{T}s_{ijk} \le \sum_{i' \ne i} \sum_{s' < s} TX_{i'jks'} + M \cdot \left(1 - X_{ijks}\right) \quad \forall i,j,k,s \tag{1.19}$$

With the beginning processed time, the ending time could be easily given.

$$\tilde{T}e_{ijk} = \tilde{T}s_{ijk} + T_{ijk}^{SC} \quad \forall i,j,k \tag{1.20}$$

The objective of the cyclic scheduling problem would maximize the average profit。

$$Max\ z = \sum_{i,j,k,l} \left(\begin{array}{l} PR_{l} \cdot [c_{ijl} \cdot FT_{ijk} + F_{ijk} \cdot a_{ijl} \left(e^{b_{ijl}\tilde{T}e_{ijk}} - e^{b_{ijl}\tilde{T}s_{ijk}} \right) / b_{ijl}] \\ -(CR_{i} + CP_{j}) \cdot FT_{ijk} - CC_{j} \cdot Tcl_{jk} \end{array} \right) / TC \tag{1.21}$$

Based upper bound of coking thickness and coefficient of coking velocity, the upper bound of subcycle length could be calculated. Therefore, the maximum kind of raw materials which could be processed in one subcycle could be gotten.

$$\sum_{i,s} X_{ijks} \le \frac{\tau^{U}}{\min_{i}\left\{\gamma_{ij}\right\} \cdot T^{L}} \quad \forall j,k \tag{1.22}$$

The proposed models are both MINLP with nonlinear objective function and linear constraints.

4. Solution Algorithm

There are four-index binary variables and more big-M constraints in our models. As one of general algorithms for MINLP, an improved Outer approximation(OA) algorithm with parallel strategy is designed for the presented models in order to decrease the

iterations. With the description of general OA from Grossmann(2002), a simplified description of the algorithm is as follows.
Step 1, Initialization: solve the relaxed NLP1 of primal MINLP, getting the lower bound of the problem, then solve constructed master MILP based on the solution of NLP1;
Step 2, Construct several NLP2 with the different collected integer solutions of MILP, then solve these problems concurrently, get few solutions of NLP2;
Step 3, Construct MILP master problem based on these solutions of NLP2, then solve the master problem. If the terminal condition would be not satisfied, collect few solutions of MILP, return to step 2, else stop.
The presented model is formulated with GAMS(Brooke etc, 1992). The improved OA is also programmed on GAMS platform.

5. Computational Results

One example is considered respectively for the two formulations. It is desired to determine a cyclic schedule to process three different feeds A, B, C in a furnace. Other part of related parameters are from Jain and Grossman(1998). The predefined number of subcycles is 7, and the lower bound of total cyclic length is set 135 days.
For the concurrent cracking model, the number of pipe groups is 3, An optimal solution is shown in Figure 2. Concurrent operation based on pipe-groups could release the shortage of feeds. For the serial cracking model, an optimal solution is shown in Figure 3.
Data experiments demonstrates that the presented improved OA algorithm could decrease whole iterations.

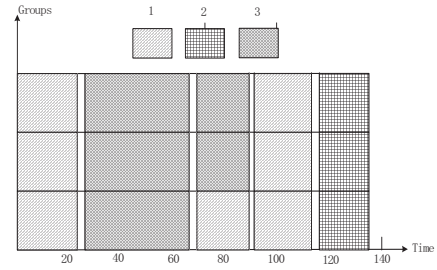

Figure 2 Optimal scheduling solution for concurrent cracking model

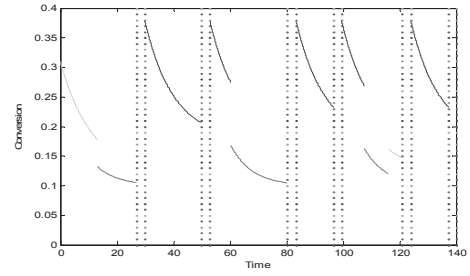

Figure 3 Optimal scheduling solution for serial cracking model

6. Conclusions

The characters of concurrent and serial operations are considered in the cyclic scheduling for multiple cracking furnaces. Continuous-time representation method, linearization and valid inequalities are used to reformulate two MINLP models. The improved OA algorithm is designed to solve the problems. Results could reflect the flexibility of production process, and better mass balance.

References

V. Jain, I. E. Grossmann, 1998, Cyclic Scheduling of Continuous Parallel-Process Units with Decaying Performance, AIChE Journal, Vol. 44, No. 7, 1623-1636.
C.W. Liu, J. Zhang, Q. Xu, K. Y. Li, 2010, Cyclic scheduling for best profitability of industrial cracking furnace system, Computers and Chemical Engineering, Vol. 34 544-554.
I. E. Grossmann, 2002, Review of nonlinear mixed-integer and disjunctive programming techniques. Optimization and Engineering, Vol.3, 227–252.
A. Brooke, D. Kendrick, A. Meeraus, 1992, GAMS: A user's guide. Palo Alto, CA: Scientific Press.

I.A. Karimi and Rajagopalan Srinivasan (Editors), Proceedings of the 11th International Symposium on Process Systems Engineering, 15-19 July 2012, Singapore.

Thermodynamic analysis and modeling for typical feed-preheating and fractionating processes in delayed cokers

Yang Lei, Bingjian Zhang, Qinglin Chen*

School of Chemistry and Chemical Engineering/Key Lab of Low-carbon Chemistry & Energy Conservation of Guangdong Province, Sun Yat-Sen University, Guangzhou 510275, China

Abstract

Delayed coking is one of the main processes for heavy oil processing with higher energy consumption in refineries. The present analysis includes the energy and exergy balance of the de-superheating section, the heat exchanging process of the feeds, etc. An approach to optimize the heat exchanger network through integrating the fractionating process is illustrated. A much higher feed temperature is usually considered better for an energy-use optimization retrofit. However, considering the limit of the energy integration within the whole plant, determining the feed preheating temperature is usually an optimization problem. Finally, a model is built that the annual cost is set as an objective function which is subject to the restrictions mentioned above.

Keywords: delayed coker; modeling; optimization; thermodynamic analysis

1. Introduction

To efficiently lower the energy consumption of a delayed coking unit (DCU), it is crucial to increase the efficiency of the coking furnace, to reasonably use the heat of the main fractionator within the unit (Chen et al., 2004). In DCUs, there exist special energy-use characteristics for the heat exchanger network (HEN) and fractionating processes (Rodriguez-Reinoso et al., 2011). So far, the existing heat integration methods are mainly based either on pinch analysis techniques or on mathematical programming (Morar et al., 2010). Most researches and engineering retrofits mainly focused on the heat integration between different plants (Plesu et al., 2003; Zhang et al., 2011). For a single plant, Al-Riyami et al. (2007) analyzed the heat integration of a HEN in a fluid catalytic cracking plant. However, it is seldom considered how to optimize the HEN of DCUs through simultaneously integrating the fractionating processes. Consequently, thermodynamic analysis results are presented for three typical processes of DCUs. Then an optimization approach is proposed in which the integration between HEN and fractionating processes is considered. An optimal model is established for the optimal feed preheating temperature.

2. Comparison and thermodynamic analysis of three processes

A conventional DCU generally consists of three sections, i.e. coking, oil and gas separation and heat exchanging. Three typical flowsheets with different feed preheating and fractionating processes are sketched in Fig. 1, in which the primary difference is within the section of preheating/steam generation. The three processes presented above

* Correspondence author, email: chqlin@mail.sysu.edu.cn.

are all simulated by using software PRO/Ⅱ.

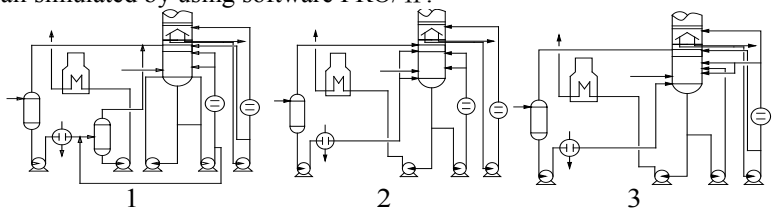

Fig. 1 Schematic representation of typical DCUs

Coking section The inlet temperature of the residual oil to the coking furnace (T_{inlet}) via energy conservation exists:

$$T_{inlet,1} < T_{inlet,3} < T_{inlet,2} \quad \text{(Eqn. 1.)}$$

Separation section The pump-around heat removal in the main fractionator is different:

$$\left(\frac{Q_t + Q_d}{Q_{all}}\right)_1 < \left(\frac{Q_t + Q_d}{Q_{all}}\right)_3 < \left(\frac{Q_t + Q_d}{Q_{all}}\right)_2 \quad \text{(Eqn. 2.)}$$

The exergy losses of the factionators are different, which is affected by the heat transfer temperature difference in the de-superheating section:

$$Ex_{loss,1} < Ex_{loss,3} < Ex_{loss,2} \quad \text{(Eqn. 3.)}$$

Heat exchanging section It is assumed that the heat exchanging sequence is same. The temperature of the preheated feed (T_{feed}) in three processes is different:

$$T_{feed,2} < T_{feed,3} < T_{feed,1} \quad \text{(Eqn. 4.)}$$

3. HEN optimization principle through integrating fractionating processes

To address the problem of the HEN optimization through integrating the fractionating process, the following strategies are presented.

1.1. Heat integration strategies

(1) All streams' data should be collected firstly. When the ratio of Q_t and Q_d to Q_{all} is less than C1 which is defined by heuristic rules, the heat removal should be changed. Thus, in the premise of Q_{all} is constant, the process simulation should be applied to increase the heat removal of the intermediate and gas oil pump-arounds. By combining with the practical operation experiences, simulations should be carried out repeatedly to make sure the optimal heat recovery.

(2) All the new hot and cold streams data must be defined. The corresponding pinch diagram can be drawn by means of ASPEN PINCH in which the minimum utility requirement can be estimated. If the difference between the actual hot utility and minimum hot utility is less than C2 which is defined by the tradeoff between the capital and energy costs involved, the HEN is optimal. Otherwise, the HEN is not the best and there exist optimization potentials.

(3) If there is a potential for HEN retrofit, there are three design objectives for HEN retrofit. The first one is to maximize the T_{feed}. So the theoretically maximum T_{feed} should be defined by pinch diagram in which the radiation oil heated by the coking furnace, and the deaerated water should not be included. The second one is to generate the maximum steam through process streams within the units. In the pinch analysis, the radiation oil is not included. The deaerated water for steam generation should be heated possibly by using hot process streams. The third one is to consider the tradeoff between the T_{feed} and the quantity of generated steam.

(4) In objective 1, or 2, three pinch principles should be carried out to retrofit the HEN.
(5) In the objective 3, to define the best HEN through calculating minimum *TAC* model.

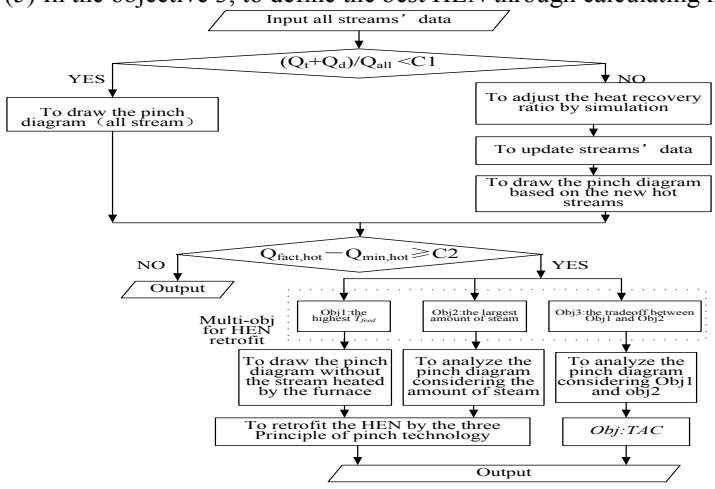

Fig. 2 Flowchart of steps for HEN optimization by integrating the fractionating process

1.2. TAC model

HEN superstructure: For the objective 3, Fig. 3 shows a superstructure with seven stages for a one-cold and four-hot stream synthesis problem. It is assumed that there is no split for feed. The order of the hot streams is defined by comparing the temperature levels. *TAC* is used as the objective function to be minimized which includes the annualized capital costs and operating costs. (Douglas JM, 1988).

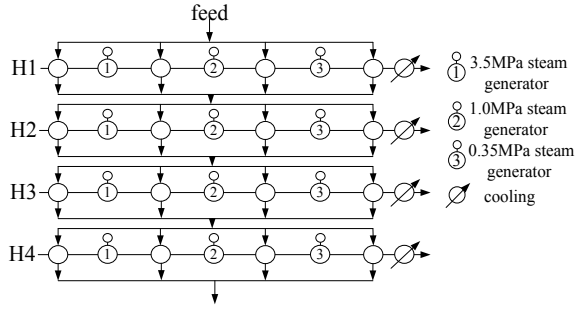

Fig. 3 HEN superstructure

Minimum TAC:

$$\frac{\sum_{j\in J}\sum_{k\in k1} Z_{jk}SS + \sum_{j\in J}\sum_{k\in k2} Z_{jk}CS + \sum_{j\in J} Z_{cuj}CS}{Payback\ period} + \sum_{j\in J} Z_{cuj}C_w + C_{hu} - \left(\sum_{j\in J} Z_{j2}C_{3.5s} + \sum_{j\in J} Z_{j4}C_{1.0s} + \sum_{j\in J} Z_{j6}C_{0.35s}\right) \quad \text{(Eqn. 5.)}$$

Overall heat balance:

$$F_j\left(T_{j,in} - T_{j,out}\right) = \sum_{k\in K} q_{jk} + q_{cuj}\ ,\ F_{feed}\left(T_{feed} - T_{f,in}\right) = \sum_{j\in J} q_{j1} + \sum_{j\in J} q_{j3} + \sum_{j\in J} q_{j4} + \sum_{j\in J} q_{j7} \quad \text{(Eqn. 6.)}$$

Assignment of superstructure inlet temperature and monotonic decrease in temperature:

$$t_{j,k} = T_{j,in},\ T_{f,in} = T_{f,1},\ T_{feed} = T_{f,out} = T_{f,5} t_{j,k} \leq t_{j,k+1}\ , j \in J, k \in K,\ t_{f,j} \leq t_{f,j+1}\quad j \in J \quad \text{(Eqn. 7.)}$$

Heat loads of hot and cold utilities:

$$Q_c = F_j\left(t_{j,8} - T_{j,out}\right)\ ,\ Q_f = F_f\left(500 - T_{feed}\right) \quad \text{(Eqn. 8.)}$$

Approach temperature and logical constraints:

$$d_{tjk} \geq \Delta T_{\min} \quad d_{tcuj} \geq \Delta T_{\min}, q_{j,k} \leq \alpha_{zjk} \quad q_{cuj} \leq \alpha_{zcuj} \tag{Eqn. 9.}$$

$$Z_{j1} + Z_{j3} + Z_{j5} + Z_{j7} \leq 1 \quad j \in J \tag{Eqn. 10.}$$

Internality conditions and bound limitations:

$$Z_{jk}, Z_{cuj} = 0,1 \quad j \in J \ , \ T_{j,out} \leq t_{j,k} \leq T_{j,in} \quad T_{f,in} \leq t_{f,j} \leq T_{feed} \quad j \in J, \ k \in K \tag{Eqn. 11.}$$

$$q_{jk} \geq 0, \ q_{cuj} \geq 0 \quad j \in J, \ k \in K \tag{Eqn. 12.}$$

4. Case study

A DCU is taken as an example to study for introducing objective 1. In Fig. 4a, the curve which includes all streams indicates that the pinch point is at T_p=149℃.

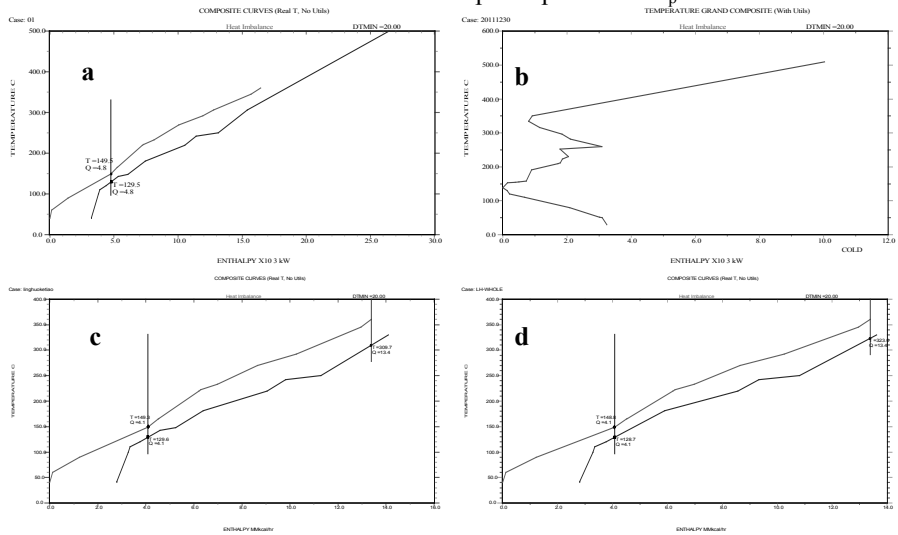

Fig. 4 DCU representation as composite and grand composite curves

From Fig. 4b, we can find that a pocket above 140℃ until 334℃ exists. The corresponding pinch diagram is shown in Fig. 4c for keeping the generated steam constant. Thus the deaerated water for steam generating is included in the streams. However, the residual oil heated by the coking furnace is used to heat the feed, so it is not included in the pinch analysis. Furthermore, a new pinch diagram is presented in Fig. 4d in which the cold streams don't include the deaerated water. On this figure, the maximum feed temperature T_{feed} is nearly 323℃. The current and new topology is presented in Fig. 5. After retrofit four heat exchangers are added, and 1435kW of hot utility can be saved. The steam generated with pressure of 1.0MPa decreased by 2.34 t/h. It is remarkable that the T_{feed} is near to the theoretical temperature.

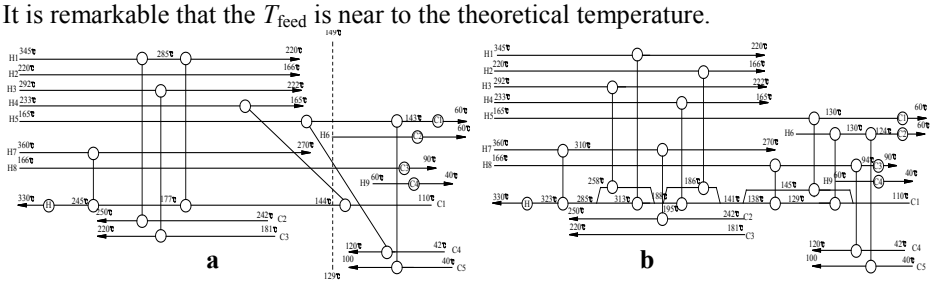

Fig. 5 Structure of the heat exchanger network of DCU

5. Conclusions

Based on a thermodynamic analysis presented for three typical flowsheets with different heat exchange and fractionating processes, the energy-use retrofit potentials are identified. An approach for retrofit design of the HEN through integrating the fractionating process in DCUs is proposed by considering the limitation of the energy integration within the whole plant, the temperature at the bottom of the main fractionator and the quantity of steam generated, etc. Three design objectives of the maximal feed preheating, the maximum quantity of steam generated and the minimum annual cost are taken for energy-use optimization of the unit. A practical delayed coker is analyzed and optimized to illustrate the performance of the design approach so as to make the feed temperature of the coking furnace T_{feed} maximal through integrating the energy-use improvement of the main fractionator. The results obtained demonstrate that the HEN of a delayed coker can be improved feasibly in accordance with the requirements of the whole unit.

Acknowledgement

The authors gratefully acknowledge the financial support from the National Natural Science Foundation of China (No. 20906016, 21076233) and the Major Science and Technology R&D Program of Guangdong Province (No. 2010A080801003).

References

Q. L. Chen, Q. H. Yin, S. P. Wang, B. Hua, 2004, Energy-use analysis and improvement of delayed coking units, Energy, 29, 12-15, 2225-2237.

F. Rodriguez-Reinoso, P. Santana, E. R. Palazon, M. -A. Diez, H. Marsh, 1998, Delayed coking: industrial and laboratory aspects, Carbon, 36, 1, 105-116.

M. Morar, P. S. Agachi, 2010, Review: Important contributions in development and improvement of the heat integration techniques, Comput. Chem. Eng., 34, 1171-1179.

V. Plesu, G. Bumbac, P. Lancu, I. Ivanescu, D. C. Popescu, 2003, Thermal coupling between crude distillation and delayed coking units, Appl. Therm. Eng., 23, 1857-1869.

B. J. Zhang, X. L. Luo, Q. L. Chen, C. W. Hui, 2011, Heat integration by multiple hot discharges/feeds between plants, Ind. Eng. Chem. Res., 50, 18, 10744-10754.

B. A. Al-Riyami, J. Klemes, S. Perry, 2007, Heat integration retrofit analysis of a heat exchanger network of a fluid catalytic cracking plant, Appl. Therm. Eng., 21, 13-14, 1449-1487.

J. M. Douglas, 1988, Conceptual design of Chemical process, McGrawHill, New York.

Nomenclature

CS--cost for lower *T* (≤200 ℃) heat exchanges

SS--cost for lower *T* (⩾ 200 ℃) heat exchanges

F--heat capacity flowrate

α-- an upper bound for heat exchange

ΔT_{min}--minimum approach temperature

Subscripts

all--total pump-around heat removal

d--diesel pump-around heat removal

j--hot stream, set $J=\{j \mid 1,2,3,4\}$

k--index for stage, and temperature location, set $K=\{k \mid 1,2,3,4,5,6,7\}$

t--top pump-around heat removal

s--steams

w--cooling water

Positive, continuous variables

d_{tjk}--temperature approach for (j, $=k$) at the hot end

$t_{j,k}$ --temperature of stream j at the hot end of k

d_{tcuj}-- temperature approach for (j, *cu*)

t_{fj} -- temperature of stream feed at the hot end heat exchanging with stream j

q_{jk} -- heat exchange between (j, *feed*) in k

q_{jcu} --heat exchange between (j, *cu*) in k

Binary variables

Z_j--existence of unit for march(j,f) in stage k

Z_{cuj}--existence of unit for march(j,*cu*)

I.A. Karimi and Rajagopalan Srinivasan (Editors), Proceedings of the 11th International Symposium on Process Systems Engineering, 15-19 July 2012, Singapore.

On an Operational Model and a Computer Support Environment for Batch Plants Based on Adaptive Scheduling –Application of simulators to obtain initial conditions for rescheduling–

Hisaaki Yamaba, Shigeyuki Tomita

University of Miyazaki, 1-1, Gakuen Kibanadai-nishi, Miyazaki, Japan

Abstract

Scheduling is one of the most important features in production management. Production systems are operated according to schedules in order to minimize production costs and complete the production of given demands by their due dates. However, production cannot be often carried out as scheduled because of problems or accidents such as reactor malfunctions and tardiness of chemical reactions. Even in such situations, production activities must continue while modifying the original schedules. In the present study, an operational model of a production system, which is used to continue production under uncertainties, was considered. A series of experiments was carried out using a computer-aided environment developed based on an object-oriented approach in order to evaluate the performance of the proposed method for various parameters.

Keywords: Batch plant, rescheduling, object-oriented

1. Introduction

In order to minimize production costs and complete production on time, production systems are operated according to a schedule. However, production cannot be carried out on a given schedule because of problems or accidents such as malfunctioning reactors or tardiness of chemical reactions. Even under such circumstances, production activities must continue while modifying the original schedule. At present, such modifications of schedules are carried out based on human experience. Therefore, a rational manner of dealing with problems and accidents is needed.

In the present study, an operational model of a production system that continues production activities under production environments with various uncertainties is considered. Concretely, the following features are of interest:

1. How to determine whether rescheduling should be performed.
2. How to determine which jobs should be rescheduled and which jobs should be processed according to the original schedule.
3. How to process jobs that should be processed according to the original schedule, which no longer works well.

These factors should be fixed depending on the configurations of target plants. In order to determine the three factors described above, a simulation-based approach was adopted. A computer-aided environment that consists of simulators and schedulers is developed based on an object-oriented approach. In the present study, a series of experiments is carried out using this environment in order to evaluate the performance of the proposed method for various parameters.

2. Basic Concept of the Operational Model

Figure 1 shows the basic concept of the operational model proposed herein.
(1) First, a scheduler makes an original schedule for a given demand. The plant starts production as scheduled. However, when it becomes difficult to continue production under the current schedule because of problems or accidents, rescheduling is carried out and the production is shifted from the original schedule to another schedule after a given switching time.
(2) In order to make out a modified schedule, the progress of production in the target time window is needed as the initial condition for the rescheduling. In order to obtain the information, a plant simulation system is introduced. The simulator works according to the conditions of the plant with the operational policy of the plant.
(3) The simulation results (e.g., the working conditions of the plant) are fed to the scheduler of the support environment. Using the information as the initial condition, the scheduler makes out a modified schedule that starts from the switching time point.
(4) By switching to the new modified schedule at the switching time, the target plant can continue seamless production.

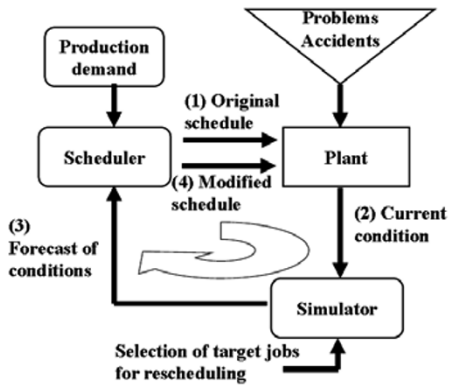

Figure 1. Concept of the proposed support method of production.

3. Class of Target Production System

In the present study, a job refers to a single process in a sequence of processes required for each final product. Production demands are sent to the plant in a periodic fashion. A schedule of demands given in the *i-1*th period is made in the *i*th period, and the demands are processed in the *i+1*th period. The productive capacity of the target plant is assumed to be balanced with the production load of given demands. Therefore, a schedule of the *i*th period has to be created under the condition that some jobs in the schedule of the *i-1*th period are pushed to the *i*th period. The concept of adaptive scheduling (Tomita 1991a) was proposed in order to cope with such production systems by iterative scheduling.

4. Operational Method

In the present study, as an example of a concrete problem, the tardiness of the operation is considered.
The basic concept of the proposed method is shown in Figure 2. In the Gantt charts for each machine, the lower rows represent schedules, and upper rows represent the corresponding progress.

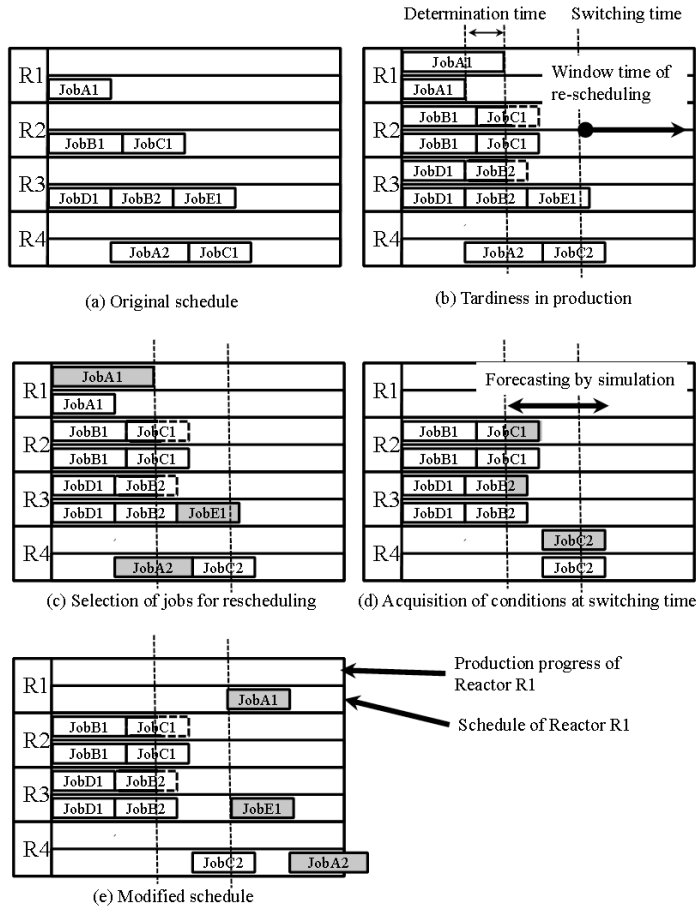

Figure 2. Proposed operational method.

1. First, the original schedule is given (Figure 2(a)).
2. When the progress of production is not in agreement with the original schedule because of problems or accidents, the plant operator must decide whether to modify the current schedule. This determination is made when a job does not end within a fixed time from the scheduled end time for the job. This fixed length of time is hereinafter referred to as the determination time (Figure 2(b)).
3. If rescheduling is performed, the switching time, which is the start time of the schedule window of the rescheduling, is first decided. In the present study, the modified schedule will start *n* time units after the determination time (Figure 2(b)).
4. Next, jobs that have not been completed are divided into two groups: jobs that are the target of rescheduling and jobs that are performed according to the current schedule. In the present study, jobs that do not start at the determination time are selected as targets for rescheduling (Figure 2(c)).
5. The jobs in the former group are performed under the policy described later in step 8.
6. A modified schedule is generated for the jobs belonging to the latter group. The target schedule span is from the switching time to the end time of the current production period. In order to create a feasible schedule, the condition of the plant in the target scheduling span must be given. A plant simulator is used to forecast the condition. (Figure 2(d)).

7. After the switching time, the plant is operated according to the new schedule (Figure 2(e)).
8. During the period from the decision time to the switching time, production is carried out according to the original schedule. However, the start time of each job is delayed according to the tardiness of the schedule. In particular, in order to synchronize the time to transfer materials between an upper reactor and a lower reactor, an additional waiting operation must be included in the process flow

The appropriate determination time and time span from the determination time to the switching time are considered to depend on the features of each production environment and each plant. In the present study, these times are decided through simulation experiments. In the next section, the performances of several candidate determination times are investigated under various production environments.

5. Experiments

The operation support environment for production systems that consists of schedulers Bpos (Tomita 1991b) and simulators was developed based on the above-described operation model using an object-oriented approach (Yamaba 2008). A series of experiments was carried out in order to evaluate the influence of the above-mentioned operational parameters on the performance of a model plant.

5.1. Conditions

The production period of the model batch plant was one day. A single experiment involved a series of seven-day simulations. The switching time was set to 30 time units after the time at which it was decided to perform rescheduling. The purpose of the experiments is to investigate the influence of the length of the determination time on the productive performance of a plant. Four delay generation environments were introduced for three candidate determination times. The results were evaluated as the total delay time of jobs that were not completed on the scheduled day. One delay was generated in one day. A delayed operation was selected at random. The duration of the delay was calculated according to the regular distributions listed in Table 1. The three candidate determination times were 50 time units, 100 time units, and never rescheduling.

Table 1. Delay generation environments

	Average	Distribution
1	30	50
2	80	50
3	100	50
4	200	50

5.2. Experimental Results

The experiments were carried out for 15 combinations of the three determination times and the four delay generation environments. Seven-day simulations were repeated five times for each set of 15 experiments. Figure 3 plots the average total delay times obtained in the experiments. In the experiments using delay generation environments 3 and 4 (respective average delay times: 100 and 200 time units), the shortest delay time was obtained when the decision time was 50 time units. Under the condition in which rescheduling was not performed, the total delay time was the longest, which means that rescheduling was effective in delay generation environments that generate longer delays. On the other hand, in environment 1 (average delay time: 30 time units), no job was delayed under the condition in which rescheduling was not executed. Moreover, some jobs were delayed when the decision time was set to 50 or 100 time units.

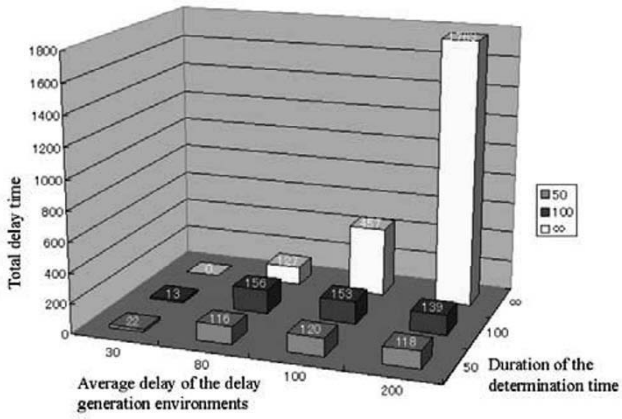

Figure 3. Experimental results.

In general, some of the jobs selected for rescheduling may have been scheduled to be processed between the determination time and the switching time in the original schedule. Since the new start times of such jobs must be postponed until after the switching time in the modified schedule, the modified schedule tends to be tight, which means that the rescheduling results in lower performance when the expected average delay time is shorter. However, for the case in which the expected delay time is longer, earlier determination of rescheduling reduces the delay in production. The boundary of the average delay time to determine whether rescheduling should be performed is indicated to be 80 time units under the conditions of the experiments.
Since the validity of knowledge obtained based on these results is limited to the conditions used in these experiments, the support environment was confirmed to be useful for obtaining the parameters of the proposed management method.

6. Conclusions

In order to manage a batch type chemical plant under uncertain conditions, a management support method was introduced along with a computer-based support system, which consists of simulators and schedulers. A series of experiments was carried out using this environment in order to evaluate the performance of the proposed method for various parameters. The experimental results demonstrate the effectiveness of this environment.

References

S. Tomita, H. Yamaba, E. O'shima, 1991a, On an Intelligent Scheduling System for a Parallel Distributed Process of Multi-Product - An attempt of developing an 'Adaptive scheduling' system -, Proceeding of 4th International Symposium on Process Systems Engineering (PSE '91), II, 19.1-19.15.

S. Tomita, H. Yamaba, E. O'shima, 1991b, Development of an intelligent Scheduling System for Managing Multipurpose Chemical Batch Plant - An attempt to exploit heuristic rules for developing an 'Adaptive' scheduling system - (In Japanese), Kagaku Kogaku Ronbunshu, 17, 740-749.

H. Yamaba, M. Hirosaki, S. Tomita, 2008, An Operational Model and a Computer Support Environment for Batch Plants Based on Adaptive Scheduling, Proceedings of 12th International Conference on Knowledge-Based and Intelligent Information and Engineering Systems, III, 33-40.

I.A. Karimi and Rajagopalan Srinivasan (Editors), Proceedings of the 11th International Symposium on Process Systems Engineering, 15-19 July 2012, Singapore.

A Comparison Study of Adjoint-Based Gradient Search Technique and Mathematical Programming for Optimal Well-Placement

R.Y. Toh[1], M.S. Tavallali[1], W.X. Leow[1], I.A. Karimi[1*]

[1]*Department of Chemical & Biomolecular Engineering*
National University of Singapore
4 Engineering Drive 4, Singapore 117576

Abstract

Optimal well placement in petroleum fields has an immense techno-economical importance. It is vital to choose the correct mathematical tool to address this important problem. Therefore, in this study we compare the adjoint-based gradient search method with a mathematical programming approach in terms of the efficiency and solution quality when addressing well placement problems.

Keywords: Adjoint-Based Gradient Search Technique, Mathematical Programming, Optimal Well Placement

1. Introduction and Previous Research

Worldwide energy demand has been steadily increasing. In order to meet energy challenges of the future, optimal recovery from all marginal, mature and any possible new hydrocarbon fields is necessary. Well placement can clearly affect the efficiency of petroleum recovery and is therefore of utmost importance.

Multiphase flow in porous media of reservoirs is represented via a set of coupled PDEs. The numerical simulators use its discrete format due to their limitations. Since wells are presented only in the cells that accommodate them (and not other grids), the problem becomes non-differentiable with respect to well location. Hence, optimal well placement is often treated as a discrete problem which will render the solutions computationally very expensive. It is therefore important to choose the right mathematical tool to solve this complicated problem.

Evolutionary methods, as the first option, are simple to use but yet are very time-consuming (Yeten et al, 2003). Gradient based approach as the second option, requires converting the problem into their compatible format and subsequently the adjoint gradient method can efficiently provide gradient information (refer to Jansen (2011)). Researchers such as Zandvliet et al. (2008) and Forouzanfar (2010) have employed pseudo well approach for this purpose. Finally, mathematical programming as the third option, has not considered the dynamic behavior of the system in details. Recently, Tavallali et al (2011) and Leow et al (2012) have modeled the dynamic well placement problem as a mixed integer nonlinear programming problem and modified the outer approximation, with equality relaxation and augmented penalty (OA/ER/AP) algorithm to solve the model.

Cleary there are both advantages and disadvantages associated with using any of above methods. This paper uses the mathematical model of Leow et al. (2012) as the

[1*] Corresponding author: Tel.: +65 6516-6359, Fax: +65 6779-1936, Email – cheiak@nus.edu.sg

main platform and solves that by both OA/ER/AP and (after customizing the model) by the pseudo-well approach of Zandvliet et al. (2008). The remaining parts of this paper are organized as follows: we start with the problem definition and formulation; we present a case study and finally provide a description of both algorithms and qualitatively compare both approaches.

2. Problem Definition

Given an oil reservoir with existing wells, the goal is to expand the production by infill drilling of new wells. Relevant petro-physical data and economical data such as projected demand curve, drilling costs, discount rate, as well as operational data such as water-cut limits, production and injection capacity expansion plan for surface facilities are also provided beforehand. It is assumed that the reservoir is a horizontal 2D plane with water and oil phases and the main driving mechanism is water-drive injection.

The objective of the mathematical programming model is to maximize the net present value (NPV) of oil production over a fixed planning horizon through the determination of new well locations.

3. Formulation

As per Tavallali et al. (2011) and Leow et al. (2012) we include the equations describing multiphase flow in a reservoir with spatial and implicit time discretization. These include water and oil mass balances and mobilities in equality form. A series of inequalities provide more information regarding the physical and operational relations and they include, ratio of water and oil flow rates, pipe flow relation for producers and injectors, water cut, demand and capacity constraints. For more information refer to the aforementioned papers. We use their MINLP model for the mathematical programming approach and for the gradient based search we slightly customize that by removing the binary variables and defining well set. A concise representation of that is as follows:

Sets:

t : Discrete time domain; n: Discrete spatial domain; W: All wells

Variables:

x_n^t : State variables (Pressure, saturation); m_n^t : Intermediate variables (Phase mobility)

u_n^t : Control variables (Total well flow rate, +ive for producer and –ive for injectors)

q_n^t : Output variables (Oil flow rate)

Objective Function:	$\min \sum_{t\geq 2} \sum_{n\in W} J_n^t(u_n^t, q_n^t)$	NPV	(1)
Subject to:			
System Equations:	$g_n^t(u_n^t, q_n^t, x_n^t, x_n^{t-1}, m_n^t) = 0;$	Mass balance	(2)
Initial Conditions:	$x_n^1 = \breve{x}_n^1$	Initial state	(3)
Intermediate Constraints:	$c_n^t(x_n^t, m_n^t) = 0$	Mobility	(4)
Output Constraints:	$h_{n\in W}^t(u_n^t, x_n^t, q_n^t, m_n^t) \leq 0$	Pipe flow	(5)
Other Inequality Constraints:	$d_n^t(u_n^t, q_n^t, m_n^t) \leq 0$	Water Cut, etc	(6)

4. Algorithm

4.1. Gradient based search

Figure 1-a presents this algorithm. Given a set of proposed injectors and producers (an initial guess), Zandvliet et al. (2008) introduced a set of pseudo-wells with negligible flow rate into the eight adjacent grid-blocks of each proposed well. Their flow rates should have minimal impact on reservoir states. The gradient of the objective function over the simulation time with respect to flow rate of each pseudo-well can be determined via adjoint gradient calculation approach. Each potential well would then move into the pseudo-well grid-block with the largest value among the eight adjacent cells. This process is repeated for the new potential well location until selected wells alternate between two different positions. There are no binary variables in this method.

To use the adjoint gradient calculation method, Euler-Lagrange function is constructed with all constraints being adjoined to the objective function. A forward simulation (reservoir production simulation) provides the value of gradient of each constraint with respect to different variables and a backward LP simulation calculates the Lagrangian multipliers and the targeted derivative. For more information about this method, refer to the review paper of Jansen (2011).

4.2. Mathematical Programming and Outer approximation

Figure 1-b shows this approach. As before, the master MILP problem is responsible for the search and the primal NLP problem evaluates the proposed solution. However, method of Tavallali et al (2011) adds few steps to the outer approximation, with equality relaxation and augmented penalty (OA/ER/AP) algorithm. Firstly, considering the dynamic nature of the problem, they solve the primal problem sequentially by marching into the time domain. Secondly, before terminating the search procedure, they perform series of local searches to partially check the local optimality.

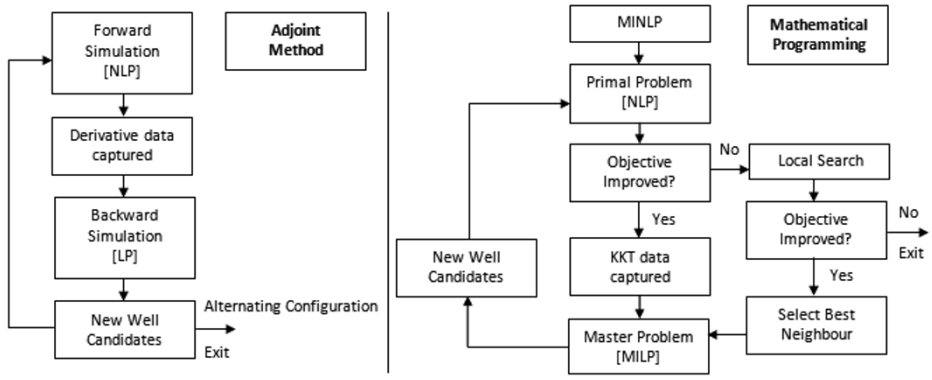

Figure 1-a. Adjoint-based technique flowchart Figure 1-b. Mathematical Programming flowchart

5. Case Study

Considering a 20x20 reservoir with 3 existing producers and 2 existing injectors labeled as “PRO” and “INJ” in figure 2. Computation was performed in an identical manner as described by Leow (2012) with the addition of the CPLEX solver for the backward simulation. The goal is to locate the best drilling site for a new producer in this oil field. To do the gradient dependant search, we had to develop our own in-house adjoint gradient evaluator tool box that can consider the inequality constraints. For this purpose we used the value of slack variables and only considered the binding inequalities.

A brute force search was conducted by introducing new producers at every possible location with the exclusion of the existing wells; the heat map of Figure 2 denotes its outcome. Both mathematical programming and adjoint-based gradient search technique approaches were utilized by identical initial guesses and in the diagram above we present 2 sets of them. The numbered configurations represent the steps that the gradient search method takes from an initial guess "1"; termination involves alternating configurations represented by the curved arrows. Additionally, the straight black arrows denote the initial and final well location as determined by the OA/ER/AP algorithm from the same initial guesses. Convergence criteria as described by Zandlivet et al. (2008) involved alternating between two well configurations. This was shown to be the case for the majority of our tests (the pair of curved arrows). However, there are instances where cycling would occur. The unpaired curved arrows denote such an occurrence. For example the initial guess at [4,11] would result in a series of new well candidates that would eventually return [4,11] and thus repeatedly cycle. Cycling can be easily dealt with by storing all previous well candidates and terminating if any candidate is selected twice. With suitable initial guesses both methods converge to their global optimal location as determined by the brute force search.

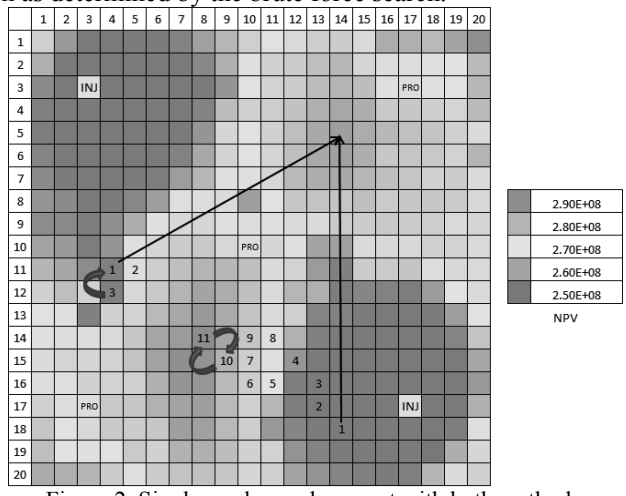

Figure 2. Single producer placement with both methods

To our knowledge there is no comparison of these two approaches, specifically for optimal well placement problem in literature. Therefore, based on both available literature and mainly our own experience, we provide a comparison both approaches:

Table 1. Comparison between Mathematical Programming and Adjoint-Based Gradient Search Technique for well placement problem

	Mathematical Programming	**Gradient Method**
Problem type	Primal – NLP	Forward – NLP
	Master – MILP	Backward – LP
Preliminary preparation	MILP model preparation	Backward LP preparation
Inequality handling	Simple	Might be difficult
Information collected from Reservoir Sim.	Values of all variables and Lagrangian multipliers	Values of all variables (and slack variables if required)

Search engine	Master MILP section	LP backward and steepest ascent method
Reducing number of wells	By setting the well binary variable to zero	By merging two or more wells into a same cell
Optimum no. of wells	Can check, but maximum number should be specified	Can check, but maximum number should be specified
Well configuration constraints	The background MINLP model handles implicitly	The algorithm should intervene during iterations
Initial guess	Important	Very important
Objective value improvement	Is assured	Not guaranteed
Cycling	Integer-cut prevents that	Can happen
Termination criteria	Heuristic, deterioration of objective value	Alternating or cycling heuristic
Search time duration	Longer, keeps increasing per each iteration	Shorter, may decrease per iteration as two well merge

6. Conclusion

In this paper we provided a qualitative comparison between mathematical programming and an adjoint-based gradient search method for optimal well placement. Both approaches are currently at research stage and require improvement to be able to handle uncertain and large size problems. However, in a general comparison with evolutionary search methods, they are faster and might be able to handle more detailed problem such as scheduling the drilling order, and simultaneous well placement and well optimal control.

7. Acknowledgements

We would like to extend our gratitude to Schlumberger for the provision of the VFPi software to aid us in our work.

References

Forouzanfar Fahim**,** Gaoming Li & A.C. Reynolds (2010): A two-stage well placement optimization method based on adjoint gradient , 2010 SPE Annual Technical Conference and Exhibition , Florence, Italy

Jansen, J.D. (2011). "Adjoint-based optimization of multi-phase flow through porous media – A review." Computers & Fluids **46** (1): 40-51

Leow, W.X., Tavallali, M.S., Karimi, I.A., & Teo, K.M. (2012). Simultaneous Optimal Placement of Injector and Producer Wells Using Mathematical Programming. 11th International Symposium on Process Systems Engineering, Singapore.

Tavallali, M.S., Karimi, I.A., & Teo, K.M. (2011). Dynamic Optimal Well Placement In Oil Reservoirs. Annual Meeting of AICHE. Minneapolis, USA.

Zandvliet, M.J., Handels, M., van Essen, G.M., Brouwer, D.R. & Jansen, J.D. (2008). Adjoint-based well-placement optimization under production constraints. SPE Journal **13** (4): 392-399.

Yeten B., Durlofsky, L.J., & Aziz, K. (2003). Optimization of Nonconventional Well Type, Location, and Trajectory. SPE Journal **8** (3): 200-210.

I.A. Karimi and Rajagopalan Srinivasan (Editors), Proceedings of the 11th International Symposium on Process Systems Engineering, 15-19 July 2012, Singapore.

Minimization of storage requirement in a batch process using pinch analysis

Nitin Dutt Chaturvedi* and Santanu Bandyopadhyay

Department of Energy Science and Engineering, Indian Institute of Technology Bombay, Powai, Mumbai 400 076, INDIA
**corresponding author's E-mail: nitin.chaturvedi@iitb.ac.in*

Abstract

In this paper an algebraic algorithm, based on the concepts of pinch analysis, is proposed to determine the minimum storage requirement for a batch process, while satisfying the minimum resource requirement. The proposed algorithm can be applied to any fixed flow rate and fixed scheduled batch process involving single quality. The proposed algorithm is proved for optimality on basis of rigorous mathematical arguments and also provides physical insight to the problem.

Keywords: batch process; pinch analysis; storage optimization; resource minimization.

1. Introduction

In recent years, significant research efforts are directed to minimize resources (such as: energy, freshwater, cooling water, hydrogen, raw materials, etc.) in batch processes. Most of the work is directed towards water minimization (Gouws et al., 2010). The methods are often categorized as mathematical based optimization (Almató et al.,1999; Majozi, 2005; Chen et al., 2010) and pinch based optimization (Wang and Smith, 1995; Kim, 2011). Recently, a hybrid approach, known as automated targeting technique, has been developed by Foo (2010). Although networking is considered as more important than targeting part but still in batch process it is less focused. Optimizing the storage requirement is also an important aspect considering network complexity, space limitation as well as capital investment. In this paper a mathematically rigorous algorithm is proposed to determine the minimum storage requirement to satisfy the minimum resource requirement for a single batch process The methodology is based on concepts of pinch analysis so provides physical insight understanding of problem.

2. Problem definition

A general problem to determine the minimum storage requirement, for a batch process satisfying the minimum resource requirement, may be given as follows: (i) A set of internal demands is given. Each demand requires a defined flow at a given maximum allowable quality for a fixed interval of time. (ii) A set of internal sources is also given. Each source produces a fixed flow at a given quality for a fixed interval of time, which can be used in internal demands appearing during or after the availability of source flows. (iii) An external source, called resource, is also available to satisfy the requirement of internal demands, at a given quality (q_{rs}). (iv) The objective is to determine the minimum storage requirement while satisfying the minimum resource requirement.

3. Minimum storage algorithm (MSA)

The following algorithm is proposed to determine the minimum storage requirement

while satisfying the minimum resource requirement.

1. Divide the entire time horizon of batch process into several time intervals (say T_1, T_2, T_3, ..., T_n) considering start and end time of each source and demand.
2. Integrate the sources and demand within each interval to calculate pinch location and waste profile (maximum possible flow available at each source quality after integration) of each interval.
3. Add the waste profile from time interval T_1 as sources to next time interval T_2. Recalculate resource requirement, waste profile, and pinch location (say end pinch location, q_{Pte2}) at the end of interval T_2 .Calculate the storage requirement as the wastes of time interval T_1 utilized in time interval T_2 as follows:
   Storage requirement at given quality level can be calculated using Equation (1).
   $$Storage\ \ requirement = W_T - W_{ie} \quad (1)$$
   W_T is the waste transferred at that quality level from other intervals and W_{ie}, is the net waste generated after the transfer in interval T_i at a given quality level. It may be noted that if $W_T - W_{ie}$ is negative than storage is considered to be zero.
4. Repeat Step 3 and 4 to calculate individual pinch location (q_{PTi}), waste profile at the end of the time interval and the end pinch location (q_{PTei}) for all the subsequent time intervals.
5. Apply the following three rules to reduce the storage requirement:
   Rule 1: Waste transfer is to be carried out directly from interval T_i and T_{i+1} to T_{i+2} for the case where $q_{PT_{i+2}} \geq q_{PT_{i+1}} \geq q_{PTe_i}$, till the overall resource requirement till T_{i+2} is unaffected.
   Rule 2: For the cases where waste transfer only leads to its redistribution into higher and lower qualities but does not affect the resource requirement, then this redistribution is skipped if it does not give any resource reduction on transferring to subsequent time intervals.
   Rule 3: For the cases where, $q_{PTe_{n-l}} \geq q_{PT_{n-l+1}} \geq ..... \geq q_{PT_n}$ any indirect waste-transfer is not required.
6. List out storage requirement at each quality level and its duration. Select the highest value of storage requirement on same quality level having completely different duration of requirement of storage. Sum up individual storage requirements to get total storage requirement.

It may be noted that source composite method (Bandyopadhyay et al., 2006) is used to calculate minimum resource requirement and waste profile.

4. Mathematical proof

Mathematical induction method is used to prove minimum storage algorithm (MSA). For any resource allocation network it is proved by Pillai and Bandyopadhyay (2007), that minimization of the external resource requirement (R) is equivalent to the minimization of the total waste generation (W). Therefore, it is sufficient to minimize the overall waste generation to minimize the overall resource requirement. To calculate the change in waste flow, expression for the minimum waste generation, as derived by Pillai and Bandyopadhyay (2007), is utilized in this paper. However, detailed calculations are not shown for brevity.

A batch process containing only two time intervals (T_1 and T_2) is considered first. Let q_{PT1} and q_{PT2} be the individual pinch qualities respectively, when these time intervals are solved without integration. Let δ amount of flow is transferred (at a quality of q_{si}) from interval T_1 to interval T_2 such that the pinch qualities of both the time intervals

remain same. The changes in overall waste generation for all possible cases are expressed as follows:

$$\Delta W = \begin{cases} 0 & \text{when } q_{si} \geq q_{PTt1}, q_{PT2} \\ \delta \dfrac{q_{PT1} - q_{si}}{q_{PT1} - q_{rs}} & \text{when } q_{PT1} \geq q_{si} \geq q_{PT2} \\ -\delta \dfrac{q_{PT2} - q_{si}}{q_{PT2} - q_{rs}} & \text{when } q_{PT2} \geq q_{si} \geq q_{PT1} \\ \delta(q_{si} - q_{rs}) \dfrac{(q_{PT1} - q_{PT2})}{(q_{PT1} - q_{rs})(q_{PT2} - q_{rs})} & \text{when } q_{PTt1}, q_{PT2} \geq q_{si} \end{cases} \quad (2)$$

It may be concluded that change in waste (ΔW) is negative (implies a reduction in overall waste generation) only when q_{PT1} is less than q_{PT2} which is Rule 3 of MSA.

A batch process containing three time intervals is considered now. There could be two options for transferring the waste: sequentially or directly. In sequential transfer, wastes of interval T_1 are transferred to interval T_2 and then combined wastes at the end of interval T_2 are transferred to interval T_3. In direct transfer, wastes of interval T_1 and T_2 are directly transferred to interval T_3. Let δ_{T1} amount of flow from pinch quality source (q_{PT1}) of interval T_1 and δ_{T2} amount of flow from pinch quality source (q_{PT2}) of interval T_2 are transferred to interval T_3 using both of these options. The change in waste generation, are calculated for sequential (ΔW_S) and direct transfer (ΔW_D) and their differences are summarized as follows:

$$\Delta W_S - \Delta W_D = \begin{cases} 0 & \text{Case 1} : q_{PT3} \geq q_{PT2} \geq q_{PT1} \\ -\delta_{T1} q_{PT1} \left(\dfrac{q_{PT2} - q_{PT3}}{(q_{PT2} - q_{rs}())(q_{PT3} - q_{rs})} \right) & \text{Case 2} : q_{PT2} \geq q_{PT3} \geq q_{PT1} \\ -\delta_{T1} \left(1 - \dfrac{q_{PT2} - q_{PT1}}{q_{PT2} - q_{rs}} \right) & \text{Case 3} : q_{PT2} \geq q_{PT1} \geq q_{PT3} \\ 0 & \text{Case 4} : q_{PT1} \geq q_{PT2} \geq q_{PT3} \end{cases} \quad (3)$$

Therefore, sequential waste transfer always leads to the minimum resource requirement. Cases 1 and 4 bring about Rule 1 and Rule 3 of MSA, respectively. There are two more cases to be considered: Case 5 ($q_{PT1} \geq q_{PT3} \geq q_{PT2}$) and Case 6 ($q_{PT3} \geq q_{PT1} \geq q_{PT2}$). In these cases, there is a possibility of waste profile change without any change in overall waste generation. Let δ_{T1} amount of flow (q_{PT1}) gets distributed in two different sources: a flow δ_u is added to higher quality source (q_u) and δ_l flow is added to lower quality source (q_l). The differences of the waste flows are expressed as follows:

$$\Delta W_S - \Delta W_D = \begin{cases} 0 & \text{Case 5a} : q_u, q_l \leq q_{PT3}, q_{PT3} \geq q_{PT1} \geq q_{PT2} \\ 0 & \text{Case 5b} : q_u, q_l \geq q_{PT3}, q_{PT3} \geq q_{PT1} \geq q_{PT2} \\ -\delta_u \left(\dfrac{q_u - q_{PT3}}{q_{PT3} - q_{rs}} \right) & \text{Case 5c} : q_l \leq q_{PT3} \leq q_u, q_{PT3} \geq q_{PT1} \geq q_{PT2} \\ 0 & \text{Case 6a} : q_u, q_l \leq q_{PT3}, q_{PT1} \geq q_{PT3} \geq q_{PT2} \\ 0 & \text{Case 6b} : q_u, q_l \geq q_{PT3}, q_{PT1} \geq q_{PT3} \geq q_{PT2} \\ -\delta_u \left(\dfrac{q_u - q_{PT3}}{q_{PT3} - q_{rs}} \right) & \text{Case 6c} : q_l \leq q_{PT3} \leq q_u, q_{PT1} \geq q_{PT3} \geq q_{PT2} \end{cases} \quad (4)$$

This signifies that when waste is redistributed across the pinch quality of interval T_3 (q_{PT3}) then sequential transfer leads to more or same reduction in waste as compared to direct transfer. These cases result in Rule 2 of MSA.

The MSA is assumed to be true for a batch process involving 'n' time intervals. Let us consider a batch process with '*n+1*' time intervals. There are two possible cases for $n+1^{\text{th}}$ time interval. For case A ($q_{PTe_n} \geq q_{PT_{n+1}}$) by our assumption, MSA guarantees the minimum storage requirement to satisfy resource requirement up to time interval T_n. This reduces our problem to an equivalent batch process involving only two time

intervals T_n and T_{n+1}. So as discussed in earlier section there is no reduction in resource requirement via waste transfer which is included in MSA via Rule 3. For case B ($q_{PTe_n} \le q_{PT_{n+1}}$), the role of the time interval prior to n^{th} time interval have to be investigated. For $n\text{-}1^{th}$ time interval again there could be two possible cases, for the case $q_{PTe_{n-1}} \le q_{PT_n}$, where the problem reduces to case 1 of batch process containing three intervals and such cases are included in Rule 1 of MSA. For the other case $q_{PTe_{n-1}} \ge q_{PT_n}$ the problem essentially reduces to case 5 and case 6 of the batch process having three intervals which are included in Rule 2. This proves the result.

5. Illustrative example: batch water network

Limiting water data for this example are given in Table 1. All the sources and demands are segregated into six time intervals T_1,T_2, T_3,T_4, T_5 and T_6 (0-1h, 1-2h, 2-3h, 3-4h, 4-5h and 5-6h) based on their start and end time points. Initially sources and demands lying within each time interval are integrated and individual pinch location (q_{PTi}) and waste generation (W_i) are calculated. Then, resource requirement and waste generation are for each interval is recalculated considering waste up to preceding interval as additional sources (Table 2) and storage requirement is calculated as 72.83 t using Equation (1).

Table 1: Limiting water data for the example

Source	Flow rate (t/h)	Conc. (ppm)	Duration (h)	Demand	Flow rate (t/h)	Conc. (ppm)	Duration (h)
S1	5	25	0.0-1.0	D1	10	0	0.0-1.0
S2	5	15	0.0-1.0	D2	40	27.5	1.0-2.0
S3	51.34	37.5	1.0-2.0	D3	5	15	1.0-3.0
S4	20	93.75	2.0-3.0	D4	5	25	2.0-3.0
S5	12.5	150	3.0-4.0	D5	100	84.375	3.0-4.0
S6	90	75	3.0-4.0	D6	100	33.75	3.0-4.0
S7	12.5	60	3.0-5.0	D7	35	10	4.0-5.0
S8	90	30	3.0-4.0	D8	20	5	5.0-6.0
S9	50	10	5.0-6.0				

Table 2: Storage calculation using sequential transfer

C (ppm)	W_1	W_2	W_3	W_4	W_5	W_6	W_1	W_{2e}	W_{3e}	W_{4e}	W_{5e}	W_{6e}
150	0	0	0	0	0	0	0	0	0	5	5	5
93.75	0	0	17.87	0	0	0	0	0	20	0	0	0
84.375	0	0	0	0	0	0	0	0	0	0	0	0
75	0	0	0	2.5	0	0	0	0	0	17.5	17.5	17.5
60	0	0	0	0	6.67	0	0	0	0	5	17.5	17.5
37.5	0	20	0	0	0	0	0	25.33	20	0	0	0
30	0	0	0	2.5	0	0	0	0	0	17.5	0	0
25	5	0	0	0	0	0	5	0	0	0	0	0
15	5	0	0	0	0	0	5	0	0	0	0	0
10	0	0	0	0	0	40	0	0	0	0	0	40
Cum. FW(t)	-	-	-	-	-	-	10	19	23.7	23.7	45.8	55.8
Storage								10	5.33	40	17	**Tot. 72.8**

Rule 1 ($q_{PTe1} \le q_{PT2} \le q_{PT3}$) of MSA is applicable to first three intervals (step 6). Hence, individual waste generation of interval T_1 and T_2 can be transferred directly to the interval T_3 instead of sequential supply from T_1 to T_2 and then to T_3 to reduce the storage requirement. Note that the cumulative resource requirement up to interval T_3 is unaffected while this transfer. Total 40 t of waste is generated (20 t at each 37.5ppm

and 93.75 ppm) at the end of third time interval. It can be observed from Table 2 that both wastes get redistributed when transferred to fourth interval without affecting resource requirement. But according to Rule 2 of MSA the transfer of 20 t at 93.75 ppm is not required as its distribution does not affect the overall resource requirement when transferred subsequent interval while skipping the waste redistribution of other one gives a penalty of 1.83 ton in resource requirement. The pinch at the end of time interval T_5 is higher than the pinch location of interval T_6. Hence, according to Rule 3 of MSA waste transfer from interval T_5 to T_6 is not required. Therefore, minimum 47.5 t of storage is required to satisfy the minimum resource requirement. (see Table 3).

Table 3: Storage calculation using MSA

C(ppm)	W_1	W_2	W_{3e2}	W_{4e2}	W_{5e2}	W_{6e2}
93.75	0	0	***20***	***20***	***20***	20
84.375	0	0	0	0	0	0
75	0	0	0	2.5	2.5	2.5
60	0	0	0	5	17.5	17.5
37.5	0	20	20	0	0	0
30	0	0	0	17.5	0	0
25	5	0	0	0	0	0
15	5	0	0	0	0	0
10	0	0	0	0	0	40
Cum FW	10	23.7	23.7	23.7	45.8	55.8
storage			10	20	17.5	**Tot. 47.5**

6. Conclusion

An algorithm is proposed to determine minimum storage requirement while satisfying targeted minimum resource requirement for a fixed flow rate and fixed scheduled batch process with single quality. The algorithm based on pinch analysis and proved rigorously using mathematical results therefore, guarantees the optimum solution. The methodology is applicable when single batch operation is carried out and cannot be applied when operation is carried out in cyclic mode. Such aspect is addressed as future work.

References

Almató, M.; Espuña, A; Puigjaner L. Optimisation of water use in batchprocess industries. Computers and Chemical Engineering, 1999 23, 1427-1437.

Bandyopadhyay, S.; Ghanekar, M.D.; Pillai, H.K. Process water management. Ind Eng Chem Res 2006 45, 5287-5297.

Chen, C.L; Lee, J.Y.; Ng, D.K.S.; Foo, D.C.Y. A unified model of property integration for batch and continuous processes. AIChE J. 2010 56, 1845-1858..

Foo, D.C.Y. Automated targeting for batch process integration. Ind. Eng. Chem. Res. 2010 49 (20), 9899-9916.

Gouws, J.F.; Majozi, T; Foo, D.C.Y.; Chen, C.L; Lee, J.Y. Water Minimization Techniques for Batch Processes, Ind Eng Chem Res 2010 49, 8877-8893.

Kim, J.K. Design of discontinuous water using systems with a graphical method. Chemical Engineering Journal 2011 172 799– 810.

Majozi, T. Wastewater minimization using central reusable storage in batch plants. Comput. Chem. Eng. 2005 29, 1631–1646.

Pillai, H.K.; Bandyopadhyay, S. A rigorous targeting algorithm for resource allocation networks. Chem. Eng. Sci. 2007 62, 6212–6221

Wang, Y.P., Smith, R. Time pinch analysis. Transaction of the Institute of Chemical Engineers 1995 73 Part A, 905—914.

I.A. Karimi and Rajagopalan Srinivasan (Editors), Proceedings of the 11th International Symposium on Process Systems Engineering, 15-19 July 2012, Singapore.

Targeting Minimum Heat Transfer Fluid Flow for Multiple Heat Demands

Mukund H. Bade* and Santanu Bandyopadhyay

Department of Energy Science and Engineering, Indian Institute of Technology Bombay, Powai, Mumbai 400 076, INDIA
**corresponding author's E-mail: mukundbade@gmail.com*

Abstract

In this paper, an algorithmic procedure, called resource targeting algorithm (RTA), is proposed to target the minimum flow rate of heat transfer fluid (HTF) used to supply heat from a single heater to multiple heat demands. The proposed methodology is based on the principles of pinch analysis. The applicability of RTA is demonstrated through an illustrative example.

Keywords: Pinch analysis; Targeting; Heat transfer fluid; Indirect heating

1. Introduction

Heat transfer fluid (HTF) is primarily used as an intermediate fluid to transfer heat from a heat source to other heat demands (or cold streams). Single heater can provide heat to any number of cold streams through HTF. The HTF is recirculating fluid that transfers heat through heat exchangers to cold streams and returns to the heat source (heater). Selection of HTF is based on the type of industrial applications, stable temperature range for safe operation and life of the HTF (Guffey 1997; Krishanan, 2005). Mckechnie (1927) proposed the design and manufacturing guidelines for HTF system. Design and operating problems of HTF system have been the main attention of manufacturers and process engineers. However, research related to HTF focused on individual components and not on the overall system. Traditionally, heat exchangers are arranged in parallel and hence, the inlet temperature of HTF is same in all the exchangers (Stoecker, 1989). However, such a parallel arrangement of heat exchangers need not guarantee the minimum flow rate of the circulating HTF. Determination of the minimum circulating HTF flow rate is important as the capital cost of the HTF can be reduced significantly. Use of HTF for process heating application may reduce number of fired heaters (Varghese and Bandyopadhyay, 2012). In this paper, an algorithmic methodology, called resource targeting algorithm (RTA), is proposed to target the minimum HTF flow rate to supply heat from single heater to multiple heat demands.

2. Minimum HTF flow rate targeting

The methodology to target the minimum HTF flow rate is analogous to the methodologies for analyzing cooling water system (Kim and Smith, 2001) and water management systems (Wang and Smith, 1994). Similar to cooling duties (Kim and Smith, 2001), all heat demands do not require HTF to supply at maximum stable temperature of HTF. This allows to change the heat exchanger network from parallel to

a series-parallel arrangement in most cases. A series-parallel arrangement of heat exchangers allows reuse of HTF so that the circulation flow rate of HTF can be reduced significantly. Sahu and Bandyopadhyay (2010) proposed an energy recovery algorithm (ERA) to target minimum hot and cold utilities requirement for heat integrated water network problems where the effects of contaminants can be neglected. ERA is suitably modified in this paper to target the minimum flow rate of HTF.

Capacity rate of HTF is the product of mass flow rate and specific heat at constant pressure. In this paper, specific heat of HTF is assumed constant and thus, minimizing mass flow rate is equivalent to minimizing capacity rate of HTF. Minimum temperatures of HTF for each process stream are determined by adding minimum approach temperature ($\Delta T_{\min}$) to the respective temperatures of cold fluids.

Steps of the proposed RTA are given as follows:

Step 1: Convert all cold streams temperatures (T_i) to minimum temperature for HTF by adding suitable minimum approach temperature ($\Delta T_{\min}$).

Step 2: Tabulate temperature of all the streams, including the maximum stable temperature of HTF, in decreasing order in the first column. If particular temperature occurs more than once, the same need not to be repeated. Without loss of generality, it can be said that a temperature for i^{th} row is denoted as T_i such that

$$T_1 > T_2 > \cdots > T_i > \cdots > T_n \tag{1}$$

Typically, T_1 represents the maximum stable temperature of the HTF (T_{rs}). The HTF is heated up to this temperature in the heater.

Step 3: Tabulate net capacity rates (i.e., product of mass flow rate and specific heat) in the second column. Consider capacity rate of inlet stream as negative and outlet stream as positive. As the HTF capacity rate is not known a priori, capacity rate for T_1 is assigned as zero in the second column. For i^{th} row, net capacity rate ($C_{i\text{Net}}$) at T_i may be expressed as:

$$C_{i\text{Net}} = \sum C_{\text{in}T_i} + \sum C_{\text{out}T_i} \tag{2}$$

Step 4: Tabulate the cumulative capacity flow rates in the third column. Summation of net capacity flow rates for all previous rows $(C_{Ti} = \sum_{l=1}^{i} C_{l\text{Net}})$ denotes the cumulative capacity flow rate for i^{th} row. Last entry in this column gives zero, as mass flow rates are conserved and specific heats are assumed constant in this algorithm.

Step 5: First entry in the fourth column is assigned zero. For all subsequent rows in the fourth column, heat load (Q_i) for temperature interval (i, i-1) can be calculated using Equation 3.

$$Q_i = \begin{cases} 0 & for \quad i = 1 \\ (T_i - T_{i-1}) \sum_{l=1}^{i-1} C_{l\text{Net}} & for \quad \text{i} > 1 \end{cases} \tag{3}$$

Step 6: Cumulative heat loads are addition of heat loads for all previous rows $\left(\sum_{l \le i} Q_l\right)$ and tabulated in the fifth column. Using Equation 3, cumulative heat load till i^{th} row may be expressed as (Equation 4).

$$\sum_{l=1}^{i} Q_l = \begin{cases} 0 & for \quad i = 1 \\ \sum_{l=1}^{i-1} [(T_i - T_l) C_{l\text{Net}}] & for \quad i > 1 \end{cases} \tag{4}$$

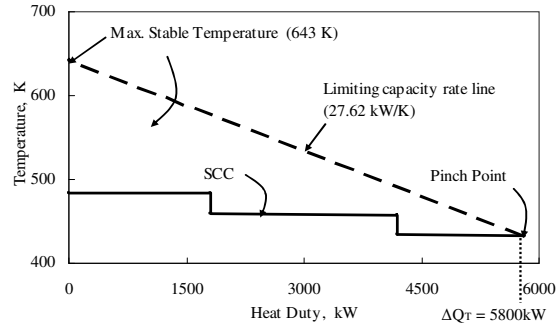

Figure 1: Resource targeting algorithm for minimum HTF flow rate (ΔTmin = 10K)

Now, cumulative heat load may be plotted against temperature to obtain source composite curve (SCC) as shown in Figure 1. Physically, SCC is equivalent to grand composite curve (GCC) in heat-exchanger synthesis. Bottom entry in the fifth column signifies total heat load (ΔQ_T) to be supplied by the heater through HTF.

$$\Delta Q_T = \sum_{l=1}^{n} Q_l = \sum_{l=1}^{n-1} (T_n - T_l) C_{l\text{Net}} \tag{5}$$

Step 7: Capacity rate of HTF is calculated using Equation 6:

$$C_i = \frac{\sum_{l=1}^{i} Q_l}{T_{rs} - T_i} \qquad for \quad T_i < T_{rs} \tag{6}$$

Largest entry in the sixth column is the minimum capacity rate of HTF required for the problem. This procedure can be explained geometrically as follows.
Any line with a negative slope on temperature (T) versus heat load (ΔQ) diagram, passing through a point (0, T_{rs}), represents a capacity rate line. Equation for capacity rate line is

$$\Delta Q = \Delta Q_T - C_T (T_{rs} - T) \tag{7}$$

Note that slope of capacity rate line is inversely proportional to mass flow rate of HTF. It should also be noted that at any point, capacity rate line cannot cross SCC i.e., it cannot transfer more heat load than required (as given by SCC or cumulative heat load available at any given temperature). Therefore, the minimum flow rate can be targeted by rotating a capacity rate line with (0, T_{rs}) as the pivot point such that it just touches the SCC. A point at which, capacity rate line touches the SCC denotes the pinch point (see Figure 1) and the line may be called the limiting capacity rate line (Figure 1). Temperature corresponds to the minimum capacity rate represents the pinch temperature.

3. Illustrative example

A simple example from Stoecker (1989) is used to demonstrate methodology of the RTA. The heating system (Figure 2) has three different reboilers using HTF to heat three process fluids. The heat duty, heating temperature and minimum temperatures of HTF for all process fluids are given in Table 1 (Stoecker, 1989). The heat evolved by the combustion of fuel in fired heater is transferred to reboilers through HTF (Figure 2). HTF is heated in fired heater up to the maximum stable temperature of 643K and then it is passed through reboilers transferring heat to process fluids. Subsequently it is circulated back to the fired heater at a lower temperature. The objective is to minimize the capacity rate of HTF (or equivalently the mass flow rate of the HTF).
Table 2 summarizes step-by-step calculation procedure given for RTA. The minimum approach temperature ΔT_{min} is assumed as 10 K for this problem. Process temperatures are converted to minimum inlet/outlet temperatures for HTF and arranged in descending order (column 1, Table 2). As process fluids are heated at constant temperature, 1 K temperature difference between inlet and outlet temperatures is considered to avoid the problem of infinite capacity rate. For example, the stream 1 is heated at 473 K by HTF in reboiler, so the minimum temperatures for HTF at inlet and outlet are calculated as 484 K and 483 K respectively. Similarly, temperatures of all the process streams are converted to HTF temperatures (column 3, Table 1). First entry in column 1 of Table 2 is the maximum stable temperature of HTF (i.e., 643 K). Column 2 gives cumulative heat capacity for a particular temperature interval.

Table 1: Process data given in Illustrative Example (Stoecker, 1989)

Reboiler No.	Duty, kW	Temperature of fluid being heated, K	Minimum approach temperature of HTF ΔT_{min} = 10 K	
			T_i K	T_o K
1	1800	473	484	483
2	1600	423	434	433
3	2400	448	459	458

In Table 2, last entry of column 3 is zero, as explained validation of mass conservation. Last entry of fifth column suggests that 5800 kW of total heat load is to be supplied by fired heater (ΔQ_T = 5800 kW). Column sixth of Table 2 gives minimum HTF capacity rate 27.62 kW/K at a pinch temperature of 433 K.

Table 2: RTA to target minimum Capacity applied to Example

Temperature K	Heat Capacity kW/K	Cumulative Heat Capacity kW/K	Heat Flow kW	Cumulative Heat Flow kW	Heat Capacity kW/K
643	0	0	0	0	0
484	-1800	-1800	0	0	0
483	1800	0	1800	1800	11.25
459	-2400	-2400	0	1800	9.78
458	2400	0	2400	4200	22.70
434	-1600	-1600	0	4200	20.096
433	1600	0	1600	5800	**27.62**

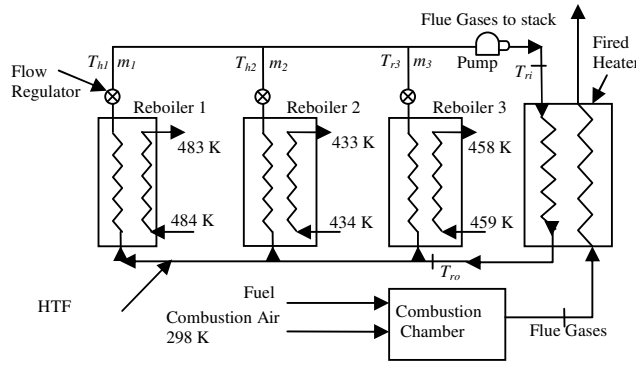

Figure 2: Heating system containing reboilers, fired heater and HTF

A source composite curve (SCC), temperature Vs. heat duty (Table 2, column 1 vs. column 5) is plotted as shown in Figure 1. The limiting capacity rate line shown in Figure 1, dictates minimum HTF capacity rate. For the same problem and data, instead of series-parallel configuration of reboilers, parallel configuration is used then HTF capacity rate can turn out to be 31.84 kW/K. Thus total HTF capacity rate is least for series-parallel configuration. This is targeted before actual design of reboilers.

4. Conclusions

Pinch technology, initially proposed as a thermodynamics-based approach to energy conservation, has evolved over the years to become a powerful tool for process integration and resource optimization. The tools of pinch technology are extended to target the minimum HTF flow rate. As the pinch analysis recognizes the importance of setting targets before design, similarly it sets the minimum HTF capacity rate target using RTA. The proposed RTA for the minimum HTF capacity rate shows 15.3% less capacity rate than the parallel configuration for 10 K approach temperature. Future work focuses on the overall optimisation of the HTF system by integrating radiator and heat exchangers.

References

Guffey E.G. II. 1997. Sizing up heat transfer fluids and heaters, Chemical Engineering, 126- 131.

Kim J.K. and Smith R. 2001. Cooling water system design, Chemical Engineering Science 56(12), 3641-3658

Krishnan S. 2005. Get the Most from High-temperature Heat-transfer-fluid Systems, Chemical Engineering, 46- 50.

Mckechnie A.B. 1927. Industrial Heating by Oil Circulation, Industrial & Engineering Chemistry 19(6), 691-693.

Sahu G.C. and Bandyopadhyay S. 2010. Energy Conservation in Water Allocation Networks with Negligible Contaminant Effects, Chemical Engineering Science 65(14), 4182-4193.

Stoecker W.F. Design of thermal systems, 1989, Third Edition, McGraw-Hill Company, New York.

Varghes J. and Bandyopadhyay S. 2012. Fired heater integration into total site and multiple fired heater targeting, Applied Thermal Engineering, In press.

Wang Y.P. and Smith R. 1994. Wastewater minimization, Chemical Engineering Science, 49(7), 981-1006.

I.A. Karimi and Rajagopalan Srinivasan (Editors), Proceedings of the 11th International Symposium on Process Systems Engineering, 15-19 July 2012, Singapore.

A Study of Complex Distillation Arrangements for Improved Depropanizing, Debutanizing and Deisobutanizing Fractionation of NGL

Youngmi Jung, Nguyen Van Duc Long, Mesfin Getu Woldetensay, Moonyong Lee†

School of Chemical Engineering, Yeungnam University, Gyeongsan 712-749, South Korea

Abstract

The depropanizing, debutanizing and deisobutanizing fractionation steps of processing natural gas liquids were improved through studying complex distillation arrangements, including the double dividing wall column arrangement (DDWC), the sequence including a dividing wall column (DWC) and a bottom DWC (BDWC) and the sequence including a DWC and a BDWC with top vapor recompression heat pump. These arrangements offer benefits by decreasing reboiler and condenser power consumption. Reducing the number of columns and their diameters can potentially reduce construction costs. The result also showed that operating cost could be reduced most significantly through novel combinations of internal and external heat integration: bottom dividing wall columns employing a top vapor recompression heat pump.

Keywords: Dividing wall column; DWC; Heat pump; NGL recovery.

1. Introduction

The uses and processing of natural gas (NG) are still evolving since their early twentieth century origins in the United States. Although its primary use is as a fuel, NG is also a source of hydrocarbons for petrochemical feed stocks and a major source of elemental sulfur, an important industrial chemical (Kidnay, 2006). Its clean burning and ability to meet stringent environment requirements ensure demand for natural gas (Elliot *et al.*, 2005). Recovery of natural gas liquids (NGL) has become increasingly economically attractive as a number of its components are often isolated and sold separately. Consequently, numerous methods exist to increase NGL recovery from a feed gas, with potential enhancements involving integrated processes (Elliot *et al.*, 2005; Mak, 2006).

Distillation is the primary separation process used in industrial chemical processing. While it has many advantages, a drawback is its large energy requirement (Schultz *et al.*, 2002), which can significantly influence overall plant profitability. Increasing energy costs deter energy consumption as do tighter environmental regulations regarding fossil fuel use, leading to research into new and more efficient separation methods (Knapp and Doherty, 2005; Malinenand and Tanskanen, 2009).

Ternary separations typically involve either direct or indirect sequences with two conventional columns. Although the control and operation of conventional columns are simple, their use is inefficient in terms of energy due to the mixing entropy by irreversible split (Aspiron, 2010). Therefore, various methods have been developed to improve the energy efficiency of such distillation systems. Many studies confirm that the Fully Thermally Coupled Distillation System (FTCDS) or the Petlyuk column can reduce energy consumption (Halvorsen and Skogestad, 2004; Jiménez *et al.*, 2003). The

Petlyuk column allows reversible splits, with no part of the separation being performed twice (Figure 1), which gives superior separation energy efficiency over other column configurations (Poth *et al.*, 2004).

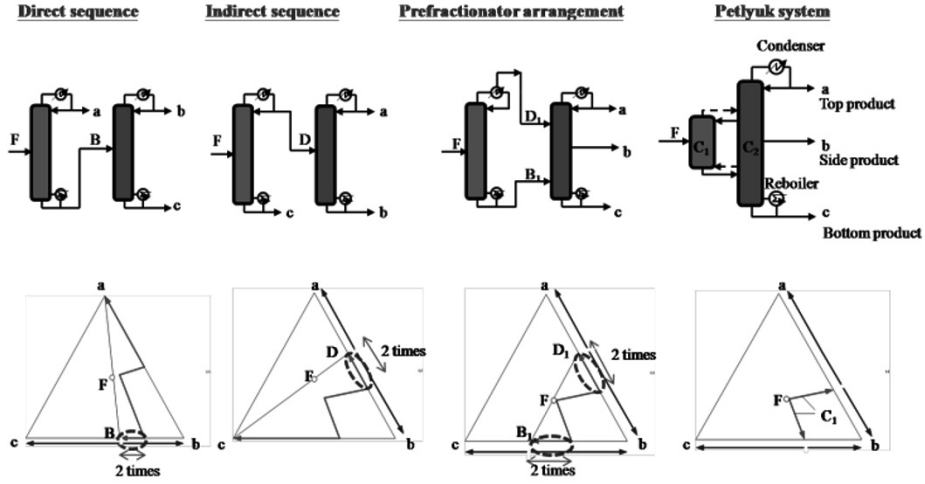

Figure 1. The ternary systems of direct sequence, indirect sequence, prefractionator arrangement, and the Petlyuk system.

Instead of having an external prefractionator, the prefractionator can be incorporated into a single shell arrangement by installing an internal wall, which divides the column into the prefractionator and the main section. This dividing wall column (DWC) is conceptually similar to the Petlyuk column, given their thermodynamically equivalent arrangements (Amminudin *et al.*, 2001), and is expected to give a similar energy saving. However, the dividing wall column requires less capital expenditure and space. Its single shell feature, single reboiler and condenser can typically reduce capital expenditure by 30% compared with conventional two column sequences. The design of the dividing wall column is more complex than a simple column because there are more degrees of freedom that need to be specified. Key variables and parameters such as the number of trays of the column, the liquid and vapor splits each side of dividing wall, and the feed and side tray locations must be established. These degrees of freedom all interact with each other and need to be simultaneously optimized to obtain the best design. Since number of stages is an integer variable, column optimization falls into a class of mixed integer non-linear programming problems (MINLP) (Dejanović *et al.*, 2010), which cannot be solved by commercially available process simulators.

Integrating three columns, whose operating pressures are so different, in such ways is impractical (Long and Lee, 2012). At least two columns are needed. This work aims to find a configuration suitable for improving the performance of the depropanizing, debutanizing and deisobutanizing fractionation steps of NGL processing.

2. Conventional column sequence

Liquid hydrocarbons recovered from NGL are typically separated into relatively pure ethane (C_2), propane (C_3), isobutane (iC_4), normal butane (nC_4), and gasoline products (C_{5+}). This is conventionally done by distilling C_2, C_3 and C_4 from gasoline in sequence

and then distilling iC_4 from nC_4. Because of the large energy consumption, there are numerous configurations and methods known to increase NGL recovery from a feed gas. The difference of operating pressures complicates columns' integration and directly affects energy consumptions and the use of refrigeration.

The depropanizer, possessing 34 theoretical trays, is operated at 17.50 bar as commercial propane can be condensed with cooling water at this pressure, as seen in Figure 2a. The debutanizer and deisobutanizer columns, with 40 and 92 trays, respectively, are operated at 3.50 and 4.40 bar, respectively (Manley, 1997; Amminudin and Smith, 2001). The final distillation of iC4 from nC4 is energy and capital intensive because these compounds' small relative volatility (Manley, 1998). Simulations were performed using the simulator Aspen HYSYS V7.1. The Peng-Robinson equation of state that supports the widest range of operating conditions and the greatest variety of systems was used to predict the vapor-liquid equilibria of these simulations (Aspen Technology, 2009). The base case simulation shows that the energy consumptions of the depropanizer, debutanizer and deisobutanizer are 21.54, 10.48 and 23.80 MW, respectively.

(a) (b)

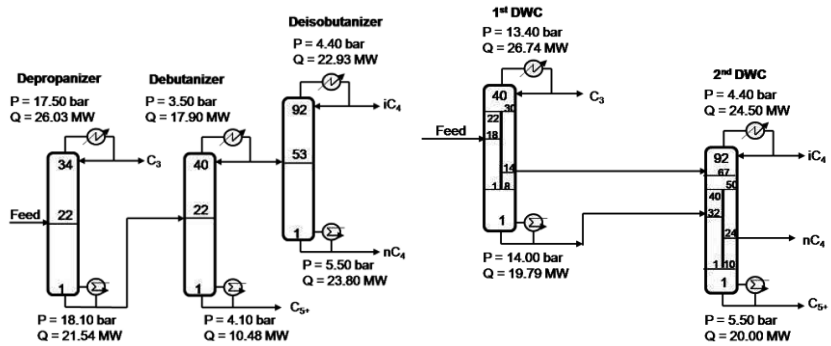

Figure 2. Simplified flow sheet illustrating (a) the separation train of three conventional columns and (b) the DDWC system.

3. Proposed base sequence

3.1. Integration by DWC and bottom dividing wall column (BDWC)

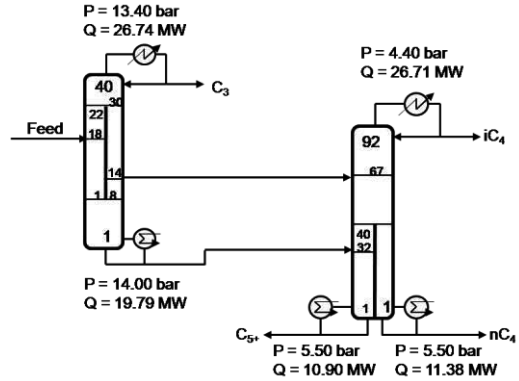

Figure 3. Simplified flow sheet illustrating the DWC and BDWC arrangement.

A double dividing wall column (DDWC) sequence was used to improve energy efficiency in NGL recovery process (Figure 2b) (Long and Lee, 2012). Instead of using the 2nd DWC, a bottom dividing wall column (BDWC) can be used as shown in Figure 3. This BDWC is created by moving the dividing wall down to the bottom of the column to separate the column to three sections: one is prefractionator section for the feeding the mixtures with its own reboiler to produce C_{5+}, another is the top section upper the divided wall, and the last is the divided wall section. Compared to the DWC, the BDWC has one more reboiler causing more investment cost. Using one DWC and one BDWC sequence could save 24.63% in terms of energy consumption. BDWC shows less advantage as compared to DWC because this kind of column could not be adjusted in terms of vapor split ratio (R_v). However, it gives a potentiality with the assistance of heat pump.

3.2. Integration by DWC and BDWC with top vapor recompression heat pump

In the former, instead of using a separate condenser and reboiler, the top product can be compressed to a higher pressure and then condensed in the reboiler of the column. As a result, the condensed vapor provides heat needed for vapor generation at the bottom of the column in the heat exchanger. Then the top outlet stream must be further cooled before being divided to two streams, which including one is recycled back the column as reflux, another is the final top products as shown in Figure 4. Note that the pressure of outlet compressor was adjusted to obtain a minimum approach in the heat exchanger of 5°C. It is possible to save 45.02% in terms of reboiler energy. But that is not the only advantage of this arrangement because, by using a heat pump, the CO_2 footprint could be reduced (Díez *et al.*, 2009). Hence, there is an environmental advantage which could become more important if CO_2 quotas are enforced by governments.

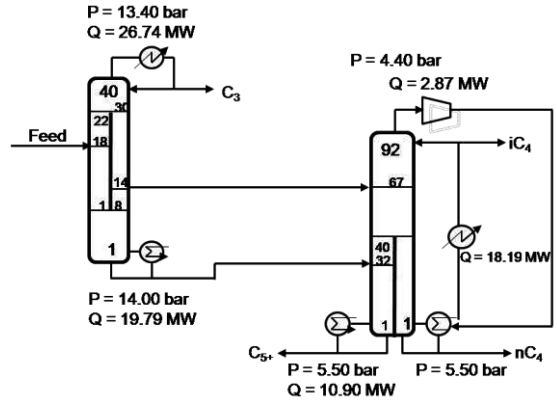

Figure 4. Simplified flow sheet illustrating the DWC and BDWC with top vapor recompression heat pump arrangement.

4. Conclusions

Complex distillation sequences were studied to improve the performance of the depropanizing, debutanizing and deisobutanizing fractionation steps of NGL processing. The sequence including a DWC and a BDWC was shown to reduce energy requirement considerably compared with conventional distillation sequence. Furthermore, operating cost could be reduced most significantly through novel combinations of internal and external heat integration: bottom dividing wall columns

employing either a top vapor recompression heat pump. Furthermore, these sequences, with a decreased number of smaller columns, could reduce investment costs. The reduced numbers of columns and reboilers could also make a plant more compact.

Acknowledgments

This research was supported by a grant from the Gas Plant R&D Center funded by the Ministry of Land, Transportation and Maritime Affairs (MLTM) of the Korean government.

References

Amminudin, K. A.; Smith, R.; Thong, D. Y. C.; Towler, G. P. Design and Optimization of Fully Thermally Coupled Distillation Columns: Part 1: Preliminary Design and Optimization Methodology. Trans. IChemE. 2001, 79 (Part A), 701-715.

Amminudin K. A., R. Smith. Design and optimization of fully thermally coupled distillation columns. Part 2: application of dividing wall columns in retrofit Trans. IChemE., 2001; 79, 716-724.

Aspen Technology. Aspen HYSYS Thermodynamics COM Interface, version number V7.1, January 2009.

Asprion N., G. Kaibel. Dividing wall columns: Fundamentals and recent advances, Chem. Eng. Process., 2010; 49, 139-146.

Dejanović I., Lj. Matijašević, Ž. Olujić. Dividing wall column-a breakthrough towards sustainable distilling, Chem. Eng. Process., 2010; 49, 559-580.

Díez E., P. Langston, G. Ovejero, M. D. Romero. Economic feasibility of heat pumps in distillation to reduce energy use, App. Ther. Eng., 2009; 29, 1216-1223.

Elliot, D.; Qualls, W. R.; Huang S.; (Roger) Chen J. J. Benefit of Integrating NGL Extraction and LNG Liquefaction Technology. AIChE Spring National Meeting, 5th topical conference on Natural Gas Utilization (TI) Session 16c-Gas, 2005.

Halvorsen I. J., S. Skogestad. Shortcut analysis of optimal operation of Petlyuk distillation, Ind. Eng. Chem. Res., 2004; 43, 3994-3999.

Jiménez A., N. Ramírez, A. Castro, S. Hernández. Design and energy performance of alternative schemes to the Petlyuk distillation system, Trans. IChemE., 2003; 81 (Part A), 518-524.

Knapp J.P., M.F. Doherty. Thermal integration of homogeneous azeotropic distillation sequences, AIChE J., 1990; 36, 969-984.

Kidnay, A. J.; Parrish W. R. Fundamentals of Natural Gas Processing; Taylor and Francis: Baca Raton, 2006.

Long, N. V. D.; Lee, S. H.; Lee, M. Y. Design and Optimization of a Dividing Wall Column for Debottlenecking of the Acetic Acid Purification Process. Chem. Eng. Process. 2010, 49, 825-835.

Long N. V. D.; Lee M. Y. Improvement of Natural Gas Liquid Recovery Energy Efficiency through Thermally Coupled Distillation Arrangements, Asia Pac. J. Chem. Eng., In Press, 2012.

Manley, D. B. Deethanizer/Depropanizer Sequences with Thermal and Thermo-Mechanical Coupling and Component Distribution. U.S. patent 5,673,571, 1997.

Manley, D. B. Multiple Effect and Distributive Separation of Isobutane and Normal Butane. U.S. patent 8,806,339, 1998.

Mak J. Configurations and methods for improved NGL recovery, U.S. Patent 7,051,552, 2006.

Malinenand I., J. Tanskanen. Thermally coupled side-column configurations enabling distillation boundary crossing. 1. An overview and a solving procedure, Ind. Eng. Chem Res., 2009; 48, 6387-6404.

N. Poth, D. Brusis, J. Stichlmair. Minimaler energiebedarf von trennwandkolonnen, Chem. Ing. Tech., 2004; 76, 1811–1814.

Schultz M.A., D.G. Stewart, J.M. Harris, S.P. Rosenblum, M.S. Shakur, D.E.O'Brien. Reduce costs with dividing wall columns, CEP, 2002, 64-71.

I.A. Karimi and Rajagopalan Srinivasan (Editors), Proceedings of the 11th International Symposium on Process Systems Engineering, 15-19 July 2012, Singapore.

Water condensate collection system by using MINLP model

Anita Kovac Kralj, [a] Jernej Hosnar[a]

[a]*Faculty of Chemistry and Chemical Engineering, University of Maribor, 2000 Maribor, Slovenia*

Abstract

This paper presents a retrofitted procedure for wastewater, or more specifically, water condensate's separate collection, using an intermediate mathematically-programmed heating design based on a MINLP (mixed-integer nonlinear programming) model. The existing separate condensate collection using an intermediate heating system may no longer be optimal; the basic intention being that minimal changes in the system can efficiently improve the separate collections of low and high-temperature condensates, and the use of available heat. This water condensate collection process was tested on an existing methanol process, by using a MINLP model, which allowed for more effective and additional 5 % water condensate collection system for steam generation.
Keywords: water condensate, MINLP-model, energy saving

1. Introduction

Water minimization within the process industry is becoming increasingly important as environmental legislation becomes more stringent, and awareness increases about the impact of industrial activities on the environment. Extensive work was carried out by Bagajewicz (2000) and Foo (2009) on water-minimization during continuous processes. They developed methodologies for wastewater minimization during continuous processes, mainly using pinch-analysis techniques.

Water condensate collection is very important during real chemical processes because it can reduce raw materials, energy-losses, and costs, and can improve the operations of energy and process systems (Richter, 1993). Water is amongst the more important raw materials and utilities, therefore, it is reasonable to collect water during the process industries' activities.

This paper presents the separate collection of low and high-temperature condensates using an intermediate heating by the mathematical techniques - MINLP model.

2. Water condensate collection with an intermediate heating by using MINLP model

Water is amongst the more important raw materials and utilities, therefore it is reasonable to collect water from process industries.

Their goal is to minimize the amount of wastewater, or more specifically reuse condensates by using a MINLP model. Condensate, as produced during a process, could be separately collected, heated, and utilized for steam-generation.

The MINLP approach deals with both continuous and discrete variables, simultaneously (Biegler et al., 1997). Whilst continuous variables are defined for the continuous optimization of parameters (mass flow-q, heat flow rate-Φ, temperatures-T, specific heat capacity-cp costs, etc.). The basic structural binary variable (y) determines the location of an exact condensate (c) into an exact reservoir (r; eq. 1). Each condensate

has the possibility of entering into any reservoir, and this selection can be determined by the binary variables. If the value is one, it means, that the condensate is selected for a particular reservoir, if zero, and then it is not selected (eq. 1).

$$\sum_{r} y_{c,r} = 1 \qquad r = 1. \ldots R \qquad c = 1, \ldots C \tag{1}$$

Different temperature condensates could be collected more efficiently with separated collections for high-temperature and low-temperature condensate collection reservoirs, according to the minimum energy-loss.

When the different temperature condensates are separately collected within a variety of different lower and higher temperature reservoirs and then followed by heating, the allocation choice for various condensates is very important.

This system of separated lower and higher temperature condensates' (c = 1, …C) collection with intermediate heating, includes different numbers of reservoirs (r = 1, …R) and heaters (h = 1,…H) using mass balance equations (Fig. 1). The mass balance for reservoir number 1 (eq. 2) includes all inlet (fresh water - q_{in} and condensates - $q_{c,r}$) and outlet streams (q_r; eqs. 2, 3):

$$q_{in}\, cp_{in}\, T_{in} + \sum_{c}(q_{c,r}\, y_{c,r}\, cp_c\, T_c) = [\sum_{c}(q_{c,r}\, y_{c,r}) + q_{in}]\, cp_r\, T_r \qquad c = 1, \ldots C \quad r = 1 \tag{2}$$

$$q_r = \sum_{c}(q_{c,r}\, y_{c,r}) + q_{in}] \qquad c = 1, \ldots C \quad r = 1 \tag{3}$$

The outlet stream from reservoir number 1 is the same as the stream into heat-exchanger number 1:

$$q_r = q_h \qquad r = 1 \qquad h = 1 \tag{4}$$

Mass balance of reservoir number two is:

$$q_h\, cp_h\, T_h + \sum_{c}(q_{c,r}\, y_{c,r}\, cp_c\, T_c) = [\sum_{c}(q_{c,r}\, y_{c,r}) + q_h]\, cp_r\, T_r \qquad c = 1, \ldots C \quad r = 2 \quad h = 1 \tag{5}$$

$$q_r = \sum_{c}(q_{c,r}\, y_{c,r}) + q_h] \qquad c = 1, \ldots C \qquad r = 2 \qquad h = 1 \tag{6}$$

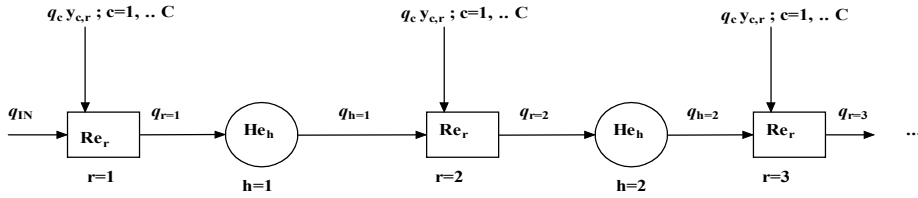

Figure 1: Collection of condensates.

General mass balance of reservoir r is:

$$q_h\, cp_h\, T_h + \sum_{c}(q_{c,r}\, y_{c,r}\, cp_c\, T_c) = q_r\, cp_r\, T_r \qquad c = 1, \ldots C \qquad r = 1, \ldots R \qquad h = 0, 1 \ldots H \tag{7}$$

The energy balance for the heater h is:

$$\Phi_h = q_r \,.\, (cp_r + cp_h)/2 \,.\, (T_h - T_r) \qquad r = 1, \ldots R \qquad h = 1 \ldots H \tag{8}$$

The objective function (OBF, eq. 9) of the MINLP model was to maximize the output temperature from reservoir number 2 by saving (C_{sav} = 100 EUR/K):

$$OBF = C_{sav}\, T_{r2} \tag{9}$$

Many constrained engineering and industrial optimization problems can be modelled as mixed integer nonlinear programming (MINLP) problems.

3. Case study

The existing methanol production had a condensate collection system using two reservoirs. The efficiency of the collection was tested using an MINLP (mixed-integer nonlinear programming) model.

During the methanol process, all the condensates (c=K1−K5) were collected as utilities for 37 bar steam-generation (Fig. 2). The collected condensates were added to the freshly- demineralization water ($q_{FR\text{-}W}$ =19791 kg/h) within the reservoir (R1). The fresh-water and condensates were heated in a heat-exchanger (E111=he-1), followed by another collection of condensates into the reservoir (R2), pumped using a pump (P1) at 50 bar, and then heated in heat-exchangers (E110, E102, REA2, E107, E104, E103). The necessary heat flow rates for the heating of a steam-generation system were obtained from synthesis gases (E111, E110, E107), the furnace-channel (E102, E104, E103), and the REA-2 reactor.

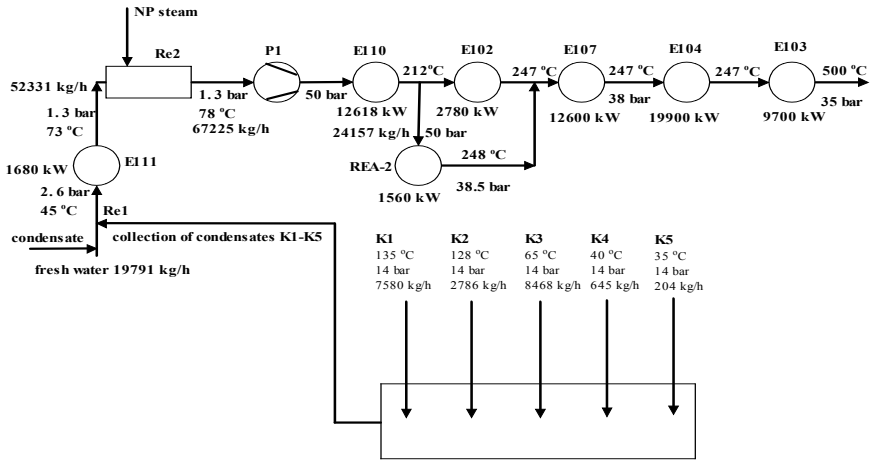

Figure 2: The existing steam-generation.

The existing steam preparation system had been modified by using an Aspen Plus simulator (Aspen Plus, 1996) without a mathematical method. The existing steam preparation system was newly-optimized by using mathematical methods. The optimal modification can be obtained by the mathematical MINLP method by using GAMS optimization tool with execution time of 4.9 s (GAMS with DICOPT, 1992). The MINLP model includes equations from 10 to 18.

Five condensates (c=K1−K5) with different constant temperatures (T_c) and mass flow rates (q_c) were collected within reservoirs (r = R1, R2). Each condensate (c=K1−K5) could be collected in reservoirs 1 or 2, but not in both (eq. 10):

$$\sum_{r} y_{c,r} = 1 \qquad r = R1, R2 \qquad c = K1, K2, K3, K4, K5 \tag{10}$$

Mass balance for the reservoir number 1 is:

$$\sum_{c}(q_{c,r1}\, y_{c,r1}\, cp_c\, T_c) + (q_{FR\text{-}W} + q_{add})\, cp_{FR\text{-}W}\, T_{FR\text{-}W} = [\sum_{c}(q_{c,r1}\, y_{c,r1}) + q_{FR\text{-}W}]\, cp_{r1}\, T_{r1} \tag{11}$$

$$q_{m\,r1} = [\sum_{c}(q_{c,r1}\, y_{c,r1}) + q_{FR\text{-}W}] \quad c = K1, K2, K3, K4, K5 \tag{12}$$

Parameter $q_{FR\text{-}W}$ denotes the heat-flow rate of the fresh water with constant inlet temperature (T_c) and heat-capacity (cp_c), which is only entering reservoir number 1. Parameter q_{add} denotes the additional heat-flow rate of the fresh water with constant

parameters (T_c, cp_c), and with an upper-limit of 3700 kg/h. This is an upper-limit where the system is not too overloaded. All existing units remain the same without additional modifications.

E111 heater (he-1= E111), which heats the outlet from reservoir number one. The energy balance for the heater is:

$$\Phi_{\text{he-1}} = q_{\text{m r1}} (cp_{\text{r1}} + cp_{\text{he-1}})/2 \ (T_{\text{he-1}} - T_{\text{r1}}) \quad (13)$$

The heat flow rate ($\Phi_{\text{he-1}}$) can be calculated using known-values for the inlet and outlet heat capacities (cp_{r1}, $cp_{\text{he-1}}$) and temperatures ($T_{\text{he-1}}$, T_{r1}) of heat exchanger number 1, by using equation 13.

Mass balance for reservoir number 2 is:

$$\sum_{c}(q_{c,\text{r2}} y_{c,\text{r2}} cp_c T_c) + q_{\text{h-w}} cp_{\text{h-w}} T_{\text{h-w}} + q_{\text{m r1}} cp_{\text{r1}}, T_{\text{r1}} = [\sum_{c}(q_{c,\text{r2}} y_{c,\text{r2}}) + q_{\text{h-w}} + q_{\text{m r1}}] cp_{\text{r2}} T_{\text{r2}} \quad (14)$$

Variables T_{r1} and T_{r2} are the denoting outlet temperatures from reservoirs 1 and 2. Parameter $q_{\text{h-w}}$ denotes the heat-flow rate of the hot water-stream with constant inlet temperature ($T_{\text{h-w}}$) and specific heat capacity ($cp_{\text{h-w}}$), which is only entering reservoir number 2. Parameter $q_{\text{m r1}}$ is the sum of all the mass-flow rates, into reservoir 1 (eq. 12), which then further enters the next reservoir number 2. All the condensates (c=K1−K5) have a constant mass-flow rate (q_c), temperature (T_c) and heat-capacity (cp_c) and, therefore, can be multiplied by the binary parameters ($y_{c,r}$).

The specific heat-capacity ($cp_{c,r}$) regarding reservoirs 1 and 2, can be calculated by using linear equation 15, depending on the outlet temperature from the tank (T_r). The parameters of specific heat capacity (a_r b_r) are known values (0.0093, and 1.1067 kJ/(kg K)) for water.

$$cp_r = a_{,r} T_r + b_r \qquad r = \text{R1, R2} \quad (15)$$

Specific heat-capacity ($cp_{c,r}$) after heating in heater he-1, can be calculated by using linear equation 16 depending on the outlet temperature from heater ($T_{\text{he-1}}$).

$$cp_{\text{he-1}} = a_{,\text{he-1}} T_{\text{he-1}} + b_{\text{he-1}} \qquad \text{he} = \text{he-1} \quad (16)$$

An equation similar to the eighteenth can be used for a further heat-exchanger, by considering the additional mass-flow:

$$\Phi_{\text{he}} = (q_{\text{m he}} + q_{\text{add}})(cp_{\text{he-in}} + cp_{\text{he-out}})/2 \ (T_{\text{he-out}} - T_{\text{he-in}}) \quad \text{he} = \text{E110, E102, E107, E104, E103} \quad (17)$$

The objective function (OBF, eq. 18) of the MINLP model maximized additional profit. The reconstruction did not include many modifications, and thus costs. The process did not operate at 100 % capacities, and so the existing process could be used without additional modification. The basic additional cost of reconstruction ($C_{\text{add-fw}}$ = 0.02 EUR/kg) was the cost of additional fresh water mass-flow rate (q_{add}), including the contingencies cost. The additional income accounted for the additional price of steam-generation ($P_{\text{st-gen}}$ = 0.1 EUR/kg). The maximum additional mass-flow rate of steam generated would be increased by 3700 kg/h (an upper-limit), including 40 % efficiency. The operational time (O) was 8000 h/a.

$$\text{OBF} = P_{\text{st-gen}} \ q_{\text{add}} \ 0.4 \ O - C_{\text{add-fw}} \ q_{\text{add}} \ O \quad (18)$$

3.1. Retrofitted system of condensate collection

The existing steam-generation system, including all hot and cold streams (Fig. 3) during the methanol process could be optimized by using MINLP.

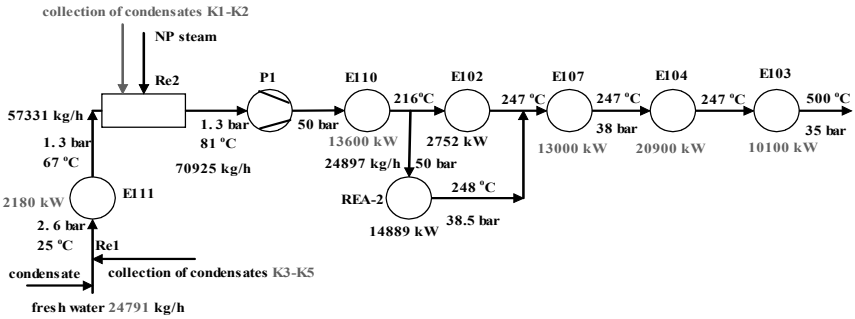

Figure 3: The retrofitted steam-generation.

The optimal result of the objective function was the selection of separate condensate collections (Fig. 3). Low-temperature condensates K3–K5 could be collected within a Re1 reservoir containing fresh-water. The high-temperature condensates K1–K2 could then be collected within a Re2 reservoir. Selection was the same as for the first objective function. The additional heat-flow rate of fresh water (q_{add}) was 3700 kg/h, which was within the lower-bound. The loss of heat-flow rate into the air-cooler was distributed into E111 and E110 heat-exchangers heated with 500 and 1000 kW higher heat-flow rates for the demineralization water, and the inlet temperature of the air-cooler was reduced to 101 °C. The demineralizated water was evaporated in E107 and E104 with additionally-available heat within the furnace-channel, followed by overheating into E103.

The reconstruction of the steam-generation-system could be more effective, as all the available-heat was used during the process. 5 % more steam could be produced by the existing system, which does not work at 100 % capacity.

4. Conclusions

The optimal allocation of condensate collection could be optimized by using a mathematical method, as such the MINLP model. The MINLP model enables both the low and high-temperature condensates to have the possibility of entering into any reservoir, and this choice of selection can be determine by the binary variables.

The existing condensate collection during the methanol process was modified in order to collect low and high-temperature condensates, separately. By modifying the existing process, very little change would be needed for a better preparation of overheated-steam, as used in steam-turbines for producing electricity. The additional profit from the retrofitted steam production system was 590 kEUR/a.

References

Aspen Plus (1996). User Guide, Cambridge.

M.J. Bagajewicz, (2000), A review of recent design procedures for water networks in refineries and process plants, Computers and Chemical Engineering 24, pp. 2093–2113.

L. T. Biegler, Grossmann I. E. and Westerberg A. W., (1997), Systematic methods of chemical process design, Prentice Hall, Upper Saddle River, New Jersey, pp. 1–408.

A Brooke., D. Kendrick and A Meeraus. (1992). GAMS: A User's Guide, Palo Alto, Scientific Press.

D. C. Y. Foo, (2009), A state-of-the-art review of pinch analysis techniques for water network synthesis, Ind. Eng. Chem. Res. 48, pp. 5125– 5159.

H.J Richter., (1993),Thermodynamics and the design, analysis and improvement of energy systems 1993, HTD-Vol. 266 ASME, New York.

I.A. Karimi and Rajagopalan Srinivasan (Editors), Proceedings of the 11th International Symposium on Process Systems Engineering, 15-19 July 2012, Singapore.

Pressure Drop Consideration in Cooling Water Systems with Multiple Cooling Towers

Khunedi V. Gololo[a,b], Thokozani Majozi[a]

[a]*Department of Chemical Engineering, University of Pretoria, Pretoria, South Africa*
[b]*Council for Scientific and Industrial Research, Advanced Modelling and Digital Science, Pretoria, South Africa*

Abstract

Pressure drop consideration has shown to be an essential requirement for synthesis of cooling water network where reuse/recycle philosophy is employed. This is due to an increased network pressure drop associated with additional reuse/recycle streams. This paper presents a mathematical technique for pressure drop optimization in cooling water systems consisting of multiple cooling towers. The proposed technique is based on the Critical Path Algorithm (CPA) and the superstructural approach. The CPA is used to select the cooling water network with minimum pressure drop whilst the superstructure allows for cooling water reuse. This technique which was previously used in a cooling water network with single source is modified and applied in a cooling water network with multiple sources. The mathematical formulation exhibits a mixed integer nonlinear programming (MINLP) structure. The cooling tower model is used to predict the exit conditions of the cooling towers, given the inlet conditions from the cooling water network model.

Keywords: Cooling water system, Pressure drop, Critical Path Algorithm, Optimization

1. Introduction

Cooling water systems are used in many industries to remove waste heat from the process to the environment. Research in this area has focused mostly on optimization and synthesis of cooling water systems in which the technique of recycle and reuse is explored. In most cases the synthesized cooling water network is more complex thus resulting in a higher pressure drop. Kim and Smith (2001) used the graphical technique to debottleneck a cooling water system with single source. Ponce-Ortega *et al.* (2010) also presented a mathematical model for synthesis of cooling water networks that was based on a stage wise superstructural approach. This work included the cooling tower model and the pressure drop for each cooler was considered. Panjeshahi and Ataei (2008) extended the work of Kim and Smith (2001) on cooling water system design by incorporating a comprehensive cooling tower model. Different approach was taken by Majozi and Moodley (2008) who developed a mathematical model for optimization of cooling water systems with multiple cooling towers. This work was later improved by Gololo and Majozi (2011) by incorporating the cooling tower model.

In all the abovementioned work the topology of cooling water network was more complex thus prone to higher pressure drop than the conventional parallel design. Kim and Smith (2003) presented a paper on retrofit design of cooling water systems in which pressure drop was taken into consideration. The authors used graphical technique to

target the minimum circulating water flowrate and mathematical technique to design a cooling water network. This work was limited to one cooling source.
This paper presents a mathematical technique for pressure drop optimization in cooling water systems consisting of multiple cooling towers. The proposed technique is based on the Critical Path Algorithm (CPA) and the superstructural approach. The CPA is used to select the cooling water network with minimum pressure drop whilst the superstructure allows for cooling water reuse. This technique was previously used by Kim and Smith (2003) to synthesize cooling water network with single source. However in this paper CPA is adapted for a cooling water network with multiple sources. Furthermore, the detailed cooling tower model is also incorporated.

2. Model development

A two-step approach is employed to synthesize and optimize the cooling water system with multiple cooling towers considering pressure drop. The first step involves targeting of the minimum circulating water flowrate and in the second step the CPA is incorporated to synthesize the cooling water network with multiple cooling sources.
The cooling tower model developed by Kröger (2004) is used to predict the outlet conditions of the cooling towers and the overall cooling towers effectiveness. The cooling water network model by Gololo and Majozi (2011) is improved by incorporating the modified heat exchangers and pipes pressure drop correlations of Nie and Zhu (1999) shown in Eq. (1) and Eq. (4) respectively. In this paper the correlation of Nie and Zhu (1999) is expressed in terms of mass flowrate.

$$\Delta P = N_{t1} m^{1.8} + N_{t2} m^2 \tag{1}$$

where $$N_{t1} = \frac{1.115567 \mu^{0.2} n_{tp}^{2.8} A}{\pi^{2.8} \rho N_t^{2.8} d_o d_i^{4.8}} \tag{2}$$

$$N_{t2} = \frac{20 n_{tp}^{3} \rho}{\pi^2 N_t^2 d_i^4} \tag{3}$$

The line pressure drop is calculated from Eq. 4 (Kim and Smith, 2003).

$$\Delta P = N_p \frac{1}{F_p^{0.36}} \tag{4}$$

where $$N_p = \frac{188.318 \rho^{0.176} \mu^{0.2} L}{\pi^{1.8}} \tag{5}$$

The CPA is used to select the cooling water network with minimum pressure drop. Kim and Smith (2003) used the superstructure shown in Fig. 1(a). The superstructure is based on single source cooling water network. By modifying the superstructure for single source cooling water systems, a multiple sources superstructure is shown in Fig. 1(b). The CPA used by Kim and Smith (2003) is based on finding a path from source to sink with maximum pressure drop. The maximum pressure drop path is then minimized during optimization to obtain the network with minimum pressure drop. Eq. (6) is used to identify the maximum pressure drop path between the source and sink.

$$P_m - P_n \geq \Delta P_{mn} \tag{6}$$

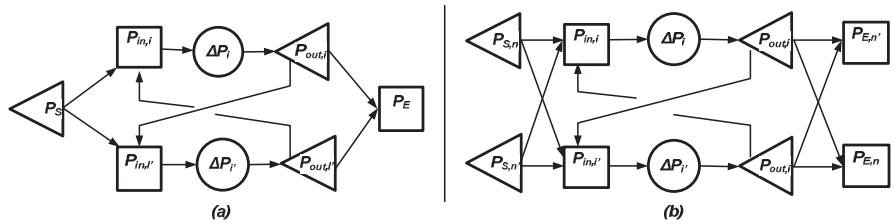

Figure 1: Cooling water system superstructure; (a) Single source (b) Multiple sources

To cater for multiple sources and sinks, the superstructure in Fig. 1(b) is modified by using single imaginary source and sink as shown in Fig. 2. Eq. (7) is then used to define the pressure of source node *n* from the imaginary source node.

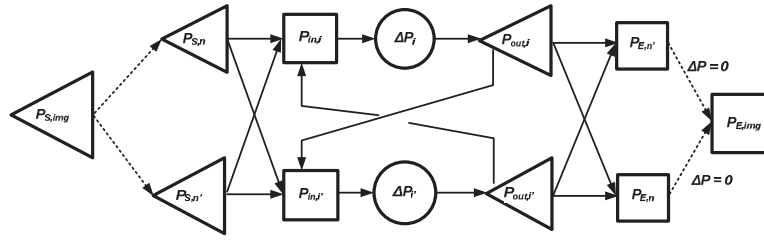

Figure 2: Multiple sources cooling water system superstructure

Eq. (8) to (11) represent the CPA adapted from Kim and Smith (2003). Eq. (12) defines the pressure at the imaginary sink node. From this equation the imaginary sink node will assume a value from all sink nodes with minimum pressure thus identifying a path with maximum pressure drop. The pressure drop of this critical path is then minimized to synthesize a cooling water network with minimum pressure drop.

Sets
$i = \{ i \mid i$ is a cooling water using operation$\}$
$n = \{ n \mid n$ is a cooling tower$\}$

$$P_{S,img} - P_{S,n} = \Delta P_{img,n} \tag{7}$$

$$P_{S,n} - P_{in,i} + LV\left(1 - x_{n,i}\right) \geq \Delta P_{n,i} \tag{8}$$

$$P_{out,i'} - P_{in,i} + LV\left(1 - y_{i',i}\right) \geq \Delta P_{i',i} \tag{9}$$

$$P_{in,i} - P_{out,i} = \Delta P_i \tag{10}$$

$$P_{out,i} - P_{E,n} + LV\left(1 - z_{i,n}\right) \geq \Delta P_{i,n} \tag{11}$$

x, y and z are a binary variables indicating the existence of stream from any source *n*/ operation *i*' *to* operation i/sink *n*. *LV* is a large value.

$$P_{E,n} - P_{E,img} \geq \Delta P_{n,img} \tag{12}$$

The network topology with minimum pressure drop is then synthesized by minimizing the pressure drop between the imaginary source and sink shown in Eq. (13).

$$P_{S,img} - P_{E,img} = \Delta P \tag{13}$$

A case study is considered which involves a cooling water system with dedicated cooling water sources and sinks. This implies that a set of heat exchanger can only be supplied by one cooling tower. No pre-mixing or post-splitting of cooling water return is allowed. However, reuse of water within the network is still allowed (Majozi and Moodley, 2008). The developed mathematical model consists of bilinear terms and binary variable thus rendering the models MINLP.

3. Solution Procedure

The solution procedure involves linearization of nonlinear terms and using results from linearized model as a starting point for the exact MINLP. The bilinear terms in the cooling water network model are linearized using the Reformulation Linearization technique by Sherali and Alameddine (1992) as shown in the paper of Gololo and Majozi (2011). However, a different technique is used to linearize the pressure drop equations. Functions are first plotted within the operating range of the heat exchangers and the piecewise linearization is then used to approximate the nonlinear function (Kim and Smith, 2003).

4. Case Study

Fig. 3 shows a cooling water system consisting of three cooling towers each supplying a set cooling water using operations. The total circulating water flowrate is 31.94 kg/s and the overall cooling towers effectiveness is 90%.

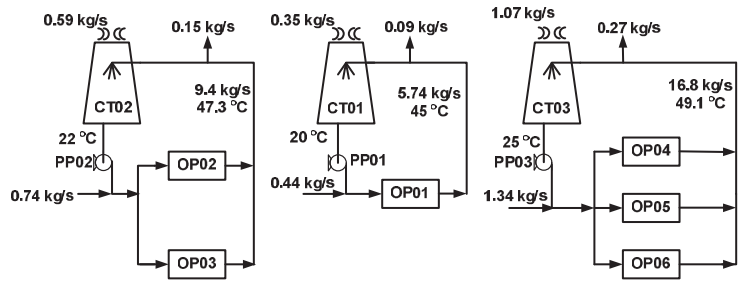

Figure 3: Cooling water system with multiple cooling towers (Majozi and Moodley, 2008)

Fig. 4 shows synthesized cooling water system after the application of the proposed technique. The total circulating cooling water decreased by 22% due to the exploitation of reuse opportunities. The overall increase in cooling tower return temperature associated with decrease in overall circulating water flowrate resulted in a 4%

improvement in effectiveness. The proposed methodology does not only debottleneck the cooling water system but also generate the network topology with the least pressure drop. This has a potential to minimize pumping cost associated with additional reuse/recycle streams. The pressure drop between sources and sinks $\Delta P_{S1,E1}$, $\Delta P_{S2,E2}$ and $\Delta P_{S3,E3}$ is 19 kPa, 31 kPa and 43 kPa respectively.

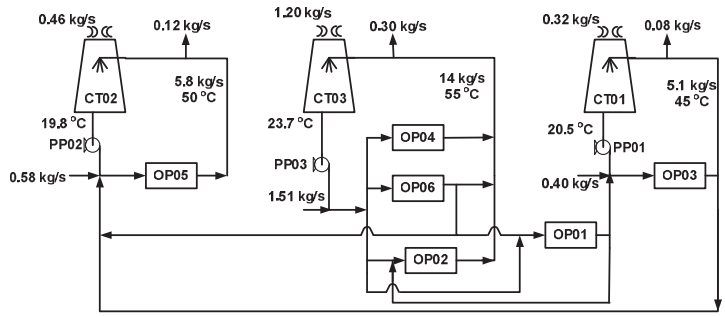

Figure 4: Debottlenecked cooling water system with the minimum pressure drop

5. Conclusion

The mathematical model for synthesis and optimization of cooling water systems with multiple cooling sources which takes into account the pressure drop is presented. The proposed technique is based on the CPA and the superstructural approach. The mathematical formulation developed yields MINLP structure. The case study showed a 22% decrease in circulating water flowrate due to the exploration of reuse opportunities. The return cooling tower temperature was increased which resulted in 4% improvement in the overall effectiveness. The proposed technique offers the opportunity to debottleneck the cooling water system with multiple cooling towers while maintaining minimum pressure drop and maximizing the overall cooling tower effectiveness.

References

J.K. Kim, & R. Smith, (2001), Cooling water system design, Chem. Eng. Sci., 56, 3641-3658

J.M. Ponce-Ortega, M. Serna-González, & A. Jiménez-Gutiérrez, (2010), Optimization model for re-circulating cooling water systems, Comput. Chem. Eng., 34, 177-195

M.H. Panjeshahi, & A. Ataei, (2008), Application of an environmentally optimum cooling water system design in water and energy conservation, Int. J. Environ. Sci. Technol., 5(2), 251-262

T. Majozi, & A. Moodley, (2008), Simultaneous targeting and design for cooling water systems with multiple cooling water supplies, Comput. Chem. Eng., 32, 540-551

K.V. Gololo, & T. Majozi, (2011), On synthesis and optimization of cooling water systems with multiple cooling towers, Ind. Eng. Chem. Res., 50,(7), 3775-3787

J.K. Kim, & R. Smith, (2003), Automated retrofit design of cooling water system, AICHE J. ,Vol 49, No 7, 56, 1712-1730

D.G. Kröger, (2004), Air-cooled heat exchangers and cooling towers: mass transfer and evaporative cooling, Penn Well Corporation, USA

X. Nie, & X.X. Xhu, (1999), Heat exchanger retrofit considering pressure drop and heat transfer enhancement, AICHE J., 45, 1239-1254

H.D. Sherali, & A. Alameddine, (1992), A new reformulation-linearization technique for bilinear programming problems, J. Global Optim., 2(4), 1992, 379-410

I.A. Karimi and Rajagopalan Srinivasan (Editors), Proceedings of the 11th International Symposium on Process Systems Engineering, 15-19 July 2012, Singapore.

New method for large-scale heat exchanger network synthesis

Christopher Brandt,[a] Georg Fieg,[a] Xing Luo,[b] Ole Engel[c]

[a]*HamburgUniversity of Technology, 21073 Hamburg, Germany*
[b]*Helmut Schmidt University, 22043 Hamburg, Germany*
[c]*XRG Simutlation GmbH, 21073 Hamburg, Germany*

Abstract

For the synthesis of large-scale heat exchanger networks a new method based on a hybrid genetic algorithm is proposed. It uses subnets in order to improve the resulting network structures and the calculation time. The application of the new method on an example from literature yielded a HEN structure with reduced total annual costs by 14% and a decreased calculation time by a factor of 18.

Keywords: heat exchanger network synthesis, genetic algorithm, MINLP.

1. Introduction

Production processes in chemical industry usually come along with a large energy consumption. Therefore, the integration of a heat exchanger network (HEN) can have a major impact on energy consumption and sustainability of a production plant. With increasing heat recovery the energy costs are decreasing whereas the investment costs are increasing. Thus, the design of a cost optimal HEN can be considered as a classical optimization problem.

Due to availability of special software and the strong sequential procedure, the most common used method for HEN synthesis is the well-known pinch design method (Linnhoff & Flower, 1978). Recent research activities have shown that specially tailored genetic algorithms are very capable of finding even better HEN structures (Luo et al., 2009), though. However, because of the large number of optimization variables the computation time is very high especially for large-scale HEN. In order to overcome this disadvantage a new method has been developed by the Institute of Process and Plant Engineering of the Hamburg University of Technology. This new method is based on the idea of subnets. A subnet represents a part of the whole network that does not have any contact to other parts of the HEN. Thus, it can be considered and treated like a single subproblem, which therefore can be easily solved by the genetic algorithm. Further, in order to increase the quality of the result, single subnets are combined and then solved again by the genetic algorithm. The application of this innovative method on industrial relevant problems yielded very promising results.

2. Formulation of the optimization problem

For structural representation of a HEN a simple stage-wise superstructure is used. This method was first introduced be Yee et al. in 1990. With this representation a wide range of theoretically possible network structures is covered. Fig. 1 illustrates the fundamental principle for an example with four hot process streams and three cold process streams.

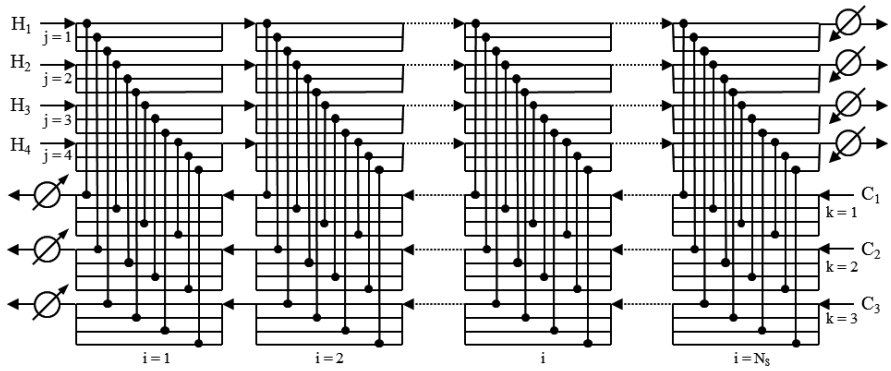

Figure 1: Stage-wise superstructure

Within a stage *i* each hot stream *j* is connected to every cold stream *k* once. The number of stages is proposed as either the amount of hot process streams or the amount of cold process streams, depending which of them is higher (Fieg et al., 2009).
The actual number of series connections of one stream to other streams in an optimal structure is usually rather small. Thus, the number of stages could be smaller. With less amount of stages valuable computational time can be saved.
With a fixed arrangement of the variables *i*, *j*, and *k* every heat exchanger (HX) in the structure has its explicit index that can be calculated by Eq. (1). The HX *ijk* in a given structure connects the hot stream *j* with the cold stream *k* in stage *i*.

$$ijk = (i\text{-}1)N_hN_c + (j\text{-}1)N_c + k \tag{1}$$

The synthesis problem of heat exchanger networks is typically given as a set of N_h hot process streams and N_c cold process streams. These streams are defined by their heat capacity flow rates $\dot{W}$, the overall heat transfer coefficients h and the supply temperatures t_{in} and the target temperatures t_{out}, respectively. For any additional heating and cooling of process streams utility streams are needed. A utility stream is defined by its inlet and outlet temperatures, heat transfer coefficient and a heat load dependent cost factor.
The given task is then to determine the network structure, which produces the minimum total annual costs. Therefore, a HEN is characterized by the heat transfer areas and heat capacity flow rates of the hot and cold streams of each existing heat exchanger within the structure. Thus, the variables to be optimized are the areas A_{ijk} and the heat capacity flow rates $\dot{W}_{h,ijk}$ and $\dot{W}_{c,ijk}$ of the stage-wise superstructure.
The total annual costs are considered as the sum of the investment costs of the heat exchangers and the costs caused by utility usage. In order to avoid binary variables it is stipulated that a positive value for a heat exchanger area indicates an existing HX within the network structure. For the calculation of the investment costs of a HX a typical area dependend approach is used:

$$C_{HX} = a + bA^c \tag{2}$$

This approach considers the fixed costs a of a HX and an area depending part bA^c. For temperature calculation an explicit analytical solution is used (Chen at al., 2007; Fieg et

al. 2009). With this method it is possible to calculate all temperatures within the network as well as the outlet temperatures of the network. In order to meet the postulated target temperatures of the process streams the excessive use of utilities proposed by Lewin et al. in 1998 is applied. A process stream that doesn't reach its target temperature at the outlet of the stage-wise superstructure will be cooled down or heated up by utility anyway. Cold utility is used if the exit temperature of this stream is higher than its target temperature and hot utility is used if its target temperature is below the exit temperature, no matter if it is a hot or a cold process stream. With this method applied the feasibility of any randomly generated HEN is ensured. The necessary heat load for additional heating or cooling is then used to calculate the costs for the utility usage. Therefore, the heat load Q_U that has to be provided by the respective utility U is linked to a cost factor c_U. The costs of each utility are calculated by:

$$C_U = c_U Q_U \tag{3}$$

Thus, the objective function is defined as the sum of the investment costs of all heat exchangers present in the HEN and the costs for the complete utility usage.

3. New synthesis method

3.1. Concept

As mentioned above specially tailored genetic algorithm are very capable of cost optimal HEN synthesis. The combination of heuristic approaches and a genetic algorithm improved the solving characteristics even further (Brandt et al., 2011). Yet, the computational time can get very high for large-scale problems. This is because of the immense amount of structural and continous variables to be optimized. Good large-scale HEN structures consist of many subnetworks, though. The main positive effect is the increasing stability of the process with increasing amount of subnetworks. Occasionally appearing disturbances like temperature changes of single process streams can only effect the respective subnetwork. Therefore, it is not necessary to optimize the whole problem in one single step. Based on this idea the concept of the new method was built up. The new algorithm decomposes the problem into as many subproblems as possible. Each of these subproblems can then be easily solved by the genetic algorithm.

3.2. The new algorithm

In a process without any heat integration each process stream can be considered as a single subnetwork. This is the starting point for the new algorithm. From this set few hot and cold streams are randomly selected to form a new subproblem definition. This subproblem is then optimized by the genetic algorithm presented in the work of Brandt et al. in 2011. From this optimization step the resulting structure is implemented back into the network. Afterwards a novel search algorithm investigates the complete HEN structure for new subnetworks and identifies them. This search algorithm is based on the depth first search method from graph theory. This ensures that all subnetworks will be identified without the need of much calculation time. The result of the search algorithm is a new set of subnetworks. From this set some subnetworks are randomly picked again in order to build a new subproblem definition for the genetic algorithm. This procedure ist carried out until the total annual costs of the complete network can not be reduced over 30 iteration steps. In order to guarantee the HEN synthesis is carried out entirely, two additional constraints are defined. The first constraint ensures that every stream has been used at least once within the optimization procedure. The

second constraint defines the minimum size of a subproblem. Each subproblem formed by several independent subnetworks must consist of more than three process streams.
In order to improve the performance of the new method further, some characteristics of the genetic algorithm are utilized. It turned out that the structural search ability of the genetic algorithm is considerable higher in comparison to the optimization of the continuous variables. Therefore, the new synthesis method runs through two stages, that mainly differs in the parametrisation of the genetic algorithm. In the first stage a rough structural search is carried out. This is to find the most promising combinations of hot and cold process streams. For this task it is reasonable to reduce the population size of the genetic algorithm. Half the size of the population compared to the normal application of the algorithm is enough for finding good first structures. Within the second stage the optimization of the subproblems is carried out more intensively. That means that at this stage the continous variables are optimized as well. Here the parametrisation is the same as for the normal application of the genetic algorithm, see Brandt et al..

3.3. Case study

In this section we demonstrate the improvement of the new method and compare the results to these from literature. For this matter we took one of the largest published examples. It was first presented in the work of Kefeng in 1998 and describes an Ethylene production plant. This example contains 55 process streams and 11 utility streams. In the respective literature a new HEN design was proposed with a claimed total annual cost of 33.1E6 $/a. However, the explicit structure of the HEN was not given. Therefore, this result has to be considered warily.
The HEN synthesis for this example was carried out ten times using the genetic algorithm introduced by Brandt et al. and ten times using the new synthesis method. The results are presented in Table 1. For each calculation run the HEN structure with the lowest total annual costs is considered. For a more practical point of view the process to process heat exchangers and the amount of subnets within these structures are presented, as well.
In order to demonstrate the improvement regarding the calculation effort the average calculation times are presented in Table 1, also. All calculations were carried out on a personal computer with an Intel Xeon 2.8 GHz CPU.

Table 1. Results for case study

	Literature	Genetic Algorithm	New Method
min. costs [$/a]	33,100,000	7,899,968	6,775,277
Number of HX [-]	51	38	32
Amount subnetworks [-]	n.a.	17	23
avg. calc. time [min]	n.a.	1,322	74

Compared to literature the results from the genetic algorithm are considerably better. Especially the costs could be reduced dramatically. On the other hand, the practicability seems also to be improved by the genetic algorithm. Although, the actual structure from literature is unknown, this is strongly indicated by the reduced number of HX. A HEN with less heat exchangers is more likely to have a higher amount of subnetworks. Furthermore, the risk of remixing of process streams due to leakages is reduced by the presence of fewer heat exchangers. Finally, by the application of the new synthesis

method these results could be improved even further. The found structure shows more subnetworks, less heat exchangers and decreased total annual costs by 14 %. A noticable reduction in the calculation time could also be observed. In comparison to the simple application of the genetic algorithm the new synthesis method is about 18 times faster.

4. Conclusion

In this work a new synthesis method for large-scale HEN was introduced. This method uses subnetworks in order to improve the solving characteristics of a genetic algorithm. The application of this method on a large scale problem with 55 process streams yielded very promising results. Compared to the simple application of a genetic algorithm the new method was 18 times faster and a HEN structure was found with 14% less total annual costs. In addition, the practicability could also be improved. The application of the new method yielded a structure with more subnetworks and less process to process heat exchangers.

References

C. Brandt et al., 2011, Efficient synthesis of heat exchanger networks combining heuristic approaches with a genetic algorithm, Heat Mass Transfer, Volume 47, Issue 8, 1019-1026

D.-Z. Chen et al., 2007, An explicit solution for thermal calculation and synthesis of superstructure heat exchanger networks, Chinese Journal of Chemical Engineering, Volume 15, Issue 2, 296-301

G. Fieg et al., 2009, A monogenetic algorithm for optimal design of large-scale heat exchanger networks, Chemical Engineering and Processing: Process Intensification, Volume 48, Issues 11-12, 1506-1516

W. Kefeng, 1998, Model and algorithm for optimal synthesis of large scale heat exchanger networks without stream splitting, Journal of south China University of Technology, Volume 26, Issue 11, 52-61

D. R. Lewin et al., 1998, A generalized method for HEN synthesis using stochastic optimization – I. General framework and MER optimal synthesis, Computers and Chemical Engineering, Volume 22, Issue 10, 1503-1513

B. Linnhoff, J. R. Flower, 1978, Synthesis of heat exchanger networks: I. Systematic generation of energy optimal networks, AIChE Journal, Volume 24, Issue 4, 633-642

X. Luo et al., 2009, A hybrid genetic algorithm for synthesis of heat exchanger networks, Computers and Chemical Engineering, Volume 33, Issue 6, 1169-1181

T. F. Yee et al., 1990, Simultaneous optimization models for heat integration – I. Area and energy targeting and modeling of multi-stream exchangers, Computers and Chemical Engineering, Volume 14, Issue 10, 1151-1164

I.A. Karimi and Rajagopalan Srinivasan (Editors), Proceedings of the 11th International Symposium on Process Systems Engineering, 15-19 July 2012, Singapore.

Dynamic characteristics of self-heat recuperative distillation process

Yasuki Kansha, Akira Kishimoto, Atsushi Tsutsumi

Collaborative Research Center for Energy Engineering, Institute of Industrial Science, The University of Tokyo, 4-6-1, Komaba, Meguro-ku Tokyo 153-8505, Japan

Abstract

Recently, self-heat recuperation technology has been developed. In this technology, whole process heat is recirculated in the process without heat addition, leading to the drastic energy saving for the process. Although the process based on this technology can achieve drastic energy saving at steady state, the dynamics of the process have not been investigated. Therefore, operators of the process have to manually switch the conventional operation mode to the operation mode by self-heat recuperation at reaching steady-state. Two stream lines for each operation mode are required and increase the capital cost. Thus, in this paper, the dynamic characteristics of the self-heat recuperative process for distillation have been investigated to design operation systems such as controllers for further energy saving and stability of this process during operation.

Keywords: Energy, modeling, self-heat recuperation, dynamics, exergy

1. Introduction

Distillation has been widely used for separation in industries owing to the simplicity of their process. Simultaneously, it is well-known process for consuming a large amount of energy, because of large latent heat between liquid and vapor phases. So far, many innovative distillation processes for energy saving purpose have been developed. A vapor recompression (VRC, Annakou and Mizsey, 1995) technology is one of the most famous technologies, in which the top vapor stream is compressed and the heat of the stream is exchanged with the heat of the bottom liquid stream in the column to recover the heat of condensation to the heat of vaporization. Another famous technology is a heat integrated distillation column (HIDiC, Huang et al., 2006). In this technology, the distillation column can be divided into two parts and the condensation heat is exchanged with the vaporization heat between these two parts by using pressure difference. However, both VRC and HIDiC are only focused on heating by the reboiler in the distillation column and are not interested in the heating of feed stream to the distillation. Recently, by incorporating compressors and heat exchangers, the authors have developed another attractive technology to reduce the energy consumption of chemical processes (Kansha et al. 2009) and applied it to the distillation process (Kansha et al. 2010a,b). In this technology, a process unit is divided into functions to analyze the process required heat and all of the self-heat of process stream is recirculated in the process without any external heat source. As a result, the energy consumption and exergy destruction of the process can be greatly reduced in the steady state. Although this technology achieved reduction of energy consumption in the steady state, only few investigations of process dynamics and operation methods for the self-heat recuperative process have been performed. Thus, to apply this technology to actual industrial processes, it is necessary to design the operation system. In fact, there is a pilot self-heat

recuperative distillation process for ethanol production in Japan. This process achieves drastic energy reduction in the steady state. However, operators are switching the operation mode and stream lines when it reaches steady state condition.
Thus, we investigated the dynamic characteristics of the self-heat recuperative process especially distillation, to design the operation systems for the process, achieve further energy savings and investigate the stability of the process during operation in this research.

2. Self-Heat Recuperative Separation Process

To Apply the self-heat recuperation technology to separation processes (Kansha et al. 2010a,b), a system including not only the separation process itself but also the preheating/cooling section, is divided on the basis of their functions, namely separation and heat circulation modules in which the heating and cooling loads are balanced, as shown in Fig. 1. This figure shows the case which has one feed and two products. The enthalpy of inlet stream (feed) is equal to that of the summation of outlet streams (products) in each module. Then, the cooling load in each module is recuperated by compressors and exchanged with the heating load by following the self-heat recuperation technology. As a result, the heat of the process stream (self heat) is perfectly circulated without any heat addition in each module, the perfect internal heat circulation in a whole separation process can be obtained.

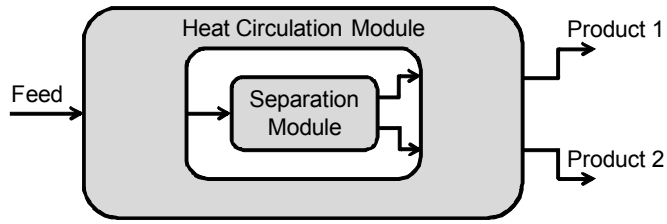

Fig. 1. Conceptual figure of Self-Heat Recuperative Separation

2.1. Self-heat recuperative distillation

To prevent the emission of CO2 by following the self-heat recuperation technology (Kansha et al. 2010b), distillation process can be divided into two sections, namely the preheating and distillation sections, on the basis of their functions. The heating and cooling load are balanced by performing enthalpy and exergy analysis, and the self-heat recuperation technology is applied in these two sections. In the preheating section, one of the streams from the distillation section is a vapor stream and the stream to the distillation section has a vapor–liquid phase. It is necessary to balance the enthalpy of the feed streams and that of the effluent streams in the section, namely heat circulation and distillation module. In balancing the enthalpy of the feed and effluent streams in the heat circulation module, the enthalpy of the streams in the distillation module is automatically balanced. Thus, the reboiler duty is equal to the condenser duty of the distillation column. Therefore, the vapor and liquid sensible heat of the feed streams can be exchanged with the sensible heat of the corresponding effluent streams and the vaporization heat can be exchanged with the condensation heat in each module as shown in Fig. 2.
Figure 2 (a) shows the structure of a self-heat recuperative distillation process consisting of two standardized modules, namely, the heat circulation module and the distillation module. Note that in each module, the summation of the enthalpy of the feed

streams and that of the effluent streams are equal. Figure 2 (b) shows the temperature and heat diagram of the self-heat recuperative distillation process. Both the sensible heat and the latent heat of the feed stream are subsequently exchanged with the sensible and latent heat of effluents in a heat exchanger. The vaporization heat of the bottoms from the distillation column is exchanged with the condensation heat of the distillate from the distillation column in the distillation module. The heat of streams are recuperated by the compressors and exchanged with the heat in the module. It can be seen that all the self-heat is exchanged. As a result, the exergy loss of the heat exchangers can be minimized and the energy required by the distillation process is reduced to 1/6–1/8 of that required by the conventional heat exchanged distillation process. Finally, to examine the feasibility of the simulation when applied to the industrial processes in petrochemical industry, Matsuda et al. (2011) provided it with practical industrial data and modified the stream lines to be suitable for the practical processes. The energy required, exergy destruction and economical efficiency are examined. From these studies, it can be concluded that the self-heat recuperative distillation process is a very promising process for energy saving.

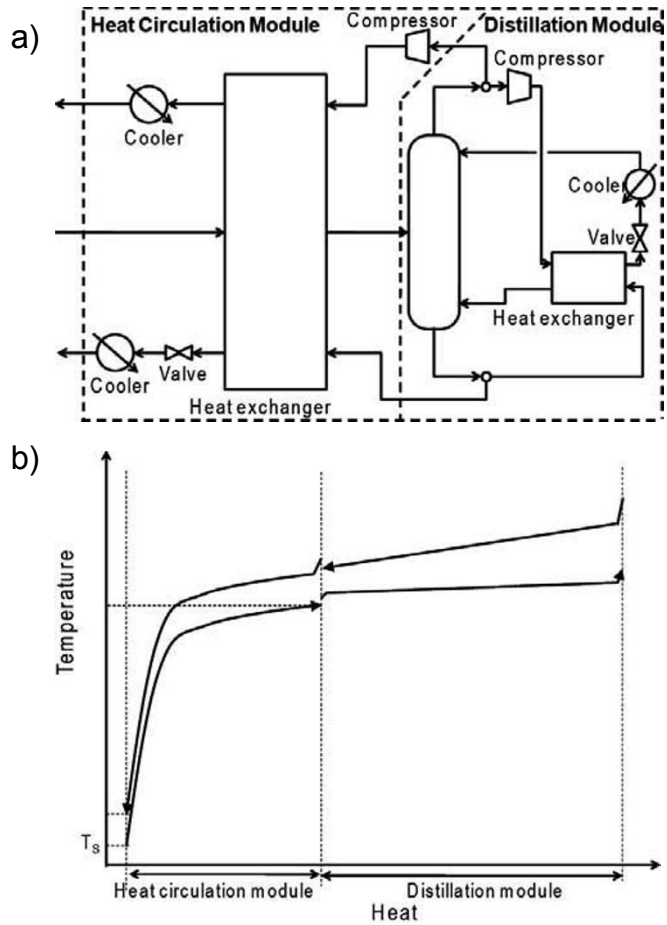

Fig. 2. A Schematic Image of Self-Heat Recuperative Distillation

3. Dynamic Characteristics of Self-Heat Recuperative Process

To investigate the dynamic characteristics of a self-heat recuperative process, step response test was conducted by HYSYS Ver. 7.3 (ASPEN Tech.). The schematic flow diagram for gas stream is shown in Fig. 3. As a real fluid, butane was used for the gas stream. The stream 1 was heated from 25 ^{o}C to a set temperature 100 ^{o}C, and the flow rate of the stream was 100 kmol/h at the initial steady state and ±10 % step changes of the flow rate were introduced to investigate the dynamics. The Soave-Redlich-Kwong (SRK) was used for the state equation. The minimum temperature difference for heat exchange was assumed to be 6 K. The efficiency of the heat exchanger and the adiabatic efficiency of the compressor were 100% (i.e., no heat loss) and 80%. A type of heat exchanger and TEMA type were assumed shell and tube and AFL. Overall heat transfer (UA) in the heat exchanger was 1.216×10^{5} kJ/K^{-1}h^{-1}. The pressure drops of both streams in this heat exchanger are 0.69 kPa. The stream pressures among the compressor are 100.6 and 120.8 kPa. Figure 4 shows the representative response curves of stream temperatures (stream 2 and 4) when the flow rate 10% increase is introduced. It can be seen that the stream temperature of stream 2 cannot reached to the set temperature (100 ^{o}C) due to the increased flow rate. This means that in the case of gas streams, this process cannot naturally keep the equal enthalpy of the feed streams to that of the effluent streams in the module without any adequate operation system under dynamic condition.

As well as the case study with gas stream, the simulation using water as a vapor/liquid stream to close the distillation process was conducted. In this simulation, water must be liquid at standard condition. Thus, it is easy to understand that this process requires the heater to produce vapor initially. Although the heater to initially heat the process stream was introduced, the super heated steam cannot be produced and vapor/liquid mixture was produced in this dynamic simulation. The feed water transforms the phase from liquid to vapor in the heat exchanger in steady state simulation. However, the hold-up in the heat exchanger is required in dynamic simulation and it cannot perfectly transform the phase in this ordinal heat exchanger. Thus, it requires other suitable heat exchanger to produce the super heated steam.

To realize the ideal heat circulation module, it is required to balance the enthalpy of the feed streams to that of the effluent streams. However, this observed phenomena caused by hold-up in the heat exchanger seem to be preferable in respect of design of the heat circulation module in the self-heat recuperative distillation, because the void fraction and enthalpy of feed stream are possible to be controlled by controlling the hold-up level in the heat exchanger.

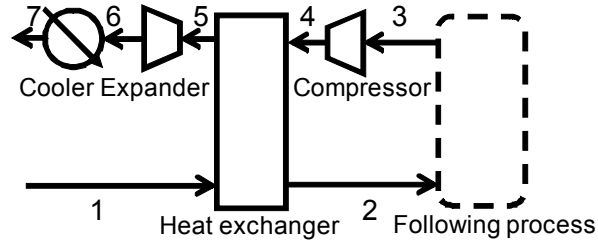

Fig. 3. Flow Diagram for Gas Stream Using Self-Heat Recuperation

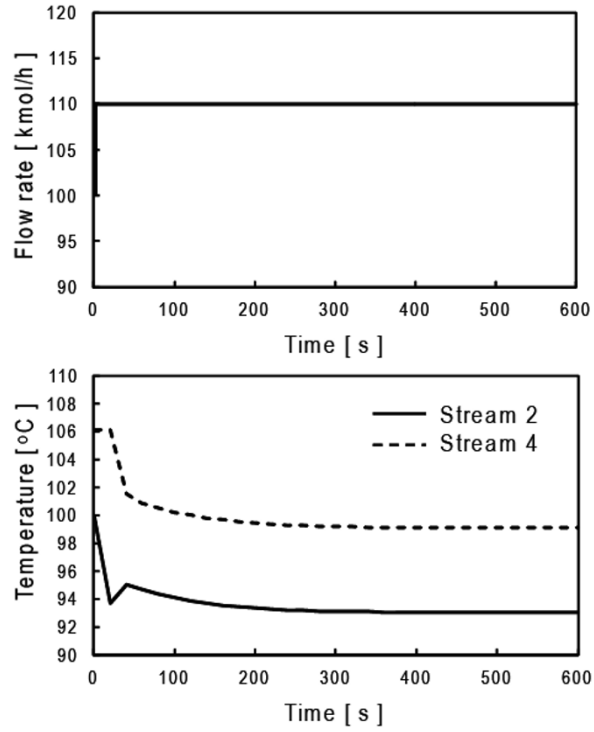

Fig. 4. Step Change of Flow Rate from 100 to 110 kmol/h and Response of Stream Temperature

4. Conclusion

The dynamic characteristics of the self-heat recuperative process to design the operation systems for the process to achieve further energy saving and to investigate the stability of the process during operation are investigated in this paper. To realize the self-heat recuperative distillation, it requires balancing the enthalpy of the feed streams to that of the effluent streams. According to these simulations, it is necessary to design the suitable operation system with further investigation to automatic operation. However, it can also be seen that this process has some potential for further energy saving.

References

O. Annakou, P. Mizsey, 1995, Rigorous Investigation of Heat Pump Assisted Distillation, Heat Recovery Syst. CHP, 15, 241–247

K. Huang, K. Matsuda, T. Takamatsu, M. Nakaiwa, 2006, The Influences of Pressure Distribution of Ideal Heat-Integrated Distillation Column (HIDiC), J. Chem. Eng. Japan, 39, 652–660

Y. Kansha, N. Tsuru, K. Sato, C. Fushimi, A. Tsutusmi, 2009, Self-Heat Recuperation Technology for Energy Saving in Chemical Processes, Ind. Eng. Chem. Res., 48, 7682–7686

Y. Kansha, N. Tsuru, C. Fushimi, K. Shimogawara, A. Tsutsumi, 2010, An Innovative Modularity of Heat Circulation for Fractional Distillation, Chem. Eng. Sci., 65, 330–334

Y. Kansha, N. Tsuru, C. Fushimi, K., A. Tsutsumi, 2010, Integrated Process Module for Distillation Processes Based on Self-Heat Recuperation Technology, J. Chem. Eng. Jpn., 43, 502–507

K. Matsuda, K. Kawazuishi, Y. Kansha, C. Fushimi, M. Nagao, H. Kunikiyo, F. Masuda, A. Tsutsumi, 2011, Advanced Energy Saving in Distillation Process with Self-Heat Recuperation Technology, Energy, 36, 4640-4645

I.A. Karimi and Rajagopalan Srinivasan (Editors), Proceedings of the 11th International Symposium on Process Systems Engineering, 15-19 July 2012, Singapore.

Model-Based Optimal Design of Experiments for Determining Reaction Network Structures

M. D. Hoang[a*], G. Wozny[a], Y. Brunsch[b], A. Behr[b], J. Markert[c], C. Hamel[c], A. Seidel-Morgenstern[c], H. Arellano-Garcia[a]

[a] *Chair of Process Dynamics and Operation, TU Berlin, Str. des 17. Juni 135, 10623 Berlin, Germany*

[b] *Technische Chemie A, TU Dortmund, Emil-Figgestr. 66, 44227 Dortmund, Germany*

[c] *Chemische Verfahrenstechnik, OvGU Magdeburg, 4120, 39016 Magdeburg, Germany*

Abstract

A new approach for optimal experimental design has been developed to support the work of chemists and process engineers in determining reaction kinetics of complex reaction networks. The methodology is applied on sub-networks of the hydroformylation process of 1-dodecene with a Biphephos-modified rhodium catalyst in a DMF-decane thermomorphic solvent system (TMS). The isomerization and hydrogenation sub-networks are systematically analyzed with respect to parameter estimability. They are determined in a sequential approach using model-based optimal experimental design via perturbations with respect to temperature and synthesis gas pressure, and subsequently used to build up the reaction network. The focus of this contribution is the parameter estimation procedure at the very early investigation stage where model uncertainties are high. Sensitivities of sensitive parameters are increased while others are suppressed, which are carried over from the estimated sub-networks or structurally more difficult to determine. This subsequently leads to more reliable parameter estimations.

Keywords: optimal experiment design, model discrimination, parameter estimation, hydroformylation, 1-dodecene

1. Problem Statement

The German Collaborative Research Centre/Transregio 63 is engaged in the development of efficient production processes based on integrated chemical processes in liquid multiphase systems (InPROMPT). Currently, the hydroformylation process of 1-dodecene with a Biphephos-modified rhodium catalyst in a DMF-decane TMS-system is investigated. The proposed complete hydroformylation reaction network is quite complex. It is well known, that side reactions can occur in the hydroformylation reaction like isomerization and hydrogenation of 1-dodecene and its isomers. These side reactions have a negative influence on the product distribution. Hower, side or subsequent reactions leading to adols, alcohol and acids have not been observed in all our experiments leading to a reaction network as proposed in Fig. 1:

* Corresponding author Tel.: +49-30-314-26901; Fax: +49-30-314-26915; E-mail: duc.hoangminh@mailbox.tu-berlin.de

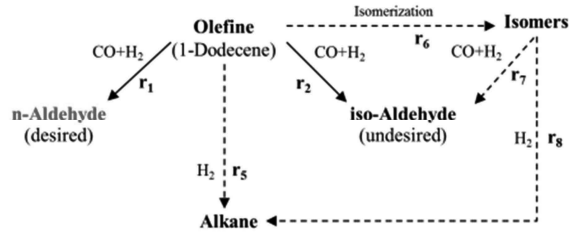

1: investigated hydroformylation reaction network

The hydroformylation network involves a large number of parameters so that it could not be estimated in an *all-in-one* approach. Therefore, an investigation series of sub-networks is suggested in order to achieve an accurate estimation of the kinetic parameters. The crucial idea is to avoid simply putting the estimated sub-networks together but to regard their estimated parameter sub-sets as uncertainties. Moreover, regarding the parameter estimation of complex reaction networks, it is usually necessary to fix some parameters in order to estimate the free parameters properly. However, most of the experimental design approaches aim at maximizing sensitivities of all parameters. It is rather recommendable to hold the sensitivities of those parameters, which are going to be held constant, as low as possible.

In both cases, the goal is to ensure an acceptable performance of the parameters to be estimated for all possible values of uncertain parameter subsets. A new robust experimental design method is proposed to implement this idea (see 2.2.2).

Notation

c_i	concentration of component i	$c^{L,I}$	g-l-interphase concentration
k_{eff}	effective mass transport coefficient	p	partial pressure
H	Henry coefficient	$\mathrm{H_{ads}}$	adsoprtion enthalpie
r	reaction rate	k_r	reaction rate coefficient
k_{ref}	normalized frequency factor	k_{eff}	effective mass transfer coefficient
c_{Cat}	catalyst concentration	z	state variable (concentrations,…)
s	sensitivity ($\partial z/\partial\theta$)	s^*	sensitivity to be suppressed
u	control variable	h	element length (OC on FEM)
N_e	number of elements(OCFEM)	N_n	number of states
N_θ	number of parameters	N_{sp}	number of sampling points
K	order of OC on FEM	Q	weighting matrix
q_r	diag. element of Q w.r.t. the r-th state	E_a	activation energy

Greek letters

θ_i	i-th parameter	ψ	polynomial base of degree K

2. Methodology

2.1. Model building

By dividing the main network into sub-networks, one can determine the parameters step by step. The isomerization and hydrogenation sub-networks are shown in figure 2a and 2b.

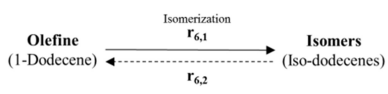

2a: Isomerization sub-network

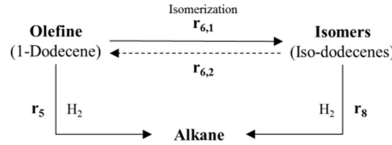

2b: Hydrogenation sub-network

The mass transfer of hydrogen through the gas-liquid interface is modeled as:

$$\dot{N}_{H_2} = k_{eff,H_2}\left(c_{H_2}^{L,I} - c_{H_2}^{L}\right)$$

Using the Henry's Law with the Van't Hoff temperature dependency, the interfacial concentration on the liquid side can be described as follows

$$c_{H_2}^{L,I} = \frac{p_{H_2}}{H_{H_2}(T)}, \qquad H_{H_2}(T) = H_{0,H_2}\, exp\left(\frac{H_{ads}}{RT}\right)$$

The ractionrate for the isomerization and hydrogenation reaction are as follows

$$r_{6_1/6_2} = c_{Cat} k_{r,6_1/6_2}\, c_{Doce/IsoDoce}^{L}, \qquad r_{5/8} = c_{Cat} k_{r,5/8} c_{H_2}^{L} c_{Doce/IsoDoce}^{L}$$

The temperature dependency of the reaction rate coefficients are described as proposed by Buzzi-Ferraris et al. [2009]:

$$k_{r,i} = k_{ref,i} ex\, p\left(-\frac{E_{a,i}}{R}\left(\frac{1}{T} - \frac{1}{T_{ref}}\right)\right)$$

2.2. Estimability analysis

If it is not possible to estimate all parameters in an *all-in-one* approach, then one would like to know, which one has to be held constant in the first estimation loops. In this step, the parameter estimability analysis proposed by Franceschini and Machietto [2008] is applied. If the rank of the estimability matrix P_E is equal to the number of parameters N_θ, then all model parameters are estimable. If not, the analysis of the P_E-matrix will give us the information of which parameter sensitivity must be taken out of the analysis. This is equivalent to identify those parameters, which must be held constant in the subsequent parameter estimation. The idea is to push the sensitivities of those parameters to zero. This aims for ensuring an acceptable performance of the "estimable" parameters for all possible values of the discarded parameters.

2.3. Optimal Experimental Design

The main idea of maximizing the divergence of competing model candidates for model discrimination or maximizing the information content of designed experiments for precise parameter estimation are the main methods of the model based experimental design community. In this work, a simultaneous approach for optimal experimental design is proposed based on the simultaneous optimization approach of Biegler et al. [1991]. Moreover, a new A_R-criterium for robust parameter estimation is discussed.

2.3.1. Problem Formulation

The defined problem (Espie and Macchietto, [1989]) can generally be written as an optimal control problem consisting of the objective function:

$$\varphi(z(t), s(t), u(t), \theta) = \sum_{l=1}^{N_{sp}} \Phi_l(z(t_l), s(t_l), u(t_l), \theta)$$

which is to be maximized, subject to a process model:

$$0 = f(z(t), s(t), u(t), \theta), \qquad 0 = g(z_{t0}, s_{t0}, u_{t0}, \theta)$$

where $0 = g(\ldots)$ is the general formulation of the initial state conditions. Furthermore the system has to follow the constraints of states and controls:

$$z_L \le z \le z_U, \qquad u_L \le u \le u_U$$

2.3.2. Robust Experimental Design Criterion

Applying the simultaneous approach with orthogonal collocation on finite elements on the A_R-criterion, one obtains:

$$\max_{u_{ik},z_{ik},s_{ik}} \varphi(u_{ik},z_{ik},s_{ik}) = \sum_{m=1}^{N_{sp}} \left(\frac{\sum_{r=1}^{N_n} \sum_{s=1}^{N_\theta} q_r \cdot (s_{ik}^{rs})^2}{\exp\left(\sum_{r=1}^{N_n^*} \sum_{s=1}^{N_\theta^*} q_r \cdot \left(s_{ik}^{*,rs}\right)^2\right)} \right)_m$$

Where x_{ik} are the fully discretized state variables, $x := [z, s]$. The equality and inquality constraints of the process model are:

$$0 = \sum_{k=0}^{K} x_{ik} \dot{\psi}_k(\tau_j) - h_i f(x_{ij}, u_{ij}, \theta), \qquad i = 1, \dots, N_e; j = 1, \dots, K$$

$$x_{10} = x_{t_0}, \qquad x_{l0} = x_{l-1K}, \qquad l = 2, \dots, N_e$$

$$x_L \leq x_{ij} \leq x_U, \qquad u_L \leq u_{ij} \leq u_U$$

In order to maximize the objective function φ, the sensitivities of the discarded parameters $s_{ik}^{*,rs}$ are suppressed.

3. Results

The methodology is described by an experimental design example for robust parameter estimation of the hydrogenation sub-network.

It is very common to identify the solubility of the gas educts separately without the reactions. Those thermodynamic parameters are fixed afterwards for the determination of the reaction kinetics parameters. Nevertheless they still represent uncertainties because of their high sensitivities towards the reaction rates and so make the kinetic parameter estimation unreliable. Now, one would like to have an experimental design which suppresses the sensitivities of the solubility parameters making the kinetic measurements more robust towards mass transfer effects.

As shown in figure 3a the sensitivity of solubility parameters could be reduced upto 50%. On the other hand the designed experiment still yields high sensitivities for the wanted kinetic parameters (fig. 3b). The difference with respect to control trajectories between classical and robust experimental design can be seen in figure 4.

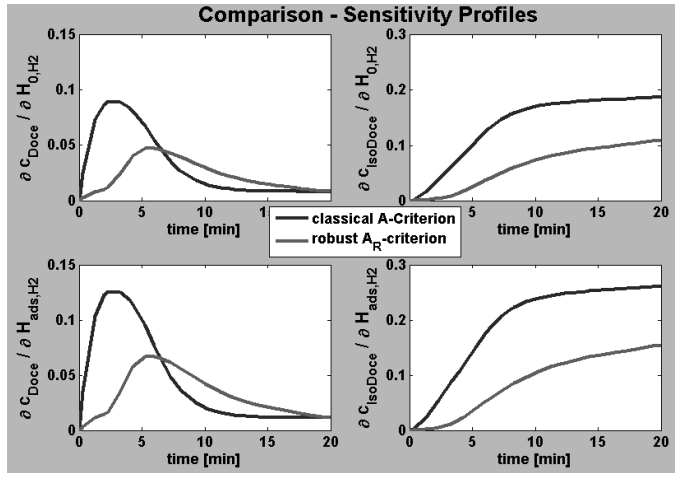

3a: sensitivities with respect to solubility parameters

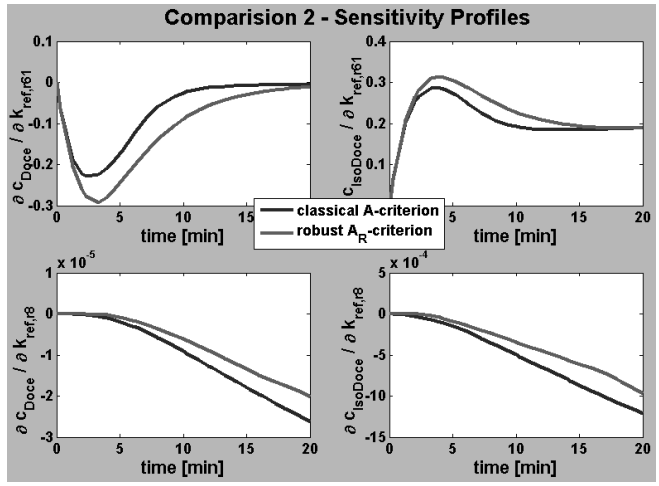

3b: sensitivities with respect to kinetic parametres

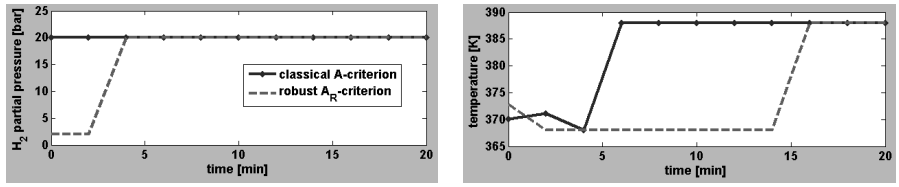

4: sensitivities with respect to kinetic parametres

4. Conclusion

The solution strategy aims at dividing a complex reaction network into sub-networks, in particular, if an *all-in-one* parameter estimation approach is not possible. The determination of the sub-networks provides parameter subsets which are transfered to the main reaction network and treated as uncertainties. The new method aims for a robust optimal experimental design which ensure an acceptable performance of the new parameters for all possible values of the carried over parameter-subsets. This subsequently leads to more reliable kinetic parameter estimations.

Acknowledgement: This work is part of the Collaborative Research Centre "Integrated Chemical Processes in Liquid Multiphase Systems" coordinated by the Technische Universität Berlin. Financial support by the Deutsche Forschungsgemeinschaft (DFG) is gratefully acknowledged (TRR 63).

References

Behr A., Obst D., Turkowski B., 2004 Isomerizing Hydroformylation of *trans*-4-octene to *n*-nonanal in Multiphase Systems: Acceleration Effect of Propylene Carbonate, Journal of Molecular Catalysis A: Chemical 226, 215–219

Biegler T. L., Tjoa B., 1991, Simultaneous Solution and Optimizazion Strategies for Parameter Estimation of DAE Systems, Ind. Eng. Chem. Res., 30, 376-385

Buzzi-Ferraris G., Manenti F., 2009, Kinetic models analysis, Chem. Eng. Sience, 64, 1061-1074

Espie D., Macchietto S., 1989, The Optimal Design of Dynamic Experiments, AIChE J., 35, 2, 223-229

Franceschini G., Macchietto S., 2008, Model-based design of experiments for parameter precision: SotA, Chem. Eng. Science, 63, 4846-4872

Koeken C.J. A., v. d. Broeke J.P.L., Deelman B., Keurentjes T.F. J., 2011,Full kinetic description of 1-octene hydroformylation in a supercritical medium. Journal of Molecular Catalysis A: Chemical, 346, 1-11

I.A. Karimi and Rajagopalan Srinivasan (Editors), Proceedings of the 11th International Symposium on Process Systems Engineering, 15-19 July 2012, Singapore.

A continuous hydroformylation process in a mini-plant scale: equipment design for the separation of three liquid phases

Michael Müller[a,*], Yasemin Kasaka[b,*], David Müller[a,*], Reinhard Schomäcker[b,*], Günter Wozny[a,*]

[a]*Chair of process Dynamics and Operation, Sekr. KWT9*
[b]*Department of Chemistry, Sekr. TC8*
[*]*Berlin Institute of Technology, Straße des 17. Juni 135, D-10623, Germany*

Abstract

A novel process concept for the hydroformylation of long chain olefins in micro emulsions is investigated and developed within the framework of a Collaborative Research Centre in Germany. In this process, the liquid feed material (C12 olefin) is brought in contact with a hydrophilic rhodium-ligand-complex, which is dissolved in an aqueous phase while forming a micro emulsion system under the use of non-ionic surfactants. The hydroformylation reaction is started by adding syngas (H_2&CO) into a continuously stirred tank reactor (CSTR). Due to phase separation into an aqueous phase (catalyst-rich) and an organic phase (product-rich), the valuable rhodium catalyst can be retrieved and recycled. This key separation step is challenging and crucial for the technical and economic feasibility of the overall process concept and plant design.

Depending on the temperature the mixture decomposes into two or even three liquid phases. Preliminary investigations have shown that product and catalyst separation in a continuous process is only attainable in the three phase state, given the required separation time and quality. However, due to the lack of thermodynamic data for micro emulsion mixtures, the design of the phase separation unit strongly depends on experimental data. Consequently, a systematic experimental approach has been developed to identify potential operating conditions and relevant design parameters. In order to classify and find these, a set of systematic experimental set-ups have been investigated to characterize impact factors on the phase separation such as type of surfactant, different concentrations of surfactant, olefin, product, and water. With the information gained through the observations the relevant composition of the investigated mixture and the separation temperature are determined for the operating conditions. Finally, necessities with regards to plant and process design are revealed.

Keywords: Hydroformylation, micellar catalysis, phase separation, process design

1. Introduction

Hydroformylation represents an important application in the field of homogenous catalysis. For short olefins, hydroformylation has already been established as a standard process in order to produce aldehydes. Due to the decreasing solubility of alkenes with an increasing length of carbon chains in the aqueous phase, hydroformylation of higher olefins is not yet performed in industry. Therefore, non-ionic surfactants are applied to

increase the miscibility of the oil- and the catalyst-containing water phase. In order to increase yield and selectivity even under mild reaction conditions, a water-soluble, hydrophilic rhodium-ligand-complex is employed. The resulting multiphase system offers the possibility to separate the valuable rhodium catalyst comparatively easy from the organic product (Bode et al., 2000). Figure 1 shows the novel process concept for the hydroformylation of long chain olefins in a micellar multiphase system.

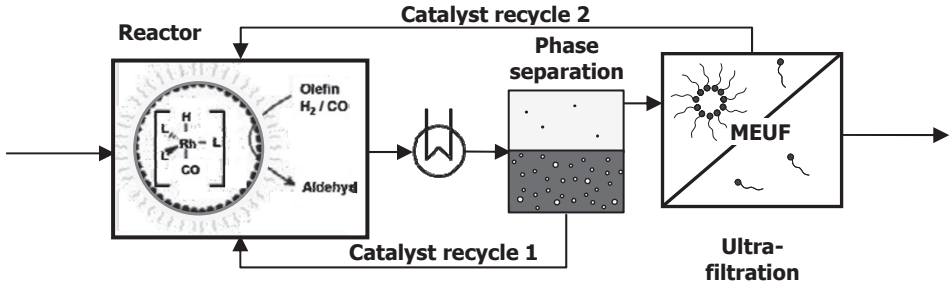

Figure 1: Novel process concept for the hydroformylation of long chain olefins

The first step is the hydroformyltion reaction of C12 olefins in a CSTR according to Figure 2. Secondly, the valuable catalyst is retrieved by means of phase separation and subsequently recycled to the reactor. Due to high catalyst costs a second separation step through ultra filtration is required to reduce the catalyst loss to a minimum (lower 1ppm) and to ensure economic feasibility.

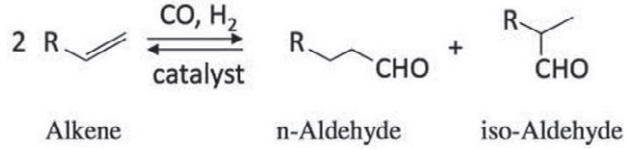

Figure 2: Basic concept of the hydroformylation reaction equation (Kupka, 2006)

The initial catalyst removal takes place in the phase separation unit (decanter), in which most of the rhodium is drawn into the aqueous phase. Preliminary investigations have shown that this is quite challenging. Phase separation itself as well as separation quality and time strongly depend on the type of surfactant and its concentration (γ, Eq. 1), on temperature, on the amount of water (α, Eq. 2), and product (λ, Eq. 3). The following three equations are employed to represent the respective concentrations after the reaction.

$$\gamma = \frac{m_{\text{surfactant}}}{m_{\text{olefin}} + m_{\text{water}} + m_{\text{surfactant}}} \tag{1}$$

$$\alpha = \frac{m_{\text{olefin}}}{m_{\text{olefin}} + m_{\text{water}}} \tag{2}$$

$$\lambda = \frac{m_{\text{aldehyde}}}{m_{\text{aldehyde}} + m_{\text{olefin}}} \tag{3}$$

2. Systematic analysis of the micro emulsion mixture for process and equipment design

Due to the lack of thermodynamic data for micro emulsion mixtures and a lack of reliable simulations, the design of the phase separation unit strongly depends on experimental data. Therefore, a systematic experimental approach is developed so as to identify potential operating conditions and relevant design parameters.

2.1. General phase separation behavior

In a first step, the general phase separation behavior is determined. There are four potential states, which depend on temperature and conversion rate. These are depicted in Figure 3 in the form of Kahlweit´s fish (Kahlweit et al., 1983) for a given composition.

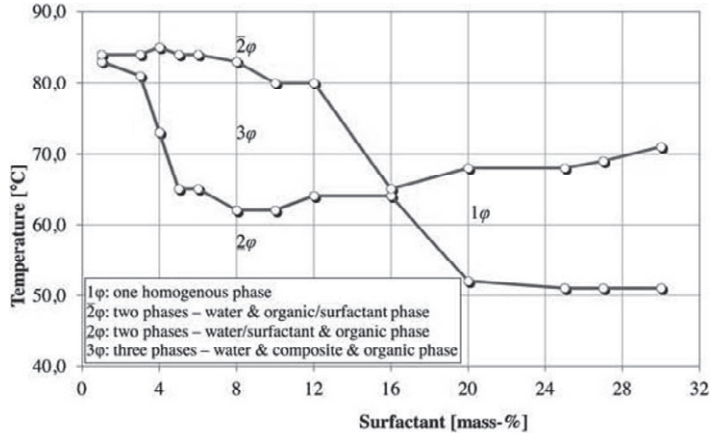

Figure 3: Kahlweit's fish for Marlophen NP9, α=0.5 and λ=0.5 conversion

Preliminary investigations of a mixture consisting of Marlophen NP9, water, and dodecene show that product and catalyst separation in a continuous process are only attainable in the three phase state, given the required separation time and quality. Hence, the initial aim is to identify the three phase region to find potential operating conditions.

2.2. Dynamics of phase separation & quality classification

In a second step the separation dynamics and quality of the three phase state has to be determined. Therefore, the mentioned composition is mixed in a tempered measuring glass and the separation progress of each single phase is recorded. In Figure 4 two graphs are shown for the dynamic separation behavior at 71°C and 74°C.

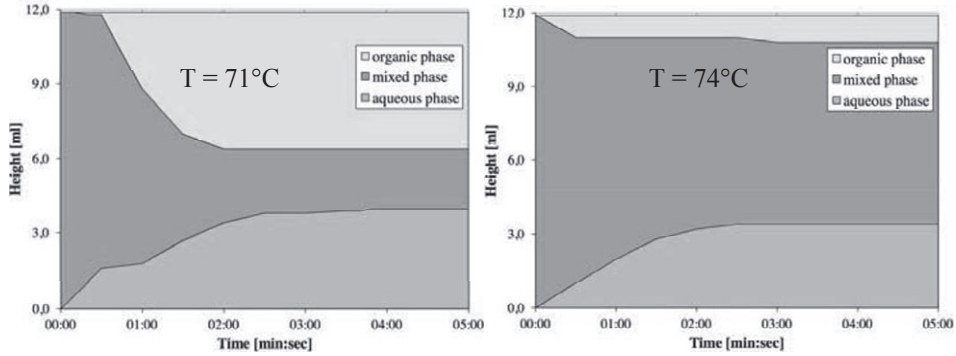

Figure 4: Dynamic phase separation behavior for γ=0.05, α=0.5, λ=0.5 at 71°C and 74°C

For 71°C the separation occurs comparatively fast, reaching a quasi steady state after around three minutes. All of the three phases appear transparent, which signifies a complete separation of the micro emulsion. A further quality criterion is a small mixed phase in comparison to the other two phases. These observations imply a qualitatively good separation. On the other hand, the graph for 74°C shows that the separation of the organic phase is poor and most of the product remains in the mixed phase. This is an example for an undesired phase separation behavior. The comparison of these two examples illustrates the difficulty in handling this multiphase system, because of the strong temperature dependency. Even within the three-phase-state, the separation quality of each phase differs strongly for small temperature changes, in this case, 3 K. This necessitates a flexible and fast temperature control.

2.3. Continuous separation

Since adequate and potential process parameters were found by means of the dynamic investigations of the mixture, the next step is the demonstration of the general applicability in a continuous separation process. Figure 5 shows the PFD-diagram and a picture of the applied experimental test set-up. The mixture consisting of γ=0.05, α=0.5, λ=0.5 is heated and stirred in the composite storage tank and pumped into the heated glass decanter, which is designed referring to the required retention time. Here, both of the heavier phases, the catalyst rich aqueous and the surfactant rich middle phase, are removed together. The lighter organic product phase is removed separately. The experimental results show that the separation of a three phase micellar multiphase system is possible for a continuous process.

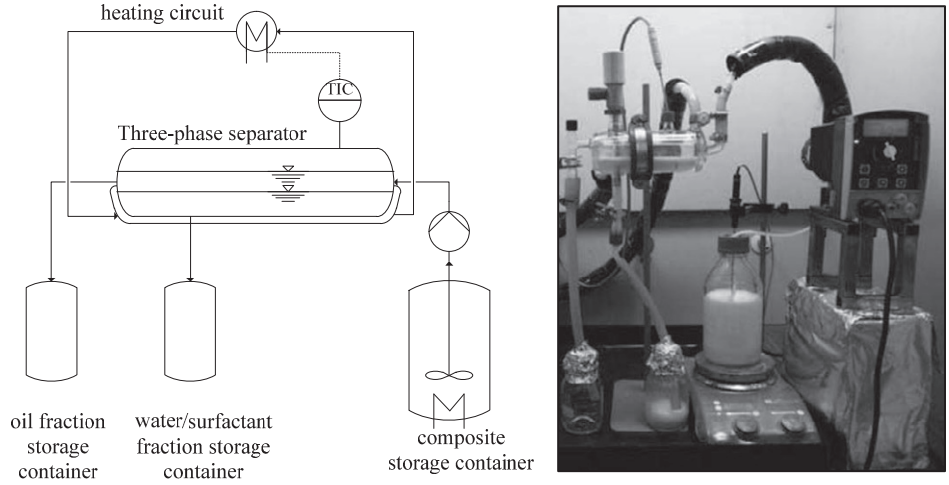

Figure 5: PFD diagram and a picture of the experimental test set-up for the continuous separation of a three phase micellar multiphase system

3. Mini-plant Design

The systematic approach discribed so far aids in designing a mini-plant to test the viability of the process concept and at the same time shows opportunities to optimize the yield of the almost pure organic product phase. The observations of the dynamic separation behavior highlight the necessity of a temperature control system in both

reactor and decanter of the mini-plant. Thus, the temperature for an optimal phase separation with respect to quality and time can be maintained. Furthermore, the results obtained during the continuous separation allow for the sizing of the actual decanter in relation to the reactor volume. The instability of the phase separation dynamics with regards to the temperature influence imply the implementation of an additional quality control of the product phase to ensure and ascertain the composition. This is achieved through an online HPLC which can be used to modify and control feed and recycle streams of the mini-plant.
To proceed, the afore mentioned investigation of the phase separation dynamics may aid in improving the control concept through the development of a short-cut model predicting the phase sizes in the decanter. This requires extensive experimental investigations of the stand-alone decanter for various temperatures and concentrations.

4. Conclusion

The removal of the valuable rhodium catalyst for recycling by means of phase separation is vital for the economical and technical feasibility of the proposed novel process concept for the hydroformylation of long chain olefins. To identify potential process and design parameters for a micellar multiphase system, a systematic approach has been successfully developed and established in three steps. First of all the general phase separation behavior was determined. Then, the dynamics of the phase separation were investigated, which basically provide information to evaluate and classify potential process parameters and to enable the design of a decanter. In the last step, the applicability of a continuous phase separation was demonstrated by means of an experimental test set-up. This systematic approach now offers the possibility to adapt the decanter operation of the mini-plant towards new developments concerning the micellar multiphase mixture and contributes to improve and develop the novel process design systematically.

Acknowledgement: The authors acknowledge the support from the Collaborative Research Center SFB/TR 63 InPROMPT “Integrated Chemical Processes in Liquid Multiphase Systems” coordinated by the Berlin Institute of Technology and funded by the German Research Foundation.

References

1. G. Bode, M. Lade, R. Schomäcker, 2000, The Kinetics of an Interfacial Reaction in Micro-emulsions with Excess Phases, Chem. Eng. Technol. 23, 405-409.
2. J. A. Kupka, 2006, Hydroformylierung von 1-Octen in Mikroemulsion, Diss. Technische Universität Braunschweig.
3. M. Kahlweit, R. Lessner, R. Strey, 1983, Influence of the Properties of the Oil and the Surfactant on the Phase Behavior of Systems of the Type H_2O-Oil-Nonionic Surfactant, J. Phys. Chem. 87, 5032-5040.

I.A. Karimi and Rajagopalan Srinivasan (Editors), Proceedings of the 11th International Symposium on Process Systems Engineering, 15-19 July 2012, Singapore.

A generic process template for continuous pharmaceutical production

Ravendra Singh,[a] Raquel Rozada-Sanchez,[b] William Dean,[b] Jacob Perkins,[b] Frans Muller,[b] Andy Godfrey,[b] Krist V. Gernaey,[a] Rafiqul Gani,[a] John M. Woodley[a]

[a]*Department of Chemical and Biochemical Engineering, Technical University of Denmark (DTU), DK-2800 Kgs. Lyngby, Denmark*

[b]*AstraZeneca Limited, Charter Way, Silk Road Business Park, Macclesfield, Cheshire SK10 2NA, UK*

Abstract

In the work reported here, a conceptual generic continuous process *template* for pharmaceutical production is presented. The template is demonstrated on a nitro reduction case study that should in principle be generic such that it can handle a series of substrates with similar molecular functionality. To assist in adoption of different substrates, a systematic substrate adoption methodology (SAM) has also been developed. The objective of the generic process *template* together with the SAM is to provide flexibility as well as increased efficiency to continuous processes while reducing inventory for safer operations (from 50 to 100 L in batch or 3 to 5 L in continuous processes). It is shown that the use of the template together with SAM can lead to potential savings in product development times through flexible and efficient production of Kg amounts of product material for clinical trials and other analyses.

Keywords: process template, API, substrate adoption, methodology, pharmaceutical.

1. Introduction

Identification of an effective and safe pharmaceutical product is based on success in clinical trials. Often, several candidate APIs (active pharmaceutical ingredients) targeting the same disease area are tested in order to identify efficacious products. This involves the manufacture of small quantities of compounds in early delivery campaigns. Of these candidates only a few are successful for which, further development is required to scale–up the process. Conventionally, for each candidate API, a whole new manufacturing system (process, reagents, process conditions etc.) needs to be developed, which is costly in terms of time and resources. One solution is to develop a generic process 'template' (a common manufacturing platform) that can be adapted for the production of a series of similar APIs for their early delivery campaigns, resulting in a reduction of time, early manufacturing cost and resource consumption.

2. A conceptual generic nitro reduction process template

A conceptual generic nitro reduction process *template* has been designed (see Figure 1). The template consists of several route alternatives as well as generic process equipments. The nitro compound (C_N) is dissolved in a solvent (S) in a stirred tank, prior to filtration to remove any un-dissolved material before feeding to the reactor. The reducing agent (R_A) can be mixed with C_N, with the catalyst or fed directly to the reactor. The suspension of catalyst may also be prepared in a stirred tank prior to being

continuously fed to the reactor. A slurry plug-flow micro-reactor is used to perform the reaction in continuous mode. The outlet stream from the reactor contains product (P_N, representing, for example, an amino compound), catalyst, any un-reacted R_A and by-product(s), P_B. The subsequent steps are to separate catalyst, reducing agent, products (P_N and P_B) and solvent.

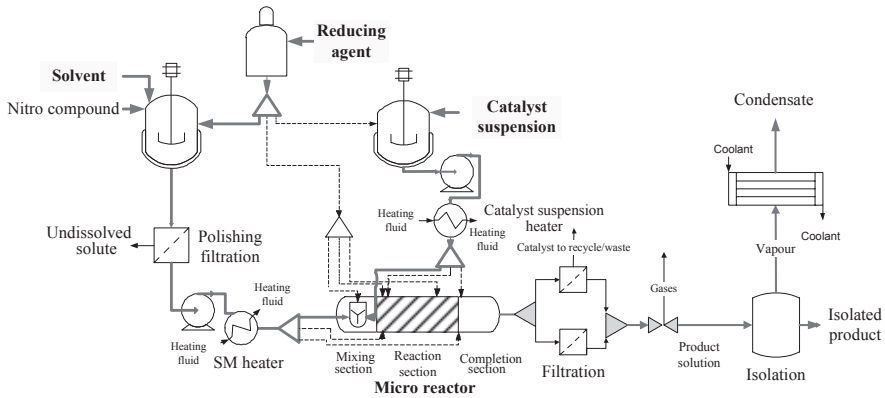

Figure 1. Nitro reduction process template (one route is highlighted)

A generic form of the nitro reduction reaction is given in Scheme 1. Through this reaction, an aromatic nitro compound (C_N) is reduced to the corresponding amine (P_N). The reducing agent, solvent and catalyst are the key materials which need to be selected for a given substrate. By-product(s) depend on the type of reducing agent used. The number of alternatives because of R and reducing agent is potentially very high.

$$R\text{-}NO_2 \quad + \quad \text{Reducing agent} \quad \xrightarrow[\text{Solvent}]{\text{Catalyst}} \quad R\text{-}NH_2 \quad + \quad \text{By-product(s)}$$

Scheme 1. Generic nitro reduction forming an amine

3. Substrate Adoption Methodology (SAM)

To adopt any new substrate in the generic process template, SAM employs 6 hierarchical steps as shown in Figure 2. In step-1 the aim is to check whether the substances involved in the process are hazardous. In step-2 a preliminary solvent list, suitable for dissolving the substrate and product is generated. The reducing agent and catalyst are selected in step-3 through reactivity and selectivity assessments. In step-4, an appropriate process flowsheet is generated from the process template and the corresponding process conditions are identified. The feasibility of the generated process is analyzed in step-5. On the basis of the outcomes of steps-1 to -5, reducing agent, catalyst, solvent, process flowsheet and the process operating conditions necessary for a new product synthesis are summarized (step-6). These can then be further validated through experiments. The data sources needed and the corresponding output from the methodology are also given in Figure 2. Each step of the methodology is described in a publication by Singh et al. (2011) – the SAM related work-flow is new.

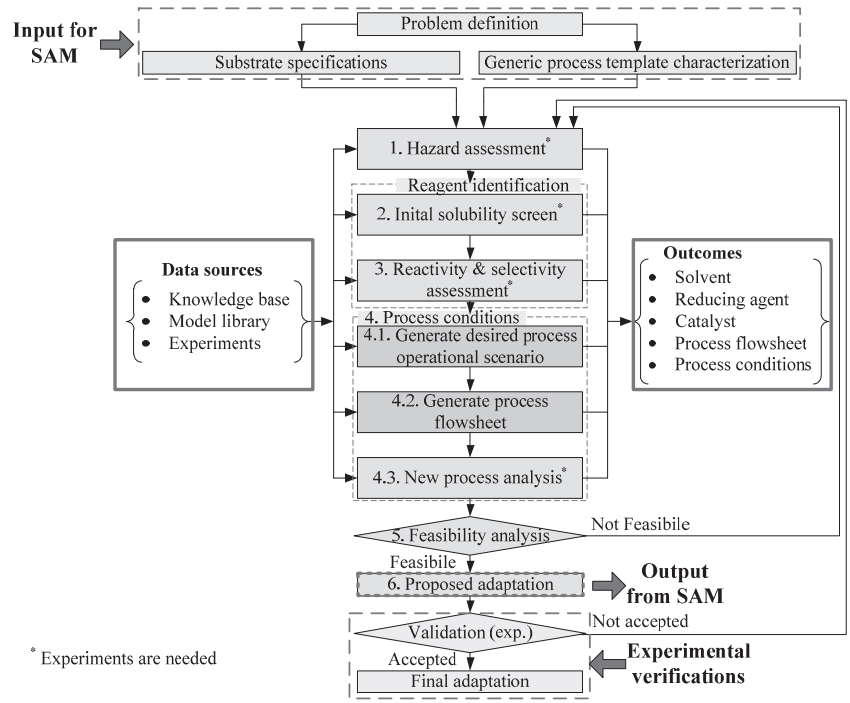

Figure 2. Substrate adoption methodology (SAM)

4. Conceptual case study

Problem definition: To adapt a generic nitro reduction process template for the production of P_N (a multi-functional organic chemical with C, H, N & O atoms) through transfer hydrogenation (for reasons of confidentiality, the actual names of the chemicals cannot be disclosed). The reaction scheme is similar to that shown in Scheme-1.

Substrate specifications: The reactant (substrate) is CN (also a multi-functional organic chemical with C, H, N & O atoms).

Generic process template characterization: Based on experimentation and analysis of several nitro compounds and the nitro reduction process template, some common information & data is generated, which are expected to be applicable to a series of nitro compounds. For example potential reducing agent candidates (e.g.: triethylammonium formate and ammonium formate), catalyst candidates (e.g. Pd/C, Pt/C) and solvent candidates (THF, IPA, NMP) are identified.

4.1. Hazard assessment (step-1)

The substrate is subjected to a hazard assessment methodology. For the purpose of this example, we will assume that based on experimental results, it was concluded that this substrate could be considered for adoption with appropriate safety measures.

4.2. Initial solubility screen (step-2)

The solubility of reactant and product in different solvent candidates is predicted using the UNIFAC group contribution model to select the appropriate solvent. For the purpose of this demonstration, the solubility order found is THF >IPA>NMP.

4.3. Reactivity and selectivity assessment (step-3)

A number of reducing agents and catalyst candidates can be used to carry out this reaction. Based on our existing knowledge, only one reducing agent candidate (for example, triethylammonium formate), one catalyst candidate (for example, Pd/C) and three solvent candidates (THF, IPA and NMP) are considered for further analysis (see Figure 3). Figure-3 shows an example of the type of information that could be generated in this step of the methodology. In the case of THF as solvent, the yield increases rapidly at first but after a certain reaction time the yield decreases, meaning that the reaction is fastest in this case but it also leads to the highest over-reduction. However, the maximum yield achieved with triethylammonium formate, Pd/C and THF is satisfactory meaning that these could be considered as reagents. Furthermore, the use of continuous reaction technology allows a better control of reaction time compared to batch operation and therefore an adaptation is proposed for this reaction with these reagents.

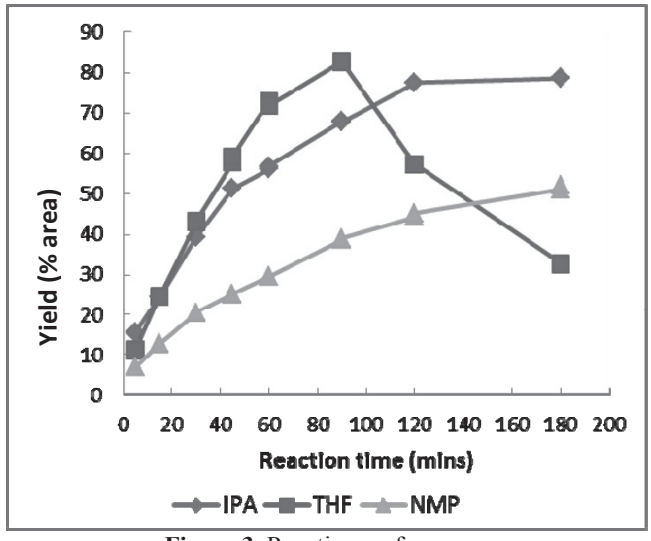

Figure 3. Reaction performance

4.4. Process conditions (step-4)

For the purpose of this demonstration, a process flowsheet is generated (indicated by the highlighted part of Figure 1) from the generic process template. The process is then analyzed and operating conditions are generated. The reactor operating window is shown in Figure 4 as an example.

4.5. Feasibility analysis (step-5)

In this step plant feasibility, operational feasibility and reagents feasibility are analyzed and could be considered satisfactory for the purpose of this demonstration.

4.6. Proposed adaptation (step-6)

On the basis of the outcomes of steps-1 to -5, the necessary reagents, process flowsheet and operating conditions are proposed as a demonstration example.

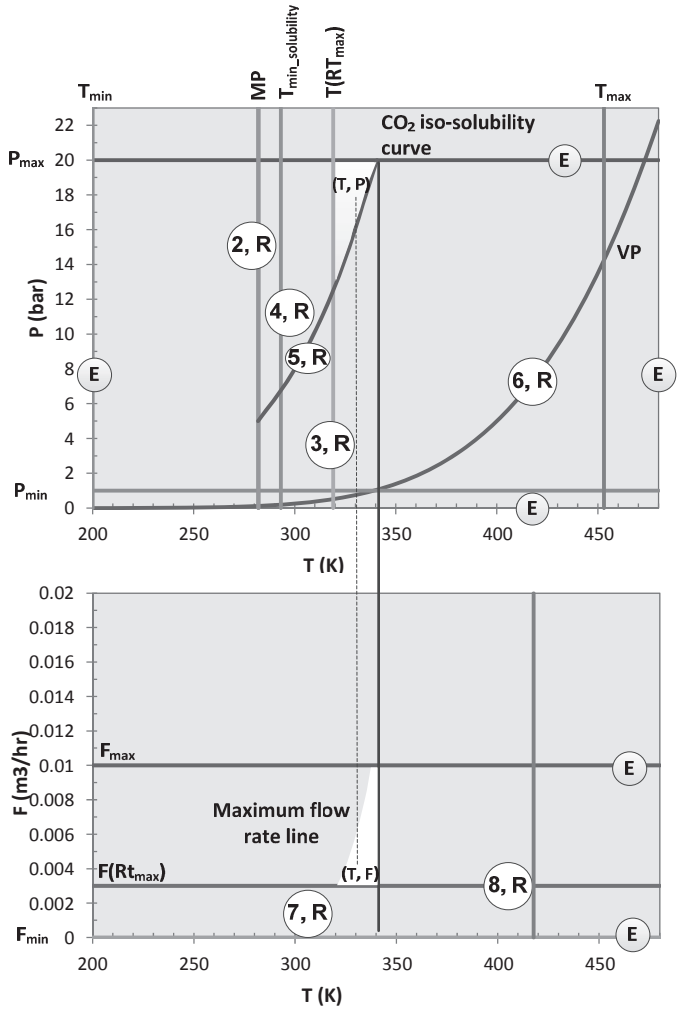

Figure 4. Reactor operating window (R: reaction dependent, E: equipment dependent)

5. Conclusions

In this paper, a generic nitro reduction process template has been reported. To assist in adaptation of the process template, a systematic substrate adoption methodology (SAM) has also been developed. The scope and significance of the process template and SAM has been demonstrated through a conceptual case study. The practical implementation of the template will now follow. The rapid and easy adaptation of the process template results in potential savings of time and resources.

Reference

R. Singh, R. Rozada-Sanchez, T. Wrate, F. Muller, K. V. Gernaey, R. Gani, J. M. Woodley, 2011, A retrofit strategy to achieve "Fast, Flexible, Future (F^3)" pharmaceutical production processes, Computer-Aided Chemical Engineering, 29, 291-295.

I.A. Karimi and Rajagopalan Srinivasan (Editors), Proceedings of the 11th International Symposium on Process Systems Engineering, 15-19 July 2012, Singapore.

Probabilistic design approach to build the litheness in an integrated process scheme

Shyamal Gondkar [a] [b], *Edwin Zondervan* [a], *Sivakumar Sreeramagiri* [b], *Andre.B. de Haan* [a], *Jan Meuldijk* [a]

[a] Eindhoven University of Technology (TU/e), Eindhoven, The Netherlands

[b] GE India Technology Centre Pvt. Ltd., Innovative Plastics Lab, Bangalore, India

Abstract

Flexibility in manufacturing processes is essential not only to handle a variety of feed stocks or to produce multiple product grades but also to accommodate process or catalyst inventions to improve productivity or quality. While designing in litheness we should ensure the robustness of the process output. In this paper, through a case study of biodiesel manufacturing, we summarize a novel technique which uses a probabilistic design approach using meta-models to evaluate the process intensification/integration scheme in a bio-refinery context.

In our methodology first we develop individual process models for a number of processes intensification alternatives where waste or non-edible vegetable oil are converted to biodiesel. These alternatives include the use of reactive distillation and a supercritical process. We integrate these process intensification schemes along with other necessary process steps to establish a plausible manufacturing process. Simultaneously we formulate high fidelity meta-models to describe the various responses of the reactive distillation column w.r.t the changes in the process conditions (or decision variables) in a given design space as an example. This simplification allows us to setup a probabilistic design using commercially available meta-heuristic optimization tools.

Keywords: process integration, reactive distillation, meta-model, probabilistic design

1. Introduction

There have been various efforts worldwide for more efficient conversion of biomass into syn-gas, chemicals, fuels etc. to overcome certain technical challenges leading to better process economics and operations. Biomass is a promising resource having lower carbon footprint compared to the existing non-renewable energy sources such as coal or petroleum based feedstocks. The areas of ongoing research include biomass pre-treatment e.g. biochemical or thermochemical routes such as biomass gasification or pyrolysis, gas treatment and cleaning, biogas to liquid conversion such as Fischer-Tropsch synthesis, transformation of bio-oil or vegetable oil into biodiesel by transesterification and esterification, fermentation of biomass to ethanol or other products, use of biogas in fuel cell for electric power. Each process or technology has its own advantages, for example, in a thermochemical path-way most of the biomass including lignin can be converted into added value chemicals, which is difficult using biochemical treatment. With the availability of many technologies and the ongoing

developments for converting variety of biomass to more useful products, integrating these technologies or processes in the most economical way has become equally important. Generally bio-refinery is referred as a facility capable of converting various types of bio-feedstock into biofuels, chemicals and energy in a sustainable way. In such a scenario, flexibility of the manufacturing unit is essential not only to handle multiple feed stocks or multiple products but also to accommodate process inventions to improve overall economics and sustainability of an integrated scheme. Our work mainly focuses on developing a tool which will enable to assess various process integration alternatives for biomass conversion. In our previous paper (Gondkar *et al.*, 2011) we discussed various types of uncertainties encountered in process engineering problems. Probabilistic design allows to quantify the fitness of a given process or component by providing a probability (likelihood) that the same will survive the operating conditions. In this paper first we discuss a case-study *i.e.* a process integration alternative for manufacturing of biodiesel and then derive a framework for probabilistic design. For this purpose we used the literature reported kinetics as mentioned in the next section. We demonstrate the power of this design with an example where the meta-model is used for optimization of a reactive distillation case.

2. Case Study

A case study for manufacturing of fatty acid alkyl esters (FAAE) of non-edible or waste vegetable oil feedstock containing higher amount of free fatty acids is investigated. In a typical heterogeneous catalytic transesterification and esterification process a fixed bed reactor is fed with a mixture of oil and methanol at a given molar ratio. Excess methanol and water formed due to esterification is removed at the exit of the reactor by partial evaporation. Esters and glycerol are separated in a settler. The reaction products are further purified and methanol can be reused after removing water. Solid acid catalysts and amphoteric metal oxides based on zinc or lanthanum are promising candidates. It is a well-known fact that heterogeneous catalyst for such reactions result in much slower volumetric reaction rates as compared to homogeneous catalysts. There is also a possibility of significant catalyst deactivation, leaching or blocking of porous solid catalyst because of its use. It is possible to overcome such limitations by further optimization of the reaction conditions, by minimizing mass transfer limitations or by carefully designing the catalyst architecture.

First we investigated the possibility of a process intensification alternative for fatty acid methyl esters (FAME) manufacturing comprising a reactive distillation using a heterogeneous catalyst. Here the oil containing higher fatty acid is continuously fed in the upper section of the distillation column containing a heterogeneous catalyst and the methanol is fed at a location a few stages above the reboiler. The bottom product obtained from the reboiler contains FAME, unreacted oil *i.e.* mixture of glycerides, glycerol and water. It is not necessary to have catalyst in the bottom stages to avoid hydrolysis. Methanol is distilled at the top which is either refluxed or recycled to the column. This concept avoids the use of a separate column to separate water and methanol and also possibly helps to improve mass transfer because of the presence of vapors bubbling on each stage. We developed Aspen Plus steady-state models for these processes. Dortmund modified UNIFAC property method is used. For the reactive distillation case we used the pseudo-homogenous catalytic reaction kinetics for tranesterification and esterification, as an approximation to demonstrate the concept. We derived the apparent kinetics from the published work of Qing *et al.,* (2011) for carbon

based solid acid catalyst as an example. Simulation results suggest that the reactive distillation alternative is useful to convert free fatty acids into esters and partial conversion of triglycerides at moderate process conditions (<125^0C). At higher temperatures the reaction would be more sensitive to solid-liquid mass transfer and requires a higher operating pressure for the reactive distillation column.

The other process intensification option we considered is a heterogeneous catalytic supercritical process. It uses CO_2 as a solvent along with methanol in a fixed bed catalytic reactor at elevated temperatures (approximately 200^0C) which needs much shorter residence times. For this case, the pseudo homogenous kinetics are derived from the reported experimental results (Macaira *et al.*, 2011) for a solid acid catalyst, Nafion SAC-13. One of the advantages of this process is that liquid to solid mass transfer under super-critical condition is so high that the reaction is still in the kinetically controlled regime. The downside of such a process is a need to separate water from the recovered solvents, which makes it energy intensive. Our simulation results suggest that if there is no water present in the recovered mixture of CO_2 and methanol, the energy requirement can be considerably reduced. So this process requires either using a feed free from fatty acids or a solvent dewatering scheme such as molecular sieves.

In order to leverage the best of both processes, it is possible to integrate the reactive distillation with the supercritical process. Reactive distillation is useful to convert free fatty acids into esters and realize partial conversion of triglycerides at moderate process conditions. The supercritical methanol and CO_2 based catalytic process is suitable for further conversion of glycerides at reasonable energy consumption. The flow-sheet of the integrated scheme is shown in Figure-1. When such processes are integrated the design and operation of individual unit are critical to obtain the optimum performance of an integrated shceme. In the next section the design philosophy is discussed using reactive distillation as an example.

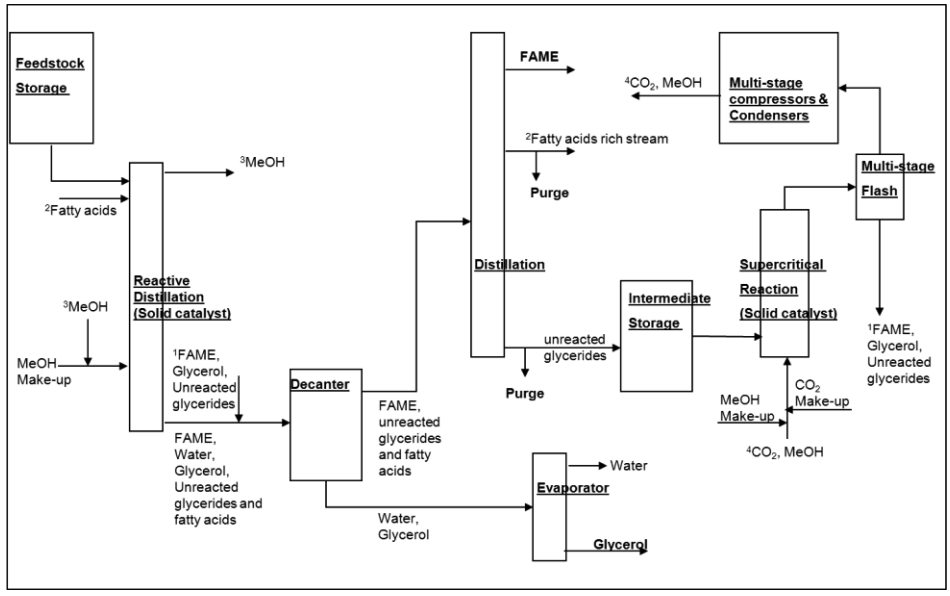

Figure-1: Integrated process (simplified block diagram)

3. Probabilistic Design

In our previous work (Gondkar *et al.,* 2011) for optimization of process intensification, we attempted the use of classical response surface methodology (C-RSM) based on a center composite design (CCD), but the errors associated with these simplified models (linear or quadratic) were resulting in wider error range on the predictions. We also directly coupled a commercially available meta-heuristic optimizer with a process simulator such as Aspen Plus. The results were satisfactory but the simulations were computationally intensive, i.e. long CPU times. This prompted us to look for an alternative methodology for model simplification. The use of meta-models is reported in structural engineering or mechanical design, but their application is very limited in process engineering (Palmer & Realff, 2002; Caballero & Grossmann, 2008; Henao & Maravelias, 2011). In the following section we will discuss the results from C-RSM and the meta-modeling exercise and the subsequent optimization of the reactive distillation for the kinetics derived from recent work by Qing *et al.,* 2011. In this example for illustration purposes, we selected 2 variables (methanol feed rate and reflux ratio), 7 responses (FAME rate, reboiler duty, condenser duty, methanol losses, liquid flow rate, gas flow rate and liquid hold-up) and the objective was set to maximize the product rate i.e. FAME rate with certain design requirements or constraints derived from the other responses.

C-RSM simulations were run at CCD design points (i.e. factorial points, center point and star points – alpha=1.41421)suggested by Design Expert software. As expected from our previous work (Gondkar *et al.,* 2011) the models suggested have very poor R^2. The diagnostic plots (*e.g.* Actual vs. Predicted) for two of the responses are shown in Figure 2. Such large residuals of the model predictions do not justify further optimization.

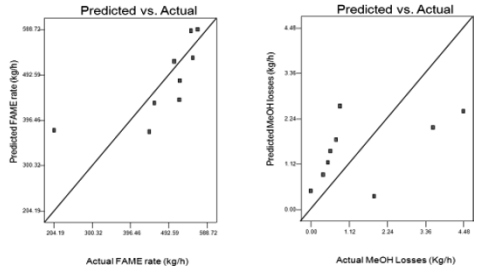

Figure 2: C-RSM model predictions (for CCD design) for reactive distillation

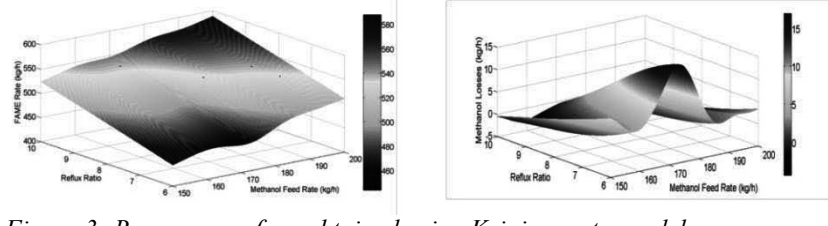

Figure 3: Response surface obtained using Kriging meta-model.

For the purpose of meta-modeling a Latin Hypercube sampling technique was preferred by keeping the same sample size as that of C-RSM and simulations were run at these points. For the fitting of the meta-models for all the responses, the Kriging toolbox implemented by Lophaven, Nielsen and Sondergaard (Nielsen, 2002) was used. The

meta-model parameters are estimated to minimize root mean squared error (RMSE). The response surface obtained using Kriging interpolation are given in Figure-3 for FAME rate and methanol losses.

For probabilistic optimization we developed a framework as follows: Crystal Ball, a spreadsheet based application is used for sampling probability density functions of decision variables as well as running simulations using above mentioned meta-models. For optimization OptQuest a meta-heuristic commercial optimization software is used. In this example for the decision variables i.e. methanol feed rate and reflux ratio standard deviation of 2% and 3% are specified to obtain the distribution of these variables at a given point. For the objective function defined and the design requirements specified the results obtained from this optimization exercise are given in Table 1. These results are further validated using Aspen Plus model.

		Objective	Requirements					Decision Variables	
		Maximize P99.87 Percentile	Certainty of 2.75-3.75 >= 95%	Certainty of 250.00-425.00 >= 95%	Certainty of 0.00-0.75 >= 95%	Certainty of -0.75-0.00 >= 95%	Certainty of 0.00-20.00 >= 95%		
Rank	Solution #	FAME rate *Kg/h*	Liquid rate *M^3/h*	Gas rate *M^3/h*	Reboiler duty per 1000 Kg FAME *Gcal/h*	Condenser duty per 1000 Kg FAME *Gcal/h*	MeOH losses per 1000 Kg FAME *kg/h*	Reflux ratio	MeOH rate *kg/h*
1	113	509.74	100.00%	95.50%	100.00%	100.00%	95.51%	8.75	173.94
2	190	509.33	100.00%	97.83%	100.00%	100.00%	100.00%	8.75	173.67
3	33	508.99	100.00%	98.16%	100.00%	100.00%	96.65%	8.72	173.94

Table 1: Results obtained from optimization for reactive distillation example for 1000 kg/h of oil feed.

4. Conclusions and Path Forward

In our case study for evaluating a possible process intensification alternative it was found that highly non-linear responses can be described by high fidelity meta-models. This simplification allowed us the probabilistic design, which otherwise was difficult using classical response surface methodology because of large error, or by integrating process model with an optimizer. The methodology discussed here can be used to design an industrial system comprising of multiple processes and products. This will be accomplished using a multi-layer hierarchical framework (Zondervan *et al.,* 2008).

References

S. Gondkar *et al.*, (2011). Chemical Engineering Transactions, 24, 355-360. Towards the assessment of robustness in an industrial process system.

S. Qing *et al.*, (2011). Chinese Journal of Chemical Engineering, 19(1), 163-168. Reaction Kinetics of Biodiesel Synthesis from Waste Oil Using a Carbon-based Solid Acid Catalyst

J. Macaira *et al.,* (2011). Fuel, 90, 2280–2288. Biodiesel production using supercritical methanol/carbon dioxide mixtures in a continuous reactor.

K. Palmer & M. Realff (2002). Chem. Eng. Res. Des., 80(7), 760-772. Metamodeling approach to optimization of steady-state flowsheet simulations: Model generation.

J. Caballero & I. Grossmann (2008). Computer Aided Chem. Eng. 25, 551- 556. Rigorous flowhseet optimization using process simulators and surrogate models.

C. Henao & C. Maravelias (2011). AIChE, 57(5), 1216-1232. Surrogate-based superstructure optimization framework.

H. Nielsen (2002). "DACE, A MATLAB Kriging toolbox", http://www.imm.dtu.dk/hbn/dace/.

E. Zondervan *et al.*, (2008). FOCAPO, 397. Flexible optimization of industrial process systems.

I.A. Karimi and Rajagopalan Srinivasan (Editors), Proceedings of the 11th International Symposium on Process Systems Engineering, 15-19 July 2012, Singapore.

Integrated optimization of the adsorption of theaflavins from black tea on macroporous resins

Miguel Monsanto, [a], Edwin Zondervan, [a] O. Trifunovic, [a] Peter M.M. Bongers [a],[b].

[a] *Eindhoven University of Technology, the Netherlands*

[b] *Unilever, Vlaardingen, the Netherlands*

Abstract

In this work the adsorption and desorption parameters for the separation of theaflavins from tea are determined. The obtained data is used for a preliminary selection of the resin with the best adsorption capacity and desorption ratio. From the four tested resins the hydrophobic A-DVB resin has the best characteristics. In addition, the data was used to fit the adsorption isotherms at different temperatures to two theoretical models. The isotherms form the basis of a more extensive model that can be used to optimize the sorption separation yield. The selected resin will be used in a follow up study to determine the optimal operating conditions of the system, using design of experiments and analysis of variance.

Keywords: macroporous resin, adsorption, food industry, polyphenols, tea.

1. Introduction

Tea polyphenols are associated with many health benefits, such as prevention of heart, inflammatory and neurological diseases, as well as cancer prevention. While in green tea mostly catechins can be found, black tea is the source of several types of polyphenols formed by enzymatic polymerisation of catechins, including theaflavins, which can only be found in black and oolong teas [1,2].

The conventional approach for large-scale polyphenols separation is solid-liquid extraction followed by column adsorption chromatography as a purification step. Although this process is not very efficient from an energy requirement and reagents consumption point of view [3], today there is no established alternative to it. Macroporous adsorption resins are economically attractive and have a large surface area combined with a hollow and layered structure [4]. The purification mechanism is based on differences in polarity, hydrophobicity, molecular size and the shape of the different solutes for adsorbent resin. While the literature reports some investigation about suitable resins for green tea polyphenols adsorption [5], information about black tea polyphenols (namely theaflavins) adsorption is scarce.

The first step in designing any adsorption system is to acquire knowledge about adsorption equilibria, kinetics and capacity for target compounds on the selected ligand. The capacity of the adsorbents is usually characterized by isotherms, where Langmuir [6] and Freundlich [7] isotherms are most often applied for phenolic compounds:

Langmuir: $$Q_e = \frac{K_L C_e}{1 + a_L C_e} = \frac{Q_m a_L C_e}{1 + a_L C_e} \quad (1)$$

Freundlich: $$Q_e = K_F C_e^{1/n} \quad (2)$$

where K_L(l/g) is the solute adsorptivity, a_L(l/mg) is a Langmuir constant that represents the ratio between the adsorption and desorption rate constants, Q_m(mg/g) is another Langmuir constant that represents the maximum adsorption capacity, K_F (l/g) is the

Freundlich constant that represents the adsorption capacity and $1/n$ (dimensionless) is an empirical constant that represents the magnitude of the adsorption driving force [8,9].

In this study both the adsorption and the desorption parameters for the separation of theaflavins from black tea were determined. Adsorption data has been analyzed with both types of isotherms to determine the best experimental fit. The results obtained will be used further as a basis for characterization and optimization of a suitable system for purifying the theaflavins from the black tea on the large scale.

2. Experimental

2.1. Reagents and adsorbents

Acetonitrile and ascorbic acid were analytical grade obtained from Sigma – Aldrich. Glacial acetic acid (HPLC grade) and ethanol absolute were purchased from Merck KGaA. Individual theaflavins standards were obtained from Unilever NV. The deionized water (< 18,2 MΩ) used in the experiments was Milli-Q gradient (Millipore). Freeze-dried dry black tea powder was supplied by Unilever R&D.

The resins used in this work and their characteristics are presented in Table 1. Prior to the adsorption-desorption experiments, all resins were pre-treated to remove the monomers and preservative agents. The resin was subsequently dried at 70°C in the oven during 24 hours. Weighted amounts of resin where then washed with ethanol and subsequently a second thorough wash with deionized water was done [10,11].

Table 1: Screened macroporous resins physical properties (manufacturer data)

Resin matrix	Surface area (m^2/g)	Particle size (mm)	Pore volume (ml/g)	Polarity
Polymethacrylic acid ester (AAE)	370	0.25-0.84	1.14	Moderate polar
Aromatic divinylbenzene copolymer (A-DVB)	700	0.6-0.75	1.4	Non polar
Styrene-divinyl benzene (S-DVB)	600	0.25-0.85	1.30	Non polar
Formophenolic (F-PHE)	150-250	0.56-0.76	0.95-1.18	Polar

2.2. Static adsorption and desorption experiments

The tea solutions used for the resin screening and for the adsorption isotherms were prepared by dissolving tea powder in 20% aqueous acetonitrile solution. The starting concentration of theaflavins used in the resin screening tests was around 0.4 mg/ml and for the isotherms experiments the theaflavins concentration range was 0.11-0.62 mg/ml.

For the desorption on the A-DVB resin at different water ethanol solutions, the tea solutions were prepared by dissolving tea powder in water (with stirring). This change in the solution preparation method was made to achieve similar properties to the tea at the process level. All future tests will be done using tea aqueous solutions.

For the static adsorption tests, the hydrated resin (with a dry weight of 1.5 g) was placed in an Erlenmeyer with a lid and 25 ml of black tea solution was added to it. The Erlenmeyer was shaken at 100 rpm at 25°C in a temperature controlled IKA KS 4000i Control Orbital Shaker, during 4 hours. After achieving the adsorption equilibrium, a desorption test was initiated by placing the resin in another Erlenmeyer and adding 25 ml of eluent. The Erlenmeyer was again shaken at 100 rpm and 25°C during 4 hours. Based on the results obtained by Huang *et al.* [12] we decided to use a 50 % (v/v) ethanol solution in this preliminary screening study. In another experiment the ethanol-water ratio was varied to study it's effect in the desorption ratio.

The adsorption capacity (Qe, in mg/g) and adsorption ratio (E, in %) of the theaflavins in the tested resins were calculated according to the following equations:

$$Q_e = \frac{(C_0 - C_e)V_i}{W} \quad (3)$$

$$E = \frac{(C_0 - C_e)V_i}{C_0} \times 100\% \quad (4)$$

where C_0 (g/l) and C_e (g/l) were the initial and equilibrium concentration of the solute in solution, respectively, V_i (l) was the volume of initial solution and W (g) was the weight of dry resin. Desorption ratio (D, in %) was calculated according to:

$$D = \left[\frac{C_d V_d}{(C_0 - C_e)V_i}\right] \times 100\% \quad (5)$$

where C_d (g/l) is the concentration of the solute in the desorption solution and V_d (l) is the volume of desorption solution.

2.3. Analytical methods: HPLC analysis of theaflavins

Individual theaflavins concentrations were determined by HPLC analysis on a Varian HPLC equipped with a Varian Prostar 310 UV Detector and on a Waters 2695 equipped with a 2487 wavelength detector. The analysis was performed in a C18 column, by isocratic elution with acetic acid/water/acetonitrile solutions. The exact method was supplied by Unilever R&D. The total amount of theaflavins was determined by a summation of the four theaflavins (theaflavin, theaflavin 3 monogallate, theaflavin 3' monogallate and theaflavin digallate).

3. Results and discussion

3.1. Static adsorption

The adsorption process during the first hour exhibits an almost linear increase (Figure 1) for all tested resins, followed by a slow increase until the equilibrium plateau was reached. The maximum adsorption capacities, adsorption and desorption ratios at room temperature can be found in Table 2. The polar F-PHE resin consistently showed

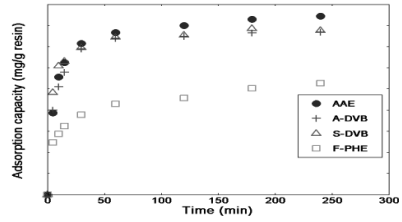

Figure 1:Adsorption kinetic curves for total theaflavins

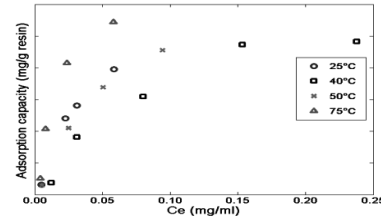

Figure 2: Adsorption isotherms of theaflavins on a A-DVB resin

lower adsorption capacity, probably due to slightly hydrophobic nature of theaflavins. Gogoi *et al.* [5] noticed a completely opposite trend when testing tea catechins adsorption capacities of different resins, where the most polar resin had the best performance. Similar results were reported for polyphenol adsorption on microporous non-ionic aliphatic ester resin by Silva *et al.* [12], where hydrogen bonding between studied polyphenols and resin active sites was the most probable adsorption mechanism. This is not surprising as the theaflavins, which are dimers of green tea catechins, are expected to have a reduced polarity compared to their monomers, i.e. hydrophobic interactions are expected to have a predominant effect for adsorption. However, a straightforward conclusion why a certain resin behaves better than the other is difficult to make at this stage, as their active surface areas (Table 1) are quite different: Although the F-PHE resin has approximately three times lower surface area when comparing to both DVB resins, it only has a ~50 % lower adsorption capacity (Table 2).

Table 2: Adsorption capacity and ratio of adsorption and desorption for theaflavins at 25 °C

Resin	Q_e (mg/g resin)	E (%)	D (%)
AAE	8.44	82	38
A-DVB	7.69	81	71
S-DVB	7.76	71	61
F-PHE	5.26	49	78

According to Table 2 the resin with the best combined adsorption and desorption characteristics was the highly hydrophobic A-DVB resin. This resin was further used to determine parameters for both isotherms. Figure 2 shows the adsorption isotherms for the theaflavins on A-DVB resin at four different temperatures. To calculate the values for both adsorption models, Eq. 1 and Eq. 2 were re-written into their linear forms:

$$\frac{1}{Q_e} = \frac{1}{K_L C_e} + \frac{1}{Q_m} \quad (6)$$

$$\log Q_e = logK_F + \left(\frac{1}{n}\right) logC_e \quad (7)$$

The parameters of the two isotherms are summarised in Table 3. The correlation coefficients are very high for the Langmuir isotherm model at all the tested temperatures and for the Freundlich isotherm model at 25°C and 50°C, suggesting that both models fit very well to the experimental data. The Langmuir model shows a better fitting than the Freundlich model and the highest correlation coefficient is obtained at 25°C for the Langmuir equation (R^2 = 0.9961). The constant (1/n) in the Freundlich equation is the degree of favorability in the adsorption. Since the value is always between 0.1 and 1, the adsorption of theaflavins on the A-DVB resin was considered to be favorable. For a value above 1 it would be very difficult for the adsorption to occur [13].

Table 3: Langmuir and Freundlich adsorption values for theaflavins on A-DVB resin

Temperature (°C)	Langmuir model	R^2	Freundlich model	R^2
25	Ce/Qe=0.0745 Ce+0.0016	0.9961	Qe= 50.81 $Ce^{0.5520}$	0.9872
40	Ce/Qe =0.0693 Ce+0.0013	0.9925	Qe= 26.91 $Ce^{0.4908}$	0.9598
50	Ce/Qe=0.0713 Ce+0.0019	0.9873	Qe= 38.48 $Ce^{0.5058}$	0.9954
75	Ce/Qe=0.0607 Ce+0.009	0.9914	Qe= 65.83 $Ce^{0.5284}$	0.9202

3.2. Static desorption on A-DVB resin

Theaflavins are soluble in water, ethanol, methanol, acetone and ethyl acetate [14]. Since the possibility of food grade operations is to be tested, the desorption study was performed with different concentrations of ethanol-water solutions.

According to Figure 3, the normalized desorption ratio (to 100% ethanol) of theaflavins increases with increasing ethanol concentrations until it reaches a maximum at 70% (v/v). At higher ethanol concentrations the desorption ratio decreased again.

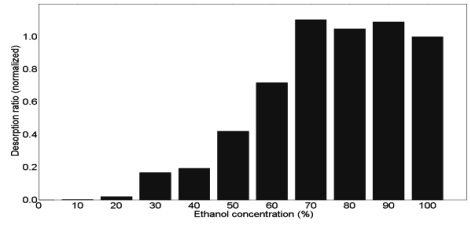

Figure 3: Normalized desorption ratio of theaflavins on A-DVB resin with different ethanol–water solutions

This ethanol-water desorption ratio is in accordance with the result obtained by Yi *et al.* [15] for eluting purified theaflavins. This is explained by a higher hydrophobicity of the theaflavins when comparing to other components present in black tea, e.g. catechins or caffeine, which have higher desorption rates at lower ethanol concentrations.

4. Future work

The selected resin will be used in a follow up study to identify the operational conditions (temperature, flow, etc.) that significantly affect the adsorption and desorption behavior of the resin. To capture the nonlinear behavior between the influence factors and the response factors a surface response methodology will be used. In addition, polynomial models can be generated from the data which can be used for optimization purposes.

5. Conclusions

Four commercial macroporous resins ranging from polar to non-polar were tested for their theaflavins adsorption characteristics from real aqueous black tea extracts. Among all resins studied, the most apolar A-DVB resin was found to have the best adsorption and desorption characteristics, probably due to chemical nature of the adsorbent. The desorption process was strongly influenced by the water content of the alcoholic solvent, as theaflavins will partition in the alcoholic phase only if their energy requirement for that phase is lower than for their sorption on the resin. The adsorption equilibrium exhibited a slightly better fit with the Langmuir model for all resins studied.

This work is the first step for a more detailed characterization and modeling study of the theaflavins adsorption process.

Acknowledgements

This work was supported by the Institute for Suistainable Processing Technology (ISPT) consortium.

References

[1] M.E. Harbowy, D.A. Balentine, (1997), *Critical Reviews in Plant Sciences*. 16(5), 415.
[2] C. S. Yang, J. Y. Chung, G.Yang, S. K. Chhabra and M.J. Lee, (2000), *J.Nutr.* 130, 472S.
[3] Y. J. Fu, Y. G. Zu, W. Liu, T. Efferth, N. J. Zhang, X. N. Liu, Y. Kong, (2006), *Journal of Chromatography A*, 1137, 145.
[4] F.Shahidi, (2007), Nutraceuticals and Functional Foods in Health Promotion and Disease Risk Reduction. Shanghai: Based on Keynote presentation at IUFoST Conference held in conjunction with Fi Asia/China.
[5] P. Gogoi, N.Dutta, P.Rao, (2010), *Indian Journal of Chenical Tecnology*, Vol.17(5),337-3.
[6] I. Langmuir, (1918), *The Journal of the American Chemical Society*.40 (9), 1361.
[7] H. Freundlich, (1907), *Z Phys Chem*, 57, 385.
[8] E.M. Silva, D.R. Pompeub, Y. Larondelle, (2007), *Sep. Purif. Technol.* 53, 274.
[9] X.L. Du, Q.P. Yuan, J.S. Zhao, (2007), *J. Chromatogr. A* 1145, 165.
[10] R.S. Juang, J.Y. Shiau, (1999), *J. Hazard. Mater*. B 70, 171.
[11] M. Scordino, A.D. Mauro, A. Passerini, (2003), *Agric. Food Chem.* 51, 6998.
[12] R. Q. Huang, N. H. Li, S.Y. Huang, (2011), Advanced Materials Research, 2957,236-238.
[13] R.E. Treybal, Mass-Transfer Operations. third ed., McGraw-Hill International, 1981.
[14] M. Naczk, F. Shahidi, (2004), J. Chromatogr. A 1054, 95–111.
[15] X. Yi, J. Yuxia, W. Yuanyuan, T. Youying, (2010), *Journal of Liquid Chromatography & Related Technologies*, 33:20, 1791.

I.A. Karimi and Rajagopalan Srinivasan (Editors), Proceedings of the 11th International Symposium on Process Systems Engineering, 15-19 July 2012, Singapore.

Influence of the organic phase fraction in the biphasic organic-aqueous reactor feed stream on the enzymatic hydrolysis of FAME in a packed bed

Przemyslaw Krause, Georg Fieg

Hamburg University of Technology, Institute of Process and Plant Engineering, Schwarzenbergstrasse 95 C, 21073 Hamburg, Germany, p.krause@tu-harburg.de

Abstract

The behavior of a differential packed-bed reactor element was investigated regarding the impact of the organic phase fraction on the reaction rate of an enzymatic hydrolysis with biphasic reactant flow. Wetting of the catalyst particles played an important role for this reaction system, and an assumed packed-bed flow pattern was examined. To cover the entire operation range varying from biphasic flow with high water excess to singular organic phase flow an integrated approach consisting of experiments and simulation was chosen. With the developed method wetting of the catalyst particles only by one liquid phase could be confirmed for the entire operation range.

Keywords: packed bed, enzyme, multiphase reactors, modeling

1. Introduction

For the development of production processes in the biochemical industry quantitative information about the behavior of reaction systems is decisive. Their knowledge enables the transfer of imaginable processes, already working in laboratory scale, to concepts suitable for production scale. The present work deals with a systematic investigation of a biotechnological reaction system. To ensure practical relevancy the procedure was developed on the basis of a model system, so that this work may be seen as an exemplary case study. The findings were obtained from knowledge-based assessment and modeling of the enzymatic hydrolysis of short-chain fatty acid (C_6–C_{10}) methyl esters using *Candida antarctica* lipase B (Novozym®435). The reacting methyl esters and water formed two liquid phases. The reaction was performed as batch run in a recycle packed-bed reactor assembly containing swollen catalyst particles. Fatty acids and methanol were obtained as products.

2. Theoretical Approach

The reaction behavior of the packed-bed element was determined from experiments and their model based analysis. For this purpose the usage of a phenomenological model based upon a decomposition of the observed reaction behavior into singular contributions was required. A mathematical model for the aforementioned hydrolysis reaction was developed by Krause and Fieg (2011) and utilized for the present study. This model assumed a pseudo-homogeneous reaction in the organic phase, whereas the kinetic expression used thermodynamic activities. The approach applied a UNIQUAC model for description of the liquid-liquid phase behavior. The biochemical reaction occurring at the active sites of the catalyst depended on the transport of the reactants and products between the bulk phase and the particles. The bulk phase composition was obtained from macroscopic balances of the entire experimental assembly. The

macroscopic balances constituted the connection between the actual (intrinsic) reaction and the observed reaction behavior. To limit the complexity of the modeling approach simplifying assumptions were made. All simplifications were justified by choosing adequate reaction conditions, e.g., to warrant ideal mixing or excluding mass transfer limitations by choosing appropriate superficial velocities.
The examination of the flow patterns showed that both liquid phases occupied the same pores of the particle bed, whereas the particles were enclosed by the organic phase. Hence, wetting of the catalyst particles only by the organic phase was assumed. The schematic representation of the determined flow pattern at biphasic flow is depicted in Fig. 1. Fig. 1 shows a strong simplification of the observed flow pattern, which exhibited a dynamic change of the flow channel positions and geometries.

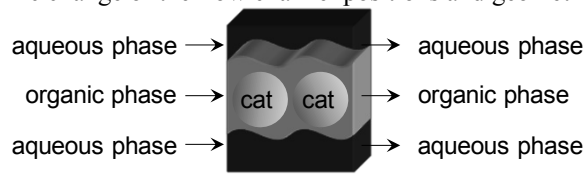

Figure 1: Schematic representation of the determined flow pattern in the packed-bed reactor at biphasic flow. (cat = catalyst particle)

At absence of mass transfer limitations a differential reaction step in the assembly can be subdivided in two separate imaginary steps (Krause and Fieg (2012)): (1) differential reaction progress in the bed element, and (2) attainment of the phase equilibrium. Assuming that for step 1 only the organic phase is required, both imaginary steps can be sterically separated from each other without the change of the observed global reaction behavior in the apparatus. From this decomposition two operation modes resulted, which could be compared: the two-phase flow operation mode in which both phases were passed through the packed bed vs. the singular phase flow operation mode with only organic phase flow through the reactor, in which the liquid-liquid phase mass transport exclusively occurred outside the reactor. In both operation modes only differential conversion per pass through the reactor was presumed.

3. Experimental Procedure

The kinetic experiments were performed in a so-called batch recycle packed-bed reactor assembly (Krause and Fieg (2011)). The schematic representation is given in Fig. 2. A similar setup was used, for example, by Kosugi and Tomizuka (1995), however without following the above described differential reactor concept. The assembly exhibited one circuit to provide the feed stream from the mixing vessel to the packed-bed reactor. To realize the decomposition of the reaction steps the experimental assembly could be run in two operation modes: either biphasic flow through the packed bed or singular phase flow. In the biphasic flow operation mode a homogeneous emulsion generated in the mixing vessel was passed through the reactor circuit. In the singular phase flow operation mode only the organic phase was passed from the mixing vessel to the reactor circuit. The liquid-liquid phase equilibrium was subsequently achieved in the mixing vessel. Within the experiments the impact of high water excess was investigated in the two-phase flow operation mode, whereas the singular phase flow operation mode was additionally used to confirm the model validity. The experimental assembly operated in the singular phase flow operation mode is depicted in Fig. 3. Fig. 3 shows that at the appropriate stirrer speed it was possible to achieve an o/w-emulsion in the aqueous phase while a clear organic phase layer on top of the emulsion was obtained.

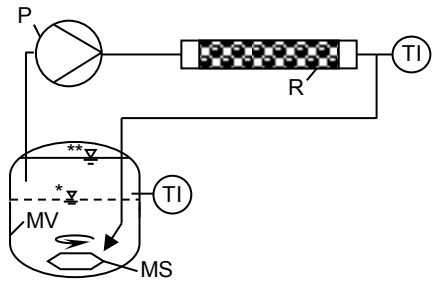

Figure 2: Schematic representation of the used reactor assembly. (MV = mixing vessel with 600 ml volume, MS = magnetic stirrer, P = circulation pump, R = 8 cm long packed-bed reactor with 1 cm i.d. containing Novozym®435 particles, TI = temperature indication, **▽ = liquid level at both operation modes, *▽ = phase boundary between the continuous organic phase layer on top of the aqueous phase in the singular phase flow operation mode)

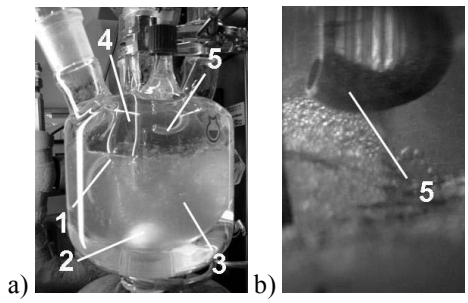

Figure 3: a) Mixing vessel in the singular phase flow operation mode. b) Magnification of the intake pipe. ((1) liquid-liquid phase boundary, (2) stirrer, (3) aqueous phase (o/w-emulsion in the mixing zone), (4) organic phase, (5) intake pipe of the reactor circuit)

4. Results and Discussion

4.1. Operation at low organic phase fractions

All kinetic parameters were determined on the basis of experimental conversion courses X_i obtained in the two-phase flow operation mode with organic phase total mass fractions of approximately 0.3, corresponding to an initial water to methyl ester mass ratio of $A_{H2O} = 2.3$. The determination of the kinetic parameters in this operation range provided advantages in the experimental procedure and a simplified mathematical evaluation. The main benefit was that the entire assembly could be treated as a stirred tank because of the comparatively small conversion per pass through the reactor, while still a sufficiently high final total conversion of the methyl esters was obtained despite the strong limitation by the reaction equilibrium (Krause et al. (2010)). From experimental runs it was found that the initial reaction rate was independent of the aqueous phase fraction and constant for a constant organic phase to catalyst ratio.

For decreasing organic phase fractions in the emulsion the conversion per pass through the packed bed increased when flow velocity and bed length remained unchanged. This caused an increasing deviation of the assembly behavior from the stirred tank assumption. The reason for not reducing the bed length was to maintain exactly the same catalyst bed throughout one experimental series. Hence, for low organic phase fractions the packed bed could not be treated as a differential reactor in the modeling

approach. To consider the integral character of the bed it was treated as a plug flow reactor.

Measuring the conversion courses X_i on the basis of the organic phase compositions was impossible at low organic phase fractions without significantly interfering with the observed system behavior. However, the reaction could be tracked by following the methanol mass fraction in the aqueous phase $w_{MeOH,aq}$, which was an adequate method to compare the experimentally determined and modeled reaction courses. For this purpose the absence of mass transfer limitations and a reliable description of the methanol distribution between the phases were required. The comparison of the obtained experimental and calculated courses is given in Fig. 4. For the cases (1) to (4) the overall methyl ester conversion increased from $X \approx 0.5$ to 0.8 (the temperature had no decisive influence). Because of the decreasing total amount of methyl ester and the increasing water excess the methanol content of the aqueous phase decreased.

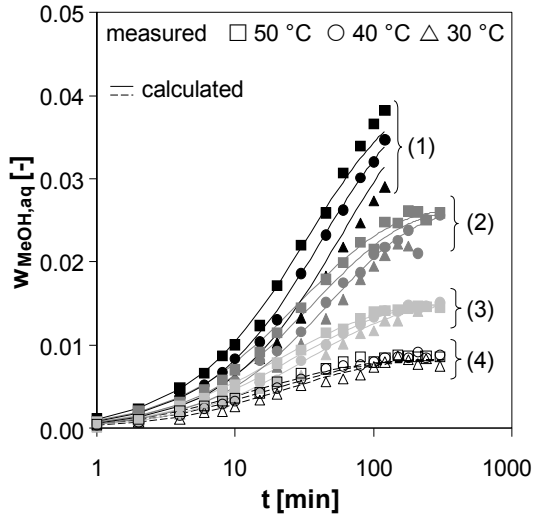

Figure 4: Influence oft the initial water to methyl ester (A_{H2O}) and catalyst to methyl ester (A_{cat}) mass ratios on the conversion course during the hydrolysis of methyl octanoate at constant total reactant mass and a packed bed superficial velocity of 0.07 m/s. (1) $A_{H2O} = 2.3$, $A_{cat} = 7\times10^{-3}$; (2) $A_{H2O} = 4.4$, $A_{cat} = 12\times10^{-3}$; (3) $A_{H2O} = 9.8$, $A_{cat} = 23\times10^{-3}$; (4) $A_{H2O} = 20.6$, $A_{cat} = 46\times10^{-3}$. Comparison of calculated and measured methanol mass fractions $w_{MeOH,aq}$ in the aqueous phase.

Within the mathematical model wetting of the entire particle bed by the organic phase irrespective of A_{H2O} and direct proportionality between the reaction rate and the catalyst mass were assumed. From the good agreement between the calculated and measured courses shown in Fig. 4 it can be concluded that the modeling assumptions were correct up to a water excess of 20:1 g/g for temperatures ranging from 30 to 50 °C.

4.2. Direct comparison of the operation modes

In section 2 the decomposition of the reaction in two steps was suggested. The purpose of the decomposition was to prove the validity of the assumptions regarding the catalyst wetting applying the sterical separation of reaction and liquid-liquid mass transfer. A direct comparison between calculated and measured courses for both operation modes is shown in Fig. 5. The calculated courses were based upon the parameter determination from two-phase flow experiments as described in section 4.1. The successful separation of both elementary steps enabled the examination of the impact of the catalyst wetting on the reaction rate from the direct comparison of experiments performed in both

operation modes for a fixed value of A_{H2O}. From the comparison it can be concluded that both operation modes gave nearly identical conversion courses, which confirmed that in both cases the same amount of catalyst was active. Thus, wetting of the entire particle bed by the organic phase at two-phase flow could be assumed.

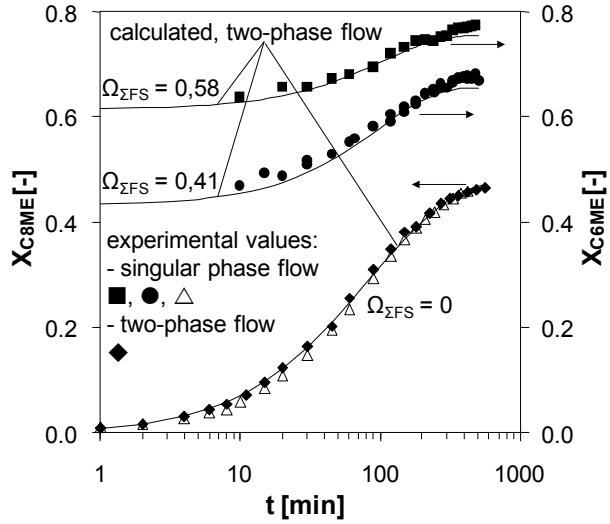

Figure 5: Comparison of experimental and calculated conversion courses obtained in the singular and two-phase flow operation mode at A_{H2O} = 2.3 exemplarily given for four independent experimental runs. (X_{C6ME}, X_{C8ME} = methyl hexanoate or methyl decanoate conversion; $\Omega_{\Sigma FS}$ = initial fatty acid to (fatty acid + methyl ester) mass ratio).

5. Conclusions

For this type of equilibrium limited reactions multistage extractive-reaction processes provide an alternative concept for shifting the equilibrium conversion toward the products (Krause et al. (2010), Samant and Ng (1998)). Either high water to methyl ester mass ratios resulting in a comparatively small number of equilibrium stages, or a moderate water excess resulting in a comparatively high number of stages are applicable. Both strategies lead to different requirements in respect of the process design. Using the suggested examination method a reliable calculation model necessary for the simulation of process alternatives was obtained.

References

Y. Kosugi, N. Tomizuka, 1995, Continuous lipolysis reactor with a loop connecting an immobilized lipase column and an oil-water separator, JAOCS, 72, 1329-1332

P. Krause, R. Macias, G. Fieg, 2010, Applicability of a Countercurrent Enzymatically Catalyzed Multistage Extractive Reaction Process for the Hydrolysis of Methyl Octanoate, Ind. Eng. Chem. Res., 49, 3217-3222

P. Krause, G. Fieg, 2011, Experiment based model development for the enzymatic hydrolysis in a packed-bed reactor with biphasic reactant flow, Chem. Eng. Sci, 66, 4838-4850

P. Krause, G. Fieg, 2012, Applicability of a simple laboratory setup for the extractive hydrolysis using immobilized enzymes, Chem. Eng. Process., submitted

K.D. Samant, K.M. Ng, 1998, Design of Multistage Extractive Reaction Processes, AIChE J., 44, 12, 2689-2702

I.A. Karimi and Rajagopalan Srinivasan (Editors), Proceedings of the 11th International Symposium on Process Systems Engineering, 15-19 July 2012, Singapore.

Statistical Monitoring of Water Systems

Marco Cedeño Viteri,[a] Leandro Rodriguez Aguilar,[a] Mabel Sánchez[a]

[a]*Planta Piloto de Ingeniería Química (UNS- CONICET,) Camino La Carrindanga Km 7, (8000) Bahía Blanca, Argentina*

Abstract

In this work a new statistical control methodology that works in the original variable space is presented. The study is focused on the performance of the detection stage, which applies the 2-order Mahalanobis distance as statistical test. Its critical-value is estimated using a kernel density estimation technique. The identification stage uses the concept of the nearest in control neighbor to calculate the variable contributions to the inflated statistic and employs the same distance measure. Application results are provided for a waste water treatment plant.

Keywords: Statistical Process Control, Mahalanobis Distance, Waste-Water Treatment Plants.

1. Introduction

Multivariate Statistical Process Control (MSPC) techniques have been widely applied for turning data into information since they are suitable to develop empirical descriptions of the process behavior based on measurements. Most of them work in latent-variable spaces. In the spirit of developing new approaches that could provide new features and capabilities to those techniques, little attention has been paid to the fact that some strategies which work in the original measurement space could also perform well when monitoring a process (Alvarez et al., 2010).

From the monitoring standpoint, determining whether the process can be considered as in-control at a given time t is just one step in the procedure, called the detection stage. The MSPC approaches that work in the space of measurements make use of the Hotelling (T^2) statistic, which is a measure of the linear Mahalanobis Distance (MD), for this purpose. Whenever one observation is believed to show an abnormal behavior, all the effort must be oriented towards finding what the root cause of the deviation is. The activities related to isolating the variable(s) that indicate(s) the faulty state conform what is known as the identification stage, which is frequently performed by calculating the variable contributions to the inflated statistic. The main purpose of evaluating those contributions is to compare the relative influence of each measured variable on the final T^2-statistic value. It is considered that those having the largest contributions reveal the faulty state. In this sense, Mason and Young (2002) presented a combinatorial strategy to decompose the T^2-statistic into the contributions of each variable. It has the limitation that a great number of possible decompositions are obtained, increasing the complexity of the identification procedure. Then a straightforward method to decompose the T^2 statistic as a unique sum of variable contributions, called OSS, was developed by Alvarez et al. (2007). Recently, Alvarez et al. (2010) proposed a new MSPC strategy for batch process monitoring, called OSSBP, based on that decomposition. For the analyzed case studies, the proposed strategy has comparable abilities regarding the detection of process failures with respect to the ones presented by the most popular latent variables-based approaches (Westerhuis et al., 2000; Ramaker et al., 2005; Yoo et al., 2004).

Moreover, identification performance indexes show better results for the OSSBP. Its satisfactory behaviour may be attributed to the fact that the number of variables involved in this type of processes is moderate and the strong non-linear relationships among them prevent the measurements from being linear combinations. These facts prevent the data correlation matrix to be singular.

When the T^2-statistic is applied for the detection stage of a MSPC procedure, it is generally assumed that measurement vectors are independent and follow a multivariate normal distribution. In this case, the T^2-statistic follows a $[J(I^2-1)/(I^2-IJ)]F_{J,I-J,\alpha}$ distribution where, $F_{N,I-N,\alpha}$ is the value of the F distribution for a level of significance α with J and $(I-J)$ degrees of freedom, I represents the number of samples in the reference population and J is the number of measurements. No assumption about the probability density function (*pdf*) is required when the threshold value T^2_C is determined as the $(1-\alpha)$ quantile of the T^2 *pdf*, which can be estimated using well-known kernel density estimation (KDE) methods. Although the computational effort increases, the extra calculations are performed offline, thus no application restrictions during the online monitoring stage arise due to the extra computational burden (Alvarez et al, 2010).

Because the OSS methodology has a comparable ability for fault detection with respect to the existing latent-variable procedures, the use of a different distance measure to indicate the out of control state is analyzed in this work. The same type of distance between the nearest in control neighbour (NICN) and the current observation (Alvarez et al., 2009) is used to determine the contribution of each variable to the out of control state. Those variables whose distance measures exceed a certain threshold value are considered as suspicious. The coordinates of the NICN are obtained by solving a minimization problem. In this work, the Polynomial Mahalanobis distance of order 2 is selected for both stages of the proposed MSPC.

The rest of the paper is structured as follows. In Section 2 the methodology is presented. Results corresponding to its application for the detection of faults in a waste water treatment plant (WWTP) benchmark are provided in Section 3. A Conclusion section ends this work.

2. Methodology

The Mahalanobis distance is a common metric that attempts to capture the non-isotropic properties of a J-dimensional feature space. It weights the distance calculation according to the statistical variation of each component using the covariance matrix of the observed sample. Grudic and Mulligan (2006) have shown that the MD may not tightly follow a learning data set, and substituted it by the Polynomial Mahalanobis distance (PMD), which is obtained by mapping the measurement space into high order polynomial terms. They use the PMD for classifying path regions in images of natural outdoor environments.

Those authors formulated the q-order PMD (q-PMD) as follows. Given a set of $\mathbf{x}_k$ observation vectors (k=1,..,I) of dimension J, the q-PMD between vectors $\mathbf{x}_i$ and $\mathbf{x}_j$ is calculated by first mapping each $\mathbf{x}_k$ into all polynomial terms of order q or less, which are included in vector $\mathbf{z}_k$, and then calculating the MD between $\mathbf{z}_i$ and $\mathbf{z}_j$ using the covariance matrix obtained from the reference population of polynomial term mappings. In this way they attempt to describe more sophisticated and nonlinear relations among feature vectors.

The T^2- statistic applied in MSPC procedures is a measure of the MD between an observation and the population mean. An out-of-control state of the process is indicated

if the T^2- statistic value exceeds the critical one. This is calculated using a KDE technique when the OSS procedure is used.
In this work a new MSPC procedure is devised whose detection stage makes use of the 2-order PMD (PMD^2) between an observation and the population mean as statistic test. That PMD^2 is formulated following the work by Grudic and Mulligan (2006) and the critical value of the statistic PMD^2_C is calculated using the KDE technique.
Regarding the identification stage, the knowledge about how far the faulty observation is from an in-control allocation gives us an idea of the directions whose distances explain the anomalous situation. This information is obtained by finding the nearest neighbour of the observation point that is in statistical control ($\mathbf{x}_{NICN}$). An optimization problem is formulated whose objective is to minimize the PMD^2 between $\mathbf{x}_{NICN}$ and the measured point $\mathbf{x}$, subject to the constraint that the PMD^2-value for $\mathbf{x}_{NICN,}$ is equal to the critical one (PMD^2_C). The comparison of the absolute difference between x_{NICN} and x for each variable j with a threshold value τ, which is obtained by simulations for a given Number of Precise Identifications (Alvarez et al., 2010), allows to identify the suspicious measurements.

3. Application Results for the WWTP Benchmark

In this section application results of the proposed strategy for the detection and identification of faults associated to a WWTP benchmark are presented. The plant layout, model equations and control strategy are not included for the sake of brevity but they are described in detail online [http://www.ensic.u-nancy.fr/COSTWWTP]. For the present study, plant layout combines nitrification with predenitrification, which is the most commonly used method for nitrogen removal. The plant is designed to treat an average flow of 20,000 m^3/day with an average biodegradable chemical oxygen demand concentration of 300 mg/l. The plant is made up of five-compartment biological tanks and a secondary settler. The first two compartments of the bioreactor are not aerated whereas the others are aerated. The nonreactive secondary settler is modeled with a series of 10 layers. There are two internal recycles: the nitrate internal recycle from the last tank to the first tank, and the activated sludge recycle from the underflow of the secondary settler to the front end of the plant. In Figure 1 a schematic diagram of the simulation benchmark is shown.

Fig 1: WWTP Layout

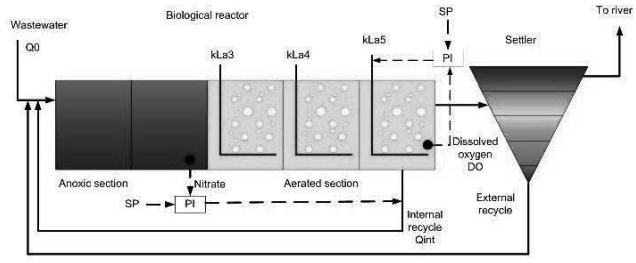

The training model is based on a normal operation period of 1-week of dry weather and a 1-week data set is used for validation. The sampling time is 15 min; therefore 96 samples are taken each 24-hour period. The data used are the influent file and outputs with noise suggested by the benchmark. The following eight variables are selected to build the monitoring system: influent ammoniac concentration, influent flow rate, total

suspended solids in reactor 4, effluent total suspended solids, dissolved oxygen concentration in reactors 3 and 4, oxygen transfer coefficient in reactor 5, and nitrate concentration in reactor 2.

In this work, three scenarios describing real situations are considered for the analysis. The first external disturbance takes the form of a storm event. It originates that the influent flow rate exceeds the maximum standardized value for normal operating conditions, which is equal to 2.67, during the following time intervals (848-857), (1049-1086), (1095-1103). The second external disturbance is the increment of the influent flow rate due to rain. This flowrate exceeds its maximum normal-operating value from samples (807-906). The third fault is a mean change in the nitrate concentration sensor noise. This fault is introduced at the beginning and maintained until the end of the simulation.

Regarding the detection capabilities of the proposed strategy, the evolution of T^2-statistic and PMD^2-statistic in time is analyzed. Both statistics are compared to their corresponding critical values obtained using a KDE technique. For a significance level α= 0.06, their values are: 16.85 for T^2, and 120.11 for PMD^2. A failure is declared after three consecutive warnings.

For the storm disturbance, the T^2-statistic gives alarms at samples 849 and 1051, and the PMD^2-statistic indicates a fault condition at samples 849 and 1049. Both statistics point out the abnormal situation for a long time. This shows the effect of the influent flowrate increment on internal variables persists in time. The evolution of the influent flowrate, the T^2-statistic and PMD^2-statistic in time is displayed in Figure 2 for the storm event.

Fig 2: Storm Events

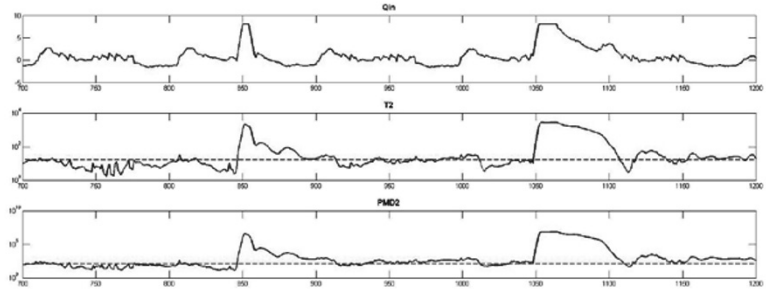

Fig 3: Rain Event

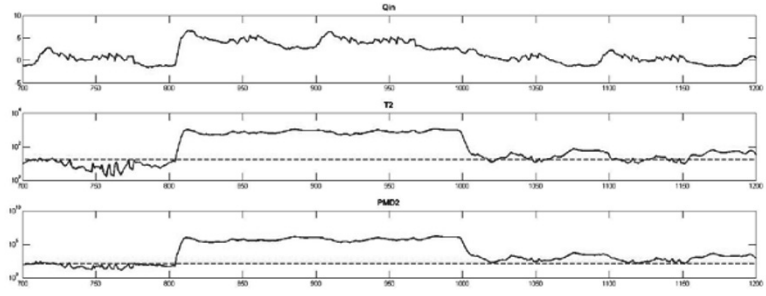

For the rain event, both the T^2-statistic and PMD^2-statistic give an alarm at sample 807, that also persist in time. The time evolution of the statistics for this event is shown in Figure 3. The next figure reports the same information for the third fault, which is

associated with a mean change of the concentration nitrate sensor noise. The T^2-statistic gives an alarm at sample 47, after 3 consecutive warnings are obtained. In contrast the PMD^2-statistic provides the first alarm signal at sample 3 and it is repeated many times during the operation. Variable contributions to the inflated statistics are obtained that properly indicate the faulty variables. Contribution plots are not included for the sake of brevity.

Fig 4: Mean change in sensor noise

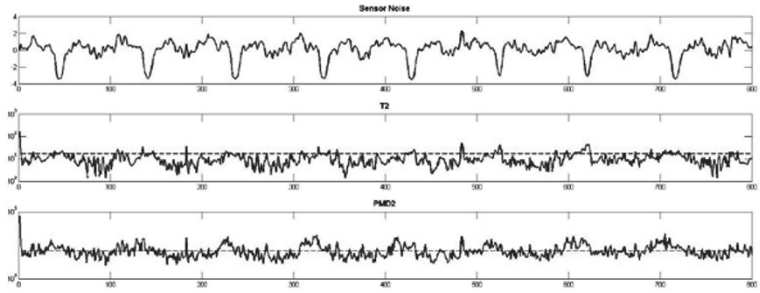

4. Conclusions

In this paper a new MSPC methodology that works in the original variable space is presented and applied for WWTP fault diagnosis. A different distance measure, the *q order-PMD*, is used as test statistic for the detection stage and to determine the variables that signal the fault.

For the fault scenarios of the WWTP analyzed in this work, the PMD^2 has shown better capabilities for fault detection with respect to the T^2-statistic. Also it has a rewarding performance with respect to the statistics used in the latent variable space methodologies reported in literature when the action to signal time is considered for comparison purposes.

The computational load of the identification stage ensures real-time results for the tested faults. Future work involves the selection of the polynomial order.

References

C. Alvarez, A. Brandolin, M. Sánchez, 2007, On the Variable Contributions to the D-statistic, Chemom. & Intell. Lab. Syst., 88, 2, 189-196.

C. Alvarez, A. Brandolin, M. Sánchez, 2009, A Neighbour in Control Technique for Batch Process Monitoring", Comp. Aided Chem. Eng. Elsevier, 27, C, 1581-1586.

C. Alvarez, A. Brandolin, M. Sánchez, 2010, Batch Process Monitoring in the Original Measurement's Space, J. of Process Control, 20, 6, 716-725.

G. Grudic, J. Mulligan, 2006, Outdoor Path Labeling Using Polynomial Mahalanobis Distance, Proceedings of Robotics: Science and Systems II, MIT Press, Cambridge, Massachusetts.

R. Mason, J. Young, 2002, Multivariate Statistical Process Control with Industrial Applications, ASA SIAM, Philadelphia.

H. Ramaker, E. Van Sprang, J. Westerhuis, A. Smilde, 2005, Fault Detection Properties of Global, Local and Time Evolving Models for Batch Process Monitoring, J. of Process Control, 15, 7, 799-805.

J. Westerhuis, S. Gurden, A. Smilde, 2000, Generalized contribution plots in multivariate statistical process monitoring, Chemom. & Intell. Lab. Syst., 51, 1, 95-114.

C. Yoo, J. Lee, P. Vanrolleghem, I. Lee, 2004, On-Line Monitoring of Batch Processes Using Multiway Independent Component Analysis, Chemom. & Intell. Lab. Syst., 71, 2, 151-163.

I.A. Karimi and Rajagopalan Srinivasan (Editors), Proceedings of the 11th International Symposium on Process Systems Engineering, 15-19 July 2012, Singapore.

Next-Generation, Integrated Fire Detection and Diagnosis Built Upon the Recent Advances in the Abnormal Situation Management

Kijun Lee[a], Seong-Hwan Han[a], Tae-Ok Kim[a], Dongil Shin[a]

[a]*Department of Chemical Engineering, Myongji University, Yongin 449-728, Korea*

Abstract

Process fault monitoring, detection and diagnosis, and fire detection and isolation technologies have many common characteristics between them, and the amount of technological overlapping is being increased. This paper compares and discusses our works in the areas of conventional abnormal situation management (ASM) as well as fire alarm generation management, as a try to show how the ASM technologies would contribute in developing next-generation fire detection and management technologies and improve the safety of process plants and the public. And the lessons from the fire detection research that could be applied for better monitoring, detection and diagnosis of processes are also discussed.

Keywords: Fire Detection, Process Monitoring and Diagnosis, Industrial Applications, Process and Public Safety, Computational Methods

1. Introduction

Fire is one of the oldest hazards and has been around the human beings with the start of the history. Process fault monitoring, detection and diagnosis and fire detection and isolation technologies have been developed separately and have rich histories individually, but there has been no study of the commonality of the both. There are many sharing characteristics between them and the amount of technological overlapping is being increased: Mitigation of sensor failures, context sensitivity, and minimization of Type I, II errors are important problems. Use of wireless sensors and merge of heterogeneous information are getting the focus en route to the next-generation technologies. This paper discusses how the abnormal situation management technologies, studied in the process systems engineering perspective, would contribute in developing next-generation fire detection and management technologies and improve the safety of process plants and intelligent buildings as well. The next sections show our works in the area of conventional abnormal situation management as well as fire alarm generation management.

2. Fault Detection, Monitoring and Diagnosis System for CNG Stations

2.1. Necessity of the Research

The compressed natural gas (CNG) among the eco-friendly energy sources already accounts for more than 10 percent of domestic energy consumption of Korea. CNG vehicles and also the gas stations are being increased. However, more than nine large and small accidents of CNG vehicle and gas stations have occurred in the past five years, which makes us aware of the need for the study for the safety and safe operations of CNG stations. A lot of non-repetitive transition sections exist during the ordinary operation of CNG gas stations. Therefore, fault detection and diagnosis are limited with

the current monitoring methods, and the advanced maintenance before failures is almost impossible and even the alarms exceeding the specified upper and lower thresholds are ignored as nuisant [1,2].

2.2. Using PCA

In this study, we developed a system (see Fig. 1) to build a monitoring model for the CNG station and perform the real-time monitoring and diagnosis using Principal Component Analysis (PCA), which is suitable for processing large amounts of multi-dimensional data for multivariate statistical analysis [3].

2.2.1. Filtering and Scaling

Filtering and scaling processes are conducted prior to the model construction and application. As shown in Fig. 2, data during the start-up and shut-down are removed from the 7 pressure sensor and 5 temperature sensor data collected per second, and the remaining data of ordinary charging operation are used for model development [4,5,7].

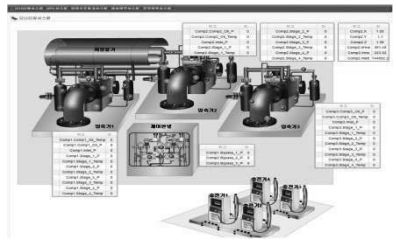

Fig. 1. Screenshot of the developed system

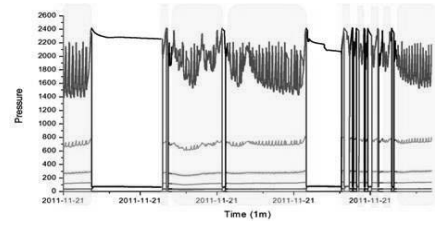

Fig. 2. Filtering of the pressure data

2.2.2. Modeling

We built the PCA model in Fig. 3 by the calculation of the new characteristics variables, called as the major component, finding the factors representing the trend of unsteady process operation. Fig. 4 represents Q residuals of model data [6].

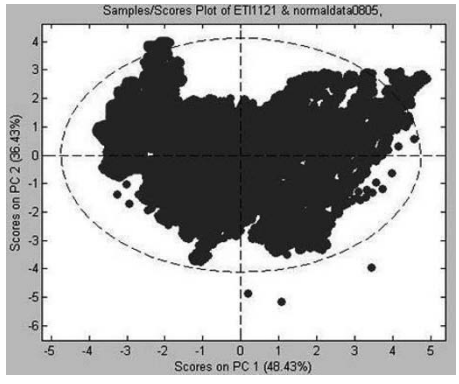

Fig. 3. Score plot of PCA model

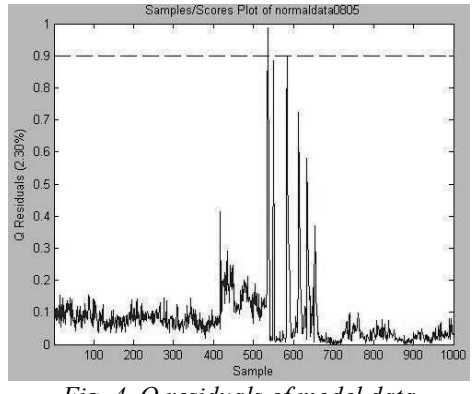

Fig. 4. Q residuals of model data

2.3. Result

The performance of real-time monitoring was measured against the data of process operations already stored in the real-time database. As a result of conducting the off-line monitoring in order to improve the accuracy of the system and verification, all data in the normal operation were distinguished as normal. And when an abnormal

phenomenon was tested by reflecting the abnormal process data, the cause of abnormality could be refined by detecting abnormality as in Fig. 5 and by tracking main contributing variables as in Fig. 6.

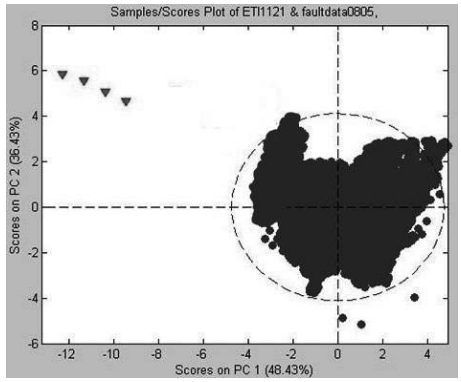

Fig. 5. Plot of detecting abnormality

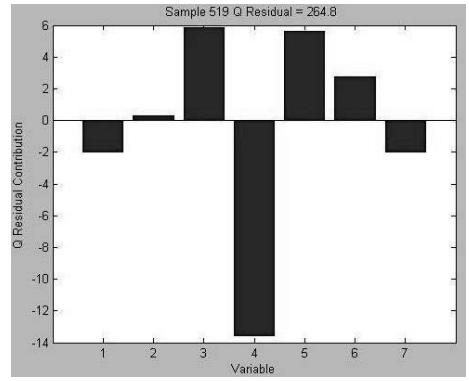

Fig. 6. Diagnosing cause of abnormality

Even though the training data of abnormal operations are rare, the proposed system is able to efficiently cope with the abnormality in process through fault detection and diagnosis with the development and building of the monitoring system for CNG gas stations using PCA. It is estimated that the optimized operation of the facility would be possible by the real time comparison of the current state of facility to the normal state of the past.

3. Fire Detection System Design Based on Multi-sensor Information for Improved Reliability

3.1. Necessity of the Research

The fire detector is used to sense and alarm the danger in an emergency, and the time it takes from the outbreak of fire and detecting the danger and its accuracy are considered critical [8]. For existing detectors, such as mechanical method (on-off), single sensor-based (heat, smoke, or flame), or dual sensor (HR combination system), malfunctions as false-positive alarms not going off in case of fire or false-negative alarms ringing when there is no fire occur frequently [9].

3.2. Improved Detection Algorithm

This study suggested an improved algorithm that senses fire by using three types of information of heat detector, smoke detector, and concentration detector, and has established a fire detecting testbed on LabVIEW, and verified algorithm by using the testbed [12]. Simulation was carried out by using the measured sensor data according to the experiments provided by Fire Research Division of NIST, and was able to verify if a fire occurs or not for a given set of data [10,11].

3.2.1. Fire Detection Algorithm

This study determined whether the temperature, smoke, or carbon monoxide values exceeded the critical value, and suggested an integrated fire detecting algorithm that determines cases of emergency based on the results as shown in Fig. 7.

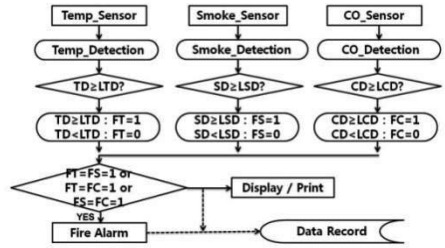

Fig. 7. Fire detection based on multiple information

3.2.2. Simulation

As shown in Fig. 8, the testbed was established on LabVIEW, implementing the suggested algorithm, and simulation was carried out by using the sensor measuring data according to the situation of Home Smoke Alarm Tests performed by the Fire Research Division of NIST from 2004 to 2008. A test scenario among Home Smoke Alarm is as shown in Table 1, and the simulation process is as shown in Fig. 9 [12].

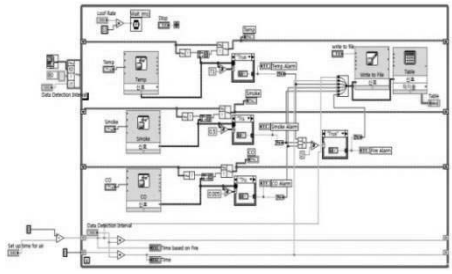

Fig. 8. Testbed implemented

Table 1. Fire place and a source of ignition [12]

Situation	Test	Ignition	Fuel Package	Fire Location
Fire	SDC02	Flaming	Chair	Living Area
	SDC05	Flaming	Mattress	Bedroom#2
	SDC08	Smoldering	Mattress	Bedroom#2
	SDC11	Smoldering	Chair	Living Area
	SDC15	Flaming	Chair	Living Area
	SDC39	Flaming	Mattress	Bedroom#2
	SDC41	Heating	Cooking Oil	Kitchen Area
Non-fire	MHN30	14 g (1 tbls) butter, cast iron pan, fan on		
	MHN31	14 g (1 tbls) butter, cast iron pan, fan off		
	MHN40	Smoldering PU foam block, fan off, (flamed)		

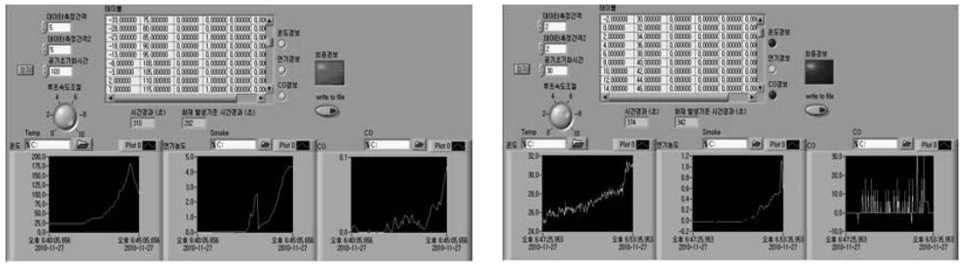

Fig. 9. Simulation: Minimization of false negative and positive errors (Scenario SDC05 at 202sec : Detected false positive / Scenario SDC05 at 342sec : Detected false negative)

3.3. Result

As a result, the elapsed time until the very first integrated generation of warning and alarm operation was identified as shown in Tables 2 and 3. Every fire emergency except for Test SDC41 was detected, and the integrated alarm method worked successfully for all non-fire situations.

The integrated fire detection system based on multiplexed information of three independent measuring data improved the accuracy of diagnosing the real and non-fire situations than the existing fire detecting systems based on single or dual information.

Improvement in more collection of quantitative data, which consider both accuracy and time of detection, and advanced algorithm built upon the recent advances in the abnormal situation management are considered to make contribution in a development of next-generation fire detection system. Performance evaluation of fire detection system which was actually restricted other than actual fire experiments is considered to be possible by expanding the suggested testbed.

Table 2. Detected all fire situations

Test	Ignition	Fuel Pkg.	Fire Location	Fire Alarm (s)	Temp Alarm (s)	Smoke Alarm (s)	CO Alarm (s)
SDC02	Flaming	Chair	Living Area	110	146	110	0
SDC05	Flaming	Mattress	Bedroom#2	117	117	67	192
SDC08	Smoldering	Mattress	Bedroom#2	3721	3721	3721	3809
SDC11	Smoldering	Chair	Living Area	4289	4303	773	3549
SDC15	Flaming	Chair	Living Area	327	313	327	417
SDC39	Flaming	Mattress	Bedroom#2	128	108	128	-
SDC41	Heating	Cooking Oil	Kitchen Area	-	-	1206	-

Table 3. Detected all non-fire situations

Test	Nuisance Sources	Fire Alarm (s)	Temp Alarm (s)	Smoke Alarm (s)	CO Alarm (s)
MHN30	14 g (1 tbls) butter, cast iron pan, fan on	-	-	324	-
MHN31	14 g (1 tbls) butter, cast iron pan, fan off	-	-	310	40
MHN40	Smoldering PU foam block, fan off, (flamed)	-	-	-	470

4. Conclusion: Integrated fire detection and diagnosis

Process fault monitoring, detection and diagnosis and fire detection and isolation technologies have many common characteristics between them, and the amount of technological overlapping is being increased: Mitigation of sensor failures, context sensitivity, and minimization of Type I, II errors are important problems. This paper discussed how the abnormal situation management technologies, shown for the case of fault detection, monitoring and diagnosis system for CNG stations, would contribute in developing next-generation fire detection and management technologies and improve the safety of process plants and public safety for the realization of better sustainable society.

References

[1] David M. Himmelblau, *Fault Detection and Diagnosis in Chemical and Petrochemical Processes*, Elsevier (1978)

[2] Kourti, T. and MacGregor, J. F., "Process Analysis, Monitoring and Diagnosis Using Multivariate Projection Methods", *Chemometrics and Intelligent Laboratory System* 28(1), 3-21 (1995)

[3] ChangKyoo Yoo, et al., "Recent Research Trends of Process Monitoring Technology: State-of-the Art", *Korean J. Chem. Eng*., 46(2), 233-247 (2008)

[4] Manabu Kano, et al., "A New Multivariate Statistical Process Monitoring Method Using Principal Component Analysis", *Computers and Chemical Engineering,* 25, 1103-1113 (2001)

[5] Jong-Min Lee, et al., "Fault detection of batch processes using multiway kernel principal component analysis", *Computers and Chemical Engineering,* 28, 1837-1847 (2004)

[6] Barry M. Wise, *PLS_Toolbox 3.5 Manual*, Eigenvector Research (2004)

[7] Hyosung Corporation, *CNG compressor package manaul system*: V1.03

[8] Mark Hunter, "False alarm reduction by use of new technology", *International fire protection,* 55-58 (2006)

[9] M. Thuillard, "New Methods for Reducing the Number of False Alarms in Fire Detection Systems", *Fire Technology J.*, 30(2). 250-268 (1984)

[10] J.A. Milke, L.A. Cestari and W. Clarence, "Advanced Fire Detection Algorithms Using Data from the Home Smoke Detector Project", *Fire Safety J*., 40(1) 1-28 (2005)

[11] A. Scheidweiler, "The Distribution of Intelligence in Future Fire Detection Systems", *Fire Safety J*., 6, 209–214 (1983)

[12] NIST, Home Smoke Alarm Tests, http://smokealarm.nist.gov/

I.A. Karimi and Rajagopalan Srinivasan (Editors), Proceedings of the 11th International Symposium on Process Systems Engineering, 15-19 July 2012, Singapore

Hierarchical proficiency evaluation system of plant operation for effective operator training

Taketoshi Kurooka,[a] * Masaki Yasuda,[b] Haruyuki Okuda,[b]
Hironobu Arakawa,[b] Hideki Manako,[b]

[a] *Department of Life Sciences & Bioengineering, Faculty of Engineering, University of Toyama, Gofuku 3190, Toyama-shi, Toyama 930-8555, Japan*
[b] *System Advanced Solutions Department, Project Division II, Mitsubishi Chemical Engineering Corporation, 4-2-8 Shibaura, Minato-ku, Tokyo 108-0023, Japan*

Abstract

We have developed a new method to evaluate plant operators' proficiency. In this method, an operating procedure is hierarchically analyzed so that the method can be applied to complicated operations. Furthermore, the method was evaluated with indices based on Levenshtein distance. The proposed method was applied to simulator training on the start-up operation of a distillation column. The results demonstrate the utility and effectiveness of the proposed method.

Keywords: Proficiency metric, Plant operation, Skill assessment, Skill transition, Simulator training

1. Introduction

Recently, plant operation has become highly complicated, and thus inexperienced operators must often learn new operational procedures in complex plants. Additionally, in Japan, many veteran operators have been retiring in recent years, forcing younger operators to assume more of a leadership role. Therefore, effective training systems are required to train inexperienced operators more efficiently and quickly. For this purpose, training simulators are often used. Training simulators have been significantly improved, and their level of realism has been greatly enhanced (Jeong et al., 2002; Barrero et al., 2003) . In particular, Mitsubishi Chemical Engineering Corporation has been developing a simulator training system called MECTRNR ®. This system is equipped with advanced functions that can evaluate an operator's proficiency and perform PKYK (Process-Kiken-Yochi-Kunren; "process risk assessment by operators" in Japanese) through simulator training. These functions are useful for developing ideal operating ability. In this paper, we present a newly developed proficiency evaluation method and apply it to the function of assessing operators' capabilities.

For effective simulator training, it is necessary to evaluate how far the operator's skill has progressed in order to check his or her present skill level and to design effective training programs. This proficiency assessment is usually done with a subjective measure such as trainers' observation records or trainees' self-evaluations such as NASA-TLX or SWAT (Hart and Staveland, 1988; Reid and Nygren, 1988; Nishitani et al., 1997). However, subjective evaluation results vary according to the judgement of the assessor. As objective measures, physiological signals, such as an electroencephalogram or heart rate, are often

*kurooka@eng.u-toyama.ac.jp

used (Kurooka et al., 1998, 2001, 2003). However, measuring physiological signals imposes a strain on subjects. Recently, a new proficiency evaluation method was proposed, which uses an operating procedure index and a process stability index, and it was shown that the method can evaluate a simple operation (Kurooka et al., 2008). However, it is still necessary to develop a proficiency evaluation method that can be applied to a complicated operation in a large-scale plant. For this purpose, we developed a hierarchical system that can analyze and evaluate an operator's proficiency in a large-scale plant.

2. Hierarchical proficiency evaluation

2.1. Operational data for evaluation

We used a message summary that consists of two types of information: "when and what kind of alarm occurs and stops" and "when and what kind of operation is executed." These data, i.e. a message summary, can be easily obtained through a distributed control system (DCS) included in the training simulator system.

2.2. Evaluation procedure

The proposed evaluation procedure is carried out as follows:

Step 1 Constructing the hierarchical structure of a standard operating procedure: :
Based on a standard operating procedure, a hierarchical structure is built as shown in Fig. 1. This is done by decomposing tasks into sub-tasks or by grouping small tasks that have the same sub-goal. For example, the activity of starting up a distillation column can be decomposed into tasks of starting feed, starting reboil-up, and so on. On the other hand, some elementary tasks, such as setting MV of FC101 and setting SV of PC103, could have the same goal, i.e. starting feed.

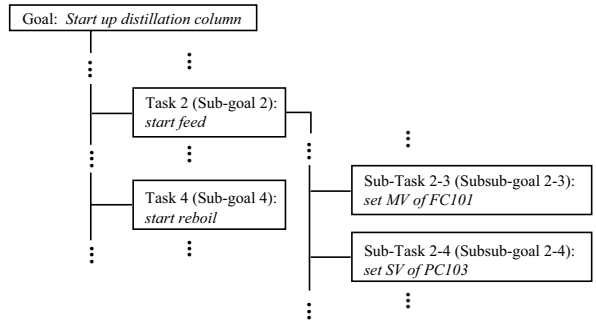

Figure 1. Example of an operation's hierarchical structure

Step 2 Building the hierarchical dictionary of a standard operating procedure: :
After constructing the hierarchical structure of a standard procedure, each task is symbolized and a layered task dictionary, i.e. a hierarchical dictionary, is built.

Step 3 Obtaining and symbolizing a trainee's operational data set:
Once the hierarchical dictionary is made, it is possible to hierarchically evaluate an operation. When a trainee is engaged in the target task on the training simulator, an alarm summary and an operating log are obtained through the distributed control system (DCS).

The obtained operating procedure is symbolized by referring to the symbols in the lowest sub-task level of the dictionary.

Step 4 Identifying higher-level tasks and calculating the task scores:
The obtained symbols of the trainee's operating procedure are divided into groups that are identified as higher-level tasks by referring to the dictionary. To identify the tasks, similarity indices are calculated. We adopted two types of similarity indices. When the sub-tasks of a task must be done in order, Levenshtein distance (*LD*) (Levenshtein, 1966) is calculated and similarity r is estimated by the following equation:

$$r = \frac{n - LD}{n} \times 100 \tag{1}$$

Here, n is the number of sub-tasks of the target task in the dictionary, and *LD* is the smallest number of insertions, deletions, and substitutions required to change one string into another, and it is applied in various areas such as spell checking, speech recognition, and DNA analysis. Through the process of calculating *LD*, we can not only analyze the extent of the difference between the trainee's operation and the standard operation but also identify the sub-tasks which produce the difference. When the sub-tasks of the task can be done in any order, r is estimated by the following equation:

$$r = \frac{n_d}{n} \times 100, \tag{2}$$

where n_d is the number of sub-tasks that are done by the operator as elements of the target task in the dictionary, and n is the total number of sub-tasks of the target task in the dictionary. The calculated r is recorded as the task score.

Step 5 Hierarchical identification:
Step 4 is done at the higher levels and repeated to the highest level of the hierarchy of the dictionary.

Step 6 Evaluating the operation:
We can evaluate and analyze the operation by observing the scores and the identification results from the highest level to the lower levels step by step.

3. Example

We applied the proposed proficiency evaluation system to actual simulator training. The target operation is starting up the distillation column shown in Fig. 2. Start-up is one of the plant's complicated operations and has many variations. The following four cases of this operation were performed by a trainee and then the results were evaluated:

Case 1) Operation according to standard operating procedure (changing the load in several steps)
Case 2) Operation while ignoring standard operating procedure
Case 3) Operation mostly according to standard operating procedure but drastically changing the load in one step
Case 4) Operation mostly according to standard operating procedure but changing the load in two steps

The evaluation results at the top of the hierarchy (Fig. 3) show that the ideal task sequence is listed in accordance with the dictionary made in Step 2. Here, r_{mean} and r_{max} are the mean and maximum values of the similarity indices of the identified sub-tasks.

More specifically, the evaluation results show that:

1) The overall scores r of operations in cases 1 and 4 indicate that those operations are similar to the standard (ideal) operation in outline.
2) The subtask scores r_{min} of case 4 are smaller than those of case 1 for task Nos. 8 and 9, which relate to loading up.
3) The overall score r of performing the operation in one's own way (case 2) is very poor.

These results are reasonable. As shown in result 2), the difference between cases 1 and 4 can be found by using a hierchical approach. If we want to analyze the difference in more detail, we can examine the lower-level evaluation results in sequence.

The r of case 1 does not show 100 due to the identified location of task No. 6. This is because the standard operation cannot describe the entire set of operations in full detail, and thus task No. 6 was difficult to identify in this example.

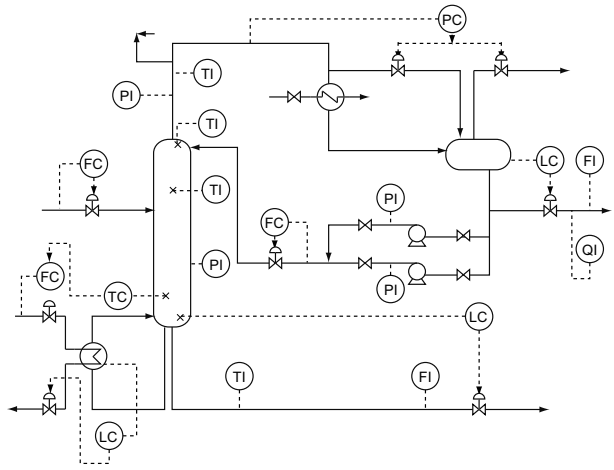

Figure 2. Example target plant

4. Conclusions

The proposed proficiency evaluation method can hierarchically evaluate and analyze an operation. This evaluation method was adopted in the simulator training system called MECTRNR, and the system was applied to a distillation column's start-up operation as an example. The results of trial evaluations show that the proposed method is useful in evaluating proficiency.

References

Barrero, L., Canales, R., Juárez-Romero, D., Mendoza, Y., Ruiz, G., Santoyo-Gutiérrez, S., 2003. Systematic building-testing of dynamic models for training simulators. Computers & Chemical Engineering 27 (10), 1421–1430.

Ideal task sequence at highest level

task No.	1	2	3	4	5	6	7	8	9

Case 1) r = 78

task No.	1	2	6	3	4	5	7	8	9
r_{mean}	87.5	15.0	10.1	40.0	40.0	50.0	3.7	54.4	40.8
r_{max}	100.0	100.0	66.7	40.0	40.0	50.0	50.0	100.0	55.6

Case 2) r = 33

task No.	1	2	6	9	7	4	5
r_{mean}	75.0	14.0	8.7	39.6	50.0	20.0	11.1
r_{max}	75.0	100.0	66.7	50.0	50.0	40.0	50.0

Case 3) r = 44

task No.	1	2	4	6	9	5	7	8
r_{mean}	87.5	12.5	40.0	9.1	40.8	50.0	50.0	83.3
r_{max}	100.0	100.0	40.0	66.7	55.6	50.0	50.0	100.0

Case 4) r = 78

task No.	1	2	6	3	4	5	7	8	9
r_{mean}	87.5	12.1	7.1	40.0	40.0	50.0	50.0	40.0	37.6
r_{max}	100.0	100.0	33.3	40.0	40.0	50.0	50.0	100.0	47.6

Figure 3. Results of evaluation at highest level

Hart, L. A., Staveland, L., 1988. Development of the NASA Task Load Index (TLX) : Results of empirical and theoretical research. Elsevier Science Publishers, Amsterdan, North-Holland, pp. 139–184.

Jeong, K. S., Kim, K. R., Jung, W. D., Ha, J. J., 2002. Development of severe accident management advisory and training simulator (SAMAT). Annals of Nuclear Energy 29, 2055–2069.

Kurooka, T., Hoshi, I., Yamashita, Y., Nishitani, H., Aug. 24-29 2003. Cascade estimation model for thinking state monitoring using plural physiological signals. In: In Proceedings of the International Ergonomics Association XVth Triennial Congress (IEA2003) and the 7th Ergonomics Society of Korea/Japan Ergonomics Society Joint Conference. Seoul, KOREA,, pp. Session HP–03–2.

Kurooka, T., Inoue, H., Watanabe, Y., June 29-July 18 2008. A new metric for evaluation of plant operators' proficiencies. In: In Proceedings of Computer-Aided Process Operations (FOCAPO 2008). Boston Massachusetts, USA.

Kurooka, T., Kisa, M., Yamashita, Y., Nishitani, H., Sept. 16-18 1998. Application of mind state estimation to plant operators. In: In Proceedings of 7th IFAC/IFIP/IFORS/IEA Symposium on Analysis, Design and Evaluation of Man-Machine Systems (IFAC-MMS'98). Kyoto, Japan, pp. 539–544.

Kurooka, T., Yamakawa, M., Yamashita, Y., Nishitani, H., 2001. Real-time monitoring of a plant operator's thinking state. Journal of Chemical Engineering of Japan 34 (11), 1387–1395.

Nishitani, H., Kurooka, T., Kitajima, T., 1997. Evaluation method of human interface in crt operation using protocol analysis. The Journal of the Society for Industrial Plant Human Factors of Japan 2 (1), 16–25.

Reid, G. B., Nygren, T. E., 1988. The Subjective Workload Assessment Technique: A scaling procedure for measuring mental workload. Elsevier Science Publishers, North-Holland, pp. 185–218.

I.A. Karimi and Rajagopalan Srinivasan (Editors), Proceedings of the 11th International Symposium on Process Systems Engineering, 15-19 July 2012, Singapore.

Simulation study of alternatives for the efficient start-up of dividing-wall distillation column sequences

Maria A. Vargas,[a] Georg Fieg[a]

[a]*University of Technology, Schwarzenbergstraße 95c,Hamburg 21071, Germany*

Abstract

The increasing interest in the use of dividing wall distillation columns demands procedures for its optimum operation. The start-up is a complicated process that requires the simultaneous and coordinated manipulation of multiple variables to take an empty column at ambient conditions to the required operation point. In the present research work is studied the start-up of a dividing-wall distillation column system (DWCSys) for the separation of a multicomponent mixture into five products using two different strategies. The implemented alternatives in the DWCSys are examined and evaluated according to the start-up time, energy consumption and accumulation of out of spec products. The results depict the influence of impurities and changes in the concentration of the feed stream on the start-up behavior of the column system. At the same time it was proven the robustness of the simulation model and the stability of the solution method to solve a very complex system of algebraic and differential equations with discontinuities that are commons in a start-up process.

Keywords: start-up, dividing-wall column, distillation sequence.

1. Introduction

The competiveness of today's market demands quality products at lower prices and thus it is required the implementation of more efficient processes. A clear example to diminish energy usage and at the same time reduce investment costs in a thermal separation process is the technology of dividing-wall distillation column (DWC). It consists of a column shell with a partition wall that separates the middle section of the column into two parts, the prefractionator and the side segment. This partition wall avoids the radial mixing of the internal vapor and liquid fluids in the prefractionator and main column, allowing the production of three pure components in a single column shell.

In recent years there have been a considerable growing interest in DWCs for industrial implementation. It demands clear procedures for the design and optimum but safe operation of the column, spanning the startup, production and shutdown periods. Numerous scientific publications have dealt with the design and control of DWCs but only few refers to the start-up process.

Start-up is a complex operation generally characterized by a long and unproductive duration. In this period, an empty column passes from ambient conditions to the required operation point. Non-specification products are produced and high amounts of energy are consumed. The economical and ecological interest to minimize the time of this non-productive period creates the necessity of developing time optimal start-up strategies which guarantee its feasibility, safety and easy implementation in columns of industrial scale. Additionally, the understanding of the process behaviour, avoids wrong

manipulations which could even retard more the start-up and create hazardous situations.
Rigorous simulation studies can be used to prepare adequate strategies and to plan a proper start-up procedure for operators.
In the simulation study of this work, start-up strategies are implemented in a dividing-wall column system (DWCSys). The system separates a mixture of linear alcohols in a direct sequence of two DWCs of industrial scale. The rigorous mathematical model used for this investigation was subject of an extensive experimental validation in a previous research in the Institute of Process and Plant Engineering (PAT) in the Hamburg University of Technology (*Niggemann et al.*). The implemented alternatives in the DWCSys are examined and evaluated according to the start-up time, energy consumption and accumulation of out of spec products.

2. Dividing-wall distillation column system

To separate a mixture into five products, three combinatorial possibilities of DWC arrangements (direct, side and indirect sequence) are feasible and the optimal column configuration is sought. The case study of this work consist of a mixture with equal mass concentration of the lineal alcohols, n-hexanol (C6), n-octanol (C8), n-decanol (C10), n-dodecanol (C12) and n-tetradecanol (C14). In a previous work from *Vargas et al.* was found that the direct connection results in the alternative with the lowest annualized total costs. A saturated liquid feed enters to the system with a mass flow rate of 5000 kg/h and is separated in products with a mass concentration > 0.99 wt.-/wt (Fig. 1). The two columns operate with a top pressure of 40 mbar which guaranteed a temperature in the condenser to cool with water and an enough low temperature in the bottom to avoid degradation.

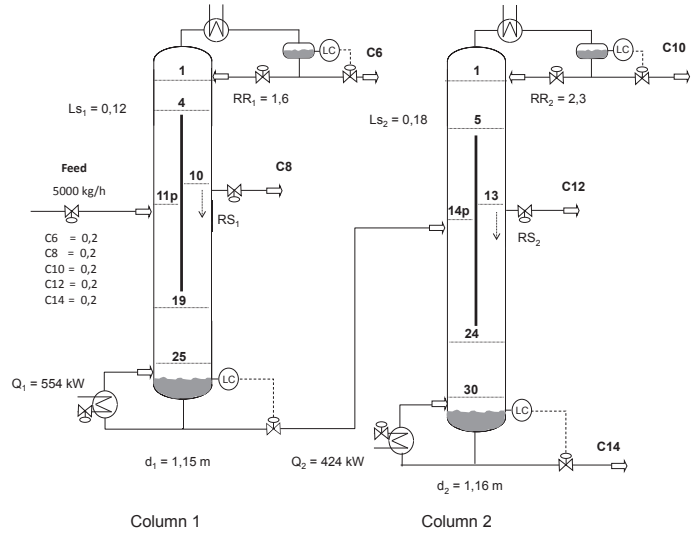

Figure 1. Dividing-wall distillation column system for five products separation.

The level in the reflux drum of both columns is controlled with the distillated stream, while the bottom level is controlled with the bottom stream respectively. The proportional controllers are set to have in the reflux drum 5 min retention time during normal operation and 5 min retention time in the bottom column. However, during the

start-up process the set point in the bottom column is doubled to avoid the dried up of the columns. Both columns are designed with Montz packing type B1-500. The column shell is of stainless steel with thickness of 0.012 m, determined according the standards AD 2000.

3. Simulation of the start-up process

A rigorous mathematical model built in the Institute of PAT capable of simulate the complete start-up process from an empty dividing-wall column at ambient temperature to steady state conditions is used. The model is composed of a system of differential and algebraic equations result of MESH balances in a column discretized in theoretical stages. Periphery equipments as reboiler, condenser and reflux drum are also integrated in the model. The simulation model also includes special features of DWCs as self adjustment of the vapour split by equalization of pressure drop in both sides of the dividing wall and heat transfer across the dividing wall.

The model is set according the column sequence design previously described, including all the design parameters, e.g., mass of packing, mass of column shell and liquids hold up which are required to simulate the heating up and filling of the column during the start-up process. Physical properties of the multicomponent mixture are determined with UNIQUAC activity coefficient model.

Typically the aim in a start-up process is to minimize the time required to achieve the steady state conditions and the production of off spec products. Several process variables can be manipulated in the attempt to speed up the process: feed flow rate, reboiler heat duty, reflux ratio, product flow rate and liquid split. These variables can vary during the start-up process within the constraints and set to the steady state value at the end of the process. In addition, during the start-up of a column system the time at which the columns are connected could have a major effect on the results.

In this work a conventional start-up strategy is implemented in the column system, in which the process variables are set to their steady state value as soon as feasible. Following the sequence of steps performed during the start-up operation:

- $t=t_0$: Begin feed input
- $t=t_1$: The liquid level set point in the bottom column is reached. Activation of reboiler (Q_i) and set to the steady state heat input.
- $t=t_2$: The boiling temperature is reached in the bottom column and the vapor starts to ascends until it reaches the condenser.
- $t=t_3$: The liquid level set point in the reflux drum is reached. The reflux ratio (RR_i), side split ratio (RS_i) and liquid split (Ls_i) are set to the steady state value.

The sequence of steps is equally performed in the two columns of the arrangements. However, during the start-up process the feed conditions to column 2 (e.g. flow rate, component concentration) may undergo changes until the stedy state conditions are reched in column 1. Two different start-up alternatives are evaluated. In the first alternative the feed to column 2 starts once the bottom product of column 1 is produced (simultaneous start-up strategy) and in the second alternative the feed to column 2 starts only after the steady state conditions in the connecting stream are reached (sequential start-up strategy).

3.1. Simultaneous start-up strategy

In the simultaneous start-up strategy the feed to column 2 starts as soon as feasible (t=0.34 h). At this moment the connecting stream (feed to column 2) still faces continues changes in composition, flow rate, temperature and pressure. Fig. 2(a) depicts

the concentration profile of the key components in the two columns of the sequence. In the first column the top and side products reach the steady state concentration relatively fast at t=1.34 h and t=1.37 h respectively (0.1 % of deviation from steady state value is accepted), but it is only at t=7.28 h when the steady state concentration is attained in the bottom stream. On the other hand in column 2, the steady state concentration of key components takes relatively longer to be reached. The low rate of increment of C10 in column 2 is mainly due to the presence of C8 impurities in the feed stream to column 2. The total start-up time of the column system is t=12.75 h limited by the bottom stream in column 2.

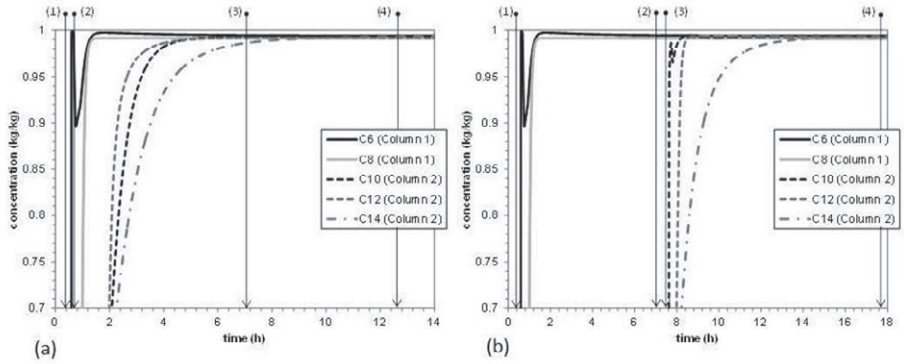

Figure 2. Concentration of key components during the (a) simultaneous and (b) sequential start-up of the dividing-wall column system, with (1) activation of reboiler (Q_1) in column 1, (2) activation of reboiler (Q_2) in column 2, (3) steady state in column 1 and (4) steady state in column 2.

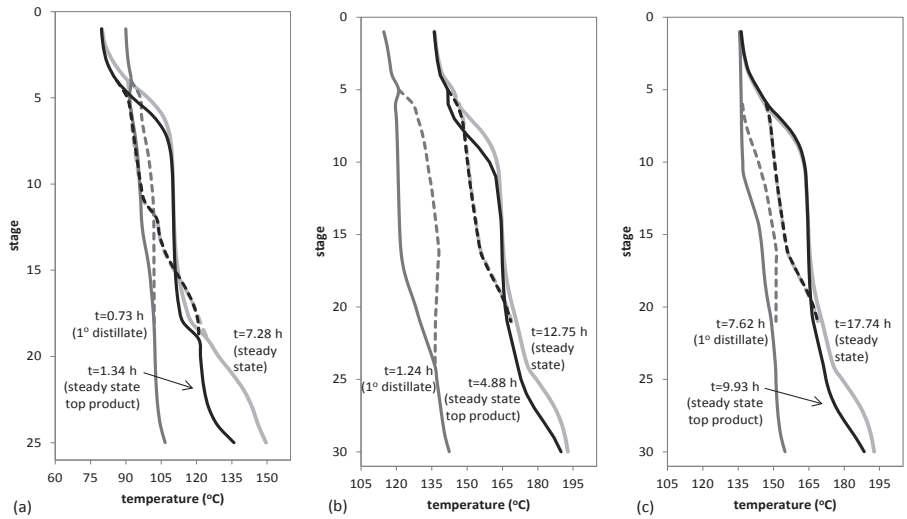

Figure 3. Temperature profile in (a) column 1 and column 2 during the (b) simultaneous and (c) sequential start-up of the dividing-wall column system. Prefractionator (- - - - -) and main column (——).

3.2. Sequential start-up strategy

In this strategy the connecting stream (feed to column 2) is deviated to a storage tank until it reaches the steady state conditions (t=7.28 h) . The concentration profile of key

components in column 2 (Fig. 2(b)) shows now a very similar behavior to the concentration profile of key components in column 1. The steady state concentrations in top and side products are reached relatively fast, once the reboiler is activated. The total start-up time of the system is t=17.74 h limited by the concentration of the bottom product in column 2.

The temperature profile during the start-up in the two columns of the sequences also reveals the consequence of impurities in the feed stream to column 2 (Fig. 3(b)). At the point the first drop of distillate is produced in column 2 with the simultaneous strategy, the temperature profile still very far from the steady state values. However, on the other hand, with both strategies is evident that after the steady state concentration in the distillate stream is reached, only in the lower segments of the column 1 and 2 there is a considerable difference with the steady state temperature profile (Fig. 3).

4. Comparison of start-up strategies

By only observing the start-up time, the simultaneous start-up strategy (t= 12.75 h) would results in the preferable alternative when compared to the sequential start-up strategy (t=17.74 h). However the total energy usage of the sequential strategy is around 13 % lower but with a higher amount of off spec product accumulation (Table 1). It evidence that in the development of start-up strategies the main objectives must be clearly define.

Table 1. Accumulated off spec products and waste energy during the start-up of the dividing wall column system.

			Strategy	
			Simultaneous	Sequential
Column 1	Accumulated off spec product, (kg)	Distillate	540	540
		Side	421	421
		Bottom	-	21253
		Q_1, (kW h)	404	404
Column 2	Accumulated off spec product, (kg)	Distillate	3475	2161
		Side	3409	574
		Bottom	13090	10882
		Q_2, (kW h)	5010	4341
	Total	Product, (kg)	20935	35831
		Q, (kW h)	5414	4745

5. Conclusion

Two different alternatives for the start-up of a direct sequence of two dividing-wall distillation columns have been presented. The results serve as the bases for the further development of optimum start-up strategies for DWCSys. In addition, it was evidenced the robustness of the model and the stability of the solution method to simulate the complex start-up process of two columns.

References

Niggemann, G., Gruetzmann, S. and Fieg, G., 2006. Distillation Startup of Fully Thermally Coupled Distillation Columns: Theoretical Examinations, In E. Sørensen, ed. Distillation and Absorption 2006 (Symp. Series No. 152). London: IChemE, 800-808.

Vargas, M. and Fieg, G., 2009. Dynamic modeling and simulation of dividing-wall distillation column systems, 10th International Symposium on Process Systems Engineering: Part A – PSE2009 (Computer Aided Chemical Engineering), Volume 27, 639-644.

Ian David Lockhart Bogle and Michael Fairweather (Editors), Proceedings of the 22nd European Symposium on Computer Aided Process Engineering, 17 - 20 June 2012, London.

Model-based system identification and PI controller tuning using closed-loop set-point response

Nataliya Baran[a], Günter Wozny[a], Harvey Arellano-Garcia[a]

[a]*Chair of Process Dynamics and Operation, Berlin Institute of Technology, Sekr. KWT-9, Straße des 17. Juni 135, D-10623 Berlin, Germany, nba@zmms.tu-berlin.de*

Abstract

In this work, a new approach to model identification and PI controller tuning based on model-based experimental design is presented. In the proposed strategy, system identification relies on a closed-loop set-point response. For this purpose, experiments are first exemplarily executed with a P-controller. Therefore, in this specific case only one design variable is considered that is represented by the controller gain. Additionally, we use the results achieved in the system identification step for the calculation of controller settings. In order to validate our approach and demonstrate the benefits of the proposed strategy, different scenarios are simulated.

Keywords: controller tuning, closed-loop, set-point response, PI controller, model-based design of experiments, model identification, parameter estimation

1. Introduction

In the chemical industry, PI controllers are widely used because of their simplicity and robust structure. However, it is still difficult to find good controller settings even though PI controllers only have a few adjustable parameters (Shamsuzzoha and Skogestad, 2010). There are basically two different methods for the calculation of controller settings. One of them is based on open-loop experiments whereas the other one uses closed-loop tests. Most tuning methods are based on information about process dynamics obtained from open-loop experiments. However, this strategy is usually time-consuming and expensive. Therefore, in this work, we focus on the determination of experimental conditions using closed-loop set-point response for the estimation of system model parameters with maximum statistical quality. For this purpose, we use a model-based optimal experimental design approach (Bauer et al., Franceschini and Macchietto, Barz et al.). The optimal experimental design strategy (OED) enables us to select experimental conditions for which the resulting data yields maximum information with respect to model parameters. The challenge of our approach is the need for model identification by closed-loop experiments. According to the concept of optimal experimental design, parameter estimation is applied in order to match the model to a real process. Therefore, our calculation of controller settings consists of two steps. First, we identify the system behavior using closed-loop set-point response and after that, we calculate the controller settings using an optimization strategy.

2. Problem Statement

We assume that a given process can be described by a set of differential-algebraic equations (DAEs) (Bauer et al., 2000)

$$\dot{y}(t) = f(t, y(t), p, u_{ED}(t)), \;\; y(t_0) = y_0(p), \tag{1}$$

where $\boldsymbol{t}$ represents the time, $\boldsymbol{y}$ denotes state variables, $\boldsymbol{p}$ is a set of parameters to be determined and $\boldsymbol{u_{ED}}$ represents the set of time-varying control variables, which are later used as design variables to plan experiments. Parameter estimation is done by fitting the results of the model simulation $\boldsymbol{y^{calc}}$ to the measured data $\boldsymbol{y^{meas}}$. We assume that measurement errors $\boldsymbol{\xi^{y}}$ are independent, normally distributed and can be characterized by a measurement-covariance matrix $\boldsymbol{MV}$. The parameter estimation is based on the minimization of a weighted least square functional

$$min_p \sum_{k=1}^{N_{exp}} \left(y_k^{meas} - y_k(u_{ED,k}, p)\right)^T \cdot MV^{-1} \cdot \left(y_k^{meas} - y_k(u_{ED,k}, p)\right). \tag{2}$$

The model-based experimental design strategy aims to maximize the accuracy of the parameter estimation that is mathematically represented by the variance-covariance matrix of the model parameters $\boldsymbol{C}$ and characterizes the statistical uncertainty of parameter estimation.

$$\min_{u_{ED}} \varphi(C)$$

$$s.t.\ \ f(\dot{y}(t), y(t), u_{ED}, p, t) = 0 \tag{3}$$

$$y(t_0) = y_0(p)$$

$$u_{ED}^{min} \leq u_{ED}(t) \leq u_{ED}^{max}$$

Statistical uncertainty is represented by the confidence region. Thus, decreasing the size of the confidence region for each model parameter leads to the minimization of the variance-covariance matrix C. The size of the confidence region (the amount of the matrix C) determines the expected information content that can be extracted from the measurement data. The form of the functional $\boldsymbol{\varphi}$ characterizes the chosen optimal criterion. Common design criteria are so-called A-, D- and E-optimal criteria whose definition can be found in (Franceschini and Macchietto, 2008). In the following we use the A-optimal criterion that represents the trace of the variance-covariance matrix and minimizes the mean parameter standard deviations.

$$\varphi(C) = \frac{trace(C)}{dim\,(C)} \tag{4}$$

The covariance-variance matrix is determined as inverse of the Fisher information matrix.

$$C = F^{-1} = \left(\sum_{k=1}^{N_{Exp}} F_k\right)^{-1} \tag{5}$$

We consider a sequential strategy, so, according to (Galvanin et al., 2007), the information matrix after N_{exp} experiments can be calculated as follows

$$F = \sum_{k=1}^{N_{exp}-1} F_k + F_{N_{exp}}\left(p, u_{ED,N_{exp}}\right) = F_C + F_{N_{exp}}\left(p, u_{ED,N_{exp}}\right) \tag{6}$$

where $\boldsymbol{F_c}$ represents a constant part of the Fisher information matrix calculated by the previous $N_{exp} - 1$ experiments. In eq. (6) only the vector $u_{ED,N_{exp}}$ can be varied during the optimization.

For one single experiment, the Fisher matrix is calculated based on the sensitivities coefficients for each estimated model output

$$F_k\left(p, u_{ED,k}, y\right) = Q_k^T MV_k^{-1}\, Q_k, \tag{7}$$

where $\boldsymbol{MV_k}$ represents the measurement-covariance matrix and $\boldsymbol{Q_k}$ characterizes the matrix of the sensitivities. Model parameters have often very different dimension. Therefore, it is convenient to use normalized sensitivity coefficients as defined in eq. (8) (Barz et al., 2010).

$$\overline{Q_k} = \left[\frac{\partial y_k(t_i)}{\partial p_j} p_j\right];\ \forall j \in N_p, \forall i \in N_{sp} \tag{8}$$

Based on these considerations, the normalized sensitivity coefficients are applied throughout this work.

3. New system identification strategy

Controller tuning requires a good process model. Therefore, our controller tuning strategy consists of two steps (s. Fig. 1). In the first step, we identify the process behavior experimentally by using closed-loop set-point response. After this, based on the results achieved in the first step, we numerically calculate the controller settings.

We assume that each process can be described by a first or second order with time delay model (Skogestad, 2003). That means that we have three or four model parameters that have to be determined. These are the process gain $\boldsymbol{K}$, the time constants $\boldsymbol{T_1}$, $\boldsymbol{T_2}$ and the time delay, $\boldsymbol{\tau}$.

Usually, an open-loop experiment is used to identify the process behavior. In the proposed strategy, we use a closed-loop set-point response (Fig. 1) for system identification. Here an experiment is executed with just a P-controller. By this method, we are able to reduce the experimental time and decrease the number of necessary experiments as well as the required amount of measured data.

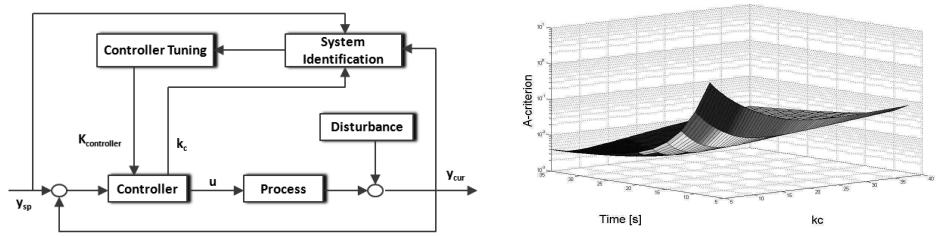

Figure 1. Controller tuning strategy (left), where $K_{controller} = [k_c, T_i]$; object function for OED over the design variable k_c for different measurement times (right)

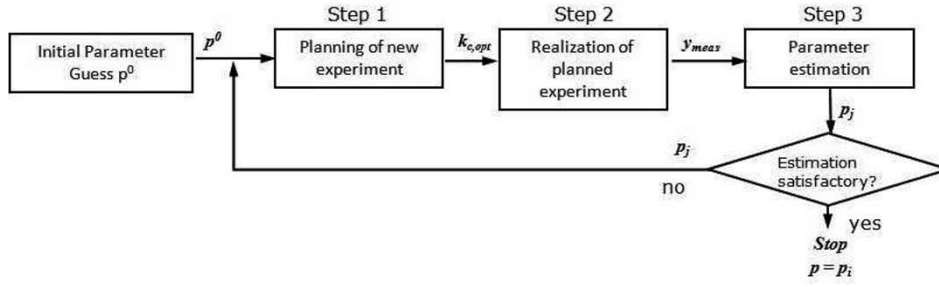

Figure 2. Model-based system identification strategy using closed-loop response

For a closed-loop system the experimental conditions are represented by controller gain $\boldsymbol{k_c}$. Here, by using the approach of OED we aim to determine the optimal value of the

controller gain $\boldsymbol{k_{c,opt}}$ for which the experimental data yields maximum information with respect to model parameters. According to the concept of OED, in the first step, the experiment is planned. Here, the optimal value of the control gain throughout the experiment is determined. Next, the planned experiment is executed and the measured data is analyzed. In the last step, the quality of the model is validated and a new set of model parameters is calculated (s. Fig. 2). These three iteration steps are executed sequentially without interruption until the required model accuracy is achieved. Important is here, that the design of a new experiment is based on the current information about model structure and parameter set obtained in the prior experiments.

4. Case Study

The strategy discussed in the previous section is applied to the first order plus time delay process (FOPTD). Based on the model reduction rule of Skogestad (Skogestad, 2003), we approximate FOPTD process with a second-order model. Here, we describe the second-order model by a model with a damping factor.

$$G_1(s) = \frac{K}{T^2 s^2 + 2dT\, s + 1} \tag{9}$$

Based on the assumed model, three model parameters have to be estimated during the model-based design. These are the process gain *K*, the time constant *T*, and the damping factor *d.* In this case study, we generate experimental data from the simulation and add a normally distributed measurement noise with the variance $\sigma^2 = 0.05$. Our goal during the parameter estimation was to get a model accuracy of 7% based on parameter standard deviations. In order to achieve the required accuracy, three experiments were executed. In the first experiment, the so called pre-experiment, the initial guess of the model parameters was identified. This experiment is unplanned and was executed with $k_c = 5$, whereas the next two experiments were designed. Table 1 shows that only two designed experiments are necessary in order to achieve the required accuracy of less than 7% for each model parameter. In addition, Fig. 3 shows the closed-loop set-point response for second designed experiment.

N_{exp}	Experimental conditions $k_{c,opt}$	Estimated parameters			Parameter standard deviations [%]		
		p_1	p_2	p_3	σ_{p1}	σ_{p2}	σ_{p3}
pre-exp	5	1.05	5.47	2.95	12.4	8.4	16.8
1st exp	15.3	0.96	5.19	2.75	7.5	4.5	7.9
2nd exp	**9.5**	**0.95**	**5.29**	**2.67**	**6.0**	**3.6**	**6.2**

Table 1. Parameter estimated during the model-based design of experiments

Once the model parameter estimation is finished, we numerically calculate the controller settings. The goal of the controller tuning is to achieve a good set-point response. Thus, our optimization problem is to minimize the overshoot while making sure that there is no undershoot. Here, the model dynamics is also represented by a second order process with a damping factor.

$$\min_{K_c,\, T_i} M$$
$$s.t.\ |\Delta y_s - \Delta y_u| \leq C, \tag{10}$$

where $\boldsymbol{M}$ represents the overshoot, $\boldsymbol{\Delta y_u}$ is the first minimum (undershoot), $\boldsymbol{\Delta y_s}$ denotes the set-point change and $\boldsymbol{C}$ is a constant. By solving of optimization problem (s. eq. (10)), we obtain the optimal controller settings that are represented by $k_c = 7.27$ and $T_i = 27.2$. Fig. 3 shows the closed-loop set-point response with the optimal controller parameters.

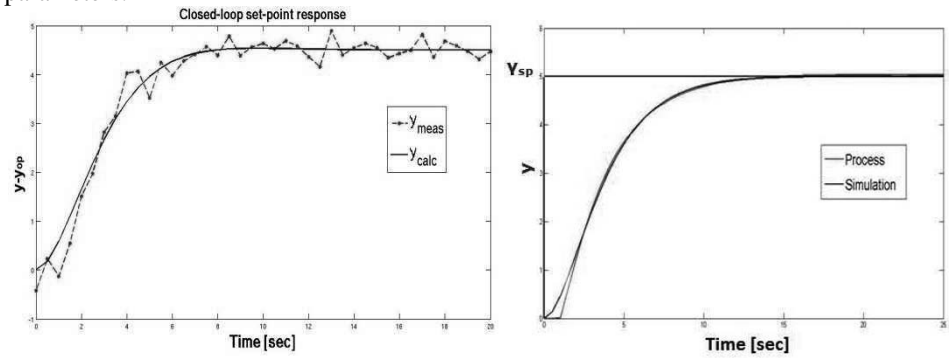

Figure 3. Closed-loop set-point response for the second designed experiment (left), where y_{op} is the operation point; closed-loop set-point response with the optimal controller settings (right).

5. Conclusions

The proposed strategy consists of two steps. In the first step, we identify the process behavior using a closed-loop set-point response. For this purpose, we first run experiments with just a P-controller. In the proposed procedure, the design variable for the optimal experimental design is represented by the controller gain k_c. After this, we calculate the controller settings by using an optimization strategy. Here, we use the model achieved in the first step for the calculation of optimal controller parameters. As the results of the case study show, one can use the second order model for calculation of the controller settings for a first order with time delay process.

Usually, a very time consuming part of the controller tuning procedure is the process identification. Here, using closed-loop set-point response leads to shorter experimental time compared to open-loop experiments. Furthermore, well designed experiments enable us to reduce the system identification effort even more. In summary, the sum of both benefits leads to reduced commissioning time in comparison to conventional methods.

References

T. Barz, H. Arellano-Garcia, G. Wozny, 2010, Handling uncertainty in model-based optimal experimental design, Ind. Eng. Chem. Res., 49, 5702-5713.

I. Bauer, H. G. Bock, S. Körkel, J. P. Schlöder, 2000, Numerical methods for optimum experimental design in DAE systems, Journal of Computational and Applied Mathematics 120, 1-25.

G. Franceschini, S. Macchietto, 2008, Model-based design of experiments for parameter precision: State of the art, Chemical Engineering Science, 63, 4846-4872.

F. Galvanin, S. Macchietto, F. Bezzo, 2007, Model-based design of parallel experiments, Ind. Eng. Chem. Res., 46, 871-882.

S. Skogestad, 2003, Simple analytic rules for model reduction and PID controller tuning, J. Process Control, 13, 291-309.

M. Shamsuzzoha, S. Skogestad, 2010, The setpoint overshoot method: A simple and fast closed-loop approach for PID tuning, J. Process Control, 20, 1220-1234.

I.A. Karimi and Rajagopalan Srinivasan (Editors), Proceedings of the 11th International Symposium on Process Systems Engineering, 15-19 July 2012, Singapore.

Optimization and control of polystyrene batch reactor using hybrid based model

Mohammad Anwar Hosen* and Mohd Azlan Hussain

Chemical Engineering Department, University of Malaya, Malaysia

Abstract

The effects of operating conditions such as initiator and monomer concentration as well as reactor temperature of polymerization reactors have been studied in this work. A recently developed hybrid model for polystyrene batch reactor was utilized in simulation study. The simulation results revealed the sensitivity of polymer properties and conversion to variation of these operating conditions. Furthermore, the study deals with the optimization of batch polymerization reactors. The optimization problem involving minimum time optimal temperature policy has been formulated and solved. Different numerical techniques have been tested and compared. The online control works were performed to validate the optimal temperature profiles. The experimental studies reveal that the calculated optimal policies were able to reduce the batch time keeping the same polymer quality.

Keywords: Polymerization reactors; Optimization; Polystyrene; Batch reactor.

***Corresponding Author,** anwar.buet97@gmail.com

1. Introduction

Recently, the use of process optimization in the control of batch reactors has received much attention in the literature (Kiparissides, 1996). This provides a useful tool for operating batch reactors efficiently and optimally. In batch polymerization, the optimization problem is identified as the time dependent control actions which maximize product quality and minimize production time(Amrehn, 1977). Different techniques have been suggested (Kiparissides, 2006) and applied to calculate and control to the optimal trajectories. Method of Pontryagin's Minimum Principle PMP) was heavily used in work of styrene polymerization in a solution batch reactor. For past seven years, researchers used solely the PMP to solve their optimal control problem (Özkan et al., 2001, Özkan et al., 2006, AltInten et al., 2003, Altinten et al., 2006, AltInten et al., 2008a, Zeybek et al., 2004, Zeybek et al., 2006, Özkan et al., 2009). The objective of optimal problem in their solution problem was to produce 50% conversion and 500 number average chain length with minimum reaction process. The temperature optimal profiles were generated using Pontryagin's Maximum Principle without any initial guess of initial costate variable. Therefore, no iteration of costate variable was initialized to obtain the time optimal temperature.

In the present work, we have considered of interest to carry out the dynamic study for a batch styrene free radical polymerization reactor theoretically and find out which variables are more effective for polymerization reactor. Later, optimization problem of minimum time optimal temperature policy has been formulated and solved for batch reactor for the solution polymerization of styrene. Finally, The generated optimal temperature profiles was used to study closed-loop control using advanced control technique which can track the process variable along the developed open-loop optimal temperature trajectory.

2. Modeling of polystyrene batch reactors.

The success of optimization efforts depends very much upon the accuracy of the process models. It has been a trend to use the simplified process models for determining the optimal control profiles, as the complexity of the process models is restricted by the methods used to determine the optimal control profiles. In this work, a simple mechanistic modelling strategy (see the AltInten et al., 2008 for details model) were used to develop optimal temperature profile (AltInten et al., 2008). However, a hybrid model (first principle-Neural network model) was used to design the controller to implement the optimum temperature profile.

Psichogios and Ungar have introduced the idea of using first principles-neural network methodology for modeling chemical processes. Such a methodology attempts to utilize all accessible process knowledge possible by implementing black-box correlations for predicting process parameters. A similar methodology was considered in the recent work of Hosen et al. (2011) for modeling the polystyrene batch reactor. In this work, the six kinetic parameters were calculated from pre-trained ANNs with high prediction capabilities (see the Hosen et al., 2011 for details hybrid model). This hybrid model was used to study the dynamic behaviour as well as to develop the advanced controller to control the polystyrene reactor.

3. Results & Discussion

First of all the simulation study was performed to study the dynamic behavior by using previously developed hybrid model (Hosen et al, 2011) and conduct the response of reactor outputs with different initial operating conditions. Secondly, developed the optimum temperature profiles based on reliable simple mathematical model (Altinten et al., 2008). Finally, an advanced controller was developed to track the optimum temperature profile.

3.1. Dynamic Open Loop Behaviour

The following simulations are performed in order to verify the sensitivity of the control system and calculate the appropriate control and system parameters. Among the simulation are:

i. Different initial initiator concentration loading to reactor (0.013, 0.016 and 0.019 mol/ltr)
ii. Different heat input to reactor system with reaction
iii. Different cooling water flow rates in cooling jacket chamber (0.5, 0.7 & 0.9 g/s).

In order to simulate these studies, the values of physical and chemical parameters used are as given in Table 1

Table 1: Operating conditions and reactor specifications

Name of the parameters	*Value*	*Units*
Reactant specific heat (C_p)	1.96886	J/g.K
Coolant specific heat (C_{pc})	4.29	J/g.K
Heat of reaction, exothermic (H)	-57766.8	J/g.K
Coolant flowrate (m_c)	0.51	g/s
Gas constant (R)	8.314	J/mol.K
Coolant inlet temperature (T_{ji})	303.14	K
Overall heat transfer coefficient (U)	55.1	W/(m^2.K)
Reactor volume (V)	1.2	ltr
Reactor jacket volume (V_c)	1	ltr
Coolant density (ρ_c)	998.00	g/ltr
Reactant density (ρ_r)	983.73	g/ltr

3.1.1. Reactor Dynamics with Different Initiator Loading

One of the control objectives in controlling the batch polymerization reactor is to control the exothermic behaviour due to the extent of reaction as the initiator is introduced to the monomer and solvent mixture in the polymerization system. It is obvious that one needs to monitor the release of heat in order to control the target specification. Moreover, the heat release may break the glass reactor depending on the temperature it can withstand. Three conditions of polymerization were used with initial initiator concentration of 0.013, 0.016 and 0.019 mol/l for this study. Each starting condition has to be maintained at fixed steady state condition. Fig. 1 represents the time trend of temperature change in terms of different initial initiator load (mol/ltr). In this case, polymer quality (X_n) highly depends on the initial initiator concentration but the conversion (X) is little affected by it.

3.1.2. Reactor Dynamic with Different Heat Loading

In the second task, the initial initiator is fixed at a value of 0.013mol/l. Five different heat input simulated the reaction in the reactor with a fixed steady state temperature at 364K. Table 2 illustrates the conversion achieved when temperature reached the steady state after high release of heat upon initiation. In addition, Fig. 2 illustrates clearly the transient behaviour of reactor temperature. As can be seen from the figure, the reactor with highest amount of heat input attains the highest overshoot. The temperature ascends from 364K to a maximum temperature of 416K and starts descending to the steady state of 403.8K completely after 500min at a heat input 150watt. In addition, it can be seen in Fig. 2 that the final polymer quality highly depends on the heat input. At lower heat input the NACL and conversion is higher than at high heat input though it requires more reaction time.

Table 2: Results of different heat input simulation

Heat, Q	Final conversion (%)	T- highest	T_{ss}
150	34.17	416	403.8
120	40.61	411	386.2
100	48.46	401	376.4

3.1.3. Reactor Dynamic with Different Jacketed Flow Rate

In the third task, the jacketed flowrate were varied three times (0.5 g/s, 0.7g/s & 0.9g/s) with the other variables kept the same as Table 1 to observe the reactor dynamics. It can be seen in Fig. 3, that the final polymer quality (NACL) highly depends on the jacketed flow rate. At lower jacketed flow rate, the NACL and conversion are higher than at higher flow rate though it requires more reaction time.

For all three conditions it can be seen that the reactor temperature profile change significantly with changing initial operating conditions or inputs. Based on these results more attention will be taken for setting the values of these operating variables at the time of experimental work. Variation in this reactor may serve as disturbances to the reactor operation.

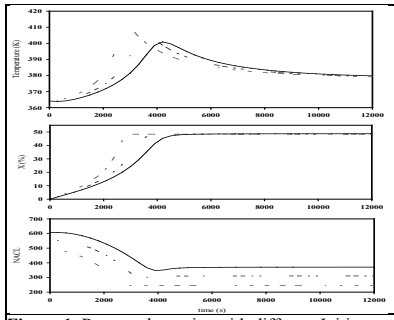

Figure 1: Reactor dynamics with different Initiator concentration. (——) at 0.013mol/ltr, (- - -) at 0.016mol/ltr and (·—·—·) at 0.019mol/ltr.

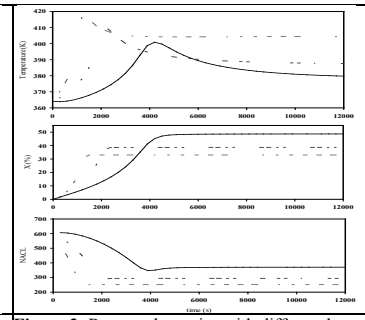

Figure 2: Reactor dynamics with different heat input. (——) at 100 watt, (- - -) at 120 watt and (·—·—·) at 150 watt.

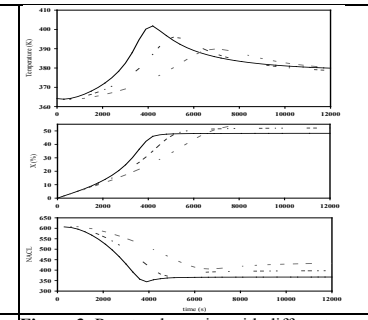

Figure 3: Reactor dynamics with different jacketed flow rate. (——) at 0.5g/s, (- - -) at 0.7g/s and (·—·—·) at 0.9g/s.

3.2. Minimum Time Optimal Temperature Profile

Recently, the offline or open loop minimum time optimal control policies were applied for the simulation of styrene polymerization in batch reactors (Altinten et al., 2008b, Zeybek et al., 2004, Zeybek et al., 2006). In this work, the optimization problem involving minimum time optimal temperature policy has been formulated and solved for a batch reactor for the solution polymerization of styrene based on previous work (Sata, 2007). This optimal temperature profile was used as set point for controller study.

The objective of optimization problem is to calculate the optimal temperature policy for a given initial initiator and monomer concentration that minimizes the reaction time, t_f, required to achieve a desired final monomer conversion, X_d. The performance target of a closed loop control minimum time optimal temperature tracking is to produce polystyrene with the specification of X_d =50% and **NACL,** $\boldsymbol{X_n}$ =500.

In order to obtain the operating conditions for minimum polymerization end-time, polymerization temperature and initiator concentration are employed as control variables. Since the temperature can be used to infer the end-quality of polymer, this work is devoted to produce specified polymer quality within the minimum time. The governing equation (Altinten et al., 2008b) for the optimal temperature profile is expressed as follows:

$$T = \frac{-(E_p + E_d/2 - E_t/2)/R}{\ln\left[E_d \Big/ \left(p_2 I^{0.5} M A_p \left(\frac{2fA_d}{A_t}\right)^{0.5} \left(E_p - \frac{E_d}{2} - \frac{E_t}{2}\right)\right)\right]} \quad (1)$$

The results of calculation for X= 50% and X_n =500 with optimal temperature T* is shown in Fig. 4. In this work, the value for initial initiator, I_0 has to be basically guessed. The procedure can determine any feasibility of the guessed value. In this study, it is found that the optimal initial initiator concentration for the initial monomer concentration of M_o=6.089 mol/l is I_o=0.016 mol/l. These optimal values are achieved within the reaction time of 138 minutes. It can be noted that the reaction time (t_f) increases with increasing I_0. Therefore, it is concluded that the optimal I_0 can be obtained by successively reducing the value of I_0 until a limiting value was reached below which the desired conversion can never be reached. Furthermore, as can be seen from the figure, as the I_0 is decreased, the gradient of the optimal temperature T* becomes more steep. The optimal temperature profile for I_0 = 0.016 will be used for tracking the set point in the control study.

3.3. Controller Design

In this work, an advanced neural network based model predictive controller (NN-MPC) was used to control the polystyrene reactor. The neural network is trained to represent the forward dynamics of the process. The experimental data of the

manipulated variable (heat load Q) and plant output (reactor temperature T) at t with two time delay units were used as inputs while the plant output reactor temperature at t+1 was used as outputs for training the neural network. The Levenberg–Marquardt method is used to train the NN based on a minimizing cost function. The mean square error (MSE) is used here as cost function. It is expressed mathematically as:

$$\mathrm{MSE} = \frac{1}{n}\sum_{k=1}^{n}\left(T_{\mathrm{tg}}(k) - T_{\mathrm{N}}(k)\right)^2 \tag{2}$$

where n is the number of training data, T_{tg} is the target/desired reactor temperature and T_{N} is the neural network output. Based on the minimizing of MSE error values, it was found that 10 hidden nodes achieve the minimum MSE value of $5.36\text{x}10^{-6}$. The design specifications for neural network model are given in Table 3.

Table 3: Design specifications of neural network model

No. of input nodes	6	
No. of hidden layer nodes	10	
No. of output nodes	1	
Total sample size	10000	
Training function	Levenberg-Marquardt Method	
	Sample size	Mean square error
Training data	5000	5.36×10^{-6}
Testing data	2500	4.13×10^{-6}
Validation	2500	4.69×10^{-6}

Before implementing the MPC controller in real time, its tuning parameters should be optimized to achieve best performance. For designing a good MPC controller it's important to specify the following controller parameters:

In this work, the developed hybrid model was utilized to determine the sampling interval and prediction and control horizon. Marlin (Marlin, 1995) general rule was used to determine the sampling interval of MPC. The prediction and control horizon were determined by trial and error method (see Dougherty and Cooper, 2003 for more details).

The performance of the controlled variable i.e. reactor temperature, was observed for a sufficient span of process dynamics time to determine the value of the prediction & control horizon. It was observed that the prediction horizon of 24 sample interval and the control horizon value of 4 sample interval provide satisfactory control performance. The other parameters of the NN-MPC controller are given in Table 4.

Table 4: Design specification of MPC

Prediction Horizon (N_2)	24
Control Horizon (N_u)	4
Control weight factor (M)	0.09
Move suppression factor(Λ)	0.003
Minimization routine	Backtracking Optimization

3.4. On-line optimal control of polystyrene reactor

In this study, the concentration of 0.016 mol/l and 6.089 mol/l for initiator and monomer loading were chosen to produce the desired target. It is noted that the benzoyl peroxide and styrene loading can produce the number average chain length (NACL) of 500 and monomer conversion of 50% at the end of 183 minutes polymerization period.

The experimental results of optimal setpoint tracking of polystyrene polymerization using NN-MPC are shown in Fig. 5. As we can see from the figure, when the initiator is introduced, the mixture temperature fell below the setpoint profile at nearly 2K. The response was realized by the controller and it acted back to increase the heat input (Q). As a result, the temperature overshot at maximum 2K and it later decayed away in decreasing oscillatory manner in 730 sec. An offset can be noted at less than .5K. This is attributed by the high exothermic load during the early course of polymerization. Nevertheless, the temperature controller performance performed well in tracking the temperature setpoint profile at the later stage of polymerization. Fig. 5 also shows the transient response of manipulated variable of heater. The regulation was smooth. It is worth mentioning that the heater regulation was initially at Q=150 Watt and it increased gradually until 200 Watt at the end of the batch-run. The final NACL and conversion can be found 496 and 52.8% respectively which is almost same as desired values.

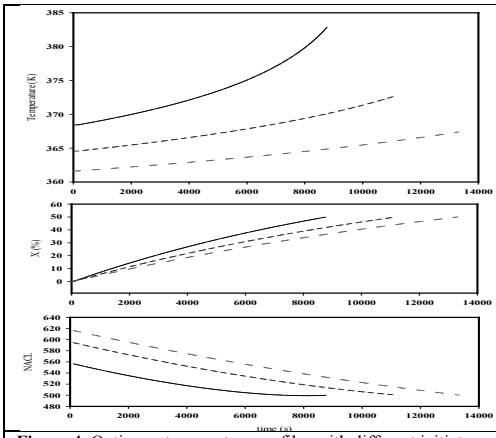

Figure 4: Optimum temperature profiles with different initiator concentration (I_o = 0.013 mol/l (—), I_o = 0.016 mol/l (- - -), I_o = 0.019 mol/l (·—·—·)

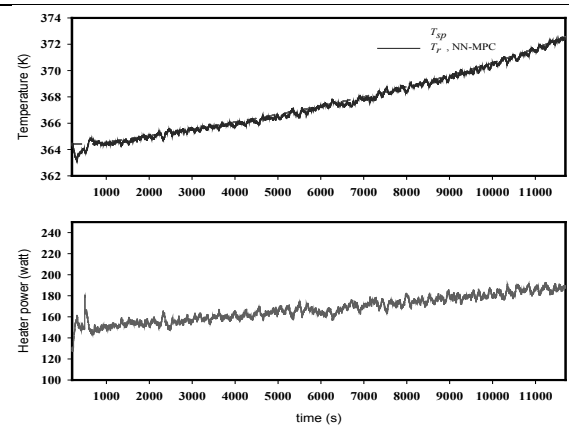

Figure 5: Optimal setpoint tracking using NN-MPC

4. Conclusion

In this work, the first principle-NN model is utilized in Matlab Simulink environment to study the dynamic behaviour of the polystyrene batch reactor. The effect of operating conditions on the properties of final product has been investigated. An optimization algorithm (Sata, 2007) was applied to optimize the reactor temperature profile based on minimal time operation. The conversion and number average chain length (NACL) was considered here as the target output for optimization. The optimized minimal time temperature profile was used as setpiont tracking for control study. An advanced controller named NN-MPC were designed and tuned for styrene polymerization batch reactor to track the optimum setpoint point experimentally. From the experimental results it can be concluded that the developed optimal temperature profile can give the desired polymer quality & quantity with the help of advanced controller.

References

ALTINTEN, A., ERDOGAN, S., HAPOGLU, H., ALIEV, F. & ALPBAZ, M. 2006. Application of Fuzzy Control Method with Genetic Algorithm to a Polymerization Reactor at Constant Set Point. *Chemical Engineering Research and Design,* 84 (11), 1012-1018.

ALTINTEN, A., ERDOGAN, S., HAPOGLU, H. & ALPBAZ, M. 2003. Control of a polymerization reactor by fuzzy control method with genetic algorithm. *Computers & Chemical Engineering,* 27 (7), 1031-1040.

ALTINTEN, A., KETEVANLIOGLU, F., ERDOGAN, S., HAPOGLU, H. & ALPBAZ, M. 2008. Self-tuning PID control of jacketed batch polystyrene reactor using genetic algorithm. *Chemical Engineering Journal,* 138 (1-3), 490-497.

AMREHN, H. 1977. Computer control in the polymerization industry. *Automatica,* 13 (5), 533-545.

DOUGHERTY, D. & COOPER, D. 2003. A practical multiple model adaptive strategy for multivariable model predictive control. *Control Engineering Practice,* 11**,** 649-664.

HOSEN, M. A., HUSSAIN, M. A. & MJALLI, F. S. 2011. Hybrid modelling and kinetic estimation for polystyrene batch reactor using Artificial Neutral Network (ANN) approach. Asia-Pacific Journal of Chemical Engineering, 6, 274-287.

KIPARISSIDES, C. 1996. Polymerization reactor modeling: A review of recent developments and future directions. *Chemical Engineering Science,* 51**,** 1637-1659.

KIPARISSIDES, C. 2006. Challenges in particulate polymerization reactor modeling and optimization: A population balance perspective. *Journal of Process Control,* 16**,** 205-224.

MARLIN, T. E. 1995. *Process control: design processes and control systems for dynamic performance,* Columbus, OH 43272, McGraw Hill Inc.

ÖZKAN, G., HAPOGLU, H. & ALPBAZ, M. 2006. Non-linear generalised predictive control of a jacketed well mixed tank as applied to a batch process--A polymerisation reaction. *Applied Thermal Engineering,* 26**,** 720-726.

ÖZKAN, G., ÖZEN, S., ERDOGAN, S., HAPOGLU, H. & ALPBAZ, M. 2001. Nonlinear control of polymerization reactor. *Computers & Chemical Engineering,* 25**,** 757-763.

ÖZKAN, G., TEKIN, Ö. & HAPOGLU, H. 2009. Application of experimental non-linear control based on generic algorithm to a polymerization reactor. *Korean Journal of Chemical Engineering,* 26**,** 1201-1207.

SATA, S. A. 2007. *Simulation and on-line control of polystyrene production in a batch reactor* PhD, University of Malaya.

ZEYBEK, Z., ÇETINKAYA, S., HAPOGLU, H. & ALPBAZ, M. 2006. Generalized delta rule (GDR) algorithm with generalized predictive control (GPC) for optimum temperature tracking of batch polymerization. *Chemical Engineering Science,* 61**,** 6691-6700.

ZEYBEK, Z., YÜCE, S., HAPOGLU, H. & ALPBAZ, M. 2004. Adaptive heuristic temperature control of a batch polymerisation reactor. *Chemical Engineering and Processing,* 43**,** 911-920.

I.A. Karimi and Rajagopalan Srinivasan (Editors), Proceedings of the 11th International Symposium on Process Systems Engineering, 15-19 July 2012, Singapore.

Modeling and stochastic dynamic optimization for optimal energy resource allocation

Go Bong Choi. Seok Goo Lee. Jong Min Lee*

School of Chemical and Biological Engineering, Institute of Chemical Processes, Seoul National University, 1 Gwanak-ro, Gwanak-gu, Seoul, 151-744, Korea

Abstract

With ever-growing global demand for energy and severe environmental regulations, optimal management of energy distribution system and policy is becoming an important problem for many countries. We present a stochastic dynamic model that describes energy resource allocation under uncertainty and derive an optimal policy for long-term investments in novel energy technologies. Probabilistic model based on Markov chain that balances the demands and supplies are developed considering the city boundaries and electric power system in South Korea. We propose an algorithmic strategy based on the framework of approximate dynamic programming and demonstrate its efficacy using a prototypic example with the available data

Keywords: Energy planning, Markov decision chain, Approximate dynamic programming.

1. Introduction

Faced with the recent challenge of meeting soaring global energy demand without damaging the environment, there has been increasing interest in a strategic approach to determining which energy sources to use and how to supply energy to demand points at optimal cost under environmental and other federal regulations. However, obtaining an optimal policy for such problems is complicated by the inherent uncertainties in demand, fuel prices, stored amount of fuels, etc. Hence, a robust dynamic optimization problem needs to be formulated and solved for deriving a meaningful optimal policy in these applications. Dynamics of such systems are stochastic because the successor state is given by a probability distribution rather than a fixed deterministic point given a current state.

When only the bounds of uncertainties are known, worst-case optimization problem set-up is introduced. If the probabilistic behavior of uncertainties can be further assumed or found from intuition or historical data, stochastic dynamic optimization problem can then be formulated.

Markov decision process (MDP) is a useful framework for modeling the problem in that it is sufficient to consider the present state only, not the past history (Puterman, 1994) and is often used to formulate most scheduling problems under uncertainty. A universal solution approach to obtain the optimal solution for MDP is dynamic programming (DP), which involves calculation of the cost-to-go value for all possible states (Bellman, 1957; Bertsekas, 2000). The main bottleneck in application of DP for

*Corresponding author. Tel. +82-2-880-1878 Email. jongmin@snu.ac.kr

practical problems is the curse of dimensionality, which refers to the exponential increase of the number of states in the state dimension. Recently, a new body of theories called Reinforcement Learning (RL) (Sutton, 2000) or approximate dynamic programming (ADP) (Powell, 2007) has attracted much attention in field of operations research due to its ability to circumvent the curse of dimensionality. The main idea of these approaches is to use closed-loop simulation with initial policies, though they may not be an optimal one, and identify relevant regions in the state space. For these identified states, Bellman's optimality equation is iteratively solved in the form of policy iteration or value iteration (Bertsekas & Tsitsiklis, 1996). In this work, we propose a Markov chain model for energy management of capital region of South Korea and apply an ADP approach to derive a nearly optimal energy management policy starting from closed-loop simulations with simple heuristics.

2. Problem description and model formulation

The objectives of this study are to develop an energy supply chain network model for the energy distribution system of capital region in South Korea and to derive an optimal policy for energy resource allocation, storage, and construction of new power plants and storage/processing facilities under demand uncertainty.

The system is composed of three types of nodes (storage, demand, and conversion nodes) and material flows. It manages energy resource flows from storage nodes (e.g., harbor, storage facility, etc.) to demand nodes such as households and corporations. It is necessary to make proper plans and minimize total cost incurred while respecting constraints. Various types of resources can be divided into primary resources and secondary resource. Resource can be carried from storage node too demand nodes directly or via conversion nodes. In this study, electricity is the only type of energy considered as the secondary energy resource and is assumed to be generated from coal, oil, natural gas, and renewable energy resources. To represent the capital region of South Korea properly, the system has two storage nodes, two conversion nodes, and three demand nodes. The data of the past 10 years on power plant constructions and consumption of energy resources in the region were obtained from KESIS (Korea Energy Statistics Information System). A prototypic energy supply chain network that represents the region is shown in Figures 1 and 2 and the details of the model are presented in the following section and summarized in Table 1.

2.1. State variable

The state vector consists of two types of variables. The first is a subset of controllable state variables that can be regulated by actions but not totally due to the existence of uncertainty. It includes the amounts of resources in the storage, the power production capacity, and the storage capacity. The second is a subset of disturbance state variables, meaning that even if it starts from the same state, its successor state cannot be always the same given the same action. The demand is only disturbance state variable in this study. Though we cannot control the demand, it is necessary to include this variable in the state vector because actions should be computed to meet the demand. The demand scenarios are constructed based on the historical data available from KESIS.

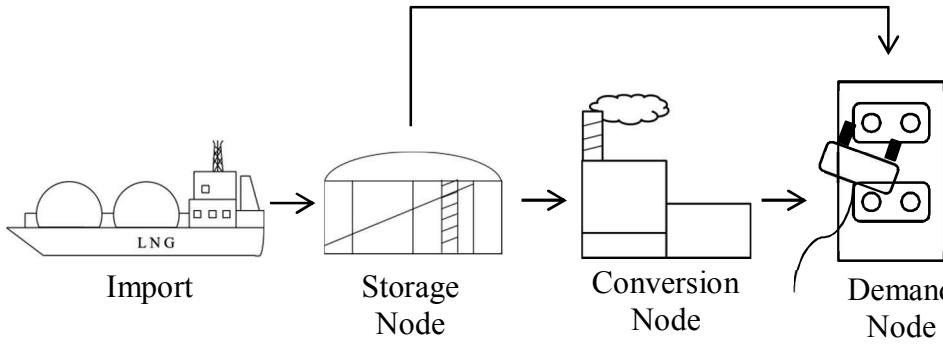

<Figure 1. Genral energy resource transit from import to demand node>

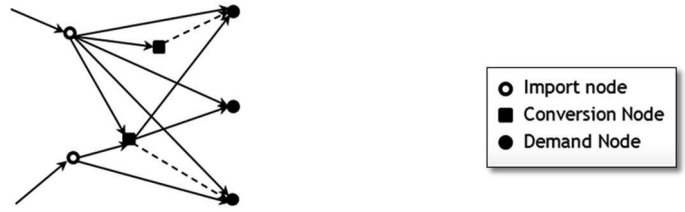

<Figure 2. Energy node network of the capital region in South Korea>

2.2. Decision variable

The decision variables are energy resource flows and capacity extension of resource facilities. The amounts of resources are divided into annual import volume and dispatch to power plants from the harbors. If the dispatch amounts are determined, the total amounts of electricity to be generated can be determined. With the assumption that all the demands should be met due to the national policy the resource flows to the households and businesses are the same with the predicted nominal demands. Capacity extension means that all the activities related to adding capacities to the current energy resource facilities. The energy resource facility has two types: power plant and storage/processing facility. Power plant capacity is defined as the maximum production of electricity from power plant for a year. Storage/processing facility capacity is the maximum volume of resources that can be stored and processed.

2.3. Objective function

The objective is to convert the available energy resources and supply the energy to meet the demand at a minimal cost. This can be cast as a stochastic dynamic optimization problem with a discounted infinite horizon cost as follows:

$$\min_{u_t} \mathrm{E}\left(\sum_{t=0}^{\infty} \alpha^t \emptyset(x_t, u_t)\right) \quad (1)$$

$$\emptyset(x_t, u_t) = \mathrm{C}(x_t, u_t) + \mathrm{X}(x_t, u_t) \quad (2)$$

, where E denotes the expectation operator and the stagewise cost $\emptyset(x_t, u_t)$ involves resource and construction expenses ($\mathrm{C}(x_t, u_t)$) and extra cost for each resource ($\mathrm{X}(x_t, u_t)$). For instance, the extra cost term can include costs for extra risk management in nuclear power plants.

2.4. State transition rule

State transition rule indicates how state evolves over one sample time given the current state and action. The state transition equation is given by simple balance equations as in

Table 1 for the controllable part. The disturbance part of the system is represented by the nominal demand scenario with additive noise based on the historical data for the capital region of South Korea from 2001 to 2010

2.5. Uncertainty

Demand is the only uncertain state variable. We represent the demand uncertainty as the fluctuation in the storage due to the constraints of meeting the demand as much as possible.

2.6. Constraints

Energy resource reservation plan is the only explicit constraint in this model. It is derived from the petroleum reservation program that a certain amount of petroleum should be secured in preparation for difficult situations to import. We assume that amount of stockpiles is bigger than a quarter of expected demand.

<Table 1.component of energy distribution model>

	Symbol	Description
State	$D_{r,t}$	Demand of resource
	$S_{r,t}$	Storage of resource
	$C_{r,t}$	Resource storage capacity of resource t
	$C_{r,t,e}$	Power plant capacity using resource
Action	$I_{r,t}$	Import of resource
	$E_{r,t}$	Extension of resource storage capacity
	$E_{r,t,e}$	Extension of power plant capacity
	$Di_{r,t}$	Dispatch to power plant of resource
State transition rule	$S_{r,t+1}$	$S_{r,t+1} = S_{r,t} + I_{r,t} - D_{r,t} - Di_{r,t}$
	$C_{r,t+1}$	$C_{r,t+1} = C_{r,t} + E_{r,t}$
	$C_{r,t+1,e}$	$C_{r,t+1,e} = C_{r,t,e} + E_{r,t,e}$
Uncertainty	$\widehat{D_{r,t}}$	
Constraint-Explicit	$S_{r,t+1} \geq \frac{1}{4} D_{r,t}$	reserves in preparation for energy crisis

2.7. Heuristics

In this study, we sample a subset of state points by performing closed-loop simulations with two simple heuristics. The first heuristic constructs a coal-fired power plant with the first priority and the nuclear and renewable energy plants are considered as a second choice. The second heuristic mainly constructs natural gas power plant. All these heuristics use a fixed value for the energy dispatch.

3. ADP-based approach for deriving an optimal policy

With the sampled state points and a function approximation scheme such as local averaging (Lee et al., 2006), the Bellman's optimality equation is solved iteratively as in Eq. (3)

$$J^{i+1}(x) = \min_{u \in U} E[\emptyset(x,u) + \alpha \tilde{J}^{i}(\mathrm{x})] \quad (3)$$

where *i* denotes the iteration index, J^{i+1} is the vector of calculated cost-to-go values for sampled state space, $\tilde{J}^{i}$ is the estimated value of cost-to-go for the successor state form the function approximator of the i^{th} iteration. The iteration is continued until (Use the infinite norm convergence criterion here. After how much iteration did you say it is converged with what criterion?) all the *J(x)* values are converged

The total number of possible state points is 1.53×10^{14} and the total number of action values is1.024×10^{7}. The number of visited state points in the proposed scheme is 1.95×10^{7}. Figure 3 shows the comparison between the converged ADP policy and two initial heuristics in terms of expected cost over five years in the future, and it shows significant performance improvement under uncertainty. The iteration scheme converged within an error tolerance $\left\| (J^{i+1} - J^{i})/J^{i} \right\|_{\infty} < 0.05$ after 2th iteration.

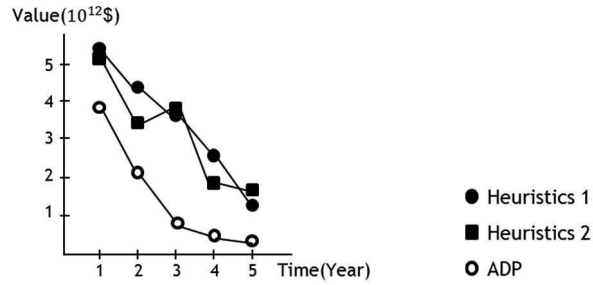

<Figure 3. Value on scenario of Heurstics and ADP>

4. Concluding Remarks

In this paper, we propose a Markov chain model for optimal energy management problem and solved it using ADP. In the revised manuscript, more comprehensive analyses and comparisons will be provided.

Acknowledgement

This subject is supported by Korea Ministry of Environment as "Projects for Developing Eco-Innovation Technologies (GT-11-G-02-001-3)".

References

Bellman, R.E. (1957). Dynamic programming. New Jersey : Princeton University Press

Bertsekas, D.P. (2000). Dynamic programming and optimal control(2nd ed.).Belmont, MA: Athena Scientific

Bertsekas, D.P., & Tsitsiklis, J.N. (1996). Neuro-dynamic programming. Belmont, Massacheusetts: Athena Scientific.

De Faria, D.P., & Van Roy, B. (2003). The linear programming approach to approximate dynamic programming. Operation Research, 51(6), 850-865

KESIS, Korea Energy Statistics Information System, from http://www.kesis.net

Lee.J.M., Kaisare, N. S., &Lee, J. H. (2006). Choice of approximator and design of penalty function for an approximate dynamic programming based control appraoch . Journal of Process Controal, 16(2), 135-156

Powell, W.B. (2007) Approximate dynamic programming : Solving the curses of dimensionality. John Wilely & Sons, Hoboken, NJ.

Puterman, M.L. (1994). Markov decision processes. New York, NY: Wiley.

Sutton, R., McAllester, D., Singh, S., & Mansour, Y. (2000). Policy gradient methods for reinforcement laernign with function approximation . In S. A. Sollar, T.K. Leen & K.-R. Muller (Eds.), Advances in neural information processing systems: 12, (pp. 1057-1063). MIT Press.

I.A. Karimi and Rajagopalan Srinivasan (Editors), Proceedings of the 11th International Symposium on Process Systems Engineering, 15-19 July 2012, Singapore.

Seawater Desalination Processes: Optimal Design of Multi Effect Evaporation Systems.

Paula Druetta[a] , Sergio Mussati[a], Pio Aguirre[a]

[a]*lNGAR - Instituto de Desarrollo y Diseño, Avellaneda 3657, Santa Fe (3000),Argentina*

Abstract

This is the first paper of a series of articles that deals with the modeling and optimization of dual-purpose desalination plants which combine thermal desalination processes and combined heat and power systems, specifically solid oxide fuel cell SOFC electricity generators. This paper presents preliminary results obtained for the multi effect evaporation (MEE) process (stand alone process). The steady state performance of the MEE system is described by a simplified and no linear programming (NLP) model. Optimal operating conditions including profiles of temperature, flow-rate and heat transfer area along the evaporator are analyzed. In addition, the influence of the effect number on the evaporation efficiency is also investigated.

Keywords: Multi-effect desalination; Optimal design; Non-Linear Programming (NLP)

1. Introduction

In many countries the most pressing issue for water security is in meeting basic provision of fresh water supply and sanitation. Sea-water desalination plays and will play in the future an important role in contributing to the provision of fresh-water since the global requirements for fresh water are increasing rapidly as the global population.

The following are the main desalination processes: a) Thermal: multi stage flash (MSF) and multi effect (MEE) distillation, vapor compression (VC) and b) reverse osmosis (RO), electrodialysis (ED), membrane distillation (MD). The thermal desalination processes are energy intensive (which global requirement is also increasing) and the efficiency is greatly improved when they are integrated with heat-power plants (co-generation power desalting plants, CPDP). Thus, the waste heat of the power plant is used as thermal source to produce fresh-water. The main drawback of such plants, however, are the high consumption of fossil fuel and high CO_2 emissions which lead to global warming and inevitable climate changes. It is essential therefore to look for cost-effective and sustainable processes that combine alternative energy sources (wind, geothermal and solar energy, fuel cells and others) with desalination technologies.

The use of high temperature fuel cells [molten carbonate fuel cells (MCFC) and solid oxides fuel cells (SOFC)] has emerged as a suitable technology for cogeneration. Certainly, electricity can be generated in a cleaner and more efficient way than with conventional technologies. In addition, the temperature of the flue gases is high enough to produce high-temperature steam to be used as heating medium in energy intensive processes.

Fig. 1 shows a schematic and feasible flow-sheet which integrates fuel cell and desalination process. The mathematical model to be presented in this work is the first basic step of a more ambitious project aimed at determining the optimal synthesis and design of the integrated process including desalination processes and SOFCs.

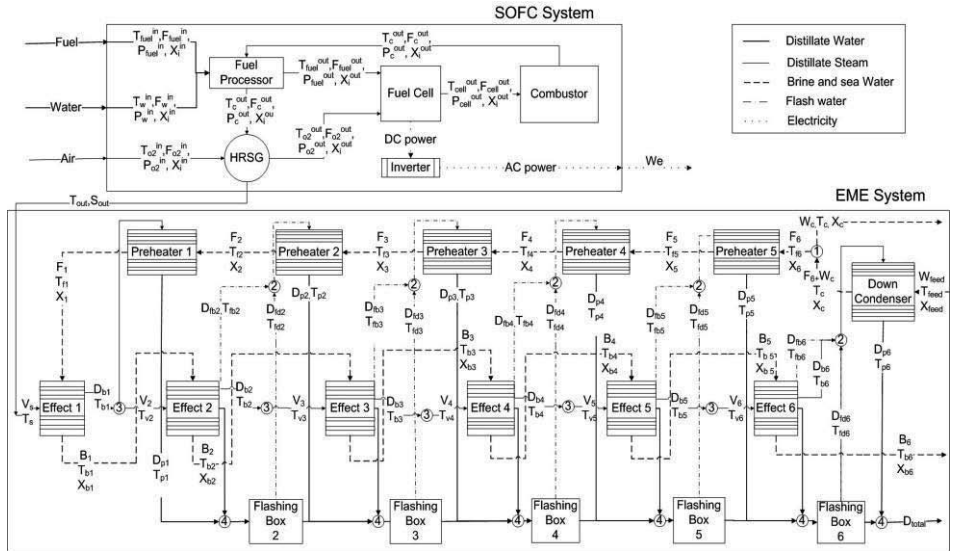

Fig. 1 Integration of SOFC and Multi-Effect Evaporation (MEE) process.

The MEE desalination system illustrated in Fig 1, which is the aim of this paper, is named "forward feed flow arrangement. As shown, each one of the effects involves a pre-heater, an evaporator and a distillate flash chamber. Feed seawater enters to the system and is preheated in the down condenser by the vapor formed in the last effect. A part of the seawater is then discharged to the sea. In the first effect, part of the vapor formed by evaporation of the brine is condensed outside the tubes of the pre-heater to heat the feed and the remaining the vapor is used in the second effect to evaporate part of the brine coming from the first effect. From the second to the last effect, the vapor formed by flashing of the brine and distillate is used to pre-heat the feed while the fresh vapor formed by evaporation is used to evaporate part of the brine in the next effect. This cycle of evaporation, condensing and heating is repeated at each effect until the last effect. The first and last stages need external heating and cooling respectively. The amount of heat removed from the last stage must nearly equal the amount of heat supplied to the first stage (Q). For sea water desalination purpose, the first stage is typically operated at a temperature below 70 °C in order to avoid scale formation.

2. Optimization Problem

The proposed optimization problem can be stated as follows. Given the sea-water conditions (composition, temperature and flow-rate), the goal is to determine the optimal operating conditions and the heat exchange values for the different heat exchangers in order to minimize the total heat transfer area in satisfying the fresh-water demand. The problem is solved for the following two cases: a) equal heat transfer areas (HTA) in all pre-heaters and evaporation effects and b) variation of HTA along the pre-heaters and evaporation effects. The output results are compared in detail. Finally, the influence of the number of effects and the steam temperature supplied in the first effect (heating utility) on the total heat transfer area is also analyzed. For this analysis, the optimization problem is systematically solved by varying both parameters.

3. Assumptions and mathematical model

The following are the main assumptions used to develop the mathematical model.

- Heat losses, non-equilibrium allowance (NEA) and Non-condensable gases effects are neglected.
- A mean value is adopted for the heat capacity coefficients (Cp), the latent heat of vaporization (λ), the overall heat transfer coefficients (U) and for the boiling point elevation of the brine (BPE), neglecting the effect of the chamber geometry, temperature, pressure and the fluid properties.
- The vapor form by flashing in the effects and the flashing boxes is used to heat the feed.
- The heat transfer equations model the HTA in each evaporator as the sum of the area for brine heating (A_b) and an area for evaporation (A_e).

3.1. Equations and computational aspects

The MEE system is represented as a No Linear Programming (NLP) model. This model consists in a set of mass and energy balances, and design equations used to compute heat transfer areas and physical-chemical properties of each one of the streams. There is mass and energy balances for each one of the pre-heaters, effects and flashing chambers. The logarithmic mean temperature difference (LMTD) is used to compute the HTA in pre-heaters. The model also includes non equality constraints which are used to avoid temperature crossover. In addition, lower and upper bounds have been imposed for each one of the variables in order to facilitate the model convergence.

The model involves non-linear constraints and bilinear terms which lead to local optimal solutions and therefore, global optimal solutions can not be guaranteed. In order to solve the optimizations, a feasible solution taken from Darwish's (2006) has been used to solve the first optimization problem. Then in order to solve the next optimization problem where some model parameters are varied, the previous solution is used as initialization. Thus, a sequence of several optimization problems is efficiently and systematically solved.

4. Results

The optimization problem described in section 3 is solved using the parameter values listed in Table 1. As mentioned earlier, the fresh-water demand (D), steam temperature (T_s), steam flow-rate (S) and seawater conditions [(X_{feed}), (T_{feed})] are given. In addition, an upper bound for the rejected brine salinity is imposed for environmental restrictions (XUp). The down condenser eject temperature (Tc) is also assumed as given.

Table 2 and Fig. 2, 3 and 4 compare the output results obtained by considering either uniform or non uniform distributions of heat transfer areas in pre-heaters and evaporation effects along the MEE system. In Table 2 are also compare same widely used variables to measure the system efficiency: the performance ratio (PR), the conversion ratio (CR), the specific total HTA (sHTA) and the specific cooling water ratio (sCWR).

Table 2 clearly shows that despite the cooling water flow-rate and the HTA in down condenser for non uniform area are greater than those required for uniform area, the total HTA required in pre-heaters and effects is considerably smaller than that required for uniform area. Fig. 2 compares the distribution of the HTA in pre-heater and evaporation effect along the MEE system (8 stages). It is possible to observe that the non uniform distribution of the HTA leads to the minimum total HTA of the process.

Fig. 3 compares the corresponding distribution of the driving force and the fresh water production in each one of the effects for both cases. It clearly shows that from the first to fifth effect the driving forces are similar in both cases and then in the last three effects the driving force for non uniform area is greater than the corresponding to

uniform distribution. In both cases, the total fresh-water production which is fixed is similarly distributed along the desaltor.

Fig. 4 compares the distribution of the temperatures in pre-heater and evaporation effect along the MEE system (8 stages) for both situations.

Table 1. Parameter values

Parameters	
Cp [KJ/Kg ºC]	4
D [Kg/s]	2500
BPE [°C]	1
λ [KJ/Kg]	2333
T_{feed} [°C]	26
T_c [°C]	40
T_s [°C]	70
X_{feed} [ppm]	45978.9
X_{Up} [ppm]	72000.0
U [kW\ m^2 ºC]	3
N	8
S [Kg/s]	600

Table 2. Optimal values

	Non uniform HTA	Uniform HTA
sHTA [m^2/Kg/s]	252.76	285.36
PR (D/S)	4.16	4.16
sCWR (Wc/D)	5.91	4.93
CR (F/D)	2.77	2.77
Cooling Water Flow [Kg/s]	14785.22	12325.65
Down Condenser HTA [m^2]	36009.02	21540.53
Total HTA [m^2]	631901.21	713408.13

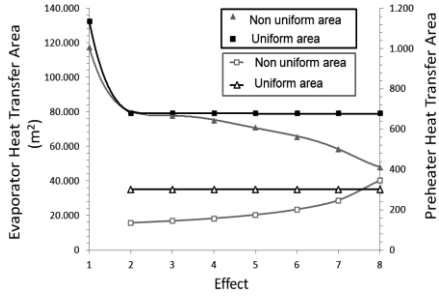

Fig. 2. Heat transfer areas vs. effect

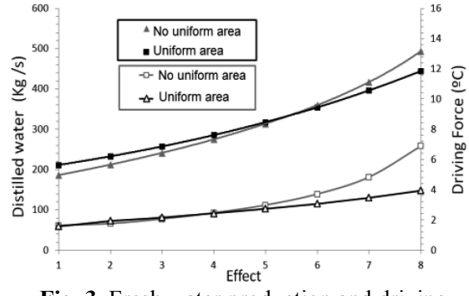

Fig. 3. Fresh water production and driving force vs. effect

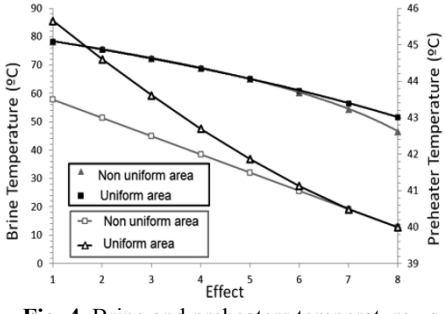

Fig. 4. Brine and preheaters temperature vs. effect

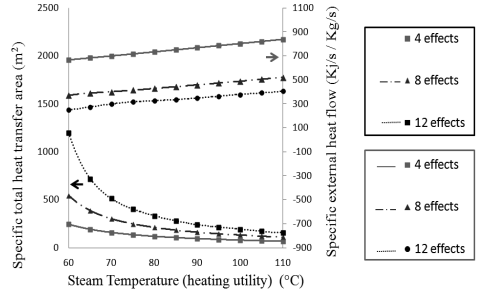

Fig. 5. Total HTA and heating utility vs. effect

The impact of the number of effects and the steam temperature used for heating utility on the total HTA and consumption of the heating utility is shown in Fig. 5. The illustrated results were obtained by minimizing the total HTA considering uniforms HTA in pre-heaters and effects and a given fresh water demand. In addition, in this case, the heating utility consumption was considered as a variable. Fig. 5 exhibits a similar behavior to those obtained via simulation by El-Dessouky (2002), instead of simultaneous optimization as is here used. As is shown, both the total HTA and heating

utility consumption are strongly influenced by the number of effects and steam temperature. The total HTA for N = 4 is not strongly influenced by the steam temperature. However, the total area is significantly increased as the number of effects increases and the steam temperature decreases. Certainly, for Ts = 65 ºC and N = 4, the total specific HTA is 192.17 m2/Kg/s, while for same steam temperature but N=12 the total specific HTA increases to 717.72 m^2/Kg/s, a 525 % higher.
By the other side, the heating utility consumption decreases as the number of effects increases and the steam temperature decreases. Certainly, for Ts = 65 ºC and N = 4, the total specific heating utility is 682.78kJ/s/Kg/s, while for same steam temperature but N=12 the total heating utility decreases to 273.57 kJ/s/Kg/s, a 59.93 % lower.

5. Conclusions and future work

A deterministic NLP mathematical model by effects for the MEE system was presented. Optimal temperature, salinity, areas dimensions and flow-rate evolutions through the equipment are obtained in order to satisfy a given fresh water demand. The proposed resulting model is a valuable tool not only to optimize the process but also to simulate the desalting process if the degree of freedom of the equation system is zero. After validation, several optimization problems using different criteria have been examined concluding that the total HTA require can be decreased a 11.4% by allowing HTA taking a non uniform distribution. It was verified that the minimization of the total HTA by fixing the fresh water demand and external heat, is equivalent to the minimization of the external heat by fixing the total HTA and fresh water demand. The effect of the number of effects and team temperature on the optimal solutions has been also investigated, obtaining similar results to those obtained by other authors. HTA and heating utility consumption are strongly influenced by the number of effects and steam temperature: the total HTA increased as the number of effects increases and the steam temperature decreases, while the heating utility consumption decreases as the number of effects increases and the steam temperature decreases.
At present, the proposed model is being expanded in order to consider the number of effects as an additional model variable (discrete decision), as well as the inclusion of the geometry, pressure drop, BPE, NEA and non-condensable gases. The coupling between the MEE system with SOFT cells and the minimization of the investment and operating costs of the entire process will be further investigated in detail. Finally, the application of a global optimum algorithm to solve the resulting model will be also addressed.

References

S. A1-Hallaj, Fuad Alasfour, Sandeep Parekh, Shabab Amiruddin, J. Robert Selman, Hossein Ghezel-Ayagh, 2004, Conceptual design of a novel hybrid fuel cell/desalination system, Desalination, 164, 19-31

M.A. Darwish, F. Al-Juwayhel, H. K. Abdulraheim, 2006, Multi-effect boiling systems from an energy viewpoint, Desalination, 194, 22–39.

H.T. El-Dessouky, I. Alatiqi, S. Bingulac, H.M. Ettouney, 1998, Steady-state analysis of the multiple effect evaporation desalination process, Chem. Eng. Technol, 21, 15±29.

H.T. El-Dessouky, H.M. Ettouney, 2002, Multiple Effect Evaporation, Fundamentals of Salt Water Desalination, Capitulo 4.2.3, ELSEVIER SCIENCE B.V., 202-205.

H.T. El-Dessouky, H.M. Ettouney, 1999, Multiple-effect evaporation desalination systems: thermal analysis, Desalination, 125, 259-276.

H.M. Ettouney, 2006, Design of single-effect mechanical vapor compression, Desalination, 190, 1–15.

P. Lisbona, J. Uche, L. Serra, 2005, High-temperature fuel cells for fresh water production, Desalination, 182, 471–482.

I.A. Karimi and Rajagopalan Srinivasan (Editors), Proceedings of the 11th International Symposium on Process Systems Engineering, 15-19 July 2012, Singapore.

An Inverse Optimization Approach to Inducing Resource Conservation in Eco-Industrial Parks

Raymond R. Tan, Kathleen B. Aviso

Chemical Engineering Department/Center for Engineering and Sustainable Development Research, De La Salle University, 2401 Taft Avenue, 1004 Manila, Philippines

Abstract

The exchange of wastes among plants within an eco-industrial park (EIP) creates potential for significant gains in sustainability through efficient use of resources and reduction of environmental discharges. If the establishment of such resource conservation networks (RCNs) is not economically optimal, intervention of an EIP authority will be necessary in order to induce companies to act in an environmentally responsible manner. This conflict of interest between the EIP authority and the industrial plants results in a Stackelberg game, which may be represented as a bi-level optimization model. In this work, a bi-level linear integer programming model for optimizing waste exchange in an EIP is developed. Then, an inverse optimization approach is used to solve it. An auxiliary model is used to determine the best set of incentives and disincentives to induce the plants in the EIP to form an optimal RCN. The methodology is demonstrated using an illustrative case study.

Keywords: Resource conservation, industrial ecology (IE), eco-industrial park (EIP), Stackelberg game, bi-level programming, inverse optimization.

1. Introduction

The concept of industrial ecology (IE) was first proposed by Frosch and Gallopolous (1989) as a means of enhancing the sustainability of manufacturing by emulating the cyclic structures of natural ecosystems. In particular, eco-industrial parks (EIPs) have been shown to be effective in developing resource conservation schemes through waste exchange and reuse. There have been significant attempts to use process systems engineering tools to provide more rigorous decision support in the design of EIPs. For example, optimal design of inter-plant water networks using mathematical programming was first proposed in the late 1990s (Keckler and Allen, 1999; Nobel and Allen, 2000); in these early models, each plant in the EIP was modeled as a "black box." Subsequent models used more detailed models describing processes within the plants themselves (Lovelady and El-Halwagi, 2009; Chew et al., 2008; Chew et al., 2010a, b; Aviso et al., 2011). Further refinements of such models were later proposed to account for potential conflicts of interest among companies (Lou et al., 2004; Singh and Lou, 2006; Piluso and Huang, 2009; Chew et al., 2009; Aviso et al., 2010a; Aviso et al., 2011; Tan, 2011; Taskhiri et al., 2011b). While many of these works have focused on water reuse, it has also been shown that the basic modeling approach may be readily extended to other streams once relevant material and energy balance considerations have been identified (Lou et al., 2004; Piluso and Huang, 2009; Aviso et al., 2011). Game theory has been proposed for resolving conflicts of interest in EIPs (Lou et al., 2004; Chew et al., 2009). In particular, some approaches have explored the role of the EIP authority (e.g.,

government) in facilitating the emergence of sustainable resource conservation networks involving different plants through incentives or disincentives (Aviso et al. 2010b; Chew et al., 2011; Tan et al., 2011a). The interaction between the EIP authority (i.e., the leader, which seeks to maximize total public good) with industry (i.e., the follower, which in turn seeks to maximize profit) results in a Stackelberg game (Aviso et al., 2010b; Tan et al., 2011a). Such games can be modeled as bi-level mathematical programs (Bard, 1998). In practice, the problem for the leader is to induce environmentally responsible behavior in the follower, despite the fact that the latter is motivated predominantly by profit. Inducement can be achieved through incentives (e.g., subsidies) or disincentives (e.g., taxes). An optimal set of incentives can then be determined, for example via inverse optimization (Ahuja and Orlin, 2001). In this work, a bi-level linear integer programming model is developed for conservation of multiple resources in an EIP. An inverse optimization solution procedure is then proposed. The methodology is demonstrated using a simple case study. Finally, conclusions and prospects for future work are given at the end of the paper.

2. Problem Statement

The formal problem statement addressed in this work is as follows:

- The EIP is assumed to be comprised of m sources, n demand, and p streams. Any given plant within the EIP can act either as a source or a demand, or both.
- Each source i (i = 1, 2, …, m) is characterized by a non-negative flowrate S_{ik} of each stream k (k = 1, 2, …, p), while each demand j (j = 1, 2, …, n) is characterized by a non-negative flowrate D_{jk} of each stream k (k = 1, 2, …, p).
- The opportunity for reuse of an given stream k between any source-demand pair is given by a constant, R_{ijk}. The decision whether or not to activate a particular link is denoted by the binary variable x_{ijk}.
- The total cost borne by industry to implement resource conservation in the EIP is assumed to be a linear function of x_{ijk}. Note that the cost may be negative.
- The total cost to the EIP authority or government to implement resource conservation in the EIP is likewise assumed to be a linear function of x_{ijk}. In general, since this cost includes externalities (e.g., monetized cost of pollution), the authority's cost function will not be the same as that of industry. However, as in the latter's case, the cost may assume negative values as well.
- Both the EIP authority and industry seek to minimize their respective cost functions, resulting in a Stackelberg game. The leader then seeks to modify both cost functions, through incentives and disincentives, so that the optimal solutions of the two decision-makers coincide. The objective is to determine the optimal set of such interventions.

3. Model

The bi-level optimization model is:

$$\min \Sigma_i \Sigma_j \Sigma_k (A_{ijk} - \alpha_{ijk} + \beta_{ijk}) R_{ijk} x_{ijk} \quad (1)$$

subject to:

$$\min \Sigma_i \Sigma_j \Sigma_k (B_{ijk} + \alpha_{ijk} - \beta_{ijk}) R_{ijk} x_{ijk} \quad (2)$$

subject to:

$$\Sigma_j R_{ijk} x_{ijk} \leq S_{ik} \qquad \forall i, k \quad (3)$$

$$\Sigma_i R_{ijk} x_{ijk} \leq D_{jk} \qquad \forall j, k \quad (4)$$

$$x_{ijk} \in \{0, 1\} \qquad \forall i, j, k \quad (5)$$

where A_{ijk} and B_{ijk} are the unit costs incurred by the leader and follower, respectively, to implement reuse of resource k between source i and demand j; α_{ijk} and β_{ijk} are the specific incentive and disincentive for the reuse of resource k from source i to demand j; R_{ijk} is the maximum amount of resource k that can be reused from source i to demand j; x_{ijk} is the binary variable denoting the decision to implement reuse of resource k between source i and demand j; S_{ik} is the amount of resource k available from source i; and D_{jk} is the amount of resource k needed by demand j. The leader's objective function is to minimize the total cost (including external costs corresponding to monetized environmental damage) associated with implementing resource reuse in the EIP (Eq. 1); likewise, the follower seeks to minimize the total cost or resource reuse (Eq. 2). The costs given by Eq. 1 and 2 may assume negative values, indicating net benefit. Source and demand balances are given by Eq. 3 and 4, while Eq. 5 restricts x_{ijk} to binary values. It can be seen that $R_{ijk} = \min(S_{ik}, D_{jk})$. Furthermore, the leader and follower will clearly have identical solutions when the terms of Eq. 1 and 2 are proportionate. Thus, when the ratio A_{ijk}/B_{ijk} is a positive constant, the leader and follower will agree on a common solution even with $\alpha_{ijk} = \beta_{ijk} = 0$. However, such a condition will rarely arise in practice, and thus it is necessary to determine what the incentives should be.

Assume that the leader seeks a set of incentives which requires the least deviation from the original cost coefficients, as proposed by Ahuja and Orlin (2001). The following auxiliary model results:

$$\min \Sigma_i \Sigma_j \Sigma_k (\alpha_{ijk} + \beta_{ijk}) \tag{6}$$

subject to:

$$\lambda (A_{ijk} - \alpha_{ijk} + \beta_{ijk}) = (B_{ijk} + \alpha_{ijk} - \beta_{ijk}) \quad \forall i, j, k \tag{7}$$

$$\lambda \geq 0 \tag{8}$$

$$\alpha_{ijk} \geq 0 \quad \forall i, j, k \tag{9}$$

$$\beta_{ijk} \geq 0 \quad \forall i, j, k \tag{10}$$

where λ is the variable proportionality ratio. Note that there are bilinear terms in Eq. 7. The procedure is illustrated in the next section with a simple case study. The optimization software Lingo 12.0 with a branch-and-bound based global optimization toolbox for non-linear models (Gau and Schrage, 2004) is used to solve the example.

4. Case Study

Consider a hypothetical EIP with three plants (i.e., a power plant, a palm oil mill and a biorefinery) and two streams (i.e., waste heat and waste biomass). The power plant may export its waste heat to the palm oil mill or the biorefinery; on the other hand, the palm oil mill generates waste biomass, which can be co-fired in the power plant or used as feedstock for the production of value-added goods in the biorefinery. The relevant stream data are shown in Table 1.

Table 1. EIP Data for Case Study

	Waste heat output (MW)	Heat demand (MW)	Waste biomass output (t/h)	Waste biomass demand (t/h)
Power plant	100	0	0	12
Palm oil mill	0	25	10	0
Biorefinery	0	20	0	5

Cost coefficients for the reuse of streams from both EIP authority and industry standpoints are given in the second and third rows of Table 2. Note that these coefficients will cause the leader and follower to seek different optimal solutions, mainly because the leader's cost coefficients account for the externalities (i.e., effects of resource conservation or pollution reduction in monetary terms).

Table 2. Cost Coefficients for Case Study

	Waste heat reuse ($/MWh)	Waste biomass reuse ($/t)
EIP Authority	–10	–1.5
Industry	2	0.2
Incentive	2	0.2

Solving the auxiliary model (Eq. 6 – 10) gives the optimal set of incentives in the last row of Table 2. The incentives in this case are just sufficient to offset the costs of implementing resource reuse, so that the industrial coalition becomes willing to accept the solution preferred for implementation by the EIP authority. Substituting these values into the main model (Eq. 1 – 5) then gives the optimal resource reuse network as shown in Table 3. The power plant exports waste heat to the two other plants for a combined recovery of 45 MW, and receives all of the available biomass (10 t/h) from the palm oil mill for co-firing.

Table 3. Optimal EIP Resource Reuse Scheme for Case Study

Source/Demand	Power plant	Palm oil mill	Biorefinery
Power plant	0	25 MW	20 MW
Palm oil mill	10 t/h	0	0
Biorefinery	0	0	0

5. Conclusion

An inverse optimization approach to inducing resource conservation in eco-industrial parks has been developed. This approach involves formulating a bi-level integer programming problem, where the EIP authority or government assumes the role of the upper-level decision maker, while the coalition comprised of participating plants acts as the lower-level decision maker. An inverse optimization strategy can be used to determine the set of incentives/disincentives that the authority should impose in order to induce the companies within the EIP to participate in resource conservation. A simple case study involving has been used to demonstrate the methodology; the model may also be tested on more complex examples in the future.

References

Ahuja, R. K. and Orlin, J. B., 2001. Inverse Optimization. Operations Research 49: 771 – 783.

Aviso, K. B., Tan, R. R., Culaba, A. B., 2010a, Designing Eco-Industrial Water Exchange Networks Using Fuzzy Mathematical Programming. Clean Technologies and Environmental Policy 12: 353 – 363.

Aviso, K. B., Tan, R. R., Culaba, A. B., Cruz, J. B., 2010b, Bi-Level Fuzzy Optimization Approach for Water Exchange in Eco-Industrial Parks. Process Safety and Environmental Protection 88: 31 – 40.

Aviso, K. B., Tan, R. R., Culaba, A. B, Foo, D. C. Y., Hallale, N., 2011, Fuzzy optimization of topologically constrained eco-industrial resource conservation networks with incomplete information. Engineering Optimization 43: 257 – 279.

Bard, J. F., 1998, Practical bilevel optimization. Algorithms and applications. Kluwer Academic Publishers, Dordrecht.

Chew, I., Tan, R. R., Ng. D. K. S., Foo, D. C. Y., Majozi, T., Gouws, J., 2008, Synthesis of direct and indirect inter-plant water network. Industrial and Engineering Chemistry Research 47: 9485 – 9496.

Chew, I. M. L., Tan, R. R., Foo, D. C. Y., Chiu, A. S. F., 2009, Game theory approach to the analysis of inter-plant water integration in an eco-industrial park. Journal of Cleaner Production 17: 1611 – 1619.

Chew, I. M. L., Foo, D. C. Y., Ng, D. K. S., Tan, R. R., 2010a, A new flowrate targeting algortihm for inter-plant resource conservation network - Part 1: unassisted integration scheme." Industrial and Engineering Chemistry Research 49: 6439 – 6455.

Chew, I. M. L., Foo, D. C. Y., Tan, R. R., 2010b, A new flowrate targeting algortihm for inter-plant resource conservation network - Part 2: assisted integration scheme." Industrial and Engineering Chemistry Research 49: 6456 – 6468.

Chew, I. M. L., Thillaivarna, S. L., Tan, R. R., Foo, D. C. Y., 2011, Analysis of inter-plant water integration with indirect integration schemes through game theory approach – Pareto optimal solution with interventions. Clean Technologies and Environmental Policy 13: 49 – 62.

Frosch, R. A., Gallopolous, N. e. 1989, Strategies for manufacturing. Scientific American 261: 94 – 102.

Gau, C.-Y. and Schrage, L. E., 2004. Implementation and testing of a branch-and-bound based method for deterministic global optimization: operations research applications. In: Floudas, C. A. and pardolos, P. M. (eds.), Frontiers in Global Optimization, p. 145 – 164, Kluwer, Dordrecht.

Keckler, S. E., Allen, D. T., 1999, Material reuse modeling; A case study of water reuse in an industrial park. Journal of Industrial Ecology 2: 79 – 92.

Lou, H., Kulkarni, M., Singh, A., Huang Y. 2004. A game theory based approach for emergy analysis of eco-idustrial systems under uncertainty. Clean Technologies and Environmental Policy 6: 151 – 161.

Lovelady, E.M. and El-Halwagi, M. M. 2009. Design and integration of eco-industrial parks for managing water resources. Environmental Progress and Sustainable Energy 28: 265 – 272.

Nobel, C. E., Allen, D. T. 2000, Using geographic information systems (GIS) in industrial water reuse modeling. Process Safety and Environmental protection 78, 295 – 303.

Piluso, C., Huang, Y., 2009, Collaborative profitable pollution prevention: An approach for the sustainable development of compex industrial zones under uncertain information. Clean Technologies and Environmental Policy 11: 307 – 322.

Singh, A., Lou, H. H. 2006, Hierarchical Pareto optimization for the sutainable development of industrial ecosystems. Industrial & Engineering Chemsitry Research 45: 3265 – 3279.

Taskhiri, M. S., Tan, R. R., Chiu, A. S. F., 2011b, Emergy-Based Fuzzy Optimization Approach for Water Reuse in an Eco-Industrial Park. Resouces, Conservation & Recycling 55: 730 – 737.

Tan, R. R., 2011, A fuzzy optimization model for source-sink water network synthesis with parametric uncertainties. Industrial and Engineering Chemistry Research 50: 3686 – 3694.

Tan, R. R., Aviso, K. B, Cruz, J. B., Culaba, A. B., 2011a, A note on an extended fuzzy bi-level optimization approach for water exchange in eco-industrial parks with hub topology. Process Safety and Environmental Protection 89: 106 – 111.

I.A. Karimi and Rajagopalan Srinivasan (Editors), Proceedings of the 11th International Symposium on Process Systems Engineering, 15-19 July 2012, Singapore.

Techno-economic analysis of ethanol production from marine biomass

Peyman Fasahati, Geongbum Yi, Jay Liu*

[a] *Department of Chemical Engineering, Pukyong National University, Busan 608-739, South Korea*

Abstract

The purpose of this study is techno-economic analysis of ethanol production from marine biomass (macroalgae), based on 10-year time frame for plant operation. This study is different from previous similar studies considering following facts: (1) Biomass considered in this study is macroalgae or seaweed, to which technologies available for conversion of biomass to fuels have been applied in limited ways. (2) This study does not provide production cost of ethanol, but target biomass cost for macroalgae production through large-scale cultivation that is a key factor for success of macroalgae as a biomass feedstock.

Currently high seaweeds price greatly limits the applicability of seaweeds as feedstocks for bioethanol production plant. To solve this issue a reduction of feedstock price seems the only option. This study develops a techno-economic model to analyze the economy of an ethanol production plant processing 100,000 MT/year (dry basis) brown algae. This study effectively defined maximum dry seaweed price (MDSP) that must be covered by large-scale seaweed production to reach a Return-On-Investment (ROI) break-even point after 10 years plant operation. The MDSP will act as target biomass cost for large-scale cultivation of macroalgae. Plant scale ups were also performed to examine the effects of plant capacity on MDSP.

Keywords: Techno-economics, Ethanol, Seaweed, Biomass, Macroalgae.

1. Introduction

Over the past 50 years, the world's population has more than doubled, coupled with an expectation of a higher standard of living and an ever-increasing economic output. This has resulted in a large increase in primary energy consumption, particularly the use of fossil fuel derived energy (BP Global, 2011).

Bio-fuels are environmentally friendly and carbon neutral, and can play a prominent role in an energy portfolio. However, if the bioenergy industry is to be successful, enough supply of biomass feedstock should be available at a low cost and on a very large scale (Antizar & Turrion, 2008).

The main obstacle of bio-energy development is stable supply of raw materials on a large scale. More than 60% of the cost for bioenergy is feedstock cost (Liu & Gu, 2008), which is a major constraint on the commercialization of algal biofuels (Johnson & Wen, 2010). It is the goal of this study to evaluate the economics of ethanol production from marine biomass, i.e., macroalgae or seaweeds (brown algae), and to calculate the maximum feed stock price based on 10-year time frame for plant operation so that industrialization of plant be economically possible. In addition, to identify most significant opportunities to decrease production costs.

* jayliu@pknu.ac.kr

An ethanol production plant from brown algae, based on a 100,000 MT/year dry feed, simulated using Aspen Plus® in order to obtain more accurate mass balance information than what typically assumed (Fasahati & Liu, 2011). Furthermore, the Aspen Plus model was used to estimate key parameters affecting the economy of the plant. Using the resulting flow rates, sizing and cost of each process unit estimated based on Aspen Process Economic Analyzer to determine the cost of bioethanol production plant. It is important to note at the outset that algal biofuel technology is still at the lab-scale or at the very early pilot stage of development; as such, the estimated cost of production may vary based on future developments on process condition and parameters change.

2. Process description

As shown in Figure 1, the simulated ethanol production process consists of three major units, feed pretreatment, simultaneous saccharification and fermentation (SSF), and finally purification. Feedstock for this plant is Saccharina Japonica, one type of brown algae, which is extensively cultivated in Korea, China, and Japan. Chemical composition for this seaweed derived from literature data (John et al., 1998; Horn S. G., 2000; Rioux et al., 2007; Jang et al., 2011). Total carbohydrates of this seaweed sum up to 66 percent of dry matter (Jang et al., 2011).

A pretreatment section carried out in two stages: The first stage is to heat up the feed stream by adding steam and H_2SO_4 for thermal acid hydrolysis. The second stage is to use enzymes for saccharification and SSF.

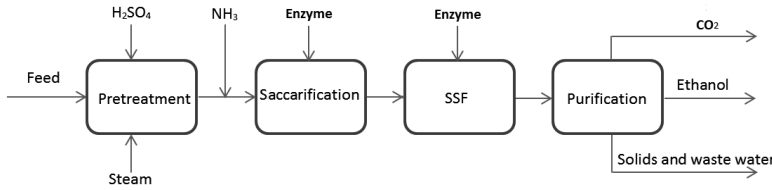

Figure 1. A simplified process flow diagram for bioethanol production plant

Slurry received from the pretreatment section first neutralized with Ammonia. Then it goes to saccharification vessels for further saccharification. Saccharified slurry, which has a reduced viscosity, goes to saccharification and fermentation vessels for SSF. Operating conditions are given in Table 1.

Table 1. Summary of plant operation conditions (Jang et al., 2011)

Unit	Condition
Thermal acid hydrolysis	10% (w/v) S. japonica, 40mM H_2SO_4, 121 °C, 60 min,
Biological saccharification	1 g dcw/L Bacillus sp. JS-1, 30 °C, 7.5 days
SSF	0.39 g dcw/L Bacillus sp. JS-1,0.45 g dcw/L P. angophorae, 30°C, 64 hr

A purification section separates the fermentation broth into water, anhydrous ethanol, and solids. Distillation and molecular sieve adsorption used to recover ethanol from the raw fermentation liquid and to produce 99.5% ethanol. Distillation accomplished in two columns. The first column, a water remover column, removes dissolved CO_2 and most of the water. The second column, an azeotropic column, concentrates ethanol from the first column to a near azeotropic composition. At the azeotropic condition ethanol products from this column goes to molecular sieves to reach 99.5 % purity. Overall process yield for ethanol production from dry seaweed is 0.25 (kg ethanol)/(kg dry seaweed).

3. Materials and methods

A list of assumptions common to all process scenarios includes the following:

- Plant base capacity is 100,000 MT/year of dry seaweed.
- Publicly available and experimentally validated literature data on reaction conversions and parameters are used.
- Equipment, chemical, and labor costs indexed to 2011 dollars.
- Contingency 18% of total project cost.
- Capital costs depreciated over 10 years of plant operation.
- Working capital 5% of total capital expense per year.
- Tax rate 24.75% per year.
- 15% internal rate of return (IRR).

The production costs include variable operating costs (such as process chemicals, bacteria, nutrients, etc.) and fixed operating costs (employee salaries, overhead, maintenance, and insurance). The chemical prices obtained from literature data and public available data such as ICIS chemical business (ICIS, 2011). Bacteria and yeast used in the process are not commercially available at a scale needed for the production plant, and this makes it difficult to obtain information needed for calculating operating costs. It is assumed that all the bacteria and enzyme will be delivered from outside to the plant and there is no onsite production. Table 2 shows material prices used in this study. CO_2 also selected as a selling material. Since this plant is capable of producing CO_2 at purity higher than 96%. We considered it as a product that can be sold.

Table 2. Raw material and product unit prices

Raw material	Cost (US$/kg)	Source
Ammonia	0.392	Humbird et al., 2011
Sulphuric acid	0.093	Humbird et al., 2011
Yeast and enzyme	0.340	Aden, 2008*
HP Steam @ 165 PSI	0.0179	Aspen utility specification
Nutrient	0.786	Aden, 2008*
Products	**Selling Price (US$/kg)**	**Source**
Ethanol 99.5%	0.891	ICIS, 2011
CO_2	0.040	Davis et al., 2011

* Nutrient and enzyme prices calculated for 2011 dollars using consumer price index, (CPI USA, 2011)

4. Results and discussions

4.1. Maximum dry seaweed price

The process model developed in Aspen Plus was sent to Aspen Process Economic Analyzer for economical evaluations. The total project capital cost is considered to depreciate, via a straight-line depreciation method, over the 10 years of economic Life of the facility. To reach a ROI break-even point after 10 years of operation, dry seaweed cost increased until net present value in 10^{th} year equals to zero. The maximum price for dry seaweed obtained was 160 $/Ton for the base case of 100,000 MT/year of dry seaweeds. Table 3 shows resulting production costs at this break-even point. Figure 2 shows a pie chart of the distribution of operating costs in 10^{th} year. From the chart, it can be seen that the raw materials constitute 68.5% of the total operating costs, and 18% of the operating cost is for utilities. This is in accordance with high raw material costs

associated for ethanol production plants using fermentation processes from biomass (Liu & Gu, 2008).

Table 3. Production costs (US$) at a ROI break-even point

Total Project Cost	12,901,300
Total operating labor and maintenance cost per year	1,466,000
Total raw material cost per year	16,302,200
Total product sales per year	26,783,400
Total utilities cost per year	4,449,870

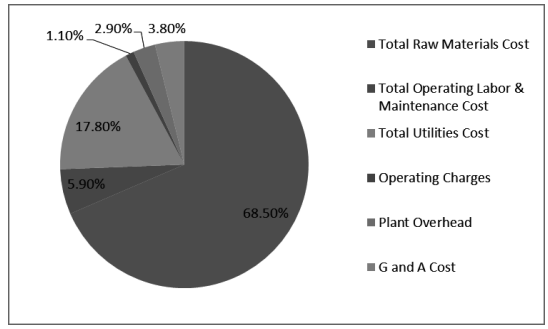

Figure 2. Operating costs break down at 10th year of plant operation

4.2. Effects of plant capacity

In order to examine the effect of plant capacity on production costs, a plant scale up from 50% to 700% of the base case (100,000 MT/Year of dry seaweeds) was performed using Aspen Process Economic Analyzer. It was found out from this study that plant economy can be improved at larger capacities. This allowed us to have increased MDSP at 10^{th} year. Figure 3 shows the trend of MDSP changes as a function of plant capacity.

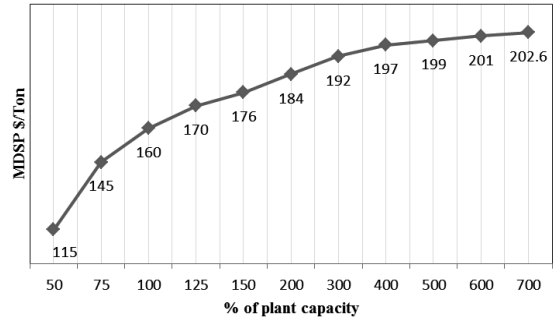

Figure 3. MDSP trend as a function of plant scale

As Figure 3 shows MDSP converge to 203 $/MT at the boundary and maximum quantity happened for plant scale up equal to 700%. Further scale ups did not affect MDSP very much and it remained constant at this value.

4.3. Conclusion

As the results of this study shows, this plant would be more economical if we can increase its capacity to five or six times of that of the base case. However, as the plant capacity increases, more biomass is needed for feed. Total production of Saccharina Japonica in South Korea in December 2011 was 43,651 MT in which 22,955 MT used

as food. This amount is much less than feedstock needed for the base case simulation. Currently, seaweeds mostly are used for food industry. Current market wholesale price of dry seaweed in South Korea is 5,622 US$/MT (December 2011) and wet seaweed price at cultivation sites is 393 US$/MT (AFL news.co.kr, 2011). Most of the seaweed available in market is wild and naturally cultivated. However, Large-scale artificial cultivation of seaweed will reduce this price. Results of this study show the necessity to perform a comprehensive study in the near future on seaweed mass cultivation procedures and efficiencies. Further technological advancements like increased conversions and process integration can further improve the plant economy and let the plant be economical even at higher seaweed prices.

Acknowledgement

This work was supported by the Ministry for Food, Agriculture, Forestry and Fisheries, and by Basic Science Research Program through the National Research Foundation of Korea (NRF) funded by the Ministry of Education, Science and Technology (2010-00003056).

• References

A. Aden, 2008, Biochemical Production of Ethanol from Corn Stover: 2007 State of Technology Model, National Renewable Energy Laboratory, NREL/TP-510-43205, Golden, CO.

BP Global: BP Energy Outlook 2030, 2011, London, UK, (www.bp.com)

L. B. Antizar and G.J.L. Turrion, 2008, Second-generation biofuels and local bioenergy Systems, Biofuels Bioprod. Bioref. 2, 455-469.

G.S. Liu and W.B. Gu, 2008, Advances in research on germplasm resources and molecular biology of the energy plants sweet sorghum, In: The proceeding of China–US workshop on bioenergy consequences for global environmental change, pp. 47-48.

M.B. Johnson and Z. Wen, 2010, Development of an attached microalgal growth system for biofuel production, Appl. Microbiol. Biotechnol. 85, 525-534.

D. Humbird, R. Davis, L. Tao, C. Kinchin, D. Hsu, A. Aden, P. Schoen, J. Lukas, B. Olthof, M. Worley, D. Sexton, and D. Dudgeon, 2011,Process Design and Economics for Biochemical Conversion of Lignocellulosic Biomass to Ethanol, In: Technical Report, National Renewable Energy Laboratory, NREL/TP-5100-47764.

R.P. John,G.S. Anisha, K.M. Nampoothiri, A. Pandey, 2011, Micro and macroalgal biomass: a renewable source for bioethanol, Bioresour Technol, 102:186–93.

P. Fasahati, J. Liu, 2012, Process simulation of bioethanol production from brown algae, ADCHEM, International Federation of Automatic Control (IFAC), Singapore.

S.J. Horn, 2000, Bioenergy from brown seaweeds, In: PhD Thesis, Norwegian University of Science and Technology, Department of Biotechnology.

L.E. Rioux, S.L. Turgeon, M. Beaulieu , 2007, Characterization of polysaccharides extracted from brown seaweeds. Carbohydrate Polymers, 69, 530–537.

S. John, T. Dunahay, J. Benemann, P. Roessler, 1998, A Look Back at the U.S. Department of Energy's Aquatic Species Program- Biodiesel from Algae, In: National Renewable Energy Laboratory, Golden, Colorado 80401-3393.

J.S. Jang, Y. Cho, G.T. Jeong and S.K. Kim, 2011, Optimization of saccharification and ethanol production by simultaneous saccharification and fermentation (SSF) from seaweed, Saccharina japonica. Bioprocess and biosystems engineering, 35, 11-18.

ICIS Chemical Business, 2011, Asia Price Report, Chemical pricing information, ICIS Pricing, 29/06/2011, Lester Teo, Lester.Teo@icis.com

AFLnews.co.kr, 2011, http://aflnews.co.kr/aflnews/news/news_contents.asp?news_code=2011011303102&c_code=0304

consumer price index, United states department of labor, 2011, Bureau of labor statistics, www.bls.gov/cpi/

R. Davis, A. Aden, P.T. Pienkos, 2011, Techno-economic analysis of autotrophic microalgae for fuel production, Applied Energy 88, 3524–3531

I.A. Karimi and Rajagopalan Srinivasan (Editors), Proceedings of the 11th International Symposium on Process Systems Engineering, 15-19 July 2012, Singapore.

Modeling and Simulation of Ship Transport of CO_2

Seok Goo Lee, Go Bong Choi, En Sup Yoon, Chonghun Han, Jong Min Lee*

School of Chemical and Biological Engineering, Institute of Chemical Processes, Seoul National University, 1 Gwanak-ro, Gwanak-gu, Seoul 151-744, Korea

Abstract

With growing concern about greenhouse gas emission, previous carbon capture and storage (CCS) research has mainly focused on efficient capture methods. However, there is a relative lack of studies on ship transport and offshore unloading. The available guidelines, if any, are simply suggested without a systematic analysis from the viewpoint of the optimal transport chain system. Thus, this study addresses the issue by modeling the ship-based transport network of CO_2. In particular, liquefaction, boil off gas (BOG) reliquefaction and offshore unloading processes are investigated to provide essential guidelines in terms of an optimal thermodynamic state (pressure-temperature: P-T). Optimal compression ratio and pressure-enthalpy flash are implemented on each compression-intercooling-separation stage, and a conceptual model for BOG reliquefaction process is also proposed.

Keywords: carbon capture and storage (CCS), CO_2, ship transport, optimal operating condition, modeling, simulation

1. Introduction

In recent years, there has been increasing demand for a significant reduction of CO_2 emissions from industrial sources to alleviate the global warming problem. Although several alternatives such as bio, wind, and solar energy are being studied to meet the huge energy demand, large amount of CO_2 emission seems to be inevitable in near future. Under the present conditions, carbon capture and storage (CCS) is considered to be the most practical approach for mitigation of CO_2 emission.

CCS technology consists of capture, transport and storage. Whereas a variety of researches have been conducted for CO_2 capture, research on systematic guidelines and technologies for transport and storage is still at its infancy.

Large amount of CO_2 can be transported via pipelines or ships. The technologies for CO_2 pipelines have been well established for many years, however this study is focused on ship transport of CO_2 due to its flexibility compared to the regional constraints of pipelines and wide range of applications. Despite the current limited knowledge and experience on ship-based CO_2 transport, there is much technical information available in the field of liquefied petroleum gas (LPG) and food grade CO_2 industries.

In order to ship CO_2, pressured-type or semi-refrigerated ship should be used for dense liquid phase conditions. Since CO_2 is in gas or solid phase at atmospheric pressure, depending on temperature, lowering the temperature at atmospheric pressure cannot liquefy CO_2 (IPCC, 2005). Hence, liquefaction of CO_2 requires a P-T condition between the triple point (T.P., 5.2 bar and -56.6 °C) and the critical point (C.P., 73 bar, 31 °C).

A key to the design for ship transport chain of CO_2 is to determine optimal P-T conditions of CO_2 because this significantly affects the system performance including liquefaction process, boil-off rate in the tank, hydrate and dry ice formation, etc. As

*Corresponding Author Tel.: +82-2-880-1878, E-mail: jongmin@snu.ac.kr

thermodynamic condition is close to the T.P., the amounts that can be transported are increased as the density rises. However, more compression energy is required for lowering the pressure for liquefaction and the amount of BOG can be increased with the temperature difference between inside and outside of the tank. If the pressure goes below the T.P., dry ice will not be necessarily formed immediately. In addition, the solubility of water in CO_2 gas decreases with higher pressure and lower temperature (Aspelund et al., 2006). For all these trade-offs, thermodynamic (P-T) conditions for liquefied CO_2 should be investigated systematically for each process.

Thus, this study systematically investigates the optimal operating condition by modeling and simulation of the major three processes, i.e., liquefaction, BOG reliquefaction, and offshore unloading.

2. Description of ship transport chain of CO_2

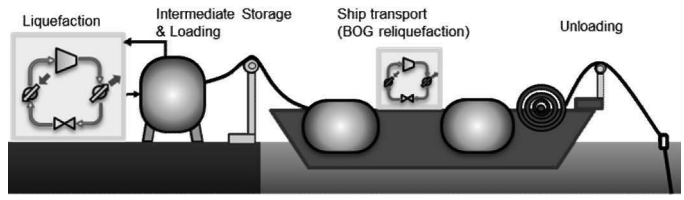

Figure 1. The ship transport chain of CO_2

As shown in Figure 1, the ship transport chain of CO_2 is divided into four parts: liquefaction, intermediate storage and loading, ship transport, and unloading. Liquefaction using Carnot cycle for volume reduction and intermediate storage tank are necessary at a terminal because CO_2 is continuously captured at the plant on shore. A loading arm or insulated flexible hose is placed between intermediate storage tank and ship. Furthermore, BOG reliquefaction process on the ship is considered in spite of much uncertainty in the amount of BOG. As the last stage, CO_2 is directly unloaded to aquifer via flexible riser (hose) which is mainly used in the field of oil/gas loading.

2.1. Liquefaction process

In the ship transport chain of CO_2, liquefaction process has the most significant influence on total cost and energy. Liquefaction of CO_2 can be classified into three categories according to the refrigeration system and refrigerant. The first is an absorption refrigeration system using NH_3. This method has the advantage of high specific heat capacity of NH_3, but is not suitable for this case due to environmental problems. The second is the method primarily used in the liquefied natural gas (LNG) industry, which lowers the temperature of CO_2 by compression-expansion loop using C_3 series refrigerant. This method has disadvantages in terms of efficiency and refrigerant cost. The last method, considered as the best, is an open cycle using the CO_2 feed as refrigerant by itself. Compared to conventional refrigerants, the most remarkable property of CO_2 is the low critical temperature of 31 °C. This means that the compression system operating at normal ambient temperatures thus works close to and even above the critical pressure of 73 bar. This leads to trans-critical cycle of CO_2 for liquefaction with favourable conditions for high compressor efficiency. In addition, most of the heat rejection at each stage takes place by air/seawater cooling instead of condenser. In other words, the refrigerant can be cooled to a few degrees above the entering coolant (air, seawater) temperature, and this contributes to the performance improvement (Neksa et al.).

As mentioned earlier, P-T condition has the most significant influence on performance for liquefaction process. This study investigates an alternative condition, which is 20 bar and -20 °C in the product stream, unlike the existing cases (7 bar, -50 °C) in the literature (Aspelund et al., 2006, 2007 & Decarre et al., 2010). Although the 20 bar and -20 °C condition may have disadvantages of high capital production cost of pressurized tank with a large volume due to the difference in density, liquefaction energy and BOG generation are smaller than the existing case (7 bar, -50 °C). This is an important problem of finding an economic optimal trade-off. However, 7 bar and -50 °C condition is unquestioningly applied to many previous studies (Aspelund et al., 2006, 2007 & Decarre et al., 2010). This study provides systematic guidelines for computing an optimal operating condition based on 20 bar and -20 °C condition.

2.2. BOG(Boil-Off Gas) reliquefaction process

With increasing fuel price, BOG reliquefaction technique has made much progress in the field of LNG transport. BOG reliquefaction for CO_2 transport is not yet reported, and there is much uncertainty about its necessity and technology. This is because there exists many difficulties in determining boil-off rate in CO_2 tank due to the uncertainties in its sensitivities with respect to insulation material and thickness, the number and size, structural shape, sloshing phenomena, impurities, etc. In addition, desirable simulation and/or experimental data for BOG reliquefaction of CO_2 has not been developed in the previous studies. Thus, to circumvent these difficulties, existing approaches in the LNG industry are applied in this study. Even though boil-off rate is determined by many variables, N_2 content is considered as a major factor in this modeling and simulation. This is because vapor-liquid equilibrium is largerly changed with N_2 content in BOG. The other variables such as insulation, surface area, and the number and size are assumed to be considered in the tank design as an economic trade-off. In addition, since N_2 is non-condensable in reliquefaction process, the amount of N_2 in BOG increases during the voyage. Thus, excessive amount of N_2 in BOG must be investigated and controlled by reliquefaction process and purge gas.

2.3. Offshore Unloading Process

There are two possible options for unloading process: indirect or direct unloading. Indirect unloading methods use a platform installed with buffer storage tank and injection facilities. Among them are submerged turret loading (STL) system and scaled-down platform (Aspelund et al., 2006). Although indirect methods can stand up to harsh condition on the sea, there are critical drawbacks that energy source for utilities on platform cannot be supplied by itself and relocation for scattered aquifers is relatively difficult.

The second method is to unload directly to aquifer without any buffer tank on ship instead of the platform. This method equips a pipeline at the bottom of ship (IPCC, 2005) or a flexible hose on the top of ship for injection. Compared with the indirect method, the direct method has many advantages such as flexibility for scattered aquifers, change of schedules and dynamic positioning. Though there are still uncertainties in choosing the best way between indirect and direct options according to given conditions, this study will focus on direct unloading methods with its economic advantages.

3. Simulation Results and Discussions

The suggested models are synthesized on process flow sheet simulator, Aspen HYSYS v7.2, and physical properties of the components were calculated by Soave-Redlich-Kwong (SRK) equation of state.

3.1. Liquefaction process

Table1. Specification of streams

	Component	Mole fraction	P-T condition	Mass flowrate
Feed gas stream	CO_2	0.95	1.1 bar, 35 °C	500 tonCO_2/hr
	H_2O	0.05		
Product stream (liquefied CO_2)	CO_2	0.9999	20 bar, -19.28 °C	475 tonCO_2/hr
	H_2O	0.0001		

Table1 shows feed flow of 500 tonCO_2/hr is used, which was determined by the thermal power plant of a unit grade 500 MW in South Korea, Boreyong city. The feed component mole fractions and P-T conditions were taken from (Aspelund et al., 2007)

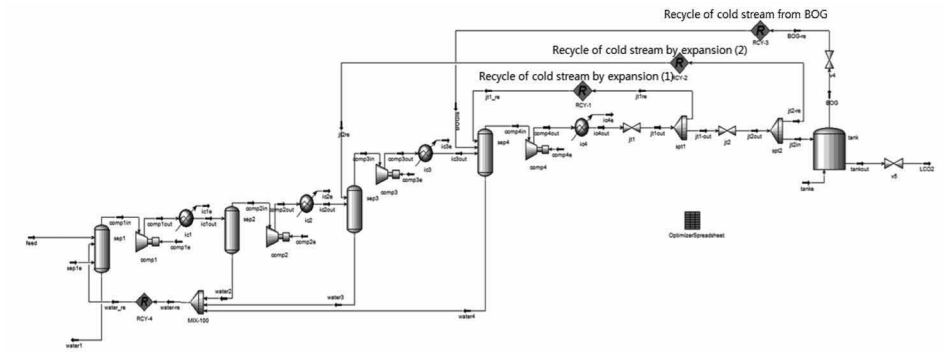

Figure 2. Process Flow Diagram of liquefaction process

For mechanical feasibility and thermodynamic efficiency, multistage compression-intercooling-separation processes are applied to increase the pressure for trans-critical cycle as shown in Figure 2, and then the liquid CO_2 is expanded over two stages to reach final specifications. The cold stream is generated by two-stage expansion and BOG from intermediate storage tank. This cold stream is recycled to pre-saturation for reducing compression power at 3 and 4 stages. Furthermore, compression pressure ratio is optimized via simulation tool satisfying mechanical constraints (i.e., in general compression ratio cannot exceed 5). As a results, the required compression power was computed as 103.42 KWh/tonCO_2. This is much more improved value compared to the previous studies (Aspelund et al., 2007 & Decarre et al., 2010). In addition, hydrate formation utility does not occur in simulation because water content is reduced to 100 ppm level in the product stream by the recycle. There are available results concerning the hydrate formation (Jakobsen et al., 2011). Hydrate will be formed at 20 bar, -20 °C when water content is contained more than 500 ppm. Thus this case does not have a problem for hydrate formation.

3.2. BOG reliquefaction process

N_2 content in the feed is contained to 500 ppm. N_2 content has a significant effect on vapor-liquid equilibrium in BOG. The boiling point of pure CO_2 at 20 bar is -19.27 °C. However the boiling point is changed to -24.35 °C when BOG contain 500 ppm N_2 content according to the SRK equation of state. The sphere tank volume and liquid volume flowrate are 10,000 m^3 and 10,000 m^3/hr, respectively. Overall heat transfer area is 2245 m^2. Heat ingress to storage tank is calculated as 64656 kJ/hr with the

overall heat transfer coefficient of 0.72 kJ/m^{2}·hr·°C. BOG massflow rate is 117.4 kg/hr containing 12 mole% N_2 content and 88 mole% CO_2 contained in BOG in the tank.

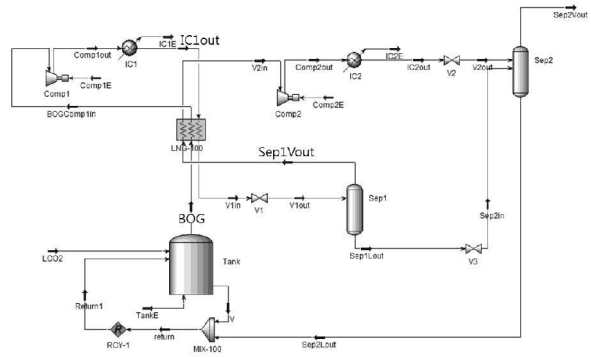

Figure 3. Process Flow Diagram of BOG reliquefaction process

Similarly, in the liquefaction process, design is proposed using CO_2 as a refrigerant by itself and two-stage compression-intercooling-expansion loop is shown in Figure 3. BOG and Sep1Vout as a cold stream pass through the multi-stream heat exchanger with hot IC1out stream after one-stage compression-intercooling. After that, the stream reliquefies via one more compression-intercooling-expansion in the last stage. Separated liquid stream containing 0.8 mole% N_2 content and 99.2 mole% CO_2 returns to the tank. It should be noted that, recovery rate is only 43%.

4. Concluding Remarks

By optimizing the compression ratio for each stage and integrating cold energy generated by expansion, the liquefaction process has been developed with 103.42 KWh/tonCO_2 of power for compression and the water content of 100 ppm level. BOG reliquefaction model for CO_2 storage tank is newly proposed to estimate the boil off rate.

Acknowledgement

This work was supported by the Industrial Strategic technology development program, 10038671, Development of Cargo Tank, Gas Dome Design, and Loading/Unloading System for CO_2 Carrier funded by the Ministry of Knowledge Economy (MKE, Korea).

References

A. Aspelund, M. J. Molnvik, G. De Koeijer, 2006, Ship transport of CO_2 - Technical solutions and analysis of costs, energy utilization, exergy efficiency and CO_2 emissions

A. Aspelund, K. Jordal, 2007, Gas conditioning - The interface between CO_2 capture and transport, International Journal of Greenhouse Gas Control, 1, 3, 343-354

The Intergovernmental Panel on Climate Change and Cambridge University, 2005, IPCC Special Report on Carbon Dioxide Capture and Storage

H. Li, J. Jakobsen, J. Stang, 2011, Hydrate formation during CO_2 transport: Predicting water content in the fluid phase in equilibrium with the CO_2-hydrate, International Journal of Greenhouse Gas Control, 5, 3, 549-554

S. Decarre, J. Berthiaud, N. Butin, J. L. Guillaume-Combecave, 2010, CO_2 maritime transportation, International Journal of Greenhouse Gas Control, 4, 5, 857-864

P. Neksa, J. Pettersen, G. Skaugen, SINTEF, CO_2 Refrigeration, Air Conditioning and Heat Pump Technology

I.A. Karimi and Rajagopalan Srinivasan (Editors), Proceedings of the 11th International Symposium on Process Systems Engineering, 15-19 July 2012, Singapore.

Design Modification Study on DME direct synthesis technology

Ik Hyun Kim, Byung Joon Kang, En Sup Yoon

School of Chemcial and Biological Engineering, Institute of Chemical Processes, Seoul National University, 1 Gwanak-ro Gwanak-gu, Seoul, 151-744, South Korea

Abstract

Korea Gas Corporation(KOGAS) has developed a process in which syngas is produced from natural gas and converted to dimethyl ether(DME) using a single-step reactor. We had conducted the study on the scale-up of the plant based on the operation experience of demo-scale plant and the numerical analysis result of the pilot-scale fixed-bed tubular reactor. Those studies didn't pay attention to the improvement of the process performance, but tended to center around the simulation of the plant with respect to development and validation of the model. In this study, we have conducted the simulation reflecting the result of a reactor modeling and the real operation data of demo-scale plant. And based on this simulation result, we make some modifications of the conceptual design of commercial-scale plant to improve its performance.

Keywords: Dimethyl-ether, One-step DME production, Conceptual Design

1. Introduction

Korea Gas Corporation(KOGAS) has developed a process in which syngas is produced from natural gas in proprietary auto-thermal reformer(Tri-Reformer) and then converted to DME in a single reactor. Based on the study of lab and pilot scale plant, KOGAS had constructed demo-scale plant since 2004 and has operated it. Scale-up study on DME plant has been carried out with the operation data of the demo plant.

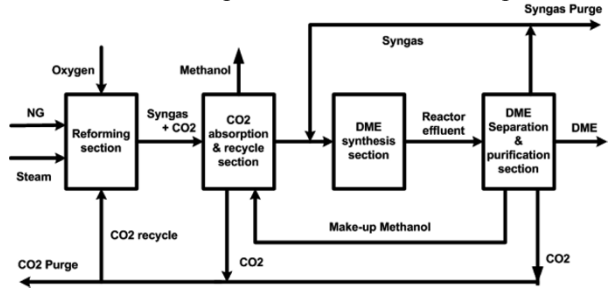

Fig.1 Simple process block diagram of one-step production of DME

The Tri-Reformer in the reforming section is an adiabatic auto-thermal reformer that is based on KOGAS' own technology. The pre-reformed natural gas (primarily methane), steam, oxygen, and carbon dioxide react to produce syngas containing the correct amount and ratio of carbon monoxide and hydrogen. The ratio of hydrogen to carbon monoxide in the Tri-Reformer outlet is set to be 1.2~1.3 to provide the correct H_2:CO ratio in the mixed feed into the DME reactor.

CO_2 absorption and recycle section uses chilled methanol as a solvent for absorbing CO_2 and serves two purposes; it removes CO_2 and water from the syngas stream going

to the DME synthesis reactor and it provides a CO_2 recycle stream being fed back to the Tri-Reformer.

The DME synthesis reactor is a tubular fixed-bed reactor with boiling water in jacket using KOGAS' catalyst. The inlet to the reactor is set to 230 C and 6.101 MPa. Given the specified feed composition and condition, the DME reactor is expected to achieve a 68% conversion of CO and provide the product profile specified by KOGAS.

DME separation and purification section is a single train that takes the combined output streams from the DME synthesis reactor, removes CO_2 to be sent back to the Tri-Reformer, recycle unreacted syngas (CO and H_2) to the DME reactor feeds, separates DME from the byproduct methanol and provides a DME product stream with the specified purity.

For the simulation of DME production plant, a commercial steady-state process simulator, Aspen Plus, has been used to model the KOGAS DME process. The previous simulation of process reflects only conceptual design of demo scale DME plants based on the pilot plant data. The revision of this simulation model should proceed for the purpose of more accurate analysis and studies.

In this paper, we have conducted simulations improved to reflect the data of experimental vapor-liquid equilibrium in the literature and the test operation data of the KOGAS' demo scale plant. And more reasonable and efficient alternatives are suggested by the modification of process.

2. Process Simulation Details

2.1. (Case1) Simulation changes by Demo plant operation data

Before this study, the simulation model had only reflected the pilot plant operation data. It should be revised to reflect the operation data of demo plant so that the simulation result of commercial plant could be correct in order for the simulation to be a useful tool for process design.

Major change from the demo plant operation is the feed and product composition changes of Tri-Reformer. This change is to increase CO_2 and O_2 composition in Tri-Reformer feed and to decrease steam demand.

This is for reasonable performance of Tri-Reformer, especially secure H_2/CO ratio in the effluent stream. As a result of this change, the demand of inlet natural gas and the flow rate of CO_2 purge stream increase since increasing demand of inlet natural gas also leads to increasing CO_2 effluent.

HP steam for supplying feed of Tri-Reformer is also serves as a preheating source of natural gas feed stream. So decreasing steam demand as a feed of Tri-Reformer causes the decreasing temperature of natural gas feed stream. As a result, the operation temperature of Sulfur Guard Bed which is required for absorbing sulfur contents in natural gas and protecting the downstream process is decreased by 10℃. Reactor performance and CO_2 absorber specification are also changed to reflect the operation data of demo plant.

2.2. (Case2) Improvement of Productivity

In the Case1, KOGAS DME plant produces DME and methanol simultaneously. KOGAS assumes that methanol produced in the DME reactor cannot be recycled due to the performance of reactor. So they allowed that the methanol needs to be purified to commercial grade and sold as a byproduct. But this means that the total capital cost and operation cost include the cost of production for not only DME but also methanol. This is not reasonable process with respect to productivity of DME.

The production of byproduct methanol also has implications for the Tri-Reformer. The amount of methanol byproduct produced impacts the H2:CO ratio required in the syngas produced by the Tri-Reformer. Methanol(CH_3OH) has an H:C ratio of 4 while DME(CH_3OCH_3) has an H:C ratio of 3. This means that as more methanols are produced, the H_2:CO ratio required in the makeup syngas will also have to increase.

To solve this problem, we added a separated methanol dehydration reactor(Fig.2). The underflow from DME separation column contains primarily methanol and water. This is sent to the primary methanol dehydration column. The reflux of methanol dehydration column is controlled so that the water content in the overhead methanol stream is maintained at 5wt%. This needs to be specified to match the feed specification for the methanol dehydration reactor. The methanol dehydration reactor is represented by a stoichiometric reactor model which converts 80% of the methanol to DME and H_2O. The reactor is assumed to be adiabatic.

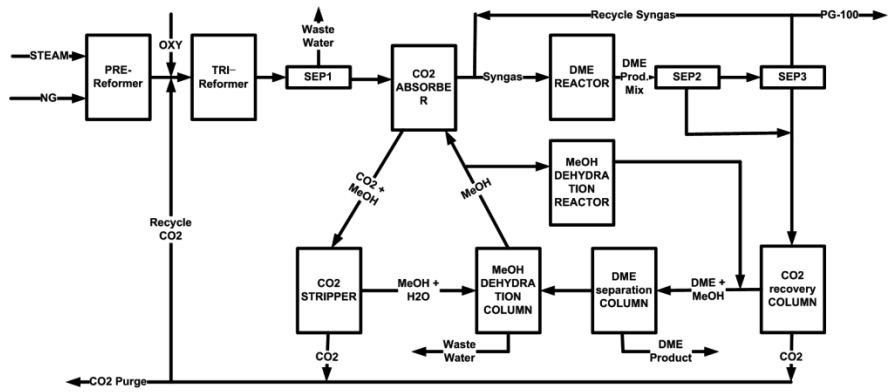

Fig. 2 Modified block diagram for Case2.

In addition, DME CO_2 absorber located between SEP3 and CO_2 recovery column in the previous cases is removed in this case. DME CO_2 absorber in DME separation and purification section is for absorbing CO_2 in the unreacted syngas recycle flow. But it seems to be unnecessary unit by the test operation of demo plant. So deleting DME CO_2 absorber from the separation process has no critical impact on the process-side streams but has an impact on the reduction of ISBL(Inside Battery Limits) and OSBL(Outside Battery Limits) fixed capital costs.

2.3. (Case3) Improvement of energy efficiency

Throughout the simulation model in the previous cases, Aspen Plus HEATER block are used to represent the process side heating and cooling. The utility side(e.g. refrigeration or steam) is not represented. In cases where process-process heat exchanger is taking place, this is represented by two HEATER blocks connected by a heat stream.

In the aspect of local energy integration, opportunities for minimizing heating and cooling utility requirements by matching hot and cold process streams were taken in all simulation cases. But the global (heat pinch type) energy integration is not conducted for 'first of a kind' plant.

In Case1 and 2, two heat exchanger blocks exist for calculating the steam generation rate in fired-heater. The fired-heater is for supplying heat duty to increase temperature of natural gas feed to 350℃. It is useful for start-up of plant, but could be substituted with an alternative reforming process scheme with respect to heat integration.

3. Result

3.1. Equipment Costs

Table 1. Equipment list in Case 1~3

	Case1	Case2	Case3
Fired-Heater	O	O	X
DME CO2 Absorber	O	X	X
Methanol Dehydration Reactor	X	O	O

The major difference of equipment costs is caused by fired heater as a reformer feed heater, DME CO_2 absorber as a CO_2 absorber in unreacted syngas recycle, and methanol dehydration reactor as an additional production of DME from byproduct methanol.

Fired-heater is the most expensive equipment but methanol dehydration reactor is the cheapest one. We can expect that Case3 can reduce about hundreds of thousands dollars of equipment cost against Case1.

3.2. Feedstock Costs

The difference of feedstock in each case is shown in Table2. Even if we only consider a natural gas feedstock, $948,000 per day can be reduced in Case3. The cost of natural gas assumed 2.0$/kg.

Table 2. Comparison of feedstock (Unit: metric ton per day)

	Case1	Case2	Case3
Natural Gas	3998	3524	3524
Oxygen	5665	4946	4946
Steam (High Pressure)	3510	3039	3162
Steam (Superheated)	1320	1193	-

3.3. Utility Costs

Table 3. Comparison of electric power requirement (Unit: kWh)

Section	Block	Case1	Case2	Case3
CO_2 Absorption and Recycle	C-2001	37087.9	34817.2	34817.2
	P-2001	3247.2	2803.0	2803.1
DME separation and purification	C-4001	1116.8	616.3	616.3
	P-4001	448.6	-	-
	P-4002	39.6	-	-
	P-4003	225.9	168.4	168.4
	P-4004	0.025	0.008	0.008
Total Costs ($/day)		50,599	46,086	46,086

Table 3 shows the electric power consumption of the whole process. Prefix ‘C’ means the compressor and ‘P’ means the pump. Case2 and Case3 consume the same electric

power which is decreased by 9% against Case 1. If the cost of electric power is 0.05 $/kWh, then the saving cost would be 4,513 $/day.

The steam requirement for reforming section is most remarkable change. This is caused by adopting methanol dehydration reactor(Case2) and deleting fired-heater from reforming section(Case3).

Table 4. Comparison of steam requirement in reforming section

Steam	Condition	Case1	Case2	Case3
SHP Steam	4.3 MPa @ 380℃	1320	1193	-
HP Steam	4.3 MPa @ Saturated vapor	3510	3039	-
HP Steam	4.3 MPa @ saturated liquid	-	-	3162

4. Conclusion

The process simulation of the commercial DME plant, which has the capacity of 3,000 metric ton per day, has been completed. The previous study on the design basis of demo plant only reflects the pilot scale plant data, but in this paper the improvement for scale-up of the commercial plant is achieved. Remarkable improvements are mainly reduction of capital costs and operating costs. This is due to adopting methanol dehydration reactor to convert the byproduct methanol to DME, removing the fired-heater as a reformer feed heater, and DME CO_2 absorber for recovery CO_2 in the syngas recycle flow. But this change of process could be influence the feasibility of operation or control. Therefore the verification of this suggestion should be performed by experiences of demo plant operation.

References

Ik Hyun Kim, Seunghyok Kim, Wonjun Cho, En Sup Yoon, Simulation of commercial dimethyl ether production plant, 2010, 20th European Symposium on Computer Aided Process Engineering

Daesung Song, Wonjun Cho, Gibaek Lee, Dal Keun Park, and En Sup Yoon, Numerical Analysis of a Pilot-scale Fixed-Bed Reactor for Dimethyl Ether(DME) Synthesis, Ind. Eng. Chem. Res, 2008, 47(13), 4553-4559.

Seung-Ho Lee, Wonjun Cho, Taekyoung Song and Young-Jun Ra, Scale up study of DME direct synthesis technology, 2009, World Gas Conf., [Pap.], 24th, WOC1

Soren Dahl, Aage Fredenslund, and Peter Rasmussen, 1991, The MHV2 Model: A UNIFAC Based Equation of State Model for Prediction of Gas Solubility and Vapor-Liquid Equilibria at Low and High Pressure, Ind. Eng. Chem. Res., 30, 1936-1945

Takashi Katayama, Kazunri Ohgaki, Goro Maekawa, Motojiro Goto, and Tamon Nagano, 1975, Isothermal vapor-liquid equilibria of acetone-carbon dioxide and methanol-carbon dioxide systems at high pressure, Journal of Chemical Engineering of Japan, Vol. 8, No. 2

Torben Laursen and Simon Ivar Anderson, 2002, High-Pressure Vapor-Liquid Equilibrium for Nitrogen+Methanol, J. Chem. Eng. Data, 47, 1173-1174

Elaine Chang, Jorge C.G. Calado, and Willian B. Streett, 1982, Vapor-Liquid Equilibrium in the System Dimethyl Ether/Methanol from 0 to 180 C and at Pressure to 6.7 MPa, J. Chem. Eng. Data, 27, 293-298

E. Brunner, W. Hultenschmidt, and G. Schlichtharle, 1987, Fluid mixtures at high pressures; Ⅳ.Isothermal phase equilibria in binary mixtures consisting of (methanol+hydrogen or nitrogen or methane or carbon monoxide or carbon dioxide), J. Chem. Thermodynamics, 19, 273-291

I.A. Karimi and Rajagopalan Srinivasan (Editors), Proceedings of the 11th International Symposium on Process Systems Engineering, 15-19 July 2012, Singapore.

Simulation of an Off-shore Natural Gas Purification Process for CO_2 Removal with Gas-Liquid Contactors Employing Aqueous Solutions of Ethanolamines

José L. de Medeiros [a], Wilson M. Grava [b], Jailton F. Nascimento [b], Ofélia de Q. F. Araújo [a], Andressa Nakao [a]

[a]*Chemical Engineering Department, School of Chemistry, Federal University of Rio de Janeiro. Av. Horacio Macedo, 2030, Bloco E, Sala E-201, CT, Cidade Universitária – Ilha do Fundão, CEP: 21949-900, Rio de Janeiro, RJ - Brazil*
[b]*Petrobras, S.A. CENPES, Ilha do Fundão Qd. 07 - Rio de Janeiro , RJ - Brazil*

1. Abstract

Brazilian Pre-Salt oil reserves present associated natural gas (NG) exhibiting high concentrations of CO_2 which requires gas purification processes for compliance with specifications imposed by the local Regulatory Agency. Due to its recognized small footprint as compared to amine based absorption route, membrane equipment show considerable potential for offshore applications. Of particular interest is the use of contactors, which combines membrane permeation with facilitated transport via liquid absorption. Process design and optimization of such innovative alternative demand flexible models to predict equipment performance at a variety of process conditions. This work presents a mathematical tool for analyzing CO_2 separation with hollow-fiber membrane contactors, using aqueous solutions of ethanolamines. The model is applied to assess the technical feasibility of offshore CO_2 separation with membrane contactors.

The developed simulator is based on rigorous principles of thermodynamics, fluid mechanics, heat transfer and mass transport. Chemical absorption modeling is approached as a typical application of the well known Chemical Theory, which aims to model chemically and/or physically complex equilibrium systems via a set of chemical equilibrium processes involving real and fictitious species. Vapor-Liquid Equilibria of real species are superimposed on the multi-reaction chemical equilibria for formation of fictitious species – non-ionic and non-volatile complexes. A process flowsheet is simulated to assert technical feasibility of this technology to offshore installations.

Keywords: CO_2 Removal, Hollow-fiber Membrane, Ethanolamines, Natural Gas Conditioning

2. Introduction

Global warming effects associated to CO_2 emissions cause societal concerns and give rise to increasing demands for clean technologies to improve sustainability of the world economy through efficient and safe usage of raw materials, and decreased CO_2 emissions (Dovi *et al*, 2009). According to Rivera-Tinoco and Bouallou (2010), among the technologies proposed to reduce CO_2 emissions, the most relevant are

associated to CCS Technologies. Ebner and Ritter (2009) state that the CO_2 removal market is dominated by amine based absorption processes. However, the authors recognize that membrane technology offers competitive advantages such as not requiring separating agent nor involving phase changes (reduced regeneration costs), which is claimed to have positive cost impacts and small footprints compared to alternative processes. Nevertheless, they state that membranes for large-scale recovery of CO_2 from natural gas are a relatively recent development.

A more innovative alternative employs gas-liquid membrane contactors for CO_2 removal from natural gas, which offers the advantages of both membrane technology and absorption processes. This hybrid-type process combines membrane separation and chemical absorption (Keshavarz *et al.,* 2008a), where the solvent (CO_2 absorbing liquid) is responsible for the selectivity of the process (typical of absorption technology) while the membrane stands as a selective barrier between the gas and the liquid. Further advantages are listed by Zhang et al. (2006), such as independent liquid and gas flow rate manipulation, much larger gas-liquid interfaces and the flexibility to scale up or down.

Differently from traditional membrane separation processes, microporous membranes used in membrane contactors are not required to be selective. The liquid phase that flows in one side of the fiber absorbs gas components physically and chemically, enhancing mass transfer therefore reducing the demand for high process pressures (Keshvarz et al, 2008b). Keshavarz and co-workers (2008a) report that the advantages depend in gas-liquid systems, types of membranes employed and applied operating conditions. The design and optimization of this innovative process suffer from a relative unavailability of experimental data and reliable mathematical representation of the impact of operational variables on process performance.

To meet this need, the present work presents a model for CO_2 separation from natural gas in membrane contactors with aqueous blends of ethanolamines. Specifically, the model treats a hollow fiber contactor configuration, based on principles of thermodynamics, fluid mechanics, heat transfer and mass transport. The tool is further applied to a conceptual process to verify the feasibility to meet natural gas CO_2 specifications.

3. Model Description

The model treats the separation of CO_2 from a stream of natural gas employing aqueous solutions of ethanolamine. Figure 1a shows the transport of the diffusing component of interest (CO_2 rich natural gas) from the gas phase through the microporous membrane into the liquid phase (aqueous amine solution) in a gas-liquid membrane contactor. The liquid absorbent flows in the lumen of the membrane while the gas mixture flows countercurrently in the shell side, configured as a fluid envelope around the hollow fiber (Figure 1b). Interaction among fibers is neglected.

Considering that the CO_2 diffusivity in the gas phase is much higher than in the liquid phase, it is reasonable to assume the gas to exhibit plug flow regime, which implies that the gas velocity and concentration distributions in the radial direction can be ignored in the shell side (Zhang et al, 2006).

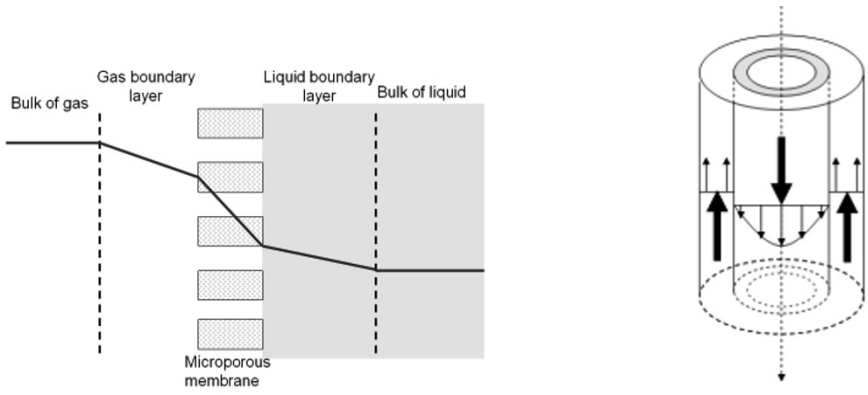

Figure 1 – Membrane Contactor. (a) mass transfer regions in membrane contactors for CO_2 absorption, (b) liquid and gas flows in a hollow fiber.

Peng-Robinson equation of state (PR EOS) has become the most popular EOS for natural gas systems (*e.g.,* Nagy and Shirkovskiy, 1982; Alfradique and Castier, 2007). The model applies rigorous thermodynamics with PR EOS to predict temperature changes associated with Joule-Thomson and dissolution effects, in a wide range of pressure, temperature and composition of multi-component gas feed stream. Chemical absorption of CO_2 in the liquid phase is represented by the *Chemical Theory* (*CT*, Prausnitz et al., 1986), which aims to model chemically and/or physically complex equilibrium systems via a set of equilibrium chemical reactions involving real and fictitious species (amine-CO_2 complexes). In the liquid compartment, multi-reactional chemical equilibria form complexes, as shown in Eqs. 1a through 1d, confined into the liquid phase, while vapor-liquid equilibria (VLE) of real species is applied.

$$CO_2 + H_2O + MEA \xleftrightarrow{K_1} CO_2 \cdot MEA \cdot H_2O \quad \text{(1-a)}$$

$$CO_2 + H_2O + MDEA \xleftrightarrow{K_2} CO_2 \cdot MDEA \cdot H_2O \quad \text{(1-b)}$$

$$H_2S + H_2O + MEA \xleftrightarrow{K_3} H_2S \cdot MEA \cdot H_2O \quad \text{(1-c)}$$

$$H_2S + H_2O + MDEA \xleftrightarrow{K_4} H_2S \cdot MDEA \cdot H_2O \quad \text{(1-d)}$$

Chemical equilibrium constants associated to the *CT* model (K_1 to K_4) were estimated via the Maximum Likelihood Criterion over VLE data of CO_2 with aqueous blends of ethanolamines (Barbosa *et al.,* 2011). The approach allows prediction of formation properties for the complexes, enthalpies and thermal effects. Barbosa *et al.* (2011) proposed an equilibrium approach for CO_2 absorption with aqueous solutions of ethanolamines using a large set of vapor-liquid CO_2/MEA/MDEA equilibrium data from the literature. The *CT* compartment was validated against the extensive databank (Barbosa *et al*, 2011) prior to application to the liquid phase of the contactor.

The *CT* model was added to the permeation model developed by Medeiros (2008), which describes the gas permeation process across a hollow-fiber membrane, with an outstanding performance when compared to the referred data bank. The combination of the two models – *CT* model and permeator model - allows investigating the performance of membrane contactors applied to CO_2 removal from natural gas. Figure 3 presents the scheme of the gas permeation module (Figure 3a) and contactors (Figure 3b). The developed contactor model is capable of describing CO_2 removal

processes using gas-liquid contactor with aqueous solutions of ethanolamines, at different process configurations.

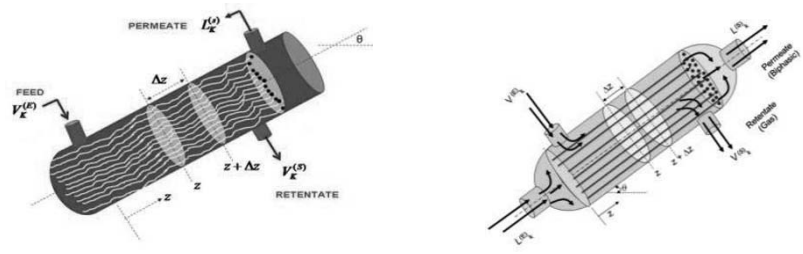

(a) (b)

Figure 3 – Equipment Schemes. (a) gas permeation module (b) gas-liquid contactor

4. Model Performance Evaluation

A process flowsheet - GN_CONTACT_1 - is used to illustrate the contactor simulator performance, shown in Figure 4, where MR1 and MR2 stand for Reacting Mixer and CGL is the gas-liquid contactor.

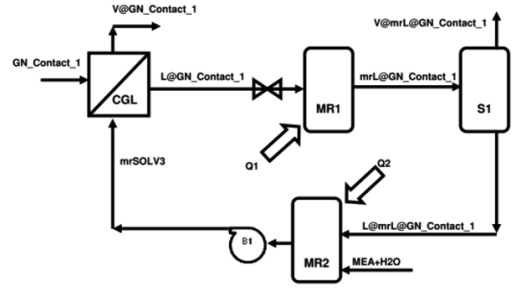

Figure 4 – CO_2 separation with Contactors

The feed stream GN_CONTACT_1 is Natural Gas with 10% of CO_2 to be purified with mrSOLV3, a stream containing an aqueous blend of MEA and MDEA. Table 1 shows a summary of stream inputs based in reported values by Formigli, 2008).

Table 1 - Summary of stream specifications and calculations for flowsheet GN_CONTACT_1

VARIABLES	STREAMS					
	GN_Contact_1	mrSOLV3	V@ GN_Contact_1	L@ GN_Contact_1	V@mrL@ GN_Contact_1	L@mrL@ GN_Contact_1
T(°C)	27	27	38.8	38.8	100.51	100.51
P(bar)	50	5	49.88	4.88	1.0	1.0
kg/h	42635	17651	33737	26549	13835	12714
MMNm³/d	1.000	---	0.829	---	0.291	---
%molCO2	10.19	0	3.49	0.437	24.895	0.096
%molCH4	73.22	0.024	76.52	0.02	33.616	0.021
%molC2H6	9.091	0.003	10.957	0.00	0.024	0.00
%molMEA	---	19.99	---	15.957	3.857	35.362
%molMDEA	---	19.99	---	11.171	0.07	49.444
%molH2O	---	59.98	---	50.595	37.523	14.482
%mol CO2H2OMEA	---	0.004	---	8.51	---	0.575
%mol CO2H2OMDEA	---	0.017	---	13.31	---	0.02
PROCESS VARIABLES						
MR1 - Q_1 (kW)	*MR2 – Q_2 (kW)*		*Make-up H2O (kg/h)*	*Make-up MEA (kg/h)*		
4300	-460		3675.3	1284.2		

Stream V@ GN_CONTACT_1 shows that the natural gas (NG) leaving the contactor meets specification on CO_2 content. Simulation results illustrate additional outputs that could support process design and optimization. Furthermore, results of the model, within a solid phenomenological framework suggest feasibility of innovative membrane contactor processes in meeting specifications of CO_2 removal from NG.

5. Conclusions

This work presents a tool to simulate processes based on innovative membrane contactors for CO_2 removal from natural gas streams. A process flowsheet employing gas-liquid contactor fed with gas stream compatible with the scenario of the Pre-Salt Pole of the Santos Basin in Brazil is presented. Simulation results show technical feasibility of this technology to offshore installations. The computational tool can be used for experimental design of pilot units to provide data for model calibration, to allow subsequent process design and optimization.

Acknowledgment

Financial support of MCT/FINEP/CTPETRO, Grant No.2460-06 is kindly acknowledged.

References

M.F. Alfradique, M. Castier, 2007, Calculation of Phase Equilibrium of Natural Gases *with the* Peng-Robinson and PC-SAFT Equations of State, Oil &Gas Science and Technology – Rev. IFP, Vol. 62, No. 5, pp. 707-714

L. C. Barbosa,; de Medeiros, J.L. ; Araujo, O. Q. F., Equilíbrio de Absorção de CO_2 e H_2S em Soluções Aquosas de Etanolaminas. Boletim Técnico da Petrobrás, v. 52, p. 21-37, 2011.

V.G. Dovi; F. Friedler; D. Huisingh; J.J. Klemes, 2009, Cleaner energy for sustainable future, J. Cleaner Production, v.17, p.889-895

A. D. Ebner, J. A. Ritter, 2009, State-of-the-art Adsorption and Membrane Separation Processes for Carbon Dioxide Production from Carbon Dioxide Emitting Industries, Separation Science and Technology, 44: 1273–1421.

J.Formigli, 2008, O Pólo Pré-Sal da Bacia de Santos – Desafios Tecnológicos para a Área de Engenharia,PETROBRAS, 2008.

P. Keshavarz, S. Ayatollahi, J. Fathikalajahi, 2008a, Mathematical modeling of gas–liquid membrane contactors using random distribution of fibers, J. Membrane Science, 325, p. 98–108.

P. Keshavarz; J. Fathikalajahi, S. Ayatollahi, 2008b, Analysis of CO_2 separation and simulation of partially wetted hollow fiber membrane contactor, J. Hazerd. Mater.,v. 152, p. 152, p. 1237-1247.

J.L. Medeiros. O. Q.F. Araujo. B. M. Versiani, 2008, Relatório 1 - Project Contact, Escola de Química, Universidade Federal do Rio de Janeiro, Brazil

Z. Nagy, A. Shirkovskiy, 1982, Mathematical Simulation of Natural Gas Condensation Processes Using the Peng-Robinson Equation of State, SPE Annual Technical Conference and Exhibition, 26-29 September 1982, New Orleans, Louisiana. 12 pages.

J.M.Prausnitz. R.N. Lichtenthaker. E.G. Azevedo, 1986, Molecular Thermodynamics of Fluid-Phase Equilibria. Englewood Cliffs, N.J., USA. 2° Edition, Prentice-Hall.

R. Rivera-Tinoco, C. Bouallou, 2010. Comparison of absorption rates and absorption capacity of ammonia solvents with MEA and MDEA aqueous blends for CO_2 capture, J. Cleaner Production, article in press.

H.Y.Zhang; R.Wang; D.T. Liang; J.H. Tay, 2006, Modeling and experimental study of CO_2 absorption in a hollow fiber membrane contactor. J. Membr. Sci., v. 279,p. 301-310.

I.A. Karimi and Rajagopalan Srinivasan (Editors), Proceedings of the 11th International Symposium on Process Systems Engineering, 15-19 July 2012, Singapore.

A Comparative Economical Analysis of Technologies for CO_2 Removal from Offshore Natural Gas

Tatiana S. Gadelha[a], Aline R. S. Guimarães[a], Andressa Nakao[a], Ofélia de Q. F. Araújo[a], José Luiz de Medeiros[a]

[a]*Departament of Chemical Engineering, Escola de Química da Universidade Federal do Rio de Janeiro. Sala R-201, Bloco E, Centro de Tecnologia, Ilha doFundão, CEP: 21949-900, Rio de Janeiro, Brazil*

Abstract

In the scenario of the Brazilian Pre-Salt fields, where associated Natural Gas (NG) shows high concentration of CO_2, gas conditioning comes out as one of the main challenges. Among the possible capture technologies available, three alternatives stand out for CO_2 sequestration: (A) gas permeation through membranes, (B) absorption columns using aqueous blends of ethanolamines and (C) application of hybrid - membrane modules in series with amine absorption and regeneration columns.

The main objective of this work is to investigate the technical and economical feasibility of applying these three separation processes on offshore platforms, given the stringent constraints on footprint and equipment weight, and for minimizing NG production and transportation costs. The methodology involves: (i) development of cases based on the Brazilian Pre-Salt gas composition. NG streams with CO_2 molar concentrations ranging from 8 to 18% are applied; (ii) Simulations of three process flowsheets, corresponding to each one of chosen technologies - A, B and C; (iii) Equipment sizing; and (iv) Analysis of economic performance through calculation of capital (CAPEX) and operational (OPEX) costs.

Keywords: CO_2, Natural Gas, Absorption, Gas Permeation

1. Introduction

In the scenario of the Pole Pre-Salt of the Santos Basin (Brazil) it has been discovered a large reserve of Natural Gas (NG) containing an expressive content of CO_2 (range: 8 to 18% mol) (Formigli, 2008). This concentration must be reduced to minimize the emission of CO_2 and to meet the National Agency of Petroleum and Biofuel (ANP) standards of marketing of NG in Brazil.

Currently, the main technologies used in industry are membrane modules and absorption equipments employing aqueous solutions of ethanolamines. Absorption of CO_2 with weak alkaline solvents is a well established technology in the chemical industry. The basic principle is a reversible chemical reaction occurring in the liquid phase between a weak alkali and the solutes (CO_2). The reaction is first impelled to solute consumption (i.e. absorption) capturing it from the raw gas stream. In the second step, the reaction is reversed releasing the separated solutes (i.e. stripping) as a gas product stream. This process involves the continuous operation of two interlinked (packing or tray) columns. The first column – the absorber – contacts the gas stream with lean solvent at moderately high pressures and moderately low temperatures. The

rich solvent (in terms of CO_2) goes to a second column – the stripper – where at expenses of lower pressures, higher temperatures and contact with a stripping agent (e.g. steam), acid gases are liberated in the top vapor product, while the lean solvent is recovered as bottom product and returned to the absorber after some cooling and making-up (Barbosa, 2010).

For gas separation in offshore platforms, membranes offer comparative advantages over other technologies – e.g. absorption and adsorption - such as: (i) process is simple requiring no heating for change in either phase, (ii) units are compact, low weight; and (iii) the modularity of membrane makes the process a flexible technology (Baker et al, 2008). These characteristics make the technology in permeation membranes more appropriate to the capture of CO_2 in offshore pre-salt conditions. However, a main obstacle to the use of membranes is the outstanding scale of separation processes required in Pre-Salt oil and gas offshore platformes, where it is possible that membrane processes lose selectivity due to high flows transfer.

This work presents a comparative economical analysis applying three separation processes on offshore platforms: (A) gas permeation through membranes, (B) absorption columns using aqueous blends of ethanolamines and (C) application of hybrid - membrane modules in series with amine absorption and regeneration columns, shown in Figures I, II and III respectively.

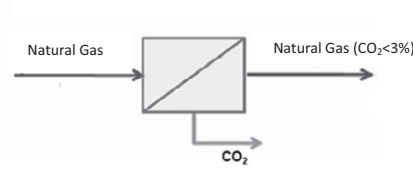

Figure I - Permeation system

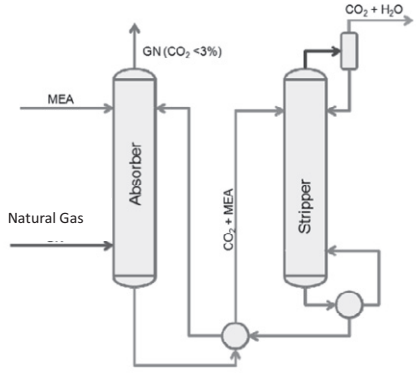

Figure II - Absorption Columns

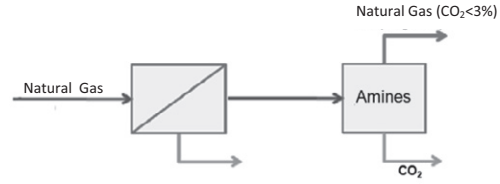

Figure III - Hybrid Process

2. Methodology

The methodology in this work deals with the following scenario:

- Development of three cases using NG streams with distinct CO_2 contents: Case 1: 8%; Case 2: 18%; and Case 3: 21%;
- Main goal of obtaining a NG stream with less than 3% of CO_2 (the standard of Brazilian Regulatory Agency);
- Operation flow is 50MMscfd;
- Three different technologies for CO_2 removal: Absorption using MEA; Membrane Permeation; and Hybrid process (Figure I, II and III);
- Processes simulations with a commercial simulator, employing a permeation module add-in developed by the Laboratory H2CIN, at Escola de Química, Universidade Federal do Rio de Janeiro, Brazil - The SPM2010 (Nakao, 2010);
- Equipment sizing.
- Calculation of Capital Expenditures (CAPEX) and Operational Expenditures (OPEX).

The economical analysis preformed is based on Turton *et al.* (2009), which was developed for chemical processes, therefore not including specifics features of the offshore environmental as modular equipments (skids), and restrictions of area and weight of these modules. However, it is emphasized that the goal of this work is the economical analysis and it is not the absolute quantification of the associated investments of each technology.

3. Results and Discussion

Compared to the absorption using amines, the hybrid process is a technology more flexible to different feeds conditions, as two different separation processes are employed.

For Cases 2 and 3, which have a process feed stream with higher CO_2 content, Baker and Lokhandwala (2008) recommend the hybrid process. In Case 1, with a feed stream with a lower concentration of CO_2, it is recommended the application of absorption column using amines. Because of this, hybrid process, in case 1, wasn't simulated.

These suggestions have been validated through the economical analysis of these three cases in this work, whose results are presented in Figure IV. The analysis shows that the flow rate and the CO_2 content have a direct influence in the technology selection for CO_2 removal.

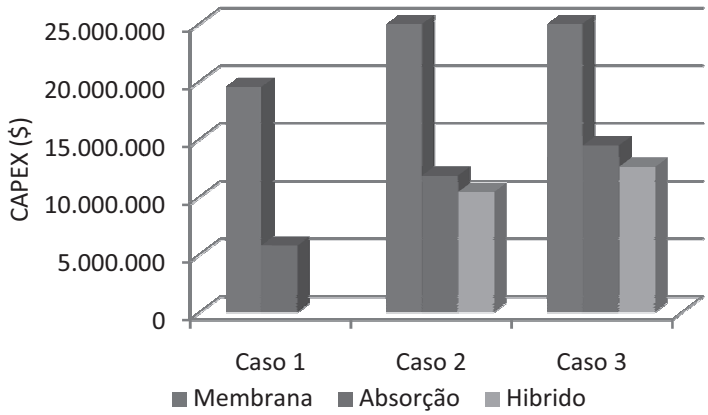

Figure IV - Capex results

Baker and Lokhandwala (2008) proposed a scheme, shown in Figure V, to guide the choice of CO_2 removal technology, based on the NG flow rate to be treated and the CO_2 content. In accordance to this scheme, this paper has conducted a preliminary economic analysis of these technologies for CO_2 removal.

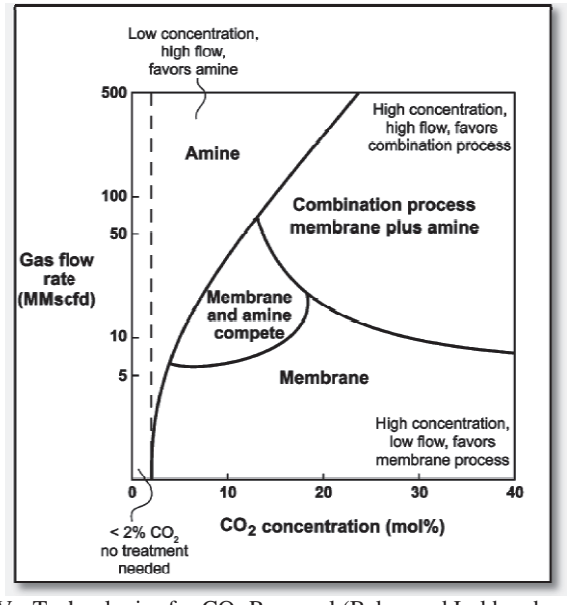

Figure V - Technologies for CO_2 Removal (Baker and Lokhandwala, 2008)

4. Conclusions

Absorption with amines showed the best results for streams with lower CO_2 content (Case 1), while hybrid process achieved better economical performance for NG streams with high concentrations (Case 2 and Case 3). These results arouse the interest in this process for the NG treatment, as proposed by Baker and Lokhandwala (2008).

5. References

R.W. Baker, K. Lokhandwala, 2008, Natural Gas Processing with Membranes: An Overview, Ind. Eng. Chem. Res., 47, p.2109-2121

L.C. Barbosa, 2010, Captura de CO_2 e H_2S com Soluções Aquosas de Alcanolaminas via Destilação Reativa; Ph.D. Thesis, Escola de Química,Universidade Federal do Rio de Janeiro.

J.M.Campbell, 2011, Gas Conditioning and Processing. Volume 2: The equipment Modules. Oklahoma: John M.Campbell and Company, 8th ed.

J.Formigli, 2008, O Pólo Pré-Sal da Bacia de Santos – Desafios Tecnológicos para a Área de Engenharia,PETROBRAS, 2008.

A. Nakao, 2010, Modelagem de Contactores Gás-Líquido para Separação de CO2 de Gás Natural com Solução Aquosa de Etanolaminas. Dissertação de Mestrado, TPQB, Universidade Federal do Rio de Janeiro

R.Turton, R. C,Bailie, W. B. Whiting, J.A. Shaeiwitz Analysis, 2002, Synthesis and Design of Chemical, Process, Prentice Hall, 2 edition

6. Acknowledgement

This work was done with the financial support from IBP - Brazilian Petroleum, Gas and Biofuels Institute and BG Group. The authors O.Q.F.Araujo and J. L. Medeiros kindly acknowledge MCT/FINEP/CTPETRO, Grant No.2460-06.

I.A. Karimi and Rajagopalan Srinivasan (Editors), Proceedings of the 11th International Symposium on Process Systems Engineering, 15-19 July 2012, Singapore.

A Systematic Approach for Optimization of an Algal Biorefinery Using Fuzzy Linear Programming

Aristotle T. Ubando[1a,c], Alvin B. Culaba[2a,c], Raymond R. Tan[3b,c],

Denny K.S. Ng[4d]

[a]*Mechanical Engineering Department, De La Salle University, Philippines*
[b]*Chemical Engineering Department, De La Salle University, Philippines*
[c]*Center for Engineering and Sustainable Development Research, De La Salle University, Philippines*
[d]*Department of Chemical & Environmental Engineering/Centre of Excelllence for Green Technologies, University of Nottingham, Malaysia*

[1]aristotle.ubando@dlsu.edu.ph, [2]alvin.culaba@dlsu.edu.ph, [3]raymond.tan@dlsu.edu.ph, [4]denny.ng@nottingham.edu.my

Abstract

In order to efficiently convert microalgae into value added products, a sustainable integrated algal biorefinery is needed. Generally, conversion of microalgae into biofuel involves several processing steps: cultivation, harvesting, dewatering, drying, oil extraction, and biofuel production. One of the main challenges in designing and optimizing an integrated algal biorefinery is determining the configuration which meets the requirements for key outputs as well as environmental and resource limits. In this work, a systematic fuzzy linear programming (FLP) approach for design and optimization of an integrated algal biorefinery which considers water footprint, land footprint, and carbon footprint is presented. A hypothetical case study is presented to illustrate the proposed approach.

Keywords: Microalgae, biofuel, biorefinery, fuzzy optimization, and process design.

1. Introduction

One of the most promising systems to convert microalgae into value-add products is the integrated algal biorefinery (IAB). An IAB combines multiple conversion pathways of microalgae to generate a range of products, such as biofuels and biochemicals (Taylor, 2008; Subhadra, 2010; Subhadra and Edwards, 2011; Tay et al., 2011a;). Such multiple pathways provide opportunities for effective utilization of process residues, thus enhancing the overall efficiency and sustainability of the biorefinery (Tan et al., 2009). Given the growing global demand for biofuels, it is necessary to assess the design of an IAB through three main environmental performance metrics: water foot print, land foot print, and carbon footprint (De Benedetto and Klemeš, 2009; Tan et al., 2009; Čuček et al., 2012). This paper presents an optimization approach for synthesis of an IAB using a fuzzy linear programming (FLP) model which considers the three main environmental performance metrics simultaneously.

2. Fuzzy Linear Programming

Fuzzy mathematical programming is used in optimization problems wherein bands of partially acceptable ranges of different objective values are considered (Zimmermann, 1978). FLP models have been used to solve multi-objective optimization problems for bioenergy systems footprint (Tan et al., 2008, Tan et al., 2009, Tay et al., 2011b). Unlike the conventional approach of identifying the Pareto optimal curve, FLP has the advantage of giving a unique solution. In this particular study, FLP approach is adapted to optimize an IAB which solves conflict of multi-objectives.

The optimization objective is to maximize the level of satisfaction (λ) of the fuzzy footprint goals:

$$\text{maximize } \lambda \tag{1}$$

Subject to:

$$\mu_i = [(f_i(x) - f_i^u) / (f_i^l - f_i^u)] \geq \lambda,\ i = 1, 2, 3 \tag{2}$$

$$f_i(x) = \boldsymbol{c_i}^T \boldsymbol{y},\ i = 1, 2, 3 \tag{3}$$

$$\boldsymbol{Ax} = \boldsymbol{y} \tag{4}$$

$$\boldsymbol{y^l} \leq \boldsymbol{y} \leq \boldsymbol{y^u} \tag{5}$$

where μ_i = degree of satisfaction of footprint goal i, $f_i(x)$ = footprint functions, i = individual footprint (i.e., water footprint, $f_1(x)$; land footprint, $f_2(x)$; and carbon footprint, $f_3(x)$), Besides, f_i^u and f_i^l are the lower and upper limits of the individual footprint i. $\boldsymbol{c_1}^T$ = water footprint coefficient vector, $\boldsymbol{c_2}^T$ = land footprint coefficient vector, $\boldsymbol{c_3}^T$ = carbon footprint coefficient vector, $\boldsymbol{A}$ is the input-output matrix , $\boldsymbol{x}$ is the process scaling vector, $\boldsymbol{y}$ is the net output vector, $\boldsymbol{y^l}$ is the lower limit for fuzzy net output vector, $\boldsymbol{y^u}$ is the upper limit for fuzzy net output vector.

The variable λ provides control to the model objective constraints which are described by the water, land, and carbon footprint that corresponds to the max-min aggregation principle (Zimmermann, 1978). The max-min aggregation ensures the optimal value of λ is the least satisfied considering the objective constraint. A value of $\lambda = 0$ indicates a state of minimum satisfaction, while a value of $\lambda = 1$ signifies a state of complete satisfaction. Partially acceptable values of λ lie in the range $0 \leq \lambda \leq 1$ as defined by the linear membership functions (Eq. 2) (Zimmermann, 1978; Lai and Hwang, 1992). Often used in a life cycle assessment, a modeling framework is used in this study based on a linear input-output (Eq. 3) (Heijungs and Suh, 2002).

Note that, unlike in Tan et al. (2008) and Tan et al. (2009); all values of $\boldsymbol{y}$ within the given limits are considered equally satisfactory for an IAB as indicated by Eq. (5). The values of the net output vector $\boldsymbol{y}$, which represents the production level of each of the outputs of the IAB, are flexibly set given a lower and upper limit.

3. Case Study

An IAB which produces biodiesel as the main product and methanol, glycerol, electricity as well as steam as by-products is used as a case study. Due to space constraints, the case study has been simplified. As biodiesel is taken as the main product, the algal residues are then separated and reprocessed to produce the by-products.

Environmental Metrics

Table 1 shows the water, land, and carbon footprint coefficients for the case study.

Table 1. Environmental metrics for the case study.

Environmental Metrics	Values
Water Foortprint	78 kg per kWh eletricity; 12,775 kg per kg algal biomass
Land Footprint	1.98×10^{-5} ha-y/ kg algal biomass
Carbon Footprint	1 kg per kWh electricity; 0.17 kg per kg steam; 3.5 kg per kg natural gas

Integrated Algal Biorefinery

The IAB can be divided into the following sections: A – Oil Extraction (including the microalgae cultivation, harvesting, and dewatering processes); B – Transesterification; C – Combined Heat and Power (CHP); D – Steam Methane Reforming (SMR); E – Residue Separator (which separates the liquid residue from the solid residue); F – Anaerobic Digester; G – Gasifier; and H – Methanol Synthesis.

In this case study, integrated algal biorefinery system consists of cultivation, harvesting, dewatering, and oil extraction of microalgae in Process A. Processes A and B can be used to extract algal oil for transesterification process to produce biodiesel. Note that a by-product glycerol is also generated in Process B. To simplify the model, these two processes can be taken as a single process unit. Process E then separates the liquid and solid residue fraction from the total algal residue from Process A. The liquid residue fraction is then processed in anaerobic digester (Process E) to produce methane which is fed into the combined heat and power (Process C) to generate electricity and steam. On the other hand, the solid residue fraction is fed into the gasifier (Process G) to produce syngas. Process D which is steam methane reforming also recycles part of the methane produced from Process E to produce syngas. The syngas produced in both Process G and D is then fed to methanol synthesis (Process H). Meanwhile, Processes G, D, and H were also combined to represent as a single cluster in the input-output matrix producing methanol from solid residue fraction of the microalgae.

Table 2. Algal Biorefinery Input-Output Coefficient Matrix.

y's	Input-Output Matrix	A-B	E	F	C	G-D-H
y_1	Microalgae (kg)	-4	0	0	0	0
y_2	Electricity (MJ)	-171	-1	-2.37	15	0
y_3	Steam (kg)	-161	-0.5	0	12.5	-0.74
y_4	Total Residue (kg)	3	-3	0	0	0
y_5	Solid Residue Fraction (kg)	0	0.6	0	0	-1
y_6	Liquid Residue Fraction (kg)	0	2.4	-2.4	0	0
y_7	Biodiesel (kg)	1	0	0	0	0
y_8	Glycerol (kg)	0.1	0	0	0	0
y_9	Methane (kg)	0	0	1.08	-1	-0.76
y_{10}	Methanol (kg)	-0.1	0	0	0	1.25

Table 2 shows the input-output coefficients of matrix A as derived from various literature sources (Singh and Gu, 2010; Khoo et al., 2011; Razon and Tan, 2011; Subhadra and Edwards, 2011; Tay et al., 2011a). Each column represents material and energy balances for a given process or cluster as discussed previously.

In the column vector, the negative values indicate the process inputs while the positive values are process outputs. For example, Figure 1 shows Process F in column vector form. The numbers indicate that 2.4 kg of liquid residue and 2.37 MJ of electricity are needed to generate 1.08 kg of methane for Process F.

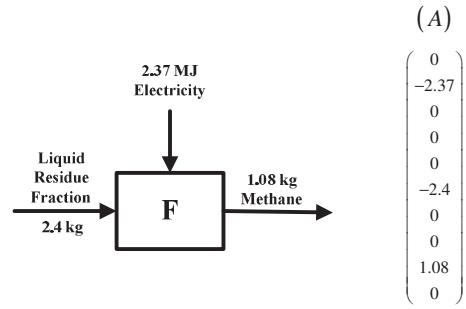

Figure 1. Example of column vector representation of a process.

4. Case Study Results and Discussion

Solving Eqn. (1) subject to Eqns. (2) – (5), the maximum λ is found as 0.95. Table 3 shows the optimized values for each desired outputs.

Table 3. Balanced process table for the optimal biorefinery configuration.

y's	Resulting Matrix	A-B	E	F	C	G-D-H	Net Outputs
y_1	Microalgae (kg/h)	-4,630	0	0	0	0	-4,630
y_2	Electricity (MJ/h)	-197,917	-1,157	-2,743	254,481	0	52,664
y_3	Steam (kg/h)	-186,343	-579	0	212,067	-514	24,632
y_4	Total Residue (kg/h)	3,472	-3,472	0	0	0	0
y_5	Solid Residue Fraction (kg/h)	0	694	0	0	-694	0
y_6	Liquid Residue Fraction (kg/h)	0	2,778	-2,778	0	0	0
y_7	Biodiesel (kg/h)	1,157	0	0	0	0	1,157
y_8	Glycerol (kg/h)	116	0	0	0	0	116
y_9	Methane (kg/h)	0	0	1,250	-16,965	-528	-16,243
y_{10}	Methanol (kg/h)	-116	0	0	0	868	752

As shown, it is noted that 4,630 kg/h of microalgae is used to produce 1,157 kg/h of biodiesel (via Processes A and B). On the other hand, the anaerobic digester (Process F) produces 1,250 kg/h of methane, which is then converted to electricity and steam in the combined heat and power system (Process C). Note that as the internally produced methane is insufficient to support the biorefinery, thus additional input of external methane (as natural gas) is needed. This external fossil-fuel supply adds to the IAB carbon footprint. Meanwhile, the resulting values of the water footprint, land footprint, and carbon footprint for the optimum case are 4.77×10^8 t/y, 792 ha-y, and 0 t/y; respectively. Note also that the resulting carbon footprint for the optimum case is 0 t/y since the negative carbon footprint from the export of electricity and steam offsets the carbon footprint required of the methane.

5. Conclusion

A fuzzy linear programming model has been developed to optimize the design of an integrated algal biorefinery. The model has been demonstrated for the case of an integrated algal biorefinery which produces biodiesel, glycerol, and methanol; as well as electricity and steam. Further work needs to be done in the future to include economic potential in the optimal design of IAB. Furthermore, fuzzy mixed integer linear programming approach with additional value-added products from microalgae such as bioethanol, biogas, and nutrient based-products are proposed for future studies.

Acknowledgement

The financial support of the University Research Coordinating Office of De La Salle University (Grant # 04 RPW AY11-12) and the Faculty Development Program of De La Salle University support of Ph.D. studies of the first author are gratefully acknowledged.

References

L. Čuček, J. Klemeš˘, Z. Kravanja, 2012, A Review of Footprint analysis tools for monitoring impacts on sustainability, Journal of Cleaner Production, (in press) DOI: 10.1016/j.jclepro.2012.02.036.

L. De Benedetto, J. Klemeš˘, 2009, The Environmental Performance Strategy Map: an integrated LCA approach to support the strategic decision-making process, Journal of Cleaner Production, Volume 17, pp. 900-906.

R. Heijungs, S. Suh, 2002, The Computational Structure of Life Cycle Assessment. (Kluwer, Dordrecht).

H.H. Khoo, P.N. Sharratt, P. Das, R.K. Balasubramanian, P.K. Naraharisetti, S. Shaik, 2011, Life cycle energy and CO2 analysis of microalgae-to-biodiesel: Preliminary results and comparisons, Bioresource Technology, Volume 102, pp. 5800–5807.

Y.J. Lai, C.L. Hwang, 1992, Fuzzy Mathematical Programming Methods and Applications, (Springer-Verlag, New York).

L.F. Razon, R.R. Tan, 2011, Net energy analysis of the production of biodiesel and biogas from the microalgae: *Haematococcus pluvialis* and *Nannochloropsis*, Applied Energy, Volume 88, pp. 3507-3514.

J. Singh, S. Gu, 2010, Commercialization potential of microalgae for biofuels production, Renewable and Sustainable Energy Reviews, Volume 14, pp. 2596-2610.

B. Subhadra, M. Edwards, 2011, Coproduct market analysis and water footprint of simulated commercial algal biorefineries, Applied Energy, Volume 88, pp. 3515-3523.

B. Subhadra, 2010, Sustainability of algal biofuel production using integrated renewable energy park (IREP) and algal biorefinery approach, Energy Policy, Volume 38, pp. 5892-5901.

R.R. Tan, A.B. Culaba, K.B. Aviso, 2008, A fuzzy linear programming extension of the general matrix-based life cycle model, Journal of Cleaner Production, Volume 16, pp. 1358-1367.

R.R. Tan, J.B. Ballacillo, K.B. Aviso, A.B. Culaba, 2009, A fuzzy multiple-objective approach to the optimization of bioenergy system footprints, Chemical Engineering Research and Design, Volume 87, pp. 1162-1170.

D.H.S. Tay, D.K.S. Ng, H. Kheireddine, M.M. Ell-Halwagi, 2011a, Synthesis of an integrated biorefinery via the C-H-O ternary diagram, Clean Technologies and Environmental Policy, Volume 13, pp. 567-579.

D.H.S. Tay, D.K.S. Ng, N.E. Sammons, M.R. Eden, 2011b, Fuzzy optimization approach for the synthesis of a sustainable integrated biorefinery, Industrial and Engineering Chemistry Research, Volume 50, pp. 1652-1665.

G. Taylor, 2008, Biofuels and the biorefinery concept, Energy Policy, Volume 36, pp. 4406-4409.

H.-J. Zimmermann, 1978, Fuzzy Programming and Linear Programming with Several Objective Functions, Fuzzy Sets and Systems, Volume 1, pp. 45-55.

I.A. Karimi and Rajagopalan Srinivasan (Editors), Proceedings of the 11th International Symposium on Process Systems Engineering, 15-19 July 2012, Singapore.

Process Analysis Using *Umberto Carbon Footprint* Tool

Pedro Chainho[a], Henrique A. Matos[a]

[a]*CPQ, Department of Chemical Engineering, Instituto Superior Técnico, Av. Rovisco Pais, 1049-001, Lisboa, Portugal*

Abstract

The software Umberto Carbon Footprint calculates CO_2 footprint of products or activities. It is based on analysis of primary and secondary footprints during the product lifecycle. It uses the ecoinvent database to analyse individual contribution of the resources consumption required for the footprint of the final product.

Umberto Carbon Footprint was applied to two processes where the streams and resources were characterized using the process simulator Aspen Plus: A) production of cumene from benzene and B) production of acetone from IPA (Isopropyl alcohol). The analysis was carried out for each process at two different scenarios (with and without simplified energetic integration).The results show an improvement on the carbon footprint value for the scenarios with energetic integration and a good agreement with ecoinvent database values

Umberto Carbon Footprint was also applied at one Portuguese chemical company to a formaldehyde process (patent Perstorp Formox®). Real industrial data was used on the streams and resources characterization. The carbon footprint obtained for F-100 (maximum production system scenario) shows a relative deviation of 1.8% comparing to ecoinvent database value.

Keywords: Modeling, Carbon Footprint, Umberto software, Industrial Process.

1. Introduction

Carbon footprint is a relative measurement of the amount of CO_2 release on the environment during the life cycle of a product or activity. Normally it's calculated from the analyses of direct and indirect emissions of resources consumed on a certain process. All streams of the industrial process must be previously characterized by a process simulation or using the industrial data. This tool could help in the discussion of different operating conditions scenarios, such as raw material diversity, process integration degree, utilities type, among others.

Nowadays this issues is has become increasingly important, and big supermarkets chains in UK and USA were wondering about putting the CO_2 footprint on the products descriptions labels, granting to the consumer the option of a more responsible choice in terms of ecologic matter.

The methodologies for carbon footprint calculations are still growing and it is emerging as an important tool for sustainability analysis. The concept of carbon footprinting has permeated and is being commercialized in all the areas of life and economy, but there is little coherence in definitions and calculations of carbon footprints among the studies. Carbon footprint is intended to be a tool to guide the relevant emission cuts and verifications, its standardization at international level are therefore necessary. Pandey et al. (2011) made a review where they describe the prevailing carbon footprinting

methods and raise the related issues. Some studies are being made as calculation of the corporate carbon footprint of the cement industry by MC3 methodology by Cagiao, et al. (2011). Yuttitham, et al., (2011) determined the carbon footprint of sugar produced from sugarcane in eastern Thailand. Graphical representation of carbon footprint reduction for chemical processes was applied by Tjan et al. (2010).
In this paper the carbon footprint calculation and analysis of chemical products with the application of software Umberto for Carbon Footprint using simulation and real industrial data.

2. Process simulator approach

2.1. Cumene process
Cumene is produced from a reaction in gas phase between benzene and polypropylene, with a main reaction (1) and parasite one (2):

$$\text{Propylene} + \text{Benzene} \longrightarrow \text{Cumene} \quad (1)$$

$$\text{Propylene} + \text{Cumene} \rightarrow \text{P} - \text{diisopropil benzene} \quad (2)$$

It was considered a minimum annual production of 120 kton of cumene with a specification of 99% in molar purity without any kind of heat integration (Scenario 1).

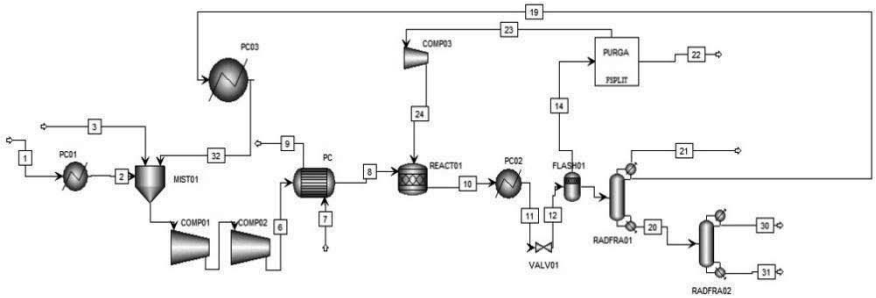

Figure 1: Cumene Process diagram in AspenPlus®. (Scenario 1)

An alternative diagram was tested with a simple energy integration of reactor effluent as hot fluid on exchanger named PC (Scenario 2).The hot utility used in Figure through stream 7 was removed.

Table 1: CO_2 Footprint and main contributions for the cumene process

Carbon Footprint (kg CO2 eq.)	
Scenario 1	Scenario 2
3.74	3.48

Contributions for the footprint			
Scenario 1		Scenario 2	
Benzene	65%	Benzene	70%
Propylene/ Propane	21%	Propylene/ Propane	22%
Others	14%	Others	8%

As expected it was noted an improvement of the CO_2 footprint of the process with simple energy integration that corresponds to a decreasing of 7% of the CO_2 footprint. The contribution of field "Others" (table 2) was smaller in the integrated process because this field includes the consumption of energetic resources that were reduced with the energetic integration.

2.2. Acetone process

The process of production of acetone from IPA contains a main reaction (3) and 2 other parasite ones (4) and (5).

$$\text{Isopropanol} \rightarrow \text{Acetone} + \text{Hydrogen} \quad (3)$$

$$\text{Isopropanol} \rightarrow \text{Propylene} + \text{water} \quad (4)$$

$$\text{Propylene} + \text{Hydrogen} \rightarrow \text{Propane} \quad (5)$$

It was considered a minimum annual production of 120 kton of acetone with a specification of 99% in molar purity (Scenario 1).

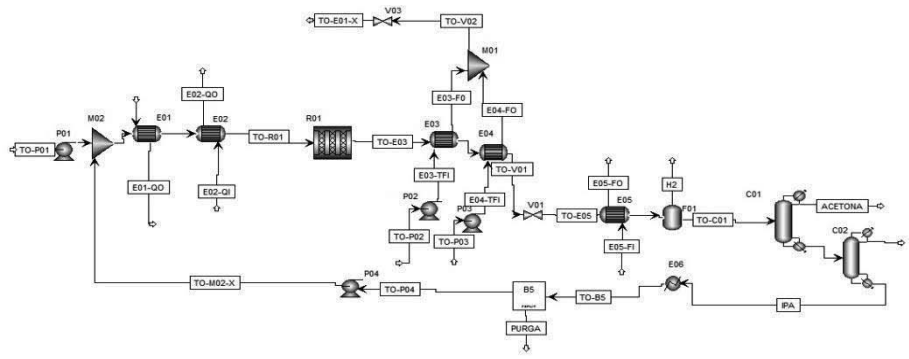

Figure 2: Acetone process diagram in AspenPlus®. (Scenario 1)

Also an alternative scenario was tested with simple energy integration. It was produced steam on the exchangers E03 and E04 and was recirculated to E01 (Scenario 2).

Table 2: CO_2 Footprint and main contributions for the acetone process

Carbon Footprint (kg CO_2 eq.)	
Scenario 1	Scenario 2
3.11	2.95

Contributions for the Footprint			
Scenario 1		Scenario 2	
IPA	77%	IPA	81%
Net steam	14%	Net steam	15%
Others	9%	Others	4%

The result is analogous of the previous process. It was verified a footprint decreasing of 5%.

3. Chemical Plant Data aproach

The carbon footprint calculation using the software Umberto for Carbon footprint is also applied to a real chemical plant data, instead of the previous approach where data was obtained by simulation with a process simulator.

This approach was applied to a process of production of formaldehyde type Perstorp Formox® of a Portuguese chemical industry. The formaldehyde production occurs on a fixed bed reactor through the partial oxidation of methanol.

The main reaction is strongly exothermic, and the heat of reaction is used to produce steam in exchanger E-2/1. The units E-18, E-22 and E-15/1 constitute the emission control system (ECS) which control the gas emissions to the atmosphere.

The equipment and streams before T-1 and T-2 are double and work in parallel, system-1 (S-1) and system-2 (S-2). The main product (F-50) is collected in T-2 and the Product F-30 on T-1.

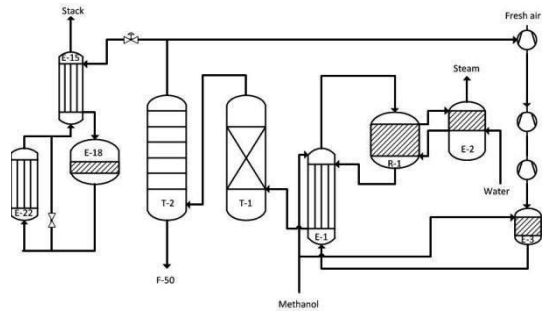

Figure 3: Simplified formaldehyde process diagram based on the Industrial site analysed.

Several production scenarios were tested:

- Scenario **3500-0**: Minimum production status, S-1 with a fresh methanol consumption of 3500 kg/h and S-2 stopped with only F-100.
- Scenario **0-4900** : S-2 with a fresh methanol consumption of 4900 kg/h and S-1 stopped;
- Scenario **3500-3500 :** S-1 with a fresh methanol consumption of 3500 kg/h and S-2 with a fresh methanol consumption of 3500 kg/h;
- Scenario **4900-4600:** S-1 with a fresh methanol consumption of 4900 kg/h and S-2 with a fresh methanol consumption of 4600 kg/h.

The scenarios with higher productions rates are the ones with smaller footprint. The carbon footprint is analysed by kg of product produced and is strongly dependent of the raw-materials utilization, and consequently in terms of process efficiency, so is expectable smaller footprints for those scenarios because they are the most efficient ones (also in observed in economical terms).

Table 3: CO_2 footprint of formaldehyde process – F100 and F-30

Methanol Consumption				
Scenario	S-1 (kg/h)	S-2 (kg/h)	CO_2 footprint (kg CO_2 eq.) F-100	CO_2 footprint (kg CO_2 eq.) F-30
3500-0	3500	0	1.11	-
0-4900	0	4900	1.22	9.91
3500-3500	3500	3500	1.07	13.45
4900-4600	4900	4600	1.09	16.49

It is predicted by ecoinvent 2.2 a carbon footprint for a formaldehyde process type Perstorp Formox® of 1.11 kg CO2 eq., for a maximum production system. Comparing this one with the value for scenario 4900-4600 is observed a relative deviation of 1.8%. The cause of deviation is explained by some differences in the calculation by ecoinvent and this one:

- Input values in ecoivent are from literature and project predicted values of several European production units.

- The ecoinvent footprint considers the contribution of final product transportation and in this project the formaldehyde was for own consumption.
- Ecoivent value uses input values from another process patent (silver catalysis) in addition to the patent Perstorp Formox®.
- Contribution of catalyst for the footprint is higher in ecoinvent because of a more regular replacement is used on the units analyzed.

Table 4: Individual contributions of Carbon footprint : F-100 and F-30

Contributions for the footprint								
Scenario	**3500-0**		**0-4900**		**3500-3500**		**4900-4600**	
	F-100	F-30	F-100	F-30	F-100	F-30	F-100	F-30
Methanol	73.3%	-	78.8%	78.9%	82.7%	83.2%	84.7%	84.5%
Electricity	3.5%	-	5.0%	4.3%	5.2%	4.2%	5.6%	6.0%
Chemical plant infrastructure	8.3%	-	6.1%	6.9%	5.2%	5.1%	3.4%	3.9%
Stack emissions	13.3%	-	9.1%	9.6%	6.9%	7.2%	5.1%	5.4%
Others	1.5%	-	1.1%	0.3%	0.1%	0.3%	1.2%	0.3%

Other causes of deviation lies on some approximations used in the footprint calculations as the assumption of CO_2 stack emissions similar for all scenarios tested and on the estimation of cooling water flows. In the future a deeper analysis will be done to overcome some practical difficulties encountered.

4. Conclusions

The Umberto for Carbon Footprint allows two different approaches for calculation of chemical processes footprints. With auxiliary data obtained for instance in a process simulator or plant data, the software becomes very easy and quick to use. The results obtained in this work show a good agreement with the ones from ecoinvent data base. In the future this contribution could be integrated with SustainPro® tool (Carvalho et al., 2008) to provide a more reliable sustainability analysis. It seems to be also an important tool to compare different process design scenarios.

References

http://www.ecoinvent.org/database/, accessed in 18/08/2011

Cagiao J., Gómez, B., Doménech, J. L., Mainar, S. G., Lanza, H. G., Calculation of the corporate carbon footprint of the cement industry by the application of MC3 methodology, Ecological Indicators, 11(6), 2011, 1526-1540

Carvalho, A., Matos, H. A., Gani. R., Design of Sustainable Chemical Processes: Systematic Retrofit Analysis Generation and evaluation of alternatives, Process Safety and Environmental Protection, 86, 2008, 328–346

Pandey, D., Agrawal, M., Pandey, J.S., Carbon footprint: current methods of estimation, Environmental Monitoring Assessment 178, 2011, 135–160

Tjan W., Tan, R. R., Foo, D.C.Y., A graphical representation of carbon footprint reduction for chemical processes, Journal of Cleaner Production, 18 (9) 2010, 848-856

Yuttitham, M., Gheewala, S. H., Chidthaisong, A., Carbon footprint of sugar produced from sugarcane in eastern Thailand, Journal of Cleaner Production, 19(17-18) , 2011, 2119-2127

I.A. Karimi and Rajagopalan Srinivasan (Editors), Proceedings of the 11th International Symposium on Process Systems Engineering, 15-19 July 2012, Singapore.

Efficient configuration/design of solvent-based post-combustion carbon capture

Zhengxiong Li, Rajab Khalilpour, Ali Abbas*

School of Chemical and Biomolecular Engineering,
The University of Sydney, Sydney, Australia
**Tel: +61 2 9351 3002; Fax: +61 2 9351 2854; E-mail: ali.abbas@sydney.edu.au*

Abstract

In this study, we analyze two design configurations for post-combustion carbon capture (PCC) namely inter-stage cooling and split flow. The results show that inter-stage cooling configuration has notable impact on improving PCC performance. It is found that, for a flue gas with 13.0 mol% of CO_2, and with objective of capturing 90% of CO_2 at purity of 98%, base case configuration imposes a 4.7GJ/ton-CO_2 reboiler duty. This energy burden decreases (about 34.8%) to 3.1 GJ/ton-CO_2 with single-stage cooling configuration. Two-stage-cooling configuration further improves the efficiency but only incrementally. Similarly, split flow design configuration shows considerable improvement in efficiency (3.8GJ/ton-CO_2 vs. 4.7GJ/ton-CO_2 for base case).

Keywords: Post-combustion carbon capture (PCC), inter-stage cooling, split flow.

1. Introduction

Solvent based PCC was evaluated by Metz et al. (2005) and described as the most mature technology for commercial scale industrial carbon capture from power plants' flue gas. The standard carbon capture process is illustrated in *Fig.1*. A stream of amine solution is continuously recycled between absorption and desorption units where the lean stream removes the CO_2 from the bulk flue gas in an absorber column and the rich stream is regenerated in the stripper column.

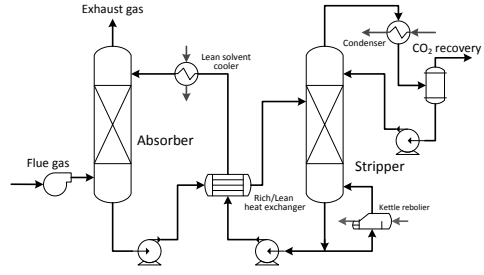

Fig.1: Schematic of standard post-combustion carbon capture process.

Despite recent progress in solvent-based PCC, the implementation of this technology still burdens a notable energy penalty mainly due to solvent regeneration. The energy penalty though varies by the type of power plant and by different techno-economic studies, is estimated to be above 20% (Khalilpour and Abbas 2011). This inevitably leads to a significant reduction in the power plant's load. The critical parameters influencing the efficiency are solvent type, solvent concentration, operating conditions

of absorption/desorption columns, percentage of CO_2 avoided, captured CO_2 purity and amount of regeneration. There are extensive research to study the impact of these parameters and their potential process improvements.

Configuration of absorption-desorption processes is also an important factor. In a conventional PCC scenario, gas enters at the bottom of the column and exists from the top. This traditional design does not exploit potential heat integration possibilities of the exothermic/endothermic absorption/desorption operation. Therefore, application of conventional simple column coupling configurations results in inefficient performances of both absorber and desorber. This leads to higher capital and operating costs. Recent studies see great potential for energy savings by introducing flow sheet innovations. Cousins et al. made an overview of several proposed configurations for PCC (Cousins et al. 2011). The purpose of this paper is to assess two improved flow schemes: Inter-stage cooling and split flow, validating their potential in relieving the energy penalty on a basis of 30wt% MonoEthanolAmine (MEA) being employed as the absorbent. Process flow diagrams of inter-stage cooling and split flow are presented in *Fig.2*. Aspen HYSYS V7.1 is used in this study.

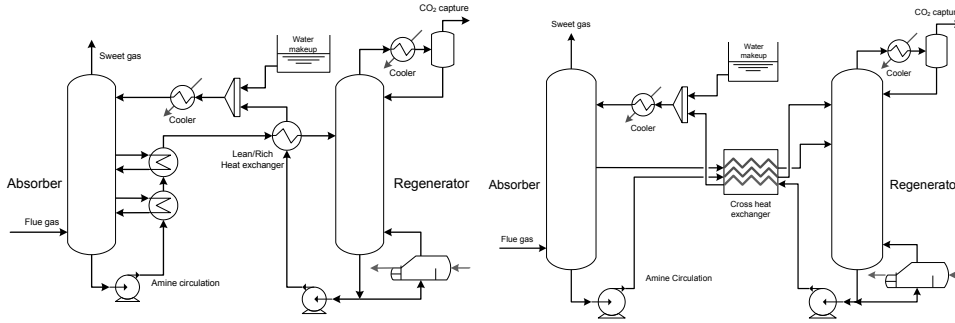

Fig. 2: Process flow diagram for (left) inter-stage cooling scheme, and (right) split flow scheme.

2. Process simulation

2.1. Fluid package

A reliable fluid package is the basis of simulation and its competency can be verified by comparing the predicted solubility of CO_2 with experimental data. Jou et al. (1995) experimentally measured the solubility of CO_2 in 30 wt% MEA solution by relating the CO_2 loading to its partial pressure. Case studies of CO_2 solubility were carried out using Amine pkg, Electrolyte NRTL respectively.

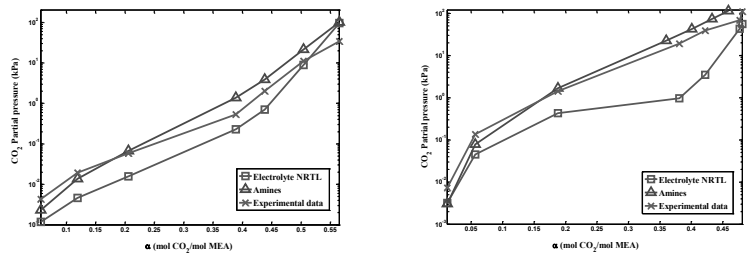

Fig.3: Validation of simulation fluid packages in terms of CO_2 solubility in 30 wt% MEA solution at (left) 60°C, and (right) 100°C.

2.2. Base case specification

The base case model was designated to achieve 90% of CO_2 removal and 98% purity of CO_2 captured. The critical operating conditions and equipment parameters are listed in *Table 1*. The composition of flue gas was set to be 12.99 mol%, after Khalilpour and Abbas (2011).

Table 1: Absorption/desorption column specifications.

Absorber		
Item	**Value**	**Reference**
Tray No.	10	
Tray Efficiency (%)	25	(Øi 2007)
Temperature (°C)	50	(Cousins, Wardhaugh et al. 2011)
Pressure (kPa)	101.3	
Stripper		
Item	**Value**	**Reference**
Tray No.	6	
Tray Efficiency (%)	50	(Øi 2007)
Reboiler pressure (kPa)	200	(Abu-Zahra, Schneiders et al. 2007)
Feed position	2	
Feed condition	Saturate liquid	

2.3. Inter-stage temperature control

The optimal temperature range for CO_2 absorption is 40-60°C since the reaction rate is highest within this range for 30 wt% MEA (Cousins et al. 2011). However the exothermic effect can raise this temperature beyond 70°C and away from the theoretical equilibrium limits, thus lowering the absorption capacity of MEA. Maintaining the temperature along the column within its optimal range could enhance the absorption performance. This idea can be realized by withdrawing a hot stream out of the column's top section (say at the third plate) and cooling it with the bottom product which is around 54°C. The cooled stream is then returned to a position below the withdrawal location (say at the fourth plate). This brings the bottom lean stream closer to the feed condition of the stripper. A temperature control strategy can further enhance the process by implementing multi-stages of cooling. In this simulation work, the side draw streams are extracted from the third and sixth trays separately and sent back to the fourth and seventh trays, respectively, after being cooled down.

2.4. Split flow

A split flow configuration provides a reduced flow to the lower section of the stripper where it can be recycled to a lower CO_2 content with the same energy input. The semi-lean solution extracted from the mid-section of the stripper removes the bulk CO_2 passing through the lower section of the absorber where partial pressure of CO_2 is sufficiently high to provide a large driving force. A side draw stream, the semi-rich amine, is extracted from the fifth plate of the absorber and sent to a cross heat exchanger where it is heated up by stripper bottom product as well as the lean amine stream from the bottom of the absorber. Then, the semi-rich amine is fed to the stripper at the fourth plate. The flow rate and the tray position where side stream is drawn from the absorber were determined by trial and error. The properties of concerned amine streams are tabulated below.

Table 2: Properties of the main process streams.

Stream properties in standard flow sheet				
	Flow rate	Temp. before HX	Temp. after HX	Loading
	tonne/hr	°C	°C	mole CO_2/mole MEA
Rich	5209	52.3	108	0.448
Lean	4980	121.3	165.5	0.241
Stream properties in split flow configuration				
	Flow rate	Temp. before HX	Temp. after HX	Loading
	tonne/hr	°C	°C	mole CO_2/mole MEA
Rich	3875	37.1	95	0.508
Semi-rich	1197	67.4	100	0.310
Lean	4843	120.7	73.6	0.252

3. Simulation Results

3.1. Temperature profile along the absorber

From *Fig.*4, it is observed that the inter-stage cooling configuration significantly levels the parabola-shaped temperature profile of the base case. It extends almost horizontally throughout the first four plates since the hot solution to be cooled down is withdrawn from the third plate. The process target is to achieve 90% of carbon capture and the ratio of amine solution to flue gas (L/G) in wt./wt. was set to be around 20. Similarly, but not as significant as inter-stage cooling, implementation of split flow also relieves the high temperature within the column (*Fig.*4).

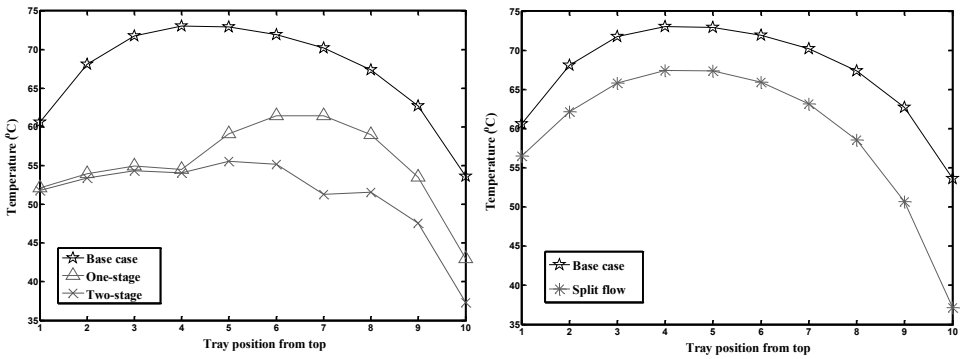

Fig.4: Temperature profile for (left) inter-stage cooling, and (right) split flow.

3.2. Improved performance in energy savings

Intensive reboiler energy consumptions in terms of GJ per tonne-CO_2-captured for base case and the new configurations were compared on a consistent basis. From Table 3, one-stage temperature control has effectively reduced the energy penalty for amine regeneration by 34.8% and split flow 18.5%.

Table 3: Reboiler duties for base case, inter-stage cooling and split flow configurations.

	L/G (tonne/tonne)	Carbon capture (%)	**Reboiler duty(GJ/tonne)**
Base Case	20.25	90.09	**4.696**
One-stage inter-cooling	20.27	90.04	**3.062**
Split Flow	20.27	90.07	**3.828**

*Fig.*4(left) shows that two-stage cooling allows a better temperature control where it has been kept below 55°C. The performances of one-stage and two-stage in terms of carbon capture with equivalent reboiler duty are compared in Table 4. With the implementation of multi-stage cooling, it yielded around 1% higher carbon capture rate with the same reboiler duty than that of single stage. These results agree well with the predicted temperature profile of *Fig.*4.

Table 4: Carbon capture rates of one-stage and two-stage inter-cooling.

	L/G (tonne/tonne)	Reboiler duty (GJ/tonne)	**Carbon capture (%)**
One-stage inter-cooling	20.25	3.008	**91.06**
Two-stage inter-cooling	20.24	3.015	**92.32**

4. Conclusion

Alternative process flowsheet models were simulated and analyzed for PCC operations. The performances with and without design changes were evaluated and analyzed on a consistent basis (90% of CO_2 removal and 98% purity of CO_2 captured). From the simulation results, we found great potential for reducing the energy consumption in PCC via the process design configurations of inter-stage cooling and split flow. Compared to the base case, both inter-stage cooling and split flow schemes successfully relieve the exothermic effect during the reaction process within the column and therefore enhance the absorption. One-stage cooling reduces the reboiler energy consumption by 34.8% while split flow reduces 18.5%. A two-stage cooling configuration was also simulated to study the performance of multistage cooling and showed 1% rise in carbon capture rate under equivalent energy consumption.

References

M. R. M. Abu-Zahra, , L. H. J. Schneiders, et al., 2007, CO2 capture from power plants. Part I. A parametric study of the technical-performance based on monoethanolamine, International Journal of Greenhouse Gas Control 1,1, 37-46.

A. Cousins, L. T. Wardhaugh, et al., 2011, A survey of process flow sheet modifications for energy efficient CO2 capture from flue gases using chemical absorption, International Journal of Greenhouse Gas Control, 5,4, 605-619.

F.Y. Jou, A. E. Mather, et al., 1995, The solubility of CO2 in a 30 mass percent monoethanolamine solution, The Canadian Journal of Chemical Engineering, 73, 1, 140-147.

R. Khalilpour, A. Abbas, 2011, HEN optimization for efficient retrofitting of coal-fired power plants with post-combustion carbon capture, International Journal of Greenhouse Gas Control, 5, 2, 189-199.

B. Metz, O. Davidson, et al., 2005, IPCC special report on carbon dioxide capture and storage, Cambridge, Cambridge University Press, for the Intergovernmental Panel on Climate Change.

L. E. Øi, 2007, Aspen HYSYS Simulation of CO2 Removal by Amine Absorption from a Gas Based Power Plant, SIMS2007 Conference, Gothenburg, Sweden.

I.A. Karimi and Rajagopalan Srinivasan (Editors), Proceedings of the 11th International Symposium on Process Systems Engineering, 15-19 July 2012, Singapore.

Effect of the microfiltration phase on pervaporation of ethanol produced from banana residues

Roger H. Bello, Ozair Souza, Noeli Sellin, Sandra H. W. Medeiros, Cintia Marangoni

University of Joinville Region (UNIVILLE) - Chemical Engineering Department, Rua Paulo Malschitzki 10 Zona Industrial, Joinville-SC 89219-710, Brazil;

Abstract

The objective of this paper is to investigate the use of microfiltration as a process of suspended solids separation in the pervaporation of bioethanol produced by banana culture residues. The composition of the fermentative broth influences on the separation, and the use of different substrates lead to a revaluation of the process, even if this is well established. Therefore, the ethanol pervaporation was studied by using polydimethylsiloxane membranes with binary mixtures (ethanol and water) as well as with fermentative broth. The fermentative broth pretreatment through microfiltration was compared to its centrifugation. It was possible to observe the reduction of the permeate flow rate, however the increasing in parameters such as the enrichment factor and the ethanol concentration in the permeate was also seen when the microfiltration was employed, comparing to the centrifugation as well as to the binary mixture.

Keywords: bioethanol, microfiltration, pervaporation, lignocellulosic residues.

1. Introduction

The need to amplify the offer of raw material for the production of ethanol without causing damage the planted areas for food, is the main factor of the development of researches using different residues for the ethanol production [1,2]. Several studies approach the use of agricultural or forest waste for the ethanol production [3]. Known as residual biomass, sugarcane bagasse and straw, or corn stover and fiber, wheat and rice straws, eucalyptus wood and residues of culture of fruits like bananas, grapes and apples are good examples. In the case of banana, although they are few, the applications are through the use of the fruits, leaves and other residues such as the stem [4].

Although the researches using banana residues show the viability of the fermentation process and consequent production of alcohol, it is important to emphasize that they are focused on the study of the hydrolysis [5] and a few of the others phases are evaluated, such as the ethanol recuperation. The use of distillation is a challenge due to its cost and the high energetic expenses [4,6]. In this context, the process of separation through pervaporation presents many advantages, because of the simplicity of its operation, use of low amounts of energy, low operational cost besides reducing the inhibition of ethanol on the fermentation [7].

Continuous fermentation processes with distillation through membranes have stood out due to the fact that they are, energetically speaking, more advantageous processes when compared to the traditional ones [8]. In this area, in the past few years pervaporation has became an alternative because of the possibility of being used coupled to the

fermentation [9,10]. However, the integrated process of fermentation and separation of the ethanol through pervaporation demands a phase of cell separation which is commonly carried out through microfiltration. There are many difficulties associated to this coupled design, related to low flows and selectivity because of the pore obstruction of the microfiltration membranes and to the swelling of the pervaporation membranes due to the presence of solids of the broth [11].
In addition, the composition of the fermentative broth influences on the separation and, the use of different substrates leads to the need of reevaluation of the process, even if it is already well established [12]. Therefore, a study of the separation of the bioethanol obtained from the residues of banana culture, employing pervaporation with commercial membranes of polydimethylsiloxane (PDMS) is proposed, aiming to evaluate the effect of the microfiltration phase as a process of separation of the solid material.

2. Materials and methods

In order to evaluate the proposal of this paper, preliminary experiments were conducted with an ethanol-water model binary mixture. This mixture was used as a pattern to analyze the results. Then, tests with the fermentative broth produced from the residues of banana pulp as a substrate were carried out. The amount of ethanol obtained in the broth was approximately 3% in mass. Two processes were compared for the cell and particulate material separation prior to the pervaporation: centrifugation and microfiltration.
The pervaporation process performance was expressed in terms of selectivity of the membrane (α) and mass flow of the permeate (J), according equations 1 and 2, where, W is the mass (g) of the permeate, A is the membrane´s effective area (m²) and, τ is the time interval (h) of the pervaporation process; y_i and y_j are the mass fractions of ethanol and water on the side of the permeate and x_i and x_j are the mass fractions of ethanol and water on the feed respectively.

$$\propto_{EtOH} = \frac{{}^{y_i}/_{y_j}}{{}^{x_i}/_{x_j}} \qquad \textit{Eq.}\ (1)$$

$$J = \frac{W}{A.\tau} \qquad \textit{Eq.}\ (2)$$

Another parameter used consisted of the enrichment factor - β_{EtOH} (Equation 3) which investigates the influence of other components on the ethanol enrichment in the permeate comparing to the feed. Yet, the index of separation through pervaporation – PSI (Equation 4) is determined by the properties of the membranes permeation and selectivity. $W_{EtOH,p}$ is the ethanol mass fraction in the permeate and $W_{EtOH,f}$ in the feed; J is the mass total flow (g/m².h) and, α the membrane´s selectivity.

$$\beta_{EtOH} = \frac{W_{EtOH,p}}{W_{EtOH,f}} \qquad \textit{Eq.}\ (3)$$

$$PSI = J.\alpha \qquad \textit{Eq.}\ (4)$$

2.1. Pervaporation

The pervaporation unit consists of a permeation removable module in PVC, with hollow membranes made of poly(dimethylsiloxane) - PDMS (PAM-PV S 0.01/PAM-Membranes), containing 50 capillaries with area of 0.04 m². The fermented broth or the model solution at approximately 22 ºC was fed with flow rates of 20 $L.h^{-1}$ from a 1 L reservoir, positioned upward the membrane, through a gear pump FE 611 (B. Braun). The vacuum pump DV 142N 250 (J/B Industries), on the permeate side, provided the pressure drop for the bioethanol vaporization (permeate pressure was lower than 5 mmHg). The vapor of permeate was collected into a reservoir refrigerated by cryogenic bath at -196 ºC, containing liquid nitrogen, for condensation. The simplified scheme of the pervaporation unity is shown in Figure 1.

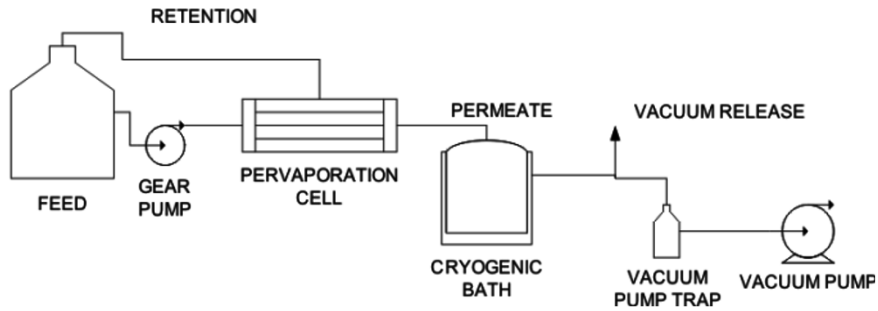

Figure 1 – Pervaporation process scheme.

The tests were carried out in duplicate, and the results presented consist on their averages. From each test, feed samples at the beginning and at the end of each experiment were taken, as well as the permeate in order to quantify the ethanol concentrations in gaseous chromatograph (GC).

2.2. Microfiltration

In natura fermented broth at environment temperature was fed from a 1 L reservoir, positioned before the membrane, by a gear pump FE 611 (B. Braun) at 90 $L.h^{-1}$. The concentrated returned to the feed in the whole microfiltration process. The microfiltration module is also made of PVC (membranes PAM) and has poly(imide) hollow membranes, with a 0.08 m^2 membrane area.

3. Results and discussion

The results obtained for the pervaporation of the ethanol and water binary model mixture are shown in Table 1. In Figure 2 the results of the flow parameters, enrichment factor and ethanol mass concentration in the permeate when centrifugation and microfiltration were used as a pretreatment are presented.

When analyzing the permeate flow, it is possible to observe that the experiments carried out with the centrifuged broth produced better results, even when they were compared to the model mixture. Those superior values can be attributed to the influence in the presence of fermentation subproducts and/or the presence of cells. In microfiltration, suspended particles may settle on the membrane surface, thus blocking feed channels and increasing friction losses (pressure drop) across the system. The result is a lower flux.

Table 1. Results of the efficiency of the separation of the ethanol and water mixture in pervaporation module with PDMS membrane

Parameter	Value
Mass Flow ($g.m^{-2}.h^{-1}$)	3.57
Selectivity (α)	8.31
Enrichment Factor (β)	7.56
PSI	29.71
Permeate Ethanol Mass Fraction % (wt/wt)	10.24

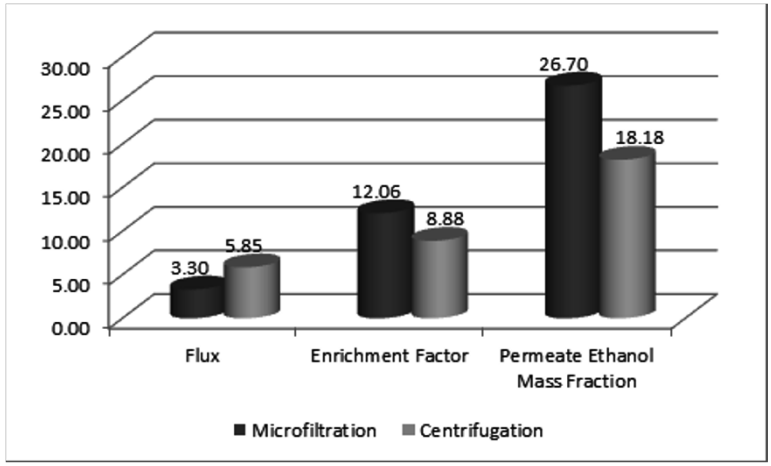

Figure 2. Comparison of the pervaporation results when the microfiltration and centrifugation processes were used as pretreatment.

On the other hand, it is possible to observe that better results for the enrichment and concentration factor of permeate were obtained when the microfiltration as pretreatments in the fermented broth cell separation was used. It was also possible to observe a 26.4% increase for the enrichment factor and 32% for the permeate ethanol mass concentration, which shows a higher potentiality in this treatment related to centrifugation. In fact, some authors [11] observed that the most used separation method for the cell segregation to be used as feed in the pervaporation process is the microfiltration, because centrifugation is widely used in liquid-solid separations at industries that produce ethanol and use distillation to recover this component.

4. Conclusions

The use of the microfiltration process coupled to the pervaporation in order to recover bioethanol from the fermentative broth produced from the lignocellulosic residues used in the banana cultivation showed itself as a very attractive alternative. The pretreatment of the fermentative broth through microfiltration presented a higher potentiality related to the centrifugation in the remaining solids separation step as well as for retaining some subproducts originated from the alcohol fermentation that influence on the pervaporation process.

References

[1] N. Sarkar; S.K. Ghosh; S. Bannerjee; K. Aikat, K., 2012Bioethanol production from agricultural wastes: An overview, Renewable Energy. *In press*.
[2] J. Swana; Y. Yang; M. Behnam; R. Thompson, 2011, An analysis of net energy production and feedstock availability for biobutanol and bioethanol, Bioresource Technology, 102, 2112-2119.
[3] M.A. Schulz, 2010, Bioethanol production from banana culture residues: Banana pulp and pell, Dissertation (Process Engineering) – UNIVILLE, Joinville, SC (In Portuguese).
[4] A.B.M.S. Hossain; S.A. Ahmed; M. A. Ahmed; M.A. Faris; M.S.M. Annua; M. Hadeel; H. Norah, 2011, Bioethanol fuel production from rotten banana as an environmental waste management and sustainable energy, African Journal of Microbiology Research, 5, 586-598.
[5] F. Lipnizki, 2010, Membrane process opportunities and challenges in the bioethanol industry, Desalination, 250, 1067-1069.
[6] R. Arumugam and M. Manikandan, 2011, Fermentation of Pretreated Hydrolyzates of Banana and Mango Fruit Wastes for Ethanol Production, Asian Journal of Experimental Biological Sciences, 2, 246-256.
[7] M. Nomura; 2002, Selective ethanol extraction from fermentation broth using a silicalite membrane, Separation and Purification Technology, 27, 59–66.
[8] M. Gryta, 2001, The fermentation process integrated with membrane distillation. Separation and Purification Technology, 24, 283–296.
[9] D.J. O'Brien; G.E. Senske; M.J. Kurantz; J.C. Craig Jr, 2004, Ethanol recovery from corn fiber hydrolysate fermentations by pervaporation, Bioresource Technology, 92, 15-19.
[10] M. Lewandowska and W. Kujawki, 2007 Ethanol production from lactose in a fermentation/pervaporation system, Journal of Food Engineering, 79, 430-437.
[11] L.M. Vane, 2005, A review of pervaporation for product recovery from biomass fermentation processes, Journal of Chemical Technology and Biotechnology, 80, 603–629.
[12] S. Chovau; S. Gaykawad; A.J.J. Straathof; B. Vand Der Bruggen, 2011, Influence of fermentation by-products on the purification of ethanol from water using pervaporation, Bioresource Technology, 102, 1669–1674.

I.A. Karimi and Rajagopalan Srinivasan (Editors), Proceedings of the 11th International Symposium on Process Systems Engineering, 15-19 July 2012, Singapore.

Virtual and Augmented Reality as Viable Tools to Train Industrial Operators

Davide Manca, Roberto Totaro, Salman Nazir, Sara Brambilla, Simone Colombo

Dipartimento di Chimica, Materiali e Ingegneria Chimica "Giulio Natta", Politecnico di Milano, Piazza Leonardo da Vinci 32, 20133 Milano, Italy

Abstract

The sensitivity and significance of operator training increased profoundly with the increase in automation of industrial plants. The paper proposes and discusses the use of Virtual Reality and Augmented Virtual Reality to train industrial operators. A detailed and immersive 3D model of the plant allows the operators understanding the details of equipment and operating conditions. Both the dynamic behavior and the control strategies of the process can be reproduced with a 3D immersive virtual environment by implementing and coupling a dynamic process simulator and a dynamic real-time accident simulator. The AVR feature enhances the VR by adding further information and analysis that result in better understanding of operators that work either in control room or in the field. The proposed training methodology allows achieving significant improvements in reliability, cost effectiveness, environmental friendliness, and process safety.

Keywords: Virtual Reality; Augmented Virtual Reality; Operator training; Dynamic process simulation; Accident simulation.

1. Introduction

The increase in complexity, technological improvement, automation, and environmental and safety constrains in the process industry, are tightly interconnected to the following demanding features:

- Retrofitting and revamping of chemical processes;
- Operators retiring and lack of viable tools to preserve their expertise, skill, experience, and knowledge without dispersing the know-how;
- Training of new operators that do not have any experience of the process since they come from different jobs and therefore are practically unaware of the specific plant features;
- Meeting quality, safety, and environmental requirements, which are difficult to achieve and preserve dynamically;
- Optimization of plant productivity, with respect to both law and process constraints.

Operator Training Simulators (OTSs) can play a major role in addressing these challenges and allowing companies to remain competitive and updated in terms of workforce. OTSs comprise both hardware devices and software tools that allow simulating the dynamic evolution of the plant and therefore allow training the operators before going on-line in the real plant. Conventional OTSs are mainly focused on replicating the control room environment by means of a mock-up of the Distributed Control System (DCS). Consequently, such OTSs (see also Figure 1) allow training

control-room operators (CROPs) whilst field operators (FOPs) are rather neglected and not looked after satisfactorily.

Figure 1: A conventional session of Operators Training.

According to the Authors, current OTSs can be expanded into three main directions:

1. Extend and improve the participation of FOPs. This allows increasing the knowledge of the field and allows facing unexpected process conditions in the shortest time while preserving the operators' safety.
2. Simulate accident events and their consequence and interaction with the plant equipment. This feature allows increasing the operator responsiveness and effectiveness (of both FOPs and CROPs) when facing real accidents.
3. Use OTSs for both business decisions and plant management to improve process performance and enhance overall safety.

These open issues are quite challenging not only in terms of single pieces of software but also in terms of effective tools to improve the skill and understanding degree of both FOPs and CROPs. Actually, one of the main objectives of modern OTSs is improving the situation awareness of operators and assessing quantitatively the training level (Endsley and Garland, 2000).

2. OTS extension to FOPs through virtual reality

The field operator section in conventional OTS is either absent or relegated to an approximated and simplified adaptation respect to the core module of the control room. Consequently, the training of FOPs, in most cases, is done on the job, *i.e.* in the real plant where the novice FOP is trained by a more experienced colleague. However, this procedure appears to be limiting, since the novice is trained to operate usually under normal operating conditions. Most of the transients (*e.g.*, startups, shutdowns, and grade changes), abnormal conditions, alarms, failures, and accidents are not easily replicable in a real plant. Actually, these scenarios are quite rare and it may happen that working in real conditions a field operator does not attend or take part to any of previous events for years.

The training of FOPs by means of a specifically designed and properly developed OTS represents a promising, and challenging solution to the aforementioned problems. However, such a feature requires the development of dedicated tools, whose function consists in building and improving the knowledge, concerning not only the process principles, but also the plant and equipment characteristics, as well as their position in the field and the interaction with the sub-assemblies, devices, valves, switches that complete the physical structure of the plant. As far as the FOP's training is concerned,

learning the plant structure means knowing not only the signs and symbols, but also the location of the equipment and devices, together with the operating procedures to run the plant under normal conditions as well as startups, shutdown, transients.
FOPs work in a complex reality where the main senses, especially sight and hearing, are called to capture every single operating detail. FOPs are able to decide and set the appropriate actions by projecting the expected results based on their choices.
In order to achieve this goal, it is recommended creating an environment based on a virtual plant, which is virtually identical to the real one. In this environment, the operator can be trained adequately without any risks for his/her safety and that of his/her colleagues. This allows avoiding any risks of economic losses and any impacts on buildings, population, and environment in case of errors done during the training session.
In order to build such a virtual environment, VE, the following features are recommended if not mandatory:

- Each process unit and device must be reproduced in the VE by using appropriate 3D editors to reconstruct its exact geometry and location. The required 3D data can be retrieved from either plant CAD drawings or laser scans of the real plant.
- A detailed photographic recognition on the plant is necessary, to achieve an accurate reconstruction of the details of the equipment in terms of external skin and usage degree. By accomplishing this step, the operator can recognize the plant as perfectly realistic. Through this measure, the gap between physical reality and the virtual one can be reduced and even dissolved.
- The operator should recognize the plant not only through the sense of sight but also of hearing. Therefore, it is advisable to implement a spatialized audio system that reproduces the surround sounds of the real plant. Using appropriate audio systems allows the operator identifying the proper source distance and the noise power.
- To increase the participation of the FOP to the VE it is possible to surround the FOP with the plant by exploiting the concept of stereoscopy, thereby, creating an immersive environment. Appropriate 3D glasses for stereoscopic vision allow the trainee to live the perception of being immersed in what s/he is observing. Using large screens allows increasing the immersivity and the sense of participation of the FOP to the training session.
- In order to increase the usability and the realism of the solution, some simple and intuitive interaction devices must be used to recognize the movements and actions done by the FOP within the chemical plant (*e.g.*, walking, looking around, climbing a vertical ladder, opening a valve, selecting and pressing a button). These devices (also known as natural interfaces) are connected to the 3D graphics engine, and present the advantage of not altering significantly the interaction between the FOP and the plant.

These recommended features of a VE represent a necessary but not sufficient condition for the training of industrial operators. Actually, the ultimate goal of a training tool is to transfer the operator a deep knowledge and understanding of the chemical process, not just to drive him/her inside an environment that is similar to the real one. To bring the OTS to a higher level of realism, the VR solution must be connected to a simulation tool capable of reproducing the dynamics of the plant. Both process and accident features should complement the simulation tool so to be able to reproduce either normal or abnormal/accident conditions. By coupling a dynamic accident simulator to a dynamic process simulator, it is possible to simulate the causes, evolution, and consequences of an accident on the equipment, the FOPs, and the environment (see also Figure 2).

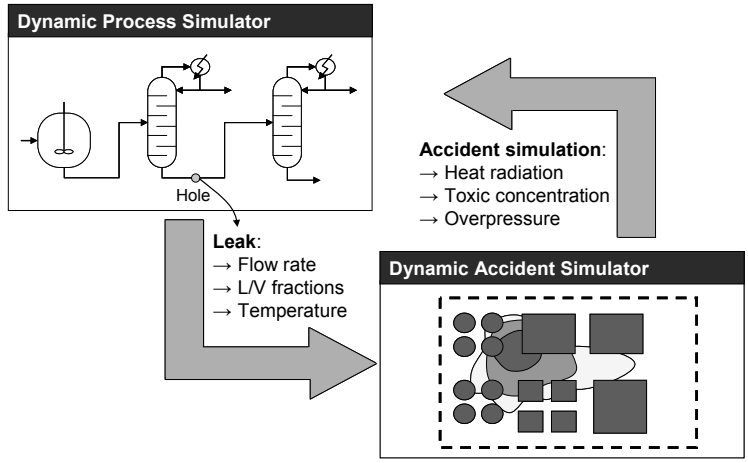

Figure 2: Two-way interaction between dynamic process and dynamic accident simulators.

3. Accident events simulation in OTS

To increase the situation awareness of operators respect to possible accident events, it is advisable to couple a dynamic process simulator to a real-time dynamic accident simulator (Brambilla and Manca, 2009). This two-way interaction was effectively implemented in an OTS for training of both CROPs and FOPs (Brambilla and Manca, 2011). The accident simulator can assess, as a function of the process variables evaluated by the process simulator, the event dynamics, which has some feedback effects on both the plant response and the FOPs' actions. The accident simulator can manage a wide range of accident scenarios, using literature models whose computation time is lower than the wall-clock time. The two-way dynamic interaction between the process and the accident simulators is carried out by considering the output variables of the process simulator (*e.g.*, flowrate) as input variables for the accident simulator, and *viceversa* (*e.g.*, the heat flux emitted by a pool fire that radiates to the surrounding equipment). In order to increase the situation awareness of FOPs about accidents, it is useful to provide the trainee(s) with some pieces of information that otherwise could not be easily visualized and understood. These details and variables fall under the realm of Augmented Virtual Reality (AVR).

4. Augmented Virtual Reality

In order to increase the operators' understanding of the process and also the effects and consequences of possible industrial accidents it can be of real help to show some additional bits of information during the training session. These bits of information are usually unavailable in real conditions but can augment the virtual reality scene by showing precious values that otherwise could not be quantified. This concept can be summarized by the AVR acronym that stands for Augmented Virtual Reality.

All the process and accident data evaluated by the corresponding dynamic simulators can be shown (according to the trainer decision) to the trainee so to increase the depth of understanding and supply statistics and records that otherwise would remain unknown. For instance, the AVR feature allows displaying the process variables that characterize the plant equipment (*e.g.*, temperatures, pressures, compositions, flowrates). The AVR feature allows also presenting the data related to the simulated accident (*e.g.*, pool diameter, jet length, cloud concentration, radiative flux, fire length, flame tilt, thermal

load, inhaled dose). These data can be shown by means of dynamically changing values, diagrams, schematics of the equipment (as shown in Figure 3). The combination of VR and AVR within the 3D VE is appealing and promising. For the sake of example, the proposed enhanced OTS (also named Plant Simulator, PS) can reproduce a process malfunction that may lead to a severe accident. Such accident event may imply the release of a liquid jet that forms a pool that spreads on the ground and that may either evaporate or be ignited with a subsequent pool fire. The PS allows displaying not only the physical features such as the liquid jet, the pool, and the fire (that are shown in the VR environment) but also the additional variables of AVR such as the radiative heat flux, the thermal load, and the consequences on the exposed FOP(s) in terms of time to reach the I, II, and III degree burns and eventually the death (Figure 3).

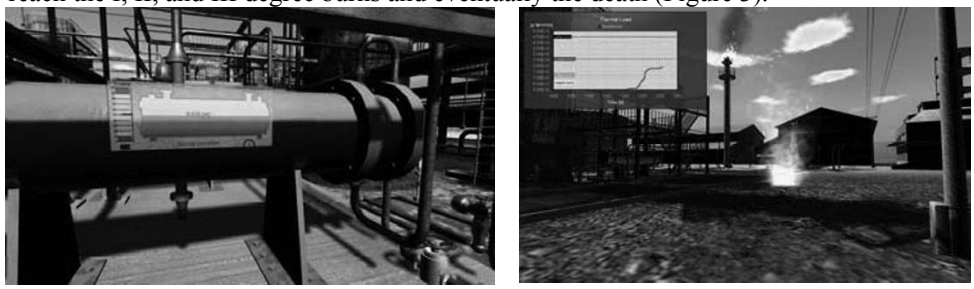

Figure 3: Two examples of AVR showing variables from the process simulator (left, reboiler level and corresponding alarms) and from the accident simulator (right, thermal load with I, II, and III degree burns).

While VR replaces the real plant, AVR is added to VR and represents a valid tool for training and increasing the conscience of operators which also refers to situation awareness. It is worth underlining that during assessment procedure, in order to make the training session consistent with what is available in the reality, the AVR tool is removed.

6. Conclusions

The challenging task of modern industrial OTSs was presented and discussed. Both VR and AVR were proposed as practical tools to improve the training level of operators and increase their situation awareness. The positive effects of an enhanced OTS and specifically of a PS consist in experimenting rather rare events such as startups, shutdowns, process transients, alarms, abnormal situations, and possible accidents. These features allow reducing the impact of human errors and human factors when running a plant by increasing the process understanding and conscience of both CROPs and FOPs.

References

Brambilla S., D. Manca, 2009, "Accidents Involving Liquids: a Step Ahead in Modeling Pool Spreading, Evaporation and Burning", Journal of Hazardous Materials, 161, 1265-1280.

Brambilla S., D. Manca, 2011, "Recommended features of an industrial accident simulator for the training of operators", Journal of Loss Prevention in the Process Industries, 24, 4, 344-355.

Coleman M.J., 1994, "Industry, school, government cooperate in model training for operators", Tappi Journal, 77, 3, 113-114.

Endsley M., D. Garland, (Eds.), 2000. Situation awareness analysis and measurement. Mahwah, NJ: LEA.

I.A. Karimi and Rajagopalan Srinivasan (Editors), Proceedings of the 11th International Symposium on Process Systems Engineering, 15-19 July 2012, Singapore.

Semantic similarity for case-based reasoning in the context of GMP

Yuske Tsujioka[a], Suriati Akmal[a], Yukihiko Takada[a], Hirofumi Kawai[b], and Rafael Batres[a]

[a]*Toyohashi Tech, Tempaku-cho, Toyohashi 441-8580, Japan*
[b]*Tokyo Institute of Technology, Nagatsuta-cho, Yokoyama 226-8503, Japan*

Abstract

The use of incident information in GMP-regulated manufacturing environments has been impeded by the lack of an effective approach to extract information. Case-based reasoning provides opportunities to extract incident information by considering an incident and its resolution as a case. Case-based reasoning relies on good similarity measures which have largely been proposed for numerical similarities. However, little has been reported for semantic similarities that can be used in case-based reasoning systems that represent part of its information using ontologies. This paper investigates semantic similarity measures based on the comparison of classes in a taxonomy by using attribute information obtained with formal concept analysis.

Keywords: semantic similarity, case-based reasoning, GMP, ontologies

1. Introduction

Good Manufacturing Practice (GMP) regulations apply to pharmaceutical, medical device, and food manufacturers to ensure that their products are processed reliably, repeatedly, consistently, safely and to a high quality. Current GMP regulations (CGMPs) require manufacturers to investigate near-misses, and other incidents that have an impact on the product quality and safety. GMP requires the result of an incident-investigation to be reported with data about the incident, including the materials and equipment involved in the incident (e.g. process lines, products, batches and raw materials), possible or actual consequences, possible causes, products made prior to and during the event and corrective or preventive actions. However, as incident reports are stored in text-form, it becomes difficult to extract information that can be used to avoid similar incidents while improving product quality and productivity.

One approach to extract information is to use case-based reasoning (CBR) in which problems are solved "by using or adapting solutions to old problems". In CBR, a case is both a representation of the problem and a solution to that problem. In this paper, a case is made up with information contained in an incident report. Incident reports are stored in a case base where incident information follows a predefined structure based on domain ontologies. When a new problem arises (for example when new incident occurs), the information that is available about this target incident is entered to retrieve similar cases from which the best matching case is selected.

Case-based reasoning uses similarity measures to identify cases which are more relevant to the problem to be solved. Approaches such as the Euclidian distance are used to evaluate the similarity of numerical attributes. Traditionally, syntax-based approaches such as the Levenshtein distance are used to calculate the similarity between

character strings. However, syntax-based similarity measures often fail to produce good matches when confronted with the meaning associated to the words they compare. For example, although pump and compressor are objects that are semantically close, a low degree of similarity is obtained.

Class hierarchies can be used in similarity measures that are based on semantics as a way to overcome the limitations of syntactic similarity measures. Thus, the similarity between two objects is based on the comparison between the classes to which the object belongs.

Unfortunately, lacking systematic approaches for their design, class hierarchies are often developed in an ad-hoc manner. Consequently, the resulting taxonomies lack the justification of the decisions that led to their creation.

To remediate this problem, we employ Formal Concept Analysis (FCA) during the taxonomy development. FCA is an analysis technique for knowledge processing based on applied lattice and order theory. FCA works by processing a collection of objects and their properties to identify hidden relationships.

2. Semantic similarity

Semantic similarity is the similarity between two classes of objects in a taxonomy (Lin, 1998). A class C_1 in the taxonomy is considered to be a subclass of C_2 if all the members of C_1 are also members of C_2. Therefore, the similarity between two classes is based on how closely they are related in the taxonomy. Wu and Palmer (1994) proposed the following similarity measure based on use of subclass links between classes:

$$\mathrm{sim}(C_1, C_2) = \frac{2N_3}{N_1 + N_2 + 2N_3} \tag{1}$$

where N_1 and N_2 are the number of subclass edges from C_1 and C_2 to their closest common superclass; N_3 is the number of subclass edges from the closest common superclass of C_1 and C_2 to the root class in the taxonomy. Note that the measure of Wu and Palmer fails when the closest common ancestor of both classes happens to be the root class.

3. Proposed approach

Based on the concept of ontology (Sowa, 2000), a class is considered to be equivalent to another class if both classes have exactly the same attributes. Similarly, for a given class *C*, all attributes of *C* are also attributes of any subclass of *C*. Therefore, similarity measures can be developed based on the number of common attributes that are shared between two classes.

However, for any taxonomy-based similarity, the correctness of a given similarity between two classes depends on the structural correctness of the taxonomy. This statement equally applies to ontologies, in which the taxonomy is a fundamental part. Here we propose the use of Formal Concept Analysis (FCA) as a way of designing the ontology as it is based on attribute information.

Equations (2)-(6) represent some attribute-based similarity measures. These equations were obtained by combining the equations given by van der Weken *et al.* (2004) but replacing fuzzy sets with attribute sets.

$$\mathrm{sim}_{Union}(C_1, C_2) = \frac{|A_1 \cap A_2|}{|A_1| + |A_2|} \tag{2}$$

$$\mathrm{sim}_{Max}(C_1, C_2) = w_1 \frac{|A_1 \cap A_2|}{|A_1| + |A_2|} + w_2 \frac{|A_1 \cap A_2|}{\max(|A_1|, |A_2|)} \quad (3)$$

$$\mathrm{sim}_{CMax}(C_1, C_2) = w_1 \frac{|A_1 \cap A_2|}{|A_1| + |A_2|} + w_2 \frac{|A_1' \cap A_2'|}{\max(|A_1'|, |A_2'|)} \quad (4)$$

$$\mathrm{sim}_{Min}(C_1, C_2) = w_1 \frac{|A_1 \cap A_2|}{|A_1| + |A_2|} + w_2 \frac{|A_1 \cap A_2|}{\min(|A_1|, |A_2|)} \quad (5)$$

$$\mathrm{sim}_{CMin}(C_1, C_2) = w_1 \frac{|A_1 \cap A_2|}{|A_1| + |A_2|} + w_2 \frac{|A_1' \cap A_2'|}{\min(|A_1'|, |A_2'|)} \quad (6)$$

where A_1 and A_2 are the sets of attributes of classes C_1 and C_2, $|A_1 \cap A_2|$ is the total number of attributes shared by C_1 and C_2, $|A_1|$ and $|A_2|$ represent the number of attributes of C_1 and C_2, A_1' and A_2' are the complements of sets A_1 and A_2 respectively. w_1, and w_2 are weights.

4. Case Study

The case study focuses on comparing the similarity measures presented in the previous section for equipment used in therapeutic protein processes.

4.1. Taxonomy construction

The equipment-class taxonomy was developed using FCA. The attributes in the context table were selected based on: (1) the behavioral characteristics of each device, (2) type of components in the device, (3) materials used or transformed by the device. ConExp (2009) was used to generate the concept lattice which is shown in Fig. 1. After analyzing and correcting the lattice, the resulting lattice and attribute information were converted to OWL format and then used in the similarity calculations. The nodes labeled with *A*, *B*, *C* and *D* represent classes obtained by the FCA analysis, which are identified by their attributes. For example, *B* represents a class of devices that contain semi-permeable membranes.

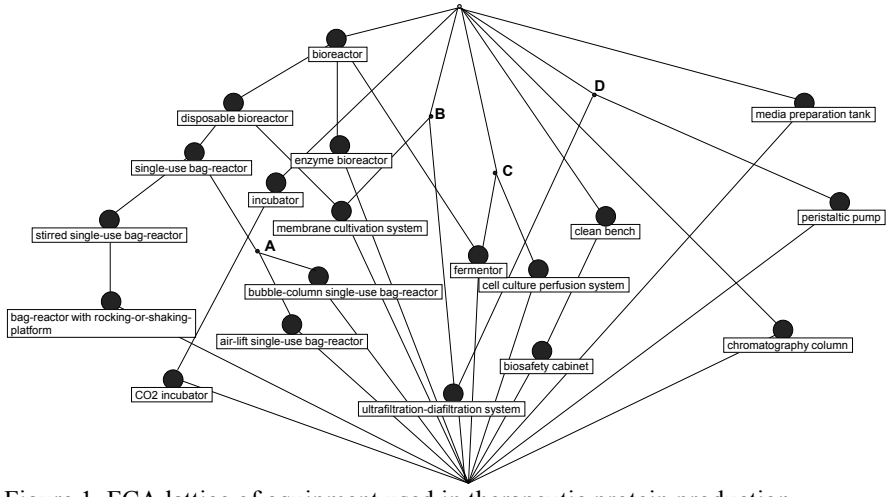

Figure 1. FCA lattice of equipment used in therapeutic protein production

4.2. Similarity calculation

A program was developed in Java to calculate similarities using the proposed approach. The program reads the OWL file and calculates the similarity between classes using equations (4) to (8). Calculations were carried out for several values of w_1, and w_2. Specifically, we focused on the similarity between *enzyme bioreactor* with the rest of the equipment classes.

Table 1. Semantic similarity measures and their correlation against human judgment

Object pair	Human judgment	Wu & Palmer	Eq. (2)	Eq. (3)	Eq. (4)	Eq. (5)	Eq. (6)
air lift single use bag reactor	0.67	0.44	0.50	0.40	0.93	0.67	0.97
Bioreactor	1.00	0.80	0.80	0.67	0.98	1.00	1.00
bioreactors with rocking or shaking platform	0.56	0.44	0.50	0.40	0.93	0.67	0.97
biosafety cabinet	0.28	0.33	0.18	0.13	0.83	0.33	0.94
bubble column single use bag reactor	0.61	0.44	0.57	0.50	0.95	0.67	0.98
cell culture perfusion system	0.72	0.33	0.25	0.20	0.90	0.33	0.95
chromatography column	0.17	0.40	0.33	0.33	0.95	0.33	0.95
clean bench	0.22	0.40	0.25	0.20	0.90	0.33	0.95
CO_2 incubator	0.44	0.29	0.18	0.13	0.83	0.33	0.94
disposable bioreactor	0.89	0.57	0.80	0.67	0.98	1.00	1.00
Fermentor	0.94	0.67	0.50	0.40	0.93	0.67	0.97
Incubator	0.39	0.33	0.22	0.17	0.88	0.33	0.95
media preparation tank	0.33	0.40	0.40	0.33	0.95	0.50	0.98
membrane cultivation system	0.50	0.57	0.50	0.40	0.93	0.67	0.97
peristaltic pump	0.06	0.33	0.22	0.17	0.88	0.33	0.95
single use bag reactor	0.83	0.33	0.80	0.67	0.98	1.00	1.00
stirred single use bag reactor	0.78	0.29	0.57	0.50	0.95	0.67	0.98
ultrafiltration diafiltration system	0.33	0.22	0.17	0.88	0.33	0.95	0.22
Correlation with human judgment	1.000	0.57	0.79	0.76	0.59	0.81	0.77

In the analysis of the results, we utilized the method proposed by Lin (1998) who compares semantic similarity measures by correlating their similarity scores with assessments made by human subjects. For this purpose, we relied on the evaluation that was carried out by a plant engineer who is knowledgeable about the use and characteristics of all the devices considered in this case study.

The results are shown in Table 1. The calculated similarities are also compared against the similarity of Wu and Palmer. Equation (5) yielded the highest correlation with a correlation coefficient of $r = 0.81$ ($w_1 = 0$, $w_2 = 1$). Using traditional statistics, it was found that the similarities against *cell culture perfusion system*, *CO_2 incubator*, *fermentor*, and *stirred single use bag reactor* performed poorly in all similarity measures, possibly due to missing attributes in the FCA analysis. This observation was also corroborated with hierarchical clustering which was carried out on both the results obtained with equation (5) and the reference data (Figure 2). The comparison of the results of the clustering analysis shows that the same four similarities are clustered differently. For example, with the propose similarity measure the similarity between *enzyme bioreactor* and *fermentor* is put closer with the similarity of the pair *enzyme bioreactor – air lift single use bag reactor* while the human expert perceives it as being closer to the similarity of the pair *enzyme bioreactor – disposable bioreactor*. After omitting these points a much higher correlation coefficient $r = 0.95$ ($w_1 = 0$, $w_2 = 1$) is obtained.

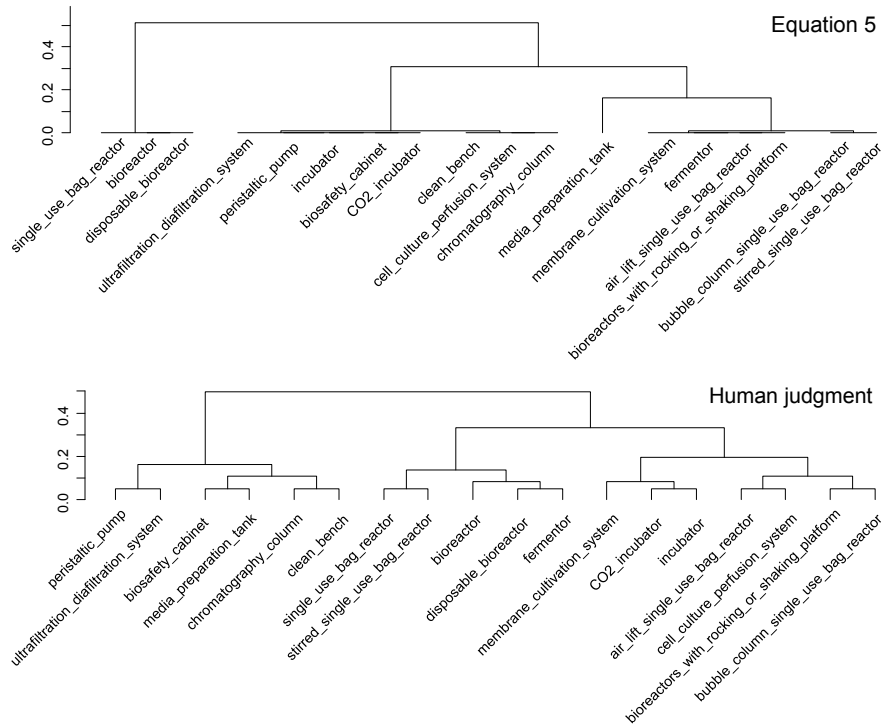

Figure 2. Comparison of the clustering of the two similarity results

5. Conclusions

This paper presented semantic similarity measures based on ontology to determine the degree of similarity of two classes. The results of the experiment show that the cardinality of the intersection between the sets of attributes of the two classes divided over the minimum cardinality performs better when compared against other semantic similarity measures. Furthermore, while Wu-Palmer's similarity is only defined for trees, our approach can be applied to taxonomies containing a class with multiple direct-superclasses (multiple-inheritance). This is because the proposed similarity measures are not only based on the taxonomy but also on the properties that characterize each class in the ontology.

References

D. Lin, (1998), An information-theoretic definition of similarity," in Proc. 15th International Conference on Machine Learning, Morgan-Kaufmann: Madison, WI, pp.296-304

J. F. Sowa, (2000), Knowledge Representation: Logical, Philosophical, and Computational Foundations, Brooks Cole Publishing Co.

D. Van der Weken, M. Nachtegael, and E. E. Kerre, (2004), Using similarity measures and homegeneity for the comparison of images, Image and Vision Computing , pp.695-702

Z. Wu and M. Palmer, (1994), Verbs semantic and lexical selection, in Procs. of the 32nd Annual Meeting of the Associations for Computational Linguistics, pp. 133-138, New mexico

S. Yevtushenko, (2009), Concept Explorer, Open source java software. (Release 1.3.) [Online]. Available: http://sourceforge.net/projects/conexp

I.A. Karimi and Rajagopalan Srinivasan (Editors), Proceedings of the 11th International Symposium on Process Systems Engineering, 15-19 July 2012, Singapore.

Computational Fluid Dynamics at work – Design and Optimization of Microfluidic Applications

Ulrich Krühne,[a] Vijaya K. Bodla,[a] Jacob Møllenbach,[b] Steen Laursen,[b] Naseem Theilgaard,[c] Leif H. Christensen,[d] Krist V. Gernaey[a]

[a] *Center for Process Engineering and Technology, Department of Chemical and Biochemical Engineering, Technical University of Denmark (DTU), DK-2800 Kgs. Lyngby, Denmark, corresponding author ulkr@kt.dtu.dk.*
[b]*Smart Biosystems ApS, Hvildkildevej 48, DK-2400 Copenhagen NW, Denmark*
[c]*Danish Technological Institute, Center of Plastics Technology, Gregersensvej 1, DK-2630 Høje Taastrup, Denmark*
[d]*Danish Technological Institute, Center of Microtechnology and Surface analysis, Gregersensvej 1, DK-2630 Høje Taastrup, Denmark*

Abstract

Computational Fluid Dynamics (CFD) is presented as a powerful tool to support design and optimization of microfluidic reactors. This is demonstrated by means of three case studies. First a three-dimensional scaffold for tissue engineering purposes is investigated using a combination of CFD and a simple biological model. The result is a suggestion of an improved geometry design. In the second case study a microfluidic cartridge of a novel automated in vitro fertilization device is presented, where the CFD model has supported the fluidic design of the microfluidic network in which the stem cells are grown. In the last case study a biocatalytic microfluidic reactor design is presented in which the material characteristics of substrates and products of the catalytic reaction can be investigated. As model system the transaminase catalyzed formation of methylbenzylamine (MBA) from acetophenone is investigated and it is demonstrated how the experimental investigation along with the CFD model can be used for the characterisation of the performance of the reactor system.

Keywords: computational fluid dynamics (CFD), microfluidics, biocatalytic reaction, in vitro fertilisation, optimisation

1. Introduction

Computer aided process engineering has many potential applications. One of the most eloquent ways of applying computational tools is to predict the performance of systems and to use the predictions for optimization of future designs. This can for instance be the configuration of single unit operations or complex process plant designs. Computational fluid dynamics (CFD) has throughout the last decades undergone a breathtaking development and is used increasingly in industrial applications. The prediction quality has indeed reached such a level of maturity that many scientific and industrial users increasingly apply the method for a broad range of applications. Often the companies are performing virtual investigations rather than experiments, or at least they are trying to reduce the number of experiments as much as possible. Typical application areas are for instance the automotive industry [1], the ship building industry [2 and 3] or turbine optimization [4]; where often the improvement of a fraction of a percent of the efficiency is guaranteeing a multimillion Euros return on investment.

A well suited field of application for CFD supported design or analysis is in the area of fluid dynamic conditions with low Reynolds numbers. Typical applications can be found where the flow channel geometries are in the range of micrometers, giving the field the name microfluidics. From a mathematical point of view the equation system is reduced to the Navier Stokes equation and hence no turbulent terms have to be implemented. Therefore the prediction quality of the CFD models is expected to supply excellent qualitative and quantitative results for such systems. In this article three different case studies of the use of CFD in designing microfluidic systems are presented.

2. Materials and Methods

2.1. Software and Modelling

In all presented cases the CFD simulations have been performed by using the ANSYS CFX software. For meshing of the geometry ICEM CFD has been used for the generation of structured hexahedral meshes. In the first case a simple biological model has been implemented with help of the CFX Command Language (CCL). This model is described in [5]. The model considers the growth of biomass with help of a Michaelis Menten kinetic and involves the growth of biomass based on the consumption of substrates and oxygen respiration. Furthermore an additional weight factor is considered in which the existence of a specific shear strain rate (SSR) will have a positive influence on the growth rate of the biomass.

2.2. Scaffold 3D Geometry Design and Optimization

The main hypothesis in this case study is that a biological model is known, which can describe the growth of autologous bone stem cells in an artificial support scaffold in which cells are cultivated in a perfusion type reactor. Besides the material transport of the substrates, the oxygen and the biomass it is assumed that a certain physiological stress level due to the laminar flow around the cells will be beneficial and is known. This assumption is made in order to consider the ongoing discussion in the medical community working in this field [6] and giving therewith the opportunity to design an optimal scaffold from a theoretical point of view.

With help of this model an automatic procedure is started in which a geometry is simulated and a cost function is calculated which is basically the squared sum of the deviation of the actual SSR from the optimal SSR. Then a change of the geometry is proposed and the new value of the cost function is calculated. If the new result is more optimal this geometry will be stored and will serve as the basis for proposing a new change to the geometry again. Otherwise the new solution will be discarded and the old version will still serve as the starting point for the search. This procedure is placed in a loop, programmed with help of a *Practical Extraction and Report Language* (PERL) routine and is automatically actuated over a specified number of runs (ca. 500). A similar evolutionary strategy has been used and is described in [7].

2.3. CFD as software sensor

In the second example a new microfluidic in vitro fertilisation chip [8] is investigated with help of a CFD model. In this chip a series of cultivation chambers are connected by means of a microfluidic channel. An automated flow is generated in this channel due to a hydrodynamic height difference between a medium reservoir and the outlet chamber, where a piston pump is removing the surplus cultivation medium with help of a capillary. A second medium reservoir can be actuated by opening and closing of an equilibration inlet. This system has been modelled by the introduction of an additional

component to the fluid which has a diffusion coefficient of $0.67 \cdot 10^{-9} m^2 s^{-1}$, corresponding to glucose in water.

2.4. The design of a microfluidic biocatalytic reactor

In this last example a biocatalytic reaction has been chosen for a microfluidic reactor system. As model system the transaminase catalyzed formation of methylbenzylamine (MBA) from acetophenone is investigated. This reaction is in detail described in [9] and is expected to be inhibited by the formed MBA or by material transport limitations of the substrate acetophenone. A reactor design in which the produced MBA can be removed simultaneously along with its formation will be desirable, and hence a simulation study of an interdigitated channel system was performed, where short diffusion distances will contribute to the fast product removal. In most cases the material characteristics such as diffusion velocities, solubilities or reaction rates are not documented. It is therefore desirable to have a mathematical tool to design experiments for verification of such key information. Similar to *2.3,* different reaction components have been modelled as additional components with different diffusion coefficients. The performance of a first experimental setup was investigated with the help of dyes, which are mixed with the different flows.

3. Results and Discussion

3.1. The optimal 3D scaffold geometry

As a starting point of the simulation it was expected that the resulting optimal geometry would be a tubular system with the corresponding diameter, which will induce the appropriate SSR at all points of the tubular wall system. In Figure 1a the starting geometry is presented with a gradient surface plot of the SSR. Figure 1b shows an intermediate result of the simulations, where it can be observed that the SSR has already considerably changed. In Figure 1c the final geometry is illustrated as a 3D surface and it can be seen that the optimal geometry is not a tubular system, as anticipated. It is rather a tube, which is squeezed in the middle and then again squeezed twice in the start and the end in a direction that is perpendicular to the first diameter reduction. In this way a larger surface is obtained along with the appropriate SSR at this increased surface area.

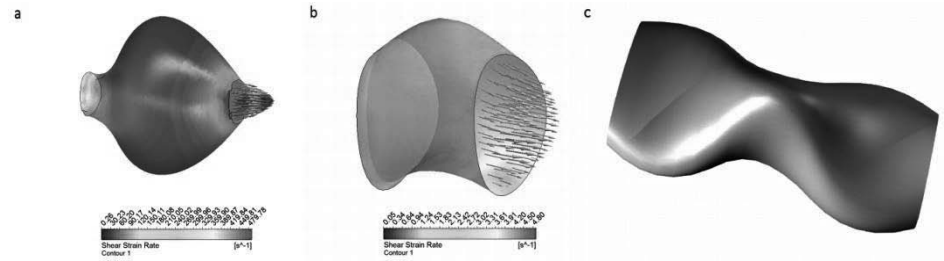

Figure 1.a. Starting geometry with SSR plot; b. intermediate result; and, c. the final 3D geometry in the optimized form.

3.2. CFD as software sensor

In this case study the IVF Chip [8] has been modelled and a transient simulation has been performed. In Figure 2a the qualitative concentration is shown in the middle plane of the flow channels and cultivation chambers. It can be seen that the upper part of the fluid domain is filled rather quickly, while the lower part, where the cells are located will not be filled as fast as the compartments above. A visual experiment with help of image analysis, shown in Figure 2b, cannot be used for the determination of the

concentration level at different depths of the system. In Figure 2c the streamlines of the flow through a cultivation compartment are presented and the worst case scenario for the placement of the embryo cell is indicated as a red cross. Finally the transient concentration profile of the averaged outlet concentration is presented in Figure 2d along with the concentration profile corresponding to the location indicated by the red cross on Figure 2c in the most downstream well. It can be seen that the transient build up of new medium at the bottom of the last well behaves much more sluggish than the outlet average concentration. But after approximately 12 minutes also the worst case placement of the cell has reached a concentration level corresponding to 95% of the desired concentration.

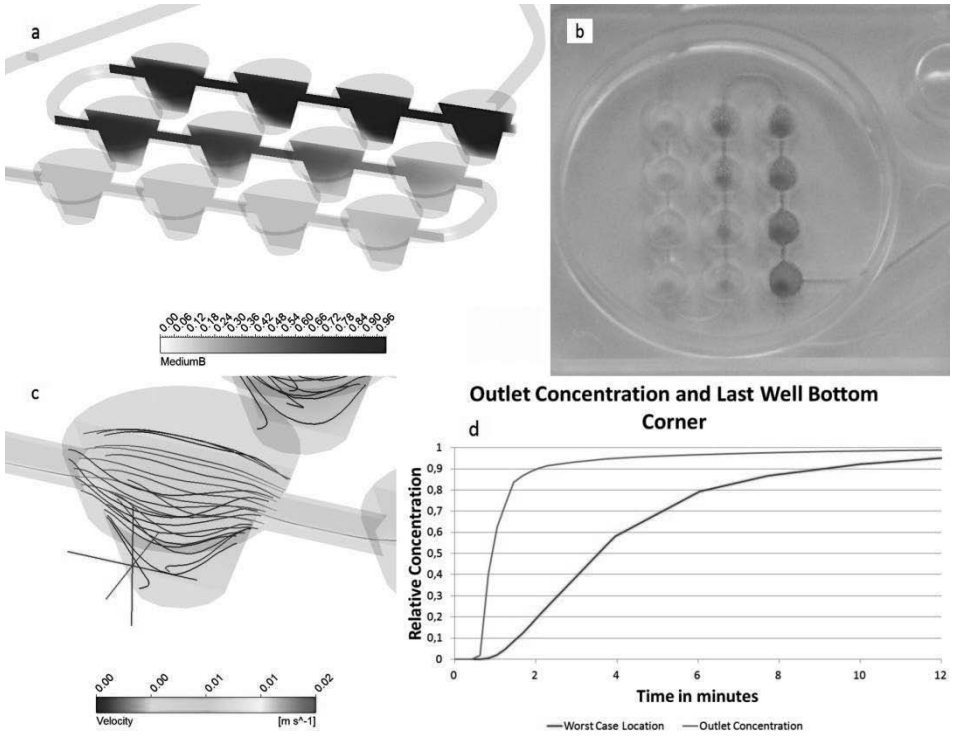

Figure 2.a. intermediate concentration profile; b. photograph of a medium change experiment with a blue dye; c. streamlines in the last cultivation chamber with the worst case placement of the cells (red cross); and, d. the transient dimensionless concentration at the outlet (averaged) and worst case placement (red cross)

3.2.1. Design of a biocatalytic reactor

In the presented simulation results in Figure 3.a the diffusion pattern of two substrate streams are shown which result from introducing alternating flows into a flow reactor (on the right hand side of figure 3a). It can be seen that the mixing due to fast diffusion coefficients ($2 \cdot 10^{-9} m^2 s^{-1}$) leads to a relatively equilibrated concentration profile already after a short distance. When performing the experimental investigation in an experimental setup with red and blue dyes with a much slower diffusion coefficient no mixing can be observed (Figure 3b). This information can be used consequently for a detailed investigation of the material properties which are predicted and observed, yielding new reactor designs, mathematical tools and simulation experiments for

optimisation of the biocatalytic reaction. Even though this result is only for demonstration purposes, the subsequent extraction of side streams at different positions of this reactor system combined with subsequent HPLC analysis will yield the exact concentration levels of the respective components. The latter will then result in a more detailed understanding of material characteristics, reaction kinetics or other information that is relevant for the specific biocatalytic reaction.

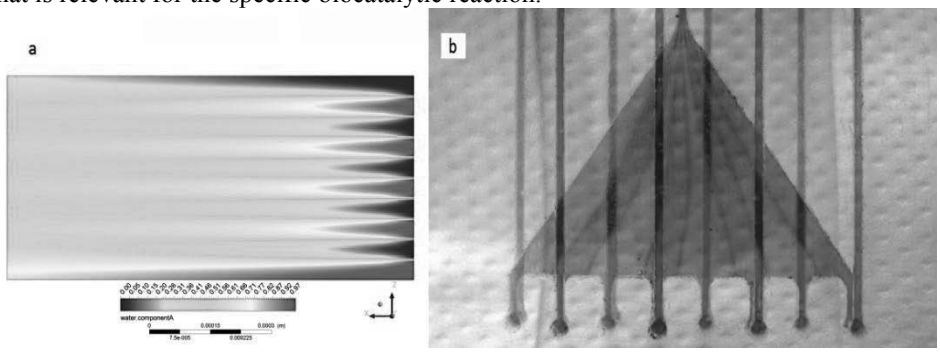

Figure 3.a. Simulation of the interdigitated fluidic array (fast diffusion coefficients for both media); b. Experimental setup with dyed liquid streams.

4. Conclusions

CFD has been demonstrated as a powerful tool for development of new theoretical qualitative insight or quantitative understanding of difficult measurable key components in microfluidic applications. Due to the lack of turbulent flow conditions in miniaturized systems the CFD results have a high predictive quality and can be obtained with relatively small effort.

Acknowledgements The work was partly financed by the Danish Research Council for Technology and Production and the 'AUTOBONE' Strep RTD project supported by the EC under the 6th Framework Programme under contract number 505711-1.

References

[1] R.Tilch et. al., 2008, Combination of body-fitted and embedded grids for external vehicle aerodynamics, Engineering Computations, 25 (1), 28-41.
[2] R. Leidenberger and K. Urban, 2011, Automatic differentiation for the optimization of a ship propulsion and steering system: a proof of concept, Journal of Global Optimization, 49 (3), 497-504.
[3] I.M. Viola, 2009, Downwind sail aerodynamics: A CFD investigation with high grid resolution, Ocean Engineering, 36 (12-13), 974-984.
[4] Y. Li et al., 2012, Dynamic overset CFD simulations of wind turbine aerodynamics, Renewable Energy 37 (1), 285-298.
[5] U. Krühne et. al., 2010, A transient 3D-CFD model incorporating biological processes for use in tissue engineering, Micro and Nanosystems, 2 (4), 249-260.
[6] C.V. Gemmiti and R. Guldberg, 2009, Shear stress magnitude and duration modulates matrix composition and tensile mechanical properties in engineered cartilaginous tissue, Biotechnology and Bioengineering, 104 (2), 809-820.
[7] D. Schäpper et. al., 2010, Topology optimized microbioreactors, Biotechnology and Bioengineering, 108 (4), 786-796.
[8] www.smartbiosystems.com
[9] P. Tufvesson et. al., 2011, Process considerations for the asymmetric synthesis of chiral amines using transaminases, Biotechnology and Bioengineering, 108 (7), 1479-1493.

I.A. Karimi and Rajagopalan Srinivasan (Editors), Proceedings of the 11th International Symposium on Process Systems Engineering, 15-19 July 2012, Singapore.

Modeling the Superovulation stage in IVF

Kirti M. Yenkie, [a,b] Urmila M. Diwekar, [a,b] Vibha Bhalerao [c]

[a]*Department of Bio Engineering, University of Illinois, Chicago, IL 60607 - USA*
[b]*Center for uncertain Systems: Tools for Optimization & Management (CUSTOM), Vishwamitra Research Institute, Clarendon Hills, IL 60514 – USA*
[c]*Jijamata Hospital, Nanded, Maharashtra, India*

Abstract

In-vitro fertilization (IVF) is the most common technique in assisted reproductive technology and in most cases the last resort for infertility treatment. It has four basic stages: superovulation, egg retrieval, insemination/fertilization and embryo transfer. Superovulation is a drug induced method to enable multiple ovulation per menstrual cycle. The success of IVF majorly depends upon successful superovulation, defined by the number and similar quality of eggs retrieved in a cycle. Hence, modeling of this stage in terms of distribution of eggs (oocytes) obtained per cycle involving the chemical interactions of drugs used and the conditions imposed on the patient during the process would provide a basis for predicting the possible outcome. This is the focus of current endeavor. The model will be made more robust by considering uncertainties; like the response of a patient depending upon previous medical history, suitability of medicine and type of protocol used. This model will then be used to decide optimal drug delivery so as to maximize good quality egg formation. Thus, a phenomenon currently based on trial and error will get a strong base. It will help the patient to decide whether to undergo superovulation or start the IVF from donor eggs, which in turn would save the patient from financial loss as well as emotional distress.

The aim of crystallization is to get maximum crystals of similar size and purity, while superovulation aims at eggs of similar quality which include the properties of size and number of chromosomes to enlist a few. The rate of crystallization and superovulation are both dependent on the process conditions and varies with time. Thus, model formulation for multiple ovulation will be on parallel lines to crystal formation in a batch process and will be modeled such.
Keywords: superovulation, batch crystallization, protocol, infertility treatment

1. Introduction

Around 80 million people in the world are suffering from infertility issues. The rate of fertility is constantly declining in the developed nations due to late marriages, postponed childbearing and primary infertility. On the contrary, in the developing world the reasons for infertility involve prevalence of sexually transmitted diseases, infections increasing the rate of secondary infertility. Childlessness is often stigmatized and leads to profound social suffering for women in the developing nations. In 1995, United Nations included rights of men and women to choose the number, timing and spacing of their children by calling reproductive health programs to include prevention and treatment of infertility (de Melo Martin, 1998).

In most countries cost is a major hurdle for access of infertility services. Most centers offering treatment for infertility operate outside of government financed health facilities. The treatment is only accessible to elites who can afford to pay for such high tech therapies. Even in a country like United States, the cost for an IVF cycle amounts

to 20% of the total annual income of a median American family. In developing nations, the cost of an IVF cycle is about 50% of the total annual income (Pennings, 2008).

2. In-vitro fertilization:

It is a process by which oocytes or egg cells are fertilized by a sperm outside the body in a laboratory simulating similar conditions in the body and then the fertilized eggs are implanted back in the uterus for full term completion of pregnancy.

2.1. Four stages in IVF:

1. Superovulation: It is method to retrieve multiple eggs using drug induced stimulation. In normal female body only one egg is ovulated per menstrual cycle, but with the use of fertility drugs and hormones, more number of eggs can be ovulated per cycle.
2. Egg collection (retrieval): On the maturation of the multiple eggs produced in the previous stage, the eggs are retrieved through special techniques like ultrasonically guided transvaginal oocyte retrieval.
3. In vitro fertilization (inseminaton/fertilization): This stage is accomplished in the IVF laboratory. Fertilization is done in the incubator using the retrieved oocytes and sperms. The conditions are maintained so as to mimic the invivo environment.
4. Embryo transfer: It takes place after several days of oocyte retrieval and after the fertilization stage is successful. The fertilized embryos are implanted into the uterus via a non-surgical technique using ultrasound guidance.

IVF treatment is an expensive treatment. There are a lot of complications associated with each stage and hence the success is highly unpredictable. The major cost of IVF is associated with the superovulation stage where expensive drugs are used and almost daily monitoring is required. Success of this stage in terms of number and quality of eggs affects the outcome of IVF and hence is a very important stage. In this work, we concentrated on modeling this stage and the approach is presented in the next section.

3. Superovulation:

In this work, we follow the analogy between batch crystallization and superovulation.

3.1. Analogy between Superovulation and Batch crystallization:

The moment model for follicle number and size is adapted from the concept of batch crystallization (Q. Hu. et. al., 2005) based on the analogy between batch crystallization and superovulation presented in Table 1.

Table 1: Analogy between batch crystallization and IVF superovulation stage

Batch Crystallization	Superovulation (IVF stage I)
Production of multiple crystals	Production of multiple oocytes or eggs
Crystal quality is determined in terms of size distribution and purity	Oocyte quality is determined in terms of no abnormalities, similar size.
The rate of crystallization or crystal growth varies with time and process conditions	The rate of ovulation or oocyte growth varies with time and drug interactions
Process is affected by external variables like agitation, and process operating variables like temperature, pressure, etc.	Process is affected by externally administered drugs and body conditions of the patient undergoing the process

The superovulation follicle growth model in general resembles greatly to the growth of seeded batch crystals. The aim of seeded batch crystallization is to allow the

seeds added to the solution to grow to desired shape and size and truncate the process of nucleation by maintaining certain process conditions. The numbers of seed added to the solution are constant and hence the zeroth moment of seeded batch crystals which corresponds to its number is constant. Similarly, when we look at superovulation, the number of follicles activated during an IVF cycle is constant. Thus, the moment model for both the processes remain the same the growth term which is a function of process variables like temperature and supersaturation in batch seeded crystallization will become a function of medicinal dosage in case of superovulation process.

4. Model details

Due to ovarian stimulation using externally injected hormones the number of follicles activated to enter into the ovulation stage are more in number as compared to a single follicle in a normal menstrual cycle. From the current data on successful superovulation for patient 1, organized in Table 2; it can be observed that during FSH dosage regime, as the time progresses the size of the eggs increase.

Table 2: Variation of Follicle size (diameter) with time and FSH dose

Sr. No	Size range (mm) / Days →	Day 1	Day 2	Day 5	Day 7	Day 9
1.	0-4	15	8	6	0	0
2.	4-8	3	6	4	2	0
3.	8-12	0	4	10	14	4
4.	12-16	0	0	0	2	11
5.	16-20	0	0	0	0	3
	FSH dose	0	300	300	300	225

4.1. Model Assumptions:

The rate expression for follicle growth is dependent on FSH administered. Thus, we can write the growth term as;

$$G=kC_{fsh}{}^{\alpha} \quad (1)$$

Assuming moment model, we consider the first six moments; zeroth moment corresponding to follicle number, the first moment corresponding to follicle size and the other 4 moments. Since, we have assumed follicle number to be a constant, hence the zeroth moment will have a constant value. Also, 1st to 5th moments are being used since they help in recovering the size distributions more precisely as against lower number of moments.

4.2. Model equations (Q. Hu. et. al., 2005):

$$\mu_0=\text{constant} \quad (2)$$

$$\frac{d\mu_1}{dt}=G(t)\mu_0(t) \quad (3)$$

$$\frac{d\mu_2}{dt}=2G(t)\mu_1(t) \quad (4)$$

$$\frac{d\mu_3}{dt}=3G(t)\mu_2(t) \quad (5)$$

$$\frac{d\mu_4}{dt}=4G(t)\mu_3(t) \quad (6)$$

$$\frac{d\mu_5}{dt} = 5G(t)\mu_4(t) \qquad (7)$$

Conversion of the data available on follicle number and size to moment using the expression given in literature by Flood, 2002:

$$\mu_i = \sum n_i(r,t) r_i^n \Delta r_i \qquad (8)$$

Here, $\mu_i = i^{th}$ moment

$n_i(r,t)$ = number of follicles in bin of mean radius 'r' at time 't'.

r_i = mean radius of i^{th} bin

Δr = range of radii variation in each bin

4.3. Moment evaluation:

Table 3: Experimental moments evaluated using equation 8

Sr. No	Time (day)	μ_0	μ_1	μ_2	μ_3	μ_4	μ_5	FSH	Cumulative FSH
1.	2	36	92	324	1340	5988	27932	300	300
2.	5	36	146	584	2728	13160	64456	300	1200
3.	7	36	180	932	4980	27428	155700	300	1800
4.	9	36	248	1764	12920	97188	749048	225	2025

5. Results:

We integrate the equations 2-7 for predicting the kinetic constants in the follicle growth expression. Later we use non-linear optimization algorithm to predict the values of these kinetic constants along with the integration constants obtained after integrating the set of moment equations. The moment values obtained from the model equations and the experimentally evaluated moments are compared and it is observed that the lower moments show some deviations, while the fit is much better for higher moments. In real practice, the model will be calibrated with the first two days of data and then used for prediction of the complete cycle.

5.1. Model Validation:

The current moment model predicts the moment values, however our final output desired is the follicle size distribution, thus in model validation the approach to obtain follicle size distribution from moment values are shown. For predicting the size distribution it is essential to have atleast 5 orders of moments to be known. The method is adapted from the literature by Flood 2002; where he shows the method to recover particle size distribution from moments in batch crystallization. Using the model predicted moment values we evaluate *n(r,t)* and compare with the actual data to check the model accuracy. We plot the follicle size distribution for four patients for various days. The experimental size distribution is shown by symbols while the continuous curve shows the model predicted values after using the inversion method. It can be seen that the predicted values are close to experimental size distribution.

6. Conclusion

The moment model developed for IVF superovulation predicts the follicle size distribution which is in well agreement with the actual size distribution seen in the IVF cycle data. The model can be used to predict the outcome. This will reduce the almost daily requirement of testing. The model can also provide a basis for predicting the optimum dosage for the desired outcome from the superovulation stage. The model used

here is a very basic model and the complexities present in the patient are not considered. Later, we aim to include these complexities and model the system uncertainties, using more data for analysis, modeling and validation.

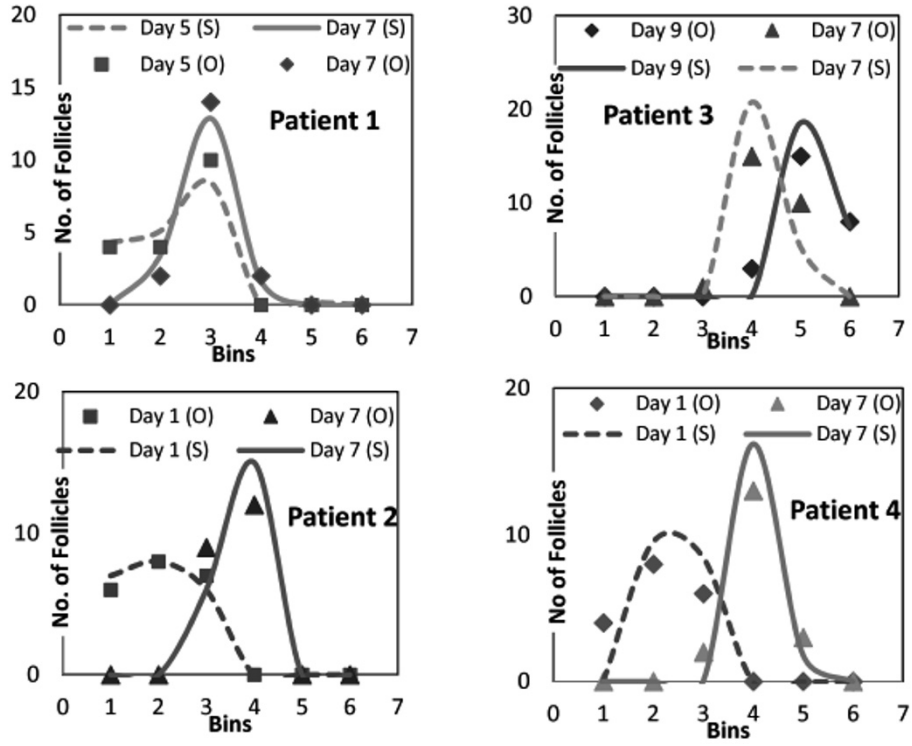

Fig 1. Follicle size distribution for four patients for various days

References

Nachtigall, R. D., 2006. "International disparities in access to infertility services", *Fertility and Sterility,* Vol. 85, No. 4, pp. 871-875.

Ombelet, W., Cooke, I., Dyer, S., Serour, G., and Devroey, P., 2008. "Infertility and the provision of infertility medical services in developing countries" *Human Reproduction Update,* Vol. 14, No. 6, pp. 605-621.

Pennings, G., 2008. "Ethical issues of infertility treatment in developing countries." *European Society of Human Reproduction and Embryology,* pp. 15-20.

Flood, A. E., 2002. "Thoughts on recovering particle size distributions from the moment form of the population balance." *Dev. Chem. Eng. Mineral Process,* Vol. 10, No. 5/6, pp. 501-519.

Commentary: The importance of fertility treatment in the developing world, 2005. *BJOG: an International Journal of Obstetrics and Gynaecology,* Vol. 112, pp. 1174 - 1176.

Baird, D. T., 1987. "A model for follicular selection and ovulation: Lessons from Superovulation." *J. steroid Biochem,* Vol. 27, No. 1-3, pp. 15-23.

Q. Hu, S. Rohani, A. Jutan, 2005. "Modelling and optimization of seeded batch crystallizers" *Computers and Chemical Engg.* Vol. 29, pp. 911-918.

de Melo-Martin, I., 1998. "Ethics and Uncertainty: In Vitro Fertilization and Risks to Women's Health" Risk: Health, Safety & Environment 201.

I.A. Karimi and Rajagopalan Srinivasan (Editors), Proceedings of the 11th International Symposium on Process Systems Engineering, 15-19 July 2012, Singapore.

Computational fluid dynamics simulation of the feed distribution system of a falling film distillation device

Joel G. Teleken,[a] Leandro O. Werle,[b] Iaçanã G. B. Parisotto,[b] Cintia Marangoni,[c] Ana P. Meneguelo,[d] Ariovaldo Bolzan,[b] Ricardo A. F. Machado[b]

[a]*Campus Palotina, Parana Federal University, Mail Box: 5153, Palotina-PR, Brazil, ZIP CODE 85950-000*
[b]*Department of Chemical Engineering, Santa Catarina Federal University, Mail Box: 476, Florianópolis-SC, Brazil, ZIP CODE 88040-970*
[c]*Process Engineering Master Program, University of the Joinville Region, University Campus, Bom Retiro, Joinville-SC, Brazil ZIP CODE 89219-905*
[d]*Federal University of Espírito Santo, Univ Center North of Espírito Santo, Department of Eng and Computing, km 60, BR101, São Mateus-ES, Brazil ZIP CODE 29932-540*

Abstract

This paper addresses the analysis of a distillation process by descending liquid film, more specifically the feed distribution system. This system offers simple construction, low resistance to liquid flow high capacity and. In this new equipment configuration the feed distribution system directly influences the efficiency of the separation. The objective of this study is to determine the best configuration of the feed distribution system through Computational Fluid Dynamics (CFD) simulations. The results obtained for this system indicate the formation of a thin liquid film on the walls of the distillation tube. The observed flow pattern oscillates between intermittent and gush, with a predominance of intermittent. Results were also obtained for the same geometry but with rotational movement.

Keywords: falling film, CFD, feed distribution system.

1. Introduction

Distillation by falling liquid film is a process with a low residence time and simple structure when compared to conventional distillation. It basically consists of a vertical unit, through which the liquid flows downwards, creating a film. Also, when the construction details are optimized, it is possible to obtain high heat and mass transfer rates [1]. However, this is an inherently non-equilibrium process, where the effect of the vapor generated by the liquid has almost no influence on the separation factor and rate. Due to the non-existence of convection by ebullition, the distillated flow is extremely limited, requiring frequent renovation. However, the process presents a simple construction, low resistance to the liquid discharge and high separation ability. As a consequence of the construction and phenomenological characteristics of this process, its effectiveness is intrinsically related to the feeding system.

In recent years, there has been considerable academic and industrial interest in the use of computational fluid dynamics (CFD) to model two phase flows in some chemical engineering processes. The volume-of-fluid (VOF) technique can be used for an initial determination of multiphase flows on structured packing. Szulczewska et al. [2] simulated the gas-liquid counter-current flow on plate-type structured packing. Gu et al.

[3] developed a two-phase flow CFD model using the VOF method to predict the hydrodynamics of falling film flow in structured packing. Ataki et al. [4] simulated the liquid flow structure in a structured packing element and liquid redistribution at the node of structured packing with the VOF model.
The hydrodynamics of the liquid-vapor contact has an essential function in the falling liquid film distillation design, since it determines the column fluid dynamics limits and controls the mass transfer rates. Computational fluid dynamics (CFD) has been used successfully to model the multiphase discharge in many chemical engineering systems [5-7]. It has become a powerful tool for the design and analysis of chemical processes. Due to the characteristics of the falling film distillation process, it is necessary to use feeding devices that allow a uniform distribution and adequate formation of a liquid film on the entire wall area of the unit. The simulations carried out allowed the evaluation of two different systems, one static and another with rotational movement using two rotation frequencies. The aim of this study is to evaluate the influence of the feeding system (rotational or static cone) on the film formation. The CFD technique was used as an auxiliary design tool due to its notable ability to represent systems. It is important to note that in this study only the flow of the water/air system will be analyzed. However, this is sufficient to characterize the flow as a whole, where the liquid mixture is represented by water vapor and the gas mixture is represented by air. Thus, an analysis of the fluid dynamics of the gas/liquid flow was carried out. The mass and heat transfer will the subject of a future study.

2. Methodology

This section is divided into three subsections. The first contains a brief description of the pilot distillation unit; the second describes the mathematical model used in these simulations; and the third presents the boundary conditions.

2.1. Geometric Characteristics of the System

The geometry for the feeding distribution system was proposed based on a study by Batistella [1]. Figure 1 shows the experimental apparatus which consists of a vertical tube and a mesh. Figure 1 (a) shows the liquid inlet at the top of the distillation tube and the design initially used to run the experimental tests with the rotational and static cones. The distribution system consists of a hollow steel cone which promotes a liquid film near the glass tube wall. Gas flows up through the inner part from the base.

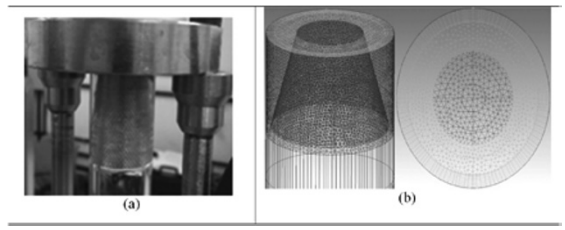

Figure 1. (a) Distribution and feeding part and (b) Hybrid mesh.

Figure 1(b) shows a hybrid mesh (with tetrahedral and prismatic volumes) built to represent the equipment and power distribution system used to perform the simulations. It should be noted that this mesh configuration gave the best numerical results with respect to convergence and time required to perform the simulations. It was built with a refined hybrid mesh comprising the prismatic walls of the distillation tube since this is the region of greatest interest in the study, *i.e.*, the area where formation of the film occurs.

2.2. Mathematical Model

The model considers the flows of gas and liquid in a Eulerian-Eulerian framework, where the phases are treated with transport equations. The equations used to solve this problem were the mass continuity and momentum equations. In order to solve these the equation of momentum flow was also required [7]. It was considered that the fluctuation (turbulence) consists of the formation and dispersion of small swarms of bubbles, and that the Reynolds stresses can be linearly related to the mean velocity gradients (eddy viscosity hypothesis), as in the case of the relation between the stress and strain tensors in laminar Newtonian flow. The shear stress transport (SST) turbulence model for multiphase flow was assumed [6].

2.3. Boundary Conditions

Dirichlet boundary conditions were used in these simulations, as follows:

1) Liquid inlet: Inlet conditions, with normal flow to the surface. A uniform liquid inlet velocity profile is recommended. Only liquid enters through the liquid inlet area, so the liquid volume fraction is taken as unity;

2) Liquid outlet: outlet condition, with normal flow to the surface. The liquid outlet boundaries were specified as pressure boundaries with volume fraction specifications. The specifications assumed that only liquid or gas leaves the simulation geometry;

3) Opening of the upper part of the cone: open condition, that is, it allows the air and/or liquid to enter and exit at the top of the cone. Entry/exit is determined by the pressure equalization;

4) Wall: All walls for the two phases are specified as no-slip wall boundaries;

5) The values of the variables of interest, such as liquid volumetric fraction, and air and water superficial velocities, were investigated at three different heights of the distillation unit and horizontal lines were drawn for this purpose. Considering the lower base of the feeding cone as zero (0) the lines were drawn at 10, 65 and 165 mm from the cone bottom. The studies were focused on the analysis of the water volumetric fraction, liquid film uniformity and thickness and formation of dry points throughout the distillation unit. The simulation conditions analyzed in this paper are listed in Table 1.

Table 1. Simulation Conditions

	Mixture water/air		
Mass Flow	50 ($kg.h^{-1}$)	50 ($kg.h^{-1}$)	50 ($kg.h^{-1}$)
Rotational Speed	-	750 rpm	1000 rpm
Wall Temperature	25ºC	25ºC	25ºC

The code used to model the computational fluid dynamics was CFX 12.0. The finite volume numeric method was used for the discretization of the equations, with a high-order interpolation scheme (high resolution) in order to avoid problems of oscillation and numerical diffusion. The pressure-velocity coupling was obtained using the phase-coupled SIMPLE algorithm. The total number of unstructured cells within the computational space was 1135238 and these are shown in Figure 1(b). Air and water were used as the gas and liquid phases, respectively, at ambient pressure. The time step was 0.01 s and the convergence criterion adopted was an average error of 10^{-5}.

3. Results and Discussions

In this section the main results obtained in the simulations carried out using the CFX 12.0 software will be reported. In Figure 2 the development of the liquid volumetric fraction profiles across the entire radius for the three height levels is shown.

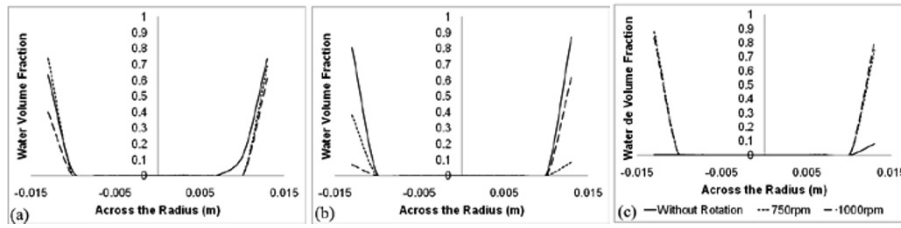

Figure 2. Liquid volumetric fraction profiles (a) 10 mm (b) 65 mm and (c) 156 mm below the feeding cone for a 50 (kg.h^{-1}) mass flow with tetrahedral mesh, cone with 750 and 1000 rpm rotation.

As can be observed in Figure 2, there were no significant differences between the liquid volumetric fractions, that is, the profiles followed a pattern formation related to the liquid volumetric fraction on the walls. On further analyzing Figure 2 it can be observed that the thickness of the film formed varies as the discharge takes place.
Figure 3 shows the Reynolds values found for each of the simulations with the power supply off and rotating at 750 and 1000 rpm.

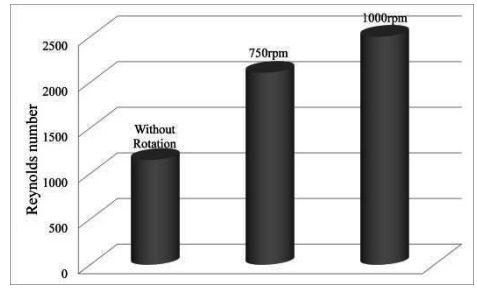

Figure 3. Average Reynolds number for each of the simulations.

It can be observed in Figure 3 that the Reynolds number increases on moving from a stationary power system to a rotation of up to 1000 rpm. This occurs because the liquid undergoes a centripetal acceleration due to the rotation of the cone and the flow has a greater velocity when in contact with the walls of the distillation tube. Figure 4 shows the volume fraction of the liquid on the distillation tube wall, over its entire length for the three simulated cases. Observing the volume fraction of the liquid on the walls of the tube distillation shown in Figure 4 (a, b and c), there is the formation of some preferential paths and also some dry spots as previously observed in experimental studies.

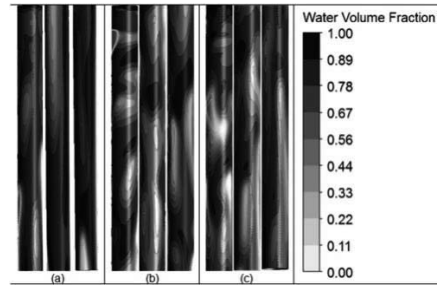

Figure 4. Profile of the volume fraction of liquid on the walls of the distillation tube for a feed flow rate of 50 (kg.h^{-1}), (a) cone without rotation, (b) cone rotating at 750 rpm and (c) cone rotating at 1000 rpm.

The formation of dry spots is not desirable from the standpoint of the distillation process by descending liquid film, because in places where there is no evaporating liquid film in contact with the steam that rises inside the tube the processes of heat and mass transfer will not occur. From the liquid volumetric fraction on the distillation unit walls in Figure 4 a slight difference can be perceived between the distributions in different parts of the unit. However, it is not possible to state that the rotational system provided a significant gain or improvement in the film formation on the distillation unit walls, and thus its use cannot be recommended.

4. Conclusions

In a rotational system the film formation is more uniform throughout the distillation unit compared with a static system. However, the formation of dry spots occurs in a similar way in both the static and rotational systems. Thus, we can conclude that this system has an impact on the film renovation. This difference becomes more evident in the case of viscous fluids. For a system with the characteristics of an air/water mixture the feeding carried out through the static device was found to be more appropriate. Studies are being carried out in order to evaluate the use of this feeding distribution system for a highly viscous mixture. The processes of heat and mass transfer through distillation using a falling liquid film are also currently being analyzed. With respect to the flow regime, two regimes were observed in full flow with a transition in the range of turbulent flow which, according to the literature, is good for the process as mass transfer can occur in a laminar flow because the film is stagnant. Regarding the maintenance of the film, it is not possible to state that the use of a rotational system substantially improved the quality of the film.

5. Acknowledgements

The authors are grateful for the financial support of the CNPq (Brazil).

6. References

[1] C.B. Batistella, (1999), Tecnologia da destilação molecular: da modelagem matemática à obtenção de dados experimentais aplicada a produtos de química fina. 216 f. (Tese de Doutorado) – Faculdade de Engenharia Química, Universidade Estadual de Campinas.
[2] B. Szulczewska, I. Zbicinski, A. Gorak, (2003), Liquid flow on structured packing: CFD simulation and experimental study, Chem. Eng. Technol., 26, 580–584.
[3] F. Gu, C. J. Liu, X. G. Yuan, G.C. Yu, (2004), CFD simulation of liquid film flow on inclined plates, Chem. Eng. Technol., 27, 1099–1104.
[4] A. Ataki, H. J. Bart, (2006), Experimental and CFD simulation study for the wetting of a structured packing element with liquids, Chem. Eng. Technol., 29, 336–347.
[5] D. Noriler, H. F. Meier, A. A. C. Barros, M. R. Wolf Maciel, (2008), Thermal fluid dynamics analysis of gas–liquid flow on a distillation sieve tray, Chem. Eng. Journal, 136, 133-143.
[6] M. R. K. Nikou, M. R. Ehsani, (2008), Turbulence models application on CFD simulation of hydrodynamics, heat and mass transfer in a structured packing, International Communications in Heat and Mass Transfer, 35, 1211-1219.
[7] X.G. Li, D. X. Liu, S. M. Xu, H. Li, (2009), CFD simulation of hydrodynamics of valve tray. Chemical Engineering and Processing: Process Intensification, 48, 145-151.

Author Index

ELSEVIER

11TH INTERNATIONAL SYMPOSIUM ON PROCESS SYSTEMS ENGINEERING

PART B

Edited by

I.A. KARIMI AND R. SRINIVASAN

COMPUTER-AIDED CHEMICAL ENGINEERING, 31

PSE 2012

11th INTERNATIONAL SYMPOSIUM ON PROCESS SYSTEMS ENGINEERING

COMPUTER-AIDED CHEMICAL ENGINEERING
Advisory Editor: R. Gani and E.N. Pistikopoulos

Volume 1: Distillation Design in Practice (L.M. Rose)
Volume 2: The Art of Chemical Process Design (G.L. Wells and L.M. Rose)
Volume 3: Computer Programming Examples for Chemical Engineers (G. Ross)
Volume 4: Analysis and Synthesis of Chemical Process Systems (K. Hartmann and K. Kaplick)
Volume 5: Studies in Computer-Aided Modelling. Design and Operation
Part A: Unite Operations (I. Pallai and Z. Fonyó, Editors)
Part B: Systems (I. Pallai and G.E. Veress, Editors)
Volume 6: Neural Networks for Chemical Engineers (A.B. Bulsari, Editor)
Volume 7: Material and Energy Balancing in the Process Industries - From Microscopic Balances to Large Plants (V.V. Veverka and F. Madron)
Volume 8: European Symposium on Computer Aided Process Engineering-10 (S. Pierucci, Editor)
Volume 9: European Symposium on Computer Aided Process Engineering-11 (R. Gani and S.B. Jørgensen, Editors)
Volume 10: European Symposium on Computer Aided Process Engineering-12 (J. Grievink and J. van Schijndel, Editors)
Volume 11: Software Architectures and Tools for Computer Aided Process Engineering (B. Braunschweig and R. Gani, Editors)
Volume 12: Computer Aided Molecular Design: Theory and Practice (L.E.K. Achenie, R. Gani and V. Venkatasubramanian, Editors)
Volume 13: Integrated Design and Simulation of Chemical Processes (A.C. Dimian)
Volume 14: European Symposium on Computer Aided Process Engineering-13 (A. Kraslawski and I. Turunen, Editors)
Volume 15: Process Systems Engineering 2003 (Bingzhen Chen and A.W. Westerberg, Editors)
Volume 16: Dynamic Model Development: Methods, Theory and Applications (S.P. Asprey and S. Macchietto, Editors)
Volume 17: The Integration of Process Design and Control (P. Seferlis and M.C. Georgiadis, Editors)
Volume 18: European Symposium on Computer-Aided Process Engineering-14 (A. Barbosa-Póvoa and H. Matos, Editors)
Volume 19: Computer Aided Property Estimation for Process and Product Design (M. Kontogeorgis and R. Gani, Editors)
Volume 20: European Symposium on Computer-Aided Process Engineering-15 (L. Puigjaner and A. Espuña, Editors)
Volume 21: 16th European Symposium on Computer Aided Process Engineering and 9th International Symposium on Process Systems Engineering (W. Marquardt and C. Pantelides)
Volume 22: Multiscale Modelling of Polymer Properties (M. Laso and E.A. Perpète)
Volume 23: Chemical Product Design: Towards a Perspective through Case Studies (K.M. Ng, R. Gani and K. Dam-Johansen, Editors)
Volume 24: 17th European Symposium on Computer Aided Process Engineering (V. Plesu and P.S. Agachi, Editors)
Volume 25: 18th European Symposium on Computer Aided Process Engineering (B. Braunschweig and X. Joulia, Editors)
Volume 26: 19th European Symposium on Computer Aided Process Engineering (Jacek Je owski and Jan Thullie, Editors)
Volume 27: 10th International Symposium on Process Systems Engineering (Rita Maria de Brito Alves, Claudio Augusto Oller do Nascimento and Evaristo Chalbaud Biscaia, Editors)
Volume 28: 20th European Symposium on Computer Aided Process Engineering (S. Pierucci and G. Buzzi Ferraris, Editors)
Volume 29: 21st European Symposium on Computer Aided Process Engineering (E.N. Pistikopoulos, M.C. Georgiadis and A.C. Kokossis, Editors)
Volume 30: 22nd European Symposium on Computer Aided Process Engineering (David Bogle and Michael Fairweather)

COMPUTER-AIDED CHEMICAL ENGINEERING, 31

11th INTERNATIONAL SYMPOSIUM ON PROCESS SYSTEMS ENGINEERING

PART B

Edited by

Iftekhar A. Karimi
Department of Chemical & Biomolecular Engineering
National University of Singapore, Singapore

Rajagopalan Srinivasan
Department of Chemical & Biomolecular Engineering
National University of Singapore, Singapore

ELSEVIER

Amsterdam – Boston – Heidelberg – London – New York – Oxford
Paris – San Diego – San Francisco – Singapore – Sydney – Tokyo

Elsevier
Radarweg 29, PO Box 211, 1000 AE Amsterdam, The Netherlands
The Boulevard, Langford Lane, Kidlington, Oxford OX5 1GB, UK

First edition 2012

British Library Cataloguing in Publication Data
A catalogue record for this book is available from the British Library

Library of Congress Cataloging-in-Publication Data
A catalog record for this book is available from the Library of Congress

ISBN (Part B): 978-0-444-59506-5
ISBN (Set): 978-0-444-59505-8
ISSN: 1570-7946

Printed and bound in Great Britain

12 13 14 15 16 10 9 8 7 6 5 4 3 2 1

Contents

Bioprocessing & Biotechnology

Computational Fluid Dynamics

Parameter Estimation

Education

Energy

Enterprise Optimization

Planning & Scheduling

Industrial Applications

Pharmaceutical Systems

Process Design

Process Simulation

Process Monitoring

Process Operations

Product Design

Sustainability & Environment

Water

Oil & Gas

Optimization

Alarms & Sensors

Heat Integration

Distillation

Model Predictive Control

Control Strategies

Modeling and Analysis

Process Synthesis

Biomedical Applications

I.A. Karimi and Rajagopalan Srinivasan (Editors), Proceedings of the 11th International Symposium on Process Systems Engineering, 15-19 July 2012, Singapore.

Integration of market dynamics into the design of biofuel processes

Anna Voll,[a] Giovanni Sorda,[b] Felix Optehostert,[a] Reinhard Madlener[b] and Wolfgang Marquardt[a]

[a]*Aachener Verfahrenstechnik – Process Systems Engineering, RWTH Aachen University, Turmstr. 46, 52064 Aachen, Germany*
[b]*Institute for Future Energy Consumer Needs and Behavior (FCN), E.ON Energy Research Center, RWTH Aachen University, Mathieustr. 6, 52074 Aachen, Germany*

Abstract

Wood is considered one of the main future feedstocks in the production of second generation biofuels in Europe. While feedstock cost has a major impact on production cost, wood prices are expected to change significantly once biorefineries enter the raw material market as new high volume consumers. Therefore, wood market dynamics and approximate price forecasting should be integrated into decision-making during the design phase. In this contribution we show how such an integration could be realized by combining a preliminary process model to determine the raw material demand and a spatial partial equilibrium model of the wood market to predict the price development. This approach is illustrated on a case study examining the production of 2-methyltetrahydrofuran (MTHF) as a novel biofuel component, which is converted from deciduous wood grown in Germany.

Keywords: biorenewables processing, process design, partial equilibrium model, biofuel

1. Introduction

New ways of using wood as a raw material in the chemical and fuel industries would contribute to crucial changes in the fuel as well as in the wood-based sectors. The availability of wood is characterized by seasonal differences and long-term re-growth patterns such that a sustainable supply can only be adapted over extended time intervals. As such, supply constraints and an increased demand would significantly affect the wood market price dynamics. Furthermore, the relatively low energy density and organic nature of wood leads to high transportation costs and expensive supply logistics. Different methods used in process systems engineering have been utilized to address some of these issues. Especially, supply chain optimization strategies have been applied recently to examine various aspects of the new bio-economy (see [1] for an overview). Most of the case studies focus on the identification of the ideal location, number and capacity for (biofuel) production facilities based on economic or sustainability criteria. Sometimes connections to scheduling and decision making frameworks are included, but long-term changes in raw material costs induced by an increasing installed capacity of bio-based processes are mostly neglected. Other research concentrates on the modeling of biomass cultivation (e.g. [2]) to enable the estimation of feedstock prices. Moreover, partial equilibrium models are widely used to describe the wood market primarily to support policy making [3] by providing a rough prediction of wood price dynamics. However, price developments are usually not considered in conceptual

process design. Steady-state market conditions are assumed instead, irrespectively of the impact a new technology may have on resource availability and cost. Yet, especially in terms of biorenewables processing, the price of the raw material often dominates the profitability of the entire production and at the same time might vary massively in cases where biorefineries enter the raw material market as new high volume consumers. In this paper, we show how wood market and process models could be combined to overcome the above mentioned shortcomings. A better understanding of the mutual influence of markets and technologies can also facilitate enterprise-wide optimization and portfolio management [4].

2. Modeling approach

A spatial partial equilibrium model is implemented to represent the wood market, while reaction network flux analysis (RNFA) is chosen for preliminary process modeling because of few required input data. In the following sections we briefly introduce the main features of these models, highlight the necessary adaptations and show the results of their integration.

The market model has to account for all industries competing for wood resources, incorporate a realistic raw wood supply and endogenously predict the evolution of wood price dynamics over the planning horizon. In addition, the modeling framework has to allow for the introduction of future wood-based technologies. A spatial partial equilibrium model has therefore been chosen, which expresses the interaction across final product markets and resources via the simultaneous maximization of a "quasi-welfare" objective function of three representative agents (consumer, producer and trade agent) spread across regions endowed with different resources and production facilities [5]. Following the notation of Kallio *et al.* [6], the optimization problem results in

$$\max_{q,h,y,e} \sum_{i,f} \int_0^{q_{i,f}} \left(\alpha_{i,f} + \beta_{i,f} q_{i,f}\right) \mathrm{d}q_{i,f} - \sum_{i,w} \int_0^{h_{i,w}} \left(\alpha_{i,w} + \beta_{i,w} h_{i,w}^{\gamma_{i,w}}\right) \mathrm{d}h_{i,w} - \sum_{i,l} c_{i,l} y_{i,l} - \sum_{i,j,k} D_{i,j,k} e_{i,j,k} \quad (1)$$

$$s.t. \quad \mathbf{\Gamma}(\mathbf{q},\mathbf{h},\mathbf{y},\mathbf{e}) \geq 0,$$

where the dependence on time t has been dropped for clarity. The first term is a linear approximation of consumers' inverse demand function for quantity $q_{i,f}$ of final product f in region i; $h_{i,w}$ refers to the supply of wood type w in region i; $c_{i,l}$ measures the unit marginal cost for a given production level $y_{i,l}$ of technology l in region i (though it excludes raw wood, intermediate wood product inputs and marginal transport costs, which are endogenously accounted for by the model); and $D_{i,j,k}$ refers to the transportation cost for shipping the amount $e_{i,j,k}$ of commodity k from region i to region j. The production and supply of the final commodities are included in the set of constraints $\boldsymbol{\Gamma}$, which ensures material balances and reflects current production capacity limitations for all model variables ***q, h, y, e***. The evolution in time t is represented by a discrete-time recursion [6], where the next period's wood growing stock $g_{i,w,t+1}$ is affected by the growth rate $\delta_{i,w}$ of its current stock level and the wood harvest $h_{i,w,t}$ at time t

$$g_{i,w,t+1} = \left(1 + \delta_{i,w}\right) g_{i,w,t} - h_{i,w,t}. \quad (2)$$

The availability of wood resources affects in turn the tightness of the wood supply, and hence its prices. In each period the model parameters related to prices, supply and demand are then re-calibrated based on the outcome of the previous period. Even though such models already exist ([7], [8]), they fail to represent the current German

market with sufficient detail, and instead aggregate it into a larger block of countries (i.e. Western Europe). The more detailed model of the German wood market developed in this work is divided into three regions, namely West, North and South. It distinguishes between coniferous and deciduous wood and includes the main wood consuming sectors by accounting for the production and consumption of sawnwood, wood-based panels (chipboard, oriented strand board and medium density fiberboard), pulp (mechanical, sulphite and sulphate), fuel wood and, ultimately, biofuels. The model accounts for the current and forecasted production capacity of the German wood-based industry [9], while data concerning the available wood growing stock and the corresponding growing rates are taken from the National Forest Inventory [10]. In order to summarize the raw material demand of all the different sectors, so called input-output tables are used to represent the production sectors and to relate the amount of feedstock required per unit of product ([11], [12]), and are included in the material balance conditions $\boldsymbol{\Gamma}$.

The input-output relation for fuel production, a novel technology to be introduced into the market, is calculated by a separate optimization problem via RNFA, which is an optimization-based screening method for the selection of reaction routes in the early stage of design focusing on the entire value chain rather than on an individual process plant ([13], [14]). In this methodology, all possible reaction steps are summarized in a network such that linear material balances can be formulated easily for each substance. Optimal reaction pathways can be detected by solving the optimization problem

$$\begin{aligned} &\min_{\boldsymbol{f},\boldsymbol{b}} \ \phi \\ &s.t.\ \boldsymbol{A}\cdot\boldsymbol{f} = \boldsymbol{b}, \\ &\quad \boldsymbol{f},\boldsymbol{b} \geq 0. \end{aligned} \tag{3}$$

The matrix $\boldsymbol{A}$ contains the stoichiometric coefficients of all reactions, while $\boldsymbol{f}$ represents the reactive molar flows through the network (including the amount of the raw material wood, an aggregate of the supplies $h_{i,w}$ for fuel production) and $\boldsymbol{b}$ indicates product and by-product formation. If desired, yield constraints and additional performance criteria can also be considered. In fact, a rough economic evaluation can be integrated by balancing raw material costs and product sales. In addition, investment costs can be estimated according to a correlation estimated by Lange [15] based on the energy loss of the process. The objective function ϕ can be chosen according to the actual application; here, the minimization of the amount of biomass feedstock is targeted. In order to cover the evolution of price and also demand, the RNFA model has to be solved repeatedly on a receding planning horizon (embedded into the market model).

The optimization of both the RNFA and the forest market models is performed as bi-level optimization problem via the General Algebraic Modeling System (GAMS) platform. Overall, the interaction between the two models is as follows: the market model predicts the raw material cost for RNFA (i.e. the cost of deciduous wood and changes thereof after the introduction of biorefineries), while RNFA determines the flux distribution of the input-output requirements of the new biorefinery technology implemented in the partial equilibrium model. The RNFA model is solved as a subproblem of the market model at discrete times t, where the net present value (NPV) of a representative biorefinery is calculated for the most favorable processing route at fixed plant capacities in relation to the varying raw material prices.

3. Case study: the production of MTHF from deciduous wood

2-methyltetrahydrofuran (MTHF) is considered as a novel biofuel component, which could potentially replace standard fuel. It can be produced from woody biomass (e.g. beech wood) via levulinic acid followed by a consecutive series of hydrogenations and dehydrations [16]. In this case study, deciduous wood chips are used as raw material inputs of the fuel synthesis for a plant in West Germany with an expected lifetime of 20 years including a building phase of 5 years. For simplicity, fuel demand and fuel price are not yet calculated by a market model, but instead assigned according to reasonable estimates. In particular, the plant capacity is varied between $50 \cdot 10^3$ and $500 \cdot 10^3$ tons of biofuel per year in order to identify the influence of different production scales on the wood market. The pre-tax fuel price of MTHF is fixed to 0.59 €/l based on current diesel prices in Germany under the assumption of fuel price parity based on energy content. Moreover, the price of (deciduous) wood chips is calculated to be 13 €/m^3 in the base case scenario. If we assume fixed price levels, the NPVs would range between 13 Mio € for the smallest facility and 598 Mio € for the largest one. In the alternative scenarios, the price of the raw materials changes over time according to the response of the wood market model to the introduction of the new biofuel technology. The price predictions for each period are then included in the updated NPV estimation of the plant. As it can be seen in Fig. 1, the price of wood chips increases significantly due to the high demand depending on the plant capacity. These changes in raw material cost affect the profitability of the production process even more strongly. Most notably, none of the production facilities can retain a positive NPV after the cost increase, whereas the impact on large production is more severe.

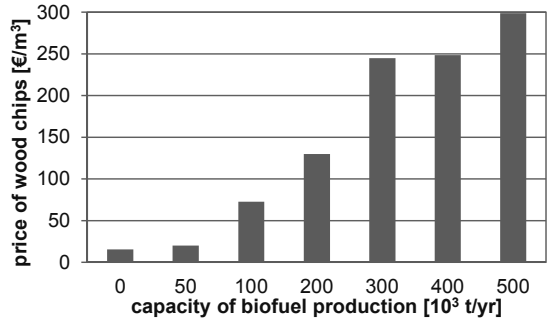

Figure 1: Prices of wood chips after the introduction of biofuel plants with different capacities.

4. Conclusions

The case study presented clearly indicates that the development of biorefineries has an enormous impact on wood market dynamics, which in turn affect the profitability of wood-based biofuel production. Consequently, market dynamics must be considered during conceptual process design and product portfolio management. The combination of RNFA and a spatial partial equilibrium model of the wood market provides a feasible framework to assess these mutual influences, even though the results are based on a rather coarse model of the German wood industry, which still needs further validation. Currently, the main drawback of the study is the lack of an adequate representation of international trade in wood products. As a consequence, on the one hand, the supply of wood is limited to the available national resources, thus possibly presenting steeper price responses to an increased demand for wood products. On the other hand, the market is also isolated from demand or supply shocks originating from abroad. At the

moment we are looking for alternatives to integrate the German market model into a larger framework to account for international trade. In addition, both the wood market and the process models incorporate several (uncertain) parameters, which call for a comprehensive sensitivity analysis to assess the validity and robustness of the results.

Acknowledgements

This work was performed as part of the Pathfinder Project "Forests In The Tank" (FITT) and of the Cluster of Excellence "Tailor-Made Fuels from Biomass" (TMFB) at the RWTH Aachen University. Key insights and helpful comments from Dr. A. Maarit Kallio (Meetla, Finnland) are also gratefully acknowledged.

References

[1] You, F., Tao, L., Graziano, D., Snyder, S., 2012, Optimal design of sustainable cellulosic biofuel supply chains: Multiobjective optimization coupled with life cycle assessment and input–output analysis. AIChE Journal 58, 1157.
[2] McEniry, J., O'Kiely, P., Crosson, P., Groom, E., Murphy, J., 2011, The effect of feedstock cost on biofuel cost as exemplified by biomethane production from grass silage. Biofuels, Bioprod. Bioref. 5, 670.
[3] Sohngen, B., 1998, An assessment of four large scale timber market models. Paper originally presented at the Workshop to Examine Models Needed to Assist in the Development of a National Fiber Supply Strategy for the 21th Century, October 3-4 1996, Washington.
[4] Varma, V., Reklaitis, G., Blau, G., Pekny, F., 2007, Enterprise-wide modeling and optimization – An overview of emerging research challenges and opportunities. Computers and Chemical Engineering 31(5-6), 692.
[5] Samuelson, P., 1952, Spatial price equilibrium and linear programming. The American Economic Review 42(3), 283.
[6] Kallio, A.M., Moiseyev, A., Solberg, B., 2004, The Global Forest Sector Model EFI-GTM – The Model Structure. European Forest Institute, Internal Report No.15, Joensuu, Finland.
[7] Kallio, M., Dykstra, D., Binkley, C., 1987, The Global Forest Sector – An Analytical Perspective. John Wiley & Sons, Chichester, United Kingdom.
[8] Buongiorno, J., Zhu, S., Zhang, D., Turner, J., Tomberlin, D., 2003, The Global Forest Products Model. Elsevier Science, London, United Kingdom.
[9] Sörgel, C., Mantau, U., 2005 and 2006, Standorte der Holzwirtschaft, Abschlussberichte, Sägeindustrie, Holzwerkstoffindustrie, Holz- und Zellstoffindustrie. Zentrum Holzwirtschaft, Universität Hamburg, Hamburg, Germany.
[10] Bundesministerium für Ernährung, Landwirtschaft und Verbraucherschutz, 2002, National Forest Inventory – Bundeswaldinventur, Bonn, Germany.
[11] UNECE, United Nations Economic Commission for Europe, 2010, Forest products conversion factors for the UNECE region. Geneva Timber and Forest Discussion Paper 49, UNECE, Geneva, Switzerland.
[12] European Commission, 2001, Integrated Pollution prevention and control (IPPC) – Reference document on the best available techniques in the pulp and paper industry. European Commission, Joint Research Center, Institute for Prospective Technological Studies, Brussels, Belgium.
[13] Voll, A., Marquardt, W., 2011, Reaction network flux analysis: Optimization-based evaluation of reaction pathways for biorenewables processing. AIChE Journal doi: 10.1002/aic.12704 (in press).
[14] Voll, A., Marquardt, W., 2012, Benchmarking of next-generation biofuels from a process perspective. Biofuels, Bioprod. Bioref. doi: 10.1002/bbb.1325 (in press).
[15] Lange, J.-P., 2001, Fuels and chemicals manufacturing – Guidelines for understanding and minimizing the production costs. Cattech 5, 82.
[16] Geilen, F., Engendahl, B., Harwardt, A., Marquardt, W., Klankermayer, J., Leitner, W., 2010, Selective and flexible transformation of biomass-derived platform chemicals by a multifunctional catalytic system. Angewandte Chemie International Edition 49(32), 5510.

I.A. Karimi and Rajagopalan Srinivasan (Editors), Proceedings of the 11th International Symposium on Process Systems Engineering, 15-19 July 2012, Singapore.

Design methodology for bio-based processing: Biodiesel and fatty alcohol production

Lida Simasatitkul,[a] Amornchai Arpornwichanop,[a] Rafiqul Gani[b]

[a] *Computational Process Engineering, Department of Chemical Engineering, Faculty of Engineering, Chulalongkorn University, Bangkok,10330, Thailand*

[b] *CAPEC, Department of Chemical & Biochemical Engineering, Technical University of Denmark, DK-2800 Kongens Lyngby, Denmark*

Abstract

A systematic design methodology is developed for producing two main products plus side products starting with one or more bio-based renewable source. A superstructure that includes all possible reaction and separation operations is generated through thermodynamic insights and available data. The number of alternative processes is systematically reduced through a screening procedure until only feasible alternatives are obtained. As part of the methodology, process intensification involving reaction-separation tasks is also considered to improve the design by shifting the equilibrium reactions. Economic analysis and net present value are determined to find the best economically and operationally feasible process. The application of the methodology is presented through a case study involving biodiesel and fatty alcohol productions.

Keywords: Methodology, Superstructure, Process intensification, Biodiesel, Fatty alcohol production

1. Introduction

Various methods for synthesis and design of chemical processes are available. The most commonly used method is heuristic by nature. Seider *et al*. (2004) proposed a step by step method for design of chemical processes. Since the physical and chemical properties of the involved chemical system play a very important role for the design/synthesis of a process, a thermodynamic insights based hybrid method was proposed by Jaksland *et al*. (1995). Hostrup *et al*. (2001) further developed this method by including a reverse design approach where process design variables are "back-calculated" for known design targets. The proposed method was applied to methyl acetate and cyclohexane productions. All these methods, however, focus on processes with one main product for a fixed reaction-catalyst and do not consider process alternatives in terms of diversion of resources to another product within the same overall process. In this paper, a systematic step by step methodology is developed for design, synthesis and analysis of a flexible process that can economically produce multiple main products plus side products according to demand and economic states. According to this methodology, all possible flowsheet configurations are first generated from a generic superstructure. Then through a systematic screening procedure, applying constraints in a hierarchical manner, the number of alternatives is reduced to identify only the feasible ones. These are further reduced in terms of productivity, consumption of raw material and process intensification. For the remaining alternatives, the optimal fractions (diversion of source) to produce multiple products is determined by solving a non-linear optimization problem. The application of design methodology is presented

through a case study involving the production of biodiesel integrated with fatty alcohol, that is, two main products and waste edible oil is employed as a feed source.

2. Methodology

The objective of the methodology is to design a chemical process to convert a renewable source to multiple main products with associated side products. The main-steps of the methodology are shown in Fig. 1, where the work-flow is structured in terms of levels (0-5) after problem definition. The starting point is problem definition where the number of available renewable sources, the number of desired main products, the qualities of the products, the performance criteria for the desired process, among others, is defined. At level-0, search of available data (in a database as well as open literature) is made, and based on this, the generic superstructure is created. Levels 1-4 involve screening of alternatives, where constraints are ordered in a hierarchical manner; the computationally easier constraints are considered first. Consequently, as the number of alternatives reduces, computationally more intensive constraints are considered. In level-0, the full set of alternatives available in the superstructure is generated, while, at the end of level-4, only a few (5-10) alternatives are considered for further analysis (for example, economic). The methodology is generic in nature (can handle any number of main products); flexible (method of solution can be changed through another order of constraints, including all at the same time). Note, however, in this paper the option for two main products and a fixed hierarchical order for constraints is used.

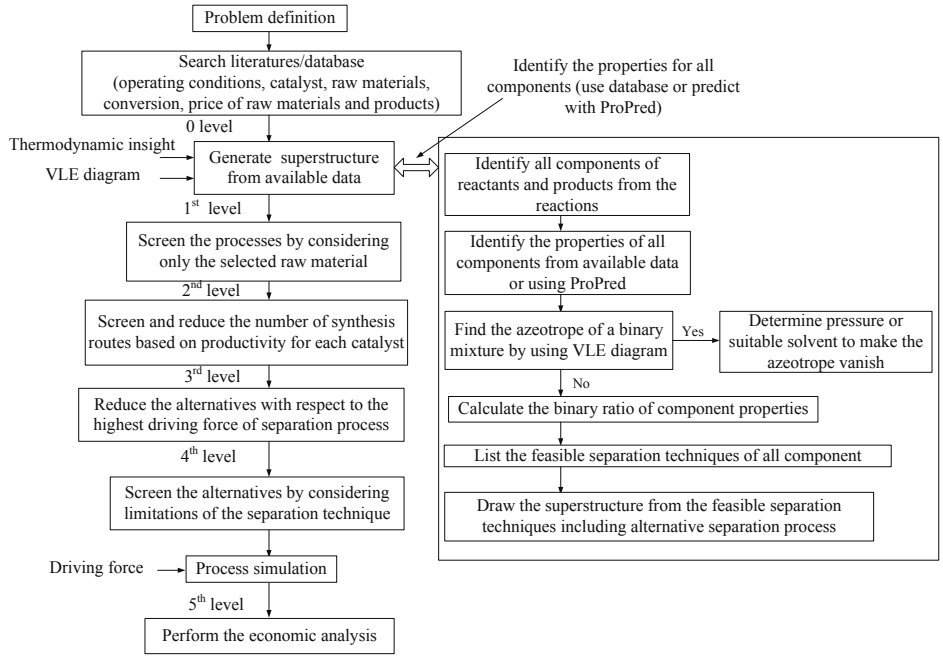

Fig. 1 Work-flow diagram for methodology for producing two main products plus side products.

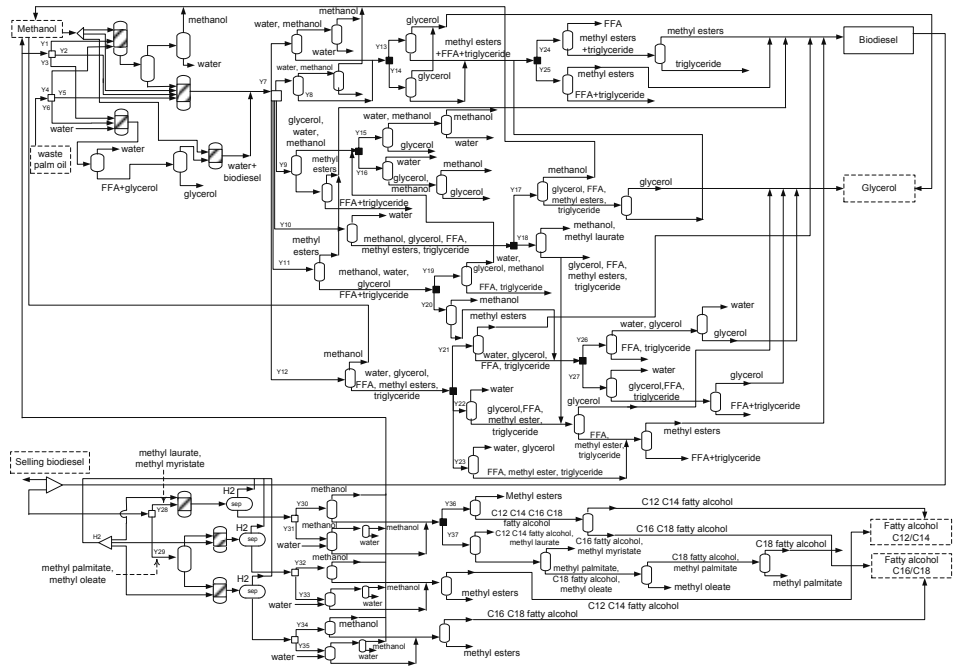

Fig. 2 Superstructure of biodiesel production process integrated with fatty alcohol production.

3. Case study

The application of the design methodology is presented through a case study involving the production of biodiesel integrated with fatty alcohol, that is, the problem defined is to produce biodiesel and fatty alcohol at a purity of 99.5 wt.%, respectively. The performance criterion is to maximize the net present value (NPV) of the process.

$$\text{Max NPV} = f(\underline{X}, \underline{Y}) \quad (1)$$

subject to design variables $\underline{X}$, binary integer (decision) variables $\underline{Y}$, process model equations (*i.e.*, mass and energy balance equations), product purities and other design targets. NPV in Eq. 1 is the summation of total capital investment, revenues, and depreciation and operating costs with interest rate (15% assumed) and lifetime (20 years assumed). In level-0, information on the type of catalysts, operating conditions, conversions for biodiesel from waste palm oil are collected. For the identified chemicals present in the system, binary ratios of properties for all components are computed and using this information and the collected data, a superstructure for the production of biodiesel integrated with fatty alcohol is generated (Fig. 2). The superstructure contains 6 separation operation types (such as flash separator, decanter, distillation, stripper and absorber) and conversion reactors (one for each type of catalyst considered; 7 types of catalysts have been considered).The number of alternatives is reduced at level-1 for the given renewable source (waste palm oil); at level-2 for the highest productivity (the reactor and catalyst that give the highest product yields); at level-3 for the easiest separations (the separation techniques employing the maximum driving force); at level-4 for the limitations on separation tasks. At the end of level-4, 7 process alternatives (such as alkali catalyzed process, acid catalyzed process, heterogeneous catalyzed process, enzyme catalyzed process, supercritical process and hydrolysis of triglyceride then esterification of free fatty acid) are obtained and then, rigorous steady-state process

simulations are performed before their performance are computed in level-5 for economic analysis and final selection. In the simulation step, the UNIQUAC model is used for phase equilibrium calculations, while the percentage recoveries of separators and distillations are specified at 90% and 99%, respectively. The driving force technique is used to design distillation columns by considering the energy consumption and total capital cost and using the reverse approach, the number of stages and the feed location that matches the driving force target are determined. The driving force diagram for separating methyl oleate from palmitic acid is shown in Fig. 3. The results for screening procedure are given in Table 1. In the last step of the methodology, seven processes are analyzed through profitability indicators such as NPV and ROI (return on investment). At the end, the best process is found to be the heterogeneous acid catalyzed process and the suitable fraction of biodiesel to produce fatty alcohol is 1. That is, most of biodiesel should be diverted to fatty alcohol because currently the price of fatty alcohol is higher than biodiesel (note that this is a constrained optimal solution and by adding a maximum amount of allowed diversion of biodiesel, both main products are obtained). Process intensification (reactive distillation) combining separation of water and methanol from biodiesel with the reaction step to improve the conversion of equilibrium-limited reaction is considered. Methanol and water are obtained at the top of the column, while methyl esters and glycerol are obtained at the bottom. The results with and without process intensification are compared in Table 2. Due to its low fraction, water derived from the esterification process (the pre-treatment section of waste palm oil) is assumed to be an inert component. From the element concept, there are 4 components with 3 elements. The ternary reactive phase diagram of the transesterification process for a biodiesel production system at 438 K is shown in Fig. 4. It shows that pure methyl ester is obtained at W_A and W_B of 50%, at AB point, while pure triglyceride is obtained at W_A and W_C of 50% at AC point. This implies that methyl ester, methanol and glycerol are found at the bottom of the reactive distillation column. As the W_A and W_B do not equal to 50% at the end of the liquid line, the bottom product is not pure methyl ester; methanol is mixed with the biodiesel product.

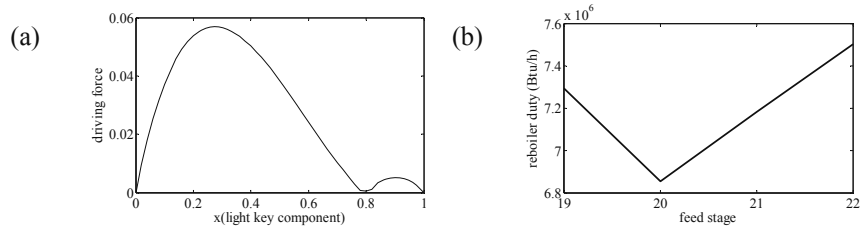

Fig. 3 (a) a driving force diagram for separating methyl oleate from palmitic acid and (b) effect of feed stage location of distillation for separating methyl oleate from palmitic acid on reboiler heat duty (Btu/h), for biodiesel production integrated with fatty alcohol production.

Table 1. Reducing alternative processes from constraint consideration

Level	Criteria	Method	No. of alternative processes
0,1	Waste palm oil is considered as raw material	Review literature such as conditions, conversion, catalysts, separation tasks then generate the overview superstructure	95,040

2	Highest productivity	Compute biodiesel yield	7,392
3	Highest driving force	Calculate the adjacent properties ratios	14
4	Limitation of separation task	LLE diagram	7
5	Highest NPV	Economic analysis	1

Table 2. Comparison of design with and without process intensification for heterogeneous acid catalyzed process for biodiesel production

Parameters	Process without intensification	Process with intensification
NPV ($/year)	2.3×10^9	2.75×10^9#
Duty (kJ/h)	9.15×10^7	8.16×10^7

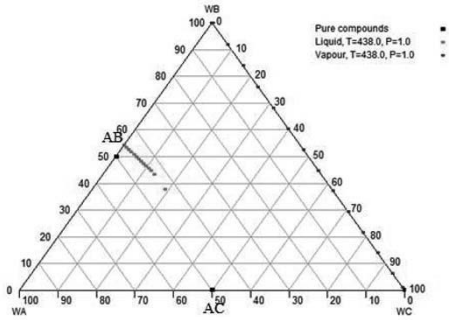

Element A: $CH_2(CH_2)_{14}CH{=}CHCO$
Element B: CH_3OH
Element C: $(CH_2)_2CH(OH)_3$.
Compound representations:
Methyl ester: A+B
Methanol: B
Glycerol: C
Triglyceride: A+C

Fig. 4 Ternary phase diagram for three elements.

4. Conclusions

The systematic design of processes for multiple main products plus side products has been presented and applied for biodiesel production integrated with fatty alcohol production. Although the methodology has been highlighted in this work for two main products, it is generic, in principle. By increasing the number of renewable sources and main products, the model for an optimal biorefinery is obtained. The mathematically complex problem has been managed by decomposing it into different hierarchical levels. This technique, in principle, also includes the simultaneous approach. Current and future work will incorporate the simultaneous approach at different levels. According to the methodology, a heterogeneous acid catalyzed process for biodiesel production integrated with fatty alcohol production is better than other process alternatives. Process intensification improves the process by reducing heat duties and production costs.

5. Acknowledgement

This work was supported by the Thailand Research Fund (RGJ-PhD Program), CAPEC of Technical University of Denmark (DTU) and Chulalongkorn University.

References

Hostrup, M., Gani, R., Kravanja, Z., Sorsak, A., Grossmann, I., 2001. Integration of thermodynamic insights and MINLP optimization for the synthesis, design and analysis of process flowsheets. Computers and Chemical Engineering 15, 73-83.

Jaksland, C., Gani, R., Lien, K., 1995. Separation process design and synthesis based on thermodynamic insights. Chemical Engineering Science 50, 511-530.

Seider, W.D., Seader, J.D., Lewin, D.R., 2004. Conceptual Design of Chemical Processes, McGraw Hill, New York.

I.A. Karimi and Rajagopalan Srinivasan (Editors), Proceedings of the 11th International Symposium on Process Systems Engineering, 15-19 July 2012, Singapore.

Multi-objective Optimization of a Fermentation Process Integrated with Cell Recycling and Inter-stage Extraction

Shivom Sharma,[a] G.P. Rangaiah[a]

[a]Department of Chemical & Biomolecular Engineering
National University of Singapore, Singapore 117576, Singapore

Abstract

Bio-fuels are clean, renewable energy with potential to replace fossil fuels. Bio-ethanol is the widely used bio-fuel, which can be produced from a variety of agricultural feed-stocks. Its production from fermentable sugars is well established. Production of bio-ethanol from starchy and cellulosic materials requires hydrolysis as an additional step to produce fermentable sugars. In SHF (separate hydrolysis and fermentation) process, hydrolysis and fermentation are performed at their respective optimal temperatures, but end products (i.e., glucose and cellobiose) inhibit hydrolysis. SSF (simultaneous saccharification and fermentation) process removes product inhibition by immediate consumption of end products of hydrolysis. Ethanol concentration also inhibits glucose to ethanol conversion in the fermentor, which results in low ethanol productivity and yield. To avoid this, ethanol can be continuously removed from the fermentor using either extraction or perm-selective membrane. In this study, a three-stage fermentation process integrated with cell recycling and inter-stage extraction is considered, for producing ethanol from the lignocellulosic feed-stocks. The integrated process is optimized using a multi-objective differential evolution algorithm for two objectives simultaneously. Finally, improvement in the performance of the fermentation process due to inter-stage extraction is evaluated quantitatively.
Keywords: Fermentation Process; Inter-stage Extraction; Multi-objective Optimization.

1. Introduction

Cellulosic ethanol production can use non-food crops and inedible waste products to produce bio-ethanol that causes less air pollution compared to conventional fuels. Cellulosic bio-ethanol production requires hydrolysis as an additional step to produce fermentable sugars. Lignocellulosic feed-stocks produce both glucose and xylose after hydrolysis. Feed concentration, fermentation temperature and time affect the conversion of these feed-stocks into glucose and xylose. Hydrolysis is faster in SSF than in SHF due to reduced end-products inhibition. Furthermore, conversion of fermentable sugars (i.e., glucose and xylose) into ethanol is inhibited by ethanol concentration inside the fermentor. Hence, several researchers have improved the fermentation process by in-situ removal of ethanol using different processes (e.g., extraction, pervaporation, etc.).

Bio-ethanol production using first generation feed-stocks (e.g., glucose, xylose, etc.) has been optimized in the recent years. Silva et al. (1999) used solvent extraction for partial removal of ethanol from the fermentor; they have maximized both yield and productivity using response surface analysis. Wang and Lin (2010) studied fuzzy multi-objective optimization (MOO) of a three-stage fermentation process with cell recycling using glucose as feed. Chen and Wang (2010a) optimized a fermentation process using lignocellulosic feed-stocks, which involves co-fermentation of glucose and xylose. Chen and Wang (2010b) have studied a three-stage fermentation process coupled with cell recycling and inter-stage extraction, and solved a fuzzy multi-objective

optimization (MOO) problem as a single objective optimization (SOO) problem using hybrid differential evolution.

Fuzzy MOO approach requires prior knowledge, such as preference interval for each objective and constraint; and also its solution as SOO problem gives single solution. Further, in the literature, several Pareto-optimal front generating techniques are available to find the trade-offs among conflicting objectives. Hence, in this work, a three-stage fermentation process integrated with cell recycling and inter-stage extraction is optimized for ethanol productivity and xylose conversion using multi-objective differential evolution (MODE) algorithm. In order to assess the usefulness of inter-stage extraction for three-stage fermentation process with cell recycling, a three-stage fermentation process with cell recycling only (base case) is also optimized for ethanol productivity and xylose conversion using MODE algorithm.

The rest of this article is organized as follows. Next section of this article briefly presents the integrated fermentation process and its mathematical model. Section 3 describes the MOO problem formulation, whereas MODE algorithm is briefly described in Section 4. Section 5 presents and discusses the optimization results. Useful insights from this study are drawn at the end of this article.

2. Integrated Fermentation Process and its Model

A schematic diagram of the three-stage fermentation process coupled with cell recycling and inter-stage extraction is presented in Figure 1. Three fermentors are placed in series, and feed enters the first fermentor. A small part of mother liquor from a fermentor goes directly to the next fermentor while remaining mother liquor goes through a cell separator and an extractor. A cell separator is used after each fermentor to separate the cell mass and recycle it to the fermentor, whereas an extractor is used to remove ethanol using a solvent.

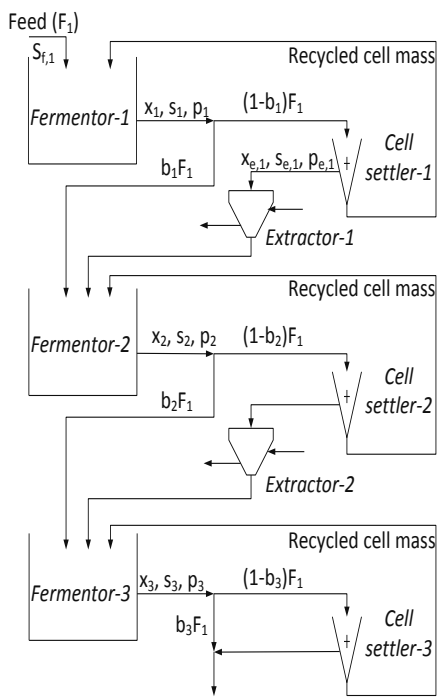

Figure 1: a schematic diagram of a 3-stage fermentation process coupled with cell recycling

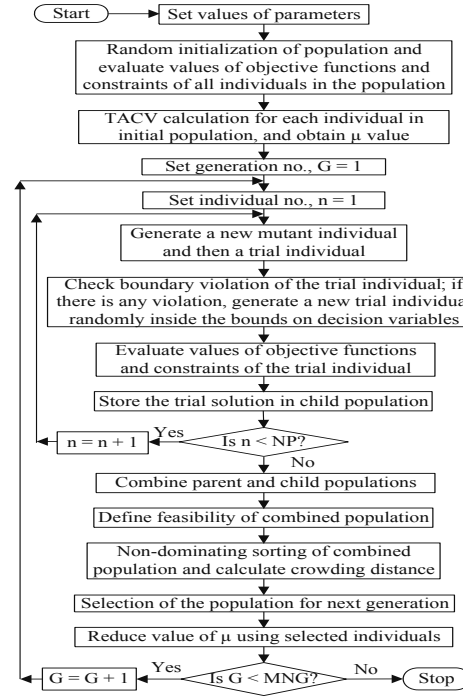

Figure 2: flowchart of the MODE algorithm

The model of the three-stage fermentation process integrated with cell recycling and extraction is taken from Chen and Wang (2010b). Steady-state material balances for cell mass, glucose, xylose and ethanol around k^{th} stage are given by equations 1-4 respectively.

$$D[b_{k-1} + (1 - b_{k-1})\zeta_x]x_{k-1} - D[b_k + (1 - b_n)\zeta_x]x_k + r_{x,k} = 0 \quad (1)$$

$$D\lambda s_{f,k} + D[b_{k-1} + (1 - b_{k-1})\zeta_s]s_{g,k-1} - D[b_k + (1 - b_k)\zeta_s]s_{g,k} - r_{sg,k} = 0 \quad (2)$$

$$D(1 - \lambda)s_{f,k} + D[b_{k-1} + (1 - b_{k-1})\zeta_s]s_{x,k-1} - D[b_k + (1 - b_k)\zeta_s]s_{x,k} - r_{sx,k} = 0 \quad (3)$$

$$D\left[b_{k-1} + (1 - b_{k-1})\frac{\zeta_p}{1+E_{k-1}}\right]p_{k-1} - D[b_k + (1 - b_k)\zeta_p]p_k + r_{p,k} = 0 \quad (4)$$

Here, D is the dilution rate. x, s_g, s_x and p are respectively cell mass, glucose, xylose and ethanol concentration (kg/m^3) in the fermentor indicated by the subscript. b_k, E_k and $s_{f,k}$ are bleed ratio, extraction efficiency and substrate concentration in feed to k^{th} stage. λ is the mass fraction of glucose in substrate, and remaining is xylose. ζ_x, ζ_s and ζ_p are cell discard/separation factor ($= x_{e,1}/x_1$), substrate condensed factor ($= s_{e,1}/s_1$) and ethanol condensed factor ($= p_{e,1}/p_1$) respectively (see Figure 1). The rate expressions for cell mass growth (r_x), glucose consumption (r_{sg}), xylose consumption (r_{sx}) and ethanol production (r_p) can be found in Chen and Wang (2010b). The kinetic parameters used in this study are taken from Krishnan et al. (1999).

3. Multi-objective Optimization Problem Formulation

In this study, ethanol productivity and xylose conversion are used as two objectives, which ensure efficient utilization of production capacity and substrate respectively. Glucose conversion is not considered as an objective since it is higher than xylose conversion (Chen and Wang, 2010b).

$$\text{Ethanol productivity}, \frac{D}{3}\left[b_3 + (1 - b_3)\zeta_p\right]p_3 + \sum_{k=1}^{2}(1 - b_k)\frac{\zeta_p E_k}{(1+E_k)}p_k \text{ [kg/(m3.h)]} \quad (5)$$

$$\text{Xylose conversion}, 1 - \frac{[b_3 + (1-b_3)\zeta_s]s_{x,3}}{(1-\lambda)s_{f,1}} \quad (6)$$

Decision variables for this optimization include dilution rate, substrate concentration in feed and cell mass recycling for different stages.

$$0.3 \le D \le 0.8 \text{ [1/h]}; \; 40 \le s_{f,1} \le 130 \text{ [kg/m}^3\text{]}; \; 0.1 \le b_k \le 0.2 \text{ for } k = 1, 2, 3 \quad (7)$$

In addition to mass balances for different stages (Equations 1 to 4), positive values of ethanol productivity of each stage (π_k), glucose and xylose conversions ($\chi_{g,k}$ and $\chi_{x,k}$) in each stage are physical constraints. Other constraints are total sugar supply (s_T) and limits on the residual glucose and xylose concentrations ($s_{g,3} < 0.1$ and $s_{x,3} < 1$) in the mother liquor from the third fermentor. These constraints can be obtained from Chen and Wang (2010b).

4. Multi-objective Differential Evolution Algorithm

Integrated fermentation process is optimized for multiple objectives using MODE, which is similar to GDE3 presented by Kukkonen and Lampinen (2009). Figure 2 presents the flowchart of this algorithm. An initial population of NP individuals is randomly generated inside the bounds on decision variables, and values of objectives and constraints are calculated for them. In each generation, for each target individual in the current population, a mutant individual is generated by mutation using three random individuals from the current population. Then, a trial individual is produced by crossover of mutant and target individuals. Similarly, NP trial individuals are generated,

and each trial individual is evaluated for its values of objectives and constraints. These trial individuals are mixed with the current population, and non-dominated sorting of the combined population followed by crowding distance calculations are performed to select NP individuals as the population for the next generation. Constrained dominance or feasibility approach (Deb et al., 2002) is used for handling inequality constraints in the optimization problem; this approach modifies the selection rule for individuals in MODE algorithm, to give higher priority for feasible individuals over infeasible individuals with better objective values. MODE algorithm has been implemented in MS-Excel (for user interface and model calculations) and VBA (for optimization steps).

5. Results and Discussion

MODE parameters used in this study are: population size = 100, crossover probability = 0.3, mutation rate = 0.5, DE/rand/1 mutation strategy and maximum number of generations (MNG) = 200. The steady state model for each stage of fermentation process (equations 1 to 4) has to be solved numerically to compute values of objectives and constraints for each decision variable vector (or individual) provided by the MODE algorithm. In this work, 'Solver' in MS-Excel has been used to solve the steady state model equations by minimizing sum of squares. Feed to the fermentation process contains 65% glucose and 35% xylose, and extraction efficiency of solvent is assumed to be 6.93 (Chen and Wang, 2010b).

Initially, a three-stage fermentation process with cell recycling but without extraction (base case) has been optimized for ethanol productivity and xylose conversion simultaneously, for the same range of decision variables stated in Equation 7. Figure 3(a) shows the Pareto-optimal front obtained for this base case. The obtained Pareto-optimal front is well distributed, which means MODE performs well and successful for this problem. As expected, ethanol productivity and xylose conversion are conflicting in nature. The quantitative trade-off in Figure 3(a) is interesting and useful. The obtained Pareto-optimal front can be analysed into two parts: (i) a steep increase in ethanol productivity from 2.6 to 5.5 kg/(m^3.h) with little decrease in xylose conversion, and (ii) a nearly linear decrease in conversion from 0.995 to 0.955 as ethanol productivity increases from 5.5 to 7 kg/(m^3.h). The significant improvement in ethanol productivity in the first part is due to steady increase in substrate concentration in feed and followed by increase in dilution rate (Figures 3c and 3e). In the second part, variation in ethanol productivity is mainly due to dilution rate. All the bleed ratios are nearly constant at their lower bounds (i.e., 0.1), and so these are not shown for brevity.

Pareto-optimal front obtained for three-stage fermentation process integrated with both cell recycling and inter-stage extraction, using MODE algorithm is shown in Figure 3(b). In this case too, optimal values of dilution rate and substrate concentration in feed vary with the objectives (see Figures 3d and 3f), and all the bleed ratios are nearly constant at their lower bounds. The obtained Pareto-optimal front in Figure 3(b) shows some discontinuity near ethanol productivity of 5 kg/(m^3.h), due to changes in dilution rate and substrate concentration (Figures 3d and 3f). In order to check the global optimality of the obtained solution, this case has been run several times with fixed bleed ratios (= 0.1 as these are nearly constant); the Pareto-optimal solutions obtained in different runs are practically same. This indicates that MODE algorithm has converged to the global Pareto-optimal front.

In the fermentation process integrated with both cell cycling and extraction, ethanol productivity has improved significantly compared to the base case (Figures 3a and 3b); maximum value of productivity has increased from 7 to 13.3 kg/(m^3.h). Furthermore,

xylose conversion has also improved, closer to one. In both cases (i.e., with and without extraction), optimal dilution rate is varying between its bounds. In the extraction case, substrate concentration in feed is mostly near to its upper bound (130 kg/m^3), which means three-stage fermentors integrated with inter-stage ethanol removal can convert larger amount of fermentable sugars into bio-ethanol, for the same capacity of plant.

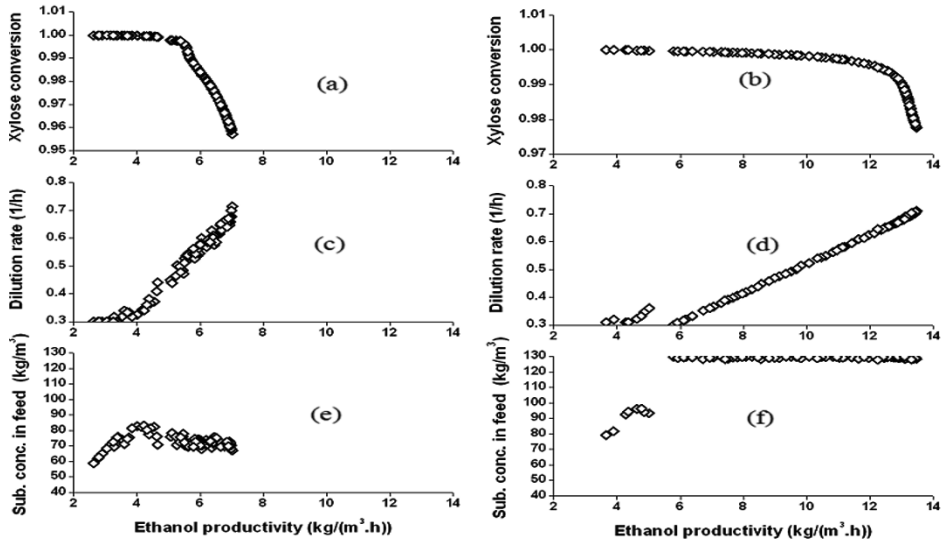

Figure 3: Selected optimization results for the three-stage fermentation process integrated with cell recycling only (plots a, c and e in the left column), and with cell recycling and inter-stage extraction (plots b, d and f in the right column)

6. Conclusions

This study optimizes a three-stage fermentation process with cell recycling and inter-stage extraction, and using glucose and xylose as the feed-stocks. The MODE algorithm is used to generate the trade-off solutions. The obtained Pareto-optimal front gives better insights by providing a range of alternatives with different ethanol productivity and substrate conversion. Low values of bleed ratios are favorable for both objectives. Finally, optimization results show that inclusion of inter-stage extraction improves the fermentation process significantly (e.g., ethanol productivity nearly doubles).

References

1. F.L.H.D. Silva, M.I. Rodrigues, F. Maugeri, 1999, Dynamic modeling, simulation and opt. of an extractive continuous alcoholic ferm. process. J. Chem. Tech. & Biotech., 74, 176-182.
2. F.S. Wang, H.T. Lin, 2010, Fuzzy optimization of continuous fermentations with cell recycling for ethanol production. Ind. Eng. Chem. Res., 49, 5, 2306-2311.
3. K. Deb, A. Pratap, S. Agrawal, T. Meyarivan, 2002, A fast and elitist multi-objective genetic algorithm: NSGA-II. IEEE Trans. Evol. Comp., 6, 182-197.
4. M.L. Chen, F.S. Wang, 2010a, Opt. of a fed-batch simultaneous saccharification and co-fermentation process from lignocellulose to ethanol. Ind. Eng. Chem. Res., 49, 12, 5775-5785.
5. M.L. Chen, F.S. Wang, 2010b, Optimal trade-off design of integrated fermentation processes for ethanol production using genetically engineered yeast. Chem. Eng. J., 158, 271-280.
6. M.S. Krishnan, Y. Xia, N.W.Y. Ho, G.T. Tsao, 1999, Fermentation kinetics of ethanol production from glucose and xylose by recombinant saccharomyces 1400 (pLNH33). A. Biochem. Biotech., 77/79, 373-388.
7. S. Kukkonen, J. Lampinen, 2009, Perform. assessment of generalized differential evolution 3 with a given set of constrained MO test problems. IEEE Cong. Evol. Comp., pp. 1943-1950.

I.A. Karimi and Rajagopalan Srinivasan (Editors), Proceedings of the 11th International Symposium on Process Systems Engineering, 15-19 July 2012, Singapore.

Integrated Design of High Temperature Steam Electrolysis and Biomass to Liquid Fuel Process

Quentin Bernical,[a1,a2,b] Xavier Joulia,[a1,a2] Isabelle Noirot-Le Borgne,[b] Pascal Floquet,[a1,a2] Pierre Baurens,[b] Guillaume Boissonnet[b]

[a1] *Université de Toulouse, INPT, UPS, Laboratoire de Génie Chimique, 4 allée Émile Monso, F-31432 Toulouse, France*
[a2] *CNRS, Laboratoire de Génie Chimique, F-31062 Toulouse, France*
[b] *CEA, Liten, DTBH, F-38054 Grenoble, France*

Abstract

This work addresses the integrated design of the High Temperature Steam Electrolysis (HTSE) and Biomass to Liquid (BtL) hybrid process.
The comprehensive gate-to-gate analysis includes BtL and hydrogen production on-site operations. Simulations are carried out using a commercial process simulation software – ProSimPlus® – to allow physical modeling and mass and energy balances; modeling is based on standard elementary and user modules and supported by various CEA (French Atomic Energy and Alternative Energies Commission) previous works.
The framework for assessment is proposed. Considering productivity, efficiency, cost and environmental issues, five criteria have been chosen: carbon matter yield; energy efficiency; greenhouse gas emissions; water use; levelized biofuels production cost.
Preliminary results verify that hydrogen input is almost doubling the productivity (biofuels/biomass). They bring out significant secondary energy saving for HTSE compared to standard process; and clear advantages over alkaline electrolysis considering technical and environmental criteria.

Keywords: integrated design, Biomass to Liquid, High Temperature Steam Electrolysis, hybrid, multicriteria.

1. Introduction

1.1. Context: enhanced BtL processes with extra hydrogen input

The second generation liquid biofuels are promising regarding substitution of petroleum: they offer both interesting energy efficiency and potential for GreenHouse Gas Emissions (GHGE) cut. The Biomass to Liquid (BtL) thermochemical route – based on biomass gasification then Fischer-Tropsch Synthesis (FTS) – is the most often considered, because it can produce fuels similar (even of higher quality) to conventional liquid fuels. However, lignocellulosic resources are significant but not plentiful: in Europe, the primary energy feedstock is about the third of the final energy consumption [1]. As a consequence advanced use of biogenic carbon is necessary. This increase in productivity is possible with optimized efficiency of the standard process, but also by providing extra hydrogen input, therefore coupled hydrogen production is studied [2–4].
Referring to chemical equations, biomass gasification is roughly $C_6H_9O_4 + 3\ O_2 + H_2O \rightarrow 4\ CO + 2.5\ H_2 + 2\ CO_2 + 3\ H_2O$ while FTS is ($n \in [5, 20]$), $n\ CO + (2n+1)\ H_2 \rightarrow C_nH_{2n+2} + n\ H_2O \approx n\ (CH_2) + n\ H_2O$. With extra hydrogen input the process equation is then roughly $C_6H_9O_4 + 3\ O_2 + H_2O + 6H_2 \rightarrow 4\ (CH_2) + 2\ CO_2 + 7\ H_2O$ instead of $C_6H_9O_4 + 3\ O_2 + 3\ H_2O \rightarrow 2\ (CH_2) + 4\ CO_2 + 5\ H_2O$.

1.2. Objective: the relevance of High Temperature Steam Electrolysis

Water electrolysis produces both hydrogen for extra input and oxygen for gasification – in the required *3:6* ratio shown above –: $H_2O \rightarrow H_2 + ½\ O_2$. Furthermore, water recycling could theoretically lead to $C_6H_9O_4 \rightarrow 4\ (CH_2) + 2\ CO_2$ for the integrated process. High Temperature Steam Electrolysis (HTSE) is notably relevant because it puts free heat (from BtL) to work, as well as it offers high energy efficiency [3] (Fig. 1).

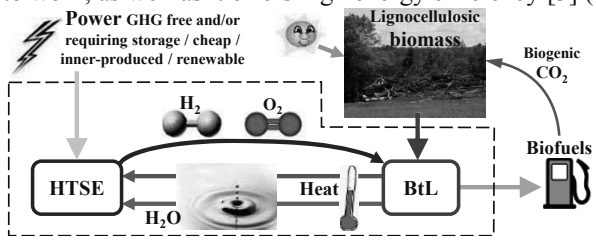

Fig. 1: Principle and interest of BtL and HTSE hybrid process to produce biofuels.

This paper aims at defining the framework for assessment, validation and quantification of the relevance of the HTSE and BtL hybrid process. Both optimal coupling of the two processes and comprehensive optimization of the new process require a detailed modeling: the selected technologies and method used are presented in §2. Challenges of energy system – and particularly second-generation biofuels processes – lead to select several criteria which are presented in §3. These modeling and criteria are suitable for multicriteria optimization.

2. Process description

2.1. BtL process

The BtL process rests on two main steps: gasification of the biomass into syngas then FTS of naphtha, gasoline, kerosene and diesel. In addition, the complete process includes preparation or recovery operations that impact process performance data and therefore the criteria. Operations involving heat or matter are simulated, from raw biomass to liquid fuels (in bold in Fig. 2).

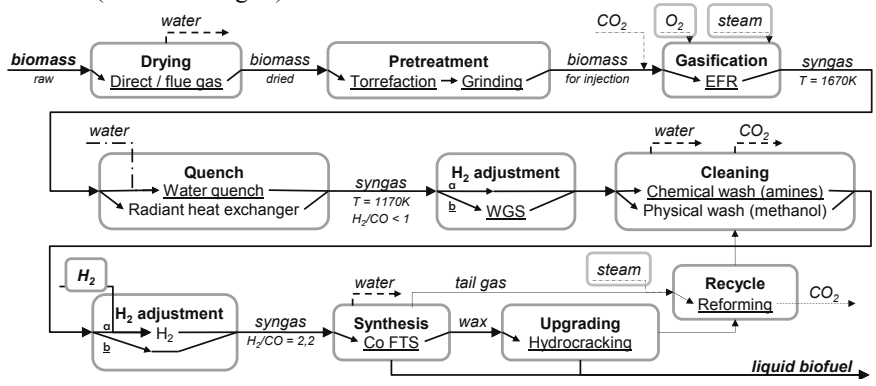

Fig. 2: Block diagram of the BtL process.

Simulations are carried out using a commercial process simulation software (ProSimPlus®) to allow physical modeling, mass and energy balances; it also generates data for complete heat integration. The process model is built from standard elementary and user modules, supported by various CEA (French Atomic Energy and Alternative Energies Commission) previous works, including modeling work [5,6] and selection of relevant

elementary processes and technologies [4]. This selection is mainly based on cost and productivity for high capacity BtL plants, e.g. adiabatic pressurized oxygen-blown Entrained Flow Reactor (EFR) is used for biomass gasification. Selected technologies are shown in the block diagram (Fig. 2, WGS: Water Gas Shift; Co FTS: cobalt catalyzed FTS. Base case is underlined). Concerning reaction models, equilibrium is considered when possible (gasification, WGS – with methane as an inert – and reforming); in case of non-standard kinetics (torrefaction, FTS) conditions and conversions are fixed; electrolysis are user-built modules.

In this paper only base case simulation results and a preliminary comparison are proposed. Three options for hydrogen ratio adaptation are presented: HTSE, Alkaline Electrolysis (AE) and WGS.

2.2. Hydrogen ratio adaptation

Adaptation is required to bring H_2/CO ratio of the syngas (<1) to stoichiometric conditions (>2) for FTS. Hydrogen can come either from a conversion of a part of the syngas using WGS reaction ($CO + H_2O \rightarrow H_2 + CO_2$) or an extra hydrogen input in order to increase carbon yield; in this case the hybrid process obtained uses both biomass and another raw energy. Using steam reforming of Natural Gas (NG) to produce hydrogen creates GHGE. With low-carbon content electricity (e.g. renewable or nuclear power), the AE (consuming only electricity) can reduce these GHGE, but with an increase in production cost and a poor equivalent primary energy efficiency. Finally, HTSE (using heat both to vaporize water and to maintain the electrochemical reaction at 1000-1200 K) brings the advantage of better energy efficiency of the process, but along with an increase in cost. WGS, NG reforming and AE are touchstones for HTSE performance and suitability. Scope, coupling issues, computing input/output and parameters are summarized in Fig. 3.

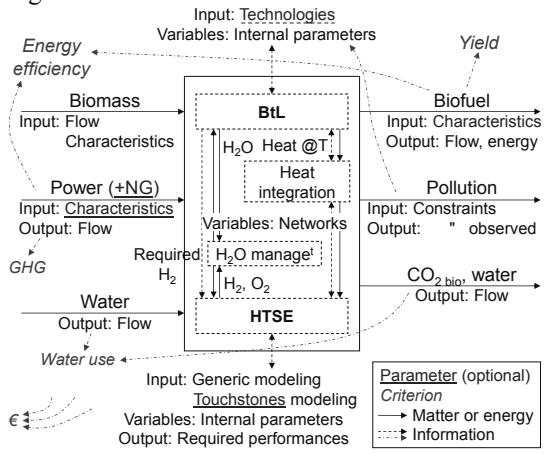

Fig. 3: Framework for BtL and HTSE hybrid process evaluation.

2.3. Heat integration

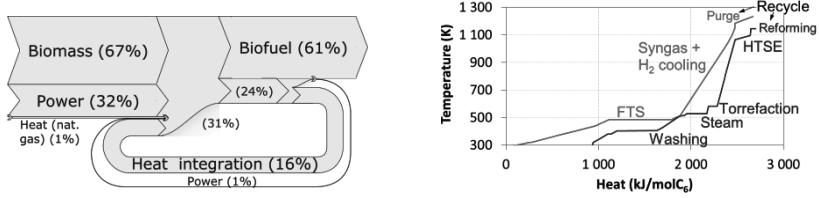

Fig. 4: Heat integration (case HTSE): Grassmann (exergy flow) diagram and composite curves.

Complete heat integration is performed after each simulation (so it does not impact the operations shown in Fig. 2). Temperatures are corrected using half matching typical ΔT_{min} (minimum temperature difference in exchangers) values [7] (Fig. 4).

3. Criteria and preliminary results

Issues of energy system – and particularly second-generation biofuels – lead to select several criteria as performance data or compliance constraints. Two technical criteria (yield or efficiency; to maximize) are used for the two main functions of the process and three other criteria (expressed per unit of energy in the liquid biofuels; to minimize) are selected: the standard economic criterion (not described for space limitation) and two environmental criteria. Criteria are italicized in Fig. 3.

3.1. Biogenic carbon criterion

The main function of the coupling is to enhance the conversion of biogenic carbon into liquid biofuels. Biogenic carbon yield is therefore selected as a technical performance criterion. Flow diagrams are presented for WGS and both electrolysis (HTSE and AE) cases. CO_2 (including part of CO_2 in the gas) is shown in grey; CO_2 formations – that are losses of biogenic carbon – are framed in Fig. 5: *6%* of the input biogenic carbon is lost at torrefaction, *12%* at the EFR, *16%* at the quench and possibly *31%* at WGS.

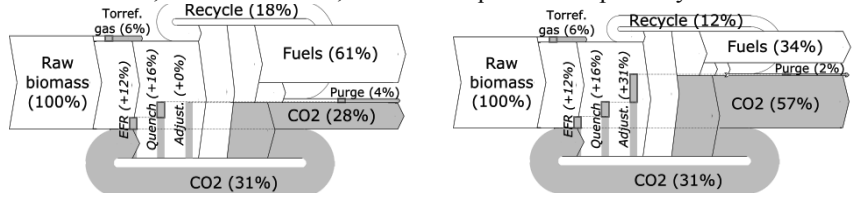

Fig. 5: Biogenic carbon flow diagrams: HTSE and AE cases (left) and WGS case (right).

3.2. Energy criterion

Energy criterion is expressed as exergy (work equivalent) efficiency in recent papers [8–10]. Exergy is particularly useful to consider heat value, that is why it is used in Fig. 4. However, secondary (i.e. without power production yield) exergy results do not provide relevant input/output data given that exergy of fuels is higher than Lower Heating Value (LHV) – biomass: 113%, liquid fuels: 107% [11] – but exergy equals power for electricity. On the contrary, we must account for upstream power production and inferred technical energy efficiency of this prior conversion. That is why the energy criterion is expressed as the yield of equivalent primary energy (heat equivalent: $[\sum(flowrates_{in} \times LHV_{in}) + power \times 2.6] / \sum(flowrates_{out} \times LHV_{out})$) in this work*.

3.3. Greenhouse gas emissions criterion

GHGE are calculated for the process (from NG consumption for hot utility), including indirect emissions for power production (French electricity mix for industrial applications: $55 g_{\text{equivalent of fossil } CO2} / kWh$); indirect GHGE for forestry is not counted due to high variability. Avoided emissions are directly related to productivity, therefore raw emissions are preferred.

3.4. Electrolysis water use criterion

Fresh water consumption is used in life cycle analysis, but it is not calculated in studies using a process engineering approach. As electrolysis uses water as raw material, the additional fresh water consumption due to electrolysis is counted in this study.

* Primary energy is found in nature (e.g. wind, biomass or NG); secondary energy has been converted (e.g. electricity) and thus it has been affected at least once by a conversion efficiency.

First results show that the process is always globally a net producer of water (due to moisture of raw biomass) and that consumption of fresh water by HTSE can be notably reduced (almost by half) using the water byproduced by the FTS. This water meets specifications for HTSE catalysts (simulations carried out using specifications for FTS from [12]) and hydrocarbons are harmless for HTSE.

3.5. Discussion

First results (Table 1) are consistent with expectations: electrolysis can nearly double the biogenic carbon conversion, but this leads to lower performance data regarding other criteria; HTSE can limit this drop compared to the AE.

It appears that characterization of power strongly impacts the results. Concerning energy, the secondary energy efficiency increases with HTSE but the equivalent primary energy efficiency is still lower than with WGS. This is due to poor efficiency of power production: the criterion in equivalent primary energy is indeed necessary. Concerning GHGE, they are strongly linked to power consumption in case of electrolysis, given that little NG is used compared to power.

Table 1: Criteria values of BtL processes for different hydrogen adaptation options.

	WGS	AE	HTSE
Biogenic carbon (Fig. 5)	34%	61%	61%
Secondary energy ($\frac{\sum(flowrates_{in} \times LHV_{in}) + power}{\sum(flowrates_{out} \times LHV_{out})}$)	50%	51%	62%
Equivalent primary energy	46%	30%	41%
GHGE (in $g_{\text{equivalent of fossil } CO2} / kWh_{\text{liquid biofuels}}$)	10	50	35
Water (in $kg / GJ_{\text{liquid biofuels}}$)	no extra	+43	+11

4. Conclusion

The first concluding elements in studying integrated HTSE-BtL process verify that hydrogen input is almost doubling the biogenic carbon conversion compared to the standard BtL process. They bring out significant secondary energy saving for HTSE; and clear advantages over AE considering technical and environmental criteria. HTSE is therefore suitable and promising, although its performance data is strongly linked to power characterization.

Next step is implementation and use of multicriteria optimization. In addition to trade-offs, multicriteria parametric optimization is expected to make the proposed structural comparison more accurate by providing adapted operating points for the integrated design under study.

References

[1] E.E.A., How much biomass can Europe use without harming the environment ? (2005)
[2] R. Agrawal et al., PNAS 104 (2007) 4828
[3] G. Hawkes et al., AIChE Annual Meeting (2009)
[4] J.-M. Seiler et al., Energy 35 (2010) 3587
[5] G. Boissonnet et al., 16th European Biomass Conference and Exhibition (2008) 1875
[6] G. Boissonnet et al., International Freiberg Conference on IGCC & XtL Technologies (2010)
[7] Introduction to Pinch Technology, Linnhoff March (1998)
[8] A. Sues et al., Energy 35 (2010) 996
[9] L. Tock et al., Biomass Bioenergy 34 (2010) 1838
[10] M.J. Prins et al., Fuel Process. Technol. 86 (2005) 375
[11] J. Szargut et al., Exergy analysis of thermal, chemical and metallurgical processes (1988)
[12] C.N. Hamelinck et al., Energy 29 (2004) 1743

I.A. Karimi and Rajagopalan Srinivasan (Editors), Proceedings of the 11th International Symposium on Process Systems Engineering, 15-19 July 2012, Singapore.

Model-based assessment of algal ponds for biomass production under temperate climates

Mohammed K Mohammed, Aidong Yang, Adel Sharif

Division of Civil, Chemical, and Environmental Engineering, Faculty of Engineering and Physical Sciences, University of Surrey, UK

Abstract

Computer modelling of open ponds for producing algal biomass in wastewater was utilised to evaluate the potential of such algal ponds in a temperate climate. Simulations were performed with the solar radiation and temperature regime of a UK location representing temperate regions, in comparison with a Qatar location representing hot regions. Simulation results indicated low cold season performance at the UK location although a peak of algal biomass production in the summer was observed. In contrast, the Qatar location was shown to have consistently high biomass productivity all year round. Further simulations suggested that the enhancement of light supply is very likely more effective than increasing temperature for improving the algal pond productivity in a temperate climate.

Keywords: algal pond, biomass yield, temperate climate, mathematical modelling.

1. Introduction

Cultivation and utilisation of microalgae have recently received much attention due to their potential roles in the production of renewable fuels as well as chemical, health and medical products, and in environmental mitigation (Demirbas, 2010). Cultivation of algae currently occurs in open ponds and closed photobioreactor (PBR) systems (Chisti and Yan, 2011). The latter is preferable as it allows for more control and vitally reduces the possibility of contamination. However, the high cost of this technology still prevents it from being economically viable for large-scale production (Kovacevic and Wesseler, 2010). Currently, open ponds are the more economic option, although they suffer from various problems stemming from the nature of being open to the environment. These particularly include the effect of natural conditions, most notably temperature and solar radiation. Generally, open ponds tend to be more productive when located in warm areas with plenty of sunlight; their performance under temperate climatic conditions is still a matter that requires investigation.

The aim of this paper is to utilise a mathematical model to evaluate algal ponds located in temperate climates, by means of a comparison with those in warm regions. Specifically, two different geographical regions were chosen: Camborne (UK) and Al Kharsaah (Qatar), representing a temperate region and a warm region, respectively. Data for each area was obtained from the Atmospheric Science Data Centre (ASDC) at NASA Langley Research Centre (NASA, 2012). This paper will report the key mathematical model components and the climatic data utilised in the simulations, as well as the observations made based on the simulation results.

2. Mathematical Model

A mathematical model was created to assess algal biomass production in a continuously operated open pond fed with wastewater, where photosynthetic algae and aerobic

bacteria co-exist with symbiosic exchange of CO_2 (produced by bacteria and utilised by algae) and O_2 (produced by algae and utilised by bacteria). A raceway type of design has been assumed for the algal pond. Key design and operation parameters such as pond volume and depth, wasterwater flow rate and nutrient level were taken into consideration (Table 1).

Table 1 Design and Operating Parameters of Simulated Algal Pond

Parameter	Nominal Value
Pond Depth (m)	0.4
Pond Volume (m^3)	350
Influent Flow Rate (m^3/day)	50
Influent BOD (g/m^3)	500

In terms of the supply of CO_2, two sources were considered by the model, namely the atmosphere and aerobic digestion of the nutrients in the wastewater. Additional CO_2 supply by gas sparging was not considered in this paper as it represents a separate level of complexity in terms of the design and operation of the pond. Other nutrients were assumed to be at levels which have no limiting or inhibitory effects. The modelling framework previously developed by Yang (2011) has been used, which particularly includes kinetic modelling of algal growth affected by temperature and light supply:

$$r_{gA} = \mu_A X_A \tag{1}$$

$$\mu_A = \hat{\mu_A}\left(\frac{CO_{2_D}}{K_c + CO_{2_D}}\right)\left(\frac{N_T}{K_{NA} + N_T}\right)f_I \tag{2}$$

$$f_I = \frac{I_a}{I_s}\exp\left(1 - \frac{I_a}{I_s}\right) \tag{3}$$

$$\hat{\mu_A} = 9.46 \times 10^5 \exp\left(\frac{-4034}{T}\right) \tag{4}$$

$$I_a = \frac{1}{Z}\int_0^Z I_0 \exp(-K_e z)\,dz \tag{5}$$

$$I_0(t) = \left(\frac{\pi}{2}\frac{I_d}{f_P}\right)\sin\left(\frac{\pi t}{f_P}\right) \tag{6}$$

The notations are explained below:

r_{gA}	Growth Rate
μ_A	Specifc Growth Rate
X_A	Mass Concentration of Algae
CO_{2D}	Dissolved CO_2
N_T	Total Nitrogen
$\hat{\mu}_A$	Constant
K_C	Constant
K_{NA}	Constant
f_I	Light Intensity Factor
I_a	Average Light Intensity in the Pond
I_s	Saturated Light Intensity (350Cal/cm^3)
T	Temperature
I_0	Surface Light Intensity
K_e	Extinction Coefficient
Z	Depth of Pond
I_d	Daily Total Light Intensity at Pond Surface
f_p	Fraction of the Photoperiod in a Day
t	Time in Days

3. Selected Locations and Climate Conditions

To avoid extremes, a relatively warm area in the UK (Camborne, latitude: 50.22; longitude; -5.33) was selected to represent temperate regions where open pond based algal cultivation might be practical. To offer a contrast, an area in central Qatar (Al Kharsaah, latitude: 25.5; longitude: 51.25) was also selected to represent hot regions, which are normally considered ideal for operating algal ponds. Data for each territory was gathered from ASDC (NASA, 2012), which provided averaging months over a 22-year period from 1983 to 2005 based on data gathered from various Earth orbiting satellites. To conduct a preliminary test on the reliability of the NASA data, a comparison was made with the measurement data collected by the Met Office in the UK for Camborne (WRDC, 2012), averaged over the period of 2005-10. This comparison gave only an average difference of 1.69%, suggesting reasonable reliability of the NASA data set. The NASA data for both sites is shown in Figure 1. It can be seen that there is an expected variation in temperature within the year with a predictable difference between the two selected locations (Fig 1c). With respect to solar radiation data, the Direct Normal Radiation follows a seasonal pattern similar to temperature with regards to variation and the expected difference (Fig 1b). Greater variation in Daily Photoperiod is apparent between the two localities, with the UK location being lower during the colder seasons and eclipsing the Qatar location during the summer period (Fig 1a).

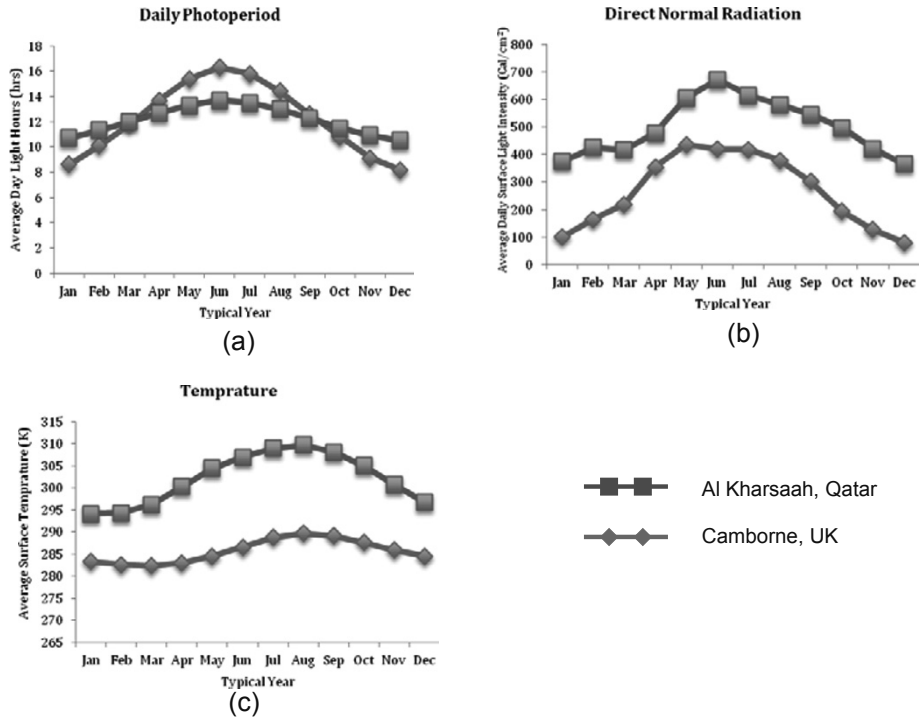

Figure 1. Comparison of (a) Daily Photoperiod, (b) Direct Normal Radiation and (c) Temperature between Camborne (UK) and Al Kharsaah (Qatar).

4. Simulation Results and Discussion

The process modelling software gPROMS was used to carry out a number of simulations, with all results presented in Figure 2. Each simulation covered a two year period and the result of the second year was taken for analysis. This is to allow for stabilisation of the (simulated) pond in the first year and subsequently to achieve in the second year a more accurate representative estimation of what would be expected in a typical year of operation.

The first two simulations were dedicated to the climate conditions of the two locations respectively, without any modification to the data presented in Section 3. The results clearly show that algal biomass production is much more favoured in the Qatar location than the UK location overall in a typical year. It can be seen that during the mid summer period the algal biomass concentration in the pond was almost identical for both countries with average figures of 301g/m^3 and 299g/m^3, respectively, for the month of June. However, gaps appear significantly in the performance between the two locations during the UK's cold seasons, suggesting inadequate solar radiation and/or temperature conditions for high biomass yield during these periods in a typical year within the UK.

The pond at the Qatar location on the other hand was shown to have a stable and relatively high level of algal biomass concentration throughout the year, suggesting the region being a good location for algal biomass production via open ponds.

To further understand the relative importance of temperature and light supply for operating open algal ponds under a temperate climate, further simulations were performed using modified climate data for the UK location. These include: (1) two tests with UK's real temperature data coupled with year-round light supply at the level of UK's April (photoperiod = 13.7 hrs, average surface light intensity = 355.20 Cal/cm^2) and June (photoperiod = 16.3 hrs, average surface light intensity = 419.71 Cal/cm^2), respectively; and (2) two tests with UK's real light data coupled with year-round temperature of 20^{o}C and 30^{o}C, respectively. As shown in Figure 2, for simulations carried out with June light data, the algal biomass concentration was similar to that obtained within Qatar throughout the year, hovering around a biomass concentration of 295g/m^3. Results for April light data showed a similarly stable but lower concentration of biomass with a peak of 275g/m^3, which however, still represent a significant improvement during the cold seasons. On the other hand, temperature at both 20^{o}C and 30^{o}C saw medium improvement of the overall productivity compared to the performance under the real temperature profile, however still with low biomass concentration yielded during the cold periods of a year. Furthermore, the improvement brought by increasing temperature from 20^{o}C to 30^{o}C is visible but not significant. The above results of these additional simulations together tend to suggest that light supply is a factor more important than temperature for improving the performance of algal ponds located in a temperate region like the UK location studied in this work.

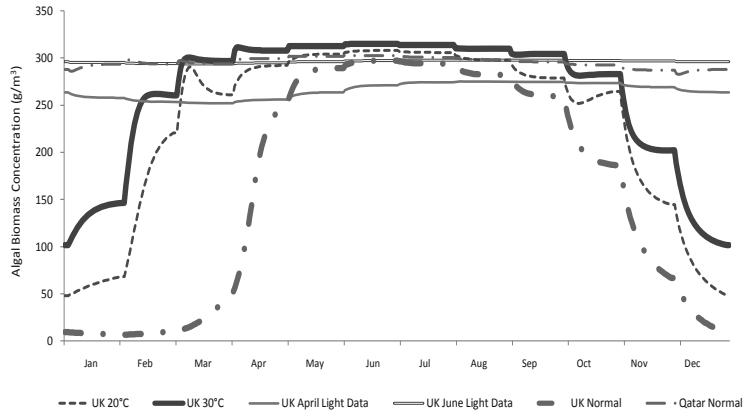

Figure 2. Model-predicted algal biomass concentration in a typical year temperature conditions at constant solar data taken from April, June as well as constant temperature of 20^{o}C and 30^{o}C.

5. Conclusion

Computer simulations were carried out to assess and compare the algal biomass production by an open pond at two geographical locations selected within the UK and Qatar to represent the temperate and hot climates respectively. Both original (i.e. actual) and modified climate data sets have been used as the input to the simulations. Results showed that in comparison to a hot region, a temperate region possesses a much inferior viability for open pond based algal biomass production. It was further shown that the importance of light supply is greater than temperature for improving the performance of an open algal pond operated in a temperate region, suggesting that additional light supply rather than heating is likely a more effective direction of intervention. It should be noted that experimental validation of the kinetic parameters currently taken from the literature is a critical step to follow, which is the ongoing work.

References

Y. Chisti and J. Yan, 2011, Energy from algae: Current status and Future trends, Applied Energy, 88, 3277-3279.

A. Demirbas, 2010, Use of algae as biofuel sources, Energy Conversion and Management, 51, 2738-2749.

V. Kovacevic and J. Wesseler, 2010, Cost-effectiveness analysis of algae energy production in the EU, Energy Policy, 38, 5749 – 5757.

NASA, 2012. NASA Langley Research Centre's Atmospheric Sciences Data Centre Homepage. [Online]. Available: http://eosweb.larc.nasa.gov.

WRDC, 2012. World Radiation Data Centre Homepage. [Online]. Available: http://wrdc.mgo.rssi.ru.

A. Yang, 2011, Modelling and Evaluation of CO_2 Supply and Utilization in Algal Ponds, Industrial & Engineering Chemical Research, 50, 11181-11192.

I.A. Karimi and Rajagopalan Srinivasan (Editors), Proceedings of the 11th International Symposium on Process Systems Engineering, 15-19 July 2012, Singapore.

PSE opportunities in biocatalytic process design and development

Pär Tufvesson,[a] Ulrich Krühne,[a] Krist V. Gernaey,[a] John M. Woodley[a]
[a]*PROCESS, Department of Chemical and Biochemical Engineering, Technical University of Denmark, DK-2800 Lyngby, Denmark*

Abstract

Biocatalysis (the use of one or more isolated enzymes in soluble or immobilized form, as well as enzymes contained within resting whole-cells) is a rapidly growing area of process technology. The introduction of biocatalysis presents new opportunities to develop 'green' synthetic routes to pharmaceuticals and other chemical products, since enzymes usually work in an aqueous solution and under mild conditions. Nevertheless the implementation of a biocatalytic reaction and the integration of a biocatalytic reaction into an otherwise chemical catalytic sequence is a complex task where PSE tools have a particularly important role to play. In this paper we will present a variety of PSE tools including computational fluid dynamics (CFD), operating windows, kinetic modelling, economic analysis and environmental assessment to support the development of economically viable biocatalytic processes.

Keywords: process template, substrate adoption, methodology, pharmaceutical.

1. Introduction

Biocatalysis, the use of cells, enzymes (or parts thereof), is increasingly used in industry for the production of chemicals [1,2]. The technology is primarily used in the pharmaceutical and fine chemicals industries, but increasingly also in the production of lower value chemicals where high reaction selectivity can be exploited to yield a more competitive process. The main limitations are the limited operating space (e.g. temperature < 100°C) and potentially low productivity (kg product / kg catalyst). Successful processes need to be carefully balanced to give optimal process performance, while at the same time exploiting the capability of the biocatalyst to the maximum extent possible. Consequently, when developing a biocatalytic reaction or process it is necessary to have an understanding of the factors that determine the activity, stability and selectivity of the biocatalyst as well as the process requirements and constraints, and the interconnection between the biocatalyst and process performance. A number of biocatalytic processes have been successfully implemented in industry. Commonly these are developed on a case-by-case basis. However, for biocatalysis to achieve its full potential it would be highly desirable to introduce systematic process design methodologies and tools similar to those that are widely used in the development of conventional chemical catalytic processes. Further, although modern biotechnology offers huge possibilities to improve the biocatalyst, e.g. by directed evolution, to increase tolerance to solvents and temperature, as well as increasing the activity, this is a time consuming and expensive activity. Therefore, clear targets for the catalyst and the process are very important in order to develop an effective and competitive process. This is a complex task due to the many factors influencing the effectiveness of the catalyst and the process. In this paper we will illustrate how a Process Systems

Engineering (PSE) approach, and associated tools, can be used to facilitate this development.

2. The development procedure

The purpose of a structured framework for the development procedure is to simplify decision making and to direct work towards collecting the data required for these decisions as efficiently as possible. A simplified development procedure is shown in Figure 1 indicating the interactions between the process and catalyst development efforts and the PSE tools that could potentially be used. For example, CFD investigations in microfluidic reactor systems, offer excellent opportunities for assessment of kinetic parameters, material characteristics and in understanding of transport and reaction details [3,4]. The understanding gained by the virtual experiments can then be used in simulations of large-scale designs of new reactor layouts or operating strategies. The framework can address challenges such as what type of product removal system to integrate, how to supply reactant, how to choose the biocatalyst format, when to integrate operations and most importantly, how to set targets for protein engineering [5]. It is this latter challenge in particular which presents a new and exciting opportunity for PSE.

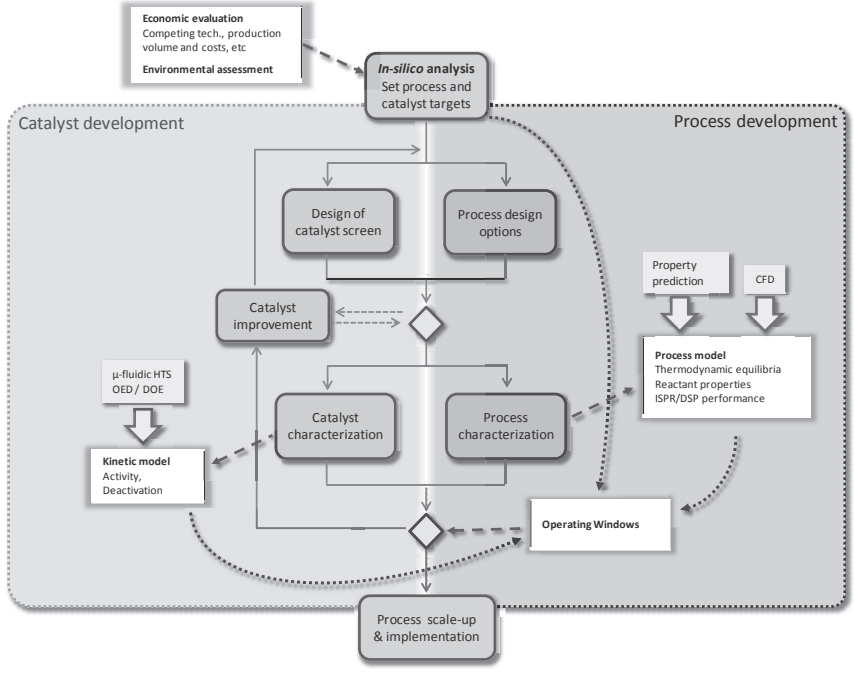

Figure 1. Biocatalytic process development procedure.

The procedure consists of different stages of development and strategic points, where a decision has to be made concerning: (1) whether to go on (or discontinue the project); and/or (2) if the catalyst needs to be developed further instead of spending additional efforts on the process. The so called 'Operating Windows' form a useful and easy to understand tool in order to facilitate the decision-making, to visualize the interactions between the biocatalyst and the process and to identify knowledge gaps [6].

3. Operating windows

An operating window is a tool to illustrate the interaction of multiple constraints on the feasibility of a process. There are four main classes of constraints that will define the operating window in the processes discussed here: (1) Economic – Allowed process cost; (2) Physico-chemical –Solubilities, reaction thermodynamics, etc.; (3) Biocatalyst – Activity and stability under different conditions, etc.; (4) Process – Separation, mixing, mass transfer. An example is given in Figure 2, indicating some of the limits for operation based on reaction product and co-product concentration, in this case for a transaminase catalyzed reaction.

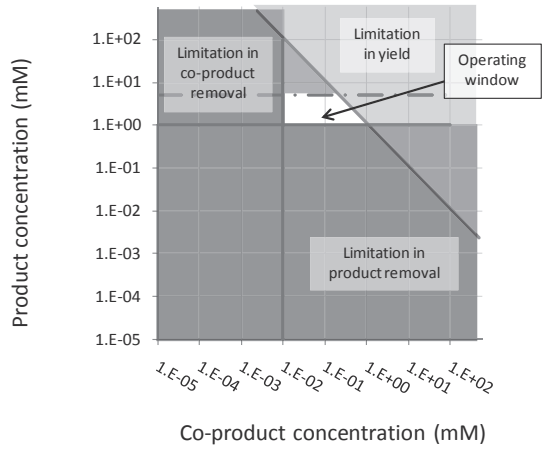

Figure 2. Operating window for the synthesis of an optically pure chiral amine based on simultaneous removal of product and co-product from the reactor.

Windows such as this can be used to dictate the requirements on the biocatalyst in an individual case - information that will be very valuable in early development. The data required for building the window will depend on the development stage. In order to be effective in choosing between the many different process options in early development, being able to make decisions based on rapidly available data is crucial. Experimental data are by their nature time consuming to acquire, which is why prediction tools for physico-chemical properties (e.g. thermodynamic equilibrium), computational fluid dynamics (CFD) simulations, as well as automated microreactor platforms and experimental protocols for rapidly collecting the relevant biocatalyst, as well as process data, would be highly valuable. Once sufficient data are available, the operating window can be refined on the basis of mechanistic process models [7,8].

4. Property prediction

Reaction and process characteristics such as the solubility of the compounds involved, the reaction equilibrium and stability of the compounds involved are independent of the biocatalyst but constitute essential information for selection of biocatalysts and operating methods. However, frequently reaction characteristics cannot be obtained from literature since the compounds involved when developing a new biocatalytic process are most often new compounds which frequently have not been studied before. Hence the required data must be obtained via experimentation. As the number of reaction and process options might be very large, the idea of property prediction is therefore to assist in narrowing down the search space for experimentation. For

biocatalytic reactions we have identified that predictive tools for water-solubility and thermodynamic properties are amongst the most important. The conditions under which a specific biocatalytic step operates make such predictions particularly challenging. In a recent study, a group contribution methodology for predicting metabolic fluxes *in-vivo* was developed, which could potentially be applied also for *in-vitro* biocatalytic reactions run in aqueous media [9]. However, this method proved to yield estimates with an unacceptable accuracy in a study of reaction sets relevant to biocatalytic transamination reactions, thereby clearly showing the need for substantial further research in this area [10].

5. Micro-scale reactors and Computational Fluid Dynamics (CFD)

The use of miniaturized systems to collect experimental data enables the benefits of parallelisation to save time. Indeed an increasing number of applications can be found in the scientific literature based on microfluidic principles. Miniaturized systems offer a range of important characteristics: (1) Use minute amount of samples and other expensive process materials (enzyme, substrate, etc.); (2) perform the experimental investigations faster than bench scale setups; (3) introduce favourable effects for the detailed investigation of material properties like diffusion coefficients or reaction kinetics due to the laminar nature of the fluid dynamic conditions; (4) can be easily automated; (5) can be more easily analysed numerically due to the absence of turbulence in the microchannels. An example of high content screening and numerical analysis by use of CFD is given in Figure 3a and b.

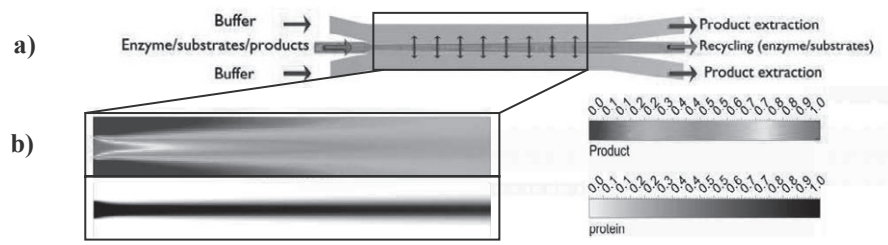

Figure 3 a) Principle of hydrodynamic focussing. Channel width 250 µm, depth 50 µm. **b)** CFD calculated concentration profiles for different components. Diffusion coefficients: Protein $1 \cdot 10^{-10}$ m^2/s Product $2 \cdot 10^{-9}$ m^2/s

Figure 3a shows an example of a miniaturized system in which the process stream of an upstream biocatalytic reactor is guided in between two buffer flows. By choosing the appropriate flowrates the residence time in the total system can be adjusted, as well as the sample width in the main channel. When the liquids flow through the channel a perpendicular material transport will take place due to concentration gradients (diffusion). The reaction medium will be composed of the enzyme, the reaction substrates and products. Each component will most likely have different diffusion characteristics, which commonly are poorly documented and might be different in an environment with changing liquid characteristics. According to the different diffusion rates different amounts of the respective substances will therefore be found in the three outlet channels. Varying the total flowrate and hence the residence time, the diffusion rates can thereby be determined. In Figure 3b a CFD simulation is shown for the investigated product, which is assumed to have a diffusion coefficient which is one order of magnitude larger than the diffusion coefficient of the biocatalyst. Selecting the

appropriate channel geometries along with the flowrate for the biocatalyst to be recycled into the reactor, a part of the product can be directly extracted through the side channels. This demonstrates one of the advantages of miniaturized systems in the field of accessing the process characteristic information. Setting up the systems with automated analytical equipment will furthermore contribute to the rapid assessment of key design information.

6. Economic assessment

For effective process development the use of economic assessment tools should be considered. Although full cost assessment is not possible at early process development stages due to a lack of reliable information about the final process, it is possible to identify critical process parameters and set development targets for the process and biocatalyst based on previous experience or literature data for similar processes. It has previously been shown how such an assessment could be used to set biocatalyst productivity targets for different types of biocatalytic reactions, ranging from small scale high value processes (pharmaceuticals) to high volume low value processes (bulk) [11]. The guidelines developed in such analyses have great value in serving as a first approximation for the process and biocatalyst development.

7. Future perspectives

In this paper we have discussed a number of PSE tools to potentially assist in the development of biocatalytic processes. The future will see the integration of such PSE tools which will enable more rapid and effective implementation of new biocatalytic processes. Collaborative efforts will be essential to further develop the tools. The testing of new methodologies will also be an important activity together with those that implement changes to the biocatalyst and those that design and implement new and retrofit processes.

References

[1] De_Wildeman et al., 2007, Biocatalytic reductions: from lab curiosity to ‘‘first choice’’, Acc Chem Res, 40, 1260-1266.
[2] Pollard and Woodley, 2007, Biocatalysis for pharmaceutical intermediates: the future is now. Trends Biotechnol, 25, 66-73.
[3] Jones et al., 2007, The effects of engineering design on heterogeneous biocatalysis in microchannels, Appl Biochem Biotechnol, 137-140, 859—873.
[4] Cantu-Perez et al., 2011, Hydrodynamics and reaction studies in a layered herringbone channel, Chemical Engineering Journal, 167, 657-665.
[5] Turner, 2009, Directed evolution drives the next generation of biocatalysts. Nat Chem Biol,, 5, 567-573.
[6] Woodley and Titchener-Hooker, 1996, The use of windows of operation as a bioprocess design tool, Bioprocess Eng, 14, 263-268
[7] Gernaey et al., 2010, Application of mechanistic models to fermentation and biocatalysis for next generation processes. Trends Biotechnol, 28, 346-354.
[8] Santacoloma et al., 2011, Multi-enzyme catalyzed processes: Next-generation biocatalysis. Org Process Res Dev, 15, 203-212.
[9] Jankowski et al, 2008, Group contribution method for thermodynamic analysis of complex metabolic networks, Biophys J, 95, 1487-1499
[10] Tufvesson et al, 2012, Experimental determination of thermodynamic equilibrium in biocatalytic transamination, Biotech Bioeng (*In-press*),
[11] Tufvesson et al, 2011, Guidelines and cost analysis for biocatalyst production in biocatalytic processes, Org Process Res Dev, 15, 266-274

I.A. Karimi and Rajagopalan Srinivasan (Editors), Proceedings of the 11th International Symposium on Process Systems Engineering, 15-19 July 2012, Singapore.

Optimal Design of an Algae Oil Transesterification Process

C. Silva[a], L. A. Fabiano[a], G. Cameron[a], and W. D. Seider[a]

[a]*Department of Chemical & Biomolecular Engineering, University of Pennsylvania, 220 South 33rd St, Philadelphia 19103, USA*

Abstract

An optimization strategy for designing processes to convert algae oils to biodiesel is introduced. In this brief paper, just a typical oil sample is used, grown experimentally using *Nannochloropsis salina* algae in salt water by Solix and transesterified using the Catilin solid T-300 acid catalyst. NIST thermophysical property data in ASPEN PLUS and literature data were used to estimate the properties of the chemical species. Approximate group contribution methods were used to estimate missing properties.

A transesterification process was synthesized and simulated using ASPEN PLUS. For the transesterification reactor design, three reversible reactions were assumed. Because kinetic data were unavailable, pre-exponential factors and activation energies for the transesterification of palm oil were used, adjusted using residence-time data from Catilin for transesterification of an algal oil[1]. A USER2 FORTRAN subroutine was written to solve the CSTR mass balances.

The process was heat integrated to reduce energy consumption. Next, the Aspen Process Economic Evaluator was used to estimate equipment sizes and purchase and installation costs. In this brief paper, just the results for a single case study are presented. In a full manuscript, the optimization strategy for selecting the best algal oil is presented.

Keywords: Biodiesel, *Nannochloropsis salina*, Transesterification

1. Introduction

1.1 Background

Because of their compatibility with conventional combustion engines, biofuels are being considered as replacements for petroleum-based, liquid transportation fuels. Originally, beef tallow, plant-derived oils, and waste oils, were transesterified to biodiesel; however, in recent years, various strains of algae have been explored as sources of oil because algae grow in much higher density, using land and water that are unfit for terrestrial plant cultivation.

Because salt water is significantly cheaper and more plentiful than fresh water, the *Nannochloropsis salina* strain of algae, which is cultivated in salt water, is an excellent candidate for the production of biodiesel. This strain yields oil levels in excess of 50% (on a dry basis[2]), using mixotrophic conditions[3].

After the algae are grown, they can either be transesterified directly under super-critical conditions, or the oil can be extracted from the cells and converted at milder conditions using an acidic or basic catalyst; we have chosen the latter approach for this initial study. During the extraction, the triglycerides are separated from an algae-sludge using a standard hexane extraction procedure, yielding relatively pure triglycerides and a byproduct of residual algae biomass.

1.2 Transesterification Kinetics

One kinetic model for converting triglycerides to biodiesel is the three-reaction mechanism in Figure 1. In each reaction step, a fatty-acid group, attached to the glycerol backbone, is reacted with methanol to form a fatty-acid, methyl ester (FAME). First, the triglycerides are converted to diglycerides, which become monoglycerides, finally yielding glycerin.

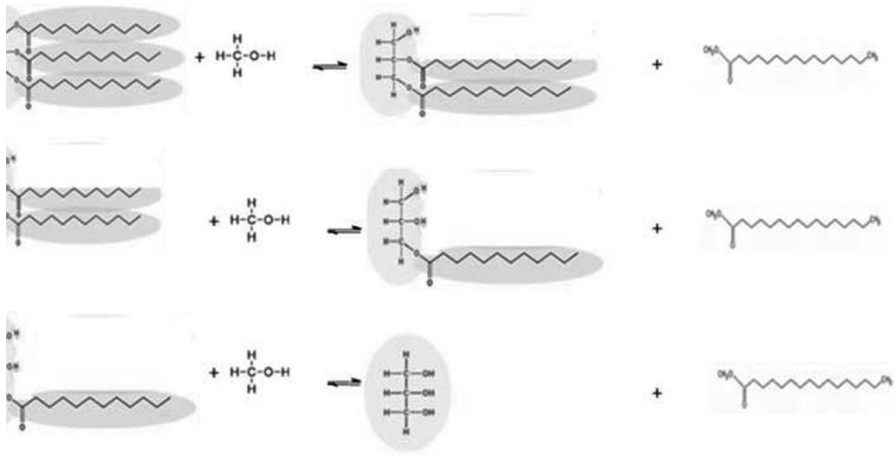

Figure 1. Transesterification Kinetics

This kinetic model is based upon the bench-scale Catilin process, which uses their proprietary T-300 solid-metal, acid catalyst for the conversion of triglyceride to FAME. We are using kinetic data for palm oil[1] (with modified activation energies to match Catilin-reported conversions for the transesterification of algae oil) to size the reactors.

1.3 Species Data

The thermophysical property data for triglycerides and their derivatives within ASPEN PLUS were extremely limited. ASPEN's databanks were supplemented with information from the NIST databank, which is interfaced with ASPEN PLUS for easy data-sharing; however, many important properties remained absent for key chemical species. Therefore, an extensive literature search was performed to obtain the missing properties.

Three sources were used for the Antoine equation parameters for the triglyceride and FAME molecules[4,5,6]; these data were nonexistent for the monoglycerides and diglycerides. Unsaturated bonds were assumed not to affect the Antoine constants or boiling points. When Antoine constants could not be found or regressed, boiling-point data were used[10,11]. When there was a disparity between two sources, the more recent source was used.

A similar search was conducted for density data, returning five sources[7,8,9,10,11]. Because ASPEN PLUS only accepts the density data at 60°C, whenever possible, the density was adjusted using linear interpolation. If an adjustment was not possible, and the data were at temperatures within 20°C of 60°C, the density was assumed constant over this range.

When pure component data were unavailable, they were estimated by ASPEN PLUS using the JOBACK group-contribution method[12]. Liquid-Liquid interaction parameters were calculated using the UNIFAC-LL group-contribution method, and

vapor-liquid interaction parameters were calculated using the traditional UNIFAC group-contribution method.

2. Process Analysis

2.1. Process Description

A process flowsheet based upon the Catilin bench-scale process is shown in Figure 2. Eventually, alternative syntheses will be considered. Algal-extracted triglycerides are mixed with excess methanol (7 mol methanol/mol triglycerides – containing catalyst pellets), heated, and sent to a CSTR, where they are converted to the FAME product and glycerol byproduct. The effluent is filtered to remove the catalyst (which is recycled to the reactor) before being sent to a decanter. The decanter separates the FAME (light phase) and glycerol (heavy phase) by gravity; methanol distributes itself between the two phases.

The light phase is sent to a second CSTR for further conversion. Its effluent is subjected to the same separation techniques, and is then sent to a distillation column, where the FAME (biodiesel) is recovered from methanol. The glycerol effluents from the decanters are combined and sent to a distillation column, where nearly-pure glycerol is recovered from methanol. The methanol effluents are recycled.

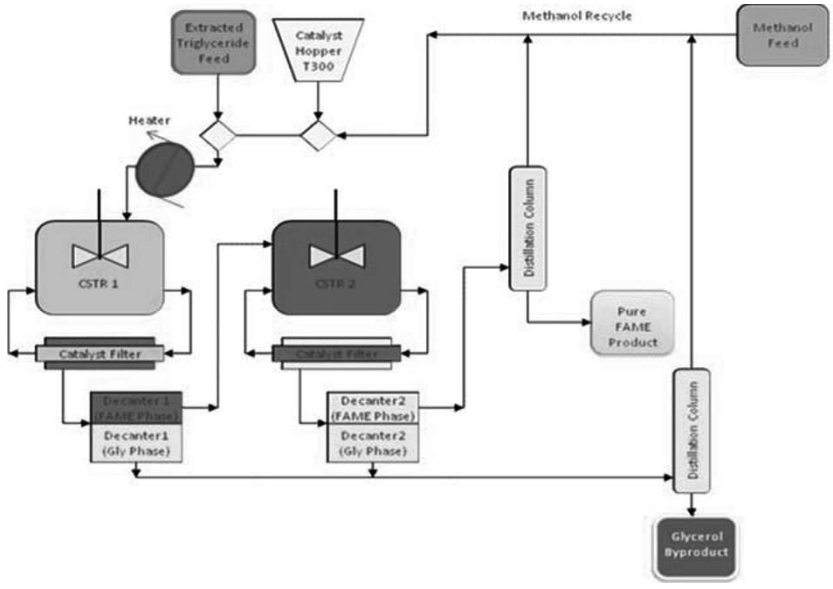

Figure 2. Modified Catilin Transesterification Process

The major material inputs and outputs from the process are shown in Table 1. Due to space limitations, stream data (temperatures, compositions, heat capacities, etc.) computed by ASPEN PLUS must be obtained from the authors. Note that 39,993 kg/hr is 0.003% of the biodiesel consumed daily in the United States in 2010[17].

Table 1. Major Process Inlet and Outlet Flow Rates

Stream	Triglyceride Inlet	Methanol Inlet	FAME Outlet	Glycerol Outlet
Flowrate (kg/hr)	39,735	4,623	39,993	4,364

2.2. Heat Integration

The heat capacities were averaged between the source and target temperatures for each stream, and then assumed constant. A pinch-analysis spreadsheet, produced by ICHEME, was used to determine the minimum utility targets. Stream matching was done using methods described in the literature[13]. Although the glycerol and FAME product streams were a source of heat for the "cold" streams, they were not cooled to room temperature (77°F); therefore, cooling water was not used to cool them.

The resulting system has 14 heat exchangers, including the condensers and reboilers for the two distillation columns: yielding hot and cold utility requirements of 2,450 KW and 1,820 KW, respectively.

2.3. Process Economics

Using Aspen's Economic Process Evaluator (AEPE), cost estimates for the transesterification process were computed. The total depreciable capital was estimated to be approximately 9 million USD. The key results are in Tables 1 and 2. The auxiliary costs include the costs of concrete and setting, structural steel, instrumentation, piping, insulation, electrical wiring, and paint.

Table 2. Costing Results for Process Equipment.

Equipment	# of items	Purchase Cost	Auxiliary Cost	Installation	Total Cost
Centrifugal Pumps	5	$ 22,700	$ 93,400	$ 67,200	$ 183,300
Decanters	2	$ 46,300	$ 213,500	$ 63,900	$ 323,700
Distillation Towers	2	$ 95,200	$ 286,000	$ 112,200	$ 493,400
Heat Exchangers	14	$ 192,700	$ 670,100	$ 327,500	$ 1,190,300
Pressure Vessels	2	$ 46,300	$ 213,500	$ 63,900	$ 323,700
Reactors	2	$ 178,200	$ 509,900	$ 103,500	$ 791,600
Total Cost of Equipment		**$ 581,400**	**$ 1,986,400**	**$ 738,200**	**$ 3,306,000**

Table 3. Costing Results for Yearly Recurring Costs.

Utilities per year		**Labor Costs per Year**	
Cooling Water	$ 15,300	Operating Labor	$ 320,000
Electricity	$ 35,900	Maintenance	$ 21,300
Heating Oil	$ 709,000	Supervision	$ 280,000
Total Utilities	**$ 760,200**	**Total Cost of Labor**	**$ 621,300**

Shell-and-tube heat exchangers, with surface areas estimated using overall heat-transfer coefficients of 730.87 kcal/hr-m^2-K (default in ASPEN PLUS), were used. The CSTR's were 95 m^3 (using a 1-hr residence time provided by Catilin). No costs for the T-300 catalyst were available. Also, the filter costs were neglected.

Cooling water (at 90°F, heated to 120°F) and heating oil were provided by a nearby utilities plant. Costs were \$0.075/1000gal and \$1.50/gal, respectively. A heating value of 146,100 kJ/gal was used to determine the amount of oil needed[14].

The hourly labor costs for operators and supervisors were estimated at \$20/hr and \$35/hr, respectively, with 330 operating days per year.

In terms of product and raw material costs, the diesel price (\$1.90/gal) was set at the wholesale price in 2009[15], and the price of methanol (\$1.16/gal) was extrapolated from a graph provided for 2008 and 2009[16]. The glycerol by-product is assumed to yield no profit; it is recycled to the cultivation process as feed for the mixotrophic algae. At

an investor's rate of return (IRR) of 20%, a triglyceride purchase price of $1.78/gal was estimated, very close to the diesel wholesale price, $1.90/gal. Clearly, to obtain diesel, this transesterication process adds a small increment to the cost of triglyceride oil.

3. Conclusion

In this brief paper, a strategy for designing transesterification processes is presented. In a full manuscript, the strategy is applied to select the best algal oil for production of biodiesel. The design optimization is based upon data for the transesterification of various algae strains using the Catilin T-300 acid catalyst. A combination of the ASPEN PLUS database, the NIST database, and an extensive literature search was used to obtain data to rigorously estimate thermophysical and transport data of the triglycerides and fatty-acid methyl esters (FAMEs). Herein, results for just a typical process are illustrated, prior to optimization. This process was heat integrated to reduce its utilities cost. Lastly, a profitability analysis shows that this transesterification process, using the T-300 catalyst, doesn't add significant capital or utilities costs.

References

1. A. Chang, Y.A. Liu, 2010, Integrated Process Modeling and Product Design of Biodiesel Manufacturing, *Ind. Eng. Chem. Res.*, **49**, 1197-1213
2. S. Boussiba, A. Vonshak, Z. Cohen, Y. Avissar, A. Richmond, 1987, Lipid and Biomass Prod. by Halotolerant Microalga *Nannochloropsis salina*, *Biomass*, 12, 37-47
3. T. Heredia-Arroyo, W. Wei, B. Hu, 2010, Oil Accumulation via Heterotrophic/ Mixotrophic *Chlorella protothecoides*, *Appl Biochem Biotechnol*, **162**, 1978-1995
4. W. Yuan, A.C. Hansen, Q. Zhang, 2005, Vapor pressure and normal boiling point predictions for pure methyl esters and biodiesel fuels, *Fuel*, **84**, 943-950
5. J.W. Goodrum, D.P. Geller, 2002, Rapid thermogravimetric measurements of boiling points and vapor pressure of saturated medium- and long-chain triglycerides, *Bioresource Technology*, **84**, 75-80
6. E.S. Perry, W.H. Weber, B.F. Daubert, 1949, Vapor Pressures of Phlegmatic Liquids. I. Simple and Mixed Triglycerides, *J. Am. Chem. Soc*., **71** (11), 3720–3726
7. J.C. Phillips, G.J. Mattamal, 1978, Effect of Number of Carboxyl Groups on Liquid Density of Esters of Alkylcarboxylic Acids, *J. Chem. and Eng. Data*, **23**, 1, 1-6
8. Y. Su, Y.A. Liu, C.A.D. Tovar, R. Gani, 2011, Selection of Prediction Methods for Thermophysical Properties for Process Modeling and Product Design of Biodiesel Manufacturing, *Ind. Eng. Chem. Res*., **50**, 6809–6836
9. A.K. Sum, M.J. Biddy, J.J. Pablo, 2003, Predictive Molecular Model for the Thermo. and Transport Properties of Triacylglycerols, *J. Phys. Chem. B*, **107**, 14443–14451
10. D.R. Lide, David R. Lide, 2006, *CRC Handbook of Chemistry and Physics*, Internet Version, <http://www.hbcpnetbase.com>, *Taylor and Francis*
11. R.H. Perry, D.W. Green, 1999, *Perry's Chemical Engineer's Handbook*, *McGraw-Hill*
12. B.E. Poling, J.M. Prausnitz, J.P. O'Connell, 2001, *The Properties of Gases and Liquids*, Fifth Edition, *McGraw-Hill*
13. W.D. Seider, J.D. Seader, D.R. Lewin, S. Widagdo, 2008, *Product and Process Design Principles: Synthesis, Analysis, and Design*, Third Edition, Section 9.3, *Wiley*
14. North American Combustion Handbook: *A Basic Reference on the Art and Science of Industrial Heating with Gaseous and Liquid Fuels*, 1952, *North American Manufact*.
15. Oil Price Information Service, <http://www.opisnet.com/tfi.asp>
16. ICIS < http://www.icis.com/Articles/2010/02/01/9330323/southeast-asia-methanol-prices-surge-on-short-supply.html>
17. Soystats <http://www.soystats.com/2011/page_24.htm>

I.A. Karimi and Rajagopalan Srinivasan (Editors), Proceedings of the 11th International Symposium on Process Systems Engineering, 15-19 July 2012, Singapore.

Potential for Bio-based Chemicals Production in Singapore's Petrochemical Cluster

Josephine Jie Min Tay[a], Cassandra Tian Hui Seto[a], Arief Adhitya[b], Iskandar Halim[b], Balaji Balagurunathan[b], Rajagopalan Srinivasan[a,b]

[a]*Department of Chemical and Biomolecular Engineering, National University of Singapore, 10 Kent Ridge Crescent, Singapore 119260*
[b]*Institute of Chemical and Engineering Sciences, A*STAR, 1 Pesek Road, Jurong Island, Singapore 627833*

Abstract

Singapore's petrochemical industry plays an integral part in the nation's economy. The industry is highly dependent on crude oil as the major feedstock. This could prove increasingly unsustainable with depleting fossil fuels resources and growing environmental concerns over greenhouse gases emissions. Using renewable feedstocks such as biomass is one possible solution. This paper evaluates the potential for bio-based chemicals production in Singapore's petrochemical cluster, focusing on polylactic acid (PLA). Cost and carbon footprint assessment of the PLA supply chain using various bio-renewable feedstocks sourced from the region is presented.

Keywords: sustainability, biomass, renewable materials, supply chain, carbon footprint.

1. Introduction

Singapore is one of the major centers for oil, gas, and petrochemicals in the world. This sector of industry has played an integral part in the growth of Singapore's economy. The centerpiece of Singapore's petrochemical industry is Jurong Island complex, which houses many of the world's leading petroleum and petrochemical companies. As of today, the total refining capacity of Singapore is 1.3 million bpd [1] and projected to increase by 300,000 to 500,000 bpd in the near future [2]. The current ethylene capacity is 2.1 million tons per year and projected to reach 4 million tons by 2014 [3]. The petrochemical industry in Singapore is heavily dependent on fossil fuel-based feedstock, mostly crude oil and natural gas. While Jurong Island is undergoing continual growth and expansion, depleting fossil fuels resources and increasing environmental concerns over the emissions (such as greenhouse gases) leads to a perception that, in the long run, a petrochemical industry solely reliant on fossil fuels is unsustainable.

The negative environmental impact the use of fossil fuels has on our earth is well-known. When fossil fuels are burned, carbon dioxide is emitted. As carbon dioxide is a gas which traps heat in the earth's atmosphere, the intensive use of fossil fuels is believed to have contributed to the increase in global surface temperatures over the past century. Another crisis arising from overdependence on fossil fuels is their rapid depletion. Fossil fuels are non-renewable, which means they are finite and might well run out in the near future – a study found that fossil fuels reserve depletion times for oil, coal, and gas are approximately 35, 107, and 37 years, respectively [4]. This rapid depletion might render petrochemical production increasingly unsustainable as fossil fuels prices continue to rise. Thus, alternative sources have to be found for continued production and growth of the petrochemical industry.

One possible solution is renewable feedstock such as biomass. This is due to the following reasons. Firstly, biomass in the forms of plants and organisms is abundantly available on earth. Secondly, biomass is considered to be carbon neutral [5]. Finally, due to the complex carbon backbone and existing chemical functionality, the processing of biomass along the chemical synthesis chain can significantly reduce the energy requirement as compared with the fossil fuels-based feedstock [6]. In this paper, we investigate the feasibility of incorporating renewables into the slate of feedstocks available for chemicals production in Jurong Island. We survey the chemicals currently produced in the cluster and identify potential bio-based chemicals that can be produced. A techno-economic assessment based on current technology is then conducted taking into account production quantities, costs, and conversion yields. The necessary supply chain is established and its cost and carbon footprints estimated.

2. Bio-based chemicals production

First generation feedstocks for bio-based chemical production are mainly derived from food biomass. Feedstocks used to produce bio-chemicals include vegetable oils/fats and sugars/starches. Examples include corn, sugarcane, cassava, soybean oil, castor oil, etc. Many of the bio-products derived from these first generation feedstocks are already in the market. Examples include NatureWorks' Polylactic Acid (PLA) and Cargill's BiOH® soy-based polyols. There was concern over first generation feedstocks due to their competition with food and land as food prices have been on the rise, and it was seen as irresponsible to grow food crops for energy or chemical use [7]. Hence, second generation feedstocks looked into lignocellulosic biomass, which can be found in plants, including crop residues. Examples include corn stover, sugarcane bagasse, and pulp and paper waste. Lignocellulosic crops are seen as better alternatives to first generation feedstocks as they not only have higher crop productivities, but are also widely available and do not compete with human food products. The main problem with lignocellulosic feedstocks, however, is in breaking down the chemical and structural biomass complex into sugars required for fermentation [8]. Most of the initiatives in producing bio-chemicals from second-generation feedstocks are currently only in advanced R&D or pilot scale [9].

The chemicals currently produced in Jurong Island were surveyed to determine which can be produced from biomass. This can be achieved in two ways:

1. Bio-based chemicals directly supplement existing chemicals derived from petroleum, e.g. bio-ethylene from sugarcane ethanol vs. ethylene from naphtha.
2. Bio-based chemicals possess new and improved properties for replacement of existing functionality or new applications, e.g. PLA derived from glucose sources vs. polyethylene from petroleum-based ethylene.

The shortlisted chemicals from the survey and their possible bio-alternatives are listed in Table 1. Due to space constraint, this paper focuses on PLA, which supplements petroleum-based polyethylene and polypropylene. PLA compares favorably to high density/low density polyethylene (HDPE/LDPE) and polypropylene (PP) in terms of its aroma barrier and grease resistance. It is also stiffer and has a higher modulus, but is more expensive. PLA compares unfavorably in terms of its water barrier. The two bulk producers of PLA, NatureWorks and PURAC, agree that PLA is likely to have partial technical substitution for HDPE, LDPE, and PP in terms of applications for resultant products. PLA also has potential for applications in other areas that do not commonly utilize polyethylene or polypropylene [10].

Table 1. Possible bio-alternatives for chemicals produced in Jurong Island [11]

Chemical	Current Route	Bio-alternative(s)
Acetic acid	Syngas	Converting biomass feedstock (e.g. cassava) to ethanol (using yeast) then to acetic acid
Ethylene	Cracking of naphtha/LPG	Distillation of ethanol derived from sugar/starch sources
Polyethylene (PE) and Polypropylene (PP)	Ethylene derived from naphtha/ LPG	a. Cellulosic plastics – from cellulosic biomass b. Polylactic acid (PLA) – from polymerization of lactic acid derived from glucose c. Polyhydroxyalkanoates (PHA) – from fermentation of naturally-occurring carbon substrate (e.g. cane sugar, corn, tapioca etc) d. PE from bio-ethylene
Polyurethane systems and Polyols	Ethylene glycol derived from naphtha-obtained ethylene	Vegetable oil-based polyols

Table 2. Yields of various feedstocks, in mass unit [11]

Feedstock (Intermediate)	Yields (in mass unit)			
	Feedstock	Intermediate	Glucose	PLA
Sugarcane (Molasses)	1000	43	23	17.2
Fresh cassava roots (Dry chips)	1000	450	299	227
Corn whole (Kernels)	1000	636	433	329
Sweet sorghum whole (Syrup)	1000	793	325	247

3. PLA production

PLA is an aliphatic polyester produced via polymerization of lactide, produced from lactic acid, which can be produced from sugars through fermentation. The physical and mechanical properties of PLA make it a good candidate for replacing petrochemical thermoplastics from polyethylene and polypropylene [10]. Raw materials that can be used include sugars and starches. Table 2 lists the yields from the various feedstocks to their intermediates, glucose, and PLA.

Lactic acid is produced from the fermentation of sugars. Sugar or starch is first extracted from the feedstock intermediates and then fermented by microorganisms. Fermentation of the obtained glucose produces lactic acid. The efficiency of this conversion is typically greater than 95% on carbohydrate substrate and can be either a batch or continuous process. The obtained lactic acid will then be purified to yield the product quality required for chemical synthesis [10].

There are two main routes to convert lactic acid to PLA. The first one is by direct polycondensation of lactic acid, and is carried out under high vacuum and high temperature. The product obtained tends to have low to intermediate molecular weight (MW 10,000 – 20,000) due to difficulties in removing water and impurities. The second method, utilized by NatureWorks and PURAC, the two largest producers of lactic acid, is a continuous process using ring-opening polymerization (ROP) of lactide. This method results in a higher molecular weight polymer and uses milder conditions [10].

4. PLA supply chain economic and environmental assessment

In this section, the supply chain for producing PLA in Jurong Island is established and the associated cost and carbon footprint estimated. Ten different combinations of feedstock and sourcing locations are considered: 1) cassava-Thailand, 2) cassava-Vietnam, 3) cassava-Indonesia, 4) cassava-China, 5) sugarcane-Thailand, 6) sugarcane-India, 7) sugarcane-Philippines, 8) sweet sorghum-China, 9) sweet sorghum-India, and 10) corn-China. For each, two different supply chain configurations are evaluated: A) Local (in the country of origin) processing of crops to intermediates, which are transported to Singapore via ocean freight, and converted to PLA in Jurong Island; and B) Crops are transported to Singapore via ocean freight, and converted to intermediates and then to PLA in Jurong Island.

Cost and CO_2 emission from each stage in the supply chain (i.e. cultivation, transport of crop, processing to intermediate, transport of intermediate, ocean transport to Singapore, and PLA production) are estimated using data gathered from literature sources [11, 12]. For carbon footprint, the CO_2 absorbed by the crops during their cultivation (carbon sink effect) is also included in the assessment [13].

Figure 1 shows the overall carbon footprint of the PLA supply chains from the 10 different feedstock sources. The carbon footprint of conventional petroleum-based PP is 5.43 kg CO_2/kg PP [12]. All the supply chains have better carbon footprint than the conventional PP. Furthermore, supply chains 5-10 (sugarcane, sweet sorghum, and corn) are carbon-neutral with negative carbon footprint. In Case B, the crops are transported instead of the intermediates, so more materials are transported and the carbon footprint is higher than Case A. Sugarcane has the lowest overall carbon footprint due to its low yield (Table 2); more sugarcane is required to make the same amount of PLA, thus resulting in a higher carbon sink effect.

Figure 2 shows the overall PLA supply chain cost from the 10 different feedstock sources, compared to the conventional petroleum-based PP cost of SGD1.94/kg [12]. It can be seen that under current conditions, PLA costs almost double the conventional PP and is not cost-competitive. It may become competitive if crude oil price increases or better technology gives higher PLA yield.

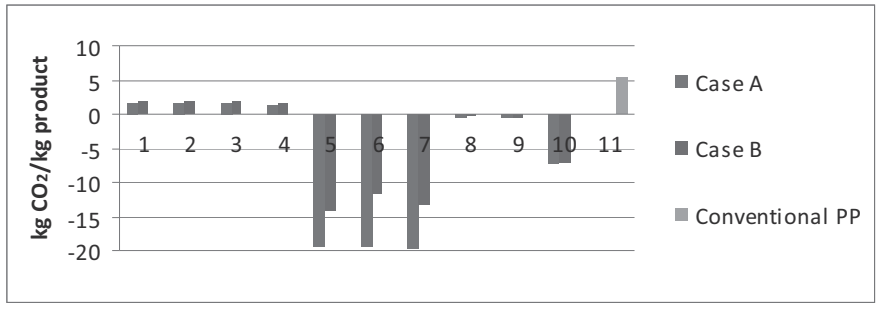

Figure 1. Carbon footprint of PLA supply chain with various feedstock sources

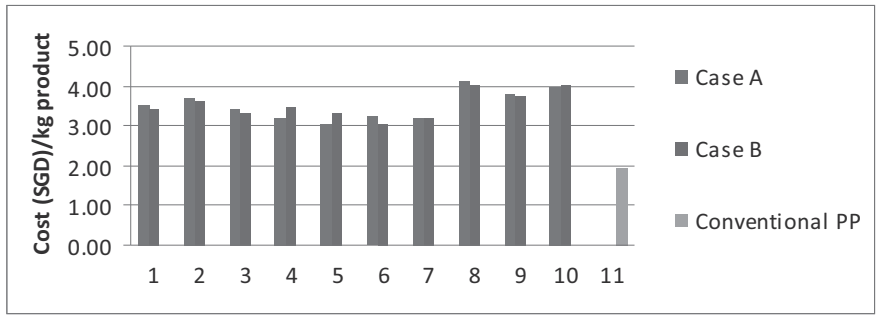

Figure 2. Cost of PLA supply chain with various feedstock sources

5. Conclusions

Bio-based chemicals production is a potential solution for increasing the sustainability of Singapore's petrochemical cluster. This paper particularly evaluates the potential for PLA production in Jurong Island using various feedstocks sourced from the region and assesses the overall cost and carbon footprint of the supply chain. It is found to be environmentally favorable but not economically competitive under current conditions. Further studies could involve other first and second-generation feedstocks and higher added-value chemicals. Also, the role of parametric uncertainty (such as conversion yields and processing costs) on the overall supply chain cost and the carbon footprint needs to be explored, given that most of the necessary technologies are in early stages of development.

References

1. http://www.edb.gov.sg/edb/sg/en_uk/index/industry_sectors/energy/industry_background.html, accessed on 18 Jan 2012.
2. http://sh.cippe.com.cn/cippeen/html/content_730.html, accessed on 18 Jan 2012.
3. http://www.siew.sg/energy-perspectives/energy-singapore/singapores-role-global-ethylene-production, accessed on 18 Jan 2012.
4. Shafiee, S. and Topal, E. (2009). Energ Pol, 37(1), 181-189.
5. Boom, R., Brehmer, B., and Sanders, J. (2009). Maximum fossil fuel feedstock replacement potential of petrochemicals via biorefineries. The Institution of Chemical Engineers. Elsevier B. V.
6. Sanders, J., Scott, E., Weusthuis, R., and Mooibroek, H. (2007). Macromol Biosci, 7(2), 105-117.
7. Keim, W. (2010). Petro Chem, 50(4), 298-304.
8. Ritslaid, K., Küüt, A., and Olt, J. (2008). State of the Art in Bioethanol Production. Institute of Technology, Estonian Institute of Life Sciences.
9. Vijayendran, B. (2010). J Bus Chem, 7(3), 109-115.
10. Shen, L., Haufe, J., and Patel, M. K. (2009). Product overview and market projection of emerging bio-based plastics. Copernicus Institute for Sustainable Development and Innovation, Utrecht University.
11. Tay, J. M. J. (2011). Assessing the feasibility of bio-based production in Singapore's petrochemical cluster. Department of Chemical and Biomolecular Engineering, National University of Singapore. Final Year Thesis.
12. Seto, T. H. C. (2011). Evaluating the feasibility of bio-based chemicals in Singapore's petrochemical cluster. Department of Chemical and Biomolecular Engineering, National University of Singapore. Final Year Thesis.
13. Groot, W. J. and Boren, T. (2010). Int J LCA, 15(9), 970-984.

I.A. Karimi and Rajagopalan Srinivasan (Editors), Proceedings of the 11th International Symposium on Process Systems Engineering, 15-19 July 2012, Singapore

Multi-Objective, Multi-Period Optimization of Renewable Technologies and storage system Using Evolutionary Algorithms and Mixed Integer Linear Programming (MILP)

Samira Fazlollahi[a,b *] Stephane Laurent Bungener[a,b] Gwenaelle Becker[a] François Maréchal[b]

a Veolia Environnement Recherche et Innovation (VERI), 291 avenue Dreyfous Ducas, 78520 Limay, France,
b Industrial Energy Systems Laboratory, Ecole Polytechnique Fédérale de Lausanne, CH-1015 Lausanne, Switzerland

Abstract

In the present work a systematic procedure, including process design and integration techniques, for sizing and operation optimization of a poly-generation plant integrated with heat storage systems is presented.
The storage system is used to balance energy demand fluctuation during 24 hours of a day. Adding thermal storage capacity allows for better utilization of equipments and avoiding over estimation of installed capacity. The integration of heat storage systems with poly-generation technologies in a multi objective and multi-period optimization model is the novelty of this work.

Keywords: Heat storage, Mixed Integer Linear Programming, Evolutionary algorithm, Renewable conversion technologies, CO_2 mitigation

1. Introduction

Poly-generation technologies, joined with the storage system, have a good potential for CO_2 emissions reduction in the district heating networks. A systematic optimization procedure is needed to select and size equipments and storage tanks.
The optimization of energy systems that include one or more technologies is extensively studied by many authors. It is referred to D.Connolly et al. (2010) for a detailed review. Most of these publications carried out only simulations, while system design optimization is neglected. For a detailed overview, the role of optimization modeling techniques in power generation is reviewed in Bazmi and Zahedi (2011). However, most of these optimization models only consider a mono economic objective function, completed with environmental and energetic targets as constraints.
On the other side, the integration of heat storage devices and conversion technologies in the energy system is studied in several publications. Soderman and Pettersson (2006) proposed a mixed integer linear model with mono objective function to integrate the storage tank with the cogeneration units in a district energy system. The MIP optimization model for sizing the heat storage tanks and a combine heat and power plant with mono

*samira.fazlollahi@epfl.ch

objective function is presented by Christidis et al. (2011) and Collazos et al. (2009), while long-term thermal storage is studied by Tveit et al. (2009).
To sum up, the energy system optimization with storage systems are studied by many authors. However, a systematic procedure including the heat storage systems and energy integration techniques with simultaneous consideration of multi-periods and multi-objectives aspects for optimizing a district energy system is needed. A multi-objective optimization model with evolutionary algorithms (EMOO) and MILP based on the decomposition approach was developed by Fazlollahi and Marechal (2011). It is extended with the integration of the thermal storage optimization model in the present work. The goal is to integrate heat storage system with other conversion technologies for optimizing a district energy system design.

2. Methodology

The multi-objective optimization techniques are used in order to investigate sizing and operating effects of poly-generation technologies and heat storage systems on CO_2 emissions. The basic concept of the developed model is the decomposition of the problem into several parts, as illustrated in Figure 1. Three major parts (Weber et al. (2006)) are; a **Structuring phase** in which required data will be collected and manipulated. Secondly the **Multi-objective nonlinear optimization phase** will solve the system configuration and produce results in the form of a Pareto frontier. In the third step, the **Post-Processing phase**, the Pareto frontier and associated results will be studied in details by doing a more details process operation simulation.

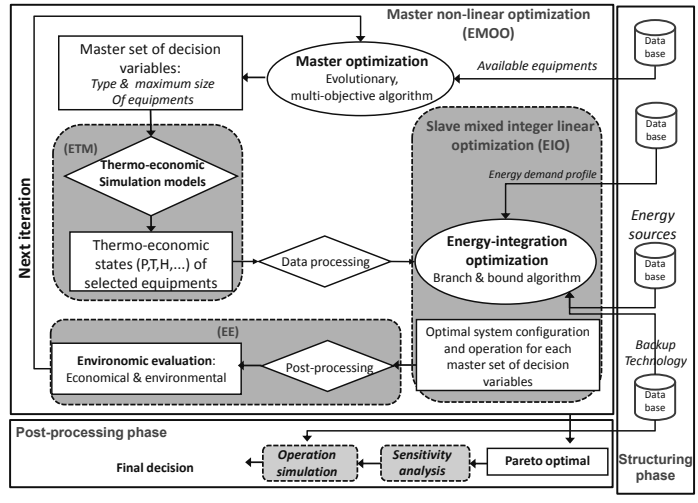

Figure 1. Illustration of the process optimization strategy

2.1. Multi-objective nonlinear optimization phase

The optimization algorithm has the aim of solving a complex non linear problem consisting of minimizing the investment costs (CAPEX), operational costs (OPEX) and CO_2 emissions simultaneously. The goal of this step is to optimize the system configuration and size the selected equipments including the storage system. This phase is decomposed in four major parts, a **master optimization (MOO)**, a **thermo-economic simulation (ETM)**, a **slave optimization (EIO)** where the best usage of equipments in the selected superstructure is calculated, and the **environomic evaluation (EE)**. For detail explanation on these steps, it is refer to the previous work of authors Fazlollahi and Marechal (2011). In the present work the slave optimization is extended by adding the heat storage model (Part.3). The storage model is considered as an equipment option to optimize the operation schedule.

3. Storage optimisation model

Heat for the district heating can be stored in heat storage tanks. The storage is used to manage the energy demand fluctuation during 24 hours of a day. Adding thermal storage capacity allows for better utilization of equipments and avoiding over estimation of installed capacity. There should be a trade off between the investment cost of additional capacity of conversion technologies and the storage system. Economical data of storage system were taken from Becker and Marechal (2012).

In the present work the thermal storage is divided into several temperature intervals, $S = 1,...,N_S$, between its maximum and minimum temperature limits. Each intervals is going to charge with the available excess heat by considering its corresponding temperature level during each time periods. When there is a heat deficit in the district networks the tank will be discharged to supply the heat requirement. For the heat storage tanks, it has been assumed that the total volume of the storage tanks is constant (Q^{max}) and the losses from radiation are negligible. Charging or discharging flow are activated throw the following two equations:

$$Fmin_S * \mathbf{y}_{S_c,t} \leq \mathbf{f}_{S_c,t} \leq Fmax_S * \mathbf{y}_{S_c,t} \qquad \forall S = 1,...,N_S \quad , \quad \forall t = 1,...,T \tag{1}$$

$$Fmin_S * \mathbf{y}_{S_h,t} \leq \mathbf{f}_{S_h,t} \leq Fmax_S * \mathbf{y}_{S_h,t} \qquad \forall S = 1,...,N_S \quad , \quad \forall t = 1,...,T \tag{2}$$

Where $Fmin_S$ and $Fmax_S$ are two parameters for showing the minimum and the maximum available capacity of each interval S. $\mathbf{y_{S_c,t}}$ and $\mathbf{y_{S_h,t}}$ are binary variables for activating the inlet flow and outlet flow of each storage's interval S in time t. $\mathbf{f_{S_c,t}}$ and $\mathbf{f_{S_h,t}}$ are continuous variables for showing the filling rate and discharging rate of each interval S in time t.

Input and output flows of each interval S should not be activated at the same time, as the heat content in the storage can vary. Eq.3 is used to present this condition:

$$1 - \mathbf{y}_{S_h,t} - \mathbf{y}_{S_c,t} >= 0, \qquad \forall S = 1,...,N_S \quad , \quad \forall t = 1,...,T \tag{3}$$

The net heat flow into each storage interval S at time t is shown by $(\mathbf{f}_{S_c,t}\dot{Q}^{-}_{S_c,t} - \mathbf{f}_{S_h,t}\dot{Q}^{+}_{S_h,t})$. Where $\dot{Q}^{+}_{S_h,t}$ is a parameter for representing the reference heat discharging of each storage interval, while $\dot{Q}^{-}_{S_c,t}$ shows the reference heat charging of the storage interval S at time t. The total charging load of the storage in the interval S is shown by $\mathbf{f}_{S_c,t}\dot{Q}^{-}_{S_c,t}$.

In this work a daily storage with 24 operating hours is defined. The heat content in the

storage must be the same at the beginning and the end of a day. This cyclic constraint is shown as following:

$$\sum_{t}^{N_t}\sum_{S}^{N_S}(\mathbf{f}_{S_c,t}\dot{Q}^{-}_{S_c,t} - \mathbf{f}_{S_h,t}\dot{Q}^{+}_{S_h,t}) * \triangle t = 0 \tag{4}$$

The heat load available in each storage interval S during each time period t, should be positive:

$$\mathbf{Q^0_S} + \sum_{p=1}^{t}(\mathbf{f}_{S_c,t}\dot{Q}^{-}_{S_c,t} - \mathbf{f}_{S_h,t}\dot{Q}^{+}_{S_h,t}) * \triangle t >= 0, \qquad \forall S = 1,...,N_S \quad , \quad \forall t = 1,...,T \tag{5}$$

Where $\mathbf{Q^0_S}$ shows the initial heat load (MWh) of each storage interval S. It is optimized by the optimization model. As mentioned before, the maximum size of the storage is constant and set by the user as an input data, while the size of each interval S is optimized through the optimization model.

$$\sum_{S}\mathbf{Q^0_S} =< Q^{max}, \tag{6}$$

3.1. Illustrative example

The proposed model is demonstrated by means of a case study, where the district heating demand should be supplied by a central plant. Available equipments in the central plant are; fuel-oil, biomass, coal and natural gas boilers, gas turbine and incinerator. Economical and technical data of each technology were taken from Fazlollahi and Marechal (2011). The first graph in Fig.2 gives the optimal outlet power of each equipments with-

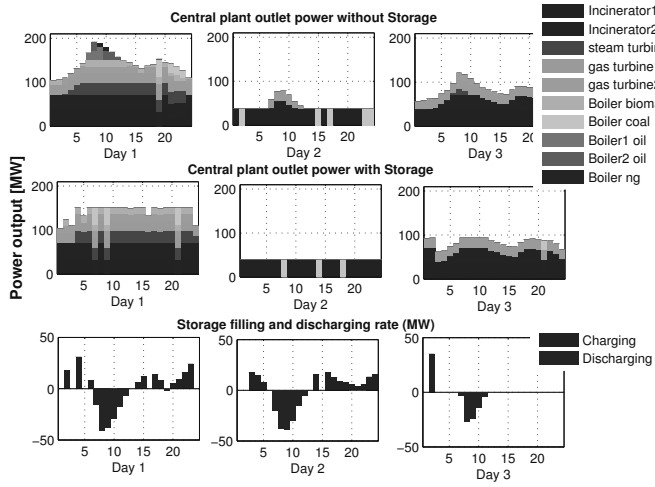

Figure 2. Comparison between a plant's operation condition with and without storage tank

out storage tanks for 3 typical days of a selected year. While the second graph shows

the optimal outlet power of each equipments integrated with storage tanks. Finally, The third graph gives the storage tank level for the second situation. The number of tanks, the volume and the initial level of storage tank are optimized by using the developed model. From the results it appears adding thermal storage capacity allows for better utilization of equipments, avoiding over estimation of installed capacity and managing the energy demand fluctuation during 24 hours of a day.

4. Conclusion

A systematic procedure including the storage system, process design and energy integration techniques with simultaneous consideration of multi-periods and multi-objective aspects, economic and environment targets, for energy system design and operation is explained. A decomposition approach is used to deal with this complexity. The heat storage optimization model is introduced in the optimization phase in order to manage the energy demand fluctuation during 24 hours of a day. Adding thermal storage capacity allows for better utilization of equipments and avoiding over estimation of installed capacity.

5. Acknowledgments

Authors would like to acknowledge Veolia Environnement Recherche et Innovation (VERI) for the financial support.

References

Bazmi, Zahedi, G., 2011. Sustainable energy systems: Role of optimization modeling techniques in power generation and supply-a review. Renewable and Sustainable Energy Reviews 15 (8), 3480 – 3500.

Becker, H., Marechal, F., 2012. Targeting industrial heat pump integration in multi- period problems. Proceedings of the 11th International Symposium on Process Systems Engineering.

Christidis, A., Koch, C., Pottel, L., Tsatsaronis, G., 2011. The contribution of heat storage to the profitable operation of combined heat and power plants in liberalized electricity markets. Energy (0), –.

Collazos, A., Marechal, F., Gohler, C., 2009. Predictive optimal management method for the control of polygeneration systems. Computers & Chemical Engineering 33 (10).

D.Connolly, Lund, H., Mathiesen, B., Leahy, M., 2010. A review of computer tools for analysing the integration of renewable energy into various energy systems. Applied Energy 87 (4), 1059 – 1082.

Fazlollahi, S., Marechal, F., 2011. Multi-objective, multi-period optimization of biomass conversion technologies using evolutionary algorithms and mixed integer linear programming (milp). Applied Thermal Engineering.

Soderman, J., Pettersson, F., 2006. Structural and operational optimisation of distributed energy systems. Applied Thermal Engineering 26 (13), 1400 – 1408.

Tveit, T.-M., Savola, T., Gebremedhin, A., Fogelholm, C.-J., 2009. Multi-period minlp model for optimising operation and structural changes to chp plants in district heating networks with long-term thermal storage. Energy Conversion and Management 50 (3), 639 – 647.

Weber, C., Marechal, F., Favrat, D., Kraines, S., 2006. Optimization of a sofc-based decentralized polygeneration system for providing energy services in an office-building in tokyo. Applied Thermal Engineering 26 (13), 1409 – 1419.

I.A. Karimi and Rajagopalan Srinivasan (Editors), Proceedings of the 11th International Symposium on Process Systems Engineering, 15-19 July 2012, Singapore.

Improved Strains for Biological Treatment of Wastewater

Shilpi Aggarwal[a], Chia Pei Lyn[a], I A Karimi[a]

[a]*Dept. of Chemical & Biomolecular Engineering, National University of Singapore, Singapore 117576*

Abstract

Nitrogen is one of the most abundant nutrients present in wastewater. The removal of excess nitrogen is a crucial step in wastewater treatment because of its detrimental effects on the human health and environment. Biological nitrogen removal processes are widely used owing to their flexibility and lower operating costs. *Nitrosomonas europaea* is widely used in the nitrification step of the biological nitrogen removal process. However, these biological treatments are unable to efficiently reduce nitrogen content to the desired low levels required to meet the discharge quality standards that are becoming stringent over time. Two of the main reasons for the lower efficiency of these processes are the low growth and nitrogen removal rates exhibited by *N. europaea*. Efforts to improve the efficiency of *N. europaea* are hindered by the lack of information about its integrated metabolic network. In this work we report the first genome-scale metabolic network of *N. europaea*. The model consists of various metabolic pathways and activities based on the organism's genome annotations and biochemical literature. The model has been validated using growth and nitrite production data taken from the existing literature.

Keywords: Wastewater Treatment, *Nitrosomonas europaea*, Metabolic Model.

1. Introduction

The stringent water quality standards prescribed by the environmental agencies for safe disposal of wastewater have made its pretreatment an essential operation. The increasing population and industrialization have further intensified the problem of wastewater generation and the need for its intensive treatment. Nitrogen is one of the most abundant nutrients present in waste water (Zhu et al., 2008). It occurs commonly in the form of ammonium ions resulting from the degradation of organic nitrogen (such as urea and fecal material) and other nitrogenous substrates. The wastewater treatment to reduce nitrogen content to safer levels is crucial as any excess of it can exert harmful effects on both the human health and environment. One of the main concerns of the presence of nitrogen in wastewater is eutrophication – a natural phenomenon in which water bodies, such as lakes and ponds, becomes eutrophic typically due to runoff of minerals and organics (Abeliovich, 1992). Nitrogen has been identified as one of the important rate-limiting nutrients in the eutrophication process. Further, if wastewater is recycled for potable purposes, the presence of excessive nitrogen in drinking water can initiate a variety of health issues in humans such as methemoglobinemia or blue-baby syndrome, a condition in which the presence of nitrates interferes with the body's ability to take up oxygen from the bloodstream. This can lead to neurologic and cardiac symptoms, and even brain damage or death under severe conditions. Considering these harmful impacts of excess nitrogen in wastewater, several biological and physiochemical processes have been devised for nitrogen removal. Of them, biological

treatments for nitrogen removal are preferentially used owing to their flexibility and low cost.

The biological process for nitrogen removal from wastewater is carried out in two steps i.e., nitrification followed by denitrification (Zhu et al., 2008). The nitrification step in turn involves two steps. The first step in nitrification involves oxidation of ammonium to nitrite via the intermediate compound hydroxylamine while the subsequent step is the oxidation of nitrite to nitrate. The denitrification step involves conversion of the nitrate to nitrogen gas that is released in the air. The first step of nitrification i.e., oxidation of ammonium to nitrite is carried out by ammonia oxidizing bacteria (AOB). *N. europaea* is identified as the one of the most suitable and widely employed bacteria owing to its relatively higher growth rates than other possible AOB such as *Nitrospira* (Wells et al., 2009). However, the nitrification and growth rates exhibited by *N. europaea* are usually lower than the desired levels which lead to inefficient nitrogen removal. Moreover, the low growth rates and long generation times prevent detailed biochemical studies of *N. europaea*'s metabolic network. Since the various cellular phenotypes arise as a result of integrated functioning of various biochemical activities, it is essential to study the entire metabolism as a whole. The complexity of metabolic networks makes it difficult to study and comprehend their integrated properties intuitively. Genome-scale modelling provides an easy way to study the properties of complex metabolic networks and biochemical activities of an organism using mathematical modelling. However, any such model or a holistic study of *N. europaea* is unavailable in literature.

In this work, we present the first genome-scale metabolic model of *N. europaea*. It incorporates the information about *N. europaea*'s metabolic network based on its genome annotations and other biochemical literature. It has been successfully validated using the data available in literature (Schmidt, 2009) for growth on two different carbon sources namely pyruvate and lactate. It also successfully predicts the nitrite production data taken from a published article (Güven and Schmidt, 2009). We have used the model to compare effects of different carbon sources on its growth.

2. Model Development

Generation of an *in silico* metabolic model requires the complete information on metabolites and their associated reactions relevant to the domain of the model, inclusion of transport reactions, biomass composition of the microorganism under consideration and a gene-enzyme association (Suthers et al., 2009). The reported model is based on the stoichiometry and biochemistry of reactions that describe the overall metabolic and biosynthetic functions of *N. europaea*. The KEGG (Kanehisa and Goto, 2000) and MetaCyc (Caspi et al., 2008) biochemical database were used to obtain genome annotations and the associated reactions for the first draft of the model. Due to the unavailability of biomass composition for *N. europaea* in literature, we have adapted the biomass equation from *E. coli*, the model organism (Edwards et al., 2001). Transport reactions are included to account for the uptake and release of nutrients from the medium. Constraints on these transport reactions are applied by restricting the uptake or release of the metabolites into or out of the metabolic system respectively. However, due to gaps and broken pathways several reactions are included from literature to bridge these gaps and enable *in silico* growth. During model reconstruction several possible new genome annotations are identified during the gap filling process. The final reconstructed model accounts for 516 open reading frames (ORFs)

corresponding to 651 reactions (633 intercellular, 18 transport) associated with 332 genes. Flux balance analysis (Raman and Chandra, 2009) is used to solve the model using the metabolic network management software tool MetaFluxNet (Lee et al., 2003).

3. Model Validation

Experimental data is indispensable for model validation. The reconstructed genome-scale model of *N. europaea* is validated by simulating the experiments of Schmidt (2009) and Güven et al.(2009). The model has been solved by simulating the various experimental conditions defined in above studies and the model predictions are compared against the reported experimental observations.

Schmidt (2009) studied the growth of *N. europaea* on pyruvate and lactate as the sole carbon sources under anoxic conditions. During their experiments they measured the carbon source and nitrate uptake rates, cell growth and CO_2 excretion rates at different times. We used their data to measure the specific uptake, excretion and growth rates. We simulated their anoxic conditions in the experiments by constraining the supply of oxygen to zero. Further, the model was solved by constraining the specific carbon source uptake and specific growth rates while maximizing the CO_2 production rates. As seen in Figures 1 and 2, the model predictions are in close agreement with the experimental data for both carbon sources.

In another study (Güven and Schmidt, 2009), the authors have investigated the nitrite formation under aerobic conditions using carbon dioxide as the sole carbon source. We inferred that the nitrogen source, ammonium was limiting as its depletion triggered the stationary phase in their experiments. Therefore, we simulated their experiment by constraining the specific ammonium uptake rate at their experimental values while allowing unrestricted supply of CO_2. We solved the model by setting the maximization of nitrite formation as the objective function. It was also reported by the authors that all of the ammonia supplied was not converted to nitrite. According to them, approximately 20% of nitrogen was lost in the form of gaseous nitrogen compounds which the model predictions do not account for. Thus, the results predicted by the model were adjusted to account for these losses and are found to be in comparable to the experimental data as seen in Figure 3.

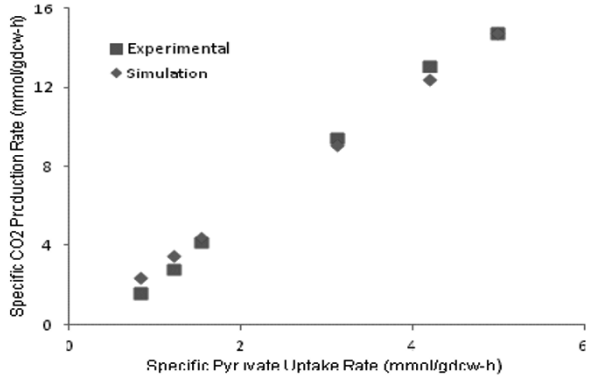

Figure 1: Specific carbon dioxide production rate vs. specific pyruvate uptake rate based on experimental data from Schmidt (2009)

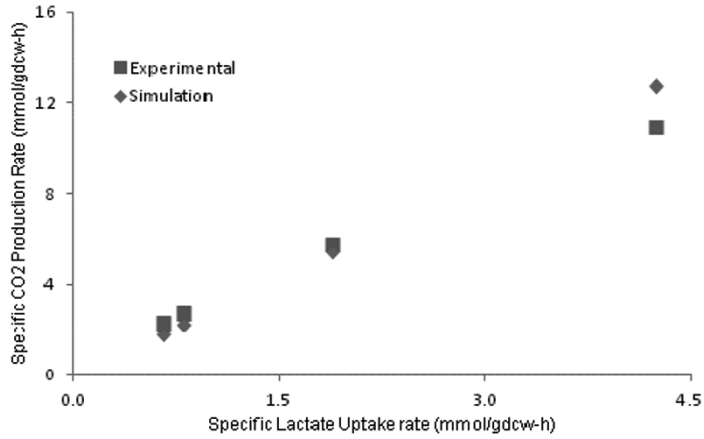

Figure 2: Specific carbon dioxide production rate vs. specific lactate uptake rate based on experimental data from Schmidt (2009)

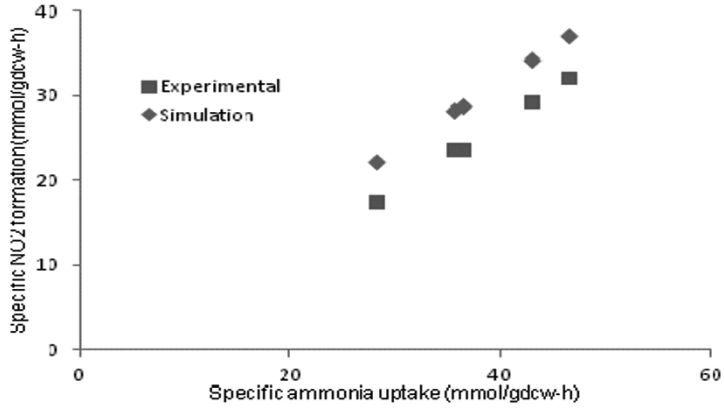

Figure 3: Specific NO_2 formation rate vs. specific ammonia uptake rate based on experimental data from Güven et al.(2009)

4. Model Analysis

Consistent with the findings of Schmidt (2009), the model exhibits growth under anaerobic conditions with nitrite as an electron acceptor using pyruvate, lactate, acetate, serine, succinate or α-ketoglutarate and fructose as the sole carbon source. It also shows that serine can replace ammonia as a nitrogen source by conversion to pyruvate and ammonia, in which the latter is liberated into the medium, as postulated by Schmidt (2009). We used our reconstructed model to compare the effects of various carbon sources on the growth of *N. europaea* under experimental conditions described by Schmidt (2009). We calculated maximum specific growth rate obtained for fixed uptake rate (20mg/gdcw-h) of each carbon source. The model predicted the suitability of carbon sources for growth per carbon atom in the following order, pyruvate (0.058 1/h-C atom as 100%) > lactate (97.7%) > serine (83.8%) > succinate (74.6%) > α-ketoglutarate (60.2%) > fructose (48.8%). This trend is fairly consistent with the published data(Schmidt 2009). We also noticed that under unrestricted conditions when

biomass maximization is used as the objective function, there is no excretion of CO_2 by the model. However, in the experiments, *N. europaea* has been found to excrete considerable amounts of CO_2 as a byproduct of respiration while growing on any of these carbon sources. This shows that there is a considerable diversion of carbon flux towards undesirable CO_2 formation than the desired growth. This observation is of high importance and can be used to improve *N. europaea*'s growth rate by altering or redesigning its respiration.

5. Conclusion

This work presents the first genome-scale metabolic model of the nitrifying bacterial strain, *N. europaea* and provides key information on the organism's cellular metabolism. Several possible new genome annotations have been identified that account for the missing functionalities in the existing annotations. The model is successfully validated using the experimental data available in literature. The proposed genome-scale model of *N. europaea* can greatly complement experimental efforts by providing concise explanations for the observed metabolic phenotypes and establishing links between metabolic entities on a genomic level. More importantly, the versatility of the reconstructed model gives it the potential to serve as a reliable platform for proposing new hypotheses and devising metabolic engineering strategies to redesign the interactions among the various host functions in *N. europaea*. It can therefore, aid the design of improved strains with enhanced nitrogen removal.

References

Abeliovich, A. Transformations of ammonia and the environmental impact of nitrifying bacteria 1992. Biodegradation, **3**(2), 255-264.

Caspi, R., H. Foerster, et al. The MetaCyc Database of metabolic pathways and enzymes and the BioCyc collection of pathway/genome databases 2008. Nucleic Acids Research, **36**(SUPPL. 1), D623-D631.

Edwards, J. S., R. U. Ibarra, et al. In silico predictions of Escherichia coli metabolic capabilities are consistent with experimental data 2001. Nature Biotechnology, **19**(2), 125-130.

Güven, D. and I. Schmidt. Specific activity and viability of Nitrosomonas europaea during discontinuous and continuous fermentation 2009. Process Biochemistry, **44**(5), 516-520.

Kanehisa, M. and S. Goto. KEGG: Kyoto Encyclopedia of Genes and Genomes 2000. Nucleic Acids Research, **28**(1), 27-30.

Lee, D. Y., H. Yun, et al. MetaFluxNet: The management of metabolic reaction information and quantitative metabolic flux analysis 2003. Bioinformatics, **19**(16), 2144-2146.

Raman, K. and N. Chandra. Flux balance analysis of biological systems: Applications and challenges 2009. Briefings in Bioinformatics**, 10**(4), 435-449.

Schmidt, I. Chemoorganoheterotrophic Growth of Nitrosomonas europaea and Nitrosomonas eutropha 2009. Current Microbiology**, 59**(2), 130-138.

Suthers, P. F., M. S. Dasika, et al. Genome-scale metabolic reconstruction Of mycoplasma genitalium, iPS189 2009. PLoS Computational Biology, **5**(2).

Wells, G. F., H. D. Park, et al. Ammonia-oxidizing communities in a highly aerated full-scale activated sludge bioreactor: betaproteobacterial dynamics and low relative abundance of Crenarchaea 2009. Environmental Microbiology, **11**(9), 2310-2328.

Zhu, G., Y. Peng, et al. Biological Removal of Nitrogen from Wastewater 2008. Reviews of Environmental Contamination and Toxicology. Springer New York, **192,** 159-195.

I.A. Karimi and Rajagopalan Srinivasan (Editors), Proceedings of the 11th International Symposium on Process Systems Engineering, 15-19 July 2012, Singapore.

In silico Simulation for Enhancing Production of Organic Acids in *Zymomonas mobilis*

Hanifah Widiastuti[a], Dong-Yup Lee[a,b], and Iftekhar A. Karimi[a*]

[a]*Department of Chemical and Biomolecular Engineering, National University of Singapore, 4 Engineering Drive 4, Singapore 117576*

[b]*Bioprocessing Technology Institute, Agency for Science, Technology and Research (A*STAR), 20 Biopolis Way, #06-01, Centros, Singapore 138668*

**E-mail: cheiak@nus.edu.sg*

Abstract

The anaerobic *Zymomonas mobilis* has been acknowledged as a promising microorganism for bioethanol production due to its numerous advantages over the popular bioethanol producer, *Saccharomyces cerevisiae. Z. mobilis* has higher sugar uptake, higher ethanol yield, and tolerance to higher ethanol concentration. Despite of many advantages of *Z. mobilis*, the wild strain ferments only glucose, fructose, and sucrose. Nevertheless, recent studies have successfully engineered strains, which were capable of fermenting xylose and arabinose. Several advanced studies were conducted to acquire more information regarding the physiology data that can be used to improve the production yield. These studies have so far been limited to time and resources consuming experimental work. Therefore, the use of biological model can enable a systematic approach for *Z. mobilis* strain improvement

To this end, we developed a complete model of *Z. mobilis* by reconstructing a genome-scale metabolic network. We built the stoichiometric model of *Z. mobilis* ATCC31821 (ZM4), based on its annotated genome and biochemical information. The reconstructed model successfully predicts the experimental observations of *Z. mobilis* ZM4 growht on glucose. The intracellular flux distribution obtained from the model analysis is in close agreement with NMR-measured fluxes in engineered strain fueled by various carbon sources (glucose, fructose and xylose). Further, comparative performance analysis with other ethanol producers (*E. coli* and *S. cerevisiae*) and gene essentiality analysis have also allowed us to confirm the functional role of *pdc* and *adh* genes in the ethanologenic activity of *Z. mobilis*, thus leading to better understanding of this natural ethanol producer.

Subsequently, we explored the *Z. mobilis* metabolic capacity for organic acids production, particularly lactic acid, acetic acid, and succinic acid. We performed gene deletion analysis on central metabolic reactions and the results suggested that pyuvate is the key metabolite in *Z. mobilis* fermentation and knocking out the competing pyruvate-consuming reactions could lead to increased production of desired product. Thus, this finding could be used as assistance for conducting strain improvement to enhance organic acids production in Z. mobilis.

Keywords: Genome-scale metabolic network, *Zymomonas mobilis*, acetic acid, lactic acid, succinic acid, systems biotechnology

1. Introduction

Zymomonas mobilis is known to have high catabolic rate and high glucose uptake rate for anaerobic fermentation. It produces ethanol as its main fermentation product and

several organic acids, such as acetic acid, lactic acid, and succinic acid as a minor fermentation product under anaerobic conditions (Johns et al., 1991). As minor by-products, the aforementioned organic acids are typically produced at the yield of 0.0025-0.014 (g/g). The high catabolic rate and high glucose uptake rate of *Z. mobilis* is expected to tackle the low organic acid productivity issue in anaerobic fermentation. Moreover, the low biomass yield of *Z. mobilis* could also benefit the production process, as most carbon fluxes would be directed for metabolites production instead of biomass growth.

As *Z. mobilis* produces low yield of organic acids, it requires strain improvement to increase its production. Recent studies have shown that genome-scale models could be useful to investigate the metabolic behavior of the strain of interest, to formulate hypothesis, and to evaluate *in silico* the potential genetic modification for strain improvements (Blazeck and Alper, 2010; Patil et al., 2004). Several methods have been designed to select the genes candidates that could give the best result in metabolite production target, namely OptKnock (Anthony P. Burgard, 2003), OptStrain (Pharkya et al., 2004), OptFlux (Rocha et al., 2010), OptForce (Ranganathan et al., 2010). The achievement of those studies utilizing genome-scale model to assist experimental studies for genetic engineering has prompted us to explore the possibilities of employing genome-scale model of *Z. mobilis* to provide metabolic engineering strategis to enhance *Z. mobilis* capability as an organic acids producer. In this study, we evaluated *Z. mobilis* metabolism for organic acids production, using constraint-based flux analysis of the genome-scale metabolic model. In particular, we carried out the knockout simulation to propose optimization strategies for overproducing organic acids in *Z. mobilis*.

2. Materials and Methods

2.1 Genome-Scale In silico Z. mobilis Metabolic Model

We have developed the genome-scale metabolic model for *Z. mobilis* ZM4 (ATCC31821), *iZM*411 based on its genome annotations (Widiastuti et al., 2011). This model comprises of 748 reactions and 704 metabolites, classified into 48 specific pathways or subsystems based on their functional role. It includes the metabolic pathways i.e. central metabolism, amino acid metabolism, lipid metabolism, cell wall metabolism, and vitamin and cofactor metabolism along with the necessary transport reactions for extracellular metabolites. Biomass equation is derived from the drain of various biosynthetic precursors and relevant cofactors into *Z. mobilis* biomass at their appropriate ratios to quantify the cell specific growth rate.

2.2 Constraint-Based Flux Analysis

Mass balance on various metabolites under the steady state assumption gives a set of linear equations with reactions fluxes as unknown quantities. It leads to an underdetermined system, as the number of metabolites constraints is less than the number of unknown fluxes to be determined. Thus, unknown flux distribution can then be evaluated by applying linear programming to find optimum value for a given cellular objective by using known uptake rates as the constraints in the model. In this study, the objective function considered was maximization of biomass growth. The modeling and simulation for flux distribution calculation were carried out by using the metabolic

network management program MetaFluxNet (Lee et al., 2003) and General Algebraic Modeling System (GAMS) 23.2 platform (McCarl, 2009). For the simulation, we assumed anaerobic growth by setting oxygen uptake to zero and set glucose uptake rate to be 10 mmol/gDCW/hr.

2.3 Gene Deletion Analysis

Gene deletion analysis was performed by applying additional constraints to the current linear flux model. This analysis was carried by deleting individual reactions associated with the genes from *in silico* models, and the alteration in flux distribution as the consequence of the absence reaction was evaluated. For the simulation, we assumed anaerobic growth on glucose by setting glucose and oxygen uptake rates at 10 mmol/gDCW/h and zero, respectively. Biomass maximization for a steady-state metabolic network, comprised of a set N = {1,…, *N*} of metabolites and a set M = {1,…, *M*} of reactions, can be expressed in the following linear program ,

maximize $v_{biomass}$

$$\text{subject to} \quad \sum S_{ij} v_j = 0 \qquad \forall\, i \in \text{N},\ \forall\, j \in \text{M}$$

$$y_j.lb_j \le v_j \le y_j.ub_j,\ \forall\, j \in \text{M},\ y_j = \{0,1\}$$

$$M - \sum_{j=1}^{M} y_j = n \quad \forall\, \text{j} \in \text{M},\ \text{n} = \text{number of genes deleted}$$

where S_{ij} is the stoichiometric coefficient of metabolite i in reaction j, v_j is flux value reaction j, and y_j is binary variable with 0 for deleted reaction and 1 for active reaction. Gene deletion conducted in this study was for single (n=1), double (n=2), triple (n=3), and quadruple (n=4).

3. Results and Discussion

From the central metabolism (presented in Figure 1) that consists of glycolysis, pentose phosphate pathway, tricarboxylix acid (TCA), and anaplerotic reactions, we narrowed down the genes candidate for disruption and further enumerated the gene deletion analysis on metabolite reactions of the central carbon metabolism of *Z. mobilis*. The 59 genes corresponded to 66 central metabolite reactions was sequentially disrupted in gene deletion analysis (as described in Method). The simulation results are presented in Figure 2. The maximum yield obtained for acetic acid, formic acid, lactic acid, and succinic acid was 0.98, 0.8, 1.9, and 1.4 mol/mol respectively. it is interesting to see that different number of genes knockout required for oveproducing each organic acid. Maximum acetic acid yield was resulting from three genes knockout of pyrucate decarboxylase (*pdc*), acetaldehyde dehydrogenase (*adh*), and lactate dehydrogenase (*ldh*) while maximum lactic acid yield could be obtained by double knockout of pyrucate decarboxylase (*pdc*) and acetaldehyde dehydrogenase (*adh*). Succinic acid overproduction required higher number of knockout genes as its maximum yield could be reached by quadruple genes knockout of acetaldehyde dehydrogenase (*adh*), pyruvate formate lyase (*pfl*), lactate dehydrogenase (*ldh*), and citrate lyase (*cl*) and slight increase of production could be obtained by additional knockout of pyruvate decarboxylase (*pdc*) gene.

From these results, we could also observe the simulated fermentation profile of *Z. mobilis*. Knocking out one of two genes required for ethanol production (*pdc* or *adh*), which is *Z. mobilis* main fermentation product, was the first step to overproduce other fermentation products. Next preferred fermentation product after ethanol was lactic acid that could be produced at its maximum yield by inactivation of ethanol production related genes (*pdc* and *adh*). This observation could be explained by similar fermentation profile of ethanol and lactic acid. Both ethanol and lactic acid production required one mol NADH for every mol product. .

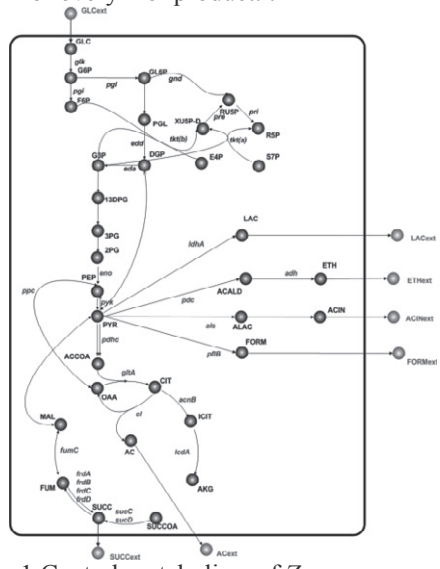

Figure 1 Central metabolism of *Zymomonas mobilis*

Different observation could be seen from the formic acid fermentation. Eventhough formic acid is also a direct product conversion from pyruvate, its maximum yield is lower than lactic acid. Formic acid production involved ACCOA and OAA in the conversion reaction from pyruvate. Thus, these two cofactors balancing in the cell might be the reason why formic acid cannot be produced in high amount as lactic acid.

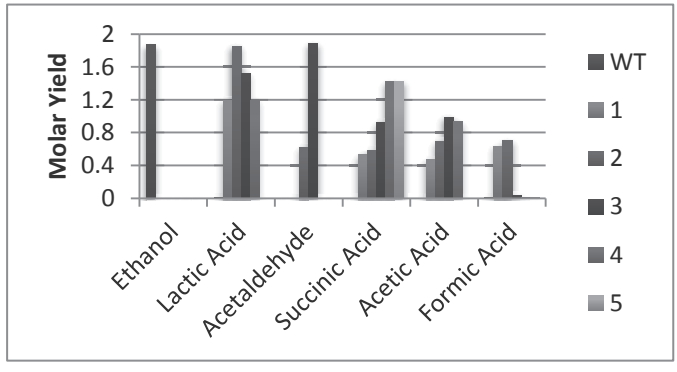

Figure 2 Simulation results for gene deletion analysis on central metabolism reactions of *Zymomonas mobilis*

Cofactor balancing might also pay important roles in acetic acid and succinic acid production as these two acids could only be produced in lower yield than lactic acid. Moreover, these two acids production required more reaction steps compared to lactic acid production.

It was concluded from the gene deletion analysis that all overproducing of organic acids in *Z. mobilis* required the inactivation of pyruvate decarboxylase (*pdc*) gene. Therefore, the deletion of the competitive pyruvate-consuming fluxes is very important for desired organic acid acid production.

4. Concluding Remarks and Future Work

Based on the *in silico* simulation results, it was shown that competing pyruvate-consuming reactions need to be inactivated for the enhanced production of desired organic acid in *Z. mobilis*. In addition, it was also observed that cofactors might affect the *Z. mobilis* fermentation performance particularly for the switching from ethanol to organic acid production. Thus, we would further evaluate the *Z. mobilis* fermentation characteristic from the metabolites point of view by incorporating flux sum analysis in the form of attenuation analysis and intensification analysis. This analysis could be useful to investigate particular metabolites that could play important roles in organic acid production, which could then be applied for medium formulation.

References

Anthony P. Burgard, P. P., Costas D. Maranas,, 2003. Optknock: A bilevel programming framework for identifying gene knockout strategies for microbial strain optimization. Biotechnology and Bioengineering. 84**,** 647-657.

Blazeck, J., Alper, H., 2010. Systems metabolic engineering: Genome-scale models and beyond. Biotechnology Journal. 5**,** 647-659.

Johns, M., et al., 1991. Byproducts from *Zymomonas mobilis*. Bioreactor Systems and Effects. pp. 97-121.

Lee, D.-Y., et al., 2003. MetaFluxNet: the management of metabolic reaction information and quantitative metabolic flux analysis. Bioinformatics. 19**,** 2144-2146.

McCarl, B. A., McCarl's GAMS User Guide. GAMS Development Corporation, 2009.

Patil, K. R., et al., 2004. Use of genome-scale microbial models for metabolic engineering. Current Opinion in Biotechnology. 15**,** 64-69.

Pharkya, P., et al., 2004. OptStrain: A computational framework for redesign of microbial production systems. Genome Research. 14**,** 2367-2376.

Ranganathan, S., et al., 2010. OptForce: An optimization procedure for identifying all genetic manipulations leading to targeted overproductions. PLoS Comput Biol. 6**,** e1000744.

Rocha, I., et al., 2010. OptFlux: an open-source software platform for in silico metabolic engineering. BMC Systems Biology. 4**,** 45.

Swings, J., De Ley, J., 1977. The biology of *Zymomonas*. Microbiology and Molecular Biology Reviews. 41**,** 1-46.

Widiastuti, H., et al., 2011. Genome-scale modeling and in silico analysis of ethanologenic bacteria *Zymomonas mobilis*. Biotechnology and Bioengineering. 108**,** 655-665.

I.A. Karimi and Rajagopalan Srinivasan (Editors), Proceedings of the 11th International Symposium on Process Systems Engineering, 15-19 July 2012, Singapore.

CFD simulation of cracking tube with internal twisted slices

Nan Zhang, Bingzhen Chen, Tong Qiu

Institute of Process System Engineering, Chenical engineering, Tsinghua University, Beijing 100084, P. R. China

Abstract

This work investigated the effectiveness and limitation of twisted slices applied in thermal cracking process. Stiff cracking kinetics was first integrated into a 3D simulation of specially configured cracking tube with twisted slices, through a comprehensive rigorous computational fluid dynamics (CFD) approach. The CFD analysis indicates that reasonable placement of twisted slices could efficiently make changes at the micro scale and flow behaviors within a certain tube length. This leads directly to thinner boundary layer, and further increasing the capacity of cracking furnace, inhibiting coke formation, extending the operating cycle but slightly postponing reaction start-up. Simulation results can be used as scientific guide for further technical retrofit and operation improvement.

Keywords: twisted slice;CFD; cracking tube; heat transfer intensification; cracking kinetic

1. Introduction

In the radiant section of cracking furnace, the thermal cracking process is highly coupled with turbulent flow, heat transfer and mass transfer. The cracking tube is both the heating load carrier and the cracking reaction channel. The undesirable coke formation and thermal fatigue damage of tube wall are two major factors restraining operating period that have aroused concerns of heat transfer intensification. At present most cracking furnaces adopt the smooth tube design, thus methods of transfer intensification are limited to changes in tube arrangement, diameter and number. This work investigated the effectiveness and limitation of twisted slices recently applied in thermal cracking process. This technique performed well in recent pilot experiments, but the transfer and reaction behaviors are temporarily unavailable due to measurement limitations. We adopted the CFD technique to inspect the influence of twisted slices on transfer behaviors. The major difficulty is to incorporate the complete cracking kinetics into severely turbulent process gas in the 3-D simulation since the cracking mechanism is invariably stiff and computationally costly.

Simulations of smooth cracking tube were given by Joo [1] , Heynderickx et al. [2], and Oprins et al. [3]. Lan et al.[4] investigated the influence of tube diameter and spacing on ethylene furnace. As to the special tube type, Han[5] investigated the local flow field of a 2.1m tube section with one twisted slice. Yuan [6] studied the plum blossom-shape tube, mixing element and swirling element in a 5.1m tube with cracking reactions ignored.

Compared with aforementioned papers, this work first integrated the stiff kinetic cracking scheme with a rigorous CFD model of a plant level *CBL-I* cracking tube successfully. Results are compared to industrial data with verification. The effectiveness and limitations of twisted slices was illustrated. Besides the change of flow pattern and the capacity enhancement, the introduction of stiff kinetics has made it possible to analyze the mutual interaction between temperature distribution and the control of cracking reactions. Results can be used as scientific guide for further technical retrofit and operation improvement.

Fig.1. showed schematic representation of the North CBL-I Cracking Furnace. The 16-group tube design and 2-1-1-1 type are adopted. Each coil tube takes four passes through the furnace. Detailed structural Parameters of the cracking tube and feedstock composition are presented in Tab.1~2.

Tab.1. Structural Parameters of *CBL-I* cracking tube

Type	*Number of passes*	*Wall thickness* （*mm*）	*Internal tube diameter(mm)*	*Length* （*mm*）	*Tube spaces*
2-1-1-1	4	6.5/7/8/8	67/94/102/102	14100/13600/13600/14100	124/176/188/188

Tab.2. The feedstock composition of cracking tube

Feedstock composition	C_2H_2	C_2H_4	C_2H_6	C_3H_6	C_3H_8	C_4H_8	C_4H_{10}	C_5H_{12}	*Aromatics others*
v/v%	0.21	0.03	69.03	1.39	13.39	0.52	13.7	1.49	0.23

2. Modeling Approach

2.1. Turbulence-chemistry interaction model

We simulated the turbulent cracking gas based on a Reynolds-averaged k-ε model and used a control-volume-based method in Fluent to convert the non-linear governing equations of mass, momentum, energy, turbulence and species to discretized and linearized scheme which were further solved in implicit Gauss-Seidel linear solver. A molecular cracking mechanism[7] involves 23 reactions is implemented and it's valid over a wide range of operating conditions and feedstock especially for light hydrocarbons. Finite-rate/eddy-dissipation model is adopted to take into account of turbulence-chemistry interactions based on the work of Magnussen and Hjertager[8].

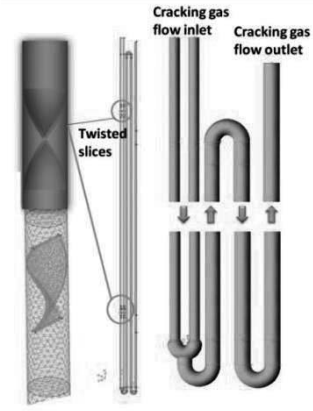

Fig.1.Schematic representation of the cracking tube and inserted twisted slices

2.2. Grid construction and boundary conditions

The platform of gambit 2.2.30 is used to create a 3D full geometry of the plant level CBL-I furnace coil tube. Unstructured tetrahedral cells are used for the complex grid around twisted slices, elbows and T-joint pieces. The number of grid varied from 0.5 to 0.7 million depending on the number of twisted slices. The inlet boundary condition is determined as mass flow inlet and specified as 24000kg/h for total 32 coils inlets. Non-slip condition is specified both on the tube wall and the surface of twisted slices. Industrial data of heat flux profiles are written in Scheme language and compiled into the Fluent solver.

2.3. Grid independent test and model validation

We utilized the initial solution and perform reasonable mesh refinement and adaption based on the work. Tab.3 represented the comparison between our simulation results of smooth tube and industrial data. They coincide well with regard to yields, cracking tube outlet temperature (COT) and inlet/outlet pressure.

Tab.3. Comparison between Industrial smooth tube data and simulation results

Yields(%)	H_2	CH_4	C_2H_4	C_2H_6	*Aromatics Others*	COT (K)	Coil Outlet/Inlet pressure (Mpa)
Simulation results	2.09	10.17	34.74	12.43	3.78	1109.78	0.1284/0.2094
Industrial data	1.85	10.60	33.13	12.67	3.56	1115.15	0.1287/0.2187
Absolute error	0.24	-0.43	1.61	-0.24	0.22	-5.37	-0.0003/-00093
Relative error(%)	12.97	-4.06	4.86	-1.89	6.18	-0.48	-0.23/-4.25

3. Result and discussion

3.1. Flow behavior of the cracking gas system

The enhancement of heat transfer inherently links to the change of flow pattern of cracking gas. Simulation results have proved the internals could efficiently turn the flow pattern

within a certain tube length. Fig.2 showed the tangential velocity distribution and effective disturbing distance. Two groups of slices (at the height of 3m and 11m, L=147.5mm, twisted ratio=2.2) were placed into the abreast tubes of the 1st pass.

It was found that the tangential velocity increased rapidly from 0.1202m/s to a peak value of 68m/s while cracking gas enters into the vortex generation area. The swirl intensity of the cracking gas comes to its maximum at the terminal of the twisted slice before the flow gradually moved out of the vortexes, with facet average tangential velocity of 20.27 m/s. Then the axial velocity augmented along the tube until almost reaches almost the same value of the scalar velocity magnitude of 144.32 m/s. At the same time the disturbance brought by the twisted slice gradually faded away while the tangential velocity returned back to 0.07924m/s. Compared with previous simulation of smooth tube, the radial velocity distribution of downstream cracking flow has a more flat shape, and larger gradients value near the tube wall region.

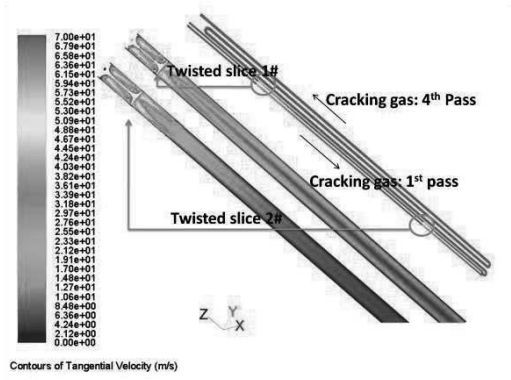

Fig.2. Tangential velocity distribution and effective distance of twisted slices

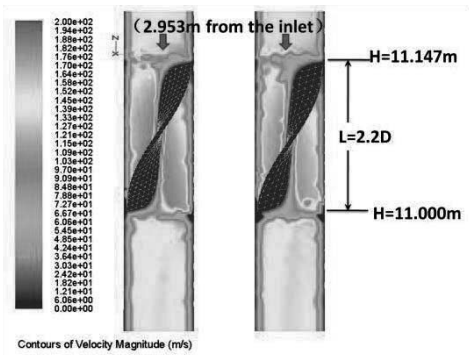

Fig.3. Velocity magnitude around the first twisted slice: (a) X=0 cross-section (b) Y=0 cross-section

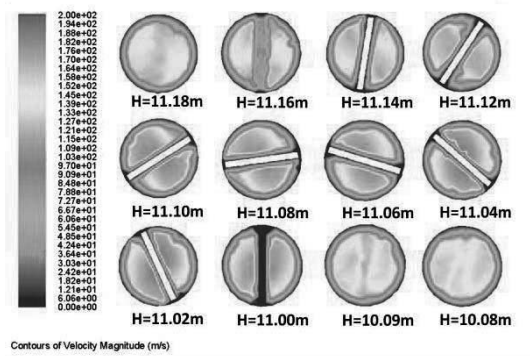

Fig.4. Distribution of velocity magnitude around the first twisted slice at different cross sections

In the present simulation, the above process occurs at both two groups of twisted slices in a like manner. However, the effective distances of the two appear to be significantly different. For the slice near the inlet(1#), the downstream cracking gas undergoes longer affected distance of 3.16m (≈47D) , while in contrast, the slice near the tube joint part (2#), the effect only lasts for 1.88m (≈28D) and quickly faded away. This difference can be explained by the mutual disturbance between the slice and the T-joint part, and is partially due to a larger upstream velocity before the cracking gas flow through twisted slice 2#.

While the twisted slices efficiently change the local plunger flow to swirling pattern and brought a desirable thinner boundary layer, the undesirable body resistance is unavoidable. The gas flow become constricted as the area available for flow decreased and transformed into two transient vortex parts as depicted in Fig.4. However, in Fig.3 we notice that the gas does not undergoes obvious drop in velocity magnitude and the resistance loss is mostly reflected on the pressure drop. The sustained velocity is meaningful since it suggests twisted slices

won't increase the residence time of cracking gas, which in turn won't decrease the reaction depth.

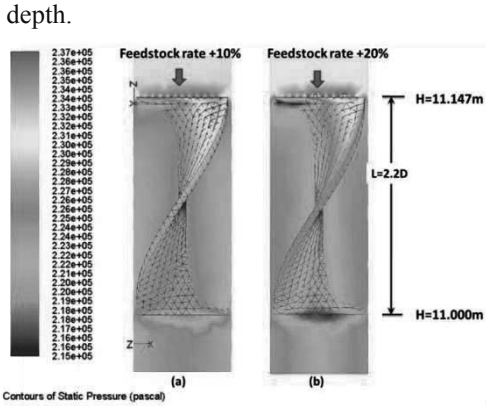

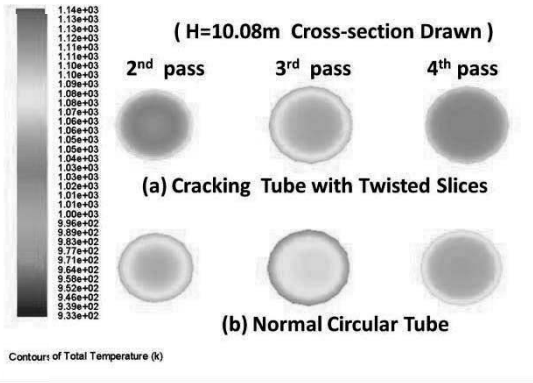

Fig.5. Pressure drop around the twisted slice section: (a) +10% feedstock rate; (b)+20% feedstock rate

Fig.6. Reduction of temperature gradient and thickness of boundary layer

3.2. Analysis of furnace capacity and pressure drop

Under the general operating conditions, the full length overall pressure drop of the base case is 0.081Mpa. The increase of the feedstock rate is accompanied with extended pressure drop (0.098Mpa for 10% more capacity and 0.110Mpa for the one of 20% more capacity). Fig.5 showed that the higher capacity case has experienced a more severe pressure loss and the low-pressure area is wider. With the existence of twisted slice, the facet averaged pressure has experienced a steep drop of 9.9Kpa in case (a), while in case (b) the pressure loss spread to 12.2Kpa. Large feed stock capacity directly brought a rise in Re number, and further increasing the pressure loss brought by the body resistance of twisted slices.

3.3. Temperature distribution and coking delay

Smaller temperature grads are of great importance of extending operating cycle and decreasing fuel consumption of the furnace. Simulation results showed a visualized alleviation in temperature distribution near the wall region. The symmetrical vertical vortexes generated by the twisted slices can serve as a source of flatting temperature distribution and the effect could last in the subsequent three passes. Fig.6 showed the comparison and the color variation revealed the sustained effect on lowering temperature grads in vicinity of tube wall. Specifically, at the cross-section of H=10.08m the coil wall with slices only have to bear a wall temperature of 1083.4K, 1106.7K and 1097.7K in following 3passes, compared with a 13.9 ~18.9 K higher wall temperature of 1102.3K, 1120.6K and 1114.0K in the absence of twisted slices. This decrease coincides with the industrial reported value of 10~20K[9].

3.4. Analysis of Kinetics Control

The integration of detailed reaction mechanism in present work makes it possible to analyze the complete interaction between heat transfer behavior and cracking reaction in a deep insight. Reactions generating C_2H_4 are the first to start up and its mass concentration reaches 0.062 at the end of 1st pass, 0.201 and 0.286 for the 2nd and the 3rd pass, respectively. At the terminal of 4th pass, the concentration of C_2H_4 is maximized with a outlet facet average value of 0.3474. Similar analysis is applied to C_3H_6 and C_4H_6. A similar trend with a initial notable start-up at the bottom of the 1st pass and an equilibrium in the middle of the 4th pass has been observed. From the perspective of technical retrofit, this analysis indicates the 1st pass hasn't been sufficiently utilized, while the 4th pass is too longer in the investigated CBL-I furnace.

A kinetic control analysis also revealed the interaction between temperature alleviation and

kinetic control. Take the consumption rate of C_3H_8 for example, among all reactions that directly involving C_3H_8 consumption, $C_3H_8 \rightarrow C_2H_4+CH_4$ and $C_3H_8 + C_2H_4 \rightarrow C_2H_6+C_3H_6$ contribute most and dominates the profile of C_3H_8 concentration along the total tube length. Fig.7 contours the reaction rate of the two reactions. We utilized the symmetric structure of 1st pass and pick off the slices in right side tube while keeping slices in left side, the results suggested that the side tube without slices insertion can start up cracking reactions prior to the other side. And a neutralization of the reaction rate is observed at the joint part. This point is in good agreement with the alleviated temperature profile and means that a trade-off between long operating cycle and quickly start-up reactions is needed.

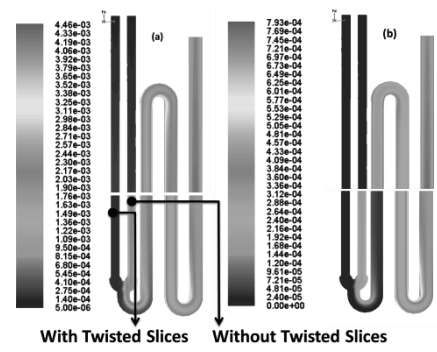

Fig.7.Reaction rate of $C_3H_8 \rightarrow C_2H_4+CH_4$ and $C_3H_8+C_2H_4 \rightarrow C_2H_6+C_3H_6$

4. Conclusion and prospect

This work presented a 3D simulation of a plant level cracking tube with twisted slices. Stiff cracking kinetic was first integrated to CFD model of this specially configured tube type. The model scheme was validated. Simulation results proves the sustainable effectiveness of twisted slices in turning flow pattern and illustrates the reasonable placement of the slices. The resistance loss brought by the slices is mostly reflected on pressure drop and the reaction depth won't be influenced. A visualized alleviation in temperature distribution near the tube wall and a sustained effect of reducing boundary layer, aiming at delayed coke formation and extended operating circles, are demonstrated. Analysis of kinetic control suggests that the 1st pass hasn't been sufficiently utilized, while the 4th pass is too longer in the investigated CBL-I furnace. The trade-off between long operating cycle and quickly start-up reactions is needed, due to the slightly delayed reaction start-up brought by the twisted slices. Multi-objective optimization of cracking tube with twisted slices could be necessary for further research.

References

E. Joo , et al., 2000, CRACKER- a PC based simulator for industrial cracking furnaces[J], Computers & Chemical Engineering, 24(2-7): 1523-1528.

G. J. Heynderickx, et al., 2001, Three-dimensional flow patterns in cracking furnaces with long-flame burners [J], AIChE Journal, 47(2): 388-400.

A. J. M. Oprins, G.J. Heynderickx, 2003, Calculation of three-dimensional flow and pressure fields in cracking furnaces. Chemical Engineering Science, 58(21): 4883 - 4893.

X. Lan, et al., 2007, Numerical Simulation of Transfer and Reaction Processes in Ethylene Furnaces [J]. Chemical Engineering Research and Design, 85(12): 1565 - 1579.

M. Han, W. J. Zhang, F. H. Liu, 2007, Numerical Simulation of Flow Field in Tube of Ethylene Cracking Furnace with Twisted Slice [J], ACTA Petrol Sinica, 63(7), 63-69

X. F. Yuan, 2011, Numerical Simulation of Flow And Heat Characters of Three Strenghted Heat Transfer Tubes [J], Petrochemical technology, 40(7): 743-748

Petroleum information office, 1976, A collection of translated essays in petrochemical industry-Volume Ⅵ.cracking of petroleum hydrocarbon [M], Beijing, Petroleum industry press

B. F. Magnussen, 1981, On the structure of turbulence and a generalized eddy dissipation concept for chemical reaction in turbulent flow [C], in Aerospace Science Meeting, 19th., St. Louis, Missouri

C. H. Ma, 2010, Trial Application of Twisted Tube Enhanced Heat Transfer Technology in SRT-Ⅳ Cracking Furnace, 15(10): 83-87

I.A. Karimi and Rajagopalan Srinivasan (Editors), Proceedings of the 11th International Symposium on Process Systems Engineering, 15-19 July 2012, Singapore.

All of the contribution has been created under contract no DE-SC0005315, with the US Department of Energy

CFD-Based Optimization of a Flooded Bed Bioreactor for Algae Production

Justin Smith,[a] Selen Cremaschi,[a] Daniel Crunkleton[a]

[a]*Department of Chemical Engineering, The University of Tulsa, 800 South Tucker Drive, Tulsa, OK 74104, USA*

Abstract

Algae show great potential for use as a feedstock for energy applications, but the cost of production must be reduced to compete with traditional feedstocks. One method of doing so is to optimize the algae production photobioreactor. This study presents the method of obtaining, and results of, such an optimization using a model derived from computational fluid dynamics simulations.

Keywords: Computational Fluid Dynamics, Optimization, Algae Bioreactor, Neural Networks

1. Introduction

Traditional biomass sources such as wood, corn, and sugarcane can be problematic as replacements for fossil fuel feedstocks because they require land currently used for other purposes. These traditional fuel crops can take from months to years to grow and be harvested, at which point the cycle must be repeated if more biomass is to be obtained. As an alternative, algae-based biofuels have been suggested because they can produce more than 100x as much oil as traditional fuel crops, while growing on low-quality land and brackish or salt water [1].

To realize algae's full potential for energy applications, it is necessary to determine the best growth methods and conditions. In principle, one can develop a mathematical programming model with the objective of maximizing algal oil production, constrained by processing and growth models to determine the optimum growth method and conditions. Algae growth could be, and has been, modeled with overall mass, momentum and energy balance equations, though using no more than these equations provides only a top-level view of the growth, which does not capture many important small-scale phenomena that may contribute to large-scale changes in algae biomass production. One such small-scale phenomenon is hydrodynamics, because many algae growth techniques, such as open ponds and photobioreactors, use geometries in which fluid flow and the resulting nutrient concentrations are important. Therefore, computational fluid dynamics (CFD) models which capture the fluid flow in an algae growth reactor, combined with algae growth models, such as the Monod equation [2], are useful tools to model the algae growth in ponds and/or photobioreactors. However, the use of CFD models as part of the optimization problem is computationally expensive, because each CFD simulation can take from several hours to several weeks on a multiprocessor workstation for convergence.

Two possible methods of large-scale algae production are open ponds and enclosed photobioreactors. While it is possible to create an open pond with a very large surface

area exposed to light, ponds, being open to the atmosphere are much easier to become contaminated, compared with enclosed photobioreactors [3]. Therefore, a column type reactor [3] was chosen as the model for algal growth in this study. Packing was included to increase the mass transfer from air to the liquid phase. We developed an artificial neural network (ANN) to replicate a packed bubble column CFD model outputs, formulated a nonlinear program with the objective of algae growth rate maximization using the developed ANN, and obtained the optimum packed bubble column design and operating conditions, which include column geometry, packing geometry, gas and liquid flow rates, and carbon dioxide (CO_2) concentration.

2. Algae Growth Model

2.1. Photobioreactors

Algae growth in the photobioreactor is modeled by the Monod equation, Eq.(1), because it is widely used to model growth of single celled organisms [4], including algae [2]. For a carbon limited environment, the molar concentration of inorganic carbon species CO_2 and H_2CO_3, *i.e.,* the total molar inorganic carbon concentration expressed as C_T, in Eq. (2), is used as the [*S*] for the Monod Equation [2]. The values for M_{max}(0.07 hr^{-1}) and k_s(2.3*10^{-6} mol/L) in Eq. (1) were chosen for *Chlorella sp.* at 27°C and 600 foot-candles of light [2].

$$M = M_{\max}([S]/([S]+k_s)) \tag{1}$$

$$[C_T]_{water} = \underbrace{0.002*[CO_2]_{water}}_{[H_2CO_3]_{water}} + \underbrace{\xi*[Air]_{water}}_{[CO_2]_{water}} \tag{2}$$

The total molar inorganic carbon concentration was calculated based on the amount of air bubbled through the photobioreactor using CFD, combined with known equilibrium relationships for the different carbon species [5]. A custom user-defined function (UDF) was developed to determine the mass transfer of air into the liquid phase separately for the packed and unpacked regions of the reactor. Specchia's [6] correlation was used for the packed region, while the correlation of Akita and Yoshida [7], was used to determine mass transfer in the unpacked regions.

2.2. CFD Simulations

The packed column photobioreactor CFD model was developed in FLUENT 6.3 as a transient 2D simulation with per-phase k-ε turbulence and full Eulerian multiphase model with a uniform mesh of 0.005 m x 0.005 m nodes. Column hydraulic diameter and boundary turbulence intensity as defined in equation 7.2-1 of the FLUENT 6.3 manual [8] were used to define turbulence boundary conditions. Gas and liquid enter the column at the bottom and exit at the top, with the packed region centered on the midline of the column. Each simulation was performed twice, once with no mass transfer to estimate the pressure drop in the packed region for use in the Specchia mass transfer correlation, and again with the diffusion UDF turned on to determine the concentrations of gas in the liquid phase. The second simulation for each case was run with second order discretization for each equation other than volume fraction and a phase coupled semi-implicit method for pressure-linked equations (SIMPLE) pressure-

velocity coupling [8]. Simulations were terminated when the volume average growth rate for the column is constant to within 5 x 10^{-5} hr^{-1} over 10 time steps, sized to ensure that the Courant number is less than one, a necessary condition for convergence.

3. Optimization Models

3.1. CFD Simulations Test Ranges

The design variables considered in this study are given in Table 1. While literature refers to the optimal column height as approximately 4 m [9], heights of 0.5 - 6 m were chosen as the minimum and maximum in this study to ensure the variable space would contain the true ideal column height. The minimum physically possible column diameter was taken to be 5 cm, with 0.5 m chosen as the maximum based on light penetration studies [10]. The ranges for the packing parameters, void fraction, and packing diameter were chosen to cover many different packing geometries. The liquid Reynolds number ($Re_L = (\rho U_L D)/\mu$) range covers both laminar and turbulent flow regimes, while the concentration of CO_2 in the gas phase ranges from atmospheric to a slightly CO_2-enriched conditions.

After the range of each input variable was determined, Latin Hypercube sampling was used to generate the test matrix for the CFD simulations to understand the impact of different levels of each variable on algae growth.

3.2. Optimization Model and Results

The concentration of air in the liquid phase ($[Air]_{water}$) for all nodes in each column was extracted from its respective FLUENT simulation and systematically reduced to the same number of nodes as the simulation with the fewest nodes. For example, if the least number of nodes was 3, and a simulation had 9 nodes, simulation nodes 3, 6, and 9 were kept and the rest were removed. The value of $[Air]_{water}$ at each node was used to calculate the maximum possible algae growth rate by Eqns. (1, 2). The concentrations of inorganic carbon species other than CO_2 and H_2CO_3 were assumed to be insignificant as they are 10^7 times smaller than $[CO_2]$ [5]. The values of M for all nodes were averaged to find the mean algae growth rate for each column.

Table 1.Minimum and Maximum Values of the Photobioreactor Design Variables

Parameter	Minimum	Maximum
Height (m)	0.623	5.89
Diameter(m)	0.093	0.5
Packing Void Fraction	0.259	1
Packing Height (as % of Column Height)	6.56	90
Liquid Reynolds Number (Re_L)	1114	25000
Superficial Gas Flow Rate (m/s)	0.013	0.149
Gas CO_2 Concentration (%)	0.127	0.889
Packing Diameter (m)	0.004	0.049

The average algae growth rate data was then used to create the vector $\boldsymbol{V}$, in which each simulation corresponds to a column. The test matrix was used to create a matrix $\boldsymbol{X}$, where each variable corresponds to a row and each sample corresponds to a column.

Both $\boldsymbol{V}$ and $\boldsymbol{X}$ were rescaled so that the entire range of each individual variable was over the range of [-1, 1].

Matlab 7.8.0 was used with vector $\boldsymbol{V}$ as targets and $\boldsymbol{X}$ as inputs for Matlab's ANN training tool with the Levenberg-Marquardt backpropagation training algorithm to train an ANN with a mean square error (MSE) of 0.0362 for the training data, and 0.1748 for the test data. Of the 23 CFD simulations, 74% was used for training the ANN, 13% was used for validation, and the remainder was used for testing. The final ANN consists of 8 inputs, 1 hidden layer consisting of 3 neurons using a tangent sigmoid function, and one output layer using a linear function. The weights and biases of the ANN are given below in Table 2.

Table 2: Weights and Biases of the trained ANN

$W_1(i,r)$	1	2	3	4	5	6	7	8
1	0.539	-1.969	0.089	-2.143	1.011	-0.576	0.454	0.257
2	-0.805	-0.740	0.626	-1.597	-0.560	-1.051	1.227	0.929
3	-0.106	-0.379	-1.192	0.425	1.207	2.776	-0.058	0.399

	W_2		B_{1r}	B_2
1	-0.911	1	-2.698	-0.459
2	0.108	2	0.012	
3	0.524	3	2.926	

The generated ANN was used to formulate a nonlinear program (NLP) (Eq. (3)) to maximize average algae growth. The NLP was formulated in GAMS version 23.6 and solved using BARON version 9.0.6.

$$\begin{aligned} &\text{Decision variables} && x_i && \forall i \in \{1,2,\ldots,8\} \\ &\text{MAX} && y = B_2 + \sum_r \left(W_{2,r} * \left\{ \frac{2}{1+\exp\left(-2 * \sum_i \left(W_{1,ir} * x_i\right) + B_{1,r}\right)} \right\} \right) && \\ &\text{Subject to} && -1 \le x_i \le 1 && \forall i \end{aligned} \tag{3}$$

where i is the index of the decision variables, B is the input bias, and W is the weight. The neurons in the hidden layer are represented by r, 1 represents the hidden layer, and 2 the output layer. The optimum solution ($M = 0.07$), indicates that the maximum algae growth occurs at the conditions given in Table 3. When a CFD simulation was run with these parameters, average growth rate was found to match the ANN to within 1.33%.

Table 3. Design Variable Values of GAMS solution

Height (m)	Diameter (m)	Porosity	Packing Height (%)	Re_L	Superficial Gas Flow Rate (m/s)	$[CO_2]_G$ (%)	Packing Diameter (m)
0.623	0.496	0.614	13.89	1114	0.149	0.889	0.049

3.3. Conclusions and Future Directions

While a solution for the "highest" growth rate is given for the tested portions of the experimental space, several of the runs gave average growth rates within less than 1% of M_{max}. As the amount of dissolved carbon dioxide, and therefore theoretical growth rate increase within a column along its height, it is plausible that algae growth rate may not have much of a dependence on the amount of carbon present or that the dependence may become much more pronounced at lower levels of carbon.

Future work will involve development of a reduced order model for algae growth which maintain the accuracy of the CFD solutions while using only a fraction of the time and computational power that would be required for a new CFD simulation, as is the case with using the average algae growth rate. Work will also be directed towards testing 3D simulations of the same columns, and determining the effects of using both light and carbon as limiting substrates.

4. Nomenclature

M	specific growth rate	M_{max}	maximum specific growth rate
[S]	limiting nutrient coefficient	k_s	half saturation coefficient
ξ	% CO2 in Air	H_2CO_3	carbonic acid
CO_2	carbon dioxide	$[C_T]$	total inorganic carbon concentration

5. Acknowledgments

The research was supported by US Department of Energy grant DE-SC0005315.

References

[1] A. Demirbas, M. Dermibas, 2011, Imporatance of algae oil as a source of biodiesel, Energy Conversion and Management., 52,1, 163-170
[2] D. Brune, 1978, The Growth Kinetics of Freshwater Algae
[3] J. Ogbonna. 2003, Photobioreactors., Biomaterials and Bioprocessing, 9, 315-348
[4] G. Okpokwasili, C. Nweke, 2005., Microbial growth and substrate utilization kinetics, African Journal of Biotechnology, 5,4, 305-317
[5] D. Harris, 2009, Buffers, Exploring Chemical Analysis, 195-211
[6] V. Specchia, S. Sicardi, A. Gianetto, 1974, Absorption in Packed Towers with Concurrent Upward Flow, AIChE Journal, 20,4, 646-653
[7] Y. Shah, et. al. , 1982, Design Parameters Estimations for Bubble Column Reactors, AIChE Journal, 28,3, 353-379
[8] FLUENT User's Manual, 2006, FLUENT 6.3, Fluent Inc.
[9] A. Miron, et. al., 1999, Comparative evaluation of compact photobioreactors for large-scale monoculture of microalgae. Journal of Biotechnology, 70, 249-270
[10] M. Janssen, et. al. , 2003, Encosed Outdoor Photobioreactors: Light Regime, Photosynthetic Efficiency, Scale-Up, and Future Prospects., Biotechnology and Bioengineering, 81,2,193-210

I.A. Karimi and Rajagopalan Srinivasan (Editors), Proceedings of the 11th International Symposium on Process Systems Engineering, 15-19 July 2012, Singapore.

CPFD Simulation for Particle Deposit Formation in Reactor Cyclone of RFCC

Hyungtae Cho[a], Bumjoon Cha[a], Jaewook Ryu[b], Sungwon Kim[b], Il Moon[a]

[a]*Department of chemical and biomolecular Engineering, Yonsei University, 50 Yonsei-ro, Seodaemun-gu, Seoul 120-749, Korea*
[b]*SK Innovation Global Technology, 325 Exporo, Yuseong-gu, Daejeon 305-712, Korea*

Abstract

In general, growing particle deposit in reactor cyclone duct has caused operational safety problems as well as a decrease of the cyclone efficiency. In this paper, Computational Particle Fluid Dynamics (CPFD) simulation for forecasting the behaviors of particle deposit formation in cyclone duct in Residue Fluidized Catalytic Cracking (RFCC) process is carried out. The CPFD simulation based on Multi-Phase Particle In Cell (MP-PIC) method in which particle phase is based on a stochastic particle model using the Lagrangian method and fluid phase based on an Eulerian method. We aim at analyzing the flow patterns of both particles and fluids, depending on the different sizes and shapes of the cyclone duct. As a result, we found that low speed zone existed on the duct 90° (inlet position 0°) at the initial time. Some particles passing out of main flow path tend to stick to the wall of the cyclone duct due to its low speed. A set of regions where particle deposit formation takes place are set as a start point for CPFD simulation. The deposit grew up to the size of 90mm thick, and sometimes fell off due to scouring phenomenon, which results in plugging in the dipleg, leading to serious problems such as carryover.

Keywords: RFCC, CPFD, cyclone, deposit, MP-PIC

1. Introduction

The atmospheric distillation process of crude oil, the atmospheric residue, and valueless products are produced about 50% of the amount of crude oil. The upgrading process produces valuable liquid products such as LPG, kerosene and gasoline from the residue cracking reaction. Residue Fluidized Catalytic Cracking (RFCC) process is a typical upgrading process. The cracking reactions of the residue are done by injection of catalysts in the riser. After the cracking reactions the product gases go to the reactor cyclone with catalysts. The reactor cyclone for RFCC process is used to separate catalysts from product gas.

However, a serious problem was reported that a deposit formation took place at the duct of the reactor cyclone, which has negative effects on the efficiency of the reactor cyclone and safety of operation. The deposit formation mechanism reveals that wetted catalysts with heavy hydrocarbon stick to the wall. The catalysts usually flow along their way with clumping together. The deposit formed in the low speed zone of the cyclone duct with some escaped particles from a clump of particles.

We knew that velocity magnitude of gas-solid has a decisive effect on the deposit formation in the reactor cyclone. So we analyzed flow pattern of gas-solid. In the previous CFD-DEM model for the simulation, K.W. Chu et al. (2011) developed to describe the gas–solid flow in the gas cyclone. It is verified by its successful capturing the flow features in the cyclone such as the flow pattern of particles along the cylinder wall in strands, and the decrease of pressure drop and tangential velocity after loading solids.

We analyzed velocity magnitude of particles depending on the different design of cyclone duct. It is important that the particle velocity of the cyclone duct has consistency with the level of inlet velocity. It decreases the deposit growth rate and improves the efficiency of the cyclone. This study suggests that the effective design of the cyclone duct by CPFD simulation of particle velocity.

2. CPFD governing equations

The fluid dynamics is described by averaged Navier–Stokes equations with strong coupling with the particle phase. The particle momentum equation follows the multi-phase-particle-in-cell (MP-PIC) formulation (Andrews and O'Rourke, 1996; Snider, 2001) with the addition of a relaxation-to-the-mean term to represent damping of particle velocity fluctuations due to particle collisions (O'Rourke and Snider, 2010).
The fluid-phase mass and momentum equations (Jackson, 2000) are

$$\frac{\partial(\theta_f \rho_f)}{\partial \mathrm{t}} + \nabla \cdot \left(\theta_f \rho_f u_f\right) = \delta \dot{m}_p \tag{1}$$

and

$$\frac{\partial(\theta_f \rho_f u_f)}{\partial \mathrm{t}} + \nabla \cdot \left(\theta_f \rho_f u_f u_f\right) = -\nabla p + F + \theta_f \rho_f g + \nabla \cdot (\theta_f \tau_f) \tag{2}$$

where θ_f is the fluid volume fraction, ρ_f is fluid density, u_f is the fluid velocity vector, p is fluid pressure, τ_f is the fluid stress tensor, g is the gravitational acceleration, and F is the rate of momentum exchange per volume between the fluid and particles.
The constitutive equation for the non-hydro part of the stress,τ_f, is

$$\tau_{f,ij} = \mu\left(\frac{\partial u_i}{\partial x_j} + \frac{\partial u_j}{\partial x_i}\right) - \frac{2}{3}\mu\delta_{ij}\frac{\partial u_k}{\partial u_k} \tag{3}$$

where μ is a shear viscosity, which is the sum of laminar and turbulence shear viscosity. In CPFD scheme, an ideal gas equation of state is used, where the partial pressure of gas i and total pressure are

$$p_i = \frac{p_i RT}{MW_i} \tag{4}$$

$$\mathrm{p} = \sum_{\mathrm{i}} \mathrm{p_i} \tag{5}$$

where R is gas constant, T is temperature, and MW_i is molecular weight of gas species.
The acceleration of a particle is

$$\frac{du_p}{dt} = D_p\left(u_f - u_p\right) - \frac{1}{\rho_p}\nabla p - \frac{1}{\theta_p \rho_p}\nabla \tau_p + g + \frac{\overline{u_p} - u_p}{\tau_D} \tag{6}$$

where θ_p is the particle volume fraction, ρ_p is particle density, $\bar{u}_p$ is the local mass-averaged particle velocity, τ_p is the particle contact stress tensor D_p is the drag coefficient, τ_d is a particle collision damping time.

3. Simulation conditions

The flow pattern of the reactor cyclone is simulated for the actual operating data. Fig. 1 shows the geometry of the cyclone. The other simulation conditions are listed in Table 1. All calculations were run for the fully developed three-dimensional mesh.

Table 1. Cyclone simulation conditions

Pressure = 2.4 atm		Temperature = 520 ℃		Inlet velocity = 16 m/s	
Product gas		RFCC Catalyst		Particle size distribution	
Molecular weight	67 g/mol	Molecular weight	78 g/mol	Fraction	Size (μm)
				0.23	30.00
Density	2.85 kg/m^3	Density	1964 kg/m^3	0.35	37.50
				0.64	45.00
Viscosity	0.019 cp	Mass flow rate	1.25 kg/s	0.95	52.50
				1	62.50

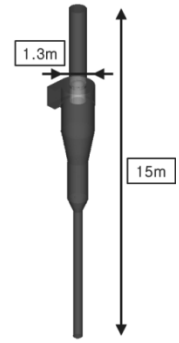

Figure 1. Cyclone geometry

4. Result and discussion

4.1. Cyclone flow pattern of the particles and fluid

In this study, we analyzed flow pattern of particles and fluid at overall and the duct in the no deposit formation case. Fig 2 shows the particles flow pattern of overall the cyclone up to 10 seconds and shows that macroscopically steady state is reached at 3.5 seconds. Fig. 2 (a) shows that the particles flow along their way with clumping together and go around the way four times and decrease their velocity magnitude. Fig. 2 (b) shows that the large-sized particles fall earlier than small-sized particles.

Fig. 3 can be seen the velocity magnitude of (a)particles and (b)fluid and (c)pressure at cross section of the duct. Escaped particles from their own way are observed in Fig. 3 (a) and the low speed zone, less than 8m/s of fluid velocity magnitude, is detected into 34mm size at duct 90° in Fig. 3 (b) When the escaped particles reach in the low speed zone, the deposit is formed. After the deposit formation, the deposit will grow backwardly on the previous formed one. That can be seen in Fig. 5 (b).

4.2. The flow pattern of the different size and shape of the expected deposit on the duct.

We found that the deposit formation started at duct 90°, so the wall was assumed the expected regions of the deposit formation for simulation. In this study, flow pattern of particles and fluid is analyzed by the duct depending on the different sizes and shapes of the expected deposit region. We knew that the deposit formed on the duct from 90° to 220° from actual the deposit shape in Fig 4 (a). Geometry of the cyclone ducts of difference maximum thickness of the expected deposit region from 30mm to 180mm can be seen in Fig. 4. Fig. 5 shows that as the deposit region gets larger, overall velocity magnitude decreases under the influence of pressure increase. There is the prospect of the hindrance of deposit growth by scouring phenomena at 90mm in Fig. 5 (d). The expected deposit region is forecasted merged (b) and (d) from Fig. 5.

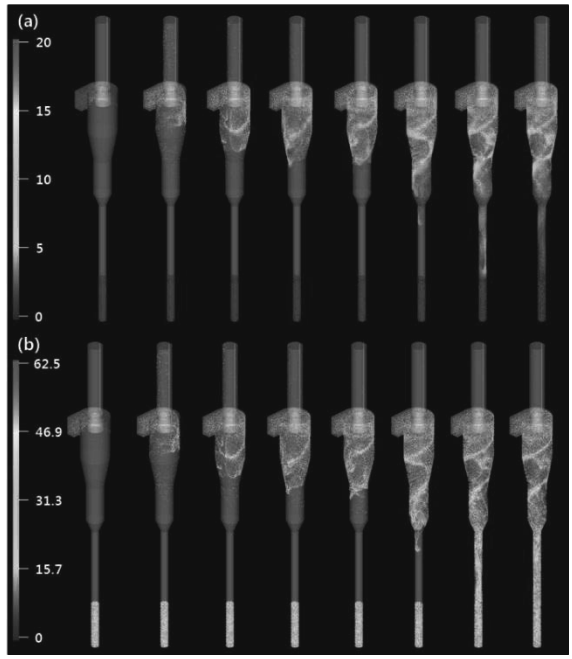

Figure 2. The dynamic flow to 10 seconds of particles in the cyclone: (a) velocity magnitude of particles (inlet velocity is 16m/s) and (b) radius of particles.

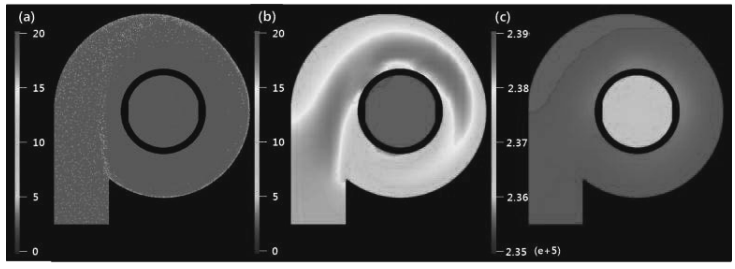

Figure 3. The flow pattern at 10seconds of duct: (a) velocity magnitude of particles, (b) velocity magnitude of fluid, and (c) pressure.

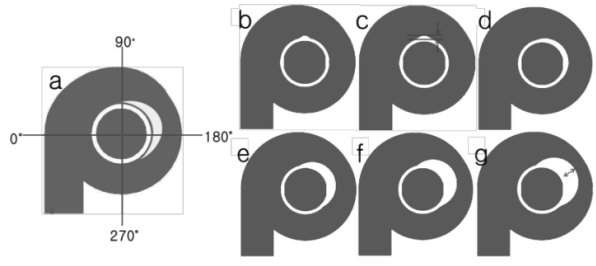

Figure 4. (a) Actual the deposit shape and Geometry of duct depending on the maximum thickness is: (b)34mm, (c)55mm, (d)30mm, (e)90mm, (f)150mm, and (g)180mm.

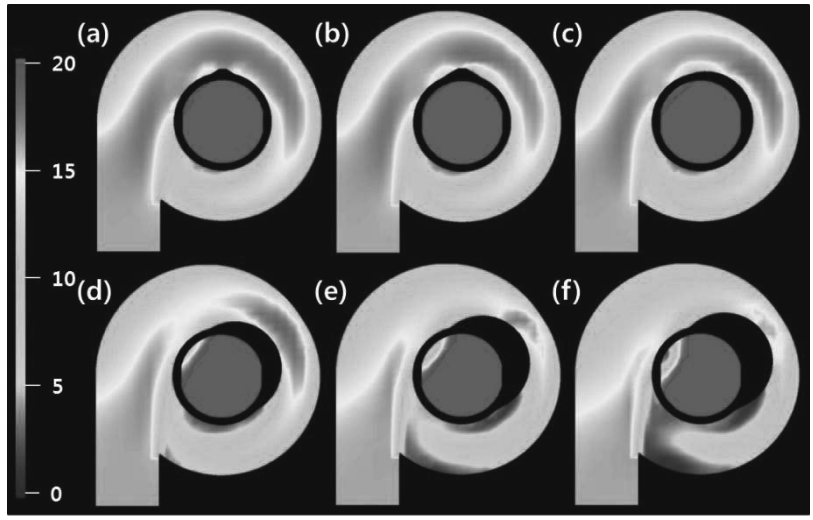

Figure 5. Velocity magnitude of fluid at 10seconds of duct depending on the maximum thickness is: (a)34mm, (b)55mm, (c)30mm, (d)90mm, (e)150mm, and (f)180mm.

5. Conclusion

We analyzed the flow pattern of particles and fluid using CPFD simulation with the actual process data. The result is verified by similarity of the overall flow features between simulation result and the cold model, and separation efficiency, 98.9%. We forecasted shape and size of the deposit formation on cyclone duct. Size and shape of expected deposit on duct was validated with the actual deposition behavior in commercial plant. We will develop a model for the deposit velocity depending on operating conditions and other parameters.

References

O'Rourke, 1996, The Multiphase Particle-in-Cell Method (MP-PIC) Method for Dense Particle Flow, Int. J. Multiphase Flow, 22, 379-402

O'Rourke, 2009, A model for collisional exchange in gas/liquid/solid fluidized beds, Chemical Engineering Science, 64, 1784 - 1797

Dale M. Snider, 2011, Eulerian–Lagrangian method for three-dimensional thermal reacting flow with application to coal gasifiers, Chemical Engineering Science, 66, 1285 - 1295

Jackson, 2000, The dynamics of fluidized particles, Cambridgw University Press, Cambridge, UK

K.W. Chu, 2008, Numerical simulation of complex particle–fluid flows, Powder Technology, 179, 104–114

K.W. Chu, 2011, CFD-DEM simulation of the gas-solid flow in a cyclone separator, Chemical Engineering Science, 66, 834 - 847

Wei Yaodong, 2000, Flow analysis of coking on the riser external wall of cyclone separator in the disengager of heavy oil catalytic cracker, Petroleum Processing and Petrochemicals, 2000-12, 017

Valery. A. Danilov, 2006, Gas Management in Flow Field Design Using 3D DMFC Model under High Stoichiometric Feed, Korean Journal of Chemical Engineering, Vol. 23, No 5, pp. 753-760.

I.A. Karimi and Rajagopalan Srinivasan (Editors), Proceedings of the 11th International Symposium on Process Systems Engineering, 15-19 July 2012, Singapore.

CFD-Mass transfer Simulation of an RDC Column

Mark. W. Hlawitschka,[a,b] Hans-Jörg Bart,[a,b]

[a]*University of Kaiserslautern, Erwin-Schrödinger-Str., 67663 Kaiserslautern, Germany*
[b] *Centre of Mathematical and Computational Modelling (CM)[2], Erwin-Schrödinger-Str., 67663 Kaiserslautern, Germany*

Abstract

A combined computational fluid dynamics (CFD), population balance modeling (PBM) and mass transfer code is used to simulate a rotating disc contactor pilot plant column. Droplet breakage and coalescence is accounted by a one group model and literature models for the breakage frequency, coalescence propability and efficiency. Mass transfer is described based on the two-film theory. The simulation results as droplet size, hold-up and concentration profile along the column height are compared to experimental data. The simulated droplet size shows a slight increase underneath the first compartment whereas it is in good agreement to experimental data in the active height of the column. Also the solute concentrations profiles could be good represented by the simulations.

Keywords: CFD, Mass Transfer, Extraction, RDC.

1. Introduction

Liquid-liquid extraction (LLE) is an important unit operation based on the different solubility of the components and is widely used in chemical industries, metals and nuclear industries (hydrometallurgy), petrochemical and coal industry as well as in the pharmaceutical and agricultural chemistry. The layout of LLE columns consists of the solvent and column selection as well as an appropriate description of the processes taking place in the column (hydrodynamics, breakage and coalescence of the droplets). State of the art models as the HTU-NTU model or axial dispersion model do not account for the complex droplet-droplet interactions and are of limited predictability. In the recent years, axial dispersion models were coupled with population balance modeling (PBM) to account for the droplet interactions. Nevertheless, parameters as the axial dispersion, energy dissipation and hold-up must be determined experimentally for each column type. The CFD coupled with PBM can overcome this handicap. For example Drumm et al. [1] used a coupled solver to predict the flow field and droplet size in a rotating disc contactor (RDC) column, where the computational time could be decreased by using a two dimensional rotational symmetrical case. Hlawitschka & Bart [2] investigated a more complex miniplant Kühni column, which only can be simulated using a three dimensional mesh. For an appropriate simulation, the influence of mass transfer on the system parameters (e.g. density, interfacial tension) has to be included in the simulation. Investigations on mass transfer combined with CFD were until now mainly performed for stirred vessel [3,4] and focused on the determination of the mass transfer coefficient. In this article, a CFD-PBM solver was extended to describe the concentration along the column height of an RDC column that was investigated experimentally by Garthe [5].

2. Numerical Background

The commercial CFD code FLUENT (version 12.1) is used for the simulations. The Eulerian multiphase model was chosen to simulate the two phase flow, whereas the phases are treated as interpenetrating continua and are described by the phase fraction in each cell. The used governing equations as continuity and momentum equations for each phase are described in Hlawitschka & Bart [2]. Due to the mass transfer calculations, the constant density of each phase is replaced by the mixture density $\rho_{q,m}$, which depends on the concentration of the transition component Y_q in each phase q and on the density of each component ($\rho_{q,1}$, $\rho_{q,2}$):

$$\rho_{q,m} = \rho_{q,1}\left(1 - Y_q\right) + \rho_{q,2} Y_q \tag{1}$$

As turbulence model, the standard k-ε-model is used that was also chosen by Drumm et al. [1] for the simulation of the hydrodynamics in a RDC column.

2.1. Species Transport

The concentration Y_q of each phase q is accounted by the species transport equation consisting of an accumulation term and convection term on the left hand side and of the transferred mass on the right hand side. The phase fraction of each phase is described by α_q, whereas the velocity of the phase is represented by $\vec{v}_q$:

$$\frac{\partial}{\partial t}\left(\alpha_q \rho_{q,m} Y_q\right) + \nabla\left(\alpha_q \rho_{q,m} \vec{v}_q Y_q\right) = \dot{m}_q^{\,i} \tag{2}$$

The generated mass is calculated based on the two film theory:

$$\dot{m} = A \rho_d \beta_{od}\left(m^* \cdot x_b - y_b\right), \tag{3}$$

where m^* is the distribution coefficient and A is the interfacial area, which is calculated for each cell by:

$$A = \frac{6\alpha}{d} \tag{4}$$

The overall mass transfer coefficient β_{od} is based on the individual mass transfer coefficients of the dispersed phase β_d and continuous phase β_c and the mixture densities for the dispersed phase $\rho_{d,m}$ and continuous phase $\rho_{c,m}$:

$$\frac{1}{\beta_{od}\rho_{d,m}} = \frac{1}{\beta_d \rho_{d,m}} + \frac{m}{\beta_c \rho_{c,m}} \tag{5}$$

As mass transfer model, the model of Kumar & Hartland [6] was chosen and implemented as user defined functions (UDF). The model was developed for droplet swarms and shows an overall accuracy of 14.1% to experimental data. The mass transfer models are coupled to the CFD, whereas the velocity, phase fraction and droplet size are given to the mass transfer equations and the resulted mass is given back to the CFD code to recalculate the phase fraction and density.

3. Droplet Size Calculation

The droplet size is calculated using a one-group model, called OPOSPM [1], which is based on the calculation of the volumetric diameter in each cell. The model of

Coulaloglou & Tavlarides [7] is used to describe coalescence and breakage of the droplets, whereas the breakage term is given by:

$$g(d) = c_1 \frac{\varepsilon^{1/3}}{d^{2/3}(1+\alpha)} \exp\left(-\frac{c_2 \sigma (1+\alpha)^2}{\rho_{c,m} \varepsilon^{2/3} d^{5/3}}\right) \tag{6}$$

Hereby, ε is the energy dissipation and d is the droplet size. The interfacial tension is described by σ. The coalescence term consists of the coalescence rate $h(d_1,d_2)$ and the collision efficiency $\lambda(d_1,d_2)$. Due to the use of the one group model, the droplet sizes d_1 and d_2 of the colliding droplets are equal to d .

$$h(d_1, d_2) = c_3 \frac{\varepsilon^{1/3}}{1+\alpha} (d_1 + d_1)^2 \left(d_1^{2/3} + d_2^{2/3}\right)^{1/2} \tag{7}$$

$$\lambda(d_1, d_2) = \exp\left(-c_4 \frac{\mu_c \rho_{c,m} \varepsilon}{\sigma^2 (1+\alpha)^3} \left(\frac{d_1 d_2}{d_1 + d_2}\right)^4\right) \tag{8}$$

The viscosity of the continuous phase is defined by μ_c. The four model parameters were adjusted to the test system of toluene/acetone/water (c_1=0.266, c_2=0.078, c_3=0.003, c_4=1.0e11), whereas c_2 was taken from Steinmetz [8].

4. Mesh Generation and Simulation Setup

A numerical grid was created that corresponds to the RDC pilot plant column, which was used by Garthe [5]. The grid consists of 46 896 cells and whereas the inflow and outflow region were reduced compared to the real column. The full column and a part of the column grid showing the principle flow direction of the dispersed and continuous phase is shown in Fig. 1 and the geometry data is summarized in Tab. 1. The inlet of the dispersed phase at the bottom of the column is defined as velocity inlet, whereas the outlet at the top of the column is defined as pressure outlet. The stators and the column wall were defined by the wall boundary condition, whereas the stirrer and shaft are described by the moving boundary condition. The simulation is based on the boundary conditions chosen by Garthe [5]. The inlet flow of the continuous phase flow is 40 L/h and the inlet flow of the dispersed phase is 48 L/h. The stirring speed is set to 200 rpm.

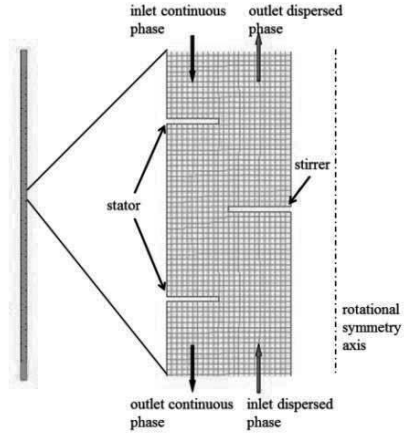

Figure 1: Mesh of the column (left) and part of the column (right) visualizing the main details of the used grid.

A detailed description of the inlet droplet size is not given. In this work, the inlet droplet size was set to 3 mm, which corresponds to the closest measured value. The acetone concentration in the continuous phase was set to the measured concentration of the continuous phase at the inlet (5.68%). The acetone concentration of the dispersed phase inside the column was set to zero. The concentration of the dispersed phase at the inlet was set to the measured value of 0.10%. The acetone concentrations at the outlets of each phase were defined as zero gradient by the use of user defined functions.

Table 1. RDC geometry

Column diameter	80 mm	Agitator diameter	45 mm
Compartment height	50 mm	Active column height	2650 mm
	10 mm	Rel. free. cross-sectional area	0.40 m²/m²

5. Simulation Results and Discussion

The simulated dispersed phase hold-up reaches a value of 6.8% in the active height (stirring zone) of the column. Compared to the results of Garthe [5], the simulated hold-up is 4.2% lower than the averaged measured value of 7.1%, which can result from an overpredicted droplet size in the inflow zone (Fig. 2, left). The simulated droplet size increases in the inflow zone due to recirculation and low energy dissipation. Due to the lack of experimental data, a direct comparison of the droplet size in the inflow zone is not possible. The increase could also be caused by an overpredicted coalescence kernel. Nevertheless, the droplet size corresponds to the experimental data in the active height. Also a slightly decreased droplet size at the column top due to a lower interfacial tension in this area can be observed. The acetone concentration in the dispersed and continuous phase is plotted versus the experimental data in Fig. 2 (right). Small deviations from the experiments can be seen for the continuous and dispersed phase acetone concentrations. The continuous phase concentration is underpredicted, whereas the dispersed phase concentration is overpredicted along the column height.

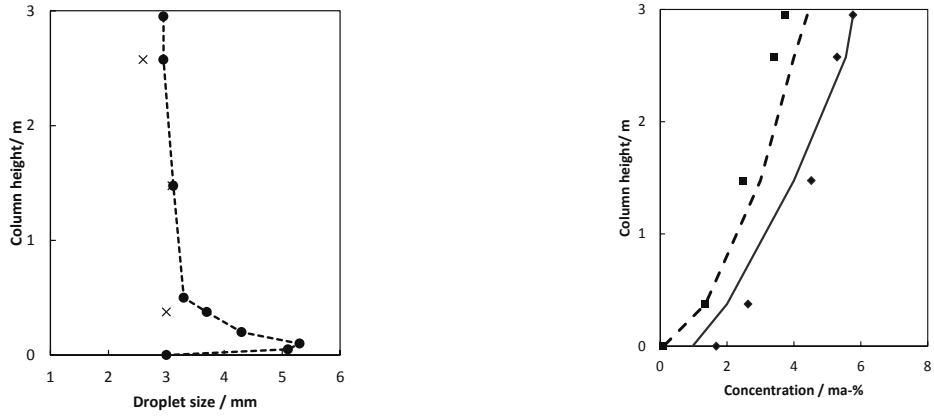

Figure 2: Left side: Droplet size (measured: **x**, simulated: ●) along the column height.
Right side: acetone concentration for the dispersed phase (measured: ■, simulated: - -) and for the continuous phase (measured: ♦, simulated: -) along the column height

The simulated values are in good agreement to the experimental data, taking the accuracy of the experimental data (higher than 5%) and the accuracy of the mass transfer coefficient model (14.1%) into account.

6. Conclusion and Outlook

A CFD-PBM simulation accounting mass transfer in a pilot plant liquid-liquid extraction column of type RDC was performed and compared to literature data. Mass transfer was described by the two-film theory and coupled to the CFD-PBM simulation. The model of Kumar and Hartland [2] was used to calculate the mass transfer coefficients. The simulation shows an over prediction of the transferred mass, which results in a lower predicted acetone concentration in the continuous phase at the column bottom and higher predicted acetone concentration in the dispersed phase at the column top. The mass transfer has an impact on the interfacial tension along the column height, which results in a slightly reduced droplet size at the column top. It can be concluded that the combination of CFD-population balance modeling with mass transfer modeling improves the accuracy of each model. Compared to state of the art models, the CFD allows a geometrical independent simulation of stirred liquid-liquid extraction columns without experimentally determined correlations for the hydrodynamics for each column type. Hence, investigation of new column types or optimizations of the geometry are possible. Further optimization of the inflow zone of each phase in the CFD simulation is required to reduce recirculation of the phases at the bottom and top of the column. Other models, as the model of Kronig and Brink [9] show a reduced mass transfer coefficient compared to the model of Kumar and Hartland [6] and could improve the prediction of the concentration along the column height in each phase.

Acknowledgement

The authors would like to acknowledge the financial support from DFG (Deutsche Forschungsgemeinschaft) and the State Research Centre of Mathematical and Computational Modelling $(CM)^2$.

References

[1] Drumm, C., Attarakih, M., Hlawitschka, M. W. and Bart, H.-J., 2010. One-group reduced population balance model for CFD simulation of a pilot-plant extraction column. Ind. Eng. Chem. Res., 49 (7), pp. 3442–3451

[2] Hlawitschka, M. W. and Bart, H.-J., 2010. Simulation of the two-phase flow in a stirred Kühni extraction miniplant column. 7th International Conference on Multiphase Flow - ICMF 2010; Tampa; University of Florida; ufdc.ufl.edu/UF00102023, Article-Nr. 1.3.1, 19.03.2012.

[3] Ranganathan, P., Sivaraman, S., 2011. Investigations on hydrodynamics and mass transfer in gas–liquid stirred reactor using computational fluid dynamics. Chem. Eng. Sci., 66, pp. 3108-3124.

[4] Gimbun, J., Rielly, C.D. , Nagy, Z.K., 2009. Modelling of mass transfer in gas–liquid stirred tanks agitated by Rushton turbine and CD-6 impeller: A scale-up study. Chem. Eng. Res. & Des., 87 (4), pp. 437-451.

[5] Garthe, D., 2006. Fluiddynamics and mass transfer of single particles and swarms of particles in extraction columns. PhD thesis, Technische Universität München, München, Germany.

[6] Kumar, A., Hartland, S., 1999. Correlation for drop size in liquid-liquid spray columns. Chem. Eng. Comm., 31, pp. 193-201.

[7] Coulaloglou, C. A. , Tavlarides, L. L., 1977. Description of interaction processes in agitated liquid-liquid dispersions. Chem. Eng. Sci., 32, pp. 1289–1297.

[8] Steinmetz, T., 2007. Tropfenpopulationsbilanzgestütztes Auslegungsverfahren zur Skalierung einer gerührten Miniplant-Extraktionskolonne. Fortschr.-Ber., VDI Verlag, Düsseldorf, Germany.

[9] Kronig, R. and Brink, J. C., 1950. On the theory of extraction from falling droplets. Appl. Sci. Res., A2, pp. 142-154.

I.A. Karimi and Rajagopalan Srinivasan (Editors), Proceedings of the 11th International Symposium on Process Systems Engineering, 15-19 July 2012, Singapore

Estimation of Primary Variables from Combination of Secondary Measurements: Comparison of Alternative Methods for Monitoring and Control

Maryam Ghadrdan,a Chriss Grimholt,a Sigurd Skogestad,a * Ivar J. Halvorsen,b

a Department of Chemical Engineering; NTNU; Trondheim, Norway
b SINTEF ICT, Trondheim, Norway

Abstract

In this work, we propose a method to estimate the primary variables based on a combination of measurements. Our method is a reformulation of the Loss method. We will compare our method with the other well-known estimators.

Keywords: Static estimator, Loss method, Partial Least Squares, Kalman Filter

1. Introduction

It happens frequently in process control that some important variables are not measurable. Sometimes they are expensive to measure and include delay. The value of primary variable can be inferred by using some secondary variable measurements. The task of soft sensors is the maximal exploitation of transforming the information of secondary measurements into more useful process knowledge.

In multi-component distillation system, a certain temperature profile exists for a specified feed component recovery and feed condition. The idea is to use temperature measurements from several locations in order to estimate the recovery of product composition, which is also good for some variation in feed properties. In this work, we propose an approach for designing a static estimator which is inspired from the loss method by Skogestad (2000). This work is a continuation of the work done by Hori et al. (2005). Measurement noise is included. The optimal static estimator is designed for two categories: "open-loop" performance (estimator used for monitoring) and "closed-loop" performance (estimator used for control). It is optimal in the sense that it gives the smallest prediction error which is defined as the difference between the true value and the estimated value. This approach will be compared with the Partial Least Square (PLS) approach and steady-state kalman filter.

2. Loss method for estimation

The objective is to find a linear combination of measurements such that keeping these constant indirectly leads to nearly accurate estimation with a small loss $\mathbf{L}$ in spite of unknown disturbances, d, and measurement noise, n^x. Figures 1-4 show four different scenarios we have considered. Linear models are assumed for the primary variables y,

*skoge@nt.ntnu.no

measurements x, and secondary variables z. It is also assumed that $\dim(\mathrm{y}) = \dim(\mathrm{x}) = \dim(\mathrm{z})$.

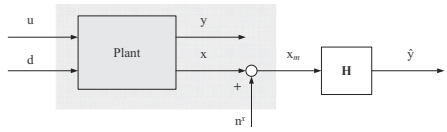

Figure 1: u is a free variable

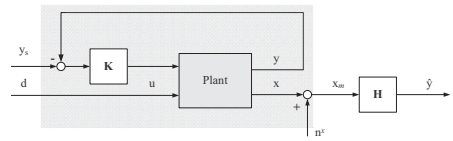

Figure 2: Control of primary variable y

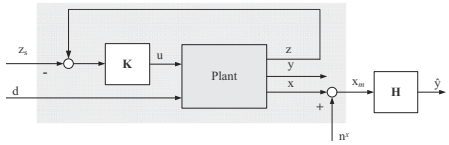

Figure 3: Control of secondary variable z

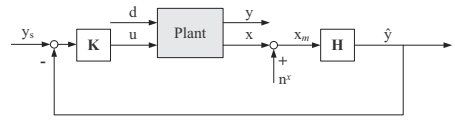

Figure 4: Control of the predicted variable $\hat{y}$

The optimal $\mathbf{H}$ is a matrix which follows the linear relationship $\hat{\mathrm{y}} = \mathbf{H}\mathrm{x}_m$, and derived by minimizing $\|\mathrm{e}(\mathbf{H})\|_{2,exp}$. We assume some expected values for disturbances and noise which come from engineering wisdom. The normalized values of disturbances and noise are used in the calculations. Table 1 shows the final expressions for obtaining $\mathbf{H}$ for different scenarios. The problem is easy for "open-loop" cases. The final expression looks like ordinary least square problems. For "close-loop" case (Figure 4), the Frobenius norm should be minimized subject to $\mathbf{H}\mathbf{G}_x = \mathbf{G}_y$ as constraint. We need to obtain the optimal sensitivity matrix $\mathbf{F}$ which is defined as $\mathbf{F} = \left(\frac{d\mathrm{x}_{opt}}{d\mathrm{d}}\right) = \mathbf{G}_x^d - \mathbf{G}_x\mathbf{G}_y^{-1}\mathbf{G}_y^d$, is simply obtained numerically by re-optimizing the model for different disturbances.

Table 1: Optimal $\mathbf{H}$ values for different scenarios

$\mathbf{H}_1 = \mathbf{Y}_1\mathbf{X}_1^{\dagger}$	$\mathbf{Y}_1 = \begin{bmatrix} \mathbf{G}_y\mathbf{W}_u & \mathbf{G}_y^d\mathbf{W}_d & 0 \end{bmatrix}$ $\mathbf{X}_1 = \begin{bmatrix} \mathbf{G}_x\mathbf{W}_u & \mathbf{G}_x^d\mathbf{W}_d & \mathbf{W}_{n^x} \end{bmatrix}$
$\mathbf{H}_2 = \mathbf{Y}_2\mathbf{X}_2^{\dagger}$	$\mathbf{Y}_2 = \begin{bmatrix} \mathbf{W}_{y_s} & 0 & 0 \end{bmatrix}$ $\mathbf{X}_2 = \begin{bmatrix} \mathbf{G}_x^{cl}\mathbf{W}_{y_s} & \mathbf{F}\mathbf{W}_d & \mathbf{W}_{n^x} \end{bmatrix}$
$\mathbf{H}_3 = \mathbf{Y}_3\mathbf{X}_3^{\dagger}$	$\mathbf{Y}_3 = \begin{bmatrix} \mathbf{G}_y^{cl}\mathbf{W}_{z_s} & \mathbf{F}_y'\mathbf{W}_d & 0 \end{bmatrix}$ $\mathbf{X}_3 = \begin{bmatrix} \mathbf{G}_x^{cl}\mathbf{W}_{z_s} & \mathbf{F}_x'\mathbf{W}_d & \mathbf{W}_{n^x} \end{bmatrix}$
$\mathbf{H}_4$	$\min_{\mathbf{H}} \left\|\mathbf{H}\begin{bmatrix} \mathbf{F}\mathbf{W}_d & \mathbf{W}_{n^x} \end{bmatrix}\right\|_F$ s.t. $\mathbf{H}\mathbf{G}_x = \mathbf{G}_y$

Note that $\mathbf{W}$'s are the diagonal scaling matrices which contain the standard deviations of the elements. We can consider u to be any variable from the process. $\mathbf{G}_y$ and $\mathbf{G}_y^d$ become so trivial if we choose $\mathrm{u} = \mathrm{y}$ ($\mathbf{G}_y = \mathbf{I}$ and $\mathbf{G}_y^d = 0$), and $\mathbf{G}_x^d$ will be equal to the sensitivity matrix $\mathbf{F}$.

3. Partial Least Square (PLS) Method

In chemometrics, Partial Least Squares (PLS) regression has become an established tool for modeling linear relations between multivariate measurements. This method is used to compress the predictor data matrix X, into a set of latent variable or factor scores. The orthogonal factor scores are used to fit a set of observations to dependent variables Y. The main attraction of the method is that it finds a parsimonious model even when the

predictors are highly collinear or linearly dependent. The final fitting equation will be

$$\mathbf{Y} = \mathbf{BX} + \mathbf{B_0} \tag{1}$$

with B and B_0 as optimization variables. B_0 is close to zero because of centering the data. The main drawback of this method is that there are several realization of the same method which do not lead to the same result for a specific problem (for PLS2 cases).

For data preparation we have two ways: If we have data, small directions in the measurement space should be deleted by SVD. We should ensure that all important directions are sufficiently exposed. We can also use exactly the same data that we get in loss method. $\mathbf{X}$ and $\mathbf{Y}$ in PLS method are the first and second row of $\mathbf{Y}_{all}$ matrix respectively.

$$\mathbf{Y}_{all} = \begin{bmatrix} \mathbf{Y} \\ \mathbf{X} \end{bmatrix} = \begin{bmatrix} \mathbf{G}_y & 0 \\ \mathbf{G}_x & \mathbf{X}_{opt} \end{bmatrix} \tag{2}$$

where $\mathbf{X_{opt}} = \begin{bmatrix} \mathbf{FW}_d & \mathbf{W}_{n^x} \end{bmatrix}$.

We need to know the expected "optimal variation" in $\mathbf{X}$ as given by the matrix $\mathbf{X}_{opt}$. Here "optimal" means that y is constant (see the second column in $\mathbf{Y}_{all}$). In addition, we also need to obtain $\mathbf{G}_x$ and $\mathbf{G}_y$ from the data, which means that the data must contain "non-optimal" variations in u, and not only contain optimal data where $\mathrm{u} = \mathrm{u}_{opt}\,(\mathrm{d})$- see the first column in $\mathbf{Y}_{all}$. This is called Closed-Loop Regressor (CLR) (Skogestad et al., 2011). CLR suffers from the same weakness as LS, giving poor results for ill-conditioned matrices and underdetermined systems. Performing a principal component analysis on the $\mathbf{X}$ data will remove the weaker directions containing noise resulting in a well-conditioned matrix. Then, CLR can be applied to the data. We call this "truncated CLR".

4. Kalman filtering

The Kalman filter estimates process states by using a form of feedback control. The linearity of state dynamics and observation process, as well as the normal distribution of noise in state dynamics and measurements are the assumptions of kalman filter. A linear difference equation $x_k = Ax_{k-1} + Bu_{k-1} + w_{k-1}$ with a measurement that is $z_k = \mathbf{C}x_k + v_k$, define the linearized process. The random variables w_k and v_k represent the process and measurement noise respectively. They are assumed to be independent of each other and with normal distributions.

$$p\,(w) \sim \mathcal{N}\,(0, Q) \tag{3}$$

$$p\,(v) \sim \mathcal{N}\,(0, R) \tag{4}$$

The objective is to minimize the estimation error. By writing a posteriori state estimate as a linear combination of an a priori estimate and the difference between actual measurement and measurement prediction weighted by kalman gain, K is calculated to minimize the a posteriori estimation error covariance. Since the focus of our work is on chemical processes, the time scales at which the sensor noise characteristics change are much larger than the time scale at which we study the system. Thus we assume the system and noise covariances are time-invariant. In addition, as mentioned previously, our proposed estimator is categorized as static estimator. So, the steady-state of kalman filter is interesting. The steady-state kalman gain is calculated as $K_\infty = P_\infty^- H^T \left(HP_\infty^- H^T + R\right)$. Figure 5 shows the block diagram of kalman filter estimation.

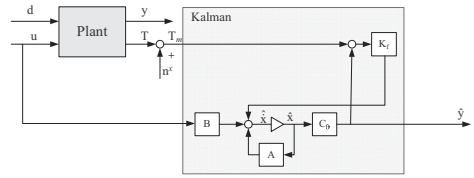

Figure 5: Block diagram of Kalman filter

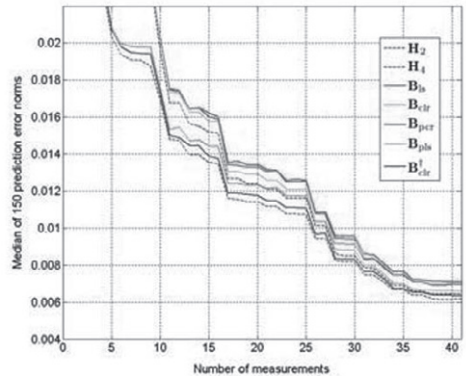

Figure 6: Median Prediction error

The algorithm of Kalman filter requires knowledge of the process noise variance W and the measurement noise variance V (Nakamura, 1982). If state-feedback control is used, the overall controller is optimal because of the separation principle. If an output-feedback controller ($u = \mathbf{K}y$) is used, then it is generally not optimal to use the $\hat{y} = \mathbf{C}\hat{x}$ estimated by Kalman filter. In loss method, the primary variable comes directly from combination of measurements ($c = \mathbf{H}y$). Since the measurements do not contribute similarly in the estimation of primary variable, it is expected that by putting weights on the state error terms, the estimation of primary variable will be improved. Another point is that we should think of what to use the estimation for. KF is said to be used for control,but if R approaches infinity, then it means that there is no control. Mejdell and Skogestad (1993) have shown that the kalman-filter might be better than a simple PCR in open-loop performance, which is because of the recursive nature of the filter, but PCR performs similarly if it is used for closed loop. We can model slowly-varying disturbances by adding states of the noise model. This gives the augmented kalman filter (Brown and C., 1997). Here, we use non-stationary noise. So zero steady-state is not reached.

5. Example

A binary distillation column model - Column A (Skogestad, 1997) - is used to demonstrate the performance of different estimators. There are two inputs, namely the reflux flow and the boilup, and two disturbances, which is the change in feed composition.

Table 2 shows the results of validation for estimators for different scenarios. Calibrating with one scenario and validating with another is mostly applicable to the last scenario. So, the shaded cells are actually showing the more interesting data. As it was expected,

the optimal estimator is obtained when it was calibrated and validated for its intended scenario. Note that all the scenarios are not comparable to each other because of different variances for different scenarios. Since there is no control in the first scenario, a small standard deviation in u was selected to give a small standard deviation in y.

Figure 6 shows the performance of estimators. Calibration data was generated by drawing random values for $\mathrm{u} \sim \mathcal{N}\left(0, 0.005^2\mathbf{I}_2\right)$, $\mathrm{d} \sim \mathcal{N}\left(0, 0.05^2\mathbf{I}_2\right)$, $\mathrm{y}_s \sim \mathcal{N}\left(0, 0.005^2\mathbf{I}_2\right)$ and $z_s \sim \mathcal{N}\left(0, \begin{bmatrix} 0.05^2 & 0.5^2 \end{bmatrix}\mathbf{I}_2\right)$, and calculating the corresponding output variables x_m and y for the respective scenarios (except scenario 4). The median of the prediction error for 150 runs are used to assess the estimators' performances because noise and variation in input variables resulted in a distorted picture of estimator performance by outliers. By increasing the number of regressors, the error decreases. All estimators are trained on calibration data from scenario 2 and validated on scenario 4.

Table 2: The mean prediction error of the model-based estimators applied to four operation scenarios

Caliberation Data \ Validation Data	S1	S2	S3	S4
S1	0.0085	0.2749	0.0215	0.0506
S2	0.0591	0.0093	0.0104	0.0104
S3	0.0599	0.0166	0.0098	0.0132
S4	0.0099	0.0099	0.0099	0.0099

6. Conclusions

In this paper, we introduced a new static estimator. Four scenarios have been used to get the calibration data and were validated for the closed-loop scenario. Our emphasis was on the fact that we should be aware of what we want to use the estimator for.

References

Brown, R. G., C., H. P. Y., 1997. Introduction to Random Signals and Applied Kalman Filtering. John Wiley & Sons.

Hori, E. S., Skogestad, S., V., A., 2005. Perfect steady-state indirect control. Ind. Eng. Chem. Res. 44, 863–867.

Mejdell, T., Skogestad, S., 1993. Output estimation using multiple secondary measurements. AIChE J. 39 (10), 1641–1653.

Nakamura, M., 1982. Relationship between steady state kalman filter gain and noise variances. J. of Systems Science 13, 1153–1163.

Skogestad, S., 1997. Dynamics and control of distillation columns: A critical survey. J. Modeling, Identification and Control 18 (3), 177–217.

Skogestad, S., 2000. Plantwide control: the search for the self-optimizing control structure. J. Proc. Control 10, 487–507.

Skogestad, S., Yelchuru, R., Jäschke, J., 2011. Optimal use of measurements for control, optimization and estimation using loss method: Summary of existing results and some new. In: Selected Topics on Constrained and Nonlinear Control Workbook. STU Bratislava and NTNU Trondheim.

I.A. Karimi and Rajagopalan Srinivasan (Editors), Proceedings of the 11th International Symposium on Process Systems Engineering, 15-19 July 2012, Singapore.

Validation of an absorber model of carbon dioxide capture in an aqueous amine solvent developed based on the SAFT-VR framework

C. V. Brand, J. Rodríguez, A. Galindo, G. Jackson and C. S. Adjiman

Department of Chemical Engineering, Centre for Process Systems Engineering, Imperial College London, London SW7 2AZ, U.K. c.adjiman@imperial.ac.uk

Abstract

The development of a model of an absorber for the removal of carbon dioxide (CO_2) from flue gas using aqueous solutions of monoethanolamine (MEA) is presented. This novel model incorporates state-of-the-art SAFT-VR thermodynamics into a rate-based process model. A characteristic of the proposed approach is that all the reactions are treated within a thermodynamic description, assuming chemical equilibrium throughout. This greatly reduces the amount of experimental data required to model the behaviour of CO_2 in the solvent. Furthermore, in contrast with traditional treatments of reactive systems of this type, no enhancement factor is used in the process model. The absorber process model is implemented in the gPROMS software platform and validated using published pilot plant experimental data. The predictive capabilities of the mass transfer correlations used in this model are assessed through a sensitivity analysis and a scaling of the diffusivity in the liquid phase is proposed. The scaling of the diffusivity is transferable to different operating conditions and good predictions are obtained for the composition profiles in the gas and liquid phases.

Keywords: CO_2 capture, reactive separation, SAFT-VR, monoethanolamine.

1. Introduction

Carbon dioxide (CO_2) emissions are largely considered to play a major role in climate change and particularly in global warming. Fossil fuel power plants are the major fixed point-source emitters of CO_2. In order to abate global warming, the UK Committee on Climate Change suggested reducing the emissions from 500 gCO_2/kWh to 100 gCO_2/kWh in the electricity sector by 2050. In this context, the development of carbon capture systems is a necessity that must be addressed in the short term, and amine-based post-combustion capture processes are seen as the most promising technology in terms of development and applicability. The major advantage of this technology is that it can be retrofitted to existing power plants.

There are, however, several concerns with amine capture processes, including large energy requirements, solvent degradation, and the environmental and health impact that may result from solvent leaks and solvent degradation products. Modelling studies can play an invaluable role in addressing some of these issues, including the choice of solvent and operating conditions that yield optimal performance.

A key challenge is to develop models that can accurately predict the behaviour of the process under different conditions. In our current study study, we address this challenge by developing a model of the CO_2 absorber that incorporates an advanced thermodynamic model of the physical properties *and* reactions into a rate-based process model. We use a version of the statistical associating fluid theory (SAFT) to model the

complex physico-chemical interactions between CO_2 and the solvent. Pilot plant data is used to validate the absorber model. The thermodynamic framework used is presented briefly in the next section and the process model is then described. In section 3, the model is validated against pilot plant data. A discussion of the results is presented in section 4.

2. Proposed model of a CO_2 absorber

The rate-based model of the absorber and the SAFT-VR [1, 2] formalism used to model the physico-chemical interactions within the absorber are presented here.

2.1. Thermodynamic treatment

In SAFT-VR, a molecule i is modelled as a chain of m_i segments. These segments are hard-cores of diameter σ_{ii} tangentially bonded to form the molecule. The attractive interaction between two segments is described by a square-well potential of range λ_{ii} and depth ε_{ii}. Off-centre and short range square-well association sites can be used to represent association interactions (hydrogen bonding and complex formation), also characterised by an energy and a range. The specificity of SAFT-VR is that the parameter λ_{ii} can be used to account for the variable range (VR) of intermolecular interactions.

In the SAFT framework, the Helmholtz free energy of a model mixture of associating chain molecules can be written as a sum of ideal, monomeric segment, chain and associative contributions. The thermodynamic properties needed to determine phase and chemical equilibrium, namely the pressure and chemical potential, are obtained as the corresponding derivatives of the Helmholtz free energy.

The reactions involved in aqueous amine solutions of CO_2 can be accounted for implicitly within the SAFT-VR thermodynamic model, with the products of the chemical reaction treated as associated aggregates of the reactant molecules [3]. This greatly reduces the number of parameters needed to describe the system as only the site-site interactions between the reactant molecules need to be specified. An accurate representation of the vapour-liquid phase equilibria of MEA + CO_2 + H_2O can be obtained in this manner. The principal reaction of interest between CO_2 and MEA is the formation of a carbamate [4]:

$$CO_2 + 2HOCH_2CH_2NH_2 \rightleftarrows [HOCH_2CH_2HCO_2^- + HOCH_2CH_2NH_3^+] \quad (1)$$

A schematic representation of how the carbamate formation is modelled in SAFT-VR is presented in figure 1.

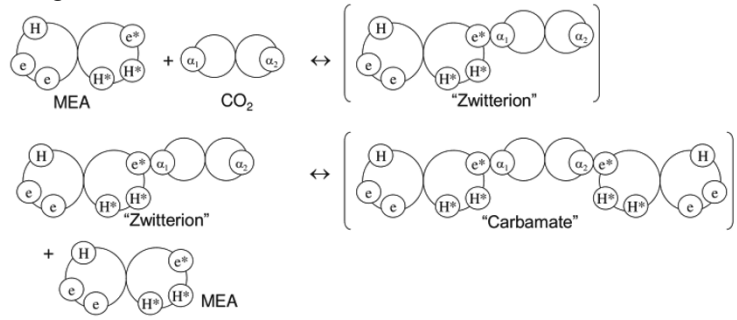

Figure 1. Schematic representation of the association scheme between MEA and CO_2 showing two reaction products. The bonding sites α_1 and α_2 on the molecular model of CO2 mediate the formation of the zwitterion and the carbamate by bonding to the e* site (of the NH_2 group) on MEA.

It can be shown that, under certain assumptions, treating the overall reaction as the generation of aggregates of the reactants is equivalent to assuming that chemical (reaction) equilibrium holds [5]. An important implication of using this approach is that the reaction products (and intermediates) do not need to be modelled explicitly. This reduces the number of components required in the overall model. We have recently shown that the concentration of carbamate is very well predicted with this method [6].
Every column stage is treated using a two-film model [7]. Each phase is split into two parts: a bulk phase and a film within which the chemical reaction and heat and mass transfer occur. In the bulk phase, the concentration, pressure and temperature are assumed to be uniform, while there may be a gradient in composition, temperature and pressure in the film. A schematic of the two-film model is shown in figure 2, with the profiles for compositions, temperature and pressure. The SAFT-VR thermodynamic model is used in the bulk phase to determine the chemical equilibrium state, and at the interface to determine the chemical equilibrium and phase equilibrium.

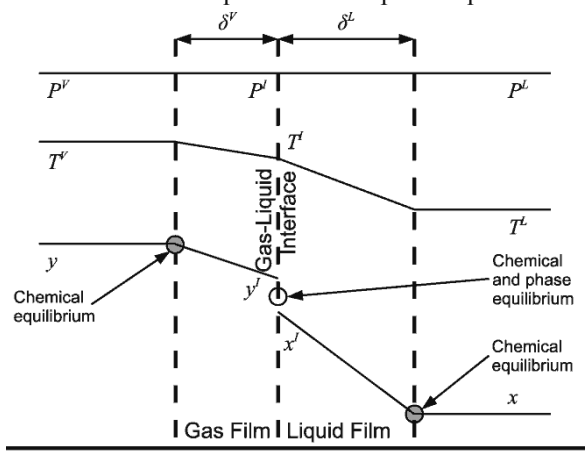

Figure 2. A schematic of the two-film model of a theoretical column stage. δ^V and δ^L represent the thickness of the gas and liquid films, respectively. P^V, P^I, and P^L are the pressures in the bulk vapour phase, at the gas-liquid interface, and in the bulk liquid, respectively. As can be seen, an isobaric profile is assumed in our current work. The temperatures of the bulk gas phase, of the gas-liquid interface, and of the bulk liquid are denoted by T^V, T^I, and T^L, respectively. Finally, y and x are the mole fractions in the bulk gas and liquid phases, respectively, and y^I and x^I are the corresponding mole fractions at the gas-liquid interface for the gas and the liquid phases.

2.2. Absorber model

The absorber column is divided into 50 stages, each representing a section of the packed column. Two widely used mass transfer correlations from Onda *et al.* [8] and Rocha *et al.* [9] are implemented in the model to compare their predictive capabilities.
The following assumptions are made in the steady-state model of the absorber:

- the bulk phases and film are at chemical equilibrium everywhere (i.e., the reaction rates are far faster than the mass transfer rates [4]).
- the interface is at phase and chemical equilibrium.
- the interfacial surface area is the same for both heat and mass transfer.
- the effective area is equal to the wetted area.
- the absorption column is considered to be adiabatic.
- there is no pressure drop along the column.

3. Model Validation

The absorber model developed in the current work is validated by comparing the model predictions with the pilot plant experimental data obtained by Tontiwachwuthikul *et al.* [10]. These include measurements at different points along the column, which have been successfully reproduced by other researchers. The validation is performed according to the operating conditions of Run T22 [10].

In preliminary calculations the model was found to over-predict the rate of absorption of CO_2 along the column. This is observed with the correlations of both Onda *et al.* [8] and Rocha *et al.* [9], which provide a very similar description. For the sake of clarity and conciseness, only results obtained with the Onda *et al.* [8] correlations are presented here. In order to investigate the nature of the over-prediction, a sensitivity analysis is performed. From this analysis, it transpires that the most influential parameter for the prediction of the composition profile is the diffusivity of the CO_2 in the liquid phase. In the reaction-implicit model, the CO_2 in the liquid phase represents CO_2, bicarbonate and carbamate. In effect, this is mostly carbamate, a much larger species than CO_2. A scaling of the CO_2 diffusivity in the liquid phase is therefore undertaken to account for the larger size of the carbamate; a good estimate of the rate of absorption of CO_2 is then obtained. The extent of rescaling is estimated from the experimental data obtained from Run T22 [10] for the gas and liquid composition profiles. On the basis of this estimation, the value that results in the least deviation between the pilot plant data and the model corresponds to a scaling of CO_2 diffusivity in the liquid phase to 4% of its original value. The liquid-phase temperature, gas-phase CO_2 concentration, and liquid-phase CO_2 concentration profiles for Run T22, with and without diffusivity scaling, are presented in Figure 3.

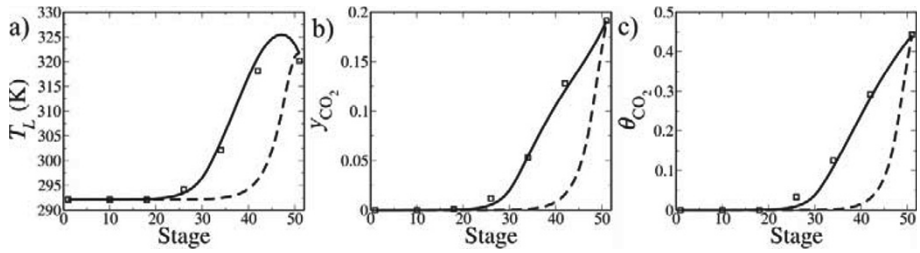

Figure 3. Comparison between pilot plant data (squares) and model results (curves) for Run T22 for the absorption of CO_2 in an 18%wt solution of MEA [10]. The dashed curves represent the results obtained without scaling of the diffusivity and the continuous curves the results obtained by scaling the CO_2 diffusivity in the liquid phase to 4% of its original value ($D' = 0.04D$) . a) Temperature profile for the liquid phase, b) gas-phase CO_2 concentration profile, and c) liquid-phase CO_2 concentration expressed in terms of loading $\theta_{CO2} = x_{CO2}/x_{MEA}$. Stage 50 corresponds to the bottom of the column.

4. Results

Other Runs from the same pilot plant absorber [10] are simulated using the same relative scaling of the diffusivity. The predictions for the temperature profile in the liquid phase, gas phase CO_2 concentration, and liquid phase CO_2 concentration for Run T20 are presented in figure 4. Runs T13, T14, T15, T16, T17, T19 and T21 have also been simulated and a similar description obtained. These runs represent a wide range of conditions in terms of amine concentration, inlet liquid phase CO_2 loading, inlet gas phase CO_2 concentration and gas-to-liquid flow-rate ratio.

Good agreement is found between the model predictions and the pilot plant data in relation to the liquid-phase temperature and the liquid- and gas-phase composition

profiles along the entire length of the column, which demonstrates that the scaling procedure can be applied in a transferable manner to different operating conditions. The temperature bulge at the bottom of the column is predicted well in terms of amplitude and location, despite the fact that no enhancement factor is used. To the best of our knowledge, no other published model predicts this bulge with such accuracy [11, 12].

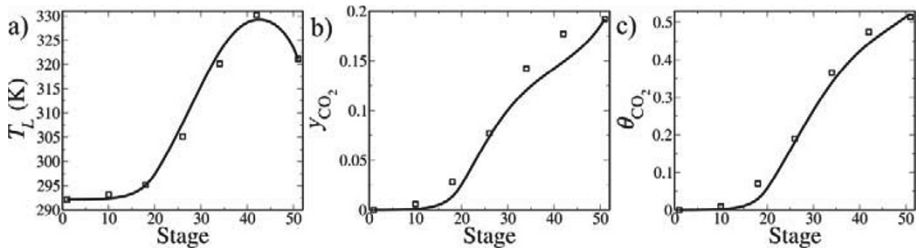

Figure 4. Comparison between pilot plant data (squares) and model results (curves) for Run T20 for the absorption of CO_2 in a 12%wt solution of MEA. Caption as in Figure 3.

5. Conclusions

A rate-based CO_2 absorber model incorporating a SAFT-VR thermodynamic treatment has been developed. The model combines physical and chemical interactions within a consistent thermodynamic framework, under the assumption that the chemical reactions are at equilibrium. The chemical reactions are treated implicitly in this formalism. Thus there is no need to incorporate an enhancement factor or to use experimental data on the rate of reaction. This greatly simplifies the description and provides a considerably more transferable model. A simple scaling of the CO_2 diffusivity in the liquid phase is proposed to account for the formation of carbamate. We show that, unlike an enhancement factor, the scaling is constant all along the entire length of the column and is transferable over a wide range of operating conditions. Our methodology allows for good predictions of the temperature and composition profiles in the gas and liquid phase along the absorber column.

Acknowledgments

The authors acknowledge financial support from EPSRC (EP/G062129/1, EP/E016340, EP/H500227/1) and invaluable discussions with L. Faramarzi and G. Kontogeorgis.

References

[1] A Gil-Villegas, A Galindo, PJ Whitehead, SJ Mills, G. Jackson, and AN Burgess. *J. Chem. Phys.*, 106(10):4168–4186, 1997.
[2] A Galindo, LA Davies, A Gil-Villegas, and G Jackson. *Mol. Phys.*, 93(2):241-252, 1998.
[3] N Mac Dowell, F Llovell, CS Adjiman, G Jackson, and A Galindo. *Ind. Eng. Chem. Res.*, 49:1883-1899, 2010.
[4] PMM Blauwhoff, GF Versteeg, and WPM Van Swaaij. *Chem. Eng. Sci.*, 39(2):207-225, 1984
[5] IG Economou and MD Donohue. *AIChE J.*, 37(12):1875-1894, 1991.
[6] J Rodriguez, N Mac Dowell, F Llovell, CS Adjiman, G Jackson and A Galindo. *Mol. Phys.,* 2012, *in press*
[7] R Krishnamurthy and R Taylor. *AIChE J.*, 31(3):449-456, 1985.
[8] K Onda, E Sada, and H Takeuchi. *J. Chem. Eng. Japan*, 1(1):62-66, 1968.
[9] JA Rocha, JL Bravo and JR Fair. *Ind. Eng. Chem. Res.,* 32(4):641-651, 1993.
[10] P Tontiwachwuthikul, A Meisen and CJ Li. *Chem. Eng. Sci*., 47(2):381-390, 1992.
[11] L Kucka, I Müller, EY Kenig, A Górak. *Chem. Eng. Sci*.,58: 3571-3578, 2003.
[12] HM Kvamsdal and GT Rochelle. *Ind. Eng. Chem. Res.,*47:867-875, 2008.

I.A. Karimi and Rajagopalan Srinivasan (Editors), Proceedings of the 11th International Symposium on Process Systems Engineering, 15-19 July 2012, Singapore

EM Algorithm for Parameter Estimation in Batch Process

Zhonggai Zhao,a,b Biao Huang,b * Fei Liu,a

a Key Laboratory of Advanced Process Control for Light Industry (Ministry of Education), Jiangnan University, Wuxi, China, 214122.

b Department of Chemical and Materials Engineering, University of Alberta, Edmonton, AB, Canada, T6G 2G6

Abstract

This paper investigates the parameter estimation problem for batch processes through the maximum likelihood method. Unlike continuous processes, a batch process has short operating period and each batch repeats the same procedure but with different raw materials. Therefore, states and measurements in different batches are not same and should be considered individually. However, the feed of material is often adjusted according to the performance of previous batches, thus the initial states of the next batch are related to the states of the previous batch. The proposed algorithm takes individuality and commonality across different batches into account and develops likelihood functions accordingly. By treating the unmeasured states and the parameters as missing variables , the maximum likelihood estimation is accomplished by expectation-maximization (EM) algorithm. In the expectation step, due to the complexity of posterior density function (PDF), particle filtering methods are employed for the implementation of filtering and smoothing. Through iterative optimization, the unknown parameters along with the states are estimated. Simulation example illustrates feasibility of this method and demonstrates its effectiveness.

Keywords: Batch process, EM algorithm, parameter estimation, particle filter

1. Introduction

Batch process plays an important role in the production of food, medicine, and so on. In the last decade, 2-dimensional (2-D) models were often used for the simulation of the batch process dynamics, along the dimensions of both time and batches [Y. Yao et al., 2008]. Most of these models are data-driven ones. However, in some batch processes, first principle models are available for the accurate description of their behaviors [T. Liu et al., 2010], but the parameters are typically unknown or partially unknown. Consider a state space model with known structure given by,

$$\begin{cases} x_k = f(x_{k-1}, \theta) + \omega_{k-1} \\ y_k = h(x_k, \theta) + v_k \end{cases} \tag{1}$$

where x_k, y_k, θ, ω_{k-1}, v_k represent the state, measurement, parameter, state noise and measurement noise, respectively. Equation (1) provides a known model structure but the parameter θ needs to be estimated according to process data.

However, this model only reflects the dynamic behavior within one batch, and fails to capture the batch-to-batch dynamics. Most of the estimation methods have tried to solve

*bhuang@ualberta.ca.

parameter estimation problem of batch processes in the same way as continuous processes [J. T. Leppavuori et al., 2011], which cannot capture the relations between batches. Considering that the initial states of each batch have similarity but also with some slight variation in many batch processes, such as fed-batch fermentation processes, $x_{i,1} = x_{i-1,1} + \gamma_{i-1,1}$ is usually used for the assignment of the initial states and defines relationship between batches [Y. Yao et al., 2008], where i represents the batch number. However, in practice, the operator often adjusts the initial states of the current batch according to the terminal performance of the last batch. For instance, in batch fermentation process, substrate is added into the fermenter only once to ensure existence of sufficient but not too much nutrition during fermentation. If the substrate concentration remains large at the end of fermentation, the initial substrate concentration of next batch will be decreased [M. Boonmee et al., 2003]. Therefore, with consideration of relations between terminal states, a practical dynamic model to describe the batch process can be written as

$$\begin{cases} x_{i,k} = f(x_{i,k-1},\theta) + \omega_{i,k-1} \\ y_{i,k} = h(x_{i,k},\theta) + v_{i,k} \\ x_{i,1} = f(x_{i-1,T},x_{i-1,1}) + \gamma_{i-1,T} \end{cases} \tag{2}$$

where k denotes the sample number. Denote $\mathbb{X} = \{X_1, X_2, \cdots, X_I\}$ and $\mathbb{Y} = \{Y_1, Y_2, \cdots, Y_I\}$ as the states and the measurements for I batches, where X_i and Y_i are all the states and measurements of the i^{th} batch, respectively. Note that the third equation of (2) defined here is more general than $x_{i,1} = x_{i-1,1} + \gamma_{i-1,1}$ [M. Boonmee et al., 2003].

This paper investigates the parameter estimation given the model structure as (2), and maximum likelihood (ML) method is employed to solve the problem. Due to the distinct features of batch process, the individuality and commonality of batches are both considered, where likelihood function of each batch process is individually set up and batches are related through terminal states during implementation of the ML method. Moreover, since states are unmeasured, expectation-maximization (EM) algorithm is introduced to accomplish the ML estimation. In the expectation step of EM algorithm, particle filters are used for the smoothing and filtering of the nonlinear and non-Gaussian processes.

2. Maximum likelihood estimation

Given the measurements $\mathbb{Y}$, the log-likelihood is $logp(\mathbb{Y}|\theta)$ and θ can be derived by maximizing the log-likelihood: $\theta = argmax\ \ logp(\mathbb{Y}|\theta)$. However, it is difficult to calculate the log-likelihood according to (2) without knowing the state. Treating $\mathbb{X}$ as "observations", the parameter estimation using ML method can be written as below

$$\theta = argmax\ \ L_\theta(\mathbb{X},\mathbb{Y}) = argmax\ \ logp_\theta(\mathbb{X},\mathbb{Y}) \tag{3}$$

where $p_\theta(\mathbb{X},\mathbb{Y}) = p_\theta(\mathbb{X})p_\theta(\mathbb{Y}|\mathbb{X})$, $p_\theta(\mathbb{X}) = p_\theta(X_1)\prod_{i=2}^{I} p_\theta(X_i|X_{1:i-1})$ and $p_\theta(\mathbb{Y}|\mathbb{X}) = p_\theta(Y_1|\mathbb{X})\prod_{i=2}^{I} p_\theta(Y_i|Y_{1:i-1},\mathbb{X})$. In order to compute the log-likelihood shown in (3), several assumptions are made as follows.

Assumption 1: state within a batch or across batches follows a first-order Markov process, satisfying $p_\theta(X_i|X_{1:i-1}) = p_\theta(X_i|X_{i-1})$ and $p_\theta(x_{i,j}|x_{i,1:j-1},X_{1:i-1}) = p_\theta(x_{i,j}|x_{i,j-1})$.

Assumption 2: observations are conditionally independent given the states, satisfying $p_\theta(Y_i|Y_{1:i-1},\mathbb{X}) = p_\theta(Y_i|X_i)$ and $p_\theta(y_{i,j}|y_{i,1:j-1},x_{i,1:j}) = p_\theta(y_{i,j}|x_{i,j})$.

Therefore, $p_\theta(\mathbb{X}) = p_\theta(x_{1,1})(\prod_{j=2}^{T} p_\theta(x_{1,j}|x_{1,j-1}))\prod_{i=2}^{I}[(\prod_{j=2}^{T} p_\theta(x_{i,j}|x_{i,j-1})]p_\theta(x_{i,1}|x_{i-1,1},x_{i-1,T})$, $p_\theta(\mathbb{Y}|\mathbb{X}) = \prod_{i=1}^{I}\prod_{j=1}^{T} p_\theta(y_{i,j}|x_{i,j})$. For models with missing or hidden

data, EM algorithm is a valid method for parameter estimation through maximizing the likelihood. Since the state is actually unknown, EM algorithm is employed to maximize (3), and the expectation of log-likelihood according to [R. B. Gopaluni, 2008] is

$$\begin{aligned} Q(\theta_i,\theta) &= \int logp_\theta(x_{1,1})p(x_{1,1}|\mathbb{Y},\theta_i)dx_{1,1} + \sum_{i=2}^{I}\sum_{j=2}^{T}\int logp_\theta(x_{i,j}|x_{i,j-1}) \\ &\quad p(x_{i,j-1:j}|\mathbb{Y},\theta_i)dx_{i,j-1:j} + \sum_{i=2}^{I}\int logp_\theta(x_{i,1}|x_{i-1,1},x_{i-1,T}) \\ &\quad p(x_{i,1},x_{i-1,1},x_{i-1,T}|\mathbb{Y},\theta_i)dx_{i,1}dx_{i-1,T}dx_{i-1,1} + \sum_{j=2}^{T}\int logp_\theta(x_{1,j}|x_{1,j-1}) \\ &\quad p(x_{1,j-1:j}|\mathbb{Y},\theta_i)dx_{1,j-1:j} + \sum_{i=1}^{I}\sum_{j=1}^{T}\int logp_\theta(y_{i,j}|x_{i,j})p(x_{i,j}|\mathbb{Y},\theta_i)dx_{i,j} \end{aligned} \quad (4)$$

From (4), the likelihood function needs to be computed for each batch, and the third term of the right side reflects the interaction of batches. In the maximization step, the gradient of $Q(\theta_i,\theta)$ with respect to θ is calculated to estimate θ, where smoothing of $p(x_{i,j}|\mathbb{Y})$ and joint distribution $p(x_{i,t},x_{i,t+1}|\mathbb{Y})$, $p(x_{i,1},x_{i,T},x_{i+1,1}|\mathbb{Y})$ need to be resolved to obtain the Q function. Since nonlinearity and non-Gaussianity are usually involved in states and measurements, particle filters are employed to estimate the posterior density function of states following the approach of [N. Gordon et al., 1993, M. Klaas et al., 2006].

3. Implementation of EM algorithm for parameter estimation

3.1. Smoothing in batch process

Assume each batch has T samples. If $j < T$, the smoother is derived as [R. B. Gopaluni, 2008]

$$p(x_{i,j}|\mathbb{Y}) = p(x_{i,j}|Y_{1:i-1},y_{i,1:j})\int \frac{p(x_{i,j+1}|\mathbb{Y})p(x_{i,j+1}|x_{i,j},\theta)dx_{i,j+1}}{\int p(x_{i,j}|Y_{1:i-1},y_{i,1:j})p(x_{i,j+1}|x_{i,j})dx_{i,j}} \quad (5)$$

According to the Monte Carlo method, $p(x_{i,j}|\mathbb{Y}) = \sum_{n=1}^{N}\omega_{i,j|IT}^{(n)}\delta(x_{i,j}-x_{i,j}^n)$. Therefore, the smoother weights are $\omega_{i,t|IT}^{(n)} = \omega_{i,t}^{(n)}\sum_{j=1}^{N}\omega_{i,t+1|IT}^{(j)}\frac{p(x_{i,t+1}^j|x_{i,t}^n,\theta)}{\sum_{k=1}^{N}\omega_{i,t}^{(k)}p(x_{i,t+1}^j|x_{i,t}^k,\theta)}$.

If $j = T$, the smoother is transformed into

$$p(x_{i,T}|\mathbb{Y}) = \int p(x_{i+1,1}|\mathbb{Y})\frac{p(x_{i,T}|Y_{1:i})p(x_{i,1}|Y_{1:i})p(x_{i+1,1}|x_{i,T},x_{i,1})}{p(x_{i+1,1}|Y_{1:i})}dx_{i,1}dx_{i+1,1} \quad (6)$$

It should be noted that there is an assumption in (6): Owing to the fact that the effect of initial value of a stable filter fades out and has little effect on the final value, $p(x_{i,T}|x_{i,1},Y_{1:i}) = p(x_{i,T}|Y_{1:i})$. The smoother weights are $\omega_{i,T|IT}^{(n)} = \omega_{i,T}^{(n)}\sum_{j=1}^{N}\omega_{i+1,1|IT}^{(j)}\frac{p(x_{i+1,1}^j|x_{i,T}^n,x_{i,1}^j)\omega_{i,1|iT}^j}{\sum_{k=1}^{N}\omega_{i,T}^{(k)}p(x_{i+1,1}^j|x_{i,T}^k,x_{i,1}^k)\omega_{i,1|iT}^k}$, where $\omega_{i,1|iT}^j$ represents the smoother weights satisfying $p(x_{i,1}|Y_{1:i}) = \sum_{k=1}^{N}\omega_{i,t|iT}^k\delta(x_{i,1}-x_{i,1}^k)$. Similar to the calculation of $\omega_{i,t|IT}^{(n)}$, the smoother $p(x_{i,j}|Y_{1:i})$ is computed as

$$p(x_{i,j}|Y_{1:i}) = p(x_{i,j}|Y_{1:i-1},y_{i,1:j})\int \frac{p(x_{i,j+1}|Y_{1:i})p(x_{i,j+1}|x_{i,j})dx_{i,j+1}}{\int p(x_{i,j+1}|x_{i,j})p(x_{i,j}|Y_{1:i-1},y_{i,1:j})dx_{i,j}} \quad (7)$$

Therefore, the smoother weights are $\omega^n_{i,t|iT} = \omega^n_{i,t|iT} \sum_{j=1}^N \omega^j_{i,t+1|iT} \frac{p(x^j_{i,t+1}|x^n_{i,t})}{\sum_{k=1}^N \omega^k_{i,t} p(x^j_{i,t+1}|x^k_{i,t})}$.

3.2. Smoothing for joint distribution

If $t < T$, the joint distribution is [R. B. Gopaluni, 2008]

$$p(x_{i,t}, x_{i,t+1}|\mathbb{Y}) = p(x_{i,t+1}|\mathbb{Y}) \frac{p(x_{i,t+1}|x_{i,t}) p(x_{i,t}|y_{i,1:t}, Y_{1:i})}{\int p(x_{i,t+1}|x_{i,t}) p(x_{i,t}|y_{i,1:t}, Y_{1:i}) dx_{i,t}} \tag{8}$$

Then the smoother weights are $\omega^{(n)}_{i,t,t+1} = \frac{\eta^n_{i,t}}{\sum_{n=1}^N \eta^n_{i,t}}$, where $\eta^n_{i,t} = \omega^{(n)}_{i,t} \omega^{(n)}_{i,t+1|IT} \frac{p(x^n_{i,t+1}|x^n_{i,t})}{\sum_{k=1}^N \omega^{(k)}_{i,t} p(x^n_{i,t+1}|x^k_{i,t})}$.

If $t = T$, the joint distribution involves the initial states as

$$\begin{aligned} p(x_{i,1}, x_{i,T}, x_{i+1,1}|\mathbb{Y}) &= p(x_{i+1,1}|\mathbb{Y}) \frac{p(x_{i+1,1}|x_{i,1}, x_{i,T}) p(x_{i,T}|Y_{1:i}) p(x_{i,1}|Y_{1:i})}{\int p(x_{i+1,1}|x_{i,1}, x_{i,T}) p(x_{i,T}|Y_{1:i}) p(x_{i,1}|Y_{1:i}) dx_{i,1} dx_{i,T}} \\ &= \sum_{n=1}^N \omega^n_{i,T,1} \delta(x_{i+1,1} - x^n_{i+1,1}) \delta(x_{i,1} - x^n_{i,1}) \delta(x_{i,T} - x^n_{i,T}) \end{aligned} \tag{9}$$

The smoother weights are $\omega^{(n)}_{i,T,1} = \frac{\eta^n_{i,T}}{\sum_{n=1}^N \eta^n_{i,T}}$, where $\eta^n_{i,T} = \omega^{(n)}_{i,T} \omega^{(n)}_{i,1|iT} \omega^{(n)}_{i+1,1|IT} \frac{p(x^n_{i+1,1}|x^n_{i,T}, x^n_{i,1})}{\sum_{k=1}^N \omega^{(k)}_{i,1|iT} \omega^{(k)}_{i,T} p(x^n_{i+1,1}|x^k_{i,T}, x^k_{i,1})}$.

To summarize, the Q function can be expressed as

$$\begin{aligned} Q(\theta_i, \theta) &= \sum_{k=1}^N \omega^k_{1,1|IT} log p_\theta(x^k_{1,1}) + \sum_{i=2}^I \sum_{j=2}^T \sum_{k=1}^N \omega^k_{i,j-1,j} log p_\theta(x^k_{i,j}|x^k_{i,j-1}) + \\ &\quad \sum_{i=2}^I \sum_{k=1}^N \omega^k_{i-1,T,1} log p_\theta(x^k_{i,1}|x^k_{i-1,T}, x^k_{i-1,1}) + \\ &\quad \sum_{j=2}^T \sum_{k=1}^N \omega^k_{1,j-1,j} log p_\theta(x^k_{1,j}|x^k_{1,j-1}) + \sum_{i=1}^I \sum_{j=1}^T \sum_{k=1}^N \omega^k_{i,j|IT} log p_\theta(y_{i,j}|x^k_{i,j}) \end{aligned} \tag{10}$$

If an analytical solution of θ to maximize (10) is intractable, numerical methods can be employed to obtain the parameter estimation. Computations of (10) and θ are iterated until the convergence of θ.

4. Simulation

Consider a batch process given by the following model:

$$\begin{cases} x_k = a * x_{k-1} + \omega_{k-1} \\ y_k = a * b * x_k + \nu_k \end{cases} \tag{11}$$

and the initial state of each batch is dependent on the initial state and last state of the previous batch as $x_{i+1,1} = -0.01 * (x_{i,T} - 20) + x_{i,1} + \gamma_{i,T}$. The true values of a and b are 1.1 and 1.5, and the initial state of the initial batch is $x_{1,1} = 1.5$. Let the batch length equal to 20, and simulate data of 10 batches according to the model. The initial guesses of a, b and $x_{1,1}$ are 2.0, 1.0 and 1.0, and the number of particles for particle filtering is 20. All $\gamma_{i,T}$, ω_{k-1} and ν_k satisfy Gaussian distribution with mean values of 0 and the variances of 0.000001, 0.000001, 0.000001, respectively. Since the actual variances are unknown in the filtering process and their guessed variances are taken as 0.001, 0.03, 0.1 to simulate performance under the mismatch. The estimation results are shown in Fig 1. One can see that the estimations of both parameters asymptotically converge to the true ones.

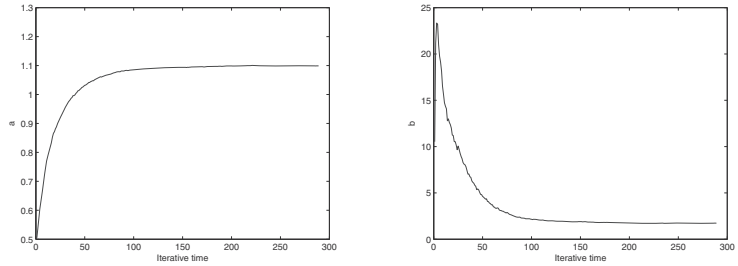

(a) The estimation of a (b) The estimation of b

Figure 1: Estimation Results

5. Conclusion

The maximum likelihood method for parameter estimation is developed for batch process, which takes the individuality and commonality property of batch processes into account. Since the state is hidden, the expectation-maximization algorithm is employed to solve the maximum likelihood estimation problem. Due to the speciality of batch processes, smoothing algorithms for the terminal state of each batch and the joint posterior distributions are derived. In addition, in view of nonlinearity and non-Gaussian property of the process and noise, particle filtering methods are applied for filtering and smoothing.

6. Acknowledgements

The authors would like to acknowledge the support in part by the support of Chang Jiang Scholar Program. The first author would also like to acknowledge the supports by Natural Science Foundation of Jiangsu Province (No. BK2010149) and National Natural Science Foundation of China (No.60904045, NSFC 61134007).

References

Y. Yao, F. Gao, 2008, Subspace identification for two-dimensional dynamic batch process statistical monitoring. Chemical Engineering Science, 63, 13, 3411-3418.

T. Liu, F. Gao, 2010, Robust two-dimensional iterative learning control for batch processes with state delay and time-varying uncertainties. Chemical Engineering Science, 65, 23, 6134-6144.

J. T. Leppavuori, M. M. Domach, L. T. Biegler, 2011, Parameter estimation in batch bioreactor simulation using metabolic models: sequential solution with direct sensitivities. Ind. Eng. Chem. Res., 50, 21, 12080-12091.

M. Boonmee, N. Leksawasdi, W. Bridge, P. L. Rogers, 2003, Batch and continuous culture of Lactococcus lactis NZ133: experimental data and model development.Biochemical Engineering Journal, 14, 127-135.

R. B. Gopaluni, 2008, A particle filter approach to identification of nonlinear process under missing observations. The Canadian Journal of Chemical Engineering, 86, 1081-1092.

N. Gordon, D. Salmond, A.F.M. Smith, 1993, Novel approach to nonlinear non Gaussian Bayesian state estimation. IEE Proceedings-F, 140, 2, 107-113.

M. Klaas, M. Briers, A. Doucet, S. Maskell, 2006, Fast particle smoothing: if I had a million particles. The 23rd International Conference on Machine Learning, 25-29.

I.A. Karimi and Rajagopalan Srinivasan (Editors), Proceedings of the 11th International Symposium on Process Systems Engineering, 15-19 July 2012, Singapore

Continuous Discrete Unscented Kalman Filtering for Nonlinear Differential Algebraic Equations Systems

S. C. Kadu[a,b] Mani Bhushan[a *] Kallol Roy[c]

a Department of Chemical Engineering, IIT Bombay, Mumbai-400076, India
b Reactor Projects Division, BARC, Mumbai-400085, India
c Research Reactor Maintenance Division, BARC, Mumbai- 400085, India

Abstract

In this paper, we propose a filtering approach for state estimation of nonlinear continuous-discrete differential algebraic equations (DAE) systems. In such systems, while the process dynamics is a set of continuous time differential algebraic equations, the measurements are discrete time. We propose continuous-discrete unscented Kalman filter (UKF) for estimating states for such systems. The proposed approach is an extension of the work of Särkkä (2007), which considered nonlinear continuous-discrete ordinary differential equations (ODE) systems. The key idea in approach is that the mean and covariance of the differential states are integrated directly using continuous time differential equations. This is in contrast to the prevalent discrete time approach in literature, which involves propagating individual sigma points through noise free model and then computing the mean and covariance of the states. In our proposed approach, the algebraic states are computed from differential states by solving the algebraic equations separately. This idea of handling algebraic states is borrowed from Mandela et al. (2010). We demonstrate the applicability of the proposed continuous-discrete UKF approach by applying it for state estimation of a well known simulation case study.

Keywords: UKF, DAE, Continuous discrete system

1. Introduction

Nonlinear differential algebraic equations (DAE) systems are frequently obtained while modeling chemical processes. For example, while mass and energy balances typically result in differential equations, consideration of thermodynamics and equilibrium relationships result in algebraic equations. These dynamics are best modeled as continuous time DAE. However, measurements in such processes are usually available at discrete times due to sampling required for computer based data acquisition and control systems, thereby resulting in an overall nonlinear continuous-discrete DAE system. Hence, problem of state estimation for nonlinear continuous-discrete DAE systems is quite relevant for chemical industries.

In literature, the various extensions of Kalman filter such as extended Kalman filter (EKF) (Jazwinski, 1970) and UKF (Julier et al., 1995) have been mainly developed for state estimation of nonlinear ODE systems. Most of these techniques are widely used for discrete

*mbhushan@iitb.ac.in

time filtering problem. A few extensions of such approaches available for continuous-discrete filtering problem for nonlinear ODE systems are: continuous-discrete versions of EKF (Jazwinski, 1970), UKF (Särkkä, 2007) and cubature Kalman filter (Arasaratnam et al., 2010).

For DAE systems, extensions of EKF and UKF are available for state estimation of nonlinear but discrete time DAE systems. Becerra et al. (2001) extended EKF approach for estimating states of nonlinear DAE. However, their approach does not utilize the algebraic state measurements while computing algebraic states estimates. Recently, Mandela et al. (2010) proposed a modified EKF approach to overcome this problem. Further, they also proposed extension of UKF approach for state and parameters estimation of DAE systems. All these approaches are applicable for discrete time nonlinear DAE systems. However, most of the problems encountered in chemical processes are continuous-discrete DAE in nature. To the best of our knowledge, extensions of EKF and UKF for directly dealing with such continuous-discrete DAE systems are not available. In this article, we propose continuous-discrete UKF (CDUKF) approach for performing state estimation in nonlinear continuous-discrete DAE systems. The proposed approach is discussed in section 2 and is applied to a case study in section 3. The conclusions are presented in section 4.

2. Continuous Discrete Unscented Kalman Filter

In this section, the proposed CDUKF formulation for state estimation of nonlinear continuous discrete DAE systems is presented. Such systems have continuous time process model but the measurements are available at discrete time intervals. The proposed approach is an extension of the CDUKF formulation presented by Särkkä (2007) for handling nonlinear continuous-discrete ODE systems. In our approach, the differential states are handled in the same manner as in Särkkä (2007). During the prediction step, the mean and the covariance matrix of the differential states are integrated directly (with continuous noise contribution). This is in contrast to discrete UKF, where individual sigma points are propagated through the noise free model and noise contribution is considered only at the measurement sampling times while obtaining the covariance matrix. The method for handling algebraic states in our proposed approach is similar to that of Mandela et al. (2010), where algebraic states are computed separately by solving the algebraic equations using a nonlinear root finding solver. The issue of solving algebraic states separately from the differential states has been discussed in Mandela et al. (2010). The estimation step is similar to that of standard UKF (Julier et al., 1995) for computing estimated mean and covariance but only for the differential states. Algebraic equations are then solved separately to compute the mean of algebraic states. The exact procedure for the proposed CDUKF for nonlinear DAE is summarized next. More details are available in Kadu (2011). Consider the following continuous-discrete time DAE model:

$$\frac{dx(t)}{dt} = f(x(t),z(t),t) + L(t)e(t);\;\; g(x(t),z(t),t) = 0;\;\; y_k = h_d(x(t_k),z(t_k)) + v_k \qquad (1)$$

where t and k represent the continuous time and discrete sampling instant respectively, $x \in \mathbf{R}^{n_d \times 1}$, $z \in \mathbf{R}^{n_a \times 1}$ and $y_k \in \mathbf{R}^{r \times 1}$ are the differential states, algebraic states and the measurement vectors. n_d and n_a represent number of differential and algebraic states respectively. Process noise $e(t)$ represents the unmodelled process dynamics in Eq. (1) and is assumed to be white, Gaussian, continuous time stochastic process with mean zero and covariance $Q_c(t)$. The measurements are corrupted by noise v_k which is assumed to be

be white, Gaussian discrete time stochastic process with mean zero and covariance R_k. Further, v_k and $e(t)$ are assumed to be uncorrelated. Functions $f()$ and $g()$ represent the differential and algebraic equations in the DAE model and $h_d()$ represents the measurement model. $L(t)$ is the matrix associated with process noise. Further, without loss of generality inputs are not considered in the above model. $x(t_k)$ represents the value of $x(t)$ at k^{th} measurement instant. For given estimated states $(\hat{x}(t_k^+))$ and associated covariance $(P(t_k^+))$ at k^{th} measurement instant, the CDUKF formulation is summarized below. Here, $+$ and $-$ indicate the time instances just after and before the measurements.

Prediction or forecast step:
The predicted mean of differential states $(\hat{x}(t_{k+1}^-))$ and its covariance $(P(t_{k+1}^-))$ are computed by directly integrating following equations:

$$\frac{d\hat{x}(t)}{dt} = f(\hat{X}(t),\hat{Z}(t),t)w; \quad g(\hat{X}(t),\hat{Z}(t),t) = 0 \tag{2}$$

$$\frac{dP(t)}{dt} = \hat{X}(t)Wf^T(\hat{X}(t),\hat{Z}(t),t) + f(\hat{X}(t),\hat{Z}(t),t)W[\hat{X}(t)]^T + L(t)Q_c(t)L^T(t) \tag{3}$$

where $\hat{X}(t) \in \mathbf{R}^{n_d \times N_p}$ is the matrix of sigma points of differential states, which is given as (Särkkä, 2007):

$$\hat{X}(t) = [\hat{x}(t) \ \ ...\hat{x}(t)] + \sqrt{n_d + \kappa}\left[[0]_{n_d \times 1} \ \ \sqrt{P(t)} \ \ -\sqrt{P(t)}\right] \tag{4}$$

with κ as a tuning parameter and $w \in \mathbf{R}^{n_d \times 1}$ being the vector of sigma points weights specified as: $w_0 = \frac{\kappa}{(n_d+\kappa)}$ and $w_i = \frac{1}{2(n_d+\kappa)}, \ i = 1 \ to \ 2n_d$. Matrix $W \in \mathbf{R}^{N_p \times N_p}$ is defined as (Särkkä, 2007):

$$W = \left[I - [w \ \ ... \ \ w]_{N_p \times N_p}\right] w_{diag} \left[I - [w \ \ ... \ \ w]_{N_p \times N_p}\right]^T \tag{5}$$

where, $w_{diag} \in \mathbf{R}^{N_p \times N_p}$ is the diagonal matrix form of vector of sigma points weights and $N_p = 2n_d + 1$ is the number of sigma points. Corresponding to the vectors in matrix $\hat{X}$ (sigma points for differential states), the vectors for the algebraic states are obtained by solving the algebraic equations for the given differential states. These vectors make-up the matrix $Z \in \mathbf{R}^{n_a \times N_p}$ and are compactly represented by the algebraic equations: $g(\hat{X}(t),\hat{Z}(t),t) = 0$. Similarly, the notation $f(\hat{X}(t),\hat{Z}(t),t)$ indicates a matrix (size $n_d \times N_p$) of function evaluations, such that the j^{th} column is the function vector f (Eq. 1) evaluated for the j^{th} sigma point (i.e. j^{th} column of $\hat{X}(t)$ and $\hat{Z}(t)$ matrices). Eq. (2) is integrated from initial conditions $\hat{x}(t_k^+)$ and $P(t_k^+)$ to time t_{k+1}. The predicted differential state mean and state prediction error covariance matrix are then given as $\hat{x}(t_{k+1}^-) = \hat{x}(t_{k+1})$, and $P(t_{k+1}^-) = P(t_{k+1})$ respectively. The consistent predicted algebraic state mean $(\hat{z}(t_{k+1}^-) = \hat{z}(t_{k+1}))$ is obtained by solving algebraic equation $g(\hat{x}(t_{k+1}),\hat{z}(t_{k+1})) = 0$. The sigma points matrix $\hat{X}(t_{k+1}^-)$ is generated by using Eq. (4) in which the terms $\hat{x}(t)$ and $P(t)$ are replaced with $\hat{x}(t_{k+1}^-)$ and $P(t_{k+1}^-)$ respectively. The consistent matrix of algebraic states is computed by solving equation $g(\hat{X}(t_{k+1}^-),\hat{Z}(t_{k+1}^-),t) = 0$. These sigma points matrices are used in the next (estimation) step.

Estimation or data assimilation step:
The matrices of sigma points are propagated through measurement model to predict the matrix of measurement sigma points:

$$Y_{k+1}^- = h_d(\hat{X}(t_{k+1}^-),\hat{Z}(t_{k+1}^-)) \tag{6}$$

The predicted observation $(\hat{y}_{k+1}^-)$, the total covariance in innovation sequence $(P_{ee,k+1}^-)$ and the cross covariance between the state prediction error and innovation sequence $(P_{se,k+1}^-)$ are computed as:

$$\hat{y}_{k+1}^- = Y_{k+1}^- w; \quad P_{ee,k+1}^- = Y_{k+1}^- W [Y_{k+1}^-]^T + R_{k+1}; \quad P_{se,k+1}^- = \hat{X}(t_{k+1}^-) W [Y_{k+1}^-]^T \tag{7}$$

The Kalman gain (K_{k+1}), estimated mean $(\hat{x}(t_{k+1}^+))$ of differential state, associated state estimation error covariance matrix $(P(t_{k+1}^+))$ and estimated mean of algebraic state $(\hat{z}(t_{k+1}^+)$ are computed as:

$$K_{k+1} = P_{se,k+1}^- [P_{ee,k+1}^-]^{-1}; \quad \hat{x}(t_{k+1}^+) = \hat{x}(t_{k+1}^-) + K_{k+1}[y_{k+1} - \hat{y}_{k+1}^-] \tag{8}$$

$$P(t_{k+1}^+) = P(t_{k+1}^-) - K_{k+1} P_{ee,k+1}^- K_{k+1}^T; \quad g(\hat{x}(t_{k+1}^+), \hat{z}(t_{k+1}^+), t) = 0 \tag{9}$$

This completes one cycle: going from measurement instant k to $k+1$. This procedure is then repeated for the next measurement instance.

3. Results and Discussions

The applicability of the proposed CDUKF approach is demonstrated on a nonlinear DAE case study given by Becerra et al. (2001). The case study is based on a kinetic model of an isothermal batch reactor system represented using nonlinear DAE involving six differential (mass balances) equations and one algebraic electro-neutrality condition as:

$$\begin{aligned}
&\dot{x}_0 = -k_2 x_1 \frac{K_2 x_0}{K_2 + 10^{-z_0}}; \; \dot{x}_1 = -k_1 x_1 x_5 + k_{-1} \frac{K_1 x_4}{K_1 + 10^{-z_0}} - k_2 x_1 \frac{K_2 x_0}{K_2 + 10^{-z_0}} \\
&\dot{x}_2 = k_2 x_1 \frac{K_2 x_0}{K_2 + 10^{-z_0}} + k_3 x_3 x_5 - k_{-3} \frac{K_3 x_2}{K_3 + 10^{-z_0}}; \; \dot{x}_3 = -k_3 x_3 x_5 + k_{-3} \frac{K_3 x_2}{K_3 + 10^{-z_0}} \\
&\dot{x}_4 = k_1 x_1 x_5 - k_{-1} \frac{K_1 x_4}{K_1 + 10^{-z_0}} \\
&\dot{x}_5 = -k_1 x_1 x_5 + k_{-1} \frac{K_1 x_4}{K_1 + 10^{-z_0}} - k_3 x_3 x_5 + k_{-3} \frac{K_3 x_2}{K_3 + 10^{-z_0}} \\
&\left[Q^+\right] - x_5 + 10^{-z_0} - \frac{K_2 x_0}{K_2 + 10^{-z_0}} - \frac{K_3 x_2}{K_3 + 10^{-z_0}} - \frac{K_1 x_4}{K_1 + 10^{-z_0}} = 0
\end{aligned} \tag{10}$$

Hence, the model consists of six differential states $(x_0 - x_5)$ and one algebraic state (z_0). The measurement vector is $y_k = [x_0(t_k), x_1(t_k), x_2(t_k), x_3(t_k)]^T$. The values for the initial states and associated covariance matrix are taken from Becerra et al. (2001). Here, entire simulation is carried out at constant temperature of $98^o C$. The true differential states were generated using 500 steps of Euler-Maruyama scheme (Kloeden and Platen, 1999) between time interval of 0.01 h. The corresponding consistent algebraic state was obtained by solving the algebraic equation at each step of Euler scheme. The proposed CDUKF was implemented by integrating the mean and covariance of differential states using 300 steps of fourth order Runge-Kutta integration between measurement intervals. The consistent algebraic state at any stage is obtained by solving the algebraic equation. The following parameter values were used: Q_c is taken to be $1e-5$ times Identity matrix (of size 6×6), R_k is also taken to be a diagonal matrix with entries 4e-5,4e-5,1e-5,1e-5 on the diagonal, and $\kappa = 1$. The measurement sampling time was taken as 0.05 h. The true and CDUKF estimated values for five differential states $(x_0, x_1, x_2, x_4, x_5)$ and the algebraic state (z_0) are plotted in Figure (1) for illustration. It can be seen from the Figure that CDUKF tracks differential as well as algebraic states very well. All the computations were performed in MATLAB® version 7.4.

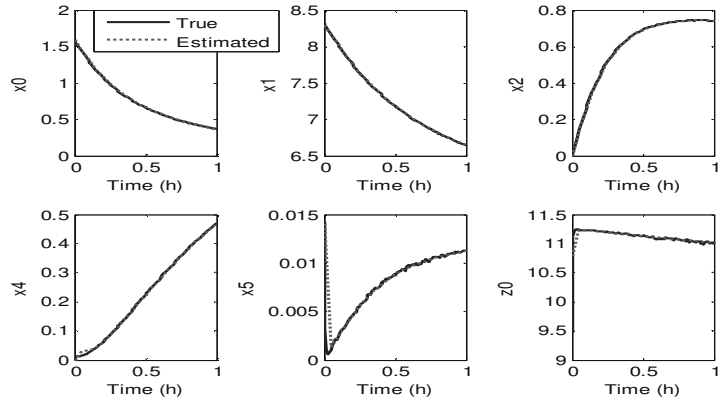

Figure 1. State estimation by CDUKF

4. Conclusion

A continuous-discrete extension of UKF (labeled CDUKF) for nonlinear continuous-discrete DAE systems has been proposed in this paper. This has the potential to provide more accuracy from modeling point of view compared to completely discrete time implementations and from estimation point of view compared to other types of continuous-discrete implementations, such as those based on EKF.

References

Arasaratnam, I., Haykin, S., Hurd, T. R., 2010. Cubature kalman filtering for continuous-discrete systems: Theory and simulations. IEEE Trans. on Signal Processing 58 (10), 4977–4993.

Becerra, V. M., Roberts, P. D., Griffiths, G. W., 2001. Applying the extented kalman filter to systems described by nonlinear differential-algebraic equations. Control Engg. Practice 9, 267–281.

Jazwinski, A., 1970. Stochastic Processes and Filtering Theory. Academic Press, New York, USA.

Julier, S. J., Uhlmann, J., Durrant-Whyte, H. F., 1995. A new approach for filtering nonlinear systems. In: Proceedings of Am. Control Conf. pp. 1628–1632.

Kadu, S. C., 2011. Nonlinear observer based approaches for fault detection and diagnosis. Ph.d. research progress seminar- iv, Indian Institute of Technology Bombay, India.

Kloeden, P. E., Platen, E., 1999. Numerical Solution to Stochastic Differential Equations. Springer, New York, USA.

Mandela, R. K., Rengaswamy, R., Narasimhan, S., Sridhar, L. N., 2010. Recursive state estimation techniques for nonlinear differential algebraic systems. Chemical Engineering Science 65, 4548–4556.

Särkkä, S., 2007. On unscented kalman filtering for state estimation of continuous-time nonlinear systems. IEEE Trans. on Automatic Control 55 (9), 1631–1641.

I.A. Karimi and Rajagopalan Srinivasan (Editors), Proceedings of the 11th International Symposium on Process Systems Engineering, 15-19 July 2012, Singapore.

Systematic identification of crystallization kinetics within a generic modelling framework

Noor Asma Fazli Abdul Samad, Kresten Troelstrup Meisler, Krist V. Gernaey, Nicolas Smit von Solms, Rafiqul Gani

Department of Chemical and Biochemical Engineering, Søltofts Plads, Building 229, Technical University of Denmark, DK-2800 Lyngby, Denmark

Abstract

A systematic development of constitutive models within a generic modelling framework has been developed for use in design, analysis and simulation of crystallization operations. The framework contains a tool for model identification connected with a generic crystallizer modelling tool-box, a tool for data handling and translation as well as model application features. Through this framework it is possible, for a wide range of crystallization processes, to generate the necessary problem-system specific models; to identify the parameters for constitutive models; and to handle or translate raw crystallization data. Application of the systematic framework is highlighted through a sucrose crystallization case study, for which the parameters for nucleation and crystal growth are first estimated from the available measured data and are then applied to study the crystallization operation.

Keywords: Crystallization, generic modelling, model identification, data handling.

1. Introduction

Crystallization is often applied in the production of salts and active pharmaceutical ingredients (API), and the crystallization step is an essential part of the manufacturing process for many chemicals-based products. Recently the monitoring and analysis of crystallization operations has received increased attention due to the growing need to control more sophisticated production lines as well as to measure/monitor the final product characteristics [1]. Usually crystallization operations involve a combination of several phenomena, and different kinetic models are required for their modelling. For example, growth of the crystals occurs in multiple dimensions and the relative rates of different growth and other kinetic phenomena control the shape and size distribution of the final product [2]. A full representation of the crystallizer operation therefore requires a combination of different constitutive (kinetic) models representing different aspects (nucleation, growth, agglomeration, breakage, etc.) of crystallization together with the population balance and other equations. The constitutive models, however, have parameters that need to be identified, for which measured data is necessary. The measured data can be in different form and dimension. For example, crystal size distribution (CSD) data could be available in the form of chord length distribution that is obtained through Focused Beam Reflectance Measurement (FBRM) equipment [3]. Use of this data for modelling purposes requires a translation procedure.

The objective of this paper is to present a framework for systematic development of constitutive models within a generic modelling framework for use in design, analysis and simulation of crystallization operations. The framework has three main options: a) crystallization model development and constitutive model identification, b) data

handling, and c) model application. For different crystallization operation scenarios, the measured data are translated to create an image of the crystallized product. Through the model identification option, the parameters of the constitutive models (embedded within the crystallizer model) are regressed to match the image of the translated data. With the models identified, they can be applied for model-based design and/or analysis of crystallization operations. The different features are highlighted through a sucrose crystallization case study involving crystallization model generation, model identification and the use of the model in analysis of crystallization operations.

2. Systematic identification of crystallization kinetics

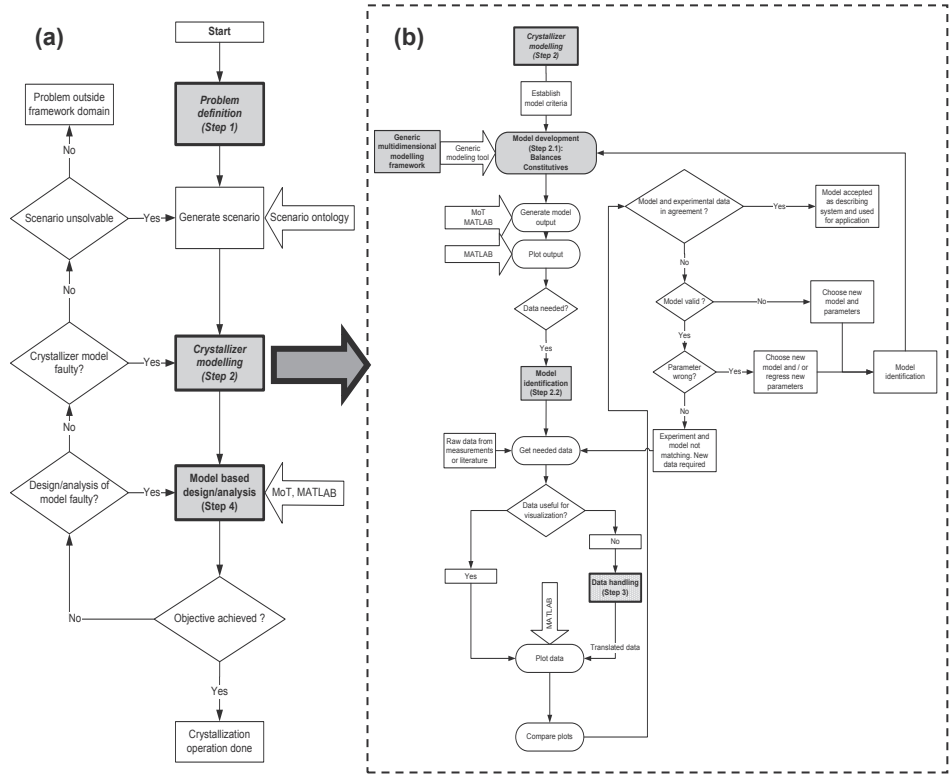

Figure 1. Systematic identification within a generic modelling framework

An overview of the different steps to be taken for systematic identification of crystallization kinetics within a generic modelling framework is shown in Fig. 1(a). The first step is the problem definition for the crystallization process under study where the overall objective is defined. Then the crystallization process scenario that needs to be investigated is generated from a scenario ontology tool-box. Step 2, crystallization model development, involves the model generation to represent the defined scenario. Here, the model identification and data handling frameworks have been integrated with the generic multi-dimensional modelling framework [4] as shown in Fig. 1(b). In step 2.1, the balance and constitutive equations are selected from the developed balances and kinetics model library in the generic multi-dimensional modelling framework [4] based on the specified assumptions and conditions. If the parameters are available, the generated problem-system specific model is then ready for use for the defined application. If not, data need to be supplied for model identification (step 2.2), for

example from experimental measurements. As such data may not come in the correct digital form for the corresponding model variable for example the CSD data shown in Fig. 2, a data handling step (step 3), which translates the data is employed. The model identification is completed by solving a parameter regression problem, including a consistency test for the data and a verification of the regressed parameters. After model identification, the complete model together with the estimated parameters is ready for use in model-based studies of crystallization operations (step 4).

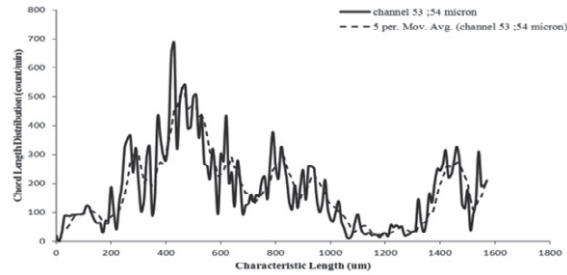

Figure 2. CSD data measured as chord length distribution

The data handling framework (step 3), as shown in Fig. 3, is used to translate the available/collected data to a form that can be employed for the parameter regression step. Here, different types of measured data are translated using an established data translation policy. Then the data are checked for consistency, after which, they are ready for parameter regression or model validation. New measured or collected data are needed if the available data fail the consistency test, while, the available model parameters are re-estimated if there is a mismatch between consistent data and model. Process-product knowledge is used for consistency check of data and evaluation of data-model mismatch.

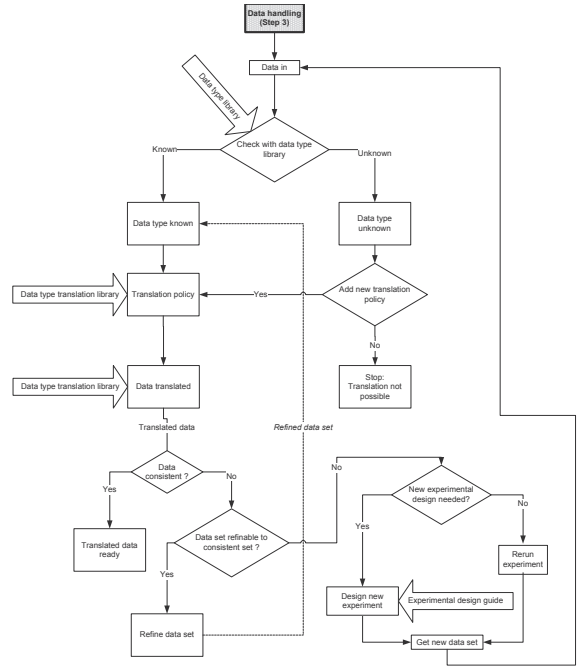

Figure 3. Data handling framework

3. Application of the systematic identification framework

The application of the frameworks for model identification and data handling is highlighted through a sucrose crystallization case study.

3.1. Problem definition (step 1)

The overall objective here is to develop a sucrose crystallization model for use in the design and analysis of crystallization operations. The operation scenario which consists of phase 1 (cooling operation), phase 2 (nucleation) and phase 3 (crystal growth) is then generated from the scenario ontology tool-box.

3.2. Crystallization model development and model identification (step 2)

The problem-system specific model for sucrose crystallization (see Table 1) is generated using the generic multi-dimensional modelling framework [4] by using similar conditions and assumptions as reported in the literature [5] (step 2.1). Before the generated model equations can be solved, the set of known variables (parameters and design variables) needs to be selected and specified. In this case study, values of the parameters k_{b0}, ΔE_b, b and m for nucleation (see Eq. (9) in Table 1) as well as k_{g0}, ΔE_g and g for crystal growth rate (see Eq. (10) in Table 1) are not available. Therefore, raw data need to be supplied. Measured data for temperature, concentration, supersaturation and total crystal mass were found in the literature [5]. Based on an analysis of the collected data, it is established that data handling and translation is not necessary as the data are found to be consistent and directly useable. The model identification step (step 2.2) is then performed in order to regress the parameters for the nucleation and crystal growth kinetic (constitutive) models.

Table 1. List of model equations for sucrose crystallization

No.	Equations	No.	Equations
1	$\frac{d\mu_0}{dt} = B_{nuc}$	6	$c^{sat} = a_{i1} + b_{i1}T + c_{i1}T^2 + d_{i1}T^3$
2	$\frac{d\mu_j}{dt} = jG\mu_{j-1}$ for $j = 1,2,3,4$	7	$S = \frac{c - c^{sat}}{c^{sat}}$
3	$\frac{dc}{dt} = -3\rho_c k_v G\mu_2$	8	$M_c = \rho_c k_v \mu_3$
4	$\rho V c_p \frac{dT}{dt} = -\Delta H_c \rho_c k_v V\ 3G\mu_2\ - U_1 A_1\ T - T_w$	9	$B_{nuc} = k_{b0} \exp\ -\ \Delta E_b / RT\ \ S^b M_c^{\ m}$
5	$\rho_w V_w c_{pw} \frac{dT_w}{dt} = \rho_w F_{win} c_{pw}\ T_{win} - T_w$ $+ U_1 A_1\ T - T_w\ + U_2 A_2\ T_{ex} - T_w$	10	$G = k_{g0} \exp\ -\ \Delta E_g / RT\ \ S^g$

The parameter estimation is performed based on the experimental data for temperature ($T_{i_{exp}}$), sucrose concentration ($c_{i_{exp}}$), supersaturation ($S_{i_{exp}}$) and total crystal mass ($M_{c,i_{exp}}$) as functions of time. The objective function for parameter regression takes the form:

$$F_{obj} = \min_{\theta} \left\{ w_T \sum_{i=1}^{n} \left\{ \frac{T_{i_{calculated}} - T_{i_{exp}}}{T_{i_{exp}}} \right\}^2 + w_c \sum_{i=1}^{n} \left\{ \frac{c_{i_{calculated}} - c_{i_{exp}}}{c_{i_{exp}}} \right\}^2 + w_S \sum_{i=1}^{n} \left\{ \frac{S_{i_{calculated}} - S_{i_{exp}}}{S_{i_{exp}}} \right\}^2 + w_{Mc} \sum_{i=1}^{n} \left\{ \frac{M_{c,i_{calculated}} - M_{c,i_{exp}}}{M_{c,i_{exp}}} \right\}^2 \right\} \quad (1)$$

Subject to: All model equations in Table 1 and $\theta_{\min} \le \theta \le \theta_{\max}$

Where $\theta = [k_{b0}, b, \Delta E_b, k_{g0}, g, \Delta E_g, m]$ is the set of parameters for the nucleation and crystal growth kinetics models, $\theta_{\min}$ and $\theta_{\max}$ are the specified lower and upper bounds for each parameter, respectively. The parameter regression problem is solved with the ICAS-MoT modelling tool and the resulting model parameters for the sucrose crystallization are given in Table 2 (F_{obj} =1.15x10^{-8}), where the values obtained are consistent with the estimated ones reported by Ouiazzane et al. [5].

Table 2. Optimum kinetic parameters for sucrose crystallization

Kinetic parameters	k_{b0}	b	ΔE_b	k_{g0}	g	ΔE_g	m
This work	3.2365x10^{13}	1.5	80.2765	2.4121x10^{6}	1	44.5618	0.4211
Ouiazzane's work	3.1512x10^{13}	1.5	78.752	2.2439x10^{6}	1	46.550	0.4136

Comparison of the simulation results with the identified sucrose model and the available experimental data shows a very good agreement (see Fig. 4). It is concluded that the sucrose crystallization model with the identified nucleation and crystal growth parameters is able to describe the temperature and sucrose concentration for the entire batch operation. Therefore the model is accepted to describe the system and is ready for use in the model-based studies.

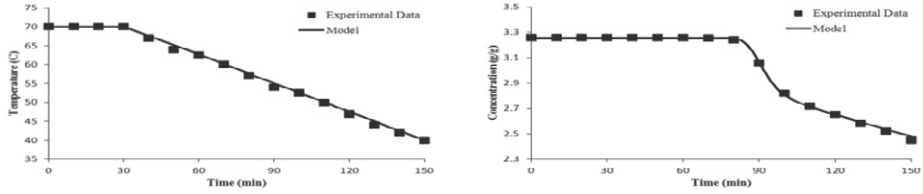

Figure 4. Model predictions and data (temperature and concentration) for sucrose crystallization

3.3. Application (step 4)

The model is now ready for design and analysis of crystallization operations. The open loop simulation results obtained are shown in Fig. 5, where the transient concentrations are plotted for 1-3 operational phases. Phase 1 indicates that the simulated sucrose concentration, initially at 3.26 g sucrose/g water is saturated from t = 30 min onwards. The sucrose (saturated) concentration is still maintained in phase 2 because most crystal nuclei are relatively small. The sucrose concentration only starts to decrease at t = 76 min during phase 3 (crystal growth): the crystal nuclei grow and a sucrose concentration of 2.46 g sucrose/g water is obtained by the end of the operation.

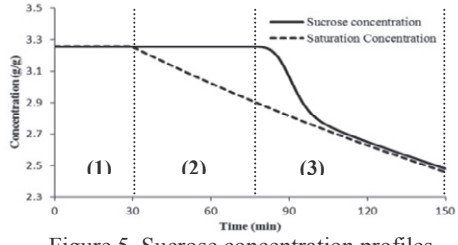

Figure 5. Sucrose concentration profiles

4. Conclusions

A systematic identification of crystallization kinetics within a generic modelling framework has been developed for operation and study of crystallization processes. The application of the newly developed framework for model identification has been highlighted through a sucrose case study. The sucrose crystallization model is generated through the generic crystallization modelling framework and the parameters for crystallization kinetics have been successfully estimated. Application of the data handling framework could not be highlighted because of the page limitation. Currently, this framework is able to handle and translate FBRM data into a one-dimensional CSD. Current and future work is focused on expanding the databases for operational scenarios, data measurement techniques and data translation policies that will allow a broader range of applications of the total modelling framework.

References

[1] E. Aamir, Z.K. Nagy, C.D. Rielly, (2010), Chem. Eng. Sci., 65, 3602-3614.
[2] H. Breisen, (2006), Chem. Eng. Sci., 61, 104-112
[3] E.J. Hukkanen, R.D. Braatz, (2003), Sensor Actuat, B-Chem., 96, 451-459.
[4] N.A.F.A. Samad, R. Singh, G. Sin, K.V. Gernaey, R. Gani, (2011), Comput. Chem. Eng., 35, 828-843.
[5] S. Ouiazzane, B. Messnaoui, S. Abderafi, J. Wouters, T. Bounahmidi, (2008), J. Cryst. Growth, 310, 798-803.

I.A. Karimi and Rajagopalan Srinivasan (Editors), Proceedings of the 11th International Symposium on Process Systems Engineering, 15-19 July 2012, Singapore.

Generation of first and higher order derivative information out of the documentation level

Victor Alejandro Merchan, Robert Kraus, Tilman Barz,

Harvey Arellano-Garcia, Günter Wozny

Chair of Process Dynamics and Operation, Berlin Institute of Technology, Sekr KWT-9, Str. des 17.Juni 13, D-10623 Berlin,Germany

Abstract

The accurate and efficient evaluation of first and higher order derivative information of mathematical process models plays a major role in the field of Process Systems Engineering. Although it is well known that the chosen methods for derivative evaluation may have a major impact on solution efficiency, a detailed assessment of these methods is rarely made by the modeler. Since standard modeling tools and some solvers normally only support own default methods for derivative evaluation, the evaluation of further methods can be a tedious work, and thus requiring the connection of different tools.

In this contribution the implementation of a general method for generation of derivative information out of the documentation level is presented. Exploiting the possibility of code generation given by the web-based modeling environment MOSAIC (Kuntsche et al. 2011), derivative information of model equations is generated either by symbolic derivatives or by coupling the models with state of the art automatic differentiation (AD) tools. This offers the modeler different methods of getting exact derivative values and opens the possibility of integrating the assessment of derivative evaluations within the modeling and simulation workflow.

Keywords: Code generation, symbolic derivatives, automatic differentiation.

1. Introduction

The numerical evaluation of derivative information plays a major role in the solution of mathematical models in Process Systems Engineering. Typical problems like the solution of nonlinear equation systems (NLEs), the integration of dynamic systems described by stiff ordinary differential equations (ODEs) and differential algebraic equations (DAEs), or the solution of optimization problems do not only require derivative information of first and perhaps higher-order but also benefit from its efficient evaluation.

However, the evaluation of derivative values may not only be related to eventual higher robustness and rate of convergence but also to a big and not always justifiable, computational effort. The latter depends strongly on the suitability of the specific model to the employed method for derivative evaluation. The most popular methods for approximation or evaluation of derivatives are finite differences (FD), symbolic differentiation (SD), and algorithmic differentiation (AD). Good overviews about these and further techniques for derivative evaluation are given in (Tolsma and Barton 1998) and (Griewank 2009).

Following the literature of the last years, it is clear that AD has several significant advantages over FD and SD, since it offers the possibility of calculating exact tangents

and gradients of a procedure with a computational effort given by a small multiple of the effort required for the evaluation of the procedure itself (Griewank and Walther 2008). New algorithms for solution of ODEs (Schlenkrich et al. 2006) and optimization problems (Vekuturi et al. 2010) take advantage of this exact and efficient evaluation of tangents and gradients provided by AD, giving up the evaluation of full Jacobians and Hessians, but showing a high solution efficiency. However, many popular solvers for NLE, DAE and optimization still rely on full Jacobians and Hessians, which in some cases can be evaluated more efficiently with SD or FD. Furthermore, models are often coded in formats that can only be differentiated by specific methods.

Although the choice of the derivative evaluation method may have a major impact on solution efficiency, a detailed assessment of the different methods is rarely made by the modeler. Standard modeling tools and some solvers normally support only default or own methods and the implementation of further methods would result in a tedious work requiring the connection of different tools. In order to give the modeler the possibility of evaluating different derivative concepts on the solution of own models, a modeling environment should offer the modeler this possibilities automatically.

This work describes the implementation of flexible derivative generation based on modeling in the documentation level. Based on a documentation conform representation of model equations and the code generation capabilities of the web modeling environment MOSAIC (Kuntsche et al. 2011), solution code for NLEs and DAEs for different numerical solvers and modeling environment is generated along with derivative information provided either by FD, SD or standard AD tools. A direct assessment of different alternative methods for derivative evaluation is integrated into the modeling and simulation workflow.

2. Modeling in the documentation level with MOSAIC and derivatives

2.1. Documentation-level-modeling with MOSAIC

When modeling with the web-based modeling environment MOSAIC, the focus lies on the problem formulation and not on the implementation of a model to any specific programming or modeling language. Model equations coupled with an own notation are entered using LaTeX expressions allowing an equation representation conform to scientific papers or further types of model documentation. Internally the LaTeX expressions are transformed automatically to a well defined subset of presentation MathML that build the basis of model analysis and code generation: Out of the MathML expressions, program code can be generated for the solution with different numerical environments. Currently, models expressed by NLEs, ODEs, and DAEs are supported and thus solver code for these type of problems can be generated. To mention a few, code can be created for high level modeling languages like gPROMS and Aspen Custom Modeler, but also for MATLAB, and FORTRAN or C/C++ programs linked with standard numerical libraries.

A common fact concerning the different solvers supported by MOSAIC is that these may benefit from derivative information given by the user. This is especially interesting for the code generation for programming languages (Matlab, C/C++, FORTRAN), since high level modeling languages normally build own symbolic derivative objects. The implementation of derivative generation out of the documentation level as proposed by MOSAIC is shown in Fig. 1. Based on the MathML/XML representation of user defined models, not only code for symbolic derivatives can be created, so as to be provided or compiled along with solver code, but also derivative information can be obtained by adapting the solver code or code of symbolic derivatives to state of the art

AD tools. In the next section the implementation of symbolic derivatives and AD tools is discussed. Since FD is supported by all major solvers by default, when no further derivative information is given, it will not be treated in this work.

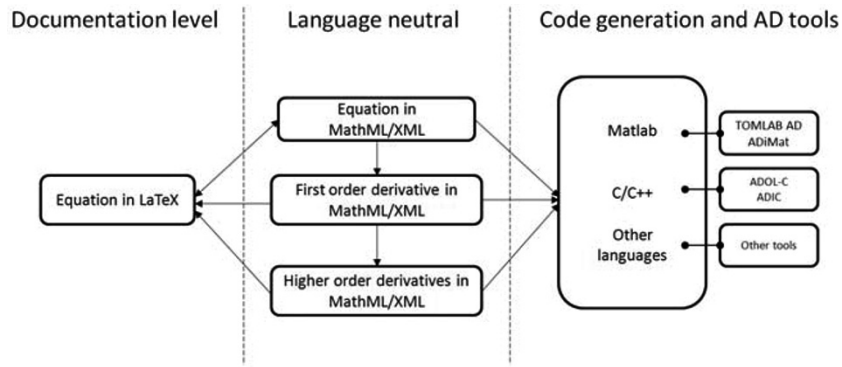

Fig. 1: Implementation of derivative generation out of the documentation level in MOSAIC

2.2. Symbolic derivatives in MOSAIC

The generation of symbolic derivatives implemented in MOSAIC is based on a recursive application of the differentiation rules on a tree representation of the respective equation object. Since the resulting derivatives are given by a further equation object, its respective MathML/XML representation can be used either to generate code for the evaluation of derivatives or it can be analyzed again in order to produce higher order derivatives.

Using the available MathML/XML expressions for equations and derivatives tailored Jacobians, Hessians or single derivative information can be generated that fulfill the format requirements of different solvers. Currently derivative code and sparsity patterns are generated for their use with Matlab and for C/C++ programs linked to the numerical libraries BzzMath (Buzzi-Ferraris) and CGSL.

2.3. Currently implemented AD-Tools

In addition to the symbolic derivatives, for some languages supported by MOSAIC, derivative information can be generated automatically by coupling the model equations with some standard AD tools. Compared to a MOSAIC specific, tool independent realization of AD, the generation of tailored code for different AD tools has the advantage of letting the user choose between different implementations, which provide the best of current AD tools. AD packages based on operator overloading and source transformation are supported. Further, depending on the chosen code generator and AD package further options are offered, e.g. forward or reverse mode.

Currently, the code generation has been adapted to generate BzzMath compatible derivatives with ADOL-C (Walther and Griewank 2008) and ADIC (Bischof et al. 1997), and derivative information for MATLAB either by the operator overloading package TOMLAB/MAD (Forth 2006) or the source transformation tool AdiMat (Bischof et al. 2002). By using the language specification tool, the user can adapt the structure of the solver code in order to use further AD tools. This is especially simple for tools based on operator overloading.

By looking at the generated code, the user may learn directly the specific needs and usage of the different AD tools. Solving the problem online, as it is offered when using the BzzMath library, the user has furthermore the possibility to compare different

standard tools or derivative evaluations methods (FD, SD and AD) without needing to install all libraries or tools in the own computer. The following results show a comparison of the influence of different derivative evaluation methods on the solution of a NLE as obtained by integration of derivative evaluation in MOSAIC's workflow.

3. Some numerical results

For the numerical test, we consider the distillation column test problem for a 20-stage column, also known as Hydrocarbon-20, a well known benchmark problem from the collection by (More 1991). In order to enhance the complexity of our case, all relations were entered in MOSAIC as single equations and thus resulting in a system with 280 equations while in the original formulation some of the equations are rearranged to form a reduced system with 99 equations.

For the tests the code generators for MATLAB and BzzMath are used, which create default implementations of the function fsolve and BzzMyNonLinearSystemObject respectively. The calculations with four different types of Jacobians are considered, the default implementation of finite differences, symbolic derivatives generated by MOSAIC, and derivatives gotten by coupling the model equations with AD operator overloading and source transformation tools. In MATLAB automatic differentiation was evaluated with TOMLAB/MAD using the sparse identity matrix as seed matrix, and ADiMat generating a compressed Jacobian in the forward mode. In case of the C++ code linked with BzzMath, standard methods for ADOL-C and ADIC are used.

Fig. 2 and 3 show the corresponding CPU-time required for the solution of the test problem with the different solvers and derivative evaluation methods. The MATLAB calculations were performed with MATLAB 2008b on a PC with Intel Core Duo CPU (3.00 GHz) and 2 GB RAM. The BzzMath results were calculated online by the MOSAIC server with an Intel Xeon CPU (2.67 GHz) and 504 MB RAM. Both solvers were executed with default settings, so that the resulting differences in CPU-time can be traced back to the influence of the derivative evaluation methods. The results should in no way be considered as comparison between different solvers, derivative evaluation methods of AD tools.

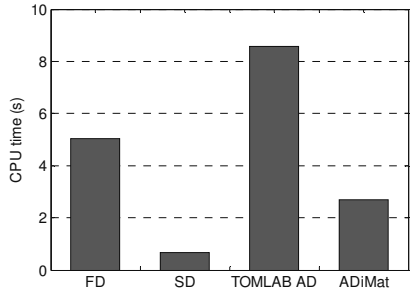

Fig. 2: CPU time for MATLAB solution

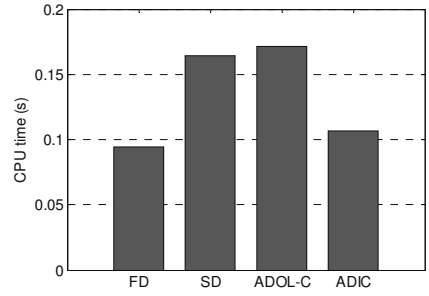

Fig. 3: CPU time for BzzMath solution

In both cases, an influence of the derivative evaluation method is well recognizable. However, while in the case of the BzzMath the influence of the derivative evaluation methods is almost no noticeable and FD results in the fastest execution, for MATLAB a stronger influence of the type of derivative evaluation can be noticed and the symbolic derivatives lead to a much faster execution. In spite of the fact that these results are only valid to the specific case above, they emphasize the central role of a proper choice of derivative evaluation methods and show in fact how a modeler can profit from having

the chance to test different methods of derivative evaluation on different environments. It is important to remark that following this strategy, the models need only to be defined once in the documentation level in order to enable the assessment of different solvers and derivative evaluation methods.

4. Conclusions and outlook

This contribution presents a general method for generation of derivative information out of the documentation level as implemented in the modeling environment MOSAIC. By this means an integration of the assessment of different derivative evaluations within the modeling and simulation workflow is achieved. So far the derivative generation has been used by the kind of problems supported by MOSAIC, currently NLEs and DAEs. With the extension of MOSAIC for the formulation and solution of optimization problems, a wide field for the application and assessment of derivative evaluation methods will be opened. The evaluation of higher order derivatives and the use of solution algorithms based on directional derivatives (tangents and adjoints) are of special interest.

5. Acknowledgement

The authors acknowledge the support from the Collaborative Research Centre SFB/TR 63 InPROMPT “Integrated Chemical Processes in Liquid Multiphase Systems” coordinated by the Berlin Institute of Technology and funded by the German Research Foundation.

References

C.H. Bischof, H.M. Bücker, B. Lang , A. Rasch and A. Vehreschild, 2002, Combining Source Transformation and Operator Overloading Techniques to Compute Derivatives for MATLAB Programs, Proceedings of the (SCAM 2002), 65-72

C.H. Bischof, L. Roh and A. Mauer, 1997, ADIC: An Extensible Automatic Differentiation Tool for ANSI-C ,Software: Practice and Experience,1427-1456

G. Buzzi-Ferraris, BzzMath: Numerical libraries in C++ , Politecnico di Milano: www.chem.polimi.it/homes/gbuzzi

S.A. Forth, 2006, An Efficient Overloaded Implementation of Forward Mode Automatic Differentiation in MATLAB, ACM Transactions on Mathematical Software, 32, 2, 195-222

A. Griewank, 2009, Complexity of Gradients, Jacobians and Hessians, In: Encyclopedia of Optimization,425-435

A. Griewank and A. Walther, 2008, Evaluating derivatives: Principles and Techniques of Algorithmic Differentiation, SIAM, Philadelphia 2002

S. Kuntsche, T. Barz, R. Kraus, H. Arellano-Garcia, G. Wozny, 2011, MOSAIC a web-based modeling environment for code generation, Computers & Chemical Engineering, 35, 11, 2257-2273

J. Moré, 1990, Acollecion of nonlinear model problems, In: Computational solution of nonlinear systems of equations, 723-762

S. Schlenkrich, A. Walther and A. Griewank, 2006, Application of AD-based Quasi-Newton Methods to stiff ODEs, In: Automatic Differentiation: Applications, Theory, and Implementations, 89-98

J.E. Tolsma and P.I. Barton, 1998, On computational differentiation, Computers & Chemical Engineering, 22, 4, 475-490

S. Vetukuri, L. Biegler and A. Walther, 2010, Industrial & Engineering Chemistry Research, 49, 23, 12004-12013

A. Walther, A. Griewank, 2008, ADOL-C: A Package for the Automatic Differentiation of Algorithms Written in C/C++ Version 2.0.0. Tech. rep., Institute of Scientific Computing, Technische Universität Dresden

I.A. Karimi and Rajagopalan Srinivasan (Editors), Proceedings of the 11th International Symposium on Process Systems Engineering, 15-19 July 2012, Singapore.

Dynamic Model Identification with Uncertain Process Variables using Fuzzy Inference System

Raony M. Fontes[a], Cristiano H. Fontes[a], Ricardo A. Kalid[a]

[a]*Research Group on Measurement Uncertainty at the Federal University of Bahia, Rua Aristides Novis ,nº02, sala 6.1.18, Federação, Salvador CEP 40210-630, Brazil*

Abstract

This paper presents a methodology for the identification of dynamic models using fuzzy logic that considers the inclusion of the measurement uncertainty in the process variables (described by the probability density function) directly in the model structure. The model comprises a type-2 fuzzy inference system, based on Takagi-Sugeno, together with the use of inputs and outputs in the non-singleton form (represented by membership functions) in both antecedent and consequent of each rule. Transformations of possibility measures into probability measures and conversely were also considered. A case study comprising a CSTR was analyzed and the results predicted by the fuzzy model were compared with Monte Carlo simulation. The proposed method presented good performance and provides a potential way to predict the dynamic propagation of measurement uncertainty through the process.
Keywords: Dynamic Identification, Dynamic Uncertainty, Fuzzy Model.

1. Introduction

Among the structures used in the identification of empirical models, particularly for the dynamic case, the fuzzy inference systems [1,2] represent a potential alternative, relatively simple, and provide the possibility of explicit inclusion of measurement uncertainty of process variables directly in the identification problem. The fuzzy inference systems (FIS) can be singleton fuzzification type (SFIS-Singleton Fuzzy Inference System) or non-singleton fuzzification type (NSFIS - Non-Singleton Fuzzy Inference System) [3]. The last case is suitable to cope with measurement uncertainties in the variables. In general, measurement uncertainties are evaluated in the form of probability density functions (pdf) instead of fuzzy sets (possibility distributions). In this case, the use of fuzzy sets represents an alternative to overcome the limits of probability theory and enables the modeling of the uncertainty of measurement [4]. Thus the transformation of probability into possibility, or conversely, provides an interchange between pdf and fuzzy sets. Mauris et al. and Dubois et al. [5,6] present an efficient method to transform the most common pdf's (Gaussian, Uniform, Triangular and Laplace) in a convex membership function called "truncated triangular possibility distribution" (tpd). Mauris et al. [5] also show the uncertainty propagation of input variables, represented by tpd, based on the extension principle [7]. The authors present algebraic equations which provide, in a simplified manner, the parameters of the output variable when it is represented by a linear combination of inputs represented by tpd Ferrero and Salicone [4] propose a new type-2 fuzzy set, RFV (Random Fuzzy Variables), to represent jointly the random and systematic effects on the process measurement. Also based on the type-2 fuzzy sets, a simplified analysis is performed using the law of propagation of uncertainty [8]. Algorithms for model identification have been proposed to incorporate measurement uncertainties in the formulation of the identification problem. Mouzouris and Mendel [3,9] present an application of NSFIS

and show a comparison with the SFIS, both based on the Mamdani structure [10]. Ferrero et al. [11–13] present a modified version of NSFIS capable to use variables in RVF form for use in dynamic identification. This structure does not consider the recurrence of uncertainty in the output variable. A recurring approach must be followed when the dynamic feature of the uncertainty is analyzed [14].This paper presents a methodology for identification of dynamic models based on a type-2 inference system fuzzy with Takagi-Sugeno structure capable to predict the uncertainty in the output variable at each time instant. The model structure comprises the use of non-singleton antecedents and the consequent of each rule is based on a NARX (Nonlinear Auto Regressive with eXogenous inputs) structure in which the input and output variables are represented by fuzzy sets. A continuous stirred tank reactor (CSTR) is adopted as case study. The fuzzy model results were compared with Monte Carlo simulation [14] in order to evaluate the capability of the proposed approach for the predict the dynamic uncertainty.

2. Fuzzy Inference System (FIS) and dynamic uncertainty

In general, the FIS comprise two types of structure (Mamdani and Takagi-Sugeno-TSK). Both structures are formed by rules of type IF-THEN, which represent, the connection of logical propositions by conjunction and implication operators. Unlike the structure of Mamdani, TSK considers a function that relates the output variable of the FIS with inputs [7] in the consequent of each rule.

In this paper we adopted the structure TSK, where the function in the consequent of each rule is a NARX (Nonlinear Auto Regressive with exogenous inputs) model (Eq. (1)), characterized more specifically by an ARX structure with nonlinearity generated by the feedback of the output predicted at previous time.

$$R^i\text{: IF } \tilde{\hat{y}}\left(k-n_y+1\right) \textit{ is } A_{n_y}^i \text{ AND } \tilde{x}_1\left(k-\theta_{x_1}-n_{x_1}+1\right) \textit{ is } B_{1,n_{x_1}}^i \text{ AND ... AND } \tilde{x}_j\left(k-\theta_{x_j}-n_{x_j}+1\right) \text{ é } B_{j,n_{x_j}}^i$$
$$\text{THEN } \tilde{\hat{y}}^i(k+1) = \sum_{m=1}^{n_y} a_{i,m}\cdot\tilde{\hat{y}}(k-m+1) + \sum_{l=1}^{n_{u_1}} b_{l,1}^i\cdot\tilde{x}_1\left(k-\theta_{x_1}-l+1\right) + \sum_{o=1}^{n_{u_j}} b_{o,j}^i\cdot\tilde{x}_j\left(k-\theta_{x_j}-o+1\right) + c_i \quad (1)$$

n_y and n_{x_j} are the number of past values of the output and each input x_j, respectively. θ_{x_j} is the delay from the input j. a_i, $b_{l,1}^i$ and c_i are the consequent parameters. k denotes discrete time samples. $A_{n_y}^i$ and $B_{j,n_{x_j}}^i$ are type-1 fuzzy sets corresponding to the output y and input x_j in the antecedent of rule i, respectively. $\tilde{x}_j$ is the non-singleton fuzzy set for each input j. $\tilde{\hat{y}}^i$ is the non-singleton fuzzy set predicted for each rule i. The final value predicted for to the output is given by equation (2):

$$\tilde{\hat{y}}(k+1) = \frac{\sum_{i=1}^{r}(\omega^i(\tilde{\mathbf{x}}(k))\cdot\tilde{\hat{y}}^i(k+1))}{\sum_{i=1}^{r}\omega^i(\tilde{\mathbf{x}}(k))} \quad (2)$$

where ω^i is the firing-level of rule i, $\tilde{\hat{y}}(k+1)$ is the predicted output (non-singleton) and the $\tilde{\mathbf{x}}(k)$ is the input vector. The data used for identification include measurement uncertainty that was inserted directly in the model. Each input variable was inserted in the antecedents in tpd form [5,6] allowing the direct insertion of the pdf of each input in the model. The truncated triangular possibility distribution (tpd) is a fuzzy set (possibility distribution) directly obtained through the pdf that represents the uncertainty model of the variable.

The law of propagation considers the pdf of each input $\left(g_{\mathbf{X}_1,\ldots,\mathbf{X}_N}(\xi_{1,1},\ldots,\xi_{N,m})\right)$ to obtain the pdf of the output $\left(g_{\mathbf{y}}(\boldsymbol{\eta})\right)$ using the Monte Carlo method (MCM) (Eq. (3)) in order to evaluate its uncertainty [15]. The advantage of this methodology compared to traditional approaches [8] is that it is not limited to linearity of the measurement function, symmetry of the pdf output and the Gaussian behaviour of the variables involved [14].

$$g_y(\boldsymbol{\eta}) = \int \ldots \int \delta\left(\boldsymbol{\eta} - f(\boldsymbol{\xi_1},\ldots,\boldsymbol{\xi_N})\right) \cdot g_{X_1,\ldots,X_N}(\xi_{1,1},\ldots,\xi_{N,m}) d\xi_{1,1},\ldots,\xi_{N,m} \tag{3}$$

$\boldsymbol{\eta}$ are possible values of the measurand $\boldsymbol{y}$, $\boldsymbol{\xi_i}$ are possible values of the input variable $\boldsymbol{X_i}$, f is the multivariate measurement model and $\delta(\cdot)$ denotes the Dirac delta function.
The propagation of dynamic uncertainty through MCM requires, at each time instant, the uncertainties of input variables and process parameters, based on their respective pdf. Thus, the pdf of output variables is obtained, from a measurement function, at each time instant [14].

3. Results

The case studied comprised a typical CSTR that transforms the reagent A into product B through a homogeneous catalysis (liquid phase). The reaction is endothermic and heating is required.
The model comprises a dynamic system with 4 ordinary differential equations (mass balance for reagent and product, energy balance in reactor and energy balance in the jacket) [14]. Uncertainty data for inputs, parameters and outputs are obtained applying MCM using the phenomenological model [14]. These data was used as reference for the identification of the NSFIS. A SISO (single input single output) case was considered. The concentration of the product (C_B) was the output and the flow of catalyst (F_{cat}) was the input. The consequent of each rule is represented by equation (4) ($\theta_{\text{F}_{\text{cat}}} = 0$, and the $n_{C_B} = n_{\text{F}_{\text{cat}}} = 1$).

$$\hat{\tilde{C}}_B^i(k+1) = c_i + b_{1,1}^i \cdot \tilde{F}_{cat}(k) + a_{i,1} \cdot \hat{\tilde{C}}_B(k) \tag{4}$$

$\tilde{F}_{\text{cat}}$ is the fuzzy set (tpd form) associated to the flow of catalyst, $\hat{\tilde{C}}_B$ is the fuzzy set (tpd form) associated to the concentration of the product B predicted by NSFIS.
Two trapezoidal fuzzy sets (high and low) were considered to represent both variables (C_B, F_{cat}) in the antecedents and the fuzzy model comprised 4 rules with 12 parameters.
Figures 1a and 1b present the estimate and the uncertainty of the input and output variables, both obtained through MCM. It was assumed Gaussian behavior over time and the transformation probability-possibility was applied.
According to equation (4), NSFIS identification comprises a nonlinear identification problem. The following objective function was adopted:

$$J = \sqrt{\frac{1}{N}\sum_{k=1}^{N}\left(\bar{y}(k) - \hat{\bar{y}}(k)\right)^2} + \sqrt{\frac{1}{N}\sum_{k=1}^{N}\left(\sigma(k) - \hat{\sigma}(k)\right)^2} \tag{5}$$

N is the number of measurements, $\bar{y}(k)$ and $\sigma(k)$ are the mean and uncertainty of the output at each instant, respectively (both estimated by MCM). $\hat{\bar{y}}(k)$ and $\hat{\sigma}(k)$ are the mean and uncertainty of output predicted by NSFIS at each instant, respectively.
It was applied a perturbation (+150%) in F_{cat}, at time 40 min. However, its uncertainty was not changed, as shown in Figure 1a. This perturbation was propagated to $u_c(C_B^{MCM})$ and the uncertainty of this measurand is changed during the transient (Figure 1b).

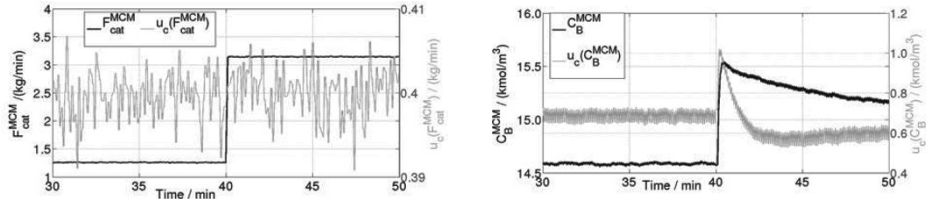

(a) (b)

Figure 1: (a) Flow of catalyst and uncertainty $\left(F_{cat}^{MCM}, u_c(F_{cat}^{MCM})\right)$. (b) Concentration of the product B with uncertainty $\left(C_B^{MCM}, u_c(C_B^{MCM})\right)$ MCM results.

Despite the identification procedure, an initial guess for the parameters was obtained through the linearization of NSFIS considering one-step ahead prediction and singleton variables [7,16].

The figure 2 shows the comparison between the NSFIS and MCM applied to evaluation the dynamic uncertainty. The coverage intervals were calculated considering the same coverage probability (95%) for the NSFIS and the MCM.

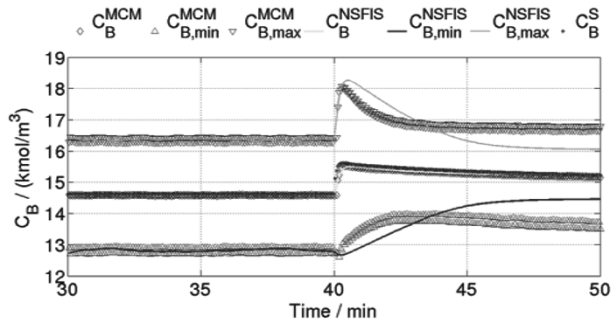

Figure 2: Simulated results (values and limits) predicted by the NSFIS $\left(C_B^{NFIS}, C_{B,min}^{NFIS}, C_{B,max}^{NFIS}\right)$ and the results (values and limits) obtained by MMC $\left(C_B^{MCM}, C_{B,min}^{MCM}, C_{B,max}^{MCM}\right)$ and the measured values for the concentration of the product B $\left(C_B^S\right)$.

The NSFIS has a good performance in the prediction of the concentration of the product B and the model described well the dynamic behavior. The NSFIS has an excellent prediction in the first stationary state ([30, 40[min). However, there was a difference between the NSFIS and MCM results during the transient period ([40 50] min) and also in the secondary stationary state. During the transient, the NSFIS found a longer interval than MCM probably due to the recurrence of predicted values in the NSFIS, i.e., recurrence of model uncertainty. However, in the second state stationary, the NSFIS found a shorter coverage interval than MCM. The causes of these differences are being analyzed.

4. Conclusion

This paper presented a method for predict dynamic systems using a Non-Singleton Fuzzy Inference System (NSFIS), capable to insert the measurement uncertainty of variables directly in the identification problem. A case study comprised a typical CSTR and the results were compared with the Monte Carlo Method (MCM), a well-known approach to predict the uncertainty propagation. The NSFIS represents a potential alternative to predict the dynamic uncertainty of output and can overcome the complex problem of dynamic measurement uncertainty, with a lower computational effort that

MCM. The time of processing of the NSFIS was 0.31×10^4 seconds, while the MCM took 1.09×10^4 seconds, both were processed in a computer with two CPU Intel Xeon E5620 2.4 GHz and 8 Gb of RAM.

Despite the restrictions associated to the transformation approaches of probability-possibility, and conversely, other general procedures can be applied considering any type of non-singleton inputs and the direct application of Extension Principle.

References

[1] L.A. Zadeh, Fuzzy sets, Information and Control. 8 (1965) 338-353.

[2] L.A. Zadeh, Fuzzy sets as a basis for a theory of possibility, Fuzzy Sets and Systems. 100 (1999) 9-34.

[3] G.C. Mouzouris, J.M. Mendel, Nonsingleton Fuzzy Logic Systems: Theory and Application, IEEE Transactions on Fuzzy Systems. 5 (1997) 56-71.

[4] A. Ferrero, S. Salicone, The Random-Fuzzy Variables: A New Approach to the Expression of Uncertainty in Measurement, IEEE Transactions on Instrumentation and Measurement. 53 (2004) 1370-1377.

[5] G. Mauris, V. Lasserre, L. Foulloy, A fuzzy approach for the expression of uncertainty in measurement, Measurement. 29 (2001) 165-177.

[6] D. Dubois, L. Foulloy, G. Mauris, H. Prade, Probability-Possibility Transformations, Triangular Fuzzy Sets, and Probabilistic Inequalities, Reliable Computing. 10 (2004) 273-297.

[7] J.M. Mendel, Uncertain rule-based fuzzy logic system: introduction and new directions, 1st ed., Prentice Hall, Upper Saddle River, NJ, USA, 2000.

[8] BIPM, IEC, IFCC, ILAC, ISO, IUPAC, et al., Evaluation of measurement data — Guide to the expression of uncertainty in measurement, Joint Committee for Guides in Metrology - JCGM 100:2008, 2008.

[9] G.C. Mouzouris, J.M. Mendel, Dynamic non-Singleton fuzzy logic systems for nonlinear modeling, IEEE Transactions on Fuzzy Systems. 5 (1997) 199-208.

[10] E.H. Mamdani, Application of Fuzzy Logic to Approximate Reasoning Using Linguistic Synthesis, IEEE Transactions on Computers. C-26 (1977) 1182-1191.

[11] A. Ferrero, S. Salicone, G. Todeschini, Accounting Measurement Uncertainty in Fuzzy Inference, in: Advanced Methods for Uncertainty Estimation in Measurement, 2007: pp. 74 - 79.

[12] A. Ferrero, A. Federici, S. Salicone, A Method for Considering and Processing Measurement Uncertainty in Fuzzy Inference Systems, in: International Instrumentantion and Measurement Techonology Coference, 2009: pp. 5-7.

[13] A. Ferrero, A. Federici, S. Salicone, Instrumental Uncertainty and Model Uncertainty Unified in a Modified Fuzzy Inference System, IEEE Transactions on Instrumentation and Measurement. 59 (2010) 1149-1157.

[14] M.A.F. Martins, R. de A. Kalid, Metodologia para avaliação da incerteza de medição em regime dinâmico de sistemas contínuos, in: XVIII Congresso Brasileiro De Engenharia Química, 2010.

[15] BIPM, IEC, IFCC, ILAC, ISO, IUPAC, Evaluation of measurement data — Supplement 1 to the "Guide to the expression of uncertainty in measurement" — Propagation of distributions using a Monte Carlo method, 1st ed., Joint Committee for Guides in Metrology - JCGM 101:2008, 2008.

[16] R.M. Fontes, I.L.S. Rodrigues, C.H. Fontes, R.A. Kalid, Obtenção de parâmetros ótimos para um modelo dinâmico fuzzy TSK considerando incerteza de medição nas entradas., in: VI Congresso Brasileiro De Metrologia, INMETRO - Instituto Nacional de Metrologia Normalização e Qualidade Industrial, Salvador - Bahia, 2011.

I.A. Karimi and Rajagopalan Srinivasan (Editors), Proceedings of the 11th International Symposium on Process Systems Engineering, 15-19 July 2012, Singapore.

Coalescence Parameter Estimation in Liquid Extraction Column using OPOSPM

Hanin B. Jildeh,[a,b] Menwer Attarakih,[a,c] Hans-Jörg Bart[a,b]*

[a]*Chair of Separation Science and Technology, TU Kaiserslautern*
[b]*Centre of Mathematical and Computational Modelling, TU Kaiserslautern, P.O. Box 3049 - 67653 Kaiserslautern, Germany*
[c]*University of Jordan, Department of Chemical Engineering, 11942 Amman, Jordan*
**Corresponding author's e-mail: bart@mv.uni-kl.de*

Abstract

The One Primary and One Secondary Particle Model (OPOSPM), which is a reduced population balance model, is used to estimate the optimum droplet coalescence parameters using steady state experimental data. The data is obtained from a pilot plant liquid extraction column of 80 mm diameter and 4.4 m height. The OPOSPM model is derived from the Sectional Quadrature Method Of Moments (SQMOM) with two identifiable parameters. These parameters are identified using a weighted nonlinear least square method with simple bounds. In this contribution, different coalescence models and correlations are studied for two different chemical test systems by solving a population balance inverse problem. The estimated droplet coalescence parameters are found to be dependent on the system physicochemical properties at a given rotor speed. After the droplet coalescence parameters had been optimized under specified column operating conditions, the OPOSPM is used effectively in full column simulation. The OPOSPM was found to predict accurately the mean dispersed phase holdup and mean droplet diameter along the extraction column height.

Keywords: Droplet coalescence, Population balance, OPOSPM, Simulation, RDC extraction column.

1. Introduction

Liquid-liquid extraction is considered one of the main important chemical industrial processes. Therefore, mathematical modeling and simulation of liquid extraction equipment is necessary for scale-up, model predictive control and optimization. However, because of their complex hydrodynamics, it is difficult to predict their performance using simple mathematical models owing to the discrete character of the dispersed phase. Hence, droplet population balance model (DPBM) has to be used. This takes into account droplet transport (rise and backmixing), and droplet interactions at macro-scale (droplet breakage and coalescence) and micro-scale (interphase mass transfer).

Due to the lack of experimental data at industrial scale, the only available data are inlet and outlet conditions and few intermediate data along column height. In contrast to previous work, where laboratory scale devices are used, an inverse population balance problem is solved to estimate the coalescence parameters using a pilot scale Rotating Disk Contactor (RDC). This optimization process is now possible from computational point of view by using the One Primary and One Secondary Particle Model (OPOSPM) as an alternative to the full DPBM [1]. The present liquid extraction model captures all the essential physical information contained in the detailed one and still tractable from

computational point of view. The model consists simply of two transport equations: namely, the number and volume concentration continuity equations. The model is derived from the Sectional Quadrature Method Of Moments (SQMOM), where only one primary and secondary particles are used. For reduction purposes, the model has two learning parameters for breakage and coalescence kernels respectively. These values can be easily determined using the full PBM model as an offline reference when the experimental data is not available. This model is considered suitable for online dynamic or steady state simulations, which can be viewed as the solution of an online inverse problem. Once the OPOSPM is learnt (two adjustable parameters are optimized) under specified column operating conditions, it can be used effectively to identify the unmeasured droplet coalescence parameters without significant loss of information.

2. Mathematical Model and Parameter Estimation

2.1. Population Balance Model

The general population balance equation (PBE), which describes hydrodynamics of liquid-liquid extraction columns (LLECs) in a one spatial domain can be written as [2]:

$$\frac{\partial f(\psi)}{\partial t}+\frac{\partial\left[u_y f(\psi)\right]}{\partial z}=\frac{\partial}{\partial z}\left[D_y\frac{f(\psi)}{\partial z}\right]+\frac{Q_y^{in}}{A_c}f_y^{in}(d;t)\delta(z-z_y)+S \tag{1}$$

In this equation f is number density function and (ψ) represents the droplet diameter (d) and the external coordinate at location (z) and time (t). The droplet velocity (u_y) is relative to the column walls. The first term on the right hand side is the droplet axial dispersion characterized by the dispersion coefficient (D_y). The second term is the droplet feed rate to LLEC with volumetric flow rate (Q_y^{in}) that is perpendicular to the column cross-sectional area (A_c) at a location (z_y) with an inlet number density (f_y^{in}). S represents the source term, which expresses the net number of droplets produced by breakage and coalescence per unit volume and unit time.

In practice, the size of equipment in process industries is large enough to prohibit the use of full DPBM given by Eq.(1). This is because the number of equations that have to be solved simultaneously is considerably large, which places a limit on the acceptable computational time. For this reason, the recently developed OPOSPM [1] presents a promising reduced version of Eq.(1):

$$\frac{\partial N}{\partial t}+\frac{\partial(u_y N)}{\partial z}=\frac{1}{A_c}\frac{Q_y^{in}}{\upsilon_{in}}\delta(z-z_y)+K_b(\vartheta(d_{30})-1)\Gamma(d_{30})N-\frac{1}{2}K_c\omega(d_{30},d_{30})N^2 \tag{2}$$

$$\frac{\partial\alpha}{\partial t}+\frac{\partial(u_y\alpha)}{\partial z}=\frac{Q_y^{in}}{A_c}\delta(z-z_y),\quad d_{30,i}=\sqrt[3]{\frac{6}{\pi}\frac{\alpha_i}{N_i}} \tag{3}$$

where υ_{in} is the feed mean droplet volume, the mean-mass droplet diameter (d_{30}) is an adaptive Gauss-Christoffel quadrature node. The breakage and coalescence frequencies are Γ and ω respectively, while ϑ is the mean number of daughter droplets produced by breakage. This model is able to capture the essential physical information contained in the full PBM and is still tractable from computational point of view. The model conserves the total number (N) and volume (α) concentrations of the population by solving directly two transport equations for N and α. For reduction purposes, the model has been expanded by introducing two learning parameters (K_b and K_c) for breakage and coalescence kernels respectively. These values can be easily determined using the full PBM model as an offline reference when the experimental data is not available.

Once the OPOSPM is learnt (K_b and K_c are optimized), it can be used efficiently to solve the inverse problem associated with droplet coalescence parameters without

significant loss of information. For this purpose, popular droplet coalescence models with adjustable parameters are carefully selected from the recent review on this topic by [3]. At this stage, a careful algorithm design is required in order to estimate these parameters with an accepted statistical error. This leads to apply the inverse problem approach to a full pilot plant RDC extraction column of 80 mm diameter and 4.4 m height. The measured dispersed phase holdup and mean droplet diameter at steady state for this column are taken from Garthe (2006) [4].

2.2. Coalescence Models

Despite the intensive work and published literature on population balance equation modeling, there are few studies on optimization packages, which can be used for coalescence parameter identification, when experimental data is available. Such an optimization package should be flexible to accommodate the chemical test system, column internal geometry and direction of mass transfer. In this regard, work is under way to develop such a package. In the present work, five different coalescence models are selected from the literature and are shown in Table 1.

Table 1. Summary of droplet coalescence models with adjustable parameters

(1)	$\omega(d,d',\phi_d)=\left[c_1\frac{\varepsilon^{1/3}}{1+\phi}(d+d')^2(d^{2/3}+d'^{2/3})^{1/2}\right]\times\left[\exp\left(-\frac{c_2\eta_x\rho_x\varepsilon}{\sigma^2(1+\phi)^3}\right)\left(\frac{(dd')}{(d+d')}\right)^4\right]$
(2)	$\omega(d,d',\phi_d)=\left[c_3\frac{\varepsilon^{1/3}}{1+\phi}(d+d')^2(d^{2/3}+d'^{2/3})^{1/2}\right]\times\left[\exp\left(-\frac{c_4\eta_x\rho_x\varepsilon}{\sigma^2(1+\phi)^3}\right)\left(\frac{(d^2+d'^2)\times(d^3+d'^3)}{(dd')\times(d^{2/3}+d'^{2/3})}\right)\right]$
(3)	$\omega(d,d',\phi_d)=\left[c_5\frac{\pi^2}{36}(d\times d')^3\right]+\left[c_6\frac{\pi^2}{6}\left(\frac{d+d'}{2}\right)^2\left\lvert d^3-d'^3\right\rvert\right]$
(4)	$\omega(d,d',\phi_d)=c_7\left(\frac{\pi d^3}{6D_R^3}\right)^{-0.49}We^{-0.51}\phi_d^{\,0.9}Oh^{-0.05}$
(5)	$\omega=c_8\varepsilon^{1/3}d^{7/3}n^2\exp\left(-\sqrt{\frac{We}{8}}\right)\exp\left(-c_9\frac{d^3}{\varepsilon}\right)$

In Table (1), model (1) is the Coulaloglou and Tavlarides (1977) model, which is developed for droplet coalescence in stirred vessel based on the kinetic theory of gases and drainage film theory [5]. Model (2) is due to Sovova, where in this model uses a different formula for the efficiency of collisions, where the coalescence of drops mechanism described by film drainage of Coulaloglou and Tavlarides model (second term) is replaced by a mechanism that is based on collision impact on coalescence efficiency [3]. Casamatta and Vogelpohl in (1985) proposed a semi-empirical model, in which the first term on the right hand side of Model (3) is the coalescence frequency caused by random motion, which is assumed to be proportional to the drop volumes. The second term represents the coalescence induced by difference in rise velocities [3]. A simplified coalescence model, with one adjustable parameter, is proposed by Laso (1986) as shown by model (4) in Table 1 [6]. The last model in Table 1 is due to Lane et al., where this model suggests that the droplet coalescence is related to the rate of binary collisions between droplets moving with a random velocity equal to the turbulent fluctuating velocity of eddies of the same size in the inertial subrange [7].

3. Results and Discussion

The mathematical model described above is programmed using MATLAB to simulate LLECs using the OPOSPM and the detailed DPBM for comparison. For optimization of

coalescence parameters the tolerance was set to 1.00E-6. The optimization algorithm is shown in Figure (1).

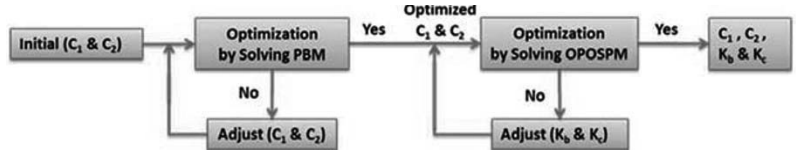

Figure 1: Optimization algorithm

The two EFCE test systems of a two-phase flow, butyl acetate-acetone-water (b-a-w) and toluene-acetone-water (t-a-w) are used. The pilot plant RDC extraction column internal and external geometry are shown in Table 2. The rotor speed is constant at 200 rpm, the volumetric flow rate for continuous and dispersed phase is 40 l/hr and 48 l/hr, respectively for both chemical tested systems.

Table 2. Geometries and specifications of the RDC extraction column

Internal geometry		External geometry	
Compartment height	50 mm	Column height	4.40 m
Internal stator diameter	50 mm	Column diameter	0.08 m
Rotator diameter	45 mm	Inlet of dispersed phase	0.85 m
Rotating shaft diameter	10 mm	Inlet of continuous phase	3.80 m
Relative free cross sectional stator	0.40 m²/m²		

The values of droplet coalescence parameters for different coalescence models (c_1-c_9) are estimated by solving the inverse problem for (b-a-w) and (t-a-w) as shown in Table 3. Using these optimized parameters, the simulated mean dispersed phase holdup and droplet diameter along column height as compared to the experimental data are shown in Figures (2) and (3) for (b-a-w) and (t-a-w) respectively.

Table 3. Optimized coalescence parameters ($c_1 - c_9$)

Liquid System	Coulaloglou & Tavlarides	Sovova	Casamatta & Vogelpohl	Laso	Lane
(b-a-w)	c_1=1.59E-02	c_3=9.15E-03	c_5=4.00E-01	c_7=2.50E-09	c_8=1.00E-09
	c_2=1.33E+10	c_4=8.84E+01	c_6=5.50E-01		c_9=5.49E+06
(t-a-w)	c_1=7.23E-03	c_3=4.02E-03	c_5=4.00E-01	c_7=1.45E-09	c_8=1.00E-09
	c_2=1.33E+10	c_4=1.12E+01	c_6=5.50E-01		c_9=5.49E+06

Note: The learning parameters values for both liquid test systems: K_b= 0.905 and K_c= 0.999.

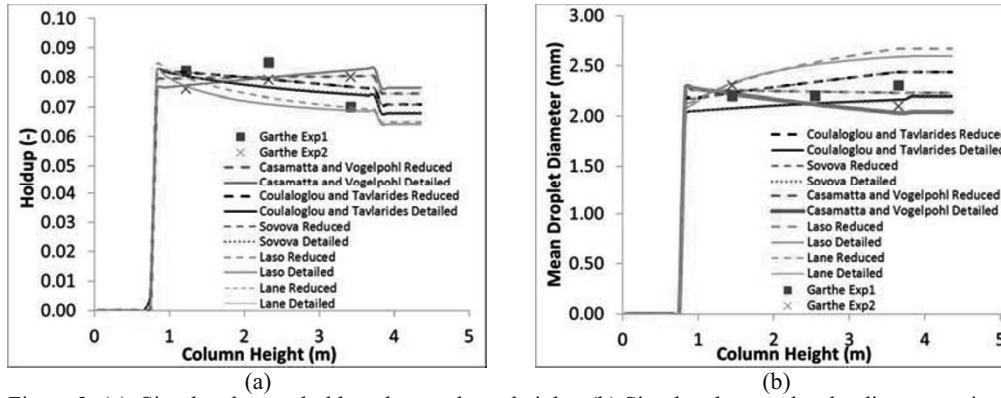

(a) (b)

Figure 2: (a). Simulated mean holdup along column height. (b) Simulated mean droplet diameter using the OPOSPM and the full PBM compared to the experimental data for (b-a-w) system.

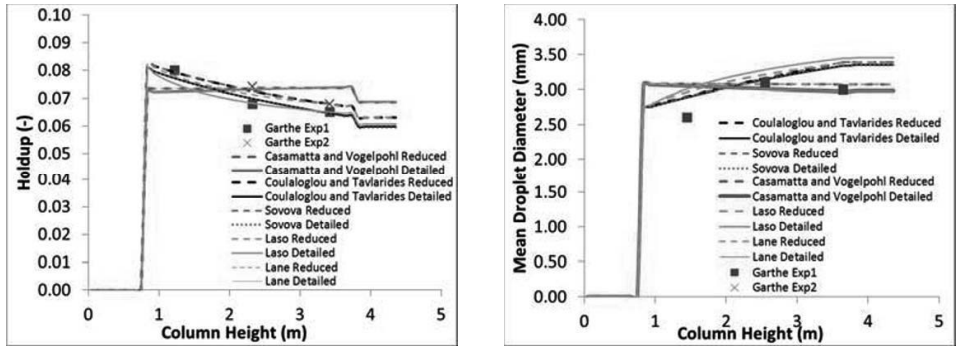

(a) (b)

Figure 3: (a). Simulated mean holdup along column height. (b) Simulated mean droplet diameter using the OPOSPM and the full PBM compared to the experimental data for (t-a-w) system.

By referring to Table 3, two main points are concluded: First, the values for the coalescence parameters are found dependent on the chemical test system. Second, the learning parameters in the reduced model are found insensitive to changes in the chemical test system and constant for this column geometry. Moreover, the reduced model reproduces accurately the information offered by detailed PBE at steady state [8] and dynamic behaviors [9] of Kühni extraction column. Further studies will be done to test the estimated parameters using different operating conditions.

4. Conclusions

In this work the OPOSPM is found to be a promising model for designing, simulating, controlling and optimizing an industrial pilot RDC extraction column when it is learnt using the detailed PBM. It gives a good prediction of the mean dispersed phase holdup and mean droplet diameter along the height of extraction column. The reduced OPOSPM can be used for online predictive control by solving an online inverse problem. From solving the inverse problem, Coulaloglou and Tavlarides model is found to be the best model to describe the coalescence of droplets using two different liquid systems.

Acknowledgements

The authors would like to acknowledge Fraunhofer Institute for Industrial Mathematics ITWM, Centre of Mathematical and Computational Modelling (CM)² and Max Buchner Research Foundation for the financial support.

References

[1] M. M. Attarakih, M. Jaradat, C. Drumm, H.-J. Bart, S. Tiwari, V. K. Sharma, J. Kuhnert and A. Klar, Computer Aided Chemical Engineering, 26 (2009) 1333.
[2] M. M. Attarakih, H.-J Bart and N. M. Faqir, Chemical Engineering Science, 61 (2006) 113.
[3] Y. Liao and D. Lucas, Chemical Engineering Science, 65 (2010) 2851.
[4] D. Garthe, PhD Thesis, Technical University of Munich, Germany (2006).
[5] C. A. Coulaloglou and L. L. Tavlarides, Chemical Engineering Science, 32 (1977) 1289.
[6] G.L. Lane, M.P. Schwarz and G. M. Evans, Chemical Engineering Science, 60 (2005) 2203.
[7] M. Laso, PhD Thesis, ETH Zürich, Zürich (1986).
[8] H. B. Jildeh, M. Attarakih, M. Mickler and H.-J. Bart, Accepted to appear in the proceeding of ESCAPE 22nd, 17-20 June 2012, London/UK (2012).
[9] M. Attarakih, H. B. Jildeh, M. Mickler and H.-J. Bart, Accepted to appear in the proceeding of PSE 11th, 15-19 July 2012, Singapore (2012).

I.A. Karimi and Rajagopalan Srinivasan (Editors), Proceedings of the 11th International Symposium on Process Systems Engineering, 15-19 July 2012, Singapore.

Constraint Programming based Input Signal Design for System Identification

Prakash Kotecha,[a] Mani Bhushan, [b] Ravindra Gudi, [b] Sridharkumar Narasimhan,[c] Raghunathan Rengaswamy [c]

[a]*Department of Chemical Engineering, IIT Guwahati, Guwahati - 781 039, India*
[b]*Department of Chemical Engineering, IIT Bombay, Mumbaii - 400 076, India*
[c]*Department of Chemical Engineering, IIT Madras, Chennai - 600 036, India*

Abstract

The selection of appropriate input harmonics in a multi-harmonic signal for the identification of nonlinear systems leads to a nonlinear, combinatorial optimization problem. Lack of efficient optimization tools for solving such problems had previously led to the development of an explicit Integer Linear Programming (ILP) based lexicographic optimization formulation. However, the dimensionality of such a formulation increases considerably with an increase in the number of frequencies and the problem has been reported to become intractable for higher frequencies. In this article, we demonstrate the ability of Constraint Programming (CP) to efficiently model and solve the original nonlinear problem to guaranteed global optimality. We successfully demonstrate the ability of CP to determine the optimal solutions much faster and also solve problems that have so far remained intractable. In addition, we also show the ability of CP to determine all the multiple optimal solutions and near best optimal solutions in a single optimization run.
Keywords: Input Signal Design, Combinatorial Optimization, Constraint Programming

1. Introduction

The design of input signals for the identification of nonlinear systems is a combinatorial optimization problem and has received considerable attention in literature (Boyd et al., 1983; Chua and Liao, 1989; Schoukens et al., 2002; Evans et al., 1996). For weakly nonlinear systems, it is beneficial to minimize the highest and lowest harmonics of the input signal for system identification. Moreover, the fact that no measurement of the linear kernel can be made below the first harmonic also necessitates the minimization of the first harmonic. The selection of such small yet evenly spaced input set for a higher number of harmonics is considered to be non trivial. Some of the previous research work addressing this problem includes the suggestion to use odd-odd sines or special odd sines (Schoukens et al., 2002). A solution procedure involving the use of several sets of frequencies such that the inter-harmonic distortion between these sets is distinct has also been proposed (Boyd et al., 1983; Chua and Liao, 1989). An intelligent search algorithm has also been proposed (Evans et al., 1996) but this algorithm was not guaranteed to determine the optimal solutions. Recently, an ILP formulation was proposed (Narasimhan and Rengaswamy, 2003) which could be used to solve problems of lower frequencies to global optimality. However, this procedure substantially increases the dimensionality of the problem and was found to be prohibitive for higher frequencies due to a very high computational cost.

From the above discussion, it can be seen that the selection of input harmonics for process friendly system identification is severely hampered by the non availability of a

robust solution technique which can solve the original nonlinear integer programming problem to global optimality. To overcome this drawback, the use of a robust optimization technique that can handle nonlinear constraints without compromising on its ability to reach the optimal solution is required. In this article, we show the ability of Constraint Programming (CP) to solve such nonlinear integer programming problems to global optimality without increasing the dimensionality of the optimization problem. The expressive modeling power of CP combined with strong constraint propagation techniques has helped us to solve the problems which have been previously reported to be intractable in literature. In addition to the determination of the globally optimal solutions, we also show the ability of CP to determine other valued added solutions. The benefits of using CP to solve these optimization problems are demonstrated for determining input harmonics of two different frequencies.

2. Constraint Programming

CP has been developed by the Artificial Intelligence and Computer Science community to solve Constraint Satisfaction Problems (CSPs). In an article (Biegler and Grossmann, 2004) on the future perspective of optimization, logic based methods such as disjunctive programming and CP have been identified as promising techniques for efficiently solving discrete optimization problems. CP has found applications in diverse areas and has enjoyed tremendous success in areas involving combinatorial optimization such as assignment and scheduling problems. For the sake of brevity, only brief descriptions of the various aspects of CP are discussed here. Additional details can be obtained from the literature (Kotecha et al., 2010).

The solution of an optimization problem by CP begins with the conversion of the optimization problem to an appropriate CSP which treats the objective function as a constraint and evaluates the objective function value at every feasible solution. This is followed by the elimination of the infeasible values from the domain of the variables by propagating the set of constraints. In case of problems with only one feasible solution, this initial propagation would lead to the optimal solution. However, if the constraint propagation does not reduce the domains of all variables to singleton, a decision variable is randomly selected and arbitrarily assigned a value from its updated domain. This non deterministic selection of the variable and a value from its domain is often referred to as choice point. After the selection of a choice point, the set of constraints are once again propagated for potentially reducing the domain of the other variables. Additional choice points are made on the other variables whenever necessary throughout the search procedure. This would eventually lead to a situation where either the domain of at least one of the decision variables becomes null or the domain of all the decision variables become singleton. The domain of a decision variable becoming null would indicate that the latest choice point leads to an infeasible solution and necessitates backtracking wherein the value of the latest choice point is revised. On the other hand, if the domain of all the variables becomes singleton it would indicate that a feasible solution has been reached and the bound on the objective function is updated. The choice points that lead to failures are removed from the domain of the decision variables thereby continuously reducing the domain of the variables. This procedure is continued till the complete search space is explored thereby guaranteeing the determination of the globally optimal solution without being trapped at suboptimal solutions.

Two of the most important features of CP are its expressive modeling power and the ability to guarantee the determination of globally optimal solutions even for non-convex

& nonlinear integer programming problems. The expressive modeling power enables the development of compact and "natural" models whereas the domain reduction by constraint propagation ensures the determination of the globally optimal solution without being trapped at local optimal solutions. Additional features like the efficient determination of the multiple solutions and near best solutions makes CP an attractive optimization technique (Kotecha et al., 2010). However, CP requires an explicit optimization framework for the propagation of constraints to reduce the domain of the variables; it may also occasionally require considerable amount of computational resources for the confirmation of the optimal solution as it does not rely on bounds/relaxations or derivative information.

3. Input signal Design – Problem Formulation:

Let the set of distinct harmonics that need to be selected be $S = \{x_1, x_2, ..., x_n\}, x_i \in \mathbb{N}$. The different objectives for the design of a plant friendly input signal are (i) minimization of the lowest harmonic (x_n), (ii) minimization of the highest harmonic (x_1), (iii) ensuring well-spaced grid; this is quantified by minimizing σ where $\sigma = \max_{\forall i=1,...,n-1}(x_{i+1} - x_i) - \min_{\forall i=1,...,n-1}(x_{i+1} - x_i)$. In the formulation next, the set of constraints represented in (2) ensure that the Type II contributions are distinct from the input frequencies whereas the set of constraints represented by (3) and (4) ensure that the Type II contributions are distinct from each other (frequency separation). The constraints in (5) define the bounds and domains of the harmonics. Additional details about the formulation can be obtained from literature (Narasimhan & Rengaswamy, 2006)

$$\min \quad \left\{\lambda_1 x_n + \lambda_2\left(\max_{\forall i=1,...,n-1}(x_{i+1} - x_i) - \min_{\forall i=1,...,n-1}(x_{i+1} - x_i)\right) + x_1,\right\} \tag{1}$$

$$s.t \quad x_k - (x_i + x_j) \neq 0,\ i = 1...,n; j = i,...,n; k = j+1,...,n \tag{2}$$

$$(x_l + x_i) - (x_j + x_k) \neq 0, \begin{cases} i = 1,...,n; j = i+1,...,n; \\ k = j,...,n; l = k+1,...,n \end{cases} \tag{3}$$

$$x_l - (x_i + x_j + x_k) \neq 0, \begin{cases} i = 1,...,n; j = i,...,n; \\ k = j,...,n; l = k+1,...,n \end{cases} \tag{4}$$

$$0 < x_i < x_{i+1} \leq N, \quad i = 1,...,n-1; \quad x_i \in \mathbb{N}, \quad i = 1,...,n \tag{5}$$

In the above equations, N is an upper bound for x_n and is given by $N=kn^2$ and λ_1, λ_2 are lexicographic constants. An optimization procedure based on standard optimization algorithms is not possible because the set of constraints represented in equation (2) to (4) are not in the conventional form. To overcome this issue, the problem was reformulated as an ILP formulation (Narasimhan & Rengaswamy, 2006). Results of this ILP formulation (not presented here) are compared with the results of CP. In addition to the objective function in (1), we will also be using the following objective function with a different precedence ordering

$$\min \quad \left\{\lambda_1\left(\max_{\forall i=1,...,n-1}(x_{i+1} - x_i) - \min_{\forall i=1,...,n-1}(x_{i+1} - x_i)\right) + \lambda_2 x_n + x_1,\right\} \tag{6}$$

The objective function in (1) and (2) will be referred as T1 and T2 respectively.

4. Results & Discussion

The results reported in this section have been generated on an Intel Core Duo CPU 2.00GHz with 3.00GB RAM machine running Windows Vista. ILOG OPL Studio 3.7.1 was used to model both the ILP and CP formulations. The ILP formulations were solved by ILOG CPLEX 9.1 whereas the CP formulations were solved by ILOG Solver 6.1. Additional discussion on the implementation procedures of the various algorithms can be obtained from literature (Kotecha et al., 2010).

Table 1 shows the dimensionality of the explicit ILP and CP optimization formulations. It can be seen that the number of binary variables increases drastically with an increase in the number of frequencies for the ILP formulation whereas the CP formulation does not have any binary variables irrespective of the number of frequencies to be selected. Also, due to the ability of CP to model the min-max constraints directly, the number of integer variables is reduced by 2 when compared with the ILP formulation. It can also be seen that an increase in the number of frequencies leads to a very large increase in the number of constraints for the ILP formulation as compared to the CP formulation.

Table 1: Dimensionality of the ILP & CP formulation

No. of frequencies	No. of binary variables		No. of integer variables		No. of constraints	
	ILP	CP	ILP	CP	ILP	CP
n = 7	252	0	9	7	522	258
n = 10	900	0	12	10	2007	996

The 100% reduction in binary variables and over 50% reduction in the number of constraints in the CP formulation are to be attributed to the highly expressive modeling power of CP.Table 2 shows the computational time required for the determination of a single global optimum solution.

Table 2: Computational performance of ILP & CP formulation

No. of frequencies	Obj. func.	Optimal solution		Computational time (secs)	
		ILP	CP	ILP	CP
n = 7	T1	{7 8 18 31 35 37 40}	{7 8 18 31 35 37 40}	134.6	2.29
	T2	{13 17 25 32 35 41 46}	{13 17 25 32 35 41 46}	31.18	1.12
n = 10	T1	-	{8 14 29 48 53 71 73 80 83 84}	> 24 hrs	6486
	T2	-	{34 36 40 51 60 67 79 89 92 97}	> 24 hrs	1204

For n = 7, it can be seen that CP is able to determine the globally optimal solution much faster than ILP for both the different objectives. For n = 10, it can be seen that ILP was not able to reach the global optimum solution whereas CP was able to determine the globally optimum solution in less than 2 hrs. Table 2 also shows that the time required for determining the optimal solution varies with the precedence ordering of various objectives. The optimal solution obtained in each case has also been shown in Table 2. As expected due to the lexicographic ordering, the solution in T1 (for both n = 7 & n = 10) has a lower highest input harmonic than T2. Similarly, the grid spacing for T2 is better than T1 as minimization of the grid spacing is given a higher precedence.

The objective function in T1 and T2 has only one globally optimum solution and hence CP was able to determine only this solution. To demonstrate that CP is indeed capable of determining all the globally optimal solutions, we solved the optimization problem to minimize the highest harmonic with 10 frequencies. This problem is characterized by

287 multiple solutions but only five of these solutions [{1 14 31 50 56 74 85 90 94 97}, {1 20 32 47 58 76 83 86 92 100}, {1 20 34 50 61 76 86 89 93 98}, {1 20 35 47 64 73 78 86 89 96}, {1 20 37 51 61 66 84 93 96 100}] are reported here for brevity. Table 3 shows the first five best solutions for the objective shown in T1 which prioritizes the minimization of the highest harmonic followed by grid spacing and the lowest harmonic respectively. For n = 7, it can be seen that the first solution has the lowest harmonic whereas the next four solutions have identical highest harmonic but the grid spacing increases. Between the last two solutions which have identical highest harmonic and grid spacing, the solution with objective function value 76240 is prioritized over 76253 as it has a smaller lowest harmonic. Thus it can be seen that CP can help in identifying value added solutions which can help the designer in making informed choices.

Table 3: Near best solutions:

No. of frequencies	Objective function value	Input harmonics	Grid spacing
n = 7	74483	{7 8 18 31 35 37 40}	12
	76121	{11 16 23 31 37 40 41}	7
	76211	{ 15 17 27 33 36 40 41}	9
	76240	{1 10 16 29 34 37 41}	10
	76253	{14 16 19 23 29 40 41}	10
n = 10	697250	{8 14 29 48 53 71 73 80 83 84}	18
	706531	{7 20 29 32 62 66 67 77 83 85}	29
	713456	{16 30 33 42 57 67 78 80 85 86}	14
	721725	{4 13 28 42 48 64 75 82 85 87}	14
	722005	{11 20 32 39 57 73 81 83 86 87}	17

In this article, we have shown that CP is suitable for solving combinatorial problems arising in system identification: in addition to determining globally optimal solutions, it can also be used to determine value added solutions and help in making informed decisions. Future work can potentially include exploring various multiple objectives without assigning any precedence ordering to the objectives.

References

Narasimhan, S., Rengaswamy, R., 2006, Multiobjective input design for system identification – frequency selection for identification of nonlinear systems, 14th IFAC Symposium on System Indetification, Newcastle, Australia

Schoukens, J., R. Pintelon, and T. Dobrowiecki, 2002, Linear modeling in the presence of nonlinear distortions. IEEE Transactions on Instrumentation & Measurement, 51,4, p.786-792.

Boyd, S., Y. Tang, and L. Chua, 1983, Measuring Volterra kernels, IEEE Transactions on Cicuits and Systems,30,8, p.571-577.

Chua, L.N.O. and Y. Liao, 1989, Measuring volterra kernels (II). International Journal of Circuit Theory and Applications, 17, 2, p. 151-190.

Evans, C., Rees, D., Jones, L., Weiss, M., 1996, Periodic signals for measuring nonlinear volterra kernels. IEEE Transanctions on Instrumentation & Measurement, 45, 2, p. 362–371.

Grossmann, I.E. and L.T. Biegler, 2004, Part II. Future perspective on optimization. Computers & Chemical Engineering, 28, 8, p. 1193-1218.

Kotecha, P.R., Bhushan, M., Gudi, R.D., 2010, Effcient optimization strategies with constraint programming, AIChE Journal, 56, 2, p. 387-404.

I.A. Karimi and Rajagopalan Srinivasan (Editors), Proceedings of the 11th International Symposium on Process Systems Engineering, 15-19 July 2012, Singapore.

Industry Embedded Training in (Bio)Process Systems

Elaine Martin,[a] Gary Montague,[b] Bryn Jones [c]

[a]EngD Director, [b]Professor of Bioprocess Control, [c]Dean of Postgraduate Studies, Newcastle Univesity, Newcastle-Upon-Tyne, NE1 7RU

Abstract

The traditional doctoral training approach for bioprocess systems engineers has been the conventional University based PhD. In some instances a degree of industrial interaction occurs but the predominant motivator has been academic lead rather than industrial demand. The traditional PhD programme has shortcomings in this context, both in terms of its support for multidisciplinary research and, with its focus on research rather than the researcher, its development of skills and attributes which align to the post-PhD industrial need. In response to industrial demand, a Doctoral Training Centre has been established to both foster multidisciplinary training and ensure the needs of industry are specifically addressed. This paper describes how a fundamentally different approach to doctoral training has been developed and how the academic / industrial collaboration is proving to be successfully changing the nature of the industrial interactive doctoral experience in bioprocess systems engineering.

Keywords: Industrial Training; Bioprocess Systems

1. Introduction

Industry leaders have successfully relied on the implementation of advanced science and technical capability to remain ahead in fields such as drug development and manufacturing. However in the UK for instance, the Sector Skills Council for Science, Engineering and Manufacturing Technologies report stated that over a quarter of bioscience companies do not have sufficient science skills. 39% of bioscience/ pharmaceutical companies have long-term vacancies; with 22% having skill shortages in the science arena (five times that for other sectors). Given the international nature of the sector these shortages are a worldwide constraint. Our objective in terms of the submission and award of an Industry / Government funded Industrial Doctorate programme (EngD) in Biopharmaceutical Process Development was to directly address this shortfall through the training of graduates who have the necessary skills set to address this gap. The key motivation and technical focus of the EngD is the utilization of process systems techniques for process development and improvement. Equally important is the development, in EngD graduates, of the broader skill portfolio required by successful industrial leaders. In meeting these needs the EngD provides in-depth training in research and project management, coupled with business and commercial awareness and is supported by large multinational pharmaceutical companies through to equipment suppliers and SMEs.

Bioprocess development is an activity that can be categorised as data rich and information poor. Whilst fundamental science and engineering knowledge provides some capability in terms of interpretability of results, predicting performance is more difficult given the complex interactions between biological behaviour and bioprocess

engineering environments. Utilising heuristic knowledge from prior process developments goes some way to assisting in predicting likely outcomes, but supporting this with data from experiments throughout the development programme is essential. Data characteristics include high dimensionality arising for example from -omic and spectroscopic devices, varying sampling rates, end point only measurements or time course data. Whilst these data characteristics in themselves raise usage challenges, the predominant problem in bioprocessing is that typically data measurements are a significant, but small subset of all the influencing factors and states of the system. To date the development team has typically relied on their ability, i.e. human understanding, to extract from limited dimensional data and also focus on a snap-shots in time without taking account of previous history or unit-to-unit interactions.

The challenge is how to utilise the information spread across a number of data constructs by extracting pertinent information using appropriate tools in conjunction with heuristic knowledge and fundamental bioscience and engineering knowledge. Consequently the EngD research projects embrace to some degree each of the following elements: *Information Sources:* The forms of knowledge available regarding process behaviour is diverse and includes heuristic experience, fundamental science and engineering and process data encompassing that recoverable from devices now employed as a consequence of the acceptance and growth of measurement technologies through Process Analytical Technology (PAT). *Systems Analysis and Representation*: From the diversity of knowledge structures, process relationships can be captured in a form that can be used for process and product characterisation and subsequent process improvement. This philosophy is at the heart of Quality by Design (QbD). *Enhanced Development and Operation*: To gain benefit in bioprocess development, appropriate process representations need to be exploited within procedures that allow more informed decisions to be made for example in experimental design, scale-up and scale-down techniques, process monitoring approaches and process control methods.

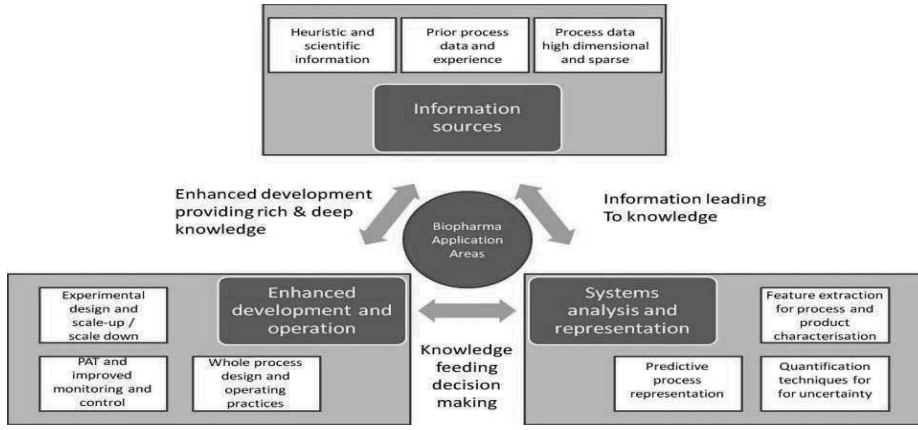

2. Programme Objectives

The ultimate objective of the Centre is to respond to a critical industrial need in bioprocess development and produce Research Engineers who are skilled in research and project management, and who combine technical excellence with a high degree of business awareness. In fulfilling this overarching objective, three sets of sub-objectives

are being addressed, (i) those relating to the training programme, (ii) those relating to industry, (iii) those relating to academia.

With respect to the training programme, the prime objective is to provide EngD students with a unique, well-rounded, multi-disciplinary research training which promotes the development of skills in bioengineering, bioprocessing and biopharmaceuticals. Alongside this technical training, it is important to provide training in the complementary skills and attributes (presentation, project management, inter-personal, business awareness etc.) which will help EngD graduates fulfil their potential and succeed in their research careers.

With respect to industry the objective is to strengthen existing relationships and develop new collaborations between academia and industry and to realize the uptake and exploitation of the research undertaken by the EngD students. It is providing access to a pool of bioscience engineers who enable bio-manufacturing concerns to compete at international levels and importantly also it is ensuring that in the longer-term academic research addresses industrial need.

With respect to academia the objective is to establish the Centre as nationally leading and internationally recognized and for it to be the preferred location for the training of students who have competencies in commercial biopharmaceutical process development with respect to QbD and PAT. To do so it is necessary to further develop the existing collaborations between engineering, biology, computing science and to promote new collaborations that will realize major breakthroughs in the characterization and scale up of emergent technologies

3. Programme Design

To satisfy the programme objectives it has been necessary to adopt a very different approach to doctoral training. In contrast to a standard UK PhD, the three key differentiators are the cohort element, the modular component and the focus on working on industrially shaped research challenges, through which the EngD student develops at first hand the skills necessary to work in an industrial environment. The cohort element is core to the success of the programme as it is the medium through which the students learn how to work in inter-disciplinary teams and with colleagues whom they may not elect to work with. By requiring all students to take a number of compulsory modules, it has enabled a diverse group of engineers, biologists and chemists to address open-ended problems that require them to pool their skills to address the problem. This is a key feature of the taught component and one that industry has strongly advocated as they have clearly stated that PhD students do not have such opportunities.

The opportunity to work within an industrial environment for a significant proportion of the EngD provides students with all round training and exposes them to the constraints imposed by a company's business drivers. It is for this reason that the student has the opportunity to tackle a number of problems within the overarching theme of their research and hence the final output is a thesis by portfolio. This approach enables them to consider transferability of concepts to similar problems and exposes them to different technical areas, providing them with a breadth of experience. Industrial placement also brings management challenges as the placement of EngD's in a company to undertake their research projects necessitates a management structure that ensures the quality of

the research is of a standard commensurate with a PhD and also that students are not facing difficulties out with their control in terms of the execution of their project or on the pastoral side. Rigorous monitoring procedures have been implemented to ensure that any issues are captured early and can be managed appropriately.

The modular component is spread throughout the 4-year duration although there is an exponential drop in the number of modules attended by the students during this period. The taught component of the modular programme was developed through consultation with industry, external academics and other stakeholders including Research Institutes and the bioProcess Knowledge Transfer Network, a Government sponsored community of interested groups. It has thus been tailored to meet the technical challenges of industry alongside ensuring that the programme draws on areas of recognized expertise within Newcastle and satisfies academic quality processes. A degree of flexibility exists in the provision of modules with students able to select ones outside of the course that are specific to their needs but these form a small component of the overall delivery.

An additional feature of this programme is that the modular element is collaborative with other universities. The diversity of the industrially focussed projects necessitates the students studying a range of modules that enable them to tackle the multi-disciplinary nature of their research challenges. Economy of scale is thus an issue and recognising that not all the expertise necessary to deliver key topics resides in one university has resulted in the modular programme becoming collaborative. For example, formulation engineering is not a recognized area of expertise In Newcastle but for some projects the students require knowledge of specific aspects. This issue has been addressed through the setting up of Collaborative Provision with the EngD Formulation Engineering at Birmingham University.

4. Programme Recruitment

Twelve EngD researchers commence their studies annually to address the longer term training requirements of the UK and the industrially embedded nature of the programme serves to deliver research that satisfies industrial need. The EngD students typically spend approximately 75% of their time based in industry over the four years of their study and receive an enhanced stipend when compared to University based doctoral students. It has been essential to link the stipend level to engineering graduate starting salaries in the UK to recruit the required calibre of students.

Working with industry raises a number of challenges including company recruitment, ensuring that the research project is of a standard commensurate with the award of an EngD and intellectual property rights (IPR). The securing of 60 industrially supported projects over a 5-year period is fundamental to the programme. The current economic landscape could potentially impact on company recruitment but the shortfall in trained personnel in the area of the Centre has resulted in this not being an issue to date. Additionally the EngD model is seen by industry as a powerful tool as the student is typically based in the company full-time and thus are exposed to the challenges of working in industry and delivering against medium term goals. This aspect differentiates the students from their PhD counterparts. A further challenge with regard to placements is that they must align with the expectations of the EngD students themselves. This includes identifying whether an SME or large multi-national is more appropriate as the two groups provide contrasting experiences for the students. Student

recruitment is thus intrinsically linked to industrial placements. In summary, the student must satisfy three criteria (i) academic excellence, (ii) ability to work in an industrial environment and (iii) excellent communication skills. This has resulted in the most academically and outfacing students being recruited onto the programme.

The inter-disciplinary nature of the Centre has attracted applications from a range of backgrounds across science and engineering including chemical, process, biochemical and mechanical engineering, biotechnology, biochemistry, biomedical science, drug chemistry, applied biology, pharmaceutical science and mathematics and statistics. The female / male split re applications is 40% /60%. Recruitment statistics differ – cohort 1 comprised 5 females / 2 males whilst this trend was reversed in cohort 2 with the split being 4 females / 8 males. The most recent cohort is 7 males / 5 females. With respect to diversity, there is a significant difference between engineering and science subjects re male/female split, with science being dominated by females. One unique feature is the recruitment of EngD students who have worked in companies and have resigned from their jobs to do the EngD. This is not a feature observed often for PhDs.

The quality of serious applications is approximately a 50/50 split between 1st and 2.1 level degrees or distinction/merit for all 3 cohorts to date. In terms of recruitment, the split has remained consistent at approximately 50/50 re 1st/2.1. The rationale behind this 1st/2.1 split is that in terms of recruitment, we are seeking students who have the academic qualifications, excellent communication skills and who have undertaken additional activities over and above their degree. It is this latter feature that truly differentiates between the students. Unfortunately a significant number of projected 1st class honours students do not fulfil the additional criteria.

5. Concluding Comments

The establishment of the Industrial Doctoral Training Centre has required a fundamental re-appraisal of how industrially collaborative process systems engineering research is undertaken, particularly taking into account training needs and the benefits to the industrial partner. A number of challenges setting up and executing the EngD programme, combining a pedagogical element alongside the requirement to undertake research within an industrial environment arose. Challenges facing such a programme include (i) University procedures and alignment with current quality assurance policies, (ii) industrial participation, and (iii) student recruitment / monitoring. Establishing a set of procedures to ensure the appropriate progression of the individual projects results and making sure that all are adhered to is essential. Indeed, one of the most difficult challenges that was not appreciated at the outset was how only a limited number of academics found the industrial collaborative nature of research to their liking. While the challenges from an academic perspective merit careful attention, the rewards of the EngD programme have proved significant for the University, the company and particularly the student.

Acknowledgements

The authors would like to acknowledge the financial support of the UK Engineering and Physical Sciences Research Council through the Industrial Doctoral Centre in Biopharmaceutical Process Development (EP/G037620/1).

I.A. Karimi and Rajagopalan Srinivasan (Editors), Proceedings of the 11th International Symposium on Process Systems Engineering, 15-19 July 2012, Singapore.

Chemical Engineering Education and Industry Megatrends

Victor Heinänen, Timo Seuranen, Markku Hurme

Aalto University, Department of Biotechnology and Chemical Technology, P.O.Box 16100, FIN-00076 Aalto, Finland

Abstract

The traditional chemical engineering paradigms have been the unit operations approach and later transport phenomena. Most of the education of chemical engineering has been based on these two basic approaches. The question raised is what is the next paradigm and further, how it should be taken into account in the education on chemical engineering? There have been several proposals for the next paradigm, such as process systems engineering, integrated multidisciplinary and multi-scale process engineering, chemical product design and sustainable chemical engineering.

Keywords: Education of chemical engineering, megatrends, paradigms, curriculum

1. Introduction to Paradigms and Megatrends in Chemical Engineering

Paradigm is a constellation that defines a profession and an intellectual discipline (a pattern or model). Commonly recognized paradigms are: *Pre-paradigm* - engineers with no formal education; *0^{th} paradigm* - formal engineering education, end of 1800 (beginning of chemical engineering education, MIT 1888); *1^{st} paradigm* - unit operations, 1908 concept proposed by Arthur D. Little, 1923 first textbook; *2^{nd} paradigm* - transport phenomena, 1960; and *3^{rd} paradigm* - innovative/creative product design/engineering, starting at 21^{st} century. [1], [2]

In the previous century, the generic concepts of "unit operations" and "transport phenomena", often referred to as the first and second paradigm in chemical engineering, were developed. In the 1980's, there were some main innovations e.g. process and heat integration and mass integrations in the plant value chain, also referred as industrial ecology. Now global scales are sought out, greenhouse gases as a topical example.

In the last decade, the design and development of chemicals-based products has been discussed by several authors as the "emerging third paradigm in chemical engineering" [2], [3], [4]. On the contrary, Siirola has made a proposal that an electrically dominated chemical processing could be a new chemical processing paradigm. He also points out that sustainability attributes when selecting and optimizing among alternatives during design are considered but very rarely these same objectives are controlled during operations [5].

Megatrends which have had the largest impact to the field of chemical engineering are the Industrial Revolution (18th Century to the present), WW I and WW II, the post war period (1945-1965), the greatest economic growth, massive inflation during the late sixties and the energy crisis, economic recession of the early seventies, Internet, globalization, green chemistry, LCA and sustainability. In addition, social and political megatrends, e.g. environmental regulations and governance, have also significant impact on the process industry and chemical engineering education. Some of the aforementioned paradigms and megatrends are presented in Figure 1 with US inflation rate, unemployment rate and change of GDP relative to previous year.

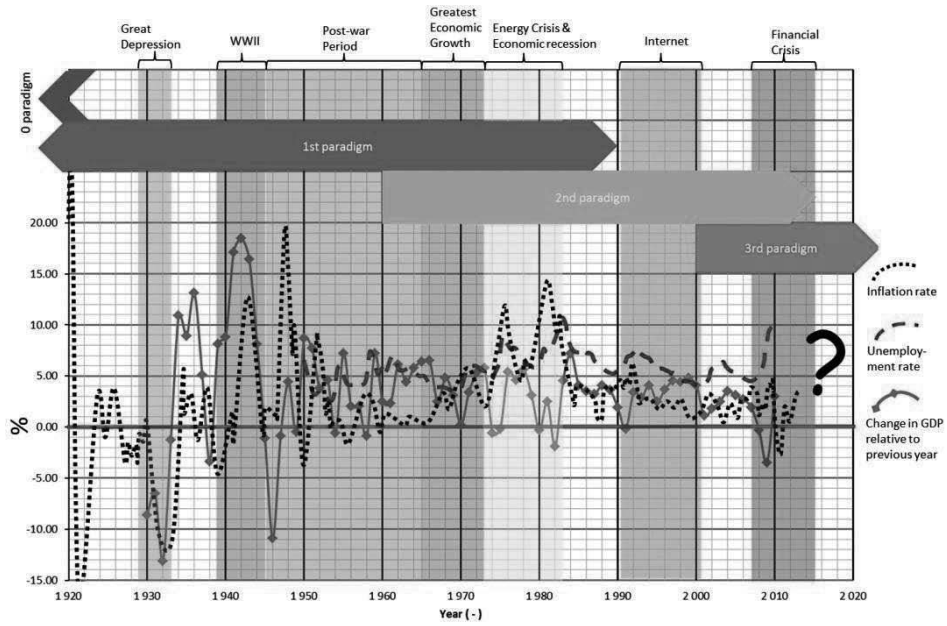

Figure 1. Graph of some paradigms and megatrends. In addition the inflation rate, unemployment rate and change in GDP relative to previous year in USA. [6], [7], [8]

2. Predicting the Future Megatrends and Paradigms

There are many predicting methods which have broad purpose of creating and/or strengthening awareness about the future by offering alternative future images and choices of action based on those images. They are used to generate, present, manipulate, and evaluate information about the future. Qualitative trend-analysis methods such as environmental scanning and monitoring involve keeping track of developments. Naisbitt's Megatrends [9], [10], for example, are based on a form of environmental scanning called content analysis. The approach is based on the premise that a small number of innovators start trends becoming popular with more and more people. Trend analyses share also the assumption that the future will in some way be an extension of the past [11]. Delphi analysis is perhaps the best known qualitative, structured futures method in use today [12]. Scenario development as an aid to planning is focused on developing alternative visions of the future. Visioning exercises typically look farther into the future (i.e., 10 years or more) than other futures methods. Scenario planning (or scenario learning) has proven to be a disciplined method for imagining possible futures in which decisions may be played out, and a powerful tool for asking "what if" questions to explore the consequences of uncertainty [13]. Cross-impact analysis is often thought of as an extension of the Delphi method. It involves identifying and evaluating the impact of trends or events upon each other [14].

The megatrends already playing a role or emerging are in our opinion: the era of (financial) uncertainty, urbanization and demand for municipal water technologies, innovative product development, new energy sources and energy efficiency, and finally generation Y, which is classified as people born between years 1980-2000.

The last few years the economic situation has globally been challenging and stigmatized by miss-trust and uncertainty accompanied with fear of a double-dip. Recent develop-

ment indicates a prolonged era of slow growth and uncertainty. As the population of Earth grows, demand for fresh water and energy increases. This results in to development of innovative new solutions to processes and products. This is suitable for generation Y. This generation has grown up during the ICT revolution and thus is quite familiar with new technologies and media. The generation Y is driven by an urge to change the world.

3. Profile of the Future Chemical Engineering Professional

Factors driving the education of chemical engineering are the changing needs of industry and society. Generally, they are linked to megatrends which have major effects on industry and employment. Much of the manufacturing industry of bulk products has already moved from the traditional industrial countries to developing countries, where the rising markets are. In addition, manufacturing industry has moved to the countries where the raw materials, like the oil, gas, minerals, forest resources and inexpensive labor, exist abundantly. This means the closures of old industrial production sites, such as steel industry in Europe. As a result, a market differentiation has taken place, e.g. Asia has a growing basic chemical industry, America is focusing on biofuels, fertilizer industry and shale gas, Middle East on oil and petrochemical industry and Europe on conglomerates industry.

These issues mentioned above have not been much discussed in the designing of the chemical engineering curriculum. The changes and shifts in megatrends and globalized economics have also been reflected on the labor force. In several industrial countries it has been estimated that an average person changes jobs 5-8 times during the work career. This may involve also changing the profession in some cases. Many of the existing job titles did not exist 30 years ago. Since a career lasts about 40 years or more, it is clear that the life-long learning is essential for chemical engineers, as well as, for chemical engineering curriculum. This has been recognized by many organizations that have developed several forms of part-time education and in-house courses.

The traits of the ideal 2020 worker according to Finnish journalist Petri Korhonen are: entrepreneurial working style (ownership of their work, as if working for themselves, also independence and responsibility), communication and presentation skills (articulates mutual interests and listens to counterparts), self-awareness (recognizing ones strengths and weaknesses, knowing own motivators), extended language portfolio (one or two main languages, such as English and German, and one or two languages of developing economies, such as Polish, Turkish or Spanish), international or ex-pat experience (flexibility, ability to tolerate uncertainty), IT-skills (incl. finding information and social media), general education and awareness (what is in the world news and causalities of global and local events, literature and culture), good overall fitness (coping with stress, better cognitive abilities) and finally, the courage to change ones field of work. [15]

Taking into consideration these traits and demands, the skill profile of the future process engineers can be compiled as in Figure 2. It consists of technical competences, personal characteristics, interactive traits and ability to work as a part of society. Each of these sections can be broken down to more detailed lists of concepts, such as natural sciences, applied engineering sciences and engineering applications. These in turn can also be broken down in individual pieces, such as mathematics, physics and chemistry in natural sciences.

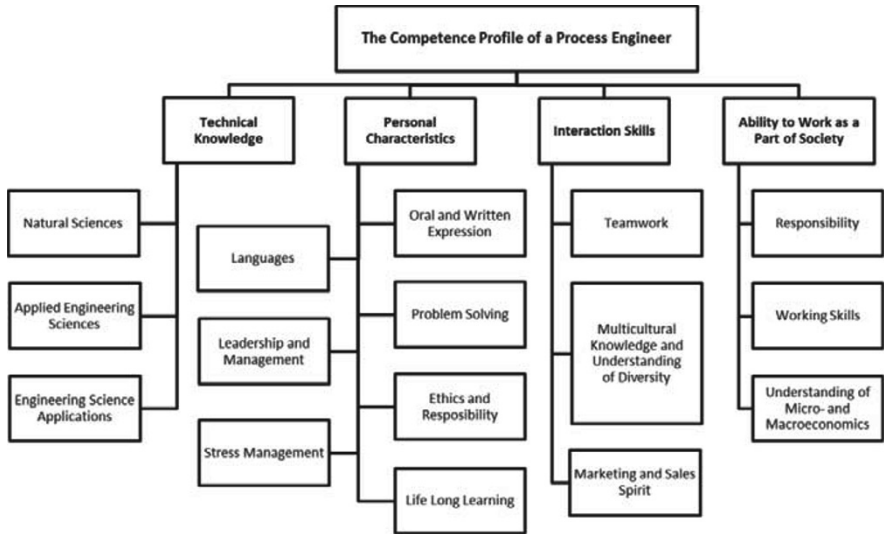

Figure 2. The competence profile of a process engineer.

4. Teaching Chemical Engineers to Face the Challenges of the Future

In recent past, it was adequate to prepare the graduate to a single task or a series of predefined assignments needed in the industry. The industry is now evolving from manufacturing to an information society i.e. an experience society or an adventure society, where the value earning logic of companies depends on innovations and developing new ways of working. The key factor is the ability to evolve and disrupt the daily work routines. In the future, working by the book is a subsiding resource. Strict rules and precise instructions are replaced by vague guidelines. Goals are becoming more abstract. The content and rules of work must be defined in an individual level. [16], [17]

These changing needs of the occidental innovation industry affect the higher education sector dramatically. Combining this with the Y generation, the educational system is forced to change. The best ways of teaching this generation is probably not strict class room discipline and thousand-page books. The video-gaming generations or virtual-life generations are highly skilled in IT, intuitive optimization and learning-by-playing.

Higher education should evolve as the world around it has evolved and embrace new technologies rather than see them as threats. Teaching should consist of design projects, which at best are real life problems from the industry. The design projects (i.e. problem based learning) are the best form of inspiring entrepreneurial attitudes and attributes of participants. Simulators are used too rarely even though they are the everyday tools in the chemical engineer graduates life. In fact, simulators can be associated with an interactive video gaming experience reinforcing the learning experience of theory and enhancing the future engineers' intuitive knowledge. This is especially true to dynamic simulators. Social media and other e-learning possibilities are also used quite rarely. With these the students can learn where ever and whenever they want (this translates to: when they are at their best performance level). At best, e-learning and social media enable mass-customization of courses to the client, namely to the student.

The basic toolbox of an engineer is something, which does not change dramatically in time and is always needed. The tools include technical principles and unit operations, natural sciences (mathematics, thermodynamics, chemistry, physics, etc.) and qualitative and quantitative evaluation. Regulations and laws are always changing and thus

there is no sense in teaching these in more detail than in a nice-to-know basis and the new developments and niche data can be adopted at work and thru life-long learning. Though, the tools are general and must be adopted to each situation. These problem solving skills require sometimes little or even dramatic creativity and innovations.

5. Conclusion and discussions

As the World, with new global connections and dependencies, is changing, the industry is evolving and perceptions of these changing, the knowledge and information needed in succeeding should meet new ways of segmenting education. The skills sought after can be identified as basic engineering skills, ability to life-long learning and skills to adapt and create.

Our claim is that not only the industry is differentiated but also the education should differentiate to comply with the changes of industry and society taking place. For example, the chemical engineering curriculum should be different in industrializing countries than in the traditional industrial countries, since also the industries and work tasks are different. The chemical engineer curriculum in Europe should be focusing on science skills, new product development and creativity whereas Asian chemical engineering education should focus to high-quality engineering and design.

References

[1] E. Favre,V. Falk, C. Roizard, E. Schaer, Trends in chemical engineering education: Process, product and sustainable chemical engineering challenges, Ed. Chem. Eng. 3(2008) 22–27.
[2] S.F. de Azevedo, Towards the European Higher Education Area: Curricula and Methods in Chemical Engineering, Proceedings of European Congress of Chemical Engineering, 2007.
[3] L.T. Biegler, I. E. Grossmann, A.W. Westerberg, Issues and Trends in the Teaching of Process and Product Design, AIChE Journal, Vol. 56 5(2010).
[4] M. Hill, Chemical Product Engineering—The third paradigm, Comp.Chem. Eng. 33(2009) 947–953.
[5] J.J. Siirola, 2011, Chemical Engineering *Megatrends* – Future Challenges and Opportunities, http://www.tnengineering.net/AICHE/Siirola-Megatrends-29sep2011.ppt.
[6] Anon., 2011, Percent Change From Preceding Period in Real Gross Domestic Product, Bureau of Economic Analysis, Avalable from http://www.bea.gov/national/index.htm#gdp
[7] Anon., 2012a, United States Unemployment Rate, Trading Economics, Avalable from http://www.tradingeconomics.com/united-states/unemployment-rate
[8] Anon., 2012b, United States Inflation Rate, Trading Economics, Avalable from http://www.tradingeconomics.com/united-states/inflation-cpi
[9] J. Naisbitt, Megatrends: ten new directions transforming our lives, New York, 1982.
[10] J. Naisbitt, P. Aburdene, Megatrends 2000: ten new directions for the 1990s,New York,1990.
[11] M. Skumanich, M. Silbernagel, Foresighting around the world, Seattle, WA: Battelle Seattle Research Center, 1997.
[12] G. Rowe, G. Wright, The Delphi technique as a forecasting tool: issues and analysis, International Journal of Forecasting 15 (1999) 353–375.
[13] P.J.H. Schoemaker, Scenario planning: a tool for strategic thinking, Sloan Manag Rev, 36 (1995) 25-40.
[14] W. Weimer-Jehle, Cross-impact balances: A system-theoretical approach to cross-impact analysis, Technological Forecasting and Social Change, Volume 73, 4(2006) 334–361.
[15] P. Korhonen, This kind of people succeed (in Finnish), Taloussanomat 22.11.2010, http://www.taloussanomat.fi/tyo-jakoulutus/2010/11/22/tallaisesta-tyypista-tuleemenestyja/201015996/139.
[16] K. Juva, Oivallus, Final report, Confederation of Finnish Industries, Helsinki, 2011.
[17] M. Pajarinen, P. Rouvinen, P. Ylä-Anttila, 2010, Where is value generated? Finland in the Global Economy (in Finnish), Taloustieto Oy, Helsinki, 2010.

I.A. Karimi and Rajagopalan Srinivasan (Editors), Proceedings of the 11th International Symposium on Process Systems Engineering, 15-19 July 2012, Singapore

Use of Podcasts for Teaching Process Control

Srinivas Palanki,*
Department of Chemical & Biomolecular Engineering; University of South Alabama; Mobile, AL, USA

Abstract

In the past decade there has been interest in quantifying teaching effectiveness in technology-mediated lectures in the science, technology, engineering and mathematics (STEM) fields. We developed podcasts for an undergraduate process control course and used two different mechanisms for delivering these lectures. Student performance was assessed via the department's student outcomes assessment procedure for ABET accreditation. It was found that podcasts were an effective tool to prepare students, especially when combined with active learning techniques.

Keywords: podcasts, process control, active learning

1. Introduction

In the past decade there has been interest in quantifying teaching effectiveness in technology-mediated lectures in the science, technology, engineering and mathematics (STEM) fields. The major motivation for these studies is the fact that STEM fields have high attrition rates compared to other fields such as humanities and business. One major reason for high attrition is the fact that most of STEM education is currently delivered via traditional lectures to classes with a large number of students, which affords a very limited amount of exchange of ideas and students have a difficult time grasping the relevance of what they should be learning [Tobias, 1990]. It has been shown that after roughly ten minutes of a typical lecture, about fifty percent of the class is inattentive [Horowitz, 1988]. Many recent studies show that students learn better when they are engaged in an instructor-guided problem-solving environment [Lewis and Lewis, 2005; Moog and Spencer, 2008]. Student performance represents a key aspect of teaching effectiveness and reviews of research comparing the effectiveness of interactive video versus face-toface instruction have found that student achievement in video-enriched courses is the same or better than courses involving face-to-face interaction [Wetzel et al., 1994; Storck and Sproull, 1995]. Webster and Hackley [1997] studied the influence of technology mediated distance learning in a variety of fields and demonstrated both qualitatively as well as quantitatively the benefits of using a media-rich, technologically savvy instruction medium over a conventional chalkboard. Toto and Booth [2008] studied the effects and implications of mini-lectures on learning in a first-semester general chemistry course. In this study, mini-lecture videos on general chemistry topics were prepared and delivered to students in a Web-based format instead of traditional 50 minute lectures three times a week. In each video, one core concept was described. Students with access to these videos scored 11.2% higher than students who attended traditional lectures. In addition, when concepts that were traditionally perceived to be difficult were tested, students who viewed mini-lecture videos scored 21.8% higher than traditional students. This marked improvement clearly shows the potential advantages of web-based videos in teaching STEM concepts. Falconer et

*spalanki@usouthal.edu

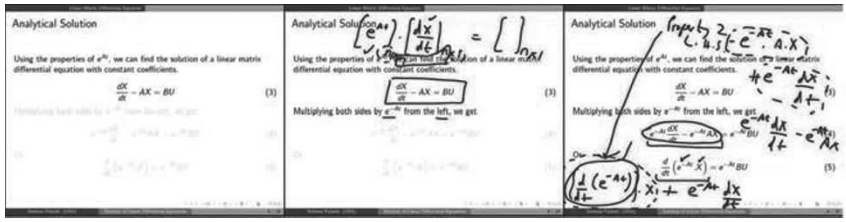

Figure 1. Screenshots of Lecture Video Annotated with Instructor's Comments

al. [2009] implemented this concept of using screencasts in five chemical engineering courses in the University of Colorado. It was observed that a significant majority of the students were in favor of this mode of instruction [e.g. 91% of the graduate reaction engineering class and 83% of the undergraduate material and energy balances class said that screenshots are useful for learning].

2. Development of Podcasts

Pen-tablet technology to annotate slides has been available for the past two decades. The availability of inexpensive desktop-based screen-capture software that is easy to use in the past five years makes it possible to make podcasts. These podcasts provide the look-and-feel of a traditional in-class lecture and when coupled with synchronized audio, allows the instructor to (a) emphasize key points in the lecture and (b) do calculations and derivations on the side using the pen-tablet technology just as he would in a chalkboard. This also makes the lecture more lively and avoids the problem of "death by PowerPoint".

We developed a series of podcasts for a traditional undergraduate process control class. The slides were made using the "beamer" style of LaTeX. Annotations on the slides were made using a Wacom Bamboo tablet and electronic pen as shown in Figure 1. The podcasts were made on a Pentium PC in the instructor's office. The software Camtasia was used to capture the audio and video part of the lecture.

3. Classroom Implementation

Two different approaches were used to test the efficacy of the podcasts in learning: (a) passive learning and (b) active learning. These approaches are described below:

Passive Learning: In Spring 2010, students taking the process control class were given a choice between attending traditional lectures along with access to podcasts or viewing the podcasts on their own without coming to class. In the traditional lecture setting, we used the same slides that were used in the podcasts; however the students had an opportunity to interrupt the lecture and ask questions. They also had access to the podcasts that they could view at their leisure. Students who chose to not attend the traditional lectures had to view the podcasts (which could be rewound and heard multiple times) and then make an appointment to see the instructor if they had questions. Half the class opted to attend the traditional lectures while the other half chose to only view the podcasts. There were very few questions asked on a regular basis during the traditional lecture by students attending the lectures or during office hours by students viewing the podcasts.

Active Learning: In Spring 2011, we used a different approach to encourage students to view the podcasts and ask questions in the process control class. Students were *required* to attend every lecture. However, they were required to view the podcast associated with each lecture, *prior* to attending the class. We divided the class into teams of two students each and we randomly picked the name of a student team out of a cup at the beginning of each class. The team whose name was picked was required to give a 30 minute presentation on that day's lecture material. The team was allowed to use the instructor's slides or could use the chalk board. The instructor (as well as the rest of the class) would assist the student team if they were stuck at any point in the lecture.

4. Assessment

In both semesters the following fixed grading scale was used to assign overall grades in the process control class: F = below 40%, D = 40% to 49%, C = 50% to 69%, B = 70% to 84% and A = 85% to 100%. Student performance was assessed via the department's student outcomes assessment procedure for ABET accreditation. The student outcomes are listed below:
Graduates of the Department of Chemical Engineering at the University of South Alabama will:

1. Have demonstrated knowledge of the mathematical, science, and engineering principles fundamental to the practice of chemical engineering. (a)
2. Be able to design and conduct experiments and analyze and interpret data related to chemical engineering. (b)
3. Demonstrate the ability to accomplish design problems to meet desired needs. (c)
4. Demonstrate an ability to function successfully in a team environment accommodating the contributions of team members having a variety of skills and perspectives. (d)
5. An ability to identify, formulate, and solve chemical engineering problems. (e)
6. Have been encouraged to develop high personal standards of integrity and ethical responsibility. (f)
7. Have demonstrated proficiency in written, graphical, and oral communications. (g)
8. Have a broad enough education to understand the impact of engineering solutions in a global and societal context. (h)
9. Indicate a motivation to continue developing knowledge and skills after graduation. (i)
10. Have knowledge of contemporary issues related to chemical engineering. (j)
11. Demonstrate an ability to use techniques, skills, and modern computational and analytical tools necessary for engineering practice. (k)

Table 1 lists the instruments where each outcome was assessed. It should be noted that some outcomes (e.g. Outcome 1) were assessed in almost all the instruments used in the course (e.g. home assignments, quizzes, tests, final project) while some outcomes (e.g. Outcome 3) were assessed only in a few instruments. For each outcome, a numerical score from 1 to 5 was assigned based on the average performance of the class for that particular outcome. The numerical scores indicated the following assessment: 1 = performance far below expectation, 2 = performance below expectation, 3 = performance meets expectations, 4 = performance exceeds expectations, and 5 = performance far exceeds expectations. The average performance of the class was computed for each outcome and compared with the overall grading scale used in the course and used for assigning the numerical score. For example, the class average for Outcome 1 was 66% in Spring 2010 and this is a C grade in the fixed grading scale described above. Thus Outcome 1 was assigned a numerical score of 3. The departmental objective for accreditation purposes is to get a score of 3 or better for each outcome; otherwise action has to be taken to make changes to the way the course is taught.

Table 1. Assessment Instruments for Student Outcomes

Outcome	Asssessment Tool
1	Home Assignments 2-7, Quizzes 1-2, Tests 1-3, Final Project
2	Laboratory Assignments 1-2
3	Home Assignment 3, Final Project
4	Laboratory Assignments 1-2
5	Home Assignments 2, 3, 6, 7, Quizzes 1-2, Tests 2-3, Final Project
6	Design Project
7	Design Project
8	Home Assignment 1
9	Design Project
10	Home Assignment 1
11	Home Assignments 2, 3, 6, 7, Quizzes 1-2, Tests 2-3, Laboratory 1, Final Project

It was observed that in both 2010 as well as 2011, each outcome received an average score of 3 or higher thereby indicating that the minimum requirement for each outcome in this course was met. Table 2 shows the outcomes assessment results (the maximum score for each outcome is 100%) for Spring 2010 and Spring 2011. It is observed that in each outcome assessed, the Spring 2011 class did much better than the Spring 2010 class. The results of Table 2 are very encouraging as these results clearly show that when students are involved in teaching the lecture, their performance is better. The podcasts were, in general, effective in preparing students to give class lectures. Furthermore, since student teams did not know *in advance* if they would be selected to present in class, all student teams came prepared for every class and this helped ensure that students reviewed the course material at frequent intervals and not just before a test. We are now utilizing this methodology to develop podcasts for teaching nanotechnology concepts in several core engineering courses in Chemical, Mechanical and Electrical Engineering via a project funded by the National Science Foundation.

Table 2. Outcomes Assessment Results

Outcome	Spring 2010	Spring 2011
Outcome 1	66%	80%
Outcome 2	66%	94%
Outcome 3	71%	81%
Outcome 4	59%	94%
Outcome 5	70%	82%
Outcome 6	70%	77%
Outcome 7	70%	82%
Outcome 8	77%	92%
Outcome 9	70%	77%
Outcome 10	77%	92%
Outcome 11	70%	83%

5. Conclusions

Podcasts can be an effective means to enhance the student learning experience. However, the mere availability of podcasts does not necessarily improve student learning. In this paper, it was observed that when podcasts were utilized with active learning techniques, there was a significant improvement in student learning outcomes.

6. Acknowledgment

Funding from the National Science Foundation Grant EEC 1042054 is acknowledged.

References

[1] Falconer, J.L., DeGrazia, J., Medlin, J.W., and Holmberg, M.P., 2009. Using Screencasts in ChE Courses, Chem. Eng. Educ., 43, 4, 302-305

[2] Horowitz, H.M., 1988. Student Response Systems, Proc. 6th Annual Conf. on Interactive Instruction Delivery, Society for Applied Learning Technology, Warrenton

[3] Lewis, S.E., and Lewis, J.E., 2005. Departing from Lectures: An Evaluation of a Peer-led Guided Enquiry Alternative, J. Chem. Educ., 82, 135-139

[4] Moog, R.S., and Spencer, J.N., 2008. POGIL: Process Oriented Guided Inquiry Learning, Oxford University Press, New York

[5] Storck, J., and Sproull, L., 1995. Through a Glass Darkly. What Do People Learn in Videoconferences, Human Communication Research, 22, 197-219

[6] Webster, J., and Hackley, P., 1997. Teaching Effectiveness in Technology-Mediated Distance Learning, Acad. Management J., 40, 6, 1282-1309

[7] Tobias, S., 1990. They're Not Dumb, They're Different: Stalking the Second Tier, Tucson: Research Corporation

[8] Wetzel, C.D., Radkte, P.H., and Stern, H.W., 1994. Instructional Effectiveness of Video Media, Hillsdale, NJ: Erlbaum

I.A. Karimi and Rajagopalan Srinivasan (Editors), Proceedings of the 11th International Symposium on Process Systems Engineering, 15-19 July 2012, Singapore.

Synthesis of Heat-Integrated Resource Conservation Networks

Y. L. Tan[a], D. K. S. Ng[c], M. M. El-Halwagi[b], Y. Samyudia[a], D. C. Y. Foo[c],

[a]*Department of Chemical Engineering, Curtin University Sarawak Campus CDT 250 98009 Miri, Sarawak, Malaysia.*
[b]*Department of Chemical Engineering, Texas A&M University, Jack E. Brown Engineering Building, College Station, TX 77843-3122 USA.*
[c] *Department of Chemical and Environmental Engineering/Centre of Excellence for Green Technologies, University of Nottingham Malaysia, Broga Road, 43500 Semenyih, Selangor, Malaysia.*

Abstract

The current drive towards environmental sustainability, the rising costs of energy, fresh resources as well as waste treatments have forced process industries to pay much attention on the improvement of their processes. Consequently, significant efforts have been devoted to develop systematic techniques for heat conservation and waste reduction. In the past, the synthesis of optimal resource conservation network (RCN) has been dealt independently for single resource. To date, very little has been accomplished on the use of heuristic techniques for simultaneous heat and resource conservation. In this work, a novel methodology is developed for the synthesis of RCN, focusing on simultaneous heat and mass integration. With the newly developed methods, the minimum resources consumption and waste generation can be identified. A case study is utilised to demonstrate the applicability of the methodology.

Keywords: Energy minimisation, resource conservation, waste reduction, simultaneous.

1. Introduction

Process integration has been commonly used as an effective tool for resource conservation and waste reduction. El-Halwagi (2006) defines process integration as *a holistic approach to process design, retrofitting and operation which emphasis the unity of the process*. Process integration can be categorized as *heat integration* and *mass integration*. *Heat integration* is a systematic methodology that provides a global understanding of heat utilization within the process and employs this understanding in identifying the utility targets and optimising heat recovery as well as energy-utility systems (El-Halwagi, 2006). On the other hand, *mass integration* is a systematic approach that provides a fundamental understanding of the global flow of mass within the process and employs the understanding in identifying performance targets and optimizing the generation and routine of species throughout the process (El-Halwagi, 2006). Extensive reviews on energy and mass integration can be found in Furman and Sarhinidis (2002) and Dunn & El-Halwagi (2003).

Most of the studies in the area of process integration have been mainly focused on either heat or mass integration separately. However, in many cases, simultaneous consideration of heat and mass integration is needed. For example, when solvent is utilised in the industry for extraction purpose, heating or cooling is needed to meet the process operating conditions. In such cases, mass and heat management need to be

considered simultaneously as both the quality and temperature of solvent are equally important. In this work, the main objective is to develop a novel methodology to optimize heat-integrated resource conservation network (RCN) using a simultaneous approach of heat and mass integration.

2. Problem Statement

The problem to be addressed is given as follow: Given a process with a set of process sinks j with a given flowrate (G_j), contaminant compositions (C_j) and temperature (T_j), and a set of process sources i which can be consider for in-plant reuse/recycle. Each source is given flowrate (W_i), contaminant composition (C_i) and temperature (T_i). In addition, fresh resources r are readily available to supply to the process sink. Streams mixed from fresh resources and process sources are categorised as hot or cold streams for heat integration. Heat exchangers are used to recover heat from hot streams to cold streams. Heaters and coolers may be used to provide external hot (Q_h) and cold (Q_c) utilities. The objective of the work is to develop a systematic procedure for the synthesis of heat-integrated RCN with minimum total annualized cost (TAC).

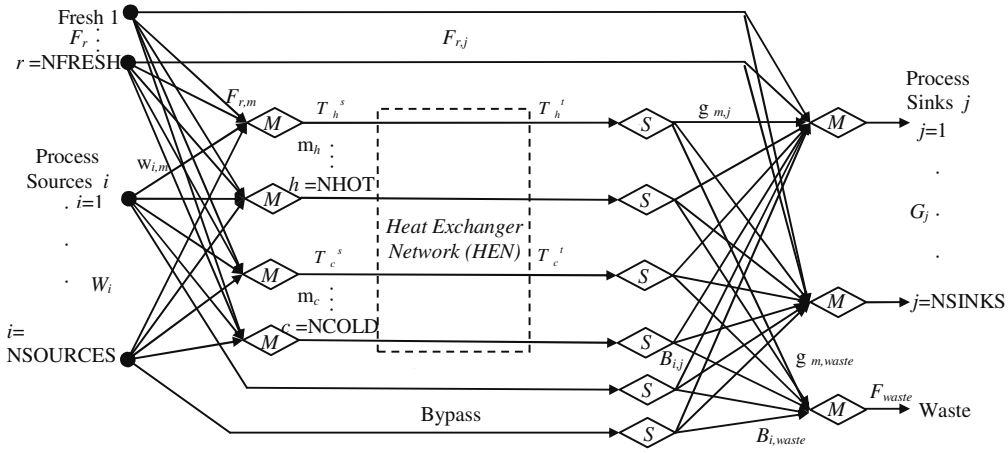

Figure 1: Superstructure of heat-integrated RCN

3. Model Formulation

Based on the problem statement, the optimization problem can be formulated as below:

$$\min_{F_r, Q_h, Q_c} TAC = k * \left\{ \sum_{r=1}^{NFRESH} Cost_r F_r + Cost_h Q_h + Cost_c Q_c \right\} \quad (1)$$

$$s.t.$$

$$HIRCN$$

$$CONSTR$$

where $Cost_r$, $Cost_h$ and $Cost_c$ are the costs of fresh resources, hot and cold utilities. HIRCN is the heat-integrated RCN model and CONSTR is the process constrained imposed in the network optimization. Meanwhile, k is referred to the operating hour per year. In the following section, HIRCN and CONSTR are presented in detail. Based on mass and energy balances of each node in the heat-integrated RCN (Figure 1), HIRCN model can be obtained as follows:

Splitting of fresh sources:

$$F_r = \sum_{j \in NSINKS} F_{r,j} + \sum_{n \in NHOT,NCOLD} F_{r,n} \quad r \in NFRESH \tag{2}$$

where $F_{r,j}$ and $F_{r,n}$ are the flowrate of fresh sources to sink *j* and HEN respectively.

Splitting of process sources:

$$W_i = \sum_{n \in NHOT,NCOLD} w_{i,n} + \sum_{j \in NSINKS} B_{i,j} + B_{i,waste} \quad i \in NSOURCE \tag{3}$$

where $w_{i,n}$, $B_{i,j}$ and $B_{i,waste}$ are the flowrates of source *i* supply to HEN, by-pass of HEN and waste respectively.

Mass balance at the inlet of HEN for hot and cold streams*:*

$$m_n = \sum_{i \in NSOURCES} w_{i,n} + \sum_{n \in NHOT,NCOLD} F_{r,n} \quad n \in NHOT, NCOLD \tag{4}$$

Composition tracking at the inlet of HEN:

$$m_n C_n = \sum_{i \in NSOURCES} w_{i,n} C_i + \sum_{r \in NFRESH} F_{r,n} C_r \quad n \in NHOT, NCOLD \tag{5}$$

where C_n is the contaminant concentration for mixture of source *i* and fresh *r* while C_r is the contaminant concentration if fresh *r*.

Energy balances at the inlet of HEN:

$$m_n Cp_n T_n^s = \sum_{i \in NSOURCES} w_{i,n} Cp_i T_i + \sum_{r \in NFRESH} F_{r,n} Cp_r T_r \quad n \in NHOT, NCOLD \tag{6}$$

where Cp_n, Cp_i and Cp_r are the heat capacities of mixture of source *i* and fresh *r*, source *i* and fresh *r* while T_n^s and T_r are the temperatures of hot and cold stream, and fresh resources, respectively.

Mass balances in the splitting point at the exit of the HEN:

$$m_n = \sum_{j \in NSINKS} g_{n,j} + g_{n,waste} \quad n \in NHOT, NCOLD \tag{7}$$

where $g_{n,j}$ and $g_{n,waste}$ are the flowrate from HEN to sink *j* and waste.

Mass balances at the mixing point before the sinks:

$$G_j = \sum_{n \in NHOT,NCOLD} g_{n,j} + \sum_{i \in NSOURCES} B_{i,j} + \sum_{r \in NFRESH} F_{r,j} \quad j \in NSINKS \tag{8}$$

Composition tracking at the mixing point before the sinks:

$$G_j C_j = \sum_{n \in NHOT,NCOLD} g_{n,j} C_n + \sum_{i \in NSOURCES} B_{i,j} C_i + \sum_{r \in NFRESH} F_{r,j} C_r \quad j \in NSINKS \tag{9}$$

Energy balances at the mixing point before the sinks:

$$G_j Cp_j T_j = \sum_{n \in NHOT,NCOLD} g_{n,j} Cp_n T_n^t + \sum_{i \in NSOURCES} B_{i,j} Cp_i T_i + \sum_{r \in NFRESH} F_{r,j} Cp_r T_r \quad j \in NSINKS \tag{10}$$

where Cp_j and T_n^s are the specific heat capacity for sink and target temperature for hot and cold streams in HEN respectively.

Mass balance of the waste:

$$F_{waste} = \sum_{i \in NSOURCES} B_{i,waste} + \sum_{n \in NHOT,NCOLD} g_{n,waste} \tag{11}$$

CONSTR for the optimization problem is listed as below:

Process Constraints for contaminant concentration (Eq. 12) and temperature (Eq. 13) of process sink *j*:

$$C_j^{\min} \le C_j \le C_j^{\max} \quad j \in NSINKS \tag{12}$$

$$T_j^{\min} \le T_j \le T_j^{\max} \quad j \in NSINKS \tag{13}$$

where $C_j^{\min}, C_j^{\max}, T_j^{\min}, T_j^{\max}$ are the minimum and maximum concentration and temperature of process sink *j*.

Based on the concept of *floating pinch* (El-Halwagi and Manousiothakis, 1990) for mass integration, the following binary integer constraints ($\lambda_{h,p}^t, \lambda_{h,p}^s, \eta_{c,p}^t$ and $\eta_{c,p}^s$) are included in the model.

$$\lambda_{h,p}^t = \begin{cases} 1 \ if \ T_h^t < T_p & h \in NHOT \\ 0 \ if \ T_h^t \ge T_p & p \in NPINCH \end{cases} \tag{14}$$

$$\lambda_{h,p}^s = \begin{cases} 1 \ if \ T_h^s < T_p & h \in NHOT \\ 0 \ if \ T_h^s \ge T_p & p \in NPINCH \end{cases} \tag{15}$$

$$\eta_{c,p}^t = \begin{cases} 1 \ if \ T_c^t < T_p & c \in NCOLD \\ 0 \ if \ T_c^t \ge T_p & p \in NPINCH \end{cases} \tag{16}$$

$$\eta_{c,p}^s = \begin{cases} 1 \ if \ T_c^s < T_p & c \in NCOLD \\ 0 \ if \ T_c^s \ge T_p & p \in NPINCH \end{cases} \tag{17}$$

where, T_p is the potential pinch candidates and is calculated using minimum temperature difference (ΔT_{min}) as follow:

$$T_p = \begin{cases} & h \in NHOT \\ T_h^s - \Delta T_{\min} & c \in NCOLD \\ T_c^s + \Delta T_{\min} & p \in NPINCH \end{cases} \tag{18}$$

where T_h^s and T_c^s are the supply temperature of the hot and cold streams in HEN.

Meanwhile, Q_c can be calculated via Equation 19.

$$\begin{aligned} Q_c \ge & \sum_{h \in NHOT} m_h Cp_h \left\{ \lambda_{h,p}^t (T_p - T_h^t) - \lambda_{h,p}^s (T_p - T_h^s) \right\} - \\ & \sum_{c \in NCOLD} m_c Cp_c \left\{ \eta_{c,p}^s (T_p - T_c^s) - \eta_{c,p}^t (T_p - T_c^t) \right\} \ p \in NPINCH \end{aligned} \tag{19}$$

where m_h, m_c, Cp_c, Cp_h, T_h^t and T_c^t are the flowrate, specific heat capacities and the target temperature for the hot and cold streams in HEN respectively.

The overall energy balance to calculate Q_h is expressed as below:

$$\sum_{h \in NHOT} m_h Cp_h (T_h^s - T_h^t) - \sum_{c \in NCOLD} m_c Cp_c (T_s^t - T_s^s) + Q_h - Q_c = 0 \tag{20}$$

Note that the optimization problem presented above is an MINLP problem. In this work, Extended Lingo v.11 with Global Solver is used to solve the optimization problem.

4. Case Study

A case study of vinyl acetate monomer plant taken from El-Halwagi (2006) is modified and adapted to illustrate the proposed approach. In this case study, $Cost_r$ (fresh acetic acid cost), $Cost_h$ and $Cost_c$ are given as \$0.625/kg, \$3.758/kW.h and 0.005\$/kW.h respectively. In addition, k, ΔT_{min} and all Cp values (Cp_n, Cp_i, Cp_r and Cp_j) are taken as 8000 h/yr, 10°C and 2.5kJ/kg.K respectively. Besides, two hot streams (T_h^s of 360K and 470K with T_h^t of 300K and 370K) and one cold stream (T_c^s of 360K with T_c^t of 460K) are also given. The proposed model is solved in 10s on a PC machine (2.66 GHz, 1GB RAM) and leads to the global optimal solution as presented in Figure 2. The minimum TAC is determined as \$62.7 million/year with the optimal F_r, Q_h and Q_c values of 9633 kg/h, 0 MW and 364.12 MW respectively. For comparison, solving the model with sequential approach (reuse/recycle network followed by HEN) leads to a TAC of \$1,355 million/ year (F_r, Q_h and Q_c values are 9584 kg/h, 43 MW and 372.4 MW respectively) which is much higher than the optimal solution of the proposed model.

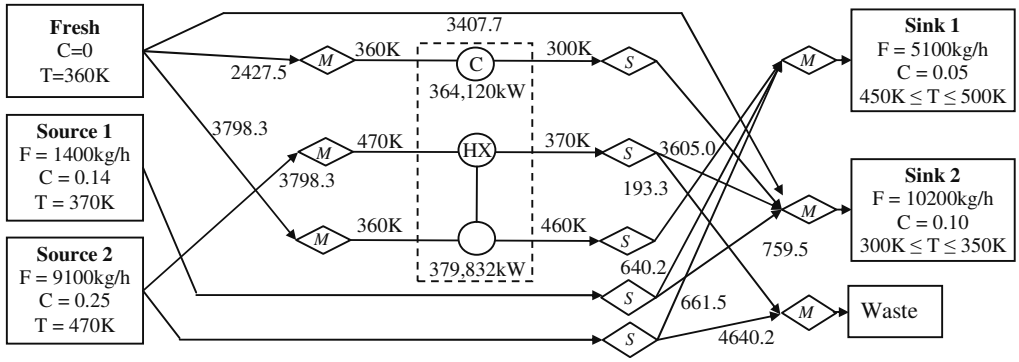

Figure 2: Optimal solution for vinyl acetate monomer plant.

5. Conclusion

In this work, a novel systematic methodology for synthesis of heat-integrated RCN is presented. An MINLP formulation has been developed to identify the minimum TAC of a heat-integrated RCN while satisfy the process constraints. A case study of vinyl acetate plant is solved to illustrate the applicability of the proposed approach.

References

R.F. Dunn, M.M. El-Halwagi, 2003, Process integration technology review: background and applications in the chemical process industry. Journal of Chemical Technology and Biotechnology, 78, 1011–1021

M.M. El-Halwagi, 2006. Process integration,. New York: Academic Press

M.M. El-Halwagi, V. Manousiouthakis, 1990, Simultaneous Synthesis of Mass Exchanger and Regeneration Networks, AIChE Journal, 36, 8, 1209-1219

K.C. Furman, N.V. Sahinidis, 2002, A critical review and annotated bibliography for heat exchengers network synthesis in the 20th century, Ind Eng Chem Res, 41, 10, 2335-2370

I.A. Karimi and Rajagopalan Srinivasan (Editors), Proceedings of the 11th International Symposium on Process Systems Engineering, 15-19 July 2012, Singapore.

Impacts of equipment off-design characteristics on the optimal design and operation of combined cooling, heating and power systems

Zhe Zhou [a], Pei Liu [a,*], Zheng Li [a], Efstratios N. Pistikopoulos [b], Michael C. Georgiadis [c]

[a] *State Key Laboratory of Power Systems, Department of Thermal Engineering, Tsinghua University, Beijing 100084, China*

[b] *Centre for Process Systems Engineering (CPSE), Department of Chemical Engineering, Imperial College London, London SW7 2AZ, UK*

[c] *Department of Chemical Engineering, Aristotle University of Thessaloniki, Thessaloniki 54124, Greece*

** Corresponding author. Email: liu_pei@tsinghua.edu.cn (Pei Liu).*

Abstract

The design and operation of combined cooling, heating and power (CCHP) systems are complicated due to the fluctuating demands that the system faces. Many mathematical models for the design and/or operation of CCHP systems have been developed to obtain better performances of such systems. Most of these models adopt a constant efficiency assumption, while others take equipment off-design characteristics into account. In this paper, we present two mathematical models for the optimal design and operation of CCHP systems with the target of minimizing the total annual cost. For comparison purposes, one model is formulated to represent the performance of a CCHP system running at design conditions, *i.e.*, with constant energy efficiency. In the other model, both the design and off-design characteristics of all key equipments in a CCHP system are considered. These two models were applied to different CCHP systems. Comparative studies of overall costs and operation schedules of different CCHP systems were performed to examine the impacts of equipment off-design characteristics on the optimal design and operation of CCHP systems. Results show that introduction of thermal storage facilities, connection to power grid and a well designed operation strategy can diminish the negative impacts of adopting the constant efficiency assumption.

Keywords: CCHP; off-design; internal combustion engine; absorption chiller

1. Introduction

Combined cooling, heating and power (CCHP) system is broadly regarded as an efficient and economic approach for simultaneous provision of cooling, heating and electricity. CCHP can increase the overall energy efficiency of an energy system by recovering a large proportion of waste heat produced in power generation. However, the expected performance of CCHP cannot be achieved without appropriate combination and operation of machinery, due to the fluctuating heating, cooling and electricity demands that the system faces. Many mathematical models for the design and/or operation of CCHP systems have been developed to obtain a better performance of such systems. A key difference amongst these models lies in their different methods in dealing with the off-design characteristics of equipment. Most models assume that the

efficiency or coefficient of performance (COP) of equipment do not change while operating at off-design levels (Arcuri, Florio et al. 2007; Cho, Mago et al. 2009; Ren and Gao 2010). This assumption can greatly simplify modelling work, but it also leads to less accurate results based on which systems design or operation strategies are made. In some other studies, more complex models are developed considering off-design characteristics of equipment (Li, Nalim et al. 2006). However, these models usually pose significant or even formidable computational challenges due to their nonlinear nature.

In this work, we illustrate the extent of negative impacts of the constant efficiency assumption on the accuracy of CCHP modelling. We present two mathematical models for the optimal design and operation of CCHP systems with the target of minimizing the total annual cost. For comparison purposes, one model is formulated to represent the performance of a CCHP system running at design conditions, *i.e.,* with constant energy efficiency. The other model considers both the design and off-design characteristics of all key equipment in a CCHP system. These two optimization models are applied to configure an optimal CCHP system for a hotel in Beijing. The impacts of equipment off-design characteristics on the optimal design and operation of CCHP systems are discussed based on the modelling results.

2. System configuration of a CCHP system

A typical configuration of CCHP systems is shown in Fig. 1. In the system, internal combustion engines (ICE) are used in the power generation unit (PGU) for simultaneous production of electricity and heat. Recovered heat in the PGU is used to meet the heating and cooling demands together with gas boilers (GB). Cooling demand is met via absorption chillers (AC). When the amount of electricity generated by the PGU is not enough, extra electricity can be drawn from a power grid. A thermal storage unit (TSU) is employed to achieve a proper utilization of energy.

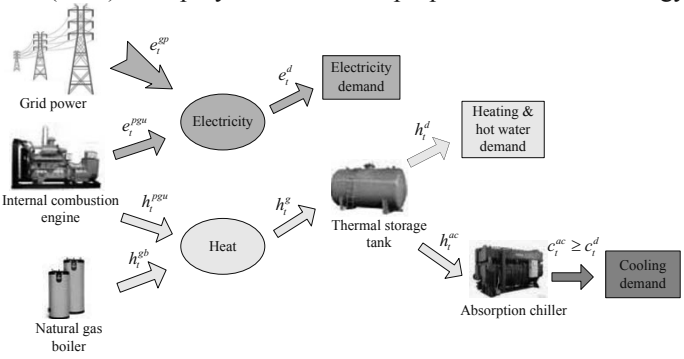

Fig. 1. Energy flow diagram of CCHP system

3. Mathematical formulation of the optimization models

Two mathematical models are developed with the target of minimizing the total annual cost of a CCHP system, covering capital cost, operation and maintenance (O&M) cost and fuel cost. One model adopts the constant efficiency assumption, whilst the other one considers the off-design characteristics of equipment. Equipment performance curves adopted in this study are obtained from (Li, Nalim et al. 2006). Sizes of equipment are standardized thus cannot be changed, but installation of multiple pieces of equipment is allowed.

The model with the constant efficiency assumption is a mixed integer linear programming (MILP) problem, whilst the other is a mixed integer nonlinear programming (MINLP) problem due to nonlinear terms introduced by equipment performance curves. However, this MINLP problem can be converted to a MILP problem through certain linearization techniques. The proposed problems are solved on the platform of GAMS with CPLEX as the MIP solver (GAMS Development Corporation 2008).

4. Case study

The baseline case is a typical hotel in Beijing with an area of 60 thousand square meters. We also include a 30 thousand square meters case and a 90 thousand square meters case for sensitivity analysis. The hourly electricity, heating, cooling and hot water demands of three representative days in winter, summer, and transitional seasons of the baseline case are shown in Fig. 2 (Jin, Zheng et al. 2008).

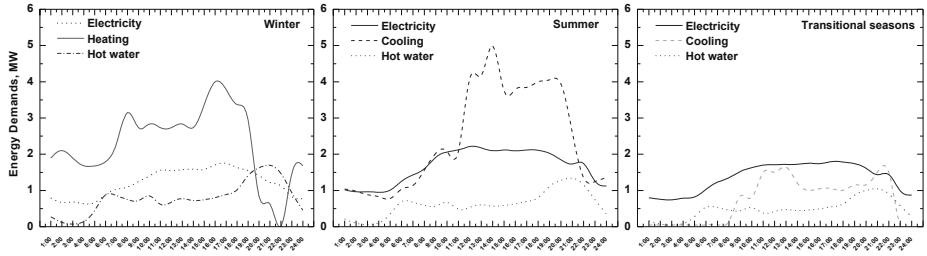

Fig. 2. The energy demands profile of a typical hotel in Beijing

Besides the demands information, both models also require technological and economic information of different technologies, as shown in Table 1, as well as energy prices information as exogenous inputs (Lu 2007; Ren, Zhou et al. 2010). Natural gas price and average time-of-use electricity price are published by Beijing government, 2.05 RMB/m^3 and 0.746 RMB/kWh, respectively (Beijing Municipal Commission of Development & Reform 2011).

Table 1. Technological and economic information of different technologies

Technology	Capacity	Unit capital cost	O&M cost	Lifetime	Rated efficiency
ICE	1.46 MW	5.2 million RMB	72 RMB/MWh	20 yr	41.4%
GB	0.96 MW	0.82 million RMB	2.16 RMB/MWh	20 yr	89.6%
AC	1.3 MW	1.6 million RMB	8 RMB/MWh	20 yr	1.26 (COP)
TSU	-	90.06 RMB/kWh	-	20 yr	90%

5. Results and discussions

The optimal total annual costs generated by both models are presented in Fig. 3. It shows that the constant effiency assumption has a rather small impact on the optimal results, and the relative differences between these two types of models in the three cases are all less than 5 percent. Moreover, the relative difference gets smaller as the building area increases. The reasons for this small difference and the dimishing relative difference are explained next.

5.1. Effect of multiple pieces of equipment

Fig. 4 shows the the joint efficiency curve of a PGU installed with multiple internal combustion engines. If the PGU faces a low electricity demand, only one engine will be employed, therefore it is easy to fall into an inefficiency zone. However, when the electricity demand is large and multiple engines work together to satisfy the large demand, the overall efficiency of the PGU can remain close to its rated efficiency.

The number of equipment pieces adopted in the three cases are listed in Table 2. As a larger building area needs more energy, more equipments are installed, allowing them operating in the efficient zone. The relative gap of the total annual costs provided by two models with different assumptions becomes smaller as the building area increases, because flexibility in opreating multiple equipments can improve the overall efficiency.

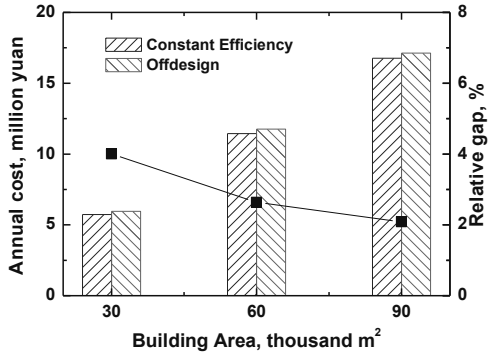

Fig. 3. The total annual costs and relative gaps of the costs generated by two different optimization models

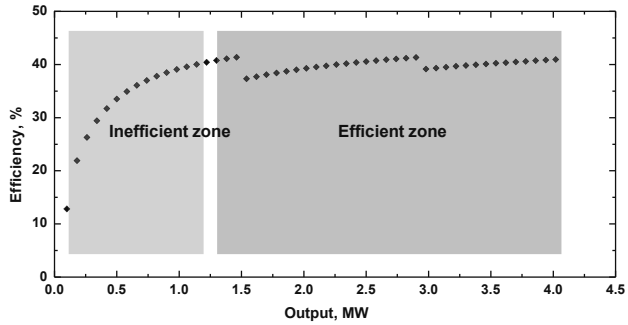

Fig. 4. The joint efficiency curve of a PGU with multiple internal combustion engines

Table 2. The number of equipment pieces employed in three different cases

Building Area, thousand m^2	30	60	90
Gas engine	1	2	2
Gas boiler	1	2	3
Absorption chiller	2	4	6

5.2. Effect of thermal storage and grid connection

The introduction of thermal storage technologies and grid connection can prevent energy generation technologies from operating in the inefficient zone. Thermal storage

technologies can shift extra heat generated during low demand periods for consumption during peak hours. Therefore, energy generation technologies can choose to produce more energy when demand is high and stop working when demand is low. The power grid plays a similar role as an effective electricity storage technology.

5.3. Implications

The aforementioned effects can guarantee that the efficiency of energy generation technologies won't significantly diverge from their rated efficiency. Therefore, the results generated by an optimization model with the constant efficiency assumption are credible. This also indicates that in the planning of a CCHP system, it is desired to employ several small scale equipments instead of only equipment with a large capacity. The introduction of thermal storage and grid connection can also contribute to the improvement of the overall efficiency.

6. Conclusions

The constant efficiency assumption of the optimization model for the design and operation of CCHP systems has a small impact on the optimization results. Multiple pieces of equipment operate together and thermal storage and grid connection can prevent energy generation technologies from working in inefficient zone in a CCHP system. This proves that the results generated by an optimization model with the constant efficiency assumption are credible.

Acknowledgements

The authors gratefully acknowledge the financial support from National Natural Science Foundation (project No. 51106080), from BP company in the scope of the Phase II Collaboration between BP and Tsinghua University, and from the IRSES ESE Project of FP7 (contract No: PIRSES-GA-2011-294987).

References

P. Arcuri, G. Florio and P. Fragiacomo, 2007, A mixed integer programming model for optimal design of trigeneration in a hospital complex, Energy 32(8), 1430-1447.

Beijing Municipal Commission of Development & Reform, 2011, Current Prices for Public Commodities. 2011, from http://www.bjpc.gov.cn/ywpd/wjgl/jgcx/syjg/syjg_ggspxxjg/

H. Cho, P. J. Mago, R. Luck and L. M. Chamra, 2009, Evaluation of CCHP systems performance based on operational cost, primary energy consumption, and carbon dioxide emission by utilizing an optimal operation scheme, Applied Energy 86(12), 2540-2549.

GAMS Development Corporation, 2008, GAMS - A user's guide. 2011, from http://www.gams.com/

H. Jin, D. Zheng and J. Xu, 2008, Distributed combined cooling heating and power system - devices and applications, Beijing, China Electric Express

H. Li, R. Nalim and P. A. Haldi, 2006, Thermal-economic optimization of a distributed multi-generation energy system—A case study of Beijing, Applied Thermal Engineering 26(7), 709-719.

W. Lu, 2007, Optimal Planning of Distributed CCHP System in Urban Energy Environment, Beijing, Graduate School of Chinese Academy of Sciences

H. Ren and W. Gao, 2010, Economic and environmental evaluation of micro CHP systems with different operating modes for residential buildings in Japan, Energy and Buildings 42(6), 853-861.

H. Ren, W. Zhou, K. i. Nakagami, W. Gao and Q. Wu, 2010, Feasibility assessment of introducing distributed energy resources in urban areas of China, Applied Thermal Engineering 30(16), 2584-2593.

I.A. Karimi and Rajagopalan Srinivasan (Editors), Proceedings of the 11th International Symposium on Process Systems Engineering, 15-19 July 2012, Singapore

Storage of Renewable Energies via Chemical Conversion using CO_2: Energy Systems Analysis

Alexander Zinser,[a] * Liisa Rihko-Struckmann,[a] Kai Sundmacher,[ab]

[a] *Max-Planck-Institute for Dynamics of Complex Technical Systems, Magdeburg, Germany*

[b] *Otto-von-Guericke University, Process Systems Engineering, Magdeburg, Germany*

Abstract

Production of fuels from carbon dioxide as carbon source may contribute positively to the global carbon balance. However, technologically, alternative fuels can be produced from CO_2 and, thus, a systematic appoach is needed in order to select the optimal energy carrier in terms of energetical efficiency. The evaluation of the production routes is an excellent task to apply the methods from process systems engineering, e. g. superstructure-based process design (Liu et al., 2011). In this contribution, we present an approach that takes the topology of the process as independent variable. This methodology is applied to the methanation of CO_2 and a comparison of methane and methanol as chemical storage of renewable energy is presented.

Keywords: Process Design, Energy Systems Engineering, Methane, Renewable Energy

1. Introduction

The sequestration of carbon dioxide (CO_2) has been seen as a way to reduce the CO_2 emissions to atmosphere but unfortunately this approach handles the concentrated CO_2 stream only as a waste to dispose. The highly complex CO_2 removal causes significant additional costs and remarkable efficiency deficit for the power plant (Haszeldine, 2009).

Recently, an energetical analysis of the processes, where CO_2 is used as a carbon source for the production of fuels, such as methanol or methane, has been published (Rihko-Struckmann et al., 2010). The reuse of exhaust CO_2 could contribute positively to the global carbon balance.

The renewable wind and solar energy sources suffer from intermittent and fluctuating character, and therefore it is necessary to find an efficient chemical storage for electricity produced from these energy sources. In this contribution we want to assess the potential of competitive production routes to store the electrical energy chemically by applying CO_2 as carbon source in terms of methane (CH_4) or methanol (MeOH). The discussed alternative processes utilise CO_2 from fossil power plants and hydrogen (H_2) produced by electrolysis from renewable energy sources.

The considered overall energy conversion-storage routes are shown in Fig. 1 (left). Fluctuating energy sources are used to produce hydrogen via electrolysis. In the next step, CO_2 is utilised to convert the hydrogen to methane or methanol, which can be stored much easier than hydrogen. In this contribution, we will focus on the conversion of H_2 into methane (1).

$$CO_2 + 4\,H_2 \leftrightarrow CH_4 + 2\,H_2O \qquad \Delta_R H^\circ = -164.7\,\mathrm{kJ/mol} \tag{1}$$

*zinser@mpi-magdeburg.mpg.de

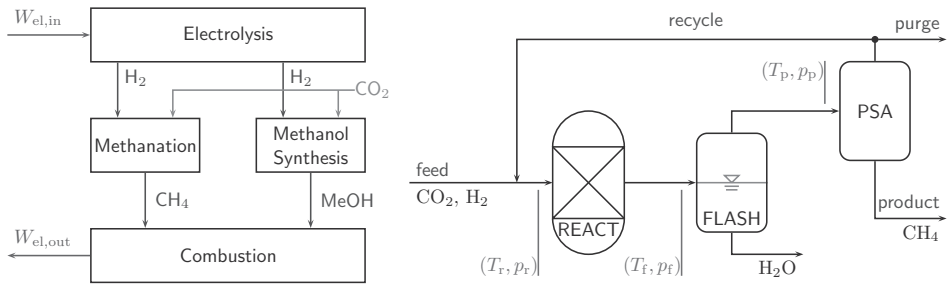

Figure 1. Competitive routes: methane and methanol as chemical storage of renewable energy (left). Basic scheme of the methanation process (right).

2. Methanation Process

A scheme of the overall methanation process is given in Fig. 1 (right). The methanation reaction (1) – originally discovered by Sabatier and Senderens (1902) – is performed in the methanation reactor REACT. Besides methanation, the reverse water-gas-shift reaction (RWGS)

$$CO_2 + H_2 \leftrightarrow CO + H_2O \qquad \Delta_R H^\circ = 41.2\,\mathrm{kJ/mol} \tag{2}$$

is considered. The reaction equilibria assumed to be established at the reactor outlet depend on the operating temperature and pressure.

The resulting mixture of CO_2, H_2, CH_4, H_2O and CO in the outlet stream of the reactor has to be splitted into the product CH_4, the side product water, and a recycle stream. This can be done by a flash evaporation (FLASH) and a downstream pressure swing adsoption unit (PSA).

3. Modeling

The reactor outlet composition is determined at given (T, p) by the Gibbs energy minimization method (Lwin, 2000)

$$\min_{n_i} nG = \min_{n_i} \sum_{i=1}^{N_c} n_i \Delta_f G(T) + RT \sum_{i=1}^{N_c} n_i \ln x_i + RTn \ln \frac{p}{p^\circ} + RT \sum_{i=1}^{N_c} n_i \ln \phi_i \tag{3}$$

subject to $\mathbf{An} = \mathbf{An}^0$ and $n_i > 0 \forall i$ where $\mathbf{A}$ is the atomic matrix that describes the elemental balances of the participating atoms, $\mathbf{n} = [n_1, \ldots, n_{N_c}]^T$ is the vector of moles at equilibrium conditions, and $\mathbf{n}^0$ represents the initial composition of the reactor feed stream.

Fig. 2 (left) shows the temperature-dependent chemical equilibria at $p = 1\,\mathrm{MPa}$ assuming ideal gas behaviour ($\phi_i = 1$) for an initial composition of $n_{CO_2} = 1\,\mathrm{mol}$ and $n_{H_2} = 4\,\mathrm{mol}$,

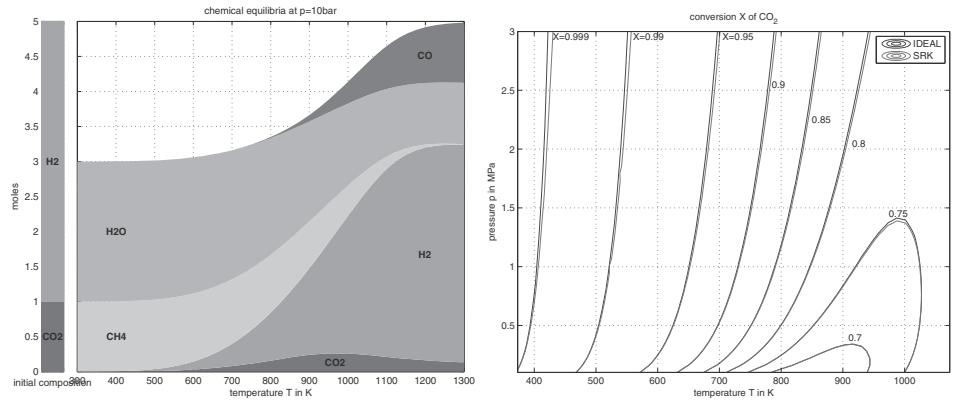

Figure 2. Temperature-dependent chemical equilibria at $p = 1\,\mathrm{MPa}$ (left). Conversion of CO_2 at different temperatures and pressures for the ideal gas law and the Soave-Redlich-Kwong equation of state (right).

respectively. Furthermore, the non-ideality of the system was assessed by use of fugacities calculated from the Soave-Redlich-Kwong (SRK) equation of state (Soave, 1972). The obtained results for ideal as well as non-ideal gas phase behaviour are depicted on the right hand side of Fig. 2. In our study, we fixed the reaction conditions to $T_\mathrm{r} = 450\,\mathrm{K}$ and $p_\mathrm{r} = 1\,\mathrm{MPa}$ and used the ideal gas law for further computations.

The vapor-liquid separation in the flash evaporator is computed by solving the vapor-liquid equilibrium (VLE) condition $x_i\phi_i^\mathrm{L} = y_i\phi_i^\mathrm{V}$ directly using the SRK equation of state. The inlet conditions of the flash were fixed to $p_\mathrm{f} = 0.5\,\mathrm{MPa}$ and $T_\mathrm{f} = 310\,\mathrm{K}$.

The PSA separation was modeled as a simple split fraction unit, where the product stream consists of 99% of the CH_4 at the inlet and 5% of the feed of the other components. The rest of the feed stream is conducted to the recycle stream. The inlet condition of the PSA unit was fixed to be at $T_\mathrm{p} = 310\,\mathrm{K}$ and $p_\mathrm{p} = 0.5\,\mathrm{MPa}$. The outlet streams of the PSA unit were fixed to have a pressure of $p_\mathrm{p}^\mathrm{out} = 0.15\,\mathrm{MPa}$.

The purge gas stream is set to 0.2% of the recycle stream.

4. Optimization

The superstructure of the methanation process is given in Fig. 3. For the inlet streams of the reactor, flash and PSA well defined states (T, p) have to be attained. This can be achieved by a general "state changer" (SC). Three different types of state changer units were defined (Fig. 3, bottom): Type 1 units realize only a pressure change of the system, type 2 and type 3 units realize a change in pressure and temperature. Compared to type 2, the type 3 state changer introduces an additional free continuous variable, the temperature prior to the compression step, which is freely optimizable.

In the case of the methanation process, the state changers SC_1 and SC_5 can be any of the available types (1, 2 or 3), as the outlet temperature is not necessarily fixed. For the

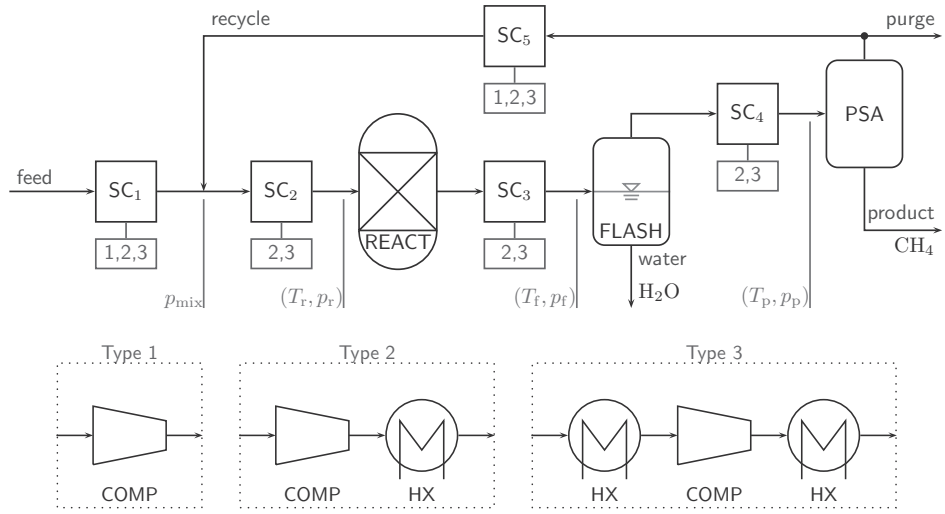

Figure 3. Superstructure of the methanation process and possible types of state changers (top). Different types of the state changers (bottom).

other state changers, the outlet temperature is fixed, because the units REACT, FLASH and PSA are defined to work in a certain state (T, p) as described above.

Each state changer SC_X has to be one of the given types $t_X \in \mathbb{T}_X$ where t_X is the type of state changer SC_X and the sets of possible state changers $\mathbb{T}_X$ are given in Fig. 3 (blue boxes). This leads to $\prod_X |\mathbb{T}_X|$ different process topologies where $|\mathbb{T}_X|$ is the cardinality of $\mathbb{T}_X$.

In general, the optimization task can be formulated as a mixed-integer nonlinear programming (MINLP) problem:

$$\min_{\{c_i\},\{t_X\}} \quad f(W, Q, \{Y_j\}) \qquad \text{s.t.} \quad c_i \in \left[c_i^{\min}, c_i^{\max}\right] \qquad t_X \in \mathbb{T}_X \tag{4}$$

where the objective function f depends on the required electrical work W of the overall process, the required heat duty Q of the process and some additional properties of interest $\{Y_j\}$, e. g. the purity of the product.

Continuous variables c_i are process conditions like temperatures and pressures.

5. Results

In the first study, the objective function includes only the required electrical energy, i. e. $f(W) = W$. The free variables for optimization were the pressure p_{mix} at the point where the feed stream and the recycle stream are mixed, the outlet temperatures $T_{\text{SC}X}$ of the state changers SC_1 and SC_5 and the intermediate temperature $T^{\star}_{\text{SC}X}$ of type 3 state changers.

Table 1. Some selected optimization results for different process topologies. The valid values of the temperatures were limited to the range $T \in [300\,\mathrm{K}, 500\,\mathrm{K}]$.

process topology (t_1,t_2,t_3,t_4,t_5)	continuous variables at optimum p_{mix} [MPa]	$T^{\star}_{\mathrm{SC1}}$ [K]	T_{SC1} [K]	$T^{\star}_{\mathrm{SC2}}$ [K]	T_{SC5} [K]	el. work / heat W [kW]	Q [kW]
(1,2,2,2,1)	0.2513	—	—	—	—	30.7	–169.7
(2,2,2,2,1)	0.3195	—	300	—	—	24.7	–164.6
(2,3,2,2,2)	0.3199	—	316	300	377	24.7	–164.5
(3,3,2,2,2)	0.3165	300	309	300	395	24.8	–164.5

The feed stream of the process was set to a CO_2:H_2 ratio of 1:4 and $9.5\,\mathrm{mol\,H_2\,h^{-1}}$ which corresponds to 1 MW power input into a electrolyzer.

Some selected results of the process optimization are given in Table 1. For a process with a minimum demand of electrical energy, the topology $(t_1,t_2,t_3,t_4,t_5) = (2,2,2,2,1)$ is a good choice.

6. Outlook

In this contribution, we initiated a superstructure based approach for process optimization with regard to the process topology. Next, this methodology will be applied to the methanol synthesis and a systematical comparison of both routes as options for chemical storage of renewable energy will be done.

A previous study already indicated that the efficiency of the overall route (electrical energy $\rightarrow$ chemical storage $\rightarrow$ electrical energy) is around 29% for methane and 18% for methanol (Zinser et al., 2011).

References

Haszeldine, R. S., 2009. Carbon Capture and Storage: How Green Can Black Be? Science 325, 1647–1652.

Liu, P., Georgiadis, M., Pistikopoulos, E., 2011. Advances in Energy Systems Engineering. Ind. Eng. Chem. Res. 50, 4915–4926.

Lwin, Y., 2000. Chemical Equilibrium by Gibbs Energy Minimization on Spreadsheets. Int. J. Engng Ed. 16 (4), 335–339.

Rihko-Struckmann, L., Peschel, A., Hanke-Rauschenbach, R., Sundmacher, K., 2010. Assessment of Methanol Synthesis Utilizing Exhaust CO_2 for Chemical Storage of Electrical Energy. Ind. Eng. Chem. Res. 49, 11073–11078.

Sabatier, P., Senderens, J.-B., 1902. Nouvelles synthèses du méthane. Seances Acad. Sci. 134, 514–516.

Soave, G., 1972. Equilibrium constants from a modified Redlich-Kwong equation of state. Chem. Eng. Sci. 27 (6), 1197–1203.

Zinser, A., Rihko-Struckmann, L., Sundmacher, K., 2011. Energetic Comparison of the Utilization of CO_2 for the Production of Methanol or Methane as a Chemical Storage for Renewable Energy. In: 11^{th} International Converence on Carbon Dioxide Utilization.

I.A. Karimi and Rajagopalan Srinivasan (Editors), Proceedings of the 11th International Symposium on Process Systems Engineering, 15-19 July 2012, Singapore.

Integrated Biomass Power Plant and Storage for Peak Load Management

Wai Shin Ho, Haslenda Hashim*, Zarina A. Muis
Process System Engineering Centre(PROSPECT), Faculty of Chemical Engineering, Universiti Teknologi Malaysia, 81310, UTM JB, Johor, Malaysia

Abstract

This paper presents a simulation based linear programming model of a biomass power plant integrated with energy storage (ES) system for peak load demand management. The integrated biomass power plant using biomass bubbling fluidized bed technology (BBFB) with ES is then compared to a biomass power plant without ES. The results revealed that the integrated BBFB with ES can significantly increase the economics of the system from a total deficit of $195528 (without ES) to a total profit of $227072.70 (with ES) over a 20 years period. The optimum size of BBFB power plant is 140 kW, while the capacity of NaS battery is 257 kWh with a maximum discharge rate (power) of 107.0 kW.

Keywords: *Distributed Generation; Renewable Energy; Biomass; Peak Load Management; Energy Storage*

1. Introduction

Interest in distributed generation (DG) had been proliferating over the decades and Distributed generation (DG) is not new and in fact, the first grid was DG based. This scenario then changes when centralized electricity generation of fossil fuel was found to be more economical. Since then, the development of electricity grids shifted to centralized system. Due to environmental issue, consideration for DG has reemerged with renewable energy (RE) as its generation source. Nevertheless, the economics of the grid is still a major concern. Many researches had been developed to design DG systems especially for rural areas where grid connectivity is not viable. DG system is also one of the most promising ways to transform a specific community to an eco- community. For grid-connected communities, the electricity should be drawn from local power plant to minimize the loss of energy through the transmission line. Most of the researches focused on a hybrid system of RE such as solar, and wind integrated with a back-up generator [1][2]. However, in countries where biomass is found abundant, biomass alone is able to meet the energy demands. Biomass is advantageous to solar and wind due to its constant availability. Nevertheless, similar to any thermal power plant, biomass faces issues on load variation (off peak and peak period) resulting in low capacity factor which leads to higher cost of electricity. As a solution to the mentioned issue, the economics of energy storage (ES) as a tool for peak load management of a biomass power plant is studied for an existing residential community. This study is carried out by developing a simulation base linear programming model which applies the cut and branch algorithm.

2. Distributed Energy System

The amount and type of biomass resources is different at different location and therefore, in order to obtain consistent results, Malaysia is selected as the case study due to abundant biomass resource such as palm oil, rice husk and wood residue. Moreover, the Malaysian Government has been promoting RE utilization through the establishment of feed-in tariff (FIT) policy where a fixed remuneration is provided per kWh of electricity injected to the grid. In this study it is assumed that the government would consider utilizing locally generated electricity without relying on the national grid except during time of maintenances and breakdowns. Biomass bubbling fluidized bed (BBFB) technology with palm kernel shell (PKS) as the biomass fuel source is applied in this study. The main criteria for selecting this setting is due to its low cost compare to other available technology and biomass fuel [3]. For the ES device, sodium sulfur (NaS) is chosen due to its suitability as a bulk storage device and its cheap price compare to other type of batteries.

2.1. Biomass System Design

The system is designed in such that BBFB power plant is the only power generator to meet the system's energy demand while generating excess energy during off-peak period for storage. The accumulated energy in the storage will be regenerated during peak hours depending on economic constraints. The current generated from BBFB power plant is an alternating current (AC) and thus, required to be converted to direct current (DC) for storage, while the energy from storage would be reconverted to AC before delivered to the load. The configuration of the system is as shown in Fig 1.

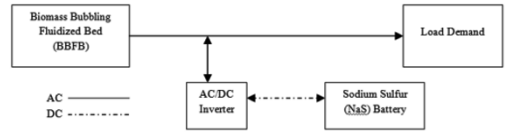

Fig. 1 Configuration of Isolated Biomass System

2.2. Data Collection

Table 1 and Table 2 shows BBFB and NaS battery specification and its cost respectively.and shows.

Table 1. BBFB power plant parameter [3].

Capital cost ($/kW)	Fixed operating and maintenance (O&M) cost ($/kW)	Variable O&M Cost ($/MWh)	Heat rate (GJ/MWh)	PKS fuel price ($/GJ)	Feed-in tariff ($/kWh)
3860.00	100.50	5.00	14.24	1.35	0.11

Table 2. NaS battery parameter [4]

Energy capacity related cost ($/kWh)	Power related cost ($/kW)	Fixed O&M cost ($/kW)	Charging and discharging efficiency (%)	Inverter efficiency (%)	Depth of discharge (%)	Battery life (yr)
346.00	173.00	23	88.3	90	80	10

The simulation based LP model is formulated based on an eco-community of 200 energy consumers with load demand as shown in Fig 2.

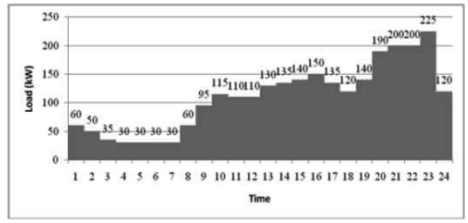

Fig 2 shows the load profile of 200 customers. [5]

3. Mathematical Model

In Malaysia, most of the RE projects are targeted for investors and as such, the objective function built in this model is to maximize the net profit of the system. The variables in this model are as shown in Table 3.

Table 3. List of Variables

Variables	Description
L^B_t	BBFB generation to meet the load at time, *t*
$L^S t$	Power from NaS battery at time, *t*
T^B_t	Total power generated at time, *t*
S^B (integer)	BBFB capacity
S^E (integer)	NaS battery energy capacity
P^E (integer)	NaS battery power
B^E_t	Power generated from BBFB for storage at time, *t*
D^B_t	Excess electricity injected to the grid
E^B_t	Accumulated energy from BBFB in NaS battery

The objective function of the integrated system is given in Eq. 1.

$$Max\ P = P_B - C_{NaS} \tag{1}$$

P_B is net profit from BBFB given by Eq. (2) and C_{NaS} is the cost of NaS battery given by Eq. (3):

$$P_B = \sum_t ((L^B_t + (L^S_t \times n^D \times n^I)) \times d \times f \times FIT) - \sum_t (T^B_t \times d \times f \times (V^B + (U^B \times H^B))) - S^B(C^B + (F^B \times f)) \tag{2}$$

t is the set of time from 1 to 24 hour, including a made-up time, 25 hour; L^B_t, BBFB generation to meet the load at time, *t*; $L^S t$, power from NaS battery at time, *t*; n^D, NaS battery discharging efficiency; n^I, AC/DC converter efficiency (90 %); *d*, amount of day in a year; *FIT*, FIT for biomass electricity generation; T^B_t, total power generated at time, *t*; V^B, BBFB variable O&M cost; U^B, PKS fuel cost; H^B, heat rate of BBFB; S^B, BBFB capacity; C^B, BBFB capital cost; F^B, BBFB fixed O&M cost; *f*, project life (20 yr). From Eq. (2), only utilized biomass energy in meeting the load is considered for remuneration, therefore, instead of the total biomass generation, the amount of direct generation to load plus the discharge of earlier stored energy from NaS battery to load is

equated in Eq. (2). Excess generated energy which is dumped or injected to the national grid in this case is not included for remuneration. This is to illustrate the condition of this case study of not relying on the national grid.

$$C_{NaS} = (S^E \times C^E \times f^{fac}) + (P^E \times PC^E \times f^{fac}) + (P^E \times F^E \times f) \quad (3)$$

S^E is the NaS battery energy capacity; C^E, NaS energy capacity related cost and BoP; P^E, NaS battery power; PC^E, NaS battery power related cost; F^E, NaS battery fixed O&M cost; f^{fac}, life factor of NaS battery life to project life given by Eq. (4**), where** f^E is the NaS battery life. The energy balance model for BBFB, NaS battery, and meeting the load on the other hand is shown in Eq. (5), Eq. (6), and Eq. (7) respectively.

$$f^{fac} = f / f^E \quad (4)$$

$$T^B_t = L^B_t + B^E_t + D^B_t \quad (5)$$

$$E^B_{t+1} = E^B_t + (B^E_t \times n^C \times n^I) - L^S_t \quad (6)$$

$$L^D_t = L^B_t + (L^S_t \times n^D \times n^I) \quad (7)$$

B^E_t is the power generated from BBFB for storage at time, t; D^B_t is excess electricity injected to the grid; E^B_t is the accumulated energy from BBFB in NaS battery; n^C, NaS battery charging efficiency; L^D_t is the load demand of the 200 customers. Several constraints are also developed for the model. To ensure the stability of the battery in a daily cycle basis, the accumulated energy is the storage at time, t = 25 (made-up) must be equal to time, t = 1 as shown in Eq. (8):

$$E^B_{t=25} = E^B_{t=1} \quad (8)$$

Constraint to prevent the accumulated energy in the battery to be more than its capacity (after considering the battery's depth of discharge, D^E) and the discharge rate of the battery to be more than its maximum discharge limit is given in Eq. (9), Eq. (10), and Eq. (12) respectively. In addition, as BBFB technologies in this study uses the steam turbine which require long response time if fluctuation were allowed during power generation. An additional constraint to force the system to generate a constant amount of power is as given in Eq. (11).

$$E^B_t \leq D^E \times S^E \quad (9)$$

$$L^S_t \leq PC^E \quad (10)$$

$$T^B_t = S^B \quad (11)$$

4. Results and Discussions

In this study, mathematical models for integrated biomass with and without energy storage are developed and coded into GAMS. To achieve optimal solution, CPLEX 12 solver which applies the cut and branch algorithm was employed. It was found that the optimum configuration of the BBFB-NaS battery system would generate a total profit of

$227072.70 over 20 years with payback period of 12.38 years. Under this configuration, the required size of BBFB power plant is 140 kW, while the capacity of NaS battery is 257 kWh with a maximum discharge rate (power) of 107.0 kW. For the system without ES, instead of profit, the total deficit calculated is $195528 while the required size of BBFB power plant is 225 kW. This indicates ES can play a significantly role to increase the economics of the system. The energy utilization profile for a) biomass system and b) integrated BBFB and NaS battery system is shown in Fig. 3. It can be seen from this figure that the excess energy generated from the system with ES is less than the system without ES. It is noted that the stored energy as shown in Fig. 3b from time 5:00 to 15:00 and from 16:00 to 19:00 will be utilized to meet the peak demand at night. This study however does not consider energy shortage during maintenances and breakdowns period. Nevertheless, it is recommended that during maintenances and breakdowns period, the electricity supply should be drawn from the national grid.

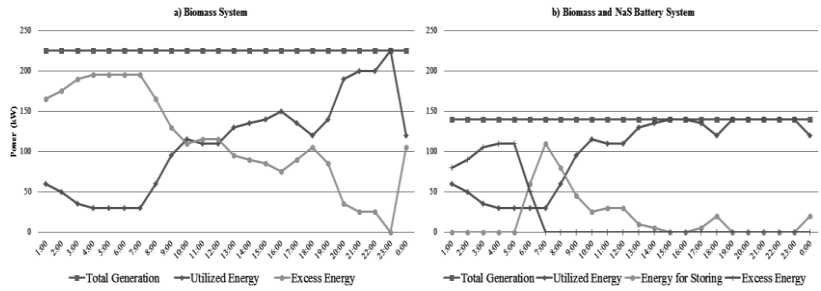

Fig. 3. Power Utilization Trend a) Biomass System b) Biomass and Sodium Sulphur Battery System

5. Conclusion

The simulation based LP model is able to determine the optimal size of integrated biomass power plant with and without ES. The optimization results convinced that ES device can indeed function as a tool for peak load demand management as well as increasing the profit gain from thermal power plant project while improving the stability and reliability of the electricity network.

Acknowledgement

Thanks to UTM, the Ministry of Higher Education (MOHE) and the Science and Technology Research Partnership for Sustainable Development (SATREPS) of the Japan International Cooperation Agency (JICA) for the funding provided.

References

[1] Haidar AMA, John PN, Shawal M. *Optimal configuration assessment of renewable energy in Malaysia*. Renewable Energy 36 p. 881-888; 2011.

[2] Sreeraj ES, Chatterjee K, Bandyopadhyay S. *Design of isolated renewable hybrid power system*. Solar Energy 84, p.1124-1136; 2010.

[3] U.S. EIA. *Updated capital cost estimates for electricity generation plants*. p.115-121; 2010.

[4] Steward D, Saur G, Penev M, Ramsden T. *Lifecycle cost analysis of hydrogen versus other technologies for energy electrical storage*. National Renewable Energy Laboratory, NREL/TP-560-46719. p.36-37; 2009.

[5] Nizar AH, Dong ZY, Zhao JH. *Load profiling and data mining techniques in electricity deregulated market*. IEEE 1-4244-0493-2; 2006.

I.A. Karimi and Rajagopalan Srinivasan (Editors), Proceedings of the 11th International Symposium on Process Systems Engineering, 15-19 July 2012, Singapore.

An optimization procedure for retrofitting process energy systems in refineries

Bingjian Zhang, Shengyuan Wu, Qinglin Chen*

chool of Chemistry and Chemical Engineering, Key Lab of Low-carbon Chemistry & Energy Conservation of Guangdong Province, Sun Yat-Sen University, No. 135, Xingang West Road, Guangzhou, 510275, China

Abstract

An optimization procedure is proposed in this paper for total site energy systems and is applied to industrial refinery complexes based on the insight of process production and energy utilization. Firstly, all process plants in the total site are optimized to target the minimum individual utilities, where processes and HENs are improved for better energy utilization and recovery. As a result, the efficiency of energy utilization is guaranteed for a single plant. Secondly, heat integration between plants is employed to recover surplus heat, which can transfer some heat below the pinch points of supplier plants into other receiver plants to decrease utility requirements. This may not change the first step, but can reduce the cold utilities of the supplier plants and the hot utilities of the receiver plants. Thirdly, low-temperature heat recovery and utilization systems are established with considering the layout and distribution of energy sources and sinks. The recovered low-temperature heat can be used to heat storage tanks and pipelines, preheat boiler feed water, and even to be low-temperature electricity generation. Finally, steam power systems are optimized in the new condition of steam and firedamp balance in the total site. A real industrial example for total site energy optimization is taken to demonstrate the performance of the presented method, and the energy requirement decreases more than 16%.

Keywords: energy system, optimization, heat integration, energy conservation

1. Introduction

Petrochemical industries intend to transform a large amount of crude oils into gasoline, diesel and other chemical pieces to meet the need of people's life while consuming a lot of energy that includes fuels, steam, electricity, etc. China government pays attention to the energy efficiency in such energy-intensive industries. Heat exchanger networks (HENs), heat integration between plants and utility systems are deployed in the total site in order to distribute the energy resources for process operations and to get better energy utilization. Therefore, it is exposed to us how to optimize such a complex energy system for realistic application?

Process synthesis and systematical optimization are effective ways that can be applied in optimizing process energy systems for better energy efficiency and economic benefits. These methodologies and technologies are based on thermodynamics or mathematical programming, and involve heat integration (Zhao, et al. 2006; Verheyen, 2006; Ponce-Ortega, et al. 2008), utility system optimization (Kim, et al. 2001; Luo, et al. 2011), total site integration (Bagajewicz, et al. 2003; Zhang, et al. 2006), and even integration of an industrial area (Matsuda, et al. 2009).

An optimization procedure is proposed in this paper for total site energy systems and is applied to industrial refinery complexes based on the insight of production process and

energy utilization. The optimization procedure is divided into four steps from process optimization to total site integration. A real industrial example for total site energy optimization is taken to demonstrate the performance of the presented method, and the energy requirement decreases more than 16%.

2. The procedure of total site optimization

A refinery is, in general, made up of many process plants, auxiliary plants, storage tanks and utility systems to separate crude oil into specified fuel oils and chemical products. Meanwhile, there are many chemical reactions and separations in refining processes. Therefore, it is very difficult to optimize such a complex process system simultaneously for better energy efficiency. Three link model presented by Hua (2000) decomposes the complex process system into three subsystems: Energy use link, energy recovery link and energy conversion link. The three subsystems are optimized independently, and then coordinated to get a globally optimal result. The optimization procedure is shown as Fig. 1.

An optimization procedure for the energy system in a total site indicated as Fig. 2 is proposed here to extend the three link model. The optimization procedure divides the optimization procedure into four steps. Firstly, chemical reactions and separations are optimized and flowsheets are restructured to decrease the total process energy requirement E_N. Secondly, heat exchanger networks (HENs) and heat integration between processes or plants are deployed to decrease the hot or cold utility demands, in other words, increasing recycled energy E_R. Thirdly, the surplus heat below the pinch points of process plants are collected by medium streams, and then used to keep the fluids in storage tanks at predetermined temperatures or to preheat boiler feed waters in utility systems. As a result, recovered energy export E_E increases. Fourthly, steam power system is optimized to satisfy the new utility requirements of process plants, reducing energy import E_P and decreasing the requirements of primary energy sources, such as fuel oils, firedamp gas, etc. Furthermore, the energy streams saved can be transformed into high value added chemical products.

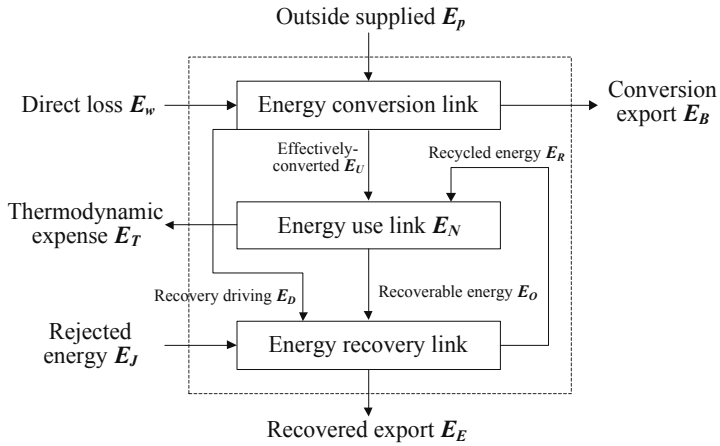

Fig. 1. A diagram of the three link model

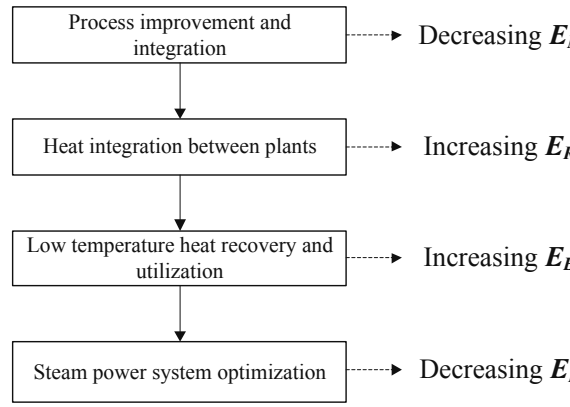

Fig. 2. An optimization procedure for process energy system

2.1. Process improvement and integration

Chemical reactions and separations are the cores of process systems indicated as Union model (Linnhoff, et al. 1982). Therefore, chemical reaction and separation improvements and process flowsheet restructure can essentially reduce the energy requirements of process system. The objective of chemical process optimization is to minimize the total process energy requirement E_N under the condition of satisfying product specifications.

$$\min E_N \tag{1}$$

$$E_N = f(d,z,x) \tag{2}$$

$$h(d,z,x) = 0 \tag{3}$$

$$g(d,z,x) \le 0 \tag{4}$$

Where d is the vector of design variables, z is the vector indicating the structure, and x is the vector of state variables. For example, over-vaporized oil in a vacuum distillation unit (VDU) can be recycled to the vacuum heater to decrease the outlet temperature of the vacuum heater when the distillate rate is kept constant, and then the heat load of the vacuum heater is decreased.

2.2. HEN optimization and heat integration between plants

The optimal chemical processes fix the boundary conditions of all hot and cold streams in plants, and then the maximum recoverable energy E_O is determined. Therefore, HEN optimization can be done in a process plant to reduce the utility requirements, and heat integration between plants can be employed to decrease the cold utility of supply plant and the hot utility of receive plant. More detailed heat integration between plants can be found in the open literatures (Morar, et al. 2010; Zhang, et al. 2011).

2.3. Low-temperature heat recovery and utilization

On the one hand, there is often some surplus heat at a relative low temperature after heat integration between or in process plants. On the other hand, boiler feed water in steam power system and temperature keeping for storage tanks are low-temperature heat sinks in a refinery. Additionally, there is a long distance between utility facilities and process plants. Therefore, a low-temperature heat recovery and utilization system can be introduced after process improvements and heat integration for process plants. A medium stream is employed in the system to collect the surplus heat in process plants

and then to transfer it into storage tank areas or into steam power system. The low-temperature heat recovery and utilization system can be simplified as Fig. 3.

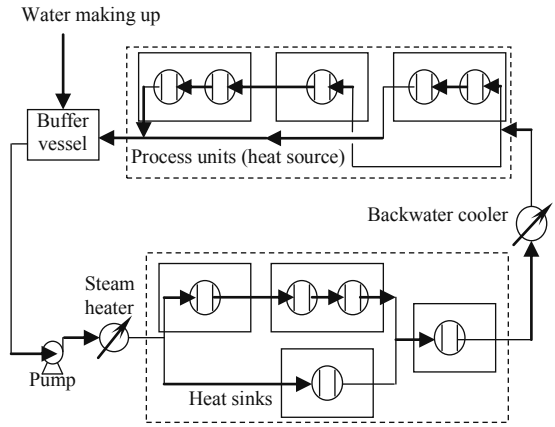

Fig. 3. The simplified flowsheet of low-temperature heat recovery and utilization system

2.4. Utility balance and optimization

Energy savings in three former steps should be finally reflected in decreasing the energy input from outside the system. Outside supplied energy E_P feeds into energy conversion link, so steam power system is the final agent of energy savings for total site energy optimization.

There are new balances of energy streams in a total site when process improvements and heat integration have been done for process plants, and steam power system should be optimized to adapt the new utility requirements. Steam power system has been widely investigated in last several decades, and these open technologies can be used to optimize steam power systems.

3. Example

A 5 Mt/a refinery is taken out as an example to demonstrate the proposed procedure for optimizing the energy system in the total site. The refinery includes a crude distillation unit (CDU), a fluid catalytic cracking unit (FCCU), a hydrotreating unit (HU) and a steam power system.

According to the proposed optimization procedure, in the first step, process improvements and flowsheet reconstruction are motivated to decrease E_N, The options involve optimizing the pumparound heat removals in atmospheric and vacuum towers, selecting high efficiency packing to reduce the pressure drop and decreasing the over-vaporizing rate in the vacuum tower, transferring the cold high-pressure segregator into hot high-pressure segregator in HU. In the second step, heat integration is investigated. The retrofit measures involve hot discharge/feed between CDU and FCCU and transferring the recycle slurry oil in FCCU into CDU to preheat the crude oil. In the third step, a recycle medium water system is set up to collect waste heat in CDU and FCCU and to use it preheating the boiler feed water for the steam power system. In the forth step, the steam power system is optimized to meet the new requirements of steam and fuel gas in the total site. The retrofit results are shown in Table 1. The dynamic

capital pay-off time is less than four years, and the specific refining energy requirement decreases from 81.0 to 68.3 kgEO/t.

Table 1 The economic evaluation for the retrofit program of energy system.

Item		Value
Energy requirement before retrofit / (kgEO/t)		81.0
Energy requirement after retrofit / (kgEO/t)		68.3
Gross investment / (10^6 RMB)		134.7
Annual profit / (10^6 RMB)	Before-tax	94.3
	After-tax	65.4
Internal rate of return / %	Before-tax	82.5
	After-tax	55.3
Capital pay-off time / year	Static	2.9
	Dynamic	3.4

4. Conclusions

Energy system in a refinery can be divided into energy conversion, utilization and recovery subsystems. In order to get a profitable retrofit program for the total energy system, an optimization procedure is presented and motivated for industrial applications. The optimization procedure involves four steps those are outlined based on the insight of energy utilization in refining processes. The application in the example indicates that the proposed optimization procedure is engineering-practical and can be carried out to retrofit the energy system to get better economic benefits.

References

B. Linnhoff, D.W. Townsend, D. Boland, G.E. Hewitt, B.E.A. Thomas, A.R. Guy, R.H. Marsland, **1982**, User Guide on Process Integration for the E|cient Use of Energy. IChemE, Rugby, UK.

B.J. Zhang, X.L. Luo, Q.L. Chen, C.W. Hui, **2011**, Heat Integration by Multiple Hot Discharges/Feeds between Plants. Ind. Eng. Chem. Res., 50(18): 10744-10754.

G.X. Zhang, B. Hua, Q.L. Chen, **2000**, Exergoeconomic methodology for analysis and optimization of process systems, Computers & Chemical Engineering, 24: 613-618.

J.H. Kim, C.H. Han, **2001**, Short-Term Multiperiod Optimal Planning of Utility Systems Using Heuristics and Dynamic Programming, Ind. Eng. Chem. Res., 40, 1928-1938.

J. M.Ponce-Ortega, A. Jiménez-Gutiérrez, I.E. Grossmann, **2008**, Simultaneous Retrofit and Heat Integration of Chemical Processes, Ind. Eng. Chem. Res., 47, 5512-5528.

K. Matsuda, Y. Hirochi, H. Tatsumi, T. Shire, **2009**, Applying heat integration total site based pinch technology to a large industrial area in Japan to further improve performance of highly efficient process plants, Energy, 34: 687-692.

M.J. Bagajewicz, A.F. Barbaro, **2003**, Financial Risk Management in the Planning of Energy Recovery in the Total Site, Ind. Eng. Chem. Res., 42, 5239-5248.

M. Morar, P.S. Agachi, Review: Important contributions in development and improvement of the heat integration techniques, Comput. Chem. Eng., **2010**, 34: 1171-1179.

N. Zhang, X.X. Zhu, **2006**, Novel modeling and decomposition strategy for total site optimization, Comput. Chem. Eng., 30: 765-777.

W. Verheyen, N. Zhang, **2006**, Design of flexible heat exchanger network for multi-period operation, Chem. Eng. Sci., 61: 7730-7753.

X.L. Luo, B.J. Zhang, Y. Chen, S.P. Mo, **2011**, Modeling and optimization of a utility system containing multiple extractions steam turbines, Energy, 36: 3501-3512.

Z.H. Zhao, G. Liu, X. Feng, **2006**, New Graphical Method for the Integration of Hydrogen Distribution Systems, Ind. Eng. Chem. Res., 45, 6512-6517.

I.A. Karimi and Rajagopalan Srinivasan (Editors), Proceedings of the 11th International Symposium on Process Systems Engineering, 15-19 July 2012, Singapore.

Optimization of Performance of Phosphoric Acid Fuel Cell (PAFC) Stack using Reduced Order Model with Integrated Space Marching and Electrolyte Concentration Inferencing

Saibal Ganguly,[a] Sonali Das, Kajari Kargupta,[b] Dipali Bannerjee[c]

[a] *Chemical Engineering Department, University Teknologi Petronas, Perak Darul Ridzuan, Tronoh, 31750, Malaysia.*
[b]*Department of Chemical Engineering, Jadavpur University, Kolkata 700032, India.*
[c] *Department of Physics, Bengal Engineering and Science University, Shibpur, India.*

Abstract

A hierarchical optimization structure is proposed for PAFC Stack. The performance of a PAFC stack is mapped with an easy to implement, low CPU usage consuming reduced order model, used as constraint equation block for the optimizer. The model is validated using different sets of experimental polarization data. Effect of variation of operating variables like hydrogen flow rate, humidifier and cell temperature on the load current versus voltage and power profiles are simulated. Finally, an economic optimization of a PAFC stack is carried out to get the optimum set of operating variables.
Keywords: PAFC, Optimization, Reduced order Model, Electrolyte Concentration

1. INTRODUCTION

In the wake of increasing energy demands and environmental concerns, fuel cells offer an innovative alternative to current power sources since they are highly efficient with renewable fuels and environment friendly. A fuel cell is an electrochemical device that converts chemical energy of a fuel directly into electricity. Of the several classes of hydrogen fuel cells, Phosphoric Acid Fuel Cells (PAFCs) represent one of the most mature technologies. Mathematical modeling and simulations are essential tools for the performance mapping of fuel cells and stacks over varying ranges of operating conditions like temperatures, partial pressures, humidity, flow rates etc. The major application of a mathematical model is online optimization for maximum utilization of the available resources for maximum profitability. Though hierarchical optimization has been used for industrial applications (Ganguly et. al, 1992; Basak et al, 2002 etc), hierarchical scheme for PAFC optimization is hardly available in international literature. A novel hierarchical scheme with Successive Quadratic programming based optimization is proposed for PAFC stack operation in the present work.

2. PAFC – WORKING PRINCIPLE

A phosphoric acid fuel cell (PAFC) is composed of two porous gas diffusion electrodes, namely cathode and anode

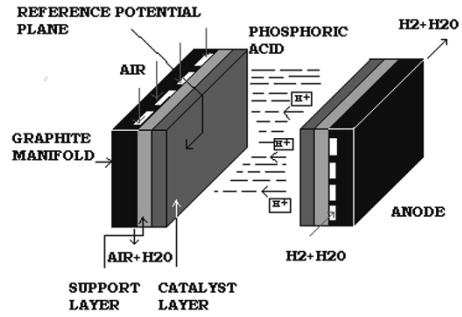

Fig 1. Schematic of a PAFC

juxtaposed against a porous electrolyte matrix. The gas diffusion electrodes are composed of a porous substrate (carbon or cloth) facing the gas feed and a reactive catalyst layer consisting of platinized fine carbon powder, facing the electrolyte. At the anode, hydrogen ionizes to H^+ and migrates towards the cathode to combine with oxygen, forming water. The free energy of reaction is converted to electrical energy, which is available in the form of a potential difference developed between the two electrodes. The reactions at anode and cathode are as follows:

Anode: $H_2 = 2H^+ + 2e^-$ Cathode: $½O_2 + 2H^+ + 2e^- = H_2O$

3. HIERARCHICAL OPTIMIZER FOR PAFC STACK

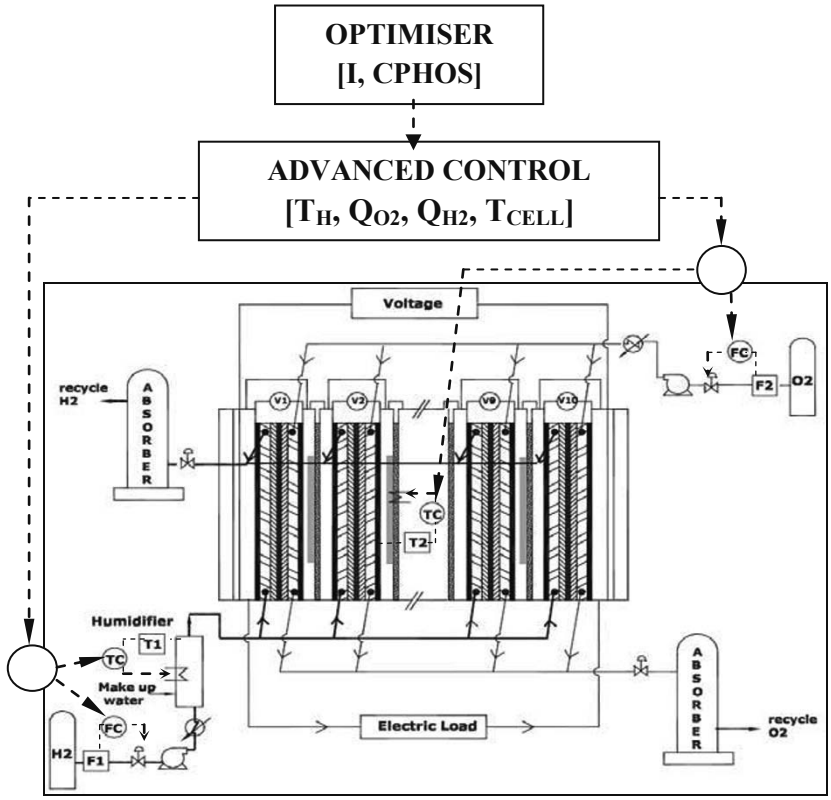

Fig 2. Hierarchical Optimization Structure for PAFC Stack

A stack consists of a number of fuel cells connected in parallel across which a given electrical load is applied. Hydrogen supplied is humidified in order to prevent drying of electrolyte by evaporation of water. In place of oxygen, air can also be used for oxidation.

4. STRUCTURAL BLOCKS FOR OPTIMIZATION

4.1 CONSTRAINT EQUATION BLOCK FOR OPTIMIZATION

The constraint equation block for optimization comprises of variable bounds, computed variable blocks, single cell simulation block and inferential prediction block. Computed variable block computes and maps the input variables to simulation block from the experimental raw data. Single cell simulation block computes the current versus individual cathode, anode overpotential, moisture transport rates from cathode and anode sides and more importantly the electrolyte concentration for each cell of the stack. Finally the inferential block computes the output variables from PAFC stack using the simulation output data from all the individual cells.

The simulation block consists of a cathode model and an anode model. For a particular overpotential, the cathode model calculates the current density and water flux. For this calculated current density, the anode model calculates the anode overpotential and anode side water flux. From a moisture balance of anode and cathode water flux, the concentration of phosphoric acid electrolyte are calculated and updated. Using this new value of electrolyte concentration, the computation is repeated until concentration of two successive steps are equal.

This steady-state model uses a one dimensional integrated cathode-electrolyte-anode model as the base model. Gas diffusion resistance and Tafel kinetics using flooded agglomerate approach for catalyst layer is considered for cathode modeling. Gas diffusion through support layer and through liquid electrolyte encapsulation along with Nernst equation for anode overpotential is used for anode modeling. Overall moisture balance over the cathode-electrolyte-anode assembly is used to obtain steady state electrolyte concentration. Finally, space marching is carried out along the direction of gas flow to take into account the variation of partial pressure and flow rate of inlet gases. Space marching of a 1-D base model instead of solving a full-fledged 2-D model considerably reduces the computational load. Current versus total over potential, rate of moisture transport and steady state electrolyte (phosphoric acid) concentration are obtained as model output. The detailed model equation development for single cell PAFC is presented in Kargupta et al (2012).

4.2 OBJECTIVE FUNCTION

The power generated by the fuel cell stack is a function of load current (I), hydrogen and oxygen flowrates (Q_{H2}, Q_{O2}), cell temperature (T_{cell}), humidity of inlet hydrogen stream and electrolyte concentration ($Cphos$), Humidity of inlet hydrogen is a function of humidifier temperature (Th), hydrogen flow rate. In phosphoric acid fuel cell the electrolyte, (phosphoric acid) concentration determines the proton conductivity and thus the power generation. For normal operation of fuel cell the electrolyte concentration must be controlled at optimal value. Drying of electrolyte due to moisture evaporation and excess dilution of electrolyte (due to low cell temperature/high humidifier temperature) drastically decreases the power generation. In the present work, a steady state optimization scheme for PAFC stack has been proposed which can be utilized in the hierarchical structure (Fig. 2). At the top most level, the process optimization variables considered, are the load current and electrolyte concentration. The set points of variables $Qh2$,$Qo2$,Th and TFC in the advanced control level are determined by the I and $Cphos$. The disturbance variables are considered in the lower most frontend control level. The present paper deals with the steady state optimization layer only.

The objective function is to maximise the profit which can be expressed mathematically as follows:

Maximize $\varphi = P_1 - P_2 - P_3 - P_4$

with respect to the operating variables where φ is the profit based objective function. P_1 is the selling price of power generated by stack

P_1 = (power x price x wt x flag) = function of (I, cphos)

where, electricity generated is in terms of kW-min, price is the selling price of power per kW-min, wt is the weighting of this term in the objective function and flag is a parameter whose value depends on the zone of operation of fuel cell. The purpose of flag is to prevent the optimum solution from being in the undesirable operation zones, namely acid drying and flooding. In some cases penalty is introduced in terms of flag. Acid drying may be caused by low humidity of inlet hydrogen stream, very low hydrogen flow rate whereas flooding is caused by high hydrogen flow rates, 1ow fuel cell temperature etc.

P_2 is the cost price of raw materials consumed defined as follows

$P_2 = Q_{hyd}$-consumed *C_{hyd}*wt_i + Qoxygen-reacted*C_{ox}*wt_j = function of (I)

where, C_{hyd} and C_{ox} are cost of hydrogen and oxygen respectively per litre, *wti* and *wtj* are the weight functions. For the unutilized fuel and oxygen a loss function is defined:

$P_3 = Q_{hyd}$-excess *C_{lh2}*wt_i + Qoxygen-reacted*C_{lo2}*wt_j = function of (Qh2,Qo2,I)= function of (I,Cphos)

P_4 is the operating cost which includes the fuel cell heater cost, compressor cost and humidifier heat load.

P_4 = price * [(H*wt_1) + ($H_{humidifier}$*wt_2) + ($W_{compressor}$*wt_3)]

where H is the heater plate input, $H_{humidifier}$ is the heat input to humidifier and $W_{compressor}$ is the power input to gas compressor in terms of kW-min and price of power per kW-min. ,

4.3. OPTIMIZATION METHODOLOGY: Nonlinear programming based steady state optimization is carried out using Sequential Quadratic Programming (SQP) algorithm with quasi newton line search to enhance convergence. The dependant variables Y, namely power, ***Q_{hyd}-consumed, Qoxygen-reacted, Q_{hyd}-excess, Qoxygen-reacted, $H_{humidifier}$*** required in the objective function are found as function of optimization variables X, namely current and Cphos. The computed variable equations obtained using the model act as the equality constraints. Variables bounds are used as inequality constraints. The converged solution depicts the optimum variables values.

5. OPTIMIZATION RESULTS

5.1. CONSTRAINT BLOCK VALIDATION WITH EXPERIMENTAL RESULTS:

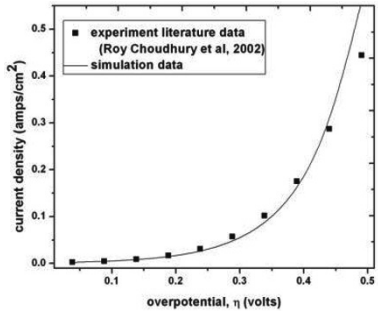

Fig 3. Comparison of Polarization curves.

To validate the model, simulated current density vs. overpotential is plotted in fig 3 and compared to published experimental data by Roy Choudhury et al. (2002). The values match quite well and as expected current density increases rapidly as the overpotential increases since the reaction increases exponentially with respect to the overpotential.

5.2. EFFECT OF OPERATING VARIABLES:

Figs. 4 and 5 show the effect of hydrogen flowrate and humidifier temperature on the electrolyte concentration.

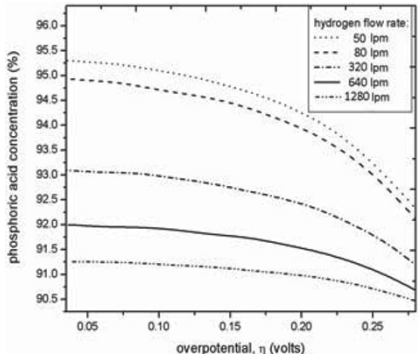

Fig 4 Effect of hydrogen flowrate on electrolyte. concentration

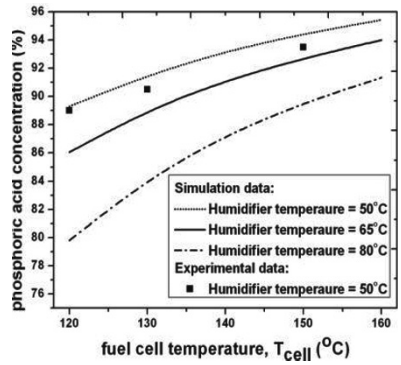

Fig 5. Effect of humidifier temperature on electrolyte concentration

5.2 *CONTOURS FOR ECONOMIC OPTIMIZATION*

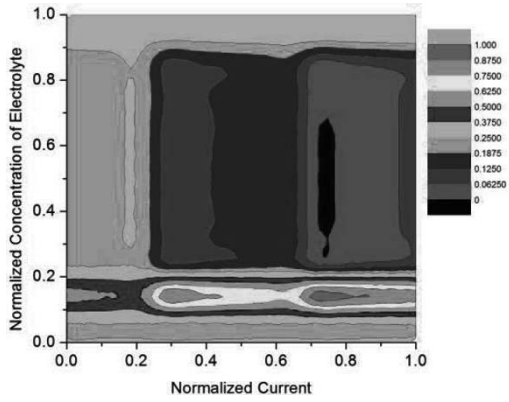

Fig 6. Contour plot of objective function

Fig. 6 shows the contour plot of the negative of objective function (cost function to be minimized) with respect to normalized current and phosphoric acid concentration. At the optimum value of current for a set of electrolyte concentration, the cost function reaches the minima.

CONCLUSIONS

A hierarchical optimization structure is proposed for PAFC Stack. The profit is maximized with respect to the optimizer variables namely load current and electrolyte concentration. A reduced order model validated with experimental data is used as the constraint block of the optimizer. The optimizer shows promising potential for real-life industrial applications..

References

Roy Choudhury, S., Deshmukh, M.B., Rengaswamy, R., 2002. A two-dimensional Steady State model for phosphoric acid fuel cells (PAFC). Journal of Power Sources 112 , 137-152.

K. Kargupta, S. Das, S .Ganguly et al., 2012, 'Reduced Order Model with integrated space marching and electrolyte concentration inferencing for Phosphoric Acid Fuel Cell Systems', communicated to Chemical Engineering Science, March 2012.

K. Basak, K. S. Abhilash, S. Ganguly, D. N. Saraf, 2002, On-Line Optimization of a Crude Distillation Unit with Constraints on Product Properties, 41, 1557-1568.

S. Ganguly and D. N. Saraf, 1992, "Online Optimization : A Hierarchical Scheme for Distillation Column", Chem. Engineering & Processing, 31, 6, 337.

I.A. Karimi and Rajagopalan Srinivasan (Editors), Proceedings of the 11th International Symposium on Process Systems Engineering, 15-19 July 2012, Singapore

Platform development for studying integrated energy conversion processes: Application to a power plant process with CO_2 capture

Laurence Tock,a * François Maréchal,a
a Industrial Energy Systems Laboratory, EPFL, Lausanne, Switzerland

Abstract

This paper presents the development of a platform for studying, designing and optimizing complex integrated energy systems. Technology models representing the physical behavior are separated from thermo-economic analysis and multi-objective optimization including energy integration, economic evaluation and environmental impact assessment. Through a Matlab based platform, structured data is transfered between different models. The advantage of dissociating the technology models from the analysis models is that process unit models developed with different software can be assembled in a superstructure for subsequent large processes design and optimization. The approach is illustrated by the thermo-economic modeling and optimization of a power plant with CO_2 capture.

Keywords: Thermo-economic modeling, Process design, Multi-objective optimization, Power plant, CO_2 capture

1. Introduction

In the context of climate change mitigation and energy supply, the development of competitive power plants with CO_2 capture is challenging. To design such complex integrated energy conversion systems taking into account energetic, economic and environmental considerations a systematic approach is developed. The approach relies on previous developments presented in Bolliger et al. (2009, 2010), Gassner and Maréchal (2009) and Gerber et al. (2011). Bolliger et al. first presented a generic approach to analyze energy conversion systems by separating the process unit models from the data needed to model the energy and mass integration in the system. Following this approach, models can be assembled in large superstructures from which system configurations can be extracted and optimized systematically with regard to competitive objectives. Dissociating system models from the system design methods is the main advantage compared to other platforms such as DOME (Pahng et al. (1998)) and CAPE-OPEN (Dickinson (2008)) dealing essentially with the flowsheeting and requiring an explicit definition of the interconnections.

This project is motivated by the need of developing a flexible tool for the conceptual process design combining thermodynamic analysis, energy integration, performance evaluation and multi-objective optimization strategies. Such a platform is particularly useful when studying the design of energy conversion systems, like power plants with CO_2 capture where the quality of the energy integration is a key factor defining the system's efficiency.

*laurence.tock@epfl.ch

2. Methodology

The process design methodology combines process modeling using established flowsheeting tools and process integration models in a multi-objective optimization framework as explained in Gassner and Maréchal (2009). The main features of the methodology are summarized in Figure 1. Chemical and physical models of process units are used to generate the heat transfer requirement of each building block of the process superstructure. The energy-integration model optimizing the heat recovery in the system and the combined heat and power production by applying the pinch analysis concepts is used to calculate the best integration of the process units. The optimal solution is calculated by minimizing the operating cost using a linear programming model as described in Maréchal and Kalitventzeff (1998). Knowing the flows and operating conditions in the selected units of the energy system, the size and equipment cost are estimated in order to calculate the economic and environmental performances of the system. The trade-off between competing performance indicators is assessed by sensitivity analysis and multi-objective optimization defining the optimal values of the decision variables of the system design. The platform consists hence of different layers: the model, the computation type (optimization, sensitivity analysis, one run) and the results extraction.

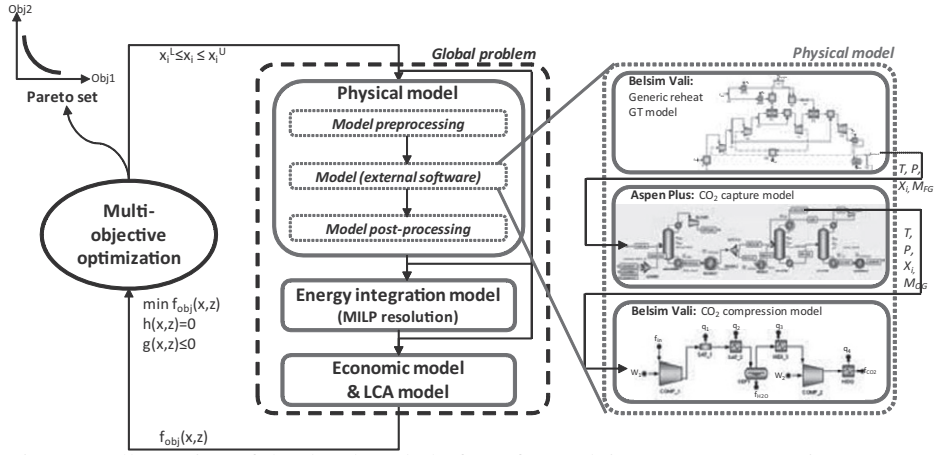

Figure 1: Illustration of the developed platform for studying energy conversion systems

2.1. Physical model

Process models are developed within specially tailored modeling languages using numerical solvers to solve the set of equations describing the thermo-physical and chemical conversion operations of the technology for a given set of decision variables and unit model parameters. Each model follows this calling sequence: the pre-processing phase selects the process model, collects necessary parameters and transfers the decision variables to the model, the simulation phase calculates the process unit using an external flowsheeting software and the post-processing phase extracts from the simulation results the data needed to define the unit interface with the rest of the process. Since each model is organized as an input (decision variables) -output entity, the internal mathematical formulation appears as a black box for the process synthesis model. The communication between different models, the calculation sequence and the process synthesis model set-up is organized in a Matlab code.

2.2. Process synthesis and optimization

From the physical model the platform extracts the data required for the synthesis methods such as the hot and cold streams for the energy integration, the size, the material and the pressure and temperature for the cost estimation and the data required for the life cycle inventory. Aggregating cost and/or environmental impact allows to calculate the performance indicators used as objective function in the optimization. Each process unit carries decision variables that are identified by degree of freedom analysis and whose value will be fixed by optimization. Combined with integer decision variables related to the technology choice (unit existence) and the interconnections, the problem becomes of a mixed integer non linear programming and differentiable problem that is solved with an evolutionary multi-objective optimization algorithm (Molyneaux et al. (2010)). The use of an evolutionary algorithm makes the approach less sensitive to non-convergence problems and the proper definition of the decision variables allows to stabilize the robustness of the model. During the Pareto font generation infeasible solutions are avoided through heuristics embedded in the sizing and cost estimation models.

3. Application: Power plant with CO_2 capture

To illustrate the approach, the integration of CO_2 capture in power plants is studied. Multi-objective optimization is performed to assess the trade-offs between investment and CO_2 emissions. Figure 2 presents the superstructure of different CO_2 capture concepts. It is focused on the study of the potential power plant performance improvement with CO_2 capture by flue gas recirculation (FGR).

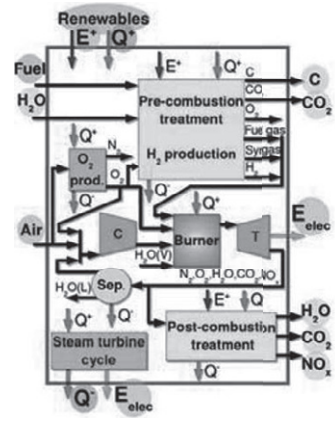

Figure 2: Conceptual superstructure of power plants with CO_2 capture

Process description: The studied process is a natural gas combined cycle with flue gas recirculation and CO_2 capture. The power plant and the CO_2 capture and compression are modeled with different flowsheeting software (Figure 1), while the optimal steam network integration is defined in the energy integration model as explained in Girardin et al. (2009).

Power plant model: The natural gas reheat gas turbine model is developed with the *Belsim-Vali* software. To address the flame stability concerns at high FGR, syngas can be injected. The syngas production is modeled by a high temperature oxygen separation membrane autothermal reforming reactor.

CO_2 capture model: The CO_2 generated in the combustion is separated from the N_2 and excess O_2 contained in the exhaust gas by chemical absorption with monoethanolamine

(MEA). The flowsheet of the CO_2 capture process is described in detail in Bernier et al. (2010). The model is based on the Aspen-Plus rate-based model adapted from the default model available from *AspenTech*. A CO_2 purity over 98%wt is targeted. The CO_2 capture rate is defined by the columns design and the operating conditions. CO_2 compression to 110[bar] for subsequent CO_2 transport and storage is modeled separately in *Belsim-Vali*. The connection between the different models is done by the material streams characteristics, namely composition, massflow, temperature and pressure (Figure 1). Table 1 summarizes the decision variables with their variation ranges. Based on the developed simulation models, the hot and the cold streams are computed for subsequent process integration and the equipment sizes are calculated for cost estimation.

Table 1: Decision variables and feasible range for optimization.

Operating parameter	Range	Operating parameter	Range
FG recirculation [-]	[0-0.56]		
ATR temperature [K]	[1050-1300]	S/C [-]	[1.5-4]
Lean solvent CO_2 loading [kmol/kmol]	[0.18-0.25]	Split fraction [-]	[0-0.7]
Rich solvent CO_2 loading [kmol/kmol]	[0.4-0.5]	Nb stages absorber	[10-17]
Rich solvent pre-heat T [^oC]	[95-105]	Nb stages HP stripper	[8-15]
Rich solvent re-heat T [^oC]	[115-125]	Nb stages LP stripper	[6-10]
LP stripper pressure [bar]	[1.7-2.1]	Absorber diameter [m]	[6-12]
HP / LP pressure ratio [-]	[1-1.5]	HP stripper diameter [m]	[3-6]
MEA % in solvent [-]	[0.3-0.35]	LP stripper diameter [m]	[2-5]
Absorber steam out [kg_{H2O}/t_{FG}]	[306-309.5]		

3.1. Optimal process performance analysis

The energy and economic cost of capturing CO_2 and the impact of CO_2 recirculation on the compressors, turbines, combustion, CO_2 capture and the steam network is assessed. The performance is expressed by the energy efficiency, the electricity production cost, the CO_2 capture rate and the CO_2 avoidance cost $\frac{COE_{CC}-COE_{ref}}{CO_{2,emit,ref}-CO_{2,emit,CC}}$ $\left[\frac{\$/MWh_e}{t_{CO2}/MWh_e}\right]$. Sensitivity analysis have revealed that FGR does not considerably impact the process efficiency but improves the economics of CO_2 capture by increasing the CO_2 concentration in the flue gas and reducing therefore the CO_2 capture cost as reported in Table 2. The multi-objective optimization minimizing the electricity production cost and maximizing the CO_2 capture rate with regard to the decision variables in Table 1, reveals the trade-off between the CO_2 capture rate and the electricity production cost (COE). This is explained by the reduced electricity output due to the energy demand for solvent regeneration and CO_2 compression, and the increased capital cost for the capture equipment. CO_2 capture with 50% FGR reduces the efficiency by around 8% and increases the electricity production cost up to 20% leading to CO_2 avoidance cost in the range of 47\$/$t_{CO2,avoided}$ with a natural gas price of 35\$/MWh_{NG}.

Table 2: Performance results (natural gas price 35\$/MWh_{NG}, operation 8000h/y)

	no CO_2 capture		85% CO_2 capture	
FGR [%]	0	50	0	50
ε [%]	58.88	58.07	49.89	50.04
$CO_{2,emitted}$ [kg/MWh_e]	379	359	64	47
Investment [\$/kW_e]	588	589	949	900
COE [\$/MWh_e]	69.4	69.7	86	84.9
\$/$t_{CO2,avoided}$	-	-	52.5	46.7

4. Conclusion

A Matlab based platform for studying, designing and optimizing complex integrated energy systems is presented. The main goal is to have a flexible tool for the conceptual process design combining flowsheeting models using commercial packages, energy integration, performance evaluation (economic and environmental) and multi-objective optimization strategies. In the proposed approach physical models are separated from the design and integration methods. A key feature is the possibility to connect process unit models developed with different software. The developed platform is applied to study the thermo-economic and environmental impacts of the integration of a CO_2 capture unit in a gas turbine combined cycle.

Acknowledgment

The authors thank Swisselectric research for their financial contribution of the project "Technologies for gas turbine power generation with CO_2 mitigation".

References

AspenTech, last visited 12/2011. http://www.aspentech.com.

Belsim SA, last visited 12/2011. http://www.belsim.com.

Bernier, E., Maréchal, F., Samson, R., 2010. Multi-objective design optimization of a natural gas-combined cycle with carbon dioxide capture in a life cycle perspective. Energy 35 (2), 1121–1128.

Bolliger, R., 2010. Méthodologie de la synthèse des systèmes énergètiques industriels. Ph.D. thesis, EPFL, Lausanne.

Bolliger, R., Becker, H., Maréchal, F., 2009. New generic approach for the analysis of energy conversion system models. In: Process Systems Engineering, PSE09. Computer Aided Chemical Engineering. Elsevier.

Dickinson, R., 2008. Expanding process modelling capability through software interoperability standards: Application, extension and maintenance of cape open standards. Computer Aided Chemical Engineering 25, 537 –.

Gassner, M., Maréchal, F., 2009. Methodology for the optimal thermo-economic, multi-objective design of thermochemical fuel production from biomass. Computers & Chemical Engineering 33 (3), 769–781.

Gerber, L., Gassner, M., Maréchal, F., 2011. Systematic integration of LCA in process systems design: Application to combined fuel and electricity production from lignocellulosic biomass. Computers & Chemical Engineering 35 (7), 1265 – 1280.

Girardin, L., Bolliger, R., Marechal, F., 2009. On the use of process integration techniques to generate optimal steam cycle configurations for the power plant industry. In: Pres'09. Vol. 18 of Chemical Engineering Transactions. Aidic Servizi Srl, Milano, Italy, pp. 171–176.

Maréchal, F., Kalitventzeff, B., 1998. Process integration: Selection of the optimal utility system. Computers & Chemical Engineering 22, 149–156.

Molyneaux, A., Leyland, G., Favrat, D., 2010. Environomic multi-objective optimisation of a district heating network considering centralized and decentralized heat pumps. Energy 35 (2), 751–758.

Pahng, F., Senin, N., Wallace, D., 1998. Distribution modeling and evaluation of product design problems. Computer-Aided Design 30 (6), 411 – 423.

I.A. Karimi and Rajagopalan Srinivasan (Editors), Proceedings of the 11th International Symposium on Process Systems Engineering, 15-19 July 2012, Singapore.

Robust Optimization of Microgrids – An Application to Taichung Industrial Park

Jin-Su Kang,[a] Chung-Chuan Chang,[b] Dong-Yup Lee,[c] Tai-yong Lee[d]

[a]*Institute of Business and Management, National Chiao Tung University, 118, Chung-Hsiao W. Rd., Taipei City 10044, Taiwan, ROC*
[b]*Global MBA, National Chiao Tung University, Tashueh Rd. 1001, Hsinchu 30010, Taiwan, ROC*
[c]*Deparment of Chemical and Biomolecular Engineering, National University of Singapore, Singapore 117576, Singapore*
[d]*Department of Chemical Engineering, Hongik University, 72-1, Sangsu-Dong, Mapo-gu, Seoul 121-791, Korea*

Abstract

Despite a number of studies of a microgrid, robust optimization of a microgrid has not been studied yet. This is critical to a microgrid because it has lots of uncertainties concerning main grid failure, power quality issues, estimates of demand, energy price, regulation change, etc. It is therefore of importance to study and develop robust optimization strategies that take the uncertainty into account at planning a microgrid. The current study aims at developing a robust optimization model for a microgrid which provides set of robust solutions and decision-making procedure for a best solution. The model enables us to consider various uncertainties including energy price, regulation change, and estimates of demand using scenario based approach. The proposed model is validated with Taichung Industrial Park in Taiwan.

Keywords: Microgrid, Robust Optimization, Taichung Industrial Park

1. Introduction

Nowadays, there is no argument that global climate change is one of most serious global issues that we face with. Among many factors, the electricity sector is a major source of carbon dioxide (green house gas) emissions that contribute to global climate change. Switching a substantial portion of electricity generating capacity away from fossil fuels to renewable energy technologies could have a significant effect in reducing greenhouse gases. In addition, increasing frequency of natural disasters put forward the flexibility and independence of electricity generation from the central generation. In this context, a "microgrid," a local generation of heat and electricity, with renewable energy resources is considered as one of the most promising options to provide a more secure, clean, and efficient energy supply.

There have been many researches on a microgrid regarding autonomous operations (Katiraei et al., 2005; Lopes et al., 2006), control schemes (Barsali et al., 2002; Piagi & Lasseter, 2006), scheduling (Morais et al., 2010), planning (Sayyaadi, 2009 ; Gholap & Khan, 2007; Gebreslassie et al., 2009; Aki et al., 2005; Alarcon-Rodriguez et al., 2010; Ren et al., 2010), etc. However, robust optimization of a microgrid planning has not been studied yet although a microgrid itself has lots of uncertainties concerning main grid failure, power quality issues, estimates of demand, energy price, regulation change, etc. Thus this study aims at developing robust optimization model that take the uncertainty the uncertainty into account at planning utilizing robustness measures.

There has been countless number of researches regarding robust optimization in the field of process engineering. Among them, Kang et al.(2012) propose to consider robustness separately depending on the nature of a variable such as scenario-independent variables, scenario-dependent technical variables (e.g., temperature, pressure, flow rate, liquid holdup, etc.), and scenario-dependent monetary or economic variables (e.g., cost, profit, production yield, etc.). The current study applies the robust optimization model proposed by Kang et al.(2012), a comprehensive robust optimization model which considers both economic and technical robustness together with decision making process. The proposed model was applied to the industrial example, Taichung Industrial Park in Taiwan.

2. Proposed Microgrid Model

The proposed microgrid model produces electricity from solar panels, wind turbine, incineration of municipal solid waste (MSW), internal combustion engine, fuel cells and microturbine (Figure 1). Trigeneration, where the waste heat from electricity production used for heating and cooling is also considered for applicable sources. Excess electricity will be stored in the battery and/or sold to the national grid while the fuels used are natural gas, hydrogen and biofuel. It is assumed that it is a smart microgrid whereby the controller allocates the nearest source to the nearest load.

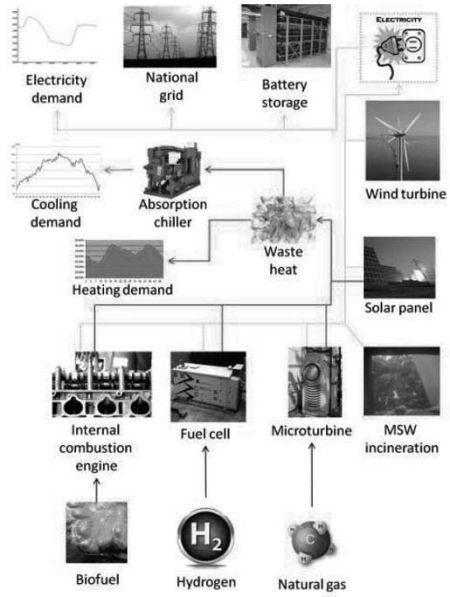

Figure 1. Scehmatic Diagram of the Microgrid

The proposed model employs possible scenarios for prices and demand of electricity concerning uncertainties. The objective is to generate the set of robust alternatives which consider both cost with minimal reliance on the national grid and carbon generated. Thus, three different objective functions will be considered in this paper namely economic robustness, technical robustness, and expected cost.

$$\min_{\mathbf{x},y_1,\cdots,y_N} (U_E(\mathbf{C}), U_{WC}(\mathbf{C}), U_T(\mathbf{y})) \tag{1}$$

where $U_E(\mathbf{C})$ is expected cost, $U_{WC}(\mathbf{C})$ is the worst-case cost of scenario, and $U_T(\mathbf{y})$ is the technical robustness which is the half interval of a technical variable. In principle, there can be many technical robustness functions depending on the number of scenario-dependent technical variables considered in the robust optimization. In this model, we consider the amount of carbon as a technical variable to consider technical robustness. Thus, the objective functions in Equation (1) are expressed as follows:

$$\text{Economic Robustness: } U_{WC}(\mathbf{C}) = \max\{C_s | s = 1, \cdots, N\} \tag{2}$$

where

$$\begin{aligned} C_s = {} & P_{\mathrm{BF}s} * Biofuel_s + P_{\mathrm{H2}s} * Hydrogen_s + P_{\mathrm{NG}s} * NGas_s + \\ & Penalty * \sum_t BuyElecN_{t,s} + Solar_s * ElectricityS_s + \\ & Wind_s * ElectricityW_s + MSW_s + ElectricityM_s \end{aligned} \tag{3}$$

$$\text{Technical Robustness: } U_T(Carbon) = \frac{1}{2}\left(\max_s Carbon_s - \min_s Carbon_s\right) \tag{4}$$

where

$$Carbon_s = \sum_i \sum_t Carbon_{i,t,s} + CarbonSolar_{t,s} + CarbonWind_{t,s} \tag{5}$$

$$\text{Expected Cost: } U_E(\mathbf{C}) = \sum_s p_s C_s \tag{6}$$

We should note that both expected cost and worst case cost of scenario have the same monetary unit and similar range while the technical robustness might have quite different unit and range. It sometimes requires to adjust the range of technical robustness according that of expected cost to implement multiobjective optimization.

The model utilizes predicted demand for electricity and incineration of MSW (assuming that 1% of MSW is incinerated at Taichung Industrial Park and an equal amount of MSW is burnt per day). Regarding to the electricity from solar and wind energy, it will be different depending on the situation including the amount of sun, velocity of wind, and pricing of input materials, expressed as scenarios. The proposed model ensures meeting local demand for electricity, heating and cooling and diversity of the sources of trigeneration with preventing idling of sources. Also, battery has enough power stored to handle power spikes, cannot charge and discharge at the same time and cannot discharge more than the amount stored. Environmental concerns are considered with carbon credits to satisfy regulations.

3. Taichung Industrial Park, Taiwan

In June 2009 Taiwan finally passed its Renewable Energy Development Act, the key legislative framework that is designed to achieve a 16% share of installed capacity for renewables by 2025 against an estimated 8% (dominated by hydropower) in 2010, according to figures from Taiwan's Bureau of Energy, part of its Ministry of Economic Affairs. This has become a key obstacle for an industrial complex, in which the competitive of firms heavily relies on operation efficiency, that is, cheap operating cost. Thus the current study attempts to apply the robust optimization model of a microgrid to Taichung Industrial Park, one of major industrial complex in Taiwan, as a preliminary step for realizing cleaner electricity generation.

The proposed layout of the microgrid for Taichung Industrial Park is described in Figure 2. The wind turbines are located at the south-west in order to capture the winds blowing from sea and not to be obstructed by any buildings. Since Taichung has relatively strong sun all year around with less raining and strong wind, this place can be a good candidate to utilize solar and wind energy efficiently.
The proposed model assumes one day with possible scenarios with a different portion of energy produced by renewable energies. Table 1 describes the hypothesized data.

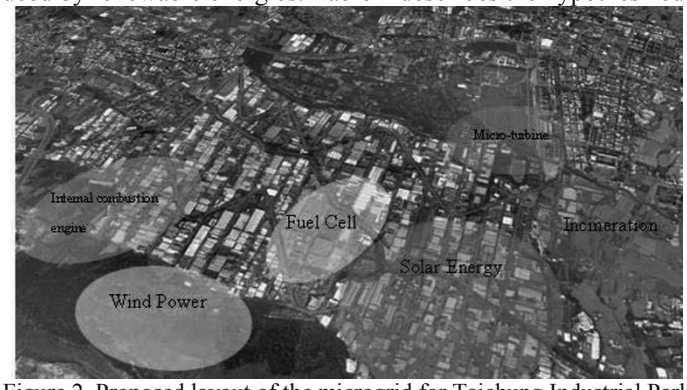

Figure 2. Proposed layout of the microgrid for Taichung Industrial Park

Table 1. Comparison of four scenarios

	Scenario 1	Scenario 2	Scenario 3	Scenario 4
Probability	0.2	0.3	0.3	0.2
P_{BF} (USD/kg)	0.2	0.23	0.26	0.3
P_{H2} (USD/MJ)	0.336	0.37	0.4	0.43
P_{NG} (USD/kg)	0.275	0.3	0.33	0.37
Renewable portion (<=)	20%	30%	40%	50%

4. Results and Conclusion

Figure 3 shows the set of robust alternatives with applying the microgrid model to Taichung Industrial Park in Taiwan attained from the robust optimization model proposed.

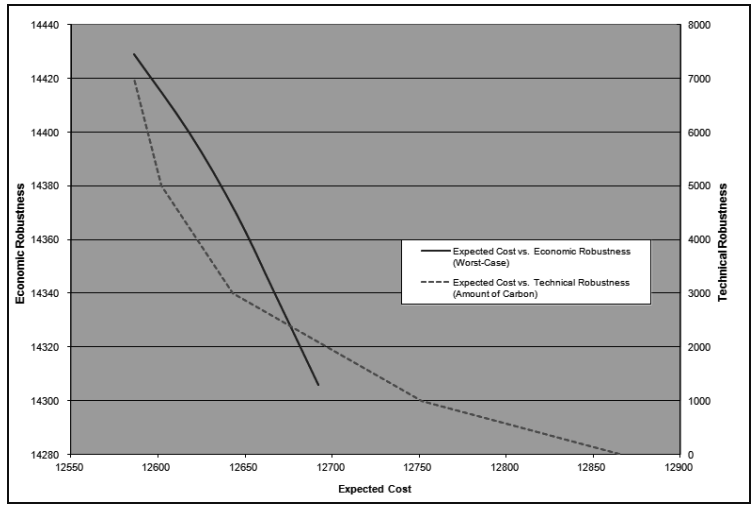

Figure 3. Ranges of robust optimization objectives

Pareto curves show trade-off relationship between expected cost and worst scenario cost (economic robustness) and expected cost and environmental regulation (technical robustness). The results describe that 1about 1% of reduction in worst scenario cost can be achieved by increasing expected cost by 0.1% while 5.5% reduction in technical robustness can be obtained by increasing expected cost by 2.2%. This implies that under the microgrid proposed, reducing technical variability (i.e., reducing the difference in the amount of carbon generated) among scenarios appears requiring more increment in expected cost than reducing economic variability (i.e., reducing worst-case scenario cost). This means that it is more expensive to keep the consistent level of carbon generated under price uncertainty. It calls for the careful consideration to exercise environmental regulation on the industrial complex like Taichung industrial park, in which the competitiveness of firms heavily relies on cost competitiveness.

The current study proposes the robust optimization model for microgrid app

The current study shows how to generate set of robust alternatives with uncertainty in the microgrid. Although limitations exist (e.g. considering limited number of uncertain parameters or using definite probability information), the results obtained can be helpful for planning a microgrid both for economic and technical consideration.

Acknowledgement

Jin-Su Kang acknowledges the financial support from National Science Council in Taiwan (NSC 100-2221-E-009 -136).

References

A. Alarcon-Rodriguez, G. Ault, and S. Galloway, 2010, Multi-objective planning of distributed energy resources: a review of the state-of-the-art, Renew Sust Energy Rev, 14(5), 1353-1366.

H. Aki, A. Murata, S.Yamamoto, J. Kondoh, T. Maeda, and H. Yamaguchi, 2005, Penetration of residential fuel cells and CO2 mitigation—case studies in Japan by multi-objective models, Int J Hydrogen Energy, 30(9), 943–52.

S. Barsali, M. Ceraolo and P. Pelacchi, 2002, Control Techniques of Dispersed Generators to Improve the Continuity of Electricity Supply, Proc. 2002 IEEE Power Engineering Society Winter Meeting, 789-794.

B. H. Gebreslassie, G. Guillen-Gosalbez, L. Jimenez, and D. Boer, 2009, Design of environmentally conscious absorption cooling systems via multi-objective optimization and life cycle assessment, Appl Energy, 86(9), 1712–22.

A. K. Gholap and J.A. Khan, 2007, Design and multi-objective optimization of heat exchangers for refrigerators, Appl Energy, 84(12), 226–1239.

J.-S. Kang, T.-y. Lee, and D.-Y. Lee, 2012, Robust optimization for Engineering Design. Engineering Optimization, 44, 217-225.

F. Katiraei, M.R. Iravani and P. Lehn, 2005, Microgrid Autonomous Operation during and Subsequent to Islanding Process, IEEE Trans, Power Delivery, 20, 248-257.

J. Lopes, C.L. Moreira, and A.G. Madureira, 2006, Defining Control Strategies for Microgrids Islanding Operation, IEEE Trans. Power Systems, 21, 916-924.

H. Morais, P. Kadar, P. Faria, Z. Vale, and H.M. Khodr, 2010, Optimal scheduling of a renewable micro-grid in an isolated load area using mixed-integer linear programming, Renewable Energy, 35, 151-156.

P. Piagi and R.H. Lasseter, 2006, Autonomous Control of Microgrid, Proc. 2006 IEEE Power Engineering Society General Meeting, 789-797.

H. Ren, W. Zhou, K. Nakagami, W. Gao, and Q. Wu, 2010, Multi-objective optimization for the operation of distributed energy systems considering economic and environmental aspects, Applied Energy, 87, 3642-3651.

H. Sayyaadi, 2009, Multi-objective approach in thermoenvironomic optimization of a benchmark cogeneration system, Appl Energy, 86(6), 867–79.

I.A. Karimi and Rajagopalan Srinivasan (Editors), Proceedings of the 11th International Symposium on Process Systems Engineering, 15-19 July 2012, Singapore.

An optimization of the food quality products throughout the supply chain

Ali Mehdizadeh[a], Nilay Shah[a], Neha Raikar[a], Peter M.M. Bongers[b]
[a]*Centre for Process Systems Engineering, Department of Chemical Engineering, Imperial College London Technology and Medicine, United Kingdom*
[b]*Unilever Research Vlaardingen, Oliver van Noortlaan 120, POBox 114, 3130 AC Vlaardingen, TheNeherlands*

Abstract

Quantitative supply chain modelling has contributed substantially in fields such as automotive, logistic, hardware, etc. However, these methods and optimization have not been employed widely in the food industry despite all the potential benefits they may bring to this sector. The reason is integration of quantitative supply chain models into food industry brings difficulties into the optimisation approaches. The objective of this work is to develop a supply chain model for the food industry based on the relationships between raw material quality, processing conditions and final product quality and customer satisfaction. Moreover, based on the developed model, we have determined key factors in the whole chain that are most likely to affect customer satisfaction and consequently overall demand. Optimum conditions to minimize overall cost and energy consumption have been determined. New methodology has been developed that simplifies and enables the model to find the optimum processing conditions to obtain maximum quality across all quality indicators with minimum cost and energy usage by developing the interrelationships between quality and processing conditions.
Keywords: supply chain management, quality modelling, mixed-integer linear programming, food processing.

1. Introduction

In the FMCG (Fast Moving Consumer Goods) sector the product improvement process is based on fundamental research and development, which is the key factor for the customer satisfaction. Hence a new methodology is developed from time to time to improve the existing product and services, and parallel to this the process is controlled to reduce the cost of the production. Supply chain management is the research area that develops a technique, which finds the bottleneck and optimizes all the steps from supplier to distribution. The supply chain is a series of logistic internal and external activities between companies to increase the efficiency by sharing information between entities to gain customer satisfaction at the lowest possible costing (Shah, 2005).
Integrating the quality and energy control models and food supply chain together would bring difficulties to the system. The reason is the complication of quantifying the food quality and managing the product quality during the process. Controlling the product quality is the most essential food product characteristics to consider (e.g. Smith et al, 2004), and maintaining the high quality product during various processes and processing conditions is an important matter in the food supply chain. The work done by Rong et al (2011) is on optimizing the food quality degradation in the production and distribution planning. This model optimizes the quality of the raw materials throughout the supply chain. The work considered a kinetic model to measure for the quality degradation. It considers only a single raw material and product and generates linear and non-linear results in the case of zero and first order reactions, respectively. This kinetic

model is integrated into the supply chain and mixed –integer linear programming is used for production and distribution. However in this work energy consumption has not been considered as a key factor.

An important factor in food industry is to have flexibility in products and not to have a seasonality problem to satisfy the given demand. Therefore the preparation process is added to the production system to increase the shelf-life of the raw materials. The focus of this paper is on the preparation processes, where it reduces the inventory wastage produced by expired materials. Fresh food materials are source of vitamin, minerals and other bioactive compounds such as pigments and volatile compounds that undergo degradation during drying process (Gregory, 1996). Therefore a quality model is developed to control for the variation in these quality indicators.

The goal of this project is to introduce a new methodology to model and optimise the food quality whilst controlling and minimizing the process energy consumption in such a way that it can be integrated in a mixed-integer linear programming model used for the production system throughout supply chain.

2. Mathematical Model

Two preparation processes are used here, namely freezing and drying processes. The freezing process is a benchmark and will be compared with the drying process. One type of freezing process and two different types of drying processes are used (figure, 1). Therefore in the case of drying processes an optimal blending task is added to achieve the optimum product quality and energy usage wise. As a result two quality models are developed and applied to the drying process, the linear quality model and the quality model with correction factor. This blending model is only applied to the drying process, but the linear quality model as well as energy model is applied to the whole process and all states throughout the system for supply chain scheduling. The following equations are used to measure and constrain the quality:

$$q_{i,s} = B_i + C_i . q_{i,s-1} + \sum_j \gamma_j \sum_D A_{i,D} . u_{j,D} \quad (1)$$

Where $q_{i,s}$ represents the quality of the product after each task of the specific indicator. The $q_{i,s}$ at each state becomes an input quality of the next state. In this model different processes will have different effects. The material processed in the task goes through transformations described by parameters *A, B* and *C*. The variable set *u* is introduced in the model which captures how the quality of the product is also affected by the process degrees of freedom (e.g. temperature, processing time). γ_j is a binary variable and it is 1 if certain task is operating.

$$q_B^k = x_A^k . q_{AD} + (1 - x_A^k) . q_{FD} + M(1 - y_A^k) + Correction^k, \quad \forall k \quad (2)$$

$$q_B \leq q_B^k - M(1 - y_A^k), \quad \forall k0 \quad (3)$$

q_{AD} & q_{FD} are the quality of the product after preparation process, Air-Dry and Freeze-Dry respectively. q_B^k, is the blended quality at every data point. *k* are the data points, these are the fixed points in the model, chosen to apply the correction and calculate the differences between the linear model and the model with correction. The data points suggest what portion of each processing type should be taken. x_A^k is the set of allowed blend fractions of *A* and y_A^k is 1 if and only if the k^{th} value of x_A^k is chosen. *Correction* is a factor which has to apply to the model to increase the accuracy of the results.

Kinetic models are used to measure the quality model parameters. Some of the litriture work used for this are Devahastin & Niamnuy (2010); Kaminski and Tomczak (2000); Giannakourou et al (2002); Martins et al (2006); Simal et al (1996) and Suvarnakuta et al (2007). The quality level of a product at a certain location in the production based on

an initial quality (q_0) and subsequent periods *i=1,...,m* with time interval t_i and degradation rate k_i (depending on temperature T_i), leads to:

$q = q_0 - \sum_{i=1}^{m} k_i t_i$ and $q = q_0 . \exp\left(-\sum_{i=1}^{m} k_i t_i\right)$ (4)

For zero and first-order reaction, where the degradation rate is measured by The Arrehenius equation:

$$k = k_0 \exp\left(-\frac{E_a}{RT}\right) \quad (5)$$

These models together with empirical data are used to develop approximate linear quality models.

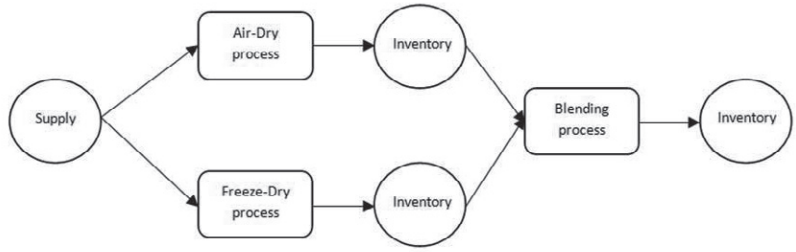

Figure 1. Drying process

The energy of each task on the other hand is modelled as follows:

$Energy_s = \sum_j \gamma_j \left(\sum_D a_{s,D} . u_{j,D} + E_j^{base}\right)$ (6)

Where *a* is the slope of the degree of freedom (e.g. process time or temperature) and *u* is the set variable and is same as the *u* in quality models. E_j^{base} is the base energy required for each task. At the blending state:

$E_b^k = x_A^k . E_{AD} + (1 - x_A^k) . E_{FD}$ (7)

E_b^k is energy after blending. Here *k* is the data point and *x* is the blending fraction.

Parameters *a* are calculated using the experimental data as well as following equation.

$Energy_j = Power_j . t_j$ (8)

This equation states; the electrical energy (kWh) consumed for the process is equal to electrical power supplied (kW) for the process multiplied by the process time in hours (Xu et al 2005). Therefore objective 1 is as follows:

$max\ [\alpha . \sum_s q_s - \beta . \sum_s Energy_s]$ (9)

This objective optimising the quality of the product while minimising the energy. The weightings α and β are given to the variables quality and energy which are 0.9762 and 0.0238, respectively. This is calculated using the ratio of quality and energy at each task and minimum quality and maximum energy. The raw materials stay for sometime in inventory before being used to overcome the seasonality. At this stage scheduling for the supply chain model is applied to measure for how long the materials should stay until they fulfil the given demand with the optimum quality and costing of products. Each time period in the horizon is one week. A coefficient *R* is introduced here for inventory to satisfy the demand. Therefore the inventory state is modelled as follows:

$I_{st} = I_{s,t-1} + \sum_j PR_{j,t} . \propto_{j,s} - D_{s,t} - w_{s,t} + R_{s,t}$ (10)

Where *R* is the residual and it would compensate for the shortage of supply. *D* and *w* are the demand and waste of each state at a time and *PR* is the production rate.

All these constraints are applied to the model to solve for the overall cost minimisation of the whole system to achieve the best quality product with minimum energy consumption, waste and cost.

$min\left(\sum_{s,t} S_{st} . PC_s + \sum_{s,t} I_{st} . SC_s + \sum_{s,t} w_{st} . DC_s + \sum_{s,j,t} PR_{jt} . TC_{sj}\right)$ (11)

3. Sample Results

The regression fitting is used for the linear quality model. Some sample results are generated using literature data for the key feedstocks. These indicate the quality following primary processing. Four raw materials have been used in this example, potato, carrot, onion and green peas. At the initial state the optimisation generates results for optimum quality and energy usage. The optimum results for the variable set *u* generally suggest using the process with low processing time and high/ low temperature in the case of drying/ freezing process. In the case of the drying process however a blending state is added therefore *M* and correction factor is calculated and variable *x* applied to find the optimum solution quality and energy wise. The model suggests blending the products from Freeze- and Air-Dry by portions of 60 and 40 % respectively for potato, 40 and 60% respectively for carrot and green peas and 100% of Air-Dry process for onion. The optimum quality of all products across all indicators after blending is shown in the figure 2.

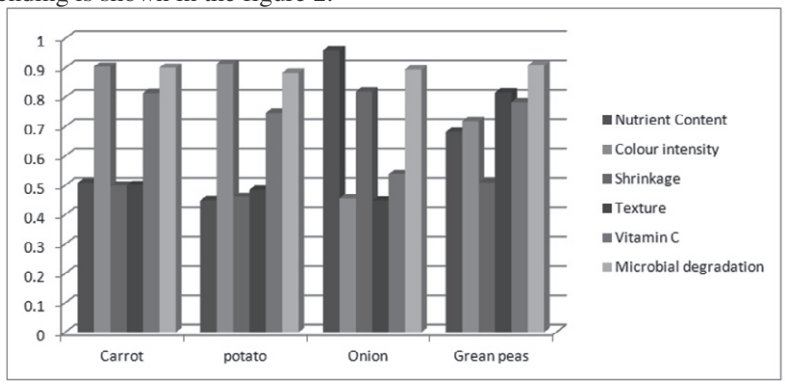

Figure 2, products quality after blending.

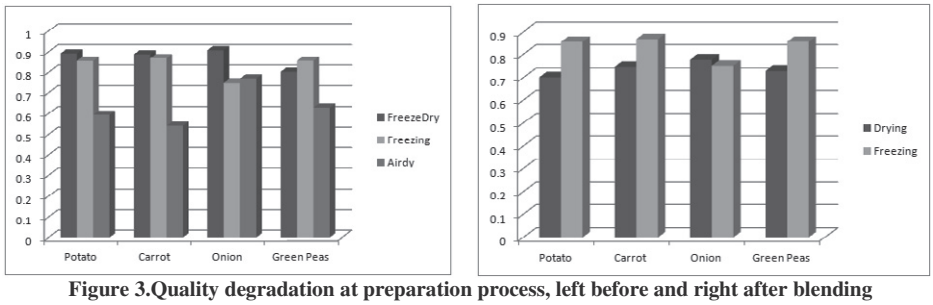

Figure 3.Quality degradation at preparation process, left before and right after blending

Figure 3 and 4 compare the quality and energy usage of the processes before and after blending the drying processes with freezing process. Air-Dry process generates the lowest quality products, but it consumes the lowest energy as well. The Freeze-Dry process on the other hand generates the best quality product for most of materials by using the highest energy. After blending the two drying processes to obtain the optimal material, quality and energy wise, the process is compared with the freezing process. The results show generally the freezing process generates better quality product. The energy consumed for carrot after blending is higher in drying process compare to freezing process. However the fact is by going through the system the energy usage for the frozen material would be much higher. The reason is, at the inventory state the frozen materials have to be stored at low temperature freezers while the dried materials

would be stored at room temperature storage. After the preparation task, the linear quality and energy models are applied to all tasks.

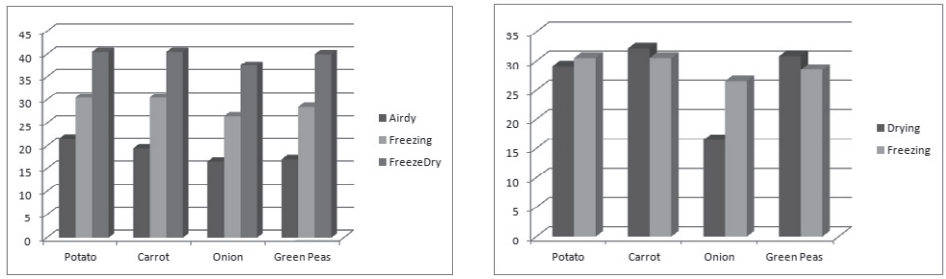

Figure 4. Energy usage at preparation process left before blending and right after blending (*MJ/Kg*).

4. Conclusion

This paper presented a mixed-integer linear programming model for the food processing and manufacturing system with the focus on product quality at the preparation process, which is strongly related to the process degrees of freedom (e.g. temperature and processing time). This is based on quality degradation and energy consumption of the food product raw materials during preparation processes, in order to increase their shelf-life, and inventory. A new methodology is applied to simplify the existing models. These are (*i*) linear quality model, which linearises the quality model and optimises the product quality across all quality indicators and is applied to the process and could also be applied to inventory. (*ii*) Base delta model to relate the energy consumption at every process to the linear quality model. (*iii*) Blending quality and energy model, which show by how much the processes should mix in order to have a product with a maximum quality and minimum energy usage. The quality and energy models are integrated into supply chain model to optimise the costing and wastage of the product throughout the system. Therefore the main contribution is introducing new methodology to simplifying the ways of optimising the quality and parallel to this controlling the energy consumption of the products, where the managing the product quality, energy consumption and controlling the temperature and processing time can be integrated in decision making on production in supply chain management. Also the interrelationships between quality and processing conditions have been developed. The model presented therefore is a useful tool in production and manufacturing in food industry.

References

Devahastin, S. & Niamnuy, C (2010). International Journal of FST 2010, 45, 1755–1767.
Giannakourou, M, C, and Taoukis , P, S (2003). Food Chemistry, volume 83, Pages 33-41
Gregory, J.F . (1996). Vitamins. In: Food chemistry, pp. 531-616. New York: Marcel Dekker.
Kaminski, W. & Tomczak, E. (2000). Drying Technology, 18, 777–790.
Martins, R, C., Silva, C, L, M (2006). Journal of food science, volume 68,pp 2232–2237,
Rong, A., Akkerman, R., and Geunow, M (2011). Int. J. Production Economics 131, 421–429
Shah, N., Pantelides, C. C., and Sargent, R (1993). Comput. Chem. 17, 229-244
Simal, S., Mulet, A., Tarrazo, J. & Rossello, C. (1996). Food Chemistry, 55, 121-128
Suvarnakuta, P., Devahastin, S. Mujumdar, A.S. (2007).Chem Eng and Processing,46,675-683.

I.A. Karimi and Rajagopalan Srinivasan (Editors), Proceedings of the 11th International Symposium on Process Systems Engineering, 15-19 July 2012, Singapore.

Single- & Multi-site Production & Distribution Planning in Food Processing Industries

Georgios M. Kopanos,[a,b] Luis Puigjaner,[b] Michael C. Georgiadis[c]

[a]*Imperial College London, Department of Chemical Engineering, Centre for Process Systems Engineering, London SW7 2AZ, UK*
[b]*Universitat Politécnica de Catalunya, Department of Chemical Engineering, Av. Diagonal 647, Barcelona 08028, Spain*
[c]*Aristotle University of Thessaloniki, Department of Chemical Engineering, Thessaloniki 54124, Greece*

Abstract

The production and logistics operations planning in real-life single- or multi-site semicontinuous food industries is addressed in this work. A mixed discrete/continuous-time mixed integer programming model, based on the definition of families of products, is devised. A remarkable feature of the proposed approach is that in the production planning problem timing and sequencing decisions are taken for product families rather than for products. However, material balances are realized for every specific product, thus permitting the detailed optimization of production (including changeovers), inventory, and transportation costs. Additionally, alternative transportation modes are considered for the delivery of final products from production sites to distribution centers. Finally, the efficiency of the proposed approach is demonstrated by solving to optimality an industrial-size case study, for a real-life Greek dairy industry.

Keywords: production planning, distribution, mixed integer programming, case study.

1. Introduction

In this work, we focused on the Food Processing Industry (FPI) sector that has received little attention in the open literature so far. FPIs acquire agricultural raw materials and then process them before further distribution. Processing is defined in a broad sense; ranging from simple packing of fresh products to extensive reforming operations. In food supply chains, logistics management normally refers to the physical material flows and the inventory of products from production facilities to Distribution Centers (DCs) or customers. Here, we consider the simultaneous detailed production and distribution planning in multi-site multiproduct semicontinuous FPIs. McDonald and Karimi (1997) and Verderame and Floudas (2009) addressed a relevant problem, but for chemical industries. Here, a real-life yogurt industry (Kopanos et at., 2010) is studied, and a linear Mixed Integer Programming (MIP) model is developed. In every planning period, the key decisions to be made are: (i) the assignment and sequencing of products (and families) to processing units, (ii) the produced product quantity in each processing site, (iii) the inventory levels for each product, (iv) the assignment of transportation trucks to production sites-DCs, (v) the selection of the available alternative transportation mode, and (vi) the detailed transportation load composition for every truck. The objective is to fully satisfy customer demand at minimum total cost, including production, changeover, inventory and transportation costs. To the best of our knowledge, there is no previous work in the literature presenting an exact method for addressing the challenges of the underlying semicontinuous food processing and distribution planning problem.

2. Mathematical Formulation

In this section, some representative and significant constraints of the proposed modeling approach are presented.

2.1. Material Balance & Distribution Operations Constraints.

The transportation of final products to DCs or customers can be done by three potential transportation modes: (a) trucks owned by the customers, (b) transportation trucks owned by the industry, and (c) contracted transportation trucks from third party logistics companies. Final products $p \in P^a$ whose final destination is the international market or big national supermarket customers are transported to their customers by transportation mode (a). The transportation of final products to the DCs owned by the enterprise can be performed by any of the other two transportation modes (b), and/or (c).

The total quantity of product p produced in production plant s in period n-λ_p, which is ready to ship to DCs (or customers) in period n, is given by:

$$Q'_{spn} = \sum_{j \in (J_s \cap J_p)} Q_{psjn-\lambda_p} \quad \forall s, p, n > \lambda_p \tag{1}$$

where λ_p denotes the days that packed product p should be kept in storage (e.g., for cooling or refrigeration purpose). Q'_{psjn} corresponds to the quantity of product p processed in unit j of production site s during period n. Note that $Q'_{psjn}=0 \ \forall \ s,p,n \leq \lambda_p$. Constraint set (2) expresses the material balance for products $p \in P^a$ whose destination is the international market or big national supermarket clients.

$$I_{spn} = I_{spn-1} + Q'_{spn} - U^a_{spn} \quad \forall s, p \in P^a, n \tag{2}$$

where U^a_{spn} denotes the quantity of product $p \in P^a$ transported from production site s to the international market or big national supermarket clients by customer trucks, at period n, in order to fully meet the demand. I_{spn} corresponds to the inventory level of product p in production plant s at time point n. Note that I_{spn}=0 reflects the initial inventory for product p in production site s. The multiperiod material balance constraints for products $p \notin P^a$ transported to company's DCs are given by:

$$I_{spn} = I_{spn-1} + Q'_{spn} - \sum_{d \in D_s} \sum_{l \in L_{sd}} U_{sdlpn} \quad \forall s, p \notin P^a, n \tag{3}$$

where U_{sdlpn} denotes the quantity of product p transported from production site s to DC d by transportation truck l at period n. Once final products reach DCs, they are stored for a day due to product quality purpose before sending them to final customers. The total load for any transportation truck l that transfers products from production facility s to DC d in period n is given by:

$$U'_{sdln} = \sum_{p \notin P^a} U_{sdlpn} \quad \forall s, d \in D_s, l \in L_{sd}, n \tag{4}$$

Hence, every truck l has a specific minimum and maximum capacity (ε_l^{min} ,and ε_l^{max}, respectively) as given by:

$$\varepsilon_l^{\min} Z_{sdln} \leq U'_{sdln} \leq \varepsilon_l^{\max} Z_{sdln} \quad \forall s, d \in D_s, l \in L_{sd}, n \tag{5}$$

Binary variables Z_{sdln} denote the use of truck l for transporting products from production site s to DC d at period n. Any transportation truck l can transfer products only between one production site s and one DC d during any period n, according to:

$$\sum_{s \in S_l} \sum_{d \in (D_s \cap D_l)} Z_{sdln} \leq 1 \quad \forall l, n \tag{6}$$

2.2. Families of Products Modeling.
Production planning in semicontinuous process industries, such as the FPI, typically deals with a large number of products with similar characteristics. That allows us to group products with similar characteristics into product families. In the proposed approach, *products belong to the same family if and only if* : (i) they come from the same batch recipe, and (ii) there is no need for changeover operations among them. Thus, the production planning problem under question could be partially focused on families rather than on each product separately. Also, sequencing and timing decisions are taken for families and not for each separate product, as Figure 1 shows. The definition of families significantly reduces the size of the underlying MIP model without sacrificing feasibility or optimality. Product lot-sizing, family allocation, sequencing and timing, and batch recipe stage constraints are similar to those presented in Kopanos et al. (2010).

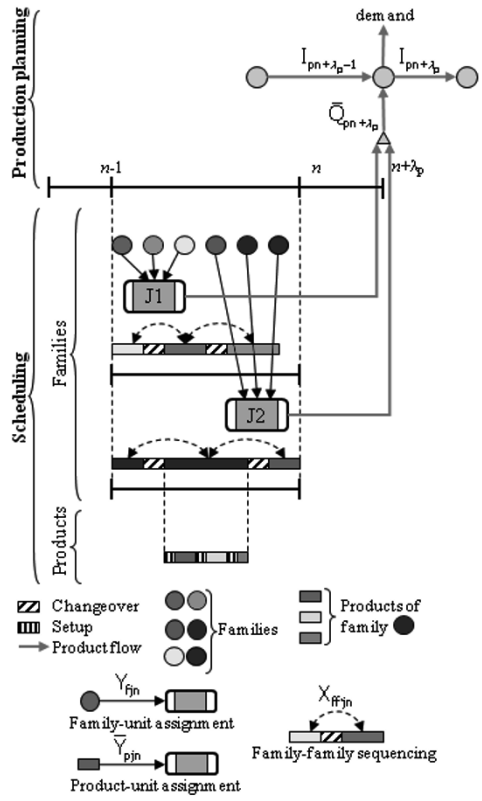

Figure 1. Modeling approach.

A salient feature of the proposed modeling approach is that allows products that belong to the same family to have different: (i) processing rates, (ii) operating costs, (iii) setup times, (iv) inventory costs, (v) transportation costs, and (vi) customer type

2.3. Objective Function.
The optimization goal is the minimization of the total cost including several factors such as: (i) inventory costs, (ii) operating costs, (iii) batch recipes preparation costs, (iv) unit utilization costs, (v) families changeover costs, and (vi) transportation costs.

3. Case Study

An industrial-size multi-site production and distribution planning problem of a real-life Greek dairy industry, producing yogurt, is considered and solved by the proposed MIP model. The production and distribution network under consideration consists of two production sites (located in Serres, and Karditsa) and five DCs, as shown in Figure 2. Processing unit types *J1* to *J4* are installed on the production plant located in Serres while processing units types *J1* to *J3* are installed on the production site of Karditsa. Each production site in owns a pair of transportation trucks, while ten and six third party logistics trucks are available in the plant of Serres and Karditsa, respectively. The production facilities have to fully meet the demand for all products. The relative sequences among families are predetermined. The remaining data are available upon request from the authors.

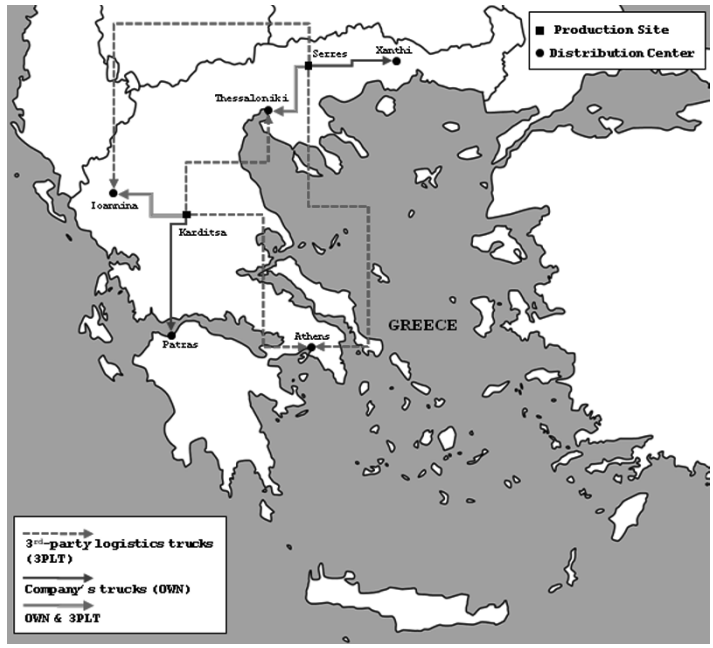

Figure 2. Production and distribution network of the dairy industry.

This case study has been solved to global optimality in a Dell Inspiron 1520 2.0 GHz with 2 GB RAM using CPLEX 11 via a GAMS 22.8 interface. The resulting MIP model consists of 19,371 constraints, 4,070 binary variables, and 35,614 continuous variables. The optimal solution reports 520,047€ of total cost, and it was reached in 379.2 CPU s after exploring 1,837 nodes in the branch-and-bound tree.

Figure 3 illustrates the total, and per production facility, cost breakdown as well as the contribution of each cost term on the total cost. Inventories costs represent 14.5% of the total cost while transportation costs stands for the 35.7% of the total cost. Production costs (i.e., operating, recipe, unit utilization, and changeovers costs) represent 49.8% of the total cost. Also, noted that 62.5% of the total inventory cost, and the 57.5% of the total transportation cost is occurred in production site of Serres; due to the fact that the plant in Serres (wherein 4 units are installed) appears higher overall production capacity than that of the plant in Karditsa (wherein 3 units are installed). The profile of total produced quantities, inventories, and transported quantities for each planning period are shown in Figure 4. The production plants operate from *n0* to *n5* period, where period *n0* is an overtime period (i.e., higher operating costs). The highest production is observed in period *n5*, with 129,723 kg of production. On average, inventory levels are maintained low throughout the planning horizon, with an exception in period *n6* where a relatively high inventory level of 64,702 kg is detected; due to the high demand requirements of the last period. Transportation operations from production facilities to DCs are realized from *n3* to *n7* period, observing the peak in period *n7*, wherein a total of 124,171 kg of products is transferred from the production sites to the DCs. Finally, the proposed MIP model also generates: the detailed production plan for both production plants, and the detailed transportation plan for each product (i.e., assignment of product to truck, assignment of truck to DC, and quantity of product transported by each truck); which are omitted here due to lack of space.

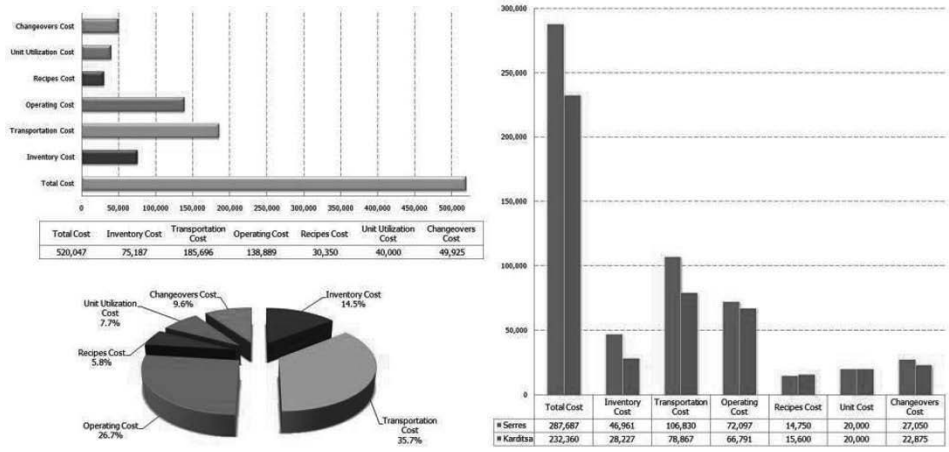

Figure 3. Total cost breakdown (€) and cost terms contribution.

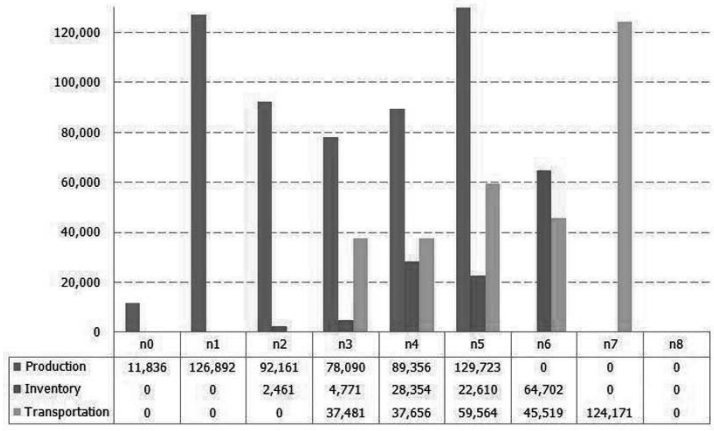

Figure 4. Total production, inventory and transportation profiles (kg) per period.

4. Concluding Remarks

The proposed integrated framework serves as a tool for negotiations between production and logistics departments, allowing them to collaborate more easily to find the best balance between inventory levels, production and distribution efficiency. The proposed approach was successfully validated and approved by the dairy industry considered, and its further improvement and implementation in the firm is currently on the way.

Acknowledgments

Financial support from the Spanish Ministry of Education and Spanish project DPI2006-05673 is gratefully acknowledged. The authors would like to thank Mr. Nikolas Polydorides, production manager at KRI-KRI S.A., for the provision of data and the fruitful comments.

References

G. M. Kopanos, L. Puigjaner, M. C. Georgiadis, 2010, Industrial Engineering & Chemical Research 49, 701-718.

C.M. McDonald, I. A. Karimi, 1997, Industrial Engineering & Chemical Research 36, 2691-2700.

P.M. Verderame, C.A. Floudas, 2009, Computers & Chemical Engineering 33, 1036-1050.

I.A. Karimi and Rajagopalan Srinivasan (Editors), Proceedings of the 11th International Symposium on Process Systems Engineering, 15-19 July 2012, Singapore.

Hybrid Approach for Multi-stage Logistics Network Optimization under Disruption Risk

Yoshiaki Shimizu[a] and Muhammad Rusman[a]

[a]*Department of Mechanical Engineering, Toyohashi University of Technology, 1-1 Hibarigaoka, Ten-paku-cho, Toyohashi 441-8580, Japan*

Abstract

Modern supply chains are subject to a wide range of risks, such as demand uncertainty, natural disasters, and terrorist attacks. Based on some prospects for risk management, this study investigates a logistics network design problem with facility disruption that will be caused by various risks. To find a solution for this design issue, we have formulated a probabilistic programming problem, and propose an effective hybrid method composed of meta-heuristic method and graph algorithm to offset potential losses from the network disruptions. Through numerical experiments, effectiveness of the proposed method is validated.

Keywords: Multistage logistics network design, Hybrid method, Disruption risk, Probabilistic programming problem.

1. Introduction

Under today's global and agile manufacturing, modern supply chains are subject to a wide range risk such as the demand uncertainty, natural disasters, terrorist attacks and so on. Recent disruptions by earthquake and tsunami in Japan (2011) and the massive flooding in Thailand (2011) had dramatic impacts on the supply chains and logistic distribution of many companies. The resulting slowdowns and cessation of operations affected seriously some companies.

Against this, we can anticipate the disruption by considering preventive action viewed as mitigation planning. Toward such mitigation plan, supply chain must build a resilient system that can minimize the impact of the disruption in future by having appropriate backup facilities.

In this study, therefore, we focus on the issue related to facility disruption risk for multistage logistic networks and present a hybrid approach that will provide a resilient design in practice. Finally, effectiveness of such approach will be examined through numerical experiments.

2. Problem Formulation

Among some previous studies, Tomlin (2006), Snyder and Daskin (2005) and Chopra and Sodhi (2004) investigate the impact and/or risk management perspective for two echelon logistic problems. Considering the risk associated with demand fluctuation, Shimizu et al. (2011) give a solution procedure by recourse model for a three echelon logistic problem.

This study takes three echelon networks for which Shimizu and Rusman (2011) carried out a morphological analysis. The network is consisted of distribution centre (DC), relay station (RS) and customer (RE). For RS, we consider two kinds of RS, i.e.,

reliable RS (RRS) and unreliable RS (URS). URS is no longer available for serving customers when the disruption would occur. In contrast, RRS is the hardened one and can continue the business even after the incident.

Figure 1 illustrates the case where RS is potentially being disrupted. Thereat, two DCs distribute products to three relay stations (RSs), which are consisted of two RRSs and one URS. If the demand of the customer is satisfied by RRSs, then only single assignment is sufficient. On the other hand, if the customer is assigned to URS, backup assignment is required besides the primary assignment. This means when the disruption occurs at URS, the demand of customer will be distributed from the backup RRS.

Here, we assume that each facility has the same probability of disruption q ($0<q<1$). Primary assignments occur with probability 1-q under the normal cost while backup assignments occur with probability q under the abnormal cost. Moreover, we consider each RS is possible to receive the product from multiple DCs and customer also from multiple RSs depending on the respective demand of the customer. In the model, we use the following notations for index sets, parameters, and decision variables.

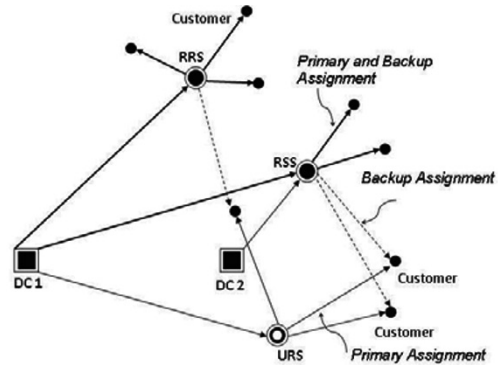

Fig.1 Logistic network under disruption risk

Index sets

I : set of distribution centres (DC)
J : set of relay stations (RS)
K : set of customers (RE)

Parameters

F^U_j : Fixed cost for opening URS j
F^R_j : Fixed cost for opening RRS j
C^P_i : Shipping cost at DC i as primary assignment
C^B_i : Shipping cost at DC i as backup assignment
H^P_j : Handling cost at RS j as primary assignment
H^B_j : Handling cost at RS j as backup assignment
$T1^P_{ij}$: Transport cost from DC i to RS j as primary assignment
$T1^B_{ij}$: Transport cost from DC i to RS j as backup assignment
$T2^P_{jk}$: Transport cost from RS j to customer k as primary assignment
$T2^B_{jk}$: Transport cost from RRS j to customer k as backup assignment
U_j : Upper bounded capacity of RS j
PU_i : Maximum supply ability of DC i
PL_i : Minimum supply ability of DC i
d_k : Demand of customer k
q : Probability of disruption ($0<q<1$)

Decision variables

f^P_{ij} : Shipped amount from DC i to RS j as primary assignment
f^B_{ij} : Shipped amount from DC i to RS j as backup assignment
g^P_{jk} : Shipped amount from RS j to customer k as primary assignment
g^B_{jk} : Shipped amount from RS j to customer k as backup assignment

$$x_j^U = \begin{cases} 1, if\ RS\ j\ is\ opened \\ as\ unreliable\ assignment \\ 0,\ otherwise. \end{cases}$$

$$x_j^R = \begin{cases} 1, if\ RS\ j\ is\ opened \\ as\ reliable\ assignment; \\ 0, otherwise. \end{cases}$$

After all, we can formulate the model as a probabilistic mixed-integer programming problem as follows.

Minimize

$$\sum_{j\in J} F_j^U x_j^U + \sum_{j\in J} F_j^R x_j^R + (1-q)\left(\sum_{i\in I}\sum_{j\in J}\left(C_i^P + T1_{ij}^P\right)f_{ij}^P + \sum_{j\in J}\sum_{k\in K}\left(H_j^P + T2_{jk}^P\right)g_{jk}^P\right)$$
$$+ q\left(\sum_{i\in I}\sum_{j\in J}\left(C_i^B + T1_{ij}^B\right)f_{ij}^B + \sum_{j\in J}\sum_{k\in K}\left(H_j^B + T2_{jk}^B\right)g_{jk}^B\right)$$

subject to

$$x_j^U + x_j^R \le 1, \quad \forall j \in J \tag{1}$$
$$\sum_{j\in J} x_j^R \ge 1 \tag{2}$$
$$\sum_{i\in I} f_{ij}^P \le U_j\left(x_j^U + x_j^R\right), \forall j \in J \tag{3}$$
$$\sum_{i\in I} f_{ij}^B \le U_j x_j^R, \forall j \in J \tag{4}$$
$$\sum_{j\in J} f_{ij}^P \le PU_i, \forall i \in I \tag{5}$$
$$\sum_{j\in J} f_{ij}^B \le PU_i, \forall i \in I \tag{6}$$
$$\sum_{j\in J} f_{ij}^P \ge PL_i, \forall i \in I \tag{7}$$
$$\sum_{j\in J} f_{ij}^B \ge PL_i, \forall i \in I \tag{8}$$
$$\sum_{i\in I} f_{ij}^P - \sum_{k\in K} g_{jk}^P = 0, \forall j \in J \tag{9}$$
$$\sum_{i\in I} f_{ij}^B - \sum_{k\in K} g_{jk}^B = 0, \forall j \in J \tag{10}$$
$$\sum_{j\in J} g_{jk}^P = d_k, \forall k \in K \tag{11}$$
$$\sum_{j\in J} g_{jk}^B = d_k, \forall k \in K \tag{12}$$
$$x_j^R \in \{0,1\}, \forall j \in J \tag{13}$$
$$x_j^U \in \{0,1\}, \forall j \in J \tag{14}$$
$$f_{ij}^P \ge 0, \forall i \in I, \forall j \in J \tag{15}$$
$$f_{ij}^B \ge 0, \forall i \in I, \forall j \in J \tag{16}$$
$$g_{jk}^P \ge 0, \forall j \in J, \forall k \in K \tag{17}$$
$$g_{jk}^B \ge 0, \forall j \in J, \forall k \in K \tag{18}$$

The objective function is expected costs that consist of fixed cost for opening RS, shipping cost at DC, transportation costs between facilities and handling cost at RS.
Equation (1) requires that either of RRS or URS can be open, but not both; Eq.(2) at least one RRS must be opened; Equations (3) and (4) are capacity constraints for RS as primary and backup assignment, respectively; Eqs.(5) and (6) upper bounds for available supply as primary and backup assignment, respectively; Eqs.(7) and (8) lower bounds for available supply as primary and backup assignment, respectively; Eqs.(9) and (10) balances of product flow as primary and backup assignment, respectively: Equations (11) and (12) mean demand of every customer must be satisfied as primary and backup assignment, respectively.
Due to some undisrupted reasons, it makes sense to assume such a relation for each cost parameter that $F_j^R > F_j^U$, $T1_{jk}^B > T1_{jk}^P$, $T2_{jk}^B > T2_{jk}^P$, $C_i^B > C_i^P$ and $H_k^B > H_k^P$.
Since thus formulated problem belongs to a NP-hard class, its solution becomes extremely difficult according to the increase in problem size.

3. Hybrid Approach for Solution

Taking a similar hierarchical logistic network mentioned above, we proposed a method termed hybrid tabu search (Shimizu et al., 2004) and applied its variants both to the

certain and uncertain cases. It is a two-level method whose upper level problem decides the locations of distribution centre and the lower derives the routes among the facilities. At the upper level, evolutionary search is carried out so that the neighbor location is updated by the sophisticated tabu search, in turn. On the other hand, the location pegged problem at the lower level refers to a linear program (LP) that is possible to transform into the minimum cost flow problem (MCF). Finally, we can apply the graph algorithm such as CS2 or Relax 4 to solve the resulting problem extremely fast compared with solving directly the original LP. These procedures will be repeated until a certain convergence criterion has been satisfied. This basic idea is possible to straightforwardly extend to the present solution just by solving the lower level problem both for normal and abnormal cases, respectively and combining them together to compute the expected cost (See right hand side of Fig.2).

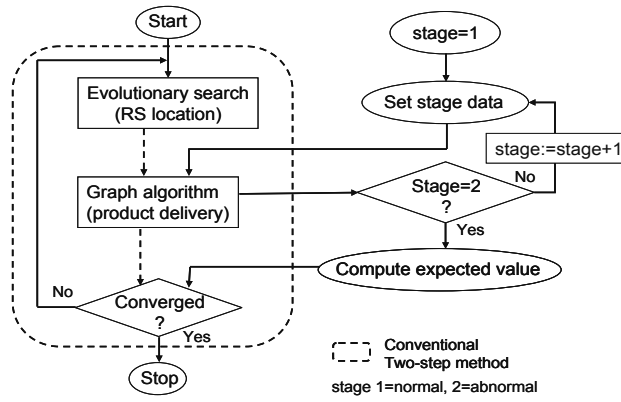

Fig.2 Flowchart of the proposed procedure

4. Numerical Experiment

To verify the effectiveness of the proposed approach, we provide a few benchmark problems whose system parameters are given randomly within the respective upper and lower bounded values.

Result of the hybrid approach for a small model (number of DC/ RS/ Customer = 2/ 5/ 50) is given in Table 1. This coincides with the one derived from commercial software known as CPLEX 12. From this, we know DCs will distribute products from three open RSs (RS#2, RS#4 and RS#5) for every disruption probability except for q=0.4. It is interesting to see that RS#4 is used as the unreliable RS when q is low while it appears as the reliable one at the higher q after it disappears during the middle range of probability. This is because the opening cost of RS#4 is quite cheap among RSs. Hence, opening this RS as URS can save the transportation cost greatly when q is low. In contrast, when q becomes higher, it makes sense to open this RS as RRS to cope with the disruption as well as transportation cost saving. The situation when q=0.4 appears as the transient status of these two cases. These facts can confirm the adequateness of the proposed model.

Relying on this preliminary experiment, we solved several problems with such larger sizes that makes extremely difficult to solve by the commercial software from our previous experiences. For example, Table 2 summarizes the results for different numbers of customer up to 5000 when q=0.1. We also know that the rising rate with the increase in q is almost constant for the primal cost while most remarkable for the backup cost. From Fig.3, as expected a priori, we can observe a rapid increase in CPU time with the problem size.

Table 1 Result for a small problem: DC/ RS/ Customer = 2/ 5/ 50

Probability (q)	0.01		0.1		0.4		0.5	
Relay station (RS)	URS	RRS	URS	RRS	URS	RRS	URS	RRS
Number of RS	1	2	1	2	0	2	0	3
Facilities (RS #)	(#4)	(#2,5)	(#4)	(#2,5)		(#2,5)		(#2,4,5)
Expected cost unit [-]	4,454,105		4,644,056		5,276,776		5,484,457	

URS: unreliable relay station RRS: reliable relay station

Table 2 Results for larger problem size when q=0.1

Problem size (DC/ RS/ Customer)	Expected cost unit	Primal cost unit	Backup cost unit	RRS	URS
10/ 30/ 500	2.75E7	2.61E7	3.95E7	9	5
10/ 30/ 1000	5.70E7	5.44E7	8.11E7	15	2
10/ 30/ 2000	1.43E8	1.37E8	2.00E8	14	1
10/ 30/ 3000	1.94E8	1.83E8	2.95E8	16	8
10/ 30/ 5000	3.24E8	3.08E8	4.68E8	17	7

5. Conclusion

Concerning with supply chain, this study investigates the multi-stage logistics network design that are exposed to various risks. The problem under disruption risk is formulated as a probabilistic programming model. Then to find the optimal solution of this problem in practice, a hybrid method is employed which combines a meta-heuristic method and a graph algorithm in a hierarchical manner. Through the numerical experiment, we have shown the proposed approach is promising to design the resilient logistic networks available for the real world mitigation planning. Future studies should be devoted to enhance the solution ability and consider the more realistic conditions suitable for business continuity plan/management that will provide .

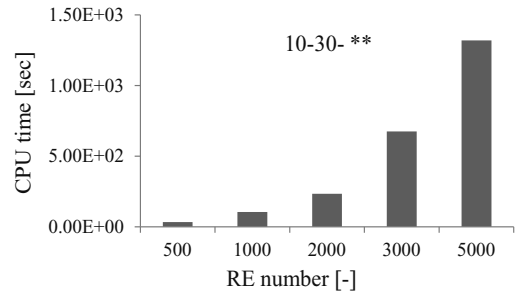

Fig.3 CPU time vs. problem size

References

S. Chopra and M.S. Sodhi, 2004, Managing risk to avoid supply-chain breakdown, MIT Sloan Management Review, Vol.46, 53-61

Y. Shimizu, H. Fushimi and T. Wada, 2011, Robust Logistics Network Modeling and Design against Uncertainties, Journal of Advanced Mechanical Design, Systems, and Manufacturing, Vol.5, No.2, 103-114

Y. Shimizu and M. Rusman, 2012, Morphological Analysis for Multistage Logistic Network Optimization under Disruption Risk, Proc. International Symposium on Semiconductor Manufacturing Intelligence, Hsinchu, Taiwan

L.V. Snyder and M.S Daskin, 2005, Reliability models for facility location: the expected failure cost case, Transportation Science, Vol.39, No.5, 400-416

B. Tomlin, 2006, The value of mitigation and contingency strategies for managing supply chain disruption risks, Management Science, Vol.50, No.5, 639-657

I.A. Karimi and Rajagopalan Srinivasan (Editors), Proceedings of the 11th International Symposium on Process Systems Engineering, 15-19 July 2012, Singapore.

Supply Chain Optimization of Biomass Production Improvement

Mingyen Yu[a] , Franjo Cecelja[a], Seyed Ali Hosseini[a]

[a]*PRISE Center for Process and Information Systems Engineering, Faculty of Engineering and Physical Science, University of Surrey, Guildford, GU2 7XH, UK*

Abstract

Renewable energy, especially biofuels, is seen as a viable solution to replace the depleting fossil fuels. Moreover, tighter environmental regulations across the world force many countries to develop strategic approaches to target and screen relevant replacement of resources and technologies. Because there are significant variations in types of biomass and conversion methods, determining the economical effectiveness of overall supply chain (SC) is a complex task. Thus, a holistic approach which accounts for economic, environmental and production aspects across the SC, starting from cultivation to the final products, and establishing appropriate links among them at each stage is imperative in analyzing overall chain efficiency.

In this work, for analysis of SC, mathematical modelling is paired with linear programming (LP), which accounts for the variability of technologies that uses biomass as input. The analysis includes economic and environmental factors along the SC. Green House Gases (GHG) is analysed in terms of carbon-equivalent units and converted into monetary values to form financial objective. In addition, incentives for each party in the SC to have economical gain have also been considered.

To validate the developed methodology, a case study from Northern Italy is investigated that takes corn stover as a feedstock and targeting production of ethanol with ash, carbon dioxide and DDGS being by-products. It should be highlighted that different types of ethanol conversion technologies are analyzed in terms of overall SC and compliance of GHG emission with existing regulation is also taken into account in the case study.

Keywords: Supply chain management, Optimization, Renewable energy

1. Introduction

With the world's population passed the seven billion mark [1], resources are getting scarce. This is especially true for fossil fuels. At the same time, the increasing emission of Green House Gases (GHGs) is recognized as a problem with climate consequences. Thus, biofuels such as ethanol from corn stover are seen as one of the solutions with respective to supply chain (SC) analysis and design in their core.

So far, the main focus of SC has been on intra-chain issues, e.g. distribution network design, inventory planning, logistics management and production coordination [2] [3]. Also, mathematical analysis for biomass SC has been recognized in the literature. Shah *et al.* [4] demonstrated the use of Mixed Interger Linear Programming (MILP) model to determine production capacity allocation, optimized layout and flow of distributed network for a biomass to heat SC system using a state-task-network (STN) approach. You *et al.* [5] developed a Mixed Interger Non-Linear Programming (MINLP) optimization model framework for economics and responsiveness of multi-site and multi-echelon process SC networks, to consider the trade-offs between net present value

(NPV) and lead time. Bezzo *et al*. [6] [7] addressed the design of bioethanol SC under multiple technological options with the help of MILP optimization and Abedpour *et al*. [8] described the key challenges in bioenergy SC modelling and developed a framework and methodology to show how multi-scale modelling can answer these SC questions.
Recently, because of the ISO 14000 environmental management standards, more attention is given to Environmental SCM (ESCM) and Life Cycle Analysis (LCA) which is seen as the main tool for ESCM. It is a technique for gathering data on environmental care issues which can be used to restructure SC in order to improve the environmental performance [9]. Kumaran *et al.* [10] further proposed the concept of life cycle environmental cost analysis (LCECA), to include eco-costs into the total cost of the products. Ultimately, it aims to reduce the total cost with the help of green or eco-friendly alternatives in all the stages of the life cycle of any product.
In this paper, we present the development and comparison of strategic overall SC, beginning from the supplier to the end customer. The design process is set as an optimized problem, intending to maximize financial performance, which is the NPV, and to minimize environmental effects with focus on GHG emissions.
The paper is organized as follows. Following the analysis and problem statement, SC financial model and LCECA model are developed. A case study on biomass for Northern Italy is presented, as well as the results. Finally, conclusions together with proposed future work are suggested.

2. Model Development

2.1. Supply Chain Financial Model

The SC financial model is defined as a LP optimization problem to maximize NPV, which is used to calculate the final profit of the SC as sum of profit after tax (PAT) for conversion technology k and biomass i, with discount factor df in terms of time t:

$$Obj_{NPV} = (\sum_{k,t} PATtk_{k,t} \times df_t) + (\sum_{i,t} PATbi_{i,t} \times df_t) \tag{1}$$

PAT for technology k and biomass i are given as:

$$PATtk_{k,t} = PBTtk_{k,t} - TAXtk_{k,t} + Subtk^{T}_{k,t} - EnvCos_{k,t} \quad \forall k,t \tag{2}$$

$$PATbi_{i,t} = PBTbi_{i,t} - TAXbi_{i,t} + Subbi^{T}_{i,t} \quad \forall i,t \tag{3}$$

It is obtained by taking the profit before tax, *PBTtk*, and total subsidies given, *Subtk*, for technology k, less the taxation, *TAXtk*, and the environment cost, *EnvCos*, at time t. Similar function is also used to calculate PAT for biomass i, *PATbi*. As environmental cost has already been considered in k in (2), it is not being re-considered again in (3). *PBTtk* and *PBTbi* are given by:

$$PBTtk_{k,t} = Inctk_{k,t} - VarCtk_{k,t} - FixCtk_{k,t} \quad \forall k,t \tag{4}$$

$$PBTbi_{i,t} = Incbi_{i,t} - VarCbi_{i,t} - FixCbi_{i} \quad \forall i,t \tag{5}$$

which is the income for technology k, *Inctk*, and biomass i, *Incbi*, less fix costs, *FixC*, and variable costs, *VarC*, of k and i respectively. It is assumed that the fix costs consist of infrastructure costs only in this model. Only one biomass site, *bs*, is used and the distance between the biomass site and the technology, k, is being considered in terms of variable costs. Next, income for k and i are given by:

$$Inctk_{k,t} = \sum_{j} TIpj_{j,k,t} + \sum_{l} TIpl_{l,k,t} \quad \forall k,t \tag{6}$$

$$Incbi_{i,t} = \sum_{bs} (Capbi_{i,bs,t} \cdot USPbi_{i}) \quad \forall i,t \tag{7}$$

The income for k is calculated by adding the sales of the main product, *TIpj*, and the by-products, *TIpl*. Income for the biomass i is the sum of the capacity of biomass, *Capbi*, with the unit sale price of biomass, *USPbi*, for the biomass site, *bs*.

2.2. Life Cycle Environmental Cost Analysis Model

The environment cost, *EnvCos*, for technology k is calculated as:

$$EnvCos_{k,t} = ETS \cdot (\frac{T\,\mathrm{Im}_{k,t}}{1000}) \quad \forall k,t \tag{8}$$

where *ETS* is the emission trading scheme, which is the price of carbon in the open market. The total environmental impact, *Tim*, is the sum of all the impacts of biomass, *Impbi*, with stages *sbi* (biomass production, *bp,* biomass pre-treatment, *bpt*, and biomass transportation, *bt*) and sum of all the impacts of technology, *Imppl*, with stages *spl* (fuel production, *fp*, and fuel transportation, *ft*), less the sum of all the impacts of carbon credit, *Impec*, with stage *ccd* (emission credit, *ec*):

$$T\mathrm{Im}_{k,t} = \sum_{sbi} \mathrm{Im}\,pbi_{sbi,k,t} + \sum_{spl} \mathrm{Im}\,ppl_{spl,k,t} - \sum_{ccd} \mathrm{Im}\,pec_{ccd,k,t} \quad \forall k,t \tag{9}$$

2.3. Constraints

In order for the SC to be operational, the PBT for technology k and biomass i should be greater than zero to ensure economical gain for all parties in the SC:

$$PBTtk_{k,t} \geq 0 \quad \forall k,t \tag{10}$$

$$PBTbi_{i,t} \geq 0 \quad \forall k,t \tag{11}$$

The conversion of biomass i to main product j and by-products l are given by:

$$MPfbi_{i,j,k,t} = (Captk_{i,k,t} \cdot ConFa\_ij_{i,j}) \quad \forall i,j,k,t \tag{12}$$

$$BPfbi_{i,l,k,t} = (Captk_{i,k,t} \cdot ConFa\_il_{i,l}) \quad \forall i,l,k,t \tag{13}$$

where main product, *Mpfbi*, is obtained by taking the capacity of biomass in k, *Captk*, and conversion factor of biomass to main product, *ConFa_ij*. By-products, *Bpfbi*, is also obtained by converting the capacity of biomass in k with conversion factor of by-products, *ConFa_il*. It is assumed in the model that by-products do not use excess resources when being produced.

The capacity of biomass in k, *Captk*, should be greater than the minimum capacity, *CapMin* of conversion technology, but less than the maximum capacity, *CapMax*, that the plant can hold to ensure that the plant is not either underloaded or overloaded:

$$CapMin_{i,k} \leq Captk_{i,k,t} \leq CapMax_{i,k} \quad \forall i,k,t \tag{14}$$

2.4. Case Study

We use a case study to show the applications and the potential capabilities of the research method proposed. Actual economic and environmental data are used, as

proposed by Bezzo *et al* [6] [7] for biofuel production in Northern Italy, and they have been adopted to evaluate specific modeling parameters. This is compared against the data obtained by Solda *et al* [11]. who also studied different biofuel technologies in Northern Italy. The environmental assessment of the stover-to-ethanol uses the LCECA model, as well as work by Luo *et al* [12] and Bezzo *et al* [6] [7].

The optimization problem is addressed by comparing two SCs in terms of different biomass conversion technologies (Ligno-Cellulosic Ethanol Process (LCEP) and Traditional Dry Milling (C+TDM)), and followed by analyzes of which SC is more profitable for a total duration of three years. In this case study, some factors such as transportation costs for biomass and products are deliberately kept the same so as to hightlight the effects of different technologies on the overall SC.

3. Result Analysis

The case study set up is solved using CPLEX solver in GAMS® modeling tool. It is then plotted into Microsoft Excel 2010® for further verification. As predicted, the result shows conflict between the environmental and the economic objectives understudy.

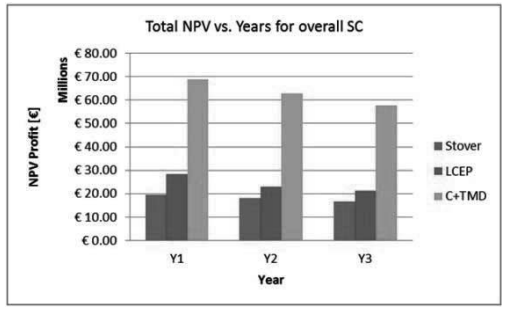

Fig 1 Total NPV vs. Years for overall SC

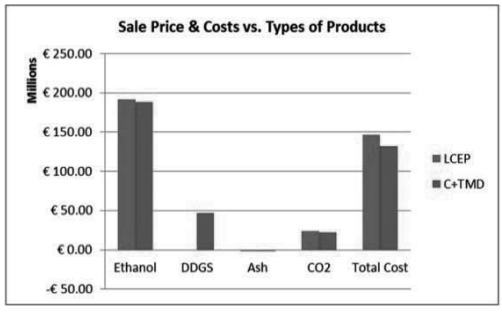

Fig 2 Sale Price & Costs vs. Types of Products

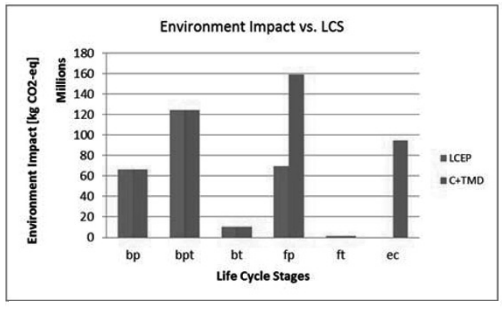

Fig 3 Environmental Impact vs. LCS

Based on the result obtained, the optimized capacity for both SCs are in the ratio of 52.27% for LCEP and 47.73% for C+TDM. The total NPV for the overall SC are shown in Fig 1.

It can be seen that C+TMD has higher NPV profit. Some possible reasons are:

- It has higher conversion factor (0.267 for LCEP vs. 0.288 for C+TDM) on ethanol.
- Compared to LCEP, C+TDM has an additional by-product, DDGS, which helps to generate extra income for the plant (Fig 2).
- As emission credit is only given to C+TDM, the overall GHG impact is lowered, and the environmental cost for C+TDM is reduced. Thus the total cost for C+TDM is lower than LCEP. This is shown in Fig 2.

In terms of environmental impact, stages *bp*, *bpt*, *bt* and *ft* are assumed to have the same GHG emission factor for both technologies, thus the impact for these four stages look identicial. However, without considering the emission credit, life cycle stage *fp* for C+TDM immediately rises to more than 160 million kg CO_2-eq, which is about 2.5 times the amount for LCEP.

At the same time, the emission credit ec for C+TDM is high as well (almost 100 million kg CO_2-eq), which effectively helps to lower the total GHG emission for the conversion technology, as well as increase the profit. This is shown in Fig 3.

4. Conclusion

In this research, different technologies of corn stover to ethanol SC are compared in terms of financial and environmental objectives. The mathematical models for the research as well as a case study comaring LCEP and C+TDM conersion technologies are presented.

Based on the result of the case study, it can be concluded that C+TDM is a more profitable conversion technology compared to LCEP, with the help of the emission credits. Thus for this case study, the maximum capacity of C+TDM is fulfilled before LCEP is used for ethanol conversion.

However, if the emission credit were removed, C+TDM may not have the advantage to be the preferred technology, as the GHG emissions for LCEP is much lower than C+TDM, even though the fixed cost for setting up the LCEP technology is higher than that of C+TDM.

The concept used in this research can be expanded into generic SC model, which can be applied to different SC scenarios other than biomass, to calculate the impact of finance against environment of the whole SC. Other performance criterias may also be added into the model for accessment in future.

References

[1] BBC NEWS, 2011. Population seven billion: UN sets out challenges.

[2] Beamon, B. M. (1998). Supply chain design and analysis: Models and methods. *International Journal of Production Economics, 55*(3), 281-294.

[3] Bramel, J., Simchi-Levi, D., 1997. *The logic of logistics: theory, algorithm and applications of logistics management.* New York: Springer.

[4] Shah, N., Dunnett, A., Adjiman, C., Biomass to Heat Supply Chains Application of Process Optimization. *IChemE,* 85, pp. 419-429.

[5] You. F., G.I.E., 2008. Optimal Design and Operational Planning of Responsive Process Supply Chain.

[6] Franceshin, G., Zamboni, A., Bezzo, F., Bertucco, A. (2008). Ethanol from corn: A technical and economical assessment based on different scenarios. *Applied Microbiology and Biotechnology,* (67), 19-25.

[7] Franceshin, G., Zamboni, A., Bezzo, F., Bertucco, A. (2011) Supply Chain Design and capacity planning: from First to Second Generation Biofuel Systems. *Chemical EngineeringTransactions,* **24**(ICheaP-10), pp. 253-258.

[8] Abedpour, A., Hosseini, S., Yu, M., (2012) Multi-scale process and supply chain modelling: from lignocellulosic feedstock to process and products.

[9] Geoffrey J.L.F. Hagelaar., Jack G.A.J. van der Vorst, 2002. Environmental supply chain management: using life cycle assessment to structure supply chains. *International Food and Agribusiness Management Review,* (4), pp. 399-412.

[10] Kumaran, D. S., Ong, S. K., Tan, R. B. H. Nee, A. Y. C. (2001). Environmental life cycle cost analysis of products. *Environmental Management and Health, 12*(3), 206-276.

[11] Solda, M., Cecelja, F., Yang, A., Manakit, P. (2011). Ethanol from corn: Screening options and power supply improvement to ethanol plant in italy

[12] Luo L, van der Vote E, Huppes G, Udo De Haes Ha, 2009. Allocation issues in LCA methodology: a case study of stover-based fuel ethanol. *The International Journal of Life Cycle Assessment,* (14), pp. 529-539.

I.A. Karimi and Rajagopalan Srinivasan (Editors), Proceedings of the 11th International Symposium on Process Systems Engineering, 15-19 July 2012, Singapore.

Modular Optimization Approach for Process Synthesis and Integration of an Integrated Biorefinery

Douglas H. S. Tay, Rex T. L. Ng, Denny K. S. Ng

Department of Chemical and Environmental Engineering/Centre of Excellence for Green Technologies, University of Nottingham Malaysia, Broga Road, 43500 Semenyih, Selangor, Malaysia

Abstract

An integrated biorefinery is a processing facility that converts biomass feedstocks into a wide range of value added products which include biofuels and specialty chemicals. In order to synthesize a sustainable integrated biorefinery, the environmental and economic performances should be taken into consideration. Via heat and power integration within integrated biorefinery, both performances can be improved. Due to the complexity of the process synthesis and integration problem, it is a need for a systematic approach to address the problem. In this work, modular optimization approach which breaks a large optimization problem into small models is proposed. Each model consists of a process unit and its alternatives (i.e., biomass drying, gasification, synthesis processes, etc.) in different degree of modeling details (i.e., white-, grey- or black-box). This allows designer to 'zoom in' on specific key process units, while, the rest of the model remain as black boxes. Thus, it will be able to reduce the computational effort significantly as compared to pure white-box modeling. By using an effective objective function to maximize the economic potential of the overall preliminary conceptual design, selection of the optimum process alternatives/technologies and products as well as integration of heat and power between process units can be performed simultaneously. A case study is solved to illustrate the approach.

Keywords: Integrated biorefinery, process integration, process synthesis, optimization

1. Introduction

Many existing industries, such as pulp and paper, wood and palm oil have the potential to be converted into integrated biorefineries. The most recent development in the synthesis of integrated biorefinery is focusing on the systematic process synthesis and integration (Kokossis and Yang, 2010). In addition, materials and utilities recovery via process integration are also presented (Tock et al., 2010; Baliban et al., 2011). Although the previous works provide reliable solutions to the problem, complex mathematical models and integration approaches are computationally intensive, labourous and required detailed process data. To address these issues, modular optimisation approach is further extended in this work. Modular optimization approach breaks the process synthesis and integration problem of integrated biorefineries into smaller models, each with different level of modeling details (i.e., white-, grey- or black-box). Each process and its alternatives are independent models which linked with the upstream and

downstream processes. With this approach, the complexity of the overall model can be reduced.

In this work, a large retrofit integrated biorefinery problem is decomposed into six distinct simplified material and energy balance models (i.e., existing processing facilities; biomass pre-treatment processes; production of intermediates processes; conditioning of intermediates processes; synthesis of final products; heat and power integration), as shown in Figure 1. Based on the sensitivity of the overall result to the process parameters or based on the amount of process data available, each part can be modeled at different level of detail (i.e., white-, grey-, or black-box). Each model is then linked with another through the material and energy streams. In this work, black-box process model of the existing processing facility is first developed and then linked to the model for an integrated biorefinery.

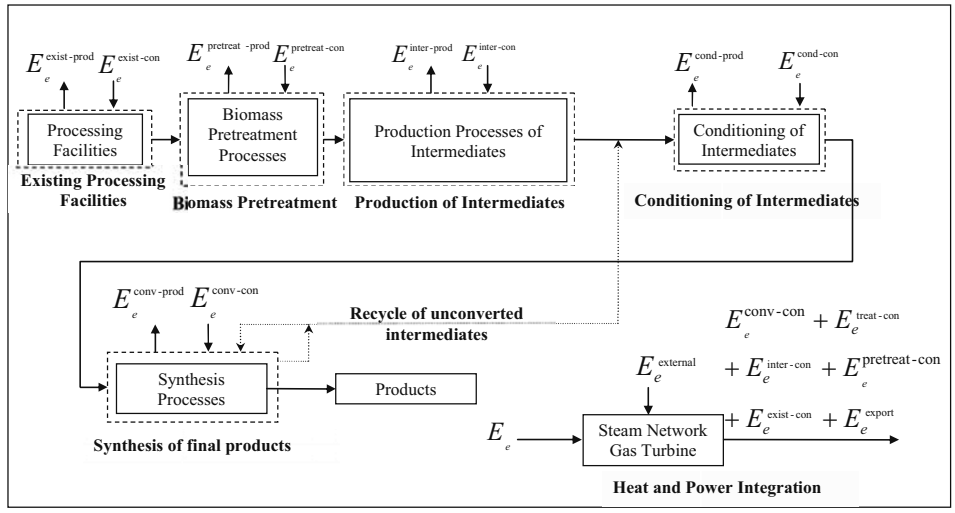

Figure 1: Superstructural Representation of the Retrofit Integrated Biorefinery

2. Problem Statement

Given an existing processing facility with a set of raw material $i^{\text{RM}} \in I^{\text{RM}}$ with the flowrate of $F_{i^{\text{RM}}}^{\text{exist}}$. At a predefined conversion Y_i^{exist} for the raw material processing process to produce the desired product, the existing processing facilities generate a set potential biomass, $i \in I$ with flowrate of F_i. F_i is to be distributed to different biomass pre-treatment technologies $j \in J$ to produce pre-treated biomass $i' \in I'$ at a conversion of biomass to pretreated biomass, $Y_{iji'}$. The flowrate of pre-treated biomass that is ready for production of intermediates is given as $F_{i'}$. In the pre-treatment processes, energy can be consumed or generated. The consumption and generation of energy $e \in E$ per unit of biomass i processed through technology $j \in J$ are given as Y_{ije}^{con} and Y_{ije}^{prod} with the total energy consumed and generated at $E_e^{\text{pretreat-con}}$ and $E_e^{\text{pretreat-prod}}$.

The pre-treated biomass $i' \in I'$ with flowrate of $F_{i'}$ is to be distributed to different biomass conversion technologies $j' \in J'$. Biomass is converted into useful intermediates $p \in P$ at given mass conversion $Y_{i'j'p}$ and the flowrate of intermediates is denoted as F_p. The consumption and recovery of energy $e \in E$ per unit of pre-treated biomass $i' \in I'$

processed through technology $j' \in J'$ are specified as $Y_{i'j'e}^{\text{con}}$ and $Y_{i'j'e}^{\text{prod}}$. The total energy consumption and generation rates of energy at the existing mill are given as $E_e^{\text{inter-con}}$ and $E_e^{\text{inter-prod}}$. In the case where unconverted intermediates p from the synthesis processes or intermediates p that do not meet the requirement of the synthesis processes, they need to be re-conditioned in processes $j' \in J'$ in order to meet the process requirement of the synthesis process. The total flowrate that send for re-conditioning process is denoted as F_p^{Rec}. In most cases, conditioning processes involved additional reactions, separations or pressurisation. Thus, a mass conversion $Y_{pj'',p'}$ is included for the production of conditioned intermediates $p' \in P'$ that meet the specification of synthesis processes. The consumption and generation of energy $e \in E$ per unit of raw intermediates $p \in P$ processed through technologies $j'' \in J''$ are specified as $Y_{pj''e}^{\text{con}}$ and $Y_{pj''e}^{\text{prod}}$. The total energy consumption and generation rates of energy at the existing mill are given as $E_e^{\text{cond-con}}$ and $E_e^{\text{conv-con}}$.

In order to meeting the process requirement of process j''', conditioned intermediates $p' \in P'$ can then be converted to final products, $p'' \in P''$ through synthesis processes $j''' \in J'''$, at the given mass conversion of $Y_{p'j''',p''}$. The consumption and generation of energy $e \in E$ per unit of conditioned intermediates $p' \in P'$ processed through technology $j''' \in J'''$ are specified as $Y_{p'j'''e}^{\text{con}}$ and $Y_{p'j'''e}^{\text{prod}}$. The total energy consumption and generation rates of energy at the existing mill are given as $E_e^{\text{conv-con}}$ and $E_e^{\text{conv-prod}}$.

3. Study Case

In year 2004, Asian Development Bank (2004) found that large part of the wood waste generated by sawmills are disposed as waste. Approximately 50% of the total log processed, in the form of log ends, bark, slabs, saw dusts and lumber edges in wood mills ended up as waste. Therefore, wood industry has huge potential to be converted into integrated biorefinery which produces value-added products (e.g., biofuels, biochemicals), as well as heat and power. Since biomass gasification able to handle various type of feedstock, it is recognized as one of the most promising options for the initial processing of biomass in an integrated biorefinery. To illustrate the propose approach, a gasification-based integrated biorefinery case study adapted from Tock et al. (2010) and Larson et al. (2006) is solved.

3.1. Existing Wood Mill - In this case study, a wood mill with the capacity of 90,000 kg log per day (= 1 kg log/s) is considered. Electricity is consumed in the cutting, debarking and sawing process at 273.6 kJ per kg log processed.

3.2. Wood Waste Pre-treament - As wood waste has high moisture content at 50 wt%, therefore, prior to the gasification process, the wood waste needs to be pre-dried to a moisture content of 25 wt%. As shown in Figure 1, different options of pre-treatment j (i.e., air drying and steam drying) can be taken into consideration.

3.3. Dried Wood Waste Generation - Various biomass gasification technologies are available to convert biomass into syngas. In this case study, different gasification technologies are to be assessed. According to Gassner and Marechal (2009), the product composition and yield of the syngas are often fixed based on type of

gasification technologies. Two types of gasification process *j*' (i.e., direct heated (DHG) and indirect-heated gasification (InDHG)) are taken into consideration.

3.4. Conditioning of Syngas - Syngas produced from biomass gasification may not meet the downstream requirement. Thus, conditioning of the syngas is required. In this case study, water-gas shift and CO_2 removal are identified as the key syngas conditioning processes, apart from the physical cleaning (i.e., filtration) which is not modeled in this work. As syngas composition is crucial for its further use in synthesis processes, water-gas shift (WGS) process is included to adjust the composition of syngas to meet the specification required (i.e., H_2/CO ratio) by additional input of steam.

3.5. Synthesis of Final Products - To further convert the conditioned syngas into final product, synthesis processes such as Fischer-Tropsch (FT) liquids, Dimethyl-ether (DME) and mixed alcohol (Mix-OH) are included in this study. Larson et al. (2006) has carried out an extensive work to simulate various synthesis processes, and their alternative configurations, to produce key biofuels. The synthesis processes consume steams. However, heat from the synthesis reactions can also be recovered to generate ultra-high pressure steam (HHP).

3.6. Heat and Power Integration - With the available data on processes and their alternatives from Sections 3.1 to 3.5, the model can be used to perform heat and power integration. In this case study, electricity (elec), HHP, high pressure steam (HP), medium pressure steam (MP) and low pressure steam (LP) are considered as energy *e*. Excess steam of a higher pressure allowed to be sent to a steam turbine to generate electricity and produce a lower pressure steam.

4. Result and Discussion

The case study is optimized for simultaneous synthesis and integration of a wood mill with integrated biorefinery via commercial optimization software (LINGO, version 10.0, with Global Solver). The result of this case study is presented in Figure 2. As shown, DME is selected as the optimum product. With 1 kg log/s wood mill capacity (0.50 kg/s wood waste), 0.2658 kg/s of DME can be produced. The model simultaneously synthesizes an optimum integrated biorefinery configuration and generates a steam network consisting of HHP, HP, MP and LP steams and gas turbine. Based on the optimum result, the maximum EP is targeted as US$ 0.073/s. Note that 889.8 kW electricity, 0.186 kg/s MP steam and 1 kg/s LP steam are imported in order to meet the demand in the retrofit integrated biorefinery. Note that this model is able to determine the economic performance and serves as benchmark for the detailed design.

5. Conclusion

The modular optimization approach is extended for the simultaneous process synthesis and integration of a sustainable integrated biorefinery with existing processing facilities. The approach allows the overall formulation to be simplified without losing the insights of interest for the effective design and integration of the processes. Based on different optimization objective, the conceptual design of an integrated biorefinery, including the optimum steam and electricity networks can be synthesized.

6. Acknowledgement

The financial support from University of Nottingham Research Committee through New Researcher Fund (NRF 5021/A2RL32) is gratefully acknowledged.

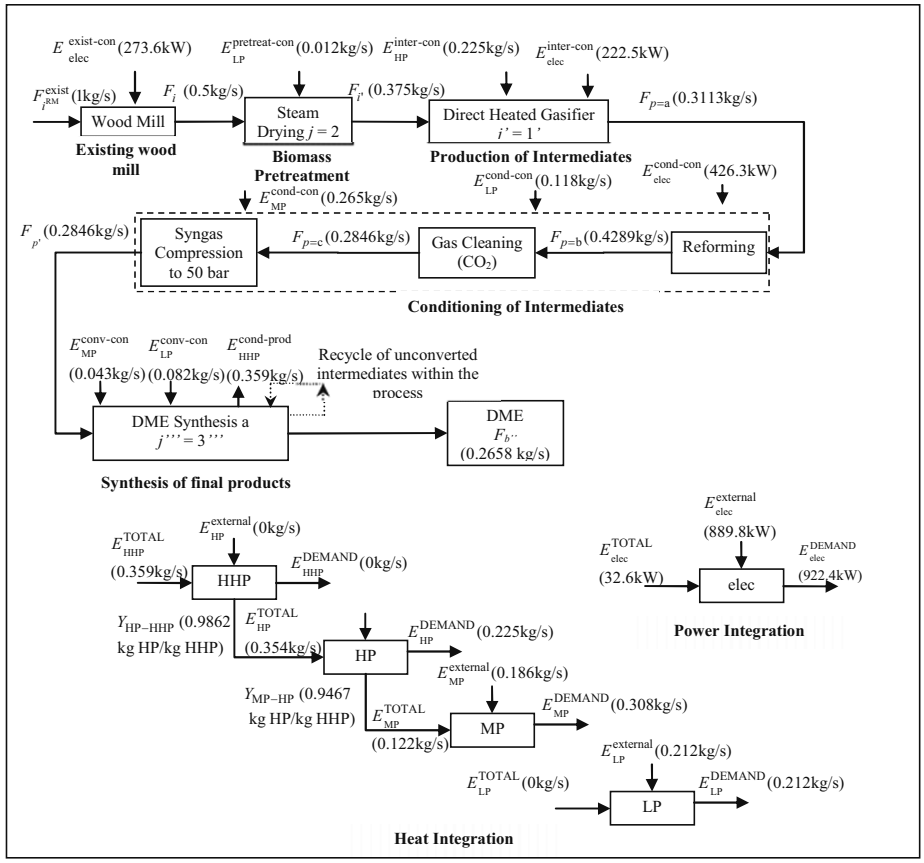

Figure 2: Result of the retrofit of wood mill into an integrated biorefinery

References

R.C. Baliban, J.A. Elia and C.A. Floudas, 2011, Optimization framework for the simultaneous process synthesis, heat and power integration of a thermochemical hybrid biomass, coal, and natural gas facility. Computer and Chemical Engineering, 35, 1647-1690.

M.Gassner and F. Maréchal, 2009, Thermo-economic process model for thermochemical production of Synthetic Natural Gas (SNG) from lignocellulosic biomass. Biomass and Bioenergy, 33(11): 1587-1604.

A.C. Kokossis and A.Yang, 2010, On the use of systems technologies and a systematic approach for the synthesis and the design of future biorefineries. Computers and Chemical Engineering, 34, 1397-1405.

E. D. Larson, S.Consonni, R. E. Katofsky, K. Iisa and W. James Frederick Jr., 2006, A cost-benefit assessment of gasification-based biorefining in the Kraft pulp and paper industry, Volume 1. Princeton, NJ: Princeton Environmental Institute.

L. Tock, M. Gassner and F. Marechal, 2010, Thermochemical production of liquid fuels from biomass: Thermo-economic modeling, process design and process integration analysis. Biomass and Bioenergy, 24, 1838-1854.

I.A. Karimi and Rajagopalan Srinivasan (Editors), Proceedings of the 11th International Symposium on Process Systems Engineering, 15-19 July 2012, Singapore.

Integrated production and distribution management with cross docking in supply chains

M.E. Cóccola[a], C.A. Méndez[a], M. Zamarripa[b], A. Espuña[b]

[a] *INTEC (UNL-CONICET), Santa Fe, Argentina*
[b] *Chemical Engineering Department, Universitat Politècnica de Catalunya (UPC), Barcelona, Spain*

Abstract

In the current context of a global and very competitive economy, multiple production and distribution activities must be properly coordinated in order to satisfy strict market requirements at the right time and with minimum cost. In typical multi-site systems, products are usually manufactured in one or more factories, moved to warehouses for intermediate storage, and subsequently shipped to retailers or final consumers. In turn, cross-docking platforms may be also used to consolidate multi-product customer demands without storing at intermediate depots. Consequently, the effective operation of complex production and distribution networks involves the management of activities performed in multiple factories, distribution centers (DCs), retailers and end users, which are usually geographical spread in many different cities, countries and/or continents. To optimally manage such complex multi-site systems, an integrated MILP-based framework for production and distribution scheduling with cross-docking in supply chains is proposed. In order to illustrate the applicability and effectiveness of the proposed method, a complex example taken from literature is solved to optimality with modest CPU times.
Keywords: MILP-based approach, supply chain management, cross-docking, logistics.

1. Introduction

Production and transport issues constitute a central activity to be considered within any multi-site manufacturing system. From the operational perspective, both problems have been traditionally treated separately and independently from any supply chain (SC) environment. Numerous efficient methodologies have been proposed in the literature to address the short-term production scheduling problem in the chemical industry. Also, a wide variety of vehicle routing problems have been extensively analyzed and solved by the communities of Operations Research and Process Systems Engineering. Numerous exact and heuristic algorithms have been proposed, focusing mainly on the individual and geographical aspects to reduce high delivery costs. The decoupled production and distribution processes rely on finished goods inventory to buffer both operations. However, higher inventory costs and the trend to operate in a just-in time manner are putting pressure on firms to reduce stocks in their distribution chains. Besides this, many big companies are not only manufacturing the demanded products but also distributing them to the customer location at a given due date, which implies a proper consideration of complex temporal and capacity interdependencies arising between production processes and transportation activities. The efficient synchronization of these complex systems remains as an open and challenging area for research. Only few contributions have been reported so far in this direction, and most of them are mainly focused on the integration at the strategic and tactical levels.

This paper introduces a new optimization approach to the integrated operational planning of multi-echelon multiproduct production and transportation networks with cross-docking platforms for shipment consolidation.

2. Problem Description

Distribution systems comprising multiple factories and warehouses as supply points with product stocks located at both kinds of facilities and the shipments going directly from manufacturers or via warehouses to customers. Thus, the problem addressed in this work is focused on a two-echelon distribution system where a set of nodes involving factories, warehouses and customer locations is considered. The warehouses act as intermediate locations between factories and end customers to both facilitate the consolidation of shipments from different suppliers and meet customer demands. Consolidation consists of combining shipment of similar or different products from several origins at the distribution center -DC-. A customer order may include several products often available at different production sites. Then, the consolidation of shipments from multiple suppliers to intermediate DCs should be made before reaching the customer location. In this work, a transportation infrastructure that allows: (i) direct shipping (ii) shipping via DC, including cross docking and (iii) combination of both types of shipment, is considered. Only one vehicle can stop at each customer site to satisfy every request but several vehicles can stop at the same manufacturing site or warehouse to accomplish pickup or delivery operations. The cross-docking facilities are located in intermediate sites. In turn, this work may also consider flexible time windows. The proposed approach provides a detailed set of coordinated production and distribution schedules to meet all product demands at minimum total transportation cost. In the following section we will introduce a new MILP-based continuous time formulation for the integrated production and distribution problem with cross-docking in supply chain.

3. Problem Formulation

The MILP-based model is divided in three blocks of constraints. The first one corresponds to production scheduling constraints where general allocation, sequencing and timing constraints are considered. The second block comprises the set of constraints to integrate both production and distribution schedules. Finally, the last one considers constraints for dealing with the distribution scheduling problem. In this paper, only the constraints related with cross-docking operation will be developed.

In the integration of production and distribution, the amount of product p loaded by vehicle v is computed by Eq.(1):

$$LOAD_{p,v} \leq \left(\sum_{b \in B} A_{b,v}\right) + AI_{p,v} + \left(\sum_{v' \in V} AV_{p,v,v'}\right) \tag{1}$$

The amount of product p unloaded by vehicle v in warehouse i can be used by all vehicles housed in node i, which is represented by Eq.(2). Eq.(3) defines a new binary variable to determine whether vehicle v' pick-ups goods delivered by vehicle v.

$$UNLOAD_{i,p,v} \geq \sum_{v' \in VB_i} AV_{p,v',v} \tag{2}$$

$$bm * BAV_{v',v} \geq AV_{p,v',v} \qquad \forall\, p \in P, v \in V, v' \in V: v \neq v' \tag{3}$$

The Eq. (4) and (5) computes the earliest start time of every trip.

$$STV_v \geq \left(\sum_{p\in P} LOAD_{p,v} * vvt_v\right) + FT_{b,i} - bm * (1 - Z_{b,v}) \qquad \forall\, i \in F_i, v \in VB_i, b \in B \tag{4}$$

$$STV_{v'} \geq TV_{i,v} + \left(\sum_{p\in P} UNLOAD_{i,p,v} * vvt_v\right) + vft_v + \left(\sum_{p\in P} LOAD_{p,v'} * vvt_{v'}\right) - bm * (1 - BAV_{v',v}) \tag{5}$$

$$\forall\, i \in W_i, v \in V, v' \in VB_i : v \neq v'$$

To maintain the inventory level, the total amount of product *p* loaded by vehicle *v*' in warehouse *i* is enforced to be equal to the amount of product *p* unloaded by other vehicles in node *i*, which is represented by Eq. (6).

$$\sum_{v\in V} UNLOAD_{i,p,v} = \sum_{v' \in VB_i} LOAD_{p,v'} \qquad \forall\, i \in W_i, p \in P \tag{6}$$

The Eq. (7) is the objective function which aims at minimizing the total cost of production and distribution as well as the total tardiness.

$$\begin{aligned} Min \left(\sum_{b\in B}\sum_{u\in U}\sum_{i\in F_i} setupC_u * X_{b,u,i}\right) + \left(\sum_{p\in P}\sum_{u\in U}\sum_{b\in BP_p} TB_{b,u} * pc_{p,u}\right) + \left(\sum_{r\in R}\sum_{v\in V} H_{r,v} * vfc_v\right) \\ + \left(\sum_{i\in(F_i\cup W_i)}\sum_{r\in R}\sum_{v\in V}\sum_{ii\in I}\left(IN_{ii,r,v} * dist_{i,ii} * vvc_v + FI_{ii,r,v} * dist_{i,ii} * vvc_v + \sum_{iii\in I} PR_{ii,iii,r,v} * di.\right.\right. \\ + \sum_{i\in I} co * TSB_i \end{aligned} \tag{7}$$

3.1. Nomenclature

Sets: B batches; BP_p batches of product p; I nodes; F_i factories; FU_i set of production units that operate in i; S_i customers; P products; U production units; V vehicles; VB_i set of vehicles housed in operational base i; W_i warehouses.
Parameters: $dem_{i,p}$ amount of product p demanded by node i; $dist_{i,ii}$ distance between node i and node ii; $inv_{i,p}$ initial stock of product p in node i; $pc_{p,u}$ processing cost of product unit p in production unit u; $setupC_u$ setup cost of production unit u; vvc_v unit distance cost for vehicle v; vfc_v fixed cost of using vehicle v; vft_v fixed stop time of vehicle v in every visited node; co represents the penalty cost per unit tardiness at each node.
Positive Variables: CTV_v overall traveling cost for vehicle v; $CV_{i,v}$ travel cost up to node i for vehicle v; $FT_{b,i}$ end time of batch b in the node i; $ST_{b,i}$ initial time of batch b in node i; STV_v departure time of vehicle v; TSB_i time window constraint violation to arrivals after delivery date; $TV_{i,v}$ travel time up to node i for vehicle v; TTV_v total routing time for vehicle v; $A_{b,v}$ amount of product p from batch b loaded in vehicle v; $AI_{p,v}$ initial stock of product p allocated to vehicle v; $AV_{p,v,v'}$ amount of product p unloaded by vehicle v' and then loaded by vehicle v; $LOAD_{p,v}$ amount of product p allocated to vehicle v; $TB_{b,u}$ batch size of b in processing unit u; $UNLOAD_{i,p,v}$ amount of product p unloaded by vehicle v in node i. Binary Variables: $BA_{v,v'}$ the vehicle v loads goods delivered by vehicle v'; $FI_{i,v}$ node i is the last one visited by vehicle v; $IN_{i,v}$ node i is the first one visited in the route of vehicle v; H_v vehicle v is used; $PR_{i,ii,v}$ node i is visited right before node ii in the route of vehicle v; $VA_{i,v}$ node i is visited by vehicle v; $X_{b,u,i}$ determines if batch b is processed in the production unit u of node i; $Y_{b,bb,i}$ sequencing of batches processing in factory i; $Z_{b,v}$ batch b is assigned to vehicle v.

4. Computational Results

The example presented here corresponds to a supply chain comprising 16 locations (2 factories, 2 DCs and 14 end customers) geographically spread in six European countries. Up to six vehicles are available to carry out the required distribution activities of three different products (P1, P2 and P3) in a cost-effective way.

Each manufacturing plant has two production units to process batches with variable size. The factory housed in Barcelona can manufacture products p2 and p3 whereas in the factory located in Bratislava only p1 and p2 are produced. Production features are described in the Table 1.

Table 1. Production Features

factory	*production unit*	*capacity*		*setup cost (€)*	*production cost (€/units)*			*setup time (h)*	*production time(h/units)*		
		min	*max*		*p1*	*p2*	*p3*		*p1*	*p2*	*p3*
Barcelona	A	50	600	10	-	10	15	0.5	-	0.1	0.1
	B	50	600	10	-	10	15	0.5	-	0.1	0.1
Bratislava	C	50	600	10	18	9	-	0.5	0.1	0.1	-
	D	50	600	10	18	9	-	0.5	0.1	0.1	-

The distribution centers are situated in Madrid and Stuttgart. Six vehicles V1-V6 are available to transport lots of three different products from the bases where they are housed. Each type of product has a different weight and volume. Finally, an initial inventory of finished goods is available in both manufacturing plants and distribution centers. Besides, each end customer has a specific demand that must be satisfied. Problem data is summarized in Table 2.

Table 2. Vehicles Features

vehicle	*operational base*	*capacity*		*average speed (km/h)*	*operative cost*		*loading/unloading time*	
		volume (m^3)	*weight (kg)*		*fixed (€)*	*variable (€/km)*	*fixed (h)*	*variable (h/unit)*
v1	Barcelona	30	200000	70	5000	4	1	0.003
v2	Bratislava	30	200000	70	5000	4	1	0.003
v3-v4	Madrid	20	100000	90	2000	1.5	0.5	0.003
v5 – v6	Stuttgart	20	100000	90	2000	1.5	0.5	0.003

The optimal integrated logistics program generated by the proposed MILP-based model is depicted in Fig. 1. Detailed coordinated production and distribution schedules are also tabulated. The example was solved with modest computational effort using GAMS 23.5.2 and CPLEX 12 in a Core Quad PC. A relative optimality tolerance of 0.001 was adopted.

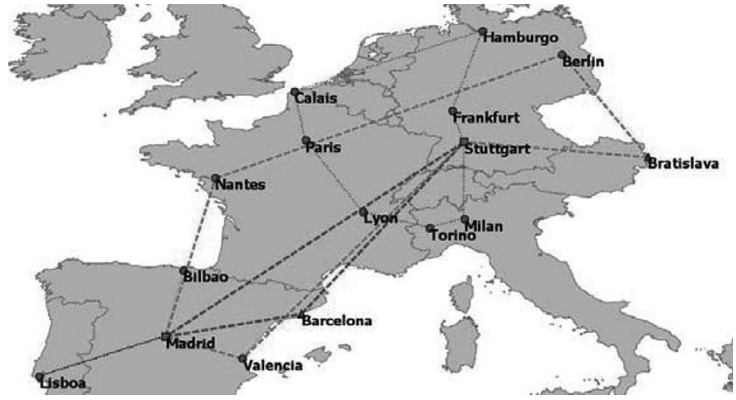

Fig.1. Optimal distribution schedule

Table 3. Optimal production and distribution schedules

factory	unit	processing time	p1	p2	p3	production cost (€)
Barcelona	A	26.00	-	+260	-	20255.00
		86.50	-	-	+600	
	B	57.50	-	-	+575	
Bratislava	C	60.00	-	+600	-	37095.00
		74.20	-	+137	-	
		134.70	+600	-	-	
	D	24.10	+241	-	-	
		84.48	+599	-	-	
		134.76	-	+498	-	

vehicle	site	arrival time	p1	p2	p3	used capacity		routing cost (€)
						%weight	%volume	
v1	Barcelona	92.01	-	+460	+1375	48.18	68.83	20028.00
	Stuttgart	110.08	-	-460	-875			
	Madrid	141.7	-	-	-500			
	Barcelona	153.18						
v2	Bratislava	143.98	+1640	+1435	-	67.65	99.08	28452.00
	Stuttgart	154.75	-770	-15	-			
	Valencia	181.06	-120	-120	-			
	Madrid	187.88	-500	-1000	-			
	Nantes	208.16	-200	-100	-			
	Berlin	230.50	-50	-200	-			
	Stuttgart	241.96						
v3	Madrid	3.00	+250	+500	+250	50.00	56.25	3884.00
	Lisbon	9.98	-250	-500	-250			
	Madrid	20.46						
v4	Madrid	195.58	+250	+500	+250	50.00	56.25	3194.00
	Bilbao	200.00	-250	-500	-250			
	Madrid	207.92						
v5	Stuttgart	164.47	+770	+475	+875	95.35	98.63	6747.50
	Frankfurt	166.72	-50	-150	-100			
	Hamburg	173.60	-200	-	-200			
	Calais	183.67	-100	-50	-50			
	Paris	188.00	-200	-50	-250			
	Lyon	195.18	-120	-0	-150			
	Torino	199.95	-50	-75	-75			
	Milan	202.63	-50	-150	-50			
	Stuttgart	207.49						

5. Conclusions

In this work an integrated MILP-based framework for production and distribution scheduling with cross-docking in supply chains has been proposed. The formulation developed can be applied to solve complex logistics problems in a reasonable computational time, providing a very detailed set of coordinated production and distribution schedules to meet all products demands at minimum total production and transportation cost.

6. Acknowledgements

Financial support received from AECID under Grant PCI-A1/044876/11, from UNL under Grant PI-66-337 and ANPCyT under grant PICT-2010-1073 is acknowledged.

References

R. Dondo, C. Méndez, & J. Cerdá, 2011, The multi-echelon vehicle routing problem with cross docking in supply chain management, Computers and Chemical Engineering, 35, 3002-3024.

R. Dondo, C. Méndez, & J. Cerdá, 2009, Managing Distribution in Supply Chain Networks, Ind. Eng. Chem. Res, 48, 9961-9978.

C. Méndez, A. Bonfill, A. Espuña, & L. Puigjaner, 2006, A rigorous approach to coordinate production and transport scheduling in a multi.site system, Computer Aided Chemical Enginnering, 21B, 2171-2176.

I.A. Karimi and Rajagopalan Srinivasan (Editors), Proceedings of the 11th International Symposium on Process Systems Engineering, 15-19 July 2012, Singapore.

Semantically-enabled Formalisation to Support and Automate the Application of Industrial Symbiosis

Tara Raafat[a] , Nikolaos Trokanas [a], Franjo Cecelja [a], Antonis Kokossis [b], Aidong Yang [a]

[a]*PRISE, FEPS, University of Surrey, Guildford, Surrey, GU2 7UB, UK*
[b]*School of Engineering, National Technical University of Athens, Zografou Campus, 9, GR-15780, Athens, Greece*

Abstract

Industrial Symbiosis (IS) is an innovative approach that brings together companies from different sectors in an effort to improve resource efficiency. This paper introduces a semantically enabled web platform that supports and automates the application of IS. The platform is based on the semantic formalisms for the waste and processing technology classifications, further supported by the semantic web services technology in the process of establishing synergies.

Keywords: Ontology, Semantic Web Services, Industrial Symbiosis.

1. Introduction

Industrial Symbiosis (IS) is an innovative approach that brings together companies from different business sectors to process waste into energy and/or material, including water. The process is done with a view to generate revenue and, at the same time, allow for a sustainable management of industrial waste and by-products, as well as municipal waste. Creating a synergy between these companies to form economically, environmentally and socially viable supply chains is a challenging task that requires in-depth knowledge on waste and respective processing technologies. A research study on existing IS systems (Grant et al. 2010) shows that the current process of IS is practiced manually with performance which intuitively depends on practitioners' ability and hence is difficult to apply in rapidly increasing industrial diversity. The input/output matching is mainly accomplished through brute force investigation, serendipitous discovery, organized workshops or coordinated search (Chetrow et al, 2000). The manual operation also results in higher costs and is prone to high inaccuracy in identifying opportunities for synergies. This paper presents the design of a semantically enabled web platform ("eSymbiosis[1]") that supports and automates the operation of IS with the focus on opportunity identification and synergy management. The platform is based on the semantic formalisms for waste and processing technology classifications and characterization which is further expanded by Semantic Web Service (SWS) technology to support the process of establishing synergies. As such, the platform is an affordable and customizable service which improves the companies' planning and decision making for establishing synergies. Industries are presented with more potential choices and opportunities for processing, re-using and replacing their resources and reducing operational costs.

[1] partly funded by eSymbiosis LIFE09 ENV/GR/000300 Project

challenging task (Massard et al., 2006). Current knowledge bases only represent what is known as explicit knowledge and fail to capture the tacit knowledge which is essential for identifying symbiotic synergies. The eSymbiosis platform exploits Semantic Web Technologies in general and ontologies in particular as its "backbone" to enable the presentation of both explicit and implicit knowledge which would allow for intelligent synergy identification. Ontologies, as formalism for knowledge representation, are used to model domain knowledge of IS with a view to support both user registration process and the process of matching partners and ranking the potential synergies by their semantic relevance. SWS technologies are used to describe all participants semantically as services and hence enable semantic and automated matching and possibly composition to form viable synergies. eSymbiosis adopts the Ontology Web Language(OWL) to represent both ontologies and SWS descriptions.

1.1. Ontologies and knowledge representation

An ontology O is defined by its set of concepts C organized in corresponding subsumption H_C, established relation R_C between concepts also organized in a hierarchy H_R, entities I with respective fillers R_I for relations, and axioms A used to infer knowledge from existing ones:

$$O=\{C,H_c, R_c, H_r, I, R_I, A\}$$

Here, the subsumption of concepts has four levels of abstraction; the meta ontology, the upper ontology, the domain ontology and the application specific ontology, as shown in Figure 1 (Trokanas et al, 2011).

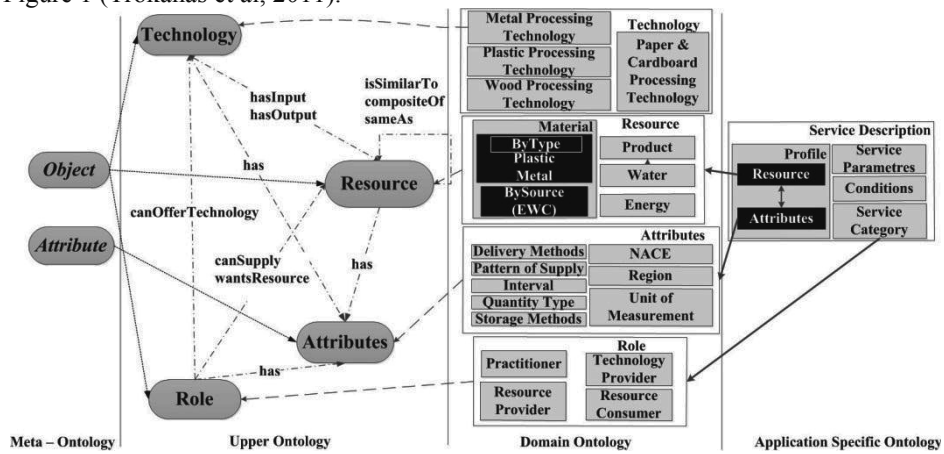

Figure 1 The Conceptual Model

1.1.1. Meta-Ontology

The meta-ontology makes the whole ontology easier to share and reuse (Marquardt et al., 2010). This is achieved by defining general purpose concepts that are independent of the domain and can be applied universally (Action, Role, Entity etc.).The eSymbiosis meta-ontology consists of two general concepts "Object" and "Attribute". Objects are all the tangible assets related to IS practice i.e. a waste or technology. Attributes are the information that define the objects such as physical form, industry codes etc.

1.1.2. Upper Ontology

The upper level of the eSymbiosis ontology includes abstract and general concepts that have application in the IS domain, but also in wider domains such as Industrial Ecology. Resources are the materials, waste, energy, products, water and expertise that a user

might have or want. The Technology concept represents the processing technologies that can process resources (inputs) and produce some others (outputs). The Role concept is very "IS specific" as it represents the different types of users that can take part in the establishment of a symbiotic synergy. Finally, the Attributes concept represents all the additional necessary information of the IS domain including units of measurement and geographical information. This level also includes high level properties that provide the relationships between those concepts such as Technology "hasInput" Resource, which links a technology with the possible inputs (materials, energy, water or products).

1.1.3. Domain Ontology

The domain of IS knowledge is represented with the use of two main ontology models; the Resource and the Processing Technology. The Resource ontology is the core concept of IS practice as it is currently in use and consists of three different classifications. The first (classification by source) is currently in use by IS practitioners. The two other classification are based on products and type of materials. The former helps users with no expert knowledge to classify their waste such as plastic bottle and the latter serves as the main classification of the system as all other concepts are linked to this classification by object properties such as "*hasComposite*". These two classifications are an innovation of eSymbiosis which aim to provide a better service, user experience and identify synergies that would otherwise remain unexplored. The Technology ontology aims in helping IS practice advance by moving one step further, taking into account not only available or requested resources, but also available technologies that can process certain resources into different type of material or energy. The combined use of these two models constitute eSymbiosis as an important planning and decision making tool for sustainable development.

1.1.4. Application Specific Ontology

This level serves features of a specific application. In the case of eSymbiosis, this level includes the service description ontology as explained in the following section.

1.2. Registration Process and the Service Description Ontology

Registration with the eSymbiosis platform is done through a dynamic web portal which is created "on the fly" from the domain ontology which coordinates the whole process. Users are provided with a set of standardized vocabulary (ontology concepts) to describe their resource or technology. While this approach eliminates any syntactic issues that might arise by the use of synonyms, acronyms and "jargon" terminology, it also provides users with greater amount of data than could help them explain their resources. The user can choose one of the three different ways available to classify a resource as explained in section 2.1.3 and from there is navigated through the ontology concepts and properties along with the restrictions on every concept. The data entered by the user is stored as instances within the ontology. The system then creates a semantic service description for every user based on those instances. The eSymbiosis Ontological formalism used for semantic service description is based on universally recognized OWL-S framework (Martin et al. 2004). Every user will be an instance of the OWL-S ontology which has been modified to incorporate properties related to the IS resources, specifically the ones which will be used for finding potential synergies. Some of these properties include the type of resource, quantity, pattern of supply, storage method, annual cost, period of availability, validity format, delivery method and the location where the resource resides. This information is presented in the format of data properties attached to the resource concept. The value assigned to these properties are either numerical or point to a concept within the domain ontology. The semantic service

description for every user results in a machine understandable representation of industries and therefore allows the automation of processing their information

1.3. Synergy Identification (matching)

The process of creating a synergy between two different industries to enable reuse of by-products could be translated to a "matching " process within the eSymbiosis environment. Semantic relevance between waste and technology providers is established by matching respective description ontologies using the purposely designed inference engine and ontology matchmaker (Tara Raafat et al ,2011). The Matching process is performed in stages and includes different levels, as shown in Figure 2. The subsumption matching is pure logical match and the distance measurement is based on graph theory distances. Both of these levels work directly on the domain ontology and take into consideration the resource concepts which are provided or processed by the user. The data property matching takes into account all attributes associated with the resource as explained in 2.2. Based on semantics, the matching process will extract/discover not only the ideal matching industries (e.g. a technology that processes exactly what the requester produces as waste) but also matches which are able to partially satisfy the requirement or if combined with other results are capable of fulfilling the requirement. Furthermore using inferred knowledge from the ontology through properties such as "*hasApplicationIn*"; where material is associated with industries that could benefit from it, the system is capable of offering the user with alternative synergy possibilities. Final ranking of discovered synergies accounts for economic, environmental and social factors. Requesters are also provided with estimations on performance improvement prior to the establishment of the synergy to aid their decision making.

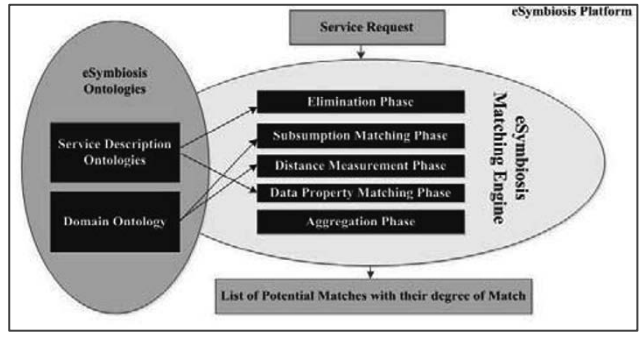

Figure 2 eSymbiosis Matching Engine

2. Use Case Validation

The platform has been validated against a set of test cases that have been developed based on data extracted from representative process industries located in the target region. One Scenario is represented in Figure 2. We assume a region with four different types of available waste registered with eSymbiosis and four available processing technologies. The platform can identify synergies between the users that have a high semantic relevance and rank them based on the degree of relevance. In the case of the Canteen Food waste for example, the food recycling technology gives a 60% match while the composting only a 40%. Both scores are low which is due to the fact that the waste cannot be completely processed by any of these technologies but each technology is capable of processing part of this waste which means they can be presented as a partial match. The use of the platform as a planning tool also supports the introduction

of new processing technologies in areas that have an excess of certain types of waste. In this case the canteen food waste does not have a match that can be turned into a synergy and therefore, the system suggests the introduction of an anaerobic digestion processing technology - a technology that can process both food and packaging waste. The introduction of such a technology will lead to a symbiotic synergy with a high matching score. Moreover, this technology will also have the potential to process other waste such as municipal waste that are not fully exploited. The results indicate that the eSymbiosis platform can be used as management tool for environmental planning and also for the promotion of sustainable development which is the aim of IS.

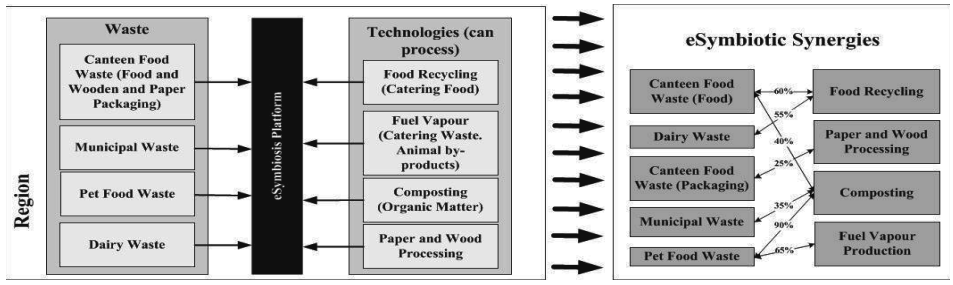

Figure 3 Symbiotic Synergies and innovative solutions

3. Conclusions and Future Work

The eSymbiosis system aims to enhance the semantic matching process and increase the accuracy of matches to the maximum possible level, to enhance and automate the creation of synergies between potential industries aiming to reduce the consumption of natural resources (raw materials, energy, and utilities), the environmental strain and the waste stream to landfills. The semantic approach furthermore allows coping with the constant emerging and changing systems. The current system will be expanded to allow feeding new knowledge gained through successful synergies into the ontology achieving continuous improvement and update of the system.

References

D. Martin, (2004). *OWL-S: Semantic Markup for Web Services* . Available: http://www.w3.org/Submission/OWL-S/. Last accessed 18/01/2012.

Grant, G. B., T. P. Seager, G. Massard, and L. Nies. (2010). Information and communication technology for industrial symbiosis. Journal of Industrial Ecology.

M.R Chertow. (2000) Industrial symbiosis: literature and taxonomy. Ann Rev Energy Environ;25:313–37

Massard, G., C. Adoue, and S. Erkman. (2006). Methodology for building industrial symbiosis networks in the Geneva region, Switzerland. *Frontiers in Research in Industrial Ecology, ScientificWorkshop, Universit´e de Lausanne*, 27 November–1 December, Lausanne, Switzerland.

N. Trokanas, T. Raafat, F. Cecelja, A. Yang, & A. Kokossis., (2011), "Semantic Formalism for Waste and Processing Technology Classifications Using Ontology Models", *Manuscript accepted for publication at ESCAPE22*, London, June 2012.

NISP UK *, NISP : What is IS?* . Available at: http://www.nisp.org.uk/what_is.aspx (Accessed: 11/24/2011)

T. Raafat, F. Cecelja, A. Yang, & N. Trokanas. (2011) 'Semantic Web Support for Industrial Symbiosis'. *Manuscript accepted for publication at ESCAPE22*, London, June 2012.

W. Marquardt, J. Morbach, A. Wiesner & A. Yang. (2010) 'Design Principles of OntoCAPE', *OntoCAPE,* , pp. 353-368.

I.A. Karimi and Rajagopalan Srinivasan (Editors), Proceedings of the 11th International Symposium on Process Systems Engineering, 15-19 July 2012, Singapore

All of the contribution has been prepared for Sandia National Laboratories Corporation, under Contract No. DE-AC04-94AL85000

Modeling and Optimization of Superstructure-based Stochastic Programs for Risk-aware Decision Support

John D. Siirola,* Jean-Paul Watson

Discrete Math and Complex Systems Department; Sandia National Laboratories; Albuquerque, NM, USA

Abstract

This manuscript presents a unified software framework for modeling and optimizing large-scale engineered systems with uncertainty. We propose a Python-based "block-oriented" modeling approach for representing the discrete components within the system. Through the use of a modeling components library, the block-oriented approach facilitates a clean separation of system superstructure from the details of individual components. This approach also lends itself naturally to expressing design and operational decisions as disjunctive expressions over the component blocks. We then apply a Python-based risk and uncertainty analysis library that leverages the explicit representation of the mathematical program in Python to automatically expand the deterministic system model into a multi-stage stochastic program, which can then be solved either directly or via decomposition-based solution strategies. This manuscript demonstrates the application of this modeling approach for risk-aware analysis of an electric distribution system.

Keywords: Superstructure optimization, Generalized disjunctive programming, Stochastic programming

1. Introduction

Process design and expansion planning are cornerstones of the Process Systems Engineering literature. While there are many challenges involved in design and planning, a central issue is managing discrete choices throughout the process: which chemical pathway to exploit, how many trays in a distillation column, how to arrange columns in the separation train, where to build the plant, where to site the distribution system, et cetera. In each of these examples, one approach to the problem is to systematically construct a superstructure of all possible discrete alternatives and then rely on a numerical optimization algorithm to select the best realization (Grossmann, 1996). While conceptually straightforward, actually implementing the superstructure as a mathematical program is an arduous task that requires careful bookkeeping. Further complicating the design problem is that the decision-maker must at some point make these discrete decisions in the face of uncertainty (e.g., material prices, demands, and construction times). Again, while systematic approaches exist for expanding the deterministic model into a stochastic model, the process is rather tedious and typically implemented by hand as a "one-off" activity.

In this manuscript we present a unified, systematic infrastructure for modeling and solving superstructure-based stochastic optimization problems based on the Pyomo[1] open source

*jdsiiro@sandia.gov

[1]Pyomo: *Python Optimization Modeling Objects:* `http://software.sandia.gov/pyomo`

optimization modeling environment (Hart et al., 2011). Pyomo provides native Python support for expressing structured models, and includes extensions for Generalized Disjunctive Programming (Raman and Grossmann, 1994) with standard automated transformations for both Big-M and Convex Hull relaxations (Lee and Grossmann, 2000). Pyomo provides "block-oriented" algebraic modeling facilities that allow the modeler to explicitly represent the superstructure and connections independently of the actual equations and variables employed within the individual sub-components. This separation greatly simplifies model management, allowing the modeler to easily substitute different component representations or propose new superstructures. Further, the open nature of the modeling environment facilitates the construction of custom optimization algorithms that can directly leverage the block structure of the superstructure model. Finally, we address model uncertainty via the PySP[2] stochastic programming package (Watson et al., 2012). PySP is built on Pyomo and can automatically generate the extensive form of a stochastic program given a deterministic Pyomo model and a characterization of parameter uncertainty. Additionally, it provides a general implementation of the Rockafellar and Wets (1991) Progressive Hedging scenario-based decomposition algorithm, including extensions for problems with discrete decision variables (Watson and Woodruff, 2011).

We demonstrate our approach through a series of operational and planning models for the electricity grid: (stochastic) unit commitment, $N-1$ reliability, and combined generation/transmission multi-period expansion planning. In these examples, we model both operational and investment decisions as disjunctive alternatives. Both generating technologies and transmission segments are modeled as discrete blocks, completely separating the distribution superstructure from the individual components. This separation allows us to rapidly explore alternative transmission approximations (e.g., DC or AC power flow, with or without line loss) and different generation technologies (e.g., new carbon sequestration and/or renewable generation technologies). Our approach also facilitates the rapid conversion of the superstructure to different structural simplifications (e.g., single bus, aggregated buses, full network model).

2. Modeling Approach

A significant challenge in constructing optimization models for engineering decision support is the dichotomy between the graph-like structured representation used to describe the engineering problem and the general algebraic form required by most optimization algorithms. To address this challenge, we formulate superstructure optimization models using "equation blocks" in Pyomo. A Pyomo equation block is a collection of modeling components (e.g., variables, parameters, constraints, and sub-blocks), and has many features in common with other block-oriented optimization modeling environments (notably JModelica.org[3]; Åkesson et al., 2010). A block represents a single component in the system and consists of the constraints, parameters, and variables that describe the behavior of that component. Individual blocks then form the "nodes" in the graph-like engineering representation of the superstructure. To facilitate connecting a block (component) to other blocks in the superstructure model, each block declares a series of "connectors" and associates each connector with one or more variables local to the block. Arcs in the original superstructure are simply equality constraints between two block connectors.

[2]PySP: *Python Stochastic Programming:* `http://software.sandia.gov/trac/coopr/wiki/PySP`
[3]JModelica.org: `http://www.jmodelica.org/`

This mechanism provides a powerful separation of concerns: the definition of the system superstructure relies only on the list of blocks and connectors, and is independent of both the component constraints and the variables that are associated with the connectors. Modelers can then develop and leverage libraries of components and substitute different component models using the same superstructure definition, provided the components all declare the same set of connectors.

We additionally leverage the Pyomo block modeling capabilities to implement key switching decisions within the superstructure model using Generalized Disjunctive Programming. Conceptually, a disjunct (single term within a disjunction) is a block of constraints that are enforced based on the logical value of an associated indicator variable. The `coopr.gdp` extension to Pyomo implements this as a specialized type of block and provides an additional constraint type for expressing the "exclusive or" relationship among the blocks in a disjunctive expression. This supports both directly modeling the switching decisions in the superstructure using disjunctive programming and creating specialized switchable components using disjunctions nested within a component block.

Given a superstructure model, Pyomo transforms the nested block structure into a "flattened" mixed-integer (non-)linear program via two steps. First, Pyomo expands expressions involving block connectors by replicating the expression for corresponding variables within the connectors. The `coopr.gdp` extension then relaxes each disjunction using either a Big-M or Convex Hull transformation (as specified by the user). The result is a deterministic mathematical program equivalent to the original superstructure optimization problem, suitable for input to a standard solver.

To capture uncertainty in the superstructure model, we leverage the PySP package to convert the (single scenario) deterministic model into a multi-scenario stochastic model. PySP takes as input a deterministic Pyomo model and a description of the system uncertainties expressed as a scenario tree. PySP then creates individual instances of the superstructure model corresponding to each scenario. If the problem is sufficiently small, PySP can generate the extensive form of the stochastic problem by including each scenario instance as a sub-block in a master problem and adding the appropriate constraints to enforce non-anticipativity. For larger problems, PySP provides an implementation of Progressive Hedging that iteratively and gradually enforces non-anticipativity across the scenario sub-problems.

3. Case Study: Electric Grid Operation and Planning

To demonstrate the utility of the proposed framework, we consider the case of electricity grid operation and expansion planning. This illustrative example possesses many of the features observed in process industries, including multiple candidate component models (e.g., AC and DC power flow models), multiple potential design and operational goals (e.g., cost and reliability), and significant system uncertainty (e.g., demand and production from renewable sources). This example also has a significant advantage as a case study: there are accepted constituent models that vary in complexity from linear (DC power flow) to non-convex nonlinear (full AC power flow). For this case study, we will consider the following aspects of the problem: short-term unit commitment (UC), $N-1$ reliability constraints, and combined generation-transmission expansion (CGTE).

Three fundamental modeling components are common to each of these problems: a node (bus), a transmission line, and a generation/load entity. Given an assumed underlying constituent model (e.g., DC power flow), we form a block definition for each component.

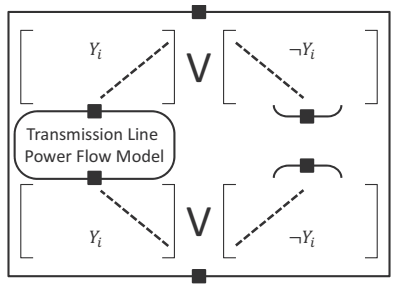

(a) conceptual disjunctions

```
def switchable_line(model, line):
  line.pf_model = Block(rule=DC_line_model)
  line.IN = Connector(dup=line.pf_model.IN)
  line.OUT = Connector(dup=line.pf_model.OUT)
  def active_rule(model, disjunct):
    disjunct.line_in = Constraint(
        expr=line.IN == line.pf_model.IN )
    disjunct.line_in = Constraint(
        expr=line.OUT == line.pf_model.OUT )
  line.active = Disjunct(rule=active_rule)
  def inactive_rule(model, disjunct):
    disjunct.line_in = Constraint(
        expr=line.IN == model.NO_FLOW )
    disjunct.line_in = Constraint(
        expr=line.OUT == model.NO_FLOW )
  line.inactive = Disjunct(rule=inactive_rule)
  line.switch = Disjunction(
      expr=[line.active, line.inactive] )
```

(b) implementation in Pyomo

Figure 1: General switchable components. Forming disjunctions over the connections preserves the separation between the component models and the network superstructure.

Node models are perhaps the simplest, as they must only enforce Kirchhoff's current law (conservation of charge). Transmission line models range from a simple 3-variable linear equality constraints (in the case of DC power flow) to multiple non-convex non-linear expressions (for AC power flow with line losses). Similarly, generator models may range from a simple constant power injection term to a full active / reactive power model with internal constraints for ramp rates, costs, emissions, and environmental impacts.

For the first problem (UC), we construct a straightforward optimal power flow (OPF) model by connecting these basic building blocks into a network through the use of connections (equality constraints between component block connectors). To model unit commitment, we replicate (index) the OPF model for each scheduling time period. An additional set of connections associate generator blocks across time, allowing the generators to enforce time-dependent constraints (e.g., ramp rates). We note that the UC model is completely independent of the model selected to represent the base OPF components.

For the second problem ($N-1$ reliability), we begin with the UC model and replace the transmission and generation component models with corresponding *switched* component models. However, unlike other power flow switching models (e.g., Hedman et al., 2010), we do not modify the model equations directly. Instead, we form disjunctive constraints over the *block connections* (e.g., see Figure 1), preserving the separation between the model structure and the component implementation. Following Hedman et al. (2010), we replicate the switched UC model for each contingency, with the disjunctive indicator variables fixed to *True* or *False* corresponding to the failure state of each component in each contingency. While the use of "fixed" disjunctions and numerous equality constraints yields a significantly larger raw MI(N)LP model, this complexity is easily reduced through the application of relatively straightforward presolve steps before handing the model to the optimization engine.

The third example addresses combined generation-transmission expansion planning. For this problem, we posit a superstructure of possible generators and transmission by adding additional switched components (transmission lines and generators) to the base OPF

model. Replicating the superstructure model similarly to the method used for generating the UC model (using significantly longer time steps) results in a deterministic multi-period CGTE model. Finally, we combine demand and cost forecasts to generate a family of potential expansion scenarios. Using PySP, we combine the scenario data with the deterministic model to form a large-scale stochastic expansion planning model.

4. Summary

This paper presents a unified software infrastructure for posing and solving large-scale superstructure-based optimization problems. Block-oriented modeling concepts facilitate re-use of core model components and yield model representations that can more closely reflect the "graph-like" nature of the original superstructure. Native support for generalized disjunctive programming expressions and automated transformations simplify the management of switching components in and out of the superstructure. Finally, a general purpose stochastic programming environment facilitates the automated transition from a deterministic superstructure model to a stochastic model for risk-aware analysis.

Acknowledgments

The Sandia National Laboratories Laboratory-Directed Research and Development Program and the U.S. Department of Energy Office of Science funded portions of this work. Sandia National Laboratories is a multi-program laboratory managed and operated by Sandia Corporation, a wholly owned subsidiary of Lockheed Martin Corporation, for the U.S. Department of Energy's National Nuclear Security Administration under contract DE-AC04-94AL85000. SAND 2012-0287C.

References

Åkesson, J., Årzén, K.-E., Gäfvert, M., Bergdahl, T., Tummescheit, H., 2010. Modeling and optimization with optimica and jmodelica.org - languages and tools for solving large-scale dynamic optimization problems. Comp.Chem.Engng 34 (11), 1737 – 1749.

Grossmann, I. E., 1996. Mixed-integer optimization techniques for algorithmic process synthesis. Vol. 23 of Advances in Chemical Engineering. Academic Press, pp. 171–246.

Hart, W. E., Watson, J.-P., Woodruff, D. L., 2011. Pyomo: modeling and solving mathematical programs in Python. Mathematical Programming Computation 3, 219–260.

Hedman, K., Ferris, M., O'Neill, R., Fisher, E., Oren, S., 2010. Co-optimization of generation unit commitment and transmission switching with n-1 reliability. IEEE Transactions on Power Systems 25 (2), 1052–1063.

Lee, S., Grossmann, I. E., 2000. New algorithms for nonlinear generalized disjunctive programming. Comp.Chem.Engng 24 (9-10), 2125–2141.

Raman, R., Grossmann, I. E., 1994. Modelling and computational techniques for logic based integer programming. Comp.Chem.Engng 18 (7), 563–578.

Rockafellar, R. T., Wets, R. J.-B., 1991. Scenarios and policy aggregation in optimization under uncertainty. Mathematics of Operations Research 16 (1), 119–147.

Watson, J.-P., Woodruff, D. L., 2011. Progressive hedging innovations for a class of stochastic mixed-integer resource allocation problems. Comp.Mgmt.Sci 8 (4), 355–370.

Watson, J.-P., Woodruff, D. L., Hart, W. E., 2012. PySP: Modeling and solving stochastic programs in Python. Mathematical Programming Computation (*to appear*).

I.A. Karimi and Rajagopalan Srinivasan (Editors), Proceedings of the 11th International Symposium on Process Systems Engineering, 15-19 July 2012, Singapore.

Accessing Direct and Indirect Effects within a LCA Based Multiobjective Synthesis of Bioproducts Supply Chains

Lidija Čuček,[a] Jiří Jaromír Klemeš,[b] Zdravko Kravanja[a]

[a]*Faculty of Chemistry and Chemical Engineering, University of Maribor, Smetanova ulica 17, 2000 Maribor, Slovenia, e-mail: lidija.cucek@uni-mb.si*
[b]*Centre for Process Integration and Intensification – CPI², Research Institute of Chemical and Process Engineering, Faculty of Information Technology, University of Pannonia, Egyetem utca 10, 8200 Veszprém, Hungary*

Abstract

This contribution proposes the integration besides direct effects of systems on the environment, also indirect effects caused by system's substitution. The direct effects of systems on the environment represent direct burden of the systems. The indirect effects are set of impacts causing indirect unburden or benefit on the environment.
This approach is applied within two Life Cycle Assessment (LCA)-based concepts - relative sustainability index (*RSI*) and eco-profit (*EP*). Within *RSI* different sustainability indicators are composed using certain weights. *EP* is defined as a difference between unburdening (eco-benefit - *EB*) and burdening (eco-cost - *EC*) the environment. *EP* and economic profit (*P*) can be merged together and the preferred solutions are those with maximal total profit (*TP*). Both concepts are illustrated on the biogas production from different raw materials under different anaerobic conditions. The results indicate that considering total effects enable the obtaining of more realistic solutions, than in those cases when only direct effects are considered.

Keywords: relative sustainability index, eco-profit, LCA, optimisation.

1. Introduction

Sustainability and especially environmental indicators are usually defined on the LCA based principles. LCA is commonly referred to as a "cradle-to-grave" analysis and takes into account the system's full life-cycle. However, LCA methodology still has certain major limitations. Among the limitations are i) the high degree of uncertainty arising from the life-cycle inventory, and ii) the lack of a systematic method for generating and identifying sustainable solutions (Grossmann and Guillén-Gossálbez, 2010; Mele et al., 2011).
This contribution presents two approaches based on sustainability metrics, which overcome the second limitation of LCA. Beside the direct, also indirect effects are included. One approach is based on the relative direct sustainability index (*RDSI*), replaced by relative total sustainability index (*RTSI*). *RDSI* is only composed of direct impacts on the environment and society, whilst *RTSI* also includes the unburdening relating to the substitution of harmful products by newly-produced benign products, and refers to current situations. Note that with this approach, subjective weighting between different environmental and/or social indicators cannot be avoided.
The second approach is an absolute approach and is based on the concept of *EC* (Vogtländer et al., 2010), and on a novel concept of *EP* (Čuček et al., 2012). *EC* is a

measurement for expressing the amount of environmental burden by a product on the basis of preventing that burden, where the calculations are based on LCA. On the other hand, *EP* includes besides burden (*EC*) also unburden (*EB*) on the environment, and is defined as a difference between *EB* and *EC*. The preferred solutions are those with maximal *TP*. *EC*, *EB*, *EP*, and *TP* are expressed in a monetary value per time unit.
Both approaches are illustrated through a case study that is comprised of integrated bioprocesses for the production of biogas from organic and animal wastes, with or without the rendering plant (Drobež et al., 2009, 2011).

2. Direct, Indirect and Total Effects

The direct effects of systems on the environment and society represent the direct burdens of those systems due to the extraction of resources, preprocessing and processing, maintenance, product use, and product recycling and/or disposal, including all transportation and distribution steps. On the other hand, the indirect effects are those sets of impacts that indirectly unburden or benefit the environment. The total effect is the sum of direct and indirect effects.

2.1. Relative Sustainability Index (RSI)

Sustainability usually considers three dimensions: environmental, economic, and social dimensions. Therefore, the *RSI* is composed of economic, environmental, and social indicators (Tallis et al., 2002).

2.1.1. Economic, environmental and social indicators

A key element of sustainability is usually the economic performance of a system. As economic indicators, either yearly profit (*P*) or the net present value (*NPV*) can be used, and maximised, or operating cost, which is minimised.
Environmental indicators are typically grouped into resource usage (material, energy, water and land), and pollution indicators as global warming, atmospheric acidification, photochemical smog formation, human health effect, etc. (Tallis et al., 2002).
The social indicators deal with measuring the quality of life. Social indicators relate to housing and ecology, employment, human rights, poverty, education, health and safety etc., and are usually overlooked since their assessment is not a straightforward task.

2.1.2. Relative sustainability index

Different indicators are expressed within different units, e.g. environmental indicators are usually expressed as a burden per some functional unit. Since their units are different, they cannot be composed unless they are normalized.
A two-level mixed-integer (non-)linear programming (MI(N)LP) system synthesis is performed. At the first level, an economically-effective synthesis is carried out in order to obtain a solution which is then considered as a base-case or reference solution for the multi-objective MI(N)LP synthesis, performed at the second level. The ε-constraint method is applied, and a set of Pareto optimal solutions are generated. When the indicators (I_f) of a studied alternative are compared to those of the selected base-case (I_f^0), relative indicators are obtained, which can then be composed into a *RSI*, by suitable weighting factors (w_f, $\sum_{f \in F} w_f = 1$):

$$RSI = \sum_{f \in F} w_f \cdot \frac{I_f}{I_f^0} \tag{1}$$

where $f \in F$ is a sustainability (economic and/or environmental and/or social) indicator. If only the direct effects on the environment and society are considered, then the *RDSI* is obtained (Eq. 2), and if in addition indirect effects are considered, than the *RTSI* is

obtained (Eq. 3), which shows how much better is *RTSI* than *RDSI* because of the substitution effect:

$$RDSI = \sum_{f \in F} w_f \cdot \frac{I_f^d}{I_f^{d,0}} \tag{2}$$

$$RTSI = \sum_{f \in F} w_f \cdot \frac{I_f^{\mathrm{d}} + I_f^{\mathrm{ind}}}{I_f^{\mathrm{d},0}} = \sum_{f \in F} w_f \cdot \frac{I_f^t}{I_f^{\mathrm{d},0}} \tag{3}$$

where I_f^{d} stands for the direct indicator, I_f^{ind} for the indirect indicator, and I_f^{t} for the total indicator.

Values of *RSI* < 0 are beneficial, while *RSI* > 0 are bad for the environment, and the higher the value, the worse for the environment.

2.2. Eco-Cost, Eco-Benefit and Eco-Profit

The *EC*, *EB*, and *EP* coefficients, defined in monetary unit/time unit, have the advantage of being directly incorporated into the objective function, together with a given economic objective. Therefore the weighting step is not required in the eco-costs system.

EC is an indicator based on LCA and describes an environmental burden on the basis of preventing it. It is a sum of the marginal prevention costs during the life-cycle, the sum of *EC* regarding materials' depletion, the *EC* of energy and transport, and the *EC* of emissions. *EC* are those costs which should be made in order to reduce environmental pollution and material depletion to a level which is in line with the carrying capacity of the Earth (Vogtländer et al., 2010).

EB is defined as a sum of the positive impacts of unburdens on the environment. Positive impacts are related to i) raw materials that mainly benefit the environment when used; e.g. the utilization of waste, since their direct harmful impact on the environment is thus avoided, and to ii) products that benefit the environment, e.g. if they are substitutes for harmful products. They are defined by the substitution factor, as the ratio between the quantity of conventional and produced product.

EP is defined as an analogy with *P*, as the difference between unburdening (*EB*) and burdening (*EC*) the environment, (*EP* = *EB* - *EC*). In the synthesis problem, where i) *P* and *EC* are summed, the preferred solutions are those with maximal net profit (*NP, NP* = *P* – *EC*), and where ii) *P* and *EP* are maximised simultaneously, the preferred solutions obtained are those with maximal *TP* (*TP* = *P* + *EP)*.

3. Industrial Case Study of Biogas Processes

The two above described LCA-based approaches are applied to a case study of the synthesis of biogas processes with the option of rendering plant. The mathematical model of these integrated processes developed by Drobež et al. (2009, 2011) was now upgraded by the *RDSI*, *RTSI*, *EC* and *EP*.

3.1. Relative Sustainability Index

Since the ε-constraint method was applied with *P* in the objective function, the *RSI* was composed only of environmental indicators. For this case study, the social indicators were undefined. A new set *R* for environmental indicators was defined using the elements $r \in R$ = {carbon footprint (CF), agricultural land footprint (ALF), water consumption (WS), nitrogen footprint (NF)}. The environmental indicators were mostly obtained using the LCA software package GaBi® (PE, LBP, 2011) and the Ecoinvent database (Frischknecht et al., 2007). The intention was to obtain solutions with considerably smaller CF; therefore it was decided to take a weighting factor for the CF

1/2 and the same also for the rest of environmental indicators together (ALF, WS and NF):

$$RSI = \frac{1}{2}\cdot\frac{CF}{CF^0} + \frac{1}{2}\cdot\frac{1}{3}\cdot\left(\frac{ALF}{ALF^0} + \frac{WS}{WS^0} + \frac{NF}{NF^0}\right) \quad (4)$$

All the indicators are normalized by their values as obtained at the first level MI(N)LP synthesis (superscript 0). The Pareto optimal solutions were obtained for *RDSI* (Fig 1) from the maximum *P* (3.668 M€/y) and *RDSI* (*RDSI*=1), to a solution with the *RDSI* by the zero *P* (*RDSI* ≈ 0.05). The most economically-optimal solution was the environmentally the worst one, and vice versa. By considering the direct effects only, the obtained solutions were wrong since they indicated that biogas production is unsustainable. By taking into account also indirect effects in *RTSI*, the 'opposite' solutions were obtained, namely biogas production is sustainable alternative along the whole set of non-trade-off solutions within the whole range of *P* – from the maximum *P* (3.668 M€/y) and minimal *RTSI* (*RTSI* ≈ -3.74), to a solution with the *RTSI* by the zero *P* (*RTSI* ≈ -0.15). Those solutions were non-trade-off solutions, since with increasing *P*, even more and more sustainable solutions were obtained. The optimal solution comprised the selection of the thermophilic process and the closed water system.

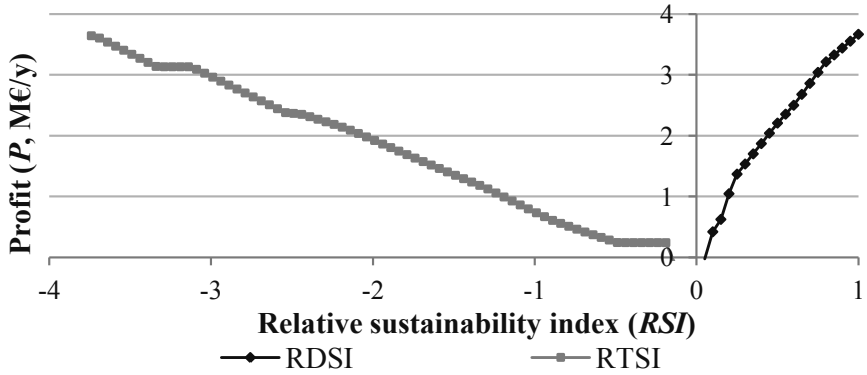

Figure 1. A Pareto curve for *RDSI* and a set of non-trade-off solutions for *RTSI*

3.2. Eco-cost and Eco-profit

Three single-objective optimisations were performed where i) the *P*, ii) the *NP*, and iii) the *TP* were maximised. The obtained results are shown in Table 1.

Table 1: Solutions obtained by maximisation of different profits

	Maximised *P*	Maximised *NP*	Maximised *TP*
Economic profit (M€/y)	**3.668**	0	3.591
Eco-cost (M€/y)	5.306	0	/
Eco-profit (M€/y)	2.667	/	2.917
Net profit (M€/y)	-1.638	0	/
Total profit (M€/y)	6.336	/	**6.508**
Income (M€/y)	7.354	0	7.249
Biogas production (m^3/d)	43,281	0	42,623
The amount of used waste (t/y)	122,861	0	121,180
RDSI | *RTSI*	1 | 1	0 | 0	0.989 | -3.725

In contrast to the non-trade-off solutions of *RDSI*, with *EP* the optimal trade-off could be established at the point of maximal *TP* (*TP* = 6.508 M€/y, with *P* = 3.591 M€/y and *EP* = 2.917 M€/y). The optimal solution included the use of a thermophilic process

converting the liquid pig manure and other substrates with no additional water and the open water system. Also, those raw materials far away from the plant were not selected because of the considerable *EC* of transportation. Note that by the maximisation of *NP*, considering direct effects only, a zero solution with no biogas production was obtained, which indicates that without considering indirect effects, as in *EP*, wrong or even no solutions can be obtained.

4. Conclusion

This contribution presented two multi-objective approaches for sustainable system synthesis based on sustainable metrics: i) a relative approach based on a *RDSI* and *RTSI*, and ii) an absolute approach based on the concept of *EC* and *EP*. These approaches have been performed through a case study of an integrated biogas process and rendering plant. All the results when considering only direct effects on environment showed that biogas production is unsustainable alternative, whilst when considering also indirect effects, the biogas production is a sustainable alternative that benefits the environment. The selection of alternatives that unburden the environment the most would have higher priority than the rejection of those with only smaller burdening impacts.

Acknowledgements

The financial support from the Slovenian Research Agency (Program P2-0032 and PhD research fellowship contract No. 1000-08-310074) and from the Hungarian project TÁMOP- 4.2.2/B-10/1-2010-0025 is gratefully acknowledged.

References

L. Čuček, R. Drobež, B. Pahor, Z. Kravanja, 2012, Sustainable synthesis of biogas processes using a novel concept of eco-profit, Computers and Chemical Engineering, doi: 10.1016/j.compchemeng.2012.01.010

R. Drobež, Z. Novak Pintarič, B. Pahor, Z. Kravanja, 2009, MINLP synthesis of processes for the production of biogas from organic and animal waste, Chemical and Biochemical Engineering Quarterly, 23, 445–459

R. Drobež, Z. Novak Pintarič, B. Pahor, Z. Kravanja, 2011, Simultaneous heat integration and the synthesis of biogas processes from animal waste, Asia-Pacific Journal of Chemical Engineering, 6, 734-749

R. Frischknecht, N. Jungbluth, H. J. Althaus, G. Doka, T. Heck, S. Hellweg, R. Hischier, T. Nemecek, G. Rebitzer, M. Spielmann, G. Wernet, 2007, Overview and Methodology, Ecoinvent Report No. 1, Swiss Centre for Life Cycle Inventories, Dübendorf, Switzerland

I. E. Grossmann, G. Guillén-Gosálbez, 2010, Scope for the application of mathematical programming techniques in the synthesis and planning of sustainable processes, Computers and Chemical Engineering, 34, 1365-1376

F. D. Mele, A. M. Kostin, G. Guillén-Gosálbez, L. Jiménez, 2011, Multiobjective Model for More Sustainable Fuel Supply Chains. A Case Study of the Sugar Cane Industry in Argentina, Industrial and Engineering Chemistry Research, 50, 4939-4958

PE, LBP, 2011, GaBi 4: Software-System and Databases for Life Cycle Engineering, Stuttgart, Echterdingen, Germany; 1992-2008 <www.gabi-software.com>

B. Tallis, A. Azapagic, A. Howard, B. Parfitt, C. Duff, C. Hadfield, C. Pritchard, J. Gillett, J. Hackitt, M. Seaman, R. Darton, R. Rathbone, R. Clift, S. Watson, S. Elliot, 2002, The sustainability metrics, Sustainable development progress metrics recommended for use in the process industries, IChemE, Rugby, UK

J. G. Vogtländer, B. Baetens, A. Bijma, E. Brandjes, E. Lindeijer, M. Segers M, F. Witte, J. C. Brezet, Ch. F. Hendriks, 2010, LCA-based assessment of sustainability: The Eco-costs/Value Ratio (EVR), VSSD, Delft, The Netherlands

I.A. Karimi and Rajagopalan Srinivasan (Editors), Proceedings of the 11th International Symposium on Process Systems Engineering, 15-19 July 2012, Singapore.

Mitigating Supply Disruption for a Global Chemical Supply Chain- Application of Agent-based Modeling

Behzad Behdani [a], Arief Adhitya[b], Zofia Lukszo [a], Rajagopalan Srinivasan [b, c]

[a] *Delft University of Technology, Faculty of TPM, the Netherlands*
[b] *Institute of Chemical and Engineering Sciences, A*STAR, Singapore*
[c] *National University of Singapore, Dept of Chemical and Biomolecular Eng, Singapore*

Abstract

In today's global and competitive markets, managing supply chain disruptions is a key factor in the success of any business. Disruption management, however, can be a challenging issue as disruptions can occur for a wide variety of reasons and the approaches to handle these risks are also ample. Moreover, evaluating the disruption impact and possible treatments is not a trivial task for a complex supply chain with many actors and different types of interactions. This calls for appropriate modeling and simulation frameworks. This paper presents a simulation-based risk analysis approach using an agent-based model and its application for a specific case of a lube oil supply chain.

Keywords: Agent based modeling, risk management, disruption, supply chain.

1. Introduction

A global supply chain faces many types of disruptions in the daily operation. One of suppliers might have an emergency shutdown which leads to the late delivery of raw materials to the plants; the transportation of raw material might be delayed due to difficulties in the shipment or the unexpected rise in customer orders might interrupt the planned operation of a supply chain. All these disruptions can have a significant impact on the performance of supply chain. To make the necessary actions to mitigate supply chain risks, a company needs to have an evaluation of the extent of this impact and also the effectiveness of different alternatives for managing disruptions. This evaluation, however, can be a great challenge; firstly because modern supply chains are highly complex systems consisting of many actors with many forms of interdependencies (physical/social/informational). Moreover, supply chain disruptions can occur for a wide variety of reasons. Likewise, the possible approaches to handle disruption are also ample. For example, to handle the risk of supplier failure, multiple sourcing (Tang, 2006), extra inventory carrying (Wilson, 2007) and demand management (Stecke and Kumar, 2009) are some of possible actions suggested in the literature. With these two challenges, a profound modeling and simulation, which provides decision makers with a flexible test-bed to model different disruptions and disruption management strategies, is a necessity.

Handling disruptions in supply chains takes two different forms: "Mitigation" vs. "Reaction" (Thun and Hoenig, 2009). Some activities and measures are taken by companies beforehand to minimize the exposure to potential disruptions (Mitigation Phase). However, despite all the efforts, disruptive events happen and the influence on the supply chain operation must be managed by defining and implementing appropriate

response (Reaction Phase). The modeling and simulation approaches can be used to support the disruption management process in both phases. The application of agent-based modeling for disruption reaction has been discussed before by Behdani et al. (2009,2010). In this paper, the focus is on mitigation of risk in supply chains. We discuss how an agent-based model can support the disruption assessment and treatment decisions in a chemical supply chain for cases in which the probability distribution of disruption occurrence and an estimation of its duration is available –e.g., based on historical data. The rest of the paper is organized as follows. Section 2 describes a simulation-based supply chain risk analysis approach followed by an illustrative case to elaborate the presented approach. Finally, Section 4 gives some concluding remarks.

2. Simulation-based Risk Analysis Approach

Supply chain disruptions are generally uncertain events happening randomly during the operation of supply chain. Of course, some sources of information such as expert opinion and statistical time series are sometimes available to assess the probability distributions for specific disruptions; however, the exact time of occurrence and the level of severity (e.g., the duration of supplier failure) are uncertain parameters. Considering this issue, the risk analysis approach of this paper is based on repeated simulation of different possible scenarios with an agent-based model (Figure 1). Firstly, based on a probabilistic description of the disruption, we generate disruption scenarios that define the day of occurrence and the duration of a potential disruption. For each scenario, the agent-based model is then used to model different possible disruption management actions and assess the impact of disruption on the supply chain performance. The steps of this approach are discussed in more details in the following.

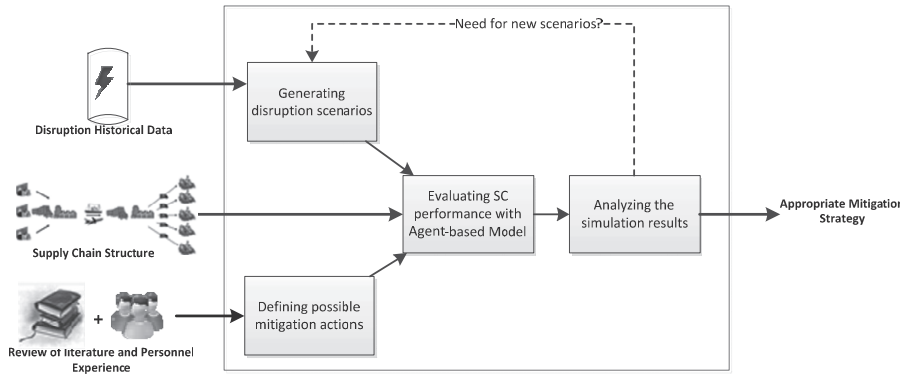

Figure 1. Simulation-based Risk Analysis Approach

Generating disruption scenarios:

A disruption scenario is a description of a particular event and how it is expected to happen and evolve in time in order to be a basis for experimentation with the model. For instance, one disruption scenario could be that a supplier has an emergency shutdown for a 10-day period starting at day 118 and another production stoppage at day 312 which lasts for 5 days. Therefore, each scenario defines the time of disruption occurrence and the severity of disruption.

To define the disruption scenarios, we assume that an estimation of disruption likelihood and its expected magnitude (e.g, the duration) is available. Historic information on supply, demand, cost, lead times etc. can be used to estimate the probability distribution for disruptive events.

As the number of plausible scenarios can be infinite, we start with a random sample of scenarios and based on analysing the simulation results, the decision for defining more scenarios can be made.

Defining possible mitigation actions:
To manage each potential disruption in supply chain, many different responses can be defined and implemented. A good review of supply chain risk mitigation strategies can be found in Tang (2006) and Stecke and Kumar (2009). Expert opinion and personnel brainstorming are other possible sources for defining the risk mitigation actions (Norrman and Jansson, 2004).

Evaluating SC performance with Agent-based Model:
Once a list of mitigation actions is generated, the agent-based model can be used to estimate the impact of disruption under different mitigation actions in each disruption scenario. The structure of model is out of scope of this paper and extensively described in Behdani et al. (2010).

Analysing the simulation results:
With a primary set of disruption scenarios, decision makers can compare the alternative responses and choose the best one for each scenario. Subsequently, the disruption response which is dominant in most scenarios must be determined. However, to be sure that the chosen strategy is a robust strategy and is generally dominant, it is necessary to generate a new sample of disruption scenarios and study the appropriate disruption management action for this new set of scenarios. If new set of scenarios leads to similar best disruption response, it can be selected as the final option to implement. Otherwise, the process must continue with defining a new set of disruption scenarios. With such an iterative process, the final disruption management action can be determined.

3. An Illustrative Case

In this section, the risk analysis approach is illustrated with a case of global lube oil supply chain (Adhitya and Srinivasan, 2010). The supply chain consists of three main components: the focal enterprise, its customers and (raw material) suppliers. This multi-plant enterprise has a global sales department (GSD) that directly interacts with customers and three production plants in different geographical locations. Each production plant itself has several functional departments, each with a specific role and performing certain tasks. Receiving a new order from one customer, the GSD passes the order to the scheduling department of each plant. Consequently, different production plants send their first possible time (FPT) for fulfilling this new order. The GSD then assigns the order to the production plant with the minimum of FPT. If none of the plants is able to produce and deliver the product on time, the GSD starts negotiation with customers for extending the order's due date. Within each plant, the operations department manages the conversion of raw materials to product based on the pre-specified recipe for each product. Following this production step the transportation of the finished order is arranged by the logistics department. Based on this description, an agent-based model with 10 agent types (customer, GSD, production plant, scheduling department, operations department, storage department, packaging department, procurement department, logistics department and supplier) has been developed in Java using Repast simulation platform. The developed model can be used to formulate many experiments related to potential disruptions, study the performance of supply chains

under different scenarios and find effective strategies to handle the effects of possible disruptions. In this paper, we specifically focus on the "Supplier Disruption" which results in the late delivery of raw material orders to the production plants.

3.1. Disruption scenarios

The supply chain is subject to random supplier disruptions. These supplier disruptions are assumed to occur with probability 0.01. The duration of a disruption is also sampled from a triangular distribution with a minimum value of 5 day, a most likely value of 10 days, and a maximum value of 20 days. With these inputs, different scenarios for disruption occurrence are generated. The procedure to generate a disruption scenario is given in Figure 2. First, the occurrence of disruption for each "day" in the simulation horizon (which is one year) is checked and in the case of disruption occurrence, the random duration of disruption is determined. Consequently, each scenario describes the starting date(s) and the duration of supplier failure in one year.

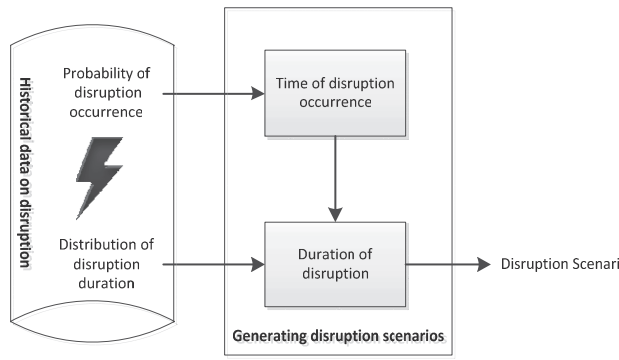

Figure 2. Procedure for scenario generation

3.2. Disruption management practices

Three strategies to handle supplier disruptions are modelled:

- **Inventory mitigation:** the production plants source exclusively from one supplier but carry some excess inventory to mitigate disruptions (the reorder point is considered 30% instead of 25% for other cases).
- **Sourcing mitigation:** the production plants source from two suppliers; one global low-cost supplier and a second backup supplier for the cases that there is an interruption in the raw material delivery from main supplier (the raw material price for local supplier is assumed 20% higher than main supplier).
- **Order reassignment:** to handle the disruption in supplier, GSD collects the orders from all plants and re-assigns them to the plants considering the new raw material constraint for affected plant.

3.3. Analysis of results

To understand the average system behavior, we started running the model for 20 disruption scenarios. For each scenario, all three strategies are compared with each other and also with the case of no action. Each simulation run yields different results; however, in general the sourcing mitigation strategy was the best choice for managing supplier disruptions in most scenarios (Figure 3). To evaluate the robustness of choosing this strategy, we generated 10 new disruption scenarios and ran the model for each scenario. In these new set of scenarios, the sourcing mitigation was again the best option in 6 disruption scenarios. With this analysis, it can be concluded that sourcing mitigation is the proper strategy to handle supplier disruptions in lube oil supply chain.

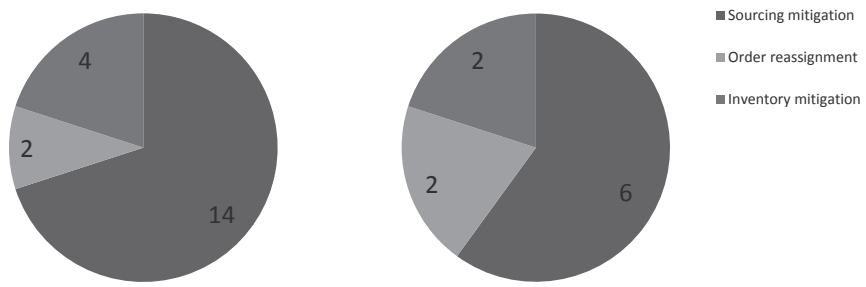

(a) (b)

Figure 3. The distribution of best mitigation strategy for: (a) first 20 scenarios; (b) for 10 extra scenarios

Table 1. Effect of disruption management on the enterprise profit (standard deviation in brackets)

	No disruption management	**Sourcing mitigation**	**Order reassignment**	**Inventory mitigation**
Average profit for 20 scenarios	9614726 (1576567)	10822740 (643339)	9730474 (1379282)	10116794 (1098405)
Average profit for 30 scenarios	9520082 (1384050)	10781721 (581979)	9792676 (1287398)	10196026 (947985)

Table 1 shows the mean value for enterprise profit over 20 and 30 scenarios. As can be seen the mean profit for sourcing mitigation is higher comparing with two other options in both cases. Moreover, the "mean" profit is relatively similar for 20 and 30 scenarios which reinforce the argument of selecting *sourcing mitigation* as final choice.

4. Concluding Remarks

In this paper a simulation-based approach for mitigating supply chain disruptions is presented. The presented approach can be used to define different disruption scenarios and evaluate the alternative mitigation strategies for a specific disruption in supply chain. The approach is, however, flexible to include multiple disruptions in defining scenarios if the probability of occurrence and an estimation of the magnitude of disruption are available for all disruptions. This is especially important as in some real cases, one specific mitigation strategy may address more than one potential disruptions. For instance, carrying extra inventory may reduce the risk of supplier emergency shutdown and also transportation disruption due to a port strike.

References

A.Adhitya and R. Srinivasan, 2010, Ind Eng Chem Res, 49(20), 9917-9931.
B. Behdani, Z. Lukszo, A. Adhitya and R. Srinivasan, 2010, Comp & Chem Eng,34(5), 793–801.
B. Behdani, Z. Lukszo, A. Adhitya and R. Srinivasan, 2009, Comp Aid Chem Eng, 26, 979-985.
A. Norrman and U. Jansson, 2004, Int J of Phys Dist & Log Man, 34(5), 434-456.
K.E. Stecke and S. Kumar, 2009, J Market Channel, 16(3), 193-226.
C. Tang, 2006, Int J Log: Res & Appl 9(1), 33-45.
J. Thun and D. Hoenig, 2009, Int J of Prod Econ 131(1), 242-249.
M.C. Wilson, 2007, Trans Res Part E: Log & Trans Rev, 43(4), 295-320.

I.A. Karimi and Rajagopalan Srinivasan (Editors), Proceedings of the 11th International Symposium on Process Systems Engineering, 15-19 July 2012, Singapore.

A Novel Multi-Grid Formulation for Scheduling Semi-Continuous Plants

Naresh Susarla,[a] Jie Li,[b] and I A Karimi[a]

[a]*Department of Chemical and Biomolecular Engineering, National University of Singapore, 4 Engineering Drive 4, Singapore 117576*
[b]*Department of Chemical Engineering, Princeton University, Princeton, New Jersey 08544*

Abstract

Semi-continuous plants are abundant in bulk manufacturing chemical process industries. However, scheduling of semi-continuous plants has received rather lower attention as compared to batch plants in the literature. In this paper, we develop a novel continuous–time formulation for short-term scheduling of semi–continuous processes using a multi–grid approach. For this, we adopt the unit-slots framework proposed by Susarla et al. (2010) to ensure accurate resource balances. We allow a number of storage configurations (no, constrained, and unconstrained) with either dedicated or multipurpose storage units. Also, we consider various wait policies (no, limited, and unlimited) for all materials. In addition, we consider resources such as utilities, equipment, etc. and allow operational scenarios such as sequence-dependent transition times. Numerical evaluation shows gains in solution efficiency as compared to the literature models in terms of better solutions, fewer variables, constraints and computation time.

Keywords: Semi-continuous plants; unit slots; multi-grid formulation; short-term scheduling.

1. Introduction

Semi-continuous plants are abundant in bulk manufacturing chemical process industries such as consumer goods, polymer, solvent extraction, bulk pharmaceuticals manufacturing, food processing, and beverage. These plants usually produce multiple products in bulk quantities using a pool of shared resources. Dealing with large material quantities and multiple products, semi-continuous plants pose various challenges mainly pertaining to inventory handling, product transitions, and resource utilizations on the manufacturer. Given such a scale and intense of operations, it is not surprising that a large share of total costs are associated with the production operations. Thus, it becomes imperative for the plant management to continuously seek the best operational schedules and strategies for optimally utilizing the plant resources.

Scheduling of batch plants has received a fair amount of attention from the researchers around the globe. On the other hand, scheduling of semi-continuous plants has rather received a limited attention in the academic research. Lim and Karimi (2003) improved and extended the model of Karimi and McDonald (1997) for short-term scheduling of semi-continuous processes based on a multi-grid slot-based approach and introduced the concept of "checkpoints" to ensure correct resource balance. Shaik and Floudas (2007) improved the continuous-time and unit-specific event-points based model of Ierapetritou and Floudas (1998). They imposed a number of timing constraints to ensure correct resource balance and to eliminate violation of storage capacities. Later, Li et al.

(2010) and Shaik and Floudas (2009) showed that many unit-specific based models including Shaik and Floudas (2007) may fall short in ensuring accurate resource balance for a number of scenarios. This creates a need for scheduling models that can efficiently handle both shared resources and industrial scale problems.

In this paper, we develop a novel continuous–time formulation for short-term scheduling of semi–continuous processes using a multi–grid approach. For this, we adopt the unit-slots framework proposed by Susarla et al. (2010) to ensure accurate resource balances. We allow a number of storage configurations (no, constrained, and unconstrained) with either dedicated or multipurpose storage units. Also, we consider various wait policies (no, limited, and unlimited) for all materials. Although we consider only materials and equipments as resources in this paper, our model is also capable of handling other resources such as utilities, manpower, etc. To demonstrate the performance of our model, we solve a number of examples from the literature (including the benchmark example from a consumer goods company) and compare results with other existing models.

2. Problem Statement

A semi-continuous plant (F) comprises of **J** semi-continuous units ($j = j1, j2, \ldots, J$) that perform **I** tasks ($i = i1, i2, \ldots, I$) involving **S** material states ($s = s1, s2, \ldots, S$). A recipe diagram (Susarla et al., 2010) of F gives the information on processing tasks, tasks to unit suitability $\mathbf{I}_j = \{i \mid \text{unit } j \text{ can perform task } i\}$, and mass ratios ($\sigma_{sij}$). R_{ij}^{L} (R_{ij}^{U}) denote the minimum (maximum) rate (mass per unit time) at which unit j can process task i. In case of a task changeover (say, i to i') in a unit j, a sequence-dependent transition time ($\tau_{ii'j}$) is required for cleaning, setup, and attaining steady state or desired output quality. $\tau_{ii'j} = 0$ for $i \notin \mathbf{I}_j$ or $i' \notin \mathbf{I}_j$. With this, the short-term scheduling problem in this paper can be stated as follows. Given (1) the scheduling horizon [0, H], (2) J processing units, their suitable tasks, limits on processing rates, minimum run lengths, transition times, and clean up times, (3) intermediate storage units, intermediate storage policies, initial inventories, and limits on their holdups, (4) cost of or net revenue from the sale of products, we determine (1) the sequence of tasks that each processing unit should perform over time, processing rates, and production quantities, (2) the inventory profiles of all material states and storage units, assuming (1) deterministic operations with no unit failures or operational interruptions, and (2) supply of all raw materials is instantaneous and unlimited. The objective is to maximize a weighted function of product sales.

3. MILP Formulation

We postulate **K** ($k = 1, 2, \ldots, K$) contiguous time-slots (Figure 1) of unknown lengths for each processing unit (j) and storage ($s = s1, s2, \ldots, S$) during [0, H]. Let T_{jk} ($k = 0, 1, \ldots, K$; $T_{j0} \geq 0$, $T_{jK} \leq H$) denote the end time of slot k on processing unit j. The time before the start of slot 1 is slot 0 ($k = 0$). A slot k on a unit j starts at $T_{j(k-1)}$, ends at T_{jk}, and has a slot length $T_{jk} - T_{j(k-1)}$. While each unit or storage has K slots, the slot times (T_{jk} and T_{sk}) may vary across different units and storages. Thus, we use a multi-grid approach, also known as unit-slots approach (Susarla et al., 2010).

We assume that the transfer to a unit or storage always begins at the start of a slot, but may end at any time during the slot. δ_{jk} / δ_{sk} denote the idle time within a slot.

$$T_{jk} \geq T_{j(k-1)} + \delta_{jk} \qquad j1 \leq j \leq J,\ k1 \leq k \leq K \tag{1a}$$

$$T_{sk} \geq T_{s(k-1)} + \delta_{sk} \qquad s1 \leq s \leq S,\ k1 \leq k \leq K \tag{1b}$$

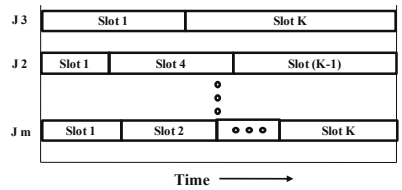

Figure 1 Design of unit-slots

We use the following binary variable (y_{ijk}) and 0-1 continuous variable (ye_{jk}) to denote the allocation of a task to a slot and its end within a slot, respectively.

$$y_{ijk} = \begin{cases} 1 & \text{if task } i \text{ is allocated to slot } k \text{ of unit } j \\ 0 & \text{otherwise} \end{cases} \qquad i \in \mathbf{I}_j,\ i = 0,\ 0 \le k \le K$$

$$ye_{ijk} = \begin{cases} 1 & \text{if the current task allocation ends during slot } k \text{ of unit } j \\ 0 & \text{otherwise} \end{cases} \qquad i \in \mathbf{I}_j,\ i = 0,\ 0 \le k \le K$$

Now, every slot in a unit j must have a task and any slot in a unit cannot have more than one task. So, we write,

$$\sum_{i=0, i \in I_j} y_{ijk} = 1 \qquad k1 \le k \le K \tag{2}$$

Note that we do not write Eqs. 2 for $k = 0$ because y_{ij0} can be fixed based on the status of a unit at time zero. Then, a task may continue its run from k to (k+1), only if it is allocated to both. Here, $ye_{jK} = 1$, as we do not allow any unfinished task at the end of the scheduling horizon.

The length of a slot must be equal to the sum of the processing time (PT_{ijk}) and the idle time (δ_{jk}, if any) within that slot. This gives us,

$$\sum_{i \in I_j} PT_{ijk} + \delta_{jk} = T_{jk} - T_{j(k-1)} \qquad j1 \le j \le J,\ k1 \le k \le K \tag{3}$$

If a task i is not allocated to a slot k of a unit j (i.e., $y_{ijk} = 0$) then the corresponding processing time must be zero. Also, if a task i does not end in a slot k and continues from slot k to k+1, then the idle time in that slot must be zero. Furthermore, we ensure that the length of each run of a task is greater than or equal to the desired minimum.

Next, we define the following 0-1 continuous variable to denote the latest allocation.

$$x_{ijk} = \begin{cases} 1 & \text{if is the latest/current allocation in slot } k \text{ of unit } j \\ 0 & \text{otherwise} \end{cases} \qquad i \in \mathbf{I}_j,\ 0 \le k \le K$$

As a unit processes only one task in any slot, there can be only one latest allocation at any slot. According to the definition of x_{ijk}, if a non-idle task i ($i \neq 0$) is allocated to a slot k of unit j, then i must be the latest allocation in that unit. However, if an idle task (i = 0) is allocated to a slot k of unit j, then the latest task is the last non-idle or a real task ($i \neq 0$) allocated in unit j before slot k. Thus, we write,

$$x_{ijk} \ge y_{ijk} \qquad i \in \mathbf{I}_j,\ k1 \le k \le K \tag{4}$$

$$x_{ijk} \ge x_{ij(k-1)} + y_{0jk} - 1 \qquad i \in \mathbf{I}_j,\ k1 \le k \le K \tag{5}$$

Then, we demand that the idle time in the slot preceding the start of a new task is sufficiently longer to accommodate an appropriate transition time. So, we write,

$$\delta_{j(k-1)} \ge \tau_{i\prime ij}(y_{ijk} + x_{i\prime j(k-1)} - 1) \qquad i, i' \in \mathbf{I}_j,\ i \neq i',\ k1 < k \le K \tag{6}$$

Following the discussion in Susarla et al. (2010) for shared resources, we write the following constraints for material transfers with dedicated intermediate storage.

$$T_{j(k-1)} \ge T_{s(k-1)} - H(2 - ye_{j(k-1)} - \sum_{i \in I_j, \sigma_{sij} < 0} y_{ijk} \qquad j1 \le j \le J,\ k1 \le k \le K,\ s: \sum_{i \in I_j} \sigma_{sij} < 0 \tag{7a}$$

$$T_{j(k-1)} \le T_{s(k-1)} + H(2 - ye_{j(k-1)} - \sum_{i \in I_j, \sigma_{sij} < 0} y_{ijk} \qquad j1 \le j \le J,\ k1 \le k \le K,\ s: \sum_{i \in I_j} \sigma_{sij} < 0 \tag{7b}$$

$$T_{jk} - \delta_{jk} \geq T_{sk} - H(2 - ye_{jk} - \sum_{i \in I_j, \sigma_{sij} > 0} y_{ijk} \quad j1 \leq j \leq J, k1 \leq k \leq K, s: \sum_{i \in I_j} \sigma_{sij} > 0 \tag{8a}$$

$$T_{jk} - \delta_{jk} \leq T_{sk} + H(2 - ye_{jk} - \sum_{i \in I_j, \sigma_{sij} > 0} y_{ijk} \quad j1 \leq j \leq J, k1 \leq k \leq K, s: \sum_{i \in I_j} \sigma_{sij} > 0 \tag{8b}$$

For multipurpose storage vessels v (v = 1, 2, …, V) capable of storing a set $\mathbf{S}_v$ of materials, we ensure that only a material that is stored has a non-zero amount and rest all are zeros. For this, we define the following binary variable.

$$z_{svk} = \begin{cases} 1 & \text{if } s \text{ is stored in vessel } v \text{ during slot } k \\ 0 & \text{otherwise} \end{cases} \qquad s \in \mathbf{S}_v,\ 1 \leq v \leq V, k1 \leq k \leq K$$

Now that materials are stored exclusively in a vessel, only one material is allowed at any given time. Thus, we demand,

$$\sum_{s \in S_v} Z_{svk} = 1 \qquad 1 \leq v \leq V, k1 \leq k \leq K \tag{9}$$

Also, only a material s that is stored in a vessel v during slot k may have a non-zero amount present in the storage. So, we set the amount (A_{svk}) of all other materials to zero whenever they are not stored in the vessel v. So, we write the following,

$$A_{svk} \leq A_v^U Z_{svk} \qquad s \in \mathbf{S}_v,\ 1 \leq v \leq V, k1 \leq k \leq K \tag{10}$$

Let $q_{ijk} = R_{ij}^L PT_{ijk} + dq_{ijk}$ ($j1 \leq j \leq J$, $i \in \mathbf{I}_j$, $k1 \leq k \leq K$) be the total amount of all the materials that task i processes in unit j during slot k. Here, R_{ij}^L is the minimum material processing rate of task i in unit j. If a task i is not allocated to unit j during a slot k, then we set $q_{ijk} = 0$. Also, if a task i is allocated to unit j during a slot k, then the total amount of materials processed must not exceed the maximum capacity of the unit. In other words, the material processing rate of task i in unit j must not exceed the maximum allowable processing rate (R_{ij}^U). Therefore, we have,

$$dq_{ijk} \leq \left(R_{ij}^U - R_{ij}^L\right) PT_{ijk} \qquad i \in \mathbf{I}_j, j1 \leq j \leq J, k1 \leq k \leq K \tag{11}$$

Aforementioned discussion and constraints allow us to write the following inventory (I_{sk}) balance for each material s, at the end of a slot k.

$$I_{sk} = I_{s(k-1)} + \sum_j \sum_{i \in I_j, \sigma_{sij} \neq 0} \sigma_{sij} (R_{ij}^L PT_{ijk} + dq_{ijk}) \qquad s1 \leq s \leq S, k1 \leq k \leq K \tag{12}$$

One of the most widely used objectives in the literature is revenue maximization. Here, it is assumed that all the products produced are sold and they must either satisfy a minimum demand or must fall within a given range of the demand. So, we have the following demand constraint applicable as required,

$$D_s^L \leq \sum_k \sum_j \sum_{i \in I_j, \sigma_{sij} > 0} (R_{ij}^L PT_{ijk} + dq_{ijk}) \leq D_s^U \qquad s1 \leq s \leq S \tag{13}$$

where, D_s^L and D_s^U are the lower and upper limits of the demand for a material s.

The total revenue through sales (SR) of the products is given as the following.

$$SR = \sum_s \sum_k \sum_j \sum_{i \in I_j, \sigma_{sij} > 0} p_s \sigma_{sij} (R_{ij}^L PT_{ijk} + dq_{ijk}) \tag{14}$$

where, p_s is the market price for a material s. $p_s = 0$, if s in not a product.

This completes our model (Eqs. 1 – 14) for scheduling semi-continuous plants.

4. Numerical Evaluation

We consider two scenarios of an industrial case study from fast moving consumer goods (FMG) manufacturing plant, which is extensively studied in the literature. The plant follows a common production sequence: mixing, storage, and packing. All examples are solved on a Dell precision PWS690 (Intel® XeonR 5160 with CPU 3 GHZ and 16 GB memory) running Windows 7 using CPLEX 11/GAMS 23.7.

4.1 Example 1

In this example, we consider four raw materials (S1-S4), 4 mixers (M-101 to M-104), and 3 packing lines (PL-101 to PL-104, 5 intermediates (S5-S9), and 5 final products

Each intermediate has its dedicated storage tank and the maximum capacities are 60 ton of S5, 200 ton of S6, 200 ton of S7, 200 ton of S8, and 200 ton of S9, respectively. Storage bypassing is allowed. While the model of Shaik and Floudas (2007) found a solution that is not feasible, our model obtains a feasible solution with objective value of 360.27 k$.

4.2 Example 2

In this case, we consider one raw material (S1), 1 mixer (M-101), 3 packing lines (PL-101 to PL-104, two intermediates (S2-S3), and 5 final products. Two flexible storage tanks (ST-101 and ST-102) are available with a maximum capacity of 40 ton. Storage tank ST-101 can store states S2 and S3, while ST-102 can hold only S3. Storage bypassing is not allowed. Both our model and the model of Shaik and Floudas (2007) attain the optimal solution of 268.7 k$ with 4 slots. Table 1 lists the model and solution statistics.

Table 1 Model and Solution Statistics

	Example 1		Example 2	
	Ours	S & F	Ours	S & F
Events/ Slots	6	-	4	4
Binary Variables	236	-	108	108
Continuous Variables	445	-	301	337
Constraints	1137	-	908	1249
MILP	360.27	-	268.70	268.70
CPU time (s)	8	-	190	540

S & F: Shaik and Floudas (2007)

5. Conclusion

We have successfully developed and demonstrated a new multi-grid MILP formulation based on unit slots for scheduling semi-continuous plants. Our model showed a better performance over the literature models. In addition, our model features many features such as sequence-dependant transition times, various storage policies, etc. We are currently working on further reduction of variables and constraints in our model to improve its performance.

References

Susarla N, Li J, Karimi IA, A novel approach to scheduling multipurpose batch plants using unit-slots 2010. AIChE Journal, 56 (7), 1859-1879.

Shaik MA, Floudas CA. Improved unit-specific event-based continuous-time model for short-term scheduling of continuous processes: Rigorous treatment of storage requirements. Industrial and Engineering Chemistry Research 2007;46(6):1764-79.

Ierapetritou MG, Floudas CA. Effective continuous-time formulation for short-term scheduling. 2. Semi-continuous processes. Industrial and Engineering Chemistry Research 1998;37(11):4341-59.

Karimi IA, McDonald CM. Planning and scheduling of parallel semicontinuous processes. 2. Short-term scheduling. Industrial and Engineering Chemistry Research 1997;36(7):2701-14.

Lim M-F, Karimi IA. Resource-Constrained Scheduling of Parallel Production Lines Using Asynchronous Slots. Industrial and Engineering Chemistry Research 2003;42(26):6832-42.

Li J, Susarla N, Karimi IA, Shaik M, Floudas CA. An Analysis of Some Unit-Specific Event-based Models for The Short-term Scheduling of Non-continuous Processes. Industrial and Engineering Chemistry Research 2010; 49, 633-647.

Shaik M, Floudas C. Novel Unified Modeling Approach for Short-Term Scheduling. Industrial and Engineering Chemistry Research 2009;48(6):2947-64.

I.A. Karimi and Rajagopalan Srinivasan (Editors), Proceedings of the 11th International Symposium on Process Systems Engineering, 15-19 July 2012, Singapore.

A Continuous-Time Approach for Scheduling Bidirectional Pipeline Operations

Vanina G. Cafaro,[a] Diego C. Cafaro,[a] Jaime Cerdá[a]

[a]*INTEC (UNL-CONICET), Güemes 3450, (3000) Santa Fe, Argentina*

Abstract

Scheduling pumping operations in multiproduct pipelines is a complex logistic task that requires efficient supporting tools. Several approaches have been proposed for solving the pipeline scheduling problem for different pipeline configurations, but up to now the problem of sizing and sequencing oil product batches moving through bidirectional pipelines could not be tackled by continuous-time representations. This work introduces a mixed integer linear programming formulation standing for the first rigorous approach effectively solving the short-term operational planning of bidirectional pipelines.

Keywords: Bidirectional pipelines, Continuous-time formulation, MILP approach.

1. Introduction

For the logistics of crude oil and refined products, pipeline transportation offers superior reliability at relatively low cost. Since different products are transported through the same line without separation devices, the mixing of adjacent batches produces volumes of degraded products that increase the operative costs. Hence, planning the size and sequence of new batches to be pumped into the pipelines, and the simultaneous deliveries to depots located across the system is a complex logistic task that requires efficient supporting tools. In the last decade, a considerable amount of work has been done for solving the multiproduct pipeline scheduling problem for different pipeline configurations. From the simplest case comprising a unidirectional pipeline with a single origin and a single destination, to mesh-structured pipeline networks connecting refineries, distribution centers and customers' facilities, a broad class of problems has been tackled by using decomposition approaches,[1] heuristic-based techniques,[2] discrete representations,[3] and continuous-time optimization models.[4-8] The latter appears to be the most efficient choice in terms of the computational burden required. However, up to now, the problem of sizing and sequencing oil product batches moving through bidirectional (also called reversible) pipelines has not been solved in a rigorous way.

Bidirectional pipelines normally connect a refinery tank farm to a harbour, or inland distribution terminals between themselves. The same pipeline is used to convey products either from the refinery to the harbour, or from the harbour to the refinery, and the flow can be inverted during the planning horizon according to terminal demands and tank availability. A key aspect of bidirectional pipelines is the fact that after sending all the demanded products in one direction, it is necessary to fill the pipeline with another product to push the batches out of the line into the terminal tanks at the other extreme. A large batch of a filler product is usually inserted to push the batch sequence in the line. Once the inputted batches have reached their destination, the flow direction can be switched. At that moment, the receiving terminal turns to be the input terminal and begins to pump batches at the other extreme, in the opposite direction. Then, the filler product gradually returns to the assigned tanks. This procedure is repeated each time the flow is inverted, thus resulting in undesirable time delays and higher costs. To the best

of our knowledge, only approximate approaches have been proposed for solving the bidirectional pipeline scheduling problem.[1,9,10] They rely on discrete MILP models that divide both the pipeline volume into single-product packs, and the planning horizon into time intervals of fixed duration. As a result, they will not provide feasible schedules unless a fine discretization is adopted. Besides, the starting flow direction is not a model decision but a user specification, and it can be inverted only once over the time horizon. Contrary to previous techniques, this work introduces the first rigorous approach for the operational planning of reversible pipelines. It consists of an MILP continuous-time formulation that accounts for the possibility of inverting the flow direction many times, at the proper time instants. Batch movements are rigorously traced along the line in both directions, and inventory levels are efficiently monitored in a continuous way. The model can optimally select pump rates and choose the most convenient product to be pumped as the filler batch. The problem goal is to find the optimal sequence of pumping and delivery operations that permits to satisfy terminal requirements at minimum total cost, including pumping, mixing, backordered demand, and inventory carrying costs.

2. Mathematical Formulation

Similar to previous formulations of the pipeline scheduling problem,[6] the continuous-time model for bidirectional pipelines is based on the following sets: the ordered set of batches $I = \{i_1 \ldots i_n\}$, the sequence of future pumping runs $K = \{k_1 \ldots k_m\}$ and the terminal set $J = \{j_1, j_2\}$ comprising the depots at both extremes of the pipeline. The set of batches I is built as follows: (i) The first r elements $\{i_1 \ldots i_r\}$ stand for new batches to be pumped from node j_2 (in reverse flow) during the future horizon; (ii) the following l elements $\{i_{r+1} \ldots i_{r+l}\}$ represent the old bathes initially into the pipeline at the start of the time horizon; and (iii) the last d elements $\{i_{r+l+1} \ldots i_{r+l+d}\}$ are new bathes to be subsequently pumped in direct flow in future runs. Hence, $I = I^{rev} \cup I^{old} \cup I^{dir}$, as shown in Fig. 1.

Fig. 1. Ordered set of batches to be transported through the bidirectional pipeline.

Besides, the MILP model comprises the following 0-1 variables: (a) $y_{i,p}$ assigning product p to batch i; (b) $x_{i,j}^{(k)}$ stating that a portion of batch i is delivered to terminal j during run k; (c) $u_{i,k}$ denoting that terminal j_1 pumps product into batch $i \in I^{dir}$ during run k (direct flow); and (d) $v_{i,k}$ denoting that terminal j_2 pumps product into batch $i \in I^{rev}$ during run k (reverse flow). The following sections present the main model constraints.

2.1 Pumping run sequence. The execution of a new pumping run should start after completing the previous operation. Variable C_k is the completion time for run k, L_k is the run duration, and $h_{\max}$ is the length of the scheduling horizon, all measured in time units.

$$C_k - L_k \geq C_{k-1} \quad ; \quad L_k \leq C_k \leq h_{\max} \quad \forall k \in K \tag{1}$$

2.2 Determining the flow direction. At every active run, products move in direct or reverse flow, depending on the terminal demands at one or the other extreme of the pipeline. Contrary to previous approaches,[1,9] the flow direction is a model decision, and can be inverted as many times as necessary over the planning horizon. Besides, if the pipeline is operated in direct flow, the model selects a single batch to pump at terminal j_1. On the contrary, in reverse flow, a single batch departs from terminal j_2.

$$\sum_{i\in I^{dir}} u_{i,k} + \sum_{i'\in I^{rev}} v_{i',k} \le 1 \qquad \forall k \in K \tag{2}$$

Every fictitious operation k verifies $u_{i,k} = 0$ and $v_{i',k} = 0$ for all $i \in I^{dir}$ and $i' \in I^{rev}$.

2.3 Sizing lot injections. If $Q_{i,k}$ denotes the volume of lot i injected during the pumping run k, its value is bounded by Eq. (3), either in direct or reverse flow operation.

$$u_{i,k}\, q_{dir}^{\min} \le Q_{i,k} \le u_{i,k}\, q_{dir}^{\max} \quad \forall i \in I^{dir}, k \in K \quad ; \quad v_{i',k}\, q_{rev}^{\min} \le Q_{i',k} \le v_{i',k}\, q_{rev}^{\max} \quad \forall i' \in I^{rev}, k \in K \tag{3}$$

2.4 Time duration of a new pumping run. Depending on the flow direction, the pipeline admits different pump rates that must be controlled at every operation. If the interval $[vb_f^{\min}; vb_f^{\max}]$ represents the feasible pump rate range for direction f, then:

$$\sum_{i\in I^{dir}} Q_{i,k} / vb_{dir}^{\max} + \sum_{i'\in I^{rev}} Q_{i',k} / vb_{rev}^{\max} \le L_k \le \sum_{i\in I^{dir}} Q_{i,k} / vb_{dir}^{\min} + \sum_{i'\in I^{rev}} Q_{i',k} / vb_{rev}^{\min} \quad \forall k \in K \tag{4}$$

2.5 Product sequence. Every non-fictitious lot i will contain a single refined petroleum product. Depending on the source node, the set of available products to be inputted may be different. If the set P_j stand for all the products that can be pumped from node j, then:

$$\sum_{k\in K} u_{i,k} = \sum_{p\in P_{j1}} y_{i,p} \le 1 \quad \forall i \in I^{dir} \quad ; \quad \sum_{k\in K} v_{i',k} = \sum_{p\in P_{j2}} y_{i',p} \le 1 \quad \forall i' \in I^{rev} \tag{5}$$

The aim of Eq. (5) is twofold: (a) every new batch that is injected into the pipeline must contain a single product; and (b) every non-fictitious batch can be injected only once over the planning horizon. Moreover, the chronological order of product injections should be established. In direct flow, the injection of lot i must precede the pumping of lot i+1, as usual. But in reverse flow the injection of lot i' must succeed the pumping of lot i'+1, because of the order given for the set I (see Fig. 1). Therefore:

$$u_{i,k} \le \sum_{l<k} u_{i-1,l} \quad \forall i \in I^{dir} \quad ; \quad v_{i',k} \le \sum_{l<k} v_{i'+1,l} \quad \forall i' \in I^{rev} \tag{6}$$

In this way, fictitious lots never pumped into the pipeline (featuring $y_{i,p} = 0\ \forall p \in P$), in direct or reverse flow, lay at the end of the associate batch sequence I^{dir} or I^{rev}. Finally, the injection of a new batch i produces a new interface, whose size can be estimated by:

$$\begin{aligned} &WIF_{i,p,p'} \ge ifd_{p,p'}\,(y_{i,p} + y_{i-1,p'} - 1) && WIF_{i',p,p'} \ge ifr_{p,p'}\,(y_{i',p} + y_{i'+1,p'} - 1) \\ &\qquad \forall i > first(I^{dir}), (p,p') \in P_{j1} && \qquad \forall i' < last(I^{rev}), (p,p') \in P_{j2} \end{aligned} \tag{7}$$

Parameters $ifd_{p,p'}$ and $ifr_{p,p'}$ stand for the size of the interface between products p' and p when sequentially pumped in direct or reverse flow, respectively. However, these estimations should be adapted for the first injection reversing the pipeline flow. This issue is left for an extended version of the work.

2.6 Batch tracking. The size of a batch i at time C_k ($W_{i,k}$) can be updated by:

$$W_{i,k} = W_{i,k-1} + Q_{i,k} - \sum_{j\in J} D_{i,j}^{(k)} \quad \forall i \in I, k \in K \tag{8}$$

For $k = 1$, $W_{i,k-1}$ is the size of the batches in the initial linefill (wo_i), and is equal to zero for $i \in I^{dir} \cup I^{rev}$. For old batches $i \in I^{old}$, variable $Q_{i,k}$ should not be considered. Besides, the last term in Eq. (8) accounts for two possible situations: (a) a batch first injected at terminal j is later discharged into the opposite terminal j' (common movement), and (b) a batch first injected at j later returns to j after a pipeline flow reversal. On the other hand, the continuity of the flow into the pipeline is imposed by Eq. (9). Moreover, each operation (in direct or reverse flow) must respect the input/output material balance.

$$F_{i,k} - W_{i,k} = F_{i+1,k} \;\; \forall i \in I, k \in K$$
$$\sum_{i \in I^{dir}} Q_{i,k} = \sum_{l \in I} D_{l,j2}^{(k)} \quad ; \quad \sum_{i' \in I^{rev}} Q_{i',k} = \sum_{l \in I} D_{l,j1}^{(k)} \qquad \forall k \in K \tag{9}$$

Note that an injection from j_1 only admits diversions into terminal j_2, and vice-versa.

2.7 Diversion feasibility. In direct flow, a product lot i can be discharged into j_2 during run k only if the end of the pipe is reached by such lot during the same run, i.e. $F_{i,k} \geq pv$, where pv stands for the overall pipeline volume. But in reverse flow, the possibility of diverting a lot i into terminal j_1 implies the condition $F_{i,k}$ - $W_{i,k} \leq 0$, given that the lot is moving in the opposite direction and the terminal j_1 is located at the pipeline origin (zero coordinate). Both conditions are imposed through Eq. (10).

$$d_{\min} x_{i,j}^{(k)} \leq D_{i,j}^{(k)} \leq d_{\max} x_{i,j}^{(k)} \qquad \forall i \in I, j \in J, k \in K$$
$$F_{i,k} \geq pv \; x_{i,j2}^{(k)} \quad ; \quad F_{i,k} - W_{i,k} \leq pv \, (1 - x_{i,j1}^{(k)}) \qquad \forall i \in I, k \in K \tag{10}$$

2.8 Injected and diverted products. To identify the product p that is injected into or diverted from the pipeline during a single run k we introduce the variables $QP_{i,p}^{(k)}$ and $DP_{i,p,j}^{(k)}$. Just in case product p is assigned to lot i ($y_{i,p}$ = 1) both variables can take positive values. Otherwise, they will be null, as stated by Eqs. (11) and (12).

$$QP_{i,p}^{(k)} \leq q_{dir}^{\max} \; y_{i,p} \quad \forall i \in I^{dir}, k \in K, p \in P_{j1} \quad ; \quad Q_{i,k} = \sum_{p \in P_{j1}} QP_{i,p}^{(k)} \quad \forall i \in I^{dir}, k \in K$$
$$QP_{i',p}^{(k)} \leq q_{rev}^{\max} \; y_{i',p} \quad \forall i' \in I^{rev}, k \in K, p \in P_{j2} \quad ; \quad Q_{i',k} = \sum_{p \in P_{j2}} QP_{i',p}^{(k)} \quad \forall i' \in I^{rev}, k \in K \tag{11}$$

$$DP_{i,p,j}^{(k)} \leq d_{\max} \, y_{i,p} \quad \forall i \in I, j \in J, k \in K, p \in P \quad ; \quad D_{i,j}^{(k)} = \sum_{p \in P} DP_{i,p,j}^{(k)} \quad \forall i \in I, j \in J, k \in K \tag{12}$$

2.9 Inventory control and demand fulfillment. If $DM_{p,j}^{(k)}$ stands for the total amount of product p sent from depot j to local markets (usually by truck) during the time interval $[C_{k\text{-}1} ; C_k]$, its value is limited by the maximum discharge rate admitted by terminal j, i.e. $vm_{p,j}$. Moreover, the total amount of p delivered from j to customers during the time horizon should be high enough to fulfill market demands. Otherwise, a backorder of size $B_{p,j}$ will arise, thus delaying the order completion and increasing operational costs.

$$DM_{p,j}^{(k)} \leq (C_k - C_{k-1}) \, vm_{p,j} \quad \forall p \in P, j \in J, k \in K; \quad \sum_{k \in K} DM_{p,j}^{(k)} = dem_{p,j} - B_{p,j} \quad \forall p \in P, j \in J \tag{13}$$

On the other hand, we assume that both terminals receive a continuous flow of certain products from neighboring refineries and/or harbors all over the time horizon at a fixed rate of $vp_{p,j}$ units per hour. As a result, the inventory level of product p in tanks of depot j at the end time of every operation k, i.e. $ID_{p,j}^{(k)}$, can be determined through Eq. (14).

$$ID_{p,j}^{(k)} = ID_{p,j}^{(k-1)} + \sum_{i \in I} DP_{i,p,j}^{(k)} - \sum_{i \in I^*} QP_{i,p}^{(k)} + vp_{p,j}(C_k - C_{k-1}) - DM_{p,j}^{(k)} \quad \forall p \in P, j \in J, k \in K \tag{14}$$

The set I^* stands for direct lots $i \in I^{dir}$, when $j = j_1$, and reverse lots $i' \in I^{rev}$, when $j = j_2$. Finally, the stock level of product p at terminal j should remain within the admissible range during the entire horizon. Hence, $(id_{\min})_{p,j} \leq ID_{p,j}^{(k)} \leq (id_{\max})_{p,j}$ for every run $k \in K$.

2.10 Objective function. The goal of the proposed MILP model is to minimize the total operational cost of the pipeline schedule including: (a) pumping costs, (b) backorder costs, (c) interface costs, (d) inventory carrying costs, and (e) the fixed cost paid for every pipeline flow reversal (see Eq. 15). Term (d) is based on the average inventory levels, whose values are estimated by summing product stocks at the end of every run,

and dividing the result by the number of runs $|K|$. Besides, term (e) can be derived from the values of the binary variables $u_{i,k}$ and $v_{i',k}$ at subsequent injections k-1 and k. Hence, a continuous variable w_k is introduced to detect a flow reversal at the start of run k, by imposing: $w_k \geq u_{i,k} + v_{i',k-1} - 1$, and $w_k \geq u_{i,k-1} + v_{i',k} - 1$, for all $i \in I^{dir}$, $i' \in I^{rev}$, and $k > 1$.

$$z = \sum_{j\in J}\sum_{p\in P_j} cp_{p,j} \sum_{i\in I^*} QP_{i,p}^{(k)} + \sum_{p\in P}\sum_{j\in J} cb_{p,j}\, B_{p,j} + \sum_{p,p'\in P} cf_{p',p} \sum_{i\notin I^{old}} WIF_{i,p,p'} + \sum_{j\in J}\sum_{p\in P} \frac{cid_{p,j}}{|K|} \sum_{k\in K} ID_{p,j}^{(k)} + cr \sum_{k\in K} w_k \quad (15)$$

3. Case study

The proposed MILP formulation was applied to a modified version of a case study first introduced by Magatao et al. (2011)[5] comprising a time horizon of 129 h. Though the flow direction can be reversed as many times as necessary, results show that the model naturally tends to reverse the flow only once over the time horizon, to reduce pumping costs. Fig. 2 illustrates the optimal sequence of product injections, similar to the one reported by previous authors.[5] In this case, however, lots are first pumped in direct flow, and then in the opposite direction, requiring no "plugs" to separate incompatible products. *P4* and *P5* are automatically chosen as filler products in direct and reverse flow, respectively. Batch sizes and pump rates take continuous values, since no time nor volume discretization is required. The model, with 315 binary vars, was solved in 197 s on an Intel Xeon CPU using GAMS/ GUROBI 3.0. Optimal solutions to larger problems can also be obtained in reasonable CPU times.

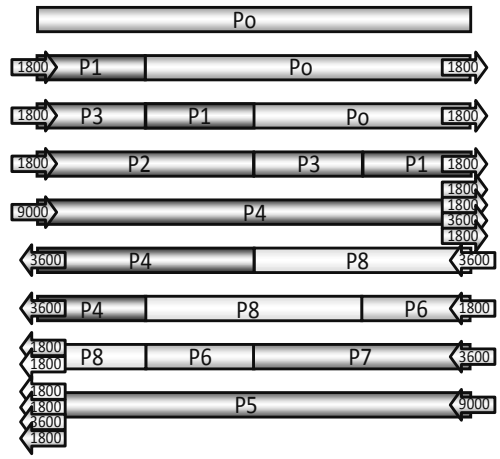

Fig. 2. Optimal pipeline schedule.

4. Conclusions

We presented the first rigorous approach effectively solving the short-term operational planning of reversible pipelines through an MILP continuous-time formulation. Batch sizes, product sequences, pump rates, and flow directions can be determined all at once, and product stocks at depots can be continuously controlled. Additional problem features like high-cost energy periods will be included in future works.

References

[1] L. Magatao, L.V.R. Arruda, F. Neves, 2011, Journal of Scheduling, 14, 47-87.
[2] S.N. Boschetto, L. Magatão, W.M. Brondani, F. Neves, L.V.R. Arruda, A.P. Póvoa, S. Relvas, 2010, Ind. Eng. Chem. Res., 49, 5661-5682.
[3] R. Rejowski, J.M. Pinto, 2004, Comput. Chem. Eng., 28, 1511-28.
[4] S. Relvas, H. Matos, A. Barbosa, Fialho, Pinheiro, 2006, Ind. Eng. Chem. Res., 45, 7841-55.
[5] D.C. Cafaro, J. Cerdá, 2008, Ind. Eng. Chem. Res., 47, 9941-9956.
[6] D.C. Cafaro, J. Cerdá, 2010, Comput. Chem. Eng., 34, 1687-1704.
[7] D.C. Cafaro, J. Cerdá, 2011, Ind. Eng. Chem. Res., 50, 5064-5085.
[8] D.C. Cafaro, J. Cerdá, 2011, In press, doi:10.1016/j.compchemeng.2011.11.007.
[9] L. Magatao, L.V.R. Arruda, F. Neves, 2004, Comput. Chem. Eng., 28, 171-185.
[10] A. Herrán, A.; J.M. de la Cruz, B.A. de Andrés, 2010, Comput. Chem. Eng., 34, 401-413.

I.A. Karimi and Rajagopalan Srinivasan (Editors), Proceedings of the 11th International Symposium on Process Systems Engineering, 15-19 July 2012, Singapore.

An iterative MILP-based approach to automated multi-product multi-stage manufacturing systems

A. M. Aguirre,[a] C. A. Méndez,[a] C. De Prada[b]

[a]*INTEC (UNL - CONICET), Güemes 3450, 3000 Santa Fe, Argentina.*
[b]*Universidad de Valladolid, c/ Real de Burgos s/n, 47011 Valladolid, Spain.*

Abstract

An efficient MILP-based approach is presented to solve flow shop scheduling problems in automated manufacturing systems. The problem comprises complex production constraints and stringent storage policies in a multiple product multistage batch process. Automated transfers accross the entire system, recicle flows and different production recipes are also considered in the process scheme. The proposed decomposition approach was able to solve the entire problem in a sequential manner by dividing it into two major stages that are iteratively solved to find near optimal results with an acceptable CPU time. The effectiveness of this method is tested and compared with a monolithic MILP formulation by solving a real-world problem.
Keywords: MILP-based model, Automated Manufacturing System, Multiple products multistage batch process, Flow shop scheduling problems, Industrial applications.

1. Introduction

Most common automated manufacturing systems consist in a complex flow shop production process in where a set of units, as machines, baths or tanks, are arranged in a single production line for processing batches of different jobs in a sequential way under specific intermediate storage policies (Crama, 1997). Automated material-handling devices, like hoists or robots, are used to move wafer's lots between units and buffers.

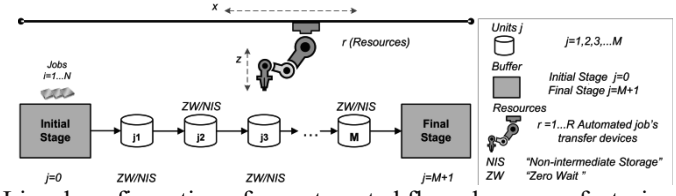

Fig. 1: Lineal configuration of an automated flow shop manufacturing system.

This type of modern automated production facilities is used in many different practical applications such as surface treatments of metal components or in the manufacture of printed circuit boards (PCBs) in electronics plants (Phillips & Unger, 1976; Shapiro & Nuttle, 1988). In these plants material handling devices, called hoists, are used to move parts from one to another machine undergoing a sequence of different operations in successive tanks. This type of production operations are also found in the automated wet-etch station (AWS) in semiconductor manufacturing facilities (Bhushan & Karimi, 2003; Aguirre et al., 2011; Zeballos et al., 2011; Castro et al., 2011). In this station, automated rail-guide vehicles (AGVs), like robots, are used to perform transfer operations by following a predefined sequence of chemical and water immersion processes between consecutive baths. Many research works have been developed in this area in recent years by using several methods like heuristic and meta-heuristics

procedures, full-space mathematical models (Bhushan & Karimi, 2003; Aguirre et al., 2011), constraint programming formulations (Zeballos et al., 2011) and also hybrid approaches (Castro et al., 2011).

One of the major assumptions that have been taken into account in these problems is the consideration of a unique production sequence for all jobs. But in most of industrial applications this simplification does not exist. Usually, a set of jobs with different production recipes, also called products, must be processed following a series of stages with a single processing unit per stage. Also, re-entrant and possible recycle flows can be found in these processes. Flexible timing operations depends on the job processed and the production stage followed. According to this, every job has a minimum processing time and a limited residence time that has to be strictly fulfilled in every stage. After the processing time, every lot has to be immediately transferred to the following stage in the recipe. The transfer operations in the system must be exactly coordinated due to no intermediate buffer exists between these stages. In order to perform transfer activities, automated material handling devices with finite capacity, are available.

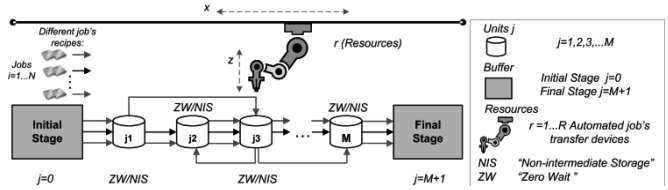

Fig. 2: Process scheme in automated manufacturing systems.

As we can see, the use of different processing recipes and shared transportation resources forces, the decision maker, to do a more detailed and synchronized schedule of all the processing and transportation activities in the system. These practical limitations faced by many real-life industries nowadays become the automated flow shop scheduling problem of multiple products in a real complex challenge for researches and practitioners.

In this work, a novel computationally efficient MILP-based mathematical formulation for the multiple product scheduling problems in a real-world automated manufacturing system is proposed. The principal aim is to find a robust solution approach for industrial scale application problems that provides good-quality results with an acceptable computational effort.

2. Flow shop MILP-based model

The model presented in this work lies on the MILP-based approach proposed by Aguirre et al., (2011) to AWS scheduling problems. The new model is devised to flow shop scheduling problems with an automated material-handling robot in a single production line. The multi-product multistage batch process under study has reentrant and possible recycle flows to the same unit. In addition, flexible processing times and transferring times are also considered.

2.1. Notations

I, S, J	Jobs $(i=i_1,...,N)$, Stages $(s=s_1,...,L)$, Units $(j=j_1,...,M)$
S_i , L_i	Stages belonging to the production sequence of job i
$j_{i,s}$	Unit j belonging to job i in production stage s
$Seq_{(i)}$	Product recipe of job i
$Ts_{(i,s)}$, $Tf_{(i,s)}$	Start time and Final time of job i in stage s

$t^{min}_{(i,s)}$, $t^{max}_{(i,s)}$	Minimum and Maximum processing time of job *i* in stage *s*
$\pi_{(i,s)}$,	Transfer time of job *i* from stage *s-1* to *s*
$\pi^{min}_{(i,s)}$, $\pi^{max}_{(i,s)}$	Minimum and Maximum transfer time of job *i* from stage *s-1* to *s*
$X_{(i,i',s,s')}$, $Y_{(i,i',s,s')}$	Job sequencing and Transfer sequencing decisions
M_T , MK	Large value (Big-M parameter); Makespan Criterion

2.2. Main Features

In the following model, Eqs. 1-2 and Eqs. 3-5 are defined to handle flexible processing times $t_{(i,s)}$ in a single unit and flexible transferring times $\pi_{(i,s)}$ for the robot. Then, Eqs. 6-7 and Eqs. 8-9 are proposed to manage job's sequencing $X_{(i,i',s,s')}$ and transfer's sequencing $Y_{(i,i',s,s')}$ decisions. Finally, Eqs. 10-11 are developed to reduce the computational complexity of the model by fixing certain variables of jobs belonging to the same production recipe $Seq_{(i)}$. The objective function *(MK)* is presented in Eq. 12. Then, Eq. 13 is proposed to provide alternative job's sequences to the entire problem.

2.3. Flexible processing times

$$Tf_{(i,s)} \geq Ts_{(i,s)} + t^{\min}{}_{(i,s)} \qquad \forall i \in I, s \in S_i \tag{1}$$

$$Tf_{(i,s)} \leq Ts_{(i,s)} + t^{\max}{}_{(i,s)} \qquad \forall i \in I, s \in S_i \tag{2}$$

2.4. Flexible transferring times

$$Ts_{(i,s)} = Tf_{(i,s-1)} + \pi_{(i,s)} \qquad \forall i \in I, s \in S_i : s > 1 \tag{3}$$

$$Ts_{(i,s)} \geq \pi_{(i,s)} \qquad \forall i \in I, s \in S_i : s = 1 \tag{4}$$

$$\pi^{\min}{}_{(i,s)} \leq \pi_{(i,s)} \leq \pi^{\max}{}_{(i,s)} \qquad \forall i \in I, s \in S_i \tag{5}$$

2.5. Sequencing decisions in the same unit

$$X_{(i,i',s,s')} = \begin{cases} 1 & \text{if task } i,s \text{ is processed after task } i',s' \text{ in the same unit } j \\ 0 & \text{otherwise} \end{cases}$$

$$Ts_{(i,s)} \geq Tf_{(i',s')} + \pi_{(i,s)} + \pi_{(i',s'+1)} - M_T(1 - X_{(i,i',s,s')}) \;\; \forall i,i' \in I : (i > i'), s \in S_i, s' \in S_{i'}, j_{i,s} = j_{i',s'} \tag{6}$$

$$Ts_{(i',s')} \geq Tf_{(i,s)} + \pi_{(i',s')} + \pi_{(i,s+1)} - M_T(X_{(i,i',s,s')}) \;\; \forall i,i' \in I : (i > i'), s \in S_i, s' \in S_{i'}, j_{i,s} = j_{i',s'} \tag{7}$$

2.6. Sequencing decisions in different units

$$Y_{(i,i',s,s')} = \begin{cases} 1 & \text{if transfer } i,s \text{ is processed after transfer } i',s' \text{ in different units} \\ 0 & \text{otherwise} \end{cases}$$

$$Ts_{(i,s)} \geq Ts_{(i',s')} + \pi_{(i,s)} - M_T(1 - Y_{(i,i',s,s')}) \;\; \forall i,i' \in I : (i > i'), s \in S_i, s' \in S_{i'}, j_{i,s} \neq j_{i',s'} \tag{8}$$

$$Ts_{(i',s')} \geq Ts_{(i,s)} + \pi_{(i',s')} - M_T(Y_{(i,i',s,s')}) \;\; \forall i,i' \in I : (i > i'), s \in S_i, s' \in S_{i'}, j_{i,s} \neq j_{i',s'} \tag{9}$$

2.7. Reducing the computational complexity of the problem

$$X_{(i,i',s,s')} = 1 \qquad \forall i,i' \in I : (i > i'), s \in S_i, s' \in S_{i'}, Seq(i) = Seq(i') \wedge s \geq s' \wedge j_{i,s} = j_{i',s'} \tag{10}$$

$$Y_{(i,i',s,s')} = 1 \qquad \forall i,i' \in I : (i > i'), s \in S_i, s' \in S_{i'}, Seq(i) = Seq(i') \wedge s \geq s' \wedge j_{i,s} \neq j_{i',s'} \tag{11}$$

2.8. Objective Function: Makespan Minimization

$$MK \geq Ts_{(i,s)} \qquad \forall i \in I, s \in S_i : s = L_i \tag{12}$$

Additional integer cuts to provide alternative job's sequences

$$\left(\sum_{\substack{i,i'>i \\ X^{old}_{(i,i',s,s')}=1}}^{N} \sum_{s \in Si}^{Li} \sum_{s' \in Si'}^{Li'} X_{(i,i',s,s')} \right) \leq \left(\sum_{i,i'>i}^{N} \sum_{s \in Si}^{Li} \sum_{s' \in Si'}^{Li'} 1 \right) + \left(\sum_{\substack{i,i'>i \\ X^{old}_{(i,i',s,s')}=0}}^{N} \sum_{s \in Si}^{Li} \sum_{s' \in Si'}^{Li'} X_{(i,i',s,s')} \right) - 1 \tag{13}$$

3. Two-Stage MILP-based solution approach

An MILP-based iterative solution method is presented here for dealing with this complex optimization problem in a sequential manner. Thus, an adapted version of bi-level approach, developed by Bhushan and Karimi (2003) and later used by Aguirre et al. (2011) for flow shop scheduling problems in the AWS, is proposed in Figure 3. The solution algorithm allows solving the whole problem in two stages. In the first stage, a relaxed model is solved without considering transfer constraints and the best job's sequence of this problem is provided. Then, in the second stage, transfer constraints are added into the model and then a reduced model is solved by fixing the job's sequencing decisions provided before. Here, it is worth to remark that the job's sequence of the first stage may not always provide a feasible solution in the second stage when sequencing transfer decisions are included. According to this, additional integer cuts are applied in each iteration to provide alternative job's sequences that generate feasible solutions and also improved results. In addition, variable $Ts_{(i,s)}$ and $Tf_{(i,s)}$, are copied in each sub-model to accelerate the convergence. The algorithm ends when an iteration limit is reached.

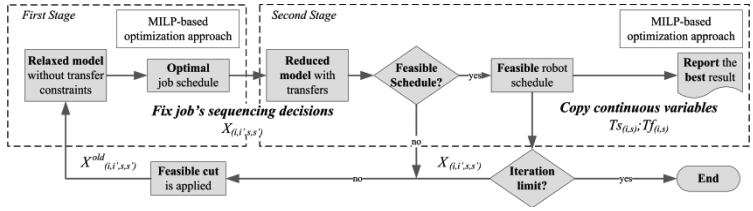

Fig. 3: Sequential procedure followed

4. Application example

An application example of real-life operations in a metal industry is presented here. In this process, jobs i_1-i_{10} have to be schedule in units j_1-j_{35} following their own production recipes $Seq_{(i)}$. The information on processing times $t_{(i,s)}$ of every task i,s and sequences $Seq_{(i)}$ of units j followed by each job i is presented in Table 1. Flexible transfer times between $\pi^{min}_{(i,s)} = 3'$ and $\pi^{max}_{(i,s)} = 6'$ are considered for every transfer.

Solutions obtained for this particular example by our iterative method and by a monolithic model, computing the CPU time and the *MK*, are compared in Table 2.

Table 1. Minimum $t^{min}_{(i,s)}$ and Maximum $t^{max}_{(i,s)}$ processing times of task i,s in unit j

Seq	jobs	s_1	s_2	s_3	s_4	s_5	s_6	s_7	s_8	s_9
1	i_1-i_5-i_6 -i_9-i_{10}	j_3:12-15'	j_5:5-15'	j_7:1'	j_9:10-15'	j_{35}:30-60'	-	-	-	-
2	i_2-i_3	j_3:12-15'	j_5:5-15'	j_4:6-10'	j_5:5-10'	j_7:1'	j_9:10-15'	j_{35}:30-60'	-	-
3	i_4-i_7-i_8	j_3:12-15'	j_5:5-15'	j_7:8-10'	j_8:5-10'	j_9:5-10'	j_{16}:56'	j_{18}:5-10'	j_{30}:5-15'	j_{35}:30-60'

Table 2. Statistics and Results of the example analyzed

Units x Jobs	Statistics	Monolithic MILP-based model with transfers	Iterative Solution Method	
			Relaxed model	Reduced model
35x10	Binary Var.	2485	203	2282
	Cont. Var.	335	335	538
	Equations	5505	941	5505
	MK*(min)*	**404**	**400**	**404**
	CPUtime(s)*	360	19.5	0.5

**Total CPU time by using Gurobi 6.0 in a PC Intel Core 2 Quad 2,5 GHz with parallel processing (4 threads)*

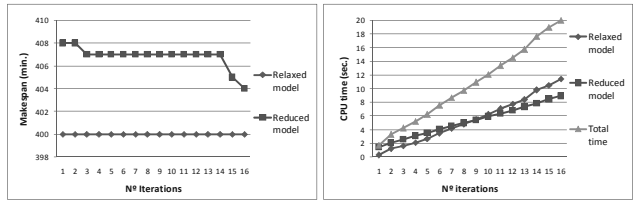

Fig. 4: Behavior of the Sequential approach

Figure 4 shows that the initial feasible solution of our iterative approach $(MK_{(min.)}=408)$ can be progressively enhanced, generating alternative job sequences with the same objective value $(MK_{(min.)}=400)$. The results in Table 2 and Figure 4, illustrate that the sequential procedure is able to provide an optimal solution $(MK_{(min.)}=404)$ in a few number of iterations even with less computational time (20 sec.) than the full-space model (360 sec.) A detailed schedule of this optimal solution is provided in Figure 5.

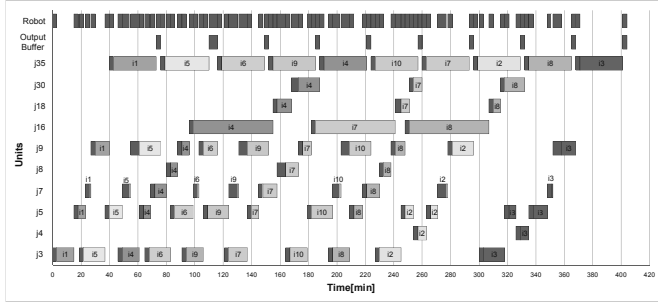

Fig. 5: Integrated manufacturing and transfer schedule

5. Conclusions

An MILP-based procedure was developed for the scheduling of multiple products in automated manufacturing systems. The sequential approach allows finding near-optimal schedules of processing and transfer operations with a reasonable computational effort, by using an adapted version of a widely known two-stage solution method, previously proposed to AWS scheduling problems. Finally, our solution method was compared favorably with an exact mathematical approach in a real-world example, providing an optimal result in few iterations with modest CPU cost.

6. Acknowledgments

Financial support received from AECID under Grant PCI A1/044876/11, from CONICET under Grant PIP-2221, from UNL under Grant PI-66-337 and ANPCyT under grant PICT-2010-1073 is acknowledged.

References

Aguirre, A. M., Méndez, C. A., Castro, P. M., 2011. Comp. Chem. Eng., 35(12), 2960-2972.
Bhushan, S., Karimi, I.A., 2003. Ind. Eng. Chem. Res., 42(7), 1391-1399.
Castro, P.M., Aguirre, A.M., Zeballos, L.J., Méndez, C.A., 2011. Ind. Eng. Chem. Res., 50,10665-10680.
Crama, Y., 1997. European Journal of Operational Research 99 (1), 136-153.
Phillips, L.W., Unger, P.S., 1976. AIIE Transactions 28(2), 219-225.
Shapiro, G.W., Nuttle, H.L., 1988. IIE Transactions 20(2), 157-167.
Zeballos, L. J., Castro, P.M., Méndez, C.A., 2011. Ind. Eng. Chem. Res., 50, 1705-1715.

I.A. Karimi and Rajagopalan Srinivasan (Editors), Proceedings of the 11th International Symposium on Process Systems Engineering, 15-19 July 2012, Singapore.

Integrated Scheduling and Control of Continuous-Time Blending Processes

Kathrin Frankl, Josef Beenken, Wolfgang Marquardt

AVT - Process Systems Engineering, RWTH Aachen University, Turmstr. 46, 52056 Aachen, Germany

Abstract

Scheduling and control of multiproduct blending processes is important in many fields of process systems engineering. It is characterized by nonlinear process dynamics, numerous product specifications and discrete state variables. Due to the high complexity of the resulting mixed-integer dynamic model, integrating all these properties simultaneously in continuous time has not been addressed for blending processes in literature so far. In this contribution, a novel modeling framework for integrated scheduling and control of continuous-time multiproduct blending problems is presented. The framework incorporates the flexible handling of production and transition stages. Moreover, product demand is treated as continuous-time specification of the production process with possible discrete demand due dates. The resulting non-convex mixed-integer dynamic optimization problem is solved by means of a single-shooting method embedded in a branch & bound framework. The novel methodology is illustrated by means of a blending case study with a variety of feed streams with different property compositions and numerous specifications for each of the three manufactured products.

Keywords: optimal control, nonlinear dynamic systems, mixed-integer dynamic optimization, blending, scheduling.

1. Introduction

Integrated scheduling and control of multiproduct blending processes is a difficult task in process operations. The overall model includes (i) discrete decisions for determining the optimal production sequence, (ii) nonlinear process dynamics of the blender and associated units and (iii) a variety of product specifications. The scheduling of blending processes has been addressed in literature for medium-scale plants comprising several blenders and other up- or down-stream units. However, the dynamics of the blenders are neglected and nonlinearities are often reformulated as linear problems, as, e.g., by Mendez et al. (2006). Tousain (2002), for example, considered the integrated scheduling and optimal control of a small-scale blending process in continuous time. However the nonlinearities are avoided by linear reformulations. Nevertheless, integrated scheduling and control has been successfully applied to continuous, nonlinear multiproduct processes before (e.g., Prata et al. (2008)).

In this contribution an integrated approach for scheduling and optimal control of continuous-time blending processes is presented. In addition to the characteristics (i)-(iii) above the proposed modeling framework allows a more flexible handling of the production sequence, and takes continuous-time demand variations as well as discrete demand due dates into account. The resulting nonlinear mixed-integer dynamic optimization problem is solved by a single-shooting method embedded in a branch & bound framework to handle the discrete decisions.

This contribution is structured as follows: Section 2 states the problem class considered. Section 3 introduces the modeling formulation, which is applied to a case study in Section 4. The blending process consists of a blender with 9 feed streams. Three products may be manufactured, each specified by 17 grades. Section 5 presents some conclusions.

2. Problem class

A single, well-mixed blender constitutes the core of the blending process. Let *C* denote the set of components fed to the blender and *P* the set of products to be manufactured in the blender. The multistage modeling approach of Oldenburg et al. (2008) is used. To this end, the time horizon is divided into stages $k \in K$ with final times t_k. Each stage $k \in K$ is either a production or a transition stage. The binary $y_{k,p}$ is true, if product $p \in P$ is manufactured in stage *k*. The binary $w_{k,p}$ is true, if product $p \in P$ is manufactured in stage *k+1*; hence, stage *k* is a transition stage. The $F_{k,c}^{in}$ denote the volumetric flow rate of the stream of component $c \in C$ and F_k^{out} the outlet stream of the blender in stage *k*. Figure 1 illustrates the nomenclature. $F_{k,p}^{out}$ denotes the inflow volume stream into the storage tank for product *p*. The availability of components *c* is assumed to be unlimited. The blender is assumed to hold a constant volume *V* which is completely filled during the whole time horizon, thus $\sum_{c \in C} F_{k,c}^{in} = F_k^{out}$ if additive mixing is assumed. The time-dependent volume of component *c* during stage *k* is denoted by $V_{k,c}$. Each component $c \in C$ is characterized by a set *E* of properties $\rho_{c,e}, e \in E$. The grade of the blend is specified by the volume fraction of component *c*, $\phi_{k,c} = V_{k,c} / V$ and the average property $\pi_{k,e} = \sum_{c \in C} \rho_{c,e} \cdot \phi_{k,c}, e \in E$, in the blender. The degrees of freedom are the volumetric flow rates of the feed streams $F_{k,c}^{in}$, the final times t_k and the production sequence, i.e., $y_{k,p}$ and $w_{k,p}$.

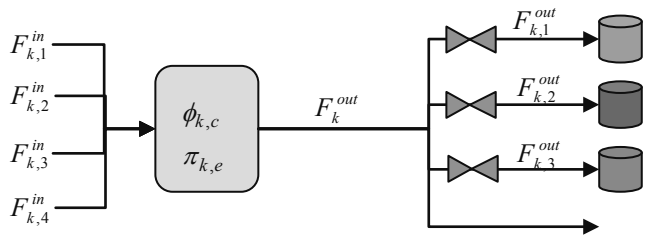

Figure 1: Schematic illustration of a continuous blender with 3 storage tanks and 4 feed streams.

3. Problem formulation

3.1. Blender and product specifications

The volume $V_{k,c}$ of component $c \in C$ inside the blender is determined by the differential equation $\dot{V}_{k,c}(t) = F_{k,c}^{in} - \phi_{k,c} \cdot F_k^{out}$. If product *p* is manufactured in stage *k*, the volume fraction $\phi_{k,c}$ and the medium property $\pi_{k,e}$ have to fulfill certain quality

bounds during the stage. $\underline{\phi}_{c,p}, \overline{\phi}_{c,p}$ denote the lower and upper bounds of $\phi_{k,c}$ and $\underline{\pi}_{e,p}, \overline{\pi}_{e,p}$ the respective bounds of $\pi_{k,e}$. Thus the following path constraints are formulated in each stage *k:*

$$-M_{\phi} \cdot (1-y_{k,p}) + \underline{\phi}_{c,p} \le \phi_{k,c} \le \overline{\phi}_{c,p} + M_{\phi} \cdot (1-y_{k,p}) \quad \forall t \in [t_{k-1}, t_k], \forall c \in C, \forall p \in P$$

$$-M_{\pi} \cdot (1-y_{k,p}) + \underline{\pi}_{e,p} \le \pi_{k,e} \le \overline{\pi}_{e,p} + M_{\pi} \cdot (1-y_{k,p}) \quad \forall t \in [t_{k-1}, t_k], \forall e \in E, \forall p \in P$$

with M_{ϕ}, M_{π} being sufficiently large and suitably chosen constants. If product p is manufactured in stage *k+1*, analogous equations have to hold with respect to $w_{k,p}$ at the final time of stage *k*.

3.2. Storage and product demand

The demand of product p may be continuous or discrete with respect to time. If the demand is continuous in time for $p \in P$, $d_{k,p}$ specifies the time-dependent demand on stage *k*. Then, the storage volume $V_{k,p}$ for product p is determined by the differential equation $\dot{V}_{k,p} = F_{k,p}^{out} - d_{k,p}$. Path constraints have to guarantee a storage hold-up between bounds $\underline{V}_p, \overline{V}_p$, i.e. $\underline{V}_p \le V_{k,p} \le \overline{V}_p, \forall t \in [t_{k-1}, t_k], \forall p \in P, \forall k \in K$. If the demand is discrete, the slot-based approach of Mendez et al. (2006) is applied. Hence, the discrete due date is assumed to coincide with the final time of a certain stage $\widetilde{k} \in K$. The $d_{k,p}$ denote the demands of product p at discrete due date at the end of stage $k = \widetilde{k}$; for other stages, $d_{k,p}$ is zero. Thus $V_{k,p}$ is determined by $\dot{V}_{k,p} = F_{k,p}^{out}$ and the endpoint constraint $V_{k,p} \ge \sum_{\hat{k} \le k} d_{\hat{k},p}, \forall t \in \{t_0, ..., t_k\}$ has to be included in the model.

3.3. Synchronization

Each stage has to be either a production or a transition stage, thus $\sum_{p \in p} y_{k,p} + w_{k,p} = 1$. If the current stage is a transition stage, then the respective product has to be manufactured in the next stage, thus $y_{k+1,p} - w_{k,p} \ge 0$. Hence, a product may be manufactured during several stages in sequence. If product p is manufactured in stage *k*, the outlet stream of the blender is directed to the respective feed stream to the storage tank, thus $F_{k,p}^{out} = y_{k,p} \cdot F_k^{out}$. All differential variables are mapped continuously across the stage borders.

3.4. Objective function

The goal is to minimize Ψ, the overall costs of consumed components $c \in C$, fed to the blender. Thus $\Psi = \sum_{k \in K} \int_{t_{k-1}}^{t_k} \sum_{c \in C} D_c \cdot F_{k,c}^{in}$, where the D_c denote the cost of component *c*.

4. Case Study

The model formulation is illustrated by means of a slightly modified case study taken from Mendez et al. (2006). The volume of the blender considered is *V=2500 l.* 9 components are fed to the blender and each component owns 8 properties, thus */E/=8* and */C/=9*. The blender manufactures 3 products, thus */P/=3*. The desired product specifications as well as the initial values and other constants are summarized below in

Section 4.1. The time horizon of *140 h* is divided into 10 stages. For products 1 and 2, the demands of *50 l/h* and *30 l/h,* respectively, are continuous in time. An amount of *5000 l* of product 3 has to be delivered at a discrete due date of *100 h*. The due date coincides with the final time of stage 6. To allow a cyclic behavior of the production process, the constraints $V_{1,p}(t_0) = V_{|K|,p}(t_{|K|}),\ p \in \{1,2\}$, are added. The control variables $F_{k,c}^{in}$ are discretized by two piecewise constant functions. The overall mixed-integer dynamic optimization problem is solved by a branch & bound algorithm, which handles the discrete decisions and the software DyOS, developed at AVT.PT, to solve the underlying optimal control problems.

4.1. Product specifications and other constants

The bounds of the average properties of the blend and the component properties are displayed in Table 1 and 2. The lower bounds of the volume fraction are defined as follows: $\underline{\phi}_{1,p} = \underline{\phi}_{2,p} = \underline{\phi}_{3,p} = \underline{\phi}_{5,p} = \underline{\phi}_{6,p} = 0,\ \forall p \in P$. Moreover, $\underline{\phi}_{4,p} = 0\ \forall p \in \{1,2\}$ and $\underline{\phi}_{7,p} = \underline{\phi}_{8,p} = \underline{\phi}_{9,p} = 0\ \forall p \in \{2,3\}$ and $\underline{\phi}_{4,3} = 0.1$, $\underline{\phi}_{7,1} = \underline{\phi}_{8,1} = \underline{\phi}_{9,1} = 0.05$. The upper bounds of the volume fraction are defined as $\overline{\phi}_{3,p} = 0.1$, $\overline{\phi}_{5,p} = 0.25$, $\overline{\phi}_{6,p} = 0.1$, $\forall p \in P$. Moreover, $\overline{\phi}_{1,p} = 0.25$, $\overline{\phi}_{2,p} = 0.24$, $\overline{\phi}_{4,p} = 0.23$, $\overline{\phi}_{7,p} = \overline{\phi}_{8,p} = \overline{\phi}_{9,p} = 0.02$ $\forall p \in \{2,3\}$ and $\overline{\phi}_{1,1} = 0.22$, $\overline{\phi}_{2,1} = 0.2$, $\overline{\phi}_{4,1} = 0.06$, $\overline{\phi}_{7,1} = \overline{\phi}_{8,1} = \overline{\phi}_{9,1} = 1$. The initial values of the volume in the product storage tanks are $V_{1,p}(t_0) = 5000l,\ p \in \{1,2\}$, $V_{1,3}(t_0) = 0l$ and of the volumes of component c in the blender are $V_{1,c}(t_0) = V/|C|, c \in C$. The bounds of the storage tanks are $\underline{V}_1 = 2500$, $\underline{V}_2 = 3000$ and $\overline{V}_1 = 8000$, $\overline{V}_2 = 7500$. The component prices are $D_1 = 24$, $D_2 = 20$, $D_3 = 26$, $D_4 = 23$, $D_5 = 24$ and $D_6 = D_7 = D_8 = D_9 = 50$ €/l.

$\underline{\pi}_{e,p} : \overline{\pi}_{e,p}$	e=1	e=2	e=3	e=4	e=5	e=6	e=7	e=8
p=1	0.72:0.775	20:50	46:71	85:1000	45:60	00:42	00:18	00:01
p=2	0.72:0.775	20:48	46:71	85:1000	45:60	00:42	00:18	00:01
p=3	0.72:0.775	22:50	46:71	85:1000	70:90	00:42	00:18	00:01

Table 1: Lower and upper bounds of the average properties of the blend

	c=1	c=2	c=3	c=4	c=5	c=6	c=7	c=8	c=9
e=1	0.7069	0.8692	0.6167	0.6731	0.654	0.746	0.756	0.8187	0.7339
e=2	3.6	1	100	94.9	91.5	15	0	1.3	34.3
e=3	16.3	4.5	100	97.1	95.5	100	0	1.3	57.1
e=4	94.3	93.5	100	100	100	100	0	93.9	95.9
e=5	35	22.7	351.1	117.1	93	31.3	63.3	16	52.4
e=6	0	88.6	0	2.3	0.2	0	48.98	65.3	21.3
e=7	0	0.1	61.3	48.9	36	0	1.04	0.6	33.3
e=8	0	3.3	0	1.1	0.1	0	3.33	0.9	0.8

Table 2: Component properties $\rho_{c,e}$ used in the case study

4.2. Results

The optimal objective function is 667,59 € with the production sequence l-2-3-1-2. This is about 9% better than, for example, the objective of the sequence 2-1-3-1-2. Figure 2

displays the optimal control functions $F_{k,c}^{in}$ for $c=2,4,7$ and the product specifications $\pi_{k,5}$ and $\phi_{k,7}$. The vertical dotted lines denote the stage boundaries. Odd stages are transitions, while even stages are production stages. As shown in Figure 2, the product specifications are not constant in general during the production phases, but vary inside their boundaries depending on the products manufactured in the preceding and next stage. The control profiles strongly differ in the transition and production phases. This suggests using finer discretized control variables for future works. The computing time is at most 5 minutes for a branch & bound node. All-in all, 22 nodes were calculated, which is of similar complexity than for total enumeration, since this example is of small integer complexity.

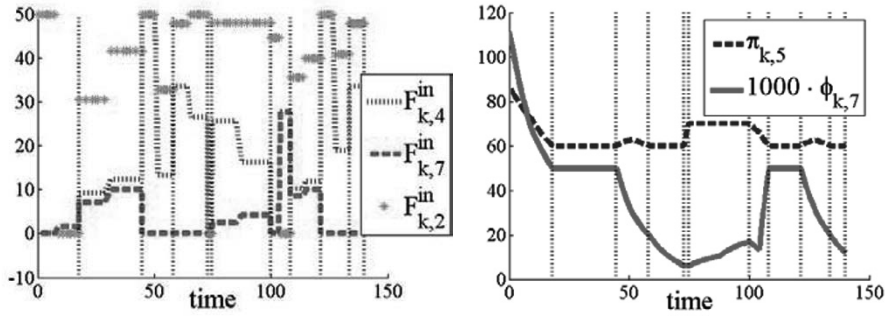

Figure 2: Control functions $F_{k,c}^{in}$ for c=2,4,7 and product specifications $\pi_{k,5}$ and $\phi_{k,7}$ for the optimal production sequence 1-2-3-1-2.

5. Conclusions

This contribution incorporates for the first time both nonlinearities and process dynamics into the modeling framework for continuous-time multiproduct blending processes, to allow a better control of the transition and production phases. Case studies with increasing complexity, in particular in product scheduling, as considered e.g. in Mendez et al. (2006), require further research for efficiently solving large-scale mixed-integer dynamic optimization problems.

Acknowledgments

We appreciate financial support by the European Commission under grant agreement CP-IP 228867-2, F^3-Factory.

References

C.A. Mendez, I.E. Grossmann, I. Harjunkoski, P. Kabore, 2006, A simultaneous optimization approach for off-line blending and scheduling of oil-refinery operations, *Comp. Chem. Engg.*, **30**, 4, 614-634

J. Oldenburg, W. Marquardt, 2008, Disjunctive modeling of optimal control of hybrid systems, *Comp. Chem. Engg.*, **32**, 10, 2346-2364

A. Prata, J. Oldenburg, A. Kroll, W. Marquardt, 2008, Integrated scheduling and dynamic optimization of grade transitions for a continuous polymerization reactor, *Comp. Chem. Engg.*, **32,** 3, 463-476

R.L. Tousain, 2002, Dynamic optimization in business-wide process control, PhD. Thesis, TU Delft.

I.A. Karimi and Rajagopalan Srinivasan (Editors), Proceedings of the 11th International Symposium on Process Systems Engineering, 15-19 July 2012, Singapore.

De-risking Scale-up of a High Shear Wet Granulation Process Using Latent Variable Modeling and Near Infrared Spectroscopy

Koji Muteki, Ken Yamamoto, George L. Reid, Mahesh Krishnan

Pfizer Worldwide Research & Development, Eastern Point Rd, Groton, CT 06340, United States

Abstract: In the development of wet granulated drug products, two primary sources of variance (disturbance) include the operational scale of the high shear wet granulation (HSWG) process and active pharmaceutical ingredient (API) lot-to-lot variability, particularly for formulations containing a high drug load. This paper presents a novel Process Analytical Technology (PAT) strategy using latent variable modeling (LVM) with near infrared spectroscopy (NIRS) to reduce risk in scale-up operations of the HSWG process while simultaneously accounting for API lot-to-lot variability, even with limited manufacturing history. The process involves building a partial least square (PLS) model among the API material properties, the HSWG process parameters and the NIRS end points of the HSWG process based on small scale design of experiment (DOE) batches. The PLS model is then used in an optimization framework to find suitable small scale mechanical process parameters (impeller/chopper speed) that approximate a previous large scale operation so as to keep the NIRS end point of large scale operation constant. Prior to making additional large scale batches with a new lot of API, NIRS end points of large-scale HSWG with the new API lot are predicted based on the PLS model developed from the small-scale operation. If the predicted NIRS end point for the HSWG using the new API lot is not within the target region, the risks associated with the scale-up operation can then be significantly reduced by modifying other HSWG process parameters such as the total amount of water added or total granulation time to achieve the target region. A case study is presented that demonstrates the effectiveness of this methodology during development and scale-up of a drug product manufactured using a HSWG process. The detailed full paper of this study has been published in (Muteki et al., 2011).
Keywords: Latent Variable Modeling, Process Analytical Technology, Quality by Design, Scale-up, Optimization, High Shear Wet Granulation

1. Introduction

In the development of wet granulated drug products, two primary sources of variance (disturbance) are the operational scale of the high shear wet granulation (HSWG) process and raw material lot-to-lot variability, particularly with respect to active pharmaceutical ingredient (API) material. Due to a limited supply of API in the early stages of development, it is often challenging to obtain adequate manufacturing experience and understanding of granular and tablet properties. Clinical supply requirements often necessitate rapid scale-up to intermediate or higher scale (e.g. 10L, 70L, 250L, 900L, etc). Under such circumstances, it is valuable to de-risk scale-up operations of the HSWG process while simultaneously accounting for raw material lot-to-lot variability to ensure timely clinical supply of drug products during development. This paper presents a novel process analytical technology (PAT) strategy using latent

variable modeling (LVM) with NIRS to de-risk scale-up operations of the HSWG process when there is limited batch experience while simultaneously accounting for API lot-to-lot variability. The goal is to scale-up and supply drug product that meets target tablet properties with minimum number of batches, i.e., minimal API consumption.

2. Modeling methodology

This methodology is developed based on small scale DOE batches with various combinations of process parameters and API material lots and with a minimum of one large scale batch manufacture. The models were utilized to de-risk additional large scale-up operations using a new lot of API with different physical properties. The mechanical process parameters (impeller/chopper speed) used for the additional large scale batches are fixed to those used for previous large scale operations.

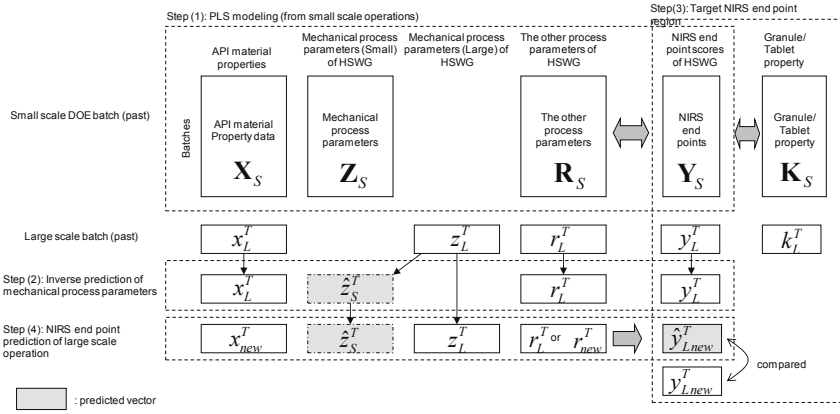

Fig. 1 Overall data structure and procedure of de-risking scale-up operations

The overall data structure and procedure of the proposed methodology are shown in Fig.1, which consists of the following four steps: ***Step (1)*** A PLS model is built with small scale DOE batches to represent the quantitative relationship among API material properties $\mathbf{X}_S$, the mechanical process parameters (impeller/chopper speed) of small scale $\mathbf{Z}_s$, other process parameters (a total amount of water, total batch time) of small scale $\mathbf{R}_s$ and NIRS end points of small scale operations $\mathbf{Y}_s$ (represented as scores by principal component analysis (PCA) using only NIRS data in advance).; ***Step (2)*** The mechanical process parameter (impeller/chopper speed) of small scale operation $\hat{z}_S^T$ approximating that of the previously run large scale batch (with z_L^T) is inversely predicted based on the PLS model built in Step (1) through an optimization computation to keep the NIRS end point of large scale operation (y_L^T) constant.; ***Step (3)*** A suitable target region of NIRS end points is determined from the desired downstream properties such as flow and tablet properties (small scale granule/tablet properties $\mathbf{K}_S$ and large scale tablet properties k_L^T).; ***Step (4)*** The NIRS end-points of additional large scale batches using a new API lot (x_{new}^T), the predicted mechanical process parameters of small scale $\hat{z}_S^T$ (the mechanical process parameter of a past large scale z_L^T is actually used) and the other process parameters (r_L^T or r_{new}^T) are predicted based on the PLS model built in Step (1), on the condition that additional large scale mechanical process

parameters (impeller/chopper speed) are kept fixed to the past large scale operation z_L^T. The predicted NIRS end-points of additional large scale operations are investigated whether they can achieve the target NIRS end point region determined in Step (3). If the predicted NIRS end points are not contained within the target region, the scale-up operation can be then de-risked by suitably updating process parameters such as the total amount of water or total batch time (r_L^T or r_{new}^T) to achieve the desired NIRS end point for the wet granulation process.

3. Experimental

The tablet formulation used for this study consists of 76% API and 24% excipients. As the API is the largest formulation component its properties could potentially be a major source of variance. A total of nine API properties $\mathbf{X}_S$ were used for the PLS model: 4 particle size distribution parameters (*D10, D43, D50, D90*), 1 bulk density, and 4 moisture sorption parameters (GAB model coefficients *Xm, K, C* and moisture sorption at relative humidity 90%). A Collette Ultima PRO^{TM} equipped with a 10L bowl and a MGT-70S model with a 70L bowl were used to conduct the HSWG experiments. Note, these granulators are dissimilar relative to their impeller diameter, shape, blade type and wall friction, etc. It was not possible to apply the previously reported scale-up rules (e.g. tip speed, Froude number, shear stress, etc.) due to lack of geometrical similarity. The HSWG process was executed sequentially: dry mixing, water addition, and wet massing. A MPA^{TM} (Bruker Optics Inc) was used to collect the NIRS spectra at a 8cm^{-1} spectral resolution and 240 co-adds per spectra. A 13 batch DOE (designed by Plackett-Burman method) was conducted to investigate four process variables and API lot-to-lot effects (3 lots) using a small scale (10L) equipment.

4. Results

4.1. PLS modeling (Step(1))

A PLS model was built to investigate the effect of 9 API properties $\mathbf{X}_S$, 2 mechanical process parameters (impeller/chopper speed) ($\mathbf{Z}_S$), 2 additional process parameters $\mathbf{R}_S$ (total amount of water and total batch time) on 2 NIRS end point scores ($\mathbf{Y}_s$ = [NIRS-PC1 NIRS-PC2]).

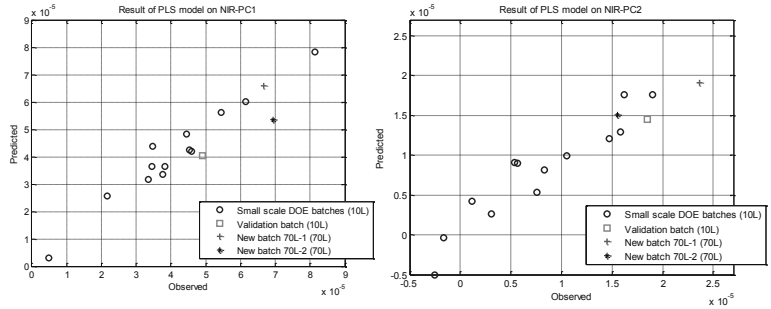

(a) (b)

Fig. 2 Result of PLS modeling and validation on: (a) NIRS-PC1; (b) NIRS-PC2

The observed vs. predicted plots on the NIRS-PC1 and NIRS-PC2 are shown in Fig. 2(a) and Fig. 2(b), respectively. The R2 of the PLS models on NIR-PC1 and NIR-PC2 are 95.6% and 88.6%, respectively. The four PLS components for these models were selected to maximize the Q2 value (result of cross validation) and avoid over-fitting.

The PLS model ability is good enough to predict the NIRS end point scores $\mathbf{Y}_s$. Note the four PLS components used are much smaller as compared to the total variable dimensions of $\mathbf{X}_{all}$(i.e. 13).

4.2. Impeller speed relationship across scale (Step (2))

The prediction result of small scale (10L) impeller speed approximating the large scale (70L) is shown in Fig. 3. The NIRS end point score plots of small scale DOE batches are labeled blue "o" with the batch number in Fig. 3(b), the NIRS end point score of the past large scale (70L) batch is labeled green "*" in Fig. 3(b), and the impeller speeds used in the small scale DOE batches are labeled blue "o" in Fig. 3(a). The simulated results of the suitable impeller speed for the 10L scale to achieve the desired NIRS end point score range (depicted by black square) were labeled red "□"in Fig. 3(a). An impeller speed of 450 rpm for the 10L granulator will be used to predict HSWG conditions for the 70L granulator having an impeller speed of 225 rpm.

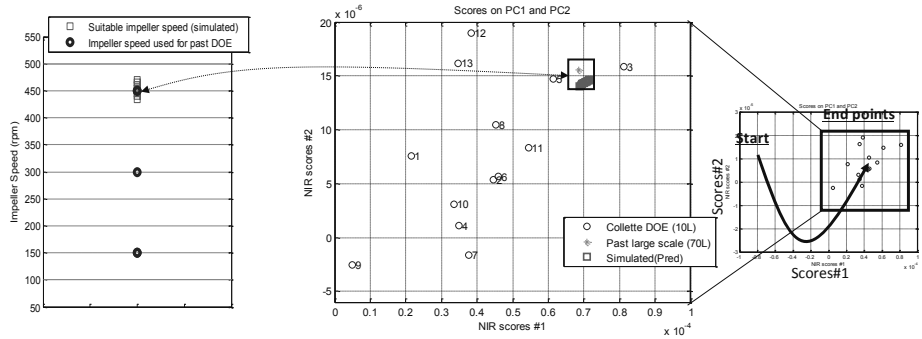

(a) (b)

Fig. 3 Result of suitable impeller speed of small scale to achieve the NIRS end point of past large scale operation: (a) Impeller speed; (b) NIRS-PC1 vs. NIRS-PC2 plot

4.3. De-risking further large scale (70L) batches (Step(3),(4))

The target NIRS end point region was therefore determined based on the FFC (flowability), as shown in Fig.4. Prior to manufacturing additional large scale (70L) granulations, a developmental small batch (10L) using the new API lot (x_{new}^T) was manufactured in order to validate the PLS model. The prediction results and observed are shown in Fig.2 and Fig.4. The PLS model provided good prediction on both NIRS-PC1 and NIRS-PC2. This small scale batch manufacture was necessary not only to validate the PLS model but also to investigate any possible risk (effect) of unknown (unmeasured) API property which was not accounted for in the PLS model. Performing just one small scale (10L) batch prior to the large scale (70L) operation greatly de-risks and increases the confidence level of scale up process. Prior to performing the 70L batches with the new API lot, a simulation was performed. The process condition used in the past large scale batch (38% total water, 18 minute batch granulation time) was first selected. The predicted NIRS end point scores with the new API lot ("new batch 70L-1") was outside the target NIRS end point region (over-granulated area), as labeled red "+"in Fig. 4. To achieve the target NIRS end point region, the total amount of water and the total batch granulation time were reduced to 34% and 16 minutes, respectively ("new batch 70L-2"). The predicted NIRS end point scores of the updated batch achieved the target NIRS end point region, as labeled by black "+" mark in Fig. 4. Both batches ("new batch 70L-1" and "new batch 70L-2") were performed to demonstrate the

effectiveness of the methodology. The results of these two large scale batches on NIRS-PC1 and NIRS-PC2 (observed vs. predicted) are shown in Fig. 2 and Fig. 4. The PLS model provided good prediction on both NIRS-PC1 and NIRS-PC2. As expected, the observed "new batch 70L-1" resulted was outside the target NIRS end point region, and the actual granules were slightly larger than desired from visual observations of appearance and particle size. The observed "new batch 70L-2" was inside the target NIRS end point region, and the resulting tablets were robust. These results indicate that the proposed methodology worked well and the models are useful and predictive in decreasing the risk during manufacture at the higher scale using a new API lot.

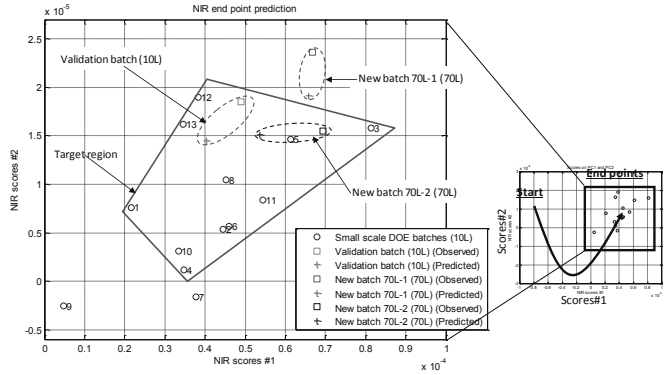

Fig. 4 Result of NIRS end point prediction of validation batch (10L) and two new batches (70L)

5. Conclusion

A scale-up methodology simultaneously accounting for both HSWG scale and API lot-to-lot variability has been successfully applied to de-risk the development of a drug product. The PLS model was built using small scale DOE batches, and provided good prediction on NIRS end points for not only the small scale DOE batches, but also small and large scale batches with a new API lot. This approach provides three advantages from an industrial perspective (1) No requirement of geometric similarity across scales and therefore, a more practical methodology unlike other scale-up models based on dimensionless analysis, and constant tip speed, Froude number, and shear stress. (2) Multiple large scale batches are not required and therefore, a more cost effective method. (3) Using small scale DOE batches to build a PLS model to predict a large scale operation reduces API usage and makes effective use of company assets (historic data), thus providing a useful Science of Scale tool for efficient scale-up in drug product development.

Acknowledgements: The authors wish to thank Stephanie Dolph, Beverly Nickerson, Mike Pelletier, Brent Maranzano, Peter Larkin, Angela Liu, Gregory W. Sluggett, Salvador García Muñoz, William Ketterhagen, Fasheng Li, Kim Vukovinsky, Julien Boccadoro, Karl Bratin, Michael Hawley, Joseph F. Krzyzaniak, Weili Yu, Sonja Sekulic, Peter Jones, Ian Clegg, Andreas Muehlenfeld, Jens Thiele, Cristoph Wabel, Bianka Wuensche in Pfizer Inc for providing the data and useful discussion.

Reference :

K. Muteki, K. Yamamoto, G. L. Reid, M. Krishnan , "De-risking Scale-up of a High Shear Wet Granulation Process Using Latent Variable Modeling and Near Infrared Spectroscopy", Journal of Pharmaceutical Innovation, Volume 6, Number 3, 142-156, 2011

N. Rahmanian, M. Ghadiri, Y. Ding, Effect of scale of operation on granule strength in high shear granulators. Chem Eng Sci. 2008;63:915-923.

H.G. Kristensen, Particle agglomeration in high shear mixers. Powder Technol. 1996;88:197-202

I.A. Karimi and Rajagopalan Srinivasan (Editors), Proceedings of the 11th International Symposium on Process Systems Engineering, 15-19 July 2012, Singapore.

Performance Assessment and Benchmarking of Desalination Plants

N. Bhutani,[a] M. Srinivas,[a] Senthilmurugan S.,[b]

[a]*ABB Corporate Research, Bangalore, Karnataka, India*
[b]*ABB Water ISI, Bangalore, Karnataka, India*

Abstract

ABB has developed a generic "technology" based tool for Energy Assessment and Benchmarking of desalination plants. It facilitates systematic and quick opportunity identification of energy efficiency improvements along with cost-benefit estimation in typical Multi-Stage Flash (MSF) and Reverse Osmosis (RO) based desalination Plants. The tool (i) calculates energy flow distribution, efficiency, losses in equipments and various performance indices (ii) recommends measures/proposals to improve efficiency based on energy assessment and key performance indices (KPIs) based benchmarking (iii) recommends proposals with cost-benefit analysis and (iv) generates energy assessment report. As a test bed, the energy assessment study performed on MSF desalination plant with this tool is presented.

Keywords: Energy efficiency, energy assessment, desalination, reverse osmosis, multi-stage flash, cost-benefit estimation

1. Introduction

Desalination plants play an important role in producing potable water. Multi stage flash (MSF) and reverse osmosis (RO) desalination plants are two pre-dominant seawater desalting systems in the world, constituting more than half of the total desalination capacity. These plants present major opportunities to improve *energy efficiency,* plant *production* and *profitability* [1]. Many authors have applied concept of exergy analysis [2-4] to assess various industrial processes [5-7] but the industrial application of these concepts for energy assessment and benchmarking is very limited. To overcome above limitations, a generic, 'technology' based, graphic user interface (GUI) enabled tool for *"performance assessment and benchmarking"* of desalination systems is developed.

2. Energy Assessment and Benchmarking - Methodology

Conventionally, the energy assessment for industrial processes is performed by domain experts, based on their experience, by – recording, analysis, benchmarking, targeting, and reporting and control respectively. This onsite energy assessment exercise is quite tedious, prone to human errors and sometimes lacks thorough analysis. However, by means of automated energy assessment tool the overall procedure for energy assessment is simplified to these key functionalities: (i) Exergy analysis (ii) KPI calculations (iii) Cost-benefit estimation, explained by means of an application on MSF plant.

3. MSF Desalination Plant

3.1. Process

The schematic flow diagram of an MSF desalination process is shown in Figure 1. The system consists of Heat recovery section (HrecS), Heat reject section (HrejS), a brine

heater, vacuum system, and couple of pumps. The HrecS and HrejS consists 19 and 3 flashing units respectively. The seawater enters the condenser tubes of HrejS where its temperature is raised by absorption of the latent heat of the condensing water vapor on other side of tubes. Partly, the sea water is rejected back to the sea and the rest makes feed, which is chemically treated and then mixed to the brine pool of the last flashing stage of HrejS. The brine, partly extracted from HrejS, is introduced to HrecS (condenser tubes) where it first absorbs latent heat of condensing vapors, and then of the steam in brine heater. The heated brine is then introduced to HrecS first stage where it flashes off, in the subsequent flash columns and gets condensed to form the distillate product stream, which is extracted from the last stage of HrejS. The main thermal energy input to MSF results from use of LP steam in brine heater. Partly, excess steam is vented off or sent to dump condenser (if existing) for steam condensate recovery. MP steam, in small quantity compared to LP steam, is used in vacuum system (not shown in diagram) to remove non-condensable from Flash column. The electricity is consumed to run pumps for Sea water (SW) supply, brine recirculation (R/C pump), distillate product, condensate return (Cond pump) and brine blowdown (B/D pump) etc.

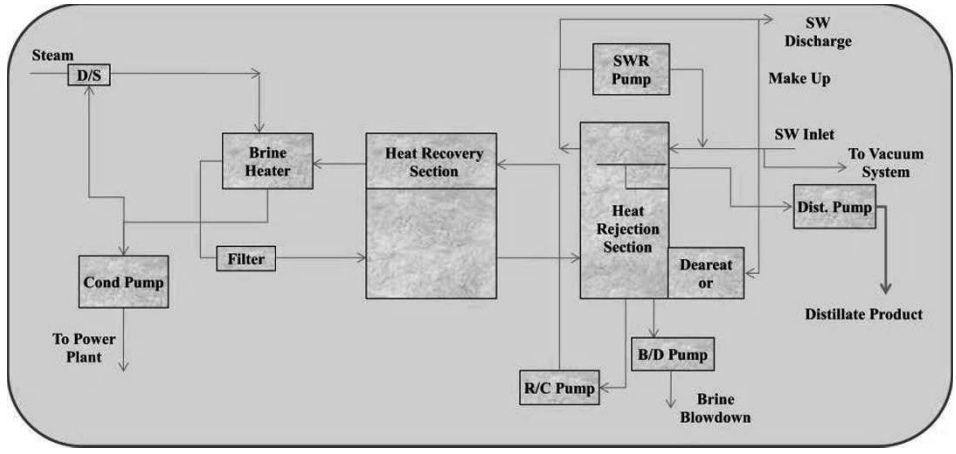

Figure 1 Simplified Process Flow Diagram for MSF desalination Plant

4. Case Study Results

As a pilot case study, the above industrial MSF desalination plant configuration was analyzed using this tool. The steady state operating data collected from the plant for a year of operation was preprocessed by data preprocessor and used for energy assessment in following steps.

4.1. Exergy Analysis

By exergy analysis, it was found that energy was mainly consumed in useful work, destroyed due to inefficiency (of mechanical or thermal process type) in process equipments like heat exchangers, pumps, flash stages, desuperheater or lost to environment with boundary streams (like brine blowdown, sea water reject) etc. The average distribution of exergy destruction in various equipments in the MSF desalination plant (Figure 2) reveals that almost 57% of the thermal energy is destroyed in MSF stages due to irreversible throttling and expansion in multiple flash stages,

followed by 20.7 % energy loss in desuperheater (D/S) due to mixing of superheated steam with condensate spray and 12.1 % loss in brine heater due to inefficiency. On an average 4 % of the energy is lost due to dumping of steam to dump condensers. Though the condensate is fully recovered from dump condensers, the latent heat of steam is still lost in the process. About 2.8 % of energy, in the form of electrical energy, is lost due to inefficiency of brine recirculation pumps. It is found that brine recirculation pump is the biggest pump in MSF desalination section and consumes more than 80% of total electrical input power to MSF section. About 1.8 % of the total energy is lost due to throttling in brine recirculation valve. Energy destruction in other equipments (like brine blowdown pump, distillate pump, condensate pumps etc) and direct losses to environment with brine blowdown stream, distillate product delivery, etc were negligible and therefore combined together into "Others" which makes 1.5 % of the total energy destruction/loss.

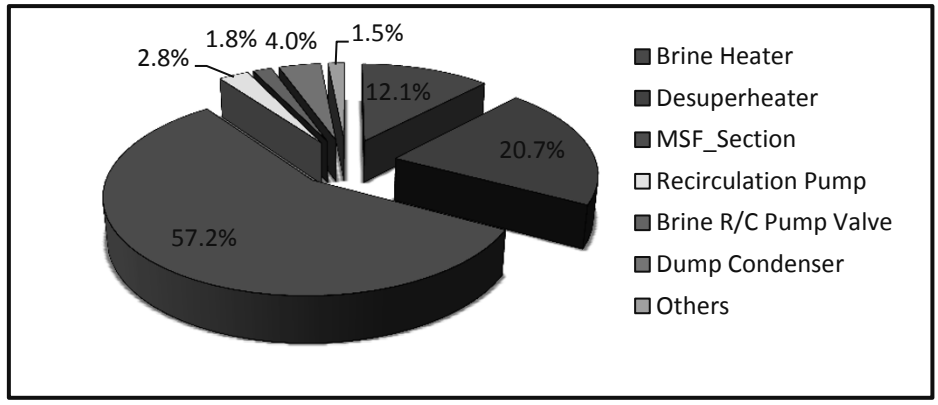

Figure 2 Exergy destruction in MSF desalination Plant

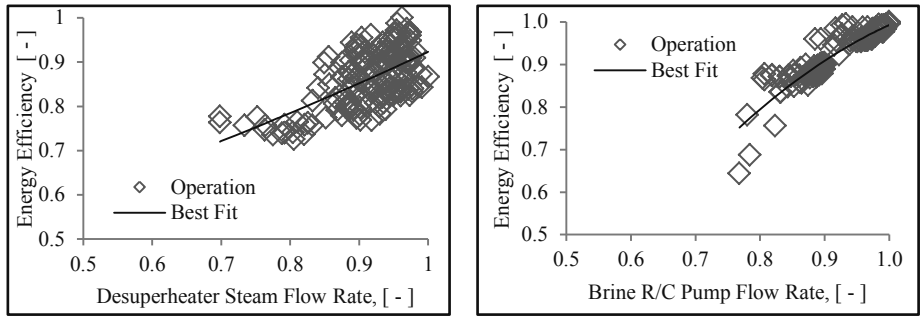

Figure 3 Energy efficiency of Desuperheater (left) and brine recirculation pump (right)

The dimensionless exergy efficiency of brine recirculation (R/C) pump and desuperheater are plotted in Figure 3. The exergy efficiency of desuperheater increases from 0.7 and 0.90 when the steam flow rate is increased from 0.7 to 1. Similarly, the exergy efficiency of brine recirculation pump increases from 0.8 to 1 when the flow is increased from 0.8 to 1, signifying opportunities for improvement in energy efficiency of both the equipments by increasing load on both the equipments. Also, for the fixed

flow conditions, the variations in efficiency are huge in case of desuperheater, signifying possible improvements in energy efficiency by reduced variations.

4.2. KPI Calculator

Various KPIs, defined in the tool, were configured to plant data and calculated for MSF desalination plant configuration. Trend plots were generated for these KPIs to evaluate their impact on plant performance. The specific steam consumption and specific electricity consumption in desalination plant can be reduced by increasing load factor (Figure 4). This would result in a maximum improvement in plant profit of ~ 0.2 kUSD/h (Figure 5, left). Note that a maximum total profit of 650 kUSD/year is possible based on the current plant production distribution profile. The specific steam consumption in plant can also be reduced by reducing the losses due to excessive dumping of steam to dump condenser (Figure 5, right). The mean values of some of the KPIs, defined in **Error! Reference source not found.**, were also compared against recommended values to identify improvements. As shown, by comparison in **Error! Reference source not found.**, a few KPIs are operating within permissible limits while others can be improved further to improve plant performance.

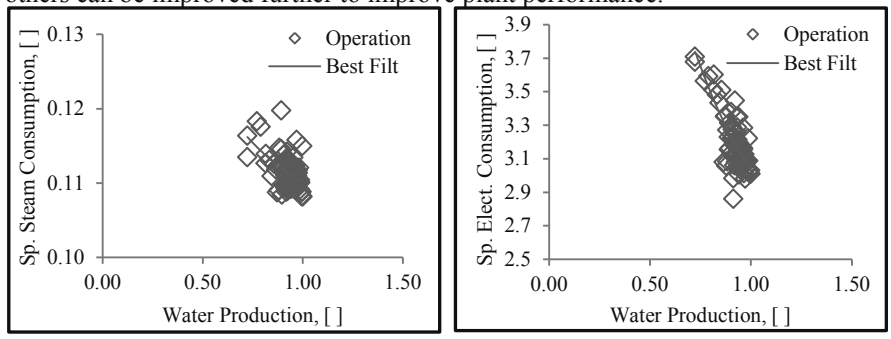

Figure 4 Specific steam consumption (left) and specific electricity consumption (right) with respect to water production.

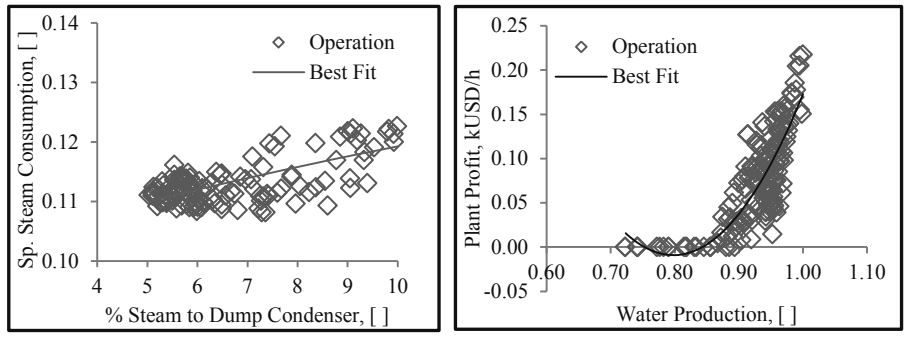

Figure 5 % Steam consumption vs. Specific steam consumption (left) and Water production vs. Plant profit (right) in an MSF desalination Plant.

4.3. Cost-Benefit estimation

In this section, the efficiency estimates of equipments from exergy analysis and improvements in KPIs were translated into cost savings. The estimated cost savings resulting from improved equipments efficiency of brine heater, desuperheater and brine

recirculation pump by improving load factor were 17, 21 and 30 kUSD/year, brine blowdown heat recovery was 19 kUSD and reduced steam losses by no dumping of steam to dump condenser was 104 kUSD respectively. Note that savings are tuned to current production of the pilot plant. Further, cost-benefit analysis is feasible with this tool for replacement of fixed drive with variable frequency drive (VFD) for pumps or other capital investments.

Table 1 Calculated KPI for MSF desalination Plant

KPI Definition	Mean Value	Recommended
Sp. Steam Consumption in major consumers, tons/m^3 water	0.12	Least Possible
Sp. Electricity Consumption in major consumers, kWh/m^3 water	3.22	Least Possible
% Brine Blowdown, %	62.56	Least Possible
Distillate To Makeup Ratio, [ ]	0.36	b/w 0.3-0.4
% Steam To Dump Condenser, %	8.18	Equal to 0 or Least Possible
Degree Superheat of LP steam, ^oC	30.12	Less than equal to 10-15 ^oC
Degree Superheat of Brine Heater steam, ^oC	10.64	Less than equal to 5 ^oC
Delta T Flash MSFSection, ^oC	57.20	Highest Possible
Delta T, SeaWater (Inlet – Reject), ^oC	7.87	Less than equal to 10 ^oC
Delta T BrineHeater (for Brine), ^oC	6.90	Less than equal to 5 ^oC

5. Conclusions

The energy assessment and benchmarking tool was used to identify opportunities for energy efficiency improvements and translate them into potential cost savings for the pilot customer. With a user-friendly graphic user interface (GUI), a wide range of industrial desalination plants/configurations (thermal, hybrid, membrane based) can be analyzed very quickly.

References

[1]. Z. Elimelech M and Philip WA., The Future of sea water desalination: Energy, Technology, and the environment, Science, vol. 333, no. 6043, pp. 712-717, August 2011.
[2]. Sharqawy M H., et. al., On exergy calculation of sea water with applications in desalination systems, International Journal of Thermal Science, vol. 50, pp. 187-196, 2011.
[3]. Kahraman N., and Cengel Y. A., Exergy analysis of a MSF distillation plant, Energy conservation and management, vol. 46, pp. 2625-2636, 2005.
[4]. Cerci Y., Exergy analysis of a reverse osmosis plant in California, Desalination, vol., 142, pp. 257-266, 2002.
[5]. Macedonio F. and Drioli E., An exergy analysis of membrane desalination system. Desalination, vol. 261, pp. 293-299, 2010.
[6]. Ataei A. and Yoo C., Combined pinch and exergy analysis for energy efficiency optimization in a steam power plant, International Journal of the Physical science, vol. 5(7), pp. 1110-1123, 2010.
[7]. Rosen M. A. and Bulucea C. A., Using exergy to understand and improve the efficiency of Electrical power technologies, Entropy, vol. 11, pp. 820-835, 2009.

I.A. Karimi and Rajagopalan Srinivasan (Editors), Proceedings of the 11th International Symposium on Process Systems Engineering, 15-19 July 2012, Singapore.

Process Modeling of Bio-Based Production on Interdisciplinary Analysis across Agriculture and Engineering: A Case Study of Sugarcane-Derived Ethanol Production

Satoshi Ohara[a], Yasunori Kikuchi[b], Rumiko Suginobe[b], Yoichi Kanzaki[b], Masahiko Hirao[b]

[a]*Asahi Group Holdings, Ltd., 1-1-21 Midori, Moriya-shi, Ibaraki, 302-0106 Japan*
[b]*Department of Chemical System Engineering, The University of Tokyo, 7-3-1 Hongo, Bunkyo-ku, Tokyo, 113-8656 Japan*

Abstract

We specified modeling requirements for biomass-derived production. An integrated modeling on interdisciplinary analysis across agriculture and engineering can become a key mechanism for enabling the clarification and fulfillment of the potential of biomass for sustainability. A modeling case study on sugarcane-derived ethanol production shows proposed integrated model can be used in the analysis of the environmental impacts associated with different conditions in agricultural and industrial process systems such as sugarcane cultivar and agricultural operation.

Keywords: sugarcane-derived ethanol, greenhouse gas, life cycle assessment, cultivar improvement, food production.

1. Introduction

Biomass resource and biotechnology have become key technologies for sustainable bioethanol production. In the previous studies, the environmental impacts of sugarcane-derived ethanol have been analyzed and its advantages on greenhouse gas emission have been confirmed (Macedo et al 2008; Sánchez and Cardona 2008). At that time, it was also confirmed that the composition of sugarcane have high sensitivities to the result of environmental assessments and process performance (Ohara et al 2009). Such detail features of sugarcane are strongly dependent on cultivars (Ohara et al 2009), the conditions of climate and soil, and the agricultural operations. To design a whole life cycle system of bioethanol appropriately, an integrated modeling from agriculture and engineering perspectives can be an effective approach.

Although modeling approaches for biomass-derived products have been discussed (Nguyen et al 2010; Kikuchi et al 2010), the process data of biomass cultivation was based on specific literature and biomass cultivar was not considered. Experimental results on yield and component of various cultivars of sugarcane planted in various types of soil have been cumulated as reports in agriculture (Okinawa Agricultural Experiment Station 1991; National Agriculture and Food Research Organization, National Agricultural Research Center for Kyushu Okinawa Region 2010).

In this study, we tackle with the integrated modeling of a whole production process of sugarcane-derived bioethanol. The modeling is based on the interdisciplinary approach to combine the knowledge from agriculture and engineering fields. The ethanol production system from sugarcane includes sugarcane cultivation, sugar and ethanol productions. The process parameters and conditions influencing on the environmental impacts due to the production of biomass-derived materials were specified and mathematical models were developed for such cradle-to-grave life cycle.

2. Specification of modeling requirement

To concretely identify the relationship among biomass related technologies and their impacts on social, economics, and environment, information-modeling approach based on unified modeling language (UML) (Objective Management Group 2011) was applied. UML has a large potential to visualize modeling requirements clearly for tools from design stages to maintenance and sustainment stages in agriculture and industrial processes. In UML class diagram, information categories are structured and characterized by specifying their properties and relationships. In addition to the static modeling by UML class diagram, dynamic information flows among stakeholders involved in agriculture and engineering processes can be discussed on UML activity diagram.

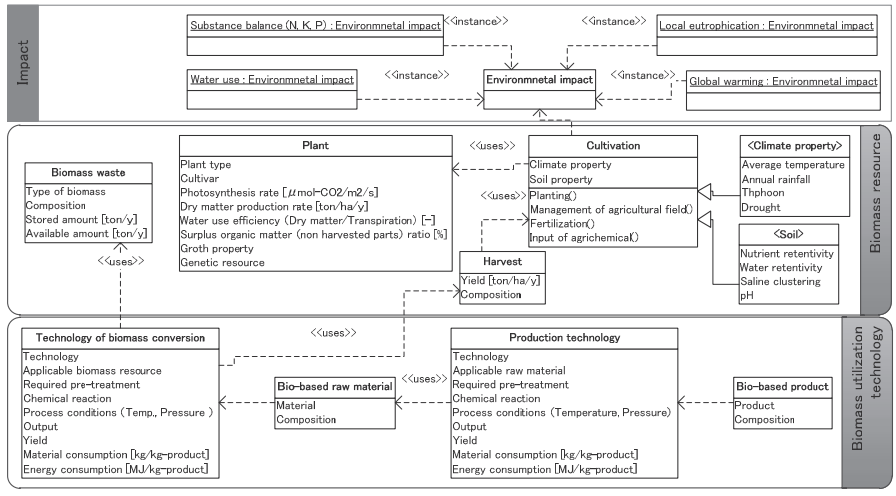

Figure 1.Overview of specified information relationships associated with agricultural and industrial processes

Figure 1 shows the overview of specified information relationships associated with agricultural and industrial processes by UML class diagram. In this diagram, the elements related with biomass resource and utilization technology. For example, biomass resources can be obtained as the result of cultivation. The composition of harvest is related with the properties of plant, agricultural operations, climate, and soil. It has also links to the biomass utilization technologies. Required pretreatment processes and available bio-based raw materials or products are strongly related with such resource conditions. Based on this diagram, we can systematically discuss the requirement on the modeling for designing agriculture and industrial processes in an integrated manner.

3. Case study: Sugarcane-derived ethanol production

3.1. Settings

Using developed modeling requirement as shown in Figure 1, an integrated model on sugarcane-derived bioethanol production was constructed as a case example. Data required for process modeling was based on the operation results of a pilot plant of sugar crystallization and ethanol fermentation constructed in Ie island in Okinawa prefecture, Japan (Ohara 2009). Heuristics and empirical data on biomass cultivation, sugar crystallization and ethanol fermentation were collected through investigations on existing literature and agricultural reports (Okinawa Agricultural Experiment Station 1991; National Agriculture and Food Research Organization, National Agricultural Research Center for Kyushu Okinawa Region 2010; Rein 2007; Okinawa Prefecture, Agriculture, Forestry and Fisheries Division 2010; Okinawa Prefecture 2006) and interviews to experts. In the development of an agricultural process model, the relationship among the process parameters on sugarcane cultivar, farm operation such as fertilization, and the conditions of cultivation area such as climate and soil was modeled on the basis of the results of the existing studies or cultivar evaluation. Depending on the composition of sugarcane such as sucrose, glucose, fiber, water-soluble materials, and water, the performance of sugar crystallization and ethanol fermentation processes are changed. For example, the sucrose and glucose are the raw material for ethanol fermentation, although glucose is an inhibitor of sugar crystallization. Fiber is not raw materials for sugar and ethanol production, but can be fuel for these processes and a green manure for agricultural field. Syrup is obtained after pretreatment of sugarcane, e.g., milling, fining and filtration treatments. Sugar crystallization is started by crystal seed, and crude sugar in massecuite is separated from molasses by centrifuge. 1st molasses includes about 70 %-sucrose in absolute dry mass. To increase sugar yield, sugar crystallization may be continued three times in Japan. The empirical relationships between sucrose purity and crude sugar yield were obtained from literature (Rein 2007) and operation results in Ie pilot plant. Molasses is the raw material for fermentation producing ethanol. Through interviews to experts and analysis on operation results of the Ie pilot plant, representative fermentation process was modeled.

In this case study, a life cycle assessment was performed by using developed integrated model. The settings of cases are organized in Table 1. The current situation of sugarcane cultivation and sugar crystallization in Japan is defined as the setting of base case. In case 1, the step number of sugar crystallization is decreased from 3 to 1. New cultivar of sugarcane is applied in case 2. Case 3 applies the new cultivar of sugarcane with one-step sugar crystallization. Based on these cases, the production amount of crude sugar and bioethanol, and greenhouse gas (GHG) emission due to their productions are evaluated with an assumption that produced bioethanol can be used as a fuel instead of gasoline.

Table 1. Case settings

	Base case	Case 1	Case 2	Case 3
Sugarcane cultivar	Current	Current	New	New
Crystallization step	3	1	3	1

3.2. Results and discussion

Table 2 organizes the results of agricultural processes. NiF8 is a cultivar of sugarcane widely planted in Japanese sugarcane field. KY01-2044 is called as “monster cane”,

which is a new cultivar of sugarcane developed in Japan. Slightly lower sugar-content than NiF8, but higher yielding is the characteristics of KY01-2044 as shown in Table 2.

Table 2. Results of agricultural processes

Cultivar	Yield	Composition [%]				
	[10^3 kg· $(10a)^{-1}$]	Sucrose	Glucose	Mineral	Fiber	Water
NiF8 (Current)	7.7	14.3	0.6	1.6	11.4	72.1
KY01-2044 (New)	10	13	0.7	2.4	14.7	69.2

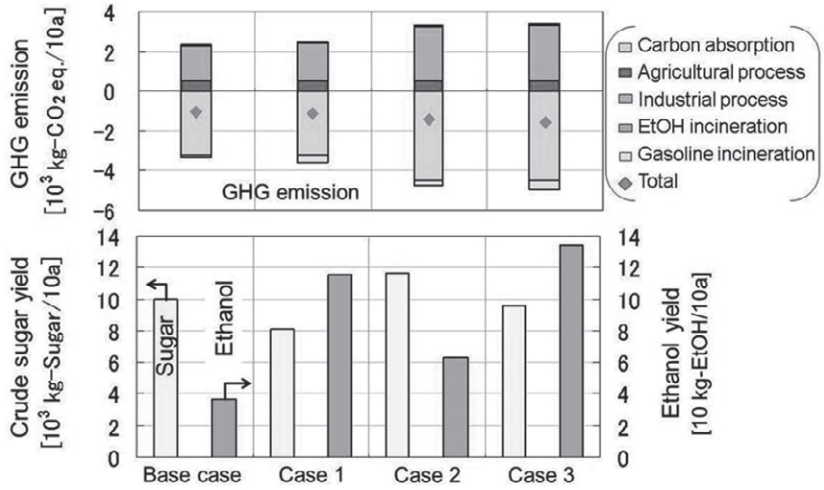

Figure 3. Total results of case study

Figure 3 shows the evaluation results of four cases. Comparing the results of base case and case 1, the decrease of crystallization step increases the production of bioethanol resulting in low GHG emission by applying bioethanol as a fuel. Case 2 demonstrates that new cultivar of sugarcane can increase sugar and bioethanol, because of its high-yielding characteristics. The new cultivar can produce nearly equal amount of sugar obtained in base case, as shown in the results of case 3.

The results of this case study reveals that new cultivar of sugarcane can increase the production amount of sugar and bioethanol in unit land area, simultaneously. It means that it may be able to increase sugarcane-derived bioethanol without the change in the production amount of food. In this regard, however, the results of agricultural process should be carefully checked, because they are highly sensitive to soil, climate conditions, and agricultural operations.

4. Discussion and conclusion

The developed model in case study on sugarcane-derived bioethanol can be used in the design of agriculture and industrial process systems to specify preferable sugarcane cultivars, agricultural operations, and production conditions for certain place under various constraints such as the demand or targeted amount of ethanol and sugar. Considering climate conditions and the prices of sugar and ethanol, the model can

propose alternatives on operations in cultivation and industrial processes. This kind of integrated agriculture and engineering model may become a strong tool for solving issues occurred in Asian countries, for example, the reduction in the land suitable for agriculture, the high frequency of abnormal weather, and the wild fluctuation of the prices of food and energy. Their conditions differ by year and counter measures must be planned constantly. The model can become a key mechanism for supporting analysis, alternative generation, and decision making on such issues. Note that the developed model is based on limited Japanese evidence. Further modeling on the relationships among impacts on environment, social and economics, amount and quality of biomass-derived products, and detail conditions on agricultural and industrial processes such as soil, climate, and so on are strongly needed.

Acknowledgement

The authors would like to thank Dr. Akira Sugimoto, Dr. Shotaro Ando and Dr. Yoshifumi Terajima in Japan International Research Center for Agricultural Sciences, Dr. Takashi Saiki in The Japan Association of Rural Resource Recycling Solutions, and Japan Alcohol Association for their cooperation in the collection of data and knowledge on sugarcane cultivation, sugar crystallization and fermentation processes.

References

Y. Kikuchi, K. Mayumi, M. Hirao, 2010, Integration of CAPE and LCA Tools in Environmentally-Conscious Process Design: A Case Study on Biomass-Derived Resin, Computer-Aided Chemical Engineering: Proc.ESCAPE-20., 28, 1051-1056

JLCA-LCA database 2011 1st Edition

I. C. Macedo, J. E. A. Seabra, J. E. A. R. Silva, 2008, Green house gases emissions in the production and use of ethanol from sugarcane in Brazil: The 2005/2006 Averages and a prediction for 2020. Biomass Bioenergy, 32, 582-595.

National Agriculture and Food Research Organization, National Agricultural Research Center for Kyushu Okinawa Region, 2010, Reference results on new variety of sugarcane: KY01-2044

T. T. H. Nguyen, Y. Kikuchi, H. Sugiyama, M. Noda, M. Hirao, 2010 Techno-economic and Environmental Assessment of Bioethanol Based Chemical Process: A Case Study on Ethyl Acetate, Environmental Progress & Sustainable Energy, in press, DOI: 10.1002/ep.10517.

S. Ohara, Y. Fukushima, A. Sugimoto, Y. Terajima, T. Ishida, A. Sakoda, 2009, Reduction in greenhouse gas emissions from process retrofitting andcultivar improvement in combined sugar-ethanol production from sugarcane, J Life Cycle Assess Jpn, 5(4) 439-445

S. Ohara, 2009, Experimental results of sugar-ethanol co-production process in Ie island, Proc. Midterm Reporting of Research Project by Ministry of Agriculture, Forestry and Fisheries of Japan, 26-27

Objective Management Group (OMG), 2011, Unified Modeling Language (UML) ® Resource Page. Available at www.omg.org/technology/documents/modeling_spec_catalog.htm (Access 20/03/2012)

Okinawa Agricultural Experiment Station, 1991, Reference results on new variety of sugarcane: NiF8

Okinawa Prefecture, Agriculture, Forestry and Fisheries Division, 2010, 2009/2010 Sugarcane and cane sugar production results,

Okinawa Prefecture, 2006, Sugar Industry and Agricultural Products Division, Cultivation guidelines of Sugarcane (*original title in Japanese*), http://www3.pref.okinawa.jp/site/view/contview.jsp?cateid=117&id=12060&page=1 (in Japanses) (Accessed in 2011/11/17)

P. Rein, 2007, *Cane Sugar Engineering*, Bartens, Berlin

J. Sánchez, C. A. Cardona, 2008, Trends in biotechnological production of fuel ethanol from different feedstocks. Bioresour. Technol. 99, 5270-5295.

I.A. Karimi and Rajagopalan Srinivasan (Editors), Proceedings of the 11th International Symposium on Process Systems Engineering, 15-19 July 2012, Singapore.

Planning and Scheduling as a Part of a Control System – Implementation Aspects

Iiro Harjunkoski

ABB Corporate Research, Wallstadter Str. 59, 68526 Ladenburg, Germany

Abstract

This paper discusses some aspects that need to be taken into account when designing and implementing solutions for scheduling real industrial production processes. It highlights certain characteristics that may complicate the practical implementation and focuses on typical requirements stemming from everyday life at a production facility. The paper concludes with some necessary system development steps and reflects those using experiences from a few real-life implementation cases.

Keywords: Scheduling, industrial, integration, control system.

1. Introduction

The activity of scheduling results in a detailed and realistic production plan based on the production targets (orders) often provided by ERP systems. The detailed schedule is then dispatched to the plant floor, where automation and control systems ensure a smooth and efficient production. Scheduling of an industrial production process is complex due to several reasons, among others:

- The problem size may grow exponentially when scaled up to industrial size.
- There are often interruptions or disturbances in the process, which impact the goodness of an existing production plan.
- Normally, the underlying process is monitored, controlled and optimized by several systems, the targets of which may conflict with each other.
- The data available is mostly reflecting the past – access to up-to-date information is crucial as well as selecting which data to use and not to use for optimization.
- Manual interaction is often necessary. It must be clear which decisions need to be optimized and which ones should be made by the operator.

A proper level of integration is very important to any type of automation component. Even the most advanced and efficient planning and scheduling solution can never see the daylight in a real production environment, unless it can be tied into the real-world situation. Normally, the production schedule is generated on demand by composing a varying set of input data in a proper way. Scheduling is thus neither an isolated nor a one-off computational exercise.

The deployment topic was also discussed at the PSE2009 meeting e.g. by Henning (2009), also raising some challenges. For overcoming these, it is crucial that the method developers (often academics) and the implementers (industrial practitioners) collaborate seamlessly with a clearly defined common goal in mind. By using scalable methods where critical sets and parameters are easily configurable through user friendly interfaces, a well-balanced compromise between problem size, solution efficiency and solution quality may be found. Such approach may also help to balance various solution targets. Ensuring that the solution is capable of adapting to frequent changes (both at a model and SW-level) makes it functional in varying situations treating disturbances as

"everyday life". A well-defined relation between each model and solution component and their connection to the real process also contributes to increasing the overall understanding of a holistic system.

2. Production environment

A planning and scheduling (P&S) system needs a large number of data in order to work properly and fulfill its purpose. To access, monitor and analyze the relevant data in a useful way, Process Information Management Systems (PIMS), Manufacturing Execution Systems (MES) or Collaborative Production Management (CPM) systems exist to fill the gap between the process control systems and ERP systems. A planning and scheduling solution must have a well-defined role and work seamlessly within an existing production system in order to be able to support operations.

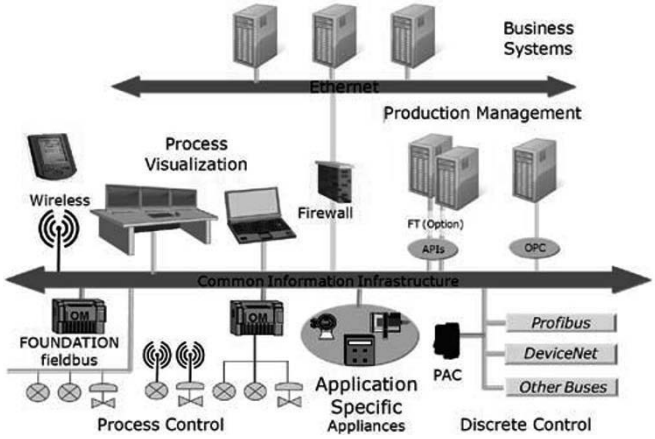

Figure 1. Logical view of a production system (Source: ARC, 2010)

Figure 1 shows a simplified view of a production system with the different hierarchical layers. Commonly a P&S solution is located in the production management layer and needs information both from the planning (ERP) as well as the process / distributed control systems (DCS) levels. Thus it is important to have a common information infrastructure that enables easy and efficient communication and management of data.

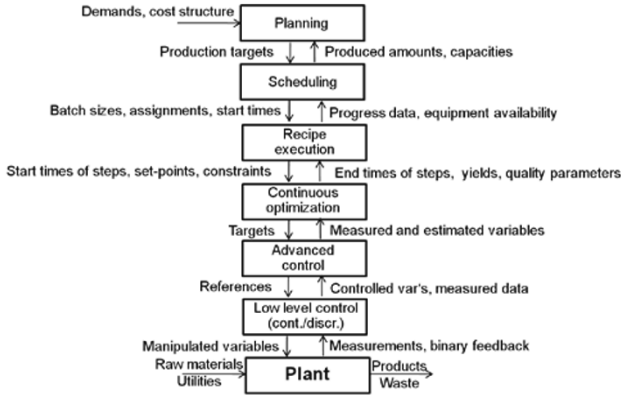

Figure 2. Functional hierarchy of batch production (Engell & Harjunkoski, 2012)

Another view on the decision landscape is seen in Fig. 2, which presents the functional hierarchy of a production system. It contains six main layers: A planning layer setting

the production targets, a scheduling layer generating the detailed schedule, a recipe execution layer governing the batch or production recipes, a continuous optimization layer optimizing the trajectories during the phases and an advanced control layer implementing the optimal trajectory e.g. through model-predictive control (MPC), and providing reference values to the low-level control layer, which is directly connected to the process.

A challenge is to ensure that information can be exchanged smoothly, e.g. information such as equipment availability is transmitted through this functional hierarchy up to the scheduling layer. This also puts more pressure on improving the interfaces and plug-ability of any kind of industrial scheduling solution. Standards such as ISA-88 and ISA-95 (ANSI/ISA, 2005) are often recommended as they can be expected to reduce problems in integrating different solutions. It is today physically possible to link every functional IT-component within a plant, as modern DCS also enable this. Nevertheless, because of the multitude of options it is very important to carefully investigate and analyze which factors can bring added value to the production process. Collaborative Process Automation Systems (CPAS, Hollender, 2009) expand the vision beyond the traditional DCS scope, and present an environment designed for agility and adaptability.

Main challenges for the implementation of P&S solutions are:

- Modeling. The cost and required time for modeling is often much too high, sometimes hindering even the exploration of potential benefits.
- Optimization algorithms. Solution times and robustness is crucial especially for online solutions.
- Interaction with the user / human operator. A solution that is not accepted by the operators will not be used in the long term, even if a benefit could be demonstrated.
- Automation systems and components. Integration of different software systems for different functions acting on a common open data structure is needed.
- Systems engineering. The design of integrated systems is a challenge for which no generic guidelines are available.

3. Example cases

Typical daily scheduling use cases that every P&S solution must be able to handle are:

- Rush customer orders (re-scheduling with priorities)
- Late deliveries or customer pickup (material & inventory considerations)
- Equipment breakdown or process delays (re-scheduling with possible re-routing)
- Scheduled maintenance (important to respect while maximizing productivity)
- Product quality problems (lower productivity, normally detected at the control level)

This also highlights the needs of good integration, user interfaces and rescheduling strategies. The core scheduling model or algorithm, often developed e.g. by a university or research laboratory, is only a part of the overall scheduling application. Production scheduling is a data intensive exercise and the success of an implementation relies on the quality of the data used by the model and on the effective transfer of data to and from the model. Before any implementation several issues must be confirmed:

- Separation of data and parameters from the model equations
- Full scalability of the models based on the provided data
- Ability of an advanced scheduling approach to solve the problem
- Availability of data needed for the advanced solution
- Possibility to integrate into the existing scheduling process and information system

In this paper we consider two concrete scenarios of integrating a P&S solution: One where the scheduling is added into an existing system and another one without a “host”.

3.1. Adding a P&S module into an existing CPM system

If the scheduling optimization solution needs to be embedded into an already existing and well-defined system, the integration effort is fairly low. The main focus on the implementation is to ensure that the solution works for all possible instances and has a way to react to unreasonable requests, i.e. fallback strategies or communication by failures. The hosting solution will be responsible for collecting all required input data (e.g. from databases, ERP and control system), converting it and providing it in a defined data format. It must be highlighted that often there are several programs involved, even written in different programming languages, so the responsibilities need to be clearly assigned to simplify the definition of roles within an integration team.

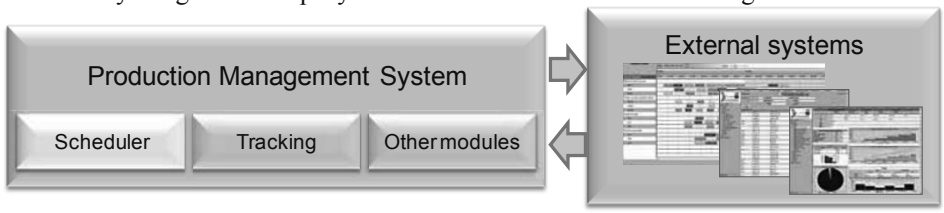

Figure 3. Scheduler as a part of an existing system

Although the integration is more or less trivial, the implementation work still requires lots of efforts, e.g.: Collection of requirements, modeling, constructing test cases, proof-of-concept in full scale, interface definition (data exchange format, how to actually invoke the solution), solution implementation (programming), comprehensive testing (never underestimate this) and finally detailed system documentation explaining the solution structure, use and possible enhancement. Through this strategy all existing connections to external systems (e.g. Gantt Chart) can be used without new efforts (see Fig. 3). It is still fairly realistic to say that the implementation easily takes about 5-10 times the amount spent on building a first prototype on for instance GAMS or AMPL, especially if these are not going to be part of the final system.

3.2. Implementing scheduling solution as a standalone module

In this scenario, the efforts of implementing a solution as a standalone module are huge: All data exchange, user interfaces, accessibility, security and backup policies must be defined separately. In this case applying standards can result in significant time savings at the implementation but also enable various future expansions, integrate-ability and it also makes it easier for a third person to work with further system development in the future. An example of such as solution is shown in Fig. 4, where the optimization models have been isolated in a modular structure and all data and parameter exchange is done using the ISA-95 standard with certain extensions.

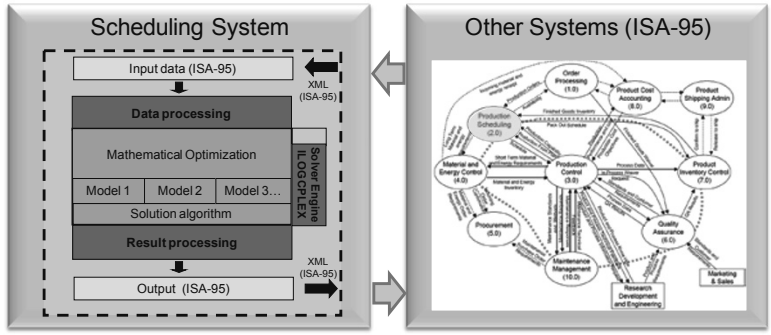

Figure 4. Modular solution and the ISA-95 Purdue Reference Model

The approach in Fig. 4 can be integrated in various ways, e.g. as a web-service (available through the internet), as a console or windows application or as a windows service. In all cases, the main system features remain the same and the data exchange is always based on the XML-file format.

4. Conclusions

The focus of this paper is on the integration and implementation, omitting the main mathematical challenges. Nevertheless, the original problem formulation must naturally comply with real requirements and be fully expandable through parameters. Along the proof-of-concept, models will continually be modified and enhanced also later as a more comprehensive understanding of the problem emerges through systematic testing and validation. Often the early use of a scheduling solution also tends to uncover necessary changes to account for unanticipated circumstances. Even when the model is robust and has been proven, it may need to be developed further due to possible changes in the production process or surrounding solution landscape as a scheduling solution must play a part in a complex IT-infrastructure. Thus, ideally the scheduling model should automatically adapt itself to most changes in the neighboring system, which may result in performance issues. Implementing a scheduling optimization solution in real life is challenging:

- In running production, every schedule is, in fact a re-schedule building upon a previous schedule. One important question is how to re-schedule in case of sudden disturbances?
- The solution should be maintainable for at least a 10-20 year time horizon (update models, adapt to major software updates).
- It should be possible to easily integrate the solution and link it to other applications.
- Implementing the solution should also ensure a good return-on-investment (ROI), which is directly affected by the related software license and development costs.
- Measuring the real performance or achieved improvement is not trivial as often the given schedule cannot be realized to 100% exactness.

Maintaining an industrial scheduling solution requires collaboration between various skills. Taking some steps towards integrated solutions already in the early model development phase may significantly reduce the required efforts (and costs) of implementing a theoretical method in practice. The ideal goal is that state-of-the-art academic models and algorithms could be tested in a plug-and-play manner on challenging industrial problems. This would speed up the development on both ends and enhance the success of optimization methodologies in the industry. But is this still a utopia? Not necessarily.

References

ANSI/ISA-95.00.03-2005 (2005). Enterprise-Control System Integration. Part 3: Activity models of manufacturing operations management, ISBN: 1-55617-955-3

ARC Advisory Group (2010). The Collaborative Process Automation System for the 21st Century CPAS 2.0

Engell, S. and Harjunkoski I., 2012, Optimal Operation: Scheduling, Advanced Control and their Integration, Proceedings of FOCAPO/CPC 2012

Henning, G.P., 2009, Production Scheduling in the Process Industries: Current Trends, Emerging Challenges and Opportunities, Proceedings 10th International Symposium on Process Systems Engineering - PSE2009, pp. 23-28

Hollender, M. (Ed.) (2009). Collaborative Process Automation Systems. ISA, ISBN 978-1936007103

I.A. Karimi and Rajagopalan Srinivasan (Editors), Proceedings of the 11th International Symposium on Process Systems Engineering, 15-19 July 2012, Singapore.

Advances in Procedural Automation in the Chemical Industry

Maurice Wilkins[a], Marcus Tennant[a]

[a]Yokogawa Corporation 2155 Chenault Dr. Carrollton TX, 75006 U.S.A.

Abstract

Over the past 20 years there has been significant advancement in automating batching processes in the Chemical industry. Many of the principles, models, and best practices outlined in the ISA-88 standard have lead to better control systems, more efficient designs, increased flexibility and safer operation of Batch processing plants.
Recently, ISA 106 was formed and now is working towards producing a standard for automating procedural operations in continuous processes. We review the concept of Modular Procedural Automation and a case study of how a company implemented procedural automation and the direct benefits they have achieved.

Keywords: Procedure, Safety, Operating Efficiency

The Chemical Industry- The tale of two business drivers and production systems.

The Chemical Industry is estimated to generate approximately three trillion US dollars a year in annual sales and supplies many markets with essential materials that are critical to making each a success through utilizing different processes, material, and operations. In classification of the chemical industry there are several ways of examining the sub segments. From a business perspective, it has been often been useful to analyze the chemical industry into two primary segments 1) Bulk Chemicals and 2) Specialty and Fine Chemicals.

Bulk chemicals produces material at the lowest cost with a focus on production innovation while specialty and fine chemicals focuses on product innovation and responding to rapid time to market product lifecycles. In general, the production process for manufacturing that supports the business driver in bulk chemicals is continuous process applications and with fine and specialty chemical, it has traditionally been batch process applications.

As global competition intensifies, the chemical industry is becoming more polarized along these two models. Material intermediates and their corresponding supply chains in the chemical industry are increasingly losing their margins at intermediate materials production. Every business segment in the Chemical industry must determine if their chemical product is either a commodity with a focus on a becoming a low cost producer and optimizing a production system that produces cost competitive material or if they

are a specialized materials solution provider maintaining a production system with maximum flexibly to meet rapidly changing market demands.

1. Advances in Procedural Operations in Specialty and Fine Chemicals

In the late 1980's specialty and fine chemical manufacturers faced a problem. In the previous decade, rapid advances in control technology from sensors, meters and distributed control systems had provided significant benefits to many process industries including the chemical industry. However, using these new technologies in automating batch processes often created problems and unintended consequences.

Due to non standard definition of terms that varied between companies and industries, it was often difficult to convey requirements to control vendors and system integrators. Terms like Procedure, Unit, and Recipe meant different things to different companies.

Improvements in automation and control often limited production flexibility. Many chemists, process engineers, and formulation scientists found it frustrating that when they had to make a procedural or formulation changes to their products they had to call in the control engineer to make the changes in the control system and often had to face significant delays. This directly impacted an important business driver in batch processing – production flexibility. Sometimes a plant would abandon the control system and revert to manual operations where they would make a change to a paper process sheet and hand it to the process operator

Lack of consistent programming methodology- Often a control engineer would build an Ad hoc batching program that would be initially well accepted by the operational staff. Eventually the control engineer would move on to a different job within the organization or leave the company altogether. The program would usually lack documentation and a consistent structure that a new control engineer could go in an easily make changes to meet the ever changing requirements of the process.

In light of these issues in 1988 the ISA (International Society of Automation) formed a standards and practices committee that focused on the automation of batch processes (ISA88). In 1995, the committee issued ISA 88 part 1- models and terminology for batch process applications. Since its issuance the ISA-88 standard has provided manufacturers in batch focused applications tremendous benefits, not only in Chemical but also in Pharmaceutical and Food & Beverage. Many papers have been written in the past 12 years that have highlighted the benefits of the standard and the business values such as: 1)Reduction in production cycle time. 2)Reduced Engineering Costs in initial implementation and in modifying systems. 3)Reduction in cost for Validation in cGMP applications. 4)Increased process plant throughput. 5)Improved Safety and risk reduction

2. Safety, Operational efficiency, and aging workforce – Bulk Chemicals emerging focus on procedural operations

As continuous process plants have taken advantage of the changes in process controls technology, it has helped make unprecedented gains in production efficiency. Most of

these benefits have occurred by optimizing steady state operations. All chemical plants spend a majority of their time at steady state but other conditions occur on a regular basis and require the most attention from the operational staff.

Startup & Shutdown-Safe and efficient startup of a continuous process unit or activity is critical to its overall operation. Startup frequency can vary, from once every day to once every five years. When startups occur often, they can occur on different shifts, and the time and skill of the operator on duty can determine the efficiency of the startup. If startups occur at longer intervals, companies run the risk of not having experienced personnel available to run and oversee the startup. Orderly and safe shutdown of a continuous process unit or operation is just as critical as a startup. One key item in the shutdown procedures is recognizing that a shutdown might not be scheduled. System problems, severe weather conditions, or power outages can require a shutdown of process operations at very short notice.

Feedstock and product output transitions- Many chemical processing units regularly operate at more than one optimum steady state. In refineries and petrochemical operations, for example, many facilities purchase feedstock of different properties from different sources and vendors. As the process runs out of one type of feedstock, operations must be adjusted to process correctly the next lot of feedstock. Similarly, in many chemical plants, it will often be a requirement to make a variety of products in a campaign fashion by changing operations to meet the new product specification.

Recovery from Abnormal Conditions- In the course of plant operations, process conditions from time to time enter abnormal operating regions where a plant is producing off spec or low quality material. Additionally, the process conditions may approach a critical condition that could cause a safety system shut down or worse a serious plant incident. This could be caused by a previous operational error or an equipment malfunction. Procedures are available for an operator execute to bring a process to normal operating conditions or to a safe state.

In most continuous process Chemical plants in the world these operations are performed by operators completing manual steps interfacing with a control system or instructing a field operator to manipulate a valve. Efficiency and accuracy in executing these operational procedures requires an experienced operational staff. Often through years of hands on experience the knowledge in a plant is no longer documented and resides in operators heads. One issue facing process plants worldwide is the loss of these knowledge based operational skills due to an aging workforce and retirements. This has already begun to affect many process manufacturers around the world.

Another issue is safety incidents caused by operational error. A study by J & H Marsh & McLennan that the shows that in an examination of major incidents by the average loss per incident indicates that operational error represents the largest average dollar loss[a]

3. The emergence of a procedural automation standard for the continuous process industries

Since the development of ISA 88, many practitioners of the standard have applied the model and principles to continuous process applications with various degrees of success, many process operations such as ethylene production, distillation, and polymer extrusion have had ISA 88 concepts applied, however there was never any whole scale adaptation of the standard to continuous process industries. Many Process manufactures have felt that ISA 88 was too rigid in its approach and did not take into account many other standards and practices that have emerged since ISA 88 was developed such as alarming, safety systems, security, and HMI interface design.

In view of the need for an industry standard to focus on continuous process operations, the International Society of Automation approved the formation of a new standards committee in April 2010, the committee, ISA106 adopted the title Procedural Automation for Continuous Process Operations. The purpose of the committee at its first meeting in June 2010 was to develop a standard, recommended practices and technical reports for the lifecycle of automated procedures for process operations in industries. So far, the standard has input and support from over 40 chemical manufacturers, refiners and suppliers. The initial goal is to publish a technical report based on the good practices that are used today, with a target release in 2012. Following that, the committee plans to refine the material and publish a standard

4. **Application of Procedural Automation & Case Example**

Yokogawa Corporation over many years has followed best practices in ISA-88, and often applied the lessons for the standard to continuous process applications. To capture the embedded knowledge and to convey to owner/operators the benefits, Yokogawa introduced an integrated solution concept called Modular Procedural Automation (MPA). MPA addresses industry needs to improve operating procedures and to apply a uniform approach to the standard using different technology tools. It is a consultative methodology whose purpose is to document and automate procedural operations in continuous processes. This approach optimizes user acceptance and reduces deployment costs by:

Establishing a hierarchy of Procedures: MPA breaks large and complex procedures into smaller modules and organizes them into a hierarchy. This modularization provides easier documentation, verification, and implementation of the discrete pieces of procedural logic and knowledge.

Re-use of Procedural Logic: Whether implemented with manual, prompted, or automated procedures, MPA can help re-use the same procedures and logic in different parts of the plant and with different products. When procedural logic (that is portions or modules of procedures) is re-used, the business gains repeatability, reliability, and it lowers the cost of developing duplicate procedures.
Use a Scalable Approach: MPA provides a flexible and scalable approach to automation; it avoids the “one size fits all” approach. Different types of procedure implementations contain scalability for manual, prompted, and automated control. The hierarchy of modular procedures is easily adjusted to fit the application requirements which can vary the level of complexity;

For example Evonik Industries operates an Acrylic Acid production facility in Germany that has integrated into the process two reactors, four distillation columns, and a

crystallizer for the manufacturing process. A regular system shutdown of the production of Acrylic Acid is required for cleaning and maintenance. The startup procedure for Acrylic Acid manufacturing requires the skills of experienced operators to bring the process up to steady state. Any additional time to bring the process to full production results in unnecessary rework and waste of production utilities.

Evonik developed their requirements and worked with Yokogawa engineers utilizing an MPA approach and determined the correct procedures and technology to automate the process. The results were
1) Process operators were able to start up their distillation columns 30% faster
2) Reactors were able to come on stream 70% faster
3) Process safety margins, of explosive conditions during startup, were increased significantly

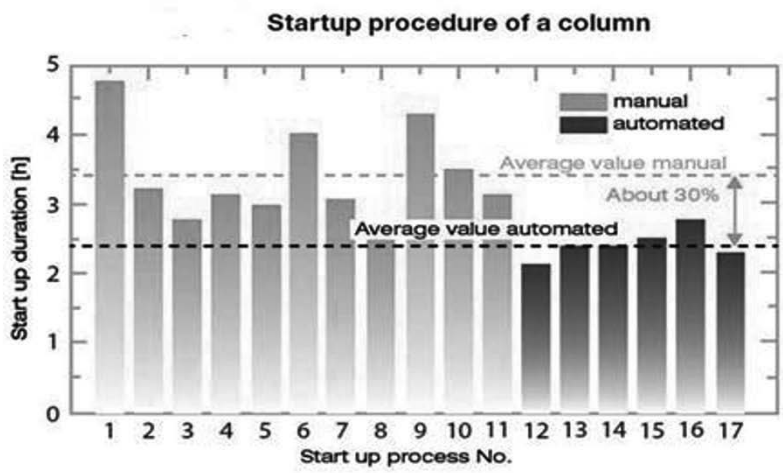

5. Conclusion

Today many procedural operations in both continuous and batch processes are performed manually, often inefficiently and sometimes unsafely. With an aging workforce and business pressure to reduce cost, improve quality and reduce safety and environmental incidents, automating procedures offers the ability to preserve and manage a plant's and company's operational and procedural knowledge and improve safety performance. Modularizing the design and implementation also provides cost savings while allowing the flexibility to make changes without impacting production. The general need for procedural automation has been shown with the formation of the ISA106 standard committee and the strong industry support for it from both users and suppliers alike.

References

a. Referenced in ARC(Automation Research Corp) Why we need a better approach to procedural automation- Larry O'Brien September 2010

I.A. Karimi and Rajagopalan Srinivasan (Editors), Proceedings of the 11th International Symposium on Process Systems Engineering, 15-19 July 2012, Singapore.

Retrofit design of a pharmaceutical batch process improving green process chemistry & engineering principles

Alireza Banimostafa*, Stavros Papadokonstantakis, Konrad Hungerbühler
Swiss federal institute of technology (ETH),Zurich 8093,Switzerland

Abstract

Rapid globalization during the last decades and increasing regulatory efforts from governments forced the chemical industry to meet up the rising concern about sustainability aspects of chemical process design. Besides these non-monetary issues, the economic performance is still a very crucial aspect of design. Therefore, considering the capital intensive nature of chemical industry, redesign of existing production plants has been recently regarded as a key strategic decision. This retrofitting task has been extensively performed in continuous processes for the production of bulk chemicals, however in the case of batch processes and specialty chemicals only few studies address the importance of retrofitting, especially including multi-criteria sustainability assessment.

The objective of this paper is to address retrofitting actions to enhance both monetary and non-monetary aspects of chemical process design. This is done using a systematic Path Flow Decomposition (PFD) method, multi-dimensional process assessment indicators, heuristics, and model based methodologies for generation of design alternatives. In this study a set of Environmental, Health, and Safety (EHS) hazard assessment and Life Cycle Impact Assessment (LCIA) indicators is newly introduced in the PFD method and evaluated in parallel with previously developed indicators. This set of indicators has been associated with a set of heuristics based on hazard and life cycle impact assessment rules and established principles of green chemistry and engineering.

The developed methodology is applied to an existent batch production plant from pharmaceutical industry by addressing three process flowsheet structural alternatives for waste solvent management, pressure swing distillation, extractive distillation, and extraction for the separation of the THF/Water azeotrope. It is found that the suggested structural alternatives result in improved EHS, LCIA, and cost metrics compared to the base case of solvent incineration.

Keywords: Retrofit design, Batch operation, Path flow decomposition, EHS, LCIA

* Corresponding author: alireza.banimostafa@chem.ethz.ch

1. Introduction

Referring to sustainability in process design, the first thing to take into account is the fact that sustainable development is a complex concept and today there is still ongoing effort to find common terms for describing it. In fact, as discussed in several approaches, one should not focus only on a single aspect (Jimenez-Gonzalez & Constable, 2011) without addressing aspects from all three main pillars of sustainability, i.e., economic, environmental and social ones. For pursuing sustainability in chemical industry it is advantageous to develop specific indicators for different sustainability aspects (Azapagic & Pedran, 2000). For instance, social aspects are partially captured by safety and health hazard indicators (Kletz & Amyotte, 2010). Moreover, the term sustainability comprises several different paradigms such as inherent safety, green chemistry, and green engineering to name the most relevant ones. Besides the non-monetary issues, considering the capital intensive nature of chemical industry, the economic performance remains a very crucial aspect of sustainable process design. As a result, redesign of existing production plants has been recently regarded as a key strategic decision in chemical industry. So far in the scientific literature and industrial practice several motivations have been considered for retrofitting tasks, the economic ones being the most prominent. However there has been little effort to systematically use green chemistry and engineering principles as an incentive. This study attempts to bridge this gap by combining an existing systematic retrofit framework based on PFD with a broad set of EHS and LCIA metrics and respective heuristics originated by green chemistry and engineering principles (Anastas & Zimmerman, 2003; Anastas & Eghbali, 2010).

2. Methodology

2.1. Path Flow Indicators (PFIs)

The original PFD method (Uerdingen et al., 2003) is based on a source-to-sink approach and includes a set of indicators focusing mainly on economic efficiency i.e. Material Value Added (*MVA*), Energy and Waste Cost (*EWC*), Reaction Quality (*RQ*), Accumulation Factor (*AF*) and Renting Cost (*RC*). In addition to these previously defined indicators, two new PFIs, namely *EHS* and *LCIA,* were newly introduced into the PFD methodology in order to consider more systematically green chemistry and engineering principles. *EHS* is appropriate for both open and cycle path flows and is defined by:

$$EHS_p = m_P . N_P . \sum_{dp=1}^{DP} \underset{u}{Max}(Ind_{p,dp}(T_u, P_u)) \quad \text{(Eq.1)}$$

where $Ind_{p,dp}(T_u, P_u)$ is the index value of path flow (p), calculated according to nine different dangerous properties (dp) , (i.e. Air effect, Water effect, Accumulation, Irritation, Acute toxicity, Chronic toxicity, Mobility, Fire/Explosion, Reaction/Decomposition) depending on temperature (T_u) and/or pressure (P_u) of the respective unit operation that affects the path flow, N_p is the number of unit operations that the path flow passes through, and m_p is the respective mass flow.

LCIA is only valid for open path flows and here is calculated based on Cumulative Energy Demand (CED), but in principle any LCIA metric could be used (e.g., Global Warming Potential, Eco-indicator, etc):

$$LCIA_{op,CED} = m_{op} . (CED_{op,pr} + CED_{op,tr}) \quad \text{(Eq.2)}$$

where *pr* and *tr* are the respective values for production and treatment (incineration or waste water treatment) of the open path respectively, and m_{op} is the respective mass flow. These two new indicators are used in combination with the existing ones in the framework of the PFD and are mainly related to four out of twelve principles of green chemistry, i.e., prevention of waste, design for energy efficiency, safer solvents and auxiliaries, and inherently safer chemistry for accident prevention. Additionally, four principles of green engineering are governed by the newly defined indicators namely, inherent rather than circumstantial, prevention instead of treatment, design for separation, and efficiency maximization.

2.2. Environment, Health, and Safety(EHS) hazard assessment

In this study, the original EHS hazard assessment framework (Koller et al., 2000) consisting of eleven Dangerous Properties (*DPs*) has been updated and condensed into nine *DPs* to provide a more versatile hazard assessment within chemical process design. Property parameters of the substances were the basis for an index calculation ranging between [0-1], 1 being the most hazardous. For each substance and each *dp* the most reliable data were selected from a variety of sources, such as databases and estimation tools.

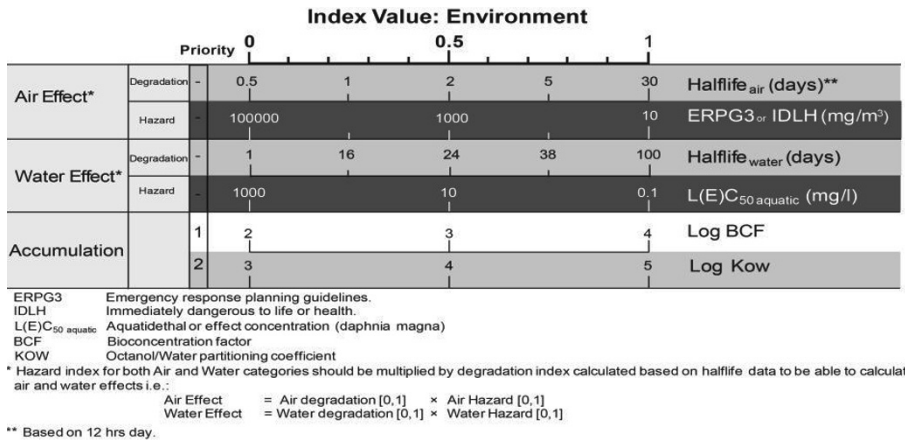

Figure 1: Dangerous properties of environmental category (E) within EHS framework

In addition, priorities were defined from the most available and reliable quantitative property to qualitative parameters such as risk phrases or generic material safety datasheets statements (MSDS). Fig.1 above depicts an example of an index calculation for the environmental (*E*) category. The air effect and water effect were based upon multiplication of the properties degradation and hazard in air and water respectively. For the index calculation of both degradation classes a probability distribution based on available data was considered. On the other hand, for the calculation of the accumulation index, only expert knowledge was considered and no statistical analysis was performed.

2.3. Life Cycle Impact Assessment (LCIA)

In order to measure if a retrofitted process is in fact green, it is crucial to determine the impacts of the process throughout its entire life cycle. There are several impact categories relevant for this kind of analysis, choosing the right impact category might be dependent on industry sector as well as company's interest. In this study, Cumulative

Energy Demand (CED) was chosen based on the industrial partner's interest in energy related impacts and the fact that typically waste management systems need to satisfy legal emission limits constraints, leaving energy consumption as the most important degree of freedom for the process design from LCIA perspective. Cradle-to-gate as well as gate-to-gate analysis were carried out for reactants, auxiliaries, and process utilities. For those streams which ended up in treatment facilities, i.e., incineration or waste water treatment , the impact categories were respectively calculated based on previously established studies(Seyler et al., 2005; Kohler et al., 2006).

3. Case study

A case study from Swiss pharmaceutical industry was performed to examine the application of the method on a batch production facility with a relatively high degree of complexity. Upstream process consisted of a semi-batch reactor with a first order reaction which was carried out in THF solution, and an extraction unit. Each batch represented approximately 100 kg of an essential intermediate in pharmaceutical production and the base case was defined based on 300 batches per year.

4. Results

The Highest Impact Potential Values (HIPVs) were chosen from the list of all calculated PFIs. Path flows with the highest number of occurrences (Highlighted column in Table 1) of HIPVs (Underlined values in Table 1) were chosen for retrofit actions. These HIPVs were connected to a table of EHS and LCIA generic heuristics. As an example by looking at separation specific heuristics, distillation with no entrainer is suggested for separation of path flows with a volatility ratio of a >1.1. However, by performing a sensitivity analysis regarding different process operating parameters and process layout settings, for separation of azeotropic mixtures, structural alternatives with no entrainer (e.g. pressure swing distillation) were not necessarily more efficient compared to those with an entrainer (e.g. extractive distillation).

Table 1: Example of normalized PFIs matrix with underlined HIPVs (Calculated based on modified PFIs ; OC refers to number of occurrences of HIPVs for each open path)

	MVA	EHS	LCIA	EI	AF	RQ	RC	OC	RANK
OP3	0.36	<u>0.73</u>	<u>1.00</u>	<u>0.87</u>	0.00	0.00	<u>0.82</u>	4	1
OP8	0.04	<u>1.00</u>	0.18	0.00	0.00	0.00	<u>1.00</u>	2	2
OP9	0.03	<u>0.64</u>	0.00	0.00	0.00	0.00	0.00	1	3

Therefore, sensitivity analysis facilitated the generation of meaningful Applicable Heuristics (AHs) to be able to suggest relevant retrofit actions. As mentioned earlier, for practicing green chemistry and engineering principles in chemical industry, it is essential to compare the generated alternatives in a multiobjective way. Therefore, all alternatives chosen by the PFD method were evaluated according to Pareto-front curves to highlight the trade-offs between different objectives along with those alternatives having the lowest objective values of LCIA , EHS, and cost.

Fig.2 illustrates an example of a structural alternative based on continuous extractive distillation using ethylene glycol as an entrainer. The base case represents the incineration option of a THF/Water azeotropic mixture currently performed in the plant. The respective values are normalized between [0, 1] and as depicted the base case represents the worse case in terms of all objectives. Two extreme points in Pareto-front 1 are cases with different recoveries (Similar THF purity). As depicted, the scenario

with higher recovery of THF is more profitable and needs less cumulative energy. On the other hand, higher recovery requires more amount of entrainer, which is the reason for higher column hold-up and EHS scores.

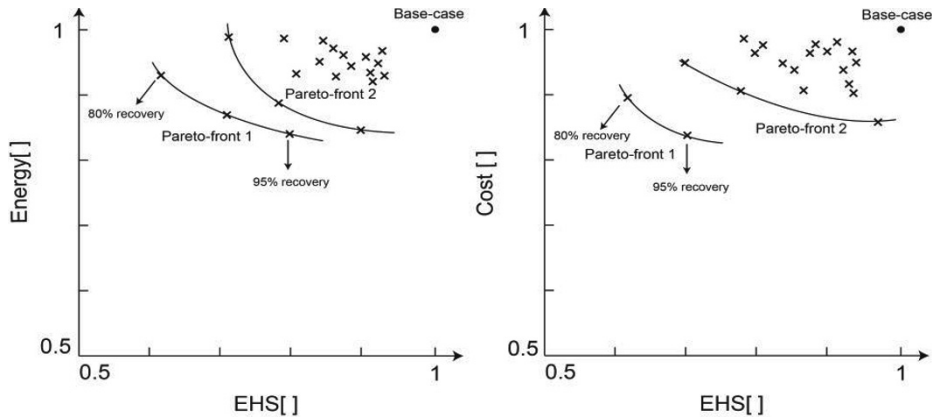

Figure 2: Multiobjective assessment of continuous extractive distillation with ethylene glycol as an entrainer compared to incineration (base case).

Furthermore, based on generic heuristics a sensitivity analysis was also performed regarding substitution of entrainers in case of extractive distillation. Finally, the results of different structural alternatives (Extractive distillation, pressure swing distillation, and extraction) were compared based on three objectives mentioned above. The comparison highlighted the fact that for downstream process, extractive distillation with ehtylene glycol was slightly advantageous compared to rest of alternatives.

References

P. Anastat, & N. Eghbali, 2010, Green Chemistry: Principles and Practice, Chemical Society Reviews, 39, 1, 301-312.

P. Anastat, & J. B. Zimmerman, 2013, Design through the 12 principles of green engineering, Environmental Science & Technology, 37, 5, 94A-101A.

A. Azapagic, & S. Perdan, 2000, Indicators of sustainable development for industry: A general framework, Process Safety and Environmental Protection, 78, B4, 243-261.

C. Jiménez-González , & D. J. C. Constable, 2011, Green Chemistry and Engineering: A Practical Design Approach, John Wiley & Sons.

T. A. Kletz , & P. Amyotte, 2010, Process plants: a handbook for inherently safer design, Taylor and Francis .

A. Kohler , & S. Hellweg, B. I. Escher, K. Hungerbuhler, 2006, Organic pollutant removal versus toxicity reduction in industrial wastewater treatment: The example of wastewater from fluorescent whitening agent production, Environmental Science & Technology, 40, 3395-3401.

G. Koller , & U. Fischer, K. Hungerbuhler, 2000, Assessing safety, health, and environmental impact early during process development, Industrial & Engineering Chemistry Research, 39, 960-972.

C. Seyler , & T. B. Hofstetter, K. Hungerbuhler, 2005, Life cycle inventory for thermal treatment of waste solvent from chemical industry: a multi-input allocation model, Jornal of Cleaner Production, 13, 1211-1224.

E. Uerdingen , & U. Fischer, K. Hungerbuhler, 2005, Screening for profitable retrofit options of chemical processes, AIChE J., 49, 2400-2418.

I.A. Karimi and Rajagopalan Srinivasan (Editors), Proceedings of the 11th International Symposium on Process Systems Engineering, 15-19 July 2012, Singapore.

Parallel design of pharmacodynamic experiments for the identification of antimicrobial-resistant bacterial population models

Carlo C. Ballan, Federico Galvanin*, Massimiliano Barolo, Fabrizio Bezzo

CAPE-Lab, Dipartimento di Ingegneria Industriale
Università di Padova, via Marzolo 9, Padova, I-35131, Italy
**E-mail: federico.galvanin@unipd.it*

Abstract

The use of detailed pharmacokinetic (PK) and pharmacodynamic (PD) models in order to investigate drug resistance and the susceptibility breakthrough by means of *in-vivo* or *in-vitro* trials is a widespread practice in the preliminary stages of drug development. However, complex PK-PD models are usually affected by identifiability issues typically related to their specific model structure and to the strong correlation among the model parameters. Model-based design of experiments (MBDoE) techniques can be successfully adopted to design multiple experiments to be executed simultaneously, detecting a proper set of experimental settings improving the identifiability of the model parameters. The preliminary results presented in this paper show that designing experiments in parallel, rather than sequentially, can substantially decrease the time and effort required by the model identification task for a microbial growth model.

Keywords: model-based design of experiments, time-kill study, parallel experiments.

1. Introduction

Pharmacokinetics (PK) and pharmacodynamics (PD) experiments are required for the development of new antimicrobial therapies and the preclinical assessment of antibacterial agents in the preliminary stages of drug development [1]. Pharmacokinetics is concerned with the time course of antimicrobial concentrations in the body, while pharmacodyamics is concerned with the relationship between those concentrations and the antimicrobial effect. Thanks to *in-vivo* and *in-vitro* trials, allowing for the definition of the dose and the proper selection of the dosing interval, it is possible to study the susceptibility breakthrough and the antimicrobial resistance of a single individual, as well as of an entire population [2]. Antibiotic resistance observed in nosocomial infection is strictly related to the treatment strategies: when the resistance to antibiotics appears, PK-PD models may provide needful indications to correct the therapy by means of time-kill studies (bacterial burden variation with time and antimicrobic concentration). In the clinical practice, trials are usually performed to determine the antibiogram of an infective pathogen, which is identified by several heuristic indicators (area under the curve, minimum inhibitory concentration, minimum bactericidal concentration) on which the therapy is currently based. The adoption of such indicators gives only descriptive and semi-quantitative information on the system and it cannot exactly predict the effects of antibiotic concentration in time. A PK-PD modeling effort is thus required to improve the ability of prediction of time-kill phenomena, and several models have been proposed in the literature to describe the dose-response to antibiotic agents [3-4]. However, structural complexity and high

correlation among model parameters may expose these models to severe identifiability issues [5], such that unplanned or ill-conceived experiments may not allow estimating the entire set of model parameters in a statistically sound way, prolonging the time and effort required by the model identification task. Structural identifiability can be assessed *a priori* for relatively simple PK-PD models at given experimental conditions [6], but its assessment is related to the level of excitation provided by the identification experiments. Furthermore, the possibility to detect a subspace of experimental conditions yielding local identifiability is strictly related to the way in which experiments are executed in time, e.g., in case multiple equipment is available and parallel experimentation is thus possible [7]. Model-based design of experiments (MBDoE) techniques represent a valuable tool to design optimally informative experiments, providing a set of experimental conditions ensuring the local identifiability of the system. Multiple experiments can be designed according to different experimental configurations, adopting parallel or sequential MBDoE techniques, and exploiting conventional and advanced design criteria [8]. In this paper, experiments are designed by MBDoE with the purpose to identify the set of parameters of a PD model of *in-vitro* bacterial growth [4]. Identifiability issues are tackled through the design of parallel experiments allowing for a progressive reduction of the initial uncertainty affecting model parameters. The resulting design permits to exploit the total duration of the experimental campaign in a more efficient way, improving the accuracy and precision of obtained parameters providing easier experimental protocols to be implemented.

2. The methodology

Conventional MBDoE techniques for parameter identification usually involve a sequential procedure: 1) the design of the experiment (based on current knowledge on model structure and parameters); 2) the execution of the designed experiment, where new data are collected; 3) the estimation and statistical assessment of model parameters. Iteration of steps 1 to 3 generally leads to a progressive reduction of the uncertainty region of model parameters. Complex PD models are usually described by systems of differential and algebraic equations in the form

$$\begin{cases} \mathbf{f}\left(\dot{\mathbf{x}}(t), \mathbf{x}(t), \mathbf{u}(t), \mathbf{w}, \boldsymbol{\theta}, t\right) = 0 \\ \hat{\mathbf{y}}(t) = \mathbf{g}\left(\mathbf{x}(t)\right) \end{cases} \tag{1}$$

where $\mathbf{x}(t)$ is the N_x-dimensional vector of time dependent state variables, $\mathbf{u}(t)$ and $\mathbf{w}$ are, respectively, the model time dependent and time invariant control variables (manipulated inputs), $\boldsymbol{\theta}$ is the set of N_θ unknown model parameters to be estimated, and t is the time. The symbol ^ is used to indicate the estimate of a variable (or a set of variables): $\mathbf{y}(t)$ is the M-dimensional vector of measured values of the outputs, while $\hat{\mathbf{y}}(t)$ is the vector of the corresponding values estimated by the model. MBDoE procedures aim at decreasing the model parameter uncertainty region by acting on the experiment design vector $\boldsymbol{\varphi}$:

$$\boldsymbol{\varphi} = \left[\mathbf{y}_0, \mathbf{u}(t), \mathbf{w}, \mathbf{t}^{sp}, \boldsymbol{\tau}\right]^T \tag{2}$$

The design vector $\boldsymbol{\varphi}$ in the most general form may contain a N_y-dimensional set of initial conditions for the measured variables ($\mathbf{y}_0$), the manipulated input variables ($\mathbf{u}$ and $\mathbf{w}$), the duration of the single experiment ($\boldsymbol{\tau}$) and the N_{sp}-set of time instants at which the output variables are sampled $\mathbf{t}^{sp}$. Usually the variables that can be optimized for design purposes in PK-PD experiments ($\boldsymbol{\varphi}$ elements) are: the allocation of samples, the initial

bacterial/antibiotic concentration, (possibly) the procedure for the administration of antimicrobial agents in time, and the duration of each single experiment. Conventional MBDoE procedures aim at decreasing the model parameter uncertainty region predicted *a priori* by the model by acting on the n_φ-dimensional experiment design vector $\boldsymbol{\varphi}$ and solving the following NLP optimization problem:

$$\boldsymbol{\varphi}^{\text{opt}} = \arg\min_{\boldsymbol{\varphi}} \left\{ \psi\left[\mathbf{V}_\theta(\boldsymbol{\theta}, \boldsymbol{\varphi}) \right] \right\} = \arg\min_{\boldsymbol{\varphi}} \left\{ \psi\left[\mathbf{H}_\theta^{-1}(\boldsymbol{\theta}, \boldsymbol{\varphi}) \right] \right\} \tag{3}$$

subject to the set of model equations (1) and to a set of constraint equations in the form

$$\mathbf{F}(\mathbf{x}) - \mathbf{G}(t) \le 0 \tag{4}$$

$$\mathbf{H}(\hat{\mathbf{y}}) - \mathbf{D}(t) \le 0 \tag{5}$$

given the set of initial conditions $\mathbf{x}(0) = \mathbf{x}_0$. In (3), $\mathbf{V}_\theta$ and $\mathbf{H}_\theta$ are the variance-covariance matrix of model parameters and the dynamic information matrix, respectively (usually evaluated from discrete forms of the Fisher information matrix), while ψ is an assigned measurement function of the variance-covariance matrix representing the chosen design criterion [9]. Among the set of constraint conditions (4-5) a distinction is made between constraints involving unmeasurable states (4) and estimated outputs (5). The formulations are expressed through a set of (possibly time-varying) constraints $\mathbf{G}(t)$ and $\mathbf{D}(t)$ on the state variables, while $\mathbf{F}$ and $\mathbf{H}$ are two sets of selection functions, allowing to choose the variables being actually constrained.

2.1. Sequential Vs Parallel design of experiments

If a sequential MBDoE approach is considered, the information matrix is defined as:

$$\mathbf{H}_\theta = \sum_{k=1}^{N_{exp}-1} \mathbf{H}^*_{\theta|k} + \mathbf{H}^*_{\theta|N_{exp}}(\boldsymbol{\theta}, \boldsymbol{\varphi}) = \mathbf{K} + \mathbf{H}^*_{\theta|N_{exp}}(\boldsymbol{\theta}, \boldsymbol{\varphi}) \quad , \tag{6}$$

where $\mathbf{K}$ is a constant matrix defined by the previously performed (N_{exp}–1) experiments. In the above information matrix, only the vector $\boldsymbol{\varphi}$ of the experimental conditions for the new experiment (N_{exp}) is available for optimization. If multiple equipment is available, as it frequently happens when time-kill experiments are carried out *in vitro*, N_{exp} new experiments can be designed simultaneously adopting a parallel design approach [8]. In this case, the information matrix becomes:

$$\mathbf{H}_\theta = \sum_{k=1}^{N_{exp}} \mathbf{H}^*_{\theta,k}(\boldsymbol{\theta}, \boldsymbol{\varphi}_k) \quad . \tag{7}$$

Here, all vectors $\boldsymbol{\varphi}_k$ (one for each experiment k) are optimized simultaneously, adopting classical alphabetic design criteria [9] or advanced criteria based on singular value decomposition of $\mathbf{V}_\theta$ [8], where each single experiment is designed so as to optimize a specific component of the overall predicted information. The $\mathbf{V}_\theta$ thus obtained will not be the same as the sum of the variance-covariance matrices obtained by optimizing each individual experiment N_{exp} times in a sequential way, and the N_{exp} new optimal experiments will normally be distinct.

3. Case study

The case study presented in this study concerns the identification of the model proposed by Tam and coworkers [4] to investigate the relationship between microbial burden and antimicrobial agent concentrations by means of *in-vitro* time-kill experimentation:

$$\frac{dN}{dt} = G\big(N(t)\big) - K\big(C(t), N(t), t\big) \qquad G\big(N(t)\big) = K_g\left[1 - \frac{N(t)}{N_{\max}}\right]N(t) \tag{8}$$

$$K\big(C(t), N(t)\big) = \left[\frac{K_k \cdot C(t)^H}{C(t)^H + \big(\alpha\big(C(t), t\big)C_{50k}\big)^H}\right]N(t) \qquad \alpha = 1 + \beta\left(1 - e^{-C(t)\cdot t\cdot\tau}\right) \quad .$$

In the model, $N(t)$ is the concentration of bacterial population over time, $C(t)$ is the concentration of meropenem (the antibiotic agent) over time, $G(t)$ is the intrinsic growth rate and $K(C(t), N(t),t)$ is the kill rate by antimicrobial agent. The purpose of the study is to design an experimental session lasting at maximum $\tau = 24$ h in order to identify the set of parameters $\boldsymbol{\theta} = [C_{50k}\ K_g\ K_k\ H\ N_{\max}\ \beta\ \tau]^T$ in the most precise and accurate way. It is supposed that a maximum number of 3 experiments can be executed simultaneously in distinct bacteria cultures. There is only one measured response, namely the concentration of bacterial population over time ($x_1 = y = N$). Measurements are possible only if taken above a detectability threshold of $D = 500$ cfu/mL, which represents a design constraint in the (5) form.

Three distinct design configurations have been compared:

- SD1: D-optimal design of a single experiment ($N_{sp} = 21$);
- PD3: parallel D-optimal design of $N_{exp} = 3$ experiments ($N_{sp} = 7$ for each experiment).

The variables being optimised by design are: the allocation of samples, the initial concentration of meropenem ($C_0 = C(0)$) and the administration of meropenem in time (SD1 configuration only). Measurements are obtained by simulation of the model with $\boldsymbol{\theta} = [0.888\ \ 1.848\ \ 3.744\ \ 1.336\ \ 7.2E9\ \ 3.580\ \ 0.0083]^T$ as the "true" parametric set and by adding Gaussian noise with zero mean and relative deviation of $\omega = 0.05$. The initial guess on model parameters is $\boldsymbol{\theta}^0 = [0.739\ \ 2.310\ \ 3.119\ \ 1.670\ \ 9.0E9\ \ 4.475\ \ 0.0069]^T$.

3.1 Results and comments

Parameter estimation results in terms of estimate values (normalized with respect to $\boldsymbol{\theta}$) and *a-posteriori* statistics (*t*-values and confidence intervals) are given in Table 1.

Table 1 Comparison of different experiment design configurations. Superscript * indicates *t*-values failing the *t*-test ($t < t_{ref}$).

Design	Parameter Estimate	Conf. Int. (95%)	*t*-values	t_{ref}
SD1	[1.03 1.04 1.04 0.90 0.99 0.95 0.91]^T	[4. 36 7.13 4.63 4.05 5.35 2.94 3.40]^T	[0.23* 0.15* 0.23* 0.22* 0.18* 0.32* 0.27*]	1.78
PD3	[1.01 1.00 0.99 1.06 0.98 1.17 0.80]^T	[0.15 0.02 0.05 0.29 0.05 5.88 4.59]	[6.75 40.13 19.01 6.63 19.86 0.20* 0.17*]	1.86

SD1 shows a poor estimation of model parameters in terms of precision on the estimate (low *t*-values) even if a higher excitation level is realized during this experimental protocol (Figure 1a) by managing the antibiotic administration in time. Even if not shown here for the sake of conciseness, it has been verified that, independently of the number of samples, the structural identifiability of the model cannot be achieved if a single experiment is executed and no antibiotic administration is undertaken, because the phases of bacterial growth, death and re-growth cannot be observed in the same trial. Conversely, PD3 allows managing the initial meropenem concentration ($\mathbf{C}_0 = [0.00\ 2.12\ 7.16]$) in such a way as to observe these phases in separate experiments executed simultaneously (Figure 1b), with great improvement in terms of precision and accuracy of the estimate for C_{50k}, K_g, K_k, H, $N_{\max}$. In fact, it can be verified that one key advantage of parallel experiment design is that it is possible to plan experiments building up the

information in a complementary way, i.e. each experiment is capable of maximizing the information specific to a subset of parameters. Notwithstanding this, the sound estimation of parameters β and τ require an additional (sequential) set of parallel experiments (adding more parallel experiments was proved to be insufficient for satisfactory estimation). Note how a specific advantage of parallel configurations is their ease of implementation, since they do not require the management of antibiotic administration in time.

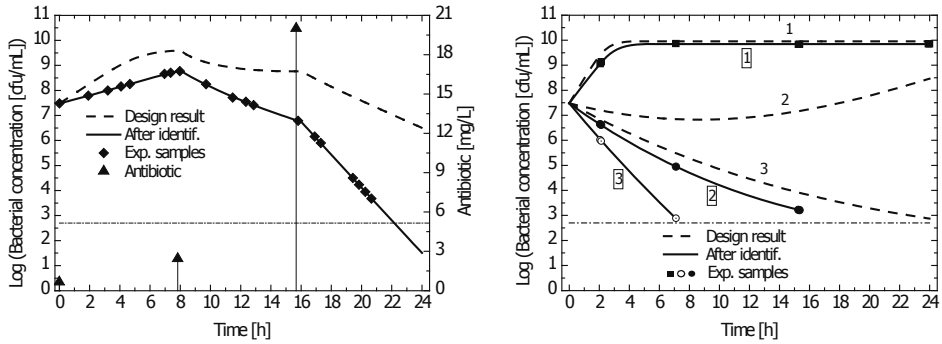

Figure 1. Bacterial concentration profiles before and after identification as obtained by (a) SD1 and (b) PD3 design configurations. The antibiotic administration for SD1 is indicated by triangles.

4. Final remarks

A parallel design approach for the optimal design of pharmacodynamic experiments has been presented in this paper. Preliminary results show the capability of the technique to improve the information content of the trials, exploiting in a more efficient way the available experimental time, designing experiments that can be optimally informative for parameter estimation purposes and easy to be implemented in the experimental practice. Future work is required to extend the applicability of parallel design techniques to larger systems by exploiting advanced design criteria.

Acknowledgements

The authors gratefully acknowledge the financial support granted to this work by the University of Padova under Project CPDR110403 on "Optimal design of pharmacodynamic and pharmacokinetic experiments for the identification of physiologically-based models for drug development".

References

[1] L. Zhang, V. Sinha, S. T. Forgue, S. Callies, L. Ni, R. Peck, S. R. B. Allerheiligen, 2006, J. Pharmacokinet. Phar., 33, 369-393.
[2] A. C. Hooker, M. Foracchia, M. G. Dodds, P. Vicini, 2003, Ann. Biomed. Eng., 31, 98-111.
[3] D. Andes, W. A. Craig, 2002, Int. J. Antimicrob. Agents, 19, 261-268.
[4] V. H. Tam, A. N. Schilling, M. Nikolaou, 2005, J. Antimicrob. Chemother., 55, 699-706.
[5] K. R. Godfrey, M. J. Chapman, S. Vajda, 1999, J. Pharmacokinet. Biopharm, 22, 229-251.
[6] M. P. Saccomani, S. Audoly, L. D'Angiò, 2010, Comput Biol Med, 40, 402-407.
[7] J. N. Bazil, G. T. Buzzard, A. E. Rundell, 2011, Bull. Math. Biol., 1, 1-29.
[8] F. Galvanin, S. Macchietto, F. Bezzo, 2007, *Ind. Eng. Chem. Res.*, 46, 871-882.
[9] F. Pukelsheim, 1993, Optimal Design of Experiments, J. Wiley & Sons, New York, U.S.A.

I.A. Karimi and Rajagopalan Srinivasan (Editors), Proceedings of the 11th International Symposium on Process Systems Engineering, 15-19 July 2012, Singapore.

Integral Formulation of the Smoluchowski Coagulation Equation using the Cumulative Quadrature Method of Moments (CQMOM)

Menwer Attarakih[a,b,*] and Hans-Jörg Bart[b,c]

[a]*The University of Jordan, Faculty of Engineering & Technology, Department of Chemical Engineering, 11942 Amman, Jordan*
[b]*Chair of Separation Science and Technology, TU Kaiserslautern*
[c]*Centre of Mathematical and Computational Modelling, TU Kaiserslautern, P.O. Box 3049 - 67653 Kaiserslautern, Germany*
**Corresponding author's e-mail: attarakih@yahoo.com*

Abstract

The integral formulation of the nonlinear continuous Smoluchowski coagulation equation (CSCE) using the CQMOM presents a hierarchical method to couple the QMOM and the physically evolving particle size distribution. This hierarchical nature of the CQMOM can be utilized in process system engineering and at individual unit operation as well. Here, not only the cumulative particle size distribution is reconstructed, but also its low-order cumulative moments. Numerical analysis shows two desirable properties of the CQMOM: First, it can be considered as a mesh-free method, since the solution of each integral equation at the current grid point does not depend on the other ones. Second, the accuracy of the targeted low-order cumulative moments depend only on the nodes and weights of the continuous Gauss-Christoffel quadrature, and not on sampling the continuous low-order cumulative moments. Moreover, at the upper particle size limit, the QMOM is imbedded as a limiting case.

Keywords: Integral Population Balance, CQMOM, Numerical Solution.

1. Introduction

The continuous Smoluchowski coagulation equation (CSCE), which is known also as the population balance equation for particle coagulation, is a nonlinear integro-partial differential equation with no general analytical solution, especially when coupled with complex CFD solvers or process system simulation at the flowsheet level. Fluid phases which are discrete either at the molecular or particle levels can be described by a statistical Boltzmann-type equation or the CSCE as a special case [4, 5]. The CSCE finds many scientific and engineering applications with mono and multivariate number density functions. Such applications include multiphase flows and turbulence modelling, aerosol science and kinetic theory [1,3-7]. The general CSCE is a hyperbolic integro-partial differential equation, which is characterized by a nonlinear integral source term. This source term accounts for interactions with which particles of a specific state can either form or disappear from the system [6]. These interactions can describe the system behavior up to any degree of detail. Thus, the CSCE is suitable for understanding and investigating many single processing units such as crystallizers, turbulent flame reactors, polymerization reactors, bubble phase reactors, and extraction columns [5, 7, 9]. However; due to its complexity and the lack of general robust numerical solution, the CSCE is hard to be used in flowsheeting programs to simulate whole plants made up of many interacting units or CFD simulations using complex

equipment geometry [3, 4, 6-8]. Therefore, there is a need to have a simple reduced model for discrete phases, without losing the detailed description of single phenomena inherently embedded in the CSCE. One of the popular model formulations is the transformation of the CSCE into a set of self-contained integral equations that describe the moments' evolution of the particle size distribution. In general, these methods belong to the moment transformation of the CSCE at the expense of destroying the distribution itself [2-4]. In contrast to the classical method of moments, where closure problem is overcome by a priori assumed distribution or simplified kernel functions [10], the Quadrature Method Of Moments (QMOM) provides not only an efficient closure to the moment problem, but also an extremely efficient Gauss-like integration quadrature [2-4]. The QMOM is based on the global low-order moments of the weight function and requires only a few nodes (two or three) to converge. However; the major drawback of the moment methods in general and the QMOM in particular is their inability to reconstruct the particle size distribution (PSD). The PSD plays a decisive role in the determination of the physicochemical and mechanical product properties made of particulate systems [6, 9, 10]. Recent advances and development in online measurements and control provide real-time access to system parameters, which are estimated, based on the whole size distribution [1, 6]. John et al. [9] investigated rigorously the PSD reconstruction from its low-order moments, where they addressed the theoretical and practical difficulties in solving the ill-posed inverse moment problem. This ill-posedness and uniqueness of the PSD are still open problems and are recently addressed by Mnatsakanov and Hakobyan [11]. This work presents a method, which obviously overcomes the above shortcomings. The present method uses a hierarchical novel formulation of the CSCE, in which the *r*th (with respect to particle property space) cumulative distribution is reconstructed at given arbitrary grid points. Here, the *r*th cumulative moment is function of the particle internal property and evolves in time and physical space. Since the *r*th cumulative moment at any grid point along the particle property space is not expected to affect the global moments, the number and structure of the grid points are not going to affect the accuracy of the cumulative integration quadrature. The present method provides a continuous Gauss-Christoffel quadrature for which a two-node quadrature with equal and unequal weights is derived analytically. For the *n*th-node quadrature, the standard Product Difference Algorithm (PDA) is used [3].

2. The Cumulative Quadrature Method Of Moments (CQMOM)

Let $\omega(x;z,t)$ be a nonnegative integrable function on the interval $[a,b]$ and all its cumulative moments exist. This function can be expanded at any given point x as a sum of Dirac delta functions (with weights $\lambda_j(x;.)$ and nodes $\zeta_j(x;.) \in [0,x]$). Now, let the cumulative moments of $w(x;.)$ be defined as:

$$\mu_r(x;.) = \int_{a=0}^{x} \zeta^r w(\zeta;.)d\zeta, \quad r = 0,1,2...2N_q - 1 \tag{1}$$

and substitute $w(x;t) = \sum_{j=1}^{N_q} \lambda_j(x;t)\delta(\zeta - \zeta_j(x;t))$ in Eq.(1) to get:

$$\mu_r(x;.) = \sum_{j=1}^{N_q} \lambda_j(x;.)\left[\zeta_j(x;.)\right]^r \tag{2}$$

The above continuous cumulative integration quadrature is exact for integrands that are polynomials of degree at most $2N_q-1$. Note that in contrast to the QMOM, the CQMOM is formulated using nodes and weights that are functions of the particle property space. This quadrature has continuous nodes and weights as long as the cumulative moments are also continuous. The global Gauss-Christoffel quadrature can be viewed as a special case when the limits of integration given by Eq.(1) are from zero to infinity. Note that $\mu_0(x) = W(x)$, which is the cumulative distribution of $w(x)$ and the other cumulative moments (for $r = 1, 2, \ldots 2N_q-1$) are all monotone and at least right continuous functions. These functions satisfy two important properties: they tend to zero as the particle property (x) tends to zero and their change with respect (x) tends to zero as (x) goes to infinity. These properties help in eliminating the so called finite domain error during the solution of the CSCE and force the numerical schemes to be conservative (with respect to x). Eq.(2) can be inverted analytically for a two-node quadrature and using the PDA For the nth-node quadrature.

3. Integral formulation of the Continuous Smoluchowski Equation

The CQMOM described in section 2, when applied to the CSCE with particle growth provides not only the cumulative number distribution, but also the required cumulative moments of higher order:

$$\frac{\partial \mu_r(x;t)}{\partial t} + G(x;c)\frac{\partial(\mu_r(x;))}{\partial x} = r\int_0^x \zeta^{r-1} G(\zeta;c)w(\zeta;t)d\zeta + S_{c,r}(x) \tag{3}$$

Where G is the particle growth rate and $S_{c,\mathrm{r}}$ is the nonlinear integral source term of Smoluchowski equation. In the above equation as the limit of the particle size tends to infinity $\partial\mu_r/\partial x \to 0$. This leaves the CSCE divergence free with respect to particle size. Using the CQMOM (Eqs.(1) & (2)), the integral source term of Eq.(3) is written as:

$$\begin{aligned} S_{c,r}(x) = \frac{1}{2}\int_0^x w(\zeta;t)d\zeta \int_0^{\eta(x,\zeta)} \psi(\zeta,u,\varphi)\left(u^3 + \zeta^3\right)^{r/3} w(u;t)du \\ - \int_0^x \zeta^r w(\zeta;t)d\zeta \int_0^{\infty} \psi(\zeta,u,\varphi)w(u;t)du \end{aligned} \tag{4}$$

Where $\eta^3(x,u) = x^3 - u^3$ and ψ is the aggregation frequency. Now by formal substitution of the $w(x)$ expansion given in section 2 and making use of the Dirac delta function properties, one gets the following semi-discrete closed source term for Eq.(3):

$$\begin{aligned} S_{c,r}(x) = r\sum_{j=1}^{N_q} \zeta_j^{r-1}(x;t)G(\zeta_j(x;t);c)\lambda_j(x;t) \\ + \frac{1}{2}\sum_{j=1}^{N_q}\sum_{n=1}^{N_q} \lambda_j(x;t)\lambda_n(\eta(x,\zeta_j);t)\Psi_{j,n,r}(x;t) \\ - \sum_{j=1}^{N_q} \zeta_j^r(x)\lambda_j(x)\sum_{n=1}^{N_q} \lambda_n(x_\infty)\psi(\zeta_n(x),\zeta_n(x_\infty),\varphi) \end{aligned} \tag{5}$$

Where Ψ is an aggregation frequency matrix to conserve the rth population moment. The source term in Eq.(5) is closed since ζ and λ are found by inverting Eq.(2). Note that the closure used above does not depend on particular values of x. So, the

cumulative moments can be reconstructed by sampling arbitrary the particle size x. This makes the CQMOM a mesh-free method and the mesh can be easily refined in the regions of sharp cumulative moments.

4. Numerical Results and Discussion

In this section numerical results are presented and analyzed to illustrate the implementation of the CQMOM using the CSCE for the homogenous case to isolate the interaction of complex flow field numerical algorithms with the CQMOM solver.

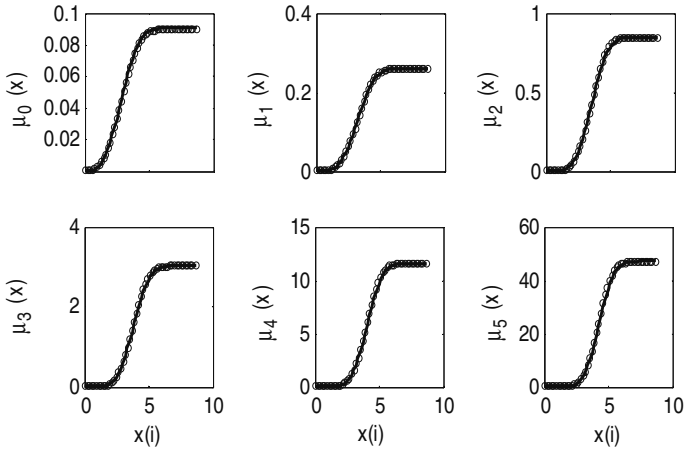

Figure (1): Comparison between analytical [12] (solid line) and numerical (open circles) solutions for the case of simultaneous particle aggregation and growth in batch vessel.

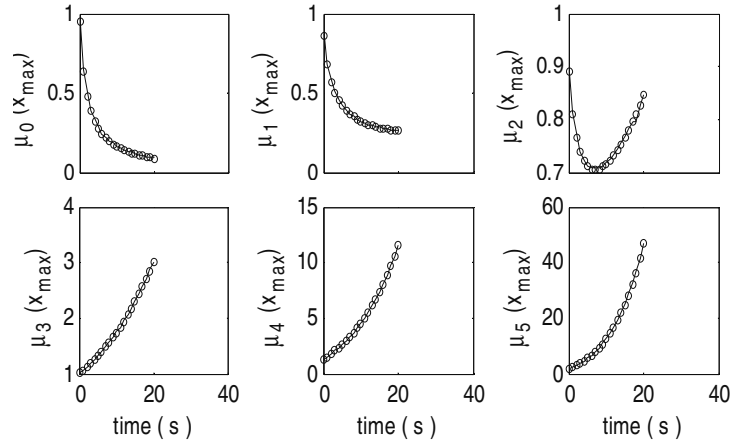

Figure (2): Simultaneous particle coagulation and growth in batch vessel (τ = 20 & number of grid points = 50) with solid line is analytical [12] solution and open circles is numerical one.

Fig.(1) compares the analytical [12] and numerical solutions using the CQMOM of three quadrature nodes for simultaneous particle coagulation and growth in a homogeneous batch vessel ($\psi = \psi_0$, G= G_0x/3 and $w_0 = exp(- x^3)$). As can be seen, Not only the PSD (cumulative number of particles) is reproduced correctly as function of particle size, but also all the other low-order cumulative moments, which are involved

in the inverse moment problem given by Eq.(2). For this case the Product Difference Algorithm (PDA) [3] is used to construct the weights and abscissa to close the source term of Eq.(5). It is clear that Eq.(3) is in the standard Lagrangian form, which is Hyperbolic PDE with a source term given by Eq.(5). It is solved using a Lagrangian moving grid with a velocity equals to the particle growth rate $G(x)$. The solution on the moving grid is projected back after each time step using polynomial interpolation on an Eulerian fixed grid. It is worthwhile to mention that the solution accuracy does not depend on the number of grid points, but only on the number of quadrature points (here $N_q = 3$). This reflects one of the important properties of the CQMOM, which is the free-mesh property. The global moments as predicted by the CQMOM are also compared to the analytical ones as can be seen from Fig.(2). These are obtained by setting the particle size to a largely enough value ($x_\infty = x_{\max} = 10$) such that $\partial \mu_r / \partial x \to 0$. For this special case the classical QMOM and the CQMOM are identical. More interestingly, the inflection point (third panel in the first row of Fig.(2)) in the surface area of the particles due to simultaneous particle coagulation and growth is predicted correctly at $\tau \approx 8$ units. This inflection point represents the balance between particle area decrease due to particle coagulation and particle area increase due to growth process. Therefore, particle coagulation is dominant for $\tau < 8$. Concerning implementation complexity, when compared to sectional methods (e.g. SQMOM [2]), the CQMOM is easier in implementation and coding and it offers a sequential solution of the ODEs, thanks to the mesh-free property. The CPU time is found also less than that of the SQMOM [2], in particular for number of grid points less than four. Consequently, since large increase in the number of grid points is decoupled from the prediction of global quantities, using small number of grid points is sufficient to infer about the shape of the distribution.

5. Conclusions

The derivation of the cumulative Gauss-Christoffel quadrature as a continuous closure rule makes it possible to derive and solve the CSCE. This continuous formulation is used to reproduce consistently any finite number of low-order cumulative moments. In contrast to the QMOM, which destroys the number density function, the present CQMOM reproduces not only the cumulative number density function, but also its low-order cumulative moments. The CQMOM can be considered as a mesh-free method since the grid structure is independent of the integration quadrature. The CQMOM is reduced simply to the standard QMOM when only one grid point is placed at infinity.

References

[1] P.L.C. Lage (2011), Comp. Chem. Eng. **35**, 2186.
[2] M.M. Attarakih, C. Drumm & H.-J. Bart (2009), Chem. Eng. Sci. **64**, 742.
[3] R. McGraw (1997), J. Aeros. Sci. Tech. **27**, 255.
[4] R.O. Fox (2008), J. Comp. Phys. ***227***, 6313.
[5] Z. Zhu, C.A.Dorao. & H. A. Jakobsen. (2010), Ind. Eng. Chem. Res., ***49***, 6204.
[6] I.T. Cameron, F.Y.Wang, C.D. Immanuel & F. Stepanek (2005). Chem. Eng. Sci. **60,** 3723.
[7] M. A. Hjortso (2004), Population Balances in Biomedical Engineering. McGraw-Hill Co., New York
[8] C. Drumm, M. Attarakih, M. W. Hlawitschka & H.-J. Bart (2010), Ind. Eng. Chem. Res., **49,** 3442.
[9] V. John, I. Angelov, A. A. Öncülc & D. Thévenin (2007), Chem. Eng. Sci. **62**, 2890 – 2904.
[10] R. B. Diemer, & J. H. Olson (2002), Chem.Eng. Sci. **57**, 2211.
[11] R. M. Mnatsakanov & A. S. Hakobyan (2009), IMS Lect. Notes–Monograph Series, **57**, 252.
[12] F. M. Gelbard & J. H. Seinfeld (1978). J. Coll. Interface Sci. **1978**, *63*, 472.

I.A. Karimi and Rajagopalan Srinivasan (Editors), Proceedings of the 11th International Symposium on Process Systems Engineering, 15-19 July 2012, Singapore.

Capacity Planning for Continuous Pharmaceutical Manufacturing Facilities

Arul Sundaramoorthy,[a] Xiang Li,[a] James M.B. Evans,[b] Paul I. Barton[a]

[a]*Process Systems Engineering Laboratory, Department of Chemical Engineering, Massachusetts Institute of Technology, 77 Massachusetts Ave, Cambridge, MA 02139, USA*

[b]*Department of Chemical Engineering, Massachusetts Institute of Technology, 77 Massachusetts Ave, Cambridge, MA 02139, USA*

Abstract

In this work, we develop an integrated optimization under uncertainty framework to address the problem of capacity planning in pharmaceutical supply chains that employ novel integrated continuous production schemes. Since the outcomes of clinical trials are uncertain, the problem naturally leads to a stochastic programming problem, which is formulated as a scenario-based multi-period mixed-integer linear programming (MILP) model. The number of scenarios grows exponentially with the number of potential products, resulting in large-scale MILP models that are intractable with standard solvers. We propose a novel solution method to solve the above industrial-scale problems that contain up to 10 potential products and nearly 60,000 scenarios.

Keywords: Capacity Planning, Pharmaceutical, Decomposition Algorithm.

1. Introduction

The single most important driver in the pharmaceutical industry is the time-to-market since the large players of the industry have relied on so-called "blockbuster" drugs for their sustained growth (Shah, 2004). Since new products must be introduced into the market as early as possible, strategic decisions such as the building of new facilities and/or expansion of existing facilities must be made when the new products are still in the development stage. Thus, one of the key challenges that decision makers routinely encounter is to ensure the availability of enough production capacity to meet the demands of products through efficient capacity planning.

Traditionally, production in the pharmaceutical industry takes place in two major steps: i) primary production, and ii) secondary production (see Figure 1a). In primary production, the raw materials are converted into active pharmaceutical ingredients (APIs) through multiple intermediate production stages, while in secondary production, the APIs are formulated into different final drug products. The above traditional two-echelon production scheme leads to inefficient supply chain operations. In addition, the pharmaceutical industry has embraced the batch mode of operation for decades, which potentially contributes to inefficiencies in the supply chain.

Recently, the Novartis-MIT Center for Continuous Manufacturing has embarked on an innovative project to develop technology for a shift from the batch mode of operation to the continuous mode, where raw materials through the APIs to the drug products are produced seamlessly in an integrated facility (see Figure 1b). Such an integrated end-to-end production scheme is more promising for several reasons: a) low costs of inventory, logistics, and production, b) short supply-chain cycle times, and c) resilient supply chain. In a recent work, Schaber et al. (2011) performed an economic comparison of

integrated continuous and batch pharmaceutical manufacturing, where the authors quantified the cost savings achieved through integrated continuous manufacturing.

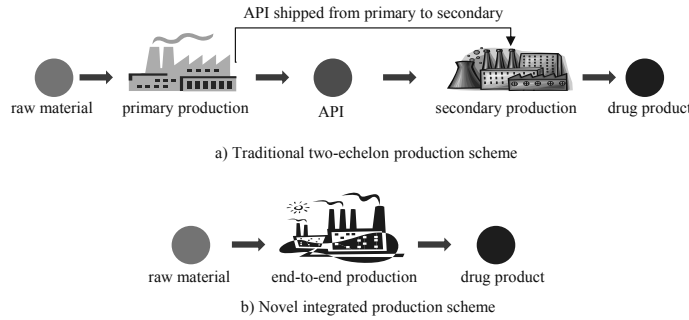

Figure 1. Traditional vs. integrated production schemes in the pharmaceutical industry.

Variants of capacity planning and drug development problems for pharmaceutical manufacturing have been addressed by several researchers in the past. For a review of various existing methods, see the work of Colvin and Maravelias (2008). The novel integrated end-to-end production scheme based on continuous manufacturing brings in additional challenges and opportunities towards better investment strategy. The aim of this work is to develop a framework for capacity planning that addresses the above challenges and exploits the benefits of novel integrated production schemes while taking into account the uncertainty in the outcome of clinical trials.

2. Problem Description

The formal statement of the problem is: given, i) a planning horizon which is divided into a number of time periods, T, defined by a set of time points $t \in \mathbf{T} = \{0,1,2,\ldots,T\}$, ii) a set of potential products $i \in \mathbf{I}$ that have passed Phase I clinical trials (PI), iii) a set of potential greenfield integrated facilities $p \in \mathbf{P}$ that are either dedicated or multipurpose, iv) success probabilities of trials Phase II (PII) and Phase III (PIII), and v) demand, price and cost details, the goal of the capacity planning problem is to decide: i) when to build a new facility and/or to expand an existing facility, ii) how much capacity to build/expand, iii) which product(s) to produce in which facilities, and iv) how much to produce and store at different time periods.

We consider potential products that have already passed trial PI, and thus we are only interested in the outcomes of trials PII and PIII. Thus, if ξ_i denotes the discrete random variable associated with the clinical trial outcome of product i, then the sample space Ω_i = {IIF, IIIF, IIIP}, where IIF corresponds to trial PII failure, IIIF to trial PIII failure, and IIIP to trial PIII success. Furthermore, if $s \in \mathbf{S}$ denotes a set of scenarios corresponding to the Cartesian product of the sample spaces, then the total number of scenarios $|\mathbf{S}| = 3^{|\mathbf{I}|}$.

To address the above problem, we propose a two-stage stochastic programming (TSSP) approach in which the first-stage decisions are when to build a new facility and/or to expand the existing facility, while the second-stage decisions are the sizes of facilities, assignment of products to facilities, and production and inventory levels at different time periods from the product launch to the peak demand. We assume that the sum of the durations of clinical trials PII and PIII is the same for all the potential products. In addition, we also assume that there are no resource constraints at the development stage. Therefore, the clinical trials are carried out simultaneously, and the uncertainties in the outcomes of clinical trials are realized for all the products by the launch period.

3. Mathematical Formulation

The proposed formulation contains the following optimization decisions: i) building new facility: W_{pt} = 1 if construction of new facility p is started in period t, ii) capacity expansion: V_{pt} = 1 if capacity expansion of existing facility p is started in period t, iii) assignment: X_{ipts} = 1 if product i is assigned to facility p in period t in scenario s, iv) production rate: R_{pts} denotes the production rate in facility p in period t in scenario s, v) incremental production rate: ΔR^N_{pts} / ΔR^E_{pts} denotes the incremental production rate installed due to new/existing facility p in period t in scenario s, vi) production amount: Q_{ipts} denotes the production amount of product i in facility p in period t in scenario s, vii) inventory: H_{ipts} denotes the inventory amount of product i in facility p in period t in scenario s, viii) order delivery: F_{ipts} denotes the supply of product i from facility p in period t in scenario s, ix) backlog: B_{its} denotes the backlog amount of product i in period t in scenario s.

The MILP model contains the following constraints:

$$\sum_t W_{pt} \le 1, \quad \forall p, \tag{1}$$

$$V_{pt} \le \sum_{t' \le (t-\theta^N)} W_{pt'}, \quad \forall p,t, \tag{2}$$

$$\sum_{t'=t-\theta^E+1}^{t} V_{pt'} \le 1, \quad \forall p,t, \tag{3}$$

$$\sum_t V_{pt} \le \sigma_p, \quad \forall p. \tag{4}$$

$$R_{pts} = R_{p(t-1)s} + \Delta R^N_{pts} + \Delta R^E_{pts}, \quad \forall p,t,s, \tag{5}$$

$$\lambda_p^{\min} W_{p(t-\theta^N)} \le \Delta R^N_{pts} \le \lambda_p^{\max} W_{p(t-\theta^N)}, \quad \forall p,t,s, \tag{6}$$

$$\varphi_p^{\min} V_{p(t-\theta^E)} \le \Delta R^E_{pts} \le \varphi_p^{\max} V_{p(t-\theta^E)}, \quad \forall p,t,s, \tag{7}$$

$$\rho_p^{\min} X_{ipts} \le Q_{ipts} \le \rho_p^{\max} X_{ipts}, \quad \forall p, i \in \mathbf{I}_p, t,s, \tag{8}$$

$$\sum_{i \in \mathbf{I}_p} Q_{ipts} \eta_{is} \le R_{pts} \Delta t, \quad \forall p,t,s, \tag{9}$$

$$H_{ipts} = H_{ip(t-1)s} + Q_{ipts} - F_{ipts}, \quad \forall p, i \in \mathbf{I}_p, t,s, \tag{10}$$

$$B_{its} = B_{i(t-1)s} + \eta_{is}\omega_{it} - \sum_{\{p: i \in \mathbf{I}_p\}} F_{ipts}, \quad \forall i,t,s, \tag{11}$$

$$H_{ipts} \le \upsilon_{ip}, \quad \forall p, i \in \mathbf{I}_p, t,s, \tag{12}$$

where $\mathbf{I}_p$ is the set of products that can be assigned to facility p. Eqs. (1-4) are capacity related constraints, where θ^N/ θ^E is the construction lead time for a new/existing facility, and σ_p is the maximum number of expansions on an existing facility. While (5)-(7) are

constraints that correspond to the production rates and amounts subject to some upper and lower limits, (8) and (9) are the capacity utilization constraints. Furthermore, the inventory, supply, and backlog constraints are given by (10)-(12). Finally, the objective is to maximize the expected net present value (ENPV), which is given by the sales revenue in each scenario RV_s, total operating cost in each scenario OC_s, fixed investment cost FIC, and variable investment cost per scenario VIC_s:

$$\max ENPV = \sum_s \kappa_s RV_s - \sum_s \kappa_s OC_s - FIC - \sum_s VIC_s. \quad (13)$$

4. Solution Method

The special structures of TSSP with recourse are well-exploited by duality-based decomposition methods (Birge and Louveaux, 1997). In Benders decomposition, or its extension to nonlinear problems, generalized Benders decomposition (GBD), the original problem is projected onto the space of first-stage variables and then reformulated into a dual problem (Geoffrion, 1972). Because the dual problem contains an infinite number of constraints, it is relaxed into a lower bounding problem with a finite subset of these constraints.

Li et al. [2011] extended the GBD framework to a more general framework, called nonconvex generalized Benders decomposition (NGBD), to handle nonconvex recourse problems in TSSP rigorously. In NGBD, nonconvexity in the form of nonlinear functions participating in the objective and/or constraints are effectively handled using McCormick's relaxation technique (McCormick, 1976; Scott et al., 2011).

In this work, we extend the NGBD framework to address TSSP with integer recourse, where the nonconvexity in recourse problems arises from binary variables. We employ continuous relaxation of the second-stage binary variables by treating them as [0,1] continuous variables. While the sequence of lower bounds on the original problem solution value is generated by a sequence of solutions of lower bounding problems, the sequence of upper bounds on the original problem solution value is obtained by a sequence of solutions of upper bounding problems, which are generated by fixing the first-stage decisions to the solutions of the lower bounding problems. When the sequences of upper and lower bounds converge, we obtain an optimal solution to the original problem. It should be noted that when the first-stage decisions are fixed, the upper bounding problem can be decomposed into smaller subproblems for each of the scenarios, which can then be solved in parallel, thus making this method computationally very attractive.

5. Results and Discussion

Consider a pharmaceutical company that has a portfolio of new products in the beginning of the PII trial. The expected launch date of these products is five years from now, and the planning horizon is 15 years, which is divided into 30 time periods of six months each. The company would like to consider building of two greenfield continuous facilities (F1 and F2) and their possible expansions in the future. We are given the probability of the outcome of PII and PIII trials for each product. The decisions of interest to the company are when to build the greenfield facilities and when to expand them, and in each scenario, how much capacity, which product to produce in which facility, and in what amounts to produce, store, etc.

We consider nine different examples, which varied in terms of the number of products in the portfolio and thus the number of scenarios addressed. For the largest example, we

consider 10 products and nearly 60,000 scenarios. We used GAMS 23.7/CPLEX 12.3 on a 3.2GHz Intel Xeon CPU with 12GB RAM on a Windows platform. The full-space model was solved within a time limit of 10,000 CPU s for examples containing up to six products (< 1000 scenarios). However, when the number of products is increased to more than six, the full-space model was not solved due to a time limit and/or memory limit. The NGBD algorithm, on the other hand, solved all the examples within the time limit. Furthermore, with the NGBD algorithm, the solver time scales linearly with the number of scenarios, and thus the largest 10-product example with nearly 60,000 scenarios comprising about 212 million variables (36 million binary and 176 million continuous variables) and over 150 million contraints was solved in less than 3 hr of solver time.

6. Conclusion

In this work, we addressed an important strategic problem faced by major pharmaceutical companies. We developed a mathematical framework for capacity planning problem under clinical trials uncertainty based on TSSP. Since the proposed formulation resulted in a large-scale MILP model, whose size increases exponentially with the number of products, the existing state-of-the-art commercial solvers are not sufficient to solve such massive problems. This motivated us to develop an efficient decomposition algorithm, which efficiently solved problems with up to 10 products and nearly 60,000 scenarios in less than 3 hr of solver time. The solution time of the NGBD algorithm scales linearly with the number of scenarios in the problem, which makes it attractive to solve industrial-scale problems. Furthermore, one can achieve an increased speedup using the NGBD algorithm by employing massively parallel computing since the subproblems can be solved in parallel.

Acknowledgment

This work was funded by Novartis Pharmaceuticals as part of the Novartis-MIT Center for Continuous Manufacturing. The authors specially thank the Executive Director of the Novartis-MIT Center for Continuous Manufacturing, Dr. Stephen R. Sofen, for insight into the problem.

References

J.R. Birge; F. Louveaux, 1997, Introduction to Stochastic Programming. Springer, New York.

M. Colvin; C.T. Maravelias, 2008, A stochastic programming approach for clinical trial planning in new drug development, Computers and Chemical Engineering, 32, 2626-2642.

A.M. Geoffrion, 1972, Generalized Benders decomposition, Journal of Optimization Theory and Applications, 10, 237-260.

X. Li; A. Tomasgard; P.I. Barton, 2011, Nonconvex generalized Benders decomposition for stochastic separable mixed-integer nonlinear programs, Journal of Optimization Theory and Applications, 2011, 151, 425-454.

G.P. McCormick, 1976, Computability of global solutions to factorable nonconvex programs: Part I - Convex underestimating problems, Mathematical Programming, 10, 147-175.

S.D. Schaber; D.I. Georgiorgis; R. Ramachandran; J.M.B. Evans; P.I. Barton; B.L. Trout, 2011, Economic analysis of integrated and batch pharmaceutical manufacturing: A case study, Industrial and Engineering Chemistry Research, 50, 10083-10092.

J.K. Scott; M.D. Stuber; P.I. Barton, 2011, Generalized McCormick relaxations, Journal of Global Optimization, 51, 569-606.

N. Shah, 2004, Pharmaceutical supply chains: key issues and strategies for optimization, Computers and Chemical Engineering, 28, 929-941.

I.A. Karimi and Rajagopalan Srinivasan (Editors), Proceedings of the 11th International Symposium on Process Systems Engineering, 15-19 July 2012, Singapore.

Multivariate Analysis of API Particle Size Distribution Variation in a Manufacturing Environment

Keeley Stepney,[a] Elaine Martin,[a] Gary Montague[a]

[a]*Biopharmaceutical and Bioprocessing Technology Centre, Newcastle Univesity, Newcastle-Upon-Tyne, NE1 7RU*

Abstract

The particle size distribution (PSD) of an active pharmaceutical ingredient (API) can influence important properties of the final product, such as the content uniformity of tablets and the dissolution rate of the drug to the patient. The purpose of this study is to characterise the PSD of a particular API product using laser diffraction measurements and then assess how multivariate data analysis methods can be applied to PSD data. Results show that a similar PSD is produced from the main and product recovery process, but there are differences between samples that are collected on two different plants. These findings are emphasised by applying principal component analysis to the PSD: clusters of samples are seen for each plant and the loadings show areas of the PSD where the differences materialise. By reducing the dimensionality of the PSD data through principal component analysis, the data can be summarised in a scores plot enabling the trends in the data to be more easily identifiable.

Keywords: Particle size distribution, multivariate analysis, active pharmaceutical ingredient

1. Introduction

When an active pharmaceutical ingredient (API) is manufactured it may be in the form of a solid powder. The particle size distribution (PSD) of the API will affect a number of important properties of the product, both during the formulation of the API into tablets and the quality of the final product that is taken by the patient [1]. For example, smaller particles may produce a greater uniformity of the drug content within tablets [2]. A greater overall surface area of the API particles will lead to more rapid dissolution and a higher release rate of the drug [3].

Laser diffraction (LD) is a commonly used method of particle size measurement in the pharmaceutical industry [1]. To take a measurement on a sample of powder, laser light is scattered by the particles and the angle of the light scatter is measured and interpreted to give a particle size distribution. Data is produced of the frequency densities of a number of size measurements. The frequencies will be correlated for similar size measurements and hence the data is appropriate for multivariate data analysis.

To compare the PSDs of several samples, the distributions can be overlaid onto a line graph. An example is shown in Figure 1. Additionally, a set of percentiles, such as the 10^{th}, 50^{th} and 90^{th}, can be found for each sample, to summarise the information contained within the PSD. However percentiles are coarse measures of PSD information content and do not capture the detail contained within the distribution. An alternative

approach is the application of multivariate data analysis techniques to analyse the complete distribution and compare the PSDs of a number of samples.

1.1. Multivariate Data Analysis

Principal component analysis is a technique of reducing the dimensionality of a dataset comprising of many variables to a smaller set of principal components that represent the majority of the variation in the data [4]. A principal component is a linear combination of the original variables that represents some of the variation within the data. Principal component analysis (PCA) summarises the data into scores and loadings that represent the trends in the observations and variables respectively.

Multivariate data analysis techniques have been widely applied in process analysis. For example in spectroscopic data, which contains many highly correlated variables (wavenumbers), PCA can be used to identify the important trends by summarising the data into a small number of principal components. This allows the data to be analysed more efficiently without losing information that is contained in the data. For example, Gabrielsson et al [5] applied PCA to a combination of process and ultra-violet spectroscopy data and by monitoring the scores, the evolution of a hydrogenation reaction could be followed. Brülls et al [6] applied PCA to near infrared spectroscopy data from a freeze drying process. They showed that the scores from the first PC indicated the rate of the drying process and step changes between drying phases.

Multivariate analysis has previously been applied to data generated from particle size distribution measurements. Typically when laser diffraction measurements are made, several repeats are taken and the data are averaged to give the PSD. Ma et al [7] applied PCA to the raw data from laser diffraction measurements, to detect small quantities of large particles that were only detected in a small number of repeats. Furthermore Mattila et al [8] applied PCA to online laser diffraction data from a mineral processing plant to detect disturbances in the process.

1.2. Aims and Objectives

The aim of this study is to characterise the PSD of the API for Rosuvastatin Calcium, manufactured by AstraZeneca and to understand the causes of the variation of the PSD. More specifically the goal was to assess the effect of different manufacturing plants and process streams on the PSD. Understanding more about the particle size distribution of the product enables the manufacturer to determine the range of particle sizes that are acceptable for the API that is to be formulated into tablets. Therefore when changes are to be made to improve the process, the PSD of new batches can be compared to that of the baseline set of samples to determine whether the change has impacted on the PSD.

Furthermore this study presents an opportunity to apply multivariate data analysis techniques to PSD data, to assess the effectiveness of using principal component analysis to compare PSD profiles through summarising the data into score and loadings.

1.3. Overview of the Industrial Process

The data forming the basis of the paper are taken from the industrial manufacturing process that produces the API. A solid powder is formed from a precipitation reaction and is isolated on a filter dryer. The powder is then milled to reduce and homogenise the particle size distribution. The API manufacture is a batch process that takes place in one

of two processing plants. Plant 1 is primarily used for the manufacture of the API, but a second plant is brought into operation when greater capacity is required. Product can be recovered from the liquors from the filter dryers and reprocessed in the recovery process, through acidification, extraction into solvent and basification and precipitation. This process can be run in either manufacturing plant.

2. PSD Baseline Study

Samples were taken from a number of batches after the product was milled to analyse the particle size distribution of the product. Each sample was analysed by laser diffraction to create a baseline dataset of the current PSD distribution. Most of the samples were taken from the main process on plant 1, but batches from plant 2 and the recovery process were also analysed. The particle size distribution measurements were taken with a Sympatec Dry Dispersion Laser Diffractor.

The study was carried out in two stages as two different particle size analysers were used. Firstly study A was run with batches from the main processes on plants 1 and 2. Subsequently study B was run with a new set of batches, including both the main and recovery processes from both plants. The two machines have been shown to produce differences in the PSD measurements, so results from the two studies cannot be compared. Each study includes one sample from each of 41 batches.

2.1. Plant 1 and Plant 2

The batches analysed in study A include a number of main batches from each plant. Figure 1 shows that after milling there are differences in the PSD of the material from the two plants, in particular the material from plant 2 has a higher level of fine particles than the material from plant 1. Although the stages of the manufacturing processes are the same for each plant, the batch sizes are different, so the precipitation vessels are not identical. The speed of the agitator in the vessel varies across the two plants, causing the rate of the precipitation reaction to differ and leading to differences in the particle sizes. Although they differ, in both cases the PSDs are within the specification limits for the product.

2.2. Main and Recovery Processes

Study B includes three batches from the plant 1 recovery process. The main and recovery processes differ at the start of the process, since different starting material is used, but the same steps are followed from the precipitation stage, as described in 1.3. The PSD profiles appear to be similar for samples from the two contrasting processes (Figure 2). This suggests that although there are differences between the main and recovery processes, this does not materialise in a difference in the particle size distribution of the final product.

3. Principal Component Analysis

An alternative approach to comparing the particle size distribution data is through the use of principal component analysis. Strong correlations exist within the data so principal component analysis can be used to summarise the data into a small number of principal components, to assess the underlying trends and identify potential outliers or unusual behaviour.

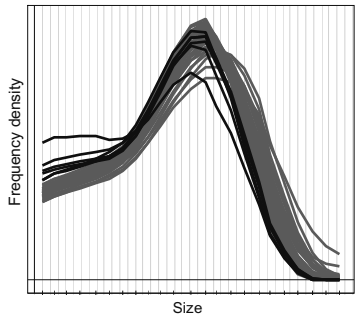

Figure 1: Plant 1 (grey) and plant 2 (black) main batches analysed from study A

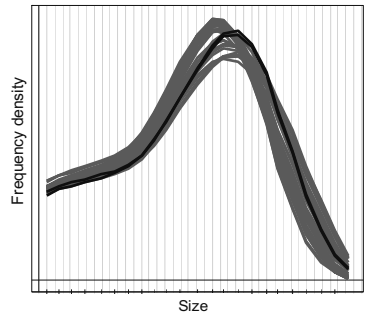

Figure 2: PSD of plant 1 main (grey) and recovery (black) process batches from study B

From the dataset for study B, the batches from the plant 1 main process were used to create a PCA model. Three principal components were retained, explaining 99% of the variability in the data. Batches from the plant 1 recovery process and both processes on the second plant were introduced as a prediction set to the PCA model. All of the data was from study B. The scores from the plant 1 recovery batches fit fairly closely with the plant 1 main batches that were used to build the model, although they do form a cluster to one side (Figure 3). However the plant 2 batches from both product streams have low scores for PC2, which corresponds to a high level of fine particles (Figure 4), agreeing with the trend observed in Figure 2.

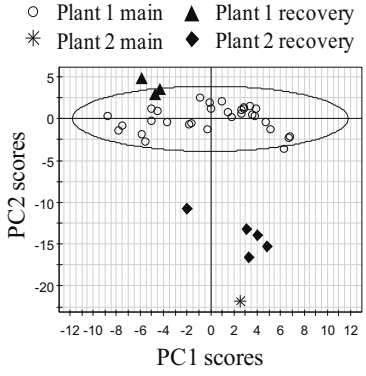

Figure 3: Scores for PC2 vs. PC1, with plant 2 and recovery batches as a prediction set

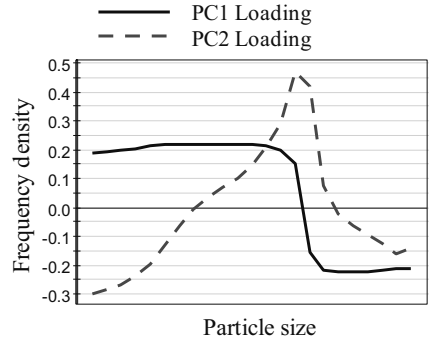

Figure 4: Loadings for PC1 and PC2

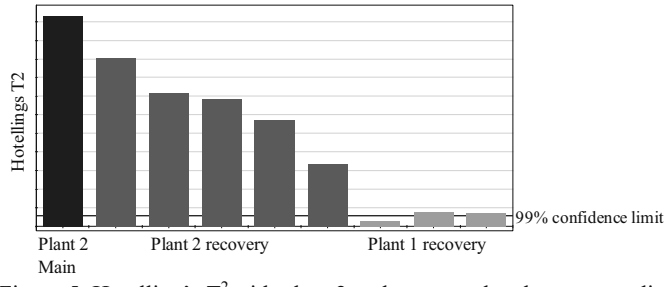

Figure 5: Hotelling's T^2 with plant 2 and recovery batches as a prediction set. Process representation built from plant 1 main process batches

From Hotellings T^2 it is evident that the plant 2 batches are significantly different to the plant 1 main batches. The baseline model was constructed from the plant 1 main batches. The benefit of this representation is that the information from the three retained principal components is presented in one representation, clearly illustrating the differences between both the plants and the recovery processes.

4. Conclusions

An assessment has been made of the particle size distribution of an API and how the PSD varies across two plants and processes. Differences have been found in the particle size of material produced on two different plants, but not between the main and recovery processes. This suggests that it is the plant where the particles are formed and the size of the batch that affects the PSD, rather than the process that is used before the precipitation stage. It is important to state that the PSD always remained within product specification, and all of the batches were successfully formulated, showing the range of particle size that is acceptable.

Principal component analysis of the PSD data was able to capture 99% of the variation in three principal components and emphasises the differences between the batches manufactured on the two plants using a scores plot. PCA is potentially an effective method for comparing the distributional behaviour of PSD data.

When the information for each batch can be compressed into a principal component representation, the batch-to-batch variation can be compared on a scores plot. The plot shows clusters of similar batches that were manufactured on the same plant, and also allows unusual batch behaviour to be detected. When several batches are to be compared, it is more efficient to compare batches on a scores plot rather than overlaying several PSD curves onto a line graph. The loadings allow the differences in the scores to be explained, for example they show that batches produced on plant 2 have a higher level of fine particles. Since 99% of the variation is explained by the principal component representation, very little information of the PSD will be lost.

Acknowledgements

The authors would like to acknowledge the financial support of the UK Engineering and Physical Sciences Research Council through the Industrial Doctoral Centre in Biopharmaceutical Process Development (EP/G037620/1), and the industrial partner, AstraZeneca, for providing funding and process data and information.

References

[1] R. G. Iacocca, C. L. Burcham, L. R. Hilden, J. Pharmaceutical Sciences, 99 (2010) 51.
[2] N. A. Orr, Analytical Proceedings, 19 (1982) 368.
[3] S. Simões, A. Sousa, M. Figueiredo, International Journal of Pharmaceutics, 127 (1996) 283.
[4] S. Wold, K., Esbensen, P. Geladi, Chemometrics and Intelligent Laboratory Systems, 2 (1987) 37
[5] J. Gabrielsson, H. Jonsson, J. Trygg, C. Airiau, B. Schmidt, R. Escott, AIChE Journal, 52 (2006) 3164.
[6] M. Brülls, S. Folestad, A. Sparén, A. Rasmuson, Pharmaceutical Research, 20 (2003) 494.
[7] Z. Ma, H. G. Merkus, J. G. A. E. de Smet, P. J. T. Verheijen, B.Scarlett, Particle and Particle Systems Characterization, 16 (1999) 71.
[8] M. Mattila, K. Saloheimo, K. Koskinen, Particle and Particle Systems Characterization, 24 (2007) 173.

I.A. Karimi and Rajagopalan Srinivasan (Editors), Proceedings of the 11th International Symposium on Process Systems Engineering, 15-19 July 2012, Singapore.

Long-term Scheduling of a Multi-stage Multi-product Bio-pharmaceutical Process

Shaurya Kabra, Munawar A. Shaik, Anurag S. Rathore

Department of Chemical Engineering, Indian Institute of Technology Delhi, Hauz Khas, New Delhi – 110016, India. E-mail: munawar@iitd.ac.in

Abstract

There have been several works in the literature for scheduling of multi-product continuous processes with significant attention laid on short-term scheduling. This work presents a continuous-time model for long-term scheduling of a multi-stage multi-product process from bio-pharmaceutical industry. The overall model is a mixed-integer linear programming (MILP) formulation based on State-Task-Network (STN) representation of the process using unit-specific event-based continuous-time representation. The proposed model is an extension of model by Shaik and Floudas (Ind. Eng. Chem. Res., 2007, 46, 1764-1779) with several new constraints to deal with additional features such as unit and sequence dependent changeovers, multiple intermediate due dates, handling overproduction, shelf-life and waste disposal, and penalties on backlogs and delayed order fulfillment. Improved tightening and sequencing constraints have been presented leading to better relaxed objective values. The validity of the proposed model has been illustrated through an example from the literature.

Keywords: Long-term Scheduling, Multi-stage, Multiproduct Plants, Optimization, Bio-pharmaceutical Process.

1. Introduction

Scheduling in the industrial context deals with optimal allocation of limited resources in a plant comprising multiple stages to maximize the performance (generally profit) in terms of efficiently meeting the demands of multiple products with several due dates. There has been lot of attention in the literature for scheduling of batch processes compared to semi-continuous/continuous processes. While short-term scheduling typically deals with shorter time horizons of the order of several hours to days, medium-term scheduling deals with time horizons of the order of several days to weeks, and long-term scheduling (or mid-term planning) deals with longer time horizons ranging from several weeks to months. Finding optimal solutions to scheduling problems with longer time horizons has been generally found to be difficult compared to short-term scheduling problems. Therefore, in the literature either heuristic based or decomposition based approaches have been reported for solving medium-term and long-term scheduling problems. Dogan & Grossmann (2006, 2008) presented bilevel decomposition algorithm for solving simultaneous planning and scheduling of single-stage multi-product continuous plants. Lima *et al*. (2011) proposed rolling horizon algorithms for long-term scheduling of single-unit multi-product continuous process to manufaure high performance glass.

2. Problem Statement

The problem in this study may be defined as follows: the objective is to develop a production schedule that maximizes profit, given a multi-stage processing plant with several parallel units at each stage with the following information: (i) unit/stage dependent production rates, (ii) minimum processing times, (iii) sequence dependent transition times for product changeovers, (iv) finite dedicated storage capacities, (v) shelf-life of intermediates or products, (vi) selling price of finished products, (vii) costs of manufacturing, inventory, transitions, backlogs for late deliveries and waste disposal, and (viii) multiple intermediate due dates and demands for each product for each customer. It is assumed that overproduction is not allowed and backlogs are penalized. Product selling is feasible only at the demand date. There are specific constraints that are often encountered in scheduling of bio-pharmaceutical processes to monitor the processing of a product before its expiry as governed by its shelf-life and also to effect any waste disposals due to rejections during any clinical trials and/or other product wastage.

3. Mathematical Model

The proposed model is an extension of the short-term scheduling model for continuous processes developed by Shaik and Floudas (2007) to cater to long/medium-term scheduling problems. Additional constraints are formulated by introducing binary variables for handling sequence-dependent changeovers and to keep track of total number of changeovers taking place within each unit, based on similar equations presented in Shaik *et al.* (2009). New constraints are written to monitor and track the demands at intermediate due dates using the production and time variables. Within each time period several sub-events are postulated and the above constraints are checked only at sub-events. This way there is no need to use slack variables, as employed in Shaik *et al.* (2009) to monitor the inequalities at the time of intermediate demands, hence there are fewer number of variables. New constraints are also written to deal with specific needs of shelf-life expiry and waste product management for the case of scheduling of bio-pharmaceutical processes. If a product is within its shelf-life it can be either stored or processed, else it is considered as waste product and disposed off. The objective is maximization of profit that includes various costs for manufacturing, storage, changeovers, waste disposal, and penalties for late deliveries. The objective function also includes penalty on the total number of binary variables used in the model. The proposed constraints are not given here due to space limitations.

The following are the enhancements and improvements in the proposed model as compared to the earlier works. The proposed constraints effectively handle sequence-dependent changeovers. New constraints are written to meet multiple intermediate due dates effectively for both the cases of overproduction being allowed or not, without the use of any slack variables. Additional tightening constraints on processing duration and changeovers have been incorporated to make the overall model tighter and give improved RMILP solution. These tightening constraints are more efficient as they make use of exact transition times in a unit compared to previous works. The sequencing constraints are also improved by removing the big-M terms. The proposed model is demonstrated on a two-stage example from a bio-pharmaceutical industry with two fermentation and two purification suites at each stage, to produce three products with multiple orders of each product during a year-long time horizon.

4. Example

The proposed model is applied to a scheduling problem taken from Lakhdar *et al.* (2005). This example caters to a general problem in bio-pharmaceutical industry that includes most common features of long-term scheduling/mid-term planning. The problem consists of a two-stage facility, with two fermentation (J1, J2) and two purification suites (J3, J4) at each stage, to produce three products (P1, P2, and P3) with multiple orders of each product during a year-long production time horizon. The STN represenation is shown in Fig. 1. Data for production rates, lead times, different costs, production and storage related parameters are taken from Lakhdar *et al.* (2005). Lakhdar *et al*. (2005) used prefixed time periods of 60 days and employed a discrete-time model to solve this problem. In their model the demands were not met on time although there were few unutilized days in different time periods.

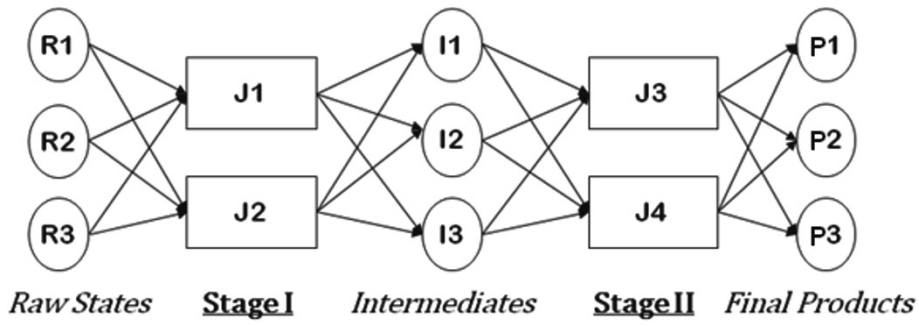

Figure 1. State-Task-Network for example

The proposed model is impelmented using GAMS 23.5/CPLEX 12.2 on 2.66 GHz Intel Core 2 Duo Processor with 3 GB RAM running on windows operating system. The model statistics such as number of binary and coninuous variables, constraints, CPU time and so on are shown in Table 1. The proposed model is solved to zero optimality gap and results in a better objective function of 517 compared to 487 reported by Lakhdar *et al.* (2005). Further, there is zero wastage and all the demands are met and were on time leading to zero backlogs and zero late deliveries. The resulting Gantt chart is shown in Fig. 2 and the demand-supply profile is shown in Fig. 3.

Table 1. Results and Model Statistics using Proposed Model

Statistics	Proposed model
Binary variables	255
Continuous variables	760
Constraints	2416
CPU time (s)	85.5
MILP solution	517

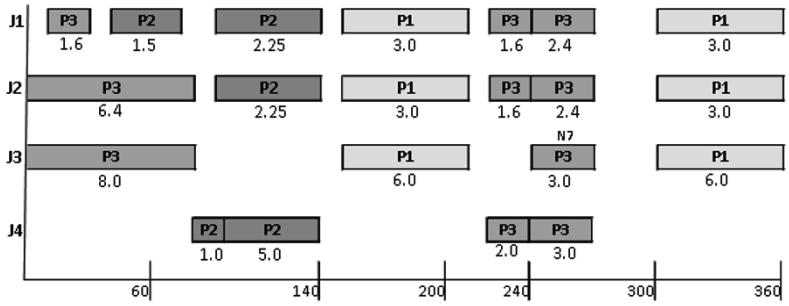

Figure 2. Gantt Chart using the Proposed Model

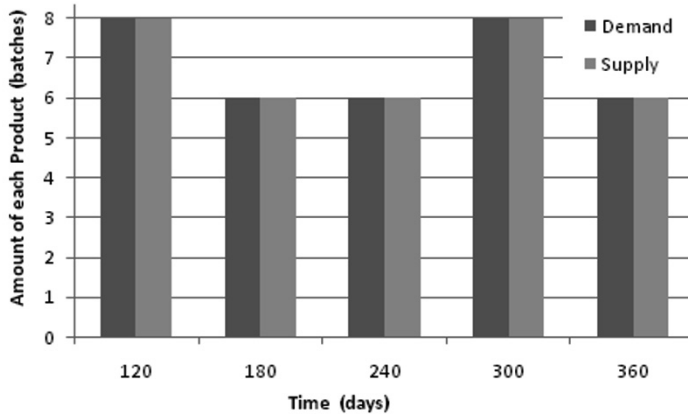

Figure 3. Demand-supply Profile using the Proposed Model

5. Conclusion

In this work, an MILP model has been proposed for solving long-term scheduling problem of a multistage multiproduct facility from bio-pharmaceutical industry. The proposed model is based on STN representation using unit-specific event-based continuous-time representation. It has been demonstrated on a literature example involving two stages with parallel units for producing three products over a year-long time horizon giving better objective values compared with results reported in the literature.

References

M. E. Dogan, I. E. Grossmann, 2006, A Decomposition Method for the Simultaneous Planning and Scheduling of Single-Stage Continuous Multiproduct Plants. Ind. Eng. Chem. Res., 45, 299-315.

M. E. Dogan, I. E. Grossmann, 2008, Simultaneous Planning and Scheduling of Single-stage Multi-product Continuous Plants with Parallel Lines. Comp. Chem. Eng., 32, 2664-2683.

K. Lakhdar, Y. Zhou, J. Savery, N.J. Titchener-Hooker, L. G. Papageorgiou, 2005, Medium-Term Planning of Biopharmaceutical Manufacture using Mathematical Programming, Biotechnol. Prog., 21, 1478-1489.

R. M. Lima, I. E. Grossmann, Y. Jiao, 2011, Long-term Scheduling of a Single-unit Multi-product Continuous Process to Manufacture High Performance Glass. Comp. Chem. Eng., 35, 554-574.

M. A. Shaik, C. A. Floudas, 2007, Improved Unit-Specific Event-Based Continuous-Time Model for short-term Scheduling of Continuous Processes: Rigorous treatment of Storage Requirements, Ind. Eng. Chem. Res., 46, 1764-1779.

M. A. Shaik, C. A. Floudas, J. Kallrath, H.-J. Pitz, 2009, Production Scheduling of a Large-Scale Industrial Continuous Plant: Short-Term and Medium-Term Scheduling. Comp. Chem. Eng., 32, 670-686.

I.A. Karimi and Rajagopalan Srinivasan (Editors), Proceedings of the 11th International Symposium on Process Systems Engineering, 15-19 July 2012, Singapore.

An advanced model for controlled oral drug delivery

Naresh Pavurala,[a] Luke E.K. Achenie,[b]

Department of Chemical Engineering, Virginia Polytechnic Institute and State University, Blacksburg, Virginia 24060

Abstract

A drug release mechanism is combined with the Compartmental Absorption and Transit (CAT) model to develop a complete pharmaco-kinetic model for predicting orally administered drug release profile. Within an optimization framework, the developed model has been used for evaluating optimal values for key parameters including the size of the tablet and pharmacokinetic parameters like peak plasma concentration (C_{max}), area under the curve (AUC) and bioavailability needed to obtain plasma concentration profiles within the therapeutically required range.

Keywords: oral drug delivery, ACAT model, dissolution model, pharmaco-kinetic simulation, optimization

1. Introduction

The oral administration route is by far the most common way of administering pharmacological substances. It is estimated that 90% of all medicines are oral formulations and oral drug delivery systems comprise more than half the drug delivery market. In 2008, the oral drug delivery market was a USD 35 billion industry and was expected to grow as much as 10% per year until at least 2012 (Gabor, Fillafer et al. 2010). Oral drug products are also profitable for the pharmaceutical industry. With recent developments in manufacturing technology, large quantities of oral formulations are produced with short production times. By following good manufacturing practices (GMP regulations), high quality oral delivery products are prepared in a reliable and reproducible manner.

Among liquid and semi-solid formulations, the tablet is still the preferred drug product for oral administration, offering several advantages. It is also a given fact that oral administration is the most comfortable mode of therapy for patients (Gabor, Fillafer et al. 2010). However, biopharmaceutical issues such as physicochemical requirements of the drug and physiological conditions make oral delivery one of the most challenging routes.

The delivery of drugs, peptides or proteins, occurs through a process of continuous swelling of the polymer carrier that is associated with simultaneous or subsequent dissolution of the polymer carrier. The drug is usually molecularly dispersed or dissolved in a polymer matrix at low or high concentrations. As water penetrates the polymer, swelling occurs and the drug is released to the external environment (Narasimhan and Peppas 1997).

Dissolution and absorption of drugs from the gastrointestinal (GI) tract is a very complex process, influenced by many factors that not only vary among drugs but also between different regions in the GI tract. However, since, nearly one third of the blood from cardiac output flows through the gastrointestinal organs, it serves a good absorption surface for the drug into the system (Gabor, Fillafer et al. 2010).

Mechanistic models try to represent the physiological and pharmacological processes as accurately as possible. Mechanism-based models help in testing hypothesis of suggested mechanisms and for learning about system processes which are not easy to test experimentally (Marshall, Macintyre et al. 2006). An effective mathematical model, which can predict the drug release profile and the optimal blood plasma concentration, helps in reducing the expense, time and effort involved in drug design.

There are dispersion models that define the GI tract as a single tube with spatially varying properties (pH, surface area, etc.) along the tube (Ni, Ho et al. 1980). The movement of drugs through the intestine was described by Willmann and co-workers (Willmann, Edginton et al. 2007) by introducing an intestinal transit function. However, assumptions such as negligible first-pass effect and passive intestinal permeability do not appear justified.

A typical CAT model (Yu and Amidon 1999) divides the GI tract into three segments namely, stomach, small intestine and colon, while the transit flow in the small intestine is separated into seven compartments. The model considers simultaneous small intestinal transit flow and drug absorption. The model assumes instantaneous dissolution and equal transit times in all the compartments. It also does not account for the first-pass effect.

The Grass Model (Huang, Lee et al. 2009) is a physiologically based compartmental model. It describes the gastric emptying, transit in the GI tract based mainly on solubility, permeability, and tissue surface area and calculates the drug absorption in each compartment.

2. ACAT Model

In this work, an Advanced Compartmental and Transit (ACAT) model (Agoram, Woltosz et al. 2001) was used as a basis for developing the pharmacokinetic model. It includes linear transfer kinetics, six plausible states of the drug component (unreleased, undissolved, dissolved, degraded, metabolized and absorbed), nine compartments (stomach, seven segments of the small intestine, and colon), and three states of the excreted material (unreleased, undissolved and dissolved). Physiological factors such as gastric emptying, intestinal transit rate, first-pass metabolism, luminal transport and physicochemical factors (e.g. pKa, solubility, particle size, particle density, permeability) and dosage factors including dosage form and dose are taken into account in predicting the oral drug absorption (Huang, Lee et al. 2009).

In the ACAT model, the drug passing through the small intestine has transit times specific to each compartment. The rate of drug transit is determined by a transfer rate constant, k_t, which is a reciprocal of the mean transit time between each compartment. The dissolution process is defined by a simple rate constant, k_d, which is calculated from the solubility of the drug (C_S) (as a function of pH), lumen concentration (C_L), its effective particle size (r_0), particle density (ρ), molecular diffusion coefficient (γ) and diffusion layer thickness (T) (Equation 1.1). Hence it does not account for the process of dissolution as in (Narasimhan and Peppas 1997) where the disentanglement of the polymer is also taken into account along with the drug dissolution, clearly explaining the dissolution process. The time scale for the absorption process is set by a rate constant, k_a, which is expressed in terms of the effective permeability (Peff) of the drug and absorption scale factor (α) for each compartment (Equation 1.2).

$$k_{(i)d} = 3\gamma \frac{C_{(i)S} - C_{(i)L}}{\rho r_0 T} \qquad (1.1) \qquad k_{(i)a} = \alpha_i P_{eff(i)} \qquad (1.2)$$

Here, 'i' is the compartment number, which in our case varies from 1 to 9.

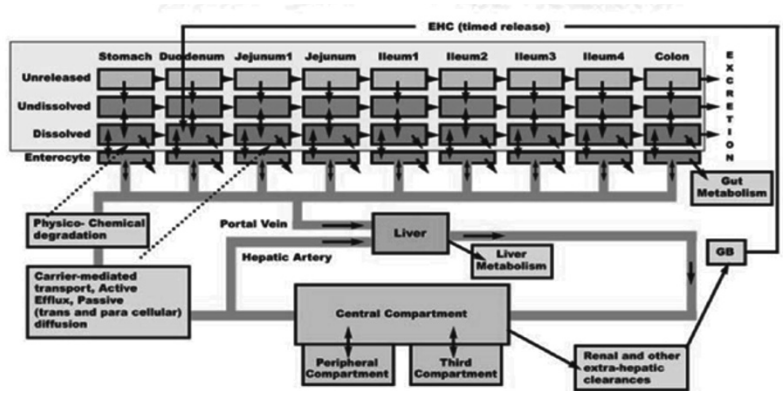

Figure 1:ACAT model schematic (Huang, Lee et al. 2009).

3. Dissolution Model

The Dissolution Model (Narasimhan and Peppas 1997) explains the release of a water soluble, crystalline drug enclosed within a swellable, hydrophilic glassy polymer, placed in contact with water or a biological fluid. It is a moving boundary problem formulated using a system of partial differential equations (pde's) and ordinary differential equations (odes) which describe the diffusion of (i) water into the system; (ii) drug out of the system; (iii) polymer chain disentanglement through the boundary layer; (iv) the left and right moving boundaries.

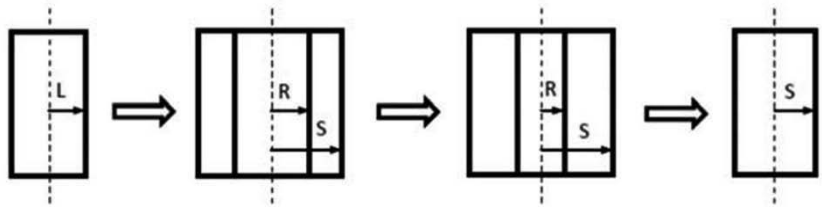

a b c d

Fig. 2: One-dimensional solvent diffusion and polymer dissolution process(Narasimhan and Peppas 1997).

In this model, when water comes in contact with the glassy polymer of initial diameter 2L (Figure 2a), the polymer starts to swell and two distinct fronts are formed: the swelling interface at position R, and the polymer-water interface at position S (Figure 2b). Initially, front R moves inwards since the drug starts moving out of the gel layer, and front S moves outwards till the polymer keeps swelling. When the concentration of water inside the polymer gel layer exceeds a critical value, v_1^*, polymer disentanglement begins and both R and S diminish. Hence, during the latter stage of dissolution process, both R and S move towards the center of the tablet (Figure 2c). The process continues, till the glassy core disappears and only front S exists, which continues to diminish till the entire polymer is dissolved (Figure 2d).

The developed pharmaco-kinetic model employs linear transfer kinetics with two plausible states of the drug component (dissolved and absorbed). The first two layers in the ACAT model (Figure 1) representing the unreleased, released states of the drug component are replaced by input from the dissolution model. The basic approach is that,

the amount of dissolved drug, which enters into each of the compartments in the ACAT model, is evaluated using the dissolution model. The latter uses the initial radius of the tablet as input to evaluate the radius of the tablet at the beginning of each compartment of the ACAT model. Hence, the drug feed into each of the compartments is evaluated using the density of the drug and the thickness of the tablet. The drug feed determines the plasma concentration profile of the drug. An optimization model is also employed into the pharmaco-kinetic model, in order to evaluate the optimal thickness of the tablet by minimizing the error between the predicted plasma concentration and the desired plasma concentration profiles.

In this paper, Cimetidine is used as a model drug to test the pharmaco-kinetic model. Cimetidine is an antagonist of the Histamine H_2-receptor that inhibits the secretion of gastric glands. The drug is available in a variety of oral dosage forms for the treatment of duodenal and gastric ulcers (Somogyi and Gugler 1983). Plasma concentration-time profiles of Cimetidine in 12 healthy patients following oral administration of a commercially available immediate release formulation (Tagamet) as well as three extended release formulations was presented in Jantratid *et al*(Jantratid, Prakongpan et al. 2006). Bioavailability and pharmacokinetics of cimetidine in 10 healthy volunteers after administration of oral doses (100,400, and 800 mg) is studied in Grahnen *et al* (Grahnén, Bahr et al. 1979).

4. Results and Discussions

A desired plasma concentration profile for cimetidine was obtained from Jantratid *et al* (Jantratid, Prakongpan et al. 2006) in which, a 400 mg cimetidine tablet was used as the initial dosage in the experiment which contained 40% of drug and 7.5% of polymer. A plasma profile with peak plasma concentration (C_{max}) of 2100 ng/ml and a bioavailability of 64% (well within the range of experimental results) was considered for the model. The optimization was started with an initial dosage of 190 mg (considering just the mass of drug and polymer). The density of cimetidine is taken as 1.4 g/cc and the effective human permeability as 0.287×10^{-4} cm/s. The total time of simulation is taken as 12 hours. The transit times, volumes and radii of each compartment were taken from (Table I) in (Bolger 2009). The radius of the tablet was fixed at 7.00 mm and the thickness of the tablet was varied during the optimization.

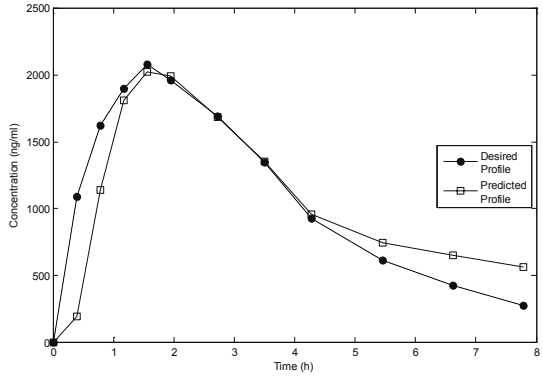

Fig. 3: Predicted and desired plasma concentration profiles of cimetidine oral dose. The dotted line represents the desired plasma concentration profile obtained from literature and the solid line represents the predicted plasma concentration profile using the pharmaco-kinetic model.

The optimal thickness of the tablet was obtained as 1.37 mm. The value of Cmax was obtained as 2024.8 ng/ml, which is comparable to the experimental value. The area under the curve (AUC) values obtained for the desired and predicted profiles in Fig. 3 are 8399.4 ng.hr/ml and 8435.4 ng.hr/ml respectively. In both profiles, the peak plasma

concentration (C_{max}) was achieved within 1.5 – 2 hours. The initial dosage (just the drug and polymer) calculated after obtaining the optimal thickness was 292 mg, which gives a bioavailability of 41%.

5. Conclusions

This paper presents effective models for drug release, drug absorption and transit. Coupling ideas from the ACAT model and the dissolution model, we have developed a complete pharmacokinetic model. The values of the pharmacokinetic parameters such as C_{max}, AUC calculated from the model are comparable to experimental results. The value of initial dosage calculated from the obtained optimal tablet thickness is slightly higher than the experimental values, which in turn results in a lower bioavailability. The advantage of the suggested approach is that it can be used to test hypothesis about the mechanism involved in drug delivery into the blood circulatory system; these are included in the next stages of our research. The model also evaluates the optimal thickness for the drug tablet in order to obtain the required plasma concentration profile. We are currently employing the composite model to hypothesize the optimal diffusion coefficient (and other physico-chemical properties) that a new drug needs in order to obtain a desired drug release profile. This is expected to be useful for drug design.

6. References

Agoram, B., W. S. Woltosz, et al. (2001). "Predicting the impact of physiological and biochemical processes on oral drug bioavailability." Advanced Drug Delivery Reviews **50, Supplement 1**(0): S41-S67.

Bolger, M. B. B. (2009). "Simulations of the Nonlinear Dose Dependence for Substrates of Influx and Efflux Transporters in the Human Intestine." The AAPS Journal **11**(2): 353-363.

Gabor, F., C. Fillafer, et al. (2010). Improving Oral Delivery

Drug Delivery. M. Schäfer-Korting, Springer Berlin Heidelberg. **197:** 345-398.

Grahnén, A., C. Bahr, et al. (1979). "Bioavailability and pharmacokinetics of cimetidine." European Journal of Clinical Pharmacology **16**(5): 335-340.

Huang, W., S. Lee, et al. (2009). "Mechanistic Approaches to Predicting Oral Drug Absorption." The AAPS Journal **11**(2): 217-224.

Jantratid, E., S. Prakongpan, et al. (2006). "Feasibility of Biowaiver Extension to Biopharmaceutics Classification System Class III Drug Products: Cimetidine." Clinical Pharmacokinetics **45**(4): 385-399.

Marshall, S., F. Macintyre, et al. (2006). "Role of Mechanistically-Based Pharmacokinetic/Pharmacodynamic Models in Drug Development: A Case Study of a Therapeutic Protein." Clinical Pharmacokinetics **45**(2): 177-197.

Narasimhan, B. and N. A. Peppas (1997). "Molecular analysis of drug delivery systems controlled by dissolution of the polymer carrier." Journal of Pharmaceutical Sciences **86**(3): 297-304.

Ni, P. F., N. F. H. Ho, et al. (1980). "Theoretical model studies of intestinal drug absorption V. Non-steady-state fluid flow and absorption." International Journal of Pharmaceutics **5**(1): 33-47.

Somogyi, A. and R. Gugler (1983). "Clinical pharmacokinetics of cimetidine." Clinical Pharmacokinetics **8**(6): 463-495.

Willmann, S., A. Edginton, et al. (2007). "Development and Validation of a Physiology-based Model for the Prediction of Oral Absorption in Monkeys." Pharmaceutical Research **24**(7): 1275-1282.

Yu, L. X. and G. L. Amidon (1999). "A compartmental absorption and transit model for estimating oral drug absorption." International Journal of Pharmaceutics **186**(2): 119-125.

I.A. Karimi and Rajagopalan Srinivasan (Editors), Proceedings of the 11th International Symposium on Process Systems Engineering, 15-19 July 2012, Singapore.

Model and analysis of pharmaceutical manufacturing system with government intervention and emergency supply

Chen Wang[a], Michael Pishko[a], and Carl Laird[a]

[a]*Texas A&M University, 3122 TAMU, College Station, TX 77845, USA*

Abstract

Recurring drug shortages continue to be a significant problem, and one major cause is the desire for manufacturers to leave the business due to the high-risk associated with uncertain demand. Guaranteed orders from government and the existence of flexible-by-design rapid manufacturing facilities can decrease manufacturing risk and ensure production of necessary products. In this paper, we model the production choices of a pharmaceutical manufacturer, assuming that the manufacturer attempts to maximize its expected profit with conditional-value-at-risk constraints on the loss. The resulting linear programming problem is analyzed to determine the optimal production level as a function of the government order amount. Including the possibility of emergency production allows for increased manufacturing flexibility and reduces the required government order costs.

Keywords: rapid therapeutics manufacturing, conditional-value-at-risk, optimization.

1. Introduction

Recurring drug shortages remain a significant problem, demonstrating limitations in the current pharmaceutical manufacturing infrastructure. In December of 2000, a single manufacturer of tetanus and diphtheria (Td) vaccine ceased production, causing a severe shortage that disrupted the routine immunization program until June of 2002. Again in 2004, the closure of a single production facility caused a shortage of influenza vaccine, and the US supply of influenza vaccine was nearly half of the desired doses. One of the major causes of these drug shortages is the desire for pharmaceutical manufacturers to avoid high-risk products with uncertain demands. Such risks can be reduced by government intervention, including for example, contract orders and guaranteed inventory buy-back (Nevel *et al.*, 2005). By doing this, the financial risk to the manufacturer is reduced, and a certain amount of a steady production is maintained.

There has also been significant interest in the development of a national infrastructure for rapid pharmaceutical manufacturing in the form of emergency production facilities, such as the National Center for Therapeutics Manufacturing (NCTM) in Texas. The NCTM is a flexible-by-design prototype of multi-product, multi-technology, flexible pharmaceutical manufacturing facility. An emergency rapid manufacturing capability provides the possibility for production recourse when demand is higher than expected.

In this paper, we consider a planning problem where the government wants to determine the appropriate guaranteed order amount to ensure continued production of a particular therapeutic. The manufacturer is assumed to be risk-averse and it attempts to maximize its expected profit while satisfying constraints on financial return and risk. A popular

financial risk measure, the Conditional Value-at-Risk (CVaR), is used to quantify the manufacturer's risk. The loss function is a convex piecewise linear function of the planned production amount, and the decision-making process of the manufacturer can be formulated as a linear programming problem. Using this model, government entities can evaluate the minimum fixed order amount that is required to ensure that a particular demand will be met. We further quantify the savings possible with the existence of an emergency rapid production facility.

2. System model

A detailed description of each entity in the model is as follows.

Manufacturer: The pharmaceutical manufacturer has to plan and schedule its manufacturing resources among multiple products at a general level. In this model, we assume that the manufacturer attempts to maximize its expected profit subject to constraints on its financial risk to determine general-level plans and therefore some "risky" products may be underproduced and lead to shortage problems in the future. The associated parameters and variable are as follows.

x_H – output of high-risk product
x_L – output of low-risk product
C_H^F – fixed cost of high-risk product
C_L^F – fixed cost of low-risk product
C_H – unit cost of high-risk product
C_L – unit cost of low-risk product
R_p – ratio of profit to investment
R_r – ratio of risk to investment

Market: Each product of the manufacturer has a known and fixed price and an unrealized demand. The underlying distribution of the demand is assumed available.

P_H – price of high-risk product
P_L – price of low-risk product
$\tilde{d}_H$ – demand of high-risk product
$\tilde{d}_L$ – demand of low-risk product

Emergency supply: The emergency suppliers such as the NCTM can take orders when drug shortages occur or are expected. The emergency supplier has its own production capacity and a reasonably higher production cost.

P_E – emergency supply price
Cap_E – emergency supply capacity

Government authorities: Government authorities can affect the manufacturers' decision in two ways. One is contract order at a price equivalent to or lower than the market price. The other is through inventory buy-back, i.e. the government authorities buy back a portion or all of the manufacturers' unsold inventory at a price lower than the manufacturing cost.

P_B – government buy-back price
γ_B – government buy-back ratio
O_G – government contract order amount of the high-risk product

According to the proposed model, the profit of the high-risk product is composed of three parts: 1) profit due to regular selling, 2) profit due to government buy-back, 3) profit due to emergency selling with the support of emergency supply. Using the above notations, the total profit can be expressed as follows.

$$Profit_H := min\{x_H, \hat{d}_H\} P_H + P_B \gamma_B \left(x_H - \hat{d}_H\right)^+ + (P_H - P_E) S_E - (C_H^F + C_H x_H) \quad (1)$$

where for any $\alpha \in \mathbb{R}, \alpha^+ := \max\{\alpha, 0\}, \alpha^- := \max\{-\alpha, 0\}$, and $\hat{d}_H := \max\{O_G, \tilde{d}_H\}$ is the order that the manufacturer finally take and

$$S_E \coloneqq min\{(x_H - \hat{d})^-, Cap_E\} \tag{2}$$

is the amount that is to be ordered from the emergency supplier. As S_E is neither a convex nor a concave function of x_H, $Profit_H$ in (1) is not directly convex or concave in x_H. However, its reformulation for computational purpose is given later. Similar to the profit of the high-risk product, the profit of the low-risk product without government interventions and emergency supplies is

$$Profit_L \coloneqq min\{x_L, \tilde{d}_L\} P_L - (C_L \cdot x_L + C_L^F) \tag{3}$$

which is concave piecewise linear function of x_L.

3. Risk measure

The conditional value-at-risk (CVaR) of the manufacturer's loss is used to measure the risk of its production plan. In this section, the loss function of the manufacturer and its convex formulation is given followed by a brief review of CVaR.

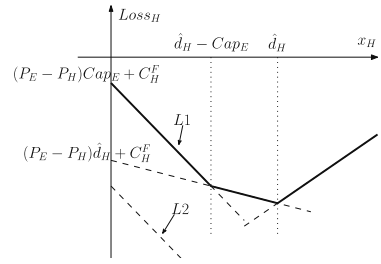

Figure 1: Loss function

3.1. Loss function and its convex formulation

As a function of the decision variable $x_H(x_L)$ and the stochastic demand $\tilde{d}_H(\tilde{d}_L)$, the associated profit is also a random variable and the loss of a product is defined as the opposite of profit, i.e.

$$Loss_H = -Profit_H,\ Loss_L = -Profit_L \tag{4}$$

As mentioned in section 2, $Loss_H$ is not directly convex. However, it can be reformulated as a convex piecewise linear function and this result is given in the following theorem.

Theorem 1: The loss function of high-risk product defined in (1) is equivalent to

$$Loss_H = max\begin{Bmatrix} (C_H - P_H)x_H + (P_E - P_H)Cap_E + C_H^F \\ (C_H - P_H)x_H + (P_E - P_H)\hat{d}_H + C_H^F \\ (C_H - P_B \cdot \gamma_B)x_H + (P_B \cdot \gamma_B - P_H)\hat{d}_H + C_H^F \end{Bmatrix} \tag{5}$$

under the condition $P_H \geq P_E \geq C_H \geq P_B \cdot \gamma_B$.

Proof: 1) Consider the case $Cap_E \leq \hat{d}_H$: i) when $x_H \leq \hat{d}_H - Cap_E$, $Loss_H = (C_H - P_H)x_H + (P_E - P_H)Cap_E + C_H^F$; ii) when $\hat{d}_H - Cap_E < x_H \leq \hat{d}\_H$, $Loss_H = (C_H - P_E)x_H + (P_E - P_H)\,\hat{d}_H + C_H^F$; iii) when $x_H \geq \hat{d}_H$, $Loss_H = (C_H - P_B \cdot \gamma_B)x_H - (P_H - P_B \cdot \gamma_B)\hat{d}_H + C_H^F$. Note that $P_H \geq P_E \geq C_H \geq P_B \cdot \gamma_B$, $Loss_H$ in case i)-iii) is roughly shown in Figure 1 and clearly equivalent to (5).

2) Consider the case $Cap_E > \hat{d}_H$: i) when $x_H \leq \hat{d}_H$, $Loss_H = (C_H - P_E)x_H + (P_E - P_H)\,\hat{d}_H + C_H^F$; ii) when $x_H > \hat{d}_H$, $Loss_H = (C_H - P_B \cdot \gamma_B)x_H - (P_H - P_B \cdot \gamma_B)\hat{d}_H + C_H^F$. Note that in case 2) $f(x_H) = (C_H - P_H)x_H + (P_E - P_H)Cap_E + C_H^F$ shifts from *L1* to *L2* in Figure 1 and $(C_H - P_H)x_H + (P_E - P_H)Cap_E < (C_H - P_E)x_H + (P_E - P_H)\,\hat{d}_H$ for all $x_H \geq 0$, hence $Loss_H$ in case 2) can also be expressed by (5). Combination of case 1) and 2) completes the proof. □

The requirement that $P_H \geq P_E \geq C_H \geq P_B \cdot \gamma_B$ is quite reasonable. If the condition is not satisfied, the optimization problem becomes trivial and the solution can be determined simply by observation. With (4), the total loss is

$$Loss\left(x_L, x_H, \tilde{d}_L, \tilde{d}_H\right) \coloneqq Loss_H\left(x_H, \tilde{d}_H\right) + Loss_L\left(x_L, \tilde{d}_L\right). \tag{6}$$

3.2. Risk measure and the whole formulation

In this work, the CVaR of the loss function (6) is used to measure the risk associated with the manufacturer's production plan. CVaR is a coherent risk measure (Artzner *et al.*, 1999) and hence yields nice properties such as subadditivity and convexity. Additionally, the associated computation is also straightforward The definition and properties of CVaR is briefly reviewed below. For more results and detailed proofs, refer to (Rockafellar & Uryasev, 2002). Given $\alpha \in (0,1)$ and a loss $L(x, \tilde{d})$ as a function of the decision variable x and the random variable $\tilde{d}$, CVaR is defined as

$$CVaR_\alpha(x) \coloneqq (1-\alpha)^{-1} \int_{L(x,\tilde{d}) \geq VaR_\alpha(x)} L\left(x, \tilde{d}\right) p\left(\tilde{d}\right) d\,\tilde{d}, \tag{7}$$

where $VaR_\alpha(x) \coloneqq \min\{\xi \in \mathbb{R}: \int_{L(x,\tilde{d}) \leq \xi} p\left(\tilde{d}\right) \mathrm{d}\tilde{d} \geq \alpha\}$ is the Value-at-Risk of the loss. It has been proven that,

$$CVaR_\alpha(x) = min_{\beta \in \mathbb{R}}\, F_\alpha(x,\beta) \coloneqq \min_{\beta \in \mathbb{R}} \{\beta + (1-\alpha)^{-1} \int \left[L\left(x, \tilde{d}\right) - \beta\right]^+ p\left(\tilde{d}\right) d\tilde{d}\}. \tag{8}$$

If enough samples $d_1, \cdots, d_k$ of $\tilde{d}$ are available, $F_\alpha(x,\beta)$ can be approximated by

$$\hat{F}_\alpha(x,\beta) \coloneqq \beta + [k(1-\alpha)]^{-1} \sum_{i=1}^{k} [L(x, d_i) - \beta]^+ \tag{9}$$

4. Simulation results and analysis

The final optimization problem is given by,

$$\begin{aligned} \max_{x_H, x_L, \beta} \quad & \mathrm{E}[Profit_H + Profit_L] \\ \text{s.t.} \quad & \mathrm{E}[Profit_H + Profit_L] \geq R_p(C_H^F + C_H x_H + C_L^F + C_L x_L) \\ & \mathrm{CVaR}_\alpha\left\{Loss\left(x_L, x_H, \tilde{d}_L, \tilde{d}_H\right)\right\} \leq R_r(C_H^F + C_H x_H + C_L^F + C_L x_L) \end{aligned} \tag{10}$$

where the first constraint is on the expected return of the initial investment which can be approximated using sampling approach, the second constraint restricts the financial risk of the initial investment. *CVaR* can be approximated using (9).

Based on (10), two simulations are done on an example system to analyze the impact of the government order amount. Demand $\tilde{d}_H$ is assumed to be truncated normally distributed on the interval [20 150] and the original normal distribution has mean $\mu_H = 100$ (million) and variance $\sigma_H^2 = 25^2$. Other parameters include $C_H^F = 120$, $C_H = 10$, $P_H = 15$, $\gamma_B = 1$, $Cap_E = 20$, $P_E = 12$, $R_p = 1.2$, $R_r = -0.2$ and $\alpha = 0.95$. The simulation results are shown in Figure 2. With no government order amount, the problem is infeasible (i.e. the manufacturer will not plan to produce any of the high risk production). The left hand chart in Figure 2 quantifies the increase in the feasible range for production as the government order increases. The existence of an emergency supply facility increases the flexibility of the system. The right hand chart in Figure 2

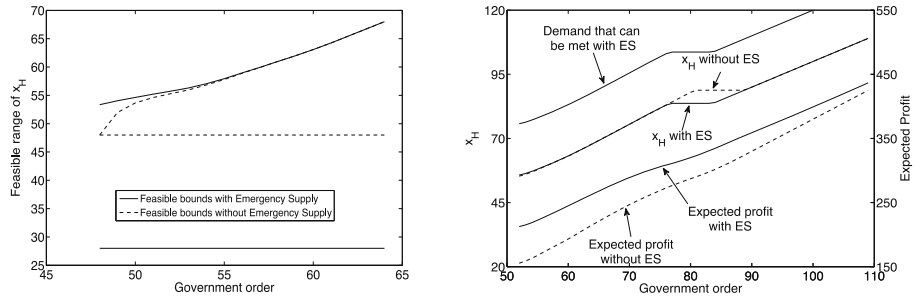

Figure 2: Simulation results

quantifies the optimal production level for the manufacturer as a function of the government order amount. This figure provides the necessary information for government planners to determine the necessary order amount. Furthermore, it quantifies the possible reduction in government costs that are possible because of the availability of an emergency rapid manufacturing facility.

5. Conclusions

Drug shortages continue to be a recurring problem. One of the major reasons for drug shortages is the exit of key manufacturers from the business due to the high-risk associated with uncertain demand. Assuming that therapeutics manufacturers is risk averse and operates according to some optimization formulation, continued production of a high-risk product can be ensured by reducing the manufacturers risk through guaranteed government orders. The existence of an emergency rapid therapeutics manufacturing facility further increases the demand that can be met for a given government order amount. In this paper, we have proposed a simple optimization formulation that represents the manufacturers' decision-making process. The manufacturer is assumed to maximize profit with conditional value-at-risk constraints on the loss. We show that the loss function is convex under reasonable conditions for the problem parameters. Sampling the demand, the CVaR condition is approximated, producing a linear programming problem. For a given set of system parameters, simulations show that the government intervention and the emergency supply can both reduce the manufacturer's risk while keeping a steady drug supply. Including an emergency rapid therapeutics facility in the system provides a much better solution since the facility allows for recourse after the demand is realized, resulting in a lower government order cost for a particular guaranteed demand.

References

Nevel, A., Layton, C., & Lenfestey, N. (2005). *Influenza Vaccine Manufacturing.* RTI International.

Rockafellar, T. R., & Uryasev, S. (2002). Conditional value-at-risk for general loss distributions. *The Journal of Banking and Finance , 26* (7), 1443-1471.

Stokley, S., Santoli, J. M., Willis, B., Kelley, V., Vargas-Rosales, A., & Rodewald, L. E. (2004). Impact of vaccine shortages on immunization programs and providers. *American Journal of Preventive Medicine , 26* (1), 15-21.

I.A. Karimi and Rajagopalan Srinivasan (Editors), Proceedings of the 11th International Symposium on Process Systems Engineering, 15-19 July 2012, Singapore.

Optimization and Control of Crystal Shape and Size in Protein Crystallisation Process

Jing J. Liu[a,b], Yang D. Hu[b] and Xue Z. Wang[a*]
[a] Institute of Particle Science and Engineering, School of Process, Environmental and Materials Engineering, University of Leeds, Leeds LS2 9JT, UK
[b] School of Chemical Engineering, Ocean University of China, Qingdao, China, 266001

Abstract

The purpose of the current work is to develop optimization techniques for protein crystallisation processes for controlled manufacture of protein crystals with desired shape. Based on a newly developed morphological population balance model for protein crystallisation that can simulate the multidimensional size distributions of a population of crystals, known as shape distribution, an optimisation technique is applied to investigate and control the growth of individual faces with the aim of obtaining desired crystal shape. Using a target shape distribution as the objective function, optimal temperature and supersaturation profiles leading to the desired crystal shape were derived. Genetic algorithm was investigated and found to be an effective optimisation technique for the current application.

Keywords: Multidimensional and morphological population balance model; Crystal shape distribution； Hen-Egg-White lysozyme crystallisation； Protein crystallisation control.

1. Introduction

Large molecule protein crystals have shown significant benefits in the delivery of biopharmaceuticals to achieve high stability, high concentration of active pharmaceutical ingredients (API), and controlled release of API. However, among the about 150 biopharmaceuticals on the market by 2004, only insulin has been marketed in crystalline form (Basu. et al, 2004). A technical challenge is that protein crystallisation has a very complicated environment and is affected by many factors. There is currently a lack of knowledge on commercial scale production of protein crystals. Therefore, in contrast to the majority of previous work on experimental and computational studies of protein crystallisation that was centered on single crystal scale, the focus of the research reported in this paper is placed on computational study of protein crystallisation at process scale, investigating the growth behavior of the population of crystals in a crystallizer.

The morphology and size distribution of protein crystals are key measures in quality control. However, research on population balance modelling of protein crystallisation processes is still very limited and restricted to simulation of crystal size distribution (Shi et al, 2005), ignoring crystal shape information because the size of a crystal is simply defined as the diameter of a sphere having the same volume as the crystal. A new morphological population balance model was proposed for modelling protein crystallisation processes (Liu et al, 2009; Liu et al, 2010a; Liu et al, 2010b). In the model, the shape of a crystal is quantitatively defined by the distances of all crystal faces to the geometric centre of the crystal. For all the crystals in the crystalliser, a

* Correspondence author, x.z.wang@leeds.ac.uk

concept of multi-dimensional size distributions, which we call shape distribution for the crystal population, was proposed. In principle, the morphological population balance model for protein crystallisation can be applied to control of the growth of individual faces with the aim of obtaining desired crystal shape and size. Therefore in this paper, process optimisation is introduced to the model for optimising the product crystal shape distribution. Optimal temperature and supersaturation profiles leading to the desired crystal shape distribution is derived. Genetic algorithm was investigated for optimisation. Since tracking an optimum temperature or supersaturation trajectory can be easily implemented by manipulating the coolant flowrate, the methodology provides a feasible closed-loop mechanism for protein crystal shape tailoring and control.
The case study protein is Hen-Egg-White (HEW) lysozyme for which the thermodynamics and kinetics of crystallisation were discussed in previous publications (Liu et al, 2009; Liu et al, 2010a; Liu et al, 2010b). The focus here is on optimisation in order to obtain desired shape for a population of protein crystals.

2. Morphological PB model and the optimisation problem

2.1. Morphological PB model for crystallisation of HEW Lysozyme

The morphological PB model of HEW Lysozyme has been presented in literature (Liu et al, 2009; Liu et al, 2010a; Liu et al, 2010b), so it is only briefly introduced here. In the current study, seeded crystallisation at a given operating condition, i.e. fixed buffer, fixed pH value and salt concentration, is considered. Supersaturation is created by reducing the temperature at constant cooling rates. As indicated in previous publications (Liu et al, 2009; Liu et al, 2010a; Liu et al, 2010b), crystal shape is modelled in two size dimensions x and y, which are the distances from the geometric crystal centre to the identified independent faces. The mathematical formulation for two-dimensional PB modelling is given in eq.(1).

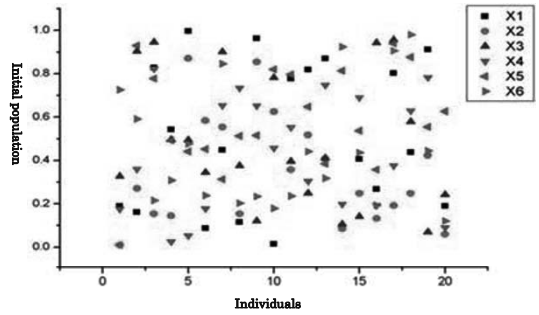

Figure 1 The initial 20 populations, each represented by six linear cooling rates, x1 ~ x6.

$$\frac{\partial f(x,y,t)}{\partial t} + \frac{\partial [G_{101}(x,t) f(x,y,t)]}{\partial x} + \frac{\partial [G_{110}(y,t) f(x,y,t)]}{\partial y} = 0 \tag{1}$$

The mass balance equation and facet growth rates are given in equations (2) and (3)

$$\frac{dC}{dt} = -\rho_c K_V \int_0^\infty \int_0^\infty f(x,y,t)\left(G_{101}(8\sqrt{2}y^2) + G_{110}(16\sqrt{2}xy - 12\sqrt{2}y^2)\right)dxdy \tag{2}$$

$$G_{101} = k_{101}\left(\frac{C - C_{sat}}{C_{sat}}\right)^{n_{101}} = k_{101}\sigma^{n_{101}} \quad G_{110} = k_{110}\left(\frac{C - C_{sat}}{C_{sat}}\right)^{n_{110}} = k_{110}\sigma^{n_{110}} \tag{3}$$

$$\sigma = \frac{C - C_{sat}}{C_{sat}} \tag{4}$$

where C is the solute concentration, *kg/l*, C_{sat} is the saturated solute concentration, *kg/l*, σ is the relative supersaturation, defined by equation (4), and k_{101}, k_{110}, *m/s*, n_{101}, n_{110} are facet kinetic parameters (Liu et al, 2009; Liu et al, 2010a; Liu et al, 2010b).

2.2. The optimization problem and genetic algorithm

For a population of HEW Lysozyme crystals, in here, the shape is described in equation (5) as a ratio of two distances, where x and y are the distances from the crystal geometric centre to the two independent faces, (101) and (110).

$$\mathrm{x} / y = ds \tag{5}$$

ds is identified as the objective function for optimising the shape of the crystal population. If the objective is to get plate shaped crystals, then the objective is to make *ds* approach 1. So the optimization function considering HEW Lysozyme crystal shape can be defined as:

$$\min_{CR(\mathrm{t})} \sum_{\mathrm{x},y} (\psi(\mathrm{x}, y, \mathrm{t})[(\mathrm{x} / y - ds)^2]) / \sum_{\mathrm{x},y} \psi(\mathrm{x}, y, \mathrm{t}) \tag{6}$$

$$\text{Contraints:} \quad CR_L \le CR(t) \le CR_U \tag{7}$$

where CR_L and CR_U are the lower and upper boundaries of the cooling rate during crystallization; $\psi(\mathrm{x}, \mathrm{y}, \mathrm{t})$ is the number population density function at the moment 't' based on population balance model; $\sum_{x,y} \psi(\mathrm{x}, \mathrm{y}, \mathrm{t})$ denotes summary of all particles density function in discrete space which can be derived from PB models. In this work, genetic algorithm (GA) is investigated since GA has features (Chiu & So, 2003) that fit the current problem well. Details of its application are described below.

3. Results and discussion

Suppose crystals with plate shape are desired, that is $x/y = ds = 1$. Cooling rates considered are CR_L= 0.01 °C/day and CR_U=8 °C/day. Five segments with six cooling rates: $x_1, x_2, x_3, x_4, x_5 x_6$, are divided within the whole process. Initial population (20 individuals) distribution is plotted in Figure 1, different colours mean different cooling rates. Morphological population balance is applied to simulate the process and scores fitness function for each individual. The maximum generation is 250 because it was found that the fitness function no longer decreases after 250 generations. The initial condition for the simulation is listed in Table 1.

Table 1 Initial condition for Lysozyme crystallization

pH	Precipitate	Concentration of precipitate	Concentration of solution	Temperature initial
4.5	NaCl	2.5% (w/v)	40 (mg/ml)	25°C

Individuals in the final generation are shown in figure 2, each variable (cooling rate) with the same colour in different individuals are quite close to each other, meaning all approaching the same solution. Figure 3 shows the change of fitness function vs. generations, clearly showing a quickly decreasing trend.

The optimal temperature and supersaturation profiles are shown in Figure 4. The shape of a typical crystal varies following the optimal temperature curve as shown in Figure 5. It can be seen that the crystal shape changed clearly from the beginning to the end of crystallization, and the crystals grow gradually from needle-like to plate-like. The value of the shape objective function $(x/y-1)^2$ decreases gradually to zero. However, facet $\{110\}$ of HEW Lysozyme is becoming diamond, shape changed totally if the value of objective function $(x/y-1)^2$ decreased to be zero. So the point should be avoided in the process of simulation and shape control. Gaussian-type distribution is kept as initially but the peak value of the distribution has dropped a little within the whole evolution, as shown in Figure 6. The changes of peak value are caused by the coefficient of variation,

which can be described as the full width at half maximum (FWHM), however, the full width at half maximum of the initial size distribution is given smaller, the increase of FWHM is not obvious compared to the decrease of peak value after optimisation.

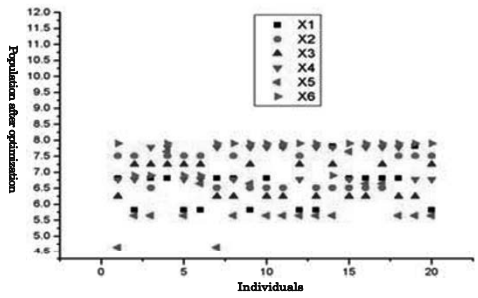

Figure 2 Final populations

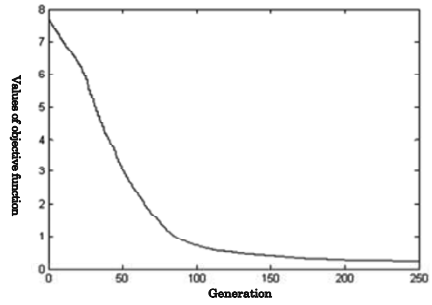

Figure 3 Objective function vs. generations

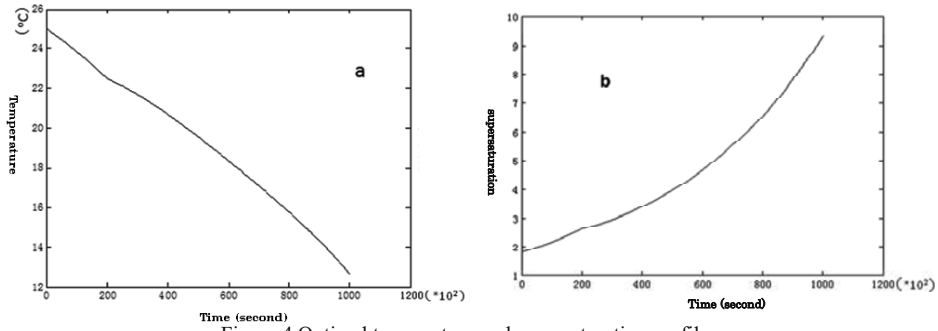

Figure 4 Optimal temperature and supersaturation profiles

4. Concluding remarks

Optimisation is applied to a morphological PB model for HEW Lysozyme crystallisation with the aim of obtaining operating conditions that lead to desired shape of crystals. Genetic algorithm proves to be an effective method for the optimization. The results demonstrated that by tracking the optimal temperature or supersaturation profile, crystals of desired shape can be obtained. The current work only represents a small step forward towards the ultimate goal of successfully manufacturing high quality protein crystals in large scale. Test of the optimization control techniques on real laboratory and industrial crystallizers should be discussed in the future work.

References

Basu., S. K., Govardhan., C. P., & Jung., C. W. (2004). Protein crystals for the delivery of biopharmaceuticals. *Expert Opinion on Biological Therapy*, *4*, 301-317.

Chiu, T.-L., & So, S.-S. (2003). Genetic Neural Networks for Functional Approximation. *Quantitative Structure Activity Relationships and Combinatorial Science*, *22*, 519-526.

Liu, J. J., Ma, C. Y., Hu, Y. D., & Wang, X. Z. 2009. Morphological Population Balance Models for the Dynamic Evolution of Particle Shape and Size Distribution in Protein Crystallization. In *Computer Aided Chemical Engineering*, ed. CAOdNaECBJ Rita Maria de Brito Alves, pp. 1911-1916: Elsevier

Liu, J. J., Ma, C. Y., Hu, Y. D., & Wang, X. Z. (2010a). Effect of seed loading and cooling rate on crystal size and shape distributions in protein crystallization--A study using

morphological population balance simulation. *Computers & Chemical Engineering*, *34*, 1945-1952.

Liu, J. J., Ma, C. Y., Hu, Y. D., & Wang, X. Z. (2010b). Modelling protein crystallisation using morphological population balance models. *Chemical Engineering Research and Design*, *88*, 437-446.

Shi, D., Mhaskar, P., El-Farra, N. H., & Christofides, P. D. (2005). Predictive control of crystal size distribution in protein crystallization. *Nanotechnology*, *16*, S562-S574.

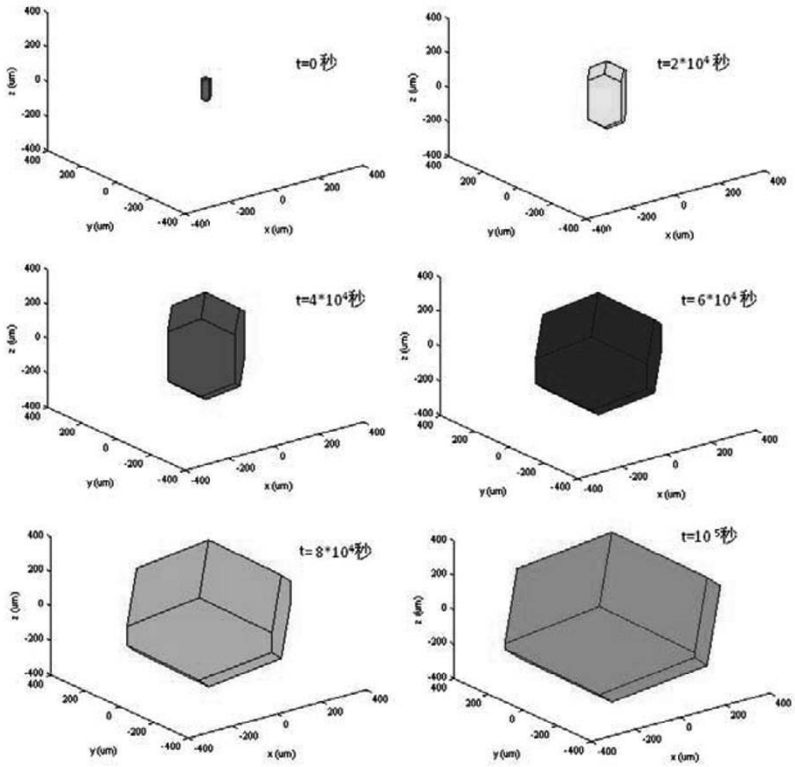

Figure 5 Shape and size change of a selected crystal

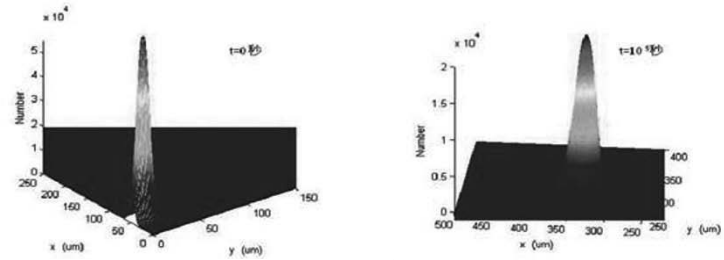

Figure 6 (a) Number density function of seed crystals, and (b) Number density functions of finial crystals.

I.A. Karimi and Rajagopalan Srinivasan (Editors), Proceedings of the 11th International Symposium on Process Systems Engineering, 15-19 July 2012, Singapore.

Intelligent Decision-Support Tools for Effective and Integrated Operational Planning in Pharmaceutical Plants

Naresh Susarla and I A Karimi

Department of Chemical and Biomolecular Engineering, National University of Singapore, 4 Engineering Drive 4, Singapore 117576

Abstract

Fierce market competition, peaking patent cliffs, mounting R&D costs, shrinking product pipelines and stringent regulatory protocols have brought a complete paradigm shift in the way pharmaceutical enterprises are operated. Motivated by an immediate need of efficient decision–support aids in pharmaceutical companies, we have devised 2 smart tools: PlanPerfect and DRplan. These tools are designed in association with Singapore based plants of multi-national pharmaceutical companies to find their application for production planning at manufacturing facilities and for requirement planning at distribution hubs. Our tools aid decisions pertinent to (i) campaign lengths with number of batches in each campaign, (ii) campaign sequencing and sequence-dependent cleaning and setups, (iii) plant maintenance, (iv) NCEs testing and production, (v) material outsourcing, (vi) resource allocation, (vii) manpower handling, (viii) inventory management, (ix) plant utilization, (x) waste generation, (xi) generate optimal size and numbers of material orders, (xii) forecast management, and (xiii) requirement planning.

Keywords: Integrated production planning, pharmaceutical plants, resource allocation, decision-support tools.

1. Introduction

The global pharmaceutical industry is now facing unprecedented challenges. Fierce market competition, peaking patent cliffs, mounting R&D costs, shrinking product pipelines and stringent regulatory protocols have brought a complete paradigm shift in the way pharmaceutical enterprises are operated. In addition, the management of global supply chains for such multinational pharmaceutical enterprises is highly complex and vital. Thus, companies are now grappling with an intensive need to optimize their manufacturing operations and improve sustainability by reducing operational costs, optimizing operations, and conserving resources. To remain competitive and economically sustainable, companies seek new and innovative technologies to reduce costs and improve profit margins. In this regard, several studies[1-3] estimated that the possible savings in the manufacturing of pharmaceutical products are in the range of $20 to $50 billion every year.

Unique characteristics of pharmaceutical plants and criticality of effective decision making demands sophisticated support tools for efficient resource allocation and production planning to achieve an optimal plan. The existing software applications such as – advanced planning and scheduling (APS), manufacture resource planning (MRP 2), or the literature models tend to be too generic to satisfy the specific needs and constraints of the pharmaceutical plants. Also, the existing tools and technologies for

the aforementioned planning problem often fall short in evaluating different scenarios and their effect on the overall profit of the plant. In addition, such commercially available tools are difficult to use and require special trainings. They offer less freedom to the planners in altering process parameters or plant configurations. As a result of this, planners in most companies either make ad hoc decisions or tend to use simple spreadsheets[9] for planning that are time consuming (usually, 2 to 3 days for a scenario) and often yield solutions with ample room for improvement.

In this paper, we present a blueprint for a smart production planning and resource allocation tool that addresses the specific needs and constraints of planners and other stakeholders in a pharmaceutical plant. We then present our decision-support tools PlanPerfect and DRplan. Our tools are specifically customized for their application in pharmaceutical plants. PlanPerfect aids decisions pertinent to (i) campaign lengths with number of batches in each campaign, (ii) campaign sequencing and sequence-dependent cleaning and setups, (iii) plant maintenance, (iv) NCEs testing and production, (v) material outsourcing, (vi) resource allocation, (vii) manpower handling, (viii) inventory management, (ix) plant utilization, and (x) waste generation. Also, PlanPerfect allows a planner to choose (add) an appropriate mode (e.g. slow/high throughput mode, vacation mode, etc.) of operation from (to) an in-built list of modes. DRplan facilitates decision making in generating optimal size and numbers of material orders, inventories, forecast management, and requirement planning. In addition to gross profit and minimum cost, which are the most comprehensive planning objective, our tools also allow the planners to choose other planning objectives such as minimum waste, maximum plant utilization, minimum production time, and maximum order fulfillment. Furthermore, they permit the user to explore and evaluate different combinations of variations in plant or process configurations, parameters, demand profiles, and operational constraints using a 'what-if' approach. Specifically, our tools embody a uniquely designed GUI keeping in view the needs of its users and stakeholders, manage a specially structured database, and employ a customized mathematical model to optimize production plans.

2. Motivation and Challenges

The procurement, manufacturing, and distribution process in a global pharmaceutical company is extremely complex. It involves a number of manufacturing stages (active pharmaceutical ingredients, drug formulation and packaging) and distribution configurations. Now, the production stages and configurations require multiple raw materials and a number of other resources (e.g. manpower, utilities, electricity, and equipments), to produce different intermediates / products or to distribute them to the consumers. Usually, the resources involved in the production and the distribution process are both limited and expensive. Thus, an efficient manufacturing / distribution process requires an effective allocation and usage of resources to meet desired targets. For this, the plant management regularly plans resource allocations and schedules process operations in the best interest of the company. The planning of operations and material requirements in a pharmaceutical plant or a distribution house involve a plethora of decisions, usually, for a period of 2 or 3 years. This primarily consists of determining campaign lengths and their sequences, cleaning and set-up times, resource allocation, inventory management, material procurement, maintenance plan, new product introductions (NPIs), waste generation, plant utilization, requirement planning, forecast management, and size and number of orders. Also, the planning activity demands collaboration with different departments[4] (process, maintenance, laboratory, sales, and suppliers) for various inputs such as demands, supplies, resource availability,

and maintenance (Figure 1). As most of the decisions and the related inputs are estimates or forecasts, their values keep changing with time. This requires regular changes and modifications to the existing plan. Given the importance of the planning problem and non-suitability of existing methods to address the specific characteristics, development of effective tools and technologies is critical.

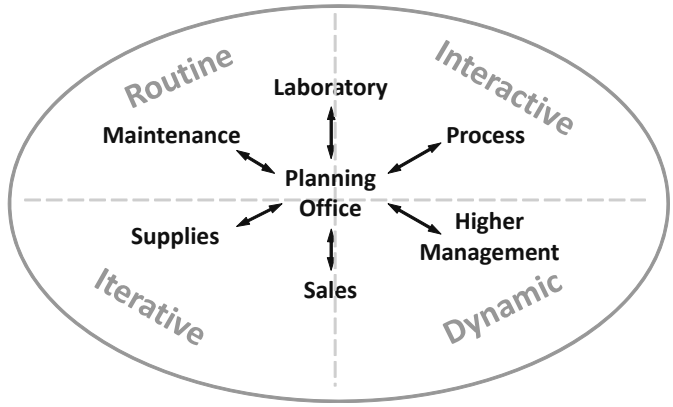

Figure 1. Schematic of collaboratove planning in pharmaceutical plants

3. Decision Support Framework

The key idea here is that the availability and allocation of the limited resources directly affects the productivity of a plant. For instance, as pharmaceutical plant operations are human intense, a limited availability of operators directly affects the number of batches that can be processed. Also, under the limited availability of operators, production of some products can be expedited by allocating sufficient operators at the cost of impeding the production of other products. Clearly, without the consideration of resource allocation and availability, a given plan may either underestimate or overestimate the total production. Typically, plant managers deal with limited resources by making ad-hoc and *in-prompt* decisions. The plant is then operated in a mode different from normal. A mode of operation can then be defined as the plant operating procedure under the limitation of one more resources with a specific resource allocation and usage profile. There can be m (m = 1, 2, …, M) such modes, e.g. low/high throughput mode, vacation mode, lab constrained mode, etc. In the normal mode of operation all resources are assumed to be available in sufficient quantities. Each mode differs from the other because the plant's productivity (number of batches processed/produced in a week/month) is a function of its mode of operation. Clearly, planning models must consider this variation in productivity for generating realistic targets.

$$\text{Plant productivity} = f(\text{mode of production, m}) \quad \text{(a)}$$

To capture the variation in productivity, we consider the knowledge and experience of the planners in modeling productivity for different modes of operation. Stake holders of a plan (planners, process engineers, laboratory officials, maintenance engineers and technicians, etc.) provide important insights of the entire process. Figure 2 represents the framework used to construct our tools.

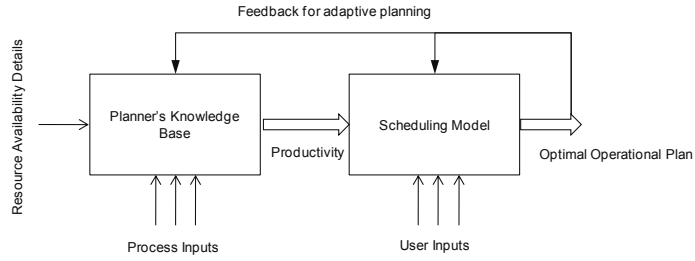

Figure 2. Framework used to construct our tools

Another important aspect is an effective adaptive planning framework to absorb any change in the planning scenario (with respect to resource availability or user inputs), as soon as a new information is available. Thus, a feedback mechanism that evaluates the current plan against the revised scenario and communicates useful information back to the scheduling model is critical.

4. Principal Features: PlanPerfect

The main feature of PlanPerfect is that it is specifically tailored for application to the pharmaceutical plants. Our copyrighted tool is developed in association with a Singapore-based plant of a multi-national pharmaceutical company and has a competitive advantage on intelligence, speed, versatility, cost, and ease-of-use. Given the plant configuration data and planning scenario data, PlanPerfect aides decisions such as campaign scheduling, inventory management, material procurement, cleaning and set-ups, waste generation, and plant utilization. The tool features constraints regarding maintenance planning, new product testing, different modes of operation, and resource allocations that are specific to the pharmaceutical companies. While gross profit may be the most comprehensive planning objective, the tool also allows the planner to specify other planning objectives such as minimum waste, maximum plant utilization, minimum production time, minimum cost, maximum order fulfilment, etc. A key feature of PlanPerfect is its smart GUI (Figure 3), which is based on popular MS Excel spreadsheet. This makes it very easy to use and so, does not require any prior training for its use. The user has a complete freedom in changing various plant parameters and configurations, to generate various scenarios for scenario planning. In addition, the tool embodies a state-of-the-art interactive help feature for quick reference and troubleshooting.

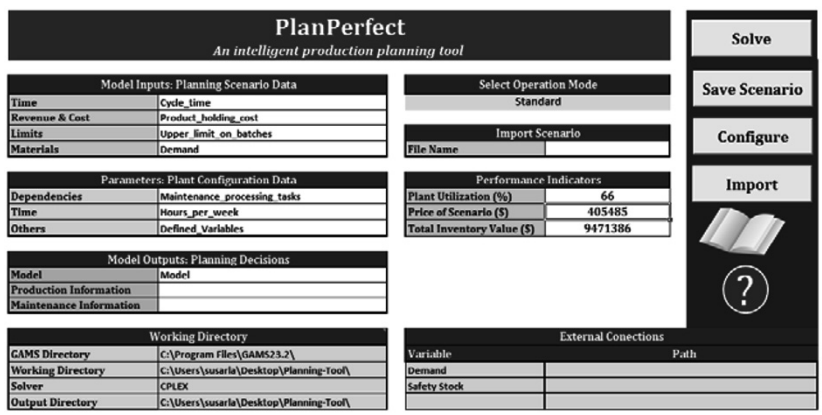

Figure 3. GUI for PlanPerfect

5. Performance Demonstration: PlanPerfect

Here, we consider an active pharmaceutical ingredient manufacturing (API) plant F, involving 10 products with up to 6 stages each and handling around 48 materials. F tests 6 new chemical entities (NCEs), consists 4 shared resources, and incorporates a given maintenance plan. For a planning horizon of 3 years, PlanPerfect gives an optimal plan with an objective value (gross profit) of $405485 and total inventory value of $9471386 within 15 minutes of CPU time. The optimal plan is represented as a gantt chart on a calendar and inventory profiles are generated for each product. Figure 4 shows a part of this solution. We then evaluate 3 different scenarios with limited resources at different mode if operations.

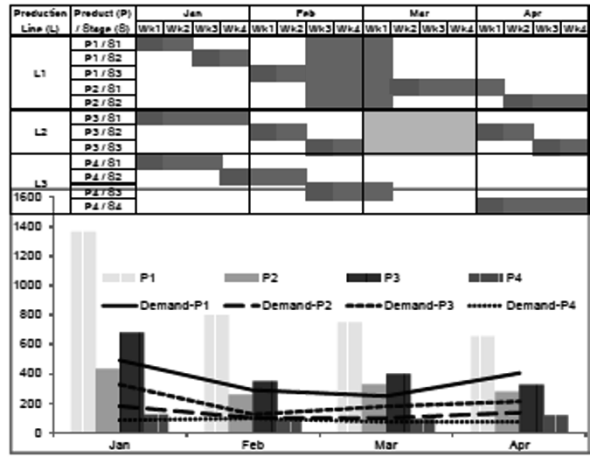

Figure 4 Gantt chart and inventory profiles obtained from PlanPerfect for the optimal solution

6. Conclusion

Resource allocation and operational planning (manufacturing and distribution) are critical for efficient operations of pharmaceutical plants. We successfully presented an intelligent framework for effective and efficient planning tools. Also we explained and demonstrated a smart, holistic, realistic, and use-friendly decision support tool (PlanPerfect) based on such a framework. PlanPerfect is specially designed for application in pharmaceutical plants.

References

Basu P, Joglekar G, Rai S, Suresh P, Vernon J. Analysis of manufacturing costs in pharmaceutical companies. Journal of Pharmaceutical Innovation 2008;3(1):30-40.

Nickerson J. Pharmaceutical industry wastes $50 billion a year due to inefficient manufacturing. http://news-info.wustl.edu/tips/page/normal/7912.html 2006.

Suresh P, Basu PK. Improving pharmaceutical product development and manufacturing: Impact on cost of drug development and cost of goods sold of pharmaceuticals. Journal of Pharmaceutical Innovation 2008;3(3):175-87.

Susarla N, Karimi IA, Integrated campaign planning and resource allocation in batch plants 2011. Computers and Chemical Engineering, 35 (12), 2990-3001.

I.A. Karimi and Rajagopalan Srinivasan (Editors), Proceedings of the 11th International Symposium on Process Systems Engineering, 15-19 July 2012, Singapore.

Embedding Methane Steam Reformer and Methanol Reactor into a Single Reactor

Amjad Riaz, [a] Gholamreza Zahedi[a,]*

[a] *Process Systems Engineering Centre (PROSPECT), Department of Chemical Engineering, Faculty of Chemical Engineering, Universiti Teknologi Malaysia, Skudai 81310, Johor Bahru (JB), Malaysia.*
** Corresponding author: Tel.: +607-5535583; Fax: +607-5581463, Email address: grzahedi@cheme.utm.my (Gholamreza Zahedi)*

Abstract

Non-incremental reductions in process plant size, cost reduction, safety, environment, and energy are some of the major objectives that currently drive the process industry towards intensifying the existing and future installations. In the present study, direct coupling of methane steam reformer and methanol reactor has been proposed. The synthesis gas produced in reformer was directly fed to methanol reactor skipping secondary reformer and shift convertors. A heterogeneous steam reformer model was developed and embedded with heterogeneous methanol reactor model. The set of differential algebraic equations was solved in MATLAB. Steady state and dynamic simulation results were validated against real plant data. The results showed gradual increase in the methanol mole fraction along the reactor length with a simultaneous decrease in CO and CO_2 levels. Although, the methanol yield achieved through this new reactor scheme remained unchanged, but the reduction in number of equipment and heat integration may help lower operational and capital cost and overall energy demand of the plant.
Keywords: Energy, Methanol, Modeling, Reactor Coupling, Synthesis gas

1. Introduction

Methanol is among few renewables which have the potential to replace or at least minimize dependency on fossil fuels. Commercially, methanol is produced in a three step process; Steam reforming, Methanol conversion, and Product separation. Like every other alternative fuel, the major constraint is end user product cost or market competency in terms of economic benefits. Basini [1] estimated that in most applications of synthesis gas such as methanol, about 60-70% of the cost of the overall process is associated with syngas generation, 20-25% for liquid fuel production and the rest of 5-15% for final product upgrading and purification.

Environmentally benign technical solutions, sustainability, efficient plant design, optimization of process schemes and development of new technologies are only few of the methods that may be adopted to hold decrease in the capital cost of any process in general [2; 3] and methanol in particular McGuire et al. [4]. In the present study, a new scheme is proposed that has the potential to not only save energy but can also help to considerably reduce capital investment. The main objective of this research is to model the novel idea of merging steam reformer and methanol convertor in a way to save on energy and capital investment.

2. Hybrid Reactor Concept

Multifunctional reactors integrate one or more transport processes and reaction systems in a single vessel resulting savings in capital and operational costs. Khademi et al. [5] applied differential evolution method for optimization of methanol synthesis reaction and cyclohexane dehydrogenation in a thermally coupled reactor. Methane Steam Reformer (MSR) was modeled in a parallel plate micro-reactor with alternating channels carrying out reforming and catalytic combustion [6]. Mahajan and Goland [7] integrated methanol synthesis and CO_2 sequestration for application in integrated gasification combined cycle plants. But no work on the integration of steam reformer and methanol reactor is available.

In this study, coupling of MSR and methanol reactor is proposed. The syngas generated from MSR was directly fed to methanol reactor. The difference in temperature of both reactors (~700 K) and the heat content are used to raise high-pressure steam separately. The same may partly be used to preheat reformer feed thus making process more integrated and energy efficient. Secondary reformer and shift convertors that are used to maintain CO to CO_2 ratio were skipped. There can be a number of combinations but as a first step we considered a series arrangement similar to one proposed byHasar [8] for operating two membrane processes. Fig. 1 portrays the concept outlined above. The present work shall be novel in the sense that work of this scope has not been part of any previous study.

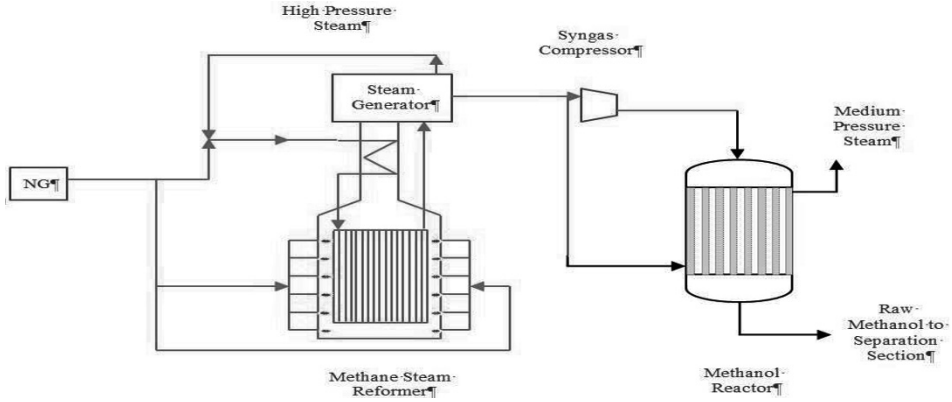

Fig. 1 Schematic of Proposed Reactor

3. Model Development

The following model considers process side of MSR but accounts for outside heat transfer effects. One dimensional plug flow was considered. Axial dispersion of heat, external mass and heat transfer resistances, radial concentration and temperature gradients were neglected.

For fluid phase:

$$\varepsilon_b c_t \frac{\partial y_i}{\partial t} = -c_t \frac{\partial (u y_i)}{\partial z} - K_{g_i} a_V c_t \left(y_i - y_{is}\right) \quad i = 1, 2, ..., N-1 \tag{1}$$

$$\varepsilon_b C_{p_g} c_t \frac{\partial T}{\partial t} = -C_{p_g} c_t \frac{\partial T}{\partial Z} - h a_V \left(T - T_s\right) + \frac{4\pi U_{tube}}{D_{in}} \left(T_{tube} - T\right) \tag{2}$$

For the solid phase:

$$\varepsilon_s c_t \left(1-\varepsilon_b\right)\frac{\partial y_{is}}{\partial t} = K_{g_i} a_V c_t \left(y_i - y_{is}\right) - a\, r_i \eta_i \rho_b \tag{3}$$

$$C_{p_s}\rho_b \frac{\partial T_s}{\partial t} = h a_V \left(T - T_s\right) + \sum_{i=1}^{3}(-\Delta H_r) a\, r_i \eta_i \rho_b \tag{4}$$

Where y_{is} and T_s are the mole fraction and temperature of the catalyst surface; and y_i and T are the mole fraction and temperature of gas phase respectively

The boundary conditions and initial conditions are as follows:

$$\text{At } z = 0\ ;\quad y_i = y_{i_o} \text{ and } T = T_o \tag{5}$$

$$\text{At } t = 0;\ y_i = y_i^s,\ y_{i_s} = y_{i_s}^s,\ T = T^s,\ T_s = T_s^s,\ a=1 \tag{6}$$

Where y_i^s, y_{is}^s are steady state mole fractions, and T_s, T_s^s is temperature of fluid phase and solid phase, respectively.

The kinetic model of Xu and Froment [9] and Catalyst deactivation model presented by Fuentes and Gamas [10] were employed. The output of syngas model comprises of gas composition and temperature both in the fluid and solid phase.

A one-dimensional heterogeneous dynamic model for methanol synthesis was simulated by Zahedi et al. [11] and is used for linking with the developed MSR model. For details of methanol model, reference may please be made to PhD work of Zahedi [12]. The techniques currently in practice for sub model routines in a single program have been adopted and the composition of syngas from MSR was exported to methanol program.

3.1. Numerical Solution

Various expressions used and the model assumptions form a system of differential algebraic equations for the two heterogeneous models. In order to avoid numerical instability [13], the reactor was divided into 50 separate sections and the discrete nonlinear algebraic equations at each section were solved. Partial differential equations were discretized by means of backward finite difference to algebraic and ordinary differential equations for each node of reactor. All of the model equations were implemented in MATLAB (R2010b).

4. Results And Discussions

Composition of natural gas used for the process is obtained from [14] and given in Table 1. Feed enters the reactor at 893 K temperature, 24 barg pressure and steam to carbon ratio 2.78 [15].

Table 1. Natural gas composition

Sr. No.	Component	Composition (mol %)	
		Dry basis	Wet basis
1.	Methane, CH_4	90.00	25.01
2.	Carbon dioxide, CO_2	2.69	0.75
3.	Carbon monoxide, CO	0.80	0.22
4.	Water, H_2O	0.00	72.21
5.	Hydrogen, H_2	3.00	0.83
6.	Nitrogen, N_2	3.51	0.98

Fig. 2 shows a gradual but exponential increase in the concentration of methanol and water in early part of the reactor but show a steady behaviour in the later sections. It was observed that CO conversion to methanol is the major reaction near the exit section of the reactor as it continues to show a decreasing trend. The contributors of carbon show a slow, steady and smooth decline in concentration owing probably to the low reaction rate and that both CO_2 and CO are tied up by shift reaction. The exothermic nature of methanol synthesis reactions causes an increase in temperature in the initial part of the reactor. The sharp rise is then compensated in the later sections of the reactor owing to endothermic nature of shift reaction. The catalyst deactivates at a faster rate during the initial phases of operation. After the fast deactivation phase, the process tends to stabilize itself and the less steep slopes are supportive of this fact.

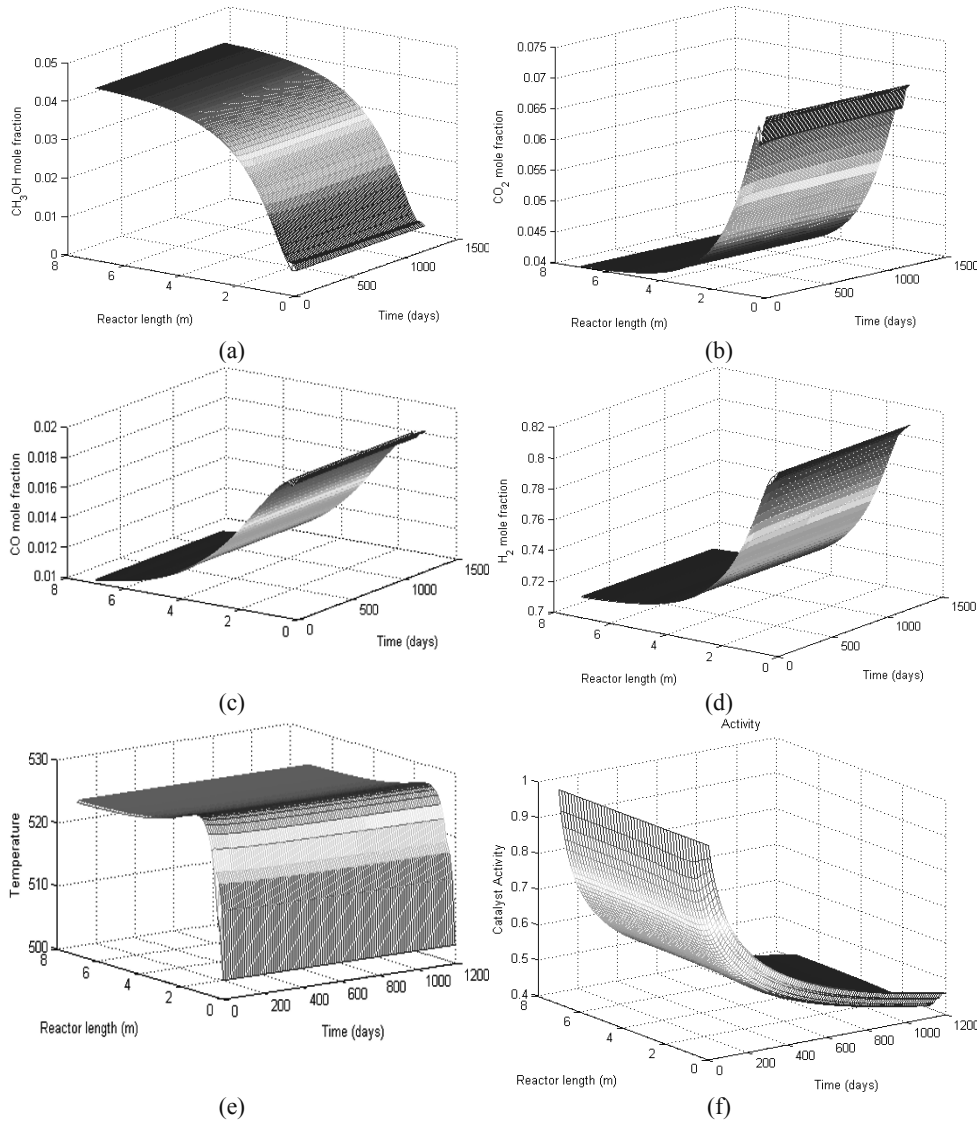

Fig. 2 Dynamic simulation results of MSR and Methanol coupled reactor

The dynamic as well as steady state results obtained from coupling steam reformer and methanol reactor are similar to the results of conventional methanol reactor widely reported in literature [16-20]. No real increase in the production rate of methanol is achieved but our objective to devise an energy efficient reactor is definitely accomplished and at no extra cost. The excess heat from reformer was used to generate high pressure steam that is one of the raw materials of the process, and later for preheating feed gas. By directly coupling the two reactors, many a vessel, equipment, process piping, instrumentation and process control items were skipped without compromising methanol production rate. Heat requirements of secondary reformer and cooling duties were minimized. This not only reduces the operational cost but capital investment as well.

5. Conclusion

A new hybrid reactor was proposed that couples together MSR and methanol reactor. The results of the coupled reactor simulation showed similarity with existing methanol model. The new scheme do not include secondary reformer, shift convertors, and other process equipment that are an integral part of the existing system; hence saving in terms of maintenance and capital cost. The proposed scheme utilizes system heat to produce steam and preheat the reformer feed. Therefore, in this context, the proposed reactor definitely improves the energy efficiency of the plant and may help methanol compete as a potential alternative fuel.

Acknowledgement

Financial support of Universiti Teknologi Malaysia (UTM) under grant no 4D042 is gratefully acknowledged.

References

[1] L. Basini, 2005, Catal. Today, 106,1-4, 34.
[2] J. A. Velasco, L. Lopez, M. Velásquez, et al. , 2010, J. Nat. Gas Sci. Eng., 2,5, 222.
[3] K. Aasberg-Petersen, J. H. B. Hansen, T. S. Christensen, et al. , 2001, Appl. Catal., A, 221,1-2, 379.
[4] N. E. McGuire, N. P. Sullivan, R. J. Kee, et al. , 2009, Chem. Eng. Sci., 64,24, 5231.
[5] M. H. Khademi, M. R. Rahimpour and A. Jahanmiri, 2010, Int. J. Hydrogen Energy, 35,5, 1936.
[6] G. D. Stefanidis and D. G. Vlachos, 2010, Chem. Eng. Sci., 65,1, 398.
[7] D. Mahajan and A. N. Goland, 2003, Catal. Today, 84,1-2, 71.
[8] H. Hasar, 2009, Bioresour Technol, 100,10, 2699.
[9] J. Xu and G. F. Froment, 1989, AlChE J., 35,1, 88.
[10] G. A. Fuentes and E. D. Gamas, 1991, Stud. Surf. Sci. Catal., 68, 637.
[11] G. Zahedi, A. Elkamel and A. Lohi, 2007, Energy & Fuels, 21,5, 2977.
[12] G. Zahedi, 2011, .
[13] W. Press, S. Teukolsky, W. Vetterling, et al. , 2007, Numerical Recipes: The Art of Scientific Computing.
[14] Y. H. Yu and M. H. Sosna, 2001, Korean J. Chem. Eng., 18,1, 127.
[15] M. Tarin, 2009, M.Sc., M. Sc. Thesis, Razi University.
[16] F. Askari, M. R. Rahimpour, A. Jahanmiri, et al. , 2008, Chem. Eng. Technol., 31,4, 513.
[17] E. J. van Lier, D. Posarac, K. E. Kwok, et al. , 2008, Chem. Prod. Process Model., 3,1.
[18] P. Parvasi, A. Khosravanipour Mostafazadeh and M. R. Rahimpour, 2009, Int. J. Hydrogen Energy, 34,9, 3717.
[19] E. V. Pisarenko and V. N. Pisarenko, 2007, Theor. Found. Chem. Eng., 41,2, 105.
[20] G. Zahedi, A. Jahanmiri and M. R. Rahimpor, 2005, Int. J. Chem. React. Eng., 3, Article A8.

I.A. Karimi and Rajagopalan Srinivasan (Editors), Proceedings of the 11th International Symposium on Process Systems Engineering, 15-19 July 2012, Singapore.

Characterization and design of a new crystallization process using a model-based approach

Benny Harjo,[a] Yoshio Fukui,[a] Sean Bermingham[b]

[a]*Mitsubishi Chemical Corp., 17-1 Towada, Kamisu-shi, Ibaraki 314-0102, Japan*
[b]*Process System Enterprise Ltd., 26-28 Hammersmith Grove, London W6 7HA, U.K.*

Abstract

The design and operation of crystallization processes pose many challenges, especially where new processes are involved. This work describes the use of model-based approach to efficiently and comprehensively characterize crystallization kinetics (nucleation and growth) from experimental data. The developed and validated model was used to perform exploratory simulation case studies and to optimize the process with respect to the required crystal size. Furthermore, effort to capture hydrodynamic effects for reliable scale-up by linking with computational fluid dynamics (CFD) models will be discussed.

Keywords: Crystallization, Modeling, Parameter estimation, Optimization, Design,

1. Introduction

The purification process in the manufacture of crystal X (the exact chemical name is undisclosed due to confidentiality) in Mitsubishi Chemical Corporation (MCC) is based on crystallization. It is necessary to obtain desired crystal size as it will affect subsequent downstream process. In order to analyze, optimize, and scale-up this process, crystallization modeling is indispensable. Based on lab scale crystallizer data, crystal growth and nucleation kinetics parameters will be estimated. The validated model will subsequently be used to carry out simulation case studies to study the effect of operating conditions on crystal size and to optimize the process. The objective of this article is to illustrate the value that a model-based approach (Bermingham et al., 2000 and Ward et al., 2010) can bring to the development of an industrial crystallization process. gCRYSTAL[1] from PSE Ltd. was used for model development, parameter estimation and optimization.

2. Crystallization Modeling and Experiments

gCRYSTAL employs a population balance approach to represent and describe the evolution of the crystal size distribution resulting from the prevailing crystallization mechanisms and hydrodynamics. The first step is to account for the thermodynamics of the system, in particular the solubility of the solute. The next step is to select appropriate kinetic models to represent the crystallization behavior. Considering the limited experimental data available, it was decided to begin with the simplest crystallization kinetic model or rather the kinetic model with the smallest number of parameters), namely power law model. The employed nucleation and growth kinetic models are:

[1] http://www.psenterprise.com/products/gcrystal/index.html

$$B = k_{n0} M t^m \sigma^n \tag{1}$$

$$G = k_{g0} \exp\left(\frac{-E_{ag}}{RT}\right)\sigma^g \tag{2}$$

$$\sigma = \frac{C - C_{eq}}{C_{eq}} \tag{3}$$

Where, B is the secondary nucleation rate, G is the growth rate, and σ is the relative super-saturation. There are 6 parameters (k_{n0}, k_{g0}, m, n, g, and E_{ag}) that need to be fitted from experimental data.

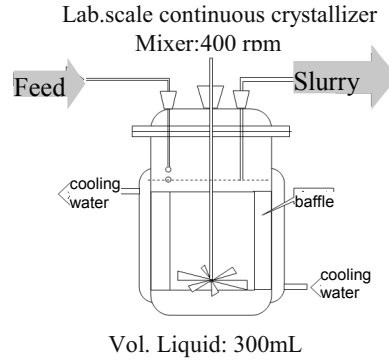

Figure 1. Lab scale experimental setup.

The experimental setup is shown in Figure 1. Crystal size distribution and slurry density data were measured at steady state. Operating conditions varied from one experiments to another include the crystallizer temperature, residence time, and feed concentrations. In addition to crystallization kinetics, solubility data (which were obtained in other experiments not mentioned here) are also necessary.

3. Parameter Fitting and Model Validation

gCRYSTAL's built-in parameter estimation capability was used to estimate the crystallization kinetic parameters described in the previous section. Parameter fitting results showing the effect of residence time and feed concentration are depicted in Figure 2.

τ =2hr	τ =1hr
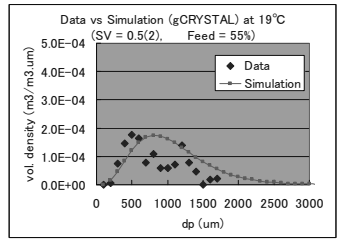	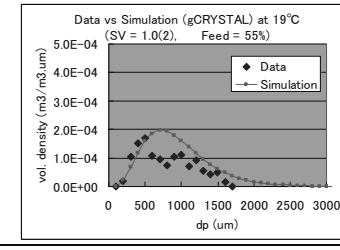
(a)	(b)

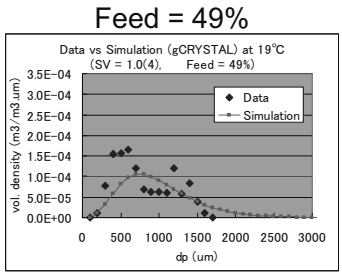

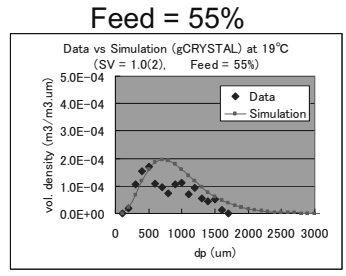

(c) (d)

Figure 2. Parameter fitting results.

PSD measurements used for parameter estimation are the dp_{25}, dp_{50}, dp_{75}. Comparisons with experimental data show that the developed model is able to represent effect of operating conditions under study. The biggest deviation of median crystal size (dp_{50}) between data and simulation is 100 μ m. This is acceptable because it is within the range of experimental error.

4. Process Simulations and Simple Optimization

Simulation results showing the effect of slurry concentration and crystallization temperature on median crystal size is given in Figure 3. Based on these results, the largest crystal size could be obtained under higher temperature and lower slurry concentration (i.e. maintaining high crystal growth rate, while suppressing nucleation rate). However, this condition will result in low crystal yield and therefore knowledge of optimum operating conditions is necessary.

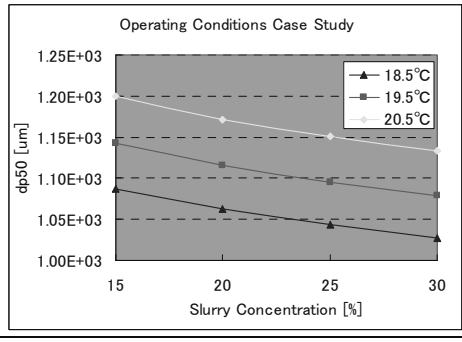

Figure 3. Process simulation results.

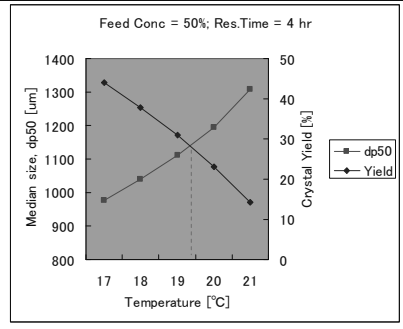

Figure 4. Simple optimization of operating conditions.

The relationships between temperature, median crystal size, and crystal yield are shown in Figure 4. It is obvious from this result that a higher temperature could lead to a bigger crystal size, but at the same time lower yield. Since a median crystal size of around 1100 μ m is desired, crystal yield of around 30% can be obtained by setting the crystallizer temperature to around 19.5℃.

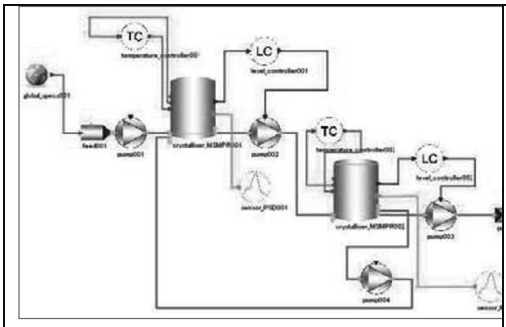

Figure 5. gCRYSTAL flowsheet of 2-stage crystallization process.

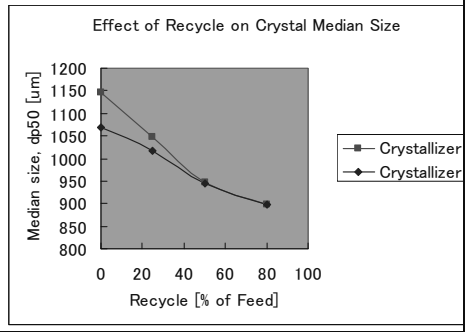

Figure 6. Median size in the first and second crystallizer as a function of recycle rate.

A two-stage crystallization process is also being investigated (Figure 5). This introduces several degrees of freedom that can be used to optimize the process, such as operating temperature of the first crystallizer, the volume of the two crystallizer stages and the recycle policy. Here we illustrate the impact of the recycle rate on the median particle size in the two stages (Figure 6). The bigger the recycle rate, the smaller the crystal size. Based on the simulation results presented here, the second stage does not seem appropriate as the median size without recycle is already less than the desired 1100 μ m . However, the use of a recycle has the advantage of lower growth rates, which may be of importance for product purity.

5. Combining hydrodynamics and crystallization kinetics for scale-up

The validated will subsequently be combined with flow information from a CFD model to construct a so-called Multizonal model (Urban and Liberis, 1999; Bezzo et al., 2004) as shown in the figure below. This multizonal modelling approach allows prediction of local nucleation and growth rates by separating macroscopic hydrodynamics and intrinsic kinetics.

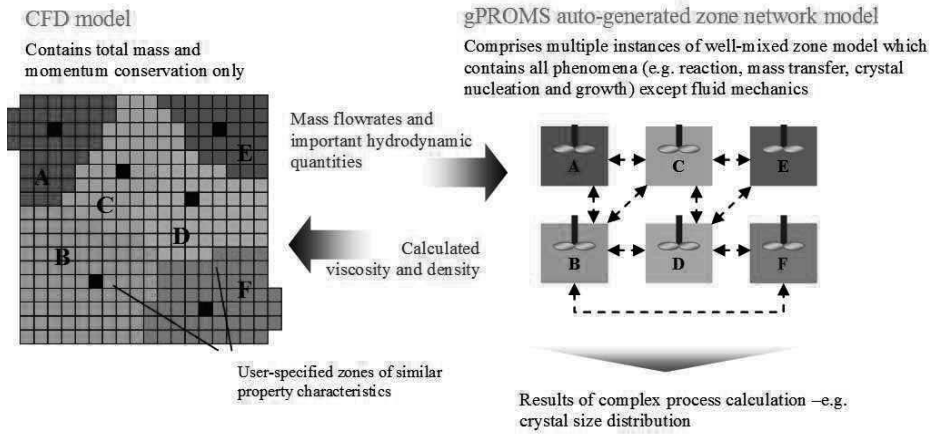

Figure 7. Multizonal interface approach.

In addition, gravity induced particle segregation can be captured by classification functions acting upon the flow rates between the zones. This phenomenon only needs

to be considered when there is a significant density difference between the liquid and solid phase and when the particles in the system are sufficiently large.

6. Concluding Remarks

The application of gCRYSTAL in characterizing crystallization kinetics (nucleation and growth) from experimental data has been demonstrated. Our procedure is summarized by the workflow shown in Figure 8. gCRYSTAL is a very useful tool in most of the crystallization development stages. Instead of performing simulation and optimization of single crystallizer, we will use the model to simulate a whole purification process flowsheet. Furthermore, scale-up investigations based on the hybrid CFD-gCRYSTAL model will also be applied. Efforts in these directions are currently underway.

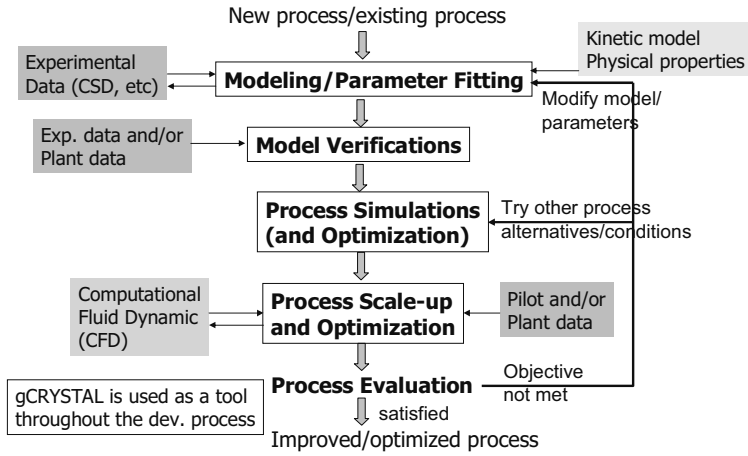

Figure 8. Summary of workflow for crystallization process modeling and development.

References

Bermingham, S.K., Neumann, A.M., Kramer, H.J.M. Verheijen, P.J.T., van Rosmalen G.M., Grievink, J. 2000. A design procedure and predictive models for solution crystallisation processes. AIChE Symposium Series No. 323, 96, 250-264.

Bezzo, F., Macchietto, S., Pantelides, C.C., 2004. A general methodology for hybrid multizonal/CFD models. Part I. Theoretical framework. Comput. Chem. Engng 28, 501-511.

Urban, Z., Liberis, L., 1999. Hybrid gPROMS-CFD modelling of an industrial-scale crystalliser with rigorous crystal nucleation and growth kinetics and a full population balance. Proc. Chemputers 1999, Düsseldorf, Germany.

Ward, J.D., Yu, C.-C., Doherty, M.F., 2010. Plantwide dynamics and control of processes with crystallization. Comput. Chem. Eng. 34, 112–121.

I.A. Karimi and Rajagopalan Srinivasan (Editors), Proceedings of the 11th International Symposium on Process Systems Engineering, 15-19 July 2012, Singapore.

A new graphical representation of exergy applied to low temperature process design

Danahe Marmolejo-Correa[a], Truls Gundersen[a]

[a]*Department of Energy and Process Engineering, Norwegian University of Science and Technology, Kolbjoern Hejes vei 1B; Trondheim NO-7491, Norway*

Abstract

The paper introduces a novel representation of exergy as well as its application in low temperature process design. This thermodynamic diagram uses a new energy quality parameter called *exergetic temperature* that is also introduced. Processes operating below ambient temperature commonly require the use of refrigeration and therefore compression work. Low temperature cooling corresponds to large requirements of compression work. The novel representation can be used in parallel with the Extended Pinch Analysis and Design (ExPAnD) methodology which uses pressure as an important design variable for networks with heat exchange, compression and expansion.

Keywords: Subambient processes, pinch analysis, exergy analysis, process integration

1. Introduction

The combination of Exergy Analysis (EA) and Pinch Analysis (PA) for the design of Heat Recovery Systems (HRSs) is not a new idea. The traditional PA is characterized by two graphical representations, Composite Curves (CCs) and the Grand Composite Curve (GCC) (Linnhoff et al., 1982) that show the minimum energy requirements for a given HRS. The CCs show the temperature profiles of energy sources (hot curve) and energy sinks (cold curve). However, traditional PA only uses temperature as a design variable and thereby ignoring the possibility to integrate the heat generated in compression or the cooling obtained in expansion. Exergy Analysis, on the other hand, uses temperature, pressure and composition to calculate the energy quality (exergy) of a material stream. A new methodology developed in our research group called ExPAnD (Extended Pinch Analysis and Design) is based on utilizing the heating and cooling generated by changing the pressure of the streams for reducing or eliminating the heat and power requirements (Aspelund et al., 2007). The traditional Composite Curves (*T-H* diagram) were used for illustrating the changes made to the HRS during the stages of the methodology. ExPAnD was applied for developing a novel natural gas liquefaction process for offshore applications (Aspelund and Gundersen, 2009).
The main objective of this paper is to introduce an alternative diagram for representing the exergy transfer in HRSs that can be used in parallel with the ExPAnD method. This diagram will then be applied in an illustrative example of an HRS operating below ambient temperature (T_0) where both temperature and pressure of the streams change.

2. Exergy of material streams

The total exergy of a material stream is equal to the sum of its kinetic, potential, chemical and thermo-mechanical exergies. For streams in an HRS, kinetic and potential exergies can be neglected (do not change much), while chemical exergy can be omitted (no change in composition since there is no reaction, mixing or separation). Thus in an

HRS, the thermo-mechanical exergy is the only one that is transferred. The thermo-mechanical exergy $\dot{E}^{TM}$ of a material stream at temperature T and pressure p relative to ambient conditions (T_0, p_0) is calculated by Eq. (1). The thermo-mechanical exergy can be decomposed into temperature based exergy $\dot{E}^{T}$ and pressure based exergy $\dot{E}^{p}$.

$$\begin{aligned}
\dot{E}^{TM}(T,p) &= \dot{H}(T,p) - \dot{H}(T_0,p_0) - T_0\left[\dot{S}(T,p) - \dot{S}(T_0,p_0)\right] \\
\dot{E}^{T}(T,p) &= \dot{H}(T,p) - \dot{H}(T_0,p) - T_0\left[\dot{S}(T,p) - \dot{S}(T_0,p)\right] \\
\dot{E}^{p}(T,p) &= \dot{H}(T_0,p) - \dot{H}(T_0,p_0) - T_0\left[\dot{S}(T_0,p) - \dot{S}(T_0,p_0)\right]
\end{aligned} \tag{1}$$

This decomposition is not unique and has no fundamental meaning; however, it is commonly accepted despite its inherent arbitrariness. Normally, this decomposition is used for better understanding of temperature and pressure based exergy contributions in processes when one exergy component is transformed into the other (i. e. processes below ambient temperature). Marmolejo-Correa and Gundersen (2011) among other authors have shown this decomposition in an Exergy-Enthalpy thermodynamic diagram. It is worth mentioning that $\dot{E}^{T}$ is positive in the complete temperature range and that its rate of change below T_0 is steeper (asymptotic to 0 K) than above. Thus, process streams that are initially at T_0 require more exergy for taking them below T_0 than above.

3. Exergetic Temperatures

The relationships between the exergy of material streams and their pressure and temperature are non-linear, and therefore not easily visualized. Thus, a specific heat capacity relation in terms of temperature and pressure for $\dot{E}^{T}$ and $\dot{E}^{p}$, and an equation of state for $\dot{E}^{p}$ are needed. If constant specific heat capacities and ideal gas conditions are assumed, then the exergy components can be rewritten as in Eq. (2)

$$\begin{aligned}
\dot{E}^{T} &= \dot{m}c_p\left[T_0\left(\frac{T}{T_0} - \ln\frac{T}{T_0} - 1\right)\right] = \dot{m}c_p T^{E^T} \\
\dot{E}^{p} &= \dot{m}c_p\left[T_0 \ln\left(\frac{p}{p_0}\right)^{\frac{\kappa-1}{\kappa}}\right] = \dot{m}c_p T^{\dot{E}^p}
\end{aligned} \tag{2}$$

The factors enclosed in brackets for both exergy components (Eq. (2)) are called the *exergetic temperatures*. These exergetic temperatures are: (*i*) in a linear relation with exergy; (*ii*) alternative energy quality parameters, and (*iii*) in absolute temperature units (K). In addition, notice that T^{E^p} is intimately related to T^{E^T} i. e. any change in the stream pressure results in a change in temperature. It is possible to take advantage of this to reduce external heating and cooling requirements. For instance, consider a stream with an initial condition (T_s, p_s) that needs to be heated and compressed to (T_t, p_t). If the compression is done first in an isentropic compressor ($\Delta S = 0$), the change in $\dot{E}^{p}$ is given by Eq. (3). After the compression, the stream has raised its pressure and without using any external heating also its temperature, thus the heating requirement has been reduced. The change in temperature based exergy in an isentropic device is given by Eq.

(3). A simple relation between the changes of the two exergetic temperatures (T^{E^T} and T^{E^p}) is also provided in Eq. (3). It is important to mention that the isentropic work $\left(-W_{\Delta s=0} = \dot{m} c_p \left(T_{\Delta s=0} - T_s\right)\right)$ consumed or obtained by manipulating stream pressure depends only on the pressure ratio and the device inlet temperature.

$$\Delta \dot{E}^p_{\Delta s=0} = \dot{m} c_p T_0 \left[\ln\left(\frac{T_{\Delta s=0}}{T_s}\right)\right]$$
$$\Delta \dot{E}^T_{\Delta s=0} = \dot{m} c_p \left[\left(T_{\Delta s=0} - T_s\right) - T_0 \ln\left(\frac{T_{\Delta s=0}}{T_s}\right)\right] \rightarrow \Delta T^{E^T}_{\Delta s=0} = \Delta T_{\Delta s=0} - \Delta T^{E^p}_{\Delta s=0} \quad (3)$$

Notice that for this simple example, the process was divided into two parts: the compression part and the heating part. Depending on at what operating condition the compression is made, the heating requirement can be reduced, and this is exactly where the heuristic rules proposed by the ExPAnD methodology are utilized.

4. New graphical representation of exergy

By only using the supply and target temperatures, the proposed diagram plots exergy sources and exergy sinks as linear composite curves in a $T^{E^T} - \dot{E}^T$ diagram as illustrated in Figs. 1*a* and 1*b*. This means that the new diagram does not require multiple calculations and the exergy targets are explicitly shown. This is in contrast to previous graphical representations of exergy for HRSs such as the Exergy Composite Curves (ECCs) (Linnhoff and Dhole, 1992). For HRSs above T_0, the exergy sources are the hot streams and the exergy sinks are the cold streams while for HRSs below T_0, the cold streams are the exergy sources and the hot streams are the exergy sinks, thus exergy and heat flows have opposite directions below T_0.

Some characteristics of the new diagram are: (*i*): The minimum value of T^{E^T} (zero) is at ambient temperature. Thus, T^{E^T} is positive for the complete temperature range, in contrast with the ECCs where the Carnot factor is negative below T_0. The state with the highest exergy is always placed at the top of the curves while the lowest (closest to T_0) is at the bottom. For streams below T_0, the coldest temperature is the largest *exergetic temperature*. (*ii*): If the minimum temperature approach (ΔT_{min}) between CCs is set, a corresponding exergetic temperature approach ($\Delta T^{E^T}_{min}$) is also obtained. Then, the exergy deficit and surplus are calculated from the exergy cascade by only using the stream data, similar to how minimum external heating and cooling are obtained from the traditional heat cascade. Since exergy destruction is related to heat transfer, it does not influence the exergy deficit and surplus figures. These are based on stream temperatures only. The *heat* and *exergy* pinch points are placed in corresponding enthalpy and exergy intervals, thus if the pinch rules are followed, then exergy is neither imported below nor exported above the *exergy* pinch, and exergy is not transferred across this pinch. (iii): Exergy destruction is graphically shown by transforming the boundary temperatures of the overlapping region obtained in *the traditional CCs* into exergetic temperatures (squares and circles in Figs. 1*a* and 1*b*). (*iv*): The maximum exergy recovery for a given ΔT_{min} is the maximum amount of exergy that the exergy sink curve can accept in the overlapping region, and the minimum process-to-process exergy destruction is the

difference between the process-to-process exergy transferred from the exergy source curve and the maximum exergy recovered by the sink curve. The calculation of exergy targets is given by Eq. (4). Notice that while exergy destruction increases the exergy requirements above *exergy* pinch, it reduces exergy rejection below *exergy* pinch.

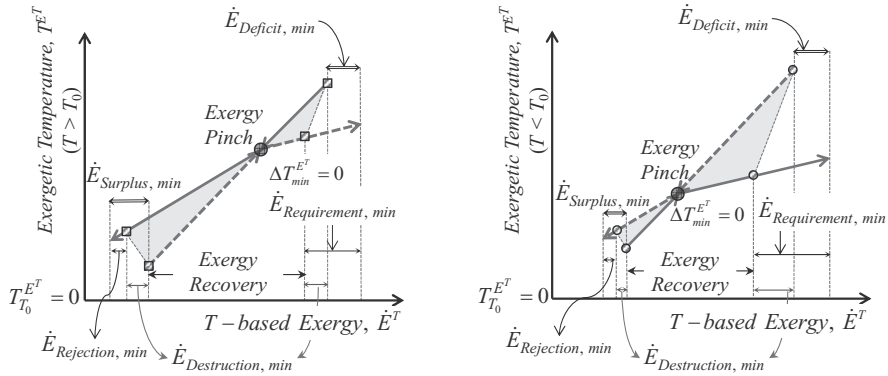

Fig. 1 $T^{E^T} - \dot{E}^T$ diagram (*a*) above T_0 and (*b*) below T_0

$$\text{Above exergy pinch: } \dot{E}_{Requirement,\,min} = \dot{E}_{Deficit,\,min} + \dot{E}_{Destruction,\,min}$$
$$\text{Below exergy pinch: } \dot{E}_{Rejection,\,min} = \dot{E}_{Surplus,\,min} - \dot{E}_{Destruction,\,min} \quad (4)$$

5. Illustrative example of using the new diagram

Table 1 shows the stream data for an HRS that operates entirely below T_0. C1and C2 are cold streams and H1 and H2 are hot streams. C1 and H1 are to be expanded and C2 should be compressed. The heat capacity flow rates (kW/K) are 0.325 for C1, 0.185 for H1, and 0.35 for C2 and H2. The specific heat ratios (κ) are 1.41 for C1 and C2, and 1.30 for H1 and H2. The ambient conditions are assumed to be 15°C and 1 bar.

Table 1 Stream data: T_s, $T_t[=]°C$, p_s, $p_t[=]bar$, $T_s^{E^T}$, $T_t^{E^T}[=]K$ and $\Delta\dot{E}_{T_s\to T_t}^T, \Delta\dot{E}_{p_s\to p_t}^p[=]kW$

	T_s	T_t	p_s	p_t	$T_s^{E^T}$	$T_t^{E^T}$	$\Delta\dot{E}_{T_s\to T_t}^T$	$\Delta\dot{E}_{p_s\to p_t}^p$
C1	-173.15	-43.15	7.00	2.50	160.80	6.80	-35.75	-27.55
C2	-83.15	6.85	1.20	3.00	21.85	0.12	-7.61	26.40
H1	6.85	-123.15	4.50	2.00	0.12	49.97	9.22	-9.98
H2	-23.15	-158.15	1.20	1.20	2.77	91.53	31.06	0.00

Eq. (2) is used for calculating T^{E^T} for supply and target temperatures and the change in exergy components ($\Delta\dot{E}_{T_s\to T_t}^T$, $\Delta\dot{E}_{p_s\to p_t}^p$). Notice that (*i*) the largest T^{E^T} corresponds to the lowest temperature and vice versa, (*ii*) $\Delta\dot{E}_{T_s\to T_t}^T$ is negative for cold streams (exergy sources) and positive for hot streams (exergy sinks), (*iii*) for C1 and H1, $\Delta\dot{E}_{p_s\to p_t}^p$ is negative (exergy sources) and this exergy is transformed into temperature based exergy and shaft work, and (*iv*) for C2, both shaft work and part of the temperature based

exergy are consumed (exergy sources), producing a positive $\Delta \dot{E}^{p}_{p_s \to p_t}$ (exergy sink) (Marmolejo-Correa and Gundersen, 2011). Fig. 2*a* shows the $T^{E^T} - \dot{E}^T$ diagram before changing the pressures. The minimum hot and cold utilities are 6.85 kW (cooling water) and 4.40 kW (refrigeration) for a theoretical ΔT_{min} of 0 K. The *heat* pinch is at -83.15°C. Notice that the *exergy* pinch (21.85 K) corresponds to the *heat* pinch temperature. The theoretical minimum process-to-process exergy destruction (ΔT_{min} of 0 K) is 7.99 kW. In this example, the exergy requirement is smaller than the destruction (exergy surplus prior to destruction). If ΔT_{min} is specified and heat (and exergy) is not transferred across pinch, then the process-to-process exergy destruction is fixed. For HRSs below T_0, exergy destruction can be considerable; even larger than the exergy requirement. Fig. 2*b* illustrates a non-optimized but improved solution where the exergy requirement (refrigeration or cold utility) is eliminated and the total exergy destruction is reduced by 30%. However, hot utility (cooling water) has increased from 6.85 to 10.12 kW. This was achieved by using the ExPAnD method and manipulating the stream pressures.

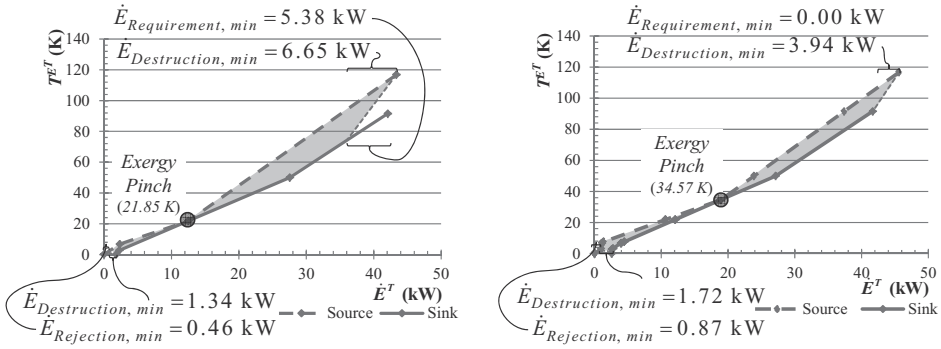

Fig. 2 $T^{E^T} - \dot{E}^T$ diagram (*a*) before pressure manipulation and (*b*) after pressure manipulation

6. Remarks

In this paper, a new diagram for exergy targeting is introduced that uses a novel energy quality parameter called *exergetic temperature*, thereby making the plots linear to reduce computational efforts, while exergy targets are obtained directly. This new thermodynamic diagram and the exergetic temperature are illustrated with an example.

References

A. Aspelund, D. O. Berstad and T. Gundersen, 2007. An Extended Pinch Analysis and Design procedure utilizing pressure based exergy for subambient cooling, Applied Thermal Engineering, 27(16): 2633-49.

A. Aspelund and T. Gundersen, 2009. A liquefied energy chain for transport and utilization of natural gas for power production with CO_2 capture and storage – Part 1, Journal of Applied Energy, 86: 781-92

B. Linnhoff et al., 1982. User Guide on Process Integration for the Efficient Use of Energy, IChemE, Rugby (UK).

B. Linnhoff and V. R. Dhole, 1992. Shaftwork targets for low-temperature process design, Chemical Engineering Science, 47(8): 2081-91.

D. Marmolejo-Correa and T. Gundersen, 2011. Low Temperature Process Design: Challenges and Approaches for using Exergy Efficiencies, in 21st European Symposium on Computer Aided Process Engineering − ESCAPE 21, Thessaloniki, Greece, 2011,vol. 2, pp. 1909-13.

I.A. Karimi and Rajagopalan Srinivasan (Editors), Proceedings of the 11th International Symposium on Process Systems Engineering, 15-19 July 2012, Singapore

Model based optimal reactor design applied to a free radical polymerization process

P. Klimantos*, and M. Hillestad
Department of Chemical Engineering; NTNU; Trondheim, Norway

Abstract

A computational framework is presented for model based optimal design of chemical reactors and applied to a multistage ethylene polymerization process. Design alternatives are generated on the basis of a state space composite model, accounting for fluid mixing, heat transfer, multiple and distributed feeds, initiator efficiency and others. A free radical polymerization kinetic mechanism is superimposed into the framework to describe the molecular and morphological polymer properties.The complexity of the kinetic mechanism due to the associated infinite dimensional population balance model (large stiff system of ODEs) is reduced by applying a continues variable approximation scheme over the discrete chain length domain. Finally an optimization problem is formulated by discretizing the resulting differential algebraic equation (DAE) system into an NLP model by applying a complete parametrization (CP) technique. Optimal reactor designs and operating modes are identified that minimize an objective function subject to technical and product quality constraints.

Keywords: reactor design, optimization, free-radical mechanism

1. Indroduction

A broad range of methods for process design appears in the literature which can be classified based on the chosen strategy for representing the design alternatives or the design space. In the field of reactor design the methods that have made considerable contributions can be classified into attainable region methods or targeting, and optimisation methods involving either construction of superstructures that are formulated as MINLP problems or state space design representation that exploit analogies from dynamic optimization techniques. Attainable region methods is a representation of the attainable concentration space when reaction and mixing take place and its theoretical framework has been extensively further by Hildebrandt and Glasser (1990). Given a chemical reaction, the method constructs graphically the consecration space based on the fact the all points in its boundaries are represented by the convex hull of combination of ideal reactor (PFR and CSTR) trajectories. The constructed convex hull contains the entire attainable region in the concentration space and given the reaction kinetics one can predict upper bounds of the performance of reaction system. The attainable region can be considered as a fundamental contribution in the area of reactor design since it provides critical insights into the properties of reaction and mixing. However, the applicability of the method has some limitations inherently imposed by the graphical approach considered restricting the designer to analyse problems in two or three dimensions. Superstructure approaches were developed by several authors , Achenie and Biegler (1986) formulated the reactor synthesis problem as a NLP optimisation problem with split fractions, source

*paris.klimantos@.ntnu.no

points and sink points that determine the mixing pattern, this network has been extended also to non isothermal reactors. Kokossis and A. (1990) proposed a reactor representation that utilizes as a basis the continuous stirred tank reactor (CSTR) and approximates the plug flow reactor as a cascade of CSTRs. A reactor network superstructure is presented in which all possible structural configurations of interconnected reactors are embedded. The combinatorial nature of the MINLP superstructure formulations result in a computational intractable problems and most of the aforementioned contributions focused on developing efficient optimisation algorithms and less focus has been given to the practical implementation in real industrial applications.

An alternative formulation for reactor design, based on the model of Hillestad (2010), is presented in this contribution. The main idea is to represent basic operation such a reaction, fluid mixing and heat transfer, through a continues state space model describing a reaction path. A fluid element is tracked along a reaction path and optimal conditions are generated that satisfy a design objective subject to process and product quality constraints. We investigate the proposed formulation for the design of LDPE (low density polyethylene) reactors, a rather complex reactive system of industrial interest.

2. Model Formulation

2.1. Reactor Model

A general state space reactor model accounting for fluid mixing, feed distribution and heat transfer is presented. Consider a fluid mixture of N species S_n described as the $n-$dimensional composition vector $\mathbf{c}^T = \begin{bmatrix} c_1, & \dots & c_n \end{bmatrix}$ of molar concentrations. Any change in composition due to occurrence of chemical reactions can be characterized through a predescribed set of reaction kinetics and denote $\mathbf{R}(\mathbf{c}) = \begin{bmatrix} R_1(\mathbf{c}), \dots, R_n(\mathbf{c}) \end{bmatrix}$ the vector of species molar formation rates $R_i(\mathbf{c})$ per unit volume, usually expressed as the stoichiometric mapping of the species reaction rates [1]. We describe variations in composition due to reaction, mixing and heat transfer through the well known equations describing ideal plug flow volumes (PFR) and perfectly mixed volumes (CSTR), expressed as a function of space time $\tau = \frac{V_R}{F_{v,0}}$. By expressing the well known CSTR component mole balance and temperature equations in a differential form a composite model describing both completely mixed and plug flows models is derived:

$$
\begin{aligned}
&\frac{dc_i}{d\tau} = R_i(\mathbf{c}) + \tau \frac{dR_i(\mathbf{c})}{d\tau} = R_i(\mathbf{c}) + \tau \sum_{k=1}^{n} \frac{\partial R_i(\mathbf{c})}{\partial c_k} \frac{dc_k}{d\tau} \implies \\
&\frac{dc_i}{d\tau} - \tau \sum_{k=1}^{n} \frac{\partial R_i(\mathbf{c})}{\partial c_k} \frac{dc_k}{d\tau} = R_i(\mathbf{c}) \implies \\
&\frac{dc_i}{d\xi}(1 - \xi \tau_R \frac{\partial R_i(\mathbf{c})}{\partial c_i}) - \xi \tau_R \sum_{\substack{k=1 \\ k \neq i}}^{n} \frac{\partial R_i(\mathbf{c})}{\partial c_k} \frac{dc_k}{d\xi} = \tau_R R_i(\mathbf{c})
\end{aligned} \tag{1}
$$

[1] For a set of m reactions and n species $\mathbf{R}(\mathbf{c}) = \nu^{\mathbf{T}} \mathbf{r}(\mathbf{c})$, ν is the $n \times m$ stoichiometric matrix and $\mathbf{r}(\mathbf{c})$ the $m-$dimensional vector of reaction rates

The final form of Eq.(6) is derived by introducing the dimensionless space time $\xi = \frac{\tau}{\tau_R}$. Based on Eqs. 5 we can writte the mole balance for the n species in a matrix form:

$$\left(\begin{bmatrix} 1 & 0 & \cdots & 0 \\ 0 & 1 & \cdots & 0 \\ \vdots & \vdots & \ddots & \vdots \\ 0 & 0 & \cdots & 1 \end{bmatrix} - \xi \tau_R \begin{bmatrix} \frac{\partial R_1(\mathbf{c})}{\partial c_1} & \frac{\partial R_1(\mathbf{c})}{\partial c_2} & \cdots & \frac{\partial R_1(\mathbf{c})}{\partial c_n} & \frac{\partial R_1(\mathbf{c})}{\partial \vartheta} \\ \frac{\partial R_2(\mathbf{c})}{\partial c_1} & \frac{\partial R_2(\mathbf{c})}{\partial c_2} & \cdots & \frac{\partial R_2(\mathbf{c})}{\partial c_n} & \frac{\partial R_2(\mathbf{c})}{\partial \vartheta} \\ \vdots & \vdots & \ddots & \vdots & \vdots \\ \frac{\partial R_n(\mathbf{c})}{\partial c_1} & \frac{\partial R_n(\mathbf{c})}{\partial c_2} & \cdots & \frac{\partial R_n(\mathbf{c})}{\partial c_n} & \frac{\partial R_n(\mathbf{c})}{\partial \vartheta} \end{bmatrix} \right) \begin{bmatrix} \frac{dc_1}{d\xi} \\ \frac{dc_2}{d\xi} \\ \vdots \\ \frac{dc_n}{d\xi} \end{bmatrix} = \tau_R \mathbf{R}(\mathbf{c})$$

$$\Longrightarrow \frac{d\mathbf{c}}{d\xi} = (\mathbf{I} - \xi \tau_R \mathbf{J})^{-1} \tau_R \mathbf{R}(\mathbf{c}) \tag{2}$$

Following the same procedure for the heat balance equation of a complete mixed volume dV, Eq. 5 is transformed to a similar format with Eqs. 6:

$$\frac{d\vartheta}{d\xi} = \tau_R \big(1 - \xi \tau_R (\frac{\partial R_T(\mathbf{c})}{\partial \mathbf{c}} \frac{d\mathbf{c}}{d\xi} - N_{st} \frac{dA}{d\xi})\big)^{-1} (R_T - N_{st} \frac{dA}{d\xi} (\vartheta - \vartheta_c) \tag{3}$$

with $R_T = \frac{-\Delta \mathbf{H^T r(c)}}{\rho c_p}$. Eqs (6) and (7) consist an intital value problem with initial values $\mathbf{y}_{\xi=0} = \mathbf{y}_o$ and $\vartheta_{\xi=0} = \vartheta_o$. The abovementioned reactor model formulation exhibits an interesting property equivalent to that of the one-dimensional axial dispersion model where convective mixing effects are lumped in one parameter the dispersion coefficient. By introducing the function $u_M(\xi)$ we observe that when $u_M \to 0$, Eq. (8) and (9) is reduced to the plug flow model reactor while integrating Eqs (8) and letting the function u_M to increase proportionally with the space time we obtain the compositional and temperature variations of completely mixed volumes with respect to the reactor space time. Any intermediate slope of u_M can be interpreted as a flow with a equivalent degree of dispersion. Feed distribution is introduced through the design function u_F wich is a function of the volume fractions of the added feeds. This additions is equivalent with the notion of the differential side stream reactor DSR, Feinberg and Hildebrandt (1997), and have been considered in various related studies. The final mixing model allows one to represent simultaneously the three main ideal reactors PFR, CSTR and DSR, a desirable task for the process engineer at the early stages of the design. In addition parameterization of the heat transfer area distribution along the reactor coordinate is introduced by defining the desing function $u_H = N_{st} \frac{dA}{d\xi}$. The final form of equations take the following form:

$$\frac{d\mathbf{c}}{d\xi} = (\mathbf{I} - u_M \tau_R \mathbf{J})^{-1} \tau_R \mathbf{R}(\mathbf{c}) + u_F (\mathbf{c} - \mathbf{c}_F) \tag{4}$$

$$\frac{d\vartheta}{d\xi} = \tau_R \big(1 - \xi \tau_R (\frac{\partial\, R_T(\mathbf{c})}{\partial \mathbf{c}} \frac{d\mathbf{c}}{d\xi} - u_H)\big)^{-1} (R_T - u_H(\vartheta - \vartheta_c) + u_F(\vartheta - \theta_F) \tag{5}$$

The reactor design problem is addressed by solving an optimal control problem in the following form :

$$\min_{\mathbf{u}} J \tag{6}$$

s.t.

$$\frac{\mathrm{d}\mathbf{z}}{\mathrm{d}\xi} = \mathbf{f}(\mathbf{z}, \mathbf{u}), \quad \mathbf{z}(0) = \mathbf{z}_0 \tag{7}$$

$$\mathbf{h}(\mathbf{z}, \mathbf{u}) \leq 0 \tag{8}$$

$$lb \leq \mathbf{u} \leq ub \tag{9}$$

Table 1: General Free Radical Homopolymerization Mechanism

Initiation	Chain Transfer to Polymer
$I \xrightarrow{k_d} 2P^*$	$P_p + D_y \xrightarrow{k_{TP}} P_y + D_p$
Chain Initiation Reactions	Termination by Disproportionation
$P^* + M_1 \xrightarrow{k_I} P_1$	$R_n + P_y \xrightarrow{k_{TD}} D_n + D_y$
Propagation Reactions	Termination by combination
$P_n + M_1 \xrightarrow{k_P} P_{n+1}$	$P_n + P_y \xrightarrow{k_{TC}} D_{n+y}$
Chain Transfer to Monomer	Intramolecular Transfer
$P_n + M_1 \xrightarrow{k_{TM}} P_1 + D_n$	$P_n \xrightarrow{k_b} P_n$
Chain Transfer to Solvent	β-scission
$P_n + S \xrightarrow{k_{TS}} P_1 + D_n$	$P_p \xrightarrow{k_{\beta'}, k_{\beta''}} D_{n-y} + P_y$

The new state vector is the vector of molar concentration augmented with the temperature $\mathbf{z} = [\mathbf{c}^T, \vartheta]$ and the model consists of the ordinary differential equations (8) and (9). Thus the proposed model formulation with the parameterized design functions along the reactor coordinate represents a reactor network consisting of a series of CSTR , PFR or DSR volume elements. Process and product design constraints are represented as non -linear inequality constraints on the state variables.

3. Reaction mechanism

3.1. Net formation Rates

Ethylene polymerization is initiated by the generation of free radicals through the decomposition of a thermal initiator and proceed through a mechanism involving, propagation, termination, and transfer reactions. A general accepted mechanism involves the reactions as depicted in Table 1. The net formation rates of the polymer radicals (P_n) and dead polymer chain (D_n) are:

$$\begin{aligned} R_{Pn} = {} & \delta(n-1)\left\{2fk_dI + (k_{tm}M + k_{ts}S)\sum_{m=1}^{\infty} P_m\right\} \\ & + k_pM(P_{n-1} - P_n) \\ & - \left\{k_{tm}M + k_{ts}S + (k_{tc} + k_{td})\sum_{m=1}^{\infty} P_m + k_\beta \sum_{m=1}^{\infty} mD_m\right\} P_n \\ & + k_{tp}nD_n \sum_{m=1}^{\infty} P_m - k_{tp}P_n \sum_{m=1}^{\infty} mD_m \end{aligned} \tag{10}$$

$$\begin{aligned} R_{Dn} = {} & \left\{k_{tm}M + k_{ts}S + k_{tp}\sum_{m=1}^{\infty} mD_m + k_{td}\sum_{m=1}^{\infty} P_m + k_\beta \sum_{m=1}^{\infty} mD_m\right\} P_n \\ & - k_{tp}nD_n \sum_{m=1}^{\infty} P_m + \frac{1}{2}k_{tc}\sum_{m=1}^{n-1} P_mP_{n-m} - k_\beta D_n \sum_{m=1}^{\infty} P_n \end{aligned} \tag{11}$$

The Kronecker delta function accounts for the generation of new radicals and the terms used for transfer to polymer assume that the propabiliy chain trasfered to a cetrain polymer chain D_n is proportional to the chain length n.

3.2. Continues Variable Approximation

The solutions of equations (14) and (15) which are of infinite dimension in the chain length represents the full molecular weight distribution (MWD). Several reduction techniques have been applied to deal with calculation of molecular weight properties, such as continuous approximation, statistical averaging using moments, stochastic methods, discrete weighted residuals etc. When a continues variable approximation is applied the discrete variables P_n and D_n are related to their continuous differentiable functions $P(n)$ and $D(n)$. By taking a Taylor series approximation of live radical concentration the difference term can be written:

$$R(n,t) = R(n-1,t) + \frac{\partial R(n,t)}{\partial n} + \frac{1}{2}\frac{\partial^2 R(n,t)}{\partial n^2} + H.O.T \tag{12}$$

In an analogous way discrete sums of live and dead polymer chains are related to their corresponding integrals by the Euler-McLauring summation formula. The resulting integro-partial differential equations are discretized on the variable n using orthogonal collocation, the integrals are approximated by Gauss quadrature, and the derivatives on the variable n are discretized using Lagrange polynomials.

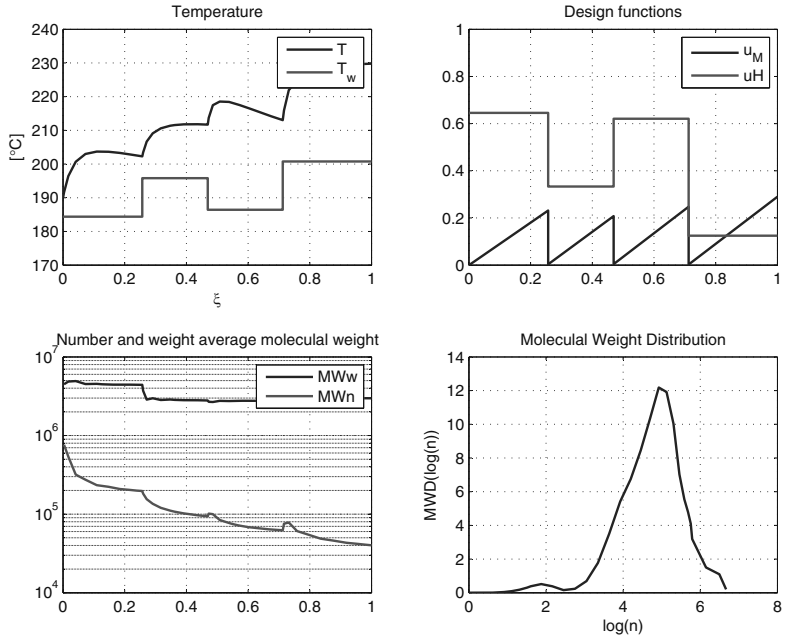

Figure 1: Case with 4-stage reactor path subject to optimization

4. Results and Discussion

For the solution of the optimal control problem of Eqs(10)-13, a direct simultaneous method based on discretization of the state variables using orthogonal collocation on finite elements is applied. The resulting NLP optimization problem is solved to local

optima using a sequential quadratic programming solver available in Matlab (fmincon). For demonstration purposes we present a hypothetical case using kinetic constants from Kim and Iedema (2004). A constant reactor space time of 40s is divided in 4 stages (elements) and an objective function that maximize the monomer conversion at the end of the reactor path has been chosen. For a given kinetic scheme the optimizer select optimal mixing profiles, heat area distribution and coolant temperature. For the hypothetical case presented a sequence of four equal volume CSTRs exhibit the highest conversion with varying temperature profiles and heat transfer area distribution at each stage as shown in Figure 1.

5. Conclusions

A model formulation for the design of reactor systems is presented. Fluid mixing, heat transfer, and distribution of feed are considered through parameterized design functions thus avoiding the combinatorial problem if otherwise discrete decision variables were included. Based on a given chemistry

the reactor path (volume or space time) is divided into a number of stages and the design is subject to optimization. The method was applied to the ethylene polymerization through a relative simple model reduction scheme for the calculation of the full molecular weight distribution and some preliminary results are presented.

References

Achenie, L. E. K., Biegler, L. T., 1986. Algorithmic synthesis of chemical reactor networks using mathematical programming. Industrial Engineering Chemistry Fundamentals 25 (4), 621–627.

Feinberg, M., Hildebrandt, D., 1997. Optimal reactor design from a geometric viewpoint i. universal properties of the attainable region. Chemical Engineering Science 52 (10), 1637 – 1665.

Hildebrandt, D., Glasser, D., 1990. The attainable region and optimal reactor structures. Chemical Engineering Science 45 (8), 2161 – 2168.

Hillestad, M., 2010. Systematic staging in chemical reactor design. Chemical Engineering Science 65 (10), 3301 – 3312.

Kim, D.-M., Iedema, P. D., 2004. Molecular weight distribution in low-density polyethylene polymerization; impact of scission mechanisms in the case of a tubular reactor. Chemical Engineering Science 59 (10), 2039 – 2052.

Kokossis, A. C., A., F. C., 1990. Optimization of complex reactor networks i. isothermal operation. Chemical Engineering Science 45 (3), 595 – 614.

I.A. Karimi and Rajagopalan Srinivasan (Editors), Proceedings of the 11th International Symposium on Process Systems Engineering, 15-19 July 2012, Singapore.
2012 Published by Elsevier B.V.

Optimization of carbon dioxide-assisted nanoparticle deposition process with uncertain design space

Michael J. Casciato[a], Sungil Kim[b], J.C. Lu[b], Dennis W. Hess[a], Martha A. Grover[a]

[a]*School of Chemical & Biomolecular Engineering,* [b]*H. Milton Stewart School of Industrial & Systems Engineering, Georgia Institute of Technology, Atlanta, GA 30332*

Abstract
A sequential design of experiments methodology with adaptive design space has been applied to optimize a nanoparticle deposition process using elevated pressure, elevated temperature carbon dioxide. This methodology is termed Layers of Experiments (LoE) with Adaptive Combined Design (ACD). Optimizing the CO_2-assisted nanoparticle deposition system presents significant challenges: uncertainty in the design region, uncertainty in model structure, a lack of information regarding the process from mechanistic considerations and/or empirical studies, significant costs related to materials processing and characterization, and an engineering tolerance requirement on the characteristics of the products. The contribution of the LoE/ACD methodology presented here is that it *systematically* finds the optimum of a process while robustly managing the aforementioned challenges.
Keywords: Optimization under uncertainty; sequential experimental design; nanoparticle deposition

1. Introduction
Advanced technology processes such as nanomanufacturing present unique challenges not inherent in more traditional materials fabrication techniques. Since nanomanufacturing processes exhibit complicated relationships between process inputs and outputs, reliable mechanistic and/or empirical models are not readily available for process optimization[1, 2]. Moreover, there are often significant uncertainties in the design region for nanofabrication[3]. Lastly, nanomanufacturing processes are expensive in terms of time and money and must still meet engineering tolerance requirements on the products. All of these issues represent unexplored challenges that must be overcome for advanced technology processes.
In this work, we present a systematic methodology to optimize a nanofabrication process that addresses uncertainty in design region and model structure while ensuring that the process meets a strict engineering tolerance requirement. This method is termed Layers of Experiments (LoE) with Adaptive Combined Design (ACD). This LoE/ACD algorithm was able to find the process optimum for a nanoparticle deposition process using the CO_2-assisted process by conducting 8 experiments in two layers. In the first layer, the target mean nanoparticle size was not achieved, exemplifying uncertainty in design region for this process. Consequently, the LoE/ACD algorithm redirected the second layer of experiments to a new design region, resulting in the successful optimization of the process at 69°C.

2. Materials and methods

2.1. Layers of Experiments with Adaptive Combined Design
The LoE/ACD algorithm begins by conducting a set of experiments and collecting data. Then, an empirical model is chosen and the model is fit using the experimental data.

Next, the accuracy of the predictions made by the model is assessed. If the accuracy is within the engineering tolerance set by the experimenter, the model is deemed acceptable and used to optimize the process. If not, the next subregion for experiments is selected using the LoE technique, design points are chosen using the ACD methodology, and the algorithm iterates until the accuracy of the model falls within the engineering tolerance set by the experimenter. Each of these steps is detailed below.

2.1.1. Model selection

Polynomial models for data were selected using the Akaike information criterion (AIC) and Bayesian probability (P_B). Methods for calculating these metrics are given elsewhere[4, 5].

2.1.2. Assessment of model accuracy

A target size T = 20nm and an engineering tolerance d = 5nm were chosen with surface enhanced Raman spectroscopy (SERS) as the motivating application[6]. A novel evaluation metric, L, is implemented to assess the model accuracy and is defined as[7]:

$$L = \max\{|T - (\hat{y}(\mathbf{x}) + CI(\mathbf{x}))|, |T - (\hat{y}(\mathbf{x}) - CI(\mathbf{x}))|\} \quad (1)$$

where $\hat{y}(\mathbf{x})$ is the fitted model and $CI(\mathbf{x})$ is the confidence on the model prediction. If $L > d$, the LoE algorithm specifies that a new layer with additional experiments is necessary. If $L \le d$, the model is sufficiently accurate and the LoE/ACD algorithm stops.

2.1.3. Selection of next layer

The next step in the LoE algorithm is choosing the location and size of the next layer (subregion). To choose the center of the next layer, the optimization problem

$$\min_x |T - \hat{y}(\mathbf{x})| \quad (2)$$

is solved n_j times for each candidate model j by calculating residuals of the model $\hat{y}(\mathbf{x})$ and experimental responses $y(\mathbf{x})$, randomly resampling (bootstrapping) these residuals to formulate synthetic response variables, fitting each candidate model to these synthetic responses, and solving Eq. (2). A histogram of the center points calculated from each optimization of each candidate model, $\tilde{c}_{lj}$, is created; the mean of the most frequent bin in the histogram is chosen as the center point for the next layer, c^*. To choose the size of the next layer, the histogram of potential center points is used: as the size of the subregion increases, the probability for the subregion to include the true optimum with respect to a distance r from the center is given by[7]:

$$\psi(r) = \frac{1}{N}\sum_{j=1}^{m}\sum_{l=1}^{n_j} I(c^* - r \le \tilde{c}_{lj} \le c^* + r) \quad (3)$$

where N is the total number of optimizations performed (i.e. $N = \sum_{j=1}^{m} n_j$) and m is the number of candidate models used in the optimization routine.

2.1.4. Adaptive combined design

A combined design methodology is implemented to choose design points in the layers used in the LoE/ACD methodology. This combined design uses a constrained approach to weight and optimize the design based on two criteria: one for a model free, minimax design, and one for a model dependent, D-optimal design. Let ξ be the design of N design points; then we define $\rho(\xi)$ as the metric to be minimized that yields a design minimizing the maximum distance between adjacent design points. A D-optimal design

seeks to minimize the determinant of the inverse of the information matrix for the most probable model, that is, $\left|\mathbf{M}(\xi)^{-1}\right|$. Thus, the weighted combined design metric to be optimized is[7]:

$$\kappa\left|\mathbf{M}(\xi)^{-1}\right|+(1-\kappa)\rho(\xi) \tag{4}$$

where $0 \le \kappa \le 1$ is the weighting factor between these two design metrics. The parameter κ is calculated as[7]:

$$\kappa = 1-\frac{max\{0, L_{t-1}^{*}-d\}}{L_{0}^{*}-d} \tag{5}$$

where L_{t-1}^{*} is the L^{*} metric from the previous layer and L_{0}^{*} is the L metric calculated fitting a simple mean model $\hat{y}(\mathbf{x})=\mu+\epsilon$.

2.2. Experimental procedure

The silver nanoparticle deposition method by elevated pressure, elevated temperature CO_2 has been detailed elsewhere[8], so only a brief description is presented here. A 2cm x 3cm silicon wafer ((100), p-type, 10-20Ωcm) was purchased from University Wafer and cleaned in an oxygen plasma to populate the surface with reactive silanol groups. The substrate was loaded into a stainless steel high pressure reactor with the organometallic precursor, silver hexafluoroacetylacetonate cyclooctadiene, hydrogen as reducing agent, and carbon dioxide. The reaction was run at 103bar at the specified temperature. Products were characterized by a Zeiss Ultra60 scanning electron microscope (SEM), and mean nanoparticle sizes were extracted from SEM images using automated image analysis in MATLAB 2010a.

3. Results

3.1. First layer

A space-filling experimental design was chosen for the first layer of experiments in the region [120°C, 150°C]. Results from these experiments are shown in Table 1. The AIC and P_B indicated that a linear model was the best fit for the data. Using a linear model, the L^{*} metric was calculated to be L^{*} = 38.8nm at x^{*} = 130°C. Since $L > d$, the LoE/ACD algorithm dictated that another experimental layer was necessary to optimize the process.

Table 1. Results of experiments and model selection criteria in first layer

Temperature (°C)	Mean AgNP size (nm)	Model order	AIC	P_B
120	44.0	1	26.1	0.59
130	41.6	2	28.1	0.41
140	55.2			
150	51.8			

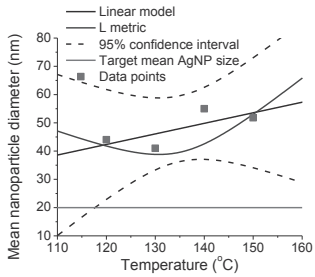

Figure 1. Linear model fit of data collected in first LoE with 95% confidence interval and L metric

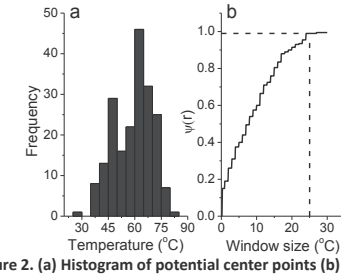

Figure 2. (a) Histogram of potential center points (b) ψ(r) vs. r; dashed lines indicate 99% confidence level and window size

3.2. Second layer

The center and size of the next subregion were calculated using the procedures described above. The histogram of center points is shown in Figure 2a; the mean of the most frequent histogram was $c^* = 63°C$, which was chosen as the center of the next region. The size of the next window was chosen using Eq. (3) to be 25°C, corresponding to a ψ level chosen to be $\psi = 0.99$ in Figure 2b so that there is a higher degree of confidence in the design region than in the model prediction (with confidence interval of 95%). The value for kappa was calculated to be $\kappa = 0.01$ from Eq. (5); using this value in the ACD algorithm resulted in an experimental design that is essentially minimax due to the weighting. Results from this design are given in Table 2; the AIC and P_B metrics indicated a linear model should be fit to the data in this window. Using this model, L^* was calculated to be $L^* = 2.49$nm. Since $L^* \le d$, the model was sufficiently accurate to within engineering tolerance and accepted; the plot of this model is shown in Figure 3, along with the 95% confidence interval and the L metric. Figure 4 shows a typical SEM image with silver nanoparticles deposited on a silicon wafer surface.

Table 2. Results of experiments and model selection criteria in second layer

Temperature (°C)	Mean AgNP size (nm)	Model order	AIC	P_B
44	12.1	1	39.9	0.54
56	17.3	2	40.3	0.46
69	19.2			
82	24.1			

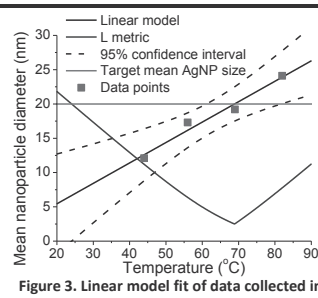

Figure 3. Linear model fit of data collected in second LoE with 95% confidence interval and L metric

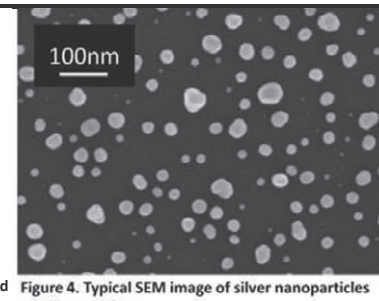

Figure 4. Typical SEM image of silver nanoparticles on silicon wafer

4. Discussion

The goal of the LoE/ACD methodology was to rapidly and systematically optimize the epet-CO_2 AgNP deposition process under uncertainty in model structure, design space, and an engineering tolerance requirement on the mean AgNP size, T = 20nm. The

investigators chose the design region [120°C, 150°C] as the initial layer in which to conduct experiments; however, results indicated that this was a poor choice for the chosen target. This is an example of how uncertainty in the design region for a system can affect process optimization. Nonetheless, the LoE/ACD algorithm was able to efficiently redirect the second layer of experiments to a region that was likely to contain the process optimum. However, due to the uncertainty in model structure from the previous layer of experiments (i.e. the relatively large L^* value in the first layer), the weighting parameter between the minimax design and D-optimal design was weighted significantly toward the minimax design in the ACD algorithm. This is because a space-filling design like a minimax design is model free, so it will not suffer bias from a poor model choice in constructing an experimental design; consequently, the design points chosen for the second layer were well "spread out" in order to locate the process optimum.

The results of these experiments indicated that the process optimum did indeed fall within the design region explored in the second layer. Furthermore, the small L^* metric (L^* = 2.49nm) indicated that the linear model structure selected for the specified target in this region was acceptable. If a further layer of experiments were to be conducted, the weighting factor κ would be $\kappa = 1$, weighted completely toward the D-optimal design since there is a higher degree of confidence in the linear model in this region of the design space. These experiments based on the model dependent D-optimal design would refine the model parameters. Last, the method can be generalized to multiple independent variables (such as pressure or reaction time).

5. Conclusion

A sequential experimental design methodology termed Layers of Experiment with Adaptive Combined Design (LoE/ACD) was proposed and implemented to optimize a silver nanoparticle deposition process under structural uncertainty, design region uncertainty, and an engineering tolerance requirement. After eight experiments conducted in two sequential layers, the algorithm found the process optimum at x = 69°C for a target mean nanoparticle size of T = 20nm with a tolerance of d = 5nm.

6. Acknowledgments

We thank NSF-CBET-0933430 and the NSF Graduate Research Fellowship Program (GRFP) for financial support.

References

[1] Xu S, Adiga N, Ba S, Dasgupta T, Wu CFJ, Wang ZL. ACS Nano. 2009;3:1803-12.
[2] Wissmann PJ, Grover MA. AIChE Journal. 2009;55:342-53.
[3] Wissmann PJ, Grover MA. Industrial & Engineering Chemistry Research. 2010;49:5694-701.
[4] Burnham D, Anderson KP. Model selection and inference: A practical information-theoretic approach: Springer-Verlag; 1998.
[5] Stewart WE, Shon Y, Box GEP. AIChE Journal. 1998;44:1404-12.
[6] Stamplecoskie KG, Scaiano JC, Tiwari VS, Anis H. The Journal of Physical Chemistry C. 2011;115:1403-9.
[7] Kim S. Experimental design methods for nanofabrication processes. Atlanta: Georgia Institute of Technology; 2011.
[8] Casciato MJ, Levitin G, Hess DW, Grover MA. Journal of Nanoparticle Research. 2011;Submitted.

I.A. Karimi and Rajagopalan Srinivasan (Editors), Proceedings of the 11th International Symposium on Process Systems Engineering, 15-19 July 2012, Singapore.

Modeling and Simulation of Multi-stream Heat Exchanger Using Artificial Neural Network

Mohd Shariq Khan , Yuli Amalia Husnil , Mesfin Getu & Moonyong Lee*

School of Chemical Engineeing, Yeungnam University Gyeongsan, 712-749, Korea

Abstract

A multi-stream heat exchanger (MSHE) is the heart of LNG plant where 40% of the entire energy is consumed in this section. Moreover, the plant operation is subject to number of variations from the plant inlet such as ambient temperature, pressure, feed flow or composition. In industrial application, the mitigating of these variations is usually performed using trial and error approaches. Thus developing a competent and accurate model to predict the performance of the MSHE is an inevitable step to overcome those variations. In this study, a model for the MSHE operation is developed using artificial neural network. The modeling is made in such a way that the information about the internals of heat exchanger could allow the MSHEs from any variation that arises from the process itself or upstream conditions. A number of simulation runs have been made by taking a case study for the MSHE operation. The developed model can predict and provide prior information for the MSHE in order to take action during the plant performance.

Keywords: Artificial Neural Network, Multi-Stream Heat Exchanger, liquefaction, Natural gas

Introduction

Multi-stream heat exchanger (MSHE) is the principal piece of heat transfer equipment in many industrial and cryogenic processes. MSHE compact design enables reduction of material, space and is popular in many cryogenic applications. MSHE typical application includes air separation, natural gas processing, liquefied petroleum gas (LPG), Helium recovery, Petrochemicals and refrigeration systems. The desired properties of MSHE include high heat transfer area with minimum approach temperature as small as 1-3^{o}C [1], large number of complex channels, and high flexibility in flow arrangement, high reliability with capability to withstand a range of pressure. Plate & fin type and Spiral wound are two common type of MSHE. The diversified application of MSHE ranging from sub ambient operation to energy improvement in chemical plant gives the motivation for developing efficient and accurate predictive model. For instance, the predictive MSHE model in LNG operation where 40% of entire energy is consumed in liquefaction gives good prospects of energy saving. MSHE Predictive model reduces the trail & error work in LNG plant operation where most deviations are mitigated by changing operations of cryogenic exchanger. Model building is also necessary for system wide optimization and for implementation of advance control schemes such as MPC. A validated model of MSHE enables the plant operators to predict the possible outcome of any control action before actually executing any control move. Modeling of MSHE can be achieved principally in two ways (i) using rigorous physiochemical model where the information about internal is required and the other is (ii)

operational data model where no information about the internal is needed and the only information needed is inlet and outlet streams temperature, pressure and flow rates, etc. Both methods has their pros and cons for instance, physiochemical model would be time consuming and computer intensive conversely, operational data model would be less time consuming but compromise would be made at the rigorousness of the model. MSHE is proprietary equipment and almost nothing is known about the internal geometry and configuration in public domain thus, we aim to develop operational data model of MSHE using artificial neural network (ANN). ANN is used because of its information processing characteristics such as nonlinearity, high parallelism, fault tolerance and the capability to generalize and handle imprecise information. ANN, over the last few decades has established their reputation in process engineering as alternative approach to information processing. The utility of ANN was demonstrated in Bhat *et al* [2, 3] where the technique was successfully used to characterize nonlinear chemical system and also to interpret biosensor data. ANN has also been used in model based predictive control methodology where neural network model effectively represent the complex nonlinear systems. Some other specific application of ANN includes the auto-tuning of PID controllers [4] and fault diagnosis and the development of intelligent system [5]. From its introduction ANN has gained sufficient maturity and successfully applied in many different fields of engineering [6][7] and their ability to solve process engineering problems has already been illustrated and studied [8].

In this paper, we aim to develop ANN model of MSHE using operational data from Natural gas liquefaction plant, which has been generated by using rigorous Hysys first principal model. To capture the star-up, shutdown and the intermittent dynamics of the MSHE several scenario were created (see section 2.2) and the most representative data were used for ANN training, testing & validation. Finally the simulation results are presented in results and discussion section.

1. First Principal MSHE Model

1.1. Dynamic Model of MSHE

The dynamic model of MSHE was developed in Aspen Hysys® V.7.2 platform as illustrated in *Fig 1.* Due to strong thermodynamic database the developed model in Hysys considered to be the most rigorous one. Peng-Robinson equation of state was used for property calculation and pre-cooled and lean NG was used as feed for MSHE. Steady state model was first developed and the steady state properties of inlet and outlet streams are summarized and presented in *Table. 1.* Once the steady state model has been configured properly, sizing were made which includes calculating the volume of flash drum, the flow coefficient of the valve (*Cv*) and most importantly the geometry of exchanger. To mimic the behavior of real Cryogenic exchanger, heat transfer between hot and cold streams is divided into several zones. Every zone is further partitioned into several layers where the actual heat transfer took place between hot and cold stream. Present model has 10 zones having 38 set of each 4 layers in it. Finally both steady-state and dynamic simulation mode are utilized to validate the developed model and mass & energy balances are checked to verify the interaction between the variables. MSHE is conceptually divided into two sections Precooling Bundle (PCB) and sub-cooling bundle (SCB) where the heavy component of mixed refrigerant provides cooling in PCB and light component of mixed refrigerant provide cold energy in (SCB). PI controller was used to control the Mixed refrigerant (MR) liquid level in flash drum by opening JT1 value whereby the flow rate of LNG is controlled by VLV-100

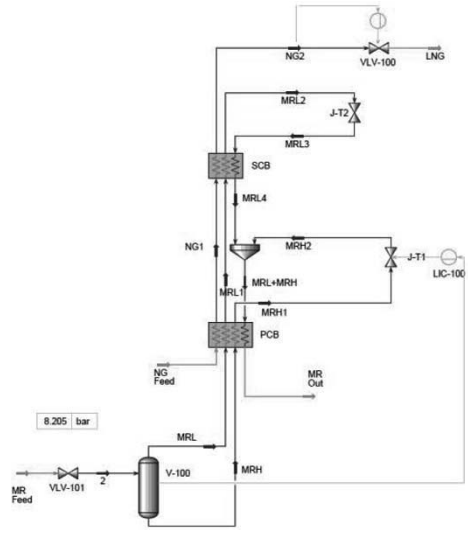

Figure 1. MSHE model in Natural gas liquefaction plant.

Table.1 Steady State properties of inlet streams

	Inlet		Outlet	
	NG feed	MR feed	LNG	MR out
Pressure (bar)	61.7	60.2	60.7	3.9
Temperature (^{o}C)	-32.7	-32.8	-153.2	-35.7
Flowrate (kmole/hr)	286.2	529.1	286.2	529.1

1.2. Data Generation

The data for both neural network training and validation were obtained by the Hysys dynamic simulation model of LNG plant. To obtain the representative data various control actions and disturbances were imposed on the cryogenic exchanger model. To capture startup and the intermittent dynamics six scenarios were created for generating representative data points, scenarios comprises of variations in NG feed temperature & pressure and increase in throughput. After giving disturbance, 3000 data points were generated for every scenario; 2500 were used for training and 500 for independent testing. Cryogenic exchanger in Hysys model is represented by two sections; PCB & SCB and both are treated as separate MSHE for data generation and simulation.

2. Artificial Neural Network Model Development

The application of ANN in chemical engineering began with the pioneering works [9] and in the subsequent years the research work has steadily increased. Process control, dynamic modeling, forecasting fault diagnosis and optimization were few areas in chemical engineering that benefits the most. In this paper the ability of ANN to store knowledge about the process and learn from the quantitative historical data information, has been exploited to develop ANN model of MSHE. The general NN structure that is used in this study is illustrated in *Fig. 2*

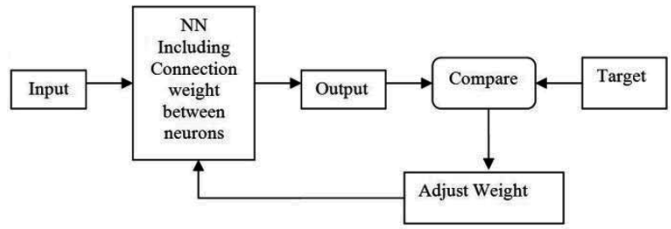

Figure 2. Neural Network Structure used in MSHE Modeling

2.1. Modeling Parameters

Modeling of PCB and SCB has done separately (see section 2.2 & 2.3) hence the modeling parameter used for both the cases are different. In general a two layer feed forward network with sigmoid hidden neuron and linear output neurons are used. The networks for both PCB & SCB were trained with Levenberg-Marquardt back-propagation algorithm. The performance evaluation of trained network was done by using mean square error (MSE) and regression analysis. In training PCB 25 hidden neurons were used whereby 20 hidden neurons in SCB case. The stopping criterion used is either total number of iterations reached or the mean square error reached the specified limit.

3. Results & Discussion

Modeling of MSHE was carried out using ANN and the simulation results are listed in *Fig. 3* to *Fig 6*. PCB and SCB bundles are simulated separately (see section 1.1). *Fig 3* & *Fig 4* represents the training, testing and validation of ANN in both bundles. Mean square value was used as the performance criterion for ANN model. In PCB the training proceeds until 24 epochs and the best validation point happen to be at 17. Training and validation curves are near and the MSE value of 10^{-2} was achieved. Training stopped when no improvement in MSE was achieved in subsequent epochs. Similarly in SCB training proceeds until 37 epochs and best validation happened at 31. Linear regression was also performed for both bundles and R^2 value of 0.9995 was achieved which represents that output tracks the target very well. Finally, ANN response was compared with the actual model developed in Hysys and illustrated in *Fig. 5* & *Fig 6*. PCB has four output temperatures that were predicted by ANN almost closely *(Fig 5)*. In SCB three output temperatures were predicted and their performance was also exceptional. Excellent prediction of ANN can be attributed to its leaning property when exposed to know data. However, this model application is limited to historical plant data and cannot be used for imaginary situations like unusual events not included in training. Considering the normal operation of process plant it will be helpful to get some rough estimate and a rigorous model should be used for real plant operation. In view of the time consumed and prediction results, this kind of model will be helpful since almost instant results can be obtained and can be used in parallel with rigorous model.

4. Conclusions

A neural network based model of MSHE for NG liquefaction is developed using operational data generated by inhouse Hysys dynamic simulator. Data generation was made by considering the possible scenarios in LNG process plant like variation in feed gas, ambient conditions fluctuations etc. The results obtained demonstrate the model behavior within and outside the training data, which is exceptionally good in predicting

behavior. This type of modeling is inexpensive and does not require difficult theories and the previous knowledge of the system moreover, modeling can be achieved in real time performing mapping by parallel distributed processing.

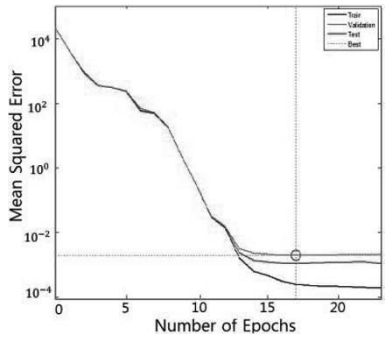

Figure 3. Performance of PCB

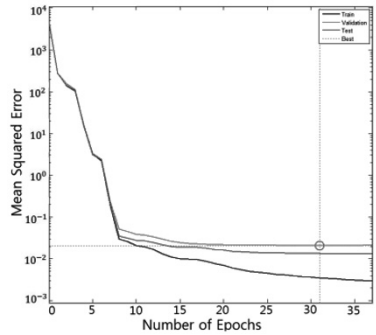

Figure 4. Performance of SCB

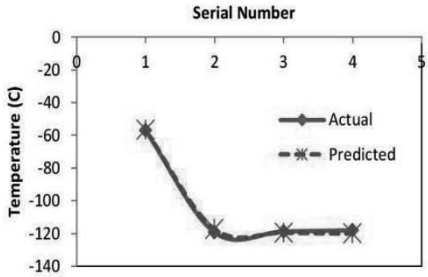

Figure 5. ANN predictions in PCB

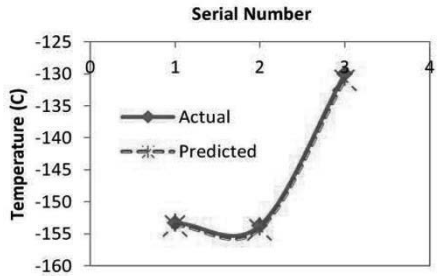

Figure. 6 ANN predictions in SCB

Acknowledgement

This research was supported by a grant from the Gas Plant R&D Center funded by the Ministry of Land, Trasnporation and Maritime Affairs(MLTM) of the Korean government.

References

I.A. Basheer and M. Hajmeer M., 2000, "Artificial Neural Network:Fundamentals, Computing, Design, and Application", Journal of Microbiological Methods., n. 43, pp.3-31,.

Bhat, N., Minderman, P., McAVOY, T., and WANG, N., 1989, "Modeling chemical process systems via neural computation'. Proc. 3rd Int. Symp. 'Control for Profit", Newcastle

Bhat, N., Minderman, P., and McAVOY, T.J.: 'Use of neural nets for modeling of chemical process systems'. Preprints IFAC Symp. Dycord , Maastricht, The Netherlands, Aug. 21-23,

Morris AJ, Montague GA, Willis MJ, 1994, "Artificial neural networks: studies in process modeling and control." Trans Inst Chem Engng, UK -- Part A ;72:3-19.

Bavarian, B.: 'Introduction to neural networks for intelligent control', IEEE *Control Syst. Mag.,* April 1988, pp. 3-7

H.H.Jui, 2007, "Hybrid Matlab and LabVIEW with neural network to implement a SCADA system of AC servo motor", Journal of Advance in Engineering Software, 39, 149-155.

J.F.D.Canete, S.G.Perez and P.D.S. Orozo., 2008, "Artificial Neural Network or Identification and Control of a Lab-Scale Distillation Column Using LABIEW", World Academy of Science, Engineerng and Technology, 47.

M.J.Willis, C.D.Massimo, G.A.Montague, M.T.Tham, A.J.Morris.,1991, "Artificial neural network in process engineering", IEEE PROCEEDINGS-D,Vol. 138, No.3

J.C.Hoskins and D.M Himmelblau, D.,1988, "Artificial Neural Network Models of Knowledge Representation in Chemical Engineering", Computers and Chemical Engineering. n. 12, 9, pp. 881-890.

I.A. Karimi and Rajagopalan Srinivasan (Editors), Proceedings of the 11th International Symposium on Process Systems Engineering, 15-19 July 2012, Singapore.

Modeling and Analysis of Novel Reactive HiGee Distillation

Gudena Krishna[a], Tay Haw Min[a], G.P. Rangaiah[a]
[a]*Department of Chemical & Biomolecular Engineering*
National University of Singapore, Singapore 117576, Singapore

Abstract

Reactive distillation (RD) is a well studied process-intensified technology where the interaction of chemical kinetics and vapor-liquid equilibrium is exploited through integration of reaction and separation in a single column. The in-situ removal of products for an equilibrium-limited chemical reaction in RD helps in realizing enhanced conversion, increased selectivity and reduced recycles. However, in spite of many benefits achievable through RD, several issues typical of a conventional column/packed bed still persist in RD; these include vapor-liquid mass-transfer limitations, inefficient catalyst wetting and constrained flooding limits, and need to be addressed. In this work, we propose a novel, intensified, reactive HiGee distillation (RHD) technology that addresses many of the issues stated above. Design of an industrial-scale, conventional RD column and the proposed RHD technology for methyl acetate (MeAc) esterification is employed as the case study. Rigorous modeling and simulation of RHD process, besides RD process, in Aspen-Plus™ is described. Obtained results suggests that nearly 13.6% reduction in equivalent annualized operating cost (EAOC) and more than 4-fold reduction in packed bed volume can be achieved by RHD over conventional RD.

Keywords: Process Intensification (PI); Reactive HiGee Distillation (RHD); Reactive Distillation (RD); Methyl Acetate Esterification; Modeling

1. Introduction

Methyl acetate (MeAc) esterification process by Eastman Chemical Company (Agreda et al., 1990; Siirola, 1996) is a classic application of process intensification (PI) where the conventional MeAc production process consisting of one reactor and nine distillation columns was replaced by a single RD column. MeAc is a valuable and high-volume commodity chemical, and its production throughput for a typical plant ranges from 18,000 to 200,000 metric tons per year (Celanese Chemicals Co., 2000; Harmsen, 2007). It is primarily used as a solvent, and as an intermediate feedstock in the manufacture of a variety of polymers such as photographic film base, cellulose acetate, Tenite cellulosic plastics and Estron acetate (Hiwale et al., 2004). However, in spite of the benefits achieved, several issues typical of a conventional packed bed still persists in RD; these include vapor-liquid mass-transfer limitations, inefficient catalyst wetting, lower catalytic bed density, excessive pressure drop for small-sized catalysts, and constrained flooding limits.

HiGee (acronym for High Gravity) or rotating packed bed (RPB) involves the rotation of a torus packed bed where liquid and gas interact counter-currently (Ramshaw, 1981). Under the high centrifugal field, liquid forms thin films and tiny droplets, leading to enhanced inter-phase mass transfer. In addition, high centrifugal acceleration raises the flooding limit of the packed bed, allowing for the use of high gas flow rates and high specific surface area of packing (500-4,000 m^2/m^3 compared to 100-1,000 m^2/m^3 in conventional columns). Different packing configurations employed in RPB are single packing (Ramshaw, 1981) and split-packing (Chandra et al., 2005). In a split-packing

RPB, the two coaxial packed disks rotate in opposite directions resulting in large vapor-liquid slip in the gap between the adjacent annular rings. Hence, radical enhancement in vapor side mass transfer coefficient over single packing can be obtained. Furthermore, split-packing RPB permits the introduction of intermediate feed between the packed disk (Agarwal et al., 2010), which is difficult in single packing RPB. Wang et al. (2011) proposed non-packing rotating zigzag bed that reduced the need for liquid distributor and dynamic seal, and allowed intermediate feed and multi-rotor configuration.

The current study proposes a novel reactive HiGee distillation (RHD) process (with split-packing configuration), and its performance is assessed for MeAc esterification using modeling and simulation approach. Rigorous analysis for plant-scale conventional packed bed RD and the novel RHD is performed, and they are compared based on equivalent annual operating cost (EAOC). A new approach to simulate HiGee in Aspen Plus process simulator is also demonstrated. Obtained results are encouraging, and suggest that further research on RHD would be promising.

2. Design and Simulation of Novel RHD Process

2.1 Reaction Kinetics

The esterification of acetic acid with methanol to form MeAc is a reversible and acid-catalyzed (here, Amberlyst 15 catalyst) reaction, and is given as:

Acetic acid (1) + Methanol (2) ⇔ Methyl acetate (3) + Water (4)

Psuedohomogeneous (PH) activity (a_i) based reaction rate (mol/g_{cat}-s) model is (Pöpken et al., 2000):

$$r = m_{cat}\left(2.961\times10^{4}\exp\left(\frac{-49{,}190}{RT}\right)a_1a_2 - 1.348\times10^{6}\exp\left(\frac{-69{,}230}{RT}\right)a_3a_4\right) \quad (1)$$

2.2 Validation of Thermodynamic Property Method

UNIQUAC model is used to determine the liquid phase activity coefficient. Due to the dimerization of acetic acid, Hayden-O'Connell (HOC) second viral coefficient model is used for the vapor phase. Validation of the UNIQUAC-HOC thermodynamic package in Aspen Plus was done with experimental data of Horsley (1973). Absolute errors in temperature and composition predictions are less than 0.5°C and 0.04 mole fraction, respectively (Table 1).

Table 1: Experimental and Predicted Azeotropic Data for MeAc System

	Experimental Value	Simulation Value	Deviation
1	Methanol – MeAc 54.0°C, (0.3590, 0.6410)	Methanol – MeAc 53.6°C, (0.3382, 0.6618)	Temperature: -0.4°C Mole fraction: (-0.0208, 0.0208)
2	MeAc – Water 56.4°C, (0.8804, 0.1196)	MeAc – Water 56.6°C, (0.9107, 0.0893)	Temperature: 0.2°C Mole fraction: (0.0303, -0.0303)

2.3 Modeling and Validation of HiGee Separation Process in Aspen Plus

Aspen Plus does not have a built-in module for HiGee unit. Hence, a novel approach for simulating HiGee using rate-based model in Aspen Plus is proposed in this work. For this purpose, the ability of Aspen Plus to carry out rigorous rate-based calculations by discretizing the process unit into segments and then solving the material balance, energy balance, mass transfer, energy transfer, phase equilibrium and summation equations simultaneously was utilized. RADFRAC module in Aspen Plus has rate-based approach implemented for conventional vertical columns, but HiGee is similar to a horizontal column. Hence, the proposed approach approximates a coaxially oriented horizontal HiGee unit by converting the differential annular rings in HiGee into a series of sequentially attached vertical cylinders (Figure 1). Variable transformation is thus

carried out based on conservation of material flux and volume (Equations 2 and 3) for different differential segments within RPB. Hence, for an annular segment within RPB (with $r_{s,i}$, $r_{s,o}$ and $h_{s,RPB}$ as the section inner radius, outer radius and height, respectively) that is approximated as a cylinder (with diameter, D and height, $h_{cylinder}$), calculations are shown as follows, and validation of the proposed approach is shown in Section 3.1:

1) Conservation of area for constant material flux for a differential segment:

Area for material flow in RPB = Area for material flow in cylinder

$$2\pi r_{lm} h_{s,RPB} = \frac{\pi D^2}{4} \rightarrow D = \sqrt{8 r_{lm} h_{s,RPB}} \text{ where, } r_{lm} = \frac{r_{s,o} - r_{s,i}}{\ln\left(r_{s,o}/r_{s,i}\right)} \quad (2)$$

2) Conservation of volume for a differential segment:

Volume of the annular ring = Volume of the cylindrical block

$$\pi\left({r_{s,o}}^2 - {r_{s,i}}^2\right) h_{s,RPB} = \frac{\pi D^2}{4} h_{cylinder} \rightarrow h_{cylinder} = \frac{4\left({r_{s,o}}^2 - {r_{s,i}}^2\right) h_{s,RPB}}{D^2} \quad (3)$$

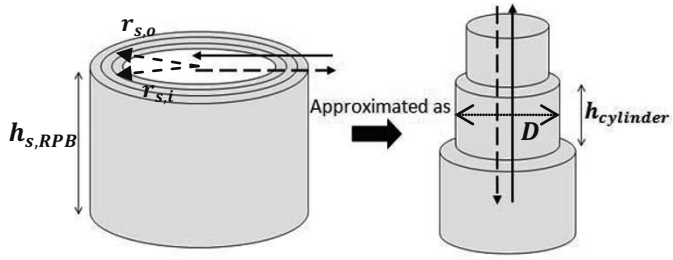

Figure 1: Schematic showing the approximation method of HiGee (left sketch) as a conventional column (right sketch) in Aspen Plus. The arrows represent the direction of material flow (solid line: vapor flow, dashed line: liquid flow).

2.4 Design of a Plant Scale Split-Packing RHD Unit

The novel split RHD unit comprises of both solid catalytic (reactive section) and non-catalytic packing (rectifying and stripping sections), and vapor-liquid-solid mass-transfer happens under high centrifugal field. Main steps for designing a RHD unit are to find the three dimensions of the entire HiGee unit, namely, inner packing radius (r_i), outer packing radius (r_o), and packing axial height (h_{RPB}).

Inner radius: Minimum inner radius of RHD is given as (Agarwal et al., 2010):

$$r_i = \left(\frac{\bar{V}}{\pi v_{jet}(1-f_d)}\right)^{0.5} \left(\frac{\rho_V p}{\rho_L}\right)^{0.25} \quad (4)$$

where, $\bar{V}$= volumetric vapor flow rate (m^3/s), v_{jet}= liquid jet velocity (4-5 m/s), f_d = fraction of packing inner radius occupied by liquid distributor (0.25-0.33), p= liquid jet to exit vapor kinetic energy ratio, ρ_V= vapor density (kg/m^3), ρ_L= liquid density (kg/m^3).

Axial height: The axial height of the split-packing HiGee unit is found for operating the unit below flooding limit. Generalized flooding correlation is (Wallis et al., 1969, Agarwal et al., 2010):

$${C_V}^{0.5} + 1.51{C_L}^{0.5} = 130{N_g}^{0.434}{a_p}^{-0.9343} \quad (5)$$

$$C_V = \bar{V}_S\left(\frac{\rho_V}{\rho_L - \rho_V}\right)^{0.5},\ C_L = \bar{L}_S\left(\frac{\rho_L}{\rho_L - \rho_V}\right)^{0.5}, \text{ and } N_g = \frac{r_i \omega^2}{g}$$

where, a_p= specific packing area (m^2/m^3), ω = angular velocity of the packed bed (rpm), N_G= dimensionless centrifugal acceleration, $\bar{L}_S$ = liquid superficial velocity (m/s), $\bar{V}_s$ = vapor superficial velocity (m/s).

Outer radius: Due to mechanical constraints on HiGee, a conservative ratio of $h_{RPB}/2r_o$ < 0.5 (Trent, 2003) is assumed. Feasible range of r_i/r_o for a HiGee unit is determined by

collecting 30 sets of experimental data on the dimensions of RPBs in the literature, and is between 0.1 and 0.7. A constraint of $0.2 < r_i/r_o < 0.6$ is set in the present study for a conservative design. Moreover, based on an industrial scale RPB, maximum limit on the outer radius was set as 1 m (Trent, 2003). In summary, outer radius of HiGee is determined under the following three constraints: $r_o > h_{RPB}$, $5r_i > r_o > 1.67r_i$ and $r_o \leq 1$ m. Mass transfer coefficient correlations for split-packing from Agarwal et al. (2010), and correlation of Onda et al. (1968) for effective interfacial area for heat and mass transfer, were used for this study.

3. Results and Discussion

3.1 Validation of Modeling HiGee Separation and Conventional RD in Aspen Plus

Verification of the proposed methodology for simulating a HiGee unit in Aspen Plus was done for lab-scale experimental data on HiGee stripping for O_2-water-N_2 system (Chen et al., 2005). Aspen Plus does not have built-in liquid and vapor side mass transfer correlations for HiGee, and hence they were calculated using correlations of Chen et al. (2005) and Onda et al. (1968), respectively. Figure 2a compares the experimental and simulation results (R^2= 0.9774). The results justify the proposed approximation method for modeling HiGee in Aspen Plus. Validation of conventional RD process simulation using rigorous rate-based approach in Aspen Plus is done using experimental data of Pöpken et al. (2001). As can be seen in Figure 2b, simulated profiles of liquid phase composition are close to the experimental data.

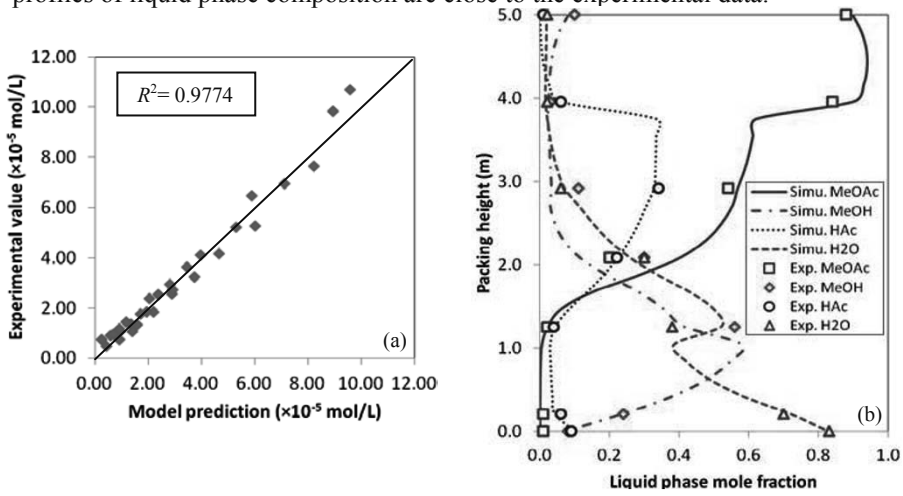

Figure 2: (a) Parity plot for experimental and simulated outlet O_2 concentration in HiGee, and (b) Experimental and simulated liquid phase composition profile in RD.

3.2 Techno-economic Analysis of Plant Scale Conventional RD & Novel RHD Process

Process conditions: Acetic acid and methanol feed flow rates are 30 kmol/hr each (for a throughput of ~21,000 metric tons/yr), and process product specifications are set as 99 wt% for MeAc in the product stream and 97 wt% for water in the bottom stream.

RD and RHD comparison: EAOC is the indicator selected to compare the performance of RD and RHD process. A FORTRAN code was built within Aspen Plus for estimating EAOC. Optimization for conventional RD column was done by employing SQP method available in Aspen Plus. Optimization of RHD has not been performed for the current study. However, the dimensions obtained from the procedure detailed in Section 2.4 provides a reasonable design for RHD, and used for this study. Table 2 shows the

techno-economic comparison between non-optimized, novel RHD process and optimized, conventional RD process for MeAc production. Obtained results show that 3 integrated RHD units ([inner radius, outer radius, height (all in m)] as [0.2, 1, 0.18], [0.2, 1, 0.2] and [0.17, 0.85, 0.18] for the 1st, 2nd and 3rd RHD unit, respectively) can replace a 8.6 m tall (1.2 m, 6 m, and 1.4 m for rectifying, reactive and stripping section, respectively) and 1 m diameter of a conventional RD column. Hence, packed bed-size reduction of 4.4 folds and EAOC reduction of 13.6% can be achieved by split-packing RHD over RD process (Table 2). Rotation of the packed bed would incur additional operating cost for RHD. Hence, in the present study of MeAc production process, extra electricity power of 133 kW is needed for RHD over RD (Table 2). However, there is further scope to reduce the EAOC of RHD by performing the process optimization (as done for RD), and is the subject of our future work.

Table 2 Comparison of Volume and EAOC for RD and Split-packing RHD Units

	Conventional RD	Split-packing RHD
Total bed volume (m^3)	6.75	1.54
Reboiler duty (W)	692,100	798,100
Electricity power (W)	-	132,800
AOC, Annual Operating Cost ($)	298,400	351,200
TCI, Total Capital Investment ($)	831,800	251,600
EAOC ($)	**464,700**	**401,500**

4. Conclusions

Although RD has many advantages over conventional reactor-followed-by-separator approach, it still has several limitations inherent to conventional gravity-driven packed beds. Novel RHD process proposed in this work reduces many of these limitations in RD. Both the conventional RD and split-packing RHD were simulated in Aspen Plus and were analyzed for MeAc production. Results show that 4.4-fold reduction in bed volume and 13.6% reduction in EAOC can be achieved by the proposed RHD over conventional RD.

5. References

L. Agarwal, V. Pavani, D.P. Rao, N. Kaistha, 2010, Ind. Eng. Chem. Res., **49**, 20, 10046-10058.
V.H. Agreda, L.R. Partin, W.H. Heise, 1990, Chem. Eng. Prog., **86**, 2, 40-46.
Celanese Chemicals Co., 2000, http://www.chemvip.com/ma_prod.pdf (13th October, 2010).
A. Chandra, P.S. Goswami, D.P. Rao, 2005, Ind. Eng. Chem. Res., **44**, 11, 4051-4060.
Y.S. Chen, C.C. Lin, H.S. Liu, 2005, Ind. Eng. Chem. Res., **44**, 20, 7868-7875.
G.J. Harmsen, 2007, Chem. Eng. Proc.: Proc. Int., **46**, 9, 774-780.
R.S. Hiwale, N.V. Bhate, Y.S. Mahajani, S.M. Mahajani, 2004, Int. Journ. Chem. Reac. Eng., **2**, 1-52.
L. Horsley, 1973, Azeotropic Data-III, ACS.
K. Onda, H. Takeuchi, Y.Okumoto, 1968, Journ. Chem. Eng. Jap., **1**, 1, 56.
T. Pöpken, L. Götze, J. Gmehling, , 2000, Ind. Eng. Chem. Res., **39**, 7, 2601-2611.
T. Pöpken, S. Steinigeweg, J. Gmehling, 2001, Ind. Eng. Chem. Res., **40**, 6, 1566-1574.
C.M. Ramshaw, H.Roger, 1981, U. S. Patent, 4,283,255.
J.J. Siirola, 1996, Adv. Chem. Eng., **23**, 1-62.
D.L. Trent, 2003, Marcel Dekker Inc., 33-68.
G. Wallis, 1969, McGraw-Hill.
G.Q. Wang, Z.C. Xu, J.B. Ji, 2011, Chem. Eng. Res. Des., **89**, 8, 1434–1442.

I.A. Karimi and Rajagopalan Srinivasan (Editors), Proceedings of the 11th International Symposium on Process Systems Engineering, 15-19 July 2012, Singapore.

Simulation and Analysis of Carbon-in-Leach (CIL) Circuits

Divyamaan Wadnerkar, Ranjeet P. Utikar, Moses O. Tade, Vishnu K. Pareek

Department of Chemical Engineering, Curtin University
Perth, WA 6102

Abstract

Carbon in leach (CIL) is an important process in gold processing involving simultaneous leaching and adsorption. The process holds the key to profitability in gold extraction. While the mechanism of leaching and adsorption are well known, the effect of different operating and design parameters on the CIL circuit performance is still empirical. The focus of this paper is to study the effect of parameters like cyanide concentration, oxygen concentration and mean particle diameter on the overall efficiency of CIL circuit. A dynamic model based on first principles is developed for the entire CIL circuit. Suitable kinetic models for both leaching and adsorption are adopted from the literature. Customizable simulator is written in MATLAB to simulate the model. Simulation results are first validated using previously published results. The validated model is then used to perform sensitivity studies on different parameters that affect the gold extraction process. The model can be used for controlling the operating parameters and to optimize the CIL circuit in order to achieve higher efficiency.

Keywords: Carbon-in-Leach, gold, cyanide concentration, particle diameter, oxygen concentration

1. Introduction

CIL process is widely used in the mining industry and in particular, it is an integral part of gold extraction plant. It is a continuous process in which gold is recovered by cyanide leaching of ore slurry and simultaneous adsorption on activated carbon in agitated tanks (Figure 1). From the time CIL process was introduced in the gold processing, a lot of progress and modifications have been made in the industry. However, the dynamics of the process are not yet studied in depth. Various operating parameters like cyanide and oxygen concentration, particle size, competitive adsorption, preg-robbing, carbon transfer cycle affect the dynamics and for the industry to increase the recovery rate, a clear understanding of kinetic mechanism and dynamics is necessary. While a lot of effort has been focused on understanding the kinetic mechanism of leaching and adsorption, the system dynamics has not received due attention. In order to increase the recovery rate, understanding real time response to changes in the operating parameters is essential. In this paper, we discuss a dynamic model for simulating CIL circuits. Transient simulations are carried out to understand the dynamic behavior of the system. The effect of various operating parameters on the performance of the system is also assessed. In the next section the model development is described.

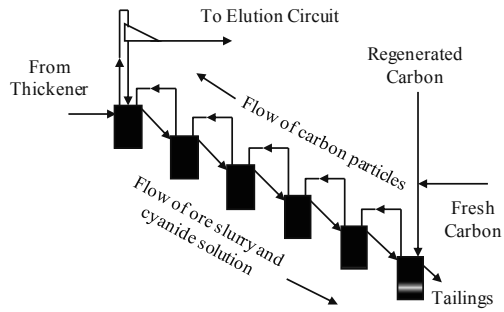

Figure 1. Carbon-in-Leach (CIL) process

2. Kinetics of leaching and adsorption

Table 1 summarizes various models that have been reported for the leaching and adsorption kinetics. Habashi (1966) devised a leaching rate equation that demonstrated the dependence of the leaching on the concentration of oxygen and cyanide. Schubert et al. (1993) modified this equation by including a dimensionless occlusion factor, s, and reduced the reaction rate to a realistic one. Kinetic equation proposed by Crundwell et al. (1997) dependent on electrochemical mechanism, surface passivation and the shrinkage of gold particle. The limitation of all these rate equations is the high probability of error in the exact determination of exposed and passivated surface area through experiments. Moreover, the practical use of such equations in the plant design, scale-up and optimisation is limited (Lima et al. 2005). Particle diameter and reagents concentration are critical for the leaching rate kinetics. But, these parameters were not considered in the models proposed by Brittan (1975), Nicol et al. (1984), Wadsworth et al. (2000) and Coetzee et al. (2005). Ling et al. (1996) developed an empirical equation which included cyanide and oxygen concentration. This work was followed by Lima et al. (2005) in which the particle diameter was also included in the rate equation. Since, this rate equation includes most of the critical process parameters, this equation was used for the calculation of leaching rate.

Adsorption is dependent on the gradient between the gold in liquid and the equilibrium concentration of gold on carbon. But, Kn models are independent of the gold loading on carbon and the model is based on assumption of a constant gold concentration in liquid. It provides highly inaccurate adsorption rate especially in CIL circuits, where, the gold concentration in liquid changes considerably. First order rate equation was only found to be applicable in the initial lower gold concentrations (Le Roux et al. 1991). Freundlich isotherm, Langmuir isotherm and Dixon model provided better fit over a range of data, but only deviated for a comparatively large values of gold concentration, which is practically not faced in the industry (Woollacott et al. 1990). Since there is no significant difference in the adsorption rate calculated using these three models, Langmuir isotherm was used for the adsorption rate kinetics in this paper.

Table 1. Leaching and adsorption rate kinetic models

Author and year	Leaching Rate Equation	Author and year	Adsorption Rate Equation
Habashi (1966)	$\frac{dn_{Au}}{dt} = \frac{2A_{Au}D_{CN^-}C_{CN^-}D_{O_2}C_{O_2}}{\delta\left(D_{CN^-}C_{CN^-} + \chi D_{O_2}C_{O_2}\right)}$	First Order Rate (Fleming et al. 1984)	$\frac{dq}{dt} = k_1 C$
Brittan (1975)	$\frac{dC_{Au}}{dt} = -\exp\left(b_1\left(C_{Au} - C^*_{Au}\right) - b_2\right) \times \left(C_{Au} - C^*_{Au}\right)$	Kn model (Fleming et al. 1980; La Brooy et al. 1986)	$q = k_2 C t^n$
Nicol et al. (1984)	$\frac{dC_{Au}}{dt} = -k\left(C_{Au} - C^*_{Au}\right)^2$	Linear isotherm(Nicol et al. 1984)	$\frac{dq}{dt} = A_c k_3 (C - q/K)$
Schubert et al. (1993)	$\frac{dn_{Au}}{dt} = -k_{Au} n_{Au}\left[\frac{1}{C_{O_2}} + \frac{1.5\chi}{C_{CN^-}}\right]^{-1}$	Freundlich isotherm (Woollacott et al. 1990)	$\frac{dq}{dt} = A_c k_4\left(C - \left(\frac{q}{q_f}\right)^{1/n}\right)$
Ling et al. (1996)	$\frac{dC_{Au}}{dt} = -k\left(C_{CN^-}\right)^{\beta}\left(C_{O_2}\right)^{\beta}\left(C_{Au} - C^*_{Au}\right)^{\varepsilon}$	Langmuir isotherm (Woollacott et al. 1990)	$\frac{dq}{dt} = A_c k_5\left(C - \frac{K_L q}{q^+ - q}\right)$
Wadsworth et al. (2000)	$\frac{dC_{Au}}{dt} = -k_1\left(\frac{K_3\left(C_{CN^-}\right)^{\beta}}{1 + K_3\left(C_{CN^-}\right)^{\beta}}\right)$	Dixon model(Dixon et al. 1976)	$\frac{dq}{dt} = k_6\left(C\left(q^+ - q\right) - K_L q\right)$
Coetzee and Lalloo (2005)	$\frac{dC_{Au}}{dt} = -k_1\left(K_L C_{Au} - \frac{C_{Au(CN)_2^-}}{C_{Au}}\right)^2$		
Lima and Hodouin (2005)	$\frac{dC_{Au}}{dt} = -k\left(C_{CN^-}\right)^{\beta}\left(C_{O_2}\right)^{\beta}\left(C_{Au} - C^*_{Au}\right)^{\varepsilon}$		

3. CIL model and kinetics

A dynamic model based on the first principles for the CIL tanks was written. Following assumptions were made in developing the governing equations: Perfect mixing; negligible back-mixing with previous tank; negligible deterioration or fouling of carbon; no carbon loading profile; carbon transfer occurs simultaneously at regular intervals; constant pH; no pregrobbing and absence of competitive species. Based on these assumptions, the equations for CSTRs were framed and the mass balance equations were written incorporating leaching and adsorption. The reaction kinetics of Lima et al. (2005) were used. A MATLAB program was written for simulating the behavior of the CIL battery. The balance of flow on a reactor i can be written as follows:

$$Q_{fs_i^*} = Q_{f^*} + Q_{s^*_{i+1}} \tag{1}$$

where Qfs is the downflow stream, Qf is the slurry feed stream, Qs is the flow rate of slurry with carbon transfer.

The balance equations for Gold in liquid phase, in ore and on carbon are given by equations 2, 3, and 4 respectively.

$$\varepsilon_{li} V_i \frac{dC_i}{dt} = \frac{\varepsilon_{l(i+1)}}{\varepsilon_{l(i+1)} + \varepsilon_{o(i+1)}} Q_{s^*_{i+1}} C_{(i+1)} + \frac{\varepsilon_{l(i-1)}}{\varepsilon_{l(i-1)} + \varepsilon_{o(i-1)}} Q_{fs^*_{i-1}} C_{(i-1)} - \frac{\varepsilon_{li}}{\varepsilon_{li} + \varepsilon_{oi}}\left(Q_{s_i^*} + Q_{fs_i^*}\right) C_i + r_{leach} - r_{ads} \tag{2}$$

$$M_i \frac{dG_i}{dt} = \frac{\varepsilon_{o(i+1)}}{\varepsilon_{l(i+1)} + \varepsilon_{o(i+1)}} Q_{s^*_{i+1}} \rho_o G_{(i+1)} + \frac{\varepsilon_{o(i-1)}}{\varepsilon_{l(i-1)} + \varepsilon_{o(i-1)}} Q_{fs^*_{i-1}} \rho_o G_{(i-1)} - \frac{\varepsilon_{oi}}{\varepsilon_{li} + \varepsilon_{oi}}\left(Q_{s_i^*} + Q_{fs_i^*}\right) \rho_o G_i - r_{leach} \tag{3}$$

$$W_i \frac{dQ_i}{dt} = \frac{\varepsilon_{c(i+1)}}{\varepsilon_{l(i+1)} + \varepsilon_{o(i+1)}} Q_{s^*_{i+1}} \rho_c Q_{(i+1)} - \frac{\varepsilon_{ci}}{\varepsilon_{li} + \varepsilon_{oi}} Q_{s_i^*} \rho_c Q_i + r_{ads} \tag{4}$$

The rate equations are:

Leaching: $$r_{leach} = k\left(C_{CN^-}\right)^{\beta}\left(C_{O_2}\right)^{\beta}\left(C_{Au} - C^*_{Au}\right)^{\varepsilon} \tag{5}$$

Adsorption: $$r_{ads} = \frac{6 k_{fj} W_i}{\rho_c d_c}\left(C_i - C_{i,s,c}\right) \tag{6}$$

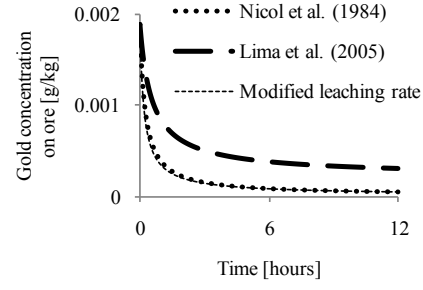

Figure 2. Comparison of leaching rates.

Cyanide Consumption: $$-r_{CN^-} = \left(\frac{1.69 \times 10^{-8}}{\frac{0.547}{\bar{d}} - 6.40} \right) [CN^-]^{3.71} \quad (7)$$

where ε is the volume fraction, C is the gold concentration in leaching tank, Q is the gold concentration on carbon, G is the gold concentration in ore, ρ_o is the ore density and ρ_c is the carbon density, W is the mass of carbon in tank, M is the mass of ore in tank, $C_{i,s,c}$ is the equilibrium concentration on carbon given by Langmuir isotherm.

There is a significant difference in the leaching rate calculated using different kinetic equations. In lieu of valid plant data, Mintek rate equation (Nicol et al. 1984) was used as a reference. The leaching rate calculated from Lima and Hodouin (2005) is slower compared to the Mintek rate equation (see Figure 2). This deviation can be attributed to the dependence of the leaching kinetics parameters, especially residual gold concentration on ore type. The leaching rate was modified so that the predicted reaction rate closely resembled Mintek rate equation. The modified residual gold concentration and k values are given by:

$$C^*_{Au} = 0.357 \times 10^{-4} \left(1 - 1.49 \exp\left(-0.0176 \bar{d}_{ore}\right)\right) \quad (8)$$

$$k = 0.00513 \left(1 - 2.28 \times 10^{-10} \exp\left(-2.93 \bar{d}_{ore}\right)\right) \quad (9)$$

4. Results and Discussion

4.1. Comparison with the literature Data

Due to lack of industrial data on the process, the simulation results were compared to previous studies of Deventer et al.(2004). Deventer et al. (2004) used Mintek leaching rate in their simulations which does not consider the effects of oxygen concentration and particle diameter. Simulations carried out using this rate equation (Figure 3a) closely agree with Deventer's results. Simulations were also carried out using modified Lima and Hodouin (2005) kinetics. These simulations shown in Figure 3b match with Deventer's data.

The Carbon-in-leach process is a countercurrent leaching-adsorption process. The slurry containing ore, lime and cyanide enters the CIL circuit from the first tank and carbon enters from the last tank. The concentration of gold in the solution was observed to decrease across the tanks. This is due to the simultaneous adsorption by the carbon particles in the tank with countercurrent flow. The countercurrent flow ensures a consistent high concentration gradient of gold between the carbon particles and the liquid throughout the circuit. Consequently, according to Le Chatelier's principle, high adsorption rates are observed. Consequently, as the carbon moves countercurrently across the circuit, the loading on the carbon increases exponentially with maximum loading observed in first tank. After the first tank the carbon is removed and is sent to the elution circuit. Even though the gold concentration in the liquid is low, the carbon is able to remove the remaining small quantity of gold leaving a low residual gold concentration.

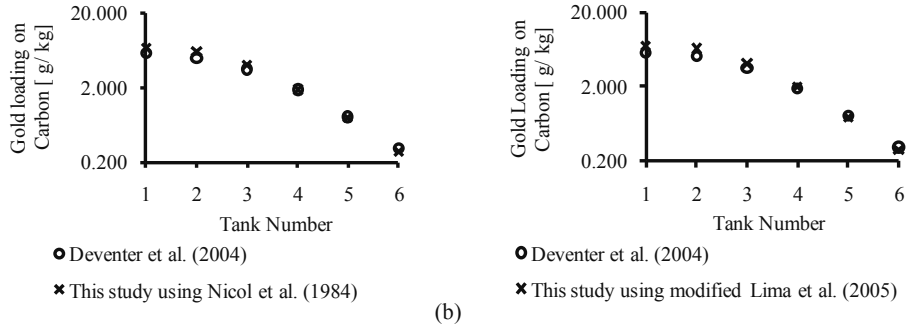

Figure 3. Comparison with literature data

4.2. Dynamic Simulation of CIL in Series

Figure 4 shows the dynamic behavior of gold loading on carbon for in different tank. Simulations were carried out using validated model with the initial gold concentration in liquid = 5 g/m^3 and initial gold loading on carbon = 0 g/kg. While the ore and liquid flow was continuous through the circuit from tank 1 to tank 6, carbon was transferred countercurrently (from tank 6 to tank 1) in a semi batch mode. The carbon transfer cycle was 12 hours with a loading time of 30 minutes.

For any given cycle, in any particular tank, the gold loading on carbon increased with time. It tends to attain an equilibrium value corresponding to the gold concentration in liquid. A reverse trend is observed for gold on ore. As the ore and liquid flow concurrently, the leaching rate decreases along the CIL circuit. Therefore a lower

gold concentration in liquid is observed. Therefore, a decrease in gold loading is observed throughout the circuit.

In general, the concentration in the initial tanks increases with time periodically dropping down as the transfer cycle kicks in. The loading vacillated within a band as a pseudo-steady state is reached. In the later tanks (tanks 4, 5, and 6), the loading first increases quickly (due to the high gradient in initial guess) and then dampens to reach a pseudo steady state value. For the first tank pseudo steady state is achieved within 108 hours (9 cycles). Longer time is required for the other tanks to achieve pseudo steady state with the 6th tank taking longest time.

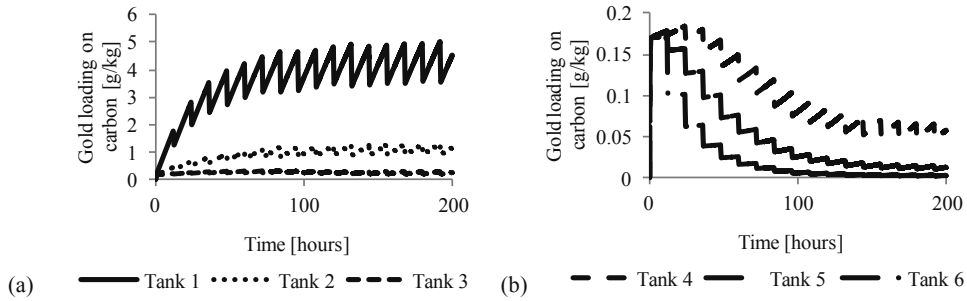

Figure 4. Gold loading on carbon as a function of time for the six tanks of CIL circuit.

4.3. Effect of Process Parameters

Ore particle diameter, cyanide and oxygen concentration have an effect on gold recovery. In order to assess their effect, dynamic simulations were carried out. The values reported below are the time averaged values after steady state was achieved. The results of the simulations with respect to the influence of these process parameters on the efficiency of gold recovery are discussed in the subsections below.

4.3.1. Cyanide Concentration

Cyanide concentration has a prominent effect on the efficiency of the CIL circuit as shown in Figure 5a. With the increase in the cyanide concentration, the efficiency of the CIL circuit increases. The positive impact of cyanide on leaching is due to the Le Chatelier's principle of equilibrium. For a particular particle diameter, the recovery was seen to increase initially with increase in cyanide concentration. Further increase in cyanide concentration did not have any effect on recovery as a plateau was observed. Thus, increasing the cyanide concentration over a certain limit only results in incurring losses.

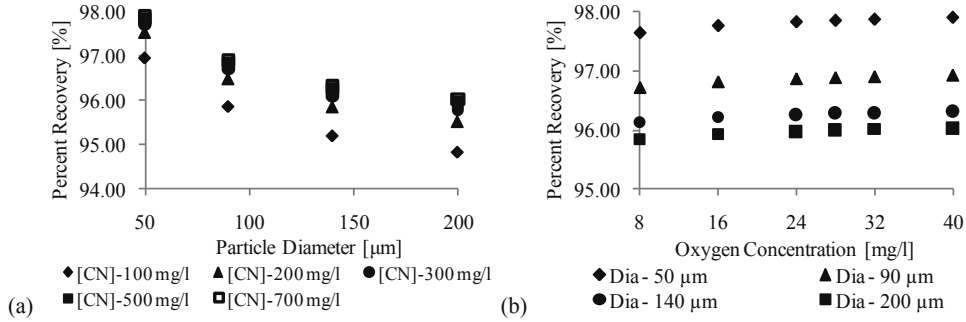

Figure. 5. Effect of (a) cyanide concentration and (b) oxygen concentration on gold recovery.

For low cyanide concentration (100 mg/l), a significant 2.5% change in the percent recovery with respect to particle diameter was observed. At the low cyanide concentration, although the percent recovery was low, the effect of particle diameter was dominant and rate was found to be more sensitive to the particle diameter. This shows that the impact of particle diameter on the CIL process is prominent. For the highest cyanide concentration studied (700 mg/l), although the improvement in percent recovery was 1.9% as compared to the maximum of 2.5%, but the recovery was also much higher. The rate of decrease in cyanide concentration is dependent on particle diameter. The rate of consumption of cyanide decreases with the increase in particle diameter. Therefore, the residual cyanide present is higher for the case of larger particles. This gives the reason for the change in the percent recovery that is slightly higher for the bigger particle than that for the smaller particle for any two cyanide concentrations.

Size reduction increases the surface area of particle and hence, increases leaching. Therefore, decrease in particle diameter increases leaching and so the efficiency of CIL process is increased. The effect of particle

diameter is incorporated in the model through rate constant and the residual gold concentration. The difference in the percent recovery is substantial, but the curve approaches a plateau value for higher particle diameter. That means, the decrease in particle size highly increases the recovery rate. Various size reduction operations in industry, i.e. crushing, grinding, etc. are cost intensive, and in order to obtain a cost effective output, it becomes necessary to conduct an optimization study to obtain an appropriate value of particle diameter, as the size reduction cost increases with the fineness of the particle. Similar case applies for the cyanide concentration, where excess cyanide will only result in excessive running cost. As is clear from the plot, the optimum CN^- concentration for the process lies around 300 mg/l.

4.3.2. Oxygen Concentration

Oxygen is involved in the cyanidation reaction; therefore, its availability is necessary for gold dissolution. The oxygen is incorporated in the leaching kinetic equation and its concentration is assumed to be independent of particle diameter. That is, a constant supply of oxygen is assumed for each CIL tank. Figure 5b shows the effect of oxygen concentration at different particle diameters. For a given particle diameter, increasing oxygen concentration marginally improves gold recovery. The increase in recovery diminishes as the oxygen concentration is increased beyond a certain level. Hence, similar to cyanide, excess oxygen will not result in any significant increase in the recovery. The oxygen is supplied in the CIL tanks through spargers. The flow rate through the sparger can be regulated in order to maintain the oxygen concentration in the CIL tank. To increase the air flow rate in order to gain only a marginal increase in the percent recovery only adds up to the running cost of the plant without any significant profit. Therefore, it is necessary to conduct such study for the ore used and run the plant in the optimized limits.

5. Conclusion

Gold extraction process in a CIL circuit was modeled and simulated. A dynamic model for the CIL circuit was developed and used to study the variation in gold concentration in the liquid and on carbon. The impact of various process parameters on the residual gold in the ore was studied. The results obtained by the model were compared with existing literature and were found to be in close agreement. The main conclusions of this study are summarized below:

1. The particle size and cyanide concentration are critical for the gold leaching. Decrease in the particle size and increase in cyanide concentration result in increase in the efficiency of the process.
2. It is necessary to obtain an optimized value of particle size and cyanide concentration with respect to the cost associated with it in order to save the running cost and obtaining higher efficiency of the process.
3. Oxygen concentration did not show significant effect on the efficiency. Although, a similar optimization study for the oxygen concentration is needed for the prevention of loss due to running costs or increasing the efficiency of the process.

The conclusions from the study will help device suitable strategies for optimizing gold extraction process.

References

Brittan, MI 1975, International Journal of Mineral Processing, vol. 2, no. 4, pp. 321-31.
Coetzee, JW & Lalloo, S 2005, Minerals Engineering, vol. 18, no. 8, pp. 845-8.
Crundwell, FK & Godorr, SA 1997, Hydrometallurgy, vol. 44, no. 1-2, pp. 147-62.
Dixon, S, Cho, EH & Pitt, CH 1976, in AIChE Meeting, Chicago, IL.,. November 26-December 2
Fleming, CA & Nicol, MJ 1984, Journal of the South African Institute of Mining and Metallurgy, p. 85.
Fleming, CA, Nicol, MJ & Nicol, DI 1980, in.,
Habashi, F 1966, Transactions of the Society of Mining Engineers of AIME, vol. 235, pp. 236-9.
La Brooy, SR, Bax, AR, Muir, DM, Hosking, JW, Hughes, HC & Parentich, A 1986, in vol. 100, pp. 123-32.
Le Roux, JD, Bryson, AW & Young, BD 1991, Journal of the South African Institute of Mining and Metallurgy, vol. 91, no. 3, pp. 95-103.
Lima, LRPdA & Hodouin, D 2005, Hydrometallurgy, vol. 79, no. 3-4, pp. 121-37.
Ling, P, Papangelakis, VG, Argyropoulos, SA & Kondos, PD 1996, Canadian Metallurgical Quarterly, vol. 35, no. 3, pp. 225-34.
Nicol, MJ, Fleming, CA & Cromberge, G 1984, Journal of the South African Institute of Mining and Metallurgy, vol. 84, no. 3, pp. 70-8.
Schubert, JH, Barker, IJ & Swartz, CLE 1993, J. S. Afr. Inst. Min. Metall., vol. 93, no. 11/12, pp. 293-9.
van Deventer, JSJ, Kam, KM & van der Walt, TJ 2004, Chemical engineering science, vol. 59, no. 21, pp. 4575-89.
Wadsworth, ME, Zhu, X, Thompson, JS & Pereira, CJ 2000, Hydrometallurgy, vol. 57, no. 1, pp. 1-11.
Woollacott, L, Stange, W & King, RP 1990, Journal of the South African Institute of Mining and Metallurgy, vol. 90, no. 10, pp. 275-82.

I.A. Karimi and Rajagopalan Srinivasan (Editors), Proceedings of the 11th International Symposium on Process Systems Engineering, 15-19 July 2012, Singapore.

The Numerical Simulation of Pneumatic Drying of Polycarbonate in Vertical Tube

Lingqi Kong*, Shiqing Zheng

Research center of Computer and Chemical engineering, Qingdao university of science and Technology,Qingdao 266042 China

Abstract

The mathematical model of pneumatic drying of polycarbonate material in vertical tube was established based on particle dynamics and Eulerian multiphase fluid model. The numerical solution of the model showed a good agreement with experimental data obtained from polycarbonate pilot production on particle moisture and air humidity along the length. Analyses of influencing factors of gas inlet temperature, gas velocity and particle size on moisture of polycarbonate material along tube length were given. The distributions of radial parameters of gas velocity and particle temperature were illustrated. The model can be used for further investigation of the drying of particulate material of industry.

Keywords: Particle dynamics; Eulerian multiphase model; Pneumatic drying; Numerical Simulation.

1. Introduction

Polycarbonate (PC) is a transparent synthetic resin which widely used in fields of electronics, construction, aircraft, security, medical and so on(Yang Wen-hua, et al., 2010). But PC is difficult to convey and dry for two reasons, one is its thermo sensitivity (S M Liu&Y Z Zhou, 2006), the other is that many factors have important influence on the pneumatic drying process. This problem is mainly depends on experimental measurements which consume lots of valuable resource and manpower (W Namkung & M Cho, 2004). These experiments are benefit for solving some practical problems. However, the mechanisms underlying the flow regimes identified and their transition are not clearly understood, which has hindered the development of a general method for reliable scale-up, design, control, and optimization of this technology.Recently, only a few literatures dealing with pneumatic drying modeling or simulation have been published(T J Jamaleddine & M B Ray, 2010). However, no publication presents the comparison between experimental data and theoretical calculation and analysis of pneumatic drying process. In this work, pneumatic drying was conducted experimentally at the pilot scale capacity of PC.

2. Experimental Setup

Use pneumatic drying of a PC pilot as an example, the vertical tube of 15 meters length and its diameter of 0.05 meters, and there are 6 sampling points with 2, 4, 6, 8, 10, 12 meters far from its feed inlet. The experiment was conducted with the following conditions: The flow rate of PC crude material is 88.2kg/h with about 20% water content by weight; air flow rate is 50Nm^3/h with its inlet temperature 373-423K. The

* To whom correspondence should be addressed.Tel.+086(532)84022515. Fax：+086(532)84859913.E-mail: konglingqi@qust.edu.cn

water content of the sample point is the average of particle moisture which sampled and analyzed 12 times with samples interval of 0.5 hour. The temperature can be calibrated by precise instrument with 0.5K accuracy. Three different particle sizes were used: 12-18 mesh(d_S=1.5mm), 18-35 mesh(d_S=1.0mm), and >35 mesh(d_S=0.5mm).

3. Description of Model

3.1. Model Assumption

The model in this work based on the Eulerian multiphase model which assumes both phases as an interpenetrating continuum and permits the solution of the Navier-Stokes equation with the assumption of incompressibility for both the gas and dispersed phases. The other assumptions as follows: (1) the gas phase is a mixture of air and water vapor, while the dispersed phase is a mixture of PC material and liquid water, and both phases are considered incompressible. (2) There is no shrinkage of PC material, only water evaporation during the drying process. (3) The dispersed phase is of uniform size and spherical in shape. (4) Electrical and surface tension forces are absent.

3.2. Hydrodynamic Model Equations

The mass conservation equation(I Skuratovsky et al., 2003) for phase (q=g, s) is

$$\frac{\partial}{\partial \mathrm{t}}\left(\rho_q \alpha_q\right)+\nabla \cdot\left(\rho_q \alpha_q \overline{V}_q\right)=\sum_{\mathrm{p}=1}^{n} S_{pq} \tag{1}$$

Here, S_{pq} represents source term which represents the mass transfer from the *p*th phase to the *q*th phase. The momentum balance equations for the gas (g) and solid(s) are:

$$\frac{\partial}{\partial t}(\rho_g \alpha_g \overline{V}_q)+\nabla \cdot(\rho_g \alpha_g \overline{V}_q \overline{V}_q)=-\alpha_g \nabla P+\nabla \cdot \tau_g+\rho_g \alpha_g \overline{g}+\overline{\beta}_{gs}+S_{sg} \overline{V}_{gs}+\overline{F}_{vm} \tag{2}$$

$$\frac{\partial}{\partial t}(\rho_s \alpha_s \overline{V}_s)+\nabla \cdot(\rho_s \alpha_s \overline{V}_s \overline{V}_s)=-\alpha_s \nabla P+\nabla \cdot \tau_s+\rho_s \alpha_s \overline{g}-\overline{\beta}_{gs}-S_{sg} \overline{V}_{gs}+\overline{F}_{vm} \tag{3}$$

Here, $\overline{V}_{\mathrm{gs}}=\overline{V}_g-\overline{V}_s$. Wen&Yu's formula(Wen C Y & Yu Y H, 1996) was used for the drag force. Drying Model Equations:

$$\frac{\partial}{\partial \mathrm{t}}(\rho_q \alpha_q H_q)+\nabla \cdot(\rho_q \alpha_q \overline{V}_q H_q)=-\alpha_q \nabla P+\tau_q \cdot \nabla \overline{V}_q+Q_{pq}+S_{\mathrm{pq}} H_q \tag{4}$$

The species transport equation (convection-diffusion equation) was used t:

$$\frac{\partial}{\partial t}(\rho_g \alpha_g Y_g)+\nabla \cdot(\rho_g \alpha_g \overline{V}_g Y_g)=\nabla \cdot(\alpha_g \rho_g D_v \nabla Y_g)+S_{sg} \tag{5}$$

The modified k- ε model equations for the continuous phase are:

$$\frac{\partial}{\partial t}(\rho_g \alpha_g k)+\nabla \cdot(\rho_g \alpha_g \overline{V}_g k)=\nabla \cdot(\alpha_g \frac{\mu_{t,g}}{\sigma_k} \nabla k_g)+\alpha_g G_{k,g}-\alpha_g \rho_g \varepsilon_g \tag{6}$$

$$\frac{\partial}{\partial t}(\rho_g \alpha_g \varepsilon_g)+\nabla \cdot(\rho_g \alpha_g \overline{V}_g \varepsilon_g)=\nabla \cdot(\alpha_g \frac{\mu_{t,g}}{\sigma_k} \nabla \varepsilon_g)+\alpha_g \frac{\varepsilon_g}{k_g}(C_{1\varepsilon} G_{k,g}-C_{2\varepsilon} \rho_g \varepsilon_g) \tag{7}$$

$$G_{k,g} = \mu_{t,g}(\nabla \cdot \overline{V}_g + (\nabla \cdot \overline{V}_g)^T)\nabla \overline{V}_g \tag{8}$$

$$\mu_{t,g} = \rho_g C_\mu k_g^2 / \varepsilon_g \tag{9}$$

$$\tau_g = -\frac{2}{3}(\rho_g \alpha_g k_g + \rho_g \alpha_g \mu_{t,g} \nabla \cdot \overline{V}_g) I + \rho_g \alpha_g \mu_{t,g}(\nabla \cdot \overline{V}_g + (\nabla \cdot \overline{V}_g)^T) \tag{10}$$

3.3. Solution Method

3.3.1. Calculated Regional Grids

In the pneumatic drying process with high gas velocity along the vertical tube, the velocity of gas and solid particles in radial and tangential direction, cannot be affected by gravity and drag force, and be taken for zero. And the simulation of the process can be handled for a two-dimensional problem. The computational domain of the two-dimensional vertical tube was divided into non-uniform grid, with finer grid at the entrance and the maximum one less than 0.05m at the exit in the axial direction, and the finest grid was used at the wall and the coarsest one at the center with the thickness less than 0.005m in the radial direction.

3.3.2. Boundary Conditions

Uniform velocity-profile for the gas phase at the riser inlet is oriented vertically upward in the axial direction of the flow; pressure-outlet condition is specified at the riser exit. The turbulent kinetic energy for the gas phase is set as $K = 1.5(V_q I)^2$, where I is the turbulent intensity set at $I = 0.16(Re_{D_H})^{-0.125}$. The turbulent dissipation rate: $e = \rho C_u^{3/4} K^{\frac{2}{3}} / l$ C_u=0.09, l = 0.07 L, in the full turbulent development of hydraulic diameter is equal to the L. Particles are assumed to collide with the wall with a specularity coefficient φ of 0.01. There are nonslip and nonpenetrating wall conditions for the gas phase. An inelastic collision between the particle and wall is assumed with a restitution coefficient e_w of 0.6.User-defined subroutines were added to extend FLUENT capability to account for mixture properties and to simulate the drying rate for surface moisture evaporation and moisture diffusion inside the particulate phase.

4. Results and discussion

4.1. The comparisons of the model and experimental data

Fig. 1 shows the comparisons of numerical solution and experimental data about the particle moisture and air humidity along the tube length. See from Fig. 1, the drying process can be divided into two processes of constant and falling drying rates, which is dominated by the temperature difference, relative velocity, heat and mass transfer of hot gas and particles around. It can be seen that the numerical solution showed a good agreement with the experimental data.

4.2. The effect of gas temperature, gas velocity and particle size on drying

4.2.1. The effect of gas temperature on drying

Fig. 2 illustrated the variation of particles moisture along the tube length with different inlet gas temperature. The higher the inlet gas temperature the faster the drying rate during the constant-rate period and the lower the particles moisture at the entrance. So the inlet gas with higher temperature is favor of drying. But PC is prone to degradation at higher temperature. Here the inlet gas temperature 150℃ is preferable.

4.2.2. The effect of gas velocity on drying

Fig. 3 illustrated the variation of particles moisture along the tube length with different inlet gas velocity. It showed that the inlet gas with higher velocity is favor of drying. This is because the elevation of gas-solid relative velocity enhanced heat and mass transfer. But too high gas velocity makes large consumption of hot gas and energy, so the gas velocity 25m/s is reasonable in Fig. 3.

4.2.3. The effect of particle size on drying

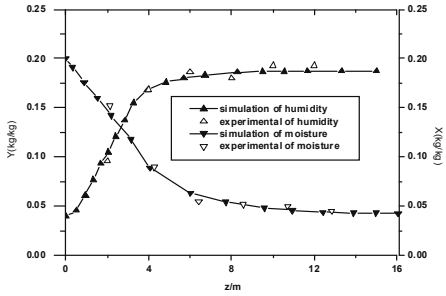

Fig. 1 Comparison of humidity and moisture

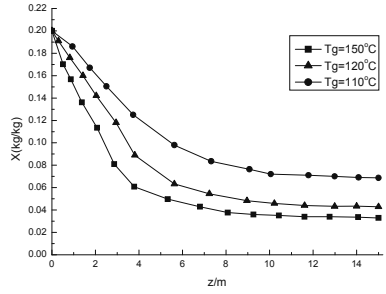

Fig. 2 Particles moisture of different T_g

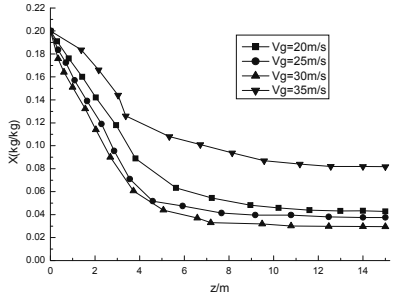

Fig. 3 Particles moisture of different Vg

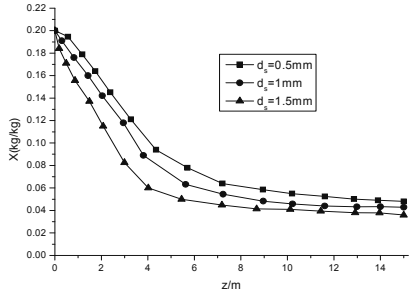

Fig. 4 Particles moisture of different d_S

Fig. 4 illustrated the variation of particles moisture along the tube length with different particle size. It showed that the smaller particle (d_S=0.5mm in Fig. 4) is favor of drying for its larger specific surface area, which intensifies the mass and heat transfer process. But at the end of tube the decrease amplitude of particles moisture is not obvious as that of the initial point. This is because larger particle, with lower velocity of upward moving and longer residence time, offsets part of the effect of contact area. But at the conveying process of higher gas velocity, the effect of gravity is secondary factor compared with drag force of hot gas.

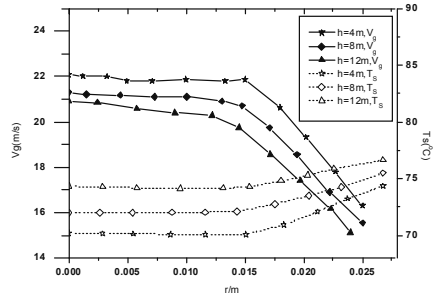

Fig. 5 The radial distributions of Vg and T_S

4.3. The analysis for distribution of radial parameters

The radial distribution of gas velocity and particle temperature is shown in Fig. 5 with different distance apart from inlet (h=4, 8 and 12 meters). It showed the gas velocity is the minimum at the wall with higher velocity gradient because the friction force of tube wall and particle surface reduces it, and on the contrary the gas velocity in the center is the maximum and has a slightly decrease around. It also showed that the gas velocity is decreased along the tube length because of the decrease of the gas temperature. It also showed the particle temperature is the maximum at the wall with higher temperature gradient. This is because the particles near the tube wall has a lower velocity and longer residence time to transfer heat and mass with gas, and has a higher temperature. It can also be deduced that particle moisture near the tube wall is lower。

5. Conclusions

The mathematical model of pneumatic drying of PC material in vertical tube was established based on Eulerian multiphase model. Model predictions showed a good agreement with experimental data, which proved that the model is reasonable and credible. The model was also used for the analysis of the effect of gas temperature, gas velocity and particle size on particles moisture along tube length in drying process and the distribution of gas velocity and particle temperature in radial direction, and reasonable explanation was given. Since the 15m vertical tube is pneumatic dryer used for the drying of PC material of a pilot production, the model can also be used for further investigation of the drying of various other materials of relative importance to the industry.

List of symbols

α_q	volume fraction of phase q	C_d	drag coefficient
d_s	particle diameter (m)	D_v	diffusion coefficient of vapor (m^2/s)
e_w	particle-wall restitution coefficient	$\overline{F}_{vm}$	virtual mass force per unit volume (N/m^3)
I	turbulence intensity	K_q	turbulence quantity of the phase q (m^2/s^2)
k_{cond}	thermal conductivity (W/(m K))	k_c	convective mass transfer coefficient (m/s)
S_{pq}	source term	X	mean particle moisture content
Y	mass fraction of vapor	V_q	velocity vector of phase q (m/s)
β	drag force of the phases (N/m^3)	ε_q	turbulent dissipation rate (m^2/s^3)
μ_q	shear viscosity of q (Pa · s)		

References

I Skuratovsky, A Levy, I Borde, 2003, Two-fluid two-dimensional model for pneumatic drying,Drying Technol.,21(9),1649-1672

S M Liu,Y Z Zhou, 2006, Study on Flame-Retardant Mechanism of Polycarbonate Containing Sulfonate-Silsesquioxane-Fluoro Retardants by TGA and FTIR, Polymer Degradation & Stability, 91,8,1808-1814

T J Jamaleddine, M B Ray, 2010, Application of Computational Fluid Dynamics for Simulation of Drying Processes: A review, Drying Technol., 28,120-154

Wen C Y and Yu Y H, 1996, Mechanics of Fluidization, Chem. Eng. Prog. Symp. Series, 62, 100-111

W Namkung and M Cho, 2004, Pneumatic Drying of Iron Ore Particles in a Vertical Tube, Drying Technol., 22,877–891

Yang Wen-hua, Yang Xia, Zheng Shi-qing, 2010, Application and Production of Polycarbonate, Guangzhou Chemical Industry,38,8,76-79

I.A. Karimi and Rajagopalan Srinivasan (Editors), Proceedings of the 11th International Symposium on Process Systems Engineering, 15-19 July 2012, Singapore.

The OPOSPM as a Nonlinear Autocorrelation Population Balance Model for Dynamic Simulation of Liquid Extraction Columns

Menwer Attarakih[a,b,*], Hanin B. Jildeh,[b,c] Matthias Mickler,[b,c] Hans-Jörg Bart[b,c]

[a]*The University of Jordan, Faculty of Engineering & Technology, Department of Chemical Engineering, 11942 Amman, Jordan*
[b]*Chair of Separation Science and Technology, TU Kaiserslautern*
[c]*Centre of Mathematical and Computational Modelling, TU Kaiserslautern, P.O. Box 3049 - 67653 Kaiserslautern, Germany*
**Corresponding author's e-mail: attarakih@yahoo.com*

Abstract

Dynamic simulation and online control problems in liquid extraction columns are still unresolved issues due to the two-phase flow and the particulate character of the dispersed phase. In this work, the One Primary and One Secondary Particle Model (OPOSPM) with two autocorrelation parameters is used as an alternative to the full population balance model. The model presents the base hierarchy of the SQMOM and consists only of two transport equations for droplet number and volume concentrations. Using the full population balance model or online experimental data, the autocorrelation parameters are identified using a constrained weighted nonlinear least square method. Compared to the experimental data in RDC and Kühni columns, the autocorrelated OPOSPM predicts accurately the dynamic and steady state mean population properties with a simulation time amounts to only 3% of that required by the detailed model.

Keywords: Autocorrelation, OPOSPM, Liquid Extraction, Image Analysis.

1. Introduction

Steady state design of chemical equipment is confronted by dynamic and controllability issues. In this regard, it is often easy to design a chemical process based on steady-state conditions, which is practically uncontrollable and unrealistic. In order to avoid any wrong assumption during process synthesis and design, and to ensure safe and stable plant operation, the dynamic behavior of the relevant units should be known. Two-phase flow liquid extraction equipment is widely used in the chemical industries, which is characterized by varying time constants, inherent nonlinearities and different time scales. Population Balance Modeling (PBM) is a fast emerging mathematical framework, which takes into account different physical and chemical phenomena that lead to the evolution of the discrete particulate (droplet) phase. Despite recent progress in model development, numerical methods and the computational power of modern computers, PBM is still not widely used in process control, dynamic analysis, online and model predictive control. In this contribution we present a novel One Primary One Secondary Particle Model (OPOSPM) as the simplest case of the hierarchical SQMOM [1,2]. The OPOSPM consists only of two transport equations; namely, the continuity equations of the volume and number concentrations of the particulate phase. The source term of the number concentration transport equation contains two adjustable constants, which takes into account model deviation from the reference (detailed) population balance model. These constants compensate for model deviation due to breakage and

coalescence events and can be correlated offline using prescribed changes in the major input variables such as inlet phase flow rate and rotor speed. These constants are identified by formulating the system at hand as a nonlinear minimization problem with simple bounds on the two identified parameters. For this purpose, experimental facilities are designed to measure droplet size distribution and population mean properties under different disturbance [3,4].

2. The OPOSPM as a nonlinear autocorrelation PBM

Online autocorrelation and parameter identification using full population balance models is extremely difficult and complicated due to the increase in the size of the differential algebraic system, which governs the system dynamic behaviour. The OPOSPM [2] is modified using two autocorrelation parameters: $\boldsymbol{\theta} = [K_b \quad K_c]^{\mathrm{T}}$. In one-dimensional space the model is given by:

$$\frac{\partial \mathbf{U}}{\partial t} + \frac{\partial (u\mathbf{U})}{\partial z} = \mathbf{S}(\mathbf{U}, \boldsymbol{\theta}),\ \mathbf{U} = \begin{bmatrix} N & \alpha \end{bmatrix}^T$$
$$\mathbf{S} = \begin{pmatrix} \dfrac{u^{in}}{v_{in}} \delta(z - z_{in}) + K_b(\vartheta(\bar{d}) - 1)\Gamma(\bar{d})N - \dfrac{1}{2} K_c \omega(\bar{d}, \bar{d}) N^2 \\ u^{in} \delta(z - z_{in}) \end{pmatrix} \tag{1}$$

In the above equations, N and α are the total number and volume concentrations, which are equivalent to zero and third moment of the droplet population in the extraction column. The mean-mass droplet diameter ($\bar{d}$) is an adaptive Gauss-Christoffel quadrature node or position of the secondary and primary particles. This mean droplet diameter couples the two state variables (N and α) through the mean droplet volume. The dispersed phase velocity relative to the column walls is u, while $u^{in}$is the superficial velocity of the dispersed phase. The breakage and coalescence frequencies are $\Gamma$and ωrespectively, which are functions of rotor speed, column internal geometry and system physical properties. Due to breakage of liquid droplets by internal (turbulent) and external (rotor blade) forces, a mean number of daughter droplets (ϑ) can be statistically estimated. The reduced model above can be derived from the SQMOM by setting the number of primary and secondary particles and $\boldsymbol{\theta}$ equal to one [1,2]. As phenomenological reduced model, it is able to capture most the essential physical information contained in the full PBM and is still computationally tractable. The respective autocorrelation (learning) parameters (K_b and K_c) for breakage and coalescence kernels can be estimated off or online. In the above model, both α and $\bar{d}$ are amenable to on- and off line measurements [3,5]. However, due to the complication of optical droplet size distribution, the uncertainty in droplet mean diameter is higher than that in measured holdup. To take this into account and during model learning, a weighted least square method is used where the measured $\bar{d}$ and α are combined by forming the weighted sum of residuals:

$$\begin{aligned} &\min_{\theta} \mathbf{e}^T \mathbf{W} \mathbf{e}^T, \\ &s.t.\ \ \mathrm{Eq.}(1), \\ &\mathbf{e} = (\Delta\alpha_1 ... \Delta\alpha_{N_\alpha} ... \Delta\bar{d}_1 ... \Delta\bar{d}_{N_d}), \mathbf{W} = diag(w_1^\alpha ... w_{N_\alpha}^\alpha .. w_1^d ... w_{N_d}^d) \end{aligned} \tag{2}$$

With appropriate model functions and parameters, the model is learnt according to the formulation in (2), which can be viewed as a solution of an online inverse problem. The

diagonals in the weight matrix **W** are chosen to give less weight to the uncertain mean droplet diameter residuals. The steady state sensitivity of the model to changes in the parameters vector **θ** is derived and is found to be:

$$S_{\alpha,j} = \frac{\partial \alpha}{\partial \theta_j} = -\alpha u \frac{\partial u}{\partial \theta_j}, \; H_{j,k} \approx 2 \sum_i \frac{\partial \alpha_i}{\partial \theta_j} \frac{\partial \alpha_i}{\partial \theta_k} \tag{3}$$

where **H** is the Gauss-Newton approximation of the Hessian matrix. The Hessian matrix itself is used to estimate an order-of-magnitude confidence intervals of the learning parameters. It is interesting to note that the model sensitivity is a strong function of explicit droplet velocity [6] and is damped by the continuous phase velocity ($u = u_r - u_x$) and α. By referring to the source term of Eq.(1), it is also interesting to notice that droplet breakage tends to increase model sensitivity with respect to $K_b\Gamma$. The eigenvalue analysis of H indicates the importance of $K_b\Gamma$ and its strong dependence on the rotor speed. The detailed PBE is resolved using an extended fixed-pivot technique [6] with respect to droplet diameter and finite volume method with respect to physical space. Since droplet coalescence is highly sensitive to the hydrodynamics and physicochemical properties, interfacial dynamics and mass transfer [6], Coulaloglou and Tavlarides (1977) coalescence model had been studied to identify the two coalescence parameters, which are named here as C_1 and C_2 [7, 9]. The first parameter (C_1) appears in the droplet coalescence frequency, while the second one (C_2) is used to adjust the droplet coalescence efficiency. In the second phase, data acquisition system is needed for both dynamic and steady state measurements. Accordingly, experimental facilities are developed for online measurement of droplet size distribution and dispersion mean properties using different types of columns (Kühni and RDC). Once the OPOSPM is learnt under specified column operating conditions, it can be used effectively to predict the mean dispersed phase properties due to different external disturbances.

3. Experimental setup and particle image processing

The experimental setup is designed for online measurement and prediction of droplet size distribution and in particular transient process changes using stirred columns. For experimental determination of droplet size distribution, two techniques are used: An optical measurement and a conductivity based method. The stirred column used here is a Kühni column of 1.0 m height and 0.15 m internal diameter. The column has seven conductivity measurement points and two optical measurement points. With the optical measurement technique [4], droplets can be captured locally and temporally while conductivity technique is used to measure integral holdup. The images obtained by the image analysis method are evaluated by algorithms based on population moments. The core elements are a segmentation followed by Euclidean distance transformation [8]. The centres of the circles are allegorised by the maximum distance to the background. Because of separation difficulties of overlapping circles, an implementation of watershed segmentation algorithm is used. Thus the setting, position and radius of droplets in the image can be found. The approach allows reliable online analysis of more than 300 droplets per image in transmitted light mode and up to 3-5 pictures per second (online, single-core) with concentrations up to 15% (vol./vol.) with a relative error less than 5% [3]. Due to restrictions of image analysis and camera speed, duration of measurement is in the range 5-10 seconds per measurement point. This corresponds to 15-50 pictures in online and 150-300 pictures in offline mode per measurement point.

4. Results and Discussion

In the steady state learning phase of the model, the OPOSPM and the full PBM are both tested using the chemical system toluene-water in a pilot plant RDC column (80 mm diameter). The steady state experimental data [5] on α and $\bar{d}$ are used first in the detailed PBM to estimate the Coulaloglou and Tavlarides (1977) model parameters. This results in values of $3.41\times10^{-2} \pm 2\times10^{-3}$ and $1.33\times10^{11} \pm 1\times10^{6}$ m^{-2}, which corresponds to 95% confidence interval for C_1 and C_2 respectively. The eigenvalues of the Hessian matrix are 1.0 and 4.6×10^{3} approximately, indicating that the objective function is not very sensitive to changes in the parameter C_2. Following the published literature on C_2, this parameter is held constant [7].

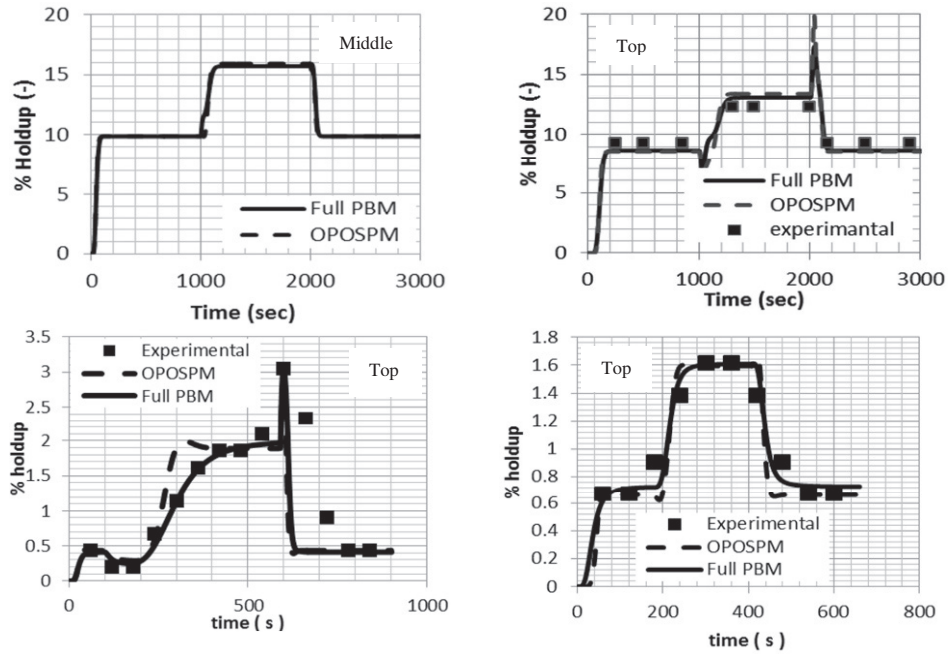

Figure 1: Simulated mean holdup using the OPOSPM compared to the full PBM and experimental data in RDC (upper panel) and Kühni (lower panel) extraction columns.

In the second phase, the model with optimal C_1 and C_2 is learnt using Eq.(2) at two different steady states along the column height with 200 and 400 rpm rotor speed. The weights, which appear in Eq.(2) are set to 0.65 for α and 0.35 for $\bar{d}$. The estimated parameter vectors $\boldsymbol{\theta}$ are [0.10 2.4] and [0.21 2.4] respectively. It is clear that droplet breakage increases due to the increase of the energy dissipated in the continuous phase at high rotor speed. The upper panel of Figure (1) shows the response of the dispersed phase holdup (α) due to rectangular pulse (200-400-200 rpm) in rotor speed. The OPOSPM of Eq.(1) follows accurately the detailed model at the middle and top of the column. The sharp changes in the dispersed phase are due to the hyperbolic structure of the system (1). At the beginning, the sudden decease of the droplet size at the distributer results in increased phase holdup at the bottom of the column, which results in a decrease of the effective continuous phase velocity. This in effect increases the effective velocity of the continuous phase and hence the holdup is decreased. As the disturbance propagates along the column, the dispersed phase increases everywhere and rises

gradually to its final steady state. The reverse occurs due to a negative step change in rotor speed(at ≈ 2000 s). The experimental data of Garthe (2006) are at steady state, and therefore the inverse response due to step changes in the rotor speeds could not be verified. To verify this interesting behavior, a dynamic experiment is designed using 150 mm diameter Kühni column with column geometry as stated in the previous section. While the column is at steady state (80 rpm, 170 & 11.2 liter/h for the continuous and dispersed phases respectively) a rectangular pulse (80-160-80 rpm) in the rotor speed is introduced. The OPOSPM was learnt at steady state with parameters: $K_b = 1.4$ and $K_c = 2.551$ using the measured holdup (α). The mean inlet diameter is held approximately constant at 1.8 mm using toluene as the dispersed phase in water and the optimal C_1 is $4.5 - 250.0 \times 10^{-3}$ and C_2 is held constant as in the first case. Note that the change in breakage frequency as function of rotor speed compensates for any extra change in K_b, while C_1 reflects the change in coalescence frequency. Fig.(1, lower panel) compares the experimental and the OPOSPM simulation of the dispersed phase holdup. The inverse response is clear at both corners of the rectangular step change and the OPOSPM follows the experimental data fairly well. In the last panel of Fig.(1), the dynamic response of the dispersed phase holdup due to a rectangular pulse in the dispersed phase rate (7.5-14.9-7.5 liter/h) is measured. The rotor speed is kept constant at 120 rpm. The solid line is the OPOSPM simulation with constant learning parameters $K_b = 1.4$ and $K_c = 2.551$ and $C_1 = 3.55 \times 10^{-2}$. As can be seen, the agreement between the dynamic data and model prediction is excellent. Furthermore, K_b, K_c and C_1 are clearly insensitive to the dispersed phase flow rate as expected [9]. This is because both breakage and coalescence frequencies are not strong functions of the dispersed or continuous flow rates. The simulation shows that the OPOSPM can simulate the column mean properties with a simulation time amounts to only 3% of that required by the full model. Furthermore, the optimization algorithm based on the interior-point method in MATLAB, is found to converge in a few iterations (5-8) with CPU time about 1.3 seconds on a laptop of 2.4 GHz speed.

5. Conclusions

The OPOSPM with two learning parameters is used for off- and online dynamic and steady state simulation of particulate flow in liquid extraction columns. These learning parameters are successfully autocorrelated using a weighted nonlinear least square optimization subject to a nonlinear differential system constraint. The OPOSPM can easily predict the mean dispersed phase holdup along the height of extraction column, with a simulation time not greater than 3 percent of that required by the detailed model. The the present reduced OPOSPM with autocorrelation parameters can be used for solving online inverse problems and model predictive control strategies.

References

[1] M. M. Attarakih, C. Drumm and H.-J. Bart, Chemical Engineering Science, 64 (2009) 742.
[2] M. M. Attarakih, M. Jaradat, C. Drumm, H.-J. Bart, S. Tiwari, V. K. Sharma, J. Kuhnert & A. Klar, Computer Aided Chemical engineering, 26 (2009) 1333.
[3] M. Mickler, S. Didas and H.-J Bart, ISEC 03.-07.10.2011, Santiago, Chile, (2011).
[4] M. Mickler, S. Didas, M. Jaradat, M. Attarakih and H.-J. Bart, Chem. Ing. Tech., 83 (2011) 226.
[5] D. Garthe, PhD Thesis, Technical University of Munich, (2006).
[6] C. A. Coulaloglou and L. L. Tavlarides, Chemical Engineering Science, 32 (1997) 1289.
[7] M. M. Attarakih, H.-J Bart and N. M. Faqir, Chemical Engineering Science, 61 (2006) 113.
[8] R. Fabbri, L. Da F. Costa, J. C. Torelli and O. M. Bruno, ACM Computing Surveys 40, No. 1 (2008).
[9] H. Jildeh, M. M. Attarakih, M. Mickler and H.-J. Bart (2012). To appear in the proceedings of ESCAPE 22, 17-20 June 2012, London/UK.

I.A. Karimi and Rajagopalan Srinivasan (Editors), Proceedings of the 11th International Symposium on Process Systems Engineering, 15-19 July 2012, Singapore.

The Simulation and Analysis of Coal to Liquids Processes

Li Sun, Robin Smith

Centre for Process Integration, School of Chemical Engineering and Analytical Science, University of Manchester, Manchester, M13 9PL, UK

Abstract

Coal to liquids process is becoming industrially important for chemicals production and the cogeneration of electricity. The tail gas treatment and process syngas consumption lead to different polygeneration arrangements. In this paper, CTL process integrated with the utility system are simulated, and three configurations with different tail gas treatment are analyzed. The tail gas as fuel in the utility plant can satisfy process power and energy demands and create a surplus.
Keywords: CTL, polygeneration, Fischer-Tropsch, reforming, tailgas

1. Introduction

With the rapid rise in the crude oil price, coal to chemicals and liquids oil (CTL) through Fischer-Tropsch (FT) synthesis is increasingly being exploited and becoming a priority, especially in the United States and China [1].

CTL process basically includes raw synthesis gas production, syngas purification for to meet FT synthesis requirement and the liquids oil production. The tail gas from FT synthesis, mainly containing CH_4, CO, H_2, CO_2, can be used as fuel and combusted in gas turbines or boilers for power and heat generation in the utility plant. Coal to chemicals production with cogeneration of electric power means polygeneration. In addition, the components CO and H_2 in the tail gas are syngas key compositions for FT synthesis, and their recovery and recycle would be beneficial for liquids production.

In this paper, based on the simulation of CTL integrated with the utility system, different CTL configurations are analyzed from the view of liquids oil production, process power demands, and power generation in the utility plant.

2. Process configurations

Figure 1 shows the CTL flowsheet blocks. Syngas consumption and tail gas treatment would allow various CTL configurations.

2.1. Syngas for power generation and chemicals production

The syngas for the FT liquids production is involved in the typical CTL process. If the syngas is only for power generation, it is so called Integrated Gasification Combined Cycle (IGCC) [2]. In this paper, only the first case is studied.

2.2. FT process tail gas treatment

FT process tail gas contains CO, H_2, C1-C4 light alkanes, and a small amount of heavy alkanes. There are three ways to treat this tail gas.

1) The tail gas is fully burnt as fuel in gas turbines for power generation or in boilers for very high pressure (VHP) steam generation in the utility plant.

2) The components CO and H_2 in the tail gas are recovered and recycled to the FT synthesis by separation units. H_2 recovery is carried out by membrane separation, and CO by pressure swing adsorption (PSA) [3]. This recycle can be achieved because there

are no components in the tail gas to poison FT catalysis reaction. It is beneficial for FT production profit with the recourse of supplying extra fuel in the utility plant.
3) The tail gas is fed to the reforming process to regenerate more CO and H_2 from C1-C4 alkanes in the tail gas, and recycle these CO and H_2 to the FT synthesis.

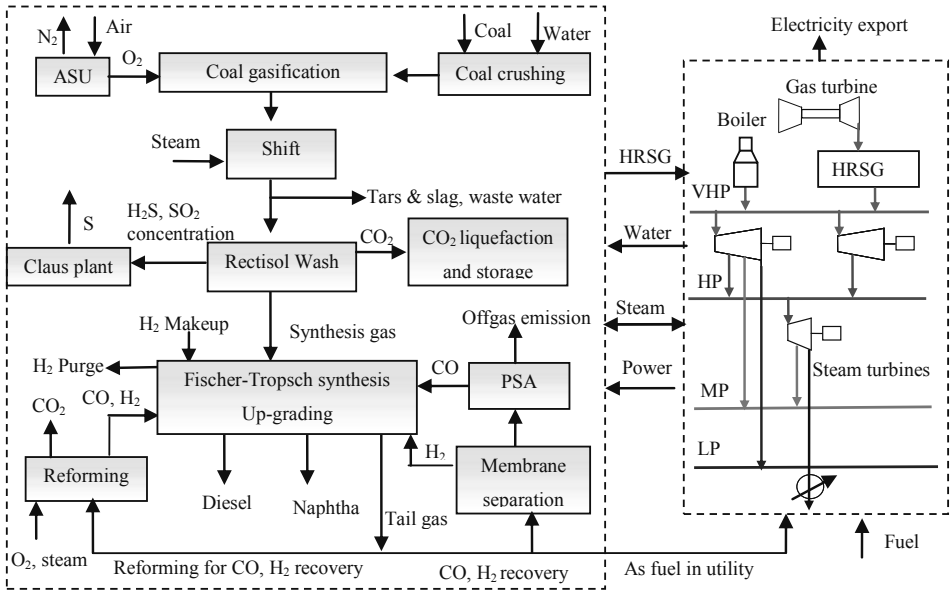

Figure 1 CTL flow sheet blocks

3. Process simulation

In this paper, both the liquids oil production process and utility system are simulated as an integrated system to provide streams detail, process heat and power demands, utility system energy and energy supply or further process analysis and optimization.
The CTL production and tail gas recovery processes are simulated and fully converged using Aspen Plus. The utility system simulation is carried out with the software 'STAR' developed by Centre for Process Integration, University of Manchester[4], which has been verified and utilized in industrial projects.

3.1. Liquids oil production

An air separation unit (ASU) supplies O_2 for the coal gasification and N_2 mainly as diluent gas for NO_x control in gas turbines for power generation. ASU contains units of air pre-treatment, air cooling, liquefaction, and cryogenic air separation.
Coal gasification is operated for the syngas production from the coal slurry and oxygen in the gasifyer at a pressure of 5.6MPa [5]. The gasification temperature is about 1350°C. Before the coal is fed to the gasifyer, it is crushed to the required particles sizes. The gasification reactions are shown in equations (1). The raw syngas consists primarily of H_2, CO, water steam, CO_2, with small amounts of H_2S, COS, CH_4, Ar and N_2.

$$C + 0.5\ O_2 \rightarrow CO$$

$$C + O_2 \rightarrow CO_2$$

$H_2 + 0.5\ O_2 \rightarrow H_2O$
$C + H_2O \rightarrow H_2 + CO$
$C + 2H_2O \rightarrow 2H_2 + CO_2$ (1)

A 2-stage sour shift unit is for the syngas production with the required molar stoichiometric ratio (SR) of about 2. SR is a key value for the syngas composition for the following liquids FTproduction. Equation (2) shows the shift reaction.

Molar Stoichiometric Ratio, SR $=H_2/CO$

The shift reaction: $CO + H_2O \leftrightarrow H_2 + CO_2$ (2)

Raw syngas purification includes acid gas removal by Rectisol wash technology, and sulphur recovery in a Claus plant [6]. Rectisol wash is a physical absorption process by removing H_2S, COS and CO_2 at very low temperature (-54°C) and higher pressure (33 MPa) with methanol as solvent[7]. It consists processes of sour components absorption, solvent regeneration and dehydration. In terms of the units operation, they are flashing, stripping, rectification, and heat exchange. The purified syngas is FT synthesis feed. The H_2S and SO_2 concentration stream is converted to sulphur by high temperature thermal reaction and lower temperature catalytic reaction (equations (3-4)) in the Claus plant. CO_2 offgas, almost free of H_2S, is compressed to 8.0 MPa for underground storage.

Oxidation stage: $H_2 + 0.5O_2 \rightarrow H_2O$
$CO + 0.5O_2 \rightarrow CO_2$
$CH_4 + 2O_2 \rightarrow CO2 + 2H_2O$
$H_2S + 1.5O_2 \rightarrow SO_2 + H_2O$
$2NH_3 + 1.5O_2 \rightarrow N_2 + 3H_2O$
$COS + 1.5O_2 \rightarrow CO_2 + SO_2$ (3)

Catalytic stage (Sulphur forming) : $2H_2S + SO_2 \rightarrow 3S + 2H_2O$ (4)

FT synthesis plus product upgrading is to produce liquid transportation oils from the cleaned syngas. To obtain long-chain alkane products (more diesel and Naphtha oil production), the high-temperature FT synthesis with Fe or Co catalyst is carried on at about 320°C[8].

3.2. Tail gas recovery

For the tail gas direct recovery and recycle process, H_2 is recovered through a membrane module made from Polyimide (PI) at the permeating pressure 2.9 kPa(g). PSA for CO recovery adopts 5-1-1/RP VPSA technology with Cu^+Y sorbent at the entrance pressure of 0.8 MPa(g). The recovery efficiency of H_2 and CO is 93.3% and 85.6% respectively.

The auto thermal reforming reaction would convert C1-C4 alkanes in the tail gas into extra CO and H_2 reacted with pure oxygen and steam at 300°C, 3.0Mpa. C1-C4 alkanes conversion ratio is 97.3%. The mol fraction of CO in the tail gas rises from 12% to 28% after reforming, and H_2 from 16% to 56%. The gas after reforming would remove H_2O by flashing and CO_2 by Rectisol wash before recycled to the FT synthesis. The followings are reforming equations.

$CH_4 + H_2O \rightarrow CO + 3H_2$
$CH_4 + 0.5O_2 \rightarrow CO + 2H_2$ (5)

3.3. Utility system

The utility system is the process of fuel combustion for steam and power generation. The fuel would be natural gas, coal, tail gas, etc.

The tail gas or fuel is fully burnt in gas turbines (GT) for power generation or in boilers for very high pressure (VHP) steam generation. The exhaust from GT generates VHP steam in heat recovery steam generators (HRSG) and distributes to multi-pressure-level

steam network through steam turbines and letdowns for the process heating demands or expands in steam turbines (ST) for extra power generation.

4. Process analysis

For the different options in a polygeneration arrangement, the liquids production processes are similar, but the tail gas treatments and utility fuel consumption would result in variations of process steam and power demands, chemicals production, CO_2 capture and storage, and utility system power and heat generation.

The feed coal contains carbon 58.9%, ash 5.6%, moisture 20.0%, and others 15.5%. Main feeds and products data are listed in Table 1. Table 2 gives the tail gas data. Power demands in the CTL process are shown in Table 3.

Table 1 Main feeds and products data

		Mass Flow, kg/h
Feed	Coal	1.05×10^5
	O_2 from ASU	7.36×10^4
Semi product	Syngas (FT Feed)	7.26×10^4
Liq products	Diesel	1.47×10^4
	Naphtha	6.81×10^3
Tail gas from FT	As fuel in utility plant	1.88×10^4
CO_2	CO_2 storage	1.136×10^5

Table 2 Tail gas data

Fuel gas export, kg/h		18850
Net heatign value - kJ/kg		26291
Composition mol%	N_2	3.96
	H_2	15.61
	CO	12.47
	CO_2	16.4
	Methane	41.22
	Ethane	2.82
	Propane	2.37
	N-Butane	2.45
	C5-C10	0.95
	Others	1.75

Table 3 Power demands data in the CTL process

Unit	Description	Power, kw
Coal crushing	Coal particles crushed to be 12mm	1.3×10^3
ASU	Air /N_2 compression	2.56×10^4
Rectisol Wash	Solvent recycle compression, solvent pumps	1.13×10^3
CO_2 liquefaction	CO_2 compression	1.16×10^4
Refrigerant Power	Refrigerants generation	1.01×10^4
FT	Process pumps. etc	3.22×10^3
Site demand	Pumps of BFW, CW, effluents, air fans,etc.	3.73×10^4
Total		5.67×10^4

Table 4 Products prices

	Price
Diesel, US$/ton	1234
Naphtha, US$/ton	1277
Coal, US$/ton	159
Electricity, US$/kwh	0.087

Three CTL configurations with different tail gas treatment are analyzed from the view of liquid products, CO/H_2 recovery, process power demands, fuel supply to the utility plant, and power export to the grid.

Table 4 lists the products prices data. Table 5 gives the comparisons of CTL with different polygeneration arrangements.

From Table 5, it is clear that the tail gas as fuel can satisfy the CTL process power and heat requirement and export extra power to the grid. It is also the simplest flowsheet compared with other two configurations without extra tail gas separation units. Considering products benefit and utility costs, the last configuration of tailgas reforming for more CO and CH recovery would generate 2287 US$/h more than the first

configuration with the compensation of extra reforming unit and complex operation. What is more, CO_2 emission in the 3rd configuration increasing 8.4% with the comparison of the 1st configuration means greater environmental burden and less carbon conversion. However, with flexible products prices and fuel supply, the last two configurations could also challenge.

Table 5 Comparisons of CTL with different polygeneration arrangements

Tail gas treatment		As fuel	CO, H_2 Direct recovery	Reforming + CO, H_2 recovery
Liq products, kg/hr	Diesel	1.47×10^4	1.47×10^4+413	1.47×10^4+3596
	Naphtha	6.81×10^3	6.81×10^3+187	6.81×10^3+1664
Tail gas recovery, kg/hr	H_2	0	2.34×10^2	2.08×10^3
	CO	0	2.43×10^3	1.42×10^4
Process power demands, kw		5.67×10^4	5.67×10^4+0.5×10^4	5.67×10^4+1.18×10^4
Fuel supply to utility plant, kg/hr		0	5.81×10^3	6.60×10^3
Power export to grid, kw		35400	0	0
CO_2 storage, kg/hr		1.136×10^5	1.136×10^5	1.136×10^5+9.60×10^3
Tail gas recovery units		N/A	Mem sep + ASP	Reforming process
Process income*, US$/hr		3224	-180	5511

* Process income=Liquids benefit (Diesel, Naphtha) + Power export income –fuel supply cost

5. Conclusions

Considering the Integration of the CTL process with the utility system, different tail gas treatment would cause several of polygeneration arrangements. The CTL configuration of the tail gas as fuel in the utility plant is energy/power self sufficient. The tail gas recovery is beneficial for liquids production with additional fuel supply to the utility plant as pension. The tail gas reforming process can realize more CO and H_2 conversion and recycle with extra reforming units as recourse.

The choice of the available configurations would be helpful for the products and power production balance to meet flexible market changes.

Acknowledgments

The authors wish to express their appreciation to the funding from BP International Limited, UK.

References

1 Chris Knudsen, etc, 2007, Process Economics Program Report 154B, Coal gasification, SRI consulting,

2 F. Emun, etc., 2010, Integrated gasification combined cycle (IGCC) process simulation and optimization,Computers and Chemical Engineering, 34: 331-338

3 Y Fang, 2009, The study on the FT offgas recovery [D]， Dalian university of technology

4 www.manchester.ac.uk/ceas/cpi/software

5 G Liu, etc., 2011,Making Fischer-Tropsch fuels and electricity from coal and biomass: performance and cost analysis, Energy Fuels, 25: 415-437

6 Abraham P. Gelbein, 2008, Acid gas removal, SRI consulting

7 Aspen Technology, Inc. 2008. Rate-Based Model of the CO_2 Capture Process by Methanol using Aspen Plus

8 H.S.Song , etc., 2004, Operating strategies for Fischer-Tropsch reactors: A Model-Directed Study, Korean J. Chem. Eng., 21(2): 308-3175

I.A. Karimi and Rajagopalan Srinivasan (Editors), Proceedings of the 11th International Symposium on Process Systems Engineering, 15-19 July 2012, Singapore.

Agent-Based Simulation Framework for Public Bus Fleet Electrification Investment Analysis

Shisheng Huang[a], Rajagopalan Srinivasan[b], Joseph F. Pekny[c], Gintaras V. Reklaitis[c]

[a]*Singapore-MIT International Design Centre, Singapore University of Technology and Design, 20 Dover Drive, Singapore 138682*
[b]*Department of Chemical and Biomolecular Engineering, National University of Singapore, 4 Engineering Drive 4, Blk E5, Singapore 117576*
[c]*School of Chemical Engineering, Purdue University, Forney Hall of Chemical Engineering, 480 Stadium Mall Drive, West Lafayette, IN 47907, USA*

Abstract

The electrification of vehicles presents a viable solution towards the reduction in reliance on fossil fuels and greenhouse gas emissions. However, the electrification of public bus transportation requires making several key decisions on the form of technology selection, operation requirements and cost management. An agent-based multi-paradigm modelling framework is proposed to enable detailed analysis to support this decision process. In this work, a framework for the modelling of a bus depot undergoing electrification is presented along with a modest example.

Keywords: Electric Vehicles, Public Buses, Agent-Based Modeling, Electrification

1. Introduction

Historically, gasoline and diesel fuels have been used for transportation, but the possible decline of oil supplies in the future is forcing nations to consider alternative fuels. Electric Vehicles (EVs) are viable options that can help reduce the dependence on these fossil fuels. Public transportation is an integral part of the transportation network in most major cities. The electrification of this network could potentially help both to generate significant cost savings and to achieve reduction in greenhouse gas emissions.

The electrification of this system represents a major investment and careful management of this transition is crucial in avoiding unwanted costs. Furthermore, the management of an electrified fleet poses increased challenges in resource management, requires new approaches to bus scheduling, and careful selection and maintenance of these new technologies. Although there have been abundant research conducted in the operations and management of traditional bus depots and interchanges, the electrification of such systems may require new and innovative ways in analysis.

2. Background

A literature search reveals that the body of literature available that is related to the electrification of public transportation systems, especially mass transport systems like public buses is quite limited. Most of the literature on the electrification of the transportation fleet has focused on the electrification of private vehicles or more conventional hybrid vehicles. Certain niche markets such as transforming school buses(Sadiq et al., 2007) and trolley buses(Leo, 2010) into Plug-in Hybrid Electric

Vehicles (PHEVs) have been examined, although the operation and optimization of such systems have not been analyzed. Sinhuber et al. have discussed the conceptual technical requirements of electric buses needed for public transport electrification. They have found that the shallow cycling of batteries would be the optimal for the preservation of the batteries and allow for lower overall costs, analysis of bus schedules could further help in reducing operational costs(Sinhuber et al., 2010).

3. Methodology

Agent-based modelling approaches are composed of interacting, autonomous agents; which through their interactions can give rise to patterns, structures and behaviours that were not explicitly programmed into the models(Macal and North, 2010). The electrification of a bus depot allows for a natural formulation in which electric buses and the charging stations are treated as intelligent agents capable of making charging and route decisions. Eventually, the framework could be extended to passengers and bus drivers allowing for even more in-depth analysis into operations management.

An agent based, multi-paradigm modelling approach is proposed for the analysis of the electrification of a public bus depot. This approach has been successfully used in the analysis of energy systems (Hodge et al., 2011). In this study we are proposing to adapt that framework to the analysis of a bus depot. The overarching framework for the analysis of such a scenario can be seen in Figure 1. The depot would consist of a fleet of public buses that could either be an electric vehicle or conventional diesel bus. Charging structures would need to be installed to ensure smooth operation of the vehicles. A central scheduling agent would seek to optimize and coordinate vehicle flows in and out of the depot. An overall optimization engine for the simulation would be used to determine optimal policy and operational parameters.

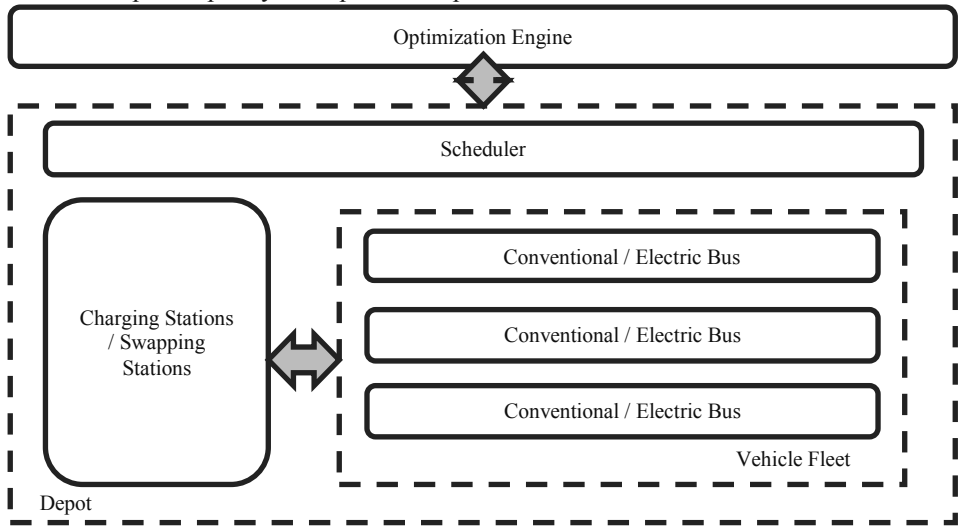

Figure 1: Simplified framework for the analysis of the electrification of a bus depot

In this paper, we would examine in detail the framework for the electrification of an agent based bus depot, specifically the framework for the buses and charging stations. There are several competing technologies that would be available for such an analysis and the model should provide for such competing alternatives.

3.1. Buses

A basic schematic diagram of an electric bus is shown in Figure 2. The agent at any time could be in any of the four states. It starts a daily cycle in a home bus depot until its scheduled departure for a route. It could be assigned an inter bus depot route which brings it to another bus depot or a loop service which brings it back to the bus depot. Once back at the home depot, it would check if it would need to replenish its battery charge or go back to waiting for another scheduled departure. A central planning agent could modify its pre-determined schedules to meet certain operational benchmarks.

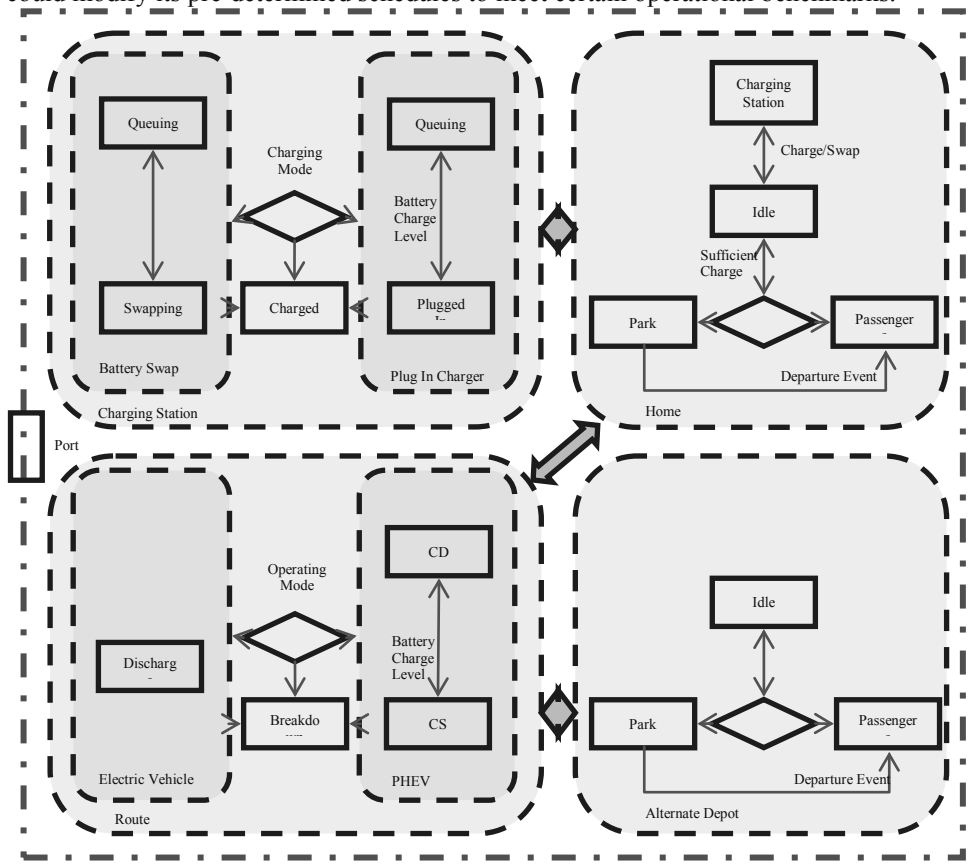

Figure 2: Schematic diagram of an agent electric bus

the form of a decision variable during optimization. a pure Electric Vehicle (EV) or a plug-in version (PHEV). An EV has the advantage of potentially not emitting any greenhouse gases. However, an EV could be hampered by its limited range which restricts its applicability in long-distanced routes originating from the bus depot. A PHEV has an alternative fuel supply on board which it could tap on to extend its electricity range; however, it potentially does this through consuming fossil fuel which produces greenhouse gas emissions. The PHEV operates on two modes, a Charge Depleting (CD) mode which utilizes only electricity for mobility and a Charge Sustaining (CS) mode which uses an alternative fuel for locomotion. There could be two configurations for a bus, a 12 meter conventional bus or an 18 meter articulated bus. A 12 meter electric bus would consume on average 1.8 kWh/km while an articulated one would consume about 2.75 kWh/km (Sinhuber et al., 2010). During its

CS mode, a PHEV bus can be assumed to consume similar amounts of fuel as a PHEV school bus at about 8 miles per gallon or 3.4 kilometers per liter (Pritchard and Johnson, 2004).

3.2. Batteries and Charging Infrastructure

The batteries considered in this study are lithium-ion based technologies, however at the level of detail appropriate for this study, consideration of specific chemistries is not of primary importance (Dinger et al., 2010). Battery costs are estimated to be around US$1000 per kWh at the moment but are expected to reach US$500 by 2020 (Dinger et al., 2010). Due to weight limitations, the capacity of batteries would be limited to 200 – 250 kWh(Sinhuber et al., 2010). It has been suggested that the optimal Depth Of Discharge (DOD) of batteries should not be more than 16%(Sinhuber et al., 2010); however, this may not be applicable to all battery chemistries(Peterson et al., 2010). Efficiency of batteries were assumed to be 95%(Joos et al., 2010). Charging of batteries could be either through level 2 or level 3 chargers and their specifications can easily be found in literature(Santini, 2010). Potential costs for level 2 charging stations could range from $700 to $4000 while level 3 stations could cost upwards of $35,000 each (Santini, 2010). Battery swapping is another viable alternative to plug-in chargers with the potential of recharging a bus in just several minutes. The estimated cost for a vehicle swapping station could be as high as $500,000 (Yarow, 2009).

4. Applications

4.1. System Policy Applications

Investment planning problems could be investigated using this framework. An example case would be the comparison of investment options between public transport alternatives such as public buses and taxi fleets. Utility level analysis such as capacity planning, transmission planning and rate tariff formulations could be conducted. Secondary usage policies, such as battery leasing strategies, peak energy management which can help subsidize these investments could also be examined.

4.2. Operational Applications

Operational issues related to the operation of an electrified bus depot could also be studied. These studies could be related to optimal resource allocation in investment planning, such as the number of buses to retrofit/procure, number of charging points, stations to build, number of routes to electrify and even additional manpower resources needed. All these parameters could be optimized such that operational benchmarks for a bus depot like punctuality, breakdown rates, are maintained when compared to a conventional bus depot.

4.3. Sample Scenario

A conventional bus depot in Singapore was used as a sample case for the framework. The bus depot selected was the Woodlands bus depot in Northern Singapore (SMRT, 2012). The depot has 21 routes that could be electrified. As a demonstration case, 7 routes with short loops were selected to be electrified. In order to maintain operational benchmarks, different numbers of charging stations were compared with the minimum charge level required for buses during operation. The benchmark that was considered was the percentage of missed or late departures to within 5 minutes of scheduled departures from the depot. Table 1 shows a summary of results with different operational parameters.

Table 1: Percentage of missed or late departures from depot with different operational parameters

		Minimum Charge Level				
		0.9	**0.8**	**0.7**	**0.6**	**0.5**
Charging Stations	**5**	4.37%	3.30%	3.04%	2.85%	2.50%
	4	11.63%	4.83%	3.81%	3.17%	2.78%
	3	26.97%	16.13%	11.32%	8.15%	7.77%

The operational target was 15% in 2008, with actual operations at 0.06% (SMRT, 2009). With 7 routes electrified, 4 charging stations are needed to bring the operational figure below 5% but not to current levels. This could represent a challenge to the optimization problem and would be discussed in more detail in a future publication.

5. Conclusion

Electric vehicles have the potential of replacing diesel powered public transportation in the future. In order to aid in the transition of this sector while conserving resources, detailed analysis of electrification is not only needed, but crucial. In developing such a tool, an adaptation of our previous agent-based multi-paradigm modeling framework is proposed. In this work, the approach is illustrated with the case of a bus depot undergoing electrification is presented.

References

Dinger, A., Martin, R., Mosquet, X., Rabl, M., Rizoulis, D., Russo, M., Sticher, G., 2010. Batteries for Electric Cars: Challenges, Opportunities, and the Outlook to 2020. The Boston Consulting Group.

Hodge, B.-M.S., Huang, S., Siirola, J.D., Pekny, J.F., Reklaitis, G.V., 2011. A Multi-Paradigm Modeling Framework for Energy Systems Simulation and Analysis. Computers & Chemical Engineering 35, 1725-1737.

Joos, G., de Freige, M., Dubois, M., 2010. Design and Simulation of a Fast Charging Station for Phev/Ev Batteries, Electric Power and Energy Conference (EPEC), 2010 IEEE, pp. 1-5.

Leo, R., 2010. Potential Solutions for Electric Vehicles in Bus and Delivery Traffic, Faculty of Electronics, Communications and Automation. AALTO University, p. 95.

Macal, C.M., North, M.J., 2010. Tutorial on Agent-Based Modelling and Simulation. Journal of Simulation 4, 151-162.

Peterson, S.B., Apt, J., Whitacre, J.F., 2010. Lithium-Ion Battery Cell Degradation Resulting from Realistic Vehicle and Vehicle-to-Grid Utilization. Journal of Power Sources 195, 2385-2392.

Pritchard, E.G.D., Johnson, R.R., 2004. Hybrid Electric School Bus Preliminary Technical Feasibility Report. N.C. Energy Office, North Carolina.

Sadiq, S., Pritchard, E., Dulaney, K., Emadi, A.H., 2007. Plug-in Hybrid Market Transformation by Leveraging a Niche Market: School Buses, Vehicle Power and Propulsion Conference, 2007. VPPC 2007. IEEE, pp. 483-492.

Santini, D.J., 2010. Cost-Effective Phev Range: Battery Costs Versus Charging Infrastructure Costs, Transportation Research Board Annual Meeting, Washington, DC.

Sinhuber, P., Rohlfs, W., Sauer, D.U., 2010. Conceptional Considerations for Electrification of Public City Buses - Energy Storage System and Charging Stations, Emobility - Electrical Power Train, 2010, pp. 1-5.

SMRT, 2009. Annual Report 2009. SMRT, Singapore.

SMRT, 2012. Buses - Woodlands Town Map. SMRT.

Yarow, J., 2009. The Cost of a Better Place Battery Swapping Station: $500,000. Business Insider.

I.A. Karimi and Rajagopalan Srinivasan (Editors), Proceedings of the 11th International Symposium on Process Systems Engineering, 15-19 July 2012, Singapore

Modeling and Control Challenges in the development of Discrete Microfluidic Devices

Jeevan Maddala,a Raghunathan Rengaswamy,a *
a Department of Chemical Engineering; Texas Tech University; Lubbock, Texas, USA

Abstract

Droplet-based microfluidics is an emerging area that has important applications in chemical engineering and several other disciplines. For example, these devices have applications in the areas of bubble computers, cancer diagnostics and development of microfactories on a chip. Some of the challenges that need to be overcome to realize the potential of this area are related to experimental uncertainties and development of devices that offer multiple functionalities, thereby reducing the footprint and aiding in miniaturization. Achieving precise functionalities in microfluidics is challenging because droplets exhibit complex dynamic behavior in these devices due to hydrodynamic interactions and discontinuities that are a result of discrete decision-making at junctions. Remarkably, transitions from periodic to aperiodic/chaotic behavior based on input conditions can be witnessed even in a simple loop device. Hence rational design frameworks that handle this complexity are required to make significant progress. Further, passive designs that achieve such functionalities might entail large footprint. As a result, active control might become a necessity for developing efficient device designs. The main purpose of this paper is the identification of the challenges and opportunities for the PSE community in this area of emerging importance. Further, our work in the area model predictive control (MPC) for active control in a microfluidic loop device will also be briefly described.

Keywords: Droplet microlfuidics, modeling and control, model predictive control

1. Introduction

Droplet based microfluidics forms the basic building block for lab on chip devices. In droplet microfluidics, discrete volumes (droplets) are produced using immiscible fluids. These droplets provide a unique environment for conducting reactions or producing concentration gradients with high precision. Droplet based microfluidic devices have been used in protein crystallization (Zheng et al., 2004), high throughput screening of cells (Brouzes et al., 2009) and single cell analysis (Huebner et al., 2007). The attractiveness of these droplet microfluidic devices vis a vis microfluidic devices stems from the fact that droplet based devices offer precise control of flow without the attendant scaling issues of general microfluidic devices, where the device size scales linearly with the number of experiments/tasks that need to be performed. Since droplet microfluidic devices use discrete flows, a large number of reactions/experiments can be performed without increase in size or complexity (Teh et al., 2007). As a result, several lab-on-a-chip applications with reduced footprint can be realized. From a chemical engineering perspective, these devices could provide breakthroughs in the development of microprocessing facilities that are relevant for high value and hazardous applications. For such applications, development of

*raghu.rengasamy@ttu.edu

rational design and control frameworks is still in its infancy. Almost, all of the developments in the area of systems engineering are likely to find applications in this exciting new area. The aim of this brief conference paper is to discuss some of the promising PSE tools that are directly relevant in the area of discrete droplet based microfluidics. Given the limited space, it is not possible to provide an exhaustive account of the various themes in PSE that we believe are relevant in this area. The intention is then to describe some of the interesting application concepts and also tie that with our ongoing work in this field.

2. Modeling opportunities

We envisage a microfactory in a discrete microfluidic platform to consist of a large of number of operational units that are tightly interconnected and form a network akin to a large chemical engineering processing facility. Similar to the tremendous impact simulation and modeling tools such as ASPEN/gPROMS have had in typical chemical engineering facilities, we expect discrete bubble microfluidic simulation tools to have an analogous significance. One of the main challenges is to conceptualize a discrete microfluidic network as consisting of repeating model fragments similar to the mass, momentum and energy transfer devices that one routinely encounters in chemical engineering problems. There are unique challenges that are related to the identification of a compact set of fundamental unit operations. One set of basic operations in droplet based microfluidic systems consists of droplet generation, droplet sorting, droplet merging, droplet splitting, droplet transporters and droplet storing units. These operations can be combined to produce various microfactory designs. An associated challenge is the development of computationally tractable models for these operations. One direction is the development of CFD models for these operations but that might not be very useful for design and control studies. Another approach is to develop conceptually simple models that are able to capture the rich dynamic behavior of these systems. A striking example of such a model development is the network model for droplet dynamics in a simple loop device that was proposed by Schindler and Ajdari (2008). This simple model based on resistive network ideas is able to explain complex and rich nonlinear behaviors that are experimentally observed (Jousse et al., 2006). This model is also extremely useful for design studies as discussed in Maddala and Rengaswamy (2012). However, this simple model might not be sufficient for online control, where the impact of the so called "thinking time" (Epstein, 2007) at the entrance of the loop device might be significant. A challenge and an opportunity then is to be able to enhance these models to higher fidelity levels without losing their computational tractability. Further, such simple models need to be developed for other operations that are relevant from the viewpoint of microfactory design.

3. Control opportunities

Control challenges abound in this area. Precise control is required in almost all the unit operations such as droplet generation, droplet sorting and droplet merging. In case of droplet generation, achieving uniform droplet size is contingent on achieving precise control over the size and shape of the droplets. Since droplets are used for drug discovery and biosensing, uniform dosing and concentrations must be ensured (Teh et al., 2007). Traditional approaches in particle formation result in broad particle size distribution, whereas droplet based systems produce monodisperse droplets with less than 1% size variations (Teh et al., 2007). Most of the droplet generation techniques use syringe pumps, where the oscillations in the pump can affect the droplet production. Further, the droplets present

in the channel can affect the upstream droplet production due to the resistance change that the syringe pump encounters. As a result, producing a large number of uniform size droplets is a challenging problem. A good model for this system and a feedback control strategy to manipulate the bulk and dispersed phase flows could be a worthwhile research direction.

Similar to droplet production, droplet sorting is an important task for high throughput screening of cells. The maneuvering of droplets to various branches of a network either by an external force or by incorporation of a moving component in the network are classified as active techniques. In droplet microfluidics either external valves or electrodes are used as active components. Valve mechanism demonstrated by Abate and Weitz (2008) is an example of active sorting. The valve constricts the flow in the channel thereby modulating the instantaneous flow the droplets face as they move through the channel. This idea can then be used to sort the droplets to different arms by manipulating the differential resistance that they encounter. Through this approach (Abate and Weitz, 2008), sorting error was shown to be less than 0.001% and droplets are sorted at a rate of 250Hz (Abate et al., 2010). Only basic on/off control is performed using this valve. To perform more complex tasks a good model of the valve needs to be developed and the droplet motion in the bifurcating channels needs to be studied. A passive device to sort droplets is developed by Cristobal et al. (2006). This device sorts the droplets alternately into the right and left branches. The article highlights the importance of incorporating a bypass near the bifurcation, which impacts the sorting scheme. When more droplets enter the channels, the decision is based on the least resistance branch. Having bypasses ensures that the decision is based only on one droplet at a time as once the droplets move past the bypasses, the resistances of both the branches as viewed from the bifurcation point are equal. Passive techniques such as these, while appealing due to their simplicity, might lack the ability to handle broad range of flow rates and disturbances in the input flows.

We now discuss MPC implementation for a particular application system to highlight the opportunities and challenges in the design and validation of model-based active control strategies in this area (Maddala et al., 2011a,b). We consider the task of sorting and synchronization of droplets to explain the model predictive control framework. We do so by considering a simple fluidic loop with two actuators and develop model predictive control strategies to achieve droplet sorting, synchronizing and merging tasks similar to that depicted in Fig. 1. The passive synchronizer (Prakash and Gershenfeld, 2007) design assumes that the black and white droplets arrive in two arms, whereas a single arm delivers the droplets into the loop device. Hence, the loop is required to perform a more complicated function which is a combination of sorting and synchronization. Clearly, a loop device with no active control will not perform either the sorting or synchronization. There are several questions that need to be answered for a solution to this active control problem. The first pertains to the mea-

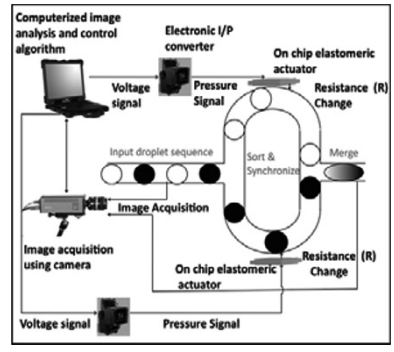

Figure 1. Possible implementation of model predictive control on loop device

surement and actuation strategy. As shown in Fig. 1 we propose an image processing system as the measurement technology. This system would allow online calculation of all droplet positions in the loop within the viewing area of the microscope. This measurement system will be able to sense the two critical parameters that are required for the sort-synchronize operation. The system will be able to specify which droplet (B/W) is entering the system and will also provide all the droplet positions in the system. From this, the controlled variable, which is the projected time difference between the exit times of the droplets at the upper and lower arms, can be calculated. The actuation for this problem will be realized using on-chip elastomeric valves. Given that valve control can be achieved experimentally, hydrodynamic resistance of any section in the loop can be actively manipulated. The next question relates to the choice of an appropriate algorithm for active control. We argue below that standard PID type control is not suitable for our purpose. First it becomes apparent that sorting control requires modulation of resistances in both the arms. This is because it is not possible for the microvalve to decrease the resistance below the inherent branch hydrodynamic resistance, but only increase. As a result, the sort-synchronize control would require two types of actuation. One is logic actuation where a resistance change is made whenever a droplet is at the entrance. Based on the current hydrodynamic resistances, the resistance in the arm that the droplet is not supposed to enter is increased than the other arm. It is clear that precise estimate of resistances through a physics-based model can help reliably perform this control. We further note that the idea of steady-state gain and time constant used in typical PID tuning are not applicable to this problem. This is because output time periods can show multiplicities in response to changes in the inputs. Further, the notion of steady-state is not valid as the output switches between different periods. Lastly, the system is highly interactive in the sense that changing the resistance in any one of the arms affects the droplet behavior in both the arms. All of these reasons basically rule out any simple PID type control and also any purely data driven model based control. A predictive controller is required. The main objective in MPC is to maintain outputs at their set points through the use of manipulated variables (actuators). MPC possesses the following important attributes: (i) simplicity, (ii) richness to solve a variety of control problems, and (iii) constraints handling (equipment constraints, operational constraints) These attributes make MPC an attractive choice for control of discrete microfluidic systems.

Notice that while the preliminary work published by Maddala et al. (2011a) demonstrates the promise of MPC based active control, there are several aspects that need to be studied further. These are: (i) How robust is the MPC to uncertainties in the droplet sequences and inlet arrival times? If one used an enhanced model would the MPC still work? What effects of the physical process (such as droplet resistance varying with flow, thinking time) are important to be included in the internal model that the controller uses yet still generate acceptable control results? These are computational questions that require considerable further work before resolution. Another major challenge is that the MPC approach has to be experimentally verified with microvalves in the loop device. While doing so, experimental issues related to droplet breakage due to active control might have to be considered. Further, concerns related to actuator dynamics and computational complexity of MPC calculations need to be addressed. For the loop structure, the droplets exit at around 40 milliseconds (ms) time intervals. The time required for one actuator move is about 10 ms. If the sampling time is chosen to be 10 ms, then about four actuator moves can be made before the exit of droplet. However, other systems might require faster dynamics and this needs to be taken into account. Further, computational complexity in terms

of the ability of the MPC approach to identify the actuations in milliseconds needs to be addressed. Parametric programming approaches (Sakizlis et al., 2004) might play an important role here.

4. Conclusions

In summary, the modeling and control opportunities in the field of discrete droplet microfluidic systems were identified. The idea of breaking down a discrete microfluidic network into discrete model fragments and modeling approaches for such fragments were discussed. From the context of control, the application of MPC for the control of discrete bubble microfluidic systems was discussed.

References

Abate, A. R., Agresti, J. J., Weitz, D. A., 2010. Microfluidic sorting with high-speed single layer membrane valves. Applied Physics Letters. 96 (203509), 1–3.

Abate, A. R., Weitz, D. A., 2008. Single-layer membrane valves for elastomeric microfluidic devices. Applied Physics Letters. 92 (243509), 1–3.

Brouzes, E., Medkova, M., Savenelli, N., Marran, D., twardowski, M., Hutchison, J. B., Rothberg, J. M., Link, D. R., Perrimon, N., Samuels, M. L., 2009. Droplet microfluidic technology for single-cell high throughput screening. Pnas 106 (34), 14195–14200.

Cristobal, G., Benoit, J.-P., jaonicot, M., Ajdari, A., 2006. Microfluidic bypass for efficient passive regulation of droplet traffic at a junction. Applied Physics Letters. 89 (034104), 1–3.

Epstein, I. R., 2007. Can droplets and bubbles think? Science 315 (5813), 775–776.

Huebner, A., Srisa-Art, M., Holt, D., Abell, C., Hollfelder, F., deMello, A. J., Edel, J. B., 2007. Quantitative detection od protein expression in single cells using droplet micrfluidics. Chem. Commun., 1218–1220.

Jousse, F., Farr, R., Link, D. R., Fuerstman, M. J., Garstecki, P., 2006. Bifurcation of droplet flows within capillaries. Physical Review E. 74 (036311), 1–6.

Maddala, J., Rengaswamy, R., 2012. A genetic algorithm (GA) based rational approach for design of discrete microfluidic networks. In: 22nd European Symposium on Computer Aided Process Engineering. Elsevier, pp. 1–5.

Maddala, J., Srinivasan, B., Bithi, S. S., Vanapalli, S. A., Rengaswamy, R., 2011a. Design of a model-based feedback controller for active sorting and synchronization of droplets in a microfluidic loop. AIChE Journal, –.

Maddala, J., Vanapalli, S. A., Rengaswamy, R., 2011b. Sort-synchronization control in microfluidic loop devices with experimental uncertainties using a model predictive control (MPC) framework. International Federation of Automatic Control (IFAC), 4886 – 4891.

Prakash, M., Gershenfeld, N., 2007. Microfluidic bubble logic. Science 315, 832–835.

Sakizlis, V., Kakalis, N. M., Dua, V., Perkins, J. D., Pistikopoulos, E. N., 2004. Design of robust model-based controllers via parametric programming. Automatica 40 (2), 189 – 201.

Schindler, M., Ajdari, A., 2008. Droplet traffic microfluidic networks: A simple model for understanding and designing. Physical Review Letters. 100 (044501), 1–4.

Teh, S.-Y., Lin, R., Hungb, L.-H., Lee, A. P., 2007. Droplet microfluidics. Lab Chip 8 (4), 198–220.

Zheng, B., Tice, J. D., Ismagilov, R. F., 2004. Formation of droplets of alternating composition in micrfluidic channels and applications to indexing of concentrations in droplet based assays. Anal Chem. 76 (17), 4977–4982.

I.A. Karimi and Rajagopalan Srinivasan (Editors), Proceedings of the 11th International Symposium on Process Systems Engineering, 15-19 July 2012, Singapore.

Simulation of Hydrodynamics and Heat Transfer in Confined Jet Reactors of Different Size Scales for Nanomaterial Production

Cai Y Ma[1], Xue Z Wang[1]*, Christopher J Tighe[2], Robert I Gruar[2] and Jawaad A Darr[2]

[1]*Institute of Particle Science and Engineering, University of Leeds, Leeds LS2 9JT, United Kingdom (* x.z.wang@leeds.ac.uk)*
[2]*Department of Chemistry, University College London, London WC1H 0AJ, United Kingdom*

Abstract

Continuous hydrothermal flow synthesis (CHFS) is an attractive process for producing high quality inorganic nanoparticles. The direct collection of detailed data about the CHFS process during experiments is not always feasible due to the supercritical conditions, hence affecting optimisation and control and scale-up. In this paper, computational fluid dynamics models are developed for confined jet reactors of a CHFS system for nanomaterial production at both laboratory and pilot-plant scales. The flow, mixing and temperature profiles in the reactors were simulated using the ANSYS Fluent package. The predicted temperature profiles were compared with the available experimental data and the mixing between supercritical water and precursor streams was examined in detail. The hydrodynamic and thermodynamic features of the reactors at both size scales were also compared.

Keywords: Confined Jet Reactor, Computational Fluid Dynamics, Supercritical Water, Scaling-up, Mixing

1. Introduction

Supercritical water (ScW) hydrothermal synthesis has been used to produce metal oxides that have a wide range of applications. Continuous hydrothermal flow synthesis (CHFS) method was developed to overcome the limitations of hydrothermal batch reactions since CHFS is easy to implement automatic control, relatively green, and able to produce very fine nano-particles for a number of functional materials. However, the laboratory and pilot-plant scale systems cannot produce the required amount of nanomaterials for commercial use. Therefore scaling-up and optimization of the system becomes very important.

In scaling up a process from laboratory to pilot plant and industrial scale, direct collection of detailed experimental data in order to study and optimise scaling-up factors is difficult due to the huge number of experiments that need to be conducted and the extreme conditions of the experiments. Computational fluid dynamics (CFD) modelling is a useful tool to study the potential effects of these factors at different size scales and to evaluate alternative designs. CFD modelling has been used to study ScW oxidation processes by some researchers (Bermejo and Cocero, 2006; Lester et al., 2006; Moussiere et al., 2007; Narayanana et al., 2008; Aimable et al., 2009; Kawasaki et al., 2010; Demoisson et al., 2011; Ma et al., 2011a; Ma et al., 2011b; Sierra-Pallares et al., 2011). The application of CFD modelling to ScW hydrothermal synthesis for production of nanoparticles is limited in literature. Lester et al. (2006) used CFD to

simulate the velocity distributions of a nozzle reactor. However, the simulation was based on a pseudo ScW reactor with methanol and sucrose being used to represent ScW and metal salt. Aimable et al. (2009) carried out prediction in the mixing zone of a reactor and obtained temperature and velocity profiles but with little details being given. Kawasaki et al. (2010) studied ScW hydrothermal process in a T-shaped mixer using experiment and CFD simulation. CFD simulation was performed to understand the mixing behaviour in the mixer. Sierra-Pallares et al. (2011) attempted to quantify the nixing efficiency in ScW hydrothermal reactors, but without comparisons to experimental data. Demoisson et al. (2011) performed CFD simulations for the design of a reactor operating in ScW conditions but without detailed comparisons with measurements.

In this paper, CFD models were developed to predict the process in confined jet reactors at different size scales of a CHFS system. The predictions of flow, mixing and temperature profiles in the reactors were carried out using the ANSYS Fluent package (2010). The predicted temperature profiles were compared with the available experimental data and the mixing between ScW and precursor streams was examined. The hydrodynamic and thermodynamic features at both size scales were also compared.

2. Mathematical formulation

2.1. Hydrodynamic and mixing models

The Reynolds-averaged continuity, momentum and enthalpy equations are numerically solved to obtain hydrodynamic and heat transfer profiles (Ma et al., 2011a). The most commonly used turbulence model is the k - ε model (Jones and Launder, 1972) where the turbulent kinetic energy k and its dissipation rate ε are solved using k and ε equations with standard empirical constants. Simulation of mixing was carried out by introducing an inert tracer into the primary liquid in the reactor. The tracer concentrations were obtained from the solution of the species transport equation:

$$\frac{\partial \rho Y_i}{\partial t} + \frac{\partial \rho u_j Y_i}{\partial x_j} = \frac{\partial}{\partial x_i}\left(\Gamma_{i,eff}\frac{\partial Y_i}{\partial x_j}\right) \quad (1)$$

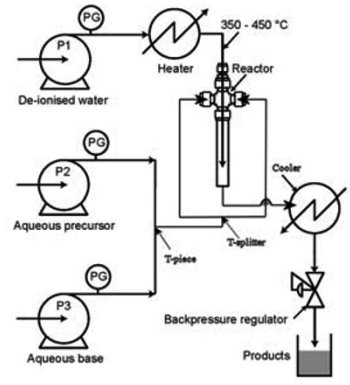

Figure 1 Flow diagram of a confined jet CHFS system.

where the effective diffusion coefficient of species i, $\Gamma_{i,eff} = \Gamma_i + \mu_t / Sc_t$, ρ is the mixture density, u_j the mixture velocity, p the pressure, τ_{ij} the viscous stress, Y_i the species mass fraction, Γ_i the species diffusion coefficient, μ_t the turbulent eddy viscosity, and Sc_t the turbulent Schmidt number.

2.2. Thermodynamic properties

In this study, the water properties obtained from National Institute of Standard and Technology (2009) using the 1995 IAPWS formulation for the thermodynamic properties of ordinary water substance (Wagner and Pruß, 2002) were piece-wise curve-fitted in polynomial forms over several temperature ranges at 24.1 MPa, and used to calculate water properties efficiently and accurately. The diffusion coefficient correlation from Liu and Macedo (1995) was used to estimate water diffusivity.

3. Experimental study

The flow diagram of a CHFS confined jet reactor system used for temperature profiling and also nanoparticle production experiments is shown in Figure 1. Deionised water was pumped through a heater system using pump P1 at 24.1 MPa and constant flowrates of 20 and 400 mL/min for the laboratory and pilot-plant scale reactors. Aqueous precursor and base streams were pumped using P2 and P3 at 24.1 MPa with fixed flowrates of 10 and 200 mL/min for the laboratory and pilot-plant scale reactors from each pump. The fluids from P2 and P3 were mixed thoroughly and the resulted mixture was split equally into two streams before entering the reactor through two inlets. The streams mixed with the stream from P1, and reacted to generate nanoparticles. The generated product stream leaves the reactor and enters a tubular heat exchanger. In order to study the effect of scaling-up on fluid flow and heat transfer in the reactors, the mixture stream from P2 and P3 was mimicked by deionised water during experiments and CFD modelling.

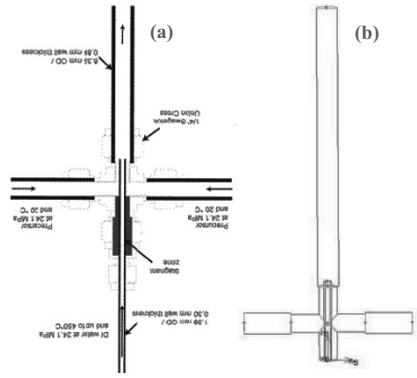

Figure 2 (a) Schematic diagram of a confined jet reactor at laboratory size scale; (b) Computational domain.

The schematic diagram of a typical reactor is shown in Figure 2(a). The reactor consists of an inner tube inserting into an outer tube. The superheated water flows in the inner tube to the mixing point to mix with the metal salt solution. Several fine J-type thermocouples were inserted into the reactors at different locations along the z direction. The tips of the thermocouples were floated in the bulk flow with an estimated tip position variations of ≤ 2 mm across the tube cross-section.

4. Simulation of confined jet reactors

4.1. Computational details

Figure 2(b) shows the computational domain of the laboratory scale reactor and similar reactor configuration was used for the pilot-plant scale reactor with the tube diameters being about 4 times bigger than those in the laboratory scale reactor. The inner diameters (D_i) of ScW are 0.99 and 3.87 mm for the

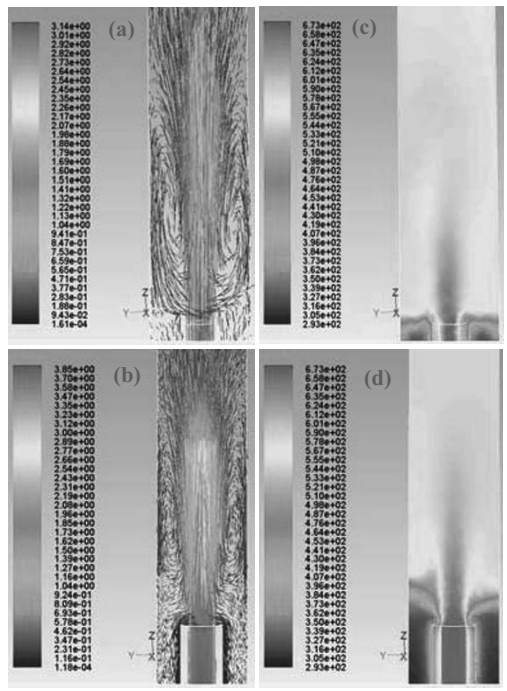

Figure 3 Velocity vectors (a, b) and temperature contour (c, d) in the ScW exit regions of confined jet reactors at laboratory scale (a, c) and pilot-plant scale (b, d).

laboratory and pilot plat scale reactors. The three-dimensional domain was discretised with 1.32×10^5 and 8.06×10^5 cells for the laboratory and pilot-plant scale reactors. The inlet conditions for the simulations were taken from experiments with the inlet temperatures of ScW and precursor streams being fixed at 400 and 15°C. For the study of mixing, a tracer identical to the ScW was introduced into the ScW stream. The flowrates of the tracer and ScW streams were 1% and 99%, respectively, of the total ScW flowrate used in the confined jet reactors.

4.2. Solution method

The mass, momentum, energy and species equations, together with the k and ε equations, are solved using ANSYS Fluent software (2010). The species equations were solved with the obtained steady-state flow and temperature profiles as the initial values. SIMPLE pressure-velocity coupling was used with a second order upwind scheme being employed for the discretisation of the convection terms. A turbulent intensity of 10% and the corresponding hydrodynamic diameters were used for the turbulence inlet conditions. Standard non-slip wall boundary conditions were applied with a standard turbulent wall function.

5. Results and discussion

Figure 3 shows the contours of velocity vectors and temperature contour around the ScW exit region. The ScW stream ejected from the inner tube and entrained the co-flowing precursor from the annual section to form a recirculation zone surrounding the ScW jet, which enhanced the mixing between the ScW and precursor streams. Even temperature distribution after the exit for the laboratory reactor (Figure 3c, d) is found which indicates that the recirculation zone in the laboratory reactor is stronger and closer to the exit as shown in Figure 3a, b. The predicted and measured temperatures along the z direction were compared in Figure 4. It can be seen that the predicted results are in good agreement with measurements.

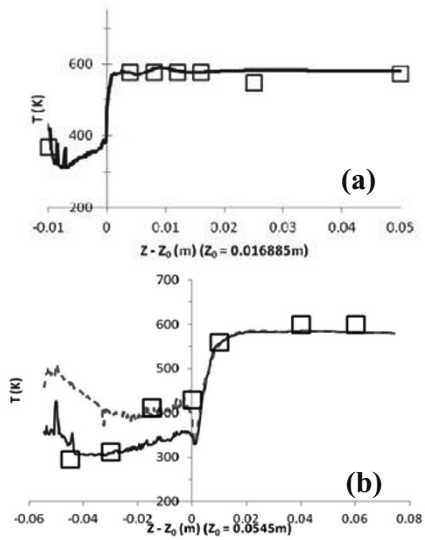

Figure 4 Predicted and measured (□) temperatures along the z direction of a mixer (a) at laboratory scale (solid line); (b) at pilot-plant scale (solid line – y=3.8mm; dashed line – y=3.4mm).

The monitored tracer mass fraction distributions were normalized by their local fully mixed mass fraction, c_∞. The mixing times, defined as the time required for the local tracer mass fraction to reach 99% of c_∞ , for the 5 monitoring points ($\triangle L/D_i$ = 0, 1, 2, 5, 8 with $\triangle L$ being the distance between the ScW exit point and monitoring point) were estimated from simulations with values of 1.0, 2.0, 2.2, 2.4, 2.5s, and 0.6, 0.7, 0.9, 1.6, 2.1s, for the laboratory and pilot plat scale reactors, respectively. However, the local tracer mass fraction reaches the fully mixing level at the reactor outlet (mass fraction of 0.005) after $\triangle L/D_i$ = 5 and 8 for the laboratory and pilot plat scale reactors, which indicates that stronger mixing happened in the reactor at laboratory scale.

6. Concluding remarks

In this study, CFD modelling was used to predict the fluid flow and heat transfer profiles in confined jet reactors of a CHFS system. The predicted temperatures along the z direction were compared with experimental data with good agreement. The mixing study indicates that strong mixing happened in the shear layer between the recirculation zone and ScW jet stream. However, scaling-up led to weaker mixing at pilot plant scale.

Acknowledgements

Financial support from the UK Engineering and Physical Sciences Research Council for the EngNano project (EP/E040624, EP/E040551) is acknowledged. We thank the industrial collaborators: Corin Group, Johnson Matthey, Resource Efficiency Knowledge Transfer Partnership, Coates Lorilleux, AMR Technologies, Malvern Instruments, and Nanoforce Technology.

References

A. Aimable, H. Muhr, C. Gentric, F. Bernard, F. Le Cras, D. Aymes, 2009. Continuous hydrothermal synthesis of inorganic nanopowders in supercritical water: Towards a better control of the process. Powder Technol. 190, 99-106.

ANSYS Fluent Package 2010. www.fluent.co.uk.

M.D. Bermejo, M.J. Cocero, 2006. Supercritical Water Oxidation: A Technical Review. AIChE J. 52, 3933-3951.

F. Demoisson, M. Ariane, A. Leybros, H. Muhr, F. Bernard, 2011. Design of a reactor operating in supercritical water conditions using CFD simulations. Examples of synthesized nanomaterials. J. Supercrit. Fluids 58, 371-377.

W.P. Jones, B.E. Launder, 1972. The prediction of laminarization with a two-equation model of turbulence. International J. Heat Mass Transfer 15, 301–314.

S.I. Kawasaki, K. Sue, R. Ookawara, Y. Wakashima, A. Suzuki, Y. Hakuta, K. Arai, 2010. Engineering study of continuous supercritical hydrothermal method using a T-shaped mixer: Experimental synthesis of NiO nanoparticles and CFD simulation. J. Supercrit. Fluids 54, 96-102.

E. Lester, P. Blood, J. Denyer, D. Giddings, B. Azzopardi, M. Poliakoff, 2006. Reaction engineering: The supercritical water hydrothermal synthesis of nano-particles. J. Supercrit. Fluids 37, 209-214.

H.Q. Liu, E.A. Macedo, 1995. Accurate correlations for the selfdiffusion coefficients of CO_2, CH_4, C_2H_4, H_2O, and D_2O over wide ranges of temperature and pressure. J. Supercrit. Fluids 8, 310-317.

C.Y. Ma, T. Mahmud, X.Z. Wang, C.J. Tighe, R.I. Gruar, J.A. Darr, 2011a. Numerical simulation of fluid flow and heat transfer in a counter-current reactor system for nanomaterial production. Chemical Product Process Model. 6, Article 6.

C.Y. Ma, C.J. Tighe, R.I. Gruar, T. Mahmud, J.A. Darr, X.Z. Wang, 2011b. Numerical modelling of hydrothermal fluid flow and heat transfer in a tubular heat exchanger under near critical conditions. J. Supercrit. Fluids 57, 236-246.

S. Moussiere, C. Joussot-Dubien, P. Guichardon, O. Boutin, H.-A. Turc, A. Roubaud, B. Fournel, 2007. Modelling of heat transfer and hydrodynamic with two kinetics approaches during supercritical water oxidation process. J. Supercrit. Fluids 43, 324-332.

C. Narayanana, C. Frouzakisa, K. Boulouchosa, K. Prıkopsky, B. Wellig, P. Rudolf von Rohrb, 2008. Numerical modelling of a supercritical water oxidation reactor containing a hydrothermal flame. J. Supercrit. Fluids 46, 149-155.

National Institute of Standard and Technology 2009. www.nist.gov.

J. Sierra-Pallares, D.L. Marchisio, E. Alonso, M.T. Parra-Santos, F. Castro, M.J. Cocero, 2011. Quantification of mixing efficiency in turbulent supercritical water hydrothermal reactors Chem. Eng. Sci. 66, 1576-1589.

W. Wagner, A. Pruß, 2002. The IAPWS formulation 1995 for the thermodynamic properties of ordinary water substance for general and scientific use. J. Phys. Chem. Ref. Data 31, 387-535.

I.A. Karimi and Rajagopalan Srinivasan (Editors), Proceedings of the 11th International Symposium on Process Systems Engineering, 15-19 July 2012, Singapore.

Modeling, Simulation and Experimental Investigation of a Reactive Hybrid Process for the Production of Dimethyl Carbonate

Johannes Holtbruegge, Philip Lutze, Andrzej Górak,

TU Dortmund University, Laboratory of Fluid Separations, Emil-Figge-Str. 70, 44227 Dortmund, Germany

Abstract

Process intensification has been identified as a main tool to achieve higher efficiencies leading to a more sustainable production. Especially hybrid as well as reactive separations allow for increased separation efficiency at the same time reducing the energy consumption. Integrating reactive and hybrid separations within one process may create even larger positive synergy effects. However, by this integration several process configurations exist and the identification of the best process operation remains unsolved. Hence, a process analysis tool has been developed to identify the most promising intensified process configuration based on simple calculations and secondly, to identify the influence of the process parameters on the target variables. To underline the potential of this tool, the equilibrium-limited transesterification of propylene carbonate forming dimethyl carbonate is investigated. For this system, a reactive hybrid process integrating reactive distillation and vapor permeation is designed in this work.

Keywords: process analysis, hybrid separation, reactive distillation, vapor permeation

1. Introduction

Due to decreasing fossil fuel reserves, the development of new and innovative processes leading to improvements in energy efficiency and sustainability is necessary. Process intensification (PI) is considered to be a key to realize this for the present and future chemical and petrochemical industry. Two main groups within PI, which have the potential to achieve this target, are hybrid and reactive separations.

Hybrid separations are the combination of two unit-operations which offer substantial synergy effects for each operation compared to the stand-alone operation, leading to increased separation efficiency and a decreased energy use [1]. Besides, the separation of multi-component mixtures with non-ideal behavior (e.g. azeotropes) is possible.

Reactive distillation is a process in which chemical reaction and distillation occur at the same time within one apparatus. Continuous product removal out of the reaction zone leads to a higher yield of equilibrium-limited reactions (e.g. transesterifications) [2].

Hence, in case of strongly non-ideal reacting systems a hybrid process which makes use of reactive distillation (RD) has a high potential for process improvement.

Despite all advantages, reactive hybrid processes are not yet fully established in industry. The reason is a lack of process know-how and process design tools. Additionally, industry was not interested in improving energy efficiency in the past which is the main advantage of reactive hybrid separations. This paper presents a process analysis tool for the selection and design of those processes, thus contributing to a broader application of hybrid reactive processes.

The potential of these processes is demonstrated for different hybrid alternatives for the transesterification of propylene carbonate consisting of RD and vapor permeation (VP).

2. Process analysis tool for the design of reactive hybrid systems

The aim of the presented process analysis tool is to identify the best reactive hybrid process for a specified reaction and separation task. A 5-step approach, shown in Figure 1, is used. First, the objective function and process constraints are defined. In the second step, a detailed investigation of the thermodynamics as well as of the reaction properties of the system is performed to identify the possible equipment and their feasible configuration. Third, the influence of important process parameters on the process configuration is investigated. Especially the influence of the feed properties is analysed by simple performance indicators to identify the best suited reactive hybrid process. Fourth, a rigorous model of the reactive hybrid process, which is validated experimentally, is set-up to perform a detailed analysis of this process using the objective function defined in step 1. After this, an optimisation is performed to identify the optimal process variables for the hybrid alternative. Currently the investigation considers RD, distillation and VP.

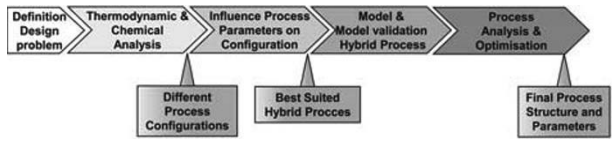

Figure 1: Workflow of the process analysis tool

3. Case-Study

In this case-study, we analyse the equilibrium-limited transesterification of propylene carbonate (PC) with methanol (MeOH) forming the target product dimethyl carbonate (DMC) and 1,2-propanediol (PDO). The reaction scheme is given in Eq. (1).

The product DMC can be used as biodegradable octane enhancer because it decomposes to carbon dioxide and methanol in contact with water [3]. Further applications of DMC are the production of polycarbonates and the use as an alkylation agent [4].

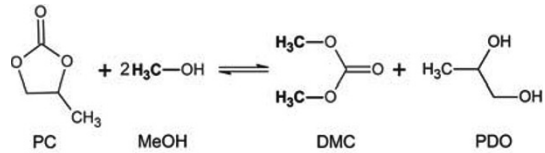

(1)

3.1. Definition of the design problem

In the first step, the design problem is defined with respect to the fixed product specifications and process boundaries as well as the objective. We fixed the total mass flow of DMC to 1700 kg/h and its purity to 99.9 wt.-%. The byproduct PDO should have a purity of 99 wt.-%. The objectives are to minimize the production costs and to have a simpler process as the base case. The base case for producing and purifying DMC consists of a continuous reactor and a sequence of four distillation columns including a pressure swing distillation to overcome the azeotrope (see Figure 2) [5].

3.2. Thermodynamic and chemical analysis

Here, the thermodynamics and the reaction of this system are investigated. Analyzing the vapor-liquid equilibrium of the system, the purification of the target product DMC is hindered by the formation of a low boiling azeotrope between DMC and MeOH shown at a pressure of 1.013 bar (see Figure 2). The diagram was computed using the UNIQUAC model and was validated with experimental results from literature [6]. For MeOH fractions higher than 0.868 mol/mol, the purification of DMC using a simple distillation is not possible. In those cases, the use of a membrane separation is advisable.

The chemical equilibrium concentration and reaction kinetics using the homogeneous catalyst sodium methoxide have been measured in our batch reactor. The equilibrium constant is in the region of K_x = 0.2 indicating that chemical equilibrium lies on the side of reactants. To overcome this equilibrium limitation the use of an RD for this chemical system is recommendable. Based on this analysis, different process concepts consisting of an RD column, a VP membrane and a distillation column are proposed and investigated with the aim to increase economics of DMC production. Using the information of the operating windows of each of these units, three promising configurations are identified. These configurations are shown in Figure 3. The first process configuration is a combination of an RD column and a distillation column for the purification of dimethyl carbonate. This configuration works for top products with a methanol mole fraction lower than the azeotropic mole fraction. Configurations 2 and 3 that additionally consist of a vapor permeation membrane are designed for the case, that the methanol mole fraction in the distillate stream of the RD column is higher than the azeotropic mole fraction. In this case, the membrane is used to overcome the azeotrope allowing the purification of DMC.

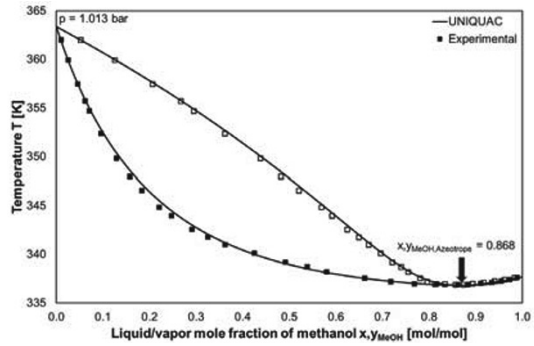

Figure 2: Vapor-liquid equilibrium for MeOH/DMC

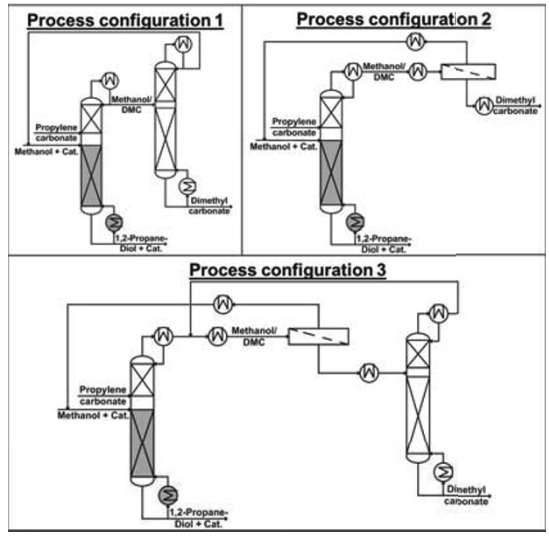

Figure 3: Process alternatives for DMC production

3.3. Influence of the process parameters on the process configuration

A simple sensitivity analysis shows, that the operational parameter with the highest influence on the distillate composition of the RD column is the molar reactant ratio χ in the feed (see Figure 5), defined as follows:

$$\chi = \dot{n}_{MeOH,Feed} \Big/ \dot{n}_{PC,Feed} \tag{2}$$

Focusing on the RD column first, the influence of the reactant ratio on the PC conversion and the PDO mole fraction in the bottom stream of the RD column is investigated (see Figure 4). The MeOH mole fraction in the distillate stream of the RD column is shown on the second y-axis.

The diagram shows, that a full PC conversion in the RD column is only possible by ensuring a reactant ratio higher than 19. Lowering this reactant ratio leads to a contamination of the bottom product PDO with PC and thus requires a further

distillation column for the bottom product. Due to the high methanol concentration in the azeotrope, a large amount of methanol is drawn in the distillate stream. This amount is not available for the chemical reaction and thus needing for high reactant ratios in the feed stream of the RD column. The diagram also shows that the reactant ratio has a minor influence on the distillate composition. For all investigated reactant ratios, the distillate stream is on the right side of the azeotrope. To purify DMC, a VP membrane allowing to overcome the azeotrope is necessary so that configuration 1 is excluded from the investigation.

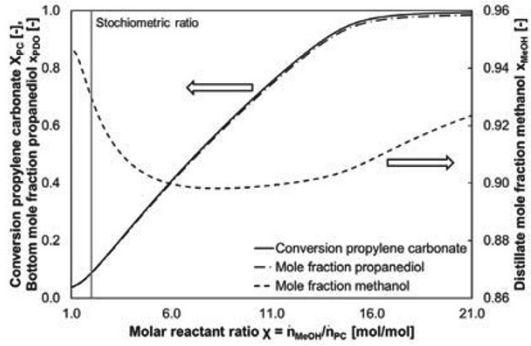

Figure 4: Influence of the reactant ratio on the performance of the RD column

An economic analysis performed on the remaining process alternatives (not shown here), shows that configuration 3 promises more benefits since the purification of the target product up to the required specification using only a membrane separation needs a large membrane area and causes higher costs. Hence, only configuration 3 is further investigated.

3.4. Process modeling and experimental model validation

The model of the RD column is based on a rate-based approach and was developed by Klöker [7]. The separation of the azeotropic mixture using the VP membrane is described using a model developed by Kreis [8] which is based on an empirical solution-diffusion model. For the determination of model parameters, lab-scale permeation experiments using the membrane Sulzer PERVAP^{TM} 1255-30 were performed. Furthermore, functions for cost calculation were taken from literature [9]. A simplified simulation flow sheet of the hybrid process is shown in Figure 5. The parameters that are varied within the simulation studies are printed in bold italic letters.

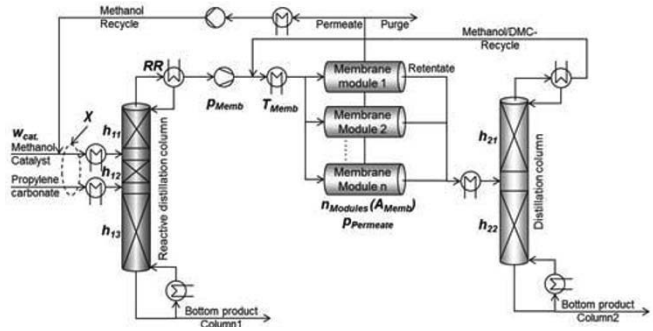

Figure 5: Scheme of the simulation flow sheet for configuration 3

3.5. Detailed process analysis for the design of the hybrid process

A detailed process analysis has been carried out for process configuration 3 to identify the best process operation. Here, membrane area, PC conversion and membrane selectivity are analyzed to identify the best savings in the costs (objective function).

The left part of Figure 6 shows the influence of the MeOH mole fraction in the retentate stream on the required membrane area and the production costs per ton of DMC. The membrane area increases exponentially with a decrease of the MeOH mole fraction. A large membrane area is necessary due to the low driving force for methanol permeation at low concentrations. This underlines the high benefit of configuration 3 in comparison to configuration 2 (see Figure 3). The reboiler duty of the second distillation column

increases with increasing MeOH mole fraction. Due to this, the DMC costs which are also shown in the diagram have a minimum for a membrane area of 2580 m².

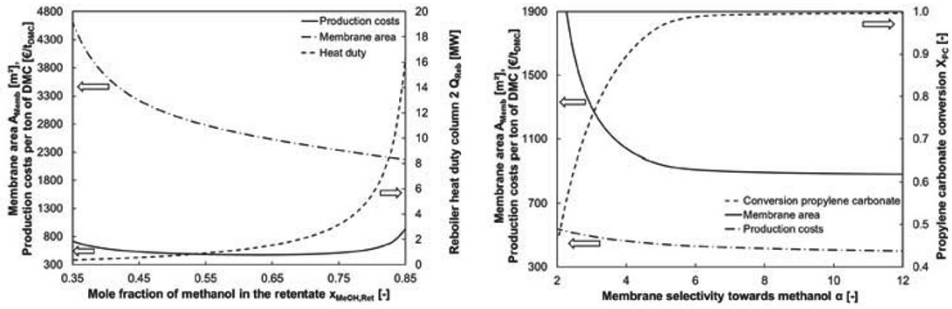

Figure 6: Influence of the membrane separation on the hybrid process

The right part of Figure 6 shows the influence of the membrane selectivity towards methanol on the membrane area, the PC conversion and the DMC costs. As expected, the membrane area and the DMC costs decrease with increasing membrane selectivity due to low DMC losses through the membrane. The more important point is the PC conversion in the RD column that decreases with decreasing membrane selectivity because a higher amount of DMC is recycled to the RD column shifting the chemical equilibrium. This leads to increasing impurities of propylene carbonate in the bottom stream of the RD column. These diagrams show the high complexity of the hybrid process and the difficulty of the selection of suitable membrane materials. Based on these results the initialization of an optimization routine to solve the final optimization problem for final tuning of the process, which is not shown here, was possible. Savings in the economics and energy consumption compared to the base case are achieved.

4. Conclusion and Outlook

A process analysis tool for the simple, quick and reliable identification of the best configuration of a reactive hybrid process was shown within this work. Within this process analysis tool a new simulation model of the hybrid process has been developed incorporating cost evaluation at early stages. For the production of dimethyl carbonate, the economically best reactive hybrid process consists of a reactive distillation column, a vapor permeation membrane and a distillation column. It was shown, that this process is able to overcome thermodynamic and chemical limitations, making savings in capital and energy use and also an increase in sustainability possible.
In further studies, pilot-scale reactive distillation experiments as well as pilot-scale hybrid experiments will be performed with this system to validate the obtained solution.

References

[1] F. Lipnizki *et al.*, 1999, *J. Membr. Sci.*, 153, 2, 183–210.
[2] A. Stankiewicz, 2003, *Chem. Eng. Process*, 42, 3, 137–144.
[3] M.A. Pacheco *et al.*, 1997, *Energy Fuels*, 11, 1, 2–29.
[4] D. Delledonne *et al.*, 2001, *Appl. Catal., A*, 221, 1-2, 241–251.
[5] J.S. Buchanan *et al.*, 2002, Patent US 6,407,279 B1.
[6] A. Rodríguez *et al.*, 2002, *Fluid Phase Equilib.*, 201, 1, 187–201.
[7] M. Klöker *et al.*, 2005, *Chem. Eng. Process*, 44, 6, 617–629.
[8] P. Kreis *et al.*, 2006, *Chem. Eng. Res. Des.*, 84, 7, 595–600.
[9] J.M. Douglas, 1988, Conceptual design of chemical processes, McGraw-Hill.

I.A. Karimi and Rajagopalan Srinivasan (Editors), Proceedings of the 11th International Symposium on Process Systems Engineering, 15-19 July 2012, Singapore.

Estimation of Predictive Accuracy of Soft Sensor Models Based on One-Class Support Vector Machine

Hiromasa Kaneko[a], Kimito Funatsu[a]

[a]*Department of Chemical System Engineering, The University of Tokyo, Bunkyo-ku, Tokyo, Japan*

Abstract

Soft sensors are widely used to estimate process variables that are difficult to measure online. By using soft sensors, analyzer faults can be detected by estimation errors. However, it is difficult to detect abnormal data and determine the reasons because estimation errors increase not only due to analyzer faults but also due to variations caused by changes in the state of chemical plants. To separate those factors, we previously proposed to construct the relationships between distances to soft sensor models (DMs) and the accuracy of prediction of the models quantitatively and estimate the prediction accuracy of new data online. In this paper, we employed a one-class support vector machine (OCSVM) to estimate data density and the output of an OCSVM as a DM. The proposed method was applied to real industrial data and the superiority of the proposed DM to the traditional ones was demonstrated by comparing their results.

Keywords: Soft sensor; Predictive accuracy; Applicability domains; Distances to models; One-class support vector machine.

1. Introduction

Soft sensors have been widely used to estimate process variables that are difficult to measure online [1]. An inferential model is constructed between those variables that are easy to measure online and those that are not, and an objective variable is then estimated using that model. Through the use of soft sensors, the values of objective variables can be estimated with a high degree of accuracy. Their use, however, involves some practical difficulties.

One of the difficulties is the degradation of soft sensor models. The predictive accuracy of soft sensors gradually decreases due to changes in the state of chemical plants, catalyzing performance loss, sensor and process drift, and so on. In order to reduce the degradation of the soft sensor model, a regression model is updated with new data or a time difference model, which is constructed between time difference of explanatory variables, **X**, and that of an objective variable, **y**, is employed, for example.

Meanwhile, if the degradation is reduced and the accuracy of soft sensor models is maintained, a **y**-analyzer fault can be detected by prediction errors. In actual plants, a threshold value of the prediction errors of **y** is set and fixed with training data, and when the prediction error of **y** exceeds a threshold value, it is considered to be abnormal. However, it is difficult to detect abnormal data and determine the reasons [2]. Prediction errors increase not only due to a **y**-analyzer fault but also due to variations in the process variables caused by changes in the state of chemical plants. In fact, reliability of a soft sensor model is affected by process conditions.

Kaneko et al. introduced applicability domains (ADs) and distances to models (DMs) [2] concepts, which are researched mainly in the field of quantitative structure-activity relationship analysis and obtained the relationships between a DM and prediction accuracy quantitatively using the distances to the average of training data as a DM. False alarms could be prevented by estimating large prediction errors when the state was different from that of training data and actual **y**-analyzer faults could be detected with certain accuracy.

The distances to the average of training data, however, cannot handle a nonlinear relationship among process variables. Additionally, if distributions of data are multiply separated, the distances cannot represent the true DM appropriately. Improvement of the ability for estimating the prediction errors or the predictive accuracy of soft sensor models is desired for process control.

We therefore propose to apply data density to a DM of soft sensors. A soft sensor model will be well trained in data regions where data density is high and the predictive accuracy of the model will be high in the same regions. On the other hand, a model will not be trained enough in data regions where data density is low and the predictive accuracy of the model will be low in the same regions. In this research, we employ a one-class support vector machine (OCSVM) [3] to estimate data density and the output of an OCSVM as a DM.

The proposed method is applied to real industrial data and the superiority of the proposed DM to the traditional ones is demonstrated by comparing their results.

2. Method

2.1. OCSVM

An OCSVM is a method in which an SVM is applied to a domain description problem. Given a set of training data in a high–dimensional input space, the objective of an OCSVM is to learn a function that will take the value +1 in the region where the majority of the data is concentrated and the value –1 everywhere else. The function to be learned is modeled as a hyperplane in a transformed space, and the hyperplane parameters are estimated so that its margin with respect to the training data is maximized, as dictated by the data–driven distribution–free paradigm.

The maximum margin solution of the OCSVM problem is obtained by solving the following quadratic optimization problem:

Minimize

$$\frac{1}{2}\|\mathbf{w}\|^2 + \frac{1}{\upsilon l}\sum_i \xi_i - b \tag{1}$$

subject to

$$\mathbf{w}\cdot\Phi(\mathbf{x}_i) \geq b - \xi_i$$
$$\xi_i \geq 0 \tag{2}$$

where $\mathbf{w} \in R^n$ denotes a weight vector; b, a bias; ξ_i, slack variables; and υ, the parameter that represents the upper bound on the fraction of outliers in the data. Finally, the decision function inferred by the learned hyperplane is as follows:

$$f(\mathbf{x}) = \mathbf{w}\cdot\Phi(\mathbf{x}) - b \tag{3}$$

In our application, a kernel function is a radial basis function:

$$K(\mathbf{x},\mathbf{x}') = \exp\left(-\gamma|\mathbf{x}-\mathbf{x}'|^2\right) \tag{4}$$

where γ is a tuning parameter that controls the width of the kernel function. By using (4), a nonlinear model can be constructed because the inner product of **x** and **w** in (3) is represented as the kernel function of **x**. The output of an OCSVM f(**x**) is the proposed DM of soft sensors.

2.2. Area under coverage and RMSE curve (AUCR)

The relationship between the coverage and the root-mean-square error (RMSE) is used to compare the performance of DMs [2]. First, data are sorted in ascending order of each DM and we calculate the coverage that is the rate of the number of the data within each AD to the total number of the data N_{all}. Then, the coverage of the i^{th} data is defined as follow:

$$coverage_{\,i} = i / N_{\text{all}} \tag{4}$$

The i^{th} RMSE value is calculated with the i data as follows:

$$RMSE = \sqrt{\frac{\sum \left(y_{obs} - y_{calc,\,pred} \right)^2}{i}} \tag{5}$$

where y_{obs} is the measured **y**-value; $y_{calc,pred}$ is the calculated **y**-value for the i data in training data or the predicted **y**-value for the i data in test data. It is desired for ADs that the smaller the values of the coverage are, the smaller the RMSE values are and vice versa. To compare DMs quantitatively, area under coverage and RMSE curve (AUCR) is introduced in this paper. The basic concept of AUCR is shown in Figure 1. The relationship between the coverage and the RMSE of A is a more desired curve than that of B, which is mentioned above and the AUCR of A is smaller than that of B. It can be said that the performance of A as a DM is better than that of B.

3. Case Study

We applied the proposed method to actual industrial data obtained during an industrial polymer process at Mitsui Chemicals, Inc. to verify the performance of DMs. There can be a nonlinear relationship between a polymer quality variable (**y**) and other process variables (**X**). Accordingly, it is difficult to estimate the predictive accuracy of the soft sensor model between **X** and **y**. We therefore attempted to model a relationship between a DM and the predictive accuracy of the model.

First, we collected data recorded for many grades and constructed support vector regression [3] models between **X** and **y** by considering the dynamics of process variables in this study. The **y**-variable is density and the melt flow rate (MFR), and the

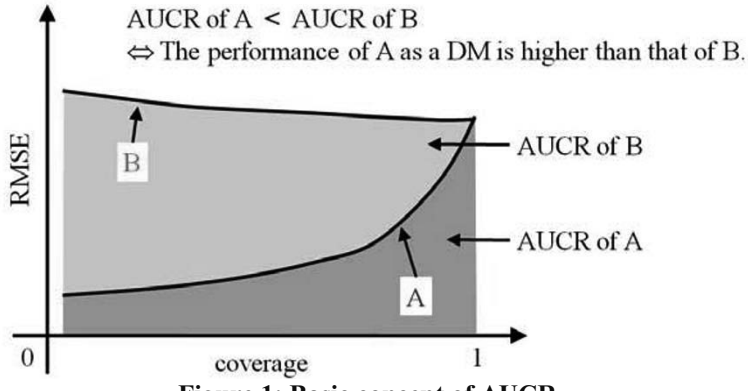

Figure 1: Basic concept of AUCR

X-variables are 37 process variables such as the temperature in the reactor, the pressure, and concentrations of the monomer, comonomer, and hydrogen. Then, we calculated relationships between DMs and calculation or prediction errors. The Euclidean distance (ED) and the Mahalanobis distance (MD) to the average of training data, and the output of an OCSVM (the proposed method) were applied as DMs.

Figure 2a shows the relationships between AUCR of training data and that of test data for each DM when **y** is density. In OCSVM modelling, a parameter ν was changed from 2^{-20} to 2^{-4} by squaring and from 0.1 to 0.9 in steps of 0.1; the other parameter γ was changed from 2^{-20} to 2^{10} by squaring; and accordingly 806 OCSVM models were constructed. The blue points represent the results of OCSVM; the red circle represents that of ED; and the green triangle represents that of MD. The distribution of the results of the proposed method locates at the bottom left compared with those of ED and MD, reflecting that the proposed DM had the better performance in most OCSVM parameters than the traditional DMs did. The OCSVM models could represent the nonlinearity among process variables. In addition, the OCSVM model having the smallest value of AUCR of training data in the all parameters had also high performance for test data. We can say that an optimal OCSVM parameter can be decided using training data.

Then, when **y** is MFR, the relationships between AUCR of training data and that of test data for each DM are shown in Figure 2b. In this case, the AUCRs of both training data and test data were relatively small when ED was used as a DM. This will come from a physical relationship between MFR and **X** and even ED of **X** could represent some information on MFR. Meanwhile, the some results of OCSVM were more left and lower than that of ED, indicating the high performance of the proposed method.

The relationships between the coverage and the RMSE of test data are shown in Figure 3. In each figure, the OCSVM parameters γ and ν were the ones where the AUCR value of training data was smallest. The blue continuous lines represent the results of OCSVM; the red dashed lines represent the results of ED; and the red chain lines represent the results of MD. As shown in the results of OCSVM, the smaller the values of the coverage are, the smaller the RMSE values are. By comparing the values of the RMSE for each coverage, at only small coverage for MFR, the values of the RMSE calculated with the proposed method were smaller than those of the other methods. This means that the model could predict more number of data with higher predictive accuracy by using the proposed index.

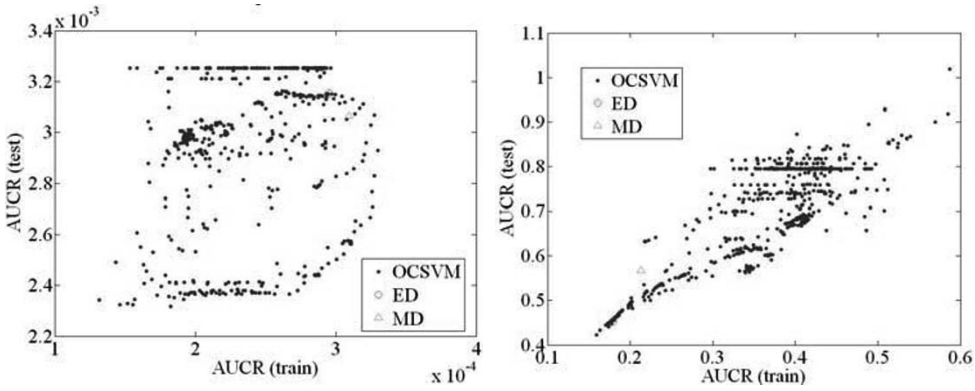

(a) Density (b) MFR

Figure 2: Relationships between AUCR of training data and that of test data

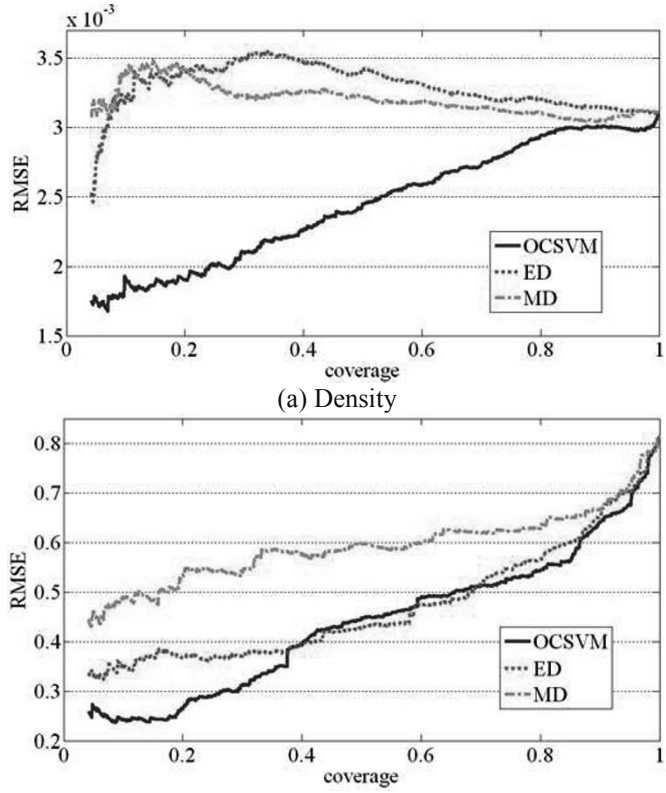

Figure 3: Relationships between the coverage and the RMSE

4. Conclusion

In this paper, we proposed a DM calculated by using OCSVM to estimate prediction errors of soft sensor models accurately. Then, AUCR was introduced as a comparative indicator, and hence, the performance of DMs could be compared quantitatively. Through the analysis of real industrial data, we confirmed that the predictive accuracy of each data could be estimated with high accuracy by using the proposed method even when there is a nonlinear relationship between **X** and **y**. By applying this method to process control, industrial plants will be operated stably.

Acknowledgement

The authors acknowledge the support of Mitsui Chemicals, Inc..

References

[1] P. Kadlec, & B. Gabrys, S. Strandt, 2009, Data-driven soft sensors in the process industry. Comp. Chem. Eng., 33, 795–814.
[2] H. Kaneko, M. Arakawa, & K. Funatsu, 2011, Applicability domains and accuracy of prediction of soft sensor models. AIChE J., 57, 1506–1513.
[3] V.N. Vapnik, 1999, The nature of statistical learning theory. Springer, New York.

I.A. Karimi and Rajagopalan Srinivasan (Editors), Proceedings of the 11th International Symposium on Process Systems Engineering, 15-19 July 2012, Singapore

Methodology for Emergency Shut-Down of Multi-Megawatt Wind Turbine Generators

Sébastien Gros,[a] Benoît Chachuat,[b,*]

[a] *Optimization in Engineering Center (OPTEC), K.U. Leuven, Belgium*
[b] *Centre for Process Systems Engineering (CPSE), Imperial College London, UK*

Abstract

This paper describes an optimization-based approach to reducing the fatigue caused by structural loads during emergency shut-down (EST) of multi-megawatt wind turbine generators. A low-order, dynamic model is developed, which accounts for the first fore-aft tower mode. This model is used to cast the EST problem as an optimal control problem that involves switched dynamics and can be solved using direct solution approaches. The optimized EST strategies are validated against a high-fidelity model in the simulation environment Bladed™ for an industrial 3MW wind turbine generator. Fatigue reductions as high as 45-60% can be obtained at various above-rated wind speeds compared to standard, constant pitch rate EST procedures.

Keywords: wind turbine, emergency shut-down, fatigue reduction, optimal control

1. Introduction

With the size of wind turbine generators (WTG) increasing steadily, there has been a growing interest in alleviating structural fatigue through better control (Bossanyi, 2003). For multi-megawatt WTG (MMWTG), transient operation such as emergency shut-down (EST) has received far less attention than normal power production operation, despite the fact that EST events can contribute significantly to the overall structural fatigue. Current practice still relies on a set of *ad hoc* rules, whereby the collective pitch control is ramped to feather, while maintaining the generator torque at its maximum value (which is itself dependent on the generator speed) (Burton et al., 2011). Systematic methodologies are still lacking for fatigue minimization during EST procedures.

Reducing fatigue during EST events is challenging because good reference trajectories for the collective pitch rate and for the generator torque are hard to assess. Besides, the dynamics are highly nonlinear, and limitations on the actuators are likely to become saturated as well as other process constraints. Such problems are naturally addressed under the framework of optimal control (Bryson and Ho, 1975). In particular, direct solution methods, whereby the optimal control problem (OCP) is converted into a nonlinear program (NLP) through parameterization of the control and/or the state trajectories can efficiently tackle such problems with point and path constraints as well as switched dynamics (Vassiliadis et al., 1994; Biegler et al., 2002). This is the approach used in this work.

In the remainder of the paper, a low-order model is presented in §2 and the optimal control problem for reduction of the tower fatigue during an EST event is given in §3. The results of a case study are presented and analyzed in §4, including a validation in the high-fidelity simulation environment Bladed™. Finally, conclusions are drawn and directions for future investigations are discussed in §5.

*b.chachuat@imperial.ac.uk

2. Low-Order Model for Wind Turbine Generators

In order to make the optimization of EST events tractable, a low-complexity, differentiable model is developed, which captures only the first fore-aft tower mode. Subsequent modes are neglected, as well as the out-of-plane blade modes corresponding to the three blades oscillating together in the fore-aft direction. Therefore, this model may only predict the behavior of WTGs accurately in the lower frequency range, below the influence of the neglected modes. A complete description of the model parameters and values can be found in (Gros and Chachuat, 2012).

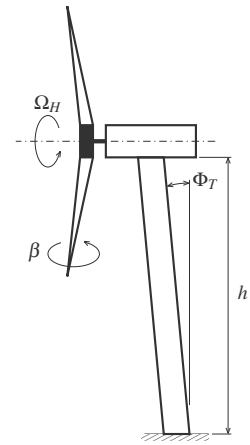

$$\dot{\Omega}_H(t) = \frac{Q_a(t) - T_G(t)}{I_{DT} + J} \tag{1}$$

$$\ddot{\Phi}_T(t) = \frac{Q_t(t) - \xi^2 M_{rn} h^2 w_t^2 \Phi_T(t) - Q_m(t)}{\xi^2 (M_{bl} h^2 + J_t)}, \tag{2}$$

where Φ_T [rad] stands for the tower fore-aft displacement relative to the vertical axis; Ω_H [rad/s], for the rotor angular velocity; and T_G [Nm], for the generator torque.

The rotor aerodynamic torque is $Q_a(t) = \frac{1}{2}\rho\,\pi R^3 \frac{C_p}{\lambda(t)} V(t)^2$ [Nm], the thrust moment is $Q_t(t) = [\frac{1}{2}(1+C_s)h\rho\,\pi R^2 C_t + C_X]V(t)^2$ [Nm], and the structural moment is $Q_m = Q_{ov} + B_t\dot{\Phi}_T(t)$ [Nm]. Moreover, the wind speed at the hub position is $V(t) = V_\infty - \xi\,h\dot{\Phi}_T(t)$ [m/s], with V_∞ [m/s] the free-flow wind speed, and $\lambda(t) = \frac{R\Omega_H(t)}{V(t)}$ is the tip-speed ratio. The aerodynamic coefficients $C_{p\lambda}(\beta,\lambda)$ and $C_t(\beta,\lambda)$ are defined in look-up tables, as obtained from combined blade element and momentum theory.

Regarding the collective pitch position β [deg], the actuator dynamics relating β to the pitch reference β_R [deg] are approximated as 2nd-order dynamics with limited bandwidth,

$$\ddot{\beta}(t) = K_P[\beta_R(t) - \beta(t)] - K_D\dot{\beta}(t). \tag{3}$$

The focus in this paper is on EST events triggered under above-rated conditions, which typically cause higher structural fatigue. In this scenario, the rotor velocity Ω_H^{r} during normal power production mode is dictated by the WTG design requirements, while the generator torque T_G^{r} is adjusted to meet the rated power value. In particular, this requires that a constant rotor velocity is maintained by pitching the blades so as to control the aerodynamic torque. A set of initial conditions for the EST is given by $Q_a(0) = T_G^{\mathrm{r}}$, $\Omega_H(0) = \Omega_H^{\mathrm{r}}$, $\dot{\Phi}_T(0) = 0$, $\ddot{\Phi}_T(0) = 0$, $\dot{\beta}(0) = 0$, $\ddot{\beta}(0) = 0$.

Note that (1)-(3) is a fifth-order model, but as many as six initial conditions are defined; therefore, the system is over-specified at initial time, which implies that only $T_G(0)$ can be set freely, whereas $\beta_R(0)$ has to be equal to $\beta(0)$ according to (3). Note also that the proposed optimization-based methodology remains applicable under below-rated conditions subject to minor modifications of the initial conditions.

3. Emergency Shut-Down Optimization formulation

The problem of minimizing the tower fatigue during an EST procedure is now cast as an optimal control problem. In order to make the problem amenable to a numerical solution, the optimization horizon is taken finite, with the final time t_{f} taken equal to the time

needed by the blades to reach the feathered position in a standard EST procedure with constant pitch rate of $\dot{\beta}^R = 5.5$ rad/s.

An approximation of the actual rainflow counting (RFC) (Burton et al., 2011) is considered as the cost functional. Since the RFC is independent of T_G and β_R and the model (1)-(3) is affine in the controls, this OCP is singular, which could invalidate the low-order model due to the presence of high frequencies such as bang-bang arcs. To remedy this, a secondary objective that penalizes high-frequencies in the collective pitch dynamics is added, leading to the following regularized cost functional:

$$J = \int_0^{t_\mathrm{f}} |\dot{\Phi}_T(t)|\,dt + \omega \int_0^{t_\mathrm{f}} \ddot{\beta}(t)^2\,dt \approx \int_0^{t_\mathrm{f}} \frac{\dot{\Phi}_T(t)^2}{\sqrt{\dot{\Phi}_T(t)^2 + \varepsilon^2}}\,dt + \omega \int_0^{t_\mathrm{f}} \ddot{\beta}(t)^2\,dt, \qquad (4)$$

with $\omega \geq 0$ the regularization parameter, and $\varepsilon \ll 1$ a numerical perturbation.

The following path constraints are imposed to represent the limitations imposed by the actuators on the pitch position, pitch rate and pitch acceleration, and in order for the pitch angles to be in (a neighborhood of the) feathered position at t_f:

$$\beta^{\mathrm{br}} \leq \beta(t) \leq 90\ [\mathrm{deg}], \qquad \beta(t_\mathrm{f}) \geq \beta_\mathrm{f},$$
$$-\dot{\beta}^{\max} \leq \dot{\beta}(t) \leq \dot{\beta}^{\max}, \qquad -\ddot{\beta}^{\max} \leq \ddot{\beta}(t) \leq \ddot{\beta}^{\max}.$$

The generator torque T_G and power $P_G := T_G \Omega_H$ too are restricted along the path as

$$0 \leq T_G(t) \leq T_G^{\max}, \qquad T_G(t)\,\Omega_H(t) \leq 1.1\,T_G^{\mathrm{r}}\,\Omega_H^{\mathrm{r}}.$$

Finally, the maximum torque that can be reclaimed from the generator typically decreases with the rotor speed due to power electronics restrictions, and no torque can be reclaimed below the so-called cut-in rotor speed Ω^{ci}. A conservative approximation of these limitations is considered next in disjunctive form as

$$T_G(t) \leq \begin{cases} a\,\Omega_H(t)\,[\Omega_H(t) + b], & \text{if } \Omega_H(t) \geq \Omega^{\mathrm{ci}} \\ 0, & \text{otherwise,} \end{cases} \qquad (5)$$

where the constants a and b are determined based on the power electronics of the WTG. Direct incorporation of (5) would make the control problem nonsmooth and may cause standard numerical solution procedure to abort prematurely. To remedy this, a multi-stage formulation (Vassiliadis et al., 1994) of the problem is adopted next, which relies on the observation that the rotor speed $\Omega_H(t)$ decreases monotonically from its rated value Ω_H^{r} at $t = 0$ down to zero at t_f during a typical EST procedure; that is, $\Omega_H(t)$ may cross the cut-in rotor speed Ω^{ci} only once.

A direct numerical procedure is considered to solve the OCP, where the control trajectories are parameterized over 100 stages as (continuous) piecewise affine functions. Because the response of the reduced-order model is non-stiff, the so-called simultaneous approach (Biegler et al., 2002) is well suited. Lagrange polynomials with 4-point Radau collocation are used for the state variables and the resulting large-scale NLP has about 4,800 variables and 4,900 equality/inequality constraints.

4. Optimal EST Procedures: Case Study

A 3 MW WTG is considered, for which a Bladed model was first developed for detailed performance and structural fatigue simulation, as well as a low-order model (1)-(3). The parameter values for the low-order model and the OCP are in (Gros and Chachuat, 2012).

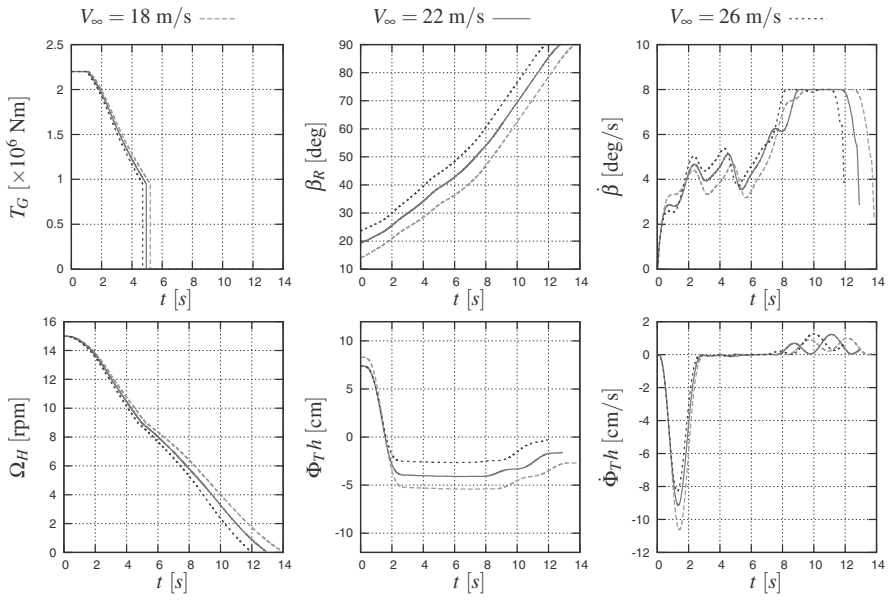

Figure 1. Optimal control and response with regularization $\omega = 10^{-6}$ *for above-rated wind speeds* $V_\infty = 18$*,* 22 *and* 26 m/s*.*

Optimal solutions of the OCP computed for various above-rate wind speeds $V_\infty = 18$, 22 and 26 m/s and a regularization of $\omega = 10^{-6}$ are shown in Fig. 1. While it is clear that the optimal trajectories are quite sensitive to V_∞, it is also seen that the general structure or pattern of these trajectories is conserved across different V_∞ values. The major effect of different wind speed values V_∞ appears to be shifting the optimal collective pitch reference trajectories $\beta_R(t)$. In all cases, the pitch trajectories reach the specified feathered position after a rather regular increase from their respective rated pitched angles. The choice of $\omega = 10^{-6}$ for the regularization yields a good compromise between performance loss and pitch rate ($\dot{\beta}$) aggressiveness across various above-rated wind speeds.

Regarding fatigue reduction, it is seen from the middle and right lower plots in Fig. 1 that the optimal control strategies are particularly efficient at dampening the fore-aft tower displacement. The first compressive peak brings the tower back to nearly vertical position, where it stays during the remaining of the EST horizon. Observe also from the lower right plot that the tower shows small fore-aft oscillations close to the end of the horizon, which are due to a loss of controllability—see below.

4.1. Validation in Bladed Simulation Environment

The Bladed simulation environment is used as a means to validate the optimized EST strategies and compare them with the constant pitch rate (standard) procedures. One such comparison is shown in Fig. 2, where the optimized EST procedures is computed for $V_\infty = 22\,\mathrm{m/s}$ and $\omega = 10^{-6}$. Large reductions in the fore-aft displacement oscillations (left plot) and in the corresponding tower root moment (right plot) are obtained. In terms of the RFC (computed over an extended horizon of 240 s), the fatigue reductions at above-rated wind speeds of 18, 22 and 26 m/s are 45%, 56% and 61%, respectively.

It should be noted that the oscillations predicted by Bladed are larger than those initially predicted by the reduced-order model (compare Fig. 1); such discrepancy is the result of

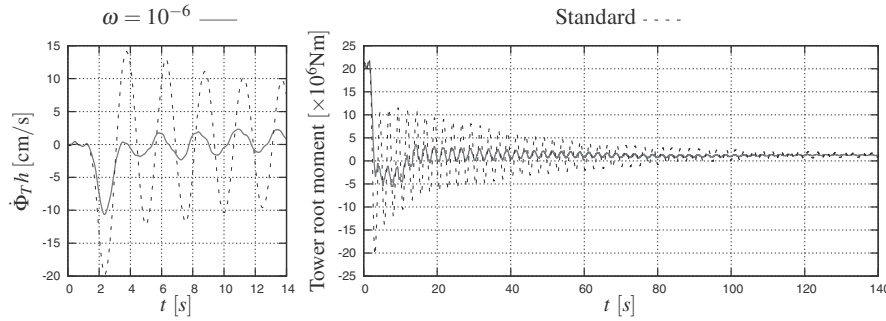

Figure 2. Comparison between constant pitch rate (standard) and optimized EST strategies for $V_\infty = 22$ m/s in the Bladed simulation environment.

the neglected out-of-plan blade modes and higher fore-aft tower modes, as noted earlier. Note also that the residual oscillations can last over several minutes. This is because once the pitch has reached its feathered position and the rotor speed is below its cut-in value, neither aerodynamic nor mechanical damping is possible anymore; that is, the WTG is left essentially uncontrolled.

5. Conclusions and Future Directions

An optimization-based approach has been proposed to tackle the problem of structural fatigue reduction during EST of WTGs. A low-order model has been developed and used for the optimal control problem formulation and solution. The resulting EST strategies have been validated in the Bladed simulation environment, and comparisons with constant pitch rate (standard) EST procedures have revealed that reductions as high as 45-60% in structural fatigue can be obtained at various above-rated wind speeds.

Because EST procedures are subject to large disturbances due to wind speed variation and turbulence, and since the mathematical models carry uncertainty, direct application of the computed optimal control trajectories in open loop may lead to poor performance or violate some operating constraints. Pivotal to the success of an optimization methodology for EST is therefore a closed-loop strategy that adapts the control trajectories in real time using on-line measurements. Such strategies are currently under investigation.

Acknowledgments. Most of the work in the paper was done when SG was with MLS Intelligent Control Dynamics, Glasgow (UK). The authors are grateful to MLS for lending them a Bladed license.

References

Biegler, L. T., Cervantes, A. M., Wächter, A., 2002. Advances in simultaneous strategies for dynamic process optimization. Chem. Eng. Sci. 57 (4), 575–593.

Bossanyi, E. A., 2003. Wind turbine control for load reduction. Wind Energy 6 (3), 229–244.

Bryson, A. E., Ho, Y. C., 1975. Applied Optimal Control. Hemisphere, Washington DC.

Burton, T., Sharpe, D., Jenkins, N., Bossanyi, E. A., 2011. Wind Energy Handbook, 2nd Edition. John Wiley & Sons, Chichester, UK.

Gros, S., Chachuat, B., 2012. Optimization-based load reduction during emergency shut-down of multi-megawatt wind turbine generators, submitted to: Wind Energy.

Vassiliadis, V. S., Sargent, R. W. H., Pantelides, C. C., 1994. Solution of a class of multistage dynamic optimization problems–2. Problems with path constraints. Ind. Eng. Chem. Res. 33 (9), 2123–2133.

I.A. Karimi and Rajagopalan Srinivasan (Editors), Proceedings of the 11th International Symposium on Process Systems Engineering, 15-19 July 2012, Singapore.

Data-driven causal inference based on a modified transfer entropy

Yidan Shu, Jinsong Zhao*

State Key Laboratory of Chemical Engineering, Department of Chemical Engineering, Tsinghua University, Beijing, China
**Email: jinsongzhao@tsinghua.edu.cn*

Abstract

Causality inference and root cause analysis are important for fault diagnosis in the chemical industry. Due to the increasing scale and complexity of chemical processes, data-driven methods become indispensable in causality inference. This paper proposes an approach based on the concept of transfer entropy which was presented by Schreiber in 2000 to generate a causal map. To get a better performance in estimating the time delay of causal relations, a modified form of the transfer entropy is presented in this paper. A case study on a simulated chemical process is performed to illustrate the effectiveness of this approach.
Keywords: Causal inference, Transfer entropy, Process safety

1. Introduction

Elucidation of the cause-and-effect relationships among variables or events is the central aim of many studies in physical, social, behavioral and biological sciences (Pearl, 2009). In the chemical process industry, knowing the cause-and-effect relationships means knowing the propagation path of fault or disturbance, which is critical for alarm management, fault diagnosis, and incident/accident investigations. As a result, it is of great significance to develop an effective and reliable method of causal inference and root cause analysis.

There exists some techniques that are to some extent similar to causal inference and root cause analysis, like HAZOP analysis (Dunjó, 2010), and signed digraph (SDG)-based methods (Maurya, 2004). But methods that rely on only process knowledge are often difficult to use because of the increasing complexity and size of modern industrial processes. Meanwhile, data-driven methods like cross-correlation function (Bauer, 2008), and transfer entropy (Schreiber, 2000, Bauer, 2007) can overcome such difficulties. However, data-driven methods needs to be improved to avoid mbiguities or false results. This paper is focused on causal inference based on an improved transfer entropy.

2. Introduction to transfer entropy and proposed midification

2.1. Introduction to transfer entropy

Based on the concept of information theory and information entropy (Shannon and Weaver, 1949), Schreiber proposed the concept of transfer entropy in 2000 to measure the asymmetric interactions in a system. Unlike mutual information, transfer entropy is in an asymmetric form, which makes it possible to measure cause-and-effect relationships. To consider time delay, which is common in many practical situations, Bauer in 2007 incorporated h, the prediction horizon, and rewrote the transfer entropy as equation (1).

$$t(x \mid y) = \sum_{x_{i+h}, x_i^{(k)}, y_i^{(l)}} p(x_{i+h}, x_i^{(k)}, y_i^{(l)}) \log \frac{p(x_{i+h} \mid x_i^{(k)}, y_i^{(l)})}{p(x_{i+h} \mid x_i^{(k)})} \tag{1}$$

x and y represent two variables while x_i and y_i represent their values at time i. $x_i^{(k)} = [x_i, x_{i-1}, \cdots, x_{i-k+1}]$ and $y_i^{(l)} = [y_i, y_{i-1}, \cdots, y_{i-l+1}]$. The probability density function (PDF) is estimated by a kernel estimator. In 2010, Yang applied the Bauer's form of transfer entropy equation (1) to validate SDGs. In his work, the prediction horizon was changed to maximize the transfer entropies and the transfer entropies that are large enough will validate the existence of the corresponding SDG arcs that represent the causal relationships between process variables.

2.2. Modification of transfer entropy

In the Bauer's transfer entropy, the reference of future uncertainty's decrease is $x_i^{(k)}$. As a result, as prediction horizon varies, the reference also varies. Such phenomenon seems unreasonable to determine the actual maximized improvement of prediction.

In our modified transfer entropy, the $x_i^{(k)}$ in equation (1) is replaced by $x_{i+h-1}^{(k)}$. As a result, the reference is fixed and doesn't change with h. In our opinion, such modification will make the maximization more reliable and make it possible to estimate time delay with prediction horizon. The modified form of transfer entropy is as below:

$$t(x \mid y) = \sum_{x_{i+h}, x_{i+h-1}^{(k)}, y_i^{(l)}} p(x_{i+h}, x_{i+h-1}^{(k)}, y_i^{(l)}) \log \frac{p(x_{i+h} \mid x_{i+h-1}^{(k)}, y_i^{(l)})}{p(x_{i+h} \mid x_{i+h-1}^{(k)})} \tag{2}$$

$x_{i+h-1}^{(k)} = [x_{i+h-1}, x_{i+h-2}, \cdots, x_{i+h-k}]$ and other symbols are the same as equation (1).

To illustrate our idea, suppose an auto-regressive model (see equation (3)). y is random and normally distributed at each moment i. x is determined by both y and x itself:

$$x(i) = x(i-1) + y(i-5) \tag{3}$$

We can expect the time delay from y to x to be 5. Both Bauer's form and our modified form of transfer entropy are applied, and let k=l=1 and h be an integer between 1 to 10. Fig. 1 (a) and (b) show transfer entropies as a function of h under both forms.

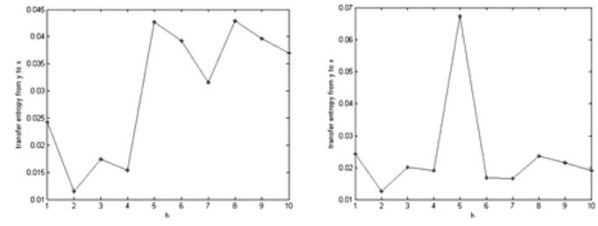

(a) (b)

Fig. 1 Transfer entropy vs. h under (a) Bauer's form (b) the modified form

From Fig. 1(a) we can see Bauer's form can find two local maximums at h= 5 and h=8 respectively. Moreover, the latter one is a little bit larger than the former one. That means this form cannot find time delay exactly for this example. However, our modified form finds only one maximum at the right h.

3. Causal inference based on the modified transfer entropy

To obtain a causal map based on the time series of process variables, the following four steps are proposed based on the modified transfer entropy.

3.1. Parameter selection

k, l, and the range of h in equation (2) should be decided before calculation. The threshold of the transfer entropy to extract the significant results also need to be chosen.

k is set to be both 1 and 0. When k=1, most transfer entropies will be smaller than those when k=0. The transfer entropies that remain above the threshold can be considered to represent the strong relations. When k=0, the transfer entropies obtained generally represent the weak relations which are still worth considering to build the causal map.

l is set to be 1. If l=0, the equation (2) is meaningless. Larger l will make the calculation more difficult, and generate many transfer entropies with similar large values which makes it hard to extract the significant part.

The choice of the range of h depends on the estimation of the actual time delay. The choice of the transfer entropy threshold is worth studying. In our proposed approach the threshold is set to be 0.1 for k=1, and 0.15 for k=0.

3.2. Strong relations extraction

With k=1, the strong relations are expected to be found. Since there exist some relations that may be the combinations of other relations, elimination of such redundant relations is necessary to avoid generation of a messy causal map. However, ambiguity may occur when we try to decide which relation is redundant. For example, for the time delay map Fig.2 (a), the following three causal maps could be all reasonable:

1. Causal chain map (Fig.2 (b)), i.e. A causes B, B causes C. This map is generated based on the fact the causal relation from A to C is redundant.
2. Common cause map (Fig.2 (c)), i.e. A causes B and C simultaneously. Due to the common cause A, it looks as if there exists a relation between B and C.
3. Straightforward causal map (Fig.2 (d)) derived based on the transfer entropy values. It is a coincidence that the sum of the time delays from A to B and from B to C approximately equals the time delay from A to C.

Here we use a strategy based on the assumption that a large transfer entropy implies high degree of significance. More specifically, the causal arcs are added in the order of the values of their corresponding transfer entropies from high to low. The causal arcs with larger transfer entropies are added first. If a causal arc to be added can be regarded as combinations of existing causal arcs, then it is a redundant relation that should be omitted. The table in Fig.2 shows the result of this strategy.

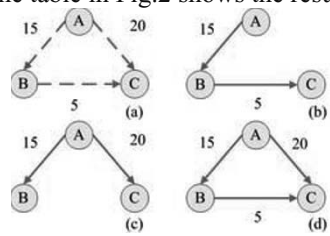

The smallest transfer entropy scenarios	Causal map inferred
from A to C	(b)
from B to C	(c)
from A to B	(d)

Fig. 2 Time delay map and causal maps of the three time-series example (a) Time delay map (b)Causal chain map (c)Common cause map (d)Straightforward causal map

3.3. Weak relations extraction

The transfer entropies with k=0 are also worth considering because they can also predict some information of causal relations. The same process of elimination of redundant relations as above should be performed then.

3.4. Reciprocal causation consideration

For k=0, if two variables have a significant maximized transfer entropy to each other at h=0, their relations may be either that they cause each other or that one is cause to the other with a time delay that is very close to 0, but not vice versa. To decide which assumption is the fact, the transfer entropies of k=1 are referred to once more. If their transfer entropies to each other are similar no matter whether they are above threshold, the former assumption will be considered as the fact, otherwise the latter.

4. Case study

The chemical process with 14 process variables simulated by UniSim Design R390.1 includes two CSTRs in series where cold water and hot water are mixed. All of the control loops are proportional controls. The Process Flow Diagram (PFD) is shown in Fig. 3.

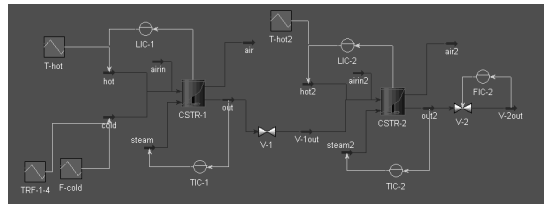

Fig. 3 PFD of the simulated process

200 samples with 0.5 second sampling interval are collected for the case study. A significance threshold of 0.1 is chosen to decide whether a transfer entropy can represent the existence of a cause-effect relationship.

With k=1, the generated causal map is shown in Fig. 4(a) with each node representing a process variable. The labels in the form of (A, B) on the arrows between two nodes indicate the maximized transfer entropy A and the corresponding time delay B. The nodes are named in the way "equipment/stream tag name" – "the variable type abbreviation" (F: flow rate, T: temperature, L: level, H: heat flow).

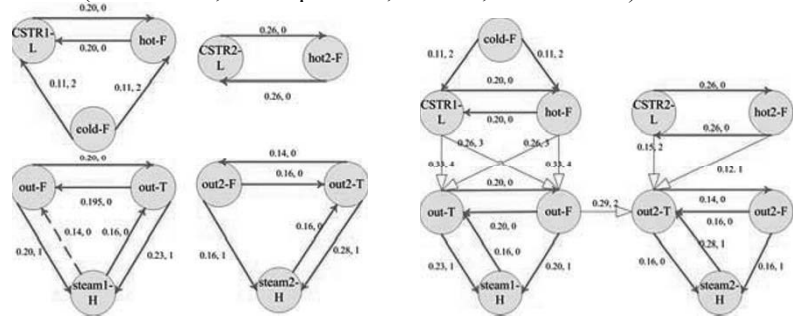

Fig. 4 (a) Strong relations in simulated case (b) Causal map with weak relations added

There are no significant transfer entropy values relevant to the three variables - stream 'hot' temperature, stream 'hot2' temperature and stream 'cold' temperature. The reason is that they belong to input flows and have only weak impact on other variables.

The other 11 variables are divided into 4 clusters in the causal map in Fig. 4(a), which exactly correspond to the 4 control loops. Dotted lines in Fig. 4 means the causal relations are omitted through examination of redundancy.

After step 3.3 and 3.4 are finished, the causal map becomes what is shown in Fig. 4(b). The fine arrows with hollow heads are added after these two steps.

It can be seen that the level of CSTR1 and the flow rate of the stream 'hot', and the level of CSTR2 and the flow rate of the stream 'hot2', make two special variable pairs. The two variables in each of the two pairs have similar transfer entropy to each other when k=1 and h=0, and interact with other variables in the same way. To make the causal map brief, such a variable pair is merged into one single node. The final simplified causal map is shown in Fig. 5.

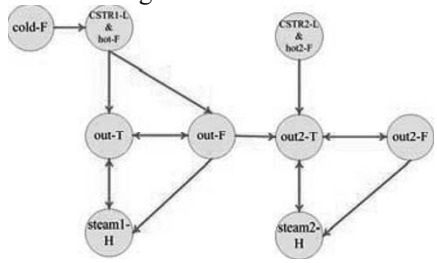

Fig. 5 Final simplified causal map

5. Conclusion

Causal inference is of great value for alarm management, fault diagnosis, and incident investigation. Due to the increasing size and complexity of modern industrial process, data-driven methods of causal inference show its advantage over knowledge-based ones. This paper modifies the Bauer's form of transfer entropy proposed and improves its performance in estimating time delay of causal relations. A causal inference approach based on transfer entropy is also proposed in this paper. A case study on a simulated chemical process is performed and illustrates the effectiveness of the proposed approach. However, some issues still need to be solved. The choice of the threshold should be considered further. Ambiguities and wrong causal relationships cannot be avoided fundamentally. A systematic procedure to bring in process topological knowledge to improve the performance of the data-driven method will be studied in the future.

6. Acknowledgements

The authors gratefully acknowledge financial support from the National Basic Research Program of China (973 Program, Grant No. 2012CB720500).

References

Bauer, M. et al, 2007. Finding the direction of diturbance propogation in a chemical process using transfer entropy. IEEE Transactions on control systems technology, 15(1), 12-21

Bauer, M. et al, 2008. A practical method for identifying the propagation path of plant-wide disturbances. Journal of Process Control 18, 707-719

Dunjó, J. et al, 2010. Hazard and operability (HAZOP) analysis. A literature review. Journal of Hazardous Materials 173, 19-32

Maurya, M. et al, 2004. Application of signed digraphs-based analysis for fault diagnosis of chemical process flowsheets. Engineering Applications of Artificial Intelligence 17, 501-518

Pearl, J., 2009. Causality: models, reasoning, and inference, second edition. Cambridge University Press, New York (Preface to the First Edition)

Schreiber, T., 2000. Measuring information transfer. Physical Review Letters, 85(2), 461-464

Shannon, C., Weaver, W., 1948. A mathematical theory of communication. The Bell System Technical Journal 27, 379-423, 623-656

Yang F. et al, 2010. Signed directed graph modeling of industrial process and their validation by data-based methods. Conference on Control and Fault Tolerant Systems, Nice, France, ThA2.1, 387-392

I.A. Karimi and Rajagopalan Srinivasan (Editors), Proceedings of the 11th International Symposium on Process Systems Engineering, 15-19 July 2012, Singapore.

Data-based Method for Diagnosing Multiple Blockage Locations in a Microreactor with Parallelized Microchannels

Masaru Noda[a] and Nobuhide Sakamoto[a]

[a]*Nara Institute of Science and Technology, 8916-5 Takayama, Ikoma 630-0192, Japan*

Abstract

Microreactors with parallelized microchannels are widely used in chemical industries because a single microchannel processes only a small amount of raw material. Any blockage in parallelized microchannels causes poor uniformity of the residence time distribution among microchannels and thus leads to degraded product quality. To address this issue, we developed a data-based identification method that can cope with blockages in multiple microchannels. The method identifies multiple blockage locations by comparing measured pressure-distribution data with pressure-distribution data calculated by computational fluid dynamic (CFD) simulation when blockage occurs. To avoid a combinatorial explosion of CFD simulations for database construction, the proposed method identifies blocked locations using only pressure-distribution data obtained when a single channel is blocked. The results of CFD simulations showed that the method can accurately identify three blocked locations using fewer pressure sensors than there are microchannels.

Keywords: Microreactor, Diagnosis, Channel blockages, Computational fluid dynamics, Correlation coefficient

1. Introduction

Microreactors have received both industrial and academic attention as a new type of production technology for specialty chemicals that are difficult to produce with conventional reactors. However, blockage in the microchannels of microreactors is a serious problem that limits their practical usage. It is therefore essential to detect and identify blockage locations to ensure more effective and stable microreactor operation.

Kano *et al.* (2007) proposed data-based and model-based blockage diagnosis methods using temperature sensors that identify blockage locations in stacked microchemical processes. Tanaka *et al.* (2011) developed a blockage detection and diagnosis system for parallelized microreactors with split-and-recombine-type flow distributors. This system can isolate a blocked microreactor with a small number of flow sensors. Simulation and experimental results showed that these methods can diagnose a single blockage location using fewer pressure sensors than microchannels.

In previous studies, we proposed a method for detecting blockage locations in a microreactor with parallelized microchannels. The method makes use of pressure sensors when blockages occur in two microchannels simultaneously (Yamamoto *et al.*, 2009, Noda *et al.*, 2010). It identifies the two blockage locations by comparing measured pressure-distribution data with pressure-distribution data calculated by computational fluid dynamic (CFD) simulation before the blockages occurred. The method can easily be extended to apply to cases in which there are three or more

blocked microchannels without incurring any combinatorial explosion of CFD simulations for database construction.

In this paper, we apply the method to a blockage identification problem where blockages occur in three microchannels simultaneously. We used CFD simulation in this study to generate the validation data for our method in case studies.

2. Microreactor

Figure 1 shows the structure of the microreactor used for the study. It is a point symmetrical microreactor consisting of three parts: an inlet manifold for flow distribution, parallelized microchannels for the reaction, and an outlet manifold for mixing. Pressure sensors are set up at all or some of the microchannel inlets. We assume that the total number of sensors and their locations have been given in advance.

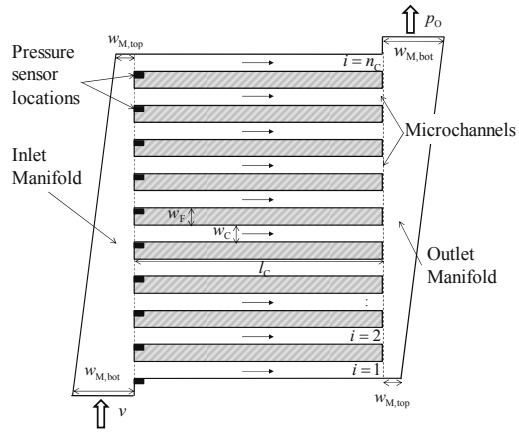

Fig. 1 Microreactor structure

The blockage degree BD_i of microchannel i is defined by Eq. (1), where $f_{B,i}$ and $f_{N,i}$ are the flow rates of microchannel i with and without blockage, respectively (Kano *et al.*, 2007).

$$BD_i = \left(1 - \frac{f_{B,i}}{f_{N,i}}\right) \times 100 \ [\%] \tag{1}$$

3. Identification method of blockage locations

The pressure drop distribution in a microreactor changes when a blockage occurs. Figure 2 shows an example of the pressure drop distribution when blockages simultaneously occur in three microchannels ($BD_1 = 15\%$, $BD_2 = 35\%$, $BD_8 = 35\%$) in a microreactor with ten microchannels.

As the figure shows, the pressure distribution has certain patterns with regard to blockage locations. Therefore, the locations can be identified by comparing the measured pressure distribution data with pressure distribution data prepared before the blockages occurred. However, to construct a database for identifying multiple blocked channels, it is necessary to calculate a large amount of pressure distribution data for all multiple channel combinations under various degrees of blockage. This calculation must be done by using CFD simulation, which is a very time-consuming process.

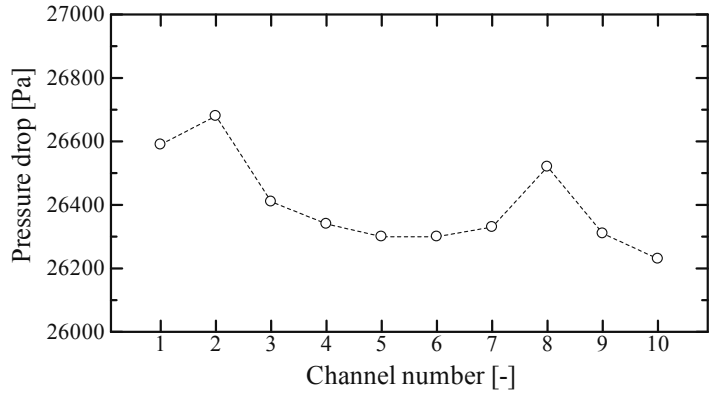

Fig. 2 Example pressure distribution data when blockage occurs in three microchannels

To avoid this combinatorial explosion of CFD simulations, we propose a method for identifying multiple blockage locations by using only pressure distribution data obtained when a single channel is blocked. In the example described here, the three blocked microchannels are identified through the following steps.

(1) Calculate the pressure difference data vector $\Delta\hat{P}_{B,i}$ defined by Eq. (2). Here, $\hat{P}_{B,i}$ is the pressure data vector at sensor locations when x% (>0) blockage occurs in microchannel i, which is calculated by CFD simulation. $\widetilde{P}_N$ is the pressure data vector measured at sensor locations under normal conditions.

$$\Delta\hat{P}_{B,i} = \hat{P}_{B,i} - \widetilde{P}_N \quad (i \in I) \tag{2}$$

Any blockage degree can be selected for x because the direction of the pressure difference vector between normal and abnormal conditions changes very little with regard to blockage degree.

(2) Measure the pressure difference data vector $\Delta\widetilde{P}$ defined by Eq. (3). Here, $\widetilde{P}_B$ is the actual pressure data vector measured at sensor locations. $\widetilde{P}_N$ is for normal conditions and $\widetilde{P}_B$ is for abnormal conditions.

$$\Delta\widetilde{P} = \widetilde{P}_B - \widetilde{P}_N \tag{3}$$

(3) Calculate the orthogonal projection vector $\Delta\overline{P}_{i_1,i_2,i_3}$ of $\Delta\widetilde{P}$ to the projection plane spanned by vectors $\Delta\hat{P}_{B,i_1}, \Delta\hat{P}_{B,i_2}$ and $\Delta\hat{P}_{B,i_3}$ $(i_1, i_2, i_3 \in I)$ by Eq. (4), where $\langle\cdot,\cdot\rangle$ denotes the inner product and $\|\cdot\|$ denotes the 2-norm.

$$\Delta\overline{P}_{i_1,i_2,i_3} = \alpha_{i_1}\Delta\hat{P}_{B,i_1} + \alpha_{i_2}\Delta\hat{P}_{B,i_2} + \alpha_{i_3}\Delta\hat{P}_{B,i_3} \tag{4}$$

$$\begin{bmatrix} \alpha_{i_1} \\ \alpha_{i_2} \\ \alpha_{i_3} \end{bmatrix} = \begin{bmatrix} \left\| \Delta\hat{P}_{B,i_1} \right\|^2 & \left\langle \Delta\hat{P}_{B,i_1}, \Delta\hat{P}_{B,i_2} \right\rangle & \left\langle \Delta\hat{P}_{B,i_1}, \Delta\hat{P}_{B,i_3} \right\rangle \\ \left\langle \Delta\hat{P}_{B,i_1}, \Delta\hat{P}_{B,i_2} \right\rangle & \left\| \Delta\hat{P}_{B,i_2} \right\|^2 & \left\langle \Delta\hat{P}_{B,i_2}, \Delta\hat{P}_{B,i_3} \right\rangle \\ \left\langle \Delta\hat{P}_{B,i_1}, \Delta\hat{P}_{B,i_3} \right\rangle & \left\langle \Delta\hat{P}_{B,i_2}, \Delta\hat{P}_{B,i_3} \right\rangle & \left\| \Delta\hat{P}_{B,i_3} \right\|^2 \end{bmatrix}^{-1} \begin{bmatrix} \left\langle \Delta\tilde{P}, \Delta\hat{P}_{B,i_1} \right\rangle \\ \left\langle \Delta\tilde{P}, \Delta\hat{P}_{B,i_2} \right\rangle \\ \left\langle \Delta\tilde{P}, \Delta\hat{P}_{B,i_3} \right\rangle \end{bmatrix}$$

(4) Identify blocked microchannels i^*_1, i^*_2, and i^*_3 by using Eq. (5), whose microchannels have the highest correlation between $\Delta\tilde{P}$ and $\Delta\overline{P}_{i_1,i_2,i_3}$.

$$(i_1^*, i_2^*, i_3^*) = \arg\max_{i_1,i_2,i_3 \in I} \frac{\left(\Delta\tilde{P} - \Delta\tilde{P}^m\right)^{\mathrm{T}} \left(\Delta\overline{P}_{i_1,i_2,i_3} - \Delta\overline{P}^m_{i_1,i_2,i_3}\right)}{\left\|\Delta\tilde{P} - \Delta\tilde{P}^m\right\| \left\|\Delta\overline{P}_{i_1,i_2,i_3} - \overline{P}^m_{i_1,i_2,i_3}\right\|} \tag{5}$$

Here, all elements of $\Delta\tilde{P}^m$ and $\Delta\overline{P}^m_{i_1,i_2,i_3}$ are the means of all elements of $\Delta\tilde{P}$ and $\Delta\overline{P}_{i_1,i_2,i_3}$, respectively.

4. Case study

The proposed method was applied to a blockage diagnosis problem for a microreactor with 10 microchannels. Table 1 summarizes the geometric parameters in Fig. 2 and the microreactor's operating conditions. Four pressure sensor configurations (Conf. A–D) were implemented for use in different case studies.

Conf. A: $n_S = 10$, $S = \{1, 2, 3, 4, 5, 6, 7, 8, 9, 10\}$
Conf. B: $n_S = 6$, $S = \{1, 3, 5, 6, 8, 10\}$
Conf. C: $n_S = 5$, $S = \{1, 3, 5, 7, 9\}$
Conf. D: $n_S = 4$, $S = \{1, 4, 7, 10\}$

Pressure sensors were set up at the inlet of the microchannels $i \in S$. The sensors' measurement accuracy was assumed to be 10 Pa, which was determined in accordance with the best measurement accuracy of commercial MEMS pressure sensors.

In the case study, the following blockage diagnosis problem was considered to assess the proposed method's effectiveness.

$$BD_1 = 15\%,\ BD_2 = 35\%,\ BD_8 = 35\%$$

Table 1 Geometric parameters and operation conditions of microreactor

Name	Parameter	Value	Unit	Name	Parameter	Value	Unit
Number of channels	n_C	10	-	Widths of manifold	$w_{M,top}$	5.0	mm
Channel width	w_C	100	μm		$w_{M,bot}$	1.4	mm
Channel depth	z_C	100	μm	Inlet velocity	v	0.01	m/s
Channel length	l_C	20	mm	Outlet pressure	p_O	101.3	kPa
Width of fin	w_F	284	μm	Viscosity	μ	0.1	Pa·s

Simulation results are summarized in Table 2, in which the combinations of identified numbers of blocked channels are shown. The proposed method correctly identified the blocked microchannels #1, #2, and #8 when there were five or more sensors. These results demonstrate that a small database with pressure distribution data for the blockage in a single microchannel can correctly identify multiple blockage locations in a microreactor when the number of pressure sensors is more than half of the number of microchannels.

Table 2 Simulation results

Sensor configuration (n_s)	A(10)	B (6)	C (5)	D (4)
Identified blockage locations	1, 2, 8	1, 2, 8	1, 2, 8	1, 5, 8

5. Conclusion

A data-based identification method that can cope with blockages in multiple microchannels was proposed. To avoid a combinatorial explosion of CFD simulations for database construction, the proposed method identifies blocked locations by using only pressure distribution data when a single channel is blocked. The results of CFD simulations showed that the method can accurately identify three blockage locations using fewer pressure sensors than there are microchannels. In this study we focused on a case in which three microchannels were blocked, but our method can easily be extended to apply to cases in which there are four or more blocked microchannels without incurring any combinatorial explosion of CFD simulations for database construction.

References

Hessel, V. H., H. Lowe, A. Muller, and G. Kolb, 2005, Chemical Micro Process Engineering, Viley-VCH Verlag, Weinheim.

Kano, M., T. Fujioka, O. Tonomura, S. Hasebe, and M. Noda, 2007, Data-Based and Model-Based Blockage Diagnosis for Stacked Microchemical Processes, *Chem. Eng. Sci.*, 62, 1073-1080

Noda, M., N. Kurihara, and H. Nishitani, 2010, Blockage Diagnosis of Stacked Microreactor Using Pressure Sensors, *Proc. of PSE Asia 2010*, 413-418

Tanaka, Y., O. Tonomura, K. Isozaki and S. Hasebe, 2011, Detection and Diagnosis of Blockage in Parallelized Microreactors, *Chem Eng. J.*, 167, 483-489

Yamamoto, R., M. Noda and H. Nishitani, 2009, Blockage Diagnosis of Microreactors by Using Pressure Sensors, *Kagaku Kogaku Ronbunshu*, 35(1), 170–176 (in Japanese)

I.A. Karimi and Rajagopalan Srinivasan (Editors), Proceedings of the 11th International Symposium on Process Systems Engineering, 15-19 July 2012, Singapore.

Conceptual Framework for Security Hazard Management in Critical Infrastructures

Yoshihiro Hashimoto, Takeshi Toyoshima, Shuichi Yogo, Masato Koike,

Sun Jing and Ichiro Koshijima

Dept. of Civil and Managegement Engineering, Nagoya Institute of Technology, Nagoya 466-8555, Japan

Abstract

In this paper, the security improvement approaches for process plant instrumentation and process information systems are proposed. By dividing control and information systems into plural zones considering process dynamics under the proposed framework, higher possibility of cyber-attacks detection and operational accident prevention can be attained. Based on this framework, accidents caused by cyber-attacks are evaluated as a form of FTA created from detectability and reachability matrices made from process, operation and control (management) constraints. An example also illustrated to understand the proposed approach.
Keywords: plant security, hazard management, plant safety, design methodology

1. Introduction

Current Industrial Control Systems (ICS: from sensors to SCADA, MES) are connected to Internet for many purposes such as information exchange for business oriented plant operations and remote maintenance. The open system movement, though, shows great promise for certain benefits through COTS (commercial off the shelf) products, it also causes various risks as the results of open architectures and network technologies. Recently, a very specific threat for process plants has come in reality. Stuxnet is acknowledged as the first malware, which attacked continuously to a uranium enriching plant in Iran, targeting specific Programmable Logic Controllers (PLCs). This malware has been spread out all over the world to many process plants with and without Internet connection. As the most serious effect from Stuxnet, demonstration by followers might be occurred with high possibility over automatically operated critical infrastructures. In this situation, ICS require highly reliable security and safety services with urgent priority.

In this paper, the authors discuss about a new protection profile for process plant that covers not only safety but also security. Under this profile, even if some invasion to the ICS is succeeded, plant operators might be able to handle the attacks with intangible and autonomous ICS. Design methodologies of secured process plant and PIS (Plant Information Systems) are also discussed with an illustrative example.

2. Characteristics of ICS security problem

The serious security holes of personal computer systems are frequently reported, and security patches thereto are distributed almost every day. In some cases, the security patches make uncertain troubles from conflicts among installed applications. Full security patches, therefore, are rarely applied to ICS for maintaining their security. For

the ICS security, particular approaches are necessary in addition to ones for information systems.

2.1. Schemes for enhancement of ICS Security

Evaluation of security assurance level of ICS is discussed in ANSI/ISA99. Security zones and conduits shown in Fig. 1 are important concepts in ISA99 (Uehara, 2011). The security of the system is evaluated based on the zones and their interfaces. The firewalls between zones must not have the same vulnerability. In this standard, however, safety is not discussed at all. For the process plants, the zone design approach to improve safety should be discussed with security of ICS.

2.2. Schemes for enhancement of ICS Safety

The design approaches of Safety Instrument Systems (SIS) are described in IEC61508 (IEC61511 is the standard for process industry). Safety integrity and reliability are evaluated using Hazard and operability studies (HAZOP), layers of protection analysis (LOPA), risk graphs, FTA and so on. However there are very few papers that consider the threats of the cyber attaches (NRC, 2010). Although, the effects of single failure are discussed in these approaches, attacks of cyber terrorists cause multiple failures. They invade the system via Internet and/or malwares and steal, manipulate and conceal process and control information.

Cyber terrorists can attack the plural layers in IPL (cf. 2, 3, 4, 6, 7 layers in Fig. 2).Especially, when emergency shutdown system in IPL4 that is constructed with PLC, is attacked, service of the plant can be stopped immediately. Against such undesirable shutdown, a fail-safe system shown in Fig. 3 is necessary. This additional logic system is attached to check the trigger conditions of the manipulation (It is not necessary to check the all conditions). The manipulation is activated only when the both outputs are identical. The design scheme of SIS should be reconsidered from security perspective.

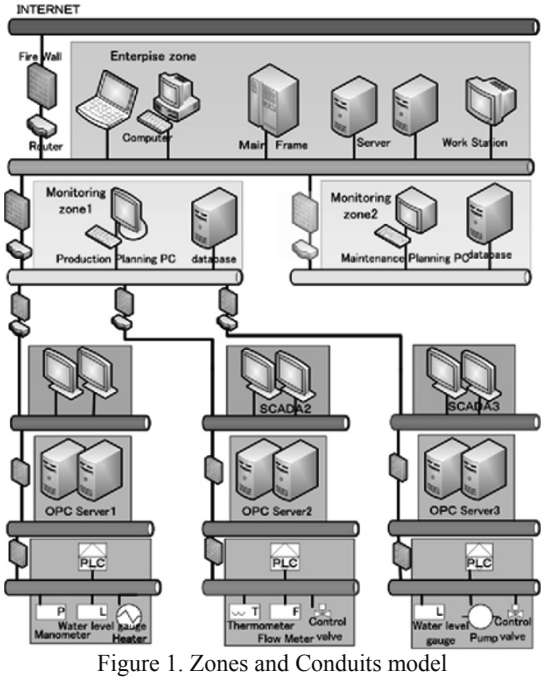

Figure 1. Zones and Conduits model

Figure 2. Independent Protection Layers

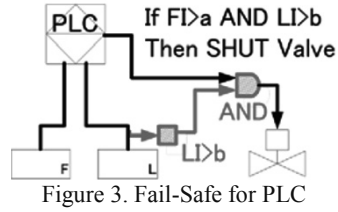

Figure 3. Fail-Safe for PLC

3. Fault Tree Analysis for threats of cyber terrorism

Fault tree is very popular method to evaluate risks. Because it can deal with multiple failures, it can be applied to evaluate the threats of cyber terrorism. Attacks of cyber terrorists are parts of causes of accidents. Manipulation sequences by terrorists are similar to sets of mal-operation. Concealment of their manipulation is similar to a set of sensor malfunctions. In safety assessment, they are evaluated based on human factors and equipment failures. In security problems, the probability of their occurrence is not independent. Cyber terrorists combine the causes to ensure their attacks. The countermeasures against cyber terrorism must appear in FTA to evaluate their efficiency. Invalidation of a countermeasure is one of the conditions, which are combined by AND, to occur a trouble state in FTA. Countermeasures are activated after the detection of abnormality. If the trigger information is concealed, countermeasure is invalidated. The effects of concealment must be considered as well as manipulation.

How to construct Fault Tree for evaluation of security threats were discussed in our previous papers (Shindo, 2000, Toyoshima, 2011, Yogo, 2011). In this paper, a systematic, qualitative and quantitative scheme is proposed to evaluate the effects of manipulation and concealment by cyber terrorists. The efficiency of the scheme to divide the plant instrument into plural zones is evaluated on the view of invalidation of cyber-attacks.

4. Effects of manipulation and concealment in a zone

The main threats of cyber terrorists are all sorts of accidents (i.e. explosion and contamination of drinking water) and/or sabotage against service continuity (i.e. power outage and water outage). In industrial plants, they are caused by manipulations of valves and/or switches. If actual process data can be observed by operators, such intentional manipulation should be detected because of spontaneous delay in process dynamics and some countermeasure can be applied before said manipulation affects. Terrorists, therefore, conceal their manipulations to disable countermeasures.

In industrial plants, many controllers are utilized. If they are divided into plural zones and the same scheme cannot be applied to invade the zones, some zones can survive against cyber-attack. As the result, possible manipulations are limited in the invaded zones. If plural manipulation is necessary to activate multiple accidents in other zones simultaneously, the probability of accident can be reduced.

Although the signals from the sensors in the invaded zones can be forged, the controller in the surviving zones may be affected by the said manipulation. When certain cyber-attack is detected, field devices and local signals such as glass gauges of tanks should be checked. The controllers in the invaded zones are switched into local backup controllers as shown in Fig. 4 or turned into manual operation mode. If the dynamics of the controller is slow, the local backup might not be necessary. When the detection is succeeded immediately, the controllers can be recovered from the attacked state. Even if the state of the invade zones becomes dangerous, certain manual sequence to shut down the plant is safely adopted.

The detection in the surviving zone also affects controllers. The controllers in the surviving zones manipulate valves based on the sensed signals. If the manipulation is manual, the action of operator based on the sensor can be considered as a controller. If the caused manipulation is a cause of an accident, the risk of the control in surviving zones should be considered.

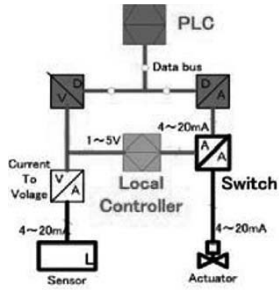

Figure 4. Backup controller

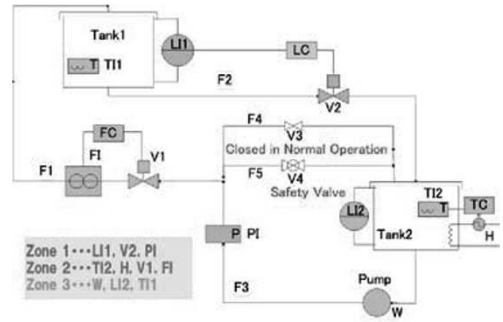

Figure 5. Two tank system for Example

In this paper, the effects of zones on detection and risk reduction of cyber-attack are discussed. A simple plant shown in Fig. 5 is utilized to illustrate the evaluation scheme of effects of zones. It has 10 process variables and 10 sensed variables. Manipulated variables are 6. Two of them are local valves, which cannot be operated by cyber attackers. One is a remote operable valve, which is not connected with a controller. Three of them are actuators of controllers. They are divided into three zones as shown in Fig. 5.

The relationships between the variables are expressed using Boolean matrices as shown in Table 1. They are square matrices, whose rows and columns contain all variables. All of their diagonal elements are one. Tables from 2 to 4 show a part of the matrices.

Matrix P in Table 1 shows the process dynamics. Matrix C in Table 2 shows control actions. It can express not only controller but also manual operations based on the observation. The columns M_{23} in Table 3 correspond to the manipulated variables in the invaded zone (zones 2 and 3 in this case). The columns of A_{23} in Table 4 correspond to the information which can be forged by cyber-terrorists. These matrices are arranged according to the selection of invaded zones. S_1 is the diagonal matrix to express the effects of concealment. The diagonal elements corresponding to the invaded sensors are zeros. O_1 is the matrix to extract the surviving sensors.

Detectability matrix and reachability matrix are defined by eq. (1) and (2), respectively.

Table 1. Cause Effect Matrix of Process dynamics [P] (26x26)

	Process Variables										Manipulated Variables						Observed Variables									
											Local		Man	Auto												
	LI	FI	F2	F3	F4	F5	TI	L2	T2	P	V3	V4	W	V1	V2	H	L1i	L2i	F1i	T1i	T2i	V1i	V2i	Pi	Hi	Wi
LI	1	1	1	0	0	0	0	0	0	0	0	0	0	0	0	0	0	0	0	0	0	0	0	0	0	0
FI	0	1	0	1	0	0	0	0	0	1	0	0	0	1	0	0	0	0	0	0	0	0	0	0	0	0
F2	0	0	1	0	0	0	0	0	0	0	0	0	0	0	1	0	0	0	0	0	0	0	0	0	0	0
F3	0	0	0	1	0	0	0	1	0	1	0	0	1	1	0	0	0	0	0	0	0	0	0	0	0	0
F4	0	0	0	0	1	0	0	0	0	0	1	0	0	0	0	0	0	0	0	0	0	0	0	0	0	0
F5	0	0	0	0	0	1	0	0	0	0	0	1	0	0	0	0	0	0	0	0	0	0	0	0	0	0
TI	0	1	0	0	0	0	1	0	1	0	0	0	0	0	0	0	0	0	0	0	0	0	0	0	0	0
L2	0	0	1	1	0	0	0	1	0	0	0	0	0	0	0	0	0	0	0	0	0	0	0	0	0	0
T2	0	0	1	0	0	0	1	0	1	0	0	0	0	0	0	0	0	0	0	0	0	0	0	0	0	0
P	0	1	0	1	1	1	0	0	0	1	0	0	1	1	0	0	0	0	0	0	0	0	0	0	0	0
V3	0	0	0	0	0	0	0	0	0	0	1	0	0	0	0	0	0	0	0	0	0	0	0	0	0	0
V4	0	0	0	0	0	0	0	0	0	0	0	1	0	0	0	0	0	0	0	0	0	0	0	0	0	0
W	0	0	0	0	0	0	0	0	0	0	0	0	1	0	0	0	0	0	0	0	0	0	0	0	0	0
V1	0	0	0	0	0	0	0	0	0	0	0	0	0	1	0	0	0	0	0	0	0	0	0	0	0	0
V2	0	0	0	0	0	0	0	0	0	0	0	0	0	0	1	0	0	0	0	0	0	0	0	0	0	0
H	0	0	0	0	0	0	0	0	0	0	0	0	0	0	0	1	0	0	0	0	0	0	0	0	0	0
L1i	1	0	0	0	0	0	0	0	0	0	0	0	0	0	0	0	1	0	0	0	0	0	0	0	0	0
L2i	0	0	0	0	0	0	0	1	0	0	0	0	0	0	0	0	0	1	0	0	0	0	0	0	0	0
F1i	0	1	0	0	0	0	0	0	0	0	0	0	0	0	0	0	0	0	1	0	0	0	0	0	0	0
T1i	0	0	0	0	0	0	1	0	0	0	0	0	0	0	0	0	0	0	0	1	0	0	0	0	0	0
T2i	0	0	0	0	0	0	0	1	0	0	0	0	0	0	0	0	0	0	0	0	1	0	0	0	0	0
V1i	0	0	0	0	0	0	0	0	0	0	0	0	0	1	0	0	0	0	0	0	0	1	0	0	0	0
V2i	0	0	0	0	0	0	0	0	0	0	0	0	0	0	1	0	0	0	0	0	0	0	1	0	0	0
Pi	0	0	0	0	0	0	0	0	0	1	0	0	0	0	0	0	0	0	0	0	0	0	0	1	0	0
Hi	0	0	0	0	0	0	0	0	0	0	0	0	0	0	0	1	0	0	0	0	0	0	0	0	1	0
Wi	0	0	0	0	0	0	0	0	0	0	0	0	1	0	0	0	0	0	0	0	0	0	0	0	0	1

Table 2. Controller Matrix [C](26x26)

	Manipulated Variables						Observed Variables											
	Local		Man	Auto														
	V3	V4	W	V1	V2	H	L1i	L2i	F1i	T1i	T2i	V1i	V2i	Pi	Hi	Wi
W	0	0	1	0	0	0	0	0	0	0	0	0	0	0	0	1
V1	0	0	0	1	0	0	0	0	1	0	0	1	0	0	0	0
V2	0	0	0	0	1	0	1	0	0	0	0	0	1	0	0	0
H	0	0	0	0	0	1	0	0	0	0	1	0	0	0	1	0

Table 3. Manipulation $[M_{23}](26x3)$

	V1	H	W
W	0	0	1
V1	1	0	0
V2	0	0	0
H	0	1	0

Table 4.Attack $[A_{23}](26x7$

	F1i	T2i	V1i	Hi	L2i	T1i	Wi
L1i	0	0	0	0	0	0	0
L2i	0	0	0	0	1	0	0
F1i	1	0	0	0	0	0	0
T1i	0	0	0	0	0	1	0
T2i	0	1	0	0	0	0	0
V1i	0	0	1	0	0	0	0
V2i	0	0	0	0	0	0	0
Pi	0	0	0	0	0	0	0
Hi	0	0	0	1	0	0	0
Wi	0	0	0	0	0	0	1

Table 5. Detectability Matrices

$[D_{23}(26)]$

	V1	H
L1i	1	0
V2i	1	0
Pi	1	0

$[D_2(3)]$

	V1	H
L2i	1	0
T1i	1	1
Wi	0	0
L1i	1	0
V2i	0	0
Pi	1	0

$$D_{23}(m) = \sum_{k=1}^{m} O_1 \, (S_1 \cdot P \cdot C)^{k-1} S_1 \cdot P \cdot M_{23} \quad (1)$$

$$R_{23}(\mathrm{n}) = \sum_{k=1}^{n} (P \cdot C)^{k-1} P \cdot A_{23} \quad (2)$$

If non-zero elements appear in each column of the detectability matrix, it can be judged that the effects of the manipulation can be detected under concealment by cyber attackers. If manipulation cannot be detected, all elements of the column corresponding to it remain zero even when the order of detectability matrix (i.e. *m* in eq. (1)) is larger than the size of variables.

Table 5 shows the detectability matrices in two cases. $D_{23}(26)$ shows that manipulation of heater cannot be detected when zones 2 and 3 are invaded. $D_2(3)$ shows every manipulation in zone 2 can be detected in three steps of propagation. In this case, the manipulation of heater can be detected in the temperature change of the other tank, T1. It is easy to calculate the detectability matrices for all cases of invasion by cyber attackers. It can be confirmed that only the case, in which zone 2 and zone 3 are invaded and heater is manipulated, is undetectable. Needless to describe, if all zones are invaded, any manipulation under concealment cannot be detected from sensed information. In order to detect the heater manipulation in such a case, the temperature analog signal must be duplicated and be transferred to zone 1.

Table 6 shows reachability matrix R_{23}. It shows the effects of forgery in invaded zones. While forgery of T1i doesn't affect others, T2i can affect as similar to H. The change of T2i can cause heater manipulation by its controller. If operator manipulation is described in controller matrix, C, the effect of the operators' countermeasures against the forged situation can be considered.

Table 6. Reachability Matrices[R_{23}]

	F1i	T2i	V1i	Hi	L2i	T1i	Wi
L1	1	0	1	0	0	0	1
F1	1	0	1	0	0	0	1
F2	1	0	1	0	0	0	1
F3	1	0	1	0	0	0	1
F4	0	0	0	0	0	0	0
F5	0	0	0	0	0	0	0
T1	1	1	1	1	0	0	1
L2	1	0	1	0	0	0	1
T2	1	1	1	1	0	0	1
P	1	0	1	0	0	0	1
V3	0	0	0	0	0	0	0
V4	0	0	0	0	0	0	0
W	0	0	0	0	0	0	1
V1	1	0	1	0	0	0	1
V2	1	0	1	0	0	0	1
H	1	1	1	1	0	0	1

5. Conclusion

Evaluation method of security zoning for Industrial Control Systems is proposed by defining detectability matrix and reachability matrix. This approach shows an example of the cooperation of information engineers and process engineers for security improvement of control systems.

Acknowledgment

The authors wish to express sincere appreciation to the METI's Task Force on ICS security for their valuable feedback.

References

National Research Council (2010) Review the Department of Homeland Security's Approach to Risk Analysis, National Academy of Sciences, 49-50

Shindo A., H. Yamazaki, A. Toki, I. Koshijima and T. Umeda (2000) An Approach to Potential Risk Analysis of Networked Chemical Plants, Comp. &Chem. Eng., 24, 2, 721-727(7)

Toyoshima, T., J. Sun, I. Koshijima and Y. Hashimoto (2011) Risk analysis and countermeasure planning against cyber-attacks, J. of Human Factors in Japan, 15, 2,4-9

Uehara, T. (2011)SCADA system and cyber security, J. of Human Factors in Japan, 15, 2,10-13

Yogo, S., T. Toyoshima, J. Sun, I. Koshijima and Y. Hashimoto(2011) Design of safe plants considering cyber security, Proceedings of 43rd Autumn Meeting of S. Chem. Engr. Japan, Q101

I.A. Karimi and Rajagopalan Srinivasan (Editors), Proceedings of the 11th International Symposium on Process Systems Engineering, 15-19 July 2012, Singapore.

A simulation based engineering method to support HAZOP studies

Rasmus Enemark-Rasmussen[2], David Cameron[3], Per Bagge Angelo[4] and Gürkan Sin[1]

[1]*CAPEC, Department of Chemical and Biochemical Engineering, Technical University of Denmark, Soltoft Plads, Lyngby, 2800, Denmark, email: gsi@kt.dtu.dk*
[2]*DONG Energy E&P, Agern Allé 24-26, Hørsholm, 2970, Denmark.*
[2]*Kongsberg Oil & Gas Technologies AS, Hamangskogen 60, 1338 Sandvika.*
[3]*Maersk Oil & Gas AS - Maersk Oil, Esplanaden 50, DK-1263 Copenhagen, Denmark*

Abstract

HAZOP is the most commonly used process hazard analysis tool in industry, a systematic yet tedious and time consuming method. The aim of this study is to explore the feasibility of process dynamic simulations to facilitate the HAZOP studies. We propose a simulation-based methodology to complement the conventional HAZOP procedure. The method systematically generates failure scenarios by considering process equipment deviations with pre-defined failure modes. The effect of failure scenarios is then evaluated using dynamic simulations -in this study the K-Spice® software used. The consequences of each failure scenario are summarized using a sensitivity measure, which forms the basis for ranking the significance of failure scenarios. The ranking then reveals the most critical process parameters as well as equipment in a system. The methodology is successfully highlighted using part of gas-reinjection process model as case study.

Keywords: HAZOP, Dynamic Simulation, Process Control, Process Model, Safety, gas-reinjection

1. Introduction

Due to increasing public awareness, legal demands (such as Seveso II directive) for safety systems and many severe accidents within the oil, gas and chemical industry, much research has been invested in developing effective hazard and safety analysis methodologies. One of the most commonly used process hazard analysis for risk assessment is the hazard and operability (HAZOP) analysis. The HAZOP method systematically covers the entire process by taking a deviation, which is generated by a combination of a relevant guide word (e.g. MORE OF, LESS OF, …) with a key process parameter (e.g. Flow, Temperature, etc.) to identify possible causes and consequences in a given section of a plant (Cameron et al. 2005). Based on a qualitative risk assessment of the identified causes and consequences of a hazard (e.g. using the ALARP principle), recommendations are then made by HAZOP team to improve the base case design (and or retrofit/upgrade the existing plant). One of the drawbacks of the HAZOP method is that it is time-consuming and purely depends on human experience and the knowledge of the multidisciplinary HAZOP team. These and other drawbacks motivated the development of computer-aided HAZOP methods and accompanying software tools to facilitate carrying out HAZOP analysis in industry.

Research in the area of computer-aided HAZOP accounts for approximately 40% of the publications in the last decade as reported in 2010 by (Jordi et al. 2010).
Most computer-aided HAZOP methods uses expert systems based on qualitative reasoning engines, logic representation and symbolic manipulation type artificial intelligence techniques. Examples of such methods include QUEEN, HAZOPexpert, STOPHAZ, functional HAZOP among others (Jordi et al., 2010; Enemark-Rasmussen, 2011). It is noted that most of these methods require the translation of a P&ID of plant into an appropriate HAZOP model (as needed by the expert system in question) and an extensive database, which consists of known facts, rules and characterization of process equipment on basis of type of operation and process variables. This information base draws on knowledge from experiences and studies of process deviations, causes and consequences of these deviations and hence needs to be adapted or extended for the specific application. Industry acceptance of such HAZOP software is rather low, due to need for new skills and expertise in learning the HAZOP modelling language.
In this contribution, our aim is to develop a methodology that provides support for incremental improvement of the HAZOP studies by using readily available dynamic models. The premise is two-fold: (i) dynamic models are increasingly used in the chemical industry –most if not all projects in the oil and gas industries use dynamic models for verifying design capacity and evaluating instrumentation, control and automation strategies. These models are available for hazard and operability analysis at no additional cost, (ii) the dynamic models are based on laws of conservation for mass, energy and momentum and a set of constitutive equations such as physical properties calculations. This provides objective credible and scientifically sound decision making in HAZOP analysis. The methodology is explained below and highlighted using the gas-reinjection process as a case stud -commonly used in offshore oil and gas industry.

2. Dynamic simulations based Methodology for HAZOP studies

The simulation methodology used for operability and safety analysis (Enemark-Rasmussen, 2011) uses a combination of failure mode effect analysis and HAZOP procedures as described by (Skelton, 1997). Generation and dynamic simulation of failure scenarios allows the user to follow the changes in the critical process variables when a failure scenario is introduced in equipment. The analysis was carried out following the steps in the methodology, as seen in Figure 1 and Figure 2:

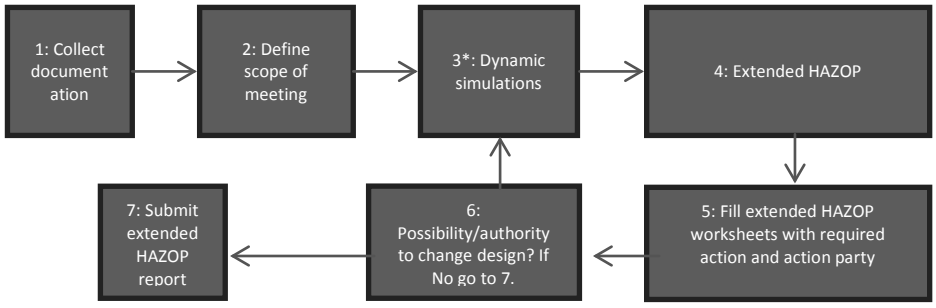

Figure 1: Extended HAZOP methodology using dynamic simulations

2.1. Scenario generation

The system is described by the simplified differential state equations (1) which are based on the conservation of mass, energy and momentum equations. The variables

defining the state of the system are the critical process parameters, *x*, the time, *t*, and the variable equipment settings, θ.

$$\frac{df}{dx} = f(x,t,\theta) \; and \; y = g(x,t,\theta) \tag{1}$$

A failure scenario is thus defined as a deviation, *i*, of the process equipment variable, θ_i, resulting in a failure mode of the process system, g_i. A failure scenario is mathematically simulated using the state equation (1) by varying the nominal values of the parameters of equipments (e.g. valve) according to the failure (e.g. valve fails to close or fails to open).

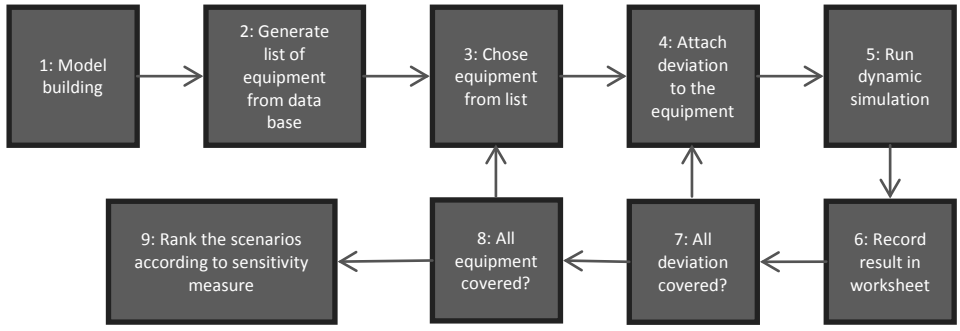

Figure 2: Detailed structure of the dynamic simulation step used in the methodology

2.2. Failure scenario ranking

The significance of the consequences of the failure scenarios are ranked based on sensitivity analysis (SA) given in equation (2) (Sin et al., 2009). The normal operation value (e.g. Pressure) at a given position and time in the process is defined by y(θ) and the failure scenario value at the same position and time is defined by y(θ-Δθ) both generated by the dynamic simulation of the failure mode, $f_i(\theta_i)$.

$$If \; \theta > \theta_i \Rightarrow SA = \frac{\Delta y}{\Delta \theta} = \frac{y(\theta) - y(\theta - \Delta\theta)}{\Delta \theta} \; and \; If \; \theta < \theta_i \Rightarrow SA = \frac{\Delta y}{\Delta \theta} = \frac{y(\theta + \Delta\theta) - y(\theta)}{\Delta \theta} \tag{2}$$

2.3. Process equipment deviations

The deviations or malfunctions included at this stage is limited to the most common process equipment used in the upstream oil and gas industry, such as separators, valves, piping and process control. Deviations are defined in the range zero to one by equations or by logical meaning. As example, plugging is defined by the admittance equation, $A_v^{new} = A_v^{normal}(1 - plugging \; fraction)$, where the admittance, A_v, is proportional to the flow through the pipe and the flow coefficient, C_v. Deviations such as fully closed/fully open are logic-based, and receive values of zero or one.

The following type of deviations considered for the process equipments in the case study: Fully closed, Fully open, Plugging low, Plugging high, Fail high, Fail low, Fouling low, Fouling high, Rupture/leakage, Power failure, Deterioration and wear. This list can be extended if necessary for different equipments or scenarios.

2.4. Summary of results: ranking of failure scenarios

The results obtained during simulations of the failure scenarios are recorded in a pre-generated worksheet which includes scenario number, j = 1…N, failure mode, f_i, values for both θ and θ_i, normal operation and failure values of the critical process parameters as well as the sensitivity measurement used for ranking.

3. Results and discussions Case study of gas re-injection process

To validate the methodology a case study of an offshore gas re-injection process is investigated. Process instrumentation and flow diagram is given in Figure 3.

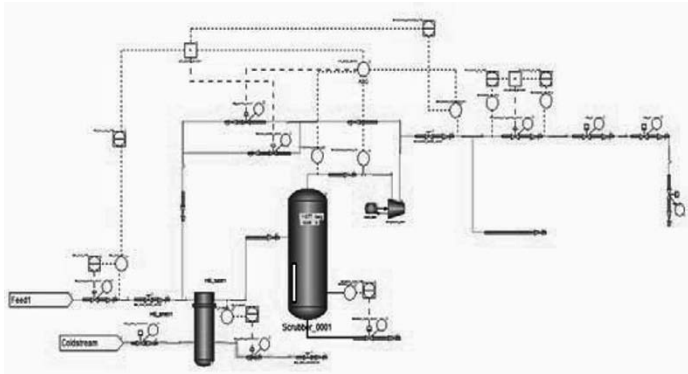

Figure 3: Process instrumentation and flow diagram for gas re-injection process

The K-Spice® software uses built-in functionality to introduce equipment deviations, in the software called equipment malfunctions. After introducing an equipment deviation, the behavior of critical process variables is displayed over time at mass or energy transfer points or other locations of interest, such as production outlets. Each failure scenario is simulated over enough time to capture any changes that might occur during the transient phase when going from normal to failure operation conditions. The system typical reaches peak values within a short time span, before the control systems react to counter e.g. pressure increase. For each failure scenario simulation any peak values are recorded together with the stabilized process parameter values to be used for sensitivity measurement ranking. The results of each failure are recorded as shown in Table 1.

Table 1: Failure scenario result from Gas feed control valve fully closed.

Scenario	**Failure scenario**				**T [°C]**	**u [kg/h]**	**P [barg]**	**Sensitivity measure (SA)**			**Consequences**
J = 1...N	Failure mode f_i	Parameter (θ)		$y_i(\theta)$	Normal value			$\frac{\Delta T}{\Delta \theta}$	$\frac{\Delta u}{\Delta \theta}$	$\frac{\Delta P}{\Delta \theta}$	
		Default	Failure		Failure value						
1	Gas_feed control valve1 fully closed	0.715	0	Recycle loop	76.5	0	189.3	107	0	264.8	No flow in system.
					0	0	0				
		0.715	0	Compressor	79.8	244110	189	112	341413	264.3	
					0	0	0				
		0.715	0	Reinjection P2	76.2	209385	169.6	107	292846	237.2	
					0	0	0				
		0.715	0	Reinjection P1	76.2	34725	169.6	107	48566	237.2	
					0	0	0				
		0.715	0	Gas feed	70	244133	120	0	341445	0.0	
					70	0	120				
		0.715	0	Sea Water outlet	37.7	697475	15.5	10	975456	-0.6	
					30.2	24	15.9				

In Table 2 the five highest ranked scenarios are displayed for Temperature, Flow and Pressure parameters based on the quantitative sensitivity measure obtained by forward or backward differentiation (equation 2). Using the methodology, 68 failure scenarios were identified and ranked based on the sensitivity ranking. The most severe failure was found to be: the re-injection control valve failed closed. This resulted in a pressure peak

above design values at the compressor and pressure build-up at gas feed inlet. Other high ranked failure scenarios resulted in loss of re-injection and possible damage to equipment due to pressures reaching above design pressure.

Table 2: Failure scenarios ranked by sensitivity measure of critical process parameters

Sc	Temp ranking Failure mode f_i	SA $\frac{\Delta T}{\Delta\theta}$	Sc	Flow ranking Failure mode f_i	SA $\frac{\Delta u}{\Delta\theta}$	Sc	Pres ranking Failure mode f_i	SA $\frac{\Delta P}{\Delta\theta}$
67	Motor_0001 fail low	226	14	Sea_water outlervalve1 fully open	3973929	60	Reinjection_P1 PT2 fail high	-530
5	Reinjection control valve1 fully closed	152	52	Compressor discharge_PT1 fail high	3345466	56	Gas_feed_PT1 fail high	-350.6
56	Gas_feed_PT1 fail high	-148	64	Cooler_outlet_TT1 fail high	2715518	5	Reinjection control valve1 fully closed	339.2
1	Gas_feed control valve1 fully closed	112	5	Reinjection control valve1 fully closed	-2679734	15	WCV_01 fully closed	339.2
65	Cooler_outlet_TT1 fail low	-91	65	Cooler_outlet_TT1 fail low	1743688	67	Motor_0001 fail low	331.9
35	Reinjection pipe1 rupture	-90	45	HE_shell1 fouling high	1630320	1	Gas_feed control valve1 fully closed	264.8

4. Conclusion and perspectives

The methodology based on dynamic simulations captures the strengths of the conventional HAZOP by being systematic in approach. It uses rigorous equipment and deviation models to generate and simulate failure scenarios. The outcomes of the simulations are recorded, which quantitatively indicate the deviations in the critical process parameters. Using the sensitivity measure, the failure scenarios are ranked and the significant ones are identified. In this way, the methodology reduces the time needed and complements the skills of the analysis team in HAZOP. The advantage of the methodology is two folds: (i) no additional skills required to use our method as HAZOP teams consist of design and control engineers familiar with the process simulations and, (ii) no need for HAZOP model building as the method *reuses* dynamic process models already available for use in the oil & gas industry. From practical experiences, it is the opinion of the authors that much time and resources can be saved with the use of dynamic simulation methodology as input to the HAZOP meeting by prioritizing the focus area for discussion in the HAZOP team. The method requires a regularly updated process model prior to use in simulations and proper selection of points in the process for recording as such the results still depend on user's process insight.

References

J. Dunjó, V. Fthenakis, J. A. Vilchez and J. Arnaldos, 2010, Hazard and operability (HAZOP) analysis. A literature review, Journal of Hazardous Materials, 173, 19-32.

I. Cameron and R. Raman, 2005, Process Systems Risk Management, Elsevier, 2005.

R. Enemark-Rasmussen, 2011, A framework for computer-aided HAZOP studies supported by dynamic simulations, Copenhagen, DTU Chemical Engineering, 64 pp.

R. Skelton, 1997, Process safety analysis: An Introduction, IChemE, UK.

G. Sin, A. Eliasson Lantz, K.V. Gernaey, 2009, Good modelling practice (GMoP) for PAT applications: Propagation of input uncertainty and sensitivity analysis, Biotechnol. Prog., 25,1043-1053.

I.A. Karimi and Rajagopalan Srinivasan (Editors), Proceedings of the 11th International Symposium on Process Systems Engineering, 15-19 July 2012, Singapore.

Optimal layout of chemical process using risk index approach to minimize risk to human

Kyusang Han, [a] Inhyuck Choi, [a] En Sup Yoon[a,b]

[a]*School of Chemical and Biological Engineering, Seoul National University, 1 Gwanak-ro, Gwanak-gu, Seoul 151-742, Korea*
[b]*Automation and Systems Research Institute, Seoul National University, 1 Gwanak-ro, Gwanak-gu, Seoul 151-742, Korea*

Abstract

Many chemical processes are constructed within very compact areas due to the limitation of resources including land and cost although many of their units are dangerous and vulnerable to accidents such as fire or explosion. There have been many researches to make chemical processes safer by modifying the layout of process to ensure the safety distance among hazardous equipment. Even the safety among units is secured, however, this situation can get worse if the process site is near residential areas or the workspace of employees is located in the site because of the risk to human, which is usually not concerned for process layout. In this study, quantitative risk to human as well as the risk of equipment itself is considered to give more reliable layout of chemical processes. Among various quantitative risk approaches, modified individual risk index has been adopted. Individual risk counts for the risk that a person near the dangerous environment can take. With this index, optimal process layout is designed by minimization of cost and land area to consider the limitation of resources, also. The proposed methodology can provide the guideline to designing safe layout of chemical process concerning the various safety distance measures including equipment-equipment distance, equipment-employees distance and equipment-the public distance.

Keywords: Process layout, Individual risk, Safety distance, MILP

1. Introduction

In 2005, there was fire and explosion at the refinery of BP Products North America in Texas City which claimed 15 deaths and more than 170 injuries. In 1998, an explosion at the LPG filling station in Bucheon, Gyeonggi province of Korea caused 1 death and 96 injuries. Apart from the direct cause of the accident, high casualties of both accidents arouse from the existence of dangerous equipment or device near the people.

Above accident cases show that the proper safety distance between process areas and public or worker residential areas is crucial to minimize the effects of accident and the damages to human. There were not many researches, however, about the safe layout of hazardous facilities considering public residence or workspace of employees from the early part of process design. Previous researches about the process layout optimization include 2-dimensional layout of processes using heuristic rules (Suzuki, 1991) and MILP modeling for multi-floor layout optimization (Patsiatzis, 2002). Researches considering safety factors and accident scenarios also have been carried out. Dow Fire & Explosion Index was used to evaluate effective radius and damage costs of accident and to optimize process layout by MILP (Patsiatzis, 2004), and scenario-based optimization using statistical method for toxic chemical release was implemented for

layout (Diaz-Ovalle, 2010). These approaches have some limitations due to the subjectivity of indices and the uncertainty of scenarios.
In this study, mathematical modeling for process layout optimization is used together with the consideration of process safety to secure safety distances, especially to human. Optimal layout of process is arranged by satisfying the separation distances and minimizing costs. To ensure the minimum effect of accident, following three types of distances must be considered: distance between equipment; distance between equipment and workspace (e.g. control room); distance between equipment and process boundary (i.e. public area). The first one is determined from previous researches about the safety distance between equipment. The second and third types of distance were calculated to meet the allowable limit of individual risk for worker and public.

2. Individual Risk

A risk index is a comprehensive, integrated representation of accident frequency and consequence. Among various risk indices, IR (Individual risk) is an effective measure for quantifying the risk from chemical process equipment to human, since it is the risk to a person in the vicinity of a hazard and includes the nature, the likelihood, and the time period of the possible injury to the individual (CCPS, 1988).
The basic calculation of risk is usually done by the product of frequency and consequence of accident that came from various quantitative risk analysis methods like Fault Tree Analysis, but IR reflects more elements.
To get IR index (Franks, 2007), first the frequency of fatality of a person at the location of interest *i*, considering the accident frequency, fatality rate, weather effect and directional effect is calculated for all the accident scenarios about the event outcome *j*.

$$FoF_i = \sum_j f_{eo,j} \cdot p_{fatality,i,j} \cdot p_{weather,i,j} \cdot p_{direction,i,j} \quad (1)$$

Then, fraction of time and probability of presence of people are multiplied to give IR for the group of people *k* at the location *i*.

$$IR_{i,k} = \theta_k \cdot p_{location,i,k} \cdot FoF_i \quad (2)$$

For certain allowable limit, IR can be used as constraint of layout optimization problem. In this study, we use IR limit to estimate the minimum safety distance of equipment.

3. Process Layout Optimization based on Risk Analysis

The optimization of process layout was carried out through two sections: calculation of IRs and safety distances of process equipment and cost optimization of process under distance constraints.
In risk boundary section, target process is analyzed and related hazards are identified to select appropriate accident scenario. Then, frequency and consequence analysis (FA and CA) for selected scenario are performed and IR of equipment is calculated. We can obtain the safety distances of equipment that satisfy the allowable limit of IR since IR can be expressed as a function of distance from the equipment.
The layout optimization section employs typical constraints of layout problem of MILP form such as dimension and orientation, non-overlapping of equipment and separation distances (Patsiatzis, 2004). In this study, however, there are three types of separation distance constraints not just one: (1) distances between equipment, ED_i (Prugh, 1988) (2) equipment – workspace distances, $RD_{work,i}$, calculated from IR of equipment to worker (3) equipment – process boundary distances, $RD_{pub,i}$, calculated from IR to public people. The process is economically optimized under these constraints by

minimization of cost including pipeline, land and equipment cost. Therefore, the objective function is expressed in three terms:

$$minimize \sum_i \sum_{j \neq i} C_{ij} D_{ij} C_{pipe} + C_{land} \sum_k AR_k Q_k + \sum_i E_i \quad (3)$$

Fig. 1 summarizes the overall procedure described above.

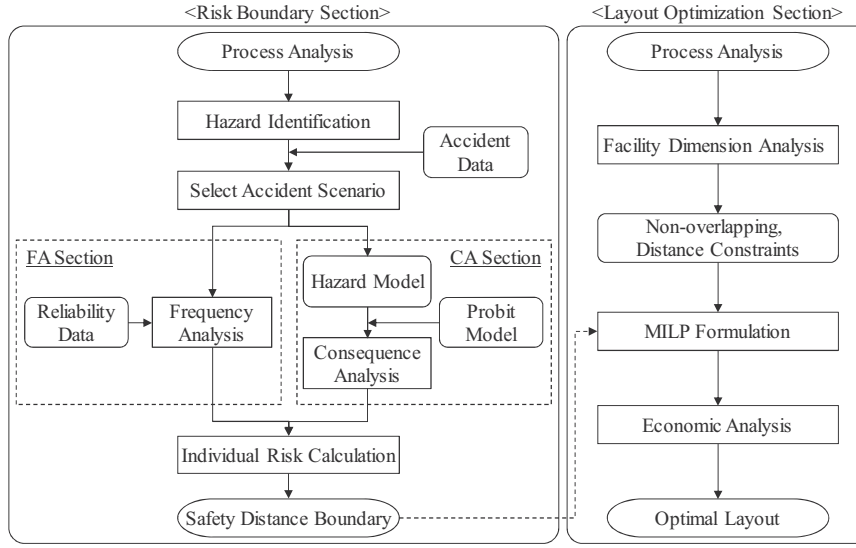

Figure 1. Overall procedure for layout optimization from risk analysis

4. Case Study

The proposed methodology is applied to a DME (dimethyl ether) filling station as an example. DME is one of the promising next-generation fuels, which has been researched as the substitute of LPG or diesel. Since the equipment required for filling station are vulnerable to fire or explosion, appropriate layout is necessary to ensure the safety for human and process itself.

4.1. Problem Description for DME Filling Station

In its filling station, there are four main units after the loading section: compressor, storage tank, pump and dispenser. Connectivity among them is shown in Fig. 2. Besides them, a control room is considered for workspace.

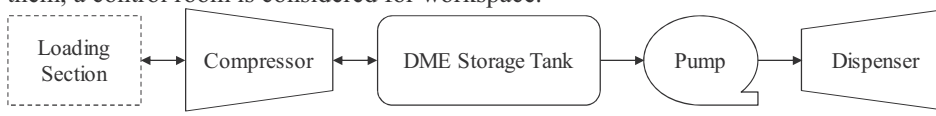

Figure 2. Scheme of DME filling station

Here, we optimize the layout of DME filling station to minimize the total cost under following assumptions:

- Worst-case accident scenarios (θ_k =1, $p_{location,i,k}$ =1)
- No directional and meteorological effects ($p_{weather,i,j}$ =1, $p_{direction,i,j}$ =1)
- Square process site and rectangular equipment
- Rectilinear pipeline connections between units

Operation condition of each unit was obtained from that of the LPG filling station since DME has similar physical properties with it and DME-LPG mixture can utilize the existing LPG facilities. To compare the economic result, various combinations of storage tank sizes with the same total capacity are considered.

4.2. Calculation of Safety Distances

From the accident records of LPG filling station in Korea (1987~2003), 3 major types of accident – flash fire, BLEVE (boiling liquid expanding vapor explosion) and VCE (vapor cloud explosion) – were considered to evaluate the accident effect. Then, risk indices are obtained with the frequency analysis using K-RDB (Korea Reliability DataBase) and the consequence analysis from probit analysis. Allowable limit of risk index (IR) is 10^{-3} for workers in control room and 10^{-4} for public people outside the process area. Safety distances that meet these criteria are listed in Table 1 for equipment.

Table 1. Minimum separation distances

Equipment		From workspace		From boundary		Between equipment
		$RD_{work,i}$ [m]	IR ($<10^{-3}$)	$RD_{pub,i}$ [m]	IR ($<10^{-4}$)	ED_i [m]
Storage tank	5ton	26	0.000942	39	0.000072	7.7
	10ton	31	0.000974	49	0.000093	
	15ton	37	0.000956	56	0.000096	
	20ton	40	0.000988	62	0.000083	
Pump		15	0.000659	17	0.000042	8.8
Compressor		18	0.000420	19	0.000042	9.6
Dispenser		25	0.000882	29	0.000086	8

4.3. Process Layout Result

Five combinations of storage tanks with total capacity of 20ton were optimized using CPLEX solver in GAMS and one of the layout results is shown in Fig. 3. Storage tanks are located near the center of the process site for all cases because they are the most hazardous equipment. Control room is on a corner to minimize the risk from other units while it does no harm to public.

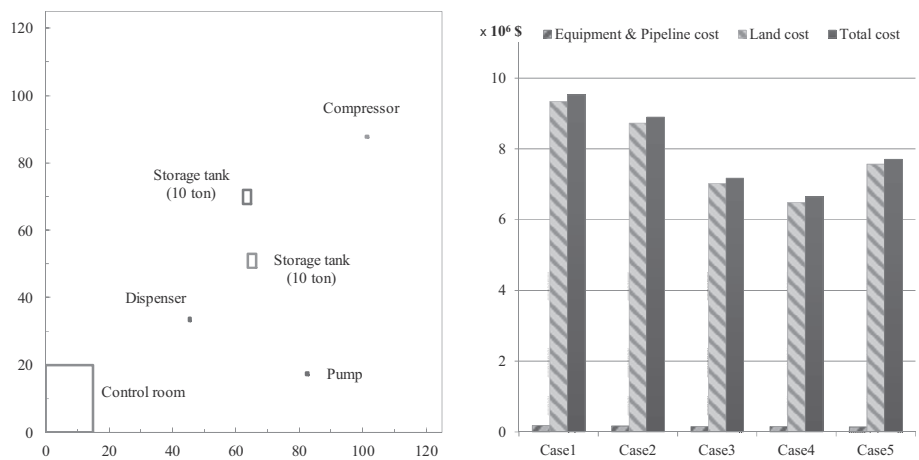

Figure 3. (left) Layout result of Case4 (right) Cost comparison of cases

Land area and costs of each case are compared in Table 2 and Fig. 3. For all cases, land cost affects the total cost much more than the cost of equipment and pipeline, and therefore, Case4 which requires the smallest land area shows the lowest total cost.

Table 2. Layout optimization result

	Case1	Case2	Case3	Case4	Case5
Combination	5ton x4	5ton x2 & 10ton	5ton & 15ton	10ton x2	20ton
Land area [m^2]	22500	21025	16900	15625	18225
Equipment& Pipeline cost [$]	181273	166127	151873	151873	138291
Land cost [$]	9343636	8731109	7018109	6488636	7568345
Total cost [$]	9524909	8897236	7169982	6640509	7706636

5. Conclusion

In this work, optimization of chemical process layout considering the inherent safety of the process was proposed. The risk of process equipment to human was divided into two categories, i.e. risk to workers and risk to public, and assessed through individual risk (IR) index approach based on the accident frequency and consequence analysis. Then, optimization of process layout minimizing the cost under safety distance constraints comes from IR value was carried out by mixed-integer linear programming (MILP). As an example case, layout of a DME filling station was optimized with the consideration of risk to workers in control room and people outside the process boundary.

With this method, economic feasibility of chemical process can be enhanced by a proper layout while ensuring the safety for human in the early stage of process design. In addition, land area required to satisfy the economic and safety constraints could be estimated. If the consideration of safety devices available for equipment were added, the reliability of resulted process layout would be improved.

References

CCPS, Center for Chemical Process Safety, 2000, Guideline for chemical process quantitative risk analysis, Center for Chemical Process Safety/AIChE, pp.153-203.

C.Diaz-Ovalle, R. Vazquez-Roman, M. Sam Mannan, 2010, An approach to solve the facility layout problem based on the worst-case scenario, Journal of Loss Prevention in the Process Industries 23(3), pp.385-392.

A.Franks, 2007, A Simplified Approach to Estimating Individual Risk, Research report for Heath and Safety Executive.

D.I. Patsiatzis, G. Knight, L.G. Papageorgiou, 2004, An MILP approach to safe process plant layout, Chemical Engineering Research and Design 82(5), pp.579-586.

D.I. Patsiatzis, L.G. Papageorgiou, 2002, Optimal multi-floor process plant layout, Computers and Chemical Engineering 26(4-5), pp.575-583.

R.W. Prugh, 1988, Quantitative evaluation of 'BLEVE' hazards, American Institute of Chemical Engineers, National Meeting, pp.74E 20p.

A.Suzuki, T. Fuchino, 1991, An Evolutionary Method of Arranging the Plot Plan for Process Plant Layout, Journal of Chemical Engineering Japan 24(2), pp.226-231.

Acknowledgments

This work was supported by Man-made Disaster Prevention Research Center of the NEMA of Korea and Institute of Chemical Process in Seoul National University.

I.A. Karimi and Rajagopalan Srinivasan (Editors), Proceedings of the 11th International Symposium on Process Systems Engineering, 15-19 July 2012, Singapore.

Optimal channel design and sensor placement in flow distributors for detecting blockage of parallelized microreactors

Osamu Tonomura, Atsushi Nishida, Lin Wang, Shnji Hasebe

Dept. of Chemical Engineering, Kyoto University, Nishikyo, Kyoto 615-8510, Japan.
E-mail: tonomura@cheme.kyoto-u.ac.jp (O. Tonomura)

Abstract

When the production capacity of micro chemical plants is increased by numbering-up approach, it is important to realize the uniform flow distribution among the parallelized microreactors. In addition, a blocked microreactor needs to be identified as early as possible to achieve the stable long-term operation of micro chemical plants. In this research, a system that can detect a blocked microreactor by using just two flow sensors is developed. The performance of the developed system is maximized by adjusting the channel size and sensor placement in the flow distributors. The effectiveness of the developed system and the optimal design result is demonstrated by computational fluid dynamics simulation.

Keywords: microreactor, flow distributor, design, sensor placement, blockage detection.

1. Introduction

Microreactors engage the attention of researchers and engineers in the pharmaceutical and chemical industries. Microreactors can achieve the high yield and selectivity of a product owing to their advantages of rapid mixing, high heat transfer, and precise residence time control (Hessel et al., 2005). The numbering-up approach, which means the parallelization of microreactors, is effective at increasing the production capacity of microreactors and opens up the possibility of a direct transfer from laboratory scale to production scale. However, some difficulties are left behind. When the numbering-up approach is applied to micro chemical plants (MCPs), it is important to realize the uniform flow distribution among the parallelized microreactors, which are connected by flow distributors. The flow maldistribution is caused by the inadequate design of the flow distributors and deteriorates the performance of MCPs. In addition to the flow uniformity, it is necessary to take measures against blockage, which is the most recognized trouble with MCPs. For example, Bayer et al. (1999), who developed a continuous radical polymerization process having micro pre-mixers, mentioned that poor mixing conditions cause blockage in a reactor. Ju et al. (2006) applied a stainless steel microchannel reactor for the continuous synthesis of zeolite NaA, and they found that aging the synthesis solution was a key procedure for avoiding blockage of the microchannel. In these literatures and others, one of the critical operation problems was blockage in microreactors, which negatively affects the flow distribution in the whole MCPs with numbering-up structure. Therefore, a blocked microreactor needs to be detected as early as possible to achieve the stable long-term operation of MCPs. However, it is not practical to install the sensors in all the microreactors from the viewpoint of cost or space. Therefore, the goals of this research are to develop a flow

distributor suitable for MCPs and to propose a blockage detection method with the limited measurement.

2. Flow Distribution in Parallelized Microreactors

This section shows the basic structure and characteristics of MCPs with parallelized microreactors. The characteristics of a specific flow distributor developed by Tonomura et al. (2008) are also analyzed through computational fluid dynamics (CFD) simulations.

2.1. Split-and-recombine-type flow distributors (SRFDs)

A schematic diagram of a MCP with externally parallelized microreactors is shown in Fig. 1. The parallelized section where microreactors are running in parallel is connected to a distribution section and a confluence section. The distribution section carries out a function of distributing a reactant flow among the parallelized microreactors. The distributed flows pass through microreactors and are collected into one flow at the confluence section. A lack of uniformity in the flow distribution lowers the MCP's performance.

Flow distributors, which are used at the distribution section in Fig. 1, are typically classified into two types: manifold-type and bifurcation-type. Unlike such flow distributors, Tonomura et al. (2008) have developed split-and-recombine-type flow distributors (SRFDs). Figure 2 shows an example of SRFDs, in which one flow is divided into four flows. The SRFD consists of channels having a length of L [mm] and a width of d [mm]. It is assumed that $L_1 = L_4 = L$ and $L_2 = L_3 = \alpha L$. α is introduced to achieve the uniform flow distribution among the parallelized microreactors under a normal operating condition and determined by CFD simulation. u_{in} [m/s] is the averaged flow velocity at the inlet, and u_k [m/s] (k is channel number) is the averaged flow velocity at the outlet of each channel. The outlet of SRFD is opened to atmosphere. In this research, the commercial CFD software "COMSOL Multiphysics® 3.4" is used to estimate the flow distribution of water (293 K) in the SRFD. The normalized flow velocity u^*_k, which is given by u_k/u_{in}, is used to evaluate the flow distribution.

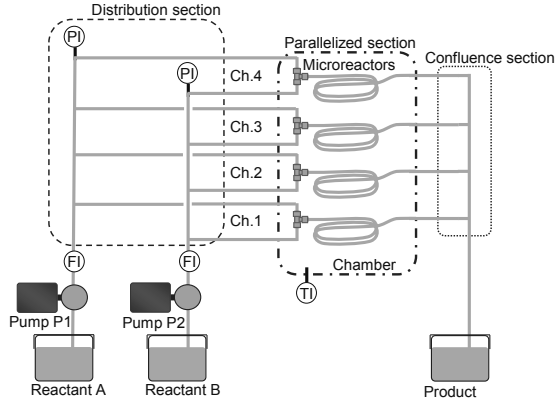

Figure 1 A MCP with parallelized microreactors.

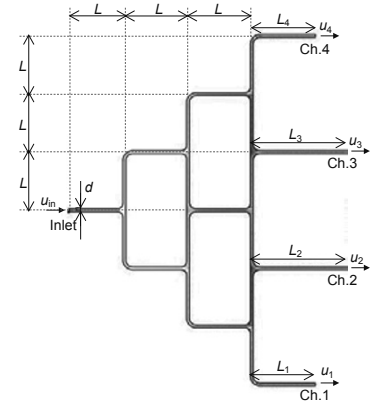

Figure 2 A developed SRFD.

2.2. Design modification of SRFD

It is preferable that the uniform flow distribution in the SRFD is maintained even when the inlet flow velocity or the material properties of the fluid change. The effects of

design parameters on the flow distribution are investigated by using CFD simulation. Table 1 shows the representative simulation conditions for SRFDs. When a circular channel having L = 10 mm and d = 1.0 mm is adopted, u_{in} = 0.2 m/s corresponds to inlet volumetric flowrate V_{in} = 10 mL/min. Figure 3 shows the results of CFD simulation. The vertical axis denotes the differences between two normalized flow velocities, u^*_2 and u^*_1, and the flow distribution is highly uniform when each plotted point in Fig. 3 is located near zero. The uniform flow distribution is achieved independently of L/d, when Reynold number (Re) is less than 100. At higher Re, the difference in flow velocity between Ch. 2 and Ch. 1 becomes large. In such a case, the SRFD needs to be re-designed so as to realize the uniform flow distribution. The alternative approach is to use flow controllers. However, the installation of flow controllers in all the channels requires high cost and extra space.

Figure 3 indicates that the difference between u^*_2 and u^*_1 is reduced at higher Re, according as L/d becomes large. An increase in L/d usually leads to a larger pressure drop of flow in the SRFD (ΔP_{SRFD}). To further improve the uniformity in the flow velocities without increasing ΔP_{SRFD}, the modified SRFD (mSRFD) where the channel width of Ch. 0 is enlarged, as shown in Fig. 4, is proposed in this research. CFD simulation result of mSRFD (L/d = 20) is added to Fig. 3, and it is clarified that mSRFD gives a more uniform flow distribution in the wide range of Re.

Table 1 Representative simulation conditions for SRFDs.

L/d	L [mm]	d [mm]	α	u_{in} [m/s]	Re
5	10	2.0	1.80	0.05	100
10	10	1.0	1.75	0.2	200
20	10	0.5	1.78	0.8	400
40	40	1.0	1.67	0.2	200

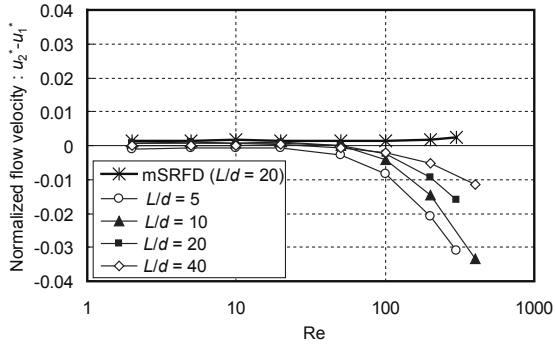

Figure 3 CFD simulation results.

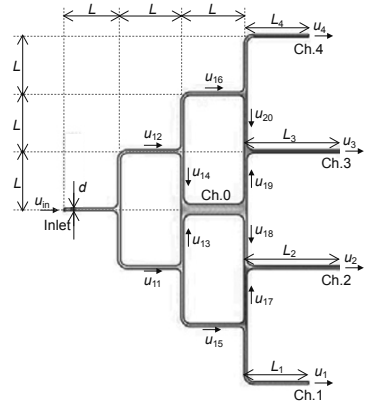

Figure 4 A modified SRFD.

3. Blockage Detection in Parallelized Microreactors

Blockage is the most recognized problem in MCPs, because the diameter of microchannels is less than 1 mm. A process monitoring system that can detect blockage is indispensable for effective and stable operation of MCPs. In this research, just two flow sensors are embedded in SRFDs, and a blockage diagnosis system (BDS) is

developed to identify a blocked microreactor among the parallelized microreactors. In addition, the performance of the developed system is maximized by adjusting the channel size and sensor placement in the flow distributors.

3.1. Blockage diagnosis system

Reactants are supplied to MCPs at a constant flowrate. MCPs have a symmetric structure and are designed beforehand so that flow distribution is uniform. Under these assumptions, the developed BDS uses the ratios of flow velocity (or flowrate) differences between normal and abnormal operating conditions at one sensor to those at the other sensor. In this research, two sensors are located in SRFDs. The procedure for building BDS is as follows: (1) obtain flow velocity data under normal operating conditions, (2) obtain flow velocity data under blockage in each microreactor, (3) calculate the flow velocity difference between normal and abnormal operating conditions at two sensors, and (4) calculate the ratio of flow velocity differences. After blockage is detected, the blockage location is identified through the following procedure: (1) calculate the flow velocity difference between normal and abnormal operating conditions at two sensors, (2) calculate the ratio of flow velocity differences, and (3) identify the microreactor that has the smallest difference between the prepared ratio and the actual ratio as a blocked reactor.

3.2. Application to four parallelized microreactors

The performance of the developed BDS is evaluated with its application to four parallelized microreactors, which are connected to SRFD. Through the system development, the results of flow velocity measurements are plotted in the two dimensional Δu_{15} and Δu_{16} space (Fig. 5). In this figure, ΔP_{MR} and ΔP_{mSRFD} represents the pressure drop of microreactors and mSRFD, respectively. The ratios of flow velocity differences under the blockage in microreactor connected to Ch.i (i = 1, 2, 3, 4) correspond to square, diamond, triangle, and circle, respectively. As each point deviates from the origin, the total flowrate in the process becomes large. Figure 5 shows that the

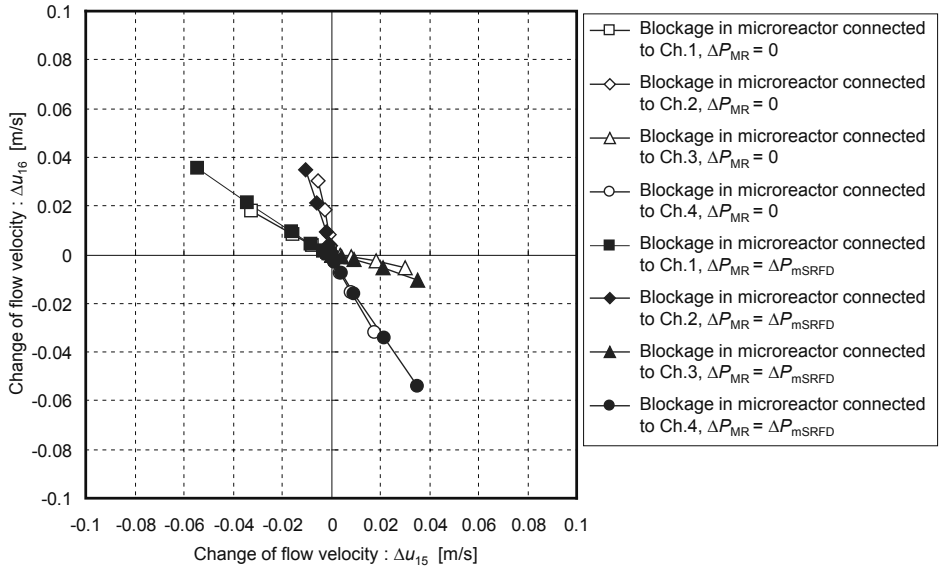

Figure 5 Blockage diagnosis results (Flow sensors are located at u_{15} and u_{16}).

ratio of two flow velocity differences remains unchanged even when total flow rate of the process varies, without reference to ΔP_{MR}. In addition, it is clarified that the blockage location is successfully identified on the basis of the ratios of two flow velocity differences. These simulation results suggest that the developed BDS has robustness to changes in the total flowrate and ΔP_{MR}.

3.3. Optimization of channel size and sensor placement

Flow distribution in MCPs with/without blockage can be estimated by CFD model or pressure balance (PB) model (Amador et al., 2004). In this research, an optimal channel design and sensor placement problem is solved on the basis of PB model, which requires less computational time than CFD model. Channel diameters and sensor placement are determined to maximize the adjacent angles between lines in Fig. 5 within constraints on the total flowrate, the flow uniformity under normal operating condition, the number of available sensors, the number of parallelized microreactors and their pressure drop, and the channel size boudaries. As a result of optimization by using gPROMS®, the maximum angle is obtained when the diameters of horizontal and vertical channels of the SRFD are 2.8 mm and 2.1 mm, respectively, and the two sensors are located at channels of u_{17} and u_{20}. The effectiveness of the optimal design result is confirmed by CFD simulation.

4. Conclusions

The flow uniformity in SRFDs, which have three or more bifurcation points and one or more junction points, was examined through CFD simulation, and the design of SRFDs is modified to achieve a uniform flow distribution in the wide range of Re. In addition, the blockage detection and diagnosis system that can identify a blocked microreactor by using a small number of flow sensors was developed, and its effectiveness was demonstrated numerically. The results showed that the developed system has high robustness to changes in the fluid properties and the microreactor characteristics such as pressure drop. In addition, the performance of the developed system was maximized by adjusting the channel size and sensor placement in the flow distributors. The developed system will be applicable to various types of microchemical plants with parallelized microreactors.

References

C. Amador, A. Gavriilidis, and P. Angeli, 2004, Chem. Eng. J., 101, 379-390.

T. Bayer, D. Pysall, and O. Wachsen, 1999, Proc. of the 3rd International Conference on Microreaction Technology (IMRET3), Frankfurt, Germany, 165–170.

V. Hessel, S. Hardt, and H. Loewe, 2005, Chemical Micro Process Engineering: Fundamentals, Modelling and Reactions, Wiley, VCH, Weinheim.

J. Ju, C. Zeng, L. Zhang, and N. Xu, 2006, Chem. Eng. J. 116, 115–121.

O. Tonomura, S. Nagahara, M. Kano, and S. Hasebe, 2008, Proc. of 10th International Conference on Microreaction Technology/AIChE Spring National Meeting, New Orleans, US, 128d.

I.A. Karimi and Rajagopalan Srinivasan (Editors), Proceedings of the 11th International Symposium on Process Systems Engineering, 15-19 July 2012, Singapore.

Batch process analysis and monitoring based on an automatic phase identification method utilizing process dynamic information

Yuan Yao,[a]* Weiwei Dong,[b] Chien-Ching Huang,[a] Yuan-Jui Liu[a]

[a]*Department of Chemical Engineering,National Tsing Hua University, Hsinchu, Taiwan*
[b]*National Engineering Research Center for Industrial Automation (South China), Guangzhou HKUST Fok Ying Tung Research Institute, Nansha, Guangzhou, China*

Abstract

Multiphase is an inherent nature of many batch processes, which should be taken into consideration to achieve efficient process monitoring. Although there have been several methods for phase identification, yet process information, especially process dynamic information, is not fully utilized. In this paper, an automatic phase identification method is proposed, which not only captures the differences in variable cross-correlations, but also explores the changes in process dynamics and model-explained variance. Accordingly, better phase identification, deeper process understanding and more efficient fault detection results are obtained. The practical application to an injection molding process verifies the effectiveness of the proposed method.

Keywords: multivariate statistical modeling, batch processes, multiphase, principal component analysis, process monitoring

1. Introduction

In today's manufacturing industry, batch processes play an important role in producing low-volume and high-value-added products. In order to achieve consistent quality and operation safety, the multivariate statistical process monitoring (MSPM) methods have attracted great research interests. Among them, multiway principal component analysis (MPCA) (Nomikos and MacGregor, 1994; Nomikos and MacGregor, 1995) is the most popular method in batch process monitoring. Nevertheless, since MPCA takes the entire batch data as a single object, the multiphase nature of many batch processes cannot be well modeled. For better monitoring, it is desired to model each phase separately.

In batch processes, different phases may have different features, while the process characteristics within the same phase are usually similar. Based on such finding, various types of phase identification and modeling methods have been proposed (Yao and Gao, 2009). Specifically, sub-PCA identifies phases by revealing the changes in cross-correlations among variables (Lu *et al.*, 2004); while, alternatively, the data distribution information also provides indications on phase division (Yao *et al.*, 2011). Nevertheless, these methods ignore the information about process dynamics, which certainly reduces the accuracy of phase identification. The multiphase PCA (MP-PCA) method (Camacho and Picó, 2006) is capable to provide a dynamic model. In spite of that, MP-PCA detects phase switch points based on model predictions, which may not lead to satisfactory phase division results consistent with the changes in process characteristics.

To overcome such shortcomings, an automatic phase identification method is proposed in this paper, not only capturing the differences in variable cross-correlations, but also exploring the changes in process dynamics and model-explained variance. As a result,

* To whom correspondence should be addressed:

Tel: 886-3-5713690, Fax: 886-3-5715408, Email: yyao@mx.nthu.edu.tw

more accurate and more stable phase identification results are obtained, on the basis of which process analysis is conducted to enhance the understanding of the batch operation, while more efficient monitoring is achieved.

2. Methodology

2.1. MPCA

After arranging the batch process data into a two-dimension matrix $\mathbf{X}(I \times JK)$ and normalizing the data, MPCA decomposes **X** as following:

$$\mathbf{X} = \mathbf{T}\mathbf{P}^T = \sum_{m=1}^{JK} \mathbf{t}_m \mathbf{p}_m^T \tag{1}$$

where *I*, *J* and *K* are the total numbers of batches, variables, and sampling intervals within each batch; $\mathbf{T}(I \times JK)$ and $\mathbf{P}(JK \times JK)$ are the score matrix and the loading matrix, respectively; $\mathbf{t}_m(I \times 1)$ are principal component (PC) vectors orthogonal to each other; and $\mathbf{p}_m(JK \times 1)$ are orthonormal loading vectors projecting data into score space and contains variable correlation information. Algebraically, $\|\mathbf{t}_m\|$ is equal to the *m*th largest eigenvalue λ_m of the matrix $\mathbf{\Sigma}=\mathbf{X}^T\mathbf{X}$, and $\mathbf{p}_m$ is the corresponding eigenvector.

2.2. Automatic phase identification

In batch processes, process variables are not only cross-correlated with one another at each sampling interval, but also autocorrelated over time. Since MPCA treats the entire batch trajectories as a single object, the loading matrix **P** extracts both the cross-correlations among variables and the dynamic correlations between different sampling intervals. Moreover, the amount of variance accounted for by each PC as function of time also provides insight into the process operation. In this paper, these two types of information are combined to provide reliable phase identification results.

Without losing generality, it is reasonable to assume that the matrix **X** is organized as $\mathbf{X} = \left[\tilde{\mathbf{X}}^1 \quad \tilde{\mathbf{X}}^2 \quad \cdots \quad \tilde{\mathbf{X}}^k \quad \cdots \quad \tilde{\mathbf{X}}^K \right]$, where $\tilde{\mathbf{X}}^k(I \times J)$ is a time-slice data matrix containing all measurements at the *k*th sampling interval in different batches, and $k = 1, \cdots, K$. Hence, the loading matrix **P** of the MPCA model has the structure as $\mathbf{P} = \left[(\tilde{\mathbf{P}}^1)^T \quad (\tilde{\mathbf{P}}^2)^T \quad \cdots \quad (\tilde{\mathbf{P}}^k)^T \quad \cdots \quad (\tilde{\mathbf{P}}^K)^T \right]^T$, where the portion-loading matrix $\tilde{\mathbf{P}}^k(J \times JK)$ containing all rows in **P** corresponding to the *k*th time interval. Consequently,

$$\tilde{\mathbf{X}}^k = \mathbf{T}(\tilde{\mathbf{P}}^k)^T = \sum_{m=1}^{JK} \mathbf{t}_m (\tilde{\mathbf{p}}_m^k)^T , \tag{2}$$

where the vector $\tilde{\mathbf{p}}_m^k(J \times 1)$ is the *m*th column in $\tilde{\mathbf{P}}^k$, containing all elements corresponding to the *k*th time interval in $\mathbf{p}_m$. To reveal the changes in process correlation structure along operating time, the explained variance of each PC with respect to time can be derived as following. At each time interval *k*, the variance can be summarized as:

$$(\sigma_{\text{time}}^k)^2 = \text{trace}\left(\frac{(\tilde{\mathbf{X}}^k)^T \tilde{\mathbf{X}}^k}{I-1}\right) = \sum_{m=1}^{JK} \text{trace}\left(\frac{(\tilde{\mathbf{X}}^k)^T (\mathbf{t}_m (\tilde{\mathbf{p}}_m^k)^T)}{I-1}\right) = \sum_{m=1}^{JK} (\sigma_{\text{time},m}^k)^2 , \tag{3}$$

where $(\sigma^k_{\text{time},m})^2$ is the extracted variance at time interval k by the mth PC. Thus, the explained variance of the mth PC at the kth time interval is obtained in terms of ratio as:

$$EVT^k_m = \frac{(\sigma^k_{\text{time},m})^2}{(\sigma^k_{\text{time}})^2} = \frac{\text{trace}((\tilde{\mathbf{X}}^k)^T(\mathbf{t}_m(\tilde{\mathbf{p}}^k_m)^T))}{\text{trace}((\tilde{\mathbf{X}}^k)^T\tilde{\mathbf{X}}^k)}. \tag{4}$$

Such explained variance EVT^k_m (m=1, ..., JK) and the portion-loading matrix $\tilde{\mathbf{P}}^k$ at each sampling interval k are then combined into a process feature matrix $\mathbf{F}^k$, where

$$\mathbf{F}^k = \left[\tilde{\mathbf{p}}^k_1 \cdot EVT^k_1 \quad \tilde{\mathbf{p}}^k_2 \cdot EVT^k_2 \quad \cdots \quad \tilde{\mathbf{p}}^k_{JK} \cdot EVT^k_{JK}\right], (k = 1, 2, \cdots K). \tag{5}$$

Hence, $\mathbf{F}^k$ not only summarizes the static and dynamic variable correlation information, but also reflects the process characteristics contained in the model-explained variance. In the meantime, $\mathbf{F}^k$ takes the different importance of each PC into consideration. Such feature matrices should be similar to each other for the time intervals within the same phase; while in different phases, the feature matrices are significantly different. Therefore, it is a natural idea to identify the phases by clustering $\mathbf{F}^k$ ($k = 1, 2, \cdots K$).

The K-means algorithm has been adopted for phase identification based on sub-PCA (Lu *et al.*, 2004). However, it suffers a major shortcoming: the total number of the clusters is usually subjectively determined by the user. To overcome such shortcoming, the X-means clustering algorithm (Pelleg and Moore, 2000), which automatically estimates the number of clusters, is adopted for phase identification in this paper.

2.3. Process analysis and monitoring

After phase identification, the model-explained variance with respect to variable can be used for process analysis in each phase. Supposing matrix $\breve{\mathbf{X}}^c_j$ contains the entire trajectory information of the jth process variable measured in phase c, the percentage of variance accounted for by each PC as function of variable is expressed as

$$EVP^{c,j}_m = \frac{\text{trace}((\breve{\mathbf{X}}^c_j)^T(\mathbf{t}_m(\breve{\mathbf{p}}^j_m)^T))}{\text{trace}((\breve{\mathbf{X}}^c_j)^T\breve{\mathbf{X}}^c_j)}, \tag{6}$$

where c, j, m are the indices of phase, variable and PC, respectively. The utilization of $EVP^{c,j}_m$ in process analysis will be illustrated in the next section.

For online monitoring, one should first determine which phase the new data belong to. Since each operation phase occupies a certain time span in the cycle duration, the current phase can be identified by checking which time span the current sample falls in. Then, various types of modeling methods, such as phase-MPCA (Dong and McAvoy, 1996), batch dynamic PCA (Chen and Liu, 2002), etc., can be adopted to build the phase models. Since the process characteristics are more stable within each phase, the phase models can provide better monitoring results. For illustration, in the following case study, phase-MPCA models are built for process monitoring.

3. Application results

Injection molding, a well-established technique, which is widely applied in the polymer processing industry, is utilized to verify the effectiveness of the proposed method. The normal operation conditions are same as the ones described in (Yao *et al.*, 2011).

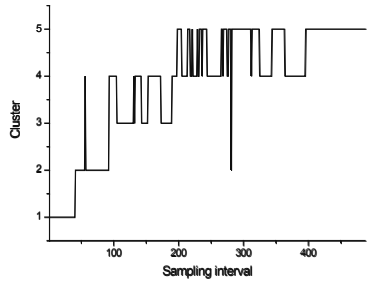

Fig. 1 Phase identification based on sub-PCA

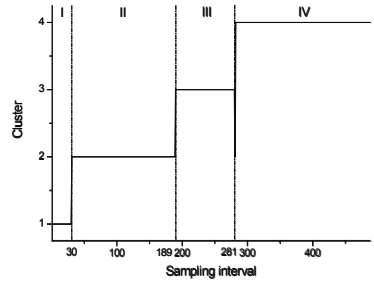

Fig. 2 Phase identification based on the proposed automatic identification method

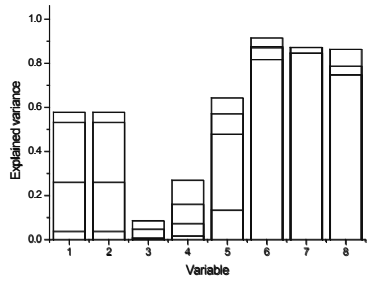

Fig. 3 Cumulative percent of the explained variance with respect to variable in phase 1

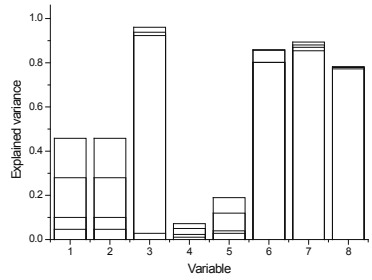

Fig. 4 Cumulative percent of the explained variance with respect to variable in phase 2

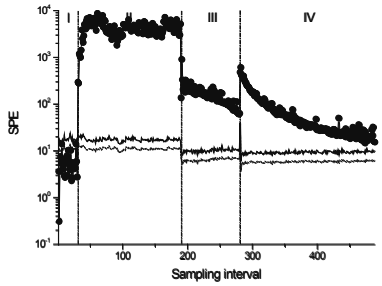

Fig. 5 SPE control chart based on the conventional MPCA model

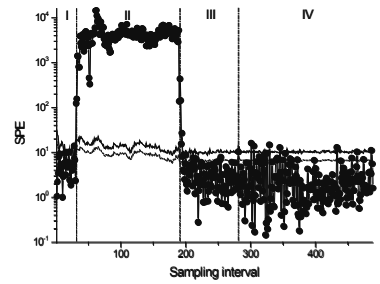

Fig. 6 SPE control chart based on the phase models

For comparison, phase identification is conducted based on sub-PCA and the proposed method, respectively. Fig. 1 and Fig. 2 show that the proposed method provides a clearer and more stable identification. Such results are expectable, since sub-PCA only focuses on the changes in static cross-correlation structure among variables, while the proposed method better utilizes process dynamic information. The identified phases correspond to filling, packing and holding, plastication, and cooling steps, respectively, well reflecting the process characteristics.

After phase identification, more process features can be explored with the model-explained variance with respect to variable in each phase. In Fig. 3 and Fig. 4, the lowest line in each bar indicates the percent explained by the first PC, the second lowest

line represents the cumulative percent explained by the first two PCs, and so on and so forth. It is observed that the first PC mainly consists of three bands of barrel temperatures throughout the whole cycle duration, while the other PCs have varying contributors in different phases. Such observation is reasonable. In the injection molding process, the barrel temperatures are continuously controlled. Therefore, the phase effects are not obvious in these variables. Because of closed-loop control, these variables are tightly correlated to each other and relatively independent to other variables. This explains why they barely share the first PC with other variables.

The monitoring results of an abnormality in the packing pressure are plotted in Fig. 5 and Fig. 6. Such fault only affects the second phase. However, Fig. 5 shows that the conventional MPCA keeps alarming in all the last three phases, making the diagnosis more difficult. In contrast, the phase models provide a more accurate monitoring result.

4. Conclusions

Multiphase is an inherent nature of many batch processes, which should be carefully considered in process modeling and monitoring. Up to the present, most existing methods for batch process phase identification ignore the dynamic information contained in process data. In this paper, an automatic phase identification method is proposed, which involves more process information. On the basis of more accurate and more reliable phase division, more efficient monitoring and deeper process understanding is achieved. The effectiveness of the proposed method is verified with the application to an injection molding process.

Acknowledgements

This work was supported in part by the National Science Council of Taiwan under Grant NSC 100-2218-E-007-018- and in part by Grant No. 100N7072E1 of the Advanced Manufacturing and Service Management Research Center of National Tsing Hua University, Taiwan.

References

Camacho, J. and J. Picó (2006). Online monitoring of batch processes using multi-phase principal component analysis. *Journal of Process Control*, **16**, 1021-1035.

Chen, J. and K. Liu (2002). On-line batch process monitoring using dynamic PCA and dynamic PLS models. *Chemical Engineering Science*, **57**, 63-75.

Dong, D. and T. McAvoy (1996). Batch tracking via nonlinear principal component analysis. *AIChE Journal*, **42**, 2199-2208.

Lu, N., F. Gao and F. Wang (2004). Sub-PCA modeling and on-line monitoring strategy for batch processes. *AIChE Journal*, **50**, 255-259.

Nomikos, P. and J. MacGregor (1994). Monitoring batch processes using multiway principal component analysis. *AIChE Journal*, **40**, 1361-1375.

Nomikos, P. and J. MacGregor (1995). Multivariate SPC charts for monitoring batch processes. *Technometrics*, **37**, 41-59.

Pelleg, D. and A. Moore (2000). X-means: extending k-means with efficient estimation of the number of clusters. *Proceedings of the 17th International Conference on Machine Learning,* San Francisco.

Yao, Y., W. Dong, L. Zhao and F. Gao (2011). Multivariate statistical monitoring of multiphase batch processes with between-phase transitions and uneven operation durations. *The Canadian Journal of Chemical Engineering*. DOI: 10.1002/cjce.21617.

Yao, Y. and F. Gao (2009). A survey on multistage/multiphase statistical modeling methods for batch processes. *Annual Reviews in Control*, **33**, 172-183.

I.A. Karimi and Rajagopalan Srinivasan (Editors), Proceedings of the 11th International Symposium on Process Systems Engineering, 15-19 July 2012, Singapore.

Data driven fault detection using multi-block PLS based path modeling approach

Manoj Kandpal, Prem Krishnan, Lakshminarayanan Samavedham *

National University of Singapore

Abstract

Early detection of process faults (while the plant is still operating in a controllable region) can save billions of dollars and enhance safety by minimizing the loss of productivity and preventing the occurrence of process mishaps. This has encouraged researchers to develop methods for improved monitoring of industrial units. This work is based on a pathway modeling approach using multi-block PLS as the mathematical machinery. The proposed approach is a multivariate data analysis procedure which divides the process data into different blocks, determines relationships among the blocks, which are then used for fault detection. In the developed methodology, an extension of multi-block PLS, a special modification of the PLS technique is realized by incorporating the H-Principle in the algorithm. This renders it different from PLS as the analysis is done in steps, maximizing the product of size of improvement of fit and associated precision at each step. The T^2 statistic is primarily used as an indicator of normalcy or fault in the system. This new technique is illustrated via application to two industrial-scale, high-fidelity simulated systems namely the Tennessee Eastman Process (TEP) and a Depropanizer Process (DPP).

Keywords: Fault Detection, Multi-Block PLS, Path Modeling, H-Principle.

1. Introduction

Significant advances in sensing technology, computer processing power and cheaper data storage have all meant that process data can be obtained, stored, analyzed and put to good use (for controller design, process improvement, fault detection and diagnosis etc.). With processes becoming more complex & tightly integrated and increased concerns over safety and environmental impact, the need to monitor and operate processes by leveraging on knowledge about their current state through the data they generate has become exigent. Just to put things in context, the size of data available for analysis has increased dramatically from a mere 1000 × 20 in the 1970's to 500000 ×1000 in this decade (Kettaneh, Berglund et al. 2005).

Various modeling methodologies have been developed for achieving efficient monitoring and control system for such processes. These methodologies are broadly divided into three types: quantitative model-based methods; qualitative model-based methods; and process history based methods (Venkatasubramanian 2003). The last type concerns with the transformation of large amounts of historical data into a particular form of knowledge representation that will enable proper detection and diagnosis of abnormalities. Availability of vast amounts of plant data has encouraged researchers to develop and improve process history based methods, such as PCA, PLS, CA, etc., for better operation and control of such industrial units. The present work deals with monitoring of faults in industrial chemical processes, using the multi-block PLS modeling approach and the H-Principle concept developed by Höskuldsson and is tested on three case studies. The various terms and abbreviations used in this work are based

on standard terms used in chemometrics literature and in the work of Höskuldsson *et al.*(Höskuldsson 1992), unless otherwise stated.

2. Methodology

2.1. H-Principle

The methodology, suggested by Hoskuldsson (Höskuldsson 1992), is similar to PLS where at each step the method maximizes the following measure,

$$[(\text{Size of improvement of fit}) \times (\text{associated precision in terms of variance})]$$

$$\text{i.e. } \boldsymbol{max}(\Delta\, fit) \,/\, (\Delta\, variance)$$

For two blocks, X and Y, the improvement in fit for given t is,

$$E = \left(\frac{1}{t^T t}\right) t\, q^T, \quad \text{such that,} \quad Q = Y^T t$$

Also, size of fit is, $\quad tr(E^T E) = \left[\frac{|Y^T t|^2}{t^T t}\right]$

The H-principle suggests that these two terms should be balanced as follows:

$$\max \left[\frac{|Y^T t|^2}{t^T t}\right] \times \frac{\left[1/|\sum|\right]}{t^T t} = \max \frac{w^T X^T Y Y^T X w}{|\sum|}$$

Assuming that $|\sum|$ is constant, the solution is to choose w as the eigenvector associated with the leading eigenvalue of the eigenproblem,

$$X^T Y Y^T X w = \lambda w \qquad \text{(similar to PLS)}$$

For a system with four blocks, we maximize the fourth block's (X_4) loading vector q_4 s.t. $|w_1|=1$; where, w_1 is calculated from

$$X_1^T X_2 X_2^T X_3 X_3^T X_4 X_4^T X_3 X_3^T X_2 X_2^T X_1 w_1 = \lambda w_1$$

This weight vector, 'w_1', is used to obtain the scores for the first block which are in turn used for detection purposes.

2.2. Multiblock PLS

In chemometrics, data from industrial and laboratory systems are typically of varied nature and come from different sub-systems. In such cases it is a better option to treat such data as being composed of multiple blocks rather than a single one. The technique applied to the case studies is also very useful in reducing the number of variables required for the monitoring scheme as only data related to variables in the first block is required to facilitate detection. The division into blocks can be done either on the basis of the nature or source of data. Several researchers have worked on multi-block PCA/PLS methodology for monitoring the operating performance of large continuous processes, such as the low-density polyethylene reactor (MacGregor, Jaeckle et al. 1994) and for various other chemical processes (Reinikainen and Höskuldsson 2007; Kohonen, Reinikainen et al. 2008) similarly. The flowchart for the general multi-block process employed is summarized in figure 1.

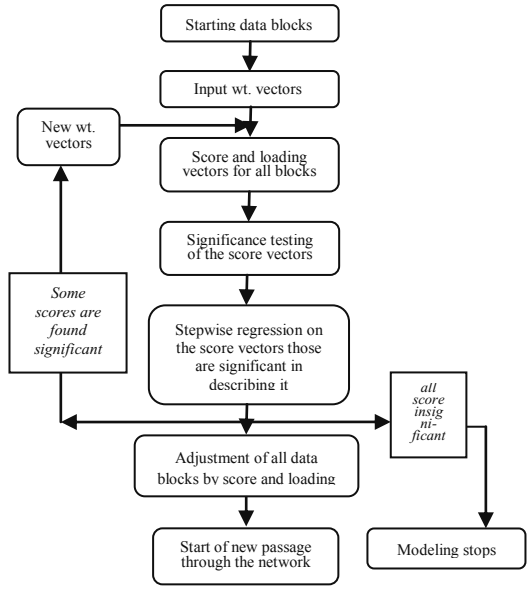

Figure 1. Multiblock PLS

3. Case studies

To test the developed methodology, we grouped the variables into blocks on the basis of the source of variable, i.e. based on orientation and arranged in a linear fashion such as

$$X_1 \rightarrow X_2 \rightarrow \ldots X_n$$

3.1. Depropanizer process (DPP)

The process schematic for DPP, as provided by EnVision System Ltd., is shown in figure 2. The unit comprises of a fractionation tower, a condenser, reflux drum and the reboiler, comprising a total of 36 variables that are monitored. The simulation data is collected for a total of 15 faults over a period of three hours for each of the normal and fault conditions and the samples are recorded at a regular interval of 12 seconds. A total of 901 samples were collected for the normal operating region as well as the faults with each fault being introduced at the 51st sample. The normal operating data was divided into training (initial 60% of the samples) and testing datasets (remaining 40%).

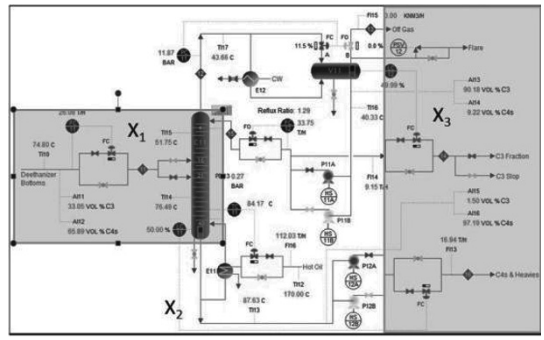

Figure 2. Block representation of DPP

3.2. Eastman's Tennessee plant 52 variables

For the second case, we consider the well-known TE process as described by Downs et al (Downs and Vogel 1993). The process includes a total of 52 variables. Data is available for 20 different faults. The data set for the process was obtained from the *Multiscale Systems Research Laboratory (Braatz 2010)* and was divided into 4 blocks (similar to DPP in figure 2) on the basis of source of data as shown in Table 1 and arranged in a linear manner. The variables were divided such that blocks X_1, X_2, X_3 and X_4, have 19,10, 10, 13 variables respectively.

3.3. Eastman's Tennessee plant 25 variables

For this case study, we considered the study of only 25 variables and placed them in the 4 blocks respectively. These 25 variables are chosen from 16 important variables as reported by Chen et al (Chen and McAvoy 1998) plus additional variables in the path. The total set included 18 CVs and 7 MVs (Table 2).

TE 52 variables				**TE 25 variables**			
Block 1	Block 2	Block 3	Block 4	Block 1	Block 2	Block 3	Block 4
XMV 1-4 XMV 10 XMEAS 1-4 XMEAS 6-9 XMEAS 23-28	XMV 5-6 XMV 11 XMEAS 5 XMEAS 10-13 XMEAS 20 XMEAS 22	XMV 7-9 XMEAS 14-21	XMEAS 29-41	XMV 1-3 XMV 10-11 XMEAS 1-3 XMEAS 6	XMEAS 7-9 XMEAS 21	XMEAS 11-14 XMEAS 22 XMV 7	XMEAS 15-19 XMV 8

Table 1: Variables for different block in TE process

4. Results and discussions

Statistical methods of PCA, CA and our proposed technique were applied to the test problems. The detection is done using T^2 and Q statistics limits at 99% and 95% confidence interval. For this work, the best result from both these measures has been taken and corresponding detection rates (DR) and false alarm rate (FAR) have been reported in Table 2-3.

4.1. Depropanizer process (DPP)

The results show that both T^2 and Q stat were able to detect faults; however, Q stat for PCA (not shown) appeared to have larger false alarm rates (0.102 – 0.2653) for all the faults. Otherwise, the false alarm rate in all other methodologies were almost nil, thus only detection rates have been shown (Table 2). The result shows that the proposed methodology was able to perform better in 10 out of the 15 cases.

Fault No.	PCA	CA	Multi-block PLS
F1	0.9918	0.9894	0.9941
F2	0.9977	0.9988	1.0000
F3	0.9977	0.9988	0.9988
F4	0.9965	0.8931	0.9988
F5	0.9965	0.9871	0.9988
F6	0.9977	0.9988	0.9941
F7	0.9918	0.9671	0.9906
F8	0.9883	0.9871	0.9918

Fault No.	PCA	CA	Multi-block PLS
F9	0.9977	0.9988	1.0000
F10	0.9977	0.9988	1.0000
F11	0.9977	0.9882	1.0000
F12	0.9977	0.9401	0.9271
F13	0.9918	0.9802	0.9941
F14	0.9883	0.953	0.9800
F15	0.9977	0.953	0.9671

Table 2: Detection rates for the faults in DPP

It can be noted that these fault were not too difficult to detect, with detection rates exceeding 92%.

4.2. Tennessee Eastman Process

The methodology was tested on the two case studies carved out from the TEP data. Table 3 gives an estimate of all the detection and false alarm rates using the 25 variable case study and Table 4 shows how the methodology will perform in different scenarios.

No.	PCA		CA		Multi- Block		**No.**	PCA		CA		Multi- Block	
	FAR	DR	FAR	DR	FAR	DR		FAR	DR	FAR	DR	FAR	DR
F_1	0	0.9900	0	0.9875	0.0063	0.9875	**F_{12}**	0.3500	0.9962	0	0.9125	0.0187	0.7488
F_2	0.1000	0.9975	0	0.9025	0.0375	0.9875	**F_{13}**	0.1000	0.9775	0	0.9413	0.0187	0.7775
F_3	0.4250	0.3538	0	0	0.0500	0.0413	**F_{14}**	0.1250	0.9988	0	0.9725	0.0375	0.7788
F_4	0.1625	1.0000	0	0	0.0500	0.6412	**F_{15}**	0.1125	0.3925	0	0.0025	0.0313	0.0437
F_5	0.1625	0.6625	0	0.1913	0.0500	0.2662	**F_{16}**	0.5188	0.6100	0.1	0.0063	0.0437	0.0975
F_6	0.0938	1.0000	0	0.9738	0.1250	0.9812	**F_{17}**	0.2062	0.9788	0	0.7800	0.0187	0.3925
F_7	0.0938	0.5813	0	0.3237	0.0375	0.3225	**F_{18}**	0.1625	0.9300	0	0.8875	0.0437	0.8788
F_8	0.2813	0.9975	0	0.8500	0.0437	0.7612	**F_{19}**	0.2188	0.3038	0	0	0.0187	0.0537
F_9	0.3500	0.3425	0.01	0	0.0500	0.0512	**F_{20}**	0.1375	0.7362	0	0.1487	0.0125	0.0450
F_{10}	0.1437	0.8187	0	0.1688	0.0313	0.1437	**F_{21}**	0.2687	0.5938	0	0.4238	0.0187	0.0288
F_{11}	0.2375	0.8750	0	0.1750	0.0250	0.4288							

Table 3. Detection and false alarm rates using 25 variables

Increase in detection rates usually implies increasing false alarm rates. Thus the use of methods depends on the type of performance we expect or accept. For example, in case of fault detection using all variables, if low FAR (< 10%) and low detection rate (> 80 %) are prefererd, the number of faults detected by PCA , CA and multi-block methods would be 4, 8 and 9 respectively; thus, multi-block method looks more promising. If the limit for FAR and detection rate were chosen as (< 10%) and (> 90%) respectively, the number of faults detected by the methods are found to be 4, 6 and 5 respectively. In this

case, CA seems to perform better. If the FAR limit is higher (< 20%), the results are 8, 6 and 9 favoring the use of multi-block methods.

FAR	DR	For 25 variables			For all 52 variables		
		PCA	CA	Block	PCA	CA	Block
<10	>99	3	0	0	3	3	3
< 10	> 95	4	3	**5**	5	6	6
<10	>90	4	**6**	5	6	6	6
< 10	> 80	4	8	**9**	**10**	7	7
< 20	> 90	8	6	**9**	**9**	6	6

Table 4. Comparison of cases for 25 and 52 variables

5. Conclusions

The developed methodology is able to detect faults with high reliability. It outperformed CA and PCA in the DPP case study. The methodology, along with PCA and CA, was also able to detect all but 5 faults (fault 3, 5, 15, 16, & 19) with good DR & low FAR in the 25-variable TEP case study. These five faults are difficult to detect even with all 52 variables. From Table 3, it can be seen that the multi-block method was able to detect more number of faults for three important scenarios in both the TEP case studies. PCA, despite giving the best detection rates with its Q statistic, also suffered from higher FARs. The performance of CA was found to be somewhere in between PCA and the multi-block methodology. The multi-block methodology was found to be more effective with lower number of variables in TEP (Table 4) leading us to believe that choosing the right variables in each of the blocks is an important factor. To this end, an optimization scheme can be applied to find out the best possible set of variables to be placed(based on post-analysis of data and using the results in an online monitoring scheme) in different blocks such that maximum effective detection is possible with minimum error. Further work would involve applying this new approach on other large scale simulated processes as well as on real time data from industrial processes.

References

Braatz, R. D. (2010). "Software and data for fault detection and diagnosis, based on the code for the Tennessee Eastman Process by Downs and Vogel." from http://brahms.scs.uiuc.edu/.

Chen, G. and T. J. McAvoy (1998). "Predictive on-line monitoring of continuous processes." Journal of Process Control **8**(5-6): 409-420.

Downs, J. J. and E. F. Vogel (1993). "A plant-wide industrial process control problem." Computers & Chemical Engineering **17**(3): 245-255.

Höskuldsson, A. (1992). "The H-principle in modelling with applications to chemometrics." Chemometrics and Intelligent Laboratory Systems **14**(1-3): 139-153.

Kettaneh, N., A. Berglund, et al. (2005). "PCA and PLS with very large data sets " Computational Statistics & Data Analysis **48** 69 – 85.

Kohonen, J., S.-P. Reinikainen, et al. (2008). "Multi-block methods in multivariate process control." Journal of Chemometrics **22**(3-4): 281-287.

MacGregor, J. F., C. Jaeckle, et al. (1994). "Process monitoring and diagnosis by multiblock PLS methods." AIChE Journal **40**(5): 826-838.

Reinikainen, S. P. and A. Höskuldsson (2007). "Multivariate statistical analysis of a multi-step industrial processes." Analytica Chimica Acta **595**(1-2): 248-256.

Venkatasubramanian, V. (2003). "A review of process fault detection and diagnosis Part III: Process history based methods." Computers & Chemical Engineering **27**(3): 327-346.

I.A. Karimi and Rajagopalan Srinivasan (Editors), Proceedings of the 11th International Symposium on Process Systems Engineering, 15-19 July 2012, Singapore.

Optimisation of a Power Plant Utility System Using Process Integration

Mkhokheli Ndlovu, Thokozani Majozi

Department of Chemical Engineering, University of Pretoria, Lynnwood Road, Pretoria 0002, South Africa

Abstract

This paper looks into the optimisation of a power plant utility system. The system consists of a boiler and a cooling tower which constitute a comprehensive utility system. These two systems, although complementing each other in real operations, have been treated separately in published literature, thus creating a false dichotomy between the boiler and cooling water systems. Such individual treatment of the system components gives suboptimal results. In this work, a holistic method of analysis and optimisation of the comprehensive utility system in presented. Nonlinear programming (NLP) models are formulated first for each system and these are then combined to give the comprehensive utility system model. In the mathematical models nonlinear equations are extensively used in the mass and energy balances and in calculating performance in terms of thermodynamic parameters which include enthalpy, entropy and efficiency. The comprehensive utility system model is solved using a specially formulated performance index as an objective function; which is a function of both the heat removed in the cooling tower and the electricity produced in the power plant. The model accurately predicts that the steam turbine efficiency decreases with increasing cooling tower effectiveness. The results further show that better performance of the utility system is achieved (1.7 % improvement in the performance index) when the system is modeled as a single utility system as opposed to treating the system's components separately.

Keywords: Optimization, process integration, cooling tower, boiler, rankine cycle

1. Introduction

1.1. Background

Process integration is no longer a new subject, having started from the pioneering work of Linnhoff and Flower (1978) in the 1970's, who developed systematic procedures for the optimisation of both grassroots and retrofit designs. Their work led to the development of pinch analysis, which was later extended to the optimisation of mass integration networks by El Halwagi and Manousiouthakis (1989). The success of the principles then developed led to a number of applications in the chemical and allied process industries and even in nontraditional chemical industries. The traditional industries include refineries and power plants, which use huge volumes of water and electricity. The cost of producing and delivering water of suitable quality and electricity has increased over the years, thus affecting the economic viability of such process plants. The result has been a continued pursuit of improving the efficiency of these industries. Kim and Smith (2001) recently realised the importance of combined heat and mass transfer and presented a technique for optimisation of a cooling water system comprising a cooling tower and its associated heat exchanger network. They showed

that improved system performance is obtained from a complete system analysis as opposed to focusing on the individual components of the cooling water system. In this work, a holistic method for the optimisation of a power plant utility system is presented, following the principles of Process Integration.

1.2. Problem Definition

Figure 1 below shows a standard Rankine cycle for power production. This is a basic cycle consisting of four main components; the boiler, the turbine, the condenser and the boiler feed water pump. The standard cycle is different to the Rankine cycles found in modern power plants, where additional components are usually added as a means of enhancing the performance of the cycle, e.g. reheat and regenerative cycles. Such advanced cycles are not considered in this paper; however the treatment of such systems follows the same principles presented in this work. Also shown in the figure is the cooling water system which supplies water used as cooling medium in the condenser. The water system consists of the cooling tower, and the circulating system including the water pump.

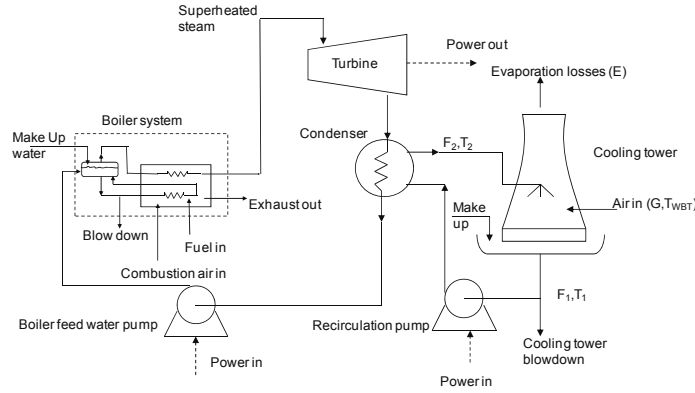

Figure 1: Standard Rankine cycle for power generation

The above figure combines two utility systems, the boiler and the cooling tower, which constitute a comprehensive utility system. These two systems, although complementing each other in real operations, have been treated separately by a number of researchers, e.g. Rodriguez et al (2001), Dincer et al. (2001), Zubair et al. (2003) and Gutierrez et al. (2010). Thus a lot of work has been done previously on optimising the standard Rankine cycle and similarly on optimising the cooling tower system. However no such work is available for the comprehensive system and it is this realisation that led to this work - the focus being to develop an integrated model for the optimisation of the complete system as shown in Figure 1.

2. Mathematical model formulation

The comprehensive utility system was modeled by first developing individual models for the Rankine cycle and for the cooling tower systems and later combining these to give a single integrated system model. The mathematical models formulated in the work have a form:

$$\min Z(x), x = [x_1, x_2, ...x_n]^T \in R^n \quad (1)$$

or

$$\max Z(x), x = [x_1, x_2, ...x_n]^T \in R^n \quad (2)$$

subject to the constraints:

$$g_j(x) \le 0, j = 1,2.....,m$$
$$h_j(x) = 0, j = 1,2.....,r \quad (3)$$

where $Z(x)$, $g_j(x)$ and $h_j(x)$ are scalar functions of the real column vector $x^{\mathbf{T}}$ and x is the vector of optimisation variables. The constraints in the model were the mass, energy and momentum balance equations and these together with the performance indices presented below as objective functions where solved in both the GAMS® and Matlab® programming environments.

2.1. Steam Turbine Model

The steam turbine model used in this work is an adaptation of the model by Rodriguez et al. [2001]. The objective was to maximize the thermal efficiency:

$$\eta_{th} = \frac{\text{Cycle Net Work}}{\text{heat supplied from external sources}} \quad (4)$$

Table 1 below shows the optimisation results from the steam turbine model for a specified circulating water flowrate of 15 kg/s with turbine inlet conditions of 500°C and 186 bar.

Table 1: Optimization results – single condensing steam turbine model

Final value of $Z(x^*)$,%	35.9
Number of iterations	48
Variables	64
Equations	69
Turbine Outlet Pressure (bar)	0.057
Condenser Heat Duty (kW)	-23230

2.2. Cooling Tower Model

The cooling tower model follows the formulation of Kim and Smith (2001). The model gives, the cooling water return flowrate and temperature, evaporation loss and outlet air temperature for a specified cooling tower height and inlet conditions. These parameters are functions of the air wet bulb temperature, cooling tower return temperature and the air and water flowrates:

$$T_1 = f(F_2, T_2, G, T_{WBT}) \quad (5)$$
$$F_1 = f(F_2, T_2, G, T_{WBT}) \quad (6)$$
$$E = f(F_2, T_2, G, T_{WBT}) \quad (7)$$

These parameters are defined in Figure 1. The objective was to maximise the cooling tower effectiveness defined as:

$$\eta_{eff} = \frac{Q_{ACT}}{Q_{MAX}} \quad (8)$$

where Q_{ACT} is the actual heat removed and Q_{MAX} is the maximum possible heat removed by the cooling tower. Figure 2 below shows the cooling tower model validation using

the experimental data of Bernier (1994). Also shown in Figure 2 is the predicted cooling tower performance in graphical form.

Cooling Tower Model Validation				
Case	*1*	*2*	*3*	*4*
Water flowrate (kg/s)	0.2	0.3	0.398	0.495
Air flowrate (kg/s)	0.67	0.656	0.664	0.658
CW inlet temperature (°C)	36.7	32	29.3	27.9
CW outlet temperature (°C)	19.8	20.4	20.7	20.8
Model Result CW Inlet Temperature	36.7483	32.0287	29.3418	27.9832
Model Result CW outlet temperature(°C)	19.500	20.00	20.24	20.52
Error (%) in CW Inlet Temperature	0.13	0.09	0.14	0.30
Error (%) in CW Outlet Temperature	-1.5	-1.9	-2.2	-1.35

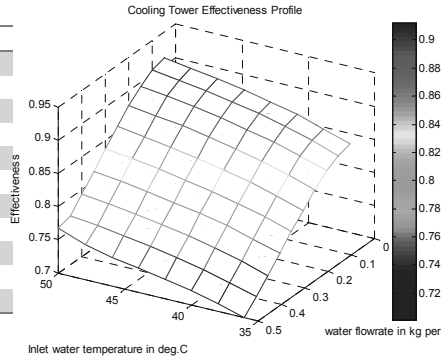

Figure 2: Cooling tower model validation and predicted performance

The model results show that high effectiveness in the cooling tower is obtained when the inlet conditions are high temperature and low flowrate.

2.3. Comprehensive system Model

The comprehensive utility system model was obtained by combining the above two models and was solved using different objective functions which were functions of both the steam turbine thermal efficiency and the cooling tower effectiveness. For the work presented in this paper, the following comprehensive system performance index (PI) was used:

$$PI = \frac{\text{Heat rejected to atmosphere by cooling tower}}{\text{Net power generation}} \tag{9}$$

The objective of the optimisation was to minimise the above performance index.

3. Results and Discussion

Figure 3 and Table 2 below show the performance of the comprehensive system.

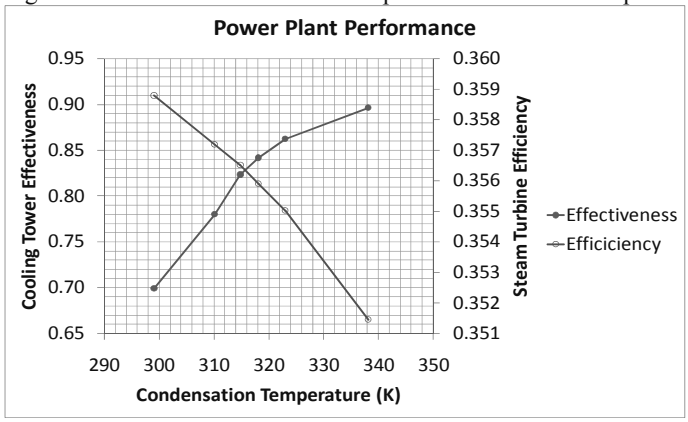

Figure 3: Comprehensive utility system performance

The data shows the effect of treating the system as a single integrated utility system as opposed to individual system component models. The comprehensive system model accurately predicts that the steam turbine efficiency decreases with increasing cooling tower effectiveness (Figure 3), a situation which is well borne out in practice as an increase in the cooling tower effectiveness occurs when conditions at the inlet of the cooling tower are high temperature and low flowrate. Consequently, the resultant high cooling tower inlet temperature translates to a high condensation temperature in the Rankine cycle and hence a reduction in the steam turbine efficiency. The results also showed that the comprehensive system PI increases with the condensation temperature. The cooling tower experimental data of Bernier (1994) was combined with data from the steam turbine model to give a comprehensive system dataset which was used as a basis for the analysis. Table 2 below shows the values of the performance index for different data sets.

Table 2: Optimisation results of the comprehensive utility system

Dataset	1	2	3	4
Individual system optimisation	1.7094	1.7094	1.7094	1.7094
Comprehensive system optimisation	1.6806	1.6840	1.6795	1.6803
% Change in comprehensive system performance index (PI)	-1.7%	-1.5%	-1.7%	-1.7%

As seen from the table, the overall system performance improves by an average of 1.7% when the system is treated as an integrated unit.

4. Conclusion

This paper presented the optimisation results of a comprehensive utility system found in power plants. The main conclusion from the work is that better performance of the system is achieved when the system is modeled as a single utility system as opposed to treating the system components individually.

References

Bernier, M A, (1994), " Cooling Tower Perfomance: Theory and Experiments", ASHRAE Transactions, Vol 100, pp 114 – 121

El Halwagi, MM and Manousiouthakis, V, (1989), "Synthesis of Mass Exchange Networks:, AIChE Journal, Vol 35, pp 1233 – 1244

Gutierrez, AF, Ponce-Ortega, JM, Serna-Gonzalez, M, (2010), " MINLP optimisation of mechanical draft counterflow wet-cooling towers, Chem.Eng Res and Design, Vol 88, pp 614-625

Kim JK, Smith R, (2001), "Cooling Water System Design", Chemical Engineering Science, Vol 56, pp 3641 – 3658

Linhoff, B and Flower, JR, (1978), " Synthesis of Heat Exchanger Networks:, AIChE Journal, Vol 24, pp 633 – 654

Rodriguez MA, Morton W and Mitchell DR, (2001), "The use of SQP Methods for the Optimisation of Utility Systems", Computers and Chemical Engineering, Vol 25, pp 287 -300.

Dincer Ibrahim, Al-Muslim H, (2001), "Thermodynamic analysis of reheat cycle steam plants", International Journal of Energy Research, Vol 25, pp 727 -739.

Zubair SM, Khan JUR,Yaqub M, (2003), " Performance Characteristics of counterflow wet cooling towers", Energy Conversion and Management, Vol 44, pp 2073 – 2091.

I.A. Karimi and Rajagopalan Srinivasan (Editors), Proceedings of the 11th International Symposium on Process Systems Engineering, 15-19 July 2012, Singapore.

Simplified MFE with power-change adaption strategy for the dynamic optimization of HTR-PM*

Sen Huang[a], Kexin Wang[a], Weifeng Chen[a], Jianghong You[a], Xi Chen[a], Jixin Qian[a], Zhijiang Shao[a], Lorenz T. Biegler[b]

[a]*State Key Laboratory of Industrial Control Technology, Institute of Industrial Control, Zhejiang University, 38 Zheda Road, Hangzhou 310027, China*
[b]*Chemical Engineering Department, Carnegie Mellon University, 5000 Forbes Avenue, Pittsburgh 15213, USA*

Abstract

Appropriate discretization is a key point of simultaneous strategies for dynamic optimization. Inappropriate discretization mesh may cause slow convergence, or even failure in the solution of the resulting NLP problem. Based on the observation that the level of power change of HTR-PM and mesh configuration is related to each another, the current paper proposes a simplified MFE strategy to discretize and solve efficiently the dynamic optimization problems arising from frequent HTR-PM load transition. The strategy develops offline and online phases to generate at low cost the appropriate discretization meshes for problems corresponding to any level of power change. The example of online optimal operation of HTR-PM demonstrates that the performance for real-time applications is significantly improved.
Keywords: High-Temperature gas-cooled Reactor (HTR), Dynamic Optimization, Moving Finite Element (MFE), Simplified MFE, Power-change adaption

1. Introduction and motivation

High-temperature gas-cooled reactor (HTR) is one of the promising nuclear power technologies, that is expected to be inherently safe and capable of integrating with advanced hydrogen, electricity, and process heat production (Idaho National Laboratory, 2009). The Shidaowan HTR plant built in Shandong, China will be the first commercial HTR plant in the world. The 200 MWe plant (two reactor modules, each with 250 MWt) will drive a single steam turbine at about 40% thermal efficiency. Modular design of HTR is of great difference from traditional light water reactors. Power change, unit shutdown, and load balance between modules could be frequent and significant.

HTR pebble bed module (HTR-PM) has a lumped parameter DAE model (Li et al., 2008) with 1,019 algebraic equations and 62 differential equations, based on which an optimization problem is formulated to ensure smooth and quick response to load transition. The simultaneous approaches that discretize both the state and control profiles using the collocation of finite elements are expected to solve the problem efficiently, as they directly couple the solution of the DAE system with the optimization problem. On the other hand, the element mesh has a great influence on the convergence and efficiency of the solution to the dynamic problem. The resulted nonlinear programming (NLP) problem after discretization may converge slowly, or even fail, due to inappropriate element meshes.

*This work was supported by the 973 Program of China(2012CB720500) and the NSF Program of China(61104134). E-mail address: zjshao@iipc.zju.edu.cn

The strategy of moving finite elements (MFE) (Russell and Christiansen, 1978; Biegler, 2010) treats the length of elements as a part of NLP variables. The variable elements allow the catching of breakpoints in the optimal control profile and the changes in the active set, and the error estimate at non-collocation points is imposed to guarantee discretization accuracy. However, the MFE strategy leads to a more constrained and difficult NLP. Furthermore, the NLP needs to be solved for each instance of the dynamic optimization problem. Therefore, the MFE strategy can be too expensive for online applications. Simplified strategies need to be developed, especially for the family of problems with similar scenarios.

2. Opportunity: Observation of element meshes for the optimization of HTR-PM load transition

For the frequent load transition of HTR-PM, a family of optimization problems arises with the same objective of control performance and based on the same process model and operating requirements, aims to provide fast and smooth power transition:

$$\begin{aligned} &\min_{z(t),y(t),u(t),p} \int_0^{t_f} \left[(x(t)-x_{sp})^T Q(x(t)-x_{sp}) + (\Delta u(t))^T R \Delta u(t)\right] dt \\ &s.t.\ \frac{dz(t)}{dt} = f(z(t), y(t), u(t), p) \\ &\quad c(z(t), y(t), u(t), p) = 0 \\ &\quad g(z(t), y(t), u(t), p) \le 0 \\ &\quad z(0) = z^0,\ t \in [0, t_f] \end{aligned} \tag{1}$$

where $z(t)$ and $y(t)$ are the differential and algebraic variables, respectively; controlled variables $x(t) \in z(t) \cup y(t)$ include the power ratio (w.r.t. full power (FP)) of the reactor, outlet helium temperature, outlet pressure of the steam header, and outlet temperature of the steam generator; manipulate variables $u(t)$ include the feedwater flowrate, helium flowrate, control rod reactivity, and turbine valve opening; and p is the time-independent parameters. Additionally, x_{sp} is the set points of $x(t)$, and Q and R are weight matrices. Note that the power operation ratio limit is $\pm 2.5\%$ FP/min. The constraints in (1) describe the system dynamics, operational path constraints, initial value, and time horizon of the optimization problem.

The simultaneous approach that uses Radau collocation on finite elements discretizes (1) into the following NLP problem (Kameswaran and Biegler, 2006):

$$\begin{aligned} &\min_{z_{ij}, y_{ij}, u_{ij}, p} \sum_{i=1}^{NE}\sum_{j=1}^{K} (x_{ij}-x_{sp})^T Q (x_{ij}-x_{sp}) + \\ &\qquad \sum_{i=1}^{NE}\sum_{j=2}^{K} (u_{ij}-u_{i,j-1})^T R (u_{ij}-u_{i,j-1}) + \sum_{i=1}^{NE-1} (u_{i+1,0}-u_{i,K})^T R (u_{i+1,0}-u_{i,K}) \\ &s.t. \sum_{k=0}^{K} \dot{\ell}_k(\tau_j) z_{ik} - h_i f(z_{ij}, y_{ij}, u_{ij}, p) = 0 \\ &\quad c(z_{ij}, y_{ij}, u_{ij}, p) = 0, i = 1..NE, j = 1..K \\ &\quad g(z_{ij}, y_{ij}, u_{ij}, p) \le 0, i = 1..NE, j = 1..K \\ &\quad z_{i+1,0} = z_{i,K},\ i = 1..NE-1 \\ &\quad z_{1,0} = z^0 \end{aligned} \tag{2}$$

where *NE* is the number of finite elements; in each element $t \in [t_{i-1}, t_i]$ ($0 < t_1 < ... < t_{NE} = t_f$), *K* is the number of Radau points, $\dot{\ell}(\tau)$ ($\tau \in (0,1]$) is the derivative of Lagrange interpolation polynomial, and $h_i = t_i - t_{i-1}$ is the element length.

We appoint four groups of power change demands, ranging from 10% FP to 40% FP. Figure 1 presents the appropriate element meshes that lead to the successful solution of the corresponding optimization problems. As shown in the figure, with the increasing level of power change, placing more elements at the beginning of the time horizon is necessary. Additionally, the similar placement of mesh points can be observed for the same level of power change. Therefore, if the MFE strategy can be parameterized with the level of power change of HTR-PM, the appropriate element mesh for any optimization problems arising from load transition can be obtained quickly after the power change demand is provided.

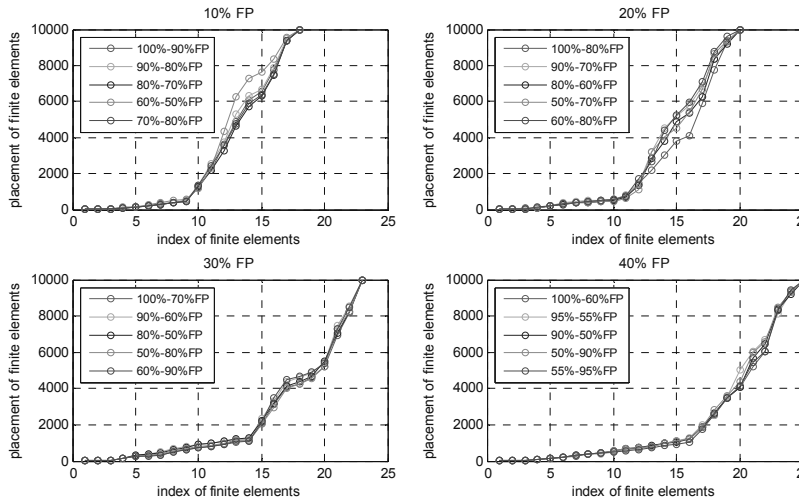

Figure 1. Mesh configuration corresponding to different levels of power change

3. Simplified MFE with power change adaption strategy

The strategy is composed of offline and online phases. The offline phase is a time-consuming but robust bi-level algorithm, which solves optimization problems for different levels of power change demands, and adjusts the element meshes to guarantee discretization accuracy. The discretization error estimate is given by:

$$e = \max\{\| \dot{z}(t_{i,nonc}) - h_i^{opt} f(z(t_{i,nonc}), y(t_{i,nonc}), u(t_{i,nonc}), p) \| \mid i = 1..NE\} \tag{3}$$

where $t_{i,nonc}$ are the non-collocation points in each element. This phase can be terminated when enough meshes have been obtained for each typical level of power change demand. Below is the more detailed description of the bi-level algorithm.

Element Mesh Generation:

For the given initial mesh $\bar{h}$, initialize the placement of mesh points $h^{opt} \leftarrow \bar{h}$, discretization error $\varepsilon^{rd} \leftarrow +\infty$; give the amplitude of mesh point disturbance d, tolerence on discretization error ε_c.

1. Upper-level: Generate an element mesh for dynamic optimization:

- Disturb placement of mesh points by uniform distribution $h_i^{opt} \leftarrow U[h_i^{opt} - d, h_i^{opt} + d]$.
- Adjust the mesh to match the given time horizon $h_i^{opt} \leftarrow t_f \cdot h_i^{opt} \Big/ \sum_{i=1}^{N_{\max}} h_i^{opt}$.

2. Lower-level: Solve problem (2) using mesh h^{opt}.
3. Check error estimate (3) at the solution:

- If $e \le \varepsilon_c$, save mesh h^{opt}, and the algorithm can stop while enough meshes, say 50 meshes, are obtained; otherwise, if $e \le \varepsilon^{rd}$, update $\varepsilon^{rd} \leftarrow e$.
- Go to step 1.

Note that different from the MFE strategy, which solves problem (2) together with the following error estimate:

$$\begin{cases} \| \dot{z}(t_{i,nonc}) - h_i f(z(t_{i,nonc}), y(t_{i,nonc}), u(t_{i,nonc}), p) \| \le \varepsilon_c \\ \sum_{i=1}^{NE} h_i = t_f, h_i \ge 0 \end{cases} \tag{4}$$

the simplified MFE does not involve solving such a more constrained and difficult NLP. Instead, the simplified MFE exploits a derivative-free method to look for meshes for accurate discretization.

Let *M* denote the set of the obtained meshes. The online phase takes advantage of *M* to generate at low cost the discretization mesh for the current power change demand *p*. A straightforward way is to use regression methods. A profile can then be obtained, which represents the configuration of the newly generated element mesh. Let *config* denote the configuration, the placement of the mesh points can be calculated by *config(index)*, where *index = 1..NE* is the index of mesh points and *config(NE)* = t_f.

4. Numerical results

For power changes ranging from 10% FP to 50% FP, the offline phase of the simplified MFE strategy generates five groups of element meshes with 50 meshes for each group, by solving the related dynamic optimization problems. Figure 2 shows the configuration of these meshes.

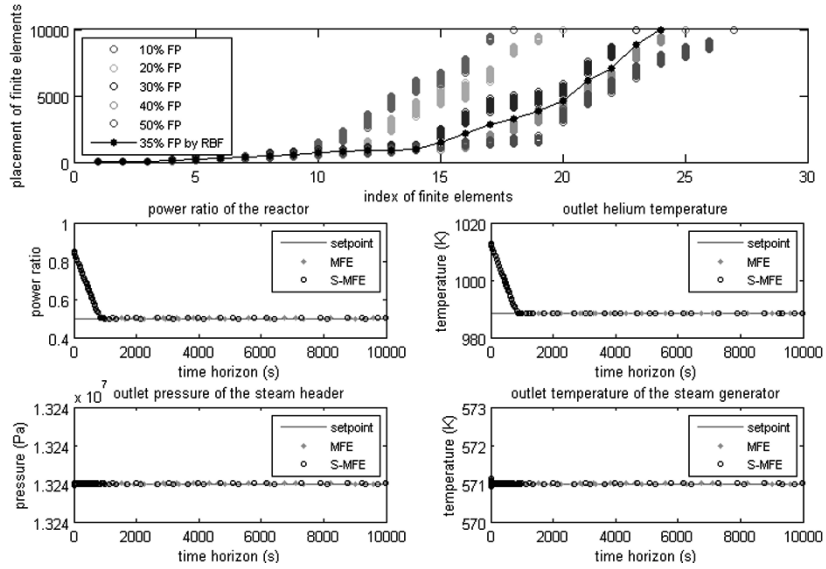

Figure 2. Online generated element mesh and optimization results

The online phase is triggered when a power change demand comes, for example, a demand that changes the load of HTR-PM from 85% FP to 50% FP. In this numerical experiment, the MATLAB toolbox function *newrbe*, which is an implementation of RBF interpolation method, is applied for regression. The configuration of the resulting element mesh is illustrated in the first plot of Figure 2, and the placement of the mesh points is obtained subsequently.

This newly obtained mesh is used to solve the dynamic problem. The resulting profiles of the controlled variables are presented in other plots of Figure 2. All the variables reach their set points as desired, and the operation ratio limit is satisfied. These plots also present the profiles using the MFE strategy. Apparently, solutions from these two strategies are almost the same.

Table 1 lists the solution-related data of both strategies, where columns #var, #eq, and #ineq are the numbers of variables, equality constraints, and inequality constraints of the resulting NLP problem, respectively. The primial-dual interior-point method code IPOPT (Wächter and Biegler, 2006) v3.8.1 is used as the NLP solver. Column *accuracy* is the error estimate according to (3). The results are obtained on a PC with 3.16GHz Core 2 processor and 4GB of RAM running Windows XP. The results indicate that the MFE strategy takes 21 times longer to solve the problem.

Table 1. Numerical results by simplified MFE and MFE strategies

Strategy	*NE*	#var	#eq	#ineq	accuracy	CPU (sec)
Simplified MFE	24	60466	59962	708	6.83736e-4	61.203
MFE					9.36438e-4	1373.969

5. Conclusion

The current paper presents a simplified MFE strategy to solve efficiently the dynamic optimization problems arising from HTR-PM load transition. By taking advantage of the relationship between the level of power change of HTR-PM and the configuration of element mesh, which leads to the successful solution of the dynamic problem, the simplified MFE can generate discretization meshes quickly for problems corresponding to any level of power change. Numerical results demonstrate that the simplified MFE strategy obtained the same optimization results as the MFE strategy, but with much faster online performance.

References

L. T. Biegler, 2010, Nonlinear Programming: Concepts, Algorithms, and Applications to Chemical Processes, SIAM, Philadelphia, USA

Idaho National Laboratory, 2009, Next Generation Nuclear Plant Project, 2009 Status Report

S. Kameswaran, L. T. Biegler, 2006, Simultaneous Dynamic Optimization Strategies: Recent Advances and Challenges, Computers and Chemical Engineering, 30, 10-12, 1560-1575

H. Li, X. Huang, L. Zhang, 2008, Operation and Control Simulation of a Modular High Temperature Gas Cooled Reactor Nucler Power Plant, IEEE Transactions on Nuclear Science, 55, 4, 2357-2365

R. D. Russell, J. Christiansen, 1978, Adaptive Mesh Selection Strategies For Solving Boundary Value Problems, SIAM Journal on Numerical Analysis, 15, 1, 59-80

A. Wächter, L. T. Biegler, 2006, On the Implementation of an Interior-Point Filter Line-Search Algorithm for Large-Scale Nonlinear Programming, Mathematical Programming, 106, 1, 25-57

I.A. Karimi and Rajagopalan Srinivasan (Editors), Proceedings of the 11th International Symposium on Process Systems Engineering, 15-19 July 2012, Singapore.

A methodology to forecast the price of commodities

Davide Manca

Dipartimento di Chimica, Materiali e Ingegneria Chimica "Giulio Natta"
Politecnico di Milano, Piazza Leonardo da Vinci 32, 20133 Milano, Italy

Abstract

A feasibility study of a new plant or even of a revamped one bases the forecast for incomes and outcomes on a discounting back approach. This means that both prices and costs of commodities are assumed constant for long periods. The paper tries to solve the "discounting back" problem that sees a coming apart between the dynamics of real market prices/costs (subject to fluctuations, volatility, and the "supply and demand" law) and the constant prices/costs assumed in conventional feasibility studies. The manuscript presents and discusses a methodology to model the time evolution of prices and costs of commodities.

Keywords: Market and demand fluctuations; Feasibility study; Price and cost forecast; Commodities; Plant design.

1. Introduction

Both the design from scratch and the revamping of a chemical plant are based on some kind of off-line optimizations where a suitable economic potential is maximized (Douglas, 1998; Manca and Grana, 2010). Such economic potential accounts for the positive contributes coming from products (and byproducts), and for the negative terms of capital and operating expenses (respectively known as CAPEX and OPEX) that include also the cost of raw materials.

To be effective, the economic assessment of the design procedure calls for an updated evaluation of both equipment and commodity costs. On the equipment side, there are tools, such as the Guthrie's formulas (Guthrie, 1969) and the cost indexes (*e.g.*, Marshall and Swift; Nelson-Farrar; Chemical Engineering, CEPCI; Vatavuk, VAPCCI), that allow evaluating up-to-date values of the CAPEX terms. On the OPEX and commodities side, the discounting back approach of feasibility studies simplifies excessively the economic assessment due to the lack of tools to forecast the prices/costs of products/byproducts and utilities.

The commodity market dictates the oscillations of both raw and product materials according to the "supply and demand" law. Unfortunately, conventional feasibility studies base the forecast for incomes and outcomes on the discounted-back approach. This means that the prices/costs of commodities and utilities are assumed constant for long periods with the reference point being usually the date when the economic assessment is performed. This calls for a further issue about the availability or estimation of updated values of prices/costs of commodities and utilities.

Going back to the discounted-back issue, it is rather evident the significant limitations of this approach that neither accounts for price/cost volatilities nor contemplates features such as market oscillations and fluctuations. The paper focuses on the price/cost of commodities and on possible modeling of their dynamics. Once this procedure is proposed, analyzed, modeled, and validated, it can be implemented to accomplish improved and more realistic feasibility studies of the designed plant (this

last feature is out of the scope of the paper).

2. The Methodology

The feasibility study of a chemical plant is based also on buying costs of raw materials and on selling prices of products. It is rather limiting assuming the price/cost of commodities either constant or characterized by a straight-line trend. These coarse approximations may play a role in the short-term forecasts but become unreliable when long-term economic assessments must be performed. Actually, during the life-cycle of a chemical plant (that can last a few tens of years) there may happen bull-and-bear periods, *i.e.* positive and negative economic situations. For instance, the price of crude oil in the 2006-2011 five-year period has seen large and sudden fluctuations from as high as 140 US$/bbl to as low as 30 US$/bbl in few months. These edgy fluctuations cannot be modeled by a simply averaged trend line. Conversely, a detailed analysis of the time series of commodity prices/costs is mandatory to extract the pieces of information that are required by the detailed statistical assessment of an improved feasibility study of a chemical plant.

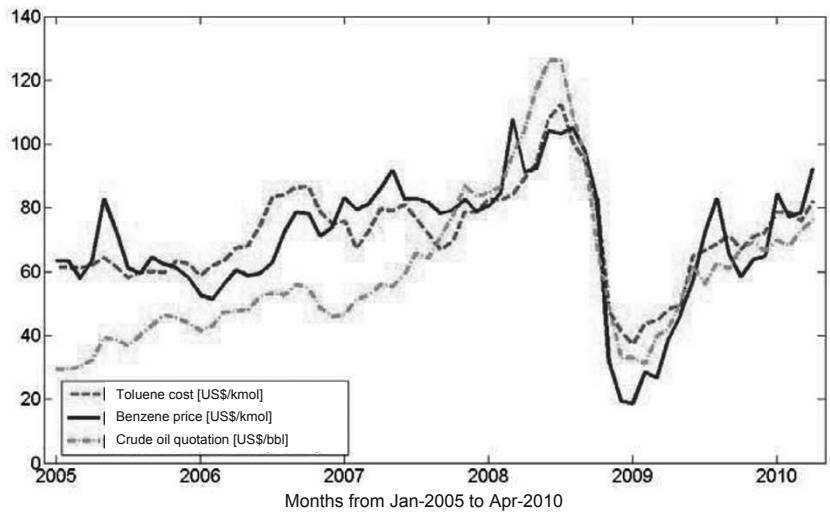

Figure 1: Prices of benzene, toluene, and crude oil in the 2005-2010 five-year period.

2.1. The Reference Component

Instead of tracking the dynamic evolution of prices and costs of each commodity of a chemical process, it is worth adopting an Archimedean approach based on the relative comparison of components respect to a reference one. By doing so, the price/cost of commodities will be referred to the price/value of a reference component and the economic dynamics of these commodities will be a suitable function of the time series of the quotation of the reference component. The reference component must be chosen according to the market field of the chemical plant. It should be a key component for either the chemical process or the sector where the plant operates. The availability of frequent and updated values of the reference component is a further recommended feature. For instance, as far as the Oil&Gas sector is concerned, an appropriate key component is crude oil.

Being the raw material and precursor of a number of chemical processes, crude oil is a

good candidate to the role of reference component. In addition, its price is well-known, largely available, and periodically updated on the main trading markets. Finally, crude oil, besides being a reference component for all its derived commodities, plays a similar role also respect to industrial utilities such as steam and electric energy.

2.2. The Process

As far as the process is concerned and for the sake of simplicity, let us focus on a well known and extensively discussed chemical process such as the hydrodealkylation (HDA) of toluene to benzene (Douglas, 1988; Luyben *et al.*, 1998; Manca and Grana, 2010). All the main components involved in the HDA, such as methane, hydrogen, benzene, toluene, and biphenyl (representative of the aromatic heavier byproducts) at some extent depend economically from the crude oil quotation. For further sake of simplicity, we will focus on the main components of the process, *i.e.* toluene (raw material) and benzene (the final product) to describe and discuss the proposed methodology to forecast the price/cost of commodities. Figure 1 shows the significant dependence of benzene price and toluene cost (on a monthly basis) from the crude oil reference quotation in the Jan-2005, Apr-2010 period.

2.3. The Correlation Role

To assess numerically the economic dependence between the commodities price/cost and the reference component quotation, it is worth considering a statistical index such as the covariance that measures the interaction intensity between the stochastic variables X and Y:

$$\sigma_{X,Y} = \mathrm{cov}(X,Y) = E\left[(X-\mu_X)(Y-\mu_Y)\right] \tag{1}$$

$\sigma_{X,Y}$ allows understanding if there are any correlations between the fluctuations of X and Y respect to their expected (*i.e.* average) values μ_X, μ_Y. To understand better the interaction between X and Y variables, the correlation index measures in a non-dimensional way the interaction between these variables:

$$\mathrm{corr}(X,Y) = \frac{\mathrm{cov}(X,Y)}{\sqrt{\mathrm{var}(X)\,\mathrm{var}(Y)}} = \frac{\sigma_{X,Y}}{\sigma_X \sigma_Y} \tag{2}$$

where $\mathrm{corr}(X,Y) \in -1,\ldots,+1$. Therefore, two variables are completely correlated if $\mathrm{corr}(X,Y) = +1$, anticorrelated if $\mathrm{corr}(X,Y) = -1$, and they are not dependent if $\mathrm{corr}(X,Y) = 0$. As a matter of fact, $\mathrm{corr}(X,Y)$ allows assessing quantitatively the dependence of the commodity prices/costs from the quotation of the reference component. Therefore, the higher the correlation index (between each single commodity price/cost, Y, and the reference component quotation, X) the better the identification of the reference component and, eventually, the better the functional dependency of prices/costs of commodities from the quotation of the reference component.

With reference to the diagrammed values of Figure 1, the following correlation indexes: $\mathrm{corr}(CO,T) = 0.8119$, $\mathrm{corr}(CO,B) = 0.7231$, where CO is crude oil, T is toluene, and B is benzene, show a high dependency degree (as expected) of benzene and toluene from the crude oil fluctuations of market quotations.

2.4. Time Dependence

Once the dependence of commodity prices/costs from the quotation of the reference component has been assessed, it is necessary to determine if there are any time delays between those time series. Possible time delays play, indeed, a role in the definition of the functional dependency between X and Y series. Correlograms can be of real help

in quantifying the time shift between such series. Correlograms are diagrams that report the correlation index of two time series X and Y as a function of the progressively increasing time shift introduced between them. For the sake of clarity, the correlogram of toluene costs respect to crude oil quotations for the monthly values of the 2005-2010 five-year period allows pointing out that the price of toluene mainly depends on the price of crude oil at the same month and at the previous one.

A further step towards the definition of the functional dependence of the commodity prices/costs from the reference component quotation consists in understanding if there are any autocorrelations for each time series of the prices/costs of commodities. In other words and with reference to the HDA plant and specifically to the toluene cost (the same can be done for the benzene price), the question is about the dependence of the toluene cost from previous values (*i.e.* prior months) of the toluene cost. How many previous values should be accounted for? What is the memory degree of the toluene cost respect to its previous quotations? The fast decreasing trend of autocorrelation bars (after the first month time shift) shows that there are not any seasonal or other peculiar trends. The negligible values of the autocorrelation index, for time delays of 4-5 months, show that the toluene cost loses any memory of the past after such a time interval. Same considerations can be drawn for the benzene price.

2.5. Dynamic Model

Both the correlograms and autocorrelograms (respectively of $X-Y$ and $Y-Y$ time series) play a major role in the definition of the functional dependence of the commodities price/cost. The objective is indeed to identify a functional time-dependence of the price/cost of each commodity from its previous value(s) and that/those of the quotation(s) of the reference component. In econometric terms, we are speaking of mixed autoregressive models based on two variables (*i.e.* X and Y). In general, a mixed autoregressive model with p delays of the dependent variable, Y, and q delays of the independent variable, X, is defined as an Autoregressive Distributed Lag model (Stock and Watson, 2003) and denoted as $ADL(p,q)$. According to the results produced by the correlograms and autocorrelograms analysis, the dynamic price/cost models for the HDA commodities assume the rather simple structure $ADL(1,0)$ and specifically:

$$P_{T,i} = a_{T,0} + a_{T,1}P_{CO,i} + b_{T,1}P_{T,i-1} \quad P_{B,i} = a_{B,0} + a_{B,1}P_{CO,i} + b_{B,1}P_{B,i-1} \tag{3}$$

where P is the price/cost of commodities, a and b are some appropriate linear regression coefficients, and subscript i refers explicitly to the monthly quotation of either the commodity or the reference component. The rather simplified linear model of equation (3), based on only one contribute from both the dependent and independent variables (respect to the actual price/cost), is chosen first of all to keep the things as simple as possible (while satisfying the findings of the correlation analysis) but also to avoid overfitting problems produced by possible overparameterizations of the identification model. The evaluation of the regression parameters a and b of equation (3) goes through a linear regression procedure based on a multidimensional unconstrained optimization algorithm. With reference to the experimental data, gathered from the market monthly quotations of Jan-2005, Apr-2010 period (*i.e.* 64 values for benzene, toluene, and crude oil), it is a good operating rule to run the identification procedure (*i.e.* the linear regression) on a subset of data (we chose 50 values), leaving the remaining ones to the cross validation procedure (*i.e.* 14 values).

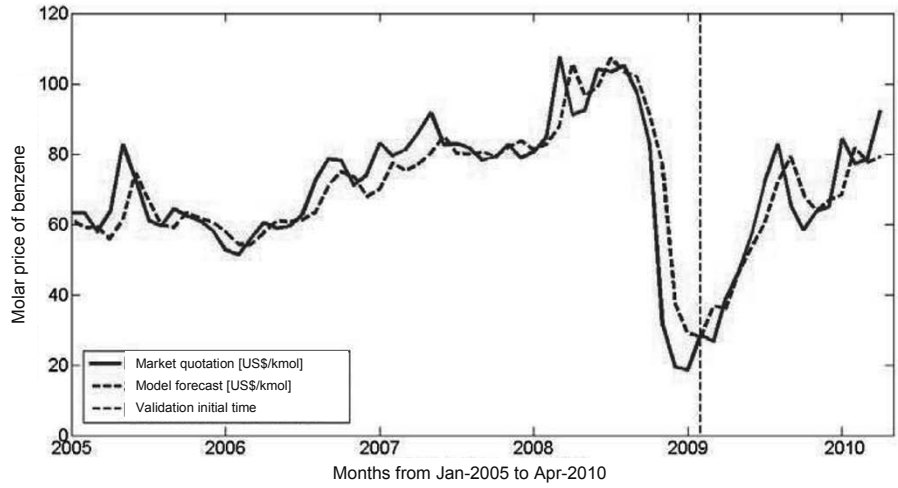

Figure 2: Comparison between market quotations and model forecasts for the price of benzene.

Figure 2 shows a comparison of the price of benzene between the effective market quotations (straight line) and the model forecasts (dashed line). There is a good agreement in the dynamic model of benzene price. The discrepancies between the market model values are due to the stochastic variability of prices and costs that cannot be accounted for by the deterministic model of equation (3). Same results and considerations can be drawn for the toluene cost.

Conclusions

Once the dynamic model of the commodity prices/costs has been determined and validated respect to past market values, it can be used for predictive purposes. The predictive feature of the dynamic model allows implementing a new approach to the feasibility study of industrial plants. For sure, the *ADL* model cannot be used in a deterministic way but a stochastic contribute, based on Monte Carlo methods, must be accounted for and implemented to obtain a suitable distribution of future price/cost of commodities. This feature allows dismissing the classical "discounting back" approach in favor of the dynamic tracking of both commodities and operating expenses to forecast through a stochastic approach the fan of alternatives (*i.e.* statistical distributions) for more consistent feasibility studies of the designed plant. Forthcoming papers will deal with the cost modeling of utilities and specifically of electric energy (again related to a proper reference component) and on the methodology to cope with the stochastic predictions of both commodity and utility prices/costs based on regressive models equal/similar to those reported in equation (3).

References

Douglas, J.M. (1988). Conceptual design of chemical processes. New York: McGraw-Hill.
Guthrie, K.M. (1969). Capital cost estimating. Chemical Engineering, 76 (6), 114.
Luyben, W.L., Tyreus, B.D., Luyben, M.L. (1998). Plantwide Process Control. New York: McGraw-Hill.
Manca, D., Grana, R. (2010). Dynamic Conceptual Design of Industrial Processes. Comp. & Chem. Eng., 34 (5), 656-667.
Stock, J.H., Watson, M.W. (2003). Introduction to Econometrics. London: Pearson Education.

I.A. Karimi and Rajagopalan Srinivasan (Editors), Proceedings of the 11th International Symposium on Process Systems Engineering, 15-19 July 2012, Singapore.

Numerical study of mixed-feedstock pyrolysis

Ka Leung Lam, Adetoyese O. Oyedun, Chi Wai Hui

Department of Chemical and Biomolecular Engineering, The Hong Kong Unviersity of Science and Technology, Clear Water Bay, Kowloon, Hong Kong

Abstract

In light of the processing difficulties and constraints in pyrolysing certain types of bulk feedstock alone, a mixed-feedstock pyrolysis approach is proposed in this work. The pyrolysis progress of some common biomass and plastic materials were first studied by common thermal analysis techniques and were then modelled. Using a mix of wood and polyethylene as an example, the proposed approach was evaluated with the aid of two models – a particle pyrolysis model and a CFD rotary kiln model. Based on the evaluation of three areas - heat transfer, secondary reaction and reactor operation, the proposed approach can possibly be used to cope with certain processing difficulties and constraints by enabling a more uniform heating across a cross-section plane, promoting secondary reaction for biomass pyrolysis volatiles, increasing the solid retention time and reducing the extend of char deposition on the reactor wall.

Keywords: modelling, CFD, pyrolysis, mixed-feedstock, kiln

1. Introduction

Pyrolysis is the thermal conversion of organic matter at elevated temperature in the absence of oxygen and yields combustible gas, pyrolysis tar and char. It is a complex process with the outcomes governed by the choice of feedstock and the processing conditions such as the heating profile, solid and vapour residence time, and feedstock size. A considerable amount of work has been on the study of those relations, and the physical and chemical processes involved. For the design, scaling up and optimization of pyrolysis processes, not only the understanding of feedstock characteristics is important, but also the practical consideration of processing efficiency is essential.

On an operational level, one categories of feedstock that has been investigated extensively is plastics. Generally, there exists great difficulties in pyrolysing plastic feedstock because of, for examples, difficulty in loading the feedstock, accumulation of char residue on reactor surface, difficulty in handling the residue and poor heat transfer [1]. It partly attributes to the fact that molten plastic has a low thermal conductivity and a very high viscosity. Another type of commonly investigated feedstock is biomasses. The tar from biomass pyrolysis, in contrast to those produced from plastics, are generally oxygenated, corrosive and unstable, so it is challenging to upgrade the liquid or separate useful chemicals out [2].

2. Problem Statement

For mixed-feedstock pyrolysis studies in the literature, it is common to focus on the possible synergetic effects between certain feedstocks from a chemical interaction prospective using milligram size well-mixed fine powder samples. This numerical study focuses on a macroscopic reactor level to evaluate on the possible processing benefits for a proposed mixed-feedstock pyrolysis approach.

3. Methodology

3.1. Overview

This work evaluates on the proposed mixed-feedstock pyrolysis approach using two mathematical models developed on separate platforms.

3.2. Experimental study

Thermogravimetric analysis (TGA) and differential thermal analysis (DTA) were used for the kinetic study and modelling of the pyrolysis of some biomass (wood and bamboo) and plastic feedstocks (polyethylene and polystyrene). It also serves as a direct approach to observe the pyrolysis progress under constant heating rate condition.

3.3. Numerical study

3.3.1. Modelling particle pyrolysis

Based on the kinetic parameters obtained from the experiment, a pyrolysis model has been developed to describe transiently the pyrolysis progress of a bed of shrinking particles with heat transfer interaction. The model is built on MATLAB® platform. The detail description of similar particle pyrolysis models has been given in earlier works [3-4]. Wood and polyethylene are used as the mixed-feedstock in this study. The shrinking factor (δ) for wood is estimated from the pyrolysis of wood piece with a bench-scale pyrolysis unit.

Table 1 Set of equations for modelling particle pyrolysis

Kinetic model
$\frac{d\alpha_i}{dt} = A_i \exp\left(-\frac{E_i}{\bar{R}T}\right)(1-\alpha_i)^{n_i}$
$\frac{d\gamma_j}{dt} = A_j \exp\left(-\frac{E_j}{\bar{R}T}\right)(1-\gamma_j)^{n_j}$
$\alpha_T = \sum_i \omega_i \alpha_i$
Heat transfer model
$\frac{\partial T}{\partial t} = \frac{\lambda}{\rho C_p}\frac{\delta^2 T}{\delta r^2} + \frac{2}{r}\frac{\lambda}{\rho C_p}\frac{\partial T}{\partial r} + \frac{1}{C_p}\sum_i\left(H_i\frac{\partial \alpha_i}{\partial t}\omega_i\right) + \frac{1}{C_p}\sum_i\left(H_j\frac{\partial \gamma_j}{\partial t}\right)$
B.C. 1: $-\lambda\frac{\partial T}{\partial r} = h(T_R - T_{bulk})$ B.C. 2: $\frac{\partial T}{\partial r}\vert_{r=0} = 0$
$C_p = \frac{(\alpha_{T,f}-\alpha_T)}{\alpha_{T,f}}C_{p,f} + \frac{\alpha_T}{\alpha_{T,f}}C_{p,c}$
$\lambda = \frac{(\alpha_{T,f}-\alpha_T)}{\alpha_{T,f}}\lambda_f + \frac{\alpha_T}{\alpha_{T,f}}\lambda_c$
Particle shrinking model
$\frac{dV}{dt} = -V_0\frac{d\alpha_T}{dt}(1-\delta)$

3.3.2. Modelling pyrolysis reactor environment with CFD

Without the necessity of shreding the feedstock into fine powders, rotary kiln is capable of handling bulk piece of feedstock and is the subject of study in this work. ANSYS ICEM CFD was used to construct the geometry and the mesh of a cross-section of a kiln. The solid bed was defined as a number of discrete bulk spherical particles that are isolated by void space in between. The unstructured triangle mesh composing of over 300000 elements was then introduced to ANSYS FLUENT 12.0 for developing a model to simulate on the heat transfer and volatiles evolving phenomena for the bed of bulk pyrolysis feedstock during a particular short time interval and to make some qualitative comparisons. Build-in volume of fluid (VOF) phase model and standard k-epsilon turbulence flow model were utilized. To simplify the model, physical process is the main focus and chemical reaction during the short time interval is neglected.

4. Result & discussion

4.1. Thermogravimetric analysis (TGA) result

Thermogravimetric analysis serves as a fundamental technique to study the pyrolysis behaviour and pyrolysis kinetics of different feedstock. The profiles in figure 1 indicate a distinct difference in the pyrolysis behaviour between biomass and plastic. This forms a key basis of the proposed mixed-feedstock approach.

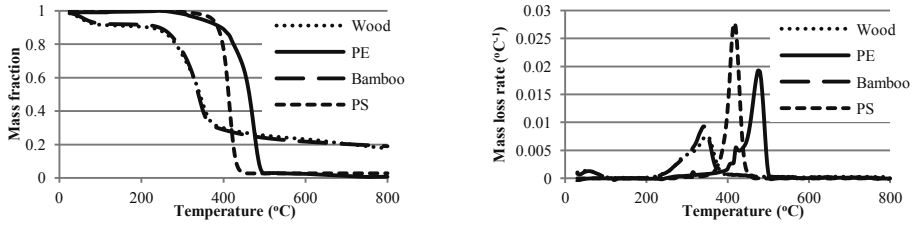

Figure 1 TG profile and DTG profile for the pyrolysis of different feedstocks at 10°C/min

4.2. Evaluation on the proposed mixed-feedstock pyrolysis approach

4.2.1. Overview and scenario

A mixed-feedstock pyrolysis approach is proposed and illustrated by figure 2. By assuming a constant heating for a 1:1 mix of wood and polyethylene particles in the particle pyrolysis model, a volatile evolving profile is obtained to give a basic idea of the pyrolysis volatile generation situation. Table 1 summarizes the simulation results, which will be discussed in the next few sections. In this approach, biomass and plastic feedstock are mixed and pyrolyzed in a rotary kiln reactor. The progress can basically be divided into five zones. In zone A, the mixed-feedstock is being heated up slowly. The moisture and extractives of the biomass is gradually releasing and it marks a minor mass loss. In zone B, polymer melting occurs and results in shrinkage of the solid bed. In zone C, major pyrolysis process for biomass feedstock occurs giving out a lot of volatiles. Further down to zone D, as the temperature increases, plastic pyrolysis contributes to another major mass loss. In zone E, further devolitization of the biomass feedstock is ongoing at this higher temperature zone. The pyrolysis char leaves the kiln at the end. This approach is evaluated in the following sections from three prospective.

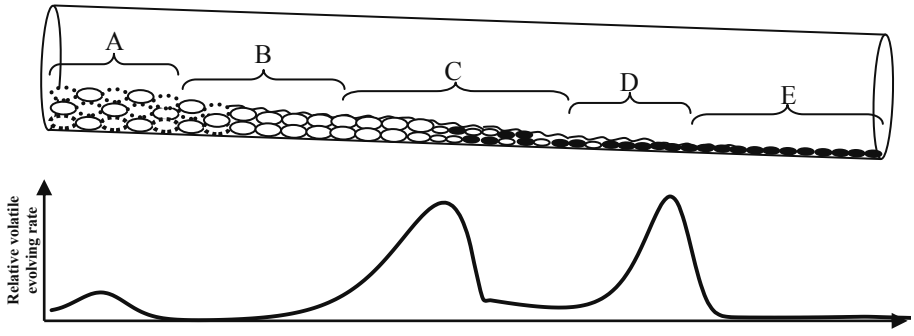

Figure 2 Illustration of a mixed-feedstock pyrolysis approach and its volatile evolving profile

Table 1 Summary of simulation results from the particle pyrolysis model

Feedstock	Relative major mass loss positions	Final volume fraction
Wood	-	0.8678
PE	-	0.0640
1:1 wood-PE mix	0.47 for wood, 0.73 for PE	0.5616

4.2.2. Heat transfer prospective

Heat transfer performance is one of the key considerations for the operation of a pyrolyzer. To achieve an uniform heating for the solid bed material in a rotary kiln, it is essential to have thorough mixing of particles in the transverse plane [5]. This is especially important when there is a significant variation in the size of the particles. A phenomenon referred as segregation occurs in which smaller particles tend to concentrate at the core and received less heating. Because of the fact that the main pyrolysis of biomass occurs at a lower temperature than that of plastic, it is possible that the evolving pyrolysis volatiles from the earlier pyrolysis of biomass material helps make the temperature of the solid bed more uniform. From the simulation shown by figure 3, the heating to the overall bed zone provided by the evolving volatiles from the bottom of the kiln is greater than by without any evolving volatiles. It tends to make the temperature in the transverse plane more uniform.

Figure 3 Contours of temperature for the transverse kiln bed (Left: with evolving volatiles, Right: without evolving volatiles)

4.2.3. Secondary reaction prospective

The pyrolysis volatile generation situation within a short time interval is studied and shown in figure 4. It is observed that the presence of a viscous molten plastic that fill up the void space of the solid bed increases the residence time of the primary pyrolysis products in the solid bed. A longer residence time of primary pyrolysis products in a high temperature zone usually favours secondary reaction. Given sufficient residence time, thermodynamically more stable compounds tend to be formed [6]. It can be an advantage for biomass pyrolysis because of the fact that the primary pyrolysis products, also referred as tar, formed are generally oxygenated, corrosive and unstable. Breaking down these undesirable compounds, formed mainly at zone C's temperature range in figure 2, to gas fraction or more stable compounds is beneficial for later product upgrading and the operation of the reactor.

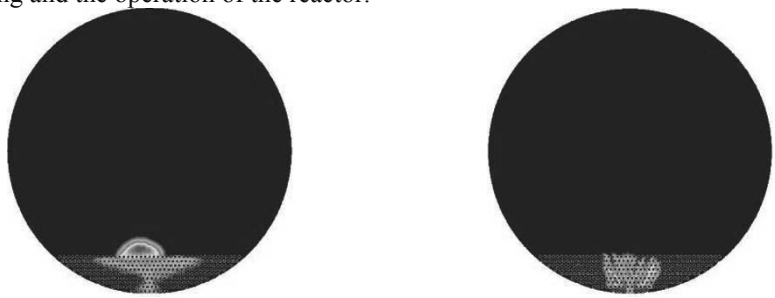

Figure 4 Contours of tracked volatile generated from the bottom of the solid bed (Left: void space not filled, Right: void space filled by molten polyethylene)

Possibly, the approach not only increases the vapour residence time within the solid bed zone, but also enables a different volatile evolving position compared to single feedstock pyrolysis. As observed in figure 2 and table 1, majority of volatiles generated from biomass pyrolysis evolve in the middle of the kiln and therefore, these volatiles have to travel for a longer time in the high temperature zone before condensing and it results in a more severe secondary reaction. On the other hand, the volatiles from plastics pyrolysis tend to be produced near the end of the kiln for faster removal.

4.2.4. Reactor operation prospective

The final residue volume from the pyrolysis of individual feedstock and mixed-feedstock were studied and presented in table 1. Obviously, a mixed-feedstock would yield a char residue with the volume between that of pyrolysing the feedstock alone. From the operation point of view for a rotary kiln, a great reduction in the solid bed size approaching the end of the kiln would generally reduce the solid residence time. The introduction of biomass feedstock is possible to counteract that. In addition, the presence of bulk biomass feedstock reduces the extent of direct contact of viscous molten plastics with the kiln surface to minimize coking from plastic pyrolysis.

5. Conclusion

A mixed-feedstock pyrolysis approach is proposed and evaluated in this work. The proposed approach is found to allow a more uniform heating in the transverse plane, promote secondary reaction for reducing undesirable tar formation from biomass pyrolysis, increase the solid residence time and reduce the extend of char deposition on the reactor wall. These processing improvements can possibly cope with the existing processing difficulties and constraints in single-feedstock pyrolysis.

Nomenclature

α, γ	extent of reaction	α_T	overall mass loss fraction
$\alpha_{T,f}$	final total mass loss fraction	t	reaction time (s)
T	temperature (K)	k	rate constant (s^{-1})
n	order of reaction	A	pre-exponential factor (s^{-1})
E	activation energy (J/mol)	$\bar{R}$	universal gas constant (J/mol-K)
ω	mass loss contribution	H	heat of reaction (J/kg)
C_p	specific heat capacity (J/kg-K)	λ	thermal conductivity (W/m-K)
r	radius of a discrete layer (m)	ρ	density of feedstock (kg/m^3)
T_R	particle surface temperature (K)	T_{bulk}	bulk temperature (K)
V	particle volume (m^3)	δ	shrinking factor
h	convective heat transfer coeff. (W/m^2-K)	i	mass loss reaction i
j	non-mass loss reaction j	f	feedstock c char

Acknowledgement

The authors gratefully acknowledge the support from Hong Kong RGC research grant (No. 613808, 614307), Hong Kong PhD Fellowship Scheme for Oyedun Adetoyese Olajire (PF09-05997) and the Global Power and Energy Company Limited.

References

[1] J. Scheirs and W. Kaminsky, Feedstock Recycling and Pyrolysis of Waste Plastics : Converting Waste Plastics into Diesel and Other Fuels, J. Wiley & Sons, Chichester, 2006.

[2] P. Basu, Biomass Gasification and Pyrolysis : Practical Design and Theory, Academic Press, Burlington, 2010.

[3] K.Y. Cheung, K.L. Lee, K.L. Lam, C.W. Lee and C.W. Hui, Fuel Process. Technol., 92 (2011) 856.

[4] K.L. Lam, A.O. Oyedun, K.Y. Cheung, K.L. Lee and C.W. Hui, Chem. Eng. Sci., 66 (2011) 6505.

[5] A.A. Boateng, Rotary Kilns : Transport Phenomena and Transport Processes, Butterworth-Heinemann, Amsterdam, 2008.

[6] C. Pasel and W. Wanzl, Fuel Process. Technol., 80 (2003) 47.

I.A. Karimi and Rajagopalan Srinivasan (Editors), Proceedings of the 11th International Symposium on Process Systems Engineering, 15-19 July 2012, Singapore.

Generating operating procedures using a micro genetic algorithm

Rafael Batres

Toyohashi Tech, Hibarigaoka, Tempaku-cho, Toyohashi 441-8580, Japan

Abstract

This paper explores the use of the so called micro genetic algorithms coupled with variable-length chromosomes and a seeding scheme based on tabu search. The problem is to find the sequence of actions that have to be executed in the shortest time possible, but also in a way that minimizes the possibility of situations that may endanger the plant personnel and plant facilities. The proposed approach was tested on the generation of the optimum sequences for startup and shutdown of a mixing vessel similar to the equipment used in the synthesis of acrylic acid. The results show that the proposed method outperforms the traditional GA algorithm both in terms of the quality of the solution and computational effort.

Keywords: operating procedures, micro genetic algorithms, tabu search

1. Introduction

A significant number of serious incidents occur in the process industry during shutdown or startups operations (IChemE, 2006). However, contrasting to industrial applications of scheduling algorithms, the generation of operating procedures is left to expert engineers and plant personnel (Batres, 2002).

The generation of operating procedures can be described as a planning problem where the objective is to find an ordered sequence of plant actions to take the process from an initial state to a goal state. In general, the sequence of actions needs not only to be carried out in the shortest time possible, but also in a way that minimizes the possibility of situations that may endanger the plant personnel or cause damages to the plant.

Existing work for determining operations sequences in the presence of quantitative safety constraints are based on mixed-integer dynamic optimization (MIDO) which combines dynamic optimization with discrete variables for a N_2,O_2,CH_4 mixture changeover. Such approach is useful in situations where a globally optimal solution is not required and one can settle for plan feasibility. In another work, Asprey *et al.* (1999) proposed a two-layer method that combined simulated annealing (SA) and the artificial-intelligence search-method A* to generate startup sequences for a mixing problem. Despite the fact that the two-layer method has the ability to generate a global optimal solution, it does so at the expense of a high number of function evaluations.

This paper investigates an approach based on micro genetic algorithms (μGAs) to generate startup and shutdown operating procedures. μGAs are characterized by a small population size which is restarted several times while keeping the very best fit individual. Krishnakumar (1989) found that μGAs converge faster to the near-optimal solution.

Another aspect of the proposed approach is the use of variable-length chromosomes. Variable-length chromosomes have been applied with success in artificial intelligence planning. In a planning problem, the objective is to find an ordered sequence of actions that achieve a goal given an initial state provided that templates for those actions are

available. For example, Westerberg and Levine (2001) use variable-chromosomes to represent feasible but not necessarily optimum plans. Their GA implementation extends traditional algorithms by incorporating an extra shrinking operator that deletes a randomly selected action from the parent chromosome. Brie and Morignot (2005) describe a genetic algorithm that besides the shrinking operator it also uses an operator for enlarging a chromosome (by inserting new actions) and an operator that modifies a parameter of a randomly selected action. In these two implementations, the respective algorithms are applied to the so-called blocks-world problem.

2. Problem definition

We adopt time optimality as a performance criterion. Therefore, the problem for generating operating procedures for startup or shutdown can be written as follows:

$$\begin{aligned} \text{Min} \quad & A\int_{t_0}^{t_f} dt + B\left\|\boldsymbol{x}_f - \boldsymbol{x}(t_f)\right\| \\ \text{subject to} \quad & \dot{\boldsymbol{x}}(t) = f(\boldsymbol{x}(t), \boldsymbol{u}(t)) \\ & \boldsymbol{x}(t_0) = \boldsymbol{x}_0 \\ & \boldsymbol{x}(t_f) = \boldsymbol{x}_f \\ & \boldsymbol{g}(\boldsymbol{x}) \leq 0 \\ & \boldsymbol{u}(t) \in U,\ U = [u_1, u_2, \ldots, u_n]^T \end{aligned} \tag{1}$$

where $\int_{t_0}^{t_f} dt$ is the time that the system takes to get from the initial state to the final state, $\boldsymbol{x}_0$ and $\boldsymbol{x}_f$ are vectors that represent the initial state and final state respectively, $\boldsymbol{u}(\mathrm{t})$ is a vector that represents a set of operations performed at time $\boldsymbol{t}$, $\boldsymbol{g}(\boldsymbol{x})$ is a vector of inequalities representing process, safety and other constraints, U represents a set of predetermined operations such as specific valve positions, and A and B are constants. When $A = 0$ the problem is reduced to finding the sequence of operations that result in a feasible trajectory.

The system under study is a mixing vessel that belongs to the kind of equipment normally used in the synthesis of acrylic acid. The mixing vessel is a stirred-tank with three inlet valves and one outlet valve. There is one inlet valve for the admission of propylene, one for air, and another for steam. The outlet valve is for the discharge of the mixture. The inlet valves can be operated in a bang-bang fashion or with multiple valve positions. The outlet flow is regulated with a local controller that keeps the pressure constant during startup or shutdown. In the startup operations, the vessel is initially filled with air and the final state is determined by a specified molar composition of the steam-air-propylene mixture outside the flammable region. Conversely, the shutdown operations have the goal of transferring the system to a state that is 100 % air by mass.

As a safety requirement, the valve operations should not take the process through the flammable range. Therefore, a feasible trajectory for the mixing vessel is that in which the final state is reached and the valve operations are carried out to avoid the flammable range. The initial, intermediate, and final states are all expressed in terms of mass fraction.

3. Methodology

The methodology consists of the following steps:

Step 1. Generate a random population.

Step 2. Use tabu search to find a *good* feasible solution and insert it to the population.

<<< Inner loop>>>>

Step 3. Evaluate the fitness of each member of the population.

Step 4. Use crossover and mutation operations to generate a new population.
Step 5. Select the best individual.
Step 6. If the stopping criteria of the inner loop are achieved then go to Step 7. Otherwise go to Step 3.
Step 7. If the stopping criteria of the outer loop are achieved then finish. Otherwise continue with Step 8.
<<< Outer loop>>>>
Step 8. Create a new random population and transfer the best individual from the previous population obtained at Step 6.
Step 9. Restart the inner loop by going to Step 3.

3.1. Procedure for obtaining the good feasible solution

Obtaining a good solution is carried out by formulating the problem as an AI planning problem in which the objective function considers the *distance* of the path from the initial state to the current node and the distance of the path from the current node to the goal. It was found that the Chebyshev distance performs best among other distance approaches considered. Therefore, the objective function is formulated as:

$$f(\boldsymbol{y}_n, n) = w(n)D\exp\left(\max_i\left|y_{n,i} - y_{n,i}^{goal}\right|\right) + E\max_i\left|y_{n,i} - y_{n,i}^{start}\right| + P(\boldsymbol{y}_n, n) \quad (2)$$

where $\boldsymbol{y}_n$ is a state vector containing the mass fractions that resulted from executing an operation, n is the number of operations in list R which is less or equal to the final number of operations that reach the goal state, $w(n)$ is an exponential decay function that reduces its value as the solution progresses towards the goal state, $y_{n,i}$ is the i^{th} component of $\boldsymbol{y}_n$ and represents the mass fraction of component i, y_i^{start} represents the mass fraction at the initial state, y_i^{goal} represents the mass fraction at the goal state, and P is a penalty function that is active when the flammability constraint is violated and whose value decreases as the solution reaches the goal state. The neighborhood used in the tabu search is obtained from a random selection of different combinations of valve positions and the *operator time duration* (the time duration for which a combination of valve positions is maintained). P is given by

$$P(\boldsymbol{y}_n, n) = F\left(1 + q(\boldsymbol{y}_{n-1}, \boldsymbol{y}_n)\right)\left(1 - \frac{n}{N}\right) \quad (3)$$

where $q(\boldsymbol{y}_{n-1}, \boldsymbol{y}_n)$ is the maximum difference between the gas concentration and the flammability envelope for all the concentrations that fall in the flammability region as part of the path that results from moving from state *k-1* to *k*. If moving from state *k-1* to *k* results in a path that is on all its segments outside the flammability region $q(\boldsymbol{y}_{n-1}, \boldsymbol{y}_n) = 0$. The flammability region is approximated by an eighth-degree polynomial. Tabu search is used as the optimization algorithm to obtain the good feasible solution.

3.2. Objective function of the inner loop

The objective function of the inner loop is implemented as a penalty function with a positive term added when the flammability constraint is violated.

$$f(n) = w_1 t_{total} + w_2\varphi + av + bq \quad (4)$$

where t_{total} is the total time that takes from the initial state to the last state, φ is a function of the difference between the last state and the goal which also takes into account the difference between the last state and the goal; v and q are penalty functions that are zero if no violation occurs and positive otherwise; and w_1 and w_2 are weights. w_1 is linearly decreased as the iteration progresses.

3.3. Chromosome structure

Each gene in the chromosome represents an operation defined in terms of the three valve positions and the operator time duration. Each operation is indexed and stored in an operation pool before the actual optimization begins. For example the chromosome shown in Fig. 1 has two genes with index 59 each of which represents an operation in which the steam valve is fully closed, the propylene valve is 10% open, the air valve is fully open, and these positions are kept during 30 seconds.

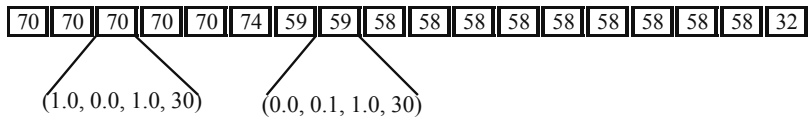

Figure 1. Example of a chromosome

3.4. Crossover and mutation

In addition to traditional crossover and mutation, the growth, shrink and parameter-change mutation (Brie and Morignot, 2005) were implemented. The shrink mutation consists of picking one random point in the chromosome of the parent and then removing the operation at that specific point. The growth mutation is carried out by selecting a random point in the chromosome of the parent and then inserting one operation from the operation pool at that point. The operation from the operation pool is also selected at random. The parameter-change mutation is similar to the traditional mutation, except that the operation from the operation pool has the same valve positions as the mutation target but different time duration.

4. Numeric experiments

All the experiments were carried considering a 50 ℓ tank with a pressure of 1 atm and a temperature of 500 K. The maximum flow rates of each inlet stream were set to 0.1 kg/s. The operator time duration was set for 15, 21, or 30 seconds. Valve positions were considered as completely-open, completely-closed, or 10% open. In the startup case, the initial state was 100 % air by mass, and the goal state was 10% steam by mass, 15% of propylene by mass and the balance was air. Other goal states were explored but this one resulted the most challenging in terms of the number of local minima. In the shutdown case, the initial and goal states were selected as the inverse of those of the startup. In order to evaluate the repeatability of the results, 10 runs were carried out for each experiment. Subsequently, the average and best values were compared with a traditional GA that is initialized with randomly generated populations. Both methods were implemented in Java using JDK 6. The experimental results were obtained on a 3.2 GHz Intel Xeon computer with 8GB of RAM and Windows 7.

The traditional GA contained a population of 100 individuals. The termination criterion for the traditional GA was defined based on a maximum number of generations after exploratory runs showed that convergence for the traditional GA stabilized at 250 generations. For the μGA, the population consisted of 5 individuals. The termination criteria for the inner and outer cycle were set to a maximum of 40 generations and 20 epochs respectively.

Figure 2 compares the process trajectories for the startup case. The operation profiles of the trajectory obtained with the proposed method are shown in Figure 3. Table 1 summarizes the results of the numerical experiments. It can be observed that the proposed method generates operating procedures that take less amount of time to reach the

goal. The results also show that the proposed method presents better repeatability. It can also be noted that the proposed method is more efficient in terms of computation time.

Table 1. Average and best values for startup and shutdown. Best values are in parenthesis.

		Startup Operations		Shutdown Operations	
		Traditional GA	Proposed method	Traditional GA	Proposed method
Computation time [s]		609.3321 (636.2360)	80.5708 (76.1150)	1288.0815 (1308.5160)	255.9522 (251.8470)
Total operations time [s]		523.0909 (498)	481.2 (450)	1575.9 (1731)	1515.0 (1515.0)
Final State	Steam [kg/kg]	0.1012 (0.1008)	0.1017 (0.1005)	0.0321 (0.0064)	0.0011 (0.0011)
	Propylene [kg/kg]	0.1498 (0.1494)	0.1505 (0.1505)	0.0029 (0.0005)	0.0009 (0.0009)
	Air [kg/kg]	0.7490 (0.7498)	0.7478 (0.7490)	0.9650 (0.9931)	0.9980 (0.9980)
Mean squared concentration error		0.0021 (0.0009)	0.0038 (0.0012)	0.0476 (0.0094)	0.017 (0.017)
Fitness		188.1390 (198.9356)	202.7944 (219.4857)	700.6392 (727.2074)	592.4112 (592.4112)

5. Conclusions

A method has been presented which uses a μGA to generate operating procedures. The proposed approach is characterized by (1) creating a good solution that is placed in the initial population; (2) chromosomes of variable size; (3) small population sizes. Numeric results show that the proposed method surpasses traditional genetic algorithms both in terms of the quality of the solution and computational effort. In addition to the advantage in convergence speed, less memory is required to store the population.

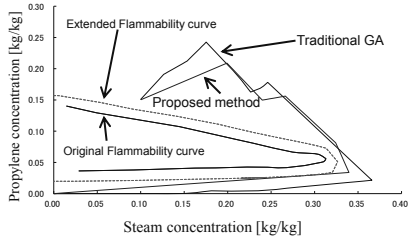

Figure 2. Startup operation trajectories

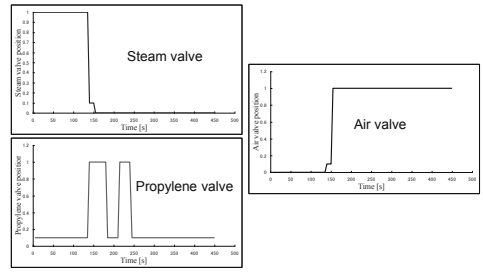

Figure 3. Valve operation profiles

Acknowledgement. This paper is dedicated to Prof. Yuji Naka on the ocassion of his retirement as professor and head of the PSE Division at Tokyo Institute of Technology.

References

A. H. Brie, P. Morignot, (2005), Genetic planning using variable length chromosomes, ICAPS

S. P. Asprey, R. Batres, T. Fuchino, Y. Naka, (1999), Optimal Simulation-based Operations Planning with Quantitative Safety Constraints, Ind. & Eng. Chem. Res., 36:6, pp. 2364-2374

R. Batres, J. Soutter, S. P. Asprey, P. Chung, (2002), Operating Procedure synthesis: science or art? The Knolwedge Engineering Review, 17:3, 261-294

IChemE, (2006), BP Process Safety Series: Safe Ups and Downs for Process Units (Sixth Edition). IChemE.

K. Krishnakumar, (1989), Micro-Genetic Algorithm for Stationary and Non-stationary Function Optimization, SPIE: Intelligent Control and Adaptive Systems, 1196, 289-296

C. H. Westerberg, J. Levine, (2001), Optimizing Plans using Genetic Programming, UK Workshop on Computational Intelligence, Edinburgh

I.A. Karimi and Rajagopalan Srinivasan (Editors), Proceedings of the 11th International Symposium on Process Systems Engineering, 15-19 July 2012, Singapore.

Optimal Operation of a Membrane Reactor Network

E. Esche[a], H.Arellano-Garcia[a], G. Wozny[a], L.T. Biegler[b]

[a]*Chair of Process Dynamics and Operation, Berlin Institute of Technology, Sekr. KWT-9, Str. des 17. Juni 135, D-10623 Berlin, Germany*
[b]*Dept. of Chemical Engineering, Carnegie Mellon University, 5000 Forbes Avenue, Pittsburgh, PA 15213-3890, USA*

Abstract

In this work, a two-dimensional model for a conventional packed-bed membrane reactor (CPBMR) is developed for the oxidative coupling of methane, which uses a non-selective porous membrane to continuously feed oxygen to the catalytic bed. The model incorporates radial diffusion and thermal conduction and assumes convective transport for the axial direction. In addition, two 10cm long cooling segments for the CPBMR were implemented based on the idea of a fixed cooling temperature outside the reactor shell. The resulting model is discretized using two-dimensional orthogonal collocation on finite elements with a combination of Hermite polynomials for the radial and Lagrangian polynomials for the axial coordinate. The simulation study shows that it is necessary to make all transport coefficients dependent on local temperatures and compositions. This leads to a simulation with roughly 130,000 variables, which is then used to generate initial points for the optimization of the CPBMR stand-alone operation. In addition, inequality constraints and variable bounds are introduced so as to avoid potentially hazardous mixtures of methane and oxygen in both shell and tube as well as to keep the temperatures below levels stressing reactor materials (< 1,100°C). Moreover, membrane thickness, feed compositions, temperatures at the reactor inlet and for the cooling segments, diameters of tube and shell, and finally the amount of inert packing in the reactor are considered as decision variables. The optimization procedure uses IPOPT as a solver. Afterwards, the 2D model is integrated into a membrane reactor network (MRN) proposed by H. Godini et al. in 2010 which is simulated. Finally, attempts are made to optimize its operation.

Keywords: OCM, MRN, CPBMR, large-scale NLP, IPOPT

1. Motivation and Problem Statement

For remote, isolated wells of natural gas, an energy-intensive combination of steam reforming and Fischer-Tropsch synthesis is often applied to turn methane into more easily transportable and chemically processable hydrocarbons. An alternative to this process is the oxidative coupling of methane (OCM), which has the potential to become a key technology in the chemical industry. The OCM process allows for direct production of alkenes (olefins) or alkanes from methane (CH_4).Fig. 1 shows the network proposed by H. Godini et al. in 2010. Many different types of catalysts and reactor configurations have been discussed in previous works. This paper will focus on the afore-mentioned network and the application of the La_2O_3/CaO-catalyst, which has shown promising behavior for OCM to C_2 products both in fixed-bed (FBR) and packed-bed membrane reactors (PBMRs). Thus, a fixed-bed reactor and a conventional packed-bed membrane reactor are run alongside each other in the network and

connected through a proposed packed-bed membrane reactor (PPBMR). The latter differs from a CPBMR only with respect to the feeding of nitrogen and methane to its shell-side. The proposed network allows for an increase in both yield and selectivity in C_2 hydrocarbons. To further investigate the network, this work will employ non-isothermal models and start with a two-dimensional model of the CPBMR to reevaluate the reported findings.

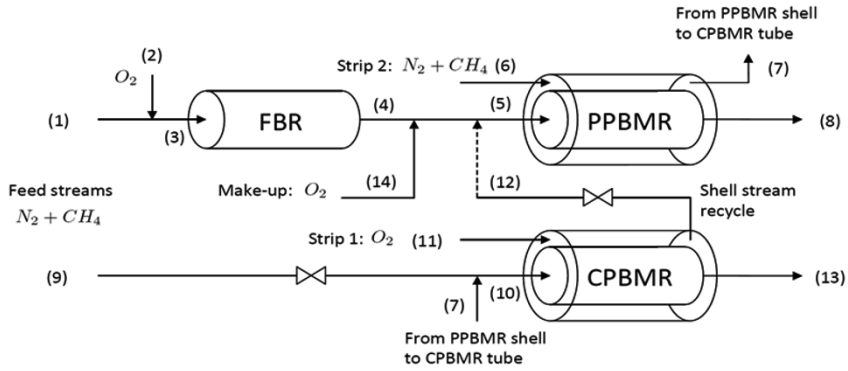

Figure 1: Membrane reactor network (**MRN**) proposed by H. Godini et al., 2010. The network consists of a fixed-bed reactor (**FBR**), a conventional packed-bed membrane reactor (**CPBMR**) and a proposed packed-bed membrane reactor, which is run with an alternative feeding policy (**PPBMR**).

2. Model for the CPBMR

The CPBMR is modeled two-dimensionally incorporating radial diffusion and thermal conduction, as well as common convective transport along the axis. In addition, a basic heating/cooling concept is introduced in all three reactors. A fixed temperature outside the reactor's lateral shell is used to generate a heat flux from or into the reactor.

In accordance with findings by D. Lafarga et al., 1994, Knudsen flux describes the diffusion through the membrane. Heat transfer through the membrane and the outer shell are described using heat transfer coefficients for the membrane derived from deliberations by V. Specchia et al., 1980, and for the outer shell initially assumed to be similar to the heat transfer coefficient in a tubular heat exchanger. In addition, the enthalpy flow caused by the molar flow through the membrane is calculated. Thermal conductivities and effective radial diffusivities are implemented as functions depending on local temperatures and compositions based on correlations published by R.J. Kee et al., 2003, E. Tsotsas et al., 1988, B.E. Poling et al., 2001, and R. Bauer et al., 1978.All reactor models need to be discretized in order to turn the set of differential and algebraic equations into a solely algebraicone. Because of its advantageous stability properties collocation on finite elements is chosen. The one-dimensional models are discretized using third order Lagrangian polynomials on finite elements employing shifted Radau roots so as to guarantee for the continuity of the collocated variable across finite elements. All two-dimensional models appearing in this work contain second order radial derivatives. Therefore, it is required to include the continuity of the first order radial derivative. This is usually achieved by introducing further equality constraints. An alternative approach is the usage of Hermite polynomials instead of Lagrangian for the radial coordinate, which through the forwarding of two collocation coefficients to an adjoining finite element automatically provide the continuity of the collocated variable itself and the first derivative.

3. Stand-alone Operation of the CPBMR

Given its configuration, radial effects can be expected to be most important in the CPBMR. Therefore, the new proposed two-dimensional model is closely examined and optimization studies are carried out to estimate the performance of the stand-alone operation. Starting with two different feeding configurations, isothermal, adiabatic, and heated/cooled models are first compared. The difference between all three models is not negligibly small. For an initial reactor configuration, the isothermal case shows the best possible performance. However, the adiabatic model proves, how unstable this performance is, if no heat is removed from the system as the yield in C_2 hydrocarbons drops from 39% to 6%. Two cases with a fixed heating/cooling temperature along the entire radius show a performance of the CPBMR almost as good as promised by the isothermal case.

In general, the one-dimensional (1D) case features a methane conversion, which is compared to the two-dimensional system considerably higher (up to 20 percentage points), whereas selectivity in C_2 hydrocarbons differs by only a few percentage points.

Given the dependence of most transport coefficients and fluid properties on local temperatures and concentrations, the equation system describing the CPBMR will always be a large-scale NLP. Because of the lack of second order derivatives in the axial direction, this does not cause much of a problem for the simulation as axial finite elements may be simulated sequentially. For any optimization, however, a too large system will slow down the solver or even make it impossible to find any optimal solution at all. For this reason, simulation studies are carried out varying the number of both radial and axial finite elements while examining their influence on the calculated performance of the reactor and the size of the errors of both mass and atom-balances. In addition, simple optimization studies with a degree of freedom of one were carried out to investigate whether any optimal solution could be found in the respective set-up. This procedure led to five radial and 12 axial finite elements so as to describe the reactor with a length of 20cm, a width of the tube-side of 7mm, and a diameter of 10mm. 10 of the 12 axial finite elements have a length of 2cm each, while the other two are 0.1mm long: one positioned at the inlet, the other one at the switching point between cooling temperatures I and II. This leads to an NLP with roughly 130 000 variables describing the CPBMR. Both the simulations and the subsequent optimization studies are carried out using IPOPT as a solver. Given the second order derivatives, fluid properties, and transport parameters appearing in the NLP, the problem is badly scaled. Attempts to fix this problem were unsuccessful. Nevertheless, IPOPT's internal gradient based scaling in contrast to CONOPT copes well with this system despite numerous line searches and regularization efforts.

3.1. Optimization Studies of the CPBMR

The simulation of the CPBMR is used to generate initial values for the general optimization of the reactor. To avoid the formation of unsustainable temperature hot-spots, inequality constraints are introduced to keep the temperature at any point in the reactor below 1100°C. On top of that, precautions need to be taken to avoid explosive mixtures of oxygen and most of all methane in the reactor. Therefore, further equality constraints ensure that the molar methane concentration is either below or equal to 5% of the oxygen concentration or greater than or equal to the oxygen concentration. Membrane thickness, the afore-mentioned feed compositions, feed and heating/cooling temperatures, diameters of both tube- and shell-side, amount of catalyst, and inert packing are considered as decision variables. A pressure difference between shell- and tube-side of 1bar is assumed and the superficial velocity is set to 1m/s.

Table 1. Optimization results – decision variables

	Temp., inlet, shell	Temp., inlet, tube	Temp.,cooling,I	Temp., cooling, II	Mol. frac., O_2, shell	Mol. frac., CH_4, tube
	[K]	[K]	[K]	[K]	[–]	[–]
Initial	1023	1023	1023	1023	0.128	0.170
Final	970	1013	970	970	0.157	0.128
	Diameter, tube	Diameter shell	Catalyst density	Catalyst vol.frac.	Membrane thickness	
	[mm]	[mm]	[kg/m^3]	[–]	[μm]	
Initial	7.0	10.0	3600	0.64	50	
Final	6.0	7.8	3700	0.70	65	

In this final optimization step, the stand-alone operation of the CPBMR shows a yield of 46.9%, a selectivity of 63.3%, and a methane conversion of 74.0%.The reactor's tube-side shows an almost isothermal performance. Apart from the cooling and the modified inlet temperatures, this is made possible by the slightly higher dilution with nitrogen in the packed-bed and the thicker membrane, which reduces the amount of oxygen passing to the tube-side. Sensitivity analyses show that influences of catalyst density and volume fraction are negligibly small. Further relaxation of decision variable bounds could yield even better performance, but the process becomes too time-consuming.

4. Simulation of the Membrane Reactor Network

Despite the surprisingly good performance of the CPBMR, the reactor is integrated into the entire network.

4.1. Implementation of FBR and PPBMR Models and Network Integration

One-dimensional models are used for both FBR and PPBMR. As the CPBMR examination showed that the 1D model overestimates Knudsen flux through the membrane, the flux is reduced by a fixed factor of 0.30 for the PPBMR. As methane and oxygen are co-fed to the catalytic bed of both reactors, hot-spot formation becomes a problem. Hence, a denser collocation is required: 25 finite elements prove to be sufficient for the PPBMR (0.5cm long) and 100 for the FBR (1cm long). On top of that, both reactors require a dilution with nitrogen greater than 85% and a reduction of the catalyst density to 900kg/m^3, which is achieved by more inert packing so as to avoid unsustainable temperature levels or hot-spots, which cause the entire amount of oxygen to react. For the integration into the network, a methane-to-oxygen ratio for the FBR inlet of 1:1 is chosen and the superficial velocity is reduced to 0.4m/s such that the entire stream no.7 (Fig. 1) can be fed to the tube-side of the CPBMR. Only 5% of stream no.12 is initially injected into the PPBMR's tube-side.

4.2. Simulation of the Membrane Reactor Network

Given the size of the NLP describing the MRN, a sequential approach is developed for the simulation of the network. All three reactors are calculated step by step starting with each first axial finite element while all other equality constraints are dropped and variables are fixed to their previous values. Afterwards, the network part, meaning all outlets and streams are calculated providing new inlets for the reactors, which then have to be recalculated. This is done until all sub-problems converge in the 0th iteration step.

Lastly, the entire system is handed over to IPOPT, which should converge to the optimal solution instantly. Table 2 contains the performance of the MRN and individual reactors in that set-up.

Table 2. Performance of reactors and network in initial simulation

Component	Yield in C2 hydrocarbons	Selectivity in C2 hydrocarbons	Methane conversion
FBR	4.77%	19.47%	24.48%
PPBMR	0.86%	14.22%	6.02%
CPBMR	41.83%	60.39%	69.27%
MRN	29.39%	43.05%	68.26%

5. Conclusions and Outlook

Several conclusions can be drawn from this work: First of all, a two-dimensional, non-isothermal model for the CPBMR is required and shows a considerably different behavior compared to previous studies. Secondly, the stand-alone operation of the CPBMR can be improved by further increasing the dilution of the catalytic bed with nitrogen, increasing the cooling, and reducing the oxygen flux through the membrane. Thirdly, yield and selectivity found for the CPBMR are higher than expected and make it debatable whether there is actually any point in considering a further network integration. However, there is one issue, which certainly has to be discussed in future work, and that is the accuracy of the kinetic system at low oxygen levels. Most kinetics are derived from experiments in micro-catalytic packed-beds and it has to be examined in what way the low oxygen influx, meaning permanently low oxygen concentrations along the reactor, might cause a different outcome.

Acknowledgements

This work is part of the Cluster of Excellence “Unifying Concepts in Catalysis” coordinated by the Technische Universität Berlin. Financial support by the Deutsche Forschungsgemeinschaft (DFG) within the framework of the German Initiative for Excellence is gratefully acknowledged. E. E. would like to thank the Ernest-Solvay-Stiftung for their financial support for a research stay at Carnegie Mellon University.

References

H. Godini, 2010, Model-based analysis of reactor feding policies for methane oxidative coupling. Ind. Eng. Chem. Res., 49:3544 – 3552

S. Jašo, 2010, Analysis of attainable reactor performance for the oxidative methane coupling process, Chem. Eng. Sci., 65, 6341 – 6342

D. Lafarga, 1994, Methane oxidative coupling using porous ceramic membrane reactors – I. reactor development, Chem. Eng. Sci., 49, 12, 2005 – 2013

V. Specchia, 1980, Heat transfer in packed bed reactors with one phase flow, Chem. Eng. Commun., 4, 361 – 380

R.J. Kee, 2003, Chemically Reacting Flow, Wiley-Interscience

E. Tsotsas, 1988, On axial dispersion in packed beds with fluid flow, Chem. Eng. and. Proc., 24, 1, 15 – 31

B.E. Poling, 2001, The Properties of Gases and Liquids, McGraw-Hill

R. Bauer, 1978, Effective radial thermal conductivity of packing in gas flow – Part I and II , Int. Chem. Eng., 18, 2, 181 – 204

I.A. Karimi and Rajagopalan Srinivasan (Editors), Proceedings of the 11th International Symposium on Process Systems Engineering, 15-19 July 2012, Singapore.

Dynamic Optimization of Solution Polymerization Process of Methyl Methacrylate in Batch Reactors

Wan Hanisah B.Wan Ibrahim[b], Iqbal M. Mujtaba[a*]

[a]*School of Engineering, Design & Technology, University of Bradford, Bradford BD7 1DP, UK. Email: I.M.Mujtaba@Bradford.ac.uk*
[b]*Faculty of Chemical Engineering and Natural Resources,Universiti Malaysia Pahang, Lebuhraya Tun Razak, 26300 Kuantan, Pahang, Malaysia.*

Abstract

In this paper, *maximum conversion (Xn)* dynamic optimization problem is formulated and solved for solution polymerization of Methyl Methacrylate (MMA) in batch reactors. Control Vector Parameterization (CVP) technique is used to pose the dynamic optimization problem as nonlinear programming problem and to find the optimal temperature profile that will maximize the monomer conversion (*Xn*) for a given number average molecular weight (*Mn*) at fixed batch time within gPROMS (general Process Modelling System) software. Note, the decomposition of initiator molecules at the beginning of the process (to form very active primary radicals) depends on the initiator efficiency, *f*. The effect of constant and time-varying *f* on the performance of the batch reactors is also evaluated.

Keywords: initiator efficiency, batch reactors, Methyl Methacrylate

1. Introduction

Solution polymerization uses solvent in the reactor to enhance heat transfer (Odian, 2004). At the beginning of the process, the initiator and the solvent are added into the reactor. Initiator will initiate the polymerization process by decomposition to form primary free radicals. These free radicals will then react with the monomer added in the reactor in homogeneous solution until the end of the process. The decomposition of the initiator molecules depends on the initiator efficiency, *f*. Not all the initiator molecules decompose to form primary radicals since some of them might either have self-terminate or react with other reactants in the system which make the initiator efficiency less than 100%. In the past some used a constant value for *f* in their studies (Achilias and Kiparissides, 1992) while others used variable *f* (Xia and Matyjaszewski, 1997; Achilias, 2007). In this work, the process model from the work of Ekpo and Mujtaba (2008) is improved for the solution polymerization of MMA by using the free volume theory to calculate the initiator efficiency based on Fan et al. (2003).
The optimal temperature profiles that will maximize the monomer conversion (X_n) for a given number average molecular weight (M_n) and fixed batch time are determined for both constant and time varying value of *f*. The batch time is divided into a finite number of intervals, and a piecewise constant temperature is used in each interval. In each interval, the temperature and length of the interval are optimized.

2. Reaction Kinetics and Dynamic Model

The process model used for the solution polymerization of MMA in batch reactors, using 2,2 azobisisobutyronitrile catalyst (AIBN) as the initiator and Toluene as the

solvent by Ekpo and Mujtaba (2008) is presented in Figure 1 in compact form. Further details can be found in Fan et al. (2003) and Ekpo and Mujtaba (2008).

$$k_d = 1.58\ x\ 10^{15} exp\left(-1.2874\ x\ 10^5/R_gT\right) \qquad \frac{dC_i}{dt} = -k_dC_i$$

$$k_{p0} = 7.0\ x\ 10^6 exp\left(-2.6334\ x\ 10^4/R_gT\right) \qquad \frac{dC_m}{dt} = -\left(k_p + k_{fm}\right)C_m\xi_0$$

$$k_{t0} = 1.76\ x\ 10^9 exp\left(-1.1704\ x\ 10^4/R_gT\right) \qquad \frac{d\xi_0}{dt} = 2fk_dC_i - k_t\xi_0^2$$

$$k_{fm} = 4.661\ x\ 10^9 exp\left(-7.4479\ x\ 10^4/R_gT\right) \qquad \frac{d\xi_1}{dt} = 2fk_dC_i - k_pC_m\xi_0 + \left(k_{fm}C_m + k_{fs}C_s\right)(\xi_0 - \xi_1) - k_t\xi_0\xi_1$$

$$k_{fs} = 1.49\ x\ 10^9 exp\left(-6.6197\ x\ 10^4/R_gT\right) \qquad \frac{d\xi_2}{dt} = 2fk_dC_i - (2\xi_0 - \xi_1)k_pC_m + \left(k_{fm}C_m + k_{fs}C_s\right)(\xi_0 - \xi_1) - k_t\xi_0\xi_2$$

$$k_{\theta p} = 3.0233\ x\ 10^{13} exp\left(-1.1700\ x\ 10^5/R_gT\right) \qquad \frac{d\mu_0}{dt} = \left(k_{fm}C_m + k_{fs}C_s\right)\xi_0 + (0.5k_t)\xi_0^2$$

$$k_{\theta t} = 1.4540\ x\ 10^{20}\ C_{i0}\ exp\left(-1.4584\ x\ 10^5/R_gT\right) \qquad \frac{d\mu_1}{dt} = \left(k_{fm}C_m + k_{fs}C_s + k_t\xi_0\right)\xi_1$$

$$k_p = k_{p0}/\left(1 + k_{p0}/Dk_{\theta p}\right) \qquad \frac{d\mu_2}{dt} = \left(k_{fm}C_m + k_{fs}C_s\right)\xi_2 + k_t\xi_0\xi_2 + k_t\xi_1^2$$

$$k_t = k_{t0}/(1 + k_{t0}/Dk_{\theta t}) \qquad PD = \frac{M_w}{M_n}$$

$$\frac{dT}{dt} = \frac{(-\Delta H_r)R_p}{C_p\rho_{mix}} - \frac{UA\left(T - T_J\right)}{C_pV\rho_{mix}} \qquad \frac{dT_J}{dt} = \frac{\left(T_{Jsp} - T_J\right)}{\tau_J} - \frac{UA\left(T - T_J\right)}{C_{pJ}V_J\rho_J}$$

$$D = exp\left[\frac{2.303\left(1 - \emptyset_p\right)}{0.168 - 8.21\ x\ 10^{-6}(T - 387)^2 + 0.03\left(T - \emptyset_p\right)}\right]$$

Figure 1: Process model

T_{Jsp} is the jacket temperature set point and is used as the control variable in place of reaction temperature in the energy balance model (as considered by Ekpo and Mujtaba, 2008). τ_J is the jacket time constant while R_p is the rates of polymerization. Table 1 shows the constants and values used in this model.

Achilias and Kiparissides (1992) had reported that there are quite a lot of published paper has treated the initiator efficiency, f as a constant value. However, it may decrease significantly with the high viscosity of reaction mixture (Russell et al., 1988). Ekpo and Mujtaba (2008) used a constant value of 0.53 for the initiator efficiency. However, it is believed that the initiator efficiency is not constant and will decrease as the viscosity inside the reactor increases (Ghosh et al., 1998). Dube et al. (1997) have used the free volume theory to model the changing of initiator efficiency as shown below:

$$f = f_0 exp\left(-C_f\left(\frac{1}{V_F} - \frac{1}{V_{F,crit}}\right)\right) \tag{1}$$

Where f_0 is the initial initiator efficiency, C_f is a parameter which modifies the rate of change of the efficiency, V_F is free volume and $V_{F,crit}$ is critical free volume. The value of C_f and f_0 are 0.006 and 0.53 respectively (Fan et al., 2003). The free volume (V_F) and critical free volume ($V_{F,crit}$) equations were given by Fan et al. (2003) as below:

$$V_F = 0.025 + 0.001(T - 167)\emptyset_m + 0.00048(T - 387)\emptyset_p + 0.00048(T - 249)\emptyset_s \tag{2}$$

$$V_{Fcrit} = 0.1856 - 2.965x10^{-4}(T - 273) \quad (3)$$

where $\boldsymbol{\emptyset_m}, \boldsymbol{\emptyset_p}$ and $\boldsymbol{\emptyset_s}$ are the volume fraction of monomer, polymer and solvent which can be obtained by the equations below:

$$\emptyset_s = C_m MW_m/\rho_m \quad (4)$$
$$\emptyset_p = \mu_1 MW_m/\rho_p \quad (5)$$
$$\emptyset_s = 1 - \emptyset_m - \emptyset_p \quad (6)$$

Table 1: Constants and values from the detail model of MMA polymerization

A = 0.0774 m2	*ρm = 915.1 kg/m3*	*VJ = 1.5 L*
CP,J = 4.184 kJ/kg.K	*ρp = 1200 kg/m3*	*-ΔHr = 5.78 x 104*
CP,m = 1.648 kJ/kg.K	*MWs = 106.17 kg/kmol*	*kJ/kmol*
CP,P = 1.47 kJ/kg.K	*MWm = 100.12 kg/kmol*	*ρJ = 997 kg/m3*
CP,S = 1.70 kJ/kg.K	*V = 2 L*	*U = 2.55 kJ/s.m2.K*
MWi = 164.21 kg/kmol	*τJ = 50s*	

3. Dynamic Optimization Problem Formulation

Mathematically the optimization problem for *maximum conversion* problem can be represented as:

$$\begin{aligned} &\textit{Max} && \textit{Xn} \\ &\textit{Tjsp(t), Ci0} && \\ &\textit{s.t.} && f(t, x'(t), x(t), u(t), v) = 0, \quad [t_0, t_f] \quad \textit{model equations} \\ & && \textit{Mn} = \textit{Mn}^* \\ & && t_f = t_f^* \\ & && 0.0001 < \textit{Ci0} < 0.150 \\ & && 1.5 < \textit{PD} < 1.8 \\ & && 320\ \textit{K} < \textit{Tjsp} < 373\ \textit{K} \\ & && 320\ \textit{K} < \textit{T} < 398\ \textit{K} \end{aligned}$$

The total batch time is discretized into 3 control intervals within which *Ci0* (initial initiator concentration) and *Tjsp* are assumed to be piecewise constant and are optimized for maximum conversion problem for fixed (denoted by *) number average molecular weight (M_n^*) at fixed batch time (3000s, 5000s and 10000s). PD denotes polydispersity. Note, more than 3 control intervals can also be chosen.

4. Results and Discussions

Results are presented in Table 2 and Figure 2. As expected, monomer conversion increased with increased final batch time since more time is available for the monomer to react inside the reactor. Initial initiator concentration also increased with increased final batch time to ensure that there are more initiators to initiate the polymer process and for the propagation process to happen at longer batch time.

Figure 2 show the optimum reactor temperature set point (*Tjsp*) profile and the monomer conversion (*Xn*) profile of run 7, 8 and 9 (batch time 10000s). The optimum *Tjsp* profiles (Figure 2a) show that the temperature is higher for lower molecular weight. This higher temperature is required to decompose higher concentration of *Ci0*.

Monomer conversion decreased with increased molecular weight (Figure 2b), because to achieve higher molecular weight, low initial initiator are needed at the beginning of the process so the monomer will continue the propagation process rather than initiate a

new polymerization process with the initiator. This can be seen where initial initiator concentration (C_{i0}) decreased with increased molecular weight (Table 2).

Table 2: Results for maximum conversion at fixed batch time, t_f*

Run	*Xn, %*	*Mn (kg/kmol)*	*Mn*(kg/kmol)*	*t_f*(s)*	*PD*	*Ci0 (x10^{-3})*
1	*76.5*	*50 000*	*50 000*	*3000*	*1.8*	*2.898*
2	*72.5*	*100 000*	*100 000*	*3000*	*1.8*	*1.729*
3	*56.1*	*150 000*	*150 000*	*3000*	*1.8*	*1.448*
4	*91.7*	*50 000*	*50 000*	*5000*	*1.8*	*3.171*
5	*81.3*	*100 000*	*100 000*	*5000*	*1.8*	*2.378*
6	*69.3*	*150 000*	*150 000*	*5000*	*1.8*	*1.907*
7	*95.5*	*50 000*	*50 000*	*10 000*	*1.8*	*4.646*
8	*91.6*	*100 000*	*100 000*	*10 000*	*1.8*	*3.378*
9	*81.8*	*150 000*	*150 000*	*10 000*	*1.8*	*2.859*

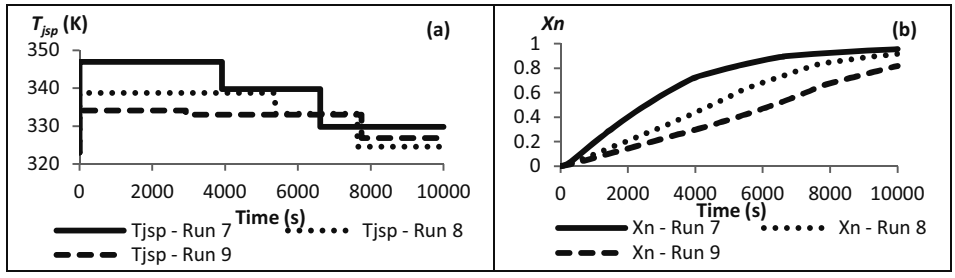

Figure 2: Optimum reactor temperature set point profiles (T_{jsp}) and monomer conversion (X_n) profiles for Run 7, 8 and 9.

The same optimization problem is solved to achieve number average molecular weight (M_n) 150000 kg/kmol in fixed batch time of 5000s using constant value of f (0.53) (F1) and time varying f (F2). The original process model of Ekpo and Mujtba (2008) and the revised model are used for this purpose. This case is same as that in Run 6 of Table 2 but with wider polydispersity. The results are shown in Table 3 and Figure 3.

Table 3: Results for different initiator efficiency, f

Run	*f*	*X_n*	*M_n*	*M_n**	*t_f(s)*	*PD*	*C_{i0} (x10^{-3})*
1	*F1*	*96.64*	*149901.5*	*150000*	*5000*	*2.249012*	*1.00*
2	*F2*	*90.18*	*149989.8*	*150000*	*5000*	*2.048531*	*1.00*

The results, clearly shows the effect of constant and variable f on X_n and PD even though C_{i0} was same. The use of constant f in the model will mislead the expected results as it does not represent the real phenomenon in the process.
The optimum profile for jacket temperature set point (T_{jsp}) for three control intervals is shown in Figure 3a. The figure clearly shows that T_{jsp} for time varying f (F2) is higher than that for constant f (F1) for each interval. Figure 3b shows that f (F2) decreases as the monomer conversion increases. Figure 3c and 3d provide corresponding reactor and jacket temperatures.

5. Conclusions

Dynamic optimization of solution polymerization process of methyl methacrylate in batch reactors is considered here. Conversion is maximized for different batch times by

controlling reactor temperature. Monomer conversion (X_n) is found to increase with the increasing batch time as expected. The results show that initiator efficiency, f is not constant but decrease with the increase of monomer conversion along the process in the solution polymerization of MMA when the free volume theory was applied. The effects of different initiator efficiency, f was also examined. The results were compared between two approaches which confirm that T_{jsp} for time varying f (F2) is higher than that for constant f (F1) for each time interval.

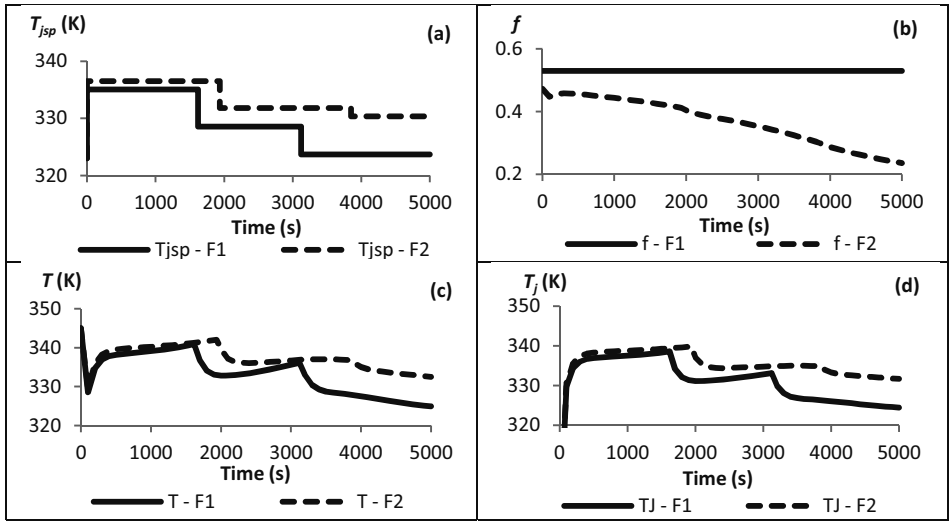

Figure 3: Results for case study 4 (Run 1 and Run 2): (a) Optimal profile of jacket temperature set point (T_{jsp}); (b) initiator efficiency (f); (c) reactor temperature T; (d) jacket temperature (T_j)

References

D. S. Achilias, (2007) A review of modeling of diffusion controlled polymerization reactions. *Macromolecular Theory and Simulations,* 16, 319-347.

D. S. Achilias and C. Kiparissides, (1992) Development of a general mathematical framework for modelling diffusion-controlled free-radical polymerization reactions. *Macromolecules,* 25, 3739-3750.

M. A. Dube, J. B. P. Soares, A. Penlidis and A. E. Hamielec, (1997) Mathematical Modeling of Multicomponent Chain-Growth Polymerizations in Batch, Semibatch, and Continuous Reactors: A Review. Industrial & Engineering Chemistry Research, 36, 966-1015.

E. E. Ekpo, and I. M. Mujtaba, (2008) Evaluation of neural networks-based controllers in batch polymerisation of methyl methacrylate. *Neurocomputing,* 71, 1401-1412.

S. Fan, S. P. Gretton-Watson, J. H. G. Steinke and E. Alpay, (2003) Polymerisation of methyl methacrylate in a pilot-scale tubular reactor: modelling and experimental studies. *Chemical Engineering Science,* 58, 2479-2490.

P. Ghosh, S. K. Gupta and D. N. Saraf, (1998) An experimental study on bulk and solution polymerization of methyl methacrylate with responses to step changes in temperature. *Chemical Engineering Journal,* 70, 25-35.

G. G. Odian, (2004) *Principles of polymerization,* New Jersey, Wiley-Interscience.

G. T. Russell, D. H. Napper and R. G. Gilbert (1988) Initiator efficiencies in high-conversion bulk polymerizations. *Macromolecules,* 21, 2141-2148.

J. Xia and K. Matyjaszewski, (1997) Controlled/"living" radical polymerization. Homogeneous reverse atom transfer radical polymerization using AIBN as the initiator. *Macromolecules,* 30, 7692-7696.

I.A. Karimi and Rajagopalan Srinivasan (Editors), Proceedings of the 11th International Symposium on Process Systems Engineering, 15-19 July 2012, Singapore.

Optimization of multi-refinery hydrogen networks

Anoop Jagannath[a], Ali Elkamel[b] and I.A.Karimi[a]

[a]*Department of Chemical and Biomolecular Engineering, National University of Singapore, Singapore 117576, Singapore*
[b]*Chemical Engineering Department, University of Waterloo, Waterloo, Ontario N2L 3G1, Canada*

Abstract

Hydrogen is an important feedstock and fuel in the refining and petrochemical industries. In this paper, we address the optimal synthesis of inter-plant hydrogen networks by modifying the superstructure-based one-plant model of Elkamel et al. (2011). The bilinear terms involved in the component balance equations of this model give rise to a nonconvex mixed integer nonlinear program (MINLP). A specialized outer-approximation algorithm is developed for solving this optimal synthesis problem to global optimality, where the lower bound on the global optimum is obtained by means of piecewise under-and-over estimators for the bilinear terms. We propose and compare several integration schemes to demonstrate significant cost savings.

Keywords: Hydrogen networks, global optimization, superstructure

1. Introduction

The escalating prices of crude oil and petroleum products have forced the refiners and petrochemical producers to operate under tight margins. In a bid to reduce costs, these industries continually seek innovative methods to conserve and manage their resources. Hydrogen is an important utility that is acquiring significant importance due to its cost and stringent environmental regulations. In a refinery, it is critical to design and operate the individual hydrocracker and hydrotreater units so as to minimize waste. However, it is equally or even more critical to optimize the usage of hydrogen throughout the whole refinery network. One common technique for optimal hydrogen management in a refinery is to perform a hydrogen pinch analysis to set targets for minimum hydrogen need. Recently, mathematical superstructure-based optimization methods have also been applied for optimizing the hydrogen consumption within a refinery. Most work so far has addressed hydrogen management within a single refinery. In refining / petrochemical complexes such as Jubail, Jurong Island, Houston, and Rotterdam, where multiple refineries and petrochemical plants exist in close proximity, it is better to expand the scope of integration and coordination from intra-plant to inter-plant. This may allow one to exploit inter-plant synergies and reduce costs.

Resource/utility conservation and process integration have attracted much interest in the process industries to improve process sustainability. A properly designed inter-plant hydrogen network could play a significant role in reducing costs (economics), minimizing energy consumption (energy), and also conserving the environment by reducing the CO_2 emissions associated with hydrogen production. Such integration efforts are in line with the flurry of research activities involving the integration of various utilities in a refinery such as fuel gas (Hasan et al., 2011) and water (Chew et al.

(2008), Chen et al. (2010)). Chew et al. (2010a, 2010b) have also considered inter-plant resource conservation. The benefits of integration in refinery planning (Al-Qahtani and Elkamel 2008, 2009) has also prompted many researchers to work in the area of resource conservation owing to its potential benefits.
In this work, we address retrofit-design and operation of optimal inter-refinery or multi-plant hydrogen networks. However, the approach is also extendable to grass-root design as well. The objective is to minimize the total annualized cost of the entire system with the help of a mathematical superstructure-based optimization. We also propose and evaluate several schemes of this integration using a realistic case study.

2. Problem statement

A petrochemical complex has several plants with processing units that produce, consume, or purify hydrogen. Let *i* denote a source that produces hydrogen, *j* denote a sink that uses hydrogen gas as fuel, *u* denote a hydroprocessing unit that needs hydrogen as feed, and *k* denote an existing compressor that can pressurize a hydrogen stream to supply to various consumers. The plants may also have some PSA (Pressure Swing Adsorption) units that can separate relatively pure hydrogen from a hydrogen-containing feed. Let *m* denote a PSA unit that could be installed in these plants. The goal is to determine (1) the PSA units to install and their sizes, (2) interconnections among various sources, sinks, and units, and (3) distribution of hydrogen flows among various units, so as to meet the hydrogen demands of all plants at minimal total annualized cost. The superstructure for this hydrogen network study can be obtained from Elkamel et al. (2011)

3. Model Formulation

Let F_{ij}, F_{ik}, F_{iu} and F_{im} represent the gas flows (MMscfd) from source *i* to sink *j*, compressor *k*, hydroprocessing unit *u*, and PSA unit *m* respectively. Similarly, let F_{kj}, F_{ku} and F_{km} denote the gas flows from compressor *k* to fuel gas sink *j*, hydroprocessing unit *u*, and purification unit *m* respectively. If $Fout_i$ is the total gas flow from source *i*, then the mass balance around source *i* gives us,

$$Fout_i = \sum_j F_{ij} + \sum_k F_{ik} + \sum_u F_{iu} + \sum_m F_{im} \tag{1}$$

Similarly, the mass and component balance around compressor *k* whose capacity FC_k is given by Eq. (2)-(5).

$$\sum_i F_{ik} + \sum_u F_{uk} + \sum_m F_{mk} = \sum_j F_{kj} + \sum_u F_{ku} + \sum_m F_{km} \tag{2}$$

$$\sum_i F_{ik}\, yout_i + \sum_u F_{uk}\, youtu_u + \sum_m F_{mk}\, yPPSA_m = (\sum_j F_{kj} + \sum_u F_{ku} + \sum_m F_{km})\, ycomp_k \tag{3}$$

$$Pwr_k = {CpT}/{\eta}\left(\left(\frac{P_o}{P_i}\right)^{\frac{\gamma-1}{\gamma}} - 1\right)(\sum_i F_{ik} + \sum_u F_{uk} + \sum_m F_{mk}) \tag{4}$$

$$\sum_i F_{ik} + \sum_u F_{uk} + \sum_m F_{mk} \le FC_k \tag{5}$$

Pwr_k is the power of the compressor which is directly related to the flow and the parameters namely inlet P_i and outlet pressures P_o, heat capacity Cp ,temperature T and

efficiency η and γ be the adiabatic index. F_{kj}, F_{ku}, F_{km} be the flow out from the compressor to fuel gas sink *j*, hydroprocessing unit *u*, and purification unit *m* respectively. F_{uk}, F_{mk} are the flows from the hydroprocessing unit *u* and purification unit *m* to the compressor *k*. The purity of hydrogen out from compressor, source and process unit are $ycomp_k$, $yout_i$, $youtu_u$ respectively. The hydroprocessing unit modeling equations is given in Eq. (6)-(8) where F_{uj} and F_{um} the flow from unit *u* to fuel gas sink *j*, and purification unit *m*. $F_{uu'}$ is the corresponding recycle stream to the processing unit. The flow and purity demand into the hydroprocessing unit is given by $Finu_u$ and $yinu_u$ respectively and flow out is denoted by $Foutu_u$. The equations for the purification unit are in Eq (9)-(12). F_{mk} and F_{mu} are the streams from the purification unit, whose recovery is $Rcvr$ and purity is $yPPSA_m$, going to existing compressor and hydroprocessing unit. F_{mj} is the residue stream from the purification unit whose purity is $yRPSA_m$. Eq.(13) and (14) is for fuel gas system.

$$Finu_u = \sum_i F_{iu} + \sum_k F_{ku} + \sum_m F_{mu} + \sum_{u'} F_{uu'} \tag{6}$$

$$Finu_u yinu_u = \sum_i F_{iu} yout_i + \sum_k F_{ku} ycomp_k + \sum_m F_{mu} yPPSA_m + \sum_{u'} F_{uu'} youtu_u \tag{7}$$

$$Foutu_u = \sum_j F_{uj} + \sum_k F_{uk} + \sum_m F_{um} + \sum_{u'} F_{uu'} \tag{8}$$

$$\sum_i F_{im} + \sum_u F_{um} + \sum_k F_{km} = \sum_j F_{mj} + \sum_k F_{mk} + \sum_u F_{mu} \tag{9}$$

$$\sum_i F_{im} yout_i + \sum_u F_{um} youtu_u + \sum_k F_{km} ycomp_k = \sum_j F_{mj} yRPSA_m + yPPSA_m (\sum_k F_{mk} + \sum_u F_{mu}) \tag{10}$$

$$Rcvr(\sum_i F_{im} yout_i + \sum_u F_{um} youtu_u + \sum_k F_{km} ycomp_k) = yPPSA_m (\sum_k F_{mk} + \sum_u F_{mu}) \tag{11}$$

$$(1 - Rcvr)(\sum_i F_{im} yout_i + \sum_u F_{um} youtu_u + \sum_k F_{km} ycomp_k) = \sum_j F_{mj} yRPSA_m \tag{12}$$

$$Finj_j = \sum_i F_{ij} + \sum_k F_{kj} + \sum_m F_{mj} + \sum_{u'} F_{uj} \tag{13}$$

$$Finj_j yinj_j = \sum_i F_{ij} yout_i + \sum_k F_{kj} ycomp_k + \sum_m F_{mj} yRPSA_m + \sum_{u'} F_{uj} youtu_u \tag{14}$$

Since the hydrogen network problem is a gas network, the flow from any source *p* in general to any sink *q*, is possible only when the pressure of source P_p is greater than or equal to sink pressure P_q. In case of units whose pressure is known, the flows between them are fixed to zero when the pressure of source P_p is less than pressure of sink P_q. In case of equipments which need to be retrofitted, the pressure is unknown and hence a binary variable X_{pq} is required to model the pressure difference between them. Elkamel et al.(2011) had not considered the piping cost in their model, so used only one type of binary variable to model the flow and pressure difference between the units. In our case, the piping cost becomes significant when considering refinery network integration. Hence we will require two levels of binary variables in our model one to show the existence of pressure difference X_{pq} and other depicting the flow between them XF_{pq}. Second, since we are interested in solving the model to global optimality, we

introduce redundant cut into the model which aids to solve the model to global optimality given by Eq. (15). Moreover the constraint to depict the inter-plant/refinery connection is given by Eq. (16) where the connection between source and sink among refineries may or may not exist based on type of integration and *r* is index for refinery. By modeling the system using Eq.(1)-(14), we reduce the number of bilinear terms in comparison to the model of Elkamel et al. (2011) by $[|K|+|U|+|M|]$ where $|K|$, $|U|$ and $|M|$ are the number of compressors, hydroprocessing units and purification units respectively. Inclusion of piping cost, solving model to global optimality, introduction of redundant bound strengthening cuts, reduction in number of bilinear terms and multi-refinery network integration represent significant additions to the previous work (Elkamel et al. (2011)).

$$Fout_i yout_i + Foutu_u youtu_u = Finu_u yinu_u + Finj_j yinj_j \tag{15}$$

$$\sum_{p\in p_r}\sum_{q\in q_{r'}} XF_{pq} = 0 \quad \forall r \neq r' \tag{16}$$

$$TAC = AF\Big(\sum_m (a_{PSA}X_{PSA} + b_{PSA}(\sum_i F_{im} + \sum_u F_{um} + \sum_k F_{km})) + \sum_{pq\in O_{new}} (a_{pipe}X_{pipe} + b_{pipe}F_{pq})\Big)$$

$$OD((Fout_i OCH_i) + OCE\sum_k Pwr_k) \tag{17}$$

Eq. (17) gives the total annualized cost as objective with a_{PSA}, b_{PSA}, a_{pipe}, OCH_i and OCE as cost coefficients for PSA, pipeline, hydrogen cost and electricity cost. OD and AF are operating days in year and annualization factor respectively. Eq.(1)-(17) is globally optimized using the specialized outer approximation framework (Karuppiah et al. (2007)) where the lower bound on the global optimal is is obtained by the piecewise under-and-over estimators by the convexification of bilinear terms (Wicaksono and Karimi, 2008). A bivariate partitioning scheme is employed based on the Incremental Cost formulation for bilinear terms (Hasan and Karimi, 2009). When the gap between the lower bound and upper bound is below specific tolerance, then the algorithm is terminated.

4. Case Study

Consider three existing different hydrogen networks. In this, we seek to retrofit these three hydrogen networks with purifier units namely the pressure swing adsorption unit. The objective used in all the comparison studies is the minimal total annualized cost (TAC). For the sake of convenience the results in Table 1 shows the costs as the total cost of three networks.

Table 1. Optimization results for the case study

Cost(k$)	No Integration	Indirect Scheme 1	Indirect Scheme 2	Indirect Scheme 3	Direct Integration
H_2	106036.150	104415.185	104328.315	104269.550	104236.700
Elect	4198.960	4138.370	4124.500	4121.580	4200.780
Operational	110235.110	108553.920	108452.815	108391.130	108437.120
Piping	861.508	4190.125	4390.770	4686.059	3418.491
PSA	23512.636	20457.954	20315.696	20046.700	19894.848
Capital	24374.144	24648.079	24706.465	24732.759	23313.339
TAC	112672.261	111018.670	110923.608	110864.576	110768.534
H_2(MMscfd)	53018.075	52207.775	52164.340	52134.775	52118.350
Gas to fuel gas(MMscfd)	6286.595	6016.295	5972.860	5943.295	5926.870

In case of direct integration, the entire combined network is solved in which all possible interconnections exist among all the refineries. The decrease in the requirement of hydrogen in all the integration schemes shows a significant step towards the conservation of environment and energy. Secondly, there is also an effective usage of the hydrogen gas in the combined integrated network. Hence, an advantage could be seen in the operational cost and also in the hydrogen consumption when the refinery hydrogen networks are integrated. In the indirect integration scheme, there exists a centralized purification unit (pressure swing adsorption) through which the refinery interactions take place. In the first case of indirect integration (scheme 1), all the refineries are connected to only the centralized pressure swing adsorption unit and no connections exist among the refineries. In the indirect integration scheme (scheme 2), the hydrogen producers namely the hydrogen plant is allowed to connect with the other units of other refineries. In the final case of indirect integration (scheme 3), all the sources are allowed to connect with the sinks. From the different patterns of the integration, we observe that the both direct and integration offers better cost savings when compared to the case of no integration.

5. Conclusion

A superstructure based mathematical optimization approach is developed for inter-plant/refinery hydrogen networks. Different integration schemes were studied and the results were analyzed. All the problems were solved to global optimality with specific tolerance. The results showed that significant savings could be achieved in case of integrated network in comparison to individual networks optimized separately.

References

Al-Qahtani, K.; Elkamel,A., 2008**,** Multisite facility network integration design and coordination:An application to the refining industry, *Computers and Chemical Engineering***,** *32* (10), 2189-2202.

Al-Qahtani, K.; Elkamel,A., 2009**,** Multisite refinery and petrochemical network design :Optimal integration and coordination:An application to the refining industry, *Industrial and Engineering Chemistry Research***,** *48* (2), 814-826.

Chen, C. L.; Hung, S. W.; Lee, J. Y., 2010,Design of inter-plant water network with central and decentralized water mains, *Computers and Chemical Engineering***,** *34* (9), 1522-1531.

Chew, I. M. L.; Tan, R.; Ng, D. K. S.; Foo, D. C. Y.; Majozi, T.; Gouws, J.,2008, Synthesis of direct and indirect interplant water network, *Industrial and Engineering Chemistry Research***,** *47* (23), 9485-9496.

Chew, I. M. L.; Foo, D. C. Y.; Ng, D. K. S.; Tan, R. R., 2011**,** Flowrate targeting algorithm for interplant resource conservation network. Part 1: Unassisted integration scheme, *Industrial and Engineering Chemistry Research***,** *49* (14), 6439-6455.

Chew, I. M. L.; Foo, D. C. Y.; Tan, R. R., 2011**,** Flowrate targeting algorithm for interplant resource conservation network. Part 2: Assisted integration scheme,*Industrial and Engineering Chemistry Research***,** *49* (14), 6456-6468.

Elkamel, A.; Alhajri, I.; Almansoori, A.; Saif, Y., 2011**,** Integration of hydrogen management in refinery planning with rigorous process models and product quality specifications, *International Journal of Process Systems Engineering***,** *1* (3/4), 302-330.

Hasan, M.M.F.; Karimi, I.A.; Avison, C.M., 2011**,** Preliminary Synthesis of Fuel Gas Networks to Conserve Energy and Preserve the Environment,*Industrial and Engineering Chemistry Research***,** *50* (12), 7417-7427.

Hasan, M.M.F.; Karimi, I.A.,2009**,** Piecewise linear relaxation of bilinear programs using bivariate partitioning**,** *American Institute of Chemical Engineering Journal***,** *56* (7), 1800-1893.

Karuppiah, R.; Furman, K. C.; Grossmann, I. E., 2008**,** Global optimization for scheduling refinery crude oil operations, *Computers and Chemical Engineering***,** *32* (11), 2745-2766.

I.A. Karimi and Rajagopalan Srinivasan (Editors), Proceedings of the 11th International Symposium on Process Systems Engineering, 15-19 July 2012, Singapore.

Optimizing the PSA process of propylene/propane using Neuro-Fuzzy modeling

Mona Khalighi, S. Farooq, I.A. Karimi

Department of Chemical and Biomulecular Engineering, National University of Singapore, 4 Engineering Drive 4, Singapore 117576

Abstract

Cryogenic distillation is the common method for separating propylene/propane mixtures, but this is highly energy intensive. Some 8-ring silica zeolites, especially pure silica chabazite (SiCHA), are known to show high diffusivity ratio for propylene over propane. In this work, we study the separation of propylene/propane using pure silica chabazite (SiCHA) in a simple 4-step pressure swing adsorption process. An isothermal isobaric micropore diffusion model with concentration-dependent diffusivity has been developed to simulate this kinetically controlled separation. It is first developed and implemented in the multi-physics software COMSOL to simulate different modes of PSA process. In this study, we present a sequential optimization strategy based on neuro-fuzzy model and genetic algorithm (GA) with synergistic combination of COMSOL simulation model to maximize the purity of propylene and propane productions.

Keywords: propylene/propane separation, PSA, neuro-fuzzy model, optimization

1. Introduction

The recovery of light olefins from the off-gas of catalytic crackers is an important process in the petrochemical industry. This includes the separation of propane/propylene mixtures. In most applications, it is desirable to obtain propylene and propane with high purities. For instance, 99% propylene is the raw material for polypropylene production, a polymer of extensive applications. Propane can be either recycled to the cracking step or used separately for various purposes such as fuel for engines, oxy-gas torches, barbecues, etc.

Recently, Grande et al. (2010) proposed a new strategy to separate propane and propylene stream by VPSA technology producing polymer-grade propylene (PGP) at high recovery. In this separation process, they used dual-VPSA units operating in series using 4A zeolite. The first VPSA unit (front unit) was designed to achieve PGP. The 3-column front VPSA unit consisted of feed, depressurization, and rinse with purified propylene, second depressurization, evacuation, pressure equalization, and pressurization with feed. The simulation of the front unit predicted 99.6% purity and 67% recovery for propylene. In order to improve propylene recovery, they utilized an additional VPSA tail unit. The second VPSA unit had two columns operated on a modified Skarstrom cycle (feed, depressurization, evacuation, purge, pressure equalization, and pressurization). This unit produced purified propane and recycled the recovered propylene as feed to the front unit. The set-up with the two VPSA units in series produced PGP with recovery of 95.9% propylene. Moreover, the size of the separation unit could be reduced with this new strategy compared to the traditional

distillation process. However, the power consumption of this process was higher (~20% more) than the distillation process indicating the need for further research.

Most studies on propylene/propane separation have not been able to produce high purity propylene and propane simultaneously with low energy consumption. In other words, significant room exists for improving and optimizing adsorption-based processes for this separation. This work represents the first attempt, to our knowledge, to study the feasibility of separating propylene/propane mixture by SiCHA to obtain high purity products. We propose a 4-step PSA process with the following steps: pressurization, high-pressure adsorption, rinse with propylene rich product and counter-current evacuation. Since the pore size of SiCHA is small, we expect micropores to control the diffusion process. Thus, we develop and implement a micropore diffusion model with concentration-dependent diffusivity (Farooq and Ruthven, 1991) to simulate our proposed process.

To realize the full potential of a PSA process using SiCHA as the adsorbent to separate propylene/propane mixture, it is imperative to optimize its performance. However, this optimization poses many challenges due to the highly nonlinear algebraic and partial differential equations. This rigor along with the computational time required for the PSA process to reach the cyclic steady state make rigorous optimization difficult. Agarwal et al. (2010) presented a novel PSA superstructure to design optimal PSA cycle configurations and evaluate CO_2 capture strategy. They used a complete discretization methodology to convert partial differential equations (PDEs) to nonlinear algebraic equations for post-combustion CO_2 capture. Their proposed model is very complicated and they just consider LDF model to simulate the PSA process. Faruque Hasan et al. (2011) used sequential optimization strategy based on response surface models with design and analysis of computer experiments (DACE). They minimized the total cost of CO_2 capture in a VSA-based CO_2 capture and sequestration chain. Their method is time consuming and it has less accuracy with higher number of input parameters. Lewandowski et al. (1998) used artificial neural network (ANN) model to simulate the nitrogen unit and they minimized the nitrogen production cost using nonlinear optimization. ANN method needs more number of samples to be well trained and its accuracy depends on the number of input variables.

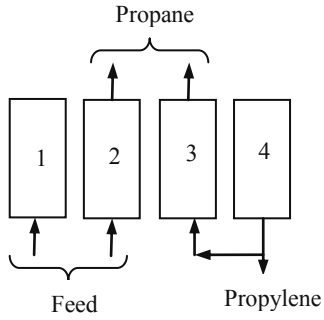

Optimum process parameters:

$p_H = 1.0$ atm	$t_{re} = 377$ s
$p_L = 0.06$ atm	$t_{bd} = 259$ s
$t_{pr} = 442$ s	$v_0 = 1.89$ cm/s
$t_{ad} = 778$ s	

Figure 1. Schematic diagram of the PSA cycle: 1) Pressurization 2) high pressure adsorption 3) rinse 4) countercurrent evacuation. Column length = 90 cm, ID = 2.1 cm.

Since optimization using the full-fledged simulation model is not feasible, we replace the simulation model by an approximate neuro-fuzzy model. The operating parameters such as step durations, operating pressures, and feed velocity are changed in this black box model to reach the optimum process using GA. The objective is to maximize the

propylene productivity of the process subject to the purity requirements of 99 mol% propylene and 90 mol% propane.

2. PSA Modeling and Simulation

We propose a 4-step PSA process (Figure 1) involving (1) pressurization, (2) high-pressure adsorption, (3) rinse with recycle product from step 4, and (4) countercurrent evacuation. Since micropore diffusion is expected to control the adsorption process, we implemented the pore diffusion model of Farooq and Ruthven (1991) with concentration-dependent diffusivity in COMSOL to simulate this process (Table 1).

Table 1. A comprehensive micropore diffusion model using Langmuir isotherm.

Model equations:	Boundary conditions:
Fluid phase mass balance: $-D_l\frac{\partial^2 c_i}{\partial Z^2}\pm v\frac{\partial c_i}{\partial Z}\pm c_i\frac{\partial v}{\partial Z}+\frac{\partial c_i}{\partial t}+\frac{1-\varepsilon}{\varepsilon}(\frac{\partial \overline{q}_{pi}}{\partial t})=0$ Mass balance inside the macropore: $\frac{\partial \overline{q}_{pi}}{\partial t}=\varepsilon_p\frac{\partial c_i}{\partial t}+(1-\varepsilon_p)\frac{\partial \overline{q}_{ci}}{\partial t}$ Mass transfer rate in micropore: $\frac{\partial \overline{q}_{ci}}{\partial t}=\frac{3}{r_c}D_i\left.\frac{\partial q_{ci}}{\partial r}\right\|_{r=r_c}$ Overall mass balance: $\pm C\frac{\partial v}{\partial Z}+\frac{1-\varepsilon}{\varepsilon}\sum_i\frac{\partial \overline{q}_{pi}}{\partial t}=0$ High pressure adsorption and rinse steps $\pm C\frac{\partial v}{\partial Z}+\frac{\partial C}{\partial t}+\frac{1-\varepsilon}{\varepsilon}\sum_i\frac{\partial \overline{q}_{pi}}{\partial t}=0$ Pressurization and evacuation steps Particle balance: $\frac{\partial q_{ci}}{\partial t}=\frac{1}{r^2}\left[\frac{\partial}{\partial r}\left(r^2D_i\frac{\partial q_{ci}}{\partial r}\right)\right]$ $D_i=\frac{D_{i0}}{1-\theta_i-\theta_j}\left[(1-\theta_j)+\theta_i\frac{\partial q_j/\partial r}{\partial q_i/\partial r}\right]$ For the variable pressure steps, we use exponential function as proposed by Farooq et al. (1993): Pressurization $P=P_H-(P_H-P_L)exp(-a_1t)$ Blowdown $P=P_L+(P_H-P_L)exp(-a_2t)$	Pressurization, feed, rinse steps: $D_l\left.\frac{\partial^2 y_i}{\partial z^2}\right\|_{z=0}=-v\|_{z=0}(y_i\|_{z=0^-}-y_i\|_{z=0})$ $\left.\frac{\partial y_i}{\partial z}\right\|_{z=L}=0$ Evacuation steps: $\left.\frac{\partial y_i}{\partial z}\right\|_{z=0}=0$ $\left.\frac{\partial y_i}{\partial z}\right\|_{z=L}=0$ Boundary conditions for velocity: $v\|_{z=L}=0$ step 1 $v\|_{z=1}=v_0$ step 2 $v\|_{z=1}=Gv_0$ step 3 $v\|_{z=L}=0$ step 4 Particle boundary conditions (Langmuir isotherm): $\left.\frac{\partial q_i}{\partial r}\right\|_{r=0}=0$ $\frac{q_i\|_{r=R_c}}{q_{is}}=\theta_i=\frac{b_ic_i\|_{r=R_c}}{1+\sum_i b_ic_i\|_{r=R_c}}$

3. PSA Optimization Using Neuro-Fuzzy

We choose the upper and lower bounds of design and operating variables such as, cycle pressures (p_H, p_L), cycle durations (t_{pr}, t_{ads}, t_{re}, t_{bd}) and feed velocity (v_0) considering the

minimum and maximum range of practical operating conditions. Then, we simulate the process in COMSOL to get cyclic steady state (CSS) and obtain purity, recovery and productivity of propylene and propane for several combinations of the variables well distributed within the chosen range. Then, we train our neuro-fuzzy model using 33 points of synthesized data. Neuro-fuzzy model is generated from a hybrid intelligent system that combines artificial neural network (ANN) and fuzzy logic using the human-inspired reasoning style of fuzzy systems (Amin et al., 2010). In this method, a layer of hidden neurons corresponds to the task of a fuzzy inference system. Jang (1993) implemented Takagi-Sugeno fuzzy rules by adaptive network-based fuzzy inference system (ANFIS). Finally, we use genetic algorithm (GA) method and our trained ANFIS structure to optimize our PSA process. The objective function that we use in this work is:

$$\max \; Productivity_{C_3H_6} - \lambda_1 \left[max(purity_{C_3H_6} - 99.0)^2 \right] - \lambda_2 \left[max(purity_{C_3H_8} - 90.0)^2 \right]$$

where productivity (mol.kg^{-1}.hr^{-1}) is amount of gas products per hour and weight of adsorbent in the PSA process, λ_1 and λ_2 are chosen as 50 and 40, respectively.

4. Optimization Results

We use ANFIS and ANN methods to model our PSA process. We check and compare the obtained results from the two models with simulation results from COMSOL. The mean square errors (MSE) of the performance of proposed PSA process for ANFIS and ANN are 2% and 10%, respectively. It seems that predictions from ANFIS are closer to COMSOL results than ANN. Therefore, we use ANFIS prediction results as the objective of our optimization. Using trained ANFIS model and GA searching method, we obtain 98.5% purity and 0.36 productivity (mol.kg^{-1}.hr^{-1}) for propylene and 90.46% purity for propane. The purity, recovery and productivity calculated by COMSOL using the optimum operating parameters for propylene are 97.6%, 92.1% and 0.31 (mol.kg^{-1}.hr^{-1}), respectively and for propane are 91.2%, 95.3% and 0.34 (mol.kg^{-1}.hr^{-1}), respectively.

In Table 2, we compare the performance of our proposed PSA process using SiCHA with the other results available in the literature for other adsorbents. We can see that our results is as good as those using 4A zeolite studied by Grande and Rodrigues (2005), where the kinetic selectivity was 811 compared to 26 in SiCHA at 353K. In 4A zeolite the propylene to propane Henry's constant and micropore diffusivity ratios are 45.3 and 321, respectively. In contract, these ratios in SiCHA are 0.36 and 5014, respectively (Grande and Rodrigues, 2005; Olson et al., 2004). Moreover, our proposed PSA process is 4-step however, Grande and Rodrigues (2005) used 5-step PSA process. Therefore, the energy consumption and cost of their process could be higher.

It may be argued that the reported literature results are not optimized and are likely to improve further. It nevertheless raises the following two important issues related to adsorbent screening for a given separation application: i) Is ideal selectivity *(= Henry's constant ratio * (diffusivity ratio)$^{0.5}$)*, calculated using uncoupled limiting equilibrium and kinetic parameters, adequate for ranking adsorbents? ii) Is it appropriate to report performance of an adsorbent without optimizing the process?

Majumdar et al. (2011) have discussed the limitation of the ideal selectivity to represent the separation factor of an adsorbent and shown that time dependent effective selectivity taking into account equilibria and diffusional interactions should be calculated for

assessing the potential of an adsorbent. We agree that the later is a better indicator than the former, but suggest that full optimization of the process is the most unambiguous way to assess an adsorbent. In this regard, our optimization approach discussed in this article provides the necessary speed and efficiency that was preventing the implementation of this route as a routine procedure.

Table 2. Purity and recovery of propylene from different adsorbents for an equimolar feed of propylene/propane.

Adsorbent	PSA process	%Purity	%Recovery
4A (Grande and Rodrigues, 2005)	5-step	99	84
SiCHA (This work)	4-step	98	92
AgNO3-SiO2 (Rege and Yang, 2002)	4-step	98	71
AlPO4-14 (Rege and Yang, 2002)	4-step	98	63
13X (F.A. Da Silva and Rodrigues 2001)	5-step	98	19

5. Conclusion

In this study, we propose the 4-step PSA process using SiCHA for propylene/propane separation. We used micropore model with concentration-dependence diffusivity to simulate the PSA process. Moreover, to realize that the proposed PSA process can produce pure propylene and propane we optimize the process using GA method. To speed up the optimization, we use ANFIS model as a black box instead of COMSOL simulation model. The objective of this optimization was to reach 99% pure propylene and 90% pure propane. This optimization could improve by minimizing the energy consumption of the PSA process in the future. Moreover, our proposed model can complement the existing and future experimental studies considerably. The resulting knowledge can then guide the design of better PSA cycles for enhancing the purity and recovery of products with lower energy consumption.

References

Agarwal, A., Biegler, L. T. and Zitney, S. E. (2010). *AIChE Journal* 56, 1813-1828.

Amin, T., Lloyd, H. C. C. and W., W. T. S. (2010). *Journal of Hydrology* 391, 248–262.

Farooq, S., Rathor, M. N. and Hidajat, K. (1993). *Chemical Engineering Science* 48, 4129-4141.

Farooq, S. and Ruthven, D. M. (1991). *Chemical Engineering Science* 46, 2213-2224.

Faruque Hasan, M. M., Karimi, I. A., Farooq, S., Rajendran, A. and Amanullah, M. (2011). *In* "Computer Aided Chemical Engineering", vol. 29, pp. 402-406. Elsevier.

Francisco A. Da Silva and Alírio E. Rodrigues. (2001). *AIChE Journal* 47, 341-357.

Grande, C. A., Poplow, F. and Rodrigues, A. E. (2010). *Separation Science and Technology* 45, 1252 - 1259.

Grande, C. A. and Rodrigues, A. E. (2005). *Industrial & Engineering Chemistry Research* 44, 8815-8829.

Jang, J.-S. R. (1993). *IEEE Transactions on Systems, Man, And Cybernetics* 23, 665-685.

Jari Lewandowski, Norberto O. Lemcoff and Seppo Palosaari. (1998). *Chemical Engineering & Technology* 21, 593-597.

Majumdar, B., Bhadra, S. J., Marathe, R. P. and Farooq, S. (2011). *Industrial & Engineering Chemistry Research* 50, 3021-3034.

Olson, D. H., Camblor, M. A., Villaescusa, L. A. and Kuehl, G. H. (2004). *Microporous and Mesoporous Materials* 67, 27-33.

Rege, S. U. and Yang, R. T. (2002). *Chemical Engineering Science* 57, 1139-1149.

I.A. Karimi and Rajagopalan Srinivasan (Editors), Proceedings of the 11th International Symposium on Process Systems Engineering, 15-19 July 2012, Singapore.

Rigorous Generation and Model-Based Selection of Future Biofuel Candidates

Manuel Hechinger, Manuel Dahmen, Juan J. Victoria Villeda, Wolfgang Marquardt

AVT – Aachener Verfahrenstechnik, Process Systems Engineering, RWTH Aachen University, 52064 Aachen, Germany

Abstract

Future liquid energy carriers should not only be synthesized sustainably from biomass, but they should also exhibit optimal properties for their application in future combustion engines. Due to the large amount of potential organic molecules, the identification of most promising fuel candidates in the entire molecular search space can only be realized by a model-supported approach. To this end, a novel fuel design framework is presented which combines a rigorous generation of molecular structures with a stepwise reduction to a set of promising candidates based on fuel-relevant properties. Predictive quantitative structure-property relations (QSPR) are employed to assess molecular structures in order to reduce necessary experiments to high potential fuel candidates. Although some of the property prediction models employed are still of limited predictive quality, the feasibility of the proposed approach is successfully shown for gasoline fuels. In particular, a significant reduction of the space of candidate fuel molecules is achieved, thus demonstrating the potential of the novel framework.

Keywords: biofuel, QSPR, property modeling, structure generation, CAMD.

1. Motivation for a model-based fuel design framework

The inevitable future depletion of fossil resources requires the premature identification of alternative value chains which are based on the renewable carbon source of biomass [1]. While often considered as a burden, this raw material shift rather represents a unique opportunity to tailor novel value chains towards pre-defined products exhibiting ideal properties with respect to their application. Identifying suitable products is thus a fundamental prerequisite for realizing optimal future value chains, and biofuels play a major role in this context. They have to replace common fossil fuels exhibiting given, but not necessarily optimal properties due to fixed crude oil composition. In contrast, the new raw material basis allows the identification of innovative, tailored biofuel structures showing superior properties with respect to both, sustainable producibility as well as clean combustion in future engines. And while these requirements ask for an integrated product and process design [2], the present contribution just focuses on product design aspects.

Obviously, the large amount of possible molecular structures renders a solely experimental search for ideal fuel compounds infeasible. This necessitates a model-supported product design approach, which could be based on one of the existing promising frameworks for chemical product design [3,4]. However, the identification of most appropriate biofuels represents a more specific product design problem which calls for a tailored framework regarding problem formulation and solution strategy. Such a frame-

work should exploit both, the well-defined atomic composition of the raw material biomass and property constraints emanating from combustion engine requirements.
The present contribution proposes a novel, fuel-specific product design framework which combines a comprehensive generation of molecular structures with critically assessed, predictive fuel property models for a stepwise reduction of the initially large molecular space towards a selection of most promising biofuel candidates. By directing experimental effort to these high-potential structures, this approach allows a targeted identification of future liquid energy carriers.

2. Fuel requirements and proposed fuel design process

The goal of a model-based fuel design is the identification of molecules with promising characteristics in all relevant aspects of a fuels' life cycle. Thus, a novel fuel should be efficiently synthesizable from biomass resources and chemically stable under ambient conditions to allow for storage and safe handling. Moreover, in order to be applicable in combustion engines, various property constraints stemming from injection, mixture formation and combustion have to be fulfilled. Focusing on these engine relevant aspects in a first step, thermophysical properties such as normal boiling point, heat of vaporization and liquid density as well as surface tension and liquid viscosity are of primary interest. Moreover the combustion kinetic characteristics like laminar burning velocity for gasoline and ignition delay time for diesel fuels have to be considered.
Model-based identification of promising fuels requires an assessment of all possible molecular structures with respect to the aforementioned properties, which results in two main questions:

1. What are all possible molecular structures and how can they be determined?
2. Which modeling approach should be used to reliably determine the fuel relevant properties of all candidates?

While the first question asks for a rigorous molecular structure generator, the second question concerns the development of predictive property models which are of reasonable accuracy over the diverse molecular range of generated structures. Since some of the fuel-relevant properties can be estimated easier from molecular structure than others, a proper cascading of "property filters" for a stepwise reduction of the initially large set of candidates becomes important. This insight leads to the staged approach illustrated in Figure 1.

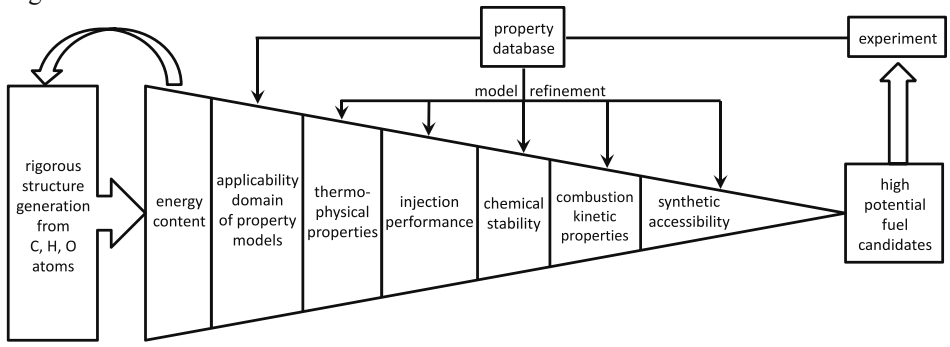

Figure 1: Workflow of model-based biofuel identification. Starting from rigorous structure generation, the molecular space is gradually decreased towards high potential fuel candidates by a combination of models and experiments.

The fuel design process starts with the rigorous generation of all possible molecular structures, where only organic molecules containing carbon (C), oxygen (O) and hydrogen (H) atoms are considered to reflect the major atomic constituents of the biomass feedstock. To this end, the software package Molgen [5] is employed, which combines valence rules with graph theory to identify all mathematically possible atomic arrangements of a given sum formula. Moreover, Molgen allows for various types of constraints on the generated structures, such as number and types of atoms and bonds.

The large number of generated fuel candidates is subsequently reduced in a stepwise fashion. In each step, a certain fuel-relevant property is predicted for all candidates first. Then, structures with a property value outside the desired range are removed from further consideration. The approach is thus similar to the one proposed by Gani et al. [3,4], who also apply property constraints to identify promising chemical compounds. However, while Gani et al. generate and assess structures based on a group contribution (GC) framework [4], the atom-based generation allows a comprehensive enumeration of all instances in the molecular space. In contrast, molecules generated from groups, i.e. molecular fragments, are constrained by the sub-graphs of each group as well as the limited number of available groups. However, the higher flexibility of an atom-based generation might lead to unrealistic structures if insufficient or inappropriate generation constraints are considered. This potential drawback is largely circumvented when only groups derived from existing molecules are employed.

This also implies that GC methods are unfavorable to assess molecules that were generated on an atomic level, as just few known groups are likely to occur in the generated molecular space. Although methods for estimating new GC parameters have been proposed [6], their general applicability is still under debate [7]. Thus, for an assessment of the molecular structures generated from atoms, quantitative structure-property relations (QSPR) [8] represent a suitable alternative as they employ molecular descriptors which can be evaluated for any molecular graph.

The cascading of the QSPR in Figure 1 is chosen such that each QSPR has the largest applicability range or confidence region possible at the respective level of structure refinement. That is, a reliable property prediction for the entire range of the very diverse molecular space of generated structures is generally not feasible, since the QSPR models are developed on the basis of available measurement data which capture only a confined molecular subspace. The resulting neglect of promising candidates due to a limited model applicability domain has to be accepted to ensure a reliable identification of final fuel candidates (see Figure 1). Obviously, their estimated properties have to be experimentally validated afterwards, and the obtained measurement data adds to the available property database, which in turn allows refining the property models and extending their applicability domains (see Figure 1). This allows gradually increasing the reliable search space, such that also the initially neglected, but promising structures will be identified correctly, however, at much lower experimental effort.

The first refinement step shown in Figure 1 is based on energy content, which is measured by the lower heating value H_u. To this end, a QSPR based on the measurement data of all 939 organic compounds in the DIPPR property database [9] showing an experimental error of less than 5% has been developed. This model explains the heating value by only two molecular descriptors with high accuracy (R^2 = 0.9994); its extrapolative capabilities have been critically assessed by cross validation. Since both descriptors can be deduced from the molecular graph, the QSPR can be translated into a constraint for the structure generation in Molgen. This way, a property-constrained generation of candidates exhibiting a minimal desired energy content is achieved (see Figure 1).

For the generated structures, property-specific applicability domains are determined by evaluating the structures' distances to database training compounds in the molecular space spanned by latent variables. These latent variables are extracted from the original descriptor database by partial least squares analysis in order to model the property under investigation. The number of significant latent variables is determined by cross-validation, and the models' predictive capabilities are further assessed by evaluating their performance on an external validation set of compounds not used during model development. Only the properties of those generated molecules sufficiently "close" to the training compounds are considered to be reliably predicted. For these molecular structures, the thermophysical properties of interest are subsequently evaluated by a combination of the empirical QSPR approach with the Peng-Robinson cubic equation of state (EoS) [10]. First, the inputs to the EoS, i.e., the critical temperature and pressure as well as the acentric factor, are estimated by QSPRs. The EoS is then evaluated for the vapor-liquid equilibrium properties. Rather than directly using QSPRs, the so-called hybrid model improves the models' physical foundation, which in turn enhances its extrapolative capabilities towards novel structures.

The next refinement step in Figure 1 comprises injection-related properties, in particular viscosity, which, however, cannot yet be predicted by means of QSPR with sufficient accuracy. The same applies for chemical stability, which cannot be predicted reliably to the authors' knowledge. While standard heat of formation has been sometimes used to predict chemical stability, our own investigations have shown that this indicator is often misguiding. More rigorous thermodynamic assessment criteria based on Gibbs free energy could provide better estimations. Moreover, stability is not only thermodynamically determined, but also influenced by combustion kinetics, which still suffer from insufficient measurement data. While a first QSPR for the laminar burning velocity has been proposed previously [11], the applicability range of those models still needs to be considerably extended in order to be included in the proposed framework. Here, optimal design of experiment techniques should be applied to achieve broad model applicability at minimum experimental cost. Finally, the synthetic accessibility [12] of the remaining structures from biomass feedstock is assessed as a first indicator of their producibility. However, the framework presented in [12] has been developed for large pharmaceutical molecules; hence, the applicability to smaller fuel molecules still has to be investigated.

Despite the fact that the latter four refinement criteria of the fuel design framework in Figure 1 still require further improvement, a first application of the framework to gasoline fuels considering only the first three criteria is presented in the following to explore the feasibility of the suggested fuel design framework.

3. Application of the fuel design framework to the gasoline fuel range

Due to the combustion process of spark ignited gasoline engines, typical gasoline fuels comprise up to eight carbon atoms. Hence, organic structures in this carbon range with up to 30 wt% oxygen have been generated and refined with respect to heating value, normal boiling point and heat of evaporation as shown in Table 1. Both, oxygen content and thermophysical property constraints stem from engine requirements [13]. Table 1 shows that the molecular search space can be reduced by more than 99% compared to the unconstrained generation if only those structures are considered which exhibit a minimum heating value and do not contain both, unstable bonds (three- and four-membered carbon rings, oxygen-oxygen single bonds) and unfavorable bonds (triple bonds, carbon bound to four other carbons). The additional refinement based on model applicability domains and property constraints leaves a final set of 122 fuel candidates

only. Although around 57 % of the generated molecules lie outside the property models' applicability domains – thus highlighting the need for further guided experiments – the strong reduction of the initial molecular space clearly illustrates the potential of the proposed framework to identify most promising fuel candidates.

Table 1: Size of generated and refined organic molecular space, C_1 - C_8

	constraint	C_1-C_6	C_7	C_8	search space
unconstrained generation	-	340,088	28,402,888	153,690,076	100.00 %
constrained generation	H_u > 30 MJ/kg[1]	2,262	15,083	172,528	0.104 %
normal boiling point	< 100 °C	492	615	533	0.000899 %
heat of vaporization	< 60 kJ/kg air[2]	13	27	82	0.000067 %

[1] and exclusion of structures with unfavorable/unstable bonds; [2] at stoichiometric fuel to air ratio

4. Conclusions

A novel framework for the identification of future biofuels is presented, which combines rigorous structure generation on an atomic level with a stepwise reduction of the fuel candidates by prediction and assessment of fuel-relevant properties. To this end, quantitative structure-property relations (QSPR) are developed and their validity range is critically evaluated before fuel properties are predicted. While the majority of building blocks for the complete framework already exist, reliable prediction methods of some remaining fuel properties still have to be established and refined in ongoing work. However, the successful demonstration of the framework in this work clearly illustrates its potential for a reliable identification of future liquid energy carriers.

Acknowledgement

This work was performed as part of the Cluster of Excellence "Tailor-Made Fuels from Biomass", which is funded by the Excellence Initiative by the German federal and state governments to promote science and research at German universities.

References

1. Marquardt, W., Harwardt, A., Hechinger, M., Kraemer, K., Viell, J., Voll, A., 2010. AIChE J. 56, 2228-2235.
2. Hechinger, M., Voll, A., Marquardt, W., 2010. Comput. Chem. Eng. 34, 1909-1918.
3. Gani, R., 2004. Comput. Chem. Eng. 28, 2441-2457.
4. Conte, E., Gani, R., Ng, K. M., 2011. AIChE J. 57, 2431-2449.
5. Laue, R., Grüner, T., Meringer, M., Kerber, A., 2005. DIMACS Ser. Discrete Math. Theoret. Comput. Sci. 69, 319-332.
6. Gani, R., Harper, P. M., Hostrup, M., 2005. Ind. Eng. Chem. Res. 44, 7262-7269.
7. Mohs, A., Jakob, A., Gmehling, J., 2009. AIChE J. 55, 1614-1625.
8. Katritzky, A., Kuanar, M., Slavov, S., Hall, C., 2010. Chem. Rev. 110, 5714-5789.
9. DIPPR®801 database, 2009. Design Institute for Physical Properties, UT, USA, http://dippr.byu.edu.
10. Peng, D., Robinson, D., 1997. ACS Pub. 15, 59-64.
11. Hechinger, M., Marquardt, W., 2010. Comput. Chem. Eng. 34, 1507-1514.
12. SYLVIA sofware package. http://www.molecular-networks.com/products/sylvia.
13. Janssen, A., Institute for Combustion Engines, RWTH Aachen University, personal comm.

I.A. Karimi and Rajagopalan Srinivasan (Editors), Proceedings of the 11th International Symposium on Process Systems Engineering, 15-19 July 2012, Singapore.

Reducing drying energy consumption by adsorbent property optimization in multistage systems

James C. Atuonwu,[a] Gerrit van Straten,[a] Henk C. van Deventer,[b] Antonius J. B. van Boxtel[a]

[a]*Systems and Control Group, Wageningen University, P O Box 17, Wageningen 6708WG, the Netherlands*
[b]*TNO, P O Box 360, Zeist 3700AJ, the Netherlands*

Abstract

This work presents a mixed integer nonlinear programming method for the design of energy efficient multistage adsorption dryers within product temperature and moisture constraints. The aim is to find the adsorbent type and properties that minimize specific energy consumption. The results show that the adsorbents chosen in each stage have highest sorption capacities for corresponding drying air conditions. Heat requirements are matched so, zero utility energy is spent regenerating the second stage adsorbent. The adsorbent flow speeds are such that the first stage is optimized for dehumidification and the second for heat recovery. Overall, the optimal system reduces specific energy consumption by about 64% compared to a conventional system at the same drying temperature. Also, drying capacity is improved which permits the use of smaller dryers.

Keywords: Multistage adsorption drying, Mixed integer nonlinear programing, Energy

1. Introduction

Drying is a major industrial energy consumer. Hence, reduction of drying energy consumption remains important in view of the cost and environmental implications. One major method of reducing energy consumption in convective drying is heat recovery. Apart from using heat exchangers and heat pumps, heat recovery can be accomplished by multistage and adsorption drying. In multistage drying, sensible and latent heat in the exhaust air from the earlier drying stages is regained by reusing the air for drying in latter stages. Reheating is necessary to regain drying capacity lost due to moisture uptake. In adsorption drying, moisture is removed from ambient air so latent heat is recovered while sensible heat is gained by adsorption heat release. The high drying capacity air so derived is used for drying. When optimized (for one-stage zeolite systems without exchanger heat recovery), energy consumption reduces by about 20% (Atuonwu et al., 2011). Multistage adsorption drying combines the advantages of both methods as the sensible and latent heat of both inlet and exhaust air of the drying stages are recovered by passing them through adsorbent stages with no need for reheating. Previous studies on this type of drying have focused on the use of a single adsorbent in all stages. To extend the energy efficiency it is important to explore several adsorbent options. In this work, an energy optimization problem is formulated in which adsorbent choice per-stage is a superstructure of alternatives. Specific adsorbents are not defined but the discrete variable of adsorbent choice is specified by isotherm type. Properties like sorption capacity, sorption heat and other isotherm model parameters constitute continuous optimization variables with constraints specified to avoid situations where some parameters become unrealistically high or low (compared to literature values).

2. Process description, superstructure modeling and optimization

In the adsorption drying process (Fig. 1) an adsorbent-coated rotary wheel with adsorption and regeneration sections (A and R respectively) is an add-on to the basic conventional dryer. Ambient air is dehumidified in the adsorber and used in the dryer for drying the wet product. The dehumidification is accompanied by the release of adsorption heat. The dryer exhaust air is passed through a second-stage adsorber and reused in drying. The product flow direction could be co- or counter-current to the airflow direction and the number of stages can be greater than two. Meanwhile, for each stage, there is regeneration of spent adsorbent by hot air. The mass and energy balances describing each stage of the system are available in Atuonwu et al. (2011). In that work, zeolite was considered in a one-stage system and so, the adsorption isotherm and all other constitutive equations were based on zeolite. In this work, all adsorbent constitutive equations are lumped into a superstructure model derived based on a general adsorbent isotherm structure. The dehumidification performance, ease of regeneration, sorption heat and other adsorbent properties that determine adsorption dryer energy performance depend on the nature of the adsorbent-water vapour sorption isotherm. For practical purposes, these isotherms, regardless of the particular adsorbent involved have been classified into types 1 to 5 (Brunauer, et al., 1940). The type 1 isotherm is largely described by the Langmuir equation while the types 2 and 3 are well-fitted by the BET equation (Thibodeux, 1996). Similarly, the types 4 and 5 are well-described by the Dubinin-Astakhov equation (Stoeckli, 1998). Hence, in this work, all isotherms are categorized in three as shown in the superstructure (Fig. 2). Category 1 corresponds to type 1; category 2 to types 2 and 3; and category 3, to types 4 and 5.

Let $I=\{i:i=1...M\}$ and $J=\{j:j=1...N\}$ be the set of adsorbent categories i and drying stages, j, then, we formulate the energy consumption minimization problem as

$$\min Q_{in}(x_{ij}, y_{ij}) = \sum_{i=1}^{i=M}\sum_{j=1}^{j=N} y_{ij} F_{aRj}\left(C_{pa} + Y_{aRin\,j} C_{pv}\right)\left(T_{aRinij} - T_{aRout_{j-1}}\right)\ i \in I, j \in J, T_{aRout0} = T_{amb} \quad (1)$$

subject to constitutive, coupling equations (Atuonwu et al., 2011) and the constraints:

$$x_{ij} = \left[X_{01ij} \quad X_{02ij} \quad X_{03ij} \quad X_{04ij} \quad b_{0ij} \quad E_{ij} \quad F_{ij} \quad G_{ij} \quad H_{ij} \quad n_{ij}\right] \quad i \in I \quad j \in J \quad (2)$$

$$y_{ij} \in \{0,1\} \qquad i \in I \quad j \in J \quad (3)$$

$$X_{ads} = \left[X_{01} bP/1+bP \quad X_{02} Fw/\left[(1-w)(1+(F-1)w)\right] \quad X_{03}\exp(-A/G)^n + X_{04}\exp(-A/H)^n\right] \quad (4)$$

$$b = b_{0ij}\exp(-E_{ij}/RT_{ij}) \quad (5)$$

$$w = P/P_{sat} \quad (6)$$

$$A = RT\ln(P_{sat}/P) \quad (7)$$

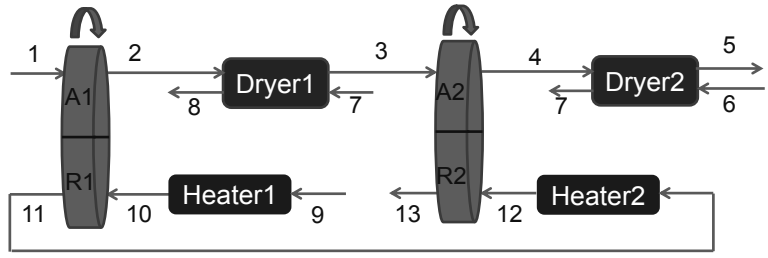

Fig. 1. Two-stage adsorption drying process

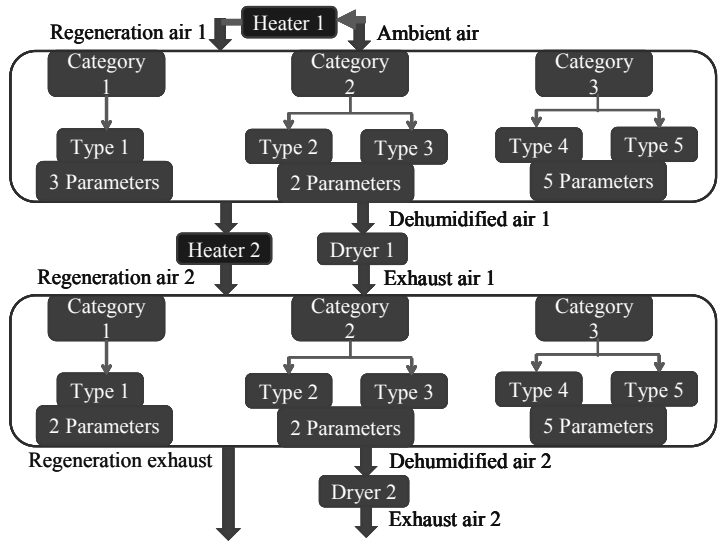

Fig. 2. Superstructure model of a two-stage adsorption drying process

$$H_{ads} = -RT^2\left(\partial \ln P/\partial T\right)_{X_{ads}\ \ constant} \tag{8}$$

$$\sum_{i=1}^{i=M} y_{ij} = 1 \qquad j \in J \tag{9}$$

$$L_j = \sum_{i=1}^{i=M} y_{ij} L_{ij} \qquad j \in J \tag{10}$$

$$Y_{outij} = Y_{inij} - \frac{F_{Sij}}{F_a}\left(X_{Soutij} - X_{Sinj}\right) \tag{11}$$

$$T_{outij} = \frac{F_{aij}\left(\left(C_{pa} + Y_{anij}C_{pv}\right)T_{ainij} + \left(\Delta H_v + H_{ads}\right)\left(Y_{ainij} - Y_{aoutij}\right)\right) + F_{Sij}\left(\left(C_{pSij} + X_{Sinij}C_{pw}\right)T_{Sinij}\right)}{F_{aij}\left(C_{pa} + Y_{aoutij}C_{pv}\right) + F_{Sij}\left(C_{pSij} + X_{Soutij}C_{pw}\right)} \tag{12}$$

The symbols are designated as follows: Q_{in} is the regeneration air heat input (kJ/s), C_p is specific heat capacity (kJ/kgK), x represents continuous optimization parameters of which X_{01}-X_{04} are sorption capacities, E-H, energy constants, n is the heterogeneity parameter, y, the adsorbent choices, Y, air absolute humidity (kg/kg), T, temperature (K), F, flowrates (kg/s), P is vapour pressure (Pa), w is water activity. X_{ads} is the equilibrium adsorbent loading vector (kg/kg), R, gas constant (J/molK), P_{sat}, saturation pressure (Pa), H_{ads}, the adsorption heat, ΔH_v, water latent heat of vaporization (kJ/kg) and L, is a general lumped variable for the air flow in and out of the sorption system (e.g. temperature, humidity). For the subscripts, *amb* represents the ambient, *in*, the inlet, *out*, the outlet, *w* for water, *a* for air, *R* for regenerator and *S* for solid (adsorbent or dried product). Equation (1) minimizes the total regeneration energy which approximates the net system energy input for low-temperature drying. Equation (2) contains the continuous optimization variables while (3) defines the discrete variables. (4) is a vector containing the three categories of equations defining the superstructure of sorption isotherms; (5), (6) & (7) are definitions of variables within (4); while (8) is the Claussius-Clapeyron equation which defines the adsorption heat which appears in the

energy balance (12). (9) ensures that only one adsorbent is chosen per-stage, (10) states that the state variable (temperature, humidity, loading, etc) of the air and solid outputs of each sorbent system is a binary-weighted sum of all the possibilities. (11) is the mass balance. (11) and (12) apply to both the adsorption and regeneration sections of the wheel. They also apply to the dryer except that the sorption heat term in the energy balance is negligible. The product is at a dry mass flowrate of 72kg/h, initial moisture content of 10kg water/kg dry matter. The outlet moisture content is constrained to be 0.05kg/kg while the product temperature is less than 50°C. For comparison, a 2-stage conventional dryer is also optimized. Here, the wheels in Fig. 1 are replaced by heaters that heat up the air to the same dryer inlet temperatures as the optimal adsorption dryer.

3. Results and Discussion

A sensitivity analysis shows that the optimal adsorbent choices depend strongly on the parameter (x) upper and lower bound constraints. The active sets are: $\{b_0, n\}$ for the lower bound and $\{X_{01}, X_{02}, X_{03}, X_{04}, E, F, G, H\}$ for the upper bound constraints. Thus, in choosing among adsorbents of known isotherm parameters for drying applications, the lower the values of $\{b_0, n\}$ and the higher the values of $\{X_{01}, X_{02}, X_{03}, X_{04}, E, F, G, H\}$, the more suitable the adsorbent. When the upper and lower bound constraints are set to within ±50% of typical values for adsorbents as reported in the literature (Atuonwu et al., 2011; Mihoubi and Bellagi, 2006; Moore and Serbezov, 2005), the optimal choice of adsorbents is as shown in Fig. 3. Ambient air dehumidification which occurs in the first stage requires a type 1 adsorbent (example, zeolite) while exhaust air dehumidification in the second uses a type 4 or 5 isotherm-based adsorbent (example, silica-gel). The following is observed: first, sorption capacity-vapour pressure matching. The adsorbent chosen for ambient air dehumidification has a higher sorption capacity at lower drying air vapour pressures while for the moister higher vapour pressure 1st stage dryer exhaust air, another adsorbent of higher sorption capacity is chosen. Second, there is heat requirement matching. The optimal operating conditions (Table 1) shows the required regeneration air temperature for the second stage adsorbent equals the first stage regenerator exhaust air temperature (streams 11 & 12). Thus, Heater2, Fig. 1 is redundant. Third, the flowrate (speed) of the second-stage adsorbent is 3701 kg/h which is much higher than that of the first stage which is returned as 2139 kg/h. This implies the second-stage wheel behaviour is optimized for dryer and regenerator exhaust heat recovery while the first stage is optimized for air dehumidification. Overall, these effects ensure a highly energy-efficient system that improves further with heat recovery.

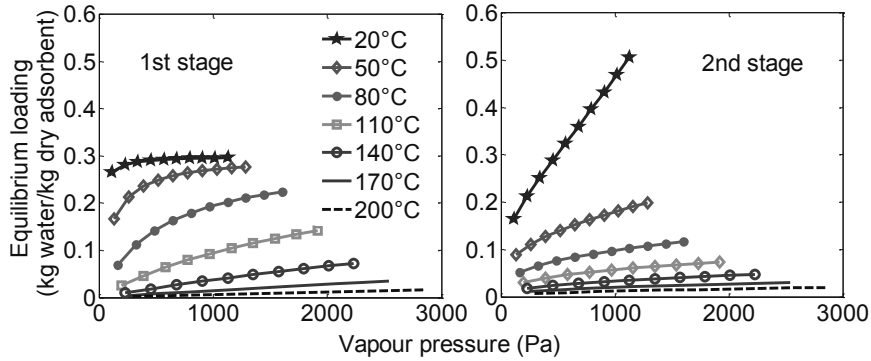

Fig. 3. Adsorbent-water vapour sorption isotherms for optimal adsorbent choices per stage showing type 1 in first stage and type 4 (or 5) in second stage

Table 1. Process variables for optimal adsorption dryer

No.	*Flow(kg/h)*	*Temp.(°C)*	*Humidity(kg/kg)*	*No.*	*Flow(kg/h)*	*Temp.(°C)*	*Humidity(kg/kg)*
1	54000	25	0.0100	8	72	46	0.0500
2	54000	46	0.0020	9	3794	25	0.0100
3	54000	24	0.0109	10	3794	400	0.0100
4	54000	34	0.0061	11	3794	229	0.1232
5	54000	23	0.0105	12	3794	229	0.1232
6	72	23	10.0000	13	3794	130	0.1918
7	72	34	6.6765				

Table 2. Process variables for conventional dryer

No.	*Flow(kg/h)*	*Temp.(°C)*	*Humidity(kg/kg)*	*No.*	*Flow(kg/h)*	*Temp.(°C)*	*Humidity(kg/kg)*
1	71067	10	0.0100	5	71067	28	0.0141
2	71067	46	0.0100	6	72	10	10.0000
3	71067	29	0.0108	7	72	29	3.2894
4	71067	36	0.0108	8	72	28	0.0500

The specific energy consumption of the system is 2040 kJ/kg of water evaporated. With heat recovery where stream 13 is used to preheat stream 9, it becomes 1565 kJ/kg. For a conventional two-stage dryer at the same drying air temperatures, the operating conditions when energy consumption is optimized are shown in Table 2. The drying capacity is much less and so, the required air flowrate is much higher (Compare stream 1, Tables 1 & 2). The energy required to heat this high air flow increases and the scope for heat recovery is very low as the exhaust air (stream 5) temperature is very close to ambient. The specific energy consumption is 4310 kJ/kg. In comparison therefore, the optimal adsorption drying system reduces energy consumption by about 64%.

4. Conclusion

Adsorbent property and operational optimization ensures matching of system needs with adsorbent material properties and operating conditions thus yielding significant energy savings. Improved drying capacity is observed. Based on the optimal adsorbent properties, the use of zeolite in the first stage and silica gel in the second is proposed.

Acknowledgment

This work is funded by the Energy Research Program EOS of the Dutch Ministry of Economics under Project EOSLT07043.

Referencess

F. Stoeckli, 1998, Recent developments in Dubinin's theory, Carbon, 36, 4, 363-368.

J.C. Atuonwu, G. van Straten, H.C. van Deventer, A.J.B. van Boxtel, 2011, Model-based energy efficiency optimization of a low temperature adsorption dryer, Chemical Engineering and Technology, 34, 10, 1723-1732.

S. Brunauer, L. Deming, W. Deming, E. Teller, 1940, On the theory of the van der Waals adsorption of gases, Journal of American Chemical Society.

J.D. Moore, A. Serbezov, 2005, Correlation of adsorption equilibrium data for water vapour on F-200 activated alumina, Adsorption, 11, 65-67.

L.J. Thibodeux, 1996, Environmental chemodynamics: movement of chemicals in air, water and soil, 2nd ed., John Wiley & Sons, NY.

D. Mihoubi, A. Bellagi, 2006, Thermodynamic analysis of sorption isotherms of bentonite. Journal of Chemical Thermodynamics, 38, 1105-1110.

I.A. Karimi and Rajagopalan Srinivasan (Editors), Proceedings of the 11th International Symposium on Process Systems Engineering, 15-19 July 2012, Singapore.

Optimizing Protein-Excipient Interactions for the Development of Aggregation-Reducing Lyophilized Formulations

Brock C. Roughton,[a] Anthony I. Pokphanh,[b] E.M. Topp,[c] and Kyle V. Camarda[b]

a University of Kansas, Bioengineering Graduate Program, 1520 W. 15th Street, Lawrence, KS 66049
b University of Kansas, Department of Chemical and Petroleum Engineering, 1530 W. 15th Street, Lawrence, KS 66049
c Purdue University, Department of Industrial and Physical Pharmacy, 575 Stadium Mall Drive, West Lafayette, IN 47907

Abstract

As protein drugs become increasing popular therapeutic approaches, formulations must be developed to ensure stability of the final drug product. Lyophilization, or freeze-drying, is an approach commonly used to produce stable protein drugs, yet protein aggregation may still occur in lyophilized formulations. Excipients in the formulation may be selected to reduce the propensity of a protein to aggregate through interaction with aggregation prone regions. In the following work, molecular docking simulations were used to predict the regions on a protein where different excipients were most likely to interact. Simulation results compared variably with experimental hydrogen/deuterium exchange experiments used to determine regions of protein-excipient interactions. The results were used to design formulations for lyophilized calmodulin (PID #1CLL). Sugar and surfactant pairs were selected that would maximize protection of different aggregation prone regions through direct interactions.

Keywords: protein aggregation, lyophilization, formulation design.

1. Introduction

Protein aggregation is an active problem in the development of protein drug formulations. Aggregation can occur either from unfolding of proteins leading to interaction or surface interactions between hydrophobic regions on proteins. Lyophilization, or freeze-drying, is used to improve stability but aggregation can still occur (Costantino*, et al.*, 1995). Stabilizing additives, or excipients, are often included in lyophilized formulations to reduce aggregation.

Nonionic surfactants have been shown to bind with weak affinity to proteins (McNally and Hastedt, 2008). Such binding could interact with hydrophobic regions on the protein and limit access to aggregation prone “hot spots”. Nonionic surfactants such as Tween 80 have been shown to decrease aggregation in lyophilized protein formulations (Kerwin, 2008). However, use of surfactants can cause difficulty during the lyophilization process due to the low glass transition temperatures exhibited by surfactants (McNally and Hastedt, 2008). A successful formulation using surfactants requires the presence of glass formers, such as sugars or polymers.

Sugars are widely used as protein stabilizers in lyophilized products. Sugars usually have high glass transition temperatures which lead to stable glass formation during freezing and subsequent drying. Sugar molecules have also been shown to exhibit site-specific effects on proteins during lyophilization through use of hydrogen-deuterium exchange mass spectroscopy (Li*, et al.*, 2008), indicating that interaction between sugars and proteins occur in the lyophilized state. Such interactions can be exploited to provide better coverage of aggregation prone "hot spots" on the protein.

By selecting excipients that interact preferably with aggregation prone regions, a lyophilized formulation can be developed to reduce aggregation. In this work, a sugar and surfactant pair is selected to optimally provide the most interaction with an aggregation prone region on the protein calmodulin (PID #1CLL). By choosing a formulation with maximal protein-excipient interactions, the potential for aggregation is reduced. While surfactants may interact more than sugars on a per molecule basis, a sugar was included to ensure that a stable glass could be formed.

2. Methods

2.1. Determination of Protein-Excipient Interactions

To predict the amino acids of calmodulin most likely to interact with a given excipient, molecular docking simulations were performed using Autodock (http://autodock.scripps.edu/). Each simulation provided ten docking conformations that provided the lowest free energy. Five simulations were done for each excipient with calmodulin, providing fifty docking conformations total for each excipient. Each conformation was analyzed to determine which resides were in contact, either through van der Waals forces or hydrogen bonding, with the excipient molecule.

The computation results from Autodock were compared to experimental hydrogen-deuterium exchange (HDX) mass spectroscopy experiments using lyophilized formulations of calmodulin and either trehalose, sucrose, raffinose, or mannitol (Li*, et al.*, 2008). Regions of the protein that are able to freely exchange hydrogen for deuterium are exposed and are not protected by protein-excipient interactions. Experimentally, protein-excipient interactions are indicated by low deuterium uptake.

2.2. Optimal Selection of Excipients

Contact information provided by the docking simulations was used to optimally select excipients that have the highest number of interactions with aggregation prone "hot spots". The hot spots were predicted using Aggrescan (Conchillo-Sole*, et al.*, 2007).

For each hot spot, a sugar and a surfactant molecule were chosen to maximize protein-excipient interactions. For selection purposes, whichever excipient had the most interactions with a particular residue was chosen as the best candidate. It was assumed that the molecule with the most interactions with a residue would have the dominant effect and thus contribute the most to the protection of the residue of interest. At each residue in the hot spot, the best sugar candidate and the best surfactant candidate were compared. Whichever excipient had the most interactions was selected and the process was repeated for the entire hot spot sequence. The sugar-surfactant pair that provided the maximum number of interactions was selected as the optimal drug formulation. The formulation of the optimization problem is given in Equation (1). The problem is

formulated as a MINLP and was solved using the DICOPT solver in GAMS (http://www.gams.com/).

$$\max \sum_{i}^{n} \text{interaction score}(i) \tag{1}$$

s.t.

$$\text{interaction score}(i) = y_{sugar}(i) \cdot \text{sugar score}(i) + y_{surfactant}(i) \cdot \text{surfactant score}(i)$$

$$\text{sugar score}(i) = \sum_{j=1}^{4} y_j \cdot score_j(i)$$

$$\text{surfactant score}(i) = \sum_{k=1}^{3} y_k \cdot score_k(i)$$

$$y_{sugar}(i) \le \frac{\text{sugar score}(i)}{\text{surfactant score}(i)}$$

$$y_{surfactant}(i) \le \frac{\text{surfactant score}(i)}{\text{sugar score}(i)}$$

$$y_{sugar}(i) + y_{surfactant}(i) = 1$$

$$\sum_{j=1}^{4} y_j = 1$$

$$\sum_{k=1}^{3} y_k = 1$$

$$y_{sugar}, y_{surfactant}, y_j, y_k = \{0,1\}$$

Where i is a residue location, n is the number of residues in the hot spot of interest, j is a specific sugar, and k is a specific surfactant. The $score_j(i)$ and $score_k(i)$ are input as parameters based on the results from molecular docking. The scores are integer values, but are not explicitly defined as such in GAMS. The constraints ensure that the highest interaction score between a sugar and a surfactant is chosen for each residue. The constraints provide an interaction score that is summarized below, without the need for disjunctive programming:

$$\text{interaction score}(i) = \begin{cases} \text{sugar score}(i) & \text{if sugar score}(i) \ge \text{surfactant score}(i) \\ \text{surfactant score}(i) & \text{if surfactant score}(i) > \text{sugar score}(i) \end{cases} \tag{2}$$

3. Results and Discussion

3.1. Docking Simulation Results

Docking simulations providing fifty conformations were performed individually for mannitol, trehalose, sucrose, raffinose, octyl glucoside, tween 40, and tween 80 with the protein calmodulin. The results for the sugars were compared to experimental HDX results. Overall, the docking results compared favorably with the HDX results. Regions of high interactions in the docking simulations corresponded to regions that were protected from hydrogen/deuterium exchange. The histogram of interactions versus residue location is provided in Figure 1 for trehalose. Residues that interacted frequently with trehalose match well with the shaded regions indicating protection from hydrogen/deuterium exchange.

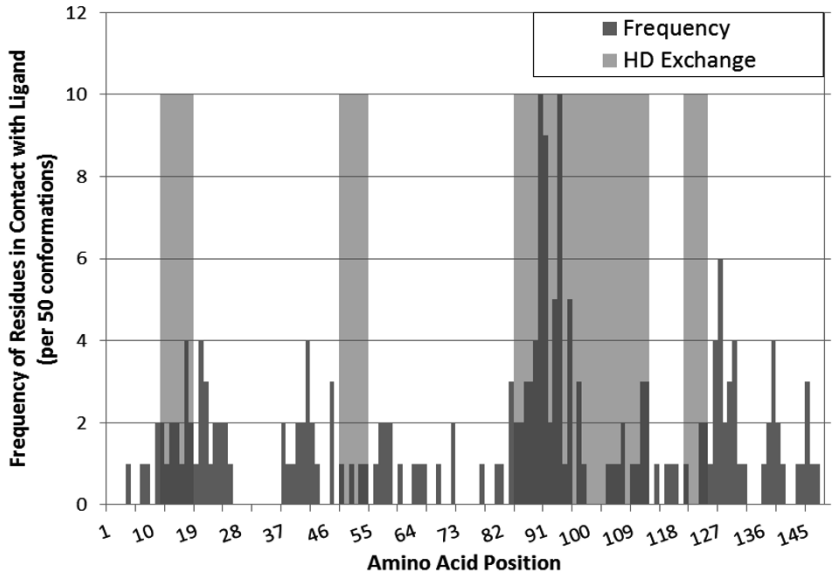

Figure 1. Frequency of amino acid residues of calmodulin in contact with trehalose. Results are given for 50 docking conformations. The shaded regions indicate amino acids that were protected by trehalose in the lyophilized state, as determined by HDX experiments (Li*, et al.*, 2008).

Figure 2 provides a visual comparison of the regions with high interaction and the regions protected from exchange for the trehalose-calmodulin system. From the comparison of the computational and experimental results, the docking simulations provide a reasonable prediction of the residues involved in protein-excipient interactions and provide a useful tool for selecting excipients for lyophilized protein formulations.

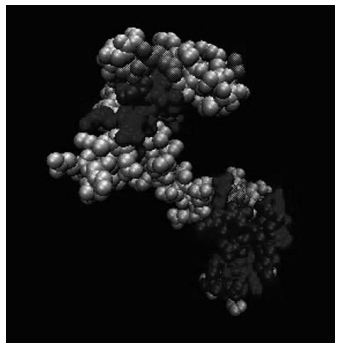

Figure 2. Trehalose interaction regions mapped to the surface of calmodulin. Blue regions indicate residues that interacted with trehalose in more than three conformations. Red regions indicate regions that were protected by trehalose in the lyophilized state, as determined by HDX experiments. Purple regions are the intersect of the computationally predicted high interaction regions and the experimentally determined protected regions.

3.2 Formulation Selection for Maximizing Protein-Excipient Interactions

Using the docking simulation results and the previously described optimization problem formulation, sugar-surfactant pairs were selected for each hot spot region on calmodulin. The hot spots were predicted using Aggrescan (Conchillo-Sole*, et al.*, 2007). Due to the proximity of hot spots 4 and 5, a formulation was also selected for the combined region. The results are given in Table 1. The interaction scores provided correspond to the number of interactions exhibited in the docking simulations.

Table 1. Sugar-surfactant formulations selected for maximum interaction with hot spot regions.

Hot Spot	*Amino Acids*	*Sugar*	*Surfactant*	*Combined Interaction Score*	*Sugar Interaction Score*	*Surfactant Interaction Score*
1	15-19	Trehalose	Tween 40	24	10	24
2	33-38	Mannitol	Tween 40	13	10	7
3	67-73	Sucrose	Tween 40	17	9	15
4	99-103	Raffinose	Octyl Glucoside	10	7	8
5	106-111	Raffinose	Tween 80	17	11	13
6	141-145	Raffinose	Octyl Glucoside	26	15	26
4 & 5	99-111	Raffinose	Octyl Glucoside	29	18	22

The results show that the excipients providing maximal interactions vary from hot spot to hot spot. All available excipients were selected at least once. The addition of a sugar provided no additional interactions for the formulations selected for hot spots 1 and 6 and thus was not beneficial from a protein-excipient interaction standpoint. A sugar would be necessary to ensure a stable glass was formed during the lyophilization.

The procedure outlined above could be used for any number of excipients and proteins to predict formulations with maximal protein-excipient interactions. By maximizing protein-excipient interactions, the aggregation propensity is reduced and a safer, more effective drug product is produced. The fact that the sugar-surfactant pair providing maximal interactions differed between hotspots speaks to the complexity of selecting beneficial excipients for a lyophilized protein formulation.

References

Conchillo-Sole, O., de Groot, N., Aviles, F., Vendrell, J., Daura, X. and Ventura, S., 2007, AGGRESCAN: a server for the prediction and evaluation of "hot spots" of aggregation in polypeptides. BMC Bioinformatics, 8, 1, 65.

Costantino, H. R., Langer, R. and Klibanov, A. M., 1995, Aggregation of a Lyophilized Pharmaceutical Protein, Recombinant Human Albumin: Effect of Moisture and Stabilization by Excipients. Nat Biotech, 13, 5, 493-496.

Kerwin, B. A., 2008, Polysorbates 20 and 80 used in the formulation of protein biotherapeutics: Structure and degradation pathways. Journal of Pharmaceutical Sciences, 97, 8, 2924-2935.

Li, Y., Williams, T. and Topp, E., 2008, Effects of Excipients on Protein Conformation in Lyophilized Solids by Hydrogen/Deuterium Exchange Mass Spectrometry. Pharmaceutical Research, 25, 2, 259-267.

McNally, E. J. and Hastedt, J. E., 2008, Protein formulation and delivery, 2nd, New York: Informa Healthcare.

I.A. Karimi and Rajagopalan Srinivasan (Editors), Proceedings of the 11th International Symposium on Process Systems Engineering, 15-19 July 2012, Singapore.

Signature Descriptors for Process and Molecular Design in Reactive Systems

Nishanth G. Chemmangattuvalappil[a,b], Christopher B. Roberts[a], Mario R. Eden[a]

[a]*Department of Chemical Engineering, Auburn University, USA*
[b]*Department of Chemical and Environmental Eng., University of Nottingham, Malaysia*

Abstract

The reverse problem formulation is a technique used for the solution of integrated process and product design problems from a properties perspective. In this work, an algorithm has been introduced for reverse problem formulations using property operators based on molecular signature descriptors. Current molecular design algorithms are applicable only in non-reactive systems. Here, a general framework is introduced for integrated design of systems where chemical reactions are taking place.

Keywords: Signature Descriptors, Reactive Systems, Molecular Design.

1. Theoretical background

1.1. Reverse problem formulation (RPF) technique and property operators

In most design problems, it is important to consider the aspects of process and molecular designs simultaneously because of their mutual relationships. However, some model equations are non-linear in nature which makes integrated problems computationally challenging. The reverse problem formulation (RPF) is a technique used to reduce the complexity of such integrated problems [1]. In RPF, the integrated problem is decomposed into two reverse problems. The first reverse problem identifies the property targets to achieve optimum process performance and the second reverse problem generates the molecular structures that meet the identified property targets. To track properties, property operators are used which are functions of the original properties tailored to obey linear mixing rules. The normalized property operator, Ω_{js} is obtained by dividing it by a reference value [2]. If $\psi_j(P_{js})$ is the property operator of the j^{th} property P_{js} of stream s, x_s is the fractional contribution, N_s is the number of streams:

$$\Omega_{js} = \frac{\sum_{s=1}^{Ns} x_s \psi_j\left(P_{js}\right)}{\psi_j^{ref}} \tag{1}$$

1.2. Molecular signatures

Molecular signature is a descriptor used for representing the atoms in a molecule using extended valencies of atoms to a pre-defined height [3]. If G is a molecular graph and x is an atom of G, the atomic signature of height h of x is a canonical representation of the subgraph of G containing all atoms that are at a distance h from x. Faulon *et al.* identified the relationship between TIs and signatures [4]. If k is a constant, ${}^h\alpha_G$ is the vector of occurrences of atomic signature of height h and TI (root (${}^h\Sigma$)) is the vector of TI values calculated for each root of atomic signature:

$$TI(G) = k.{}^h\alpha_G.TI\left(root\left({}^h\Sigma\right)\right) \tag{2}$$

2. Signature descriptors for molecular design

There are a number of property models that make use of different topological indices for predicting properties from molecular structures. These relationships are known as quantitative structure activity/property relationships (QSAR/QSPR). Algorithms have been developed that make use of molecular signature descriptors to represent topological indices for the molecular design [5]. Since many existing QSPR expressions can be reformulated in terms of signatures, algorithms based on signatures will be able to track a wide variety of property targets.

2.1. Signature descriptors for reactive systems

Most computer-aided molecular design algorithms can be applied only to systems where no chemical reactions take place. However, the clustering technique has been shown to have the ability to track the properties for stoichiometric conversion reactors [6]. The normalized property operator of the outlet stream of a stoichiometric conversion reactor, Ω_{j2} can be calculated using eq. (3):

$$\Omega_{j2} = \frac{F_1}{F_2} \cdot \left(\Omega_{j1} + X.y_{Key1} \cdot \sum_{i=1}^{NC} \theta_i \cdot \Omega_{ji}^{*} \right) \tag{3}$$

Where F_1 and F_2 are the flowrates of inlet and outlet steams respectively, θ_i is the stoichiometric coefficient, X is the conversion, Ω_{ji}^{*} is the property operator corresponding to the individual components. To track the same set of target properties, the signature of a reaction, $\sigma(R)$ can be defined as shown in eqs. (4) and (5):

$${}^{h}\sigma(R) = f(\sigma(A)\sigma(B)) \tag{4}$$

$$\Delta\Omega_{f2} = f({}^{h}\sigma(R)) \tag{5}$$

Where $\sigma(A)$ and $\sigma(B)$ are the signatures corresponding to the reactants and products. During a reaction, one or more of the molecular groups in the compound will be replaced by a new group(s). The change in groups results in changes in the molecular signatures. The height of the signature considered for tracking the target property will determine the signatures from the original molecular groups that will be repeated in the product as well. For instance, consider the esterification of alcohols with acetic acid:

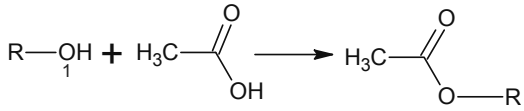

According to eq. (2), the signatures of atoms originating from the last two groups in 'R' will be changed because of the esterification reaction. Therefore, the change in property function will be represented as the changes in atomic signatures of the atoms that are at a height 2 from the signature marked as '1'. In general, the difference in property contributions of different signatures can be represented using eq. (6):

$$\Delta\Omega = \Delta\left[\left(\sum {}^{h}\alpha_{h-k} \right)_{reactant} - \left(\sum {}^{h}\alpha_{h-k} \right)_{products} \right] \tag{6}$$

where, $({}^{h}\alpha_{h\text{-}k})_{\text{reactants}}$ is the sum of property operators for the signatures of the atoms that are at height '*h*-*k*' from the group that would be replaced, $({}^{h}\alpha_{h\text{-}k})_{\text{products}}$ is the sum of

property operators for the signatures of the atoms that are at height '*h-k*' from the group that is formed after the reaction and $\Delta\Omega$ is the difference in property operator value as a result of the reaction. Since the atomic signatures of molecular building blocks that are farther from height '*h-k*' will be the same even after the reaction, the property operators will be same for the rest of the molecule. Now, the property operator corresponding to the molecule formed after a specific type of chemical reaction can be estimated:

$$\Omega_{reaction} = \Delta\Omega + \Omega(P) \tag{7}$$

where, $\Omega_{reaction}$ is the property operator corresponding to the final molecule when the initial compound used has a property operator value of $\Omega(P)$.

2.2. General problem statement

Design the molecules with the best dominant property that satisfy a set of property constraints identified during the process design when the molecule is formed after a chemical reaction.

2.3. Problem formulation

The property operator of a property P is a function, θ, of the actual property which obeys linear mixing rules [5]:

$$\theta = f(TI) \tag{8}$$

$$TI = \sum_{i=1}^{N} {}^{h}\alpha_i \cdot TI(root({}^{h}\Sigma)) = \sum_{i=1}^{N} {}^{h}\alpha_i L_i \tag{9}$$

$$\Omega(P) = \sum_{i=1}^{N} x_i L_i \tag{10}$$

$$\left(\Omega_{reaction}\right)_j = \Delta\Omega + \Omega(P) \tag{11}$$

This problem can be formulated as a bilevel optimization problem. The first level is to identify the right sets of atomic signatures that change after the reaction and the second level is to identify the right combination of those atomic signatures along with the atoms whose signatures would not change with the reaction. To solve the first level, the groups can be represented as a set of binary variables:

$$\Phi = \sum {}^{h}\alpha_{h-k}.e_i \tag{12}$$

where e_i is the number of appearances of each signature that will change because of the reaction. Φ will be optimized to get the optimum value of Ω_j. The components of $\Delta\Omega$ can be estimated corresponding to the type of reaction. Since the difference is restricted to the atoms that are at height *h-k* from the group on which the reaction can take place, this modification will add only a small number of additional parameters in the final problem formulation. The dominant property, which is expressed in terms of the occurrences of atomic signatures, can be optimized subject to the property constraints. If Ω_j is the property operator corresponding to the dominant property and Ω_{ij} is the normalized property operator of molecule *i*, an optimization problem can be formulated as follows:

$$Max / Min \ \ \Omega_j \tag{13}$$

$$\Omega_j^{\min} \le \Omega_j \le \Omega_j^{\max} \tag{14}$$

The principles of graph theory are applied to ensure that the signatures connect together to form feasible molecules [7]. To do that, a number of structural constraints that ensure the consistency of signatures are introduced in terms of the number of appearances of atomic signatures [5].

2.4. Stepwise procedure

- The property targets for the input molecules to provide the optimum process performance will be calculated using eq. (1).
- Identify the QSAR/QSPR/group contribution models that predict the properties corresponding to the optimum performance.
- Identify heights of molecular signatures corresponding to the TIs used in QSPR
- Estimate the property operators corresponding to the changes possible on the molecular groups because of the reaction.
- Estimate the property operator values corresponding to potential types of reactions.
- Based on the structural constraints and transformation techniques explained in section 2.4, identify the signatures and generate candidate molecules using the algorithm by Faulon *et al*. [8].

3. Proof of Concept Example

In this case study, the target is to identify an alcohol that produces an ester with a given set of properties. The property targets for the ester are given in Table 1, while the property models that are used to predict the target properties are given in Table 2.

Table 1. Property Constraints

Property	Upper Bound	Lower Bound
Boiling Point, *BP* (°C)	170	110
log(*TLC*) (ppm)	-	1
log(K_{oc})	Minimum	

Table 2. Property Models

Property	Property Model
log(K_{oc}) [9]	$\log(K_{oc}) = 0.53({}^1\chi) - 1.25(\Delta^1\chi^v) - 0.72(\Delta^0\chi^v) + 0.66$
Boiling Point, *BP* [10]	$T_b = t_{b0}.\ln\left[\sum_{g=1}^{n_g} n_i t_{b1} + \sum_{s=1}^{N_s} n_s t_{b2} + \sum_{t=1}^{N_t} n_t t_{b3}\right]$
log(*TLC*) [11]	$\log(TLC) = 4.066 - 0.9915({}^1\chi^v)$

The molecular descriptors used in the equations presented in Table 2 are transformed into the corresponding molecular signatures. The maximum signature height appearing

in this case is 2. The following signatures (and the similar signatures from the C4 root) have the potential to form a different signature because of the reaction:

O1(C2(OC)),O1(C3(OCC) O1(C4(OCCC)) C2(O1(C)C2(CC)) C2(O1(C)C3(CCC)) C3(O1(C)C1(C)C2(CC)) C3(O1(C)C2(CC)C2(CC)) C3(O1(C)C3(CCC)C2(CC)) C3(O1(C)C3(CCC)C3(CCC))

An optimization problem has been set up using eqs. (8)-(14) and relevant structural constraints and solved for the minimum value of soil sorption coefficient. The best three candidates along with their predicted property are given in Table 3:

Table 3. Final molecules

Molecule	*BP* (K)	log *TLC* (ppm)	log K_{oc} (ppm)
$(CH_3)_2CH(CH_3)CHOH$	114	1.762	1.892
$(CH_3)_2CH(CH_2)CH_2OH$	125	1.707	1.921
$CH_3CH_2CH(CH_3)CH_2OH$	125	1.609	1.941

4. Conclusions

An algorithm has been developed for solving property based product design problems when chemical reactions are involved during the process. The algorithm is formulated to track the changes in the properties during different types of reactions. The developed algorithm focuses on the changes in the reaction sites of the molecules to design the components involved.

5. Acknowledgements

The authors gratefully acknowledge the financial support provided by the Southeastern Regional Sun Grant Program, and the USDA-AFRI (Award# 2011-67009-20077).

References

[1] M.R. Eden, S.B. Jørgensen, R. Gani and M.M. El-Halwagi, (2004), Chemical Engineering & Processing 43, 595-608
[2] M.D. Shelley and M.M. El-Halwagi, (2000), Computers & Chemical Engineering, 24
[3] D.P. Visco Jr., R.S. Pophale, M.D. Rintoul, J.L. Faulon, Journal of Molecular Graphics and Modeling 20 (2002) 429-438
[4] J.L. Faulon, D.P. Visco Jr., R.S. Pophale, J. Chem. Inf. Compt. Sci. 2003a, 43, 707-720
[5] N.G. Chemmangattuvalappil, C.C. Solvason, S. Bommareddy, M.R. Eden (2010), Computers & Chemical Engineering, 34
[6] M.R. Eden (2003), Technical University of Denmark, PhD Thesis
[7] N. Trinajstic, Chemical Graph Theory, 2nd Edition, CRC press, Boca Raton, FL, 1992
[8] J.L. Faulon, C.J.Churchwell, D. P. Visco Jr., J.Chem. Inf. Compt. Sci. 2003, 43, 721-734
[9] D.A. Bahnick and D.J. Doucette (1988), Chemosphere, 17
[10] J. Marrero and R. Gani, (2001), Fluid Phase Equilibria, 183/184, 183-208.
[11] R. Koch (1982), Chemosphere, 11(9)

I.A. Karimi and Rajagopalan Srinivasan (Editors), Proceedings of the 11th International Symposium on Process Systems Engineering, 15-19 July 2012, Singapore.

Optimization of Product Formulation through Multivariate Statistical Analysis

Subin Hada[a], Nishanth G. Chemmangattuvalappil[a,b], Christopher B. Roberts[a], Mario R. Eden[a]

[a]*Department of Chemical Engineering, Auburn University, USA*
[b]*Department of Chemical and Environmental Eng., University of Nottingham, Malaysia*

Abstract

The property integration framework is combined with multivariate statistical techniques and applied in a reverse problem formulation on chemical product design problems by systematic and insightful use of past data describing the properties of the raw materials, their blend ratios, and the process conditions during the production of a range of product grades to achieve new and improved products. The method is illustrated using a polymer blending problem.

Keywords: Mixture Design, PCA, PLS, Property Clustering, Reverse Problems.

1. Introduction

Correlation is inherent in the data of chemical processes which requires the use of multivariate statistical tools for visualization and identification of important relationships in the data. The product formulation design problem in industrial research and development is one such area where the analysis of mixture data is a common problem, especially in pharmaceutics, cosmetics, oil, and biotechnology. Such mixture design problems are traditionally formulated as *mixed integer non-linear programs* (MINLPs) which can be difficult to formulate and solve.

2. Methodology

Projection methods like principal component analysis (PCA) and partial least squares (PLS) are employed to extract and utilize the necessary information from three degrees of freedom that are available to control the properties of any product manufactured in blending operations. This information forms the basis for models that can be used to simultaneously explore the effects of the raw material properties data (**X**), their blend ratios (**R**), and process conditions (**Z**) on the product quality (**Y**). These methods capture information about the variance and correlation structure within predictor and quality variables that were present during the production of previous grades and that are important for the consistency of the desired process conditions with past operating procedures.

The empirical models are used in a reverse problem formulation to ensure that a complete set of candidate materials and their mixtures are found which match the design target subject to the predictive power of the model. Mapping the design problem onto the lower dimension cluster space utilizing the property clustering algorithm facilitates simultaneous visualization and solution of the problem and also avoids combinatorial explosion when dealing with multi-component mixtures [1]. The solution methodology can be summarized as follows:

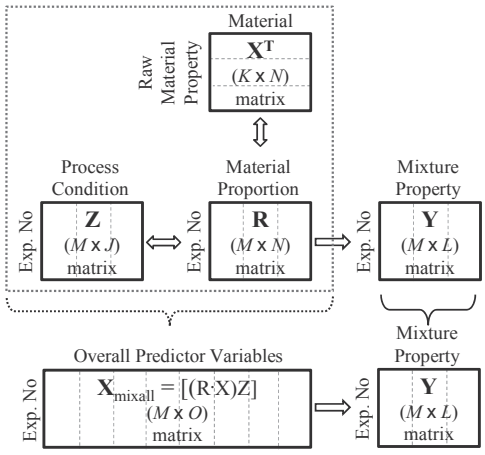

Figure 1. Data structure for three predictor variable matrices and a quality matrix. (The dotted lines in the blocks indicate the mean centering and scaling direction.)

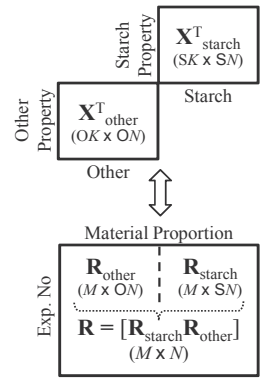

Figure 2. Data structure of **X** and **R** Matrix for the polymer blend problem.

1. Acquire original training data matrix generally available on mixture design. The structure of the raw material properties matrix, $\mathbf{X}_{NxK}$, consists of N available raw materials with K number of properties. The blend ratio matrix, $\mathbf{R}_{MxN}$, consists of M number of blends of N materials used in the blend formulation such that $\sum_{i=1}^{N} r_i = 1$, where $r_i \geq 0 \; \forall \; \mathrm{i} = 1,2,\ldots,N$. The process conditions matrix $\mathbf{Z}_{MxJ}$, consists of J process conditions. The response or product quality matrix $\mathbf{Y}_{MxL}$, consists of L properties measured on the final product. Using ideal mixing rules the raw material properties matrix (**X**) and the blend ratios matrix (**R**) can be combined in order to relate all (**Z**, **R**, $\mathbf{X}^T$) to the **Y** matrix with a common dimension M [2]. The model to relate **Y** with all three **Z**, **R** and $\mathbf{X}_{mix\ all}$ variables can be of the form:

$$\mathbf{Y}_{M\times L} = f(\mathbf{X}_{mix\ all\ M\times O}) + \varepsilon \qquad \text{where, } \mathbf{X}_{mix\ all} = \left[\mathbf{X}_{mix}\mathbf{Z}\right] = \left[\left(\mathbf{R}\cdot\mathbf{X}\right)\mathbf{Z}\right] \tag{1}$$

$\mathbf{X}_{mix\ all}$ is a matrix combining $\mathbf{X}_{mix}$ and **Z** in parallel and contains O (=K+J) number of predictor variables. This simplifies the analysis and design by not having to differentiate between mixture and process variables and not having to assume independence of the factors [3]. This data structure illustrated in Fig. 1.

2. Mean centre and unit variance scale $\mathbf{X}_{mix\ all}$ and **Y** variables.
3. Perform PCA to achieve a qualitative analysis of the data and PLS to develop the calibration model. Using PCA, a large number of correlated variables can be transformed into a smaller number of uncorrelated variables called *principal components* (PCs). Choose A number of PCs based on cumulative percentage variance explained. The PLS projection to lower dimensional subspace gives:

$$\mathbf{X}_{mix\ all,M\times O} = \sum_{i=1}^{A} t_i \cdot p_i^T + \mathbf{E}_{M\times O} = \mathbf{T}_{M\times A}\cdot\mathbf{P}_{A\times O}^T + \mathbf{E}_{M\times O} \qquad \text{where, } \mathbf{T} = \mathbf{X}_{mix\ all}\cdot\mathbf{W}^* \tag{2}$$

In this way, the data matrix $\mathbf{X}_{mix\ all}$, containing O highly correlated predictive variables is transformed into the *score* matrix, **T**, containing only A (where, A<K) independent *latent variables* (LVs), which are linear combinations of the original

manipulated variables. Thus, further design work can be conducted in the reduced subspace. The prediction of **Y** can be obtained from the PLS model as:

$$\hat{\mathbf{Y}}_{M\times L} = \sum_{i=1}^{A} t_i \cdot q_i^T = \mathbf{T}_{M\times A} \cdot \mathbf{Q}_{A\times L}^T = \mathbf{X}_{mix\ all,M\times O} \cdot \mathbf{W}_{O\times A} \cdot \mathbf{Q}_{A\times L}^T = \mathbf{X}_{mix\ all,M\times O} \cdot \hat{\mathbf{B}}_{O\times L} \tag{3}$$

P, **W*** and **Q** are the *loading* matrices, **E** is a *residual* matrix, and **B** is the regression coefficient matrix. The scores from PCA can also be used for a development of a regression model (PCR) as:

$$\hat{\mathbf{Y}}_{M\times L} = f\left(\mathbf{T}_{M\times A}\right) \qquad \text{where, } \mathbf{T} = \mathbf{X}_{mix\ all} \cdot \mathbf{P} \tag{4}$$

If new raw material properties, x^T_{new}, have to be predicted from the desired product quality specifications, y^T_{des}, then the inversion of the latent variable model gives:

$$\hat{x}^T_{new,1\times K} = \hat{y}^T_{des,1\times K} \cdot (\hat{\mathbf{B}}^T \cdot \hat{\mathbf{B}})^{-1} \cdot \hat{\mathbf{B}}^T_{L\times A} \cdot \mathbf{P}^T_{A\times K} \tag{5}$$

where, $(\hat{\mathbf{B}}^T \cdot \hat{\mathbf{B}})^{-1} \cdot \hat{\mathbf{B}}^T$ is the generalized inverse or pseudo-inverse of $\hat{\mathbf{B}}$.

Note: It is important to check and remove outliers prior to the calibration of a model. *Hotelling's* T^2 is a powerful measure of a multidimensional outlier.

4. Convert all the physico-chemical attribute properties of interest to *principal properties* (PP) [4] by using the regression coefficients from the calibration model as

$$\mathbf{T}_{M\times A} = \mathbf{Y}_{M\times L} \cdot \mathbf{B}^T_{L\times O} \tag{6}$$

5. In order to utilize the LVs in the property clustering algorithm, it is important that the LV structures follow a linear mixing rule. This can be achieved by standardizing the data structure to obtain a new $\mathbf{Q}_{MxA}$ matrix [4].

$$\mathbf{Q}_{M\times A} = \left(\sum_{i=1}^{M} \mathbf{S}^T_{O\times M}\right)^{-1} \cdot T_{M\times A} \qquad \text{where, } \mathbf{S}_{M\times O} = \mathbf{T}_{M\times A} \cdot \mathbf{P}^T_{A\times O} \tag{7}$$

6. Using the property clustering algorithm, map the problem from conserved principal property domain to the conserved componentless cluster domain [5].

$$\Psi_l\left(y_l\right)_{mix} = \sum_{u=1}^{U} x_u \cdot \Psi_l\left(y_l\right)_u \qquad \text{where, } \Psi_l\left(y_l\right)_u = Q_u \tag{8}$$

where, $\Psi_l(y_l)_u$ is an operator on the *j*'th property of stream/material, *u,* involved in the mixing. For systems of up to three properties, each vertex in a ternary diagram represents a pure latent property cluster.

7. Apply the property integration solution approach within the cluster domain by formulating and solving two reverse problems, one for identification of the synthesis/design feasibility target region (reverse of simulation problem) and another for identification of materials, blends, or plant operation conditions that match the target values identified earlier (reverse of property prediction problem) [1,5].
8. Compute the performance index based on cost, environmental impact, solubility, etc. for all feasible solutions from step 7 and rank to determine the optimal solution.

Following the above steps, one can avoid the difficulties involved with formulating and solving mixed integer non-linear programming (MINLP) problems.

3. Proof of Concept Example – Polymer Blending

The development of thermo-plastic from a mixture of starches, lactic acids and additives using latent variables in cluster space is presented as a case study to illustrate the method and concept described in this paper. The data consists of properties of starch (**X**), blend ratios of starch and other materials (**R**), molding temperature (**Z**) and final product properties (**Y**) for 28 blends. Fig. 2 represents a more complex extension of the data structure for the **X** and **R** matrixes involved in this problem than shown in Fig. 1. More details can be found in Muteki [2]. Using PCA, the first three PCs obtained captured about 87% of the total variance of the mean centered and unit variance scaled $\mathbf{X}_{mix\ all}$ [=($\mathbf{R}_{starch}$:$\mathbf{X}_{starch}$)$\mathbf{R}_{other}$**Z**] data. Latent variable models were developed stepwise by minimizing the *Bayesian Criterion* (BIC) using the PCs obtained from PCA to predict three product properties: tensile strength (TS), elongation at break (EB) and density (Rho). The general form of the model is

$$\hat{y} = \beta_0 + \sum_{i=1}^{3} \beta_i t_i + \sum_{i<j}^{3} \sum_{j>i}^{3} \beta_{ij} t_i t_j + \sum_{i=1}^{3} \beta_{ii} t_i^2 \tag{9}$$

It is desirable to cover a wide range of product properties with a minimum number of products, thus the desired product properties could be independently selected in the *cluster space* (Fig. 4 (left)) as well as in the *score space* (Fig. 4 (right)) that spans the desired property space. A mixture feasibility region in cluster space also ensures that the products within its boundary are physically feasible, consistent with past operating strategies and expected to yield the desired product qualities. LV models can be inverted to obtain mixture conditions that give the desired product quality after selecting an appropriate point or region in cluster space. Table 1 shows the calculated mixture conditions that yield the desired product properties for a target blend point that was not part of an existing product grade. Fig. 3 shows how the starch properties, the polylactic acid, the additives and the molding temperature influence the final product properties.

Table 1. Target product properties and mixture conditions

	Y			$\mathbf{R}_{starch}$			$\mathbf{R}_{other}$			**Z**
	TS (MPa)	EB (%)	Rho (g/cm^3)	Starch 1	Starch 2	Starch 3	PLA	Add 1	Add 2	Temp ^{o}C
Target	15.53	1.58	1.35	0.171	0.132	0.053	0.404	0.223	0.016	159.5

Coefficient	Tensile Strength	Tensile modulus	Elongation at Break	Density
Intercept	0	0	0	0
Amylose %	-0.25549	-0.110519	-0.273004	0.2356439
Mn	-0.108938	-0.082517	-0.080511	0.272358
Mw	-0.036264	-0.053488	0.0201779	0.1763707
Mz	-0.091851	-0.082306	-0.031031	0.2440896
PDI	-0.140953	-0.118622	-0.027782	0.282538
PLA	0.3861019	0.3455124	-0.003243	-0.252159
Additive1	-0.326327	-0.424744	0.2981036	-0.110699
Additive2	0.02548	0.1375219	-0.112882	0.1742941
Mold Temp	-0.049204	-0.033337	-0.408832	-0.09632

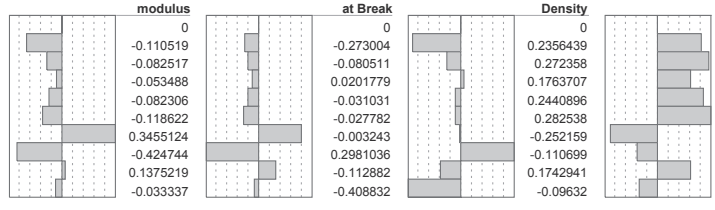

Figure 3. PLS model coefficients for blend property matrix **Y** using four latent factors**.**

Moreover, if two polymer product grades are compatible, i.e. miscible, they can be mixed together to get a polymer with properties somewhere between those of the two polymers mixed. In latent property cluster space, one can rapidly screen out inherently

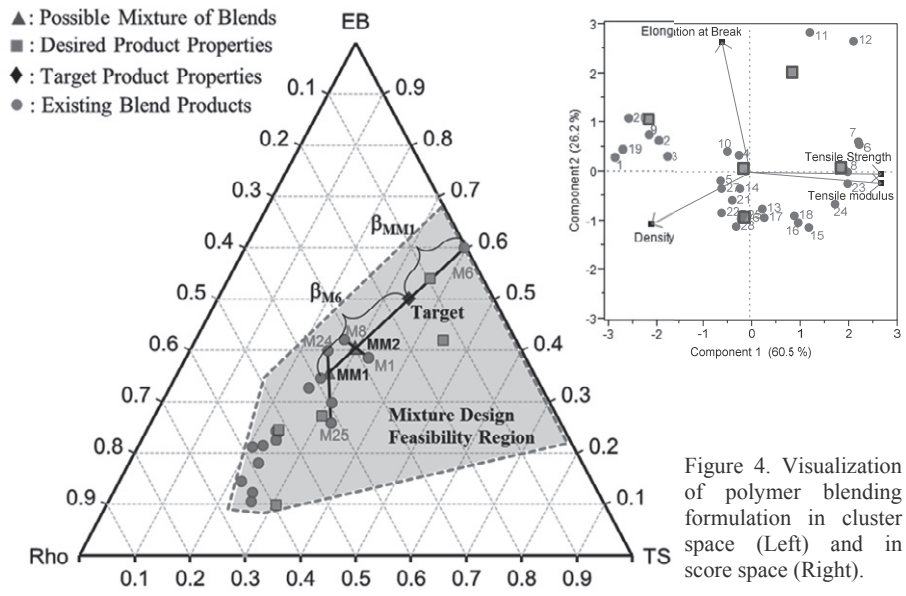

Figure 4. Visualization of polymer blending formulation in cluster space (Left) and in score space (Right).

infeasible combinations of candidate constituents visually. The reduced search space can then be explored for the feasibility of formulating binary, ternary and multi-component mixtures to achieve optimum products based on *lever-arm analysis* without extensive enumeration. For example, the same target product that can be blended from the information in Table 1 can also be formulated by mixing products M6 with MM1 (binary mixture product of M24-M25) in a proportion 0.648 and 0.352 respectively.

4. Conclusions

This research effort has been focused on formulation and solution of product design problems by systematic and insightful use of past data describing the properties of the raw materials, their blend ratios, and the process conditions to predict and enhance the performance of target product. Such a practice in industry results in fewer trials and experiments to run, thereby saving resources, capital and most importantly the product development time.

5. Acknowledgements

The authors gratefully acknowledge the financial support provided by the Southeastern Regional Sun Grant Program, and the USDA-AFRI (Award# 2011-67009-20077).

References

[1] M.R. Eden, S.B. Jørgensen, R. Gani, M.M. El-Halwagi (2003), Computer Aided Chemical Engineering, 15B, 1175-1180.
[2] K. Muteki (2006), Mixture Product Design using Latent Variable Methods, Ph.D. Thesis.
[3] N. Kettaneh-Wold (1992). Chemometrics and Intelligent Laboratory Systems, 14, 57-69.
[4] C.C. Solvason, N.G. Chemmangattuvalappil, M.R. Eden (2009), Computers and Chemical Engineering, 33, 977.
[5] M.D. Shelley, M.M. El-Halwagi (2000), Computers and Chemical Engineering, 24, 2081.

I.A. Karimi and Rajagopalan Srinivasan (Editors), Proceedings of the 11th International Symposium on Process Systems Engineering, 15-19 July 2012, Singapore.

Control strategies for flexible operation of power plant integrated with CO2 capture plant

Yu-Jeng Lin[a], Chun-Cheng Chang[a], David Shan-Hill Wong[a] Shi-Shang Jang[a] * and Jenq-Jang Ou[b]
a National Tsing-Hua University, Hsin-Chu 30013, Taiwan
b China Steel Corporation, Kaohsiung, 80012, Taiwan

Abstract

About 20% power output penalties will be incurred for implementing CO2 capture from power plant. This loss can be partially compensated by flexible operation of capture plant. However, daily large variations of liquid and gas flows may cause operation problems to packed columns. Control schemes were proposed to improve the flexibility of power output without causing substantial hydraulic disturbances in capture plant is presented. Simulations were implemented using ASPEN Plus. In varying lean solvent flow strategy, the flow rate of recycling solvent was manipulated to control the CO2 capture rate. The liquid flow of the absorber and gas flow of the stripper will vary substantially. In an alternative strategy, the lean solvent loading will be varied. Variation of gas throughput in the stripper is avoided by recycling part of CO2 vapor to stripper. This strategy provided more stable hydraulics condition in both columns and is recommended for flexible operation.

Keywords: Plantwide control, CO2 scrubbing, ASPEN PLUS, heat integration, flexible operation

1. Introduction

In recent years, global warming and climate change caused by greenhouse gases have received widespread concern. The majority of CO_2 emission comes from flue gas emitted from electricity generation, coal-fired power plant especially. The most mature technology for post combustion CO_2 capture is amine scrubbing. Pilot-scale plants of various sizes have been constructed and operated to investigate the design and operability of such processes. However, Implementing CO_2 capture incurs penalties of electric power output. Coal-fired power plant usually performs as a base load power plant that produces a steady electricity output. However, power demands fluctuate on daily and seasonal basis. Electricity has higher prices in peak load periods. It was suggested that electric power output can be increased to meet higher electricity demand by turning off CO_2 capture plant in peak hours (Cohen et al. 2010). Chalmers et al.(Chalmers, Leach et al. 2009) showed that if CO_2 trading price is included, bypassing CO_2 capture is valuable when \$/MWh electricity selling price are 2~3 times higher than \$/ton CO_2. Thus flexibility added to the power plant was proclaimed as one of the advantages of post-combustion CCS by amine scrubbing. However, a continuous process such as the amine scrubbing and regeneration process commonly used in CCS cannot be shut down and turned on at will. It should be recognized that when flue gas bypasses the CO_2 capture plant, hydraulics conditions of the absorber and the stripper will change substantially. Flooding and poor wetting will occur when the throughput

rate is too high or too low. Normal operation cannot be maintained if the throughput is turned down much beyond this limit because of poor wetting. It was also suggested that rich solvent is stored during peak load period and will be regenerated later in off-peak period (Chalmers, Lucquiaud et al. 2009). This strategy could avoid CO_2 emission penalty because CO_2 is captured all the time. However, this strategy requires huge additional tanks and solvent inventory for buffering between peak and off-peak load period. The additional cost and safety hazards can be staggering (Haines and Davison 2009). Using this strategy, a normal gas and liquid throughput can be maintained in the absorber; but large changes in throughput can still be found in the stripper. In this work, we suggested that flexible operation can be achieved by implementation of proper control strategies. The feasibility of this approach is verified using dynamic simulation of an integrated system with power generation and heat recovery sections of a power plant and the corresponding CO_2 capture plant by Aspen Plus and Aspen Dynamics.

2. 2. Process description

2.1. Power plant

A power plant model is required so that interaction between multi-stage compressor, turbine output and the CCS capture plant can be simulated. In this work, a reference 580MW power plant burning bituminous coal with 36.3% net efficiency (HHV) (NETL R&D Solutions 2007) was selected. Boiler supplies high pressure steam at 170 bar/560oC and reheated steam at 38 bar/560oC for power generation. Flue gas out from boiler then is sent to flue gas desulfurization (FGD) process for removing sulfur dioxide. After that, about 2300 ton/hr flue gas containing 13mol% CO_2 will head to CO_2 capture plant. Power extractions from steam are simulated by series of turbines with different outlet pressures. The outlet steam of each turbine is available for preheating condensate or providing heat for the reboiler in the CO_2 capture plant. To facilitate heat transfer, saturate temperature of heating steam should be at least 10^oC approach above reboiler temperature (Alie 2004).

2.2. CO_2 capture plant

The CO_2 capture plant includes two columns, absorber and stripper, and one lean/rich solvent cross heat exchanger. Flue gas carrying CO_2 generated from power plant is delivered into bottom of packed absorber to contact with lean solvent, an aqueous solution containing 30 wt% MEA. Treated gas is vented to atmosphere from top of absorber. After absorption, the rich solvent is preheated to 100^oC by heat exchanger before being sent to stripper. In the stripper, low pressure steam from power plant is injected into reboiler for CO_2 desorption.

2.3. Multi-stage compressor

CO_2 product accompanying with water vapor is about 100^oC while being stripped out from top of stripper. Before being compressed, CO_2 product is cooled to 40^oC by overhead condenser and part of water will be condensed. Further, the CO_2 is compressed from 2 to 110 bar through multi-stage compressor, which includes intercoolers to cool the exhaust gas back to 50oC before entering next stage. Each stage is simulated by compressor, heat exchanger, and condenser, responsible for compressing, cooling, and knocking water out respectively.

2.4. Heat integration

Romeo et al.(Romeo, Espatolero et al. 2008) showed that heat integration of intercoolers can save about 2% of electricity output. To implement heat integration,

first, heat acquired from cooling CO_2 in overhead condenser and intercoolers of the CCS plant is used to preheat condensate coming out of the condenser of the power plant. Part of condensate is delivered to intercoolers in parallel to cool CO_2 vapor to 50^oC before entering each compressor.

2.5. Flexible operation strategies

The actual optimal operating strategy depends on the pricing, duration of the peak load period and the trading price of CO_2 emission. In this study, we assume that an average capture rate 70% should be attained. If the peak load period is 10 hours per day, electricity output can be increased during peak load period by decreasing CO_2 capture rate to 50%; then, to balance overall capture rate to 70%, CO_2 removal rate has to increase to 90% in the next 14 off-peak load hours. The purpose is to show that we can adjust the CO_2 capture rate without causing large disturbances in the capture plant.

2.5.1. Variation of Lean Solvent Flow (VLSF)

A plantwide control strategy of CO_2 capture plant was proposed by Lin et al (Lin, Pan et al. 2011). As figure 1(a) shows, CO_2 capture rate is controlled by variation of lean solvent flow (VLSF), and reboiler temperature is controlled by manipulating reboiler steam flow rate. In VLSF control structure, flexible operation can be implemented by adjusting setpoint of CO_2 capture rate controller. Lean solvent circulating rate is varied to meet the capture rate target. In the VLSF strategy, reboiler temperature is controlled at a fixed value. Reboiler temperature is an indicator of lean loading. Hence the residual loading of CO_2 in the recirculating solvent is approximately constant during flexible operation.

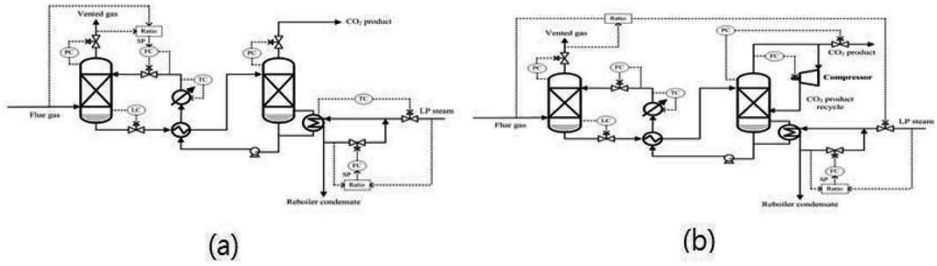

Figure 1(a) Control structure of CO_2 capture plant in variation of lean solvent flow strategy.(b) Control structure of CO_2 capture plant in variation of lean solvent loading strategy.

2.5.2. Variation of Lean Solvent Loading (VLSL)

To avoid the potential fluctuations in liquid flow in the absorber and gas and liquid flow in stripper, we propose an alternative control strategy that stabilizes the hydraulic conditions of both columns during flexible operation.

First, if the circulating lean solvent rate is fixed, lean solvent loading can be used to meet different CO_2 capture rate. The lean solvent loading can be reduced so that more CO_2 can be captured in the absorber with a steady lean solvent flow. Conversely, if we wish to reduce CO_2 capture rate, a higher the lean solvent loading can be allowed, thus reducing the load of the reboiler. Hence the scheme is based on variation of lean solvent loading, VLSL. The control scheme of variation of lean solvent loading is shown in Figure 1b. Lean solvent flow rate is controlled at a given value by a flow controller. CO_2 capture rate is controlled by manipulating reboiler steam flow rate.

2.5.3. Dynamic simulation results and discussions

To understand dynamic behaviors while implementing flexible operation, the integrated system modeled in Aspen Plus is exported to Aspen Dynamics and then simulated dynamically. After being exported to Aspen Dynamics, basic controllers that maintain steady operation are installed. There are several pressure controllers and level controllers in columns and vessels. To implement heat integration between intercoolers when CO_2 vapor flow rate is changing, condensate should be adequately distributed to overhead condenser and intercoolers. So, temperature controllers are installed to manipulate condensate flow rate to each intercooler and rest condensate is sent to overhead condenser.

A base case with 70% capture is used to demonstrate flexible operation decreasing capture rate to 90% and decreasing to 50% in two operating strategies. Fractional capacity is 63% in absorber and 54% stripper in base case.

2.5.4. Results of variation of lean solvent flow

To demonstrate operability, setpoint of capture controller is changed in ramp rate of 1% capture rate/min. Setpoint given is from 70% to 50% or 90% in 20 minutes to increase or decrease power output. Figure 2(a-b) shows dynamic responses of flexible operation implemented by VLSF strategy. CO_2 capture rate starts to change at 5th minute. When CO_2 capture rate is changing, lean solvent rate is manipulated to track correct capture rate. To cope with the changing circulating solvent rate, reboiler steam is manipulated to maintain reboiler temperature. We can see that lean solvent loading is keeping nearly at 0.37 mol CO_2/mol MEA. Using this operation strategy, fractional capacity in absorber varied in a relatively smaller range compared to simple bypass, between 55% in peak hours and 70% in off-peak hours. However, the fluctuation in stripper still exists. Fractional capacity decreases to below 40% when CO_2 capture rate is reduced to 50%.

2.5.5. Results of variation of lean solvent loading

Figure 2 (c-d) shows dynamic responses of flexible operation implemented by VLSL strategy. In this operating strategy, system successfully attains CO_2 capture targets of 50% and 90%. Lean solvent flow rate is fixed at 14000 m^3/hr. The reboiler temperature was increased to 118 ^oC to meet a higher CO_2 capture rate target of 90% and reduced to 110^oC to meet a lower CO_2 capture rate target of 50%. Lean solvent loadings also change from 0.37 to 0.41 and 0.33 mol CO_2/mol MEA at 50% and 90% capture rate respectively. Comparing new steady state value of reboiler duty obtained by two operating strategies, VLSL has slightly lower energy requirement at 90% capture and slightly higher at 50% capture rate.

In VLSL strategy, 30% of CO_2 product is recycled to stripper initially and then fractional capacity increases to 63%. Recycle rate is manipulated to maintain the gas flow rate out from top of stripper constant. By stabilize throughput of absorber and stripper in constant value, we can see that the fractional capacities in both columns are almost unchanged. Fluctuations in both columns due to large variations of liquid and vapor rate during flexible operation are avoided in this control strategy.

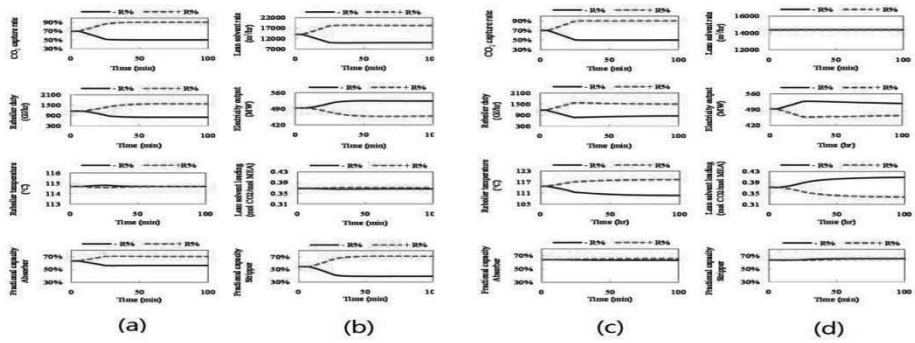

Figure 2. Dynamic responses of flexible operation adjusting capture rate from 70% to 50% and 70% to 90% implemented by variation of lean solvent flow strategy (a-b), and variation of lean solvent loading strategy (c-d).

2.6. Conclusions

Certain degree of flexibility is built in by manipulating the target of CO_2 capture in peak-load and off peak-load periods. However, large changes in hydraulic conditions absorber and stripper will occur if the amount of flue gas entering the capture plant and the amount of circulating solvents change substantially. To implement flexible operation but avoid potential fluctuations in packed columns due to large variation of liquid and gas flow rate, two operating strategy are proposed. In variation of lean solvent flow strategy, instability in absorber is partly reduced by delivering all flue gas to absorber. Capture rate is controlled by manipulating lean solvent rate and reboiler temperature is controlled at constant to maintain a nominal lean loading. In variation of lean solvent loading strategy, lean circulating solvent rate is unchanged to reduce fluctuations in both packed columns. Further, part of CO_2 product is recycled to stabilize stripper's operation. This strategy is able to maintain stable hydraulic conditions in both the absorber and stripper during both peak and off-peak load hours.

References

Alie, C. F. (2004). CO_2 Capture With MEA: Integrating the Absorption Process and Steam Cycle of an Existing Coal-Fired Power Plant, University of Waterloo. Master.

Chalmers, H., M. Leach, et al. (2009). "Valuing flexible operation of power plants with CO(2) capture." Greenhouse Gas Control Technologies 9 1(1): 4289-4296.

Chalmers, H., M. Lucquiaud, et al. (2009). "Flexible Operation of Coal Fired Power Plants with Postcombustion Capture of Carbon Dioxide." Journal of Environmental Engineering-Asce 135(6): 449-458.

Cohen, S. M., G. T. Rochelle, et al. (2010). "Turning CO_2 Capture On and Off in Response to Electric Grid Demand: A Baseline Analysis of Emissions and Economics." Journal of Energy Resources Technology-Transactions of the Asme 132(2): -.

Haines, M. R. and J. E. Davison (2009). "Designing Carbon Capture power plants to assist in meeting peak power demand." Greenhouse Gas Control Technologies 9 1(1): 1457-1464

Lin, Y. J., T. H. Pan, et al. (2011). "Plantwide Control of CO_2 Capture by Absorption and Stripping Using Monoethanolamine Solution." Industrial & Engineering Chemistry Research 50(3): 1338-1345.

NETL R&D Solutions (2007). Bituminous Coal and Natural Gas to Electricity. Cost and Performance Baseline for Fossil Energy Plants, National Energy Technology Laboratory. 1.

Romeo, L. M., S. Espatolero, et al. (2008). "Designing a supercritic/al steam cycle to integrate the energy requirements of CO_2 amine scrubbing." International Journal of Greenhouse Gas Control 2(4): 563-570.

I.A. Karimi and Rajagopalan Srinivasan (Editors), Proceedings of the 11th International Symposium on Process Systems Engineering, 15-19 July 2012, Singapore.

A framework for water footprint optimisation in the bioethanol supply chain

Andrea Bernardi, Sara Giarola and Fabrizio Bezzo*

CAPE-Lab, Dipartimento di Principi e Impianti di Ingegneria Chimica, Università di Padova, via Marzolo 9, 35131, Padova, Italy
**Corresponding Author. E-mail: fabrizio.bezzo@unipd.it*

Abstract

The transition towards more sustainable biofuels systems might be conveniently driven by purpose-devised quantitative decision-making tools based upon the optimisation of the entire Supply Chain (SC). In this work, a moMILP (multi-objective Mixed Integer Liner Programming) modelling framework is proposed to support strategic investments on bioethanol infrastructures considering both economic and environmental sustainability (e.g., impact on global warming and water resource). Corn grain and stover are accounted for as feedstocks for ethanol production; Northern Italy is taken as a geographical reference. Results show that investments strategies are affected by the trade-off between environmental and financial objectives.

Keywords: MILP optimisation, bioethanol, water footprint.

1. Introduction

In the search for a viable solution to the global energy question, bioethanol has been gaining ever greater attention as alternative energy source. Although starch-based ethanol (first generation) has greater economic profitability and currently dominates the market, second generation (cellulose-based) ethanol seems to represent the technology that may lead to substantial greenhouse gas – GHG – emissions reduction. However, a paradigm shift towards sustainable transport systems needs to account for other urgent issues. In particular, water consumption has become a major concern: its demand is expected to grow significantly, and recent occurrences of local scarcity have showed its supply vulnerability (EU, 2011). Only a few works have addressed water footprint (WF) assessment in the context of biofuels (Hoekstra *et al.*, 2011); some bioethanol production technologies have been recognised as water intensive processes (UNESCO-IHE, 2009). In order to help managing the transition towards sustainable biofuels production, WF assessment needs integrating in a comprehensive financial and environmental framework. Mathematical programming techniques can provide decision makers with the necessary quantitative tools to optimise the overall water requirement guaranteeing an efficient use of the resource. Environmental aspects (carbon and water footprint) should be coupled with economic ones within a Multi-Objective Mathematical Programming (moMP) framework involving the overall SC, to offer an effective approach to explore trade-offs between conflicting objectives. Mixed Integer Linear Programming (MILP) allows addressing alternative configurations simultaneously.

Here, a moMILP modelling framework is proposed to design long-term ethanol SCs, involving both first (from corn) and second (from stover) generation technologies, considering also the possibilities of their mutual integration within hybrid

infrastructures. This work aims at delivering an environmentally conscious decision-making tool for the optimal design of bioethanol production systems where WF assessment along the entire SC is explicitly dealt with. Several technological alternatives are characterised by varying biomass mix between corn grain and stover for bioethanol production. In addition, valuable by-products (i.e. DDGS, Distiller's Dried Grains with Solubles) and stover use to produce energy is investigated.

2. Assumptions and methods

The core task of this work is the development of a design tool to steer investment decisions on general biofuel SCs over the long-term. The objective is to determine the optimal system configuration which maximises the financial profitability while minimising the environmental impacts (i.e., GHG emissions, WF). The key variables to be optimised deal with the best bioethanol SC design in terms of: feedstock mix, plant conversion technology and by-products end-use options. The economics have been assessed by means of SC analysis techniques. Only the upstream SC is considered, involving biomass cultivation and delivery as well as fuel production. The environmental performance is evaluated by adopting LCA (Life Cycle Assessment) techniques for the whole SC according to ISO standards (ISO 14040). The energy unit is taken as a reference for the environmental analysis. In the absence of a universally recognised method to cope with the effect of by-products end-use, three approaches have been assessed: a substitution method as well as a price- and energy-based allocation procedures. The substitution method, in particular, involves that credits derived from the displacement of alternative goods with by-products are subtracted from the primary product (ethanol) overall impact. For instance, in the corn-based bioethanol system, DDGS could be used either as a substitute for cattle feed or as a fuel for CHP generation; in cellulose-based processes, lignin is exploited to produce electricity and a power excess can be sold to the national grid. In case of allocation, the overall SC impact (i.e., GHG emissions, WF) is divided among the products according to their corresponding sharing quota determined either on price or energy content.

Table 1. Ethanol technologies assessed in the study.

Process	Feedstock		Fuel to CHP			Output		
	corn	stover	NG	DDGS	stover	EtOH	CHP	DDGS
DGP	X		X			X		X
DGP-CHP	X			X		X	X	
DGP-stover	X				X	X	X	X
DAP		X				X	X	
Hybrid*	X	X			X	X	X	X
Hybrid-CHP*	X	X		X	X	X	X	

*each hybrid technology comprises three instances at varying biomass mix.

Referring to the conversion phase, ten technologies are taken into account for ethanol production (Table 1), according to the work by Giarola *et al.* (2011): first generation from corn (dry-grind process, DGP), second generation from stover (lignocellulosic process, DAP), and hybrid technologies (Hybrid), where the feedstock mix describes three corn to stover ratios (1:1, 1:2, 1:3). The use of by-products (DDGS) and stover as alternative fuels to natural gas (NG) for the power station (CHP) is then investigated.

3. Mathematical features

The problem is formulated as a moMILP model based on the mathematical approaches commonly adopted in the strategic design of multi-echelon SCs (Tsiakis *et al.*, 2001). It also embodies different features to address the capacity planning and technology selection (Liu *et al.*, 2007) of fuel systems design at the strategic level. The environmental frame is approached as in Giarola *et al.* (2011).

The economic objective function (Obj_{NPV} [€]), is estimated in terms of the Net Present Value (NPV) of the system and needs being maximised in configuring the production network to optimise business profitability. It is calculated by summing up the discounted annual cash flows ($CF_{k,t}$ [€/y]) for each technology k and time period t minus the capital investment (TCI_k [€]) when a production facility of technology k is established. Accordingly:

$$Obj_{NPV} = NPV = \sum_k \left(\sum_t \left(CF_{k,t} \cdot df_t \right) - TCI_k \right) \tag{1}$$

where df_t is the discount factor related to the year t of production considered.

Two environmental objective functions are embedded within the formulation. The former concerns minimisation of the impact on global warming, estimated in terms of the total GHG emissions due to SC operation during time, (Obj_{GHG} [kg CO_2-eq]), $TIOT^{GHG}$. This is estimated by summing up the annual impact related to technology k, $TI_{k,t}^{GHG}$ [kg CO_2-eq/y] over time:

$$Obj_{GHG} = TIOT^{GHG} = \sum_t TI_{k,t}^{GHG} \tag{2}$$

The second environmental objective function (Obj_{WF}, m^3_{H2O}) refers to the minimisation of the overall water footprint due to SC operation over time ($TIOT^{GHG}$) and determined by summing up the annual impact on water resource $TI_{k,t}^{WF}$ [m^3_{H2O}/y] of technology k for ethanol production:

$$Obj_{WF} = TIOT^{WF} = \sum_t TI_{k,t}^{WF} \tag{3}$$

In the environmental model (Eq. (4)), the total impact, $TI_{k,t}^{l}$ ($l \in \{GHG, WF\}$) accounts for both carbon and water footprints per each LCA stage s, $Imp_{k,s,t}^{l}$, [kg CO_2-eq/y or m^3_{H2O}/y]. The impact rate $Imp_{k,s,t}^{l}$ is determined by applying a properly devised impact factor, $f_{i,s}^{l}$, [kg CO_2-eq/unit or m^3_{H2O}/unit], to a reference flow, $F_{i,k,s,t}$ [units/y], specific for biomass i, technology k and LCA stage s. Accordingly:

$$TI_{k,t}^{l} = \sum_s Imp_{k,s,t}^{l} = \sum_s \sum_i f_{i,s}^{l} \cdot F_{i,k,s,t}, \qquad \forall k,t \quad l \in \{\text{GHG,WF}\} \tag{4}$$

4. Case study

The emerging ethanol production system in Northern Italy was chosen as a case study. The problem refers to a single bioethanol production plant of fixed scale (160 kt/y of ethanol) which is supplied with the necessary biomass (corn, stover or both) cultivating a hypothetical land surface of limited extension. The approach proposed by Giarola *et al.* (2011) has been adopted to evaluate the modelling parameters related to the ethanol SC and LCA issues. WF assessment has been defined according to the methodology

proposed by Hoekstra *et al.* (2009) and the modelling parameters reveal the current level of technology development (base case). In addition, three scenarios have been analysed involving improved efficiency of agricultural irrigation (A), process water consumption reduction (B) and both of them (C). Finally, alternative approaches to by-products end-use account affecting total LCA results (e.g., allocation), are evaluated.

5. Results and discussion

The optimisation problem was solved with the CPLEX solver of the GAMS® modelling tool. The resulting set of Pareto optimal solutions (P1, P2, P3) obtained with the substitution method is shown for the base case and scenario C: Figure 1.a presents the trade-off between WF and the NPV; Figure 1.b illustrates the trade-off between the two environmental objectives. In the following, the base case results is first discussed, then the effects of increased efficiency in water consumption outlined. Finally a discussion is provided about the allocation procedure consequences on the optimisation results.

The economic optimum (point P1 in Figure 1.a) involves the establishment of the standard DGP process with DDGS sold as animal fodder. This option allows for more revenues coming from the by-product selling and results in a normalised NPV of 0.54 €/GJ. The environmental outcomes show a high impact on global warming (78.03 kg CO_2/GJ, Figure 1.b) as well as on WF (about 6.16 m^3/GJ). This configuration results in a medium stress of water withdrawals over resource availability (UNESCO-IHE, 2009).

Moving down towards a better environmental performance, (point P2 in Figure 1) the strategic investment involves the establishment of a hybrid technology with a corn/stover ratio of 1/3, where DDGS is sold as animal fodder. This solution has a lower profitability (NPV equal to 0.03 €/GJ, Figure 1.a), but leads to great improvements in the environmental performance (e.g., WF is about 1.71 m^3/GJ and GHG emissions drop down to 13.59 kg CO_2-eq/GJ).

The environmental optimum (point P3 in Figure 1) involves the establishment of a standard DAP process. The negative value for the WF (-0.046 m^3/GJ) is due to the amount of credits from electricity displacement which exceeds the water consumed along the entire SC. The carbon footprint is reduced down to 1.8 kg CO_2-eq/GJ (Figure 1.b). This is mainly due to the lower emissions resulting from stover production and conversion to ethanol when compared to conventional first generation biomass. However, this solution is not economically sustainable: the normalised NPV drops down to -4.31 €/GJ (Figure 1.a), which clearly shows the scarce competitiveness of the business due to the consistent capital costs.

The improvement of water efficiency in scenarios A, B and C does not change the optimal solutions, in terms of technology selection for the business to be established. WF changes considerably, however, dropping down to 4.1 and 0.72 m^3/GJ for solutions P1 and P2 of scenario C (with about 33% and 58% of reduction with respect to the base case). A complete cellulose-based facility (P3) will lead to a negative WF (-0.19 m^3/GJ, Figure 1), thus providing water use savings up to four times greater than the base case. The water use decrease characterising scenario C, is mainly due to improvements of irrigation efficiency for solutions P1 and P2, accounting for about 31% and 49% of WF reduction (scenario A). Being corn stover a residual feedstock, according to the substitution method, which attributes the overall water consumption to the main crop, a complete stover-based WF, solution P3 (Figure 1), is not affected by increasing efficiency of irrigation, but from process water usage optimisation, only (scenario B).

Two allocation methods have also been considered to estimate the impacts in terms of WF and GHG emissions. Price allocation gives the same trade-off between

environmental and economic purposes as those obtained with the expansion method in terms of technological selection. According to an energy allocation method, the DAP process, while minimising the GHG emissions, produces a greater WF than first generation, which becomes the most suitable solution not only on economic terms but also when considering water use impact.

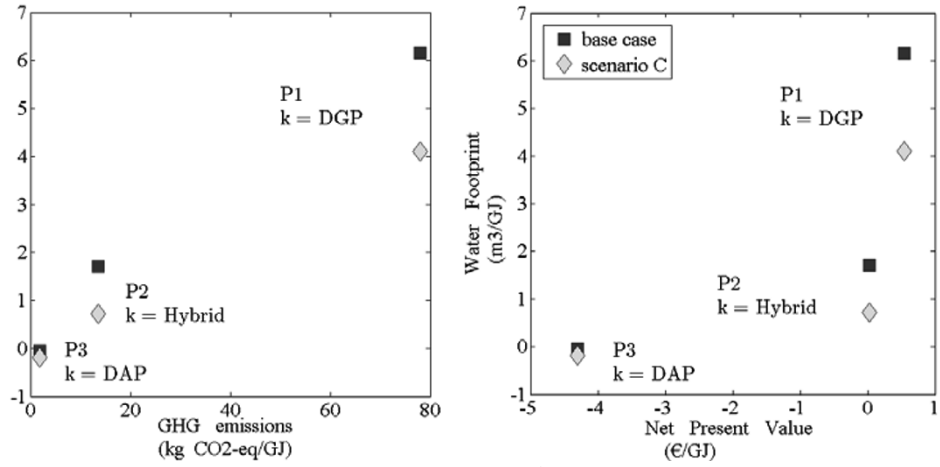

Figure 1: Pareto frontier: impact on water footprint against a) NPV, and b) GHG emissions.

6. Final remarks

A moMILP modelling framework to support strategic design and planning of biofuel systems has been developed in steering the transition towards more sustainable generation productions under both economic and environmental criteria. Results show that business strategies are influenced by the trade-off between profitability and sustainability. Some ethanol production processes (first generation) involve intensive use of water resource, but results are significantly affected by the procedure used to account for by-products end-use effect on the overall environmental SC performance.

Acknowledgements

Fondazione Cariparo is acknowledged for Progetti Dottorati di Ricerca 2008 and 2011.

References

EU, 2011, Third Follow up Report to the Communication on water scarcity and droughts in the European Union COM (2007) 414 final (2011).

UNESCO-IHE, 2009,Value of water, Research Report Series, n.38.

S. Giarola *et al.*, 2011, Spatially explicit multi-objective optimisation for design and planning of hybrid first and second generation biorefineries. Comput Chem Eng, 35, 1782-1797

A.Y. Hoekstra *et al.*, 2011, The water footprint assessment manual, London: Earthscan.

P. Liu *et al.*, 2007, Modelling and optimisation of polygeneration energy systems, Catal Today, 127, 347-359.

P. Tsiakis *et al.*, 2001, Design of multi-echelon supply chain networks under demand uncertainty, Ind Eng Chem Res, 40, 3585-3604.

I.A. Karimi and Rajagopalan Srinivasan (Editors), Proceedings of the 11th International Symposium on Process Systems Engineering, 15-19 July 2012, Singapore

Steady-state multiplicity of a biogas production system based on anaerobic digestion

Astrid Bornhöft[a], Richard Hanke-Rauschenbach[b,*], Kai Sundmacher[a,b]

[a]*Otto-von-Guericke University Magdeburg, Process Systems Engineering, Universitätsplatz 2, 39106 Magdeburg, Germany*

[b]*Max Planck Institute for Dynamics of Complex Technical Systems, Sandtorstraße 1, 39106 Magdeburg, Germany*

Abstract

In the present contribution a biogas production system is systematically analysed based on the Anaerobic Digestion Model No.1 (ADM1). Steady-state solutions as well as dynamic responses after disturbances are taken into account. The stationary solutions give insights in the qualitative difference of operation conditions. Conclusions are drawn from the analysis of the transient behaviour regarding intervention strategies after disturbances.

Keywords: biogas production system, anaerobic digestion, steady-state multiplicity, ADM1

1. Introduction

Currently, the complex problems of energy supply become increasingly important. The world is faced with two main difficulties: the limitations of fossil resources, while the energy demand is rising, as well as the problems caused by increasing CO_2 emissions. In this context, the utilization of biomass is a promising option for a sustainable energy supply, because it is a renewable and easily available resource.

One technology following this direction is anaerobic digestion for biogas production. Fig. 1 shows a scheme of such a biogas plant. The essential component is the biogas fermenter, where organic matter, such as wastes or energy crops as well as cattle manure, is biochemically degraded to biogas. The biogas contains carbon dioxide and methane and can be used in power plants or fuel cells to produce electricity and heat. The remaining digestate can be used as a natural fertiliser and closes the nutrient cycle.

The anaerobic digestion process, like every biological system, is characterized by large complexity. It arises from different aspects such as a large number of metabolites and its heterogeneity with selective interactions (Kitano, 2000). Furthermore macroscopic phenomena like different phases and physical effects play an important role. In particular anaerobic digestion is a complex multi-step degradation process (see illustration Fig. 1 right hand side). Due to its structure the system shows strongly nonlinear behaviour such as steady-state multiplicity (Shen et al., 2007). Therefore a detailed stationary and transient analysis of the anaerobic digestion process is performed in the present study. The findings are applied for operation issues of biogas plants.

2. Model based approach

In the present contribution the Anaerobic Digestion Model No. 1 (ADM1) is analysed to study the complex system of anaerobic digestion. ADM1 was introduced in 2002 by

*hanke-rauschenbach@mpi-magdeburg.mpg.de

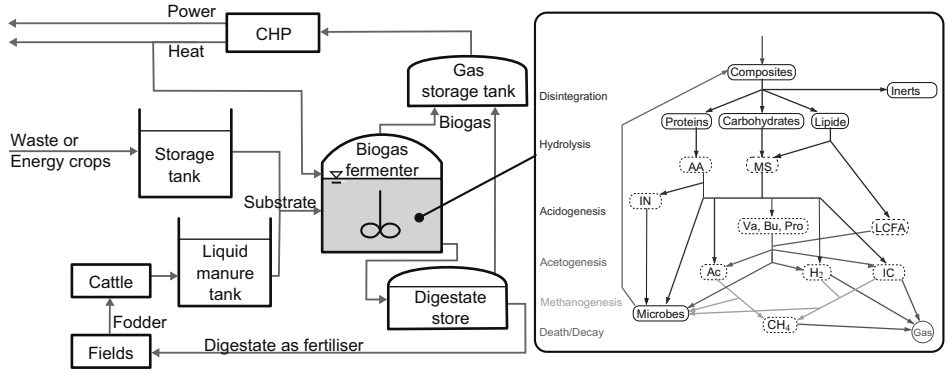

Figure 1. Scheme of components of a biogas plant (left) and reaction steps within the anaerobic digestion (right).

Batstone et al. (2002) and since then successfully used in several analyses (see e.g. review of Batstone et al. (2006)). The application not only to waste water but also to agricultural waste and energy crops has been demonstrated e.g. by Koch et al. (2010) and (Zhou et al., 2011).

ADM1 is a kinetic model and considers two compartments, namely a liquid and a gas phase. For each of them spatially lumped material balances are formulated. The biochemical reactions and the liquid-gas transfer are included through sink and source terms in the material balances. For the different processes first order kinetics and Monod kinetics are assumed. The microbial degradation processes can be inhibited by different mechanisms (e.g. pH and ammonium), which are modelled by nonlinear inhibition factors. Furthermore acid base reactions are included and assumed to be in equilibrium to determine the pH value. The liquid-gas transfer is modelled as first order kinetics with respect to Henry's law.

The complete model consists of 15 algebraic and 29 ordinary differential equations. This differential algebraic equation system was implemented in MATLAB and analysed using bifurcation theory. The results of the stationary analysis and the study of the dynamic effects are described in the next section.

3. Results

The biogas reactor has typically two input parameters which can be influenced by the operator. The first one is the dilution rate D, which can be easily changed by the flow rate of the substrate. The second one is the inlet substrate concentration $X_{\mathrm{C,in}}$. The output variables of interest are for example the methane flow rate G_{CH4}, the biogas flow rate q_{gas} or the pH value.

3.1. Steady-state operating boundary

In a first step of the analysis only the dilution rate is changed whereas the inlet substrate concentration is kept constant. It was found that depending on the operation condition

the system can reach up to ten different steady-states (not shown here). One relevant output value is the methane flow rate at the different steady-state solutions. It is shown in Fig. 2 (a). There it can be seen, that at branches III–X no methane is produced, consequently they are not desirable for the operation. Since branch II is unstable, indicated by the dashed line in Fig. 2 (a), it is also not a feasible working point. The only meaningful solution of the system is branch I, as it is stable and methane is produced.

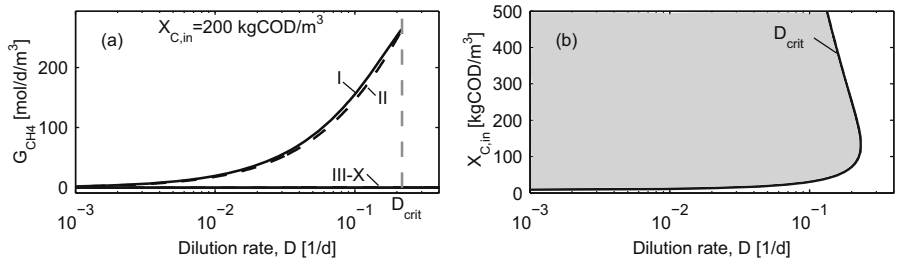

Figure 2. (a) Molar methane flow rate at steady-state solutions depending on dilution rate D and for a given inlet substrate concentration $X_{\mathrm{C,in}} = 200\,kgCOD/m^3$. *(b) Dependency of critical dilution rate* D_{crit} *on inlet substrate concentration* $X_{\mathrm{C,in}}$. *The grey area shows the feasible operating range.*

Furthermore it can be seen, that branch I ends at a critical dilution rate D_{crit}. For larger dilution rates no methane can be produced, this state is commonly known as the washout state and is obviously undesired for the system operation.

In the second step of the analysis the influence of the inlet substrate concentration on the critical dilution rate is analysed, the results are shown in Fig. 2 (b). The resulting curve is very important for the operation, since only on the left hand side (grey area) a methane producing working point is feasible. To determine a favourable operating point within that area, Fig. 3 shows the methane flow rate (3a) and the methane yield (3b).

It becomes obvious that for the operation of a biogas plant, there is a trade-off between high yield and high methane production rates. That corresponds to the considerations of higher investment costs for larger reactors against higher operation costs for a larger amount of feedstock. Typically the investment costs for the reactor are much higher than the costs for the substrate. Consequently, the biogas plants are intended to operate as close as possible to the washout line (Liu et al., 2004).

3.2. Critical disturbances: Analysis and intervention

As discussed before, the operation near the boundary curve is favourable. However, this kind of operation is risky, because the exact location is a priori unknown and due to disturbances the boundary can be crossed eventually. One can divide possible disturbances into two classes: On the one hand disturbances within the operation area, which lead to a desirable new operating point, and on the other hand the boundary crossing disturbances, that lead to washout states.

Both kinds of disturbances are systematically analysed. It was found, that they differ qualitatively in the dynamic response. Here only one example is shown (Fig. 4), namely

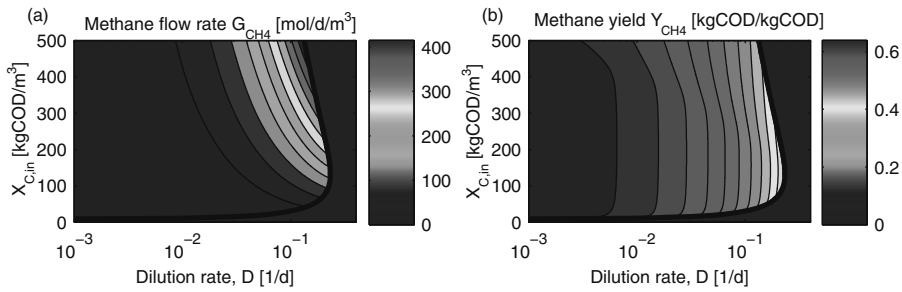

Figure 3. Steady-state solutions with respect to dilution rate D and inlet substrate concentration $X_{C,in}$: (a) Molar methane flow rate, (b) Methane yield.

an increase of the dilution rate to a higher value than the critical dilution rate at t=0 days (see Fig. 4 (b)). Fig. 4 (c) shows the transient of the volumetric flow rate of the biogas (in black). It initially increases and then rapidly decreases to a new lower value. The pH value in Fig. 4 (d) shows a continuous decrease.

The analysis of different disturbances indicates that the overshoot of the biogas flow rate in conjunction with the decrease of the pH value is typical for critical disturbances. The

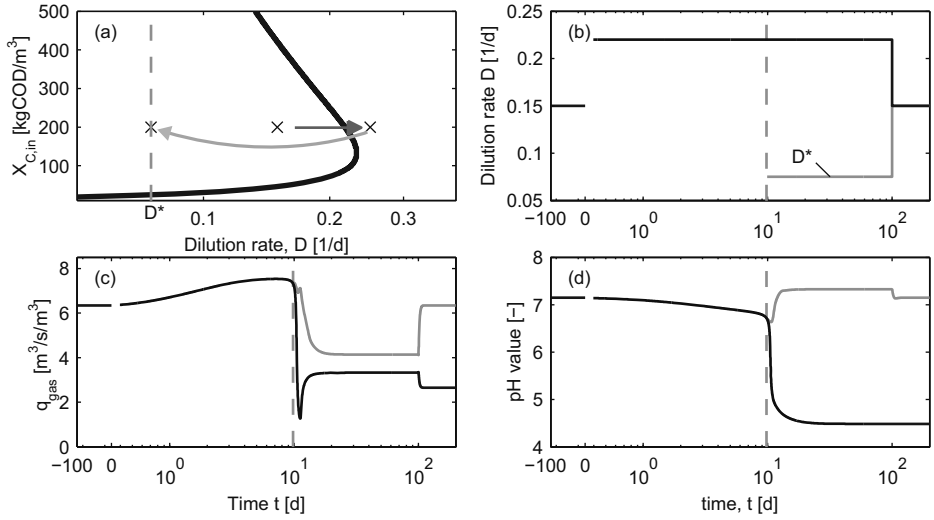

Figure 4. Dynamic system response: (a) Red arrow disturbance; grey arrow intervention, (b) Dilution rate over time, (c) Volumetric flow rate of biogas over time, (d) pH value over time.

following deduced diagnosis rule can be used as a tool to detect critical disturbances before the undesired washout state is reached.

$$\frac{\mathrm{d}q_{\mathrm{gas}}(t)}{\mathrm{d}t} = 0; \qquad \frac{\mathrm{d}q^2_{\mathrm{gas}}(t)}{\mathrm{d}^2t} < 0; \qquad \frac{\mathrm{dpH}(t)}{\mathrm{d}t} < 0 \tag{1}$$

Once the critical disturbance is detected, the operator can intervene to avoid the washout state. An example for an intervention is a reduction of the dilution rate. It is illustrated in Fig. 4 (grey lines). It can be seen, that after the intervention the old operating point can be reached again. In contrast to that without an intervention the system remains in the washout state and is not producing any methane (black line in Fig. 4).

4. Conclusions

In the present contribution ADM1 is analysed with respect to steady-state multiplicity and up to 10 coexisting stationary solutions were found depending on the input parameter. Furthermore different disturbances and intervention strategies were systematically analysed and qualitative operating diagrams were generated. They give information in what way the suggested strategy acts and whether and in which region it is successful. In a next step this theoretical considerations will be validated experimentally.

References

Batstone, D. J., Keller, J., Angelidaki, I., Kalyuzhnyi, S. V., Pavlostathis, S. G., Rozzi, A., Sanders, W. T. M., Siegrist, H., Vavilin, V. A., 2002. The iwa anaerobic digestion model no 1 (adm1). Water Science and Technology 45 (10), 65–73.

Batstone, D. J., Keller, J., Steyer, J. P., 2006. A review of adm1 extensions, applications, and analysis: 2002-2005. Water Science and Technology 54 (4), 1–10.

Kitano, H., 2000. Perspectives on systems biology. New Generation Computing 18 (3), 199–216.

Koch, K., Lubken, M., Gehring, T., Wichern, M., Horn, H., 2010. Biogas from grass silage - measurements and modeling with adm1. Bioresource Technology 101 (21), 8158–8165.

Liu, J., Olsson, G., Mattiasson, B., 2004. Monitoring and control of an anaerobic upflow fixed-bed reactor for high-loading-rate operation and rejection of disturbances. Biotechnology and Bioengineering 87 (1), 43–53.

Shen, S. W., Premier, G. C., Guwy, A., Dinsdale, R., 2007. Bifurcation and stability analysis of an anaerobic digestion model. Nonlinear Dynamics 48 (4), 391–408.

Zhou, H. D., Loffler, D., Kranert, M., 2011. Model-based predictions of anaerobic digestion of agricultural substrates for biogas production. Bioresource Technology 102 (23), 10819–10828.

I.A. Karimi and Rajagopalan Srinivasan (Editors), Proceedings of the 11th International Symposium on Process Systems Engineering, 15-19 July 2012, Singapore.

A Unified Approach for the Optimization of Energy and Water in Multipurpose Batch Plants

Omobolanle Adekola[a], Jane D. Stamp[a], Thokozani Majozi[a,b*], Anurag Garg[c], Santanu Bandyopadhyay[d]

[a]*Department of Chemical Engineering, University of Pretoria, Lynnwood Road, Pretoria, 0002, South Africa*
[b]*Modelling and Digital Science, CSIR, Meiring Naude Road, Pretoria, 0002, South Africa*
[c]*Centre for Environmental Science and Engineering, Indian Institute of Technology Bombay, Powai, Mumbai, 400076, India*
[d]*Department of Energy Science and Engineering, Indian Institute of Technology Bombay, Powai, Mumbai, 400076, India*
**Corresponding Author:* thoko.majozi@up.ac.za

Abstract

Presented in this paper, a unified framework to optimize both water and energy usage simultaneously, together with the scheduling problem, is developed. In this manner, the timing of tasks remains a variable throughout optimization. Due to the fact that a flexible process schedule is employed, an improved result in the form of a better overall production schedule compared to the schedules obtained from optimizing water and energy separately is achievable. Opportunities for direct water reuse and indirect water reuse, using wastewater storage, were explored. Both direct and indirect heat integration were explored for reducing external utilities. The objective was to improve the profitability of the plant by minimizing wastewater generation and utility usage. The results from a case study show that the profit using only external utilities and freshwater was 18 537 cu with requirements of 390 kWh for cooling water, 240 kWh for steam and 816 kg for freshwater. The profit improved to 22 235 cu when opportunities for both direct and indirect water reuse as well as direct and indirect heat integration were explored. In this case, the requirements for cooling water, steam and freshwater were 190 kWh, 10 kWh and 896 kg, respectively.

Keywords: Wastewater minimization, heat integration, heat storage, multipurpose

1. Introduction

Utility and water requirements in many batch plants, such as in the food industry, breweries, dairies, biochemical plants and agrochemical facilities, contribute largely to their overall running costs. Heating and cooling are unavoidable aspects of many plant facilities, with operations where heat is generated and others where heat is required. It is because of this occurrence that heat integration becomes a possibility. Process equipment cleaning is usually associated with large amounts of water, due to the inherent sharing of equipment by different tasks. Hence, efficient use of water for process equipment cleaning is pursued to ensure that the amount of freshwater consumed as well as the amount of wastewater generated is minimized.

Published literature exists for the independent consideration of wastewater minimization (Gouws *et al.,* 2010; Liu *et al.,* 2009; Adekola & Majozi, 2011) and heat integration (Halim & Srinivasan, 2009; Stamp & Majozi 2011) in batch plants. The simultaneous consideration of both wastewater minimization and heat integration has been largely ignored, due to the potential complexities of such a model.

Halim and Srinivasan (2011) developed a framework that integrated scheduling, direct heat integration and direct water reuse optimization based on sequential steps. Firstly, the process schedule was optimized to meet an economic objective. This was followed by the generation of alternate schedules through a stochastic search-based integer cut procedure. These alternate schedules were used to optimize energy and water consumption with the aim of retaining the optimality of the scheduling solution. Next, heat integration analysis and water reuse synthesis were each performed to optimize water and energy requirements on each schedule.

2. Problem Statement

The problem considered in this paper can be stated as follows.
Given:

(i) Scheduling data (production recipe for each product, available units and their capacities, time horizon of interest, costs of raw materials and products)
(ii) Heat integration data (hot and cold duties of tasks, operating temperatures of tasks, minimum allowable temperature differences, design limits on heat storage, cost of utilities)
(iii) Wastewater minimization data (mass load of contaminant, maximum inlet and outlet concentration of contaminants, washing time for each unit, storage capacity for water, cost of freshwater and effluent treatment)

Determine the production schedule that achieves the maximum profit with the minimum amount of external utility and freshwater use.

3. Mathematical Formulation

The mathematical formulation consists of three modules: production scheduling, heat integration and wastewater minimization. For production scheduling, the objective is profit maximization. During production, certain tasks require cooling or heating, for instance, exothermic reactions that require cooling or endothermic reactions that require heating. The requirements for heating or cooling afford opportunities for heat integration. In multipurpose batch plants, particularly at the completion of a processing task in a unit, the equipment unit is washed before performing subsequent tasks. This is to ensure product quality and prevent contamination. The washing operations present an opportunity for wastewater minimization. For the sake of brevity, only the objective function, maximization of profit, is presented in Equation (1). The first term is product revenue, the second term is the cost of freshwater, the third term is the cost of effluent treatment, the fourth is the cost of cooling water and the last term is the cost of steam. The complete description of the heat integration constraints used in this model can be found in literature (Stamp & Majozi, 2011) and also the complete description of the wastewater minimization constraints (Adekola & Majozi, 2011). These two formulations were embedded in a production scheduling framework based on the state sequence network representation of Majozi and Zhu (2001). The overall formulation resulted in a mixed integer nonlinear problem, MINLP.

$$Max\ profit = \sum_{s}\sum_{p} CP(s)d(s,p) - CF\sum_{s_{in,j}}\sum_{p} mw_f\left(s_{in,j},p\right) - CE\sum_{s_{in,j}}\sum_{p} mw_e\left(s_{in,j},p\right) - Cost\_cw\sum_{s_{in,jh}}\sum_{p} cw\left(s_{in,jh},p\right) - Cost\_st\sum_{s_{in,jc}}\sum_{p} st\left(s_{in,jc},p\right) \quad (1)$$

4. Case Study

Consider the multipurpose batch facility in Figure 1 popularly referred to as Batch1 in literature (Kondili *et al.,* 1993), which has been adapted to suit the problem at hand. The heat integration data are given in Table 1. The production data and wastewater minimization data can be obtained from literature (Adekola & Majozi, 2011). The time horizon of interest is 12 h. The costs of steam, cooling water, freshwater and effluent treatment are 10 cu, 2 cu, 2 cu and 3 cu (cost units) respectively.

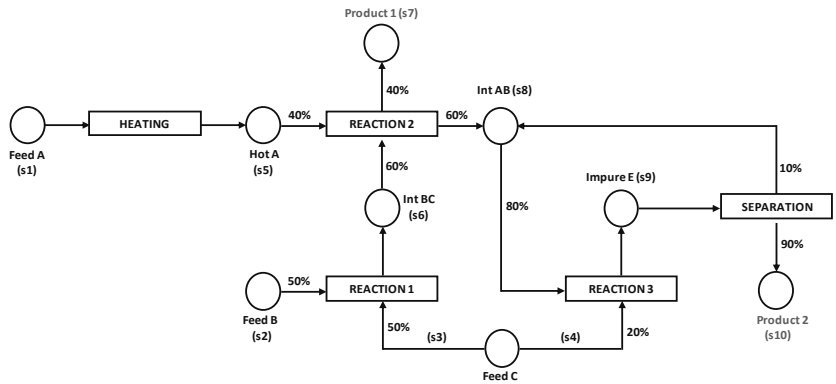

Figure 1.Multipurpose batch facility, Batch1.

Table 1.Heat integration data.

Reaction	Type	Heating/cooling requirement (kWh)	Operating Temperature (°C)
RX1	exothermic	60 (cooling)	100
RX2	endothermic	80 (heating)	60
RX3	exothermic	70 (cooling)	140

The case study was solved with GAMS 22.0 using the DICOPT2 algorithm, with CPLEX 9.1.2 as the MIP and CONOPT3 as the NLP solvers. Different variations of the case study were solved to demonstrate the capabilities of the developed model, the results of which are provided in Table 2. These variations are as follows:

- Production scheduling + freshwater + hot and cold utilities
- Production scheduling + freshwater + direct water reuse + hot and cold utilities + direct heat integration
- Production scheduling + freshwater + direct/indirect water reuse + hot and cold utilities + direct/indirect heat integration

Direct water reuse refers to the use of an outlet wastewater stream from a processing unit in another processing unit. Indirect water reuse refers to the use of previously stored wastewater in a procesing unit. Similarly, direct heat integration refers to the use of heat generated from a processing unit, in a processing unit requiring heat. Indirect

heat integration refers to the use of heat previously stored in a heat storage vessel by a processing unit requiring heat. The storage capacity for indirect water reuse was given to be 200 kg. In the case of indirect heat integration, heat is stored through a fluid medium. The storage capacity and the initial storage temperature of the storage vessel are variables to be optimized (Stamp & Majozi 2011). Heat losses were not considered.

Table 2.Results of the case study.

	Freshwater and utilities	Direct water reuse and direct heat integration	Direct/indirect water reuse and direct/indirect heat integration
Profit (cu)	18 537	19 836	22 235
Cooling water (kWh)	390	250	190
Steam (kWh)	240	180	10
Freshwater (kg)	816	1 020	896
Time points	11	11	13
CPU time (s)	9.9	110.7	176 705
Binary variables	128	508	954
Initial storage temperature (ºC)			82.9
Heat storage capacity (ton)			2.024

From Table 2 it can be observed that the inclusion of both indirect water reuse and indirect heat integration lead to a substantial decrease in both the utility and freshwater requirements. The resulting process schedule for the results in column 4 is illustrated in Figure 2.

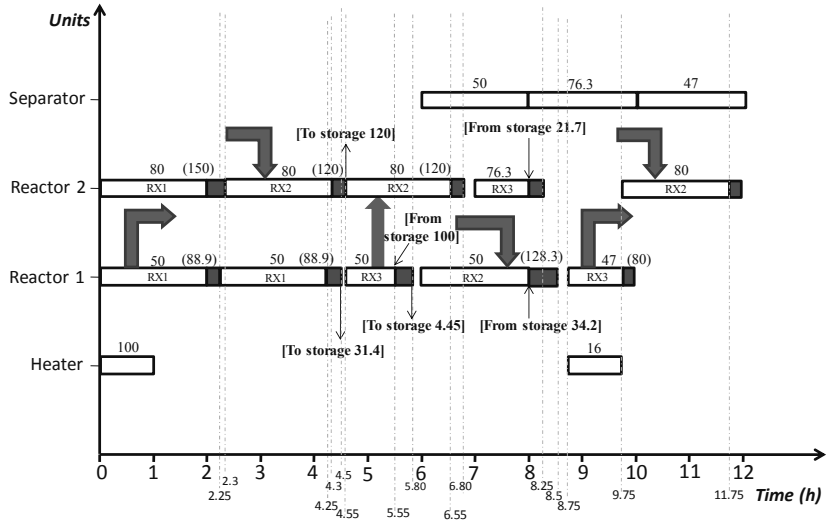

Figure 2. Resulting process schedule when both direct/indirect heat integration and wastewater minimization are possible.

The clear blocks represent the production operation in the unit while the dark blocks represent the washing operations which take place after tasks are completed. The numbers above the clear blocks represent the amount of raw material used in the unit for

production and the numbers in brackets represent freshwater. Water transfer to and from storage has been clearly labelled. The straight arrows represent direct heat integration, while the bent arrows represent indirect heat integration to or from the heat storage unit.

A comparison was made between the simple sequential profit maximization problem from Halim and Srinivasan (2011). The results can be seen in Table 3. The overall profit improved in the simultaneous case when compared to the sequential method.

Table 3.Statistics of profit maximization comparison.

	Halim & Srinivasan (2011)	Proposed formulation
Profit ($)	4 764	4 773
Cooling water duty (MJ)	313.9	319
Steam duty (MJ)	43.9	11.5
Freshwater (kg)	1238.4	1086
Time points	7 (slots)	9
CPU time (s)		500

5. Conclusions

In the presented method, wastewater minimization and heat integration are both embedded within the scheduling framework, thus leading to a truly flexible process schedule. Results from a case study show that profit maximization together with heat integration and wastewater minimization were achieved. The profit using only external utilities and freshwater was 18 537 cu with requirements of 390 kWh for cooling water, 240 kWh for steam and 816 kg for freshwater. The profit improved to 22 235 cu when opportunities for both direct and indirect water reuse as well as direct and indirect heat integration were explored. In this case, the requirements for cooling water, steam and freshwater were 190 kWh, 10 kWh and 896 kg, respectively. The optimality of the case study solution was determined using the procedure used by Adekola and Majozi (2011) and Stamp and Majozi (2011).

References

O. Adekola and T. Majozi, 2011, Wastewater minimization in multipurpose batch plants with a regeneration unit: Multiple contaminants, *Comp. Chem. Eng.,* 35 (12) 2824-2836.

J.F. Gouws, T. Majozi, D.C.Y. Foo, C.L. Chen and J.Y. Lee, 2010, Water minimization techniques for batch processes,*Ind. Eng. Chem. Res.,* 48 (19), 8877-8893.

I. Halim and R. Srinivasan, 2009, Sequential methodology for scheduling of heat-integrated batch plants, *Ind. Eng. Chem. Res.*, 48 (18), 8551-8565.

I. Halim and R. Srinivasan, 2011, Sequential methodology for integrated optimization of enegy and water use during batch process scheduling, *Comp. Chem. Eng.* 35, 1575-1597.

E. Kondili, C.C. Pantelides and R.W.H. Sargent, 1993, A general algorithm for short-term scheduling of batch operations – I. MILP formulation, *Comp. Chem. Eng.*, 17 (2), 211-227.

Y. Liu, G. Li, L. Wang, J. Zhang and K. Shams, 2009, Optimal design of an integrated discontinuous water-using network coordinating with a central regeneration unit, *Ind. Eng. Chem. Res.,* 48 (24), 10924-10940.

T. Majozi and X. X. Zhu, 2001, A novel continuous-time MILP formulation for multipurpose batch plants. 1. Short term scheduling, *Ind. Eng. Chem. Res.,* 40 5935-5949.

J.D. Stamp and T. Majozi, 2011, Optimum heat storage design for heat integrated multipurpose batch plants, *Energy,* 36 5119-5131.

I.A. Karimi and Rajagopalan Srinivasan (Editors), Proceedings of the 11th International Symposium on Process Systems Engineering, 15-19 July 2012, Singapore

Evaluation of coal-based dimethyl ether production system using life cycle assessment in South Korea

Seunghyok Kim[a], Jaeha Kim[a], En Sup Yoon[a,b] *

[a] *School of Chemical and Biological Engineering, Institute of Chemical Processes, Seoul National University, Seoul, Republic of Korea*

[b] *Automation System Research Institute, Seoul National University, Seoul, Republic of Korea*

Abstract

Dimethyl ether is one of the sustainable energy sources because it is clean and easy to handle. DME can be produced from various materials such as coal, natural gas (NG), and biomass. Actually, NG-based DME plant is in operation in Korea. Many studies have also investigated NG-based processes and reactor design needed for use of dimethyl ether. Unlike the previous studies, this study focuses on DME production system using coal as a raw material. Coal is drawing attention as the upcoming energy source due to the depletion of oil in Korea. Whereas Korea depends entirely on imports for crude oil, coal can be supplied by domestic production. To decide coal as a raw material, we need to assess the competitiveness of coal. A life cycle assessment of coal-based DME production system was performed to evaluate environmental impact and energy consumption. The assessment of coal-based DME production system with respect to the environment and energy use is essential for sustainable DME production in Korea. The aim of this study was to analyze the amount of CO_2 emission and energy consumption of coal-based DME production. The life cycle of DME production includes the mining of coal, pretreatment of the mined coal, transportation to the DME production plant, and DME conversion. Related data and the assumptions pertinent to South Korea are introduced and adopted as a case study.

Keywords: life cycle assessment, dimethyl ether, coal-based DME production

1. Introduction

Ensuring of energy security may be major challenges to secure national competitiveness. The current crisis regarding the depletion of oil resources around the world demands the development of a next generation energy system in many countries. Korea is no exception; actually Korean government has invested many efforts to control its energy situation for sustainable development. Among the candidates for upcoming energy resources, dimethyl ether (DME) is one of the most favorable because it can easily replace conventional fuels and is more eco-friendly than traditional fuels.

DME can be synthesized in at least two steps. The first is the synthetic gas (syngas) generation step; hydrocarbons obtained from natural gas, coal, or biomass are converted to synthetic gas (syngas), which is a combination of carbon monoxide (CO) and hydrogen gas. The second is the DME conversion step; the obtained syngas is converted to

*esyoon@pslab.snu.ac.kr

DME by several processes. DME conversion process has two different methods. These methods are indirect synthesis and direct synthesis. Indirect synthesis requires two reactors for methanol synthesis and dehydration whereas direct synthesis produces DME directly from syngas and does not include the intermediate steps of methanol production and purification.

The commercial DME plant using direct synthesis method have been in operation in Korea. The natural gas (NG) is now used as a raw material for DME production. Meanwhile, a coal is in the limelight for DME production because the domestic consumption of NG is growing rapidly. Korean government needs to seek alternatives to replace the NG as the price of NG grows. In this study, a DME production system from coal is analyzed for an entire life cycle. For sustainability, the analysis considers the factors of energy and carbon dioxide emission, and the life cycle of DME production includes the mining of coal, pretreatment of the mined coal, transportation to the DME production plant, and DME conversion. All processes for DME synthesis are simulated using an ASPEN Plus simulator. Recent technologies pertinent to practical plant in Korea and Korean energy situation data are introduced in the case study.

2. LCA of DME production processes

2.1. Life cycle assessment (LCA)

Life cycle assessment (LCA) is a technique used to identify the environmental load and lessen environmental impact, and a critical factor determining policy decisions. The main aim of LCA is to quantify and compare the full range of environmental impacts of materials and/or processes. In this study, LCA is used to evaluate coal as a raw material for DME production. Obtaining raw materials, pretreatment, manufacture, transportation, use and disposal are all involved in the life cycle. As a rule, LCA is comprised of four phases with include goal and scope definition, inventory analysis, impact assessment, and interpretation.

2.2. Goal and scope definition

The goal of this study is to assess the environmental impact (e.g. CO_2 emission) and energy impact of the entire DME production process. The prospective raw material in this study is coal. The scope of the DME production process includes the pretreatment of coal, transportation, and conversion. The main structure of the system is shown in Figure 1, and a detailed description will be presented in subsequent sections.

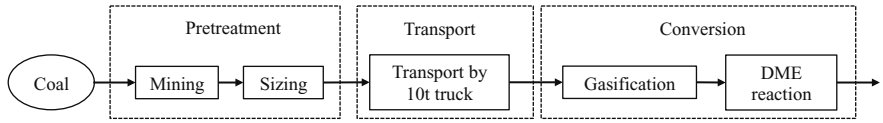

Figure 1. Block diagram of DME production

2.3. Inventory analysis

As previously mentioned, a coal is treated in accordance with the defined scope. The pretreatment process represents improvement of the quality of raw coal for DME conver-

sion. The transportation process includes movement of coal to the DME production plant, and the conversion process includes syngas production and the DME reaction. These inventories are simulated using an Aspen Plus simulator based on some assumptions. The capacity of a DME plant is assigned as 1,000 t/day, which is the practical target in a Korea Gas Corporation (KOGAS) DME plant (Baek et al., 2010). The amount of CO_2 emission and energy consumption is adopted for inventory analysis, the intensity term is introduced. The intensity parameters can be calculated by Equations (1) and (2).

$$\text{CO}_2 \text{ emission intensity}_{inv} = \frac{w_{CO_2,inv}}{PE_{DME}} \tag{1}$$

$$\text{Energy intensity}_{inv} = \frac{\sum_{inv}(FE+RE)}{PE_{DME}} \tag{2}$$

where *inv* represents each inventory. In the numerator terms of two impact parameters, w indicates weight of materials while FE and RE are consumed fuel energy and required energy in process, respectively. In the denominator, PE_{DME} stands for total produced DME energy.

Coal is assumed to be obtained by mining at Taebaek in Korea. The methods of mining are open-cut mining and underground mining. In Korea, most mines are in mountainous districts, and underground mining is favored. Table 1 shows the energy consumed and the amount of CO_2 produced by coal mining.

Table 1. Energy consumption and CO_2 emission for mining coal

	Coal mining	Unit
Electricity	19.4	[kWh/t coal]
Diesel	0.66	[L/t coal]
CO_2 emission	0.228	[gCO_2/MJ coal]

Coal is mined in an irregular size, and should be sized uniformly. Sizing process can be simulated by Aspen Plus. The coal is mixed with water and sent to a crusher that pulverizes the coal to a maximum particle diameter of 0.0002m. Then, coal is moved to the Incheon base by 10 t-trucks. For truck transportation, CO_2 emissions and the required energy are related to the fuel consumption of the truck, which can be expressed as a function of the loading rate of weight (Dowaki and Genchi, 2009) (Equations (3)-(5)).

$$f_{FC}(\lambda) = a\lambda + b \tag{3}$$

$$\lambda_{avg} = \frac{w_{material}}{10N_{material}} \tag{4}$$

$$N_{material} = \left(\frac{w_{material}}{24.7\rho}\right) + 1 \tag{5}$$

where a(=714 gCO_2/km) and b(=508 gCO_2/km) are constants on the fuel consumption, ρ indicates bulk density of materials and N is total number of transportation (Dowaki and Genchi, 2009). The data for coal transportation in Korea is listed in Table 2.

Table 2. Data of coal transportation

	Transportation	Unit
Bulk density (coal)	1,056	[kg/m^3]
Distance (round trip)	540	[km]
CO_2 emission	3.015	[gCO_2/g diesel]
Fuel efficiency	2.4	[km/L diesel]

In conversion process, the gasification for generating syngas is required. The gas cleaning process should be included to remove sulfur and CO_2 in the feed stream. The CO_2 removal process removes CO_2 in the generated syngas stream using methanol as a solvent. After the gas cleaning process, DME synthesis and DME purification process are required. The block diagram of proposed process is shown in Figure 2.

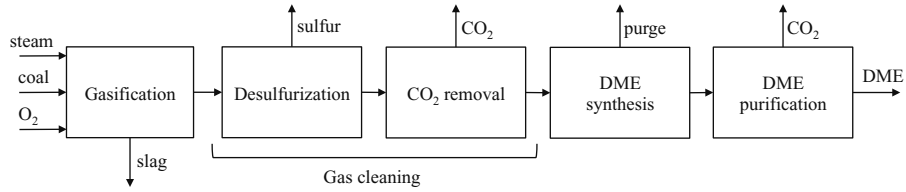

Figure 2. Block diagram of conversion processes of DME production from coal in Aspen Plus environment

In the DME synthesis block, which is for DME reaction, the direct method (one-step) is used. The products of the DME reaction, which are DME, syngas, methanol, water, and CO_2, pass through the DME purification section to separate DME. The property methods for simulation are SRK when substances have a vapor phase behavior and RKSMHV2 when substances have a vapor-liquid phase behavior (Kim et al., 2010).

3. Results of impact assessment and its interpretation

Table 3 shows simulation results. As previously mentioned, the Incheon plant produces DME of 1,000 t/day. Energy efficiency means produced DME energy per each feed potential energy.

Figure 3 shows the resulting CO_2 emission intensity and energy intensity of the inventories for coal. The conversion process plays an important role in both intensities. This implies that a CO_2 capture system used for DME production from coal should be developed and added in conversion process.

4. Conclusion

DME is widely used as a commercial fuel, and therefore, Korea does need to develop DME production technologies and cultivate the market for sustainable development. In

Table 3. Results of energy consumption and CO_2 emission in DME production

	DME [ton]	Feed [ton]	Total CO_2 [ton]	Energy efficiency	CO_2/DME [gCO_2/MJ]	Required energy [MJ]
Coal	1,000	1,956	1459.15	0.475	48.23	1,977,528

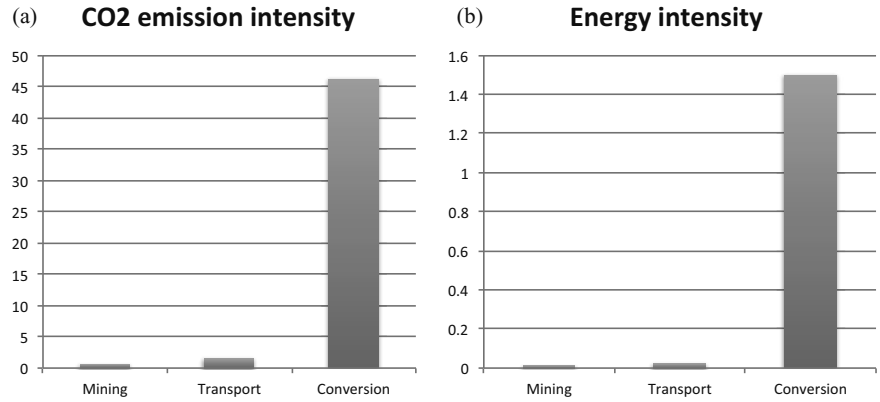

Figure 3. Results of (a) CO_2 emission intensity and (b) energy intensity in life cycle

this study, life cycle assessment of DME production using coal was conducted in terms of CO_2 emission and energy consumption. The goal, scopes, and inventories were defined to implement life cycle assessment. Practical data from Korea and several assumptions were adopted for this case study, the pretreatment process and DME conversion process were simulated using an Aspen Plus simulator to evaluate the amount of feed, CO_2 emission, and energy consumption. Results showed that the conversion process should be improved in terms of CO_2 emission.

References

Baek, Y., Cho, W., Lee, H. C., 2010. The status of DME development and utilization as a fuel. Korean Ind Chemistry News 13, 1–11.

Dowaki, K., Genchi, Y., Jul. 2009. Life cycle inventory analysis on Bio-DME and/or Bio-MeOH products through BLUE tower process. Int J LCA 14, 611–620.

Kim, I. H., Kim, S., Cho, W., Sup, E., 2010. Simulation of commercial dimethyl ether production plant. In: Computer Aided Chemical Engineering. Vol. 28. Elsevier B.V., pp. 799–804.

I.A. Karimi and Rajagopalan Srinivasan (Editors), Proceedings of the 11th International Symposium on Process Systems Engineering, 15-19 July 2012, Singapore.

Analysis and Modeling of Information Required for Process Assessment on Environment, Health, and Safety by IDEF0 and UML

Yasunori Kikuchi[a], Stavros Papadokonstantakis[b], Alireza Banimostafa[b], Hirokazu Sugiyama[b], Konrad Hungerbühler[b], Masahiko Hirao[a]

[a] *Department of Chemical System Engineering , The University of Tokyo, 7-3-1 Hongo, Bunkyo-ku, Tokyo, 113-8656, Japan*
[b] *Institute for Chemical- and Bioengineering, Safety & Environmental Technology Group, Swiss Federal Institute of Technology Zurich (ETHZ), Switzerland, Wolfgang Pauli-Strasse 10, 8093 Zurich, Switzerland*

Abstract

We present a systematic approach of information modeling towards more systematic consideration of environmental, health and safety aspects during process design. Unified modeling language (UML) and type zero method of integrated definition (IDEF0) are applied for analyzing and defining required information in the comprehensive process evaluation. The proposed model visualizes the procedures of multiple assessments on various aspects of process system with data acquisition in process design and operation. Collaborated information modeling by UML and IDEF0 enables the discussion of integrated software system supporting process assessment within process development.

Keywords: activity modeling, information modeling, life cycle assessment, risk assessment, process development.

1. Introduction

In the development of chemical processes, it has become a common practice to consider various consequences of decisions, i.e. not only direct profit, but also non-monetary aspects. Among others, environment, health, and safety (EHS) issues have been gaining increasing attentions, for preventing short term as well as long term damages to companies. Various methods have been developed, which can be used for identifying weak points needing technical countermeasures, or comparing different process options for prioritized investment of resources. The scope differs between methods, e.g., hazard assessment focuses more on the accidental issues around the place where chemicals are used, while life cycle assessment (LCA) highlights longer term and steady-state impacts via the environment. Ideally, multiple assessment methods should be applied in order to reflect impacts on various areas into decisions. However in practice, companies are facing challenges in (1) collecting required data for executing non-conventional assessment such as LCA (2) combining various assessment results in making a decision (3) systematizing tools, data and activities across different units/departments.

The key steps to close these gaps are to precisely (re)define required data, information, simulation tools and mechanisms at different stages of assessment and to present the entire as a business model. Several contributions can be found in the field of PSE/CAPE, such as extensive application of information technology (Schneider and Marquardt

2002), or effective connection of various computer-aided design tools by developing design ontology for sharing data over different design tools (Marquardt et al. 2010; Wiesner et al. 2011).

In this study, we present a business-model based approach for analyzing information required for multiple assessment methods, with a specific focus on environmental LCA and EHS hazard assessment. In the business process analysis, we have applied type zero method of integrated definition (IDEF0) (Ross 1985) and unified modeling language (UML) (OMG 2011) in a combined manner to exploit strength of both methods. For EHS hazard assessment, where various contributions can be found, a method by Koller et al. (2000) was selected as an example.. Having understood characteristics of required data, difficulty will still remain in operationalizing multiple assessment methods, especially in data collection and information/tool integration. To guide a gradual development for industry, four levels of maturity have been defined according to the degree of tool and information integration, which could be distinguished in the collaborative use of IDEF and UML.

2. Method

2.1. Information required for process assessment

Figure 1 presents the syntax of IDEF0 and UML. In industry, IDEF0 is widely used especially in the field of business process reengineering (BPR). The feature of IDEF0 is the hierarchical break down of "activities" into "sub activities" with keeping consistency of input and output on all different levels. Here, three types of "input" are differentiated: (1) input – can be transformed to "output" (2) constraint – unchangeable input and (3) mechanism – required in executing an activity. Several authors applied IDEF0 in integrating new or existing engineering methods and tools for environmental protection and EHS risks in chemical process design (Sugiyama et al. 2008) and other industrial process design (Kikuchi and Hirao 2009). UML for systems modeling has a large potential to visualize data requirements clearly for software tools from design stages to maintenance and sustainment stages in companies' activities. In UML class diagram, information categories are structured and characterized by specifying their properties and relationships. In addition to the static modeling by UML class diagram, dynamic information flows among information providers involved in process assessment such as assessment engineers, operators, and process designers can be discussed on UML activity diagram.

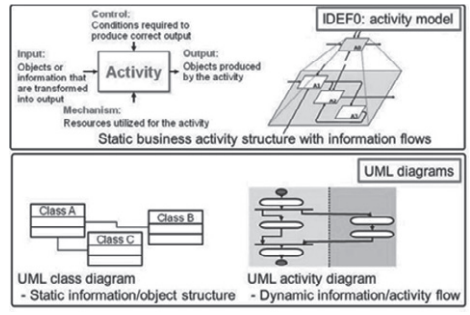

Figure 1 Syntax and basic features of IDEF0 and UML

Activity model by IDEF0 can be a highly re-usable concept of implementing multiple assessments into practice. It can be a strong rationale of business model. UML is

capable of showing more usable models, which are static structure of elements included in information system and dynamic work flow. We attempt to apply both methods in order to analyze truly required activity and information conceptually and practically.

2.2. Analyzed process assessment method

LCA quantifies various environmental impacts throughout the "life cycle" of a product or a service, e.g. from raw material production to the final disposal. Although there are ongoing researches mainly in individual impact assessment methods, e.g. global warming, or acidification, it is commonly agreed that an LCA of a chemical process requires mass and energy balances. On contrary, input information for EHS hazard differs from method to method (Adu et al. 2008). The EHS method is data-intensive, in order to cover wide range of hazard elements, and thus was selected for analyzing the complexity of information transfer as well as creating a robust business process model.

3. Results and discussion

3.1. Information required for process assessment

Figure 2 shows a general activity model of process assessment utilizing multi assessment methods on the basis of an activity modeling template (Sugiyama et al. 2008) and existing process improvement framework (Kikuchi and Hirao 2009). Figure 3 shows the example of developed information models of assessment method, where EHS method is analyzed. Based on the developed IDEF0 and UML models, the process assessment using LCA and EHS method was analyzed. While LCA considers only material and energy input/output per functional unit (e.g., kg-product), hazard assessment methods can also require additional properties such as temperature of stream, as expressed in conditions of steam in Figure 3. This can lead to disagreement of results in LCA and hazard assessment.

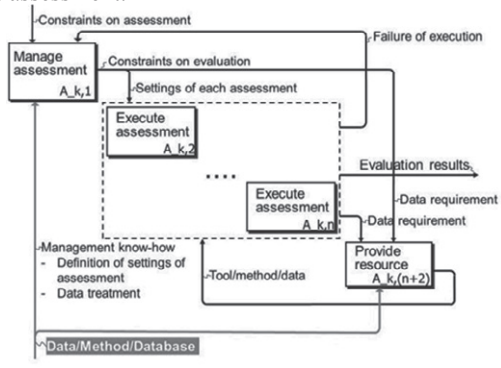

Figure 2 A part of developed general-activity model of process assessment utilizing multiple assessment methods

In our proposed model, information required in process assessment is differentiated into three categories; general, assessment-specific and technical data. Technical data is a set of information specific to the process, which can be represented by "condition of streams" such as flow rates and "condition of units" such as reaction conversions or structure of unit operations such as reactor, distillation column, and tank in chemical process. Typically, these data are primarily available to process engineers and thus technical data must be collected by process engineers for hazard assessment and LCA.

Assessment-specific data e.g., normalization methods of quantifying process hazards or life cycle impact factors, is independent of the process to be evaluated, i.e. can be

separately stored. Some existing databases on assessment methods (Swiss Centre for Life Cycle Inventories 2011) are applicable. All other related data for assessment is categorized into general data. It includes not only physicochemical data such as properties of chemical substances, but also plant-specific conditions and project-specific settings such as local regulation, ambient surroundings, budget and timeline.

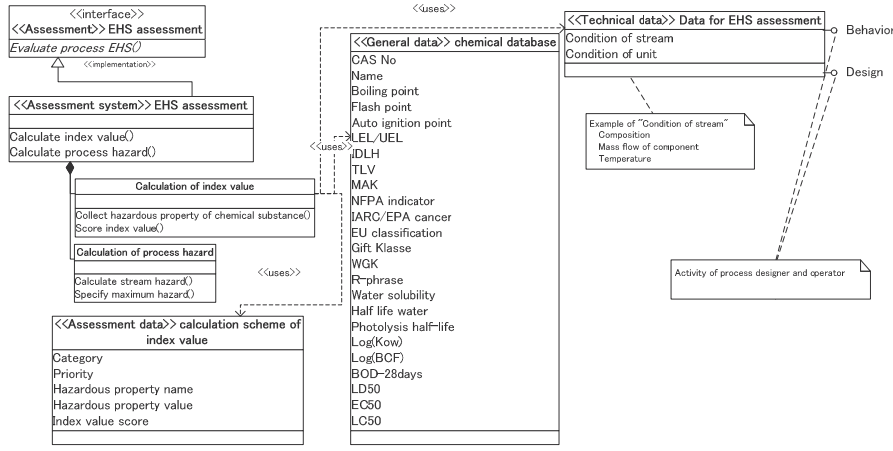

Figure 3 UML class diagram of assessment method: an example of EHS assessment methods

3.2. Maturity level of systematic process assessment

Figure 4 presents different levels of organization from poor to matured status, considering the degree of integrating and sharing process information, simulation software and assessment data. At an initial level or Level 0, no systematic information sharing exists on process assessment; therefore engineers, being responsible for process assessment, must collect all required data for each assessment method, i.e. general, assessment-specific and technical data. In some cases, engineers have to study and understand the assessment method to extract required process data and to create a calculation model. At Level 1, all methods are understood and data requirements are listed up. This unifies the data collection procedure for each design cases. However, the collection itself is repeated at each design project. Process manager can facilitate process assessment with process design and behavior in Level 2 by sharing knowledge on assessment methods. At Level 2, knowledge from past design cases or other sites are well shared within process engineering group. However, the group manager has to trigger the assessment activity, i.e. actively collect data and information. Finally at Level 3, tools and assessment methods are systematically connected during all activities of the design. This means, for example, a full and online integration of process simulator with LCA or hazard assessment. As shown in Figure 4, the combination of static and dynamic models by IDEF0 and UML enabled distinction of different maturity levels, which serves as a guidance to companies for organizational development. This application is not limited to incorporation of LCA and EHS but to any other assessment methods.

4. Conclusion

We developed information models described by a unique combination of UML and IDEF0 for systematizing process assessment methods. These models visualize the procedures of multiple assessments on various aspects of process system with data

acquisition in process design and operation. Through this study, we concluded that visualization of information and activities enables detail indication of process information required for assessment methods. Collaborated information modeling by UML with business activity modeling by IDEF0 enables the discussion of integrated software system used in process assessments within plant life cycle.

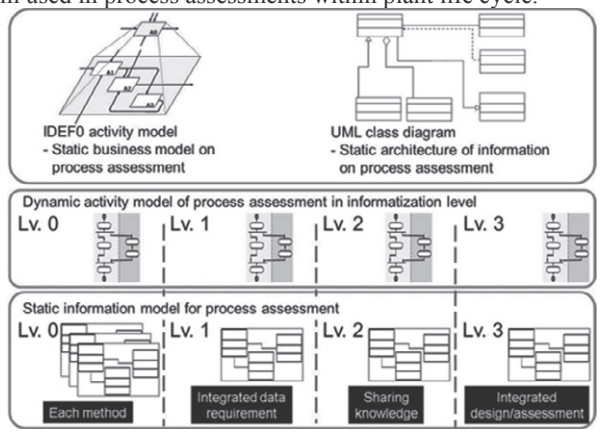

Figure 4 Proposed framework of analyzing maturity level of organization for systematic process assessment

Acknowledgement

The author (Yasunori Kikuchi) was supported through the Japan Society for Promotion of Science Institutional Program for Young Researchers Overseas Visits and Young Researchers Overseas Study Program for Mechanical Systems Innovation managed by the Global COE Program by the Ministry of Education, Culture, Sports, Science and Technology, Japan.

References

I.K. Adu, H. Sugiyama, U. Fischer, K. Hungerbühler, 2008, Comparison of methods for assessing environmental, health and safety (EHS) hazards in early phases of chemical process design. Trans. IChemE: PartB Proc. Saf. Environ. Protec. 86 (B2), 77-93.

Y. Kikuchi, M. Hirao, 2009, Hierarchical Activity Model for Risk-Based Decision Making Integrating Life Cycle and Plant-Specific Risk Assessments, J. Ind. Ecol. 13(6), 945-964.

W. Marquardt, J. Morbach, A. Wiesner, A. Yang, 2010, OntoCAPE: A Re Usable Ontology for Chemical Process Engineering: RWTH Edition, Springer-Verlag

Objective Management Group (OMG), 2011, Unified Modeling Language (UML) ® Resource Page. Available at www.omg.org/technology/documents/modeling_spec_catalog.htm (Access 20/03/2012)

D.T. Ross, 1985, Application and Extensions of SADT, Computer, 25-34

R. Schneider, W. Marquardt, 2002, Information technology support in the chemical process design life cycle, Chem. Eng. Sci. 57(10) 1763-1792

H. Sugiyama, M. Hirao, U. Fischer, and K. Hungerbühler, 2008, Activity Modeling for Integrating Environmental, Health and Safety (EHS) Consideration as a New Element in Industrial Chemical Process Design, J. Chem. Eng. Japan., 41(9) 884-897

Swiss Centre for Life Cycle Inventories (2011), database ecoinvent, http://www.ecoinvent.ch/

A. Wiesner, J. Morbach, W. Marquardt, 2011, Information integration in chemical process engineering based on semantic technologies. Comput. Chem. Eng. 35, 692-708

I.A. Karimi and Rajagopalan Srinivasan (Editors), Proceedings of the 11th International Symposium on Process Systems Engineering, 15-19 July 2012, Singapore.

Correlations among Footprints within Biomass Energy Supply-Chains

Lidija Čuček,[a] Jiří J. Klemeš,[b] Petar S. Varbanov,[b] Zdravko Kravanja[a]

[a]*Faculty of Chemistry and Chemical Engineering, University of Maribor, Smetanova ulica 17, 2000 Maribor, Slovenia, e-mail: zdravko.kravanja@uni-mb.si*
[b]*Centre for Process Integration and Intensification – CPI², Research Institute of Chemical and Process Engineering, Faculty of Information Technology, University of Pannonia, Egyetem utca 10, 8200 Veszprém, Hungary*

Abstract

In this contribution correlations among different direct footprints are studied within a multi-objective optimisation (MOO) where profit is maximised vs. footprints in the synthesis of biomass energy supply-chains. We investigate correlations among two-dimensional (2D) Pareto projections of carbon footprint (CF), energy footprint (ENF), water footprint (WF), water pollution footprint (WPF), land footprint (LF) and food-to-energy footprint (FEF). 'Dependent' footprints are i) linearly and ii) nonlinearly correlated with respect to a chosen 'independent' one (CF). The MOO is performed only for one footprint, the 'independent' one, rather than for all of them whilst the rest of the 'dependent' footprints are evaluated after the optimisation from the independent one. In this way, the number of optimisation runs in the MOO can be substantially reduced.

Keywords: footprint, multi-objective optimisation, bioenergy supply-chain, correlations among footprints.

1. Introduction

Environmental and social concerns are becoming increasingly important in many areas (Guillén-Gosálbez, 2011). Plenty of indicators measuring environmental and social issues have been developed, amongst them also footprints. They are usually measured in units of area, and one of the most well-known is the ecological footprint. However, the data expressed in units of area show high variability and the high inherited inaccuracy since they could be based on a variety of different assumptions (Wiedmann and Minx, 2008). Converting some of the footprints to area units can prove to be even problematic, especially for processes that are not primarily area-based (De Benedetto and Klemeš, 2009). In many studies only one footprint is considered and evaluated, which most likely leads to inaccurate conclusions. It is much more realistic when more impacts are considered. However, the reduction and aggregation of different objectives have mostly relied on the decision-makers' preferences rather than on a systematic mathematical approach (Guillén-Gosálbez, 2011).

This contribution presents the MOO method of reduced dimensionality (2D) with emphasis on environmental footprints. The correlations among 2D projections of footprints are investigated. 'Dependent' footprints are aggregated and expressed through one, selected as independent, footprint only. This approach with correlated footprints is applied to the aggregated regional biomass supply chain (Čuček et al., 2010, 2012).

2. Description of the Proposed Methodology

2.1. The Multi-Criteria Approach

The conventional way of obtaining 2D projections for footprints is to perform the MOOs by the use of ε-constraint method. A sequence of constrained single-objective mixed-integer non-linear programming $(\mathrm{MINLP}_j)_f$ problems is thus solved for each footprint $f \in F = \{\mathrm{CF}, \mathrm{ENF}, \mathrm{WF}, \mathrm{WPF}, \mathrm{LF}, \mathrm{FEF}\}$ as the maximisation of the profit (P) subjected to a relative footprint, $f^r_{j,f}$, where $f^r_{j,f}$ is defined as the footprint obtained by MOO, divided by its reference value obtained at the maximal profit. During the sequence of $(\mathrm{MINLP}_j)_f$ the footprint is forced to decrease sequentially from its maximal value $(f^r_{j,f} = 1)$ by a suitable step size $\Delta\varepsilon$ until there is no feasible solution. Different sets of non-inferior Pareto optimal solutions are generated, one for each footprint:

$$\max_{x,y} \; P = \boldsymbol{c}^{\mathrm{T}}\boldsymbol{y} + f(\boldsymbol{x}) - \sum_f 10^{-6} \cdot ENVB_f - \sum_f 10^{-6} \cdot SOCB_f$$

$$\text{s.t.} \quad \boldsymbol{A}\boldsymbol{y} + \boldsymbol{h}(\boldsymbol{x}, \boldsymbol{y}) = 0$$

$$\boldsymbol{B}\boldsymbol{y} + \boldsymbol{g}(\boldsymbol{x}, \boldsymbol{y}) \le 0 \qquad (\mathrm{MINLP}_j)_f$$

$$f^r_{j,f}(\boldsymbol{x}, \boldsymbol{y}) \le \varepsilon_{j,f}$$

$$(\boldsymbol{x}^{\mathrm{LO}} \le \boldsymbol{x} \le \boldsymbol{x}^{\mathrm{UP}}) \in \boldsymbol{X} \subset \boldsymbol{R}^n, \quad \boldsymbol{y} \in \boldsymbol{Y} = \{0,1\}^m$$

$$\varepsilon_{j-1,f} = \varepsilon_{j,f} - \Delta\varepsilon, \quad \Delta\varepsilon = \frac{1}{N}, \quad \varepsilon_{j,f} = \frac{1}{N} \cdot (j-1), \quad j = \{1,\ldots,N+1\}$$

With the above described approach two-criterion optimisation is performed for each footprint in all the points defining the Pareto curves, which is a time-consuming task especially if complex MINLPs have to be solved. The intention of this work is to replace the reiterated generation of two-dimensional (2D) projections by linear or more accurate quadratically-based correlations. If we select CF as an 'independent' footprint $(i \in I \subset F$, I = {CF}), and perform ε-constrained $(\mathrm{MINLP}_j)_{\mathrm{CF}}$, then all other 'dependent' footprints' 2D projections ($d \in D \subset F$, D = {ENF, WF, WPF, LF, and FEF}) can be evaluated from the CF' projection.

2.2. Methodology for Obtaining Linear Correlations among Footprints' 2D Projections

For 'independent' footprint the MOO is performed in order to obtain sets of Pareto optimal solutions defined at points $\left(f^r_{j,f}, P_{j,f}\right)$, $j = \{1,\ldots,N+1\}$. For the rest of 'dependent' footprints only two MINLPs are performed, one at zero and one at unit value of relative footprints. In this way, two data points can be defined: $\left(f^r_{1,f}, P_{1,f}\right)$ and $\left(f^r_{N+1,f}, P_{N+1,f}\right)$. From the first and last points the following linear function for each footprint can be derived:

$$P_{j,f} = k_d \cdot f^r_{j,f} + P_{1,f}, \quad f \in F, \quad f^r_{j,i} = (1/N) \cdot (j-1), \quad j = \{1,\ldots,N+1\} \tag{1}$$

where k_d is the slope of the line, and N is e.g. 20.

The profit of the linearly-correlated 'dependent' footprint, $P_{j,d}$, should be equal to the one of the 'independent' footprint, $P_{j,i}$:

$$k_d \cdot f^r_{j,d} + P_{1,d} = k_i \cdot f^r_{j,i} + P_{1,i}, \quad \forall d \in D \wedge \forall i \in I \wedge d \ne i, \quad f^r_{j,i} = (1/N) \cdot (j-1), \quad j = \{1,\ldots,N+1\} \tag{2}$$

The line equations Eq. (3, 4) for each 'dependent' footprint can be expressed through 'independent' footprint from Eq. (2):

$$f_{j,d}^r = \frac{k_i}{k_d} \cdot f_{j,i}^r + \frac{P_{1,i} - P_{1,d}}{k_d} = \frac{P_{j,i} - P_{1,d}}{k_d}, \forall\, d \in D \wedge \forall\, i \in I \wedge d \neq i, f_{j,i}^r = (1/N) \cdot (j-1), j = \{1,\ldots,N+1\} \quad (3)$$

$$f_{j,d}^r = \max\left\{0, \frac{P_{j,i} - P_{1,d}}{k_d}\right\}, \quad \forall\, d \in D \wedge \forall\, i \in I \wedge d \neq i, \quad j \leq \{1,\ldots,N+1\} \quad (4)$$

Note that max operator is introduced in order to prevent negative values.

2.3. Methodology for Obtaining Quadratically-Based Correlations among Footprints

In order to obtain quadratically-based correlations among footprints, now three data points were selected, at zero, half and unit values of footprints: $\left(f_{1,f}^r,\, P_{1,f}\right)$, $\left(f_{(N+1)/2,f}^r,\, P_{(N+1)/2,f}\right)$ and $\left(f_{N+1,f}^r,\, P_{N+1,f}\right)$. The profits for quadratically-based correlated footprints are defined as:

$$P_{j,f} = b_f \cdot (f_{j,f}^r)^2 + c_f \cdot f_{j,f}^r + e_f, \ \forall f \in F, f_{j,f}^r = (1/N) \cdot (j-1), \ j = \{1,\ldots,N+1\} \quad (5)$$

Parameters b_f, c_f and e_f are obtained through the following relations: $b_f = a_{f,2}$, $c_f = a_{f,1} - a_{f,2} \cdot (f_{1,f}^r + f_{(N+1)/2,f}^r)$ and $e_f = a_{f,0} - a_{f,1} \cdot f_{1,f}^r + a_{f,2} \cdot f_{1,f}^r \cdot f_{(N+1)/2,f}^r$, where:

$a_{f,0} = P_{1,f}$, $a_{f,1} = \dfrac{P_{(N+1)/2,f} - P_{1,f}}{f_{(N+1)/2,f}^r - f_{1,f}^r}$, and $a_{f,2} = \dfrac{1}{(f_{N+1,f}^r - f_{(N+1)/2,f}^r)} \cdot \left(\dfrac{P_{N+1,f} - P_{1,f}}{f_{N+1,f}^r - f_{1,f}^r} - \dfrac{P_{(N+1)/2,f} - P_{1,f}}{f_{(N+1)/2,f}^r - f_{1,f}^r}\right)$.

Since the profit of the correlated 'dependent' footprint must be equal to the one of the 'independent' footprint, it follows:

$$b_d \cdot (f_{j,d}^r)^2 + c_d \cdot f_{j,d}^r + e_d = b_i \cdot (f_{j,i}^r)^2 + c_i \cdot f_{j,i}^r + e_i, \quad \forall\, d \in D \wedge \forall\, i \in I \wedge d \neq i, f_{j,i}^r = (1/N) \cdot (j-1), \ j = \{1,\ldots,N+1\} \quad (6)$$

Each 'dependent' footprint is then expressed from Eq. (6) through the 'independent' one as:

$$(f_{j,d}^r)_{1,2} = \frac{-c_d \pm \sqrt{(c_d)^2 - 4 \cdot b_d \cdot (e_d - (b_i \cdot (f_{j,i}^r)^2 + c_i \cdot f_{j,i}^r + e_i))}}{2 \cdot b_d}, \ f_{j,d}^r = \max\left\{0, f_{j,d_{1,2}}^r\right\} \quad (7)$$

It should be noted that besides MINLPs needed to define the Pareto curve of the chosen 'independent' footprint we have to perform now three additional MINLPs for each 'dependent footprint in order to generate 2D projections of 'dependent' footprints.

3. Case Study of Biomass Energy Supply-Chains

The simple methodology described above was applied on a case study of biomass energy supply-chains (Čuček et al., 2010, 2012) to derive 2D Pareto projections for a multi-criteria problem.

Biomass and bioenergy supply chains involve harvesting (agricultural layer), storage and pre-treatment (pre-processing layer), conversion steps (processing layer), distribution and usage of products (use layer), and transport amongst their activities. The total area of the region was assumed as 1,000 km^2. Several biomass types, technology options, and bio-products have been considered in the synthesis. The biomass types utilised were corn, corn stover, wood chips, municipal solid waste (MSW), manure, and timber. The technologies for converting biomass were the dry-grind process, anaerobic digestion, MSW incineration, timber sawing and incineration, and the produced bio-products were bioelectricity, bioheat, bioethanol, boards, organic

fertiliser, and distiller dried grains with solubles. The required data for obtaining correlations among footprints are presented in Table 1.

Table 1. Required data for obtaining linear and quadratically-based correlations among footprints

Footprint	$P_{1,f}$ (M€/y)	$P_{(N+1)/2,f}$ (M€/y)	$P_{N+1,f}$ (M€/y)
CF	$0.162 \cdot 10^{-6}$	19.743	34
ENF	0	20.937	34
WF	$-7.259 \cdot 10^{-2}$	20.536	34
WPF	0.748	19.388	34
LF	2.360	19.429	34
FEF	26.104	30.050	34

From the above data, the obtained linear and nonlinear (based on quadratic function) correlations among footprints are shown in Table 2.

Table 2. Obtained linear and nonlinear correlations among footprints

Footprint	Linear correlation	Nonlinear correlation based on quadratic function
ENF	$f^r_{j,\mathrm{ENF}} = f^r_{j,\mathrm{CF}} + 4.77 \cdot 10^{-9}$	$f^r_{j,\mathrm{ENF}} = 1.58 \pm \sqrt{0.70 \cdot (f^r_{j,\mathrm{CF}})^2 - 2.86 \cdot f^r_{j,\mathrm{CF}} + 2.50}$
WF	$f^r_{j,\mathrm{WF}} = 0.10 \cdot f^r_{j,\mathrm{CF}} + 2.13 \cdot 10^{-3}$	$f^r_{j,\mathrm{WF}} = 1.69 \pm \sqrt{0.77 \cdot (f^r_{j,\mathrm{CF}})^2 - 3.15 \cdot f^r_{j,\mathrm{CF}} + 2.86}$
WPF	$f^r_{j,\mathrm{WPF}} = 1.02 \cdot f^r_{j,\mathrm{CF}} - 2.25 \cdot 10^{-2}$	$f^r_{j,\mathrm{WPF}} = 2.56 \pm \sqrt{1.36 \cdot (f^r_{j,\mathrm{CF}})^2 - 5.58 \cdot f^r_{j,\mathrm{CF}} + 6.67}$
LF	$f^r_{j,\mathrm{LF}} = 1.08 \cdot f^r_{j,\mathrm{CF}} - 7.46 \cdot 10^{-2}$	$f^r_{j,\mathrm{LF}} = 3.67 \pm \sqrt{2.20 \cdot (f^r_{j,\mathrm{CF}})^2 - 9.00 \cdot f^r_{j,\mathrm{CF}} + 13.92}$
FEF	$f^r_{j,\mathrm{FEF}} = 4.31 \cdot f^r_{j,\mathrm{CF}} - 3.31$	$f^r_{j,\mathrm{FEF}} = -680.23 \pm \sqrt{-1{,}891.38 \cdot (f^r_{j,\mathrm{CF}})^2 - 7{,}753.45 \cdot f^r_{j,\mathrm{CF}} + 458{,}216.00}$

Then MOO for CF was performed and its Pareto 2D 'independent' projection was obtained, from which all the rest 'dependent' projections were derived by the above defined linear (Figure 1) and nonlinear (Figure 2) correlations. Note that nonlinearities in Figure 2 are better preserved than in Figure 1. At N=20, only about 30 MINLPs with linear and 35 MINLPs with nonlinear correlations have to be performed instead of 120.

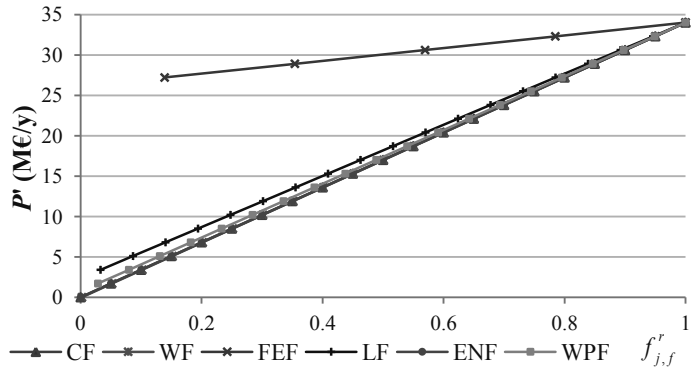

Figure 1. Linearly-correlated curves

For the estimation of the error we used the mean difference measure (Δf' for linear and Δf'' for nonlinear correlation) and standard deviation measure (σ' for linear and σ'' for nonlinear correlation). The mean differences and standard deviations between footprints obtained by MOO and those correlated ones are presented in Table 3.

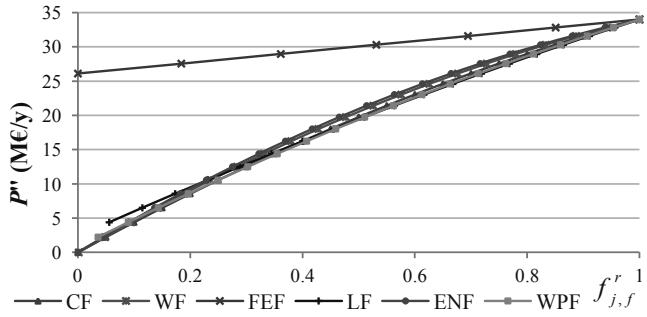

Figure 2. Nonlinearly-correlated curves

From Table 3 it can be seen that errors are especially small for quadratically-based correlated footprints (usually around 1 % or less). Similar results as by the MOO can be obtained by nonlinearly-correlated footprints.

Table 3. Mean differences and standard deviations between obtained and correlated footprints

Footprint	$\Delta f'$	σ'	$\Delta f''$	σ''
CF	6.59 %	2.81 %	1.20 %	1.18 %
ENF	9.20 %	4.37 %	1.02 %	2.23 %
WF	8.92 %	3.30 %	2.11 %	2.02 %
WPF	4.85 %	2.75 %	0.61 %	1.91 %
LF	2.83 %	1.76 %	0.14 %	0.98 %
FEF	0.12 %	0.86 %	0.10 %	0.87 %

4. Conclusions

The current contribution presents the development of the correlations among different footprints within an MOO approach. Different footprints have been investigated on the case study of the biomass energy supply-chain. The nonlinearly-correlated curves fit well to the 2D Pareto projections obtained by maximising the profit against each footprint. The number of MINLPs to be solved has been significantly reduced by applying those correlations yet yielding solutions of acceptable accuracy, thus enabling a large number of footprints to be considered in the LCA-based MINLP synthesis approach.

Acknowledgements

The financial support from the Slovenian Research Agency (Program P2-0032 and PhD research fellowship contract No. 1000-08-310074) and from the Hungarian project TÁMOP- 4.2.2/B-10/1-2010-0025 is gratefully acknowledged.

References

L. De Benedetto, J. J. Klemeš, 2009, The Environmental Performance Strategy Map: an integrated LCA approach to support the strategic decision-making process, J Cleaner Prod, 17(10), 900-906

L. Čuček, H. L. Lam, J. J. Klemeš, P. S. Varbanov, Z. Kravanja, 2010, Synthesis of regional networks for the suppy of energy and bioproducts, Clean Technol Environ Policy, 12, 635-645

L. Čuček, P. S. Varbanov, J. J. Klemeš, Z. Kravanja, 2012, Total footprints-based multi-criteria optimisation of regional biomass energy supply chains, Energy, doi: 10.1016/j.energy.2012.01.040

G. Guillén-Gosálbez, 2011, A novel MILP-based objective reduction method for multi-objective optimization: Application to environmental problems, Comput Chem Eng, 35, 1469-1477

T. Wiedmann, J. Minx, 2008, A definition of 'carbon footprint'. In: C. C. Pertsova, Ecological Economics Research Trends: Ch 1, 1-11, Nova Science Publisher, Hauppauge, NY, USA

I.A. Karimi and Rajagopalan Srinivasan (Editors), Proceedings of the 11th International Symposium on Process Systems Engineering, 15-19 July 2012, Singapore.

Energy Generation and Carbon Footprint of Waste to Energy: Centralised vs. Distributed Processing

Petar S. Varbanov[a], Hon Loong Lam[b], Ferenc Friedler[a], Jiří Jaromír Klemeš[a]

[a]*Faculty of Information Technology, University of Pannonia, Egyetem u. 10, H-8200 Veszprém, Hungary*
[b]*Department of Chemical and Environmental Engineering, The University of Nottingham, Malaysia Campus, Jalan Broga, 43500 Semenyih, Selangor, Malaysia*

Abstract

Waste to Energy (WTE) carries a trade-off between energy generation and the energy spent on collection, transport and treatment. Major performance indicators are cost, Primary Energy Savings (PES), Carbon Footprint (CFP). This presentation analyses the trade-off introducing a new indicator – the Waste Energy Potential Utilisation (WPU). The results indicate that the impact of logistics and energy distribution can be significant, and distributed WTE architectures may be good candidates for optimal solution, subject to further economical and environmental assessment.

Keywords: Waste-to-Energy, Waste Energy Potential Utilisation, optimisation processing distribution

1. Introduction

Waste management has become a significant problem due to its environmental impact (Eurostat, 2011). It mainly relates to atmospheric emissions and aqueous effluents from landfills, waste collection, transport, and processing. The growing demands for securing cleaner energy supplies (EIA, 2011) make necessary to achieve maximum savings of fossil fuels at minimum Carbon Footprint (CFP) in an economically viable way.

Studies of Waste-to-Energy (WTE) at the level of equipment and process design (Stehlík, 2011; Fodor and Klemeš 2012; Tabasová et al., 2012) and integrated waste utilisation (Singhabhandhu and Tezuka, 2010) have been published. There have been also studies on Carbon-Constrained economy targeting from New Zealand (Atkins et al., 2010) and Malaysia (Wong et al., 2011). Bastin and Longden (2009) compared fuel costs and CO_2 emissions of waste logistics networks with centralised vs. distributed location of UK waste processing, indicating 30 % higher fuel consumption for the centralised arrangement. A systematic evaluation of the CFP, energy saving and utilisation trends of WTE networks is important as well. One step in this direction for the synthesis of regional bioenergy networks has been the work by Čuček et al. (2010).

This contribution extends the analysis of WTE processing by defining a new performance indicator of the significance of the centralised versus distributed networks. The former allow larger and more efficient WTE plants but involve longer distances for waste transportation and energy distribution, while the latter feature the opposite trends.

2. Problem Description

The problem is to select a waste management network utilising the waste energy value optimally. The objective functions are typically minimum total cost, maximum waste energy utilisation or minimum environmental impact. Other criteria are also possible

(Zhang et al., 2011). The system includes households and intermediate WTE nodes, all connected with links for waste transportation and energy distribution (Figure 1).

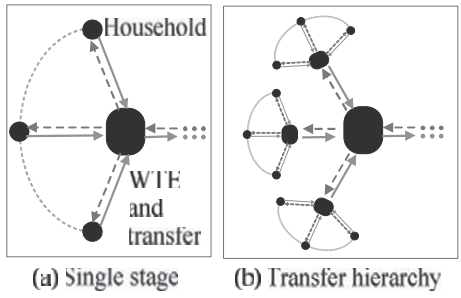

Figure 1. Nodes connectivity

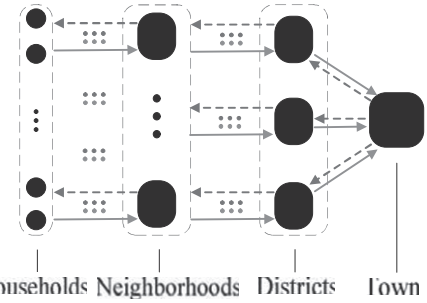

Figure 2. Network topology

WTE networks can be classified as reverse-logistics supply chain problems (Zhang et al., 2011). This work assumes that the household waste is separated to obtain a biomass fraction for anaerobic digestion to biogas. This is only one possible technology selected for the illustration the spatial development aspect. Other WTE technologies could be used too (Fodor and Klemeš, 2012).

2.1. Major Factors and Degrees of Freedom

The main activities in WTE processing include waste generation, collection, separation, transportation, conversion, energy distribution. The separation and WTE conversion may be performed at any network layer (Figure 2). The most significant factor in selecting the distribution of the processing activities within the WTE network is the CFP reduction. It is represented by the Primary Energy Savings (PES) concept. Other indicators are the waste volume sent to landfills, the type of WTE technologies and their environmental and health impacts, and the operating and investment cost of the system.

The main degrees of freedom are the choices of the technologies and locations for WTE and separation plants. It is important which WTE technologies will be selected. It is a common misconception to identify WTE as only waste incineration with heat recovery, which is the most common application to date (Stehlík, 2011). Other options as anaerobic digestion to biogas with further use as a fuel can also be applied.

Other implications concern capital cost (equipment and vehicles) and land cost. Situating WTE plants closer to the waste sources (households) may impose higher land cost and emission problems, but could reduce transport cost. Building the WTE plants at a distance, outside cities, would tend to reduce the land cost and increase transport cost.

2.2. Constraints and Trade-offs

WTE location and technology have significant public acceptance implications affecting the project feasibility– e.g. incineration is frequently resisted in populated areas. A comprehensive solution must account for this. The current study focuses on the energy trade-off aspect. An interesting constraint of WTE lies in the duality of its goals. Firstly it is needed to safely treat the waste and minimise landfilling. But with increasing concerns for energy security and CFP minimisation (Dovì et al., 2009), energy recovery can be considered equally important. There is a maximum distance, at which the energy for transporting the waste becomes equal to its energy value. It depends on the ratio of the waste specific heating value and the energy consumption for transport.

2.3. General Solution Algorithm

The general solution to the problem can be carried out using various algorithms. Examples are the inexact reverse logistics (Zhang et al., 2011), an adaptation of the

synthesis of biomass-based energy supply chains (Čuček et al., 2010; Iakovou et al., 2010), which involve rigorous mathematical models. The algorithm should be able to adapt to the size and circumstances accounting for the trade-off of centralised vs. distributed processing. It has to define the following stages: (i) System identification – boundaries, sizes, zones, waste generation rates and energy value, transportation distances, main constraints; (ii) Scoping, identification of the system interactions, trends limitations; (iii) Formulation of the network architecture using clustering (Lam et al., 2010); (iv) Detailed supply chain modelling and optimal synthesis inside each cluster.

3. Utilisation of the waste energy potential

Municipal Solid Waste (MSW) potential (Step ii above) can be utilised at several stages (Figure 2) – households, neighbourhoods, districts, city, regional level. Transport decreases its energy value. Heat and power distribution are associated with losses proportional to the distance. The appropriate indicator for evaluating these options is the Primary Energy Savings – PES (Pavlas et al., 2010), and the Waste Potential Utilisation (WPU) – defined in this work:

$$\mathrm{PES} = \mathrm{FDD} - \mathrm{FTr} \tag{1}$$

$$\mathrm{FDD} = \frac{\mathrm{Q_{rep}}}{\mathrm{FQ} \cdot \mathrm{DQ}} + \frac{\mathrm{W_{rep}}}{\mathrm{FW} \cdot \mathrm{DW}} \tag{2}$$

$$\mathrm{WPU} = \frac{\mathrm{PES}}{\mathrm{WEV}} \left[\frac{\mathrm{GJ}}{\mathrm{GJ}} \right] ; \mathrm{WPU}^{*} = \mathrm{WPU} \cdot 100 \, [\%] \tag{3}$$

FDD is the fuel saving from displaced demand; FTr is the transport fuel, Q_{rep} and W_{rep} – the replaced heat and power user demands, FQ and FW – efficiency factors for conversion to heat and power, DQ and DW – distribution efficiency factors. WPU is the ratio of PES to the waste energy value (WEV) before conversion or transportation. Using these indicators, a task is to evaluate at which stage the WTE facilities would yield the best effect – maximum WPU.

4. Illustrative Example

The defined framework is illustrated on an example of a town of 100,000 inhabitants, with an average of 4 persons per household (HH). The town has 3 districts with 4 neighbourhoods (NH) in District 1 (D1), 3 NH in D2 and 4 NH in D3. The average waste generation is 450 kg/y per inhabitant (Eurostat, 2011). From that 30 % is suitable for energy generation, LHV = 0.01 GJ/kg, translating to waste heating value WHV = 135,000 GJ/y for the town. Each HH has an average demand of 4,500 kWh/y for power and 12,000 kWh/y for heat. Fuel consumption for waste transport is 0.02 GJ/(t·km). The performance of the energy conversion plants is specified in Table 1. It is assumed that WTE processing takes place at only one of the four potential levels – HH, NH, D, town. In this case the WEV is completely offset after transportation to 500 km, so this is not constraining for the scale of the system (smaller than 100 km). The energy trends for the network are summarised in Figure 3.

It can be seen from Figure 3 that the WPU features a trend with a maximum, explained on by the trade-off between two factors as follows. The increasing distance from the waste source tends to decrease the PES via FTr. Also the WTE conversion efficiency increases with the plant scale to a saturation point. The WPU can be above 100 %, which means that more fossil fuel energy can be saved than the energy value of the

utilised waste. This is caused by the distribution losses for heat and power, associated with the fossil based reference system for central utility supply and of the WTE options.

Table 1. Performance factors for the WTE plants

	BGD	**FQ**	**FW**	**DQ**	**DW**
	GJ/GJ	GJ/GJ	GJ/GJ	GJ/GJ	GJ/GJ
Reference system (fossil based CHP)	-	0.55	0.30	0.88	0.95
Biogas based heating at HH level	0.58	0.8	0	1	1
Biogas based CHP – NH level	0.58	0.55	0.24	0.92	0.98
Biogas based CHP – districts	0.58	0.55	0.24	0.90	0.96
Biogas based CHP – town	0.58	0.55	0.24	0.88	0.95

CHP: Combined Heat and Power generation; BGD: BioGas Digester efficiency

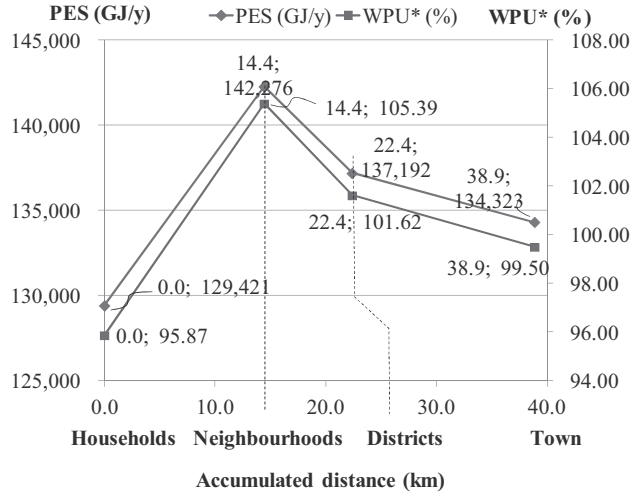

Figure 3. Energy trends for the illustrative example

5. Conclusions and Further Work

This work analyses the trend of utilising the waste energy value between distributed and centralised WTE processing. A new indicator – the WPU, has been formulated. The impact of the waste transport and energy distribution distances can be significant, reaching up to 10 % WPU variations even for smaller urban systems. The results also indicate that the WTE processing location between completely centralised or completely distributed arrangements has to be explored systematically with further indicators, as even an intermediate level such as neighbourhood-scale WTE facilities may be optimal. It should be also considered that the problem is not static, but developing with changing conditions as population growth, fuels prices increase, more efficient transport means.

Future work should involve a more detailed formulation of a systematic procedure for optimal WTE networks synthesis within the context of the waste management priorities and more accurate specification of the efficiency for energy conversion. It should include additional indicators – such as CFP and the other footprints as well as economic performance – especially the economy of scale (Čuček et al, 2012). A number of constraints should be satisfied – social acceptance, health regulations, availability of land for the WTE plants as well as for landfills. To solve this extended problem a multi-objective optimisation would be an obvious approach.

Acknowledgements

The acknowledge the financial support of the Hungarian project Társadalmi Megújulás Operatív Program "Tudományos képzés műhelyeinek támogatása" TÁMOP-4.2.2/B-10/1-2010-0025 and the Slovenian Research Agency (Program No. P2-0032).

References

M.J. Atkins, A.S. Morrison, M.R.W. Walmsley, 2010. Carbon Emissions Pinch Analysis (CEPA) for emissions reduction in the New Zealand electricity sector. Applied Energy, 87(3), 982-987.

L. Bastin, D.M. Longden, 2009. Comparing transport emissions and impacts for energy recovery from domestic waste (EfW): Centralised and distributed disposal options for two UK Counties. Computers, Environment and Urban Systems 33, 492–503.

L. Čuček , H.L. Lam, J.J. Klemeš, P.S. Varbanov, Z. Kravanja, 2010. Synthesis of regional networks for the supply of energy and bioproducts. Clean Technologies and Environmental Policy, 12(6), 635-645.

L. Čuček, J.J. Klemeš, Z. Kravanja, 2012, Footprints as Measures for Burdens and Impacts on Sustainability, Journal of Cleaner Production, under review

V.G. Dovì, F. Friedler, D. Huisingh, J.J. Klemeš, Cleaner energy for sustainable future. Journal of Cleaner Production, 17 (10) 2009, 889-895.

EIA, 2011. AEO2011 Early Release Overview, 2011, <www.eia.gov/forecasts/aeo/pdf/0383er%282011%29.pdf>, accessed 09.02.2011.

Eurostat, 2011, Waste statistics, <epp.eurostat.ec.europa.eu/statistics_explained/index.php/Waste_statistics>, accessed 09.02.2011

Z. Fodor, J.J. Klemeš, Waste as alternative fuel – Minimising emissions and effluents by advanced design, Process Safety and Environment Protection, 2012, doi:10.1016/j.psep.2011.0

E. Iakovou, A. Karagiannidis, D. Vlachos, A. Toka, A. Malamakis, 2010. Waste biomass-to-energy upply chain management: A critical synthesis. Waste Management, 30(10), 1860-1870.

H.L. Lam, P. Varbanov, J. Klemeš, 2010. Minimising Carbon Footprint of Regional Biomass Supply Chains. Resources, Conservation & Recycling, 54(5), 303-309.

M. Pavlas, M. Touš, L. Bébar, P. Stehlík, 2010. Waste to energy - An evaluation of the environmental impact. Applied Thermal Engineering, 30, 2326–2332.

A. Singhabhandhu, T. Tezuka, 2010. The waste-to-energy framework for integrated multi-waste utilization: Waste cooking oil, waste lubricating oil, and waste plastics. Energy, 35(6), 2544-2551.

P. Stehlík, 2011. Computational support as efficient sophisticated approach in waste-to-energy systems. Computer Aided Chemical Engineering 29, 1954-1958.

A. Tabasová, J. Kropáč, V. Kermes, P. Stehlík, A. Nemet, 2012,Waste-to-Energy Technologies: Impact on Environment, Energy, 10.1016/j.energy.2012.01.014

W.H. Wong, D.C.Y. Foo, R.R. Tan, 2011. Chronologically constrained composite curves for carbon constrained agricultural planning. Biomass and Bioenergy, 35(5), 1716-1720.

Y.M. Zhang, G.H. Huang, L. He, 2011. An inexact reverse logistics model for municipal solid waste management systems. Journal of Environmental Management, 92(3), 522–530.

I.A. Karimi and Rajagopalan Srinivasan (Editors), Proceedings of the 11th International Symposium on Process Systems Engineering, 15-19 July 2012, Singapore.

Assessing the environmental potential of carbon dioxide utilization: A graphical targeting approach

Marie-Noëlle Dumont,[a,b] Niklas von der Assen,[b] André Sternberg, [b] André Bardow [b]

[a] *Chemical Engineering Department, University of Liege, Sart-Tilman, allée de la chimie, B6A, 4000 Liège, Belgium, mn.dumont@ulg.ac.be*
[b] *Lehrstuhl für Technische Thermodynamik, RWTH Aachen University, Schinkelstr. 8, 52062 Aachen, Germany*

Abstract

Carbon Capture and Utilization (CCU) has the potential to reduce both greenhouse gas emissions and fossil fuel use. However, the conversion of CO_2 is intrinsically difficult due to its low energetic state. Thus, a positive environmental effect of a CO_2-consuming reaction cannot be taken for granted. In this work, we therefore present a graphical method to identify promising reaction schemes using CO_2 as a feedstock. Reactant mixtures leading to minimal life-cycle greenhouse gas (GHG) emissions are determined. The optimal reaction schemes strongly depend on the reactants' global warming potential (GWP); in the case of CCU, the future GWP values of CO_2 and H_2 are particularly critical and subject to major uncertainty today. The graphical method therefore provides GWP targets for CO_2 capture and H_2 production technologies. The method is demonstrated for the production of methanol. Five optimal reaction schemes are identified depending on the GWP values of CO_2 and H_2. Thus, four threshold relations for the GWP of CO_2 and H_2 are derived showing directly under which conditions the utilization of CO_2 as a feedstock is environmentally preferential.

Keywords: Carbon Capture and Utilization, LCA, Methanol, CO_2 Conversion

1. Introduction

The utilization of captured CO_2 is drawing increasing attention [1]. With progress in capture technologies, high purity CO_2 can become abundantly available, e.g. from fossil fueled power plants. Using CO_2 as a feedstock for the production of chemicals and fuels might allow for a reduction of both greenhouse gas emissions and fossil fuel depletion. However, major challenges have to be overcome to implement CCU on a large scale: new products and pathways have to be identified and the reaction must be exergonic [2]. Systematic methods to identify promising candidate reactions are therefore desirable. Patel et al. [3] recently introduced a thermodynamic process design framework. The framework can directly be employed to identify promising CO_2-based reactions from a thermodynamic perspective. But the utilization of CCU is most often motivated environmentally. Therefore, we extend the framework from Patel et al. [3] by an optimization step based on ecological criteria such as the GWP. This extension enables the identification of the ecologically optimal composition of reactants and products. In a further step, the method can be used to determine GWP targets for CO_2 capture and H_2 production technologies.

In Section 2, the graphical method is introduced for the example of methanol production. In Section 3, results are presented before conclusions are given in Section 4.

2. Graphical Targeting Approach

After a short description of methanol production, the graphical design framework by Patel et al. [3] is briefly summarized and then extended for environmental analysis.

2.1. Methanol production from CO_2

Methanol production from CO_2 has been evaluated both from a thermodynamic [4] and a simplified environmental [2] perspective, mostly for one particular reaction, namely:

$$CO_2 + 3\ H_2 \rightarrow CH_3OH + H_2O \tag{1}$$

Although reaction (1) is thermodynamically feasible, it might not be environmentally optimal. The following section will provide a graphical method to obtain an ecologically optimal scheme for the production of methanol. The approach is directly applicable to any other compound of the form $C_xH_yO_z$.

2.2. Obtaining an ecologically optimal reaction scheme

From a thermodynamic perspective, a reaction must fulfill the mass, energy and entropy (in terms of Gibbs energy) balances. Patel et al. [3] use these balance equations as constraints for a linear program (LP). We adopt the approach for the production of any compound of the form $C_xH_yO_z$ at standard conditions (298K, 1 bar). The considered components (reactants or by-products) are limited to methane (CH_4), water (H_2O), oxygen (O_2), carbon dioxide (CO_2) and hydrogen (H_2):

$$\nu_{CH_4}\,CH_4 + \nu_{H_2O}\,H_2O + \nu_{O_2}\,O_2 + \nu_{CO_2}\,CO_2 + \nu_{H_2}\,H_2 \rightarrow C_xH_yO_z \tag{2}$$

The stochiometric coefficient of the product $C_xH_yO_z$ is always fixed to 1. The other components are reactants for negative and by-products for positive stochiometric coefficients ν_i. The mass, energy and entropy balances can be written as follows [3]:

$$0 = \nu_{CH_4} + \nu_{CO_2} + x \tag{3}$$

$$0 = 4\,\nu_{CH_4} + 2\,\nu_{H_2O} + 2\,\nu_{H_2} + y \tag{4}$$

$$0 = \nu_{H_2O} + 2\,\nu_{O_2} + 2\,\nu_{CO_2} + z \tag{5}$$

$$\Delta h^{R,0} = \Delta h^{f,0}{}_{CxHyOz} + \sum_i \nu_i\,\Delta h^{f,0}{}_i \leq 0 \tag{6}$$

$$\Delta g^{R,0} = \Delta g^{f,0}{}_{CxHyOz} + \sum_i \nu_i\,\Delta g^{f,0}{}_i \leq 0 \tag{7}$$

In this work, a reaction with a minimal environmental impact is sought after. Since the focus of CCU is on greenhouse gas emissions, the method is exemplified using the GWP as an environmental impact category. Only the supply of the reactants is considered to contribute to the GWP of the reaction whereas no benefit, i.e. no avoided burden, is given to any of the by-products.

For the methanol example, the GWP values for CH_4, H_2O and O_2 are taken from the ecoinvent database [5] whereas those of CO_2 and H_2 are treated as variable. The resulting optimization problem can be formulated as follows:

$$\min \quad OF = -\sum_i \nu^R{}_i\,GWP_i \tag{8}$$

$$\text{s.t.} \quad (3)-(7) \ \text{ where } \ \nu_i^R = \begin{cases} \nu_i, \text{ if } \nu_i < 0 \\ 0, \text{ if } \nu_i \geq 0 \end{cases} \tag{9}$$

Due to the discontinuity (9) of the objective function (OF), the problem is not an LP. A formulation as a mixed-integer linear program (MILP) is possible. However, it is insightful to decompose the solution space into regions with different, but continuous

OFs leading to several LPs. These regions are particularly conveniently determined by the graphical approach by Patel et al. [3] using so-called zero lines.

The procedure is demonstrated for the example of methanol synthesis where CO_2 and/or CH_4 act as potential carbon sources ($v_{CH_4} \leq 0$, $v_{CO_2} \leq 0$). Figure 1 shows the amount of H_2 produced or required as a function of the CO_2 amount used as feedstock. The zero lines represent stochiometries with zero amounts of a certain compound ($v_i=0$), zero reaction enthalpy ($\Delta h^{R,0}=0$) or zero Gibbs energy ($\Delta g^{R,0}=0$). Here, the $\Delta h^{R,0}=0$ constraint (6) is dominated by the $\Delta g^{R,0} \leq 0$ constraint (7) due to a negative reaction entropy and is neglected for clarity in Figure 1.

The objective function OF_k is continuous within each region k bounded by the zero mass balance lines. In Figure 1, four reasible regions ($k=1,...4$) exist, hence four LPs are solved. For example in region $k=3$, the following objective function is used:

$$OF_3 = - (v_{CH_4} GWP_{CH_4} + v_{O_2} GWP_{O_2} + v_{CO_2} GWP_{CO_2} + v_{H_2} GWP_{H_2}) \quad (11)$$

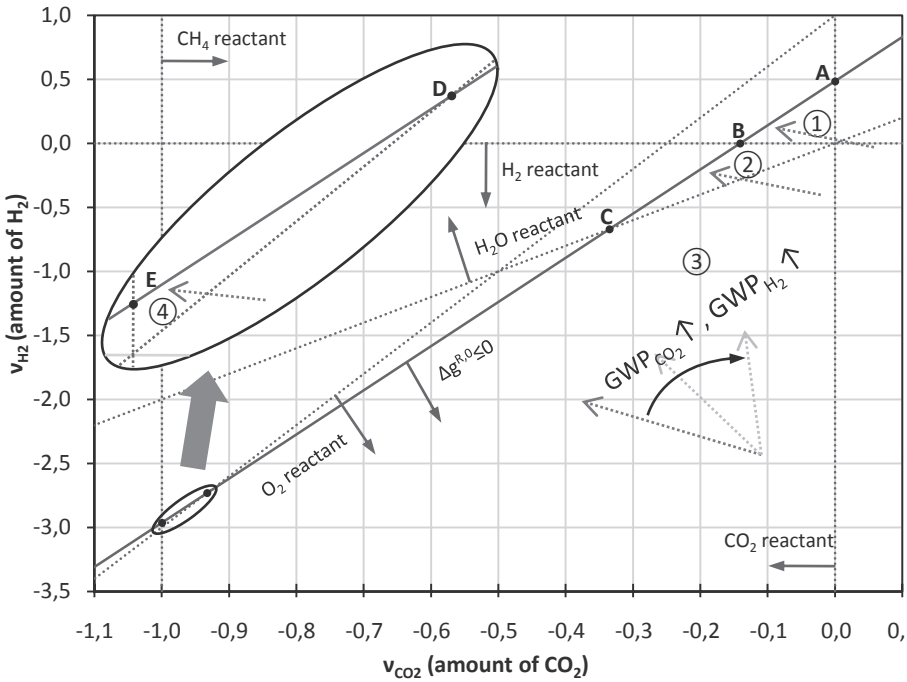

Figure 1: Solution space of (MI)LP for methanol synthesis with CO_2 as a potential feedstock. The (qualitative) dotted vectors pointing towards the regional optimal solution turn clockwise with increasing GWP values of CO_2 and H_2.

As for any LP, the optimal solution of every region is at a corner. A vector $\vec{n}_{OS,k}$ pointing towards the local (minimal) optimal solution (OS) can be defined as:

$$\vec{n}_{OS,k} = \begin{pmatrix} n_{OS,1,k} \\ n_{OS,2,k} \end{pmatrix} = \begin{pmatrix} -\partial OF / \partial v_{CO_2} \\ -\partial OF / \partial v_{H_2} \end{pmatrix} \quad (12)$$

For region 3, the vector $\vec{n}_{OS,3}$ is given by

$$\vec{n}_{OS,3} = \begin{pmatrix} \frac{\partial \nu_{CH_4}}{\partial \nu_{CO_2}} GWP_{CH_4} + \frac{\partial \nu_{O_2}}{\partial \nu_{CO_2}} GWP_{O_2} + GWP_{CO_2} \\ \frac{\partial \nu_{CH_4}}{\partial \nu_{H_2}} GWP_{CH_4} + \frac{\partial \nu_{O_2}}{\partial \nu_{H_2}} GWP_{O_2} + GWP_{H_2} \end{pmatrix} \approx \begin{pmatrix} -GWP_{CH_4} - 2GWP_{O_2} + GWP_{CO_2} \\ \frac{1}{2} GWP_{O_2} + GWP_{H_2} \end{pmatrix} \quad (13)$$

The global optimal solutions for given GWP values are obtained as follows: the vectors $\vec{n}_{OS,k}$ are plotted and the local optimal corners are identified. With the corners' reactant mixtures computed from (3) – (5), the objective function values OF_k (8) are compared to determine the global optimal solution.

2.3. Threshold values for the GWP of CO_2 and H_2

The GWP of CO_2 and H_2 are the critical factors in determining the environmental potential of a CCU scheme: How much additional CO_2 was produced in preparing the CO_2 feedstock? How was the – usually required – hydrogen produced? Most CCU proposals rely on projections about the future supply of the required feedstock. The presented graphical method allows for a convenient determination of GWP target values for future CO_2 capture and H_2 production technologies.

Eq. (13) shows, exemplary for k=3, that the vectors $\vec{n}_{OS,k}$ depend on the variable values GWP_{CO_2} and GWP_{H_2}. All vectors turn clockwise if GWP_{CO_2} or GWP_{H_2} increase. Only vector $\vec{n}_{OS,1}$ does not depend on GWP_{H_2}. This general behavior can be used to identify possible optimal corners. For example, the vector $\vec{n}_{OS,3}$ always points upwards in positive direction of ν_{H_2} since $(\frac{1}{2} GWP_{O_2} + GWP_{H_2}) \geq 0$.

The optimal solution moves from its current to a neighboring corner if the vector $\vec{n}_{OS,k}$ is orthogonal to the zero-line connecting these corners. This condition is fulfilled if:

$$m_{zero-line} = -\frac{n_{OS,k,1}}{n_{OS,k,2}} = -\frac{\partial OF_k / \partial \nu_{CO_2}}{\partial OF_k / \partial \nu_{H_2}}, \quad (14)$$

where $m_{zero\text{-}line}$ denotes the slope of the zero line. The derivatives of the OF depend on the GWP_i values. The GWP_i values fulfilling Eq. (14) are called *local GWP threshold values* since values just below or above the threshold values result in different optimal solutions in a region *k*. For the two degrees of freedom (GWP_{CO_2} and GWP_{H_2}), it is convenient to compute threshold lines.

The procedure for obtaining global GWP threshold values is as follows: the potential local optimal corners are identified using (12) with variable values for GWP_{CO_2} and GWP_{H_2}. By applying (14) to the zero-lines that connect these corners, relations for the local GWP threshold values are derived. Whether these local values are also global threshold values can be checked in analogy to the procedure in 2.2.

3. Results

The proposed method is used to determine the global GWP threshold values for CH_3OH production. In this case, five global environmentally optimal solutions can be found in dependence of GWP_{CO_2} and GWP_{H_2} (corners A to E in Figure 1). Hence, four threshold lines can be computed, see Figure 2. If GWP_{CO_2} is above 0.276 kg CO_2eq./kg CO_2, the use of CO_2 as a feedstock for methanol synthesis is environmentally not advisable and methane should be employed as carbon source. If GWP_{CO_2} is below that value, it is always preferential to (partially) use CO_2 as a feedstock. How much CO_2 should be used, depends also on GWP_{H_2}, see Figure 2.

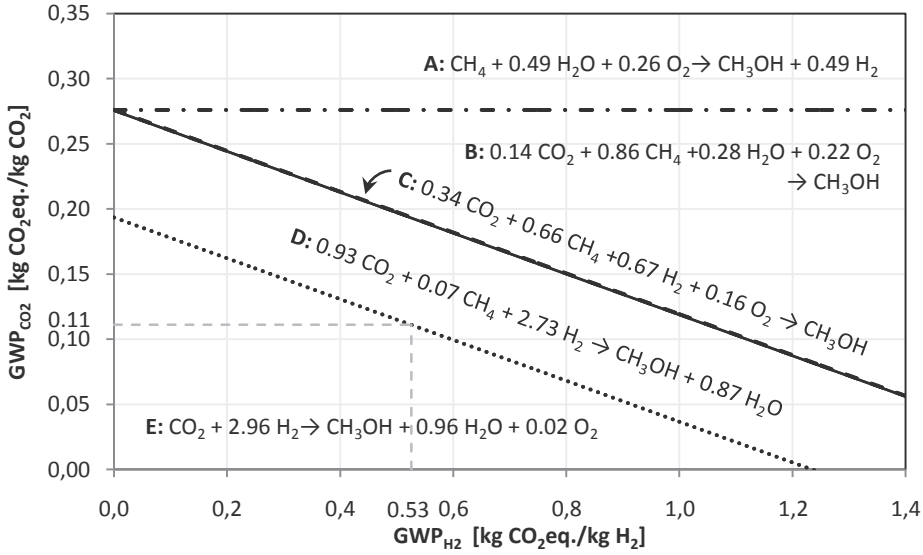

Figure 2: Environmentally optimal reactions as a function of the GWP of CO_2 and H_2.

Figure 2 can be used to define GWP targets for technologies. For example, in a power plant with a 90% CO_2 capture rate where all of the remaining 10% are allocated to the captured CO_2 stream, the GWP of CO_2 is 0.11 kg CO_2eq./kg CO_2 (=0.1/0.9). Please note that this allocation procedure provides a worst case value for GWP_{CO_2}. Still, with this worst case value, CO_2 should always be used as a feedstock. Moreover, CO_2 should be the only carbon source if GWP_{H_2} is below 0.53 kg CO_2eq./kg H_2.

4. Conclusions

Environmentally optimal reaction schemes for CCU can be obtained by introducing environmental impact coefficients into the process design framework by Patel et al. [3]. The resulting graphically-based targeting method gives further valuable insight into the process: threshold values for the GWP of CO_2 and H_2 can be derived that are tipping points between different reaction schemes. A worst case analysis shows that methanol production from CO_2 captured from power plants is a promising CCU scheme.

Acknowledgments

Niklas von der Assen and André Sternberg acknowledge financial support by the German Federal Ministry of Economics and Technology (ref. no.: 01RC1005B and 01RC1006B, respectively).

References

[1] G. Centi, S. Perathoner, Catal. Today, 148 (2009) 191
[2] M. Peters, B. Köhler, W. Kuckshinrichs, W. Leitner, P. Markewitz, T.E. Müller, ChemSusChem, 4 (2011) 1216
[3] B. Patel, D. Hildebrandt, D. Glasser, B. Hausberger, Ind. Eng. Chem. Res., 46 (2007) 8756
[4] L.K. Rihko-Struckmann, A. Peschel, R. Hanke-Rauschenbach, K. Sundmacher, Ind. Eng. Chem. Res., 49 (2010) 11073
[5] Ecoinvent Centre, The life cycle inventory data version 2.2., Switzerland (2010)

I.A. Karimi and Rajagopalan Srinivasan (Editors), Proceedings of the 11th International Symposium on Process Systems Engineering, 15-19 July 2012, Singapore.

Simultaneous Water and Energy Minimization for Brown Stock Washing System

Irene Mei Leng Chew,[a]Dominic Chwan Yee Foo,[b]Jean-Christophe Bonhivers,[c] Paul Stuart, [c]Alberto Alva-Argaez, [d]Luciana Elena Savulescu[d]

[a]*School of Engineering, Monash University Sunway Campus, Jalan Lagoon Selatan, 46150 Bandar Sunway, Selangor, Malaysia*
[b]*Department of Chemical and Environmental Engineering, Centre of Excellence for Green Technologies, University of Nottingham Malaysia, Broga Road, 43500 Semenyih, Selangor, Malaysia*
[c]*Department of Chemical Engineering, NSERC Chairholder in Process Integration for the Pulp and Paper Industry, École Polytechnique de Montreal, Montreal, Canada*
[d]*Natural Resources Canada, CANMET Energy Technology Centre, Varennes, 1615 Lionel-Boulet Blvd., Varennes, QC, Canada J3X 1S6*

Abstract

Pulp and paper mills are huge consumers of water and energy. Hence, much research works have been dedicated to simultaneous reduction of water and energy in the past decades. However, none of those works are addressing the brown stock washing system (BSWS), which is the core processing section that determines the amount of energy required in black liquor (BL) concentration. The latter is the largest energy consumption in a typical pulp and paper mill. Therefore, minimizing water consumption in the BSWS will lead to energy saving too. In this work, mass balances of the BSWS is first analyzed in a process simulation software (Cadsim), and adopted as the base case model for the study. Next, a mixed integer non-linear programming (MINLP) optimization model is developed to minimize the total annualized cost incurred in the project. The synthesized water network features significant reduction in both energy and water consumption in the BSWS.

Keywords: water minimization; pulp and paper mill; optimization; process integration.

1. Introduction

In recent decades, the large-scale exploitation of resources i.e. energy and water by the process industries has exacerbated the imbalance between economic growth and environmental protection (OECD, 2008). Being one of the biggest consumers of these resources, the process industries are urged to adopt sustainable resource management strategies to minimize overexploitation and pollution (UNEP, 2009).

Energy is used for heating purposes in the process plants. Energy embedded in water creates an inextricable link between both resources, in which the conservation of water will directly translate into energy savings (Tellinghuisen, 2009). Various attempts have been reported on the application of process integration techniques for simultaneous energy and water reduction in pulp and paper mill. Wising et al. (2005) identify the potential of excess heat recovery in the mill utilising the grand composite curve. On the other hand, Nordman and Berntsson (2006) introduce a “tank curve” to identify the maximum excess heat in the mill. Savulescu and Alva-Argáez (2008) investigated the non-isothermal mixing point and direct heat transfer to achieve water and energy efficiency.

In this work, water network for a brown stock washing system (BSWS) in an existing pulp and paper mill is optimized. An MINLP is developed to minimize the total cost associated with water consumption in the BSWS and its piping cost incurred in the proposed water network design.

2. Problem Statement

By referring to Figure 1, a set of washers with fixed flowrates and displacement ratio (DR), is optimized for its water network system by effectively reused/recycled the filtrate (water source) in the showers (water sink) and in the dilution of pulp inlet stream (water sink). Table 1 tabulates the water flowrates and DR of each washing equipment in the base case (Bonhivers and Stuart, 2007).

Table 1.Washers flowrates and displacement ratio (DR)

Washers, k	**DR**	**Water flowrates, (kg/t pulp)**			
		Pulp inlet D_k	**Shower S_k**	**Filtrate F_k**	**Pulp outlet P_k**
Emcc	0.65	9457	4998	10505	3950
Diffuser 1	0.90	7612	12494	12852	7254
Diffuser 2	0.90	7254	12494	12494	7254
Decker	0.75	57439	9500	59803	7136
Washer 1	0.70	61981	4500	60681	5800
Washer 2	0.72	71662	6000	70869	6793
PreDO	0.70	71662	6000	71614	6048

3. Mathematical Model for Brown Stock Washing System

BSWS is the most important washing section in a pulp and paper mill. The main function of BSWS is to remove dissolved solids (DS) from the pulp. The filtrate generated during the washing process is known as black liquor (BL) and is concentrated in evaporator to become strong BL for recovery. The mathematical model for BSWS optimization is formulated as follows:

The objective function is set to minimize the total annualized cost, obj_{COST} as shown in Equation (1). This includes the fresh water (first term) cost which has been annualized to 330 operation days per year, with 600 ton of pulp produced daily and the annualized piping (second term) cost.

$$\min obj_{\mathrm{COST}} = \left(F_{\mathrm{FW}} \times F_{\mathrm{COST}} \times 600\ \text{ton pulp/day} \times 330\ \text{day/year}\right) + P_{\mathrm{COST}} \tag{1}$$

3.1. Washers Mass Balances

Equations (2) – (4) stated the flowrate balances for shower, dilution point and filtrate, respectively, while Equation (5) is the overall flowrate balance at washer k.

$$S_k = FW_k^S + \sum_{k' \in K} R_{k',k}^S + T_k^S \qquad k \in K \tag{2}$$

$$D_k = FW_k^D + \sum_{k' \in K} R_{k',k}^D + P_{k-1} + T_k^D \qquad k \in K \tag{3}$$

$$F_k = \sum_{k' \in K} R_{k,k'}^D + \sum_{k' \in K} R_{k,k'}^S + R_k^T + BL_k \qquad k \in K \tag{4}$$

$$D_k + S_k = P_k + F_k \qquad k \in K \tag{5}$$

where $R^{S}_{k',k}$ and $R^{D}_{k',k}$ denote filtrate flowrate sent for reused/recycled at the shower and pulp dilution point (from another washer *k'* to washer *k*), respectively. It is worthy of note that, in case of filtrate self-recycle, *k'* = *k*. Variables T^{D}_{k} and T^{S}_{k} denote the pressate flowrate from TRP; P_{k-1} represents flowrate of pulp liquor from washer *k*-1 entering into washer *k*; variable $BL_k$is the lean black liquor which will be sent for heat treatment; FW^{S}_{k} and FW^{D}_{k} denote fresh water that makes up shower and pulp dilution point, respectively.

On the other hand, DS balances for the shower stream and pulp dilution point are given by Equations (6) – (7), respectively. Equation (8) states the DR parameters in relationship with DS concentration.

$$FW^{S}_{k} C_{\mathrm{FW}} + \sum_{k' \in K} R^{S}_{k',k} C^{F}_{k'} + T^{S}_{k} C_{T} \le S_{k} C^{S}_{k} \qquad k, k' \in K \quad (6)$$

$$FW^{D}_{k} C_{\mathrm{FW}} + \sum_{k' \in K} R^{D}_{k',k} C^{F}_{k'} + P_{k-1} C^{P}_{k-1} + T^{D}_{k} C_{T} \le D_{k} C^{D}_{k} \qquad k, k' \in K \quad (7)$$

$$\mathrm{DR}_{k} = \left(C^{D}_{k} - C^{P}_{k}\right) / \left(C^{D}_{k} - C^{S}_{k}\right) \qquad k \in K \quad (8)$$

where $C^{S}_{k}, C^{F}_{k}, C^{D}_{k}, C^{P}_{k}, C_{T}, C_{\mathrm{FW}}$ represent the concentration at shower, filtrate, pulp dilution, pulp outlet, TRP and fresh water, respectively.

3.2. Twin Roll Press (TRP) Mass Balance

Pressate from TRP is sent for reuse/recycle, and Equations (9) and (10) stated the flowrate and DS balances, respectively. The total flow rate of fresh water, F_{FW} is given in Equation (11).

$$D_{\mathrm{T}} = FW^{T} + \sum_{k \in K} R^{T}_{\mathrm{k}} + P^{in}_{\mathrm{T}} \quad (9)$$

$$FW^{\mathrm{T}} C_{\mathrm{FW}} + \sum_{k \in K} R^{T}_{\mathrm{k}} C^{F}_{k} + R_{T} C^{out}_{T} + P^{in}_{\mathrm{T}} C^{P}_{Dec} \le D_{T} C^{in}_{T} \quad (10)$$

$$F_{\mathrm{FW}} = \sum_{k \in K} FW^{S}_{k} + \sum_{k \in K} FW^{D}_{k} + FW^{T} \quad (11)$$

where variables D_{T} and C^{in}_{T} denote the inlet flowrate and concentration at TRP, respectively. Variable FW^{T} denote the fresh water flowrates at TRP. It is further note that P^{in}_{T} is identical to $P_{k\text{-}1}$ in Equation (3), where in this case P^{in}_{T} and C^{P}_{Dec} are referring to the pulp outlet flowrate and DS concentration from decker washer.

3.3. Energy Consumption

Energy is consumed in three identified sections, e.g. multiple-effect evaporator (MEE), H_{evap}, BL concentration heater, H_{conc} and O_2 delignification reactor, H_{react} (see Fig. 1); their respective energy balance equations are shown in Equations (12) – (14). Equation (15) denotes the total BL sent to the MEE for heat treatment. As shown in Equation (13), the lean BL is preheated to 100 °C whereas in Equation (14) the pulp stream is heated to the reaction temperature of 115 °C.

$$H_{\mathrm{Evap}} = \left(BLE - SBL\right) \times \overline{H} \div a \quad (12)$$

$$H_{\mathrm{conc}} = \left(BLE - BL_{EMCC}\right) \times C^{\mathrm{BL}}_{\mathrm{P}} \left(100 - T_{BL}\right) \quad (13)$$

$$H_{\mathrm{React}} = F_{\mathrm{R}} \times C^{\mathrm{R}}_{\mathrm{P}} \left(115 - T_{R}\right) \quad (14)$$

$$BLE = \sum_{k \in K} BL_k - RBL \tag{15}$$

where parameters *RBL* and *SBL* denote the recycled BL to the EMCC washer, and strong BL exit at the MEE; parameters $\overline{H}$ and *a* represent the specific heat and efficiency of the MEE. Variable BL_{EMCC} is the BL flowrate at the EMCC washer, while variable T_{BL} is the average BL inlet temperature at the concentration heater while T_R is the inlet temperature at the reactor. Variable F_R denotes the pulp outlet flowrate at TRP (before entering the reactor). In this work, heat capacity for black liquor, C_P^{BL} and pulp mat in reactor, C_P^R are assumed at 3.5 kJ/kg°C and 4 kJ/kg°C, respectively.

3.4. Annualized Piping Cost

Equations (16) - (17) give the upper (UB) and lower (LB) bounds of the reused/recycled filtrate. Binary variable $x_{k',k}$in Equation (16) indicates the existence of piping connection between the filtrate of washer *k'* and shower of washer *k*; binary variable $y_{k',k}$ in Equation (17) indicates the existence of piping connection between the filtrate of washer *k'* and dilution point of washer *k*. Note that in this case, the *LB* is set at zero while the *UB* is set at the filtrate flowrate, F_k (see Table 1).

$$LB \times x_{k',k} \le R^S_{k',k} \le UB \times x_{k',k} \qquad k, k' \in K,\ k \ne k' \tag{16}$$

$$LB \times y_{k',k} \le R^D_{k',k} \le UB \times y_{k',k} \qquad k, k' \in K,\ k \ne k' \tag{17}$$

Capital cost for piping (P_{COST}) in Equation (1) is adapted from Kim and Smith (2004) and is given in Equation (18). The piping cost considers the use of carbon steel pipes (given in USD), with the cost parameters of p = 7200 and q = 250 (CE plant index = 318.3). It is further assumed that the stream flowrate velocity, ν = 1 m.s^{-1} and water density, ρ = 1000 kg.m^{-3} throughout this study. An equal Manhattan distance, *D* is assumed for all pipelines.

$$P_{\text{COST}} = D\left[\left(p \sum_{k' \ne k \in K} \frac{R^S_{k',k}}{3600\rho\nu} + q x_{k',k}\right) + \left(p \sum_{k' \ne k \in K} \frac{R^D_{k',k}}{3600\rho\nu} + q y_{k',k}\right)\right] AF \tag{18}$$

An annualised factor (*AF*) is used to annualise the piping capital cost, defined as:

$$AF = \frac{m(1+m)^n}{(1+m)^n - 1} \tag{19}$$

where m = fractional interest rate per year, n = number of years.

4. Case Study

In the case study illustratation, the following assumptions are in place:-

F_{COST} is set at \$ 1/ton; C_{FW} = 0; *RBL* = 2000 kg/ton pulp; *SBL* = 2900 kg/ton pulp; $\overline{H}$ = 2200 kJ/kg; a = 4; D = 10 m; TRP pulp inlet, filtrate and pulp outlet flowrates are 26829, 23807 and 3022 kg/ton pulp, respectively; T_R and T_{BL} are set at 80 °C; The upper limit of DS concentration leaving PreDO washer ≤ 0.094 %.

The MINLP model in this work entails a total of 221 continuous variables, 119 binary variables and 441 constraints with solution found in 3 CPU second.

5. Conclusion

Objective function in Equation (1) is solved subject to the constraints in Equations (2) – (19) yields the minimum total annualized cost of USD$1.94 million. Fig. 1 shows one of the possible optimal water network configurations. Table 2 summarizes the total fresh water, BL and heat consumption of the base case and the optimized BSWS.

Table 2. Comparison of fresh water and energy consumption

	Base case (Cadsim simulation)	MINLP
Fresh water (kg/ton pulp)	12321	9644
Black liquor (kg/ton pulp)	13948	13053
Energy (GJ/ton pulp)	6.74	5.05

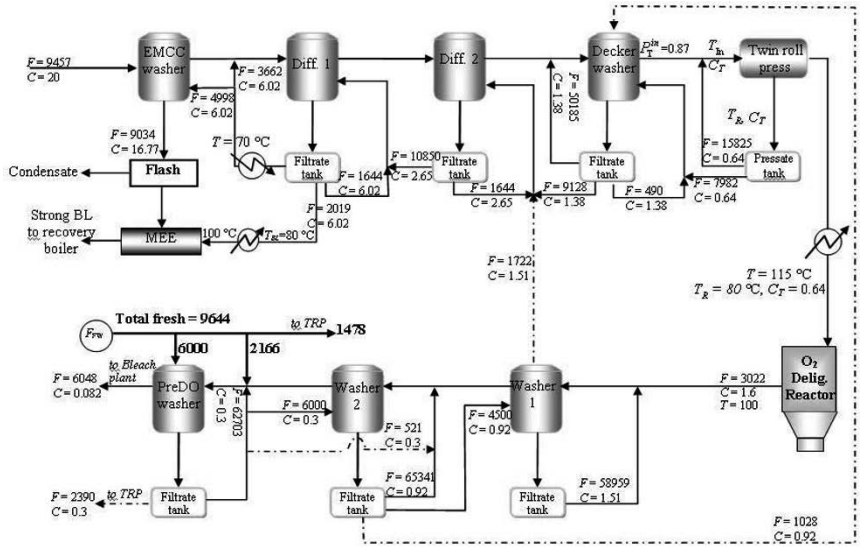

Figure 1: Process layout for optimized BSWS with F (kg/ton pulp), C (%) and T (°C)

References

J.C. Bonhivers, P. Stuart,(2007), Study on the brown stock washing configuration of the softwood line at Espanola mill, NSERC PhD research report.

J. Kim, R. Smith, (2004), Automated design of discontinuous water systems, Trans IChemE, Part B 82(B3), 238–248.

R. Nordman, T. Berntsson, (2006), Design of kraft pulp mill hot and warm water systems-A new method that maximizes excess heat, Appl. Therm. Eng., 26, 363-373.

OECD, (2008), OECD Environmental Outlook to 2030, Organisation for economic co-operation and development, Paris.

L. Savulescu, A. Alva-Argáez, (2008), Direct heat transfer consideration for improving energy efficiency in pulp and paper Kraft mills, Energy, 33, 1562-1571.

S. Tellinghuisen, Water conservation = Energy conservation, Western Resource Advocates, 2009, http://www.circleofblue.org/waternews/wp-content/uploads/2010/08/CWCBe-wstudy.pdf, accessed on October 11, 2011.

UNEP Year Book, (2009), United Nations Environment Programme. www.unep.org/geo/yearbook/yb2009/, accessed on October 11, 2011.

U. Wising, T. Berntsson, P. Stuart, (2005), The potential for energy savings when reducing the water consumption in a kraft pulp mill, Appl. Therm. Eng., 25, 1057-1066.

I.A. Karimi and Rajagopalan Srinivasan (Editors), Proceedings of the 11th International Symposium on Process Systems Engineering, 15-19 July 2012, Singapore.

A heuristic approach to design batch water-using networks with multiple contaminants

Bao-Hong Li,[a] You-Kang Liang,[b] Chuei-Tin, Chang[b1]

[a]*Department of Chemical Engineering, Dalian Nationalities University, Dalian 116600*
[b]*Department of Chemical Engineering, National Cheng Kung University, Tainan, 70101*

Abstract

A heuristic design method is presented in this paper for batch water-using networks with *multiple* contaminants. A systematic procedure is developed on the basis of the performance measures originally used for evaluating the continuous systems. Specifically, the well-established *concentration indices*, i.e., Concentration Potential of Demand (CPD) and Concentration Potential Source (CPS), are adopted as primary criteria and the *time priority* as secondary criterion to match the water sources with demands sequentially. For illustration purpose, an example is given at the end of this paper. The results show that this manual approach can be easily implemented to produce a near optimal batch water-using network, which consumes a reasonable amount of freshwater with relatively low level of storage capacity.

Keywords: Batch water-using network, Multiple contaminants, Concentration index.

1. Introduction

Water integration in the batch plants has gained increasing attention in recent years(Gouws et al., 2010). The available integration methods can be classified into two kinds. The first can be considered as the graphic-based(Chen & Lee, 2008) or pinch-based(Hallale, 2002; Majozi et al., 2006; Kim, 2011) approach which can be applied only to the single-contaminant systems, while the other is the model-based strategy(Li & Chang, 2006; Chen et al., 2008). The main feature of the pinch-based approach is that the target amount of freshwater is first determined and the network design can then be synthesized accordingly. With a graphic-based approach(Chen & Lee, 2008), the design task can be performed directly without a targeting step, while the minimum freshwater consumption and the maximum water recovery is ensured by following the necessary condition of optimality(Salvelski & Bagajewicz, 2000) and the nearest neighbors algorithm(Prakash & Shenoy, 2005). On the other hand, since in general time limitation of unmatched operation periods may be the primary barrier for resource integration in batch processes, storage facilities are often installed to enhance the opportunities for water recovery. As a result, the corresponding NLP or MINLP models can be very difficult to solve(Chen et al., 2008).

[1] To whom correspondence should be addressed. E-mail: ctchang@mail.ncku.edu.tw

The objective of this study is to develop a systematic heuristic procedure for designing the batch systems with multiple contaminants, which is analogous to the aforementioned graphic-based approach with *single* contaminant(Chen & Lee, 2008). Such an analogy is possible primarily owing to the fact that two concentration indices, i.e., Concentration Potential of Demand (CPD) and Concentration Potential Source (CPS), can be used to order the degrees of contamination of various water demands and sources respectively in a way just like that for the single-contaminant water streams(Liu et al., 2009). Two kinds of water-using units, *i.e*., the *fixed load* and *fixed flow rate* operations, are considered in this work. The concentration constraints are adopted as primary criteria and time priority as secondary criteria to match the water demands and sources sequentially and the needed storage facilities are simultaneously determined in the network synthesis process.

2. Problem Statement

A batch water-using network may consist of several different types of unit operations, and each consumes and/or generates certain quality and quantity of water. In addition, the starting and finishing times of every operation should be predefined. To overcome the mismatch between the operating periods of two chosen batch processes, a buffer tank may be introduced to facilitate water integration. It is assumed that freshwater is available at any time and wastewater can be discharged to the environment. The primary design objective is to minimize freshwater consumption by maximizing water reuse among water-using units. As a secondary objective, the total number of buffer tanks and the sum of their capacities should both be reduced as much as possible so as to cut down the overall capital investment. Finally, water recycle is forbidden in this work to avoid accumulation of trace contaminants that may result in operational difficulties.

3. Concentration Potentials

Liu et al.(2009) proposed to use the *concentration potentials* for characterizing the reuse capabilities of sources and demands. The concentration potential of demand D_j (CPD) was defined as

$$CPD(D_j) = \sum_{i=1}^{NS} R_{i,j} = \sum_{i=1}^{NS} \min_{k=1,2,\cdots NC} \left[\frac{C_{D_j,k}^{\lim}}{C_{S_i,k}} \right] \qquad (i \neq j) \tag{1}$$

where, the subscripts i, j and k represent the labels of demands, sources and contaminants respectively; NS and NC denote the total numbers of sources and contaminants respectively; $R_{i,j}$ is the maximum amount of S_i that can be used to satisfy 1 ton of D_j; $C_{D_j,k}^{\lim}$ is the maximum allowable concentration of contaminant k in demand D_j; $C_{S_i,k}$ is the concentration of contaminant k in source S_i. Here $i \neq j$ because it is forbidden to recycle a water stream to the process where it is produced. Obviously, the overall reuse capability of demand D_j is proportional to CPD(D_j). On the other hand, the concentration potential of source S_i (CPS) was defined as

$$\frac{1}{CPS(S_i)} = \sum_{j=1}^{ND} R_{i,j} = \sum_{j=1}^{ND} \min_{k=1,2,\cdots NC} \left[\frac{C_{D_j,k}^{\lim}}{C_{S_i,k}} \right] \quad (i \neq j) \tag{2}$$

where, *ND* is the total number of demands. It can be inferred that the overall reuse capability of S_i is inversely proportional to CPS (S_j).

From equations (1) and (2), it can be observed the concentration potentials are functions of the contaminant concentrations only. Note also that multiple demands (or sources) with the same concentrations should be treated as one stream in calculating these potentials.

4. Allocation Principles

When the demands are satisfied by sources in a cyclic batch process, a total of seven allocation principles should always be observed, only two of principles are given below because of space limitation and interested readers are referred to our full paper(Li et al., 2012):

(1) When there are multiple source streams available, the source with largest value of maximum R should be reused first to reduce the freshwater usage. If there is more than one source with identical R value, the source with the highest CPS should be reused to reduce downstream freshwater consumption, where the CPS value of the sources should be calculated only for the unmatched processes.

(2) If a demand cannot be totally satisfied with a single source, another source should be used. The remainder of the mass loads in the demand can be calculated by subtracting the mass load in the allocated source from the maximum mass load of the demand. Similarly, the remainder of the limiting flow rate of the demand can be calculated by subtracting the flow rate of the allocated source from the present limiting flow rate, and the allowable maximum concentration can be calculated by dividing the remainder of the mass load by the remainder of the limiting flow rate. The allocation procedure will continue till the concentrations of at least one contaminant reach the maximum(s) or the reminder of the limiting flow rate becomes zero.

5. A Case study

This example is adopted to illustrate the effectiveness of the proposed design method. The processing data considered in this case study is given in Table 1. From the starting and ending times given in this table, it can be observed that units 1, 2 and 4 are operated in truly batch mode while units 3 and 5 in semi-batch mode.

Before exploring water reuse, let us consider a base case in which all units are satisfied with freshwater. For the fixed-load operations (i.e., units 1, 2 and 4), the required amounts of water can be determined to be 30, 55 and 15 ton respectively. On the other hand, both units 3 and 5 require 40 ton of water. Therefore, the freshwater consumption level in the base case is 30+55+15+40+40=180 ton in a single period (8.5h).

Let us next arrange these five units in ascending order of the limiting inlet concentration potential (CPD) which are calculated by using the limiting concentration values. By applying the proposed allocation principles, the network configuration in Figure 1 can be identified. The detailed implementation steps are omitted here due to space limitation, interested readers are referred to our full paper(Li et al., 2012). Note that in this figure

the duration of each batch operation is expressed in a color bar and, moreover, the time periods of water intake and discharge are indicated by the shaded and blank bars. The charging and discharging periods of the storage tanks are also marked with angled solid lines. Notice that the total freshwater usage has been reduced to 83.1 ton, which means a 53.8% saving from the base case. Certainly, three buffer tanks must be installed to achieve this goal. The required storage capacities can be easily determined to be 30, 75 and 26.9 ton respectively according to the corresponding time profiles of their inventories.

In order to check the optimality of Figure 1, the minimum freshwater usages for the case study when only one contaminant is considered and time is entirely ignored can be obtained by any availble method(Foo et al., 2005), which are all 80 ton. So the low bound of minumu freshwater usage is 80 ton and the freshwater consumption in Figure 1 is really near to this low bound value and the error is only 4%.

Table 1: Process data for the example problem

Unit	Time(h)		Contaminant	$C_{in,k}^{max}$	$C_{out,k}^{max}$	m^{load}	F^{lim}
	intake	discharge		ppm	ppm	kg	ton
1	0.0-1.0	1.0-5.0	A	0	100	3.0	30
			B	0	90	2.7	
			C	0	50	1.5	
2	0.0-0.5	4.5-5.0	A	40	150	8.25	75
			B	60	80	1.5	
			C	20	70	3.75	
3	5.0-6.5	5.0-6.5	A	170	170	0	40
			B	120	120	0	
			C	100	100	0	
4	2.0-2.5	6.5-7.0	A	110	210	3.0	30
			B	135	200	1.95	
			C	60	120	1.8	
5	7.0-8.5	7.0-8.5	A	170	170	0	40
			B	120	120	0	
			C	100	100	0	

6. Conclusions

A systematic heuristic design procedure for batch water-using network with multiple contaminants is proposed in this paper. Two allocation principles and the corresponding network synthesis steps are illustrated with a simple example. The implementation results show that this manual design strategy is quite effective for producing near optimal water-using networks.

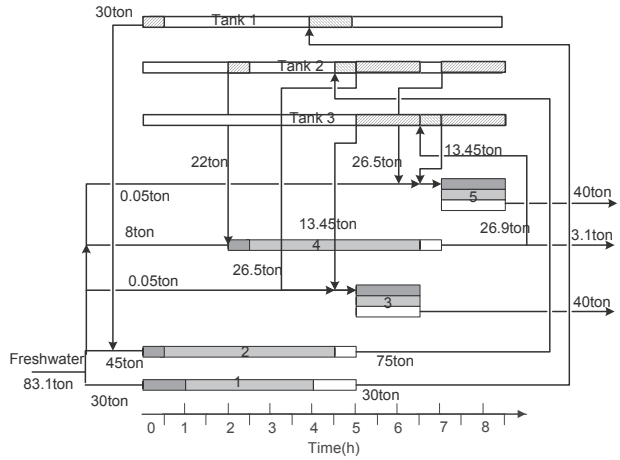

Figure 1: The network configuration for the case study

7. Acknowledgement

Financial support provided by National Natural Science Foundation of China under Grant NO. 20806015 and The Independent Research Fund of Dalian Nationalities University under Grand No. DC110104 are is gratefully acknowledged.

References

C. L. Chen,, C. Y. Chang, & J. Y. Lee, 2008, Continuous-time formulation for the synthesis of water-using networks in batch plants. Ind. Eng. Chem. Res., 47, 7818–7832.

C. L. Chen, & J. Y. Lee, 2008, A graphical technique for the design of water-using networks in batch processes. Chem. Eng. Sci., 63, 3740–3754.

C. Y. Foo, Z. A. Manan, & Y. L. Tan, 2005, Synthesis of maximum water recovery network for batch process systems. J. Clean Prod., 13, 1381-1394.

J. F. Gouws, T. Majozi, D. C. F. Foo, C. L. Chen, & J. Y. Lee, 2010, Water minimization techniques for batch processes. Ind. Eng. Chem. Res., 49, 8877–8893.

N. Hallale, 2002, A new graphical targeting method for water minimization. Adv. Eng. Res., 6, 377-390.

J. K. Kim, 2011, Design of discontinuous water-using systems with a graphic method. Chem. Eng. J., 172, 799-810.

B. H. Li, & C. T. Chang, 2006, A mathematic programming model for discontinuous water-reuse system design. Ind. Eng. Chem. Res., 45, 5027–5036.

B. H. Li, Y. K. Liang, & C. T. Chang, 2012, Manual design strategies for multi-contaminant water-using networks in batch processes. Chem. Eng. J., submitted.

Z. Y. Liu, Y. Yang, L. Z. Wan, X. Wang, & K. H. Hou, 2009, A heuristic design procedure for water-using networks with multiple contaminants. AIChE J., 55, 374-382.

T. Majozi, C. J. Brouckaert, & C. A. Buckley, 2006, A graphic technique for wastewater minimization in batch processes. J. Environ. Manage., 78, 317-329.

R. Prakash, & U. V. Shenoy, 2005, Targeting and design of water networks for fixed flowrate and fixed contaminant load operations. Chem. Eng. Sci., 60, 255-268.

M. J. Salvelski, & M. J. Bagajewicz, 2000, On the optimality conditions of water utilization systems in process plants with single contaminants. Chem. Eng. Sci., 55, 5035-5048.

I.A. Karimi and Rajagopalan Srinivasan (Editors), Proceedings of the 11th International Symposium on Process Systems Engineering, 15-19 July 2012, Singapore.

Synthesis of Sustainable Property-Based Water Networks

Luis Fernando Lira-Barragán,[a] José María Ortega-Ponce,[a]* Medardo Serna-González,[a] Mahmoud M. El-Halwagi[b].

[a] *Universidad Michoacana de San Nicolás de Hidalgo, Morelia, Mich., México*
[b] *Chemical Engineering Department, Texas A&M University, College Station, TX, USA*

Abstract

This work presents a new mathematical programming model for the optimal integration of an industrial water network and its supporting watershed. In particular, the model determines the optimal location of a new industrial facility considering the sustainable integration of its wastewater discharges with the surrounding watershed through a disjunctive formulation. The behavior of the watershed impacted by the new discharges is described by the material flow analysis (MFA) technique in terms of property balances. The MFA technique considers all inlet and outlet streams in the watershed (i.e., residential, sanitary, industrial discharges and extractions). Therefore, for a new industrial plant, the proposed model allows to track the water properties throughout the watershed and determine the allowable level of discharges. The objective function involves the minimization of the total annualized cost that includes the costs for the installation of the new plant (including the transportation for raw materials, products and services, as well as the land cost), wastewater treatment, piping, and the purchase of the fresh sources. The resulting model is a mixed-integer nonlinear program (MINLP) and a case study for one of the most important watersheds of Mexico is presented to demonstrate the advantages of the proposed formulation. The results show that the environmental regulations are not enough to satisfy the sustainability of the integrated system (i.e. new industrial plant, watershed and other elements of the environment). Hence, unlike previous approaches, the proposed model yields sustainable water networks by taking into consideration simultaneously in-plant water integration and its interaction with the surrounding watershed including various environmental elements such as neighboring plants, cities and agricultural areas.
Keywords: Property-Based, Material Flow Analysis, Optimal Plant Location, Sustainable Systems, Watershed, Water Integration.

1. Introduction

Industrial facilities consume large quantities of fresh water and, at the same time, produce considerable amounts of wastewater. Over the last years, economic competition, scarcity of fresh water and the increasingly strict environmental regulation on industrial effluents have driven the process industry to develop a variety of techniques for the integrated management of water resources. Among them, the water process integration, which is based on water reuse/recycle and wastewater regeneration strategies, has been proven as an effective approach to reduce both fresh water consumption and wastewater discharge of industrial facilities (El-Halwagi, 2011). While this approach is beneficial, its application has only focused on water integration in individual plants and eco-industrial parks without explicitly addressing the sustainability problem of the surrounding watersheds. Recently, Lira-Barragán et al.

*jmponce@umich.mx

(2010a; 2011b) presented two mathematical programming models to account simultaneously for the optimum water integration of a new industrial plant and the sustainability of its watershed. It should be noted that this integrated approach is based on mass concentration of water streams (i.e. constraints for environment and process units are in terms of composition of the pollutants). Therefore, it cannot handle constraints (i.e. environmental regulations) imposed on water quality in terms of properties such as pH, toxicity, turbidity, chemical oxygen demand (COD) and others.
Therefore, this work presents a mathematical programming formulation based on properties for water network synthesis of new plants with multiple pollutants, which allows the simultaneous consideration of the integration of their discharges with macroscopic watershed systems. The Material Flow Analysis (MFA) technique is used to determine the environmental impacts of material flows caused by new plants on the watersheds. Since different plant locations will have different environmental impact and may entail different treatment costs, the plant location is incorporated as a design variable into the model using disjunctive programming and a set of discrete variables. The proposed formulation identifies the optimal property-based water network and location of a new plant that meet the sustainability requirements of the watershed system.

2. Model Formulation

The model proposed in this paper is based on the representation shown in **Figure 1**, where the integration of the wastewater effluent from the new plant is integrated with the surrounding watershed through the determination of the optimal location of the new plant and the quantity and quality (given in terms of specific values for the properties) of the wastewater discharged to the watershed. Notice in this figure that each process source inside the new industrial plant is segregated to be treated for a set of interceptors in several treatment stages. Once the treatment is completed, these streams and the fresh sources are sent to the process sinks and to the wastewater discharge. The process sinks and the wastewater discharge include property constraints. This allows to integrate the process wastewater discharge with other discharges to the watershed (i.e., water for agricultural use, wastewater discharged to the river with and without treatment, industrial and residential effluents, etc.), in addition to natural phenomena like precipitation, filtration and vaporization, as well as the quality for the water in the final disposal to avoid accumulation of hazardous pollutants.
To determine the properties of the water in different sections of the watershed, the river is sectioned in parts (reaches) where the properties can be considered constant (ovals in **Figure 1**). The discharges to the watershed contain compounds that interact chemically and biochemically with the system thought the flora and fauna established in the watershed; in addition, the properties of these discharges modify the properties of the water in the watershed. To ensure the sustainability of the surrounding watershed, it is required to carry out an analysis prior to the optimization respect to the capacity of the final disposal to decompose chemically and biochemically the pollutants and, as consequence, it is necessary to quantify these processes in terms of properties. The analysis yields the sustainability constraints, which ensures that the pollutants will not be accumulated in the system and to maintain the properties of the watershed under reasonable limits.
To solve this problem, the mathematical programming model consists of four main elements: the material flow analysis model for the watershed, the water network inside the new industrial facility, the disjunctive model to integrate the new discharge to the watershed and the objective function.

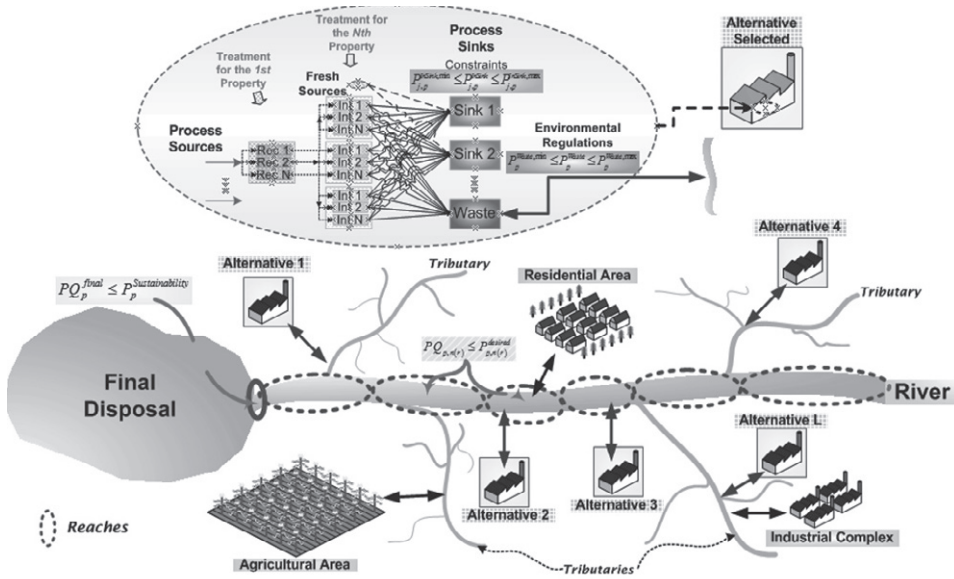

Figure 1: Problem addressed in this paper including the mass integration inside the new plant.

Watershed model based on properties. The overall and component balances for the different sections of the river (**Figure 1**) state that the outlet flowrate in a reach Q_r is equal to the inlet flowrate Q_{r-1} plus precipitation P_r, direct discharge D_r, residential discharges H_r, the sum of tributaries $FT_{r,t}$ and the possible discharge from the new plant $QPNEW_r$ minus the losses L_r and uses U_r.

$$Q_r = Q_{r-1} + P_r + D_r + H_r + \sum_{t=1}^{N_{t(r)}} FT_{r,t} + QPNEW_{r(l)} - L_r - U_r, \quad \forall r \in R \tag{1}$$

The property balances of each reach are based on equation (1), but this also includes a reactive term $r_{p,r}$ to account for the chemical and biochemical reactions that change the properties of the streams. In addition, the mixing rules for different properties are stated in similar way that the component balances (i.e., proportional to the flowrate). However, some properties do not follow a direct relation with the flowrate, so specific property operators ψ_p determined experimentally are used for these cases (see Shelley and El-Halwagi, 2000).

$$\psi_p\left(P_{p,r}^{Reach}\right)Q_r = \psi_p\left(P_{p,r-1}^{InReach}\right)Q_{r-1} + \psi_p\left(P_{p,r}^{Prec}\right)P_r + \psi_p\left(P_{p,r}^{Ind}\right)D_r + \psi_p\left(P_{p,r}^{Resid}\right)H_r + \sum_{t=1}^{N_{t(r)}}\psi_p\left(P_{p,r,t}^{Trib}\right)FT_{r,t} \tag{2}$$

$$+\psi_p\left(P_{p,r(l)}^{PNEW}\right)QPNEW_{r(l)} - \psi_p\left(P_{p,r}^{Loses}\right)L_r - \psi_p\left(P_{p,r}^{Uses}\right)U_r - \int_{V=0}^{V_r} r_{p,r}\,dV_r, \ \forall p \in P, r \in R$$

Similar balances are established for the tributaries of the river.

Location of the new plant. There are several alternatives (L) to locate the new industrial facility specified prior to the optimization process. For each alternative, it is necessary to consider the possible discharge of the new wastewater ($QPNEW_l$) with its properties. Thus, if the new industrial plant is located in the alternative 1, the wastewater flowrate and their property associated to this site must be greater than zero; otherwise, if the new plant is not located in the position 1, the wastewater flowrate and their property operators discharged are zero. This is included in the following disjunction:

$$\begin{bmatrix} Y_1 \\ \psi_p\left(P_{p,1}^{PNEW}\right) \geq 0, QPNEW_1 \geq 0 \\ \psi_p\left(P_{p,2}^{PNEW}\right) = 0, QPNEW_2 = 0 \\ \vdots \\ \psi_p\left(P_{p,I}^{PNEW}\right) = 0, QPNEW_I = 0 \end{bmatrix} \vee \begin{bmatrix} Y_2 \\ \psi_p\left(P_{p,1}^{PNEW}\right) = 0, QPNEW_1 = 0 \\ \psi_p\left(P_{p,2}^{PNEW}\right) \geq 0, QPNEW_2 \geq 0 \\ \vdots \\ \psi_p\left(P_{p,I}^{PNEW}\right) = 0, QPNEW_I = 0 \end{bmatrix} \vee \cdots \vee \begin{bmatrix} Y_I \\ \psi_p\left(P_{p,1}^{PNEW}\right) = 0, QPNEW_1 = 0 \\ \psi_p\left(P_{p,2}^{PNEW}\right) = 0, QPNEW_2 = 0 \\ \vdots \\ \psi_p\left(P_{p,I}^{PNEW}\right) \geq 0, QPNEW_I \geq 0 \end{bmatrix}, \quad \forall p \in P$$

The previous disjunction is reformulated using the convex hull technique.

In-plant water integration. The in-plant mass integration is based on **Figure 1**. The size of this formulation increases exponentially according to the number of treated properties (*N*); however, the major advantage for the model obtained from this representation is that it is linear. As it can be seen in **Figure 1**, for each property to be treated there is a set of treatments units; therefore, there are *N* treatment units. The balances for describing the in-plant water integration include the overall and property balances in the segregating and mixing points as well as the models for the property interceptors.

Environmental constraints. The model requires a set of constraints that include upper and lower limits for specific properties in the wastewater discharged to the environment (i.e., pH, COD, toxicity, color, etc.). These are stated in form of property operators as:

$$\psi_p\left(P_p^{Waste,\min}\right) \leq \psi_p\left(P_p^{Waste}\right) \leq \psi_p\left(P_p^{Waste,\max}\right), \quad \forall p \in P \tag{3}$$

Constraints for the quality of specific reaches. It is necessary a set of property constraints for some reaches of the river where water is required for specific uses:

$$\psi_p\left(P_{p,m(r)}^{DesiredMIN}\right) \leq \psi_p\left(P_{p,m(r)}^{\text{Re}ach}\right) \leq \psi_p\left(P_{p,m(r)}^{DesiredMAX}\right), \quad \forall p \in P, m(r) \in M(R) \tag{4}$$

Sustainability constraints. The model considers the following constraints to assure the sustainability of the watershed and avoid environmental risks of the final disposal:

$$\psi_p\left(P_p^{SustainableMIN}\right) \leq \psi_p\left(P_{p,final}^{\text{Re}ach}\right) \leq \psi_p\left(P_p^{SustainableMAX}\right), \quad \forall p \in P \tag{5}$$

Objective Function. The objective function consists in the minimization of the total annual cost (*TAC*), which is constituted by the installation cost for the new plant, the fresh sources cost, the treatment cost (including operational cost, variable and fixed capital cost) and the piping cost. The installation cost ($Cland_l$) takes into account the land cost and the transportation costs for raw materials, products and services.

$$\begin{aligned} Min\ TAC = & \sum_{l \in L} Cland_l y_l + H_Y \sum_{k \in K} FreC_k F_k + H_Y \sum_{i \in I} \left[\sum_{int^1 \in INT^1} VarC_{op}^{int^1} w_i^{int^1} + \cdots \sum_{int^N \in INT^N} \left(VarC_{op}^{int^N} w_i^{int^1, \cdots, int^N} \right) \right] \\ & + H_Y \sum_{i \in I} \left[\sum_{int^1 \in INT^1} VarC_{cap}^{int^1} w_i^{int^1} + \cdots \sum_{int^N \in INT^N} \left(VarC_{cap}^{int^N} w_i^{int^1, \cdots, int^N} \right) \right] + k_f \sum_{i \in I} \left[\sum_{int^1 \in INT^1} FixC_{cap}^{int^1} z_i^{int^1} + \cdots \sum_{int^N \in INT^N} \left(FixC_{cap}^{int^N} z_i^{int^1, \cdots, int^N} \right) \right] \\ & + H_Y \left[\begin{array}{l} TrPipC \sum_{i \in I} \left(\sum_{int \in INT} w_i^{int^1} + \cdots \sum_{int^N \in INT^N} w_i^{int^1, \cdots, int^N} \right) + WaPipC \sum_{i \in I} \sum_{int^1 \in INT^1} \cdots \sum_{int^N \in INT^N} g_{i,Waste}^{int^1, \cdots, int^N} \\ + EqPipC \sum_{i \in I} \sum_{int^1 \in INT^1} \cdots \sum_{int^N \in INT^N} \sum_{j \in J} g_{i,j}^{int^1, \cdots, int^N} + FrPipC \sum_{k \in K} \sum_{j \in J} f_{k,j} \end{array} \right] \end{aligned} \tag{6}$$

3. Results and Discussion

This case considers the Balsas watershed that is one of the biggest systems in Mexico (**Figure 2**). This system transports several types of discharges until the Pacific Ocean (CONAGUA, 2010). The properties restricted for the stream discharged to the environment are composition, toxicity, COD, odor and color, while the process sinks limit the composition and density. In this sense, the environmental regulations for the properties restricted in the wastewater stream are the following: for composition is 50, for the toxicity is 0.1, for COD is 75, for odor is 2.7 and for color is 100. The system has twenty possible locations to install the new industrial facility. This example was

implemented in GAMS using the solver DICOPT and the optimal solution found by the proposed model shows that the new facility must be placed in alternative 6 with a total annual cost of $\$14.9x10^6$/yr, composed by $\$9x10^6$/yr for installation cost, $\$3.6x10^6$/yr for treatment cost, $\$1.52x10^6$/yr for fresh source cost and \$779,040/yr for piping cost. In this solution, the mass integration shows that the values for some of the properties in the discharged wastewater stream need to be lower than their corresponding environmental regulations to fulfill the constraints in the watershed. For example, the value of toxicity in the wastewater stream is zero, satisfying the constraint in the reach 8, where is not allowed the existence of this property.

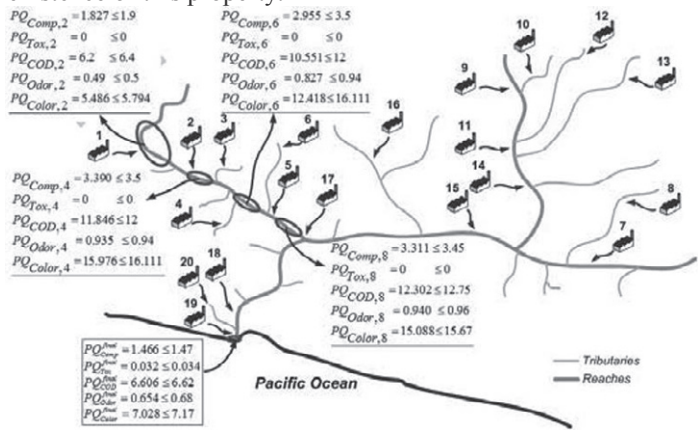

Figure 2. Balsas watershed system.

4. Conclusions

This work presents a new water integration approach to consider simultaneously the water integration inside a new plant and the sustainability of the associated watershed. The results show that the traditional water integration schemes that do not consider the watershed system yield inappropriate solutions, because the environmental regulations are not enough to satisfy the sustainability of the system. To satisfy the sustainability, the interaction of the wastewater streams discharged to the environment with other discharges through the watershed must be considered in conjunction to the chemical and physical phenomena that happen in the watershed. In addition, a model based on properties like the one proposed is suited for this problem because the large set of compounds present in these macroscopic systems.

References

CONAGUA, 2010, Mexican National Water Commission, Water Statistics, 2009, http://www.conagua.gob.mx/OCB07/Temas/EstadisticasBALSAS-FINALago09.pdf

L. F. Lira-Barragán, J. M. Ponce-Ortega, M. Serna-González, and M. M. El-Halwagi, 2011a, An MINLP model for the optimal location of a new industrial plant with simultaneous consideration of economic and environmental criteria, Industrial Engineering and Chemical Research, 50(2), 953–964.

L. F. Lira-Barragán, J. M. Ponce-Ortega, M. Serna-González, and M. M. El-Halwagi, 2011b, Synthesis of water networks considering the sustainability of the surrounding watershed, Computers and Chemical Engineering, 35(12), 2837–2852.

M. D. Shelley, M.M. El-Halwagi, 2000, Componentless design of recovery and allocation systems: A functionality-based clustering approach, Computers and Chemical Engineering, 24(9-10), 2081-2091.

M. M. El-Halwagi, 2011, Sustainable Design Through Process Integration, Butterworth-Heinemann.

I.A. Karimi and Rajagopalan Srinivasan (Editors), Proceedings of the 11th International Symposium on Process Systems Engineering, 15-19 July 2012, Singapore.

Modeling and optimization of water-based polygeneration system

Triana Prihatin, Shuhaimi Mahadzir and M. Ibrahim Abdul Mutalib*
Process Development Research Group, Chemical Engineering Department, Universiti Teknologi PETRONAS, Bandar Seri Iskandar, 31750, Tronoh, Perak, Malaysia
**shuham@petronas.com.my*

Abstract

The impact of climate change, particularly drought, places an enormous pressure on the synthesis of process systems that use freshwater resources efficiently. This paper presents the synthesis of water-based polygeneration system to minimize freshwater consumption. A comprehensive model is formulated through a superstructure, featuring the possible configurations of simultaneous heat and power generations, re-circulating cooling water system, wastewater treatment options, as well as reaction and separation technologies for chemical production. Process units are modeled using Aspen Hysys 2006. A case study on the synthesis of optimum water polygeneration system is developed for an ethylene glycol production. The superstructure model is a mixed integer non-linear programming problem (MINLP) consisting of 305 equations, 326 variables and 20 binary variables. The objective of the model is to minimize freshwater make-up subject to 85 constraints. The model is subsequently solved using DICOPT++ in GAMS 20.7 with the optimum solution showing nearly 50% savings of freshwater consumption.

Keywords: water conservation, heat and power, cooling water, 3R, ethylene glycol.

1. Introduction

Climate change creates pressure on the sustainability of future water supplies. The problem of declining freshwater resources due to population and industrial needs is further elevated by the impact of climate change such as drought. The problem is further compounded with the generation of industrial waste water. A recent strategy to address the problem of declining resources, such as water, is polygeneration. Polygeneration is an integrated approach to generates multiple products from a single resource [1-2]. In the case of water-based polygeneration, water is the main input material for the generation of multiple outputs from a single industrial plant, such as hot utility, power, cold utility and chemical products. As a result, water-based polygeneration minimizes the consumption of limited natural resources and energy as well as reducing the generation of waste water [2].

Previous works have addressed the design and analysis of polygeneration system from the perspective of energy conservation [3-4]. The search for an optimum polygeneration energy system is computationally demanding due to the complex combination of options that are built in large superstructure representation. Liu et al. [5-8] developed mathematical programming models for the design and analysis of polygeneration energy systems. The investment planning for the polygeneration system was formulated as a mixed integer linear programming (MILP) model and solved in GAMS [5]. The authors later developed mixed-integer nonlinear programming (MINLP) models to address design and operational variables [6] with multi-objective optimization function [7] and

polygeneration energy systems design under uncertainty using decomposition based stochastic programming approach [8]. Optimum polygeneration system of a combined energy and water production has been presented by Rubio-Maya et al. [9]. Choices of possible technologies are represented using MINLP superstructure. Although the focus of the work was on desalinated and cooling water production associated with the production of heat and power, it did not investigate the minimization of freshwater consumption and wastewater generation.

In this study, optimum polygeneration system incorporating 3R water conservation concept, i.e. regenerate, reuse and recycle, is investigated. An MINLP model is developed through a superstructure that simultaneously addresses heat and power generations, re-circulating cooling water system, wastewater treatment options, and reaction and separation technologies for chemical production. A water polygeneration system for ethylene glycol production is presented as a case study.

2. Superstructure Representation

The mathematical programming problem for a process network synthesis is formulated using a superstructure that incorporates many alternative design paths. The idea of a superstructure is to establish the interaction between intermediate inputs and outputs for every unit operation represented as a network comprising process streams and equipment. Yeomans and Grossmann [10] presented a state-task-network (STN) in which three basic elements of superstructure syntheses are states, tasks, and equipment. As shown in Fig. 1, a circle represents the state of a process stream, such as raw material composition, or product flow rate. In addition, a task corresponds to momentum, mass and energy transfer that take place in equipment such as heat exchanger, reactor, or absorber. States and tasks are connected with arrow lines building the network superstructure. The identification of states and tasks helps in determining the type of equipment to be applied for each task. For complex process synthesis problem, such as the water-based polygeneration system, the superstructure is further divided into subsystems comprising different unit operations.

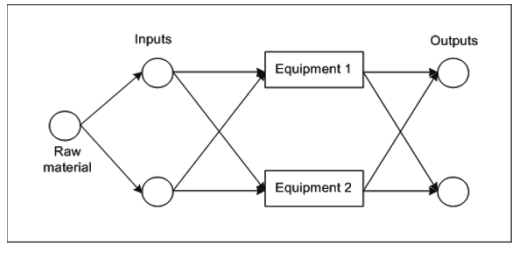

Fig.1. General superstructure representation.

3. Model Formulation

A mixed integer nonlinear programming (MINLP) model for the selection of optimum water-based polygeneration system is formulated based on superstructure representation. Binary variable, $y \in Y = \{0,1\}$, is introduced as a logical constraint that provides yes-no decision. The selection of process technology option is represented as

$$\sum_{i \in I} y_i = 1 \qquad (1)$$

where i is index of unit operation. For a specific unit operation i, variable $y_i = 1$ if unit i is selected in the optimal structure or 0 otherwise.

For heat and power generation subsystem, mass and energy balances are expressed as

$$\sum_j \sum_i F_{j,i}.y_i - \sum_k \sum_i F_{k,i}.y_i = 0 \tag{2}$$

$$\sum_j \sum_i F_{j,i}.H_j.y_i - \sum_k \sum_i F_{k,i}.H_k.y_i = 0 \tag{3}$$

where F and H are flowrates and enthalpy values of inlet streams j and outlet streams k, respectively. For the energy balance around steam boiler, an efficiency factor, η_B, is also included. For the energy balance around steam turbine, the power demand, $W_{st,i}$, and the steam enthalpy at steam pressure level, $\Delta H_{st,i}$, is correlated to the flowrate intake of the steam turbine, $FT_{st,i}$, as shown below [11]:

$$F_{stB} - \sum_{i \in I} FT_{st,i} = 0 \tag{4}$$

$$FT_{st,i} = W_{st,i} / \Delta H_{st,i} \tag{5}$$

In Eq. (4), F_{stB} refers to steam flowrate coming from the boiler of the selected steam generation technology.

In the cooling water subsystem, mass balance around the cooling tower is given by

$$F_{in} + F_m - F_{out} - F_b = 0 \tag{6}$$

where F_{in} is the inlet water flowrate to cooling tower, F_{out} is outlet water flowrate of cooling tower, F_m is the cooling water makeup and F_b is the cooling tower blowdown. Water loss through evaporation, F_{ev}, is correlated to blowdown and makeup as per Eq. (7) and (8), in which π_c is the cooling tower cycles of concentration.

$$F_b = F_{ev} / (\pi_c - 1) \tag{7}$$

$$F_m = F_{ev} \left[\pi_c / (\pi_c - 1) \right] \tag{8}$$

The chemical production subsystem is simulated in Aspen HYSYS 2006 using the UNIQUAC property model. The constraints for the supply of cooling, heating and power requirement in the chemical production are formulated as per process demands. For example, the steam supply to a distillation column, St_{supply}, is equal to the steam demand by the reboiler, St_{Dem}.

$$ST_{supply} \geq ST_{Dem} \tag{9}$$

The objective for the water-based polygeneration system is to optimize the flowrate of freshwater consumption (FW) at minimum total annualized cost. The objective function (z) includes the cost of freshwater intake, C_{fw}, and the cost of water recovery, $OP_{recovery}$, as shown in Eq. (10).

$$\min z = \left[(FW \times C_{fw}) + OP_{recovery} \right] \times AOT \tag{10}$$

The cost of water recovery takes into consideration the pumping cost as well as cost associated with water recycle, reuse and regeneration (3R). Water recycling involves post-treatment process of the water quality to meet the next water-user specification.

However, water reuse does not require additional treatment and is possibly sent to the next user in its water effluent condition. The cost is calculated on annual basis assuming annual operation time, *AOT*, of 8000 hrs/year.

4. Case Study: Water-based polygeneration system in ethylene glycol production

An ethylene glycol production follows the reaction between ethylene oxide and water at temperature of 200^{o}C and pressure of 20 bars to produce mono-ethylene glycol and other higher glycols derivatives. The product recovery and purification consume water for the heating and cooling of the separation processes. An MINLP model based on the superstructure generated in Fig. 2. is demonstrated for the synthesis of an optimum water-based polygeneration system in an ethylene glycol production.

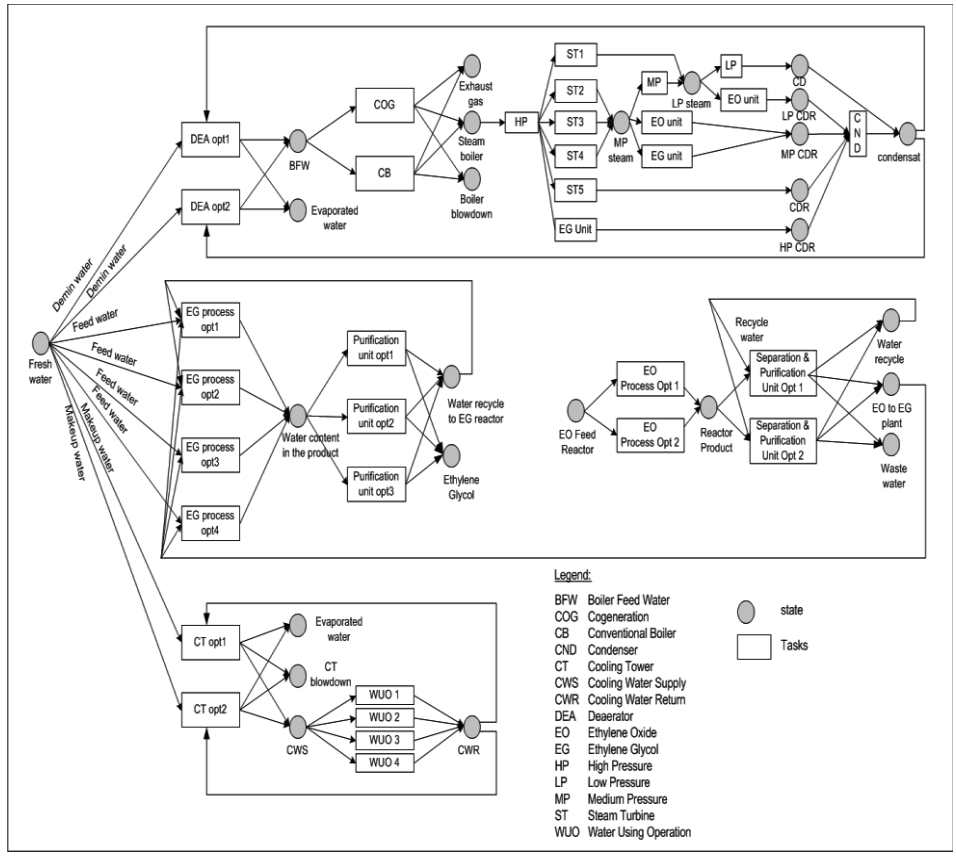

Fig.2. Superstructure representation of water-based polygeneration system.

The superstructure for water-based polygeneration system is presented with three subsystems, namely heat and power generation, recirculating cooling water and chemical production. The heat and power generation subsystem features power generation option from either gas turbine or steam turbine, while the option for boilers include a conventional boiler or a cogeneration system that recovers hot gas turbine exhaust to raise steam. Gas turbines options are simple or regenerative gas turbines, while steam turbines options are back-pressure or condensing steam turbines. For recirculating cooling water system, choices of cooling tower include the forced or the

induced mechanical drafts types. For the chemical production subsystem, two options of ethylene glycol (EG) synthesis are ethylene oxide (EO) hydrolysis and the Shell's OMEGA process. Options for the separation system include direct sequence, indirect sequence or dividing wall distillation column.

The model is developed in GAMS and solved using DICOPT++. It is a nonconvex MINLP model comprising 20 binary variables, 326 continuous variables and 305 equations. The optimum results indicate the power generation unit employs a cogeneration system comprising a gas turbine with HRSG and three steam turbines. Simple gas turbine cycle and back-pressure steam turbine are selected to meet the heat and power demands. For EG production, the EO hydrolysis process is selected with minimum freshwater consumption. For separation unit, the dividing wall column is selected resulting in significant reduction in capital cost from the distillation columns arrangement and considerable energy savings in condenser and reboiler loads.

Table 1. Optimum results of water-based polygeneration system

	Freshwater consumption (t/hr)	Wastewater generation (t/hr)	Objective Function ($/yr)
Base case	447.674	228.453	931,161.08
Optimised case	219.221	0	637,587.84

The 3R strategy for water recovery is also implemented in the optimum solution. As shown in Fig. 2, freshwater is consumed as makeup for demineralized water in the heat and power subsystem, feed to the EG reactor, and makeup water for the cooling tower. The cost of water consumption is minimized through water regeneration and recycle from boiler and cooling tower blowdown as well as from wastewater produced in the EG plant. Comparison between the base case and the optimized case is summarized in Table 1. The optimized case showed a significant reduction of freshwater consumption by almost 50% and total elimination of wastewater generation.

5. Conclusion

A comprehensive model for the synthesis of an optimum water-based polygeneration system was formulated through superstructure representation. The application of the model was demonstrated on an ethylene glycol production case study. The optimum solution highlighted that water-based polygeneration system may potentially bring significant savings in freshwater consumption.

References

[1] K.H. Kaggerud, et al, 2006, Applied Thermal Engineering, 26, 1345-1352.
[2] L.M. Serra, et al, 2009, Energy, 34, 575-586.
[3] H. Li, et al, 2010, Applied Energy, 87, 2846-2853.
[4] T.A. Adams II, and P.I. Barton, 2011, Fuel Processing technology, 92, 639-655.
[5] P. Liu, et al, 2007, Catalysis Today, 127, 347-359.
[6] P. Liu, et al, 2009, Computers & Chemical Engineering, 33, 759-768.
[7] P. Liu, and E.N. Pistikopoulos, 2010, Process System Eng AIChE Journal, 56, 1218-1234.
[8] P. Liu, et al, 2010, Ind. Eng. Chem. Res., 49, 3295-3305.
[9] C. Rubio-Maya, et al, 2011, Energy Conversion & Management, 52, 2861-2896.
[10] H. Yeomans and I.E. Grossmann, 1999, Computers & Chemical Engineering, 23, 709-731.
[11] R. Smith, 2005, Chemical Process Design and Integration, England: John Wiley & Sons.

I.A. Karimi and Rajagopalan Srinivasan (Editors), Proceedings of the 11th International Symposium on Process Systems Engineering, 15-19 July 2012, Singapore.

Multi-objective Optimization for Integrated Water Network Synthesis

Iskandar Halim,[a] Arief Adhitya,[a] Rajagopalan Srinivasan[a,b]

[a]*Institute of Chemical and Engineering Sciences, A*STAR, 1 Pesek Road, Jurong Island, Singapore 627833*
[b]*Department of Chemical and Biomolecular Engineering, National University of Singapore, 10 Kent Ridge Crescent, Singapore 119260*

Abstract

This paper proposes a multi-objective genetic algorithm for optimal synthesis of integrated water networks. The framework is based on formulating a superstructure that incorporates all feasible design alternatives for the water network and solves it for minimum freshwater and treatment costs. It considers also selection of treatment units and piping cost in the formulation. The framework is illustrated by solving a literature case study.

Keywords: water reuse, wastewater minimization, superstructure, NSGA-II.

1. Introduction

In chemical plants, the water that is used for processing and non-processing purposes would lead to wastewater that needs to be treated to acceptable level prior to being discharged to the environment. With growing pressure to become more sustainable, chemical plants are looking for alternatives to minimize their freshwater consumption as well as wastewater generation. This is especially important in region with constrained water resources. In this regard, process modifications through water saving technologies and optimal design of water networks need to be promoted.

The problem of optimal synthesis of an integrated water network can be described as follows: given a set of processing units that requires water, synthesize an optimal network of water flows over the set of processing units subject to contaminant mass load, allowable contaminant concentrations, maximum flowrates, and wastewater treatment efficiencies. This optimization problem is known to be highly nonlinear and nonconvex. Over the past decades, various solution methods have been proposed and these can be differentiated into deterministic and stochastic. The former formulates the water network synthesis problem as MINLP and solves it for global optima. The drawback of this approach is that it is limited to formulating the water network synthesis as single objective problem involving either minimization of freshwater or cost. Further, solution to MINLP problem is difficult and cannot be guaranteed by the conventional gradient-based algorithm (Hul et al., 2007). To mention a few, Karuppiah and Grossmann (2006) proposed an advanced search strategy by combining deterministic spatial branch and contract algorithm and General Disjunctive Program for optimizing water network superstructure. Rubio-Castro et al. (2010) solved the MINLP superstructure by first discretizing it to MILP (mixed integer linear programming).

Stochastic optimization techniques such as genetic algorithm (GA) have been applied to solve the integrated water network problem. Tsai and Chang (2001) applied a GA technique to identify minimum freshwater consumption and cost-optimal water usage and treatment network. Tudor and Lavric (2011) proposed a GA method for

simultaneous minimization of freshwater consumption and piping cost. The advantage of stochastic approach over the deterministic method is that the former is able to explore the trade-off surface of multiple objectives efficiently. Another advantage of stochastic technique is its ability to solve the inherently nonlinear and nonconvex problem with optimal consistency (Thunyawart et al., 2011). However, such advantage comes at the expense of longer computing time (Hul et al., 2007).

In this paper, we apply a multi-objective GA for simultaneous minimization of freshwater consumption and total water treatment cost including the piping cost. We include a choice for selection of treatment units in the formulation and explore the trade-off surface of the two objectives.

2. Integrated water network model

The water network model is based on the superstructure shown in Figure 1 (Karuppiah and Grossmann, 2006). It shows an integrated water network with four process units (PUs) and two groups of treatment units (TUs). Each PU requires water and would pick up a certain load of contaminants from the processing. The resulting wastewater stream from each PU must be treated in the TUs prior to discharge. In this case, one TU from each treatment group needs to be selected. To minimize the amount of freshwater usage, water from the TUs needs to be reused. However, this is subject to maximum allowable inlet contaminant concentrations of the PUs.

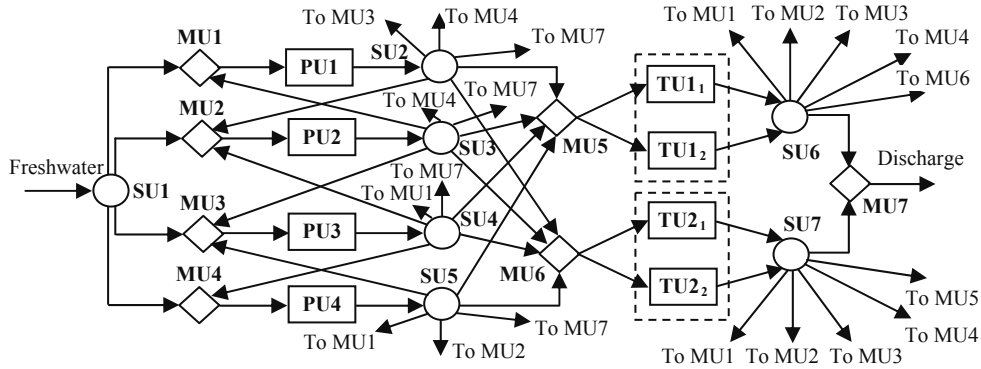

Figure 1. Superstructure of water network with selection of treatment units

The mass balance over a process unit p is written as:

$$F_i\, C_{i,j} + L_j \times 1000 = F_k\, C_{k,j} \tag{1}$$

where F_i and F_k are the flowrates of the input i and output k streams of unit p (ton/h), $C_{i,j}$ and $C_{k,j}$ are the concentrations of contaminant j in the input i and output k streams of unit p (ppm), and L_j is the loading of contaminant j in unit p (kg/h). In this case, F_i and F_k are assumed as equal. The removal of contaminant j from a treatment unit t is described as:

$$C_{i,j} = (1 - RR_j) C_{k,j} \tag{2}$$

where RR_j is the removal ratio for contaminant j in unit t.

The objective functions are described as follows:

$$\text{Min } HC_{FW} FW \tag{3}$$

$$\text{Min } \Phi = AR \sum_{t=1}^{T_{total}} IC_t F_{out,t}^{\ \alpha} + H \sum_{t=1}^{T_{total}} OC_t F_{out,t} + PC \tag{4}$$

where FW is the freshwater flowrate to all process units (ton/h), C_{FW} is the freshwater cost ($/ton), H is plant operating hours per annum (h/yr), AR is the annualized

investment factor (/yr), IC_t is the investment cost coefficient for treatment unit t, $F_{out,t}$ is the flowrate of wastewater from treatment t (ton/h), OC_t is the operating cost coefficient for treatment unit t (ton/h), and PC is the piping cost expressed as follows (Rubio-Castro et al., 2010):

$$PC = AR \times PP \times [\frac{D_{k,i}F_{k,i}}{3600\rho\upsilon} + D_{k,i} \times CU_p] \quad (5)$$

where PP is the pipe parameter, $D_{k,i}$ is the piping distance between point k and i (m), $F_{k,i}$ is the flowrate between point k and i (kg/h), ρ is the water density (kg/m^3), υ is the velocity of water inside the pipe (m/s), and CU_p is the unit cost of the pipe ($). Here, we set a minimum flow of 0.1 ton/h in each pipe, except for the flow to the discharge.

3. Multi-objective Genetic Algorithm

We have applied Non-Dominated Sorting in Genetic Algorithm-II, NSGA-II, (Deb et al., 2002) for multi-objective optimization. The procedure is as follows:

Step 1. A random initial population of size N is generated within the variable ranges and the objective functions for each chromosome are evaluated.

Step 2. The initial population is sorted based on the objective values using fast sorting method to generate several non-dominated fronts. Each member in each front is assigned a fitness value (rank).

Step 3. The crowding distance for each member in each front is calculated and sorted according to its objective values.

Step 4. Based on the rank and crowding distance, the parent population is selected from the initial population using binary tournament selection.

Step 5. Crossover and mutation are performed to the parent population to generate offspring population.

Step 6. The parent and offspring population are combined to generate a population size of 2N. Elitism is performed to select the best population of size N according to its objective function value.

Step 7. The stopping criterion is checked. Step 2 to 7 is repeated if necessary.

The decision variables in this water network problem are various water flows – Freshwater to PU, PU to another PU, PU to TU, PU to Discharge, TU to PU, TU to another TU, and TU to Discharge. Other decision variable is selection of treatment technology for each treatment group. These flows together with treatment selection constitute a chromosome. The GA is coded in such a way that mass balance constraints will always be satisfied. As concentration limits may be violated, a penalty function proportional to the difference from the limit is applied on the objective values.

4. Case study

We have solved the case study of Karuppiah and Grossmann (2006) shown in Figure 1. It involves two contaminants A and B, for which the PU and TU data are shown in Table 1 and 2, respectively. The discharge limits for both contaminants are 10 ppm. The freshwater cost is $1/ton and the annualized factor for investment is taken to be 0.1/yr. The plant is operated for 8000 h/yr. Table 3 shows the distances between PUs and TUs.

The Pareto plot in Figure 2 shows a trade-off between freshwater and treatment costs. It shows that for a network with less freshwater flow, it needs to be compensated with more flow of reused water. Consequently, this leads to higher treatment cost. The figure also shows a minimum total operating cost of $655,110 which corresponds to minimum freshwater case. Figure 3 compares two different water networks involving minimum freshwater and treatment costs. The former corresponds to freshwater flowrate of 40

ton/h while freshwater flowrate in the later is 75.16 ton/h. In both cases, the selected treatment technologies are $TU1_2$ and $TU2_1$ – this is in line with the results of Karuppiah and Grossmann (2006). Comparison between Figure 2 and 3 highlights that a change to the network structure would lead to significant repercussion in the freshwater demand. This explains a series of "jumps" in the freshwater cost shown in Figure 2.

Table 1. Process unit data

Unit	Flowrate (kg/h)	Contaminant load (kg/h)		Max. inlet concentration (ppm)	
		A	B	A	B
PU1	40	1	1.5	0	0
PU2	50	1	1	50	50
PU3	60	1	1	50	50
PU4	70	2	2	50	50

Table 2. Treatment unit data

Group	Treatment technology	α	Removal ratio (%)		Investment cost coeff.	Operating cost coeff.
			A	B		
TU1	$TU1_1$	0.7	95	0	16800	1
	$TU1_2$	0.7	90	0	4800	0.5
TU2	$TU2_1$	0.7	0	90	12600	0.0067
	$TU2_2$	0.7	0	95	36000	0.067

Table 3. Distances (in meters) between plant units

	PU1	PU2	PU3	PU4	$TU1_1$	$TU1_2$	$TU2_1$	$TU2_2$	Discharge
Fresh	150	170	180	200	–	–	–	–	–
PU1	–	50	50	50	60	60	60	60	70
PU2	50	–	50	50	60	60	60	60	70
PU3	50	50	–	50	60	60	60	60	70
PU4	50	50	50	–	60	60	60	60	70
$TU1_1$	60	60	60	60	–	–	20	20	10
$TU1_2$	60	60	60	60	–	–	20	20	10
$TU2_1$	60	60	60	60	20	20	–	–	10
$TU2_2$	60	60	60	60	20	20	–	–	10

5. Conclusions

A multi-objective optimization framework for integrated water network is proposed using NSGA-II. The framework takes into account selection of treatment technologies and piping cost. The framework is tested using a literature case study. Pareto plot of the optimization results highlights trade-off between the freshwater and treatment costs. Our future work is to extend the framework to batch process by exploring both the structural and variable aspects of the synthesis problem.

References

K. Deb, A. Pratap, S. Agarwal and T. Meyarivan, 2002, A fast and elitist multiobjective genetic algorithm: NSGA-II, IEEE Transactions on Evolutionary Computation, 6, 182-197.

S. Hul, R.R. Tan, J.Auresenia, T. Fuchino and D.C.Y. Foo, 2007, Water network synthesis using mutation-enhanced particle swarm optimization, Process Safety and Environmental Protection, 85, 507-514.

R. Karuppiah and I.E. Grossmann, 2006, Global optimization for the synthesis of integrated water systems in chemical processes, Computers and Chemical Engineering, 30, 650-673.

E. Rubio-Castro, J.M. Ponce-Ortega, F. Napoles-Rivera, M.M. El-Halwagi, M. Serna-Gonzalez and A. Jimenez-Gutierrez, 2010, Water integration of eco-industrial parks using a global optimization approach, Industrial and Engineering Chemistry Research, 49, 9945-9960.
M.J. Tsai and C.T. Chang, 2001, Water usage and treatment network design using genetic algorithms, Industrial and Engineering Chemistry Research, 40, 4874-4888.
R. Tudor and V. Lavric, 2011, Dual-objective optimization of integrated water/wastewater networks, Computers and Chemical Engineering, 35, 2853-2866.
J. Thunyawart, T. Srinophakun, W. Henwatthana, 2011, Simulation of mass exchange networks using modified genetic algorithms, Korean Journal of Chemical Engineering, 28, 332-341.

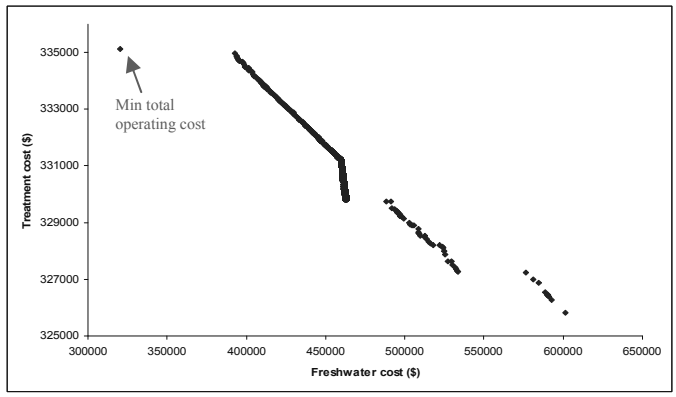

Figure 2. Pareto plot of integrated water network

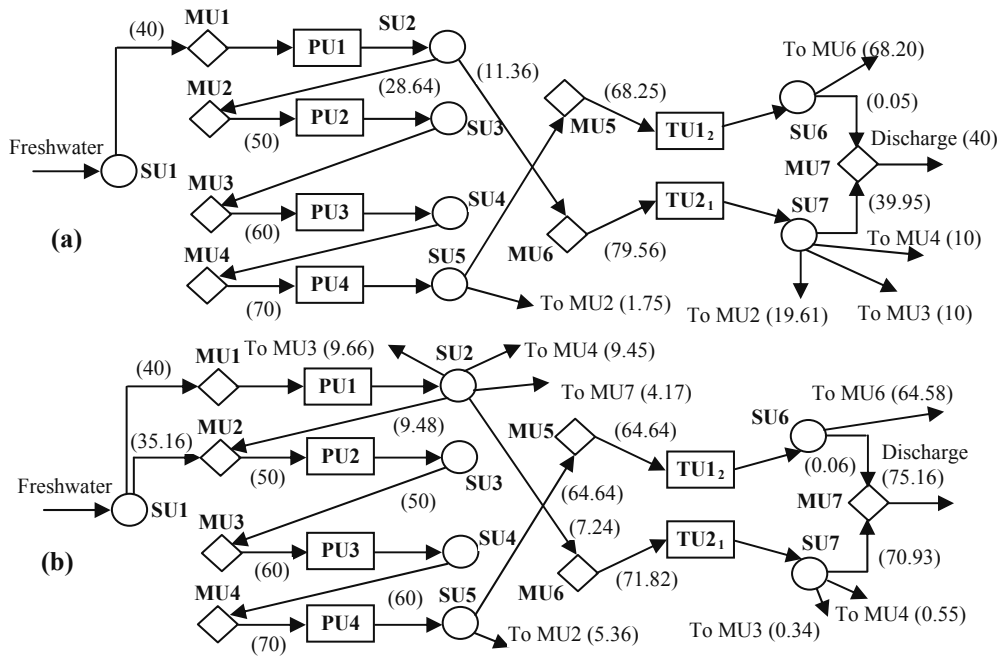

Figure 3. Optimal water network (a) minimum freshwater cost and (b) minimum treatment cost. Number in bracket denotes the water flowrate in ton/h.

I.A. Karimi and Rajagopalan Srinivasan (Editors), Proceedings of the 11th International Symposium on Process Systems Engineering, 15-19 July 2012, Singapore.

Synthesis of water networks for processes with mixed batch and continuous units

Cheng-Liang Chen, Chun-Yen Lin, Hui-Chu Chen, Jui-Yuan Lee

National Taiwan University, No. 1, Sec. 4, Roosevelt Rd., Taipei 10617, Taiwan

Abstract

This paper presents a mathematical model for the synthesis of water networks, where both batch and continuous units are involved. For cases where the number of batch units is greater than that of continuous units, a dividing approach is proposed. By treating continuous operation as a combination of batch operations, the original design problem is simplified and the remaining task is almost to synthesize a batch water network. The model is formulated as a mixed-integer nonlinear program based on a superstructure including all feasible network interconnection. A modified literature example is solved to illustrate the proposed approach.

Keywords: process integration, water network synthesis, batch and continuous units, mathematical optimization.

1. Introduction

Water is one of the most important natural resources widely used in various process industries. However, rapid industrial growth has led to serious water pollution in the world. In addition, the growing concern about high consumption and waste of water for industrial applications calls for efficient and responsible use of water in industry. Other reasons tied to this need include the predicted scarcity of industrial water, increasingly stringent environmental regulations for wastewater disposal, and the rising costs of fresh water and effluent treatment.

To make efficient use of water, water recovery via *water network synthesis* has been commonly accepted as an effective means, with *reuse*, *recycle*, and *regeneration* as options for reducing industrial water withdrawals and discharges. Over the past decades, various *process integration* techniques for water network synthesis were developed for continuous and batch processes (Foo, 2009; Jeżowski, 2010; Gouws et al., 2010) based on *pinch analysis* and *mathematical optimization* approaches. The latter is preferred when a systematic strategy leading to an optimal solution is required.

While previous works on water network synthesis are restricted to addressing systems with all continuous or batch units, there are cases where both types of units exist. In this work, a mathematical model is developed for the synthesis of water networks involving batch and continuous units, focusing on the particular case where batch units are in the majority. Application of the model is demonstrated through an illustrative example.

2. Problem Statement

Given is a set of water-using units $i \in \mathcal{I}$ consisting mostly of batch process units ($i \in \mathcal{I}^{b}$) with a few continuous ones ($i \in \mathcal{I}^{c}$). These units require water to pick up a set of contaminants $c \in \mathcal{C}$ with fixed mass loads from the process streams. Available for service are a set of fresh water sources $w \in \mathcal{W}$ supplying water of different purity levels. Prior to

the use of fresh water, reuse/recycle of effluent from the process units is considered. To facilitate water recovery, a set of storage tanks $s \in \mathcal{S}$ for intermediate water storage may be used. The objective is to synthesize an optimal water network that achieves the minimum fresh water consumption, while satisfying all process constraints.

3. Solution Approach

Since the problem addressed in this work involves batch and continuous units, the main challenge is to integrate the units of different operating modes. While continuous units operate uninterruptedly for a long duration, batch units are often operated shortly (for a few hours) and cyclically. In addition, water intake and discharge of a batch unit are found at the start and end of the operation respectively. The inlet and outlet water of a continuous unit, by contrast, is continuously fed and discharged during the operation.

To deal with the case where the number of batch units is greater than that of continuous units, it is proposed to treat continuous operation as a combination of batch operations. This can be achieved by dividing the operating time of continuous units into a number of time intervals, according to the start and end of operation of the batch units. Through water storage, in any time interval (t, $t + 1$) the inlet water of a continuous unit is treated as if charged only at time point t, as illustrated in Figure 1. Meanwhile, the outlet water from the unit is treated as if discharged only at time point $t + 1$. The original problem can thus be converted into a simpler one where only batch units are involved in water network synthesis.

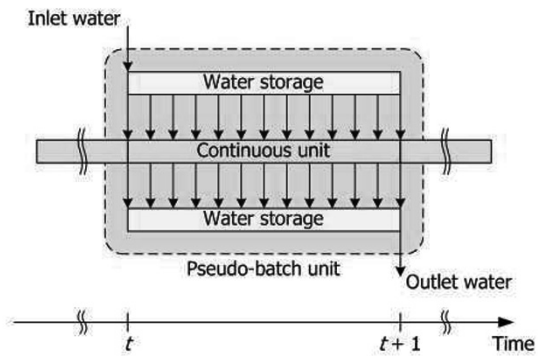

Figure 1: Illustration of a pseudo-batch unit

4. Superstructure and Model

Having treated all continuous units as pseudo-batch units, the remaining task is almost to synthesize a batch water network. In this work, the model developed by Chen et al. (2009) is extended to perform the synthesis task. The modified model consists of basic mass balance equations, flow/concentration limits of water-using units, capacity limits of storage tanks, and logical constraints, and is based on a superstructure including all feasible network connections between units and tanks. To address the time dimension in batch processes, a set of time points $t \in \mathcal{T}$ are defined.

Figure 2 shows the schematic diagram of a water-using unit i. As shown, its inlet water may come from other water-using units i', storage tanks s, and/or fresh water sources w;

its outlet water may be sent to other water-using units *i′*, storage tanks *s*, and/or waste disposal systems *d*.

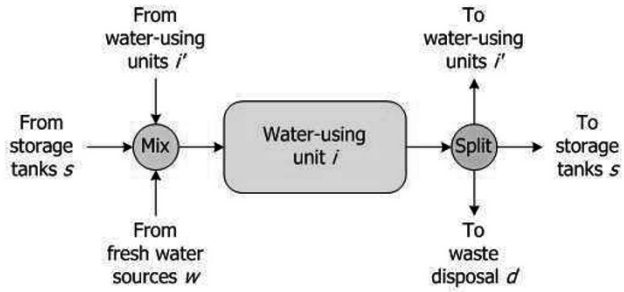

Figure 2: Schematic diagram of a water-using unit

Figure 3 shows the schematic diagram of a storage tank *s*. As shown, its inlet water may come from water-using units *i* and/or other storage tanks *s′*; its outlet water may be sent to water-using units *i* and/or other storage tanks *s′*.

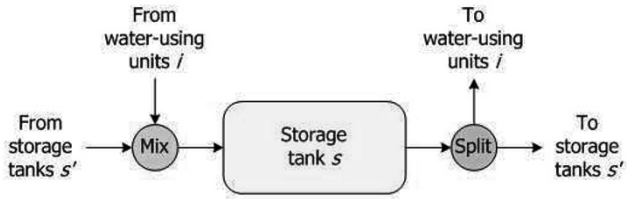

Figure 3: Schematic diagram of a storage tank

Additional constraints that need to be considered are as follows.

- No direct water reuse/recycle is allowed for the continuous units.

This is because treating continuous units as pseudo-batch units involves water storage to change the pattern of water intake and discharge (Figure 1).

- A continuous unit is not allowed to send water to a tank at a time point (t) if the unit received water from the tank at the previous time point ($t - 1$).

In other words, the inlet and outlet water flows of a storage tank must be prevented from occurring in the same time interval. This is to provide sufficient time for perfect water mixing in the tank.

- The inlet and outlet water flow rates of a continuous unit should be constant.

For maximum water recovery, the objective function is set to minimize the consumption of fresh water for water-using operations. Due to the bilinear terms in the contaminant balance equations and binary variables used to indicate the connections between units and tanks, the model is a mixed-integer nonlinear program (MINLP).

5. Illustrative Example

A two-plant example is solved to analyze in-plant and inter-plant water integration. This example involves two plants, nine batch units, and two continuous units. The operating data for the water-using units in both plants are shown in Tables 1 and 2, adapted from Majozi (2005) and Kim and Smith (2004) respectively. From the Gantt charts shown in Figs. 4(a) and (b), it can be seen that seven time points are defined for plant 1 and five time points for plant 2, according to the start and end times of the batch operations. Also,

the operation of unit F is divided into six batch sub-operations and the operation of unit K four sub-operations. A single pure fresh water source is available for use.
The optimization is carried out in the General Algebraic Modeling System (GAMS) on a Core 2, 2.00 GHz processor, with BARON as the solver for MINLP.

Table 1: Operating data for the water-using operations in plant 1

Unit	$C^{in,max}$ (kg salt/ton water)	$C^{out,max}$	M^{load} (kg)	Duration (h)
A	0	0.1	100	0-3
B	0.25	0.51	72.8	0-4
C	0.1	0.1	0	4-5.5
D	0.25	0.51	72.8	2-6
E	0.1	0.1	0	6-7.5
F	0.1	0.25	*187.5	0-7.5

Cycle time = 7.5 h. *Total mass load over the 7.5-h cycle time; the instantaneous mass load of unit F is 187.5 kg/7.5 h = 25 kg/h.

Table 2: Operating data for the water-using operations in plant 2

Unit	$C^{in,max}$ (kg salt/ton water)	$C^{out,max}$	M^{load} (kg)	Duration (h)
G	0	0.1	2	0-1
H	0.05	0.1	12.5	1-3.5
I	0.05	0.8	60	3-5
J	0.4	0.8	8	1-3
K	0.2	0.4	*100	0-5

Cycle time = 5 h. *Total mass load over the 5-h cycle time; the instantaneous mass load of unit K is 100 kg/5 h = 20 kg/h.

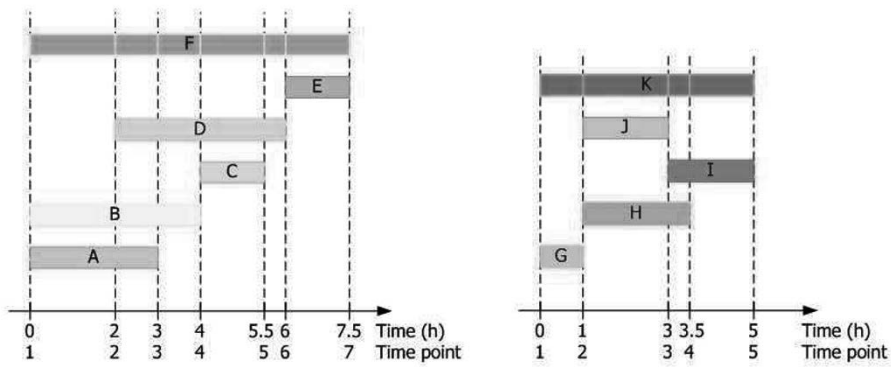

(a) (b)

Figure 4: Gantt charts for (a) plant 1 and (b) plant 2 operations

5.1. In-plant Water Integration

Two storage tanks are available in both plants to facilitate water recovery. The model for plant 1 involves 856 constraints, 746 continuous variables, and 168 binary variables, and is solved in 9 CPU s. The minimum fresh water consumption is determined as 1150 ton/cycle. This corresponds to a 56.4% reduction compared with the base case (2635.49 ton/cycle) where no water is recovered. The optimal network configuration is not shown because of space limitation. Both tanks are used and the capacities required are 1000

and 280 ton. The plant 2 model involves 527 constraints, 429 continuous variables, and 100 binary variables, and is solved in 7 CPU s. The minimum fresh water consumption is determined as 356.25 ton/cycle. This corresponds to a 25.8% reduction compared with the base case (480 ton/cycle; without water recovery). Both tanks are used and the required capacities are 125 and 20 ton.

5.2. Inter-plant Water Integration

When the two plants are considered together, a common cycle time of 15 h is assumed, where plant 1 operates two cycles and plant 2 three. Before inter-plant water integration is carried out (in-plant integration only), the total fresh water consumption over the 15-h cycle time is calculated as $1150 \times 2 + 356.25 \times 3 = 3368.75$ ton. By performing pinch analysis for the two plants, one can find out the pinch points for plant 1 and plant 2 are at 0.25 and 0.4 kg salt/ton water, respectively. This indicates sending wastewater of the pinch concentration from plant 1 to plant 2 can lead to further fresh water reduction. From the solution to plant 1, the total amount of wastewater at 0.25 kg salt/ton water is 590 ton/7.5 h. By introducing this wastewater as an additional water source into plant 2 and resolving its model, it is obtained the minimum fresh water consumption of plant 2 is reduced to 222 ton/5 h, and the minimum consumption of the additional water source is 358 ton/5 h. The total fresh water consumption now becomes 2966 ton/15 h, which corresponds to a further 12% reduction through inter-plant integration.

6. Concluding Remarks

A mathematical model has been developed for synthesizing water networks involving batch and continuous units. For the particular case where batch units are in the majority, a dividing approach is proposed. It converts the original problem into a simpler one that is almost to synthesize a batch water network. An example was solved to illustrate the proposed approach. Note that only a preliminary analysis for inter-plant integration has been performed in the present work. A more systematic method should be developed for optimizing connections and operations within individual plants and between different plants. This is the subject of future work. Other cases where the number of continuous units is large compared to that of batch units also remain for future work.

References

C.-L. Chen, J.-Y. Lee, J.-W. Tang, Y.-J. Ciou, 2009, Synthesis of Water-using Network with Central Reusable Storage in Batch Processes, Comput. Chem. Eng., 33, 1, 267–276

D. C. Y. Foo, 2009, State-of-the-Art Review of Pinch Analysis Techniques for Water Network Synthesis, Ind. Eng. Chem. Res., 48, 11, 5125–5159

J. F. Gouws, T. Majozi, D. C. Y. Foo, C.-L. Chen, J.-Y. Lee, 2010, Water Minimization Techniques for Batch Processes. Ind. Eng. Chem. Res. 49, 19, 8877–8893

J. Jeżowski, 2010, Review of Water Network Design Methods with Literature Annotations, Ind. Eng. Chem. Res., 49, 10, 4475–4516

J.-K. Kim, R. Smith, 2004, Automated Design of Discontinuous Water Systems, Process Safe. Environ. Prot., 82, 3, 238–248

T. Majozi, 2005, Wastewater Minimisation Using Central Reusable Water Storage in Batch Plants, Comput. Chem. Eng., 29, 7, 1631–1646

I.A. Karimi and Rajagopalan Srinivasan (Editors), Proceedings of the 11th International Symposium on Process Systems Engineering, 15-19 July 2012, Singapore.

Optimal operation of reverse osmosis plant driven by solar power without batteries

Senthil.K, Shankar Narasimhan, Sridharakumar Narasimhan

Department of Chemical Engineering,
Indian Institute of Technology Madras, Chennai, India

Abstract

Ensuring adequate supply of clean drinking water and electricity in several parts of the world continues to be a formidable challenge. In coastal areas facing this problem, desalination of sea water using Reverse Osmosis (RO) driven by solar power without batteries can be an appropriate technological solution. Variability in incident solar power is a significant operational issue. The focus of this work is optimal operation and control of the RO plant with guaranteed water purity. A steady state model is developed and validated using 'ROSA', a black-box software programme commonly used for simulating RO plants. Analysis of the optimal solution reveals that the feasible space (of available power) consists of two regions where different set of constraints are active. In one region salt concentration constraint is active and in another, the pressure constraint is active. Hence the optimal operation strategy can be implemented by active constraint control.

Keywords: Reverse osmosis, Desalination, Solar power, Optimization, Active constraint control, Without batteries.

1. Introduction

In remote coastal areas where electricity and drinking water are not available, reverse osmosis plants driven by non conventional energies like wind, solar are attractive. Photovoltaic cells provide power that varies with the intensity of sunlight. Since the solar incidence radiation shows significant variability during the day and across months, batteries are used as energy storage devices. However, the main disadvantage with batteries is that they require regular maintenance. This is a major drawback for the plants in remote places. Secondly, efficiency of these batteries is less than 80%. In such a situation, optimal operation of the RO plant without the use of batteries is an excellent option. Some experience of operating and simulating RO unit without batteries can be found in the works of Riffel & Carvalho (2009) and Keefer et al. (1985). Operation of such a plant with guaranteed purity and production is a challenging control problem and this is the focus of this work.

A typical solar powered reverse osmosis plant consists of solar panel, DC-DC converter, three phase bridge, three phase induction motor, reciprocating pump, and membrane unit. The DC-DC converter boosts the voltage from 50 volts to 550 volts. The three phase bridge converts 550 volts DC to a three phase AC power of variable frequency and voltage which is fed to the induction motor. Reciprocating pump driven by the induction motor delivers feed water at a pressure of 60-69 bars to the membrane unit. Permeate that diffuses through the membrane and the reject are collected in separate tanks. In a battery-less solar powered reverse osmosis plant, power available to run the plant varies with intensity of sunlight. The objective of the project is to

maximize permeate production rate for this time varying power subject to the constraint of keeping the salt concentration in permeate at any time less than 500 ppm. The various other constraints considered are water balance, salt balance, salt diffusion equation, water diffusion equation, maximum working pressure of the system and the power constraint.

2. RO membrane Model

An RO membrane model is required to solve the optimization problem. A static lumped parameter model (Dow's Technical manual) can be used for optimization purpose. The various assumptions made in the RO model are

- Temperature of the water is assumed to be 25 deg Celsius
- Frictional pressure drop in the membrane unit is assumed to be negligible

The RO model has two equations, one describing the rate of water diffusion and the other describing the rate of salt diffusion through the membrane. The rate of water diffusion is proportional to the difference between the pressure in excess of the osmotic pressure on the feed side and the pressure in excess of the osmotic pressure on the permeate side.

$$Q_p = A \times S_a \times \{(P_{af} - \pi_{avg} \times PF) - (P_{ap} - \pi_p)\} \tag{1}$$

where Q_p, A, S_a, P_{af}, π_{avg}, PF, P_{ap}, π_p refer to permeate flow rate, permeability of water, active surface area of the membrane (constant for a given membrane), absolute feed pressure, average osmotic pressure of the water on the feed side, concentration polarization factor, absolute permeate pressure and permeate osmotic pressure, respectively. Pressure on the permeate side is approximately atmospheric and so equation (1) can be rewritten as

$$Q_p = A \times S_a \times \{P_f - \pi_{avg} \times PF + \pi_p\} \tag{2}$$

where P_f is the feed water gauge pressure. The concentration polarization factor (PF) [3] is given by

$$PF = \exp\left(K \times \frac{Q_p}{Q_f}\right) \tag{3}$$

where Q_f is the feed flow rate. As water diffuse through the membrane, the concentration of salt near the surface of the membrane becomes considerably higher than the salt concentration of the bulk solution. Concentration polarization factor is used as a correction factor to account for this concentration gradient effect. The mass rate of diffusion of salt (J_s) through the membrane is proportional to salt concentration difference between the feed and the permeate side (C_p).

$$J_s = B \times S_a(C_{avg} \times PF - C_p) \tag{4}$$

where C_{avg} and B refer to average salt concentration on the feed side and salt permeability of the membrane respectively. Here also the factor 'PF' plays the same role as it did in the water diffusion equation. Equation (4) can be rewritten by dividing both sides by Q_p as follows

$$C_p = \frac{J_s}{Q_p} = \frac{B \times S_a(C_{avg} \times PF - C_p)}{Q_p} \tag{5}$$

In equation (5), C_p is very less compared to C_{avg}, and so C_p term on the right hand side is neglected and the resulting equation is

$$C_p = \frac{B \times S_a\left(C_{avg} \times PF\right)}{Q_p} \tag{6}$$

The equations (2) and (6) constitute the RO model.

3. Parameter estimation and validation

The RO model described above has three unknown parameters namely permeability of water (A), permeability of salt (B) and proportionality constant (K) which can be determined using the plant input/output data. The input data include feed water concentration (C_f), feed water pressure (P_f), feed water flow rate (Q_f) and the output data are permeate flow rate (Q_p) and the permeate concentration (C_p). Currently an experimental facility is not available with us for obtaining the data. DOW™ developed a software called 'ROSA' which is used primarily to design membrane units. This software has an inbuilt model of the membrane unit, but integration of 'ROSA' with the optimization program cannot be done easily. So 'ROSA' is used as a substitute for an RO plant in order to generate the input/output data which are then used to estimate model parameters. Feed water flows in the range of 2.4-6 m^3/day and feed pressure in the range of 50-69 bars are chosen for the simulation of the 'ROSA' software. The feed concentration is kept constant at 35000 ppm. The estimates of A, B and K are found by least squares technique and are 0.0148 m/day/bar, 0.0027 m/day and 0.0491 respectively. Then the model is simulated with test data set (within the same range of the training data set) and found to predict the permeate flow rates within an accuracy of ±2% and the permeate concentration within ±4% on an average. The cases where maximum deviation between the model and ROSA occur are shown in Fig-1 & 2.

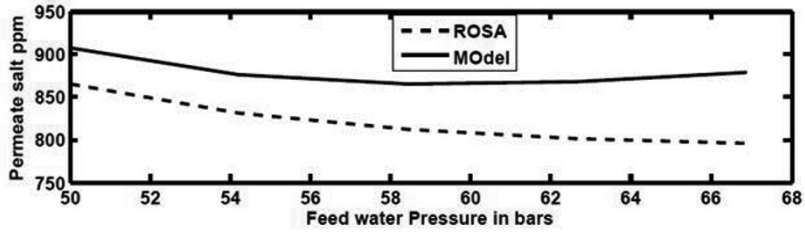

Figure-1: Comparison of permeate salt concentration prediction between the developed model and ROSA at constant feed flow of 6m^3/day.

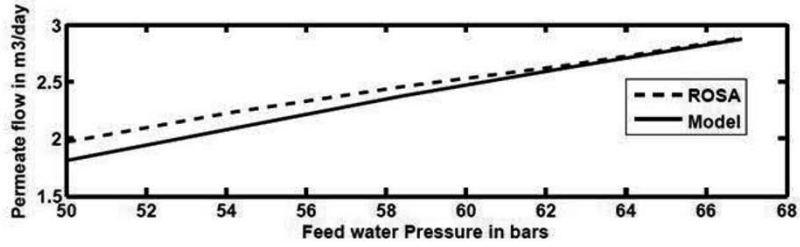

Figure-2: Comparison of permeate flow rate prediction between the developed model and ROSA at constant feed flow of 2.4 m^3/day.

4. Optimization

Given the power available, an analysis of the system shows that they are two degrees of freedom i.e. feed water flow rate and feed pressure. As the solar radiation varies throughout the day, it is not feasible to operate the plant at constant feed flow rate and constant feed pressure. So a formal optimization problem needs to be formulated and solved to determine the optimal feed flow rate and feed pressure for each solar radiation intensity. The objective of the optimization problem is to maximize permeate flow rate subject to the constraints of (i) permeate salt concentration being less than 500 ppm, (ii) power available being less than or equal to the product of feed pressure and feed flow rate, (iii) feed pressure being less than the maximum design pressure of the membrane (69 bar), and (iv) salt balance, water balance & salt diffusion equations being satisfied. The optimization problem can be formulated as follows:

$$\underset{Q_f, Q_c, P_f, C_c, C_p}{\text{Maximize}} \; Q_p = A \times S_a \times \{P_f - \pi_{avg} \times PF + \pi_p\} \tag{7}$$

Subject to

$$C_p - B \times S_a \times \frac{C_{avg}}{Q_p} exp\left(\frac{K \times Q_p}{Q_f}\right) = 0 \tag{8}$$

$$Q_f - Q_c - Q_p = 0 \tag{9}$$

$$Q_f \times C_f - Q_c \times C_c - Q_p \times C_p = 0 \tag{10}$$

$$C_p - 500 \leq 0 \tag{11}$$

$$P_f - 69 \leq 0 \tag{12}$$

$$\text{PW} - P_f \times Q_f \times \frac{100}{(24 \times 60^2)} \leq 0 \tag{13}$$

In the above formulation, equation (7) refers to the water diffusion equation of the membrane model. Equations (8), (9) and (10) refer to salt diffusion equation of the membrane, overall material balance and salt balance, respectively. Equation (12) ensures that the feed pressure does not exceed the maximum permissible pressure of the membrane Equation (13) ensures that the power consumed by the pump does not exceed the power available (PW). The above mentioned optimization problem is solved using Matlab's fmincon function which is a local optimizer. The results of the optimization presented in Fig. 3, show that the optimal policy is to maintain either the pressure or the permeate concentration active at its maximum permissible value. The critical power point at which the active constraint shifts depends on the feed water salt concentration. If the feed water concentration is 35000 ppm, the shift occurs at 0.333 kilowatt. For a feed water salt concentration of 32000 ppm and 36000 ppm, the shift occurs at 0.3060 kilowatt and 0.3430 kilowatt respectively.

In order to implement the above optimal policy, an active constraint control strategy can be used which does not require knowledge of the critical power point or the available input power. Only the feed pressure and the permeate concentration have to be measured and monitored. If the pressure is less than its maximum value, the plant is operated such that permeate salt concentration is maintained at the maximum

permissible limit. If the pressure reaches its maximum limit, the plant is operated such that the pressure is maintained at its maximum limit. The manipulated variable is the position of a valve which is placed at the reject line of the RO module whose stem position is changed to either keep the pressure or the permeate concentration at its maximum value. This optimal strategy is robust to uncertainties in the model parameters. Additionally, the feedback solution to the optimal operation problem can be implemented easily without the need to perform real time optimization

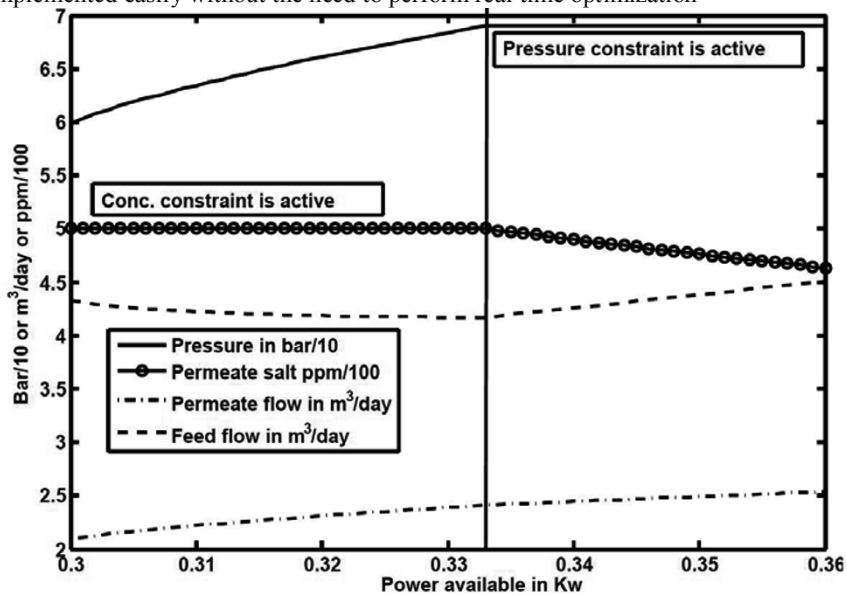

Figure-3: Optimal feed water flow rate & feed water pressure that correspond to various powers levels (at constant feed water salt conc. of 35000 ppm)

5. Conclusion

An appropriate optimization problem for operation of an RO desalination plant driven by solar power without batteries subject to input variability has been formulated and solved. Analysis of the solution reveals that a simple active constraint control strategy can realize the optimal solution. This control strategy is robust with respect to parametric changes. Replacing the present RO model with a detailed model to study whether the same concept holds good, to study the influence of a product buffer tank on permeate production, study of dynamics of the system, controller design and implementation of active constraint control in plant will constitute our future work.

References

D. B. Riffel and P. C. M. Carvalho, 2009, Small-scale photovoltaic-powered reverse osmosis plant without batteries:Design and simulation, Desalination, 247, 378-389

B. G. Keefer, R. D. Hembree and F.C. Schirack, 1985, Optimized matching of solar photovoltaic power with reverse osmosis desalination, Desalination, 54, 89-103.

Dow's Water & process solution (Technical manual). Retrieved from http://msdssearch.dow.com/PublishedLiteratureDOWCOM/dh_0885/0901b8038088586b.pdf?filepath=liquidseps/pdfs/noreg/609-00071.pdf&fromPage=GetDoc.

I.A. Karimi and Rajagopalan Srinivasan (Editors), Proceedings of the 11th International Symposium on Process Systems Engineering, 15-19 July 2012, Singapore.

Optimization of the scheduling and water integration in batch processes based on the Timed Petri net

Li Huan, Xiao Wu*, He Gaohong, Du Jian

State Key Laboratory of Fine Chemical, R&D Center of Membrane Science and Technology, Dalian University of Technology, Dalian 116024, Liaoning, China

Abstract

A approach based on the Timed Petri net (TPN) for incorporating water integration in batch process scheduling was presented in this paper. Firstly, the Petri net model of process scheduling was built and the scheduling can be obtained using the incidence matrix analysis method. Then the Petri net model of the water integration was established according to the water cascading analysis, the principles of water network design and the water matching rules. Finally, based on the facility of multiple view integrated modeling, the Petri net models of the scheduling and water-using network synthesis were combined to achieve the optimization of the scheduling and water integration in batch process. An example was presented to demonstrate the validity and advantages of the proposed approach.

Keywords: batch processes; Timed Petri net; scheduling; water integration;

1. Introduction

Batch processes are used for high-value-added products in process industries widely, and the wastewater often has a bad influence on environment, so the water integration with certain scheduling in batch processes has got more attention[1-3]. However, to a great extent, the optimal water-using network and the economic benefits in batch processes rely on the production and scheduling. So the scheduling optimization is also an important problem in batch processes[4,5]. The optimization of the scheduling and water integration of batch process, as two separate problems, were taken into consideration in recent years[6,7], and most of the approaches were based on the mathematical programming[8-10], but it was often hard to get the optimal solution due to the multiple solution of the model, which was resulted in by the no-linear and integrality constraints and the non-convexity of the problem.

With the Petri net has been the primary tool to be used in the activities of modeling, performance analysis and simulation of the discrete event systems as its outstanding ability in graphic description and mathematical analysis. The Petri net has gained widely application in the scheduling-model problem of batch processes[11,12]. As the Petri net is a good representation of conflict situations, shared resources, precedence constraints and explicit time constraints, it has been a availably modeling tool suited to model the scheduling and water integration of batch system. Hence, a new approach for optimization of the scheduling and water integration in batch process was presented based on time Petri net (TPN) in this paper, which can obtain the targets avoiding the solution complexity of the mathematical programming.

* wuxiao@dlut.edu.cn (W. Xiao).

2. Optimization of the scheduling and water integration

2.1. Scheduling model based on the time Petri net

When a Petri net was used to formulate a scheduling problem, the state equation of the Petri net model ,which was expressed by Eq. (1), calculated the new state.

$$M_k = M_0 + A^T X \tag{1}$$

where A is the incidence matrix which represents the preceding relationships between places and transitions, X is a firing sequence of transitions.

The scheduling model was built based on the TPN, the transitions t/t' respectively represent the start/stop of the operation, which is expressed by the places of the TPN. So the sub-process accomplished in the R device can be described by the subnet shown in Fig. 1. The places P'/P'' respectively represent the feed/product of the operation, the P place represents the operating procedure of the operation and its delay time is the operating time in the device R. The tokens in the places indicate the current state of the operation or device.

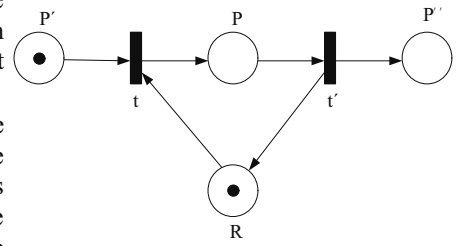

Fig. 1 PN model of the sub-process in R device.

The delayed vector was defined $DT = (d\tau_0, d\tau_1, d\tau_2, \cdots, d\tau_m)$, the element $d\tau_i$ is the delayed time of the place P_i. In the state vector $S(\tau_k) = (s_0(\tau_k), s_1(\tau_k), s_2(\tau_k), \cdots, s_m(\tau_k))$, the element $s_i(\tau_k)$ means the transient-time that the tokens arrive at the place P_i in the k step. In the enabling vector $T(\tau) = (t_0(\tau), t_1(\tau), t_2(\tau), \cdots, t_n(\tau))$, the element $t_j(\tau)$ is the earliest time that the transition t_j was triggered. As a result, the transition set T^*, which is called optimization transitions sequence, is constituted by the transitions corresponded with the minimum elements in the enabling vector. Then the N-vector X_{k+1} was determined, because the j element in the X_{k+1} is the times that the transitions appeared in T^*. And then the new state could be gained by Eq. (1). When M_k=M_0, the calculation was end. The τ_k was the make-span of the operation and the T^* was the operation sequence. In the simulation algorithm process, the heuristic scheduling rules described in the literature [13] was used to solve the conflicts.

2.2. Water integration model based on the TPN

The Petei net model of water integration was built using the water cascading analysis

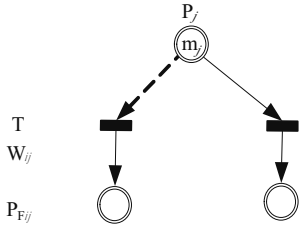

Fig. 2 PN model controlled by time interval.

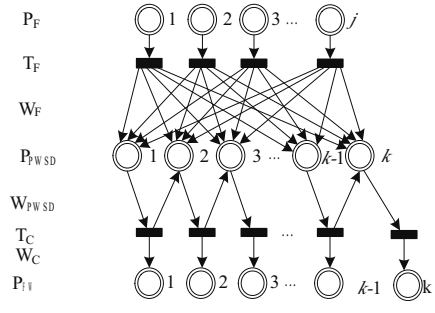

Fig. 3 PN model of pinch analysis.

(WCA)[14]. And the time is the critical factor and the same stream can be found in different time intervals in batch processes, thereby, the Petri net model controlled by time interval, shown in Fig. 2, was built then. The tokens in P_j place are the total mass

flowrate of the *j* stream and the places P_{Fj} are the *j* streams in time intervals *i*. And a common model of pinch analysis, shown in Fig. 3, was firstly established based on the time Petri net using WCA.

Once the minimum fresh water demand and the water pinch location were obtained, the Petri net model of water network synthesis can be established according to the water cascading analysis, the principles of water network design and the water matching rules[15], shown in Fig. 4, there were 3 operation units in the synthesis model, unit 1 was above the pinch purity, unit 2 was below the pinch purity and unit 3 was across the pinch purity.

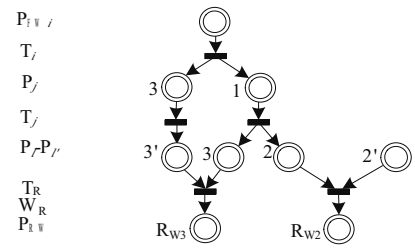

Fig. 4 PN model of water network synthesis.

2.3. Optimization model of the scheduling and water integration

To optimize the batch process scheduling and water integration, the Petri net model for incorporating pinch analysis in scheduling should be constructed first. In the Fig. 1, the tokens in place P obtained after the transition t was fired are the material in R device, while in the Fig. 2, the tokens in place P_j are the total mass flowrate of the *j* stream, which also could be treated as a material. That, in turn, makes the place P has the same physical significance to the place P_j. So the Petri net model for incorporating pinch analysis in scheduling was built by combining the place P with the place P_j, shown in Fig. 5, where m_j was the limiting mass flowrate of stream *j* and the significance of other variables are the same as the above models.

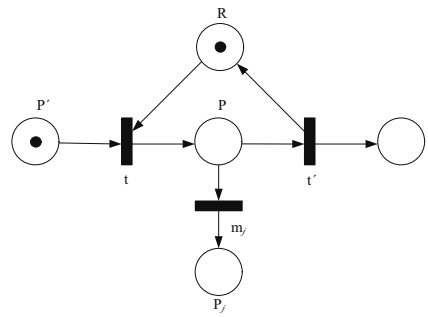

Fig. 5 Petri net for incorporating pinch analysis in scheduling

3. Example

Following an example was presented to illustrate the validity of the proposed approach.

Table 1 Stream data for the batch process example

Operation	Process	Cin	Cout	Limiting mass flowrate	Time of duration
		ppm	ppm	ton/h	h
$OP_{A,1}$	D_1/S_1	0	100	20	2
$OP_{A,2}$	D_2/S_2	50	100	250	2
$OP_{B,1}$	D_3/S_3	50	800	90	3
$OP_{B,2}$	D_4/S_4	400	800	20	2

Consider a batch process with two devices R_1 and R_2, two different products (P_A/P_B) were produced according to the same order in the devices. In the process, it need 2 hours and 2 hours respectively in devices R_1 and R_2 to produce one product, 3 hours and 2 hours respectively in devices R_1 and R_2 to produce the other product. It was assumed that every operation needed water-using process. Table 1 summarize the data for the water stream corresponding with the operation.

The Petri net model for incorporating pinch analysis in scheduling of example was built based on the model of Fig. 5, shown in Fig. 6, the meanings of the places and transitions are the same as before. The model of water integration considering the scheduling was obtained by combining the model of Fig. 6 and the model of Fig. 3.

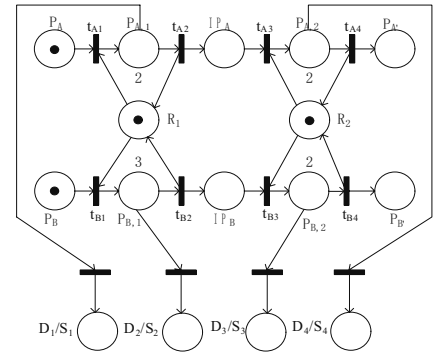

Fig. 6 Petri net model for incorporating pinch analysis in scheduling of example

The results could be obtained using the scheduling calculation and the application software of Petri net, which were shown in Table 2. In the Table 2, the operation sequences of branch 1 (Fig. 7(a)) and branch 2 (Fig. 7(b)) were shown in Fig. 7. It was known from the results in the table, although the make-span of the two branches were same, the total fresh water flow of branch 1 was much less than the branch 2. So the operation sequence corresponding with the branch 1 was adopted in this paper.

And then, based on the model of Fig. 5, according to the determined operation sequence and the total fresh water flow demanded in the example, the water-using network diagram without storage was designed shown in Fig. 8.

Table 2 The results data for the example

Branch	The total fresh water flow/t·h^{-1}	Make-span/h
1	213.13	7
2	309.38	7

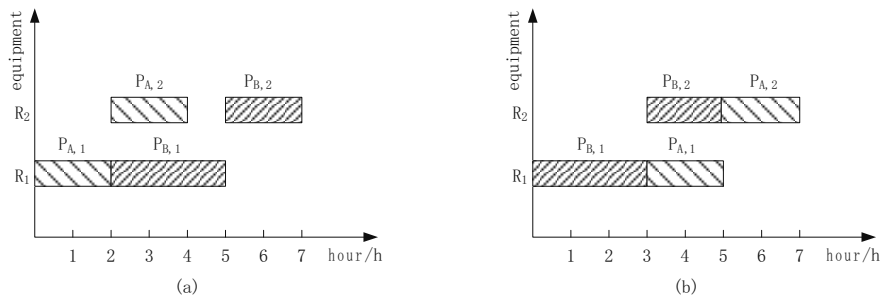

Fig. 7 The Gantt for the example of branches

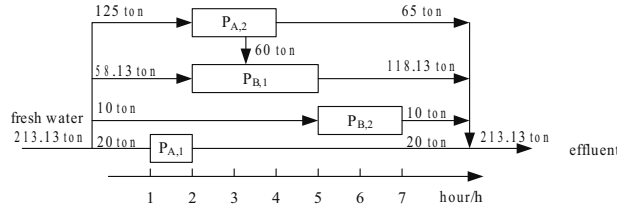

Fig. 8 Water-using network diagram for example without storage

4. Conclusion

A new approach was developed in this paper for optimizing the scheduling and water integration in batch process synchronously, the time factor in batch process was

translated into the delayed time of the places, which was one of objects in Petri net. And the optimization of the scheduling and water integration in batch process was obtained by using the simulation calculation of the Petri net model, which was validated effectively by an example. Compared with the mathematical programming, the models based on the TPN were simple and intuitive and the solution of the models was also simple and efficient avoiding the complicated calculation of the mathematical programming. Not only was the successful implementation of the approach conducive to the development of the study on the water integration but also it provided the foundation for the synchronous optimization of the scheduling and other mass transfer processes in batch process.

Acknowledgements

The research project is supported by the Program for Science and Technology of Liaoning Province of China under Contract NO.2011224005, the National Science Fund for Distinguished Young Scholars of China under Grant NO.21125628, and the Innovation Fund of Chinese Petroleum Science and Technology under Grant NO.2011D-5006-0401.

References

1. DCY.Foo et al., 2005, Synthesis of maximum water recovery network for batch process systems, Journal of Cleaner Production, 13, 1381-1394.
2. CL. Chen et al., 2009, Synthesis of water-using network with central reusable storage in batch processes, Computers and Chemical Engineering, 33, 267-276.
3. JF. Gouws et al., 2010, Water minimization techniques for batch processes, Ind. Eng. Chem. Res., 49, 8877-8893.
4. B. Roe et al., 2005, A hybrid MILP/CLP algorithm for multi-purpose batch process scheduling, Computers and Chemical Engineering, 29, 1277-1291.
5. F. Ridouard et al., 2008, On-line scheduling on a batch processing manhine with
6. unbounded size to minimize the makespan, European Journal of Operational Research, 189 (3), 1327-1342.
7. I. Halim, R. Srinivasan, 2010, Sequential methodology for simultaneous batch process scheduling and water reuse optimization, Chemical Engineering Transactions, 21, 727-732.
8. CL. Chen et al., 2011, Resource-task network approach to simultaneous scheduling and water minimization of batch plants, Ind. Eng. Chem. Res., 50 (7), 3660-3674.
9. KF. Cheng, CT. Chang, 2007, Integrated water network designs for batch processes, Industrial and Engineering Chemistry Research, Vol.46, NO.4, 1241-1253.
10. AH. Rabie, MM. El-Halwagi, 2008, Synthesis and scheduling of optimal batch water-recycle networks, Chinese Joyrnal of Chemical Engineering, Vol.16, NO.3, 474-479.
11. T. Gu, PA. Bahri, 2002, A survery of Petri-net applications in batch processes, Computers in Industry, 47 (1), 99-111.
12. M. Ghaeli et al., 2005, Petri-net based formulation and alogrithm for short-term scheduling of batch plants, Computers and Chemical Engineering, 29 (2), 249-259.
13. LI Huifang, FAN Yushun, 2002, Dynamic Scheduling of Batch Processes Based on Simulation of Petri Nets, Journal of System Simulation (in Chinese), 14 (7) , 928-931.
14. CY. Foo et al., 2004, Synthesis of mass exchange network for batch process-part I: Utility targeting, Chemical Engineering Science, 59 (5), 1009-1026.
15. YANG Xia et.al, 2007, Single contaminant water network design for batch processes, Journal of Chemical Industry and Engineering (in Chinese), 58 (1), 161-167.

I.A. Karimi and Rajagopalan Srinivasan (Editors), Proceedings of the 11th International Symposium on Process Systems Engineering, 15-19 July 2012, Singapore.

A method to find an optimal draw solute for cost-effective FO(forward osmosis) desalination process

Tae-wooKim[a],Young Kim[b], Choamun Yun[c],Hong Jang[a], Woohyun Kim[a], Sunwon Park[a*]

[a]*Department of Chemical and Biomolecular Engineering, Korea Advanced Institute of Science and Technology, 373-1 Guseong-dong, Yuseong-gu, Daejeon,305-701, South Korea*

[b]*Korea Institute of Machinery and Materials, 156 Gajeongbuk-Ro, Yuseong-gu, Daejeon, 305-343, South Korea*

[c]*Fuel Cell System Development Team, Corporate R&D Institute, Doosan Heavy Industries & Construction, 463-1, Jeonmin-Dong, Yuseong-gu, Daejeon, 305-811, South Korea*

Abstract

A method to find a draw solute for forward osmosis desalination is developed. The economics of a forward osmosis process is largely influenced by the selection of a draw solute and energy consumed for its separation from the fresh product water. The proposed method evaluates a vast number of possible draw solutes by predicting the production rate of fresh water, investment cost and energy consumption in the separation process. The possible draw solutes are confined to electrolytes and its separation processes to thermal systems. Subsequently, a cost-minimizing draw solute is determined subject to any necessary constraints. The developed method will contribute to designing commercially viable forward-osmosis desalination processes.

Keywords: Draw Solute, Forward Osmosis, Desalination, Screening, Property Database

1. Introduction

Water scarcity problem has been intensified in many regions all over the world by climate change, and expanding industrial and agricultural demand for water. In many of such areas of drought, desalination is often the only solution. Current commercial desalination technologies such as multi-stage flash (MSF) and reverse osmosis (RO), however, consume large thermal energy (200~400 MJ/ton in MSF process) (Borsani et al., 2005), or expensive electrical energy (4~6 kWh in RO process) (Fritzmann et al., 2007). In this regard, forward osmosis (FO) desalination is recently drawing attention to reduce the energy consumption in desalination processes.

An FO desalination system consists of a membrane process and a draw solute recovery process. In the membrane process, the driving force for water permeation is the chemical potential difference between draw solution and seawater. Therefore, the osmotic pressure of draw solution should be higher than that of seawater to enable spontaneous permeation of water molecules. The draw solution diluted with the permeated water then enters the recovery process to produce fresh water while reconcentrating the solution. Note that the total energy efficiency is determined by the energy requirement of the recovery process (McGinnis et al., 2007).

The design of an FO desalination system is mainly determined with selection of a draw solute. The draw solute should have high solubility and high osmotic pressure which would lead to high water flux through the membrane. At the same time, it should be readily separable from water consuming low energy.
In previous researches, several candidate compounds have been assessed for their application to desalination. The water flux at a fixed concentration is measured in those studies, often to figure out the performance of the membrane. These candidates include ammonium bicarbonate, magnesium sulfate, sodium sulfate, potassium sulfate, potassium nitrate, potassium chloride, ethanol, glucose and fructose (Cath et al., 2006) (Achilli et al., 2010). A systematic approach is proposed in this study for optimal design of a forward osmosis desalination system. This approach considers all components in the property database not to overlook any candidate of high potential. Moreover, both membrane and draw solute recovery processes are optimized for respective candidates considering water flux and energy consumption, both of which vary depending on the selection of the draw solute. In the first step, a chemical database is established to calculate solubilities and osmotic pressures. Secondly, draw solute candidates are selected by exploring the established chemical database. Lastly, the optimal desalination system is designed for each candidate draw solute and the costs of those systems are compared to find the optimal draw solute.

2. Screening method

Property information of total 4,058 compounds is gathered to establish a property database from the OLI stream analyzer which is developed by OLI systems, Inc. The analyzer provides properties such as pH, ORP, viscosity, density, enthalpy based on property models and experimental data. Subsequently, the compounds are screened in hierarchical order. The screening criteria are shown in Fig 1. At first, components whose maximum osmotic pressures are lower than that of seawater (24 bar) are screened. Then, rare metals, radioactive substances and the compounds of low solubilities below 0.5 molal concentration are screened. Boiling points of the candidates are set to be below 100°C to find the components more volatile than water because boiling water requires large latent heat energy. Finally, toxic components whose concentrations should be less than 1 ppm in drinking water are screened.

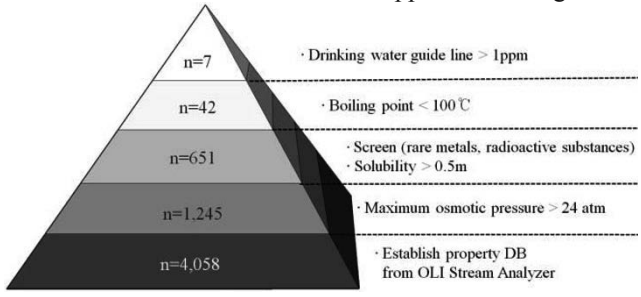

Figure 1: Screening criteria

3. Mathematical models

3.1. FO membrane process model

FO membrane consists of a selective layer and a support layer (Loeb et al., 1997). Water flux through the membrane (J_w) is proportional to the osmotic pressure difference between those of seawater and draw solution, and to the pure water permeability

coefficient (A). A can be experimentally determined. The effective osmotic pressure difference is less than that of bulk solutions($\pi_{ds.b}$-$\pi_{sw.b}$) due to the effect of internal concentration polarization (ICP) in the support layer and external concentration polarization (ECP) at the outer wall of selective layer. The actual water flux, therefore, should be calculated as below (Tan et al., 2008).

$$J_w = A\left\{\pi_{ds,b}\exp(-J_w K) - \pi_{sw,b}\exp(J_w / k)\right\} \quad (1)$$

where K is solute resistivity for diffusion within the support layer, k is the mass transfer coefficient, $\pi_{ds.b}$ is osmotic pressure of the bulk draw solution and $\pi_{sw.b}$ is osmotic pressure of the bulk seawater.

3.2. Draw solute recovery process model

In this study, the draw solute recovery is confined only to thermal separation with a distillation column. Aspen Plus® is used to simulate distillation columns. As this process only concerns about the purity of product water, i.e. the bottom product, the column is designed as a stripping column.

The minimum number of trays at the specified design pressure is calculated while the purity of bottom product is kept below the target concentration. At each tray, physical and chemical equilibrium states are assumed. The vessel height is calculated by multiplying the number of trays with the tray spacing. The vessel radius is decided from the vessel height and the flowrates of vapor and liquid.

4. System optimization

4.1. Investment cost model for the FO membrane process

To assess the integrated performance of the FO membrane process and the draw solute recovery process, a cost minimization problem needs to be established. The six-tenth rule is applied to calculate investment cost of the FO membrane process because currently there is no commercial-scale FO membrane process established (Williams et al., 1947). This relationship has been found to provide reasonable results for individual pieces of equipment and for entire plants. The investment cost for the FO membrane process ($C_{inv.M}$) is calculated from Eq. (2).

$$C_{inv.M} = C_{ref.M}\cdot\left(\frac{Q/J_w}{Area_{ref}}\right)^{0.6} \quad (2)$$

where $C_{ref.M}$ is the investment cost for the reference process, $Area_{ref}$ is the membrane area of the reference process. The term (Q/J_w) means required membrane area to meet target production.

4.2. Investment cost model for the draw solute recovery process

To calculate the investment cost for the distillation column, Mulet-Corripio-Evans's method is applied (Mulet et al., 1947). The method calculates the purchase costs of the vessel, the platform, ladders, and trays from the vessel weight and size.

4.3. Cost minimization

The cost minimization problem for unit mass of product water is as follows.

$$\min C = \frac{1}{Q}\left(\frac{C_{inv.DC}}{L_{DC}} + \frac{C_{inv.M}}{L_M}\cdot U_M\right) + \left(U_{steam}\cdot r_{steam} + U_{electricity}\cdot r_{electricity}\right) \quad (3)$$

where C is the total production cost to produce a ton of product water. U_{steam} and $U_{electricity}$ are the unit utility & maintenance costs for steam and electricity. r_{steam} and $r_{electricity}$ are the required amounts of steam and electricity to produce a ton of product water, $C_{op.DC}$ is the operation cost for the distillation column to produce a ton of product

water, L_M is the lifespan expectancy and U_M is the utility & maintenance cost coefficient for the FO membrane process which includes the costs for maintenance and operation. It is assumed that the operation cost for FO membrane process is negligible.

5. Case study

The optimal system design is also influenced by several cost parameters. The variance in the operation cost is represented by the steam price change while that in the investment cost is expressed with the production capacity. Several cases are studied for U_{steam} value of 0.008$/MJ and 0.0001$/MJ, and Q value of 1 million imperial gallons per day (MIGD : 4,546 tons per day) and 100 MIGD. Note that the capacity of a typical RO plant is 0.1~35 MIGD and that of MSF plant is 20~200 MIGD. The maximum concentration is limited to 10m(molal concentration) to compensate the negligence of the back diffusion in this model. The target purity of product water is set to follow the drinking water guidelines.

5.1. Normal steam price(0.008$/MJ), small plant capacity(1MIGD)

The best candidate in this case is 2-Butanone (methyl-ethyl-ketone : MEK) with vacuum operation of the distillation column. Although 2-Butanone offers relatively low water flux, it is selected because the energy requirement to satisfy the purity standard is less than the half of the 2nd best candidate, ammonium hydroxide. Meanwhile, ammonium hydroxide ranks higher than ammonium bicarbonate even though the carbonic acid ion provides additional osmotic pressure with low energy consumption. This is because the solubility of ammonium bicarbonate is relatively low. On the other hand, high solubility of ammonium hydroxide contributes to enhancing the water flux.

5.2. Low steam price(0.0001$/MJ), large plant capacity(100MIGD)

Desalination systems are often located close to power plants. When the waste heat from the power plants can be utilized, the utility cost may be significantly reduced. This case searches for the best solution with steam price of $0.0001/MJ which is much lower than the market price. Because the plant capacity of this case is small, investment cost becomes a dominant factor to decide the optimal draw solute and operation condition. Accordingly, ammonium hydroxide, which requires the smallest membrane area, is also selected as the optimal solute with 2-butanone.

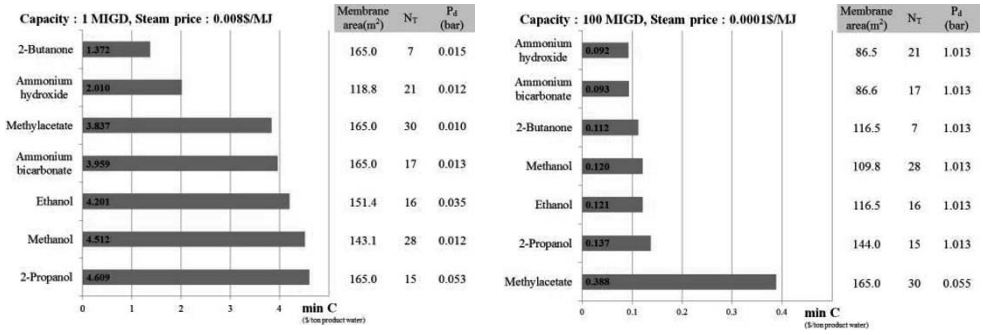

Figure 2: Optimization results.

6. Conclusions

In this study, a systematic approach has been proposed to finding the optimal draw solute and process design. Draw solute candidates have been selected by a hierarchical

screening method. Models for the FO membrane process and the draw solute recovery process have been established to calculate water permeability and energy consumption. A cost function integrating operation and investment costs have enabled comparing the production costs of the draw solute candidates. The cost is minimized to find the optimal draw solute, the diluted concentration of the draw solution, required membrane area, as well as the number of trays and pressure in the distillation column. In case studies, production costs at different steam prices and plant capacity conditions are evaluated.

The proposed approach provides an evaluation tool to compare draw solute candidates when new candidates are suggested. Moreover, the application is not limited to the production of potable water using distillation. Membrane distillation or nanofiltration can also be used in the recovery process. The target purity of product water can be set for agricultural or industrial purposes. Furthermore, this approach can be applied to systems for solution concentration or wastewater reuse with minor modifications.

References

A. Achilli, T.Y. Cathb, A.E. Childress, 2010, Selection of inorganic-based draw solutions for forward osmosis applications, Journal of Membrane Science, 364, 233–24

R. Borsani, S. Rebagliati, 2005, Fundamentals and costing of MSF desalination plants and comparison with other technologies, Desalination, 182, 29-37

T.Y. Cath, A.E. Childress, M. Elimelech, 2006, Forward osmosis: principles, applications, and recent developments, Journal of Membrane Science, 281, 70–87

B.S. Frank, 1972, Desalination of sea water, US Patent 3,670,897

C. Fritzmann, J. Löwenberg, T. Wintgens, T. Melin, 2007, State-of-the-art of reverse osmosis desalination, Desalination 216, 1–76

D.N. Glew, 1965, Process for liquid recovery and solution concentration, US Patent 3,216,930

G.T. Gray, J.R. McCutcheon, M. Elimelech, 2006, Internal concentration polarization in forward osmosis: role of membrane orientation, Desalination, 197, 1-8

I.C. Karagiannis, P.G. Soldatos, 2008, Water desalination cost literature: review and assessment, Desalination, 223, 448–456

J.O. Kessler, C.D. Moody, 1976, Drinking water from sea water by forward osmosis, Desalination, 18, 297-306

R.E. Kravath, J.A. Davis, 1975, Desalination of seawater by direct osmosis, Desalination, 16, 151–155.

S. Loeb, L. Titelman, E. Korngold, J. Freiman, 1997, Effect of porous support fabric on osmosis through a Loeb-Sourirajan type asymmetric membrane, Journal of Membrane Science, 129, 243-249

P. McCormicka, J. Pellegrinoa, F. Mantovanib, G. Sarti, 2008, Water, salt, and ethanol diffusion through membranes for water recovery by forward (direct) osmosis processes, Journal of Membrane Science, 325, 467–478

J.R. McCutcheon, R.L. McGinnis, M. Elimelech, 2005, A novel ammonia-carbon dioxide forward (direct) osmosis desalination process, Desalination, 174, 1-11

R.L. McGinnis, M. Elimelech, 2007, Energy requirements of ammonia–carbon dioxide forward osmosis desalination, Desalination, 207, 370–382

A. Mulet, A.B. Corripio, L.B. Evans, 1981, Estimate costs of distillation and absorption towers via correlations, Chemical Engineering, 77–82

C.H. Tan, H.Y. Ng, 2008, Modeling of external and internal concentration polarization effect on flux behaviour of forward osmosis, Water Science & Technology: Water Supply, 8.5, 533-539

M. Turkay, I.E. Grossmann, 1998, Structural flowsheet optimization with complex investment cost functions, Computers & Chemical Engineering, 22, 673-686

R. Williams, 1947, Six-Tenths Factor Aids in Approximating Costs, Chemical Engineering, 54, 124–125

I.A. Karimi and Rajagopalan Srinivasan (Editors), Proceedings of the 11th International Symposium on Process Systems Engineering, 15-19 July 2012, Singapore.

Optimal water network synthesis with detailed membrane-based regenerator models

Cheng Seong Khor,[a,b] Benoit Chachuat,[a] Nilay Shah[a]

[a]*Centre for Process Systems Engineering, Department of Chemical Engineering, Imperial College London, South Kensington Campus, London SW7 2AZ, UK*
[b]*Chemical Engineering Department, Universiti Teknologi PETRONAS, Bandar Seri Iskandar, 31750 Tronoh, Perak, Malaysia*

Abstract

This work addresses integrated water network synthesis problems by proposing detailed yet computationally efficient models for the design of membrane separation-based water regenerators. The resulting tighter formulation incorporates major physical parameters for the membrane regenerators. The resulting nonconvex mixed-integer nonlinear program (MINLP) based on a source–regenerator–sink superstructure is implemented on a case study and solved to global optimality using GAMS/BARON.
Keywords: Optimization; Superstructure; MINLP; Water network synthesis; Water reuse; Water regeneration

1. Introduction

Water network synthesis problems have received increasing attention in the process systems engineering literature as evidenced by a flurry of recent publications (among others, see Ahmetović and Grossmann, 2011; Faria and Bagajewicz, 2010; Misener et al., 2011), including fairly recent resurgence in water pinch analysis (see the reviews by Jezowski (2010) and Foo (2009)). We extend our recent work on the industrially-favored pressure-driven membrane separation-based water regenerators by postulating computationally-efficient models (Khor et al., in press) yet with more detailed representations (Khor et al., 2011). The approach gives rise to precise tighter formulations in investigating the interactions between non-membrane and membrane-based regenerators for an integrated water network. The goal is to synthesize an optimal water network given the three elements of: (i) water sources with fixed flowrates and contaminant concentrations; (ii) water sinks with fixed flowrates and maximum allowable inlet concentration (MAIC) limits; and (iii) water regenerators. To this end, we develop a source–regenerator–sink superstructure that allows all feasible interconnections of the elements to embed numerous alternative configurations for direct reuse/recycle, regeneration–reuse, and regeneration–recycle. The rest of the paper mainly discusses the proposed model formulation and gives a flavor of its implementation and solution on a case study.

2. Optimization-Based Model Formulation for Water Network Synthesis

The formulation adopts a fixed-flowrate representation for water-using units that caters for both mass transfer- and non-mass transfer-based operations (Foo, 2009). Such a representation is amenable to a source–sink model with the additional component of water regeneration subnetwork that pools the sources for treatment before directing them to the sinks for reuse/recycle. For non-membrane regenerators, we employ the conventional model of linear water treatment units (Karuppiah and Grossmann, 2008).

On the other hand, for membrane regenerators, the permeator and the rejector are decomposed into two separate entities, in which each is treated as a regenerator to ensure the permeator concentration is lower than that of the rejector (Khor et al., in press). To incorporate the important physical parameters for a membrane regenerator, we employ the more detailed representation afforded by knowledge-driven first-principles models (Khor et al., 2011). Figure 1 shows the superstructure around the water regeneration subnetwork that is representative of the entire network in general.

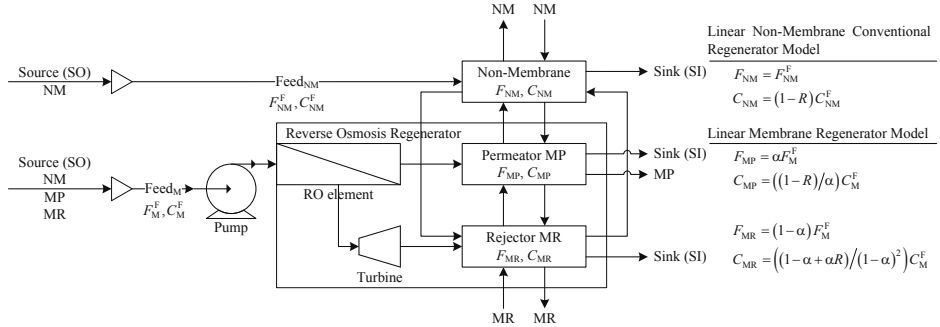

Figure 1. Superstructure for the water regeneration subnetwork

The superstructure and regenerator models lead to a nonconvex MINLP that globally optimizes the capital and operating costs for the interconnections in terms of total stream flows and concentrations. The nonlinearity is due to contaminant mixing while the integrality pertains to discrete decisions on selection of the interconnections and the regenerators.

The following notation will be used in the formulation. Flow in an interconnection from the subscript representing the origin entity A (as indexed by β) is sent to the destination entity B (as indexed by α) at the rate $F_{A,B}(\beta,\gamma)$. For example, $F_{SO,SI}(i,j)$ indicates flowrate from a source (SO) $i \in I$ to a sink (SI) $j \in J$. Concentrations for a set of contaminants $q \in Q$ is defined for each network entity. K_{NM} denotes the set of non-membrane regenerators k, while the set K_M contains ordered pairs of the permeator MP and the rejector MR of membrane regenerators k. The formulation is as follows:

(a) Linear mass balance for a source:

$$F_{SO}(i) \geq \sum_{k \in K_{NM}} F_{SO,NM}(i,k) + \sum_{k' \in K_M} \left(F_{SO,MP}(i,k') + F_{SO,MR}(i,k')\right) + \sum_{j \in J} F_{SO,SI}(i,j), \quad \forall i \in I$$

This balance is formulated as an inequality for the numerical purpose of accounting for the direct discharge flow of any excess water source into the following three terminal sinks: the waste sink representing an effluent treatment plant (ETP); the discharge sink for safe removal into the environment; and the incineration sink for handling untreated wastes that do not meet discharge regulations and contaminants whose fate do not end up in any sink for reuse/recycle.

(b) Linear mass balance around the feed point for a non-membrane regenerator:

$$\sum_{i \in I} F_{SO,NM}(i,k) + \sum_{\substack{k' \in K_{NM} \\ k' \neq k}} F_{NM,NM}(k',k) + \sum_{k'' \in K_M} \left(F_{MP,NM}(k'',k) + F_{MR,NM}(k'',k)\right) = F^F_{NM}(k), \quad \forall k \in K$$

where F^F_{NM} is the feed flowrate to a non-membrane regenerator.

(c) Nonconvex bilinear concentration balance around the feed point for a non-membrane regenerator:

$$\left(\begin{array}{l}\sum_{i\in I}F_{\mathrm{SO,NM}}(i,k)C_{\mathrm{SO}}(i,q)+\sum_{\substack{k'\in K_{\mathrm{NM}}\\k'\neq k}}F_{\mathrm{NM,NM}}(k',k)C_{\mathrm{NM}}(k',q)\\+\sum_{k''\in K_{\mathrm{M}}}\left(F_{\mathrm{MP,NM}}(k'',k)C_{\mathrm{MP}}(k'',q)+F_{\mathrm{MR,NM}}(k'',k)C_{\mathrm{MR}}(k'',q)\right)\end{array}\right)=F_{\mathrm{NM}}^{\mathrm{F}}(k)C_{\mathrm{NM}}^{\mathrm{F}}(k,q),\forall k\in K,q\in Q$$

(d) Linear mass and concentration balances for a non-membrane regenerator:

$$F_{\mathrm{NM}}^{\mathrm{F}}(k)=\sum_{j\in J}F_{\mathrm{NM,SI}}(k,j)+\sum_{\substack{k'\in K_{\mathrm{NM}}\\k'\neq k}}F_{\mathrm{NM,NM}}(k,k')+\sum_{k''\in K_{\mathrm{M}}}\left(F_{\mathrm{NM,MP}}(k,k'')+F_{\mathrm{NM,MR}}(k,k'')\right),\quad\forall k\in K$$

$$\left(1-R(k,q)\right)C_{\mathrm{NM}}^{\mathrm{F}}(k,q)=C_{\mathrm{NM}}(k,q),\quad\forall k\in K,\forall q\in Q$$

(e) Linear mass balances around the feed point to the permeator and the rejector of a membrane regenerator:

$$\sum_{i\in I}F_{\mathrm{SO,MP}}(i,k)+\sum_{k'\in K_{\mathrm{NM}}}F_{\mathrm{NM,MP}}(k',k)+\sum_{\substack{k''\in K_{\mathrm{M}}\\k''\neq k}}\left(F_{\mathrm{MP,MP}}(k'',k)+F_{\mathrm{MR,MP}}(k'',k)\right)=F_{\mathrm{M}}^{\mathrm{F}}(k),\quad\forall k\in K$$

$$\sum_{i\in I}F_{\mathrm{SO,MR}}(i,k)+\sum_{k'\in K_{\mathrm{NM}}}F_{\mathrm{NM,MR}}(k',k)+\sum_{\substack{k''\in K_{\mathrm{M}}\\k''\neq k}}\left(F_{\mathrm{MP,MR}}(k'',k)+F_{\mathrm{MR,MR}}(k'',k)\right)=F_{\mathrm{M}}^{\mathrm{F}}(k),\quad\forall k\in K$$

Note that the membrane regenerator feed flowrate $F_{\mathrm{M}}^{\mathrm{F}}(k)$ is not related to a permeator or a rejector. This is appropriate to ensure the formulation naturally and consistently represents entities of the actual physical configuration of a membrane regenerator.

(f) Nonconvex bilinear concentration balances around the feed point to a permeator and a rejector:

$$\left(\begin{array}{l}\sum_{i\in I}\left(F_{\mathrm{SO,MP}}(i,k)\right)C_{\mathrm{SO}}(i,q)+\sum_{k'\in K_{\mathrm{NM}}}F_{\mathrm{NM,MP}}(k',k)C_{\mathrm{NM}}(k',q)\\+\sum_{\substack{k''\in K_{\mathrm{M}}\\k''\neq k}}F_{\mathrm{MP,MP}}(k'',k)C_{\mathrm{MP}}(k'',q)+\sum_{\substack{k''\in K_{\mathrm{M}}\\k''\neq k}}F_{\mathrm{MR,MP}}(k'',k)C_{\mathrm{MR}}(k'',q)\end{array}\right)=F_{\mathrm{M}}^{\mathrm{F}}(k)C_{\mathrm{M}}^{\mathrm{F}}(k,q),\forall k\in K,q\in Q$$

$$\left(\begin{array}{l}\sum_{i\in I}\left(F_{\mathrm{SO,MR}}(i,k)\right)C_{\mathrm{SO}}(i,q)+\sum_{k'\in K_{\mathrm{NM}}}F_{\mathrm{NM,MR}}(k',k)C_{\mathrm{NM}}(k',q)\\+\sum_{\substack{k''\in K_{\mathrm{M}}\\k''\neq k}}F_{\mathrm{MP,MR}}(k'',k)C_{\mathrm{MP}}(k'',q)+\sum_{\substack{k''\in K_{\mathrm{M}}\\k''\neq k}}F_{\mathrm{MR,MR}}(k'',k)C_{\mathrm{MR}}(k'',q)\end{array}\right)=F_{\mathrm{M}}^{\mathrm{F}}(k)C_{\mathrm{M}}^{\mathrm{F}}(k,q),\forall k\in K,q\in Q$$

(g) Linear mass balances for a permeator and a rejector with liquid recovery factor α:

$$\alpha(k)F_{\mathrm{M}}^{\mathrm{F}}(k)=\sum_{j\in J}F_{\mathrm{MP,SI}}(k,j)+\sum_{k'\in K_{\mathrm{NM}}}F_{\mathrm{MP,NM}}(k,k')+\sum_{\substack{k''\in K_{\mathrm{M}}\\k''\neq k}}\left(F_{\mathrm{MP,MP}}(k,k'')+F_{\mathrm{MP,MR}}(k,k'')\right),\quad\forall k\in K$$

$$\left(1-\alpha(k)\right)F_{\mathrm{M}}^{\mathrm{F}}(k)=\sum_{j\in J}F_{\mathrm{MR,SI}}(k,j)+\sum_{k'\in K_{\mathrm{NM}}}F_{\mathrm{MR,NM}}(k,k')+\sum_{\substack{k''\in K_{\mathrm{M}}\\k''\neq k}}\left(F_{\mathrm{MR,MP}}(k,k'')+F_{\mathrm{MR,MR}}(k,k'')\right),\forall k$$

(h) Linear concentration balances for a permeator and a rejector with removal ratio *R*:

$$\left(1-R(k,q)\right)C_{\mathrm{M}}^{\mathrm{F}}(k,q)=\alpha(k)C_{\mathrm{MP}}(k,q),\quad\forall k,q$$

$$R(k,q)C_{\mathrm{M}}^{\mathrm{F}}(k,q)=\left(1-\alpha(k)\right)C_{\mathrm{MR}}(k,q),\quad\forall k,q$$

It is noteworthy that a more general expression for the rejector concentration is adopted.

(i) Linear mass balance for a sink:

$$\sum_{i\in I}F_{\mathrm{SO,SI}}(i,j)+\sum_{k\in K_{\mathrm{NM}}}F_{\mathrm{NM,SI}}(k,j)+\sum_{k'\in K_{\mathrm{M}}}\left(F_{\mathrm{MP,SI}}(k',j)+F_{\mathrm{MR,SI}}(k',j)\right)=F_{\mathrm{SI}}(j),\quad\forall j$$

(o) Quality requirement for a sink as dictated by its MAIC limits:

$$\sum_{i\in I} F_{\mathrm{SO,SI}}(i,j)C_{\mathrm{SO}}(i,q)+\sum_{k\in K_{\mathrm{NM}}} F_{\mathrm{NM,SI}}(k,j)C_{\mathrm{NM}}(k,q)+\sum_{k'\in K_{\mathrm{M}}}\begin{pmatrix}F_{\mathrm{MP,SI}}(k',j)C_{\mathrm{MP}}(k',q)\\+F_{\mathrm{MR,SI}}(k',j)C_{\mathrm{MR}}(k',q)\end{pmatrix}$$
$$\le F_{\mathrm{SI}}(j)\cdot C^{\mathrm{MAIC}}(j,q),\quad \forall j,q$$

(p) Logical constraints on existence of piping interconnections:

$$F^{\mathrm{L}}_{\mathrm{A,B}}(\beta,\gamma)\,y_{\mathrm{A,B}}(\beta,\gamma)\le F_{\mathrm{A,B}}(\beta,\gamma)\le F^{\mathrm{U}}_{\mathrm{A,B}}(\beta,\gamma)\,y_{\mathrm{A,B}}(\beta,\gamma),$$
$$\forall(\beta,\mathrm{A})\in(I,\mathrm{SO})\cup(K_{\mathrm{NM}},\mathrm{NM})\cup(K_{\mathrm{M}},\mathrm{MP})\cup(K_{\mathrm{M}},\mathrm{MR}),$$
$$\forall(\gamma,\mathrm{B})\in(K_{\mathrm{NM}},\mathrm{NM})\cup(K_{\mathrm{M}},\mathrm{MP})\cup(K_{\mathrm{M}},\mathrm{MR})\cup(J,\mathrm{SI})$$

where $F^{\mathrm{U}}_{\mathrm{A,B}}(\beta,\gamma)$ is the maximum capacity of the interconnection between A and B.

3. Detailed Nonlinear First-Principles Model Formulation for Membrane Regenerators

As mentioned, we consider regeneration subnetwork models based on first-principles for the membrane regenerators that account for their major physical parameters including the types, sizes, number of modules, and orientations. Such a representation is more rigorous than models considered for water treatment units in Misener and Floudas (2010) and Karuppiah and Grossmann (2008). We illustrate such a formulation for a single-stage hollow fiber type reverse osmosis network (RON). Constraints on the RON operating condition is enforced by considering pressure difference across the membrane:

$$\left(\frac{\omega}{A\gamma}\sum_{q\in Q}C^{\mathrm{F}}_{\mathrm{M}}(k,q)+\pi_{\mathrm{F}}\sum_{q\in Q}C_{\mathrm{MP}}(k,q)\right)\left(\sum_{q\in Q}C^{\mathrm{F}}_{\mathrm{M}}(k,q)+\sum_{q\in Q}C_{\mathrm{MR}}(k,q)\right)$$
$$=\left(P_{\mathrm{F}}(k)+P_{\mathrm{R}}(k)-2P_{\mathrm{P}}(k)\right)\sum_{q\in Q}C^{\mathrm{F}}_{\mathrm{M}}(k,q)\sum_{q\in Q}C_{\mathrm{MP}}(k,q),\quad \forall k\in K$$

where ω is the contaminant flux constant, A is the water permeability coefficient, γ is a membrane- and water- related physical coefficient, and π_{F} is the osmotic pressure at feed side. The additional decision variables denoted by $P_{\mathrm{F}}(k)$, $P_{\mathrm{R}}(k)$, and $P_{\mathrm{P}}(k)$ are pressures of the feed, rejector, and permeator of a membrane regenerator k, respectively.

For the total annualized costs (TAC) of the RON, the following components are taken into account:

(a) capital cost of the RO modules as a function of the shell side and stream pressures, which is nonconvex in the linear fractional terms:

$$\frac{C_{\mathrm{module}}\sum_{j\in J}F_{\mathrm{MP,SI}}(k,j)}{AS_m\gamma\left(P^{\mathrm{F}}_{\mathrm{M}}(k)-\frac{\Delta P_{\mathrm{shell}}}{2}-P_{\mathrm{MP}}(k)-\frac{b}{e(q)}\sum_{q\in Q}C_{\mathrm{MP}}(k,q)A\gamma\left(P_{\mathrm{F}}(k)-\frac{\Delta P_{\mathrm{shell}}}{2}-P_{\mathrm{MP}}(k)-\Delta\pi_{\mathrm{RO}}\right)\right)},$$

(b) capital cost of the pump as a function of the feed pressure and flow, which is bilinear and concave in the power terms:

$$C_{\mathrm{pump}}\left(\left(P_{\mathrm{F}}(k)-P_{\mathrm{atm}}\right)F^{\mathrm{F}}_{\mathrm{M}}(k)\right)^{0.65}$$

(c) capital cost of the energy-recovering turbine as a function of the pressures and rejector flow, which is bilinear and concave in the power terms:

$$C_{\mathrm{turbine}}\left(\left(P_{\mathrm{F}}(k)-\Delta P_{\mathrm{shell}}-P_{\mathrm{atm}}\right)\sum_{j\in J}F_{\mathrm{MR}}(k,j)\right)^{0.43}$$

(d) linear operating cost of pump:

$$\frac{1}{\eta_{\text{pump}}} C_{\text{electricity}} H \left(P_{\text{F}}(k) - P_{\text{atm}} \right) F_{\text{M}}^{\text{F}}(k)$$

(e) linear operating cost of using pretreatment chemicals:

$$C_{\text{chemicals}} H \cdot F_{\text{M}}^{\text{F}}(k)$$

(f) linear operating revenue of the turbine:

$$\left(P_{\text{F}}(k) - \Delta P_{\text{shell}} - P_{\text{atm}} \right) \eta_{\text{turbine}} C_{\text{electricity}} H \sum_{j \in J} F_{\text{MR}}(k, j)$$

4. Case Study: Water Network in a Petroleum Refinery

The MINLP model is applied on a refinery case study that involves 28 sources including freshwater; 2 regenerators: mud trap–corrugated plate interceptor and a single-stage RON; and 14 sinks including two terminal sinks (ETP and discharge to the environment). Full details of the case study can be found in Khor et al. (2011). We use a set of base operating values obtained from available plant data to initialize the solution procedure. We utilize the general purpose global optimization solver GAMS 23.3.3/BARON 9.0.2 to avoid obtaining an unreliable local optimal solution. Using BARON requires good variable bounds for tight relaxations, which we supply in the form of general equations based on analyzing the source–regenerator–sink network topology (Ahmetović and Grossmann, 2011). To tighten the formulation and enhance solution convergence, we add linear logical constraints using 0–1 variables on certain design and structural specifications derived from physical insights of the problem. These logic cuts remove undesirable fractional solutions in a branch-and-bound search tree by deducing as many values for the 0–1 variables as possible. An optimal water network configuration is attained in 3970 iterations requiring an acceptable CPU time of 282.5 s with promising results of more than 50% annual savings in freshwater use. Future work is geared towards solving a realistic multicontaminant problem involving uncertainty in the flowrates, concentrations, and removal ratios by employing customized strategies for handling model nonconvexities.

5. References

E. Ahmetović and I. E. Grossmann, 2011, Global Superstructure Optimization for the Design of Integrated Process Water Networks, AIChE J., 57, 434–457.

D. C. Faria and M. J. Bagajewicz, 2010, On the Appropriate Modeling of Process Plant Water Systems, AIChE J., 56, 668–689.

D. C. Y. Foo, 2009, State-of-the-Art Review of Pinch Analysis Techniques for Water Network Synthesis, Ind. Eng. Chem. Res., 48, 5125–5159.

R. Karuppiah and I. E. Grossmann, 2008, Global Optimization of Multiscenario Mixed Integer Nonlinear Programming Models Arising in the Synthesis of Integrated Water Networks under Uncertainty. Computers & Chemical Engineering, Comput. Chem. Eng., 32, 145–160.

C. S. Khor, D. C. Y. Foo, M. M. El-Halwagi, R. R. Tan, N. Shah, 2011, A Superstructure Optimization Approach for Membrane Separation-Based Water Regeneration Network Synthesis with Detailed Nonlinear Mechanistic Reverse Osmosis Model, Ind. Eng. Chem. Res., 50, 13444–13456.

C. S. Khor, B. Chachuat, and N. Shah, in press, A Superstructure Optimization Approach for Water Network Synthesis with Membrane Separation-Based Regenerators, Comput. Chem. Eng., doi: 10.1016/j.compchemeng.2012.02.020

J. Jezowski, 2010, Review of Water Network Design Methods with Literature Annotations, Ind. Eng. Chem. Res., 49, 4475–4516.

R. Misener, J. P. Thompson, and C. A. Floudas, 2011, APOGEE: Global Optimization of Standard, Generalized, and Extended Pooling Problems via Linear and Logarithmic Partitioning Schemes. Comput. Chem. Eng., 35, 876-892.

I.A. Karimi and Rajagopalan Srinivasan (Editors), Proceedings of the 11th International Symposium on Process Systems Engineering, 15-19 July 2012, Singapore

A Stochastic Programming Formulation for Disinfectant Booster Station Placement to Protect Large-Scale Water Distribution Systems

Gabriel A. Hackebeil[a], Angelica V. Mann[a], William E. Hart[b], Katherine A. Klise[c], Carl D. Laird[a*]

a Artie McFerrin Dept. of Chemical Engineering, Texas A&M University, USA
b Informatics and Data Analysis Dept., Sandia National Laboratories, Albuquerque, NM 87185, USA
c Geoscience Research and Application Group, Sandia National Laboratories, Albuquerque, NM 87185, USA

Abstract

We present a methodology for optimally locating disinfectant booster stations for response to contamination events in water distribution systems. A stochastic programming problem considering uncertainty in both the location and time of the contamination event is formulated resulting in an extensive form that is equivalent to the weighted maximum coverage problem. Although the original full-space problem is intractably large, we show a series of reductions that reduce the size of the problem by five orders of magnitude and allow solutions of the optimal placement problem for realistically sized water network models.

Keywords: optimal placement, weighted maximum coverage, water distribution systems

1. Introduction

Unintentional or malicious contamination of water distribution systems poses significant health risks to consumers. Early-warning detection systems have been proposed to detect the presence of contaminant using a fixed grid of sensors throughout the network, and several researchers have studied the problem of optimal sensor layouts within these drinking water distribution systems (Ostfeld and Salomons, 2004; Berry et al., 2005; Murray et al., 2010). However, adequate emergency response mechanisms must also be developed. If the sensor grid flags a warning, a manual water sample will be drawn and sent for laboratory analysis. Following analysis (which can take several hours or more), a positive confirmation of contaminant will likely result in a no-drink order. However, during the time between the first detection and the laboratory confirmation, contaminant will be spreading throughout the network. Disinfectant booster stations can help mitigate the effect of potential contamination by injecting additional (but safe) amounts of disinfectant immediately following the initial warning (Parks et al., 2009).

Here, we address the optimal placement of disinfectant booster stations to mitigate the effect of a contamination event. This is a particularly challenging problem for two reasons. First, the interaction between the contaminant and the disinfectant are often described using nonlinear reaction kinetics. In addition to this nonlinearity, since the particular contaminant is not known a priori, the specific structure and values for the kinetic parameters

*Corresponding Author, carl.laird@tamu.edu

are not known. Second, the water network model itself is large, and since the time and location of the contamination event is not known a priori, considering potential contamination events from every network node and all possible timesteps leads to an extremely large number of scenarios.

In this paper, we make simplifying assumptions on the contaminant-disinfectant interaction that allow us to precompute the effect of disinfectant booster stations and toxin scenarios independently, removing the need to embed the large-scale water quality model within the problem formulation. These simulations provide input data to a very large mixed-integer linear programming formulation with hundreds of thousands of scenarios and discrete decision variables corresponding to the placement of booster stations within the network. While the initial formulation is intractably large, we show a series of reductions that significantly decrease the problem size, while yielding an exact mathematical transformation of the original stochastic programming problem. With these techniques, we demonstrate effective, optimal booster station placement using a real water network model with over 3000 nodes.

2. Problem Formulation

To remove the complexities associated with the disinfectant-toxin reaction kinetics, we use the simplifying assumption that a sufficient concentration of disinfectant is injected to completely and instantaneously neutralize the toxin if they come into contact. With this assumption, the problem can be formulated using independent precomputed simulations for all possible booster station locations and all possible contamination scenarios.

The extensive form of the stochastic programming formulation is given by the following mixed-integer linear programming problem,

$$\min \sum_{s\in S} \alpha_s \sum_{\substack{n\in N\\ t\in T}} \delta_{n,t,s}\, m_{n,t,s} \tag{1}$$

$$\text{s.t.} \quad \sum_{b\in B} y_b \le \mathbf{M} \tag{2}$$

$$\delta_{n,t,s} \ge 1 - \sum_{b\in B} y_b Z_{b,n,t,s} \qquad \forall\ n\in N,\ t\in T,\ s\in S \tag{3}$$

$$0 \le \delta \le 1, \quad y \in \{0,1\} \tag{4}$$

This problem is equivalent to the weighted maximum coverage problem, where S, N, T, B are sets representing the scenarios, network nodes, timesteps, and potential booster locations, respectively. The mass of toxin consumed from node n at time t for scenario s is given by the parameter $m_{n,t,s}$ (calculated from the precomputed toxin simulations). Assuming each scenario s has probability α_s, the objective function is the expected value of the mass of toxin consumed from the entire water distribution system over all scenarios. The binary variable y_b is 1 if node b is selected as a booster station location, and Equation 2 restricts the number of booster stations that can be placed to be no more than $\mathbf{M}$. The indexed parameter Z is determined from the precomputed booster station simulations and captures the node-time pairs in each scenario that are disinfected as a result of each potential booster station location. The parameter $Z_{b,n,t,s} = 1$ only if a booster station installed at node b supplies sufficient disinfectant to node n and time t for scenario s (otherwise, $Z_{b,n,t,s} = 0$). The continuous variable $\delta_{n,t,s}$ indicates whether or not toxin is consumed at node n and time t for scenario s. Equation 3 ensures that $\delta_{n,t,s}$ is only allowed to be 0 if

at least one selected disinfectant booster station location provides neutralization of node n at time t for scenario s. This continuous indicator variable is guaranteed to have a value of either 0 or 1 at the solution (where 0 indicates the complete neutralization of toxin for that combination of n, t, and s).

The input parameters for this problem formulation are calculated using simulations computed by the Merlion (Wong et al., 2010) water quality modeling package. Given a particular sensor layout in the network we perform a toxin simulation for each scenario s to determine $m_{n,t,s}$ the mass of toxin consumed from node n at time t and the contaminant detection time. Assuming that the booster station injections begin immediately following sensor detection, we can simulate the effect of every booster station location for this scenario, starting the disinfectant injection at the detection time, and continuing injection for 8 hours (when the laboratory results would confirm a positive or false alarm).

For large water network models, the full mixed-integer linear problem formulation is still intractable. Fortunately, there are a number of reductions that significantly decrease the problem size while providing an exact mathematical transformation of the full problem.

1. For any particular contamination scenario, there are a number of node-time pairs where toxin will not be present (the value of $m_{n,t,s} = 0$) and the corresponding $\delta_{n,t,s}$ can be removed from the problem. Likewise, there are node-time pairs where toxin exists ($m_{n,t,s} > 0$), but no disinfectant can reach the node ($Z_{b,n,t,s} = 0 \; \forall \; b$). This is true, for example, for all times prior to the detection time of a particular scenario since no disinfectant is injected as yet. In this situation, we can set the corresponding $\delta_{n,t,s}$=1 and again remove the variable from the problem.

2. Consider the constraints shown in Eq. (3). When the right-hand-sides of multiple constraints are identical, we can aggregate the corresponding indices in the δ variables. This would occur, for example, if $Z_{b,1,2,3} = Z_{b,4,5,6} \; \forall \; b$. Then, the corresponding variables $\delta_{1,2,3}$ and $\delta_{4,5,6}$ are indistinguishable from each other and can be aggregated to a single variable, $\delta_{1/4,2/5,3/6}$. With this aggregation, the new coefficient in the objective function is determined using the probability weighted sum of the original coefficients ($m_{1/4,2/5,3/6} = \alpha_3 m_{1,2,3} + \alpha_6 m_{4,5,6}$). Notice also that the parameter Z is calculated using disinfectant simulations from every potential booster station location with the injection starting at the detection time of the corresponding scenario. Any two scenarios that have the same detection time will also have the same calculated values for Z. While the number of scenarios is very large, there can only be as many possible detection times as there are time discretizations (i.e. $|T|$). Therefore, we only need to perform booster station simulations, at most, over all timesteps and not all scenarios, significantly reducing both the size of the problem and the computational time required to calculate the parameters.

As seen in the numerical results presented in the next section, these reductions are necessary for reasonable memory usage and solution times for larger water network problems.

3. Numerical Results

In this case study we examine the optimal placement of 5 booster stations in the water distribution network shown in Figure 1. This network has $3,358$ nodes and $3,829$ pipes. $1,621$ nodes have been selected as booster station candidates (all nodes with non-zero demand). We assumed 20 fixed sensors in the network, which were optimally placed

using the TEVA-SPOT toolkit (Berry et al., 2008). These sensor locations are shown in Figure 1. The water quality model was generated using a 30 minute water quality timestep and a full simulation horizon of 72 hours. For contamination scenarios, we considered contaminant injections from every junction and every timestep during the first 24 hours of the simulation horizon, resulting in a total of 159,504 contamination scenarios. The Merlion water quality model (Wong et al., 2010) was used to perform all of the toxin and booster station simulations, and the total simulation time, including writing of the data files for the problem formulation, was about 2 minutes for the required 170,310 simulations.

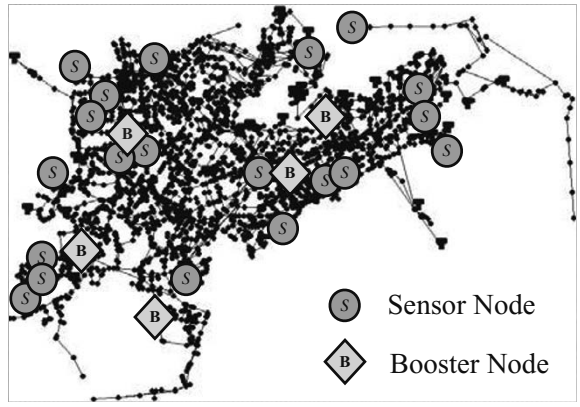

Figure 1. Network schematic showing network nodes and pipes, where sensors are indicated by `S` *and the optimal booster station locations indicated by* `B`

The size of the full problem is shown in Figure 2 (vertical axis is in logarithmic scale). The large number of scenarios results in a mixed-integer linear problem that has over 10 billion variables and constraints. Following the application of reduction (1), the problem size has been reduced by almost two orders of magnitude, but is still prohibitively large. The memory required to store the nonzeros in the constraint jacobian alone (as 8-byte doubles) is over 600 gigabytes. Applying reduction (2) reduces the problem by another three orders of magnitude, giving a reasonably sized problem with approximately half a million variables. Solving this problem using CPLEX 12.2 required approximately 45 minutes and 70 gigabytes of RAM on a machine with 8 Intel(R) Xeon(R) processors (X5570 @ 2.93GHz).

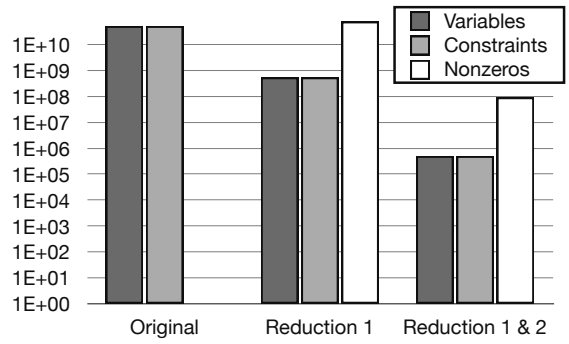

Figure 2. Problem size (log scale) for the original full space problem, the problem following reduction (1), and the problem following reductions (1) and (2).

Figure 1 shows the optimal solution for the booster station placement. With this booster station placement, the expected value of the mass of toxin consumed by the public is reduced by 62% over the value for the network with sensors only (no booster stations), where 64% of the expected consumption occurs before detection.

4. Summary and Conclusions

In this paper, we have proposed a stochastic programming formulation for the optimal placement of disinfectant booster stations in a large-scale water distribution system. This problem formulation considers uncertainty in both the time and location of contamination events. Given large water

network models and the number of scenarios, the extensive form of this problem is intractably large.

There is a tremendous amount of structure in the problem induced by the scenario-based formulation and the network model itself. This allows for a series of problem reductions that dramatically decrease the size of the formulation. Indeed, in the case study considered here, the problem size was reduced by over five orders of magnitude. This problem formulation includes an extremely large number of scenarios (all junctions and timesteps for an entire day), nevertheless, with these reductions, solution is possible considering realistic network models. While commercial modeling and solver packages have a presolve phase, the original problem is far too large to even fit in memory on a reasonable workstation. Furthermore, even with smaller test problems, we did not see significant reduction in the problem size using the presolve in both AMPL or CPLEX 12.2.

Acknowledgements

This research was supported in part by the Office of Advanced Scientific Computing Research within the Department of Energy Office of Science, as part of the Complex Interconnected Distributed Systems program. Sandia National Laboratories is a multi-program laboratory managed and operated by Sandia Corporation, a wholly owned subsidiary of Lockheed Martin Corporation, for the U.S. Department of Energy's National Nuclear Security Administration under contract DE-AC04-94AL85000. The authors would like to thank Reagan Murray and Terra Haxton from the US Environmental Protection Agency for their guidance in this research.

References

Berry, J., Boman, E., Riesen, L. A., Hart, W. E., Phillips, C. A., Watson, J. P., 2008. User's manual: TEVA-SPOT toolkit 2.2. US EPA, Office of Research and Development, EPA-600-R-08-041, National Homeland Security Research Center, Cincinnati.

Berry, J. W., Fleischer, L., Hart, W. E., Phillips, C. A., Watson, J. P., 2005. Sensor Placement in Municipal Water Networks. Journal of Water Resources Planning and Management 131, 237.

Murray, R., Haxton, T. M., Janke, R. J., Hart, W. E., Berry, J., Phillips, C. A., 2010. Sensor Network Design for Drinking Water Contamination Warning Systems: A Compendium of Research Results and Case Studies using the TEVA-SPOT-Report. US Environmental Protection Agency, Washington, DC. Tech. rep., EPA/600/R-09/141.

Ostfeld, A., Salomons, E., 2004. Optimal Layout of Early Warning Detection Stations for Water Distribution Systems Security. Journal of Water Resources Planning and Management 130 (5), 377–385.

Parks, S., VanBriesen, J., et al., 2009. Booster Disinfection for Response to Contamination in a Drinking Water Distribution System. Journal of Water Resources Planning and Management 135, 502.

Wong, A. V., McKenna, S. A., Hart, W. E., Laird, C. D., 2010. Real-Time Inversion and Response Planning in Large-Scale Networks. Computer Aided Chemical Engineering 28, 1027–1032.

I.A. Karimi and Rajagopalan Srinivasan (Editors), Proceedings of the 11th International Symposium on Process Systems Engineering, 15-19 July 2012, Singapore.

Incorporating Complex Fiscal Rules in Strategic Planning of Offshore Oil and Gas Fields

Vijay Gupta and Ignacio E. Grossmann

Dept. of Chemical Engineering, Carnegie Mellon University, Pittburgh, PA 15213, USA

Abstract

In this paper, we extend a recently proposed multi-field site strategic planning model for offshore oil and gas fields to include the complex fiscal rules, specifically sliding scale production sharing agreements (PSAs). The proposed multiperiod MINLP model maximizes NPV after paying royalties, profit share, etc. to the host government. The model can be reformulated into an MILP using linearization techniques to solve it to global optimality. It is shown that the computational cost increases significantly by adding the sliding scale PSA contracts in contrast to a simple NPV based optimization. However, the model yields improved investment and operations decisions due to the explicit consideration of the fiscal terms within development planning.

Keywords: Multiperiod Optimization, Oil exploration, Production sharing agreements.

1. Introduction

Strategic planning of offshore oil and gas fields involves capital intensive decisions pertaining to the installation of exploration and production facilities, subsea structures, pipeline connections, well drilling, etc. that are taken at the early stages of the project. However, there is a very large number of alternatives that are usually available to make these decisions under the given physical and practical restrictions. This necessitates optimizing the investment and operations decisions to ensure the highest return on the investments over the given time horizon. Furthermore, fiscal rules of the agreements between oil company and the host government usually determine the share of each of these entities in the total oil production or gross revenues and the timing of these payments. Hence, including fiscal considerations as part of the oilfield development problem can impact the optimal decisions and revenue flows over the planning horizon, as a large fraction of the total oil produced is paid as royalties, profit share, etc.

There are several deterministic (Iyer et al. 1998, Gupta and Grossmann 2011a), and stochastic (Goel and Grossmann 2004, Tarhan et al. 2009) models that have been proposed for the oil/gas field planning problem. However, the models and solutions approaches in the literature that consider the fiscal rules within development planning are either very specific or simplified. Van den Heever and Grossmann (2001) considered optimizing the complex economic objectives including royalties, tariffs, and taxes for the multiple gas field site where number of wells were used as parameters (fixed well schedule). Moreover, the fiscal rules presented were specific to the gas field site considered, but not in generic form. Based on a continuous time formulation for gas field development with complex economics of similar nature as Van den Heever and Grossmann (2001), Lin and Floudas (2003) presented an MINLP model and solved it with a two-stage algorithm. Simulation based approaches (Blake and Roberts 2006) are also considered for the analysis of the different fiscal terms.

In this paper, we address the optimal development planning of offshore oil and gas fields under complex fiscal rules considering as a basis the deterministic model for

multi-field site by Gupta and Grossmann (2011a), which includes sufficient level of details to be realistic as well as computationally efficient. We first discuss the basic elements of the various types of contracts with particular focus on the progressive PSA terms, and then the way to include these contracts in the model. Numerical results on an instance of the development planning problem with a typical PSA terms are presented.

2. Background

There are a variety of contracts that are used in the offshore oil and gas industry. These contracts can be classified into two main categories:

2.1. Concessionary System

A concessionary (or tax and royalty) system usually involves royalty, cost deduction and tax. Royalty is paid to the government at a certain percentage of the gross revenues. The net revenue after deducting costs becomes taxable income on which a pre-defined percentage is paid as tax. The total contractor's share involves gross revenues minus royalty and taxes. The basic difference as compared to the production sharing agreement, is that the oil company obtains the title to all of the oil and gas at the wellhead and pay royalties, bonuses, and other taxes to the government.

2.2. Production Sharing Agreements (PSAs)

The revenue flow in a typical Production Sharing Agreement can be seen as in Figure 1, (World Bank 2007). Some portion of the total oil produced is treated as cost oil by the oil company to recover costs after paying royalties to the government at a certain percentage of the oil produced. There is a ceiling on the cost oil recovery to ensure revenues to the government as soon as production starts. The remaining part of the oil, called profit oil, is divided between oil company and the host government at a certain percentage. The oil company needs to further pay income tax on its share of profit oil. Hence, the total contractor's (oil company) share in the gross revenue comprises of cost oil and contractor's profit oil share after tax. The other important feature of a PSA is that the government owns all the oil and transfers title to a portion of the extracted oil and gas to the contractor at an agreed delivery point. Notice that the cost oil limit is one of the key differences with a concessionary system.

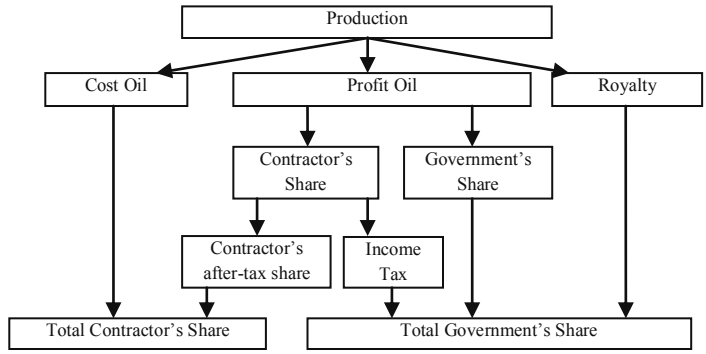

Figure 1: Revenue flow for a typical Production Sharing Agreement

The specific rules defined in such a contract (either concessionary or PSA) between oil company and host government determine the profit that the oil company can keep as well as the royalties and profit share that are paid to the government. These profit oil shares, royalty rates are usually based on the profitability of the project (sliding scale or progressive fiscal terms), where cumulative oil produced, rate of return, R-factor etc. are the typical profitability measures that determine the tier structure (levels) for these

contract terms. For instance, if the cumulative production is in the range of first tier, $L_1 \le xc_t \le U_1$, the royalty R_1 will be paid to the government, while if the cumulative production reaches in tier 2, royalty R_2 will need to be paid, and so on. In practice, as we move to the higher tier the percentage share of contractor in the total production decreases. Given that the resulting royalties and/or government profit oil share can represent a significant amount of the gross revenues, it is critical to consider these contract terms explicitly during oilfield planning to assess the actual economic potential of such a project. In the next section, we discuss how to include these sliding scale PSA rules in a development planning model which covers the key elements of the most of the available contracts, and represent one of the most general forms of fiscal rules.

3. Model

A typical offshore oilfield infrastructure consists of a set of oil fields *F = {1,2,..,f}* for producing oil using a set of FPSO (Floating, Production, Storage and Offloading) facilities, *FPSO = {1,2,...fpso},* (see Fig. 2) that can process the produced oil, store and offload it to the other tankers. Each oilfield consists of a number of potential wells to be drilled using drilling rigs, which are then connected to these FPSO facilities through pipelines to produce oil. The goal is to determine the optimum investment and operation decisions to maximize the NPV for a long-term planning horizon, which is discretized into a number of time periods *t,* typically each with 1 year of duration. Investment decisions in each time period *t* include which FPSO facilities should be installed or expanded, and their respective installation or expansion capacities for oil, liquid and gas, which fields should be connected to which FPSO facility, and the number of wells that should be drilled in a particular field *f*. Operating decisions include the oil/gas production rates from each field *f* in each time period *t*. It is assumed that the installation and expansion decisions occur at the beginning of each time period *t*, while operation takes place throughout the time period.

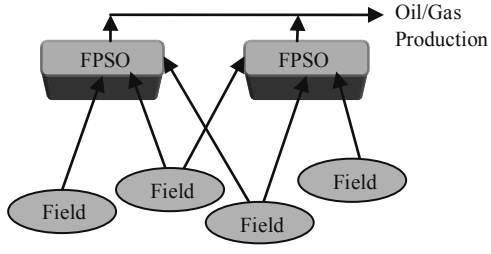

Figure 2. Typical Offshore Oilfield Infrastructure

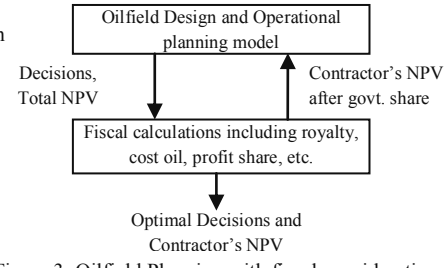

Figure 3. Oilfield Planning with fiscal considerations

Gupta and Grossmann (2011a) recently proposed an efficient multiperiod MINLP model (**Model 2**) for this development planning problem which is reformulated into an MILP (**Model 3**) to solve it to global optimality. The models were further reduced (**Model 2R** and **Model 3R**) to improve the computational efficiently in fullspace. We incorporate the sliding scale PSA terms in these MINLP/MILP models that are explained above. The proposed model considers the trade-offs involved between investment and operations decisions and resulting royalties, profit shares that are paid to the government, and yields the maximum overall NPV for the contractor, (see Fig. 3).

The objective function is to maximize the contractor's NPV where Economic Constraints, Reservoir Constraints, Field-FPSO Flow constraints, FPSO Capacity Constraints, Well drilling limitations and Logic Constraints are similar to the proposed MINLP/MILP models (see Gupta and Grossmann 2011a for details). This corresponds

to the design and operational planning model without fiscal considerations, (see Fig. 3). We describe below the constraints (1)-(8), that correspond to the fiscal part of the problem and these can be included in either of the proposed MINLP or its MILP reformulation. Notice that a detailed generic oilfield planning model with fiscal considerations and solution strategies are discussed in Gupta and Grossmann (2012).

$$TotalConSh_t = ConSh_t^{aftertax} + CO_t \qquad \forall t \qquad (1)$$

$$CO_t = \min(CR_t, f_t^{CR} \cdot REV_t) \qquad \forall t \qquad (2)$$

$$CR_t = CAP_t + OPER_t + CRF_{t-1} \qquad \forall t \qquad (3)$$

$$CRF_t = CR_t - CO_t \qquad \forall t \qquad (4)$$

$$PO_t = REV_t - CO_t \qquad \forall t \qquad (5)$$

$$\bigvee_i \begin{bmatrix} Z_{i,t} \\ ConSh_t^{beforetax} = f_i^{PO} \cdot PO_t \\ L_i \le xc_t \le U_i \end{bmatrix} \qquad \forall t \qquad (6)$$

$$Tax_t = f_t^{tax} \cdot ConSh_t^{beforetax} \qquad \forall t \qquad (7)$$

$$ConSh_t^{aftertax} = ConSh_t^{beforetax} - Tax_t \qquad \forall t \qquad (8)$$

Total contractor's share in time period *t*, (see Fig. 1), is calculated in constraint (1) as the sum of contractor's profit oil share (after paying income tax) and cost oil that it keeps to recover the expenses. We assume that there are no royalty provisions in this case. The cost oil in time period *t*, constraint (2), is calculated as the minimum of the cost recovery in that time period and maximum allowable cost oil (cost recovery ceiling), which is a given fraction f_t^{CR} of the gross revenue. Constraint (2) can further be rewritten as mixed-integer liner constraints. The cost recovery in time period *t*, constraint (3), is the sum of capital and operating costs in time period *t* and cost recovery carry forward from previous time period *t-1* which is calculated in constraint (4) as the difference between cost recovery and cost oil. Constraint (5) states that the total profit oil in time period *t* is the portion of the gross revenue that remains after subtracting the cost oil. Contractor receives a certain fraction, f_i^{PO}, of the total profit oil which is based on a sliding scale variable, for instance cumulative oil production. In particular, disjunction (6) is used to model this tier (levels) structure for profit oil fraction, which states that variable $Z_{i,t}$ will be true if cumulative oil production by the end of time period *t* lies between given tier thresholds $L_i \le xc_t \le U_i$; i.e. tier *i* is active and corresponding fraction f_i^{PO} is used to determine the contractor share in that time period. The disjunction (6) in the model is further reformulated into linear and mixed-integer linear constraints using the convex-hull formulation. The contractor pays income-tax, constraint (7), on its profit oil share at the given tax rate f_t^{tax} that is used in constraint (8) to calculate the contractor's after tax share.

4. Example

In this example, we consider 5 oilfields that can be connected to 3 FPSO's with 11 possible connections. There is a total of 31 wells that can be drilled and planning horizon is 20 years. There is a cost recovery ceiling and 4 tiers (see Fig. 4) for the profit oil fraction of the contractor linked to cumulative oil production, which defines the fiscal terms of a typical PSA. Table 1 compares the results of the proposed MILP (Model 3) and reduced MILP models (Model 3R) with PSAs, that are implemented in

GAMS 23.6.3 and run on Intel Core i7, 4GB RAM machine using CPLEX 12.2. Model 3 with PSA takes more than 10 hours with a 14% of optimality gap as compared to Model 3R, which terminates the search with a 2% gap in reasonable time (1,163.7s). In contrast, Model 3R without any fiscal terms can be solved in only 189.8 seconds. Interestingly, Model 3R with a flat 35% of the profit share of contractor is solved in 72.64s which is even smaller than model without any fiscal terms (189.8s).

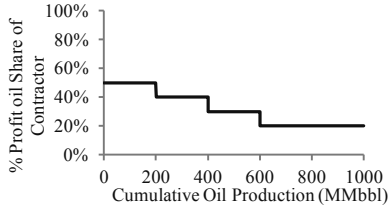

Figure 4. Contractor's Profit oil share for Example

Table 1. Computational Results for Example

	Model 3 with PSA	**Model 3R with PSA**
Constraints	9474	9363
Cont. Variables	6432	6223
Dis. Variables	727	551
NPV ($Million)	2,183.63	2,228.94
Time(s)	>36,000	1,163.7

Therefore, the increase in computational time while including fiscal rules in oilfield planning, is directly related to the number of tiers (levels) that are present in the model to determine the profit oil shares or royalties. This is due to the additional binary variables that are required to model tiers, and resulting weak relaxation, as good bounds on some of the key variables, e.g. profit oil, are not available a priori. The details of the optimal decisions for this example are discussed in Gupta and Grossmann (2011b).

5. Conclusions

In this paper, we have incorporated the complex fiscal terms of the contract between oil company and the host government in a recently proposed model for offshore oil and gas field infrastructure planning. Numerical results in an example show that the model can become expensive to solve with sliding scale fiscal terms due to the additional binary variables to model tiers. However, the model yields improved decisions due to the trade-offs involved between investments and actual contractor's profit share.

References

A. J. Blake and M. C. Roberts, 2006. Comparing petroleum fiscal regimes under oil price uncertainty. Resources Policy, 31(2), 95–105.

V. Goel and I. E. Grossmann, 2004. A stochastic programming approach to planning of offshore gas field developments under uncertainty in reserves. Comput. Chem. Eng., 28 (8), 1409-1429.

V. Gupta and I. E. Grossmann, 2011a. An Efficient Multiperiod MINLP Model for Optimal Planning of Offshore Oil and Gas Field Infrastructure. I&EC Res., Submitted for publication.

V. Gupta and I. E. Grossmann, 2011b. Offshore Oilfield Development Planning under Uncertainty and Fiscal Considerations. Optimization and Analytics in the Oil and Gas Industry, Part I, Springer Edition, Submitted for publication.

V. Gupta and I. E. Grossmann, 2012. Modeling and computational strategies for optimal development planning of offshore oilfields under complex fiscal rules. Working paper.

R. R. Iyer, I. E. Grossmann, S. Vasantharajan, A. S. Cullick, 1998. Optimal planning and scheduling offshore oilfield infrastructure investment and operations. I&EC Res., 37, 1380-1397.

X. Lin, C. A. Floudas, 2003. A Novel Continuous-Time Modeling and Optimization Framework for Well Platform Planning Problems. Optim. Eng., 4 (1-2), 65.

B. Tarhan, I. E. Grossmann, V. Goel, 2009. Stochastic programming approach for the planning of offshore oil or gas field infrastructure under decision-dependent uncertainty. I&EC,48(6),3078.

S. A. van den Heever and I. E. Grossmann, 2001. A Lagrangean Decomposition Heuristic for the Design and Planning of Offshore Hydrocarbon Field Infrastructures with Complex Economic Objectives. Ind. Eng. Chem. Res., 40, 2857-2875.

World Bank, 2007. Contracts for Petroleum Development: Part 1. Petro. Sect. Brief. Note No. 7.

I.A. Karimi and Rajagopalan Srinivasan (Editors), Proceedings of the 11th International Symposium on Process Systems Engineering, 15-19 July 2012, Singapore.

Optimization of Pure-Refrigerant Cycle Compressing Ratio on C3-MR Process

Inkyu Lee,[a] Kyungjae Tak,[a] Wonsub Lim,[a] Kwangho Choi,[b] Il Moon[a]

[a] *Department of Chemical and Biomolecular Engineering, Yonsei University, 50 Yonsei-ro, Seodaemun-gu, Seoul 120-749, Korea*
[b] *GS E&C, GS Yeokjeon Tower 537, Namdaemun-ro 5-ga, Joong-gu, Seoul, Korea*

Abstract

The natural gas liquefaction process is an energy intensive process due to its low temperature. Compressor units are one of primary factors in minimizing energy consumption of natural gas liquefaction process. Among various natural gas liquefaction processes, C3-MR (Propane Pre-cooled Mixed-Refrigerant) process is the most commonly used in LNG market. C3-MR process uses two types of refrigerants such as mixed-refrigerant and pure-refrigerant. In this study, pure-refrigerant cycle is simulated, along with different compressing ratios and different pressure levels. The simulation of case studies shows that energy consumptions mainly depend on both compressing ratios and pressure levels.. This study has achieved the energy consumption savings by 27.7% through different case studies with an emphasis on compressing ratios and pressure levels.

Keywords: LNG, pure-refrigerant cycle, liquefaction process, propane pre-cooled mixed-refrigerant process

1. Introduction

Due to the tightening regulation of greenhouse gases and instability of demands and supplies of energy, the structure of world energy market is of large fluctuations.. As an alternative energy source against typical existing fossil fuels, the role of natural gas in the world's energy market has been growing now [1]. Moreover, a number of natural gas liquefaction plant have been built or under construction. This latest trend has a consequence that interest in the development of innovative natural gas liquefaction processes is rapidly growing [2].

In general, the liquefaction of natural gas yields huge volume reduction by 1/600 approximately.. For this reason, LNG can be generally used for long distances transportation. In order to liquefy natural gas, the liquefaction temperature must be cooled down below -162°C which is boiling point of methane, a main component of natural gas[3]. Therefore, the natural gas liquefaction process requires to operation under cryogenic conditions and huge amounts of energy. A Compressor is a most important unit in natural gas liquefaction process because it consumes most of energy of the process. Because of large energy consumption, a number of researches on natural gas liquefaction process optimization have been carried out [4]. Main optimization objectives can be classified into two categories such as the improvement of efficiency of the heat exchanger and reduction of the energy consumption of the compressor. [5].

The C3-MR process uses a pure-refrigerant for cooling mixed-refrigerant and pre-cooling natural gas. Many researches on mixed-refrigerants have been conducted, however, a small number of studies on pure-refrigerants. This study simulates pure-refrigerant cycle to find optimal set of compressing ratios and pressure levels of pure-

refrigerant cycle through case studies. Furthermore, the analyses of relationships of energy consumptions with pressure levels and compressing ratios, respectively.

2. Characteristics of C3-MR Process

A schematic diagram of C3-MR process using prue-refrigenrant for pre-cooling natural gas is shown Figure 1. . Propane is used as the pure-refrigerant, and it is also used to cool a mixed-refrigerant.

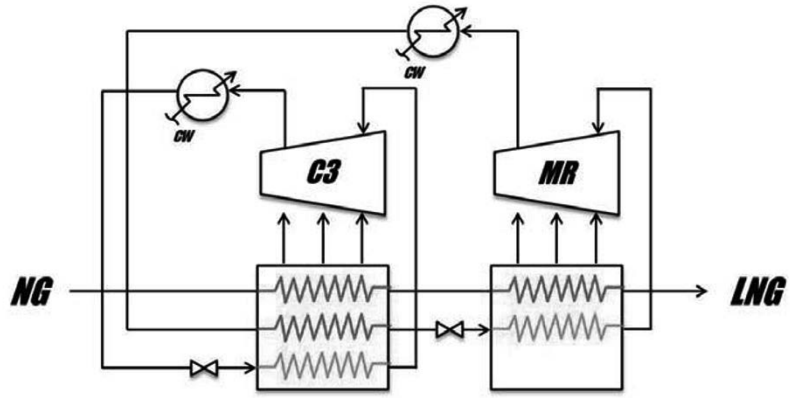

Figure 1. Propane pre-cooling mixed-refrigerant (C3-MR) process diagram

Propane is compressed through a compressor and then cooled by a cooler up to liquid sate. After that, it is expanded through valves. Cold propane is also used to cool natural gas and mixed-refrigerant, and it is vaporized again. Therefore, there is no temperature change of propane in the heat exchanger, only an evaporation heat is used for cooling natural gas and mixed-refrigerant. As shown in figure 2,Vapor propane goes to a compressor again and this series of steps are repeated. In this cycle, total energy consumption is changed by pressure levels and compressing ratios applied [6].

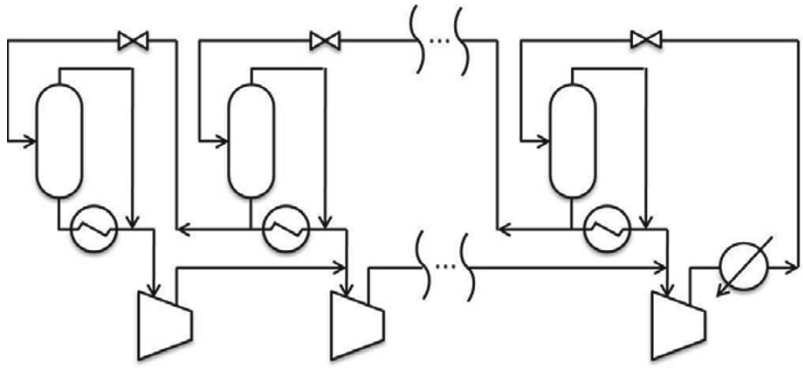

Figure 2. Propane cycle flow sheet

When using a pure-refrigerant for heat exchange, the temperature of cold stream remains constant. Due to this characteristics, heat exchange efficiency increases when using various temperatures of the cold stream. For this reason, pure-refrigerant cycle is

designed to be multi-stages. Compressor, heat exchanger, flash drum, and valves are needed to increase pressure level again. Thus, in general, 2 to 4 compressors are used for pure-refrigerant cycle due to the constraints of an investment cost and space as needed.

3. Mathematical Model

To cool a natural gas and mixed-refrigerant down to a desired temperature, flow rate of propane has to be determined. For this, the following energy balances are used.

$$\dot{Q}_h = \left(H_{h,i} - H_{h,c}\right) \times \dot{m}_h \quad (1)$$

$$\dot{Q}_c = \left(H_{c,i} - H_{c,o}\right) \times \dot{m}_c \quad (2)$$

$$\dot{Q}_h = -\dot{Q}_c \quad (3)$$

where $\dot{Q}$ denotes heat flow rate, H,enthalpy, and $\dot{m}$, mass flow rate, respectively. The subscript h represents a hot stream, c, cold stream, o an inlet and outlet streams of a heat exchanger, respectively.

4. Simulation results

4 types of compressing ratios for and 3 different pressure levels are taken into consideration. Pressure levels are divided into 3 parts; 3rd level with 2 compressors, 4th level with 3 compressors, and 5th level with 4 compressors. Peng-Robinson equation is used as the equation of state.

4.1. Operation Conditions of NG and MR for simulation

Other operating conditions remain as the same over each case. As shown in table 1, the mixed-refrigerant and natural gas conditions stay unchanged around the propane cycle. Minimum temperature difference between hot and cold streams in heat exchanger is within 5°C. Liquid propane is assumed to be perfectly vaporized through the heat exchanger.

Table 1. Conditions of natural gas and mixed refrigerant

	Feed NG	*Pre-cooled NG*	*MR In*	*MR out*
Temperature (°C)	15.00	-37.49	45.00	-37.49
Pressure (kPa)	6150	6150	6150	6150
Mass Flow (kg·mole/hr)	4973	4973	8761	8761

4.2. Simulation Conditions for Case Studies

A set of compressing ratios applied are follows. In case 1, compressing ratio is changed according to the propane temperature. Compressing ratio is high and low at lower and higher temperatures, respectivel.. Compressing ratio used in case 2 is also changed according to propane temperature, but it is used in opposite way to case 1; compressing ratio is low and high at low and high temperatures, respectively . Compressing ratio in case 3 is determined in a way that temperature differences of each pressure level

remiain same. In case 4, every compressor ratio keeps the same. Table 2 shows temperature and pressure conditions of propane.

Table 2. Temperature and pressure of propane

	Pressure Level 3		*Pressure Level 4*		*Pressure Level 5*	
	Temp. (°C)	Pressure (kPa)	Temp. (°C)	Pressure (kPa)	Temp. (°C)	Pressure (kPa)
Case 1						
Level 1	-42.49	100	-42.49	100	-42.49	100
Level 2	-19.34	250	-14.12	150	-37.28	125
Level 3	15.95	750	-32.38	300	-27.13	187.5
Level 4	-	-	15.95	750	-7.41	375
Level 5	-	-	-	-	15.95	750
Case 2						
Level 1	-42.49	100	-42.49	100	-42.49	100
Level 2	-14.12	300	-19.34	250	-25.43	200
Level 3	15.95	750	1.79	500	-5.40	400
Level 4	-	-	15.95	750	7.98	600
Level 5	-	-	-	-	15.95	750
Case 3						
Level 1	-42.49	100	-42.49	100	-42.49	100
Level 2	-13.27	308.8	-23.01	218.9	-27.88	182.2
Level 3	15.95	750	-3.54	424.4	-13.27	308.8
Level 4	-	-	15.95	750	1.34	493.2
Level 5	-	-	-	-	15.95	750
Case 4						
Level 1	-42.49	100	-42.49	100	-42.49	100
Level 2	-16.74	274	-25.97	196	-30.44	165
Level 3	15.95	750	-6.68	384	-16.74	274
Level 4	-	-	15.95	750	-1.28	455
Level 5	-	-	-	-	15.95	750

4.3. Simulation Result

Simulation has been carried out for 12 different cases and comparedin tems of total energy consumptions. The result is shown in table 3.

Table 3. Total energy consumption

	level 3	level 4	level 5
Case 1	320.08 kW	281.30 kW	248.19 kW
Case 2	308.24 kW	256.32 kW	234.00 kW
Case 3	307.31 kW	255.44 kW	231.54 kW

Case 4	312.74 kW	259.17 kW	234.36 kW

5. Conclusion

This study had an objective of finding an optimal set of compressing ratio and pressure level throughcase studies. Each case is observed to be advantageous for cooling. Case 1 can cool down natural gas and mixed-refrigerant using propane at lower temperature. Case 2 can decrease an energy load at each compressors, using lower compressing ratio at higher flow rate of propane. In case 3, the efficiency of each heat exchanger can be increased by minimizing areas between hot and cold composite curves. Case 4 can keep compressing ratios at each compressor the same.

As the result, It was found that as the compressing level is getting higher, energy consumption is getting lower. Furthermore, it is identified that using lower compressing ratio at higher flow rate of propane is better than using lower temperature of middle pressure streams. The worst case is found to be pressure level 3 in case 1 with total energy consumption is 320.08 kW. On the other hand, the best case is identified as the pressure level 5 of case 3 consuming 231.54 kW which is 27.7% lower than that of worst case.

It can be concluded that compressing ration is a primary factor for saving energy consumption and required to be optimized as more than 20% energy savings can be improved by manipulating compression ratio.This work can contribute to minimizing energy consumption of natural gas liquefaction processes which use pure-refrigerant, such as C3-MR process and CASCADE process.

6. Acknowledgement

This research was supported by a grant from GAS Plant R&D Center funded by the Ministry of Land, Transportation and Maritime Affairs (MLTM) of the Korean government.

References

Kyungjae Tak, 2011, "Optimization of Mixed-Refrigerant System in LNG Liquefaction Process", ESCAPE 21

Satish Kumar, 2011, "Current status and future projections of LNG demand and supplies: A global prospective", Energy Policy, 29, 4097-4104

Abdullah Alabdulkarem, 2011, "Optimization of propane pre-cooled mixed refrigerant LNG plant", Applied Thermal Engineering, 31, 1091-1098

Ho-Myung Chang, 2011, "An efficient multi-stage Brayton-JT cycle for liquefaction of natural gas", Cryogenics, 51, 278-286

Bengt O. Neeraas, 2004, "Experimintal data and model for heat transfer, in liquid falling film flow on shell-side, for spiral-wound LNG heat exchanger", Internatrional Journal of Heat and Mass Transfer, 47, 3565-3572

Alexandre Morin, 2011, "Using evolutionary search to optimise the energy consumption for natural gas liquefaction", Chemical Engineering Research and Design, 89, 2428-2441

I.A. Karimi and Rajagopalan Srinivasan (Editors), Proceedings of the 11th International Symposium on Process Systems Engineering, 15-19 July 2012, Singapore.

Monitoring and fault diagnosis system for LNG fractionation process

Hahyung Pyun, Hyunseok Jeong, Daeyeon Kim, Daegun Ha, Chonghun Han*

Seoul national university, Rm.712,Bldg.302, Seoul Nat'l Univ ,Gwanakgu,151-744, Korea

Abstract

LNG, the most common clean energy, has been consumed increasingly. Moreover it is expected to be over 50% of total energy source after 2030. Therefore, it is necessary for efficient monitoring and diagnosis system of LNG plant. This plant is very sensitive and correlated each other. If this plant is not operated appropriately, it causes a large amount of operating cost and damaged of equipment. Furthermore, it can propagate other process and cause its fail or risk. Previous monitoring and fault diagnosis system of this plant is based on univariate methodology. However univariate system is inconvenient to LNG plant because this system has so many sensors correlated each other.

It is necessary to apply multivariate monitoring and fault diagnosis methodology. In this study, PCA, one of the most common multivariate methodologies, is suggested as a monitoring method for a whole process. When fault is detected by this method, three steps methodology for diagnosis are suggested; fault propagation, fault magnitude and event analysis. This suggested methodology is demonstrated to application to LNG fractionation process. As a result, the application of this methodology has rapid detection and accurate performance compared to previous univariate monitoring system.

Keywords: LNG plant, PCA, Monitoring, Fault diagnosis

1. Introduction

In the future, echo-friendly energy will be spotlighted throughout the world. LNG is the most useful source of clean energy. For stable and cost-effective supply, monitoring and fault diagnosis system in LNG plant should be improved. The current system is based on univariate methodology. However, LNG plant has too many sensors to identify whole system. In order to these difficulties, multivariate statistical techniques should be applied. In this study, PCA, one of many multivariate statistical methodologies, is applied appropriately and event matrix for diagnosis is suggested.

2. Backgrounds

2.1. Propagation

Propagation is a signal path to identify a route of faults. This method is achieved by transforming new data to normalized data. Because the normalized data are different from the original data in terms of scale and deviation, the normalized data are more convenient for comparing with each sensor and visualization than the original data. After the data normalized, 3δ deviation is selected as the limit of the sensors. Exceeding the limit is recording in order. This recording is converted to the event matrix and this matrix is used for diagnosis.

2.2. PCA(Principal component analysis)

PCA is a method that reduced the dimension of a number of sensors. This method uses an orthogonal transformation to convert a set of sensors into a PC(principal components). First PC has as high a variance as possible, and each succeeding component is turn has the highest variance possible under the constraint that it be orthogonal to the preceding components. This method can properly describe the trend in whole system.

2.2.1. Fault magnitude

Fault magnitude is from PCA contribution result. This method shows which sensors contribute to the state in the spot of that time. There are two contributions; T-contribution and residual contribution. If fault is detected in T-score chart, than T-contribution interpret system. Otherwise, SPE chart detects fault, residual contribution is used to diagnosis. Fault magnitude is also converted to event matrix and used for diagnosis.

2.2.2. Correlation

PCA is based on decomposition of the covariance matrix of the process variables. So it can describe correlation sensors each other. This correlation is called loading. Loading plot is similar with contribution. The difference between contribution and loading is time-varying or one kind of indicator. So correlation is reflected trend of the system history which pre-set time interval. Likewise above methods, this method is converted to event matrix and used for diagnosis.

2.3. Event analysis

Event analysis is a method to interpret one's methodology. In other words, qualitative or quantitative result translates to standard description. Fig1 shows example of translation magnitude and correlation.

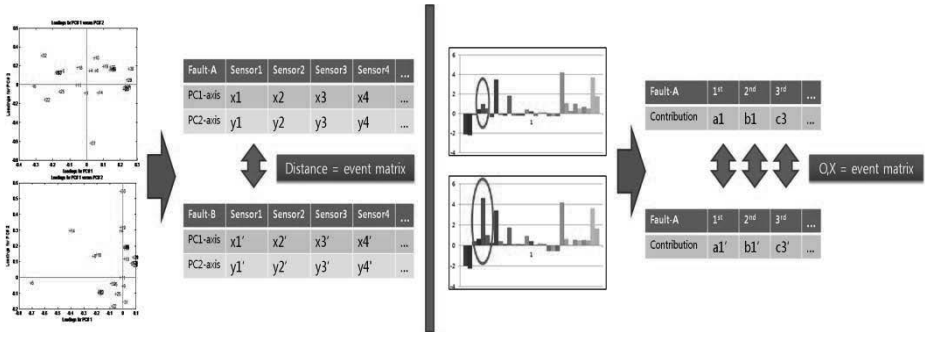

Fig 1 Event matrix for correlation(left) and magnitude(right)

2.4. Fractionation process

LNG plant has self refrigerant process to liquefy NG to LNG. Fractionation process is first section to make refrigerant. Preprocessing NG gas gets through scrubber and heavy gases become feed of the fractionation process. This process has 4 column; demethanizer, deethanizer, depropanizer, debutanizer. From each column methane, ethane, propane, butane+ are distillated. Since heat balance in liquefaction part is very sensitive as temperature of the cooling materials, high distillation performance in

fractionation is needed. In this study, dynamic simulation model for this process is used to verify the proposed methodologies.

3. Case study

3.1. Normal process

In order to monitor the process, normal state must be specified. In this study, aspen hysys simulator is used and the range of convergence dynamic model is defined as the normal state. Feed condition shows in table 1.

	Temperature [℃]	*Pressure [kPa]*	*Flow rate[kg/h]*
Normal process	-16.8~-14.8	6050~6250	51000~56000

Table 1. Normal operation condition

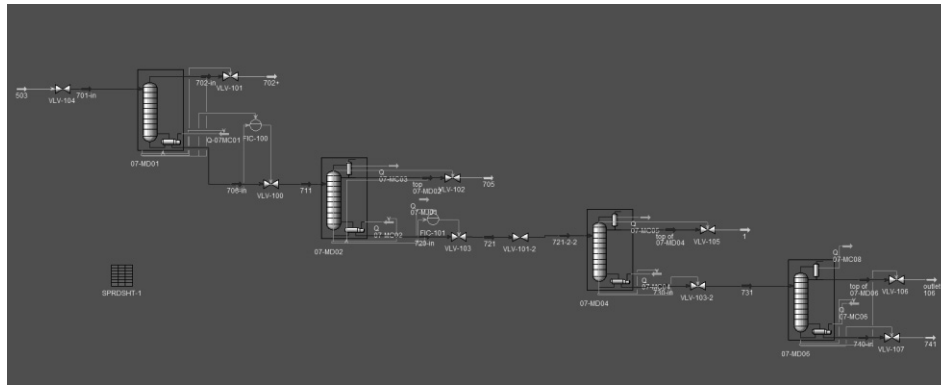

Fig 2 Dynamic model of fractionation process using aspen hysys

3.2. Abnormal process

In this study, 4 fault scenarios are used. Fist case is overheating in demethanizer's reboiler. Overheating in deethanizer reboiler is the second fault. Reboiler of deethanizer failure of the pressure controller is a third scenario. Last abnormal case is leaking of deethanizer bottom stream. Each scenario has 3 intensities; increased 5% , 10% and 20%.

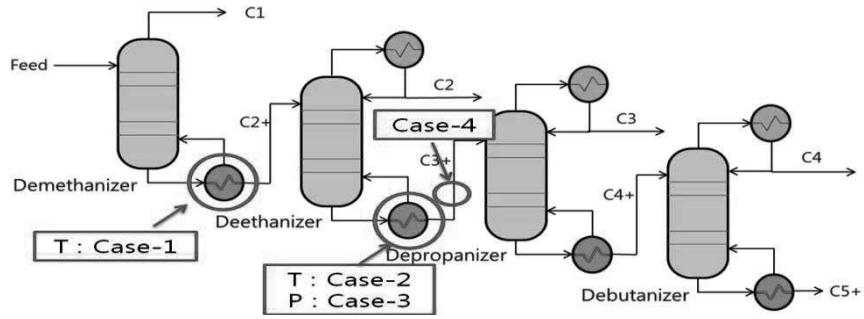

Fig 3 Fault location

4. Results

4.1. Propagation

In propagation method, case3-5% is not correct and case2-20% has a misleading. But other case has well matched to their group.

	Case1 -5%	Case1 -10%	Case1 -20%	Case2 -5%	Case2 -10%	Case2 -20%	Case3 -5%	Case3 -10%	Case3 -20%	Case4 -5%	Case4 -10%	Case4 -20%
Case1 -5%		0.5	0.5	0	0	0	0	0	0	0	0	0
Case1 -10%	0.5		0.5	0	0	0	0	0	0	0	0	0
Case1 -20%	0.5	0.5		0	0	0	0	0	0	0	0	0
Case2 -5%	0	0	0		0.75	0.5	0.5	0.25	0.25	0	0	0
Case2 -10%	0	0	0	0.75		0.5	0.5	0	0	0	0	0
Case2 -20%	0	0	0	0.5	0.5		0.5	0	0	0	0	0
Case3 -5%	0	0	0	0.5	0.5	0.5		0	0	0	0	0
Case3 -10%	0	0	0	0.25	0	0	0		1	0	0	0
Case3 -20%	0	0	0	0.25	0	0	0	1		0	0	0
Case4 -5%	0	0	0	0	0	0	0	0	0		0.75	0.25
Case4 -10%	0	0	0	0	0	0	0	0	0	0.75		0.5
Case4 -20%	0	0	0	0	0	0	0	0	0	0.25	0.5	

Table 2. Propagation result

4.2. Fault magnitude

Using fault magnitude method matches all case perfectly. But this method also has a misleading between case2 and case3.

	Case1 -5%	Case1 -10%	Case1 -20%	Case2 -5%	Case2 -10%	Case2 -20%	Case3 -5%	Case3 -10%	Case3 -20%	Case4 -5%	Case4 -10%	Case4 -20%
Case1 -5%		1	1	0.33	0.33	0.33	0.33	0.33	0.33	0	0	0
Case1 -10%	1		1	0.33	0.33	0.33	0.33	0.33	0.33	0	0	0
Case1 -20%	1	1		0.33	0.33	0.33	0.33	0.33	0.33	0	0	0
Case2 -5%	0.33	0.33	0.33		1	0.66	1	1	1	0	0	0
Case2 -10%	0.33	0.33	0.33	1		0.66	1	1	1	0	0	0
Case2 -20%	0.33	0.33	0.33	0.66	0.66		0.66	0.66	0.66	0	0	0
Case3 -5%	0.33	0.33	0.33	1	1	1		1	1	0	0	0
Case3 -10%	0.33	0.33	0.33	1	1	1	1		1	0	0	0
Case3 -20%	0.33	0.33	0.33	1	1	1	1	1		0	0	0
Case4 -5%	0	0	0	0	0	0	0	0	0		0.66	0.66
Case4 -10%	0	0	0	0	0	0	0	0	0	0.66		1
Case4 -20%	0	0	0	0	0	0	0	0	0	0.66	1	

Table 3. Fault magnitude result

4.3. Correlation

Correlation has two incorrect performances. In small intensity of fault tend to not matching correctly.

	Case1 -5%	Case1 -10%	Case1 -20%	Case2 -5%	Case2 -10%	Case2 -20%	Case3 -5%	Case3 -10%	Case3 -20%	Case4 -5%	Case4 -10%	Case4 -20%
Case1 -5%		9.11	10.55	10.58	11.78	11.00	3.17	3.36	3.94	8.50	9.83	10.89
Case1 -10%	9.11		2.24	6.15	10.18	10.06	10.84	10.47	10.38	10.30	9.61	9.95
Case1 -20%	10.55	2.24		7.07	9.75	10.00	11.54	11.28	11.08	10.76	9.94	10.29
Case2 -5%	10.58	6.15	7.07		9.38	10.04	11.80	11.37	11.06	9.95	8.97	9.33
Case2 -10%	11.78	10.17	9.75	9.38		2.81	11.81	11.84	11.65	9.22	8.04	7.06
Case2 -20%	11.00	10.06	10.00	10.04	2.81		10.62	10.62	10.46	10.37	9.23	8.17
Case3 -5%	3.17	10.84	11.54	11.80	11.81	10.62		1.15	1.81	8.40	9.89	11.06
Case3 -10%	3.36	10.42	11.28	11.37	11.84	10.62	1.15		0.79	8.09	9.52	10.39
Case3 -20%	3.94	10.38	11.08	11.06	11.65	10.46	1.81	0.79		7.73	9.15	10.40
Case4 -5%	8.50	10.30	10.76	9.95	9.22	10.37	8.39	8.09	7.73		3.05	3.09
Case4 -10%	9.83	9.61	9.94	8.97	8.04	9.23	9.89	9.52	9.15	3.05		2.70
Case4 -20%	10.89	9.95	10.23	9.32	7.06	8.17	11.06	10.76	10.40	3.09	2.70	

Table 4. Correlation result

5. Conclusions

Suggested methodology; Propagation, Fault magnitude, Correlation, matches generated fault and past history fault. It is not perfect but very high performance. Misleading or incorrect case occurs each methodology. But if these methodologies are complementary, its accuracy should be improved. In this study, multivariable statistical methodologies are applied to LNG plant. Additional algorithms and correct idea for event matrix will be developed and should be improved the monitoring and diagnosis system.

Acknowledgement

This research was supported by a grant from the LNG Plant R&D Center funded by the Ministry of Land, Transportation and Maritime Affairs(MLTM) of the Korean government.

References

D.M. Yoon, Y.H. Lee, C.H. Han, H.S. An and S.Y. Chang, 2003, “Fault Detection and Diagnosis in Film Processing Plants", HWAHAK KONGHAK, Vol.41, No.5, pp 585-591

S. Wold, E. Kim and P. Geladi, 1987, “Principal Component Analysis”, Chem. and Int. Lab. Sys., 2, 37-52

S.R. Cheng, B. Lin, B.M. Hsu and M.H. Shu, 2009, “Fault-tree analysis for liquefied natural gas terminal emergency shutdown system", Expert Systems with Applications 36, pp 11918-11924

C. Ding and X. He, 2004, “K-means clustering via principal component analysis”, Proceedings of the 21 st International Conference on Machine Learning.

H.A.Gabbar and F.I.Khan, 2010, “Design of Fault Semantic Networks to Integrate Fault, Failure, Hazard, and Accident Models for LNG Plants”, IEEE NPSS (Toronto)

S. Natarajan and R.Srinivasan, 2010, “Multi-model based process condition monitoring of offshore oil and gas production process”, chemical engineering research and design, Vol.88, No 3, pp 572-591

I.A. Karimi and Rajagopalan Srinivasan (Editors), Proceedings of the 11th International Symposium on Process Systems Engineering, 15-19 July 2012, Singapore.

Simultaneous Optimal Placement of Injector and Producer Wells Using Mathematical Programming

W.X. Leow[1], M.S. Tavallali[1], I.A. Karimi[1*], K.M. Teo[2]

[1]*National University of Singapore, Department of Chemical & Biomolecular Engineering, 4 Engineering Drive 4, Singapore 117576*
[2]*National University of Singapore, Department of Industrial & Systems Engineering, 1 Engineering Drive 2, Singapore 117576*

Abstract

Well placement is a critical step with a permanent impact, and hence, finding the best location to drill the wells will have high economic benefits. This work utilizes the previous study of Tavallali et al. (2011) as the base platform and improves their model. It considers both the injectors' and producers' locations as the optimization variables. The final formulation is a dynamic and nonconvex mixed integer nonlinear model, and is solved by a modified outer approximation method.

Keywords: Simultaneous injector and producer well placement, mixed integer nonlinear programming, PDE constraint optimization.

1. Introduction

We are in the millennium of energy. As hydrocarbon prices climb higher and higher, the optimal recovery of new and marginal/mature oil fields becomes more important. The first step in exploiting a given hydrocarbon field is well drilling. Wells play two important roles: a group of them produces oil, while another group injects another fluid (such as water). This is both to maintain the pressure of the reservoir and to increase the sweep efficiency. Well placement is a critical step with a permanent impact, and hence, finding the best location to drill the wells will have high economic benefits. This work utilizes the previous study of Tavallali et al. (2011) as the base platform and improves their model. We consider both the injectors' and producers' locations as the optimization variables. This is a complex task as further important modifications to the model are required.

Although higher oil flow rate improves the revenue, higher water injection can play a twofold role. It can both increase and decrease the economic profit of the project. Hence, the different nature of producers and injectors necessitates introducing both new binaries and new logical constraints**.**

2. Previous works

In a pioneering study, Rosenwald and Green (1974) developed a mixed integer linear programming (MILP) model to select the optimal well locations from a limited set of potential sites to best satisfy the demand targets. Later, Ierapetritou et al. (1999) formulated a MILP model and utilized a decomposition approach through a series of

[1*] Corresponding author: Tel.: +65 6516-6359, Fax: +65 6779-1936, Email – cheiak@nus.edu.sg

quality cut-offs and feasibility tests to obtain the optimal selection of vertical wells in a 3D reservoir model. In another study, Cullick et al. (2004) introduced a two stage method for determining well locations in a 3D reservoir model. The first stage determined the completions for strictly vertical wells, while the second stage determined the configuration of the wells obtained in the first stage.

Although mathematical programming is the pioneer method in addressing optimal well placement problem, it could not become common in practice in comparison with evolutionary methods (Yeten et al., 2003 and Güyagüler et al., 2002). The main reason is due to the inaccuracy of the models used to represent the reservoir response. To overcome that, Tavallali et al., used a rigorous multiphase flow model in their MINLP model to determine the optimal producer locations. They employed two mutually exclusive sets of reservoir cells: (a) already existing wells, and (b) the rest of cells. The latter formed the potential producer set. They also modified the outer approximation with equality relaxation and augmented penalty method to solve this problem.

In the current paper, we use the method of Tavallali et al as the base platform and target simultaneous producer and injector placement to extend its applicability. We improve the model; however we use their solution algorithm directly. The algorithm consists of a decomposition of the MINLP model into an iterative nonlinear programming (NLP), a local search procedure and MILP.

In contrast to their study, each cell will now be a candidate for both producer and injector well site. To achieve that, the remaining parts of this paper are organized as follows. First, the oil drilling problem is described. Subsequently, the model is presented, and illustrated through a case study. Next is a discussion of the results, and finally, the paper is closed with a conclusion and acknowledgements.

3. Problem Definition

Given an oil reservoir with existing wells, the goal is to expand the production by infill drilling of new producers and injectors to meet a projected oil demand for a given time horizon. Necessary geological and PVT data of the reservoir and the fluids are assumed to be available through preliminary studies and lab tests. Furthermore, relevant economic data such as projected demand curve, drilling costs, injection costs, discount rate, oil revenue forecasts, etc, as well as operational data such as water-cut limits, maximum injection pressure, minimum production pressure, production and injection capacity expansion plan for surface facilities are also provided. Finally the minimum allowable well-to-well distance is also specified.

The objective of the mathematical programming model is to maximize the net present value (NPV) of oil production over a fixed planning horizon through the simultaneous determination of new producer and new injector well locations.

It is assumed that the reservoir is a horizontal 2D plane with only water and oil phases, capillary pressure in the reservoir is negligible and the main driving mechanism is water-drive injection.

4. Model

The oil production plan is subjected to mass balances for each phase and should ensure that it meets the oil demand while keeping within the various plant production and injection capacities and operational water cut limits. Moreover, the number of drilled wells should match the budget and decision of the management team.

We use set $l = 1,2,\ldots,\mathrm{L}$ to refer to the discrete cell location, and $t = 1,2,\ldots,\mathrm{T}$ to represent the discrete time steps. The main decision variables are the total fluid flow rate in or out of the well and oil flow rate. They are shown by q_l^t and $q_{o,l}^t$ respectively. As is usual in the reservoir modeling field, we use negative values for the well flow rate of injectors ($q_l^t \leq 0$) and positive value for producers ($q_l^t \geq 0$). Additionally, we define two binary variables: y_l and z_l to choose the well location and its functionality (producer/injector) respectively. y_l indicates the absence ($y_l = 0$) or presence ($y_l = 1$) of a well, while z_l reflects the functionality of the well, $z_l = 1$ for a producer, $z_l = 0$ for an injector.

It is evident that should there be no well present in the cell, there cannot possibly be any flow rate:

$$q_l^t \leq z_l\left(Q_{p0} + E^t\right) \tag{1}$$

$$-y_l|Q_{i0} + I^t| \leq q_l^t \tag{2}$$

where Q_{p0} and Q_{i0} refer to the initial production and injection capacities of the reservoir. E^t and I^t are the production and injection expansion capacities of the reservoir.

Furthermore, if there is no well, it should also be reflected that there is no producer, and hence:

$$z_l \leq y_l \tag{3}$$

For any producer well, the respective flow rates must be tuned to provide the minimum required tubing head pressure (THP_l^L) behind the production choke valves. It is to facilitate the required pressure for the surface operations and separation stages:

$$q_{o,l}^t \leq \psi_l M_{o,l}^t \left(P_l^t - \left[\gamma_1 {q_l^t}^2 + \gamma_2 {q_{o,l}^t}^2 + \gamma_3 q_l^t + \gamma_4 q_l^t + \gamma_5 \frac{q_{o,l}^t}{q_l^t} + \gamma_6\right] - THP_l^L\right) + (1 - z_l) q_l^U \tag{4}$$

where, ψ_l is connection transmissibility factor for wells, $M_{o,l}^t$ is the oil mobility that combines the pressure and saturation dependency of the multiphase fluid flow. q_l^U is an upperbound for production. The γ is the regression parameter and the associated regression terms in the middle bracket, capture the pressure drop inside the well string due to hydrostatic, frictional, and acceleration effects. The binary variables are introduced to ensure the equations will be reduced to their true form only for the appropriate functionality of the well (i.e. producer well), and become loose constraints in the other cases. Similarly, ignoring frictional, and acceleration pressure drops and considering maximum possible THP_l^U for an injector, we can have:

$$q_l^t \geq \psi_l M_{w,l}^U \left(P_l^t - \rho_{w,l} g L - THP_l^U\right) - (1 - y_l)|q_l^L| - z_l|q_l^L| \tag{5}$$

Here, $M_{w,l}^U$ is the maximum water mobility. With the same idea, the ratio of q_l^t and $q_{o,l}^t$ can be modeled in a general sense, using the proper mobility and binary terms.

We maximize NPV as the well placement objective. It comprises of the following parts: drilling, oil revenues and oil processing costs, water production costs, and water injection costs:

$$Min \sum_{l \notin \boldsymbol{IW} \cup \boldsymbol{IP}} \left(c_f y_l\right) - \sum_{t>1} \sum_l \left[c_o q_{o,l}^t - c_{pw} z_l \left(q_l^t - q_{o,l}^t\right) + c_{iw}(1 - z_l) q_l^t\right] \times \frac{\Delta h^t}{\frac{h^t}{(1+\alpha)^{365}}} \tag{6}$$

The fixed costs for drilling a well are reflected in the first summation term. The second summation term consists of the variable costs and profits. c_o, c_{pw}, c_{iw} refers to the oil

production profit, water production cost and water injection cost per unit volume respectively. The final group of terms outside the summation is to account for the time value of money of the cash flows.

5. Case Study

The computations are performed on a Dell Precision T7400 mini-work station with Intel(R) Xeon (R) CPU X5492 @ 3.40 GHz Processor, 64 GB of RAM. The model and algorithm are implemented in GAMS 23.7.3. The MILP models are solved by GUROBI 4.5.1 solver. Additionally the NLP problems are mainly solved by CONOPTD 0.1 and in (rare) case of failure IPOPT and SNOPT.

The reservoir is modeled into a 20 by 20 spatial grid, with each block having the dimensions of 94.1m x 79.6m x 5.56m. There are already 3 existing producers and 2 existing injectors. They are shown by the white stars and triangles respectively in the subsequent figures. The reservoir has been producing oil for the last 250 days with an initial production capacity of 1300m^3/day and injection production capacity of 1500m^3/day. It is suggested to drill 3 new producers and 2 new injectors to plan the next production horizon of 2150 days.

Before performing the case study, a set of 10 mono-producer well placement runs were carried out to gauge the solver's performance. The solver successfully managed to converge to the global optimal solution which was verified using a brute force search to identify the NPVs of drilling a well at every single possible location.

For the case study, different sets of initial guess of 3 additional producers and 2 additional injectors are provided to the solver to begin the run. Figure 1 represents the progress of the best solution through the course of optimization with the NPV shown above each stage . Notice that after major changes in the first two iterations the rest are location refinement through local search stage.

The final solution's NPV after 7 major iterations and 25 production simulations is $504 million with 3 new producers and no new injectors, which is an improvement over the NPV of $486 million for the base case which contained only the existing wells, and no additional producers or injectors drilled.

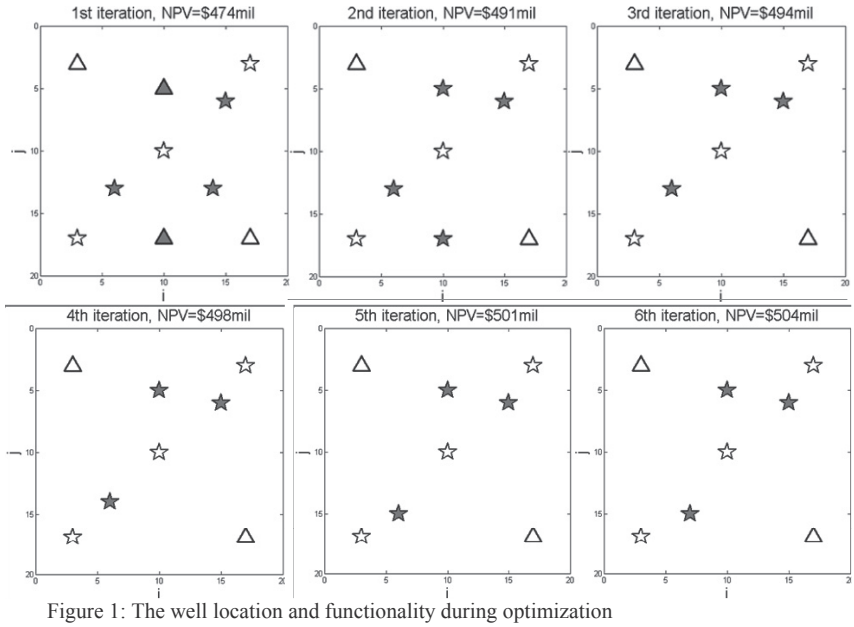

Figure 1: The well location and functionality during optimization
Stars represent producers, triangles represent injectors
Shaded shapes represent additional guesses, white shapes represent an already existing well

6. Discussion

It is notable that similar to Tavallali et al. (2011) we only used local search for the oil producer with the least production history. Owing to the non-convexity of the problem, the local search is extremely crucial in helping to find a better solution. We foresee even better results if we also include injector perturbation in the local search stage. However special care should be given to the screening criteria in the local search. Tavallali et al (2011) selected the well with the lowest level of oil production, as it is the lowest contributor to the NPV of the project, thus, possibly the best candidate to improve on. In contrast, injectors with the highest amount of water injection would have the highest injection costs. However, this may not necessarily mean that the injector has the greatest negative impact on the NPV. This injector could also be the one which provide the most effective water drive energy and sweep and drain the remaining oil zones. It is the actual role of injectors in the first place and hence contributes to the NPV positively in an indirect manner.

7. Conclusion

We have successfully improved on the previous work of Tavallali et al. (2011) by allowing each cell location to have an equal chance of becoming a producer or an injector. The remaining bottlenecks in place are a result of the large size of the problem. In addition there is a level of uncertainty regarding the well placement solutions as there is no definitive way to check whether the solutions are close to the global optimum, and hence this concern will need to be addressed through future additional testing of the model.

8. Acknowledgements

We would like to extend our gratitude to Schlumberger for the provision of the VFPi software to aid us in our work, and Maritime Industry Attachment Programme for their provision of the research grant.

References

M.S. Tavallali, I.A. Karimi, & K.M. Teo, 2011, Dynamic Optimal Well Placement in Oil Reservoirs, Annual Meeting of AICHE, Minneapolis, USA.

G.W. Rosenwald & D.W. Green, 1974, Method For Determining The Optimum Location of Wells in a Reservoir Using Mixed-Integer Programming, Society of Petroleum Engineers of AIME Journal, Volume 14(1), Pages 44-54.

M.G. Ierapetritou, C.A. Floudas, S. Vasantharajan & A.S. Cullick, 1999, Optimal Location of Vertical Wells: Decomposition Approach, AIChE Journal, Volume 45(4), Pages 844-859.

A.S. Cullick, S. Vasantharajan & M.W. Dobin, 2004, Determining Optimal Well Locations From a 3D Reservoir Model, United States Patent No. US 6,549,879.

B. Yeten, L.J. Durlofsky & A. Khalid, 2003, Optimization of Nonconventional Well Type, Location, and Trajectory, SPE Journal, Volume 8(3), Pages 200-210.

B. Güyagüler, R.N. Horne, L. Rogers, L. Livermore & J.J. Rosenzweig, 2002, Optimization of Well Placement in a Gulf of Mexico Waterflooding Project, SPE Reservoir Evaluation and Engineering, Volume 5(3), Pages 229-236.

I.A. Karimi and Rajagopalan Srinivasan (Editors), Proceedings of the 11th International Symposium on Process Systems Engineering, 15-19 July 2012, Singapore.

Contract selection under uncertainty: LNG buyers' perspective

Rajab Khalilpour,[a] I. A. Karimi[b]

[a]*School of Chemical and Biomolecular Engineering, The University of Sydney, Sydney, Australia, Tel: +61 410091600; Fax: +61 2 9351 2854; E-mail: r.kh@usyd.edu.au*
[b]*Department of Chemical & Biomolecular Engineeering, National University of Singapore, 4 Engineering Drive 4, Singapore 117576*

Abstract

As a result of the expanding global LNG market, contracts are becoming more complex due to significant variations in price formulations, flexibility, duration, lead-time, quality, capacity, commitments, discounts and other terms and conditions. The existence of various uncertainties further complicates the contract selection process. We have presented a 2-stage mixed integer linear programming formalism to select LNG contracts with minimum total procurement cost under uncertain demand and LNG price over the planning horizon.

Keywords: LNG; contract, natural gas; vendor selection.

1. Introduction

Recent increases in energy prices, the rise in natural gas demand due to the concerns over CO_2 emissions and a possible carbon tax, the development of a low-cost and high-capacity liquefied natural gas (LNG) value chain, the emergence of new suppliers with large gas reserves, the flow of uncommitted LNG capacity to the market, and the disappearance of conventional contract clauses such as destination are stimulating global LNG trade. Moreover, natural gas market liberalization is resulting in the emergence of new buyers with variable demands, which is increasing the competitiveness and dynamicity of the market. The LNG contracts are thus diversifying in price formulations, flexibility, duration, quality, quantity, commitment, discount, and other terms and conditions. Finding a combination of contracts and suppliers, which trades off various cost factors in an optimal manner, is becoming more and more challenging, where systematic optimization-based approaches can be very useful.

Recently, Khalilpour and Karimi (2011) introduced a deterministic mixed-integer linear programming (MILP) formalism to help the LNG buyers select the best combination of suppliers and contracts in an integrated manner that addresses various aspects, such as contract timings and lengths, demands, price formulations, volume discounts, delivery terms, shipment costs, purchase commitments, etc. However, in reality contract selection is associated with numerous uncertainties (e.g. LNG demand and price). In this study, we have further extended the previous formulation to consider the uncertainties in order to improve robustness of decision making. This paper introduces the new formulation followed by an example.

2. Problem Statement

Consider a company that plans to procure LNG over a given planning horizon H comprising P multiple periods (p = 1, 2, ..., P) of a given fixed length (day, week, etc.). The LNG price in the market is defined as a function (linear, S-curve, etc.) of crude oil price. LNG need or demand is function of many parameters such as energy prices, economical development of the society, etc.

The company assumes I scenarios ($1 \leq i \leq I$) for oil price. Let OP_{pi} denote the oil price for scenario i during period p. For each oil price scenario, it assumes J scenarios ($1 \leq j \leq J$) for LNG demand. Let D_{pij} denote the total LNG demand in period p with a Wobbe Index, WI, (MJ/m^3) in the range of $[WI_p^L,\ WI_p^U]$. Let Pr_{ij} be the probability of oil price scenario i and demand scenario j. Then, P_{ij} = Pr[Demand scenario j for oil price scenario i] × Pr[Oil price scenario i].

The company has access to several potential globally distributed suppliers (or sellers) and a spot market. Thus, it can purchase LNG of varying grades and qualities and then blend these purchases to meet its WI specification. Following Bansal et al. (2007), we replace each supplier with the set of its offered contracts to make this a contract (versus supplier) selection problem. Let C denote the total number of all contracts (c = 1, 2, .., C) offered by the potential suppliers. Let L_c denote the stipulated length of contract c measured in the number of periods. Each contract is of a pre-specified type, either FOB (freight on board) or DES (delivered ex-ship). For an FOB contract, the buyer is responsible for the transport. The buyer may own or charter a fleet of LNG vessels or employ a 3PL (third party logistics provider) to transport its cargo. If it has a limited fleet or does not plan to charter vessels for all its cargo needs, then it may opt for a certain desired mix of DES and FOB contracts for reasons of flexibility.

The current Sales and Purchase Agreements (SPA) enforce a clause that "LNG shall be sold or purchased in full cargo lots" (GIIGNL, 2004). Thus, the company orders its purchases in terms of the number of vessels rather than the volume or mass of LNG. Let w_{cp} (tonnes of LNG) denote cargo size under contract c for purchases in period p. If it is an FOB contract, then the company determines w_{cp}, otherwise the SPA stipulates it. The amount of LNG purchased in a period under a contract may be limited by the seller's production capacity or its non-technical policies such as customer base diversification. On the other hand, the buyer's policies may advocate multi-sourcing and supplier or energy source diversity, and result in similar limits. Therefore, let q_{cp}^U denote the given maximum number of full cargo loads that the company can purchase in period p under contract c. It is also possible to have a constraint on the total purchase under a contract over the entire contract length. Thus, let Q_c^U denote the given maximum amount (tonnes) of LNG that the company can purchase under contract c.

The aim of this problem is, therefore, to determine: the contracts that the buyer should sign with respect to stochastic conditions; the contracts start times; the amount of LNG cargo that the buyer should order under each contract in each period; the spot market sales or procurement under any stochastic scenario; and the total minimum cost for LNG procurement.

3. Formulation

The primary decisions in this problem are to select contracts and their start times. Therefore, we define the following binary variable for each contract c as follows:

$$z_c = \begin{cases} 1 & if\ contract\ c\ is\ selected \\ 0 & otherwise \end{cases} \qquad 1 \leq c \leq C$$

$$ys_{cp} = \begin{cases} 1 & if\ contract\ c\ starts\ with\ period\ p \\ 0 & otherwise \end{cases} \qquad 1 \le p \le P,\ 1 \le c \le C$$

Since a contract can begin only once in the horizon, we get:

$$z_c = \sum_{p=1}^{P} ys_{cp} \qquad 1 \le c \le C \qquad (1)$$

Equation 1 allows us to treat z_c as a continuous variable. ya_{cp} allow us to determine if a contract is active during a period by using the following 0-1 continuous variable:

$$ya_{cp} = \begin{cases} 1 & if\ contract\ c\ is\ active\ during\ period\ p \\ 0 & otherwise \end{cases} \qquad 1 \le p \le P,\ 1 \le c \le C$$

$$ya_{cp} = \sum_{p'=\max[1,\ p-CL_c+1]}^{p} ys_{cp'} \qquad 1 \le p \le P,\ 1 \le c \le C \qquad (2)$$

Let q_{cp} denote the amount of LNG cargo that the company orders during period p under contract c. If contract c is inactive during period p, then this must be zero.

$$q_{cp} \le q_{cp}^{U} y_{cp} \qquad 1 \le p \le P,\ 1 \le c \le C \qquad (3)$$

Similarly, the total purchase over the entire contract length cannot exceed its upper bound.

$$\sum_{p=1}^{P} w_{cp} q_{cp} \le Q_c^{U} z_c \qquad 1 \le c \le C \qquad (4)$$

The cumulative procurement from all contracts during a period ($\sum_{c=1}^{C} w_{cp} q_{cp}$) might be less or more than the stochastic demand, D_{pij}. In case, that the contracted quantity for a period is less than the demand, the remainder will be procured from spot market (BS_{pij}), and if there is redundancy, it will be sold to spot market (SS_{pij}). In other words,

$$BS_{pij} - SS_{pij} + \sum_{c=1}^{C} w_{cp} q_{cp} = D_{pij} \qquad 1 \le p \le P,\ 1 \le i \le I,\ 1 \le j \le J \qquad (5)$$

We have to ensure that at any period p, at most one of the variables BS_{pij} or SS_{pij} have nonzero value. We define the following binary variable, yd_{pij}, as:

$$yd_{pij} = \begin{cases} 1 & if\ the\ contracted\ LNG\ for\ period\ p\ is\ less\ than\ demand \\ 0 & otherwise \end{cases}$$

Then,

$$BS_{pij} \le yd_{pij} D_{pij} \qquad 1 \le p \le P,\ 1 \le i \le I,\ 1 \le j \le J \qquad (6)$$

$$SS_{pij} \le (1 - yd_{pij}) D_{pij} \qquad 1 \le p \le P,\ 1 \le i \le I,\ 1 \le j \le J \qquad (7)$$

The company may desire the contracted LNG quantity for any period p ($\sum_{c=1}^{C} w_{cp} q_{cp}$) to be in certain range of any demand scenario, D_{pij}. Such policies are practiced to further reduce or control supply surplus/shortage risks. Let [fD^L, fD^U] denote the desired range for the fraction of fixed contracts in the company's procurement plan.

$$fD^L D_{pij} \le \sum_{c=1}^{C} w_{cp} q_{cp} \le fD^U D_{pij} \qquad (8)$$

In addition to meeting quantity needs, the purchases must also satisfy quality requirements. Assuming that the separate shipments over each period can be mixed over time to meet the desired quality, we can write this quality constraint as:

$$WI_p^L \sum_{c=1}^{C} \frac{w_{cp}\, q_{cp}}{SG_{cp}} \le \sum_{c=1}^{C} \frac{WI_{cp}\, w_{cp}\, q_{cp}}{SG_{cp}} \le WI_p^U \sum_{c=1}^{C} \frac{w_{cp}\, q_{cp}}{SG_{cp}} \qquad (9a\text{-}b)$$

where WI_{cp} is the Wobbe index for LNG purchased under contract c during period p and SG_{cp} is the specific gravity of LNG under contract c at period p.

As discussed before, FOB contracts offer some flexibility to the company in terms of destination and trade. Unless the company has decided to use only one specific type (FOB or DES) of contract, it may desire a certain percentage of FOB contracts in the contract mix. Let [f^L, f^U] denote the desired range for the fraction of FOB contracts in the company's procurement plan.

$$f^L \sum_{c=1}^{C} z_c \le \sum_{c=1, c \in FOB}^{C} z_c \le f^U \sum_{c=1}^{C} z_c \qquad (10a\text{-}b)$$

Let $STPC_{ij}$ denote the company's total cost of LNG procurements under oil price and demand scenarios (i, j). It includes the fixed costs of contracts, the cost of contracted

LNGs transport, procurement cost of LNG from spot market, and sales price of surplus LNG to spot market. Let v_{cpi} denote the price ($/tonne) of LNG under contract c during period p and at oil price scenario i. Similarly, PB_{ci} and PS_{pi} are procurement and selling price of spot market during period p under oil price scenario i, respectively. For DES contracts the transport cost is included in the LNG price, and we do not need to compute a separate transport cost. However, if a contract is FOB, then we compute its transport cost (TC_{cp} $ per round trip of cargo shipment during period p under contract c) by considering the ship's time-charter cost, its operating expenditure, boil-off losses and port and passage fees for the entire round trip. We set $TC_{cp} = 0$ for the DES contracts.

$$STPC_{ij} = \sum_{c=1}^{C} FC_c z_c + \sum_{p=1}^{P} \left[BS_{pij} PB_{ci} - SS_{pij} PS_{pi} + \sum_{c=1}^{C} q_{cp} \left(v_{cp} w_{cp} + TC_{cp} \right) \right] \quad (11)$$

where FC_c denotes the fixed cost of signing contract c. With this, the company's goal is to minimize the Expected Total Procurement Cost, $ETPC$, given by

$$ETPC = \sum_{i=1}^{I} \sum_{j=1}^{J} Pr_{ij} STPC_{ij} \quad (12)$$

The complete formulation for LNG procurement for a single-site buyer is given by Equations 1-10 and 11-12 where q_{cp} is an integer, ys_{cp} and yd_{cp} are binary, z_c and ya_{cp} are 0-1 continuous and the rest of the variables are continuous.

4. Example

A buyer plans its LNG purchases over 14 years (H = 14 years) or 56 quarterly periods (P = 56). The company has defined three stochastic values for current crude oil prices, i.e. $70 (probability=0.25), $100 (0.50) and $150 (0.25) with assumption of a constant escalation rate of 0.74% per period. For each crude oil scenario, they have defined three demand scenarios (with equal probabilities) over the planning horizon. Figure 1 illustrates the profiles of the nine different demand projections. The buyer's facilities need LNG with a WI of 51-53 MJ/m^3.

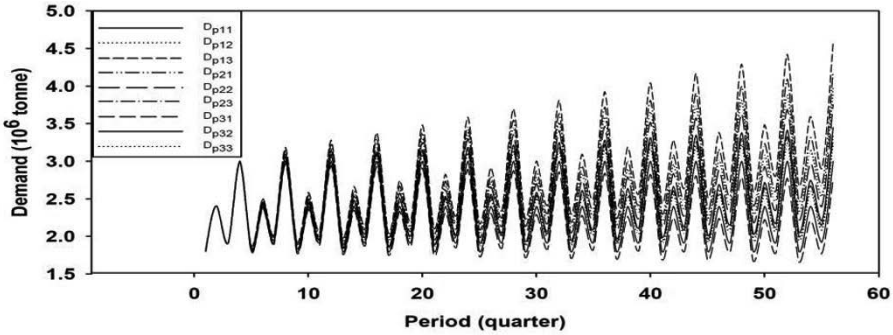

Fig. 1: The buyer's periodical LNG demand under various scenarios.

At present, it is considering C = 40 candidate contracts. Due to its internal policies, the buyer has some limits on total purchase quantities from a few contracts. Some contracts also have supply limits. Some contracts use S-curve price formulas with different price-breaks, while some others use linear formulations. Some contracts are FOB and others are DES. The detailed specifications of the contracts are elsewhere (Table 5 of Khalilpour and Karimi (2011)). The company has its own shipping fleet with the LNG carrier size of w_{cp}= 67,500 tonnes (about 150,000 m^3) for delivery of FOB LNGs.

The MILP model was solved using GAMS software with short execution time of 0.608 CPU s. Figure 2 presents the optimal purchase plan that has 11 of the 40 contracts of which seven contracts are FOB (c = 1, 11, 12, 21, 22, 31 and 32) and four contracts (c = 6, 9, 26 and 36) are DES.

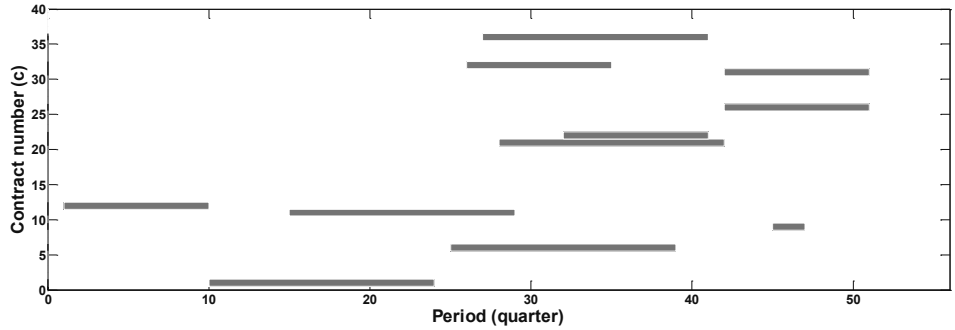

Fig. 2: Optimal contracts and their schedule.

Figure 3 presents the percentage of fixed contracts (taken as base 100%), demand under scenario (*i,j*), procured LNG from spot market and sales LNG to spot market over the entire planning horizon (14 years). The spot market procurement under the nine scenarios will vary in the range of 0.73% - 12.55% of contracted LNG quantity and the surplus LNG for selling to spot market will be in the range of 1.61-15.43 % of contracts.

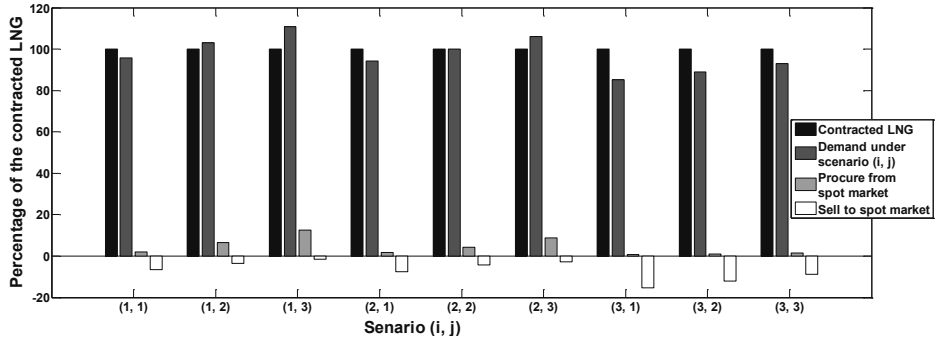

Fig. 3: Percentages of demand and spot market procumbent/sales for each scenario based on fixed contracts (taken as 100%).

5. Conclusion

In this paper, we presented a mixed integer linear programming formalism to select LNG contracts with minimum total procurement cost where the LNG demand and price are uncertain during the planning horizon. We introduced a scenario-based methodology and a 2-stage algorithm to select the here-and-now fixed contracts as first stage. The second stage involves the wait-and-see decisions. In the future if any of the stochastic demand or price scenarios happen, the company can then sell the surplus to spot market or procure if there is shortage.

References

M. Bansal, I. A. Karimi, R. Srinivasan, 2007, Optimal contract selection for the global supply and distribution of raw materials, Industrial & Engineering Chemistry Research, 46, 6522-6539.

GIIGNL, 2004, Master FOB LNG Sales Agreement, Paris, France, International Group of Liquefied Natural Gas Importers.

R. Khalilpour, I. A. Karimi, 2011, Selection of Liquefied Natural Gas (LNG) Contracts for Minimizing Procurement Cost, Industrial & Engineering Chemistry Research, 50, 10298-10312.

I.A. Karimi and Rajagopalan Srinivasan (Editors), Proceedings of the 11th International Symposium on Process Systems Engineering, 15-19 July 2012, Singapore.

A Novel Global Optimization Approach to the Multiperiod Blending Problem

Scott P. Kolodziej,[a] Ignacio E. Grossmann,[a] Kevin C. Furman,[b] and Nicolas W. Sawaya[c]

[a]*Department of Chemical Engineering, Carnegie Mellon University, 5000 Forbes Ave, Pittsburgh PA, 15213, USA*
[b]*ExxonMobil Upstream Research Company, 3120 Buffalo Speedway, Houston, TX 77098, USA*
[c]*ExxonMobil Gas & Power Marketing Company, 800 Bell Street, Houston, TX, 77002, USA*

Abstract

In this paper, we introduce a generalized multiperiod version of the pooling problem to represent time varying blending systems, and also propose novel approaches to solve these problems to global optimality. The primary difficulties in solving this optimization problem are the presence of bilinear terms inherent in blending operations, as well as binary decision variables required to impose the operational constraints over multiple time periods. A general nonconvex MINLP formulation is presented that is used to globally optimize small systems, but quickly becomes intractable as problem size increases. A novel approximation of specified precision for the nonconvex bilinear terms is developed (a radix-based discretization scheme), with which the problem can be reformulated as an MILP. Solving this new formulation requires much less computational time than when the MINLP model is solved directly with a global optimization solver such as BARON. This then allows for the global optimization of larger blending systems. A comparison of the two formulations is presented, along with detailed computational results of each approach.

Keywords: global optimization, pooling problem, MINLP, discretization, radix-based

1. Introduction

The efficient blending of liquid fuels to meet both technical and environmental specifications has been a growing research area in recent years as stricter regulations and smaller profit margins drive the need for the globally optimal blending scheme (Misener & Floudas, 2009). Specifically in refineries, the blending of different distilled fractions to meet specifications - without waste - is of great importance. Research up to this point has focused on what has become known as the pooling problem, posed by Haverly in 1978. In short, the problem is as follows: Multiple liquid streams with various properties (called qualities) are fed from supply tanks into blending tanks where they are assumed to be perfectly mixed in some proportion to meet a set of specifications, and are then fed into demand tanks. The goal is then to select the flows that minimize the overall cost of the blending process. The traditional pooling problem is assumed to operate at steady state, and thus inventory and other dynamics are neglected. In practice, however, supply and demand vary with time, and therefore the inventory in each tank varies as well. This gives rise to a multiperiod blending problem, which has received very little attention in the literature. Therefore, unlike the pooling

problem, the supply and demand flows in the multiperiod problem are specified as a function of time. Additionally, mass balances over each blending tank must allow for accumulation in the form of inventories, as flow into a tank need not equal the flow leaving the tank. Lastly, a special operational constraint is imposed: flow cannot both enter and exit a blending tank in the same time period. This avoids the dynamic change of concentration associated with filling and draining a tank at the same time. The multiperiod blending problem allows for a more accurate modeling of a blending system that varies over time, as is the case in gasoline and crude oil blending in refineries.

2. Multiperiod Blending Problem

2.1 Problem Description

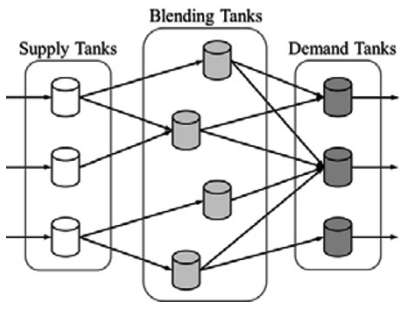

Figure 1: The pooling problem

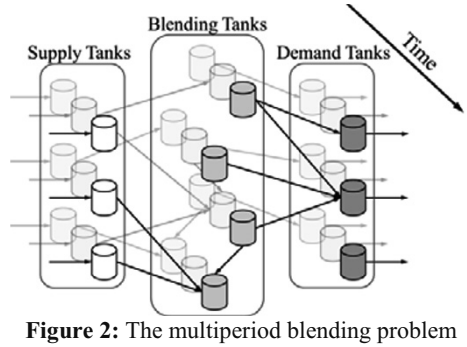

Figure 2: The multiperiod blending problem

The multiperiod blending problem can be stated as follows. A network of supply, blending, and demand tanks is given that operates over a time horizon defined by a set of time periods. At time $t = 0$, an initial inventory is specified for each tank, as well as initial values for the qualities. Given the specified network topology, the optimal flows between the tanks in each time period must be determined, as well as the corresponding inventory levels, which are carried over from one period to another. It is important to note that each time period is not independent of the others due to the coupling created by the inventories. For example, flow may be diverted to a tank for temporary storage to be used in a later period, or there may be no direct path from a source tank to a demand tank. Thus, the optimization must be performed simultaneously over all time periods.

In detailed terms, incoming supply flows ($F_{s,t}$) enter supply tanks each time period, and demand flows ($F_{d,t}$) are withdrawn from the demand tanks each time period. The supply flows to a given tank are assumed for simplicity to have the same composition over all time ($C_{q,s}$) but can vary in amount (hence the subscript t in $F_{s,t}$). Likewise, the concentration of flows leaving the demand tanks must be within specified bounds ($C^L_{q,d}$ and $C^U_{q,d}$), but the flows can also vary in amount (hence the subscript t in $F_{d,t}$). Bounds on inventories are also given for each tank (I^L_n and I^U_n) and for each flow between each tank ($F^L_{n\to n'}$, usually zero, and $F^U_{n\to n'}$). Lastly, costs for the supply flows (β_s), demand flows (β_d), and fixed and variable costs for flows within the network (α and β, respectively) are taken into account with the goal of maximizing the profit (or minimizing the costs) of the multiperiod network operation to most efficiently mix the fuels to meet demand specifications. Because of the operational constraint that flow cannot both enter and exit a blending tank in the same time period, as well as to represent the fixed costs, binary decision variables $y_{n\to n',t}$ must be introduced into the

problem such that $y_{n\to n',t}$ =1 when any flow exists between tank n and tank n' in time period t, and $y_{n\to n',t}$ = 0 otherwise.

2.2 MINLP Formulation

Given a network topology and all associated values described above, the schedule for blending the fuels is sought that maximizes total profit. As stated earlier, the multiperiod blending problem naturally involves binary variables $y_{n\to n',t}$ for all the streams in each time period, and bilinearities for the mass balance constraints involving mixing. This leads to the following nonconvex mixed-integer nonlinear programming (MINLP) model:

$$Max \sum_{t\in T}\left[\sum_{b\in B}\sum_{d\in D}\beta_d F_{b\to d,t} - \sum_{s\in S}\sum_{b\in B}\beta_s F_{s\to b,t} - \sum_{n\in N}\sum_{n'\in N}\left(\alpha_{n\to n'}y_{n\to n',t}+\beta_{n\to n'}F_{n\to n',t}\right)\right] \quad (1)$$

Subject To:

$$F_{n\to n',t} \le F^U_{n\to n'}y_{n\to n',t} \qquad \forall n,n'\in N; t\in T \quad (2a)$$

$$F_{n\to n',t} \ge F^L_{n\to n'}y_{n\to n',t} \qquad \forall n,n'\in N; t\in T \quad (2b)$$

$$C_{q,b,t} \le C^U_{q,d} + M(1-y_{b\to d,t-1}) \qquad \forall q\in Q; d\in D; t\in T \quad (3a)$$

$$C_{q,b,t} \ge C^L_{q,d} + M(1-y_{b\to d,t-1}) \qquad \forall q\in Q; d\in D; t\in T \quad (3b)$$

$$C_{q,b,t} \le C^U_{q,d} + M(1-y_{s\to d,t-1}) \qquad \forall q\in Q; s\in S; t\in T \quad (3c)$$

$$C_{q,b,t} \ge C^L_{q,d} + M(1-y_{s\to d,t-1}) \qquad \forall q\in Q; s\in S; t\in T \quad (3d)$$

$$I_{s,t} = I_{s,t-1} + F_{s,t} - \sum_{n\in N}F_{s\to n,t} \qquad \forall s\in S; t\in T \quad (4a)$$

$$I_{b,t} = I_{b,t-1} + \sum_{n\in N}F_{n\to b,t} - \sum_{n\in N}F_{b\to n,t} \qquad \forall b\in B; t\in T \quad (4b)$$

$$I_{d,t} = I_{d,t-1} + \sum_{n\in N}F_{n\to d,t} - F_{d,t} \qquad \forall d\in D; t\in T \quad (4c)$$

$$I_{b,t}C_{q,b,t} = I_{b,t-1}C_{q,b,t-1} + \sum_{s\in S}F_{s\to b,t}C_{q,s} + \sum_{b'\in B}F_{b'\to b,t}C_{q,b',t-1} - \sum_{n\in N}F_{b\to n,t}C_{q,b,t-1} \qquad \forall q\in Q; b\in B; t\in T \quad (5)$$

$$y_{n\to b,t} + y_{b\to n',t} \le 1 \qquad \forall b\in B; n,n'\in N \quad (6)$$

$$I^L_n \le I_{n,t} \le I^U_n \qquad \forall n\in N; t\in T$$

$$y_{n\to n',t}\in\{0,1\} \qquad \forall n,n'\in N; t\in T$$

$$F_{n\to n',t}\ge 0; \quad I_{n,t}\ge 0; \quad 0\le C_{q,b,t}\le 1 \qquad \forall b\in B; n,n'\in N; t\in T; q\in Q$$

To solve the multiperiod blending problem, the MINLP formulation must be solved to global optimality due to the bilinear constraints in (5).

3. Radix-based Discretization

Because the primary difficulty is the presence of bilinear terms and the difficulty in obtaining feasible solutions with MINLP algorithms, we propose an approximation for the bilinear term u = F·C by introducing a novel radix-based discretization (RBD) of C. This approach was proposed in the solution of water network problems by Teles, Castro, & Matos (2012). The approximation constraints, which can be derived using disjunctive programming and exact linearizations, replace the bilinear terms F·C in equation 5 of the MINLP formulation (I·C is treated similarly)This set of constraints essentially represents C as a discrete value based on a given radix (in this case 10) to arbitrary precision (determined by p, the smallest power of 10 allowed, and P, the

largest power of 10 allowed). Other radices (or bases) can also be used. The accuracy of the solution depends on the precision of this approximation.

$$u = \sum_{k=p}^{P} \sum_{j=0}^{9} 10^k \cdot j \cdot \hat{F}_{j,k} \tag{7}$$

$$C = \sum_{k=p}^{P} \sum_{j=0}^{9} 10^k \cdot j \cdot z_{j,k} \tag{8}$$

$$\hat{F}_{j,k} \leq F^U \cdot z_{j,k} \qquad \forall k \in \{p, \dots, P\}, j \in \{0, \dots, 9\} \tag{9}$$

$$\sum_{j=0}^{9} \hat{F}_{j,k} = F \qquad \forall k \in \{p, \dots, P\} \tag{10}$$

$$\sum_{j=0}^{9} z_{j,k} = 1 \qquad \forall k \in \{p, \dots, P\} \tag{11}$$

$$z_{j,k} \in \{0,1\}; \quad \hat{F}_{j,k} \geq 0 \qquad \forall k \in \{p, \dots, P\}, j \in \{0, \dots, 9\}$$

However, a global or near global solution can be found by fixing the binary variables to the values found by the approximation and resolving the problem with a global or local NLP solver. Also, we should note that to ensure feasible solutions, the tolerances for the satisfaction of constraints need to be adjusted accordingly.

While the proposed reformulation introduces significantly more constraints and variables, it changes the class of the problem from an MINLP to a mixed-integer linear programming problem (MILP). This class of optimization problem can generally be solved more efficiently, especially using highly refined commercial solvers such as IBM ILOG's CPLEX Optimizer (Int, 2009) and Gurobi Optimization's Gurobi Optimizer (Gur, 2011). These solvers can also take advantage of multiple computing threads, a further advantage over current MINLP solvers. It should also be noted that to avoid numerical instability, the range of powers ($P - p$) should be minimized, and robust LP solvers should be used to solve the relaxed LPs in the MILP solver.

4. Computational Results

The nonconvex MINLP model was implemented in the modeling language GAMS (Brook et al, 1988) and solved using BARON 9.3.1 (Sahinidis, 1996) to guarantee a global optimum. For comparison, the discretized MILP formulation was also implemented in GAMS and solved using Gurobi 4.5.1. Using this new radix-based discretization approach at a discretization of p = -3 and P = 0 (10^{-3} to 10^{0}), we can solve previously intractable problems (requiring BARON more than 6 hours of computational time to close the optimality gap to 0.1%) in minutes. The results of this approach and the MINLP formulation solved by BARON are shown in Table 1. All computations were performed on an Intel Core i7 processor at 2.93GHz. The Gurobi results used eight threads simultaneously, while BARON could only utilize one thread.For an 8 tank, 3 time period problem with 2 qualities selected from the test problems, the optimal schedule is shown in Figure 3 and detailed results in Table 2.

Table 1: Computational results of MINLP (BARON) and MILP (Gurobi) formulations for five test multiperiod blending problems

Tanks	6	8	8	8	8
Time Periods	3	3	3	4	4
MINLP CPU Time (s)	17.7	*>21600.0*	*>21600.0*	*>21600.0*	*>21600.0*
RBD CPU Time (s)	3.0	663.6	389.7	845.9	409.7
CPU Time Speedup	5.9x	>32.5x	>55.4x	>25.5x	>52.7x

Table 2: Computational results for 8 tank, 3 time period, 2 quality problem

	CPU Time (s)	Objective	Constraints	Cont. Vars.	Bin. Vars.
MINLP	>21600.0	*13.4517	628	136	87
RBD (MILP)	389.7	13.5268	7092	4632	855
NLP Post-Solve	0.2	13.5268	447	327	0

*Best lower bound

While the discretization approach greatly increases the problem size, the time required to solve the problem is decreased significantly. Additionally, after solving the discretized MILP, the binary variables present in the original problem were fixed and the problem was solved again with BARON acting as an NLP solver (see Table 2).

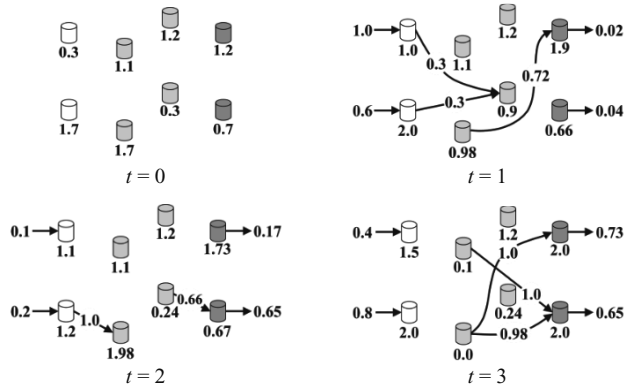

Figure 3: Optimal solution for 8 tank, 3 time period, 2 quality problem

5. Conclusion

We have addressed in this paper the multiperiod blending problem for which a nonconvex MINLP formulation was proposed. It was shown that the radix-based discretization approach has allowed the solution of larger multiperiod blending problems, with up to 8 tanks and 4 time periods, in a significantly shorter amount of time. However, as problem size increases, the discretized approach may become intractable. Thus, for future investigation, decomposition approaches will likely be required for the solution of very large systems.

Acknowledgements

We would like to thank ExxonMobil Corporation for supporting this research.

References

Brook, A.; Kendrick, D.; and Meeraus, A. 1988. GAMS, a user's guide. SIGNUM Newsletter 23:10–11.

Gurobi Optimization. 2011. Gurobi Optimizer Reference Manual Version 4.5.

Haverly, C. A. 1978. Studies of the behavior of recursion for the pooling problem. SIGMAP Bulletin 19–28.

International Business Machines Corporation. 2009. IBM ILOG CPLEX V12.1: User's Manual for CPLEX.

Misener, R., and Floudas, C. A. 2009. Advances for the pooling problem: Modeling, global optimization, and computational studies. Appl. Comput. Math. 8(1):3 – 22.

Sahinidis, N. V. 1996. BARON: A general purpose global optimization software package. Journal of Global Optimization 8:201–205.

Teles, J. P.; Castro, P. M., and Matos, H. A. Global Optimization of Water Networks Design using Multiparametric Disaggregation. Computers & Chemical Engineering, doi:10.1016/j.compchemeng.2012.02.018.

I.A. Karimi and Rajagopalan Srinivasan (Editors), Proceedings of the 11th International Symposium on Process Systems Engineering, 15-19 July 2012, Singapore

Finding an optimized set of transformations for convexifying nonconvex MINLP problems

Andreas Lundell* Tapio Westerlund
Center of Excellence in Optimization and Systems Engineering
Åbo Akademi University, Turku, Finland

Abstract

In this paper we describe a method for obtaining sets of transformations for reformulating a mixed integer nonlinear programming (MINLP) problem containing nonconvex twice-differentiable (C^2) functions to a convex MINLP problem in an extended variable space. The method for obtaining the transformations is based on solving a mixed integer linear programming (MILP) problem given the structure of the nonconvex MINLP problem. The solution of the MILP problem renders a minimal set of transformations convexifying the nonconvex problem. This technique is implemented as an part of the α signomial global optimization algorithm (αSGO), a global optimization algorithm for nonconvex MINLP problems.

Keywords: global optimization, nonconvex MINLP problems, reformulation techniques, signomial functions

1. Introduction to the αSGO-algorithm

The αSGO-algorithm is a global optimization method for nonconvex MINLP problems (Lundell et al., 2012). An αBB-type underestimator is used for nonconvex C^2-functions. In the αBB-underestimator a quadratic function $\alpha(x-\overline{x})(x-\underline{x})$, where α is large enough to guarantee convexity, is added to a nonconvex function resulting in a convex underestimator on the interval $[\underline{x},\overline{x}]$ (Floudas, 2000). In the αSGO-algorithm, instead of using a branching tree for dividing the nonconvex problem into convex subproblems, a reformulation technique based on different transformation schemes is utilized for signomial functions and an αBB-type reformulation for C^2-functions. The reformulations convexify the problem and overestimates its feasible region in an extended variable-space. The solutions to the subproblems form a converging sequence towards the global optimum when the overestimations are iteratively reduced. However, a certain amount of freedom exists in how to choose the transformations. For signomial terms, different types of transformation schemes (for positive terms: the positive power transformation (PPT), exponential transformation (ET) and mixed power and exponential transformation (MPET); for negative terms: the power transformation (PT)) can be applied term-wise (Lundell et al., 2009) in addition to the αBB-reformulation (αR). Depending on what combinations of transformations are chosen, the number of discrete and continuous variables needed in the reformulations may vary, leading to reformulated problems of different complexities. Therefore, a method for automatically obtaining an optimized set of these transformations is described in this paper. It is based on solving a MILP problem, where the parameters of the problem are specified by the nonconvex signomial terms and C^2-functions in the MINLP problem. The method was previously described in, *e.g.,* Lundell and Westerlund

*andreas.lundell@abo.fi

(2009b) for the predecessor of the αSGO-algorithm, *i.e.,* the SGO-algorithm. Here, the method is extended to allow for nonconvex C^2-functions, as well as some modifications to the transformations available for nonconvex signomial functions.

2. The optimization method for transformations

In the MILP formulation, the following sets are used for the terms and functions: J_{S_+} and J_{S_-} are the set of nonconvex positive and negative signomial terms respectively, and J_{S} is the union of these two sets, *i.e.,* all nonconvex signomial terms; J_{G} is the set of nonconvex C^2-functions (excluding the signomials); J is the union of J_{S} and J_{G}. The set I correspond to all variables in the problem and I_j, $j \in J$, is the set of variables in the j-th signomial term or nonconvex function. The set K is all nonconvex constraints in the problem. Also, some binary variables are needed: B_i indicate if the variable x_i is transformed in the problem or not and B_i^{P}, B_i^{E}, B_{ki}^{α} what type of transformation is used; ${b_{ji}}^{\mathrm{P}}$, ${b_{ji}}^{\mathrm{E}}$ and ${b_{ji}}^{\alpha}$ indicate whether a power transformation $x = X^Q$, exponential transformation $x = \exp(X)$ or αR have been applied to the i-th variable in the j-th term or function; β_j^{PPT}, β_j^{MPET} and $\beta_j^{\alpha R}$ indicate which transformation is applied to the j-th term or function. The integer variables N^{P}, N^{E} and N^{A} represent the total number of distinct transformations needed. The real variables Δ are transformation dependent penalties used for selecting numerically better transformations. The powers Q in the power transformations are in the interval $[Q_{\min}, Q_{\varepsilon}]$ if negative and in the interval $[Q_{\varepsilon}, Q_{\max}]$ if positive. Finally, the power of the variable x_i in the j-th signomial term p_{ji} is a given parameter and can be any real value.

To find an optimized set of transformations convexifying the problem at hand while keeping the reformulated problem as simple as possible, the objective function will be

$$\begin{aligned}\text{minimize} \quad & \delta_B \sum_{i\in I} B_i + \delta_I \left(N^{\mathrm{P}} + N^{\mathrm{E}} + N^{\alpha}\right) + \delta_N \sum_{j\in J_{S_+},\, i\in I} \left({b_{ji}}^{\mathrm{P}} + {b_{ji}}^{\mathrm{E}} + {b_{ji}}^{\alpha}\right) \\ & + \delta_N \sum_{j\in J_{S_-}, i\in I} \left({b_{ji}}^{\mathrm{P}} + {b_{ji}}^{\alpha}\right) + \delta_\Delta \sum_{j\in J_{S_+}} \left(\Delta_j^{\mathrm{PPT}} + \Delta_j^{\mathrm{MPET}} + \Delta_j^{\alpha R}\right) + \delta_\Delta \sum_{j\in J_{S_-}} \left(\Delta_j^{\mathrm{PT}} + \Delta_j^{\alpha R}\right). \end{aligned} \tag{1}$$

The strategy parameters δ in the objective function are δ_B, δ_I, δ_N and δ_Δ and these are normally selected such that $\delta_B \gg \delta_I \gg \delta_N \gg \delta_\Delta$. To guarantee a convex reformulation, the constraints (2–22) are also included in the MILP problem.

Only one transformation is allowed per signomial term, so therefore

$$\forall j \in J_{S_+}: \quad \beta_j^{\mathrm{PPT}} + \beta_j^{\mathrm{MPET}} + \beta_j^{\alpha R} = 1 \qquad \text{and} \qquad \forall j \in J_{S_-}: \quad \beta_j^{\mathrm{PT}} + \beta_j^{\alpha R} = 1. \tag{2}$$

The following expressions are used to determine whether the i-th variable is transformed using a power or exponential transformation in some constraint

$$\forall i \in I: \quad B_i^{\mathrm{P}} \geq \tfrac{1}{\mathrm{card} J_{\mathrm{S}}} \textstyle\sum_{j\in J_{\mathrm{S}}} {b_{ji}}^{\mathrm{P}} \quad \text{and} \quad \forall i \in I: \quad B_i^{\mathrm{E}} \geq \tfrac{1}{\mathrm{card} J_{S_+}} \textstyle\sum_{j\in J_{S_+}} {b_{ji}}^{\mathrm{E}}. \tag{3}$$

For the αR, it is necessary to determine this per constraint, since a different transformation variable is needed for each constraint

$$\forall i \in I, k \in K: \quad B_{ki}^{\alpha} \geq \tfrac{1}{\mathrm{card} J_k} \textstyle\sum_{j\in J_k} {b_{ji}}^{\alpha}. \tag{4}$$

The binary variables corresponding to whether a variable is transformed at all in the problem is determined through the following constraint

$$\forall i \in I: \quad B_i \geq \tfrac{1}{\mathrm{card} J} \Big(\sum_{j\in J_{\mathrm{S}}} {b_{ji}}^{\mathrm{P}} + \sum_{j\in J_{S_+}} {b_{ji}}^{\mathrm{E}} + \sum_{j\in J} {b_{ji}}^{\alpha} \Big). \tag{5}$$

Since a transformation variable is needed for each power transformation with different powers Q for each variable, the binary variables $\gamma_{j_1 j_2 i}$, indicating whether the transformations of the i-th variable in the j_1-st and j_2-nd terms are different, are needed

$$\forall j_1, j_2 \in J_S, j_1 \neq j_2, i \in I_j: \quad \begin{cases} \gamma_{j_1 j_2 i} \geq \frac{1}{Q_{\max}+Q_{\min}} (Q_{j_1,i} - Q_{j_2 i}) - (2 - b^{\mathrm{P}}_{j_1 i} - b^{\mathrm{P}}_{j_2 i}) \\ \gamma_{j_1 j_2 i} = \gamma_{j_2 j_1 i}. \end{cases} \tag{6}$$

The integer variables N^{P}, N^{E} and N^{α} are used to count the number of transformation variables in the reformulated problem

$$N^{\mathrm{P}} = \sum_{i \in I_j} B^{\mathrm{P}}_i + \tfrac{1}{2} \sum_{j_1, j_2 \in J_S, j_1 \neq j_2,\ i \in I_j} \gamma_{j_1 j_2 i},\ N^{\mathrm{E}} = \sum_{i \in I_j} B^{\mathrm{E}}_i, \text{ and } N^{\alpha} = \sum_{k \in K,\ i \in I_j} B^{\alpha}_{ki}. \tag{7}$$

For C^2-functions, the αR is always used for nonconvex functions (*i.e.,* with an $\alpha \geq 0$), so

$$\forall j \in J_G, i \in I_j: \alpha_{ji} > 0: {b_{ji}}^{\alpha} = 1, \beta^{\alpha R}_j = 1, \text{ and } \forall j \in J_G, i \in I_j: \alpha_{ji} = 0:\ {b_{ji}}^{\alpha} = 0. \tag{8}$$

The αR may be used for signomial terms, and in this case it should be used on all variables with positive α-values in the term.

$$\forall j \in J_S, i \in I_j: \alpha_{ji} > 0:\ {b_{ji}}^{\alpha} = \beta^{\alpha R}_j, \quad \text{and} \quad \forall j \in J_S, i \in I_j: \alpha_{ji} = 0:\ {b_{ji}}^{\alpha} = 0. \tag{9}$$

The constraints in Eqs. (10–12) should be applied to all negative signomial terms, *i.e.,* $j \in J_{S_-}$. For variables with a negative power in negative terms, the transformation power Q should be larger than $-Q_{\min}$ (which is already given by the bounds of the variable Q) and less than the parameter value $-Q_{\varepsilon}$ if the PT is used. Also, the PT should be applied to all variables in the term if used on one variable:

$$\forall j \in J_{S_-}, i \in I_j: p_{ji} < 0: \quad Q_{ji} \leq -Q_{\varepsilon} \beta^{\mathrm{PT}}_j + Q_{\max}(1 - \beta^{\mathrm{PT}}_j) \quad \text{and} \quad {b_{ji}}^{\mathrm{P}} = \beta^{\mathrm{PT}}_j. \tag{10}$$

For variables with positive powers, the transformation power should be between $Q_{\min}$ and one if the PT is used on the term. However, not all variables need always to be transformed since if $Q = 1$ no transformation occurs and then b^{P} can be zero:

$$\forall j \in J_{S_-}, i \in I_j: p_{ji} > 0: \begin{cases} Q_{\varepsilon} \beta^{\mathrm{PT}}_j - Q_{\min}(1 - \beta^{\mathrm{PT}}_j) \leq Q_{ji} \leq \beta^{\mathrm{PT}}_j + Q_{\max}(1 - \beta^{\mathrm{PT}}_j) \\ \frac{1}{\max\{Q_{\max}, Q_{\min}\}} (1 - Q_{ji}) - (1 - \beta^{\mathrm{PT}}_j) \leq {b_{ji}}^{\mathrm{P}} \leq \beta^{\mathrm{PT}}_j. \end{cases} \tag{11}$$

If the PT is used, the sum of the powers should be less than or equal to one, so

$$\forall j \in J_{S_-}: \quad \sum_{i \in I_j} p_{ji} Q_{ji} \leq M + (1 - M) \beta^{\mathrm{PT}}_j, \quad \text{where} \quad M = Q_{\max} \cdot \max_i |p_{ji}|. \tag{12}$$

For the PPT, the constraints (13–15) should be applied to all positive signomial terms, *i.e.,* $j \in J_{S_+}$. Since we can choose between three transformation schemes for positive signomial terms (PPT, MPET or αR), the constraints are somewhat more complicated. If the PPT is used, the sum of the powers in the transformed term should be greater than or equal to one, otherwise the constraint should be relaxed. This can be expressed as:

$$\forall j \in J_{S_+}: \quad \sum_{i:\ p_{ji} > 0} p_{ji} Q_{ji} + \sum_{i:\ p_{ji} < 0} p_{ji} \geq 1 - M(1 - \beta^{\mathrm{PPT}}_j), \tag{13}$$

where the parameter M can be chosen as $M = Q_{\min} \cdot \sum_{i \in I_j : p_{ji} > 0} p_{ji} + \sum_{i \in I_j : p_{ji} < 0} |p_{ji}| + 1$.

No transformations are needed for the variables with negative powers when using the PPT. Since only one variable is allowed to have a positive transformation power in each term transformed using the PPT scheme, the following condition is needed

$$\forall j \in J_{S_+}: \quad \sum_{i:\ p_{ji}>0} {b_{ji}}^{+} = \beta_j^{\mathrm{PPT}}, \quad \text{where} \quad {b_{ji}}^{+} = 1 - {b_{ji}}^{-} - (1-\beta_j^{\mathrm{PPT}}). \tag{14}$$

The transformation powers when using the PPT should be between $-Q_{\min}$ and $-Q_\varepsilon$ in all except one transformation, where the power must be between one and $Q_{\max}$:

$$\forall j \in J_{S_+}, i \in I_j : p_{ji} > 0: \quad \begin{cases} Q_{ji} \geq -Q_{\min}{b_{ji}}^{-} + {b_{ji}}^{+} - (Q_{\min}+1)(1-\beta_j^{\mathrm{PPT}}) \\ Q_{ji} \leq Q_{\max}{b_{ji}}^{+} - Q_\varepsilon {b_{ji}}^{-} + (Q_{\max}+Q_\varepsilon)(1-\beta_j^{\mathrm{PPT}}) \\ {b_{ji}}^{\mathrm{P}} \geq \frac{1}{\max\{Q_{\max},Q_{\min}\}}(Q_{ji}-1) - (1-\beta_j^{\mathrm{PPT}}) \\ {b_{ji}}^{\mathrm{P}} \geq {b_{ji}}^{-} - (1-\beta_j^{\mathrm{PPT}}). \end{cases} \tag{15}$$

For the MPET, the constraints (16) and (17) are applied to all positive signomial terms, *i.e.,* $j \in J_{S_+}$. For any variable with positive power in a positive signomial term, to which the MPET is applied, either the exponential or a power transformation, with transformation powers between $-Q_{\min}$ and $-Q_\varepsilon$, should be used. This is enforced using:

$$\forall j \in J_{S_+}, i \in I_j : p_{ji} > 0: \ {b_{ji}}^{\mathrm{E}} + {b_{ji}}^{\mathrm{P}} \geq \beta_j^{\mathrm{MPET}} \text{ and } Q_{ji} \leq -Q_\varepsilon {b_{ji}}^{\mathrm{P}} + Q_{\max}(1-\beta_j^{\mathrm{MPET}}). \tag{16}$$

The following condition assure that the correct transformation is selected

$$\forall j \in J_{S_+}: \quad \beta_j^{\mathrm{PPT}} + \beta_j^{\mathrm{MPET}} \geq \tfrac{1}{\mathrm{card} I_j} \sum_{i \in I_j : p_{ji}>0} {b_{ji}}^{\mathrm{P}} + {b_{ji}}^{\mathrm{E}}. \tag{17}$$

If only the objective function (1) and the constraints (2–17) are used in the MILP formulation, the solution would not take into consideration that different types of transformations (including power transformations with different powers Q) lead to transformations with different underestimation errors. Thus, if alternate solutions exists that lead to transformed problems with the same number of additional variables used in the transformations we are also interested in finding the transformations with better numerical properties. Results regarding the tightness of the power and exponential transformations can be found in, *e.g.,* Lundell and Westerlund (2009a). For example, it has been shown that a single-variable power transformation with positive power gives a tighter underestimator than a single-variable exponential transformation applied to the same power function x^p. The same is true for the single-variable exponential transformation with respect to a single-variable power transformation with negative powers. These facts could be used to favor the PPT over the ET and the ET over the NPT. The problem is then how to penalize the αR, since no general theoretical results are known regarding the tightness of the αBB-underestimator in comparison to the signomial transformations.

The numerical penalties can be included in the MILP formulation by adding variables Δ_j^{PT}, Δ_j^{PPT}, Δ_j^{MPET}, $\Delta_j^{\alpha R}$ to the objective function (1), corresponding to a penalty if the transformation in question is applied to the i-th variable in the j-th term or function group. The exponential transformation is selected to have a numerical penalty zero, and the power transformations are penalized as follows: a transformation with a negative power $-Q_{\min} \leq Q \leq -Q_\varepsilon$ (Eqs. (18) and (22)) has a penalty which is zero at $-Q_{\min}$ and one at $-Q_\varepsilon$; a power transformation with a positive power $1 \leq Q \leq Q_{\max}$ (Eq. (20)) has a penalty of one at one and zero at $Q_{\max}$; a power transformation with a positive power

$Q_\varepsilon \leq Q \leq 1$ (Eq. (21)) has a penalty which is one at Q_ε and zero at one; the αR has a fixed penalty of one for each variable in a term, *i.e.,* $\Delta_j^{\alpha R} = 1$:

$$\forall j \in J_{S_-}, \forall i \in I_j : p_{ji} < 0 : \ \Delta_{ji}{}^{\mathrm{PT}} \geq \tfrac{1}{Q_{\min} - Q_\varepsilon} (Q_{ji} + Q_{\min}) - (1 + Q_{\min})(1 - \beta_j^{\mathrm{PT}}) \quad (18)$$

$$\forall j \in J_{S_+}, \forall i \in I_j : p_{ji} > 0 : \ \Delta_{ji}{}^{\mathrm{PT}} \geq \tfrac{1}{Q_\varepsilon - 1} (Q_{ji} - 1) - (1 - \beta_j^{\mathrm{PT}}) \quad (19)$$

$$\forall j \in J_{S_+}, \forall i \in I_j : p_{ji} > 0 : \ \Delta_{ji}{}^{\mathrm{PPT}} \geq \tfrac{1}{1 - Q_{\max}} (Q_{ji} - Q_{\max}) - b_{ji}{}^{-} - (1 - \beta_j^{\mathrm{PPT}}) \quad (20)$$

$$\forall j \in J_{S_+}, \forall i \in I_j : p_{ji} > 0 : \ \Delta_{ji}{}^{\mathrm{PPT}} \geq \tfrac{1}{Q_\varepsilon + Q_{\min}} (Q_{ji} + Q_{\min}) - b_{ji}{}^{+} - (1 - \beta_j^{\mathrm{PPT}}) \quad (21)$$

$$\forall j \in J_{S_+}, i \in I_j : p_{ji} > 0 : \ \Delta_{ji}{}^{\mathrm{MPET}} \geq \tfrac{1}{Q_\varepsilon - Q_{\min}} (Q_{ji} - Q_{\min}) - b_{ji}{}^{\mathrm{E}} - 2(1 - \beta_j^{\mathrm{MPET}}). \quad (22)$$

3. An example

If the MILP method is applied to the nonconvex function $x_1^2 x_2 - x_2^{-1} + x_2 x_3 + 5 \sin x_2 \cos x_3$ in a MINLP problem, the total number of additional transformation variables needed in the reformulated convex MINLP problem is four. Two of the variables (x_2 and x_3) are involved in transformations so in addition two binary variable or SOS2-sets are needed. If a rigid transformation scheme is used without optimizing the transformations, the worst-case scenario is instead seven transformation variables and three binary variable or SOS2-sets. As the number of variables in the binary variable sets are increased iteratively in the αSGO-algorithm, this small decrease in initial variables will have a large direct impact on the solution process and the number of iterations required in the algorithm.

4. Results and discussion

In this paper it was shown how the MILP method from Lundell and Westerlund (2009b) could be extended to handle all the transformations schemes in the αSGO-algorithm. By including also the αBB convex reformulation technique, it is possible to obtain the set of transformations for obtaining a convex reformulation of any MINLP problem containing nonconvex twice-differentiable functions.

5. Acknowledgements

Support from the Foundation of Åbo Akademi University, as part of the grant for the Center of Excellence in Optimization and Systems Engineering, is gratefully acknowledged.

References

Floudas, C. A., 2000. Deterministic Global Optimization. Theory, Methods and Applications. No. 37 in Nonconvex Optimization and Its Applications. Kluwer Academic Publishers.

Lundell, A., Skjäl, A., Westerlund, T., 2012. A reformulation framework for global optimization. Journal of Global Optimization (available online).

Lundell, A., Westerlund, J., Westerlund, T., 2009. Some transformation techniques with applications in global optimization. Journal of Global Optimization 43 (2), 391–405.

Lundell, A., Westerlund, T., 2009a. Convex underestimation strategies for signomial functions. Optimization Methods and Software 24, 505–522.

Lundell, A., Westerlund, T., 2009b. Optimization of transformations for convex relaxations of MINLP problems containing signomial functions. In: de Brito Alves, R. M., do Nascimento, C. A. O., Biscaia, E. C. (Eds.), 10th International Symposium on Process Systems Engineering: Part A. Vol. 27 of Computer Aided Chemical Engineering. Elsevier, pp. 231–236.

I.A. Karimi and Rajagopalan Srinivasan (Editors), Proceedings of the 11th International Symposium on Process Systems Engineering, 15-19 July 2012, Singapore.

Structured regularization in barrier NLP for optimization models with dependent constraints

Kexin Wang,[a] Zhijiang Shao,[a] Lorenz T. Biegler,[b] Yidong Lang,[b] Jixin Qian[a]

[a]*State Key Laboratory of Industrial Control Technology, Institute of Industrial Control, Zhejiang University, 38 Zheda Road, Hangzhou 310027, China*
[b]*Chemical Engineering Department, Carnegie Mellon University, 5000 Forbes Avenue, Pittsburgh 15213, USA*

Abstract

Global convergence and fast performance of barrier nonlinear programming (NLP) solvers are frequently challenged by linearly dependent constraints. Such constraints arise in many process optimization models, and they often preclude finding successful NLP solutions. To deal with this problem we present a structured regularization strategy for barrier methods that identifies and excludes dependent constraints in the KKT system while leaving independent constraints unchanged. As a result, more accurate Newton directions can be obtained and much faster convergence can be expected for the KKT system over the conventional regularization approach. Numerical experiments with examples derived from the CUTE and COPS test sets as well as two refinery blending problems demonstrate the effectiveness of the proposed method and significantly better performance of the NLP solver.
Keywords: Barrier NLP Methods, Dependent Constraints, KKT Regularization, Newton's Method

1. Introduction

Practical nonlinear programming (NLP) algorithms are required to solve challenging optimization problems derived from chemical engineering applications. One of the most important challenges is the presence of dependent constraints. Regardless if this dependency is local or structural, many NLP algorithms that are based on Newton's method experience convergence difficulties. When this happens, NLP iterations produce very little progress, calculation of Lagrange multipliers is ill-conditioned, and penalty parameters for the line search become very large.

Dependent constraints are not completely avoidable in nonlinear programming, as they can arise through local linearization of nonlinear constraints. Moreover, reformulation of complementarity constraints, which may be used to describe switching behavior, can lead to linearly dependent active constraint normals at any feasible point (Fletcher et al., 2006). Also, discretized dynamic problems with path constraints can violate the linear independence constraint qualification (LICQ), as the finite element mesh is refined (Kameswaran and Biegler, 2008). Finally, poor model formulations, such as redundant or inconsistent model descriptions, induce failure of the NLP solver.

It is important for a practical NLP solver to consider the case when LICQ does not hold. This problem was considered in the framework of reduced space barrier NLP methods by taking advantage of variable decompositions to detect and remove dependent constraints (Wang et al., 2011). Here we consider a related approach for full space barrier methods, where decomposition is avoided in order to maintain sparsity. Instead, we develop a new, structured regularization method that implicitly detects and handles constraint dependency in the KKT system and leads to fast performance.

2. Barrier Method Background

Consider the NLP problem of the form

$$\min_{x\in R^n} f(x) \quad s.t.\ c(x)=0,\ x\geq 0 \tag{1}$$

where the objective function and equality constraints, $f(x): R^n \to R$ and $c(x): R^n \to R^m$ with $m \leq n$, are assumed to be twice continuously differentiable. We use the simpler form (1) for more efficient derivation, although our approach is directly applicable to double bounded problems as well. The primal-dual interior point method solves problem (1) through a sequence of barrier problems (Wächter and Biegler, 2006):

$$\min_{x\in R^n} \phi_\mu(x) = f(x) - \mu\sum_{i=1}^{n} \ln x^{(i)}, \quad s.t.\ c(x)=0 \tag{2}$$

with decreasing values of barrier parameter $\mu > 0$. Problem (2) is solved through the primal-dual equations

$$\begin{aligned} \nabla f(x) + A\lambda - v &= 0 \\ c(x) &= 0 \\ XVe - \mu e &= 0 \end{aligned} \tag{3}$$

where $A = \nabla c(x)$, $\lambda \in R^m$ is the vector of Lagrange multipliers for the equality constraints, the dual variable is $v = \mu X^{-1} e$, X and V are diagonal matrices generated from vectors x and v respectively and $e^T = [1,...,1]$. Note when $\mu = 0$ and $x, v \geq 0$, the equations (3) are the first order KKT conditions of problem (1). The Newton step to solve (3) at iteration k is calculated from the simplified linear system:

$$\begin{bmatrix} \nabla^2_{xx} L_k + \Sigma_k & A_k \\ A_k^T & 0 \end{bmatrix} \begin{pmatrix} d_k^x \\ \lambda_{k+1} \end{pmatrix} = -\begin{pmatrix} \nabla \varphi_\mu(x_k) \\ c(x_k) \end{pmatrix}. \tag{4}$$

where $\nabla^2_{xx} L_k$ is the Hessian of Lagrange function $L(x,\lambda,v) = f(x) + c(x)^T\lambda - v$, $\Sigma_k = X_k^{-1} V_k$ is a barrier term added to the Hessian, and the search direction for v is obtained from $d_k^v = \mu X_k^{-1} e - v_k - \Sigma_k d_k^x$. When Jacobian A_k^T is not full rank, the KKT matrix in (4) is singular and Newton step cannot be taken. A popular regularization approach for barrier solvers, e.g., IPOPT, is to modify the KKT matrix as:

$$\begin{bmatrix} \nabla^2_{xx} L_k + \Sigma_k + \delta_H I & A_k \\ A_k^T & -\delta_c I \end{bmatrix}. \tag{5}$$

where $\delta_H > 0$ is adjusted and $\delta_c > 0$ is a small constant. In particular, the latter correction handles rank deficient Jacobians in (5), but may greatly distort the Newton step, and can lead to much slower convergence, especially for large-scale problems.

3. Constraint regularization and inertia correction

3.1. Structured constraint regularization method

We omit subscript k in (4) and (5) and partition A to $[A_I \mid A_D]$ with dependent columns in A_D. These columns can be found through an LU factorization of A^T, i.e.

$$LA^T = \begin{bmatrix} U_1 & U_2 \\ 0 & 0 \end{bmatrix}. \tag{6}$$

Through multiplying (4) with matrix $diag(I, L)$ and defining $\lambda = L^T[\lambda_I^T \quad \lambda_D^T]^T$ and $Lc = [(Lc)_I^T \quad (Lc)_D^T]^T$, we can obtain a linear system equivalent to (4) but with its

constraint related parts organized according to their dependency. To solve the resulting system we add a regularization term corresponding to the dependent constraints to get:

$$\begin{bmatrix} \nabla^2_{xx}L+\Sigma & \begin{bmatrix} U_1^T & 0 \\ U_2^T & 0 \end{bmatrix} \\ \begin{bmatrix} U_1 & U_2 \\ 0 & 0 \end{bmatrix} & \begin{bmatrix} 0 & 0 \\ 0 & -\delta_D I \end{bmatrix} \end{bmatrix} \begin{pmatrix} d^x \\ \lambda_I \\ \lambda_D \end{pmatrix} = -\begin{pmatrix} \nabla\varphi_\mu \\ (Lc)_I \\ (Lc)_D \end{pmatrix}. \tag{7}$$

which leads to $-\delta_D\lambda_D + (Lc)_D = 0$. By choosing δ_D very large relative to $(Lc)_D$, this leads to negligible values for λ_D, which has the same effect as solving (7) with its last equation removed. Moreover, this is equivalent to

$$\begin{bmatrix} \nabla^2_{xx}L+\Sigma & A_I \\ A_I^T & 0 \end{bmatrix} \begin{pmatrix} d^x \\ \bar{\lambda} \end{pmatrix} = -\begin{pmatrix} \nabla\varphi_\mu \\ c_I \end{pmatrix} \tag{8}$$

where $\bar{\lambda} = L^{-T}\lambda_I$, and the factorization in (6) is not needed. Therefore, the regularization in (7) promotes progress toward feasibility of the independent constraints without distorting their Newton directions, but removes the dependent constraints from the current iteration. This approach works well if the dependent constraints are consistent at the optimum solution. On the other hand, inconsistent constraints are eliminated, though they remain infeasible at convergence and can be presented to the user for correction. The inconsistent case has also been discussed in Fletcher et al. (2002) and Gill et al. (2005).

3.2. Inertia correction

In addition to the structured regularization in (7), the Hessian may also need to be regularized to guarantee a descent direction and maintain positive curvature in constrained directions. Therefore, system (4) is modified to

$$\begin{bmatrix} \nabla^2_{xx}L+\Sigma+\delta_H I & A \\ A^T & -M \end{bmatrix} \begin{pmatrix} d^x \\ \lambda \end{pmatrix} = -\begin{pmatrix} \nabla\varphi_\mu \\ c \end{pmatrix} \tag{9}$$

where $\delta_H > 0$ and M is a diagonal matrix with δ_D on the columns corresponding to dependent columns of A. Both regularization terms are important for global convergence of barrier NLP algorithms. Moreover, appropriate corrections δ_H and δ_D are found when the KKT matrix in (9) has an inertia (*n, m, 0*) with *n* positive, *m* negative, and no zero eigenvalues. As modified from Wächter and Biegler (2006), the following algorithm achieves the correct inertia for (9).

Inertia Correction Logic:

Set initial values for $M := 0, \delta_{\min} > 0, \delta_H := 0, \kappa_\delta < 1$, and $\delta_H^{last} := 0$.

1. Factorize the KKT matrix in (9):
- If its inertia is $(n, m, 0)$, save the current value of regularization parameter $\delta_H^{last} \leftarrow \delta_H$ provided that $\delta_H > 0$. Continue to solve linear system (9).
- Otherwise go to step 2.
2. If the factorization has fewer than *m* negative eigenvalues or is singular, correct the lower-right corner of the KKT matrix in (9) as follows:
- Corresponding to each dependent column of A, add a large element $-\delta_D$ (say, $\delta_D = 10^{30}$) to the diagonal of M and go to step 1.
3. Determine the value of δ_H:
- If $\delta_H = 0$ and $\delta_H^{last} = 0$, set δ_H to an initial tentative value; go to step 1.

- If $\delta_H = 0$ and $\delta_H^{last} > 0$, set δ_H to $\min\{\delta_{\min}, \kappa_\delta \delta_H^{last}\}$, where $\kappa_\delta < 1$; go to step 1.
- Otherwise increase the value of δ_H. If δ_H is too large, inertia correction fails and turn to the feasibility restoration phase; otherwise go to step 1.

In this last step, the feasibility restoration phase (Fletcher et al., 2002) is designed for filter methods, as in IPOPT, to reduced infeasibility and promote successful steps.

4. Numerical results

We implemented the structured regularization strategy within the FORTRAN version of full-space IPOPT (Wächter and Biegler, 2006), and we use the MUMPS sparse solver (Amestoy et al., 2001) for the linear system (9). Also, the filter line search option in IPOPT is selected for global convergence. We demonstrate this approach on 47 examples derived from CUTE and COPS test sets as well as two large-scale refinery blending examples. These examples were designed with dependent constraints and present difficulties for current NLP solvers.

4.1. Examples from CUTE and COPS test sets

We first consider the 47 test examples from the CUTE and COPS test set, which were used with reduced-space IPOPT in our previous work (Wang et al., 2011). Curtis et al. (2009) modified these examples by making the first equality constraint $c_1(x) = 0$ dependent with an additional constraint $c_1(x) - c_1^2(x) = 0$ (consistent case) or $c_1(x) - c_1^2(x) = 1$ (inconsistent case).

We compare both regularizations (5) and (9) for these cases. First, all inconsistent examples are expected to converge to stationary points that minimize infeasibility. For the inconsistent case, both regularizations behave similarly because feasibility restoration is eventually triggered and this step dominates the calculation.

On the other hand, for the examples with consistent constraints, we see a significant improvement with the structured regularization. Using the default options in IPOPT, the conventional regularization (5) solves only 29 out of 47 problems. Failures usually occur at infeasible points with no improvement possible. The new, structured regularization solves 45% more problems and fails on only five problems. These failures occur at points of minimum infeasibility in the restoration step. Performance profiles (Dolan and Moré, 2001) are shown in Figure 1, and indicate that the structured regularization strategy is much more efficient than its conventional counterpart.

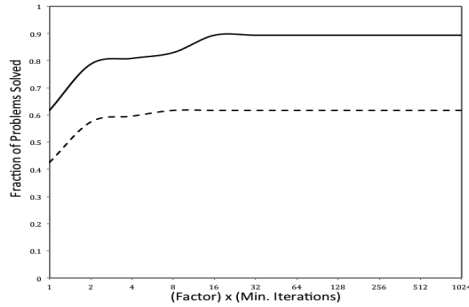

Figure 1. Performance plot for examples with consistent dependent constraints using Structured (solid line) vs. Conventional Regularization (dashed line). The plot (*fraction vs. factor*) shows the *fraction* of problems solved within a *factor* of minimum number of iterations for each example.

4.2. Refinery blending examples

The original refinery blending models have many nonconvex terms and several complementarity constraints. Reformulation of these constraints leads to linearly

dependent constraints, which were detected during solution. IPOPT with conventional regularization solves neither problem under default options. On the other hand, with the structured regularization and default options, IPOPT easily solves both examples. Problem characteristics and numerical results are presented in Table 1. In particular, #depcon represents the largest number of dependent constraints encountered by MUMPS at a given iteration; #iter is the number of iterations taken to solve the problem. It is clear that structured regularization leads to more efficient convergence for IPOPT.

Table 1. Numerical results for two refinery blending examples

	#var	#con	#depcon	conventional	structured
Blend1	833	772	5	failed with singular matrix	optimum found #iter = 75
Blend2	5176	4702	83	failed with ≥ 3000 iter.	optimum found #iter = 399

5. Conclusions

We present a new, structured regularization method to improve convergence of NLP algorithms when dependent constraints are present. Different from the conventional regularization method, which distorts Newton iterations, the structured regularization excludes dependent constraints from the current iteration. We incorporate this strategy into the inertia correction of KKT matrix and implement it within the solver IPOPT. Numerical results on degenerate examples indicate that the structured regularization method is more efficient than its conventional counterpart in handling dependent constraints, and shows significantly better performance within IPOPT.

Acknowledgement: This research is supported by the 973 Program of China (2012CB720503), NSF Program of China (61104134), and Zhejiang Provincial NSF of China (Y1110243).

References

P. R. Amestoy, I. S. Duff, J. Koster, J. L'Excellent, J. Koster, 2001, A Fully Asynchronous Multifrontal Solver Using Distributed Dynamic Scheduling, SIAM Journal on Matrix Analysis and Applications, 23, 1,15-41

F. E. Curtis, J. Nocedal, A. Wächter, 2009, A Matrix-Free Algorithm for Equality Constrained Optimization Problems with Rank-Deficient Jacobians, SIAM Journal on Optimization, 20, 3, 1224-1249

E. D. Dolan, J. J. Moré, 2001, Benchmarking Optimization Software with Performance Profiles, Technical Report, Argonne National Laboratory, Argonne, IL, USA

R. Fletcher, N. I. M. Gould, S. Leyffer, P. L. Toint, A. Wächter, 2002, Global Convergence of a Trust-Region SQP-Filter Algorithm for General Nonlinear Programming, SIAM Journal on Optimization, 13, 3, 635-659

R. Fletcher, S. Leyffer, D. Ralph, S. Scholtes, 2006, Local Convergence of SQP Methods for Mathematical Programs with Equilibrium Constraints, SIAM Journal on Optimization, 17, 1, 259-286

P. E. Gill, W. Murray, M. A. Saunders, 2005, SNOPT: An SQP Algorithm for Large-Scale Constrained Optimization, SIAM Review, 47, 1, 99-131

S. Kameswaran, L. T. Biegler, 2008, Advantages of Nonlinear-Programming-Based Methodologies for Inequallity Path-Constrained Optimal Control Problems – A Numerical Study, SIAM Journal on Scientific Computing, 30, 2, 957-981

A. Wächter, and L. T. Biegler, 2006, On the Implementation of an Interior Point Filter Line Search Algorithm for Large-Scale Nonlinear Programming, Mathematical Programming, 106, 1, 25-57

K. Wang, Z. Shao, L. T. Biegler, Y. Lang, J. Qian, 2011, Robust Extensions for Reduced-Space Barrier NLP Algorithms, Computers and Chemical Engineering, 35, 10, 1994-2004

I.A. Karimi and Rajagopalan Srinivasan (Editors), Proceedings of the 11th International Symposium on Process Systems Engineering, 15-19 July 2012, Singapore.

Portions of the contribution have been prepared for Sandia National Laboratories Corporation, under Contract No. DE-AC04-94AL85000

A Progressive Hedging Approach for Parameter Estimation via Stochastic Nonlinear Programming

Daniel P. Word[a], Jean-Paul Watson[b], David L. Woodruff[c], and Carl D. Laird[a]

[a]*Texas A&M University, 3122 TAMU, College Station, TX 77845, USA*
[b]*Discrete Algorithms and Math Department, Sandia National Laboratories, MS 1318, P.O. Box 5800, Albuquerque, NM, 87185-1318, USA*
[c]*Graduate School of Management, University of California - Davis, Davis, CA 95616-8609, USA*

Abstract

We consider the problem of estimating transmission parameters in a model of childhood disease transmission. We show the structural equivalence between parameter estimation and two-stage stochastic programming, and use the Progressive Hedging decomposition strategy to efficiently compute parameter values on large-scale, real-world observations.

Keywords: Parameter estimation, Stochastic programming, Progressive Hedging.

1. Introduction

Nonlinear programming continues to be an effective tool for parameter estimation in models of chemical engineering processes. The size of these estimation problems can become computationally prohibitive when rigorous dynamic models and many observations are considered, outstripping desktop computing capabilities. As well, we are no longer seeing continued increases in CPU clock speed. Computer chip manufacturers are focusing instead on the development of hyper-threaded and multi-core architectures to provide performance improvements via parallelism (Schenk et al., 2009). Given this paradigm shift in computer architecture, continued performance improvements on challenging nonlinear programming problems demands that we develop algorithms that can effectively utilize parallel computing architectures.

Classical parameter estimation problems are structurally equivalent to two-stage stochastic programming problems. There is a suite of decomposition strategies for solving stochastic programming problems and, in this paper, we make use of the Progressive Hedging algorithm to provide a parallel solution strategy for a large-scale dynamic parameter estimation problem. A general form of a parameter estimation problem can be written as follows:

$$\begin{aligned} \min \quad & \textstyle\sum_{s\in S} P_s f(w_s, \varepsilon_s) \\ \text{s.t.} \quad & g(x_s, y_s, w_s, \theta) = 0 \quad \forall\, s \in S, \\ & h(y_s, y_s^*, \varepsilon_s) = 0 \quad \forall\, s \in S. \end{aligned} \tag{1}$$

Here, S denotes the set of all observations. The vectors x_s are unmeasured state variables, the y_s correspond to model outputs (measured variables), and the w_s represent unknown model noise. Model parameters are denoted by θ and are to be estimated by fitting the model outputs y_s to the known measurements y_s^*. The constraints g represent the system model, and h defines the measurement errors between the calculated and

measured outputs. In the objective, P_s, where $\sum_{s\in S} P_s = 1$, is a weight for each observation, and $f(w_s,\varepsilon_s)$ represents some goodness-of-fit function given the estimated model and measurement noise.

A general formulation for the extensive form (also known as the deterministic equivalent) of a two-stage stochastic programming problem is given as follows:

$$\begin{aligned} &\min \quad \sum_{s\in S} P_s f(v_s, u_s) \\ &\text{s.t.} \quad q(v_s, u_s) = 0, \qquad u_s = \bar{u}\,, \qquad \forall\, s \in S. \end{aligned} \tag{2}$$

Here, the goal is to determine optimal values for the first-stage variables (given by $\bar{u}$) while considering uncertainty through a number of possible realizations in S. The variables v_s represent second-stage, scenario-specific decision vectors (also called recourse variables). The objective function usually computes an expected value across all possible scenarios, where P_s is the probability associated with a particular scenario.

The parameter estimation problem in Eq. (1) is structurally equivalent to the two-stage stochastic programming problem given in Eq. (2). The parameters θ are equivalent to first-stage variables, while the remaining variables can be considered second-stage variables. In parameter estimation, the goal is to determine parameter values that are common across all observations, while the measurement and model errors can be considered recourse variables that provide a mechanism for matching with the measurements from each individual observation.

This equivalency is important because a number of stochastic programming decomposition techniques have been developed to handle multi-scenario problems with a very large number of scenarios and decision variables. Progressive Hedging (PH) is one such algorithm, and decomposes a stochastic program by scenarios (Rockafellar and Wets, 1991). As discussed below, PH is also particularly amenable to parallelization.

In this work, we demonstrate the potential of PH for the efficient solution of large-scale nonlinear parameter estimation problems. Specifically, we estimate transmission parameters in an SIR disease model using pre-vaccination measles data from 60 cities in England and Wales (Grenfell, 2011). The estimation problem is formulated as a multi-scenario problem with a scenario for each city and transmission parameters as common variables. City size is used to weight the likelihood of each scenario, so larger cities receive greater weight. The following sections describe in detail the problem formulation and estimation approach, along with the resulting solutions.

2. Model Formulation

As early as 1929, researchers proposed that measles transmission is correlated with school terms (Soper, 1929). Measles data from England and Wales is used to estimate the seasonal pattern of the transmission parameter across all 60 cities. The SIR model used in this work is shown below in Eq. (3). The corresponding dynamic optimization problem is converted to a large-scale nonlinear programming problem (through the simultaneous discretization approach) using a three-point Radau collocation on finite elements (Zavala, 2008). The number of finite elements was chosen to yield one finite element per reporting interval of the data giving 26 finite elements per year.

The optimization model for a single city is as follows:

$$\min \quad \sum_{t\in T}\left(\omega_M(\varepsilon_{Mt})^2 + \omega_\phi\left(\varepsilon_{\phi t}\right)^2\right)$$

$$\text{s.t.} \quad \frac{dS}{dt} = -\left(\frac{\beta(y(t))S(t)I(t)}{N} + \varepsilon_M(t)\right) + B(t), \qquad \frac{dI}{dt} = \frac{\beta(y(t))S(t)I(t)}{N} + \varepsilon_M(t) - \gamma I(t)$$

$$\frac{d\phi}{dt} = \frac{\beta(y(t))S(t)I(t)}{N} + \varepsilon_M(t), \qquad R_i^* = \eta_i(\phi_i - \phi_{i-1}) + \varepsilon_{\phi i} \tag{3}$$

$$\bar{\beta} = \frac{\sum_{i\in\tau}\beta_i}{|\tau|} = 2.05, \qquad 0.05 \le \beta(y(t)) \le 5.0$$

$$0 \le I(t), S(t) \le N, \qquad 0 \le \phi(t)$$

Here, *S* denotes individuals with no immunity to the disease, *I* denotes individuals that are infected with the disease and are infectious, *N* denotes the total population, and *β(t)* denotes the time-varying transmission parameter. The function *y(t)* maps the overall time horizon into the elapsed time within the year, making *β(y(t))* a seasonal transmission parameter with a periodicity of one year. *B* denotes the reported births, and the recovery rate $(Y = 1/14)$ is given as a known scalar input. ε_M represents the dynamic model noise, which is assumed to be normally distributed. The index *i* denotes a point in time within the set of data reporting intervals *T*, η denotes a reporting factor accounting for under-reporting, and R_t^* denotes the actual reported incidence over a given time interval. The cumulative new incidence is ϕ, and $\varepsilon_{\phi t}$ represents the measurement noise. ω_M and ω_ϕ represent weights for the model and measurement noise terms, respectively. These weights are set to be proportional to the inverse of the assumed variance of the error terms. The $\bar{\beta}$ term denotes the average β across the yearly set of discretizations τ and is constrained here due to difficulties in simultaneously estimating *S* and β. $|\tau|$ is the cardinality of the set τ.

The England and Wales measles data contains biweekly reported measles case counts by city for the years 1944 through 1963. The number of births per year is also reported by city. We assume births are uniform throughout the year. For all cities, population is assumed to be constant throughout the time horizon. The reporting fraction was estimated for London using a susceptible reconstruction technique that is similar to those described elsewhere (Bobashev et al., 2000; Finkenstädt et al., 2000), with the exception that we restrict the reporting factor to vary linearly with time.

3. Estimation Approach

The problem shown in Eq. (3) was formulated in the algebraic modeling language Pyomo (Hart et al., 2011; Hart et al., 2012). This model is for a single city and data set. Prior to estimation, we specify a scenario tree and use PySP (Watson et al., 2011) to automatically convert this problem into the multi-city problem. PySP and Pyomo are both part of the open-source Coopr software package released by Sandia National Laboratories. PySP allows for convenient formulation and solution of multi-scenario problems. PySP takes a model formulated for a single scenario, data for multiple scenarios, constructs the multi-scenario problem, and then uses one of two approaches to solve the problem. The first approach considers the extensive form of the multi-scenario problem. This has the form of Eq. (2) and is solved using the interior-point solver IPOPT (Wächter, A. and Biegler, 2006). The other approach utilizes Rockafellar and Wets' Progressive Hedging (PH) algorithm, with IPOPT as the subproblem solver. Problem sizes and solution times for both approaches are shown in Table 1.

The PH algorithm is outlined below, where *P* is the weight placed on each observation, *C* is the set of all observations, and ρ is a tuning parameter:
For the base model Eq. (3):

1. Initialize the iterate $k \leftarrow 0$ and let $\omega_c^k = 0$
2. For all scenarios $c \in C$: $\beta_c^0 \leftarrow argmin\ f_c(\varepsilon)$
3. Update the iterate, $k \leftarrow k + 1$, and update $\bar{\bar{\beta}}$:
   $\bar{\bar{\beta}}^{k-1} \leftarrow \sum_{c \in C} P_c \beta_c^{k-1}$ where $\sum_{c \in C} P_c = 1$
4. For all scenarios $c \in C$, update ω and β: $\omega_c^k \leftarrow \omega_c^{k-1} + \rho(\beta_c^{k-1} - \bar{\bar{\beta}}_c^{k-1})$
   $$\beta_c^k \leftarrow argmin\ f_c(\varepsilon) + \omega_c^k \beta_c + \frac{\rho}{2} \left\| \beta_c - \bar{\bar{\beta}}^{k-1} \right\|^2$$
5. If termination criterion not met, go back to step 3.

Steps 2 and 4 are computationally expensive, but these steps can be solved in parallel - allowing for significant performance improvements.

4. Results & Conclusions

Figure 1 shows the estimated values of the seasonal transmission parameter. The extensive form and the PH approach yield nearly identical solutions that are consistent with published values (Finkenstädt and Grenfell, 2000). PH was terminated once the sum of differences between the first stage variables and their average reached a value less than 1×10^{-4}, indicating logical convergence.

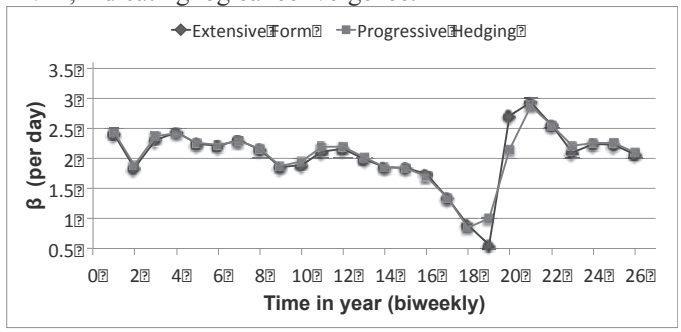

Figure 1: Estimated transmission parameters for extensive form and PH solutions.

Table 1 shows that the extensive form solution requires a total of 5.5GB of RAM. We wish to solve problems with 100s of observations, and problems of this size will not only require very long solution times but also more memory than would be available on a single computer. Using Progressive Hedging in serial requires more time but less memory. The parallel solution of this problem using PH shows good speed-up, and memory requirements remain low for each compute node.

Eqs. 1 and 2 demonstrate that two-stage stochastic programming problems are structurally equivalent to nonlinear programming parameter estimation problems. This similarity allows large-scale nonlinear parameter estimation problems to be solved using stochastic programming decomposition techniques. Our results demonstrate that Progressive Hedging can be used to solve very large parameter estimation problems in parallel with significant reductions in solution times and memory requirements.

Further improvements will allow greater speed-up for parallel PH. Currently, if even one scenario requires significantly longer to converge than the rest of the scenarios, many computing nodes remain idle for extended periods of time. Asynchronous

approaches being studied will reduce the number of idle processors by allowing the majority of computing nodes to continue with the next iteration of PH using an altered update formula. Improved strategies for the selection of the algorithm parameter ρ could also further reduce solution times.

Table 1. Timing and Memory Results

	Extensive Form	PH (serial)	PH (60 processors)
Jacobian Nonzeros	2594522	43184	43184
Variables	625948	10430	10430
Constraints	594721	9883	9883
Solver Time (min)	27.9	93.3	5.1
PySP Time (min)	6.6	8.9	2.1
Solver RAM (GB)	2.2	<0.050	<0.050
PySP RAM (GB)	3.3	3.6	<0.45

Acknowledgements

This research was supported in part by the Office of Advanced Scientific Computing Research within the Department of Energy Office of Science, as part of the Complex Interconnected Distributed Systems program. Sandia National Laboratories is a multi-program laboratory managed and operated by Sandia Corporation, a wholly owned subsidiary of Lockheed Martin Corporation, for the U.S. Department of Energy's National Nuclear Security Administration under contract DE-AC04-94AL85000.

References

Schenk, O. and Manguoglu, M. and Sameh, A. and Christen, M. and Sathe, M., 2009, Parallel Scalable PDE-Constrained Optimization: Antenna Identification in Hyperthermia Cancer Treatment Planning, Computer Science – Research and Development, 23, p. 177-183.

Soper, H.E., 1929, The Interpretation of Periodicity in Disease Prevalence, Journal of the Royal Statistical Society, 92, p. 34-73.

Zavala, V.M., 2008, Computational Strategies for the Optimal Operation of Large-Scale Chemical Processes, Carnegie Mellon University.

Finkenstädt, B.F. and Grenfell, B.T., 2000, Time Series Modelling of Childhood Diseases: A Dynamical Systems Approach, Jrnl. of the Royal Statistical Society, Series C, 49, p. 187-205.

Bobashev, G.V. and Ellner, S.P. and Nychka, D.W. and Grenfell, B.T, 2000, Reconstructing Susceptible and Recruitment Dynamics from Measles Epidemic Data, Mathematical Population Studies, 8(1), p. 1-29.

Hart, W.E., Watson, J-P., Woodruff, D.L., 2011, Pyomo: Modeling and Solving Mathematical Programs in Python, Mathematical Programming Computation, 3(3), p. 219-260.

Watson, J-P., Woodruff, D.L., Hart, W.E., 2011, PySP: Modeling and Solving Stochastic Programs in Python. (To Appear) Mathematical Programming Computation.

Wächter, A. and Biegler, LT., 2006, On the Implementation of an Interior-Point Filter Line-Search Algorithm for Large-Scale Nonlinear Programming, Mathematical Programming, 106(1), p. 25-57.

Rockafellar, R.T.and Wets, R.J.B., 1991, Scenarios and Policy Aggregation in Optimization Under Uncertainty, Mathematics of Operations Research, 16(1), p. 119-147.

Hart, W.E., Laird, C.D., Watson, J.P., and Woodruff, D.L., 2012, Pyomo: Optimization Modeling in Python, Volume 67. Springer Verlag.

Grenfell, B.T., 2011, Pathogen population dynamics, (accessed on October 3, 2011) http://www.zoo.cam.ac.uk/zoostaff/grenfell/measles.htm.

I.A. Karimi and Rajagopalan Srinivasan (Editors), Proceedings of the 11th International Symposium on Process Systems Engineering, 15-19 July 2012, Singapore

Performance Analysis of Shooting Algorithms in Chance-Constrained Optimization

S. Werk, * T. Barz, H. Arellano-Garcia, G. Wozny
Chair of Process Dynamics and Operation, Berlin University of Technology, Sekr. KWT 9, 10623 Berlin, Germany

Abstract

An important aspect for model-based design and development as well as for process monitoring and control is the consideration of uncertain process parameters. One approach for the explicit consideration of such uncertainties is the formulation of *Chance-Constrained* optimization problems. Within the last years, several different methods for the efficient solution of these problems have been presented. In this work, chance constraints are evaluated following the idea of the *variable mapping approach*.

Because the efficiency of the original approach deteriorates with an increasing number of uncertain parameters, the probability integration has been extended recently to the exploitation of sparse grids. In this work, additional techniques for improving the efficiency of the variable mapping approach are presented. Firstly, the solution of a subproblem, the so called *shooting task* is analyzed in detail and enhanced through an idea called here *result recycling*. Secondly, possible extensions are presented which make use of second order derivative information. The new methods are verified by application to an industrially validated process model of a vacuum distillation column for the separation of multicomponent fatty acids.

Keywords: Chance Constrained Optimization, uncertainty, stochastic optimization, higher order derivatives, result recycling

1. Introduction

For industrial process models it is often not possible to assign exact values to all model parameters. In model-based process optimization, different approaches for the explicit consideration of those uncertain parameters have been proposed, under these Approximated Polyhedral Dynamic Programming (Björnberg and Diehl, 2006), Robust Stochastic Programming (Nagy and Braatz, 2003) or Chance-Constrained Optimization based on the *variable mapping approach* (Arellano-Garcia and Wozny, 2009).

The latter, which is discussed here, consists mainly in two parts, the solving of a *shooting task* and the multivariate integration over a known probability distribution function. Recently, significant performance advancements have been reported through the use of sparse grids in the integration task (Geletu et al., 2011). This work focuses on enhancements of the first task, the solution of the *shooting problem*. Moreover, special attention is given to the exploitation of second order derivative information, which is getting more and more popular through solvers like IPOPT (Wächter and Biegler, 2006).

*swerk@zmms.tu-berlin.de

2. Chance Constraint Optimization

To include a Chance Constraint in an optimization problem, Eq. (1) is used, where u represents the decision variables of the optimization problem, ξ the vector of uncertain parameters and the scalar y^{max} a constraint limit. The scalar α stands for the probability, with which the term $f(u,\xi) \leq y^{max}$ has to be fulfilled. ξ is assumed to be multivariate normally distributed with the mean vector μ and the covariance matrix Σ, although a normal distribution is not presupposed.

$$\Pr\{f(u,\xi) \leq y^{max}\} \geq \alpha \tag{1}$$

In the mapping approach (see Wendt et al., 2002), the calculation of a probability $Pr\{\cdot\}$ is performed solving the integral (2), where φ represents the multivariate normal distribution density function. The integration limits are chosen as depicted in Eq. (3).

$$\Pr\{f(u,\xi) \leq y^{max}\} = \int_{-\infty}^{\infty} \dots \int_{-\infty}^{\infty} \int_{-\infty}^{\bar{\xi}_n : f\left(u,\xi_1,\dots,\xi_{n-1},\bar{\xi}_n\right)=0} \varphi(\xi_1,\dots,\xi_n) d\xi_n d\xi_{n-1} \dots d\xi_1 \tag{2}$$

$$\approx \int_{\mu_1-3\sigma_1}^{\mu_1+3\sigma_1} \dots \int_{\mu_{n-1}-3\sigma_{n-1}}^{\mu_{n-1}+3\sigma_{n-1}} \int_{\mu_n-3\sigma_n}^{\bar{\xi}_n : f\left(u,\xi_1,\dots,\xi_{n-1},\bar{\xi}_n\right)=0} \varphi(\xi_1,\dots,\xi_n) d\xi_n \dots d\xi_1 \tag{3}$$

Since the anti-derivative of the density function is not analytically available, a numerical integration is required. Therefore, the outer $n-1$ integrals are used to provide a grid of integration points. Accordingly, for each tuple $(\xi_1,\dots,\xi_{n-1})$ the upper integration limit $\bar{\xi}_n$ of the most inner integral has to be determined, such that $f(u,\xi_1,\dots,\xi_{n-1},\bar{\xi}_n) = 0$ holds. This subproblem, called *shooting task*, is a classic root-finding problem. For general nonlinear process models, the calculation of f implies the solving of a system of differential algebraic equations. This calculation can be considered as the computational time determining step, consequently a reduction of evaluations has a strong impact on the total performance. In the next two chapters, we present two different techniques to improve this part of the calculation.

3. Result recycling for initial estimations

One way to reduce the number of evaluations of f is to improve the initial estimations of the starting points for the root-finding. For the very first u, the best estimations should be μ_n, since no other information is available. For further sets of decision variables $\bar{u}$, the previous results can be reused for starting points. The circumstance that the grid of integration points is independent of u allows for good estimations. Below ξ_n is the vector of the solutions of $\xi_n : f(u,\xi) = 0$ for the whole grid.

For the following approaches the already evaluated u's are considered to be in the set U, while the current one is called $\bar{u}$. For all approaches a metric d is needed, to determine the distance of two different u's. A $\hat{u} \in U$ is called the closest $\hat{u} \in U$, if $d(\hat{u},\bar{u}) \leq d(u,\bar{u})$ for all $u \in U$.

3.1. Nearest neighbour approach

This approach determines the closest $\hat{u} \in U$ and takes its $\hat{\xi}_n$ as initial estimations. In spite of the simplicity, the initial estimations might be much better than μ_n.

3.2. Affine hull approach

For this approach, the closest subset $\{\hat{u}_1, \ldots, \hat{u}_K\} \subseteq U$ has to be determined, whose affine hull includes $\bar{u}$. Then, the linear equation system on the left side of Eq. (4) needs to be solved to obtain the different α_k as weight factors.

$$\sum_{k=1}^{K} \alpha_k \hat{u}_k = \bar{u}, \quad \sum_{k=1}^{K} \alpha_k = 1 \qquad \Rightarrow \qquad \bar{\xi}_n \approx \sum_{k=1}^{K} \alpha_k \hat{\xi}_k \tag{4}$$

Having determined them, $\bar{\xi}_n$ can be calculated according to the right side of Eq. (4).

3.3. Derivative approach

The last approach presented here is the derivative approach. It can only be used, if the derivatives $\frac{\partial f}{\partial \hat{u}}$ and $\frac{\partial f}{\partial \hat{\xi}_n}$ are available. Since $f(\hat{u}, \hat{\xi}) = 0$ holds, with the use of the implicit function theorem the derivative $\frac{\partial \hat{\xi}_n}{\partial \hat{u}}$ can be calculated. Therefore, a first order Taylor Polynomial can be formulated so as to provide an initial estimation.

$$\bar{\xi}_n \approx \hat{\xi}_n + \frac{\partial \hat{\xi}_n}{\partial \hat{u}} \cdot (\bar{u} - \hat{u}) \tag{5}$$

If the second derivatives $\frac{\partial^2 f}{\partial \hat{u}^2}$, $\frac{\partial^2 f}{\partial \hat{u} \hat{\xi}_n}$ and $\frac{\partial^2 f}{\partial \hat{\xi}_n^2}$ are also available, with the same approach $\frac{d^2 \hat{\xi}_n}{d \hat{u}^2}$ can be calculated and a second order Taylor polynomial can be constructed:

$$\bar{\xi}_n \approx \hat{\xi}_n + \frac{\partial \hat{\xi}_n}{\partial \hat{u}} \cdot (\bar{u} - \hat{u}) + \frac{1}{2} (\bar{u} - \hat{u})^T \cdot \frac{\partial^2 \hat{\xi}_n}{\partial \hat{u}^2} \cdot (\bar{u} - \hat{u}) \tag{6}$$

4. Enhanced root-finding using Halley's method

In case second order derivatives are available, the Newton-step in the root finding for the solution of the shooting task can be extended. To do so, a second order Taylor polynomial is constructed for each ξ_n, used in the root-finding process. The root of this polynomial is calculated using Eq. (7). This method is also known as Parabolic Halley's method.

$$\begin{aligned} & f(x_1) \approx f(x_0) + f'(x_0)(x_1 - x_0) + \frac{1}{2} f''(x_0)(x_1 - x_0)^2 \stackrel{!}{=} 0 \\ & \Rightarrow x_1 = x_0 - \frac{f'(x_0) - \operatorname{sgn}(f'(x_0)) \cdot \sqrt{f'(x_0)^2 - 2 f(x_0) f''(x_0)}}{f''(x_0)} \end{aligned} \tag{7}$$

The convergence of this method is cubic, while Newton's method's is only quadratic, even though, with good initial estimations or linear relation between ξ and f its effect on computational time might be low, since only one Newton-step is usually needed then.

5. Numerical tests

In the following, the different techniques presented in the preceding sections are compared by their efficiency for the evaluation of chance constraints in a practical application. To do so, an industrial packed distillation column for the separation of fatty acids is considered (Figure 1). The process model consists in a system of differential algebraic equations (179 implicit defined differential and 232 algebraic equations).

The Murphree tray efficiencies η_1 and η_2 for the rectification and stripping section are assumed to be uncertain model parameters with uncorrelated normal distributions of $\eta_1 \sim \mathcal{N}(0.55, 0.08^2)$ and $\eta_2 \sim \mathcal{N}(0.6, 0.1^2)$. The C10 stream of the bottom section is very sensitive towards the Murphree efficiencies. For the dynamic optimization problem it is assumed, that its mass concentration $f(u, \eta_1, \eta_2)$ at the end of the time horizon may not exceed 1.5 percent with a probability of 90 percent. Therefrom the Chance Constraint Eq. (8) is formulated. The objective function minimizes the reboiler duty, which is defined as decision variable u with a starting value of 610.70 MW. The reflux ratio is fixed to 1.0.

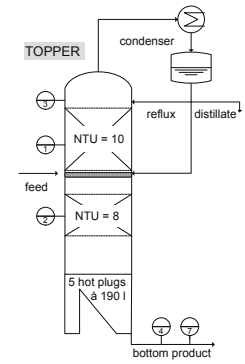

Fig. 1. Packed vacuum distillation column for the distillation of fatty acids (Barz et al., 2011).

$$\Pr\{f(u, \eta_1, \eta_2) \leq 1.5\} \geq 0.90 \tag{8}$$

All different result recycling approaches are evaluated with the classical Newton's method as well as with the Halley's method by using the Sequential Least Squares Programming solver of SciPy 0.9.0 on a Intel Core i7-2700K, running Ubuntu Server 11.10 64bit. All dynamic simulations as well as first and second order derivative generation have been realized using the numeric solver sDACl (Barz et al., 2011). To guarantee a consistent comparison, the same number of evaluations of the probability function was ensured. The results are presented in table 1.

initial estimation approach	Newton's method	Halley's method
none	548 (0.0%)	542 (1.1%)
nearest neighbour	406 (25.9%)	406 (25.9%)
affine hull	402 (26.6%)	402 (26.6%)
1st order derivative	404 (26.3%)	404 (26.3%)
2nd order derivative	404 (26.3%)	404 (26.3%)

Table 1. Number of function evaluations $f(u, \xi)$ (improvement in percent).

All of the different approaches for better initial estimations have shown significant speed improvement from 25.9 to 26.6 percent. The affine hull approach did show the highest speed improvement while the derivative approaches and the nearest neighbour approach did perform slightly slower. The use of Halley's method for the root-finding problem did not show a significant improvement over Newton's method in this case study.

To evaluate the efficiency of the initial estimation approaches in scenarios with multiple Chance Constraints, the previous example is extended as follows: The reboiler duty can be varied over time, and the C10 stream has different constraints over time. Figure 2 shows the result of an optimization with ten equally spaced time steps. The mass concentration of the C10 stream decreases from 1.95 at the end of the first time step to 1.5 at the end of the time horizon. All limits have to hold with a probability of 90 percent. The optimized reboiler duty over time is shown in the bottom diagram. To obtain the optimal solution without record recycling, the simulation had to be performed 17046 times, while the use of the 1st order derivative approach reduced this number to 9655, a performance increase of over 43 percent.

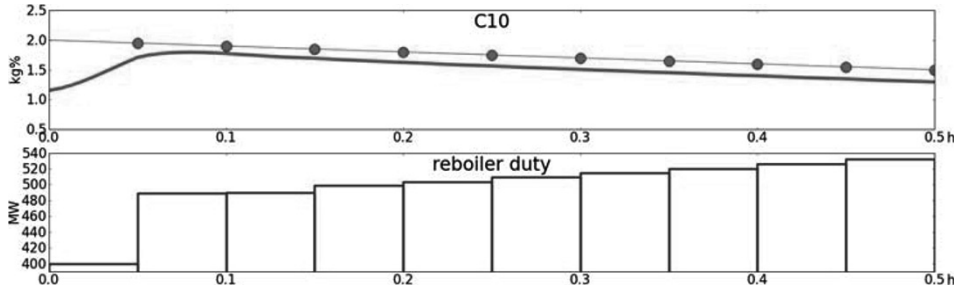

Fig. 2. Extended case study. Top: expected value of mass concentration of C10 bottom stream (bold line) and its restrictions (dots). Bottom: reboiler duty over time.

6. Conclusion

In this paper, we discussed various algorithmic improvements of a method for the evaluation of probabilities of Chance-Constraints in general optimization problems. The new approaches considered in this work aim at the reduction of the number of necessary solutions of a shooting problem, which arises when following the mapping approach.

For our industrial case study, we have shown, that recycling of previous results within the optimization can reduce the computation time up to 43 percent. A second approach based on the exploitation of available second order derivative information using Halley's root finding method did not show clear improvements. Anyhow, preliminary results indicate that problems exist for which this approach performs much better. This and further improvements of the presented strategies for a result recycling are currently under investigation. All approaches are implemented in a software framework to be easily applicable to other optimization models.

References

Arellano-Garcia, H., Wozny, G., 2009. Chance constrained optimization of process systems under uncertainty: I. strict monotonicity. Computers & Chemical Engineering 33 (10), 1568–1583.

Barz, T., Kuntsche, S., Wozny, G., Arellano-Garcia, H., 2011. An efficient sparse approach to sensitivity generation for large-scale dynamic optimization. Computers & Chemical Engineering 35 (10), 2053–2065.

Björnberg, J., Diehl, M., 2006. Approximate robust dynamic programming and robustly stable mpc. Automatica 42 (5), 777–782.

Geletu, A., Hoffmann, A., Klöppel, M., Li, P., 2011. Monotony analysis and sparse-grid integration for nonlinear chance constrained process optimization. Engineering Optimization 43 (10), 1019–1041.

Nagy, Z. K., Braatz, R. D., 2003. Robust nonlinear model predictive control of batch processes. AIChE Journal 49 (7), 1776–1786.

Wendt, M., Li, P., Wozny, G., 2002. Nonlinear chance-constrained process optimization under uncertainty. Industrial & Engineering Chemistry Research 41 (15), 3621–3629.

Wächter, A., Biegler, L. T., 2006. On the implementation of an interior-point filter line-search algorithm for large-scale nonlinear programming. Mathematical Programming 106, 25–57.

I.A. Karimi and Rajagopalan Srinivasan (Editors), Proceedings of the 11th International Symposium on Process Systems Engineering, 15-19 July 2012, Singapore.

Multiple Sensor Fault Isolation Using Contribution Plots without Smearing Effect to Non-Faulty Variables

Jialin Liu[a],* Ding-Sou Chen[b]

[a]*Department of Information Management, Fortune Institute of Technology, 1-10, Nwongchang Rd., Neighborhood 28, Lyouciyou Village, Daliao Township, Kaohsiung, Taiwan, Republic of China*
[b]*New Materials Research & Development Department, China Steel Corporation, 1, Chung Kang Rd., Hsiao Kang, Kaohsiung, Taiwan, Republic of China*

Abstract

Investigating the root causes of abnormal events is a crucial task for an industrial process. When process faults are detected, isolating the faulty variables provides additional information for investigating the root causes of the faults. Numerous data-driven approaches require the datasets of known faults, which may not exist for some industrial processes, to isolate the faulty variables. The contribution plot is a popular tool to isolate faulty variables without a priori knowledge. However, it is well known that this approach suffers from the smearing effect, which may mislead the faulty variables of the detected faults. In the presented work, a contribution plot without the smearing effect to non-faulty variables was derived. A continuous stirred tank reactor (CSTR) example was provided to demonstrate that the proposed approach is not only capable of isolating faulty variables of a simple fault but also a complex fault.

Keywords: fault detection and isolation, principal component analysis, contribution plots, missing data analysis.

1. Introduction

In modern chemical processes, the operating data are collected and stored in a historical database. However, information about process operations is hidden under the historical data. Therefore, it is more practical to develop methods that detect and investigate the root causes of process faults based on data-driven approaches, rather than to use other methods based on rigorous process models or knowledge-based approaches. Since the measured variables are correlated for a chemical process, principal component analysis (PCA) is a popular tool to extract the features of the process data that are applied to monitor the process variations. After a fault is detected, the faulty variables need to be isolated in order to diagnose the root causes of the fault. Contribution plots are the most popular tool for identifying which variables are pushing the statistics out of their control limits. Kourti and MacGregor, 1996 remarked that the contribution plots may not reveal the assignable causes of abnormal events; however, the group of variables contributed to the detected events will be unveiled for further investigation. Westerhuis et al., 2000 introduced the confidence limits of the contribution plots to enhance the capability of identifying the behaviors of faulty variables departing from the normal operating condition (NOC). They reported that there must be a careful interpretation of the contribution plots, since the residuals of the PCA are smeared out over the other variables. Yoon and MacGregor, 2000 comprehensively compared model-based and

data-driven approaches for fault detection and isolation, and summarized that the contribution plots provide for the easy isolation of simple faults, but that additional information about operating the process is needed to isolate complex faults.
The remainder of this paper is organized as follows. The proposed approach of the contribution plots without smearing effect to non-faulty variables is detailed in section 2. In section 3, a CSTR example is provided to demonstrate the effectiveness of the proposed approach. Finally, conclusions are given.

2. Proposed Approach

Yue and Qin, 2001 combined the statistics Q and T^2 of PCA to develop an index that is minimized when isolating the faulty variables, i.e., $\varphi = \mathbf{x}^{\mathrm{T}}\boldsymbol{\Phi}\mathbf{x}$ where $\mathbf{x}$ is a normalized measured vector with zero means and unit variances, and $\boldsymbol{\Phi} \equiv \tilde{\mathbf{P}}\tilde{\mathbf{P}}^{\mathrm{T}}/Q_\alpha + \mathbf{P}\boldsymbol{\Lambda}^{-1}\mathbf{P}^{\mathrm{T}}/T_\alpha^2$ in which $\boldsymbol{\Lambda}$ and $\mathbf{P}$ respectively are a diagonal matrix with first K terms of the significant eigenvalues and the respective eigenvectors and $\tilde{\mathbf{P}}$ contains the residual eigenvectors; Q_α and T_α^2 respectively are the (1-α) confidence limits of the statistic Q and T^2. For a multiple sensor fault, the reconstructed variables can be written according to the combined index: $\boldsymbol{\xi}^{\mathrm{T}}\boldsymbol{\Phi}\mathbf{x} = \mathbf{0}$ where $\boldsymbol{\xi} \equiv \begin{bmatrix} \boldsymbol{\xi}_1 & \boldsymbol{\xi}_2 & \cdots & \boldsymbol{\xi}_{nf} \end{bmatrix}$, in which nf is the number of faulty variables and $\boldsymbol{\xi}_i$ is a column vector in which the i^{th} element is one and the others are zero. The monitored variables can be decomposed as $\mathbf{x} = \boldsymbol{\Gamma}\mathbf{x} + (\mathbf{I} - \boldsymbol{\Gamma})\mathbf{x}$, where $\boldsymbol{\Gamma}$ is a diagonal matrix, in which the values of the diagonal elements are one for the faulty variables and zero for the non-faulty ones. Therefore, minimizing the combined index can be rewritten as: $\boldsymbol{\xi}^{\mathrm{T}}\boldsymbol{\Phi}\boldsymbol{\Gamma}\mathbf{x} = -\boldsymbol{\xi}^{\mathrm{T}}\boldsymbol{\Phi}(\mathbf{I} - \boldsymbol{\Gamma})\mathbf{x}$. The left-hand side of the above equation contains the data to be reconstructed by the normal data in the right-hand term. The data that to be reconstructed can be expressed as: $\boldsymbol{\Gamma}\mathbf{x} = \boldsymbol{\xi}\mathbf{x}_{nf}$ in which $\mathbf{x}_{nf}$ is the collection of the faulty variables. The reconstruction of the faulty variables can be obtained by the following equation:

$$\mathbf{x}_{nf}^{*} = -\left(\boldsymbol{\xi}^{\mathrm{T}}\boldsymbol{\Phi}\boldsymbol{\xi}\right)^{-1}\boldsymbol{\xi}^{\mathrm{T}}\boldsymbol{\Phi}(\mathbf{I} - \boldsymbol{\Gamma})\mathbf{x} \tag{1}$$

Since $\boldsymbol{\Phi}$ is a full-rank matrix, $\left(\boldsymbol{\xi}^{\mathrm{T}}\boldsymbol{\Phi}\boldsymbol{\xi}\right)$ is invertible. The reduction of the combined index (RCI) after reconstructing the faulty data can be written as follows:

$$\varphi - \varphi_{nf}^{*} = \left(\mathbf{x}_{nf} - \mathbf{x}_{nf}^{*}\right)^{\mathrm{T}}\left(\boldsymbol{\xi}^{\mathrm{T}}\boldsymbol{\Phi}\boldsymbol{\xi}\right)\left(\mathbf{x}_{nf} - \mathbf{x}_{nf}^{*}\right) \tag{2}$$

Therefore, the fault isolation task is to find subset $\mathbf{x}_{nf}$ from $\mathbf{x}$ to maximize the RCI, until the statistics Q and T^2 are under the corresponding control limits, without the information from faulty variables. The contribution of the i^{th} faulty variable to RCI can be defined as:

$$c_i^{RCI} = \left[\left(\mathbf{x}_{nf} - \mathbf{x}_{nf}^{*}\right)^{\mathrm{T}}\left(\boldsymbol{\xi}^{\mathrm{T}}\boldsymbol{\Phi}\boldsymbol{\xi}\right)^{0.5}\boldsymbol{\xi}_i\right]^2 \tag{3}$$

The proposed approach first evaluates each RCI with a reconstructed variable and inserts the variable with the maximum RCI into $\mathbf{x}_{nf}$ in the first step. Next, the RCIs are evaluated using the reconstructed data of a non-faulty variable and the selected faulty variables in $\mathbf{x}_{nf}$. The non-faulty variable with the maximum RCI is inserted into $\mathbf{x}_{nf}$. The

steps of adding a new faulty variable into $\mathbf{x}_{nf}$ is repeated until both statistics Q and T^2 are under the corresponding control limits. The algorithm is summarized as follows:

1. Set $nf = 0$ and $\mathbf{x}_{nf} = \varnothing$.
2. For $i = 1 \ldots N\text{-}nf$, which N is the number of variables,
   Reconstruct the data of $\mathbf{x}_{nf} \cup \mathbf{x}_i \notin \mathbf{x}_{nf}$ using *(1)* and evaluate the RCI using *(2)*.
3. Add the variable with the maximum RCI into $\mathbf{x}_{nf}$ and set $nf = nf + 1$.
4. If the statistics Q and T^2, without the information of the selected faulty variables, are still over their control limits, go back to step 2.
5. Decreasingly sort the selected faulty variables according to the contributions of RCI using *(3)* and retain the variables in $\mathbf{x}_{nf}$ that sufficiently reduce the statistics Q and T^2 under the corresponding control limits.

Steps 2-4 of the algorithm guarantee *(2)* to be a monotonically increasing function with the number of selected faulty variables; therefore, the statistics Q and T^2 monotonically decrease during iterations. The non-faulty variables, which may be selected in the early stage of the iterations under insufficient information about the faulty variables, are removed from $\mathbf{x}_{nf}$ in step 5. When diagnosing the root causes of process faults, the selected faulty variables do not equally contribute to the faults. The contribution plots for the reduction of statistics can be used to find the faulty variables with the most contributions, as the contributions have been confined within the selected faulty variables and the fault magnitude will not smear over to the non-faulty variables.

3. Continuous Stirred Tank Reactor Example

A nonisothermal continuous stirred tank reactor (CSTR) with feedback control systems was simulated; the schematic diagram of the CSTR and feedback control system is shown in Fig. 1 and the details of the simulated CSTR can be found in Singhal and Seborg, 2002. Data from the monitored variables (listed in Table 1) were collected every minute. PCA was applied to the dataset with a 1-day window size, and four PCs were retained using cross-validation. The PCA model captured about 81% of the total variance. Two sensor faults were considered, based on the work of Yoon and MacGregor, 2001. The simple fault data were generated by introducing a bias of 1 K to the measurement of the feed temperature (T_F) after the first day. After the simple fault was triggered, the smearing effect of the contribution plots could be observed, as shown in Fig. 2(a) where the Q contributions were normalized with the corresponding 99% confidence limits. The result was similar with what Yoon and MacGregor, 2001 reported. Figure 2(b) shows that the contributions of RCI, normalized with the sum of RCIs, indicate the third variable (the feed temperature) was over 80% responsible for this simple fault.

Table 1. Monitored Variables for the CSTR Example

ID	Variable Description	ID	Variable Description
1	Reactor temperature (T)	6	Reactor exit flow rate (Q)
2	Coolant exit temperature (T_C)	7	Coolant flow rate (Q_C)
3	Feed temperature (T_F)	8	Reactor feed flow rate (Q_F)
4	Coolant feed temperature (T_{CF})	9	Reactant concentration (C_A)
5	Reactor level (h)		

The complex fault data were generated by adding a bias of 1 K to the measurement of the reactor temperature (T) after the first day. Since the reactor temperature was regulated by the coolant flow rate (Q_C), the measured temperature would be brought back to its set point after a short period of time, as shown in Fig. 3(a). However, the actual reactor temperature was lower than its set point; therefore, the reactant

concentration (C_A) would be higher than the normal operating data due to the lower reaction rate, as Fig. 3(b) shows. The coolant flow rate reached a new steady-state condition after the fault had been compensated, as shown in Fig. 3(c), which induced the coolant exit temperature (T_C) to be lower than its normal operating values due to the excess of the coolant flow rate, as Fig. 3(d) shows. The other monitored variables were not affected by this complex fault. Figure 4(a) shows that the faulty variables were identified as variable 2, 5, 6, and 9, according to the normalized Q contribution plots. It misidentified the reactor level and the reactor exit flow rate as faulty variables and lost the faulty variable Q_C. The proposed approach repeatedly selected the variables with the maximum RCI as the faulty variable candidates until both statistic Q and T^2 were under the corresponding control limits. The normalized contributions, based on RCI in the faulty variable candidate, were then plotted. Figure 4(b) shows the correct faulty variables, T_C, Q_C, and C_A, were identified.

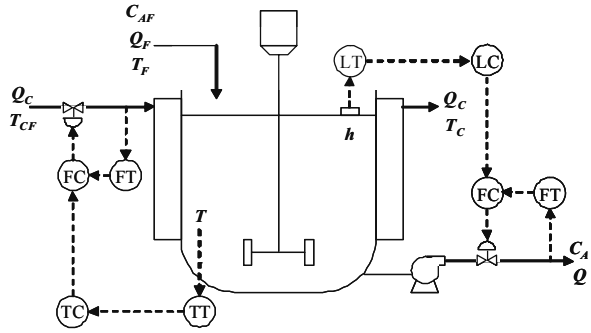

Fig. 1. Schematic of the CSTR system.

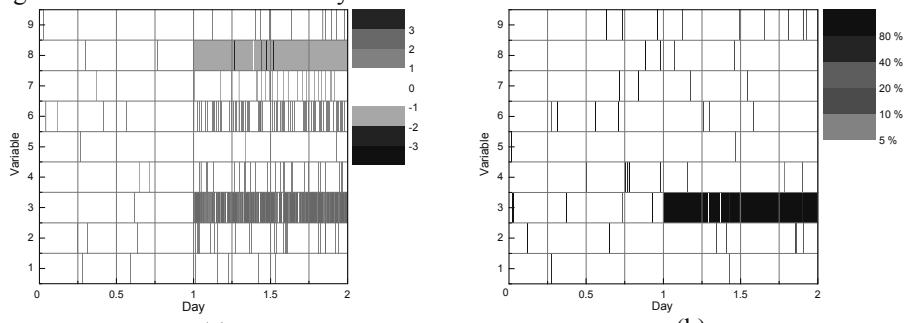

(a) (b)

Fig. 2. Isolating faulty variables for the simple fault using (a) the traditional Q contribution plots, and (b) the normalized contribution plots based on RCI.

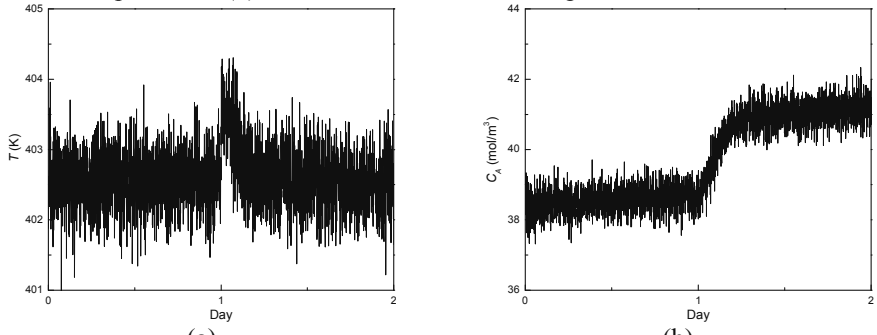

(a) (b)

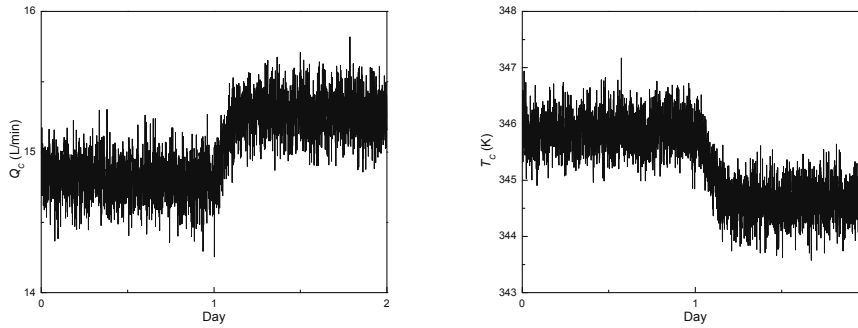

(c) (d)

Fig. 3. Trends of the monitored variables for the complex fault: (a) reactor temperature, (b) reactant concentration, (c) coolant flow rate, and (d) coolant exit temperature.

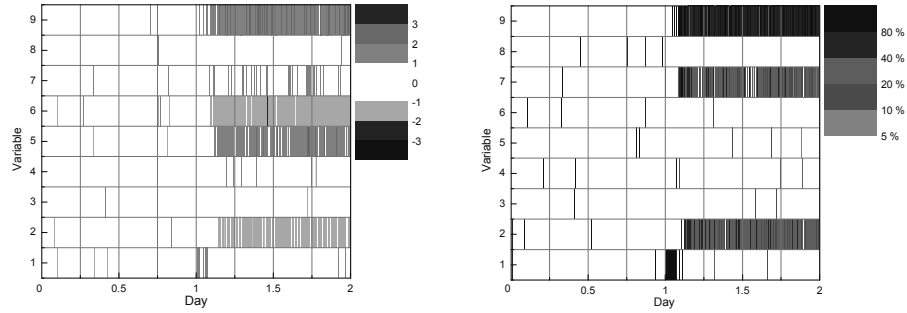

(a) (b)

Fig. 4. Isolating faulty variables for the complex fault using (a) the traditional Q contribution plots and (b) the normalized contribution plots based on RCI.

4. Conclusions

The presented work developed a contribution plot without the smearing effect to non-faulty variables. The proposed approach was shown to have the capability of isolating multiple sensor faults without predefined faulty datasets. In the CSTR example, the fault isolation results using the contribution plots of RCI were more precise than the solutions found using the traditional contribution plots. The results show that the predefined faulty datasets are not necessary for the proposed approach; in addition, the smearing effect of the traditional contribution plots is also eliminated.

References

T. Kourti and J. F. MacGregor, 1996, Multivariate SPC Methods for Process and Product Monitoring, J. Qual. Technol., 28, 4, 409.

J. A. Westerhuis, S. P. Gurden, and A. K. Smilde, 2000, Generalized Contribution Plots in Multivariate Statistical Process Monitoring, Chemom. Intell. Lab. Syst., 51, 1, 95.

S. Yoon and J. F. MacGregor, 2000, Statistical and Causal Model-Based Approaches to Fault Detection and Isolation, AIChE J., 46, 9, 1813.

H. H. Yue and S. J. Qin, 2001, Reconstruction-based Fault Identification Using a Combined Index, Ind. Eng. Chem. Res., 40, 20, 4403.

A. Singhal and D.E. Seborg, 2002, Pattern Matching in Multivariate Time Series Databases Using a Moving-window Approach, Ind. Eng. Chem. Res., 41, 16, 3822.

S. Yoon and J.F. MacGregor, 2001, Fault Diagnosis with Multivariate Statistical Models Part I: Using Steady State Fault Signatures, J Proc. Cont., 11, 4, 387.

I.A. Karimi and Rajagopalan Srinivasan (Editors), Proceedings of the 11th International Symposium on Process Systems Engineering, 15-19 July 2012, Singapore

Integrated Sensor Network Design

Nabil M, Sridharakumar Narasimhan*
Department of Chemical Engineering; Indian Institute of Technology Madras; India

Abstract

Selection of sensors is an important structural decision for the safe and optimal operation of a chemical plant. Recently, we have proposed a mixed integer cone formulation for selecting sensors for linear data reconciliation with the aim of minimizing the operational loss caused due to measurement noise. In this work, we extend our formulation to select a redundant sensor network such that the system is observable in case of sensor failures. Finally, the proposed approach is illustrated using an evaporation process.

Keywords: data reconciliation, sensor faults, convex optimization

1. Introduction

Efficient process monitoring, control and fault diagnosis are vital for optimal and safe operation of a chemical process. The success of each of the above activities depends critically on the choice of the sensor network. Although sensor network design problems have been discussed extensively in literature, they are tailored for each activity independently (Chmielewski et al., 2002; Bhushan and Rengaswamy, 2000). Since the individual design problems are incommensurable, the integration of sensor network design is difficult to account for the multi-faceted elements (observability, controllability, redundancy, accuracy, reliability, etc.,). To this end, there is an increasing interest to define performance metrics based on process economics. Despite this, a sensor network is chosen to cater to a specific objective rather than considering all objectives simultaneously. Thus, the current objective is to determine an economically optimal sensor network that considers both data reconciliation and sensor failure case.

In this work, we extend our optimization framework that was addressed for data reconciliation to account for sensor faults as well. In particular, we address the problem for the case of single sensor failure situation by defining a set of convex constraints. Hence preserving convexity of our earlier formulation and guaranteeing globally optimal solutions. The proposed approach is exemplified using an evaporator system.

2. Problem Formulation

In this section, we present a systematic approach of reformulating the sensor network selection problem based on process economics. First, we present the data reconciliation problem followed by which sensor network design formulation for data reconciliation is presented. Next, we define the set of constraints that accounts for sensor failure situation.

2.1. Data reconciliation

Data reconciliation is a method to improve the accuracy of the measurements corrupted by random noise, given the process model and description of noise. Chmielewski et al. (2002) have proposed a formulation by defining the measurement vector by incorporating

*sridharkrn@iitm.ac.in

the process model as: $y = Cz_p + v$, $v \in \mathcal{N}(0, \Sigma_v)$; where C is a process matrix and z_p denotes primary variables (defined as any set of variables that form a minimum observable network). It is important to note that the vector y denotes the set of all variables of interest which contains both measured and unmeasured variables. Also note that fixing z_p fixes the process matrix C which is independent of the sensor network to be chosen. For more details, the reader is referred to Chmielewski et al. (2002). Thus, the reformulated reconciliation problem is unconstrained and is stated as:

$$\min_{\hat{z}_p} (y - C\hat{z}_p)^T \Sigma_v^{-1} (y - C\hat{z}_p) \tag{1}$$

where $\Sigma_v^{-1} = diag\{\frac{q_i}{\sigma_i^2}\}$ and q_i is a binary variable (0 or 1) denoting that the particular variable is unmeasured or measured respectively. Unmeasured variable ($q_i = 0$) can also be inferred statistically as the sensor with infinite variance. Reconciled estimate of primary variables, $\hat{z}_p = (C^T \Sigma_v^{-1} C)^{-1} C^T \Sigma_v^{-1} y$ and hence the reconciled estimate of all variables of interest, $\hat{z} = C\hat{z}_p$. The covariance matrix of estimation error is given by

$$\Sigma_z = C(C^T \Sigma_v^{-1} C)^{-1} C^T \tag{2}$$

It is important to recall that data reconciliation adjusts the given measurement data such that the residual is minimized. However, sensor network design objective is to select those variables that result in least residual for the assumed measurement noise characteristics. Hence the formulation (1) is of direct use for sensor network design where q_i is the decision variable.

2.2. Sensor network design

Sensor network plays a significant role in the optimal and safe operation of a chemical plant. The typical objective of the sensor network design problem based on reconciliation framework is to minimize average error i.e., $Tr(\Sigma_z)$ (Narasimhan and Jordache, 2000) where $Tr(.)$ denotes the trace operator. Recalling $\Sigma_v^{-1} = diag\{\frac{q_i}{\sigma_i^2}\}$, the sensor network design problem can be mathematically stated using expression (2) as:

$$\min_{q_i} \quad Tr(C(C^T \Sigma_v^{-1} C)^{-1} C^T) \tag{3}$$

where the invertibility of $C^T \Sigma_v^{-1} C$ signifies that the system is observable. However for the average error to be minimum, $C^T \Sigma_v^{-1} C$ has to be positive definite. As discussed in section 1, to quantify in terms of process economics we have recently proposed a formulation that minimizes the weighted error variances i.e., $Tr(W\Sigma_z)$ (Nabil and Narasimhan, 2012). The sum of weighted error variances is called "average loss" as it represents the operational loss in profit caused due to measurement error. Thus, economically optimal sensor network is obtained by solving

$$\min_{\hat{q}_i} \quad \tfrac{1}{2} Tr(WC(C^T \Sigma_v^{-1} C)^{-1} C^T) \tag{4}$$

where the weighting matrix $W = RR^T$ is a function of the economic objective function J. The formulation is a non linear integer programming problem. However, it could be transformed into easily solvable Linear Matrix Inequalities (LMIs) using convex optimization

theory (Boyd and Vandenberghe, 2004). For the purpose of brevity, only the final form of the optimization formulation which is a mixed integer cone problem is presented here:

$$\min_{t,q_i,Y} \quad \overline{L} = \tfrac{1}{2}t \tag{5a}$$

$$s.t. \quad Tr(Y) \leq t \tag{5b}$$

$$Y \succ 0 \tag{5c}$$

$$\begin{bmatrix} Y & R^T C \\ (R^T C)^T & (C^T \Sigma_v^{-1} C) \end{bmatrix} \succ 0 \tag{5d}$$

$$\textstyle\sum_{i=1}^{n_z} c_i q_i \leq c^* \tag{5e}$$

where the scalar t and matrix Y are the internal variables created during convexification of the constraints. Additionally, the last constraint (5e) is imposed to restrict the number of sensors being chosen based on the maximum allowable capital cost (c^*) where c_i denotes the cost of selecting the ith sensor.

Sensor Failure Case: The primary requirement of any fault diagnostic approach is detecting and identifying the origin of faults. Hence, the selection of a suitable sensor network plays a key role in the detection of faults. Sensors should be selected such that the system is observable in case of any process faults and sensor faults. Typical fault diagnostic sensor network designs are based on digraph or signed digraph approach. Later, to handle sensor faults, the term reliability was defined based on the sensor failure probability information to quantify the unobservability value of the variables. Thus, a sensor network that maximizes the least reliability is typically chosen. However, this reliability is showed to be dual to the error variance problem (Kotecha et al., 2008). Therefore, maximizing reliability is equivalent to minimizing error variances. However, this metric is not readily deciphered by the operators as discussed earlier. Hence, our current focus is to design an economically optimal sensor network that can handle sensor failure situations in addition to data reconciliation.

To this end, we use redundant measurements which are not only useful in improving the accuracy of measurements but also helps us to observe the system when some sensor fails. Without loss of generality, it is assumed here that only one sensor can fail at a time. Although the formulation (5) could result in redundant measurements, it might not be observable in case of sensor failures. Thus, a new set of observability conditions have to be imposed that would yield a redundant sensor network of degree one (i.e., if any one of the sensor fails, the system is still observable). For the system to be observable, it is mentioned earlier that $C^T \Sigma_v^{-1} C$ has to be positive definite. Hence, with our weighted variance formulation, to account for a single sensor failure situation, the following 'n' (number of potential variables available for measurement) additional constraints have to be imposed such that all $C^T \Sigma_v^{-1} C$ is positive definite:

$$C^T \begin{bmatrix} 0 & 0 & 0 & 0 & 0 \\ 0 & \frac{q_2}{\sigma_2^2} & 0 & 0 & 0 \\ 0 & 0 & \frac{q_3}{\sigma_3^2} & 0 & 0 \\ 0 & 0 & 0 & \ddots & 0 \\ 0 & 0 & 0 & 0 & \frac{q_n}{\sigma_n^2} \end{bmatrix} C \succ 0, \text{ if first sensor fails}$$

$$C^T \begin{bmatrix} \frac{q_1}{\sigma_1^2} & 0 & 0 & 0 & 0 \\ 0 & 0 & 0 & 0 & 0 \\ 0 & 0 & \frac{q_3}{\sigma_3^2} & 0 & 0 \\ 0 & 0 & 0 & \ddots & 0 \\ 0 & 0 & 0 & 0 & \frac{q_n}{\sigma_n^2} \end{bmatrix} C \succ 0, \text{ if second sensor fails and so on.}$$

The above defined matrix inequality constraints ensures that the system is observable if that sensor fails. In other words, the formulation finds a sensor network with one degree of redundancy.

For the case of multiple sensor failures, ${}_nC^r$ additional constraints have to be imposed where 'r' denotes the number of sensors that can fail at a time. In such a case, the formulation (5) along with the suitable set of constraints would yield a degree 'r' redundant sensor network. However, multiple sensors failing at a time is less common in practice and hence not discussed further.

As the above constraints are convex in relaxed form, the mixed integer cone programming formulation of problem (5) is preserved and hence solved using a branch and bound technique to obtain a globally optimal sensor network. In this work, the problem is solved using YALMIP, a freely available software for solving convex optimization problems (Löfberg, 2004).

3. Case study: Evaporator system

Consider the forced circulation evaporation process. The details of the system including the mathematical model, operational constraints, objective function and nominal optimal values are given in Nabil and Narasimhan (2012). The process model has five degrees of freedom assuming the active constraints are enforced. Therefore, at least five variables have to be measured for the system to be observable for data reconciliation. However, if any of the sensor fails then the system is always unobservable. Hence, the redundant sensor network of at least degree one is required to handle single sensor failing at a time.

In the proposed formulation (5), redundant measurements are chosen based on the available capital cost (c^*). In this case study, the cost of flow, temperature and pressure sensors are assumed to be 100 \$, 150 \$ and 200 \$ respectively to show the effect of available monetary resource. Here we present the results of formulation (5) for two case: without and with sensor failure conditions. The corresponding economically optimal sensor networks obtained are tabulated in Table 1 and Table 2 respectively. Up to the available resource of 600 \$, only five sensors could be selected as shown in Table 1 and hence there is no feasible sensor network available to account for sensor faults. With 650 \$ of available resource, the economically optimal network obtained for both the cases are the same. However, for the available resource of 700 \$, the optimal network is different for the two cases considered. This implies that, although the sensor network $\{F_2, F_3, F_5, F_{100}, F_{200}, P_2\}$ result in a lower average loss than the network $\{F_2, F_3, F_5, F_{100}, F_{200}, T_{201}\}$, the latter can handle sensor failure situation while the former cannot. From the result obtained for the available resource of 750 \$, it can be inferred that the available resource is utilized to exploit redundancy by selecting more sensors for sensor failure situation than the one solved for reconciliation only. Indeed, the average loss is the same for both cases. It is also important to observe that increasing the number of measurements show a decrease in operational loss (due to measurement noise) which is because redundancy improves the data.

Table 1. Optimal sensor network for data reconciliation only

Available resource, c^* ($)	Sensor Network	Sensor cost ($)	Average loss ($/h)
500	$F_2, F_3, F_5, F_{100}, F_{200}$	500	12.2
550	$F_2, F_3, F_{100}, F_{200}, T_{201}$	550	10.28
600	$F_2, F_3, F_{100}, F_{200}, T_{201}$	550	10.28
650	$F_2, F_3, F_5, F_{100}, F_{200}, T_{201}$	650	9.57
700	$F_2, F_3, F_5, F_{100}, F_{200}, P_2$	700	9.48
750	$F_2, F_3, F_5, F_{100}, F_{200}, P_2$	700	9.48
800	$F_2, F_3, F_5, F_{100}, F_{200}, T_2, T_{201}$	800	9.10

Table 2. Optimal sensor network for both data reconciliation and sensor failure situations

Available resources, c^* ($)	Sensor Network	Sensor cost ($)	Average loss ($/h)
upto 600	Infeasible	-	-
650	$F_2, F_3, F_5, F_{100}, F_{200}, T_{201}$	650	9.57
700	$F_2, F_3, F_5, F_{100}, F_{200}, T_{201}$	650	9.57
750	$F_1, F_2, F_3, F_5, F_{100}, F_{200}, T_{201}$	750	9.48
800	$F_2, F_3, F_5, F_{100}, F_{200}, T_2, T_{201}$	800	9.10

4. Conclusion

Sensor network design procedure that can handle both data reconciliation and sensor failure simultaneously based on process economics was presented. The relaxed formulation is convex and thus yielding globally optimal solution. In summary, the redundant sensor network that is observable even if some sensor fail could be found using the proposed framework. The approach was successfully demonstrated using the evaporator system.

References

Bhushan, M., Rengaswamy, R., 2000. Design of sensor network based on the signed directed graph of the process for efficient fault diagnosis. Ind. & Eng. Chem. Res. 39 (4), 999–1019.

Boyd, S., Vandenberghe, L., 2004. Convex Optimization. Cambridge University Press, NY, USA.

Chmielewski, D. J., Palmer, T., Manousiouthakis, V., 2002. On the theory of optimal sensor placement. AIChE Journal 48 (5), 1001–1012.

Kotecha, P., Bhushan, M., Gudi, R., Keshari, M., 2008. A duality based framework for integrating reliability and precision for sensor network design. Jr. of Process Control 18, 189 – 201.

Löfberg, J., 2004. Yalmip : A toolbox for modeling and optimization in MATLAB. In: Proceedings of the CACSD Conference. Taipei, Taiwan.

Nabil, M., Narasimhan, S., 2012. Sensor network design for optimal process operation based on data reconciliation. Ind. & Eng. Chem. Res., under review.

Narasimhan, S., Jordache, C., 2000. Data reconciliation & gross error detection: an intelligent use of process data. Gulf Publishing Co., Houston, TX, USA.

I.A. Karimi and Rajagopalan Srinivasan (Editors), Proceedings of the 11th International Symposium on Process Systems Engineering, 15-19 July 2012, Singapore

Reallocation Index Based Sensor Network Design for Efficient Fault Diagnosis

Suryanarayana Kolluri, Mani Bhushan *

Department of Chemical Engineering, Indian Institute of Technology Bombay, Mumbai-400076, India

Abstract

A novel concept of reallocation index is proposed and incorporated in the base case design of sensor networks from a fault diagnostic perspective. Reallocation index indicates the possibilities of future reallocations of sensors. Maximization of reallocation index is added as an objective during sensor network design. The resulting design is then optimal not only for the base case, but also ensures that any future upgrade and reallocation can be carried out effectively with less cost. The proposed sensor network design approach is illustrated on the Tennessee Eastman challenge problem. It is shown that the design obtained after consideration of reallocation index performs much better than the design obtained without reallocation index.

Keywords: Sensor Locations, Reallocation Index, Fault Diagnosis, Optimization

1. Introduction

The problem of sensor network design is to choose the variables to be measured to optimize some criteria while satisfying various technical and economic constraints. Several approaches have been proposed in literature for designing sensor networks for various criteria such as those related to estimation-reliability, estimation-precision, gross error detection, data reconciliation and fault diagnostic relevant information, etc. (Bagajewicz, 2002). Most of the work in the area of sensor network design is for base case scenarios when the process does not have any existing sensors. However, over a period of time, the process usually goes through significant changes since the operating conditions of the process may change. Additionally new equipments can be added or deleted from the process. Due to these changes a design, which was optimal to begin with, may no longer be optimal or even adequate for meeting the requirements for the existing process. Hence, for existing processes a relevant problem is of sensor network retrofit, i.e. modifying an existing sensor network to meet specific requirements or improving the quality of information available about the process. Recognizing this need, Bagajewicz and Sanchez (2000) proposed a reallocation and upgrade formulation which allows optimal modification of an existing network while maximizing performance related to precision. In their formulation, new sensors can be added (termed upgrade) or existing sensors can be transferred to other variables (termed reallocation). Bhushan et al. (2003) used the upgrade and reallocation idea of Bagajewicz and Sanchez (2000) for retrofitting an existing sensor network from a fault diagnostic perspective. There are few other approaches that directly incorporate possibilities of process change during base case design. Bo and Bing-Zhen (2002) considered the notion of sensor network flexibility (ability to observe variables when new streams are added) in the base case sensor network design for linear processes.

*mbhushan@iitb.ac.in

Bhushan et al. (2008) proposed maximizing network distribution (number of measured variables) during base case design so that the resulting design is robust to future changes in the process.

In this paper, we propose a novel reallocation index based approach to integrate sensor network retrofit with the design problem. The objective is to maximize possibilities of reallocation of sensors in future without compromising on the optimality of base case design. This is possible since often there are multiple solutions for the base case design problem. So, our approach is to select, amongst those multiple solutions, the solution which enables maximum number of reallocations in future. The idea being that in case of significant variations in the process/operating conditions, it will be easy (for example, cost-wise) to retrofit the existing network while achieving the desired performance objectives. We apply our approach to the problem of sensor network design from a fault diagnostic perspective where the process is modeled as a signed digraph. However, the proposed idea of reallocation index can be easily incorporated with problem of sensor network design for other objectives and model types as well. This paper is structured as follows: in section 2 we briefly summarize the previous relevant work in the area of sensor network design and retrofit for fault diagnosis while in section 3 we propose the reallocation index based design formulation. In section 4 we apply our design idea to the well known Tennessee Eastman challenge process and compare the resulting sensor network to the network obtained from literature, before concluding in section 5.

2. Previous Related Work

The optimization formulations proposed for sensor network design for fault diagnosis are based on the concept of “unreliability of fault" which is defined as the probability of a fault occurring and remaining undetected due to simultaneous failure of sensors affected by that fault. For i^{th} fault, the unreliability is (Bhushan et al., 2008):

$$U_i = f_i \prod_{j=1}^{n} (s_j)^{(B_{ij}x_j)} \tag{1}$$

where f_i is the probability of occurrence of fault i, s_j is the failure probability of sensor placed on variable j, n is the number of variables in the process and matrix B is the fault-variable bipartite matrix such that $B_{ij} = 1$ if fault i affects variable j and is 0 otherwise. For various scenarios, such as single fault observability and resolution, the matrix B can be obtained from the cause-effect matrix A which in turn is obtained by analyzing the effect of faults on variables such as that obtained from the process signed digraph (Bhushan and Rengaswamy, 2002).

2.1. Base Case Design of Sensor Networks for Fault Diagnosis

Bhushan and Rengaswamy (2002) proposed the following optimization formulation for base case sensor network design for minimizing system unreliability:

$$\textbf{Formulation I:} \quad \min_{x_j, U, x_s} [U - \alpha x_s] \tag{2}$$

subject to:

$$U \geq \log U_i, \;\; i = 1, ...m; \;\; \sum_{j=1}^{n} c_j x_j + x_s = C^* \tag{3}$$

$$x_j \in \mathbb{Z}^+, \;\; j = 1, ...n; \;\; x_s \in \mathbb{R}^+; \;\; U \in \mathbb{R}^- \tag{4}$$

In the above formulation, the objective function U is the system unreliability defined as the maximum unreliability of detection amongst all faults (m in number). c_j is the cost of the sensor for measuring j^{th} variable, C^* is the available cost for selecting sensors, x_j is the main decision variable which indicates the number of sensors placed at j^{th} variable and variable x_s indicates the cost unused for the given C^*. Variable x_s becomes relevant since for the same optimal U different sensor networks with different costs can be obtained (multiple optimal solutions). The positive constant α in the objective function ensures that the least cost solution is chosen amongst these multiple solutions.

2.2. Reallocation and Upgrade of Sensor Networks for Fault Diagnosis

Bagajewicz and Sanchez (2000) proposed optimization formulations for reallocation and upgrade of sensor networks for improving precision of the estimated parameters. This idea was implemented by Bhushan et al. (2003) for retrofitting sensors from a fault diagnostic perspective as:

$$\textbf{Formulation II:} \quad \min_{x_j, q_j, u_{t,r}, x_s, U} [U - \alpha x_s] \tag{5}$$

subject to:

$$U \geq \log U_i, \;\; i = 1, ...m; \quad \sum_{j=1}^{n} c_j q_j + \sum_{t \in M_t} \sum_{r \in M_r} h_{t,r} u_{t,r} + x_s = C^* \tag{6}$$

$$x_j = q_j + x_j^* - \sum_{r \in M_r} u_{j,r}, j \in M_t, \notin M_r; \;\; x_j = q_j + x_j^* + \sum_{t \in M_t} u_{t,j}, j \in M_r, \notin M_t \tag{7}$$

$$x_j = q_j + x_j^* + \sum_{t \in M_t} u_{t,j} - \sum_{r \in M_r} u_{j,r}, j \in M_r \cap M_t; \;\; x_j = q_j + x_j^*, j \notin M_r \cup M_t \tag{8}$$

$$\sum_{r \in M_r} u_{j,r} \leq x_j^*, j \in M_t; \quad x_j, q_j, u_{t,r} \in \mathbb{Z}^+; \quad U_i \in \mathbb{R}^- \tag{9}$$

In the above formulation, x_j is the total number of sensors placed at j^{th} variable which is a sum of: new sensors (q_j), existing sensors (x_j^*), sensors reallocated to variable j ($u_{t,j}$) or away from variable j ($u_{j,r}$). $h_{t,r}$ is the cost for reallocating a sensor from variable t to r, M_t is the set of variables whose sensors can be reallocated to other variables and M_r is the set of variables which can receive sensors from other variables. Other constraints are as in Formulation I.

3. Reallocation Index Based Sensor Network

In the current work, we propose incorporation of reallocation index in the design of sensor networks. For a given sensor network, reallocation index (R_I) is defined as the total number of variables to which sensors can be transferred for a given sensor network:

$$R_I = \sum_{j=1}^{n} n_j \left(\sum_{k=1}^{n} M_{jk} \right) \tag{10}$$

where M_{jk} is the $(j,k)^{th}$ element of the reallocation compatibility matrix M, such that $M_{jk} = 1$ if sensor can be transferred from variable j to variable k and is 0 otherwise. The matrix M is assumed to be available during the design stage. n_j is a decision variable computed such that $n_j = 1$ if j^{th} variable is measured (irrespective of the number of

sensors placed on variable j) and is 0 if j^{th} variable is not measured. Our proposed base case design formulation is:

$$\textbf{Formulation III:} \quad \min_{x_j,U,x_s,n_j} [\lambda_1 U - \lambda_2 R_I - x_s] \tag{11}$$

subject to:

$$U \geq \log U_i, \;\; i = 1,....m; \quad \sum_{j=1}^{n} c_j x_j + x_s = C^* \tag{12}$$

$$n_j \leq x_j; \quad n_j \in \{0,1\}; \quad x_j \in \mathbb{Z}^+, j = 1,...n; \quad x_s \in \mathbb{R}^+; \quad U \in \mathbb{R}^- \tag{13}$$

with R_I as given in equation 10. In the above formulation, similar to the idea in Formulation I presented earlier, R_I is optimized while ensuring that U achieves its optimal value. The third objective x_s will minimize the cost used if the problem still has multiple solutions. The procedure for calculating weighting factors λ_1 and λ_2 to ensure this lexicographic optimization is given in Bhushan et al. (2008). The resulting optimization formulation is mixed integer linear programming (MILP) problem.

4. Case Study: Tennessee Eastman Process

The proposed optimization formulation incorporating reallocation index is applied to the Tennessee Eastman process (Downs and Vogel, 1993). The major unit operations in the process are: an exothermic two phase reactor, product condenser, flash separator, reboiled stripper and a recycle compressor. There are 50 measurable variables and 33 faults in the process (Bhushan et al., 2008). The data for sensor failure probabilities, fault occurrence probabilities, sensor costs and matrix B (bipartite matrix) which gives the information of fault affecting variables is taken from Bhushan et al. (2008). Sensor networks resulting from the proposed formulation (Formulation III) are tabulated in Table-1. These were obtained by solving the MILP optimization problems in CPLEX®. Corresponding to a given available cost C^*, the table lists the U, R_I and x_s values alongwith the sensors selected by formulation III. In the last column in the table, the number in bracket indicates the number of sensors selected. For example, 45(2) indicates 2 sensors are placed on variable 45. As expected, as the available cost C^* increases, the system unreliability of detection decreases or remains the same.

Comparison of Sensor Network Designs Obtained with and without Reallocation Index:
To demonstrate the utility of the resulting sensor networks the following numerical experiment is conducted for results obtained with $C^* = 6000$. Let S_1 be the sensor network obtained using proposed formulation for this case as listed in Table 1. Base case sensor network design without considering reallocation index (formulation I) is also obtained for $C^* = 6000$ as listed in Bhushan et al. (2008). Let this sensor network be labeled S_2. The two networks then are:

$S_1 = [1,2,3,4,5,6,8,9,13,42,43,45(2),46,47(2),48,49(2),50]$
$S_2 = [3,4,5,8,9,13,42,43,45(2),46,47(2),48,49(2),50]$

To evaluate the performance of the two networks after retrofit (using formulation II), the cause-effect matrix (A) which contains affect of original faults on variables as +1 (positive effect), -1 (negative effect), 2 (effect with unknown sign) and 0 (no effect) is randomly perturbed. This perturbation simulates unknown changes in the process. In particular,

randomly chosen +1 entries are changed to -1 or 2 and similarly randomly chosen -1 entries are changed to +1 or 2. The new fault-variable bipartite matrix B is generated again using single fault resolution procedure (Bhushan and Rengaswamy, 2002). With this bipartite matrix, reallocation and upgrade of the base case sensor networks is performed using formulation-II (with $C^* = 6000$) for two cases: first with S_1 and then with S_2 as the existing sensor network. This process is carried out for 1000 realizations. It was found that for about 73% of the cases, lower cost was used to retrofit network S_1 compared to the cost used for retrofitting S_2 while at the same time obtaining same or lower system unreliability. This demonstrates that incorporating R_I in the design stage has enabled efficient retrofit.

C^*	x_s	U	R_I	Sensors selected
1000	100	-2	8	1,2,3,4,13
4000	700	-2	11	1,2,3,4,6,7,13,22
6000	300	-5	12	1,2,3,4,5,6,8,9,13,42,43,45(2),46,47(2),48,49(2),50
10000	50	-8	12	1,2,3(2),4(2),5(2),6,8(2),9(2),13(2),42(2),43(2),45(3),46(2),47(3),48(2),49(3),50(2)

Table 1. Results for base case design with reallocation index

5. Conclusions

In this work, a novel concept of reallocation index is proposed for sensor network design. Incorporation of reallocation index during base case design ensures effective retrofit in future by creating possibilities for reallocation of sensors. The resulting optimization formulation is a mixed integer linear programming (MILP) problem. The utility of the approach is demonstrated on the Tennessee Eastman process for obtaining sensor networks that maximize fault diagnosis related criteria. Application of the proposed ideas for sensor network design for other objectives can also be investigated.

References

Bagajewicz, M., 2002. A review of techniques for instrumentation design and upgrade in process plants. Canadian Journal of Chemical Engineering 80, 3–16.

Bagajewicz, M., Sanchez, M., 2000. Reallocation and upgrade of instrumentation in process plants. Comput. Chem. Engng. 24, 1945.

Bhushan, M., Narasimhan, S., Rengaswamy, R., 2003. Sensor network reallocation and upgrade for efficient fault diagnosis. In: Fourth International Conference on Foundations of Computer-Aided Process Operations, Coral Springs, Florida, USA. pp. 443–446.

Bhushan, M., Narasimhan, S., Rengaswamy, R., 2008. Robust sensor network design for fault diagnosis. Comput. Chem. Engng. 32, 1067–1084.

Bhushan, M., Rengaswamy, R., 2002. Comprehensive design of a sensor network for chemical plants based on various diagnosability and reliability criteria: I. framework. Ind. Eng. Chem. Res. 41, 1826–1839.

Bo, L., Bing-Zhen, C., 2002. Study on flexibility of sensor network for linear processes. Comput. Chem. Engng. 26, 1363–1368.

Downs, J. J., Vogel, E. F., 1993. A plant-wide industrial process control problem. Comput. Chem. Engng. 17 (3), 245.

I.A. Karimi and Rajagopalan Srinivasan (Editors), Proceedings of the 11th International Symposium on Process Systems Engineering, 15-19 July 2012, Singapore.

A Graphic Processing Unit (GPU) Algorithm for Improved Variable Selection in Multivariate Process Monitoring

Lau Mai Chan[a], Rajagopalan Srinivasan[a,b]

[a] *Department of Chemical and Biomolecular Engineering, National University of Singapore, Singapore, 10 Kent Ridge Crescent, Singapore 119260, Singapore*
[b] *Process Sciences and Modeling, Institute of Chemical and Engineering Sciences, Pesek Road, Jurong Island, Singapore 627833, Singapore*

Abstract

Process monitoring is extremely important for producing high quality product and at the same time ensuring safe working environment in chemical process industry. Recently, it has been shown that selection of an appropriate subset of variables can improve the monitoring performance. The main contribution of this work is the development of a parallel version of the Genetic Algorithm-Principal Component Analysis algorithm which was proposed by Ghosh et al. [2] for variable selection. The developed algorithm has been implemented using NVIDIA's Compute Unified Device Architecture, CUDA parallel computing platform. Experimental results show that the proposed parallel approach is 12 times faster than the original serial code when applied to the Tennessee Eastman challenge problem.

Keywords: Genetic Algorithm, Compute Unified Device Architecture (CUDA), Graphics Processing Unit (GPU) parallel computing, Variable Selection.

1. Introduction

Process monitoring involves quick detection of process abnormal behavior as soon as the fault occurs, so that the corrective action can be taken promptly and losses can be minimized. Recently, it has been shown [1] that selection of an appropriate subset of variables can improve the monitoring performance. As the genetic algorithm-principal component analysis (GA-PCA) algorithm proposed in [2], the variable selection problem can be solved as a multi-objective optimization problem in which two objectives are (i) maximization of monitoring performance, and (ii) minimization of number of variables. This work was inspired by the successful deployment and acceleration of a wide variety of data mining and optimization problem through graphics processing unit computing. The objective of this work is to develop and evaluate the GPU version of a variable selection algorithm. Accelerated variable selection is desirable especially when large training dataset is involved. Furthermore, variable selection is required whenever process dynamics change is required. Since the variable selection problem is structured as a simulation optimization problem, the proposed parallelization approach with the use of GPU computing could be generalized and applied to a variety of simulation optimization techniques. Simulation optimization techniques are important tools in optimizing complex systems such as the supply chain management (SCM) system and decision support system (DSS), where expensive computational cost is known to be the major challenge for their practical applications. Hence, a computational efficiency improvement is highly desirable.

2. Graphics Processing Unit (GPU) Computing

GPU was originally designed for graphics rendering applications. Due to the massive parallelism of GPU by having many cores, GPU has evolved into General Purpose GPU (GPGPU) as a solution for tackling data explosion issues. Further development of GPGPU into GPU computing is done by introducing the general purpose programming interface as a replacement of the graphical programming API. Compute Unified Device Architecture (CUDA), developed by NVIDIA, is an architecture that attempts to harness the computing power of GPGPU. GPUs work as co-processors for CPU and this is done through incorporating CUDA kernels into the serial CPU program, from which computational acceleration can be achieved. A CUDA kernel is a function written in CUDA language, that when called, are executed N times in parallel by the N different CUDA threads.

Successful implementation of GPU computing include the parallel k-nearest neighbor algorithm developed in [3] which has achieved a 15 times speedup; [4] proposed the implementation of PCA on GPGPU with the use CUDA Basic Linear Algebraic Subroutines (cuBLAS) and 12 times acceleration was reported; [5] worked on an island model of GA which results in 7000 times speedup; and [6] reported the parallel GA algorithm was up to 400 times faster than the serial code. On the other hand, it has also been noticed that the application of GPU computing has been restricted to rather simple problems. The objective of this work is to study the performance of GPU computing on real life problem in the process monitoring perspective. This is done by developing and applying the parallel GA-PCA on the Tennessee Eastman challenge problem.

3. GPU implementation of GA-PCA

A PCA model for process monitoring can be constructed with all the measured process variables or a subset of these measured variables. In this work, we are interested to identify the subset of variables which is sensitive to faults; therefore a PCA model constructed using this subset is expected to have improved monitoring performance. To identify these variables, Ghosh et al. [2] proposed a multi objective GA-based stochastic optimization technique which minimizes the cumulative error rate, defined as sum of miss detection and false alarm rates, while at the same time minimizing the number of selected variables.

The main contribution of this work is the development of the parallel version of the GA-PCA algorithm which mainly involves the design of the CUDA kernel functions. Here, we propose to parallelize and include the most time consuming tasks of the serial GA-PCA code including PCA modeling and validation, in the CUDA kernels. Since the variable selection process is performed in MATLAB, the CUDA kernels are integrated into the MATLAB program through the use of MATLAB's MEX function.

The achieved computational efficiency improvement is closely related to a number of interrelated factors involved in the kernel design, and a series of experiments need to be carried so as to attain an optimal design. There are four important design factors to be discussed here in respect to GA-PCA algorithm. The first one is the execution configuration which includes both the grid size and block size. In evolutionary algorithm, it is intuitive to assume each chromosome as a block except for cases where the calculations for fitness value are extremely simple. In other words, the number of block in a grid is equal to the population size. As for the block size, as numerical methods like Jacobi transformation used for constructing PCA model are iterative

processes, it is more appropriate to have small thread block size. This is because large thread block will result in long waiting time at the point of barrier synchronization. Such waiting time becomes enormous as iteration increases. On the contrary, fitness evaluation in GA requires large thread block for optimal performance. This is because testing dataset is usually extremely large and the validation calculation on them tends to result in high computational intensity; besides the validation of testing sample is independent of each other, hence more threads are likely to provide higher parallelism without causing long waiting time. It should be noted that tasks require distinguished block size should be put into different kernels. The second design factor is the algorithmic level of parallelism. In PCA modeling step, a thread can be assigned a row or a column or a matrix element, in the case of fitness evaluation step, except for such element-level parallelism, a thread can also be assigned to a testing sample.

Memory type is another critical design factor need to be considered. In CUDA architecture, there are five memory types including global memory, texture memory, constant memory, shared memory and register. The different types of memory are characterized by memory bandwidth, lifetime, writability and the storage space. In the GA-PCA algorithm, data that is being modified repeatedly through thread cooperation such as covariance matrix, eigenvalues and eigenvectors should be stored in the shared memory if the size of data is sufficiently small. On the other hand, both training data and testing data may be too large to be stored in shared memory. In this case, global memory, texture memory or constant memory may be used since the data is for read only purpose. It should be noted that unique access patterns are required for texture and constant memory; otherwise global memory would be preferred. The last design factor to be covered here is the memory accessing pattern. Program developers should be aware that data transposition can sometime be used to take advantage of the coalesced memory access pattern of the global memory. Moreover, padding technique [7] which adds an extra column and/or row on matrix/vector may also help to reduce the occurrence of bank conflicts on shared memory. The objective of such techniques is to improve the memory transferring speed within GPU or between GPU and CPU. By considering these factors, a proposed parallel GA-PCA algorithm (in Matlab) is given in Fig. 1.

4. Application to Tennessee Eastman Challenge Process

The performance of the proposed parallel GA-PCA algorithm is evaluated by applying the algorithm to the benchmark Tennessee Eastman (TE) process. The TE process was designed for evaluating the performance of process control and monitoring, details can be found in [8]. TE process contains 52 process variables and 21 programmed faults. We have focused on 32 pre-selected variables. In this case study, the GA-PCA algorithm is used to identify the most informative variables that are affected significantly by the 21 programmed faults. The selected subset of variables is used to construct a reduced-PCA model [2] that has better monitoring performance as compared to a full PCA model with all the variables. The system used in this work is 32-bit Intel Core 2 Quad at 3.00GHz and 4.00GB of RAM, and an Nvidia Quadro2000 card.

Experimental results has shown that at the end of 1000 generations, the two objective values obtained from serial and parallel algorithm are equivalent for population size up to 1000. For instance, at population size of 100, both serial code and parallel code resulted in maximum 14 variables and the corresponding reduced-PCA models were reported to have comparable false detection rate, which is 0.26. On the other hand, the improvement in computation efficiency achieved by this parallel GA-PCA algorithm

was studied at various population sizes, as shown in Fig. 2. The optimal performance speedup was found at population size in the range of [40 80] which is about 12.4 times faster than the serial version; where the actual times are reduced from 10.3 min and 21.5 min to 0.8 min and 1.7 min at population size 40 and 80, respectively. Population size that is below this range, for instance 20 chromosomes in a population, results in only up to 10 times speedup. This is because the device resources like stream processors are not fully utilized. On the other hand, as population size increases beyond the point of 80, the computational speedup starts to decrease. There is only 3.47 times acceleration can be expected for population size equal to 1000. Such declining performance is due to the non-dominated sorting step which executes in serial fashion. This serial sorting step consumes significant amount of time when population size is large.

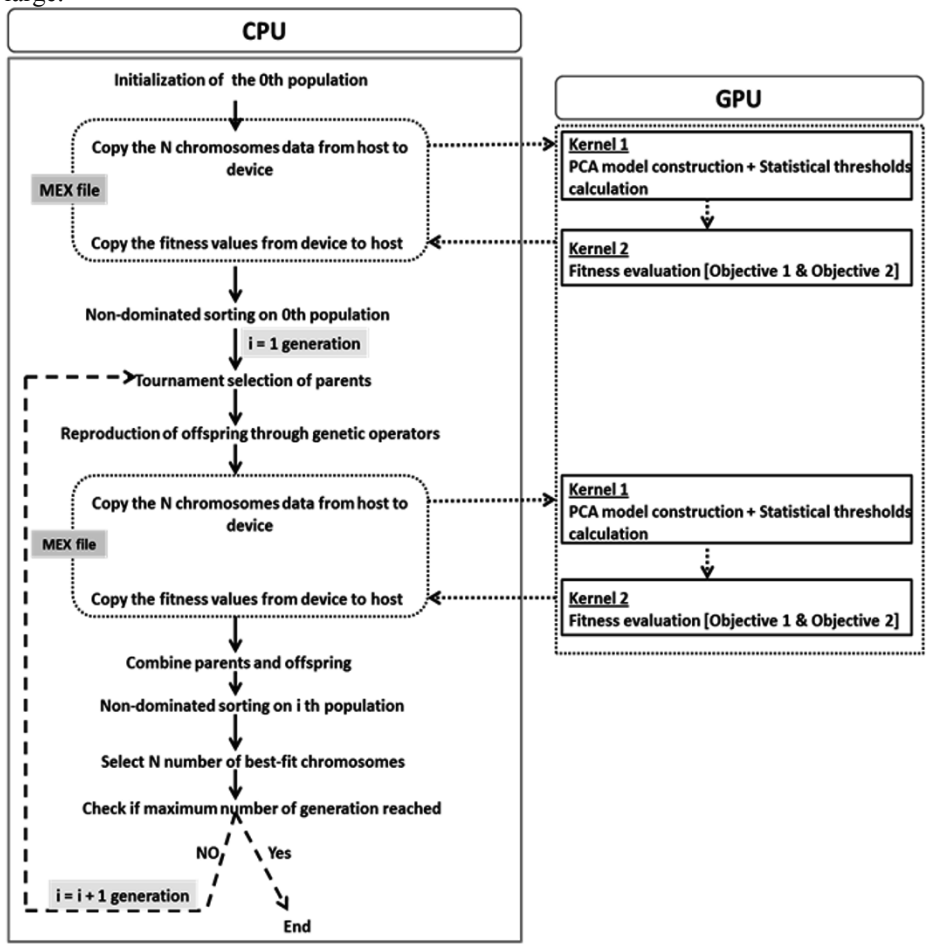

Figure 1: Heterogeneous/ parallel GA-PCA algorithm

5. Conclusions

The parallel GA-PCA algorithm proposed in this work has been shown to improve the computation efficiency of the serial program up to 12 times, when implemented on the Tennessee Eastman challenge problem which is considered as a real life process

monitoring problem. In order to identify the best computational acceleration possible with the proposed parallel GA-PCA algorithm, the effect of reducing the number of generation while keeping the same total amount of computation (by increasing population size) has to be studied and will be the subject of our future work. Future work should also extend to include applications where the size of data is too large to fit in the device memory space.

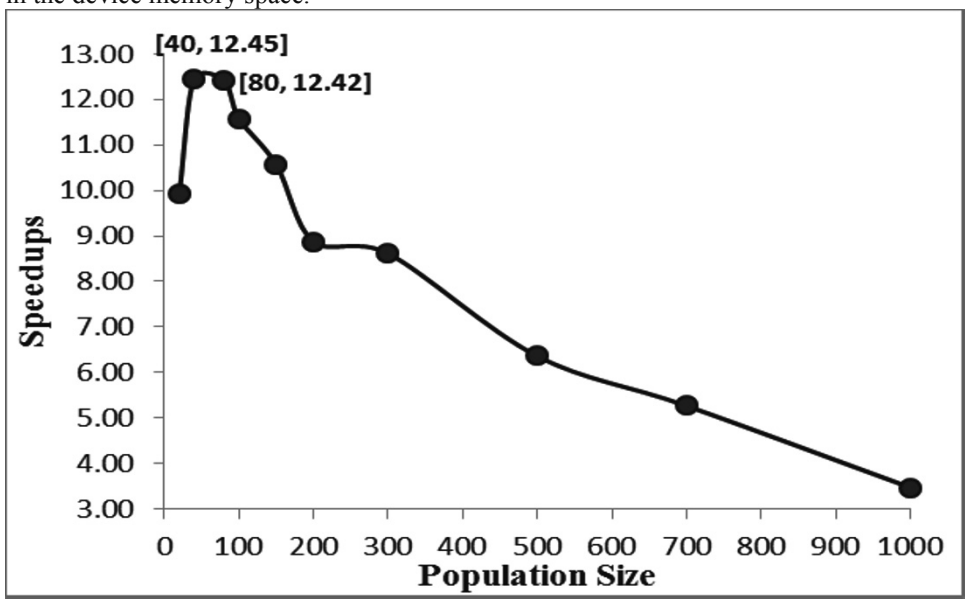

Figure 2: Speedups achieved by the parallel GA-PCA algorithm with respect to the serial algorithm. Experiments were conducted based on 1000 generations and 10 replicates of run. The relative standard deviations of the 10 runs are less than 5%.

References

[1] Q. Guo, W. Wu, D.L. Massart, C. Boucon, S. de Jong, Chemom, 2002, Feature selection in principal component analysis of analytical data, *Chemometrics and Intelligent Laboratory Systems*, Volume 61, Issues 1-2, Pages 123-132.

[2] Kaushik Ghosh, Manojkumar Ramteke and Rajagopalan Srinivasan, Optimal Variable Selection for Improving Effectiveness of Statistical Process Monitoring, Manuscript submitted for publication.

[3] S. Liang, Y. Liu, C. Wang and L. Jian, 2010, Design and evaluation of a parallel k-nearest neighbor algorithm on CUDA-enabled GPU, In: *ProceedingsIEEE 2nd Symposium on Web Society (SWS)*, Pages 53–60.

[4] M. Andrecut, 2009, Parallel gpu implementation of iterative pca algorithms, *Journal of Computational Biology*, Volume 16, Issue 11, Pages 1593–1599.

[5] P. Pospichal and J. Jaros, 2009, Gpu-based acceleration of the genetic algorithm, in *Genetic and Evolutionary Computation Conference GECCO competition*.

[6] R. Arora, R. Tulshyan and K. Deb, 2010, Parallelization of binary and real-coded genetic algorithms on GPU using CUDA, in *Evolutionary Computation (CEC), 2010 IEEE Congress*, Page 1-8.

[7] NVIDIA CUDA C Best Practices Guide. URLhttp://developer.download.nvidia.com/compute/cuda/4_0_rc2/toolkit/docs/CUDA_C_Best_Practices_Guide.pdf

[8] Downs J. J. and E. F. Vogel, 1993, A plant-wide industrial process control problem, *Computers & Chemical Engineering*, volume 17, No. 3, Pages. 245-255.

I.A. Karimi and Rajagopalan Srinivasan (Editors), Proceedings of the 11th International Symposium on Process Systems Engineering, 15-19 July 2012, Singapore.

Proactive Alarms Monitoring using Predictive Technologies

Shichao Xu[a], Shanqing Yin[b], Rajagopalan Srinivasan[a,c], Martin Helander[b]

[a] *Institute of Chemical and Engineering Sciences , A*STAR, Singapore*
[b] *Nanyang Technological University, School of Mechanical and Aerospace Eng, Singapore*
[c] *National University of Singapore, Dept of Chemical and Biomolecular Eng, Singapore*

Abstract

Chemical plants are now built to have large number of integrated and interlinked process units so as to optimize production and reduce waste. When an abnormal situation occurs, the automation systems alert the operators through alarms and help orient them to the new state. However, as most processes are highly-coupled, many simultaneous alarms can occur resulting in a flood of alarms. This can create confusion among operators, who must diagnose and rectify the fault before the condition escalates. Sometimes when the abnormal situation cannot be properly diagnosed, the operator will then activate the emergency shut-down, resulting in loss of productivity. In this work, we propose a novel alarm management framework, called *proactive alarms monitoring scheme* that provides operators with anticipatory information on incipient alarms that could happen within a certain time-window. This anticipatory information, which is built around a predictive algorithm, seeks to improve the sense-making facilities offered by the alarm system. As such, it allows plant operators to adopt a more proactive approach in managing alarm floods during various abnormal situations.

Keywords: Alarm Management; Hybrid Modeling; Process Monitoring

1. Introduction

Modern chemical plants are complex systems consisting of large number of process units. To optimize production of these plants, process operators and engineers depend on automation systems to extract information (e.g. through the thousands of sensors throughout the plant) and to assist them in the management of operations (e.g. through built-in controllers). When an abnormal situation occurs, there will be alarms which are presented on the operator monitoring screens to alert the operators. As modern chemical plants are highly interlinked and integrated (both up-stream and downstream), this may lead to many alarms occurring at the same time, causing a deluge of alarms, often called alarm flood (Liu et al., 2003, Liu et al. 2004). For inexperienced/novice operators, who rely primarily on alarms to diagnose faults, alarm flooding may lead to more confusion in the control room, resulting in information overload on the part of the operator. This causes the operators to become disoriented and when the problem cannot be promptly diagnosed, emergency shutdown would be triggered, resulting in loss of production, which is undesirable. On the other hand, experienced/expert operators, who have a more complete understanding of the process, tend to utilize trend displays to diagnose faults and predict future process states. This mental prediction helps them diagnose and rectify the abnormal situation early and prevent plant shut downs. While training novice operators to become experts can take years, one way to mitigate this performance gap is to use tools to aid young operators so that they perform just as well as experts. Expert

operators benefit from years of operational experience, which allows them to quickly understand and anticipate situations, as well as proactively initiate appropriate responses. Although younger operators may lack these knowledge and experience, technological intervention can help support and improve this manual decision-making process. One such example can be a predictive display, which provides the operator with information about the process' future state, so as to improve the operator's situation awareness and provide a longer lead time for action. In this paper, we explored a viable concept of developing a predictive alarm monitoring display to facilitate the performance of process control operators.

2. Proactive Alarms Monitoring Scheme

The utilization of predictive aids that help users anticipate future system states already exist in various other domains. For example, The Cockpit Display of Traffic Information found in modern jet airliners presents other aircrafts in the proximity and their trajectories, and alerts the pilots of any potential conflicts, thereby improving pilots' ability to anticipate and reducing their workload (Morphew & Wickens, 1998). Similar applications and benefits were also found in maritime (van Breda, 1990). A more familiar example is in hurricane forecasts, in which powerful simulations extrapolate where oncoming hurricanes will and will not strike. All these examples reflect the common technology of integrating available information in the system / environment to calculate a prediction, and present this result to the user during decision-making.

While predictive displays have been widely used in a variety of areas, it is still not practiced, particularly in the area of alarm management in chemical industries. In this work, a *proactive alarms monitoring scheme* with predictive capabilities is being developed such that control-room operators are provided with anticipatory information on incipient alarms that could happen within a certain time window. By providing this information, operators, both novice and expert, can obtain a complete sense of the true state of the process which would help them, localize and rectify the problem early before the plant reaches a dangerous operating state. Furthermore, the availability of this anticipatory information on alarms in advance of their actual occurrence reduces the confusion in the control room caused by alarm floods and allows efficient handling of abnormal situations.

The proactive alarms monitoring scheme is built around a predictive algorithm, which utilizes dynamic models of the process to anticipate the alarms. Developing dynamic models that are suitable for abnormal situations is particularly a challenge since it must take into account the structural and parametric changes to the nominal model of the process. As a result, these models do not get less and less reliable during abnormal situations when the process deviates further from the nominal operating point, something that existing models used in advanced process control systems (APC) faced. To develop these dynamic models, we proposed a new hybrid modeling strategy that utilizes both first-principles and data-driven modeling techniques. The predictive algorithm will then utilized this hybrid process model to offer an accurate short-term prediction of the rate-of-change of process variables which are then translated into predictions of time horizons for the occurrence of various alarms.

3. Case Study: A Depropanizer Unit

The development of the proactive alarms monitoring scheme is described using a simulation case study of a depropanizer unit. A schematic diagram of the unit is shown in Fig 1. The primary objective of the unit is to separate a feed mixture consisting primarily of C_3 and C_4 hydrocarbons, into two product streams. The lighter product consists primarily of C_{3s} and the heavier product consists of both C_{4s} and heavier hydrocarbons. The depropanizer unit has 24 measured process variables and each of them has its own alarm high and low limits. However, from the point of view of the operator, not all process variables have equal importance. For example, *FI16*, the flow indicator for hot oil to the reboiler, is not as important as compared to *TC11*, that control and highlight any temperature abnormalities for the 34th-tray which also dictates the temperature profile of the column. In this study, 9 process variables were selected for proactive alarms monitoring.

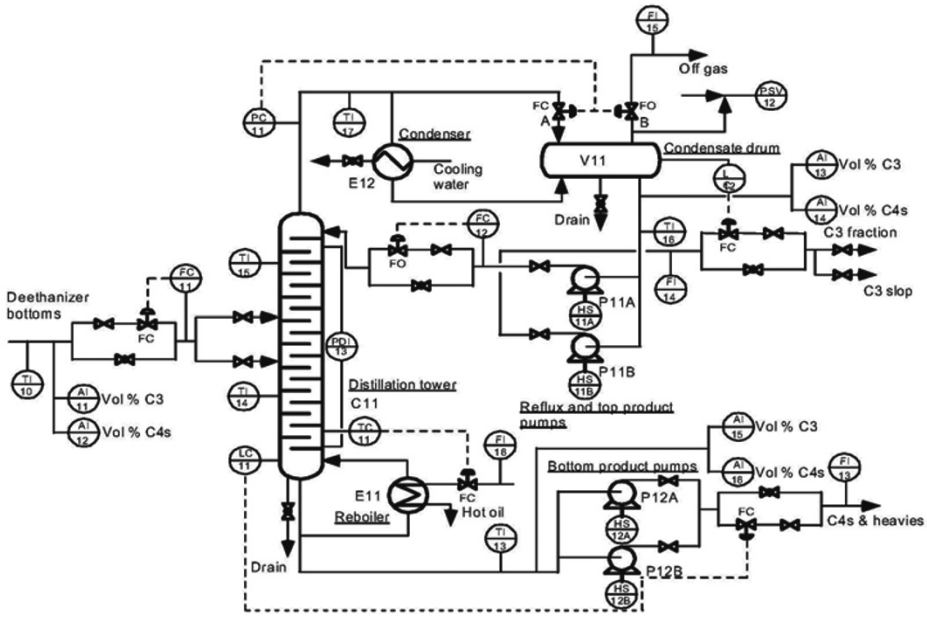

Figure 1.: Schematic diagram of a depropanizer unit

3.1. Predictive Algorithm

The predictive algorithm is built around a hybrid modeling framework that is used to predict the rate-of-change of process variables. In this case study, individual hybrid model for each process variable is developed. However, due to space constraints, only the steps for modeling of the tray temperature will be presented in this paper.

The temperature for *i*-th tray can be described by the following energy balance:

$$m_i \frac{d\Delta H_i^L}{dt} = L_{i-1}\Delta H_{i-1}^L + V_{i+1}\Delta H_{i+1}^V - L_i\Delta H_i^L - V_i\Delta H_i^V \quad (1)$$

where m, L, V, ΔH, represent the moles hold-up on the tray, liquid and vapor flowrates and the change in specific enthalpy (between a reference temperature, T_{ref} and its tray temperature) respectively. The subscript index denotes the tray number while the superscript index represents the type of flow. To facilitate the modeling development,

the following assumptions are made to Eq (1). One, it is assumed that the moles hold-up on each tray stay relatively constant and two, equimolar liquid and vapor flowrates are assumed. The terms ΔH_i^L and ΔH_i^V can be further expanded to $\Delta H_i^L = A_i^L(T_i - T_{ref}) + B_i^L(\frac{T_i^2 - T_{ref}^2}{2})$ and $H_i^V = \widetilde{V_i}\Delta P_i + A_i^V(T_i - T_{ref}) + B_i^V(\frac{T_i^2 - T_{ref}^2}{2})$, where T_i represent the temperature of *i*-th tray, ΔP_i represent the difference between the pressure of *i*-th tray (P_i) and a reference pressure (P_{ref}) and $A^L{}_i$, $B^L{}_i$, $A^V{}_i$, $B^V{}_i$ are constants describing the heat capacities of the liquid and vapour flow leaving the *i*-th tray. The above representations can be similarly used to describe ΔH_{i-1}^L and ΔH_{i+1}^V, respectively. The derivative of ΔH_i^L can be represented as $(A_i^L + B_i^L T_i)\frac{dT_i}{dt}$. The term $\widetilde{V_i}$ represent the molar volume of vapor flow which can be defined by the following equation $\widetilde{V_i} = \left(\frac{RT_i}{P_i} + \gamma_i RT_i\right)$, where γ_i is a constant that is used to account for any non-idealities in the vapour flow. It is further assumed that the heat capacities and gas properties are constant (e.g., $A^L{}_i = A^L{}_{i-1} = A$) since their variations between neighbouring trays (e.g. *i*+1, *i*-1 and *i*) are not strong. Rewriting Eq (1) based on the above assumptions, we have

$$\begin{aligned}\frac{dT_i}{dt} = & -\frac{B^L}{A^L}\left[T_i\frac{dT_i}{dt}\right] + \frac{1}{m_i}[L(T_{i-1} - T_i)] + \frac{B^L}{m_i A^L}\left[L\left(\frac{T_{i-1}^2 - T_i^2}{2}\right)\right] \\ & + \frac{1}{M_i A^L}\left[V\left(\frac{RT_{i+1}}{P_{i+1}}\right)\Delta P_{i+1} - V\left(\frac{RT_i}{P_i}\right)\Delta P_i\right] + \frac{\gamma_{i+1}}{M_i A^L}[VRT_{i+1}\Delta P_{i+1}] \\ & + \frac{A^V}{m_i A^L}[V(T_{i+1} - T_i)] + \frac{B^L}{m_i A^L}\left[V\left(\frac{T_{i+1}^2 - T_i^2}{2}\right)\right] - \frac{\gamma_i}{m_i A^L}[VRT_i\Delta P_i] \end{aligned} \quad (2)$$

Equation (2) is arranged in a way such that the terms on the left-hand side of the equation and in the square brackets are *known* while the rest of the terms are *unknown* constants. In this form, data-driven modeling techniques, such as linear regression can be performed using simulated plant data sets obtained during different abnormal situations to determine the unknown constants. Note that the training of Eq (2) using different set of plant data will generate different sets of constants, as such it is important to select the right set of plant data for training so that the set of constants that are determined offers good prediction capabilities even during abnormal situations whose plant data are not used for training. To aid us in this selection, a metric that compares the actual with the predicted times of a process variable that is about to hit its alarm limits is developed and is given as: $Metric = \frac{\left(\sum_{i=j}^{N}|\hat{t_i} - t_i|\right)}{(N-i+1)}$, where *j* represent the *j*th time instant when the prediction starts and *N* represents the time instant just before the alarm is triggered. Times $\hat{t_i}$ and t_i represent the predicted and actual times of the process variable at the *i*th time instant respectively. By using such a metric system, we can then select the set of constants with the lowest metric value to be used in Eq (2). Similar steps are used in developing the hybrid models for other process variables. Once the hybrid models for the process variables are developed, they can be used to predict a time horizon for the occurrence of each individual alarms. This information is then passed on to the operators through a proactive alarms monitoring display. A prototype of the display is shown in Fig. 2. In this display, the alarms of the depropanizer unit are grouped into various regions e.g., the level alarm for reflux drum (LC12) is placed under the "REFLUX DRUM" region while the bottom temperature (TI13) is placed under the "REBOILER" region. This helps reduce the complexity of

the display and allows operator to identify and understand the alarms in a systematic manner. The alarm display shows the temporal trends of the alarms in two panes, one showing alarms that have occurred in the recent past (e.g. 5 min) and the other showing incipient alarms as per the model prediction. An alarm summary containing the "Area of Interest" helps operators to focus on the region where the fault may originate. This will save the operators' time in identifying the problem and allow them to focus in bringing the plant back to safe operation.

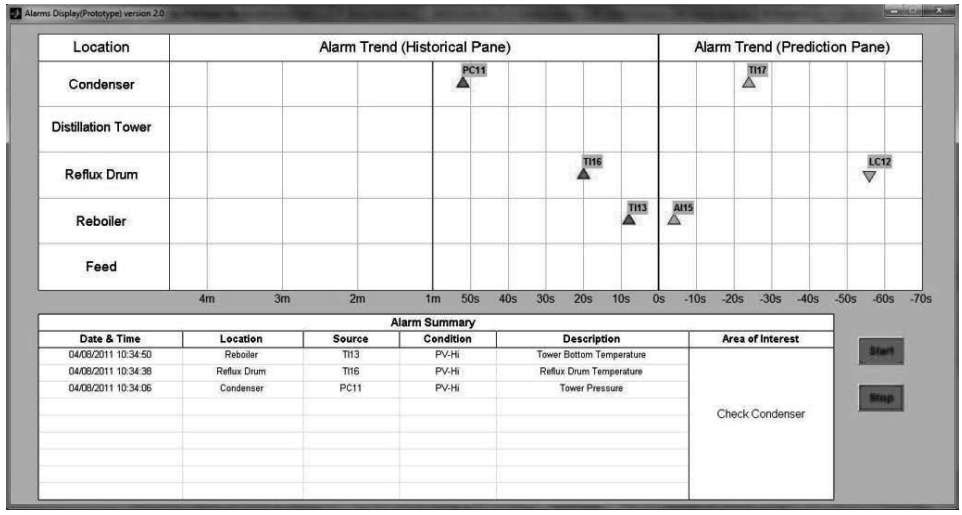

Figure 2: Prototype of proactive alarms monitoring display

4. Conclusion

In this paper, an alarm management framework, known as proactive alarms monitoring scheme is developed. This scheme has two primary objectives: (1) to provide operators with anticipatory information on incipient alarms that could happen within certain time-window and the likely abnormal situation that has occurred, and (2) to allow the operators to identify and rectify the problem early before the plant reaches a dangerous operating state. The scheme is built around a predictive mechanism that utilizes hybrid modeling techniques to predict the rate-of-change of process variables within the plant. The predicted rate-of-change of process variables are then translated into predictions of occurrence of various alarms. The historical record of alarms together with the predicted ones can be displayed to the operator to enable effective sense making. A case study of a depropanizer unit is used to illustrate the development of the proposed alarm monitoring scheme.

References

J. Liu, K.W. Lim, W.K. Ho, K.C. Tan, R. Srinivasan and A. Tay, 2003, The intelligent alarm management system, IEEE Software, 20, 2, 66-71

J. Liu, K.W. Lim, R. Srinivasan, K.C. Tan and W.J. Ho, 2004, The intelligent alarm management system, Hydrocarbon Processing , 47-53

E.M. Morphew and C.D. Wickens, 1998,. Pilot performance and workload using traffic displays to support free flight. In Proceedings of the 42nd Annual Meeting of the HFES. Santa Monica.

L. van Breda, 1999, Anticipatory behaviour in supervisory control, Delft University Press ,Delft, The Netherlands

I.A. Karimi and Rajagopalan Srinivasan (Editors), Proceedings of the 11th International Symposium on Process Systems Engineering, 15-19 July 2012, Singapore.

Synthesis of Large-scale Multi-stream Heat Exchanger Network Based on Pseudo-temperature Enthalpy Diagram Method Combined with Superstructure Method

Jilong Li, Jian Du*, Zongchang Zhao, Qingwei Meng, Pingjing Yao

Institute of Process Systems Engineering, Dalian University of Technology, Dalian, 116012, Liaoning, China

Abstract

This paper introduces a new approach for optimizing heat exchanger networks (HEN), which combines pseudo-temperature enthalpy diagram method and superstructure method. The approach focusing on the minimization of total annual cost, uses a simplified superstructure to solve the sub-networks which obtained by a pseudo-temperature enthalpy diagram, and also involves multi-stream heat exchangers as exchange units. An example taken from literature is studied here. The result of the study indicates the effectiveness and advantages of this methodology.
Keywords: pseudo-temperature enthalpy diagram; superstructure; heat exchanger network; multi-stream heat exchanger

1. Introduction

Traditional methods of heat exchanger network optimization can be generally divided into mathematical programming methods and heuristic ones. Although many studies have been done on these areas during last several decades, there are still flaws in each kind of methods. For example, the complexity of superstructure which grows with the scale of the problem exponentially limits the applicability of this method. Also a pseudo-temperature enthalpy diagram method[6] based on the pinch program can get a network that has the minimum thermodynamic area by the division of enthalpy interval with low complexity, it can rarely get the optimal solution due to the deficiency of various networks. As these are considered, a combined method is presented. Taking advantages of both methods mentioned, this method uses a pseudo-temperature enthalpy diagram to get a series of sub-networks and solve them by superstructure.

On the other hand, a multi-stream heat exchanger is used more widely in process industry thanks to the development of technology. Compared with a two-stream heat changer, a multi-stream one has higher efficiency, more compact and lower cost. There are mainly two categories of multi-stream heat exchanger, multi-channel heat exchanger and plate-fin heat exchanger. The former one can handle one cold stream and two or more hot streams or vice versa, called as one vs. more multi-stream heat exchanger, while the later one can handle both more than two cold streams and hot streams, called more vs. more multi-stream heat exchanger here. In this study, only one vs. more multi-stream heat exchanger is used because of the industry situation of the case and the convenience of program editing. A more vs. more multi-stream heat exchanger can be obtained by a further reorganization.[1,2]

2. Method representation

The method is illustrated in Sections 2.1 and 2.2. The fundamental stages are represented in Section 2.1. The practical calculation procedures are showed in Section 2.2.

2.1. Fundamental stage

Stage 1: Get a initial network by pseudo-temperature enthalpy diagram.

Get a set of ΔT_C^i as initial values according to the correlation equation (Xiao, 2005)[5]:

$$\Delta T_C^i = \sqrt{\frac{a_i h_r}{a_r h_i}} \cdot \frac{T_i^2}{T_r^2} \cdot \Delta T_C^r \tag{1}$$

This equation gives a relationship between each stream's ΔT_C^i. The best ΔT_C^i that can offer a minimum heat transfer area per heat load has been proved to relate to a_i and h_i.[3] Moreover, a later research found it also relating to the stream's temperature. To get a set of ΔT_C^i, a reference stream is needed, which is chosen by experience. However, this group of ΔT_C^i is just used as a group of initial values for the pseudo-temperature enthalpy diagram, and it still need to be optimzed by an intelligent algorithm.

Stage 2: Merge adjacent enthalpy intervals and construct sub-network.

The merging only occurs in ordinary enthalpy intervals which excluding hot/cold utility streams. First, a **Merge Array**, consisting of some Boolean variates, is defined to judge whether to merge the corresponding enthalpy intervals. The size of the merge array is one less than the number of ordinary enthalpy intervals. Each member of the array represents the judgment of merger: True means merging, while False means not.

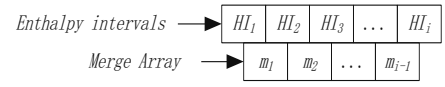

Fig. 1. Illustration for Merge Array

The merging begins with simply adding streams together. Any stream in the chosen intervals will exist in the new interval with its original property. After obtaining the new intervals, several possibilities exist:

Case 1. The number of streams is less enough (4 for cold/hot streams respectively in this study). All streams in the new intervals compose a sub-network directly.

Case 2. The number of streams is more than that. The following methods are proposed to simplified the sub-network:

Find out common streams existing in every original interval among cold and hot streams respectively. Merge these common streams according to the similarity of their heat transfer coefficient, until the number of streams becomes lower than the threshold value. A **Pseudo-stream** is named to describe the merged common stream, and its inlet and outlet temperatures are set as the lowest one if it is a hot stream, while the highest one if it is a cold stream to satisfy feasibility of heat transference. All pseudo-streams and other unmerged streams compose a sub-network. After synthesizing the network, pseudo-streams are split into real streams to match other streams if needed. All these treats are realistic thanks to the feature of multi-stream heat exchanger.

Stage 3: Optimize sub-networks by superstructure.

An improved two-stage non-isothermal mixed superstructure model (Fig. 2.) is used here. The features are illustrated as follows:

(i) There is no utility involved in this model. Obviously, the sub-network consists of several enthalpy intervals which have already attain heat equilibrium.

(ii) The outlet temperature of each branch needs not to be coincident. This extends the flexibility of candidate for structure.

(iii) One more branch without match is added in this model. This alteration covers the solution space more intuitively, and is beneficial for program editing.

Stage 4: Synthesize the finial network

Joint the results of each sub-network obtained in **Stage 3** and initial results of the intervals without merged in **Stage 1** together. Then total annual cost can be calculated, and is used as the object for optimizing.

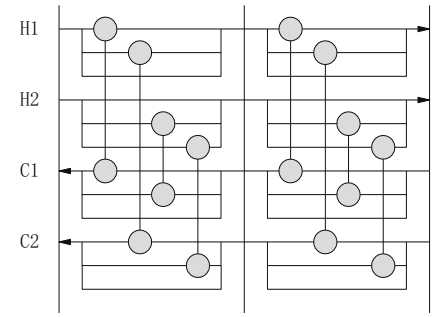

Fig. 2. A two-stage non-isothermal mixed superstructure

2.2. Practical calculation procedure

The stages above are realized in a program. Procedures are detailed as following:

(i) Generate a set of ΔT_C^i by heuristic method;
(ii) Use pseudo-temperature enthalpy diagram method to get a group of enthalpy intervals and synthesize an initial network;
(iii) Generate a merge array and initialize it randomly;
(iv) Merge certain enthalpy intervals according merge array and obtain sub-networks by the rules given above;
(v) Optimize sub-networks by superstructure method;
(vi) Optimize the merge array and repeat step iv and v until reach the convergence condition;
(vii) Optimize the set of ΔT_C^i and repeat step ii to vi until reach the convergence condition.

The optimization uses a simulated annealing and genetic algorithm (SA/GA). The convergence condition is set as: no evolution in 30 generations.

3. Case Study

An 11-stream problem (9 hot streams and 2 cold streams) is used to give an illustration of the new method. This case is taken from a reorganization project of the oil refinery system in a Chinese plant. It has been used in Wei's paper (2004)[4] and Xiao's paper (2006)[6]. The details of the process data are shown in Table 1. There is only one kind of cold/hot utility respectively. The cost of all heat exchangers (including coolers and heaters) in this case is calculated by the model: $1000A^{0.6}$\$/a, and heat transfer coefficient is calculated by $U=1/(1/h_h+1/h_c)$ kW• m^{-2}• K^{-1}.

In this study, as C2 has the largest enthalpy rate, it is selected as a reference stream. The ratios of other streams' temperature difference contribution value can be calculated by eq.(1). It can be found that C1 has the least one, so ΔT_C^i of C1 is set as 5℃, a temperature difference coefficient, and then other streams' ΔT_C^i can be obtained, as shown in Table 2. This group of ΔT_C^i is used as initial values in the calculation program. After 304 seconds' computation, an optimal solution can be obtained. It is compared with other results from literatures in Table 3, and the optimal network is shown in Fig. 3.

Details of the optimal solution gained are illustrated as following:

First, an initial network is obtained by pseudo-temperature enthalpy diagram method, and there are 12 enthalpy intervals and 19 heat exchangers. The total cost is 7,532,314\$• a^{-1}. Then the 2nd, 3rd, 4th, 5th, 6th and 7th enthalpy intervals are chosen to be merged into one and a simplified sub-network can be gained by our strategies, so as the 8th and 9th ones, and the 10th and 11th ones. (This chosen pattern is just a result due to the SA/GA.) After solving these three sub-networks by superstructure method respectively, and taking the results back to the initial network, the final result is obtained. In the final result, the number of heat exchangers decreases to 16, which mainly reduces the cost.

The total annual cost obtained by our method has a decrease by 12.49% compared with HEXTRAN's result, a decrease by 5.38% with that obtained using superstructure method by Wei[4] and a decrease by 4.91% with that obtained using pseudo-temperature enthalpy diagram method by Xiao[6]. The total area in this study is a little more than that by Wei, but quite more than that by Xiao. However, the utility cost decreases a lot. The reason is that a superstructure is used to search an optimal structure, but this disobeys the vertical match rules and leads to an increase in total area. However, a superstructure method is just a sub-optimization, and after the global optimization, the utility cost must be set to a low level to complete the optimal mission. This result also indicates the efficiency of our method for a large scale network.

Table 1 Process data for Case Study

Stream	T_{IN} (K)	T_{OUT} (K)	h (kW·m^{-2}·K^{-1})	F_{CP} (kW·K^{-1})
H1	521.2	323.2	0.9	47.67
H2	623.2	343.2	0.6	8.97
H3	541.2	343.2	0.75	44.79
H4	593.2	343.2	0.6	10.68
H5	648.2	368.2	0.45	73.18
H6	648.2	368.2	0.45	71.94
H7	388.2	313.2	1.2	33.85
H8	565.2	343.2	0.9	72.29
H9	466.2	333.2	0.9	26.26
C1	328.2	521.2	0.6	304.73
C2	516.2	633.2	0.6	318.62
S1	723.2	723.2	1.8	--
W1	303.2	323.2	1	--

Cost of hot utility ($•kW^{-1}•a^{-1}): 440; Cost of cold utility ($•kW^{-1}•a^{-1}): 40.

Table 2 Temperature difference contribution values and Ratios of that for Case Study

Stream	H1	H2	H3	H4	H5	H6	H7	H8	H9	C1	C2
Ratio	1.35	4.00	1.54	3.48	1.56	1.57	1.14	1.27	1.66	0.54	1.00
ΔT_C^i	12.46	36.87	14.15	32.01	14.36	14.48	10.52	11.67	15.34	5.00	9.21

Table 3 Comparison of the optimal solution with that in literatures for Case Study

Item	Total area (m^2)	Number of units	Equipment cost ($•a^{-1})	Utility cost ($•a^{-1})	Total cost ($•a^{-1})
HEXTRAN	39853	23	1,619,556	6,958,794	8,578,350
Wei	22751	11(4#)	637,188	7,296,336	7,933,523
Xiao	16975	14(6#)	748,832	7,145,397	7,894,229
This paper	25843	16(4#)	920,616	6,586,186	7,506,802

refers to the number of multi-stream heat exchanger

4. Conclusion

This paper has presented a combined method jointing pseudo-temperature enthalpy diagram and superstructure together. Some strategies of merging enthalpy intervals and constructing sub-networks are proposed to realize the combined method such as introducing a Merge Array and rules for simplifying sub-network. A large scale problem is turn into several small scale problems in order to decrease the complexity of calculation. Besides, some improvements are brought to the model of superstructure to make it more suitable for editing program and calculating to improve the flexibility of structures. An example has been studied in this work to show the application of the proposed methodology. A relatively better result is obtained. Because of the division,

complexity is quasi-linear with scale instead of explosive. This makes our methodology suitable for a large scale problem. Further work could aim towards the improvement of the strategies. Some heuristic rules should be proposed to synthesis a sub-network directly instead of using superstructure. Though it may lose the optimal solution, it can simplify calculation extremely.

Acknowledgements

The authors gratefully acknowledge the financial support from Natural Science Foundation of China (No. 20976022).

Notation

ΔT_C^i temperature difference contribution value of stream i
a_i cost per area of a heat exchanger including stream i
h_i heat transfer coefficient of stream i
HI_i enthalpy interval i
m_i element i of merge array
H_i hot stream i
C_i cold stream i
S hot utility stream
W cold utility stream
A heat exchange area
U total heat transfer coefficient in a match
T_{IN} inlet temperature
T_{OUT} outlet temperature
F_{CP} heat capacity flowrate
Subscripts
r reference stream

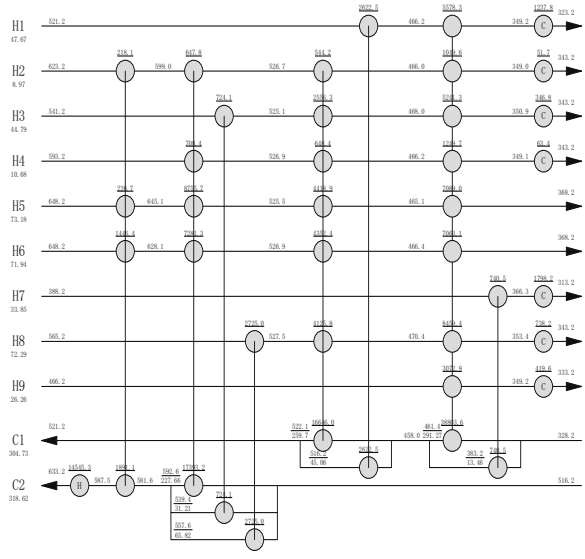

Fig. 3. Optimal heat exchanger network for Case Study.

References

[1] S. Ghosh, I. Ghosh, D.K. Pratihar, B. Maiti, P.K. Das, Optimum stacking pattern for multi-stream plate-fin heat exchanger through a genetic algorithm, International Journal of Thermal Sciences, 50(2011)214-224.
[2] Xing Luo, Meiling Li, Wilfried Roetzel, A general solution for one-dimensional multistream heat exchangers and their networks, International Journal of Heat and Mass Transfer, 45(2002)2695-2705.
[3] H.Nishimura, A Theory for the Optimal Synthesis of Heat-Exchanger Systems, 1980.
[4] Wei Guanfeng, Yao Pingjing, Luo Xing, Wilfried Roetzel, A Parallel Genetic Algorithm/ Simulated Annealing Algorithm for Synthesizing Multistream Heat Exchanger Networks, J. Chin. Inst. Chem. Engrs., 35(3)(2004)285-297.
[5] Xiao Wu, Li Xinqiang, Yao Pingjing. Synthesis of Large Scale Multi-Stream Heat Exchanger Networks by Using Genetic/Simulated Annealing Algorithms based on Stream Effective Temperature level, the China/USA/Japan Joint Chem. Eng. Conference, Beijing, 2005.
[6] Xiao Wu, Large Scale Multi-Stream Heat Exchanger Network Synthesis Based on the Stream Effective Temperature Level, Dalian, Dalian university of technology, 2006.

I.A. Karimi and Rajagopalan Srinivasan (Editors), Proceedings of the 11th International Symposium on Process Systems Engineering, 15-19 July 2012, Singapore.

A New Tool For Simultaneous Targeting And Design Of Heat Exchanger Networks

Sharifah Rafidah Wan Alwi,[a] Zainuddin Abdul Manan[a], Misrawati Misman[a]

[a]*Process Systems Engineering Centre (PROSPECT), Faculty of Chemical Engineering, Universiti Teknologi Malaysia, 81310 Skudai, Johor, Malaysia.*

Abstract

Pinch analysis is a well-established methodology for the design of processes to achieve the minimum utility requirements. The Composite Curves (CCs) is a popular pinch analysis tool to determine the minimum energy targets. An efficient alternative to CCs is a numerical technique known as Problem Table Algorithm (PTA). However, the PTA does not fully show individual hot and cold streams heat cascade profile and cannot be used for Heat Exchanger Network (HEN) design. This paper introduces the Segregated Problem Table Algorithm (SePTA) as a new and versatile numerical tool for simultaneous targeting and design of a HEN. SePTA shows profiles of heat cascade across temperature intervals for individual hot and cold streams, and can be used to simultaneously locate pinch points, calculate utility targets and perform SePTA Heat Allocation (*SHA*). The *SHA* can be represented on a new SePTA Network Diagram (SND) that graphically shows a heat exchanger network together with the amount of heat exchange on a temperature interval scale. The new method is illustrated using a case study.

Keywords: Segregated Problem Table Algorithm (SePTA); heat allocation; network diagram; numerical; heat exchanger network.

1. Introduction

Heat pinch analysis is a popular and effective technique which allows utility targets to be determined using a graphical technique such as Composite Curves (CC) [1, 2] or a numerical technique such as Problem Table Algorithm (PTA) [2]. Other latest numerical techniques include the Simple Problem Table Algorithm (SPTA) [3], geometry-based approach [4], enthalpy flowrate and temperature technique [5], PTA with multiple utilities [6], Unified Targeting Algoritm (UTA) for diverse process integration problems [7] and Grid Diagram Table (GDT) that combines numerical and visualization tools [8]. All these methods require targeting and design to be done separately. Simultaneous targeting and design using a graphical method called Segregated Temperature vs. Enthalpy Plot (STEP) has recently been proposed [9]. The key advantage of STEP is its ability to clearly show the allocation of heat sources to demands since it is constructed based on individual streams as opposed to composite streams.

This paper presents the Segregated Problem Table Algorithm (SePTA) as a new numerical tool for simultaneous targeting and design of a maximum energy recovery network. SePTA is an extension to STEP (Streams Temperature vs. Enthalpy Plot) [15] which shows the profiles of heat cascade across temperature intervals for continuous individual hot and cold streams. SePTA can be used to simultaneously locate the pinch points, calculate the utility targets and conveniently perform network

design that overcomes the limitations of PTA. Though SePTA yields the same results as STEP, it can vitally complement the STEP technique in terms of accuracy as well as speed, and in terms of its amenability to computer programming. Table 1 represents the stream data for an illustrative case study that will demonstrate the application of SePTA.

Table 1: Example 1 stream data (ΔT_{min} = 10°C).

Stream	Supply temperature, T_s (^{0}C)	Target temperature, T_t (^{0}C)	Flowrate heat capacity, FCp (MW/^{0}C)	Entalphy, ΔH (MW)	Shifted supply temperature, T_s' (^{0}C)	Shifted supply temperature, T_t' (^{0}C)
H1	170	126	9	-396	165	121
H2	270	93	7	-1239	265	88
C1	60	160	5	500	65	165
C2	116	260	8	1152	121	265

2. SePTA for simultaneous targeting and design

2.1. SePTA for targeting

The targeting procedure using SePTA is described as follows:

1. The first step is to change the original hot temperature (T_h) and cold temperature (T_c) data into shifted temperatures (T_h' and T_c'). Using shifted temperatures effectively builds ΔT_{min} into heat exchange process and allows hot and cold streams to touch during stream matching and facilitates pinch point search. Assuming a minimum temperature approach (ΔT_{min}) of 10°C, the last two columns of Table 1 show the streams' shifted temperatures for the illustrative case study.
2. These temperatures are then sorted in descending order into temperature intervals, leaving out the temperatures which are common to both hot and cold streams.
3. Draw the arrow that shows the supply and target temperatures for all the hot and cold streams.
4. Begin by choosing the largest FCp hot stream for each temperature interval to determine the set of streams that will form Hot STEP 1. For example, Table 2 shows that between temperature intervals of 244°C to 165°C, there is only H2. Hence, H2 is chosen. Between 165°C and 155°C, both H1 and H2 exist. Since H2 (FCp = 5 kW/^{0}C) has a bigger FCp as compared to H1 (FCp = 3 kW/^{0}C), H2 is chosen. This procedure is repeated for all intervals.
5. Repeat step 4 to determine the set of streams to form the next hot STEP by extracting the remaining hot streams from the intervals with multiple streams. Referring to Table 2, for example, the set of streams to form Hot STEP 2 are determined from the remaining hot streams after Hot STEP 1 has been constructed. Between the temperature intervals of 165^{0}C and 121^{0}C, the remaining hot stream is H1.
6. Repeat steps 4 and 5 to determine the streams to form the continuous cold STEPs.
7. For each hot STEP and cold STEP, calculate the net heat capacity flowrate by deducting the heat capacity flowrates of the cold stream from the hot stream (see columns 11 and 12, Table 3).
8. FCp_{net} for each STEP is then multiplied with the temperature interval to get the net heat surplus (positive value) or deficit (negative value) for a given interval (see columns 13 and 14, Table 2.

9. Starting with a zero heat input at the highest temperature, cumulatively add the net enthalpy (surpluses or deficits) down the temperature intervals, to get an overall net enthalpy cascade (see columns 15 and 16, Table 2).
10. The cascade in step 9 normally contains negative heat flows and is thermodynamically infeasible. In order to have a feasible heat cascade, take the absolute value of the largest negative heat flow from this "infeasible heat cascade" and add this amount of heat as hot utility to the highest temperature interval in the cascade shown in the next column (Columns 17 and 18). All the net heat flows in the cascade now increase by this amount, and the minimum value becomes zero. Note that if all the values in step 9 are nonnegative, then step 10 is not required and the result remain as in step 9.
11. The heat added to the first available interval is the hot utility requirement (target) $QH_{STEP\ i}$. On the other hand, the summation of the heat removed from the final interval is the cold utility target $QC_{STEP\ j}$. The pinch point is the point(s) at which there is zero net heat flow in the cascade. From Table 2, the minimum hot and cold utilities are the total from the two STEPs. Hence, the minimum hot utility is 643.5kW and the minimum cold utility is 34.5kW. The shifted pinch temperature for this problem is 88^0C.

Table 2: Targeting using SePTA.

1	*2*	*3*	*4*	*5*	*6*	*7*	*8*	*9*	*10*	*11*	*12*	*13*	*14*	*15*	*16*	*17*	*18*
										Targeting							
FCp, (kW/^{0}C)		5	3	6	3.5	**STEP selection**				**FCphot-FCpcold**		**ΔH, kW**		**Cum ΔH, kW**		**Cum ΔH', kW**	
T', °C	**ΔT, oC**	**H2**	**H1**	**C1**	**C2**	**Hot STEP 1**	**Hot STEP 2**	**Cold STEP 1**	**Cold STEP 2**	**STEP 1**	**STEP 2**	**STEP 1**	**STEP 2**	**STEP 1**	**STEP 2**	**STEP 1**	**STEP 2**
265														0		**229.5**	
	21							**C2**		-3.5		-73.5					
244														-73.5		156	**414**
	79					**H2**		**C1**	**C2**	-1	-3.5	-79	-277				
165														-153	-277	77	137.5
	10					**H2**	**H1**	**C1**	**C2**	-1	-0.5	-10	-5				
155														-163	-282	67	132.5
	22					**H2**	**H1**	**C1**	**C2**	-1	-0.5	-22	-11				
133														-185	-293	45	121.5
	12					**H2**	**H1**	**C1**	**C2**	-1	-0.5	-12	-6				
121														-197	-299	33	115.5
	33					**H2**		**C1**	**C2**	-1	-3.5	-33	-116				
88														-230	-414	0	0
	23					**H2**		**C2**		1.5		34.5					
65														-195		**34.5**	

2.2. SePTA Heat allocation

The heat allocation can be determined by constructing SePTA Heat Allocation (SHA) as follows:

1. Rewrite all the stream selected for hot and cold STEP 1 from Table 2 with enthalpy for each temperature interval as shown in columns 7, 8, 10,11 and 12, 13, 15, 16 in Table 3.

2. Starting from the top of the column, cascade available heat from hot STEP 1 down the interval temperatures (columns 7 and 8) to cold STEP 1 (columns 10 and 11) (normally, hot utility will be the first match from hot STEP). Considering the minimum driving force for heat exchange (ΔT_{min}) that is built in the heat cascade, the hot streams interval temperature can be higher than or equal to cold streams interval temperature for feasible heat transfer.
3. In order to achieve minimum utility requirement, there should be no heat transfer across the pinch.
4. Repeat all steps to construct heat allocation for STEP 2.

Table 3: SePTA Heat Allocation.

1	2	3	4	5	6	7	8	9	10	11	12	13	14	15	16
						Heat Allocation									
FCp, (kW/0C)		5	3	6	3.5	STEP 1					STEP 2				
T', °C	ΔT, oC	H2	H1	C 1	C2	Hot Stream ΔH, kW				Cold Stream ΔH, kW	Hot Stream ΔH, kW				Cold Stream ΔH, kW
265						QH	295	73.5							
	21							156	C2	73.5					
244															
	79					H2	395	318	C1	474	QH	414	276.5	C2	276.5
165								60					35		
	10					H2	50	50	C1	60	H1	30	16.5	C2	35
155								17					25.5		
	22					H2	110	65	C1	132	H1	66	77	C2	77
133								45					13.5		
	12					H2	60	27	C1	72	H1	36	66	C2	42
121								33							
	33					H2	165	165	C1	198			36		
88														C2	115.5
	23					H2	115	80.5	C2	80.5					
65								34.5	Qc	34.5					

2.3. SePTA Network Diagram

For better visualisation of the overall heat exchanger network (HEN), the SePTA heat allocation (*SHA*) can be converted into SePTA network diagram (SND) as shown in Figure 1. SND shows the heat exchanger locations for each hot and cold stream. It also shows the temperature supply and target for each heat exchanger according to scale as well as the corresponding heat load. Note that the exact stream mapping as well as the quantity of heat exchange is extracted from SePTA heat allocation (SHA) performed in the previous section.

3.Conclusion

A new numerical tool for simultaneous utility targeting and design of maximum energy recovery (MER) network known as the SePTA has been introduced as an extension for

STEP [15]. SePTA are profiles of heat cascade across temperature intervals for individual hot and cold streams, and can be used to simultaneously locate pinch points, calculate utility targets and perform SePTA Heat Allocation (*SHA*). The *SHA* can be represented on a new SePTA Network Diagram (SND) that graphically shows a heat exchanger network together with the amount of heat exchange on a temperature interval scale.

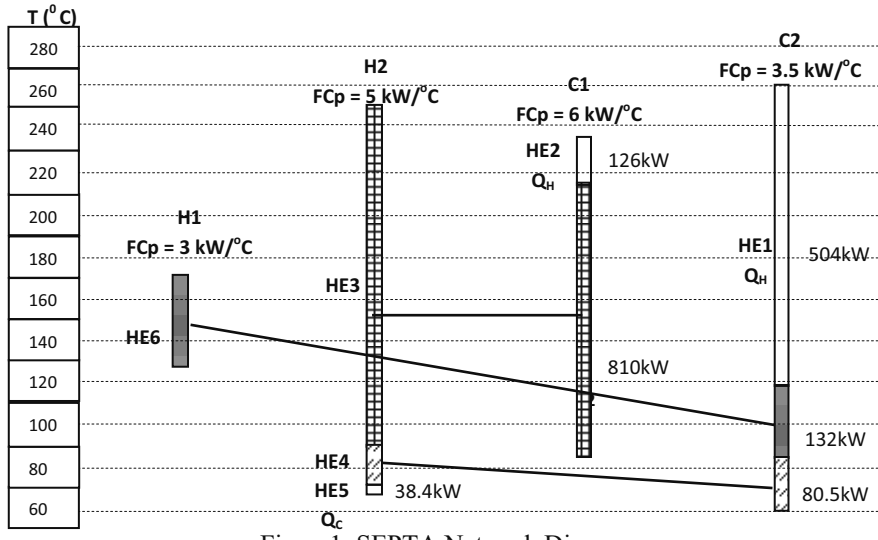

Figure1. SEPTA Network Diagram.

4. Acknowledgment

The authors would like to thank MOHE (Ministry of Higher Education) Malaysia and UTM in providing the research fund for this project under Vote No. Q.J130000.7125.00H22.

References

[1] E. C. Hohmann, 1971, Optimum networks for heat exchange, PhD Thesis, University of Southern California, Los Angeles, USA.

[2] B. Linnhoff and J. R. Flower, 1978, Synthesis of heat exchanger networks: I. Systematic generation of energy optimal networks, AIChE Journal, 24, 4, 633–642.

[3] A. I. A. Salama, 2005, Numerical techniques for determining heat energy targets in pinch analysis, Computers and Chemical Engineering, 29, 1861-1866.

[4] A. I. A. Salama, 2006, Determination of the optimal heat energy targets in heat pinch analysis using a geometry-based approach, Computers and Chemical Engineering, 30, 758-764.

[5] A. I. A. Salama, 2009, Numerical construction of HEN composite curves and their attributes, Computers and Chemical Engineering, 33, 181-190.

[6] A. L. H. Costa and E. M. Queiroz, 2009, An extension of the problem table algorithm for multiple utilities targeting, Energy Conversion and Management, 50, 1124-8.

[7] V. S. Uday, 2011, Unified targeting algorithm for diverse process integration problems of resource conservation networks, Chemical Engineering Research and Design, 89, 2686-705.

[8] N. Abbood, Z. A. Manan and S. R. Wan Alwi, 2011. A Combined Numerical and Visualisation Tool For Utility Targeting and Heat Exchanger Network Retrofitting, Journal of Cleaner Production, 21, 1, 1-7.

[9] S. R. Wan Alwi and Z. A. Manan, 2010, STEP - A new graphical tool for simultaneous targeting and design of a heat exchanger network, Chemical Engineering Journal, 162:, 106-121.

I.A. Karimi and Rajagopalan Srinivasan (Editors), Proceedings of the 11th International Symposium on Process Systems Engineering, 15-19 July 2012, Singapore.

Heat Exchanger Network Synthesis Using a Hyperstructure of Stagewise Stream Superstructures

Ke Feng Huang[a] and I. A. Karimi[a]

[a]*Department of Chemical & Biomolecular Engineering, National University of Singapore, 4 Engineering Drive 4, Singapore 117576*

Abstract

The existing hyperstructure for the simultaneous heat exchanger network synthesis (HENS) have embedded the alternative structures excluded by a stagewise superstructure. However, the existing hyperstructure-based approaches employs pinch-based transshipment model and do not simultaneously allow cyclic matching. In this work, we propose a simultaneous mixed-integer nonlinear programming formulation based on a hyperstructure of multistage stream superstructures. We include cyclic matching, avoid the pinch-based transshipment model and allow exchangers for utilities in each stage. Using several examples, we demonstrate the significant advantages of our approach compared to those from the literature.

Keywords: heat exchanger network synthesis (HENS); hyperstructure; mixed-integer nonlinear programming (MINLP); optimization; superstructure

1. Introduction

Energy is the essence of life. Without access to affordable alternative energy, how to utilize limited fossil energy efficiently will remain a key issue for the foreseeable future. The chemical process industry consumes extensive energy to produce utilities for heating and cooling process streams. Because of its holistic and optimal integration between the hot and cold process streams and utilities to reduce energy usage, heat exchanger network synthesis (HENS) has gained intense and significant attentions in both practice and research for several decades.

In general, the HENS problem is to derive a network of 2-stream heat exchangers (HEs) with minimum total annualized cost (TAC), which integrates given sets of hot and cold process streams and utilities with known flow rates, heat contents, and inlet and outlet temperatures. There are two main approaches for HENS, sequential and simultaneous. The simultaneous approach is considered as more attractive as it does not rely on the concept of pinch and holistically trade-offs the various factors (utility usage, number and areas of HEs) that impact TAC. The simultaneous approach, as a result, can increase the possibility of obtaining better networks. Most of the simultaneous synthesis methods employ a stagewise superstructure (Yee and Grossmann, 1990) of possible 2-stream matches of HEs and assume isothermal mixing to eliminate the nonlinear energy balance for substream mixing at each stage. The limitations of this multistage superstructure and isothermal mixing assumption are well established in the literature by Huang et al. (2012). Floudas and Ciric (1989) developed a hyperstructure allowing non-isothermal mixing and cross flow. Subsequently, Ciric and Floudas (1991) combined this hyperstructure with the pinch-based transshipment model of Papoulias

and Grossmann (1983) to simultaneously select optimal heat exchanger network (HEN) for a variable heat recovery approach temperature. However, unless in advance dividing those streams into two substreams based on the pinch temperature, the hyperstructure-based model does not allow cyclic matching, which may help to decrease the requirement of HE area at the expense of using more numbers of units in some cases and give superior HENs with less TAC. Furthermore, the limited attention on the hyperstructure-based approach may be attributed to the fact that applying the pinch-based transshipment model needs to partition the temperature interval, which depends on a predetermined temperature interval approach temperature (TIAT). Whenever, a poor choice of TIAT may lead to a suboptimal network. The challenge, therefore, is to establish a generalized superstructure-based model that accounts for all the possible HEN configurations.

In this work, we propose a simultaneous model based on a hyperstructure of stagewise stream superstructures to address HENS. Specially, we focus on including the certain alternatives in the HEN configurations which the stagewise superstructure neglects. We present examples in which cross flows not accounted by the existing literature eliminate superior HENs. We propose an MINLP model that avoids the pinch-based transshipment model and allows exchangers of process streams with utilities in each stage. We then solve several examples to demonstrate the significant advantage of our approach and compare the results with those from the literature.

2. MINLP Formulation

Consider the well-known HENS problem with two types of streams, process and utility, we use i for hot streams, j for cold streams, and s for any stream. Thus, we need to decide the inlet and outlet temperatures along with the flow rates for each HE in the final network with minimum TAC. We base our formulation on a hyperstructure of multistage stream superstructures shown in Figure 1. This is a combination of the one used by Huang et al. (2012) and the one proposed by Floudas and Ciric (1989). It comprises K stages $(k = 1, 2, \dots, K)$ with $I \cdot J$ potential 2-stream exchangers in each stage. Furthermore, in each stage, splitters are located at the inlet of the stream to the network and at the exits of each HE; mixers are located at the inlets of each HE, and at the exit of the stage. We let $K \geq 2$ allow possible cyclic matches between a hot and a cold process stream. Then let hot (cold) utility streams i (j) enter stage k, and also exit from stage k. Thus, hot (cold) utilities can be used to adjust the temperature of the cold (hot) process streams in each stage. In this work, as done by Huang et al. (2012), we also use similar constraints for the energy balances for each stage and each HE, and bounds for key inlet and outlet temperature variables.

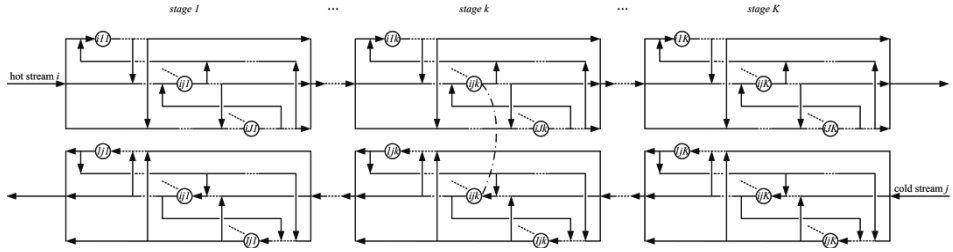

Figure 1 Hyperstructure of multistage stream superstructures

Because of mixing with cross flows, the temperatures of the substreams into the exchangers can be different from the temperature of their parent stream. Thus, we need

additional variables for the flows and temperatures of substreams and cross flows at each stage. Let f_{ijk} (g_{ijk}) denote the fractional flow of hot (cold) stream i (j) used in HE_{ijk}. Let f_{ijk}^{in} (g_{ijk}^{in}) denote the fractional flow of the substream split from hot (cold) stream i (j). let $f_{ijk}^{j'}$ ($g_{ijk}^{i'}$) denote the fractional cross flow split from the substream of hot (cold) stream i (j) following $HE_{ij'k}$ ($HE_{i'jk}$). Then, the mass balances for the mixers at the inlets of exchangers are:

$$f_{ijk} = f_{ijk}^{in} + \sum_{j'} f_{ijk}^{j'} \tag{1}$$

$$g_{ijk} = g_{ijk}^{in} + \sum_{i'} g_{ijk}^{i'} \tag{2}$$

Similarly, let f_{ijk}^{out} (g_{ijk}^{out}) be the fractional flow of the substream to reform hot (cold) stream i (j) after HE_{ijk} in stage k. Then the mass balances for the splitters at the outlets of exchangers are given by:

$$f_{ijk} = f_{ijk}^{out} + \sum_{j'} f_{ij'k}^{j} \tag{3}$$

$$g_{ijk} = g_{ijk}^{out} + \sum_{i'} g_{i'jk}^{i} \tag{4}$$

Additionally, we need the energy balance for the mixer at the inlet of HE_{ijk} to determine the corresponding flow rates of cross flows for both hot and cold streams.

Finally, the HENS objective of minimum TAC is given by,

$$\begin{aligned}\text{TAC} = {} & \sum_i \sum_j \sum_k UC_i Q_{ijk} + \sum_i \sum_j \sum_k UC_j Q_{ijk} + \\ & \sum_i \sum_j \sum_k \left[FC_{ijk} x_{ijk} + CA_{ijk} \left(\frac{Q_{ijk}}{FT_{ijk} U_{ij} LMTD_{ijk}} \right)^{\beta_{ijk}} \right]\end{aligned} \tag{5}$$

where, UC_s is the unit cost of utility s; FC_{ijk}, β_{ijk}, and CA_{ijk} are the appropriate cost coefficients for HE_{ijk}; U_{ij} is the overall heat transfer coefficient for HE_{ijk}; and $LMTD_{ijk}$ and FT_{ijk} are the LMTD and LMTD correction factor respectively for HE_{ijk}. This completes our MINLP formulation, and we call it **M**, which comprises Eqs. (1)-(5) along with the appropriate energy and mass balances, and logical constraints.

3. Examples

We now solve three examples from the published literature to demonstrate the effectiveness of our approach. We use BARON/GAMS and limit its solution time since its convergence is slow. In order to compare our approach with those existing in the literature, we assume $FT_{\text{ijk}} = 1$.

3.1. Example 1

This example from Biegler et al. (1997) involves a process with one hot process stream (H1), two cold process streams (C1-C2), one hot utility, and one cold utility. Figure 2 shows the best HENs from **M**. It has a TAC of \$76,327 with three exchangers and is the same as obtained by Huang et al. (2012). As in Figure 2(a), H1 matches first against C2 in HE_{121} at stage 1, and then it matches with C2 again in HE_{122} at stage 2. To illustrate the impact of this cyclic matching, we use $k = 1$ for this example and resolve it. **M** then gives a HEN (Figure 2(b)) with two HEs and TAC=\$77,913. Obviously, the previous optimal configuration is eliminated from the hyperstructure based model excluding cyclic matching. Thus this small example merely serves to validate our model and show the advantage by using the hyperstructure of multistage stream superstructures instead of one-stage stream superstructures.

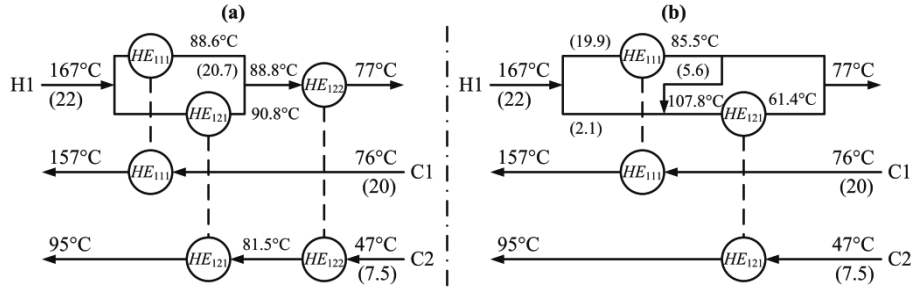

* The numbers within the brackets are heat content flows (kW/°C)

Figure 2 Final HENs from **M** for Example 1

3.2. Example 2

This is taken from Björk and Westerlund (2002). It consists of two hot (H1-H2) and four cold (C1-C4) process streams with one hot and one cold utility. **M** yields an HEN (Figure 3) with six exchangers, one heater, one cooler and TAC = \$123,398. This TAC is 3.72% and 11.3% lower than the best TACs of \$128,169 and \$139,083 reported by Huang et al. (2012) and Björk and Westerlund (2002), respectively. While the utility usage of our HEN is the same as that for the optimal HEN of Huang et al. (2012), it has lower HE areas with the same amount of exchangers.

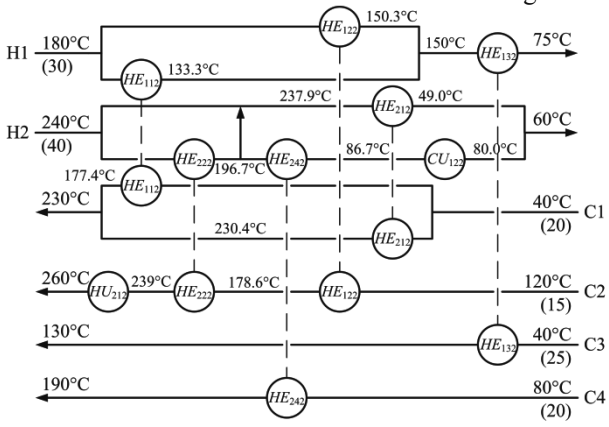

Exchanger	Heat load (kW)	Area (m^2)
HE_{112}	21.4	0.946
HE_{122}	878.6	106.0
HE_{132}	2250.0	83.9
HE_{212}	3778.6	533.6
HE_{222}	906.4	175.2
HE_{242}	2200.0	327.3
HU_{212}	315.0	7.0
CU_{122}	315.0	5.9
Total		1240.0

Annualized utility cost = \$44,100
Investment = \$79,298
Total annualized cost = \$123,398

* The numbers within the brackets are heat content flows (kW/°C)

Figure 3 Final HEN from **M** for Example 2

Note that there is a cross flow between H2's substreams from the outlet of $HE_{222}$to the inlet of HE_{212}. Thus, the existing HENS formulations based on stagewise superstructure exclude such possibly optimal structures and may give suboptimal solutions as in this example. Also it is worth mentioning that there is a cooler (CU_{122}) at H2's substream, similar scenario would be eliminated by the widely used assumption that utilities are used only adjust the final stream temperatures for the sake of simplicity. Thus, an HENS model with this assumption cannot admit the HEN in Figure 3 and may give suboptimal solutions for this example.

3.3. Example 3

This example is from Trivedi (1988). It involves four hot process streams (H1-H4) and three cold process streams (C1-C3), with heating and cooling utilities provided by steam and cooling water. The optimal network (Figure 4) from **M** features a TAC of \$105,403 for eight matches, which is 7.91% lower than that (TAC = \$114,460 with 12

matches) reported by Ciric and Floudas (1991). Although the cyclic matching is not the issue with this example, our simultaneous model indeed gives a better network, since it does not rely on pinch-based transshipment model. Furthermore, as in Example 2, our HEN allows a heater (HU_{132}) at C3's substream. This configuration is also excluded in the hyperstructure based synthesis approaches by Floudas and Ciric (1989) and Ciric and Floudas (1991). Again, this example shows that our proposed formulation can obtain better results than those reported with other methodologies.

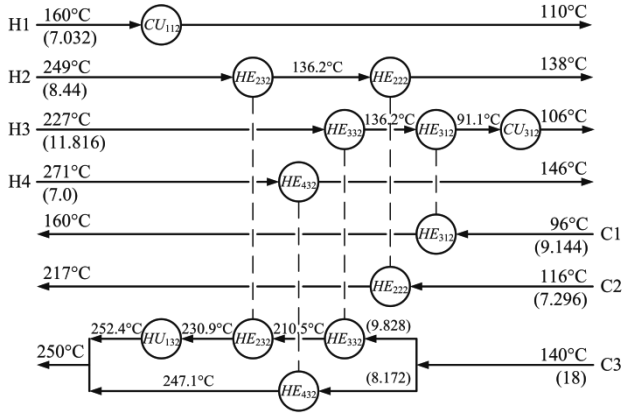

Exchanger	Heat load (kW)	Area (m^2)
HE_{222}	736.9	65.5
HE_{232}	199.9	15.2
HE_{312}	585.2	50.9
HE_{332}	693.3	39.6
HE_{432}	875.0	84.3
CU_{112}	351.6	8.2
CU_{312}	151.3	5.9
HU_{132}	211.8	4.6
Total		274.2

Annualized utility cost = \$27,000
Investment = \$78,403
Total annualized cost = \$105,403

* The numbers within the brackets are heat content flows (kW/°C)

Figure 4 Final HEN from **M** for Example 3

4. Conclusion

We presented a model based on the hyperstructure of stagewise stream superstructures for HENS. The novelties in our model include certain configurations that both the stagewise superstructure and existing hyperstructure neglect. Our model also avoids applying the pinch-based transshipment model. By solving three literature examples, we demonstrate that our model admits better solutions that existing HENS formulations cannot admit.

References

Biegler, L., Grossmann, I., Westerberg, A., 1997. Systematic methods of chemical process design. Prentice Hall PTR.

Björk, K.M., Westerlund, T., 2002. Global optimization of heat exchanger network synthesis problems with and without the isothermal mixing assumption. Computers & Chemical Engineering, 26, 1581-1593.

Ciric, A.R., Floudas, C.A., 1991. Heat exchanger network synthesis without decomposition. Computers & Chemical Engineering 15, 385-396.

Floudas, C.A., Ciric, A.R., 1989. Strategies for overcoming uncertainties in heat exchanger network synthesis. Computers & Chemical Engineering 13, 1133-1152

Huang, K.F., Almutairi, E., Karimi, I.A., 2012. Heat exchanger network synthesis using a stagewise superstructure with non-isothermal mixing. Chemical Engineering Science 73, 30-43.

Papoulias, S.A., Grossmann, I.E., 1983. A structural optimization approach in process synthesis--II : Heat recovery networks. Computers & Chemical Engineering 7, 707-721.

Trivedi K. K., 1988. The pinch design method for the synthesis of heat exchanger networks: the constrained case. Paper 8lb, AIChE Annual Meeting, Washington, DC.

Yee, T.F., Grossmann, I.E., 1990. Simultaneous optimization models for heat integration--II. Heat exchanger network synthesis. Computers & Chemical Engineering 14, 1165-1184.

I.A. Karimi and Rajagopalan Srinivasan (Editors), Proceedings of the 11th International Symposium on Process Systems Engineering, 15-19 July 2012, Singapore

Improvement in Strategy for Design of Heat Exchanger Networks using Multiagent Framework

Naoki Kimura*, Kizuki Yasue, Kei Kobayashi, Yoshifumi Tsuge
Dept. of Chemical Engineering, Faculty of Engineering, Kyushu University; 744 Motooka, Nishi-ku, Fukuoka 819-0395 Japan

Abstract

In this study, a multiagent approach was applied into design of energy-saving chemical processes using pinch technology. We have introduced various strategies for simplification of heat exchanger network (HEN) to HEN design agents. Although large and complicated processes were optimized by the multiagent system, there were several cases where the HEN simplification had stopped at the insufficient and inadequate stages. Therefore we improved the strategy to make more preferable HENs. And we showed the effectiveness of improvement and our multiagent framework.

Keywords: Heat exchanger network, Multiagent system, Pinch technology.

1. Introduction

Post-Kyoto Protocol negotiations on greenhouse gas emissions reduction have been held for sustainable environment. Although there are several problems to achieve fairness, effectiveness and reasonability of the new agreements, there is a broad international consensus that reductions of the energy consumption and the emissions of greenhouse gases are required to prevent the global warming. Pinch technology is one of the commonly used energy-saving technologies in the chemical industries. Despite pinch technology has been incorporated in the process simulation software, the skilled engineers' considerations are required to make preferable heat exchanger networks (HEN). We have introduced a multiagent oriented simulation framework Kimura et al. (2010) into the HEN design to save the energy usage and to reduce the emissions of greenhouse gases. We set up several "HEN design agents" and each had different strategy to search candidate segments to be changed through the HEN. In our previous study, it was possible to optimize the HEN for the small and medium-scale processes. But there were several cases where the HEN simplification stops at the inadequate stage. In this study, we will introduce new strategies to search candidate segments. And we will show the effectiveness of the new algorithms and our multiagent framework.

2. Multiagent Framework

2.1. Multiagent Framework for HEN-Design using Pinch Technology

To design energy-saving chemical processes, we adopted "pinch technology" (Linnhoff and Flower (1978)) in our framework. In this section, the workflow of the HEN design will be explained. Fig.1 shows a schematic diagram of our multiagent framework. The *Human Operator*— who is on the upper-left of Fig.1— gives basic process information (*i.e.* PFD, stream data profile and available utilities) to the *Project Manager*.

*nkimura@chem-eng.kyushu-u.ac.jp

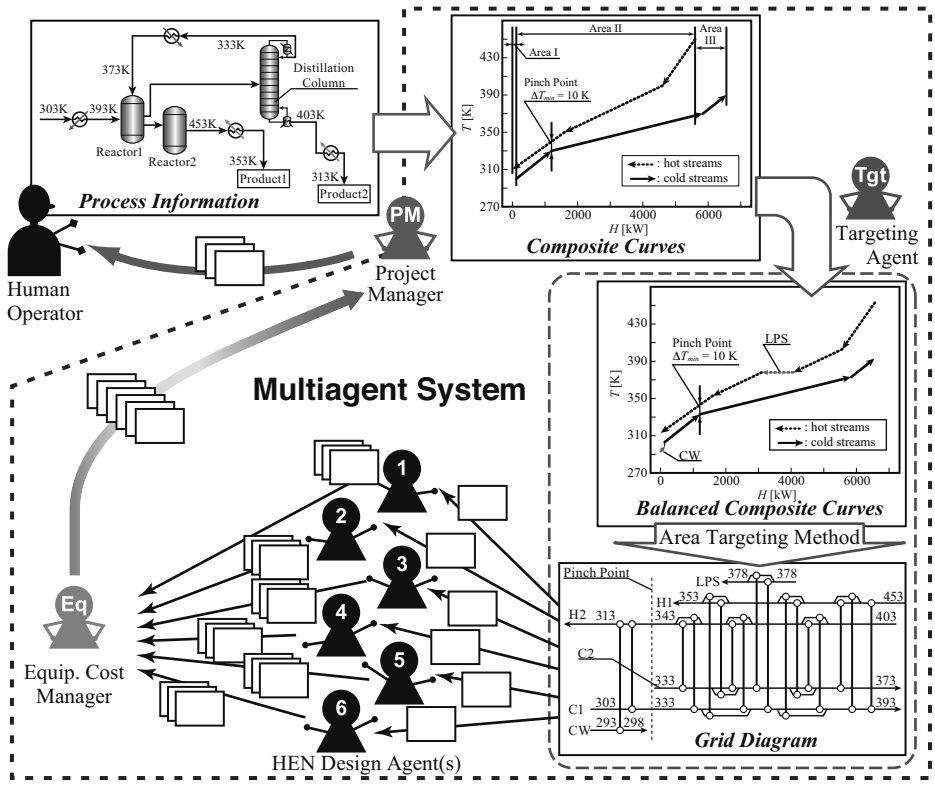

Figure 1. Schematic view of our multiagent framework.

The *Project Manager* is an interface between the human operator and the multiagent system. Then, the *Project Manager* makes "composite curves" and gives it to the *Targeting Agent* (upper-right of Fig.1) via TCP/IP communication. The *Targeting Agent* decides the utility allocation and the amount of heat recovery constrained by ΔT_{min} (minimum approach temperature). As a consequence, the *Targeting Agent* makes "balanced composite curves". Then, the *Targeting Agent* converts the "balanced composite curves" into the initial HEN—which is expressed in "grid diagram"— using "area targeting method". When using the "area targeting method", the sum of heat transfer area is minimized due to the heat transfer within the each vertical section where the balanced composite curves partitioned at each inflection points. Therefore the numbers of both the heat exchangers and the branches of the process streams increase and the network gets complicated. For example, there are 17 heat exchangers and 11 branches in the grid diagram on the lower right of Fig.1. Then it would be preferable if the HEN has been simplified. In our framework, strategies for simplification of HEN were defined and each *HEN Design Agent* has different strategy. And the *HEN Design Agents* receive the initial HEN from the *Targeting Agent*. Then, each *HEN Design Agent* respectively makes alternative HENs by simplifying step by step by following its own strategy. And they send the informa-

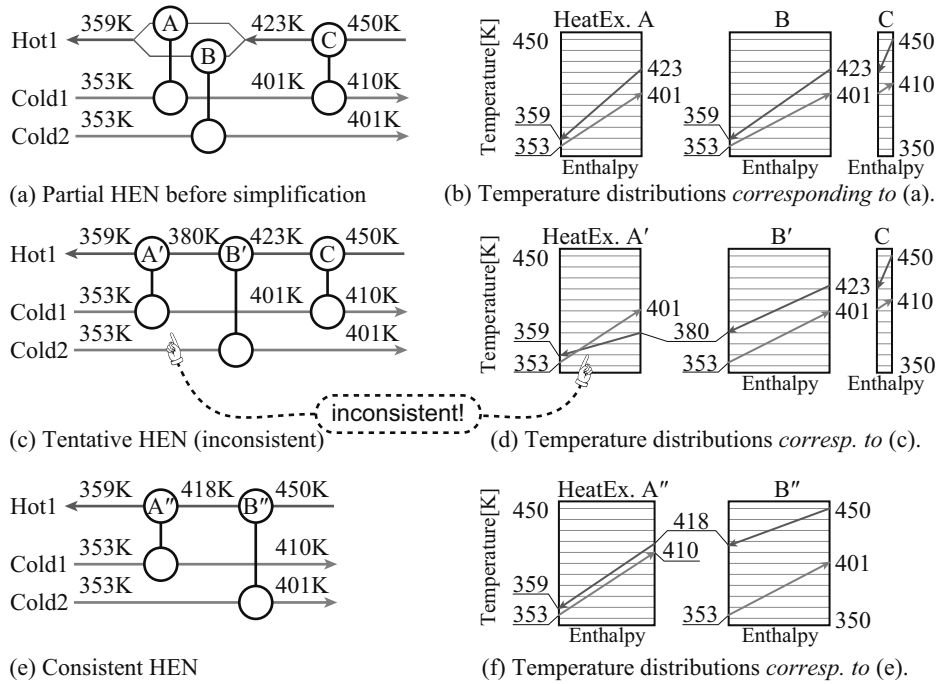

(a) Partial HEN before simplification

(b) Temperature distributions *corresponding to* (a).

(c) Tentative HEN (inconsistent)

(d) Temperature distributions *corresp. to* (c).

(e) Consistent HEN

(f) Temperature distributions *corresp. to* (e).

Figure 2. Grid diagrams and temperature distributions of partial HENs.

tion about alternative HENs to the *Equipment Cost Manager*. When the *Equipment Cost Manager* receives information about HEN, "an equipment cost (*i.e.* investment cost) of the HEN" was calculated by summing up the each estimated equipment costs of all the heat exchangers involved in the HEN. After calculating the equipment costs of all the alternatives, the *Equipment Cost Manager* makes a shortlist of HENs, whose equipment costs are low, to send to the *Project Manager*. The *Project Manager* also picks out several alternatives from the shortlist according to the other criteria such as complicacy of the network. And the *Project Manager* sends back the selected several alternatives to the *Human Operator*. Finally, the *Human Operator* is able to make decision on the HEN design based on not only the structure information of the HEN but also the estimated values of the criteria provided from the multiagent system.

2.2. Strategy for HEN simplification

There are several steps to simplify the network structure of HEN. First of all, it is necessary to search the HEN for the specific partial structures, such as "loop"(a partial structure which consists of several heat exchangers, hot and cold streams circularly traceable in the grid diagram) and "split"(a partial structure where a hot/cold stream is split into several sub-streams to feed into parallel heat exchangers). Steps such as *"DeleteLoop"*, *"DeleteWideScaleLoop"* and *"ReduceSplit"* are defined. Fig.2(a) shows a grid diagram of partial HEN—there are one heat giving stream (Hot1), two heat receiving stream (Cold1, Cold2) and three heat exchangers (HeatEx.A, B, C). There is a branch on Hot1,

Table 1. Stream data and available utilities for 4SP problem.

Stream/Utility Name		Temperature [K]		ΔH	Utility Cost
		Inlet	Outlet	[kW]	[$/kW/yr]
Heat giving streams	H1	443.0	333.0	3,300	-
	H2	423.0	303.0	1,800	-
Heat receiving streams	C1	293.0	408.0	2,300	-
	C2	353.0	413.0	2,400	-
Heating utility	Steam	450.0	450.0	-	80.0
Cooling utility	Water	293.0	313.0	-	20.0

in which the stream is split 44%:56% to change the heat with Cold1 through HeatEx.A and with Cold2 through HeatEx.B respectively. Fig.2(b) shows temperature distributions of each heat exchangers in Fig.2(a). To simplify the HEN through a step *"ReduceSplit"*, the split on Hot1 will be reduced, that is, the relationship between HeatEx.A and B will be changed from parallel connection to serial connection (the names of heat exchangers are also changed to A′ and B′). Usually, the outcome network is consistent and different from the one before the step was carried out. And the other step would be applied to the new HEN one after another. Occasionally, the new structure of the HEN brought by the step would not meet the constraints conditions such as heat balance and temperature differences. Fig.2(c) shows a tentative HEN in which HeatEx.A′ is inconsistent. Because the temperature of the heat giving stream of HeatEx.A′ is lower than that of the heat receiving stream (shown in Fig.2(d)).

In our previous study, such a step—which brings inconsistent HEN— is not permitted to be carried out. Therefore, there are few cases where the HEN simplification stops at the insufficient stage, because any of the steps could not make consistent HEN, it just come to a dead end. In this study, we improved the strategy to permit to execute the strategies even if the resultant HENs are inconsistent—it can expect that the HENs may satisfy the constraint after some series of steps were applied. Fig.2(e) shows a consistent HEN where HeatEx.A′ and HeatEx.C in Fig.2(c) are combined through a step *"DeleteLoop"*. In this partial HEN, the number of heat exchanger was reduced from 3 (in Fig.2(a)) to 2 to simplify the HEN. However, it must be noted that the inconsistent HENs could not adopted as the final solutions.

3. Simulations and Results

3.1. 4SP problem description

This process is popular problem, studied by many research groups. There are two hot streams (H1, H2) and two cold streams (C1, C2). The stream data and available utilities are presented in Table 1. And ΔT_{min} is 5.6 K.

3.2. Simulation results

Table 2 shows the comparison of energy consumption, the numbers of the heat exchangers and branches, and annualized sum of equipment cost. The given process is consuming

Table 2. Comparison among HENs for 4SP problem.

Description	Energy consumption [kW]		Num. of heat ex. [-]	Num. of branches [-]	Annualized cost [k$/kW/yr]
	Heating utility	Cooling utility			
Given problem without heat recovery.	4,700	5,100	-	-	-
The initial HEN achieved heat recovery target w/o simplification.	0	400	15	11	139.6
An example of the optimized HEN by the previous strategy.			11	5	115.7
An example of the optimized HEN by the improved strategy.			**6**	**0**	**84.5**
The optimized HEN using differential evolution by Yerramsetty et al.	0	400	6	1	83.8
The optimized HENs using randomized algorithm by Pariyani et al.	0	400	5	0	83.3
			6	1	85.3

4700 kW of heating utility and 5100 kW of cooling utility. Using pinch technology, the energy consumption is considerably reduced to no heating utility and 400 kW of cooling utility. However the numbers of heat exchangers and branches are large in the initial HEN. By using our previous strategy, the simplification was stopped at the insufficient stage—where there are still 11 heat exchangers and 5 branches. On the other hand, by using the improved strategy, the number of heat exchanger is reduced to 6 and the number of branches is also reduced to 0. Comparing the numbers of heat exchangers and branches, and the annualized cost with the results of Yerramsetty and Murty (2008) and Pariyani et al. (2006), the optimized HEN by the improved strategy was simplified sufficiently.

4. Conclusion

In this paper, the strategy of HEN simplification using pinch technology and multiagent framework was improved. The results show that the improvement was effective and adequate to get sufficiently simplified HENs.

References

Kimura, N., Yasue, K., Kou, T., Tsuge, Y., 2010. A multiagent approach for sustainable design of heat exchanger networks. LNAI 6277, 409–416.

Linnhoff, B., Flower, J. R., 1978. Synthesis of heat exchanger networks:I. systematic generation of energy optimal networks. AIChE Journal 24, 633–642.

Pariyani, A., Gupta, A., Ghosh, P., 2006. Design of heat exchanger networks using randomized algorithm. Computers and Chemical Engineering 30, 1046–1053.

Yerramsetty, K., Murty, C., 2008. Synthesis of cost-optimal heat exchanger networks using differential evolution. Computers and Chemical Engineering 32, 1861–1876.

I.A. Karimi and Rajagopalan Srinivasan (Editors), Proceedings of the 11th International Symposium on Process Systems Engineering, 15-19 July 2012, Singapore.

Process Heat Exchanger Network Integration and Decomposition via Clustering Approach

Wendy Pei Qin Ng[a], Hella Tokos[b], Hon Loong Lam[a], Yongrong Yang[b]

[a]*Department of Chemical and Environmental Engineering*
The University of Nottingham, Malaysia Campus
Jalan Broga, Semenyih, Selangor 43500, Malaysia
[b] *State Key Laboratory of Chemical Engineering*
Department of Chemical and Biochemical Engineering
Zhejiang University, Hangzhou, Zhejiang 310027, P. R. China

Abstract

This paper presents a novel method for process heat exchanger network integration and decomposition: Clustering Approach. The objective of this new approach is to reduce the complexity of the integrated structure, construction and maintenance cost simultaneously. The main idea of this approach is to divide the original system into two or more clusters (subsystems) under several optimisation constrains such as piping and other investment cost, hot and cold stream matches. The results of utilities and investment cost for both original and clustered system are compared. The outcome of this study indicates effectiveness, potential and further application of the novel method.

Keywords: process integration, decomposition, clustering, heat exchanger network, optimisation

1. Introduction

1.1. Process Integration

Heat integration was proposed by Linnhoff and Flower (1978) initially in realising the potential of energy saving through heat exchanger networks (HEN) design. Two major approaches have been developed for optimal synthesis of heat exchanger network: pinch technology (Itoh et al., 1982; Kemp, 2007; Smith, 2005) and mathematical programming methods (Biegler et al., 1997). Mathematical optimisation methods for HEN synthesis can be classified as sequential and simultaneous approaches. Works based on the simultaneous approach solve the problem without any decomposition, and can explicitly handle the trade-offs between the network's capital and operational costs.

1.2. Decomposition technique

Despite the sound development of HEN, there are deficiencies in the field of network integration that are yet to be tackled. One of which is the network complexity when dealing with large network. Long computational time and impractical remote heat exchange are resulted due to HEN complexity. Model size reduction techniques had been developed for application in various disciplines. For example, the analysis of large scale production and supply networks by Lam et al. (2011), reactive batch distillation optimisation by Khazraee et al. (2011), etc. In this paper, decomposition approach is applied to reduce the HEN complexity. Heat exchangers are grouped into two or more subsystems (clusters). A novel heat network design by integrating the decomposition approach based on heat exchanger area and network piping contribution via mathematical programming is presented.

2. Model formulation

The mathematical formulation for typical HEN optimisation can be found elsewhere in Ortega et al. (2008) and Yee and Grossmann (1990). In case of proposing decomposition method to the basic heat integration model, the following equations were added and the objective function is formulated to develop the clusters. To every heat exchangers included in the superstructure, a binary variable, y_k is associated by equations:

$$A_k \cdot y_k - A_k = 0 \qquad k \in E \tag{1}$$

where k is set of heat exchangers within the superstructure, A_k / m^2 is the area of the existing heat exchanger k, y_k is a binary variable related to heat exchanger k.

The binary variable activated by previous equations is connected with binary variable, $y_{k,c}^{Cluster}$, ensuring the heat exchanger k to be included in only one cluster c:

$$y_k - \sum_c y_{k,c}^{Cluster} = 0 \qquad k \in E \ \wedge \ c \in C \tag{2}$$

where E denotes all heat exchangers preset in the superstructure, c is a set of possible clusters and $y_{k,c}^{Cluster}$ is a binary variable connecting heat exchanger k to cluster c. It should be nothed that by fixing the value of binary variable $y_{k,c}^{Cluster}$ on zero we can forbid heat exchanger k to be included in cluster c due to the technical or operational disadvantages.

2.1. Definition of heat exchanger's contribution to a particular cluster based on the heat exchanger area

The total area of heat exchangers belonged to cluster c, $A_c^{Cluster}$ / m^2 is given by equation:

$$A_c^{Cluster} = \sum_k A_k \cdot y_{k,c}^{Cluster} \qquad k \in E \ \wedge \ c \in C \tag{3}$$

The upper and lower bound for the total area of heat exchangers in cluster c are defined to avoid the possibility to join all clusters together into one:

$$A_c^{Cluster} - A^{Cluster,UB} \leq 0 \qquad c \in C \tag{4}$$

$$A_c^{Cluster} - A^{Cluster,LB} \geq 0 \qquad c \in C \tag{5}$$

where $A^{Cluster,UB}$ / m^2 is the upper bound for the total area of heat exchangers in clusters and $A^{Cluster,LB}$ / m^2 is the lower bound for the total area of heat exchangers in clusters.

The contribution of heat exchanger k to cluster c, $a_{k,c}^A$, based on its area is calculated as a ratio between the area of heat exchanger k and the total of heat exchangers in cluster c:

$$a_{k,c}^A = \frac{A_k \cdot y_{k,c}^{Cluster}}{A_c^{Cluster}} \qquad k \in E \ \wedge \ c \in C \tag{6}$$

2.2. Definition of heat exchanger's contribution to a particular cluster based on the pipe length associated with the heat exchanger

The total length of piping connected to heat exchanger k, PL_k / m is given as:

$$PL_k = \sum_{\substack{l \\ l \neq k}} PL_{k,l}^H \cdot z_{k,l}^h + \sum_{\substack{l \\ l \neq k}} PL_{k,l}^C \cdot z_{k,l}^c + \sum_s PL_{s,k}^I \cdot y_{s,k}^{In} \qquad k,l \in \mathrm{E} \ \wedge \ c \in \mathrm{C} \ \wedge \ \mathrm{s} \in \mathrm{S} \tag{7}$$

where S denotes all hot and cold process streams in the superstructure, $PL_{k,l}^H$ / m is the length of new pipeline connecting the hot ends of heat exchangers k and l, $PL_{k,l}^C$ / m is the length of new pipeline connecting the cold ends of heat exchangers k and l, $PL_{s,k}^I$ / m is the length of new initial pipeline of stream s to heat exchanger k, $z_{k,l}^h$ is a binary variable to denote the pipeline connecting exchangers k and l at the hot ends, $z_{k,l}^c$ is a

binary variable to denote the pipeline connecting exchangers k and l at the cold ends and $y_{s,k}^{In}$ is a binary variable to denote the inlet stream s is assigned to exchanger k.

The total length of pipeline within cluster c, $PL_c^{Cluster}$ / m, is:

$$PL_c^{Cluster} = \sum_k PL_k \cdot y_{k,c}^{Cluster} \qquad k \in E \ \wedge \ c \in C \tag{8}$$

The upper and lower bound for the total length of the pipeline in cluster c are:

$$PL_c^{Cluster} - PL^{Cluster,UB} \leq 0 \qquad c \in C \tag{9}$$

$$PL_c^{Cluster} - PL^{Cluster,LB} \geq 0 \qquad c \in C \tag{10}$$

where $PL^{Cluster,UB}$/ m is the upper bound for the total length of the pipeline in clusters and $PL^{Cluster,LB}$ / m is the lower bound for the total length of the pipeline in clusters.

The contribution of heat exchanger k to cluster c, $a_{k,c}^{PL}$, based on the associated piping length is given:

$$a_{k,c}^{PL} = \frac{PL_k \cdot y_{k,c}^{Cluster}}{PL_c^{Cluster}} \tag{11}$$

The objective function for the clustering model is to minimise the contribution of heat exchangers to the clusters:

$$Obj = \sum_k \sum_c a_{k,c}^{A} + \sum_k \sum_c a_{k,c}^{PL} \tag{12}$$

3. Case study

A case study, which considers four hot and four cold non-isothermal process streams and the network pipelines, is developed. In the superstructure, 10 heat exchangers are available for service. The streams data for the case study is presented in Table 1. The piping costs parameters are tabulated in Table 2 and Table 3.

The MINLP models formulated are solved in GAMS 23.4.3 with the solver DICOPT. The HEN is first divided into 3 clusters by applying the previously described approach and then heat integration is performed within each cluster. A general model based on minimum utility requirement in Figure 1 and a clustered model in Figure 2 are presented as the outcomes of HEN optimisation. The results of the models are listed in Table 4. The resulting heat exchanger area requirement and piping cost are compared.

Table 1: Stream data for case study.

Stream	T_{IN} (°C)	T_{OUT} (°C)	FCp (kW/K)	Stream	T_{IN} (°C)	T_{OUT} (°C)	FCp (kW/K)
H1	400	120	1.0	C1	160	400	1.5
H2	340	120	2.0	C2	100	250	1.3
H3	175	75	3.5	C3	80	140	1.5
H4	100	50	2.5	C4	20	80	3.0
HU	500	500	-	CU	20	30	-

Table 2: Piping cost ($/yr) for case study: inlet stream to heat exchanger - $CO_{s,k}^{PI}$.

	1	2	3	4	5	6	7	8	9	10
H1	7018	3640	5099	2693	3606	1500	2550	2693	3500	4717
H2	4031	1118	2236	1118	2000	3354	4301	3202	4610	4031
H3	6500	2693	4123	3354	2000	1118	1581	500	1803	2500
H4	3640	3202	2236	5315	3162	6185	6519	5025	6021	3640
HU	2500	5315	4472	4924	6403	8322	9301	8139	9552	8322
C1	2500	3640	2236	5408	4000	7018	7517	6021	7159	4924
C2	2500	3354	3000	2693	4472	6103	7106	6021	7433	6500
C3	6021	3041	3606	5025	2000	3905	3808	2500	3041	500
C4	8139	4500	6000	4031	4123	1118	1581	2500	2693	4610
CU	9708	6021	7211	6946	5000	3640	2550	3202	1803	3640

Table 3: Piping cost ($/yr) for case study: heat exchanger to heat exchanger - $CO_{k,l}^{PC}$.

	1	2	3	4	5	6	7	8	9	10
1	0	3808	2500	4528	4717	7280	8078	6708	8062	6364
2	3808	0	1500	2236	1118	3536	4272	2915	4301	3162
3	2500	1500	0	3202	2236	5025	5701	4272	5590	3905
4	4528	2236	3202	0	3041	3536	4610	3808	5148	5000
5	4717	1118	2236	3041	0	3041	3536	2062	3354	2062
6	7280	3536	5025	3536	3041	0	1118	1414	2000	3536
7	8078	4272	5701	4610	3536	1118	0	1500	1118	3354
8	6708	2915	4272	3808	2062	1414	1500	0	1414	2121
9	8062	4301	5590	5148	3354	2000	1118	1414	0	2550
10	6364	3162	3905	5000	2062	3536	3354	2121	2550	0

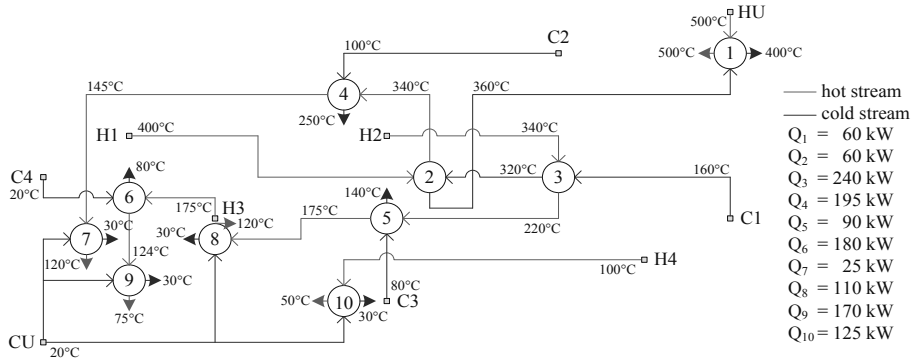

Figure 1: The existing heat exchanger network of the general model.

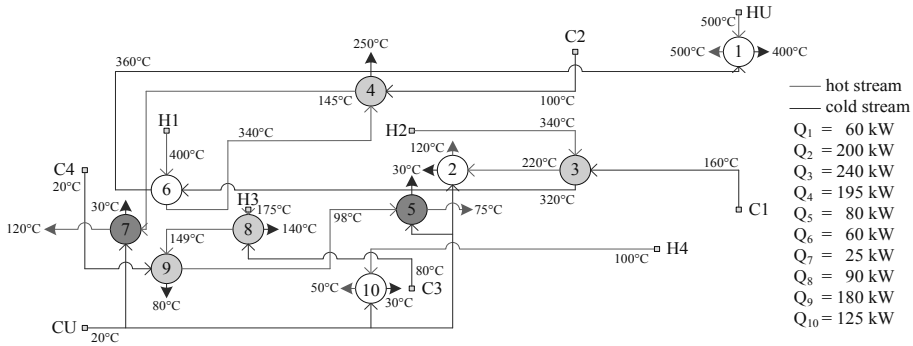

Figure 2: The clustered heat exchanger network based on optimised clustering model.

Table 4: Results comparison for case study.

	Existing model	Clustered model
Total heat exchanger area (m^2)	31.00	31.24
Total exchanger area cost ($/yr)	11778	11869
Total utility cost ($/yr)	14600	14600
Total capital piping cost ($/yr)	69278	63537
TOTAL annual cost ($/yr)	95656	90006

* Heat exchanger area cost = $380/$m^2$.yr

* Utility cost = $100/kW.yr for hot utility and $20/kW.yr for cold utility.

The clustering of the model network yields a cost saving from the reduction in piping costs incurred. However, it is noted that the clustered model brings an increment to the heat exchanger area requirement, thus incurring higher heat exchanger capital cost.

Better result may be obtained if other indicator such as maintenance cost is considered. It should be noted that the utility requirement is not static but varying with the HEN design and any additional utility allocation. The model clustering may render the annual cost saving in certain cases due to any additional utility needed.

Nevertheless, the clustering approach is effective in model size reduction. This improves the computational performance by capping a limit to the number of variables. The approach will be particularly useful for large HEN retrofit, i.e. petro-chemical refineries, as well as other outsized models, i.e. country supply chain optimisation.

4. Conclusions and Future Work

This paper investigates the effectiveness of clustering approach on heat network size reduction. A clustering method based on heat exchanger area and piping length contribution is formulated. 6% of annual cost saving is achieved through the implementation of clustering approach on HEN design, even for a small HEN.

Future work should implement the clustering approach on greater size case study that consists of more than ten hot and ten cold streams to significant the contribution of the approach. A more detailed formulation should be generated which considers more accurate piping cost, piping insulation, maintenance cost, heat exchanger incurred cost together with the utility costs. A multi-objective integration is suggested to solve this extended problem.

Acknowledgement

The financial supports from University of Nottingham Research Committee via New Researcher Fund to Ng W.P.Q. and Global Green Synergy Sdn Bhd to Lam H.L are gratefully acknowledged.

Nomenclature

s	set index for all stream	HE	heat exchanger
k	set index for all heat exchanger	$CO_{s,k}^{PI}$	piping cost: stream inlet to HE
c	set of clusters	$CO_{k,l}^{PC}$	piping cost: HE to HE

References

Biegler L.T., Grossmann E.I. and Westerberg A.W., 1997, Systematic Methods of Chemical Process Design, International Edition, Prentice-Hall, New Jersey

Itoh J., Shiroko K. and Umeda T., 1982, Extensive application of the T-Q diagram to heat integrated system synthesis. *Proc. (Technical Sessions) Int. Proc. Syst. Engng. (PSE-82)*, 92-99

Kemp I.C., 2007, Pinch Analysis and Process Integration: A User Guide on Process Integration for the Efficient Use of Energy, 2nd Edition, Butterworth-Heinemann, Great Britain

Khazraee S.M., Jahanmiri A.H., Ghorayshi S.A, 2011, Model reduction and optimization of reactive batch distillation based on the adaptive neuro-fuzzy inference system and differential evolution, *Neural Computer & Application*, doi: 10.1007/s00521-010-0364-x

Lam H.L., Klemeš J.J. and Kravanja Z., 2011, Model-size reduction techniques for large-scale biomass production and supply networks, *Energy*, 36, 4599-4608

Linnhoff B. and Flower J.R., 1978, Synthesis of heat exchanger network: I. Systematic generation of energy optimal networks, *AIChE Journal*, 24(4), 633-642, doi: 10.1002/aic.690240411

Ponce-Ortega J.M., Jiménez-Gutiérrez A. and Grossmann I.E., 2008, Simultaneous Retrofit and Heat Integration of Chemical Processes, *Ind. Eng. Chem. Res.*, 47, 5512-5528

Smith R., 2005, Chemical Process: Design and Integration, Wiley

Yee T.F. and Grossmann I.E., 1990, Simultaneous Optimization Models for Heat Integration: II. Heat Exchanger Network Synthesis, *Computers Chem. Engng.*, 14(10), 1165-1184

I.A. Karimi and Rajagopalan Srinivasan (Editors), Proceedings of the 11th International Symposium on Process Systems Engineering, 15-19 July 2012, Singapore.

Controllability of three types of dividing wall columns

Chuan-Chen Chao and Jeffrey D. Ward

Department of Chemical Engineering, National Taiwan University, No. 1, Sec. 4, Roosevlt Road, Taipei, 106, Taiwan

Abstract

We investigated the pairing of controlled and manipulatd variables and the overall controllability of three types of dividing wall columns (with the dividing wall in the upper, lower and middle section of the column; DWCL, DWCU and DWCM, respectively) using steady-state and dynamic controllability measures. Dividing wall columns were designed for the separation of a mixture of three species with constant relative volatilities, for different values of the relative volatilities and feed compositions. The steady-state processes were simulated in Aspen Plus and the relative gain arrays, non-square relative gain array and condition number were determined for each case using the steady-state model. Finally, the dynamic responses of the processes were simulated in Aspen dynamics and an integral error criteria was used to compare the performance of different control structures. The results indicate that generally DWCL is favorable if the intermediate-boiling species is most plentiful in the feed, and DWCU is preferable in other cases.

Keywords: Divided Wall Column, Process Control

1. Introduction

A dividing wall column, first proposed by Wright[1] in 1949, is a kind of integrated process in which separation between three or more species is accomplished in a single vessel through the use of one or more dividing walls. Pioneering research on the design of dividing wall columns using Underwood's method was conducted by Fidkowski and Krolikowski.[2–3] Studies have shown that in some cases dividing wall columns can significantly reduce capital and energy cost compared to conventional multi-column processes.[4–5] However, industrial application of dividing wall columns remains relatively limited, in part because of the increased difficulty of designing and controlling the integrated unit.[6]

Control of divided wall columns has received some attention in the literature.[6–18] However, almost all research conducted so far on the control of dividing wall columns has considered the case where the wall is located in the middle of the column and there is only a single reboiler and condenser. Another option which as received much less attention is for the dividng wall to extend to either the top or bottom of the column so that there are two condensers or reboilers, respectively. This changes the number of degrees of freedom and the control options.

In this work we investigate control loop pairing and controllability of three different types of dividing wall columns for a variety of feed compositions and different values of the ease of separation index (ESI).

2. Model development and column design

2.1. Thermodynamic model

In this work, a ternary system with species A, B and C is considered. All species are assumed to have constant relative volatilities. Three different cases are considered, which correspond to different values of the ease of separation index (ESI) which measures the relative difficulty of the A/B split to the B/C split: ESI>1 ($\alpha_A/\alpha_B/\alpha_C$=7.1/2.2/1), ESI=1 ($\alpha_A/\alpha_B/\alpha_C$=4/2/1) and ESI<1 ($\alpha_A/\alpha_B/\alpha_C$=4/2.4/1). This was achieved in Aspen by modeling the saturation vapor pressure using Antoine's equation and adjusting the values of the Antoine coefficient A and the normal boiling point of the species to give the desired constant relative volatility.

2.2. The three types of dividing wall columns

Three different types of dividing wall columns were considered as shown in Figure 1. For DWCL, the dividing wall is located in the lower part of the column and touches the bottom, so there are two reboilers and one condenser. DWCM is the most common type of dividing wall column, in which the dividing wall is locatd in the middle of the column and there is one condenser and one reboiler. Finally, for DWCU the dividing wall is located at the top of the column and there is one reboiler and two condensers.

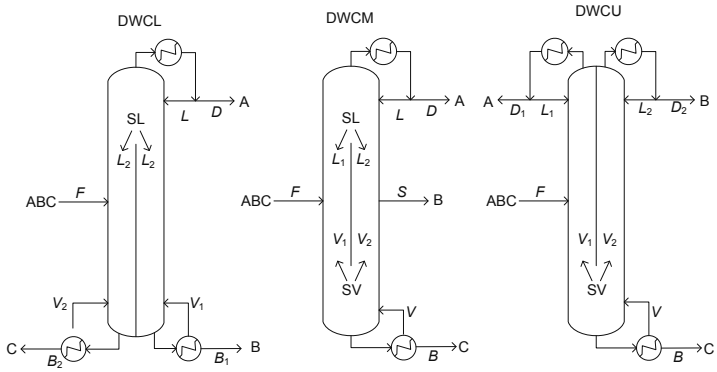

Figure 1. Three types of divided wall columns with notation.

For each reboiler there is an associated boilup ratio BR and for each condenser there is an associated reflux ratio RR. For example, for DWCL, there are two boilup ratios BR1=V_1/B_1 and BR2=V_2/B_2 and one reflux ratio RR=L/D. The liquid split SL is defined by SL=L_1/L_2, and the vapor split is defined by SV=V_1/V_2. Although some authors consider the use of SV as a manipulated variable, in practice it is difficult to measure or adjust SV with adequate precision, therefore in this work we do not consider SV as a possible manipulated variable. We further assume that flowrates D and B are used to control the inventory in the distillate receivers and reboilers respectively. The control objective is to maintain the purity of the three product streams.

For DWCL, there are four candidate manipulated variables: RR, SL, BR1 and BR2. For DWCM, there are also four candidate manipulated variables: RR, SL, S and BR, where S is the sidedraw flow rate. Finally, for DWCU, there are only three candidate manipulated variables: RR1, RR2 and BR.

2.3. Column design and analysis

For each feed composition and ease of separation index, the three dividing wall columns were designed using the method of Chu et al.[19] This method determined the

number of stages in each column section as well as the liquid and vapor splits and boilup and reflux ratios. A linear steady-state model of each column was then developed by modeling each column in Aspen plus and making small modifications to the input variables in order to determine the steady-state gain between each of the input variables and all of the controlled variables (the compositions of the product streams). It was then possible to calculate the non-square relative gain array[20] for each column and relative gain array[21] and the condition number[22] for each set of three manipulated variables. (For DWCM and DWCL, which have four possible manipulated varibles, there are four possible choices for the set of three manipulated variables.)

Finally, the steady-state models in Aspen Plus were converted into dynamic models in Aspen Dynamics. For control structures that were identified as promising based on steady-state analysis, the tuning parameters for the flow, level and pressure controllers were assigned certain fixed values, and the PI tuning parameters for the thrree composition controllers were determined using sequential relay auto tuning.[23] Finally, the dynamic response of the process was simulated for +/− 10% changes in the feed flow rate. For each control structure, the IAE and ITAE of the three composition controllers were determined and added together to determine the combined IAE and ITAE.

Table 1. Pairings recommended by RGA and CN analysis.

	0.8/0.1/0.1	0.1/0.8/0.1	0.1/0.1/0.8	0.33/0.33/0.33
DWCL ESI>1	RR-BR1-BR2	RR-BR1-BR2	RR-BR1-BR2	RR-BR1-BR2
		RR-SL-BR2	RR-SL-BR2	RR-SL-BR2
DWCL ESI=1	RR-BR1-BR2	RR-BR1-BR2	RR-BR1-BR2 RR-SL-BR2	RR-BR1-BR2
DWCL ESI<1	RR-BR1-BR2	RR-BR1-BR2	RR-SL-BR2	RR-SL-BR2
DWCM ESI>1	S-SL-BR	RR-S-BR	BR-SL-S	S-RR-BR
			RR-SL-S	
DWCM ESI=1	S-SL-BR	RR-S-BR	RR-SL-S	S-SL-BR
	S-SL-RR			RR-SL-BR
DWCM ESI<1	S-SL-BR	RR-S-BR	RR-SL-S	RR-SL-BR
	S-SL-RR			

3. Results

3.1. RGA Analysis

Table 1 shows the results of the RGA analysis. The column headings indicate the feed compositoin in mole fraction of A/B/C. The entries in the table indicate the preferred control structure or structures. For example, for a DWCL when ESI>1 and when the feed composition is 80% A, 10% B and 10% C, the preferred pairing is RR-BR1-BR2, meaning that x_A should be controlled by manipulating RR, x_B should be controlled by manipulating BR1 and x_C should be controlled by manipulating BR2. When two possible controller pairings are listed, it indicates that the two pairings gave similar results and a conclusive decision about which was better could not be made. DWCU

does not appear in the table because there is only one set of three controlled variables, and in all cases it was found that the preferred pairing is RR1-RR2-BR.

3.2. Dynamic Response Analysis

Table 2 shows the prefered pairings between controlled and manipulated variables based on the ITAE dynamic performance criteria. A star (*) indicates that the result is different from the result based on steady-state analysis. Table 3 shows the numerical value of the best achievable ITAE for each column, ESI and feed composition. Generally, DWCU performs the best, except for the case where the intermediate-boiling speices B is the most plentiful, in which chase DWCL is preferred.

Table 2. Pairings recommended by ITAE.

	0.8/0.1/0.1	0.1/0.8/0.1	0.1/0.1/0.8	0.33/0.33/0.33
DWCL ESI>1	RR-BR1-BR2	RR-BR1-BR2 RR-SL-BR2	RR-SL-BR2*	RR-SL-BR2*
DWCL ESI=1	RR-SL-BR2*	RR-BR1-BR2	RR-BR1-BR2 RR-SL-BR2	RR-BR1-BR2
DWCL ESI<1	RR-BR1-BR2	RR-BR1-BR2	RR-SL-BR2	RR-SL-BR2
DWCM ESI>1	S-SL-BR	RR-S-BR	RR-SL-S*	S-RR-BR
DWCM ESI=1	S-SL-BR*	RR-S-BR	RR-SL-S	S-SL-BR*
DWCM ESI<1	S-SL-BR*	RR-S-SL*	RR-SL-S	RR-SL-BR

Table 3. Best achievable ITAE.

	0.8/0.1/0.1	0.1/0.8/0.1	0.1/0.1/0.8	0.33/0.33/0.33
DWCL ESI>1	0.5962	0.0173	0.2087	0.2016
DWCL ESI=1	2.0973	0.0555	2.4944	0.4745
DWCL ESI<1	1.7823	0.0760	0.7393	0.5145
DWCM ESI>1	0.5617	0.4441	0.0663	1.0997
DWCM ESI=1	1.3552	1.0528	0.0960	0.2354
DWCM ESI<1	2.3915	1.2887	0.0463	0.2682
DWCU ESI>1	0.1664	0.0516	0.0274	0.0590
DWCU ESI=1	0.0533	0.0563	0.0286	0.0413
DWCU ESI<1	0.0757	0.1299	0.0421	0.0597

4. Conclusions

The controller pairings and overall controllability for three types of dividing wall columns was analyzed for different feed compositions and ESI values using steady-state and dynamic methods. The results suggest that from a controllability standpoint, DWCU is favorable in all cases except when the feed contains predominatly the middle boiling component, in which case DWCL is preferred. If a different column

configuration is preferred for economic reasons, the results can also be used to suggest the best pairing between controlled and manipulted variables.

The dynamic analysis conducted so far does not consider changes in the set-points of the composition controllers or disturbances in feed the feed composition. In the future it may be worthwhile to consider these changes. Furthermore, it has been assumed that the composition of the three streams can be measured online. It may also be interesting to compare the performance of different control structures when the product composition is inferred by temperature measurement.

References

[1] R.O. Wright and N.J.Elizabeth, Fractional apparatus, US Patent No. 2 471 134 (1949).
[2] Z. Fidkowski and L. Krolikowski, Aiche J, 32. (1986) 537.
[3] Z. Fidkowski and L. Krolikowski, Aiche J, 33. (1987) 643.
[4] G. Dunnebier and C. C. Pantelides, Ind Eng Chem Res, 38. (1999) 162.
[5] M. Emtir, E. Rev and Z. Fonyo, Appl Therm Eng, 21. (2001) 1299.
[6] S. J. Wang and D. S. H. Wong, Chem. Eng. Sci., 62. (2007) 1010.
[7] E. A. Wolff and S. Skogestad, Ind Eng Chem Res, 34. (1995) 2094.
[8] M. I. A. Mutalib and R. Smith, Chem Eng Res Des, 76. (1998) 308.
[9] M. I. A. Mutalib, A. O. Zeglam and R. Smith, Chem Eng Res Des, 76. (1998) 319.
[10] M. Serra, A. Espuna and L. Puigjaner, Chem Eng Process, 38. (1999) 549.
[11] I. J. Halvorsen and S. Skogestad, J Process Contr, 9. (1999) 407.
[12] M. Serra, M. Perrier, A. Espuna and L. Puigjaner, Comput Chem Eng, 24. (2000) 901.
[13] M. Serra, M. Perrier, A. Espuna and L. Puigjaner, Comput Chem Eng, 25. (2001) 859.
[14] M. Serra, A. Espuna and L. Puigjaner, Ind Eng Chem Res, 42. (2003) 1773.
[15] T. Adrian, H. Schoenmakers and M. Boll, Chem Eng Process, 43. (2003) 347.
[16] Y. Cho, B. Kim, D. Kim, M. Han and M. Lee, J Process Contr, 19. (2009) 932.
[17] H. Ling and W. L. Luyben, Ind Eng Chem Res, 48. (2009) 6034.
[18] R. C. van Diggelen, A. A. Kiss and A. W. Heemink, Ind Eng Chem Res, 49. (2010) 288.
[19] K. T. Chu, L. Cadoret, C. C. Yu and J. D. Ward, Ind Eng Chem Res, 50. (2011) 9221.
[20] S. Skogestad and I. Postlethwaite, Multivariable feedback control : analysis and design, Wiley, New York, 1996.
[21] E. H. Bristol, Ieee T Automat Contr, Ac11. (1966) 133.
[22] D. E. Seborg, T. F. Edgar and D. A. Mellichamp, Process dynamics and control. 2nd ed.; Wiley, Hoboken, NJ, 2004.
[23] C.-C. Yu, Autotuning of PID controllers : a relay feedback approach. 2nd ed., Springer, London, 2006.

I.A. Karimi and Rajagopalan Srinivasan (Editors), Proceedings of the 11th International Symposium on Process Systems Engineering, 15-19 July 2012, Singapore.

A systematic procedure for synthesis of intensified simple column configurations for multicomponent distillations

Ben-Guang Rong*, Massimiliano Errico

University of Southern Denmark,Institute of Chemical Engineering, Biotech. and Env. Tech., Niels Bohrs Alle 1, Odense 5230, Denmark. Email: bgr@kbm.sdu.dk

Abstract

In this work, we have presented a systematic procedure for synthesis of intensified simple column configurations (ISC) for multicomponent distillations, which constitutes a new specific subspace of distillation configurations that has not been approached in the earlier works. The intensified simple column configurations fulfill the process intensifications principle that they have reduced the number of columns as well as the number of heat exchangers. More importantly, they keep the similar features as the conventional simple column configurations, that each column produces an overhead product with a condenser and bottoms product with a reboiler. As a consequence, these new intensified simple column configurations keep the similar simplicity in terms of systems design, control and operation as the conventional simple column configurations. However, they have the potential to reduce the energy consumption and especially capital costs substantially due to the improved separation efficiency and reduced number of equipment units. The procedure can be generalized to synthesize the intensified simple column configurations for any traditional distillation configurations of an N-component mixture with both sharp and sloppy splits.

Keywords: systematic procedure, synthesis, intensified simple column configuration, process intensification

1. Introduction

To achieve N nearly pure products for an N-component mixture by distillation, it is traditionally believed that the minimum number of simple columns in a conventional simple column configuration is N-1 (Thompson and King, 1972). Each of the N-1 simple columns receives a feed and produces two products, i.e. an overhead product with a condenser in the rectifying section and a bottoms product with a reboiler in the stripping section. Such conventional simple column configurations are commonly used in the workplace of process industries, primarily due to its simple and easy in design, control and operation. However, they are energy inefficiency due to the inevitable remixings and thermodynamic irreversibility, and are characterized with high energy consumption and capital costs (Petlyuk et al., 1965). To reduce the energy consumption and capital costs, many different distillation configurations have been proposed, among others, the heat-integrated distillation systems (Rathore et al., 1974) and dividing-wall columns (Wright, 1949) are the most impressive ones, and have been successfully applied in certain cases. However, these systems are also more complex than the simple column configurations and in many cases increased the difficulty in system's design, control and operations. Moreover, they are more difficult to be used to replace the existing distillation plants. Therefore, distillation configurations with similar simplicity

as simple column configurations while have potential to reduce both energy and capital costs are desired. In this work, we present a systematic procedure to synthesize the intensified simple column configurations with such features.

2. The systematic synthesis procedure

Starting from the simple column configurations, a step-by-step procedure has been formulated which can systematically synthesize the intensified simple column configurations. The procedure is based on thermal coupling technique and is shown in Figure 1. The key mechanism is to produce the thermodynamically equivalent structures (TES) in which there exist *single-section transport side column(s)*. The transport-side-column can be eliminated and leave the submixtures transport directly between the columns. We have formulated two criteria for a TES structure that could finally lead to the ISC configurations.

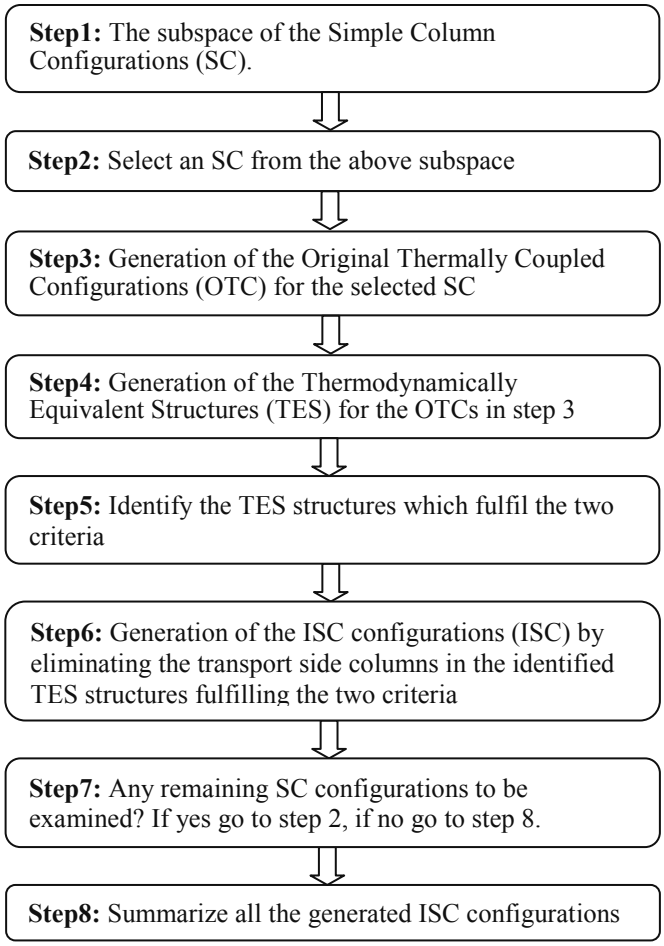

Figure 1. The procedure for synthesis of ISCs from simple column configurations

Criterion 1: The TES must contain the single-section transport-side-column.

Criterion 2: Except the transport side columns, each of the other columns in the TES must keep the simple column features that each column produces an overhead product with a condenser and a bottom product with a reboiler.

Therefore, to achieve the possible ISC configurations for an N-component mixture, we need systematically examining the TES structures and identifying those TES structures which fulfill the two criteria. In the following, the procedure is illustrated for a five-component mixture to generate the ISCs which applicable to any N-component mixture.

3. Synthesis of the ISCs for a five-component mixture

Step1. The SC configurations for a five-component mixture. In total, there are 14 simple column configurations for a five-component mixture.

Step2. Select an SC configuration. Let us select the SC configuration which is from the separation sequence of A/BCDE(1)→BCD/E(2)→B/CD(3)→C/D(4).

Step3. Generate the OTCs for the selected SC configuration. For any traditional distillation configurations, all of possible original thermally coupled configurations can be generated by replacing the heat exchangers associated with submixtures individually or combinatorially (Rong et al., 2002). For above selected SC configuration, in total 7 OTCs can be generated. Figure 2 presents 4 OTCs which would finally generate ISCs.

Steps4 and 5. Generate the TES structures and identify the TES structures fulfilling the two criteria. For any original thermally coupled configuration, there are a certain number of movable column sections, which are designated by the introduced thermal couplings. By recombining the column sections through moving the movable section individually or combinatorially, all of the TES structures can be generated (Rong et al., 2004). Figure 3 presents the identified TESs for the OTCs in Figure 2.

Step6. Generation of the ISC configurations from the identified TES structures in step 5. It is obvious that each of the identified TES structures shown in Figure 3 contains a transport side column. By eliminating the transport side columns, the corresponding ISC configurations are readily generated which are presented in Figure 4.

Step7. Select another SC and repeat from step 2 to step 6 until all of the 14 SC configurations are selected.

Step8. Summarize all the generated ISC configurations.

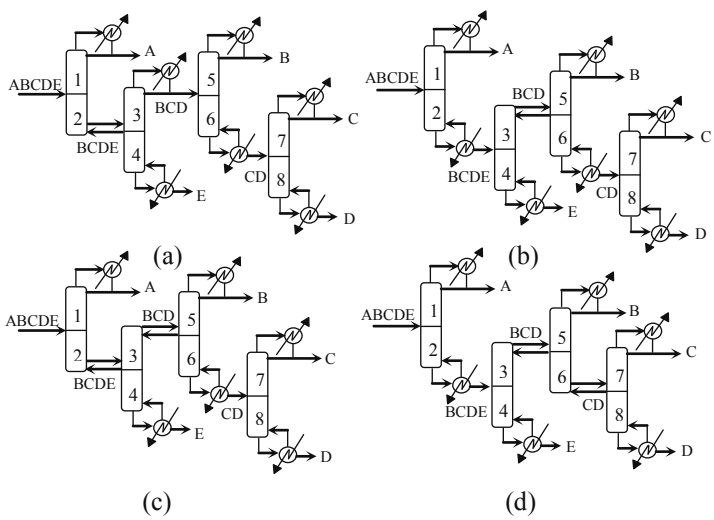

Figure 2. The original thermally coupled configurations generated from the selected SC

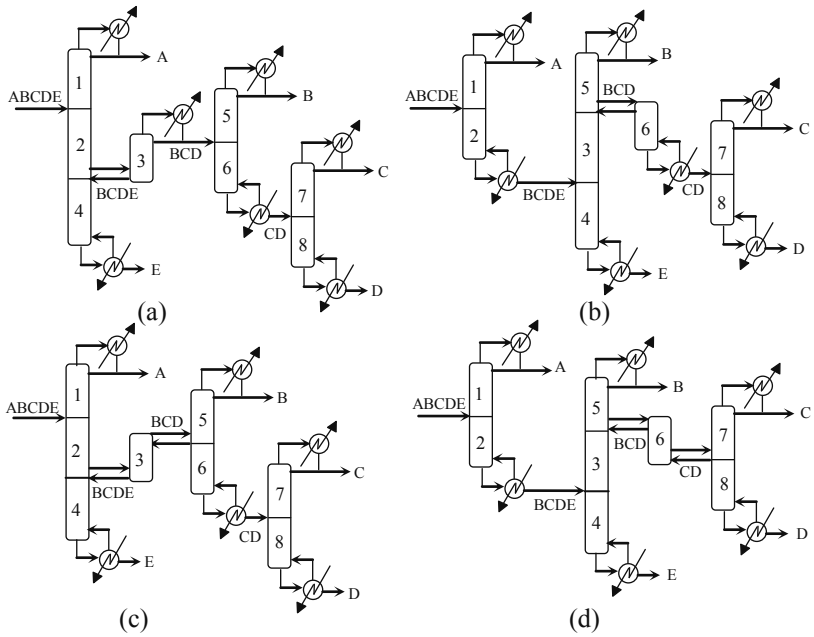

Figure 3. The identified TES structures fulfilling the two criteria for the selected SC

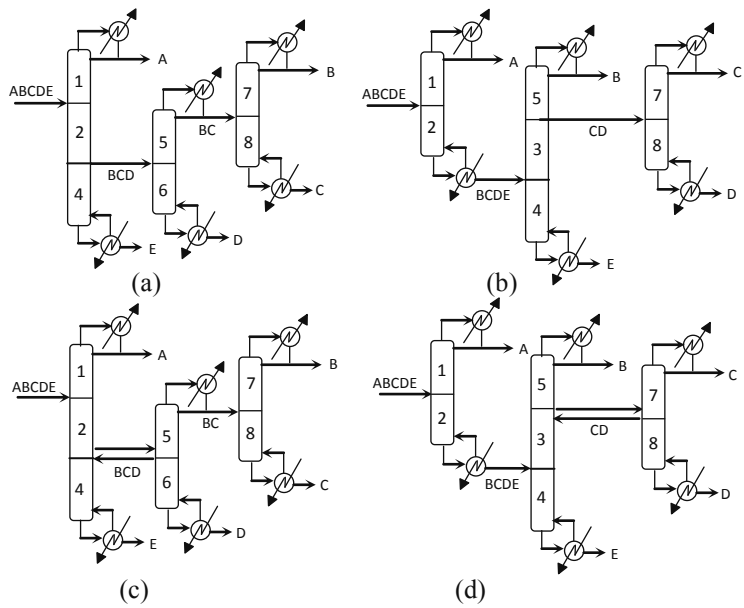

Figure 4. The ISC configurations with one-way and two-way transports from the TESs in Figure 3

Following the procedure, in total, 12 ISCs with one-way transport of a submixture between intermediate locations of two columns are generated from the 14 SCs. Correspondingly, 12 ISCs with two-way transport of a submixture between intermediate locations of two columns are generated from the 14 SCs. Compared to the SC, each of the ISCs in Figure 4 has reduced 1 column and 2 heat exchangers to obtain the same five products.

4. Discussion and Conclusion

The systematic procedure can be generalized to generate the ISCs from the SCs for any N-component mixture. It is expected that there will reduce more columns and more heat exchangers when the number of the components is increased in the feed mixture. It is observed that the similarity between the ISCs and their corresponding SCs exist in that each column produces an overhead product with a condenser and a bottoms product with a reboiler. However, the ISCs are generated by modifying the corresponding SCs, they have some different features from the SCs.

a) An ISC configuration uses less than N-1 columns for an N-component mixture.
b) Each column has an overhead condenser and a bottom reboiler.
c) There exist submixtures transporting between intermediate locations of columns in one-way or in two-way.
d) A column in an ISC can have more than two column sections.

These structural features of the intensified simple column configurations can be regarded as the relaxation to the definition of the classical simple column configurations. Now, taking these structural features into consideration, the procedure in Figure 1 can be generalized to synthesize the ISC configurations from the traditional distillation configurations (TDC) containing both sharp and sloppy splits. The generalized procedure will be introduced in a full paper which will show that a complete new subspace of ISC configurations can be generated from the TDCs with both sharp and sloppy splits for any N-component mixture. Therefore, the ISCs constitute the intensified alternatives of the corresponding TDCs. The present work has focused on the development of the systematic synthesis procedure together with the new subspace of the ISC systems. Work concerning the quantitative comparison between the intensified columns and the conventional columns is expected to develop heuristics for their selection and application. Furthermore, dynamic performance and control studies for such intensified systems are also important for their specific applications.

In conclusion, the ISCs have the potential to reduce both energy consumption and capital costs. Therefore, the ISCs should be included in the optimization search space to look for the optimal configuration for both grassroot designs as well as retrofitting existing distillation plants.

References

F.B. Petlyuk, V.M. Platonov, D.M. Slavinskii, 1965, Thermodynamically optimal method of separating multicomponent mixtures, Int. Chem. Eng., 5, 555-561.

R.N.S. Rathore, K.A. VanWormer, G.J. Powers, 1974, Synthesis strategies for multicomponent separation systems with energy integration, AIChE Journal, 20(3), 491-502.

B.G. Rong, A. Kraslawski, 2002, Optimal design of distillation flowsheets with a lower number of thermal couplings for multicomponent separations, Ind Eng Chem Res. 41(23), 5716-5726.

B.G. Rong, A. Kraslawski, 2002, Synthesis of thermodynamically efficient distillation schemes for multicomponent separations, Computer-Aided Chemical Engineering, ESCAPE-12, vol.10, 319-324.

B.G. Rong, A. Kraslawski, I. Turunen, 2004, Synthesis and optimal design of thermodynamically equivalent thermally coupled distillation systems, Ind Eng Chem Res. 43(18), 5904-5915.

R.W. Thompson, C.J. King, 1972, Systematic synthesis of separation schemes, AIChE Journal, 18(5), 941-948.

R.O. Wright, 1949, Fractionation apparatus, US Patent No. 2471134.

I.A. Karimi and Rajagopalan Srinivasan (Editors), Proceedings of the 11th International Symposium on Process Systems Engineering, 15-19 July 2012, Singapore.

Design and Control of a Reactive-Distillation Process for Esterification of an Alcohol Mixture Containing Ethanol and n-Butanol

Yi-Chang Wu[a], Hao-Yeh Lee[b], Chen-Yu Tsai[a], Hsiao-Ping Huang[a] and I-Lung Chien[a*]

[a]*Department of Chemical Engineering, National Taiwan University, Taipei 106, Taiwan.*
[b]*Department of Chemical Engineering, National Taiwan University of Science and Technology, Taipei 106, Taiwan.*

Abstract

The objective of this study is to present a feasible design and control structure for the esterifications of ethanol (EtOH) and n-butanol (BuOH) mixtures with acetic acid (HAc). This alcohol mixture is frequently obtained in semiconductor industry as a waste by-product, thus a detailed study of how to re-use this stream to produce high-value ester products is a worthy research. In our previous paper[1], the design and control of mixed-alcohol reactive-distillation process, categorized as Type-II system[2], has been developed. In this study, a new more difficult to design reactive-distillation process, categorized as mixed Type-II/Type-III system, will be studied. After comparing several alternative design sequences, an indirect design sequence containing a reactive distillation column and a stripper gives the lowest total annual cost (TAC).

In the control strategy, a traditional inventory control structure shows that this process would exhibit multiple steady states. An improved inventory control strategy is proposed to alleviate this complex dynamic behavior. The most important inventory control loop is the bottom liquid level of the reactive distillation column. A rather unusual inventory control strategy which manipulates the reboiler duty should be used. The dynamic results show that the proposed plant-wide control structure is capable of holding product specifications despite disturbances from throughput and feed composition changes. Overall control strategy with tray temperature control loops are proposed for the plant-wide control structure.

Keywords: Reactive Distillation, Inventory Control, Esterification

1. Introduction

Manufacturing processes in the semiconductor and pharmaceutical industries often produce massive organic liquid wastes including alcohol mixtures. Therefore, the esterifications of alcohol mixtures may be a beneficial strategy in reusing wastes from these industries. The purpose of this paper is that an alcohol mixture of EtOH and BuOH can be used as a feed stream for further processing. The existing literature on this topic by esterifications of either EtOH or BuOH with acid (e.g., acetic acid) to obtain ethyl acetate (EtAc) or butyl acetate (BuAc) in a RD system is relatively scarce.

In this study, the EtOH and BuOH alcohol mixture is fed in the RD process as a single stream. NRTL-HOC thermodynamic model is used for modeling the vapor-liquid and vapor-liquid-liquid equilibrium. The reactions are catalyzed by using Amberlyst-15 catalyst. Based on the thermodynamic properties and reaction kinetics, this paper

investigates two alternative design concepts which contain three kinds of feasible design flowsheets for the overall system.

2. Conceptual Design of the Process Flowsheet

This section compares the minimum TAC of two design concepts for this mixed alcohol system. The first thinking is "separation first" which means to separate the mixed alcohols from the upstream process first, and then feeds the EtOH and BuOH into different reactive distillation systems to produce EtAc or BuAc. The other thinking is "reaction first," which means feeding the mixed alcohols stream into a RD column directly, and then separates the two ester products and water. This design thinking includes two alternative flowsheets. One is "direct-sequence" design flowsheet. The other is "indirect-sequence" design flowsheet. All the conceptual design of the alternative process flowsheets are shown in Figure 1.

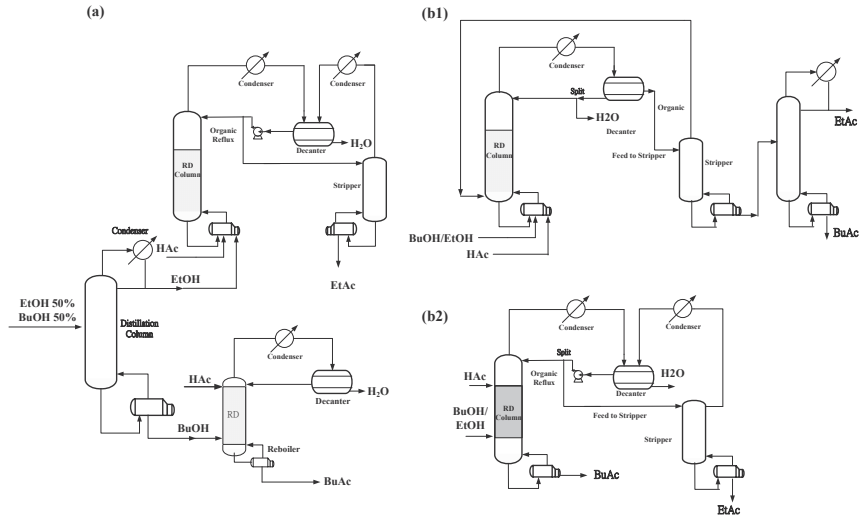

Figure 1. (a) "Separation first" flowsheet; (b1) "direct-sequence"; and (b2) "indirect-sequence" of the "reaction first" flowsheet.

2.1. "Separation First" Design

The "separation first" design flowsheet includes one traditional distillation column, two RD columns and a stripper. The first column separates the EtOH and BuOH from the feed stream as shown in Figure 1-(a). Then the purified EtOH and BuOH are fed into their own RD columns and react with HAc. The final products of EtAc and BuAc are obtained at the bottoms of the stripper and RD column, respectively. Furthermore, water is discharged from the outlet at the top of the decanter for the EtAc system and is obtained as distillate of the RD for the BuAc system. This study makes several assumptions in the following simulation: the mixed alcohols feed stream (EtOH/BuOH) is set to be equal molar, and the total flow rate is 100 kmol/h. The feed stream of pure reactant HAc is used and also set at 100 kmol/h flow rate. Product specifications are set as follows: x_{EtAc} = 99 mol %; x_{BuAc} = 99 mol %. The x_{HAc} in the EtAc and BuAc product stream must be less than 50 ppm. The results in Tang et al.[2] provided the optimal design of EtAc and BuAc RD processes. Therefore, determining the optimal design of the first distillation column is the only additional task for this design flowsheet.

There are two design variables for the distillation column: total number of stages and feed tray location. In all Aspen Plus simulation runs, the column top composition is set at 99.99 mol % EtOH by varying the reflux ratio, and the bottom BuOH composition is set at 99.99 mol % by varying the reboiler duty. High-purity EtOH and BuOH are required to use the optimal design proposed in Tang et al.[2] for the remaining two RD processes. The minimum TAC of this distillation is $588.1 ($1000/year). Upon combining the results of the other two RD processes from Tang et al.[2], the energy consumption of the overall "separation first" process is 10791.74 kW and the minimum TAC of the overall process is $ 2283.58 ($1000/year).

2.2. "Direct-sequence" of the "Reaction First" Design

Figure 1-(b1) shows the flowsheet of the "direct-sequence" design. In this design, all the reactants are fed into the bottom of the RD column. The overhead stream of the RD column enters the decanter, and the entire organic stream is fed into the stripping column. A part of the aqueous phase H_2O from the decanter is removed as the water product; the other part of H_2O is recycled back to the top of the RD column. Because of the aqueous reflux, BuOH tends to form the ternary minimum boiling azeotrope BuOH/BuAc/H_2O at top of RD column, and the separation will be easier. The stripping column separates the other components with the ester mixtures. The third column is used to separate the two products of EtAC and BuAC.

This study makes the same assumption for the feed composition and feed flow rate as in the "separation first" design. The decanter temperature is again set at 40 ° C. The EtAc and BuAc product specifications are also the same as in the "separation first" design. If the HAc composition of the stripping column bottom stream is greater than 0.3 mol %, this residue reactant affects product purity levels, and product specifications cannot be met in the third product column. Therefore, the reboiler duty of the stripping column is used to meet the HAc composition requirement of 0.3 mol % at the bottom of the stripping columns. Then the reflux ratio and reboiler duty of the third product column are used to meet the EtAc and BuAc specifications, respectively. The total TAC of "direct-sequence" design is $2542.46 ($1000/yr) and the overall reboiler duty is 13429 kW.

2.3. "Indirect-sequence" of the "Reaction First" Design

Figure 1-(b2) shows another possible flowsheet, the "indirect-sequence" design. Unlike the "direct-sequence" case, the "indirect-sequence" flowsheet collects the heaviest product, BuAc at the bottoms of the RD column. The other product, EtAc is obtained at the bottoms of another stripping column, which is fed by the organic stream from the decanter at the top of the RD column. This study proposes a design flowsheet of organic reflux with no aqueous reflux. The purpose of the organic reflux is to put ester back into the RD column, carrying water to the top by forming the ternary minimum boiling azeotrope of EtOH/EtAc/H_2O.

There are five design variables in this flowsheet which includes the stage numbers of the reactive section (N_{rxn}), the rectifying stage numbers of RD column (N_r), the HAc feed location (NF_{HAc}), the mixed alcohols feed location (NF_{OH}) and the total stage numbers of the stripping column (N_S). The product specifications are the same as in the previous two cases. The minimum TAC of "indirect-sequence" design is $1841.23 ($1000/yr) and the overall reboiler duty is 6898 kW.

Table 1 shows that the "indirect-sequence" of the "reaction first" design flowsheet is better than the "separation first" design strategy. The overall savings of the reboiler duty and TAC are 36% and 19%, respectively, in comparison with the "separation first"

design. For the mixed EtOH and BuOH esterification system, the "indirect-sequence" with organic reflux is a better process flowsheet than the "direct-sequence" flowsheet.

Table 1. Optimal TAC and Overall Reboiler Duties of Each Case

Case	Separation First	Direct-Sequence	Indirect-Sequence
Product flow rate (kmol/hr)	97.72	97.4	98.07
Total reboiler duty (kw)	10805	13429	6898
Annualized Capital cost	1232.17	1077.54	903.46
Operating cost	956.65	1373.20	720.44
Catalyst cost	94.77	91.72	217.33
TAC ($1000/yr)	2283.59	2542.46	1841.23

3. Control Strategy Design

In the following, we will investigate the proper overall control strategy of the "indirect-sequence" design flowsheet. For the RD column with the decanter, the aqueous-phase level is controlled by manipulating the aqueous outlet flow; the column top pressure is controlled by manipulating the top vapor flow; and the organic phase level is controlled by manipulating the partial organic flow where it is fed to the stripper. One important loop pairing in this system is that the column bottom level is controlled by manipulating the reboiler duty. Figure 2 shows that this process exhibiting multiple steady states if the column bottom level is controlled by manipulating the bottom BuAc product flow. For the stripping column, the column bottom level is controlled by the bottom EtAc product flow; and the column pressure is controlled by the top vapor flow.

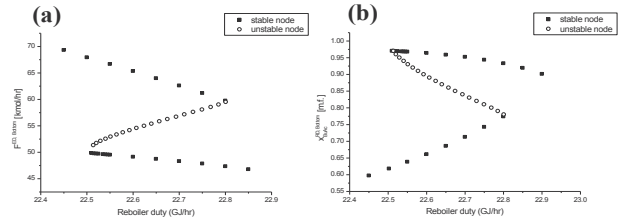

Figure 2. (a)Reboiler duty vs. RD column bottom flow; (b) Reboiler duty vs. composition of EtAc product

The remaining manipulated variables for the RD column are the feed ratio and the bottom flow, and the remaining manipulated variable for the stripping column is the reboiler duty. Close-loop sensitivity analysis is used to determine the tray temperature control point for both the RD column and the stripping column. Stage 10 and stage 33 of the RD column and stage 7 of the stripping column are selected as the temperature control points. PI control is used in these three temperature control loops. With additional open-loop test information, the control pairings should use feed ratio to control the 10th stage temperature and use bottom flow rate to control 33th stage temperature. For the stripping column, the reboiler duty is used to control the 7th stage temperature. The overall control strategy is shown in Figure 3.

Three types of disturbances will be used to test the proposed control strategy. The disturbance of unmeasured fresh feed composition changes will be considered first. A large variation of -10% changes in the feed stream of HAc composition is tested with the closed-loop results shown in Figure 4. For the second disturbance, variations of ±10% changes in the mixed alcohols composition are tested with the closed-loop results

shown in Figure 5. From these two figures, the two product compositions are all maintained at high purity. Another disturbance test is the throughput changes. Figure 6 displays the responses with ± 20% changes in the mixed alcohols flow rate. Again, the two RD controlled temperatures returned quickly to their set point values and with small deviations of the two product purities.

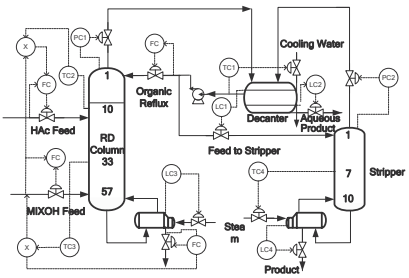

Figure 3. Proposed overall control strategy.

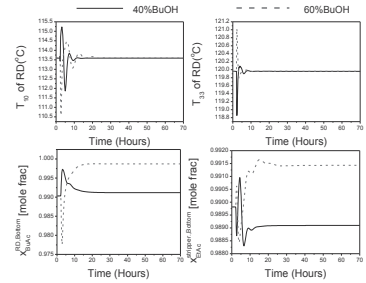

Figure 4. Dynamic responses with - 10% HAc composition changes

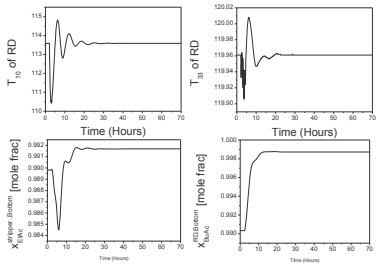

Figure 5. Dynamic responses with ±10% mixed alcohols composition changes

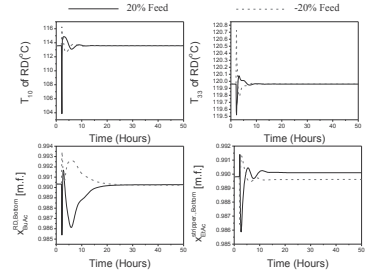

Figure 6. Dynamic responses with ±10% mixed alcohols feed flow rate

4. Conclusions

This study presents a feasible design for the esterification of EtOH and BuOH mixtures with HAc. Three design flowsheets are explored in this work: one "separation first" design and two "reaction first" designs. The best choice among these different design configurations is based on TAC savings and energy consumption. Comparing these three cases, it is shown that the "indirect-sequence" of "reaction first" design with organic reflux is the best design flowsheet having the least TAC and the energy consumption.

In the control strategy, the most important control loop is the bottom level of the RD column. This level should be controlled by manipulating the reboiler duty. Simulation results show that the proposed control strategy is capable of holding product specifications despite disturbances from throughput and feed composition changes.

5. References

1. Lee, H.Y.; Yen, L. T.; Chien, I. L.; Huang, H. P., 2009, Reactive distillation for esterification of an alcohol mixture containing n-butanol and n-amyl alcohol, *Ind. Eng. Chem. Res*, 48, 7186.
2. Tang, Y. T.; Chen, Y. W.; Huang, H. P.; Yu, C. C.; Hung, S. B.; Lee, M. J., 2005, Design of reactive distillations for acetic acid esterification, *AIChE J*, 51, 1683.

I.A. Karimi and Rajagopalan Srinivasan (Editors), Proceedings of the 11th International Symposium on Process Systems Engineering, 15-19 July 2012, Singapore.

Design and Control of Reactive Divided Wall Column for Esterification with Mixed n-Amyl alcohol and n-Hexanol Feed

Yi-Chang Wu[a], Hao-Yeh Lee[b], Chung-Han Lee[a], Hsiao-Ping Huang[a] and I-Lung Chien[a]*

[a]*Department of Chemical Engineering, National Taiwan University, Taipei 106, Taiwan.*
[b]*Department of Chemical Engineering, National Taiwan University of Science and Technology, Taipei 106, Taiwan.*

Abstract

The semiconductor and pharmaceutical industrial process often produces alcohol mixture byproducts. This study discusses the esterification process of an n-amyl alcohol (AmOH) and n-hexanol (HexOH) mixture with acetic acid (HAc). In the previous paper[1], the optimal design of the same type III mixed alcohol reactive distillation (RD) process was developed. In that paper the mixed alcohol feed contains n-butanol and n-amyl alcohol and the indirect sequence containing a RD column with heavier amyl acetate product and a second column to product bottom butyl acetate product gives the lowest total annual cost (TAC). In this study, with different mixed alcohol feed although of the same type, we find that the direct sequence design is more economically favorable. We then propose an integration of this design into a reactive divided wall column (RDWC) configuration for further savings in energy consumption. The result shows that 14% operating energy can further be saved by using RDWC configuration.

In the dynamic simulation, the RDWC is much more complicated and hard to control and operate, therefore proper selection and pairing of controlled and manipulated variables is very important. The control strategy in this study is determined by using the open loop sensitivity analysis. Dual-temperature control strategy works satisfactory for this RDWC column to indirectly hold the product specifications. The disturbances such as the throughput, the feed composition, and the vapor ratio changes are used in the closed-loop simulations.

Keywords: Reactive Dividing Wall Column, Control Strategy, Esterification

1. Introduction

Manufacturing processes in the semiconductor and pharmaceutical industries often produce massive organic liquid waste including alcohol mixture. Therefore, the esterification of the alcohol mixture may be a more beneficial way in reusing wastes from these industries. The purpose of this paper is to use an alcohol mixture of AmOH and HexOH as a feed stream to produce esters for further usage. However, existing literature on investigating the design and control of an esterification process with an alcohol mixture as a feed stream is relatively scarce.

In this study, the esterificaiton reactions of AmOH and HexOH are used to build-up the RD process. NRTL-HOC thermodynamic model is used for modeling the vapor-liquid and vapor-liquid-liquid equilibrium. The reactions are catalyzed by using Amberlyst-15 catalyst. Based on thermodynamic properties and reaction kinetics, this study presents three kinds of design alternatives for the overall RD system.

2. Conceptual Design of the Process Flowsheet

This section demonstrates and compares the minimum TAC of three kinds of design alternatives for a type III mixed alcohols system. The first is "direct-sequence" configuration. In this design configuration, the ester mixture is produced in the bottoms of RD column. This bottom stream is fed into an additional distillation column which collects the main products, AmAc and HexAc, at top and bottoms of this distillation column, respectively. The second is "indirect-sequence" configuration which collects the heaviest product, HexAc at the bottoms of RD column; the other product, AmAc, is obtained at the bottom of an additional distillation column. The feed stream of the additional distillation column comes from the organic stream of the top RD decanter. Another design configuration is to further integrate energy from "direct-sequence" configuration into a reactive dividing wall column (RDWC) configuration. All the design alternatives of the esterification process are shown in Figure 1.

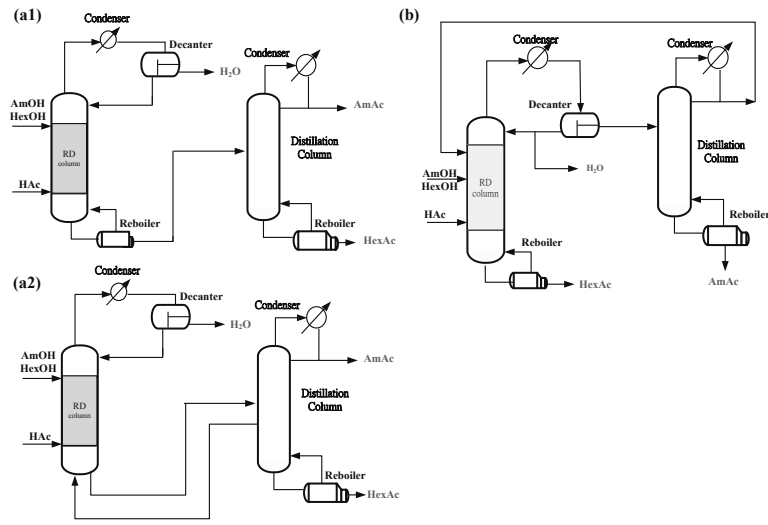

Figure 1. (a1) "direct-sequence"; (b) "indirect-sequence"; and (a2) "RDWC" configuration.

"Direct-sequence" design

Figure 1-(a1) shows the design configuration of the "direct-sequence". The major concept of this configuration is an extension of type III RD system (c.f. Tang et al.[2]) with an additional distillation column to separate two esters. Figure 2 displays a minimum boiling alcohol-ester-water azeotrope inside the large two-liquid region. In this liquid-liquid region, one end of the tie-line is directed to the pure water. The overhead stream of the RD column enters the decanter, and the organic rich stream is totally refluxed back to the RD column to carry water up the RD column. The bottom stream enters another distillation column to separate the two esters. The heaviest component, HexAc, is thus easily obtained at the bottoms of the distillation column and the AmAc product is obtained at the top of this column.

In all the Aspen Plus simulation runs, the mixed alcohols feed stream is set to equal molar, and the total flow rate of this stream and HAc feed stream are 100 kmol/h. The distillation column top composition is set at 99 mol % AmAc by varying the reflux ratio, and the bottom HexAc composition is set at 99 mol % by varying the reboiler duty. The eight design variables of this case are the stage numbers of the reactive section (N_{rxn}),

the stage numbers of the rectifying section (N_R), the stage numbers of the stripping section (N_S), the HAc feed location (NF_{HAc}), the mixed alcohols feed location (NF_{OH}), reboiler duty of the RD column, the total stage numbers of the distillation column (NT), and the feed location (NF) of the distillation column. After running the optimization procedure, the minimum TAC of "direct-sequence" configuration is \$1640.5 (\$1000/yr) and the overall reboiler duty is 4725.5kW.

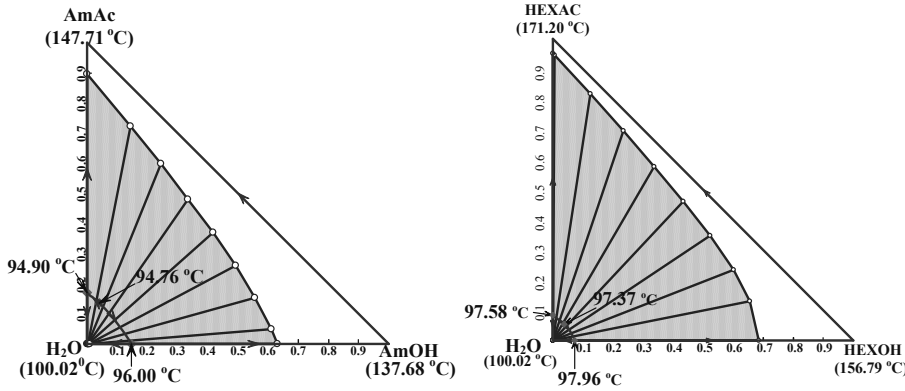

Figure 2. LLE of AmOH-AmAc-H_2O and HexOH-HexAc-H_2O ternary system under 1atm.

"Indirect-sequence" design

Figure 1-(b) shows another design configuration, of the "indirect-sequence". Unlike the "direct-sequence" configuration, the "indirect-sequence" configuration only collects the heaviest product, HexAc, at RD column bottoms. The other product, AmAc, is obtained at the bottoms of an additional distillation column which is fed by the organic stream from the top of the RD decanter. This study uses a configuration with partial aqueous reflux stream. The purpose of the partial aqueous reflux stream is to feed water back into the RD column to carry the heavier AmAc component by forming the ternary minimum boiling azeotrope of alcohol-ester-water.

The design variables considered in this configuration are nine including: the stage numbers of the reactive section (N_{rxn}), the stage numbers of the rectifying section (N_R), the stage numbers of the stripping section (N_S), the HAc feed location (NF_{HAc}), the mixed alcohols feed location (NF_{OH}), the aqueous split ratio, the total stage numbers of the distillation column (NT), the feed location (NF) of the distillation column, and the reflux ratio of this column. All product specifications are met in the optimization steps. The minimum TAC of "indirect-sequence" configuration is \$2506.8 (\$1000/yr) and the overall reboiler duty is 8045.0 kW.

Reactive Dividing Wall Column Design

Figure 1-(a2) shows a process integration of the "direct-sequence" configuration into a reactive dividing wall column (RDWC) for further savings of the operating energy. This design is similar to "direct-sequence" with the differences of removing a reboiler from the RD column and side-drawing a vapor stream from the distillation column to provide the heat source to the RD Column. Liquid and vapor streams are interchanged between the bottoms of the RD and a stage of the distillation column.

In this process, notice that the vapor flow rate is used as the design degrees of freedom to minimize the total TAC, and the reflux ratio and reboiler duty of the

distillation column are used to satisfy two purity specifications of AmAc and HexAc, respectively. Other seven design variables of this configuration are: the stage numbers of the reactive section (N_{rxn}), the stage numbers of the rectifying section (N_R), the stage numbers of the stripping section (N_S), the HAc feed location (NF_{HAc}), the mixed alcohols feed location (NF_{OH}), the total stage numbers of the distillation column (NT), and the side-draw location (NF) in the distillation column. After running optimization procedure, the minimum TAC of RDWC configuration is \$1434.2 (\$1000/yr) and the overall reboiler duty is 4065.05 kW.

Results and Discussion

Table 1 gives the comparison of the "direct-sequence", "indirect-sequence", and RDWC configurations. Unlike the result of Lee et al.[1], "indirect-sequence" seems not to provide any benefit on energy saving and TAC. Its energy requirement increases almost 70% comparing with the "direct-sequence". The reason is due to large recycle flow rate back to the RD column in the "indirect-sequence". The configuration from "direct-sequence" to RDWC results in further energy saving due to the reduction of the remixing effect in the RD bottom section. The result in Table 1 shows that the overall savings of the reboiler duty and TAC are 14.0% and 12.6%, respectively. Comparing these three designs show that the RDWC is the best configuration.

Table 1. Optimal TAC and Overall Reboiler Duties of Each Configuration

Design	"Direct-sequence"	"RDWC"	"Indirect-sequence"
Qr (kw)	4725.5	4065.0	8045.0
Qr saving	-	-14.0%	70.2%
Total capital cost/3 (\$1000/yr)	983.08	947.87	1289.22
Total operating cost (\$1000/yr)	657.42	486.33	1217.58
TAC (\$1000/yr)	1640.5	1434.2	2506.8

3. Control Strategy Development

In the following, the proper overall control strategy of the RDWC configuration will be investigated. There are nine inventory control loops included six level and three pressure loops which are shown in Figure 3. The remaining manipulated variables are the reflux flow rate and the reboiler duty of the distillation column, and feed ratio of the RD column. With the close-loop and open-loop test information, the 35th stage temperature should be controlled by the feed ratio. For the distillation column, the 11^{th} stage temperature should be controlled by the reflux flow rate. The reboiler duty is ratioed to the mixed alcohol feed.

Three types of disturbances will be used to test the proposed control strategy. For outer disturbance, the unmeasured fresh feed composition changes are considered. Changes in the mixed alcohol and the HAc compositions are tested. The results of closed-loop performance are shown in Figure 4. Another disturbance test is the throughput changes. Figure 5 displays the responses with ± 10% changes in the mixed alcohols flow rate. For inner disturbance, the vapor ratio change (to the RD vs. to the other column) is also considered. Figure 6 displays the responses with ± 10% changes in the vapor ratio. The two controlled temperatures returned quickly to their set point values and the two products are still maintained at high-purity. We are currently

investigating using dual-temperature control loops on the RD side to further improve the product composition performance.

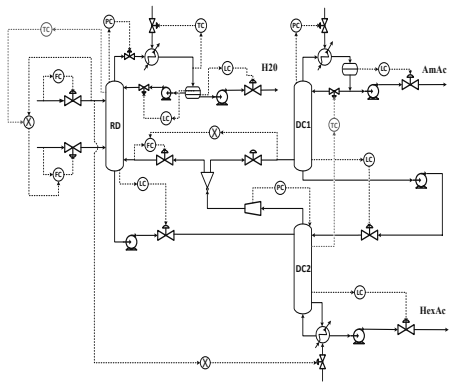

Figure 3. Proposed overall control strategy.

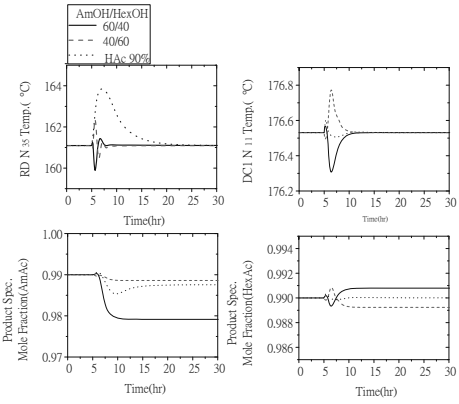

Figure 4. Dynamic responses with Feed composition changes

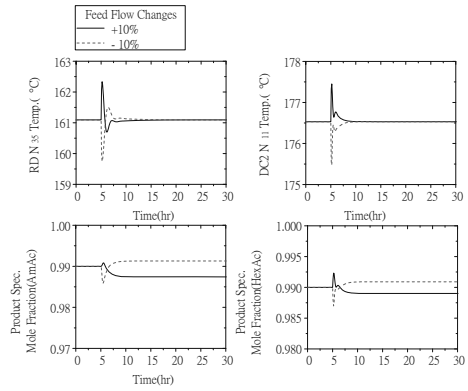

Figure 5. Dynamic responses with ±10% throughput changes

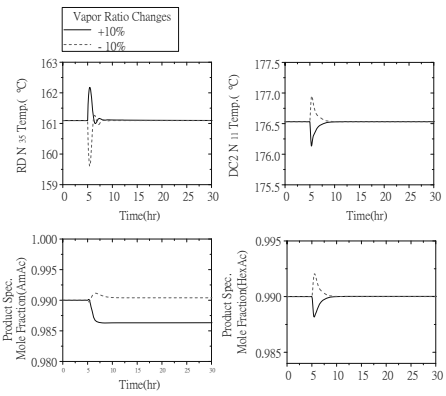

Figure 6. Dynamic responses with vapor ratio changes

4. Conclusions

This study investigated the feasible design for the esterification of AmOH and HexOH mixtures with acetic acid. Three design configurations are explored in this work: “direct-sequence”, “indirect-sequence”, and RDWC configurations. Comparing these three design configurations, it is shown that the RDWC has the best potential to provide maximum energy saving and cost reduction.

In the dynamic simulation, the results show that dual-temperature control strategy performs satisfactory to maintain high-purity of the two products in the face of three disturbances such as the throughput, the feed composition, and the vapor ratio changes.

References

1. Lee, H.Y.; Yen, L. T.; Chien, I. L.; Huang, H. P., 2009, Reactive distillation for esterification of an alcohol mixture containing n-butanol and n-amyl alcohol, *Ind. Eng. Chem. Res*, 48, 7186.
2. Tang, Y. T.; Chen, Y. W.; Huang, H. P.; Yu, C. C.; Hung, S. B.; Lee, M. J., 2005, Design of reactive distillations for acetic acid esterification, *AIChE J*, 51, 1683.

I.A. Karimi and Rajagopalan Srinivasan (Editors), Proceedings of the 11th International Symposium on Process Systems Engineering, 15-19 July 2012, Singapore.

Aggregate models based on the wave propagation theory for high-purity distillation columns

Lingyu Zhu[a], Dexin Li[a],Yichen Ren[a], Xi Chen[b], Lorenz T. Biegler[c]

[a]*College of Chemical Engineering and Materials Science, Zhejiang University of Technology, Hangzhou 310014, China*
[b]*Department of Control Science & Engineering, Zhejiang University, Hangzhou 310027, China*
[c]*Department of Chemical Engineering, Carnegie Mellon University, Pittsburgh, PA 15213, USA*

Abstract

Aggregate models are frequently used for online optimization of distillation columns because of their balance of accuracy and simplicity. When applied to high-purity distillation columns with large numbers of trays in a section, however, traditional group methods cannot accurately depict the strongly nonlinear features along the trays. On the other hand, absorption/stripping factors of the components along the trays were observed as a traveling sigmoidal wave, with the absorption/stripping factors at the top and bottom trays hardly changing with the reflux ratio. An improved group method based on the wave propagation theory is thus proposed to simulate the high-purity distillation columns. Applications are also conducted through process simulation on an argon sidearm column in a cryogenic air separation process. Excellent performance of the proposed method in terms of accuracy and converging rate is observed.

Keywords: Aggregate model; Wave propagation theory; Group methods

1. Introduction

Accurate and easy-to-converge models are always demanded for advanced control and real-time optimization of industrial processes. In many complex applications, the nonlinearity of multi-stage countercurrent gas-liquid contactors, such as high-purity distillation columns, cannot be well addressed through the shortcut method or linear correlations. Thus, rigorous tray-by-tray models are preferred for multi-stage columns. However, such models become large and expensive for high-purity columns with large numbers of trays, which hinders convergence in on-line applications. Considering the balance between model precision and difficulty in calculation, other methods, such as aggregate models (Fenske,1932; Gilliland, 1940; Kremser, 1930), are therefore investigated to describe the features of high-purity systems.

The group method is a type of aggregate method that provides reasonably accurate predictions with simple model structures. In the traditional group method, the effective absorption and stripping factors of the components, which represent the average values of the absorption and stripping factors for all trays, are applied in the model to simplify the rigorous tray-by-tray description. Usually, these factors are calculated by averaging the absorption and stripping factors at the top and bottom trays of the column. However, this method cannot accurately describe the strongly nonlinear performance of the column, especially for high-purity distillation columns with large numbers of trays. In the present paper, an improved aggregate model using the wave propagation theory to describe the nonlinear feature of the absorption and stripping factors is proposed for

high-purity distillation columns. The good performance of the proposed method is demonstrated using a high-purity argon sidearm column with 198 stages; comparisons with the traditional method are also presented.

2. Aggregate model of distillation column

The aggregate model relates the outlet stream properties to the inlet stream and other specifications by providing simplified MESH equations for a section of stages of the column. They consist of the mole balance,

$$V_{N+1}y_{N+1,i} + L_0x_{0,i} = V_1y_{1,i} + L_Nx_{N,i} \quad i \in C \tag{1}$$

the energy balance,

$$V_1H_1^V + L_NH_N^L = V_{N+1}H_{N+1}^V + L_0H_0^L \tag{2}$$

and the summation equations,

$$\sum_{i\in C} y_{1,i}/K_{1,i} = 1, \sum_{i\in C} K_{N,i}x_{N,i} = 1 \tag{3}$$

$$\sum_{i\in C} y_{1,i} = 1 \ , \sum_{i\in C} x_{N,i} = 1 \tag{4}$$

Unlike the tray-by-tray rigorous model that uses stage equilibrium equations to calculate the composition profile, the aggregate model usually correlates component recovery to key parameters through a performance equation. The group method (Kremser, 1930) provides only an overall treatment of the stages in the cascade, without considering detailed changes in temperature and composition of the individual stages. The most important contribution of the method is the derivation of the component recovery factor in the cascade by Horton (1940) and Edmister (1957). Horton (1940) gives the performance of the cascade by,

$$V_{1,i}y_{1,i} = V_{N+1,i}y_{N+1,i}\phi_{A,i} + L_{0,i}x_{0,i}(1-\phi_{S,i}) \tag{5}$$

where $\phi_{A,i}$ and $\phi_{S,i}$ denote the recovery factors for absorption and stripping, as follows:

$$\phi_{A,i} = \frac{1}{A_{1,i}A_{2,i}\cdots A_{N,i} + A_{2,i}A_{3,i}\cdots A_{N,i} + \cdots + A_{N,i} + 1} \tag{6}$$

$$\phi_{S,i} = \frac{1}{S_{1,i}S_{2,i}\cdots S_{N,i} + S_{1,i}S_{2,i}\cdots S_{N-1,i} + \cdots + S_{1,i} + 1} \tag{7}$$

$$A_{j,i} = L \big/ K_{j,i}V_j \ , S_{j,i} = 1 \big/ A_{j,i} \ , i \in C, j \in N \tag{8}$$

However, the phase equilibrium constants cannot be calculated using the aggregate model. The following effective absorption/stripper factors are normally substituted into Eqs. (6)-(8) in the Edmister group method (1957).

$$\phi_{A,i} = \frac{A_{e,i}\text{-}1}{A_{e,i}^{N+1} - 1}, \quad \phi_{S,i} = \frac{S_{e,i}\text{-}1}{S_{e,i}^{N+1} - 1} \tag{9}$$

$$A_{e,i} = \left[A_{N,i}(A_{1,i}+1) + 0.25\right]^{0.5} - 0.5 \tag{10}$$

$$S_{e,i} = \left[S_{1,i}(S_{N,i}+1) + 0.25\right]^{0.5} - 0.5 \tag{11}$$

where $A_{e,i}$ and $S_{e,i}$ are the effective absorption and stripping factors that represent the average values of the absorption and stripping factors along all trays in the cascade.

Thermodynamic methods are also applied to calculate the equilibrium constants and the vapor/liquid enthalpies,

$$K_{1,i} = f(x_1, y_1, T_1), \ K_{N,i} = f(x_N, y_N, T_N), \ i \in C \tag{12}$$

$$H_1^V = f(y_{1,i}, T_1), \quad H_N^L = f(x_{N,i}, T_N) \tag{13}$$

For the variables L_1 and V_N, which cannot be calculated using any of these equations, the approximate equation (Kamath, 2010) can be used,

$$L_1 - L_N \approx V_1 - V_N \tag{14}$$

The group methods have been used in some cases (Souders,1932; Horton,1940; Edmister,1943; Kamath, 2010), however, it sometimes fails to capture the nonlinear feature of the system with large numbers of trays. The predicted purity error can differ in orders of magnitude.

3. Modification of recovery factors in the group method

The key problem in the traditional group method is its incapability to address the nonlinear feature of the recovery factors for large numbers of trays using Eqs. (9)-(11). To overcome the precision problem in the Edmister group method, the wave propagation theory is proposed in the present study to correlate the nonlinear feature of the recovery factors. For example, using an argon sidearm column in a cryogenic air separation unit with 198 equilibrium stages, the absorption and stripping factors of the components along the trays and the change in the reflux ratio at about 40 to 50 are illustrated in Fig. 1. It can be observed that the A/S profiles are normally sigmoidal. As the reflux ratio increased, the upper front of the curve travels towards the upper boundary with an initially constant shape, as a so-called "constant pattern wave". In addition, the absorption and stripping factors at the top and bottom trays of the column hardly change, but the values in the intermediate section changed greatly, which lead to large deviations in the calculation of the effective absorption and stripping factors using Eqs. (9)-(11).

In the present paper, an aggregate model based on group method and wave propagation theory is proposed for high-purity distillation columns. The wave propagation theory (Huang, 1991; Kienle, 2000), which can give the dynamic composition profiles of distillation column, was used to describe the nonlinear feature of the recovery factors as follows,

$$A_{i,j} = A_{i,1} + \frac{A_{i,1} - A_{i,N}}{1 + \exp[-\gamma_i (j - s_i)]}, \quad j \in N \tag{15}$$

where s_i denotes the wave position, γ_i is a parameter relating to wave slope. Combining Eqs. (6), (7), and (15) to replace Eqs. (9)-(11) can provide a better correlation of the nonlinear features of high-purity columns.

Table 1 Feed conditions and specifications of column in Fig. 1

Number of trays	198	Feed composition	
Top/Bottom pressure, bar	1.244/1.39	mol fraction O_2	0.904
Reflux ratio	40 - 50	mol fraction Ar	0.096
		mol fraction N_2	210ppm

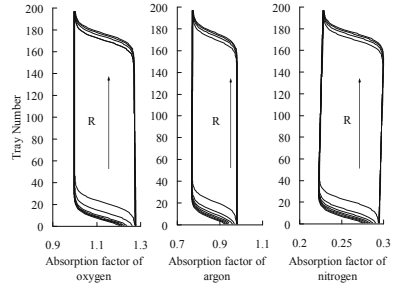

Fig. 1. Absorption factors profiles of argon sidearm column.

4. Results and discussion

An argon sidearm column in the cryogenic air separation unit was used to demonstrate the performance of the proposed method. The column is designed for the separation of oxygen from a ternary mixture of nitrogen/argon/oxygen. The column has a cascade of 198 equilibrium stages between the vapor feed at the bottom and the partial condenser at the top. The specifications and feed conditions of the column are presented in Table 1. Both the proposed wave group method and the Edmister group method were performed. For comparison, the rigorous tray-by-tray model with Soave-Redlich-Kwong equation of state was also developed in AspenPlus®.

The parameters in Eq. (15) were estimated using data at different reflux ratios generated by AspenPlus®. The oxygen recovery factors of the tray cascade, $\phi_{A,O2}$ and $\phi_{S,O2}$, at different reflux ratios were calculated. The comparison of the results between the proposed *wave group method*, the *Edmister group method* (Edmister, 1957), and the *rigorous group method* (Kremser, 1930; Horton, 1940) are illustrated in Fig. 2 using logarithmic coordinate. The absorption/stripping factor profile along the tray cascade used in the rigorous group method are generated by AspenPlus®. We can be seen that the $\phi_{A,O2}$ and $\phi_{S,O2}$ calculated by wave group method fit very well the results of rigorous group method. However, the absorption and stripping factors of the Edmister group method differ by several orders of magnitude, respectively. These results indicate that the average values derived through Eqs. (9)-(11) cannot address the nonlinear feature of the system well. On the other hand, the proposed wave method, as illustrated in Fig. 2, suits the recovery factors of the high-purity column very well.

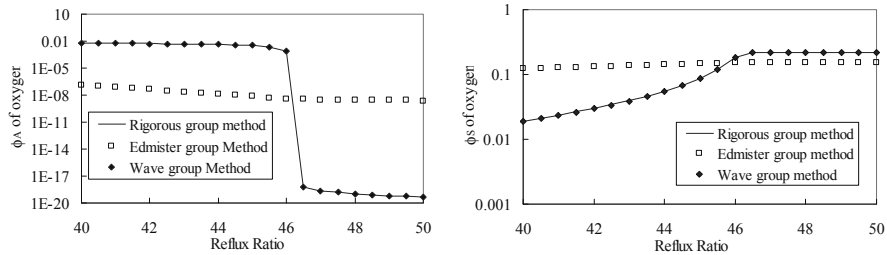

Fig. 2. Oxygen recovery factors of tray cascade.

The simulation results of the column with different aggregate models were obtained at varying reflux ratios. Comparison of the oxygen compositions at the top and bottom calculated using each method is illustrated in Fig. 3. The solutions of the wave group method, which solves 28 equations, closely resemble the results of the rigorous model. However, the Edmister group method, also with 28 equations, has obvious errors at lower reflux ratios. At the part where the reflux ratio and the purity of the products were both high, the relative error in the Edmister group method was even worse, with a difference of several orders of magnitude.

The solver performance of the aforementioned methods was also compared on the same platform. All the methods were coded in Matlab® and were solved using the function *fsolve*. The reflux ratio was changed from 40 to 45 and the solution of the former is used to initialize the solution for the latter. Both aggregate models converged very quickly; the Edmister group method required 1.06 s and the wave group method required 3.21 s as it has more intermediate variables to calculate the recovery factors. On the other hand, the rigorous method, which solves a system of 2377 equations, required a much longer period of about 7254 seconds to converge. These results further prove that our proposed

model accurately depicts the nonlinear feature of the high-purity column and is also suitable for online use.

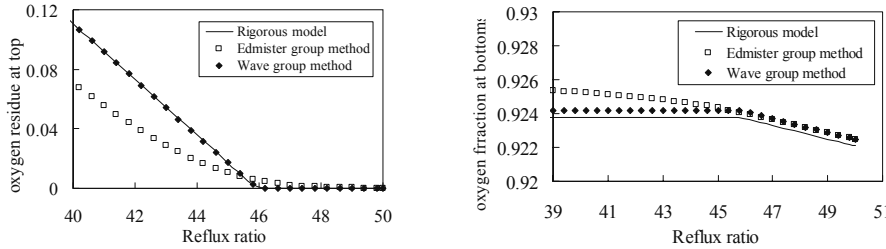

Fig. 3. Oxygen compositions of the column products.

5. Conclusion

A wave group method is proposed to improve the application of the aggregate model to high-purity distillation columns. The proposed method accurately depicts the nonlinear feature of the recovery factors using a sigmodal wave profile. The simulation results show that the proposed method is easier to converge than the rigorous model and is more precise than the Edmister group method, thereby providing good performance and potential for online use.

Acknowledgement

We gratefully acknowledge the financial support of Zhejiang Provincial Natural Science Foundation of China (No.Y4100319).

References

Edmister W. C., 1943, Design for hydrocarbon absorption and stripping, *Industrial & Engineering Chemistry Research,* 35, 8, 837-839.

Edmister W. C., 1957, Absorption and stripping-factor functions for distillation calculation by manual and digital-computer methods, *AIChE Journal*, 3, 2, 165-171.

Fenske M. R., 1932. Fractionation of straight-run Pennsylvania gasoline. *Industrial & Engineering Chemistry Research*, 24, 482-485.

Gilliland E. R.,1940, Multicomponent rectification: Estimation of the number of theoretical plates as a function of the reflux ratio. *Industrial & Engineering Chemistry Research*, 32, 1220-1223

Horton G., Frankin W. B., 1940, Calculation of Absorber Performance and Design, *Industrial & Engineering Chemistry Research,* 32, 10, 1384-1388.

Huang Y. L., 1991, Nonlinear Wave Theory for Dynamics if Binary Distillation Columns, *AIChE Journal,* 37, 5, 705-723.

Kamath R. S., Grossmann I. E., and Biegler L. T., 2010, Aggregate models based on improved group methods for simulation and optimization of distillation systems, *Computers & Chemical Engineering,* 34, 8, 1312-1319.

Kremser A., 1930, Theoretical Analysis of Absorption Process, *National Pstroleum News,* 22, 43-49.

Kienle A., 2000, Low-order dynamic models for ideal multicomponent distillation processes using nonlinear wave propagation theory, *Chemical Engineering Science,* 55, 10, 1817-1828.

Souders M., Brown G. G., 1932. Fundamental Design of Absorbing and Stripping Columns for Complex Vapors, *Industrial & Engineering Chemistry Research,* 24, 5, 519-522.

Zhu G. Y., Henson M. A., Megan L., 2001, Low-order dynamic modeling of cryogenic distillation columns based on nonlinear wave phenomenon, *Separation and Purification Technology,* 24, 3, 467-487.

I.A. Karimi and Rajagopalan Srinivasan (Editors), Proceedings of the 11th International Symposium on Process Systems Engineering, 15-19 July 2012, Singapore.

An exergy grand composite curve based procedure for arranging side exchangers on distillation columns

Zhiqiang Wei, Shengyuan Wu, Bingjian Zhang, Qinglin Chen*
School of Chemistry and Chemical Engineering/Key Lab of Low-carbon Chemistry & Energy Conservation of Guangdong Province, Sun Yat-Sen University, Guangzhou 510275, China

Abstract

This paper presents an exergy grand composite curve based procedure for arranging a side-exchanger on a distillation column. The novel method is proposed to identify the original value of the location, heat duty of the side-exchanger and the criterion of modifying the column stage number. A benzene-toluene column is used to demonstrate the performance of the procedure. The results show that the location, heat duty of the side-exchanger, stage number modification on the column can be effectively identified, and the feeding stage optimization is also considered as the stage number modified. The procedure can guide the arrangement of a side-exchanger in a relatively simple, systemic and reliable way.

Keywords: distillation column, side-reboiler, side-condenser, exergy.

1. Introduction

It is a common known that adding side-exchangers (side-reboilers and/or side-condensers) can effectively improve the thermodynamic efficiency of a distillation column. To arrange a side-exchanger, three questions must be answered firstly: (1) Where is the proper location? (Naka et al., 1980; Terranova et al., 1989; Björn et al., 2002; Pinto et al., 2011; Agrawal et al. 1996; Bandyopadhyay, 2007; Björn et al. 2006) (2) How much heat duty shoule be assigned? (Naka et al., 1980; Terranova et al., 1989; Björn et al., 2002; Pinto et al., 2011) (3) How to modify the stage number when a side-exchanger is arranged? (Pinto et al., 2011; Agrawal et al. 1996). Few researchers could provide a comprehensive answer, or the results are obtained in a comparatively complex way. Motivated to answer the questions mentioned above and facilitate for industrial applications, this paper proposes a procedure to place a side-reboiler and a side-condenser on a distillation column, in which exergy grand composite curve (EGCC) and avoidable exergy destruction curve (AEDC) are employed. A benzene-toluene column is used to demonstrate the performance of the procedure.

2. EGCC and AEDC

The major difference between column grand composite curve (CGCC) and EGCC is the parameter on the *y*-axis. Temperature (T) or stage number (*N*) is used in CGCC, while Carnot parameter (ε) is made use of in EGCC, as shown in Fig 1. It is clear that the dashed area represents the avoidable exergy destruction of the column by arranging a side-rebioler (refer to area a) or a side-condenser (refer to area b). On the energy-

* Correspondence author; email: chqlin@mail.sysu.edu.cn.

savings aspect, the optimum location to place a side-reboiler or a side-condenser is the stage where the corresponding dashed area is maximized. The corresponding heat duty is the proper heat duty of the side-reboiler or side-condenser.

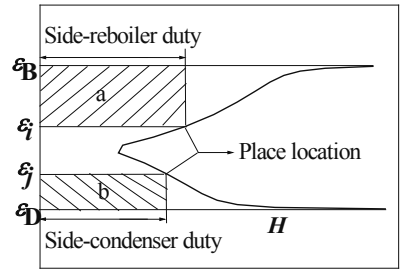

Fig. 1 Diagram of an exergy grand composite curve (EGCC)

The avoidable exergy destruction of the column through arranging a side-rebioler ($\dot{E}_{\mathrm{D,side\text{-}re}}$) or a side-condenser ($\dot{E}_{\mathrm{D,side\text{-}con}}$) is calculated as below, where H_{EGCC}, i, p represent the enthalpy value in EGCC, the stage number and the pinch point stage, respectively.

$$\dot{E}_{\mathrm{D,side\text{-}con}} = H_{\mathrm{EGCC},\,i}(\varepsilon_B-\varepsilon_i) \quad (p\le i\le n) \tag{1}$$

$$\dot{E}_{\mathrm{D,side\text{-}re}} = H_{\mathrm{EGCC},\,i}(\varepsilon_i-\varepsilon_D) \quad (1\le i\le p) \tag{2}$$

According to Eqs (1) and (2), the avoidable exergy destruction for each stage can be calculated. Changes of avoidable exergy destruction along the column are reflected in AEDC, in which the y-axis is defined as the avoidable exergy destruction, and x-axis is the stage number. The maximum value between the 1st and p-1th stage is the proper location to place the side-reboiler, and the maximum value between the p+1st and nth stage is the proper location for the side-condenser. The corresponding value of H_{EGCC} is the heat duty of the side-reboiler or side-condenser.

A benzene-toluene column is used to demonstrate the performance of AEDC. Specifications of the column are listed in Table 1, and the AEDC of benzene-toluene column is shown in Fig. 2. It can be seen that the 8th and 16th stages are the reasonable locations for the side-reboiler and side-condenser, respectively.

Table 1 Feed, product, and column specifications

Feed properties		Column characteristics		Feed molar fractions	benzene	0.50
Molar flow kmol/h	100	Stage number	20		toluene	0.50
Temperature K	365	Feed number	10	Column specifications	$x_{\mathrm{D,benzene}}$	0.99
Pressure MPa	0.1	Condenser	total		$x_{\mathrm{B,toluene}}$	0.99

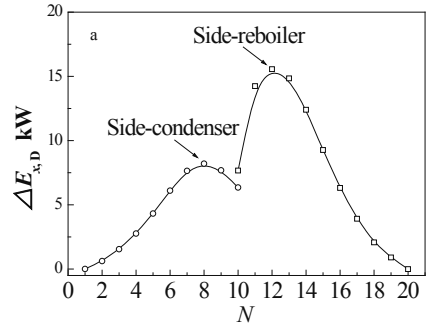

Fig. 2 AEDC of a benzene-toluene column

3. Criterion of modifying the column stage number

The relationship between placing side-reboilers or side-condensers on a distillation column and modifying the stage number is denoted in a McCabe-Thiele diagram, as shown in Fig. 3. It is clear that once the side-reboiler or side-condenser is placed, both the rectifying and stripping section operating lines are moved towards the equilibrium lines. To meet the separation requirement, more stages are needed. Otherwise, the reflux ratio should be increased. Indeed, the energy-savings of the side-reboiler and side-condenser are all at the expense of separation efficiency, and increasing the stage number or reflux ratio can re-meet the requirement of separation processes.

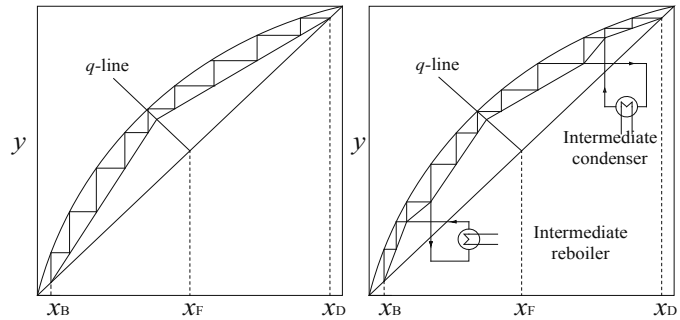

Fig. 3 McCabe-Thiele diagram of a binary system

For the existing distillation column, a balance between stage number and reflux ratio is carried out on the basis of the design process. To meet the separation requirement and maintain the balanced stage number and reflux ratio, increasing the stage number is a preferred alternative for practical industrial processes. Therefore, the criterions of modifying the column stage number are outlined as below.

(1) For a side-reboiler, the modified reflux ratio should not be larger than the existing reflux ratio.

(2) For a side-condenser, the modified reboiled ratio should not be larger than the existing reboiled ratio.

4. Calculation procedure

The calculation procedure of arranging a side-reboiler or a side-condenser on a distillation column is presented in Fig. 5, and described as below.

1) Identify the optimum feed stage $N_{F,opt}$, the optimum reflux ratio $R_{0,\,opt}$ (side-reboiler), or the optimum reboiled ratio $V_{B0,\,opt}$ (side-condenser).

2) Identify the original value of the location $N_{side\text{-}re,i}$ ($N_{side\text{-}con,i}$) and the heat duty $Q_{side\text{-}re,i}$ ($Q_{side\text{-}con,i}$) of the side-reboiler (side-condenser) through EGCC and AEDC.

3) Determine the new reflux ratio R_i' (reboiled ratio $V_{B,i}'$) after the side-reboiler or condenser arranged.

4) If R' ($V_{B,i}'$) is not larger than $R_{0,\,opt}$ ($V_{B0,\,opt}$), the option of adjusting the stage number is unnecessary, and the information of the side-reboiler or side-condenser: $N_{side\text{-}i}'$, $Q_{side\text{-}i}'$ ($_{i\,=\,re,\,con}$) can be output and the calculation is ended.

5) If R_i' ($V_{B,i}'$) is larger than $R_{0,\,opt}$ ($V_{B0,\,opt}$), add one stage to the column, and optimize the feed stage.

6) Return to the second step, recalculate until R_i' ($V_{B,i}'$) is not larger than $R_{0,\,opt}$ ($V_{B0,\,opt}$), output the information of the side-reboiler or condenser: $N_{side\text{-}j}'$, $Q_{side\text{-}j}'$, N_{add}, N_F' ($_{j\,=\,re,\,con}$)

and the procedure is ended.

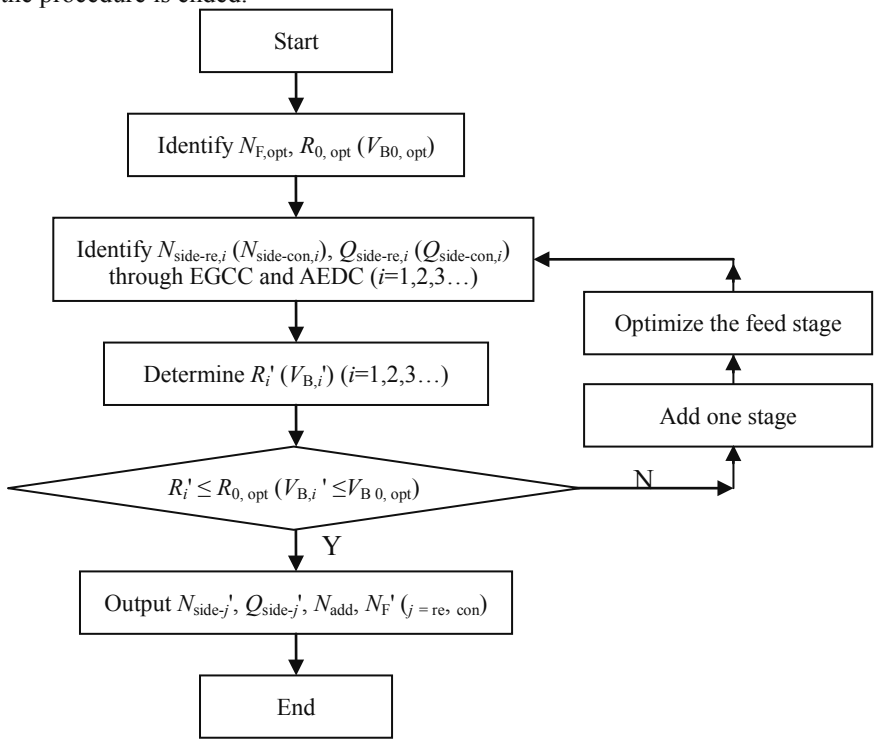

Fig. 5 Procedure for arranging side-reboilers/condensers on a distillation column

The benzene-toluene column mentioned above is used to demonstrate the performance of the proposed procedure. The detailed results of arranging a side-reboiler on the benzene-toluene column are listed in Table 3. It can be seen that in order to arrange a side-reboiler on the benzene-toluene column, three iteratives are needed to perform the calculation. With the increasing of the stage number the optimal feed stage is changed from the 10th stage to the 11th stage, and the proper location of the side-reboiler is varied from 12th stage to the 15th stage, and the heat duty is decreased from 590 kW to 520 kW. When the third stage is added to the column, the modified reflux ratio is lower than that of the original one. Then, the calculation is ended, and information to arrange the side-reboiler is output, i.e. three stages should be added, the feed stage is the 11th stage, the placing location is the 15th stage, and the side-reboiler duty is 520 kW.

Table 3 Information of arranging side-reboilers on benzene-toluene column

Iteration	R_i	$N_{F,i}$	$N_{side\text{-}re,i}$	$Q_{side\text{-}re,i}$ / kW	$N_{add,i}$
Base case	2.06	10	12	590	0
1	2.23	10	13	560	1
2	2.09	11	14	535	2
3	1.95	11	15	520	3

For placing a side-condenser, the detailed results are listed in Table 4. According to the procedure, two iteratives are needed to perform the calculation. With the stage number increased, the optimal feed stage is changed from the 10th stage to the 11th stage, and the placing stage is remained to the 8th stage, and the heat duty decreased from 390 kW to 330 kW. When the second stage is added, the modified reboiled ratio is lower than that of the original value. Then, the calculation is ended, and information to arrange the side-

condenser is output, i.e. two more stages are needed, the side-condenser duty is 330 kW, and the feed stage, the placing location are the 11th and 15th stages, respectively.

Table 4 Information of arranging a side-condenser on benzene-toluene column

Iteration	$V_{B,i}$	$N_{F,i}$	$N_{\text{side-con}}$	$Q_{\text{side-con},i}$ / kW	$N_{\text{add},i}$
Base case	2.85	10	8	390	0
1	2.95	10	8	360	1
2	2.79	11	8	330	2

As detailed above, one can conclude that the energy-savings of the side-reboiler and side-condenser are all at the expense of separation efficiency. In practical, the increasing of the stage number is the preferred alternative to re-meet the requirement of separation processes. With the stage numbers increased, the optimal feed stage, proper side-exchanger arranging location and heat duty are all changed. Therefore, re-considering those parameters is necessary. The procedure being proposed can address these issues in a simply, systemic and reliable way.

5. Conclusions

A procedure functioning to arrange a side-exchanger on the distillation column is proposed in this paper. EGCC and AEDC are used to identify the original value of location, heat duty of the side-exchanger. The criterion of modifying the column stage number is outlined, i.e. the modified reflux ratio (side-reboiler) should not be larger than the existing reflux ratio, and the modified reboiled ratio (side-condenser) should be less than the existing reboiled ratio. A benzene-toluene column is used to demonstrate the performance of the proposed procedure, and the optimal location and heat duty of the side-excahnger, stage number modification on the column are presented. The results indicate that the procedure is effective in arranging a side-exchanger on the distillation column.

Acknowledgement

The authors gratefully acknowledge the financial support from the National Natural Science Foundation of China (No. 20906016, 21076233) and the Major Science and Technology R&D Program of Guangdong Province (No. 2010A080801003).

References

B. E. Terranova, A. W. Westerberg, 1989, Temperature-Heat Diagrams for Complex Columns. 1. Intercooled/Interheated Distillation Columns, Ind. Eng. Chem. Res., 28, 9, 1374-1379.

F. S. Pinto, R. Zemp, M. Jobson, R. Smith, 2011, Thermodynamic optimization of distillation columns, Chem. Eng. Sci., 66, 13, 2920-2934.

I. N. Björn, U. Grén, F. Svensson, 2002, Simulation and experimental study of intermediate heat exchange in a sieve tray distillation column, Comput. Chem. Eng., 26, 4-5, 499-505.

I. N. Björn, U. Grén, A. P. Soemardji, 2006, Intermediate heat exchanger for fixed separation requirement Applications to a Binary Sieve Tray Distillation Column for Energy Savings, Chem. Eng. Res. Des., 84, A6, 453-464.

R. Agrawal, Z. T. Fidkowski, 1996, On the Use of Intermediate Reboilers in the Rectifying Section and Condensers in the Stripping Section of a Distillation Column, Ind. Eng. Chem. Res., 35, 8, 2801-2807.

S. Bandyopadhyay, 2007, Thermal integration of a distillation column through side-excahngers, Chem. Eng. Res. Des., 85, A1, 155-166.

Y. Naka, M. Terashita, S. Hayashiguci, S. Takamatsu, 1980, An Intermediate Heating and Cooling Method for a Distillation Column. J. Chem. Eng. Jpn., 13, 2, 123-129.

I.A. Karimi and Rajagopalan Srinivasan (Editors), Proceedings of the 11th International Symposium on Process Systems Engineering, 15-19 July 2012, Singapore.
2012 Published by Elsevier B.V.

Optimization of Complex Column Networks with Hybrid Genetic Algorithm

Seon B. Kim[a] and Andreas A. Linninger[a]

[a]*Departments of Chemical Engineering and Bioengineering, University of Illinois at Chicago, Laboratory for Product and Process Design. Chicago, IL 60607, USA*

Abstract

Complex column networks including Petlyuk, Kaibel, divided wall columns, side-stripper and rectifiers have better energy efficiency than simple separation networks. We present automatic and systematic computer-aided design and synthesis of complex column networks with heat-integrated configurations to separate multicomponent mixtures. Automatic synthesis of complex column is a challenging problem because the rigorous mass, equilibrium, summation and heat (MESH) equations lead to non-smooth fragmented search spaces. Therefore global optimization methods involving both structural and parametric degrees of freedom can currently not handle this problem and find realizable optimal energy efficiency in practice.

To tackle the network synthesis problem, we proposed the following design and optimization approaches. First we apply an inverse design methods based on temperature collocation which substantially reduces the problem dimension. This method identifies the design feasibility keeping final product purities. Second, we developed hybrid genetic algorithm, in which stochastic GA elements can be combined with a local deterministic search. At first stage, GA explores the design space until individual network solutions begin to coalesce and confines the region with niche technique. The gradient-based local optimizer refines a solution to local optimality. This hybrid scheme enables to find out all global and local solutions and thus improves computation speed and accuracy of the solutions.

Our novel methods allow the global search for feasible, effective and optimal energy efficient designs of the complex distillation column network in a fully automatic fashion. We used the rigorous commercial flowsheet simulator AspenPlus to validate the result and both results are very close each other. The automatic and rigorous flowsheet synthesis is apt to systematically address industrial-size process design problems such as the synthesis of energy-efficient separation networks, layout of biorefineries with novel feedstocks or sustainable process for reduction of greenhouse gases emissions.

Keywords: Temperature Collocation, Complex Column Networks, Hybrid Genetic Algorithm

1. Introduction

The large-case petrochemical and bio-separation process inherently contains purification structures for the final product value. One of the main units on the purification process is the distillation unit which is by far mostly utilized and prevalent in the industry. In the USA, there are approximately 40,000 distillation columns and those energy consumption is about 6% of the entire energy use of the USA (Lucia et al. 2010). Although energy consumption from distillation unit takes up great amount, industry is still operating simple column network which are built when the energy

consumption had minor impact on its consideration. However the rising energy cost and concerns over atmospheric carbon emissions redefine the design objectives for industrial separations with a new focus on energy conservation and the emission reduction associated with it.

Recently, heat-integrated complex column network have been revisited critically from several research group. The complex column configurations have the potential of achieving up to 70% energy savings over simple column networks (Hilde K. Engelien 2005). The well considered Petlyuk complex column configuration is an excellent example to realize energy efficient separations. Also Wright proposed the divided wall column, in which the prefractionator is transferred inside the second tower and its energy efficiency is better than conventional simple column configurations (Wright 1949). Linnger's group has also contributed to the systematic design method of complex column networks for last ten years (Zhang and Linninger 2004, 2006; Seon Kim et al. 2010, 2011)

However, there are no automatic and systematic algorithm to design and synthesize the entire complex column network. This challenge can be explained mathematically with two reason. First, problem size increases as the number of stages approximates infinity close to singular points of the composition space (e.g. saddle, pinch points). Secondly, in column design problems it is not known a priori whether a set of desired specifications has a feasible solution. In case of an infeasible specification, all direct performance design methods don't converge. To overcome these design problems, we have implemented a temperature collocation method specially for its use in column design including simple and complex column configuration. Also we propose two level optimization problem to meet both feasible design specification and energy efficiency criteria simultaneously. The hybrid genetic algorithm was applied to solve two level optimization problem. In the optimality of energy efficient design, the feasibility is necessary condition and lower vapor flowrate is sufficient condition for the this optimization problem. In this article, we will review the implemented collocation method and show hybrid GA optimization result with the case study.

2. Methodology

2.1. Inverse design procedure

Our design approach starts from the final product purities and inversely goes to find design parameters which was initially guessed from classical performance design approaches. Specifying required product purities, column profiles of both rectifying and stripping sections go to the stationary point named pinch points respectively. In the complex columns, we have equivalent rectifying or stripping section depending on the feed or product stream, a pair of both section constitutes one objective for the bubble point distance algorithm which should be optimized necessarily. For the sake of reduced search space of minimum distance for both profiles, our group discovered a thermodynamics transformation of the continuous model proposed by Hildebrandt's group (Tapp et al, 2003) by replacing the column stage number, n, with the equilibrium bubble point temperature, T. This thermodynamically motivated transformation offers massive size reductions in the column profile computations and is a key feature in a rigorous feasibility criterion based on minimum bubble point distance functions which eases the search (eq.1). In the case that there exists a pair of compositions with BPD = 0 at the same bubble point temperature, it guarantees feasible design and other cases vice versa.

$$\frac{\partial x_i}{\partial T} = -\left(\left(1+\frac{1}{R_\Delta}\right)\left(x_i - y_i\right)+\frac{1}{R_\Delta}\left(X_{\Delta i} - x_i\right)\right)\frac{\sum_{i=1}^{c}\left(\frac{\partial K_i}{\partial T}x_i\right)}{\sum_{i=1}^{c}\left[\left(\left(1+\frac{1}{R_\Delta}\right)\left(x_i - y_i\right)+\frac{1}{R_\Delta}\left(X_{\Delta i} - x_i\right)\right)K_i\right]} \qquad (1)$$

$$R_\Delta = \frac{L}{\Delta}, \quad X_{\Delta i} = \frac{Vy_i - Lx_i}{\Delta}$$

2.2. Two-level Optimization and Hybrid Genetic Algorithm

According to the generalization of the minimum bubble point distance approach, a complex column is feasible if the sum of all profile distances of all adjacent sections is within a small tolerance in eq. 2. This optimization is called a first level optimization and its solution is a necessary optimality condition.

$$\psi = \min_{xp,r}\left(\sum_{i=1}^{N}\sum_{j=1}^{k}\phi_{i,j} < \varepsilon\right) \qquad \begin{array}{l} i\text{: } i^{th} \text{ column for total N column network} \\ j\text{: } j^{th} \text{ pair of sections in } i^{th} \text{ column} \end{array} \qquad (2)$$

In this optimization, ε are set to 10^{-3} for the quaternary mixtures case study with reasonable match with AspenPlus simulation result. Once BPD optimization has converged, the algorithm seeks to minimize the energy requirement by reducing the vapor flowrate in the second level optimization as shown in eq. 3.

$$\omega = \min_{xp,\psi}\sum V(r) \qquad (3)$$

The design algorithm aims to achieve the final product purity with minimum energy requirement. However, in complex networks the decisions on sloppy slits in prefractionator columns as well as intermediate product purities are key variables to achieve energy efficiency. Accordingly, our algorithm explores intermediate products specifications and operating conditions for all columns. Also sloppy slits for multi-product columns are investigated, which is not possible with most existing design methods. The global approach does not optimize individual columns, but explores the entire network, since optimal conditions in a single column does not mean the network is optimal. Thus, minimum vapor flowrate for all columns in a network is solved simultaneously with two level optimization, all intermediate product purities and operating condition such as reflux ratio will be adjusted in the optimization procedure.

In the proposed two level optimization, it is critical to identify all local and global candidate solutions of the BPD criterion. Hybrid niche genetic algorithm (HNGA) was successfully implemented as a reliable multimodal optimizer with reasonable performance. It uses a niche technique to find all solutions sequentially. Basically, once one extremum is precisely located, a niche demarcating the area of attraction around the local minimum is recorded. The sequential process proceeds to search for additional extrema. The detailed description and performance test can be found elsewhere (Moon and Linninger, 2009). Figure 1 shows flowchart for the two level optimization with HNGA.

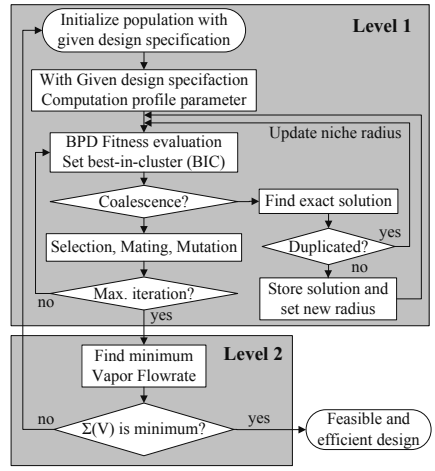

Figure 1. Hybrid niche genetic algorithm for two level optimization. The level 1 find solution for minimum BPD and level 2 seeks for minimum vapor flowrate.

3. Case Study

In mixtures with four or more components, the design problem involves the search for one or more compositional degree of freedom of any product stream. This multi-dimensional global optimization problem is solved using a hybrid method that combines stochastic genetic algorithm (i.e. product specification) with rigorous finite element collocation of column profiles (Zhang and Linninger 2006).

3.1. Separation of Quaternary Mixture

We performed case study to illustrate the potential energy saving of complex column configuration over simple column sequences for the separation of a quaternary mixture of benzene, toluene, octane and nonane. For the rigorous test to find best candidate from all 18 structures shown in Figure 2, the optimization for the least total vapor flow rates in each network was computed. The feed was set as 100 *kmol/hr* with equimolar concentration and the assumptions - constant molar overflows, no pressure drop by column height, monotonic behavior temperature, etc. - were applied for the simplification and DELPHI program was used for the numerical computation.

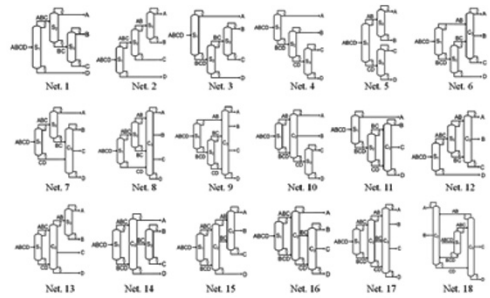

Figure 2. (a) Separation flowsheets to separate a quaternary mixture. All simple and basic Complex configurations are shown.

The selected optimization results for BPD and vapor flowrate, V, were listed in Table 1 and reboiler heat duty were obtained from the AspenPlus simulation. After rigorous testing for 18 networks, Net.10 has the minimum vapor flowrate and least reboiler heat duty. Comprehensively, all complex column networks have better efficiency than other simple column networks as shown in Table 1. From this result, net. 10 have 70% energy saving comparing to simple column net. 2.

Table 1. Selected results of design and synthesis calculation of 18 structures to separate alkane mixture (benzene/toluene/octane/nonane)

Network	10	13	16	12	4	1	3	5	2
Total BPD	1.32e-3	6.34e-4	5.22e-3	1.65e-3	2.08e-4	6.29e-3	8.49e-3	3.50e-3	8.26e-3
Total V	**202.02**	223.41	264.45	282.59	299.09	310.15	500.38	614.28	722.76
Total Q (MJ/hr)	16699	17646	20469	21980	23662	24353	38167	45160	54651

3.2. Initialization of complex distillation networks with AspenPlus

Figure 3 shows the complex network and composition profiles optimized with our temperature collocation profiles (top) and AspenPlus simulation results (Bottom). In the performance design approach, finding design variables to initialize AspenPlus simulation needs time-consuming trial and error method. However, our approach automatically finds all those variables by solving optimization with thermodynamically transformed composition profile equation (eq. 1). The AspenPlus simulation from the result of our approach converged with only one or two iterations. This result confirms the accuracy of our methodology is acceptable for a design and synthesis calculations. Our methodology using automatic interface with Aspen flowsheet simulator, will be also useful as an industrial practice for implementing this design idea of complex column networks.

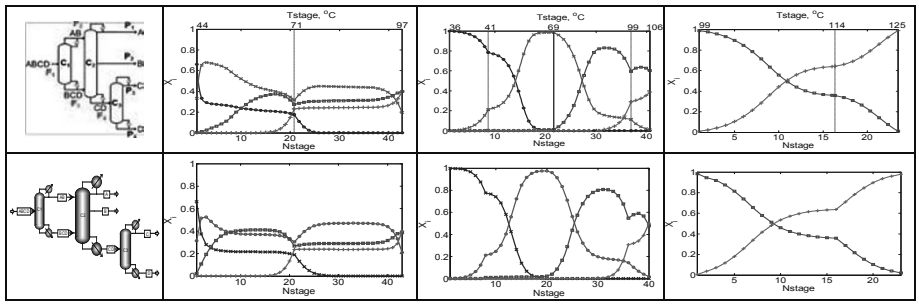

Figure 3. Liquid composition profiles in the stage domain found by temperature collocation model (top), and AspenPlus simulation results (bottom) for prefractionating complex column network NW10.

4. Conclusions

In this article, we advocated the recent progress for optimized energy efficient complex distillation networks. A two level optimization approach with hybrid genetic algorithm towards a generalized solution of the complex distillation problem is presented. This approach makes it possible the automated and systematic design procedure satisfying both feasibility and low energy consumption. Inverse design procedure fully assisted with hybrid niche genetic algorithm, thermodynamically transformed composition profiles, and minimum bubble point distance algorithm were the effective way to find a feasible separation by intercepting profiles. In finding optimal solution, two level optimization was performed to discriminate the energy efficiency. The case study demonstrates the potential to 70% of energy savings using a complex column network compared to the simple column configuration. Our design approach also demonstrates that current state of the art of separation synthesis in conjunction with computer simulations is now ready to address to fully integrate complex separation networks. In the future, this methodology will be applied for cases of nonideal mixtures such as homogeneous or heterogeneous azeotropes.

Acknowledgements

Financial support by DOE Grant: DE-FG36-06GO16104 is gratefully acknowledged.

References

K. Hilde, and S. S. Engelien, 2005, Minimum energy diagrams for multi-effect distillation arrangements, AIChE J, 51, 6, 1714-1725.

S. Kim, G. Ruiz, and A. A. Linninger, 2010, Rigorous Separation Design. 1. Multicomponent mixture, nonideal mixtures, and prefractionating column networks, 49, 14, 6499-6513.

S. Kim, and A. A. Linninger, 2010, Rigorous Separation Design. 2. Network design solutions for mixtures with various volatility differences and feed compositions, 49, 18, 8670-8684.

A. Lucia, and B. R. McCallum, 2010, Energy targeting and minimum energy distillation column sequences. Computers & Chemical Engineering, 34, 6, 931-942.

J. Moon, and A. A. Linninger, 2009, A hybrid sequential niche algorithm for optimal engineering design with solution multiplicit, Computers and Chemical Engineering, 33, 7, 1261–1271

M. Tapp, S. T. Holland, D. Hildebrandt, and D. Glasser, 2004, Column Profile Maps. 1. Derivation and Interpretation, I&EC Research, 43, 2, 364-374.

L. Zhang, and A.A. Linninger, 2004, Temperature collocation algorithm for fast and robust distillation design, I&EC Research, 43, 12, 3163-3182.

L. Zhang, and A. A. Linninger, 2006, Towards computer-aided separation synthesis, AIChE J, 52, 4, 1392-1409.

R. O. Wright, 1949, US Patent, 2,471,134.

I.A. Karimi and Rajagopalan Srinivasan (Editors), Proceedings of the 11th International Symposium on Process Systems Engineering, 15-19 July 2012, Singapore.

Using PSE to develop innovative cryogenic air separation processes

Chao Fu, Truls Gundersen

Department of Energy and Process Engineering, Norwegian University of Science and Technology, Kolbjoern Hejes vei 1.A, NO-7491 Trondheim, Norway

Abstract

The double-column distillation scheme is the basis for most existing cryogenic air separation plants. When the scheme is used for low pressure O_2 production, power is wasted in compressing O_2 in the air feed. A vapor recompression air distillation scheme has been developed to avoid O_2 compression. Distributed reboiling is used to reduce the irreversibilities in the distillation column. Column Grand Composite Curves are used to determine the load and location of the reboilers. Compared to a value published by authors representing the air separation industry, the power consumption has been reduced by 10.7% in the intermediate vapor recompression cycle presented in this paper.

Keywords: cryogenic air separation; vapor recompression; Column Grand Composite Curve

1. Introduction

Due to the increased concern about CO_2 emissions, oxy-combustion power plants represent a new large scale application of air separation units (ASUs) (Higginbotham *et al.*, 2011). Commercially available air separation technologies for large volume O_2 production are based on cryogenic distillation. For oxy-combustion power plants, the O_2 purity is around 95 mole% and the supply pressure is slightly above atmospheric pressure (around 120 kPa). These new specifications on the O_2 product provide considerable opportunities for improving the ASUs (Higginbotham *et al.*, 2011).

The double-column air separation cycle was developed by Linde in 1910 (Latimer, 1967, Kerry, 2007), and has been used as the basis for most existing air separation plants. All the air feed is compressed to a pressure high enough (usually 400-600 kPa) to allow reasonable pressure losses along the flow path and enough temperature driving forces in the condenser/reboiler exchanger. An exergy analysis of a conventional double-column air separation cycle (termed as "Cycle 1") indicates that the air compression process and the distillation system are responsible for the two largest exergy losses: 38.4% and 28.2% respectively (Fu and Gundersen, 2011). The irreversibilities in distillation columns can be reduced by using "distributed reboiling" (Gaumer, 1967). For the air compression process, the power consumption can be reduced by (i) improving the compressor efficiency, (ii) reducing the compression ratio, (iii) lowering the operating temperature, and (iv) reducing the mass flow through the air compressor. This paper focuses on the last of these measures. For oxy-combustion power plants, the O_2 product does not need to be delivered at elevated pressure, thus power is wasted in the compression of O_2 in the air feed in Cycle 1. A vapor recompression air distillation scheme has been developed in this paper to avoid the compression of O_2 (Lynd and Grethlein, 1986, Agrawal and Yee, 1994, Fu *et al.*, 2011). Furthermore, Column Grand Composite Curves (CGCCs) are applied to investigate the load and level (location) of distributed reboilers in distillation columns (Dhole and Linnhoff, 1993).

2. An innovative vapor recompression air distillation scheme

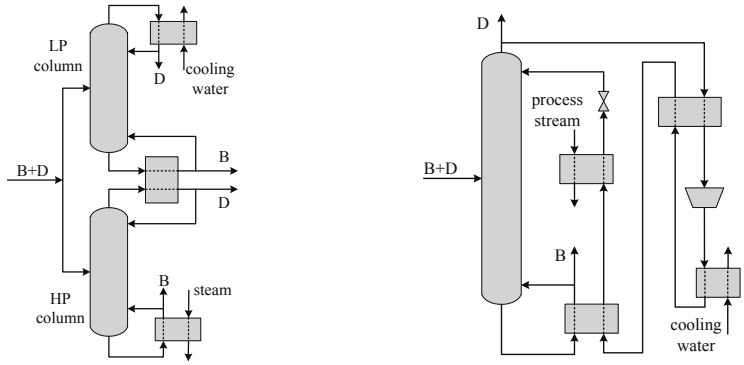

(a) Thermally coupled distillation (b) Vapor recompression distillation

Figure 1. Distillation schemes

Thermally coupled distillation is the basis of the double-column air separation scheme. Figure 1 (a) shows a typical thermally coupled distillation scheme at above-ambient temperature. The two columns are operated at different pressures so that the overhead vapor product from the higher pressure (HP) column can be condensed by the bottom liquid from the lower pressure (LP) column, thus steam is only consumed in the HP column. The feed to the HP column has to be compressed to the operating pressure of the HP column. By using a vapor recompression distillation scheme, the compression of the bottoms product (B) can be avoided. Such a scheme for sub-ambient application is shown in Figure 1 (b). A portion of the distillate product (D) is heated to ambient temperature, compressed and then condensed against the boiling liquid in the bottom of the column after cooling, and finally used as reflux for the column. When this scheme is used for air separation, one can avoid compressing the O_2.

2.1. The vapor recompression air distillation cycle

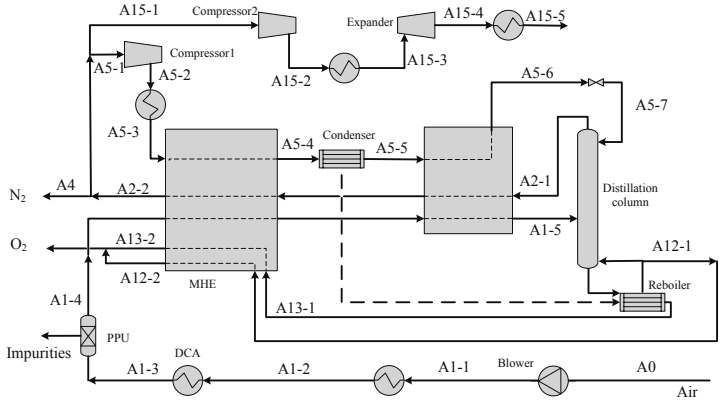

Figure 2. Cycle 2: a vapor recompression air distillation cycle

A vapor recompression air distillation cycle has been developed and is shown in Figure 2, termed as "Cycle 2". In this cycle, the air feed (A0) is slightly compressed to compensate for the pressure losses along its flow path. The compression heat and

impurities are removed from the air. The air (A1-4) is cooled to its dew point (A1-5) and separated into O_2 and N_2 in a distillation column. The O_2 (A12-1 and A13-1) and N_2 (A2-1) are heated to ambient temperature in the multi-stream heat exchangers. A portion of the N_2 product (A5-1) is compressed and cooled to its dew point (A5-4), and then condensed against the boiling O_2 at the bottom of the distillation column. The condensed N_2 (A5-5) is sub-cooled, expanded and returned back to the distillation column as reflux. Another portion of the N_2 product (A15-1) is used as the working fluid in a refrigeration cycle. This refrigeration cycle provides necessary cold energy for the main heat exchanger (MHE). Since only a portion of the N_2 is compressed for the production of reflux, one avoids compressing the O_2 in the air feed significantly, thus power consumption is reduced.

2.2. The dual-reboiler cycle

Distributed reboiling in the distillation column can reduce the irreversibilities and save energy. The Column Grand Composite Curve (CGCC) has been applied to investigate the load and level (location) of the distributed reboiling (Dhole and Linnhoff, 1993). The CGCC for the distillation column in Cycle 2 is shown in Figure 3(a). The large area between the ideal profile curve and the actual profile curve indicates the improvement potential by using distributed reboiling. A simplified dual-reboiler cycle is shown in Figure 4, termed as "Cycle 3". Only the most important parts that reflect the idea of distributing the reboiling are presented. With reference to Figure 2, the dashed lines without stream connections in the main heat exchanger (MHE) in Figure 4 are for O_2 streams. Compared to Cycle 2, the main difference is that the N_2 used for reflux is compressed to two pressures (A5-2 and A7-2). The higher pressure N_2 stream (A5-2) is cooled and condensed in the bottom reboiler of the distillation column (Condenser1/Reboiler1 exchanger), while the lower pressure N_2 stream (A7-2) is cooled and condensed in an intermediate reboiler (Condenser2/Reboiler2 exchanger). The power consumption is reduced since a portion of the N_2 for reflux production can be compressed to a lower pressure (A7-2). The CGCC for Cycle 3 is shown in Figure 3(b).

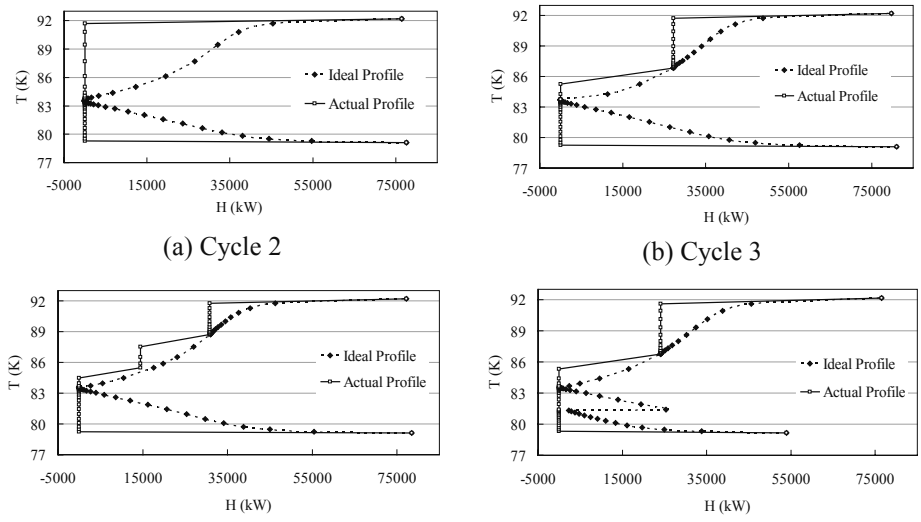

(a) Cycle 2 (b) Cycle 3

(c) Cycle 4 (d) Cycle 5

Figure 3. Column Grand Composite Curves

2.3. The three-reboiler cycle

Similar to the dual-reboiler cycle, a three-reboiler cycle, termed as "Cycle 4", has been studied but not presented in detail in this paper due to space limitations. In this cycle, the N_2 is compressed to three pressures for reflux production and condensed in a bottom reboiler and two intermediate reboilers in the distillation column. The CGCC for this cycle is shown in Figure 3(c). Compared to Figure 3(b), the area between the ideal profile curve and the actual profile curve has not been significantly reduced, thus the power saving potential by using more reboilers is limited.

2.4. The intermediate vapor recompression cycle

Figures 3(a) and (b) show that the irreversibilities of the rectifying section of the distillation column can also be reduced, even though the potential is not as large as in the stripping section. An intermediate vapor recompression cycle has been developed based on the idea of reducing the irreversibility of the rectifying section, as shown in Figure 5, termed as "Cycle 5". The main difference between this cycle and Cycle 2 is that a portion of impure N_2 (A7-1) is extracted at an intermediate location of the rectifying section of the distillation column. This N_2 stream is compressed after being heated to ambient temperature, and then condensed in an intermediate reboiler in the column after being cooled to its dew point, and finally returned back to the column. The main advantage is that the intermediate N_2 stream can be compressed to a much lower pressure (A7-3) compared to the overhead N_2 compression (A5-2). The CGCC is shown in Figure 3(d).

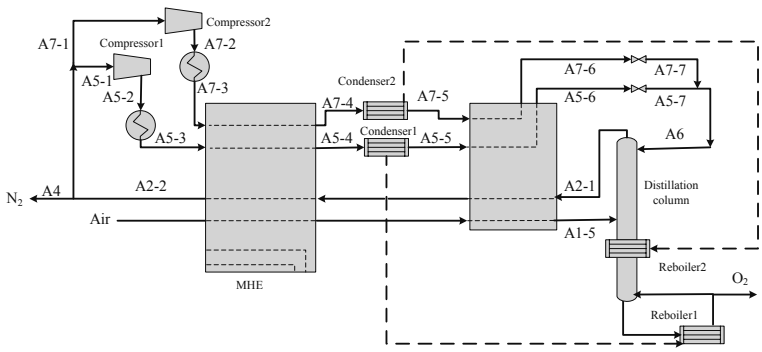

Figure 4. Cycle 3: a dual-reboiler cycle

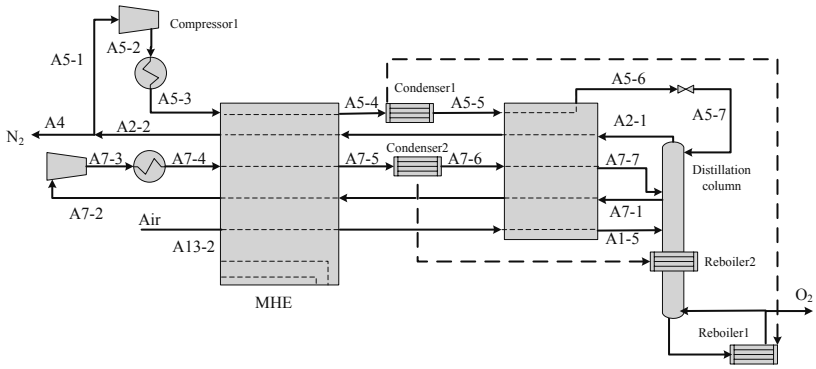

Figure 5. Cycle 5: an intermediate vapor recompression cycle

3. Plant performance comparison

All the cycles have been simulated without optimization. A three-column cycle reported by Higginbotham *et al*. (2011) has been used as the reference case (Cycle 0). The same ambient conditions (288.15 K, 101.3 kPa, 60% relative humidity) and cooling water temperature (288.15K) are used. Specific shaftwork for separation (the shaftwork for producing 1 kg O_2 contained in the O_2 product at 101.3 kPa) is compared. The plant performance data are listed in Table 1. Compared to Cycle 1, the power consumption has been reduced by 7.8% in the vapor recompression distillation cycle (Cycle 2) and by 14.0% in the dual-reboiler cycle (Cycle 3), and further reduced by 16.6% and 17.6% in Cycle 4 and Cycle 5. However, the investment cost will increase if distributed reboiling is used. The reference cycle (with three columns and two reboilers) is designed based on the double-column distillation scheme. Compared to this cycle, the power consumption has been reduced by 10.7% in Cycle 5. An economic study is necessary for further comparison of the various cycles; however, this is beyond the scope of this study.

Table 1. Plant performance comparison

	Cycle 0	Cycle 1	Cycle 2	Cycle 3	Cycle 4	Cycle5
O_2 purity, mole%	95.0	95.0	95.4	95.5	95.5	95.1
O_2 recovery rate, %	97.7	99.3	98.4	98.5	98.5	97.9
Specific shaftwork for separation, kWh/kgO_2	0.178	0.193	0.178	0.166	0.161	0.159

4. Conclusion

The double-column air separation cycle has been used as the basis for most existing air separation plants. This cycle causes unnecessary compression of O_2 when low pressure O_2 is the desired product. By applying the vapor recompression distillation scheme, the mass flow through compressors can be reduced with corresponding energy savings. The power consumption has been reduced by 7.8% in the vapor recompression cycle. When the principle of distributed reboiling is applied, the power consumption has been reduced by 14.0% and 16.6% in a dual-reboiler and a three-reboiler cycle, respectively. Compared to a value published by representatives of the air separation industry, power consumption has been reduced by 10.7% in the best of the cycles presented in this paper.

References

R. Agrawal and T. F. Yee, 1994, Heat pumps for thermally linked distillation columns: an exercise for argon production from air, Ind. Eng. Chem. Res., 33, 2717-2730

V. R. Dhole and B. Linnhoff, 1993, Distillation column targets, Computers chem. Engng, 17, 5/6, 549-560

C. Fu and T. Gundersen, 2011, Power reduction in air separation units for oxy-combustion processes based on exergy analysis, Computer Aided Chemical Engineering, 29, 1794-1798

C. Fu, T. Gundersen and D. Eimer, 2011, Air separation, GB patent, application number: GB1112988.9

L. S. Gaumer, 1967, Method for separating gaseous mixtures, US Patent 3327489

P. Higginbotham, V. White, K. Fogash and G. Guvelioglu, 2011, Oxygen supply for oxyfuel CO_2 capture, Int. J. Greenhouse Gas Control, 5S, S194-S203

F. G. Kerry, 2007, Industrial Gas Handbook: Gas Separation and Purification, Boca Raton, Florida, US, CRC Press

R. E. Latimer, 1967, Distillation of Air, Chem. Eng. Prog. , 63, 2, 35-59

L. R. Lynd and H. E. Grethlein, 1986, Distillation with intermediate heat pumps and optimal sidestream return, AIChE J., 32, 8, 1347-1359

I.A. Karimi and Rajagopalan Srinivasan (Editors), Proceedings of the 11th International Symposium on Process Systems Engineering, 15-19 July 2012, Singapore.

Heterogeneous batch distillation with variable decanter hold-up

László Hégely[a,b], Vincent Gerbaud[b,c], Péter Láng[a]

[a]*Budapest University of Technology and Economics, Dept. of Building Services and Process Engineering, Muegyetem rkp. 3-5, H-1521 Budapest, Hungary*
[b]*Université de Toulouse, INP, UPS, LGC (Laboratoire de Génie Chimique), 4 allée Emile Monso, F-31432 Toulouse Cedex 04, France*
[c]*CNRS, LGC (Laboratoire de Génie Chimique), F-31432 Toulouse Cedex 04, France*

Abstract

A general model of batch heteroazeotropic distillation is proposed, in which both liquid phases present in the decanter can be refluxed or withdrawn as distillate, their hold-up can be increased, decreased or kept constant, as well. A feasibility study is performed with the assumption of maximal separation, that is, that the composition of the condensate always equals to that of the heteroazeotrope. The still path directions are determined for all the 16 possible operation policies, and the results are validated by rigorous simulations for three cases not published yet. The still path can be steered in any direction by changing the operational parameters, allowing the recovery of a pure component in the still.

Keywords: heteroazeotropic distillation, operational policies, rigorous simulation.

1. Introduction

The separation of azeotropic and close-boiling mixtures requires the application of special distillation methods. Batch heteroazeotropic distillation is one of the possible methods: a third component (entrainer, E) is added to the mixture, leading to the formation of two liquid phases, which can be separated by decantation.
Decantation is performed in a decanter placed after the condenser. In the model of Pham and Doherty (1990) both liquid phases are refluxed. The model of Rodríguez-Donis et al. (2002) allows the reflux of any fraction of either phase; distillate is withdrawn from the E-lean phase, and the hold-up of the E-rich phase in the decanter is variable. Skouras et al. (2005) distinguished two modes of batch heteroazeotropic distillation. By Mode I, decantation and distillation are performed sequentially, and the reflux is heterogeneous. By Mode II, the phase separation and distillation are simultaneous. Mode II has two versions: Strategy A, where the E-rich phase is refluxed entirely, and Strategy B, where it is refluxed partially. In the model of Lang and Modla (2006) any fraction of either liquid phase can be refluxed, while the hold-up of both phases are constant. Distillate can be withdrawn from both phases.

2. Model description

Figure 1 shows the scheme of the heterogeneous distillation column of our generalised model. The condensate of the top vapour, which has a molar flow rate of V and molar composition of y_2, gives rise to two-phase liquid stream with a flow rate of L_0, composition of x_0, and a split ratio of ω (ratio of the E-rich phase and total flow rate).

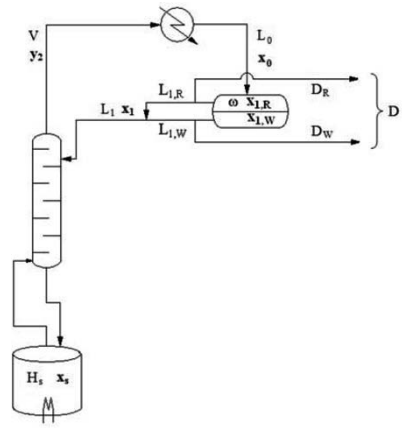

Figure 1. Heteroazeotropic distillation column scheme for the generalised model.

Both liquid phases can be refluxed or withdrawn as distillate. Besides, the hold-up of both phases can be increased, decreased or kept constant in the decanter. The change in the hold-up of the E-rich (resp. E-lean) phase is characterised by the variables θ_H (resp. φ_H), which are defined as the ratio of the amount of E-rich (resp. E-lean) phase removed from and entering the decanter:

$$\theta_H = \frac{L_{1,R} + D_R}{L_{0,R}} \qquad (1) \qquad\qquad \varphi_H = \frac{L_{1,W} + D_W}{L_{0,W}} \qquad (2)$$

where $L_{0,R}$ and $L_{0,W}$ are the flow rates of the E-rich and E-lean phase in the condensate, D_R and D_W are the flow rates of E-rich and E-lean phases withdrawn as distillate, $L_{1,R}$ and $L_{1,W}$ are those refluxed, respectively. If the value of θ_H is lower than one, the hold-up of the E-rich phase increases, if it is higher, the hold-up decreases.

The variables θ_{refl} and φ_{refl} determine the ratio of the amount refluxed and the total amount leaving the decanter for the E-rich and E-lean phases, respectively:

$$\theta_{refl} = \frac{L_{1,R}}{L_{1,R} + D_R} \qquad (3) \qquad\qquad \varphi_{refl} = \frac{L_{1,W}}{L_{1,W} + D_W} \qquad (4)$$

Multiplying θ_H and θ_{refl} (resp. φ_H and φ_{refl}), the ratio of the refluxed E-rich (resp. E-lean) phase is obtained, which value can be higher than one:

$$\theta = \theta_H \theta_{refl} = \frac{L_{1,R}}{L_{0,R}} \qquad (5) \qquad\qquad \varphi = \varphi_H \varphi_{refl} = \frac{L_{1,W}}{L_{0,W}} \qquad (6)$$

The following simplifying assumptions are applied in the feasibility analysis:

- the composition of the condensate is constant and equals to that of heteroazeotrope,
- the vapour and liquid hold-ups of the column and of the condenser are negligible,
- constant molar overflow.

The first assumption also means that ω, $x_{1,R}$ and $x_{1,W}$ are not changing in time, although they may change slightly during a real operation (Pommier et al., 2008).

The flow rate of the condensate (equal to that of the top vapour, V):

$$L_0 = L_{0,R} + L_{0,W} = \omega L_0 + (1-\omega) L_0 = V \qquad (7)$$

The total flow rate of reflux stream is the following:

$$L_1 = L_{1,R} + L_{1,W} = \theta L_{0,R} + \varphi L_{0,W} \qquad (8) \qquad\qquad L_1 = \theta\omega V + \varphi(1-\omega) V \qquad (9)$$

The component flow rates of the reflux flow:

$$L_1 x_1 = L_{1,R} x_{1R} + L_{1,W} x_{1,W} \qquad (10)$$

The evolution of the still composition is described by a differential equation, which can be derived from the total and component (differential) material balances of the still pot.
The total material balance (assuming constant molar overflow):

$$\frac{dH_S}{dt} = L_1 - V = (\theta - 1)\omega V - (1-\varphi)(1-\omega)V \tag{11}$$

The component material balance:

$$\frac{d(H_S x_S)}{dt} = L_1 x_1 - V x_0 = (\theta - 1)\omega V x_{1,R} - (1-\varphi)(1-\omega)V x_{1,w} \tag{12}$$

By applying the product rule of differentiation, the equation of the still path:

$$H_S \frac{dx_S}{dt} = \frac{d(H_S x_S)}{dt} - x_S \frac{dH_S}{dt} \tag{13}$$

The final form of the equation describing the evolution of the still composition:

$$\frac{dx_S}{dt} = (1-\theta)\omega \frac{V}{H_S}(x_S - x_{1,R}) + (1-\varphi)(1-\omega)\frac{V}{H_S}(x_S - x_{1,W}) \tag{14}$$

The two terms represent the removal of the E-rich and the E-lean phase from the system, respectively, by either withdrawal as distillate, or accumulating in the decanter.

3. Operational policies

Based on the values of two operational parameters θ and φ, 16 different cases can be distinguished, shown in Table 1. If θ (resp. φ) is 0, the E-rich (resp. E-lean) phase is not refluxed. If θ (resp. φ) is 1, the E-rich (resp. E-lean) phase is refluxed entirely. If θ (resp. φ) is greater than 1, the amount of the E-rich (resp. E-lean) phase refluxed to the column is greater than what is removed from it with the top vapour. To supply this difference in the flow rates, the hold-up of the respective phase must be decreased.
In Eq. 14, the terms related to the refluxing of a phase (θ_{refl} and φ_{refl}) and to the change in its hold-up (θ_H and φ_H) are only present with their products (θ and φ). That is, the same effect can be achieved either by accumulating one of the phases, or by withdrawal as distillate. The practical implementation of withdrawal is easier. Accumulating one of the phases in the decanter may be useful, e.g. in order to ensure the existence of two liquid phases. However θ or φ can only be greater than 1, if the hold-up is reduced. In Table 1 examples are given for some operational policies.
The still path can be characterised by the direction of the derivative vector of the still composition. This can be written (Eq. 14) as the sum of two other vectors, whose magnitude depends on θ and φ, respectively. Their direction can even be reversed, if θ or φ is greater than 1. Therefore, the direction of the resultant vector depends on the operation policy and the value of the operational parameters θ and φ. The results are illustrated with a mixture of A, B and E. A and the entrainer E form a binary heteroazeotrope, which is the only unstable node of the system.
The two vectors influencing the still path are presented in Fig. 2a. The vector corresponding to the E-lean phase points away from $x_{1,W}$, if φ<1, and towards it, if φ>1. The other vector, corresponding to the E-rich phase points away from $x_{1,R}$, if θ<1, and towards it, if θ>1. If θ or φ equals 1, the respective vector does not exist.
Fig. 2b shows the possible directions of the derivative vector, that is, the instantaneous direction of the still path for every possible operational policy shown in Table 1. By directing the still path appropriately, through choosing the right values of θ and φ, B can be recovered in the still, thus eliminating the need of a further separation step.

Table 1. The possible operational policies (reintr.: reintroduction - a greater amount of liquid is refluxed than what leaves the column as distillate).

	θ	φ	Reflux	Example
1	0	0	No reflux	
2		<1	E-lean phase (partial)	
3		1	E-lean phase (total)	
4		>1	E-lean phase (reintr.)	
5	<1	0	E-rich phase (partial)	Mode II, Strategy B (Skouras et al., 2005); Mode II, Strategies 2' and 2" (Gerbaud and Rodríguez-Donis, 2010)
6		<1	E-rich (partial) and E-lean phase (partial)	
7		1	E-rich (partial) and E-lean phase (total)	
8		>1	E-rich (partial) and E-lean phase (reintr.)	
9	1	0	E-rich phase (total)	Mode II, Strategy A (Skouras et al, 2005); Mode II, Strategy 1 (Gerbaud and Rodríguez-Donis, 2010)
10		<1	E-rich (total) and E-lean phase (partial)	Operation with reflux from E-lean phase, as well
11		1	E-rich (total) and E-lean phase (total)	Total reflux operation
12		>1	E-rich (total) and E-lean phase (reintr.)	
13	>1	0	E-rich phase (reintr.)	Mode II, Strategy 3 (Gerbaud and Rodríguez-Donis, 2010)
14		<1	E-rich (reintr.) and E-lean phase (partial)	
15		1	E-rich (reintr.) and E-lean phase (total)	
16		>1	E-rich (reintr.) and E-lean phase (reintr.)	

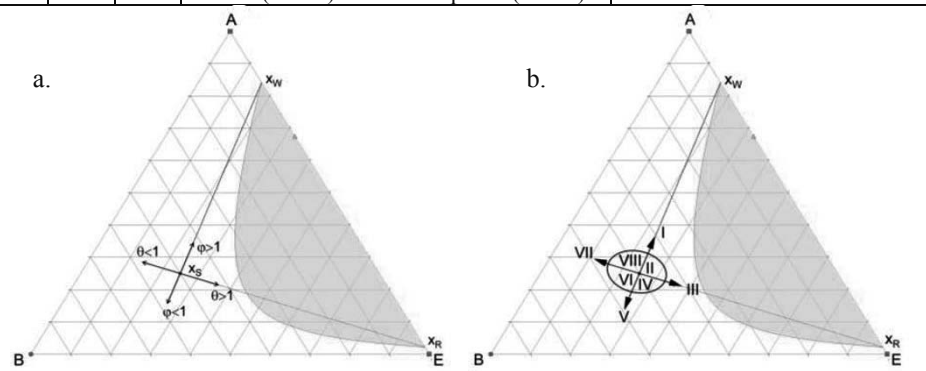

Figure 2 a. The possible directions of the vectors influencing the still path. b. The direction of the still path for the different operational policies.

4. Rigorous simulation results

In order to validate the model, rigorous simulations are performed with the professional flowsheet simulator CHEMCAD. Operational policies 8, 12 and 16 are applied in order to demonstrate that the still path can be turned into directions previously not reported, that is, towards the E-lean phase. The column has 50 theoretical plates; the mixture to be separated is water (A) – formic acid (B) – propyl formate (E). The vapour-liquid-liquid equilibria are described with the NRTL model. The mixture A – B exhibits a minimum boiling-point homoazeotrope, while A and E form a heteroazeotrope, enabling the separation of the A – B mixture.

The hold-up of the decanter is 0.5 dm^3; that of the column is 0.01 dm^3/plate. The charge has a molar amount of 160 mol and a composition of 52.5 mol% A, 40.5 mol% B and 7% E. The heat duty applied is 2 kW. The column is operated for 40 minutes under total reflux, after which one of the policies previously mentioned is applied. At the end of the total reflux period, the volumes of liquid phases in the decanter are equal. The values of the operational parameters are: $\varphi = 1.21$, $\theta = 0.986$ (Policy 8), 1.0 (Policy 12), and 1.014 (Policy 16), respectively. The respective still paths are shown in Fig. 3. Each path starts from the composition at the end the total reflux period ($x_{S,\infty}$). For Policy 12, the still composition moves towards that of the entrainer-lean phase, while for Policies 8 and 16, the path deviates from this direction as predicted: towards the edge A-B (Policy 8) or vertex E (Policy 16). That is, the still path directions are in accordance with the results of the feasibility analysis.

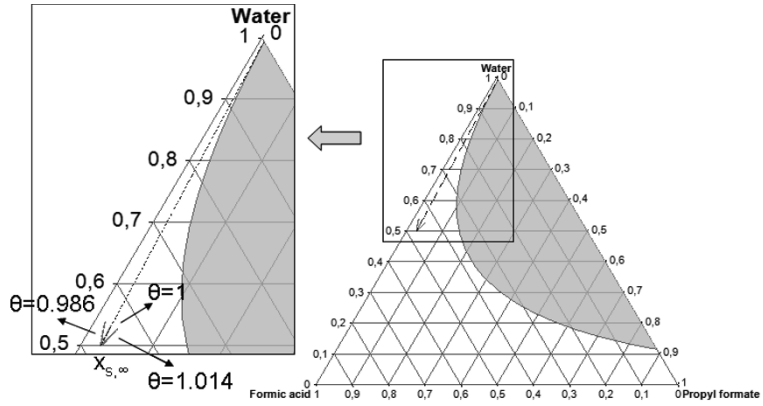

Figure 3. The calculated evolution of still composition (operational policies 8, 12, 16)

5. Conclusions

A general model of batch heteroazeotropic distillation was proposed. Both liquid phases present in the decanter can be refluxed or withdrawn as distillate, their hold-up can be increased, decreased or kept constant, as well. By assuming maximal separation, that is, that the condensate is always the heteroazeotrope, the still path equation was derived and the vectors determining the evolution of still composition were identified. The still path directions were determined for all the 16 possible operation policies. The results were validated by rigorous simulations for three cases not published yet. By using appropriate operational policies, it is possible to steer the still path in any desired direction, making possible to recover a pure component in the still.

Acknowledgement

This work was supported by TÁMOP - 4.2.2.B-10/1-2010-0009 and OTKA, proj. No.: T-049184.

References

Gerbaud, V. and Rodríguez-Donis, I., 2010, Techniques de l'ingénieur, J2 612, Tissot, Paris.
Lang P. and Modla G., 2006, Chemical Engineering Science, 61, 426.
Rodríguez-Donis, I., Gerbaud, V., Joulia, X., 2002, AIChe Journal, 48, 1168
Pham, H.N., Doherty, M.F., 1990, Chemical Engineering Science, 45 (7), 1837.
Pommier, S., Massebeuf, S., Kotai B., Lang, P., Baudouin, O., Floquet, P., Gerbaud, V., 2008, Chem. Eng. Proc., 47(3), 408.
Skouras, S., Kiva, V., Skogestad, S., 2005, Chemical Engineering Science 60, 2895.

I.A. Karimi and Rajagopalan Srinivasan (Editors), Proceedings of the 11th International Symposium on Process Systems Engineering, 15-19 July 2012, Singapore.

Economic NMPC for energy intensive applications with electricity price prediction

Rui Huang[a] and Lorenz T. Biegler[b]

[a] *United Technologies Research Center, 411 Silver Lane, East Hartford, CT, 06108*
[b] *Dept. of Chemical Engineering, Carnegie Mellon University, Pittsburgh, PA, 15213.*

Abstract

An economic nonlinear model predictive control (NMPC) framework is proposed to minimize utility cost for energy intensive applications in volatile electricity markets. In the *day ahead pricing* scheme, an economic objective function is used to minimize the future cost. On the other hand, a time series model must be incorporated to predict future electricity prices for *real time pricing*. A multicriterion objective function is proposed to minimize variation due to either pricing scheme. The proposed framework is demonstrated on an air separation unit and nearly 10% in cost reduction is observed.
Keywords: economic NMPC, electricity price prediction, Air separation unit

1. Introduction

Energy prices are often subject to high fluctuations in today's electricity markets, because electricity is not readily stored and has to be used or wasted after production. As a result, utility companies resort to complex pricing schemes to allocate resources. These schemes include *day ahead pricing* and *real-time pricing* strategies where electricity price can vary by an order of magnitude over the course of a day, especially in the latter case. This fluctuation can significantly impact the operating cost of a plant, especially for energy intensive applications. In Ierapetritou et al. (2002) and Baumrucker and Biegler (2010), short-term optimization schemes were proposed to take advantage of varying power price.

To deal with process dynamics, model predictive control (MPC) and nonlinear MPC (NMPC) have been widely used in industry, as they readily handle constraints and multi-input-multi-output systems. However, the majority of (N)MPC applications have been posed as setpoint tracking problems, where, the setpoint is normally calculated by the so-called real-time optimization (RTO) layer, based on a steady state first principle model. Furthermore, most theoretical analyses of (N)MPC are restricted to set-point tracking formulations (Rawlings and Mayne, 2009). Nevertheless, model inconsistency may lead to an unreachable setpoint or suboptimal solution by simply tracking the given setpoint as fast as possible (Rawlings and Amrit, 2009). As a result, interest has significantly increased in economically oriented NMPC, which directly optimizes the economic performance. Recently, several NMPC studies have reported good practical performance by using economically-oriented NMPC or, equivalently, dynamic RTO formulations that directly optimize the plant's economic performance (Rawlings and Amrit, 2009; Bartusiak, 2007; Diehl et al., 2011). Meanwhile, stability analyses of economic NMPC have also appeared in the literature (Aske et al., 2009; Diehl et al., 2011). In particular, our previous work (Huang et al., 2011, 2012) established the nominal and robust stability properties of NMPC for cyclic processes. Moreover, around 30% cost reduction has been achieved for an energy intensive air separation unit.

In this work, we present a framework to implement economically-oriented NMPC to control energy-intensive applications. This framework incorporates a time series model to predict prices from the volatile electricity market. This predicted price is used in the NMPC objective function to carry out the prediction in the controller. This framework is demonstrated by controlling an energy intensive air separation unit, which has been studied in our previous work (Huang et al., 2009). The rest of the paper is organized as the follows. Section 2 briefly discusses the economically-oriented NMPC formulation while Section 3 presents the time series model for the electricity price forecasting. Section 4 describes the simulation results and Section 5 concludes the paper.

2. Economically-oriented NMPC formulation

In this section, we consider the nominal discrete time nonlinear system

$$x_{k+1} = f(x_k, u_k); \qquad x_k \in \mathbf{X}, u_k \in \mathbf{U}, \tag{1}$$

where at time step k, x_k is the plant state in the domain $\mathbf{X}$ and u_k is the control input in the domain $\mathbf{U}$. As a result, the economically-oriented NMPC formulation is written as the following nonlinear programming (NLP) problem,

$$\min_{x,u} \sum_k l(x_k, u_k) \text{ s.t. } x_{k+1} = f(x_k, u_k), x_k \in \mathbf{X}, u_k \in \mathbf{U}, \tag{2}$$

where $l(x_k, u_k)$ is the economical cost function at the time step k for the plant (1). The objective of the NMPC controller is to minimize the economic cost over the predictive time horizon. Here unlike conventional setpoint-tracking NMPC, the cost function $l(x_k, u_k)$ usually does not take a quadratic form. In the following, we present two economic cost function to minimize the utility cost in the volatile electricity market. Let p_k be the electricity price at the time step k. This price information can be achieved from published data by utility companies, or from the prediction of time series model discussed in the next section. In addition, let g_k be the amount of the energy consumed at the time step k, and $g_k = h(u_k)$ is a function of the control inputs. Hence the cost function of NMPC (2) at time step k can be chosen as $l_k = p_k g_k$. Clearly, the economic NMPC (2) with the cost function (3) is to minimize the utility cost in a deterministic framework. On the other hand, the future electricity price may suffer from uncertainties, especially when the price is predicted from a time series model. In this case, the stochastic performance should also be considered in the economic NMPC formulation. Hence, the cost function is modified as

$$l_k = W_1 E(p_k) g_k + W_2 var(p_k) g_k, \tag{3}$$

where $E(p_k)$ and $var(p_k)$ are the expected value and variance of the predicted electricity price p_k at time step k, respectively, and W_1 and W_2 are the weights. As a result, the economic NMPC (2) with the objective function (3) is to minimize the utility cost in the volatile electricity market while minimizing the uncertainty of the control policy subject to the uncertainties in the predicted electricity price. Similarly, the economic NMPC formulation can be modified by choosing $l_k = E(p_k) g_k$ and adding an inequality constraint $\mathrm{var}(\mathrm{p_k}) \leq \kappa(\max\ var)$ to the optimization problem (2). In this work, we use the economic NMPC formulation (2) with objective function (3).

Finally, it is worth noting that the objective function (3) may not guarantee the stability of the NMPC controller (2) in reaching an equilibrium point. This can be avoided by introducing quadratic regularization terms in the objective function, as will be further illustrated in the simulation example in Section 4.

3. Volatile electricity pricing schemes

The price of electricity depends on many different factors such as time of day, location and so on. In this section, we focus on two complicated pricing schemes, namely *day ahead pricing* and *real-time pricing* schemes, which are commonly used in industrial sectors *Day ahead pricing* changes the electricity price every hour. Utility companies estimate the production cost and the energy demand for the next day to come up with the energy price they charge. This price is usually published 24 hours in advance, and the pricing scheme is similar to the commodities future contract price. *Real time pricing* also changes the electricity price hourly, but this is based on the real time market-balancing price, i.e., the last price paid by the utility for electricity in the time period. This is similar to the spot market price or clearing price. Since the day-ahead electricity price is available 24 hours in advance, it can be directly used in the NMPC prediction problem. However, in the real time pricing scheme, the electricity price is only available at the end of every hour, which is not suitable for the prediction problem. Hence, a price forecast model is developed to predict the future price based on the past information. There is an extensive literature in the development and application of forecasting techniques. A survey and detailed comparison of various methodologies can be found in (Box et al., 1994). Here a commonly-used Autoregressive Integrated Moving Average (ARIMA) model is used to predict the future real time electricity price over next 24 hours.

More specifically, the ARIMA model is referred to as an ARIMA(*p,d,q*) model where *p*, *d* and *q* are non-negative integers that refer to the order of the autoregressive, integrated, and moving average parts of the model respectively. An add-on Microsoft Excel statistics tool XLSTAT, from www.xlstat.com, is used for model construction. We analyze the electricity price in the period of 3/20 -3/23/2011 from Ameren (https://www2.ameren.com/RetailEnergy/realtimeprices.aspx), a utility company in St. Louis. ARIMA (2,1,1) shows the best balance of model complexity and predictability, and is characterized by the following forecasting equation

$$\hat{y}_{k+1} = \mu + y_k + \phi_1(y_k - y_{k-1}) + \phi_2(y_{k-1} - y_{k-2}) - \theta e_k \qquad (4)$$

where y_k, y_{k-1} and y_{k-2} are the actual prices of the latest three time steps, while $\hat{y}_{k+1}$ is the predicted price at the next time step. μ is a constant term which represents the moving average, $\phi_1$and ϕ_2 are the first and the second order autoregressive coefficients, repectively, θ is a constant multiplier and $e_k = y_k - \hat{y}_k$ is the lagged forecasting error, representing the integrated part. The ARIMA model is constructed by finding the set of constants μ, ϕ_1, ϕ_2 and θ that minimizes certain objectives such as Akaike information criterion (AIC) and Schwarz Bayesian criterion (SBC) over a historical data set.

New electricity price information is available at the end of each hour in the real time pricing scheme, and we update the ARIMA(2,1,1) model at the end of each hour based on moving horizon framework (Rao et al., 2003). Figure 1 shows the predicted price after moving horizon problem is solved 24 times based on 96 hrs of historical data from Ameren. In addition, covariance information of predicted electricity price is also available from XLSTA. For instance, the grey lines in Figure 1 are upper and lower bounds for the predicted price with 80% confidence interval. This information can be used in the objective function (3) where we also consider minimizing the variation of utility cost.

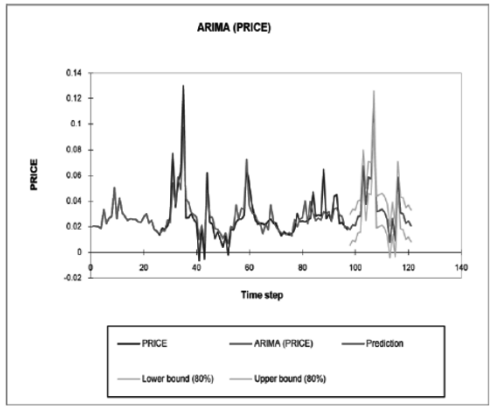

Figure 1 Predicted real time price.

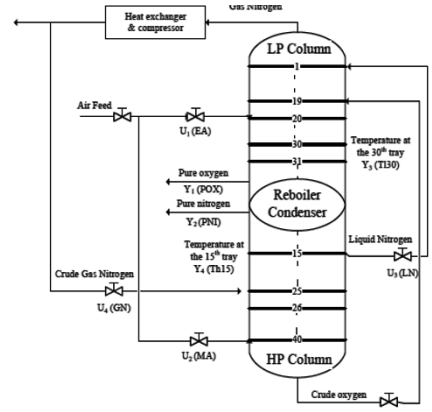

Figure 2 Air separation unit

4. Simulation results

Air separation unit is an energy intensive application because ambient air is compressed and cooled to extremely low temperature (-170℃ to -195℃). Since the raw material (ambient air) is free, the major operational cost is the energy consumed for compression. Here we revisit the ASU system (Figure 2) presented in [10] and assume that the energy used in by the ASU is proportional to the main air feed ($\boldsymbol{U_1}$-MA) and expanded air feed ($\boldsymbol{U_2}$-EA). As a result, the objective function (3) at time step *k* is chosen as $\boldsymbol{l_k = W_1 p_k \times (EA_k + MA_k) + W_2 var(p_{T_k}) \times (EA_k + MA_k) + reg_k}$, where $\boldsymbol{reg_k = (Y_k - Y_{set})^T \mathcal{Y} (Y_k - Y_{set}) + (U_k - U_{ref})^T \mathcal{U} (U_k - U_{ref})}$, $\boldsymbol{Y_k}$ represents controlled variables; $\boldsymbol{U_k}$ represents manipulated variables and $\boldsymbol{Y_{set}}$ and $\boldsymbol{U_{ref}}$ are setpoint and reference values for controlled and manipulated variables, respectively. Here, $\boldsymbol{\mathcal{Y} = diag[10^{-4}, 10^{-4}, 3\times10^{-2}, 3\times10^{-2}]}$ and $\boldsymbol{\mathcal{U} = diag[10^{-4}, 10^{-5}, 10^{-5}, 10^{-5}]}$ are diagonal weighting matrices. The regularization term, $\boldsymbol{reg_k}$ guarantees stability and improves numerical performance of the optimization problem (2). In addition, weights are set to $\boldsymbol{W_1 = W_2 = 10^{-3}}$. Therefore, the problem is strongly regulated around the equilibrium point. To achieve better economic performance, one could increase W_1 and W_2 and add inequality constraints to obtain the required performance, e.g., O_2 production and purity.

In the first scenario, the electricity price is taken from the *day ahead pricing* scheme of Ameren for 48-hour period (3/23/2010-3/24/2010). The economic NMPC formulation (2) with the objective function (3) is solved. The prediction horizon is chosen to be 120 minutes and the sampling time is 6 minutes. Fig. 3 presents the input variables in the day ahead pricing scenario. The economical NMPC renders an operational cost of $12,511 over this 48-hour period, while the operational cost of the conventional setpoint tracking NMPC with a fixed setpoint (Y_{set} and U_{ref}) is $13,042. Hence, it generates 4.25% cost reduction by using the economical NMPC. In the second scenario, the electricity price is predicted from the ARIMA(2,1,1) model and economic NMPC (2) with objective function (3) is used. Figure 4 presents the input variables in the *real time pricing* scenario. Here the operational cost in the 24-hour period (3/24/2011) is $4,347.2/day while setpoint tracking NMPC leads to a $4,768.9/day operational cost, a 9.7% cost reduction. After full discretization, the NLP has 117,140 variable, 116,900

constraints, and is solved using AMPL and IPOPT. For both scenarios, IPOPT requires from 8 to 18 iterations and 180 to 380 CPUs (Intel core i7 2.8GHz, 8 GB memory). In addition, advanced step NMPC [10] reduces computational delay to below 1 CPUs. Advanced step NMPC and ideal NMPC are identical, as seen in Figures 3 and 4.

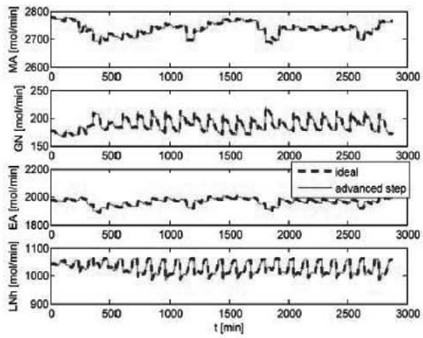

Figure 3 Input in day ahead scenario

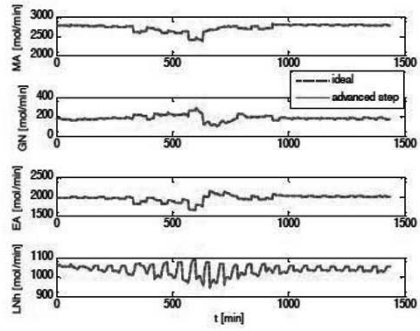

Figure 4 Input in real time scenario

5. Conclusion

This work presents a framework for economically-oriented NMPC that directly minimizes the operational cost of energy intensive applications to exploit *day ahead* and *real time pricing* electricity markets. ARIMA model based on moving horizon framework is proposed to forecast the future electricity price in a real time pricing scheme. The proposed framework is implemented on an air separation unit and more than 9% cost reduction is observed compared to the setpoint-tracking NMPC.

References

Aske, E., S. Strand, S. Skogestad, Coordinator MPC for maximizing plant throughput, Computer & Chemical Engineering, 32 (28), 195-204. 2009

Bartusiak, R. D., NlMPC: Platform for optimal control of feed- or product-flexible manufacturing, in *Assessment & Future Directions of NMPC*, Springer, 2007, 1-16.

Baumrucker, B., L. Biegler MPEC strategies for cost optimization of pipeline operations. Computer and Chemical Engineering. 34. 900-913, 2010.

Box, G., G. Jenkins, G. Reinsel, *Time series analysis: forecasting and control*, 3rd ed., Prentice-Hall. 1994.

Diehl, M., R. Amrit, J. Rawlings. A Lyapunov function for economical optimizing model predictive control, IEEE Trans. Auto. Cont. 56, 703-707, 2011

Huang, R., E. Harinath, L. Biegler, Lyapunov stability of economically oriented NMPC for cyclic processes. Journal of Process Control, 21, 501-509, 2011

Huang, R., L. Biegler, E. Harinath, Robust stability of economically oriented infinite horizon NMPC that include cyclic processes, J. Proc. Cont. 22, pp. 51-59 (2012)

Huang, R., V. Zavala L. Biegler Advanced step nonlinear model predictive control for air separation units. Journal of Process Control, 19, 678-685, 2009.

Ierapetritou, M., D. Wu, J. Vin, P. Sweeney and M. Chigirinskiy. Cost minimization in an energy-intensive plant using mathematical programming. I&EC Res 41, 5262-5277. 2002

Rao, C., J.Rawlings D. Mayne; Constrained state estimation for nonlinear discrete-time systems: stability and moving horizon approximations. IEEE TAC, 48, 246-258, 2003.

Rawlings, J., D. Mayne, Model Predictive Control:Theory & Design, Nob Hill, 2009.

Rawlings, J., R.Amrit,Optimizing economic performance using MPC, in *Future Directions of NMPC*, Springer, 2009, 119-138.

I.A. Karimi and Rajagopalan Srinivasan (Editors), Proceedings of the 11th International Symposium on Process Systems Engineering, 15-19 July 2012, Singapore.

A Multivariable Nonlinear Model Predictive Control Framework for a PEM Fuel Cell System

Chrysovalantou Ziogou[a,b], Efstratios N. Pistikopoulos[d], Spyros Voutetakis[a], Michael C. Georgiadis[a,b], Simira Papadopoulou[a,c]

[a]*Chemical Process Engineering Research Institute (C.P.E.R.I.), Centre for Research and Technology Hellas (CE.R.T.H.), P.O. Box 60361, 57001 Thessaloniki, Greece,*
[b]*Department of Engineering Informatics, University of Western Macedonia, Vermiou and Lygeris str., Kozani, 50100, Greece*
[c]*Department of Automation, Alexander Technological Educational Institute of Thessaloniki, P.O. Box 141, 54700 Thessaloniki, Greece*
[d] *Department of Chemical Engineering, CPSE, Imperial College London, SW7 2AZ London, UK*

Abstract

The aim of this work is to present an integrated framework for the on-line control of a Polymer Electrolyte Membrane (PEM) fuel cell system using an optimization-based control methodology. The framework consists of a nonlinear model predictive control (NMPC) scheme and an on-line supervisory control and data acquisition system (SCADA). The solution of the NMPC problem is achieved by a direct optimization method which involves the use of orthogonal collocation on finite elements and represents the optimal control problem as a nonlinear programming problem (NLP). The on-line application of the multivariable controller shows that the proposed framework can accomplish the desired objectives for power fulfilment in the context of a safe operating region. Furthermore the controller exhibits excellent performance in terms of computational requirements and can follow load changes with a negligible error in its response.

Keywords: on-line implementation nonlinear model predictive control, experimental fuel cell unit, dynamic optimization, power tracking, starvation avoidance, excess ratio

1. Introduction

A Fuel Cell (FC) is a complex system with various phenomena evolving while it operates, which thus posing interesting control challenges, while the appropriate determination of the operating region leads to different behavior of the system regarding its response. Characteristics such as fast time response, subsystem interactions and conflicting operating objectives can be handled through the development of an advanced control framework, which enables the adjustment of the manipulated variables according to changes in the underlying process and simultaneously ensures fast response and precise tracking of the defined set-points. Nonlinear Model predictive control (NMPC) has the ability to handle state and input constraints, dynamic nonlinearities of the process into consideration while it simultaneous satisfies economic and operating objectives under an integrated optimization methodology. Within this scope a NMPC framework along with its on-line deployment to an experimental small-scale unit is developed and analysed.

2. Experimental Unit Setup and Automation System

An integrated FC Unit consists of various electrochemical, mechanical and electronic components and subsystems and it is important to measure the variety of the physical quantities of the subsystems along with the voltage and the current density of the FC. In this context a small scale plant has been designed and constructed at CPERI/CERTH. The unit is comprised of two mass flows for the regulation of the gases flow rates, a humidification system, two PID controllers for the anode and cathode pressure control, fan assisted air cooling and an electrical heat up subsystem along with the necessary power conditioning device.

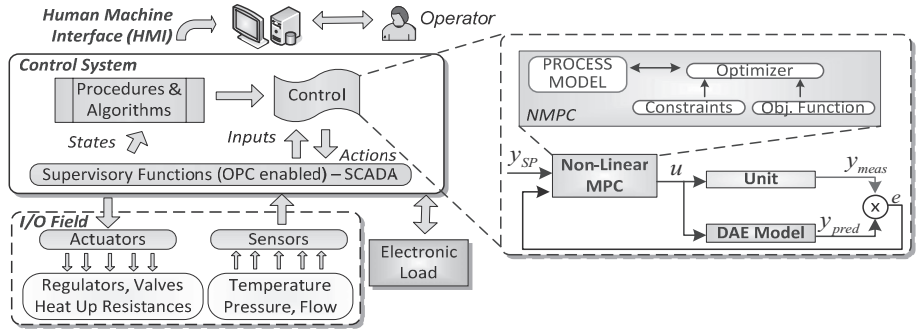

Figure 1 Information flow and NMPC structure

The automation of the unit is based on a Supervisory Control and Data Acquisition system (SCADA) which was used for the monitoring and control of the unit's input/output (I/O) field. In the SCADA system data are organized in a process database (PDB) and each I/O signal is assigned to a record named tag. Each tag can be sampled at different rates selected accordingly to the nature of the measured variables. This sampling is performed at predefined regular time intervals. Although the data from the I/O field can be acquired at smaller intervals, dictated by the communication protocol and the driver (polling time), the values at PDB are updated based on the scan period setting. The SCADA system enables us to measure the available signals and control the appropriate variables. All system components (pumps, heaters, valves, etc) are controlled by digital commands and pre-programmed procedures. The temperatures and pressures are maintained at the required set points by the SCADA system, via PID controllers, while the excess ratio level (λ_{o2}) and the power are controlled by the developed NMPC controller. The information flow from the I/O field to the operator, including the advanced control methodology approach is shown in Fig 1.

3. Nonlinear Model Predictive Control Framework

Nonlinear Model predictive control (NMPC) performs on-line optimization for future control actions over a prediction horizon. At each sampling time a finite horizon optimal control problem is solved using the current state of the process as the initial state. Using a process model, the effect of past inputs on future outputs is predicted. The deviation of the model prediction from the actual response is recorded and considered as the error of process model. The calculated error defines a bias term that is used to correct future predictions and it is assumed constant for the entire prediction horizon.

3.1. Dynamic Fuel Cell Model

A semi-empirical isothermal dynamic model was utilized in the NMPC scheme which is oriented towards process operation and control and takes into account main variables,

such as the operating temperature, the partial pressures of all gases and the fuel cell current (Ziogou, 2011). The model relies on first-principle equations and it accounts for mass dynamics in five control volumes: the gas flow channels, the gas diffusion layers and the membrane. It has been validated against experimental data generated by the PEM fuel cell unit and it provides the basis for the proposed on-line control framework.

3.2. Dynamic Optimization

The optimization method which is applied in the current work is a direct method which uses an augmented Lagrangian solver (Murtagh, 1998) and the problem formulation involves orthogonal collocation on finite elements (OCFE). The constrained optimization problem is converted into a large scale but sparse nonlinear programming problem (NLP), which is exploited to achieve an efficient solution (Biegler, 2002, Kiparissides, 2002). The method of OCFE approximates manipulated (input) and the state variables' profiles and consequently the output (controlled) variables' profiles with a family of Lagrange polynomials on finite elements (FE). The time horizon is divided into a series of finite elements ($i = 1..NE$) in such a way that wide variations of the transition profiles can be handled. Within each FE the dynamic profiles of inputs, states and outputs are further discretized around collocation points ($j = 0..N_{cop}$) determined as the shifted roots of Legendre polynomials. The solution is approximated at each FE:

$$x(t) \approx \sum_{j=0}^{Ncop} x^{i,j}\Omega_j(t),\ \ i = 1..NE\ \ ,\ \ t \in [t_i, t_{i+1}] \tag{1}$$

$$\Omega_j(t) = \prod_{k=0,k\neq j}^{Ncop} \frac{(t - t_{i,k})}{(t_{i,j} - t_{i,k})} \tag{2}$$

where *Ncop* is the total number of the internal collocation points of each element, *NE* is the number of the finite elements, $x^{i,j}$ is the value of the state vector at collocation point j of the ith finite element. Respectively the algebraic variables ($z^{i,j}$) and input (manipulated variables) variables ($u^{i,j}$) are approximated. After the discretization of the DAE model, the optimization problem (3) is expressed as an NLP problem in the form:

$$\min_{x^{i,j}, z^{i,j}, u^i} \sum_{i=1}^{NE}\sum_{j=1}^{Ncop} w_{i,j}\phi\left(x^{i,j}, z^{i,j}, u^{i,j}\right) \tag{3}$$

$$\text{s.t. :} \qquad \sum_{k=0}^{Ncop} \dot{\Omega}_k(\tau_{i,j}) x^{i,k} = h_i f_d\left(u^{i,j}, x^{i,j}, z^{i,j}\right) \tag{3a}$$

$$0 = f_a\left(u^{i,j}, x^{i,j}, z^{i,j}\right) \tag{3b}$$

$$x^{1,0} = x_0, \quad x(t_f) = \sum_{j=0}^{Ncop} x^{NE,j}\Omega_j(1) \tag{3c}$$

$$x^{i,0} = \sum_{j=0}^{Ncop} x^{i-1,j}\Omega_j(1),\ \ \mathrm{i} = 2..NE \tag{3d}$$

To enforce continuity of the states at adjacent finite elements, connecting equations are used (3d). Furthermore u, x, y are constrained within upper and lower bounds.

3.3. Problem Formulation

The control objectives of the system are to fulfil the power demand and to avoid oxygen starvation using the current and the air mass flow rate as manipulated variables. The effective control of the oxygen concentration in the cathode ensures safe operation during load changes and avoids oxygen starvation, a phenomenon which greatly affects

the lifetime of the fuel cell. The excess ratio level (λ_{o2}) is an unmeasured variable that can be expressed as the inlet flow of oxygen to the rate of oxygen consumption. The prediction (T_p) and control horizon (T_c) are set at 5s. The nonlinear model is comprised out of 8 differential equations and 1 algebraic which are discretized at 10 finite elements having 4 collocation points each. The resulting discretized system has 371 variables and 342 equations. The Jacobian matrix has 2430 non-zero elements (density = 1.915%).

3.4. On-line Implementation

Verification and validation of the framework is performed by deploying the multivariable controller on-line to the unit. An OPC-based interface was developed for the synchronization of the NMPC framework and the SCADA system. The NMPC algorithm is executed on-line on a PC which is communicating in real time with the control system, having a sampling rate of 1s. The response of the NMPC framework to various load (power) demands and different stoichiometric ratios was studied at specific operating conditions of temperature and pressure (T=338K, Pt=1Barg) with constant hydrogen flow (flows: H_2=350cc/min).

4. Results and Discussion

The proposed NMPC framework was deployed to the system and a number of on-line experiments were performed in order to verify the efficiency and the response of the controller at often power demand changes. A prerequisite for the online application of the controller is to exhibit both fast response and minimize the error towards the set-point. Therefore the analysis focuses on these two metrics through two scenarios. In the first scenario the power profile changes while the oxygen excess ratio remains at a constant level while in the second scenario both profiles are modified.

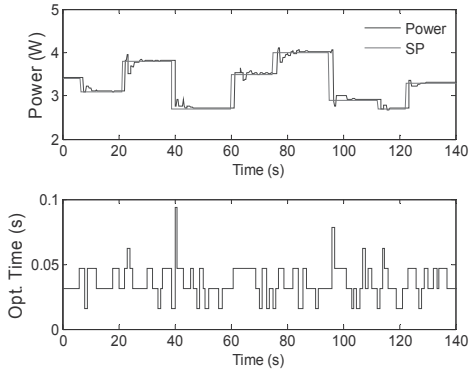

Figure 2 a)Power b)Optimization time

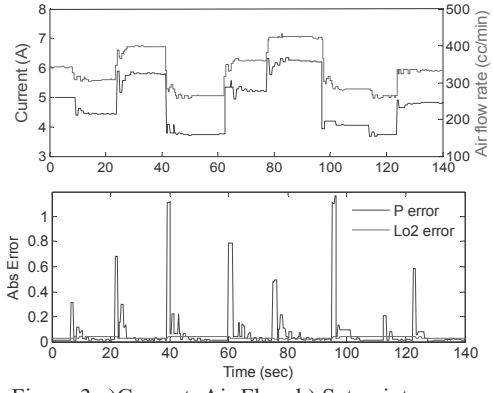

Figure 3 a)Current, Air Flow b) Set point error

Fig 2a shows the power response to the corresponding control actions of the manipulated variable (Fig 3a) as the power demand changes while the oxygen excess ratio remains at a constant set point (λ_{o2}=3). The controller is able to steer the fuel cell power to any admissible set-point while maintaining the required excess ratio level. This is better illustrated from the absolute error analysis in Fig 3b. The mean square root error is 43mW for the power and the average oxygen excess ratio error is $3*10^{-3}$. Also it is observed (Fig 2b) that the maximum optimization time is 93ms while the average optimization time is 36ms. From Fig 2 we observe that the optimization time is less the 100ms but since the scan time is 1s, the new output will be applied at that time interval. Therefore there is always a lag between the implementation of the output signal and the update of the input information, performed at the next scan interval. In the second scenario where both profiles are modified (power and oxygen excess ratio) the

same behaviour is observed (Fig 4, Fig 5). Overall the optimization time remains lower than 65ms with an average time of 39ms (Fig 5b) and it is not affected by the changes of the set points.

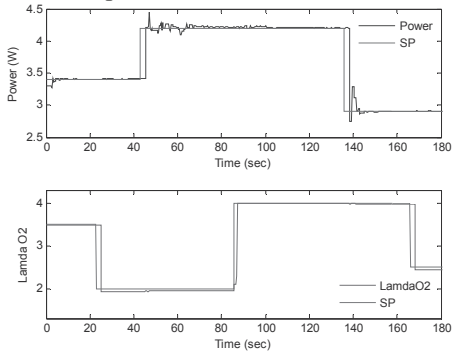

Figure 4 a)Power b)O2 excess ratio

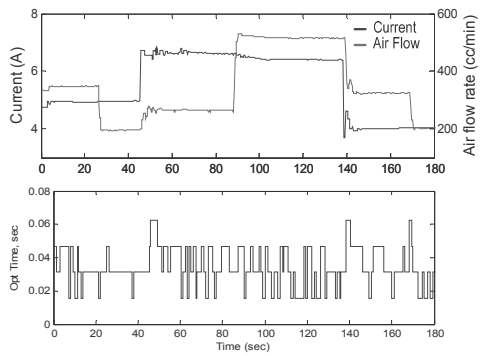

Figure 5 a)Current, Air Flow b) Optimization time

At low oxygen excess ratio ($\lambda_{o2}=2$) some fluctuations of the power profile around the new set point occur when the power demand increases, from 3.4W to 4.2W. This is caused by the fact that although the current increases in order to reach the new power set point and consequently increases the required oxygen (consumed), the air flow rate is not increased respectively due to the low oxygen excess ratio requirement (set point). As the excess ratio increases to converge to the new lamda set point ($\lambda_{o2}=4$) we observe that the fluctuation of power diminishes after a few seconds. That means that NMPC satisfies increased load demand in a smoother way when operating at higher values of oxygen excess ratio. Overall the proposed framework can efficiently provide the necessary control actions in order to follow the power set-point changes and adjust the air flow rate according to the requirement for oxygen excess ratio and thus avoid oxygen starvation.

5. Conclusions

The proposed NMPC framework combines two operational objectives and guarantees an operation that on the one hand satisfies the power demand in a safe and controlled way and on the other can adapt to sudden power demand changes. The controller was deployed to the SCADA system and on-line experimental studies showed that the control framework was able to maintain the stability of the system. The multivariable controller was successfully evaluated at the fuel cell unit under varying operating conditions leading to fast response time and negligible offset from the desired set points. Overall the NMPC approach guarantees that the PEMFC performs within its operating objectives and illustrates an excellent potential for on-line applications in order to manage the produced energy in an optimum manner.

Acknowledgments

Financial support from the DECADE IAPP Project of FP7 is gratefully acknowledged (Contract number PIAP-GA-2008-230659).

References

Biegler L.T, A.M. Cervantes, A.Wachter, Chem. Engineering Science 57 (2002) 575–593
Kiparissides C., Seferlis P., Mourikas G., A. J. Morris, Ind. Eng. Chem. Research 41 (2002) 6120-6131
Murtagh, B. A., Saunders, M. A. (1998). MINOS 5.5 User's guide, Report 83-20R, Stanford University
Ziogou C., Voutetakis S., Papadopoulou S., Georgiadis C. M., Computers & Chemical Engineering 35 (9) (2011) 1886-1900

I.A. Karimi and Rajagopalan Srinivasan (Editors), Proceedings of the 11th International Symposium on Process Systems Engineering, 15-19 July 2012, Singapore

Online Model Predictive Control of Municipal Water Distribution Networks

Gokul Siva Sankar, Sridharakumar Narasimhan * and Shankar Narasimhan
Department of Chemical Engineering, Indian Institute of Technology Madras, India

Abstract

Optimal operation of municipal Water Distribution Networks (WDNs) is based on optimizing one or more performance metrics while meeting consumer demands and satisfying supply side and storage constraints. This can be achieved by implementing advanced control schemes such as Model Predictive Control (MPC). With the alarming decrease in fresh water supplies, the primary focus of online control strategies should be to conserve water. A novel control strategy that can handle both water sufficient and deficient cases is proposed for WDNs with storage facilities. Performance of the developed model based online control strategy is tested by numerical simulations of an illustrative WDN.

Keywords: water distribution network, model predictive control, optimization, storage tanks

1. Introduction

Municipal water distribution networks supply water from sources such as dams, lakes and ponds to the consumers at the demand points through a network of pipes, valves and pumps such that their demands are met at desired pressures. WDNs have to be operated efficiently and reliably to supply the guaranteed amount of water in both directly pumped (24×7) and intermittent (possible in networks with storage facilities) modes of supply. In addition, depletion of water resources, shortage in water availability for supply and growth in demand have necessitated improved and sustainable water management practices in distribution systems. Traditionally, optimal operation of WDNs is concerned with minimizing the total cost of operation while maintaining water quality, regulating pressure in the pipelines to prevent leaks, and meeting consumer demands, assuming that sufficient water is available for meeting consumer demands (Kumar, 2008). However, in several countries such as India, overhead tanks and underground sumps are available at individual households for storage of water. These tanks can serve as intermediate storage elements when peak demand requirements cannot be met. Hence, an optimal control strategy has to be devised that considers the supply side and storage constraints to meet demand requirements. We introduce a novel MPC based control strategy for WDNs which takes into account the limitations of the actuators and storage tanks to address both water deficient and water surplus scenarios.

2. Modelling Water Distribution Networks

2.1. Pipes, Nodes and Node Resistance

A WDN consists of pipes, pumps, storage tanks, and valves. It has nodal points where water is withdrawn/supplied or where two or more pipes meet (Bhave and Gupta, 2009).

*sridharkrn@iitm.ac.in

A WDN can be modelled using mass balances for all storage tanks and nodal points, and the relations between pressure drop/rise and flow rate for pipes, pumps and valves. In addition, for a pressure-driven outflow model, relations between the pressure at the demand points and outflows are also included. The model equations are as follows.

Pressure drop in pipes is given by

$$\Delta h_j = \frac{\gamma L_j \text{sign}(Q_j)|Q_j|^{1.85}}{\lambda_j^{1.85} D_j^{4.87}}, \quad j = 1, ..., P \tag{1}$$

where λ_j is Hazen-William roughness coefficient of pipe j, Δh_j is the head loss in pipe j, L_j and D_j are the length and diameter of pipe j in m, Q_j is the flow through j^{th} pipeline in m^3/s and γ is the factor depending on the dimensional system used, is 10.7 when SI system of units is followed.

Mass balance at nodal points is given by

$$\sum_{j=1}^{p} a_{ij} Q_j - d_i = 0, \quad i = 1, ..., N \tag{2}$$

where d_i is the demand (or supply) at node i, N and P are the total number of nodes and pipes in the network respectively and a_{ij} is a coefficient that has a value 0 if pipe j is not linked to node i and has a value +1 or -1 otherwise, depending on whether the flow in pipe j is towards node i or away from it, respectively.

Outflow rate at a demand point is related to the pressure at that node by

$$p_i = k_i d_i^2 \;\; i = 1, ..., N \tag{3}$$

where p_i and and k_i are the pressure and resistance offered to outflow at node i.

2.2. Valves, Reservoirs and Tanks

A valve is a control device in a WDN that is used to vary the flow rate and/or pressure by closing and opening the stem. Head loss equation for a valve is given by

$$\Delta h_v = \frac{Q^2 G_L}{\left(C_v \frac{e^{ln\tau V}}{\tau}\right)^2} \tag{4}$$

where Δh_v is the head loss across the valve for a flow rate Q, C_v is the valve coefficient when the valve is 100% open, τ is the valve rangeability, V is the fraction of valve opening and G_L is the specific gravity of the fluid.

Tanks are storage units in WDNs and are associated with a minimum and maximum capacity. Quasi-steady state approximation is used here, wherein water level in all reservoirs and tanks are assumed to be constant in each time period and are updated at the end of the period. Mass balance expression for a reservoir/tank and physical storage limits of a tank are

$$H_z(k+1) = H_z(k) + \frac{\Delta t}{A_z}\left(Q'_{\text{in}}(k) - Q'_{\text{out}}(k)\right), \quad z = r \text{ or } t \tag{5}$$

$$0 \le H_t(k) \le H_{t\max} \tag{6}$$

where $H_r(k)$ and $H_t(k)$ are liquid levels in reservoir and tank at the end of time period k, A_r and A_t are cross sectional areas of reservoir and tank, $Q'_{\text{in}}(k)$ and $Q'_{\text{out}}(k)$ are sum of steady state rate of inflows to and outflows from the reservoir/tank respectively, Δt is the sampling time and $H_{t\max}$ represents maximum storage height.

3. Control Problem Description

Traditionally, demand outflows are the controlled variables and control can be effected by manipulations of stem positions of continuous control valves. Continuous valves provide better controllability of flow rate and/or pressure in WDNs than on-off valves. Generally, WDNs are non-square systems with one or more demand outflows being controlled by a single valve. The constraints to be satisfied represent the physical limitations of the system (limitation on the storage capacity of the tanks as in Eq. 6) and manipulated variables (valve opening in percentage can be from 0% to 100%). A suitable demand set point profile can be chosen to capture the temporal and spatial variations in the water usage pattern. To conserve water, the amount of water supplied should be just enough to meet the consumers' demand as over supply may lead to wastage of water.

3.1. Control strategy

Kumar (2008) proposed the use of MPC strategy for optimal operation of directly pumped WDNs. Control moves were calculated by minimizing the instantaneous deviation of demand outflow from the desired flow rate. However, storage facilities such as tanks or sumps, that are usually available at the demand points, were not accounted for. If it is not possible to meet peak demand requirements, water can be stored in these buffer tanks during the preceding periods and can be used to meet peak demand requirements. Thus, the use of buffer tanks allows intermittent supply and it is not necessary to meet the instantaneous demand rate. Rather, it is sufficient to schedule the supply such that the average daily requirement is met. However, in water sufficient situations, it is important not to overfill the tanks in order to conserve water. Hence, a common control strategy has to be devised which can address both these situations. The withdrawal rate from a tank is typically unknown. In the present work, it is assumed to be limited by either the amount of water in the tank or the actual demand rate, whichever is lower.

$$Q'_{\text{out}_i}(k) = \min\left(d_i^{sp}(k), \frac{H_t(k)\times A_t}{\Delta t} + Q'_{\text{in}_i}(k)\right), \quad i = 1, ..., N_d \tag{7}$$

where $d_i^{sp}(k)$ and $Q'_{\text{out}_i}(k)$ are demand set-point and the amount of water withdrawn from the tank, respectively. $Q'_{\text{in}_i}(k)$ is the flow rate into the tank and is equal to the outflow rate from the demand node to which it is linked. At any instant k, the assumed demand set profile may not match the consumers' actual consumption of water from the tanks and the cumulative deviation, $\Delta d_i(k)$ can be calculated as:

$$\Delta d_i(k) = \Delta d_i(k-1) + Q'_{\text{in}_i}(k) - (H_i(k) - H_i(k-1))A_t/\Delta_t - d_i^{sp}(k) \tag{8}$$

The second term in Eq. 8 is the actual withdrawal rate of water inferred from the liquid levels in the tank at the beginning and end of a time period. The control objective chosen in the present work is to minimize the sum square of cumulative deviations. This will try to ensure that the amount of water supplied closely matches the required amount of water over the horizon of interest. In addition, to prevent wastage of water when it is available in excess, water level in storage tank at the end of horizon is also simultaneously minimized. Hence, the control objective chosen is to minimize a weighted sum of the two terms.

3.2. MPC Formulation

MPC is an advanced control scheme that uses a model of the system to be controlled to predict its behaviour over a finite time horizon in the future (Maciejowski, 2002). The process in the basic scheme of MPC shown in figure 1, is a simulator that uses the pressure

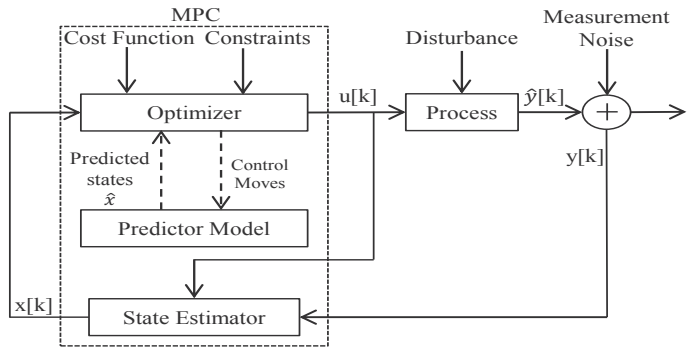

Figure 1. Basic MPC scheme

driven model to simulate the working of WDN. State estimator developed by Kumar et al. (2008) is used to estimate the current states (flow rate, pressure and outflow rate) from the corrupted measurements. The predictor model (also called extended period simulator) requires an explicit model for predicting the process output for N_p (prediction horizon) time steps ahead given N_c (control horizon) future control moves. The optimizer determines the optimal future control moves which minimizes the cost function while taking into account the constraints. Control moves for the current time period is implemented and the procedure is repeated for the next time period, based on the new set of measurements.

$$\min_{u_k,\ldots,u_{k+N_p-1}} \quad J = \sum_{i=1}^{N_d}\sum_{j=1}^{N_p} H_{t_i}^2(k+j) + \Delta d_i^2(k+j) \tag{9}$$

$$0 < u_k < 1 \tag{10}$$

$$p_j \geq p_{\min}, \quad j \in \text{demand nodes} \tag{11}$$

where u_k is the fractional control valve position at k^{th} instant, N_p is the prediction horizon, N_d is the total number of demand nodes in the network, p_j is the pressure at node j and $p_{\min}$ is the minimum pressure to be maintained.

4. Demonstration

The use of MPC strategy for online control of WDNs is tested on a sample network shown in figure 2. Elevation of all nodes is taken as zero and the source pressure is considered as 30 m of water and a minimum gauge pressure requirement of 2 m of water is imposed at the demand nodes. Cross sectional area of the storage tanks at nodes 5 and 11 are assumed to be 6 m^2 and 8 m^2 respectively, and maximum height of these tanks are taken to be 3 m. Initial water level in both tanks is assumed to be 0.1 m. The two control valves have a

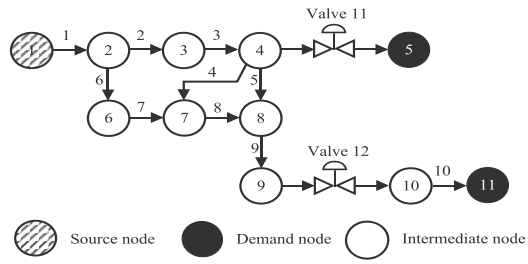

Figure 2. Schematic of the WDN used in the demonstration of MPC strategy

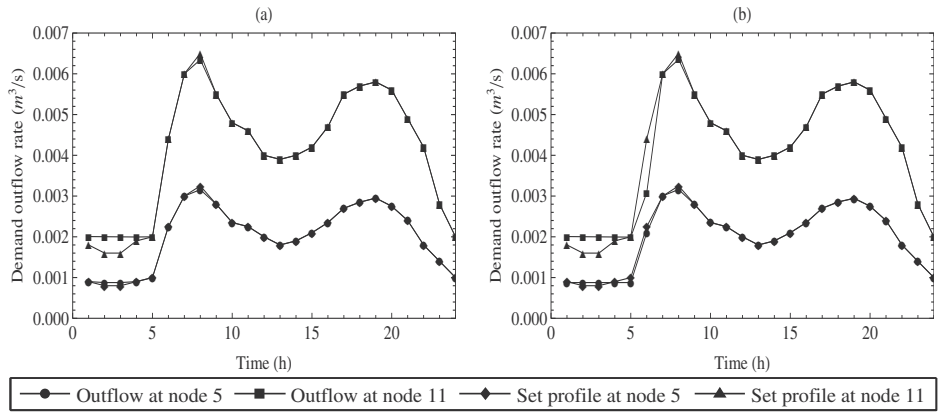

Figure 3. (a) Demand outflow profile without storage tank and (b) with storage tank

rangeability of 50 and the valve coefficient, C_v, of the valves 11 and 12 are 50 and 100 respectively. Pressure at nodes 1, 4 and 8, flow rate in pipe 1 and water level in the two tanks are measured on an hourly basis. The case when there is sufficient water to meet the need of customers is studied. MPC is applied with $N_p = 1$ and $N_c = 1$. The outflow rates at the two demand points obtained with the objective function used by Kumar (2008) without taking into account the storage tanks available at these points, are shown in 3(a). It is observed that the outflow rate matches the demand rate for most time periods, except the oversupply in the first few periods (to satisfy the pressure constraint at demand nodes). The total outflow during the 24 h period exceeds the requirement at demand node 11 by 0.97%. On the other hand, if storage facilities at the demand points and the control objective given by Eq. 9 are considered, then the solution obtained is shown in 3(b). It is observed that the initial oversupply is compensated by undersupply during the periods 5 to 8, such that the integral amount of water supplied during the 24 h period matches with the requirement. Both the tanks were empty at the end of 24 h period. In water deficient case, MPC scheme allocates water so as to meet the requirement over the 24 h period with minimal percentage undersupply. However, the results are not reported here in the interest of space.

5. Conclusions

In this work, MPC scheme was used for generating control strategies that operate WDNs with buffer tanks at demand nodes, to meet the performance goals. Sustainable operation of WDNs using a MPC control scheme was demonstrated with a sample WDN, resulting in water savings.

References

Bhave, P. R., Gupta, R., 2009. Analysis of Water Distribution Network. Narosa Publishing House.

Kumar, S. M., 2008. Monitoring and Control of Water Distribution Networks. Ph.D. thesis, Indian Institute of Technology Madras.

Kumar, S. M., Narasimhan, S., Bhallamudi, S. M., 2008. State Estimation in Water Distribution Networks Using Graph-Theoretic Reduction Strategy. Journal of Water Resources Planning and Management 134 (5).

Maciejowski, J. M., 2002. Predictive control: with constraints. Pearson Education. Prentice Hall.

I.A. Karimi and Rajagopalan Srinivasan (Editors), Proceedings of the 11th International Symposium on Process Systems Engineering, 15-19 July 2012, Singapore.

Multi-fidelity models for model predictive control

Shiva Kameswaran,[a] Niranjan Subrahmanya,[a]

[a]*ExxonMobil Research and Engineering, 1545 US22E, Annandale, 08807, USA*

Abstract

Model predictive control (MPC) is based on repeated solution of finite horizon dynamic optimization problems, where only the control decisions close to the start of the time horizon are of interest. This observation suggests the potential use of multi-fidelity models with models of reduced complexity and fidelity being used for predictions away from the current time instant. We explore this idea through theoretical analysis and simulations. We attempt to quantify the effect of (bounded) error in computing future states and controls on current control actions. The assumption of bounded error covers a number of potential approaches based on model and solution approximation techniques. One of these approaches, using reduced order models, is illustrated using a simulated process. We provide comparisons with conventional MPC in terms of the overall quality of the control as well as the computational complexity and demonstrate that MPC based on multi-fidelity models performs better than MPC based only on reduced order models.

Keywords: multi-fidelity models, model reduction, model predictive control

1. Introduction

Recent advances in computing have enabled use of high-fidelity dynamic models in technologies like model predictive control (MPC) and real-time optimization. The challenges in implementing these technologies for real-world processes are (a) computational cost associated with calculating optimal set points and controls (b) ensuring that controls are robust and execution prompt, and (c) explaining non-intuitive control actions to engineers. Such technologies employ optimization to make decisions over a prediction horizon. The prediction window is important for proactive decision-making based on understanding of the system's capabilities and stability considerations.

MPC is based on repeated solution of finite-time optimal control problems, where only the control decisions close to the start of the time horizon are of interest. This observation opens the door for approximation strategies such as ADP [4] and model reduction that attempt to capture the effects of states and controls that are farther along the prediction horizon on objective function, constraints, dynamics and stability. We explore the possibility of reducing model complexity as we move away from the start of the prediction horizon. This reduces the computational burden of carrying model detail well into the prediction horizon. This reduced complexity would improve computational robustness and allow frequent economically responsive optimization moves. In addition it becomes easier to navigate the reduced models to provide clearer interpretations of the control moves. Using such reduced order models (ROMs) farther in the prediction horizon can also facilitate computation of "cost-to-go" surrogates in methods that use reinforcement learning in MPC. While a great deal of the computational load in conventional linear MPC can be reduced through offline calculations (parametric programming), such methodologies only work for small-scale linear systems. There is also a vast body of literature on using ROMs in the context of MPC. Refer to [2] and the references therein for information on using a single ROM for MPC.

2. Analysis of the effect of using multi-fidelity models in optimal control

We begin our analysis by considering an unconstrained optimal control problem of the form shown below. Here *z(t)* are the states, *u(t)* are the controls. The objective is to minimize a scalar function of the states at the end of the time period $t \in [t_0, t_f]$. We assume that all the functions involved are sufficiently smooth and we continue to use the assumptions in [3].

$$\min_{z(t),u(t)} \varphi\left(z(t_f)\right) \tag{1a}$$

$$\frac{d}{dt}z(t) = f(z(t), u(t)); z(t_0) = z_0 \tag{1b}$$

The direct simultaneous approach [3] using Radau collocation and a uniform temporal mesh size h is used to solve the optimal control problem. We use the analytical setting in [3] to show that bounded perturbations to the rhs of the differential equation over $t \in [\tau, t_f]; t_0 < \tau$ result in bounded control moves. These perturbations to the rhs are assumed to be due to model reduction errors. While the errors due to model reduction can be well characterized [1] and have a definite structure, our analysis assumes this error to be bounded. The structure of the error is key for precise understanding of its impact on the controls and will be the subject of future research.

Let the KKT conditions for the discretized problem be written as $\emptyset(w) = -he$, where e is the error in the rhs of the state equation, and w collectively represents discretized states, controls and Lagrange multipliers. Refer to [3] for a detailed description of the structure and the components of $\emptyset$. The vector e has nonzero entries only for state collocation equations over temporal regions where a ROM is used ($t \in [\tau, t_f]; t_0 < \tau$). This nonzero sub-vector of e will be referred to as e_{state}. The true solution to (1), when discretized using same temporal mesh as in the simultaneous approach, results in an error residual r that satisfies $\emptyset(w^*) = r$. Using the mean value theorem,

$$\emptyset(w^*) - \emptyset(w) = J(w^* - w) = r + he \tag{2}$$

$$(w^* - w) = (\tilde{w} - w) + (w^* - \tilde{w}) = J^{-1}r + hJ^{-1}e \tag{3}$$

where $J = \int_0^1 \emptyset'(\delta w^* + (1-\delta)w)d\delta$ has the same symbolic form and structure as the KKT matrix of the discretized NLP, and $\tilde{w}$ satisfies $\emptyset(\tilde{w}) = 0$. In [3] it was shown that $\|w^* - \tilde{w}\|_\infty \sim \|J^{-1}r\|_\infty = O(h^K)$, where K is the number of collocation points. Consequently $\Delta w = (\tilde{w} - w)$ inherits the order property of $hJ^{-1}e$. It is important to note that the size of the vectors and matrices in (2) increase with *1/h*.

The similarity of J to the KKT matrix allows us to perform a range-and-null-space decomposition [3]. The constraint Jacobian matrix $\hat{A}$ is of the form $(\hat{C} \quad N)$ where N represents the derivatives wrt to the discretized controls and $\hat{C}$ includes derivatives wrt to the discretized states. Let Y and Z be a pair of range and null space matrices for $\hat{A}$ defined as $Y^T = (I\ 0)$ and $Z^T = (-N^T\hat{C}^{-T}\ \ I)$. It follows from [3] that error in the control variables (part of Δw corresponding to discretized controls) arising from errors in the rhs of the state differential equations is given by:

$$\Delta w_{cont} = -h(Z^T HZ)^{-1}Z^T HY\hat{C}^{-1}\begin{pmatrix} 0 \\ e_{state} \end{pmatrix} \tag{4}$$

The term $\hat{C}^{-1}h\begin{pmatrix} 0 \\ e_{state} \end{pmatrix}$ has the effect of integrating the error in the state equations forward in time. The effect of this error accumulation on the state related parts of the

objective function are partly represented by $HY\hat{C}^{-1}\begin{pmatrix}0\\ e_{state}\end{pmatrix}$. Z^T serves the role of a backward integrator where the consequence (objective fn) of all the accumulated error is communicated to the controls at various point in time. It has been shown in [3] that:

$$\|Z^T\|_\infty = O(1);\ \|Y\|_\infty = O(1);\ \|H\|_\infty = O(h);\ \|C^{-1}\|_\infty = O\left(\frac{1}{h}\right)$$

As in [3] we assume that $\|(Z^THZ)^{-1}\|_\infty = O\left(\frac{1}{h}\right)$. Given that e_{state} is *O(1)*, it follows from the above matrix norms and (4) that $\|\Delta w_{cont}\|_\infty = O(1)$. This result implies that if there is a bounded error that is added to the rhs of (1b) and the resulting problem is solved using the direct simultaneous approach then the norm of the difference between the optimal controls for the problems with and without the error term is bounded. We have not exploited the special structure of the error vector. The effect of several types of approximations can be examined using this framework and they include: model reduction error, inexact solution of state equations, and coarser / varying discretization error. All these three types of approximations can be applied as we move away from the start of the prediction horizon. The next section presents results based on an approximation that uses a ROM beyond a transition point in the prediction horizon.

3. Example

In this section, we consider a 10th order plant given by, $\dot{x} = A_p x + B_p u$

$$A_p = \begin{bmatrix}
-0.21 & 0.08 & 0.04 & -0.05 & -0.07 & -0.17 & -0.12 & 0.06 & -0.00 & -0.06\\
0.09 & -0.09 & -0.03 & 0.04 & -0.03 & 0.06 & 0.02 & 0.01 & 0.06 & 0.07\\
-0.14 & 0.04 & -0.22 & 0.02 & -0.02 & 0.01 & -0.14 & 0.03 & -0.04 & -0.02\\
0.14 & -0.04 & 0.07 & -0.25 & 0.02 & 0.01 & 0.07 & 0.02 & 0.07 & -0.00\\
0.01 & -0.07 & 0.05 & -0.03 & -0.13 & -0.05 & -0.00 & 0.04 & 0.02 & -0.01\\
0.07 & -0.04 & 0.17 & -0.09 & -0.03 & -0.22 & 0.08 & 0.10 & 0.04 & -0.02\\
-0.07 & -0.00 & 0.04 & -0.12 & -0.07 & -0.12 & -0.23 & 0.08 & -0.02 & -0.05\\
-0.05 & 0.06 & -0.04 & 0.06 & 0.03 & 0.10 & -0.01 & -0.06 & -0.03 & -0.02\\
-0.03 & 0.07 & 0.01 & 0.00 & -0.02 & -0.05 & -0.06 & 0.01 & -0.13 & -0.02\\
0.02 & 0.03 & 0.06 & -0.06 & -0.02 & -0.05 & 0.01 & -0.00 & 0.01 & -0.15
\end{bmatrix}$$

$$B_p = \begin{bmatrix}
-0.03 & 0.02 & 0.24 & 0.00 & -0.46 & 0.15 & 0.56 & -0.52 & -0.23 & 0.27\\
0.01 & -0.14 & 0.44 & -0.15 & 0.49 & -0.52 & -0.11 & -0.40 & 0.09 & 0.29\\
-0.55 & -0.15 & -0.38 & -0.09 & 0.08 & 0.24 & -0.03 & -0.06 & 0.39 & 0.55
\end{bmatrix}^T$$

The plant has 6 stable real poles, 2 stable complex poles and 2 unstable poles. We consider the problem of stabilizing all the states of the plant. The inputs are constrainted to lie within the interval [-1.5 1.5]. We consider 3 schemes for comparison.

1. MPC with the full model over the entire prediction horizon (Full model)
2. MPC with a reduced model over the entire prediction horizon (Reduced model)
3. MPC with the full model at the beginning and a ROM beyond a preset transition point (Multi-fidelity model)

For the sake of simplicity proper orthogonal decomposition [1] is used for model reduction. We vary the number of states in the ROM and report the tradeoff in terms of control accuracy and computational complexity. For multi-fidelity MPC, we also vary the fraction of the prediction horizon at which the transition to a reduced model is made (t_r). Control accuracy is measured using the frobenius norm of the difference between control and state values obtained using approximate techniques (reduced and multi-fidelity) to that obtained using the full model. The reported accuracies are normalized using the frobenius norm of the solutions from the full model and are denoted by NE_u (for normalized control error) and NE_x (for normalized state error). We consider only the initial part of the prediction horizon for computing the accuracies as this is the time-

frame that is of interest for implementation in a moving horizon implementation. In this example, we consider a prediction horizon of 15 minutes and assume that the interval between successive optimization runs is 15seconds. Therefore, the errors are measured during this 15 second interval only. The computational complexity is reported in terms of the number of optimization variables, which is used as a proxy for the true computational cost, but should suffice to demonstrate the basic idea. Let n_x be the number of states in the full model, n_r be the number of states in the reduced model, n_i be the number of inputs, N_1 be the number of elements before the transition to reduced model, N_2 be the number of elements after the transition and n_c be the number of collocation points in each element. The number of optimization variables (N_{opt}) may then be calculated as $(N_1+ N_2)* n_c *(n_x + n_i)$ for the full model, $(N_1+ N_2)* n_c *(n_r + n_i)$ for the reduced model and $N_1* n_c *(n_x + n_i) + N_2* n_c *(n_r + n_i)$ for the multi-fidelity model. In the simulations, $N_1+ N_2 = 400$, $n_c = 2$ and $n_i = 3$. The results are summarized in Table 1, Table 2 and Figure 1.For each parameter setting, simulations were run with 10 randomly chosen initial states and averages values of the error were used.

Table 1. Results for MPC based only on ROM

n_r	1	2	3	4	5	6	7	8	9	10
NE_u	0.95	0.79	0.71	0.38	0.35	0.27	0.15	0.15	0.06	0
NE_x	0.26	0.21	0.18	0.09	0.08	0.07	0.04	0.04	0.02	0
N_{opt}	3200	4000	4800	5600	6400	7200	8000	8800	9600	10400

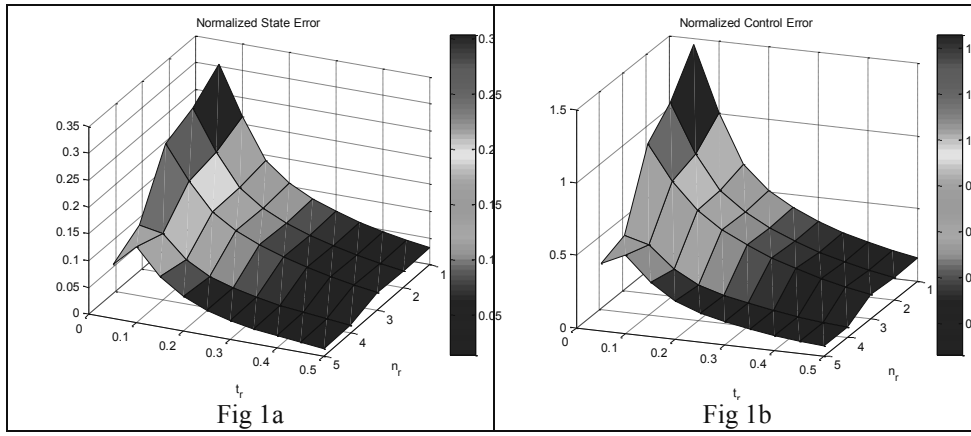

Fig 1a Fig 1b

Figure 1. a) normalized state error versus the number of reduced states and fraction of horizon at which the transition to reduced model is made for multi-fidelity MPC b) The same plot for the normalized control error

Table 2. Selected results for MPC based on multi-fidelity models

n_r	1	1	2	1	1	1	2	4	4	5
t_r	0.10	0.20	0.25	0.35	0.45	0.50	0.50	0.40	0.50	0.50
NE_u	1.01	0.51	0.40	0.28	0.19	0.16	0.16	0.10	0.07	0.07
NE_x	0.22	0.11	0.08	0.06	0.04	0.03	0.03	0.02	0.01	0.01
N_{opt}	3920	4640	5600	5720	6440	6800	7200	7520	8000	8400

Table 2 provides a numerical representation of selected information from Figure 1. Comparing, the results from Table 1 and Table 2, it can be seen that for a given number of variables, or alternatively for a given computational budget, multi-fidelity MPC

outperforms pure reduced order MPC across a broad range. From Figure 1, it can be seen that choosing the right values for the order of the reduced model and the time to transition to the reduced model is important to get the best performance for a given budget. Finally Figure 2 shows a sample of the estimated "optimal" control for the 3 approaches compared in this section. An interesting observation is that the discontinuity in model fidelity significantly distorts the optimal trajectory around the transition region, but it approximates the true optimal trajectory much better at the beginning of the prediction horizon as compared to the reduced order MPC. This confirms the intuition presented in the introduction to this paper. The nature of the control input distortion at the point of transition needs further analysis as this is the main source of error for the multi-fidelity MPC and also the main constraint on moving the transition horizon to an earlier point to further reduce computational complexity.

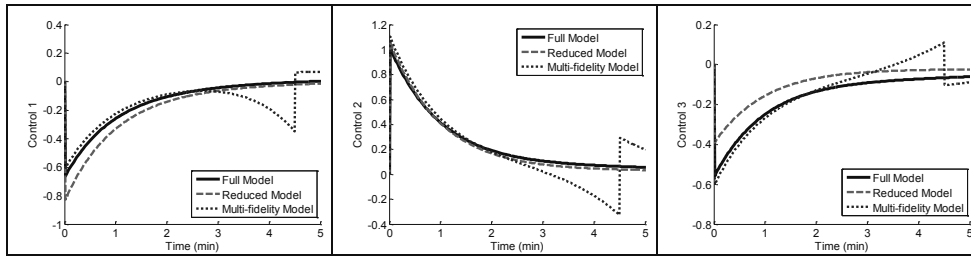

Figure 2. A comparison of "optimal" control trajectories computed by the 3 approaches. The ROM has 5 states (6400 variables). The multi-fidelity model has 3 states and transitions at 4.5 seconds (6480 variables).

4. Conclusion

In this paper we presented the idea of using accurate models near the beginning of a prediction horizon for MPC and then using models of reduced fidelity towards the end of the horizon. Theoretical analysis presented in section 2 indicates that the introduction of bounded error at later points in the control horizon will have a bounded perturbative effect on the computed control input at the beginning. Computational complexity can be traded for model error in multiple ways including using ROMs, inexact solutions and coarse discretizations. Further analysis that considers the exact structure of each of these errors is required to provide tighter bounds and guarantees for control input perturbation and will be the focus of future research. The simulation example presented in section 3 confirms the advantage of using multi-fidelity models over pure ROMs. It also emphasizes the need to use the right parameters to obtain the best approximation for a given computational budget. An interesting observation form the simulations is the fact that the difference between an approximate and optimal control inputs tends to be the highest near the point of transition from the high-fidelity model to the low-fidelity model. A better understanding and characterization of this phenomenon will be the focus of future research as well.

References

[1] C. Homescu, L.R. Petzold and R. Serban, SIAM Review, 49(2), pp. 277-299, 2007
[2] S. Hovland, J.T. Gravdahl, and K.E. Wilcox, AIAA J. Guidance, Control and Dynamics, 31(4), 2008.
[3] S. Kameswaran and L.T. Biegler, Comput. Optim. and Appl., 41(1), pp. 81-126, 2008
[4] J.M. Lee and J.H. Lee, Int. J. Control, Automation & Systems, 2(3), pp. 263-278, 2004

I.A. Karimi and Rajagopalan Srinivasan (Editors), Proceedings of the 11th International Symposium on Process Systems Engineering, 15-19 July 2012, Singapore

A Frequency Domain Approach for MPC Tuning

Leyla Özkan, a * Joris Meijs, b A.C.P.M. Backx, a
a Department of Electrical Engineering; TU Eindhoven; Eindhoven, The Netherlands
b Department of Mechanical Engineering; TU Eindhoven; Eindhoven, The Netherlands

Abstract

This paper presents a frequency domain based approach to tune the penalty weights in the model predictive control (MPC) formulation. The two-step tuning method involves the design of a favourite controller taking into account the model-plant mismatch followed by the controller matching. We implement this approach on a SISO example.

Keywords: model predictive control, tuning, robust performance, inverse optimality

1. Introduction and Preliminaries

MPC is an advanced control methodology that has been widely adopted in industry as an effective tool to drive and maintain a plant at a specified operating condition. The performance of MPC highly depends on the model accuracy and the tuning of the system. The tuning problem in MPC is the selection of weighting matrices in such a way that the resulting closed loop behaviour is a good trade-off between the performance and the robustness given the specific characteristics of the process and the model's accuracy.

There have been several attempts to achieve a systematic tuning guideline for selecting the right set of MPC weighting matrices. In D.J.Chmielewski and A.M.Manthanwar (2004) it was proposed to minimize the variance of the controlled output by making use of both the solution of the minimum variance covariance constrained control and the inverse optimality problem. Lee and Yu (1993) proposed tuning for nominal performance first and hereafter to robustify the system by evaluation of the sensitivity and complementary sensitivity function. In Rowe and J.Maciejowski (2000) it was shown that for a process in which the model uncertainty is due to normalized coprime factor perturbations, $\mathscr{H}_\infty$ loop shaping can be utilized to determine the weighting matrices of the MPC.

This paper is organized as follow. First, we introduce preliminary information below. In Section 2, the frequency domain interpretation of MPC is presented. Section 3 explains the proposed MPC tuning method and presents the illustration on a SISO system with uncertainty description. In Section 4 conclusions are given.

We assume the system is represented by the difference equations

$$x(k+1) = Ax(k) + B_1 w_p(k) + B_2 u(k) \tag{1a}$$
$$z(k) = C_1 x(k) + D_{12} u(k) \tag{1b}$$

where (A, B_2) is controllable and (A, C_1) is detectable. $x \in \mathbb{R}^n, u \in \mathbb{R}^m, w_p \in \mathbb{R}^n$ are states, inputs and unmeasured disturbances modeled as a Gaussian white noise of unit intensity respectively. We also assume that disturbance energy distribution has low pass characteristics.

$$E\left[w_p(k)\right] = 0, \qquad E\left[w_p(k+\tau)\, w_p^T(k)\right] = I\delta(\tau)$$

*l.ozkan@tue.nl

where $\delta(\tau)$ represents the Dirac function. The outputs z is constructed from the weighted input signal $z = \begin{bmatrix} \tilde{u} \\ z_p \end{bmatrix}$. The variance of z_p due to w_p is expressed as

$$\begin{aligned} \sigma^2(z_p(k)) &= E\left[z_p^2(k)\right] - (E[z_p(k)])^2 = E\left[z_p^2(k)\right] \\ &= \frac{1}{2\pi}\int_{-\pi}^{\pi} \text{Trace}\left[T_{z_p w_p}\left(e^{j\omega_n}\right) T_{z_p w_p}^*\left(e^{j\omega_n}\right)\right] d\omega_n = \|T_{z_p w_p}\|_2^2 \quad \text{(Parseval)} \end{aligned}$$

where $T_{z_p w_p}$ defines the transfer function from w_p to z_p and $\omega_n = 2\pi\omega T_s$ is the normalized frequency. We consider an MPC controller solving the finite horizon control problem

$$\mathscr{V}(x(k)) = \min_{\mathscr{U}(k)} \sum_{i=0}^{N-1} x(i|k)^T Q x(i|k) + u(i|k)^T R u(i|k) + x(N|k)^T X x(N|k) \tag{2a}$$

$$s.t.$$

$$x(i+1|k) = Ax(i|k) + B_2 u(i|k), \qquad i \geq 0 \tag{2b}$$

$$Hx(i+1|k) \leq h, \quad Du(i|k) \leq d \qquad i = 0, \ldots N-1 \tag{2c}$$

$$u(i|k) = Kx(i|k), \qquad i \geq N \tag{2d}$$

$$x(0|k) = x(k) \tag{2e}$$

where $\mathscr{V}(x(k))$ is the cost function, $\mathscr{U}(k) = [u(0|k) \ldots u(N-1|k)]^T \in \mathbb{R}^{Nm}$ is the vector to be optimized. The matrices $Q \in \mathbb{R}^{n \times n}$ and $R \in \mathbb{R}^{m \times m}$ satisfy the conditions $Q = Q^T \geq 0$, $R = R^T > 0$ and represent the state and input weight respectively. The integer N denotes the MPC horizon and $X \in \mathbb{R}^{n_x \times n_x}$ is the terminal weight. Equation (2c) defines the state and input constraints. The auxiliary controller, equation (2d), is chosen as the solution of the infinite horizon LQR problem with weights Q and R and X is the corresponding solution of the discrete algebraic Riccati equation

$$K = -\left(R + B_2^T X B_2\right)^{-1} B_2^T X A \tag{3a}$$

$$X = Q + K^T R K + (A + B_2 K)^T X (A + B_2 K) \tag{3b}$$

With this choice of K and X, the MPC controller corresponds to the constrained linear quadratic regulator introduced in Scokaert and Rawlings (1998). Assuming that the process operates away from its constraint boundary, the MPC control law equals to $u(k) = Kx(k)$.

2. Frequency Domain Interpretation of MPC Tuning

In this section, we discuss the frequency domain analysis of MPC controllers as we change the weighting matrices Q and R in the objective function. The result of this analysis in the case of plant-model mismatch is the main motivation for the proposed tuning method. For this analysis, we interpret the cost function in (2) as a measure of the output energy of the process under control (Zhou et al. (1996)). We, therefore, choose the weights Q and R as $C_1^T C_1$, $R = D_{12}^T D_{12}$ respectively where we assume that the model of the process under control is constructed such that $C_1^T D_{12} = 0$ and $D_{12}^T D_{12} = \rho I$. The

squared output energy of the process under control due to w_p is then expressed as

$$\begin{aligned}\|z(k)\|_2^2 &= \sum_{k=0}^{\infty} x(k)^T C_1^T C_1 x(k) + u(k)^T D_{12}^T D_{12} u(k) = \|z_p(k)\|_2^2 + \rho\|u(k)\|_2^2 \\ &= \frac{1}{2\pi}\int_{-\pi}^{\pi}\left(\mathrm{tr}\left[T_{z_p w_p}^*\left(e^{j\omega_n}\right) T_{z_p w_p}\left(e^{j\omega_n}\right)\right] + \rho\,\mathrm{tr}\left[T_{uw_p}^*\left(e^{j\omega_n}\right) T_{uw_p}\left(e^{j\omega_n}\right)\right]\right) d\omega_n \\ &= \|T_{z_p w_p}\left(e^{j\omega_n}\right)\|_2^2 + \rho\|T_{uw_p}\left(e^{j\omega_n}\right)\|_2^2\end{aligned}$$

By the choice of ρ, the trade-off between performance and the robustness in the frequency domain can be demonstrated. For example, for high values of ρ, the bandwidth of the closed loop system is zero and no control is applied. Incrementally decreasing ρ, the bandwidth for which the disturbance is rejected increases, hence the output variance decreases. In case of plant-model mismatch, the decrease in the output variance is achieved up to a certain bandwidth. Decreasing ρ further will result in an increase in the output variance due to model-plant mismatch becoming significant at this bandwidth. In figure 1(a) this observation is demonstrated using an SISO example with a plant-model mismatch.

3. MPC Tuning Method

The proposed tuning method involves two steps. First, a favourite controller is designed using $\mathscr{H}_\infty$ controller synthesis. Then, a solution to the problem of inverse optimality is used to determine the MPC weighting matrices Q and R.

3.1. The favourite controller

The general control configuration used for the synthesis of the favourite controller is shown in figure 1(b). The model P, is constructed from the blocks G_n, W_u and W_p representing a nominal description of the process under control, a bi-proper weight function describing the uncertainty of the nominal model and a bi-proper performance weight function respectively. The state vectors of the three individual blocks are assumed to be available for control and are stacked as the vector x. P can be described by the difference equations (1) and is used as the internal model of the MPC. The block $\triangle$ and K_{fv} represent the norm bounded perturbation matrix and the favourite controller respectively. K_{fv} satisfies the robust performance theorem 3.1.

Theorem: Assume that the plant is internally stable and is constructed by the inclusion of K_{fv} in the generalized plant P, then

$$\text{Robust Performance} \quad \leftrightarrow \quad \|W_p T_{\triangle z_p w_p}\|_\infty < 1, \qquad \forall\|\triangle\|_\infty \le 1$$

where $T_{\triangle z_p, w_p}$ represents the set of perturbed transfer function from w_p to z_p. Having found a K_{fv} that satisfies the theorem above, it follows that $\bar{\sigma}\left(T_{\triangle z_p, w_p}\right) < \bar{\sigma}\left(W_p^{-1}\right), \forall\omega_n$ (Skogestad and Postlethwaite (2005)). To synthesize K_{fv}, the following procedure is proposed. W_p is parameterized as

$$W_p^{-1}\left(e^{j\omega_n}\right) = \alpha\|T_{z_p w_p}(1)\|_\infty W_{hp}\left(e^{j\omega_n}\right) \tag{5}$$

where $W_{hp}\left(e^{j\omega_n}\right)$ is a first order stable high-pass filter characterized by $W_{hp}(1) = \beta$, $|W_{hp}\left(e^{j\omega_k}\right)| = 1$ and $W_{hp}(e^{j\pi}) = 1$. The controller designer first has to determine the amount of disturbance rejection by a combination of the parameters α and β. ω_κ has to

be determined such that disturbance rejection is only required for the frequencies where model uncertainty is insignificant. Subsequently, an iterative scheme is proposed to maximize the attained robust performance.

- Construct the model P, define A, B_1, B_2, C_1 and D_{12} and check the condition for the favourite controller to exists; find $Y = Y^T > 0$ and M that satisfy

$$\begin{pmatrix} -Y & AY + B_2M & B_1 & 0 \\ YA^T + M^TB_2 & -Y & 0 & YC_1^T + M^TD_{12}^T \\ B_1^T & 0 & -I & 0 \\ 0 & C_1Y + D_{12}M & 0 & -I \end{pmatrix} < 0 \tag{6}$$

- If a feasible Y and M are found, $K_{fv} = MY^{-1}, \omega_\kappa = \omega_\kappa + \varepsilon$. Else quit iterations.

The LMI condition (6) can be found in Gahinet and Apkarian (1993) and ε is user defined.

3.2. Inverse Optimality

In this section, we consider how to determine the weights Q, R and N in the MPC cost function such that K_{fv}, is optimal. A control law for which such Q, R and N can be found is called inverse optimal. The following theorem states the condition for inverse optimality.

Theorem: If there exists a matrix $X = X^T \geq 0$ and a matrix $R = R^T > 0$ that satisfy the constraints,

$$\left(A + B_2K_{fv}\right)^{-1} X \left(A + B_2K_{fv}\right) + K_{fv}^T R K_{fv} - X \leq 0 \tag{7a}$$

$$\left(R + B_2^T X B_2\right)^{-1} K_{fv} = -B_2^T XA \tag{7b}$$

then the control law $u(k) = K_{fv}x(k)$ is inverse optimal with respect to the cost function that is minimized by the MPC defined in section 1. The inverse optimal weights X and R can be found by the LMI problem (7) and Q can be found by (3b). The proof results from algebraic manipulations of (3).

Example: Consider the task of designing an MPC with the purpose to minimize the variance of the temperature in a swimming pool, z_p due to the unmeasured disturbance w_p. The nominal model G_n is described by the difference equations

$$G_n\left(e^{j\omega_n}\right) \begin{cases} x_n(k+1) &= 0.7788x_n(k) + w_p(k) + 0.04424\left(\triangle_{out}(k) + u(k)\right) \\ z_p(k) &= x_n(k) \end{cases}$$

and the uncertainty weight, W_u is described by

$$W_u\left(e^{j\omega_n}\right) \begin{cases} x_u(k+1) &= 0.5626x_u(k) + 0.5u(k) \\ z_u(k) &= -0.8878x_u(k) + 1.016u(k) \end{cases}$$

The parameters α, β and ω_κ to design the performance weight function are chosen as $\alpha = 1.3, \beta = 0.48$ and $\omega_\kappa = 0.5 rad/sec$.. K_{fv} resulting from the proposed iterative scheme with $\varepsilon = 0.01 rad/sec$ equals $K_{fv} = [-0.9233 \quad -1.0655 \quad -5.9393]$.

For this K_{fv} we find a feasible solution X and R from the LMI constraints expressed in theorem 3.2 and they are equal to $R = 2.7048 \cdot 10^{-4}$,

$$X = \begin{bmatrix} 1.4359 & -0.0589 & 0.4672 \\ -0.0589 & 0.1320 & 0.3654 \\ 0.4672 & 0.3654 & 3.4608 \end{bmatrix} \quad Q = \begin{bmatrix} 0.5763 & -0.0046 & 0.2222 \\ -0.0046 & 0.1282 & 0.3763 \\ 0.2222 & 0.3763 & 1.3325 \end{bmatrix}$$

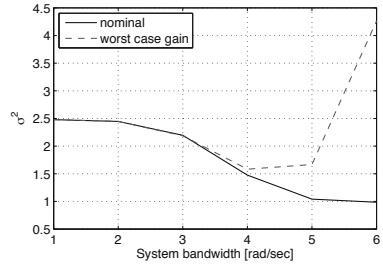

(a) The variance of the nominal and worst case gain transfer

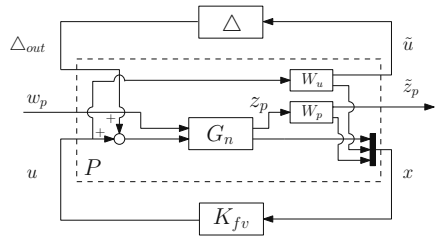

(b) The control configuration for MPC design

The variance of z_p when controlled by the MPC equals $\sigma^2(z_p) = 2.2$ obtained by a nominal simulation and $\sigma^2(z_p) = 2.25$ when simulated with worst case gain transfer from the set $T_{\triangle z_p w_p}$. The minor discrepancy between the two, 2.2 and 2.25, emphasizes the excellent robustness properties of the proposed method.

4. Conclusion

A frequency domain approach is presented to determine the set of weighting matrices Q and R in MPC formulation. An $\mathscr{H}_\infty$ control problem was constructed from the nominal model, a description of the model uncertainty and a performance weighting function. Subsequently, an iterative scheme was introduced to maximize the frequency region over which the desired rejection is achieved robustly. The static state feedback control law resulting from the scheme is denoted as the K_{fv}. An inverse optimality problem is formulated as an LMI to calculate the corresponding weighting matrices Q and R. A simple SISO example is used to demonstrate the tuning method which can be easily extended to a control problem of industrial relevance.

References

D.J.Chmielewski, A.M.Manthanwar, 2004. On the tuning of predictive controllers: Inverse optimality and the minimum variance covariance constrained control problem. Ind. Eng. Chem. Res. 43, 7807–7814.

Gahinet, P., Apkarian, P., 1993. An lmi-based parametrization of all $\mathscr{H}_\infty$ controllers with applications. Proceedings of the 32nd Conference on Decision and Control, 656 – 661.

Lee, J. H., Yu, Z. H., 1993. Tuning of model predictive controllers for robust performance. Computers and Chem. Eng. 18 (1), 15–37.

Rowe, C., J.Maciejowski, 2000. Tuning mpc using h_∞ loop shaping. Proceedings of the American Control Conference.

Scokaert, P. O. M., Rawlings, J. B., 1998. Constrained linear quadratic regulation. IEEE transactions on automatic control 34 (8), 1163–1169.

Skogestad, S., Postlethwaite, I., 2005. Multivariable Feedback Control Analysis and Design. John Wiley & Sons, Ltd.

Zhou, K., Doyle, J. . C., Glover, K., 1996. Robust and optimal control. Prentice Hall, Inc.

I.A. Karimi and Rajagopalan Srinivasan (Editors), Proceedings of the 11th International Symposium on Process Systems Engineering, 15-19 July 2012, Singapore.

Control Strategy for Thermal Budget and Temperature Uniformity in Spike Rapid Thermal Processing Systems

Jyh-Cheng Jeng,* Wen-Chung Chen

Department of Chemical Engineering and Biotechnology, National Taipei University of Technology, Taipei 106, Taiwan

Abstract

Temperature control in the rapid thermal processing (RTP) system with spike-shaped temperature profile is a challenging task, and targeting perfect servo control is almost unachievable because of the high temperature ramp-up/down rate and significant nonlinearity of the process. This study presents a novel method of control system design to provide a precise thermal budget in the spike RTP system. A nonlinear control strategy is proposed based on modeling the RTP system as a nonlinear Wiener model. Further, multivariable control is considered to maintain the temperature uniformity within wafer. Simulation results demonstrate the effectiveness of the proposed control strategy, and provide guidelines for the design of the multivariable control configuration to achieve better wafer temperature uniformity.

Keywords: Rapid thermal processing; Thermal budget control; Nonlinear control; Wiener model; Multivariable control.

1. Introduction

Single wafer rapid thermal processing (RTP) has become one of the key technologies in semiconductor manufacturing due to its faster wafer processing with precise control of the thermal budget. The thermal budget is an important process issue derived from the duration and maximum of wafer temperature beyond a specific reference value, as shown in Fig. 1. As the dimension (line width) keeps shrinking, the demand of shallow junctions requires very tiny and precisely applied thermal energy. The spike RTP system is the way to maintain scaling requirements. As a result, a triangular-shaped set-point profile for wafer temperature is usually applied for thermal budget control.

Various control designs for RTP to follow the desired temperature trajectory have been proposed in the literature. However, achieving desired thermal budget by designing a tightened servo control system is difficult and complex in spike RTP system due to high set-point ramp-up/down rate. As an alternative, our previous work (Jeng and Lee, 2011) considered targeting the control performance on the indices for thermal budget, instead of set-point tracking. In this way, the thermal budget can be precisely controlled and the controller design is much simpler. Nevertheless, the previous work used a simple first-order model to represent the RTP system. In fact, the real RTP system is more accurately modeled as a nonlinear model. To solve this problem, this study uses a nonlinear Wiener model to represent the RTP system, and proposes a nonlinear control strategy based on extensions of the previous design method. In practice, the temperature uniformity within wafer during the heating/cooling process is also a very important specification. The RTP equipment has many lamps, and these lamps are usually clustered into several adjusting zones for wafer temperature control. This study

considers the multivariable control system to achieve good temperature uniformity within wafer. Moreover, the effects of allocation of clustered lamps and location of temperature measurements on the temperature uniformity are discussed.

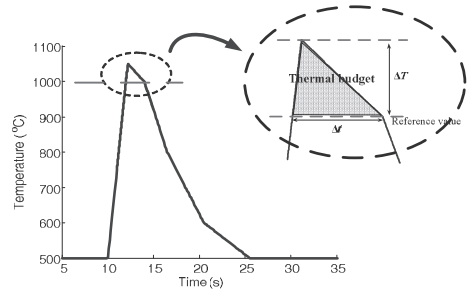

Figure 1. Thermal budget and temperature profile for the spike RTP system.

2. RTP System

A schematic diagram of the RTP system is shown in Fig. 2. In an RTP chamber, power is supplied to several rings of tungsten-halogen lamps, and energy is transferred through a quartz window onto a thin semiconductor wafer via direct or reflective paths. The wafer temperature is controlled by manipulating the lamp power sources.

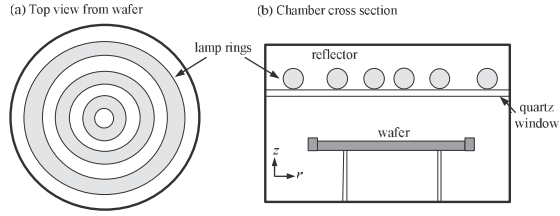

Figure 2. Schematic diagram of a RTP system: (a) top view (b) cross section.

Assume the wafer and the lamp rings are divided into several annual zones, n and m zones, respectively. Additionally, only temperatures in radius (r) direction are of interest by assuming symmetrical temperature distribution. A lumped physical model that describes the relationship between power from the jth lamp zone, P_j, and wafer temperature at the ith zone, T_i, can be formulated as follows: (Huang *et al.*, 2000)

$$\frac{dT_i}{dt} = \frac{-\sigma}{\rho C_p d}\left(\sum_{j=1}^{m}\varphi_{ij}\right)T_i^4 - \frac{h_{ci}}{\rho C_p d}\left(T_i - T_a\right) + \frac{1}{\rho C_p d}\sum_{j=1}^{m}\left(\varphi_{ij}P_j\right), \quad i = 1,\cdots,n \tag{1}$$

where ρ is the density, C_p is the heat capacity, σ is the Stefan-Boltzmann constant, d is the wafer thickness, h_{ci} is the convective heat transfer coefficient, T_a is the temperature of cooling gas, and φ_{ij} is given by

$$\varphi_{ij} = \frac{1}{\left(1-\varepsilon\right)/\varepsilon + \left(1/F_{i,j}\right)} \tag{2}$$

where ε is the emissivity and $F_{i,j}$ is the view factor from the wafer zone i to the lamp zone j. The view factor can be obtained as (Chao *et al.*, 2003)

$$F_{i,j} = \frac{1}{\pi}\int_{r_{L,j-1}}^{r_{L,j}}\int_0^{2\pi}\frac{h^2}{S_{ij}^4}r_L\,d\theta_{ij}\,dr_L \quad \text{with} \quad S_{ij}^2 = h^2 + {r_{w,i}}^2 + {r_L}^2 - 2r_{w,i}r_L\cos\theta_{ij} \tag{3}$$

where h is the distance between wafer and lamp; $r_{w,i}$ and $r_{L,j}$ are the radii of wafer zone i and lamp zone j, respectively. Equation (1) indicates that the RTP system is a nonlinear process in nature due to the radiative heat transfer (the T^4 term), and also a multivariable process. Table 1 gives the physical and system parameters used in this study.

Table 1. Parameters for RTP system

Parameter	Value	Parameter	Value
Wafer density	2330 kg/m^3	Distance between wafer and lamp	5 cm
Wafer thickness	0.0675 cm	Heat capacity (J/kg/K)	641+0.2473T
Emissivity	0.7	Stefan-Boltzmann constant	5.67×10^{-8} W/ m^2/K^4
Wafer radius	15 cm	Convective heat transfer coefficient	8.5 W/m^2/K
Lamp radius	30 cm	Temperature of cooling gas	27 ^{o}C

3. Thermal Budget Control

This study formulates the objective of thermal budget control as targeting the two thermal budget indices: time duration beyond the reference temperature, Δt, and the range between the maximum temperature and the reference value, ΔT, as shown in Fig. 1. Giving the ramp-up and ramp-down rates of set-point profile, k_1 and k_2, respectively, the controller parameters and the maximum of set-point profile are to be designed to meet these two control specifications.

3.1. Linear Model Based Design

Considering the single-input single-output (SISO) case (i.e., n=m=1), Jeng and Lee (2011) presented a design method for thermal budget control based on a first-order linearized RTP model, $K/(\tau s+1)$. The feedback controller used is a proportional-integral (PI) controller. The integral time is tuned by $\tau_I = \tau$. The controller gain K_C and the maximum of set-point profile $T_{\mathrm{sp,max}}$ are then determined to meet the specified thermal budget indices. The results are given as

$$K_C = \frac{\tau}{K}\frac{W\left(bC\exp\left(bA/B\right)/B\right)B - bA}{bB} \tag{4}$$

$$T_{\mathrm{sp,max}} = T_{ref} + \Delta T + k_2\frac{bB}{W\left(bC\exp\left(bA/B\right)/B\right)B - bA}\ln\left(\frac{k_1+k_2}{k_2}\right) \tag{5}$$

where T_{ref} is the reference temperature, $W(\bullet)$ is the Lambert W-function, and

$$\begin{aligned} &A = (k_1+k_2)(1-a);\quad B = \Delta T - k_2 b;\quad C = (k_1+k_2)e^{-a} \\ &a = 1-\left[k_2\ln\left((k_1+k_2)/k_2\right)\right]/k_1;\quad b = \Delta t - (\Delta T/k_1) \end{aligned} \tag{6}$$

3.2. Nonlinear and Multivariable Control Strategy

The heating/cooling process of RTP system is nonlinear, so that it is more accurately modeled as a nonlinear model. This study proposes using a nonlinear Wiener model to represent the RTP system for thermal budget control. In addition, this study considers multivariable control scheme to maintain better temperature uniformity within wafer.

3.2.1. Wiener Modeling for RTP System

The Wiener model, as shown in Fig. 3(a), has a linear dynamic subsystem, **G**, followed by a nonlinear static function, **F**. The input is lamp power, $\mathbf{P} = [P_1 \ \ldots \ P_m]^{\mathrm{T}}$, and the output is m wafer temperature measurements selected from n locations, $\mathbf{T} = [T_{m,1} \ \ldots \ T_{m,m}]^{\mathrm{T}}$. The physical model (1) indicates that the dynamic part of the PTP system is not coupled, and only the static part is interactive. Therefore, **G** is a diagonal matrix with element g_i, i=1,…,m; $\mathbf{F} = [f_1 \ldots f_m]^{\mathrm{T}}$ with $f_i = f_i(v_1, \ldots, v_m)$.

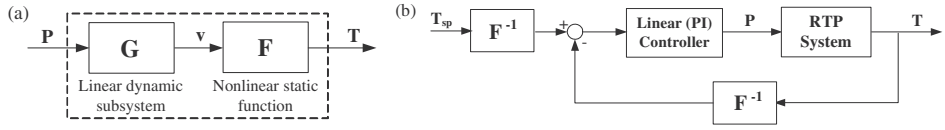

Figure 3. (a) Wiener model. (b) Control structure for RTP system based on Wiener model.

This study proposes a noniterative algorithm for the identification of Wiener model using the input-output data. The intermediate variable v_i, at time k, can be written as

$$v_i(k) = \sum_{l=0}^{L} h_i(l) P_i(k-l) \tag{7}$$

where $h_i(l)$ designates the finite impulse response model of the linear dynamics g_i. On the other hand, $v_i(k)$ can also be written in terms of the inverse function of the static nonlinearity, f_i^{-1}, described by expansion of a set of known basis function B_r as

$$v_i(k) = f_i^{-1}\left(T_{m,1}(k),\cdots,T_{m,m}(k)\right) = \sum_{r=1}^{R} c_{i,r} B_r\left(T_{m,1}(k),\cdots,T_{m,m}(k)\right) \tag{8}$$

where $c_{i,r}$'s are unknown coefficients to be determined. Because the gains of the linear dynamic subsystem and the nonlinear static function are actually not unique, it will be assumed here, without loss of generality, that $c_{i,1} = 1$. Equating the right-hand sides of (7) and (8), the following equation is obtained.

$$B_1\left(T_{m,1}(k),\cdots,T_{m,m}(k)\right) = \sum_{l=0}^{L} h_i(l) P_i(k-l) - \sum_{r=2}^{R} c_{i,r} B_r\left(T_{m,1}(k),\cdots,T_{m,m}(k)\right) \tag{9}$$

Equation (9) allows the estimation of model parameters, $h_i(l)$ and $c_{i,r}$, by the linear regression technique.

3.2.2. Wiener Model Based Design

The identified Wiener model is used to design a simple linearizing control system, as shown in Fig. 3(b), resulting in an equivalent linear control system. Because the linear dynamic subsystem is not coupled, the multivariable control design is now decomposed into m SISO design tasks. Therefore, the linear model-based thermal budget control approach can be directly applied to design the m linear controllers (PI controllers) for the linear dynamic subsystem, g_i, without considering the static nonlinearity.

4. Simulation Results

The process conditions are given as: $k_1 = 200\ ^{o}$C/sec, $k_2 = 50\ ^{o}$C/sec, and $T_{ref} = 1000\ ^{o}$C. The control targets are set as $\Delta t = 2$ sec and $\Delta T = 50\ ^{o}$C. From the linear model based design, controller parameters $\tau_{I,i} = \tau_i$, $K_{C,i} = 2.646\ \tau_i / K_i$, and $T_{\mathrm{sp,max}} = 1080.4\ ^{o}$C are resulted.

4.1. Multivariable Control: 2×2 Scheme

For the 2×2 control scheme, the lamps are clustered into two zones (with outer radius of $r_{L,1}$ and $r_{L,2} = 30$cm) to control the wafer temperature at two locations.

4.1.1. Effect of Allocation of Clustered Lamps

Assume the wafer is divided into 15 annual zones (n=15) with radius $r_{w,i} = i$ cm, and the temperatures at the 2nd and 15th zones ($r_{w,2}$ and $r_{w,15}$) are used for thermal budget control. Three cases for the allocation of clustered lamps are considered: $r_{L,1} = 10$cm, 15cm, and 20cm. Based on a steady operating point $T_{is} = 600\ ^{o}$C, the Wiener model is identified for each case using the simulated input-output data from (1). The control structure shown in Fig. 3(b) is applied for thermal budget control. Table 2 shows the percentage errors of Δt and ΔT ($E_{t,i}$(%) and $E_{T,i}$(%), respectively) resulting from the two controlled temperature profiles. To evaluate the temperature uniformity, the average of the absolute values of the error for all 15 temperatures and the standard deviation of the error for all 15 temperatures are also given in Table 2. The lamp allocation of $r_{L,1}$ = 20cm results in the best uniformity of thermal budget indices. This result can be attributed to more uniformly distributed view factors $F_{i,1}$ and $F_{i,2}$ on the wafer surface because the radius of the inner lamp zone is larger than the wafer radius.

4.1.2. Effect of Location of Temperature Measurement for Control

Using the lamp allocation of $r_{L,1} = 20$cm, various locations of temperature measurement are selected for control. The results are given in Table 3, where the results for SISO control are also given for comparison. The 2×2 control scheme shows improved

uniformity of thermal budget indices compared to SISO control scheme regardless of the locations of temperature measurement. Nevertheless, the specified thermal budget indices can be more accurately achieved when one of the temperature measurements for control is located at the most outer zone of wafer ($r_{w,15}$). The view factors at the most outer zone of wafer $F_{15,1}$ and $F_{15,2}$ are particularly lower and higher, respectively, than those at other zones, so that the dynamics of temperature at the most outer zone is quite different with those at other zones. Therefore, the temperature at the most outer zone must be directly controlled. On the other hand, the location of the other temperature measurement has no significant effect on the control performance.

Table 2. Results for 2×2 control with various allocations of lamps

Allocation	$E_{t,2}$	$E_{T,2}$	$E_{t,15}$	$E_{T,15}$	avg($\|E_{t,i}\|$)	std($E_{t,i}$)	avg($\|E_{T,i}\|$)	std($E_{T,i}$)
$r_{L,1}=10$cm	-2.0	8.99	-2.0	-0.05	8.72	6.66	28.95	19.31
$r_{L,1}=15$cm	-1.5	1.98	-2.0	6.72	3.03	2.36	11.83	8.81
$r_{L,1}=20$cm	-1.0	5.43	-2.0	2.28	1.13	0.32	4.79	0.86

4.2. Multivariable Control: 3×3 *Scheme*

The lamps are clustered into three zones to control the wafer temperature at three locations. According to the results in 2×2 control, the lamps are allocated as $r_{L,1}=20$cm, $r_{L,2}=25$cm, and $r_{L,3}=30$cm, and the locations of temperature measurement are $r_{w,5}$, $r_{w,10}$, and $r_{w,15}$. The results are given in Table 3. The uniformity of thermal budget indices is even better than that of 2×2 control scheme, especially for the ΔT index.

Table 3. Results for SISO, 2×2, and 3×3 control schemes

Location of measurement	avg($\|E_{t,i}\|$)	std($E_{t,i}$)	avg($\|E_{T,i}\|$)	std($E_{T,i}$)
2×2, $r_{w,2}$ and $r_{w,15}$	1.13	0.32	4.79	0.86
2×2, $r_{w,8}$ and $r_{w,15}$	1.23	0.33	4.87	0.81
2×2, $r_{w,5}$ and $r_{w,10}$	4.63	0.35	7.88	0.97
SISO, $r_{w,15}$	2.10	1.11	4.29	2.18
SISO, $r_{w,8}$	1.33	1.30	3.49	2.94
3×3, $r_{w,5}$, $r_{w,10}$, and $r_{w,15}$	0.37	0.30	5.04	0.25

5. Conclusions

This study proposes a nonlinear control strategy for thermal budget in the spike RTP based on Wiener modeling the RTP system. Furthermore, multivariable control is considered to maintain the wafer temperature uniformity. Simulation results have confirmed the effectiveness of the proposed control strategy, and revealed two guidelines for the design of the multivariable control configuration to achieve better wafer temperature uniformity: (1) the radius of the most inner lamp zone must be allocated larger than the wafer radius; (2) the wafer temperature at the most outer zone must be measured for feedback control.

References

C. K. Chao, S. Y. Hung, C. C. Yu, 2003, The Effect of Lamps Radius on Thermal Stresses for Rapid Thermal Processing System, J. Manufacturing Science and Engineering, 125, 504–511.

C. J. Huang, C. C. Yu, S. H. Shen, 2000, Selection of Measurement Locations for the Control of Rapid Thermal Processor, Automatica, 36, 705–715.

J. C. Jeng, B. C. Lee, 2011, Thermal Budget Control for Processes with Spike-Shaped Temperature Profile: Application to Rapid Thermal Annealing, Asian J. Control, DOI: 10.1002/asjc.435.

I.A. Karimi and Rajagopalan Srinivasan (Editors), Proceedings of the 11th International Symposium on Process Systems Engineering, 15-19 July 2012, Singapore.

Systematic Formalization of Control Requirements using Hierarchical Cause-Effect Charts[1]

Stephan Fischer, Christian Sonntag, Sebastian Engell

Process Dynamics and Operations Group, Department of Biochemical and Chemical Engineering, TU Dortmund, 44221 Dortmund, Germany

Abstract

In this paper, a hierarchically structured formalism, the *Hierarchical Cause-Effect Charts* (*HCEC*), is introduced to iteratively refine and formalize complex control requirements of industrial systems, resulting in a hierarchical tree structure of small and transparent cause-effect matrices that can be translated into Boolean formulae algorithmically. These formulae are used as input for a supervisory control synthesis tool chain, resulting in a logic controller that is correct by design. The formalization methodology is supported by a graphical software tool.

Keywords: Supervisory Control Synthesis, Cause-Effect-Matrix, Logic Control

1. Introduction

The safe operation of chemical plants requires large amounts of control logic. *Cause-Effect Matrices (CEM)* and similar formalisms have become very popular in this domain to specify control requirements in an intuitive fashion (e.g. Martinez & Enkerud (2005), Russo & Turk (2007), and Fischer & Lohmann (2009)). In addition, many *CEM* formalisms allow the algorithmic generation of control code. A major drawback of these formalisms is that the matrices become very large (up to thousands of rows and columns) and intransparent in realistic application scenarios. Thus, the validation of *CEM* of industrial-scale systems is a challenging and tedious task. A formalized representation of the specification is required for analysis and validation of the resulting logic by means of formal methods.

In this contribution, we present a hierarchically structured formalism, *Hierarchical Cause-Effect Charts* (*HCEC*), for the iterative refinement and formalization of the requirements of a control system, resulting in a hierarchical tree structure of small and well-arranged cause-effect matrices that can be translated into Boolean formulae algorithmically. These formulae are used as input for a supervisory control synthesis tool chain described in Theunissen et al. (2009), resulting in a logic controller that is correct by design. The formalization methodology is supported by a software tool that is implemented as an extension of the *DC/FT* software (see Fischer et al. (2011)) that supports the refinement of informal specifications into *Sequential Function Chart* (*SFC*) control programs.

1.1. Illustrative Example

To illustrate the formalization methodology, the example process shown in Fig. 1 is considered. The plant consists of three tanks (T1-T3) that are connected via pipes. The flow to and from the tanks is controlled by valves (represented by Boolean variables [1: open, 0: closed]). The levels in T1 and T2 are measured by two independent

[1] The research reported in this paper was (partly) funded by the European FP7 project MULTIFORM, contract number INFSO-ICT-224249, http://www.ict-multiform.eu. This support is very gratefully acknowledged.

measurements (one continuous sensor and two discrete sensors for each tank). T3 is equipped with two quality sensors, a temperature sensor, a pressure sensor, and two discrete level sensors.

For the safe operation of the plant, the following control requirements have to be implemented in the controller:

1. An overflow of the tanks must be avoided. The inflow to the tanks has to be stopped if one of the level measurements indicates the risk of an overflow.

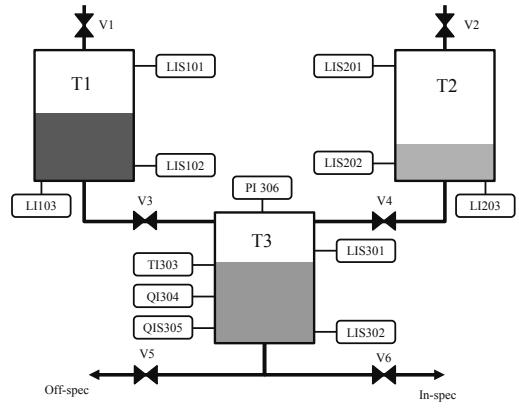

Figure 1: Example process

2. The production has to be stopped if either the pressure or the temperature in T3 reaches predefined (upper) thresholds. In both cases, T3 should be emptied via V5.
3. In addition, the following combinations of opened valves have to be avoided since the resulting (direct) material flows are undesired: V1 and V3, V2 and V4, V3 and V4, V3 and V5, V3 and V6, V4 and V5, and V4 and V6.
4. It has to be ensured that only in-spec product is transported to the downstream processing units (not shown). The valve V6 must not be opened if the quality is insufficient. The quality is determined by two independent quality measurements (QI304 and QIS305).

The inputs of the controller are the measurements via the sensors (LIS101 - PI306), operator commands (OpenV5, OpenV6) and the settings of the valves (V1-V6), the latter of which are considered to be both, input and output variables. The outputs of the controller are the settings sent to the valves (V1-V6) and two alarm variables (alarm, stop).

1.2. Supervisory Control Synthesis

The synthesis of a supervisory controller as reported in Theunissen et al. (2009) requires an automata model of the plant and a formal specification of the control requirements by a set of Boolean formulae specifying the control requirements. In this contribution, we consider the plant model as given while we focus on structuring and specifying the control requirements using the hierarchical *HCEC* formalism. The specification is then automatically translated into Boolean formulae as described in the following sections.

2. The Formalization Procedure

2.1. Cause-Effect Matrices (CEM)

The *Cause-Effect Matrix* (*CEM*) formalism is used for the specification and (partly for the) implementation of safety-related logic controllers but is not limited to this domain. An advantage of *CEM*-based formalisms is that a large amount of information can be visualized in a clearly arranged and intuitive data structure. However, neither the syntax nor the semantics of the *CEM* have been standardized yet so that different forms of *CEM* exist. The different *CEM* implementations range from very simple forms that only represent connections of sensors and actuators to complex forms that can represent more advanced control logic. All *CEM* formalisms share the basic structure that consists of four quadrants (see Tab. 1). The top-right quadrant contains the definitions of the *effects* (i.e. the actions in the control requirements), the

top-left quadrant holds information of the matrix such as author, date, name, project, etc., the bottom-left quadrant contains the definitions of the *causes* (inputs to the logic controller or internal variables), and the bottom-right quadrant defines the connections of causes and effects.

Table 1: Cause-Effect Matrix (*Quality Control* example, see Fig. 2)

Quality Control - Empty tank T3 via V5 in case of an error - Ensure product quality before opening V6		Stop	V5	V6
		Stop reaction	*Open V5*	*Open V6*
Inputs	**Comments**	OR	OR	AND
TI303 ≥ 200	*Temperature too high*	+	+	
PI306 ≥ 3.50	*Pressure too high*	+	+	
QIS305 AND QI304 ≥ 100	*Quality sufficient*			o
OpenV6	*Command to open V6*			o

The *CEM* definition here utilized for the formalization of the control requirements is defined as follows: Each cause consists of one or more inputs (plant states or events) and a logical function (AND, OR, or XOR) defining the connection of inputs in case of multiple inputs (e.g. QIS305 and QI304 in the third row in Tab. 1). The intersections define the connections of causes and effects. Each cell (= connection of one cause to one effect) can hold one of three qualifiers (+, -, o) defining if the cause is forcing (+), enabling (o) or blocking (-) the effect/event. If the cause forces the effect, the effect has to be activated whenever the cause is activated while enabling means that the effect can only be activated while the cause is activated. Blocking means that the effect must not be activated while the cause is activated. Each effect holds one output (action) that is enabled, forced, or blocked according to the connection specified in the intersections. Furthermore, effects hold a logical function defining how the intersections have to be interpreted (usually OR or AND). In addition, each cause and each effect holds a descriptive *comment* in natural language (see Tab. 1).

2.2. Hierarchical Cause-Effect Charts (HCEC)

In theory, it is possible to specify all requirements in one large matrix. However, the resulting matrix would be hardly comprehensible and maintainable (even in the case of simple requirements) so that a hierarchical approach should be utilized instead. To this end, this paper introduces the *Hierarchical Cause-Effect Charts* (*HCEC*) formalism (see Fig. 2) that introduces a hierarchical structure for *CE* matrices. It consists of a set of *causes* (inputs) on the left-hand side, a set of *effects* (outputs) on the right-hand side,

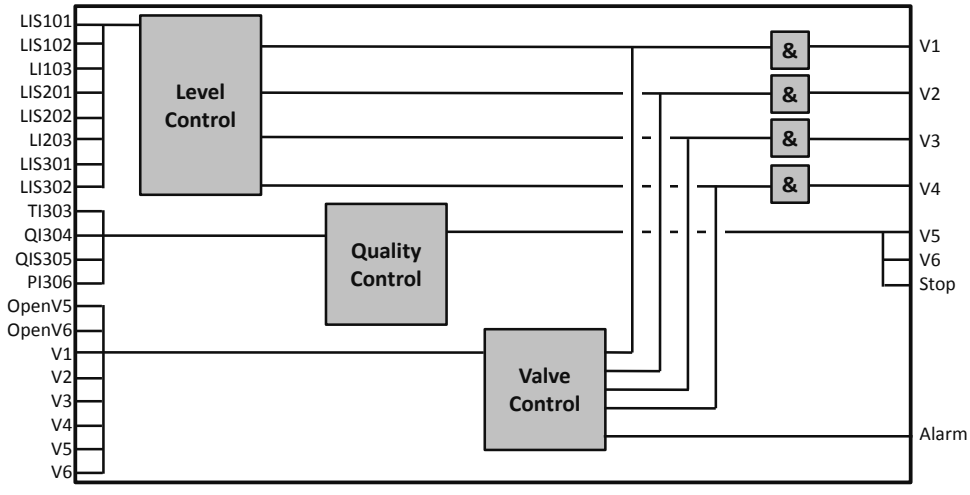

Figure 2: HCEC of the example process

and a set of *Function Blocks* that represent subsets of the control requirements. The requirements are grouped with respect to the process equipment involved, or in another appropriate way. Each of the function blocks is connected to sub-sets of causes and effects that are necessary to specify the behavior of this part of the system. The function blocks are either further refined using another *HCEC* sub-chart or by means of a *CEM*. The refinement ends if all requirements are formally defined by *CEM*.
In theory, it is possible to split the requirements into function blocks and finally CE matrices arbitrarily. However, in particular in safety-related control, requirements can usually be grouped according to the functional unit they belong to as this is highly recommended in relevant standards (see e.g. Brown (2000)).
For the example process, it was decided to group the requirements with respect to the required control tasks. Inputs to a module can be used in multiple embedded function blocks while in case of multiple function blocks accessing the value of the same output variable, an additional function block has to be introduced that specifies either the priority of one function block or how the signals are combined (e.g. for variable V1, see Fig. 2). For the example process, the set of causes consists of all sensor inputs from the plant and the current valve positions while the effects contain all actuator settings (see Fig. 2).

3. Formal Specification

3.1. Formalization of the Requirements for the Example
Initially, all outputs and inputs are assigned to the top-level *HCEC* block. During the hierarchical refinement of the control logic, three groups of interlocks are defined (*Level Control*, *Quality Control*, and *Valve Control*). Therefore, three function blocks are embedded into the top-level *HCEC* (see Fig. 2). The function block *Level Control* is further refined with another *HCEC* containing three function blocks (one for the level control of each tank). These low-level function blocks are refined by *CEM*s. For this relatively simple example, a refinement by means of *CEM*s is sufficient for *Valve Control* and *Quality Control*. The CEM of *Quality Control* is depicted in Tab. 1.

3.2. Translation of the Matrices into Boolean Formulae
The matrices are translated into a formal representation of the requirements that is suitable for the controller synthesis as follows:
Each "+" in the matrix denotes that the event should be forced when the condition is fulfilled. This can be expressed using the implication ("cause => effect"). The "-" denotes that the event is forbidden as long as one of the conditions is fulfilled. This can be expressed using a negated implication ("cause => ¬(effect)"). The third symbol, "o" denotes that the event is enabled only if the condition is true. This can be expressed by the implication ("effect => cause"). Since multiple "causes" can enable, force, or forbid a certain event/effect, the following rules apply:
1. All connections using the "-" are formulated as simple formulae ($a \Rightarrow \neg(b)$)
2. All connection using the "+" are combined using either "OR" or "AND". The utilized connector is specified in the matrix.
3. All connections using the "o" are formulated as simple formulae ($b \Rightarrow a$).

3.3. Formalized Requirements of the Example Process
After all requirements have been processed and the *HCEC* structure has been completed, the requirements are translated into Boolean formulae. As an example, the requirements implemented in the matrix shown in Tab. 1 are translated into the following four formulae:

$$(TI303 \geq 200) \vee (PI306 \geq 3.5) \Rightarrow Stop \quad (1)$$

$$(TI303 \geq 200) \vee (PI306 \geq 3.5) \Rightarrow V5 \quad (2)$$

$$V6 \Rightarrow QIS305 \wedge (QI304 \geq 100) \quad (3)$$

$$V6 \Rightarrow OpenV6 \quad (4)$$

These formulae in turn are used as inputs to the supervisory control synthesis tool chain, automatically resulting in a logic controller that fulfills the given specification. For details on controller synthesis we refer to Theunissen et al. (2009).

4. Conclusions

This paper introduces the new *Hierarchical Cause-Effect Charts* (*HCEC*) formalism for the structured representation of safety-related control logic. This formalism is embedded into an automated tool chain for algorithmic logic controller design that starts with an informal, natural-language description of the control requirements. The formalization benefits from the hierarchy which supports the design by breaking down the complexity of the system into CE matrices of manageable size that involve only small subsets of states and events of the controlled system and facilitates changes in the controller specification i.e. in the context of incremental system design or customization purposes. For the example process, the requirements are split into six matrices arranged in three levels of hierarchy with not more than seven rows and five columns each where one single matrix would consist of about 30 rows (inputs and their combinations) and a minimum of ten columns.

A formal representation of the control requirements as Boolean formulae is generated automatically from the final HCEC structure and is used as the input to the supervisory controller synthesis methodology which guarantees the correctness of the controller (according to the requirements). The HCEC formalism is generic and allows the application to other CEM formalisms used for e.g. test-case and/or code generation or as basis for formal verification. Future work will focus on this area.

References

Martinez, R., Enkerud, T., 2005. *The Importance of Single-Source Engineering of Emergency and Process Shutdown Systems*, Proc. SAFECOMP 2005, 13-23.

Russo, H., Turk, A., 2007. *Application of Interactive Cause and Effect Diagrams to Safety-Related PES in Industrial Automation*, Proc. SAFECOMP 2007, 187-196.

Fischer, S., Lohmann, S., Engell, S., 2009. *Neutral Representation, Visualization and Verification of Logic Controllers Represented by Function Block Diagrams.* Proc. Dependable Control of Discrete Systems, 45-50.

Theunissen, R.J.M., Schiffelers, R.R.H., van Beek, D.A., Rooda, J.E., 2009. *Supervisory Control Synthesis for a Patient Support System*, Proc. European Control Conference,1-6.

Fischer, S., Hüfner, M., Sonntag, C., Engell, S., 2011. *Systematic Generation of Logic Controllers in a Model-Based Multi-Formalism Design Environment*. Proc. IFAC World Congress, 12490-12495.

Brown, S., 2000. *Overview of IEC 61508. Design of electrical/electronic/programmable electronic safety-related systems*. Computing & Control Engineering Journal, 11(1), 6-12.

I.A. Karimi and Rajagopalan Srinivasan (Editors), Proceedings of the 11th International Symposium on Process Systems Engineering, 15-19 July 2012, Singapore.

Self-optimizing control for hydrogen optimization in a diesel hydrodesulfurization plant

Elena G. Sayalero,[a] Sigurd Skogestad,[b] César de Prada,[a] J. Miguel Sola,[c] Rafael González[c]

[a]*Dpt. Systems Engineering and Automatic Control, University of Valladolid, c/Dr. Mergelina, Valladolid 47011, Spain*
[b]*Dpt. Chemical Engineering, Norwegian University of Science and Technology, Trondheim N7491, Norway*
[c]*Dpt. Advanced Control, Petronor (Repsol), Edificio Muñatones, Muskiz 48550, Spain*

Abstract

The aim of this work is to apply the self-optimizing control technique (Skogestad, 2000) in order to ascertain the plantwide control structure for a hydrodesulfurization HDS plant of a petroleum refinery with regards to hydrogen consumption optimization. The resulting control structure for the HDS plant is simple, robust to uncertainty, easy to implement (feedback control) and assures the global optimum in most cases, although an upper RTO layer will be needed to guarantee the operation in the adequate region, with non frequent updates. Only in one uncommon scenario a trade-off arises regarding the unconstrained degrees of freedom, and self-optimizing control variables must be looked for. Potential application to global refinery H_2 network is also discussed.

Keywords: self-optimizing control, hydrogen optimization, hydrodesulfurization plant.

1. Introduction

Hydrogen is an expensive utility used in many operations that is gaining increasing importance in the economic balance of a refinery. In this framework, a project oriented towards the optimal management of the real-time operation of a refinery H_2 network is being undertaken in collaboration with the Petronor refinery (Vizcaya, Spain) of the Repsol group (Sarabia et al., 2009), in order to minimize H_2 production costs.

H_2 is distributed by means of a network from the producer plants to the consumer plants. Make-up H_2 to each consumer plant can be provided from different production lines, corresponding to different producer plants as well as consumer plants outlets. Accumulation of H_2 is not possible; as a deficit of H_2 is very damaging for catalyst active life, being catalysts very expensive, then always H_2 production must exceed consumption in operation. Because H_2 is expensive to produce, minimization of H_2 production has a great potential for economic profit. Furthermore, in scenarios where H_2 production is bottleneck for the refinery fuel processing capacity, the potential for profit increase is even higher. Minimization of H_2 production cost is mainly achieved by means of: a) a better H_2 redistribution at the network scale, trying to reuse as much as possible the low purity H_2 from the consumer plants outlets; b) minimization of losses to fuel gas, as a consequence of a better fitting of H_2 production to H_2 consumption in operation, while guaranteeing certain excess for pressure control purposes.

Determining a good plantwide control structure, in this case for an H_2 consumer diesel hydrodesulfurization HDS plant, is an issue of great practical importance to achieve optimal operation. Skogestad's procedure looks for a control strategy which can be

implemented in practice in a robust and simple manner. In the first place, active constraints are controlled, and then, for the remaining unconstrained economic degrees of freedom, self-optimizing variables are looked for. Self-optimizing control (Skogestad, 2000) is when close-to-optimal economic operation is obtained with a constant set-point policy. In this way it is avoided, or at least reduced, the need for an upper optimization RTO layer, being feedback control still the easiest way to implement a control strategy in industrial practice (Skogestad, 2004). Self-optimizing control design has been applied successfully to many processes (e.g. Araujo, Govatsmark and Skogestad, 2007; Lid and Skogestad, 2008).

2. Hydrodesulfurization plant description

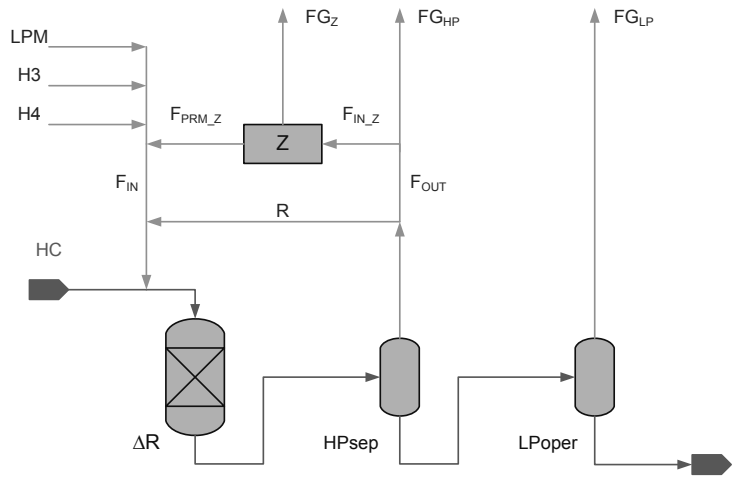

Figure 1. General H_2 consumer plant structure, with membranes unit for H_2 recovery.

A process flow diagram for the HDS plant is shown in Fig.1. Desulfurization reactions take place in fixed bed catalytic reactors (ΔR) where a minimum ratio H_2/hydrocarbon must be ensured for catalyst maintenance reasons. Reactors are fed with a blend of fuels of different qualities. The hydrocarbon (HC) feed is mixed with the recycled H_2 stream (R) and with make-up H_2 from the network. Two make-up streams (*H4*, *H3*) correspond to high purity inlets from producer plants, while the other (*LPM*) corresponds to the low purity line constituted from other plants outlets and excess. After being separated in a high pressure separation drum (*HPsep*), non reacted H_2 is partially recycled (R), partially purified and recycled in membranes Z (F_{PRM_Z}), and partially purged and burnt as fuel gas (FG_Z, FG_{HP}). Downstream of *HPsep*, several distillation columns at low pressure (*LPoper*) enable the complete separation of light gases from the desulfurized diesel stream. Light gases from low pressure separation processes (*LPoper*) are directed to fuel gas (FG_{LP}), since H_2 purity is not high enough for its recovery to be profitable. A HDS plant simplified model is available from previous work (Sayalero et al., 2010).

3. Self-optimizing control structure

The systematic procedure for plantwide control (Skogestad, 2004) will be applied to determine the self-optimizing control structure, following the steps in the top-down economic steady-state analysis.

3.1. Degrees of freedom analysis

A total of 5 degrees of freedom are available for economic optimization based on the process model. The following are natural manipulated variables (u) in operation: H_2 make-up flow rates from production plants F_{H3}, F_{H4}, membranes inlet flow rate F_{IN_Z}, membranes purge ratioed to the inlet F_{FG_Z}/F_{IN_Z}, purge to fuel gas from the high pressure recycle F_{FG_HP}. Other process variables are not truly degrees of freedom regarding H_2 optimization; that is the case for: a) pressure in separators, controlled at a fixed value according to compression ratios and security valves design; b) temperature in separators, regulated at minimum possible value by means of air exchangers, thus enabling the best relative separation of H_2 from light ends; c) quench flows between beds in the catalytic reactors, whose purpose is to maintain proper temperature gradients and to avoid high temperatures; d) reactor inlet temperature, which will always be active constraint at the minimum value enabling to achieve the sulfur specification in product.

3.2. Definition of optimal operation: cost and constraints

Only H_2 material cost is considered, as energy cost is in general an order of magnitude lower. Due to H_2 recycle flow being much greater than H_2 make-up flow, the H_2/hydrocarbon minimum ratio constraint (F_{H2}/F_{HC} > min) at reactor inlet is attained by means of recycle compressor's capacity (at minimum feasible, to minimize energy cost), and is thus decoupled from the H_2 optimization problem. Membranes operating costs can be disregarded as only low pressure steam is needed. Fuel gas value of purge streams is not considered (p_{fuel}) as this term will compete with minimization of the LPM make-up H_2 flowrate, being LPM H_2 price already a fictitious one. As a consequence, only make-up H_2 cost will be considered:

$$\min_u J = p_{H4} \cdot F_{H4} + p_{H3} \cdot F_{H3} + p_{LPM} \cdot F_{LPM} \qquad \text{(Eqn. 1.)}$$

Constraints to fulfill are the following: a) recycle H_2 purity between minimum to prevent deposition of coke over catalyst particles ensuring enough H_2 excess, and maximum to avoid surge of centrifugal compressor: min < y_{REC} < max; b) membranes operating range: min < F_{FG_Z}/F_{IN_Z} < max, and membranes capacity: min < F_{IN_Z} < max; c) producer plants capacity and LPM availability: min < F_{H3} < max, min < F_{H4} < max, 0 < F_{LPM} < max; d) compressors [reciprocating/centrifugal] capacity: min < F_C < max.

3.3. Identification of important disturbances

Regarding the plant state, disturbances in hydrocarbon feed influence: gas separated in the low pressure operations F_{FG_LP}, $y_{FG\_LP}^{H2}$, determined under pressure control according to inventory regulation; hydrogen consumption ΔR_{H2} and light ends generation ΔR_L in the reactor. Regarding different future scenarios, there are several disturbances that deserve being considered, namely: H_2 purity of certain make-up streams y_{LPM}^{H2}, y_{H3}^{H2}, and make-up availability from the low purity line F_{LPM}.

3.4. Regions of active constraints (modes of operation)

To identify the different regions of active constraints, optimization with respect to the available degrees of freedom is performed for the different operating points (19) selected corresponding to historical process conditions, for 6 case studies corresponding to different disturbances in utilities; in total 114 case studies. The model is implemented in EcosimPro® modelling and simulation environment and optimizations are performed with a NAG® SQP solver linked with EcosimPro®. In increasing order of H_2 requirements, the regions of active constraints are the following:

- **A.** Recycle H_2 purity (y_{REC}^{H2} = min) controlled with F_{IN_Z}. Manipulated variables active: F_{FG_Z}/F_{IN_Z} = min, F_{FG_HP} = 0, F_{H3} = 0, F_{H4} = 0.

The purge of H_2 is minimum (F_{FG_Z}/F_{IN_Z} = lower bound), and as a result both make-up H_2 flow and H_2 losses in the purge are also minimum.

- **B.** Recycle H_2 purity (y_{REC}^{H2} = min) controlled with F_{FG_Z}/F_{IN_Z}. Manipulated variables active: F_{IN_Z} = max, $F_{FG\_HP} = 0$, $F_{H3} = 0$, $F_{H4} = 0$.
  When H_2 requirements increase with respect to previous **A**, H_2 purge (F_{FG_Z}/F_{IN_Z}) is not at the lower bound because the membranes capacity upper bound is reached. Higher purge implies higher permeate purity, but also higher make-up H_2 flow rate.
- **C.** Recycle H_2 purity (y_{REC}^{H2} = min) controlled with F_{FG_HP}. Manipulated variables active: F_{IN_Z} = max, F_{FG_Z}/F_{IN_Z} = max, $F_{H3} = 0$, $F_{H4} = 0$.
  When H_2 requirements increase with respect to **B**, and membranes are saturated.
- **D.** Trade-off between ratio purged in membranes and HPM H_2 make-up (F_{H4}, F_{FG_Z}/F_{IN_Z}). Recycle H_2 purity controlled (y_{REC}^{H2} = min). Manipulated variables active: F_{IN_Z} = max, $F_{FG\_HP} = 0$, $F_{H3} = 0$. Case rather infrequent.
  When make-up H_2 from a producer plant (HPM H_2) is needed due to LPM H_2 shortage (small purity of 0.67 %1mol for example but not small F_{LPM} availability). The optimum is quite flat with respect to F_{FG_Z}/F_{IN_Z}, so a value can be fixed while using F_{H4} to control y_{REC}^{H2}, being $F_{FG\_Z}/F_{IN\_Z} = 0.33$ the most common by far (self-optimizing variable). According to the experiments carried out, the optimal ratio varies between 0.27-0.36, so 600 Nm^3 H_2/h is the difference for F_{IN_Z} = max, and the maximum loss in HPM H_2 is 300 Nm^3/h provided 0.33 is fixed. Cases B and D can be easily distinguished; if an increase in F_{LPM} (by allowing an increase in F_{FG_Z}/F_{IN_Z}) does not lead to an increase in y_{REC}^{H2}, then HPM H_2 will be needed. This occurs when $y_{LPM}^{H2} < y_{REC}^{H2}$. Direct purge F_{FG_HP} will be needed if membranes get saturated, besides HPM H_2.
- **E.** When the maximum make-up compressor's capacity is binding constraint besides y_{REC}^{H2} (y_{REC}^{H2} = min, F_{C1} = max), controlled with F_{FG_HP} and F_{H4}. Manipulated variables active: F_{IN_Z} = max, F_{FG_Z}/F_{IN_Z} = max, $F_{H3} = 0$.
  This situation is common in cases where $y_{LPM}^{H2} > y_{REC}^{H2}$, but only slightly greater. As a high flow F_{LPM} is needed, make-up compressor capacity gets saturated. As usual, membranes capacity is fully employed before HPM H_2 is used.
  F. When the maximum LPM H_2 availability is active constraint, besides y_{REC}^{H2} (y_{REC}^{H2} = min, F_{LPM} = max). Manipulated variables active: either F_{FG_Z}/F_{IN_Z} = min, $F_{FG\_HP} = 0$, $F_{H4} = 0$ (control with F_{IN_Z}, F_{H3}); F_{FG_Z}/F_{IN_Z} = min, $F_{FG\_HP} = 0$, $F_{H3} = 0$ (control with F_{IN_Z}, F_{H4}); F_{IN_Z} = max, F_{FG_Z}/F_{IN_Z} = min, $F_{FG\_HP} = 0$ (control with F_{H3}, F_{H4}); or F_{IN_Z} = max, $F_{FG\_HP} = 0$, $F_{H3} = 0$ (control with F_{FG_Z}/F_{IN_Z}, F_{H4}).
  Both membranes and HPM H_2 make-up are needed. With increasing H_2 demand, first F_{IN_Z} is manipulated, then F_{FG_Z}/F_{IN_Z}. Between the two HPM H_2, F_{H3} and F_{H4}, which one is used depends mainly on their respective prices and purities (very constant), but also on plant state, although no trade-off arises. An upper RTO layer will be required to know whether to use F_{H3} or F_{H4}, with very low frequent updates.

4. Discussion

Self-optimizing control is a robust technique not sensitive to uncertainty when compared with RTO (Skogestad, 2000). As i) disturbances: H_2 consumption, light gases inlet and generation, and gases solubility in hydrocarbons, are difficult to estimate accurately, and ii) gas flow measurements need to be compensated with molecular weight in operation, where the stream molecular weight is quite sensitive to light gases composition due to the low value of H_2 molecular weight (2.016 g/mol), a self-optimizing control approach can be advantageous and preferred compared to RTO.

Other major advantage is that the self-optimizing approach considered is reliable regardless of model mismatch: although model validation is not perfect quantitatively (errors up to 10% in the prediction of H_2 consumption rate), the analysis performed regarding regions of active constraints is correct.
The resulting control structure for the HDS plant is simple, easy to implement (feedback control with programmed logic) and assures the global optimum in most cases, although an upper RTO layer will be needed to guarantee the operation in the adequate region, with non frequent updates. Only in one scenario, rather uncommon, a trade-off arises regarding the unconstrained degrees of freedom, and self-optimizing control variables must be looked for to assure close to optimal operation avoiding more complex on-line optimization techniques. Main drawbacks are related to plant automation level, which needs to be high to implement this technology; in particular the membranes unit can't be operated manually. Transport delay due to reactor and dynamic effects due to separators are not negligible, therefore a MPC approach with an economic objective function could be justified, especially when the high number of regions of active constraints is taken into account, due to its potential to easily handle constraints.

4.1. Hydrogen optimal management at refinery network scale

A further step is being considered regarding the potential application of self-optimizing control design to on-line optimization of the global H_2 network operation. Although the structure at network scale is much more complex, the number of combinations allowed is usually small. Considering where it is more efficient to employ HPM H_2, and looking for self-optimizing variables when needed, consumer plants optimization with regards to H_2 consumption could be decoupled from the whole network, being the problem at network scale simplified, and thus reducing the loss between RTO executions.

Acknowledgements

The cooperation of Petronor – Repsol group, and financial support of spanish Ministry of Science and Innovation (CICYT project DPI2006-13593, FPI program) are gratefully acknowledged.

References

V. Alstad, S. Skogestad, 2007, Null space method for selecting optimal measurement combinations as controlled variables, Ind. Eng. Chem. Res., 46, 3, 846-853.
V. Alstad, S. Skogestad, E.S. Hori, 2009, Optimal measurement combinations as controlled variables, J. Proc. Control, 19, 138-148.
A.C.B. Araujo, M. Govatsmark, S. Skogestad, 2007, Application of plantwide control to the HDA process. I Steady-state and self-optimizing control, Control Eng. Pract., 15, 1222-1237.
S. Engell, 2007, Feedback control for optimal process operation, J. Proc. Control, 17, 203–219.
E. Gómez, D. Sarabia, S. Cristea, G. Gutiérrez, C.A. Méndez, J.M. Sola, E. Unzueta, R. González, C. de Prada, 2010, Simplified modelling and validation of an industrial diesel hydrodesulfurization plant, DYCOPS 9th Dynamics & Control of Systems, Louvain, Belgium.
I.J. Halvorsen, S. Skogestad, J.C. Morud, V. Alstad, 2003, Optimal selection of controlled variables, Ind. Eng. Chem. Res., 42, 14, 3273-3284.
T. Lid, S. Skogestad, 2008, Data reconciliation and optimal operation of a catalytic naphtha reformer, J. Proc. Control, 18, 320–331.
D. Sarabia, C. de Prada, E. Gómez, G. Gutiérrez, S. Cristea, J.M. Sola, R. González, 2011, Data reconciliation and optimal management of hydrogen networks in a petrol refinery, Control Eng. Pract., Article in Press, available online 18 July 2011.
S. Skogestad, 2000, Plantwide control: the search for the self-optimizing control structure, J. Proc. Control, 10, 487-507.
S. Skogestad, 2004, Control structure design for complete chemical plants, Comp. Chem. Eng., 28, 1-2, 219-234.

I.A. Karimi and Rajagopalan Srinivasan (Editors), Proceedings of the 11th International Symposium on Process Systems Engineering, 15-19 July 2012, Singapore

Reconfigurable stabilizing control applied to a neutralization process

Thiago V. Costa[a]*, Ana M. F. Fileti[a], Luís C. Oliveira-Lopes[b], Flávio V. Silva[a]

[a] *FEQ/UNICAMP -School of Chemical Engineering, University of Campinas - Av. Albert Einstein, 500 - CEP 13083-970, Campinas-SP, Brazil*

[b] *FEQUI/UFU - School of Chemical Engineering, Federal University of Uberlândia, Av. João Naves de Ávila, 2121, Santa Mônica, CEP 38408-144, Uberlândia-MG, Brazil*

Abstract

This paper presents the application of reconfigurable control strategy to a multivariable neutralization process under several fault scenarios. The combined control strategy is integrated to a reconfiguration block that uses the available signals from the remaining sensors and actuators to reconstruct a signal useful to the nominal controller leading to a stable closed-loop behavior even in the presence of faults. Simulations results show that, although the overall system performance can be compromised, the reconfigurable control strategy leads to a system that is still able to operate within acceptable performance in the studied fault scenarios.

Keywords: fault tolerant control, neutralization, reconfigurable control

1. Introduction

Modern control design aims not only to stabilize processes in normal operating conditions, but also to control them successfully in abnormal situations. In this sense, fault tolerant control (FTC) systems include taking online corrective actions to mitigate fault effects preventing plant shutdown and off-specification production. The main objective is to make the system closed-loop stable under a fault situation while accepting a reduced performance in the overall process (Blanke et al., 2001).

Reconfigurable control is a type of active fault tolerant system where the fault-handling is carried out by changing the parameters of a nominal controller, switching it, or broadly restructuring the control loop to deal with different dynamics imposed by faults. Control reconfiguration differs from the passive fault tolerant systems, where the failure modes are accounted in the design stage ensuring the control system to work under several fault scenarios considered in advance (Jiang, 2005).

This work considers the problem of achieving a fault tolerant control loop by means of a reconfigurable control based on the use of virtual instrumentation (Steffen, 2005; Richter, 2011). In order to recover closed-loop stability in the presence of actuator/sensor losses, the reconfiguration strategy uses a signal composed by the difference between nominal and faulty plant dynamics. Instead of switching the nominal controller to one designed for a specific fault, a control reconfiguration block hides the fault from the nominal controller keeping it active during the fault period. Hence, the available signals from the remaining sensors and actuators are used to reconstruct a signal useful to the nominal controller bypassing the faulty instrumentation (Richter and Lunze, 2010).

*thiagocosta@feq.unicamp.br

The studied method is used to design a FTC system applied to a multivariable neutralization process under several fault scenarios. Simulations results show that, although the overall system performance can be compromised, the reconfigurable control strategy leads to a system that is still able to operate within acceptable performance in the studied fault scenarios.

2. Neutralization Process

The studied neutralization process (Figure 1) is characterized by a continuous stirred tank reactor (CSTR) supplied by a strong acid (HNO_3) and a strong base (NaOH) lines, in addition to a third line composed by a buffering component ($NaHCO_3$). Each stream flow is locally manipulated by a dedicated slave controller that receives a reference signal from the multivariable controller output. The fault scenarios (FI and FII) considered are based on the loss of communication between master and slave controllers.

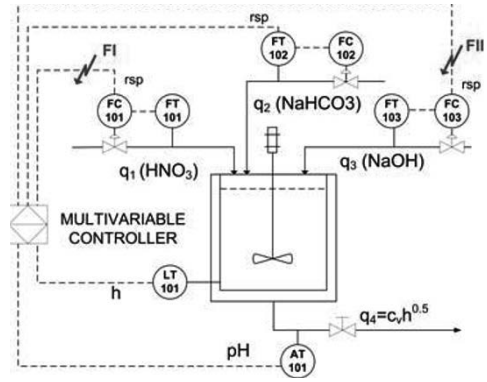

Figure 1. Neutralization process subject to faults in the signal path between master and slave controllers

The nominal plant model, without the presence of faults, is described by equations 1 – 3 and is considered as the reference model for the reconfiguration control design. It consists of three states: reactor level (h) and the invariant species concentrations W_a and W_b. Basically, system dynamics are just slightly nonlinear due to the bilinear combination between the invariant states with respect to the input flows.

$$\dot{h} = [q_1 + q_2 + q_3 - q_4]A^{-1} \tag{1}$$

$$\dot{W}_a = [(W_{a1} - W_a)q_1 + (W_{a2} - W_a)q_2 + (W_{a3} - W_a)q_3](Ah)^{-1} \tag{2}$$

$$\dot{W}_b = [(W_{b1} - W_b)q_1 + (W_{b2} - W_b)q_2 + (W_{b3} - W_b)q_3](Ah)^{-1} \tag{3}$$

The main nonlinearity is described by the static output model given by equation 4 which relates the output of the dynamic subsystem (invariants) to the system output, pH. The block oriented characteristics of the neutralization process are similar to a Wiener model. Hence, the design of the reconfiguration control based on linear techniques is considered feasible as the main process nonlinearity is located on the system static gain and not on its dynamics.

$$W_a + 10^{pH-14} - 10^{-pH} + W_b \frac{1 + 2 \times 10^{pH-pk_2}}{1 + 10^{pk_1-pH} + 10^{pH-pk_2}} = 0 \tag{4}$$

3. Control Reconfiguration Procedure

In this work, control reconfiguration operates on the use of virtual actuators as proposed in Steffen (2005). The idea builds on the use of state feedback applied to the deviation of the faulty plant from its nominal behavior represented by a new state denoted x_Δ. The reconfiguration block (Figure 2) is placed between the faulty plant and the nominal controller. The block receives the output of the faulty plant (y_p) and the output of the controller (u_c) correcting the signal sent to the nominal controller (y_c) and translating the signal from the controller to a signal (u_p) that will make use of the available actuators to handle the fault. The virtual actuator is based on two design parameters: M and N. Feedback gain M is used to stabilize the pair (A, B_f), where B_f denotes the faulty plant input matrix. The feedforward term $N = I$ is used to provide the reconfiguration block with autonomous behavior.

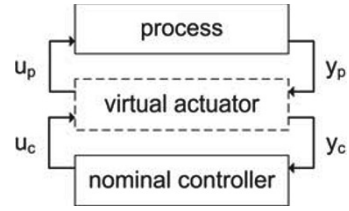

Figure 2. Reconfigurable control based on virtual actuator

$$\dot{x}_\Delta = \left(A - B_f M\right) x_\Delta + \left(B - B_f N\right) u_c; \;\; x_\Delta = x - x_f \text{ and } x_\Delta(0) = 0 \tag{5}$$

$$y_c = y_p + C x_\Delta; \; u_p = M x_\Delta + N u_c \tag{6}$$

The virtual actuator gain M is designed here by means of an optimization problem as in the design of a LQR (linear quadratic regulator). Given the system presented by equations 5 – 6 the virtual actuator is obtained by solving the following LMI (linear matrix inequality):

$$\min_P \operatorname{Tr}(P)$$

$$\text{s. t. } \begin{pmatrix} A^T P + PA + Q & PB_f \\ B_f^T P^T & R \end{pmatrix} > 0; \;\; P = P^T > 0 \tag{7}$$

4. Simulation Results

Two fault scenarios were investigated in order to demonstrate the efficacy of the studied control reconfiguration strategy: loss of communication between master and slave controllers in acid line (FI) and base line (FII). Which means that stream flow in the faulty line is fixed in steady state due to the inability of the actuator to respond. A linearized state-space model, derived from equations 1 – 3 was used for the nominal controller and the reconfiguration block design. Each fault is modeled by replacing the respective input matrix column elements to zero (actuator is bypassed). Parameters used in simulation are given in Henson and Seborg (1994). Nominal closed-loop behavior is shown in Figure 3.

Fault scenario I is presented in Figure 4. System output behaviour is shown in Figures 4(a) and 4(b) for both reconfigured (solid line) and non-reconfigured cases (thin line). Figures 4(c) to 4(e) shows the controller output (solid lines) and actual stream flow (dashed lines) in the faulty non-reconfigured case. The simulation shows that the nominal controller performance is degraded by the loss of the first actuator. Whereas, the reconfiguration block as shown in Figures 4(f) to 4(h) changes the nominal controller output (solid lines) to a signal meaningful for the faulty plant (actual stream flow – dashed lines) that uses

mainly the second input (buffer stream) to cope with the acid line loss. As in the first case, control reconfiguration after fault, FII (Figure 5), is able to recover the closed-loop system within acceptable performance based on buffer input (q_2) amplification. It is important to mention that in both situations a small offset is introduced due to the plant/model mismatch in the reconfigured case.

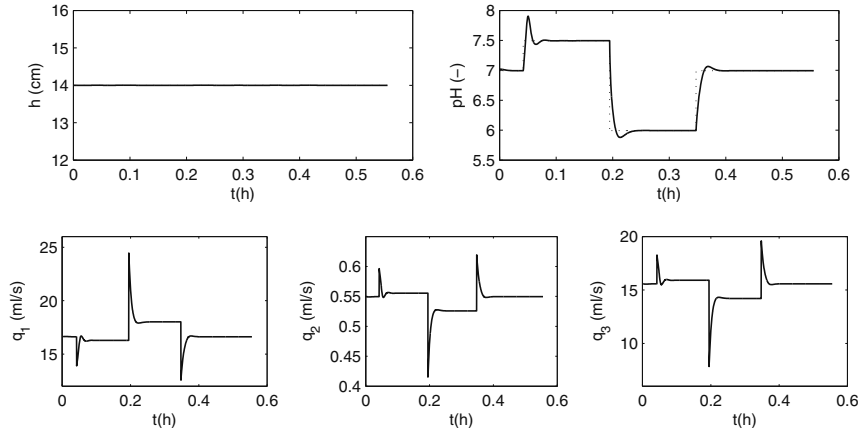

Figure 3. Closed-loop nominal behavior based on a LQR controller for the following initial conditions: $q_1 = 16.6ml/s$, $q_2 = 0.55ml/s$, $q_3 = 15.6ml/s$, $pH = 7.02$ *and* $h = 14.00cm$.

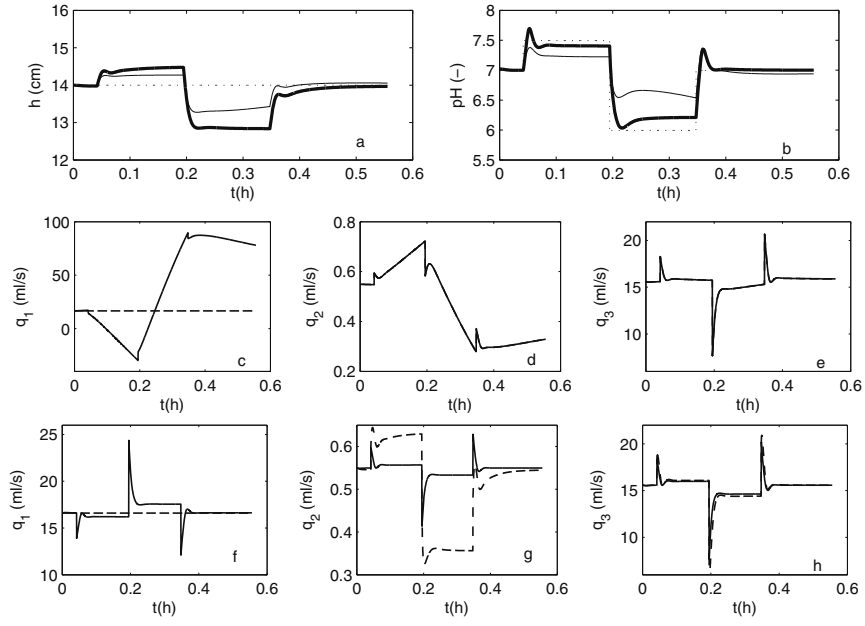

Figure 4. Fault Case I. Controlled variables (a) – (b): reconfigured (–) and non-reconfigured cases (–). Input variables for non-reconfigured (c–e) and reconfigured (f–h) cases: controller output (solid lines) and actual stream flow (dashed lines).

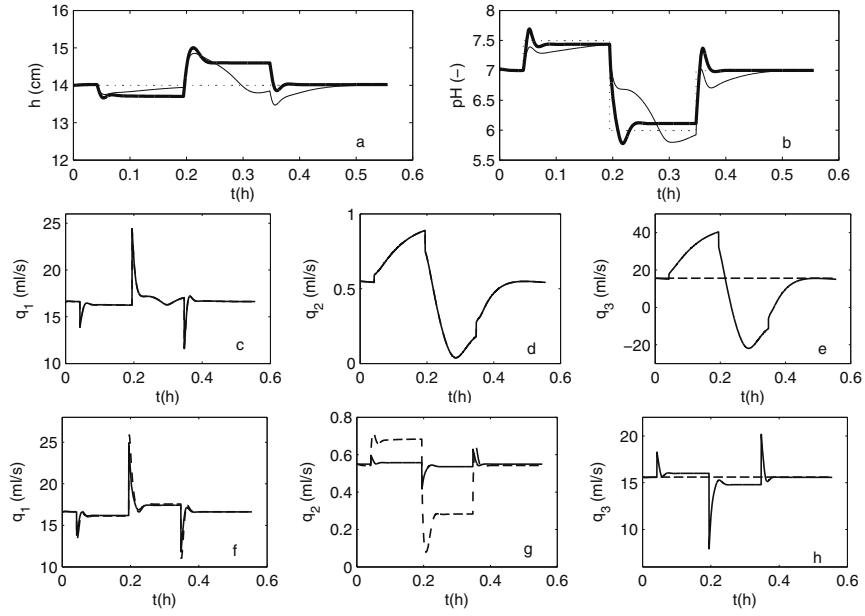

Figure 5. Fault Case II. Controlled variables (a) – (b): reconfigured (–) and non-reconfigured cases (–). Input variables for non-reconfigured (c–e) and reconfigured (f–h) cases: controller output (solid lines) and actual stream flow (dashed lines).

5. Conclusions

This paper addressed a reconfigurable stabilizing control based on the use of virtual actuators. The method applied in the control reconfiguration of a neutralization process subject to actuator losses proved feasible and efficient in the studied scenarios. Although the system overall performance has been compromised the reconfigurable control strategy led to a system within good performance/loss-recover operation as shown in the fault scenarios studied.

References

Blanke, M., Staroswiecki, M., Wu, N., 2001. Concepts and methods in fault-tolerant control. American Control Conference 4, 2606–2620.

Henson, M., Seborg, D., 1994. Adaptive nonlinear control of a ph neutralization process. IEEE Transactions on Control Systems Technology 2(3), 169–182.

Jiang, J., 2005. Fault-tolerant control systems: an introductory overview. Automatica SINCA 31(1), 161–174.

Richter, J., 2011. Reconfigurable Control of Nonlinear Dynamical Systems: A Fault-Hiding Approach. Springer.

Richter, J., Lunze, J., 2010. Reconfigurable control of hammerstein system after actuator failures: stability, tracking and performance. Internation Journal of Control 83(8), 1612–1630.

Steffen, T., 2005. Control Reconfiguration of Dynamical Systems: Linear Approaches and Structural Tests. Springer.

I.A. Karimi and Rajagopalan Srinivasan (Editors), Proceedings of the 11th International Symposium on Process Systems Engineering, 15-19 July 2012, Singapore

Robust IMC-PID Design for Optimal Closed-loop Response with Specified Gain and Phase Margins for SOPTD Systems

Keyu Li *

Department of Thermal Energy Engineering;China University of Petroleum, Beijing;Beijing, China

Abstract

A new internal model control (IMC) based robust PID tuning method for second order plus time delay (SOPTD) systems is developed to meet specified gain and phase margins (GPM). The exact open-loop amplitude ratio and phase change equations are derived based on frequency analysis. The tuning method based on IMC with constraints on GPM and closed-loop overshoot ratio is further given. The method is demonstrated in simulation examples and compared with previous work on this topic.

Keywords: Gain and phase margins, PID tuning, IMC

1. Introduction

Internal model control (IMC) Rivera et al. (1986) has been widely accepted by industry for PID tuning due to its simplicity to apply. For any model-based PID tuning algorithm like IMC, robustness plays an important role in PID design due to model mismatch. In practice, gain and phase margins serve as important indicators of system robustness, and the combination of IMC tuning and GPM has also been explored Ho et al. (2001); Kaya (2004); Chu et al. (2011). Previous work includes IMC-GPM tuning for PI controller and PID controller for FOPTD systems, but there is still no report on IMC based PID tuning for SOPTD systems with specified gain and phase margins.

In this work, the IMC tuning algorithm is used for SOPTD systems to meet specified gain and phase margins for the PID controller for the first time. Another contribution of this work is that the overshoot ratio is directly used in the controller design as the closed-loop performance criterion combined with GPM as the robustness criteria.

2. System Frequency Analysis

2.1. The Open-loop Frequency Analysis

The transfer function of a SOPTD process is given by

$$G_p(s) = \frac{K_p}{\tau^2 s^2 + 2\xi\tau s + 1} e^{-\theta s} \tag{1}$$

and the transfer function of the PID controller in parallel form is given by

$$G_c(s) = K_c(1 + \frac{1}{\tau_I s} + \tau_D s) \tag{2}$$

*likeyu@cup.edu.cn

Then the open-loop transfer function is given by

$$G_{ol}(s) = G_c(s)G_p(s) \tag{3}$$

$$= \frac{K_cK_p(\tau_I\tau_Ds^2+\tau_Is+1)e^{-\theta s}}{\tau_Is(\tau^2s^2+2\xi\tau s+1)} \tag{4}$$

With relatively simple mathematical manipulation, the frequency response amplitude ratio AR_{ol} and phase change ϕ_{ol} are explicitly given by

$$AR_{ol} = \frac{K_cK_p\sqrt{(1-\omega^2\tau_I\tau_D)^2+(\omega\tau_I)^2}}{\omega\tau_I\sqrt{(1-\omega^2\tau^2)^2+(2\omega\xi\tau)^2}} \tag{5}$$

$$\phi_{ol} = \begin{cases} \Lambda_1(\omega)-\omega\theta-\Lambda_2(\omega)+\frac{\pi}{2} & \text{if } \Lambda_1(\omega)<0, \Lambda_2(\omega)\geq 0 \\ \Lambda_1(\omega)-\omega\theta-\Lambda_2(\omega)-\frac{3\pi}{2} & \text{if } \Lambda_1(\omega)\geq 0, \Lambda_2(\omega)<0 \\ \Lambda_1(\omega)-\omega\theta-\Lambda_2(\omega)-\frac{\pi}{2} & \text{else} \end{cases} \tag{6}$$

where

$$\Lambda_1(\omega) = tan^{-1}\left(\frac{\omega\tau_I}{1-\omega^2\tau_I\tau_D}\right) \tag{7}$$

$$\Lambda_2(\omega) = tan^{-1}\left(\frac{2\omega\xi\tau}{1-\omega^2\tau^2}\right) \tag{8}$$

2.2. The Closed-loop Frequency Analysis

For open-loop system G_{ol}, the closed-loop transfer function is given by

$$G_{cl} = \frac{G_{ol}}{1+G_{ol}} \tag{9}$$

By simple mathematical manipulation, we have

$$AR_{cl} = \frac{1}{\sqrt{(\frac{1}{AR_{ol}}+cos\phi_{ol})^2+sin^2\phi_{ol}}} \tag{10}$$

Thus the overshoot ratio can be obtained by calculating the maximum amplitude ratio AR_{cl} from AR_{ol} and ϕ_{ol} in the entire frequency range $\omega\in(0,\infty)$.

3. IMC-PID Design Based on Gain and Phase Margins

From definition, the gain margin A and phase margin ϕ can be calculated from the following equations:

$$A = \frac{1}{|G_{ol}(j\omega_p)|} \tag{11}$$

$$\phi = \angle G_{ol}(j\omega_g)+\pi \tag{12}$$

where

$$|G_{ol}(j\omega_g)| = 1 \tag{13}$$

$$\angle G_{ol}(j\omega_p) = -\pi \tag{14}$$

Substituting Eq. 5 and 6 into 11-14, we have 4 equations

$$A = \frac{\omega_p \tau_I}{K_c K_p} \sqrt{\frac{(1-\omega_p^2\tau^2)^2 + (2\omega_p \xi \tau)^2}{(1-\omega_p^2 \tau_I \tau_D)^2 + \omega_p^2 \tau_I^2}} \tag{15}$$

$$\phi = \begin{cases} \Lambda_1(\omega_g) - \omega_g \theta - \Lambda_2(\omega_g) + \frac{3\pi}{2} & \text{if } \Lambda_1(\omega_g) < 0, \Lambda_2(\omega_g) \geq 0 \\ \Lambda_1(\omega_g) - \omega_g \theta - \Lambda_2(\omega_g) - \frac{\pi}{2} & \text{if } \Lambda_1(\omega_g) \geq 0, \Lambda_2(\omega_g) < 0 \\ \Lambda_1(\omega_g) - \omega_g \theta - \Lambda_2(\omega_g) + \frac{\pi}{2} & \text{else} \end{cases} \tag{16}$$

and

$$\frac{K_c K_p}{\omega_g \tau_I} \sqrt{\frac{(1-\omega_g^2 \tau_I \tau_D)^2 + \omega_g^2 \tau_I^2}{(1-\omega_g^2\tau^2)^2 + (2\omega_g \xi \tau)^2}} = 1 \tag{17}$$

$$\begin{cases} \Lambda_1(\omega_p) - \omega_p \theta - \Lambda_2(\omega_p) + \frac{3\pi}{2} & \text{if } \Lambda_1(\omega_p) < 0, \Lambda_2(\omega_p) \geq 0 \\ \Lambda_1(\omega_p) - \omega_p \theta - \Lambda_2(\omega_p) - \frac{\pi}{2} & \text{if } \Lambda_1(\omega_p) \geq 0, \Lambda_2(\omega_p) < 0 \\ \Lambda_1(\omega_p) - \omega_p \theta - \Lambda_2(\omega_p) + \frac{\pi}{2} & \text{else} \end{cases} = 0 \tag{18}$$

with 5 unknowns ω_g, ω_p, K_c, τ_i and τ_D for given gain margin A and phase margin ϕ, so we can not solve them directly. However, if we further apply the IMC-Mac tuning formula Panda et al. (2004), the tuning problem becomes 4 equations with 3 unknowns (τ_c, ω_g and ω_p), where τ_c is the tuning parameter for IMC. Then the tuning problem could be solved to meet the robustness criteria, but we also want the PID tuning to lead to required closed-loop performance, such as response time and overshoot ratio. Since τ_c is related to the closed-loop response time and the overshoot ratio could be calculated from Eq. 10, we formulate the tuning problem into an optimization problem

$$\min_{\tau_c, \omega_g, \omega_p} \tau_c \tag{19}$$

S.T.

$$A \geq A^* \tag{20}$$

$$\phi \geq \Phi^* \tag{21}$$

$$AR_{cl} \leq O^* \qquad \forall\, \omega \in [0, \infty) \tag{22}$$

where A^* and Φ^* are given gain margin and phase margin bounds respectively; O^* is the user-specified overshoot ratio.

4. Simulation Examples

4.1. Second-order System

The SOPTD example in Ho et al. (1997) is first considered and the plant model is given by

$$G_p(s) = \frac{1}{s^2 + s + 1} e^{-s} \tag{23}$$

For required gain margin $A^* = 3$ and phase margin $\phi^* = 60^\circ$, the closed-loop response results for step response and load disturbance from Ho and proposed method are shown in Fig. 1. Tuning parameters and some results are shown in Table. 1.

Table 1. PID tuning results for example 1 with different methods

Parameter	K_c	τ_I	τ_D	A	ϕ	A^*	ϕ^*	O^*	IAE
Proposed	0.5241	1.0964	0.9358	3.0145	64.6366	3	60	1.2	5.4328
Method from Ho	0.52	1	1	3.9	65	3	60	N/A	5.5765

Table 2. PID tuning results for example 2 with different methods

Parameter	K_c	τ_I	τ_D	A	ϕ	IAE	Settling Time
Proposed	0.6133	0.6309	1.0532	3.277	63.9684	3.3620	4.6883
Method from Ho	0.783	0.832	0.790	4.898	70	3.3664	8.8755
Method from Shen	0.92	1.075	0.775	3.273	46.6	3.1019	9.4844

From the results we can see that the proposed method leads to smaller overshoot and integrated absolute error (IAE) value.

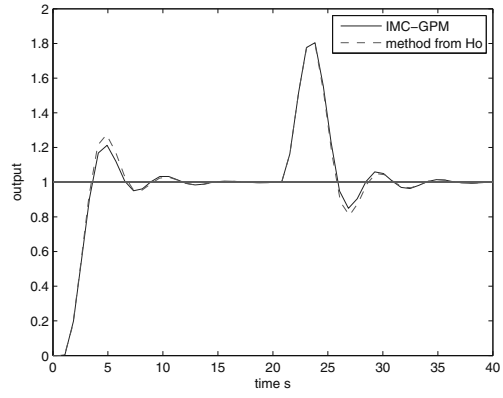

Figure 1. The Closed-loop Response from the SOPTD System

4.2. Higher Order System

Let's consider an example from Shen (2000), where Shen proposed a new PID tuning method for under-damped second order system based on dominant pole assignment. The system is given by

$$G(s) = \frac{18}{(s^2+s+2)(s+3)^2} \quad (24)$$

A step response experiment gives the model Shen (2000)

$$G_p(s) = \frac{1.52e^{-0.48s}}{s^2+0.9s+1.52} \quad (25)$$

The tuning method from Shen gives out a gain margin 3.273 and a phase margin 46.6°. Then we use the same values as the required gain and phase margin bounds, i.e. $A^* = 3.273$ and $\phi^* = 46.6°$, for proposed IMC-GPM method and Ho's method. The closed-loop responses from different methods are given in Fig. 2 and results are compared in Table 2.

From the results we can see that tuning method from Shen gives the best overall IAE, but more oscillations and the longest settling time. Our proposed method gives just slightly better IAE value than Ho's method, but far less oscillations and a much smaller settling time than the other two methods.

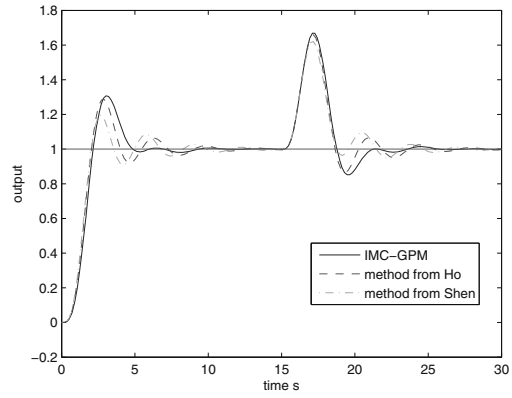

Figure 2. The Closed-loop Response from Higher Order System

5. Conclusion

The gain and phase margins are used as robustness criteria to tune the PID controller in the IMC framework. The closed-loop overshoot ratio is also explicitly used as a performance criterion by frequency analysis. The tuning algorithm is formulated as a nonlinear optimization problem to minimize the closed-loop response time τ_c, with constraints on gain margin, phase margin and overshoot ratio. The simulation results show that the new robust tuning method leads to better overall closed-loop performance (smaller IAE and settling time) than the existing GPM based PID tuning method. The proposed method also results in much smaller settling times and much less oscillations than the method based on pole assignment for examples in this paper.

References

Chu, C., Ydstie, B. E., Sahinidis, N. V., May 29-June 1 2011. Optimization of IMC-PID tuning parameters for adaptive control: Part 1. 21st European Symposium on Computer Aided Process Engineering-ESCAPE 21.

Ho, W. K., Hang, C. C., Zhou, J. H., 1997. Self-tuning PID control of a plant with under-damped response with specifications on gain and phase margins. IEEE Transactions on Control Systems Technology 5 (4), 446–452.

Ho, W. K., Lee, T. H., Han, T. P., Hong, Y., 2001. Self-tuning IMC-PID control with interval gain and phase margins assignment. IEEE Transactions on Control Systems Technology 9 (3), 535–541.

Kaya, I., 2004. Tuning PI controllers for stable processes with specifications on gain and phase margins. ISA Transactions 43, 297–304.

Panda, R. C., Yu, C., Hang, H., 2004. PID tuning for SOPTD systems: Review and some new results. ISA Transactions 43, 283–295.

Rivera, D. E., Morari, M., Skogestad, S., 1986. Internal model control. 4. PID controller design. Industrial & Engineering Chemistry Process Design and Development 25 (1), 252–265.

Shen, J., 2000. New tuning method for PID control of a plant with under-damped response. Asian Journal of Control 2, 31–41.

I.A. Karimi and Rajagopalan Srinivasan (Editors), Proceedings of the 11th International Symposium on Process Systems Engineering, 15-19 July 2012, Singapore.

A New Strategy of Locality Enhancement for Just-in-Time Learning Method

Qing Lin Su,[a] Manabu Kano,[b] Min-Sen Chiu[a]

[a]*Department of Chemical and Biomolecular Engineering, National University of Singapore, 4 Engineering Drive 4, Singapore 117576, Singapore*
[b]*Department of Systems Science, Kyoto University, Sakyo-Ku, Kyoto 606-8501, Japan*

Abstract

Just-in-Time Learning (JITL) method has recently received increasing attention, particularly its application to control and soft sensing. Unlike the conventional JITL methods, which construct a local model directly based on the relevant data selected from reference database, a novel strategy is proposed by considering the local model as a Taylor series of the global model expanded in the vicinity of a reference point. This reference point could be chosen as the most relevant data or the query data. A comparative study using a benchmark nonlinear CSTR process showed the efficiency of the proposed strategy by achieving better prediction than its conventional counterparts.

Keywords: Data-Based; Local Model; Just-in-Time Learning; Locality Enhancement

1. Introduction

Just-in-Time Learning (JITL) methodology approximates a nonlinear system with a set of local models valid in the relevant operating regimes (Atkeson et al., 1997; Bontempi et al., 1999). There are three steps, i.e., relevant data selection from database according to some similarity criterion, local model construction based on the relevant data, and model prediction using the local model and query data, associated with the JITL modeling. Recent developments include the combination of distance and angular metrics to characterize the similarity between query data and relevant data by Cheng and Chiu (2004), and the use of correlation measure proposed by Fujiwara et al. (2009). Recently, the supervised locality preserving projection was applied to the JITL modeling (Chen et al., 2011), which is capable of finding a projection vector from which both input variables and output variables can be used for similarity evaluation. However, previous local models are directly based on the relevant data. In this paper, a new strategy of locality enhancement by considering the local model as a Taylor series of the global model expanded around a reference point, which can be selected as the most relevant data or query data, is explored and applied to the JITL modeling.

2. Conventional Just-in-Time Learning Techniques

Suppose the relationship between the input $\mathbf{x} = [x_1, x_2, \ldots x_M]^T$ and output y is $y = f(\mathbf{x})$; and an available reference database given by $\boldsymbol{\psi} = [y_i, x_{i,1}, x_{i,2}, \ldots x_{i,M}]_{N\times(M+1)}$, where $i = 1, \cdots, N$, N is the number of sample data, and M is the number of input variables. In what follows, JITL method based on distance and angular metrics (Cheng and Chiu, 2004) is briefly reviewed.

When a query data $\mathbf{x}_q = [x_{q,1}, x_{q,2}, \ldots x_{q,M}]^T$ comes, the distance and angular metrics are calculated by Eqs. 1 and 2, respectively. The similarity index, S_i, between ith data in

the reference database and the query data is calculated by these two metrics as given in Eq. 3, with $0 \leq \gamma \leq 1$ as a tuning parameter.

$$d_i = \left\|\mathbf{x}_i - \mathbf{x}_q\right\|_2 \tag{1}$$

$$\cos(\theta_i) = \frac{\Delta\mathbf{x}_i^{\mathrm{T}}\Delta\mathbf{x}_q}{\|\Delta\mathbf{x}_i\|_2 \cdot \|\Delta\mathbf{x}_q\|_2}, \quad \Delta\mathbf{x}_i = \mathbf{x}_i - \mathbf{x}_{i-1} \tag{2}$$

$$S_i = \gamma\sqrt{\mathrm{e}^{-d_i^2}} + (1-\gamma)\cos(\theta_i) \tag{3}$$

After the selection of k ($k_{min} \leq k \leq k_{max}$) relevant sample data, linear or nonlinear regression model is trained accordingly, by which the prediction is made.

3. Locality-enhanced Just-in-Time Learning

It is worth to note that the aim of JITL methodology is to find a local model around the query data and make a prediction accordingly. Hereby, if the local model can be built directly at the query data, its prediction would theoretically be much more accurate than the conventional local model that is constructed directly based on the relevant dataset. In light of this, the strategy of locality enhancement by considering the Taylor series expanded at the reference point as the local model is explored in this study.

In reference to an arbitrary point, $(a_1, \cdots, a_M)$, the process model can be represented by the Taylor series as an infinite sum of terms with coefficients calculated by the corresponding derivative at this particular point as follows:

$$f(x_1, \ldots, x_M) = \sum_{n_1=0}^{\infty} \cdots \sum_{n_M=0}^{\infty} \frac{(x_1-a_1)^{n_1} \cdots (x_M-a_M)^{n_M}}{n_1! \cdots n_M!} \left(\frac{\partial^{n_1+\cdots+n_M} f}{\partial x_1^{n_1} \cdots \partial x_M^{n_M}}\right)(a_1, \cdots, a_M) \tag{4}$$

where n_i is the order of derivative with respect to x_i.

There are two possible choices for the reference point, the most relevant data, $\boldsymbol{\varphi}_n = [y_n, x_{n,1}, x_{n,2}, \ldots x_{n,\mathrm{M}}]^T$ or query data, $\boldsymbol{\varphi}_q = [y_q, x_{q,1}, x_{q,2}, \ldots x_{q,\mathrm{M}}]^T$. When the most relevant data is considered, the remaining relevant data could be normalized by Eqs. 5 and 6, whereas the corresponding local model is given by Eq. 7.

$$\tilde{y}_i = \frac{y_i - y_n}{y_n}, \quad i=2, \cdots, l_r \tag{5}$$

$$\tilde{x}_{i,j} = \frac{x_{i,j} - x_{n,j}}{x_{n,j}}, \quad j=1, \cdots, M \tag{6}$$

$$\tilde{y}_i = \sum_{n_1=0}^{\infty} \cdots \sum_{n_M=0}^{\infty} \frac{\tilde{x}_1^{\,n_1} \cdots \tilde{x}_M^{\,n_M}}{n_1! \cdots n_M!} \left(\frac{\partial^{n_1+\cdots+n_M} f}{\partial \tilde{x}_1^{n_1} \cdots \partial \tilde{x}_M^{n_M}}\right)(\tilde{\mathbf{x}} = \mathbf{0}),\ n_1 + \ldots + n_M \neq 0 \tag{7}$$

where l_r is the number of relevant data.

When query data is used as the reference point, the input variables could be normalized similarly using Eq. 6. As the output variable y_q is not available and therefore it is set equal to the predicted output, $\hat{y}_q$. The corresponding local model is represented by Eq. 8. Compare to Eq. 7, the local model in Eq. 8 has one more parameter, $\hat{y}_q$. As a result, the output prediction $\hat{y}_q$ is obtained while training the local model.

$$y_i = \hat{y}_q + \sum_{n_1=0}^{\infty} \cdots \sum_{n_M=0}^{\infty} \frac{\tilde{x}_1^{\,n_1} \cdots \tilde{x}_M^{\,n_M}}{n_1! \cdots n_M!} \left(\frac{\partial^{n_1+\cdots+n_M} f}{\partial \tilde{x}_1^{n_1} \cdots \partial \tilde{x}_M^{n_M}}\right)(\tilde{\mathbf{x}} = \mathbf{0}),\ n_1 + \ldots + n_M \neq 0 \tag{8}$$

For the purpose of comparison between traditional and the proposed locality-enhanced local models, a schematic illustration is provided in Fig. 1. As the proposed new strategy of locality enhancement can be readily applied to existing JITL methodologies. The JITL developed by Cheng and Chiu (2004) is used as the benchmark (JITL-OR), while the predictive performance of the resulting JITL methods taking into account of reference point chosen to be the nearest relevant data (JITL-RN) and query data (JITL-RQ), respectively, is compared in a case study presented in the next section.

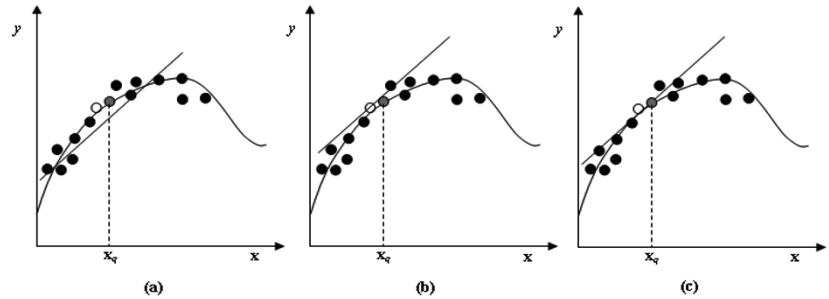

Fig. 1 Comparison of linear local model scheme: (a) JITL-OR; (b) JITL-RN; (c) JITL-RQ (● : relevant sample data; ○ : nearest relevant data; ● : query data)

4. Case Study: van de Vusse CSTR

To evaluate the proposed locality enhancement strategy, a nonlinear van de Vusse CSTR process is considered (Harris and Palazoğlu, 1998; Helbig et al., 2000). The reaction scheme is follows: $A \overset{k_1}{\rightarrow} B \overset{k_2}{\rightarrow} C$ and $2A \overset{k_3}{\rightarrow} D$. The reactor temperature T is controlled through a recirculating cooling medium in the jacket, where the medium temperature is manipulated through a heat flow Q_w. The feedstock of reactant A with concentration c_{A0} and temperature T_0 is introduced with flow rate F. The concentration of product B, c_B, is the process output which is influenced by the concentration of reactant A, c_A, and T, as well as the three process inputs, F, Q_w and c_{A0}. Five ARX local models are considered for one-step ahead prediction by the three JITL methods.

LM1 $c_B(k) = f\ [c_B(k\text{-}1), c_A(k\text{-}1), T(k\text{-}1), F(k\text{-}1), Q_w(k\text{-}1), c_{A0}(k\text{-}1)]$
LM2 $c_B(k) = f\ [c_B(k\text{-}1), c_B(k\text{-}2), T(k\text{-}1), F(k\text{-}1), Q_w(k\text{-}1), c_{A0}(k\text{-}1)]$
LM3 $c_B(k) = f\ [c_B(k\text{-}1), c_B(k\text{-}2), F(k\text{-}1), Q_w(k\text{-}1), c_{A0}(k\text{-}1)]$
LM4 $c_B(k) = f\ [c_B(k\text{-}1), T(k\text{-}1), F(k\text{-}1), Q_w(k\text{-}1), c_{A0}(k\text{-}1)]$
LM5 $c_B(k) = f\ [c_B(k\text{-}1), F(k\text{-}1), Q_w(k\text{-}1), c_{A0}(k\text{-}1)]$

To proceed to the JITL, a database containing 2000 sample data was generated by introducing random step changes in F, Q_w and c_{A0} within the ranges of ±50%, ±20%, and ±20% of their respective steady-state operating conditions, as shown in Fig. 2. The validation data was also generated in a similar fashion as shown in Fig. 3.

Each JITL method is fine tuned by choosing the parameters k_{min} and γ to give the best prediction accuracy. The results are summarized in Table 1, where RMSE represents the root mean square errors and Averaged-l_{opt} is the averaged number of relevant data selected during prediction. As k_{max} has least influence on JITL performance, k_{max} = 80 is used for all the JITL methods. It can be seen from the LM1, LM2 and LM4 cases that JITL-RN and JITL-RQ give better prediction than JITL-OR, while three JITL methods

give comparable prediction results for the LM3 and LM5 cases, where the temperature measurement is not included in the relevant data selection. Since temperature is an important variable affecting the reaction rate, advantages of the locality enhancement strategy may not be fully exploited when T is not considered in the relevant data selection. Representative prediction results using the LM2 local model are shown in Fig. 4. Furthermore, in case that relevant data are clustered near to the query data, like in LM1 and LM2 cases, fewer relevant data are utilized for the JITL with locality enhancement method, as indicated by a smaller averaged-l_{opt} in Table 1, implying that a stricter criterion on the linearity and locality around the query data, as shown in Fig. 1. Finally, as the essence of JITL-RN and JITL-RQ is similar to each other, their performance is comparable in all the tests. Based on the on-going discussions, it is evident that the proposed method indeed improves the performance of the original JITL method developed previously.

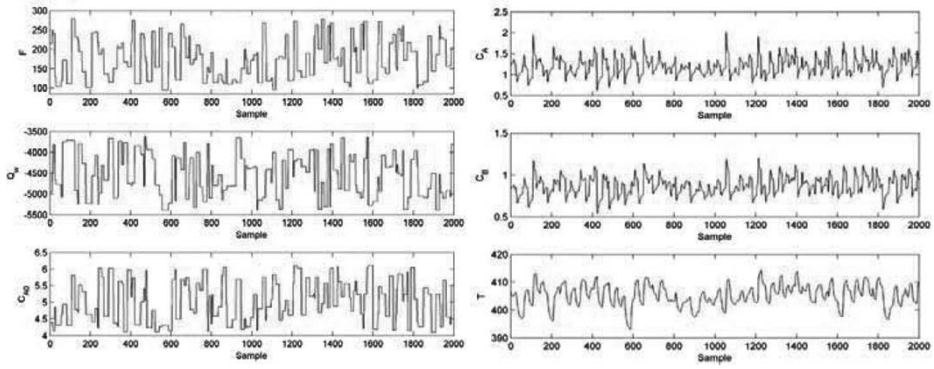

Fig. 2 Process data used to construct database for the JITL

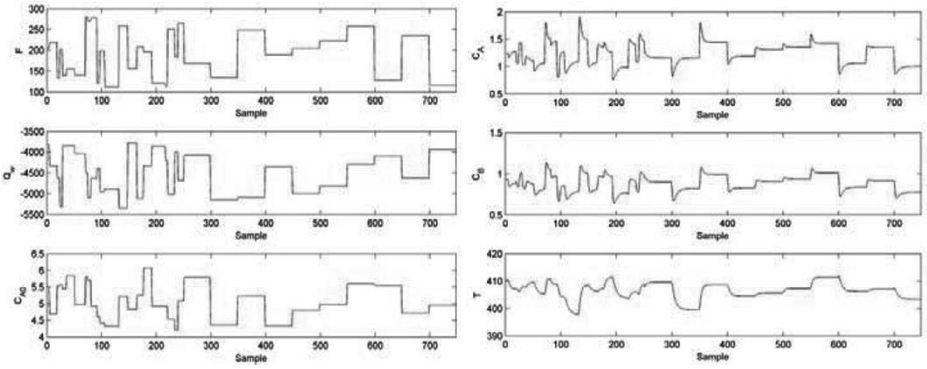

Fig. 3 Process data used for validation test

5. Conclusion

A locality-enhancement strategy for the JITL method is developed in the present study by considering the local model as a Taylor series of the global model expanded in the vicinity of the most relevant data or the query data, which focuses more on the query data rather than the whole relevant dataset. A comparative study using the van de Vusse CSTR process shows the efficacy of the proposed strategy by improving prediction accuracy compared with the conventional JITL method.

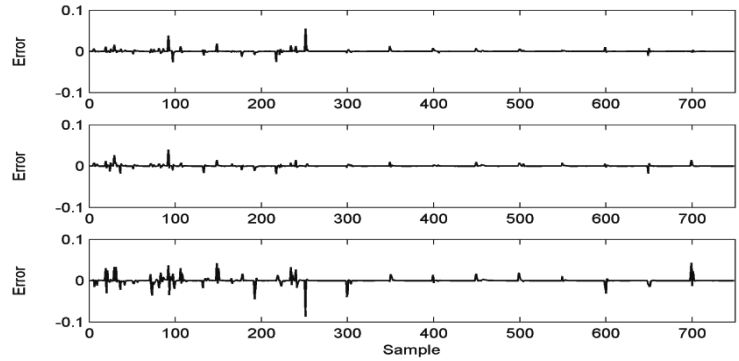

Fig. 4 Prediction errors of the JITL methods using the LM2 model

JITL-RN (top), JITL-RQ (middle), JITL-OR (bottom)

References

Atkeson C. G., Moore A. W., Schaal S. (1997) Locally weighted learning, *Artificial Intelligence Review*, **11**, 11-73.

Bontempi G., Birattari M., Bersini H. (1999) Lazy learning for local modeling and control design, *International Journal of Control*, **72**, 643-658.

Chen K., Ji J., Wang H., Liu Y., Song Z. (2011) Adaptive local kernel-based learning for soft sensors modeling of nonlinear processes, *Chem. Eng. Research and Design*, **89**, 2117-2124.

Cheng C., Chiu M. S. (2004) A new data-based methodology for nonlinear process modeling, *Chem. Eng. Sci.*, **59**, 2801-2810.

Fujiwara K., Kano M., Hasebe S., Takinami A. (2009) Soft-sensor development using correlation-based Just-in-Time Modeling, *AIChE Journal*, **55**, 1754-1765.

Harris K. R., Palazoğlu A. (1998) Studies on the analysis of nonlinear processes via functional expansions III: controller design, *Chem. Eng. Sci.*, **53**, 4005-4022.

Helbig A., Marquardt W., Allgöwer F. (2000) Nonlinearity measures: definition, computation and applications, *Journal of Process Control*, **10**, 113-123.

Table 1 Prediction performance of the three JITL methods

Local Model	Methodology	RMSE	Averaged-l_{opt}	k_{min}	γ
LM1	JITL-RN	0.002016	21.61	12	0.90
	JITL-RQ	0.002065	23.49	12	0.90
	JITL-OR	0.003375	40.79	30	0.90
LM2	JITL-RN	0.003450	23.73	12	0.65
	JITL-RQ	0.002922	31.74	20	0.70
	JITL-OR	0.007129	43.00	30	0.65
LM3	JITL-RN	0.006761	75.51	70	0.90
	JITL-RQ	0.007193	42.44	30	0.90
	JITL-OR	0.007255	42.55	30	0.90
LM4	JITL-RN	0.003155	42.20	30	0.85
	JITL-RQ	0.003894	43.23	30	0.85
	JITL-OR	0.019252	44.90	30	0.90
LM5	JITL-RN	0.012211	43.32	30	0.55
	JITL-RQ	0.011694	44.81	30	0.55
	JITL-OR	0.011392	23.84	12	0.60

I.A. Karimi and Rajagopalan Srinivasan (Editors), Proceedings of the 11th International Symposium on Process Systems Engineering, 15-19 July 2012, Singapore.

Hybrid Dynamic Modeling of 4-CBA Hydrogenation Fixed-Bed Catalytic Reactor of PTA Production Plant

Abbas Azarpour, Gholamreza Zahedi

Process Systems Engineering Centre (PROSPECT), Faculty of Chemical Engineering, Universiti Teknologi Malaysia, UTM Skudai, 81310 Johor Bahru, Johor, Malaysia

Abstract

In this paper, a dynamic hybrid model of 4-carboxybenzaldehyde (4-CBA) hydrogenation fixed-bed catalytic reactor of Purified Terephthalic Acid (PTA) production plant has been developed. At the first step, the deactivation model of the reaction system has been predicted by using artificial neural network (ANN) technique. Then, the deactivation model estimated by ANN as black box incorporated to first principle model (FPM) as white box. Therefore, the established hybrid model has been utilized to model the hydrogenation reactor of PTA plant. Finally, the simulated results have been compared with the industrial reactor data. It has been concluded that hybrid model is more precise than a FPM model.

Keywords: Terephthalic acid, hydrogenation, 4-carboxybenzaldehyde, hybrid modeling, deactivation.

1. Introduction

Purified terephthalic acid (PTA) is one of the most important chemicals as the major raw material to synthesize polyethylene terephthalate. Commercially, it is produced by the well-established process developed by the American Amoco Group. In this process, p-xylene (PX) is oxidized by air. The outlet main component of oxidation reactor which is called crude terephthalic acid (CTA) includes about 3000 ppm of 4-carboxybenzaldehyde (4-CBA) and 500 ppm of para-toluic acid (pta) as impurities. Since the amount of impurities is too high for polymerization, CTA is hydrogenated in a fixed-bed reactor (FBR) including carbon coated palladium (Pd/C) catalyst to convert the major impurity, 4-CBA, to pta. The final purified terephthalic acid contains less than 25 ppm of 4-CBA and 150 ppm of pta.

Several reports on modeling of fixed-bed reactors have been published with the aim of understanding the overall reactor performance and comparison of the predictions with experimental data among others (Goto & Smith, 1975; Levec & Smith, 1976; Herskowitz, 1985; Rajashekharam et al., 1998; Nijhuis et al., 2003; Bhaskar, 2004; Murali et al., 2007).

Shaogang et al. (2008) studied the mass transfer characteristics of the fixed-bed reactor for hydrorefining of terephthalic acid. They developed a steady state heterogeneous one-dimensional model of the reactor.

Hybrid model or gray box model (GBM)is a combination of first principle model (FPM) as white box and artificial neural network (ANN)as black box.

In this study, a hybrid model of the reactor performance consisting of FPM and the model predicting the deactivation behavior of the catalyst bed relied on ANN has been developed for the industrial fixed-bed reactor of PTA production plant. In hybrid model,

the catalytic hydrogenation reaction of 4-CBA in the three-phase reactor along with the deactivation of Pd/C catalyst implying the dynamic behavior of the system has been analyzed. A heterogeneous plug-flow model has been devised. This model is able to predict the trend of the Pd/C catalyst deactivation and components concentration distribution. Finally, the results of the dynamic model have been compared with the industrial data.

2. Hybrid Modeling of PTA Hydrogenation Reactor

In hydrogenation reactor, the feed is concurrently contacted with highly pressurized hydrogen from the top and they pass through a catalytic fixed-bed including Pd/C. Therefore, the main impurity of CTA naming 4-CBA is hydrogenated to pta.

2.1. First Principle Modeling

To develop a simplified dynamic model of the reactor for describing the hydrogenation reactions, it has been assumed that the reactor operates under unsteady state and isothermal conditions. Moreover, the chemical reactions take place on the surface of the catalyst particles. A plug flow behavior of gas and liquid phases in axial direction along the reactor has been developed. Generalized power law has been used to present the deactivation model in FPM (Bartholomew, 2001). This model is able to predict the concentration of the reaction components and the weakness of catalytic potentiality of Pd/C catalyst.

2.1.1. Reactions

Hydrogenation reaction of 4-CBA is a two-step process. At the first step, 4-CBA is hydrogenated to 4-hydroxymethylbenzoic acid (4-HMBA) which eventually converts to pta (Zhou et al., 2006). The following reactions show the mentioned steps:

$$C_8H_6O_3\,(4-CBA) \quad + \quad H_2 \xrightarrow{Pd/C} C_8H_8O_3(4-HMBA) \tag{1}$$

$$C_8H_8O_3\,(4-HMBA) + \quad H_2 \xrightarrow{Pd/C} C_8H_8O_2\,(pta) \; + \; H_2O \tag{2}$$

The kinetic rate equations of the reactions are following:

$$r_1 = k_{\circ_1} \exp\left(-\frac{E_1}{RT}\right) C_{4-CBA}^{0.96}\, C_{H2}^{0.24} \tag{3}$$

$$r_2 = k_{\circ_2} \exp\left(-\frac{E_2}{RT}\right) C_{4-HMBA}^{0.61}\, C_{H2}^{0.75} \tag{4}$$

where $k_{\circ_1}$ and $k_{\circ_2}$ are 0.04738 $\frac{m^{3.6}}{kmol^{0.2}.s.kg}$ and 0.15272 $\frac{m^{4.08}}{kmol^{0.36}.s.kg}$, respectively, and E_1 and E_2 are 16976.4 $\frac{kJ}{kmol}$ and 23438.6 $\frac{kJ}{kmol}$, correspondingly (Shaogang et al., 2008).

2.1.2 Mass Conservation

Mass balance for Hydrogen in gas phase is:

$$\varepsilon_g \frac{\partial C_{H_2,g}}{\partial t} = -u_g \frac{\partial C_{H_2,g}}{\partial z} - K_{H_2,gl} a_{gl} \left(\frac{P_{H_2}}{H_{H_2}} - C_{H_2,l}\right) \tag{5}$$

Mass balance for Hydrogen in liquid phase is:

$$\varepsilon_l \frac{\partial C_{H2,l}}{\partial t} = -u_l \frac{\partial C_{H2,l}}{\partial z} + K_{H_2,gl} a_{gl} \left(\frac{P_{H2}}{H_{H2}} - C_{H2,l} \right) - k_{H_{2,ls}} a_{ls} (C_{H2,l} - C^S_{H_2,s}) \quad (6)$$

Mass balances for other components are:

$$\varepsilon_l \frac{\partial C_{i,l}}{\partial t} = -u_l \frac{\partial C_{i,l}}{\partial z} - k_{i,ls} a_{ls} (C_{i,l} - C^S_{i,s}) \quad (7)$$

The components transported between liquid and solid phases are consumed or produced by the chemical reaction at the surface of the catalyst, according to the following differential equations:

$$\varepsilon_p (1 - \varepsilon_B) \frac{\partial C_{i,s}}{\partial t} = k_{i,ls} a_{ls} (C_{i,l} - C^S_{i,s}) \pm \sum_{j=1}^{2} r_j \eta_j \rho_B a \quad (8)$$

The following boundary and initial conditions have been considered to solve the model.

Initial Conditions:

For t = 0 at z = 0 $C_{i,g} = C^0_{i,g}$; i is hydrogen.

$C_{i,l} = C^0_{i,l}$; i are 4-CBA, 4-HMBA, pta.

$C_{i,s} = C^0_{i,s}$; i are 4-CBA, 4-HMBA, pta.

For t = 0 at z > 0 $C_{i,g} = C^{ss}_{i,g}$; i is hydrogen.

$C_{i,l} = C^{ss}_{i,l}$; i are 4-CBA, 4-HMBA, pta.

$C_{i,s} = C^{ss}_{i,s}$; i are 4-CBA, 4-HMBA, pta.

Boundary Conditions:

For t > 0 at z = 0 $C_{i,g} = C^0_{i,g}$; i is hydrogen.

$C_{i,l} = C^0_{i,l}$; i are 4-CBA, 4-HMBA, pta.

$C_{i,s} = C^0_{i,s}$; i are 4-CBA, 4-HMBA, pta.

a is the deactivation parameter of the system.

2.2 ANN Modeling

In this study, deactivation model has been derived by employing Artificial Neural Network. To train the network, Levenberg-Marquardt training algorithm was found to be suitable to estimate the deactivation parameter of the catalyst.

Time, and the concentrations of hydrogen, 4-CBA, 4-HMBA, and pta were the inputs of the ANN and the deactivation parameter was its output.

3. Hybrid Model

Hybrid or GBM model which is a combination of FPM and ANN was used to simulate the reactor. The hybrid model is able to predict the concentration values of the components and the deactivation trend of the catalyst.

4. Results and Discussions

Fig. 1 displays the profile of the concentration of reaction mixture components in the catalytic reactor. It can be realized that the concentration of pta increases continuously whilst the concentration of 4-CBA decreases along the bed. Moreover, concentration of 4-HMBA reaches at the maximum value and then reduces to the end of the bed.

Fig. 2 shows the reduction of hydrogen in solid phase through the bed. It can be figured out that the consumption of hydrogen is notable at the early parts of the bed.

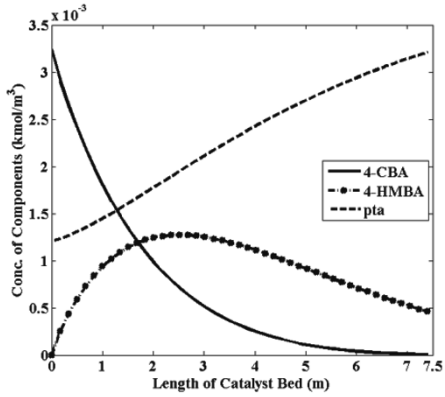

Fig. 1: Concentration profile of reaction components through the catalyst bed based on GBM.

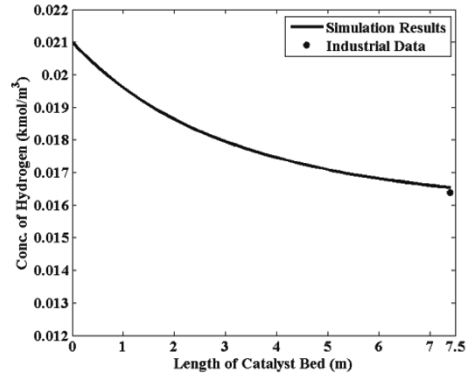

Fig. 2: Concentration profile of hydrogen through the catalyst bed based on GBM.

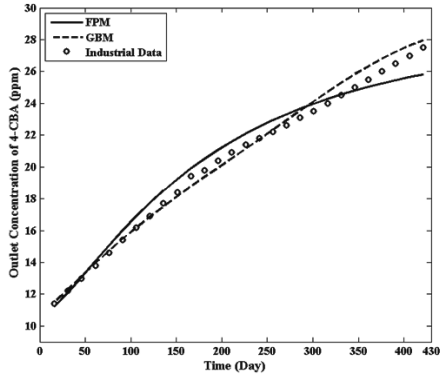

Fig. 3: Comparison of FPM and GBM with the industrial data based on the main impurity of PTA (4-CBA)

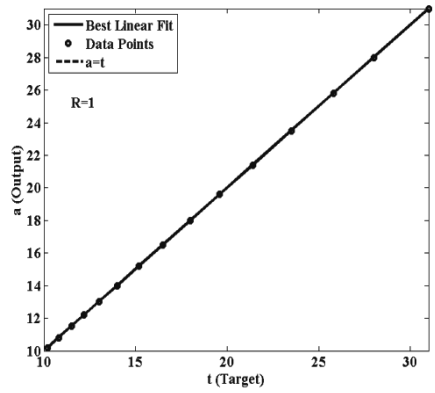

Fig. 4: ANN training regression for deactivation model

Fig. 3 compares the results of FPM with Hybrid model. It can be implied that the hybrid model is more precise than FPM.

Fig. 4 depicts the performance of the ANN which has been used for the deactivation model prediction. It is clear that the used network is very powerful to predict the required values of the deactivation model. To train the data, Levenberg-Marquardt algorithm has been employed with 70 neurons in the hidden layer.

5. Conclusion

In this paper, modeling of hydrogenation reactor of PTA plant has been carried out using gray box modeling technique. The gray box model incorporates both the ANN (black box) model and first principle (white box) model. To validate the devised gray box model, its prediction ability has been compared with the industrial reactor data. It has been concluded that the performance of gray box model is more precise than first principle model.

Abbreviations

C_i	concentration of component i (kmol/m^3)
E_j	activation energy of reaction j (kJ/kmol)
H	Henry's constant (barg.m^3/kmol)
$k_{\circ 1}$	frequency factor of reaction 1 (m$^{3.6}$/kmol$^{0.2}$.s.kg)
$k_{\circ 2}$	frequency factor of reaction 2 (m$^{4.08}$/kmol$^{0.36}$.s.kg)
$K_{i,gl}a_{gl}$	gas-liquid mass transfer coefficient of component i (1/s)
$K_{i,ls}a_{ls}$	liquid-solid mass transfer coefficient of component i (1/s)
P_i	partial pressure of component i (barg)
r_j	rate of reaction j (kmol/s.kg)
t	time (s)
T	temperature (K)
u_g , u_l	superficial velocity of gas and liquid (m/s)
Greek letters	
ε_B	bed void fraction (-)
ε_P	particle porosity (-)
ε_g	gas phase holdup (-)
ε_l	liquid phase holdup (-)
η_j	catalyst effectiveness factor (-)
ρ_B	bulk density (kg/m^3)
Superscripts and subscripts	
B	bed
g	gas phase
i	component index
j	reaction index
l	liquid phase
s	solid phase
ss	steady state
0	reactor inlet condition

ACKNOWLEDGEMENT

Financial support of Universiti Teknologi Malaysia (UTM) under grant no 4D042 is gratefully acknowledged.

References

C.H. Bartholomew, 2001, Mechanisms of catalyst deactivation, Applied Catalysis A: General, 212, 17-60.

M. Bhaskar, G. Valavarasu, B. Sairam, K.S. Balaraman, & K. Balu, 2004, Three-Phase Reactor Model to Simulate the Performance of Pilot-Plant and Industrial Trickle-Bed Reactors Sustaining Hydrotreating Reactions, Ind. Eng. Chem. Res., 43, 6654-6669.

S. Goto, & J.M. Smith, 1975, Trickle bed reactor performance Part II: reaction studies, AIChE J., 21, 714-720.

M. Herskowitz, 1985, Modelling of a trickle bed reactor: the hydrogenation of xylose to xylitol, Chem. Eng. Sci., 40, 1309-1311.

J. Levec, & J.M. Smith, 1976, Oxidation of acetic acid solutions in a trickle bed reactor, AIChE J., 22, 159-168.

C. Murali, R.K. Voolapalli, N. Ravichander, D.T. Gokak, & N.V. Choudary, 2007, Trickle bed reactor model to simulate the performance of commercial diesel hydrotreating unit, Fuel, 86, 1176-1184.

T.A. Nijhuis, F.M. Dautzenberg, & J.A. Moulijn, 2003, Modeling of monolithic and trickle-bed reactors for the hydrogenation of styreneChem. Eng. Sci., 58, 1113-1124.

M.V. Rajashekharam, R. Jaganathan, & R.V. Chaudhari, 1998, A trickle-bed reactor model for hydrogenation of 2,4 dinitrotoluene: experimental verification, Chem. Eng. Sci., 53, 787-805.

Z. Shaogang, Z. Jinghong, & Y. Weikang, 2008, Mathematical Simulation of Hydrorefining Reactor for Terephthalic Acid Stud. Surf. Sci. Catal., 24, 54-60.

J.H. Zhou, G.Z. Shen, J. Zhu, & W.K. Yuan, 2006, Terephthalic Acid Hydropurification over Pd/C Catalyst, Stud. Surf. Sci. Catal., 159, 293-296.

I.A. Karimi and Rajagopalan Srinivasan (Editors), Proceedings of the 11th International Symposium on Process Systems Engineering, 15-19 July 2012, Singapore.

Integrated Model-Based Support for the Design of Complex Controlled Systems

Martin Hüfner, Stephan Fischer, Christian Sonntag, Sebastian Engell

Process Dynamics and Operations Group, Department of Biochemical and Chemical Engineering, Technische Universität Dortmund, 44221 Dortmund, Germany

Abstract

In the model-based design of industrial controlled processes, many design data artifacts are generated, such as a variety of models in different formalisms, design-related documentation, and design parameters. This leads to several challenges: The use of model-based tools in each stage often requires remodeling due to incompatibilities of the employed model formalisms. This is costly and error-prone and may result in inconsistencies. Inconsistencies within the design data set can also arise due to the complex interdependence of design artifacts, leading to design errors that are often only detected late in the design process or even after commissioning. This paper illustrates the use of a software-based *Design Framework* for model-based design that was developed recently within the European project *MULTIFORM* (*www.ict-multiform.eu*). The goal of the *Design Framework* is to reduce the design effort, and thus the cost, while improving the quality of the designed system by *consistently integrating* the artifacts and tools that arise in model-based design processes. The set of model-based tools that can be applied in each design stage is expanded by automated model transformations via the general model exchange format *CIF* (http://se.wtb.tue.nl/sewiki/cif). To ensure that design inconsistencies and errors are detected as early as possible (i.e. when it is relatively cheap to correct them), the framework provides structured data and model management capabilities as well as automated design consistency checking and design parameter propagation. The framework is illustrated using a challenging case study, the model-based design of a pipeless plant, which employs many of the capabilities of the framework.

Keywords: Model-based design, Design support, Model exchange, Tool integration, Pipeless plants, Design consistency.

1. Introduction

The model-based design of complex systems and their control systems offers many advantages over traditional design methodologies, because it leads to shorter durations of the design process, increased reliability, and a more economical operation of the system. In recent years, sophisticated methods and tools have been developed for all stages of the design of controlled systems, ranging from requirement analysis and simulation to automatic controller synthesis and verification of the implementation of the control software. Although many of these model-based methods and tools are already used for specific tasks in industrial design projects, several challenges have to be solved to enable *integrated model-based design* in industry. The efficiency of the design process as well as the quality of the designed system crucially depend on the consistency of the design data set throughout the design process, since errors due to inconsistent design parameters or misunderstandings are costly if they are detected late in the design process. In addition, the manual management and adaptation of the design documentation, the design parameters, and of the variety of models present in modern

industrial design projects leads to duplications of work, is error-prone, and increases the duration (and thus the cost) of the design cycle. To overcome these challenges, a *Design Framework* (DF) for consistent integrated design with model-based tools has been developed in the European research project *MULTIFORM* (MULTIFORM (2008-2012)), with the Embedded Systems Institute (ESI) in Eindhoven, the Netherlands, as the main contributor (http://df.esi.nl). This framework supports a wide range of different design flows, enables the automated exchange of models between different design and analysis tools, provides design data and model management facilities, and enables a consistent representation and propagation of design parameters, including the detection of design conflicts (see Moneva et al. (2010) for more information on the DF). In this paper, the capabilities of the *Design Framework* are presented using a challenging case study, the model-based design of a pilot-scale chemical pipeless plant.

2. The Pipeless Plant

The pipeless plant (see Fig. 1) is a pilot-scale demonstration process that provides design and control challenges on different levels of the control and design hierarchies (which are also relevant in industrial design processes). It employs filling stations that feed colored water to mobile vessels. After filling, the vessels are transported by *Automated Guided Vehicles* (AGVs) to a mixing station, where plaster is added and the compound is mixed. The vessels are then transported to a storage station, where the plaster layer hardens. Several cycles of this process can be executed to obtain individually colored pieces of "plaster art". A central computer is responsible for the overall scheduling and control of the plant, while local controllers are installed on the hardware of the AGVs and of the stations. The movement of the AGVs is tracked by a camera. This flexible and dynamic production environment demands a design approach that is different to that used for traditional chemical plants, as the throughput in a pipeless plant depends not only on the production capacities, but also on their time-optimal usage. Although the chemical processes still have to be considered, the focus lies on the scheduling of the recipe steps, the coordination of the AGVs (path planning, collision avoidance, and docking control) and on a multitude of low-level control tasks. In this work, most of the design tasks are solved using model-based techniques within the *Design Framework*.

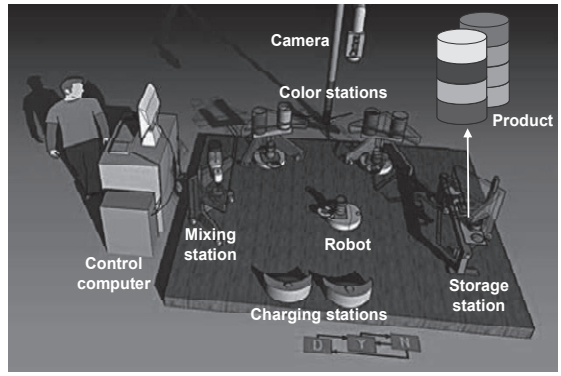

Fig. 1 Scheme of the pipeless plant.

3. The *Design Framework*

The *Design Framework* structures the overall *Design Flow* (see upper part of Fig. 2) into a number of *Design Steps* (DS), which represent the current design stage, and a number of *Design Decisions* (DD). While the *Design Flow* concept of the DF is generic and can be adapted to arbitrary design processes, the model-based design approach employed here follows the top-down approach that has been established in industrial practice. It starts with abstract models of the complete system that are used to roughly estimate the performance that can be expected from the chosen system structure, and to identify critical design problems and potential bottlenecks. In subsequent design steps,

these problems, and the system itself, are investigated and designed in more detail using refined models. To structure the plethora of design information that arises in such a design flow, each *Design Step* employs one or more *Design Views* (center part in Fig. 2), each representing a specific view on the system, e.g. structural composition or control systems hierarchy. The views are structured using *System Blocks* that may contain arbitrary design information, such as documents or models at different levels of abstraction. As different model types (possibly using different formalisms) are often employed in practical design processes, the DF provides a low-level integration and model exchange framework for the tools required in a design process. It currently supports many model-based engineering tools such as *UPPAAL* (Larsen et al (2010)), *Matlab/Simulink*, *Modelica* (MA (2011)), *gPROMS* (PSE (2011)), and *EcosimPro* (Jorrín et al. (2008)), as well as text processing tools. The exchange of models between different formalisms is achieved by automatic model transformations, enabling the designer to use the best tool for a given task. To store design information and parameters, the DF employs *System Parameters*, whose values can be propagated between the different models and design layers and whose consistency is monitored by the DF. Consistency and traceability is in addition facilitated by *Experiments* that store the parameters (i.e. the inputs, tools, tool parameters, models, and results) of any tool execution within the DF (see lower part Fig. 2). These *Experiments* can be reused, and their input parameters and results can directly be obtained from / stored in *System Parameters*.

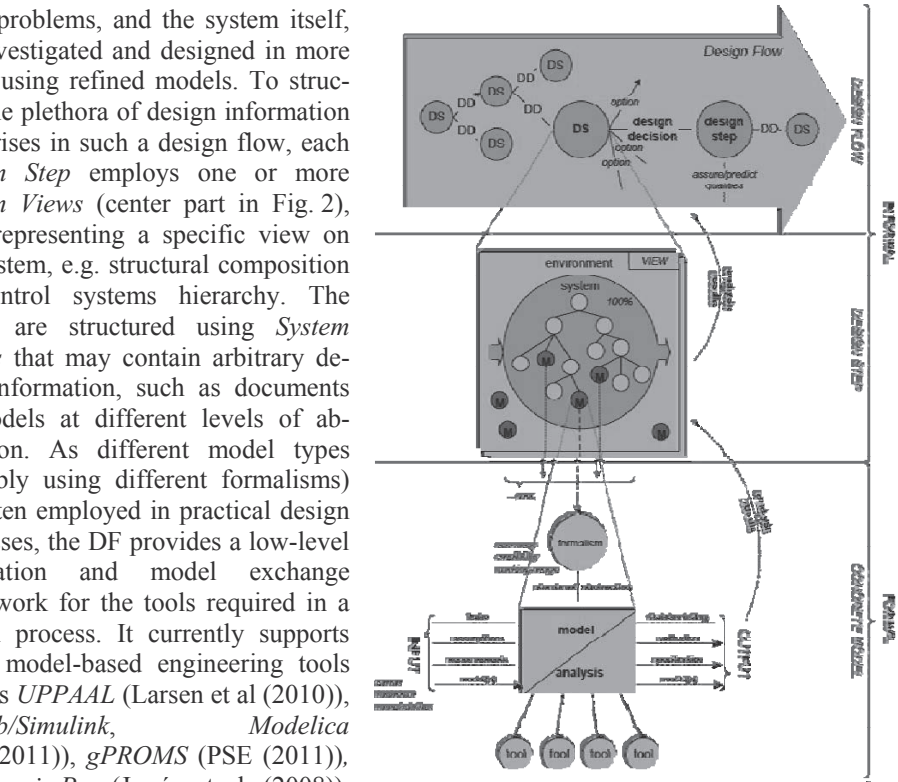

Fig. 2 Conceptual model of the *Design Framework* [2].

4. Model-based Design of the Pipeless Plant

Fig. 3 shows the design process that was developed for the pipeless plant in the *Design Framework*. The design flow starts with the ***Requirement Specification*** in which the requirements are collected and key design drivers are developed. In this step, a requirement view is created that contains a single system block that stores design parameters, such as the number of stations, the size of the plant area, the positions of the stations, and the desired throughput. In this stage, the values of these *Design Parameters* are roughly estimated since detailed information of these properties is not yet available.

In the step ***Layout Design***, rigorous model-based design based on the chosen parameters is started. A new *Design View* is created that contains a system block for the complete plant, which in turn contains sub-blocks for AGVs, the stations, and the plant area size. The design parameters from the requirement step are distributed to these new blocks, as shown in Fig. 3. In this step, the number and positions of stations and AGVs that will

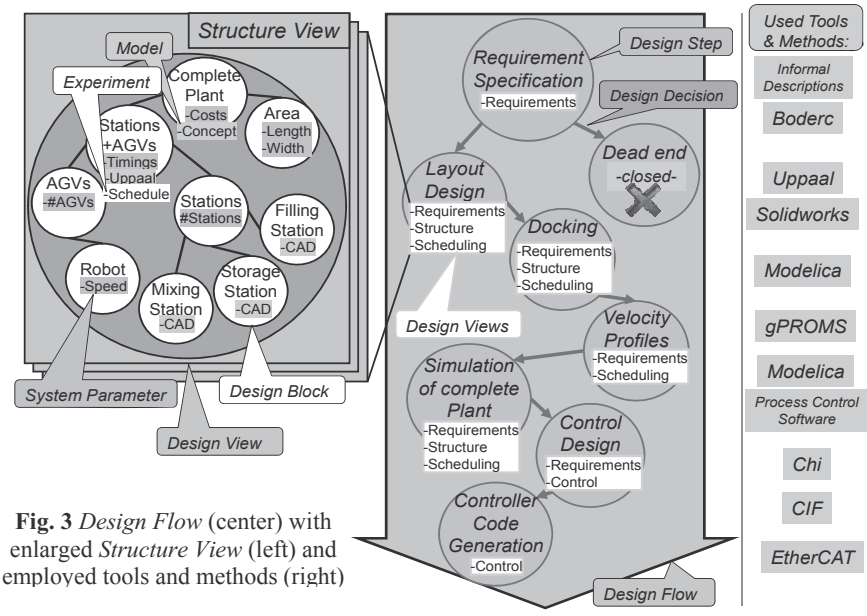

Fig. 3 *Design Flow* (center) with enlarged *Structure View* (left) and employed tools and methods (right)

provide the demanded throughput at minimal cost is determined using abstract plant models with timed dynamics, in which the durations of all plant activities are estimated based on tests at existing hardware. Then, the tool *UPPAAL* is used to derive optimal schedules for different plant configurations. All experiments are executed using parametrizable DF *Experiments*, and the results are stored in the DF database. After a suitable plant layout has been determined, its parameterization is stored in the DF parameter set (or existing parameters are updated)[1].

In the third step, the ***Docking Maneuver*** of the AGVs is explored in more detail, as it is a critical part in the operation in the plant that might have a strong impact on the throughput. To this end, a detailed spatial hybrid docking model based on differential-algebraic equation (DAE) systems is developed in *Modelica*. The results of this design step indicate that the initially assumed parameter values are valid.

To avoid the spilling of liquid during vessel transportation, in the fourth step the acceleration profiles of the AGVs are investigated. A detailed PDE *gPROMS* model of the liquid in the vessels is created, and the *gPROMS* optimization facilities are used to determine the maximally allowable acceleration of the AGVs to avoid spilling of the liquid, which also leads to the realization that the docking must be done more carefully than previously determined. Thus, the *Modelica* docking model is adapted with these results and is re-evaluated. The resulting longer docking time is propagated to the high-level *UPPAAL* model, and the scheduling *Experiment* is re-evaluated providing new values in the *Modelica* and *gPROMS* models. This circle is repeated until a fixed point of the system parameters is reached. In the fifth design step (***Simulation of Complete Plant***), a detailed plant model is created based on the design parameters determined in the previous steps, and the operation schedule determined in step 2 is validated on the detailed model, again leading to iterations through the design process in which the durations considered in the timed models used for scheduling are updated according to the

[1] Note that if any new parameter values conflict with other parts of the design, or if they invalidate previous experiment results, the consistency mechanism will notify the designer of these potential inconsistencies.

simulation results. All of the parameter propagations, experiment executions, and the design information management are handled by the *Design Framework*, ensuring a consistent design process documentation and a time-efficient design process.
After the high-level design steps, the low-level controllers are designed in the steps ***Control Design*** and ***Controller Code Generation*** using tools based on *Chi* (a process-algebraic modeling language, van Beek et al. (2008)) and *CIF* (an interchange format for hybrid systems, van Beek et al. (2009)) . The models for these steps can (partly) be transformed from the existing *UPPAAL* model via the DF, making manual model recoding mostly obsolete (Nadales et al. (2011)). The *Chi*/*CIF*-based tools employed here support the automatic generation of supervisory low-level controllers for the processing stations that can directly be connected to the pipeless plant via the *EtherCAT* protocol.

5. Conclusions and Future Work

This paper illustrates on a realistic case study that integrated software-supported model-based design can significantly speed up the design process compared to traditional design methodologies, as many of the previously manually executed tasks can be automated. In addition, it provides controlled processes of higher quality, since the integration ensures that design errors are detected very early. In future work, we will improve on the design process (e.g. by using correctness verification using tools such as *SpaceEx* (Frehse et al. (2011)) and *[mc]square* (Schlich & Kowalewski (2006)), and we are building a pipeless plant demonstrator based on the design presented in this paper.

This work has been performed as part of the MULTIFORM project, supported by the Seventh Research Framework Programme of the European Commission, grant agreement number: INFSO-ICT-224249. This support is gratefully acknowledged.

References

MULTIFORM, 2008-2012. Integrated Multi-formalism Tool Support for the Design of Networked Embedded Control Systems. EU-FP7 research project, contract number INFSO-ICT-224249, http://www.ict-multiform.eu.

Moneva, H., Hamberg, R., Punter, T., Vissers, J., 2010. Putting Chaos under Control: On how Modeling should Support Design. In *Proc. Int. Council on Systems Engineering*.

Larsen, K.G., Pettersson, P., Yi, W., 1998. UPPAAL in a Nutshell. In *Int. Journal on Software Tools for Technology Transfer* 1, 134-152.

Modelica Association, 2011. Modelica - A Unified Object-oriented Language for Physical Systems Modeling. http://www.modelica.org.

Process Systems Enterprise (PSE), 2011. gPROMS. http://www.psenterprise.com/gproms.

Jorrín, A., de Prada, C., Cobas, P., 2008. EcosimPro and its EL Object-Oriented Modeling Language. In *Proc. 2nd International Workshop on Equation-Based Object-Oriented Modeling Languages and Tools*, 2008, 95-104.

van Beek, D.A., Reniers, M.A., Schiffelers, R.R.H., Rooda, J.E., Hofkamp, A.T., 2008. Syntax and Formal Semantics of Chi 2.0. *Technical Report 2008–01*, SE, TUE, http://goo.gl/e5jxl.

van Beek, D.A., Collins, P., Nadales, D.E., Rooda, J.E., Schiffelers, R.R.H., 2009. New Concepts in the Abstract Format of the Compositional Interchange Format. In *Proc. IFAC Conf. on Analysis and Design of Hybrid Systems*, 250-255.

Nadales Agut, D.E., Reniersm, M.A., Schiffelers, R.R.H., van Beek, D.A. 2011. A Semantic-preserving Transformation from the Compositional Interchange Format to UPPAAL. In *Proc. IFAC World Congress*, 12496-12502.

Frehse, G., Le Guernic, C., Donzé, A., Cotton, S., Ray, R., Lebeltel, O., Ripado, R., Girard, A., Dang, T., Maler, O., 2011. SpaceEx: Scalable Verification of Hybrid Systems. In *Proc. Int. Conf. on Computer Aided Verification*, 379-395.

Schlich, B., Kowalewski, S., 2006. [mc]square: A Model Checker for Microcontroller Code. In *Proc. Conf. Leverag. App. of Formal Methods, Verification and Validation*, 466-473.

I.A. Karimi and Rajagopalan Srinivasan (Editors), Proceedings of the 11th International Symposium on Process Systems Engineering, 15-19 July 2012, Singapore.

Design and modeling of a new periodical-steady state process for the oxidation of sulfur dioxide in the context of an emission free sulfuric acid plant

R. Günther[a], J.C. Schöneberger[b], H. Arellano-Garcia[a], H. Thielert[b], G.Wozny[a]

[a] *Berlin Institute of Technology, Str. des 17. Juni 135, D-10623, Berlin, Germany*
[b] *ThyssenKrupp Uhde GmbH, Friedrich-Uhde-Str. 15, D-44141, Dortmund, Germany*

Abstract

The oxidation of sulfur dioxide over vanadium pentoxide catalysts represents a basic step in the sulfuric acid production process. In conventional sulfuric acid plants the SO_2 oxidation represents the limiting step with respect to the SO_2 emissions. Due to the fact that the SO_2 oxidation is an equilibrium reaction, sulfuric acid plants always have SO_2 emissions. In this work, a new process concept is presented, which uses the transient behaviour of the reaction in two reactors operating under unsteady conditions (**S**aturated **M**etal **P**hase reactor). Besides several advantages, which can increase the efficiency of the whole sulfuric acid process drastically, the SMP Reactor is a key component for an efficient operation of a sulfuric acid plant which reduces the emissions down to zero while keeping the necessary conditions for the hydrogenation unit installed downstream. For this purpose, a mathematical model is used, which describes the dynamic effects of the SO_2 oxidation. The model has been experimentally verified in a Miniplant, which works with commercial catalyst pellets.

Keywords: sulfur dioxide oxidation, unsteady state, sulfuric acid production

1. Introduction

Vanadium pentoxide based catalysts for the oxidation of sulfur dioxide to sulfur trioxide are some of the best investigated catalysts in heterogeneous catalysis. Due to the fact that sulfuric acid is one of the most important chemicals and sulfur dioxide oxidation is the basic step of the production process, research on the oxidation catalyst has been conducted for almost 40 years. Because of the equilibrium limited character of the reaction ($SO_2 + ½\ O_2 <-> SO_3$), it is impossible to reduce the SO_2 emissions down to zero at standard operating temperatures.

Investigations about the dynamic behavior of the reaction by Boreskov and Matros [1] observed a change of the catalyst structure depending on the exposed gas mixture. Also, several authors observed different behavior of the reaction between dynamic and steady state operation [1-4]. In our previous experimental kinetic studies, Schöneberger [4] observed a peak of the reaction rate whenever the catalyst is first exposed to oxygen and then to the reaction mixture that contained oxygen and sulfur dioxide. A reaction network that describes the whole catalytic cycle can explain this behavior [1]. The usage of the additional dimension of time gives the possibility to achieve a super-equilibrium which is limited by the equilibrium of one specific partial reaction in the catalytic cycle, which is then positioned far at the product side.

In the context of coking plant gas treatment, a new sulfuric acid process concept without any emissions is proposed. In this process concept, the sulfur dioxide in the sulfuric acid plant rest gas is hydrogenated to hydrogen sulfide and then recycled in the coking plant gas treatment. The use of a transient working oxidation is a promising process

alternative in order to meet the restrictions of sulfur dioxide and oxygen content in the hydrogenation reactor and the recycle gas.

2. Emission free sulfuric acid process

The simplified process concept of a classical wet sulfuric acid process in the context of coking plant gas treatment contains three basic unit operations. First, the H_2S in the sour gas is oxidized in a combustion unit to SO_2. In the following process step the SO_2 is oxidized to SO_3 over a vanadium pentoxide based catalyst. In a last step, the SO_3 is absorbed with water to H_2SO_4. The offgas of the limiting process step of the SO_2 oxidation in the vanadium pentoxide catalyst filled fixed bed reactor always contains SO_2 because of an incomplete conversion of the equilibrium reaction.

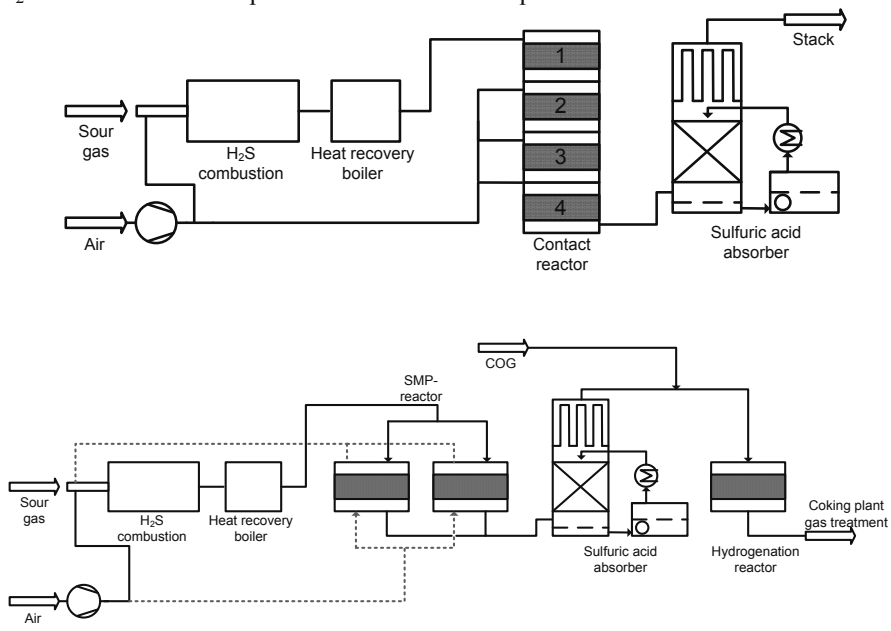

Fig. 1. Sulfuric acid plant and emission free sulfuric acid plant with SMP-reactor

In the emission free sulfuric acid plant this SO_2 will be hydrogenated completly to H_2S (SO_2+3H_2 <-> H_2S+2H_2O). Because of the intolerance of the hydrogenation reactor to high oxygen concentrations in the process gas stream, it is necessary to optimize the oxidation reactor. To achieve an oxygen free outlet stream of the oxidation reactor, the SMP reactor is implemented, which uses the transient behavior of the reaction. This effect is based on the fact that vanadium pentoxide exists as a liquid metal phase at operation temperature. In this liquid metal phase, oxygen is chemisorpt. However, in the steady state operation, this partial reaction (Eq. 3) represents the limiting step. By passing only oxygen across the catalyst, for instance in form of air, the oxygen accumulates. The oxidation is initiated by feeding the reactor with a reaction mixture (SO_2, O_2, N_2). Thereafter, the rate limiting reaction changes into another much faster reaction (Eq. 1 or Eq. 2) for the time of oxygen excess. Thus, much higher reaction rates are possible during this period. With a proposed two reactor concept, one reactor oxidizes the SO_2 in the process gas, while the other reactor is saturated with oxygen. In Fig. 1, a conventional and an emission free sulfuric acid process is shown in

comparison. In the conventional process the sour gas is oxidized hyper-stoichiometrically to set the oxygen concentration for the first bed of the oxidation reactor. In the next beds, quench air is used to set the optimal temperature and reach a higher conversion. After the sulfuric acid absorber, the rest gas is realeased into the environment via a stack. In the emission free sulfuric acid process the sour gas is oxidized nearly stoichiometrically. Behind the heat recovery boiler, the SMP reactor oxidizes the SO_2 to SO_3 with a drastically increased reaction rate compared to the steady state process. Because of the oxygen free reactor inlet stream, an oxygen free reactor outlet stream is realized, which meets the requirements of the hydrogenation unit that is installed downstream. In the oxygen saturation halfcycle, the reactor outlet stream contains decreased oxygen content because of the chemisorption of the oxygen at the catalyst. The oxygen reduced process gas stream is fed into the combustion to lower the combustion temperature and reduce NOx formation. Behind the sulfuric acid absorber coke oven gas is mixed into the gas stream so as to provide the hydrogen for the hydrogenation reaction. The process gas is fed into the hydrogenation reactor which hydrogenates the SO_2 and the remaining O_2 to H_2S and H_2O. The process concept of the emission free sulfuric acid plant can generally be applied to every sulfuric acid process. However, in the context of coking plant gas treatment it is very efficient because scrubbers for H_2S containing gas streams are already in place and the offgas stream of the emission free sulfuric acid process can easily recycled into the coking plant gas treatment.

3. Model and numerical methods

For the simulation of the SMP process, the model needs to represent the dynamic behavior of the reaction. A model based on the overall reaction of the SO_2 oxidation (SO_2 + ½ O_2 <-> SO_3) does not consider the intermediate forms of the vanadium catalyst. The SO_2 oxidation takes place in a liquid metal phase [6] with the active species. Hence, besides interphase mass transfers, the reactions inside the metal phase have to be taken into account. Balzhinimaev [6] postulates the catalytic cycle with vanadium intermediates as follows:

$$V_2^{5+}O_2^{2-} + SO_2 \leftrightarrow V_2^{5+}O^{2-} + SO_3 \qquad \Delta_R^h = 42\ kJ/mol \qquad (1)$$

$$V_2^{5+}O^{2-} + SO_2 \leftrightarrow V_2^{5+}SO_3^{2-} \qquad \Delta_R^h = 80\ kJ/mol \qquad (2)$$

$$V_2^{5+}SO_3^{2-} + O_2 \leftrightarrow V_2^{5+}O_2^{2-} + SO_3 \qquad \Delta_R^h = 63\ kJ/mol \qquad (3)$$

$$2SO_2 + O_2 \leftrightarrow 2SO_3 \qquad (4)$$

$$V_2^{5+}SO_3^{2-} \leftrightarrow V_2^{4+} + SO_3 \qquad \Delta_R^h = -42\ kJ/mol \qquad (5)$$

The capacity for the absorption of SO_2, O_2, and SO_3 in the melt is described by Henry's law because of the high adsorption velocity. The reaction rates are described by the law of mass action proposed by Bunimovich [5].

The reactor model has been implemented as a heterogeneous and transient process model of a fixed bed reactor, which considers the gas phase and the catalyst phase separately. This modeling approach is necessary to display the components of the mobile phase (SO_2, O_2, SO_3) and of the immobile phase (SO_2, O_2, SO_3, $V_2^{5+}SO_3^{2-}$, $V_2^{5+}O_2^{2-}$, V_2^{4+}, $V_2^{5+}O^{2-}$). Furthermore, it makes sense for dynamic simulations to consider the delaying effects of the interphase mass and energy transfer. According to changes in the steady state solution, they have great impact on the dynamic solution [4].

The parameters assumed by Balzhinimaev et al. [6] could not be used because of working with real catalyst and not powdered catalyst like in common kinetic investigations. The deviation is assumed to be due to transport limitations, modified catalyst compositions, and different experimental conditions. The kinetic parameters are estimated with the measurement data from the miniplant as per description in [4]. The effort has to be made for each catalyst, which is used for dynamic processes, provided that reliable predictions shall be achieved.
For the numerical calculation, the model is discretised with finite differences along the spatial coordinate. The temporal coordinate is solved by a multistep solver using Backward Differential Formulas (BDF). Because of the finite differences discretisation in space, the jacobian matrix is very sparse and has a bandstructur. Therefore, the ODE solver works with a sparse jacobian matrix, which makes it much more efficient.

4. Experimental set up and process synthesis

To reduce development time for the new process, a methodology [4] is used which skips the estimation of kinetics in a lab, which is carried out in conventional approaches. The experimental data was obtained by a miniplant which works with commercial catalyst pellets directly. Hence, the generated data could be used for industrial reactor design. After the model validation in the pilot plant at the TU Berlin under ideal conditions, the involved reactions are to be investigated with real process streams parallel to the real process. Fig. 2 shows the experimental set up and the mobile miniplant for investigation of heterogeneous catalysts under industrial conditions.

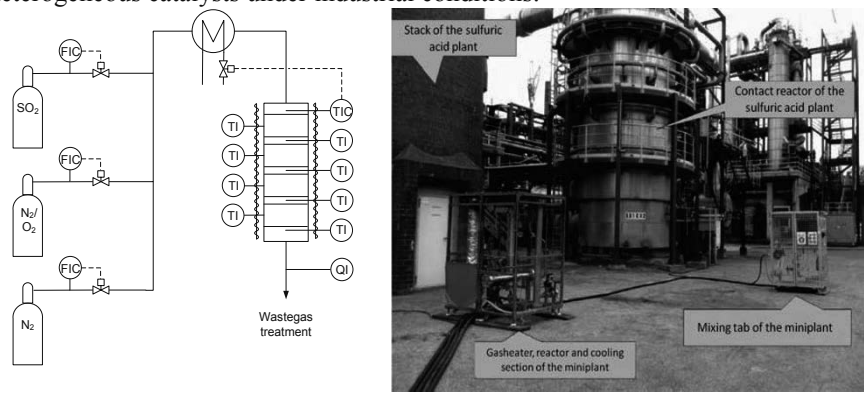

Fig. 2. Experimental set up for kinetic investigations of the sulfur dioxide oxidation and the mobile miniplant for reaserch under real plant conditions

5. Results and discussion

The obtained data is used for model validation and estimation of the kinetik parameters. Fig. 3 (left) shows the comparison between the temperature measurement behind each reactor bed and the corresponding simulation results. Each reactor bed has the same height such that measurement points are equidistantly distributed along the reactor. The reactor inlet stream contains SO_2, O_2, and N_2. Before the reaction starts, the reactor is heated up with air, which saturates the catalyst with oxygen. From t=0s to t=1500s, an increased reaction rate can be observed. During this periode a nearly sulfur dioxide and oxygen free reactor outlet stream is present. At t=3000s the steady state operation has been established.

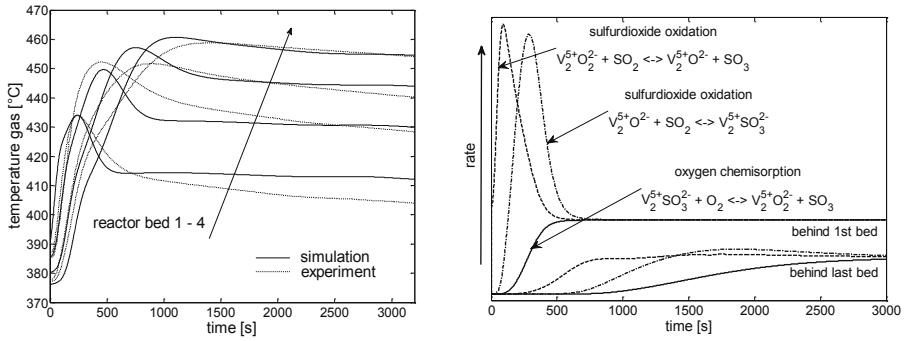

Fig. 3. Temperatures at four equidistant points in the reactor with the corresponding simulation results of the model and rates of the reactions Eq.1-3

Fig. 3 (right) gives a more detailed insight into the reaction. It displays the simulation associated reaction rates. For the sake of clarity, only the rates behind the first and the last reactor bed are shown. A large increase of the rates of reaction Eq.1 and Eq.2 can be observed during the time of $V_2^{5+}O_2^{2-}$ excess, before the rates converge to the limiting reaction of the O_2 chemisorption (Eq.3). In order to decrease the amount of kinetic parameters of the four reactions, the problem was divided into the oxygen enrichment and the oxidation of SO_2. While the model for the steady state operation could be fitted with temperature measurement data and the complimentary heat of reaction, a model considering the catalytic cycle with the elementary reactions has to be identified with concentration measurements. In both cases, a dynamically optimal experimental design has to be used so as to carry out the different phenomena of kinetics and absorption. After a fully identified model, plantwide optimization studies have to be carried out and the reaction has to be analyzed in terms of adaptability with real process gas streams at a last step in process synthesis.

6. Acknowledgement

The present work was supported by the Max-Buchner-Reserch Foundation and the Association of German Cokemaking Experts.

References

[1] Boreskov G.K., Matros Yu.Sh., 1983, Unsteady-state performance of heterogeneous catalytic reactions, Catalysis Reviews-Science and Engineering, 25, 551-590

[2] Dunn J.P., Stenger H.G., Wachs I.E., 1999, Oxidation of sulfur dioxide over supported vanadia catalysts: molecular structure - reactivity relationships and reaction kinetics, Catalysis Today, 51, 301-318

[3] Mezaki R., Kadlec B., 1972, Remarks on the reduction-oxidation mechanism of sulfur dioxide on vanadium catalyst, Journal of Catalysis, 25, 454-459

[4] Schöneberger J.C., 2010, Entwicklung und Analyse katalytischer Abgasbehandlungsprozesse am Beispiel der emissionsfreien Schwefelsäureanlage, Shaker Verlag Aachen

[5] Bunimovich G.A., Vernikovskaya N.V., Strots V.O., Balzhinimaev B.S., 1995, SO2 oxidation in a reverse- flow reactor: influence of a vanadium catalyst dynamic properties, Chemical Engineering Science, 50, 565-580

[6] Balzhinimaev B.S., Ivanov A.A., Lapina O.B., Mastikhin V.M., Zamaraev K.I.,1989, Mechanism of sulfur dioxide oxidation over supported vanadium catalysts, Faraday Discuss. Chem. Soc., 87, 133-147

I.A. Karimi and Rajagopalan Srinivasan (Editors), Proceedings of the 11th International Symposium on Process Systems Engineering, 15-19 July 2012, Singapore

Thinking Ontologies

Heinz A Preisig *
Department of Chemical Engineering; NTNU; Trondheim, Norway

Abstract

Ontologies are a means of abstraction and concentrating information. Whilst it has mostly found acceptance in the computer and information technology domain, it is an excellent thinking pattern promoting a more structural approach to chemical engineering problems on all levels, starting with the representation of functionalities, their combination to form processing units and combined again as whole plants. The concepts helps in constructing models that adhere to basic concepts as they are the foundation for physical processes: the conservation principles and the description of transport phenomena. The material models, the interaction between different chemical species or biological species form a knowledge framework suitable in in case of biological processes also intensively mapped into ontologies. When properly used, The high density of information, makes it easy to check consistency and the consistent use in all applications yields a framework that produces reliable, checkable results quickly and efficiently and consistency across applications that in the past have been without any information link.

Keywords: computer-aided modelling, software tools, process engineering

1. Structure is the Key

Ontologies have entered the chemical engineering community a couple of years ago stimulating their use as a thinking model. To the Chem Eng the concept of an ontology is almost provoking as its meaning implies foundation, in terms of knowledge and pure existence. Why provoking? Well because we all believe that we know our profession and we are using, and realising tools and solutions on the background of basic knowledge. So what about these ontologies? They do indeed provide base knowledge. They do though also offer a thinking pattern that first provides a motivation to put structure over our knowledge and secondly an abstraction lifting things up a level. Being harvested are the benefits of abstraction, namely a widening of the horizon, and a reduction of faults. Latter is mainly due to the direct use of theory in software for basic correctness checks, which also leads to the design of simpler underlying building blocks. Ontologies are not a source of new chemical engineering related information, but ontologies do add structure, which opens doors to do things differently and to do more of different things. In other words we really do not want to argue with our old fierce lady chemical engineering, but to give her a new nice chair to relax.

2. Ontologies are models

Ontologies are structures capturing the essential of a knowledge domain. The definition of a ontology is thus context dependent. Wikipedia defines ontologies in the context of computer science as: *...and information science, an ontology is a formal representation of knowledge as a set of concepts within a domain, and the relationships between those*

*Heinz.Preisig@chemeng.ntnu.no

concepts. It is used to reason about the entities within that domain, and may be used to describe the domain. In theory, an ontology is a "formal, explicit specification of a shared conceptualisation". An ontology provides a shared vocabulary, which can be used to model a domain – that is, the type of objects and/or concepts that exist, and their properties and relations. The concept of ontologies has been readily adapted by the system's biology community Courtot et al. (2011) and also chemical engineering has been working on conceptualising its knowledge Morbach et al. (2009); Yang and Marquardt (2009); Preisig (2011). These efforts focus on the representation associated with the core model, the model describing the process behaviour and its structure.

The ontology idea can though be carried further in the process involved in modelling and utilisation of models in computational engineering and it can also be expanded into the other direction, namely more towards capturing the nature of the process in terms of its basic functionalities. The ontology concept is applicable to any activity that involves abstract structures. The innovation, modelling, realisation and operation process all build on concepts, which can be thought of ontologies.

2.1. Process functionality dimension

Being confronted with a suggested process, a chemical engineer will use his experience to design a process Charpentier (2003), which involves understanding the chemistry and material properties of all chemical species involved. He will then suggest what network of unit operations will in his view produce the desired product.

But what unit operations to use? and in what network? The "basket" of operations can be seen as an ontology in which the functionality is primarily mapped into basic operations and secondarily into unit operations. For example functionality can be separation, which can be further detailed into for example co- and counter-current staged process, which in turn may be further detailed into liquid/liquid or gas/liquid separation systems leading to alternative realisations in the form of filter-like operations (membranes), crystallisation, extraction, distillation and the like. It can readily been seen that this structure is largely hierarchical where some of the layers may be interchanged but where the leave nodes are basic operations realisable as unit operations or combinations there off.

This dimension sets the industrial process in the centre, reflecting the paradigm-shift taking place in industry in which the intensified processing unit is set in the centre and all developments focus on this unit until production level is reached. The core is based on an ontology, representing the physical phenomena and process operations. Integration of these phenomena and operations results in process intensification; for example the concept of maximising surface/volume ratio, or the combination of different mechanism: e.g. diffusion and phase change. It is these set of rules and concepts, which form a type of "ontology".

Having derived an intensified unit from this core ontology, all activities focus on the development of this unit, i.e. the simultaneous development of all design and control aspects. Once developed and validated, the unit is multiplexed and embedded in the auxiliary parts of the plant providing feed preparation and product handling / separation units. In some cases the approach is different: devices are constructed such that the scale-up is solved a priori, when a series of equipment pieces exists for which the main characteristic design variable remains essentially constant. A very common one is a constant surface/volume ratio. Others multiplex in a different way, in that for example the mixing dynamics is being multiplexed, whilst dimension-related insensitive characteristics are scaled.

2.2. Modelling dimension

The units of the functionality ontology are to be modelled in order to enable studying the potential use of the unit in a network of units. The elements of the functional units are thus to be represented as mathematical objects describing their behaviour in the form of (partial) differential-algebraic equation systems. The mechanistic models are constructed on hard first principles such as the conservation principles of physics, fundamental energy functions and geometry (Preisig (2010)). The physical principles are augmented with structural principles, associated with constructing a network of systems that appropriately represents the plant. The latter is on the basis a spatial composition of the physical system augmented with the information processing system providing control. The first we term the physical topology, whilst the second is the information processing topology. The link between the physical topology and the conservation principles is formed by "what" is being "put" into the physical topology, in terms of mass and energy Preisig (2011).

For the formulation of the conservation principles one requires the information on how material, energy and momentum is crossing the surface of systems, how these quantities progress inside the system and how they are being modified. These descriptions involve material properties defining the need for material models, which, besides the exceptional ideal cases, are empirical models. These model components can also be represented as ontologies, which not only can be utilised in high-level modelling tools, but also in expert systems aiding the user to make an optimal model selection for their application.

The process-physics ontology, the material model ontology and the kinetics ontology are all having a structure that can be described as a multi-graph, which is a superstructure that combines several graphs thereby accommodating alternatives. For example for a type of transfer one may have more than one possible description, but only one can be used in an instantiated model. Thus a choice must be made. This can be done with an expert system or the user is given the opportunity to choose.

The view is that the ontologies are used in a modelling tool to assemble the plant model. They are also used to construct the modelling tool itself, so that the tool is context sensitive with the context being defined by the ontologies. The latter utilises the "rules" defined in the ontologies and implements them in the model editor.

The model then becomes an extract and a combination of elements of the involved ontologies, which is to be compiled into a target language and instantiated to form a mathematical problem. This in turn enables the use of tools for solving the problems associated with the plant: such as product design, process design all the way down to the detailed engineering design and operations design: control structure design, controller design, operator simulator, operator interface and process monitoring as well as planning and scheduling. This can also be extended to logistics. The here-defined ontology contains the structures to building models as dynamic systems represented as (partial) differential - algebraic equation systems together with structural elements such as hierarchical structure of the control volumes and control blocks, the species being involved, reactions and the like. The ontology may be hierarchical consisting of a root ontology which inherits structural information from subsidiary ontologies, examples being thermodynamic material models and kinetic models (Preisig (2010)).

The core modelling dimension must have the ability to generate, aggregate, decompose and link multi-scale application-tailored models efficiently and robustly. These models must then be made to match the applications requirements, which adds the next dimension.

2.3. Information technology dimension

The main issue in the information technology dimension is to enable a flexible exchange of information whilst avoiding duplication of information. Thus the idea comes about that there should be a centralised administration of information from which the software components required by the application can be produced through a factory.

So process information is put into the centre and parts of this information can be exchanged to various computational engineering applications. This approach builds a gear-network that links a large number of process systems and computational engineering applications together, stretching over: modelling, model simplification, approximations, different levels of design (screening, plant, engineering); but also control and operation-related activities such as: operator training, monitoring and plant scheduling, as well as alarm handling and more.

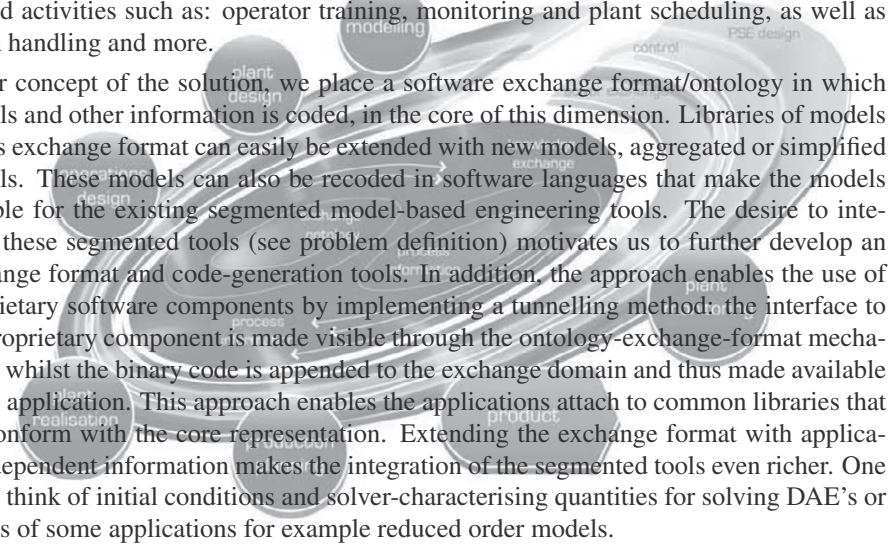

In our concept of the solution, we place a software exchange format/ontology in which models and other information is coded, in the core of this dimension. Libraries of models in this exchange format can easily be extended with new models, aggregated or simplified models. These models can also be recoded in software languages that make the models suitable for the existing segmented model-based engineering tools. The desire to integrate these segmented tools (see problem definition) motivates us to further develop an exchange format and code-generation tools. In addition, the approach enables the use of proprietary software components by implementing a tunnelling method: the interface to the proprietary component is made visible through the ontology-exchange-format mechanism, whilst the binary code is appended to the exchange domain and thus made available to the application. This approach enables the applications attach to common libraries that are conform with the core representation. Extending the exchange format with application dependent information makes the integration of the segmented tools even richer. One could think of initial conditions and solver-characterising quantities for solving DAE's or results of some applications for example reduced order models.

The top-level ontology is the one for the representation of the exchange format. It will typically use a template for the representation of all knowledge associated with the various computational engineering tasks. An ontology interfacing the exchange format with the centralised knowledge base enables the construction of a model warehouse. One such effort is reported on MODELISAR webpage (Modelisar (2012)), an effort of the Modelica Modelica (2009) community to define a simpler interface and presentation of process models and associated data. The extensions are mainly in the direction of optimisation. Whilst this effort is mainly used in the domain of megatronics applications, the idea is absolutely transferable to chemical engineering models. It is no parts specific to the application domain. The approach promises to be easier and more broadly applicable than the CAPE-OPEN approach (CoLan (2012)), which though has similar objectives.

3. Discussion

The concept of ontology can be directly projected into chemical engineering. For example we can define basic operations as elements of a plant ontology and construct new plants by generating different combinations of them. This would be a substitute of our old "bag of tricks", enabling a logical formal handling of the information and for example generate combinations automatically or in an optimal way, given a measure for quality of the design, a process which is likely to enable us to generate a very wide range of

combinations that we today term as ”intensified processes”. So this ontology would serve in the first place as our design ontology.

Collecting the theoretical pieces of chemical engineering into an ontology, capturing the basics of physical behaviour, adding the chemistry and the biology, yields a formal body of information to be used for constructing models for the processes. Obviously there is a close relation between the design ontology mentioned above and the modelling ontology, though in a quite different form, with the modelling ontology providing detailed process information.

The ontology concept applies equally well to the information processing and handling framework. Here we have a model for the plant design, plant control, operations design, plant realisation, product planning and product information as well as knowledge exchange. This ontology captures the different processes associated with design and operations on the different levels.

By clearly separating process ontology, from math model ontology and information handling ontology, we enable an integrated model-based computational engineering approach covering the range from process design to process realisation and process operations. The interlinking reduces the time from idea to realisation in all aspects whilst reducing the costs and increasing the efficiency. This in turn enables also the testing of many more alternatives in the same time, increasing the chance for finding a better solution, in terms of any objectives one may have in mind: profit, inter-operability, embedding in the environment, ecology and the like.

References

Charpentier, J.-C., 2003. Market demand versus technolgical development: the future of chemical enegineering. Int J Chem Reac Eng 1, A14. 2.1

CoLan, 2012.
URL http://www.colan.org 2.3

Courtot, M., Juty, N., Knupfer, C., Waltemath, D., Zhukova, A., Drager, A., Dumontier, M., Finney, A., Golebiewski, M., Hastings, J., Hoops, S., Keating, S., Kell, D. B., Kerrien, S., Lawson, J., Lister, A., Lu, J., Machne, R., Mendes, P., Pocock, M., Rodriguez, N., Villeger, A., Wilkinson, D. J., Wimalaratne, S., Laibe, C., Hucka, M., Le Novere, N., Oct. 2011. Controlled vocabularies and semantics in systems biology. Mol Syst Biol 7, –.
URL http://dx.doi.org/10.1038/msb.2011.77 2

Modelica, 2009. Modelica - a unified object-oriented language for physical systems modeling.
URL www.modelica.org/documents/ModelicaTutorial14.pdf 2.3

Modelisar, 2012.
URL http://www.functional-mockup-interface.org 2.3

Morbach, J., A, W., Marquardt, W., 2009. Ontocape – a (re)usable ontology for computer-aided process engineering. Comp & Chem Eng 33(10), 1546–1556. 2

Preisig, H. A., 2010. Constructing and maintaining proper process models. Comp & Chem Eng 34(9), 1543–1555. 2.2

Preisig, H. A., 2011. A multi-layered ontology for physical-chemical-biological processes. ESCAPE 21 (2011), Porto Carras, Chalkidiki, Greece 1, ISBN 978-0-444-53711-9 (ISBN 978-0-444-53711-9), 101–105. 2, 2.2

Yang, A., Marquardt, W., 2009. An ontological conceptualization of multiscale models. Comp & Chem Eng 33, 822–837. 2

I.A. Karimi and Rajagopalan Srinivasan (Editors), Proceedings of the 11th International Symposium on Process Systems Engineering, 15-19 July 2012, Singapore.

The impact of radiation on gas combustion modeling for a Kraft recovery boiler

Daniel J. O. Ferreira[a], Marcelo Cardoso[a], Song Won Park[a]

[a] *São Paulo University Av.Luciano Gualberto 380, São Paulo, Brazil*
[b] *Federal University of Minas Gerais – Av.Antônio Carlos 6627 Belo Horizonte , Brazil*

Abstract

The Computational Fluid Dynamics (CFD) has been used recently to develop comprehensive models to study and represent the largest possible number of physical and chemical process inside the equipment. The objective of present work is to evaluate two different numerical radiation method to simulate a Kraft recovery boiler by a comprehensive model on the commercial CFD code for the homogeneous combustion of the volatiles released from black liquor pyrolysis. The model considered the turbulent flow represented by the SST, and the gaseous homogeneous combustion of the volatiles CH_4 and CO by the EDM. The radiation was evaluated discussing no radiation, P1 Model and Discrete Transfer Model. As an additional result, the black liquor drops trajectories were calculated for a representative number of particles by one way coupling using the Ishii-Zuber drag particle model without any influence on the continuous phase. A detailed discussion about the radiation numerical methods is presented to pave the preliminary work aiming to reach the complete black liquor combustion with drying, devolatilization, pyrolysis and char combustion. The full discussion of the temperature and chemical composition profiles indicates several insights for better operational conditions.

Keywords: Combustion modeling, CFD, Radiation, Recovery boiler,

1. Introduction

According to the Brazilian Association of Pulp and Paper Inds, almost 91% of Brazilian pulp production are Kraft process whose chemical recovery boiler recycles reactants generating power and live steam (Vakkilainen et al., 2000). As any boiler, after bullnose there are convective heat transfer zones as economizers, pre-heaters and super-heaters. Bellow the bullnose, the in-flight black liquor drops are releasing volatiles and producing char in furnace. At the bottom of the boiler there is a porous structure called char bed where occurs the heterogeneous char combustion and reduction reactions of sodium and sulfur compounds. The control of the boiler temperature relies, basically, on the air supply strategy composed by three or four air. The specific function and impacts of each air level and *velocity profiles are detailed* in Ferreira *et al.*(2010). Under high temperatures (>1000°C) the radiation is a very significant heat transfer mechanism in the furnace (Siegel & Howell, 1992). The rates of the drying and pyrolysis of the black liquor combustion are strongly influenced by temperature, so the accurate prediction of the heat transferred by radiation is a very important task in the design and operation of combustion chambers (Carvalho & Farias, 1998). The objective of the present work is to analyze two different radiation models in the homogeneous gaseous combustion of the volatiles inside the recovery boiler furnace by CFD, aiming to obtain a comprehensive model.

2. Methods

What happens inside a boiler can be evaluated by numerical simulations for flow involving heat transfer, mixing of gaseous components, chemical reactions and particulate material drag into a computational domain representing its geometry, and it is possible to analyze a large amount of physical and chemical processes connected to the flow of combustion. Here the comprehensive modeling is adopted as the strategy to incorporate the turbulent flue gas flow, homogeneous combustion of volatiles and particulate drag. The turbulence is represented by the SST (Shear Stress Transport) model RANS because it is adequate to flow near domain walls (Versteeg & Malalasekera, 2007) and to the heat transfer between flue gases and surfaces (boiler walls and super-heaters) with heat conduction on the boundary layer. Even in regions with the lack of oxygen, the homogenous combustion of fuel gases from pyrolysis is highly dominated by gas mixing rate, with high Damköhler number, very suited for Eddy Dissipation Model (EDM), which one is simpler than Flamelet, without the needs for defining specific inputs for fuel and oxidant inlets to obtain values to mixture fraction on the β-PDF (Turns, 1996). EDM is controlled by turbulent time scales, able to represent the combustion of volatiles released by black liquor. The liquor spray is represented by the one way coupling model because the particles are very small and are diluted in the field. The flashing phenomena produces small regions of dense spray and another regions of transient diluted dispersed spray (Mikkulainen et al., 2007), promoting the insert of liquor in the boiler preferably into small droplets enough to make negligible influence on the continuous phase flow. The drag force of the flow in the droplets is represented by Ishii-Zuber model, that consider the drag on particles that could strain the shape of the droplets, it is a robust disperse phase drag model (Ishii & Zuber, 1979). The droplet size distribution for the insertion liquor chosen was the Rosin-Rammler distribution, widely adopted for liquor spary in Kraft recovery boilers (Englblom *et al.*, 2010, Bergroth *et al.*, 2010). The radiative heat transfer is described by:

$$\rho c_P \frac{DT}{Dt} = \beta T \frac{DP}{Dt} + \nabla.\left(k\nabla T - \vec{q}_r\right) + q''' + \Phi_d \qquad (1)$$

where the radioactive heat fluxes is $\vec{q}_r$. The last two terms means the heat generation per unit volume and time and the viscous dissipation function, respectively. The spectral radiation heat transfer equation (RTE) can be found in Versteeg & Malalasekera, (2007):

$$\frac{dI\left(\vec{r},\vec{s}\right)}{ds} = \kappa I_b\left(\vec{r}\right) - \kappa I\left(\vec{r},\vec{s}\right) - \sigma_s I\left(\vec{r},\vec{s}\right) + \frac{\sigma_s}{4\pi}\int_{4\pi} I_{-}\left(\vec{s}_i\right)\Phi\left(\vec{s}_i.\vec{s}'\right)d\Omega_i \qquad (2)$$

The left hand term represents the rate of variation of radiation intensity per path length. The first right hand term is the emitted radiant intensity, the second the absorbed radiant intensity, the third is the out-scattering radiant intensity and the last represents the in-scattering radiant intensity. Combining the absorbed and out scattering terms as a sum and manipulating them to define the single scattering albedo (Versteeg & Malalasekera, 2007),

$$\varpi = \frac{\sigma_s}{\kappa + \sigma_s}, \quad \text{and} \quad \tau = \int_0^s \left(\kappa + \sigma_s\right) ds' \qquad (3), (4)$$

So rewriting the eq. (2) with this variables and defining the source function as

$$S\left(\tau,\vec{s}\right) = \left(1-\varpi\right) I_b\left(\tau\right) + \frac{\varpi}{4\pi}\int_{4\pi} I_{-}\left(\vec{s}_i\right)\Phi\left(\vec{s}_i,\vec{s}\right)d\Omega_i \qquad (5)$$

the variation of radiation intensity now is :

$$\frac{dI(\tau,\vec{s})}{d\tau}+I(\tau,\vec{s})=S(\tau,\vec{s}) \tag{6}$$

Due to the complexity of the RTE integral-differential nature, analytical solutions aren't current available and the numerical models consider approximate equations for the source function. Both P_1 approximation and Discrete Transfer Method (DTM) are adequate for the radiation inside the boiler, the computational domain doesn't show high aspect ratio regions and its continuous participant medium is semi-transparent. The P_1 method provides an expression for the local divergence of the radiative flux in differential form Siegel & Howell (1992) expressing the radiative intensity field $I(\vec{r},\vec{s})=\sum_{l=0}^{\infty}\sum_{m=-l}^{l} I_l^m(\vec{r})Y_l^m(\vec{s})$ as 2-D generalized Fourier series. The radiative heat flux as function of incident radiative intensity, accordind to P_1 approximation has is:

$$\vec{q}_r=-\frac{1}{3(\kappa-\sigma_s)-A\sigma_s}\nabla I_- \tag{7}$$

Despite of the method doesn't present any restriction about isotropic emission, scattering or reflection, it presents significant errors to thin media with strongly anisotropic intensity distributions in 2D or 3D geometries (Lockwood & Shah, 1981). Higher order approximations (like P_3) can minimize, but not vanish, this problem but needs higher computation effort and implies in few increase in accuracy. The DTM uses the consideration of isotropy radiation directions and wavelengths. It was built on the concept of solving determinate rays inside the domain with specified directions solved only for paths between the determinate pairs of boundary walls (Marklund & Gebart, 2007). DTM establishes an equal division of hemispheres in N parts with azimuthal $\delta\theta=(\pi/2N_\theta)$ and polar $\delta\phi=(2\pi/N_\phi)$ angles. Each hemisphere has vectors tracing the emitted, absorbed, scattered and reflected radiation intensity distributions. The source function $(\varpi/4\pi)\int_{4\pi} I_-(\vec{s}_i)\Phi(\vec{s}_i,\vec{s})d\Omega_i$ from (5) is expressed in function of a sum of averaged intensity $I_{-,ave}(\vec{s}_i)$, so one has

$$S(\tau,\vec{s})=(1-\varpi)I_b(\tau)+\frac{\varpi}{4\pi}\sum_{i=1}^{N} I_{-,ave}(\vec{s}_i)\Phi(\vec{s}_i,\vec{s})d\Omega \tag{8}$$

The initial intensity of each ray at its originating surface element is given by:

$$I_0=\frac{q_+}{\pi} \quad \text{where } q_+=\varepsilon_s E_s+(1-\varepsilon_s)q_- \text{ and } q_-=\sum_N I_-(\vec{s})\vec{s}.\vec{n}d\Omega \tag{9}$$

The $\nabla\vec{q}_r=\frac{1}{\Delta V}\sum_{k=1}^{N}\delta Q_{gk}$ can be calculated by the net radiative heat flow with

$$Q_{si}=A_i(q_+-q_-) \quad \text{and} \quad \delta Q_{gk}=\int_{\delta\Omega}(I_{n+1}-I_n)A_i(-\vec{s}_k.\vec{n})d\Omega_k \tag{10), (11}$$

3. Simulation

The considered domain doesn't contain the superheaters ducts. The geometry and computational mesh is composed by 1,427,799 cells, refined in several regions, as shown in Figures 1 and 2. There are 5 inlet boundary conditions: air1, air2 and air3 air supplies, 12 liquor feeding ports and the char bed at bottom. The char bed where the residual char/ashes are leaving the system, is also considered as an open boundary which one allows the entrance of CO and CO_2 to the furnace as conversion of 70% this

char bed. The wall temperature was estimated on the coal boiler simulated in Butler & Webb (1991) and the Kraft recovery boiler wall ducts temperature. The volatiles are inserted directly in the liquor guns ports between the secondary and tertiary air. The surface coefficient tension comes from Adams *et al.* (1997) and the Rosin-Rammler distribution were obtained from Bergroth *et al.* (2010). As scattering effects should be considered in further particle heat transfer simulations using two-way, it was tested 8, 16, 24 and 32 ray tracing directions for DTM. One simulation considers homogeneous volatiles combustion without radiation, two simulations uses P_1 method and more 8 simulations use DTM.

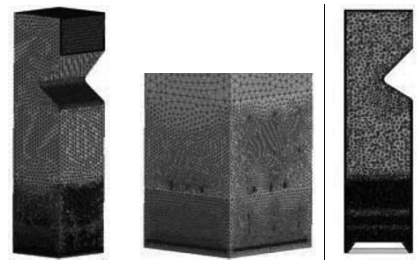

Figure 1: Cell distribution in computational mesh

4. Results

The results to the simulation without radiation show high temperatures above tertiary air level. When radiation is considered, the results showed profiles more coherent with expected behaviour presenting higher temperatures between the first tertiary air level and the bullnose in the Figure 2.

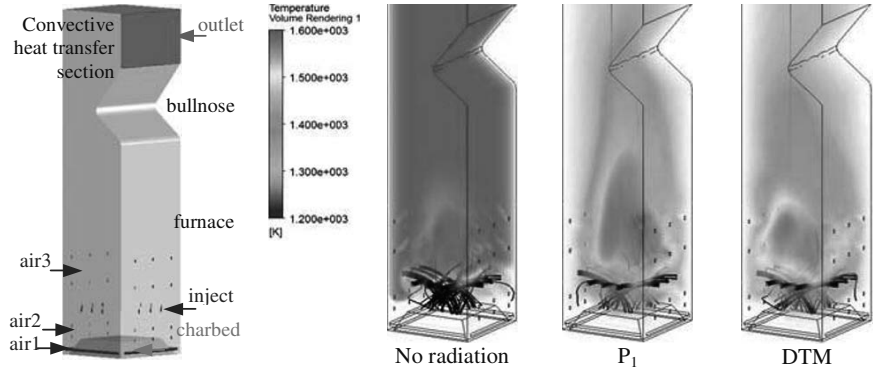

Figure 2: Geometry details and comparison of particle tracking trajectories and volume renderings to simulations a) without radiation; b) P_1 approximation; and c) DTM using 16 directions.

The P1 results showed a vertical larger region with higher temperatures than DTM results. Them temperature profiles follow the flow channeling shape observed in the velocity profiles as described in Ferreira *et al.* (2010). The obtained results to CH_4, O_2, CO, CO_2 and H_2O composition are coherent with the Eddy Dissipation Model proposal which reaction rate is strongly affected by turbulent eddies: CH_4 and CO react practically as soon as them enter the furnace. All profiles for the chemical compounds didn't present differences in all simulated cases, its consumption appears to be independent of radiation. The 90,000 liquor drop particles are represented by 70

trajectories chosen randomly. It was observed that the velocity and temperature profiles weren't affected by the number of directions, so it was chosen 16 directions to run the post processing to obtain the particle tracking trajectories. The comparison of particle trajectories and temperature volume rendering for the simulations without radiation, for P_1 approximation and DTM using 16 directions results is showed in Figure 2. The significant high value from simulation without radiation suggests that radiation works as way to distribute energy inside boiler and allows the heat loses through walls.

5. Conclusions

The presence of radiation showed influence on the velocity profile. Both velocities profiles from P_1 and DTM are similar presenting flow channeling as expected but the results without radiation showed ascendant flow near the walls. Anyway, radiation should be considered, even if there isn't disperse phase on simulations of combustion under high temperatures. According to the temperature profiles obtained, the most appropriate method among the tested to represent radiation for the comprehensive CFD model to a Kraft recovery boiler is the DTM due to its better similarity with expected and theoretical behavior. As all profiles obtained to DTM cases are equal, the choice of the amount of ray directions should be based on minimizing computational effort and to be accurate enough to represent radiation disperse particles in a further two-way coupling. A more accurate thermal profile, considering an adequate radiation heat transfer to represent the operation, can provide valuable information about a new air supply arrangement or better positions to insert the combustible or combustion air.

References

E. K. Vakkilainen, J. Gullichsen, H. Paulapuro, 2000, Kraft recovery boiler. TAPPI Press.

D. J. O. Ferreira, M. Cardoso; S. W. Park, 2010, Gas flow in a Kraft recovery boiler. Fuel Processing Technology, vol 91, pp. 789-798.

P. Mikkulainen, A. Kankkunen, M. Järvinen, C. J. Foegelhom, 2007, Significance of velocity in black liquor spraying. Tappi International Chemical Recovery Conference, pp. 403-406.

T. N. Adams, W. J. Frederick, T. M. Grace, M. Hupa, K. Lisa, A. K. Jones, H. Tran, 1997, Kraft recovery boilers. TAPPI Press, New York.

R. Siegel, R. Howell, 1992, Thermal Radiation Heat Transfer. Third Edition. Taylor & Francis Inc.

M. G. Carvalho, T. L. Farias, 1998, Modelling of heat transfer in radiating and combusting systems. Trans IchemE, vol 76, Part A, pp. 175-184.

H. K. Versteeg, W. Malalasekera, 2007, An introduction to computational fluid dynamics – the finite volume method. Second edition. Pearson Education Limited, England.

S. R. Turns, 1996, An introduction to combustion: concepts and applications. McGraw-Hill.

M. Ishii, N. Zuber, 1979, Drag coefficient and relative velocity in bubbly, droplet or particulate flows. AIChE Journal. n° 5, vol. 25, pp. 843-854.

M. Engblom, N. Bergroth, C. Mueller, A. Jones, A. Brink, M. Hupa, 2010, CFD – based modeling of Kraft char beds – part 2: a study on the effects of droplet size and bed shape on bed processes, TAPPI Journal, vol. 93 nº 2 p. 15-20.

N. Bergroth, M. Engblom, C. Mueller, M. Hupa, 2010, CFD – based modeling of Kraft char beds – part 1: char bed burning model, TAPPI Journal, vol. 93 nº 2 p. 6-13.

F. C. Lockwood, N. G. Shah, 1981 A new radiation solution method for incorporation in general combustion prediction procedures. Eighteenth Symposium (International) on Combustion. pp. 1405-1414.

M. Marklund, R. Gebart, 2007, Experiments and reactor model predictions in high temperature. black liquor gasification Tappi International Chemical Recovery Conference, pp. 147-154.

B. W. Butler, B. W. Webb, 1991, Local temperature and wall radiant heat flux measurements in as industrial scale coal fire boiler. Fuel, vol. 19, n° 12, pp. 1457-1464.

I.A. Karimi and Rajagopalan Srinivasan (Editors), Proceedings of the 11th International Symposium on Process Systems Engineering, 15-19 July 2012, Singapore.

Process development in a miniplant scale – A multilevel - multiscale PSE approach for developing an improved Oxidative Coupling of Methane process

Steffen Stünkel, Konstantin Bittig, Hamid-Reza Godini, Stanislav Jašo, Walter Martini, Harvey Arellano-Garcia, Günter Wozny

Technische Universität Berlin, Department of Process Engineering, Chair of Process Operation and Dynamics,Straße des 17. Juni 135, 10623 Berlin, Germany

Abstract

The oxidative coupling of methane (OCM) is a promising alternative route to olefins that converts methane to higher hydrocarbons and open up a new feedstock for the oil based industry. However, due to yield limitations of available catalysts and high separation costs for conventional gas processing, the OCM process has not been applied yet in the industry. Starting with process simulation and sensitivity studies a flexible mini-plant was built in this research so as to demonstrate technical feasibility of an efficient OCM process, model validity and to study long term effects. By this means a concurrent engineering approach was applied for the whole process while investigating each unit parallel. Moreover, catalyst with several reactor concepts like the fluidized bed and membrane reactor were investigated by CFD simulation, process simulation and experiments, in order to study catalyst life time, operation conditions and technical feasibility. Thus, the reaction section was improved from 16% yield to 18%. Furthermore, the separation part of the OCM process was energetically improved by an integrated down streaming unit for the CO_2. Thus, an energetic improvement of more than 40% in comparison to a benchmark absorption - desorption based CO_2 separation process was achieved. In addition to this, novel absorbents were studied starting with molecular simulation up to process simulation and experimental validation for the CO_2 separation. The results of the integrated process development and optimization process for the OCM will be presented and an overview of the multi scale and multilevel Process System Engineering (PSE) approach will be given for the case study.

Keywords: Oxidative Coupling of Methane, concurrent PSE approach, miniplant

1. Introduction

Oxidative coupling of methane to ethylene provides with natural- or biogas a new feedstock for the chemical industry and represents in combination with other alternative processes a promising alternative for the petro chemistry. However, although several process alternatives have been proposed in the literature (Lunsford, 1988), the industrial application of the stand-alone OCM process suffers in yield limitation and high separation costs for by-products, (Salerno, 2011). In a novel approach of concurrent engineering, the whole OCM process is investigated in miniplant scale, in order to study novel reactor concepts, as well as alternative separation processes and thus following new process concepts of Salerno (2011). Beside engineering aspects, the research cluster focus is also put on catalyst design. Therefore, the most promising catalysts that

tested in milligram scale under laboratory conditions by the cluster chemists (Simon et. al., 2011; Zavyalova et. al., 2011), was tested in gram scale in the miniplant under industrial close operation conditions (Jašo et. al., 2011). By this means that macro- and micro-kinetics of the catalyst are then studied.

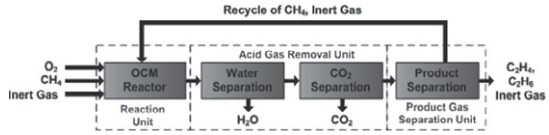

Figure 1: OCM Process flow sheet

To focus on the reaction part, fixed bed reactor (FBR), a fluidized bed reactor and a membrane reactor were investigated since they are the most common reactor types for OCM. Besides, in order to achieve high product quality, the reaction product gas has to be treated and the undesired side products have to be removed. Therefore, CO_2 has to be separated early in the process so as prevent condensation or freezing in the further product separation unit. The purpose of separation process synthesis for this design task was primarily the development of an integrated energy efficient gas treatment for 90% CO_2 removal under the particular OCM conditions of up to 25 mol% CO_2 in the raw gas with a feed pressure of 32 bar. The general flow sheet of the installed OCM process is presented in Fig. 1 and its implementation in a mini-plant scale can be seen in Fig. 5.

2. Catalyst selection – laboratory scale

In the novel multi-level PSE approach is a big emphasis of the research cluster put on catalyst design, concurrently to the process development. Thus studied Zavyalova et. al. (2011) more than 1000 full text references from about the last three decades of OCM's catalyst composition concerning their performance. Their statistical analysis of binary and ternary interactions between the elements showed, that Mg and La oxide based catalyst provides the highest performance concerning C_2 yield and selectivity.

However, the studies of Simon et. al. (2011) show, that the preparation route has a strong effect on the catalyst performance in OCM, especially for large scale heterogeneous catalyst preparation, like miniplant scale. Simon et. al. (2011) developed a homogeneous coating procedure of amorphous silica with dispersed Mn_2O_3 and Na_2WO_4 crystal layer in a fluidized bed technique. A Na–W–Mn/SiO_2 catalyst was prepared in a fluidized bed technique through which the core amorphous SiO_2 granules are homogenously coated by an injected solution containing Mn_2O_3 and Na_2WO_4 and results in a catalyst with 2wt% Mn(II) ions and 5wt% Na_2WO_4. Their catalyst remained constant performance over 24 h stability test in a packed-bed tubular reactor in laboratory scale with acceptable methane conversion and high C_2 selectivity. However, to approve the catalytic performance and to adjust the operation condition for the catalyst, it was tested in a miniplant scale fluidized bed reactor by Jašo et. al. (2011) and is discussed in detail.

3. Reactor concepts – mini-plant scale

In our miniplant scale research activity on the OCM process, the different reactor concepts were investigated from fixed bed reactor up to membrane and fluidized bed reactor. They are investigated concerning their performance in case of efficiency of selective-conversion and operability for the most promising catalyst. These reactor concepts include different feeding policies as well as safety and operating issues (Jašo et. al., 2011; Godini et.al., 2009). In this context, effect of operating parameters such as

temperature, pressure and inert gas along with the catalyst and reactor types, reactor dimension and combination of reactors not only on the performance of the reactor section, but also in the content of the downstreaming process, for the whole OCM process performance are analyzed.

3.1. Fluidized bed reactor

Fluidized bed reactors have been studied in several reactor engineering researches for OCM, also quite stable and efficient performance was reported especially in case of reactor operability and safety concerns. Due to the large exothermic of the OCM reaction, a fluidized bed reactor enables an almost isothermal reactor performance in OCM and was therefore the first investigated reactor type.

The activity and characteristics of the catalyst as well as the reactor operating conditions and taking some measures such as using inert gas diluents, affect the observed hot spot formation and therefore the reactor performance. However, the observed methane conversion was up to 45% with a C_2 selectivity of up to 84 % for a methane to oxygen ration of 10:1 and the particular ethylene yield results to 19.6 %.

Figure 2: CFD-Simulation, investigation of 4 different reactor geometries

3.2. Membrane reactor

Membrane reactors using porous inert membrane or catalytic dense membrane are among the most promising reactor concepts utilized for OCM (Godini et.al., 2009). Usually, a high selectivity toward C_2 production is achievable in a membrane reactor because of the fine dosing policy of oxygen. In the porous packed bed membrane reactor of Fig. 3, simultaneous high amount of methane conversion and C_2 yield was achieved by the fine oxygen dosing policy.

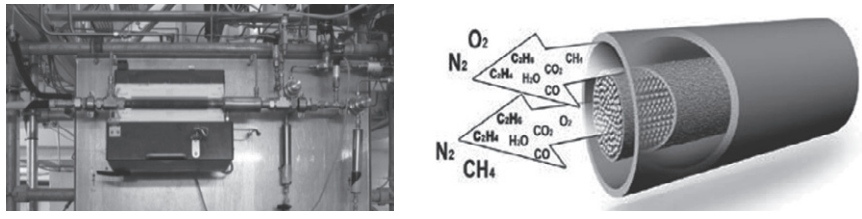

Figure 3: Experimental packed bed membrane reactor facility and principle

Moreover, the hot-spot formation is reduced by using porous membrane compared to a fixed bed reactor due to the feeding policy and its consequent low value of local methane to oxygen ratio. Although the observed nearly isothermal fluidized bed reactor performance was not reached in porous membrane reactor, the observed C_2 selectivity and yield was higher than in the fluidized bed. According to our experimental observations, porous packed bed membrane reactor shows 4-6 percent higher C_2 yield than the fixed bed reactor for the comparable set of operating conditions.

4. Downstream concept – miniplant scale

The gas purification of the reaction product gases as a major energy sink effects the overall process performance. Thus, it was improved particularly and is described in detail for the CO_2 removal. In the benchmark process for CO_2 removal was the developed rigorous process model for 30 wt% Monoethanolamine validated and a parity plot is presented in Fig. 4 for the experiments in miniplant scale. Furthermore, processes options using alternative absorbent and novel process concepts was studied concerning their energetic improvement for the OCM process and described below.

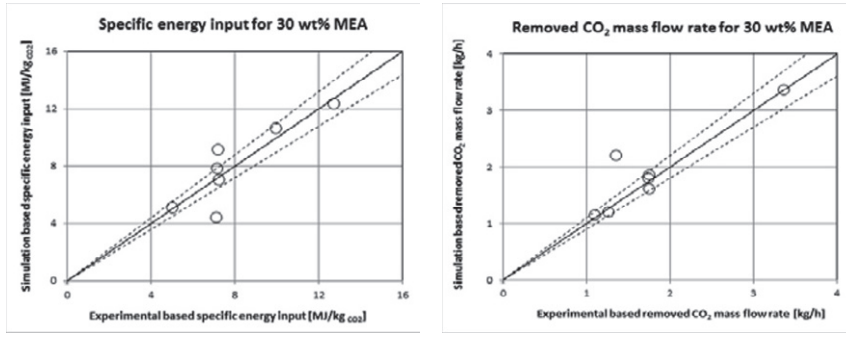

Figure 4: Parity plot of simulation results compared with the experiments for the specific energy input and CO_2 removed mass flow rate with +/- 10% relative deviation

4.1. State of the art CO_2 removal

The benchmark CO_2 gas purification unit for high purity and high selectivity consists of a chemical absorption process using an amine based absorbent. An energetic optimum for 30 wt% Monoethanolamine to achiev 90% CO_2 removal of the OCM product gas stream was found with 5 MJ/kg_{CO2}. Moreover, 37wt% N-Methyldiethanolamine (MDEA) as a ternary amine was investigated concerning the energetic advantage in the regeneration step. Due to the low reaction kinetics of the MDEA it was increased by using 3wt% of Piperazine as an activator. More than 30 % energy saving was achieved using the alternative absorbent in comparison to the benchmark absorbent.

4.2. Alternative process – membrane process

In previous studies membrane separation showed a high potential as an alternative for the OCM downstream (Stünkel et.al. 2011). The applicability and first evaluation of the separation efficiency in a OCM process was investigated using process simulation in Aspen Custom Modeler® (ACM). Therefore, a rigorous simulation model was implemented (Stünkel et. al. 2011) and several membrane materials were studied. Based on the simulation results, a matrimid based flat sheet membrane module from the HZG* with 0.5 m² membrane material was installed in the miniplant and the ACM model was validated.

4.3. Improved CO_2 removal

In order to reduce the energy demand a membrane was implemented prior to the absorption process so as to achieve a CO_2 stage cut of 0.5 with each separation principle. The CO_2 concentration was reduced from 25 vol% down to 17 vol% by the membrane. However, for further energy reduction regarding the benchmark process was Piperazine activated MDEA used in the hybrid process mode. Hence, the overall

* Helmholtz Zentrum Geestacht, Max-Planck-Straße 1, 21502 Geesthacht, Germany

specific energy demand per captured kilogram CO_2 was reduced to 2.74 MJ/kg_{CO2} with the hybrid membrane-absorption process configuration. Furthermore, the CO_2 removal rate for the hybrid process is much higher than the one of the benchmark process and a saving in column height results for the hybrid process to reach the 90% CO_2 removal. Moreover, in the hybrid process 20% of solvent flow rate was reduced in comparison to the benchmark.

5. Conclusion

An efficient state of the art OCM process was designed and improved using a multilevel, multiscale approach in a miniplant (Fig. 5). Several reactor concepts and catalysts studied in different scale, accompanied by fundamental catalyst research while using the most promising catalyst in the miniplant. Furthermore, an energy efficient CO_2 capture process for the oxidative coupling of methane was developed and compared with a benchmark process. Thereby, more than 40% energy reduction, more than 30% reduced column height and more than 20% solvent flow rate reduction was achieved experimentally with the membrane-absorption hybrid process in miniplant scale. More approach details as well as further results will be discussed in the presentation.

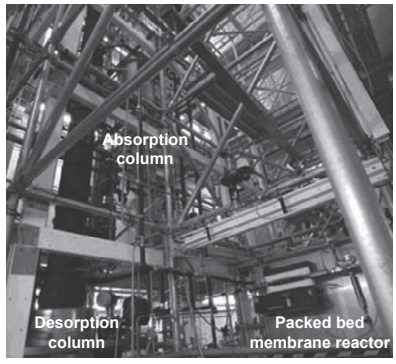

Figure 5: OCM miniplant

6. Acknowledgment

This work is part of the Cluster of Excellence “Unifying Concepts in Catalysis” coordinated by the Technische Universität Berlin. Financial support by the Deutsche Forschungsgemeinschaft (DFG) within the framework of the German Initiative for Excellence is gratefully acknowledged (EXC 314).

References

Godini H. R., Arellano-Garcia H., Omidkhaha M. R., Wozny G., (2009) Analysis of oxidative coupling of methane in membrane reactors, *Computer Aided Chemical Engineering, vol. 26*

Jašo S., Arellano-Garcia H., Wozny G., 2011, Oxidative coupling of methane in a fluidized bed reactor: Influence of feeding policy, hydrodynamics, and reactor performance, *Chemical Engineering Journal, doi:10.1016/j.cej.2011.03.077*

Lunsford J.H., (1988), Direct conversion of Methane to metahnol and higher hydrocarbons, *Studies in Surface Science and Catalysis,* Volume 36, pp. 359-371

Salerno S., Arellano-Garcia H., Wozny G., Techno-Economic Analysis for Ethylene and Methanol Production from Oxidative Coupling of Methane Process, 2011 *Computer Aided* Chemical Engineering, Volume 29, pages: 1874-1878

Simon U., Görke O., Berthold A., Arndt S., Schomäcker R., Schubert H., 2011, Fluidized bed processing of sodium tungsten manganese catalysts for the oxidative coupling of methane, *Chemical Engineering Journal, doi: 10.1016/j.cej.2011.02.013*

Stünkel S., Drescher A., Wind J., Brinkmann T., Repke J.-U., Wozny G., 2011, Carbon dioxide capture for the oxidative coupling of methane process – A case study in mini-plant scale, *ChERD, Vol. 8 9, pages: 1261–1270, doi:10.1016/j.cherd.2011.02.024*

Zavyalova U., Holena M., Schlögel R. and Bearns M., 2011, Statistical Analysis of Past Catalytic Data on Oxidative Methane Couplingt for New Insights into the Composition of High-Performance Catalysts, *ChemCatChem, doi: 10.1002/cctc.201100186*

I.A. Karimi and Rajagopalan Srinivasan (Editors), Proceedings of the 11th International Symposium on Process Systems Engineering, 15-19 July 2012, Singapore.

Phenomena-based Process Synthesis and Design to achieve Process Intensification

Philip Lutze, Deenesh K. Babi, John Woodley, Rafiqul Gani

Department of Chemical and Biochemical Engineering, Technical University of Denmark (DTU), DK-2800 Kgs. Lyngby, Denmark; rag@kt.dtu.dk

Abstract

Process intensification (PI) has the potential to improve existing processes, necessary to achieve a more sustainable production. PI can be achieved at different levels. That is, the unit operations, functional and/or phenomena level. The highest impact is expected by looking at processes at the lowest level of aggregation: phenomena. Therefore, in this paper, a phenomena-based synthesis/design methodology is presented. Using this methodology, a systematic identification of necessary and desirable (integrated) phenomena as well as generation and screening of phenomena-based flowsheet options are made using a decomposition based solution approach. The developed methodology is highlighted through a case study involving the production of isopropyl-acetate.

Keywords: Methodology, Phenomena, Process Synthesis, Process Intensification

1. Introduction

In recent years, PI has attracted much interest as a potential means of process improvement and to meet the increasing demands for sustainable production. A variety of intensified equipment have been developed, which potentially creates a large number of options to improve a process by PI. However, to date, only a limited number have achieved implementation in industry such as reactive distillation, dividing wall columns and reverse flow reactors [1]. One reason for this is that the screening of options and the identification of the best PI option is neither simple nor systematic.

In previous works [2, 3] we reported the development of a general systematic PI synthesis/design methodology in which the initial search space is defined by PI unit operations stored in a knowledge base. Even though process improvements have been achieved in several case studies, the methodology is limited to PI unit operations available in our knowledge base. In order to go beyond those and achieve even greater benefits by PI, process synthesis/design needs to be investigated at a lower level of aggregation, namely the phenomena level. The phenomena level has been considered before [4] with respect to synthesis and design of reactive distillation, but solution strategies for phenomena based design of whole processes not fixing the phenomena a priori, have not been developed, which is the objective of this paper.

In principle, synthesizing processes from phenomena may lead to a large number of process options. Thus, an efficient solution procedure for the mathematical synthesis problem is needed. The decomposition based solution approach has been selected to break down the complex mathematical synthesis problem into manageable sub-problems (steps) that allows the stepwise reduction of the search space. This approach has been used successfully in the area of computer-aided molecular design (CAMD) [5] and for synthesis of process flowsheets based on different building blocks [3, 6].

In this paper, the needed workflow to apply this methodology is presented together with illustration of its application through a new case study.

2. Methodology

In this section, the concept as well as the workflow of the phenomena-based synthesis/design methodology based on the decomposition approach is explained.

2.1. Phenomena building blocks and their interconnection/connection

Phenomena building blocks are based on mass, energy and momentum balances. They can be classified in terms of: mixing, stream dividing, phase contact, phase transition, phase change, phase separation, reaction and energy transfer phenomena [7]. The combination of phenomena to form simultaneous phenomena building blocks (SPB's in Fig.1) is governed by a set of interconnection rules. For example, a necessary interconnection of phenomena is phase transition phenomena needing a phase contact phenomenon. Integrating phase transition phenomena may be desirable for a reaction phenomenon limited to an unfavorable equilibrium. A dividing phenomenon cannot be connected to any other phenomena. SPB's may be connected in co-, cross- and counter-current forms by placing them into one or a number of stages of an operation to achieve a process task. This connection is following another set of rules based on the connectivity of inlet/outlet streams of SPB's that depend on their operating window. As shown in Fig.1, one or more phenomena form a SPB; each SPB may represent a stage; one or more stages form a unit operation; and one or more unit operations form a process flowsheet.

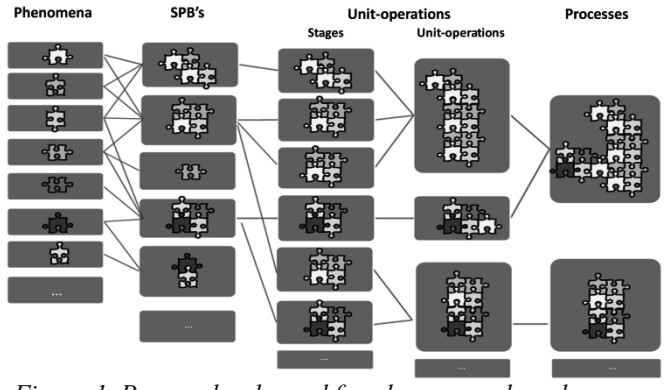

Figure 1. Process levels used for phenomena-based process synthesis/design.

2.2. Workflow of the phenomena-based synthesis/design methodology

The workflow of the methodology is given in Figure 2. The starting point of the methodology is either a base case design of an existing process or a new process.

In step-1, the synthesis/design problem with respect to PI is defined, including: the definition of the objective function; the process/operation scenario; and the constraints that the options need to match. Also, the performance metrics for evaluation of generated options are selected. In step-2, all process data, necessary to gain full understanding of the process is collected, and, based on this, limitations and their corresponding phenomena are identified. In step-3, the information from above is used for identification of suitable or desirable tasks that must be integrated to overcome the limitations. Output of this step is the search space of necessary and desirable phenomena within the process. In step-4, all phenomena are interconnected to form SPB's. Subsequently, the number of stages as well as their connections (co-, counter-, cross-current) to fulfil the necessary tasks is determined using an extended Kremser method [8]. This allows the identification of generic superstructures retrieved from a model library. SPB's can be inserted into stages of generic superstructures to form processes which are subsequently screened by logical and structural constraints (Eqs.2-3). In step-5, all PI options are screened for matching operation constraints (Eq.4-5). The remaining process options are screened for additional process constraints based on performance criteria (Eq.6).

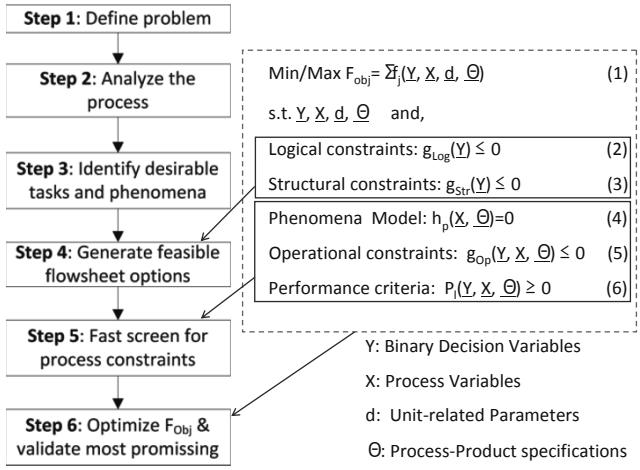

Figure 2. Workflow based on the decomposition approach.

Remaining options are transformed to unit operations using a set of integration rules. Subsequently, they are screened by operational constraints as well as performance criteria at the unit operational level. In step-6, in case after step-5 process variables are still not fixed, the remaining options are optimized (Eqs.1-6). If all variables have been already fixed in steps 1-5, the objective function (Eq.1) is calculated and all alternatives are ranked.

3. Case study

The methodology is applied to the production of isopropyl acetate (IPAc) which is an important bulk chemical product used widely as organic solvent [9].

IPAc is produced from isopropanol (IPOH) and acetic-acid (HOAc) heterogeneously catalyzed by Amberlyst 15 (Eq.7). The reaction takes place in the liquid phase.

$$CH_3COOH + C_3H_7OH \leftrightarrow C_5H_{10}O_2 + H_2O\,. \quad (7)$$

The base case design is a simple CSTR for a production of 50000 t/y of IPAc. The CSTR is assumed to run isothermal by T=330K and P=1bar. The feed is an equimolar mixture of the reactants. The reaction is not complete. In step-1, the scenario is restricted to design of a reactor with or without built-in separation for the continuous production of IPAc. The objective is to identify one apparatus with the lowest operational costs at lowest capital costs that achieves a conversion of 0.99. From the PI performance metric [2], options for energy, simplification, volume and waste are selected. Based on these, logical and structural constraints are retrieved from a knowledge base and operational constraints are set. In step-2, using a set of rules, the unit-operation based flowsheet is transformed to a task based flowsheet (necessary to identify the necessary phenomena for the process) and a phenomena-based flowsheet. The task is the conversion of IPOH and HOAc to produce IPAc. Hence, the reaction phenomenon is necessary. The involved phenomena to start with are liquid phase mixing, reaction and convective cooling for isothermal operation. Pure component, mixture and reaction analyses [2, 3] are performed to identify the limitations of the involved phenomena. The reaction analysis based on kinetics given by Lai et al. [9] confirmed the exothermic irreversibility and the equilibrium limitation of the reaction (K>1). In step-3, the knowledge base is contacted to identify possibilities for PI to overcome the identified limitations in order to achieve a conversion of 0.99. Since this case has an unfavorable equilibrium, the integration of the reaction task with a second reaction (of IPAc and/or H_2O) or a separation task (to remove IPAc and/or H_2O) using suitable phenomena are options obtained from the database. The latter is selected here because reactions converting water into a valuable product or reactions converting the target product are not recommended. The following phenomena were identified as suitable: phase transition by relative volatility

(identified by differences in boiling points) to remove H_2O and IPAc; phase transition by pervaporation (identified by differences in radius of gyration) to remove H_2O. Additional necessary phenomena are: mixing (Liquid (L): ideal, tubular flow, rectangular flow; Vapor (V): ideal; 2-phase V-L: ideal); stream dividing; convective heating and cooling; heterogeneous reaction; phase contact (ideal V-L); phase separation (ideal V-L). In total, $n_{P,tot}$=13 phenomena are in the search space. In step-4, SPB's are generated through combination of the selected phenomena. Based on $n_{P,tot}$ and the maximum number of phenomena allowed within an SPB $n_{P,max}$ (see Eq.8), a total number of 4019 SPB's ($NSPB_{max}$, see Eq.9) are generated. First, the number of competing phenomena (see Eq.8) which cannot be present within one SPB because they cannot occur at the same time and space is $n_{P,compete}$=4. Competing phenomena are heating vs. cooling; the different liquid flow mixing phenomena; and, dividing vs. all other phenomena because dividing is by definition a single phenomenon SPB.

$$n_{P,\max} = n_{P,tot} - n_{P,compete} = 13 - 4 = 9 \tag{8}$$

$$NSPB_{\max} = \sum_{k=1}^{n_{P,\max}} \left(n_{P,tot,w/oD}\,!/\left(\left(n_{P,tot,w/oD} - k\right)!k!\right)\right) + 1 = 4019 \tag{9}$$

Screening of all SPB's for feasibility: Using connectivity rules and the information of the operating window of each phenomenon, a total number of 58 SPB's are found to be feasible in terms of conditions of the operating windows of the integrated phenomena (not shown here). The potential outlets of the 58 SPB's are checked by using an extension of the Kremser method [7]. When the reaction phenomenon is coupled with phase transition by pervaporation a conversion of 0.99 may be achieved within one stage. This performance criterion together with the needed volume for the task and the simplification of the superstructure leads to the selection of the usage of up to three cross-current stages. The simplified superstructure for this form is retrieved from the model library. The insertion of a dividing phenomenon into one stage of the 3-stage superstructure points to 6 recycles of the liquid while for configurations with 2 stages, in total 3 recycles are possible. Hence, in total 218892 different process options are generated (Eq.10) based on the 58 feasible SPB's in the search space (Fig.3).

$$NOO_{\max} = 58^3 + 58^2 + 58^1 + 6 \cdot 58^2 + 3 \cdot 58^1 = 218892 \tag{10}$$

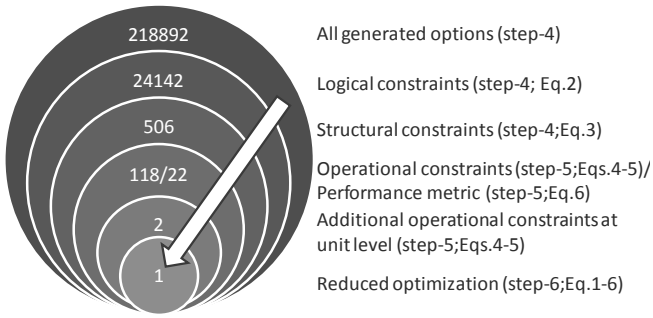

Figure 3. Search space reduction.

In step 4, all options are screened by logical constraints (Eq.2) fixing the binary variables $\underline{Y}$ for feasible processes by ensuring matching operating window of inlet/outlet streams of the SPB's and by ensuring the formation of the product. That gives 24142 remaining options. By subsequent structural screening (Eq.3), e.g. by removing energy redundant options, 506 structural promising processes are identified. In step-4 and step-5, the remaining options are screened by operational constraints (Eqs.4-5) to identify all options having a feasible set of process variables $\underline{X}$ and, subsequently, by identifying the most promising options based on a ranking by the defined performance metric (Eq.6). In total, 2 options remain in the search space which have been identified achieving the lowest operational costs (represented by raw material and

energy consumption). These two are: a tubular (#1) or a rectangular (#2) flow reactor-pervaporator with integrated heating in parallel (see Fig.4). The pervaporation has been modeled using correlations for selectivity and flux of a membrane based on experimental data from Van Hoof *et al.* [10].

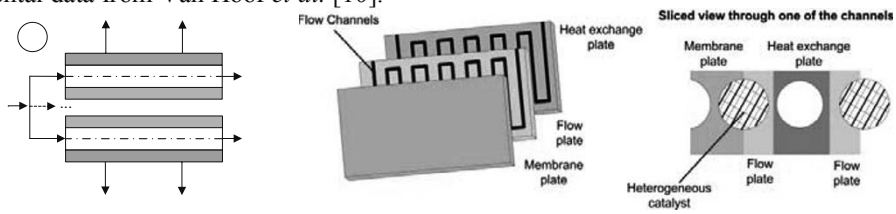

Figure 4. Tubular flow reactor-pervaporator with integrated heating (Option #1).

In step-6, a reduced NLP optimization problem involving the remaining two options is solved in which the diameter (and/or volume) of the tube/channel is optimized to achieve a conversion of 0.99 and a pressure drop $\Delta p<1$bar. The results are given in table 1. The best option is option #1 (see Fig. 4). The achieved concentration of the product in the outlet stream is 98 mol.% IPAc.

Table 1. Simulation results for both remaining process option #1 and #2 for a number of 100 reactors in parallel (W: width; H: height).

Option	T	Rectangular channel			$A_{membrane}/V$	V_{single}	r or r_h	Δp
	[K]	W/H	H [m]	W [m]	[m^{-1}]	[m^3]	[m]	[bar]
#1	373				100	1.46	0.01	1.0
#2	373	4	0.01	0.04	100	1.51	0.008	1.0

Conclusions

A phenomena-based methodology for synthesis/design to achieve PI has been developed and tested through a case study. With this approach it is possible to generate potentially novel process options. That is truly predictive models lead to reliable predictive solutions as well as the simultaneous development of the necessary process models. Current and future work is the development of necessary tools to support the workflow and the implementation of this approach into a software tool.

References

[1] J. Harmsen, 2010, Chemical Engineering and Processing, 49, 70-73.
[2] P. Lutze, R. Gani, J.M. Woodley, 2010, Chemical Engineering and Processing: Process Intensification, 49, 547-558.
[3] P. Lutze, A. Roman-Martinez, J.M. Woodley, R. Gani, 2012, Computers and Chemical Engineering, 36, 189-207.
[4] S. Hauan, K.M. Lien, 1998, Chem Eng Eng Res Des, 76, 396-407.
[5] A.T. Karunanithi, L.E.K. Achenie, R. Gani, 2005, Ind Eng Chem Res, 44, 4785-97.
[6] L. D'Anterroches, R. Gani, 2005, Fluid Phase Equilibria, 228-229, 141-146.
[7] P. Lutze, R. Gani, J.M. Woodley, 2011, Computer Aided Chemical Engineering, 29, 221-225.
[8] J.D. Seader, E.J. Henley, 1998, Separation process principles, Wiley & Sons Inc.
[9] I.K. Lai, S.B. Hung, W.J. Hung, C.C. Yu, M.J. Lee, H.P. Huang, 2007, Chemical Engineering Science, 62, 878-898.
[10] V. Van Hoof, C. Dotremont, A. Buekenhoudt, 2006, Separation & Purification Technology, 48, 304-309.

I.A. Karimi and Rajagopalan Srinivasan (Editors), Proceedings of the 11th International Symposium on Process Systems Engineering, 15-19 July 2012, Singapore.

Three-layer solution strategy for multi-objective process synthesis

Jincai Yue,* Shiqing Zheng, Xia Yang

Research Center for Computer and Chemical Engineering, Qingdao University of Science and Technology, Qingdao266042, China

Abstract

Multi-objective process synthesis can be described as a multi-objective mixed-integer nonlinear programming (MOMINLP) problem. To solve such problem, the main goal of this work is to develop a three-layer solution strategy, which includes simulation layer, synthesis layer and decision-making layer. Simulation layer is used to simulate and analyze the process system. In synthesis layer, NSGA-Ⅱ is used to deal with the process data and generate an optimized population that transfers to simulation layer. In decision-making layer, the compromise solution is generated. The computer user interface is developed to support the data transmission. As a case study, MDA brine treatment process is used to illustrate the proposed strategy. The rigid process model and the optimization model are presented. The non-inferior solution curve is obtained and the final results are used to design industrial process.

Keywords: Process synthesis; MOMINLP; MOGA; NSGA-Ⅱ

1. Introduction

Multi-objective process synthesis is a key step during designing a sustainable process and needs to solve a multi-objective mixed-integer nonlinear programming (MOMINLP). The MOMINLP model is given by

$$\begin{aligned} \min \quad & F = \left[f_1(x,y), f_2(x,y), ..., f_p(x,y) \right]^{\mathrm{T}} \\ \text{s.t.} \quad & h(x,y) = 0 \\ & g(x,y) \le 0 \\ & x \in X \subseteq R^n \\ & y \in Y \subseteq Z^q \end{aligned} \tag{1}$$

Here, x is a n dimension vector of continuous variables, y is a q dimension vector of integer variables, R and Z are decision spaces, F is a p dimension vector of objectives, and $h(x, y)$, $g(x, y)$ are the equality and inequality constrains, respectively.

Multi-objective mathematical programming and multi-objective optimization algorithm based on evolutionary strategy are two main research methods often used. It's difficult especially for complex processes to solve MOMINLP using mathematical programming, so the process model has to be simplified and the results cannot be used to design industrial process. Schaffer (1985) proposed using genetic algorithm (GA) to solve multi-objective optimization problem firstly. Up to now, many MOGA algorithms, such as NSGA-Ⅱ, are developed. Some scholars (Bhaskar et al., 2000; Ravi et al., 2000; Kasat et al., 2003; Amy et al., 2003) have done some research on process synthesis using MOGA, but the process model, based on equations, are still very simple.

* Corresponding author. Tel.: +86-532-84022000; fax: +86-0532-84856913.
E-mail address: yjc@putech.com.cn (Jincai Yue).

Integrating with module simulator such as Aspen Plus, MOMINLP will be simplified and easy to solve. Furthermore, the results can be use to design industrial process because of using rigid process model. Leboreiro & Acevedo (2004) presented GA and modular simulator to optimize sequences of distillation which has one objective. Zheng (2006) proposed mathematical programming and modular simulator to solve waste minimization problems.

A new three-layer solution strategy for MOMINLP based on NSGA-Ⅱ in modular simulator is proposed in this work.

2. Three-layer Solution Strategy

The framework of three-layer solution strategy is given in Fig.1. Three layers are simulation layer, synthesis layer and decision-making layer. Data and information are transferred by the interface program.

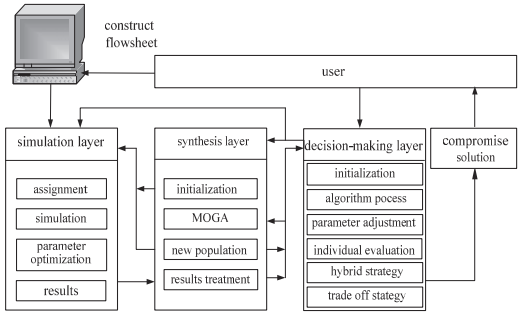

Fig.1 Framework of three-layer solution strategy

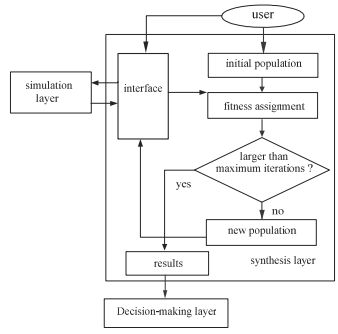

Fig. 2 Flowchart of synthesis layer

2.1. Simulation Layer

Simulation layer is the basic layer. The user constructs flowsheet on Aspen Plus according to the superstructure of the problem, and then assigns initial value data of operating parameters. Finally, the flowsheet is simulated and optimized. As long as a set of decision variables (an individual of the population) is given to Aspen Plus by synthesis layer, all the process variables can be obtained after simulation. The interested variables and simulation information are transferred to the synthesis layer and decision-making layer.

2.2. Synthesis Layer

Synthesis layer's main functions are to deal with the interested variables and simulation information returned from simulation layer. NSGA-Ⅱ is used to generate new population that is transferred to simulation layer. Fig. 2 is the flowchart of synthesis layer.

The interface(Yue et al., 2009a)is programmed using Visual Basic. The interface enables Aspen Plus to open simulation file, simulate the process, and change flowsheet structure and operating parameters. If process simulation fails to converge, the information is transferred to synthesis layer and each objective function is assigned an inferior value directly to avoid interfering with the optimization of NSGA-Ⅱ.

2.3. Decision-making Layer

The functions of decision-making layer are to (1) construct superstructure of process and MOMINLP model, (2) improve the non-inferior solutions by using local search algorithm, and (3) determine the compromise solution by using coordination strategy.

3. Case Study

3.1. Process Description and Extracting Model

Methylenedianiline(MDA) is a kind of chemical intermediate and a large amount of alkaline brine containing aniline, MDA and methanol is produced during the MDA production(Yue et al., 2009b). The brine treatment process flowsheet is given in Fig. 3. Total flow rate of brine is 20092 kg/h which contains 14.5kg/h MDA and 148.3kg/h aniline. Firstly, MDA in brine is extracted by using aniline as extractant, then the brine enters into the stripping tower, and direct steam is added into the bottom to drive off aniline and ethanol. Brine discharged from the bottom still contains a minute quantity of amines. The goal is to reduce the amines content in brine with minimum cost.

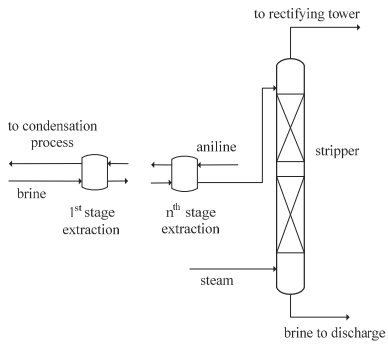

Fig. 3 Flowsheet of brine treatment process

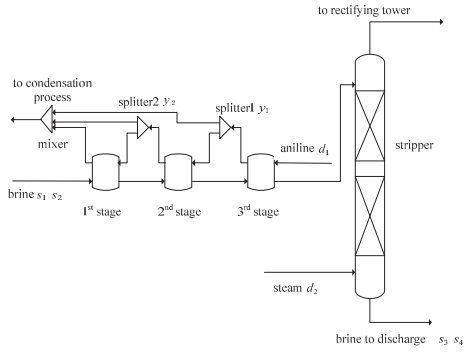

Fig. 4 Superstructure of brine treatment process

Zhang et al. (2008) studied the extraction process of MDA in brine by using aniline. The extraction distribution coefficient K is regressed. Its expression is shown as:

$$\ln K = -4.403 + 2086/T + 0.06833 \ln T + 0.01268T \tag{2}$$

Here, K is distribution coefficient, T is extracting temperature.

Equation (2) can be introduced into Aspen Plus and used to simulate the extraction process.

3.2. Process Superstructure and MOMINLP Model

For a process having maximum number of three extracting stages, the superstructure is given in Fig. 4. The split ratio of logical splitters is 0 or 1. When split ratio of splitter 1 is 0, it means one-stage extraction; when split ratio of splitter 1 and 2 are 1 and 0, respectively, it means two-stage extraction; when split ratio of splitter 1 and 2 are all 1, it means three-stage extraction. Waste w is the total flow rate of MDA and aniline in brine discharged from the stripping tower bottom. Profit p is the cost of recovered MDA and aniline minus the cost of extracting equipment and operating cost which is the sum of direct steam cost and equipment running cost. The cost of tower is fixed and not calculated in profit p. The waste minimization model is shown as:

$$\begin{aligned}
&\max \quad p = 17.5(s_1 - s_3) + 7.7(s_2 - s_4) - 0.08d_2 - 5.63(1 + y_1 + y_1 y_2) \\
&\min \quad w = s_3 + s_4 \\
&\text{s. t.} \quad 300 \le d_1 \le 2000 \\
&\qquad 3000 \le d_2 \le 6000 \\
&\qquad y_1 = [0,1] \\
&\qquad y_2 = [0,1]
\end{aligned} \tag{3}$$

Here, p is process profit (¥/h), w is waste (kg/h), $d_1$is extracting aniline flow rate (kg/h), d_2 is steam flow rate of stripping tower (kg/h), y_1 and y_2 are split ratio, s_1 and s_2 are MDA flow rate and aniline flow rate (kg/h) in feeding brine, s_3 and s_4 are MDA and aniline flow rate (kg/h) in discharged brine, respectively.

3.3. Solving Process

The first thing to do is to build the process simulation file in Aspen Plus as shown in Fig. 4 and ensure the process simulation runs normally, then to design the interface for data and information transferring between Aspen Plus and NSGA-Ⅱ. For NSGA-Ⅱ, extracting aniline flow rate and stripping steam flow rate use real type coding, and split ratio of two splitters use binary coding. The number of population scale and generations are 40 and 60 respectively. The value of mutation rate and crossover rate are 0.8 and 0.01. Finally, the non-inferior solutions obtained by NSGA-Ⅱ are weighted and coordination solution is chosen to design process.

3.4. Results and Discussion

3.4.1. Initial Population of NSGA-Ⅱ

The distribution of initial population of NSGA-Ⅱ is shown in Fig. 5. It shows that :(1) the value of profit p and waste w varies quite largely within the given range of decision variables; (2) the changing tendency for most of the points in solution set is that the profit p decreases with the increase of waste w, these points are inferior solution points; (3) the top left-hand area of Fig. 5 is enlarged which is shown in Fig. 6, the results shows that non-inferior solutions appears in this area, in which the profit p increases with the increase of waste w.

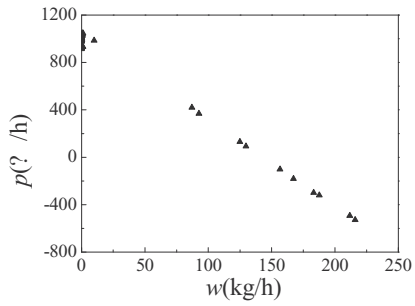

Fig.5 Initial population distribution of NSGA-Ⅱ

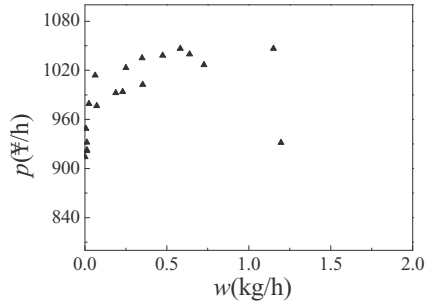

Fig. 6 Part of initial population distribution

3.4.2. Non-inferior Solutions

Fig. 7 shows the distribution of non-inferior solutions at 60th generation. The curve consists of three sections which identify three extraction structures respectively. The curve of the one-stage extraction is comparatively level, the waste w is larger and varies in a wide range, and the corresponding profit is also larger but varies in a very narrow range. The waste w and profit p both vary in a wide range for the two-stage extraction. The curve of the three-stage extraction is quite steep, the waste w is less and varies in a narrow range, and the corresponding profit p varies in a very large range.

If the amine contenting in brine is less than 0.02kg/h, it could be used to electrolyze directly. One-stage extraction process cannot meet the specification. By choosing right extracting aniline flow rate and steam flow rate, two-stage extraction process can meet the specification, but disturbance in operation may lead to fail easily. Three-stage extraction process can meet the specification in the most part of the operating range and

the operation is characteristic of robustness. To ensure the profit at a reasonable level, the choice of operating parameters is important for three-stage extraction in industrial process design. Considering the waste and profit, the operating parameters decided are as follow: the extraction aniline flow is 1875.6kg/h and stripping steam flow is 5039.6kg/h. The corresponding waste flow is 0.012kg/h and the profit is 977.8¥ /h.

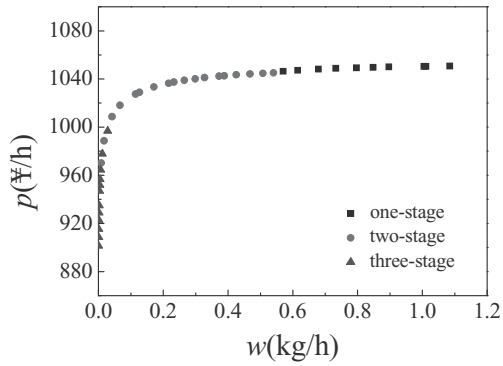

Fig. 7 Distribution of solutions at 60th generation

4. Conclusions

Three-layer solution strategy for multi-objective process synthesis based on module simulator Aspen Plus is proposed. The data and information is transferred by interface among simulation layer, synthesis layer and decision-making layer. MOGA has its advantages on solving MOMINLP which is simplified by using rigid process model in Aspen Plus. The results can be used to guide process design. The strategy was applied to a case study of the design of waste brine treatment process.

References

J. D. Schaffer, Multiple objective optimization with vector evaluated genetic algorithms// Grefenstette J J, Proceedings of the First International Conference on Genetic Algorithms and Their Application, Hillsdale NJ: Lawrence Erlbaum Associates, 1985: 93-100

V. Bhaskar, S. K. Gupta, A. K. Ray, 2000, Multiobjective optimization of an industrial wiped film poly (ethylene terephthalate) reactor, AIChE Journal, 46, 5, 1046-1058

G. Ravi, S. K. Gupta, M. B. Ray, 2000, Multiobjective optimization of cyclone separators, Ind. Eng. Chem. Res., 39, 11, 4272-4286

R. B. Kasat, S. K. Gupta, 2003, Multi-objective optimization of an industrial fluidized-bed catalytic cracking unit(FCCU) using genetic algorithm (GA) with the jumping genes operator, Computers and Chemical Engineering, 27, 9, 1785-1800

K. Y. Y. Amy, K. R. Ajay, G. P. Rangaiah, 2003, Multiobjective optimization of an industrial styrene reactor, Computers and Chemical Engineering, 27, 1, 111-130

J. Leboreiro, J. Acevedo, 2004, Processes synthesis and design of distillation sequences using modular simulators, Computers and Chemical Engineering, 28, 8, 1225-1236

Zheng Shiqing, 2001,Study on multi-objective process system process synthesis in a modular simulator. Guangzhou[D], Guangzhou:South China University of Technology

Yue Jincai, Zheng Shiqing, Han Fangyu, 2009a, Strategy of multi-objective process synthesis based on modular simulator, CIESC Journal(China), 60, 1, 177-182

Yue Jincai, Yang Xia, Cheng Huanong, Zheng Shiqing, 2009b,Waste minimization of MDA brine treatment process. Computers and Applied Chemistry(China), 26, 8, 1048-1051

Zhang Xinping, Yue Jincai, Zheng Shiqing, 2008, Simulation and analysis of diphenylmethane diisocyanate brine extract process, Chemical Engineering(China), 36, 2, 5-8

I.A. Karimi and Rajagopalan Srinivasan (Editors), Proceedings of the 11th International Symposium on Process Systems Engineering, 15-19 July 2012, Singapore.

Conceptual process synthesis for isolation and purification of natural products from plants - A case study of artemisinin from *Artemisia annua*

Chandrakant Malwade, Haiyan Qu, Ben-Guang Rong*, Lars P. Christensen

Institute of Chemical Engineering, Biotechnology and Environmental Technology, University of Southern Denmark, Niels Bohrs Allé 1, DK-5230, Odense M, Denmark; Tel. +45 6550 7481, email: bgr@kbm.sdu.dk

Abstract

A systematic method based on conceptual process synthesis for recovery of natural products from their biological sources is presented. The proposed methodology divides the task into two major subtasks namely, isolation of target compound from a chemically complex solid matrix of biological source and purification of the target compound from the crude extract. This methodology consists of three major separation techniques to achieve the task and provides a platform to generate different process alternatives by employing different combinations of separation units and with different set of key process variables. Decision making about the different combinations of separation units as well as key process variables is based upon the process information collected at every step with the help of process analytical techniques (PAT) and heuristics. The optimal combination of different separation units and set of key process variables is determined in an iterative approach. In the present work, this methodology is applied to isolate and purify artemisinin, an anti-malarial drug from the plant *Artemisia annua*.

Keywords: conceptual process synthesis, natural products, separation and purification, process flow sheet

1. Introduction

Natural products form a vast resource of compounds with unlimited chemical and functional diversity and also serve as a major resource for drug discovery. However, the isolation and purification of target compounds from their biological sources represents one of the most challenging tasks due to the presence of many other compounds in the biomass and also due to lack of basic process information. Associating compounds having similar chemical and physical properties to that of the target compound significantly influence the performance of a stand alone separation technique. In addition, the current chemical process industries face challenges like quicker development of new products and processes, making existing processes more efficient by reducing capital and operating costs, and improving the safety and environmental performance. To cater to these demands, a systematic approach in designing a commercial separation process consisting of multiple separation techniques for isolation and purification of natural products, which can evaluate different possible process alternatives within short span of time, is necessary.

The approach of conceptual process design provides such a systematic framework to rapidly evaluate different process alternatives and thus enable major decisions making at very low cost in a speedup way. It identifies the steps within a process that are the

most critical operations to determine the process economy and product quality. That will also provide insights into how costs can be reduced and what affects final product quality and thus guiding future research and development efforts. A detailed separation process design for recovery of natural products can be very time consuming and laborious, while a rapid conceptual process design can screen different process alternatives within short period of time with less resources used (Douglas J. M, 1988). A detailed description of manufacturing process design for phytochemicals along with heuristics is given by Harjo et al., while the effect of different process variables on the efficiency of different stand alone separation processes is described by Ndocko et al. However, there is scarcity of information on determination of synergistic effects between various separation processes used in combination for recovery of natural products.

The objective of this work is to perform a real case study to recover the target compound artemisinin from *A. annua*, which aims at providing a generalized model to evaluate different separation process alternatives for recovery of natural products. The methodology is expected to fit in the majority of natural product recovery problems. In the present work, the methodology is developed and formulated through evaluating different process alternatives for recovery of artemisinin from dried leaves of *A. annua*. The focus is on the interaction and synergistic effect between the chromatography and crystallization separation operations.

2. The methodology

The basic structure of the process model for isolation and purification of natural products is shown in Fig. 1. The task is divided into two subtasks of isolating the target compound from its source and then purification of the target compound from complex

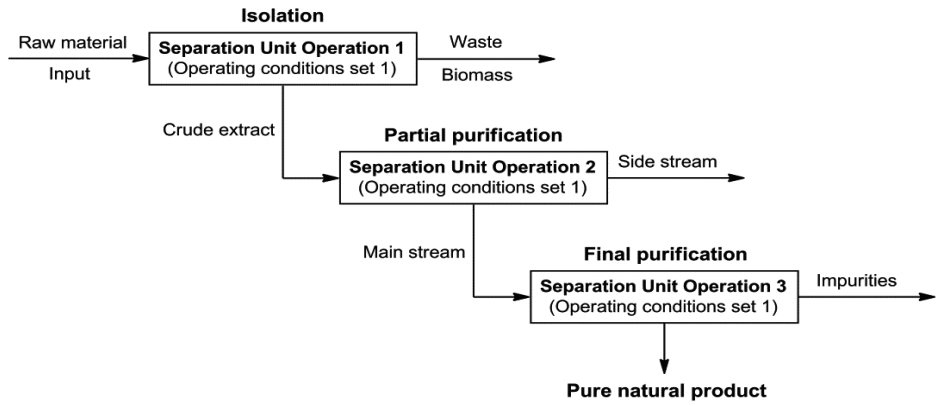

Figure 1. Basic process structure for isolation and purification of natural products.

crude extract. This methodology also emphasizes the use of process analytical technology (PAT) to analyze the process streams at various stages of the process in order to collect information about critical process parameters, which affects critical quality attributes as well as the overall design of the process.

2.1. Isolation

The process begins with the task of isolating target compound from the biomass designated by separation unit operation 1 (Fig. 1). Separation unit operation 1 can be represented by one of the numerous industrial applied separation techniques. A

comprehensive review of the separation techniques used to isolate natural products is given by Sarkar et al. The decision to pick up the best suitable one and selection of optimal operating conditions is product specific and depends upon many factors like amount of target compound present in the biomass, distribution of target compound in the source, final product specifications and also the physico-chemical properties of the target compound.

2.2. Purification

Taking into consideration the complex nature of the crude extract obtained from the previous step, the use of combined separation techniques is suggested for the purification of the target compound. In practice, high purity natural products can be obtained by highly efficient stand alone separation techniques like preparative high performance liquid chromatography (HPLC), but the cost of such process is always high. The present methodology suggests the use of preparative separation methods with less operating cost compared to, e.g. HPLC, to only partial purification of target compound combined with final purification by using cost effective techniques like crystallization. In this way, feasible process alternatives can be generated by employing different separation techniques with different arrangements in a sequence to achieve the tasks of isolation and purification of the target compound.

3. Case study of artemisinin from *Artemisia annua*

The proposed methodology is applied to generate process flow sheet alternatives to isolate and purify an anti-malarial drug, artemisinin from dried leaves of *A. annua*. In the present work, one such process flow sheet is evaluated in regard to the synergistic effect between chromatography and crystallization separation techniques. The basic process flow structure is shown in Fig. 2. Three major separation unit operations are used: solid-liquid extraction to isolate artemisinin into the crude extract, flash column chromatography (CC) to fractionate the crude extract, and crystallization to recover and purify artemisinin from the fractions of the crude extract.

3.1. Solid-Liquid Extraction

Artemisinin is extracted from the dried leaves of *A. annua* with dichloromethane (DCM) using maceration technique. DCM is chosen as the extraction solvent mainly due to the high solubility of artemisinin in DCM combined with its low boiling point that facilitates easy recovery of the solvent. The extraction procedure included immersion of 150 g of dried leaves containing 2.08% w/w artemisinin into 1 L of DCM followed by filtration after 5 hrs. The procedure is repeated one more time with 1 L of DCM. The combined DCM extract (2 L) is evaporated to obtain 12.5 g of crude extract. The concentration of artemisinin in the crude extract is determined by analytical HPLC–Charged Aerosol Detection (CAD). The yield of the extraction process in terms of artemisinin recovery using this extraction method is 90%.

3.2. Flash Column Chromatography

The crude extract obtained in the previous step is partially purified using flash CC to obtain artemisinin rich fractions with less number of other components. 15 g of crude extract is separated on a 7 cm diameter column filled with normal phase silica. Adsorbent (silica gel) to solute (crude extract) ratio of 20:1 is used. Gradient type of elution is used to run the column under the applied pressure. The eluent was selected based on the results of solvent screening by thin-layer chromatography (TLC). Column conditioned with 100% *n*-hexane and the gradient starts with 100% *n*-hexane followed by 10% stepwise gradient from 100 % *n*-hexane to 100% ethyl acetate.

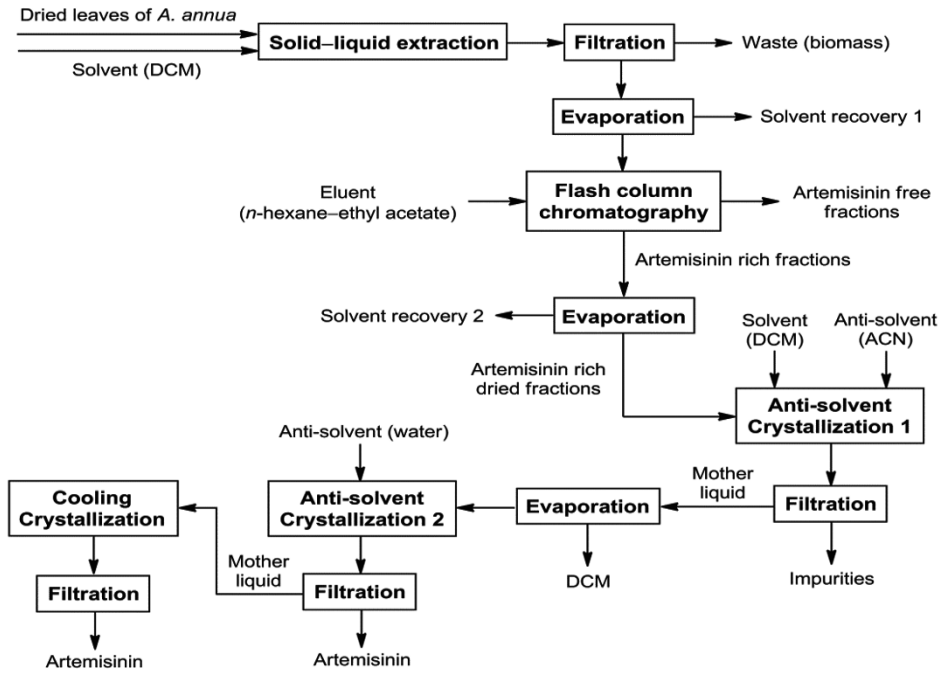

Figure 2. Process flow sheet for isolation and purification of artemisinin from dried leaves of *A. annua.* (DCM: dichloromethane, ACN: acetonitrile)

Each gradient of 900 mL is used and the size of fractions collected is 100 mL. Collected fractions were analyzed by TLC to identify the artemisinin rich fractions and these were then analyzed by HPLC–CAD for quantification of artemisinin. The results of this analysis are shown in Fig. 3.

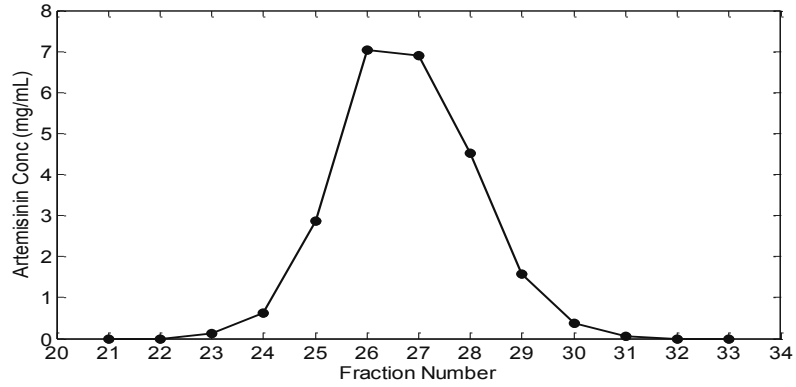

Figure 3. Concentration profile of artemisinin in fractions obtained by flash CC.

3.3. Crystallization

The artemisinin containing fractions obtained in the previous step are purified further by using a three-step crystallization process as shown in Fig. 2. The two-step anti-solvent crystallization process has been reported in our previous work by Qu et al. The artemisinin rich fractions 25-28 are processed individually, whereas fractions 23-24 and

29-31 are combined together to form two fractions. However, no artemisinin is crystallized out from these combined fractions because of the low concentration of artemisinin. Yield and purity of artemisinin crystals obtained from each fraction are shown in Table 1. Artemisinin is crystallized from fractions 25-28 with varying purity and yield. One remarkable observation from Table 1 is that the yield of artemisinin from fraction 25 is much higher than that from fractions 26, 27, and 28; regardless of the higher artemisinin concentration in the fractions 26-28. This fraction wise variation in purity and yield of artemisinin may be attributed to the associating compounds present in the fractions, which might be affecting the solubility of artemisinin and furthermore some of which may have crystallization behavior similar to artemisinin during the anti-solvent crystallization. FT-Raman spectroscopy measurement confirmed that thermodynamically stable orthorhombic polymorph of artemisinin has been obtained from all fractions.

Table 1: Purity and yield of artemisinin obtained from fractions during crystallization process.

Fraction No.	Artemisinin purity		Yield (%)
	Anti-solvent Crystallization2 (%)	Cooling Crystallization (%)	
25	91.37	100	87.4
26	84.85	92.35	45.8
27	100	100	64.0
28	66	100	28.8

4. Conclusion

The systematic method for synthesis of conceptual processes for isolation and purification of natural products from plants is investigated. A case study for recovery of artemisinin from dried leaves of *A. annua* is performed. Three major separation techniques of maceration extraction, flash CC and crystallization are selected to formulate the process flow sheet. Lab scale experiments are studied to confirm and understand the effectiveness of the separation methods. To do so, PAT is used in each step to get the necessary information and data of the process. The results showed that the formulated process flow sheet is feasible to isolate and purify the target compound artemisinin from *A. annua*. One outstanding observation is that the associating compounds in the fractions have significant effects to the purity and yield of the target compound artemisinin during crystallization steps. This indicated that seeking synergy between chromatography and crystallization to obtain optimal hybrid separation process is the key direction for commercial manufacturing process of artemisinin from *A. annua*. Effort in this direction is underway.

References

J.M. Douglas, 1988, Conceptual design of chemical processes, McGraw-Hill.

B. Harjo, C. Wibowo, K.M. Ng, 2004, Development of natural product manufacturing processes, Chemical Engineering Research and Design, 82(A8), 1010-1028.

E.N. Ndocko, W. Bäcker, J. Strube, 2008, Process Design Method for Manufacturing of Natural Compounds and Related Molecules, Separation Science and Technology, 43: 3, 642 -670.

S.D. Sarker, Z. Latif, A.I. Gray, 2006, Natural Products Isolation, 2nd ed., Humana Press, New Jersey.

H. Qu, K.B. Christensen, X.C. Fretté, F. Tian, J. Rantanen, L.P. Christensen, 2010, Chromatography-Crystallization Hybrid Process for Artemisinin Purification from *Artemisia annua,* Chemical Engineering & Technology, *33*, No. 5, 791–796.

I.A. Karimi and Rajagopalan Srinivasan (Editors), Proceedings of the 11th International Symposium on Process Systems Engineering, 15-19 July 2012, Singapore.

Synthesis and Optimization of Distributed Energy Supply Systems using Automated Superstructure and Model Generation

Philip Voll,[a] Carsten Klaffke,[a] Maike Hennen,[a] Stefan Kirschbaum,[b] André Bardow[a]*

[*]*Corresponding author: Tel.: +49 241 8095376, Fax: +49 241 80 92255, Email: andre.bardow@ltt.rwth-aachen.de*
[a]*Institute of Technical Thermodynamics, RWTH Aachen University, Schinkelstr. 8, 52062 Aachen, Germany*
[b] *Society for the Promotion of Applied Computer Sciences, Volmerstr. 3, 12489 Berlin, Germany*

Abstract

A novel approach is presented for the automated generation of models representing superstructures for the synthesis and optimization of distributed energy supply systems (DESS). Based on a basic problem description (load cases, available technologies, and topographical constraints), the proposed algorithm automatically generates a model accounting for time-varying load profiles and part-load dependent operating efficiencies. Building upon the P-graph approach, the derived superstructure is extended to include multiple redundant conversion units as required for DESS optimization. In the present implementation, a GAMS model is generated that can be readily optimized. The approach is applied to the retrofit synthesis of the energy supply system of an industrial site. It is shown that the automated procedure provides a convenient and efficient optimization framework for DESS.

Keywords: Distributed Energy Supply Systems, Synthesis and Optimization, MINLP, MILP, Superstructure generation, P-graph.

1. Introduction

Distributed energy supply systems (DESS) are highly integrated and complex systems. In particular, DESS design principles are fundamentally different from classical chemical plants as the following simple example shows: Consider the total cost optimization of a heating system for a single time-varying heat demand (Fig. 1 a).

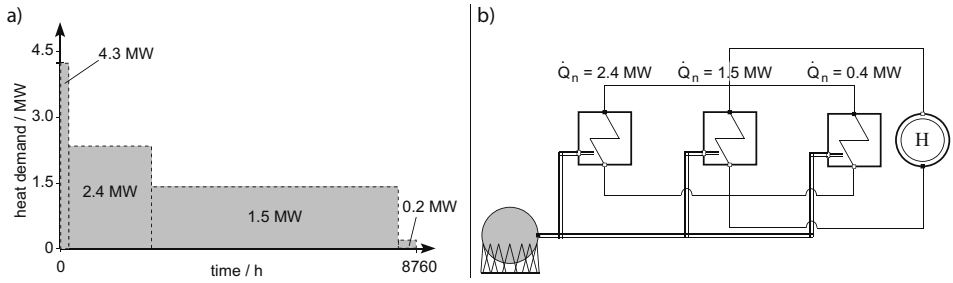

Fig. 1. Time-varying heat demand (a) and optimal heating system (b) covering this demand.

Even if only a single technology such as a simple boiler is considered, the grassroots design problem becomes challenging due to the trade-offs between

- economy of scale of the equipment investments,
- equipment performance in part-load operation, and
- minimum operation loads of the equipment.

On the one hand, the boilers' total capacity has to cover the maximum heat demand, and economy of scale favors large over small equipment; on the other hand, the boilers' efficiencies drop at part-load operation, and thus full-load operation is beneficial. Moreover, boilers must not be operated below their minimum part-loads, and therefore boilers need to be sized small enough to cover the minimum loads. For the considered example, these trade-offs enforce the installation of three redundant boilers in the optimal configuration (Fig. 1 b). This shows that multiplicity and redundancy of energy conversion units should generally be considered for DESS synthesis problems.

The intrinsic properties of DESS have to be reflected in an optimization model. Therefore, both the superstructure generation and optimization are difficult tasks leading to MINLP problems with time-dependent constraints (e.g., demand profiles). For solving these problems, algorithmic approaches rely on the use of mathematical programming techniques [1-2] to optimize a given superstructure. Thus, the designer needs to decide *a priori* which alternatives should be encoded in the superstructure, and thereby runs the risk to exclude the optimum from consideration. Since manual superstructure generation is an error-prone task, automated methods are desirable.

For process network synthesis (PNS) problems, the P-graph [3] based PNS framework has been developed. P-graphs are graph-representations of process networks enabling to employ efficient graph-theoretic algorithms for automated superstructure generation [4] and optimization [5]. Recently, the P-graph approach has been applied successfully to the synthesis of energy systems [6]. However, since the current PNS framework has been developed for synthesizing chemical plants, it does not consider time-varying boundary conditions and part-load dependent equipment performance – features that have a strong impact on the performance of DESS as demonstrated above. Moreover, in case of classical PNS problems, multiplicity and redundancy are often regarded as shortcomings of the problem formulation [7]. The current PNS framework therefore requires manual manipulations to incorporate multiple redundant equipment in the superstructure.

In this paper, an automated superstructure and model generation algorithm is presented accounting for time-dependent boundary conditions, part-load performance, as well as multiplicity and redundancy of energy conversion units as key features of DESS.

2. Automated superstructure and model generation

This section describes the proposed algorithm for automated generation of DESS superstructures represented as MI(N)LP models (Fig. 2). The starting point is a set of simple user inputs defining the synthesis problem: energy demand time series, existing equipment, available new technologies, number of redundant units n to be considered in the superstructure, and topographical constraints. Next, the P-graph based *maximal structure generation* (MSG) algorithm [4] is employed to generate a P-graph superstructure, which contains only one unit of each technology. Then, this superstructure is expanded to incorporate n redundant units: For this purpose, the generated superstructure is represented by a connectivity matrix whose rows and columns represent final energy users (e.g., demands for heating and cooling) and generators (e.g., boilers, absorption and compression chillers), respectively. Absorption

chillers take a special role as they represent both final energy users (driving heat) and generators (refrigeration). The entries of the connectivity matrix represent the connectivity between users and generators: If a generator is connected to a user, the entry in the corresponding row and column is 1; otherwise, it is 0. For superstructure expansion, all columns representing generators are copied *n*-times. The same applies to all rows representing the demand for driving heat of absorption chillers.

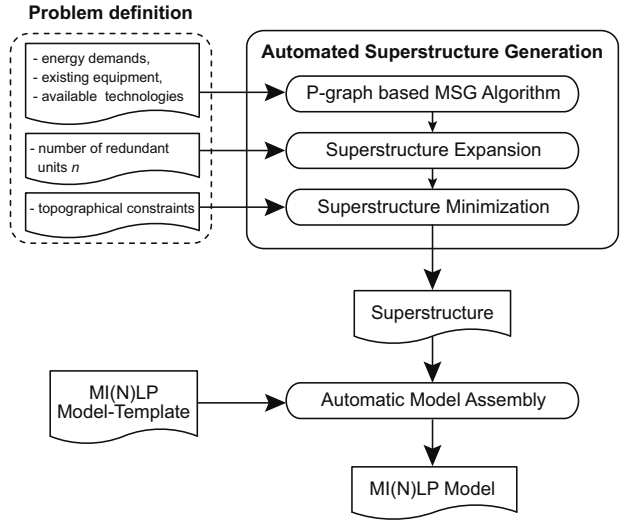

Fig. 2. Flowchart of the algorithm for automated MI(N)LP model generation.

If specified, topographical constraints are taken into account to reduce the generated superstructure by cutting infeasible connections, or more technically, assigning zeros to the corresponding matrix entries. To assemble the final model, the user can use arbitrary MI(N)LP model-templates, which are initialized by the generated connectivity matrix.
In the present implementation, a GAMS model [8] is generated that can be readily optimized using standard solvers. This model employs an MILP formulation [9] based on quasi-stationary energy balances and equipment performance functions accounting for time-varying load profiles and part-load dependent operating efficiencies.

3. Case study: Retrofit extension of an industrial site

The proposed framework is applied to the retrofit synthesis of an industrial site, which is extended by a new production facility. The available energy conversion technologies are listed in Table 1. The optimization is performed maximizing the net present value (NPV) with a cash flow time and discount rate of 10 years and 8 %, respectively.

Table 1. Available energy conversion technologies including their power and price ranges.

Technology	Thermal power range / MW	Price range / 10^3 €
Boiler	0 - 5.0	0 – 160
CHP engine	0 - 3.2	0 – 850
Absorption chiller	0 - 5.0	0 – 360
Turbo-driven chiller	0 - 5.0	0 – 790

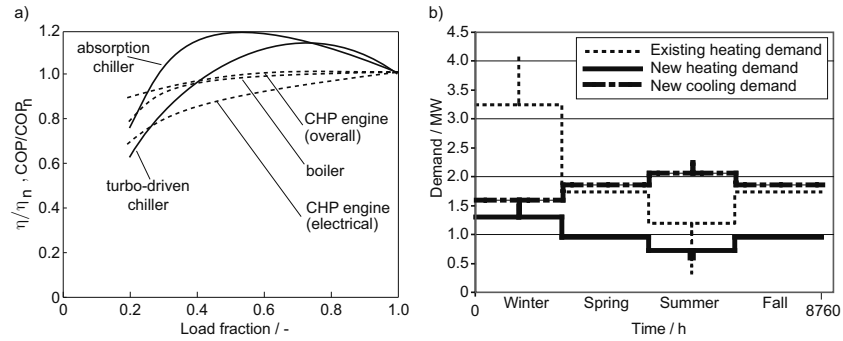

Fig. 3. Part-load performance curves (a) and simplified annual demand profiles (b).

Fig. 3 a) shows the characteristic curves of these technologies, i.e., the boiler efficiency, η, the CHP engine's overall and electrical efficiencies, η_{th+el} and η_{el}, and the chillers' coefficients of performance, COP. While boilers and CHP engines are subject to efficiency losses in part-load operation, chillers have maximum efficiencies in part-load operation. For all technologies, the minimum part-load is assumed to be 20 %. Fig. 3 b) illustrates monthly-averaged existing and new energy demands of the considered industrial site. Peak loads are modeled by spikes on top of the averaged demands.

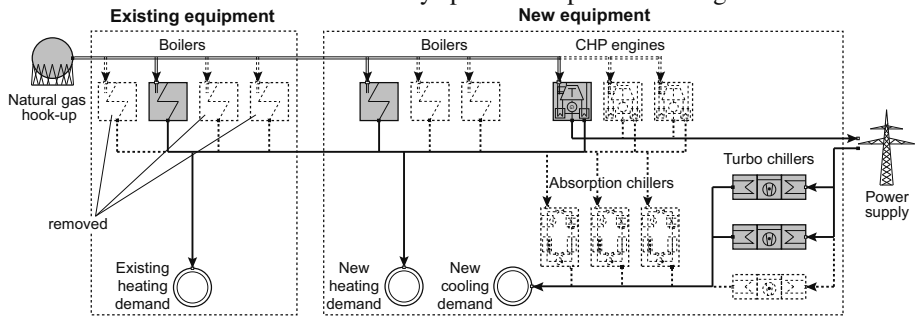

Fig. 4. Superstructure and optimal solution (units in grey) for the retrofit synthesis problem.

Fig. 4. shows the superstructure and the optimal solution obtained when the automated model generation algorithm and an MILP optimization is applied. The superstructure incorporates existing as well as new equipment. The number of redundant units considered is n = 3. In the optimal configuration (NPV = -6.15 Mio. €), three of the existing boilers are replaced by one new boiler and one CHP engine; furthermore, two turbo-driven chillers are installed on-site. Table 2 lists all units of the optimal solution including nominal powers and investments.

Table 2. Nominal thermal powers and investments of the installed equipment.

	Boiler 1	Boiler 2	CHP engine	Chiller 1	Chiller 2
Thermal power / MW	2.0	1.5	3.1	0.9	1.8
Investment / 10^3 €	0 (existing)	70	820	160	300

In optimal operation, the CHP engine covers 88 % of the total heat demand. Except during summer, it constantly runs at full load, and thus generates a considerable amount of feed-in electricity. The new boiler is operated in winter and in summer for the minimum heat loads. The existing boiler is reserved to solely meet the peak load

requirements in winter. The installation of two chiller units in the cooling system allows for load sharing enabling to run both units close to their maximum COP year-round.
Noteworthy, the optimal solution contains both redundant boilers and chillers. Since the superstructure offered even more redundant units than used in optimal configuration, the choice of $n = 3$ redundant units is considered to be sufficiently large for this problem. For comparison, a superstructure prohibiting any redundancy would lead to 10.4 % higher costs.

4. Summary and conclusions

This paper proposes a generic framework for the automated model generation for superstructures of distributed energy supply systems (DESS) incorporating multiple redundant energy conversion technologies. The generated models account for time-varying load profiles and part-load performance as key features for DESS optimization. In the present implementation, a GAMS model is generated that has been successfully applied to the retrofit extension of an industrial site. It is shown that the automated procedure provides a convenient and efficient optimization framework for DESS synthesis problems.

Acknowledgements

The authors wish to thank Prof. Petar Varbanov and Dr. Süle Zoltán from Centre for Process Integration and Intensification, University of Pannonia, for their courtesy and support on the PNS framework.
This study was funded by the German Federal Ministry of Economics and Technology (ref. no.: 0327885A).

References

1. Frangopoulos, C.A., von Spakovsky, M.R., Sciubba, E.A, 2002. *Brief review of methods for the design and synthesis optimization of energy systems*. Int Journal of Applied Thermodynamics 5 (4), 151-160.
2. Biegler, L.T., Grossmann, E., 2004. *Retrospective on optimization*. Computers & Chemical Engineering 28 (8), 1169-1192.
3. Friedler, F., Tarjan, K., Huang, Y.W., Fan, L.T., 1992. *Graph-theoretic approach to process synthesis: axioms and theorems*. Chemical Engineering Science 47 (8), 1972-1988.
4. Friedler, F., Tarjan, K., Huang, Y.W., Fan, L.T., 1993. *Graph-theoretic approach to process synthesis: polynomial algorithm for maximal structure generation*. Computers & Chemical Engineering 17 (9), 929-942.
5. Friedler, F., Varga, J.B., Fehér, E., Fan, L.T., 1996. *Combinatorially accelerated branch-and-bound method for solving the MIP model of process network synthesis*. In: Floudas, C.A., Pardalos, P.M. (Eds.), State of the Art in Global Optimization. Kluwer Academic Publishers, Boston, MA, USA, 609-626.
6. Varbanov, P.S., Klemeš, J.J., Friedler, F., 2011. *Integration of fuel cells and renewables into efficient CHP systems*. In: Bojic, M., Lior, N., Petrovic, J., Stefanovic, G., Stevanovic, V. (Eds.), Proceedings of 24th ECOS, Novi Sad, Serbia, July 3-7, 2011, 1021-1033.
7. Farkas, T., Rev, E., Lelkes, Z., 2005. *Process flowsheet superstructures: Structural multiplicity and redundancy: Part I: Basic GDP and MINLP representations*. Computers & Chemical Engineering 29 (10), 2180-2197.
8. Brooke, A., Kendrick, D., Meeraus, A., 2010. *GAMS: A User's Guide. Tutorial by Rick Rosenthal*. GAMS Development Corporation, Washington, DC, USA.
9. Yokoyama, R., Hasegawa, Y., Ito, K., 2002. *A MILP decomposition approach to large scale optimization in structural design of energy supply systems*. Energy Conversion and Management 43 (6), 771-790.

I.A. Karimi and Rajagopalan Srinivasan (Editors), Proceedings of the 11th International Symposium on Process Systems Engineering, 15-19 July 2012, Singapore.

Design of optimal disease and patient-specific chemotherapy protocols for the treatment of Acute Myeloid Leukaemia (AML)

E. Pefani[a], N. Panoskaltsis[b], A. Mantalaris[a], M.C. Georgiadis[a], E.N. Pistikopoulos[a]

[a]*Centre for Process Systems Engineering, Department of Chemical Engineering, Imperial College London, South Kensington Campus, London SW7 2AZ, UK*
[b]*Department of Haematology, Imperial College London, Northwick Park & St. Mark's Campus, London, HA1 3UJ, UK*

Abstract

The current project focuses on the design and optimization of chemotherapy protocols for Acute Myeloid Leukaemia (AML). AML is a type of blood cancer in which patients are characterized by a weakened blood and immune system due to abnormalities in the bone marrow where the tumour is located. In that respect, there is a high risk that the patient will not withstand the treatment due to life-threatening toxicities of the chemotherapeutic drug mix. Therefore the individualization and optimization of treatment dose and schedule is essential to balance the benefits of higher dose therapy against the tumour with the toxicity to normal tissue. This balance can be achieved by modelling key biological mechanisms as a means to gain insight into the effects of chemotherapy, which can then be used as a predictive tool for patient response during treatment (Dua, 2005; Dua,2008).In this work, we extend our previous model (Pefani et. al., 2011) for the first cycle of chemotherapy for the treatment of AML to include the chemotherapeutic drug action of both anticancer drugs used in current treatment protocols: cytarabine (Ara-C) and daunorubicin (DNR). The simulation and optimization results demonstrate the need for optimal treatment schedule in order to limit the life-threatening toxicities of chemotherapy-induced cytopenia in patients with AML undergoing treatment.

Keywords: Mathematical modelling, chemotherapy optimization, pharmacokinetics, pharmacodynamics.

1. Framework for the design of optimal disease and patient-specific chemotherapy protocols

Most cancers are treated with chemotherapy, anti-tumour drugs which can be equally as toxic to the patient as they are to the cancer and with effects dependent on the characteristics of the patient, the stage of disease and the type, dose and schedule of anticancer drugs used. Current treatment protocols are designed based on empirical rules from the physicians' acquired experience, usually through collection of data from clinical trials. A more systematic and efficient approach for the design of treatment protocols, such as through mathematical modeling, is required. These mathematical models should be able to adequately describe the behavior of the organism under treatment and the tumour being eradicated, leading to an optimal individualized chemotherapy treatment protocol. Such models are lacking in the open literature as most of them fail to include in detail

the above mentioned aspects and are based on empirical assumptions (Afenya, 2001; Fister, 2000; Sherer, 2006).
The models aiming to describe chemotherapy action should consist of mathematical expressions for all steps of treatment, from drug administration through to intracellular drug action. All these parts are described in fig. 1, wherein the general framework for the derivation of such a mathematical model is described.

Figure 1: Framework for the design of optimal tailor-made chemotherapy protocols

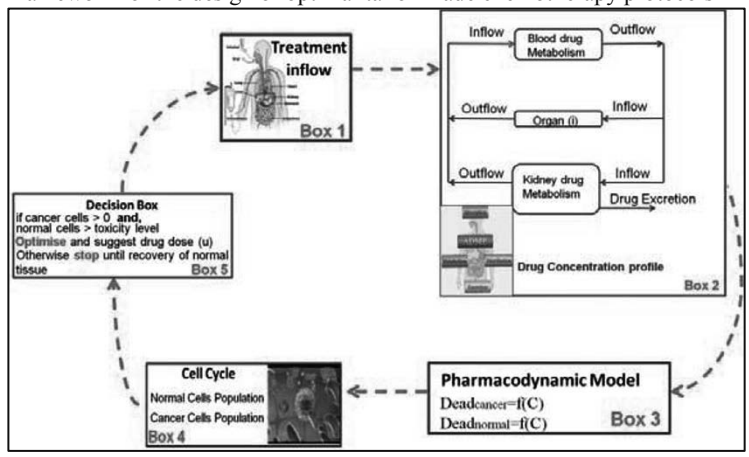

To start, the initial dose given to the patient in combination with the administration route and the injection rate will be used for the calculation of the treatment inflow (box 1: fig. 1) that is the main input for the pharmacokinetic model (PK) (box 2: fig. 1). The PK model depends on patient characteristics and is comprised of the set of drug mass balances in patient organs for calculation of the drug concentration profile. This profile is the main input for the pharmacodynamic (PD) model (box 3: fig. 1). The PD model calculates the number of both normal and cancer cells which have died due to drug administration which are then successively subtracted from the starting number of cells in order to calculate the number of each cell type which remain following the chemotherapy cycle (box 4: fig. 1). Thereafter, a new optimization problem will be introduced and solved (box 5: fig. 1) only if there are tumour cells still present (in this model) and normal cells are in sufficient number such that the patient can tolerate another chemotherapy cycle. With this framework, optimal chemotherapy cycles will be designed based on patient characteristics (data input in box 2) and disease characteristics (data input in box 4).

2. Mathematical Modeling

In accordance with the presented framework in the previous section, the mathematical model should consist of the cell cycle model combined with relevant aspects of PK and PD. The general structure of the mathematical model for the AML patients' behavior (including tumour) during treatment is presented in table 1.

Table 1: Structure of the proposed mathematical model for AML patients' response to chemotherapy

$\inf low_j = \frac{u_j}{rate_j}$	(1)	$inflow_j$:treatment inflow of drug j u_j: dose load of drug j $rate_j$: administered rate of drug j

$\dot{C}_{b,j} = Q_i \cdot C_{bj} - Q_b \cdot C_{b,j} + \inf low_j$	(2)	$C_{b,j}$: drug concentration in blood of drug j Q_i: blood flow of organ i:kidney,liver,heart,marrow e.t.c
$\dot{C}_{M,j} = Q_M \cdot C_{bj} - Q_M \cdot C_{M,j}$	(3)	$C_{M,j}$: drug concentration in marrow of drug j
$Dead_j = \frac{E_{\max} \cdot C_{M,j}^{slope}}{EC_{50}^{slope} + C_{M,j}^{slope}}$	(4)	$Dead_j$: number of dead cells because of drug j action E_{max},EC_{50},slope: drug pharmacodynamic parameters
$CancerCells = S + G_1 + G_2M$	(5)	
$\dot{S} = -\mu \cdot S + k \cdot G_1 - \lambda \cdot S - Dead_j$	(6)	S: cancer cells in proliferating phase μ,k,λ: transition rates between phases
$\dot{G_1} = -\mu \cdot G_1 - k \cdot G_1 + 2 \cdot d \cdot G_2M - Deadj$	(7)	G_1: cancer cells in growth phase d:proliferation rate
$G_2\dot{M} = -\mu \cdot G_2M + \lambda \cdot S - d \cdot G_2M$	(8)	G_2M:cancer cells in the pre-mitotic and mitosis phase
$NormalCells = P + Q$	(9)	
$\dot{P} = (a - m - n) \cdot P + b \cdot Q - Dead_j$	(10)	P:normal cells in proliferating phase a,m,n,b: transition rates between proliferating and non-proliferating phases
$\dot{Q} = m \cdot P - b \cdot Q - Dead_j$	(11)	Q:normal cells in non-proliferating phase

To start, the dose u_j of drug j is used for the calculation of treatment $inflow_j$ (eq. 1) that is the main inflow for the calculation of drug concentration in blood (eq. 2). Successively, the drug concentration in the organs (i.e. kidneys, liver, heart, bone marrow) is calculated and the drug concentration in bone marrow $C_{M,j}$ (eq. 3) (tumour location) is used by the PD model (eq. 4) for the calculation of dead cells. Dead cells are thereafter subtracted from the starting cell number (eq. 5-eq.11) for the calculation of the new state of normal and cancer cells after this dose administration. These expressions form the equations of the optimization problem wherein the objective is to minimize the number of cancer cells and maximize recovery by keeping normal cells above a certain level as required by the patient for survival of normal tissue.

3. Patient case study

A case study of a man weighting 70 kilograms and 1.80 metres in height is presented using Ara-C and DNR combination treatment. Both chemotherapy agents are cell-cycle specific. In particular, DNR is an anthracycline antitumour agent that is metabolized to daunorubicinol, an active metabolite with the ability to prevent DNA and RNA formation by interferring with cells in G_1 and S phase of the cell cycle (Huffman, 1972). Ara-C is an anti-neoplastic drug that is intracellularly activated to Ara-CTP a metabolite that acts on S-phase of the cell cycle to block DNA expression in order to cease cell proliferation (Kufe, 2006). This specificity of the drugs makes the role of cell cycle critical for the validity of the model as the cell cycle phase distribution profile is a parameter required in order to adequately assess the effects of chemotherapy on the tumour. However, this level of knowledge is limited and detailed experimental data are required for system representation. In lieu of this representation, as a first step in the current work we assume a cancer and normal cell population and the case study is solved for some assumed characteristics of these cell populations. To be more specific,

we assume that the initial distribution in the normal cell population is 75% in non-proliferating and the remaining 15% in proliferating phases (Afenya, 2001). Moreover, the percentages used for the cancer cell population are 70% of cell population will be in proliferation phase and 30% in non-proliferating phase (Wilkoff, 1967). The distribution of cells into cell phases is a parameter that varies tremendously between patients (Preisler, 1995) however the assumed distribution shares a certain amount of validity if we consider that cancer cells are characterized by a higher proliferation rate than that of normal cells (Afenya, 2001). The initial AML tumour burden is assumed to be 10^{12} leukaemic blasts with concomitant 10^{11} normal cells within the bone marrow organ at presentation (Williams, 1983). PK parameters for Ara-C are taken from (Dedrick et al., 1972) while PK parameters for DNR are from (Loveless, 1978). Lastly PD parameters for both drugs were found in the work of (Quartino, 2007).

The model is solved for the treatment protocol in (Quartino, 2007) to be in accordance with the PD data used for the two drugs. According to this protocol a total of 700mg/m^2 dose of Ara-C is given as continuous infusion over 7 days and 45mg/m^2 of DNR as daily bolus during the first three days. Simulation results are obtained from this protocol and can be seen in fig. 2 for normal and cancer cells. Normal cell population is decreasing from 10^{11} to $1.29\text{x}10^9$ cells and cancer cells from 10^{12} to $1.16\text{x}10^9$ cells.

Figure 2: Normal and cancer cell population during reference treatment protocol

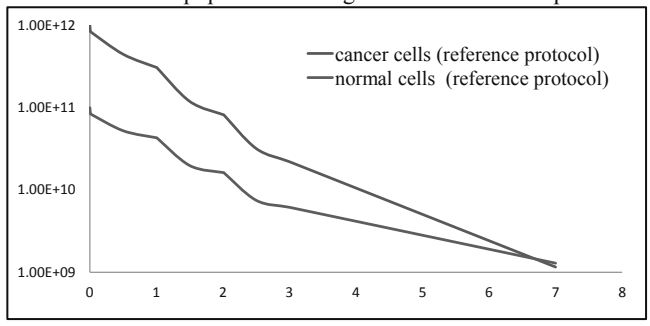

The minimum accepted level of normal cells during the induction period is set to 3-log cell destruction, which would equate to $1\text{x}10^8$ cells by the completion of induction treatment. Apart from keeping normal cells above this level, the treatment objective is to achieve more normal than cancer cells in the bone marrow. This problem was formed and solved using gOPT (gPROMS, 2003) and the optimal treatment schedule suggests an increase of Ara-C that to total dose of 1400mg/m^2 continuously given over 7 days and DNR dose to 45 mg/m^2 bolus injection during the first three days of treatment.

Figure 3: Normal and cancer cell population during reference and optimal treatment protocols

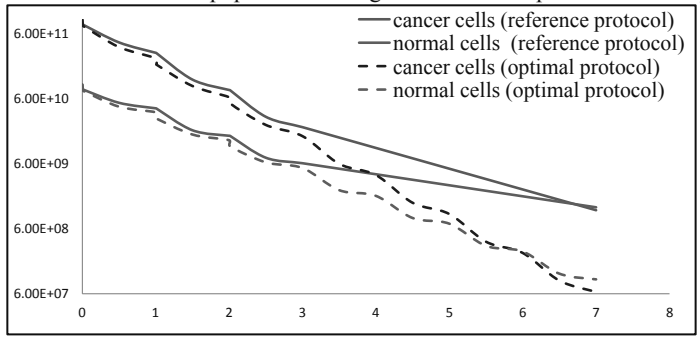

During the optimal treatment scenario cancer cells are further decreased leading to 6.42 $x10^7$ cells by the end of the treatment, while normal cells reach the minimum accepted level of 10^8 cells. Thus cancer cell population is further decreased making a difference of $1.08x10^9$ cells less comparing to the reference treatment protocol while the resulting bone marrow is of higher level of normal than cancer cells (fig 3).

4. Concluding Remark

In this paper, an optimal control model for the scheduling of AML treatment with Ara-C and DNR is proposed. A case study of an adult man of 70 kg and 1.80 m is analysed. The model is simulated for the induction period of chemotherapy only using combination of 700 mg/m^2 Ara-C continuously infused for 7 days and 45 mg/m^2 DNR given by rapid intravenous injection for 3 days.

Simulation results are obtained showing both normal and cancer cell populations decreasing during the chemotherapy treatment. An optimization problem was formulated and solved using gPROMS with objective to further minimize cancer cell population while obtaining a bone marrow with higher percentage of normal cells. Optimization results suggested higher dose of Ara-C and same dose of DNR and this treatment protocol results in $1.08x10^9$ less cancer cells during the optimal scenario comparing to the reference treatment protocol while normal cell population is higher comparing to the cancer cell population. Optimization results are satisfactory as the AML cell population has decreased enough to debulk the marrow of tumour and the normal cell population is in adequate number to allow for normal tissue recovery prior to the next cycle of chemotherapy to further decrease AML cells. The study demonstrates the clear need for optimal treatment schedule during all cycles of chemotherapy in order to limit life-threatening toxicities of long-term cytopenias in patients with AML undergoing treatment.

5. Acknowledgements

This work is supported by European Research Council (MOBILE, ERC Advanced Grant, No: 226462) and the CPSE Industrial Consortium.

References

Afenya, E.K., 2001. *Mathematical biosciences*, 172(1), 15-32.
Dedrick, et.al., 1972. *Biochemical Pharmacology*, 21, 1-16.
Dua, P. et. al., 2005.. *Computers & Chemical Engineering*, 29(11-12), 2290-2296.
Dua, P., et. al., 2008. *Computers & Chemical Engineering*, 32(1-2), 99-107.
Fister, K.R. et. al.,2000. SIAM J. Appl. Math. (60), 1059-1072.
gPROMS, 2003, Process Systems Enterprise Limited, London, U.K
Huffman, D. H., et. al., 1972. Blood, 39, 637-643.
Kufe, D. W., et al., 2006. *Cancer Medicine*. 7th ed. London: BC Decker Inc.
Loveless, H.,et. al., 1978. *Cancer Research*, 38, 593-598.
Pefani, E. et. al., 2011. *Proceedings ESCAPE 2)*, Halkidi, Greece, 2011.
Preisler, H. D., et. al., 1995. *Leukemia Research,* 19 (10), 693-698.
Quartino,A., et. al., 2007. *Journal of clinical pharmacology*, 47, 1014-1021.
Sherer, E. et al., 2006. *Journal of theoretical biology*, 240(4), 648-61.
Wilkoff, L.J., et. al., 1967. *Cancer Chemotherapy Rept*., 51, 423-429.
Williams, W.J. et. al., 1983. *Hematology.* 3rd ed. USA: McGraw-Hill.

I.A. Karimi and Rajagopalan Srinivasan (Editors), Proceedings of the 11th International Symposium on Process Systems Engineering, 15-19 July 2012, Singapore.

A Control Engineering Perspective of Calcium Homeostasis

Christopher R. Christie[a], Luke E.K. Achenie[a], Babatunde A. Ogunnaike[b]

[a] *Department of Chemical Engineering Virginia Polytechnic Institute & State University, Blacksburg, VA 24060*

b Department of Chemical Engineering, University of Delaware, Newark, Delaware 19716

Abstract

Achieving calcium homeostasis in the human body, whereby extracellular fluid calcium is maintained within a narrow range (2.4±0.25mM) necessary for normal physiological function, is the task of a biological control system that is still not completely understood. Although general information is available on several of the component processes involved in calcium homeostasis, there is currently no mechanistic understanding of the emergent characteristics of the entire system. To this end, we present an engineering control framework for understanding calcium homeostasis, which is predicated on a configuration of the physiological system in terms of appropriately connected control system components (sensor, controller and actuator). Using information from the literature, we develop mathematical models for each component and integrate them into a holistic, comprehensive dynamic model of the complete system. The framework enables a more systematic study of observable physiological responses such as hypo- and hypercalcemia; it also allows us to interpret pathologies in terms of control system component defects.

Keywords: Calcium homeostasis, mathematical model, calcium control system, parathyroid hormone, Ca-PTH,

1. Introduction

Calcium (Ca) homeostasis is a condition in which, in spite of varying physiological conditions (e.g., lactation, excess or inadequate Ca intake or excretion), the calcium concentration in the human extracellular fluid (ECF) is maintained within a narrow range of 2.45 ± 0.25mM (Parfitt, 1993). This is achieved by a sophisticated biological control system.

Under normal conditions, low Ca levels stimulate the secretion of parathyroid hormone (PTH) from the parathyroid gland (PTG). Subsequently PTH stimulates the production of calcitriol (CTL) from the kidneys, increases renal Ca reabsorption and, stimulates bone cell proliferation, leading to a net bone Ca release. High CTL levels stimulate increased intestinal Ca absorption, inhibit PTH secretion through lowering the PTG capacity, and promote bone cell proliferation. Conversely, high Ca levels cause reduced PTH secretion, increased renal Ca excretion and, net bone formation (Parfitt, 1993).

In this paper, we present a control engineering perspective of plasma Ca homeostasis. The approach provides an efficient structure for organizing the complex and detailed microenvironment information about Ca regulation and the various physiological sub-processes involved. First, we represent the regulatory organs and associated processes involved in Ca homeostasis as a control system comprising sensor (PTG), controller (PTG) and actuators (kidneys, bone and intestines). Here the process is the ECF Ca. Next we develop mathematical models for each of the control system components. Finally, we simulate clinically induced conditions in order to provide quantitative insight into (a) how ECF Ca is regulated within this narrow range, and (b) the meaning of control system component defects in the physiological context.

2. Model Development

Standard conservation of mass principles applied to each component sub-process, lead to mathematical models that represent the dynamic behavior of PTH, CTL, bone cell proliferation, ECF Ca and phosphate. The models are in the form of a system of nonlinear ordinary differential equations. We assume that all hormones and ions are uniformly distributed in the ECF; also their concentrations are similar to those in the plasma. Unless otherwise stated, the following holds: 1) the rate of secretion, production or proliferation and any hormone/ion dependencies are described by the four-parameter logistic function H_{ij} (i is the ion/hormone in the j[th] compartment); 2) in H_{ij}, estimates for the mid-point for half-maximal secretion (S_{ij}) were solved at initial conditions; 3) the literature model refers to that from Peterson and Riggs (2010); 4) Ca refers to ionized Ca; 5) phosphate transfer rates for renal excretion (ν_{23}), intestinal absorption(ν_{24}), bone (ν_{25}) and intracellular (ν_{28}) flux are as described in the literature model; and, 6) parameter were estimated and ODE solved using Simulink in MATLAB.

A detailed description of Ca homeostasis framework as a closed-loop control system with feedback follows. The relevant equations and parameters are listed in Tables 1 and 2.

Sensor/Controller: PTG – For the sensor, direct proportionality is assumed between the detected Ca (u_{12}) and the ECF Ca (x_{11}). In the controller, PTH (u_{31})

Table 1. Model Equations

Process :

$$dx_{11}/dt = \lambda_{11}(\nu_{15} + \nu_{14} - \nu_{13}) \pm \nu_{17}$$

$$dx_{21}/dt = \nu_{25} + \nu_{24} - \nu_{28} - \nu_{23}$$

Sensor :

$$u_{12} = \lambda_{12} x_{11}$$

Controller :

$$du_{31}/dt = H_{12} u_{56} - k_{31} u_{31}$$

$$du_{56}/dt = \frac{1}{u_{56,0}} \begin{cases} (1-u_{56})\left[\lambda_{56} T_{41}^{-} + (1-\lambda_{56})\right] \\ -u_{56}\left[\lambda_{56} T_{41}^{+} + (1-\lambda_{56})\right] \end{cases}$$

$$T_{41}^{\pm} = 1 \pm \tanh\left[\lambda_{41}\left(u_{41} - u_{41,0}\right)\right]$$

$$H_{ij} = \left(A_{ij} - B_{ij}\right) / \left[1 + \left(z_{ij} / S_{ij}\right)^{m_{ij}}\right] + B_{ij} \; ; \; z_{ij} = \begin{bmatrix} x_{ij} \\ u_{ij} \end{bmatrix}$$

Actuator :

$$du_{41}/dt = H_{31a} H_{21} - k_{41} u_{41}$$

$$\nu_{13} = \lambda_{13} \begin{cases} x_{11}(0.1 - 0.09 H_{31b}), x_{11} \le x_{11T} \\ (\sigma_{13} x_{11} + \beta_{13}), \qquad x_{11} > x_{11T} \end{cases}$$

$$\nu_{23} = \lambda_{23} x_{21}$$

$$\nu_{14} = \Pi_{14} \sigma_{14}\left(\mathrm{H}_{41} + \lambda_{14}\right)$$

$$\nu_{24} = \Pi_{24} \sigma_{24}$$

$$\nu_{15} = \sigma_{15} \begin{cases} \left(1-\lambda_{15}\right) + \lambda_{15}\left[H_{75}\left(u_{85}/u_{75}\right)^{\gamma_{15}}\right] - \\ \left(\frac{x_{11}}{\bar{x}_{11}}\right)\left[\left(1-\lambda_{15}\right) + \lambda_{15}\left(\frac{u_{65}}{\bar{u}_{65}}\right)\right] \end{cases}$$

$$\nu_{25} = \lambda_{25} \nu_{15}$$

$$du_{28}/dt = \nu_{28} = \lambda_{28} x_{21} - k_{28} u_{28}$$

Table 2. Model parameters and initial conditions

	Value	Units		Value	Units		Value	Units		Value	Units
λ_{11}	1.00E+0	$mmol^{-1}$	σ_{14}		-	B_{12}	6.19E+3	pmol/h	A_{31b}	1.05E+0	-
λ_{12}	1.00E+0	-	σ_{15}	9.38E-2	mmol/h	mA_{12}	-5.0E+1	-	B_{31b}	0.00E+0	-
λ_{13}	4.29E-1	h^{-1}	σ_{24}	7.00E+1	-	mB_{12}	-2.5E+2	-	m_{31b}	-6.5E+0	-
λ_{14}	1.50E-1	-	β_{13}	-5.7E+0	mmol	mm_{12}	-1.5E+2	-	S_{31b}	5.19E+1	pmol
λ_{15}	1.50E-1	-	Π_{14}	9.76E-1	mmol/h	mS_{12}	1.8E+1	mmol	A_{41}	4.15E+1	-
λ_{23}	2.38E-2	h^{-1}	Π_{24}	1.80E+0	mmol/h	A_{21}	1.03E+0	-	B_{41}	0.00E+1	-
λ_{25}	4.64E-1	-	x_{11T}	3.11E+1	mmol	B_{21}	4.18E-1	-	m_{41}	-8.4E+0	-
λ_{28}	5.18E+1	h^{-1}	$x_{11,0}$	1.72E+1	mmol	m_{21}	1.24E+1	-	S_{41}	1.31E+3	pmol
λ_{41}	2.14E-3	-	$x_{21,0}$	1.68E+1	mmol	S_{21}	1.86E+1	mmol	A_{75}	1.27E+0	-
λ_{56}	8.50E-1	-	$u_{28,0}$	4.52E+4	mmol	A_{31a}	3.23E+0	pmol/h	B_{75}	9.95E-1	-
k_{28}	1.93E-2	h^{-1}	$u_{31,0}$	5.53E+1	pmol	B_{31a}	1.00E+0	pmol/h	m_{75}	-1.2E+0	-
k_{31}	3.20E+1	h^{-1}	$u_{41,0}$	1.26E+3	pmol	m_{31a}	-2.0E+1	-	S_{75}	9.62E-1	-
k_{41}	8.66E-2	h^{-1}	$u_{56,0}$	5.00E-1	-	S_{31a}	9.82E+1	pmol			
σ_{13}	3.15E-1	-	A_{12}	3.98E+2	pmol/h						

production/secretion is dependent on the sensor output (u_{12}) and CTL-stimulated PTG capacity (u_{56}). Their expressions are from the literature. The logistic function (H_{12}) for the Ca-induced secretion is modified to ensure appropriate responses to both hypo- and hypercalcemia and is addressed in the discussion. Finally, PTH decays at a rate of k_{31}.

Actuator: Kidneys (CTL production) – CTL (u_{41}) production is tightly regulated by PTH, the CTL decay rate (k_{41}) and ECF phosphate levels (x_{21}). Parameters for PTH-dependent rate (H_{31a}) and the phosphate-dependent rate (H_{21}) were determined from data by Horwitz et al. (2005).

Actuator: Kidneys (Ca Reabsorption) – A piecewise continuous function (v_{13}) is defined for Ca excretion. Above the Ca threshold, a Ca-dependent linear relationship holds. Below the threshold, Ca reabsorption is distributed between PTH-dependent (H_{31b}) and passive amounts. The Ca threshold is the Ca level at which the PTH dependent excretion is maximum and equal to the linear excretion.

Actuator: Intestines (Ca absorption) –Intestinal Ca absorption (v_{14}) depends on daily Ca intake (Π_{14}) and occurs via both a passive (λ_{14}) and an active (H_{41}) pathway.

Actuator: Bone Formation and Resorption – The bone cell and growth factor proliferation models for osteoblasts (u_{65}), osteoclasts (u_{75}) and RANKL (u_{85}) are unaltered from Lemaire et al., (2004) and the Ca flux from bone (v_{15}) is described by the literature model. Finally, the stoichiometric ratio (λ_{25}) of phosphate to Ca in hydroxyapatite is used to determine the phosphate flux (v_{25}) between ECF and bone.

Process: ECF Ca and phosphate - are determined from the net ion transfer rates from the kidneys, intestines, bone and any disturbance (v_{17}).

3. Results and Discussion

Although we generated more simulation data (e.g. CTL, bone Ca and intestinal Ca) from our model than is published in the literature, due to space limitations, the results presented here focus on comparisons with available Ca-PTH data. Also, for ease of comparison, our results are presented as ratios relative to baseline.

From our proposed framework, we are able to replicate clinical interventions of hypo- and hypercalcemia Fig. 1 [Ca (Sim) and PTH (Sim)]. The infusion protocols, which are the disturbances in our system, are similar to those described for the trials.

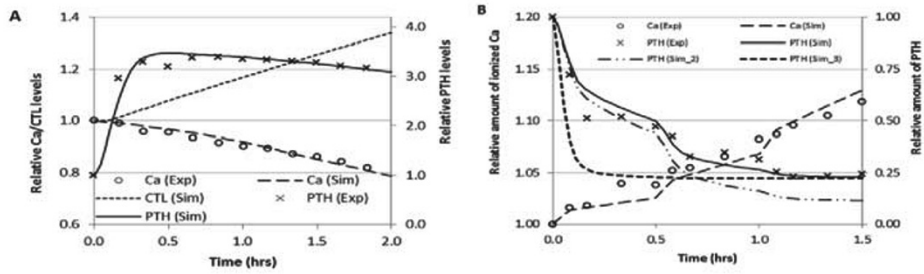

Fig. 1. Simulation of (A) hypocalcemia (Ramirez et al, 1993) and (B) hypercalcemia (Haden et al; 2000)

We estimated the parameters for H_{12} by fitting the model to data for induced hypocalcemia as shown in Fig. 1A. Using these parameters, we simulated hypercalcemia; however, we noticed that the PTH had a faster response and reached steady-state much sooner than the clinical data, [PTH (Sim_3)] in Fig. 1B.

These observations are consistent with those in Shrestha et al. (2010). Although their model was not a fully integrated Ca homeostatic model, they noted that model parameter estimates developed from hypocalcemia data could not predict hypercalcemic PTH response. This phenomenon has also been observed in clinical studies and can be attributed to hysteresis in the PTH response between hypo- and hyper-calcemia (Diaz et al., 2010). To account for this, we modeled H_{12} as an asymmetric logistic function, where the constant exponent was replaced by a Ca-dependent logistic function. This modification significantly improved the PTH response [PTH (Sim)].

We also observed that the minimal and maximal PTH secretory rates (A_{12} andB_{12}) were sensitive to different datasets. PTH (Sim_2) in Fig. 1B shows the result when the minimal secretory rate from one dataset is used to simulate another. Here, the final PTH level for PTH (Sim_2) is 50% lower than PTH (Sim) and the experimental data.

These findings are comparable to clinical observations, which suggest that there are in-group variations in Ca-PTH dynamics. Haden et al. (2000) found that ageing was associated with an increase in PTH secretory response to Ca changes. They also showed that, there were wide variations in the maximal and minimal PTH levels within the same age and ethnic groups. In the data used for comparisons, the subjects were young white men aged 26.6 ± 1.3yrs (Haden et al., 2000) and, a mix of young men and women aged 21 ± 2yrs of unreported ethnicities (Ramirez et al., 1993).

The utility in the proposed framework lies in the insight it provides with changes to control system components. To test this hypothesis, we introduced a gradual decrease in sensor gain (λ_{12}) (from 1 to 0.9) over a one-month period, and then held it steady for an additional 11 months. In Fig. 2, there is a gradual increase in the Ca level, up to a maximum of 1.1 above baseline. Likewise, the PTH level reaches a maximum of 1.1; however, this is attained over the 1-yr period rather than one month for Ca increase. As the excreted Ca is partly PTH-dependent, there is a concurrent gradual but significant 25% reduction in renal Ca with increase in PTH.

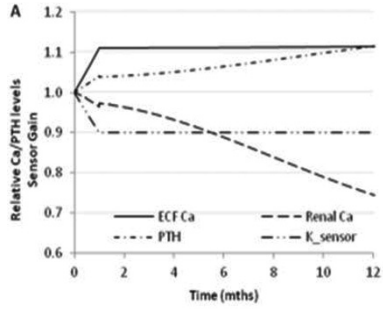

Fig. 2. Ca homeostatic response to sensor gain reduction

Again, these outcomes are in accordance with pathological cases. Familial hypocalciuric hypercalcemia (FHH), an inherited genetic condition, is characterized by mild hypercalcemia, normal-to-slightly elevated PTH levels and low urinary Ca excretion. More than two-thirds of families with FHH have inactivating mutations in the Ca-sensing receptor (CaR) gene, which result in varied levels of receptor inactivation (Yano and Brown, 2005). Therefore, this reduction in sensor gain mimics the behavior of a form of genetic mutation of the CaR.

4. Conclusions

This paper focuses on an engineering control system framework proposed for understanding Ca homeostasis that is based on developing/assembling appropriate computational models for each of the control system components. We have shown that we can simulate clinically induced hypo- and hypercalcemia with our model and account for hysteresis in the Ca-PTH secretory response. Furthermore the results show that variations in in-group demographics affect Ca-PTH response. Finally the results indicate that a gradual reduction in sensor gain is consistent with a type of genetic mutation in the CaR, which causes FHH.

References

R. Diaz, G.E. Fuleihan, EM. Brown, 2010, Parathyroid Hormone and polyhormones: Production and Export, Comprehensive Physiology, 607-62

ST Haden, EM Brown, S Hurwitz, J Scott and GE Fuleihan, 2000, The effects of age and gender on parathyroid hormone dynamics, Clinical Endocrinology, Vol 52, 329-38

MJ Horwitz, MB Tedesco, SM Sereika, MA Syed, A Garcia-Ocaa, A Bisello, BW Hollis, CJ Rosen, JJ Wysolmerski, P Dann, C Gundberg, AF Stewart, 2005, Continuous PTH and PTHrP Infusion Causes Suppression of Bone Formation and Discordant Effects on 1,25(OH)2Vitamin D, Journal of Bone and Mineral Research, Vol 20, 1792-1803

V Lemaire, FL Tobin, LD Greller, CR Cho, LJ Suva, 2004, Modeling the interactions between osteoblast and osteoclast activities in bone remodeling. J Theor Biol Vol 229, 293–309.

AM Parfitt, 1993 Calcium homeostasis, Physiology and pharmacology of bone, Vol 107,1–66

MC Peterson, MM Riggs, 2010, A physiologically based mathematical model of integrated calcium homeostasis and bone remodeling, Bone, Vol 46, 49-63

JA Ramirez, WG Goodman, J Gornbein et al., 1993, Direct in vivo comparison of calcium-regulated parathyroid hormone secretion in normal volunteers and patients with secondary hyperparathyroidism, J Clin Endocrinol Metab, Vol 76, 1489 –1494

RP Shrestha, CV Hollot, SR Chipkin, CP Schmitt, Y Chait, 2010, A mathematical model of parathyroid hormone response to acute changes in plasma ionized calcium concentration in humans, Mathematical Biosciences, Vol 226, 46-57

S Yano,EM Brown, 2005, The Calcium Sensing Receptor, Molecular Biology of the Parathyroid, Ed. 1, 44-56

I.A. Karimi and Rajagopalan Srinivasan (Editors), Proceedings of the 11th International Symposium on Process Systems Engineering, 15-19 July 2012, Singapore.

Hemodynamics of cerebral micro vasculature

Ian Gopal Gould, Thomas Marinnan, Maurice Chojecki, Masood Qader, Brian Henry, Mohammed Pervais, Nicholas Vaičaitis, Yiyi Zhu[b], Aaron Rogers[b] and Andreas Linninger

University of Illinois at Chicago, LPPD, 601 S Morgan St, Chicago, 60607, USA
[b]NSF REU fellows

Abstract

In this paper we present a novel technique for 3D micro capillary bed model reconstruction and computational fluid-dynamics (CFD) calculation to simulate morphological and blood perfusion parameters. Major arterial and venous cerebral blood vessels were reconstructed from scanning electron microscope (SEM) images and vessels whose diameters are beyond the resolution of modern imaging techniques were grown from this base structure using our novel directed interactive growth algorithm (DIGA). 3D voronoi networks were used to represent the microvasculature capillary network that joins arterial vessels to adjacent draining veins. The resulting network is morphologically accurate to *in vivo* measurements of the functional unit with accurate measurements of vessel density (3.17%) and surface area to tissue volume ratio (5.84%). Perfusion patterns of supply to the functional unit and systemic pressure drops match those expected in living tissue and indicate the model is a good candidate for exploring the hemodynamic phenomenon of autoregulation.

Keywords: micro vascular, functional blood unit, hemodynamics, cerebral vasculature

1. Introduction

Many questions regarding cerebral hemodynamics and control of cerebral blood flow remain unanswered due to the complex architecture of the cerebral vascular network. Clusters of a single draining vein surrounded by a ring of three to six arterioles were discovered to provide the blood supply to the cortex [1]. The separate independents units appear to form a functional blood unit (FBU) serving a critical physiological role in the micro vascular network of the human brain by facilitating the efficient distribution of oxygen and nutrients to their associated clusters of neurons of the cerebral cortex. Each FBU consists of single central draining vein with a diameter of 80μm to 120μm. The ring arterioles are approximately 40μm in diameter [2-3]. To better understand the ability of the brain to maintain adequate blood perfusion over a wide range of blood pressures - a phenomenon known as autoregulation - many researchers have suggested detailed fluid dynamics analyses of the micro vascular flows. However, most studies have been performed on one or two dimensional models that did not preserve the morphologic and spatial dimensions of the FBU. To accurately describe the blood flow patterns in the capillary microcirculation in the brain, a three-dimensional representation of the FBU is necessary. In this paper presents for the first time a complete three-dimensional model of a FBU in the human cortex. We will illustrate how we constructed with computer algorithms a network of micro vessels matching the morphology of the FBU (Figure 1). We also demonstrate computational results of blood flow patterns, which are a strong function of the network architecture.

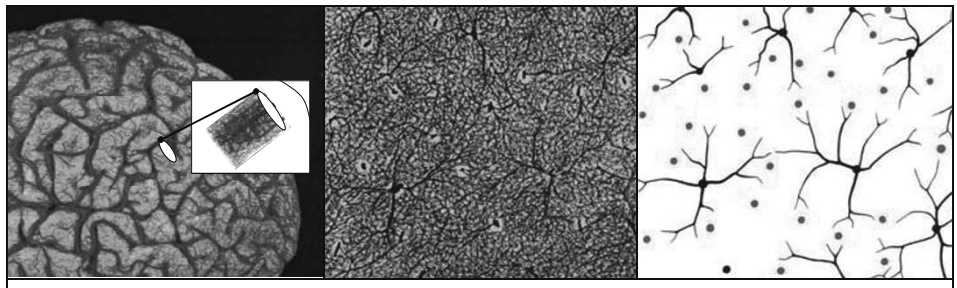

Figure 1 Morphological context of FBU. From left to right; the position of the FBU in the entire brain, SEM of micro vessel structure of the cortical surface of the brain[1], medical illustration of pattern of a draining veins surrounded by feeding ring arterioles[1].

2. Methods

We first generated a three-dimensional network representing the morphology of the FBU. The momentum equations were solved to compute pressure and flow field throughout the network. The transition times of a tracer injected into the ring arterioles were computed. The computed transition times match well with clinical values. The network construction and the computations are presented here for the first time.

2.1. Vascular network generation

Since cerebral micro blood vessels are smaller than the resolution provided by the most powerful angiography imaging techniques, the micro vascular network geometry must be generated artificially. Analysis of SEM images of cortical capillary micro vessel bed yielded the dimensions of the functional unit and the vessel diameter of the central draining vein and three ring arterioles that supply the functional unit. The draining vein and ring arterioles penetrate the cortex surface at a normal angle, then proceed to bifurcate as they enter deeper into the cerebral cortex. Artificial networks composed of cylindrical segments were generated to emulate the micro vessel structure with physiologically accurate morphometric parameters. Initially, a cylindrical domain was constructed using commercial mesh generation software (MIMICS); the surface mesh was created via the marching cubes algorithm, where an iso-surface is detailed by the voxels that enclose the domain. The volume mesh serves as a reference frame for the generation of the bifurcating trees networks of the arterial and venous systems. Large vessel backbone segments (above 50μm) were obtained manually from SEM micrographs [4]. Binary acyclic trees were generated using the novel DIGA developed by our group, which uses elements from a constrained constructive optimization perfusion algorithm used previously for synthesis of coronary arteries [5]. DIGA spawns multiple vessels within a user selected domain from a reconstructed backbone. An acyclic binary graph composed of cylindrical elements is then created by adding the segment in such a way that the total network volume – the lumen of the blood it would contain – is minimum. The addition of each new segment was the computed as the solution of a repeated global minimization problem for the entire tree volume. At each step, the volume of the network is minimized and solved as a constrained optimization problem which solves for the bifurcation coordinate (Eq. 1).

$$\underset{\vec{x},\, r_i,\, l_i}{Min}\ V = \sum_{i=1}^{N} \pi r_i^2 \cdot l_i(\vec{x}) \qquad \text{Eq. 1}$$

$$\text{s.t. } \Delta P = \alpha_i F_i \quad \forall \text{arcs on Network}$$

The relation between the diameters of parent and daughter segments obeys Murray's Law[7]. The microvasculature is not a tree and mesh-like structures were generated in a

morphologically consistent manner. Mesh-like structures were based Voronoi meshes with a vessel density of about 10542 segments per mm^3 [Table 1]. These setting achieved capillary lengths, diameters and vessel density consistent with SEM micrographs of the FBU [2]. The resulting network was constructed at physiological scale, and contained 12,292 vessels.

2.2. Hemodynamic simulations of the FBU

Network simulations were carried to solve the mass and simplified momentum balances. For each vessel, pressure and flow were computed as functions of length *L*, diameter *d* and viscosity μ by the Hagen-Poiseuille equation (Eq. 3).

$$\nabla u = 0 \qquad \text{Eq. 2}$$

$$\Delta P = \alpha u A \qquad \text{where } \alpha = \frac{128\mu L}{\pi d^4} \qquad \text{Eq. 3}$$

Where u is the average velocity through and ΔP is the pressure drop, A is the cross sectional area and α is the resistance.

2.3. Dye Infusion

To assess the validity of the model in comparison to clinical values, we dynamically simulated the infusion of dye into ring arterioles. For the network and each segment we computed the dye washout times, know in medical literature as the transient times through the functional blood unit. The dye transport was modelled by the dynamic species balance of *C* with convection as in Eq. 4 in which diffusion was neglected.

$$V\frac{dC}{dt} = u\nabla C \qquad \text{Eq. 4}$$

In this equation, *C* is the species being transported and *V* is the volume of the conservation envelope.

3. Results

3.1. Network morphology

By following the morphological patterns as described extensively in medical literature, DIGA was employed to generate a physiologically accurate function blood unit model whose morphological parameters (Table 1) agree reasonably with the characterization presented in literature[1-2, 4, 8]. Flow patterns were calculated as a function of cortical depth of the supply of arterial blood as it enters the micro vessel capillary bed. The model predicted a distribution of oxygenated blood to the neuronal capillaries that is consistent with medical understanding of grey matter organization, in which the internal granular layer, at 60% cortical depth [2] is the location of the highest activity neurons with the highest metabolic requirement (Figure 2).

	Model Parameters	Clinical Parameters
Volume Density	5.40%	3.02% [2]
Vessel Count/ Tissue Volume	10887.6/mm^3	10542.02/mm^3 [2]
Vessel Surface Area/ Tissue Volume	13.60 mm^2/mm^3	12.85 mm^2/mm^3 [2]
Mean Capillary Length	56.16 μm	52.95 μm [8]
Mean Capillary Diameter	6 μm	6.47 μm [1]
Diameter of Functional unit	0.71 mm	0.5 - 2 mm[1]
Depth of Functional unit	3.3 mm	2 – 4 mm [4]

Table 1 Morphological comparison between model and literature values.

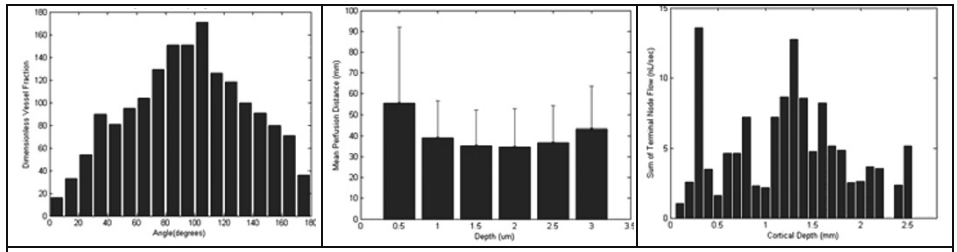

Figure 2 Functional blood unit morphological characterization. From left to right, Angle spectrum of vessels, mean perfusion distance as a function of cortical depth, and terminal node count as a function of cortical depth.

3.2. Results of Hemodynamic simulations

Fluid flow throughout the system was conserved in the arterial graph and decreased monotonically before reaching the capillary bed, than increased steadily until the venous outlet. Vessel pressure decreased monotonically from inlet to outlet (Figure 3). Simultaneous pulse injections of a dye into the three ring arterioles was computed dynamically and concentration trajectories for each vessel were recorded at each time point (Figure 4). The sharp inlet pulse of dye into three inlet arteries is attenuated as it traverses the capillary micro vessels, and the signal is much wider as it leaves the draining vein.

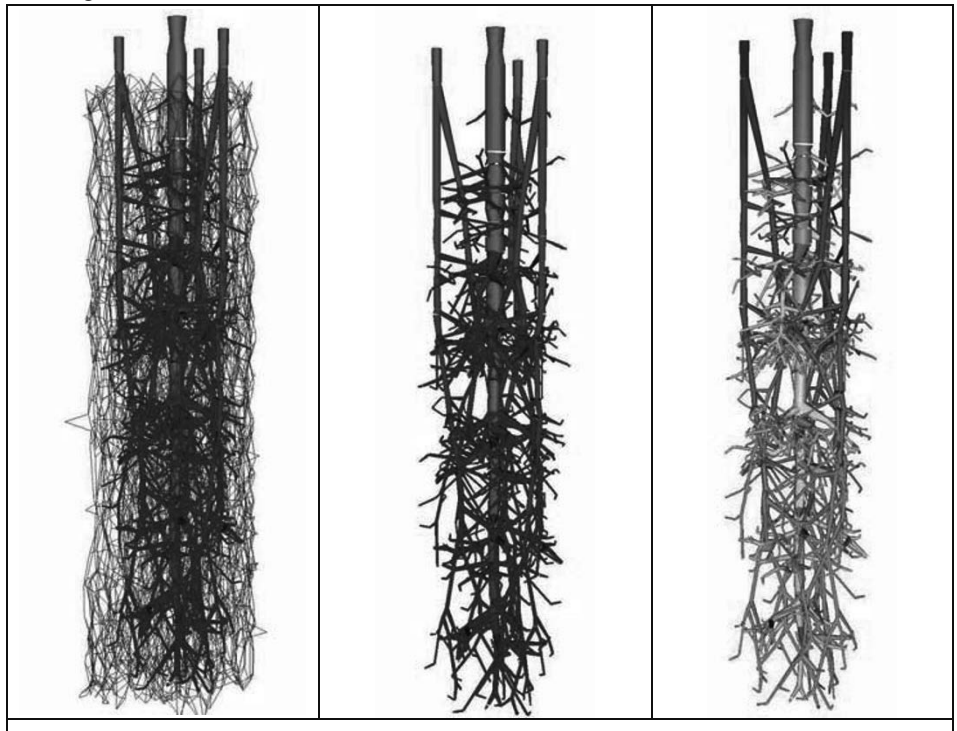

Figure 3 Hemodynamic simulation of the FBU in the human cortex. From left to right; structure of the entire functional blood unit with flow values mapped from 20 uL/sec (red) to 1 fL/sec (blue), flow through network with only large vessels shown, pressure map network rendered from 45 mmHg (blue) to 25 mmHg (red) with only large vessels shown.

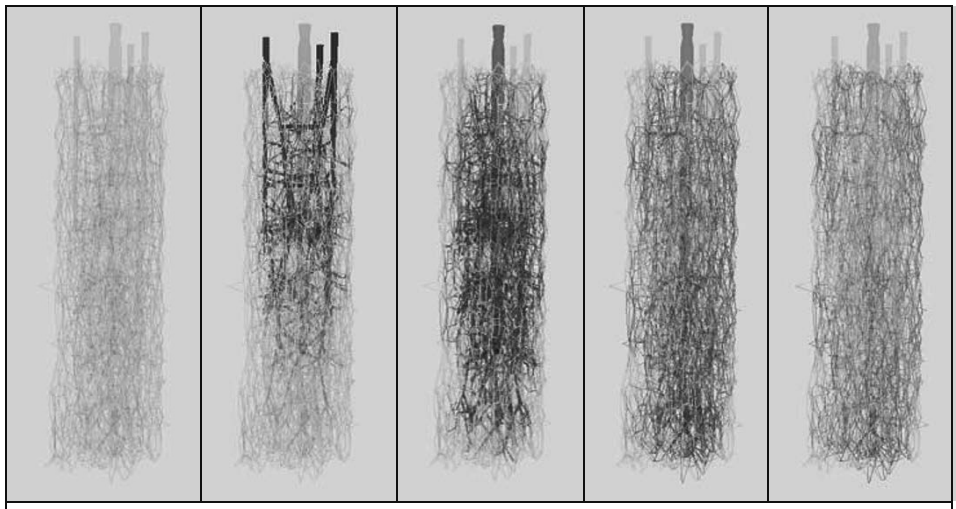

Figure 4 Dynamic dye dilution from feeding ring arterial to draining vein. Time dependent renderings of concentration profiles in the functional blood unit, from left to right. Inlet pulse of dye into three inlet arteries is flattened as it traverses the capillary micro vessels, resulting in a wider signal as the dye leaves the draining vein.

4. Discussion and Conclusions

Morphological comparisons between the functional unit and the model constructed by DIGA show favourable results in the vessel density of the model, vessel surface area to tissue volume ratios and volume density. This paper has presented an analysis of a automatically generated functional blood unit which provides insight into the morphologic and hemodynamic properties of a micro vascular network in the human cerebral cortex. Implementation of DIGA imbues the network with micro vessel architecture beyond the scope of modern reconstruction techniques and gives a fluid transition from arterioles to capillaries to veins. Future applications of this model include the effects of pulsatile flow on hematocrit distribution through a micro vessel network, investigating the biochemical transport of oxygen or the implementation of autoregulation as a response to ischemic biochemical signalling pathways.

References

1. Duvernoy, H.M., S. Delon, and J.L. Vannson, *Cortical blood vessels of the human brain.* Brain Res Bull, 1981. **7**(5): p. 519-79.
2. Lauwers, F., et al., *Morphometry of the human cerebral cortex microcirculation: general characteristics and space-related profiles.* NeuroImage, 2008. **39**(3): p. 936-48.
3. Canaud, B., et al., *Whole-blood viscosity increases significantly in small arteries and capillaries in hemodiafiltration.* Hemodial Int, 2010. **14**(4): p. 433-40.
4. Duvernoy, H., S. Delon, and J.L. Vannson, *The Vascularization of the Cerebellar Cortex.* Brain Res Bull, 1983. **11**(419-480).
5. Schreiner, W., et al., *Structural quantification and bifurcation symmetry in arterial tree models generated by constrained constructive optimization.* J Theor Biol, 1996. **180**(2): p. 161-74.
7. Murray, C.D., *The Physiological Principle of Minimum Work: I. The Vascular System and the Cost of Blood Volume.* Proc Natl Acad Sci U S A, 1926. **12**(3): p. 207-14.
8. Safaeian, N., M. Sellier, and T. David, *A computational model of hemodynamic parameters in cortical capillary networks.* J Theor Biol, 2010. **[Epub ahead of print]**.

I.A. Karimi and Rajagopalan Srinivasan (Editors), Proceedings of the 11th International Symposium on Process Systems Engineering, 15-19 July 2012, Singapore.

Medical Image-based Systematic Design of Human Gene Silencing Therapies

Ying Hsu,[a] Ashty Karim,[a] Andreas Linninger[a]

[a]*Laboratory for Product and Process Design,851 S Morgan St, Chicago, IL 60607, USA*

Abstract

Gene silencing therapies have succeeded in controlling expression levels of a desired gene in animal models. By infusing short-interfering RNAs (siRNA), these molecules target particular messenger RNA (mRNA) in the cells through sequence-specific binding, suppressing the translation for the target protein. These therapies hold great promise for treating numerous disorders of the central nervous system (CNS) including novel approaches to chronic pain management. While novel siRNA targets are being discovered rapidly, difficulties in siRNA delivery such as anatomical accessibility of the target tissue, slow diffusion and non-specific uptake make achieving a precise degree of protein downregulation nearly impossible. We propose to design optimal infusions integrating medical imaging with systems engineering principles. A novel pain management therapy is designed to suppress the expression of pain-transducing NMDA receptors in the subject's spinal cord. The coupling of biotransport equations with intracellular siRNA kinetics enables the design of siRNA gene silencing therapies. The accurate prediction of dose-response and the computation of optimal infusions are expected to accelerate clinical implementations of gene silencing therapies.

Keywords: RNA interference, medical imaging, patient-specific medicine, siRNA.

1. Introduction

Gene silencing therapies are the next generation of treatments for CNS disorders. siRNA molecules bind and destruct target mRNA in the cell, changing the expression levels of the target protein at the cellular level. This promising technique induced down-regulation of NMDA receptor subunit NR2B in the spinal cord of rats, temporarily inhibiting pain transmission.[1] The NMDA receptor mediates sensitized pain in chronic pain subjects. A design method is proposed in this article to precisely control the expression of disease-related proteins in the human CNS. High resolution medical imaging can capture fine anatomical details. The integration of medical reconstruction with mathematical models may provide quantitative answers to issues that currently delay the clinical implementation of human gene silencing therapies.

The infusion of therapeutics into the human CNS is particularly challenging due to the blood brain barrier, which prevents macromolecules from leaving the cerebrovasculature. To reach the brain or spinal cord tissue effectively, therapeutics can be instead infused into the cerebrospinal fluid (CSF), which surrounds the entire CNS. After infusion, the biodistribution and reactions of these therapeutic molecules are unknown. What is the distribution of these molecules along the spine? What percentage of the infused molecules reached the target? Can we quantify the biochemical interaction of siRNA with the tissue, such as binding, internalization, or enzymatic activation of other intracellular proteins? We provide quantitative answers to these open questions using medical image-based computational fluid dynamics, termed miCFD.

2. Methodology

2.1. Three dimensional reconstruction of the human CNS

A patient-specific model was reconstructed from magnetic resonance (MR) images of the patient's CNS through a process termed image reconstruction (Figure 1).[3] Automatic and manual segmentation were used to reconstruct the CSF, the brain and spinal cord tissues in three dimensions. This patient-specific model was converted into an unstructured computational mesh as described in Somayaji et al.[4]

2.2. Functional regions in the spinal cord

The human spinal cord is composed of the grey and white matter. Within the grey matter, our target regions are within the dorsal horns where the NMDA receptors are densely populated (Figure 1). Neurons within these target regions specialize in pain signal transduction through these receptors. Neurons outside of the dorsal horns have little or no target receptors. Therefore, siRNA molecules have no effect in neurons outside of the target regions due to the lack of NMDA receptor-encoding mRNA. The bioreactivities of siRNA molecules differ in different functional regions in the spinal cord. The application of transport and reaction equations allows the computation of infusion, biodistribution, and reactions of siRNA within different cell types.

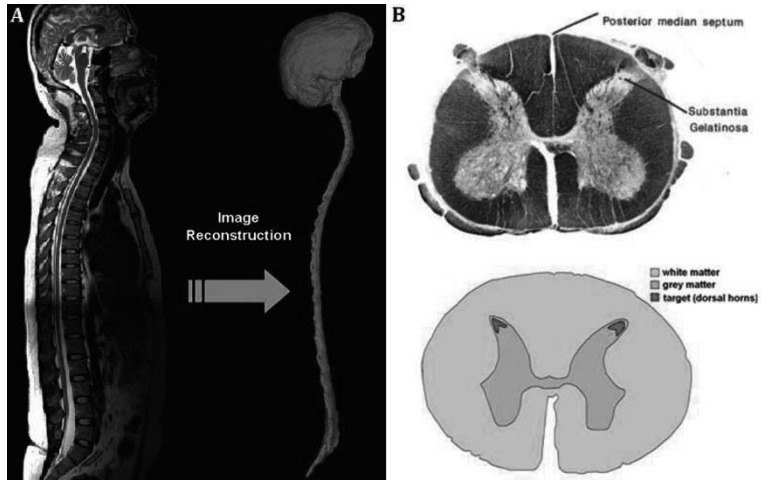

Figure 1. (A) Image reconstruction of the subject's CNS. (B) Image of the human spinal cord[2] (top frame) and the reconstructed model with different zones (bottom frame). The target zones are the dorsal horns, densely populated with NMDA receptors.

2.3. Gene silencing therapies for chronic pain

The goal of this therapy is to silence 70% of the pain-transducing NMDA receptors in the subject's spinal cord to suppress chronically heightened pain. We estimate the siRNA infusion concentration that would achieve this precise demand. NMDA receptor down-regulation in the spinal cord is computed for four different siRNA concentrations in the CSF, simulating continuous spinal infusions. The continuity (1) and species transport (2) equations compute the biotransport of siRNA.

The cells in grey and white matter of the spinal cord actively uptake siRNA molecules in the extracellular space. In untargeted cells lacking NMDA receptors and their corresponding mRNA, siRNA molecules accumulate and are merely degraded. Inside

the target cells, the activation of the gene silencing cascades is initiated by the binding of siRNA to an intracellular protein termed RNA-induced-silencing-complex (RISC). The activated siRNA binds to the NMDA receptor-encoding mRNA with high affinity and specificity. The RISC-siRNA cleaves the bound mRNA, and the translation of the receptor is suppressed for as long as an effective siRNA concentration is present in the cell. These biochemical reactions are computed for extracellular siRNA (3), intracellular siRNA (4), RISC (5), activated RISC-siRNA complex (6), bound RISC-siRNA-mRNA (7), target mRNA (8), and NMDA receptors (9).

$$\frac{\partial \rho}{\partial t} + \nabla \cdot (\rho v) = 0 \tag{1}$$

$$\frac{\partial}{\partial t}(\rho Y_i) + \nabla \cdot (\rho v Y_i) = -\nabla \cdot J_i + S_i \tag{2}$$

$$\frac{\partial \mathrm{C_{siRNAex}}}{\partial \mathrm{t}} = -\mathrm{k_1} \cdot \mathrm{C_{siRNAex}} - \mathrm{k_2} \cdot \mathrm{C_{siRNAex}} \tag{3}$$

$$\frac{\partial C_{siRNAin}}{\partial t} = +k_1 \cdot C_{siRNAex} - k_3 \cdot C_{siRNAin} \cdot C_{RISC} \tag{4}$$

$$\frac{\partial C_{RISC}}{\partial t} = \mathrm{P_{RISC}} - k_3 \cdot C_{siRNAin} \cdot C_{RISC} + k_6 \cdot C_{RISC \cdot siRNA} - k_{10} \cdot C_{RISC} \tag{5}$$

$$\frac{\partial C_{RISC \cdot siRNA}}{\partial t} = k_3 \cdot C_{siRNAin} \cdot C_{RISC} - k_4 \cdot C_{RISC \cdot siRNA} \cdot C_{mRNA} + k_5 \cdot C_{RISC \cdot siRNA \cdot mRNA} - k_6 \cdot C_{RISC \cdot siRNA} \tag{6}$$

$$\frac{\partial C_{RISC \cdot siRNA \cdot mRNA}}{\partial t} = k_4 \cdot C_{RISC \cdot siRNA} \cdot C_{mRNA} - k_5 \cdot C_{RISC \cdot siRNA \cdot mRNA} \tag{7}$$

$$\frac{\partial C_{mRNA}}{\partial t} = \mathrm{P_{mRNA}} - k_4 \cdot C_{RISC \cdot siRNA} \cdot C_{mRNA} - k_7 \cdot C_{mRNA} - k_8 \cdot C_{mRNA} \tag{8}$$

$$\frac{\partial \mathrm{C_{receptor}}}{\partial \mathrm{t}} = \mathrm{k_8} \cdot \mathrm{C_{mRNA}} - \mathrm{k_9} \cdot \mathrm{C_{receptor}} \tag{9}$$

In these equations, C is species concentration; $P_{RISC} = 5 \cdot 10^8$ is the RISC production rate, and $P_{mRNA} = 5 \cdot 10^9$ is the mRNA production rate. Reaction rate constants used were derived from experimental data by Bartlett and Davis.[5]

3. Results and Discussion

Prior to siRNA treatment, the NMDA receptors and their encoding mRNA in the target cells maintain constant levels. These steady state levels are responsible for the stable receptor expression in these cells. The number of 'cells' per cm^3 is estimated based on the extracellular volume fraction and the average cell volume. This allows us to estimate the number of molecules per cell from computed concentrations.

At steady state, there are 55,543 NMDA receptors and 900 receptor-encoding mRNA per cell. The quantities of mRNA and protein are within reported range for mammalian genes.[6] As expected, the amount of receptors per cell is much greater than its encoding

mRNA,[6] due to translational amplification. Each mRNA transcript is used for translation multiple times before its natural degradation.

After the start of a continuous siRNA infusion, the system in steady state experiences a dynamic transition. siRNA molecules diffuse into the tissue from the spinal cord surface. Cellular uptake of siRNA molecules occurs simultaneously. A small amount of siRNA molecules reach the dorsal horns and initiate gene silencing. siRNA concentration inside dorsal horn cells is several orders of magnitude smaller than the infusion concentration due to the diffusion resistance and non-specific cellular uptake.

Intracellular siRNA in a cross section of the spinal cord is shown for four hours of continuous infusion at the concentration of 10^{-6} M (top panel of Figure 2). The receptor down-regulation in the dorsal horns is shown in the bottom panel (Figure 2).

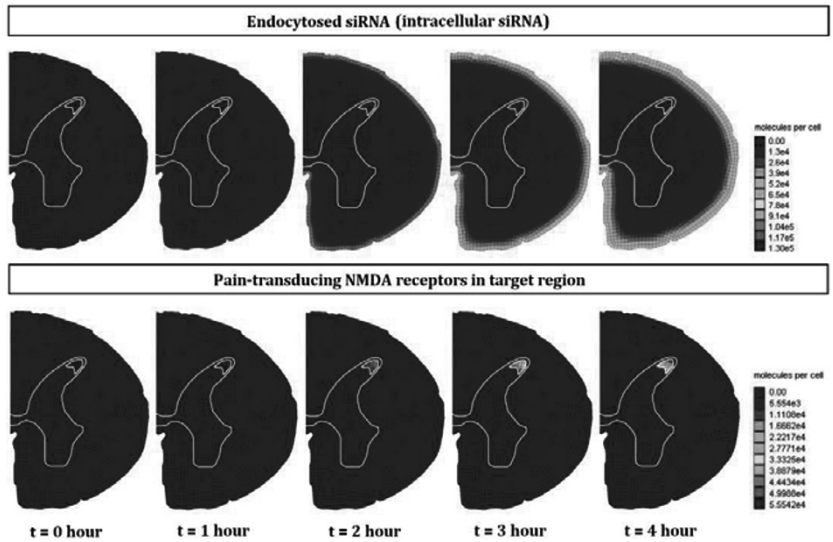

Figure 2. Intracellular siRNA (top) and NMDA receptors in the dorsal horns (bottom) in a cross section of the spinal cord over four hours of continuous siRNA infusion at 10^{-6} M. (Top panel) siRNA molecules are uptaken by cells during their diffusion. Slow diffusion and non-specific uptake of siRNA are principle barriers for effective delivery of siRNA into a targeted region in the CNS. (Bottom panel) gene silencing of pain-transducing NMDA receptors induced by intracellular siRNA molecules in the dorsal horns.

Four different infusion concentrations were compared for gene silencing efficacy using this patient-specific model. NMDA receptor down-regulation for continuous siRNA infusions into the CSF over 9 hours is shown in Figure 3. After gene silencing, the target receptors were 92.9%, 85.9% 57.6% and 29.4% of the steady state level for siRNA infusion concentrations of 10^{-7}M, $2 \cdot 10^{-7}$M, $6 \cdot 10^{-7}$M and 10^{-6}M, respectively. The therapy goal of 70% NMDA receptor suppression was met using an injectate with 10^{-6}M siRNA concentration.

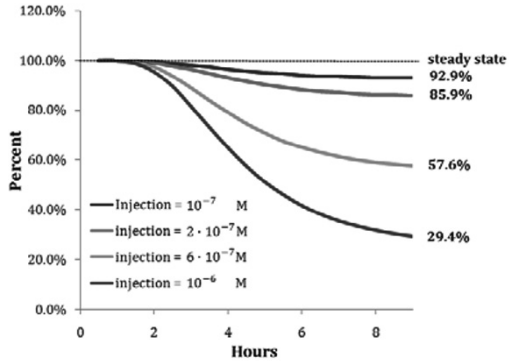

Figure 3. Pain-transducing NMDA receptor down-regulation for 9 hours of continuous siRNA infusion. The infusion concentration of 10^{-6}M induces 70.6% of receptor suppression, meeting the therapy goal. The optimal infusion concentration is determined.

4. Conclusions

Controlling the expression of disease-related genes in the CNS using gene silencing therapies is the next generation of CNS treatments. However, delivering an exact concentration of siRNA molecules to a targeted region in the CNS presents multiple challenges. CNS therapy design also poses stringent requirements. For example, a precise percent of protein down-regulation may be desired in the target region, while maintaining unaltered protein levels elsewhere. In many cases, it is not desirable to completely suppress the expression of a target gene. The use of sub-optimal infusion parameters may cause either no effect on the gene expression or the complete suppression of a gene, leading to unwanted outcomes.

The traditional trial and error animal infusion experiments do not provide quantitative answers for the optimal dosing of a human subject. This article addresses the challenge of optimal human dosing by integrating medical imaging with systems engineering principles. siRNA biochemical kinetics coupled with biotransport are fused with subject-specific anatomy to estimate drug action in vivo. The systematic design of human gene silencing therapies can generate optimal infusion parameters to precisely suppress protein expression levels as desired. Future direction includes the coupling of this patient-specific model with spatially distributed kinetic inversion technique for the determination of unknown siRNA reaction parameters.

References

1. PH Tan, LC Yang, HC Shih, KC Lan and JT Cheng, 2005, Gene Knockdown with Intrathecal Sirna of Nmda Receptor Nr2b Subunit Reduces Formalin-Induced Nociception in the Rat, Gene Therapy, 12, 1, 59-66

2. University of Oxford: Sections of Spinal Cord, http://msdlt.physiol.ox.ac.uk:8081/medlearn/1bm2t2005/Neuroanatomy/Peripheral-Nervous-System/Sections-of-Spinal-Cord-2.html,

3. Mimics Innovation Suite - Materialise, www.materialise.be/mimics/main_ENG.html,

4. MR Somayaji, M Xenos, L Zhang, M Mekarski and AA Linninger, 2008, Systematic Design of Drug Delivery Therapies, Computers & Chemical Engineering, 32, 1-2, 89-98

5. DW Bartlett and ME Davis, 2006, Insights into the Kinetics of Sirna-Mediated Gene Silencing from Live-Cell and Live-Animal Bioluminescent Imaging, Nucleic Acids Research, 34, 1, 322-33

6. B Schwanhausser, D Busse, N Li, G Dittmar, J Schuchhardt, J Wolf, W Chen and M Selbach, 2011, Global Quantification of Mammalian Gene Expression Control, Nature, 473, 7347, 337-42

Author Index